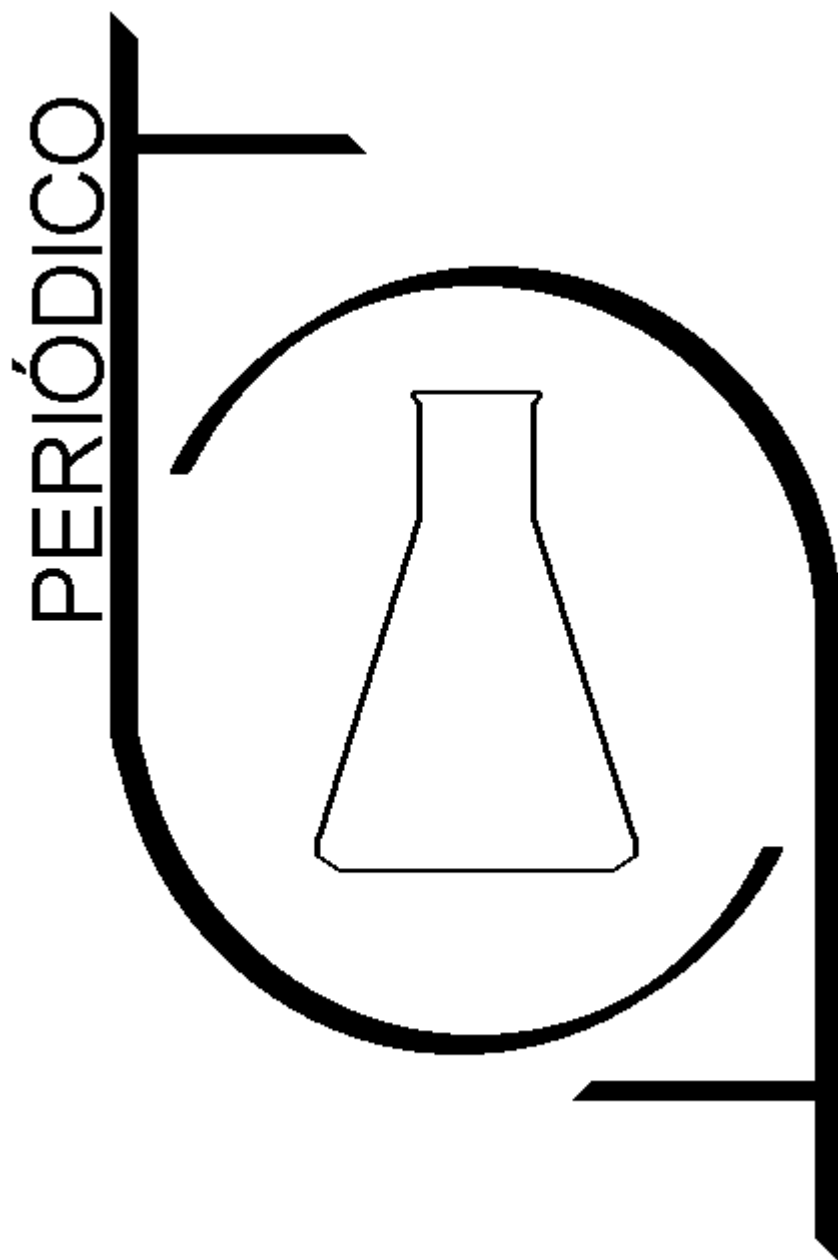


PERIÓDICO TCHÊ QUÍMICA



Volume 17

-

Número 36

-

2020 ISSN 2179-0302

Órgão de divulgação científica e informativa

www.periodico.tchequimica.com

PERIÓDICO TCHÊ QUÍMICA

ISSN - 1806-0374 (Impresso) - ISSN - 2179-0302 (Online)

Volume 17

Número 36 – 2020

ISSN 2179 - 0302

Órgão de divulgação científica e informativa.

Dados Internacionais de Catalogação na Publicação (CIP)

Periódico Tchê Química: órgão de divulgação científica e informativa [recurso eletrônico] / Grupo Tchê Química – Vol. 1, n. 1 (Jan. 2004) – Porto Alegre: Grupo Tchê Química, 2005 - Semestral.
Sistema requerido: Adobe Acrobat Reader.
Modo de acesso: World Wide Web:
<<http://www.tchequimica.com>>

Descrição baseada em: Vol. 14, n. 28 (ago. 2017).

ISSN 1806-0374

ISSN 2179-0302

1. Química. I. Grupo Tchê Química.

CDD 540

Bibliotecário Responsável

Ednei de Freitas Silveira

CRB 10/1262



Welcome to the TCHÊ QUÍMICA JOURNAL
International multidisciplinary scientific journal

*The Tchê Química Journal publishes original research papers, review articles, short communications (scientific publications), book reviews, forum articles, technical reports, articles on chemical education, interviews, announcements or letters. Articles suitable for publication in the Tchê Química Journal are those that cover the traditional fields of **Chemistry, Physics, Mathematics, Biology, Pharmacy, Medicine, Engineering and Agriculture**. We are especially interested in those submissions that are highly relevant to theoretical and applied contributions in the area of chemistry and related disciplines.*

PERIÓDICO TCHÊ QUÍMICA

Volume 17

Número 36 – 2020

ISSN 2179 - 0302

Órgão de divulgação científica e informativa.

Comissão Editorial

Editores-chefe

- Luis Alcides Brandini De Boni, Dr., labdeboni@gmail.com, Brasil, Tchê Química
- Eduardo Goldani, Dr., eduardogoldani@gmail.com, Brasil, Tchê Química.

Editores técnicos

- Ednei de Freitas Silveira
– *Bibliotecário Responsável*
- Francisco José Santos Lima, Dr., limafjs@yahoo.com, Brasil, UFRN.
- Carlos Eduardo Cardoso, Dr., prppg@universidadedevassouras.edu.br, Brasil, USS.
- Sérgio Machado Corrêa, Dr., sergiomc@uerj.br, Brasil, UERJ.

Corpo Editorial

Membros

- Teresa M. Roseiro Maria Estronca, Dr., troseiro@ci.uc.pt, Portugal, UC.
- Monica Regina da Costa Marques, Dr., mmarquesrj@gmail.com, Brasil, UERJ.
- Ketevan Kapatadze, Dr., ketevan_kapatadze@iliauni.edu, Geórgia, ISU.
- Márcio von Mühlen, Dr., marciovm@mit.edu, EUA, MIT.

- Élcio Jeronimo de Oliveira, Dr., elcioejo7@gmail.com, Suécia, Luleå Tekniska Universitet.
- José Carlos Oliveira Santos, Dr., josecos@ufcg.edu.br, Brasil, UFCG.
- Alcides Wagner Serpa Guarino, Dr., guarino@unirio.br, Brasil, UNIRIO.
- Roseli Fernandes Gennari, Dr., rgennari@dfn.if.usp.br, Brasil, USP.
- Rafael Rodrigues de Oliveira, Dr., rafa_rdo@yahoo.com.br, Brasil, Neoprospecta.
- Lívio César Cunha Nunes, Dr., liviocesar@hotmail.com, Brasil, UFPI.
- João Guilherme Casagrande Jr, Dr., jgcasajr@gmail.com, Brasil, EMBRAPA.
- Denise Alves Fungaro, Dr., dfungaro@ipen.br, Brasil, IPEN.
- Murilo Sérgio da Silva Julião, Dr., murilo-sergio@uol.com.br, Brasil, UVA.
- Amit Chaudhry, Dr., amit_chaudhry01@yahoo.com, Índia, Panjab University.
- Hugo David Chirinos Collantes, Dr., hdccoll@gmail.com, Peru, UNI.
- Carlos E. de Medeiros J., Dr., c_enrique@hotmail.com, Brasil, PETROBRAS.
- Walter José Peláez, Dr., walter.pelaez@unc.edu.ar, Argentina, UNC.
- Rodrigo Brambilla, Dr., kigobrambilla@gmail.com, Brasil, UFRGS.
- Joan Josep Solaz-Portolés, Dr., Joan.Solaz@uv.es, Espanha, UV.
- José Euzébio Simões Neto, Dr., euzebiosimoes@gmail.com, Brasil, UFRP.
- Aline Maria dos Santos Teixeira, Dr., aline.santos@ifrrj.edu.br, Brasil, UFRJ.

- Shaima R. Banoon, MsC., shimarb@uomisan.edu.iq, Iraque, Universidade de Misan.
- César Luiz da Silva Guimarães, Dr., cesarluiz66@uol.com.br, Brasil, IBAMA.
- Daniel Ricardo Arsand, Dr., daniel.arsand@gmail.com, Brasil, IFSul.
- Paulo Sergio Souza, Dr., paulosasouza@gmail.com, Brasil, Fundação Osorio.
- Moisés Rômolos Cesário, Dr., romolosquimica@hotmail.com, França, ULCO.
- Andrian Saputra, Dr., andriansaputra@fkip.unila.ac.id, Universidade de Lampung, Indonésia.
- Vanessa Barbieri Xavier, Dr., nessa.bx@gmail.com, Brasil, PUCRS.
- Oana-Maria Popa, Dr., p.oanamaria@gmail.com, IPN, Romênia.
- Danyelle Medeiros de Araújo Moura, Dr., danyelle.quimica@yahoo.com.br, Brasil, UFRN.
- Alessandra Deise Sebben, Dr., adsebben@gmail.com, Brasil
- Gabriel Rubensam, Me., rubensam_quimico@hotmail.com, Brasil, UFRGS.
- Masurquede de Azevedo Coimbra, Me., masur@pop.com.br, Brasil, Sec. de Saúde do Estado - RS.
- Flavia Maria Pompeia Cavalcanti, Me., flaviamaria@upf.br, Brasil, UPF.
- Gustavo Guthmann Pesenatto, MD., gustavoggp@gmail.com, Atenção Primária à Saúde, Brasil.
- Fábio Herrmann, MD., fabioherrmannfh@gmail.com, Hospital Santa Casa de Misericórdia de Porto Alegre, Brasil.

Periódico Tchê Química

ISSN - 1806-0374 (Print)
ISSN - 2179-0302 (Online)

LCCN: 2010240735

Divulgação *on-line* em
<http://www.periodico.tchequimica.com>
<http://www.journal.tchequimica.com>
<http://www.tchequimica.com>

Esta revista é indexada e resumida pelo CAS, EBSCO, Latindex, Sumários, Index Copernicus, Scopus, OAIJ, CAB Abstracts, EuroPub e Reaxys.

Missão

O Periódico Tchê Química (PTQ) publica artigos de pesquisa originais, artigos de revisão, notas curtas (publicações científicas), revisões de livros, artigos de fórum, editoriais e entrevistas. Pesquisadores de todos os países são convidados a publicar nas páginas do PTQ.

A responsabilidade sobre os artigos é de exclusividade dos autores.

Correspondências

Rua Anita Garibaldi, 359/603.
Bairro Mon't Serrat. CEP: 90450-001
Porto Alegre – RS. Brasil.
www.periodico.tchequimica.com
www.journal.tchequimica.com
journal.tq@gmail.com

Índice

1 – Nota dos Editores / Editors Note

DE BONI, LUIS ALCIDES BRANDINI; GOLDANI, EDUARDO

2 - Artigo / Article

FERREIRA, Mariana Babilone de Souza; DOS SANTOS, Claudio Gouvêa;

BRASIL

LIÇÕES APRENDIDAS EM 2020

LESSONS LEARNED IN 2020

BRAZIL

ESTUDO DA INFLUÊNCIA DOS MÉTODOS DE RETICULAÇÃO SOBRE AS PROPRIEDADES DO POLIETILENO

STUDY OF THE INFLUENCE OF THE CROSSLINKING METHODS ON THE PROPERTIES OF POLYETHYLENE

Página – 1

3 - Artigo / Article

HACHIM, AHMAD KHADEM; HATEET, RASHID RAHIM; MUHSIN, TAWFIK MUHAMMAD;

IRAQ

ESTUDO DE CITOTOXICIDADE, ATIVIDADE ANTIBACTERIANA E COMPOSIÇÃO POR FT-IR E GC-MS PARA O EXTRATO ORGÂNICO DA TRUFA BRANCA *TIRMANIA NIVEA* DO DESERTO DO IRAQUE

STUDY CYTOTOXICITY, ANTIBACTERIAL ACTIVITY, AND COMPOSITIONS BY FT-IR AND GC-MS FOR ORGANIC EXTRACT OF WHITE IRAQI DESERT TRUFFLE TIRMANIA NIVEA

Página – 18

5 - Artigo / Article

AKBAR, Hammar Ilham; SUROJO, Eko; ARIAWAN, Dody; PRABOWO, Aditya Rio;

INDONESIA

INVESTIGAÇÃO TÉCNICA DO REFORÇO DE AREIA DO MAR PARA NOVOS COMPÓSITOS AL6061-AREIA DO MAR: IDENTIFICAÇÃO DE DESEMPENHO E PROPRIEDADES MECÂNICAS

TECHNICAL INVESTIGATION OF SEA SAND REINFORCEMENT FOR NOVEL AL6061-SEA SAND COMPOSITES: IDENTIFICATION OF PERFORMANCE AND MECHANICAL PROPERTIES

Página – 47

Página – 7

4 - Artigo / Article

GOERITNO, Arief; NUGRAHA, Irwan; BAKTI, Prayoga;

INDONESIA

MÉTODOS CLÁSSICOS PARA PREVER O DESEMPENHO DE RELÉ BUCHHOLZ DANDO OS FENÔMENOS DE FALHA INCIPIENTE NO TRANSFORMADOR IMERSO DE ÓLEO

CLASSICAL METHODS TO PREDICT THE PERFORMANCE OF BUCHHOLZ RELAY BY GIVING THE PHENOMENA OF INCIPIENT FAULT INTO THE OIL IMMERSSED TRANSFORMER

Página – 32

6 - Artigo / Article

ABD AL-NABI, Zainab Jumhia; KASIM, Ali Abdulwaheed;

IRAQ

ISOLAMENTO E IDENTIFICAÇÃO DE FUNGOS DE DETRITOS DE PLANTAS SUBMERGIDAS EM HABITATS AQUÁTICOS NA PROVÍNCIA DE MISAN

ISOLATION AND IDENTIFICATION OF FUNGI FROM SUBMERGED PLANTS DEBRIS IN AQUATIC HABITATS IN MISAN PROVINCE

Página – 58

7 - Artigo / Article

ISLAMGULOV, Damir; ISMAGILOV, Rafael; ALIMGAFAROV, Rail; BAKIROVA, Aygul; ENIKEEV, Rafik;

RUSSIA

QUALIDADES TECNOLÓGICAS DA BETERRABA SACARINA NAS CONDIÇÕES DA REGIÃO CIS-URALS

TECHNOLOGICAL QUALITIES OF SUGAR BEETROOT CROPS UNDER THE CONDITIONS OF THE MIDDLE CIS-URAL REGION

Página – 72

9 - Artigo / Article

SURYADI, Taufik; KULSUM, Kulsum;

INDONESIA

VALIDADE DO CONTEÚDO DO INSTRUMENTO DE PESQUISA SOBRE QUESTÕES ÉTICAS NA CONDUÇÃO DA PANDEMIA DE COVID-19

CONTENT VALIDITY FOR THE RESEARCH INSTRUMENT REGARDING ETHICAL ISSUES IN HANDLING THE COVID-19 PANDEMIC

Página – 100

11 - Artigo / Article

ALANI, Ekhlas A.; ALMUSAWI, Mustafa S.; MAHDI, Amar H;

IRAQ

AVALIAÇÃO DO PAPEL DA VITAMINA C COMO AGENTE PROTETOR DE RADIAÇÃO UTILIZANDO γ -H2AX COMO SINALIZAÇÃO DE DANOS AO DNA EM TESTÍCULOS IRRADIADOS DE RATOS

EVALUATION THE ROLE OF VITAMIN C AS A RADIATION PROTECTIVE AGENT USING γ -H2AX FOR SIGNALING OF DNA DAMAGE ON IRRADIATED MICE TESTIS

Página – 128

13 - Artigo / Article

ROHAETI, ELI; PUTRI, NUR ISNA MELATI; BUDIASIH, KUN SRI; RAKHMAWATI, ANNA;

INDONESIA

O USO DO EXTRATO DE *Cyperus kyllinga* NA SÍNTESE DE NANOPARTÍCULAS DE PRATA PARA MELHORAR A QUALIDADE DE COURO DE CABRA

*THE USE OF *Cyperus kyllinga* EXTRACT IN SYNTHESIS OF SILVER NANOPARTICLE TO ENHANCE QUALITY OF GOAT LEATHER*

Página – 159

8 - Artigo / Article

COSTA, Renata Katryne Bispo da Silva; SILVA, Débora Cardoso; GUALBERTO, Simone Andrade; DA SILVA, Paulo Sávio Damásio COSTA, Matheus Andrade Rocha;

BRAZIL

COMPOSIÇÃO QUÍMICA E ATIVIDADE OVICIDA DO ÓLEO ESSENCIAL DAS FOLHAS DE *CROTON ARGYROPHYLLUS* (EUPHORBIACEAE) SOBRE O *AEDES AEGYPTI* (DIPTERA: CULICIDAE)

*CHEMICAL COMPOSITION AND OVICIDA ACTIVITY OF THE ESSENTIAL OIL OF *CROTON ARGYROPHYLLUS* (EUPHORBIACEAE) LEAVES ABOUT *AEDES AEGYPTI* (DIPTERA: CULICIDAE)*

Página – 85

10 - Artigo / Article

SERIKKYZY, Mira; AVDEENKO, Aleksei; GOULY, Yoro Ella; TYURIN, Igor; STEPANOVA, Diana;

KAZAKHSTAN / RUSSIA

EFICÁCIA DA SECAGEM POR SORÇÃO DE SEMENTES DE SOJA E TRATAMENTO PRÉ-COLHEITA COM DESSICANTES COMO UMA ABORDAGEM ABRANGENTE

EFFICACY OF SOYBEAN SEEDS SORPTION DRYING AND PREHARVEST TREATMENT WITH DESICCANTS AS A COMPREHENSIVE APPROACH

Página – 119

12 - Artigo / Article

MRAHMATINA, Desi; NUSANTARA, Toto; PARTA, I Nengah; SUSANTO, Hery; AS'ARI, Abdur Rahman;

INDONESIA

RAZÃO ESTATÍSTICA DA VARIABILIDADE NA PERSPECTIVA NARRATIVA DE ESTUDANTES

STATISTICAL REASONING OF VARIABILITY IN THE NARRATIVE PERSPECTIVE OF STUDENTS

Página – 140

14 - Artigo / Article

NURWIDIYANTO; ZHANG, Kaijun;

CHINA

ESTRATÉGIAS DE GENERALIZAÇÃO DE PADRÕES PARA MELHORAR O PENSAMENTO ALGÉBRICO DOS ESTUDANTES

STRATEGIES OF PATTERN GENERALIZATION FOR ENHANCING STUDENTS' ALGEBRAIC THINKING

Página – 171

15 - Artigo / Article

KYDYRALIYEVA, Aziza Dossymbekkyzy; BESTEREKOV, Uilesbek; NAZARBEEK, Ulzhalgas Bakytzy; BOLYSBEK, Aidar Alibekuly4; URAKOV, Kinis Nurmagambetovich;

KAZAKHSTAN**OTIMIZAÇÃO DE UMA TECNOLOGIA DE PRODUÇÃO DE NP-FERTILIZANTES**

OPTIMIZATION OF AN NP-FERTILIZER PRODUCTION TECHNOLOGY

Página – 186

17 - Artigo / Article

ZAITSOVA, Irina N;

RUSSIA**ESTIMATIVA DE ERRO DO ALGORITMO PARA A DEFINIÇÃO DO DESLOCAMENTO DE FASE DOS SINAIS HARMÔNICOS NO TEMPO MENOR QUE O PERÍODO DO SINAL UTILIZANDO AMOSTRAGEM ESTOCÁSTICA**

ERROR ESTIMATION OF THE ALGORITHM FOR THE PHASE SHIFT DEFINITION OF HARMONIC SIGNALS IN THE TIMELESS THAN THE SIGNAL PERIOD USING STOCHASTIC SAMPLING

Página – 213

19 - Artigo / Article

MARTINEZ, Fredy; MARTINEZ, Fernando; MONTIEL, Holman;

COLOMBIA**A UTILIZAÇÃO DE SIMULADORES DE FINS ESPECIAIS COMO UMA FERRAMENTA DE TREINAMENTO PROFISSIONAL AVANÇADO SOB CONDIÇÕES DE E-LEARNING**

THE USE OF SPECIAL-PURPOSE SIMULATORS AS AN ADVANCED PROFESSIONAL TRAINING TOOL UNDER E-LEARNING CONDITIONS

Página – 239

21 - Artigo / Article

ARIFIN, Zainal, HADI, Syamsul, SUYITNO, Suyitno, PRABOWO, Aditya Rio, PRASETYO, Singgih Dwi;

INDONESIA**CHARACTERIZATION OF ZnO NANOFIBER ON DOUBLE-LAYER DYE-SENSITIZED SOLAR CELLS USING DIRECT DEPOSITION METHOD**

CHARACTERIZATION OF ZnO NANOFIBER ON DOUBLE-LAYER DYE-SENSITIZED SOLAR CELLS USING DIRECT DEPOSITION METHOD

Página – 263

16 - Artigo / Article

SUPRAPTO, Nadi; ABIDAH, Azmil;

INDONESIA**USANDO O ENSAIO DIAGNÓSTICO EM TRÊS NÍVEIS PARA AVALIAR CONCEPÇÕES DE ENERGIA DE IONIZAÇÃO**

USING ONLINE THREE-TIER DIAGNOSTIC TEST TO ASSESS CONCEPTIONS OF IONIZATION ENERGY

Página – 196

18 - Artigo / Article

AL-MASAOODI, Rusul Ali; ALWALID, Shumoos H; AL-SHEMERY, Maryam Kadhim;

IRAQ**DETERMINAÇÃO DO EFEITO DA SOBRECARGA DE FERRO NA VITAMINA D E DA PERCENTAGEM DE CADA GRUPO DE SANGUE EM PACIENTES COM TALASSEMIA**

DETERMINATION THE EFFECT OF IRON OVERLOAD ON VITAMIN D AND THE PERCENTAGE OF EACH BLOOD GROUPS IN PATIENTS WITH THALASSEMIA

Página – 223

20 - Artigo / Article

DA SILVA, Edilma Elayne; BARBOSA, Maria Verônica de Sales; DE FREITAS, Jucleiton José Rufino; FREITAS, Jucarlos Rufino, DE FREITAS FILHO, João Rufino;

BRASIL**SÍNTESE, CARACTERIZAÇÃO E AVALIAÇÃO DA TOXICIDADE FRENTE A ARTEMIA SALINA DE GLICOSÍDEOS 2,3-INSATURADOS**

SYNTHESIS, CHARACTERIZATION, AND EVALUATION OF TOXICITY AGAINST SALINE ARTEMIA OF 2,3-UNSATURATED GLYCOSIDES

Página – 251

22 - Artigo / Article

BABICH, Elena Anatolyevna; OVCHINNIKOVA, Lyudmila Yuryevna; OVCHINNIKOV, Aleksandr Aleksandrovich; ZHAKSUMBAY, Zhanara Serikovna;

KAZAKHSTAN**PRODUTIVIDADE LEITEIRA E PROPRIEDADES TECNOLÓGICAS DO LEITE DAS VACAS HOLSTEIN E BLACK-MOTLEY**

MILK PRODUCTIVITY AND TECHNOLOGICAL PROPERTIES OF THE MILK FROM THE HOLSTEIN AND BLACK-MOTLEY COWS

Página – 278

23 - Artigo / Article

ASWOOD, Murtadha S.; ALMUSAWI, Mustafa S.; MAHDI, Naser K. W.; SHOWARD, Ansam F;

IRAQ**AVALIAÇÃO DA DOSE EFETIVA COMPROMETIDA DE RADÔNIO PELA INGESTÃO DE ÁGUA POTÁVEL EM AL-QADISIYAH, IRAQ**

EVALUATION OF COMMITTED EFFECTIVE DOSE OF RADON DUE TO INGESTION OF DRINKING WATER IN AL-QADISIYAH, IRAQ

Página – 291

25 - Artigo / Article

ARYNOV, Kazhimukhan T.; ZHUBATOV, Zhailaubay; AUESHOV, Abdirazah P.; SARUAROVA, Gulnur M.; NURTAZA, Nazgul M.;

KAZAKHSTAN**CRIAÇÃO E IMPLEMENTAÇÃO DE UM NOVO REGULADOR DE CRESCIMENTO ALTAMENTE EFICAZ PARA RESTAURAR A FERTILIDADE DO SOLO NAS REGIÕES ÁRIDAS DO CAZAQUISTÃO**

DEVELOPMENT AND INTRODUCTION OF NEW HIGH-POTENCY GROWTH REGULATOR FOR RESTORING SOIL FERTILITY IN ARID AREAS OF KAZAKHSTAN

Página – 315

27 - Artigo / Article

BEREZINA, Daria I.; FOMINA, Lyubov L;

RUSSIA**EFEITO DO ESTRESSE INDUZIDO POR HORMÔNIOS NO COAGULOGRAMA DE CARPA (CYPRINUS CARPIO)**

EFFECT OF HORMONE-INDUCED STRESS ON CARP (CYPRINUS CARPIO) COAGULOGRAM

Página – 346

29 - Artigo / Article

TATARKANOV, Aslan Adal'bievich; ALEXANDROV, Islam Alexandrovich; OLEJNIK, Andrej Vladimirovich;

RUSSIA**AVALIAÇÃO DOS PARÂMETROS DA SUPERFÍCIE DE CONTATO NA SUPERFÍCIE DE TROCADOR DE CALOR COM ALETAS SERRILHADAS POR SERRILHAS EM AROS VAZIOS**

EVALUATION OF THE CONTACT SURFACE PARAMETERS AT KNURLING FINNED HEAT-EXCHANGING SURFACE BY KNURLS AT RING BLANKS

Página – 372

24 - Artigo / Article

IBRAKOVA, Nurgiza F.; KUTLUGILDINA, Galiya G.; ZIMIN, Yuriy S.;

RUSSIA**COMPLEXAÇÃO DE PRAZIQUANTEL COM α -, β - E g- CICLODEXTRINAS EM SOLUÇÕES HIDROALCOÓLICAS**

COMPLEXATION OF PRAZIQUANTEL WITH α -, β - AND g- CYCLODEXTRINS IN AQUEOUS-ALCOHOLIC SOLUTIONS

Página – 302

26 - Artigo / Article

KASSIMBEKOVA, Mereke; KALIYEVA, Anar; KASSYMBAYEV, Bekbossyn; MEDEUOVA, Galiya, MAMYTOVA, Nurgul;

KAZAKHSTAN**CARACTERÍSTICAS BIOLÓGICAS DA PLANTA MEDICINAL ELAEAGNUS RHAMNOIDES CULTIVADA NO SUDESTE DO CAZAQUISTÃO**

BIOLOGICAL FEATURES OF MEDICINAL PLANT ELAEAGNUS RHAMNOIDES GROWING AT SOUTH-EAST OF KAZAKHSTAN

Página – 334

28 - Artigo / Article

JASIM, Mazin Shakir; MASHEE, Fouad Kadhum;

IRAQ**MONITORAMENTO E CÁLCULO DAS EMISSÕES DE DIÓXIDO DE CARBONO EM BAGDÁ E SEU EFEITO NO AUMENTO DAS TEMPERATURAS DE 2003-2018 USANDO DADOS DE SENSORIAMENTO REMOTO**

MONITORING AND CALCULATING THE CARBON DIOXIDE EMISSIONS IN BAGHDAD AND ITS EFFECT ON INCREASING TEMPERATURES FROM 2003-2018 USING REMOTE SENSING DATA

Página – 357

30 - Artigo / Article

SAFAROV, Eshkabal; PRENOV, Shavkat; BEKANOV, Kuatbay; SALOKHITDINOVA, Sevar; UVRAYIMOV, Sunnatilla;

UZBEKISTAN**APLICAÇÃO DE TECNOLOGIAS DE GEOINFORMAÇÃO E SENSORIAMENTO REMOTO PARA DETECTAR O USO DA TERRA E MUDANÇAS NA COBERTURA DO SOLO CAUSADA PELA SECAGEM DO MAR DE ARAL**

APPLICATION OF GEOINFORMATION TECHNOLOGIES AND REMOTE SENSING TO DETECT LAND USE AND CHANGES IN THE SOIL COVER CAUSED BY THE DRYING OF THE ARAL SEA

Página – 390

31 - Artigo / Article

ANDRINI, Vera Septi; MATSUN; MADURETNO, Tri Wahyuni;

INDONESIA**IMPLEMENTAÇÃO DE WEBINARS EM MODELOS DE APRENDIZAGEM COMBINADA PARA MELHORAR A MOTIVAÇÃO E RESULTADOS NA APRENDIZAGEM DO ESTUDO DO SISTEMA ESQUELETAL HUMANO**

IMPLEMENTATION OF WEBINARS IN BLENDED LEARNING MODELS TO IMPROVE MOTIVATION AND LEARNING OUTCOMES OF THE STUDY OF HUMAN SKELETAL SYSTEM

Página – 402

33 - Artigo / Article

AMANKULOV, Yerdos; PETUNINA, Irina; LOBANOVA, Nadezhda;

KAZAKHSTAN / RUSSIA**CONFIGURAÇÃO TRIDIMENSIONAL DE MATERIAIS COMPOSITOS COMO FORMA DE ALCANÇAR ALTAS PROPRIEDADES MECÂNICAS**

THREE-DIMENSIONAL SETUP OF COMPOSITE MATERIALS AS A WAY TO ACHIEVE HIGH MECHANICAL PROPERTIES

Página – 431

35 - Artigo / Article

MOHAMMAD, Hawraa Jabbar; ALI, Ali Khalaf; AL-ALI, Zainab Abdul Jabbar Ridha;

IRAQ**ESTUDO COMPARATIVO DAS ESTRUTURAS HISTOMORFOLÓGICAS E HISTOQUÍMICAS NO ESÔFAGO DE OVELHAS (*Ovis aries*) E COELHOS (*Oryctolagus Cuniculus*)**

*COMPARATIVE HISTOCHEMICAL AND HISTOMORPHOMETRICAL STUDY OF ESOPHAGUS STRUCTURES IN SHEEP (*Ovis aries*) AND RABBITS (*Oryctolagus Cuniculus*)*

Página – 457

37 - Artigo / Article

SAREGAR, Antomi; LATIFAH, Sri; HUDHA, Muhammad Nur; SUSANTI, Fina; SUSILOWATI, Nur Endah;

INDONESIA**DEBATE DA ABORDAGEM STEM: HABILIDADE DE PENSAMENTO CRÍTICO E CRIATIVO EM MATERIAL DE FLUIDO ESTÁTICO**

STEM-INQUIRY BRAINSTORMING: CRITICAL AND CREATIVE THINKING SKILLS IN STATIC FLUID MATERIAL

Página – 491

32 - Artigo / Article

BAHRAMI, SAAED; SAADATMAND, SARA; HAJIVAND SHOKROLLAH; FATH MOJTABA;

IRAN**MELHORANDO A TOLERÂNCIA DE ESTRESSE A FRIO EM CORYLUS AVELLANA L. USANDO VÁRIOS COMPOSTOS QUÍMICOS**

IMPROVING COLD STRESS TOLERANCE IN CORYLUS AVELLANA L. USING VARIOUS CHEMICAL COMPOUNDS

Página – 415

34 - Artigo / Article

ORTEGA-TORRES, Enric; SOLAZ-PORTOLÉS, Joan-Josep; SANJOSE LÓPEZ, Vicente;

SPAIN**PREFERÊNCIAS SENSORIAIS VARK DE ALUNOS DE ENSINO MÉDIO NA APRENDIZAGEM DE CIÊNCIAS: ELES SÃO CONFIÁVEIS?**

SECONDARY STUDENTS' VARK SENSORY PREFERENCES IN SCIENCE LEARNING: ARE THEY RELIABLE?

Página – 440

36 - Artigo / Article

FALIH, Israa Qusay; TAHIR, Noor Thair; AL-JEDDA, Walaa Ahmed;

IRAQ**AVALIAÇÃO DOS NÍVEIS DE VITAMINA D3 E DE ZINCO EM CRIANÇAS IRAQUIANAS COM DEFICIÊNCIA DO HORMÔNIO DE CRESCIMENTO E SUA RELAÇÃO COM OUTROS PARÂMETROS BIOQUÍMICOS**

EVALUATION OF VITAMIN D3 AND ZINC LEVELS IN IRAQI CHILDREN WITH GROWTH HORMONE DEFICIENCY AND THEIR RELATION WITH OTHER BIOCHEMICAL PARAMETERS

Página – 476

38 - Artigo / Article

PRISCHEPA, Oleg M.; NEFEDOV, Yuri V.; IBATULLIN, Aydar Kh;

RUSSIA**FONTE DE MATÉRIA PRIMA DE HIDROCARBONETOS DA ZONA ÁRTICA DA RÚSSIA**

RAW MATERIAL SOURCE OF HYDROCARBONS OF THE ARCTIC ZONE OF RUSSIA

Página – 506

39 - Artigo / Article

ZHUZBAY, Kassymbekov, KULYASH, Alimova, GALIMZHAN, Kassymbekov;

KAZAKHSTAN**ESTUDO DO PROCESSO DE EROÇÃO DE TURBINAS DE UMA MICRO USINA HIDRELÉTRICA (UHE) NA FORMA DE UM HIDROCICLONE**

STUDY OF THE PROCESS OF EROSION OF A MICRO HYDROELECTRIC POWER PLANT (HPP) TURBINES IN THE FORM OF A HYDROCYCLONE

Página – 527

41 - Artigo / Article

ABED, Sadeem Subhi; RASHEED, Ashraf Saad;

IRAQ**ESTIMAÇÃO SIMULTÂNEA DE CLONAZEPAM E METRONIDAZOL EM COMPRIMIDOS FARMACÊUTICOS PELO MODO DE CROMATOGRAPHIA LÍQUIDA DE ALTA EFICIÊNCIA DE FASE REVERSA COM DETECÇÃO UV**

SIMULTANEOUS ESTIMATION OF CLONAZEPAM AND METRONIDAZOLE IN PHARMACEUTICAL TABLETS BY REVERSED-PHASE HIGH-PERFORMANCE LIQUID CHROMATOGRAPHY MODE WITH UV DETECTION

Página – 554

43 - Artigo / Article

SADOON, Ahmed M.; SHEEJ AHMAD, Omar;

IRAQ / UNITED KINGDOM**ESTUDO DE ESPECTROSCOPIA DE CLUSTER $MCl_2(H_2O)_n$ USANDO CÁLCULOS AB INITIO**

SPECTROSCOPY STUDY OF $MCl_2(H_2O)_n$ CLUSTER USING AB INITIO CALCULATIO

Página – 584

45 - Artigo / Article

WIDAYANA, Gede; RATNAWATI, Dianna; ROHMAN, Mojibur; SURYAMAN, Suryaman;

INDONESIA**MULTIMÍDIA INTERATIVA PARA MELHORAR A COMPREENSÃO DOS CONCEITOS DOS ESTUDANTES NO CURSO DE ENGENHARIA**

DINTERACTIVE MULTIMEDIA TO ENHANCE STUDENTS' UNDERSTANDING OF CONCEPTS IN ENGINEERING DRAWING COURSE

Página – 608

40 - Artigo / Article

BRATANOVSKII, Sergei; AMANKULOV, Yerdos; MEDVEDEV, Ilya;

RUSSIA / KAZAKHSTAN**CÁTODO DE EMISSÃO DE CAMPO MULTIPONTO COMO GERADOR DE OSCILAÇÕES DE ALTA FREQUÊNCIA**

MULTI-POINTED FIELD-EMISSION CATHODE AS A GENERATOR OF HIGH-FREQUENCY OSCILLATIONS

Página – 542

42 - Artigo / Article

BILAUT, Dedy Adrianus; SUPARMI, A; CARL, C; FANIANDARI, Suci;

INDONESIA**ANÁLISE DAS FUNÇÕES DE ENERGIA E ONDA E DAS PROPRIEDADES TERMODINÂMICAS DA EQUAÇÃO DE SCHRODINGER 6-DIMENSIONAL SOB DUPLO OSCILADOR EM FORMA DE ANEL (DRSO) E POTENCIAIS MANNING-ROSEN USANDO MÉTODO SUSY QM**

ANALYSIS OF ENERGY AND WAVE FUNCTIONS AND THE THERMODYNAMICS PROPERTIES OF THE 6-DIMENSIONAL SCHRODINGER EQUATION UNDER DOUBLE RING-SHAPE OSCILLATOR (DRSO) AND MANNING-ROSEN POTENTIALS USING SUSY QM METHOD

Página – 565

44 - Artigo / Article

BAEHAKI, Farhan; FAJRIANI, Gita Nur; HAERANI, Ani; AENI, Suci Rizki Nurul; SARI, Ayu Yunita;

INDONESIA**MEDIÇÃO DA CONCENTRAÇÃO DE CHUMBO NO SANGUE DE MOTORISTAS DE TRANSPORTE PÚBLICO NO DOMÍNIO DE BANDUNG, WEST JAVA, INDONÉSIA**

MEASUREMENT OF LEAD CONCENTRATION IN THE BLOOD OF PUBLIC TRANSPORT DRIVERS IN BANDUNG REGENCY, WEST JAVA, INDONESIA

Página – 598

46 - Artigo / Article

BUDI, Hendrik Setia; JULIASTUTI, Wisnu Setyari; ARIANI, Winda;

INDONESIA**AValiação CITOTÓXICA BASEADA EM MTT DE SEIVA DO TRONCO DE BANANA AMBONESE (*Musa paradisiaca* var. *sapientum* (L.) Kuntze) EM FIBROBLASTOS**

*MTT-BASED CYTOTOXIC EVALUATION OF AMBONESE BANANA STEM SAP (*Musa paradisiaca* var. *sapientum* (L.) Kuntze) ON FIBROBLAST CELLS*

Página – 624

47 - Artigo / Article

SULAIMAN, Izzat Niazi, TAWFEEQ, Yahya Jirjees;

IRAQ**UM SISTEMA DE LABORATÓRIO PARA INVESTIGAÇÃO DA CAPACIDADE DE FLUXO DE FLUIDOS ATRAVÉS DE AMOSTRAS DE AREIA NÃO CONSOLIDADAS**

A LABORATORY SYSTEM FOR INVESTIGATING OF FLUIDS FLOW CAPACITY THROUGH UNCONSOLIDATED SAND SAMPLES

Página – 634

49 - Artigo / Article

FARDELA, Ramacos; SUPARTA, Gede Bayu; ASHARI, Ahmad; TRIYANA, Kuwat;

INDONESIA**MEDIDA DA TAXA DE DOSE DE RADIAÇÃO PARA PROGRAMAS DE PROTEÇÃO NO AMBIENTE DE TRABALHO PARA OS TRABALHADORES DE SAÚDE: UM ESTUDO EXPERIMENTAL**

RADIATION DOSE RATE MEASUREMENT FOR PROTECTION PROGRAMS IN THE WORK ENVIRONMENT FOR THE HEALTH WORKERS: AN EXPERIMENTAL STUDY

Página – 662

51 - Artigo / Article

SHAKIR, Safa Waleed; WIHEEB, Ahmed Daham; KHALAF, Zainab abdulmajeed; OTHMAN, Mohd Roslee;

IRAQ / MALAYSIA**CAPTURA MELHORADA DE DIÓXIDO DE CARBONO POR NANOFLUIDOS CONTENDO NANOPARTÍCULAS INORGÂNICAS E LÍQUIDO ORGÂNICO DE LIGAÇÃO**

IMPROVED CARBON DIOXIDE CAPTURE BY NANOFLUIDS CONTAINING INORGANIC NANOPARTICLES AND BINDING ORGANIC LIQUID

Página – 688

53 - Artigo / Article

RODIONOVA, Natalia Sergeevna; POPOV, Evgeny Sergeevich; KHITROV, Anatoly Anatolievich; RODIONOVA, Natalia Alekseevna; EGOROVA, Elena Ivanovna;

RUSSIA**AValiação de Impacto de Corretores Biológicos Alimentares na Eficiência Energética do Estado Nutricional**

IMPACT ASSESSMENT OF ALIMENTARY BIOLOGICAL CORRECTORS ON THE ENERGY EFFICIENCY OF NUTRITIONAL STATUS

Página – 720

48 - Artigo / Article

ONATE, Clement Atachegbe; ONYEAJU, Michael Chukwudi; ABOLARINWA, Abimbola; OKORO, Joshua Otonritse;

NIGERIA**EFEITO DE UMA BARREIRA NO AUTOVALOR ENERGÉTICO DA EQUAÇÃO DE SCHRÖDINGER NÃO RELATIVISTA E ALGUNS VALORES DE EXPECTATIVA DE POTENCIAIS COMBINADOS**

EFFECT OF A BARRIER ON ENERGY EIGENVALUE OF THE NONRELATIVISTIC (SCHRÖDINGER EQUATION) AND SOME EXPECTATION VALUES OF COMBINED POTENTIALS

Página – 646

50 - Artigo / Article

HINDAYANI, Ayu; MULYANA, Muhammad Rizky; BUDIMAN, Harry; DARMAYANTI, Nur Tjahyo Eka; ZUAS, Oman;

INDONESIA**DESENVOLVIMENTO DE MISTURAS DE GÁS DE CALIBRAÇÃO (DIÓXIDO DE CARBONO E OXIGÊNIO EM MATRIZ DE NITROGÊNIO) EM UMA FAIXA DE CONCENTRAÇÃO TÍPICA DE EMBALAGEM DE ATMOSFERA MODIFICADA**

DEVELOPMENT OF CALIBRATION GAS MIXTURES (CARBON DIOXIDE AND OXYGEN IN NITROGEN MATRIX) AT A TYPICAL CONCENTRATION RANGE OF MODIFIED ATMOSPHERE PACKAGING

Página – 674

52 - Artigo / Article

AL-MAYAH, Abdulelah Abdulhussain; AL-TAHA, Huda Abdulkreem; AL-BEHADILI, Widad Ali Abd;

IRAQ**O EFEITO DE CEPAS DE *Agrobacterium tumefaciens* EM CALOS INDUZIDAS PELOS BROTO DE GENGIBRE (*Zingiber officinale* var. Roscoe) NA PRODUÇÃO DE ALGUNS COMPOSTOS ATIVOS MEDICINAIS ESTIMADOS POR RP-HPLC**

*THE EFFECT OF *Agrobacterium tumefaciens* STRAINS ON CALLUS INDUCED FROM THE SHOOT TIPS OF GINGER (*Zingiber Officinale* var. Roscoe) IN THE PRODUCTION OF SOME MEDICINAL ACTIVE COMPOUNDS ESTIMATED BY RP-HPLC*

Página – 706

54 - Artigo / Article

QUTLIMUROTOVA, Nigora; MAHMADOLIEV, Salohiddin; SMANOVA, Zulayho; YAKHSHIYEVA, Zuhra; TURSUNKULOV, Zhasur;

UZBEKISTAN**DETERMINAÇÃO AMPEROMÉTRICA DE CÉRIO (III) USANDO SOLUÇÃO DE ÁCIDO 2,7-DINITROZO-1,8-DI-HIDROXINAFTALENO-3,6-DISSULFÔNICO**

AMPEROMETRIC DETERMINATION OF CERIUM (III) USING 2,7-DINITROZO-1,8-DIHYDROXYNAPHTHALENE-3,6-DISULFONIC ACID SOLUTION

Página – 735

55 - Artigo / Article

LEKOMTSEV, Alexander Viktorovich, KANG, Wanli, GALKIN, Sergey Vladislavovich, KETOVA, Yulia Anatolievna;

RUSSIA / CHINA**AVALIAÇÃO DE EFICIÊNCIA DA DESPARAFINIZAÇÃO DE CALOR DO POÇO DE PRODUÇÃO EQUIPADA POR SUBBOMBA COM HASTES OCAS**

EFFICIENCY EVALUATION OF THE HEAT DEPARAFINIZATION OF PRODUCING WELL EQUIPPED BY SUB PUMP WITH HOLLOW RODS

Página – 750

57 - Artigo / Article

AL-MAJIDII, Noor K. Saad; ALSAADY, Hussain A. Mhouse;

IRAQ**A PREVALÊNCIA DO PARASITA *TRICHOMONAS VAGINALIS* ENTRE MULHERES EM ALGUMAS REGIÕES DA PROVÍNCIA DE MAYSAN**

THE PREVALENCE OF TRICHOMONAS VAGINALIS PARASITE AMONG WOMEN IN SOME REGIONS OF MAYSAN PROVINCE

Página – 784

59 - Artigo / Article

KORCHAGINA, Tatyana

RUSSIA**CARACTERÍSTICAS ECOLÓGICAS E BIOLÓGICAS E COMPOSIÇÃO QUANTITATIVA DA FAUNA DE INFUSORIA EM DIFERENTES PARTES DO ESTÔMAGO DE ALCES EUROPEUS (*ALCES ALCES*) QUE VIVEM NAS REGIÕES DE OMSK E CHELYABINSK DA RÚSSIA**

*THE ECOLOGICAL AND BIOLOGICAL FEATURES AND QUANTITATIVE COMPOSITION OF INFUSORIA FAUNA IN DIFFERENT PARTS OF THE STOMACH OF EUROPEAN ELK (*ALCES ALCES*) LIVING IN THE OMSK AND CHELYABINSK REGIONS OF RUSSIA*

Página – 816

61 - Artigo / Article

SADRITDINOV, Aynur R.; CHERNOVA, Valentina V.; BAZUNOVA, Marina V.; ZAKHAROVA, Elena M.; ZAKHAROV, Vadim P.;

RUSSIA**CARACTERÍSTICAS DE FORÇA DE COMPÓSITOS DE POLÍMERO BASEADOS EM POLIPROPILENO RECICLADO PREENCHIDO DE CASCA DE ARROZ NO PROCESSO DE ABSORÇÃO DE UMIDADE E ENVELHECIMENTO NATURAL**

STRENGTH CHARACTERISTICS OF POLYMER COMPOSITES BASED ON RECYCLED POLYPROPYLENE FILLED WITH RICE HUSK DURING MOISTURE ABSORPTION AND NATURAL AGING

Página – 845

56 - Artigo / Article

HARYANI, Sri; DEWI, Siti Herlina; HARJITO;

INDONESIA**A EFICÁCIA DO TEXTO DE REFUTAÇÃO PARA MELHORAR A COMPREENSÃO DOS CONCEITOS DE ÁCIDO-BASE PARA ESTUDANTES DO ENSINO MÉDIO**

THE EFFECTIVENESS OF THE REFUTATION TEXT TO IMPROVE UNDERSTANDING OF THE ACID-BASE CONCEPTS FOR HIGH SCHOOL STUDENTS

Página – 766

58 - Artigo / Article

SAPUTRO, Sigit Dwi; TUKIRAN; SUPARDI, Zainul Arifin Imam; JATMIKO, Budi;

INDONESIA**ESTRUTURA CONCEITUAL DE HABILIDADES CRÍTICAS DE PENSAMENTO PARA TESTES DE TRABALHO E ENERGIA APLICADOS AO ENSINO DE FÍSICA**

CONCEPTUAL FRAMEWORK OF CRITICAL THINKING SKILLS FOR WORK AND ENERGY TESTS APPLIED TO PHYSICS LEARNING

Página – 798

60 - Artigo / Article

DAWOOD, Kutayba Farhan; ALFALAHI, Ayoob Obaid; NEAMAH, Shamil Ismail; DHANNOON, Omar Mahmood;

IRAQ**CARACTERIZAÇÃO BIOQUÍMICA DA PLANTA MEDICINAL DE *Ferula rutbaensis* NO DESERTO OCIDENTAL IRAQUIANO**

*BIOCHEMICAL CHARACTERIZATION OF *Ferula rutbaensis* MEDICINAL PLANT IN IRAQI WESTERN DESERT*

Página – 831

62 - Artigo / Article

ORUMBAYEV, Rakhimzhan K.; KIBARIN, Andrey A.; BAKHTIYAR, Balzhan T.; KASSIMOV, Arman S.; KOROBKOV, Maxim S.;

KAZAKHSTAN**PESQUISA DOS MODOS DE COMBUSTÃO DURANTE A QUEIMA EM GRELHA DE CARVÃO DE SHUBARKOL NA GRELHA DE COMBUSTÃO COM FORNALHA MANUAL DA CALDEIRA DE ÁGUA QUENTE KSVR-0.43**

RESEARCH OF COMBUSTION MODES DURING LAYER-BURNING OF SHUBARKOL COAL ON THE FIRE GRATE WITH THE HAND FURNACE OF THE KSVR-0.43 HOT WATER BOILER

Página – 856

63 - Artigo / Article

BASHIR, Moath Kahtan; MUSTAFA, Yasser Fakri; OGLAH, Mahmood Khudhayer;

IRAQ**SÍNTESE E ATIVIDADE ANTITUMORAL DE NOVAS CUMARINAS MULTIFUNCIONAIS**

SYNTHESIS AND ANTITUMOR ACTIVITY OF NEW MULTIFUNCTIONAL COUMARINS

Página – 871

65 - Artigo / Article

HAMODAT, Zahraa Mohammed Ali;

IRAQ**ESTIMATIVA DO NÍVEL DE ADROPINA PARA PACIENTES IRAQUIANOS COM DOENÇA CARDÍACA E ATEROSCLEROSE E OS FATORES QUE AFETAM O SEU NÍVEL**

ESTIMATION THE LEVEL OF ADROPIN FOR IRAQI PATIENTS WITH CARDIAC DISEASE AND ATHEROSCLEROSIS AND THE FACTORS AFFECTING ITS LEVEL

Página – 910

67 - Artigo / Article

RAYISYAN, Maria G.; BORODINA, Maria Anatolievna; DENISOVA, Olga Igorevna; BOGACHEV, Yuri Sergeevich, SEKERIN, Vladimir Dmitriyevich;

RUSSIA**A EFICÁCIA DA UTILIZAÇÃO DE OFICINAS DE LABORATÓRIO VIRTUAL NA EDUCAÇÃO ON-LINE DE ALUNOS QUE ESTUDAM A DISCIPLINA “QUÍMICA INORGÂNICA”**

THE EFFECTIVENESS OF USING VIRTUAL LABORATORY WORKSHOPS IN ONLINE EDUCATION OF STUDENTS STUDYING THE DISCIPLINE “INORGANIC CHEMISTRY”

Página – 934

69 - Artigo / Article

AKHMETALIYEVA, Aliya, NASSAMBAYEV, Yedige, BOZYMov, Kazybay, NUGMANOVA, Aruzhan;

KAZAKHSTAN**HABILIDADES BIOLÓGICAS E ADAPTIVAS DE BOVINOS JOVENS DAS RAÇAS HEREFORD E ABERDEEN-ANGUS E SUAS CRUZAS EM REGIÕES ÁRIDAS DO CAZAQUISTÃO OCIDENTAL**

BIOLOGICAL AND ADAPTIVE ABILITIES OF YOUNG CATTLE OF HEREFORD AND ABERDEEN-ANGUS BREEDS AND THEIR CROSS-BREEDS IN ARID TERRITORIES OF WEST KAZAKHSTAN REGION

Página – 958

64 - Artigo / Article

RIATTO, Fabrizio Belli;

BRAZIL**O EMPREGO DE UM JOGO DE PERGUNTAS E RESPOSTAS COMO UMA FORMA DE PROBLEMATIZAR E MOTIVAR O ENSINO DE FÍSICA NO ENSINO MÉDIO**

EMPLOYMENT OF A SET OF QUESTIONS AND ANSWERS AS A WAY TO PROBLEMATIZE AND MOTIVATE THE TEACHING OF PHYSICS IN HIGH SCHOOL

Página – 884

66 - Artigo / Article

TANIRBERGENOV, Samat I.; SULEIMENOV, Beibut U.; CAKMAK, Dragan; SALJNIKOV, Elmira; SMANOV, Zhassulan;

KAZAKHSTAN / SERBIA**ESTADO DE MELHORAMENTO DOS CHERNOSSOLOS CLAROS IRRIGADOS DA REGIÃO DO TURQUESTÃO**

THE AMELIORATIVE CONDITION OF THE IRRIGATED LIGHT SEROZEM OF THE TURKESTAN REGION

Página – 920

68 - Artigo / Article

FLAIH, Mohammed Hassan; AL-ABADY, Fadhil Abbas; HUSSEIN, Khwam Reissan;

IRAQUE**DETECÇÃO DE INTERLEUCINA PRÓ-INFLAMATÓRIA 17 EM PACIENTES COM L. TROPICA NA PROVÍNCIA THI-QAR, IRAQ**

DETECTION OF PRO- INFLAMMATORY INTERLEUKIN 17 IN PATIENTS WITH L. TROPICA IN THI-QAR PROVINCE, IRAQ

Página – 949

70 – Nota editorial / Editorial note

Editors

BRAZIL**PLANEJANDO A PUBLICAÇÃO NA REVISTA**

PLANNING THE PUBLICATION IN THE JOURNAL

Página – 976

71 - Artigo / Article

LURIE, Sergey A.; RABINSKIY, Lev N.; KRIVEN, Galina I.; MAKOVSKIY, Sergey. V.;

RUSSIA

SOBRE AS PROPRIEDADES DISSIPATIVAS EFICAZES DA CAMADA WHISKERIZADA EM COMPÓSITOS DE FIBRA MODIFICADOS COM FIBRAS WHISKERIZADAS

EFFECTIVE DISSIPATIVE PROPERTIES OF A WHISKERED LAYER IN MODIFIED FIBROUS COMPOSITES WITH WHISKERED FIBRES

Página – 978

73 - Artigo / Article

GORYANINA, Tatiana A.;

RUSSIA

PRODUTIVIDADE POTENCIAL DAS CULTURAS DE INVERNO NA REGIÃO DO VOLGA CENTRAL

POTENTIAL PRODUCTIVITY OF WINTER CROPS IN THE MIDDLE VOLGA REGION

Página – 1004

75 - Artigo / Article

BAIBATSHA, Adilkhan B.; KEMBAYEV, Maxat K.; MAMANOV, Erkhosha Zh.; SHAIYAKHMET, Tanirbergen K.;

KAZAKHSTAN

MÉTODOS COSMOGEOLÓGICOS PARA IDENTIFICAR DEPÓSITOS MINERAIS

REMOTE SENSING TECHNIQUES FOR IDENTIFICATION OF MINERAL DEPOSIT

Página – 1038

77 - Artigo / Article

KLASNER, Georgy Georgievich; SPIRIDONOV, Alexandr Maximovich;

RUSSIA

JUSTIFICATIVA EXPERIMENTAL DO RENDIMENTO DE PROTEÍNA DE SOJA NO EXTRATANTE DURANTE O ESMAGAMENTO DO GRÃO DE SOJA NA FORMA ENCHARCADA

EXPERIMENTAL STUDY OF THE YIELD OF SOY PROTEIN IN THE EXTRACTANT WHILE THE ABRASION-RESISTANT SOYBEANS IN SOAKED FORM

Página – 1061

72 - Artigo / Article

KHUDYAKOVA, Hatima K.; SHITIKOVA, Aleksandra V.; ZARENKOVA, Nadezhda V.; KUKHARENKOVA, Olga V.; KONSTANTINOVICH, Anastasiia V.;

RUSSIA

CONTEÚDO DE CARBOIDRATOS ESTRUTURAIS E LIGNINA EM GRAMÍNEAS FORRAGEIRAS PERENES DEPENDENDO DA FASE DE CRESCIMENTO

ASSESSMENT OF CONTENTS OF STRUCTURAL CARBOHYDRATES AND LIGNIN OF PERENNIAL FODDER HERBAGES DEPENDING ON VEGETATIVE STAGE GROWTH

Página – 994

74 - Artigo / Article

SALIKOVA, Natalya S.; TLEUOVA, Zhulduz O.; KURMANBAYEVA, Aigul S.; KHUSSAINOVA, Razya K.; KAKABAYEV, Anuarbek A.;

KAZAKHSTAN

DISTRIBUIÇÃO DE RADIONUCLÍDEOS EM ÁGUAS NATURAIS DO NORTE DO CAZAQUISTÃO E AVALIAÇÃO DAS DOSES DE RADIAÇÃO DA ÁGUA USA PELA POPULAÇÃO

DISTRIBUTION OF RADIONUCLIDES IN NATURAL WATERS OF NORTHERN KAZAKHSTAN AND ASSESSMENT OF WATERBORNE DOSES IRRADIATION OF POPULATION

PÁGINA – 1016

76 - Artigo / Article

HASHIM, Nidhal Abdullah; ABDULLAH, Younus Jasim; SHAWI, Hasan Rahman;

IRAQ

AVALIAÇÃO DE ALGUNS PARÂMETROS HEMATOLÓGICOS DE PACIENTES INFECTADOS POR *HELICOBACTER PYLORI*

*EVALUATING SOME OF THE HEMATOLOGICAL PARAMETERS FOR *HELICOBACTER PYLORI* INFECTED PATIENTS*

Página – 1052

78 - Artigo / Article

FAWZI, Mohammed; TAIFI, Ahmed; LAWI, Zahraa Kamil Kadhim;

IRAQ

HIPERMETILAÇÃO DO PROMOTOR DE SOMATOSTATINA (SST) EM ASSOCIAÇÃO COM CÂNCER COLORRETAL

SOMATOSTATIN (SST) PROMOTER HYPERMETHYLATION IN ASSOCIATION WITH COLORECTAL CANCER

Página – 1075

79 - Artigo / Article

POLYAKOV, R. Yu;

RUSSIA

**APLICAÇÃO DE SISTEMAS ROBÓTICOS MÓVEIS VOADORES
PARA DETECÇÃO PRECOCE DE UMA FONTE DE IGNIÇÃO**

*APPLICATION OF PORTABLE FLYING ROBOTIC SYSTEMS
FOR EARLY DETECTION OF AN IGNITION SOURCE*

Página – 1083

81 - Artigo / Article

SURYANI, Chatarina Lilis; WAHYUNINGSIH, Tutik Dwi;
SUPRIYADI; SANTOSO, Umar;

INDONESIA

**DERIVATIZAÇÃO DE CLOROFILA DE FOLHAS DE PANDAN
(*Pandanus amaryllifolius* Roxb.) E SUA ATIVIDADE
ANTIOXIDANTE**

*DERIVATIZATION OF CHLOROPHYLL FROM PANDAN
(Pandanus amaryllifolius Roxb.) LEAVES AND THEIR
ANTIOXIDANT ACTIVITY*

Página – 1110

83 - Artigo / Article

GOUDARZI, Zahra; HOSEINI Seyed Ebrahim; MEHRABANI,
Davood; HASHEMI, Seyedeh Sara;

IRAN / CANADA

**MUDANÇA NA QUÍMICA SANGUÍNEA, CITOCINAS PRO-
INFLAMATÓRIAS E GENES APOPTÓTICOS APÓS O USO DE
METAFETAMINA EM RATOS EXPERIMENTAIS**

*CHANGE IN BLOOD CHEMISTRY, PRO-INFLAMMATORY
CYTOKINES, AND APOPTOTIC GENES FOLLOWING
METHAMPHETAMINE USE IN EXPERIMENTAL RATS*

Página – 1147

85 - Artigo / Article

ALI, Esraa Abd Almuhsen; ALJAWADI, Hussein Fadhil;

IRAQ

**PREVALÊNCIA E FATORES DE RISCO PARA OCORRÊNCIA
DE ANOMALIAS CONGÊNITAS EM NEONATOS EM HOSPITAL
PARA CRIANÇA E MATERNIDADE NA PROVÍNCIA DE MISAN**

*PREVALENCE AND RISK FACTORS FOR OCCURRENCE OF
CONGENITAL ANOMALIES IN NEONATES AT HOSPITAL FOR
CHILD AND MATERNITY IN MISAN PROVINCE*

Página – 1176

80 - Artigo / Article

MOHAMMED, Najla Salim; AL-JAWADI, Zena Abdul Monim;

IRAQ

**O PAPEL DA VITAMINA D COMO UM NOVO MARCADOR NA
INFERTILIDADE DAS MULHERES**

*THE ROLE OF VITAMIN D AS A NEW MARKER ON THE WOMEN
INFERTILITY*

Página – 1099

82- Artigo / Article

MASLENNIKOVA, Nadezhda N.; GIBADULINA, Ilzira I.;
GAFIYATULLINA, Elvira A.;

RUSSIA

**DESENVOLVIMENTO DE HABILIDADES ESPECIAIS EM
QUÍMICA NO SISTEMA DE FORMAÇÃO PROFISSIONAL
UNIVERSITÁRIA DOS ALUNOS**

*DEVELOPMENT OF SPECIAL CHEMISTRY SKILLS IN THE
UNIVERSITY VOCATIONAL TRAINING SYSTEM OF THE
STUDENTS*

Página – 1127

84 - Artigo / Article

SAZONOV, Yu.A.; MOKHOV, M.A.; TUMANYAN, Kh.A.;
FRANKOV, M.A.; BALAKA, N.N.;

RUSSIA

**PROTOTIPAGEM DE TURBINA MALHA COM SISTEMA DE
CONTROLE DE JATO**

*PROTOTYPING MESH TURBINE WITH THE JET CONTROL
SYSTEM*

Página – 1160

86 - Artigo / Article

USMAN, Mustofa; INDRYANI N; WARSONO1; AMANTO,
WAMILIANA

INDONESIA

**MODELAGEM DINÂMICA DE USO DE DADOS DE SÉRIE DE
TEMPO MODELO BEKK-GARCH**

*DYNAMIC MODELING OF TIME SERIES DATA USING BEKK-
GARCH MODEL*

Página – 1186

87- Artigo / Article

IONI, Yulia V.

RUSSIA

NANOPARTÍCULAS DE METAIS NOBRES NA SUPERFÍCIE DE FLOCOS DE GRAFENO

NANOPARTICLES OF NOBLE METALS ON THE SURFACE OF GRAPHENE FLAKES

Página – 1199

Author instructions

INSTRUCTIONS FOR AUTHORS - PREPARATION OF MANUSCRIPTS

Página – 1225

Call for conference

Página – 1234

88 - Artigo / Article

KULYMBAYEVA, Marzhan Sh.; ORUMBAYEV, Rakhimzhan K.; SEIDALIYEVA, Aiganym B.; OTYNCHIYEVA, Marzhan T.; MUNTIS, Vladimir A.

KAZAKHSTAN /RUSSIA

ESTUDO EXPERIMENTAL DE RESISTÊNCIA HIDRÁULICA DE FLUXO TURBULENTO EM UMA CAMADA COMPACTADA

EXPERIMENTAL STUDY OF THE HYDRAULIC RESISTANCE OF TURBULENT FLOW IN THE PACKED BED

Página – 1212

ARTICLE PROCESSING CHARGES

PUBLICATION FEES (1), ADDITIONAL FEES FOR PUBLICATION (2), DISCOUNTS (3), AND FREE PUBLICATION OPPORTUNITIES (4)

Página – 1231

LESSONS LEARNED IN 2020

DE BONI, Luis Alcides Brandini^{1*}; GOLDANI, Eduardo¹

¹ Periódico Tchê Química. BRAZIL.

** Corresponding author
e-mail: journal.tq@gmail.com*



The year 2020 was unique to this Journal for several reasons, good and bad. We have received a few hundred manuscripts during this year and tried to select the best ones for publication.

After almost 20 years of adopting one publishing model, it is certainly time to do a good PDCA cycle. Some of the challenges that we are improving for 2021 are related to the Journal pre-prints, cover letter, and other minor issues.

- Regarding the Journal pre-prints, for almost 17 years, we provided pre-prints that matched very close with the final file. We noticed this year that it is better to make the pre-prints as a limited view of the final version instead of as closer as possible to the final approved version. Therefore, the authors who publish with us for many years will notice a difference in the preview files format already in the end of 2020. As the Journal does not provide ahead of print (AOP) solutions, it will avoid misunderstandings by the authors.
- Review time. As the Journal grows in new countries, the average time of review of 60 days will need to change. For some countries, the average time for the evaluation will be extended to up to 180 days as the number of manuscripts is significant, and the communication with the authors is more difficult due to linguistic challenges.
- The cover letter file was also updated and improved. The new file makes it simpler for the authors to inform if they are eligible for any available discount opportunities. Pages 2 to 6 illustrate the new version of the cover letter.
- Predicted calendar for 2021 will be March, July, and November. Plan the publication of the manuscript with sufficient review time.

On behalf of all the journal team, we are grateful to all the authors and institutions that have worked with us over the last 17 years. We hope to provide a good quality service for the next 17 years.



COVER LETTER FOR SUBMISSION OF MANUSCRIPT

Date:

Editor-in-Chief

Tchê Química Journal

359 Anita Garibaldi Street.

Mont' Serrat, Zip Code: 90450-001

Porto Alegre/RS - Brazil

Subject: SUBMISSION OF A MANUSCRIPT FOR EVALUATION

Title:

Keywords:

Authors:

Corresponding author details:

Full Name:

Full correspondence address (including):

Name of the institution:

Department Name:

Full Address:

Town/city:

State/Province:

Country:

Phone:

E-mail:

Zip Code:

Dear Editor

I, the corresponding author of the manuscript, am enclosing herewith a paper for publication in **TCHÊ QUÍMICA JOURNAL** for possible evaluation.

With the submission of this manuscript, I would like to undertake that:

- All authors of this research paper have directly participated in the planning, execution, or analysis of this study;
- All authors of this paper have read and approved the final version submitted;
- The contents of this manuscript have not been copyrighted or published previously;
- The contents of this manuscript are not now under consideration for publication elsewhere;

- The contents of this manuscript will not be copyrighted, submitted, or published elsewhere, while acceptance by the Journal is under consideration;
- There are no directly related manuscripts or abstracts, published or unpublished, by any authors of this paper;
- My Institute's representative is fully aware of this submission.
- **ATTENTION: ETHICS COMMITTEE APPROVAL ON RESEARCH WITH HUMAN OR ANIMAL PARTICIPANTS**

Research on human participants, which includes identifiable human material or identifiable data, requires ethical protection. According to the **Declaration of Helsinki** issued by the World Medical Association, research on human participants should be clearly formulated in experimental protocols, and these should be submitted to independent ethical review boards (ethics committees and institutional review boards) for approval. Additionally, every potential participant should be informed about the "aims, methods, sources of funding, any possible conflicts of interest, institutional affiliations of the researcher, the anticipated benefits and potential risks of the study and the discomfort it may entail" and should give consent to participate.

Source: S Schroter, R Plowman, A Hutchings, A Gonzalez; Reporting ethics committee approval and patient consent by study design in five general medical journals. J Med Ethics 2006; 32:718–723. DOI: 10.1136/jme.2005.015115.

- **Authors are required to describe in their manuscripts ethics committee approval and participants consent by study design from participants when research involves human participants.**

Ethics approval must be sought for research involving human participants.

A 'participant' is someone who:

- Actively provides research data. For example:
 - ✓ Completes surveys
 - ✓ Participates in interviews, discussions or observations
 - ✓ Undergoes psychological, physiological or medical treatment or testing
 - ✓ tests software
 - ✓ Grants access to personal collections of records, photographs, etc.
 - ✓ Is the person from whom tissue has been collected (including blood, urine, saliva, hair)
 - ✓ Is identified in a record, e.g., employment record, medical record, education record, membership list, electoral roll or
 - ✓ Is identified or de-identified in data banks or unpublished human research data, e.g., analysis of existing unpublished data collected by another researcher or collected for a different research project.

Source: <https://www.newcastle.edu.au/research-and-innovation/resources/human-ethics/what-needs-ethics-approval>, accessed on November 23rd, 2019

- **Authors are required to describe in their manuscripts the Animal Ethics Committee approval when the study is carried out using animals.**

Animal Ethics Committees (AECs) provide avenues for public participation in the regulation of animal research. AECs are responsible for approving and monitoring research within Accredited Animal Research Establishments, including carrying out inspections of animals and facilities.

No animal research may be carried out without AEC approval. AECs must consider and evaluate applications to conduct research on the basis of the researchers' responses to a comprehensive set of questions, including their justification for the research, its likely impact on the animals, and procedures for preventing or alleviating pain and distress.

On behalf of the establishment, AECs have the power to stop inappropriate research and to discipline researchers by withdrawing their research approvals. They can require that adequate care, including emergency care, is provided for animals. They also provide guidance and support to researchers on matters relevant to animal welfare, through means such as the preparation of guidelines and dissemination of relevant scientific literature. AECs are responsible for advising establishments on the changes to physical facilities that should be made to provide for the needs of the animals used.

Source: <https://www.animaethics.org.au/animal-ethics-committees>, accessed on November 23rd, 2019

Does your research is based on human or animal participants?

(Select one option with a cross in the appropriate box)

YES:	NO:
------	-----

If YES, please provide the Animal Ethics Committee Approval Number or Ethics Committee Approval and patient consent by study design

.....

.....

Will you require a letter of acceptance?*

(Select one option with a cross in the appropriate box)

YES:	NO:
------	-----

* The acceptance letter is an **optional service** of the Journal. If the authors need a document to prove that their article has been peer-reviewed and accepted for publication, they may request, upon payment of an additional fee of USD 40, an acceptance letter for publication of the article.

NOTE 1: THE LETTER OF ACCEPTANCE may be issued **if, and only if**, the article has undergone a complete peer-review and is considered ACCEPTED for publication. Letters will NOT be issued for newly sent articles that have not yet been appropriately evaluated and peer-reviewed.

NOTE 2: The Journal does not agree with the trade-in documents that can attest to the publication of articles that have not gone through the due process of peer-review and are legitimately considered approved for publication in the subsequent edition.

NOTE 3: THE LETTER OF ACCEPTANCE may be revoked at any time if, concerns about the manuscript emerge.

Will you require formatting services?

(Select one option with a cross in the appropriate box)

YES:	NO:
------	-----

This is an optional service. Not free of cost.

The submitted manuscript is a **(Select one option with a cross in the appropriate box)**

Research Article / Original Article	
Review Article	
Short Report	
Technical Notes	
Case Studies	
Interview	
Book review	
Forum article	
Clinical Trial	
Retrospective Chart Reviews	
Cohort Studies	
Prospective or Retrospective Data Collection	
Any other (specify the type of manuscript)	

Any other (specify the type of manuscript).....

For the Editors, I would like to disclose the following information about the project: **(If any, please write here)**

The research project was conducted under the supervision of:

(Provide the name of the Supervisor with his/her complete information)

The research project was my: **(Select one option with a cross in the appropriate box)**

Undergraduate project	
Masters project	
Ph.D. project	
Any Other (Please specify)	

Any Other (please specify).....

I am aware that the journal does not provide ahead of print publication. I will not share any type of pre-print prior to the printing of the journal.

I am aware that the journal may review my manuscript at anytime prior to the publication, and postpone or exclude it from publication if concerns are raised regarding the authorship, authenticity, or other undesirable issues that may occur.

Are you eligible for discounts and Free publication opportunities? If so, please select the appropriate check box:

- a) 50% discount for authors who support other journals from the team (Southern Brazilian Journal of Chemistry), with 1 manuscript approved for publication;
- b) 100% discount for authors who support other journals from the team (Southern Brazilian Journal of Chemistry), with 2 manuscripts approved for publication;
- c) Volume discount if you are an author of the journal, that has published with us 4 manuscripts (paid your full corresponded price), your fifth manuscript will be free of charge. Later the counting cycle restart.
- d) Young scientists that are publishing the first manuscript of their career. Requirements: Copy of the curriculum without publications; maximum of 2 authors; one manuscript previously accepted in the Southern Brazilian Journal of Chemistry (the manuscript may be from the author or from colleagues, provided that the extra purpose of the collaboration is notified at the time of submission), or two manuscripts previously accepted Journal of Law, Public Policies, and Human Sciences (manuscripts may be from the author or from colleagues, provided that the extra purpose of the collaboration is notified at the time of submission). (Last revision of the rule: 10/15/2020)
- e) All personal related to the production of the journals, from Brazil and abroad;
- f) Longtime collaborators. The authors who published four (4) articles during the first decade of the journal, will be rewarded with one (1) free publication.
- g) Paper considered by the Editors of high quality, priority, and relevance for the development of the society shall pay no fees. Note that this condition is a small recognition prize, not something that you may request. Thank you for your comprehension.
- h) **I am not eligible for discounts and Free publication**

If the manuscript is accepted for publication, and fees are applicable to it, I prefer to receive an invoice order to pay for it using:

- a) Regular bank transfer
- b) Paypal

(Signature of the corresponding author on behalf of all authors)
(A scanned signature is valid)

ESTUDO DA INFLUÊNCIA DOS MÉTODOS DE RETICULAÇÃO SOBRE AS PROPRIEDADES DO POLIETILENO.

STUDY OF THE INFLUENCE OF THE CROSSLINKING METHODS ON THE PROPERTIES OF POLYETHYLENE.

FERREIRA, Mariana Babilone de Souza^{1*}; DOS SANTOS, Claudio Gouvêa²^{1,2} Universidade Federal de Ouro Preto, REDEMAT - UFOP CEP – 35400-000, Ouro Preto, MG

* Autor correspondente

e-mail: marianababilone@hotmail.com

Received 12 June 2020; received in revised form 30 September 2020; accepted 08 October 2020

RESUMO

O polietileno (PE) é considerado um dos mais versáteis termoplásticos disponíveis na atualidade, mas possui limitações ligadas ao baixo ponto de fusão, baixa resistência ao calor, tendência à propagação de trincas e à baixa resistência à ruptura quando sob tensão. Para suprir essas deficiências, desenvolveu-se processos de reticulação da cadeia do PE, conferindo ao polímero uma rede tridimensional, que o torna mais estável às variações de temperatura. Neste trabalho, foram analisados métodos que utilizam peróxido (PEX-A) e silano (PEX-B) como agentes de modificação da cadeia do PE, visando a aplicação do PE em tubos de condução de água. Os materiais foram caracterizados por espectroscopia de infravermelho (FTIR), teor de gel e análises térmicas (TGA e DSC). Foram avaliadas propriedades mecânicas como dureza e resistência à tração e a determinação da temperatura de deflexão (HDT). Os espectros obtidos demonstraram a presença dos grupos funcionais característicos do PE e a incorporação de grupos siloxano no PEX-B. O teor de gel obtido acima de 60% demonstrou a formação de cadeias intrecruzadas entre as moléculas dos polímeros. As análises térmicas associadas aos demais dados da literatura indicam maior eficiência na formação de cadeias cruzadas pelo processo de reticulação via silano do que a reticulação via peróxido. Quanto aos ensaios mecânicos, os mesmos também demonstram melhoria nas propriedades mecânicas do polímero reticulado quando comparado ao respectivo PE original. Assim, o método via silano forneceu resultados suficientes para a conclusão de que as propriedades avaliadas são superiores quando comparado ao método de reticulação via peróxido.

Palavras-chave: *polietileno, polietileno reticulado, peróxido, silano.*

ABSTRACT

Polyethylene (PE) is considered one of the most versatile thermoplastics available today. However, it exhibits several limitations related to its low melting point, low heat resistance, tendency to crack propagation, and its low resistance to rupture under stress. In order to overcome these deficiencies, several processes for crosslinking PE chains were developed, which makes this material more stable to temperature changes. In this work, methods based on peroxide (PEX-A) and silane (PEX-B) as chemical modification agents for PE chain crosslinking were analyzed, aiming to apply PE in pipes for conduction water. The materials were characterized by infrared spectroscopy (FTIR), gel content, and thermal analysis (TGA and DSC) to achieve those objectives. Also, some mechanical properties such as tensile strength and hardness and the determination of the heat deflection temperature (HDT) were evaluated. Spectra demonstrated the presence of the functional groups characteristic of PE and the incorporation of siloxane groups in PEX-B. Gel content values obtained were above 60% and indicated the formation of crosslinked chains between the molecules of the polymers. The thermal analysis suggests a greater efficiency in forming a chain network by the silane crosslinking process compared to the peroxide process. As for the mechanical tests, they also showed improvement in the mechanical properties of the crosslinked polymer when compared to the respective original PE. Thus, the silane method provided sufficient results to conclude that the properties evaluated are superior compared to the peroxide crosslinking method.

Keywords: *polyethylene, crosslinked polyethylene, peroxide, silane.*

1. INTRODUÇÃO:

Para garantir a sobrevivência da humanidade frente às dificuldades impostas pelo planeta desde as épocas mais remotas da sociedade, o ser humano tem desenvolvido a capacidade de transformar os recursos disponíveis, em busca de novas soluções para os problemas cotidianos. Dentre estes recursos, o plástico faz parte da história da evolução humana e vem sendo utilizado em substituição a ligas metálicas e materiais cerâmicos, entre outros, tendo em vista a baixa complexidade de seu processamento, a redução de consumo de energia elétrica e a possibilidade de economia de matéria-prima, visto que a reciclagem, em muitos casos, é uma alternativa plausível. Podemos quantificar a importância desse produto no mundo ao considerarmos uma produção mundial de aproximadamente 250 milhões de toneladas de resinas termoplásticas em 2013, segundo a Abiplast (2014), para a qual o Brasil contribuiu com 6,5 milhões de toneladas, o que representa 2,7% da produção mundial, a mais significativa da América Latina.

Dentre os materiais termoplásticos, destaca-se o polietileno (PE), proveniente da transformação molecular do etileno e estudado desde 1935 na Inglaterra. Entretanto, o PE apresenta limitações quando aplicado em produtos que são submetidos a elevadas temperaturas, pois apresenta baixa temperatura de fusão. Em busca de solucionar essa deficiência do polímero, surgiu o polietileno reticulado (PEX), que apresenta uma rede polimérica mais resistente, ampliando suas possibilidades de uso. Segundo Morawetz (1995), o primeiro polietileno reticulado (PEX) foi preparado em 1930, irradiando-se um tubo extrusado, com um feixe de elétrons. Em 1960, Thomas Engel reticulou o PE misturando peróxido com um polietileno de alta densidade (PEAD) antes da extrusão, e as ligações cruzadas foram formadas durante a passagem do polímero fundido através de uma longa matriz aquecida. Em 1968, o processo Sioplás (realizado em duas etapas), usando silano, foi patenteado, seguido por outro processo baseado em silano, o Monosil (realizado em uma etapa), em 1974.

O processo de reticulação confere ao polímero uma rede tridimensional termofixa, que não pode ser processada ou dissolvida sem que ocorra a degradação do mesmo, o que torna este material mais estável às variações de temperatura, permite a incorporação de um maior

volume de carga, melhora a resistência à formação e propagação de trincas e resulta em um material com maior resistência à tração de acordo com o trabalho de Chong (2005). Atualmente, o PEX pode ser moldado por processos de injeção, compressão, extrusão e moldagem rotacional. Esse material é utilizado na construção civil em tubos para aquecimento de pisos (pisos radiantes), tubos de irrigação, tubos para o transporte de água fria, água quente e gás, espumas para isolamento térmico, vedações resistentes a produtos químicos, no setor de embalagens para fabricação de fitas e filmes diversos e em isolamento de fios e cabos. Uma nomenclatura foi definida para diferenciar os métodos de fabricação do PEX, sendo o PEX-A reticulado via peróxido, o PEX-B reticulado via silano, o PEX-c quando a irradiação é utilizada para reticular as cadeias e PEX-d quando o método AZO é empregado para reticulação.

Para transporte de água quente na construção civil, os materiais metálicos, principalmente o cobre, são historicamente os mais utilizados. Os materiais plásticos para condução de água quente chegaram ao mercado brasileiro há menos de 40 anos com a introdução do CPVC. Em seguida foram lançados o PEX e o PPR, este último com a união efetuada por termofusão, após a qual a junta passa a constituir um conjunto único com espessura reforçada. Os tubos PEX monocamada, podem ser obtidos tanto pelo método via silano, quanto pelo método via peróxido, através de processos de extrusão que variam seus equipamentos de acordo com a exigência de cada método. Esses são tubos flexíveis e maleáveis, o que fez com que se adequassem às exigências do setor de tubos para condução de água e imediatamente foram considerados como uma boa alternativa tendo em vista sua segurança e economia. É um material com alta resistência à corrosão química, baixa tendência à incrustação e perdas de carga baixa, também é leve, flexível e fácil de transportar e instalar visto que pode ser entregue em bobinas. A flexibilidade permite curvar os tubos sem uso de conexões.

Nesse contexto, este trabalho visa estudar e comparar a influência do método de reticulação via peróxido (PEX-A) e via silano (PEX-B) sobre as propriedades do polietileno, considerando sua aplicação em tubos para condução de água quente, buscando contribuir para o melhor entendimento dessa tecnologia.

2. DESENVOLVIMENTO OU MATERIAL E

MÉTODOS OU PARTE EXPERIMENTAL:

2.1. Materiais

Os materiais empregados neste trabalho foram cedidos pela empresa Karina Ind. e Comércio de Plásticos. As amostras foram preparadas e caracterizadas na mesma empresa.

Para a produção de PEX-A foram: PEAD grade 1878 produzido pela Borealis, Peróxido Trigonox produzido pela Akzo Nobel e Antioxidante Irganox 1076 do fabricante Ciba.

Para a produção de PEX-B foram utilizados os seguintes materiais: PEAD grade 4400 produzido pela Braskem, Viniltrimetoxissilano (VTMS) produzido pela Newport Industries, Catalisador grade 4/4 produzido pela Karina Ind. e Com. de Plásticos e Antioxidantes Ciba 1076 e Ciba 1010.

2.1.1 Preparação das Amostras

Foram produzidas fitas a partir da mistura dos pellets e demais componentes da formulação (Tabela 1), em uma extrusora de bancada, monorosca, com quatro zonas de aquecimento, de marca IMACON.

(I) Produção de PEX-A	
Materiais	Percentual (%)
PEAD grade 1878	99,40
Peróxido Trigonox	0,30
Antioxidante Irganox 1076	0,30
TOTAL	100
(II) Produção de PEX-B	
Materiais	Percentual (%)
PEAD grade 4400	93,45
VTMS	1,25
Catalisador grade 4/4	5,00
Antioxidante Ciba 1076	0,15
Antioxidante Ciba 1010	0,15
TOTAL	100

Tabela 01: Formulação utilizada para produção de amostras de PEX-A (I) e PEX-B (II).

Foram aplicadas as condições de processo para extrusão das fitas na extrusora de bancada (Figura 1) de acordo com o recomendado pelo fabricante dos polietilenos, sendo as temperaturas: 210°C (Zona 1), 220°C (Zona 2), 230°C (Zona 3) e 240°C (Zona 4), sendo que para esta extrusora a Zona 4 é a mais próxima à saída do material pelo cabeçote.

Foi utilizada uma tela de 80 mesh para melhorar a homogeneização da mistura. O material produzido e utilizado como amostra para este trabalho foi processado em 80 rpm.

Para a produção das fitas (Figura 1), foram utilizados no total cerca de 300 g de mistura para garantir a estabilidade da extrusora e evitar interferências relacionadas ao processo de partida da máquina na amostra. Após estabilização, amostras da fita com aproximadamente 5 g, com comprimento de 8,0 cm e largura de 2,0 cm foram cortadas e devidamente selecionadas para serem ensaiadas de acordo com cada corpo de prova necessário.

2.1.2 Processo de Reticulação

Para acelerar a reticulação do PE via silano, a amostra foi acondicionada em um béquer e imersa em água aquecida a 100°C. O conjunto foi depositado em uma estufa da marca Fanem, modelo 320/3 MP por um período de três horas, conforme NBR NM IEC 60811-2-1:2003. Nas amostras obtidas a partir de reticulação via peróxido, PEX-A não foi necessário nenhum tipo de aceleração, uma vez que o processo ocorre de maneira imediata após a passagem da mistura pela extrusora.

2.1. Técnicas de Caracterização

2.2.1 FTIR – Espectroscopia de Infravermelho

A espectroscopia no infravermelho com transformada de Fourier é uma técnica de análise vastamente utilizada por fornecer evidências da presença de vários grupos funcionais na estrutura química. A técnica é baseada na interação das moléculas ou átomos com a radiação eletromagnética em um processo de vibração molecular, fornecendo espectros de infravermelho de maneira rápida. A espectroscopia no infravermelho produz espectros de absorção (e/ou transmissão) conforme sugerido no exemplo de

Leite e Prado (2012) fazendo um feixe de luz na região do infravermelho incidir sobre a substância e determinando as frequências absorvidas por ela. As análises de infravermelho foram realizadas no modo de reflectância total atenuada (ATR) em um espectrômetro Perkin Elmer, modelo Spectrum One, com varredura de 4000 a 400 cm^{-1} .

2.2.2 Teor de Gel

A determinação do grau de reticulação (teor de gel) foi realizada por extração com solventes conforme NBR 15939, anexo F. Os corpos de prova coletados foram dispostos em um cesto com tampa, fabricado com tela metálica, com uma malha de $125 \pm 25 \mu\text{m}$. Foram submersos em xileno puro, ao qual se adicionou 1% de antioxidante CIBA 1010, e mantido em ebulição por 8 horas, em uma estufa a vácuo da marca Fanem, modelo 320/3 MP a $140 \pm 2^\circ\text{C}$.

O teor de gel foi determinado segundo a equação:

$$G = \frac{m_3 - m_1}{m_2 - m_1} \times 100 \quad (\text{Eq. 1})$$

onde G é o grau de reticulação dos corpos de prova individuais, expresso em porcentagem (%), m_1 é a massa do cesto com tampa, m_2 é a massa combinada do corpo de prova original, com cesto e tampa e m_3 é a massa combinada do resíduo, com cesto e a tampa, todas expressas em miligramas. Para este trabalho, essa análise é de grande importância, pois é necessário confirmar a presença dos percentuais de reticulação conforme estabelecidos pela norma NBR 15939.

2.2.3 Análise Termogravimétrica – TGA

A TGA é uma técnica destrutiva destinada ao monitoramento da variação da massa de uma amostra em função da temperatura ou do tempo em um ambiente de temperatura e atmosfera controladas segundo Mothé (2009). Neste trabalho, as análises termogravimétricas foram utilizadas para avaliar e comparar possíveis mudanças na estabilidade térmica do PEX. As amostras foram aquecidas a uma taxa de $20^\circ\text{C}/\text{min}$ em atmosfera de nitrogênio e em uma faixa de temperatura de 30 a 600°C , utilizando-se

um equipamento da marca TA Instruments, modelo TGA Q 500.

2.2.4 Calorimetria Exploratória Diferencial – DSC

A DSC pode ser definida de acordo com Silva e Araújo (2014) como uma técnica que mede as temperaturas e o fluxo de calor associado com as transições dos materiais em função da temperatura e do tempo. Tais medidas fornecem informações qualitativas e quantitativas sobre mudanças físicas e químicas que envolvem processos endotérmicos, exotérmicos ou mudanças na capacidade calorífica. As análises de calorimetria exploratória diferencial foram realizadas com o objetivo de avaliar o PE antes e depois da reticulação, aplicando taxa de aquecimento de $10^\circ\text{C}/\text{min}$ em atmosfera de nitrogênio e uma faixa de temperatura compreendida entre -30 e 200°C . Os ensaios foram feitos em um equipamento de análise térmica da TA Instruments, modelo DSC Q 2000.

2.2.5 Ensaio Mecânico de Tração

Esses ensaios foram realizados com o propósito de avaliar o comportamento mecânico do PEX reticulado via silano e peróxido, para fins comparativos com cada PEAD utilizado sem reticulação. Como apresentado por Cassu e Felisberti (2005), esse tipo de ensaio destrutivo, as propriedades mecânicas dos materiais são avaliadas a partir de uma solicitação, na forma de uma deformação ou na aplicação de uma tensão, com o monitoramento da resposta do material, expressa como tensão ou como deformação, respectivamente. Neste trabalho, a partir das fitas extrudadas e após a comprovação de que o percentual de reticulação está de acordo com a NBR 15939, os corpos de prova tipo borboleta foram retirados com auxílio de um molde metálico. A máquina de tração e alongamento utilizada no trabalho é da marca EMIC, modelo DL500 e os ensaios estão de acordo com a norma IEC 60811-1-1, realizados a velocidade de $50\text{mm}/\text{min}$, utilizando uma célula com carga máxima de 20 kN.

2.2.6 Ensaio Mecânico de Dureza Shore D

Nos ensaios para a verificação da dureza Shore D, utilizou-se um durômetro do fabricante

Barreis, modelo BS 61 II, com resolução de um dígito. Conforme Callister (2002) o comportamento mecânico de um material é definido pela relação entre a força aplicada e a sua resposta ou deformação gerada. Entre as propriedades mecânicas mais importantes estão a dureza e a resistência a diferentes tipos de carregamentos, justificando assim o uso desse ensaio neste trabalho.

Estas durezas são obtidas por um tipo específico de penetrador, quando forçado a entrar em um corpo de prova plano de material sob condições especificadas. Esta dureza de indentação é inversamente proporcional à penetração, dependente do módulo elástico e do comportamento viscoelástico do material, sendo uma importante fonte de conhecimento sobre as propriedades dos polietilenos reticulados estudados neste trabalho.

2.2.7 Ensaio de Temperatura de Deflexão Térmica

A temperatura de deflexão térmica (HDT) determina a temperatura em que ocorre uma deformação (deflexão) específica de uma barra submetida a tensão pré-estabelecida. De acordo com Waschburger (2006), a temperatura de deflexão térmica (HDT) corresponde a temperatura em que uma quantidade arbitrária de deflexão ocorre, sob efeito de uma carga pré-determinada e a temperatura de amolecimento VICAT corresponde à temperatura na qual uma agulha penetra 1 mm no corpo de prova, sob efeito de carga específica. Este ensaio pode ser utilizado como um ensaio comparativo entre materiais em condições especificadas por normas, corroborando com o objetivo deste trabalho na comparação do PEX-A e PEX-b.

O ensaio foi realizado em um equipamento Ceast, modelo HDT 3 Vicat com uma tensão de 1,85Mpa, taxa de aquecimento de 120°C/h. A temperatura foi determinada após a amostra ter defletido 0,25mm. Uma série de 3 amostras de cada material foi ensaiada e a temperatura de deflexão térmica medida.

3. RESULTADOS E DISCUSSÃO:

As duas resinas de PEAD e os respectivos polímeros reticulados gerados, PEX-A e PEX-B foram analisados por espectroscopia de absorção na região do infravermelho. Os espectros do PEAD 1878 antes e após a reticulação com peróxido (Figura 2) são bem semelhantes e

mostraram as bandas típicas esperadas para esse polímero. A Figura 3 mostra os espectros do PEAD 4400 antes e após a reticulação com siloxano.

A espectroscopia na região do infravermelho é uma técnica largamente utilizada para caracterização de substâncias através da identificação de grupos funcionais presentes em suas moléculas. Os espectros do PEAD 1878 antes e após a reticulação com peróxido (Figura 2) são bem semelhantes e mostraram as bandas típicas esperadas para esse polímero, quais sejam, as três bandas intensas em torno de 2900, 1460 e 730/720 cm^{-1} . Essas bandas podem ser atribuídas, respectivamente, aos modos de vibração de estiramento, deformação e dobramento das ligações C-H. No caso da Figura 3, onde são apresentados os espectros do PEAD 4400 antes e após a reticulação com silano, é possível observar algumas diferenças, sendo a principal delas o aparecimento de uma pequena banda em 1018 cm^{-1} , que pode ser atribuída ao estiramento da ligação Si-O-Si. Ainda nessa região, embora apareçam várias outras bandas de pequena intensidade, é possível destacar as bandas em 1369 e 1095 cm^{-1} , comumente atribuídas a deformações da ligação Si-CH₂, conforme trabalhos de Silverstein (1991) e Kalyanee e Sirinya (2006). Esses resultados comprovam a presença do grupo siloxano na estrutura reticulada do polímero.

Os valores obtidos nos ensaios de teor de gel foram de 73,3%, para o polietileno reticulado com peróxido e de 64,0% para o reticulado via silano. O percentual de teor de gel de PEX-A foi ligeiramente superior ao PEX-B. Os valores de teor de gel encontrados neste trabalho são similares aos obtidos em estudos de reticulação elaborados por Celine e George (1995) que também observaram valores maiores desse parâmetro para a reticulação via peróxido quando comparados com aquela via silano, o que foi associado às diferenças entre as ligações cruzadas via peróxido (C-C) que são menos volumosas que as do grupo siloxano (Si-O-Si), permitindo melhor distribuição nas cadeias poliméricas e assim, a reticulação por adição de peróxido exibe uma rede relativamente homogênea, porém mais frágil; enquanto que a reticulação por adição de silano resulta em uma rede menos homogênea, já que esse grupo é mais volumoso e a reticulação ocorre apenas na fase amorfa, sendo, porém, mais resistente. De acordo com Zumdahl (2003) a maior resistência advém da energia de ligação das ligações Si-O-Si (452 kJ/mol) que é superior à das ligações C-C (347

kJ/mol). Vale ressaltar novamente a correlação das frações de silano e peróxidos utilizadas, pois com o aumento ou diminuição dos percentuais de cada componente na mistura, diferentes valores de teor de gel podem ser encontrados, como demonstrado por Kampouris e Andreopoulos (1989) em trabalho sobre o efeito do teor de gel nas propriedades físicas do polietileno.

A caracterização térmica dos polietilenos antes e após as reações de reticulação foram feitas por análise termogravimétrica (TGA) e por calorimetria exploratória diferencial (DSC). A Figura 4 apresenta as curvas TG dos dois diferentes tipos de polietileno de alta densidade (PEAD) usados neste trabalho e dos respectivos materiais resultantes após a reação de reticulação.

Embora não sejam úteis como métodos de identificação de polímeros, as análises térmicas têm sido cada vez mais utilizadas para caracterizar polímeros, medir a dependência de algumas propriedades mecânicas ou físicas com a temperatura e correlacionar essa dependência com a estrutura do polímero, apresenta Mano (2004). Apesar das curvas TG apresentarem perfis bastante similares, é possível identificar algumas diferenças sutis para cada amostra. A degradação de todos os polímeros analisados se iniciou acima de 400°C; tanto para o PEAD 1878 como para PEAD 4400 a temperatura de degradação máxima (T_{onset}) ocorreu em torno de 455 °C. Observa-se uma pequena diferença que pode ser atribuída às diferentes fontes desses polímeros, embora ambos sejam referidos como polietileno de alta densidade. O processo de reticulação contribuiu para uma ligeira melhoria na estabilidade térmica dos polietilenos. Para o PEAD 1878 a temperatura de degradação sofreu um pequeno aumento de 454 para 461 °C, enquanto para o PEAD 4400 ela passou de 457 para 466 °C, após a reticulação.

A Figura 5 apresenta as curvas DSC das amostras de polietileno antes e após a reticulação.

As curvas de DSC mostram que as temperaturas de transição vítrea das amostras de PEAD antes da reticulação ficaram entre -44 e -43 °C, que são valores típicos para esse polímero. Embora o processo de reticulação tenha sido comprovado pelos outros métodos descritos anteriormente, não se observou um aumento significativo da Tg para nenhuma das amostras após o processo de reticulação. Em relação à temperatura de fusão, embora as variações também tenham sido pequenas, os valores observados foram ligeiramente maiores; no caso

do PEAD 1878 a temperatura aumentou de 125,5°C para 134,1°C no PEX-A e de 128,7°C no PEAD 4400 para 136,0°C no PEX-B. É importante considerar que o polietileno de alta densidade já possui temperaturas de transição vítrea e de fusão um pouco mais elevadas que outros tipos de polietileno como o PELBD e o PEBD, conforme Peacock (2000); sendo assim, mesmo que as variações daquelas temperaturas não tenham sido significativas, os aumentos observados comprovam que a mobilidade das cadeias ficou mais restrita após a reticulação, como seria de se esperar.

A fim de avaliar a influência dos diferentes métodos de reticulação sobre as propriedades mecânicas dos polietilenos estudados, foram realizados ensaios de alongamento na ruptura, resistência à tração, dureza e temperatura de deflexão térmica para as amostras antes e após os processos de reticulação, conforme apresentado na Tabela 2.

Os resultados indicaram que o processo de reticulação implicou em uma melhora das propriedades mecânicas do material original em ambos os casos. Por se tratar de um material termoplástico, o PEAD possui maior mobilidade das cadeias sendo esperado um percentual de alongamento maior quando comparado aos materiais reticulados (Ritums et al., 2006). Os valores de alongamento na ruptura e resistência à tração para os dois tipos de PEAD utilizados são comparáveis àqueles relatados por Bomtempo (1994). O maior percentual de alongamento na ruptura e, conseqüentemente a menor resistência à tração apresentados pelo PEX-B em comparação ao PEX-A, pode ser atribuído à natureza das ligações químicas geradas no processo de entrecruzamento (Moela et al., 2004). A reticulação via silano confere maior flexibilidade ao polímero, devido à presença de ligações O-Si-O; entretanto, como essas ligações são mais fortes que as ligações resultantes da reticulação via peróxido, o PEX-B apresenta maior percentual de alongamento na ruptura.

Em relação aos índices de dureza Shore D dos polietilenos utilizados, tendo-se obtido valores entre 60-72, que estão de acordo com a literatura. (Oliveira e Costa, 2010; Silva e Araújo, 2014), onde PEX-A e PEX-B apresentaram valores ligeiramente maiores que os polietilenos não reticulados.

Os resultados obtidos apontaram um aumento no valor de HDT dos polietilenos após o processo de reticulação. Para o PEAD 1878 esse aumento foi de 57,4°C para 92,6 °C no polímero

reticulado e para o PEAD 4400, de 69,6°C para 95,8°C. Esses aumentos provocados pelo processo de reticulação são bastante encorajadores e abrem novas perspectivas do ponto de vista tecnológico para as aplicações desses polímeros em tubos.

4. CONCLUSÕES:

Neste trabalho foram investigados dois métodos de reticulação para o polietileno, um envolvendo a reação com peróxido e o outro com silano. O primeiro resulta em um material denominado PEX-A e, o segundo, em outro material designado como PEX-B. Tanto os polímeros originais como os reticulados foram caracterizados por métodos clássicos de análise.

A espectroscopia na região do infravermelho permitiu identificar a presença dos grupos funcionais característicos do polietileno, bem como os resultantes da incorporação de grupos siloxano. Os polímeros reticulados apresentaram teores de gel acima de 60%, o que permite concluir que os métodos utilizados foram eficientes no sentido de obter uma quantidade adequada de ligações cruzadas entre as moléculas dos polímeros. A reticulação influenciou o comportamento dos polímeros em termos da temperatura, conforme indicado pelas curvas de termogravimetria, que mostraram uma ligeira melhoria da estabilidade térmica dos polímeros após o processo de reticulação. Através da análise termogravimétrica foi possível observar que o método silano produziu uma estrutura com interação mais forte entre as cadeias devido à presença de grupos siloxano. As temperaturas de transição vítrea e de fusão dos materiais reticulados foram moderadamente superiores em comparação aos polímeros originais, conforme observado pelas curvas obtidas pelo DSC.

As propriedades mecânicas dos materiais também foram avaliadas e observou-se uma boa melhoria dessas propriedades após efetuada a reticulação. Essas melhorias no desempenho dos materiais foi justificada em termos da maior interação entre as cadeias provocada pela reticulação.

O ganho de qualidade nas propriedades do polietileno abre novas perspectivas para ampliar o leque de aplicações desse polímero commodity, incluindo a produção de tubos para transportar líquidos a altas temperaturas.

De modo geral, o método via silano forneceu resultados mais satisfatórios em termos de promover uma melhoria das propriedades do polietileno através da reticulação. Essa observação, aliada ao fato de que o processo via silano envolve procedimentos mais simples, justifica a constatação de que esse é o método mais utilizado pelas empresas brasileiras que produzem polietileno reticulado.

As conclusões obtidas a partir deste trabalho deverão auxiliar as diversas discussões existentes no mercado de tubos no que diz respeito ao desempenho do PEX-A em comparação ao PEX-B, pois atualmente as empresas produtoras via um determinado método defendem a qualidade de seu produto levando em conta somente aspectos comerciais, e a partir do que foi apresentado, as vantagens e desvantagens de cada método, poderão ser debatidas também por meio de resultados provenientes de estudos científicos.

5. AGRADECIMENTOS:

Os autores agradecem à Karina Ind. e Com. de Plásticos pelos polímeros fornecidos e pelos experimentos realizados, à CAPES e à REDEMAT/ UFOP em parceria com Fundação Gorceix, pelo apoio financeiro.

6. REFERÊNCIAS:

1. ABIPLAST, Associação Brasileira de Plásticos (2014). Relatório anual: Perfil da Indústria Brasileira de Transformados Plásticos. Recuperado de www.abiplast.com.br.
2. ABNT NBR 15939-1:2011. Sistemas de tubulações plásticas para instalações prediais de água quente e fria — Polietileno reticulado (PE-X).
3. Bomtempo, J. V. (1994). "Innovation et organisation: le cas de l'industrie des polymeres." L' École Nationale Supérieure des Mines de Paris, Paris.
4. CALLISTER Jr. (2002) W.D. *Ciência e Engenharia de Materiais uma Introdução*, LTC. Ed. 5ª Ed., Rio de Janeiro.
5. Cassu, S. N.; Felisberti, I. M. (2005) *Comportamento Dinâmico-Mecânico e Relaxações em Polímeros e Blendas*

- Poliméricas. *Quim. Nova*, Vol. 28, No. 2, 255-263.
6. Celina, M., George, G.A. (1995). Characterization and degradation studies of peroxide and silane crosslinked polyethylene, *Polymer Degradation and Stability*, v. 48, pp. 297-312.
 7. Chong, T. S. (2005) Design and process for producing silane crosslinked polyolefin compound. University Teknologi Malaysia, Malásia.
 8. Kalyanee Sirisinha, Sirinya Chimdist. (2006) Comparison of techniques for determining crosslinking in silane-water crosslinked materials. *Polymer Testing*, v. 25, pp. 518–526.
 9. KampouriS, E. M.; AndreopouloS, A. G. (1989) "The effect of the gel content of crosslinked polyethylene on its physical properties". *European Polymer Journal*. Vol. 25, nº 3, pp. 321-324.
 10. Leite, D. O. e Prado, R. J. (2012) Espectroscopia no infravermelho: uma apresentação para o Ensino Médio. *Revista Brasileira de Ensino de Física*, v. 34, n. 2.
 11. Mano, Eloisa Biassoto. (2004) *Introdução a Polímeros*. 2ª Edição. São Paulo, Editora Edgar Blücher.
 12. Moela, Carosena, Carlomagno, Giovanni Maria, Nele, L. (2004) Chemical and irradiation crosslinking of polyethylene. Technological performance over costs. *Polymer-Plastic Technology and Engineering*, v. 43, nº 3, pp 629-646.
 13. Morawetz, Herbert. (1995) *Polymers: The Origins and Growth of a Science*. 2ª Edição. Nova York. Editora Dover.
 14. Mothé, C. G. (2009), *Análise térmica de materiais*. São Paulo. Editora Artliber.
 15. Oliveira G.L., Costa, M.F. (2010) Optimization of process conditions, characterization and mechanical properties of silane crosslinked high-density polyethylene. *Materials Science and Engineering*, v. 527, pp. 4593–4599.
 16. Peacock, Andrew J. (2000). *Handbook of Polyethylene: Structures, Properties, and Applications*. Nova York. Editora Marcel Dekker.
 17. Ritums J. E., A. Mattozzi, U. W. Gedde, M. S. Hedenqvist, G. Bergman, M. Palmlo. (2006) Mechanical Properties of High-Density Polyethylene and Crosslinked High-Density Polyethylene in Crude Oil and Its Components. *Journal of Polymer Science: Part B: Polymer Physics*, v. 44, pp. 641–648
 18. Silva, Divânia F., Araújo, Edcleide M. (2014) Análise do Comportamento Termomecânico, Térmico e Mecânico De Blendas De Pa6/Resíduos De Borracha. *Revista de Engenharia e Tecnologia*, v. 6, nº. 1, pp. 160-169.
 19. Silverstein, R. M., Bassler, G. C.; Morrill, T. C. (1991). *Spectrometric Identification of Organic Compounds*. 5 ed, New York, John Wiley & Sons.
 20. Souza, Sérgio Augusto de. (1982) *Ensaaios mecânicos de materiais metálicos. Fundamentos teóricos e práticos*. São Paulo. Blucher.
 21. WASCHBURGER, M. R. (2006) Compósito de Polipropileno com Nanocarga, Dissertação de mestrado, Programa de Pós-Graduação em Engenharia de Minas, Metalúrgica e de Materiais – PPGEM, Universidade Federal do Rio Grande do Sul, Porto Alegre.
 22. Zumdahl, S. S. (2003), *Introduction Chemistry*. 5ª Edição. Editora Houghton-Mifflin

Tabela 2. Resultados dos Ensaio Mecânicos. Fonte: o autor.

AMOSTRA	ALONGAMENTO NA RUPTURA (%)	RESISTÊNCIA À TRAÇÃO (MPa)	DUREZA SHORE D	HDT (VICAT)
PEAD 1878	593,80	22,16	63,1	57,4
PEX-A	432,60	49,70	69,3	92,6
PEAD 4400	639,50	24,18	63,7	69,6
PEX-B	532,20	41,89	71,8	95,8



Figura 1: Preparação de mistura para produção de fitas em extrusora de bancada.

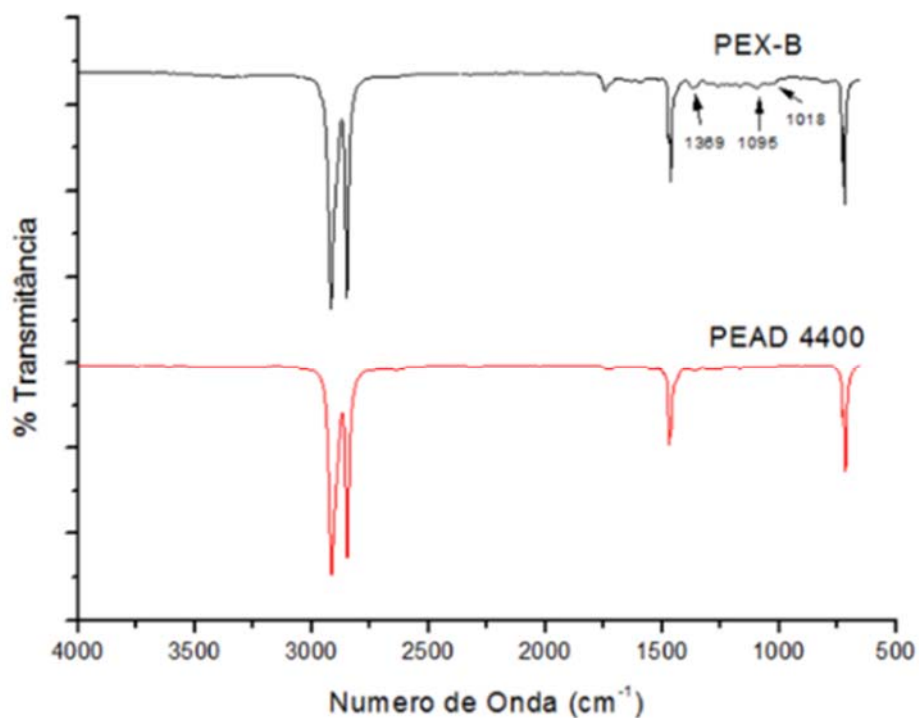


Figura 2: Espectros de FTIR das amostras de PEX-A e PEAD 1878.

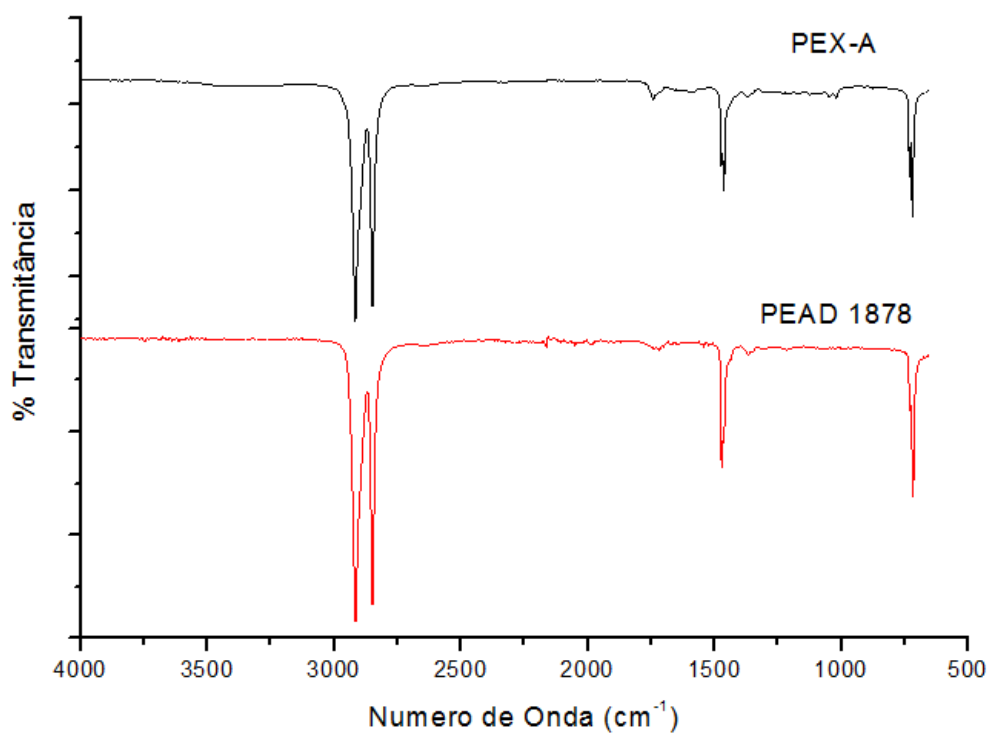


Figura 3: Espectros de FTIR das amostras de PEX-B e PEAD 4400.

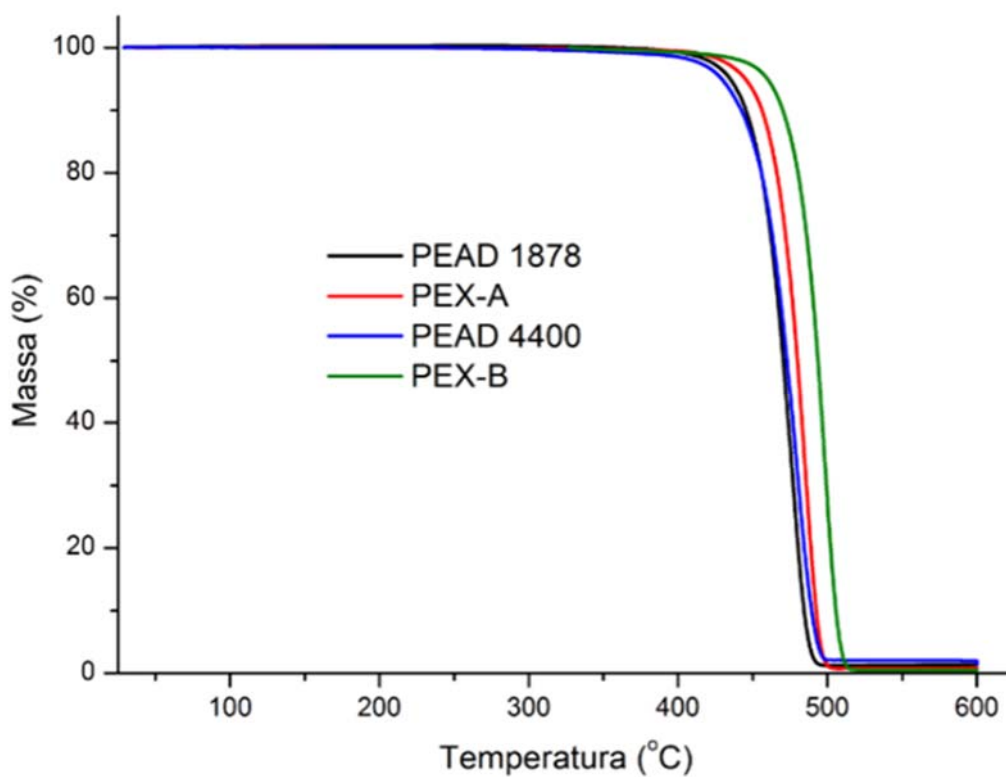


Figura 4: Curvas TG das amostras de polietilenos antes e após a reticulação.

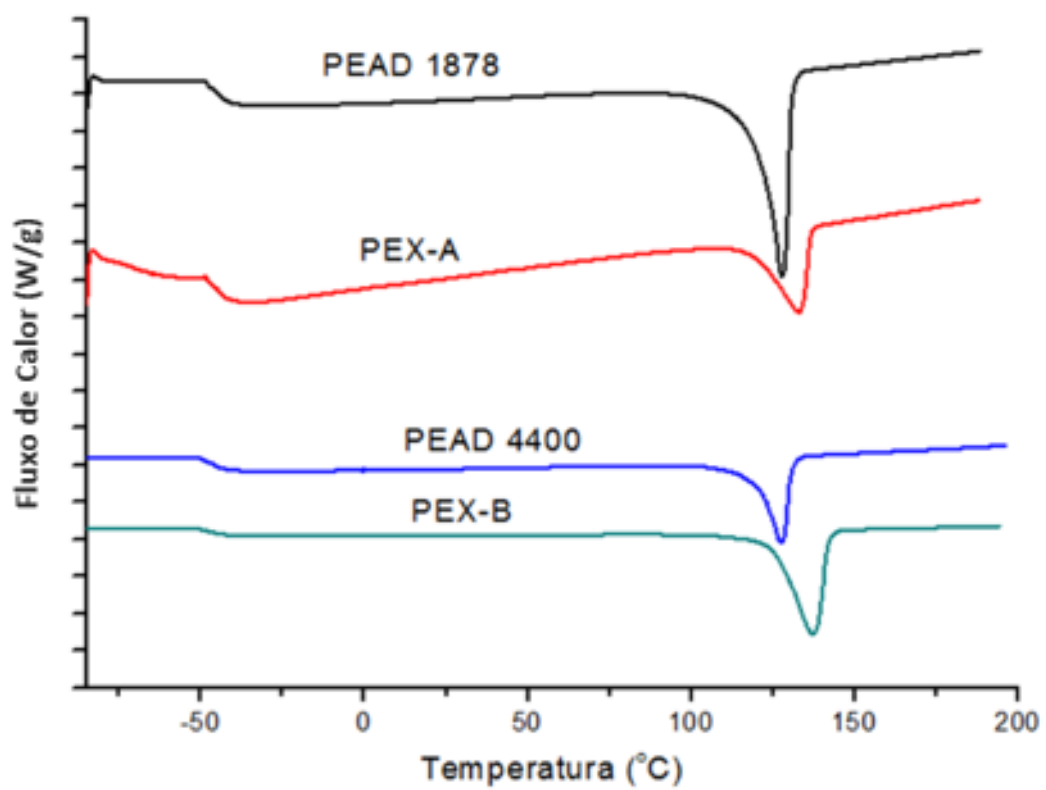


Figura 5: Curvas DSC das amostras de polietilenos antes e após a reticulação

ESTUDO DE CITOTOXICIDADE, ATIVIDADE ANTIBACTERIANA E COMPOSIÇÃO POR FT-IR E GC-MS PARA O EXTRATO ORGÂNICO DA TRUFA BRANCA *TIRMANIA NIVEA* DO DESERTO DO IRAQUE

STUDY CYTOTOXICITY, ANTIBACTERIAL ACTIVITY, AND COMPOSITIONS BY FT-IR AND GC-MS FOR ORGANIC EXTRACT OF WHITE IRAQI DESERT TRUFFLE *TIRMANIA NIVEA*

دراسة السمية الخلوية، الفعالية ضد بكتيرية، والمركبات بواسطة FT-IR و GC-MS للمستخلص العضوي من الكما الصراوية العراقية البيضاء *TIRMANIA NIVEA*

HACHIM, Ahmad khadem^{1*}; HATEET, Rashid Rahim²; MUHSIN, Tawfik Muhammad³

¹ The Directorate of Education, Basrah, Iraq.

² Department of Biology, College of Science, University of Misan, Maysan, Iraq.

³ Department of Biology, College of Education for Pure Science, University of Basrah, Basrah, Iraq.

* Corresponding author

e-mail: biorashed@uomisan.edu.iq

Received 07 May 2020; received in revised form 07 June 2020; accepted 05 August 2020

RESUMO

O objetivo do presente trabalho foi explorar os potenciais componentes bioquímicos e atividades biológicas de um extrato orgânico da trufa branca *Tirmania nivea* coletada no deserto do Iraque, posteriormente testou-se a citotoxicidade do extrato orgânico contra células de carcinoma da laringe humana e cepas selecionadas de bactérias patogênicas. A espectroscopia no infravermelho com transformada de Fourier (FTIR) e a cromatografia gasosa acoplada a espectrometria de massa (GC/MSS) foram usadas para analisar as composições micoquímicas. A atividade antibacteriana, a concentração inibitória mínima (CIM), e a concentração bactericida mínima (MBC) foram investigadas pelo método do disco-difusão em ágar. O efeito da citotoxicidade do extrato de trufa contra a linha celular da laringe (Hep-2) foi avaliado pelo ensaio MTT (*in vitro*). Os resultados do FTIR domonstraram a presença de fenol, ácido carboxílico e grupo funcional do alceno. A análise GC-MS de *T. nivea* revela a existência de dezenove compostos que podem contribuir para as propriedades farmacêuticas da trufa. Quanto ao resultado da atividade antibacteriana, foi detectada uma atividade de inibição do crescimento do extrato de trufa em (zonas de inibição de 18-40 mm) contra as cepas bacterianas patogênicas testadas, cujos valores mínimos de concentração inibitória variaram de 3,12 a 6,25 mg/mL para *Escherichia coli* (ATCC 25922) e *Staphylococcus aureus* (ATCC 25923), respectivamente. Os resultados da citotoxicidade mostraram que o extrato orgânico de trufa exibiu uma alta taxa inibitória (52.685%) contra a linha celular (Hep-2) a uma concentração de 1,56 µg/mL. Neste trabalho, os resultados mostraram que os extratos orgânicos de *T. nivea* são muito promissores como citotoxicidade do câncer e agente antibacteriano para futuras aplicações médicas.

Palavras-chave: *Tirmania nivea*, Carcinoma da laringe, Teste MTT, Bactérias patogênicas, Propriedades farmacêuticas.

ABSTRACT

The purpose of the present work aimed at exploring the potential biochemical components and biological activities of an organic extract of the white truffle *Tirmania nivea* collected from the Iraqi desert, then test the organic extract against the Cytotoxicity on Human Larynx carcinoma cells and selected strains of pathogenic bacteria. Fourier transform infrared spectroscopy (FTIR) and gas chromatography-mass spectrometry GC/MSS were used to analyze mycochemical compositions. The antibacterial activity and Minimum Inhibitory Concentration (MIC) and Minimum Bactericidal Concentration (MBC) was investigated using a disk diffusion agar method. The truffle extract's cytotoxicity effect against the larynx cell line (Hep-2) was assessed by the MTT assay (*in vitro*). FTIR results provided the presence of phenol, carboxylic acid, and

alkane's functional group, The GC-MS analysis of *T. nivea* disclose the existence of nineteen compounds that can contribute to the pharmaceutical properties of the truffle. As for antibacterial activity result, A growth inhibition activity of truffle extract at (18-40 mm inhibition zones) against the tested pathogenic bacterial strains was detected, which minimum inhibitory concentration values ranged from 3.12 to 6.25 mg/mL for *Escherichia coli* (ATCC 25922) and *Staphylococcus aureus* (ATCC 25923) Respectively. The results of cytotoxicity shown that the organic truffle extract exhibited a high inhibitory rate (52.685%) against cell line (Hep-2) at a concentration of 1.56 µg/mL. In this work, the results showed that the organic extracts of *T. nivea* are very promising as cancer cytotoxicity and antibacterial agent for future medical applications.

Keywords: Tirmania nivea, Larynx carcinoma, MTT assay, Pathogenic bacteria, Pharmaceutical properties

الملخص

الغرض من العمل الحالي الذي يهدف إلى استكشاف إمكانية المكونات البيوكيميائية والفعاليات الحيوية للمستخلص العضوي من الكمأ الأبيض الذي تم جمعه من الصحراء العراقية، بعدد اختبار المستخلص العضوي ضد السمية الخلوية على خلايا سرطان الحنجرة البشري وسلالات مختارة من البكتيريا المسببة للأمراض. تم استخدام تحويل فورييه الطيفي بالأشعة تحت الحمراء (FTIR) واستشراب غازي-مطياف كتلة GC-MS لتحليل المكونات الكيميائية الفطرية. تم فحص الفعالية ضد بكتيرية والتركيز المثبط الأدنى (MIC) والتركيز القاتل للبكتيريا (MBC) باستخدام طريقة النشر بالأقراص. تم تقييم تأثير السمية الخلوية لمستخلص الكمأ على خط خلايا الحنجرة (Hep-2) بواسطة اختبار MTT (في المختبر). أثبتت نتائج FTIR وجود الفينول، حمض الكربوكسيل والمجموعة الوظيفية للألكان، تحليل GC-MS للكمأ كشف عن وجود تسعة عشر مركباً يمكن أن تساهم في الخصائص الصيدلانية للكمأ. أما بالنسبة لنتيجة الفعالية ضد بكتيرية، فقد تم الكشف عن فعالية تثبيط نمو مستخلص الكمأ عند (18-40 ملم منطقة التثبيط) ضد السلالات البكتيرية المرضية، والتي تراوحت قيم التركيز المثبط الأدنى من 3.12 إلى 6.25 ملغم / مل لـ الإشريكية القولونية سلالة (ATCC 25922) والعنقودية الذهبية سلالة (ATCC 25923) على التوالي. أظهرت نتائج السمية الخلوية أن مستخلص الكمأ العضوي أظهر معدل تثبيط مرتفع (52.685%) ضد خط الخلايا (Hep-2) بتركيز 1.56 ميكروغرام/مل. في هذا العمل، أظهرت النتائج أن المستخلصات العضوية من الكمأ الأبيض واعدة للغاية للتطبيقات الطبية في المستقبل بأعتبارها تمتلك سمية للخلايا السرطانية وعامل مضاد للبكتيريا.

الكلمات المفتاحية: الكمأ الأبيض، سرطان الحنجرة، اختبار MTT، البكتيريا المسببة للأمراض، الخصائص الصيدلانية.

1. INTRODUCTION:

Over the past fifty years, many significant advances in medicine have come from the Kingdom of fungi. Fungi are distinct manufacturers of biologically active compounds with antibiotics, growth-regulating, toxic, mutagenic, and immunosuppressive, in addition to other biological properties (Gajos *et al.*, 2014; Manoharachary *et al.*, 2014). The first antibiotic was extracted from fungi, and the drug has been regarded as a wonder for infectious and communicable diseases. New developments in cancer treatment have recently increased in natural chemotherapy, which involves the use of adjuvants of biologically active compounds. In particular, fungi natural products may not only be used as potent immunosorbents, but it can also be used as a source of active metabolites, which penetrate the cell membranes and interfere with a specific pathway for signal transfer in processes like inflammation, cell differentiation, survival, carcinogenesis, and metastases (Liu *et al.*, 2016).

Mushroom is one of the most promising pharmaceutical applications fungi. Mushrooms and truffles are nutrient-dense, versatile foods with putative health benefits associated with fruit and vegetable consumption. China is the world leader in the production of mushrooms, followed

by the United States, Italy, the Netherlands, and Poland. Mushrooms are a rare source of ergothioneine, dietary fiber, selenium, minerals, and vitamins. The mushroom market is expected to rise because of nutritional and potential health benefits, including awareness, oral health, weight control, and reduced cancer risk. Mushrooms and truffles are also alleged to exert an immunomodulatory effect through interaction with the gut microbiota (Saritha *et al.*, 2016). Hall *et al.* (2003) describe mushrooms in a far more realistic portrait as "Every fungus has a Featured fruiting body, large enough to be picked" (Pérez-Moreno and Martínez-Reyes, 2014). The use of mushrooms in ancient eastern treatments is well known. Current researchers have confirmed and documented a significant part of the long time past data. The interdisciplinary research in medicinal mushrooms has been expanded through the last periods and demonstrated further the essential and distinct characteristics of compounds extracted from various species. The field is currently produced in an extremely productive region. Current clinical practice is dependent on mushroom extracts in Japan, China, Korea, and other Asian nations (Murat *et al.*, 2008; Elsayed *et al.*, 2014).

Desert truffle is a hypogene ascomycete obligatory for ectomycorrhizal mushrooms, formed in symbiotic relation to *Helianthemum's*

roots (Kagan-Zur and Roth-Bejerano 2008; Zdrojewicz *et al.*, 2016). It has been documented to be medicinal feeding stuff and was described as a natural miracle in ancient culture as Chinese, Greek, Egyptian and Mesopotamian civilizations (Bahrani 2006; Wang and Marcone, 2011; Badalyan 2012; Patel 2012). Truffles are one of the ancient foods; It was used as a meat replacement and consumed in large quantities because of its delicious flavor and its musky flavor (Al-Shabibi *et al.*, 1982; Mandeel and Al-Laith 2007; Dundar *et al.*, 2012). The scent of the white truffle is often identified as sulfurous or garlicky, and the presence of sulfur-containing VOCs is due to this kind of odor (Vita *et al.*, 2018). Furthermore, It was used in folk medicine for eye treatment. (Janakat and Nassar 2010; Brown *et al.*, 2016). Truffles are among the main ingredients of many favorite Middle East traditional dishes (AL-RUQAIE, 2006). Truffle contains high amounts of P, K, and fair levels of Ca, Mg, Na, Fe, Cu, Zn, and Mn (Hussain and Al-Ruqaie, 1999).

Tirmania nivea, the most known truffles in the world, are white desert truffle common names (zabidee), including Iraq, which is naturally found in the middle, south, and western areas (Gutiérrez *et al.*, 2003; Al-Laith, 2010; Stojković *et al.*, 2013; Vahdani *et al.*, 2017). After a rainy period (February, March, and April), truffles usually arise in the desert. It is periodically and socially and economically indispensable fungi. According to the quantity of rain and other environmental factors, truffle distribution, nutrition value, and therapeutic properties will differ in seasons (Owaid 2016).

Desert truffles include an unlimited but generally untapped source of new pharmaceutical products (Shavit and Shavit 2014). Truffle has a high nutritional value consisting of healthy fatty acids, vitamin supplements, protein, and minerals. There are a few truffle species reported in the genera *Terfezia*, *Tirmania*, and *Tuber* in chemical components as well as in therapeutic characteristics (Villares *et al.*, 2012; Akyüz, 2013), which is a novel exporter of anti-inflammatory, anticancer, and antioxidative compounds (Hannan *et al.*, 1989; Murcia *et al.*, 2002; Dahham *et al.*, 2015). In addition to the antiviral lectin cyanovirin-N (CVN) and fruiting body-specific lectin TBF-1 from *Tuber borchii* Vittad (Percudani *et al.*, 2005; Cerigini *et al.*, 2007).

According to our information, there is little data available on bio-compounds produced from

truffle *Tirmania*, especially Iraqi truffles. Current work has therefore been carried out to investigate the chemical compounds extracted from ascocarps of this fungus Collected from the desert of Iraq and identified using Fourier transforms infrared spectroscopy (FT-IR) and gas chromatography-mass spectrometry (GC-MSS), tested for cytotoxicity in human larynx carcinoma cells and selected pathogenic bacterial strains.

2. MATERIALS AND METHODS

2.1 Truffles Collection

A sample of truffles locally known as "Alchama" used in the present study was collected from the Al-Salman region in the Iraqi desert during the growing season (February-April) associated with the host roots of *Helianthemum sp.* (Cistaceae), were identified based on the morphological and microscopic characters using standard methods (Alsheikh and Trappe 1983).

2.2 Preparation of Truffles

Ascocarps samples were cleaned from the soil in the laboratory, peeled, sliced, and dried at Shadow (7 days). Crushed the dried slices, and the fine powder was capped in well-labeled airtight containers and stored at room temperature (Al-Laith, 2010).

2.3 Preparation of truffle extract

20 g of truffle powder was soaked for three days in 0.5 L of methanol 400 ml and distilled water (type IV) 100 ml (4:1, v/ v) at room temperature, then filtered through Whitman filter paper No.1, evaporated, redissolved in H₂O, and pH=3 by HCl (2N), separating funnel was used to extract filtrate three times with ethyl acetate (150 mL). The organic composition was obtained and dehydrated in Petri dishes using Na₂SO₄ at room temperature (Berger *et al.*, 2004).

2.4 Antibacterial bioactivity assay

2.4.1 The microorganisms test

Five bacterial strains (*Escherichia coli*, *Staphylococcus aureus*, *Streptococcus pyogenes*, *Klebsiella pneumonia*, and *Salmonella typhi*) were isolated from the clinical cases in Misan, South Iraq and have been used two standard bacterial strains; *Escherichia coli* (ATCC 25922) and *Staphylococcus aureus* (ATCC

25923) for comparison. All samples were cultivated on maintenance media until use (Hateet, 2015).

2.4.2 Discs diffusion agar method

To evaluate the antibacterial activity of the truffle crude extract, disc diffusion agar assay was employed in standard ways (Casals, 1979). Dissolved in 1 mL dimethyl sulfoxide (DMSO) solvent, 2.5 mg of the dried truffle extract from Whitman filter paper, sterilized Discs with a diameter of 0.6 mm was soaked in the fungal extract. Placed on Petri dishes containing medium Muller-Hinton Agar (MHA), inoculated by streaking process of 0.1 mL suspension of bacterial strains. Incubation of bacterial cultures at 37 °C.

2.4.3 Determination of MIC and MBC

A standard test using serial dilutions of truffle extract (100, 50, 25, 12, 6.5, 3.13, 1.56, 0.78, 0.39, 0.2, 0.1, 0.05, 0.025 µg/L) has determined values of MIC. In this assay, the lowest levels indicated that the MIC values inhibit bacterial growth. The low bactericidal (MBC) was registered as the lowest bacterial-killing concentration, and no visible bacterial growth was found (McGinnis 2012).

2.5 Cytotoxicity efficacy of the truffle extract

The potential cytotoxicity of truffle extract using cell line (Hep-2) was tested by MTT (Ibrahim *et al.*, 2011). Briefly, the Hep-2 cell line was cultivated on a specified medium enhance with antibiotics and cells grown in CO₂ and humidity conditions at a temperature of 37 °C. The cell line (Hep-2) was seeded in 96 well tissue plates in quantities of (1 to 105 cell/well). Preparation of different truffle extract concentrations ranging from (0.05-100 µg/mL) and modified to cell lines in the wells and incubated at 37 °C for 24 hours. Non-treated cells were used as control. After the incubation time, the cells were rinsed with PBS, and the viability of the cells was determined. To measurement, the absorption at 550 nm, a spectrometer (APEL PD-303, Japan) was used, and the cell viability percentage was calculated as equation no. 1 (Eq.1). IC₅₀ was identified as the concentration of truffle extract that kills 50% of cells.

2.6 Detection of Chemical Compositions

2.6.1 Fourier transforms infrared spectroscopy (FT-IR) technique

FTIR analytics were performed using the Shimadzu UV-1700 Spectrophotometer system to detect functional groups in organic truffle extracts. For the production of translucent disks, the 5 mg truffle extract was encapsulated into 100 mg of pellet (KBr) potassium bromide, which was then inserted into the sample cup of an accessory for diffuse reflection. The peak values of the FTIR were recorded, and the scanning range was set at 4 cm⁻¹ resolution from 400 - 4000 cm (Zhao *et al.*, 2006).

2.6.2 Gas Chromatography-Mass Spectrometry

The organic extract extracted from truffle *Tirmania nivea* was analyzed using GC SHIMADZU QP2010 Ultra and gas chromatography, interfaced with a Mass Spectrometer (GC-MS) equipped with the DbB5ms capillary column. The relative % amount of each component was calculated by comparing its average peak area to the total areas, software adapted to handle mass spectra, and chromatograms were a Turbomass. Interpretation of mass spectrum GC-MS was conducted using the database of National Institute Standard and Technology (NIST), having more than 62,000 patterns. The frequency of the unknown component was compared with the range of the known elements stored in the NIST library. The Name, Molecular weight, and structure of the Ingredients of the test materials were ascertained (Pacioni *et al.*, 2014).

3. RESULTS AND DISCUSSION

3.1 Truffles Collection, Preparation of the extract

The truffles ordinarily found in Iraq's desert (Ewaze and Al-Naama, 1989; Owaid 2016). Truffle's ascocarps are usually hypogynous, with the basal attachment, such as Tuber. All truffles have been identified as white *Tirmania nivea* (Zabidi) (Pezizaceae), with microscopic characteristics, musk smell, and flavored lightness, as shown in (figure 1). The truffle separate from the root of the host plant *Helianthemum* sp. (Cistaceae), the majority of plant species supporting desert truffle mycorrhizas belong to the genus *Helianthemum* (Cistaceae) (Kagan-Zur and Akyuz, 2014).

3.2 Antibacterial activity of the truffle extract

In the present research, the antibacterial organic extract activity from truffle *T. nivea* was determined using Discs diffusion agar method. The extract of *T. nivea* has antibacterial activity in all the examined pathogenic bacteria in the occurrence or absence of inhibitory zones and zone diameter (Figure 2) (Table 1). The extract of *T. nivea* antibacterial inhibitory activity was measured against *Salmonella typhi* (40 mm), *Klebsiella pneumonia* (35 mm), *Streptococcus pyogenes* (27 mm), *E. coli* (26 mm), *Staph. aureus* (NCTC6571) (25 mm), *E. coli* (ATCC25922) (24 mm), and *Staph. aureus* (18 mm) (Table 1). In contrast to the two standard bacterial strains, *E. coli* (ATCC25922) and *Staph. aureus* (NCTC6571), the values of MIC and MBC were very shallow (Table 2). Previous works confirmed the results of this research, the antimicrobial effects of different extracts from *Terfezia sp.* and *Tirmania sp.* revealed their good antimicrobial activity on different bacterial species (Fortas and Belahouel-Dieb, 2007; Neggaz and Fortas 2013; Neggaz *et al.*, 2018; Hamza *et al.*, 2016). Dib-Bellahouel and Fortas (2011) reported a potent antibacterial activity against *B. subtilis* and *Staph. aureus* with the ethyl acetate extract from *Tirmania pinoyi*. In a further study conducted by Gouzi *et al.* (2011), *Tirmania nivea* aquatic extract has antibacterial efficacy at *Staph. aureus*, *P. aeruginosa*. More recent studies indicate that *Tirmania* truffle methanol extract has higher inhibitory activity than ethyl acetate and aqueous extracts of both gram bacteria (Janakat *et al.*, 2005). However, the results obtained by using organic extract are similar or more effective than this literature. Also, the *Tirmania*-AgNPs had a promising antibacterial activity against bacteria, which consider the main infectious for the eyes *Pseudomonas aeruginosa* bacteria and gram-positive (*Staphylococcus aureus*) bacteria (Owaid *et al.*, 2018).

3.3 Cytotoxicity efficacy of the truffle extract

The *in vitro* cytotoxicity of the organic truffle extract *T. nivea* was tested at various concentrations against the cell line (Hep-2). The results indicated that the truffle *T. nivea* extract inhibition concentration (IC₅₀) of 50% of the mortality of cells was 1.56 µg/mL (Figure 3). Cytotoxicity has, however, been increased at higher truffle extract concentrations. These data suggest that *T. nivea* crude organic compound was toxic onto the cell line Hep-2. Truffle's cytotoxic activity might be clinically significant,

and further anticancer properties must be investigated. The results are similar to those observed in the American National Cancer Institute (NCI) crude extract cytotoxicity activity, which is IC₅₀ < 30 µg/mL⁻¹. Mekawey (2015) shown cytotoxicity of the various *Terfezia boudieri* extracts in Egypt on six tumour cell lines. The study showed that aqueous extract is highly toxic to four cancer lines HEP2, HCT116, MCF7, and CACO2. Dahham *et al.* (2018) reported that *Terfezia claveryi* hexane extract from the Iraq truffle showed IC₅₀ value was 50.3 µg/mL⁻¹, followed by a 72.6 µg/mL⁻¹ ethyl acetate extract from brain cell (U-87) line. Also, the cytotoxicity of ethanol and methanol extracts against U-87 MG was moderate, with IC₅₀ values of 109.25 ± 9.51 and 136.2 ± 7.4 mg/mL, respectively.

3.4 Fourier transforms infrared spectroscopy (FT-IR) technique

The organic extract from truffle *T. nivea* was passed through the FTIR in the range of 400-4000 cm⁻¹. The FT-IR peaks and functional groups in Table 3. The truffle extract showed the presence of broadband at about 3346 cm⁻¹, at 2925 cm⁻¹ and 2854 cm⁻¹ sharp bands; two large groups at about 1660 cm⁻¹ and 1595 cm⁻¹; band at about 1743 cm⁻¹, 1411 cm⁻¹, and 1039 cm⁻¹; at 991 cm⁻¹ and 804 cm⁻¹ reflect the bending vibrations of the hydroxyl bond, fatty acids, amide I and amide II protein, alkyl esters and carbohydrates respectively (Figure 4). The study showed that crude extracts of *T. nivea* have the properties of antimicrobials and antitumor and have phenol, carboxylic acid, and alkanes, functional group.

3.5 Gas Chromatography-Mass Spectrometry

GC - MS analysis showed nineteen chemical components that may relate to and participate in the truffle's pharmaceutical properties. Identify of chemical compounds with their molecular formula, retention time (RT), molecular weight (MW), and peak area value (%) is shown in Table 4 and Figure 5. Results show that methyl ester, (Z) - 13-Docosenoic acid (Erucic Acid) (19.82%), Octadecanoic acid, Stearic acid, methyl ester (15.18%), Oleic acid ester (12.94%), Palmitic acid, methyl ester (11.53%), Methyl 9,10-methylene- octadecanoic (7.04 %), 8-Octadecenoic acid, methyl ester (5.14%) were found as the major components in the methanol extract and the other minor components such as 1,3-Dioxane-2-propanol, 2-methyl-alcohol

(0.87%), isosorbide (Glucitol) (2.95%), N -[(Penta fluorophenyl, Benzeneethanamine Aromatic Compound (0.94%), 4,4'-isopropylidene di-Phenol (Biphenol A) Aromatic alcohol (4.29%), methyl ester, (Z) - 15-Tetracosenoic acid (Methyl neonate) (1.35%), I - (+) - Ascorbic acid 2,6- di hex decanoate (1.72%). Methyl ester has been reported to serve as antibacterial effects, anti-inflammatory, hypocholesterolemic, preventive, hepatoprotective, and antihistaminic properties of palmitic acid, 9,12,15-octadecatrienoic acid, and hexadecanoic acid (Kumar *et al.* 2011). Furthermore, Palmitic acid also had significant cytotoxicity against breast MCF-7, liver cancer WRL-68, colon cancer CaCO₂, Colo-320 DM, and hepatoprotection against galactosamine. Further research by Carrillo and Alonso-Torre (2012) revealed the antitumor and anti-proliferative impact of oleic acid on prostate cancer PC3.

Nevertheless, Hayshi *et al.* (1998) stated that octadecadienoic acid is also antitumoral. Recently, Wang and Marconi (2011) recently concluded in a study that hexadecanoic acid is an essential compound discovered in truffle tuber that has a smell of a truffle. As a result of the above points, the cytotoxicity and antibacterial activity of *T. nivea* can be speculated due to the presence and synergistic effect of these major chemical constituents.

4. CONCLUSIONS

This study revealed the antibacterial properties and cytotoxicity of organic extract *Tirmania nivea*, a wild truffle from the Al-Salman area of the Iraqi desert. Besides, phenolic, fatty acids, triterpenes, and vitamins have been found in truffles, which may be responsible for the antimicrobial and cytotoxic activity reported in this research. The study results showed that the crude extract exhibited inhibitory activity against all pathogenic bacteria and cytotoxicity effects against the cell line (Hep-2), and based on the results of current research, the truffle extract can be a useful source of antibacterial and cytotoxicity drugs. However, it is essential to further investigate the purification and identification of white desert truffle bioactive compounds to explore in more detail potential pharmaceutical effects.

5. ACKNOWLEDGMENTS:

The authors thank the authorities of the

University of Basrah (Iraq) for supporting this research work.

6. REFERENCES:

1. Al-Laith, A. A. A. (2010). Antioxidant components and antioxidant/antiradical activities of desert truffle (*Tirmania nivea*) from various Middle Eastern origins. *Journal of Food Composition and Analysis*, 23(1), 15-22.
2. AL-RUQAIE, I. M. (2006). Effect of different treatment processes and preservation methods on the quality of truffles: I. Conventional methods (drying/freezing). *Journal of food processing and preservation*, 30(3), 335-351.
3. Al-Shabibi, M. M. A., Toma, S. J., and Haddad, B. A. (1982). Studies on Iraqi truffles. I. Proximate analysis and characterization of lipids. *Canadian Institute of Food Science and Technology Journal*, 15(3), 200-202.
4. Alsheikh, A. M., and Trappe, J. M. (1983). Desert truffles: the genus *Tirmania*. *Transactions of the British Mycological Society*, 81(1), 83-90.
5. Badalyan, S. (2012). Medicinal aspects of edible ectomycorrhizal mushrooms. In *Edible Ectomycorrhizal Mushrooms* (pp. 317-334). Springer, Berlin, Heidelberg.
6. Bahrani, Z. (2006). Race and ethnicity in Mesopotamian antiquity. *World Archaeology*, 38(1), 48-59.
7. Berger, A., Rein, D., Kratky, E., Monnard, I., Hajjaj, H., Meirim, I., Piquet-Welsch, C., Hauser, J., Mace, K., and Niederberger, P. (2004). Cholesterol-lowering properties of *Ganoderma lucidum* in vitro, ex vivo, and in hamsters and minipigs. *Lipids in health and disease*, 3(1), 2.
8. Brown, M. A., Potroz, M. G., Teh, S. W., and Cho, N. J. (2016). Natural products for the treatment of Chlamydiae infections. *Microorganisms*, 4(4), 39.
9. Carrillo, C., and Alonso-Torre, S. R. (2012). Antitumor effect of oleic acid; mechanisms of action. A review. *Nutricion hospitalaria*, 27(6), 1860-1865.
10. Casals, J. B. (1979). Tablet sensitivity testing on pathogenic fungi. *Journal of clinical pathology*, 32(7), 719-722.
11. Cerigini, E., Palma, F., Buffalini, M., Amicucci, A. Ceccarelli, P., Saltarelli, R,

- Stocchi, V. (2007). Identification of a novel lectin from the Ascomycetes fungus *Tuber borchii*. *INTERNATIONAL JOURNAL OF MEDICINAL MUSHROOMS*, 9:287.
12. Dahham, S. S., Al-Rawi, S. S., Ibrahim, A. H., Majid, A. S. A., and Majid, A. M. S. A. (2018). Antioxidant, anticancer, apoptosis properties and chemical composition of black truffle *Terfezia clavaryi*. *Saudi journal of biological sciences*, 25(8), 1524-1534.
 13. Dahham, S. S., Tabana, Y. M., Iqbal, M. A., Ahamed, M. B., Ezzat, M. O., Majid, A. S., and Majid, A. M. (2015). The anticancer, antioxidant and antimicrobial properties of the sesquiterpene β -caryophyllene from the essential oil of *Aquilaria crassna*. *Molecules*, 20(7), 11808-11829.
 14. Dib-Bellahouel, S., and Fortas, Z. (2011). Antibacterial activity of various fractions of ethyl acetate extract from the desert truffle, *Tirmania pinoyi*, preliminarily analyzed by gas chromatography-mass spectrometry (GC-MS). *African Journal of Biotechnology*, 10(47), 9694-9699.
 15. Dundar, A., Yesil, O. F., Acay, H., Okumus, V., Ozdemir, S., and Yildiz, A. (2012). Antioxidant properties, chemical composition and nutritional value of *Terfezia boudieri* (Chatin) from Turkey. *Food science and technology international*, 18(4), 317-328.
 16. Elsayed, E. A., El Enshasy, H., Wadaan, M. A., and Aziz, R. (2014). Mushrooms: a potential natural source of anti-inflammatory compounds for medical applications. *Mediators of inflammation*, 2014.
 17. Ewaze, J. O., and AL-NAAMA, M. M. (1989). Studies on nitrogen metabolism of *Terfezia* spp. and *Tirmania* spp. *New phytologist*, 112(3), 419-422.
 18. Fortas, Z., and Belahouel-Dieb, S. (2007). Extraction des substances bioactives des terfezes d'Algérie et mise en évidence de leur activité antimicrobienne. *Rég. Arid*, 1, 280-282.
 19. Gajos, M., Ryszka, F., and Geistlinger, J. (2014). The therapeutic potential of truffle fungi: a patent survey. *Acta Mycologica*, 49(2), 305-318.
 20. Gouzi, H., Belyagoubi, L., Abdelali, K. N., and Khelifi, A. (2011). In vitro antibacterial activities of aqueous extracts from Algerian desert truffles (*Terfezia* and *Tirmania*, Ascomycetes) against *Pseudomonas aeruginosa* and *Staphylococcus aureus*. *International journal of medicinal mushrooms*, 13(6), 553-8.
 21. Gutiérrez, A., Morte, A., and Honrubia, M. (2003). Morphological characterization of the mycorrhiza formed by *Helianthemum almeriense* Pau with *Terfezia clavaryi* Chatin and *Picoa lefebvrei* (Pat.) Maire. *Mycorrhiza*, 13(6), 299-307.
 22. Hall, I. R., Yun, W., and Amicucci, A. (2003). Cultivation of edible ectomycorrhizal mushrooms. *TRENDS in Biotechnology*, 21(10), 433-438.
 23. Hamza, A., Jdir, H., and Zouari, N. (2016). Nutritional, antioxidant and antibacterial properties of *Tirmania nivea*, a wild edible desert truffle from Tunisia arid zone. *Med. Aromat. Plants*, 5(258), 2167-0412.
 24. Hannan, M. A., Al-Dakan, A.A., Aboul-Enein, H.Y., and Al-Othaimeen, A.A. (1989). Mutagenic and antimutagenic factor(s) extracted from a desert mushroom using different solvents. *Mutagenesis*, 4(2), 111-114.
 25. Hateet, R. R. (2015). Study of Susceptibility Patterns of Clinical *Staphylococcus aureus* Isolated From Patients With Otitis Media in Missan. *International journal of Comprehensive Leading Research In Science*, 1(2), 51-61.
 26. Hayshi, Y., Nishikawa, Y., Mori, H., Tamura, H., Matsushita, Y. I., and Matsui, T. (1998). Antitumor activity of (10E, 12Z)-9-hydroxy-10, 12-octadecadienoic acid from rice bran. *Journal of fermentation and bioengineering*, 86(2), 149-153.
 27. Hussain, G., and Al-Ruqaie, I. M. (1999). Occurrence, chemical composition, and nutritional value of truffles: an overview. *Paki. J. Biol. Sci*, 2(2), 510-514.
 28. Ibrahim, A. H., Al-Rawi, S. S., Majid, A. A., Rahman, N. A., Abo-Salah, K. M., & Ab Kadir, M. O. (2011). Separation and fractionation of *Aquilaria malaccensis* oil using supercritical fluid extraction and the cytotoxic properties of the extracted oil. *Procedia Food Science*, 1, 1953-1959.
 29. Janakat, S. M., Al-Fakhiri, S. M., and Sallal, A. K. (2005). Evaluation of antibacterial activity of aqueous and methanolic extracts of the truffle *Terfezia clavaryi* against *Pseudomonas aeruginosa*. *Saudi medical journal*, 26(6), 952-955.
 30. Janakat, S., and Nassar, M. (2010). Hepatoprotective activity of desert truffle

- (*Terfezia clavaryi*) in comparison with the effect of *Nigella sativa* in the rat. *Pakistan Journal of Nutrition*, 9(1), 52-56.
31. Kagan-Zur, V., and Akyuz, M. (2014). Asian Mediterranean desert truffles. In *Desert Truffles* (pp. 159-171). Springer, Berlin, Heidelberg.
 32. Kagan-Zur, V., and Roth-Bejerano, N. (2008). Desert truffles. *Fungi*, 1(3), 32-37.
 33. Kumar, B. P., Kannana, M. M., Lavanyaa, B., Suthakaranb, R., and Quinec, D. S. (2011). GC-MS analysis of methanolic extract of *Litsea decanensis* gamble and its free radical scavenging activity. *J of Pharma. Res*, 4(1), 100-103.
 34. Akyüz, M. (2013). Nutritive value, flavonoid content and radical scavenging activity of the truffle (*Terfezia boudieri* Chatin). *Journal of soil science and plant nutrition*, 13(1), 143-151.
 35. Liu, Y., Chen, D., You, Y., Zeng, S., Li, Y., Tang, Q., Han, G., Liu, A., Feng, C., Li, C., Su, Y., Su, Z., and Chen, D. (2016). Nutritional composition of boletus mushrooms from Southwest China and their antihyperglycemic and antioxidant activities. *Food chemistry*, 211, 83-91.
 36. Mandeel, Q. A., and Al-Laith, A. A. A. (2007). Ethnomycological aspects of the desert truffle among native Bahraini and non-Bahraini peoples of the Kingdom of Bahrain. *Journal of ethnopharmacology*, 110(1), 118-129.
 37. Manoharachary, C., Kunwar, I. K., and Rajithasri, A. B. (2014). Advances in applied mycology and fungal biotechnology. *Kavaka* 4379, 92.
 38. McGinnis, M. R. (2012). *Laboratory handbook of medical mycology*. Elsevier.
 39. Mekawey, A. (2015). *Terfezia boudieri* as sources of antitumor and antiviral agent. *World J Pharmac Pharmaceut Sci*, 4, 294-315.
 40. Murat, C., Mello, A., Abbà, S., Vizzini, A., and Bonfante, P. (2008). Edible mycorrhizal fungi: identification, life cycle and morphogenesis. In *Mycorrhiza* (pp. 707-732). Springer, Berlin, Heidelberg.
 41. Murcia, M. A., Martinez-Tome, M., Jimenez, A. M., Vera, A. M., Honrubia, M., and Parras, P. (2002). Antioxidant activity of edible fungi (truffles and mushrooms): losses during industrial processing. *Journal of food protection*, 65(10), 1614-1622.
 42. Neggaz, S., and Fortas, Z. (2013). Tests of antibiotic properties of algerian desert truffle against bacteria and fungi. *Journal of Life Sciences*, 7(3), 259.
 43. Neggaz, S., Fortas, Z., Chenni, M., El Abed, D., Ramli, B., and Kambouche, N. (2018). In vitro evaluation of antioxidant, antibacterial and antifungal activities of *Terfezia clavaryi* Chatin. *Phytothérapie*, 16(1), 20-26.
 44. Owaid, M. N. (2016). Biodiversity and bioecology of Iraqi desert truffles (Pezizaceae) during season 2014. *Journal of Aridland Agriculture*, 2, 22-25.
 45. Owaid, M. N., Muslim, R. F., and Hamad, H. A. (2018). Mycosynthesis of silver nanoparticles using *Terminia* sp. desert truffle, pezizaceae, and their antibacterial activity. *Jordan J. Biol. Sci*, 11(4)401-5.
 46. Patel, S. (2012). Food, health and agricultural importance of truffles: a review of current scientific literature. *Current Trends in Biotechnology and Pharmacy*, 6(1), 15-27.
 47. Pacioni, G., Cerretani, L., Procida, G., and Cichelli, A. (2014). Composition of commercial truffle flavored oils with GC-MS analysis and discrimination with an electronic nose. *Food chemistry*, 146, 30-35.
 48. Percudani, R., Montanini, B., and Ottonello, S. (2005). The anti-HIV cyanovirin-N domain is evolutionarily conserved and occurs as a protein module in eukaryotes. *Proteins: Structure, Function, and Bioinformatics*, 60(4), 670-678.
 49. Pérez-Moreno, J., and Martínez-Reyes, M. (2014). Edible ectomycorrhizal mushrooms: biofactories for sustainable development. In *Biosystems engineering: biofactories for food production in the century XXI* (pp. 151-233). Springer, Cham.
 50. Saritha, K. V., Prakash, B., Khilare, V. C., Khedkar, G. D., Reddy, Y. M., and Khedkar, C. D. (2016). Mushrooms and Truffles: Role in the Diet.
 51. Shavit, E., & Shavit, E. (2014). The medicinal value of desert truffles. In *Desert Truffles* (pp. 323-340). Springer, Berlin, Heidelberg.
 52. Stojković, D., Reis, F. S., Ferreira, I. C.F.R., Barros, L., Glamočlija, J., Ćirić, A., Nikolić, M., Stević, T., Giveli, A., and Soković, M. (2013). *Tirmania pinoyi*: Chemical composition, in vitro antioxidant and antibacterial activities and in situ control of *Staphylococcus aureus* in

- chicken soup. *Food research international*, 53(1), 56-62.
53. Vahdani, M., Rastegar, S., RAHIMIZADEH, M., Ahmadi, M., and Karmostaji, A. (2017). Physicochemical Characteristics, Phenolic Profile, Mineral and Carbohydrate Contents of Two Truffle Species. *JOURNAL OF AGRICULTURAL SCIENCE AND TECHNOLOGY*, 19(4), 1091-1101.
 54. Villares, A., García-Lafuente, A., Guillamón, E., and Ramos, Á. (2012). Identification and quantification of ergosterol and phenolic compounds occurring in Tuber spp. truffles. *Journal of food composition and analysis*, 26(1-2), 177-182.
 55. Vita, F., Franchina, F. A., Taiti, C., Locato, V., Pennazza, G., Santonico, M., Purcaro, G., De Gara, L., Mancuso, S., Mondello, L., and Alpi, A. (2018). Environmental conditions influence the biochemical properties of the fruiting bodies of Tuber magnatum Pico. *Scientific reports*, 8(1), 1-14.
 56. Wang, S., and Marcone, M. F. (2011). The biochemistry and biological properties of the world's most expensive underground edible mushroom: Truffles. *Food Research International*, 44(9), 2567-2581.
 57. Zdrojewicz, Z., Pawlus, K., and Horochowska, M. (2016). Secret life of truffles. *Medycyna Rodzinna*. 3, 133-137.
 58. Zhao, D., Liu, G., Song, D., Liu, J. H., Zhou, Y., Ou, J., and Sun, S. (2006). Fourier transform infrared spectroscopic study of truffles. In *ICO20: Biomedical Optics* (Vol. 6026, p. 60260H). International Society for Optics and Photonics.

$$\text{Viability of cells \%} = \frac{\text{absorption of samples}}{\text{absorption of control}} * 100 \quad (\text{Eq.1})$$



Figure 1. Ascocarps of *Tirmania nivea* (Zabidi)

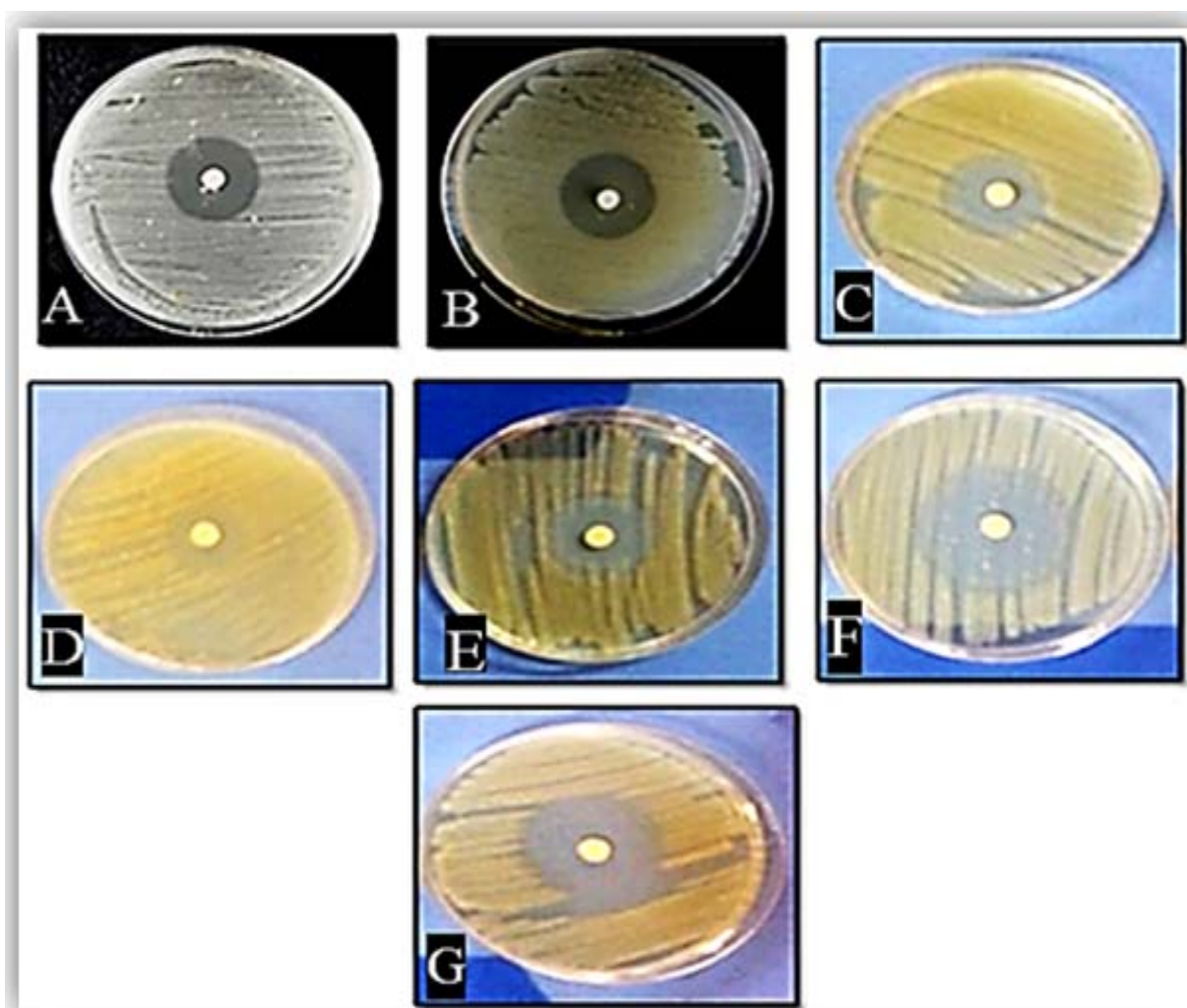


Figure 2. In vitro, the antibacterial activity of organic extracts of desert truffle at concentration 25 µg/discs. (A) *E. coli* (ATCC25922) (B) *Staph. aureus* (NCTC6571) (C) *E. coli* (D) *Staph. aureus* (E) *Streptococcus pyogenes* (F) *Salmonella typhi* (G) *Klebsiella pneumonia*.

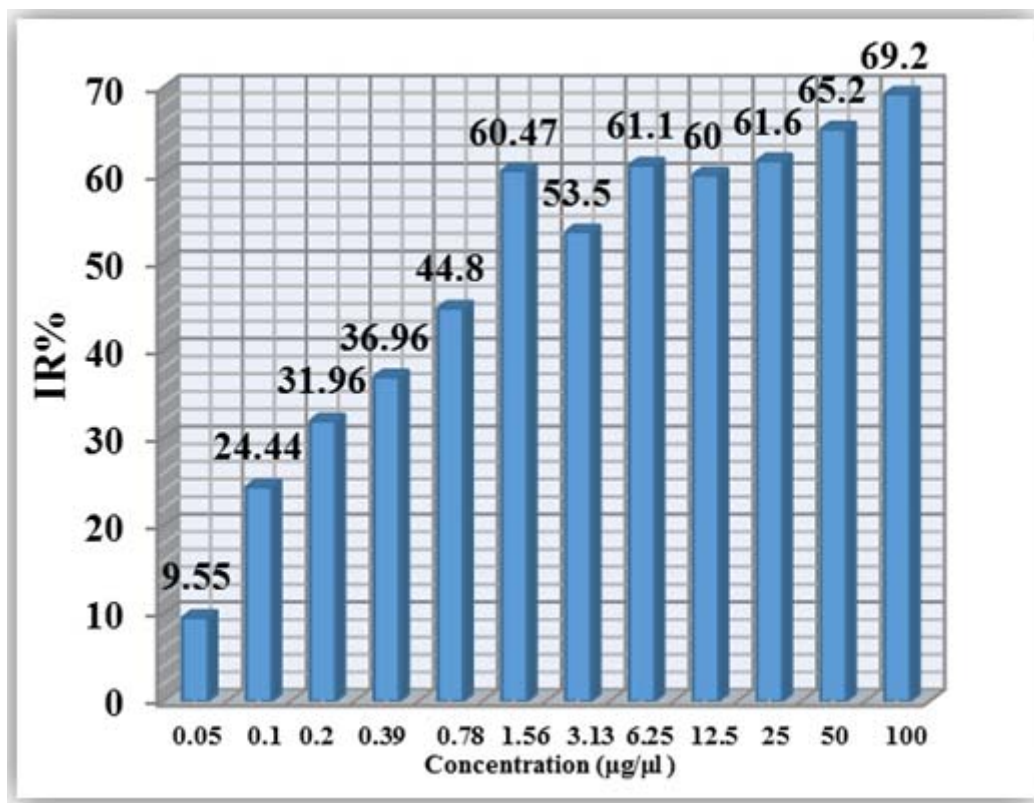


Figure 3. In vitro, the cytotoxicity efficacy of the organic truffle extract *Tirmania nivea* against Human larynx carcinoma cell-line (Hep-2).

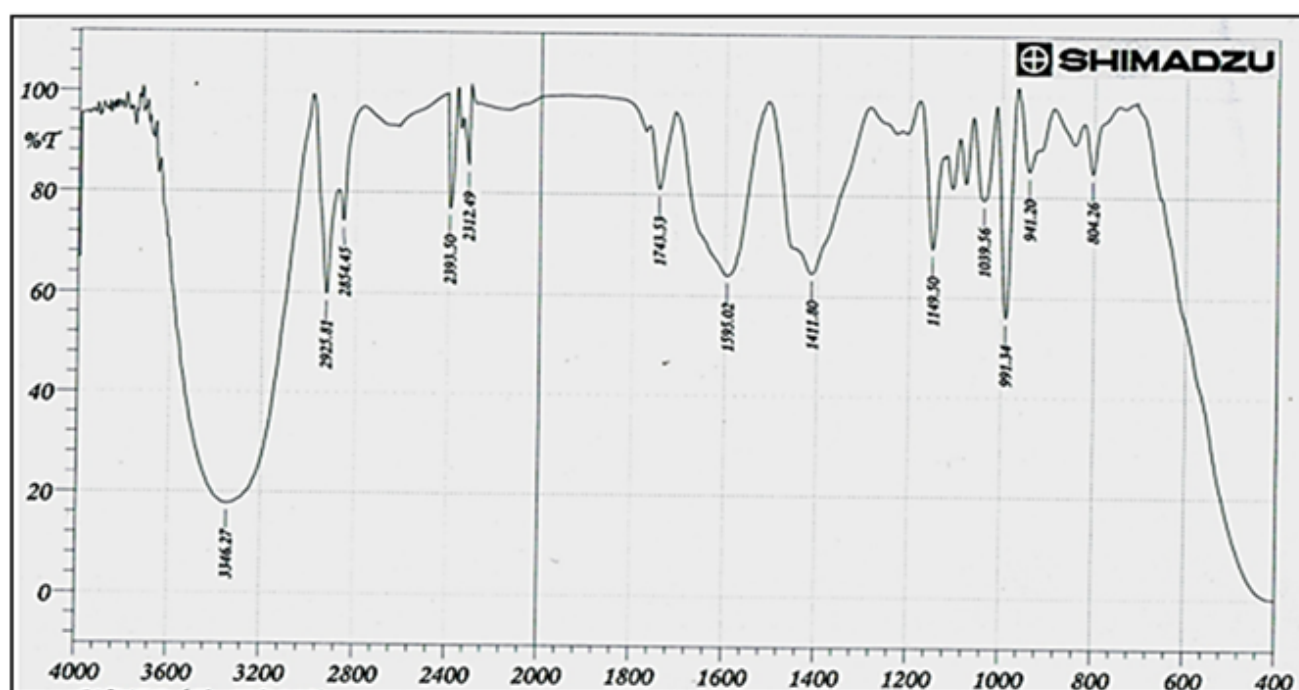


Figure 4. FTIR analysis of organic extracts of desert truffle *Tirmania nivea*.

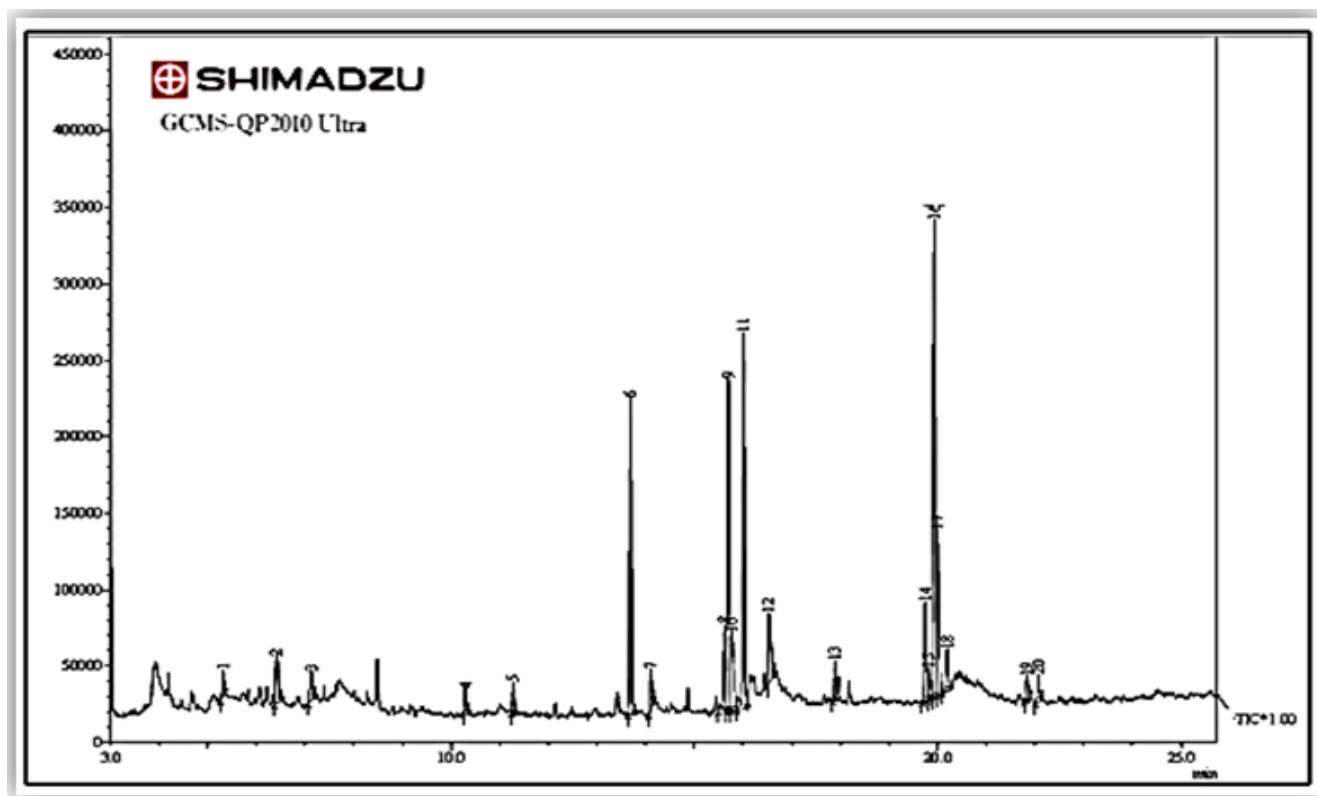


Figure 5. Gas Chromatography-Mass Spectrometry (GC-MS) analysis of an organic extract of desert truffle *Tirmania nivea*.

Table 1. The antibacterial activity of organic extract of desert truffle *Tirmania nivea*

Tests bacteria	Inhibition zone
<i>Escherichia coli</i> (ATCC25922)	24*
<i>Staphylococcus aureus</i> (NCTC6571)	25
<i>Escherichia coli</i>	26
<i>Staphylococcus aureus</i>	18**
<i>Streptococcus pyogenes</i>	27
<i>Salmonella typhi</i>	40**
<i>Klebsiella pneumoniae</i>	35**

* Values represent means of four replicates

** Significant difference at $P \leq 0.001$

Table 2. MIC values of the organic extract of desert truffle *Tirmania nivea* ($\mu\text{g/mL}$).

Bacteria	MIC ($\mu\text{g/ml}$)	MBC($\mu\text{g/ml}$)
<i>Escherichia coli</i> (ATCC25922)	3.12	6.25
<i>Staphylococcus aureus</i> (NCTC6571)	6.25	12.5

Table 3. FTIR peak values and functional groups of organic extracts of desert truffle *Tirmania nivea*

Peak Values λ (nm)	Functional group
3346.27	O-H stretch
2925.81	CH ₂ stretch asymmetric
2854.45	CH ₂ stretch symmetric
1743.53	C=O stretch
1660	C=C aliphatic
1595.02	C=C, C=N aromatic
1411.80	C-O, C-N
1149.50	C-N ₃ binding
1039.56	C-F
991.34, 941.20	C-H aromatic
804.26	C-H aliphatic

Table 4. Total ion chromatogram (GC-MS) of crude extracts of desert truffle *Tirmania nivea*

S. No.	RT	Name of the compound	Molecular formula	Molecular weight	Compound nature	Peak area%
1	5.310	1,3-Dioxane-2-propanol, 2 methyl-	C ₈ H ₁₆ O ₃	160	alcohol	0.87
2	6.416	Isosorbide (Glucitol)	C ₆ H ₁₀	146	Diol	2.95
3	7.126	dodecamethyl-Cyclohexasiloxane	C ₁₂ H ₃₆ O ₆ Si ₆	444	Cyclic silyl ether	1.50
4	10.291	N-[(pentafluorophenyl, Benzeneethanamine	C ₂₄ H ₃₄ F ₅ NO ₃	563	Aryl amine	0.94
5	11.276	Methyl tetra decanoate (Myristic acid ester)	C ₁₅ H ₃₀ O ₂	242	Saturated fatty acid ester	1.09
6	13.690	Hexadecanoic acid, methyl ester (Palmitic acid, methyl ester)	C ₁₇ H ₃₄ O ₂	270	Saturated fatty acid ester	11.53
7	14.108	l-(+)-Ascorbic acid 2,6-dihexadecanoate	C ₃₈ H ₆₈ O ₈	652	Ascorbic acid ester	1.72
8	15.617	Methyl 10-trans,12-cis octadecadienoate	C ₁₉ H ₃₄ O ₂	294	Unsaturated fatty acid ester	3.55
9	15.700	9-Octadecenoic acid (Z)- (Oleic acid ester)	C ₁₉ H ₃₆ O ₂	296	Unsaturated fatty acid ester	12.94
10	15.777	8-Octadecenoic acid, methyl ester	C ₁₉ H ₃₆ O ₂	296	Unsaturated fatty acid ester	5.14
11	16.013	Octadecanoic acid, methyl ester (Stearic acid, methyl ester)	C ₁₉ H ₃₈ O ₂	298	saturated fatty acid ester	15.18
12	16.534	4,4'-isopropylidenedi-Phenol (Biphenol A)	C ₁₅ H ₁₆ O ₂	228	Phenol	4.29
13	17.891	Methyl 11-eicosenoate	C ₂₁ H ₄₀ O ₂	324	Unsaturated fatty acid ester	1.45
14	19.745	hexadecyl- Oxirane (1,2-Epoxyoctadecane)	C ₁₈ H ₃₆ O	268	Epoxy Compound	4.40
15	19.932	methyl ester, (Z)- 13-Docosenoic acid (Erucic acid)	C ₂₃ H ₄₄ O ₂	352	Unsaturated fatty acid	19.82
16	20.002	Methyl 9,10-methylene-octadecanoate	C ₂₀ H ₃₈ O ₂	310	Unsaturated fatty acid ester	7.04
17	20.197	Methyl 20-methyl heneicosanoate(Behenate)	C ₂₃ H ₄₆ O ₂	354	saturated fatty acid ester	1.87
18	21.839	methyl ester, (Z)- 15-Tetracosenoic acid (Methyl nervonate)	C ₂₅ H ₄₈ O ₂	380	Unsaturated fatty acid ester	1.35
19	22.074	Tetracosanoic acid, methyl ester (Lignoceric acid methyl ester)	C ₂₅ H ₅₀ O ₂	382	saturated fatty acid ester	1.15

MÉTODOS CLÁSSICOS PARA PREVER O DESEMPENHO DE RELÉ BUCHHOLZ DANDO OS FENÔMENOS DE FALHA INCIPIENTE NO TRANSFORMADOR IMERSO DE ÓLEO**CLASSICAL METHODS TO PREDICT THE PERFORMANCE OF BUCHHOLZ RELAY BY GIVING THE PHENOMENA OF INCIPIENT FAULT INTO THE OIL IMMERSSED TRANSFORMER****METODE KLASIK UNTUK PREDIKSI KINERJA RELAI BUCHHOLZ DENGAN PEMBERIAN FENOMENA GANGGUAN INCIPIENT KE DALAM TRANSFORMATOR DAYA RENDAMAN MINYAK**GOERITNO, Arief^{1*}; NUGRAHA, Irwan²; BAKTI, Prayoga³¹ Bogor Ibn Khaldun University, Faculty of Engineering and Science, Electrical Engineering Study Program, Indonesia.² Sahabat Sampoerna Company; Credit Analyst, Cimanggis, Depok, West Java, Indonesia.³ Research Center for Testing Technology, Indonesian Institute of Science, Puspiptek Region, Indonesia.

* Corresponding author
e-mail: arief.goeritno@uika-bogor.ac.id

Received 19 July 2020; received in revised form 01 September 2020; accepted 17 September 2020

RESUMO

Este trabalho explica os métodos clássicos para a previsão do desempenho do relé Buchholz. Os métodos tradicionais usam simulações, dando um fenômeno de falha incipiente no transformador imerso em óleo. O relé Buchholz é um tipo de relé mecânico cujo mecanismo de operação é influenciado pelo óleo e o gás no tanque do transformador tendem a se mover para o tanque de expansão através da tubulação de interconexão. Este dispositivo é um componente crítico que está integrado na filosofia de proteção do transformador imerso em óleo. Um simulador baseado em circuito eletrônico que é integrado com um painel de controle de operação do disjuntor foi escolhido como um meio para criar condições durante o alarme ou desarme. A medição de desempenho fornece condições de falha simuladas para configuração de alarme e desarme. Fornecimento de simulação de falhas na forma de pressionar um botão uma vez para simular a existência de uma condição de alarme. Nessa condição, o painel de controle dos disjuntores não funciona, mas sim o apontamento de um sinal de alarme. Com base nisso, a sirene soa e a falha de verificação da condição ainda é normal ou "sem bloqueio". Fornecendo pressão total como uma forma de simulação para condições de disparo no relé Buchholz, o painel de controle designa a condição dos dois CBs (lado de 150 kV e lado de 20 kV) abertos, e a designação do sinal de alarme também ocorre com o som da campainha. Portanto, o status da verificação torna-se "bloqueio". O relé Buchholz serve para detectar a presença do gás oriundo do aquecimento local ou picos de pressão no óleo do transformador. Depois de fornecer todas as condições, o desempenho do relé Buchholz é conhecido.

Palavras-chave: alarme e disparo; detectar a presença de gás; simulação de condições reais.

ABSTRACT

This work explains the classical methods for predicting the performance of the Buchholz relay. The traditional methods use the simulation by giving a phenomenon of incipient fault into the oil-immersed transformer. The Buchholz relay is a type of mechanical relay whose operating mechanism is influenced by oil and gas in the transformer tank tend to move into the expansion tank through the interconnecting piping. This device is a critical component that is integrated into the oil-immersed transformer protection philosophy. An electronic circuit-based simulator that is integrated with a circuit breaker operation control panel was chosen as a means for creating conditions during alarm or trip. The performance measurement provides simulated fault conditions for setting on alarm and trip. The provision of faults simulation in the form of pressing a push-button one time to simulate the existence of an alarm condition. In that condition, the CBs control panel does not operate, but the appointment of an alarm signal. Based on that, the Buzzer sounds and the status check trip is

still normal or "no lock-out". Giving full pressure as a form of simulation for trip conditions on the Buchholz relay, the control panel designates the condition of the two CBs (side of 150 kV and 20 kV side) open, and the alarm signal designation also occurs with Buzzer sounding. Hence, the check trip status becomes "lock-out". The Buchholz relay serves to detect the presence of gas caused by local heating or pressure surges in the transformer oil. After giving all of the conditions, the Buchholz relay performance is known.

Keywords: *alarm and trip; detect the presence of gas; simulation of real conditions.*

ABSTRAK

Makalah ini berisi penjelasan metode klasik untuk prediksi kinerja relai Buchholz. Metode tradisional digunakan untuk simulasi dengan pemberian fenomena gangguan incipient ke dalam transformator rendaman minyak. Relai Buchholz merupakan relai tipe mekanis dengan mekanisme pengoperasiannya dipengaruhi oleh minyak dan gas di dalam tangki transformator yang cenderung bergerak menuju tangki ekspansi melalui pipa penghubung. Peralatan ini merupakan komponen penting pada filosofi proteksi terhadap transformator rendaman minyak yang diintegrasikan ke dalamnya. Simulator berbasis rangkaian elektronika diintegrasikan ke panel kontrol pengoperasian pemutus tenaga telah dipilih sebagai sarana untuk penciptaan kondisi-kondisi alarm atau trip. Pengukuran kinerja berupa penyediaan simulasi gangguan untuk penyetelan kondisi alarm dan trip. Pemberian simulasi gangguan melalui penekanan tombol satu kali untuk pensimulasian keberadaan kondisi alarm. Dalam kondisi tersebut, panel kontrol untuk pengoperasian pemutus tenaga tidak beroperasi, melainkan hanya penunjukan sinyal alarm. Berdasarkan hal itu, Buzzer berbunyi dan status pemeriksaan trip masih normal atau "no lock-out". Pemberian tekanan pada tombol tekan secara penuh dan berlangsung lama sebagai bentuk simulasi kondisi trip pada relai Buchholz, panel kontrol dengan penunjukan kondisi dua pemutus tenaga (sisi 50 kV and sisi 20 kV) terbuka, dan penunjukan sinyal alarm juga terjadi melalui Buzzer berdering. Sehingga, status pemeriksaan trip menjadi "lock-out". Relai Buchholz dengan fungsi untuk pendeteksian keberadaan gas akibat pemanasan setempat atau lonjakan tekanan pada minyak transformator. Setelah pemberian semua kondisi tersebut, kinerja relai Buchholz diketahui.

Kata-kata kunci: *alarm dan trip; deteksi keberadaan gas; simulasi kondisi nyata.*

1. INTRODUCTION:

The oil-immersed power transformer in each substation plays a crucial role, so it is said to be the vital apparatus of the connection between the transmission line and distribution network. The oil-insulated power transformer's role has not changed over the last decades (Godina *et al.*, 2015). Supporting equipment as an inseparable part of the power transformer is the proper adjustment of the protection relay, so there is no sympathetic phenomenon (Goeritno and Saidah, 2014) and reliable performance of the circuit breaker (Goeritno and Rasiman, 2017; Goeritno, 2020a).

Guided by the IEC 60076-1 standard, it is said that the power transformer is a static electrical apparatus with two or more windings by electromagnetic induction process, changing the voltage and current in alternating current system into other values which are usually of different values and at the same frequency value to transmit electric power (IEC 60076-1:2011, 2011: 7; Gajic, 2013: 21). The classes for power transformers range from distribution voltages of 2.5 kV to extra high voltages up to 765 kV (Choi,

2014). The power transformers are being operated beyond their designed lifetime (Energetic Incorporated, 2015: 3).

Power transformers have been grouped into three market segments based on power size ranges (Sim and Digby, 2002: 2; Choi, 2014), i.e. (i) small power transformers of 500 to 7,500 kVA, (ii) medium power transformers with the capacity start of from 7,500 kVA to 100 MVA, and (iii) large power transformers (LPT) with capacity is greater than 100 MVA. The presence of transformer oil in the power transformers of oil-immersed type with a capacity of 500 kVA or more (Sim and Digby, 2002: 2; HRTSG, 2005) has been equipped with a conservator tank to anticipate the expansion of oil from the main tank of the power transformer through the connecting pipe.

Faults in power transformers are divided into two types, namely external and internal faults (IEEE Std C37.91-2008, 2008: 8). External faults, including overvoltage, over fluxing, less frequency, and short-circuit on outside of the power transformer (Mohammadpour and Dashti, 2011: 741; Joshi *et al.*, 2012: 77). Internal faults on the power transformer is an event with a

probability ranging from 70% to 80% (Mohammadpour and Dashti, 2011: 741; Joshi *et al.*, 2012: 77) which are divided into two types of faults, namely (i) initial or incipient faults and (ii) short-circuit faults that occur on inside of the power transformer (IEEE Std C37.91-2008, 2008: 8; Wang, 2002: 500; Thangavelan, 2014: 2).

Initial faults include: I) the presence of arcs, II) presence of faults in the cooling system, or III) the existence of circulating currents in parallel operated transformers. The three faults included in the initial faults are the cause of the presence of local heating, but they do not affect the overall transformer temperature (Mishra *et al.*, 2013: 61). These faults cannot be detected from the connection of the transformer windings because the value and balance of currents and voltages that occur are not much different from the conditions when power transformer under normal conditions (Joshi *et al.*, 2012: 77-78).

Short circuit on windings that potentially occurs locally and shock pressure arises in the oil transformer, thus producing flammable gas that is flowed to the conservation tank through connecting pipes and Buchholz relay (Buchholz, 1927), can be called as a gas detector relay (HRTSG, 2005; Hartman, 2018). Although the developing fault is a form of minor detect, it can have a significant impact and be able to cause more severe damage; if not detected immediately. Short-circuit fault is a fault due to the existence of short-circuiting that can be detected; because it is the cause of the presence of abnormal currents and voltages or unbalanced loads (Lin *et al.*, 2015: 3).

Guarantees for protection relays that operate with high reliability, the tuning of the Buchholz relay must be precise so that any faults that may arise can be overcome. Installation of the Buchholz relay as a mechanical safety against power transformers from the faults of gases and oil pressure in the power transformer tank (HRTSG, 2005). This relay is not responsive to external forces. There is no servicing required throughout the function. Guided by these descriptions, then set two research objectives in the form of predicting the performance of the Buchholz relay for alarm and trip conditions. The schematic diagram of the complete structure of the oil-immersed power transformer is shown in Figure 1.

1.1. LITERATURE REVIEW:

The phenomena of switching and protecting are the two phenomenally terminology

in the electrical power system (Samonto *et al.*, 2016: 29). There are amount of components of transmission and distribution, include power transformers, cables and conductors, protection devices, and other equipment, which cannot be separated from the switching and protecting phenomena. The ability of the electrical power system in the supplying for the need of loads as a determinant of the reliability of the system, so always strived to generate the electrical power that equals the demand on the load sides and the transmission-related losses for any time condition (Goeritno, 2020b: 293).

The power transformers are essential to the transmission and distribution of electricity efficiently and reliably (Energetic Incorporated, 2015: 2). Today, the basic physical principle of power transformers is still as it was 130 years ago, but the density of energy, range of efficiency, costs of the product, their weight, and dimensions have dramatically improved. The most important function of the power transformer is transforming voltage levels, stepping them up for long-distance transmission from a power plant, and stepping them down for distribution to consumers (Energetic Incorporated, 2015: 3).

The power transformers are large, box-shaped structures connected to multiple wires and are usually the largest single item in a substation. The power transformer is usually located on one side of a substation, and the connection to switchgear is by bare conductors. Linkage with the large quantity of oil, it is essential to take precautions against fire hazards. Hence, a transformer is usually located around a sump used to collect excess oil. When oil-insulated transformers are located indoors, because of fire hazard, it is often necessary to isolate these transformers in a fireproof vault (HRTSG, 2005).

Power transformer comes in all shapes and sizes to the mammoth Extra High Voltage (EHV) power transformers that weigh several metric tones and occupy large areas (Paithankar and Bhide, 2010: 77). The power transformers are being operated beyond their lifetime, although they do not match the design results. For instance, approximately 70% of transformers are over 25 years old on their operation, while their useful life is estimated only 20 years (Energetic Incorporated, 2015: 3). A variety of faults are often in the power transformers and the most common being the winding to core faults, because of the weakening of insulation. Phase faults inside the transformer are rare (Paithankar and Bhide, 2010: 77).

Physical properties of transformer oil, including (a) thermal conductivity, (b) specific heat, (c) volume expansion coefficient, (d) density, (e) viscosity, (f) pour point, (g) solubility of other substances, (h) vapor pressure, (i) fire resistance, and (j) pollutants (contaminants) (Myers *et al.*, 1981: 158-161; HTRSG, 2005). Thermal conductivity, specific heat, and viscosity as a determinant of the rate of heat dissipation from electrical equipment to outside the tank. These characteristics are for determining the type of cooling that a power transformer needed. Viscosity and pour point also affect the mechanism of heat dissipation. The volume expansion coefficient, fire resistance, interface stress, and dissolution power of the pollutants are also important enough to determine the free space required in the transformer and conservator tank, where it is estimated for all spaces that tend to increase in temperature (Myers *et al.*, 1981: 158-161; HRTSG, 2005).

Excerpts from C. Russel Mason on his book title "The Art and Science of Protective Relays" (Mason, 1956: 3); that the function of protective relaying is to cause the prompt removal from service of an element of a power system when it suffers a short circuit or when it starts to operate in an abnormal manner that might cause damage or otherwise interfere with the effective operation of the rest of the system. A number of criteria have been established for a protection relay, in order to operate properly is related to the minimum criteria, include reacting quickly, being selective, sensitive, and reliable (Blackburn and Domin, 2006: 18-22; Ram and Vishwakarma, 2001: 11-12; Glover *et al.*, 2010: 526; Rifaat, 2016).

Reacting quickly is interpreted as the ability to terminate parts of the system with faults that are carried out quickly, so that terminations quickly also with the aim of accelerating the achievement of the system performance again, minimized the possibility of damage, and minimized the possibility of further fault due to initial fault (Glover *et al.*, 2010: 526). Selective is interpreted as the ability of the relay to determine at which point the fault occurs so that the CBs can be chosen precisely so that only the faulty part is separated from the system (Glover *et al.*, 2010: 526). Sensitive means that the protection relay must be operational even though the fault that occurs is still at a light level (is called sensitive to all levels of fault). The higher the level of sensitivity, the more complex the series is and requires more components, thus impacting on financing (Singh, 2009: 151). Reliable means that the relay must operate in the conditions that

the relay should operate on (Rifaat, 2016).

The faults on the inside of the power transformers can also occur on the outside of the power transformers, as on the transformer terminals, which fall within the power transformer protection zone (Paithankar and Bhide, 2010: 80). The incipient faults in power transformer are faults which not significant in the beginning but which slowly develop into serious faults (Paithankar and Bhide, 2010: 96-98). The placement of the Buchholz relay (Paithankar and Bhide, 2010: 96-98) is shown in Figure 2.

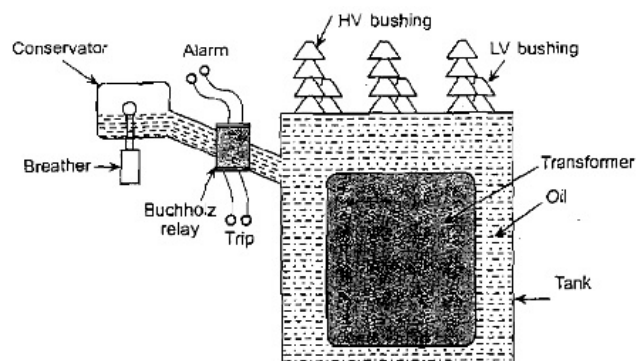


Figure 2. The placement of the Buchholz relay

Based on Figure 2, the Buchholz relay provides protection against such incipient faults. The position of the Buchholz relay with respect to the power transformer tank and the conservator. The conceptual diagram of the inner working of the Buchholz relay (Paithankar and Bhide, 2010: 96-98) is shown in Figure 3.

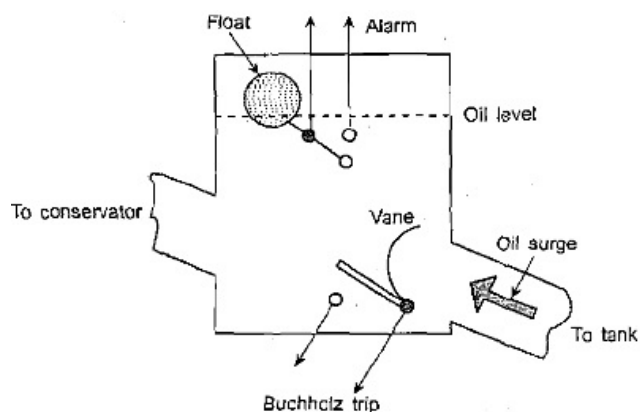


Figure 3. The conceptual diagram of the inner working of the Buchholz relay

When an incipient fault occurs in the form of a winding to the core or an interturn on the power transformer winding, there is a severe heating point of the transformer oil. One of the two faults causes the gases to be liberated from the transformer oil in the range of values 350 °C. There is a build-up of transformer oil pressure,

causing oil to rush into the conservator tank through the interconnection piping (Paithankar and Bhide, 2010: 96-98). A vane is placed in the path of a surge of oil between the main tank of the power transformer and the conservator tank. A set of contact points that conducted by the mercury and operated by this vane is used as a trip command signal from the Buchholz relay for disconnecting the CBs. This output of the Buchholz relay may be used to trip the power transformer (Paithankar and Bhide, 2010: 96-98).

The Buchholz relay also has another set of contact points that conducted by the mercury and operated by a float. These contact points stay open (uncontacted condition) when the transformer oil is filled into the power transformer tank. However, if any leak case of the transformer oil or occurred the decomposition of transformer oil, then the float sinks, so that the contact points that conducted by the mercury to close (contacted condition). Loss of the transformer oil will inevitably cause the transformer temperature to rise, but does not warrant immediate tripping. Hence, normally these contact points are fix-wired to an alarm port that alerts the operator (Paithankar and Bhide, 2010: 96-98).

The trapped gases in the conservator tank can give a valuable clue to the type of specific damage that takes place on inside the power transformer, as the damages in the burnout over insulation between the core lamination stampings and the transformer oil or in the burnout over insulation between the turns of winding. Liberating the specific gases caused by all of the damages when there is heated up that caused by a fault. The specific gases that arise can be used as a phenomenon of a particular type of damage that may have happened at a particular point on inside the power transformer. The lists of information about the analysis of trapped gases (Paithankar and Bhide, 2010: 96-98) is shown in Table 1.

The amount of gas content caused by the fault is in the form of a ratio of gas to flammable gas in percent (%) (Myers *et al.*, 1981: 158-161; HRTSG, 2005). The group of gas type, the ratio of gas to flammable gas in percent (%), and its effects are shown in Table 2.

Based on Table 2, it can be explained that some of the gases arising from faults consisted of 70% in the form of hydrogen gas (H_2), and the rest is in the form of other gases (Myers *et al.*, 1981: 158-161; HRTSG, 2005).

The existence of a several of gases is

done through the analysis of dissolved gas (dissolved gas analysis, DGA), such as acetylene (C_2H_2), methane gas (CH_4), carbon dioxide (CO_2), and propane (C_3H_8) (Duval, 1989; Sun *et al.*, 2012; Mirowski, 2012; Liepniece *et al.*, 2017). The existence of a mixture of several gases, namely (i) H_2 and C_2H_2 , as a result of arising of arcing (arching) between conductors or iron core; (ii) H_2 , C_2H_2 , and CH_4 , due to the decomposed insulation of phenols that used in the tap changer; (iii) H_2 , C_2H_2 , CH_4 , and C_2H_4 gases as a result of heating on the core connection plate; and (iv) gases H_2 , C_2H_4 , CO_2 , and C_3H_8 , due to the decomposed insulation of turns (IEEE Std C57.104-2008, 2008; Myers *et al.*, 1981: 158-161; HRTSG, 2005).

A summary of the Buchholz relay, i.e. (i) gas accumulator relay; (ii) applicable to conservator tanks equipped; (iii) operates for small faults by accumulating the gas over a period of time and typically used for alarming only; (iv) operates or for large faults that force the oil through the relay at a high velocity, used to trip, and able to detect a small volume of gas and accordingly can detect arcs of low energy; and (v) detects high-resistance joints, high eddy currents between laminations, energy arcing in low and high, and accelerated aging caused by overloading (Hartman, 2018: 28).

2. MATERIALS AND METHODS:

2.1. Materials of Research

Installing the Buchholz relay and measuring its performance mounted on the power transformer, then the protective function measurements were carried out by the Buchholz relay. A set of circuits for measuring the performance of the Buchholz relay, in the form of an analogy to the main tank of a power transformer, the connecting pipe between the main tank analogy and the Buchholz relay, the connecting pipe between the Buchholz relay and the conservator tank analogy, the analogy of an oil storage tank, a pump, and the installation of several diaphragm valves. The end of the pipe comes from the main transformer tank is connected inside the conservatory on the bottom portion. A Schematic diagram of the circuit for measuring the performance of the Buchholz relay is shown in Figure 4.

Based on Figure 4, it can be explained that the performance measurement of the Buchholz relay is carried out, namely the

installation of a solenoid valve that operated through the push button to simulate the alarm and trip conditions. When the power transformer is loaded, and when the temperature of ambient temperature, the oil volume inside the power transformer increases. A conservator tank of power transformer provides adequate space to this expanded the transformer oil. It also acts as a reservoir for the transformer insulating oil. An electronic circuit-based control panel that is integrated with a circuit breaker operation was chosen as a means for creating conditions during alarm or trip.

2.2. Methods of Research

The flowchart of research methods is shown in Figure 5.

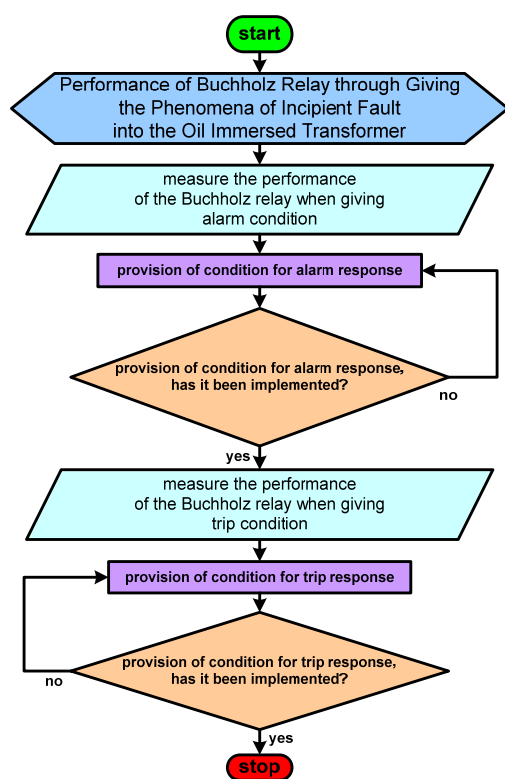


Figure 5. The flowchart of research methods

Based on the research flow diagram in Figure 5, it can be explained that the Buchholz relay performance measurement provides simulated fault conditions for setting on alarm and trip.

The stages of providing conditions for simulating an alarm or trip are guided by the experimental circuit in Figure 4. Prior to the simulation of the alarm, diaphragm valve #2 and diaphragm valve #3 was closed. The pressure indicator on the analogy of the main tank of the transformer (designated by pressure gauge #1) is higher than the designated by pressure gauge

#2, and the pressure indicator on pressure gauge #2 is higher than the designated by pressure gauge #3. The condition for the occurrence of an alarm is done by pressing the push-button switch once so that the solenoid valve is open for a moment. The momentary opening of the solenoid valve is a phenomenon of oil shock pressure, resulting in oil flow from the main transformer tank, which has a higher pressure than the oil pressure in the conservator tank. The change in oil pressure in the conservator tank results in a decrease in the position of the upper float downward, so that the contact point, which is on the upper float, is conducted by mercury. Conduction of this contact point results in sending an alarm signal to the control panel so that the buzzer sounds like an alarm signal.

Prior to the trip simulation, diaphragm valves #2 and #3 are open. The pressure indicator on the analogy of the main tank of the transformer (designated by pressure gauge #1) is higher than the designated by pressure gauge #2, and the pressure indicator on pressure gauge #2 is higher than the designated by pressure gauge #3. The provision of trip conditions is carried out by pressing the push-button switch continuously so that the solenoid valve is open for a long time. The continuous opening of the solenoid valve is a phenomenon of oil flow from the main tank of the transformer to the conservator tank. Oil flow occurs because the pressure in the main tank of the transformer is higher than the oil pressure in the conservator tank. The occurrence of oil flow to the conservator tank results in changes in the position of the lower float in the direction of the oil flow for a long time so that the contact point, which is on the lower float, is conducted by mercury. Conduction of this contact point results in sending a trip signal to the control panel so that the control panel carries out the CBs operation to the OFF condition and the buzzer also sounds.

3. RESULTS AND DISCUSSIONS:

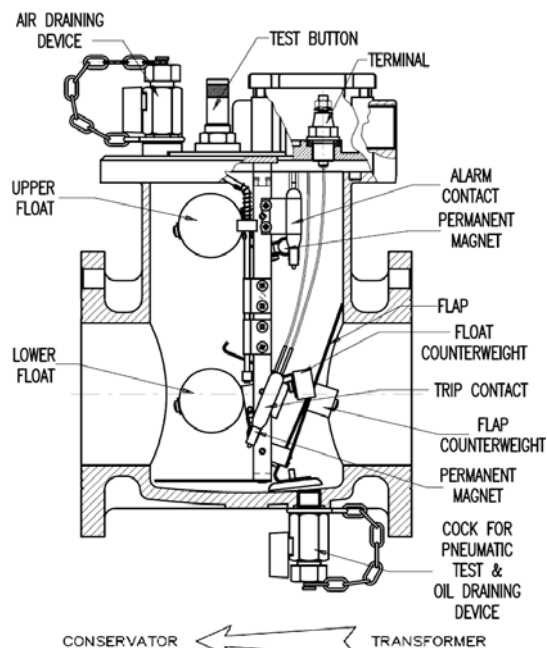
The Buchholz relay was invented and implemented in 1921 by Max Buchholz, in Kassel. The Buchholz Relay is used as a protection purpose, which is sensitive to the effects of dielectric transformer oil failure on inside the equipment and installed to monitor large power transformers for oil loss or insulation breakdown. In the Buchholz relay, there is a hollow space or chamber which is placed between the tank of the transformer and

conservator. When the winding of the transformer is heated, or there are any fault occurs, flammable gas is produced, which tries to occupy the upper segment of the space of the chamber that containing the oil. The occupation of the flammable gas in the upper segment of the space will be possible only when the level of transformer oil goes down. When a small fault occurs, then the level of transformer oil goes down slightly.

The Buchholz relay is an essential component of the oil-immersed power transformer protection philosophy. This device detects the gas accumulation that formed by (i) the oil degeneration in partial discharges and (ii) disconnecting the transformer in large faults due to the oil flow. Those two things are caused by internal electrical short-circuits and arcing. The Buchholz relay is a type of mechanical relay whose operating mechanism is influenced by oil and gas in the transformer tank. The use of the Buchholz relay functions as a protective relay on the oil-immersed power transformer to anticipate internal faults that may occur, such as the failure of the oil function as a cooling and insulation media or the failure of solid and liquid insulation on the coil, or other reasons.

The Buchholz relay is usually connected in a chain with the piping that interconnection with the main tank of the power transformers oil to the expansion tank; in this manner, the gases produced inside by eventual intermittent or persistent malfunctions tend to move into the expansion tank through the interconnecting piping. The Buchholz relay then captures and retains this gas in its chamber where a relay mechanism will be activated after the gas build-up has reached a certain level, which in turn, enables the alarm contact float (1st level).

The type of physical form and explanation of each Buchholz relay is shown in Figure 6. Based on Figure 6 can be illustrated with detail of part in the chamber of the Buchholz relay. The cross-section of details of the Buchholz relay construction is shown in Figure 7.



Source:

<https://www.electricalclassroom.com/buchholz-relay-working-principle/>

Figure 7. The cross-section of details of the Buchholz relay construction

Based on Figure 7 can be explained; that a typical Buchholz relay will have two sets of contacts that are conducted by the mercury. One is arranged to operate for the slow accumulation of gases, the other for the bulk displacement of transformer oil in the event of a substantial internal fault. When an alarm is generated for the former, but the latter is usually direct-wired to the relay contact of the trip condition for operating the circuit breaker. Therefore, the device sounds an alarm for the following abnormal conditions, all of which have a low level of urgency: (I) hot spots on the core due to short circuit of lamination insulation, (II) core bolt insulation failure, (III) faulty joints, (IV) inter-turn faults or other winding faults involving only lower power infeeds, and (V) reduced oil volume due to leakage. When a major fault on winding occurs, this causes an oil surge, which moves the lower float to a lower position and thereby causes decreasing the insulation capability of the power transformer. This action will take place for: (a) all severe winding faults, either to earth or inter-phase, and (b) loss of oil if allowed to continue to a dangerous degree.

In the invention of improved Buchholz relay (Dal Lago, 1999) explained that switches operated by fluid change pressure, by pressure waves on fluid, or by the turn of the fluid flow actuated by devices allowing the continual flow of fluid, e.g., vane the switch being of the reed switch type. A Buchholz relay comprising, to be

immersed in an oil bath, a supporting frame for magnetic switches for closing circuits which are operated by portable devices, of which at least one is of the floater type, and at least one is of the type with a flap rotatably associated with the frame. The moveable flap device, which has a surface that is sensitive to the presence of oil flows.

The movable flap device is independent of said floaters and comprises a flat member provided with a pivot that is rotatably associated with said frame by way of its ends. It also has a surface that is sensitive to the presence of oil flows, so that said movable flap device is able to rotate with respect to the said frame under the oil flow action. At least one part of the surface of the moving flap device, which is sensitive to the presence of oil flows, can also be reduced. Characterized in that device, prefractures are formed in said flat member so as to constitute said reducible surface, prefractures forming at least one detachable portion.

According to characterized in that device, including (a) said movable flap device comprises tubular support inside which a counterweight can be inserted; (b) mutually opposite guides for the sliding of the ends of the said pivot are formed in said frame, the end of each guide with an adapting seat for the snap insertion of the end; and (c) said movable flap device is made of plastics.

The steps to test the Buchholz relay is done through positioning on "test mode". Then followed by the testing stages, i.e. (a) short-circuit the alarm contacts and checked if the annunciation is received at the control room, and then short-circuit tripping contact and verified whether the trip command is issued to the circuit breaker; (b) injected the air into the Buchholz relay from the pet valve provided at the top of the relay, to simulated the gas accumulation and checked the alarm and tripping; and (c) drain the transformer oil from the relay, after closing the gate valves provided at both the sides of the relay in the interconnection piping and checked the annunciation and tripping.

The measurement results of the protective function of the Buchholz relay is shown in Table 3. Based on Table 3, it is shown that the measurement results of the protection function of the Buchholz relay are performed by the simulation of faults by pressing the push-button one time to simulate the existence of an alarm condition in which the control panel of the CBs does not operate. However, the appointment of an alarm signal, so that the Buzzer sounds and

the status check trip is still normal or "no lock-out". Giving full pressure as a form of simulation for trip conditions on the Buchholz relay, the control panel designates the status of the two CBs (150 kV side and 20 kV side) open, and the alarm signal designation also occurs with Buzzer sounding. Hence, the check trip status becomes "lock-out".

The schematic diagram and the mechanism of operation of the Buchholz relay are shown in Figure 8. Based on Figure 8, it can be explained, that the type of fault that occurs and must be overcome by the Buchholz relay, namely: (i) a mild fault that results in a gas bubble flowing to the top of the relay and pressure that results in the upper float moving downward, so that the contact mercury is connected and giving an alarm signal, so that the buzzer alarm sounds and (ii) severe disturbances that result in gas and oil shock and there is a pressure that causes the lower float to move downward, so that the contact point conducted by is mercury and the signaling occurs trip.

The Buchholz relay serves to detect the presence of gases caused by local heating or pressure surges in the transformer oil. When oil-insulated power transformers are located indoors, it is often necessary to isolate these transformers in a fireproof vault because of fire hazards. On the other hand, relays are not responsive to external pressures. No servicing required throughout the function. The illustrations for the alarm and trip phenomena are depicted in the form of a schematic diagram. The schematic depiction of the cross-section and specific parts of the Buchholz relay is shown in Figure 9. Based on Figure 9, it can be explained that specific parts of the Buchholz relay play an essential role in the alarm and tripping processes. It was also shown that maintenance is required for correct alarm and tripping conditions.

The schematic diagram explanation, under normal circumstances, the Buchholz relay is filled with transformer oil. Providing conditions with initial/minor/incipient fault, suppose that a short circuit occurs in the winding of the transformer, then gas is generated due to local heating from solid and liquid insulation. The resulting gas collects on the upper surface of the Buchholz relay, and when there are enough, there is an emphasis on the upper float, so the float changes position, which impacts the operation of the mercury contact point (alarm signal contact). The schematic diagram of the operation of contact points conducted by mercury on the Buchholz relay for alarm signal is shown in Figure 10.

A case of arc arises because of the existence of a short circuit between phases resulting in arcing arising. The inter-phase coils are located in a tank submerged by transformer oil; because the oil reacts to the heat generated by arcing arcs, then C_2H_2 gas is formed and enters the Buchholz relay; so that the presence of gas by operating alarm contacts. For conditions where the fault continues, pressure on the transformer oil arises; so that under certain pressure, a contact trip operation can occur. The schematic diagram of the operation of contact points conducted by mercury on the Buchholz relay for trip signals is shown in Figure 11.

5. CONCLUSIONS:

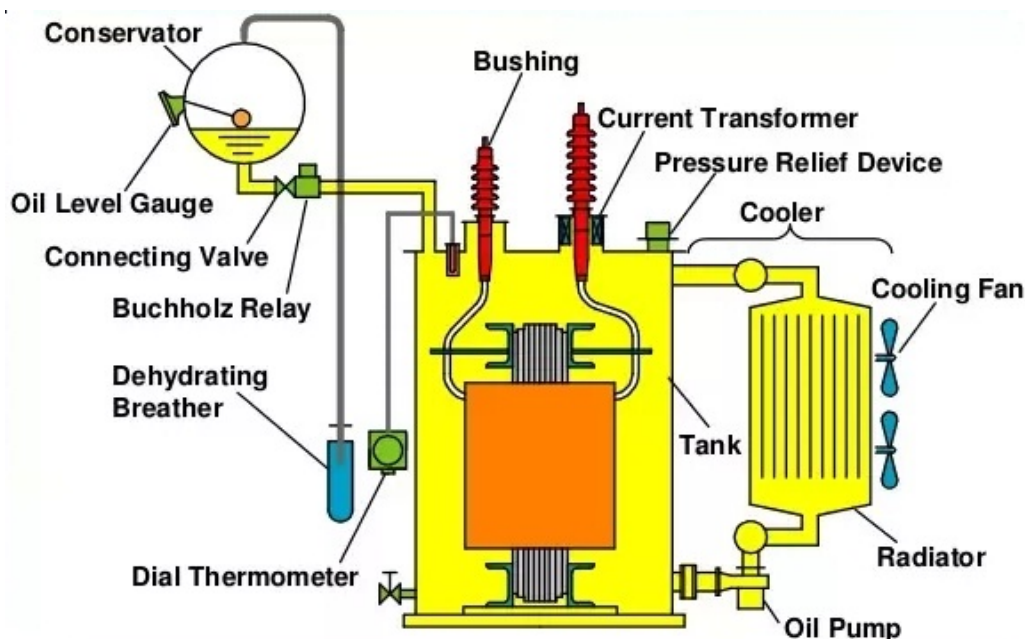
Based on the results and discussions, conclusions can be drawn according to the research objectives. The provision of faults simulation in the form of pressing a push-button 1 (one) time to simulate the existence of an alarm condition, in that condition, the CBs control panel does not operate, but the appointment of an alarm signal, so that the Buzzer sounds and the status check trip is still normal or "no lock-out". Giving full pressure as a form of simulation for trip conditions on the Buchholz relay, the control panel designates the condition of the two CBs (150 kV side and 20 kV side) open, and the alarm signal designation also occurs with Buzzer sounding. Hence the check trip status becomes "lock-out". The illustrations for the alarm or trip phenomenon are depicted in the form of a schematic diagram. The inter-phase coils are located in a tank submerged by transformer oil because the oil reacts to the heat generated by arcing arcs, then C_2H_2 gas is formed and enters the Buchholz relay; so that the presence of gas by operating alarm contacts. For conditions where the disturbance continues, pressure on the transformer oil arises; so that under certain pressure, a contact trip operation can occur.

6. REFERENCES:

1. Buchholz, M. (1927, September 13). *Method and means for protecting liquid-insulated electric apparatus*. Google APIs. <https://patentimages.storage.googleapis.com/04/df/3f/8dd3619fd8eefe/US1642397.pdf>
2. Choi, T.Y. (2014). *Large Power Transformers and the U.S. Electric Grid*. Office of Electricity Delivery and Energy Reliability. T&D World. <https://cdn.tdworld.com/files/base/ebm/tdworld/document/2020/03/LPTStudyUpdate-040914.pdf>
3. Dal Lago, S. (1999, March 12). *Improved Buchholz Relay*. Google APIs. <https://patentimages.storage.googleapis.com/81/41/ed/7ff70142235a6d/EP0944150A2.pdf>
4. Duval, M. (1989). Dissolved gas analysis: It can save your transformer. *Electrical Insulation Magazine*, IEEE, 5(6): 22-27.
5. Energetics Incorporated. (2015). *Materials Innovation for Next Generation T&D Grid Components: Scoping Document*. U.S. Department of Energy. <https://www.energy.gov/sites/prod/files/2016/06/f32/OE%20ORNL%20Materials%20Innovation%20for%20Grid%20Workshop%20Scoping%20Document%20FINAL.pdf>
6. Gajic, Z. (2008). *Differential Protection for Arbitrary Three-Phase Power Transformers*, Doctoral Dissertation Department of Industrial Electrical Engineering and Automation, Lund University.
7. Glover J.D.; Sarma, M.S.; Overbye, T.J. (2010). *Power System and Analysis*, 5th Edition. Cengage Learning, Boston, MA, 526.
8. Godina, R.; Rodrigues, E.M.G.; Matias, J.C.O.; and Catalao, J.P.S. Effect of Loads and Other Key Factors on Oil-Transformer Ageing: Sustainability Benefits and Challenges. *Energies*, 2015 (8), pp. 12147-12186.
9. Goeritno, A.; Saidah. (2014). Simulation of Single-phase to Ground Fault to Anticipate Against the Sympathetic Tripping Phenomena. The 1st International Conference on Engineering, Technology and Industrial Application (ICETIA-2014), UMS, Surakarta. <https://publikasiilmiah.ums.ac.id/xmlui/bitstream/handle/11617/4994/37-Arief%20Goeritno.pdf?sequence=1>
10. Goeritno, A.; Rasiman, S. (2017). Performance of Bulk Oil Circuit Breaker (BOCB) Influenced by Its Parameters (Case Study at the Substation of Bogor Baru). The 3rd International Conference on Engineering, Technology, and Industrial Application (ICETIA-2016). <http://aip.scitation.org/doi/pdf/10.1063/1.4985446>.
11. Goeritno, A. (2020a). Preliminary Evaluation for the Performance of Circuit

- Breaker Mediated by SF₆ Gas. *Journal of Electrical and Electronics Engineering (JEEE)*, 13(1): 35-38. https://electroinf.uoradea.ro/images/article/s/CERCETARE/Reviste/JEEE/JEEE_V13_N1_MAY_2020/07%20paper%201115%20GOERITNO.pdf
12. Goeritno, A. (2020b). Implementation of the coordination equation for determining the transport-related losses in economic dispatch phenomena. *Mathematical Modelling of Engineering Problems*, 7(2), 293-298. Retrieved from <https://doi.org/10.18280/mmep.070216>
 13. Hartman, W. (2018). Transformer Protection. 35th Annual Hands-on Relay School, March 12-16, 2018, Pullman, Washington, 28. https://na.eventscloud.com/file_uploads/fcdbd21cac1909692839b242e46c9a3c_TransformerProtection__180306.pdf
 14. HRTSG (Hydroelectric Research and Technical Services Group). (2005). Transformers: Basics, Maintenance, and Diagnostics. U.S. Department of the Interior, Bureau of Reclamation, Denver, Colorado. <https://www.usbr.gov/tsc/techreferences/mands/mands-pdfs/Trnsfrmr.pdf>
 15. IEEE Std C37.91-2008. (2008). IEEE Guide for Protecting Power Transformers. (Revision of IEEE Std C37.91-2000; Revision of IEEE Std C37.91-1985). Retrieved from <https://doi.org/10.1109/IEEESTD.2008.4534870>.
 16. IEEE Std C57.104-2008. (2009). IEEE Guide for The Interpretation of Gases Generated in Oil-Immersed Transformers. (Revision of IEEE Std C57.104-1991). <https://doi.org/10.1109/IEEESTD.2009.4776518>.
 17. Joshi, N.C.; Sood, Y.R.; Jarial, R.K., Thapliyal, R. (2012). Transformer Internal Winding Faults Diagnosis Methods: A Review. *MIT International Journal of Electrical and Instrumentation Engineering*, 2(2): 77-81. http://mitpublications.org/yellow_images/1362470798_logo_3.pdf.
 18. Liepniece, R.; Vitolina, S.; Marks, J. (2017). Study of approaches to incipient fault detection in power transformer by using dissolved gas analysis. *ENERGETIKA*, 63(2): 66-74.
 19. Lin, X.; Ma, J.; Weng, H.; Tian, Q. (2015). Principles of Transformer Differential Protection and Existing Problem Analysis. *Electromagnetic Transient Analysis and Novel Protective Relaying Techniques for Power Transformers*. John Wiley & Sons (Asia), Pte. Ltd., Singapore, 1-36.
 20. Mason, C.R. (1956). The Art and Science of Protective Relays, 1st Edition. John Wiley & Sons, New Jersey, NJ, 3.
 21. Mirowski, P. (2012). Statistical Machine Learning and Dissolved Gas Analysis: A Review. *IEEE on Power Delivery*, 27(4): 1791-1799.
 22. Mishra, V.; Prakash, S.; Singh, A. (2013). Detection of Internal Faults in Transformers by Negative Sequence Current. *Journal SAMRIDDHI (S-JPSET)*, 4(2), 61-65.
 23. Mohammadpour, H.; Dashti, R. (2011). A New Method Presentation for Fault Location in Power Transformers. *International Journal of Electrical and Computer Engineering*, 5(6), 741-746. <https://publications.waset.org/15109/a-new-method-presentation-for-fault-location-in-power-transformers>
 24. Myers, S.D.; Kelly, J.J.; Parish, R.H. (1981). The Insulation System - The Lifeline of a Transformer. A Guide to Transformer Maintenance. Transformer Maintenance Institute (Division of S.D. Myers, Inc.), Akron, OH, 139-211.
 25. Paithankar, Y.G.; Bhide, S.R. (2010). Transformer Protection. *Fundamentals of Power System Protection*, Second Edition. PHI Learning Private Limited, New Delhi, 77-103.
 26. Ram, B.; Viswakarma, D.N. (2001). *Power System Protection and Switchgear*, 2nd ed. Tata McGraw-Hill, Education (India) Private Limited, New Delhi, 11-12.
 27. Rifaat, R. (2016). Power System Protective Relays: Principles & Practices. IEEE Southern Alberta Section PES/IAS Joint Chapter Technical Seminar - November 21, 2016, 10. https://site.ieee.org/sas-pesias/files/2016/12/PowerSystemProtectiveRelays_PrinciplesAndPractices.pdf
 28. Samonto, S.; Pal, S.; Banerjee, S.; Sarkar, B. (2016). Transformer Protection by Using FL Based Artificial Intelligent Buchholz Relay against Incipient Faults. *International Journal of Engineering Science and Technology (IJEST)*, 8(03), 29-36.
 29. Sim, H.J.; Digby, S.H. (2004). Power Transformer. *Electric Power Transformer*

- Engineering, Harlow, J.H. (ed.). CRC Press, Boca Raton, FL, 1-23.
30. Singh, R.P. (2009). *Switchgear and Power System Protection*. PHI Learning Private Limited, New Delhi, 151.
 31. Sun, H.C.; Huang, Y.C.; Huang, C.M. (2012). A Review of Dissolved Gas Analysis in Power Transformers. *Energy Procedia*, 14: 1220-1225.
 32. Thangavelan, M.; Prabavathi, K.; Ramesh, L. (2014). Review on Power Transformer Internal Fault Diagnosis. *Journal of Electrical Engineering*, 14(3): (50)1-6.
<http://www.jee.ro/covers/art.php?issue=W H1390973948W52e893fc96ea7>.
 33. Wang, H.; Butler, K.L. (2002). Modeling Transformers with Internal Incipient Faults. *IEEE Transaction on Power Delivery*, 17(2): 500-509.



Source: Engineering360 (power by IEEE GlobalSpec.):
<https://cr4.global-spec.com/thread/120090/11000kV-Wires-vs-11000kV-to-220V-Transformer>

Figure 1. Schematic diagram of the complete structure of the oil-immersed power transformer

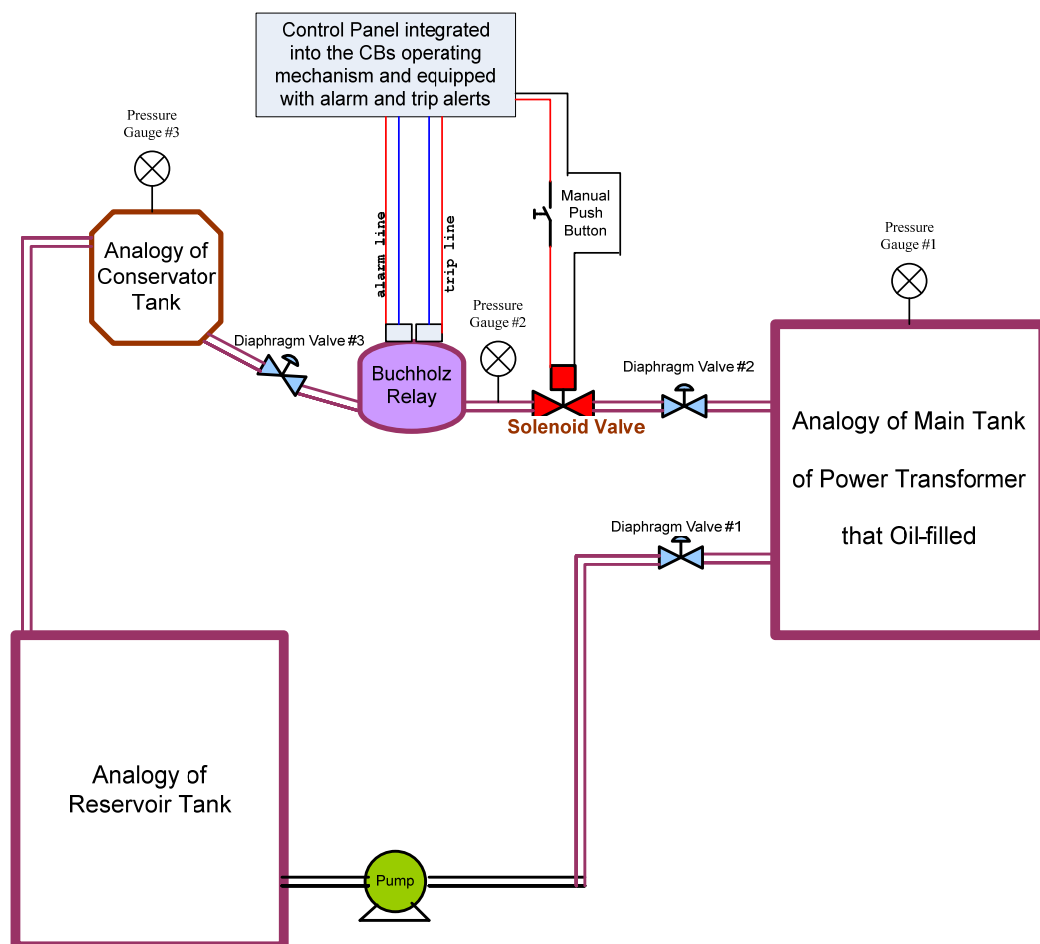
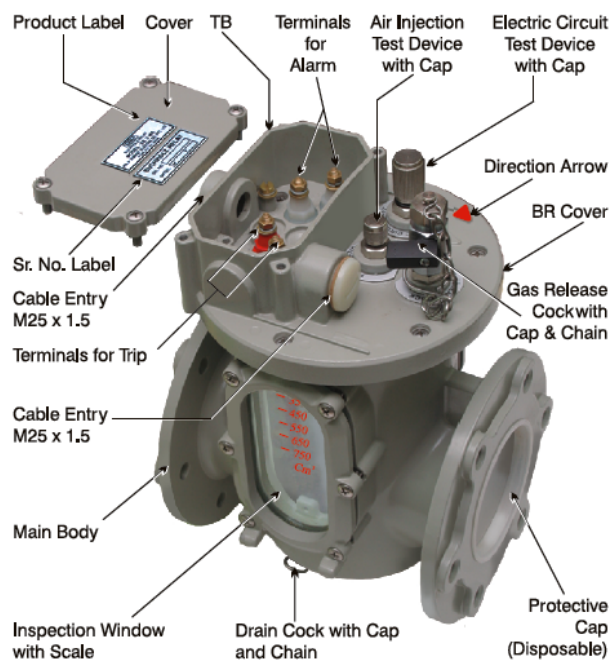


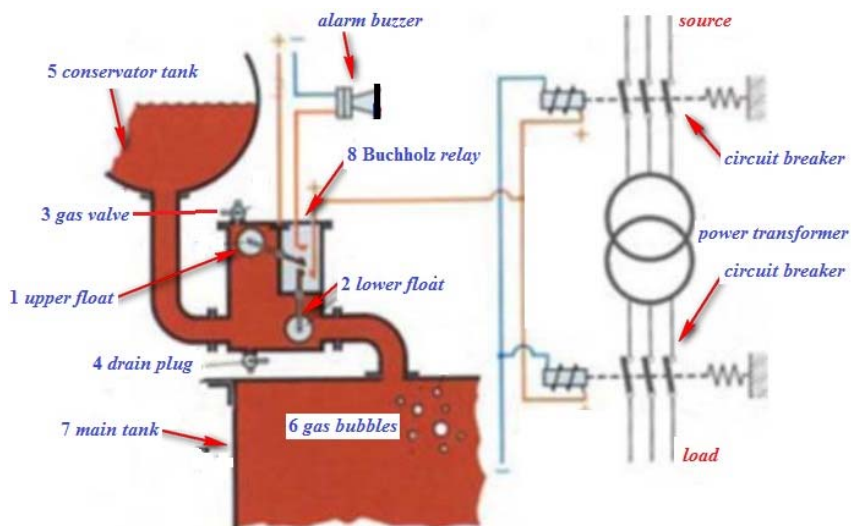
Figure 4. Schematic diagram of the circuit for measuring the performance of the Buchholz relay



Source: <https://docplayer.net/docs-images/99/143315317/images/67-0.jpg>

Source: <https://circuitpedia.com/wp-content/uploads/2020/05/buchholz-relay-construction.png>

Figure 6. The physical form and explanation of each Buchholz relay



Source: <http://electricalengineering-eg.blogspot.co.id/2014/02/buchholz-relay.html>

Figure 8. The schematic diagram and the mechanism of operation of the Buchholz relay

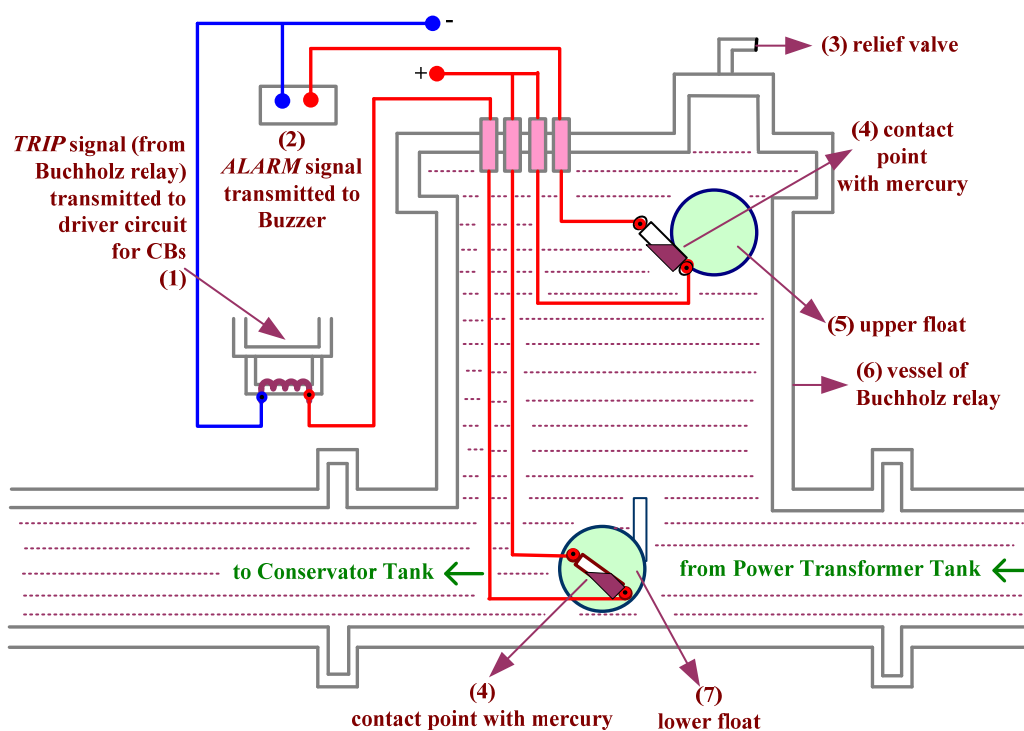


Figure 9. The schematic depiction of the cross-section and specific parts of the Buchholz relay

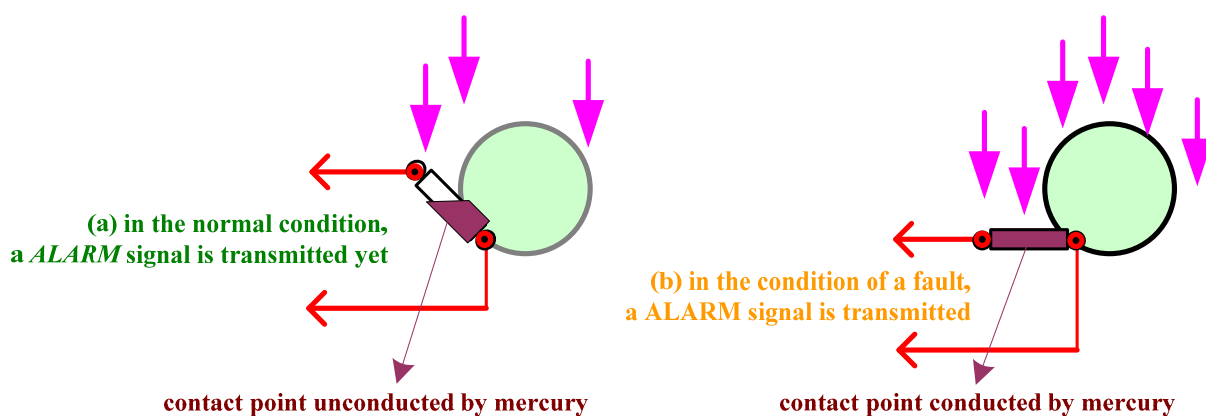


Figure 10. The schematic diagram of the operation of contact points conducted by mercury on the Buchholz relay for alarm signal

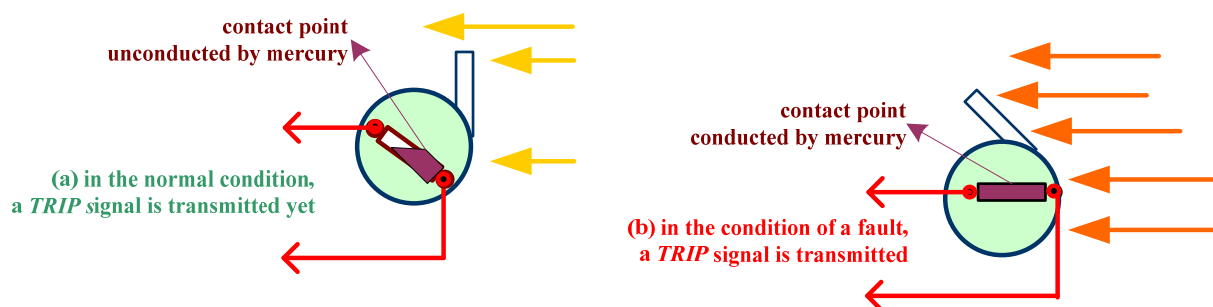


Figure 11. The schematic diagram of the operation of contact points conducted by mercury on the Buchholz relay for trip signals

Table 1. The lists information about the analysis of trapped gases

Type of Gas	Diagnosis
H ₂ and C ₂ H ₂	Arcing in oil between constructional parts
H ₂ , C ₂ H ₂ , and CH ₄	Arcing with some deterioration of phenolic insulation, e.g., fault in tap changer
C ₂ , CH ₄ , and C ₂ H ₄	Hot spot in core joints
H ₂ , CH ₄ , CO ₂ , and C ₃ H ₆	Hot spot in a winding

Table 2. *The group of gas type, the ratio of gas to flammable gas in percent (%), and its effects*

Group of Gas Type	Ratio* in (%)	Its effects
H ₂ C ₂ H ₂ CH ₄ C ₂ H ₄ C ₂ H ₆	60.0 30.0 5.0 3.3 1.6	Leap of sparks in oil (and jumps occur in the paper when there are CO and CO ₂ contents)
H ₂ CH ₄ C ₂ H ₆ CO C ₂ H ₄ C ₂ H ₆	86.0 13.0 0.5 0.2 0.2 0.1	Corona in oil (and Corona in the paper if there are CO and CO ₂ content)
C ₂ H ₄ C ₂ H ₆ CH ₄ CO H ₂	63.0 17.0 16.0 trace trace	Overheating (if there is a C ₂ H ₂ content, there may be interference or short circuit)
CO H ₂ CH ₄ C ₂ H ₆ C ₂ H ₄ C ₂ H ₂	92.0 6.7 1.2 0.01 0.01 0.01	Overheating (if there is a C ₂ H ₂ content, there may be interference or short circuit)
Ratio* = ratio of gas to flammable gas		

Table 3. *The measurement results of the protective function of the Buchholz relay*

Protecting Object	Giving the Simulation of Fault	Condition of CBs (opened)		Panel of Control	Protection Panel	Alarm	Check Trip
		150 kV side	20 kV side				
Alarm from Buchholz	pressed one time	-	-	Buchholz Alarm Indication	-	yes	-
Trip from Buchholz	fully pressed	yes	yes	Buchholz Trip Indication	MVAJ: ½ is operated	ya	lock-out

**INVESTIGAÇÃO TÉCNICA DO REFORÇO DE AREIA DO MAR PARA NOVOS
COMPÓSITOS AL6061-AREIA DO MAR: IDENTIFICAÇÃO DE DESEMPENHO E
PROPRIEDADES MECÂNICAS****TECHNICAL INVESTIGATION OF SEA SAND REINFORCEMENT FOR NOVEL AL6061-
SEA SAND COMPOSITES: IDENTIFICATION OF PERFORMANCE AND MECHANICAL
PROPERTIES**Akbar, Hammar Ilham¹; Surojo, Eko^{2*}; Ariawan, Dody³; Prabowo, Aditya Rio⁴^{1,2,3,4} Department of Mechanical Engineering, Universitas Sebelas Maret, Surakarta, Indonesia** Corresponding author
e-mail: esurojo@ft.uns.ac.id*

Received 12 June 2020; received in revised form 10 August 2020; accepted 01 September 2020

RESUMO

Materiais leves com baixo custo de produção foram desenvolvidos nos últimos anos. A adição de cerâmicas e partículas de óxidos como Al_2O_3 , SiC e SiO_2 tem melhorado as propriedades mecânicas dos compósitos com matriz de alumínio (AMCs). Como solução, o uso de material de reforço natural continua a ser investigado. Este artigo investiga a areia do mar como um reforço alternativo aos AMCs. O Al 6061 foi usado como matriz e areia do mar como reforço. A fabricação do compósito foi realizada por rota de fundição sob agitação com variação de 0, 2, 4, 6% em peso da armadura. O compósito foi testado quanto à dureza e resistência à tração, o teste de dureza foi obtido de acordo com ASTM E-10, e o teste de tração foi conduzido de acordo com a norma JIS Z2201. A densidade do composto diminui linearmente com a adição do reforço de 2% em peso a 6% em peso, e o mesmo fenômeno é obtido na porosidade, a porosidade aumenta com a adição de partículas de areia do mar de 2% em peso a 6% em peso. O declínio na densidade devido à menor densidade das partículas de areia do mar em comparação com a matriz de alumínio. Quanto maior a partícula de areia do mar que se dispersa na matriz, menor a densidade do composto. O aumento da porosidade causou uma maior fração de reforço resultando em maior contato superficial entre a matriz e o reforço que promovem a porosidade. A dureza e a resistência à tração final dos AMCs aumentam com o aumento do conteúdo de partículas de areia do mar. A presença de um composto de óxido na areia do mar aumentou as propriedades mecânicas do composto. O aumento nas propriedades mecânicas indica que a partícula de areia do mar dispersa na matriz e a areia do mar podem ser usadas como material para fins de engenharia.

Palavras-chave: *alumínio, compósito, areia do mar, resistência a tração, dureza.***ABSTRACT**

Lightweight materials with low-cost production have been developed in recent years. The addition of ceramics and oxide particles such as Al_2O_3 , SiC , and SiO_2 has been improving in the mechanical properties of aluminum matrix composites (AMCs). As a solution, the use of natural reinforcing material continues to be investigated. This paper investigates sea sand as an alternative reinforcement to AMCs. The Al 6061 was used as the matrix and sea sand as reinforcement. The manufacturing of the composite was conducted by stir casting route with variation 0, 2, 4, 6 %wt of the reinforcement. The composite was tested in hardness and tensile strength, the hardness test was obtained according to ASTM E-10, and the tensile test was conducted according to JIS Z2201 standard. Composite density decreases linearly with the addition of the reinforcement from 2 %wt to 6%wt, and the same phenomenon is obtained in porosity, the porosity increases with the addition of sea sand particles from 2%wt to 6%wt. The decline in density due to the lower density of sea sand particles compared to the aluminum matrix. Higher the sea sand particle that disperses into the matrix resulted in a lower density of the composite. Increasing porosity caused a higher fraction of reinforcement resulting in wider surface contact between matrix and reinforcement that promote the porosity. The hardness and ultimate tensile strength of AMCs increase with increasing of sea sand particles content. The presence of an oxide compound on the sea sand increased the mechanical properties of the composite. Increasing in mechanical properties indicate the sea sand particle dispersed into the matrix and sea sand can be used as engineering purpose material.

Keywords: *aluminum, composite, sea sand, tensile strength, hardness.*

1. INTRODUCTION:

The industrial demand for reliable, lightweight, and eco-friendly materials has increased in recent years. This is related to the massive, environmentally friendly campaign (Akbar *et al.*, 2018; Zheng *et al.*, 2018; Radhika *et al.*, 2015). One of the materials that have the qualifications and continuously developed is aluminum matrix composites (AMC). AMC is a combination of several materials, with aluminum matrix and reinforcing materials, which are ceramic compounds, and its mechanical properties can be achieved with specific compositions (Nagaral *et al.*, 2017). The popular matrix used in AMC is Al 6061. In the commercial, Al 6061 is an aluminum alloy that can be improved in mechanical properties after heat treatment (Giofr  *et al.*, 2017). The Al 6061 is commonly chosen as construction, automotive, aerospace, and marine application due to their characteristics such as intermediate strength, good corrosion resistance, and can be improved in mechanical properties (Gireesh *et al.*, 2018).

In the AMC manufacturing, ceramic particles such as Al_2O_3 , SiO_2 , SiC , TiO_2 , and graphite are used as reinforcements (Bisane *et al.*, 2015). The addition of ceramic particles improved the mechanical properties of the composite (Bharat *et al.*, 2014). On the other hand, manufacturing AMC with ceramic material as reinforcement in AMC limits its application due to expensive production costs (Tiwari and Pradhan, 2017). As a solution, researchers innovate to utilizing organic and eco-friendly materials to reduce production costs (Patel *et al.*, 2017; Reddy and Srinivas, 2018). One of the potential materials that contain ceramic compounds, as mentioned, is sea sand.

As the owner of 5.9 million km^2 sea area and 95,161 km coastline, which is the second-longest in the world (Lasabuda, 2013), Indonesia has abundant natural resources of sea sand. Oxide minerals such as SiO_2 , Al_2O_3 , ZnO , MgO , and TiO_2 , which are found on the south coast of Java and Aceh province, allowed the sea sand as one of the high-tech materials (Alimi *et al.*, 2016; Jalil *et al.*, 2017). Utilizing sea sand particles as reinforcement in aluminum composite materials has not been investigated. Generally, sea sand is used as a substitute for aggregate in concrete. Previous research shows that concrete with sea sand combined with fiber-reinforced polymer (FRP) has been studied by Dong *et al.* (2019). The results state that the presence of sea sand

as an aggregate in concrete results the concrete is improving strength, but tend to be a brittle fracture.

Manufacturing aluminum matrix composites with stir casting is a common process. This method is the easiest and has a significant production capability. Behind its simplicity, the stir casting also has deficiencies in particle distribution or homogeneity. Homogeneity of aluminum matrix composites is strongly influenced by several factors, including a fraction of reinforcing particles, stirring speed, and particle treatment. The fraction of particles affects the mechanical properties of aluminum matrix composites. The addition of bamboo leaf ash to aluminum matrix composite has a positive effect. The mechanical properties of the composites increase with the addition bamboo leaf ash from 0 to 4% wt, then decrease when bamboo leaf ash content increase to 6% wt (Dhanesh *et al.*, 2020). The mechanical properties of the Al_2O_3 /3Y-TZP composite increase with the increasing content of micro-alumina. The Vickers hardness dropped from 12.6 GPa to 8.9 GPa with the particle addition from 20 vol% to 50 vol%. The flexural strength increases significantly from 547.1 MPa at 0 vol% to 633.3 MPa at 20 vol% (Zhang *et al.*, 2015).

Previous research shows the addition of ceramic and oxide particles such as SiC (Hall *et al.*, 1994), red mud particle (Chinta *et al.*, 2018) resulted in increasing the mechanical strength of aluminum matrix composites. This study aims to determine the addition of sea sand particles as an aluminum matrix composite reinforcement to its mechanical properties.

1.2. Literature review

The manufacturing of AMC with alternative reinforcement has been investigated before. Reinforcement from various industrial, agricultural, and natural material wastes such as fly ash, red mud, rice husk ash, and sugar bagasse ash has been studied and improved the mechanical properties of AMC. Except to improve the mechanical properties of AMC, this innovation also has an impact on reducing production costs and increasing the value of raw materials into materials for engineering purposes (Patel *et al.*, 2017).

Hybrid composite rice husk- SiC -Al 6061 has been successfully produced (Sarkar *et al.*, 2018). Hybrid composites have porosity less than 2.86%. The composite hardness decreases with

an increasing quantity of rice husk ash. The tensile strength of hybrid composites is lower than Al composites with SiC. However, the tensile strength of hybrid composites at 110 MPa remains higher than the matrix. Investigation of mechanical properties and tribology of Al-SiC-Rice Husk Ash (RHA) hybrid composites with powder metallurgy fabrication showed excellent results (Shaikh *et al.*, 2019). Hybrid composites have a lower density of up to 9% when reinforcement is increased, and porosity increases from 3.7% in pure Al to 11% in Al-10%wt SiC-15%wt RHA. Composite hardness increased to 19% with the best SiC and RHA compositions of 10%wt, respectively. Al-10%wt SiC-10%wt RHA showed better wear resistance with a 33% increase compared to pure Al.

The addition of bagasse ash to Al 5056/SiC hybrid composites decreases the wear rate of the composites. The wear rate falls with increasing Si, which effectively blocks the movement of dislocation (Harish *et al.*, 2019). Another natural material used as reinforcement in AMCs is coconut shell ash (CSA). Studies of the effect of adding CSA to Al 6082/CSA/ZrO₂ hybrid composite has been investigated (Kumar *et al.*, 2018). Composite hardness decrease when 10 %wt CSA is added, the highest hardness and tensile strength is achieved in the composition of 8%wt ZrO₂ reinforcement and 2 %wt CSA. The decrease in composite hardness is due to the lubrication properties of CSA particles. The highest flexural strength is achieved at 2 %wt ZrO₂ and 8%wt CSA. The hardness and tensile strength of Al6061/CSA/SiC composite increased up to the addition of 8%wt CSA and compressive strength increased until the addition of CSA 6% wt. Friction resistance is increased when CSA particles are added to Al6061-SiC composites (Satheesh and Pugazhvadivu, 2019).

In addition to materials from industrial and agricultural waste, other natural based materials that have the potential to be used as reinforcement in AMC is sea sand. Sea sand has been investigated for its effect on the strength of concrete. The use of sea sand as an aggregate in concrete increases its strength (Xiao *et al.*, 2017; Zhang *et al.*, 2019). Chemical analysis shows that sea sand contains compounds such as Fe₂O₃, SiO₂, Al₂O₃, and MgO (Carranza-Edwards *et al.*, 2009) that can improve the mechanical properties of AMC.

Increasing reinforcing volume fraction increased the strength but decreased the plasticity of the composite (Raj and Thakur, 2019; Razzaq *et al.*, 2017; Song, 2009; Viswanaatha *et al.*, 2013). Figure 1 shows the comparison of the volume fraction of reinforcing particles on aluminum composites. Higher ceramic particles added increased the agglomeration in the matrix (Das *et al.*, 2014). The agglomeration caused composite porosity (Podymova and Karabutov, 2017). Agglomeration of 14 %vol SiC nanoparticles in aluminum composites is shown in Figure 2. The Figure 3 shows the surface fracture of a SiC/Al composite with various SiC volume fractions. Observation of the fracture shows the characteristics of ductile fractures with the presence of dimple on the surface fracture of the specimen (Song, 2009).

The effect of the weight fraction of ash in the aluminum hybrid composite linearly increased with the addition of ash. The maximum tensile strength, impact strength, and compressive strength are achieved on the addition of 6% wt ash. The maximum hardness of the hybrid composite is found in the addition of 4% wt of ash (Vijaybabu *et al.*, 2019). The study of mechanical characterization of aluminum E-waste composite has resulted in the tensile, yield, and compressive strength increases by addition fly ash with a constant amount of e-glass fiber. The toughness of the composite is decreased with an increasing fraction of the fly ash ((Patel *et al.*, 2017).

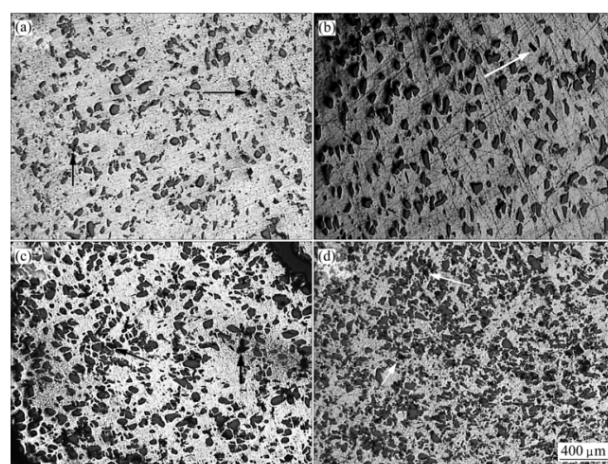


Figure 1. Optical observation of SiC various fractions in SiC/Al composite: (a) 8%vol (b) 12%vol (c) 16%vol (d) 20%vol (Song, 2009)

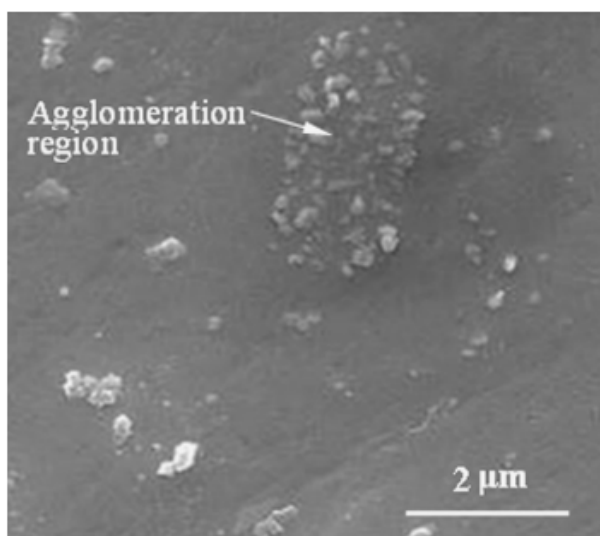


Figure 2. The agglomeration of 14%vol nanoparticles in Al composite (Xiong *et al.*, 2011)

Effect of various alumina nanofibre content on the alumina toughened zirconia composite resulted in increasing microhardness by 14% at the addition of 5% wt the alumina nanofibre, and the highest fracture toughness is reached at the addition of 1% wt of alumina fiber (Leonov, 2019). Addition ZrB₂ particle increasing mechanical properties of AA6063-ZrB₂ composite. Maximum tensile strength is achieved in addition to 10% wt of reinforcement. The hardness of the composite is increased from 52 HV to 63 HV with the addition ZrB₂ particle from 0 to 10% wt (Mohanavel *et al.*, 2018).

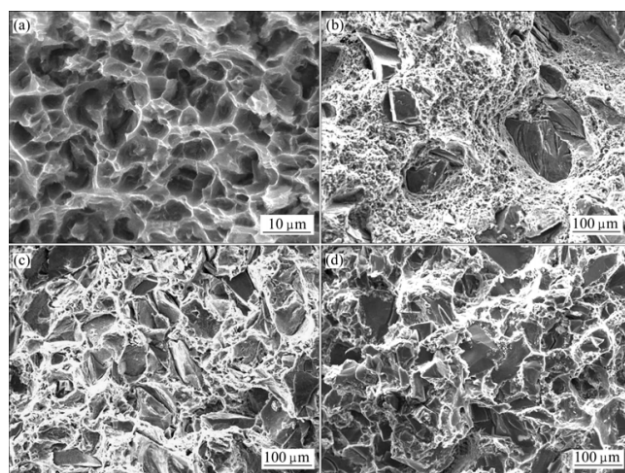


Figure 3. SEM observation of various SiC volume fractions in SiC/Al composite: (a) 8% (b) 12% (c) 16% (d) 20% (Song, 2009)

Addition of silicon nitride from 2% wt to 10% wt with 2% wt increasing on the aluminum

metal matrix composite affected increasing in hardness and ultimate tensile strength of composite with an addition 8% wt reinforcement. The composite hardness increases from 44.8 to 54.4 BHN, and the tensile strength increases from 127.1 to 178.5 MPa (Rao and Mohan, 2020). The optimum of SiO₂ addition on the aluminum composite was achieved in 20% wt. In addition, 20% of wt has an optimum intersection between hardness and ductility curve of the composite (Pattnayak *et al.*, 2018). Increasing the content of TiC ceramic particle resulted in an increase in hardness. The hardness escalated with increasing from 0% wt to 12% wt of TiC particle (Sharma *et al.*, 2020)

On the manufacturing of aluminum matrix composite, stir casting is the simplest and most effective method. On the other hand, the stir casting method has limitations, such as (1) Dispersed reinforcement is limited (usually is under 30% vol). (2) The distribution of reinforcement is not perfectly homogeneous. (3) Forming a local cluster of reinforcement (agglomeration) (Thomas *et al.*, 2014). In the stir casting, the high shear force is needed to dispersed reinforcement into the matrix, but the vortex that resulted from stirring process can increase the porosity and decreasing properties of the composite (Zhang *et al.*, 2019)

One limitation of in the aluminum matrix composite manufacturing is wettability. Wettability in aluminum matrix composite plays a crucial role in the final properties of the composite. Wettability can be defined as the ability of a molten metal to disperse on the solid surface, which represents a contact angle between the liquid and solid (Hashim *et al.*, 2001). The wetting behavior is affected by many factors, the thermodynamics characteristics, atmosphere, roughness of the reinforcement, crystallography, impurities, surface oxidation, and oxide film (Sangghaleh and Halali, 2009). Wettability can be improved with several approaches (Hashim *et al.*, 2001):

1. Addition of alloying elements
2. Coating of the reinforcement
3. Treatment on the reinforcement

The addition of alloying elements is the simplest method for improving wettability. The common is the addition of magnesium. Magnesium can be improved the wettability because magnesium has lower surface tension compared to aluminum, and magnesium can reduce the interfacial energy and forming new compounds on the interface of the reinforcement

(Hashim *et al.*, 2001). Effect of addition Mg on the wettability of SiC-Al showed that contact angel between Al and SiC decreases with increasing process temperature. The process temperature from no-wetting to wetting is decreased with the increasing content of Mg (Liu and Lin, 2017). However increasing of Mg addition more than 1% wt on the molten aluminum resulted in increasing viscosity of molten metal and more difficult to achieved a homogeneous distribution of particles (Bihari and Singh, 2017)

2. MATERIALS AND METHODS

Al 6061 was used as a matrix in the manufacture of Al 6061-sea sand composites. Sea sand particles were obtained from Samas beach, Yogyakarta, Indonesia. Before processed, the sea sand particle washed with alcohol to obtain impurities free on sea sand particles. After that, the sea sand was crushed to get a 200 mesh size using a ball milling process. The result of the ball milling process on sea sand has shown in Figure 4.

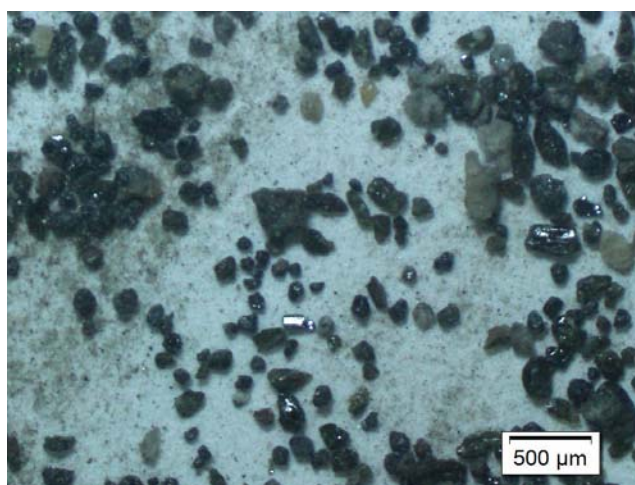


Figure 4. Sea sand particles after ball mill.

Stir casting technique has been used for composite manufacturing. The calculated Al 6061 was heated in the furnace, and the temperature was controlled at 800 °C with accuracy $\pm 25^{\circ}\text{C}$. Vortex flow was generated with a 45° four-blade impeller, which had been coated with 200 μm TiO_2 ceramics. The dimension of the impeller, as shown in Figure 5. The stirring condition was set at 720-750°C for 5 minutes and of 400 rpm. After first stirring, the 1 %wt of Mg was added as a wetting agent into the mixture, then continued stirring for 5 minutes. The composite mixture was poured into 130 x 130 x 60 mm permanent mold that has been heated at 700 °C, with pouring

temperature has controlled at 750 °C. The stir casting equipment is shown in Figure 6.

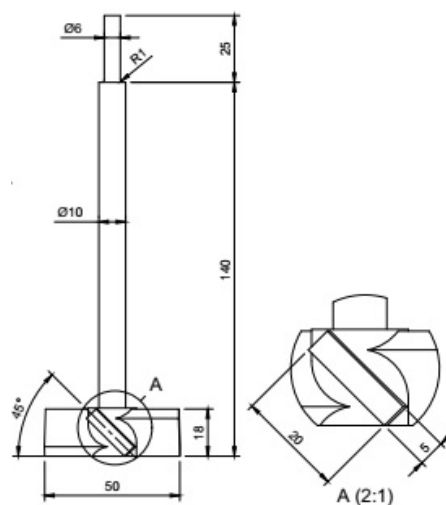


Figure 5. Impellers dimension.

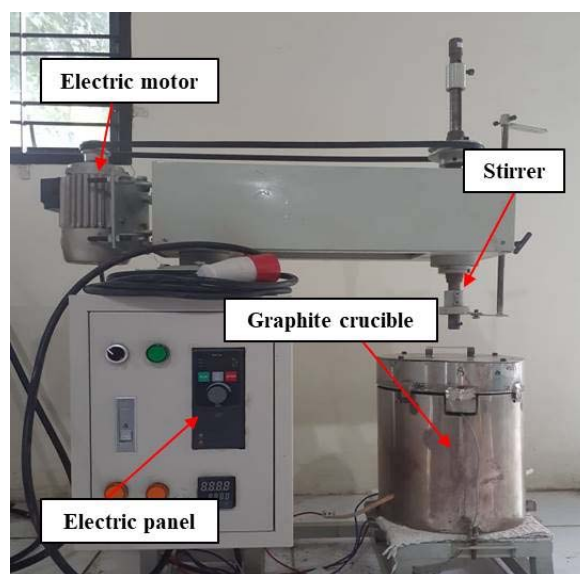


Figure 6. Stir casting equipment.

The prepared composite was mechanical and physical characterization by density, hardness, and tensile tests. The density and porosity were calculated by Archimedes's method. The hardness composite was measured using O.M.A.G AFRI ITALY MOD 100 MR, according to ASTM E-10, with a 2.5 mm steel ball indenter and 62.5 kg load. The hardness Brinell of the composite was calculated using Eq.1. Where P symbolize the load was used, D diameter of indenter and d symbolize the width of indentation diameter on the specimen. The

hardness value reported is an average of 9 readings taken at variously located of the specimen.

$$\text{BHN} = \frac{2P}{(\pi D)(D - \sqrt{D^2 - d^2})} \quad (\text{Eq.1})$$

The tensile strength test was measured using SUNPOC WEW-300D Hydraulic Universal Testing Machine according to JIS Z2201 standard with 6 mm specimen thickness. The dimension of the tensile test specimen has shown in Figure 7.

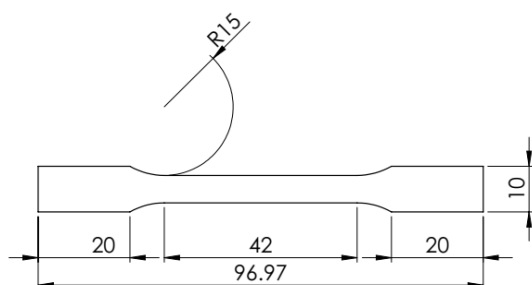


Figure 7. Tensile specimen dimension (mm).

3. RESULTS AND DISCUSSION:

3.1 Density and porosity

The theoretical, experimental density and porosity of the Al 6061-Sea sand composite are determined based on the rule of the mixture as follows Equation 2 (Kannan and Ramanujam, 2017).

$$\rho_{\text{theoretical}} = \rho_m \phi_m + \rho_r \phi_r \quad (\text{Eq.2})$$

Where ϕ_m and ϕ_r symbolize the weight fraction of the matrix and reinforcement, while ρ_m and ρ_r symbolize the density of the matrix and reinforcement, the experimental density was calculated adopting the Archimedes principle. Calculation of porosity of composites can obtain using Equation 3.

$$\text{Porosity} = \frac{(\text{Theoretical density} - \text{Experimental density})}{\text{Theoretical density}} \times 100\% \quad (\text{Eq.3})$$

The density and porosity of Al6061-sea

sand composites are shown in Figure 8 and Figure 9. The density of composite Al 6061-sea sand with a 2 %wt particle is 2.69 g/cm³. Composite density is decreased to 2.67 g/cm³ at the addition of 4%wt and 6 %wt of sea sand, respectively. This is due to the lower sea sand reinforcement density, which is 2.5-2.6 g/cm³ (Di *et al.*, 2019; Hilman *et al.* 2014), resulting in the composite density decreases with increasing reinforcement weight fraction. On the other hand, composite porosity increases with increasing reinforcement of sea sand reinforcement. The higher porosity caused by the increase in the surface of the sand sea in contact with molten aluminum, the higher the contact surface, resulted in a higher chance of porosity (Garg *et al.*, 2019).

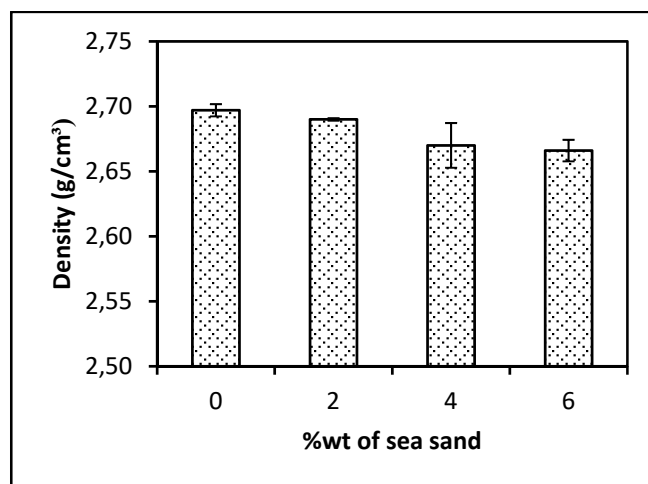


Figure 8. The density of the Al6061-sea sand composite.

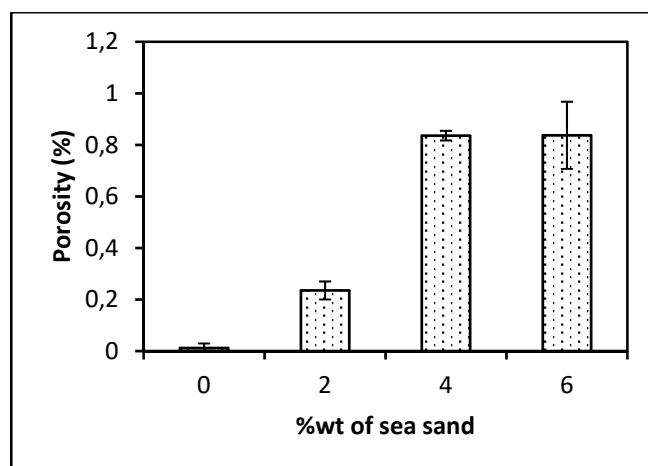


Figure 9. The porosity of the Al6061-sea sand composite.

3.2 Hardness

The hardness test of the composite is shown in Figure 10. The highest hardness is obtained in addition to 6 %wt sea sand with 119 BHN. The lowest hardness is captured in the acquisition of 2 %wt reinforcement with 107.93 BHN. Composite hardness increases with an increasing fraction of sea sand. The hardness of ceramic compounds that contain in sea sand affects the hardness of composites. Higher sea sand particles dispersed in the composite results increasing the hardness of the composite (Zhou and Xu, 1997). The dispersion of sea sand particles on the matrix causes slip disruption that limiting dislocation (Rozhbiany and Jalal, 2019). Also, ceramic compounds that contain in sea sand also increase the hardness of composites (Kumar *et al.*, 2013).

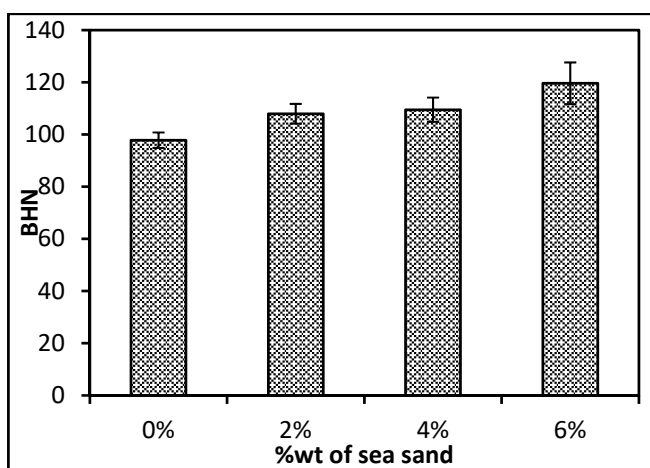


Figure 10. The hardness of the Al6061-sea sand composite

3.3 Tensile strength

The tensile strength of the Al6061-sea sand composite is shown in Figure 11. The UTS increases with an increasing fraction of sea sand. The highest tensile strength is achieved at 6% wt sea sand with 119 MPa, while the lowest tensile strength obtains at 2% wt sea sand with 98 MPa. Increased tensile strength is associated with ceramic compounds (Al_2O_3 , SiO_2 , Fe_2O_3) that contain in sea sand (Dhaneswara *et al.*, 2017). Previous research states that in composites, there are several strengthening mechanisms, including grain refinement, particle reinforcement, and reinforcement due to thermal differences (Kannan and Ramanujam, 2017). In Al6061-Sea sand composites, the strengthening mechanism that occurs is the mechanism of particle strengthening. This phenomenon is related to the

limited movement of dislocation due to the presence of sea sand particles. This is in accordance with the Orowan's mechanism (Srivastava and Chaudhari, 2018; Tang *et al.*, 2018).

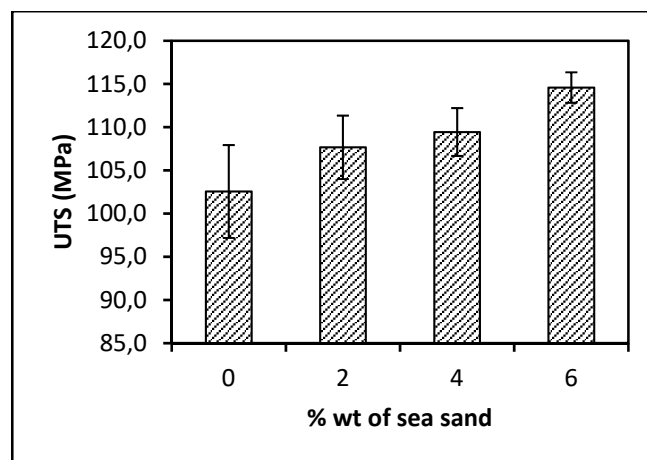


Figure 11. UTS of the Al6061-sea sand composite

4. CONCLUSIONS

In this study, Al 6061 composites with sea sand reinforcement were produced by the stir casting method. The findings of this work can be summarized:

1. Aluminum composite with sea sand reinforcement has been successfully produced by the stir casting method. The physical and mechanical properties of a composite depend on the amount of reinforcement added into the matrix.
2. Composite density decreases with increasing fraction sea sand, while porosity increases with an increasing fraction of sea sand.
3. The hardness and UTS of the composite increased due to an increasing fraction of sea sand. This phenomenon occurred due to ceramics compounds in sea sand, which gives a strengthening effect on composites.

Based on experiments, the sea sand can be used as an alternative reinforcement on aluminum composites, while also increasing the raw materials into materials for engineering purposes.

5. ACKNOWLEDGMENTS

This research was funded by the Republic of Indonesia Ministry of Research and Technology (National Research and Innovation Agency). Through research program for Ph.D. dissertation, contract No. 111/UN27.21/HK/2020.

6. REFERENCES

- 1 Akbar, H. I.; Surojo, E.; Ariawan, D. (2018). Effect of quenching agent on dimension stability of Al 6061-Al₂O₃ composite. *MATEC Web of Conferences*, 159.
- 2 Alimi, M.; Putri, S. E. (2016). Analisis Kandungan Mineral Pasir Pantai Losari Kota Makassar Menggunakan XRF dan XRD. *Jurnal Chemica*, 17(2), 19–23. (in Indonesian)
- 3 Bharath, V.; Nagaral, M.; Auradi, V.; Kori, S. A. (2014). Preparation of 6061Al-Al₂O₃ MMC's by Stir Casting and Evaluation of Mechanical and Wear Properties. *Procedia Materials Science*, 6, 1658–1667.
- 4 Bihari, B.; Singh, A. K. (2017). An Overview on Different Processing Parameters in Particulate Reinforced Metal Matrix Composite Fabricated by Stir Casting Process. *International Journal of Engineering Research and Applications*, 7(1), 42–48.
- 5 Bisane, V. P.; Sable, Y. S.; Dhobe, M.M.; Sonawane, P. M. (2015). Recent development and challenges in processing of ceramic reinforced Al matrix composite through stir casting: A Review. *International Journal of Engineering Research and Applied Science*, 21(10), 11–16.
- 6 Carranza-Edwards, A.; Kasper-Zubillaga, J. J.; Rosales-Hoz, L.; Morales-de la Garza, E. A.; Lozano-Santa Cruz, R. (2009). Beach sand composition and provenance in a sector of the southwestern Mexican Pacific. *Revista Mexicana de Ciencias Geológicas*, 26(2), 433–447.
- 7 Chinta, N. D.; Selvaraj, N.; Mahesh, V. (2018). Mechanical characterization of aluminium-Red mud metal matrix composites. *Materials Today: Proceedings*, 5, 26911–26917.
- 8 Das, D. K.; Mishra, P. C.; Singh, S.; Pattanaik, S. (2014). Fabrication and heat treatment of ceramic-reinforced aluminium matrix composites- A review. *International Journal of Mechanical and Materials Engineering*, 9(1), 1–15
- 9 Dhanesh, S.; Kumar, K. S.; Yohannan, L.; Fayiz, N. K. M.; Sajith, E. (2020). Materials Today : Proceedings Aluminium metal matrix composites reinforced with non - conventional materials: A review. *Materials Today: Proceedings*.
- 10 Dhaneswara, D.; Syahrial, A. Z.; Ayman, M. T. (2017). Mechanical Properties of Nano SiC-Reinforced Aluminum A356 with Sr Modifier Fabricated by Stir Casting Method. *Procedia Engineering*, 216, 43–50.
- 11 Di, W. U.; Yan, Q.; Wang, Y. J.; Gan, X. Q.; Dong, Z. H.; Wang, J. B.; Chen, J. J. (2019). Micro-analysis of Marine Sand from Zhoushan Seas. *IOP Conference Series: Earth and Environmental Science*, 304(3).
- 12 Dong, Z.; Wu, G.; Zhu, H. (2019). Mechanical properties of seawater sea-sand concrete reinforced with discrete BFRP-Needles. *Construction and Building Materials*, 206, 432–441.
- 13 Garg, P.; Jamwal, A.; Kumar, D.; Sadasivuni, K. K.; Hussain, C. M.; Gupta, P. (2019). Advance research progresses in aluminium matrix composites: manufacturing and applications. *Journal of Materials Research and Technology*, 8(5), 4924–4939.
- 14 Giofré, D.; Junge, T.; Curtin, W. A.; Ceriotti, M. (2017). Ab initio modelling of the early stages of precipitation in Al-6000 alloys. *Acta Materialia*, 140, 240–249.
- 15 Gireesh, C. H.; Durga Prasad, K.; Ramji, K. (2018). Experimental Investigation on Mechanical Properties of an Al6061 Hybrid Metal Matrix Composite. *Journal of Composites Science*, 2(3), 49.
- 16 Hall, J. N.; Jones, J. W. (1994). Particle size, volume fraction, and matrix strength effects on fatigue behavior and particle fracture in 2124 aluminum-SiCp composites. *Materials Science and Engineering A*, 183, 69–80.
- 17 Harish, T. M.; Mathai, S.; Cherian, J.; Mathew, K. M.; Thomas, T.; Prasad, K. V.

- V; Ravi, V. C. (2019). Development of aluminium 5056/SiC/bagasse ash hybrid composites using stir casting method. *Materials Today: Proceedings*, 27(3), 2635-2639.
- 18 Hilman, P. M; Suprpto, S. J; Sunuhadi, D. N; Tampubolon, A; Wahyuningsih, R; Widhyatna, D; Pardiarto, B; Gunradi, R; Franklin, F; Yudawinata, K; Sutisna, D. T; Dinarsih, D; Sukaesih.; Yuningsih, E.T; Candra.; Oktaviani, P; Rahmawati, R; Ulfa, R. M; Sukmayana, I; Ostman, I. (2014). Pasir besi di Indonesia: Geologi, Eksplorasi dan Pemanfaatannya, Pusat Sumber Daya Geologi, Bandung. (in Indonesian).
 - 19 Hashim, J.; Looney, L.; Hashmi, M. S. J. (2001). The wettability of SiC particles by molten aluminium alloy. *Journal of Materials Processing Technology*, 119(1–3), 324–328.
 - 20 Jalil, Z.; Rahwanto, A.; Mustanir.; Akhyar.; Handoko, E. (2017). Magnetic behavior of natural magnetite (Fe_3O_4) extracted from beach sand obtained by mechanical alloying method. *AIP Conference Proceedings*, 1862(July 2017), 8–12.
 - 21 Kannan, C; Ramanujam, R. (2017). Comparative study on the mechanical and microstructural characterisation of AA 7075 nano and hybrid nanocomposites produced by stir and squeeze casting. *Journal of Advanced Research*, 8(4), 309–319.
 - 22 Kumar, A; Lal, S; Kumar, S. (2013). Fabrication and characterization of A359/ Al_2O_3 metal matrix composite using electromagnetic stir casting method. *Journal of Materials Research and Technology*, 2(3), 250–254.
 - 23 Kumar, K. R.; Pridhar, T.; Sree Balaji, V. S. S. (2018). Mechanical properties and characterization of zirconium oxide (ZrO_2) and coconut shell ash (CSA) reinforced aluminium (Al 6082) matrix hybrid composite. *Journal of Alloys and Compounds*, 765, 171–179.
 - 24 Lasabuda, R. (2013). Development in Coastal and Ocean in Archipelago Perspective of The Republic of Indonesia. *Jurnal Ilmiah Platax*, 1, 92–101. (in Indonesian)
 - 25 Leonov, A. (2019). Effect of Alumina Nanofibers Content on the Microstructure and Properties of ATZ Composites Fabricated by Spark Plasma Sintering. *Materials Today: Proceedings*, 11, 66–71.
 - 26 Liu, Z. X.; Lin, W. S. (2017). The effect of Mg on the wetting behavior of SiC-Al system. *Materials Science Forum*, 893 MSF, 132–135.
 - 27 Mohanavel, V.; Kumar, S. S.; Sathish, T.; Anand, K. T. (2018). Effect of ZrB 2 content on mechanical and microstructural characterization of AA6063 aluminum matrix composites. *Materials Today: Proceedings*, 5(5), 13601–13605.
 - 28 Nagaral, M; Shivananda, B. K; Auradi, V; Parashivamurthy, K. I; Kori, S. A. (2017). Mechanical Behavior of Al6061- Al_2O_3 and Al6061-Graphite Composites. *Materials Today: Proceedings*, 4(10), 10978–10986.
 - 29 Patel, S; Rana, R. S; Singh, S. K. (2017). Study on mechanical properties of environment friendly Aluminium E-waste Composite with Fly ash and E-glass fiber. *Materials Today: Proceedings*, 4(2), 3441–3450.
 - 30 Pattnayak, A.; Madhu, N.; Panda, A. S.; Sahoo, M. K. (2018). A Comparative study on mechanical properties of Al-SiO₂ composites fabricated using rice husk silica in crystalline and amorphous form as reinforcement. *Materials Today: Proceedings*, 5(2), 8184–8192.
 - 31 Podymova, N. B; Karabutov, A. A. (2017). Combined effects of reinforcement fraction and porosity on ultrasonic velocity in SiC particulate aluminum alloy matrix composites. *Composites Part B: Engineering*, 113, 138–143.
 - 32 Radhika, N.; Balaji, T.V.; and Palaniappan, S. (2015). Studies On Mechanical Properties And Tribological Behaviour Of LM25/SiC/ Al_2O_3 Composites. *Journal of Engineering Science and Technology*, 10, 134–144.
 - 33 Raj, R; Thakur, D. G. (2019). Effect of particle size and volume fraction on the strengthening mechanisms of boron carbide reinforced aluminum metal matrix composites. *Proceedings of the Institution of Mechanical Engineers, Part C: Journal of Mechanical Engineering Science*, 233(4), 1345–1356.
 - 34 Rao, P. S. R.; Mohan, C. B. (2020). *Materials Today: Proceedings Study on*

- mechanical performance of silicon nitride reinforced aluminium metal matrix composites. *Materials Today: Proceedings*.
- 35 Razzaq, A. M; Majid, D. L; Ishak, M. R; Basheer, U. M. (2017). Effect of fly ash addition on the physical and mechanical properties of AA6063 alloy reinforcement. *Metals*, 7(11), 1–15.
 - 36 Reddy, B. R; Srinivas, C. (2018). Fabrication and Characterization of Silicon Carbide and Fly Ash Reinforced Aluminium Metal Matrix Hybrid Composites. *Materials Today: Proceedings*, 5(2), 8374–8381.
 - 37 Rozhbiany, F. A. R; Jalal, S. R. (2019). Reinforcement and processing on the machinability and mechanical properties of aluminum matrix composites. *Journal of Materials Research and Technology*, 8(5), 4766–4777.
 - 38 Sangghaleh, A.; Halali, M. (2009). Effect of magnesium addition on the wetting of alumina by aluminium. *Applied Surface Science*, 255(19), 8202–8206.
 - 39 Sarkar, S; Bhirangi, A; Mathew, J; Oyyaravelu, R; Kuppan, P; Balan, A. S. S. (2018). Fabrication characteristics and mechanical behavior of Rice Husk Ash-Silicon Carbide reinforced Al-6061 alloy matrix hybrid composite. *Materials Today: Proceedings*, 5(5), 12706–12718.
 - 40 Satheesh, M; Pugazhvadivu, M. (2019). Investigation on physical and mechanical properties of Al6061-Silicon Carbide (SiC)/Coconut shell ash (CSA) hybrid composites. *Physica B: Condensed Matter*, 572(August), 70–75.
 - 41 Shaikh, M. B. N; Arif, S; Aziz, T; Waseem, A; Shaikh, M. A. N; Ali, M. (2019). Microstructural, mechanical, and tribological behaviour of powder metallurgy processed SiC and RHA reinforced Al-based composites. *Surfaces and Interfaces*, 15 (December 2018), 166–179.
 - 42 Sharma, P.; Prakash, S.; Sharma, R.; Dabra, V.; Sharma, N. (2020). Materials Today: Proceedings Microstructural and mechanical behavior of aluminium alloy reinforced with TiC. *Materials Today: Proceedings*, 25, 934–937.
 - 43 Song, M. (2009). Effects of volume fraction of SiC particles on mechanical properties of SiC/Al composites. *Transactions of Nonferrous Metals Society of China (English Edition)*, 19(6), 1400–1404.
 - 44 Srivastava, N; Chaudhari, G. P. (2018). Microstructural evolution and mechanical behavior of ultrasonically synthesized Al6061-nano alumina composites. *Materials Science and Engineering A*, 724(December 2017), 199–207.
 - 45 Tang, X. C; Meng, L. Y; Zhan, J. M; Jian, W. R; Li, W. H; Yao, X. H; Han, Y. L. (2018). Strengthening effects of encapsulating graphene in SiC particle-reinforced Al-matrix composites. *Computational Materials Science*, 153 (April), 275–281.
 - 46 Thomas, A. T.; Parameshwaran, R.; Muthukrishnan, A.; Kumaran, M. A. (2014). Development of Feeding and Stirring Mechanisms for Stir Casting of Aluminium Matrix Composites. *Procedia Materials Science*, 5, 1182–1191.
 - 47 Tiwari, S; Pradhan, M. K. (2017). Effect of rice husk ash on properties of aluminium alloys: A review. *Materials Today: Proceedings*, 4(2), 486–495.
 - 48 Vijaybabu, G.; Raju, K. P.; Raju, V. V. M. K.; Sunilkumar, K. (2019). Studies on effect of ash in aluminium hybrid metal matrix composites. *Materials Today: Proceedings*, 18, 2132–2136.
 - 49 Viswanatha, B.M.; Kumar, M.P.; Basavarajappa, S.; and Kiran, T.S. (2013). A356/SiCp/Gr Metal Matrix Composites. *Journal of Engineering Science and Technology*, 8, 754–763.
 - 50 Xiao, J; Qiang, C; Nanni, A; Zhang, K. (2017). Use of sea-sand and seawater in concrete construction: Current status and future opportunities. *Construction and Building Materials*, 155, 1101–1111.
 - 51 Xiong, B; Xu, Z; Yan, Q; Lu, B; Cai, C. (2011). Effects of SiC volume fraction and aluminum particulate size on interfacial reactions in SiC nanoparticulate reinforced aluminum matrix composites. *Journal of Alloys and Compounds*, 509(4), 1187–1191.

- 52 Zhang, F.; Li, L.; Wang, E. (2015). Effect of micro-alumina content on mechanical properties of Al₂O₃/3Y-TZP composites. *Ceramics International*, 41(9), 12417–12425.
- 53 Zhang, Q; Xiao, J; Liao, Q; Duan, Z. (2019). Structural behavior of seawater sea-sand concrete shear wall reinforced with GFRP bars. *Engineering Structures*, 189(March), 458–470.
- 54 Zhang, W. Y.; Du, Y. H.; Zhang, P. (2019). Vortex-free stir casting of Al-1.5 wt% Si-SiC composite. *Journal of Alloys and Compounds*, 787, 206–215.
- 55 Zheng, K; Politis, D. J; Wang, L; Lin, J. (2018). A review on forming techniques for manufacturing lightweight complex—shaped aluminium panel components. *International Journal of Lightweight Materials and Manufacture*, 1(2), 55–80.
- 56 Zhou, W; Xu, Z. M. (1997). Casting of SiC reinforced metal matrix composites. *Journal of Materials Processing Technology*, 63(1–3), 358–363.

ISOLAMENTO E IDENTIFICAÇÃO DE FUNGOS DE DETRITOS DE PLANTAS
SUBMERGIDAS EM HABITATS AQUÁTICOS NA PROVÍNCIA DE MISAN

ISOLATION AND IDENTIFICATION OF FUNGI FROM SUBMERGED PLANTS DEBRIS IN
AQUATIC HABITATS IN MISAN PROVINCE

عزل وتشخيص الفطريات من البقايا النباتية المغمورة في البيئات المائية في محافظة ميسان

ABD AL-NABI, Zainab Jumhia¹; KASIM, Ali Abdulwaheed^{1*}

¹ Department of Biology, College of Science, University of Misan, Maysan, Iraq

* Corresponding author

e-mail: alimycol@uomisan.edu.iq

Received 12 June 2020; received in revised form 25 August 2020; accepted 08 October 2020

RESUMO

Quarenta e oito táxons de fungos saprófitos foram isolados e identificados a partir de amostras de restos de plantas submersas coletadas em diferentes locais na província de Misan, sul do Iraque, que são Maymouna, Al-Salam, Majar Al-Kabir e Amara. Dentre elas, 24 espécies pertenciam a Ascomycota (seis delas em estado sexual), 19 espécies a hifomicetos (fungos anamórficos), 4 a Zygomycota e uma a Oomycetes. Seis espécies foram isoladas e recentemente registradas no Iraque, que são *Aniptodera margaration*, *Cirrenalia iberica*, *Cordana lignicola*, *Cordana verruculosa*, *Pseudoacrodactys appendiculata* e *Scytalidium thermophilum*. No entanto, na avaliação dos métodos de câmara úmida e cultura direta, 34 espécies foram isoladas pelo primeiro método e 27 espécies pelo segundo método, entretanto, 13 espécies (9 pertenciam a Ascomycota, 2 a hifomicetos e 2 a zigomicetos) foram recuperado por ambos os métodos. *Aspergillus terrus* apareceu com maior frequência e ocorrência (11,76%, 42,55%, respectivamente), seguido por *Aspergillus horti* (10%, 36,17%, respectivamente) e, em seguida, *A. niger* com uma frequência e ocorrência de 5,29% e 19,14%, respectivamente, enquanto 17 espécies apresentaram menor frequência e ocorrência, atingindo 0,58%, 2,12%, respectivamente, para todas. Cento e sete isolados foram recuperados de todos os locais de estudo. Enquanto isso, sessenta e quatro isolados foram relatados de Majar Al-Kabir, em comparação com outros locais, seguido por Amara (43 isolados), enquanto 39 isolados foram isolados de Maymouna e 24 isolados de Al-Salam. A biodiversidade de fungos isolados de restos de plantas submersos foi comparada com estudos anteriores. Breves descrições dos novos fungos registrados foram fornecidas.

Palavras-chave: lignocelulose, restos de plantas submersas, Ascomycota, Hyphomycetes, Iraque.

ABSTRACT

Forty-eight taxa of saprophytes fungi were isolated and identified from submerged plant debris samples collected from different sites in Misan province, southern Iraq, which are Maymouna, Al-Salam, *Majar Al-Kabir*, and Amara. Among them, 24 species belonged to Ascomycota (six of which are sexual state), 19 species to hyphomycetes (anamorphic fungi), 4 to Zygomycota, and one to Oomycetes. Six species were isolated and newly recorded from Iraq, which are *Aniptodera margaration*, *Cirrenalia iberica*, *Cordana lignicola*, *Cordana verruculosa*, *Pseudoacrodactys appendiculata*, and *Scytalidium thermophilum*. However, in the evaluation of both moist chamber and direct culture methods, 34 species were isolated by the first method and 27 species by the second method, meantime, 13 species (9 belonged to Ascomycota, 2 to hyphomycetes, and 2 to Zygomycetes) were recovered by both methods. *Aspergillus terrus* was appeared in highest frequency and occurrence (11.76%, 42.55%, respectively), followed by *Aspergillus horti* (10%, 36.17%, respectively), and then *A. niger* with a frequency and occurrence of 5.29% and 19.14%, respectively, while 17 species were appeared lowest frequency and occurrence to reach 0.58%, 2.12%, respectively, for all. One hundred and seven isolates have been recovered from all study sites. Meantime, sixty-four isolates have been reported from *Majar Al-Kabir*, as compared with other sites, followed by Amara (43 isolates), while 39 isolates have been isolated from the Maymouna, and 24 isolates from Al-Salam. The biodiversity of fungi isolated from submerged plant debris was compared with previous studies. Brief descriptions of the new recorded fungi were given.

Keywords: lignocellulose, submerged plants debris, Ascomycota, Hyphomycetes, Iraq.

تم عزل وتشخيص 48 نوعاً من الفطريات المترمة والمتواجدة على البقايا النباتية المغمورة من عينات جمعت من مناطق مختلفة في محافظة ميسان/ جنوب العراق وهي الميمونة والسلام والمجر الكبير والعمارة. وجد أن من بين الأنواع المعزولة، 24 نوعاً تعود إلى الفطريات الكيسية (سنة أنواع منها بالطور الجنسي) و19 نوعاً تعود إلى فطريات hyphomycetes (الفطريات بالطور اللاجنسي) و4 أنواعاً تعود إلى الفطريات اللاقحية ونوع واحد من الفطريات البيضية. تم عزل وتسجيل ستة أنواع لأول مرة في العراق هي *Aniptodera margaration*، *Cortana* و *Cirrenalia iberica*، *Scytalidium thermophilum*، *Pseudoacrodictys appendiculata* و *Cordana verruculosa* و *lignicola* الرطبة والزرع المباشر لعزل الفطريات، فتم عزل 34 نوع بالطريقة الأولى و24 بالطريقة الثانية، ولوحظ أن 13 نوع قد تم عزلها بالطريقتين معاً (9 أنواع تعود إلى الفطريات الكيسية ونوعين من كل من الفطريات اللاقحية والبيضية). أظهر الفطر *Aspergillus terreus* أعلى نسبة تردد وظهور (11.76%) و42.55% على التوالي، تلاه الفطر *Aspergillus horti* (10% و36.17% على التوالي) ومن ثم الفطر *A. niger* والذي أعطى نسبة تردد وظهور بلغت 5.29% و19.14% على التوالي. بينما وجد أن 17 نوعاً أظهرت أقل نسبة تردد وظهور بلغت 0.58% و2.12% على التوالي لكل فطر. تم عزل 107 عذلة فطرية خلال هذه الدراسة من جميع مناطق الدراسة، ووجد أن أعلى عدد من العزلات قد تم عزلها من موقع المجر الكبير مقارنة ببقية المواقع حيث بلغت 64 عذلة، تلاه موقع العمارة (43 عذلة)، وتم عزل 39 عذلة من موقع الميمونة و24 عذلة من موقع السلام. تمت مقارنة التنوع الاحيائي للفطريات المعزولة من بقايا النباتات المغمورة بالدراسات السابقة. وأعطى وصف مختصر للفطريات التي سجلت لأول مرة في العراق.

الكلمات المفتاحية: lignocellulose، بقايا النباتات المغمورة، Ascomycota، Hyphomycetes، العراق.

1. INTRODUCTION:

Dead plant substrates (lignocellulose) are colonized and degraded by a wide variety of biological agents such as fungi, bacteria, and insects if the appropriate environmental conditions are available (Goodell et al., 2003), and are essential components in the terrestrial and freshwater ecosystems (Tsui et al., 2001). Fungi are evolutionarily and functionally diverse ubiquitous and found in the vast majority of ecosystems (Grossart et al., 2019). Fungi are characterized by tremendous environmental diversity, the majority belong to terrestrial fungi, and a few are isolated from aquatic habitats and woody submerged remains (Shearer, 1993). Nearly 3,000 fungal species and 138 non-fungal oomycetes have been reported from aquatic habitats (Ittner et al., 2018). Furthermore, the majority of these fungi have occurred in temperate regions and Asian tropical areas. Moreover, most of them belonged to the phyla ascomycetes, basidiomycetes, chytridiomycetes, zygomycetes, and oomycetes (Shearer et al., 2007; Raghukumar, 2012). The freshwater hyphomycetes (sometimes referred to as Amphibions or Ingoldian fungi) mainly belong to the ascomycetes with a small percentage in the basidiomycetes (Ittner et al., 2018).

Aquatic fungi have a vitally important role in ecosystems because they are among crucial decomposer microorganisms that fall within the food web (Rani and Panneerselvam, 2009; Daniel, 2016), and participate in the decomposition of detritus and the energy stream to the higher trophic levels (Bärlocher, 2009). Fungi from the different groups under suitable conditions will often colonize and degrade the wood material and even attack the same wood cells (Daniel, 2016). It can break down the

organic materials (Raja et al., 2018), so they play an essential functional role in the recycling of carbon, nitrogen, and other nutrients (Cai et al., 2006; Kantharaj et al., 2017) because it can produce various wood decay enzymes (Sonigo et al., 2011; Andlar et al., 2018).

In particular, ascomycete fungi and fresh aquatic hyphomycetes occur on a variety of submerged substrates (Michel et al., 2005; Sati and Pathak, 2016) and are osmoorganotrophs, absorbing nutrients via their cell wall. Moreover, the majority of them have a filamentous growth phase during their life cycle. This morphology helps them invade deep into the substance and directly decompose particles of organic matter to obtain nutrients for growth and reproduction (Christian et al., 2011).

Freshwater lignicolous hyphomycetes are a predominant and variety group, which live on submerged plant debris and decaying tree leaves (Shearer et al. 2007; Hyde et al. 2016), and are traditionally identified based on the morphology conidia (Sridhar, 2009). In addition, these fungi grow abundantly and develop large quantities of conidia (Bärlocher, 2009) and mycelia formation that develop within and outside remains of the plant (Wurzbacher and Grossart, 2012).

Several researchers have studied the occurrence and distribution of fungi from submerged wood in aquatic habitats in different sites of Iraq. Forty-two species have been isolated from Basrah in southern of Iraq (Muhsin and Kalaf, 2002). On the other hand, eight species were recorded from different sites of Iraq (Al-Saadoon and Al-Dossary, 2010). Al-Saadoon and Al-Dossary (2014) reported 67 species in several locations in southern Iraq. Al-Nasrawi (2014) Isolated tow species from Al-Huwaizah marshes in Southern Iraq. Al-Huwaizah marshes

in Southern Iraq. It is known that the water bodies, including marshes, swamps, ponds, and rivers, represent broad areas of the Misan province, so these environments are rich in aquatic plants and submerged plant debris.

Consequently, it is rich in aquatic fungi and fungi associated with plant debris. Therefore, due to the lack of studies on these fungi in such environments. Accordingly, the study aimed to isolate and identify fungi from submerged plant debris present in some sites.

2. MATERIALS AND METHODS:

2.1 Sample collection

Forty-seven samples from submerged and floating plant debris such as small branches and stem were collected from many locations in Misan province (12 samples from Maymouna, 11 samples from Al-Salam, 12 from Majar Al-Kabir, and 12 from Amara) during September 2019 to February 2020. The samples were placed in snap lock plastic bags and sent to the laboratory.

2.2 Methods for isolating fungi

2.2.1 Moist Chamber Method

The samples were washed gently with tap water and then with sterile distilled water several times, 5 pieces (1-2 cm) were put in a glass chamber contain moist filter papers, incubated at 25 °C for 8 weeks with the addition of sterile distilled water whenever needed to keep it from drying out. The samples were examined daily after 5 days of incubation for any fungal growth. Upon observing the growth of mycelium on the samples, a portion of the mycelium was transferred with a sterile loop to the Petri dishes containing Czapek-Doxe Agar and incubated at 25 °C for 7 days to for obtaining pure cultures. For ascomycetes, once the ascocarps emerged on samples, the fruit bodies were squashed on a sterile slide mounted with water to release asci and ascospores (to remove the gelatinous coats and appendages on, or around the ascospores, Indian ink (Himedia, CAS No. 0) was added), and then covered with cover slides for an initial examination, water was replaced with cotton blue lactophenol for measuring (ascocarps, asci, ascospores, conidiophores, conidia, etc.) and photography (microscope camera system, Scope Image Dynamic Pro Co.China).

2.2.2 Direct culture method

The samples were washed as the previous paragraph and cut into pieces of 1 cm. Five pieces were planted on Malt Extract Agar (MEA) and Potato Carrot Agar (PCA) plates and incubated at 25 °C for 7 to 10 days. Then, different fungal colonies were isolated and cultured separately in MEA and PCA.

To examine the fungal mycelium that appeared in both methods, slides were prepared by cutting a portion of the mycelium using a sterile surgical blade and put on a slide and stain with a drop of cotton blue lactophenol or lactophenol according to the color of the specimen. The slides were examined under a light microscope. The identification of the isolated fungi is made according to the available taxonomic keys. Permanent slides, dried samples, and pure cultures were preserved at the biology department from the College of Sciences of the University of Misan.

The percentage of frequently (Eq. 1) and the occurrence (Eq. 2) of fungal species were measured using Equations 1 and 2 (Krebs, 1978).

3. RESULTS AND DISCUSSION:

3.1 Taxonomic study

Forty-eight species of saprophytes fungal were isolated during this study from submerged plant debris from different sites (Maymouna, Al-Salam, Mgr Al-kabeer, and Amara) in the Province of Misan, comprising 24 species belonged to Ascomycota (six of which are sexual state), 19 hyphomycetes, four Zygomycota, and one Oomycota. Six species were recorded for the first time in Iraq. These are *Aniptodera margaration*, *Cirrenalia iberica*, *Cordana lignicola*, *C. verruculosa*, *Pseudoacrodictys appendiculate*, and *Scytalidium thermophilum*. The taxonomic notes on these taxa are described below.

1- *Aniptodera margaration* Shearer, (1989).

Isolate examined: from submerged stem wood, Maymonia. Isolation No. Ma3570, Figure1.

Ascocarps hyaline, globose or subglobose, immersed or superficial, with ostiole, 145 – 162 µm diam. Asci hyaline, subglobose to pyriform ovoid, rounded at the apex, 20 - 35 X 45 - 70 µm. Containing eight ascospores. Ascospores ellipsoidal or oblong-ellipsoidal, hyaline, 1-septum, not constricted at the septum, 7.5 - 10 X 20 - 25 µm.

This feature of the present isolate conforms with Shearer (1989). Jones *et al.* (2009) indicated the ability of some species of *Aniptodera* to occur in fresh and saltwater. The most important characteristic of this species is its formation of hyaline ascomate and the growth as saprobes on submerged wood.

2- *Cirrenalia iberica* Hernandez-Restrepo *et al.*, (2017).

Isolated examined: on submerged wood, Mgr Al-kabeer. Isolation No. Mg0512, Figure 2.

The colony is superficial. Mycelium hyaline, branched, septated, 2.5-5µm wide. Conidiophores micronematous, pale brown, 7.5-10 x 12.5-15 µm. Conidia straight or slightly curved, with 1-4 septa with an almost globose cell, the distal cells are much bigger and dark than others. Basal cell 7.5-12.5 µm, middle cell 10-15 µm, apical cell 25-30 µm, one conidium only produced on the apex of conidiophore

The present isolates are were precisely similar to those described by Hernandez-Restrepo *et al.*, (2017). There are 13 species of *Cirrenalia*, isolated from terrestrial and marine habitats. Based on molecular phylogenetic analysis, many species of *Cirrenalia* have been transferred to *Halazon*, *Hiogispora*, *Hydea*, and *Matsusporium* belonging to the Lulworthiales (Abdel-Wahab *et al.*, 2010).

3- *Cordana lignicola* Luo, *et al.*, (2019).

Isolated examined: submerged wood, Maymona. Isolation No. Ma1245, Figure 3.

The colonies were superficial, hairy like, brown to dark brown, and mycelium branched, septate. Conidiophore macronematous 2.5-5 x 100 - 120 µm unbranched, containing septa and intercalary nodes, dark brown, and acropleurogenous. Conidia elongated-ellipsoid, 1 - 2 septa. 1-septate conidia had slightly constricted at the septum, septate near the apex, globose or subglobose at the apex. 2-septate conidia not constricted at the septum, elongate cylindrically. Conidia hyaline when young, becoming brown when aged. 2.5 -5 x 7.5 -12.5 µm.

This present isolate feature conforms with the designated species *C. lignicola* (Luo *et al.*, 2019). This species was similar to *C. mercadiana* except that the ellipsoidal or cylindrical conidia, 0-1 septum, and conidiophores were longer in the latter species compared to *C. lignicola* the conidia elongated-ellipsoid, 1-2 septa. Phylogenetic analysis showed a difference between them

(Hernández-Restrepo *et al.*, 2014; Luo *et al.*, 2019).

4- *C. verruculosa* Hernández-Restrepo *et al.*, (2014).

Specimen examined: submerged wood, Amara. Isolation No. Am40121, Figure 4.

Colonies were superficial, brown to light brown. Mycelium growing superficial and partially immersed in the wood, branched, light brown, 2.5–5 µm diam. Conidiophore mononematous or macronematous, straight, unbranched, and distinguish present intercalary nodes and spherical basal cell, 2.5-5 x 115-120 µm. Conidia ellipsoidal, obovoid or verruculosa, light brown to brown, acropleurogenous, non-septate, 2.5-5x 2.5-7.5 µm.

The reason for naming *C. verruculosa* was due to the verruculosa shape of conidia. This species can be easily recognized from *C. solitaria* and *C. semaniae* (which are produced black, lacking septa conidia) by morphological characters. However, the conidia size is smaller and pale brown (Hernández-Restrepo *et al.*, 2014).

5- *Pseudoacrodictys appendiculata* (Ellis) Baker and Morgan-Jones, (2003).

Specimen examined: submerged wood, Maymonia. Isolation No. Ma0510, Figure 5.

Colonies were effuse, black. Mycelium branched, superficial, 2.5 – 5 µm diam. Conidiophore macro-nematous, single or in a group of two or three, bearing a single conidium, straight, black or dark brown, 2.5 – 5 x 15 – 35 µm. Conidia turbinate to pyriform, black, bearing 1 – 4 black appendages (muriform), 25 –37.5 x 30 – 57.5 µm.

The characters of the examined isolate match well with Ellis (1965) description, which was erected as *Acrodictys appendiculata* and transferred into *P. appendiculata* by Baker and Morgan-Jones (2003) due to the dark color, large size, irregular shape, and septa of conidia.

6- *Scytalidium thermophilum* (Cooney and Emerson) Austwick, (1976).

Specimen examined: submerged wood, Amara. Isolation No. Am1334, Figure 6.

Colonies white. Mycelium hyaline, branched, septated, 2-5 µm diam. Conidia as arthroconidia ellipsoidal or subglobose, 5- 7.5 x 7.5 - 17.5 µm. Chlamydospores present, 7.5 - 12.5 µm.

Our isolate matches the original description of

Austwick (1976).

3.2 Population dynamic of isolated fungi

A total of 48 fungal taxa were isolated from submerged plant debris, comprising 24 Ascomycota (50%), 19 hyphomycetes (39.58%), four species belonged to Zygomycota (8.33%), and one Oomycota (2.08%) were recorded. 34 species were isolated using the moist chamber method, and 27 by direct culture method, 13 species (9 belonged to Ascomycota, 4 to hyphomycetes) were recovered by both methods (Table 1). In the habitat of submerged plant debris, *A. terreus* was appeared in the highest frequency and occurrence (11.76%, 42.55%, respectively) followed by *A. horti* (10%, 36.17%). In comparison, the frequency and occurrence of *A. niger* and *A. oryzae* were found in less amount reaching 0.58%, 2.12%, respectively.

Thirty-four species were isolated using the moist chamber method, and 27 by direct culture method, 13 species (9 belonged to Ascomycota, 2 to hyphomycetes, and 2 to Zygomycetes) were recovered by both methods (Table 1). In the habitat of submerged plant debris, *A. terreus* has appeared in the highest frequency and occurrence (11.76%, 42.55%, respectively), followed by *A. horti* (10%, 36.17%), and then *A. niger* with a frequency and occurrence of 5.29 and 19.14, respectively. In comparison, the frequency and occurrence of 17 species were found in less amount reaching 0.58%, 2.12%, respectively (Table 1).

This study revealed that 107 isolates had been isolated from all study sites, 64 isolates were recorded from Majar Al-Kabir, 43 isolates were reported from Amara, 39 isolates from Maymouna and, 24 isolates from Al- Salam.

Many studies have also investigated the biodiversity of fungi found on submerged plant debris (Shearer *et al.*, 2007; Daniel, 2016). The most frequent fungi identified were ascomycetes and hyphomycetes (Hu *et al.*, 2010; Sati and Pathak, 2016). Anamorphic fungi were more frequent in submerged plant debris (Samson, *et al.*, 2011; Lepère *et al.*, 2019). However this due to rapid growth, the ability to produce a large number of spores (conidia) that are long and branched or filamentous; this assist their attachment to substrates in running water (Ghate and Sridhar, 2015; Raja *et al.*, 2018) and its adaptation to different ecological environments (Domsch *et al.*, 1980; Daniel, 2016).

Fungi have important roles in cycling of organic matter and food net (Grossart *et al.*, 2019). So, this study demonstrated that the most

Isolated fungi belong to the genus *Aspergillus* (8 species), *A. terreus*, *A. horti*, *A. fumigatus* isolated from all study sites. The reason for its diverse species of *Aspergillus* and has a worldwide distribution because it can adapt and grow in different ecological environments and secrete many enzymes for breaking down organic matters (Sohail *et al.*, 2009; Wurzbacher *et al.*, 2010).

C. lignicola and *C. verruculosa* were isolated from submerged plant debris samples from some sites. Anyway, Hernández-Restrepo *et al.*, (2014) indicated that the species of *Cordana* are distributed in most parts of the world and frequently found on different material, such as soil, plant debris.

A. alternate, *A. pullulans*, *C. macrocephala*, *M. varius*, *S. lignicola*, *E. rostratum*, *C. globosum*, and other sexual ascomycota were isolated by Al-Saadoon and Al-Dossary (2014) from submerged plant debris in Basrah province (southern Iraq). However, *C. globosum* was isolated from different environments such as soil, water, and plant debris (Fallah and Shearer, 2001).

N. inornata was equivalent to *N. Aquatic* but different in the way ascospores were released from Ascomate, and ascospores of *A. quatica* carrying appendices at one time (Hyde, 1992). Furthermore, Pang *et al.* (2003) demonstrated that the DNA sequence of *N. inornata* proved that it was closely related to genus *Aniptodera*. Anyway, *N. inornata* was isolated from marine habitats (Dethoup and Manoch, 2009) and from submerged dead plants (Muhsin and Kalaf, 2002; Al-Saadoon and Al-Dossary, 2014).

S. lignicola was isolated from freshwater, brackish, saltwater, and can tolerate high salinity (Hyde, 1994). Moreover, Al-Saadoon and Abdullah (2001) isolated *S. lignicola* from dead stem submerged from freshwater in Nineveh province (Northern Iraq). *S. lignicola* is similar to *S. fusiformis* and *S. Longispora* and can be distinguished by the size of ascospore as well as by genotypes. (Ho *et al.*, 1997; Boonyuen *et al.*, 2011). Furthermore, the ascospore of *S. longispora* are longer and thinner (Abdel-Wahab and Jones, 2000), and differs from *S. aquatic* with the wide of ascospore (Jones and Hyde, 1992).

Chaverri *et al.* (2011) showed that *Trichoderma* a widespread genus capable of grow in broader habitats. Therefore, two isolates of *T. harzianum* have been isolated from plant remains from Majar Al-Kabi and Amara because it able to

produce many enzymes such as cellulase, amylases, and pectinase (Sandhya *et al.*, 2004; Schuster and Schmoll, 2010; Li *et al.*, 2013)

Some species of *Aspergillus*, *Penicillium*, *Fusarium*, and *Rhizopus* appeared high-frequency value, and this result corresponded to many studies (Frisvad and Samson, 2004; Al-Saadoon and Al-Dossary, 2014; Refai *et al.*, 2015).

4. CONCLUSIONS:

In the present study, saprophytic fungi that grow on submerged plant debris were recovered. The abundance of plant remains due to the diversity of plants in aquatic environments which are a suitable source for the growth of these fungi, especially ascomycetes and hyphomycetes. The water bodies in Misan province still need further study to identify more new species and new record fungi, especially when using molecular studies.

5. ACKNOWLEDGMENTS:

The authors thank Asst. Prof. Maitham Dragh, the head of the biological Department, College of Science, University of Misan, for his help.

6. REFERENCES:

1. Abdel-Wahab, M. A., Pang, K. L., Nagahama, T., Abdel-Aziz, F. A., and Jones, E. G. (2010). Phylogenetic evaluation of anamorphic species of *Cirrenalia* and *Cumulospora* with the description of eight new genera and four new species. *Mycological Progress*, 9(4), 537-558.
2. Abdel-Wahab, M. A., and Jones, E. G. (2000). Three new marine ascomycetes from driftwood in Australia sand dunes. *Mycoscience*, 41(4), 379-388.
3. Al-Nasrawi, H. (2014). Two ascomycetes from different aquatic habitats. *International Journal Research in Environmental Studies*. (2) 24-30.
4. Al-Saadoon, A. H., and Abdullah, S. K. (2001). Some interesting ascomycetes from Iraq. *Iraqi J, Biology*, 1, 125-134..
5. Al-Saadoon, A. H. and Al-Dossary, M. A. (2010). Some fungi isolated from submerged plant debris in Southern Iraq. *Marsh Bulletin*, 5(2), 207-221.
6. Al-Saadoon, A. H., and Al-Dossary, M. N. (2014). Fungi from submerged plant debris in aquatic habitats in Iraq. *International Journal of Biodiversity and Conservation*, 6(6), 468-487.
7. Andlar, M., Rezić, T., Marđetko, N., Kracher, D., Ludwig, R., and Šantek, B. (2018). Lignocellulose degradation: an overview of fungi and fungal enzymes involved in lignocellulose degradation. *Engineering in Life Sciences*, 18(11), 768-778.
8. Austwick, P. K. C. (1976). Environmental aspects of *Mortierella wolffii* infection in cattle. *New Zealand journal of agricultural research*, 19(1), 25-33.
9. Baker, W. A., and Morgan-Jones, G. (2003). Notes on Hyphomycetes. XCI. *Pseudoacrodictys*, a novel genus for seven taxa formerly placed in *Acrodictys*. *Mycotaxon*, 85, 371-391.
10. Bärlocher, F. (2009). Reproduction and dispersal in aquatic hyphomycetes. *Mycoscience*, 50(1), 3-8.
11. Boonyuen, N., Chuaseeharonnachai, C., Suetrong, S., Sri-Indrasutdhi, V., Sivichai, S., Jones, E. G., and Pang, K. L. (2011). *Savoryellales* (Hypocreomycetidae, Sordariomycetes): a novel lineage of aquatic ascomycetes inferred from multiple-gene phylogenies of the genera *Ascotaiwania*, *Ascothailandia*, and *Savoryella*. *Mycologia*, 103(6), 1351-1371
12. Cai, L., Ji, K. F., and Hyde, K. D. (2006). Variation between freshwater and terrestrial fungal communities on decaying bamboo culms. *Antonie van Leeuwenhoek*, 89(2), 293-301.
13. Chaverri, P., Gazis, R. O., and Samuels, G. J. (2011). *Trichoderma amazonicum*, a new endophytic species on *Hevea brasiliensis* and *H. guianensis* from the Amazon basin. *Mycologia*, 103(1), 139-151.
14. Christian, W., Janice, K., and Hans-Peter, G. (2011). Aquatic Fungi. In *The Dynamical Processes of Biodiversity-Case Studies of Evolution and Spatial Distribution*. IntechOpen.
15. Daniel, G. (2016). Fungal degradation of wood cell walls. In *Secondary xylem biology* (pp. 131-167). Academic Press.
16. Dethoup, T., and Manoch, L. (2009). Diversity of marine fungi in eastern Thailand. *Kasetsart Journal (Natural Science)*, 43, 100-106.

17. Domsch, K. H., Gams, W., and Anderson, T. H. (1980). *Compendium of soil fungi. Volume 1*. Academic Press (London) Ltd.
18. Ellis, M. B. (1965). Dematiaceous hyphomycetes. 6. *Mycol. Pap.*, 103, 1-46.
19. Fallah, P. M., and Shearer, C. A. (2001). Freshwater ascomycetes: new or noteworthy species from north temperate lakes in Wisconsin. *Mycologia*, 93(3), 566-602.
20. Frisvad, J.C. and Samson, R.A. (2004). Polyphasic taxonomy of *Penicillium* Subgenus *Penicillium* A guide to identification of food and airborne terverticillate *Penicillia* and their Mycotoxines. *Studies in mycology*, 49, 1- 174.
21. Ghatge, S. D., and Sridhar, K. R. (2015). Diversity of aquatic hyphomycetes in streambed sediments of temporary streamlets of Southwest India. *Fungal Ecology*, 14, 53-61.
22. Goodell, B., Nicholas, D. D., and Schultz, T. P. (Eds.). (2003). *Wood deterioration and preservation: advances in our changing world*. American Chemical Society.
23. Grossart, H. P., Van den Wyngaert, S., Kagami, M., Wurzbacher, C., Cunliffe, M., and Rojas-Jimenez, K. (2019). Fungi in aquatic ecosystems. *Nature Reviews Microbiology*, 17(6), 339-354.
24. Hernandez-Restrepo, M., Gené, J., Castañeda-Ruiz, R. F., Mena-Portales, J., Crous, P. W. and Guarro, J. (2017). Phylogeny of saprobic microfungi from Southern Europe. *Studies in Mycology*, 86, 53-97.
25. Hernández-Restrepo, M., Gené, J., Mena-Portales, J., Cano, J., Madrid, H., Castaneda-Ruiz, R. F. and Guarro, J. (2014). New species of *Cordana* and *epitypification* of the genus. *Mycologia*, 106(4), 723-734.
26. Ho, W. H., Hyde, K. D., and Hodgkiss, I. J. (1997). Ascomycetes from tropical freshwater habitats: the genus *Savoryella*, with two new species. *Mycological Research*, 101(7), 803-809.
27. Hu, D., Cai, L., Chen, H., Bahkali, A. H., and Hyde, K. D. (2010). Fungal diversity on submerged wood in a tropical stream and an artificial lake. *Biodiversity and Conservation*, 19(13), 3799-3808.
28. Hyde, K. D. (1992). Tropical Australian freshwater fungi. II.* *Annulatascus velatispora* gen. et sp. nov., *A. bipolaris* sp. nov. and *Nais aquatica* sp. nov. (Ascomycetes). *Australian Systematic Botany*, 5(1), 117-124.
29. Hyde, K. D. (1994). The genus *Savoryella* from freshwater habitats, including *grandispora* sp. nov. *Mycoscience*, 35(1), 59-61.
30. Hyde, K. D., Fryar, S., Tian, Q., Bahkali, A. H., and Xu, J. (2016). Lignicolous freshwater fungi along a north-south latitudinal gradient in the Asian/Australian region; can we predict the impact of global warming on biodiversity and function?. *Fungal ecology*, 19, 190-200.
31. Ittner, L. D., Junghans, M., and Werner, I. (2018). Aquatic fungi: a disregarded trophic level in ecological risk assessment of organic fungicides. *Frontiers in Environmental Science*, 6, 105.
32. Jones, E. G., and Hyde, K. D. (1992). Taxonomic studies on *Savoryella* Jones et Eaton (Ascomycotina). *Botanica marina*, 35(2), 83-92.
33. Jones, E. B. G., Sakayaroj, J., Suetrong, S., Somrithipol, S., and Pang, K. L. (2009). Classification of marine Ascomycota, anamorphic taxa and Basidiomycota. *Fungal Diversity*, 35(1), 187.
34. Kantharaj, P., Boobalan, B., Sooriamuthu, S., and Mani, R. (2017). Lignocellulose degrading enzymes from fungi and their industrial applications. *Int J Cur Res Rev/ Vol, 9(21)*, 1.
35. Krebs, C. J. (1972). *Ecology: the experimental analysis of distribution and abundance/ by Charles J. Krebs* (No. 574.5 K74.).
36. Lepère, C., Domaizon, I., Humbert, J. F., Jardillier, L., Hugoni, M., and Debroas, D. (2019). Diversity, spatial distribution and activity of fungi in freshwater ecosystems. *PeerJ*, 7, e6247.
37. Li, C., Yang, Z., Zhang, R. H. C., Zhang, D., Chen, S., and Ma, L. (2013). Effect of pH on cellulase production and morphology of *Trichoderma reesei* and the application in cellulosic material hydrolysis. *Journal of Biotechnology*, 168(4), 470-477.
38. Luo, Z. L., Hyde, K. D., Liu, J. K. J., Maharachchikumbura, S. S., Jeewon, R., Bao, D. F., Bhat, D. J., Lin, C. G., Li, W. L., Yang, J., Liu, N. G., Lu, Y. Z., Jayawardena, R. S., Li, J. F., and Su, H. Y. (2019). Freshwater Sordariomycetes. *Fungal diversity*, 99(1), 451-660.
39. Michel, J. R. B., and Bärlocher, F. (2005). Molecular evidence confirms multiple origins of aquatic hyphomycetes. *Mycological research*, 109(12), 1407-1417.
40. Muhsin, T. M., and Khalaf, K. T. (2002). Fungi from submerged wood in aquatic habitats, southern Iraq. *Iraq. J. Biol*, 2, 455-463..

41. Pang, K. L., Vrijmoed, L. L., Kong, R. Y., and Jones, E. G. (2003). Lignicola and Nais, polyphyletic genera of the Halosphaeriales (Ascomycota). *Mycological Progress*, 2(1), 29-36.
42. Raja, H. A., Shearer, C. A., and Tsui, C. K. M. (2018). Freshwater fungi. *eLS*, 1-13.
43. Raghukumar, C. (2012). *Biology of Marine Fungi*. Springer Heidelberg Dordrecht, London, New York.
44. Refai M., Hassan A. and Hamed M. (2015): Monograph on the Genus *Fusarium*. Available at https://scholar.cu.edu.eg/?q=hanem/files/monograph_on_the_genus_Fusarium.pdf.
45. Rani, C., and Panneerselvam, A. (2009). Diversity of lignicolous marine fungi recorded from muthupet environs, East coast of India. *Journal of Agricultural and Biological Science*, 4, 1-6.
46. Samson, R. A., Varga, J., and Frisvad, J. C. (2011). *Taxonomic studies on the genus Aspergillus*. CBS-KNAW Fungal Biodiversity Centre.
47. Sandhya, C., Adapa, L. K., Nampoothiri, K. M., Binod, P., Szakacs, G., and Pandey, A. (2004). Extracellular chitinase production by *Trichoderma harzianum* in submerged fermentation. *Journal of Basic Microbiology: An International Journal on Biochemistry, Physiology, Genetics, Morphology, and Ecology of Microorganisms*, 44(1), 49-58.
48. Sati, S. C. and Pathak R. (2016). Anamorph (asexual stage) Teleomorph (sexual stage) Connections in Aquatic hyphomycetes. *The International Journal of Plant Reproductive Biology* 8(2), pp.128-135.
49. Schuster, A., and Schmoll, M. (2010). Biology and biotechnology of *Trichoderma*. *Applied microbiology and biotechnology*, 87(3), 787-799.
50. Shearer, C. A. (1989). Aniptodera (Halosphaeriaceae) from wood in freshwater habitats. *Mycologia*, 81(1), 139-146.
51. Shearer, C. A. (1993). The freshwater ascomycetes. *Nova Hedwigia*, 56(1-2), 1-33.
52. Shearer, C.A., Descals, E., Kohlmeyer, B., Kohlmeyer, J., Marvanova, L., Padgett, D., Porter, D., Raja, H. A., Schmit, J. P., Thorton, H. A. and Voglymayr, H. (2007). Fungal biodiversity in aquatic habitats. *Biodivers Conserv.* 16, 49-67.
53. Sridhar, K. R. (2009). Aquatic fungi—are they planktonic. *Plankton dynamics of Indian waters*. Jaipur: Pratiksha Publications, 133-148.
54. Sohail, M., Naseeb, S., Sherwani, S. K., Sultana, S., Aftab, S., Shahzad, S., Ahmad, A., and Khan, S. A. (2009). Distribution of hydrolytic enzymes among native fungi: *Aspergillus* the predominant genus of hydrolase producer. *Pak. J. Bot*, 41(5), 2567-2582.
55. Sonigo, P., De Toni, A. and Reilly, K. (2011). A review of fungi in drinking water and the implications for human health. *Report Bio Intelligent Service, France*.
56. Tsui, C. K., Hyde, K. D., and Hodgkiss, I. J. (2001). Longitudinal and temporal distribution of freshwater ascomycetes and dematiaceous hyphomycetes on submerged wood in the Lam Tsuen River, Hong Kong. *Journal of the North American Benthological Society*, 20(4), 533-549.
57. Wurzbacher, C., and Grossart, H. P. (2012). Improved detection and identification of aquatic fungi and chitin in aquatic environments. *Mycologia*, 104(6), 1267-1271.
58. Wurzbacher, C. M., Bärlocher, F., and Grossart, H. P. (2010). Fungi in lake ecosystems. *Aquat. Microbiol. Ecol.* 59: 125-149.

$$\text{Percentage of occurrence} = \frac{\text{The number of samples that appeared to show one type}}{\text{The total Number of samples}} \times 100 \quad (\text{Eq. 1})$$

$$\text{Percentage of frequency} = \frac{\text{The number of isolates of the same species}}{\text{The total number of isolates of all kinds}} \times 100 \quad (\text{Eq. 2})$$

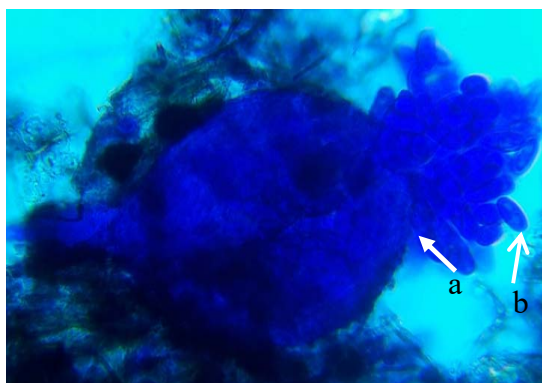


Figure 1: Ascocarp of *Aniptodera margaritana* (arrows a: Ascus b: Ascospore).

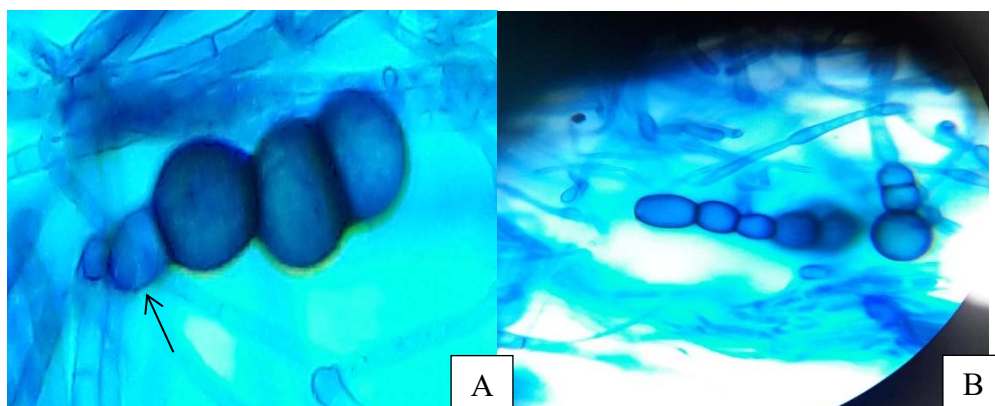


Figure 2: *C. iberica*, A: Conidia B: straight conidia, the light-colored basal cell (arrow)

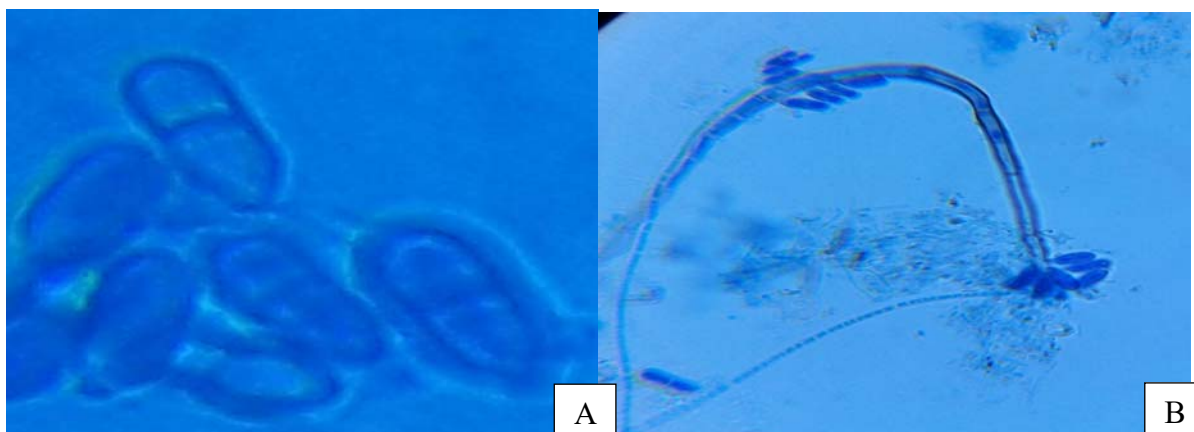


Figure 3: *Cordana lignicola* A: conidia B: conidiophore and conidia



Figure 4: *Cordana verruculosa*, A: Mycelium and conidia B: conidiophore, C: conidiogenous cells (arrow).

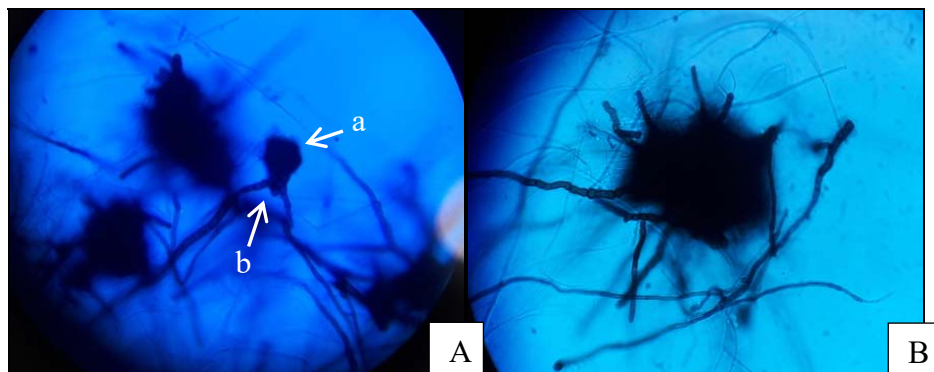


Figure 5: *Pseudoacrodictys appendiculata* A: a- conidia, b-conidiophore (arrows). B: conidia

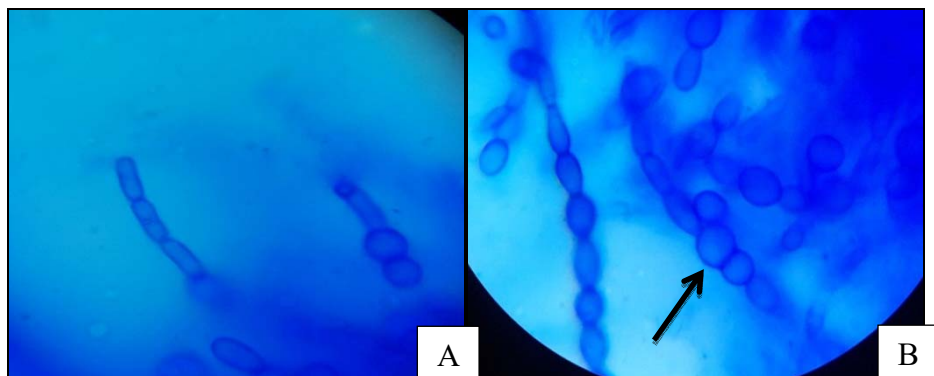


Figure 6: *Scytalidium thermophilum* A: Arthroconidia B: Clamedospore (arrow) and Arthroconidia

Table 1 List of fungal species isolated from submerged wood in Misan

Fungi species	Maymouna	Al- Salam	Majar Al-Kabir	Amara	Total	Frequency %	Occurrence %	Moist Chamber Method	Direct Culture Method
Ascomycetes									
<i>Aniptodera margiration</i> Shearer	1	-	-	-	1	0.58	2.12	+	-
<i>Arthrobotrys dianchiensis</i> (Hao and Zhang) Yu	-	-	-	1	1	0.58	2.12	+	-
<i>Aspergillus flavus</i>	1	2	1	-	4	2.35	8.51	+	+
<i>A. fumigatus</i> Fresen.	1	3	1	3	8	4.70	17.02	+	+
<i>A. horti</i> (Langeron) Dodge	3	6	6	2	17	10	36.17	+	+
<i>A. niger</i> Van Tiegham	2	-	7	-	9	5.29	19.14	+	+
<i>A. oryzae</i> (Ahlburg) Cohn	1	-	-	-	1	0.58	2.12	-	+
<i>Aspergillus sp.</i>	-	-	-	1	1	0.58	2.12	+	-
<i>A. terrus</i> Thom	10	2	3	5	20	11.76	42.55	+	+
<i>A. tubingensis</i> Mosseray	-	1	-	-	1	0.58	2.12	+	-
<i>Byssoschlamys nivea</i> Westling	-	2	-	2	4	2.35	8.51	+	+
<i>Candida tropicalis</i> (Castellani) Berkhout	-	-	-	1	1	0.58	2.12	+	-
<i>Chaetomium globosum</i> Kunze	-	-	-	1	1	0.58	2.12	+	-

<i>Exophiala jeanselmei</i> (Langeron) McGinnis and Padhye	-	-	-	-	-	1	1	0.58	2.12	+	-
<i>Geotrichum candidum</i> Link ex Leman	-	-	-	1	2	3		1.67	6.38	+	+
<i>Kirschsteiniothelia maritime</i> (Linder) Hawksworth	2	-	-	-	3	5		2.94	10.63	+	-
<i>Leptosphaeria agnita</i> (Desm.) Ces. and De Not.	-	-	-	-	1	1		0.58	2.12	+	-
<i>Nais inornata</i> Kohlmeier	2	-	-	2	-	4		2.35	8.51	+	-
<i>Pencillium chrysogenum</i> Thom	3	1	1	1	2	7		4.11	14.89	+	+
<i>P. commune</i> Charles and Thom	2	2	-	-	1	5		2.94	10.63	+	+
<i>Savoryella lignicola</i> Jones and Eaton	-	-	-	2	2	4		2.35	8.51	+	-
<i>Scedosporium prolificans</i> Hennebert and Desai) Guého and de Hoog	1	-	-	-	-	1		0.58	2.12	+	-
<i>Trichoderma harzianum</i> Rife	-	-	-	1	1	2		1.17	4.25	-	+
<i>Zopfiella latipes</i> (Lundquist) Malloch and Cain	1	-	-	2	2	5		2.94	10.63	+	-
Total	30	20	26	31	107						
Hyphomycetes											
<i>Alternaria alternate</i> (Fresen) Keissler	-	-	1	1	2			1.17	4.25	+	-
<i>A. chlamedosporia</i> Mouchacca	-	-	1	1	2			1.17	4.25	+	-
<i>Aurobasidium pullulans</i> (de Bary) Arnaud	1	-	-	-	1			0.58	2.12	-	+

<i>Cirrenalia iberica</i> Hern.-Restr. and Gene	-	-	1	-	1	-	0.58	2.12	-	+
<i>C. macrocephala</i> (Kohlm.) Meyers and Moore	-	-	3	-	3	-	1.76	6.83	-	+
<i>Cladosporium cladosporioides</i> (Fresen.) de Vries	-	-	1	-	1	-	0.58	2.12	-	+
<i>C. cucumerium</i> Ellis and Arthur	-	-	1	1	2	-	1.17	4.25	-	+
<i>Cordana lignicola</i> Luo, Hyde and Su	1	-	2	-	3	-	1.76	6.83	+	-
<i>C. verruculosa</i> Hern.-Rest., Mena., Gene and Guarro	-	-	-	1	1	-	0.58	2.12	-	+
<i>Cuvularia lunata</i> (Wakker) Boedijn	-	1	1	-	2	-	1.17	4.25	-	+
<i>Fusarium aquiseti</i> (Corde) Sacc. and Sylloge	-	-	-	1	1	-	0.58	2.12	-	+
<i>F. oxysporium</i> Schlecht	2	-	5	-	7	-	4.11	14.89	+	+
<i>F. solani</i> (Mart.) Sacc.	1	1	6	-	8	-	4.70	17.02	+	+
<i>Graphium</i> sp.	1	-	1	-	2	-	1.17	4.25	-	+
<i>Moromyces vrains</i> (Chatmala and somrith.) Abdel-wahab, Pang, Nagahama, Abdel-Aziz and Jones	-	-	2	1	3	-	1.76	6.83	+	-
<i>Pseudoacrodactys appendiculata</i> (Ellis) Baker and Morgan	-	-	1	-	1	-	0.58	2.12	-	+
<i>Ramichloridium schulzeri</i> (Sacc.) de Hoog	-	-	-	2	2	-	1.17	4.25	+	-

<i>Scytalidium thermophilum</i> (Conney and Emerson) Austwick	-	-	2	1	3	1.76	6.83	+	-
<i>Tricocladium acrosporium</i> (Meyers and Moore) Dixon	-	-	1	1	2	1.17	4.25	-	+
Total	5	4	28	10	47				
Zygomycetes									
<i>Absidia corymbifera</i> (Cohn.) Sacc. and Trotter	1	-	3	-	4	2.35	8.51	-	+
<i>Mucor circinelloides</i> Van Tieghem	-	-	-	1	1	0.58	2.12	+	-
<i>M. pseudolamprosporium</i> Nagan. and Hirahara	2	-	-	-	2	1.17	4.25	+	+
<i>Rhizopus oryza</i> Went and Prinsen Geerligs	1		7	-	8	4.70	17.02	+	+
Total	4	0	10	1	15				
Oomycetes									
<i>Saprolegina</i> sp.	-	-	-	1	1	0.58	2.12	+	-
Total	39	24	64	43	170	100			

QUALIDADES TECNOLÓGICAS DA BETERRABA SACARINA NAS CONDIÇÕES DA REGIÃO CIS-URALS**TECHNOLOGICAL QUALITIES OF SUGAR BEETROOT CROPS UNDER THE CONDITIONS OF THE MIDDLE CIS-URAL REGION****ТЕХНОЛОГИЧЕСКИЕ КАЧЕСТВА КОРНЕПЛОДОВ САХАРНОЙ СВЕКЛЫ В УСЛОВИЯХ СРЕДНЕГО ПРЕДУРАЛЬЯ**

ISLAMGULOV, Damir ¹; ISMAGILOV, Rafael ^{2*}; ALIMGAFAROV, Rail ²; BAKIROVA, Aygul ²; ENIKEEV, Rafik ²

¹ Federal State Budgetary Educational Institution of Higher Education "Bashkir State Agrarian University", Department of soil science, botany, and plant breeding. Russian Federation

² Federal State Budgetary Educational Institution of Higher Education "Bashkir State Agrarian University", Department of plant growing and agriculture. Russian Federation

* Corresponding author
e-mail: ismagilovraf@rambler.ru

Received 12 June 2020; received in revised form 10 August 2020; accepted 28 August 2020

RESUMO

O O crescimento econômico e o bem-estar do estado dependem em grande parte da eficiência do complexo agroindustrial, incluindo o subcomplexo de açúcar de beterraba. Na Rússia, incluindo a região central dos CIS-Urais, a beterraba sacarina é a principal cultura técnica que fornece matéria-prima para a indústria açucareira. Mais de 70% da área é semeada nos Distritos Federal Central e Sul. No território do médio CIS-Urais, a beterraba sacarina é atualmente cultivada em uma área de mais de 100.000 ha (Kornienko, 2014). O objetivo da pesquisa foi identificar os padrões de produtividade e qualidade tecnológica de novos híbridos de beterraba sacarina, a influência das características varietais sobre o conteúdo de substâncias molassigênicas, dosagem do fertilizante de nitrogênio, densidade da cultura e época de colheita para obter o maior rendimento de raízes com altas qualidades tecnológicas na região central CIS-Urais da Rússia. Quatro estudos de campo foram realizados. O teor de açúcares foi determinado por digestão a frio com sacarímetro-polarímetro. Para determinar o nitrogênio α -amino, foi utilizado o método de Stanek e Pavlas modificado por Wininger e Kubadinov. Os resultados mostraram que, com o aumento da dose de fertilizante de nitrogênio, o teor de açúcar das raízes diminuiu naturalmente. À medida que a densidade da cultura aumentou, o teor de açúcar também aumentou. O maior teor de açúcar nas culturas de raízes foi revelado em uma densidade de cultivo de 95.000 e 110.000 plantas/ha. Os autores propuseram recomendações para obter o maior rendimento bruto de açúcar purificado no cultivo de beterraba sacarina: para colheita precoce - cultivar um híbrido de beterraba açucareira do tipo normal-açucarado (Christella), para colheita tardia - um híbrido do tipo produtivo (HM-1820); aplicar fertilizante nitrogenado na dose de 160 kg de agente ativo/ha; cultivar beterraba sacarina com densidade de 95.000 plantas por hectare; remova as safras de beterraba açucareira com colheitadeiras modernas de beterraba em 10-25 de Outubro.

Palavras-chave: *beterraba sacarina; densidade da cultura; sujidade; dano por geada; tempo de colheita; híbridos.*

ABSTRACT

The economic growth and welfare of the state largely dependent on the efficiency of the agro-industrial complex, including the beet-sugar subcomplex. In Russia, including the middle CIS-Ural region, sugar beet is the main technical crop that provides raw materials for the sugar industry. More than 70 % of the area is sown in the Central and Southern Federal Districts. On the territory of the middle CIS-Ural region, sugar beet is currently cultivated on an area of more than 100,000 ha (Kornienko, 2014) The purpose of the research was to identify the productivity and technological quality patterns of new sugar beet hybrids, the influence of varietal characteristics on the content of molassigenic sub-stances, nitrogen fertilizer dosage, crop density and harvest time to obtain the highest yield of root crops with high technological qualities in the middle CIS-Ural region of

Russia. Four field studies were conducted. The sugar content was determined by cold digestion with saccharimeter-polarimeter. To determine the α -amino nitrogen, the method of Stanek and Pavlas modified by Wininger and Kubadinov was used. The results showed that with an increased dose of nitrogen fertilizer, the sugar content of the root crops naturally decreased. As the crop density increased, the sugar content also increased. The highest sugar content in the root crops was revealed at a crop density of 95,000 and 110,000 plants/ha. The authors proposed recommendations to obtain the highest gross yield of purified sugar in sugar beet cultivation: for early harvesting – cultivate a sugar beet hybrid of normal-sugary type (Christella), for late harvesting – a hybrid of yielding type (HM-1820); apply nitrogen fertilizer at a dose of 160 kg of active agent/ha; cultivate sugar beet with a density of 95,000 plants per hectare; remove sugar beetroot crops with modern beet harvesters on October 10–25.

Keywords: *sugar beet; crop density; dirtiness; frost-damage; harvest time; hybrids.*

АННОТАЦИЯ

Экономический рост и благосостояние государства в значительной мере зависят от эффективности функционирования АПК, в составе которого важное место принадлежит свеклосахарному подкомплексу. В России, в том числе в Среднем Предуралье, сахарная свекла является основной технической культурой, которая обеспечивает сырьем сахарную промышленность. Более 70 % площади посева приходится на Центральный и Южный федеральные округа. На территории Среднего Предуралья в настоящее время сахарная свекла возделывается на площади более 50 тыс. га (Kornienko, 2014). Цель исследований состояла в выявлении закономерностей формирования продуктивности и технологических качеств новых гибридов сахарной свеклы, степени влияния сортовых особенностей на содержание мелассообразующих веществ, установлении дозы азотного удобрения, густоты насаждения растений и срока уборки для получения наибольшей урожайности корнеплодов с высокими технологическими качествами в условиях Среднего Предуралья (Россия). Четыре полевых исследования были проведены. Содержание сахара определяли путем холодного расщепления поляриметром-сахариметром. Для определения α -аминоазота был использован метод Станека и Павласа, модифицированный Винингером и Кубадиновым. Результаты показали, что с увеличением дозы азотных удобрений содержание сахара в корнеплодах естественным образом снижается. По мере увеличения плотности посевов содержание сахара также увеличивалось. Наибольшее содержание сахара в корнеплодах выявлено при плотности посева 95000 и 110000 растений/га. Авторами предложены рекомендации по получению наибольшего валового выхода очищенного сахара при возделывании сахарной свеклы: для ранней уборки возделывать гибрид сахарной свеклы нормально-сахаристого типа Кристелла, для поздней уборки – гибрид урожайного направления ХМ-1820; вносить азотное удобрение в дозе 160 кг д.в. на гектар; возделывать сахарную свеклу с густотой насаждения 95000 растений на гектар; убирать корнеплоды сахарной свеклы современными свеклоуборочными комбайнами с 10 по 25 октября.

Ключевые слова: *сахарная свекла; густоты насаждения; загрязненность; подмороженность; время сбора урожая; гибриды.*

1. INTRODUCTION:

Sugar beet is the only source of raw materials for industrial sugar production in the Russian Federation (Islamgulov *et al.*, 2019). A significant reserve for improving the productivity of sugar beet cultivation and meeting the need for sugar through its production is the use of highly efficient hybrids and the development of sugar beet root technical qualities, which ensure timely delivery of raw materials and products while minimizing financial and environmental losses. Crop formation features and methods of increasing sugar content as one of the leading technical indicators of sugar beet quality have been studied by national scientists (Islamgulov *et al.*, 2018). It is shown that along with the variety, the main elements of sugar beet cultivation

technology affecting the yield and sugar content in root crops include the use of nitrogen fertilizers, crop density and harvest time (Bloch and Hoffmann, 2003a; Hoffmann and Kenter, 2018; Ghorbanian *et al.*, 2019).

Among all macronutrients, nitrogen has the most significant impact on sugar beet root yield and quality (Chatterjee, 2018). Insufficient nitrogen nutrition at the beginning of the vegetation reduces the root yield. Still, the use of nitrogen fertilizers in large doses stimulates growth processes and leads to a decrease in sugar content and deterioration of juice purity (Trimpler *et al.*, 2017).

Russian studies have shown that one of the most critical factors for obtaining a high yield

of sugar beet with high technological qualities is to create an optimal crop density with uniform drilling distance (Jacobs *et al.*, 2018).

Increased sugar production can be achieved by reducing the beet and sugar loss due to optimum harvest time. Early harvesting of raw beet is one of the reasons for low sugar content and decreased keeping quality of root crops (Rother, 1998). Sugar beet harvested at a relatively late date has a higher yield and technological conditions, but also high dirtiness. With a delay in harvesting the number of frozen roots increases, technical qualities reduce and weight loss of conditioned roots increases (Märlander, 1992; Bloch and Hoffmann, 2003b; DeBruyn *et al.*, 2017).

Significant progress has been made in the selection of sugar beet. Currently, hybrids with more advanced technological genotype have been developed (Hoffmann *et al.*, 2009). Along with sugar content, the indicator of root crop technical qualities determining the sugar yield per planted area is the molassigenic substance content, which reduces the sugar yield in the root crops (Hoffmann, 2006; Schnepel and Hoffmann, 2016a; Varga *et al.*, 2017). At the same time, there is practically no scientific information on the regularities of productivity formation and technological qualities of new sugar beet hybrids depending on nitrogen fertilizer dosage, crop density, and harvest time in natural conditions of the middle CIS-Ural region.

In this regard, studies aimed at increased sugar production by increasing yields and technological qualities, including the reduction of the molassigenic substance content in root crops by selecting highly productive hybrids and optimizing the parameters of technical methods of sugar beet cultivation, solve the urgent problem of the country's economy.

2. MATERIALS AND METHODS:

2.1. Field trials

Four field experiences were conducted (3 years each). The soil of the field experiment sites, as well as the soil of beet-growing enterprises in the middle CIS-Ural region, was represented by leached chernozems. In terms of humus layer thickness, leached chernozems are of medium thickness, and their particle size distribution is heavy loam.

In the first experiment, the influence of varietal characteristics on the formation of sugar beet technological qualities were studied

(Buchholz *et al.*, 1995; Schnepel and Hoffmann, 2016b). Such factors as a cultivar were experimentally investigated. The objects of the research were a sugar beet hybrid of Russian breeding – RMC-70 (control); two hybrids of Syngenta breeding – Geracl, HM-1820; two hybrids of KWS breeding – Christella, Dominica; one hybrid of Strube-Dieckmann breeding – Akhat.

The second experiment studied the effect of nitrogen fertilizer dosage on sugar beet technological qualities. The factor considered in the trial was a dose of nitrogen fertilizer application. The objects of the research were Geracl sugar beet hybrid and a dose of nitrogen fertilizer (Dosage N₄₀ (control), N₈₀; N₁₂₀; N₁₆₀; N₂₄₀ kg a.m./ha).

The third experiment was aimed at studying the effect of crop density on sugar beet technological qualities. The factor studied was crop density. The objects of the research were Geracl sugar beet hybrid and crop density (50,000 plants/ha; 65,000 plants/ha; 80,000 plants/ha (control); 95,000 plants/ha; 110,000 plants/ha).

The fourth experiment was devoted to the harvest time effect on sugar beet technological qualities. The factor studied was the harvest time. The objects of the research were RMC-120 sugar beet hybrid of Russian breeding and harvest time (8 harvest periods every ten days from 10.09 to 20.11.).

The variant replication at all points of experimentation was 4-fold. Fertilizers were introduced for the planned yield – 350 kg/ha. Sowing was carried out with a precision seeder (Mudarisov *et al.*, 2017; Khamaletdinov *et al.*, 2018). The plant stand was 90 to 95 thousand plants per ha (except for the experiments with crop density). The predecessor was winter rye. During field experiments, the weather conditions reflected the climate patterns of the natural areas of the Republic of Bashkortostan, where beet-growing enterprises are located.

2.2. Sample treatment and analyses

Sugar content was determined by cold digestion with saccharimeter-polarimeter (Figure 1), which is based on a direct method of obtaining water extract from the pulp of sugar beetroots.



Figure 1. Saccharimeter-polarimeter

To determine the α -amino nitrogen, the method of Stanek and Pavlas modified by Winingier and Kubadinov was used, which is based on the measurement of optical density using a spectrophotometer (Figure 2).



Figure 2. Spectrophotometer

Potassium and sodium content were determined by the Silin method on a flame photometer (Figure 3).



Figure 3. Photometer

Standard sugar losses when molasses was formed were calculated according to Brunswick formula (Equation 1), introduced by Buchholz *et al.* (1995) (Abyaneh *et al.*, 2017; Hoffmann, 2017; Märlander *et al.*, 2018).

The purified sugar content was calculated as the difference between sugar content and standard sugar losses in molasses. The gross sugar yield was defined as the product of yield and sugar content, and the total yield of purified sugar was calculated as the product of yield and

purified sugar content (Draycott, 2006; Koch *et al.*, 2016; Barzegari *et al.*, 2017).

In the second stage, the analysis of the experiment results was carried out in the form of mathematical processing to obtain the statistical estimate of the resulting indicators, identify the empirical dependence, mathematical confirmation of the scientific hypothesis validity and to prove the scientific conclusions. The variance to determine the significance of the results for each factor is analyzed. The essence of variance analysis is to divide the variance and the total number of degrees of freedom into parts corresponding to the structure of the experiment and to assess the significance of the studied factors' action and interaction. The use of these methods allowed to prove the reliability of the differences in the field experiment, the relationship between the studied factors, and to determine the model of the impact of one or more variable field factors (Islamgulov *et al.*, 2019).

This study was carried out following the authors' affiliated institutions recommendations from the IRB. The IRB approved the protocol of affiliated institutions of authors. Under the Helsinki Declaration, all subjects had given written, informed consent.

3. RESULTS AND DISCUSSION:

3.1. Sugar beet varietal characteristics and technological qualities

Crop yield is one of the main indicators of sugar beet productivity. In this experiment, an average of three years, HM-1820 hybrid formed the highest yield (51.8 t/ha), and RMC-70 control hybrid – the lowest (39.5 t/ha). The yield of other hybrids varied from 43.7 to 49.2 t/ha. High productivity of HM-1820 and Dominica hybrids is due to their selection assignment (producing high yield and standard yield). Akhat hybrid showed the highest sugar content (18.10%), HM-1820 hybrid – the lowest (16.70%). The remaining hybrids had a relatively similar sugar content varying from 17.00 to 17.90%.

Potassium content in root crops varied both by year and between hybrids. HM-1820 hybrid had the highest potassium content in the root crops – 4.92 mmol, Akhat hybrid – the lowest – 4.11 mmol. RMC-70 and Dominica hybrids did not differ significantly in this indicator and had 4.86 and 4.85 mmol, respectively. Thus, potassium content in root crops showed the same intervarietal variability. Hybrids of sugary and

normal-sugary types were characterized by lower potassium content in root crops than hybrids of the productive type. Sodium, like potassium, belongs to one of the main molasses makers, which adversely affect the extraction of crystallized sugar. The results showed that HM-1820 hybrid had the highest sodium content in root crops in all years of the research (0.90 mmol), Akhat hybrid – the lowest – 0.45 mmol. Among the nitrogen compounds of sugar beet roots α -amino nitrogen, or "harmful nitrogen", plays the most negative role in sugar extraction. On average, over three years of the research, the RMC-70 control hybrid had the highest α -amino nitrogen content (2.23 mmol), Akhat hybrid – the lowest (1.55 mmol). HM-1820, Dominica, and Geracl hybrids also had a high α -amino nitrogen content of 1.91; 1.87 and 1.80 mmol, respectively. Christell hybrid had a low value of this indicator, as well as RMC-70 hybrid.

Sugar loss in molasses formation is largely due to the technical qualities of sugar beet. The results of three-year studies have shown that the difference in sugar loss between hybrids was significant. The values of standard sugar losses in molasses formation ranged from 1.40 to 1.70%. The values of this indicator in hybrids of yielding and normal-yielding types were relatively higher than in sugary and normal-sugary types of hybrids, which was due to the high content of molasses-forming substances (potassium, sodium, and alpha-aminoazota). The studied hybrids differed in the content of purified sugar: in hybrids producing high yield and normal yield, it was less than in hybrids of sugary and normal-sugary types.

On average, over three years, HM-1820 hybrid had the highest gross sugar yield (8.65 t/ha), RMC-70 hybrid – the lowest (6.91 t/ha). The remaining hybrids had almost the same sugar yield (from 7.91 to 8.36 t/ha). RMC-70 control hybrid had less sugar yield than other hybrids (1.0–1.74 t/ha). The gross sugar yield in yielding hybrids was higher than that of the sugary.

On average, over three years, HM-1820 hybrid had the largest gross yield of purified sugar (7.80 t/ha), RMC-70 control hybrid – the lowest (6.24 t/ha). Dominica and Geracl hybrids formed the same sugar yield 7.57 t/ha, Christella, and Akhat hybrids – 7.62 and 7.30 t/ha, respectively. Thus, hybrids differ in the gross yield of purified sugar. Dominica hybrid exceeds Geracl in gross sugar yield, and Christella is inferior to both of them.

Sugar beet hybrids can be estimated

more objectively by the gross yield of purified sugar than by gross sugar yield (Figure 4). So, Dominica hybrid exceeded Geracl in terms of gross sugar yield, and Christella hybrid is inferior to both of them. Hybrid evaluation of the gross yield of purified sugar shows that Geracl is not inferior in productivity to Dominica, and Christella is superior to both hybrids.

All of the above points to the complex genetic nature of the characteristics determine the technological qualities of beetroots. Differences in sugar content and ash elements in hybrid root crops are probably primarily determined by differences in their heredity, determining the duration and nature of the vegetative phase of sugar beet development in the first year.

3.2. Technological qualities of sugar beet depending on nitrogen fertilizer dosage

The increase in sugar beet yield depending on the year and variant was 2.45–8.6 t/ha. The highest sugar beet yield was formed in N₂₄₀ variant – 37.4 t/ha, the lowest – in N₄₀ (30.4 t/ha). Correlation analysis of the experimental data over three years showed that there is a weak positive relationship between the dose of nitrogen fertilizer and sugar beet yield ($\eta=0.44$).

On average, over three years, the maximum sugar content in root crops was in the N₄₀ variant (17.48%), the lowest – in N₂₄₀ (16.20%). Other variants had relatively the same sugar content – 16.98–17.06%. Correlation analysis showed that there is a weak inverse relationship between the dose of nitrogen fertilizer and sugar content in sugar beetroots ($\eta=-0.41$). Thus, with an increase in the dose of nitrogen fertilizer, the sugar content of sugar beet roots decreases.

The dose of nitrogen fertilizer had an impact on potassium content in root crops. On average, over three years, potassium content in the experiment variants varied from 4.73 to 5.40 mmol per 100 g of wet weight. Correlation analysis showed a moderate positive relationship ($\eta=0.53$) with an increase in the dose of nitrogen fertilizer, potassium content increases.

The dose of nitrogen fertilizer affected the sodium content in sugar beetroots. The highest sodium content was in the N₁₆₀ variant (1.05 mmol), the lowest – in N₄₀ variant (0.8 mmol). N₈₀, N₁₂₀, N₂₄₀ variants slightly differed (0.88–0.95 mmol). The difference in comparison with the control was from 10 to 31.2% (Islamgulov *et al.*,

2019). There is a moderate dependence in the form of parabola between the dose of nitrogen fertilizer, and sodium content in sugar beetroots, (η) is 0.66. With an increase in the dose of nitrogen fertilizer (N_{160}), sodium content in the wet weight of root crops increases and then decreases.

On average, in 2008–2010, α -amino nitrogen content in the root crops was different and depended on the dose of introduced nitrogen fertilizer. The lowest content was noted in the control variant, the highest – at the maximum nitrogen dose. The content of α -amino nitrogen in the N_{160} variant exceeded the control by 1.43 times in the N_{240} variant – by 2.23 times. Correlation analysis showed that there is a strong positive relationship between these indicators ($\eta=0.96$). Increased doses of nitrogen fertilizer caused increased growth of both root crops and sugar beet tops. As a result, there was a sudden accumulation of nitrogenous matter in the root crops, especially of α -amino nitrogen.

The dose of nitrogen fertilizer significantly affects the sugar loss in molasses. Increasing the dose of nitrogen fertilizer increases the standard loss of sugar in molasses. N_{240} variant was characterized by the highest sugar losses, exceeding the control by 0.40%. Sugar losses were primarily associated with high α -amino nitrogen and potassium content in the root crops.

The dose of nitrogen fertilizer significantly influenced the purified sugar content in the root crops. The highest content of purified sugar was in N_{40} variant – 16.10%, the lowest sugar content (14.42%) was in maximum nitrogen dose of N_{240} . N_{80} and N_{120} variants had the same sugar content (15.54%). The difference between the variants ranged from –0.56 to –1.68%. With an increased nitrogen fertilizer dosage, standard sugar loss in molasses also increased.

Studies have shown that, on average, in 2008–2010, the maximum gross sugar yield was while using high doses of nitrogen fertilizers (N_{160} and N_{240} variants), exceeding the control by 14.4 and 14.6%. The increase in sugar yield ranged from 0.36 to 0.77 t/ha. Gross sugar yield increased with increasing dose of nitrogen fertilizer.

On average, over 2008–2010, the N_{160} variant showed the maximum gross yield of purified sugar (5.47 t/ha), N_{40} control variant – the minimum (4.85 t/ha). Sugar yield of N_{120} and N_{240} variants was relatively the same – 5.35 and 5.38 t/ha.

The increase in the gross yield of purified sugar ranged from 0.30 to 0.60 t/ha. The maximum high dose of nitrogen fertilizer (N_{240}) did not give an increase in the gross yield of purified sugar since the sugar loss in the molasses was high.

Studies have shown that the gross yield of purified sugar increases with an increase in nitrogen fertilizer dosage up to a certain limit. Calculations have found that to assess the sugar beet productivity, and it is more appropriate to use the gross yield of purified sugar than the total sugar yield (Figure 5). Thus, the highest gross sugar yield was obtained in the N_{240} variant – 6.04 t/ha. At the same time, the yield of purified sugar, including molasses losses, was higher in the N_{160} variant.

3.3. Crop density and sugar beet technological qualities

On average, over three years of the research, the maximum sugar beet yield was in the variant with a crop density of 95,000 plants/ha. Thinned out (50,000 plants/ha) and thick planting (110,000 plants/ha) formed a lower yield of root crops. With an increase in crop density, the yield of sugar beet increased to a certain limit and varied from 33.4 to 36.0 t/ha. At the same time, the maximum yield was 95,000 plants/ha, and in the variant of 110,000 plants/ha, it reduced due to root crop degrowth.

On average, in 2008–2010, the sugar content of the root crops in the harvest period ranged from 16.95 to 17.62%. With an increase in crop density, sugar content in root crops increased to 17.62% and then decreased. Crop density of 95,000 plants/ha provided the highest sugar content (17.62%).

Potassium content was dependent on the region of plant alimentation. The highest potassium content was found at a crop density of 50,000 plants/ha (5.57 mmol), a little less – at a density of 65,000 plants/ha (5.17 mmol). Variants with a density of 80,000 and 95,000 plantings/ha had a relatively small difference (4.97 and 4.89 mmol). The minimum potassium content was in thick planting at a density of 110,000 plants/ha. In comparison with the control, the difference was from –0.22 to 0.60 mmol. The correlation analysis of the experimental data confirmed that there is an average inverse relationship ($\eta=-0.51$) between the sugar beet density and potassium content.

The variant with a density of 50,000 plants/ha had the largest sodium content in root crops. With an increase in crop density from

65,000 to 95,000 plants/ha, the sodium content in root crops decreased from 0.62 to 0.53 mmol per 100 g of wet weight. The lowest indicator value was in the variant with a density of 110,000 plants/ha – 0.51 mmol. The difference in the variants concerning the control ranged from – 0.06 to 0.13 mmol. The correlation analysis of the experimental data confirmed that there is a very strong inverse relationship ($\eta=-0.91$) between the sugar beet density and sodium content. As the crop density increased, the sodium content decreased.

On average, over three years, the maximum α -amino nitrogen content was in the variant of 50,000 plants/ha, the minimum – in the variant of 110,000 plants/ha. With an increase in crop density from 65,000 to 95,000 plants, α -amino nitrogen content decreased from 1.47 to 1.29 mmol. The deviation from the control was from –0.13 to 0.43 mmol per 100 g of wet weight. The correlation analysis of the experimental data over three years also showed that there is a strong negative relationship between these indicators ($\eta=-0.89$). With an increase in crop density, α -amino nitrogen content in sugar beet roots is reduced.

Research results showed different standard sugar losses of 1.41 to 1.66 percent in molasses formed under different crop densities. The highest standard loss of sugar was at a density of 50,000 plants/ha in the variant. Standard sugar losses in the formation of molasses decreased with crop density increased.

On average, in 2008-2010, the content of refined sugar in root crops ranged from 15.29 to 16.18%. The lowest amount of purified sugar was in the variant with the lowest crop density of 50,000 (15.29%), the highest – with a density of 95,000 plants/ha (16.18%).

On average, in 2008-2010, the gross sugar yield varied from 5.66 to 6.34 t/ha.

The highest gross sugar yield was observed at a crop density of 95,000 plants/ha – 6.34 t/ha. The increase concerning the control was 0.20 t/ha.

In general, in 2008-2010, the value of the gross yield of purified sugar ranged from 5.11 to 5.82 t/ha. The density of 95,000 plants/ha provided the highest gross yield of purified sugar (5.82 t/ha) in comparison with other variants. It was found that a further increase in crop density, as well as its reduction, had a negative impact on the gross yield of purified sugar.

Thus, the gross yield of purified sugar

increases with an increase in crop density to a specific limit (95,000 plants/ha) (Figure 6). The calculations confirmed the correctness of the use of the gross yield of purified sugar to assess the sugar beet productivity as a more objective indicator.

3.4. Sugar beet technological qualities at different harvest time

The studied variants of sugar beet harvest time differed in root yield. On average, over three years, this figure had an increase from the first to the seventh harvest time. During the eighth harvest period, there was a slight decrease. The maximum increase was detected from the second to the fourth harvest time in all years of the research. The correlation analysis showed that there is a strong relationship ($\eta=0.85$) between the harvest time and the sugar beet yield.

Over three years of the research, the sugar content of the root crops naturally increased, and by November 10, it reached its maximum value. During the eighth harvest time, a decrease in sugar content was observed. The reduction in sugar content is associated, apparently, with a reduction of the intensity of growth processes due to a decrease in air temperature and increased sugar use for breathing. On average, over three years, the most intensive sugar formation was observed during the third and fourth harvest periods. In other variants, the accumulation of sugar occurred without any surge. There is a very strong positive relationship ($\eta=0.94$) between the harvest time and sugar content in sugar beetroots.

Potassium content in sugar beet roots changed in different harvest periods. Thus, the highest potassium content was in 2014 (4.01 mmol) in the seventh harvest period, the lowest – in 2015 (3.18 mmol) in the first harvest period. The correlation index (η) between the two indicators was 0.48.

Unlike potassium, sodium content naturally decreased from the first to the seventh harvest period. On average, over three years, it dropped from 0.93 to 0.77 mmol (by 17.2%) from the first to the sixth harvest period. When harvesting on November 10, there was an increase in sodium content to 0.80 mmol, followed by a decrease to 0.74 (November 20).

The most significant decrease in sodium content was found during the fourth and fifth harvest periods. The relationship between these indicators is inverse ($\eta=0.59$).

The changing factor in α -amino nitrogen content was similar to the one in potassium content. The increase in its content occurred until November 10 (0.97–1.46 mmol). In contrast to potassium content, α -amino nitrogen content increased by 50.5%. On average, over three years of the research, the smallest increase of α -amino nitrogen was observed during the third and fourth harvest periods. The correlation analysis showed that there is a moderate, positive relationship ($\eta=0.62$) between these parameters.

Sugar losses ranged from 1.20 to 1.46%. The increase in standard molasses loss at later harvest time was associated with an increase in potassium and α -amino nitrogen content. On average, in 2013–2015, the sugar loss between the third and sixth harvest periods was minimal concerning other harvest periods. The relationship between these indicators is moderate and positive ($\eta=0.65$).

The purified sugar content also depended on the harvest period. On average, this indicator increases over three years from the first to the last harvest period. In 2013–2015, an increase in the purified sugar content fell on the fourth harvest period. Later harvesting accounted for the highest amount of refined sugar. The relationship between these indicators is very strong ($\eta = 0.93$).

On average over three years, the highest value of the gross sugar harvest was at a later date of harvesting – 9.14 t/ha (the seventh harvest period), the intensity of the increase between the terms was maximum at the third and fourth harvest periods (0.77–0.88). There is a strong correlation between these indicators ($\eta=0.90$).

On average, over three years, the highest gross yield of purified sugar was at a later harvest time. From the average for three years, it is clear that the high increase was obtained during the fourth harvest time (October 10) – 0.83 t/ha. There is a strong positive relationship between the harvest time and the gross yield of purified sugar. The correlation index (η) is 0.90.

The main causes of beetroot mass loss, when accepted at a sugar factory, are the dirtiness and frost-damage. High dirtiness of sugar beet roots at a later harvest time was primarily due to a large amount of precipitation during that period, which affected the soil moisture in the arable layer. On average, soil moisture at a depth of arable layer ranged from 15.5 to 33.1%, from the first to the third harvest period, this figure is below normal (25%). From

the fourth to the fifth harvest periods, the soil moisture was within normal limits. In the sixth term, the soil moisture in the arable layer is slightly lower than the optimal value for sugar beet. And during the seventh and eighth harvest periods, it was much higher than in the previous ones.

On average, in 2013–2015, the sugar beet dirtiness amounted to 20.8%. Reduced dirtiness fell on the third harvest period. High sugar beet dirtiness at a later harvest time was primarily due to the amount of precipitation during that period, which affected the soil moisture in the arable layer. Sugar beet frost-damage in 2013 was recorded during the sixth harvest period – 2.4%, and at further harvest periods, it ranged from 2.4 to 3.7%. In 2014 the frost-damage from the fifth to the eighth harvest periods varied from 4.3 to 53.4%. The surge was recorded during the eighth harvest period. In 2015 the frost-damage was already observed during the fourth harvest period – 3.1%, and by the sixth period, it increased to 67.8%. The percentage increase of frost-damaged root crops was primarily due to air temperature decrease.

Losses due to beetroot dirtiness and frost-damage increased in November harvest time. From the first to the fourth harvest periods, the number of losses was not that great, unlike the further ones. The maximum loss rate (89.9%) was observed in the eighth harvest period in 2015. On average, over three years, the lowest losses fell on the third harvest period.

On average, over three years of the research, the maximum gross yield of purified sugar, including losses, was revealed at the fifth harvest period (6.66 t/ha). The minimum value of this indicator was at the seventh harvest period (2.93 t/ha) as a result of significant losses due to beetroot dirtiness and frost-damage (Figure 7).

The gross sugar harvest and the gross refined sugar harvest increased from the first to the seventh harvest period. In contrast to the previous indicators, the gross yield of purified sugar, including losses, increased from the first to the fifth harvest periods. There is a slight decrease during the sixth harvest period and a sharp decline during the seventh and eighth periods, which was due to high losses. Fig. 4 shows the possibility of choosing the most optimal harvest time to obtain the maximum yield with high technological qualities. To obtain the highest gross yield of purified sugar, the optimal harvest time is October 10–25.

The accumulation of sugar in the root

crops of sugar hybrids (Akhat, Christella) is more intense than in hybrids of yielding (HM-1820, Dominica) and normal (Geracl) types. The sugar content of the control hybrid (RMC-70) was higher than that of other hybrids of the same type. With an increased dose of nitrogen fertilizer, the sugar content of the root crops naturally decreased. As the crop density increased, the sugar content also increased. By the end of the growing season, a crop density of 95,000 and 110,000 plants/ha revealed the highest sugar content in root crops. In the fourth experiment, the sugar content of sugar beet roots increased until November 10, although there was some decrease in its intensity in early November.

The hybrids producing high yield (HM-1820) and normal yield (Dominica) formed the maximum crop productivity. With an increase in the dose of nitrogen fertilizer, the sugar beet yields also increased. The maximum yield was found in the variant with a density of 95,000 plants/ha. Thinned out (50,000 plants/ha) and thick planting (110,000 plants/ha) formed a lower yield of root crops. In the variant with a density of 110,000 plants / ha, the increase in plant number per unit area did not compensate for the decrease in an individual mass of plant. The yield of sugar beet root crops increased (by 41.6%) to the seventh harvesting period (10.11). In the eighth term (20.11), there was some decrease. The sugar beet yield within the period studied largely depended on the harvest time.

The hybrid types differ significantly in the content of molasses-forming substances in root crops. There is a significant intercultivar variability in potassium, sodium, and α -amino nitrogen content. Hybrids of sugary (Akhat) and normal-sugary (Christella) types contained less molasses-forming substances than hybrids producing high yield (HM-1820) and normal yield (Dominica). Hybrid control RMS-70 had a high content of alpha-aminatta. With an increase in the dose of nitrogen fertilizer, the content of molasses-forming substances in sugar beet roots naturally increases. The increase in the area of plant nutrition led to an increase in the content of molasses-forming substances in the root crops of sugar beet. A significant increase in α -amino nitrogen content occurred in the roots from the first (10.09) to the seventh (10.11) harvest time. Potassium content in root crops also increased from the first to the seventh harvest periods. Sodium content, on the contrary, decreased from the first to the eighth harvest periods (20.11).

Due to the high content of molasses-forming substances, standard sugar losses in

molasses formation were higher in hybrids producing high yield (HM-1820) and normal yield (Dominica) than that of sugary (Akhat) and normal-sugary (Christella) types. The purified sugar content in the root crops of hybrids producing high yield (HM-1820) and normal yield (Dominica) was less than that of sugary (Akhat) and normal-sugary (Christella) types. With an increased dose of nitrogen fertilizer, the standard sugar loss in molasses increased due to the increase of molasses-forming substances such as α -amino nitrogen and potassium. With an increase in nitrogen fertilizer dosage, the purified sugar content decreased. Standard losses of sugar decreased with increasing density of plantings. The highest content of refined sugar was at a density of 95,000 plants/ha.

Further increase in crop density led to a decrease in the purified sugar content in root crops. At a later harvest time (10.11–20.11), sugar losses increased sharply, and from the third to the sixth harvest periods (01.10–30.10), losses were minimal. There was an increase in the purified sugar content from the first (10.09) to the seventh (10.11) harvest periods, and by the eighth period (20.11), there was some decrease in the content of purified sugar.

In yielding hybrids (HM-1820, Dominica), the gross sugar yield was higher than that of sugary ones (Akhat, Christella). With an increase in the dose of nitrogen fertilizer, the gross sugar yield increased and reached the maximum value when applying N_{240} . Gross sugar yield depended on the crop density. The maximum gross sugar harvest provided sowing for the final density of 95,000 plants per 1 ha. The highest gross sugar yield was detected at the late harvest time (10.11).

The gross sugar yield of Dominica hybrid was more than that of Geracl hybrid, and the gross sugar yield of Christella hybrid was less than that of Dominica and Geracl hybrids. Evaluation of the productivity of the gross collection of refined sugar showed that Geracl hybrid is not inferior in productivity to the hybrid of Dominic, and Christella is superior in sugar collection both hybrids.

The most substantial gross sugar yield was obtained in the variant with a dose of nitrogen fertilizer of N_{240} . At the same time, the gross yield of purified sugar, including molasses losses, was higher in the N_{160} variant. The crop density of 95,000 plants/ha provided the highest gross yield of purified sugar in comparison with other variants. Further increase in crop density

(up to 110,000 plants/ha) and reduction (up to 50,000 plants/ha) resulted in a decrease in the gross yield of purified sugar. The natural increase in the gross yield of purified sugar occurred from the first (10.09) to the seventh (10.11) harvest periods. During the eighth period (20.11), there was a slight decrease.

The sugar beet dirtiness and frost-damage are important indicators in determining the optimal harvest time. Starting from the fifth harvest period (20.10), due to the increase in soil moisture, the sugar beet dirtiness increased and amounted to 89.9% during the eighth harvest period (20.11). Beetroot frost-damage occurred from October 10. The maximum frost-damage was during the eighth harvest period. Due to the dirtiness and frost-damage, the beetroot losses increased dramatically, starting from the sixth harvest period (30.10). The highest beet root yield and gross yield of purified sugar, including losses, were revealed in the fifth harvest period (20.10).

According to the suite of metrics, the optimum sugar beet harvest time in the natural conditions of the middle CIS-Ural region when using modern beet harvesters is October 10–25.

4. CONCLUSIONS:

To obtain the highest gross yield of purified sugar in sugar beet cultivation on the leached chernozem of the middle CIS-Ural region, it is recommended:

- for early harvesting – cultivate a sugar beet hybrid of normal-sugary type (Christella), for late harvesting – a hybrid of yielding type (HM-1820);
- apply nitrogen fertilizer at a dose of 160 kg of active agent/ha;
- cultivate sugar beet with a density of 95,000 plants per hectare;
- remove sugar beetroots with modern beet harvesters on October 10–25.

5. REFERENCES:

1. Abyaneh, H. Z., Jovzi, M., Albaji, M. (2017). Effect of regulated deficit irrigation, partial root drying, and N-fertilizer levels on sugar beet crop (*Beta vulgaris* L.). *Agricultural Water Management*, 194, 13-23.
2. Barzegari, M., Sepaskhah, A. R., Ahmadi, S. H. (2017). Irrigation and nitrogen management affects nitrogen leaching and root yield of sugar beet. *Nutrient Cycling in Agroecosystems*, 108(2), 211-230.
3. Bloch, D., Hoffmann, C. M. (2003a). Yield and quality of sugar beet in the course of vegetation - interaction of variety and harvest date. *Announcements from the Society for Crop Science*, 15, 258-259. (in German)
4. Bloch, D., Hoffmann, C. M. (2003b). Choice of variety - location and harvest date play a role. *Sugar beet*, 52, 228-230. (in German)
5. Buchholz, K., Märlander, B., Puke, H., Glattkowski, H., Thielecke, K. (1995). Reassessment of the technical merit of sugar beet. *Sugar industry*, 120(2), 113-121. (in German)
6. Chatterjee, A. (2018). Additions of ammonium sulfate and urease inhibitor with urea to improve spring wheat and sugar beet yield. *Archives of Agronomy and Soil Science*, 64(10), 1459-1464.
7. DeBruyn, A. H., O'Halloran, I. P., Lauzon, J. D., Van Eerd, L. L. (2017). Effect of sugarbeet density and harvest date on most profitable nitrogen rate. *Agronomy Journal*, 109(5), 2343-2357.
8. Draycott, P. (2006). *Sugar Beet*. Oxford: Blackwell Publishing Ltd.
9. Ghorbanian, A. R., Khoshgoftarmanesh, A. H., Zahedi, M. (2019). The effect of foliar-applied magnesium on root cell membrane H⁺-ATPase activity and physiological characteristics of sugar beet. *Physiology and Molecular Biology of Plants*, 25(5), 1273-1282.
10. Hoffmann, C. M. (2006). Sugar beet as a raw material. The technical quality as a prerequisite for efficient processing. Göttingen: Weender Druckerei GmbH und B Co. (in German)
11. Hoffmann, C. M. (2017). Changes in root morphology with yield level of sugar beet. *Sugar Industry*, 142(7), 420-425.
12. Hoffmann, C. M., and Kenter, C. (2018). Yield potential of sugar beet—have we hit the ceiling?. *Frontiers in plant science*, 9, 289.
13. Hoffmann, C. M., Huijbregts, T., van Swaaij, N., Jansen, R. (2009). Impact of different environments in Europe on yield and quality of sugar beet genotypes. *European Journal of Agronomy*, 30(1), 17-26.
14. Islamgulov, D. R., Ismagilov, R. R., Bakirova, A. U., Alimgafarov, R. R.,

- Mukhametshin, A. M., Enikiev, R. I., Akhiyarov, B. G., Ismagilov, K. R., Kamilanov, A. A., Yagafarov, R. G. (2018). Productivity and technological qualities of sugar beet at different times of harvesting depending on contamination and freezing of root crops. *Journal of Engineering and Applied Sciences*, 13(S8), 6533-6540.
15. Islamgulov, D. R., Alimgafarov, R. R., Ismagilov, R. R., Bakirova, A. U., Mukhametshin, A. M., Enikiev, R. I., Ahijarov, B. G., Ismagilov, K. R., Kamilanov, A.A. (2019). Productivity and technological features of sugar beet root crops when applying of different doses of nitrogen fertilizer under the conditions of the middle Cis-Ural region. *Bulgarian Journal of Agricultural Science*, 25 (Suppl. 2), 90–97.
 16. Jacobs, A., Koch, H. J., Märlander, B. (2018). Preceding crops influence agronomic efficiency in sugar beet cultivation. *Agronomy for sustainable development*, 38(1), 5.
 17. Khamaletdinov, R. R., Gabitov, I. I., Mudarisov, S. G., Khasanov, E. R., Martynov, V. M. Negovora, A.V., Stupin, V. A., Gallyamov, F.N., Farkhutdinov, I. M., Shirokov, D. Y. (2018). Improvement in engineering design of machines for biological crop treatment with microbial products. *Journal of Engineering and Applied Sciences*, 13(S8), 6500-6504.
 18. Koch, H. J., Laufer, D., Nielsen, O., Wilting, P. (2016). Nitrogen requirement of fodder and sugar beet (*Beta vulgaris* L.) cultivars under high-yielding conditions of northwestern Europe. *Archives of Agronomy and Soil Science*, 62(9), 1222-1235.
 19. Kornienko, A. V. (2014) Sustainable living systems - the basis of evolution in their development of the external world. *Eastern European Scientific Journal*, 4, 29-33.
 20. Märlander, B., Hoffmann, C., Koch, H. J., Ladewig, E., Niemann, M., Stockfisch, N., Var-relmann, M., Mahlein, A. K. (2018). Sustainable intensification a quarter century of research towards higher efficiency in sugar beet cultivation. *Sugar Industry*, 143(4), 200-217.
 21. Märlander, B. (1992). Influence of the harvest time. *Sugar industry*, 11, 79-91. (in German)
 22. Mudarisov, S., Khasanov, E., Rakhimov, Z., Gabitov, I., Badretdinov, I., Farchutdinov, I., Gallyamov, F., Davletshin, M., Aipov, R., Jarullin, R. (2017). Specifying two-phase flow in modeling pneumatic systems performance of farm machines. *Journal of Mechanical Engineering Research and Developments*, 40(4), 706-715.
 23. Rother, B. (1998). The technical quality of sugar beet under the influence of various cultivation factors. Dissertation. Cuvillier. (in German)
 24. Schnepel, K., Hoffmann, C. M. (2016a). Effect of extending the growing period on yield formation of sugar beet. *Journal of Agronomy and Crop Science*, 202(6), 530-541.
 25. Schnepel, K., Hoffmann, C. M. (2016b). Genotypic differences in storage losses of sugar beet—causes and indirect criteria for selection. *Plant breeding*, 135(1), 130-137.
 26. Trimpler, K., Stockfisch, N., Märlander, B. (2017). Efficiency in sugar beet cultivation related to field history. *European Journal of Agronomy*, 91, 1-9.
 27. Varga, I., Antunović, M., Iljkić, D. (2017). Sugar Beet Root Development with Different Nitrogen Fertilization Rate. *Listy cukrovarnické a řepařské*, 133(4), 138-141.

$$SSL = 0,12 \times (K + Na) + 0,24 \times \alpha\text{-amino N} + 0,48 \quad (\text{Eq. 1})$$

where

SSL – Standard Sugar Loss, %;

K – potassium content, mmol/100 g wet weight;

Na – sodium content, mmol/100 g wet weight;

α -amino N – α -amino nitrogen, mmol/100 g wet weight

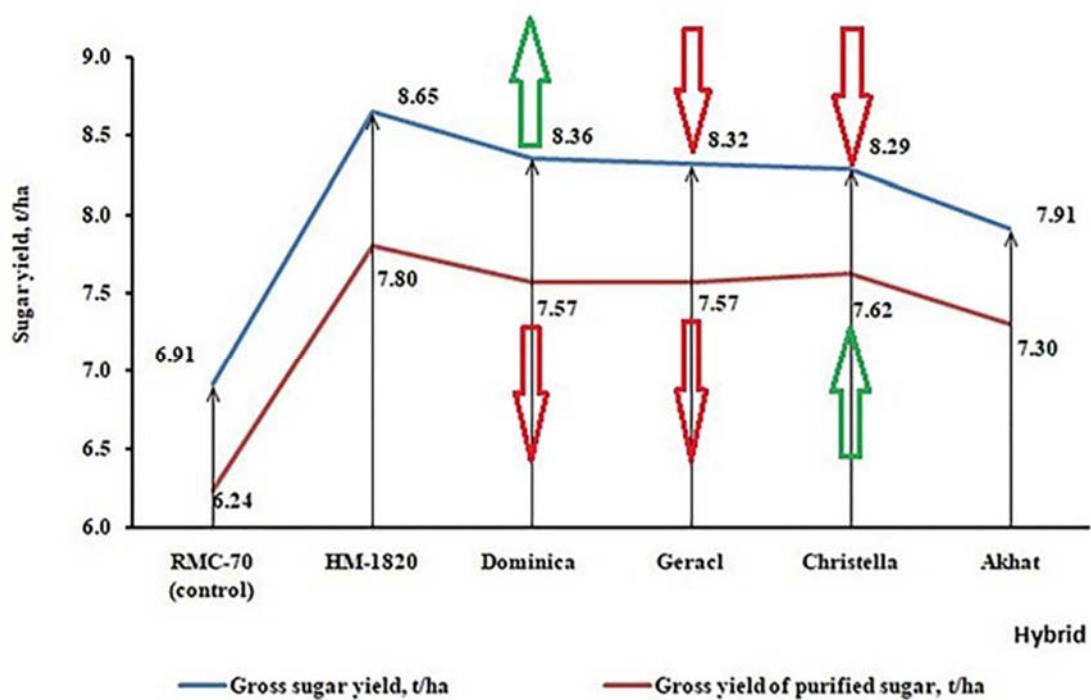


Figure 4. Hybrid sugar yield (Karmaskaly, 2007-2009)

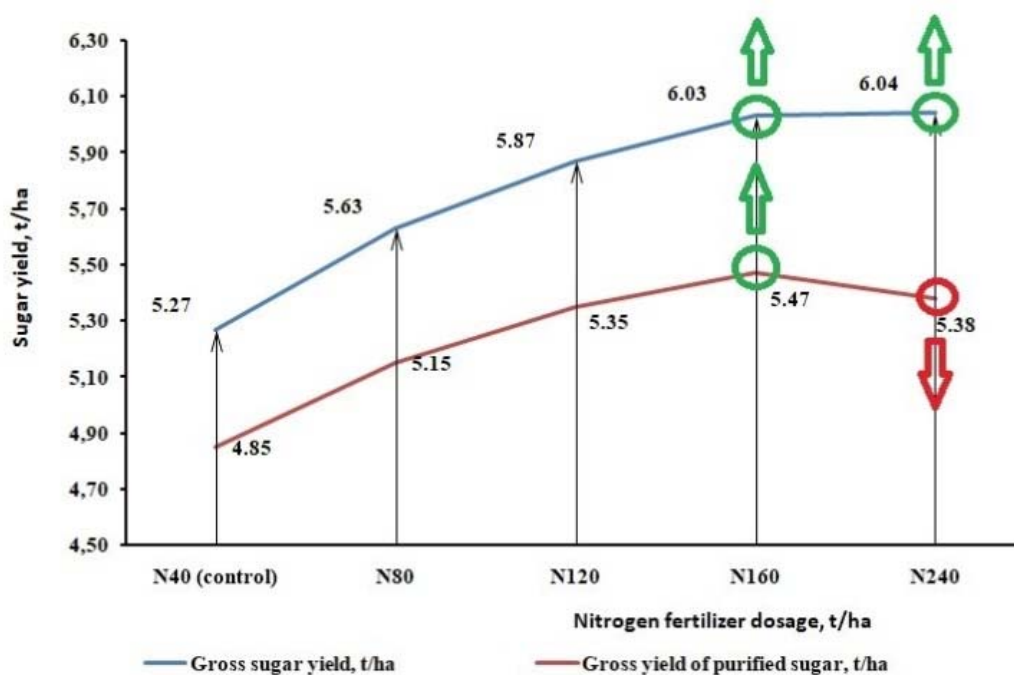


Figure 5. Sugar yield under different doses of nitrogen fertilizer treatment (2008-2010)

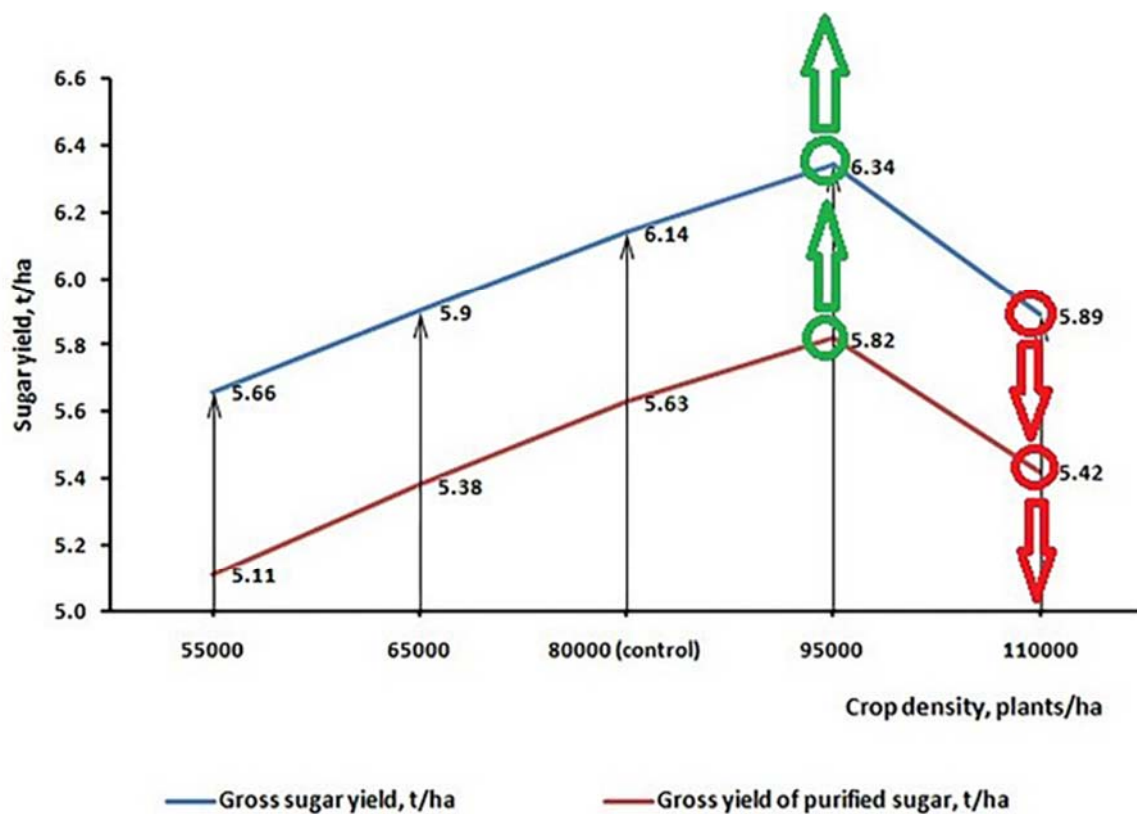


Figure 6. Sugar collection at different plant density (2008-2010)

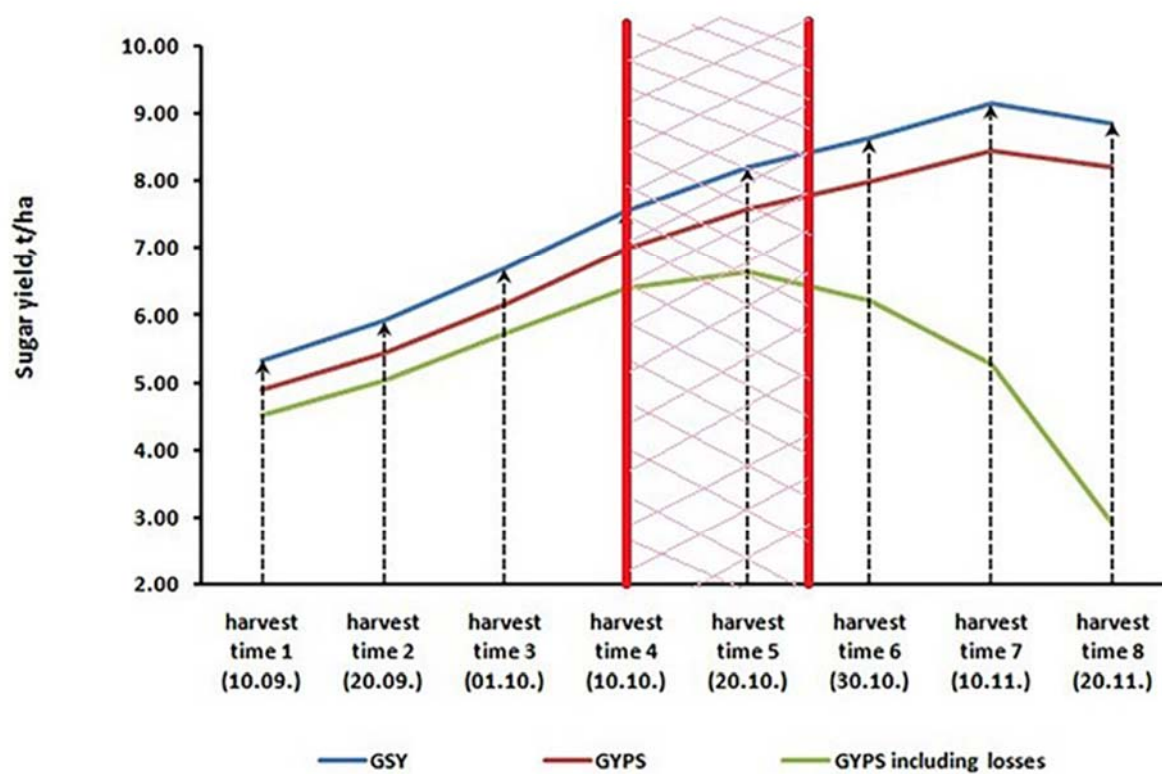


Figure 7. Changes in sugar yield by harvest time (2013-2015): GSY – Gross sugar yield, t/ha; GYPS – Gross yield of purified sugar, t/ha; GYPS including losses – Gross yield of refined sugar including losses, t/ha

COMPOSIÇÃO QUÍMICA E ATIVIDADE OVICIDA DO ÓLEO ESSENCIAL DAS FOLHAS DE *CROTON ARGYROPHYLLUS* (EUPHORBIACEAE) SOBRE O *AEDES AEGYPTI* (DIPTERA: CULICIDAE)

CHEMICAL COMPOSITION AND OVICIDA ACTIVITY OF THE ESSENTIAL OIL OF *CROTON ARGYROPHYLLUS* (EUPHORBIACEAE) LEAVES ABOUT *AEDES AEGYPTI* (DIPTERA: CULICIDAE)

COSTA, Renata Katryne Bispo da Silva¹; SILVA, Débora Cardoso^{1*}; GUALBERTO, Simone Andrade¹; DA SILVA, Paulo Sávio Damásio² COSTA, Matheus Andrade Rocha³.

¹Laboratório de Pesquisa de Inseticidas Naturais/Universidade Estadual do Sudoeste da Bahia/UESB, Praça Primavera, 40, Bairro Primavera, CEP 45700-000, Itapetinga, BA, Brasil. (Fone: +55 77 3261-8468)

²Laboratório de Biossistemática Animal/ Universidade Estadual do Sudoeste da Bahia, Estrada Itapetinga, s/n, Itapetinga - BA, 45700-000, Itapetinga, BA, Brasil.

³Centro Regional de Ciências Nucleares do Nordeste (CRCN-NE)
Av. Prof. Luís Ferreira, 200, CEP: 51740-540, Cidade Universitária, Recife, Pernambuco, Brasil

*Autor correspondente
E-mail: dcardoso_rj@hotmail.com

Received 17 October 2019; received in revised form 02 July 2020; accepted 12 August 2020

RESUMO

O controle do *Aedes aegypti*, transmissor de várias arboviroses de importância para a saúde pública, tem como estratégias a utilização de inseticidas sintéticos, integrados com o controle ambiental. Seu controle é direcionado principalmente para as fases de larva e adulto. A fase de ovo é difícil de ser controlada, pois possui grande resistência às condições ambientais. Objetivou-se avaliar o potencial ovicida do óleo essencial obtido das folhas de *Croton argyrophyllus*, sobre o *Aedes aegypti*, bem como determinar o teor da umidade, o rendimento e a sua composição química. Os ovos foram expostos à solução aquosa do óleo essencial em Tween 80 a 10%, na concentração de 12 mg mL⁻¹, por um período de 15, 30, 60 e 120 minutos. Posteriormente, os ovos foram lavados e, após 180 horas de observação, foi adicionada ração ao meio. A análise da composição química do óleo essencial foi realizada por Cromatografia Gasosa acoplada a Espectrometria de Massas. Verificou-se que até 180 horas de observação, a maior porcentagem de eclosão larvar ocorreu nos ovos expostos ao óleo essencial por 15 min (30%) e o menor percentual nos ovos expostos por 120 min (<10%). Após 180 horas houve aumento da eclosão em todos os tratamentos. O teor de umidade foi de 58,69%, o rendimento do óleo foi 0,35%, e os principais constituintes químicos encontrados foram o biciclogermacreno e β-cariofileno. Observou-se que o óleo essencial de *Croton argyrophyllus*, na concentração avaliada, afeta a eclosão das larvas do *Aedes aegypti* somente na ausência de alimento no meio.

Palavras-chave: Caatinga, Inseticidas, Parasitologia

ABSTRACT

The control of *Aedes aegypti*, which transmits several arboviruses of importance to public health, has as strategies the use of synthetic insecticides, integrated with environmental control. Its control is mainly directed to the larvae and adult phases. The egg phase is difficult to control, as it has great resistance to environmental conditions. The objective of this work was to evaluate the ovicidal potential of the essential oil obtained from the leaves of *Croton argyrophyllus*, on *Aedes aegypti*, as well as to determine the moisture content, the yield, and its chemical composition. The eggs were exposed to the aqueous solution of the essential oil in 10% Tween 80, in the concentration of 12 mg mL⁻¹, for a period of 15, 30, 60, and 120 minutes. Subsequently, the eggs were washed and, after 180 hours of observation, the feed was added. The analysis of the chemical composition of the essential oil was performed by Gas Chromatography coupled to Mass Spectrometry. It was found that up to 180 hours of observation, the highest percentage of larval hatching occurred in eggs exposed to essential oil for

15 min (30%) and the lowest percentage in eggs exposed for 120 min (<10%). After 180 hours, there was an increase in hatching in all treatments. The moisture content was 58.69%, the oil yield was 0.35%, and the main chemical constituents found were bicyclogermacrene and β -cariophyllene. It was observed that the essential oil of *Croton argyrophyllus*, at the concentration evaluated, affects the hatching of *Aedes aegypti* larvae only in the absence of food.

Keywords: *Caatinga, Insecticides, Parasitology*

1. INTRODUÇÃO

O *Aedes aegypti* Linnaeus, 1762 (Diptera: Culicidae) é um mosquito transmissor de arboviroses, como os quatro sorotipos do vírus da dengue (DENV-1, DENV-2, DENV-3 e DENV-4), o vírus do chikungunya e do zika (VEGA-RUA, 2014). Esses dois últimos causam doenças que apresentam sintomas semelhantes aos da dengue, sendo o vírus Zika associado também à Síndrome de Guillain-Barré na Polinésia Francesa (OEHLER *et al.*, 2014) e microcefalia no Brasil (MARCONDES; XIMENES, 2015). Não há vacina para chikungunya e zika, e ainda não está claro se existe uma vacina eficaz contra a dengue, portanto, o controle do *A. aegypti* continua sendo o principal instrumento para a diminuição da incidência destas doenças (FERREIRA *et al.*, 2017).

Para o controle integrado do *A. aegypti* são utilizadas estratégias que abrangem os controles mecânico, biológico e químico. O controle mecânico consiste em práticas capazes de eliminar criadouros. O biológico envolve vários predadores naturais que apresentam potencialidade para reduzir a população de mosquitos. Métodos de controle biológico estão sendo avaliados, como a modificação genética de populações de insetos selvagens (MCGRAW 2013, SLATKO 2014), a utilização da bactéria *Wolbachia pipientis* Hertig e Wolbach, 1924, e a esterilização de insetos por irradiação (BOYER, 2012). O controle químico é amplamente empregado, e é executado através da utilização dos inseticidas sintéticos, sendo este responsável pelo surgimento de populações resistentes no Brasil (MACORIS *et al.*, 2014) e em outros países, o que requer a busca por novas substâncias que sejam eficazes contra as larvas, adultos e, também, sobre os ovos do *A. aegypti*.

Com relação ao uso de substâncias químicas, os agentes utilizados no controle dos mosquitos são direcionados para a fase larval e adulta, não atuando na fase de ovo. O ovo é considerada a fase mais difícil no que diz

respeito ao controle, pois é a fase mais resistente do ciclo biológico do vetor, podendo apresentar uma sobrevivência de até um ano sem contato com a água, devido a sua capacidade de quiescência e a cutícula de cera que se forma entre doze a treze horas após a oviposição. Nas regiões onde as estações possuem invernos rígidos, esta fase é tida como estratégica para suportar o frio (SILVA; POLETO, 2012). Características como essas, conferem aos ovos do *A. aegypti* uma tolerância às condições físicas e químicas, como os inseticidas (REZENDE *et al.*, 2008). Além disso, permite o transporte a longas distâncias, tornando-se o principal meio de dispersão do mosquito (SILVA *et al.*, 2009).

Dentre as formas de controle químico que podem atuar nas diferentes fases de desenvolvimento do *A. aegypti*, inclusive na fase do ovo, podem-se citar os inseticidas botânicos, principalmente os formulados com óleos essenciais. Os óleos essenciais são produtos do metabolismo secundário das plantas, cujas funções abrangem a defesa contra agentes patogênicos, proteção contra herbívoros e atração de polinizadores (BAKKALI *et al.*, 2008). Estes produtos do metabolismo vegetal são voláteis, lipofílicos, geralmente odoríferos e líquidos (SIMÕES; SPITZER, 2004). Apresentam em sua constituição cerca de 20 a 60 componentes em diferentes concentrações (ANDRÉ *et al.*, 2018), sendo que os componentes majoritários geralmente determinam suas propriedades biológicas (PAVELA, 2015). Cruz *et al.* (2017), ao analisarem o potencial inseticida do óleo essencial obtido das folhas secas de *Croton argyrophyllus* Kunth, constataram o seu efeito tóxico sobre as larvas e adultos fêmeas do *A. aegypti*, sendo essa bioatividade atribuída, provavelmente, aos componentes majoritários do óleo essencial, como o espatulenol, β -cariofileno, α -pineno e o bicyclogermacrene. Contudo, outros estudos têm revelado o efeito larvicida de constituintes químicos presentes em baixas concentrações em extratos e óleos vegetais sobre o *A. aegypti*, seja de forma isolada ou atuando em sinergia com outros constituintes

(GOMES *et al.*, 2016).

Do ponto de vista ambiental, os inseticidas e repelentes botânicos que são constituídos por óleos essenciais se degradam rapidamente no meio ambiente, além de serem capazes de agir nas funções fisiológicas e bioquímicas dos insetos, em virtude da volatilidade e baixa persistência em condições de campo (COITINHO *et al.*, 2011). Por isso, podem ser seguros para o manejo por humanos e, é pouco provável, que ocorra intoxicação por contato com seus resíduos, como ocorre com inseticidas sintéticos. A volatilidade pode afetar também a eficiência de uma formulação que tenha na sua composição óleos essenciais, caso seja necessário um tempo de exposição prolongado para que o efeito tóxico ocorra. A utilização de óleos essenciais na formulação de inseticidas botânicos pode ser viável a nível econômico, ambiental e social, atendendo ao mesmo tempo a uma parcela da sociedade que opta por produtos naturais, que supostamente causem menor impacto sobre o meio ambiente e sobre a saúde dos indivíduos (FIGUEIREDO *et al.*, 2018).

Com relação ao gênero *Croton* Linnaeus estudos têm demonstrado o seu potencial para ser usado em programas de controle integrado do *A. aegypti*. Anjos *et al.* (2018) verificaram o efeito tóxico do óleo essencial da parte aérea de *Croton tetradenius* Baillon sobre larvas do *A. aegypti* e a influência do período de extração sobre o rendimento do óleo e a sua composição química. Carvalho *et al.* (2016) testaram a bioatividade do óleo essencial obtido das folhas de *C. tetradenius* sobre larvas e adultos do *A. aegypti*, demonstrando o seu efeito tóxico, e realizaram testes em mamíferos observando uma baixa toxicidade sobre *Mus musculus* Linnaeus, 1758. Da mesma forma, Cruz *et al.* (2017), ao avaliarem o óleo essencial obtido das folhas de *C. argyrophyllus*, constataram sua toxicidade sobre larvas e adultos fêmeas do *A. aegypti*, tendo apresentado, também, baixa toxicidade sobre *Mus musculus*.

Diante do potencial inseticida de espécies do gênero *Croton* sobre o *A. aegypti*, esse estudo teve por objetivo avaliar a toxicidade do óleo essencial obtido das folhas de *Croton argyrophyllus* sobre os ovos do *A. aegypti*, bem como determinar o teor da umidade, o rendimento e a composição química do óleo essencial.

2. MATERIAL E MÉTODOS

2.1. Material botânico

As folhas de *Croton argyrophyllus* foram identificadas e depositadas no Herbário da Universidade Estadual do Sudeste da Bahia (HUESB 4662). A coleta das folhas da espécie foi realizada no mês de maio de 2017, no período matutino, na Floresta Nacional de Contendas do Sincorá. As coordenadas geográficas do local da coleta foram S13°55.25' W041°06.88' (Figura 1).

2.2 Determinação do teor de umidade

A determinação da umidade das folhas foi realizada pelo método gravimétrico, conforme metodologia descrita por Santos *et al.* (2004), com adaptações. Inicialmente, 500 g de folhas frescas de *C. argyrophyllus* foram secas em estufa de circulação de ar a 50 °C durante 24 horas. Posteriormente, em um cadinho de porcelana, pesou-se 5 g do material vegetal previamente triturado e desidratado. Em seguida, este material foi seco em estufa de esterilização e secagem por 5 horas a uma temperatura de 110 °C. Após este período, o cadinho foi retirado da estufa com o auxílio de uma pinça, e colocado em um dessecador por 20 minutos para esfriar. Após a primeira pesagem, o cadinho retornou para a estufa por um período 1 hora. Este procedimento foi repetido até peso constante. O experimento foi conduzido em triplicata.

O teor de umidade foi expresso em porcentagem, através da diferença entre a massa perdida e a massa inicial das folhas frescas, multiplicado por 100.

2.3. Extração e rendimento do óleo essencial

Inicialmente, as folhas frescas foram alocadas em estufa de circulação de ar, pelo período de 12 horas, a uma temperatura de 40 °C.

Posteriormente, o material vegetal seco foi triturado manualmente e o óleo essencial foi extraído por hidrodestilação em aparelho de Clevenger modificado. Para cada extração foram utilizadas 60 gramas de folhas secas e trituradas, colocadas em balão de fundo redondo de 2,0 L com junta esmerilhada e adicionado a esse balão 1 L de água grau reagente (tipo II). O processo de extração foi conduzido em triplicata, à temperatura de 100 °C. O hidrolato foi extraído com éter etílico (C₄H₁₀O). A fração etérica foi seca com sulfato de sódio anidro (Na₂SO₄) e o solvente removido a baixa pressão, a temperatura de 20°C em concentrador de

amostras (Christ AVC 2-18 CD).

O óleo essencial extraído foi armazenado em frasco âmbar, vedado e armazenado em freezer a temperatura de $-4\text{ }^{\circ}\text{C} \pm 1\text{ }^{\circ}\text{C}$, até a realização das análises químicas e dos ensaios biológicos.

O teor do óleo essencial foi determinado dividindo a massa do óleo essencial (g) pela massa foliar seca utilizada (g) e multiplicando esse valor por 100.

2.3. Determinação da composição química do óleo essencial

A composição química do óleo essencial foi determinada em um Cromatógrafo Gasoso acoplado a um Espectrômetro de Massas (Shimadzu CG-EM, GC-17A/ QP2010 Plus), equipado com coluna capilar Factor Four-VF-5ms (30 m x 0,25 mm de diâmetro interno x 0,25 μm de espessura de filme), usando hélio como gás de arraste a uma vazão de 1 mL min^{-1} e pressão de 12 psi. A programação da temperatura do forno foi de $60\text{ }^{\circ}\text{C}$ a $260\text{ }^{\circ}\text{C}$ ($3\text{ }^{\circ}\text{C}\cdot\text{min}^{-1}$), depois $10\text{ }^{\circ}\text{C}\cdot\text{min}^{-1}$ até $290\text{ }^{\circ}\text{C}$, com temperatura do injetor a $220\text{ }^{\circ}\text{C}$, interface a $310\text{ }^{\circ}\text{C}$ e fonte de íons a $220\text{ }^{\circ}\text{C}$. Injetou-se $1\text{ }\mu\text{L}$ de solução da amostra em diclorometano a uma razão de split 1:30. Os espectros de massas foram obtidos na faixa de varredura de 40-500 u.m.a, com energia de impacto de elétrons de 70 eV. As análises quantitativas foram realizadas utilizando um cromatógrafo de fase gasosa (HP 5890 Series II) equipado com um detector de ionização de chamas (DIC), nas mesmas condições experimentais e temperatura do detector de $280\text{ }^{\circ}\text{C}$. Os espectros de massas foram obtidos em equipamento Modelo:GCMS-QP2010 Plus da Shimadzu Coluna: HP-5 (30X0.25X0.25), nas mesmas condições experimentais descritas anteriormente. Os cromatogramas obtidos para as amostras do óleo essencial e dos padrões de hidrocarbonetos são mostrados nas Figuras 2, 3 e 4. Os espectros de massas são apresentados como anexos.

Os componentes do óleo essencial foram identificados através de seus índices de retenção (IR), calculados para cada constituinte por meio da injeção de uma série de padrões de hidrocarbonetos lineares (C8-C20) (Sigma-Aldrich) nas mesmas condições da amostra, e comparados com o valor tabelado por Adams (2007), assim como através da comparação com o banco de dados da biblioteca Nist08.

2.4. Avaliação da atividade ovicida

Os experimentos foram conduzidos em sala climatizada a uma temperatura média de $27,7\text{ }^{\circ}\text{C}$ e umidade média de 60,13%.

Os ovos do *Aedes aegypti* utilizados foram oriundos da linhagem Rockefeller, fornecidos pelo Laboratório de Fisiologia e Controle de Artrópodes Vetores – LAFICAVE, da Fundação Oswaldo Cruz, do Rio de Janeiro, Brasil.

Para o teste ovicida foi utilizada uma solução do óleo essencial de *C. argyrophyllus* na concentração de $12\text{ mg}\cdot\text{mL}^{-1}$, obtida a partir da solubilização do óleo em uma solução de Tween 80 a 10% em água grau reagente (tipo II). Os ovos do *A. aegypti* (Figura 5) foram expostos à solução do óleo essencial de *C. argyrophyllus* por um período de 15, 30, 60 e 120 minutos. Como controles foram utilizadas a solução de Tween 80 a 10% em água deionizada e somente a água grau reagente. Após o período de exposição, os ovos foram retirados da solução e lavados com 10 mL de água grau reagente, por três vezes. Em seguida, foram selecionados aleatoriamente 30 ovos por repetição, com 5 repetições por tratamento, os quais foram colocados em recipiente de Polipropileno (PP) (3 x 3 cm) contendo 5 mL de água grau reagente (tipo II). O percentual de eclosão das larvas foi observado inicialmente a cada duas horas, por um período de 12 horas e, posteriormente, a cada 12 horas, por um período de 180 horas.

Após o período de 180 horas, com o intuito de avaliar se o óleo essencial havia causado mortalidade ou apenas inibição da eclosão das larvas, foram adicionados 0,01 g de ração para peixe triturada da marca Alcon Basic® nos recipientes de todos os tratamentos. As observações foram realizadas a cada 12 horas, por mais 144 horas. A cada 48 horas foram retirados 3 mL de água de cada recipiente e adicionados 3 mL de água deionizada limpa. Na medida em que ocorria a eclosão, as larvas eram quantificadas e retiradas dos recipientes com auxílio de uma pipeta Pasteur.

2.5. Análise estatística

Para comparar se a porcentagem média de eclosão de larvas do *A. aegypti* (%) diferiu antes e depois da adição de ração para peixes, em função do tempo de observação em minutos, nos diferentes tempos de exposição ao óleo essencial (15, 30, 60 e 120 minutos) e controles (Tween 80 e água grau reagente tipo II) foi feita a ANOVA fatorial. Para comparar as diferenças entre as médias foi realizado o teste de Tukey. A normalidade para todas as variáveis foi

investigada através do teste Lilliefors. Todas as análises foram desenvolvidas de acordo com Sokal and Rohlf (1995). Uma análise descritiva foi desenvolvida para calcular as médias e erro padrão. Neste estudo foi considerado o nível de significância de 5%. O programa utilizado para as análises foi o Do R.

3. RESULTADOS E DISCUSSÃO

No presente trabalho o rendimento médio do óleo essencial obtido das folhas de *Croton argyrophyllus*, coletadas em maio de 2017, foi de 0,35% (intervalo de confiança: 0,34-0,36) e o teor de umidade médio 58,69% (intervalo de confiança: 57,08 - 60,30).

Cruz *et al.* (2017), avaliando o rendimento médio do óleo essencial das folhas de *C. argyrophyllus*, as quais também foram coletadas na Floresta Nacional de Contendas do Sincorá/Bahia, no mês de maio de 2014, obtiveram um rendimento médio do óleo maior (0,48%) do que o encontrado nesse estudo. De acordo com os dados obtidos na estação meteorológica de Ituaçu/Bahia (OMM: 83292), do Instituto Nacional de Meteorologia, a precipitação pluviométrica total foi menor para o mês de maio de 2014 (2,8 mm), comparado a maio de 2017 (13,3 mm), o que pode ter interferido na produção dos metabólitos secundários, visto que diversos fatores relacionados ao estresse hídrico como, por exemplo, chuvas intensas e solos encharcados, podem afetar o metabolismo da planta, interferindo no rendimento do óleo essencial.

Outros fatores também podem afetar a atividade biossintética das plantas, e, conseqüentemente, o rendimento do óleo essencial, como o genético e o estágio de desenvolvimento, além das relações ecológicas intra e interespecíficas. Conhecer o rendimento do óleo essencial das espécies é necessário para determinar a viabilidade econômica e ambiental, para então, serem utilizadas como substâncias inseticidas. A variação no rendimento do óleo essencial da planta, assim como o teor de umidade nas folhas, pode ser atribuída a fatores extrínsecos abióticos, como temperatura, umidade relativa do ar, duração total de exposição ao sol, pluviosidade, o regime de ventos e as condições edáficas, assim como a fatores bióticos, através das relações ecológicas intra e interespecíficas (LIMA *et al.*, 2016; ANJOS, *et al.*, 2018).

Em relação à eclosão das larvas, com quatro e oito horas, o percentual de eclosão foi inferior a

10%, em todos os tratamentos e inclusive nos grupos controle. Com 12 horas ocorreu um aumento no percentual de eclosão, sendo que no tratamento no qual os ovos foram expostos ao óleo essencial por 120 minutos o percentual de eclosão manteve-se inferior a 10%, até 180 horas (Figura 6 (A) e (B)). Após a adição da ração (estímulo bioquímico) no meio, ocorreu um aumento na eclosão das larvas em todos os tratamentos, inclusive nos grupos controle (Figura 6 (C)). Com 336 horas de observação, a eclosão das larvas foi superior a 50% nos tratamentos cujos ovos foram expostos ao óleo essencial por 15, 30 e 60 minutos, assim como os controles, o que não ocorreu com o tratamento cujos ovos foram expostos por 120 minutos ao óleo essencial de *C. argyrophyllus* (Figura 6 (C)).

Antes da adição da ração, a porcentagem média acumulada de eclosão das larvas do *A. aegypti* foi significativamente menor para os tempos de exposição ao óleo de 60 e 120 minutos, quando comparado com 15 e 30 minutos de exposição e com os grupos controle (Figura 7). Entretanto, após a adição da ração, a eclosão das larvas não seguiu o mesmo padrão observado antes do fornecimento da ração. Constatou-se que a porcentagem acumulada de eclosão das larvas foi significativamente maior após a adição da ração (média \pm erro padrão; $54 \pm 1,02$), quando comparado ao período anterior à adição ($16,42 \pm 0,72$; $F = 992,67$; $P < 0,001$), em todos os tratamentos.

É provável que o óleo essencial de *C. argyrophyllus* tenha ocasionado a inibição do desenvolvimento larval, em virtude das condições adversas que foram geradas pela exposição dos ovos ao óleo essencial, por diferentes períodos. De Lima *et al.* (2013) testaram o óleo essencial de *Croton zehntneri* Pax et Hoffm, *Croton nepetaefolius* Kuntze, *Croton argyrophyllodes* Muell. Arg e *Croton sonderianus* Muell. Arg sobre ovos do *A. aegypti*, sendo que todos os óleos testados inibiram a eclosão dos ovos, obtendo assim resultados semelhantes ao deste trabalho. Contudo, no presente trabalho, o fornecimento da ração de peixe pode ter estimulado a eclosão das larvas, independente das condições adversas a que foram submetidas. Dessa forma, o óleo essencial obtido das folhas de *C. argyrophyllus*, na concentração e nos períodos de exposição utilizados nesse estudo, não apresentou potencial para ser usado como um produto ovicida em programas de controle do *A. aegypti*, visto que, embora tenha afetado a biologia na

fase de ovo, provavelmente ocasionando um retardo temporário da eclosão, não interferiu de forma significativa na mortalidade larval. No experimento de De Lima *et al.* (2013) não houve o estímulo bioquímico (oferecimento de alimento) após o período de observação.

Calado (2002), em um experimento realizado com ovos do *Aedes albopictus* Skuse, 1894, observou uma menor eclosão na ausência de alimento e um aumento significativo quando a ração para peixe foi adicionada ao meio líquido. Da mesma forma, Dieng *et al.* (2018), ao avaliarem a atuação de fluidos de resíduos doces, como fruto de banana, batata-doce cozida e a embalagem de alimentos doces, como lata de leite condensado, sobre a eclosão das larvas do *A. aegypti*, em condições artificiais, verificaram que o percentual de eclosão foi semelhante ao obtido no ambiente natural.

A atividade ovicida de um produto também pode ser afetada pelo tempo de exposição em razão de sua grande volatilidade, causando um efeito residual curto e sua baixa solubilidade em água (BILIA *et al.*, 2014), pela idade do ovo, pela concentração do produto aplicado (TENNYSON *et al.*, 2011), assim como pela estrutura coriônica do ovo (CAMPBELL *et al.*, 2016) e por fatores bióticos e abióticos como a temperatura, umidade (BESERRA *et al.*, 2006), pluviosidade (FORATTINI, 2003), fotoperíodo (DINIZ *et al.*, 2017) e o oxigênio dissolvido (DO), que está ligado ao crescimento bacteriano (PONNUSAMY, 2011).

Aznar *et al.* (2013) observaram que em climas temperados, chuvas intensas desencadeavam a eclosão das larvas, proporcionando um aumento na densidade larval. Por outro lado, a ausência de bactérias inibia a eclosão durante a estação de inverno e nas estações com chuvas isoladas, eclosão essa que também dependia da disponibilidade de alimento. Em ambientes naturais, as larvas do *A. aegypti* se alimentam também de bactérias, portanto, a sua presença no criadouro é um fator que estimula a eclosão das larvas.

É importante destacar que a ação dos óleos essenciais sobre os insetos não se restringe apenas a mortalidade do indivíduo. Além disso, esses produtos podem provocar alterações comportamentais, como a deterrence alimentar, conforme citado por Colpo *et al.* (2014).

Portanto, não se pode descartar o potencial do óleo essencial de *C. argyrophyllus*, pois embora não tenha atuado como um ovicida nos testes realizados, pode ter afetado outras fases

do desenvolvimento do inseto, como o potencial biótico, refletindo assim, no seu potencial reprodutivo e interferindo no crescimento populacional do *A. aegypti*.

Nesse estudo, a adição da ração ao meio aumentou significativamente o percentual de eclosão das larvas, funcionando, provavelmente, como um estímulo bioquímico, independente das condições adversas do meio, visto que as larvas eclodiram na presença de um fator essencial à sua sobrevivência, o alimento, mesmo tendo entrado em contato com uma substância potencialmente tóxica, como o óleo essencial de *C. argyrophyllus*. É necessário, portanto, estar atento ao fato de que esses fatores, em condições naturais, não são controlados e que um produto pode inicialmente demonstrar um potencial ovicida ao ser avaliado, mas em campo, em contato com diversos fatores ecológicos, a eclosão das larvas pode ocorrer.

Quanto à composição química do óleo essencial obtido das folhas de *C. argyrophyllus*, a análise indicou a presença de 57 substâncias, tendo sido identificados 24 compostos, correspondendo a 42,10% do total. Destas substâncias, 38,37% são sesquiterpenos hidrocarbonados, 15,15% são monoterpenos hidrocarbonados, 2,91% sesquiterpenos oxigenados, 1,32% monoterpenos oxigenados e 0,69% outros constituintes (Tabela 1).

Os constituintes com percentuais superiores a 1% identificados no óleo essencial de *C. argyrophyllus* foram: biciclogermacreno (15,46%), β -cariofileno (14,69%), β -pineno (7,18%), α -humuleno (4,03%), β -elemeno (3,47%), α -felandreno (1,93%), óxido de cariofileno (1,70%), p-cimeno (1,53%), γ -terpineno (1,47%), β -ocimeno (1,41%) e espatulenol (1,21%).

Corroborando com o presente trabalho, Araújo *et al.* (2014), encontraram o biciclogermacreno como o componente principal (27,78%) das folhas de *C. argyrophyllus*, e também, o β -elemeno (8,50%), β -cariofileno (6,27%) e o espatulenol (4,83%). Brito *et al.* (2018), também encontraram o biciclogermacreno como componente majoritário do óleo essencial das folhas de *C. argyrophyllus*, coletadas entre fevereiro e abril de 2016. Contudo, Cruz *et al.* (2017), ao avaliarem o óleo essencial das folhas de *C. argyrophyllus*, coletadas em maio de 2014, encontraram como componente majoritário o espatulenol (22,80%), seguido por β -cariofileno (15,41%), α -pineno (14,07%) e biciclogermacreno (10,43%).

Quanto a atividade biológica, a presença de um constituinte químico, seja majoritário ou não, pode intensificar ou até mesmo inibir a toxicidade de uma planta. Deste modo, ao avaliar o potencial de uma planta para ser usada em programas de controle de vetores e sua relação com os constituintes químicos, é preciso que seja considerado o sinergismo e o antagonismo entre os constituintes.

4. CONCLUSÕES

O óleo essencial de *Croton argyrophyllus* testado na concentração de 12 mg·mL⁻¹ interferiu na eclosão dos ovos do *Aedes aegypti*, provavelmente pela tolerância do ovo em proteger o embrião de substâncias tóxicas nesta fase. No entanto, quando os ovos foram expostos ao alimento (ração de peixe) houve eclosão.

A busca por compostos bioativos que interrompam ou evitem o desenvolvimento embriológico do *A. aegypti*, a exemplo dos inseticidas botânicos, é pertinente e urgente, em virtude da sua importância como transmissor de patógenos.

5. AGRADECIMENTOS:

Ao Programa de Pós-Graduação em Ciências Ambientais (PPGCA) e aos órgãos de fomento: CAPES, FAPESB, CNPq e a UESB.

6. REFERÊNCIAS:

1. Adams, R. P. (2007). Identification of essential oil components by gas chromatography/ mass spectrometry, 4th ed., Allured Publishing Corporation, Carol Stream, IL USA.
2. André W. P. P.; Ribeiro W. L. C.; Oliveira L. M. B.; Macedo I. T. F.; Rondon F. C. M. and Bevilacqua C. M. L. (2018). Óleos essenciais e seus compostos bioativos no controle de nematoides gastrintestinais de pequenos ruminantes. *Acta Scientiae Veterinariae*, 46: 1522.
3. Anjos, Q. Q. A.; Silva, S. L. C.; Silva, D. C.; Gualberto, S. A.; Santos, F. R.; Carvalho, M. G. and Sousa, D. L. (2018). Composição química do óleo essencial da parte aérea de *Croton tetradenius* (Euphorbiaceae) e a sua bioatividade

sobre *Aedes aegypti* (Diptera: Culicidae) em relação em diferentes períodos de coleta. *Periódico Tchê Química.*, 15(30), 364-379.

4. Araujo, S. S.; Santos, M. I. S.; Dias, A. S.; Ferro, J. N. S.; Lima, R. N.; Barreto, E. O.; Alves, P. B.; Santana A.E.G.; Thomazzi S. M.; Antonioli A. R. and Estevam C.S. (2014). Composição química e análise de citotoxicidade do óleo essencial das folhas de *Croton argyrophyllus* Kunth. *Journal of Essential Oil Research*. 26(6), 446-451.
5. Aznar V. R.; Otero M. J.; de Majo M. S.; Fischer S, and Solari H. G. (2013). Modeling the complex hatching and development of *Aedes aegypti* in temperate climates. *Ecological Modelling*. 253, 44-55.
6. Bakkali F.; Averbeck S.; Averbeck D. and Idaomar M.(2008). Biological effects of essential oil–Review. *Food and Chemical Toxicology*. 46(2), 446-475.
7. Beserra, E. B.; Castro Jr. F. P.; Santos, J. W.; Santos, T. S. and Fernandes, C. R. M.(2006). Biologia e exigências térmicas de *Aedes (Stegomyia) aegypti* (Diptera: Culicidae) provenientes de quatro regiões bioclimáticas da Paraíba. *Neotropical Entomology*. 35(6), 853-860.
8. Bilia, A. R.; Guccione C.; Isacchi B.; Righeschi C.; Firenzuoli F. and Bergonzi M. C. (2014). Essential oils loaded in nanosystems: a developing strategy for a successful therapeutic approach. *Evidence-based Complementary and Alternative Medicine: eCAM*. 651593, 29.
9. Boyer, S. (2012). Sterile insect technique: targeted control without insecticide. *Medecine Tropicale: Revuedu Corps de sante colonial*. , 72, 60-62.
10. Brito, S. S. S.; Silva, F.; Malheiro, R.; Baptista, P. and Pereira, J. A. (2018). *Croton argyrophyllus* Kunth and *Croton heliotropiifolius* Kunth: Phytochemical characterization and bioactive properties. *Industrial Crops and Products*. 113, 308-315.
11. Calado, D. C. and Silva, M. A. (2002)

- Avaliação da influência da temperatura sobre o desenvolvimento de *Aedes albopictus*. *Revista de Saúde Pública*. 36(2), 173-179.
12. Campbel, B. E.; Pereira, R. M. and Koehler, P. G. (2016) Complications with controlling insect eggs. *Insecticides Resistance*. InTech. 437p.
 13. Carvalho, K. S.; Silva, S. L. C.; Souza, I. A.; Gualberto S. A.; Cruz, R. C. D.; Santos, F. R. and Carvalho, M. G. (2016) Toxicological evaluation of essential oil from the leaves of *Croton tetradenius* (Euphorbiaceae) on *Aedes aegypti* and *Mus musculus*. *Parasitology Research*. 115 (9), 3441-3448.
 14. Coitinho, R. L. B. C.; de Oliveira J. V.; Junior M. G. C. G. and Câmara C. A. G. (2011). Toxicidade por fumigação, contato e ingestão de óleos essenciais para *Sitophilus zeamais* Motschulsky 1885 (Coleoptera: Curculionidae). *Ciência e Agrotecnologia*. 35(1), 172-178.
 15. Colpo, J. F.; Jahnke, S. M. and Füller, T. N. (2014). Potencial inseticida de óleos de origem vegetal sobre *Grapholita molesta* (Busck) (Lepidoptera: Tortricidae). *Revista Brasileira de Plantas Medicinais*. 16, (2), 182-188.
 16. Cruz R. C. D.; Silva S. L. C. E.; Souza I. A.; Gualberto S. A.; Carvalho K. S.; Santos F. R. and Carvalho M. G. (2017). Toxicological Evaluation of Essential oil from the leaves of *Croton argyrophyllus* (Euphorbiaceae) on *Aedes aegypti* (Diptera: Culicidae) and *Mus musculus* (Rodentia:Muridae). *Journal of Medical Entomology*. 54(4):985-993.
 17. De Lima, G. P. G., de Souza, T. M., de Paula Freire, G., Farias, D. F., Cunha, A. P., Ricardo, N. M. P. S. and Morais S. M. Carvalho, A. F. U. (2013). Further insecticidal activities of essential oils from *Lippia sidoides* and *Croton* species against *Aedes aegypti* L. *Parasitology Research*. 112(5), 1953-1958.
 18. Dieng H.; Satho T.; Meli N. K. K. B.; Abang F.; Nolasco-Hipolito C.; Hakim H.; Miake F.; Zuharah W.F.; Kassim N. F.A.; AbMajid A.H.; Morales Vargas R. E.; Morales N.P. and Noweg G. T. (2018). Occurrence of sweet refuse at disposal sites: rainwater retention capacity and potential breeding opportunities for *Aedes aegypti*. *Environmental Science and Pollution Research*. 25(14), 13833-13843.
 19. Diniz, D. F. A.; Albuquerque, C. M. R.; Oliva, L. O.; Melo-Santos, M. A. V. and Ayres, C. F. J. (2017). Diapause and quiescence: dormancy mechanisms that contribute to the geographical expansion of mosquitoes and their evolutionary success. *Parasites and Vectors*. 10(1), 310.
 20. Ferreira D. A. C.; Degener C. M.; Marques-Toledo C. A.; Bendati M. M.; Fetzer L. O.; Teixeira C. P. and Eiras Á. E. (2017). Meteorological variables and mosquito monitoring are good predictors for infestation trends of *Aedes aegypti*, the vector of dengue, chikungunya and zika. *Parasites and Vectors*. 10, 78.
 21. Figueiredo, R. C.; Rocha, W. C. and De Freitas, A. D. G. (2018). Efeito inseticida do óleo essencial e extratos etanólicos das folhas de mastruz (*Chenopodium ambrosioides* L.) sobre o gorgulho do milho (*Sitophilus zeamais* Mots.) *Ensaios e Ciência: Ciências Biológicas, Agrárias e da Saúde*. 22(2), 80-84.
 22. Forattini O. P. and Brito M. (2003) Reservatórios domiciliares de água e controle do *Aedes aegypti*. *Revista Saúde Pública*. 37, 676-677.
 23. Gomes, P. R. B.; Silva, A. L. S.; Pinheiro, H. A.; Carvalho, L. L., Lima, H. S.; Silva, E. F.; Silva, R. P., Louzeiro, C. H.; Oliveira, M. B. and Filho, V. E. M.(2016). Avaliação da atividade larvicida do óleo essencial do *Zingiber officinale* Roscoe (gengibre) frente ao mosquito *Aedes aegypti*. *Revista Brasileira de Plantas Medicinais*. 18(2, Suppl. 1), 597-604.
 24. Macoris M. L. G.; Andrighetti M. T. M.; Wanderley D. M. V. and Ribolla P. E. M. (2014). Impact of insecticide resistance on the field control of *Aedes aegypti* in the State of São Paulo. *Revista da Sociedade Brasileira de Medicina Tropical*. 47(5): 573-578.

25. Marcondes C. B. and Ximenes M. F. F. M. (2015). Zika virus in Brazil and the danger of infestation by *Aedes* (Stegomyia) mosquitoes *Revista da Sociedade Brasileira de Medicina Tropical*. 49(1):4-10
26. McGraw, E. A. and O'Neill, S. L.. (2013). Beyond insecticides: new thinking on an ancient problem. *Nature Reviews-Microbiology*. 11(3), 181.
27. Oehler, E.; Watrin, L.; Larre, P.; Leparc-Goffart, I.; Lastere, S.; Valor, F.; Baudouin, L.; Mallet, H.; Musso, D. and Ghawche, F. (2014). Zika virus infection complicated by Guillain-Barré syndrome – case report, French Polynesia, December 2013. *EuroSurveillance* 19, 7–9.
28. Pavea, R. (2015). Essential oils for the development of eco-friendly mosquito larvicides: A review. *Industrial Crops and Products*. 76, 174-187.
29. Ponnusamy, L.; Böröczky, K.; Wesson, D. M.; Schal, C. and Apperson, C. S. (2011) Bacteria Stimulate Hatching of Yellow Fever Mosquito Eggs. *PLoS One*. 6(9), 24409.
30. Rezende, G. L.; Martins, A. J.; Gentile, C.; Farnesi, I. C.; Pelajo-Machado, M.; Peixoto, A. A., and Valle, D. (2008). Embryonic desiccation resistance in *Aedes aegypti* presumptive role of the chitinized serosal cuticle. *BMC Developmental Biology*. 8(1), 1-14.
31. Santos, A. S.; Alves, S. M.; Figueiredo, F. J. and Rocha Neto, G. (2004). Rendimento e qualidade físico-química de óleo essencial extraído de diferentes composições da biomassa aérea de pimenta longa. *Embrapa*. 1-6.
32. Silva, O. E. and Poletto, C. (2012). Monitoramento de *Aedes albopictus* em pequenas comunidades. *Uningá Review*. 10(1), 25-32.
33. Silva, V. C.; Serra-Freire, N. M.; Silva, J. D. S.; Scherer, P. O.; Rodrigues, I.; Cunha, S.P. and Alencar, J. (2009). Estudo comparativo entre larvitrap e ovitrap para a avaliação da presença de *Aedes aegypti* (Diptera: Culicidae), em Campo Grande estado do Rio de Janeiro. *Revista da Sociedade Brasileira de Medicina Tropical*. 42, 730-731.
34. Simões C.M.O and Spitzer V. (2004). Óleos voláteis In: *Farmacognosia da Planta ao medicamento* 5.ed.Porto Alegre..467-495.
35. Sokal, R. R. and Rohlf F. J. (1995) Biometry, 3ª Edição. W. H. Freeman and Company, NewYork. 887p.
36. Slatko B. E.; Luck A. N.; Dobson S. I. and Foster J. M. (2014). Wolbachia endosymbiont and human disease control. *Molecular and Biochemical Parasitology*. 195, 88-95.
37. Tennyson, S.; Ravindran, K. J. and Arivoli, S.; (2011). Screening of plant extracts for ovicidal against *Culex quinquefasciatus* say (Diptera: Culicidae). *Elixir Applied Botany*. 40, 5456-5460.
38. Vega-Rúa A.; Zouache K.; Girod R.; Failloux AB, and Lourenço-de-Oliveira R. (2014) High level of vector competence of *Aedes aegypti* and *Aedes albopictus* from ten American countries as a crucial factor in the spread of Chikungunya virus. *Journal Virology*. 89(14), 6294-306.

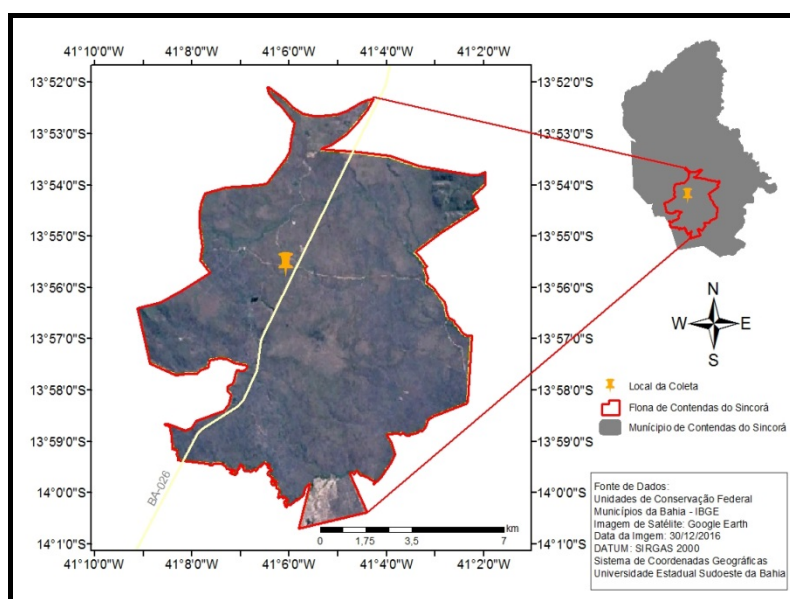


Figura 1. Mapa de localização indicando com seta amarela o local de coleta das folhas de *Croton argyrophyllus*, na Floresta Nacional de Contendas do Sincorá, Bahia, Brasil.

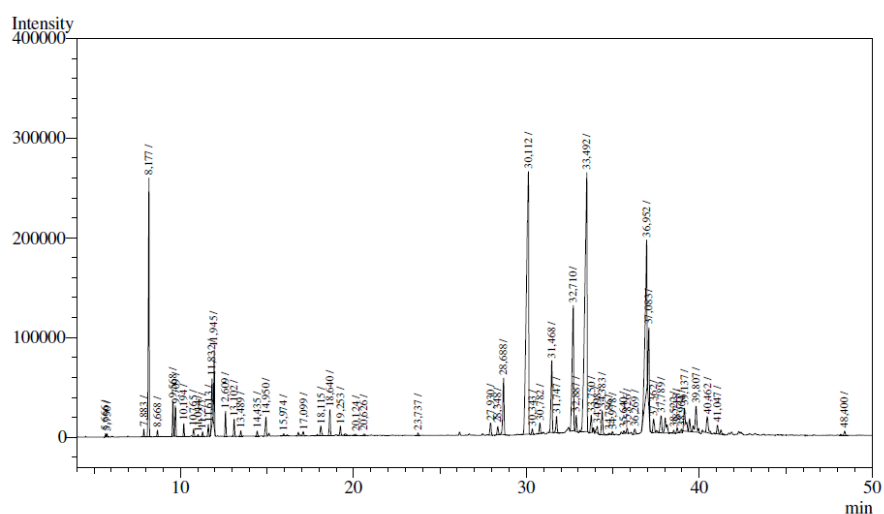


Figura 2. Cromatograma obtido com detector de ionização de chamas da amostra do óleo essencial das folhas de *Croton argyrophyllus* coletadas na Floresta Nacional Contendas do Sincorá - BA, Brasil, no mês de maio de 2017.

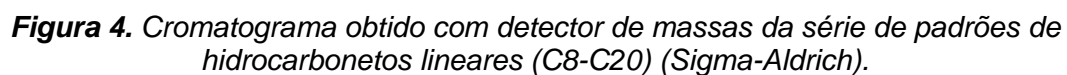
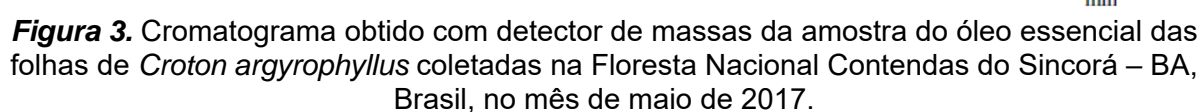




Figura 5. Ovo do *Aedes aegypti* oriundo da linhagem Rockefeller (Aumento 8 x10).

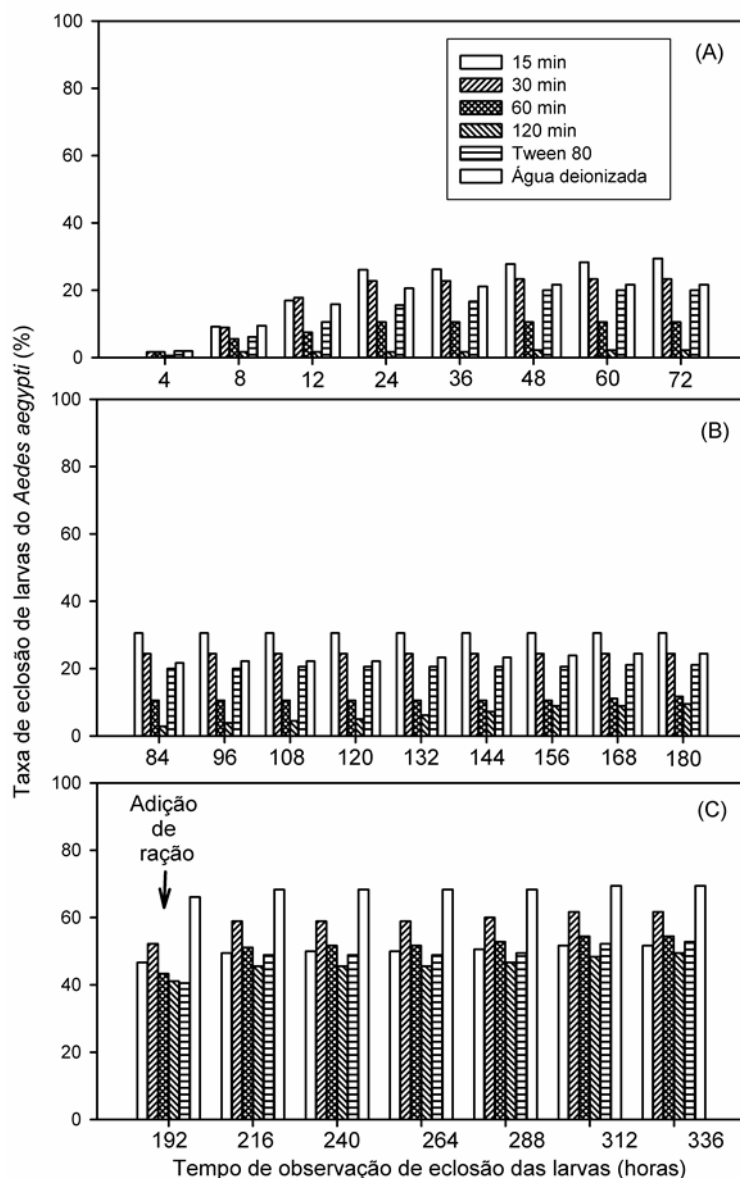


Figura 6. Taxa acumulada de eclosão de larvas do *Aedes aegypti* em função do tempo de exposição dos ovos à solução aquosa em Tween 80 a 1% do óleo essencial obtido das folhas de *Croton argyrophyllus* (12 mg mL^{-1}) e controles (água deionizada e Tween 80), com tempo de observação de eclosão das larvas reportado nas figuras (A) e (B) de 4 a 180 horas e (C) de 192 a 336 horas

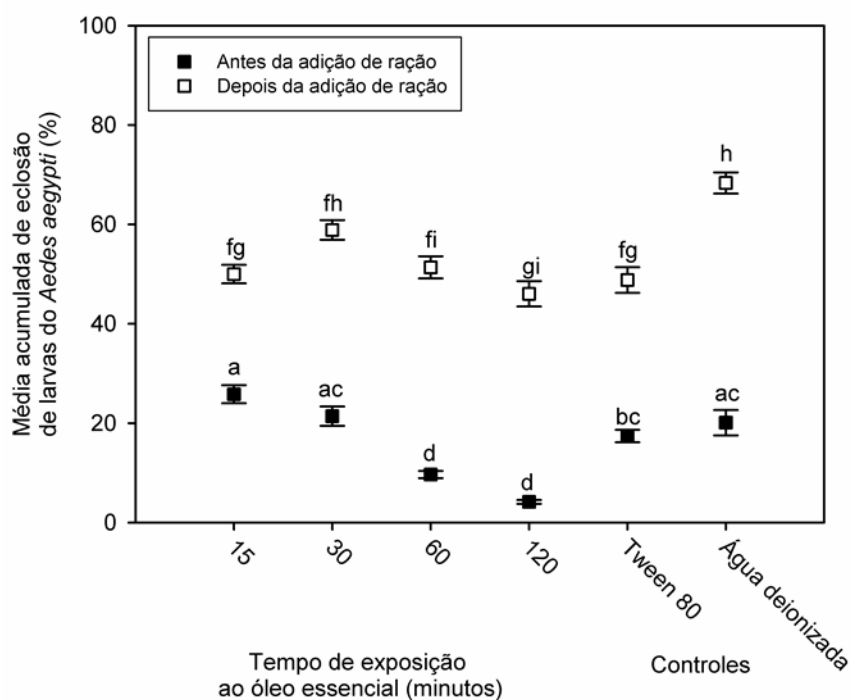


Figura 7. Média acumulada (\pm erro padrão) de eclosão de larvas do *Aedes aegypti* em função do tempo de exposição dos ovos à solução aquosa em Tween 80 a 1% do óleo essencial de *Croton argyrophyllus* (12 mg mL^{-1}) e controles antes e depois da adição de ração. Os quadrados fechados representam o período antes da adição de ração e os abertos representam após a adição da ração de peixe. As diferentes letras representam diferenças significativas baseadas no Pós-teste de Tukey.

Tabela 1. Composição química do óleo essencial obtido das folhas secas de *C. argyrophyllus*

Constituintes	IRL ¹	IKC ²	(%) ³
Monoterpenos hidrocarbonados			
Canfeno	930	954	0,03
β -Felandreno	934	1029	0,59
β -Pino	943	979	7,18
Mirceno	956	990	0,42
α -Felandreno	980	1002	1,93
p-Cimeno	1010	1024	1,53
α -Pino	1016	939	0,59
(E)- β -Ocimeno	1031	1050	1,41
γ -Terpineno	1039	1059	1,47
Monoterpenos oxigenados			
Terpineno-4-ol	1174	1177	0,73
Verbenona	1196	1205	0,59
Sesquiterpenos hidrocarbonados			
β -Bourboneno	1392	1288	0,72
β -Elemeno	1399	1390	3,47
β -Cariofileno	1432	1419	14,69
α -Humuleno	1464	1454	4,03
Biciclogermacreno	1509	1500	15,46
Sesquiterpenos oxigenados			
Óxido de cariofileno	1596	1583	1,70
Espatulenol	1603	1578	1,21
Outros constituintes			
Hexanal	804		0,05
(2E)-Hexenal	856	855	0,12
(4Z)-Hexenal	860	877	0,03
n-Hexanol	870	870	0,03
Heptanal	905	902	0,05
α -Acetato de Fenchil	1291	1220	0,19
Acetato de bornila	1345	1288	0,22
Monoterpenos hidrocarbonados			15,15
Monoterpenos oxigenados			1,32
Sesquiterpenos hidrocarbonados			38,37
Sesquiterpenos oxigenados			2,91
Outros constituintes			0,69
Rendimento do óleo essencial			0,35

¹ Índice de retenção encontrado na literatura² Índice de Kovats calculado³ Porcentagem do constituinte encontrado no óleo

VALIDADE DO CONTEÚDO DO INSTRUMENTO DE PESQUISA SOBRE QUESTÕES ÉTICAS NA CONDUÇÃO DA PANDEMIA DE COVID-19**CONTENT VALIDITY FOR THE RESEARCH INSTRUMENT REGARDING ETHICAL ISSUES IN HANDLING THE COVID-19 PANDEMIC****VALIDITAS ISI INSTRUMEN PENELITIAN TENTANG MASALAH ETIKA DALAM PENANGANAN PANDEMIK COVID-19**SURYADI, Taufik^{1*}; KULSUM, Kulsum²¹ Department of Forensic Medicine and Medicolegal, Faculty of Medicine, Universitas Syiah Kuala, Indonesia.² Department of Anaesthesiology and Intensive Care, Faculty of Medicine, Universitas Syiah Kuala, Indonesia.

* Corresponding author

e-mail: taufiksuryadi@unsyiah.ac.id

Received 12 August 2020; received in revised form 15 September 2020; accepted 26 September 2020

RESUMO

Na pandemia de COVID-19, o tratamento médico pode causar problemas éticos relacionados à disponibilidade de médicos, instalações hospitalares limitadas, problemas de exames de diagnósticos, equipamentos de proteção individual, falta de compreensão do público e falta de conscientização pública na prevenção e redução do risco de contratação do COVID-19. É necessária pesquisa relacionada a essas questões éticas, envolvendo médicos como sujeitos de pesquisa. Em todo estudo, é necessário um instrumento válido para responder ao problema de pesquisa. Um dos métodos de validade do instrumento é a validade de conteúdo. A validade de conteúdo é evidência essencial para apoiar a validade de uma ferramenta de medição, como um questionário para pesquisa. Este instrumento de pesquisa teve como objetivo determinar a capacidade dos médicos de identificar quatro princípios éticos básicos e suas atitudes em relação ao tratamento do COVID-19. Em um estudo de ética médica no tratamento da pandemia do COVID-19, um teste de validade de conteúdo foi realizado envolvendo 9 especialistas, sendo 5 bioeticistas e 4 especialistas do COVID-19. A validade de conteúdo foi realizada em 36 pontos de afirmações relacionadas a questões éticas que surgiram no manejo da pandemia COVID-19. Os resultados da validação dos 36 itens do enunciado obtiveram um IVC inicial de 0,646, mas foram eliminados 7 itens porque o CVR estava muito longe do valor crítico. Após a eliminação, havia 29 itens da afirmativa utilizados como instrumento de pesquisa com um IVC de 0,738. O valor médio da concordância entre os avaliadores nos itens do enunciado foi de 0,78, e o valor médio da proporção da relevância dos itens do enunciado foi de 0,83 (valor de recomendação 0,90). No teste de confiabilidade pelo método alfa de Cronbach, o valor do coeficiente de confiabilidade foi de 0,732 ($0,70 < r_i < 0,90$), pode-se afirmar que a validade de conteúdo do questionário é válida e confiável para este instrumento de pesquisa.

Palavras-chave: *validade de conteúdo, COVID-19, ética médica, instrumento de pesquisa.***ABSTRACT**

In the COVID-19 pandemic, medical handling can cause ethical problems related to the availability of doctors, limited hospital facilities, diagnostic test problems, personal protective equipment, lack of public understanding, and a lack of public awareness in preventing and reducing the risk of contracting COVID-19. Research is needed relating to these ethical issues by involving doctors as research subjects. In every study, a valid instrument is required to answer the research problem. One of the methods of instrument validity is content validity. Content validity is essential evidence to support the validity of a measuring tool such as a questionnaire for research. This research instrument aimed to determine the ability of doctors to identify four basic ethical principles and their attitudes towards handling COVID-19. In a study of medical ethics in managing the COVID-19 pandemic, a content validity test was carried out by involving 9 experts consisting of 5 bioethicists and 4 COVID-19 experts. The validity of the contents was carried out on 36 points of statements related to ethical issues that arose in handling the COVID-19 pandemic. The results of the validation of the 36 statement items obtained an initial CVI of 0.646, but 7 items were eliminated because the CVR was too far from the critical

value. After elimination, there were 29 statement items used as a research instrument with a CVI of 0.738. The average value of the agreement between the raters on the statement items was 0.78. The average value of the proportion of the relevance of the statement items was 0.83 (recommendation value 0.90). In the reliability test using the Cronbach's alpha method, the value of the reliability coefficient was 0.732 ($0.70 < r_i < 0.90$), it can be stated that the content validity of the questionnaire is valid and reliable for this research instrument.

Keywords: *content validity, COVID-19, medical ethics, research instrument*

ABSTRAK

Pada kondisi pandemic COVID-19, penanganan medik dapat menimbulkan masalah etika terkait ketersediaan dokter, keterbatasan fasilitas rumah sakit, masalah uji diagnostik, alat pelindung diri, kurangnya pemahaman masyarakat, serta kurangnya kepedulian masyarakat dalam mencegah dan mengurangi resiko tertular COVID-19. Diperlukan penelitian terkait isu etik tersebut dengan melibatkan dokter sebagai subjek penelitian. Dalam setiap penelitian dibutuhkan instrumen yang valid untuk menjawab masalah penelitian. Salah satu metode validitas instrumen adalah validitas isi. Validitas isi merupakan bukti esensial untuk mendukung validitas suatu alat ukur seperti kuesioner untuk penelitian. Instrumen penelitian ini bertujuan untuk mengetahui kemampuan dokter dalam mengidentifikasi empat prinsip dasar etika terkait COVID-19 dan sikapnya terhadap penanganan COVID-19. Dalam kajian masalah etika kedokteran dalam penanganan pandemi COVID-19 dilakukan uji validitas isi dengan melibatkan 9 orang ahli yang terdiri dari 5 ahli bioetika dan 4 ahli COVID-19. Validitas isi dilakukan terhadap 36 butir pernyataan terkait masalah etika yang muncul dalam penanganan pandemi COVID-19. Hasil validasi 36 item pernyataan diperoleh Content Validation Index (CVI) awal sebesar 0.646, tetapi 7 item dieliminasi karena Content Validation Ratio (CVR) terlalu jauh dari nilai kritis CVR. Setelah dilakukan eliminasi, terdapat 29 item pernyataan yang digunakan sebagai instrumen penelitian dengan CVI sebesar 0.738. Rata-rata nilai kesepakatan antar penilai pada item pernyataan adalah 0,78, dan nilai rata-rata proporsi relevansi item pernyataan adalah 0,83 (nilai rekomendasi 0.90). Pada uji reabilitas dengan menggunakan metode Cronbach's alpha didapatkan nilai koefisien reabilitas 0.732 ($0.70 < r_i < 0.90$), maka dapat dinyatakan bahwa validitas isi kuisioner ini valid dan reliabel untuk instrument penelitian ini.

Kata kunci: *validitas isi, COVID-19, etika kedokteran, instrumen penelitian*

1. INTRODUCTION:

Severe Acute Respiratory Syndrome Coronavirus 2 (SARS-CoV-2), originally named novel coronavirus or 2019-nCoV, is one of the single-stranded ribonucleic acid (RNA) viruses which are known to infect humans. This virus causes Coronavirus Disease 2019 (COVID-19), which is an infection of the lower respiratory tract that has the potential to cause the novel coronavirus (2019-nCov) - infected pneumonia (NCIP), which is severe and possibly fatal in humans. This pathogen was identified from the patient's throat swab sample. Types of diagnostic tests that can be performed currently being performed to detect coronavirus are reverse-transcription polymerase chain reaction (RT-PCR), real-time PCR (rRT-PCR), and reverse transcription loop-mediated isothermal amplification (RT-LAMP) (Nicola *et al.*, 2020; Harapan *et al.*, 2020; Jamil *et al.*, 2020).

COVID-19 was declared a pandemic on March 11, 2020 by the World Health Organization (WHO). Currently, the COVID-19 pandemic is the biggest challenge for the health sector worldwide (McGuire *et al.*, 2020). The handling of the COVID-19 pandemic has raised issues of

medical ethics that are of concern to all groups, including the general public (Montazeri, 2020). The spike in COVID-19 cases has overwhelmed health systems around the world. This increasing number of cases requires treatment in hospitals with limited facilities, the results of which may not be as expected, especially for patients with comorbidities or those over 80 years of age. (Xafis *et al.*, 2020).

From a public health view of point, the pandemic condition raises several ethical challenges in the form of public distrust of this pandemic condition, a lack of public knowledge about the dangers of this outbreak, and a lack of public awareness about the importance of preventing the spread of COVID-19 through several programs that have been delivered by health workers (Asghari and Tehrani, 2020). Several efforts to control the spread of COVID-19 were carried out with large-scale social restrictions, travel restrictions, social distancing, quarantine to lockdowns (Xafis *et al.*, 2020).

Issues related to medical ethics that arise include confirmed or probable COVID 19 patient who refuses to preventive, diagnostic and therapeutic measurement (Asghari and Tehrani, 2020), patients other than COVID-19 who are

rejected by the hospital because the hospital is full, particularly access to intensive care resources (Huxtable, 2020), personal information on COVID-19 patients, the spread of false information (Yusof *et al.*, 2020). This raises ethical challenges when the health system has reached its maximum capacity to handle the influx of patients during a pandemic (McGuire *et al.*, 2020).

In the spread of the COVID-19 pandemic throughout the region, in practice, there may be an inability to meet needs and spread it. A shortage of hospital beds, labor, medicine, and equipment is one of the limited resources in a pandemic. As the number of COVID-19 cases increases, discussions regarding ventilator allocation criteria have emerged in several countries. In making decisions about resource allocation, a balance between benefits and equity must be met. Increased balance in allocating ventilators for people who have a better chance of survival (Robert *et al.*, 2020).

The COVID-19 pandemic has caught the attention of both the medical community and the public, which has raised several problems not only related to medical but also related to medical ethics and humanities. The medical profession emphasizes ethical competence, morals, and medical professionalism. This is because these competencies will support the participation of health workers in patient safety, which is central to better medical services (Suryadi and Kulsum, 2020).

Seeing the importance of physician's knowledge regarding ethical issues in handling the COVID-19 pandemic, research on this topic is needed. To be able to do research, a valid instrument is needed so that the research results can be accounted for scientifically (Yusoff, 2019). One of the instrument validity tests is done by using content validity. Content validity is carried out by expert panels that understand the research problem (Cabatan *et al.*, 2020). Some literature requires a minimum of 5 experts to validate the instrument (Rodrigues *et al.*, 2017; Cabatan *et al.*, 2020).

Content validity is an instrument content validation technique by assessing the relevance of the questions or statements in the questionnaire to be filled in by the respondent. The results of the content validity are beneficial for researchers in ensuring that the questionnaire is following the questions, objectives and benefits of the study (Rodrigues *et al.*, 2017; Yusoff, 2019).

This paper aimed to address the following research objectives: (1) to develop a

questionnaire that will describe the relationship between a knowledge of physician regarding ethical issues and their attitude in handling the COVID-19 pandemic, (2) to determine the content validity of the questionnaire.

2. MATERIALS AND METHODS:

This study used an instrument development design to develop and determine the content validity of the questionnaire (see Appendix). The steps in determining content validity can be carried out in six stages, namely: (1) preparing content validity forms, (2) determining experts who will review content validity, (3) asking reviewers to assess the relevance of statement items, (4) reviewing domain and items, (5) determining the score of each statement item, (6) calculating Item Content Validity Index (I-CVI), Scale Content Validity Index (S-CVI), Content Validity Ratio (CVR), and Content Validity Index (CVI) (Yusoff, 2019; Cabatan *et al.*, 2020).

2.1. Preparing content validity form

The purpose of the instrument was to develop a comprehensive tool to describe the ability of a physician to identify ethical issues in handling COVID-19. The content validity form consists of 3 parts, namely the first part about statement items regarding ethical issues in handling COVID-19, the second part about four basic ethical principles (beneficence, non-maleficence, justice and autonomy), and the third part regarding the statement of the respondent's attitude towards the issues with a 5-point Likert scale, namely the value 1 = *strongly disagree*, 2 = *disagree*, 3 = *doubtful*, 4 = *agree*, 5 = *strongly agree*.

The content validity form is structured so that reviewers easily understand the contents of the questionnaire and can provide appropriate assessments and make suggestions for correcting sentences in the questionnaire. Instructions for filling in content validity, reviewers are asked to provide an assessment of the parameters/item statements by looking at the relevance (suitability) with existing aspects. For the relevancy scale, a 4-point Likert scale was used. The rating ranges from 1 to 4 with the following details: value 1 = *not relevant*, 2 = *somewhat relevant*, 3 = *quite relevant*, 4 = *very relevant*. Ratings of 1 and 2 are considered content invalid while ratings of 3 and 4 are considered content valid (Rodrigues *et al.*, 2017; Zamanzadeh *et al.*, 2017, Amaya *et al.*, 2016).

2.2. Determining experts who will review content validity

The selection of who will review and criticize the validity of the content of the research instrument is usually determined by looking at professional skills and research-related expertise (Yusoff, 2019). The experts were selected based on the following criteria: (1) holder of a master's or doctoral degree, (2) specialist or consultant in medicine, (3) five or more years of academic faculty experience, (4) had experience in the field of bioethics and had possessed national certificate as bioethics teacher, (5) had experience in handling COVID-19 pandemic (Cabatan *et al.*, 2020). In this study, content validation was carried out by involving 9 experts experienced in their fields (4 people from outside the institution where the research was carried out) consisting of 5 bioethicists and 4 medical experts in handling COVID-19. The characteristics of the 9 experts can be seen in table 1.

2.3. Asking reviewers to assess the relevance of statement items

In this questionnaire content validity test was carried out using an online system. The researcher sent the questionnaire content validity form via email or other social media. Researchers provide information related to the research conducted and ask the experts for approval to participate as validators. Before assessing the relevance of the research instrument, the researcher explains the research questions, the objectives, and the benefits of the research. In the content validity assessment carried out, experts have agreed verbally and are willing to fill in and validate the statement items in the content validation form. Experts are given the freedom to provide their views regarding the relevance of each item and are also asked to give suggestions for improvements both in grammar and the content of the statement (Masuwai *et al.*, 2016).

2.4. Reviewing domain and items

In this study, an assessment of a questionnaire that will describe the relationship between a knowledge of physician regarding ethical issues and their attitude in handling the COVID-19 pandemic was conducted. In the content validity form, an explanation has been given about what the experts should judge. Experts provide comments on each questionnaire statement according to their expertise. On the validity of the contents of this questionnaire, the experts provided an opinion on ethical issues that

arose in each statement item. Experts write their suggestions in the column that has been provided. These suggestions are used to improve the relevance of the questionnaire content (Zamanzadeh *et al.*, 2017). Some of the corrections needed to improve the questionnaire content consisted of grammatical suitability, clarification of confusing terms, correction of word choice, correction of sentence structure, the suitability of letter size, and suitability of the structure of the questionnaire content. (Masuwai *et al.*, 2016).

2.5. Determining the score of each statement item

To complete the review that has been carried out, the experts are requested to determine the score of each statement item. After the experts have finished reviewing the contents of the questionnaire, the experts are requested to send the review results to the researcher (Yusoff, 2019). Each item is declared valid if more than 70% of the number of experts assesses the content of the statement as relevant to the research objectives (Amaya *et al.*, 2016).

2.6. Calculating I-CVI, CVR, and CVI

By looking at the degree of agreement of all reviewers for each item of the questionnaire statement. Cohen's Kappa index (CKI) can be determined. CKI is often referred to as the inter-rater agreement, most easily indicated by a percentage (Masuwai *et al.*, 2016). CKI also has the same meaning as the item Content Validity Index (I-CVI) (Yusoff, 2019).

In determining the validity of the instrument, it was carried out using the content validity ratio (CVR) according to Lawshe equation. CVR is a method that aims to find out whether a test is valid so that it can measure what we want to measure. Equation 1 is used to calculate the Lawshe CVR:

$$CVR = \frac{ne - \frac{N}{2}}{\frac{N}{2}} \quad (\text{Eq.1})$$

Information: ne = number of experts who agree; N = The number of all validating experts. Based on this equation, the CVR value for each point can be obtained. The meaning of this Lawshe equation is: If the validator who agrees is less than half of the total number of validators, the CVR value is negative; if the validator who agrees is precisely half of the total number of validators, the CVR value is zero; and if the validator who agrees is more than half of the total

number of validators, the CVR value is between 0 – 1 (Hendryadi, 2017; Rodrigues *et al.*, 2017).

Each point is accepted if the point has a value greater than the critical value of CVR and/or greater than I-CVI. The CVR value obtained from the calculation results were compared with the critical value of the CVR based on the number of validators as listed in Table 2. (Ayre and Scally, 2014; Bashooir and Supahar, 2018).

Table 2. CVR Critical Value (one-tailed, $\alpha = 0,05$)

Number of Validators	Proportion agreeing essential (I-CVI)	CVR Critical Value
5	1	1
6	1	1
7	1	1
8	0,875	0,775
9	0,889	0,778
10	0,900	0,800

After identifying each point using CVR, then calculating the CVI, which is the average of the CVR value. The CVI was calculated using equation 2:

$$CVI = \frac{\sum CVR}{\text{Number of test items}} \quad (\text{Eq. 2})$$

3. RESULTS AND DISCUSSION:

3.1. Identification of ethical issues

Identification of ethical issues based on the four basic principles of ethics is beneficence, non-maleficence, justice, and autonomy. These principles have a profound effect, not only in medical ethics academically but also in their application in clinical situations to make ethical clinical decisions. Recognizing ethical issues will make it easier for doctors to deal with difficult situations and get through them well and correct according to relevant ethical principles (Henky, 2018). According to the assessment by the panelist, ethical issues related to the COVID-19 pandemic can be seen in Table 3.

Table 3. Basic ethical principles

Basic ethical principles	Number of statement items
Beneficence	S1,S2,S4,S5,S6,S8,S9
Non-maleficence	S10,S14,S15,S21
Justice	S7,S12,S16,S17,S18,S19, S20,S22,S23,S24,S25,S26, S27,S29,S30,S34
Autonomy	S3,S11,S13,S28,S31,S32, S33,S35,S36

Panelists grouped the four basic principles of ethics based on the suitability of statement items with each basic ethical principle (Page, 2012). The principle of beneficence is always related to kindness, providing benefits, convenience, affection and attention. The principle of non-maleficence relates to preventing risk, harm, damage, loss, or injury. The principle of justice relates to justice, equal rights, protection against discrimination, abuse, disease transmission, and several things related to the social context. The principle of autonomy talks about respect for human dignity, protection of vulnerable people, and granting the right to individual freedom (Afandi, 2017; Page, 2012; Pozgar, 2020).

In the context of handling the COVID-19 pandemic, many things are related to ethics, including discrimination and stigmatization of patients infected with COVID-19, patient rejection by community members, and information that is not following reality (Yusof *et al.*, 2020). From the hospital side, ethical problems that arise are limited human resources and facilities and lack of personal protective equipment (McGuire *et al.*, 2020).

3.2. Item Content Validity Index (I-CVI) and Scale Content Validity Index (S-CVI)

Content validity was determined by calculating for I-CVI and S-CVI from an experts rating (Cabatan *et al.*, 2020). I-CVI is the number of experts who agree divided by the number of experts (Yusoff, 2019; Rodrigues *et al.*, 2017). The I-CVI should be 0.889 or higher, with nine experts. I-CVI lower than 0.889 were deleted or revised (Ayre and Scally, 2014; Bashooir and Supahar, 2018; Cabatan *et al.*, 2020).

In the study, for the I-CVI calculation, twenty-nine items (80,56%) were marked as appropriate (17 items are valid and 12 items need to be revised), and the I-CVI's ranged from 0.44-1.00. Eight items had an I-CVI = 1.00, nine a score of 0.89, twelve a score of 0.78, six a score

of 0.67, and one a score of 0.44. Value range from 0 to 1 where I-CVI > 0.79, the item is relevant, between 0.70 and 0.79, the item needs revision, and if the value is below 0.70, the item is eliminated (Rodrigues *et al.*, 2017).

The S-CVI is the average of I-CVI of all items of the scale. S-CVI 0.90 or more for a scale to have excellent content validity is recommended (Cabatan *et al.*, 2020; Rodrigues *et al.*, 2017; Yusoff *et al.*, 2019). The value of relevance and agreement of each statement item can be seen in table 4. In Table 4, it is obtained that the average agreement value of all experts on statement items (S-CVI/ave) based on I-CVI is 0.78, and the average value of the proportion of relevance to statement items is 0.83.

3.3. Content Validity Ratio (CVR) and Content Validity Index (CVI)

All content validity (CVR and CVI) calculations can be seen in Table 5. For the CVR calculation, twenty-nine items (80,56%) were marked as remained (17 items are valid and 12 items need to be revised), and the CVR ranged from -0.11-1.00. Eight items had a CVR = 1.00, nine a score of 0.78, twelve a score of 0.56, six a score of 0.33, and one a score of -0.11. The CVR should be 0.778 or higher, with nine experts. CVR lower than 0.778 was deleted or revised (Ayre and Scally, 2014; Bashooir and Supahar, 2018).

In addition to calculating the CVR of each statement item, we also must calculate the CVI value. CVI value is the average result of the CVR value, namely 0.646. After calculating the CVR and I-CVI of each item, the results were several statement items that had to be eliminated even though, in fact, according to the researcher, the statement item was essential to answer the research question (can be seen in Table 6). These results indicate that of the 36 statements, there are 7 statements must be eliminated because the CVR and I-CVI are too small than the critical value (0,778). After 7 statements item was eliminated, CVI value is to be 0,738, and the S-CVI value is to be 0.814. From this CVI value, it can be stated that the instrument content validity is a high level.

3.4. Reliability test

One way to determine the reliability of the instrument is to determine the alpha coefficient value. Alpha reliability has a value range of 0 to 1, provided that an instrument is considered reliable if in preliminary research the reliability value of alpha is 0.70, in basic research is 0.80

and in medical research is 0.95 (Bashooir and Supahar, 2018). When using the Cronbach's alpha coefficient, the instrument is considered to be reliable if the coefficient value is between 0.70 to 0.90 (Yusup, 2018). In this study, the Cronbach's alpha coefficient value was 0.732, so it can be stated that the research instrument is reliable.

4. CONCLUSIONS:

The validation of the research instrument in the form of a questionnaire using the content validity conducted and assessed by experts had many advantages and the potential to be developed in various studies because the results of this validation were of very high quality. In this study, the validity of the contents of the questionnaire was found to be high in terms of the CVI value. To support the increase in content validity, it is necessary a reliability test was also obtained. With high-level content validity, it can make it easier for researchers to prepare their research, which, of course, will produce quality scientific work.

5. ACKNOWLEDGMENTS

We express our gratitude to the content experts who shared their time and expertise.

6. ETHICAL STATEMENT

Consent to participate has been obtained from the experts was verbally

7. COMPETING INTEREST

The authors declare that there are no competing interests related to the study

8. FUNDING

This study did not require funding

9. REFERENCES:

1. Nicola, M., O'Neill, N., Sohrabi, C., Khan, M., Agha, M., and Agha, R. (2020). Evidence- based management guideline for the COVID-19 pandemic - Review article. *Int J Surg*, 77, 206–216. Available from: <https://doi.org/10.1016/j.ijsu.2020.04.001>
2. Harapan, H., Itoh, N., Yufika, A., Winardi, W., Keam, S., Te, H., Megawati, D.,

- Hayati, Z., Wagner, A. L., and Mudatsir, M. (2020). Coronavirus disease 2019 (COVID-19): A literature review. *J Infect Public Health* [Internet], 13(5):667–73. Available from: <https://doi.org/10.1016/j.jiph.2020.03.019>.
3. Jamil, K. F., Winardi, W., Yufika, A., Anwar, S., Librianty, N., Prashanti, N. A. P., Sari, T. N. W., Utomo, P. S., Dwiamelia, T., Natha, P. P. C., Salwiyadi, S., Asrizal, F. W., Ikram, I., Wulandari, I., Haryanto, S., Fenobileri, N., Wagner, A. L., Mudatsir, M., and Harapan, H. (2020). Knowledge of coronavirus disease 2019 (COVID-19) among healthcare providers: A cross-sectional study in Indonesia. *Asia Pacific J Trop Med*, 13(9): 402-408.
 4. McGuire, A. L., Aulisio, M. P., Davis, F. D., Erwin, C., Harter, T. D., Jagsi, R., Klitzman, R., Maccauley, R., Racine, E., Wolf, S. M., Wynia, M., Wolpe, P.R., and The COVID-19 Task Force of the Association of Bioethics Program Directors (APBD). (2020). Ethical challenges arising in the COVID-19 pandemic: an overview from the Association of Bioethics Program Directors (ABPD) task force. *The American Journal of Bioethics*, 1-13.
 5. Montazeri, A. (2020). Some ethical concerns related to the Coronavirus disease 2019 (COVID-19). *Med J Islam Repub Iran*, 34, 53.
 6. Xafis, V., Schaefer, G. O., Labude, M. A., Zhu, Y., and Hsu, L.Y. (2020). The perfect moral storm; Diverse ethical consideration in the COVID-19. *Asian Bioethics Review*, 12, 65-83.
 7. Asghari, F., and Tehrani, S. S. (2020). Ethical issues responding to the COVID-19 pandemic; a narrative review. *Adv J Emerg Med*, 4(2s): e60.
 8. Huxtable, R. (2020). COVID -19: where is the national ethical guidance?. *BMC Medical Ethics*, 21(32), 1-3.
 9. Yusof, A. N. M., Muuti, M. Z., Ariffin, L. A., Tan, M. K. M. (2020). Sharing information on COVID-19: the ethical challenges in the Malaysian setting, *Asian Bioethics Review* 1-13.
 10. Robert, R., Barnes, N. K., Boyer, A., Laurent, A., Azoulay, E., and Reignier, J. (2020). Ethical dilemmas due to the COVID-19 pandemic. *Ann Intensive Care*, 10:84, 1-9.
 11. Suryadi, T., and Kulsum, K. (2020). Medical humanities in clinical rotation of forensic medicine and other clinical setting. *Britain Int Humanit Soc Sci J*;2:421–428.
 12. Yusoff, M. S. B. (2019). ABC of content validation and content validity index calculation. *Education in Medical Journal*, 11(2): 49-54.
 13. Cabatan, M. C. C., Grajo, L. N., and Sana, E. A. (2020). Development and content validation of the adaptation process in academia questionnaire for occupational therapy educators. *Acta Medica Philippina*, 54(2), 142-150.
 14. Rodrigues, I. B., Adachi, J. D., Beattie, K. A., and MacDermid, J. C. (2017). Development and validation of a new tool to measure the facilitators, barriers and preferences to exercise in people with osteoporosis. *BMC Musculoskeletal Disorders*, 18:504, 1-9.
 15. Zamanzadeh, V., Ghahramanian, A., Rassaoili, M., Abbaszadeh, A., Majd, H. A., and Nikanfar, A. R. (2015). Design and implementation content validity study: Development of an instrument for measuring patient-centered communication. *Journal of Caring Sciences*, 4(2), 165-178.
 16. Amaya, M. A., Paixao D. P. S. S., Sarquis, L. M. M., and Cruz, E. D. A. (2016). Construction and content validation of checklist for patient safety in emergency care. *Rev Gaucha Enferm*, 37 (spe), 1-8.
 17. Masuwai, A., Tajudin, N. M., and Saad, N. S. (2016). Evaluating the face and content validity of teaching and learning guiding principles instrument (TLGPI): a perspective study of Malaysia teacher educators. *Malaysian J Society and Space*, 12, issue 3, 11-21.

18. Hendryadi, H. (2017). Content validity: Initial stage of questionnaire development. *Journal of Management and Business Research*, 2(2), 169-178.
19. Ayre, C., and Scally, A. J. (2014). Critical value for Lawshe's content validity ratio: Revisiting the original methods of calculation. *Measurement and Evaluation in Counseling and Development*, 47(1), 79-86.
20. Bashooir, K., and Supahar, S. (2018). The validity and reliability of the STEM-based science literacy performance assessment instrument. *Journal of educational research and evaluation*, 22(2), 219-222.
21. Henky, H. (2018). Clinical Ethics Services. *Indones J Medical Ethics*; 2(2), 59.
22. Page, K. (2012). The four principles: Can they be measured, and do they predict ethical decision making?. *BMC Med Ethics*, 13:10, 1-8.
23. Afandi, D. (2017) The basic principles of bioethics in ethical clinical decision making. *Andalas Med J*, 40:2, 111-121.
24. Pozgar, G.D. (2020). Legal and ethical issues for health professions. 5th Ed. *Jones & Bartlett Learning*; 443.
25. Yusup, F. (2018). Test the validity and reliability of quantitative research instruments. *Tarbiyah Journal: Journal of education science*, 7(1), 17-23.

Table 1. Characteristics of CVR test panelists.

No.	Expertise	Field to be reviewed	Institution
1.	Doctor of Bioethics and Medical Humanities	Ethical issues	Universitas Jendral Soedirman
2.	Doctor of Bioethics and Master of Medical Education	Ethical issues	Universitas Pembangunan Nasional
3.	Doctor of Bioethics and Forensic Medicine Specialist, Ethics and Medicolegal Consultant	Ethical issues	Universitas Indonesia
4.	Doctor of Medical Science and Obstetrician Gynaecologist, Consultant	Ethical issues	Universitas Muslim Indonesia
5.	Doctor of Medical Education, Master of Disaster Management	Ethical issues	Universitas Syiah Kuala
6.	Doctor of Medical Sciences and Pulmonologist and Respiratory Medicine, Consultant	Medical aspect of COVID-19	Universitas Syiah Kuala
7.	Anaesthesiology and Intensive Care Specialist, Neuro-Anaesthesiologist Consultant	Medical aspect of COVID-19	Universitas Syiah Kuala
8.	Chair of the Task Force Handling COVID-19 and an Anatomy-Histologist	Medical aspect of COVID-19	Universitas Syiah Kuala
9.	Member of the Task Force Handling COVID-19 and Microbiologist, Tropical Disease Expert	Medical aspect of COVID-19	Universitas Syiah Kuala

Table 4. The value of relevance and agreement of each statement item

Items	Expert 1	Expert 2	Expert 3	Expert 4	Expert 5	Expert 6	Expert 7	Expert 8	Expert 9	I-CVI
S1	4	3	4	4	4	4	4	4	4	1,00
S2	1	3	4	4	4	4	4	4	4	0,89
S3	4	3	1	3	4	4	4	4	4	0,89
S4	4	4	4	4	4	4	4	4	4	1,00
S5	4	3	2	3	4	4	3	4	4	0,89
S6	1	2	3	3	4	4	3	4	4	0,78
S7	1	3	1	3	4	4	2	4	4	0,67
S8	2	2	1	2	4	4	4	1	4	0,44
S9	1	4	1	4	4	4	4	4	4	0,78
S10	4	4	1	3	4	4	4	4	4	0,89
S11	4	4	1	3	4	4	4	3	4	0,89
S12	4	4	2	3	4	4	4	3	4	0,89
S13	2	3	2	4	4	4	4	4	4	0,78
S14	2	3	2	4	4	4	4	1	4	0,67
S15	1	2	3	3	4	4	4	3	4	0,78
S16	1	4	2	3	2	4	4	4	4	0,78
S17	1	4	2	4	2	4	4	4	4	0,67
S18	1	4	2	4	2	4	4	4	4	0,67
S19	3	4	1	3	2	4	4	4	3	0,78
S20	3	4	1	3	2	4	4	4	4	0,78
S21	4	4	2	3	4	4	3	4	4	0,89
S22	3	3	3	3	4	4	4	4	4	1,00
S23	1	3	1	3	4	4	4	4	4	0,78
S24	2	3	4	3	2	4	4	4	3	0,78
S25	1	3	4	3	2	4	4	4	4	0,78
S26	3	3	4	3	2	4	4	4	4	0,89
S27	2	3	4	3	2	4	4	4	4	0,78
S28	4	4	4	3	4	4	4	4	4	1,00
S29	3	4	1	2	4	4	4	4	4	0,78
S30	3	4	1	2	4	4	4	1	3	0,67
S31	3	4	1	3	4	4	4	4	4	0,89
S32	4	4	4	3	4	4	4	4	4	1,00
S33	4	4	4	3	4	4	3	4	4	1,00
S34	3	4	3	3	4	4	4	4	4	1,00
S35	3	4	4	3	4	4	4	4	4	1,00
S36	3	4	4	3	4	4	4	4	4	1,00
S-CVI/ave: The average agreement value of all experts on statement items based on I-CVI										0,78
Proportion Relevance	0,58	0,92	0,44	0,92	0,69	1,00	0,97	0,92	1,00	
S-CVI/ave based on the average proportion of items judges as relevance across the nine experts										0,83

Table 5. Content Validity Ratio and Item-Content Validity Index

Item No.	Statement Items	Relevant (rating 3 or 4)	Not relevant (rating 1 or 2)	Number of agreement (Ne)	CVR	I-CVI	Interpretation
S1	Doctors who are not equipped with complete personal protective equipment (PPE) have the right to refuse to examine patients suspected of having COVID-19.	9	0	9	1	1,00	Appropriate
S2	Doctors who are not equipped with personal protective equipment (PPE) have the right to refuse to treat patients suspected of having COVID-19.	8	1	8	0,78	0,89	Appropriate
S3	Doctors may notify patient data to the general public to prevent the spread of COVID-19.	8	1	8	0,78	0,89	Appropriate
S4	The doctor has the right to ask about the patient's travel history for tracking purposes	9	0	9	1	1,00	Appropriate
S5	During a pandemic, using drugs on the market to treat COVID -19 patients is allowed even without going through the clinical trial stage.	8	1	8	0,78	0,89	Appropriate
S6	During a pandemic, taking drugs on the market to treat COVID -19 patients isolated independently in their homes is allowed even without a doctor's prescription.	7	2	7	0,56	0,78	Appropriate but need for revision
S7	Doctors who receive incentives (additional income) for treating COVID -19 patients do not violate the medical code of ethics.	6	3	6	0,33	0,67	Eliminated
S8	Doctors who transmit COVID-19 to their patients (who were not previously COVID-19 patients) receive ethical sanctions	5	4	4	-0,11	0,44	Eliminated
S9	Doctors have the right to receive protection while working during the COVID-19 pandemic	7	2	7	0,56	0,78	Appropriate but need for revision
S10	The doctor has the right to ask someone who is categorized as a suspect	8	1	8	0,78	0,89	Appropriate

	or close contact with a probable/confirmed COVID-19 person to self-isolate.						
S11	A person categorized as a suspect or in close contact with a probable/confirmed COVID -19 person has the right to refuse self-isolation.	8	1	8	0,78	0.89	Appropriate
S12	A person categorized as a suspect or in close contact with a probable/confirmed COVID -19 person who does not want to perform self-isolation may be forcibly picked up.	8	1	8	0,78	0,89	Appropriate
S13	A person who has been confirmed as COVID-19 and refuses to be treated can be forced into isolation.	7	2	7	0,56	0,78	Appropriate but need for revision
S14	A person who has been confirmed COVID -19 can be forcibly picked up to be hospitalized.	6	3	6	0,33	0.67	Eliminated
S15	Someone who has symptoms similar to COVID-19 but there is no result of the swab being treated for COVID-19	7	2	7	0,56	0,78	Appropriate but need for revision
S16	Screening of body temperature in all public service places is needed to reduce the risk of spreading COVID-19	6	3	6	0,33	0,67	Eliminated
S17	Washing your hands with soap or hand sanitizer is needed to reduce the risk of spreading COVID-19	6	3	6	0,33	0,67	Eliminated
S18	Wearing masks at all public service places is necessary to reduce the risk of spreading COVID-19	6	3	6	0,33	0,67	Eliminated
S19	People who reject COVID-19 patients in their environment are violating social ethics	7	2	7	0,56	0,78	Appropriate but need for revision
S20	People who reject the dead bodies of COVID-19 patients are violating social ethics	7	2	7	0,56	0,78	Appropriate but need for revision
S21	COVID-19 vaccine trials can be carried out directly on humans.	8	1	8	0,78	0,89	Appropriate

S22	New non- COVID-19 patients should not be hospitalized because hospitals need a place to treat COVID-19 patients	9	0	9	1	1,00	Appropriate
S23	Non- COVID-19 patients who have been hospitalized should be discharged because hospitals need a place to treat COVID-19 patients	7	2	7	0,56	0,78	Appropriate but need for revision
S24	All rapid tests / RT-PCR should be made free so that all people can be examined for COVID-19 detection	7	2	7	0,56	0,78	Appropriate but need for revision
S25	COVID-19 and non-COVID-19 patients deserve the same treatment	7	2	7	0,56	0,78	Appropriate but need for revision
S26	Allocation of funding for health services is prioritized for COVID-19 patients	8	1	8	0,78	0,89	Appropriate
S27	Changes in professional care providers such as doctors, nurses and other health workers for COVID-19 patients are carried out regularly according to needs	7	2	7	0,56	0,78	Appropriate but need for revision
S28	Residents with a high risk of contracting COVID-19 have the right to refuse the rapid test / RT-PCR.	9	0	9	1	1,00	Appropriate
S29	COVID-19 patients who have a history of comorbid diseases are prioritized for hospitalization.	7	2	7	0,56	0,78	Appropriate but need for revision
S30	COVID-19 patients with a weak economic level are prioritized for hospitalization.	6	3	6	0,33	0,67	Eliminated
S31	COVID-19 patients who are elderly are prioritized for getting treatment at the hospital.	8	1	8	0,78	0,89	Appropriate
S32	Each person has the right to use or not use masks during a COVID-19 pandemic because this is an individual's autonomous right.	9	0	9	1	1,00	Appropriate
S33	Personal data of COVID-19 patients may be published.	9	0	9	1	1,00	Appropriate

S34	Lockdowns during a COVID-19 pandemic violate the rights of individual freedoms.	9	0	9	1	1,00	Appropriate
S35	Families of COVID-19 patients can forcibly bring COVID-19 patients home.	9	0	9	1	1,00	Appropriate
S36	Families of COVID-19 patients can forcibly take the dead bodies of COVID-19 patients.	9	0	9	1	1,00	Appropriate
CVR and CVI values for the 36 initial statement items					\sum CVR= 23,27	\sum I- CVI= 28,08	CVI= 0,646, and S-CVI= 0.780
CVR and CVI values after 7 statements are eliminated					\sum CVR (ae)= 21,40	\sum I- CVI (ae)= 23,62	CVI (ae)= 0,738, and S-CVI (ae) = 0,814

Table 6. List of eliminated statement

Items	Statements item was eliminated	Panelist comment
S7	Doctors who receive incentives (additional income) for treating COVID -19 patients do not violate the medical code of ethics.	Too obvious
S8	Doctors who transmit COVID-19 to their patients (who were not previously COVID-19 patients) receive ethical sanctions	Debatable
S14	A person who has been confirmed COVID -19 can be forcibly picked up to be hospitalized.	The essence of the statement is the same as the previous question
S16	Screening of body temperature in all public service places is needed to reduce the risk of spreading COVID-19	Tend to be medical, not ethical.
S17	Washing your hands with soap or hand sanitizer is needed to reduce the risk of spreading COVID-19	Tend to be medical, not ethical.
S18	Wearing masks at all public service places is necessary to reduce the risk of spreading COVID-19	Tend to be medical, not ethical.
S30	COVID-19 patients with a weak economic level are prioritized for hospitalization.	Ethical issues become clearer if reasons are added

QUESTIONNAIRE SHEET

1. Respondent data

- a. Serial number :
 b. Place of duty :
 c. Gender :
 d. Age :

2. Questionnaires

Choose the answer that suits your opinion by putting a cross mark (X) on the available answer choices.

Item No.	Statement Items	The relevancy scale	What ethical principles are contained in the statement?	What is your attitude towards that statement?
S1	Doctors who are not equipped with complete personal protective equipment (PPE) have the right to refuse to examine patients suspected of having COVID-19.	<input type="checkbox"/> Not relevant <input type="checkbox"/> Somewhat relevant <input type="checkbox"/> Quite relevant <input type="checkbox"/> Very relevant	<input type="checkbox"/> Beneficence <input type="checkbox"/> Nonmaleficence <input type="checkbox"/> Justice <input type="checkbox"/> Autonomy	<input type="checkbox"/> Strongly disagree <input type="checkbox"/> Disagree <input type="checkbox"/> Doubtful <input type="checkbox"/> Agree <input type="checkbox"/> Strongly agree
S2	Doctors who are not equipped with personal protective equipment (PPE) have the right to refuse to treat patients suspected of having COVID-19.	<input type="checkbox"/> Not relevant <input type="checkbox"/> Somewhat relevant <input type="checkbox"/> Quite relevant <input type="checkbox"/> Very relevant	<input type="checkbox"/> Beneficence <input type="checkbox"/> Nonmaleficence <input type="checkbox"/> Justice <input type="checkbox"/> Autonomy	<input type="checkbox"/> Strongly disagree <input type="checkbox"/> Disagree <input type="checkbox"/> Doubtful <input type="checkbox"/> Agree <input type="checkbox"/> Strongly agree
S3	Doctors may notify patient data to the general public to prevent the spread of COVID-19.	<input type="checkbox"/> Not relevant <input type="checkbox"/> Somewhat relevant <input type="checkbox"/> Quite relevant <input type="checkbox"/> Very relevant	<input type="checkbox"/> Beneficence <input type="checkbox"/> Nonmaleficence <input type="checkbox"/> Justice <input type="checkbox"/> Autonomy	<input type="checkbox"/> Strongly disagree <input type="checkbox"/> Disagree <input type="checkbox"/> Doubtful <input type="checkbox"/> Agree <input type="checkbox"/> Strongly agree
S4	The doctor has the right to ask about the patient's travel history for tracking purposes	<input type="checkbox"/> Not relevant <input type="checkbox"/> Somewhat relevant <input type="checkbox"/> Quite relevant <input type="checkbox"/> Very relevant	<input type="checkbox"/> Beneficence <input type="checkbox"/> Nonmaleficence <input type="checkbox"/> Justice <input type="checkbox"/> Autonomy	<input type="checkbox"/> Strongly disagree <input type="checkbox"/> Disagree <input type="checkbox"/> Doubtful <input type="checkbox"/> Agree <input type="checkbox"/> Strongly agree
S5	During a pandemic, using drugs on the market to treat COVID -19 patients is allowed even without going through the clinical trial stage.	<input type="checkbox"/> Not relevant <input type="checkbox"/> Somewhat relevant <input type="checkbox"/> Quite relevant <input type="checkbox"/> Very relevant	<input type="checkbox"/> Beneficence <input type="checkbox"/> Nonmaleficence <input type="checkbox"/> Justice <input type="checkbox"/> Autonomy	<input type="checkbox"/> Strongly disagree <input type="checkbox"/> Disagree <input type="checkbox"/> Doubtful <input type="checkbox"/> Agree <input type="checkbox"/> Strongly agree
S6	During a pandemic, taking drugs on the market to treat	<input type="checkbox"/> Not relevant <input type="checkbox"/> Somewhat relevant	<input type="checkbox"/> Beneficence <input type="checkbox"/> Nonmaleficence	<input type="checkbox"/> Strongly disagree <input type="checkbox"/> Disagree

	COVID -19 patients isolated independently in their homes is allowed even without a doctor's prescription.	<input type="checkbox"/> Quite relevant <input type="checkbox"/> Very relevant	<input type="checkbox"/> Justice <input type="checkbox"/> Autonomy	<input type="checkbox"/> Doubtful <input type="checkbox"/> Agree <input type="checkbox"/> Strongly agree
S7	Doctors who receive incentives (additional income) for treating COVID -19 patients do not violate the medical code of ethics.	<input type="checkbox"/> Not relevant <input type="checkbox"/> Somewhat relevant <input type="checkbox"/> Quite relevant <input type="checkbox"/> Very relevant	<input type="checkbox"/> Beneficence <input type="checkbox"/> Nonmaleficence <input type="checkbox"/> Justice <input type="checkbox"/> Autonomy	<input type="checkbox"/> Strongly disagree <input type="checkbox"/> Disagree <input type="checkbox"/> Doubtful <input type="checkbox"/> Agree <input type="checkbox"/> Strongly agree
S8	Doctors who transmit COVID-19 to their patients (who were not previously COVID-19 patients) receive ethical sanctions	<input type="checkbox"/> Not relevant <input type="checkbox"/> Somewhat relevant <input type="checkbox"/> Quite relevant <input type="checkbox"/> Very relevant	<input type="checkbox"/> Beneficence <input type="checkbox"/> Nonmaleficence <input type="checkbox"/> Justice <input type="checkbox"/> Autonomy	<input type="checkbox"/> Strongly disagree <input type="checkbox"/> Disagree <input type="checkbox"/> Doubtful <input type="checkbox"/> Agree <input type="checkbox"/> Strongly agree
S9	Doctors have the right to receive protection while working during the COVID-19 pandemic	<input type="checkbox"/> Not relevant <input type="checkbox"/> Somewhat relevant <input type="checkbox"/> Quite relevant <input type="checkbox"/> Very relevant	<input type="checkbox"/> Beneficence <input type="checkbox"/> Nonmaleficence <input type="checkbox"/> Justice <input type="checkbox"/> Autonomy	<input type="checkbox"/> Strongly disagree <input type="checkbox"/> Disagree <input type="checkbox"/> Doubtful <input type="checkbox"/> Agree <input type="checkbox"/> Strongly agree
S10	The doctor has the right to ask someone who is categorized as a suspect or close contact with a probable/confirmed COVID-19 person to self-isolate.	<input type="checkbox"/> Not relevant <input type="checkbox"/> Somewhat relevant <input type="checkbox"/> Quite relevant <input type="checkbox"/> Very relevant	<input type="checkbox"/> Beneficence <input type="checkbox"/> Nonmaleficence <input type="checkbox"/> Justice <input type="checkbox"/> Autonomy	<input type="checkbox"/> Strongly disagree <input type="checkbox"/> Disagree <input type="checkbox"/> Doubtful <input type="checkbox"/> Agree <input type="checkbox"/> Strongly agree
S11	A person categorized as a suspect or in close contact with a probable/confirmed COVID -19 person has the right to refuse self-isolation.	<input type="checkbox"/> Not relevant <input type="checkbox"/> Somewhat relevant <input type="checkbox"/> Quite relevant <input type="checkbox"/> Very relevant	<input type="checkbox"/> Beneficence <input type="checkbox"/> Nonmaleficence <input type="checkbox"/> Justice <input type="checkbox"/> Autonomy	<input type="checkbox"/> Strongly disagree <input type="checkbox"/> Disagree <input type="checkbox"/> Doubtful <input type="checkbox"/> Agree <input type="checkbox"/> Strongly agree
S12	A person categorized as a suspect or in close contact with a probable/confirmed COVID -19 person who does not want to perform self-isolation may be forcibly picked up.	<input type="checkbox"/> Not relevant <input type="checkbox"/> Somewhat relevant <input type="checkbox"/> Quite relevant <input type="checkbox"/> Very relevant	<input type="checkbox"/> Beneficence <input type="checkbox"/> Nonmaleficence <input type="checkbox"/> Justice <input type="checkbox"/> Autonomy	<input type="checkbox"/> Strongly disagree <input type="checkbox"/> Disagree <input type="checkbox"/> Doubtful <input type="checkbox"/> Agree <input type="checkbox"/> Strongly agree
S13	A person who has been confirmed as COVID-19 and	<input type="checkbox"/> Not relevant <input type="checkbox"/> Somewhat relevant	<input type="checkbox"/> Beneficence <input type="checkbox"/> Nonmaleficence	<input type="checkbox"/> Strongly disagree <input type="checkbox"/> Disagree

	refuses to be treated can be forced into isolation.	<input type="checkbox"/> Quite relevant <input type="checkbox"/> Very relevant	<input type="checkbox"/> Justice <input type="checkbox"/> Autonomy	<input type="checkbox"/> Doubtful <input type="checkbox"/> Agree <input type="checkbox"/> Strongly agree
S14	A person who has been confirmed COVID -19 can be forcibly picked up to be hospitalized.	<input type="checkbox"/> Not relevant <input type="checkbox"/> Somewhat relevant <input type="checkbox"/> Quite relevant <input type="checkbox"/> Very relevant	<input type="checkbox"/> Beneficence <input type="checkbox"/> Nonmaleficence <input type="checkbox"/> Justice <input type="checkbox"/> Autonomy	<input type="checkbox"/> Strongly disagree <input type="checkbox"/> Disagree <input type="checkbox"/> Doubtful <input type="checkbox"/> Agree <input type="checkbox"/> Strongly agree
S15	Someone who has symptoms similar to COVID-19 but there is no result of the swab being treated for COVID-19	<input type="checkbox"/> Not relevant <input type="checkbox"/> Somewhat relevant <input type="checkbox"/> Quite relevant <input type="checkbox"/> Very relevant	<input type="checkbox"/> Beneficence <input type="checkbox"/> Nonmaleficence <input type="checkbox"/> Justice <input type="checkbox"/> Autonomy	<input type="checkbox"/> Strongly disagree <input type="checkbox"/> Disagree <input type="checkbox"/> Doubtful <input type="checkbox"/> Agree <input type="checkbox"/> Strongly agree
S16	Screening of body temperature in all public service places is needed to reduce the risk of spreading COVID-19	<input type="checkbox"/> Not relevant <input type="checkbox"/> Somewhat relevant <input type="checkbox"/> Quite relevant <input type="checkbox"/> Very relevant	<input type="checkbox"/> Beneficence <input type="checkbox"/> Nonmaleficence <input type="checkbox"/> Justice <input type="checkbox"/> Autonomy	<input type="checkbox"/> Strongly disagree <input type="checkbox"/> Disagree <input type="checkbox"/> Doubtful <input type="checkbox"/> Agree <input type="checkbox"/> Strongly agree
S17	Washing your hands with soap or hand sanitizer is needed to reduce the risk of spreading COVID- 19	<input type="checkbox"/> Not relevant <input type="checkbox"/> Somewhat relevant <input type="checkbox"/> Quite relevant <input type="checkbox"/> Very relevant	<input type="checkbox"/> Beneficence <input type="checkbox"/> Nonmaleficence <input type="checkbox"/> Justice <input type="checkbox"/> Autonomy	<input type="checkbox"/> Strongly disagree <input type="checkbox"/> Disagree <input type="checkbox"/> Doubtful <input type="checkbox"/> Agree <input type="checkbox"/> Strongly agree
S18	Wearing masks at all public service places is necessary to reduce the risk of spreading COVID- 19	<input type="checkbox"/> Not relevant <input type="checkbox"/> Somewhat relevant <input type="checkbox"/> Quite relevant <input type="checkbox"/> Very relevant	<input type="checkbox"/> Beneficence <input type="checkbox"/> Nonmaleficence <input type="checkbox"/> Justice <input type="checkbox"/> Autonomy	<input type="checkbox"/> Strongly disagree <input type="checkbox"/> Disagree <input type="checkbox"/> Doubtful <input type="checkbox"/> Agree <input type="checkbox"/> Strongly agree
S19	People who reject COVID-19 patients in their environment are violating social ethics	<input type="checkbox"/> Not relevant <input type="checkbox"/> Somewhat relevant <input type="checkbox"/> Quite relevant <input type="checkbox"/> Very relevant	<input type="checkbox"/> Beneficence <input type="checkbox"/> Nonmaleficence <input type="checkbox"/> Justice <input type="checkbox"/> Autonomy	<input type="checkbox"/> Strongly disagree <input type="checkbox"/> Disagree <input type="checkbox"/> Doubtful <input type="checkbox"/> Agree <input type="checkbox"/> Strongly agree
S20	People who reject the dead bodies of COVID-19 patients are violating social ethics	<input type="checkbox"/> Not relevant <input type="checkbox"/> Somewhat relevant <input type="checkbox"/> Quite relevant <input type="checkbox"/> Very relevant	<input type="checkbox"/> Beneficence <input type="checkbox"/> Nonmaleficence <input type="checkbox"/> Justice <input type="checkbox"/> Autonomy	<input type="checkbox"/> Strongly disagree <input type="checkbox"/> Disagree <input type="checkbox"/> Doubtful <input type="checkbox"/> Agree <input type="checkbox"/> Strongly agree
S21	COVID-19 vaccine trials can be carried out directly on humans.	<input type="checkbox"/> Not relevant <input type="checkbox"/> Somewhat relevant <input type="checkbox"/> Quite relevant <input type="checkbox"/> Very relevant	<input type="checkbox"/> Beneficence <input type="checkbox"/> Nonmaleficence <input type="checkbox"/> Justice <input type="checkbox"/> Autonomy	<input type="checkbox"/> Strongly disagree <input type="checkbox"/> Disagree <input type="checkbox"/> Doubtful <input type="checkbox"/> Agree <input type="checkbox"/> Strongly agree
S22	New non- COVID-19 patients should not be hospitalized	<input type="checkbox"/> Not relevant <input type="checkbox"/> Somewhat relevant <input type="checkbox"/> Quite relevant	<input type="checkbox"/> Beneficence <input type="checkbox"/> Nonmaleficence <input type="checkbox"/> Justice	<input type="checkbox"/> Strongly disagree <input type="checkbox"/> Disagree <input type="checkbox"/> Doubtful

	because hospitals need a place to treat COVID-19 patients	<input type="checkbox"/> Very relevant	<input type="checkbox"/> Autonomy	<input type="checkbox"/> Agree <input type="checkbox"/> Strongly agree
S23	Non- COVID-19 patients who have been hospitalized should be discharged because hospitals need a place to treat COVID-19 patients	<input type="checkbox"/> Not relevant <input type="checkbox"/> Somewhat relevant <input type="checkbox"/> Quite relevant <input type="checkbox"/> Very relevant	<input type="checkbox"/> Beneficence <input type="checkbox"/> Nonmaleficence <input type="checkbox"/> Justice <input type="checkbox"/> Autonomy	<input type="checkbox"/> Strongly disagree <input type="checkbox"/> Disagree <input type="checkbox"/> Doubtful <input type="checkbox"/> Agree <input type="checkbox"/> Strongly agree
S24	All rapid tests / RT-PCR should be made free so that all people can be examined for COVID-19 detection	<input type="checkbox"/> Not relevant <input type="checkbox"/> Somewhat relevant <input type="checkbox"/> Quite relevant <input type="checkbox"/> Very relevant	<input type="checkbox"/> Beneficence <input type="checkbox"/> Nonmaleficence <input type="checkbox"/> Justice <input type="checkbox"/> Autonomy	<input type="checkbox"/> Strongly disagree <input type="checkbox"/> Disagree <input type="checkbox"/> Doubtful <input type="checkbox"/> Agree <input type="checkbox"/> Strongly agree
S25	COVID-19 and non-COVID-19 patients deserve the same treatment	<input type="checkbox"/> Not relevant <input type="checkbox"/> Somewhat relevant <input type="checkbox"/> Quite relevant <input type="checkbox"/> Very relevant	<input type="checkbox"/> Beneficence <input type="checkbox"/> Nonmaleficence <input type="checkbox"/> Justice <input type="checkbox"/> Autonomy	<input type="checkbox"/> Strongly disagree <input type="checkbox"/> Disagree <input type="checkbox"/> Doubtful <input type="checkbox"/> Agree <input type="checkbox"/> Strongly agree
S26	Allocation of funding for health services is prioritized for COVID-19 patients	<input type="checkbox"/> Not relevant <input type="checkbox"/> Somewhat relevant <input type="checkbox"/> Quite relevant <input type="checkbox"/> Very relevant	<input type="checkbox"/> Beneficence <input type="checkbox"/> Nonmaleficence <input type="checkbox"/> Justice <input type="checkbox"/> Autonomy	<input type="checkbox"/> Strongly disagree <input type="checkbox"/> Disagree <input type="checkbox"/> Doubtful <input type="checkbox"/> Agree <input type="checkbox"/> Strongly agree
S27	Changes in professional care providers such as doctors, nurses and other health workers for COVID-19 patients are carried out regularly according to needs	<input type="checkbox"/> Not relevant <input type="checkbox"/> Somewhat relevant <input type="checkbox"/> Quite relevant <input type="checkbox"/> Very relevant	<input type="checkbox"/> Beneficence <input type="checkbox"/> Nonmaleficence <input type="checkbox"/> Justice <input type="checkbox"/> Autonomy	<input type="checkbox"/> Strongly disagree <input type="checkbox"/> Disagree <input type="checkbox"/> Doubtful <input type="checkbox"/> Agree <input type="checkbox"/> Strongly agree
S28	Residents with a high risk of contracting COVID-19 have the right to refuse the rapid test / RT-PCR.	<input type="checkbox"/> Not relevant <input type="checkbox"/> Somewhat relevant <input type="checkbox"/> Quite relevant <input type="checkbox"/> Very relevant	<input type="checkbox"/> Beneficence <input type="checkbox"/> Nonmaleficence <input type="checkbox"/> Justice <input type="checkbox"/> Autonomy	<input type="checkbox"/> Strongly disagree <input type="checkbox"/> Disagree <input type="checkbox"/> Doubtful <input type="checkbox"/> Agree <input type="checkbox"/> Strongly agree
S29	COVID-19 patients who have a history of comorbid diseases are prioritized for hospitalization.	<input type="checkbox"/> Not relevant <input type="checkbox"/> Somewhat relevant <input type="checkbox"/> Quite relevant <input type="checkbox"/> Very relevant	<input type="checkbox"/> Beneficence <input type="checkbox"/> Nonmaleficence <input type="checkbox"/> Justice <input type="checkbox"/> Autonomy	<input type="checkbox"/> Strongly disagree <input type="checkbox"/> Disagree <input type="checkbox"/> Doubtful <input type="checkbox"/> Agree <input type="checkbox"/> Strongly agree
S30	COVID-19 patients with a weak economic level are prioritized for hospitalization.	<input type="checkbox"/> Not relevant <input type="checkbox"/> Somewhat relevant <input type="checkbox"/> Quite relevant <input type="checkbox"/> Very relevant	<input type="checkbox"/> Beneficence <input type="checkbox"/> Nonmaleficence <input type="checkbox"/> Justice <input type="checkbox"/> Autonomy	<input type="checkbox"/> Strongly disagree <input type="checkbox"/> Disagree <input type="checkbox"/> Doubtful <input type="checkbox"/> Agree <input type="checkbox"/> Strongly agree

S31	COVID-19 patients who are elderly are prioritized for getting treatment at the hospital.	<input type="checkbox"/> Not relevant <input type="checkbox"/> Somewhat relevant <input type="checkbox"/> Quite relevant <input type="checkbox"/> Very relevant	<input type="checkbox"/> Beneficence <input type="checkbox"/> Nonmaleficence <input type="checkbox"/> Justice <input type="checkbox"/> Autonomy	<input type="checkbox"/> Strongly disagree <input type="checkbox"/> Disagree <input type="checkbox"/> Doubtful <input type="checkbox"/> Agree <input type="checkbox"/> Strongly agree
S32	Each person has the right to use or not use masks during a COVID-19 pandemic because this is an individual's autonomous right.	<input type="checkbox"/> Not relevant <input type="checkbox"/> Somewhat relevant <input type="checkbox"/> Quite relevant <input type="checkbox"/> Very relevant	<input type="checkbox"/> Beneficence <input type="checkbox"/> Nonmaleficence <input type="checkbox"/> Justice <input type="checkbox"/> Autonomy	<input type="checkbox"/> Strongly disagree <input type="checkbox"/> Disagree <input type="checkbox"/> Doubtful <input type="checkbox"/> Agree <input type="checkbox"/> Strongly agree
S33	Personal data of COVID-19 patients may be published.	<input type="checkbox"/> Not relevant <input type="checkbox"/> Somewhat relevant <input type="checkbox"/> Quite relevant <input type="checkbox"/> Very relevant	<input type="checkbox"/> Beneficence <input type="checkbox"/> Nonmaleficence <input type="checkbox"/> Justice <input type="checkbox"/> Autonomy	<input type="checkbox"/> Strongly disagree <input type="checkbox"/> Disagree <input type="checkbox"/> Doubtful <input type="checkbox"/> Agree <input type="checkbox"/> Strongly agree
S34	Lockdowns during a COVID-19 pandemic violate the rights of individual freedoms.	<input type="checkbox"/> Not relevant <input type="checkbox"/> Somewhat relevant <input type="checkbox"/> Quite relevant <input type="checkbox"/> Very relevant	<input type="checkbox"/> Beneficence <input type="checkbox"/> Nonmaleficence <input type="checkbox"/> Justice <input type="checkbox"/> Autonomy	<input type="checkbox"/> Strongly disagree <input type="checkbox"/> Disagree <input type="checkbox"/> Doubtful <input type="checkbox"/> Agree <input type="checkbox"/> Strongly agree
S35	Families of COVID-19 patients can forcibly bring COVID-19 patients home.	<input type="checkbox"/> Not relevant <input type="checkbox"/> Somewhat relevant <input type="checkbox"/> Quite relevant <input type="checkbox"/> Very relevant	<input type="checkbox"/> Beneficence <input type="checkbox"/> Nonmaleficence <input type="checkbox"/> Justice <input type="checkbox"/> Autonomy	<input type="checkbox"/> Strongly disagree <input type="checkbox"/> Disagree <input type="checkbox"/> Doubtful <input type="checkbox"/> Agree <input type="checkbox"/> Strongly agree
S36	Families of COVID-19 patients can forcibly take the dead bodies of COVID-19 patients.	<input type="checkbox"/> Not relevant <input type="checkbox"/> Somewhat relevant <input type="checkbox"/> Quite relevant <input type="checkbox"/> Very relevant	<input type="checkbox"/> Beneficence <input type="checkbox"/> Nonmaleficence <input type="checkbox"/> Justice <input type="checkbox"/> Autonomy	<input type="checkbox"/> Strongly disagree <input type="checkbox"/> Disagree <input type="checkbox"/> Doubtful <input type="checkbox"/> Agree <input type="checkbox"/> Strongly agree

EFICÁCIA DA SECAGEM POR SORÇÃO DE SEMENTES DE SOJA E TRATAMENTO PRÉ-COLHEITA COM DESSICANTES COMO UMA ABORDAGEM ABRANGENTE**EFFICACY OF SOYBEAN SEEDS SORPTION DRYING AND PREHARVEST TREATMENT WITH DESICCANTS AS A COMPREHENSIVE APPROACH****ЭФФЕКТИВНОСТЬ СОРЕБЦИОННОЙ СУШКИ СЕМЯН СОИ И ПРЕДУБОРОЧНОЙ ОБРАБОТКИ ДЕСИКАНТАМИ КАК КОМПЛЕКСНЫЙ ПОДХОД**

SERIKKYZY, Mira^{1*}; AVDEENKO, Aleksei²; GOULY, Yoro Ella³; TYURIN, Igor⁴; STEPANOVA, Diana⁵

¹ Almaty Technological University, Department of Food Safety and Quality. Kazakhstan

² Don state agrarian University, Department of Agriculture, and storage technologies for crop products. Russia

³ RUDN University, Department of Management. Russia

⁴ Saratov State Agrarian University named after N. I. Vavilov, Department of Technical Support of Agro-Industrial Complex. Russia

⁵ Plekhanov Russian University of Economics, Department of Finance and Prices. Russia

** Corresponding author
e-mail: serik.mira@rambler.ru*

Received 29 July 2020; received in revised form 26 August 2020; accepted 15 September 2020

RESUMO

O objetivo deste estudo foi avaliar a aplicação dos dessecantes e da secagem pós-colheita de sementes de soja em locais experimentais e de controle. Um total de 120 locais de estudo, em quadruplicada, foram divididos em dois grupos de 60, um dos grupos não foi pulverizado com dessecantes (local de controle), o outro recebeu tratamento com dessecante (local experimental). Após uma semana de experimentos, as sementes dos locais experimentais apresentavam 1,5 vezes menos umidade do que as sementes dos locais controle ($p \leq 0,05$). A atividade da lipase tornou-se evidente ao máximo no período de até 50 dias. A atividade da lipoxigenase aumentou de 50 para 100 dias de armazenamento. A atividade da lipase nas sementes aumentou significativamente a 60 °C ($p \leq 0,05$), mas com o subsequente aumento da temperatura para 80 e 100 °C, uma redução notável foi registrada ($p \leq 0,01$). Para a lipoxigenase, uma diminuição semelhante na reação de atividade foi observada em temperaturas de agentes secantes a partir de 80 °C. Para outros fatores, nenhum resultado semelhante foi registrado. Isso significa que a atividade de enzimas, em particular a lipase e a lipoxigenase, desempenha um papel fundamental nos processos fisiológicos das sementes de soja durante o armazenamento, mas pode ser inibida em temperaturas a partir de 80 °C. A aplicação de dessecantes acelera a maturação da semente até o teor de umidade necessário por duas semanas. Após sete dias de tratamento com Reglon, o amarelecimento dos grãos e folhas na parte inferior das plantas de soja foi observado, pois o teor de umidade das folhas e grãos diminuiu para 35%, enquanto no local de controle, esses valores foram de 48% ($p \leq 0,05$).

Palavras-chave: *Soja, umidade das sementes, secagem, lipase, lipoxigenase, armazenamento.*

ABSTRACT

The purpose of the study was to evaluate the efficacy of soybean seed treatment with desiccants and through post-harvest drying. A total of 120 quadruplicate study sites were divided into two groups of 60, one of which was not sprayed with desiccants (control sites), and the other received desiccant treatment (experimental sites). A week after the beginning of the experiment, seeds from experimental sites had 1.5 times less moisture content than seeds from control sites ($p \leq 0.05$). The peak lipase activity of seeds was recorded during the first 50 days of storage. The lipoxigenase activity was found to increase between 50 and 100 days of seed storage. The activity of lipase in seeds increased significantly at 60 °C ($p \leq 0.05$), but with the subsequent increase in temperature to 80 and 100 °C, a noticeable reduction was recorded ($p \leq 0.01$). For lipoxigenase, a similar

decrease in activity reaction was noticed at temperatures of drying agents starting from 80 °C. For other factors, no similar results were recorded. This means that the activity of enzymes, in particular, lipase and lipoxygenase, plays a key role in the physiological processes of soybean seeds during storage, but can be inhibited at temperatures starting from 80 °C. Desiccants application accelerates the maturation of the seed to the necessary moisture content for two weeks. After seven days of treatment with Reglon, the yellowing of beans and leaves in the lower part of soybean plants was noted as the moisture content of leaves and beans decreased almost twice to 35%, while on the control site, these values were 48% ($p \leq 0.05$).

Keywords: Soybean, seeds moisture content, drying, lipase, lipoxygenase, storage.

АННОТАЦИЯ

Цель данной работы – оценить возможности комбинированного применения десикантов и послеуборочной сушки семян сои в сравнении с контролем. В 4-х кратной повторности заложено 120 участков, 60 – контроль (без применения десикантов) и 60 – эксперимент (два десиканта – Реглон супер и РАП). Спустя 1 неделю разница во влажности между контролем и экспериментом составила 1.5 раза. При сушке семян активность липазы в максимальной степени проявляется на сроках хранения до 50 суток. Для липоксигеназы активность возрастает от 50 до 100 суток. При 60 С активность липазы в семенах возросла достоверно ($p \leq 0.05$), но с последующим повышением температуры до 80 и 100 С значительно спадала ($p \leq 0.01$). Для липоксигеназы подобная реакция спада активности зафиксирована при температурах сушильных агентов начиная с 80 С. Для других факторов подобных закономерностей не зафиксировано. Это значит, что активность ферментов, в частности липазы и липоксигеназы играет ключевую роль в физиологических процессах в семенах сои во время их хранения, но может ингибироваться при температурах от 80 С. Применение десикантов по сравнению с контролем на 2 недели ускоряет созревание семян до необходимого режима влажности, без снижения показателей урожайности. Через 7 дней при обработке Реглоном и РАП в 2.0 раза по сравнению с контролем до 35 % снизились показатели влажности семян, в контроле эти показатели были 48 % ($p \leq 0.05$).

Ключевые слова: Соя, влажность семян, сушка, липаза, липоксигеназа, хранение.

1. INTRODUCTION:

With the constant growth in the world's population, the food problem is becoming increasingly relevant. Since seeds of legumes and cereals comprise the basis of the people's food ration, not only the issues of increasing yields but also the development of effective methods for drying seeds to prevent their damage by insects or fungi remain relevant (Chen *et al.*, 2020). The task to ensure that crops and legumes production meets the world quality standards is of high importance (Kambhampati *et al.*, 2020).

Numerous factors can affect the quality of crops after harvesting. For example, post-harvest crops processing requires drying, which, afterward, might influence the quality of crops and beans (Chahtane and Lopez-Molina, 2017).

The drying of crops and legumes is a complex technological process (Gouly and Gusov, 2019). According to numerous data, the correct arrangement of the drying process results in obtaining products (crops) of high quality (Burkhead and Klink, 2018; Fraser *et al.*, 2016; Nayak and Panda, 2016). Normally, three main factors are considered, namely, the properties of the biomaterial itself (seeds of legumes and

crops), the construction of the dryer, and the mode in which the dryer operates. These factors are interrelated as they determine the result (Statsenko *et al.*, 2020).

There are two main methods known for drying crops and beans. The first is the steam drying of seeds, and the second is liquid drying (Ye *et al.*, 2008). The first involves the conversion of liquid to steam and is called heat drying. During this process, the energy that may be required by the crops or beans is transferred by applying convection, conduction, or thermo-radiation processes, as well as through the electric field of high-frequency currents. Individual crop parameters, such as the moisture bond strength of beans or crops, should be considered as well (Anand *et al.*, 2019).

The second type of drying is called sorption drying, as the mechanism is based on the contact between raw grain material or beans and a substance with sorption properties (Munder *et al.*, 2019). The sorption methods vary from dry crops to the use of granulated silica gel or other substances (Li *et al.*, 2002).

A separate place in the production of vegetable oils from other oilseeds belongs to soybean. This plant is from the family of legumes

(Fabaceae) and refers to oilseeds in world practice, although, in Russia, it is considered a grain legume agricultural crop (Petibskaya, 2012). In Russia, this crop is primarily intended for protein production despite the predominant oil production from soybeans. This is due to the lack of or high costs for the standard source of protein - meat - in Russia and practical application (Yatchuk, 2013). It is known that protein comprises 35 to 50% of soybean content, the rest are carbohydrates (23 - 25%) and fats (18 - 22%). In terms of protein content, soybean outperforms peas by 1.5-2.0 times (22 - 25% protein in peas), in fat content – by 9-10 times (2%), but is twice as lower in carbohydrate content compared to peas (55%) (Dospekhov, 2014).

The soybean is of very high importance in vegetable oil production, accounting for about 30% of the global total oil production volume. In comparison, sunflower has a share of only 15%, and slightly more (17 %) takes rapeseed (Bergimostyan and Tikhonova, 2016).

The main soybean areas are located in the United States, Brazil, and Argentina, and, together, they account for up to 80% global yield volume amounting to 20-25 cwt per hectare (Haire-Joshu and Tabak, 2016; He *et al.*, 2014). However, the maximum soybean yield is still harvested in Italy with a volume of 37 to 40 cwt per hectare (Huang *et al.*, 2018). In Russia, soybeans have recently started to gain popularity as a mass agricultural crop. Thus, in the Oryol region, the yield was 21 cwt per 1 ha. In 2011, the same amount was harvested the Chuvash Republic, and slightly less - 19 cwt per 1 ha. In the Belgorod region (Petibskaya, 2012). It should be noted that most soybeans are imported to Russia from abroad, and all products belong to genetically modified varieties. Given the controversial role of GMOs in the aspect of negative impact on human health, which is still actively discussed in the scientific community, it would be most reasonable to cultivate "clean" soybeans in Russia (Kaymak, 2014; Klose *et al.*, 2015; Liu *et al.*, 2016).

Among the disadvantages of soybeans as a crop in the Russian climate is the low yield due to the late maturation of seeds as the harvesting season begins in September - October (Bergimostyan and Tikhonova, 2016). Therefore, the issue of developing methods to regulate the processes of moisture release in grains in the period before harvesting (the use of so-called desiccants) remains quite urgent. The development of methods accelerating the maturation of soybean seeds will allow obtaining better quality and earlier terms of their harvest.

Equally important and relevant is the issue of drying seeds after harvesting. Both directions are considered in this study. The combined use of desiccants and post-harvest drying of soybean seeds is assumed to enable getting the yield of this agricultural crop in the climatic conditions of Russia in earlier terms. Besides, the research results can be applied as an example for regions with a similar climate.

The purpose of this work was to explore the possibilities of combined application of desiccants and post-harvest drying of soybeans with an emphasis on the yield of this crop. The objectives of the study were: a) to study the effect of desiccants on the yield and sown properties of soybean seeds, and b) to assess the efficacy of post-harvest drying of soybeans at different temperatures.

2. MATERIALS AND METHODS:

2.1. Research design

The research was conducted between 2017 and 2019 in the Moscow Region (Russian Federation). The fields of the Seed Science Laboratory of the Agrarian Institute of the Russian Academy of Sciences were used as pilot sites, the area of each site was 10 m². Each experiment was set in 4-times repetition with a randomized variant of placement. In total, 120 sites were set.

2.2. Equipment

Soybean seeds were sown by the seed drill SCS-6-10 (Russia) with a given width between the rows of 0.45 m. It has been considered that the normal indicator of soybean seed germination will be 600 thousand per 1 hectare. Fertilizers were applied following generally accepted norms under a scheme of nitrogen 30, phosphorus 45, and potassium 45. Harvesting was carried out simultaneously in all sites utilizing a Sampo harvester (model 130). All experimental sites had the same type of soil, which unified the data from the experiment. The same version of soybeans, the Lancet, was examined.

2.3. Field studies

The first experiment involved determining the effect of desiccants considering such factors as the application of two desiccants simultaneously (Super Reglon, RAP), the consumption rates of these desiccants, and

different terms of soybeans treatment with desiccants. The last factor included the following characteristics: a) at the seed moisture content of 60% to 65%, when the yellowing of leaves in the lower tier of the plant begins; b) at the seed moisture content of 45 to 59%, when the beans in the lower and middle tiers of soybean plants are colored in brown; c) at the seed moisture content of 30 to 44% when all the beans in each soybean plant become brown.

Plants were sprayed with the help of hand sprayer OP-1.5 under the same favorable weather conditions, namely, on dry and windless days. Among the factors influencing desiccation are the temperature of the air and soil (external), the growth course of the plants themselves (internal), and the rate of moisture loss in soybean seeds and stems (internal in response to external factors). Every day, the seeds and stems moisture content indicators were evaluated using the Wille 55 device (Ministry of Agriculture of the USSR, 2004).

The second experiment was a continuation of the first one and aimed to determine the germinating capacity of soybean seeds depending on treatment with desiccants (Dospekhov, 2014).

To assess the impact of technological processes, the harvested soybean seeds of the same variety with initial moisture indexes of 9-10 % were selected. For each study, 30 samples of seeds were taken with moisture indices were set up to 14% by humidification. Each sample was treated with toluene to prevent spoilage from bacteria and fungi in soybean seeds. Seeds were stored at the 80 % humidity regime. Each of the samples was placed on the bottom of a special dish, an exciter, which also contained a sodium chloride solution to ensure constant air humidity. Individual small containers of toluene were placed in the same excitors to prevent the development of microorganisms and fungi during storage. Seed drying was performed under 60, 80, and 100 °C temperature conditions of the drying agents. At that, seeds were actively ventilated with constant air humidity and amount that flowed through the seed layer in a unit of time. The treatment was considered completed when the moisture content indicators of the seed corresponded to those of the equilibrium moisture at the given air humidity parameters.

The impact of technological processes on seed quality was evaluated based on the activity of enzymes, namely, lipase A, lipoxygenase A, and concentrations of phospholipids, chlorophyll A, and iodine number of phospholipids. The concentration of raw oils in soybean seeds, the

peroxide, and acidic numbers of oils in seeds were also determined. To determine the activity of lipase A, lipoxygenase A, the concentration of phospholipids, chlorophyll A, the authors used the standard methods proposed by GOST (state standard) 7825-96 (Soybean oil. Specifications), and to determine the acid, iodine, and peroxide numbers, the recommendations of GOST 10858-77 were used (Oilseeds crops. Industrial raw materials. Methods of determination of acid value).

The concentrations of various substances (e.g., chlorophyll A), acid value, iodine value, and peroxide value were determined by carrying out experiments according to Ermakov (1987). The acidity or acid value was determined using a 25 cm³ sample of soybean seed filtrate titrated with 0.1 M KOH solution in the presence of phenolphthalein indicator. The difference in weight between the flask was filled with dried oil, and the empty flask was determined after heating the sample at 105 °C for 1 hour (Ermakov, 1987).

Chlorophyll A was determined through chromatography using an alcohol extract in the presence of 10 ml of gasoline. Lipids were extracted using a chloroform-methanol 1:2 (v/v) mixture. Common phospholipids were quantified by phosphorus determination after mineralization with perchloric acid (Ermakov, 1987).

The lipase and lipoxygenase activities were assayed using the different buffers: an alkaline phosphate buffer (pH 8.0) and an acidic acetate buffer (pH 4.7). The iodine value was determined with the Hubl method. For this, an ICl reagent and a reagent mixture of HgCl₂ and Cl₂ were applied. The peroxide value was determined by dissolving the soybean seed sample in a solution containing 70% acetic acid and 10% potassium iodide. The resulting iodine was titrated with sodium hyposulfite (Ermakov, 1987).

Thus, the indicators mentioned above during drying and active ventilation of seeds were determined after soybean seeds were maintained for 1 day after treatment. The storage modes of 0, 50, and 100 days were compared.

2.4. Statistical analysis

Statistical analysis of the data obtained was carried out using the Statistica program (StatSoft Inc., v. 6.0). The arithmetic mean for each parameter, like the concentration of enzymes and oils, amount of seeds, and the error of the mean, was estimated. The significance of differences was checked using the t-test for independent samples. Due to the normal

distribution of features within the sample, the methods of parametric statistics were applied.

2.5. Research limitations

Climatic conditions in different years of the research varied in terms of air and soil humidity and precipitation. Therefore, soybean maturation time could change by one week forward or backward from the average period in a given region. For this reason, Figure 1 depicts the data for the year 2018, which most corresponds to the norms in conditions of moderate continental climate in Russia.

3. RESULTS AND DISCUSSION:

3.1. RESULTS

The obtained results show that the use of desiccants allows for a significant reduction of the soybeans aging time with the possibility of earlier harvesting (Figure 1).

The first treatment with desiccants was carried out on August 11, 2018. This year was chosen for the description in Figure 1 as climatic indicators met the average norms for the research region. After seven days of treatment with Reglon, the yellowing of beans and leaves in the lower part of soybean plants was noted as the moisture content of leaves and beans decreased almost twice to 35%, while on the control site, these values were 48% ($p \leq 0.05$). The results similar to the Reglon application were observed in the accounting areas with RAP treatment as well. Another eight days later, on August 27th, leaf shattering occurred in the lower and middle parts of plants in the control sites. Moisture content here decreased to 35%. For sites treated by the Reglon and RAP, grain moisture content was recorded at 25%, which is one third less than that of the control site ($p \leq 0.05$). Finally, by September 8th, the moisture content difference between the control and the experiment remained significant - 1.5 times ($p \leq 0.05$). Crops acquired yellow color, beans became dark brown, and leaves completely crumbled. Thus, the use of desiccants is justified as it allows harvesting already two weeks earlier than in the control site, i.e., at the end of August.

No significant differences in yield between control and experimental sites were recorded. Thus, with an increase in the Reglon concentration, there is a tendency to yield reduction on the experimental sites compared to the control ones. The same tendency is noted when applying RAP preparation. Simultaneously,

the average yield values on experimental and control sites do not statistically differ from each other and can be compared with losses from insect pests or the activity of bacteria and fungi.

The data obtained on the application of desiccants are directly related to the second part of this research as the less moisture the soybean seeds contain, the less time it takes to dry them.

It has been established that with the seed storage periods of up to 50 days, a minor activity of enzymes without significant differences is observed (Table 1).

At that, lipase activity maximally manifests itself during the retention period of up to 50 days (at $p \leq 0.01$). It decreases slightly at storing for up to 100 days ($p \leq 0.05$), while lipoxygenase activity increases, on the contrary, between 50 and 100 days of storage (at $p \leq 0.01$). Throughout the experiment, no significant differences have been established in acid and peroxide numbers, in the oil concentration of the seeds, and, also, for active seed ventilation. On the other hand, significant differences occur during drying seeds at different temperatures of drying agents. Thus, lipase activity in seeds increased significantly at 60 °C ($p \leq 0.05$), but with the subsequent increase in temperature to 80 and 100 °C, a noticeable reduction was recorded ($p \leq 0.01$). For lipoxygenase, a similar decrease in activity reaction was noticed at temperatures of drying agents starting from 80 °C. For other factors, no similar results were recorded. It means that the activity of enzymes, particularly lipase and lipoxygenase, plays a key role in the physiological processes of soybean seeds during storage, but can be inhibited at temperatures starting from 80 °C.

3.2. DISCUSSION:

The established pattern of increasing physiological activity of enzymes in soybean seeds with higher moisture content is also known from other studies (Liu *et al.*, 2016, 2017a, 2017b; Bachleda *et al.*, 2017; Abatiet *et al.*, 2017). However, the physiological activity of enzymes directly determines the quality of the soybean seeds, as shown in this study and other authors (Bishawet *et al.*, 2012). The activity of lipase enzyme during storage for up to 50 days suggests different maturation degree of soybean seeds in the post-harvest period. The activity of lipase and lipoxygenase can be used as a marker and other features of soybean seed quality, particularly its moisture content, as suggested by other authors (Corbineau, 2012).

Storage conditions are also important for maintaining soybean seed quality as they determine the intensity of the physiological processes occurring in soybean seeds (Di Girolamo and Barbanti, 2012). On the other hand, the use of desiccants is justified, as shown by the data obtained through this research and other studies (Carvalho *et al.*, 2017), because it reliably shifts the harvesting time by one and a half to two weeks in a temperate continental climate. Pre-harvest seed quality plays a decisive role in seed preservation in the post-harvest period. During harvesting, the moisture content determines the necessity and duration of their further drying (Pereira *et al.*, 2015). Some studies point to the restriction factor, not climatic as considered in this study, but physiological as the content of lignin in soybean seeds determines their defective qualities (Yamashita *et al.*, 2017). In this research, standard soil conditions for Russia have been considered, namely, chernozem. Although, on saline soils, stress factor can also restrict normal development of soybeans (Shu *et al.*, 2017).

At a longer storage period from 50 days to 100 days, a significant change in the variety of seed mass occurred with increasing activity of enzymes.

Among applied technological processes, active ventilation did not initiate significant changes in the studied parameters, particularly maintaining the activity of enzymes at the same level or reducing it. Similar results were obtained by other authors (Shi *et al.*, 2016). Nevertheless, the effect of temperatures from 80 to 100 °C during drying significantly reduces the activity of enzymes, which allows prolonging the storage time of seeds. Other results obtained through this research are closely related to this process. Thus, the use of desiccants enables obtaining seeds with the given low parameters of moisture content, which will subsequently reduce the cost of drying the seeds and perform harvesting in earlier terms.

The heterogeneity of the seed mass increases with the rise in temperatures of the drying agent, which can be explained by the unevenness of the heating process in the dryer. Besides, seeds are dehydrated uneven as well. As the temperature increases up to 100 °C, the inhibition of enzymes occurs, which is also due to the uneven heating.

4. CONCLUSIONS:

The storage periods of soybean seeds for more than 50 days and modes of drying with temperatures of 100 °C, results in the deterioration of the seed mass quality. It has been established

that the lipase and lipoxygenase enzymes remain inactive at the maximum temperature values that worsen, thus, the quality features of seeds like raw oil mass, acid, and peroxide numbers. However, the activity of enzymes decreases during drying, and with active ventilation of the seed mass, such a pattern is not detected. It has been established that the use of desiccant accelerates the maturation of seeds to the required regime of humidity for two weeks compared to the control site, without a significant decrease in yield amounts.

At that, the lipase is active to the maximum extent at the storage of up to 50 days (at $p \leq 0.01$) and less active at storing for up to 100 days ($p \leq 0.05$), while the activity of lipoxygenase increases between 50 and 100 days of storage (at $p \leq 0.01$). Throughout the experiment, no significant differences have been established in acid and peroxide numbers in the oil concentration of the seeds. Significant differences occur during drying seeds at different temperatures of drying agents. The activity of lipase in seeds increased significantly at 60 °C ($p \leq 0.05$), but with the subsequent increase in temperature to 80 and 100 °C, a noticeable reduction was recorded ($p \leq 0.01$). For lipoxygenase, a similar decrease in activity reaction was observed at temperatures of drying agents starting from 80 °C. Other results obtained through this study are inextricably related to this process. Applying desiccants allows producing seeds with given low parameters of moisture content, which subsequently contributes to cost reduction at seeds drying and harvesting in earlier terms.

5. REFERENCES:

1. Abati, J., Brzezinski, C., Zucareli, C., Werner, F., and Henning, F. (2017). Seed vigor and amount of soybean straw on seedling emergence and productive performance of wheat. *Semina: Ciências Agrárias*, 38(4), 2179-2186.
2. Anand, A., Gareipy, Y., and Raghavan, V. (2019). Fluidized bed and microwave-assisted fluidized bed drying of seed grade soybean. *Drying Technology*, 38(5-6), In press.
3. Bachleda, N., Grey, T., Li, Z. (2017). Effects of high oleic acid soybean on seed yield, protein and oil contents, and seed germination revealed by near-isogenic lines. *Plant Breeding* 136, 539–547.
4. Berzhimosjan, S. I., and Tikhonova, A. O. (2016). The caloric value of soy protein.

- Molodezh and Nauka*, 4, 82.
5. Bishaw, Z., Struik, P., and Van Gastel, A. (2012). Farmers' seed sources and seed quality: 1. physical and physiological quality. *Journal of Crop Improvement*, 26(5), 655-692.
 6. Burkhead, T. R., and Klink, V. P. (2018). American agricultural commodities in a changing climate. *AIMS Agriculture and Food*, 3(4), 406-425.
 7. Carvalho, C. F., Uarrota, V. G., Souza, C. A., and Coelho, C. M. M. (2017). Physiological quality of soybean seed cultivars (Glycine max (L.) Merr.) with different maturity groups. *Research Journal of Seed Science*, 10(2), 59-72.
 8. Chahtane, H., Kim, W., and Lopez-Molina, L. (2017). Primary seed dormancy: a temporally multilayered riddle waiting to be unlocked. *Journal of Experimental Botany*, 68, 857-869.
 9. Chen, F., Zhou, W., Yin, H., Luo, X., Chen, W., Liu, X., Wang, X., Meng, Y., Feng, L., Qin, Y., Zhang, C., Yang, F., Yong, T., Wang, X., Liu, J., Du, J., Liu, W., Yang, W., and Shu, K. (2020). Shading of the mother plant during seed development promotes subsequent seed germination in soybean. *Journal of Experimental Botany*, 71(6), 2072-2084.
 10. Corbineau, F. (2012). Markers of seed quality: from present to future. *Seed Science Research*, 22(Suppl.1), 61-68.
 11. Di Girolamo, G., and Barbanti, L. (2012). Treatment conditions and biochemical processes influencing seed priming effectiveness. *Italian Journal of Agronomy*, 7(2), 178-188.
 12. Fraser, D. P., Hayes, S., and Franklin, K. A. (2016). Photoreceptor crosstalk in shade avoidance. *Current Opinion in Plant Biology*, 33, 1-7.
 13. Gouly, Y. E., and Gusov, A. (2019). Digital technologies as the factor of development of agro-industrial clusters in the countries of Africa. In *International Scientific and Practical Conference "Digital agriculture-development strategy" (ISPC 2019)*. Atlantis Press.
 14. Haire-Joshu, D., and Tabak, R. (2016). Preventing obesity across generations: evidence for early life intervention. *Annual Review of Public Health*, 37, 253-271.
 15. He, H., de Souza Vidigal, D., Snoek, L. B., Schnabel, S., Nijveen, H., Hilhorst, H., and Bentsink, L. (2014). Interaction between parental environment and genotype affects plant and seed performance in Arabidopsis. *Journal of Experimental Botany*, 65, 6603-6615.
 16. Huang, X., Zhang, Q., Jiang, Y., Yang, C., Wang, Q., and Li, L. (2018). Shade induced nuclear localization of PIF7 is regulated by phosphorylation and 4-3-3 proteins in Arabidopsis. *eLife*, 7, e31636.
 17. Kambhampati, S., Aznar-Moreno, J. A., Hostetler, C., Caso, T., Bailey, S. R., Hubbard, A. H., Durrett, T. P., and Allen, D. K. (2020). On the Inverse Correlation of Protein and Oil: Examining the Effects of Altered Central Carbon Metabolism on Seed Composition Using Soybean Fast Neutron Mutants. *Metabolites*, 10(1), 18.
 18. Kaymak, H. (2014). Potential effect of seed fatty acid profile of pepper (*Capsicum annuum* L.) cultivars on germination at various temperatures. *Zemdirbyste-Agriculture*, 101, 321-326.
 19. Klose, C., Viczián, A., Kircher, S., Schäfer, E., and Nagy, F. (2015). Molecular mechanisms for mediating light-dependent nucleo/cytoplasmic partitioning of phytochrome photoreceptors. *New Phytologist*, 206, 965-971.
 20. Li, Z., Kobayashi, N., Watanabe, F., and Hasatani, M. (2002). Sorption drying of soybean seeds with silica gel. *Drying Technology*, 20(1), 223-233.
 21. Liu, J., Yang, C. Q., Zhang, Q., Lou, Y., Wu, H. J., Deng, J. C., Yang, F., and Yang, W. Y. (2016). Partial improvements in the flavor quality of soybean seeds using intercropping systems with appropriate shading. *Food Chemistry*, 207, 107-114.
 22. Liu, X., Rahman, T., Song, C., Su, B.Y., Yang, F., Yong, T. W., Wu, Y. S., Zhang, C. Y., Yang, and W. Y. (2017a). Changes in light environment, morphology, growth, and yield of soybean in maize-soybean intercropping systems. *Field Crops Research*, 200, 38-46.
 23. Liu, X., Rahman, T., Yang, F., Song, C., Yong, T., Liu, J., Zhang, C., and Yang, W. (2017b). PAR interception and utilization in different maize and soybean intercropping patterns. *PLoS ONE*, 12, e0169218.
 24. Ministry of Agriculture of the USSR. (2004). *GOST 12038-84 Seeds of crop plants. Methods for determining germination: Inter-State Standard. Professional Referral Systems "Techexpert"*. Retrieved from

- <http://docs.cntd.ru/document/gost-12038-84>
25. Munder, S., Argyropoulos, D., and Muller, J. (2019). Acquisition of sorption and drying data with embedded devices: improving standard models for high oleic sunflower seeds by continuous measurements in dynamic systems. *Agriculture*, 9(1), 1.
 26. Nayak, B., and Panda, P. B. (2016). Modelling and optimization of texture profile of fermented soybean using response surface methodology. *AIMS Agriculture and Food*, 1(4), 409-418.
 27. Pereira, T., Coelho, C. M. M., Sobiecki, M., and Souza, C.A. (2015). Physiological quality of soybean seeds depending on the preharvest desiccation. *Planta Daninha*, 33(3), 441-450.
 28. Petibskaya, V. S. (2012). *Soybeans: chemical composition and application*. ACS "Poligraf-Yug2".
 29. Shi, H., Wang, B., Yang, P., Li, Y., and Miao, F. (2016). Differences in sugar accumulation and mobilization between sequential and non-sequential senescence wheat cultivars under natural and drought conditions. *PLoS ONE*, 11, e0166155.
 30. Shu, K., Qi, Y., Chen, F., Meng, Y., Luo, X., Shuai, H., Zhou, W., Ding, J., Du, J., Liu, J., Yang, F., Wang, Q., Liu, W., Yong, T., Wang, X., Feng, Y., and Yang, W. (2017). Salt stress represses soybean seed germination by negatively regulating GA biosynthesis while positively mediating ABA biosynthesis. *Frontiers in Plant Science*, 8, 1372.
 31. Statsenko, E. S., Nizkiy, S. E., Litvinenko, O. V., and Kodirova, G. A. (2020). Development of technology for food concentrates of culinary sauses of increased nutritional and biological value. *AIMS Agriculture and Food*, 5(1), 137-149.
 32. Yamashita, K., Sonoki, T., Maeda, H., and Kawasaki, M. (2017). Accumulation of proanthocyanidins and/or lignin deposition in buff-pigmented soybean seed coats may lead to frequent defective cracking. *Planta*, 245, 659-670.
 33. Yatchuk, P. V., and Durnev, G. I. (2013). Impact of desiccants on yield and sown properties of soybean seeds. *Leguminous and Groat Crops*, 1(5), 50-55.
 34. Ye, J., Luo, Q., Li, X., Xu, Q., and Li, Z. (2008). Sorption drying of soybean seeds with silica gel in a fluidized bed dryer. *International Journal of Food Engineering*, 4(6), 7-14.
 35. Ermakov, A. I. (1987). Biochemical research methods of plants. Agropromizdat, Leningrad, 430 p.

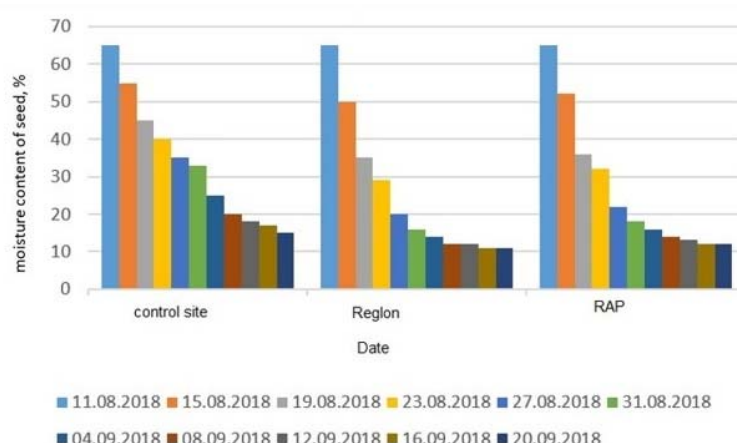


Figure 1. Changes in soybean seed moisture indices depend on treatment with two desiccant preparations (Region, RAP-600) compared to the control site (without treatment) according to data from 2018. The Region was applied in the amount of 1.5 liters per 1 ha., and RAP – 2.5 liters per 1 ha.

Table 1. Enzyme activity and oil concentration indices in soybean seeds depending on the type of technological exposure

Form of exposure	Activity of lipase *	Activity of lipoxigenase **	Acid number***	Peroxide number ****	Concentration of raw oils in seeds, %
Retention terms					
0 days, moisture content 14 %	12 ± 4 ²	24 ± 3 ¹	1.8 ± 0.3	10.0 ± 0.4	17.9 ± 0.2
50 days	22 ± 2 ²	33 ± 5 ²	1.8 ± 0.3	10.1 ± 0.3	18.0 ± 0.3
100 days	31 ± 4 ¹	66 ± 9 ²	2.0 ± 0.2	11.7 ± 0.8	18.1 ± 0.1
Active ventilation					
Ventilation of starting seeds at moisture content of 14 %	21 ± 3	26 ± 3	1.8 ± 0.4	10.1 ± 0.2	18.3 ± 0.2
Ventilation of seeds dried until moisture content of 12.5 %	29 ± 3	34 ± 7	1.8 ± 0.3	11.1 ± 0.5	18.4 ± 0.1
Drying					
Starting seeds, moisture content 14 %	22 ± 3 ¹	26 ± 4	1.8 ± 0.2	10.2 ± 0.3	18.3 ± 0.2
Dried seeds 12.5 %	35 ± 4 ¹	26 ± 4	2.1 ± 0.6	10.6 ± 0.3	18.4 ± 0.1
Temperature of the drying agent 60°C					
80 °C	28 ± 3 ²	30 ± 5 ²	2.4 ± 0.5	11.1 ± 0.4	18.3 ± 0.2
100 °C	14 ± 4 ²	12 ± 6 ²	2.6 ± 0.6	13.8 ± 0.5	18.5 ± 0.3

Note: Units of measure: * - mmol C18 / mg*min 10-3, ** - mmol O2 / mg*min *10-4, *** - mg KOH, **** - 1 / 2 mmol O / kg. Significant differences: 1 - at p ≤ 0.05, 2 - at p ≤ 0.01.

AVALIAÇÃO DO PAPEL DA VITAMINA C COMO AGENTE PROTETOR DE RADIAÇÃO UTILIZANDO γ -H2AX COMO SINALIZAÇÃO DE DANOS AO DNA EM TESTÍCULOS IRRADIADOS DE RATOS

EVALUATION THE ROLE OF VITAMIN C AS A RADIATION PROTECTIVE AGENT USING γ -H2AX FOR SIGNALING OF DNA DAMAGE ON IRRADIATED MICE TESTIS

تقييم دور فيتامين C كعامل وقائي من الإشعاع باستخدام γ -H2AX للإشارة إلى تلف الحمض النووي على خصى الفئران المشعة

ALANI, Ekhlas A.^{1,2}; ALMUSAWI, Mustafa S.^{*1}; MAHDI, Amar H.^{1,3};

¹ Unit of Medical Physics, Department of Physiology, College of Medicine / Al Mustansiriyah University, Baghdad, Iraq.

² Women and Children Hospital, Al Ramadi, Iraq. Department of Radiology.

³ National Center for Hematology, Al Mustansiriyah University, Baghdad, Iraq.

** Corresponding author*

e-mail: dr.mustafa.salih@uomustansiriyah.edu.iq

Received 29 June 2020; received in revised form 22 September 2020; accepted 14 October 2020

RESUMO

Uma característica interessante da radiação ionizante, especialmente os raios gama e dos raios-X, como indutores de dano ao DNA, é a variedade de lesões que induzem. Os focos γ -H2AX são documentados para representar quebras de fita dupla de DNA (DSBs) como um biomarcador para danos induzidos por radiação. Desenho do estudo, 42 ratos machos adultos Albino BALB/c, foram divididos aleatoriamente em 6 grupos de sete ratos cada. O Grupo 1 recebeu uma solução salina padrão também não tratada, não exposto à radiação. Os ratos do grupo 2 receberam vitamina C (200 mg/kg.dia) intraperitoneal (i.p.) injetada durante 8 dias, sem radiação. Grupo 3, controle exposto à radiação gama. O grupo 4, controle, foi exposto à radiação de raios-X. Os camundongos do grupo 5 foram administrados com vitamina C na mesma dose do grupo 2 por 8 dias, depois expostos a 4 Gy de raios gama. O grupo 6 foi administrado com uma dose de vitamina C no mesmo período anterior e, em seguida, exposto a 4 Gy de raios-X. Todos os grupos foram sacrificados por luxação cervical em 1, 3 e 24 h. Os tecidos dos testículos dos ratos foram coletados pós-irradiação. Ocorreu uma diferença significativa ($P < 0,05$) entre o grupo de vitamina C com um grupo de controle exposto a raios-X e raios gama na formação de focos, mas não houve diferença significativa ($P > 0,05$) entre raios gama e raios-X para os grupos controle e vitamina C. Os resultados demonstram que a vitamina C é um bom agente radioprotetor para os tecidos dos testículos de ratos; o efeito dos raios-X e gama tiveram quase os mesmos resultados nos tecidos dos testículo de camundongos com a mesma dose.

Palavras-chave: Radiação ionizante, DSBs, Vitamina C, focos γ -H2AX.

ABSTRACT

An interesting feature of ionizing radiation, especially Gamma and X-rays as a DNA damaging factor is the range of lesions it induces. γ -H2AX foci are documented to represent DNA double-strand breaks (DSBs) as a biomarker for radiation-induced damage. Study design 42 adult male mice Albino BALB/c, had been divided randomly into 6 groups of seven mice each. Group 1 received a standard saline solution untreated also, do not expose to radiation. Group 2 mice received vitamin C (VC) (200 mg/kg.day) intra-peritoneal (i.p.) injected for 8 days without radiation. Group 3 control was exposed to γ -radiation. Group 4 control was exposed to X-ray radiation. Group 5 mice had been administrated with vitamin C in the identical dose of group 2 for 8 days, then exposed to (4 Gy) of γ -ray. Group 6 was administrated with vitamin dose in the same above and the same period, then exposed to (4 Gy) of X-ray. All groups had been sacrificed by cervical dislocation at (1, 3, and 24 h). Post radiation testis mice tissues were collected. A significant difference ($P < 0.05$) between the group of vitamin C and with a control group exposed to both (γ , X-rays) in foci forming, but there is no significant difference ($P > 0.05$) between γ and X- rays for the control and vitamin C groups. The results demonstrate that vitamin C is a good radioprotective agent for testis mice tissues; the effect of (γ and X-rays) had almost the same results on the mice

testicle tissues with the same dose.

Keywords: Ionizing radiation, DSBs, Vitamin C, γ H2AX foci.

المخلص

السمة المدهشة للإشعاع المؤين، وخاصة أشعة جاما والأشعة السينية كعامل ضار للحمض النووي، هو مدى الأفات التي يسببها. تم توثيق بؤر γ -H2AX لتمثيل كسور الحمض النووي المزدوجة (DSBs) كمؤشر حيوي للضرر الناجم عن الإشعاع. في هذه الدراسة تم اختبار 42 من الذكور البالغين من نوع Albino BALB/c، وقد تم تقسيمها بشكل عشوائي إلى 6 مجموعات تحتوي كل مجموعة على سبع فئران. المجموعة 1 تلقت محلول ملحي قياسي بدون معالجة غير معرضة للأشعة. أما المجموعة الثانية فأن الفئران حُقنت داخل الصفاق بفيتامين C بجرعة (200 ملغم/كغم. يوم) لثمان أيام وبدون أشعة. المجموعة الثالثة عُرضت إلى أشعة جاما كمجموعة ضابطة. المجموعة الرابعة عُرضت إلى الإشعة السينية كمجموعة ضابطة. تم إعطاء فئران المجموعة 5 فيتامين C في نفس جرعة المجموعة 2 لمدة 8 أيام، ثم تم تعريضها لـ (4 Gy) من أشعة جاما. أعطيت المجموعة 6 جرعة فيتامين C في نفس الجرعة أعلاه ونفس الفترة، ثم عُرضت (4 Gy) من الأشعة السينية. بعد انتهاء التجربة تم قتل جميع المجموعات من خلال خلع الفقرات العنقية بعد (1، 3، و24 ساعة) من التشعيع. ثم جُمعت أنسجة الفئران بعد التشعيع. تُشير النتائج إلى فروق ذات دلالة إحصائية ($P < 0.05$) بين مجموعة فيتامين C والمجموعة الضابطة التي عُرضت لكل من (أشعة جاما والأشعة السينية) في تكوين البؤر، ولكن لا توجد فروق معنوية ($P < 0.05$) بين مجاميع فيتامين C. أظهرت النتائج أن فيتامين C عامل جيد للوقاية من الإشعاع لأنسجة خصى الفئران؛ تأثير (أشعة جاما والأشعة السينية) له نفس النتائج تقريبا على أنسجة خصى الفئران وبفهم الجرعة.

الكلمات المفتاحية: الإشعاع المؤين، DSBs، فيتامين C، بؤر γ H2A.

1. INTRODUCTION:

Ionizing radiation is widely used in medical diagnostics (cancer) and industrial applications (Smith *et al.*, 2017). Eventually, the human being is exposed to ionizing radiation from natural sources from cosmic rays and radioactive substances. Also, high-altitude flights and terrorism (nuclear weapons) are sources of radiation that certain populations are exposed to risk (Löbrich *et al.*, 2005).

Radiation can have direct and indirect biological effects (Hall *et al.*, 2016). If the biological material absorbs the X-ray or γ energy, the radiation can interact directly in the cell tissue. The ionization or excitation of atoms results in chain reactions culminating in biological damage (Hall *et al.*, 2016). Ionizing radiation damages the tumor microenvironment by preventing cell growth (Wu *et al.*, 2017). The radiation energy can be absorbed in tissue and induce chemical and biological changes in the cell. Double-Strand DNA Breaks are widely recognized as the most biologically important lesion that causes cancer and genetic diseases (Rothkamm and Löbrich, 2003). The Double-Strand Breaks (DSBs) are considered to be the most important DNA lesions caused by ionizing radiation. These DNA lesions are typically repaired efficiently; however, DSB miss-repair can lead to chromosomal trans-sites (Kuefner *et al.*, 2012).

DSBs can be generated indirectly through water radiolysis (decomposition of water molecules due to ionizing radiation), creating reactive chemical species damaging nucleic acids, proteins, and lipids. (Azzam *et al.*, 2012). When ionizing radiation (γ or X-ray) is directed at an

object, some photons are absorbed or scattered, while others completely penetrate the object. Penetration can be expressed as the fraction of radiation passing through the object (Anderson and Warner, 1976). Cellular tissues are made up of 80% water, so the main damage is caused by the formation of free radicals produced by radiation (Shrishrimal *et al.*, 2019).

The impacts of ionizing radiation on the biological system are the generation of Reactive Oxygen Species (ROS) containing superoxide anion, peroxides, and hydroxyl. (Azzam *et al.*, 2012; Cai *et al.*, 2001). Free radicals can be defined as molecular species that contain an unpaired electron in an atomic orbital. The presence of this unpaired electron produces unstable and highly reactive radicals (Gutteridge, 1994). A healthy organism can neutralize the formation of large amounts of harmful molecules. However, some conditions lead to a cellular imbalance resulting in oxidative stress (is an imbalance between free radicals and antioxidants in body) (Wojtunik-Kulesza *et al.*, 2016; Tan *et al.*, 2018).

The oxidative damage observed in the DNA causes mutagenesis and carcinogenesis. Cellular damage can be observed by radiation of high linear energy transfer (LET) (particle α) and radiation of low LET (γ and X-rays). The main difference between high and low LET is the appearance of free radicals during water radiolysis (Cai *et al.*, 2001).

Cytotoxic agents (ionizing radiation) can induce double-strand breaks with damage to DNA. This behavior is followed by a cellular response called histone phosphorylation (H2AX). This histone protein belongs to the H2A family. H2AX

histone, when phosphorylated, forms foci of H2AX in the lesion sites. Histone, when phosphorylated, is called γ -H2AX and is used as a biomarker for radiation-induced damage (Bassing *et al.*, 2002; Kuo and Yang, 2008; Cleaver *et al.*, 2011).

Several studies have analyzed γ -H2AX in tissue samples in mice. The objective of the research was to determine the radiation during several treatments (Rothkamm and Horn, 2009). DNA damage plays a significant role in developing atherosclerosis and other degenerative diseases, including some form of autism, Alzheimer's, Parkinson's, and cancer. The risk of radiation injuries is due to the doses received radiation (low or high LET) and the type of cell (González *et al.*, 2018; Mirończuk-Chodakowska *et al.*, 2018).

New antioxidants (water-soluble molecules) have been used to decrease radiation damage (Sukhotnik *et al.*, 2018). Small, enzymatic molecules have been tested to reduce cytotoxicity and long-term oxidative damage (Okunieff *et al.*, 2008). Antioxidants act in an oxidative series with many stages through lipid peroxidation in cell membranes (Gutteridge, 1994). Vitamin C (VC) is the most important water-soluble antioxidant (Lakshmi and Kesavan, 1993). In addition to being considered an essential micronutrient, it can donate electrons (Carr and Maggini, 2017).

Vitamin C acts as precursors to enzymes, protects food substances from the oxidative cycle, aids in the absorption of food in the intestine, and protects oxidizing agents in the blood (Rahayu *et al.*, 2019). Vitamin C protects DNA against radiation damage (Cai *et al.*, 2001). Thus, changes in the structure of DNA, caused by ascorbic acid, are closely related to its ability to defend against DSBs (Yoshikawa *et al.*, 2006). Vitamin C can eliminate ROS even before the proliferation of macromolecules (Rahayu *et al.*, 2019). Another function of vitamin C is protecting lipid membranes from oxidative damage (González *et al.*, 2018).

Unlike most mammals, humans do not have the capacity to produce vitamin C. Therefore, and it must be obtained through food (Taş *et al.*, 2014). However, in vitro experiments reveal that vitamin C has many functions (Frag *et al.*, 2018). In this sense, before being subjected to γ or X radiation, the administration of vitamin C avoids chromosomal damage in cells (Konopacka *et al.*, 1998; Mortazavi *et al.*, 2015). Many types of research show the protection of DNA by using vitamin C when it is submitted to radiation doses (Mahdi *et al.*, 2018; Yoshikawa *et al.*, 2006).

Treatment with vitamin C dramatically improved the survival of mice after total body

irradiation (TBI). Thus, vitamin C is effective and efficient in preventing DNA damage in mouse tissues. (Yamamoto *et al.*, 2010). In another study, administering vitamin C at 1, 6, 12, and 24 h after TBI improved mouse survival. The use of vitamin C was efficient in reducing cell damage by reducing free radicals (Sato *et al.*, 2015).

Thus, the administration of vitamin C before γ and X irradiation prevents chromosomal damage to cells and lethality caused by radiation. Vitamin C can prevent the adverse effects of radiation on TBI through antioxidant protection in irradiated animal tissues (Konopacka *et al.*, 1998; Mortazavi *et al.*, 2015). After ionizing radiation, DNA responds in several ways to repair the damaged structure (Mahdi *et al.*, 2018). However, the defense mechanism against radiation is not fully understood and is still a topic for discussion.

The scientific community needs answers regarding the effects of radiation and acceptable doses without harming healthy cells. The biological impact must be studied in greater depth (Hill, 2004). In this sense, this work aims to evaluate the radioprotective effect of vitamin C induced by X-rays and gamma-rays (γ -rays) in mice testis tissue.

2. MATERIALS AND METHODS:

2.1. Animals and reagents

This research was carried out at The Animal Care and Research Ethics Commission, Iraqi Centre for Cancer and Medical Genetics Research (ICCMGR) at Al-Mustansiriyah University.

All requests and treatment of animals, along with the procedures intended in this study, were confirmed. Male albino Balb/c mice with eight weeks (20 ± 2 g body weight) were obtained from (ICCMGR). The mice were isolated eight days before irradiation. The mice were separated into six groups (each group with seven) placed in cages at a temperature of 22 ± 2 °C, the relative humidity of $50 \pm 10\%$, and a 12 hour shift of the light-dark cycle, fed standard commercial rodent chow and sterile water.

2.2. γ and X-rays procedures

The mice were placed in a specially designed and well-ventilated plastic container. In the first test, the animals received a single dose of 4 Gray (Gy) of γ -ray in TBI. This experiment used

a rate of 0.3 Gy/min with energies of 1.17 and 1.33 MeV from eight rods of ^{60}Co . The tests were carried out in the Laboratory of Nuclear Sciences at the University of Baghdad/College of Science. In the second test (same methodology above) but the mice received a single dose of 4 Gray of X-ray in TBI by a linear accelerator (Electa Compact) in the Baghdad Center for Atomic Medicine at Medical City in Baghdad/Iraq. The dose rate was 2.85 Gy/min with a distance to a source sample of 120 cm. Field size 20×20 cm at room temperature (23 ± 2 °C) with 6 MeV energies. These experiments have been duplicated in both cases.

2.3. Administration of Vitamin C (Ascorbic Acid) and antibodies

Vitamin C (ALPHA CHEMIKA, India) was dissolved in physiological saline solution and administered intraperitoneally (i.p.) for 8 days at a 200 mg/kg.day dosage. Was used Anti- γ -H2AX (phospho S139) antibody [9F3] ab26350 from Abcam with 1:200 dilution.

2.4. Tissues collection and immunohistochemistry staining of γ H2AX in testis tissues

The mice were sacrificed after 1, 3, and 24 hours of irradiation with the collection of testicular tissues. The tissues were placed in formalin solution, neutral buffered, 10% for 24 hours, transferred to 70% ethanol, and embedded in paraffin. The development of this internship was carried out at the ICCMGR.

Immunohistochemistry (IHC) was performed in 5 μm sections, using the following antibodies: γ -H2AX (phospho S139) antibody [9F3] ab26350 from Abcam with 1: 200 dilution.

An optical microscope with a CCD camera (OLYMPUS OPTICAL, Model CX41RF) was used to detect the foci with 40x magnification. The images were obtained in the Unit of Medical Physics, Department of Physiology, College of Medicine / Al Mustansiriyah University, Baghdad, Iraq. The foci were divided into four tissue sites, with each site occupying 100 cells. Each cell is classified according to the number of foci in the DSB. Then, an average of the four sites was calculated, and the final result of preparing the foci was divided into mild (0-3), moderate (4-6), severe (≥ 7).

2.5. Statistical evaluation

The data were analyzed using SPSS

statistical software. A t-test was used to determine the difference between the non-irradiated sample (control) and the irradiated samples. A P-value was determined based on the difference between the non-irradiated sample and the irradiated samples. Based on these results, $P < 0.05$ is considered significant.

3. RESULTS AND DISCUSSION:

3.1. DSB detection by γ -H2AX foci on irradiated mice testis tissues with γ -ray pre and post-treatment with vitamin C

As the dose of gamma radiation interacted with the sample with vitamin C and without vitamin C, the number of foci was changed. The results are shown in Figure 1. The levels of γ -H2AX in irradiated (γ -ray) and non-irradiated samples using vitamin C did not differ significantly ($P > 0.05$).

In 1h, the foci groups (0-3), (4-6) did not show significant differences ($P > 0.05$) between irradiated and non-irradiated vitamin C. However, for the foci group (≥ 7), there was a decrease ($P < 0.01$) between non-irradiated samples (control). For 3 hours, the foci groups (0-3) and (≥ 7) showed a significant increase. Therefore, for the foci group (4-6), there was no important difference ($P > 0.05$). In turn, within 24 h, the focus groups (0-3), (4-6), and (≥ 7) do not show any significant difference ($P > 0.05$).

Figure 2 shows the endogenous damage to DNA and DSB in testicular tissues of mice (with and without vitamin C) by γ -rays. It was identified some differences in the microscopic images in the irradiated and non-irradiated samples. As the time of exposure to γ -rays increases, it was noticed a decrease in the focus groups. This behavior is not evident for the focus groups that used vitamin C.

3.2. DSB detection by γ H2AX foci on irradiated mice testis tissues with X-ray pre and post-treatment with vitamin C

Figure 3 shows the effects of X-rays on vitamin C. It was found significant differences when the testicular tissues of mice are exposed to X-rays without vitamin C (Figure 4). Thus, there was an increase in the number of foci for samples not treated with vitamin C.

Figure 3 shows the foci levels, taking into account the use or not of vitamin C combined with the time of exposure to X-ray. The results allowed us to conclude that there were no significant changes ($P > 0.05$) in the focus groups (0-3), (4-6)

with the use of vitamin C without radiation and for 1 and 3 h under the influence of X. For the focus group ≥ 7 , there were differences ($P \leq 0.01$) in the 1 and 3 h radiation. In general, in 24 hours for all focus groups, there was no significant change.

Figure 4 shows the damage to endogenous DNA and DSB in testicular tissues of mice that received doses of X-rays with and without vitamin C. In the times of 3 and 24 hours, the focus groups showed low levels using vitamin C. Significant variations occurred in 1 h. The decline rate is more evident in the groups that used vitamin C, taking into account the formation of foci of the DSB. These observations indicate that treatment with vitamin C before irradiation had positive results in reducing DSB. Thus, the decrease in the number of foci in an γ -H2AX indicator.

3.3. Comparison between foci in γ and X-rays (control and vitamin C groups) to detect DSB in DNA by γ -H2AX

To evaluate the effects of ionizing radiation (γ and X-rays) in testicular tissues of rats, vitamin C, and without vitamin (control) were used. Figures 5 and 7 reveal that the focus groups (0-3), (4-6), (≥ 7) showed no significant difference ($P > 0.05$). Figures 6 and 8 show us the images of the IHC with the γ -H2AX antibody at different times (without irradiation, 1 h, 3 h, 24 h). Microscopic images evidenced endogenous damage to DNA and DSB in tissues irradiated with γ -X rays with and without vitamin C. These results indicate that there is no apparent difference between the groups (γ , X-rays) with and without vitamin C concerning the γ -H2AX foci in the DNA.

Tissues and organs specific from individuals vary significantly when subjected to radiation. Growing male germ cells are more susceptible to disturbances and are recognized as a radiosensitive organ. (Lakshmi and Kesavan, 1993). The damaging effects of ionizing radiation on the mice testis tissues are well documented (Paull *et al.*, 2000).

This study shows that the radioprotective agent (vitamin C) acted effectively when the samples were subjected to X-rays and γ (Taş *et al.*, 2014). In addition, it decreased DNA damage in testicular tissues and the preservation of genetic material (Marjault and Allemand, 2016).

When evaluating DSBs after exposure of 4 Gy (γ -rays) for the group that administered vitamin C, tissue regeneration levels had a progressive decrease (Fig 1 and 2). However, the results were

inconsistent for the control group (without vitamin C), as there was no protection against radiation. Thus, it was concluded that the protective effect is accompanied by doses of vitamin C, as evidenced by several research groups today (Brand *et al.*, 2015; Mortazavi *et al.*, 2015; Paull *et al.*, 2000; Sato *et al.*, 2015; Sukhotnik *et al.*, 2018).

The ionizing radiation that interacted in the DSBs correlated significantly with the dose of X-rays and γ (Hill, 2004). The use of the antibody (γ -H2AX), as a marker for DSBs, was found in approximately a few minutes after irradiation (Mahdi *et al.*, 2018). The increase in DSBs, followed by a reduction, represented the repair of DSBs (Hamer *et al.*, 2003). Therefore, the number of γ -H2AX foci decreases rapidly over time (Rothkamm and Horn, 2009). This is due to the histone H2A protein presence, which acted on the DSBs and on the DNA (Jeggo and Löbrich, 2006). Figures 3 and 4 showed a similar result in Figures 1 and 2 in the amount of γ -H2AX foci, irradiated by X-rays in 1, 3, 24 h. DSBs are caused by DNA damage caused by ionizing radiation (Löbrich *et al.*, 2005; Rothkamm and Löbrich, 2003).

Imaging the foci is essential to check the effect of radiation inside cells representing DSB DNAs (Rogakou *et al.*, 1998). Previous studies have shown that damage to DSBs is correlated with X-ray and γ doses (Kuefner *et al.*, 2010). There is an increase in DSB levels between 30 and 60 minutes after radiation, followed by repairs to the DSB (Löbrich *et al.*, 2005). Therefore, studies confirm the effective role of vitamin C in reducing the risk caused by ionizing radiation. In this sense, the results obtained in this study are in line with the research carried out by several groups addressed in this work.

In this study, the effect of X-rays and γ in mouse testis, using a dose of 4 Gy, had the same effect on DNA damage with a slight difference in the proportion of foci formed due to DSBs Figures 5 – 8. This indicates that only one type of ionizing radiation will be sufficient to carry out experiments *in vivo*. Previous studies have proven that the use of 2.2 Gy of X-rays in the colon tissue in mice produces desirable effects. However, on biological tissues, a different source and energy will depend on the doses used (Graupner *et al.*, 2017).

Thus, the effective role of vitamin C in preserving testicular tissue, submitted to X-rays and γ , is evident. The probable cause of the decrease in the number of foci formed after several hours of radiation can be explained by the low production of free radicals in the DNA. Vitamin C takes some time to enter the cell's nucleus to

intercept free radicals produced near DNA. Simultaneously, the amount of γ -H2AX foci, after exposure to 4 Gy, increased without the administration of vitamin C in the control group. The use of vitamin C in a mouse had a strong inhibitory effect, which prevented damage to testicular tissues and prevented post-irradiation fertility loss.

4. CONCLUSIONS:

In view of the results obtained in this research, it was concluded that the testicular tissues of mice exposed to ionizing radiation (γ or X) suffered DNA damage. However, as a radioprotective agent, the use of vitamin C reduced the effects on the genetic code. The effect of X-rays and γ on the testicles of mice, at doses of 4 Gy, had the same effect on DNA. In this way, the use of ionizing radiation can be safe *in vivo* experiments. Although the source of energy used (photons) is different, the biological effects are similar.

5. ACKNOWLEDGMENTS:

The authors thank the staff and participants at the Unit of Medical Physics, Department of Physiology, College of Medicine/Al Mustansiriyah, Baghdad, Iraq, Iraqi Center for Cancer Research and Medical Genetics (ICCMGR), at Mustansiriyah University, Laboratory of Nuclear Sciences at the University of Baghdad/ College of Science and the Baghdad Center for Atomic Medicine at Medical City in Baghdad/Iraq.

6. REFERENCES:

1. Smith, T. A.; Kirkpatrick, D. R.; Smith, S.; Smith, T. K.; Pearson, T.; Kailasam, A.; Herrmann, K. Z.; Schubert, J.; Agrawal, D. K. (2017). Radioprotective agents to prevent cellular damage due to ionizing radiation. *Journal of Translational Medicine*, 15, 1–18.
2. Löbrich, M.; Rief, N.; Kühne, M.; Heckmann, M.; Fleckenstein, J.; Rübe, C.; Uder, M. (2005). In vivo formation and repair of DNA double-strand breaks after computed tomography examinations. *Proceedings of the National Academy of Sciences*, 102(25), 8984–8989.
3. Hall, S.; Rudrawar, S.; Zunk, M.; Bernaitis, N.; Arora, D.; McDermott, C. M.; Anoopkumar-Dukie, S. (2016). Protection against radiotherapy-induced toxicity. *Antioxidants*, 5(3), 1–18.
4. Wu, Q.; Allouch, A.; Martins, I.; Modjtahedi, N.; Deutsch, E.; Perfettini, J. L. (2017). Macrophage biology plays a central role during ionizing radiation-elicited tumor response. *Biomedical Journal*, 40(4), 200–211.
5. Rothkamm, K.; Löbrich, M. (2003). Evidence for a lack of DNA double-strand break repair in human cells exposed to very low x-ray doses. *Proceedings of the National Academy of Sciences*, 100(9), 5057–5062.
6. Kuefner, M. A.; Brand, M.; Ehrlich, J.; Braga, L.; Uder, M.; Semelka, R. C. (2012). Effect of antioxidants on X-ray-induced γ -H2AX foci in human blood lymphocytes: Preliminary observations. *Radiology*, 264(1), 59–67.
7. Azzam, E.; Jay-Gerin, J.; Pain, D. (2012). Ionizing radiation-induced metabolic oxidative stress and prolonged cell injury. *Cancer Letters*, 327(1–2), 48–60.
8. Anderson, R. E.; Warner, N. L. (1976). Ionizing Radiation and the Immune Response. *Advances in Immunology*, 24(1), 215–335.
9. Shrishrimal, S.; Kosmacek, E. A.; Oberley-Deegan, R. E. (2019). Reactive oxygen species drive epigenetic changes in radiation-induced fibrosis. *Oxidative Medicine and Cellular Longevity*, 2019, 27.
10. Cai, L.; Koropatnick, J.; Cherian, M. G. (2001). Roles of vitamin C in radiation-induced DNA damage in presence and absence of copper. *Chemico-Biological Interactions*, 137(1), 75–88.
11. Gutteridge, J. M. C. (1994). Biological origin of free radicals, and mechanisms of antioxidant protection. *Chemico-Biological Interactions*, 91(2–3), 133–140.
12. Wojtunik-Kulesza, K. A.; Oniszczuk, A.; Oniszczuk, T.; Waksmundzka-Hajnos, M. (2016). The influence of common free radicals and antioxidants on development of Alzheimer ' s Disease. *Biomedicine et*

13. Tan, B.; Norhaizan, M.; Liew, W. P.; Rahman, H. (2018). Antioxidant and oxidative stress: A mutual interplay in age-related diseases. *Frontiers in Pharmacology*, 9, 1–11.
14. Bassing, C. H.; Chua, K. F.; Sekiguchi, J.; Suh, H.; Whitlow, S. R.; Fleming, J. C.; Monroe, B. C.; Ciccone, D. N.; Yan, C.; Vlasakova, K.; Livingston, D. M.; Ferguson, D. O.; Scully, R.; Alt, F. W. (2002). Increased ionizing radiation sensitivity and genomic instability in the absence of histone H2AX. *Proceedings of the National Academy of Sciences*, 99(12), 2–7.
15. Kuo, L. J.; Yang, L. (2008). γ -H2AX – A Novel Biomarker for DNA Double-strand Breaks. *In Vivo*, 22(3), 305–309.
16. Cleaver, J. E.; Feeney, L.; Revet, I. (2011). Phosphorylated H2Ax is not an unambiguous marker for DNA double-strand breaks Phosphorylated H2Ax is not an unambiguous marker for DNA double-strand breaks. *Cell Cycle*, 10(19), 3223–3224.
17. Rothkamm, K.; Horn, S. (2009). γ -H2AX as protein biomarker for radiation exposure. *Annali dell'Istituto Superiore di Sanità*, 45(3), 265–271.
18. Mirończuk-Chodakowska, I.; Witkowska, A. M.; Zujko, M. E. (2018). Endogenous non-enzymatic antioxidants in the human body. *Advances in Medical Sciences*, 63(1), 68–78.
19. Sukhotnik, I.; Nativ, O.; Ben-Shahar, Y.; Bejar, I. N.; Pollak, Y.; Coran, A. G.; Gorenberg, M. (2018). Antioxidant treatment ameliorates germ cell apoptosis induced by a high-dose ionizing irradiation in rats. *Pediatric Surgery International*, 35(0), 137–143.
20. Okunieff, P.; Swarts, S.; Keng, P.; Sun, W.; Wang, W.; Kim, J.; Yang, S.; Zhang, H.; Liu, C.; Williams, J. P.; Huser, A. K.; Okunieff, P.; Swarts, S.; Keng, P.; Sun, W.; Wang, W.; Kim, J.; Yang, S.; Zhang, H.; Liu, C.; Williams, J. P.; Huser, A. K. (2008). Antioxidants reduce consequences of radiation exposure. *Advances in Experimental Medicine and Biology*, 614, 165–178.
21. Lakshmi, S.; Kesavan, P. C. (1993). Protective effects of vitamins c and e against yray-induced chromosomal damage in mouse. *International Journal of Radiation Biology*, 63(6), 759–764.
22. Carr, A. C.; Maggini, S. (2017). Vitamin C and Immune Function. *Nutrients*, 9(11), 1–25.
23. Rahayu, I.; Usman, E.; Reza, M. (2019). Effect of vitamin C on testosterone level, sperm count, and sperm morphology in gentamicin-induced Wistar rats. *International Journal of Research in Medical Sciences*, 7(2), 451.
24. Yoshikawa, Y.; Hizume, K.; Oda, Y.; Takeyasu, K.; Araki, S.; Yoshikawa, K. (2006). Protective effect of vitamin C against double-strand breaks in reconstituted chromatin visualized by single-molecule observation. *Biophysical Journal*, 90(3), 993–999.
25. González, E.; P.Cruces, M.; Pimentel, E.; Sánchez, P. (2018). Evidence that the radioprotector effect of ascorbic acid depends on the radiation dose rate. *Environmental Toxicology and Pharmacology*, 62, 210–214.
26. TAŞ, M.; CİRİT, Ü.; ÖZKAN, O.; Denli, M.; Zincircioğlu, S. B.; Şeker, U. (2014). Protective Role of Vitamin C on Sperm Characteristics and Testicular Damage in Rats Exposed to Radiation. *Kafkas Üniversitesi Veteriner Fakültesi Dergisi*, 20(1), 49–54.
27. Farag, H. A. M.; Hosseinzadeh-Attar, M. J.; Muhammad, B. A.; Esmailzadeh, A.; El Bilbeisi, A. H. (2018). Comparative effects of vitamin D and vitamin C supplementations with and without endurance physical activity on metabolic syndrome patients: A randomized controlled trial IRCT20161110030823N2 IRCT 11 Medical and Health Sciences 1117 Public Health and Heal. *Diabetology and Metabolic Syndrome*, 10(1), 1–12.
28. Konopacka, M.; Widel, M.; Rzeszowska-

- Wolny, J. (1998). Modifying effect of vitamins C, E, and beta-carotene against gamma-ray-induced DNA damage in mouse cells. *Mutation Research - Genetic Toxicology and Environmental Mutagenesis*, 417(2–3), 85–94.
29. Mortazavi, S. M. J.; Sharif-Zadeh, S.; Mozdarani, H.; Foadi M.; Haghani, M.; Sabet, E. (2015). Future role of vitamin C in radiation mitigation and its possible applications in manned deep-space missions: Survival study and the measurement of cell viability. *International Journal of Radiation Research*, 13(1), 55–60.
 30. Mahdi, A. H.; Huo, Y.; Tan, Y.; Simhadri, S.; Vincelli, G.; Gao, J.; Ganesan, S.; Xia, B. (2018). Evidence of intertissue differences in the DNA damage response and the pro-oncogenic role of NF- κ B in mice with disengaged BRCA1–PALB2 interaction. *Cancer Research*, 78(14), 3969–3981.
 31. Yamamoto, T.; Kinoshita, M.; Shinomiya, N.; Hiroi, S.; Sugawara, H.; Matsushita, Y.; Majima, T.; Saitoh, D.; Seki, S. (2010). Pretreatment with Ascorbic Acid Prevents Lethal Gastrointestinal Syndrome in Mice Receiving a Massive Amount of Radiation. *Journal of Radiation Research*, 51(2), 145–156.
 32. Sato, T.; Kinoshita, M.; Yamamoto, T.; Ito, M.; Nishida, T.; Takeuchi, M.; Saitoh, D.; Seki, S.; Mukai, Y. (2015). Treatment of irradiated mice with high-dose ascorbic acid reduced lethality. *PLoS ONE*, 10(2), 1–15.
 33. Hill, M. A. (2004). The variation in biological effectiveness of X-rays and gamma rays with energy. *Radiation Protection Dosimetry*, 112(4), 471–481.
 34. Marjault, H. B.; Allemand, I. (2016). Consequences of irradiation on adult spermatogenesis: Between infertility and hereditary risk. *Mutation Research-Reviews in Mutation Research*, 770(B), 340–348.
 35. Brand, M.; Sommer, M.; Ellmann, S.; Wuest, W.; May, M. S.; Eller, A.; Vogt, S.; Lell, M.; Kuefner, M.; Uder, M. (2015). Influence of Different Antioxidants on X-Ray Induced DNA Double-Strand Breaks (DSBs) Using γ -H2AX Immunofluorescence Microscopy in a Preliminary Study. *PLoS ONE*, 10(5), 1–12.
 36. Paull, T. T.; Rogakou, E. P.; Yamazaki, V.; Kirchgessner, C. U.; Gellert, M.; Bonner, W. M. (2000). A critical role for histone H2AX in recruitment of repair factors to nuclear foci after DNA damage. *Current Biology*, 10(15), 886–895.
 37. Hamer, G.; Roepers-Gajadien, H. L.; van Duyn-Goedhart, A.; Gademan, I. S.; Kal, H. B.; van Buul, P. P.; de Rooij, D. G. (2003). DNA Double-Strand Breaks and γ -H2AX Signaling in the Testis 1. *Biology of Reproduction*, 68(2), 628–634.
 38. Jeggo, P.; Löbrich, M. (2006). Radiation-induced DNA damage responses. *Radiation Protection Dosimetry*, 122(1–4), 124–127.
 39. Rogakou, E. P.; Pilch, D. R.; Orr, A. H.; Ivanova, V. S.; Bonner, W. M. (1998). DNA double-stranded breaks induce histone H2AX phosphorylation on serine 139. *Journal of Biological Chemistry*, 273(10), 5858–5868.
 40. Kuefner, M.; Hinkmann, F. M.; Alibek, S.; Azoulay, S.; Anders, K.; Kalender, W.; Achenbach, S.; Grudzenski, S.; Löbrich, M., and Uder, M. (2010). Reduction of X-ray induced DNA double-strand breaks in blood lymphocytes during coronary CT angiography using high-pitch spiral data acquisition with prospective ECG-triggering. *Investigative Radiology*, 45(4), 182–187.
 41. Graupner, A.; Eide, D. M.; Brede, D. A.; Ellender, M.; Hansen, E. L.; Houghton, D.; Brunborg, G.; Olsen, A. K. (2017). Genotoxic Effects of High Dose Rate X-ray and Low Dose Rate Gamma Radiation in ApcMin/1 Mice. *Environmental and Molecular Mutagenesis*, 58(8), 560–569.

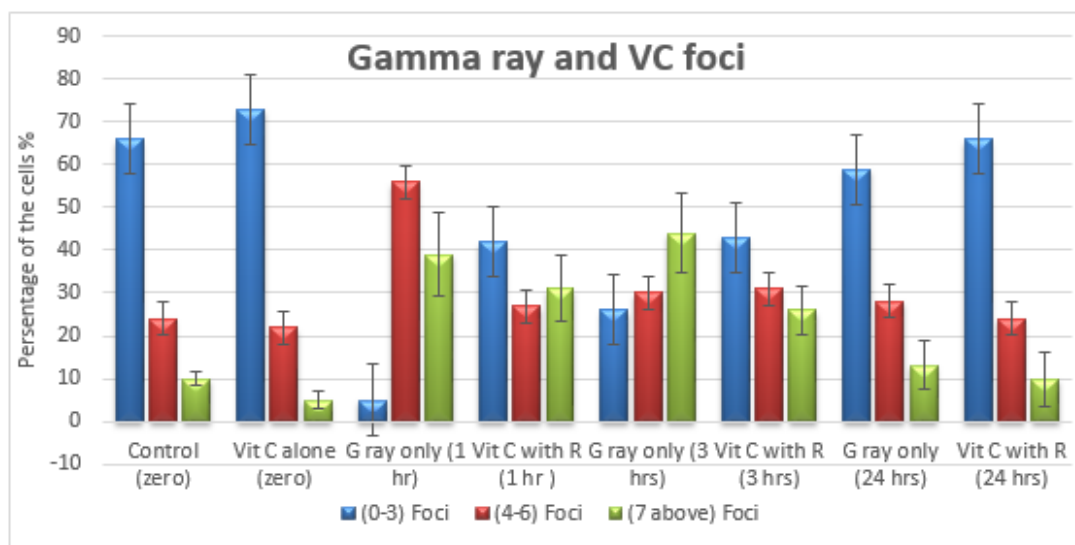


Figure 1. DSB and γ -H2AX foci in control and VC with and without IR (γ -ray) at different times.

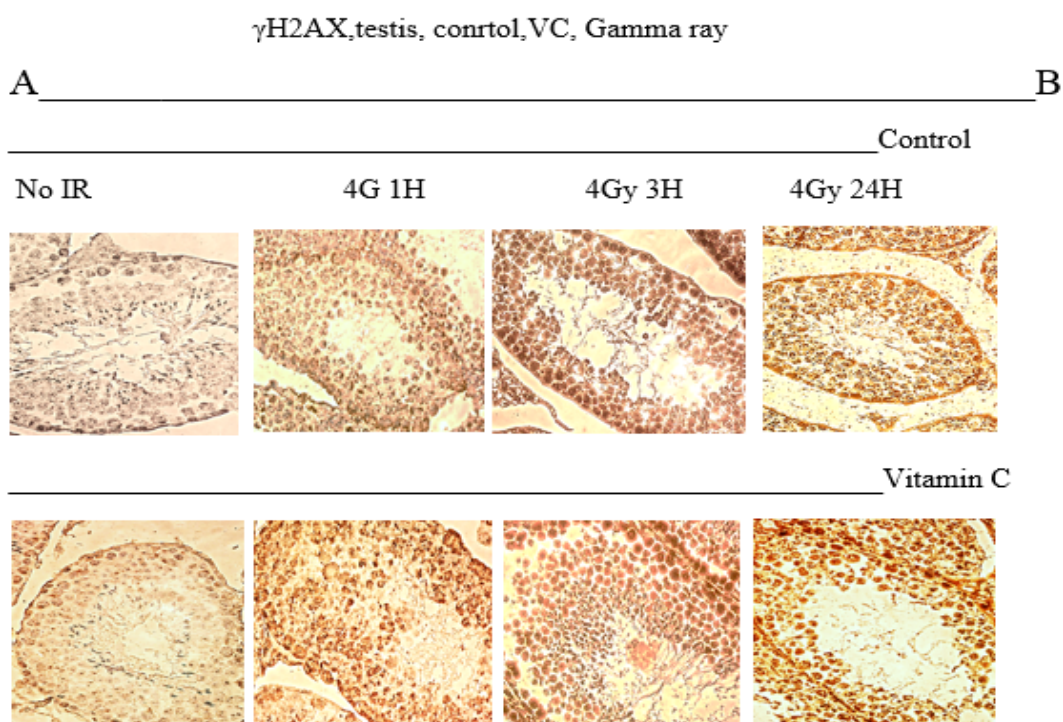


Figure 2. Endogenous DNA damage and DSB capability in control and VC groups with and without IR (Gamma-ray). A and B, Representative IHC images (A) and quantification (B) of γ -H2AX foci formation in testis tissue before and after (4 Gy) of IR in (1, 3, 24 h).

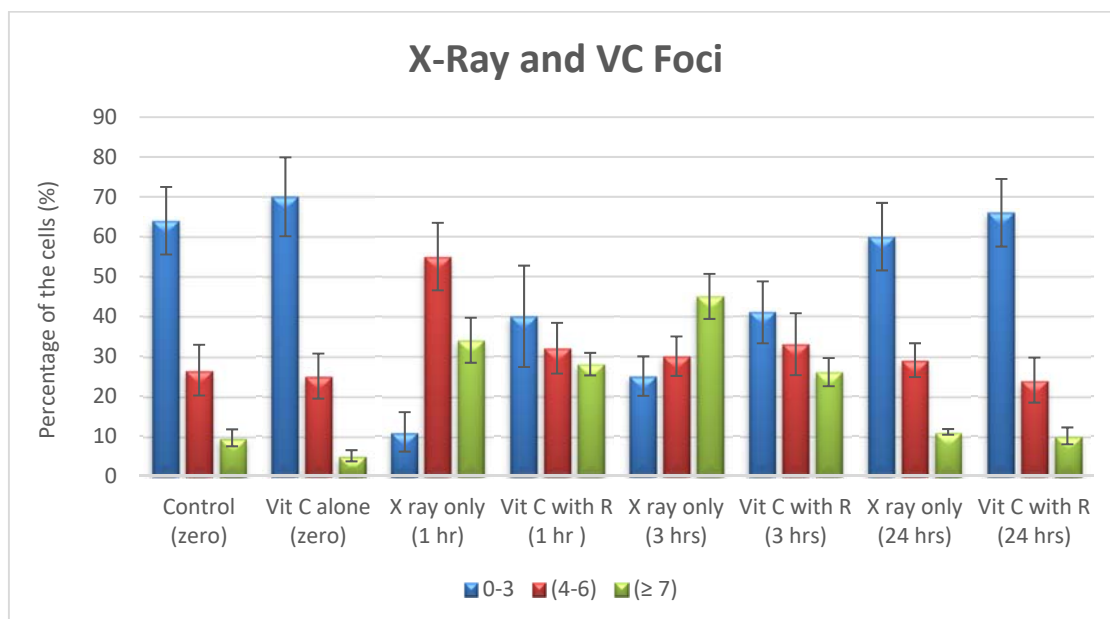


Figure 3. DSB and γ -H2AX foci in control and VC with and without IR (X-ray) in different times.

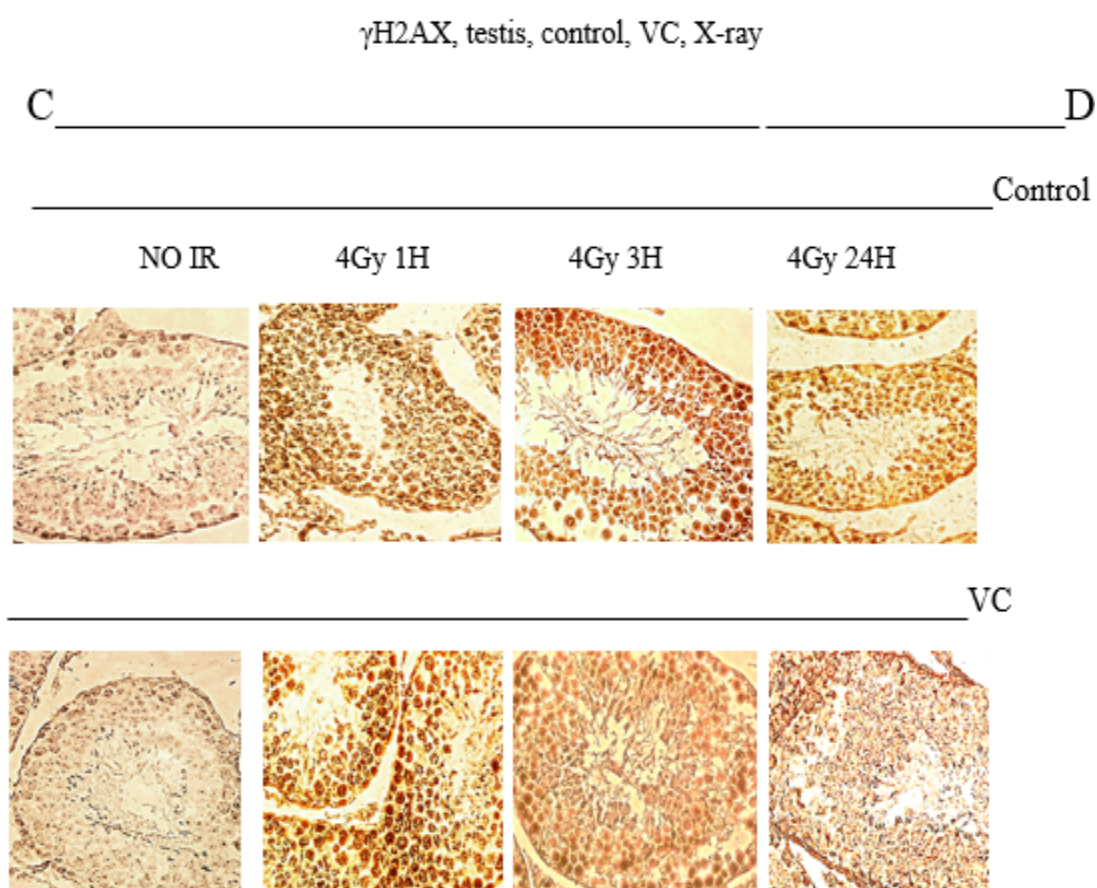


Figure 4. Endogenous DNA damage and DSB capability in control and VC groups with and without IR (X-ray). C and D, Representative IHC images (C) and quantification (D) of γ -H2AX foci formation in testis tissue before and after (4 Gy) of IR in (1, 3, 24 h).

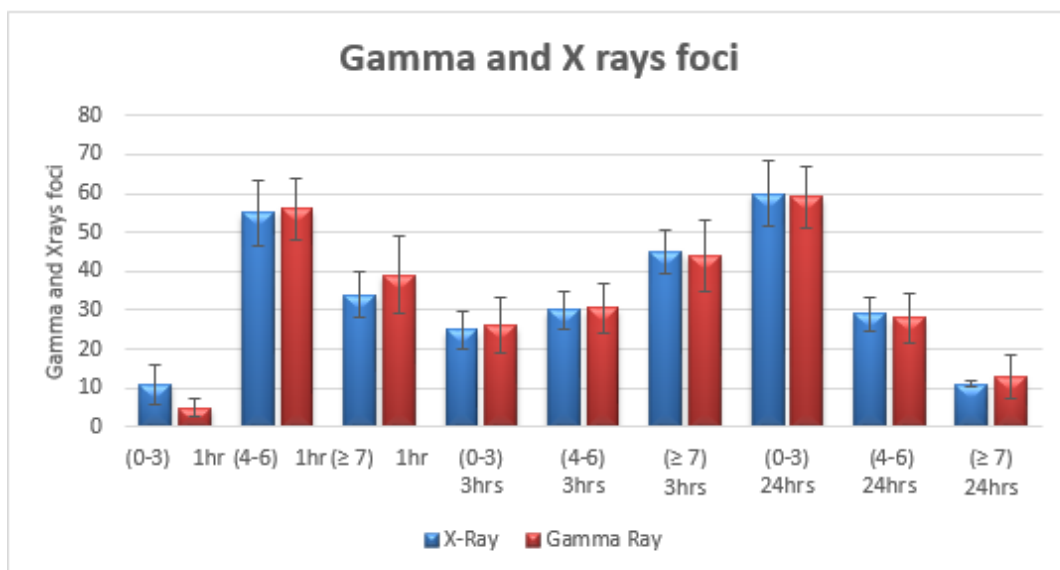


Figure 5. Comparison between Gamma and X-rays in the control group represents γ -H2AX foci of DSB in DNA.

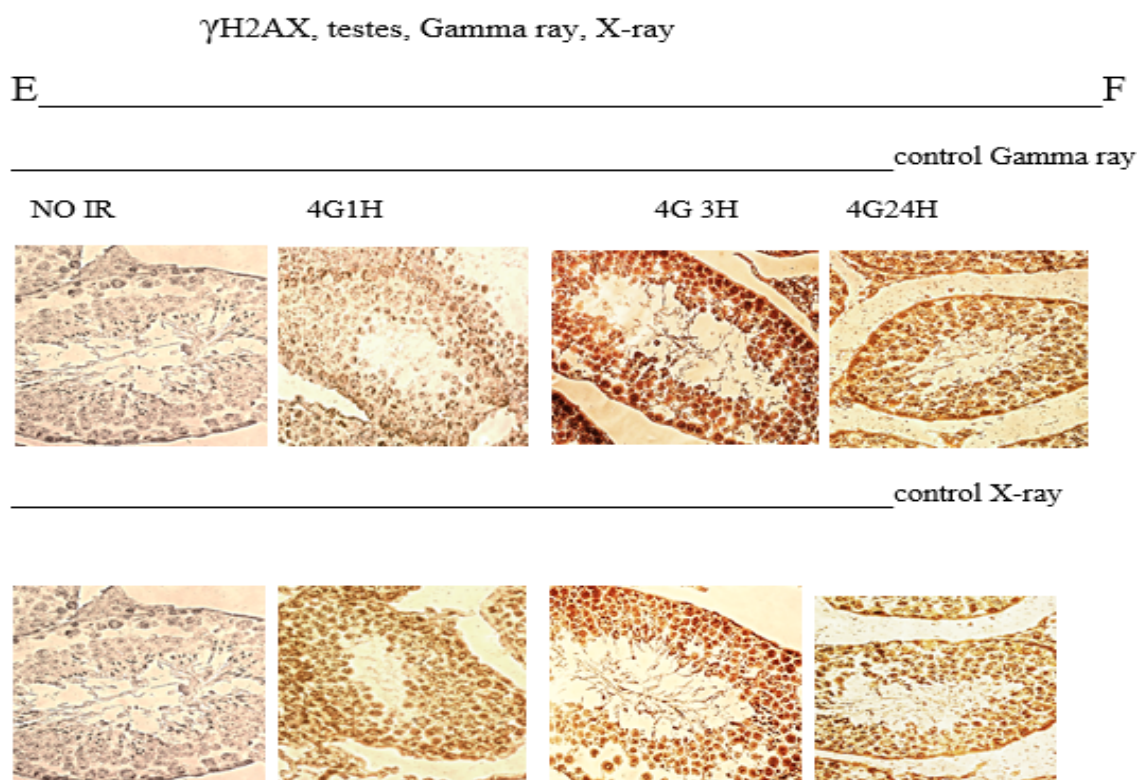


Figure 6. DNA damage and DSB capability in control groups of (γ and X-rays). E and F, Representative IHC images (E) and quantification (F) of γ -H2AX foci formation in testis tissue before and after (4 Gy) of IR in (1, 3, 24 h).

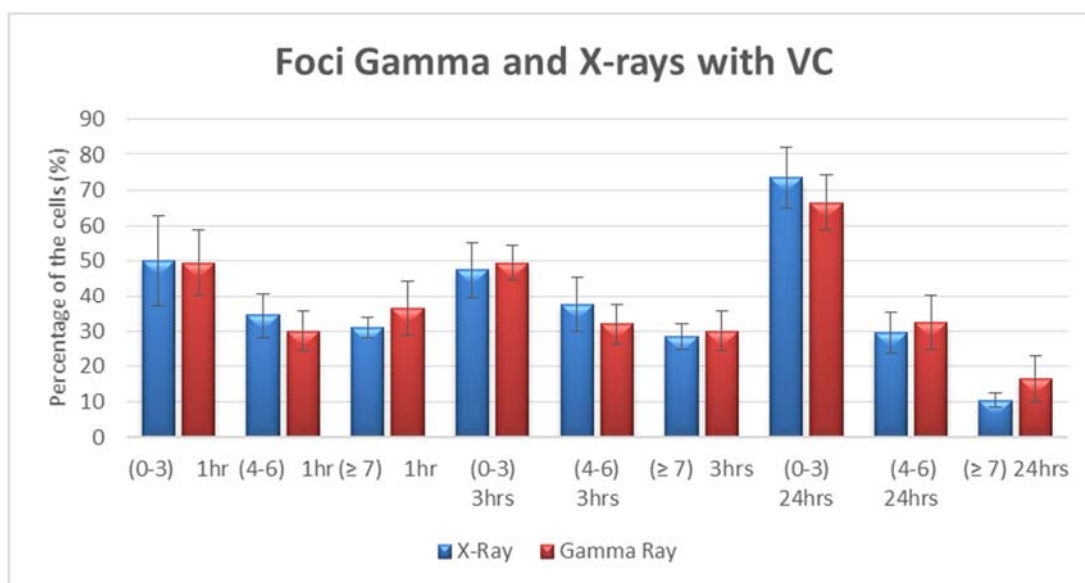


Figure 7. Comparison between Gamma and X-rays administrated with VC represent γ -H2AX foci of DSB in DNA.

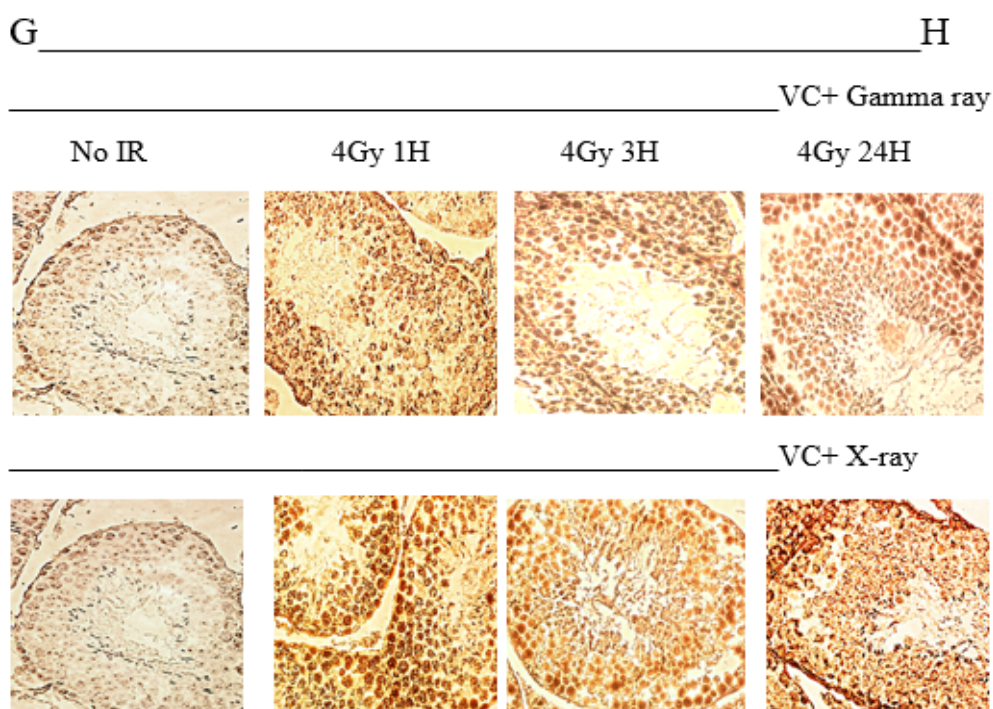


Figure 8. DNA damage and DSB capability in VC groups of (γ and X-rays). G and H, Representative IHC images (G) and quantification (H) of γ -H2AX foci formation in testis tissue before and after (4 Gy) of IR in (1, 3, 24 h).

RAZÃO ESTATÍSTICA DA VARIABILIDADE NA PERSPECTIVA NARRATIVA DE ESTUDANTES**STATISTICAL REASONING OF VARIABILITY IN THE NARRATIVE PERSPECTIVE OF STUDENTS****PENALARAN STATISTIS DALAM PERSPEKTIF NARATIF MAHASISWA TENTANG VARIABILITAS**

RAHMATINA, Desi^{1,6}; NUSANTARA, Toto^{2*}; PARTA, I Nengah³; SUSANTO, Hery⁴; AS'ARI, Abdur Rahman⁵

¹Doctorate Program of Mathematics Education, Universitas Negeri Malang, Faculty of Mathematics and Natural Sciences, Department of Mathematics, Indonesia

^{2,3,4,5} Universitas Negeri Malang, Faculty of Mathematics and Natural Sciences, Department of Mathematics, Indonesia

⁶ Universitas Maritim Raja Ali Haji, Faculty of Teacher Training and Education, Department of Mathematics Education, Indonesia.

** Corresponding author:*

e-mail: toto.nusantara.fmipa@um.ac.id

Received 19 August 2020; received in revised form 22 September 2020; accepted 23 October 2020

RESUMO

O raciocínio estatístico é a maneira como as pessoas raciocinam com ideias estatísticas e dão sentido às informações estatísticas. O raciocínio estatístico desempenha um papel importante e é essencial quando os indivíduos se deparam com fenômenos diários, como o desempenho educacional. A variabilidade é um componente fundamental do raciocínio estatístico. Este estudo teve como objetivo investigar o processo de raciocínio estatístico observado a partir da narração dos alunos a partir da tarefa de variabilidade. O processo de raciocínio estatístico utilizado neste estudo consiste na análise e interpretação dos dados. Existem três indicadores usados no processo de raciocínio estatístico, a saber, a narrativa dos alunos na comparação da variabilidade, fazendo conclusões e tomando decisões com base no gráfico ogiva. Participaram deste estudo 108 alunos da Educação Matemática, dos quais 49 foram selecionados como sujeitos da pesquisa. O sujeito foi escolhido porque havia realizado um processo de raciocínio estatístico usando narrativa com "fazer sentido" sem fazer cálculos matemáticos na conclusão da tarefa. Dois dos 49 alunos foram selecionados para serem entrevistados. Este estudo utilizou dois instrumentos, a saber, uma tarefa escrita e um roteiro de entrevista semiestruturada. Os dados foram analisados por meio de métodos qualitativos com desenho exploratório descritivo. Os resultados deste estudo indicam que duas formas de narrativa emergem quando os alunos empreendem um processo de raciocínio estatístico, a saber, uma narrativa consistente e uma narrativa inconsistente. A narrativa consistente ocorre quando os alunos podem fornecer a mesma narrativa endossada sobre a variabilidade em cada processo de raciocínio estatístico. Enquanto isso, a narrativa inconsistente ocorre quando os alunos fornecem uma narrativa endossada, que é o oposto entre comparar a variabilidade nos dois grupos de dados com a narrativa endossada na tomada de decisões. A inconsistência narrativa resulta na tomada de decisão errada na escolha de um dos dois grupos de dados. Uma narrativa consistente desempenha um papel essencial na tomada de decisão certa. A capacidade de usar conceitos estatísticos é necessária para produzir uma narrativa consistente.

Palavras-chave: raciocínio estatístico, variabilidade, narrativa, narrativa consistente, narrativa inconsistente

ABSTRACT

Statistical reasoning is the way people reason with statistical ideas and make sense of statistical information. Statistical reasoning plays a major role and is essential when individuals are faced with daily phenomena such as educational achievement. Variability is a fundamental component of statistical reasoning. This study aimed to investigate the process of statistical reasoning observed from the students' narration based on the task of variability. The statistical reasoning process used in this study is in analyzing and interpreting the data. There are three indicators used in statistical reasoning, namely students' narrative in comparing variability, making conclusions, and making decisions based on the ogive graph. There were 108 students involved in this

study in Mathematics Education; 49 were selected as research subjects. The subject was chosen because they had carried out a statistical reasoning process using narrative with "make sense" without doing mathematical calculations in completing the task. Two of the 49 students were selected to be interviewed. This study used two instruments, namely a written task and a semi-structured interview guide. The data were analyzed using qualitative methods with an exploratory, descriptive design. This study indicates that two forms of narrative emerge when students undertake a process of statistical reasoning, namely a consistent narrative and inconsistent narrative. The consistent narrative occurs when students can provide the same endorsed narrative about variability in each statistical reasoning process. Meanwhile, the inconsistent narrative occurs when students provide an endorsed narrative, which is the opposite of comparing the variability in the two data groups with the endorsed narrative in making decisions. Narrative inconsistency results in the wrong decision making in choosing one of the two groups of data. A consistent Narrative plays an essential role in making the right decision. The ability to use statistical concepts is needed to produce a consistent narrative.

Keywords: statistical reasoning, variability, narrative, consistent narrative, inconsistent narrative

ABSTRAK

Penalaran statistis merupakan cara orang menalar dengan ide-ide statistis dan membuat sense terhadap informasi statistis. Penalaran statistis memainkan peranan utama dan sangat esensial ketika individu dihadapkan pada fenomena sehari-hari, seperti pencapaian pendidikan. Variabilitas merupakan komponen penting dalam penalaran statistis. Tujuan kajian ini adalah untuk menginvestigasi proses penalaran statistis ditinjau dari naratif mahasiswa berdasarkan tugas tentang variabilitas. Proses penalaran statistis yang digunakan dalam kajian ini adalah menganalisis dan menginterpretasi data. Ada tiga indikator yang digunakan dalam proses penalaran statistis tersebut, yaitu narrative mahasiswa dalam membandingkan variabilitas pada dua kelompok data, membuat kesimpulan, dan membuat keputusan berdasarkan grafik ogive. Mahasiswa yang terlibat dalam kajian ini sebanyak 108 mahasiswa Pendidikan Matematika, 49 diantaranya dipilih sebagai subjek penelitian. Subjek tersebut dipilih karena mereka telah melakukan proses penalaran statistis menggunakan narrative dengan "make sense" tanpa melakukan perhitungan matematis dalam menyelesaikan tugas. Dua dari 49 mahasiswa dipilih untuk diwawancarai. Kajian ini menggunakan dua instrument yaitu tugas tertulis dan pedoman wawancara semi-terstruktur. Data dianalisis menggunakan metode kualitatif dengan pendekatan deskriptif eksploratif. Hasil kajian ini menunjukkan bahwa ada dua bentuk narrative yang muncul ketika mahasiswa melakukan proses penalaran statistis, yaitu narrative konsisten dan narrative inkonsisten. Narrative konsisten terjadi ketika mahasiswa dapat memberikan endorsed narrative yang sama tentang variabilitas pada setiap proses penalaran statistis. Sedangkan narrative inkonsisten terjadi ketika mahasiswa memberikan endorsed narrative yang bertolak belakang antara membandingkan variabilitas pada dua kelompok data dengan endorsed narrative saat membuat keputusan. Narrative inkonsisten berakibat kepada pengambilan keputusan yang keliru dalam memilih salah satu dari dua kelompok data. Narrative konsisten memegang peranan penting dalam membuat keputusan yang tepat. Kemampuan dalam menggunakan konsep-konsep statistis sangat diperlukan untuk dapat menghasilkan narrative yang konsisten.

Kata kunci : penalaran statistis, variabilitas, naratif, naratif konsisten, naratif inkonsisten

1. INTRODUCTION:

Statistical reasoning plays a major role and is essential when individuals are faced with daily phenomena (Bennett *et al.*, 2017) such as economic growth, the spread of diseases, production of goods, education achievement, and employment trend. Therefore, statistical reasoning has been a part of many studies, including the business field (Hoerl and Snee, 2012), education (Coladarci, 2014), law (Gastwirth, 1988), and health (Gagnier and Morgenstern, 2017). Thus, reasoning skills are necessary competencies that students must acquire in studying mathematics (NCTM, 2000).

Statistical reasoning is how people think with statistical ideas and make sense of statistical information (Garfield and Ben-zvi, 2008).

Meanwhile, Kalobo (2016) states that statistical reasoning involves making interpretations based on the collected data or summary of the statistical data. The students need to combine various ideas about data and probability to draw conclusions and interpret statistical results. Statistical reasoning is one of the pertinent learning outcomes in statistics education (Saidi and Siew, 2019). Thus, statistical reasoning can be defined as a person's logical thinking process about analyzing and interpreting data so that a conclusion is reached.

Related to that, variability is one major factor in statistical reasoning (Garfield and Ben-Zvi, 2008; Wells, 2018). Therefore, variability is essential in statistical reasoning. Due to the importance of the variability, the researchers chose the variability in this study because it is the foundation to understand other concepts in

statistics (Burrill and Biehler, 2011; Garfield and Ben-Zvi, 2008). Moreover, Ekol and Sinclair (2016) stated that reasoning about graphs, means, medians, and standard deviations in descriptive statistics requires understanding the variability.

Variability is studied in descriptive statistics at the university level (Cooper, 2018; Sánchez *et al.*, 2011). These materials are the main components in solving inferential statistics problems (Garfield and Ben-Zvi, 2008). For example, in hypothesis testing, sampling distribution, correlation, and regression tests, a good mastery of the variability concept is necessary. One example of the need for variability in hypothesis testing is when comparing the average math test scores between a group of students studying online as a form of distance learning with a group of students studying face-to-face in class, whether there is a significant difference in the average mathematics scores of the two groups of these students or not. In this case, the concept of variability is needed to determine how the variance value in the two data groups. The variance value is one of the variability measures, which is useful for calculating the appropriate statistical value in conducting the hypothesis testing process for two sample groups (Pfannkuch, 2011; Waigandt and Wang, 2010). Besides, the researchers also chose college students as research subjects (e.g., DelMas, R. C., and Liu, Y., 2007; Reading and Reid, 2007; Cooper, 2018; Ekol and Sinclair, 2016) because the concept of the variability is employed by this group of students on an ongoing basis from the lowest to the highest levels of semesters.

Nonetheless, although the reasoning is the main competence that must be possessed since the students are at school, they still have poor statistical reasoning abilities (Chan *et al.*, 2014). The students also misunderstand statistical concepts such as understanding probability (Khazanov and Prado, 2010), *p-value*, and significance (Gagnier, 2017) and random sampling (Karupiah, 2015). Furthermore, the students misunderstand the concepts of interpreting the variability (Cooper and Shore, 2010; Hjalmarsen *et al.*, 2011) in histograms, bar charts, and the values in them (Cooper, 2018).

Previous researchers have conducted studies on statistical reasoning among college students about variability (e.g., Reading and Reid, 2007; Cooper, 2018; Ekol and Sinclair, 2016). The focus of the study conducted by Reading and Reid (2007) was to reveal how the students did their reasoning about variability by using clarification, intuition, inquiry, and cognitive conflict. Meanwhile, Cooper (2018) investigated the

students' conceptions and misconceptions in interpreting variability in several groups of data displayed in the form of histograms, bar graphs, and the values of the bars. The misconceptions occurred during the observation of the height of the bars. The students predicted that higher bars represented higher variability values. The students used graph sense without performing mathematical calculations in comparing the variability of several groups of data on the histogram (Cooper, 2008), bar charts (Cooper, 2018), Chalkboard charts are based on data arising from scientific phenomena (Roth and Temple, 2014). Moreover, Ekol and Sinclair (2016) used Individual Meaning Building (IMB) to analyse the variation of data in a video. The students were able to demonstrate the ability to express standard deviations when faced with changes in graphic and numeric forms in the video. The ability to express changes in objects, as shown in the video, according to Nardi (2016), is called narrative. Lampen (2015) stated that the main factor in statistics is narrative about variation between distributions.

The narrative is a series of expressions that describe objects, processes, and relationships between objects (Sfard, 2008; Nardi, 2016) or activities with or by objects, which could be accepted or rejected within the mathematical discourse (Swidan and Daher, 2019). Objects are all types of entities related to students, teachers, and other stakeholders, while the examples of the narrative are mathematical definitions or theorems labeled with endorsed narratives (Toscano *et al.*, 2019). Furthermore, (Roberts and le Roux, 2019; Tasara, 2017) states that endorsed narrative can be in the form of theories, definitions, proofs, and theorems.

Furthermore, Few and Edge (2009) also state that narrative is to tell a story based on quantitative information, which involves numbers; this kind of narrative is called statistical narrative. Whereas, Noll *et al.* (2018) argue that statistical narrative is a story in constructing and interpreting statistical models. Noll *et al.* (2009) examine how students' narratives when confronted with the context of playing piano notes and relating them to the features of the TinkerPlots software.

Zayyadi *et al.* (2019) researched students' ability to solve mathematical problems from a commognitive perspective. The form of the narrative was indicated when the students explained the theorem of a rectangular area using the concepts of addition and subtraction. Similarly, Lampen (2015) studied the narrative of the concept of statistics in a teacher. He found that

initially, the teacher could not create narratives about the mean as a statistical object. The teacher's explanation was mixed among the mean and other measures of distribution. Through a focused discussion about the mathematical structure of the mean algorithm, the teacher could finally construct a narrative about the mean as a constant.

In carrying out statistical reasoning, the ability to narrate statistical concepts and information is necessary. When someone can perform good statistical reasoning, he/she naturally possesses expertise in narrating how to describe data, organize and reduce data, represent data, and analyze and interpret data. Kalobo (2016) states that statistical reasoning is understanding and explaining the statistical process and interpreting statistical results. In this case, it can be concluded that the ability to narrate is directly proportional to the ability to understand and explain the statistical process.

The narrative concerning this research is the expression in the form of a story or words to describe the process of statistical reasoning in analyzing and interpreting the data displayed in the form of an ogive graph. In the ogive graphic display, students provide arguments or narratives related to variability. Narratives expressed by students based on numerical information on the ogive graph are called statistical narratives.

When someone does a narrative on a concept, it can be contradictory between one statement to another. In line with the research conducted by Tasara (2018), his research shows that teachers explain different word use gradients in the learning process. As a result, students have difficulty in understanding the meaning of the gradient. Researchers suspect that the narrative's inconsistency can occur in the learning process when the teacher explains the subject matter about mathematical concepts. However, the inconsistent narrative can occur in reasoning when someone explains the concept of statistics. For example, students narrate the definition of variability correctly when comparing the variability of several groups of data. However, the rules related to the expressed variability could change when they are making decisions.

Furthermore, Tasara (2018) states that the risks arising from the inconsistent narrative by the teacher are students having difficulty in understanding a concept. Difficulty in understanding concepts results in the difficulty of students doing the process of statistical reasoning. This is because statistical reasoning is based on

understanding statistical concepts (Tempelaar *et al.*, 2006). Students who have good statistical reasoning can express the relationships between statistical concepts (Chance and Garfield, 2001). This shows that the difficulty in understanding the concept due to inconsistent narrative can properly affect someone's difficulty in statistical reasoning. Due to the risk resulting from the inconsistent narrative, the researcher needs to examine from a different perspective from the previous researcher about the narrative.

Tasara (2018) examines the teacher's narrative in explaining the gradient concept in calculus. In this study, researchers examine how students' narratives in conducting a statistical reasoning process about variability. In contrast to Tasara (2018), subjects in their research are not required to connect several concepts in narrating the gradient concept. Whereas in this study, subjects are required to link the relationship of several concepts, such as the relationship between the concept of variability with the mean, median, mode, and concept of normal distribution. The ability to connect among concepts is one characteristic of statistical reasoning (Hidayanto and Rahmatina, 2020).

The narrative plays a vital role in reasoning (Saletta *et al.*, 2020), including statistical reasoning. This is based on the fact that someone is said to have carried out statistical reasoning if they already possessed the characteristics of the statistical reasoning, including being able to connect several concepts, combining various ideas, understanding steps to solve problems, and being able to explain the statistical process (Hidayanto and Rahmatina, 2020). For example, someone who can connect several concepts must be accompanied by his ability to communicate what concepts are involved in solving a problem. Sfard (2008) named the ability to communicate what is thought as commognitive, where one of the frameworks of commognitive is narrative.

This study investigates how the process of statistical reasoning is reviewed from students' narratives based on task about variability. The task was given to students whose data display was in the form of an ogive graph. Statistical reasoning is seen from the "make sense" of students in analyzing and interpreting statistical information on an ogive graph without mathematical calculations.

This study is essentially needed, especially useful for decision-makers such as teachers, principals, and related parties in making decisions when faced with having to choose one group from

several data groups. For example, suppose a principal is given two graphs that contain information on mean, median, and equally large mode values. In that case, he/she then can decide which group of students has more equitable performance and which group should be selected. Therefore, the use of a statistical narrative of graph sense becomes an alternative to make decisions in a short time. In this case, understanding the concept of variability is certainly necessary to the endorsed narrative the form of the graph following the rules of variability.

This study aimed to investigate the process of statistical reasoning on the concept of variability by using narratives. The narrative used by students is in the form of statistical narrative because the expression or argument is based on quantitative information from the display of data in the form of an ogive graph.

1.1. Theoretical Framework

The narrative in this study refers to the Sfrad commognitive framework. Sfrad (2008) stated that thinking is communication, for example, communicating objects, the mediators used, and the rules. Furthermore, Sfrad (2008) also stated that the combination of the words: "communication and cognition" are called commognitive. The commognitive capacity is divided into two categories, namely those related to commognitive objects (such as reasoning, abstracts, and objectification) and those related to commognitive subjects (such as subjectivity and awareness).

The commognitive framework, according to Sfrad (2008), consists of Word Use, Visual Mediator, Narrative, and Routine. The researchers limit this study by only using a commognitive framework in the form of narrative to investigate students' statistical reasoning processes about variability. The statistical reasoning indicators in the narrative perspective used in this study were modified from the indicators of the statistical reasoning of Jones *et al.* (2004), as described in Table 1.

2. MATERIALS AND METHODS:

2.1 Participants

There were 108 students involved in this study (Male: 26 students; female: 82 students; aged 19-21 years) in the fourth semester (two classes) and sixth semester (two classes) of the Mathematics Education Study Program at the Raja Ali Haji Maritime University, Tanjung Pinang, Indonesia. Of the 108 students, 49 students (male:

9; female: 40; aged 19-21 years) were selected as research subjects. Garfield and Ben-zvi (2008) stated that statistical reasoning is making sense of statistical information. Therefore, in this study, the subjects were chosen based on the criterion of having carried out statistical reasoning using statistical narratives in completing tasks about variability by making sense without doing mathematical calculations. Fifty-nine participants were not used as research subjects because they could not complete the task entirely and could not make sense in completing the task. The profile of the participants and the subjects are shown in Table 2. All of the participants took a course in introduction to statistics in the previous semester, and variability was one of the subjects studied. This study was conducted in 2019.

Two of the 49 subjects were chosen to be interviewed in-depth about the narrative they expressed in the statistical reasoning process. There are 25 of the 49 subjects who have the similarity endorsed narrative in comparing variability based on the ogive graph, but having differences in the narrative in making decisions to choose a group that should receive awards. Of those the 25 subjects, there was one subject who chose group A, and 24 subjects chose group B. Therefore, the researcher chose the only one subject who chose group A (S1: female) and randomly chose one of 24 subjects who chose group B (S2: male) to be interviewed. The S2 subject selection as the second subject was due to the same narrative tendency with the other subjects in choosing group B. The procedure for taking the subjects can be seen in Figure 3.

2.2. Instrument

There were two instruments used in this study, including written task and interview guidelines. The task contained a question about variability given classically and worked individually. The task was shown in Figure 1. The task contains one question about variability that was displayed in the form of a positive ogive graph. The subjects were asked to choose one of the two data groups and conclusions obtained from the information on the ogive graph (e.g., graph form, number of students around the center of data, and the scores on the graph).

Both groups had the same mean, median, and mode, within and between the groups. Interview guidelines were made to reveal the student's statistical reasoning process about variability in the narrative perspective in depth. This study used a semi-structured interview method in which the researchers used interview

guidelines (see Table 4) and asked more flexible questions according to the information needed.

2.3. Data Collection Procedure

This study was initial research on the first researcher's dissertation. Besides being a Ph.D. student, the first researcher is also a lecturer in the mathematics education study program at Raja Ali Haji Maritime University. The first researcher requested permission verbally from the head of the Mathematics Education study program at the Raja Ali Haji Maritime University so that researcher could conduct this study. Furthermore, the first researchers asked for the lecturer's time who taught in the fourth semester and the sixth semester in the study program so that the researcher could enter the class to meet the respondents. After agreeing with the possible time, the first researcher entered the classroom to ask students for a willingness to be involved in this study. After students declared their willingness, the first researcher assigned the task to students and supervised them directly in doing the task. After the students worked on the task, the first researcher asked the willingness of two of the forty-nine students to be interviewed. After they stated their willingness, the first researcher and the students agreed regarding the time and place of the interview.

Data sources used in this study were the answers to the written task and the results of the interviews. Initially, the first researcher directly supervised the students while they worked on the task and interviewed respondents. The task was given to students to investigate students' statistical reasoning processes about variability and investigate how students expressed written narratives in this statistical reasoning. Meanwhile, interviews were conducted to obtain more in-depth information about statistical narratives used by respondents in statistical reasoning.

The procedure in collecting data was carried out through the following stages: In the first step, the researchers reduced the data by sorting out the answers of the students who did not use the process of statistical reasoning from those who used the process of statistical reasoning. In the second step, the researchers classified the answers using the statistical reasoning process of variability based on statistical narrative. Students used to make sense without doing mathematical calculations in completing the task. In the third step, the researchers collected the results of the interviews recorded using a voice recording device on the cell phone. The interviews were conducted with two students for 25-40 minutes each.

2.4. Data Analysis Procedure

This study used qualitative methods with explorative (Creswell, 2012), descriptive designs in which researchers investigate, describe, and interpret student reasoning processes about variability. The data analysis process was carried out in three stages. In the first step, the researchers investigated the students' statistical reasoning processes to analyze and interpret data about variability using statistical narrative. In the second step, the interview transcriptions were analyzed based on the task. In the third step, the researchers made conclusions based on research findings.

3. RESULTS AND DISCUSSION:

Analyzing and interpreting data are the main statistical reasoning (Jones *et al.*, 2004). The scope of this process includes identifying trends, making conclusions, data predictions (Jones *et al.*, 2004), and making decisions. Students' narratives in analyzing and interpreting data are shown when the students: 1) revealed a comparison of the variability in the two data groups displayed in an ogive graph. 2) explained conclusions from comparing the observed ogive forms, and 3) narrated a decision on which group should receive awards.

In comparing the variability of mathematics value displayed in ogive, the students' statistical narratives are shown when they explain the comparisons. The variability can be seen from the shape of the ogive curve. Only one subject (S1) narrated the small measure of variability if their frequency is mostly at around the center value and higher measure of variability if fewer students gather around the center value, as seen in Figure 2. This shows that the students can use statistical reasoning by comparing the tool of variability displayed in an ogive graph. However, subjects narrated that the measure of variability is high if the curve shape is not substantially arching; the curve rises stably in the range of 60.5-70.5.

The next process in analyzing and interpreting the data is to draw a conclusion based on variability. Some subjects used statistical narrative the conclusion that good data distribution is where the curve shape is not substantially arching, the curve rises stably. The data distribution is not only centered. Only one subject (S1) concludes that a good data distribution occurs if there were more students' scores gathered around the data center.

The last process in analyzing and

interpreting the data is to decision making. Decision making is essential in the process of statistical reasoning. Making a wrong decision would cause a mistake in giving a reward to those who do not deserve it. Many students (25 subjects) reveal the graph where the students' scores gather around the center value, receiving the awards. Besides, as many as 24 students revealed that group B should receive awards because student scores in group B were more evenly distributed in each range of student grades. Student's interpretation in making the decision is displayed in Table 3.

From Table 3, it appears that there are 25 subjects chose group A which was entitled to the award because the line shape on the ogive graph of group A rose dramatically, and more students gathered around the average. Only one student (S1) of the 25 students revealed that group A variability was smaller than group B variability. Moreover, 24 students (one of them is S2) chose group B, which was entitled to receive the award because the ogive graph of group B statically rose. The students stated that group B's variability in group B was higher than the variability in group A.

There are differences in the narrative expressed by the subjects in statistical reasoning from the two groups of subjects' answers (choosing group A and choosing group B). Three forms of endorsed narrative are used by subjects in choosing one of two data groups (group A or group B). First, the subject chose group A because group A variability was smaller than B group variability (narrative subject S1). Second, the subject chose group A because group A variability was higher than the variability of group B. Third, the subject chose group B because variability in group B was higher than variability in group A (narrative on 24 subjects). In this third narrative, all subjects had the same narrative tendency in carrying out statistical reasoning; for this reason, the researcher chose one of the 24 subjects, the S2 subject, to be interviewed. The first researcher interviewed S1 and S2 subjects to obtain in-depth information about narratives expressed by subjects related to decision making. The selection of S1 and S2 subjects was due to the same narrative tendency in comparing group A and group B's variability. The S1 and S2 subjects were equally narrated that the variability of group A was smaller than group B. However, interestingly, both subjects have different narratives in making decisions. The S1 subject chose group A to receive an award, whereas the S2 subject chose group B to receive the award. Therefore, researchers examined more deeply how the

process of statistical reasoning based on the narrative.

Based on interviews (the script was available in Appendix 1) between the first researcher and subjects, the S1 subject explains that 40 students in Group A had scores in the range of 60.5-70.5. While in Group B, 22 students had the scores in the range of 60.5-70.5. The ability of students in group A is more homogeneous than students in group B. Therefore, and the student decided that group A should be entitled to receive the awards. Meanwhile, the subject S2 revealed that the ability of students in group B was more evenly distributed than students in group A. This can be seen from the distribution of grades in group B that is not only gathered in the range of grades 60.5-70.5 but also spread in the range of other grades. Therefore, the subjects decided that group B should be entitled to receive the awards. Subjects narrative in comparing variability and making decisions are shown in Table 5.

Table 5 shows that the S1 subject provides an endorsed narrative in the form of rules related to variability. There are two endorsed narratives used by S1 subjects in the decision-making process. First, the subject used the definition of variability as a reason for selecting group A. The subject revealed that variability is a measure of the spread of data; if the data accumulates in a range of average values, then the data variability is small. Group A variability was smaller than group B. The subject chose students in group A to receive an award. Second, the subject used the interpretation of variability as a reason for choosing group A. The S1 subject revealed that the ability of students in group A was homogeneous because the students' scores accumulated in a range of average values. The subject's collecting value was seen from the form of a graph that jumped dramatically from 60.5 to 70.5.

Unlike the case with the S2 subject, he narrated that the grade of students in group B spread and not only accumulated around the average value. Thus, groups of students who have spread scores also have a large size of variability. This large variability category was the benchmark for the subject to chose group B.

In this case, there are two narratives expressed by the S2 subject, namely the first narrative about the notion of variability and the second narrative about the interpretation of variability. The subject revealed that variability was used to see the spread of data from the mean because the greater the size of the variability, the

greater the spread of data from the mean. The variability of group B was greater than group A. Thus, the subject chose students in group B to receive an award. However, in the second narrative, the subject revealed that the ability of students in class B was more evenly distributed than grade A. In the first narrative, the subject chose group B because the distribution of students' scores in group B was more varied than scores of students in group A.

Based on the narrative on the S1 and S2 subjects, it can be seen that the narrative expressed by the two subjects is the same in comparing variability. The S1 subject revealed that group A variability was smaller than group B variability because the grades of students in group A piled around the average. Whereas, the S2 subject revealed that group B's variability was higher than group A (the variability of group A was smaller than group B) because the value of group B students spread from the average and did not just accumulate around the average. This shows that the two subjects' endorsed narrative is the same in comparing the variability of the two data groups. However, the narrative difference occurred when the subject chose which group had better student ability, whether it has large variability or small variability. The narrative is important because it influences the subject to decide to choose group A or group B. Endorsed narrative expressed by S1 subject states that the distribution of good grades has a small variability because if the variability is small, the ability of students in the group is homogeneous or does not differ significantly from one student with another student. Whereas the S2 subject revealed that the distribution of good grades was in the group that had large variability because the values of students will spread across each range of grades if the variability was large. In other words, the ability of students in the group is evenly distributed.

The findings in this study indicate that students used two forms of narrative in explaining variability based on the ogive graph, namely a consistent narrative and inconsistent narrative. A consistent narrative can emerge if accompanied by a correct understanding of the concept of variability. To make good statistical reasoning, a consistent narrative is needed in each process of statistical reasoning.

Consistent narrative means that the subject can express endorsed narrative in the form of variability rules in each statistical reasoning process. For example, the subject revealed that the small size variability was interpreted as a

homogeneous data distribution. The subject looked at the small variability of student grades that accumulated in the range of average grades. Based on that thought, subjects chose group A to receive an award. In this case, the subject gave a consistent statement about variability, namely a statement of homogeneous student ability and a statement of student grades piled around an average grade. As a result, the narrative about the variability expressed by the subject is also consistent. This consistent narrative can help the subject did the statistical reasoning process correctly. Saletta *et al.* (2020) also state that narrative plays a vital role in reasoning, problem-solving, and building knowledge.

Meanwhile, inconsistent narrative means that the subject expresses endorsed narrative in the form of variability rules that change or contradict in the process of statistical reasoning. For example, the subject gives a different endorsed narrative when comparing variability in the two data groups and when the subject decides to choose one of the two data groups. When comparing variability, subjects interpret large variability measures as seen from the spread of students' value in each range of grades and not just accumulating in a range of average grades. Thus, if variability is large, students' ability in the group is evenly distributed, or the abilities of students are not too different from each other. On the contrary, in making a decision, the subject revealed that the variability of group B was greater than the variability of group A because the students' score in group B spread. Based on that significant variability, subjects chose group B to receive an award. The statement of student ability is equal, and student value spreads are what researchers consider to be two inconsistent statements about variability. As a result, the narrative about the variability he expressed was also inconsistent. In this case, the inconsistent narrative occurred when comparing the variability of two data groups and when making a decision. As a result, the subjects made the wrong decision in choosing one of two data groups. The fatal effect of this inconsistent narrative was also examined by Tasaraf (2018). The finding of his research indicated that students were confused about understanding the material due to the inconsistent narrative explained by the teacher in delivering the subject matter.

Therefore, in order to overcome the inconsistent narrative in statistical reasoning, the students need to have adequate skills in understanding and connecting the statistics concepts. Besides, students who have excellent statistics skills can do statistical reasoning well

(Rufiana *et al.*, 2018).

The researchers consider that the subject who chose group A because of the smaller variability of group A is a logical narrative compared to the one choosing group B. Information about the average value is not enough to determine which group that has more evenly distributed students' score. However, other values are needed, called variability measures, such as standard deviations and variances. A measure of variability is a measure to determine how the spread of a data set from the average (Mann, 2013; Nachmias and Guerrero, 2018). The more data gathered around the average, the smaller the size of the variability. Suppose a lot of data is gathered around the average. In that case, the ability of students in the group is more homogeneous, or it can be said that the students' ability is not much different from one student to another student. Variability can be used to choose one better group of several groups of data (Amaro and Sánchez, 2019; Kramer *et al.*, 2017). For this reason, researchers assess the narrative proposed by subjects who chose group A can do the correct statistical reasoning using a narrative that follows the rules of variability.

In this study, subjects were not only required to determine which variability is higher or smaller than some data groups (Cooper, 2018), but the subjects are also required to narrate the interpretation of large or small variability so that they can make the right decision. Also, subjects were required to connect several concepts to narrate statistical reasoning well, such as linking the variability concepts with the average, median, mode, and normal distribution. If students cannot connect among statistical concepts, it is not easy to properly carry out statistical reasoning processes. The relationship between concepts by the subjects appears when the subjects use the average concept to narrate variability between groups of data. Thus, the ability of the subjects to relate these concepts is essential so that the narratives expressed can help them carry out statistical reasoning well.

This study is limited to the use of narrative in the process of statistical reasoning. Therefore, further research can be conducted by examining statistical reasoning about variability using other commognitive frameworks such as using word use, visual mediator, and routine.

This research is limited to giving questions about variability as much as one question with the normal distribution of data. Other researchers can provide various forms of questions whose data are typically distributed and have a non-normal

distribution for further studies. Therefore, researchers can obtain more varied findings related to the statistical reasoning process of students about variability in the narrative perspective.

This study provides the implication that a consistent narrative can help students carry out statistical reasoning about variability successfully. The consistency in the narrative must be supported by understanding the correct concept of variability. Subjects who understand the concept of variability can make a logical narrative in explaining statistical reasoning.

4. CONCLUSIONS:

Based on the statistical reasoning process carried out by students in narrating variability in the two data groups on the ogive graph, it can be concluded:

1. There are three statistical reasoning processes performed by the subjects in narrating variability, namely students' narrative in comparing the variability of two data groups, making conclusions, and making decisions.
2. The narrative is a commognitive framework that can be used to investigate in detail how students carry out statistical reasoning processes about variability.
3. Narrative consistency occurs when students can provide an endorsed narrative about the same variability when comparing two groups of data, making conclusions, and making decisions.
4. Narrative inconsistency occurs when students provide an endorsed narrative about opposite variability between comparing two groups of data and choosing one of the two data groups.
5. The consistent narrative plays an essential role in making the right decision. For this reason, the ability and skills to use and connect statistical concepts are needed to produce a consistent narrative.
6. Variability can be used to make decisions in choosing one better group of several groups of data when the data for the two groups are normally distributed.

5. REFERENCES:

1. Amaro, J. A. O., and Sánchez, E. A. (2019). Students Reasoning About Variation in Risk Context. In G. Burrill and D. Ben-Zvi (Ed.), *Topics and Trends in*

- Current Statistics Education Research* (pp. 51–69). Springer Nature Switzerland AG. https://doi.org/10.1007/978-3-030-03472-6_3
2. Bennett, Jeff, Briggs, W. L., and Triola, M. F. (2017). *Statistical Reasoning for Everyday Life* (Fifth Edi). Kirby Street, London. Pearson Education Limited.
 3. Burrill, G., and Biehler, R. (2011). Fundamental statistical ideas in the school curriculum and in training teachers. In C. Batanero, G. Burrill, and C. Reading (Eds.), *Teaching statistics in school mathematics: Challenges for teaching and teacher education (A joint ICMI/IASE Study)* (pp. 57–69). New York, NY: Springer.
 4. Chan, S. W., and Ismail, Z. (2014). Developing a statistical reasoning assessment instrument for high school students in descriptive statistics. *Procedia - Social and Behavioral Sciences*, 116, 4338–4343. <https://doi.org/10.1016/j.sbspro.2014.01.943>
 5. Coladarci, T., Cobb, C. (2014). *Fundamentals of statistical reasoning in education*. (Fourth, Ed.). United States of America: John Wiley and Sons, Inc. https://www.researchgate.net/publication/267480311_Fundamentals_of_statistical_reasoning_in_education_4th_ed
 6. Cooper, L. (2018). Assessing students' understanding of variability in graphical representations that share the common attribute of bars. *Journal of Statistics Education*, 26(2), 110–124. <https://doi.org/10.1080/10691898.2018.1473060>
 7. Cooper, L., and Shore, F. S. (2008). Students' misconceptions in interpreting center and variability of data represented via histograms and stem-and-leaf plots. *Journal of Statistics Education*, 16(2). <https://doi.org/10.1080/10691898.2008.11889559>
 8. Cooper, L. L., and Shore, F. S. (2010). The effects of data and graph type on concepts and visualizations of variability. *Journal of Statistics Education*, 18(2), 1–16. <https://doi.org/10.1080/10691898.2010.11889487>
 9. Creswell, J. W. (2012). *Educational research: Planning, conducting, and evaluating quantitative and qualitative research* (P. A. Smith, C. Robb, and M. Buchholtz (eds.); Fourth Edi). Boylston Street, Boston. Pearson Education, Inc. <https://doi.org/10.1017/CBO9781107415324.004>
 10. DelMas, R. C., and Liu, Y. (2007). Students' conceptual understanding of the standard deviation. In M. C. Lovett and P. Shah (Eds.), *Thinking With data* (pp. 87–116). Mahwah, New Jersey: Lawrence Erlbaum Associates, Inc.
 11. Ekol, G., Sinclair, N. (2016). Undergraduate students' conceptions of variability in a dynamic computer-based environment. In Ben-Zvi D., Makar K. (Ed), *The Teaching and Learning of Statistics*. (pp.193-203). Springer, Cham. https://doi.org/10.1007/978-3-319-23470-0_25
 12. Few, S., and Edge, P. (2009). Statistical narrative telling compelling stories with numbers. *Visual Business Intelligence Newsletter*, 1–10. https://www.perceptualedge.com/articles/visual_business_intelligence/statistical_narrative.pdf
 13. Gagnier, J. J., and Morgenstern, H. (2017). Misconceptions, misuses, and misinterpretations of p values and significance testing. *Journal of Bone and Joint Surgery - American Volume*, 99(18), 1598–1603. <https://doi.org/10.2106/JBJS.16.01314>
 14. Garfield, J. B., and Ben-zvi, D. (2008). *Developing students' statistical reasoning*. USA. Springer New York. <https://doi.org/10.1007/978-1-4020-8383-9>
 15. Garfield, J., and Ben-Zvi, D. (2009). Helping students develop statistical reasoning: Implementing a statistical reasoning learning environment. *Teaching Statistics*, 31(3), 72–77. <https://doi.org/10.1111/j.1467-9639.2009.00363.x>
 16. Gastwirth, J. L. (1988). *Statistical*

Reasoning in Law and Public Policy (2nd ed.). Boston, San Diego, New York. Academic Press, Inc.

17. Hjalmarson, M. A., Moore, T. J., and Delmas, R. (2011). Statistical analysis when the data is an image: Eliciting student thinking about sampling and variability. *Statistics Education Research Journal*, 10(1), 15–34.
18. Hidayanto, E., and Rahmatina, D. (2020). Characteristics of student statistical reasoning in mathematical problem-solving. In *AIP Conference Proceedings* (Vol. 2215, 03002, pp. 1–11). AIP Publishing. Retrieved from <https://doi.org/10.1063/5.0003653> Published.
19. Hoerl, R., and Snee, R. (2012). *Statistical thinking: Improving business performance* (Second Edi). Hoboken, New Jersey. John Wiley and Sons, Inc.
20. Ismail, Z., and Wei, S. (2015). Malaysian students' misconceptions about measures of central tendency: an error analysis. In *The 2nd ISM International Statistical Conference. AIP Conference Proceedings* (Vol. 93). <https://doi.org/10.1063/1.4907430>
21. Jones, G. A., Langrall, C., Mooney, E. S., and Thornton, C. A. (2004). Models of development in statistical reasoning. In Ben-Zvi Dani and Garfield Joan (Ed.), *The Challenge of Developing Statistical Literacy, Reasoning, and Thinking* (pp. 97–116). Springer Science+Business Media, B.V. <https://doi.org/10.1198/tas.2006.s39>
22. Kalobo, L. (2016). Teachers' perceptions of learners' proficiency in statistical literacy, reasoning, and thinking. *African Journal of Research in Mathematics, Science and Technology Education*, 20(3), 225–233. <https://doi.org/10.1080/18117295.2016.1215965>
23. Karupiah, P. (2015). Teaching research methods: common misconceptions related to random sampling. In *USM International Conference on Social Sciences (USM-ICOSS) 2015* (pp. 280–282). https://www.academia.edu/21483523/Teaching_research_methods_common_misc
24. Khazanov, L. and Prado, L. (2010). Correcting students' misconceptions about probability in an introductory college statistics course. *ALM International Journal*, 5(June), 23–35. <https://files.eric.ed.gov/fulltext/EJ1068215.pdf>
25. Kramer, R. S. S., Telfer, C. G. R., and Towler, A. (2017). Visual comparison of two data sets: Do people use the means and the variability? *Journal of Numerical Cognition*, 3(1), 97–111. <https://doi.org/10.5964/jnc.v3i1.100>
26. Lampen, E. (2015). Teacher narratives in making sense of the statistical mean algorithm. *Pythagoras*, 36(1), 1–12. <https://doi.org/10.4102/pythagoras.v36i1.281>
27. Mann, P. S. (2013). *Introductory Statistics* (J. Dingle, E. Keohane, and B. Pearson (eds.); Eighth Edi). John Wiley and Sons, Inc. River Street, Hoboken.
28. Mueller, S. M., Schiebener, J., Delazer, M., Brand, M., and Brand, M. (2018). Risk approximation in decision making: approximative numeric abilities predict advantageous decisions under objective risk. *Cognitive Processing*, (0123456789). <https://doi.org/10.1007/s10339-018-0854-9>
29. Nachmias, C. F., and Guerrero, A. L. (2018). *Social Statistics for a Diverse Society* (J. Lasser, J. Miller, and A. Wilson (eds.); Eighth Edi). Mathura Road, New Delhi: SAGE Publications Asia-Pacific Pte. Ltd. <https://doi.org/10.2307/3211436>
30. Nardi, E. (2016). Where form and substance meet: using the narrative approach of re-storying to generate research findings and community rapprochement in (university) mathematics education. *Educational Studies in Mathematics*, 92(3), 361–377. <https://doi.org/10.1007/s10649-015-9643-x>
31. National Council of Teachers of Mathematics. (2000). Principles and standards for school mathematics.

32. Noll, J., Clement, K., Dolor, J., Kirin, D., Petersen, M., and Noll, J. (2018). Students' use of narrative when constructing statistical models in TinkerPlots. *ZDM*, 0(0), 0. <https://doi.org/10.1007/s11858-018-0981-x>
33. Pfannkuch, M. (2011). The role of context in developing informal statistical inferential reasoning: A classroom study. *Mathematical Thinking and Learning*, 13(1–2), 27–46.
34. Rahmatina, D., and Zaid, N.M.(2019). Students' misconceptions in interpreting the mean of the data presented in a bar graph. *International Journal of Insight for Mathematics Teaching*, 2(1), 57-74. <http://journal2.um.ac.id/index.php/ijoint/article/view/7114/pdf>
35. Reading, C., and Reid, J. (2007). Reasoning about variation: student voice. *International Electronic Journal of Mathematics Education*, 2(3), 110–127. <https://www.iejme.com/download/reasoning-about-variation-student-voice.pdf>
36. Roberts, A., and le Roux, K. L. (2019). A commognitive perspective on Grade 8 and Grade 9 learner thinking about linear equations. *Pythagoras*, 40(1), 1–15. <https://doi.org/10.4102/PYTHAGORAS.V40I1.519>
37. Roth, W., and Temple, S. (2014). On understanding variability in data : a study of graph interpretation in an advanced experimental biology laboratory. *Educ Stud Math*, 86, 359–376. <https://doi.org/10.1007/s10649-014-9535-5>
38. Rufiana, I. S., Sa'dijah, C., Subanji, S., Susanto, H., and Abdur Rahman Asari. (2018). Informal statistical reasoning of students taken formal statistics learning related to distribution. *International Journal of Insight for Mathematics Teaching*, 01(2), 130–140.
39. Saidi, S.S, Siew,N.M,(2019). Reliability and validity analysis of statistical reasoning test survey instrument using the rasch measurement model. *International Electronic Journal of Mathematics Education*, 14(3), 535-546. <https://doi.org/10.29333/iejme/5755>
40. Saletta, M., Kruger, A., Primoratz, T., Barnett, A., Van Gelder, T., and Horn, R. E. (2020). The role of narrative in collaborative reasoning and intelligence analysis: A case study. *PLoS ONE*, 15(1), 1–17.
41. Sánchez, E., Silva, C. B. da, and Coutinho, C. (2011). Teachers' Understanding of Variation. In C. Batanero, G. Burrill, and C. Reading (Eds.), *Teaching Statistics in School Mathematics-Challenges for Teaching and Teacher Education: A Joint ICMI/IASE Study* (pp. 211–221). México D.F., Mexico Springer Science+Business Media B.V.
42. Sfard, A. (2008). *Thinking as communicating: Human development, the growth of discourses, and mathematizing*. New York, NY: Cambridge University Press.
43. Swidan, O, and Daher, M. W. (2019). Low achieving students' realization of the notion of mathematical equality with interactive technological artifacts. *Eurasia Journal of Mathematics, Science and Technology Education*, 15(4), 1–15. <https://doi.org/https://doi.org/10.29333/ejms/103073>
44. Tasara, I. (2017). Commognitive analysis of a teacher's mathematical discourse on the derivative. In *Proceedings of the British Society for Research into Learning Mathematics* 37(3). pp. 1–6. <https://bsrlm.org.uk/wp-content/uploads/2017/12/BSRLM-CP-37-3-12.pdf>
45. Tasara, I. (2018). Making sense of the teaching of calculus from a commognitive perspective. *Proceedings of the 42nd Conference of the International Group for the Psychology of Mathematics Education*, 1, 267–274
46. Tempelaar, D. T., Gijssels, W. H., Loeff, S. S. Van Der, Tempelaar, D. T., and Gijssels, W. H. (2006). Puzzles in Statistical Reasoning Puzzles in Statistical Reasoning. *Journal of Statistics Education*

47. Toscano, Rocío, José María Gavilán-Izquierdo, V. S. (2019). A study of pre-service primary teachers' discourse when solving didactic- a study of pre-service primary teachers' discourse when solving didactic-mathematical tasks. *Eurasia Journal of Mathematics, Science and Technology Education*, (May). <https://doi.org/10.29333/ejmste/108631>
48. Waigandt, A., and Wang, Z. (2010). *An Introduction to Statistical Reasoning in Quantitative Research Third Edition* (Third Edition, Issue January 2010). Morris Publishing. Kearney, Nebraska.
49. Wells, J. F. (2018). Dot plots and hat plots : supporting young students emerging understandings of distribution, center, and variability through modeling. *ZDM*, 50(7),1125-1138. <https://doi.org/10.1007/s11858-018-0961-1>
50. Zayyadi,M, Nusantara,T. Subanji, Hidayanto, E., Sulandra, I.M. (2019). A commognitive framework: the process of solving mathematical problems of middle school students. *International Journal of Learning, Teaching and Educational Research*.18(2), pp. 89-102. <https://doi.org/10.26803/ijlter.18.2.7>

Table 1. *Statistical Reasoning Indicators Employed in this Study*

Process	Indicators	
	Jones <i>et al.</i> (2004)	This Study
Analyzing and Interpretin g data	(a) using mathematical operations to combine, integrate, and compare data (b) make inferences and predictions from the data.	(a) Narrating the differences variability two groups of data displayed in ogive form using statistical narrative (b) Narrating a conclusion of a group of data or the given data presentation (c) Narrating a decision based on the differences and conclusion among groups of data

Table 2. *Profile of participants and subjects in this study*

	Gender	Semester	The number	Subtotal	Total
Number of participants	Male	Fourth	14	26	108
		Sixth	12		
	Female	Fourth	38	82	
		Sixth	44		
Number of subjects	Male	Fourth	5	9	49
		Sixth	4		
	Female	Fourth	15	40	
		Sixth	25		

Table 3. *Narrative of subjects in making decisions*

Decision	Narrative of students on the ogive graph
Group A (25 subjects)	<ul style="list-style-type: none"> • A drastically rose (25 subjects) • Group A variability is smaller than group B (1 subject) • Group A variability is greater than group B (24 subjects)
Group B (24 subjects)	<ul style="list-style-type: none"> • B statically rose (24 subjects) • The variability of group B is greater than group A (24 subjects)

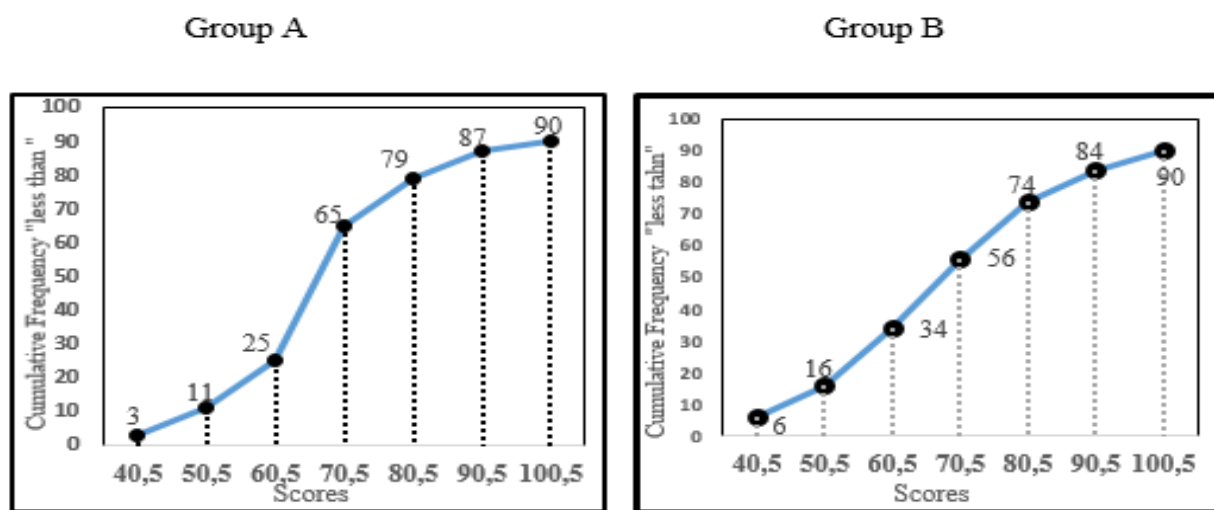
Table 4. Interview guidelines in this study

Indicators	Questions
Describing data	1. What do x and y axes mean in graphic ogive? 2. What was the initial step that came to your mind to work on the problem? 3. What do you mean by the problem that mean, median, and mode are the same in a group or between groups? 4. How did you think about the problem?
Comparing the variability of two groups	5. What is variability? 6. What is the use of variability? 7. Which group has the greatest variability?
Making conclusions about the variability of the two groups	8. Which one is better data spread or centralized?
Making decisions	9. Which group should receive the award? 10. Which group of students have the better ability?

Table 5. Subjects narrative in making comparisons and making decisions

Subject	Make a graph comparison	Make a decision
S1	The lines on the group A ogive jumped up dramatically from 60.5 to 70.5. Students score a lot in the range of grades 60.5 to 70.5. The ability of students in group A is more homogeneous than the ability of students in group B.	Awards should be given to students in group A because Group A variability is smaller than B group variability
S2	The line in group B ogive rises statically from 60.5 to 70.5. Student scores spread across each range of grades, not only piling up in a range of 60.5 to 70.5 grades. The ability of students in group B is more evenly distributed than students in group A.	Awards should be given to students in group B because B group variability is more significant than group A

The "Positive Ogive" graph below shows the distribution of mathematics test scores of two groups of students (Group A and Group B) who have the same mean, median, and mode within and between groups. The school will give an award to one of the two groups based on the of variability.



Based on the distribution of values on the "positive ogive" of the above two groups, which group should receive awards from the school? State your reason.

Figure 1. The task of variability in this study

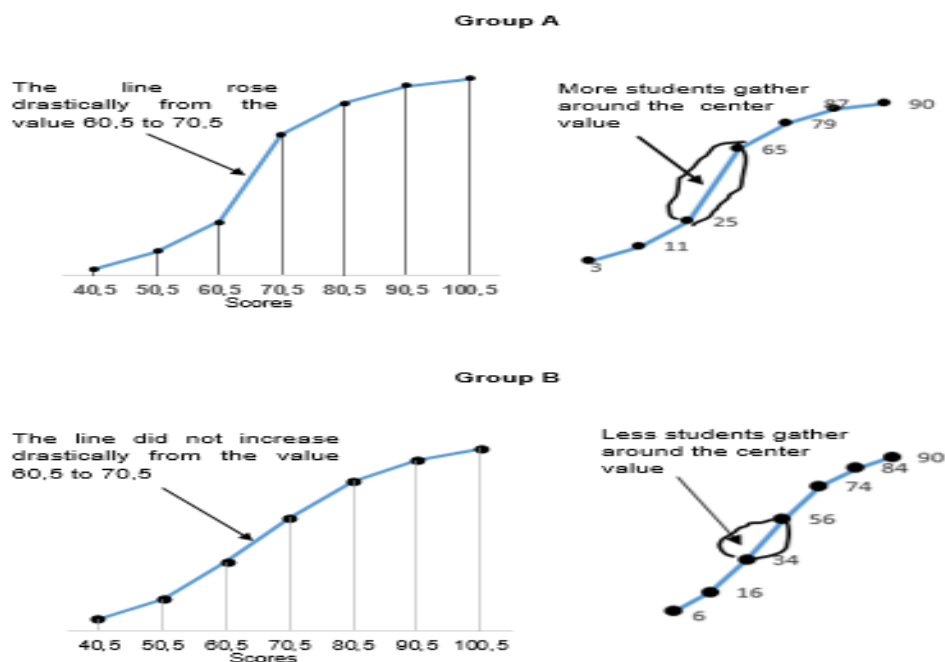


Figure 2. One of forty-nine students answer to compare the variability of two data groups

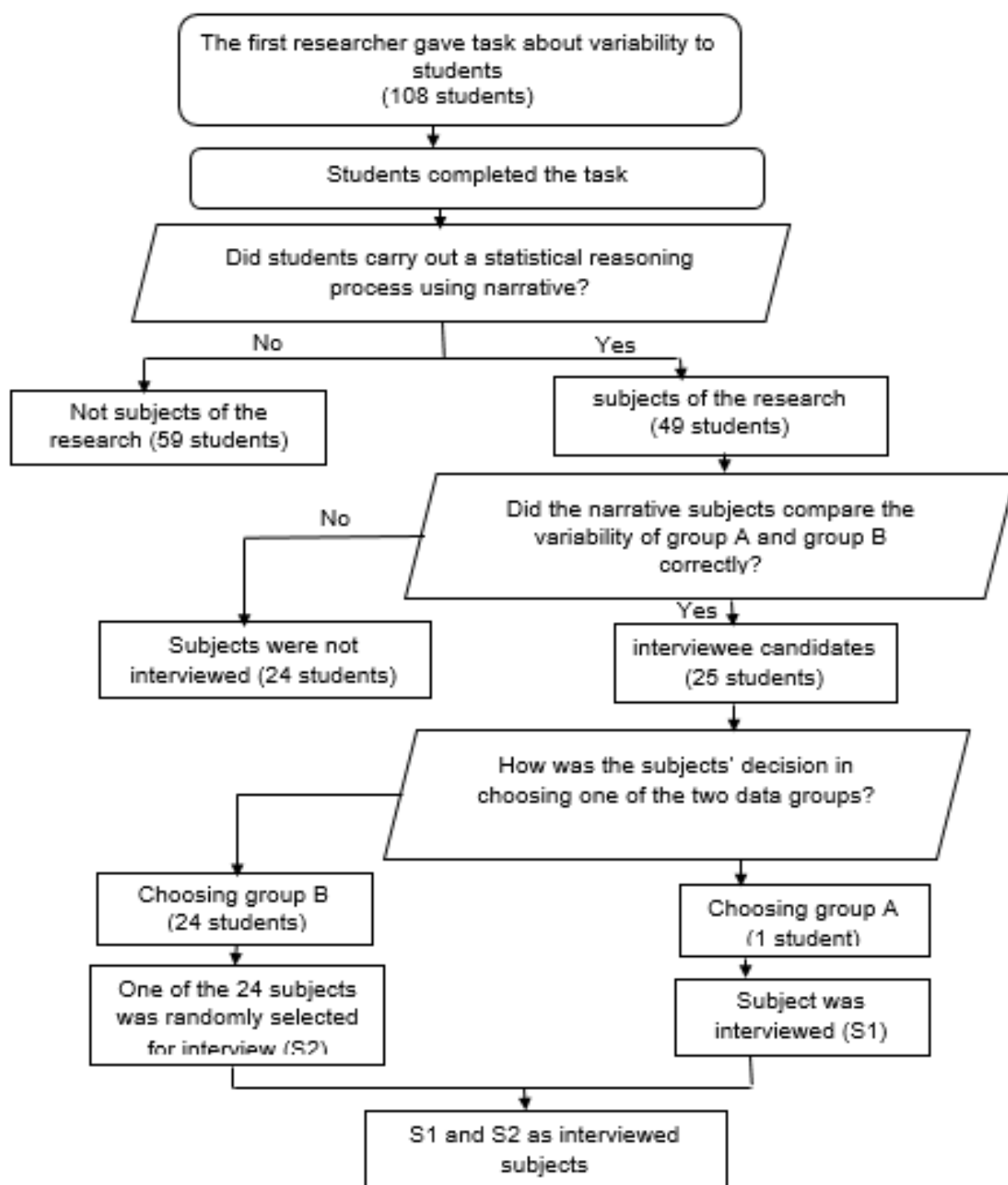


Figure 3. The procedure for selecting research subjects

APPENDIX 1

A script of the interview the first research (R) with Student S1 (S1)

R: How are you?

S1 : Fine, Ma'am,

R : I want to interview you regarding your answers to the task that you completed. Are you ready?

S1 : Yes, Ma'am,

R: I give you times to look back at the answer you wrote, Ok?

S1 : (S1 pays attention to the answer paper that she made)

R: Are you ready to be interviewed?

S1: yes, Ma'am

R: What do x and y axes mean in ogive?

S1: X axis, hmmm the upper class boundaries, Y axis number of students are less than the upper class boundaries.

R : What else can be read from ogive?

S1: Hmm what is it? Hmm.. Where the center is and how many it is, whether it increases sharply (while pointing to the graph of group A) or perhaps like this (pointing to graphic ogive of group B). Is it dynamic Ma'am, while this one increases sharply (pointing to ogive of group A), increase dramatically, there is a big gap.

R: What was the initial step that came to your mind to work on the problem?

S1: Firstly, I began with writing cumulative frequency with curvature, given a mark value of less than 40.5 is 3, less than 50,5 is 11, and so on until less than 100.5 is 90. Next, I made the frequency of each value to prove the number of students as 90. Then it was said that the school would give awards to groups based on variability.

R: How did you do it?

S1: Well 90 students means the middle value is at 45. Then I looked for the 45th student to be at what value, meaning the 45th student is in which grade, in which class, the class boundaries, so the 45th student was between frequency of 25 and 65 in the group A, and between frequency of 34 and 56 in the group B at the class boundary 60.5 - 70.5. So, more students are in group A, there are 40 students, while in group B, there are 22 students at the class boundary 60.5 - 70.5.

R: What do you mean by the problem that mean, median, and mode are the same in a group or between groups?

S1: For example, the mean is 65, and therefore the median and mode is also 65.

R: What are the measure of variability that you know?

S1: Hmmm ... there is a standard deviation, there is another range ... there is one more ... I didn't remember, Ma'am...

R: What is the use of variability?

S1: To find out whether the extent of data distribution is far or not.

R: How do we know that the distribution is far?

S1: It is far. We can see from the centre, Ma'am.

R: Which group has the greatest variability?

S1: Group B, Ma'am

R: why?

S1: because in group B fewer students were in the center of the data than group A, Ma'am

R: which one is better data spread or centralized?

S1: Center, Ma'am

R: Which group should receive the award?

S1: Group A, Ma'am.

R: Why was it decided that group A should get an award?

S1: Because it increases sharply in the centre of the data, so more students are at the class boundary 60.5 - 70.5, so that the ability is more homogeneous.

A script of interview the first research (R) with Student S2 (S2)

R: How are you?

S2 : Fine, ma'am,

R : I want to interview you regarding your answers to the task that you completed. Are you ready?

S2 : Yes, ma'am,

R: I give you times to look back at the answer you wrote, Ok?

S2 : (S2 pays attention to the answer paper that he made)

R: Are you ready to be interviewed?

S1: yes, Ma'am

R : What was the initial step that came to your mind to work on the problem?

S2: I read the problem, and I noticed the ogive graph form

R: What does number 3 mean in the ogive of group A?

S2: There are 3 students whose scores are under 40.5.

R: What does number 11 mean in the ogive in group A?

S2: There are 11 students under 50.5.

R: How did you think about the problem?

S2: I saw graphical form between groups A and B, some increase sharply.

R: What do you mean by the problem that mean, median, and mode are the same in a group or between groups?

S2 : Group A has the same mean, median, and mode. The mean, median, and mode values in group B were the same as for group A, Ma'am.

R: What is variability?

S2: The spread value is more to the standard deviation.

R: What's the function?

S2: To see the data distribution spreads widely or not.

R: which one is better data spread or centralized?

S2: Spreading, Ma'am

R: Why?

S2: If the data is spread out, it means that the distribution of the scores is balanced ma'am, students who get high, medium, and low scores are balanced, the data do not just accumulate in the middle score, ma'am.

R: What is the middle score?

S2: between the scores 60.5-70.5 Ma'am

R: Which group has better student ability?

S2 : Group B, Ma'am

R: Why?

S2: because the students' abilities were almost the same in group B, the scores were even

R: Which group has the greatest variability?

S2: Group B, Ma'am

R: Why?

S2: because of the lines in the group B graph increase in statically Ma'am. The scores do not just accumulate in the centre; however, the scores were spread out equally.

R: Which group should receive the award?

S2: Group B, Ma'am.

P: Why?

S2: Because the variability of group B was greater than group A, and the increase of ogive form of group B spreads up, ma'am, not gathering like group A

O USO DO EXTRATO DE *Cyperus kyllinga* NA SÍNTESE DE NANOPARTÍCULAS DE PRATA PARA MELHORAR A QUALIDADE DE COURO DE CABRA

THE USE OF *Cyperus kyllinga* EXTRACT IN SYNTHESIS OF SILVER NANOPARTICLE TO ENHANCE QUALITY OF GOAT LEATHER

PENGGUNAAN EKSTRAK *Cyperus kyllinga* DALAM SINTESIS NANOPARTIKEL PERAK UNTUK MENINGKATKAN KUALITAS KULIT KAMBING

ROHAETI, Eli^{1*}; PUTRI, Nur Isna Melati²; BUDIASIH, Kun Sri³; RAKHMAWATI, Anna⁴

^{1,2,3} Universitas Negeri Yogyakarta, Faculty of Mathematics and Natural Sciences, Department of Chemistry Education, Indonesia

⁴ Universitas Negeri Yogyakarta, Faculty of Mathematics and Natural Sciences, Department of Biology Education, Indonesia

* Corresponding author
e-mail: eli_rohaeti@uny.ac.id

Received 01 August 2020; received in revised form 21 August 2020; accepted 08 September 2020

RESUMO

Melhorar a qualidade do couro com propriedades antifúngicas, antibacterianas e mecânicas superiores é um esforço contínuo. Os objetivos desta pesquisa foram sintetizar nanopartículas de prata utilizando o extrato de *Cyperus kyllinga* como bioagente e depositar as nanopartículas de prata sintetizadas no couro de cabra *ex situ* e *in situ*, além de caracterizar as propriedades antibacterianas, antifúngicas, mecânicas e ângulo de contato do couro de cabra antes e depois da modificação. As nanopartículas de prata foram preparadas pelo método de redução adicionando o extrato de folha de *Cyperus kyllinga*. As nanopartículas de prata foram caracterizada utilizando espectrofotômetro UV-Vis e classificação granulométrica. A adição do composto metiltrimetoxissilano (MTMS) na amostra de couro para conhecer as propriedades de hidrofobicidade do couro. O couro foi modificado pela adição de nanopartículas de prata e compostos de silano. Os testes antibacteriano e antifúngico foram realizados pelo método de difusão e testada a significância por meio de análise estatística. Foram realizados testes de propriedades mecânicas por meio de ensaios de resistência à tração, alongamento e também módulo de Young utilizando um testador de tração. A superfície do couro de cabra modificado foi testada quanto ao ângulo de contato pelo método da gota sêssil. Os resultados da caracterização indicaram que as nanopartículas de prata foram formadas no comprimento de onda de 406,60 nm, com tamanho de partícula de 200,1 nm. Os resultados do teste antimicrobiano mostraram que o couro de cabra modificado utilizando dois métodos de preparação teve significância diferente para inibir *S. epidermidis* e *E. coli*, e também fungos de *C. albicans*. O couro, após a modificação com nanopartículas pelo método *in situ*, apresentou as maiores atividades antibacterianas contra *S. epidermidis* e *E. coli*, no entanto, o couro após a modificação com adição de nanopartículas e MTMS pelo método *ex situ* tem a maior atividade antifúngica contra *C. albicans*. O couro após modificação da nanopartícula e do MTMS via método *in situ* possui a maior resistência à tração e a maior tenacidade. Todos os couros modificados apresentaram maior atividade antimicrobiana, ângulo de contato e também tenacidade em comparação ao couro não modificado.

Palavras-chave: anti-fungo contra *C. albicans*, extrato de *Cyperus kyllinga*, bactericida para *S. epidermidis* e *E. coli*, couro de cabra, couro autolimpante.

ABSTRACT

Improving leather quality with antifungal, antibacterial, and superior mechanical properties is an ongoing effort. The objectives of this research were to synthesize silver nanoparticle using *Cyperus kyllinga* extract as a bio-agent and to deposit synthesized silver nanoparticle into goat leather by *ex situ* and *in situ*, and also to characterize the properties of antibacterial, antifungal, mechanical, and contact angle of goat leather before and after modification. Preparation of silver nanoparticles by reduction method by adding *Cyperus kyllinga*'s leaf extract. The silver nanoparticle was characterized by using spectrophotometer UltraViolet-Visible and Particle

Size Analyzer. The addition of Methyltrimethoxysilane (MTMS) compound on the leather sample to know hydrophobicity properties of the leather. The leather was modified by adding silver nanoparticle and silane compounds. The antibacterial and antifungal test was conducted by the diffusion method and tested the significance by using statistical analysis. The mechanical properties were tested through tensile strength test, elongation, and also modulus Young by using a tensile tester. The modified goat leather surface was tested the contact angle by using the sessile drop method. The characterization results indicated that silver nanoparticles were formed at a wavelength of 406.60 nm, with their particle size were 200.1 nm. The results of the antimicrobial test showed that modified goat leather using two methods of preparation had a different significance to inhibit the *S. epidermidis* and *E. coli*, and also fungi of *C. albicans*. The leather, after modification with nanoparticle via *in situ* method, had the highest antibacterial activities against *S. epidermidis* and *E. coli*. However, leather after modification with adding nanoparticle and MTMS via *ex situ* method has the highest antifungal activity against *C. albicans*. The leather after modification nanoparticle and MTMS via *in situ* method has the highest tensile strength and the largest toughness. All modified leathers had larger antimicrobial activity, contact angle, and also toughness compared to unmodified leather.

Keywords: *anti-fungi against C. albicans, Cyperus kyllinga extract, antibacterial against S. epidermidis and E. coli, goat leather, self-cleaning leather.*

ABSTRAK

Peningkatan kualitas kulit dengan karakteristik antijamur, antibakteri, dan sifat mekanik unggul merupakan usaha yang harus dilakukan. Tujuan dari penelitian ini adalah untuk mensintesis nanopartikel perak menggunakan ekstrak *Cyperus kyllinga* sebagai bioreduktor dan untuk mendepositkan nanopartikel perak terhadap kulit kambing secara *ex situ* dan *in situ*, serta untuk mengkarakterisasi sifat-sifat antibakteri, antijamur, sifat mekanik, dan sudut kontak dari kulit kambing sebelum dan sesudah modifikasi. Preparasi nanopartikel perak dilakukan secara reduksi oleh ekstrak daun *Cyperus kyllinga*. Nanopartikel perak dikarakterisasi menggunakan spektrofotometer UltraViolet-Tampak dan alat Penganalisis Ukuran Partikel. Penambahan senyawa Metiltrimetoksisilan (MTMS) pada kulit untuk mengetahui sifat hidrofobisitas kulit. Kulit dimodifikasi melalui penambahan nanopartikel perak dan senyawa silan. Pengujian antibakteri dan antijamur dilakukan dengan metode difusi dan uji signifikansi dengan analisis statistik. Sifat mekanik yang diuji meliputi kuat putus, perpanjangan, dan modulus *Young*. Permukaan kulit kambing sesudah modifikasi diuji sudut kontakannya melalui metode tetes sessile. Hasil karakterisasi menunjukkan nanopartikel perak berhasil disintesis pada panjang gelombang 406,60 nm dengan ukuran partikel 200,1 nm. Hasil pengujian antimikroba menunjukkan bahwa kulit kambing hasil modifikasi dengan kedua metode memiliki perbedaan signifikan dalam menghambat *S. epidermidis* dan *E. coli*, serta jamur *C. albicans*. Kulit hasil modifikasi dengan nanopartikel secara *in situ* memiliki aktivitas antibakteri tertinggi terhadap *S. epidermidis* dan *E. coli*. Adapun kulit hasil modifikasi dengan penambahan nanopartikel dan MTMS secara *ex situ* memiliki aktivitas antijamur tertinggi terhadap *C. albicans*. Kulit hasil modifikasi dengan penambahan nanopartikel dan MTMS secara *in situ* memiliki kuat putus dan keuletan paling tinggi. Semua kulit hasil modifikasi memiliki aktivitas antimikroba, sudut kontak, dan keuletan lebih tinggi dibandingkan dengan kulit tanpa modifikasi.

Kata kunci: *antijamur terhadap C. albicans, ekstrak Cyperus kyllinga, antibakteri terhadap S. epidermidis dan E. coli, kulit kambing, kulit anti-kotor.*

1. INTRODUCTION:

The leather and textile industry has progressed in recent years and is one of the pioneering sectors in the application of the Indonesian industry 4.0. Based on statistical data obtained from the Directorate General of Livestock and Animal Health (2018), exports of leather products reach 76.750.012 USD per the year 2017. The results of leather exports are the most significant results among other non-food animal products. Also, leather and leather products are included in the order of 10 potential export commodities in 2012-2017. As reported by the Ministry of Industry, the leather and textile industry

is one of the country's biggest foreign exchange earners and ranks third of all export commodities in Indonesia. Achievement of export value in 2018 was obtained at USD 18.96 billion or a sum of 10.52% of the total national exports in that year. The high interest in leather in the community is necessary to have an effort to improve the quality of the leather.

To improve the quality of the leather industry it is necessary to develop antimicrobial leather. Silver nanoparticles have been known to have interesting physicochemical properties. Also, the strong toxicity shown by silver in various chemical forms for a variety of microorganisms is reported to be very good. Silver nanoparticles

have been proven to have good antimicrobial properties and are also environmentally friendly (Amin *et al.*, 2009; Muliawati and Yulianti, 2018). Silver nanoparticles are also one of the antibacterial agents which are non-toxic and safe for the human body. Also, silver nanoparticles are reported to have antifungal activity (Kalishwaralal *et al.*, 2010).

In general, metal nanoparticles can be prepared by physical (top-down) and chemical (bottom-up) methods (Sharma *et al.*, 2009; Rohaeti *et al.*, 2020). Silver nanoparticles can be obtained by various methods, including the microwave irradiation method (Hasany *et al.*, 2013), photochemical method (Selvam and Sivakumar, 2015; Ahmed *et al.*, 2016), ball milling method (Maamoun and Khairy, 2013), electrochemical method (Viorel *et al.*, 2012), chemical reduction (Zhang *et al.*, 2014; Rohaeti and Rakhmawati, 2017). The method most often used is the chemical reduction method. Research in nanotechnology can use environmentally friendly processes for the synthesis of nanoscale materials such as "green" chemistry (Nanda and Saravanan, 2009; Abd-Elnaby *et al.*, 2016; Buszewski, 2016; Gopinath *et al.*, 2016). Among the many methods of nanoparticle synthesis, the biosynthetic method is more environmentally friendly, cost-effective, and safer for therapeutic use in humans (Salem *et al.*, 2015; Rohaeti *et al.*, 2020).

Plant extracts that can be used for the preparation of the synthesis of silver nanoparticles are leaves of *Cyperus kyllinga* as a reducing agent. Until now, *Cyperus kyllinga* leaves are still not widely used by many researchers. However, *Cyperus kyllinga* has been reported to have compounds that are antioxidants. Antioxidant compounds contained in *Cyperus kyllinga* extract included polyphenolic compounds, flavonoids, and tannins. The tannin compounds contained in this *Cyperus kyllinga* leaf extract were thought to play an essential role in the process of reducing Ag^+ to Ag^0 (Sindhu *et al.*, 2014).

To get a self-cleaning leather (hydrophobic) can use compounds that can give rise to the water contact angle of the material. Compounds that are often used to obtain self-cleaning properties are silane compounds and their derivatives. A material that is deposited by silane compounds with low surface energy has been shown to increase the hydrophobicity of a material. In this study, silane compounds (methyltrimethoxysilane/MTMS) are used because these compounds can produce hydrophobic leather surfaces.

Antimicrobial testing methods in a sample are divided into several types, namely the diffusion method (Kirby-Bauer and Stokes), the dilution method, and the diffusion and dilution method (Guzmán *et al.*, 2009). The antimicrobial testing method that is often done in several studies is the diffusion method. This study also used the diffusion method by measuring the diameter of the inhibitory zone or clear zone, which is used as an indicator of the effectiveness of the sample in inhibiting microbial activity. The microbial used were *Escherichia coli* as gram-negative bacteria and *Staphylococcus epidermidis* as gram-positive bacteria, and *Candida albicans* as fungi.

This research aimed to synthesize silver nanoparticles using *Cyperus kyllinga* leaf extracts to utilize the use of *Cyperus kyllinga* in improving the quality of goat leather. Characterization techniques performed on goat leather material included UV-Vis and particle size analysis to analyze the success of silver nanoparticle formation, mechanical properties (tensile strength) test, contact angle test to determine its hydrophobicity, and antibacterial and antifungal activity tests.

2. MATERIALS AND METHODS:

The types of equipment used in this study were a UV-Vis spectrophotometer, particle size analyzer (PSA), analytical scales, hot plates, magnetic stirrers, shakers, glassware, Petri dishes, autoclaves, inoculating loop, tensile test machines, cameras, and calipers. The materials used included pickle goat, turf leaves, solid AgNO_3 , starch, MTMS, distilled water, nutrient agar (NA), nutrient broth (NB), Potato Dextrose Agar (PDA), Potato Dextrose Broth (PDB), *Escherichia coli* FNCC 0048, *Staphylococcus epidermidis* DNCC 6018, *Candida albicans* ANCC 0048.

2.1. Procedure

2.1.1. Preparation of silver nanoparticle

The silver nanoparticle was prepared by biosynthesis methods using the extract of leaves. AgNO_3 solution was changed by the extract of *Cyperus kyllinga* leaves. The *Cyperus kyllinga* leaves acted as a bioreductor. The preparation of silver nanoparticles has used the leaves of *Cyperus kyllinga* begins with the preparation of a *Cyperus kyllinga* leaf extract. The *Cyperus kyllinga* leaves were washed clean and weighed as much

as 25 grams. Then put in a beaker glass and added 250 mL of distilled water, and boil for 15 minutes at a temperature of 80 °C. The cold boiled water is filtered using Whatman No.42 filter paper. The *Cyperus kyllinga* leaf extract was used to reduce silver nitrate. A total of 10 mL of turf leaves extract was put into a 100 mL Erlenmeyer, then 65 mL of $0.5 \cdot 10^{-3}$ M AgNO_3 solution was added.

Furthermore, the solution was allowed to stand for ± 2 hours to react. After that, 25 mL of 0.05% starch solution was added to the mixture while stirring for ± 2 hours. The solution was allowed to stand for two days to form a colloid and continued to be characterized using a UV-Vis spectrophotometer and PSA at a wavelength of 200-500 nm.

2.1.2. Application of silver nanoparticles on pickle goat leather (K-NP-E and K-NP-I)

Pickle goat leather was cut to size 20 x 10 cm. The deposit of silver nanoparticles was carried out by *in situ* and *ex situ* methods. In the *in situ* method, pickle goat leather was put into a mixture of 5 ml of *Cyperus kyllinga* leaf extract and then added 200 ml of $0.5 \cdot 10^{-3}$ M silver nitrate, which is placed in a 500 ml beaker glass. Pickle goat leather and mixture are heated in a temperature range of 40 °C (Ibrahim, 2015) while stirring using a stirrer. When heating takes place 15 minutes, a 0.05% starch solution of 60 ml is added to the mixed solution. The heating process is carried out for 30 minutes. In the existing method, the leather of the pickle goats soaked in colloidal silver nanoparticles is then carried out a shaker for approximately 24 hours at a speed of 154 rpm. Then the leather is dried under room temperature conditions.

2.1.3. Modification of pickle goat leather surface with MTMS compounds (L-M-e and L-M-i)

The coating of MTMS compounds on the surface of pickle goat leather is done by immersion method *in situ* and *ex situ*. Pickle goat leather is immersed in 3% ethanol-MTMS solution in 100 mL Erlenmeyer, then shaker for 1 hour with a speed of 154 rpm, then the pickle goat leather is dried at room temperature.

2.1.4. Modification of pickle goat leather surface with silver nanoparticles and MTMS compounds (L-PM-e and L-PM-i)

Pickle goat leather that has been deposited with silver nanoparticles is added with a

3% ethanol-MTMS solution. The coating of MTMS compounds in this modification was done by two methods, namely the *ex situ* and *in situ* methods. In the existing method, the leather of the pickle goat, which in the process of depositing silver nanoparticles for 30 minutes, was then added with a 3% ethanol-MTMS solution to the mixture. Immersion continued for 30 minutes, accompanied by stirring using a stirrer. Whereas *in situ* method, pickle goat leather from the deposit of silver nanoparticles was immersed in 3% ethanol-MTMS solution for 30 minutes and warmed with a temperature range of 40 °C. The same stage is continued with the addition of silver nanoparticles that will be obtained (L-MP-e and L-MP-i).

2.1.5. Contact angle test

Characterization of the hydrophobic properties of pickle goat leather is using the sessile drop method. The leather sample is placed on a table or board with a flat surface, and then the liquid is dripped from a height of approximately 1 cm from the leather sample by using a dropper. After that, the picture was taken with a camera. The photos are processed using the Corel Draw program.

2.1.6. Antibacterial and antifungal activity test

Antibacterial and antifungal activity tests are performed using the diffusion method by observing the inhibited or clear zones that form around the leather sample. A total of 9 variations of pickle goat leather were cut round using a paper hole ($d = 0.5$ cm) on the cultures of *Escherichia coli* and *Staphylococcus epidermidis* as well as on *Candida albicans* that had been planted in Petri dishes. Measurement of bacterial inhibition zone is done every 3 hours for 24 hours, while the measurement of the inhibition zone of the fungal is done every 6 hours for 72 hours of incubation time.

2.1.7. Test of mechanical properties

Mechanical properties testing is done by using a Tensile test machine. For this purpose, the leather is cut according to the standard method in Indonesia (Indonesia National Standard/SNI 06-1795-1990). The leather sample is placed on the device up to a distance of 50 mm. The withdrawal was made at a speed of 25 cm/min until the leather breaks or, if desired, only to crack the leather. Also, the stretch of the leather at the time of breaking can be calculated as a percent of its elongation. The test of mechanical properties was carried out three times for each variation of the leather sample.

3. RESULTS AND DISCUSSION:

Silver nanoparticles were synthesized using the reduction method with the principle of biosynthesis. The leaves of the puzzles (*Cyperus kyllinga*) after adding AgNO_3 solution and starch, undergo a change in color from the original colorless to brownish-orange on storage for 48 hours. The color change indicates that the nanoparticles have formed (Aldujaili and Banoon, 2020). There has been a silver nitrate reduction process that is from Ag^+ ions to Ag^0 ions (Rohaeti and Rakhmawati, 2018), and colloidal silver nanoparticles have also been formed, shown in Figure 1. The formation of nanoparticle could be caused by the H radicals formed in tannin compounds (Devi *et al.*, 2014). The hydroxyl and carboxyl groups in tannin also could form the chelate metal (Michalak, 2011). The *Cyperus kyllinga* extract effectively changed silver ions to nano-size because silver ions have high positive electrochemical potentials (Makarov *et al.*, 2014).

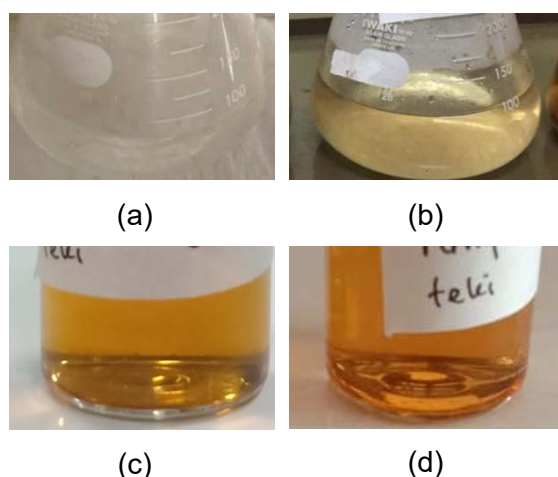


Figure 1. A mixture of a solution of the *Cyperus kyllinga* leaf extract + AgNO_3 solution $0.5 \cdot 10^{-3}$ M + Starch 0.05% (a) 0 hours, (b) 4 hours, (c) 48 hours, (d) 144 hours

Silver nanoparticles that had been left for 48 hours were then characterized using a UV-Vis spectrophotometer. In the measurement of the UV-Vis test, the measured absorption peak was 406.60 nm, as shown in Figure 2. This result was in line with the result of the previous study (Zhang *et al.*, 2014).

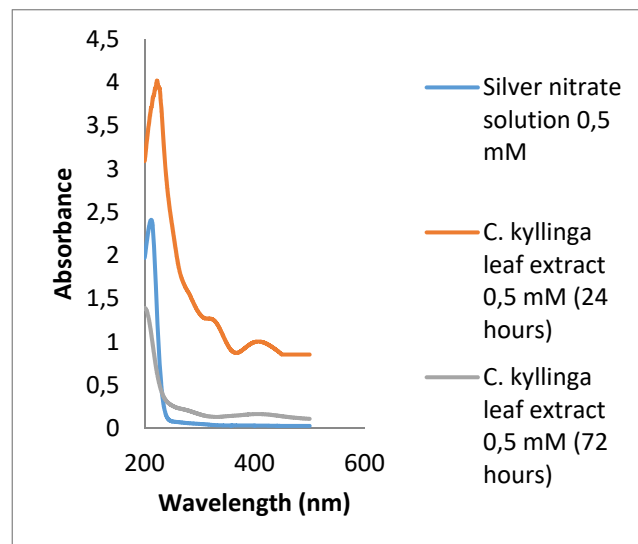


Figure 2. UV-Vis spectrum of silver nitrate solution and silver nanoparticles

From these results, the *Cyperus kyllinga* leaf extract has succeeded in reducing silver nitrate solution. *Cyperus kyllinga* leaf extracts have been known to contain chemical compounds, namely tannins. Tannin compounds are compounds that are thought to act as reducing agents, solvents, and stabilizers in the production of nanomaterials (Rohaeti and Rakhmawati, 2018; Kuppusamy *et al.*, 2016).

The results of the analysis using PSA showed that the size distribution of silver nanoparticles synthesized by the extract of *Cyperus kyllinga* leaves had an average size of nanoparticles around 200.1 nm. According to Nagarajan (2008), the optimal size of silver nanoparticles has a size range of 1 nm - 100 nm. From the measured silver nanoparticle data, it is known that silver nanoparticles have agglomerated. Silver nanoparticle solutions tend to undergo aggregation to form larger sizes (Haryono *et al.*, 2008; Rohaeti *et al.*, 2019; Shateri-Khalilabad *et al.*, 2010).

Modified pickle goat leather samples with silver nanoparticles produce brownish-orange pickle goat leather. The color change is derived from the leaves of the *Cyperus kyllinga*, a solution of silver nanoparticles. Silver nanoparticles stick to the leather surface, a possible interaction that occurs between silver nanoparticles with pickle goat leather. Goat leather has an amino-functional group ($-\text{NH}_2$) and carboxylate ($-\text{COOH}$) when silver nanoparticles interact with the surface of the goat leather, Ag^+ turns into Ag^0 , which can then interact with the NH group or O atom of the goat leather so that the surface of the goat leather is coated by nanoparticles silver (Montazer and Nia, 2015).

Table 1. The contact angle of pickle goat leather before and after modification

Methode	Contact angle value (°)				
	L0	L-P	L-PM	L-MP	L-M
<i>Ex situ</i>	25.57	73.79	66.33	90.55	50.05
<i>In situ</i>		70.16	90.46	78.82	65.29

Based on the contact angle test results in Table 1, it is known that there is a significant difference in the contact angle values in K0 samples with eight leather samples modified using silver nanoparticles, MTMS compounds, or modification of the two compounds (K-NP-MTMS and K-MTMS -NP). Unmodified leather samples only have a contact angle value of 20.57°. From the measurement results of contact angle values, all modified pickle goat leathers have higher contact angle values than the contact angle values on pickle goat leather without modification (K0). Therefore, it can be seen that the addition of silver nanoparticles (AgNP) and the addition of MTMS compounds can influence the surface properties of the leather of the goat leather, which can increase the contact angle of the leather of the goat leather.

Based on the observation of inhibition zones in the two bacteria tested showed that inhibition zones began to form, on average, at an incubation time of 3 hours. Silver nanoparticles used in this study play a role in enhancing the antimicrobial properties of pickle goat leather samples. According to Rohaeti and Rakhmawati (2017), silver nanoparticles can inhibit the growth of *Escherichia coli* and *Staphylococcus epidermidis* bacteria. Also, the antibacterial activity of 8 samples of modified goat leather of *S. epidermidis* showed an average inhibition zone that was greater than that of *E. coli*. According to Rohaeti (2017), there is a difference in the antibacterial activity between materials with modification and without modification of *E. coli* and *S. epidermidis*. This difference is influenced by the characteristics of Gram-positive and gram-negative bacterial cell walls. *S. epidermidis*, as gram-positive bacteria, has several layers of peptidoglycan, which combine to form a thick and stiff structure. At the same time, *E. coli* is a gram-negative bacterium that has a thin layer of peptidoglycan and a protected outer membrane. This results in a more effective sample of goat leather antibacterial activity against *Staphylococcus epidermidis*. Likewise, in the antifungal test, the inhibitory mechanism of bacteria and fungus has no difference. Silver nanoparticles will interfere with enzymes

(proteins) in bacterial cells and fungal cells. The difference is only in the structure of protein molecules owned by bacteria and fungi. Bacteria have a simpler structure than fungus.

The observation of inhibition zone diameter on the leather of the pickle goats against *Escherichia coli* and *Staphylococcus epidermidis* bacteria and *Candida albicans* fungus in this study carried out statistical tests which included ANOVA test and LSD advanced test using SPSS version 25.

Based on the ANOVA test results listed in Table 2 which is the test results of the *Escherichia coli* bacteria known to have a significant value of the interaction test between an incubation time and type of sample is 0,000 ($p < 0.05$), interpretation of the value of $p < 0.05$ means that there is an effect of the interaction between the incubation time with the type of sample on the antibacterial activity of *E. coli*. Whereas in the *Staphylococcus epidermidis* and *Candida albicans*, the significance value of the interaction test between the incubation time and the type of pickle goat leather sample were 0.942 and 0.762 ($p > 0.05$), the interpretation of the value of $p > 0.05$ that means no the effect of the interaction between incubation time with the type of sample on the antibacterial activity of *Staphylococcus epidermidis* and antifungal *Candida albicans*.

The advanced statistical test is the LSD test between variations of sample types against antimicrobial activity shown in Table 3. The results of the research data show a significant difference to the leather without modification (L0) with some samples of the modified goat leather in inhibiting the antibacterial and antifungal activities such as in L-P-e and L-P-i. At the same time, the L-M-e and L-M-i samples on L0 leather showed no significant difference in inhibiting antibacterial or antifungal activity.

Tensile strength, elongation, Young modulus, and toughness are mechanical properties of a material. Tensile strength indicated the strength of a material when given a vertical pull (Savitri *et al.*, 2015). The toughness of a material could be determined by using the graph of the relationship between tensile strength and elongation. The L-M-i (leather with modification by adding MTMS via *in situ*) the longest elongation at break and the highest toughness. The L-M-i has the biggest curve under the area. The highest tensile strength is shown by a sample of pickle goat leather modified by silver nanoparticles with the addition of MTMS compounds using an *in situ* preparation method (L-PM-i) as much as 5.09

MPa.

According to Sumaryono (2012), a polymer material has different physical properties, including brittle, plastic, and elastomer (highly elastic). Based on the curve of stress-strain as shown in Figure 4, samples leather with modification by adding MTMs and nanoparticle via *in situ* method (L-MP-i) is the soft and weak material, their strength at break and also elongation is very low. The leather without modification shows the lowest tensile strength and elongation compare to others. The samples L0, L-P-e, L-P-i, L-M-e, and L-M-i have soft and tough properties because stretching in a large enough plastic area and modulus Young that is not too large. The L-M sample is a sample that is very elastic compared to the others because it has the largest area of the curve. In comparison, the L-PM-i leather sample has a hard or strong nature in holding a load and is strong because it has a value of elongation that is not too small but not too big too (moderate). Furthermore, the L-MP-i leather samples are soft and weak because they have a very small area of under curve.

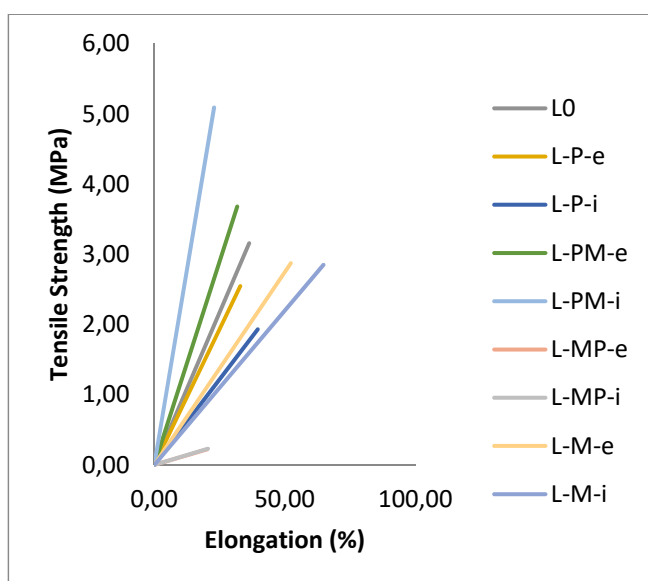


Figure 5. The curves of stress-strain of leather before and after modification.

The percentage elongation analysis is a percentage increase in the length of a test specimen when carried out vertically. Percent elongation shows the elasticity of a material, which is indicated by the elongation of the test specimen when given a certain force (Savitri *et al.*, 2015). The L-M-i leather sample had the largest elongation value, with a value of 64.82%.

Based on these results, pickle goat leather before and after the modification has different

physical and mechanical properties based on its toughness. The order of toughness in this sample variation is L-M-i > L-M-e > L-PM-e > L-PM-i > L0 > L-P-e > L-P-i > L-MP-i > L-MP-e.

4. CONCLUSIONS:

The silver nanoparticles prepared by using *Cyperus kyllinga* extract were formed at a wavelength of 406.60 nm, with their particle size were 200.1 nm. The results of the antimicrobial test showed that modified goat leather using two methods of preparation had a different significance to inhibit the *S. epidermidis* and *E. coli*, and also fungi of *C. albicans*. The leather, after modification with nanoparticle via *in situ* method, had the highest antibacterial activities against *S. epidermidis* and *E. coli*. However, leather after modification with adding nanoparticle and MTMS via *ex situ* method has the highest antifungal activity against *C. albicans*. The leather after modification nanoparticle and MTMS via *in situ* method has the highest tensile strength and the largest toughness. However, all samples of pickle goat leather after modification by impregnating silver nanoparticles have antibacterial activities, antifungal, strength at break, elongation, toughness, and also contact angles the better compared to pickle goat leather without modification.

5. ACKNOWLEDGMENTS:

Thank you to the Ministry of Education and Culture, Republic of Indonesia, through financial support from Applied Research, National Competitive Research in 2020.

6. REFERENCES:

1. Abd-Elnaby, H. M.; Abo-Elala, G. M.; Abdel-Raouf U. M.; Hamed, M. M. (2016). Antibacterial and anticancer activity of extracellular synthesized silver nanoparticles from marine *Streptomyces rochei* MHM13. *Egypt. J. Aquat. Res.*, 42(3), 301–312. DOI: 10.1016/j.ejar.2016.05.004.
2. Ahmed, S.; Ahmad, M.; Swami, B. L.; Ikram, S. (2016). Review on plants extract mediated synthesis of silver nanoparticles for antimicrobial applications: A green expertise. *J. Adv. Res.*, 7(1), 17–28. DOI 10.1016/j.jare.2015.02.007.
3. Aldujaili, N. H.; Banoon, S. R. (2020).

- Antibacterial characterization of titanium nanoparticles nanosynthesized by *Streptococcus thermophilus*. *PERIÓDICO TCHÊ QUÍMICA*, 17(34), 311-320.
4. Amin, R. M.; Mohamed, M. B.; Ramadan, M. A.; Verwanger, T.; Krammer, B. (2009). Rapid and sensitive microplate assay for screening the effect of silver and gold nanoparticles on bacteria. *Nanomedicine*, 4(6), 637–643.
 5. Buszewski, B.; Railean-plugaru, V.; Szultka-mlynska, M; Golinska, P. (2016). Antimicrobial activity of biosilver nanoparticles produced by a novel *Streptococcus thermophilus* strain. *J. Microbiol. Immun. Infect.*, xx, 1–10. DOI: 10.1016/j.jmii.2016.03.002.
 6. Devi, R. K. B.; Sarma, H. N. K.; Radhapiyari, W.; Brajakishor, C. (2014). Green synthesis, characterization and antimicrobial properties of silver nanowires by aqueous leaf extract. *Int. J. Pharm. Sci. Rev. Res.*, 26(52), 309–313.
 7. Directorate General of Livestock and Animal Health (Ministry of Agriculture). (2018). Livestock and Animal Health Statistics, 2018. Jakarta: Ministry of Agriculture. Retrieved from <https://ditjenpkh.pertanian.go.id/>
 8. Gopinath, V.; Priyadarshini, S.; Loke, M. F.; Arunkumar, J.; Marsili, E.; Mubarak Ali, D.; Velusamy, P.; Vadivelu, J. (2017). Biogenic synthesis, characterization of antibacterial silver nanoparticles and its cell cytotoxicity. *Arab. J. Chem.*, 10, 1107–1117. DOI: 10.1016/j.arabjc.2015.11.011.
 9. Guzmán, M. G.; Dille, J.; Godet, S. (2009). Synthesis of silver nanoparticles by chemical reduction method and their antibacterial activity. *International Journal of Chemical and Biomolecular Engineering*, 2(3), 104–111.
 10. Haryono, A.; Sundari, D.; Harmami, S B.; Randy, M. (2008). Sintesa nanopartikel perak dan potensi aplikasinya. *Jurnal Riset Industri*, 2(3), 156-163.
 11. Hasany, S. F.; Ahmed, I.; Rajan, J.; Rehman, A. (2013). Systematic review of the preparation techniques of Iron Oxide magnetic nanoparticles. *Nanosci. Nanotech.*, 2(6), 148–158. DOI 10.5923/j.nn.20120206.01.
 12. Kalishwaralal, K.; Barathmanikant, S.; Ram, S.; Pandian, K.; Deepak, V.; Gurunathan, S. (2010). Silver nanoparticles impede the biofilm formation by *Pseudomonas aeruginosa* and *Staphylococcus epidermidis*. *Colloids and Surfaces B: Biointerfaces*, 79(2), 340–344.
 13. Kuppusamy P.; Yusoff, M. M.; Maniam G. P.; Govindan, N. (2016). Biosynthesis of metallic nanoparticles using plant derivatives and their new avenues in pharmacological applications—An updated report. *Saudi Pharm. J.*, 24(4): 473–484. DOI 10.1016/j.jsps.2014.11.013.
 14. Maamoun, D.; Khairy, M. (2013). Improving printability of silk and polyamide substrates with madder nano-sized particles. *Am. J. Nanosci. Nanotech. Res.*, 2(1): 1–12.
 15. Makarov V. V.; Love A. J.; Sinitsyna O. V.; Makarova S. S.; Yaminsky, V.; Taliansky M. E.; Kalinina N. O. (2014). Green nanotechnologies: Synthesis of metal nanoparticles using plants. *Acta Naturae*, 6(1), 35–44.
 16. Michalak A. (2006). Phenolic compounds and their antioxidant activity in plants growing under heavy metal stress. *Plant Cell*. 15(4), 523–530. DOI 10.1016/j.fitote.2011.01.018.
 17. Muliawati, D. N.; Yulianti, E. (2018). Uji aktivitas antimikroba nanopartikel perak dari limbah perak hasil penyepuhan terhadap bakteri *Staphylococcus aureus* dan fungi *Candida albicans*. *Jurnal Prodi Biologi*, 7(2), 90-93.
 18. Montazer, M.; Nia, K.Z. (2015). Conductive nylon fabric through *in situ* synthesis of nanosilver: Preparation and characterization. *Materials Science and Engineering*, 56, 341-347.
 19. Nanda, A.; Saravanan, M. (2009). Biosynthesis of silver nanoparticles from *Staphylococcus aureus* and its antimicrobial activity against MRSA and MRSE. *Nanomedicine: Nanotechnology, Biology, and Medicine*, 5(4), 452–456. <https://doi.org/10.1016/j.nano.2009.01.012>
 20. Rohaeti, E. (2017). Kajian tentang kain poliester antibakteri dan antikotor. *Prosiding Seminar Nasional Kimia UNY*, 285–296.
 21. Rohaeti, E.; Rakhmawati, A. (2017a). Application of *Terminalia catappa* in preparation of silver nanoparticles to develop antibacterial nylon. *Oriental Journal of Chemistry*, 33, 2905–2912.
 22. Rohaeti, E.; Rakhmawati, A. (2017b). The hydrophobicity and the antibacterial activity of polyester modified with silver nanoparticle and

- hexadecyltrimethoxysilane. *Molekul*, 12(1), 78–87.
23. Rohaeti, E.; Rakhmawati, A. (2018). Application of silver nanoparticles synthesized by using *Ipomoea batatas* L. waste to improve antibacterial properties and hydrophobicity of polyester cloths. *Chiang Mai Journal of Science*, 45(7), 2715-2729.
 24. Rohaeti, E.; Budiasih, K.S.; Rakhmawati, A.; Nuraini, E.; Kusumastuti C. (2019). Assessment of extract of *Musa paradisiaca* Linn. in producing nanoparticles to enhance quality of nylon fabric. *Rasayan Journal of Chemistry*, 12(3), 1352-1359.
 25. Salem, W.; Leitner, D. R.; Zingl, F. G.; Schratter, G.; Prassl, R.; Goessler, W.; Reidl, J.; Schild, S. (2015). Antibacterial activity of silver and zinc nanoparticles against *Vibrio cholerae* and enterotoxigenic *Escherichia coli*. *International Journal of Medical Microbiology*, 305(1), 85–95. <https://doi.org/10.1016/j.ijmm.2014.11.005>
 26. Savitri; Triwulandari, E.; Haryono, A.; Syahputra, O. A. (2015). Pengaruh senyawa silan terhadap sifat mekanik material pelapis paduan hibrid epoksi termodifikasi poliuretan. *Jurnal Kimia Terapan Indonesia*, 17(1), 19–33.
 27. Selvam, G.G.; Sivakumar K. (2015). Phycosynthesis of silver nanoparticles and photocatalytic degradation of methyl orange dye using silver (Ag) nanoparticles synthesized from *Hypnea musciformis* (Wulfen) J.V. Lamouroux. *Appl. Nanosci.*, 5(5): 617–622. DOI 10.1007/s13204-014-0356-8.
 28. Sharma, V. K.; Yngard, R. A.; Lin, Y. (2009). Silver nanoparticles: Green synthesis and their antimicrobial activities. *Advances in Colloid and Interface Science*, 145, 83–96.
 29. Shateri-khalilabad M.; Yazdanshenas M. E.; Etemadifar, A. (2010). *Arab. J. Chem.*, 351(1), 293-298. DOI 10.1016/j.arabjc.2013.08.013.
 30. Sindhu, T.; Rajamanikandan, S.; Srinivasan, P. (2014). In vitro antioxidant and antibacterial activities of methanol extract of *Kyllinga nemoralis*. *Indian Journal of Pharmaceutical Science*, 3(4), 170–174.
 31. Sumaryono. (2012). Perilaku pengujian tarik pada polimer polistiren dan polipropilen. *Gardan*, 1(1), 66-80.
 32. Viorel M.; Marius, S.; Lucian, H.; Marius M.; Irina, G.; Daniela, P. (2012). Antibacterial activity of silver nanoparticles obtained by electrochemical synthesis in Poly (Amide-Hydroxyurethane) media; Available at: <https://www.technologynetworks.com/tn/posters>
 33. Zhang G.; Liu Y.; Gao X.; Chen Y. (2014). Synthesis of silver nanoparticles and antibacterial property of silk fabrics treated by silver nanoparticles. *Nanosc. Res. Lett.*, 9, 1-8. DOI 10.1186/1556-276X-9-216.




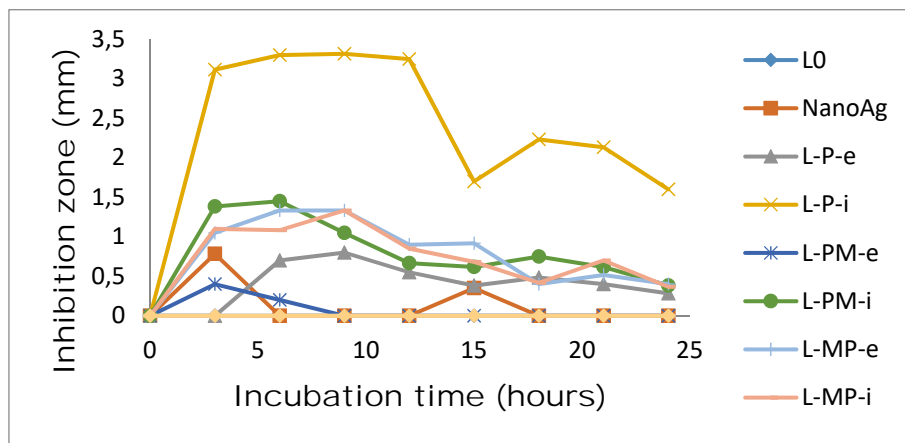
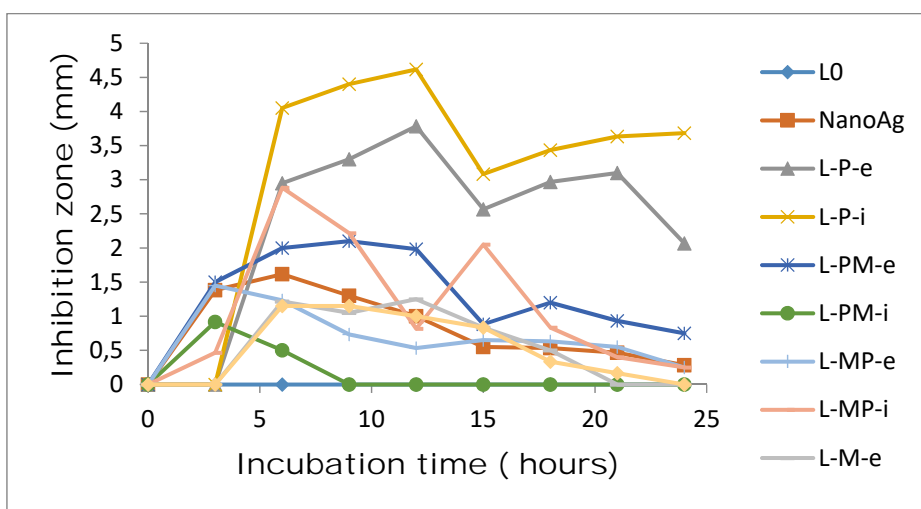
	
Leather	Leather - nanoAg
	
Leather – MTMS	Leather- nanoAg – MTMS
	
Leather – MTMS – nanoAg	

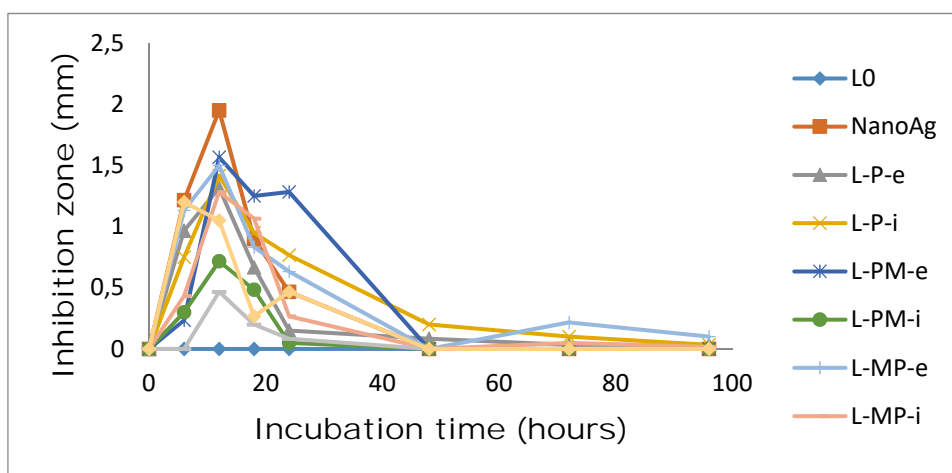
Figure 3. Images of leather before and after modification



(a)



(b)



(c)

Figure 4. The diameter of the inhibition zone to Incubation time of leather before and after modification against (a) *E. coli*, (b) *S. epidermidis*, (c) *C. albicans*

Table 2. The results of the ANOVA test for antimicrobial activity of leather against *Escherichia coli*, *Staphylococcus epidermidis*, and *Candida albicans*

<i>Escherichia coli</i>					
Variable	Sum	Df	Average	F	Sig.
Incubation	14,451	8	1,806	22,669	0,000
Pickle Leather	85,513	9	9,279	116,449	0,000
Incubation*Pickle	21,303	72	0,296	3,713	0,000
<i>Staphylococcus epidermidis</i>					
Variable	Sum	Df	Average	F	Sig.
Incubation	46,748	8	5,844	3,896	0,001
Pickle Leather	149,723	89	16,636	11,092	0,000
Incubation*Pickle	75,574	72	1,050	0,700	0,942
<i>Candida albicans</i>					
Variable	Sum	Df	Average	F	Sig.
Incubation	24,825	7	3,546	20,562	0,000
Pickle Leather	6,153	9	0,684	3,964	0,000
Incubation*Pickle	9,138	63	0,145	0,841	0,762

Table 3. Interpretation of significant differences of antimicrobial activity between 2 samples of leather against *E. coli*, *S. epidermidis*, and *C. albicans*

Variation type of leather	Interpretation		
	<i>E. coli</i>	<i>S. epidermidis</i>	<i>C. albicans</i>
L0 - LP-i	Significant	Significant	Significant
L0 - LP-i	Significant	Significant	Significant
L0 - L-PM-e	No Significant	Significant	Significant
L0 - L-PM-i	Significant	No Significant	No Significant
L0 - L-MP-e	Significant	No Significant	Significant
L0 - L-MP-i	Significant	Significant	Significant
L0 - LM-e	No Signifikan	No Significant	No Significant
L0 - LM-i	No Signifikan	No Significant	Significant

ESTRATÉGIAS DE GENERALIZAÇÃO DE PADRÕES PARA MELHORAR O
PENSAMENTO ALGÉBRICO DOS ESTUDANTESSTRATEGIES OF PATTERN GENERALIZATION FOR ENHANCING STUDENTS'
ALGEBRAIC THINKING

提高学生代数思维的模式概括策略

NURWIDIYANTO^{1*}, ZHANG, Kaijun²^{1,2} Mathematics Education, School of Mathematics and Statistics, Northeast Normal University, Changchun, Jilin, P. R. China* Corresponding author
e-mail: zil997@nenu.edu.cn

Received 17 May 2020; received in revised form 22 June 2020; accepted 30 July 2020

RESUMO

A matemática é vista como uma ciência do padrão. Identificar e usar padrões é a essência do pensamento matemático para as crianças melhorarem o pensamento algébrico desde o início da fase escolar. O padrão é um arranjo de objetos com regularidades ou propriedades que podem ser generalizadas. Portanto, é importante conhecer as estratégias usadas pelos alunos na generalização de padrões e como os alunos pensam nesses processos. Este estudo é uma pesquisa descritiva com uma abordagem quantitativa-qualitativa mista, que teve como objetivo investigar o pensamento algébrico do aluno usando várias estratégias para generalizar o padrão visual. Um instrumento sobre o padrão linear de crescimento geométrico foi administrado a 75 alunos do ensino fundamental (notas 5-6) e 81 alunos do ensino médio (notas 7-8) em duas escolas particulares em Semarang, Indonésia. Os resultados mostraram que os estudantes usaram diferentes estratégias de generalização de padrões. O aluno geralmente preferia estratégia recursiva, fragmentada e funcional em cada tarefa de generalização, enquanto poucos usavam a contagem de estratégias de desenho para generalizar o padrão. O uso da estratégia recursiva diminuiu, enquanto o uso da estratégia de chunking e da estratégia funcional aumentou nos graus 5-8 para os problemas. Os resultados também mostraram que o aluno que usou a estratégia recursiva e de fragmentação preferiu alterar os padrões visuais em linhas de números. Portanto, eles adotam uma abordagem numérica, encontrando a diferença comum do padrão visual em cada etapa.

Palavras-chave: *Pensamento algébrico, Estudo transversal, Estratégia de generalização, Padrão visual.*

ABSTRACT

Mathematics is seen as a science of pattern. Identifying and using patterns is the essence of mathematical thinking for children to improve algebraic thinking from their early schooling. The pattern is an arrangement of objects that have regularities or properties that can be generalized. Therefore, it is essential to know the strategies used by students in generalizing patterns and how students think in these processes. This study is descriptive research with a mixed quantitative-qualitative approach that aimed to investigate student's algebraic thinking using various strategies to generalize the visual pattern. An instrument about the linear geometric growing pattern was administrated to 75 upper primary school students (grades 5-6) and 81 lower secondary students (grades 7-8) in two private schools in Semarang, Indonesia. The results showed that students used different pattern generalization strategies. The student generally preferred recursive, chunking, and functional approaches in each generalization task, whereas few used counting from drawing strategies to generalize patterns. The use of the recursive strategy decreased, whereas the chunking strategy and the functional strategy increased across grades 5-8 for the problems. The results also showed the student who used the recursive and chunking strategy preferred to change visual patterns into rows of numbers. Hence, they adopt a numeric approach by finding the common difference of visible pattern in each step.

Keywords: Algebraic thinking, Cross-age study, Generalization strategy, Visual pattern.

摘要

数学被看作是一门关于模式的科学。识别和使用模式是数学思维的本质，可以促进儿童从学校教育初期开始的代数思维的发展。模式是对一类具有某些规律和属性的对象的抽象。因此，了解学生概括模式的策略以及学生的思考方式是重要的。本研究采用定性与定量相结合的方法探讨学生的代数思维发展。本研究中应用线性几何增长模型为研究工具，对印度尼西亚三宝垄的两所私立学校的75名小学高年级（5-6年级）学生和81名中学生（7-8年级）进行研究，结果表明，学生使用了不同的模式概括策略，在每个概括任务中，学生一般更倾向于递归、分块和功能策略，但很少有人从绘制策略中计数来概括模式，从5-8年级，学生对递归策略的使用逐渐减少，分块策略和功能策略逐渐增加。研究结果还显示，使用递归和分块策略的学生更喜欢将数字排成行，通过发现每一步的共同差异进行模式概括。

关键词：代数思维，跨年龄研究，概括策略，视觉模式。

1. INTRODUCTION:

Mathematics is seen as a science of pattern (Resnik, 1981), and identifying and using patterns is the essence of mathematical thinking (Booker, 2009). According to Callejo and Zapatera (2017), identifying patterns is a way for children to improve algebraic thinking from early schooling. Papic *et al.* (2009) has defined patterns as an essential skill in early mathematic learning, particularly in the improvement of spatial awareness, sequencing, and ordering. Besides, Twohill (2017) argues that shape patterns may help students develop their generalizations, represent generalizations, and have syntactic guided reasoning on generalizations. The pattern plays an essential role in improving thinking, communication, association, and problem-solving (Tanişlı and Özdaş, 2009). Besides, Fox (2005) reported patterns commonly contain the mathematical ability to calculate, classify, compare, measure, estimate, and symbolize, and these processes make the mathematical knowledge and skills of the students meaningful.

Demonstrating mathematics proficiency is a vital prerequisite for academic improvement and career readiness, which becomes the essential predictor of future academic progress (Gamoran and Hannigan, 2000).

The construction of the general term for the pattern is a vital aspect of algebraic thinking (Twohill, 2017; Walkowiak, 2014). The application of algebraic thinking is also inflexible, which leads to a lack of confidence and initiative of students in algebra learning and even the assumption that algebra is complicated. In the early algebra learning of elementary school, students' thinking is only based on "arithmetic thinking" (Radford,

2018), where more attention is in the calculation (Carpenter *et al.*, 2005). Therefore, when more symbols are involved, students will be trapped by inherent arithmetic thinking and feel that the problem cannot be solved. For instance, Demonty *et al.*, (2018) found that early secondary school students are still experiencing difficulties and continuing their mistakes in understanding algebraic thinking, especially in constructing pattern generalizations.

The students' generalization strategies using various activities such as numerical, geometric, and repeating patterns help students use symbols to express generalizations and develop meaning for symbolic generalizations (Alajmi, 2016; Lannin *et al.*, 2006). Understanding mathematical symbols and concepts are an essential component of mathematical knowledge (Skemp, 1987). Expanded vocabularies open learners to understand differences and commonalities between items by describing their attributes. For this reason, to build elementary and secondary student's skills to generalize, the researcher was encouraged to explore the strategies that students use through the examination of a linear geometric growing pattern. The approach referred to in this study focuses on what policy students use to generalize patterns and how they generalize patterns using these strategies?

Therefore, this study aimed to investigate algebraic thinking of the students using various strategies to generalize the visual pattern.

2. BACKGROUND:

2.1. Describing Algebra and Algebraic Thinking

Many people considered algebra as a

simple “symbolic game” or a short chapter in the history of mathematics. The role of algebraic thinking is not just to solve algebraic or mathematical problems. Still, the successes of developments in education, science, economics, business, and trade are also inseparable from the role of algebraic thinking (Blanton *et al.*, 2018; Booker, 2009; Moses and Cobb, 2001). Therefore, algebra is made as one of the five content principles and standards in the NCTM (National Council of Teacher of Mathematics) that students must learn from kindergarten to secondary level (NCTM, 2000) to integrate the experience of algebraic thinking from early grades on. Thus, algebra can be applied in mathematics learning in elementary and secondary schools in all countries (Wilkie and Clarke, 2016).

According to Watson (2010), Algebra is a way to express generalizations about numbers, quantities, relationships, and functions. Similarly, Taylor-Cox (2003) defined that algebra is a generalization of arithmetic ideas where unknown values and variables can be found to solve problems. Problems that can be solved by algebra are not only theoretical problems but also problems of daily life in various contexts. Algebra itself is a set of facts and techniques and a way of thinking (Lew, 2004). Therefore, algebra can be applied to develop the students' mathematical thinking abilities, called algebraic thinking. Algebraic thinking is a fundamental element of mathematical thinking and reasoning (Windsor, 2010). Algebraic thinking involves a variety of cognitive strategies to help understand more complex mathematical concepts. Algebraic thinking develops when one discovers and states structure to solve problems related to numbers or models of various situations.

2.2. Pattern Generalization

Algebra and all branches of mathematics are about pattern generalization (Lee, 1996). Several types of mathematics patterns are number patterns, geometric or pictorial growing patterns, patterns in computational procedures, linear and quadratic patterns, and repeating patterns (Zazkis and Liljedahl, 2002). This study discusses visual patterns, namely images of lines that change from one image to the next, whose changes can be predicted (Walkowiak, 2014). The teacher commonly uses a growing visual pattern in helping students predict the following pattern and generalize. Understanding of patterns, relations, and functions are a strand of algebraic reasoning that continues to exist in the principles and standards of algebra learning in schools at all

levels (NCTM, 2000).

Generalization is one of the fundamental activities in algebraic thinking (Walkowiak, 2014). Mathematical developments depend on the application of stereotypes. According to Tall (2011), generalization in mathematics is “looking for a bigger picture,” paying attention to small groups to look for larger groups, expanding concepts in larger areas. In his book, Tall (2002) also mentioned that generalization strategies are used in mathematics to show processes in a broader context and help someone know the results of problem-solving. Generalization helps one combine their experience and knowledge to solve problems in new conditions. Tall (2014) tried to encourage students in generalization by using the application of everyday issues.

Some of the results of previous studies showed that students used various strategies in predicting and generalizing patterns. The results of a study conducted by Radford (2018) showed several strategies that students carried out in solving problems, namely a strategy of naïve induction (trial and error), generalization strategies with arithmetic, and generalizations with algebra (factual, conceptual, and symbolic). The study of El Mouhayar (2018) shows that students frequently use recursive strategies and functional strategies to generalize patterns. Recursive strategies pointed the characteristic difference between pairs of consecutive terms and repetitively added the constant from term to term to extend the pattern. The functional strategy was relating parts of the pattern to the figural step number.

2.3. Algebra in Indonesian Classroom

In Indonesia, algebra does not yet formally exist in the elementary school curriculum. The Indonesian mathematics curriculum requires students to write, simplify, and substitute algebraic expressions only in secondary school. Meanwhile, in elementary school, more emphasis is given to natural numbers and fractions, geometry and measurement, and statistics. On the other hand, the Indonesian educational stakeholders are not familiar with the introductory algebra lesson. Hence, the curriculum still separates algebra and arithmetic so that secondary school students should learn algebra in a formal way (Minister of Education and Culture of Indonesia, 2016).

As a consequence of the above condition, most students rigidly learn algebra and hardly see the relationship between algebra and their previous learning in another mathematical

domain. Unlike in Indonesia, in some countries such as Singapore, South Korea, and China, algebraic thinking is implicitly inserted into the elementary school curriculum (Ferrucci *et al.*, 2004). Demonty *et al.* (2018) stressed the importance of algebraic thinking concepts to teach primary and secondary schools continuously.

2.4. Theoretical Framework

Kaput (1999) defines generalization as: “deliberately extending the range of reasoning or communication beyond the case or cases considered, explicitly identifying and exposing commonality across cases, or lifting the reasoning or communication to a level where the focus is no longer on the cases or situation themselves but rather on the patterns, procedures, structures, and the relationship across and among them” (p. 136).

El Mouhayar (2018) combined previous research on pattern generalization strategies students used to develop several category frameworks to describe pattern generalization strategies. In this framework, student's strategies in pattern generalization are (1) counting from a drawing, (2) recursive, (3) chunking, (4) whole-object, and (5) functional. In the counting from a picture, student counts the elements of a particular figural term in a pattern. In the recursive strategy, the student points out the characteristic difference between pairs of consecutive terms and repetitively adds the constant from term to term to extend the pattern. Students multiply the common difference between two terms in the pattern by the number of steps in the chunking strategy and adding the result to the starting figural term. In the whole-object strategy, students identifying the value of a term by using multiples of a previous term. Students find a general term or a term in a specific figural step in the functional strategy without the need to find the preceding figural steps.

2.5. Research Questions

The goal was to investigate the strategies that students use to examine a linear geometric growing pattern. To accomplish the goal, there was an attempt to answer the following research questions. What strategies are used by students to generalize linear geometric growing pattern? and How do they generalize linear geometric growing pattern using these strategies?

3. MATERIALS AND METHODS:

3.1. Cross-Age Study

It was employed a type of cross-sectional study to investigate the students' strategies used in generalizing patterns. The cross-sectional study was used to produce a “snapshot” of the population at one particular time (Cohen, L., Manion, L., and Morrison, 2012). In education, a cross-sectional study is used to observe changes in the physical and mental development and knowledge of students drawn from representative age levels. One type of cross-sectional study is a cross-age study. Morg and Yörük (2006) stated that the cross-age study could quickly point out the understanding levels of students from different age groups.

3.2 Participants and Instrument

The participant of this study is 156 students (average ages 11-14) from grades 5 to 8 in two private schools, which are located in Semarang city area in the Central Java province Indonesia. Every student declares to agree to participate in this study. All procedures performed in this study regarding samples taken involving human participants were in line with the local institutional of Semarang city education department as the stakeholder and/ or national research committee with the 1964 Helsinki declaration and its later amendments or comparable ethical standards. No formal consent is required for this type of study. These private schools serve students coming from a middle socio-economic status as judged by school tuition levels. The details participants' information are shown in Table 1.

The students were given a task about a linear geometric growing pattern formed of a growing number of squares problem (Figure 1) adapted from previous studies by El Mouhayar (2018). The participants were requested (a) to find the answer for small step number; (b) to find the answer for large step number, either by writing a correct mathematics rule; (c) to generalize a rule for n th step number, either by writing a correct mathematics rule. The task used for every student was the same in the form of a linear growing number of the square problem, as shown in Figure 1. It aimed to be able to compare the strategies used by upper primary school and upper secondary students in solving the problem of pattern generalization.

3.3 Data Analysis

The data were analyzed with a mixed quantitative-qualitative descriptive approach. First, frequencies and percentages were determined for each of the frequently used strategies. Second, a

cross-tabulation of strategy use by generalization type by grade level was done to explore differences in strategy use variation across grades level. A bar chart also represented the trends in students' use of strategies across the grade level. Third, Student's interview was analyzed qualitatively to understand differences in their strategies to generalize the pattern.

Semi-structured interviews were conducted to focus on the participant's general ability to solve the task and articulate a general mathematics rule. Each participant was interviewed in about 30 minutes. During the interview, participants were asked to solve the task and explain their answers and how they found those answers.

Data collected from written answers and interviews are classified according to the category of strategy in pattern generalization compiled by El Mouhayar (2018) by referring to the strategy of generalizing patterns from the results of previous studies (Lannin *et al.*, 2006; Mouhayar and Jurdak, 2014; Rivera, 2010; Stacey, 1989), as shown in Table 2. An additional category called "incorrect" is used for wrong answers without using any strategy and non-responded problems.

4. RESULTS AND DISCUSSION:

4.1. Strategies of the Students Used in Generalizing the Linear Growing Pattern

The generational activity problem is related to a linear growing pattern formed of an increasing number of square problems (Figure 1). The questions are: (1) finding how many squares would the number of the square pattern have on step 7 and explain how to obtain the answer, (2) finding how many squares would the number of the square pattern have on step 50 and explain how to obtain the answer, (3) If someone gives any step number, finding the number of squares on that step and explain how to obtain the answer. Furthermore, after the data were analyzed, the differences in the strategies obtained for each grade level students of the school are presented in Table 3 with percentages.

Table 3 shows the differences between upper primary school students and lower secondary school students in generalizing linear growing patterns. As can be seen from Table 3, The students used four strategies to solve the problem. In problem 1, the recursive category is the most frequently used strategy (27.6%) among the students, followed by the strategy (26.3%), chunking strategies (19.9%), and counting from

drawing strategies (5.1%), respectively. However, the students did not use the whole-object strategy at all. A total of 21.2 % of the respondents gave the wrong answer without using any strategy or did not respond to the problem. In problem 2, the students used four strategies to generalize the pattern. The functional strategy was the most frequently used category (26.3%) among the students, followed by the recursive strategy (18.6%), chunking strategy (18.6%), and counting from drawing (3.2%), respectively. However, the students did not use counting from drawing strategies at problem 2. Besides, (30.1%) of the students gave the wrong answers or did not respond. In problem 3, the students used four strategies to generalize the pattern. The functional strategy was the most frequently used category (21.8%) among the students, followed by the recursive strategy (19.2%), chunking strategy (18.6%), and counting from drawing (3.2%), respectively. However, the students did not use counting from drawing strategies at 1b and 1c problems. Besides, there were (21.0%) of the students in lower secondary school gave wrong answers or did not respond at all.

The results indicated that students used different pattern generalization strategies. The student generally preferred recursive, chunking, and functional strategy in each generalization task, whereas few used counting from drawing strategies to generalize patterns. For problem 1, The trend of variation of the counting from drawing strategy increased across grades 5-6, and it decreased across grades 6-8. The trend of variation of the recursive strategy decreased across grades 5-8. The trend of variation of the chunking strategy unchanged across grades 5-6, and then it increased across grades 6-8. The variation of the functional strategy increased across grades 5-6, decreased across grades 6-7 and then increased again across grades 7-8. Figure 2 shows the trends of variations in the frequency of usage of the strategies for the problems 1.

For problem 2, The trend of variation of the counting from drawing strategy decreased across grades 5-8. The trend of variation of the recursive strategy decreased across grades 5-6, increased across grades 6-7, and then it decreased across grades 7-8. The trend of variation of the chunking strategy increased across grades 5-7, and then it decreased across grades 7-8. The variation of the functional strategy increased across grades 5-6, decreased across grades 6-7, and then increased again across grades 7-8. Figure 3 shows the trends of variations in the frequency of usage of

the strategies for the problems 2.

For problem 3, The trend of variation of the counting from drawing strategy decreased across grades 5-8. The trend of variation of the recursive strategy decreased across grades 5-6, increased across grades 6-7, and decreased across grades 7-8. The trend of variation of the chunking strategy increased across grades 5-7, and then it decreased across grades 7-8. The trend of variation of the functional strategy unchanged across grades 5-6, and then it increased across grades 6-8. Figure 4 shows the trends of variations in the frequency of usage of the strategies for the problems 3.

4.2 How the Student Generalize a Linear Growing Figural Pattern

After doing the test, the students were interviewed to recheck the understanding of the researcher toward the student's written work. The interview was given to the fourth focus students, Fina (grade 5), Andi (grade 6), Lia (grade 7) and Ziki (grade 8). Figure 5 shows a sample from Fina (grade 5) using counting from drawing strategy. She tried by drawing step 7 and counting its squares without seeing the structure and the relationship between the step and the number square. Fina said if I counted the squares until step 7, I would get 17 squares. During the interview, the researcher asked what will happen with the number squares of step 50. She still uses the same strategy with drawing until step 50 to get the answer, but this strategy makes her tired if she has to draw and count the square until step 50 or more.

On the one hand, Andi (grade 6) used a recursive strategy by looking at the common differences between pairs of consecutive steps and adding the constant from step to step to get the answer. Based on Figure 6, it can be observed that Andi use a recursive strategy preferred to move from visual pattern to symbol representation by using numbers. Becker and Rivera (2006) reported that students generally tend to change visual patterns into rows of numbers. Hence, they adopt an approach numeric by finding the common difference of visual pattern in each step. Andi found the number of squares in step 7 by repeatedly adding common difference 2 from step 4 until step 7. When the researcher asked him to find the number of squares in the far step, he got difficult if he has to add 2 until any step. For example:

[1] Researcher: How you get to step 7?

[2] Andi: Look at this. I found the number of squares in step 7 by

repeatedly adding 2 from step 4 until step 7.

[3] Researcher: Why do you add 2 in each step?

[4] Andi: Here 5, 7, 9, 11, ... the difference in every step is 2.

So I add every step by 2.

[5] Researcher: How about step 50? Are you still using the same strategy?

[6] Andi: Yes, I keep adding until step 50 to get the answer. So the number of squares in step 50 is 103

[7] Researcher: How about this problem? (*pointed to the third question*) If I ask you, how about step 100, 1000, or any?

[8] Andi: I can add until any step 2, but it would be complicated.

(*Student 2 was thinking and realized to find another strategy*).

On the other hand, as shown in Figure 7, Lia observed the pattern and recognized multiplicative and additive relationships in several pattern steps. In this first problem, she used chunking strategies to solve the problem. She also described a chunking rule for the n th term. "I multiplied the number of any step minus 4 by two, and added the number of step 4. For example, to get the number of step 50, I multiply the number 50 minus 4 by two and I add the 11 of step 4. So the number of step 50 is 103." Furthermore, Ziki (grade 8) completed the problem using a functional strategy. He tried to observe the structure of the pattern and the relationship between the step. He related the number of steps to the number of above squares and bottom squares with gave an invisible marked in steps, as shown in Figure 8.

To obtain the answer in step 4, the number of above squares is 4, the number of bottom squares is 4. Then he added 3 (the different of each step). He also described a functional rule for the n th term. A common response of Ziki is shown below.

[1] Researcher: How did you get the number of squares in step 7?

[2] Ziki: This is 4 and 4 in step 4 then I added 3, this is 3 and 3 then I added 3, this is 2 and 2 then I added 3, and this is 1 and

1 in step 1 then I added 3 (gave an invisible marked in step 4 until 1). So to obtain the answer in step 7 was $7 + 7 + 3$,

[3] Researcher: How about step 50?

[4] Ziki : $50 + 50 + 3$

[5] Researcher: If I ask you to find the number of squares in any step, how do you find it?

[6] Ziki: The number of steps + the number of steps, and then I added 3.

[7] Researcher: If you use n to represent any step, how do you calculate?

[8] Ziki: I got the formula for any step is $n + n + 3$

The first result indicated that students used different pattern generalization strategies. The student generally preferred recursive, chunking, and functional strategy in each generalization task, whereas few used counting from drawing strategies to generalize pattern. According to research Mouhayar and Jurdak (2014), grades 4-11 students frequently use recursive and functional strategies in each generalizing pattern. Their study supports the results of our study of the strategies students use in generalizing patterns. On the other hand, the chunking strategy was frequently used in lower secondary school students (grades 7-8) and a few of the students used counting from drawing strategy. The explanation for this result may be due to the student's ability to observe the pattern and recognize the pattern's structure and the relationship between the step.

The second result of this study is that the trend of variation of the recursive strategy decreased, whereas, the trend of variation of the chunking strategy and the functional strategy increased across grades 5-8 for the problems, as the demands of the problem changed from constructing a step-by-step answer to finding a general formula. The explanation of this result may be due to the nature of the problem (type of generalization) and that of the strategy being used to generalize the pattern. If students can find general formulas from patterns, then they apply strategies according to their choices, but if they cannot find general formulas, then they tend to use recursive strategies to find a near step (problem 1). On the other hand, to find a far step (problem 2 and 3) the student does not use recursive because they know it is difficult for them. Compared to study

on students' strategies across generalization types, this result supports findings of research studies that suggest that while the recursive strategy is more frequently used near step generalizations, the chunking and functional strategy is more frequently used in far step generalizations. This study's results are in line with findings from the research of Mouhayar and Jurdak (2014). In general, students are inclined to use recursive strategies to get near steps while they prefer to look for general formulas and use chunking and functional strategies to get distant steps.

Another explanation for this result may be due to experience and age of the students. The present study showed that with age and experience the strategy choices of the students become more adaptive with increasingly adaptive choices of the more effective strategies. This explanation is supported with findings from the previous research of Siegler (2000). This study focused on variation of strategy to show that experience enables students to modify their strategies and ways of reasoning in a way they show a higher dependency on the more advanced strategies that exist in their repertoire (in this case the functional strategy) and lower dependency on less advanced strategy (the recursive strategy in this case). According to the Indonesian curriculum, the students in this research were indirectly exposed to pattern generalization through their exposure to algebraic concepts such as variables, equations, algebraic expressions in grade 7 and to functions and their representations starting from grade level 8. Consequently, the experience of the students to these pattern-related topics may explain the decrease of the recursive strategy and the increase of use of the chunking and functional strategy across grade level.

The third result of this study was the recursive and chunking strategy student preferred to move from visual pattern to symbol representation by using numbers. Becker and Rivera (2006) reported that students generally tend to change visual patterns into rows of numbers. Hence, they adopt an approach numeric by finding the common difference of visual pattern in each step. According to research from Akkan and Çakiroğlu (2012), students are more successful in solving patterns in the form of rows of numbers rather than visual patterns.

5. CONCLUSIONS:

The student generally preferred recursive, chunking, and functional strategy in each

generalization task, whereas few used counting from drawing strategies to generalize pattern. The trend of variation of the recursive strategy decreased, whereas, the trend of variation of the chunking strategy and the functional strategy increased across grades 5-8 for the problems, as the demands of the problem changed from constructing a step-by-step answer to finding a general formula. The student who used the recursive and chunking strategy preferred to change visual patterns into rows of numbers. Hence, they adopt a numeric approach by finding the common difference of visual pattern in each step. The student chose a recursive strategy or functional strategy to find near the step, while they prefer to use chunking and functional strategy to look for distant step.

Some students are not successful in making correct generalizations because they have very little conceptual understanding of the pattern. Therefore, the teacher must use various types of patterns and strategies to enrich student knowledge and also focus on the ability of students to understand the structure and relationships between terms to develop students' algebraic thinking. Involving students in various patterns generalization will increase their variety of more effective strategies and their skill to choose between these strategies. Future research should focus on generalizing strategies toward the generalization of linear visual pattern problem and generalizing non-linear visual pattern, which also encourages the students to think about more advanced strategy.

6. REFERENCES:

1. Akkan, Y., and Çakiroğlu, Ü. (2012). Generalization strategies of linear and quadratic pattern: A comparison of 6th-8th grade students. *Eğitim ve Bilim*, 37(165), 184-194.
2. Alajmi, A. H. (2016). Algebraic Generalization Strategies Used by Kuwaiti Pre-service Teachers. *International Journal of Science and Mathematics Education*, 14(8), 1517-1534. <https://doi.org/10.1007/s10763-015-9657-y>
3. Becker, J. R., and Rivera, F. (2006). Sixth Graders' Figural and Numerical Strategies for Generalizing Patterns in Algebra. In Alatorre, J. L. Cortina, M. Saiz, and A. Mendez (Eds.), *Proceedings of the 28th annual meeting of the North American Chapter of the International Group for the Psychology of Mathematics Education* (Vol. 2, pp. 95-101). Universidad
4. Blanton, M., Brizuela, B. M., Stephens, A., Knuth, E., Isler, I., Gardiner, A. M., Stroud, R., Fonger, N. L., and Stylianou, D. (2018). *Implementing a Framework for Early Algebra*. 27-49. https://doi.org/10.1007/978-3-319-68351-5_2
5. Booker, G. (2009). Algebraic Thinking: Generalising Number and Geometry To Express Patterns And Properties Succinctly. *Algebraic Thinking: Generalising Number and Geometry to Express Patterns and Properties Succinctly*, 10-21.
6. Callejo, M. L., and Zapatera, A. (2017). Prospective primary teachers' noticing of students' understanding of pattern generalization. *Journal of Mathematics Teacher Education*, 20(4), 309-333. <https://doi.org/10.1007/s10857-016-9343-1>
7. Carpenter, T. P., Levi, L., Franke, M. L., and Zeringue, J. K. (2005). Algebra in Elementary School: Developing Relational Thinking. *ZDM - International Journal on Mathematics Education*. <https://doi.org/10.1007/BF02655897>
8. Cohen, L., Manion, L., and Morrison, K. (2012). Research methods in education. In *Professional Development in Education* (Vol. 38, Issue 3). <https://doi.org/10.1080/19415257.2011.643130>
9. Demonty, I., Vlassis, J., and Fagnant, A. (2018). Algebraic thinking, pattern activities and knowledge for teaching at the transition between primary and secondary school. *Educational Studies in Mathematics*, 99(1), 1-19. <https://doi.org/10.1007/s10649-018-9820-9>
10. El Mouhayar, R. (2018a). Exploring teachers' attention to students' responses in pattern generalization tasks. *Journal of Mathematics Teacher Education*, 22(6), 575-605. <https://doi.org/10.1007/s10857-018-9406-6>
11. El Mouhayar, R. (2018b). Trends of progression of student level of reasoning and generalization in numerical and figural reasoning approaches in pattern generalization. *Educational Studies in Mathematics*. <https://doi.org/10.1007/s10649-018-9821-8>
12. Ferrucci, B. J., College, K. S., and Hampshire, N. (2004). Gateways to Algebra at the Primary Level. *The Mathematics Educator*, 8(1), 131-138.

13. Fox, J. (2005). Child Initiated Mathematical Patterning in Pre-Compulsory Years. In *Chick, Helen L. and Vincent, Jill L., Eds. Proceedings The 29th Conference of the International Group for the Psychology of Mathematics Education 2*, 313–320.
14. Gamoran, A., and Hannigan, E. C. (2000). Algebra for everyone? Benefits of college - preparatory mathematics for students with diverse abilities in early secondary school. *Educational, Evaluation and Policy Analysis*, 22(3), 241-254.
15. Kaput, J. J. (1999). Teaching and learning a new algebra. In T. Romberg and E. Fennema (Eds.), *Mathematics classroom that promotes understanding*. Hillsdale: Lawrence Erlbaum.
16. Lannin, J. K., Barker, D. D., and Townsend, B. E. (2006). Algebraic generalisation strategies: Factors influencing student strategy selection. *Mathematics Education Research Journal*, 18(3), 3–28. <https://doi.org/10.1007/BF03217440>
17. Lee, L. (1996). An Initiation into Algebraic Culture through Generalization Activities. In *Approaches to Algebra*. https://doi.org/10.1007/978-94-009-1732-3_6
18. Lew, H. (2004). Developing Algebraic Thinking in Early Grades: Case Study of Korean Elementary School Mathematics 1. *The Mathematics Educator (Singapore)*, 8(1), 88–106.
19. Minister of Education and Culture of Indonesia (Kemendikbud). (2016). *Curriculum 2013: Basic competence for elementary school*. Desember, 1–23. [https://doi.org/10.1016/0031-9422\(91\)83742-4](https://doi.org/10.1016/0031-9422(91)83742-4)
20. Morg, İ. İ. L., and Yörük, N. (2006). Cross-Age Study Of The Understanding Of Some Concepts In Chemistry Subjects In Science Curriculum. 3(1), 15–27.
21. Moses, R., and Cobb, C. E. (2001). Bouncing a ball. In *Radical equations: Math literacy and civil rights*. Beacon Press.
22. Mouhayar, R. El, and Jurdak, M. (2014). *International Journal of Mathematical Variation in strategy use across grade level by pattern generalization types*. January 2015, 37–41. <https://doi.org/10.1080/0020739X.2014.985272>
23. NCTM. (2000). Principles and Standards for School Mathematics. In *School Science and Mathematics*. NCTM.
24. Papic, M. M., Mulligan, J. T., and Mitchelmore, M. C. (2009). The growth of the mathematical patterning strategies in preschool children. *Proceedings of the 33rd Conference of the International Group for the Psychology of Mathematics Education*.
25. Radford, L. (2018). The Emergence of Symbolic Algebraic Thinking in Primary School. *Teaching and Learning Algebraic Thinking with 5- to 12-Year-Olds, ICME-13 Monographs*, 3–25. https://doi.org/10.1007/978-3-319-68351-5_1
26. Resnik, M. D. (1981). Mathematics as a Science of Patterns: Ontology and Reference. *Noûs*, 15(4), 529. <https://doi.org/10.2307/2214851>
27. Rivera, F. D. (2010). Visual templates in pattern generalization activity. In *Educational Studies in Mathematics* (Vol. 73, Issue 3). <https://doi.org/10.1007/s10649-009-9222-0>
28. Skemp, R. (1987). *The psychology of learning mathematics*. Mahwah, NJ: Lawrence Erlbaum.
29. Siegler, R. S. (2000). *The Rebirth of Children's Learning*. 71(1), 26–35. <https://doi.org/https://doi.org/10.1111/1467-8624.00115>
30. Stacey, K. (1989). Educational Studies in Mathematics: Editorial. *Educational Studies in Mathematics*, 20(2), 147–164. <https://doi.org/10.1007/s10649-008-9171-z>
31. Tall, D. (2002). The Psychology of Advanced Mathematical Thinking. In *Advanced Mathematical Thinking*. https://doi.org/10.1007/0-306-47203-1_1
32. Tall, D. (2011). Looking for the bigger picture. In *For the Learning of Mathematics*.
33. Tall, D. (2014). *Making Sense of Mathematical Reasoning and Proof*. https://doi.org/10.1007/978-94-007-7473-5_13
34. Tanişlı, D., and Özdaş, A. (2009). The strategies of using the generalizing patterns of the primary school 5th grade students. *Educational Sciences: Theory and Practice*, 9(3), 1485–1497.
35. Taylor-Cox, J. (2003). Algebra in the early years? Yes! In *Young Children*.
36. Twohill, A. (2017). Shape patterning tasks: An exploration of how children build upon their observations when asked to construct general terms. *Cerme* 10, 529–536. <https://keynote.conference-services.net/resources/444/5118/pdf/CERME1>

37. Walkowiak, T. A. (2014). Elementary and middle school students' analyses of pictorial growth patterns. *Journal of Mathematical Behavior*, 33, 56–71. <https://doi.org/10.1016/j.jmathb.2013.09.004>
38. Watson, A. (2010). Key understandings in mathematics learning, Paper 6: Algebraic reasoning. *Nuffield Foundation*. <https://doi.org/http://dx.doi.org/10.1016/B978-0-08-044894-7.00517-0>
39. Wilkie, K. J., and Clarke, D. M. (2016). Developing students' functional thinking in algebra through different visualisations of a growing pattern's structure. *Mathematics Education Research Journal*. <https://doi.org/10.1007/s13394-015-0146-y>
40. Windsor, W. (2010). Algebraic Thinking: A Problem Solving Approach. In L. Sparrow, B. Kissane, and C. Hurst (Eds.), *Proceedings of the 33rd annual conference of the Mathematics Education Research Group of Australasia*. MERGA.
41. Zazkis, R., and Liljedahl, P. (2002). Generalization of patterns: The tension between algebraic thinking and algebraic notation. *Educational Studies in Mathematics*. <https://doi.org/10.1023/A:1020291317178>

Table 1. Participant Information

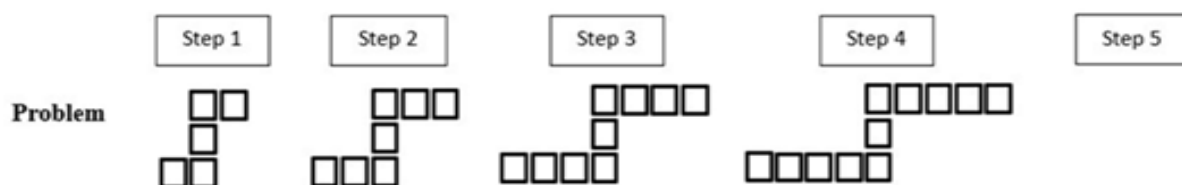
Grade	Male	Female	Total
5	15	19	34
6	19	22	41
7	20	18	38
8	18	25	43
Total	72	84	156

Table 2. A framework of Strategy In Pattern Generalization

Strategy	Description
Counting from a draw	Counting the elements of a particular figural term in a pattern
Recursive	Pointing the common difference between pairs of consecutive terms and repetitively adding the constant from term to term to extend the pattern
Chunking	Multiply the common difference between two terms in the pattern by the number of steps and adding the result to starting figural term
Whole-object	Identify the value of a term by using multiples of a previous term.
Functional	Students find a general term or a term in a specific figural step without finding the preceding figural steps.

Table 3. Strategies Used for The Linear Geometric Growing Pattern of Squares

			Grade Level				Total
			5	6	7	8	
Problem 1	Incorrect	Count	6	12	7	8	33
		% within Grade Level	17.6%	29.3%	18.4%	18.6%	21.2%
	Counting from drawing strategy	Count	3	4	1	0	8
		% within Grade Level	8.8%	9.8%	2.6%	0.0%	5.1%
	Recursive strategy	Count	8	9	8	18	43
		% within Grade Level	23.5%	22.0%	21.1%	41.9%	27.6%
	Chunking strategy	Count	4	4	11	12	31
		% within Grade Level	11.8%	9.8%	28.9%	27.9%	19.9%
	Functional strategy	Count	13	12	11	5	41
		% within Grade Level	38.2%	29.3%	28.9%	11.6%	26.3%
Total		Count	34	41	38	43	156
		% within Grade Level	100.0%	100.0%	100.0%	100.0%	100%
Problem 2	Incorrect	Count	11	18	9	9	47
		% within Grade Level	32.4%	43.9%	23.7%	20.9%	30.1%
	Counting from drawing strategy	Count	3	2	0	0	5
		% within Grade Level	8.8%	4.9%	0.0%	0.0%	3.2%
	Recursive strategy	Count	12	8	9	5	34
		% within Grade Level	35.3%	19.5%	23.7%	11.6%	21.8%
	Chunking strategy	Count	3	4	12	10	29
		% within Grade Level	8.8%	9.8%	31.6%	23.3%	18.6%
	Functional strategy	Count	5	9	8	19	41
		% within Grade Level	14.7%	22.0%	21.1%	44.2%	26.3%
Total		Count	34	41	38	43	156
		% within Grade Level	100.0%	100.0%	100.0%	100.0%	100 %
Problem 3	Incorrect	Count	11	25	10	12	58
		% within Grade Level	32.4%	61.0%	26.3%	27.9%	37.2%
	Counting from drawing strategy	Count	3	2	0	0	5
		% within Grade Level	8.8%	4.9%	0.0%	0.0%	3.2%
	Recursive strategy	Count	12	5	8	5	30
		% within Grade Level	35.3%	12.2%	21.1%	11.6%	19.2%
	Chunking strategy	Count	3	4	12	10	29
		% within Grade Level	8.8%	9.8%	31.6%	23.3%	18.6%
	Functional strategy	Count	5	5	8	16	34
		% within Grade Level	14.7%	12.2%	21.1%	37.2%	21.8%
Total		Count	34	41	38	43	156
		% within Grade Level	100.0%	100.0%	100.0%	100.0%	100%



1. What is the number of squares in step 7? show how you obtained your answer?
2. What is the number of squares in step 50? Show how you obtained your answer?
3. If someone give any step number, what is the number of squares on that step and explain how to obtain the answer?

Figure 1. A Linear growing number of square problems.

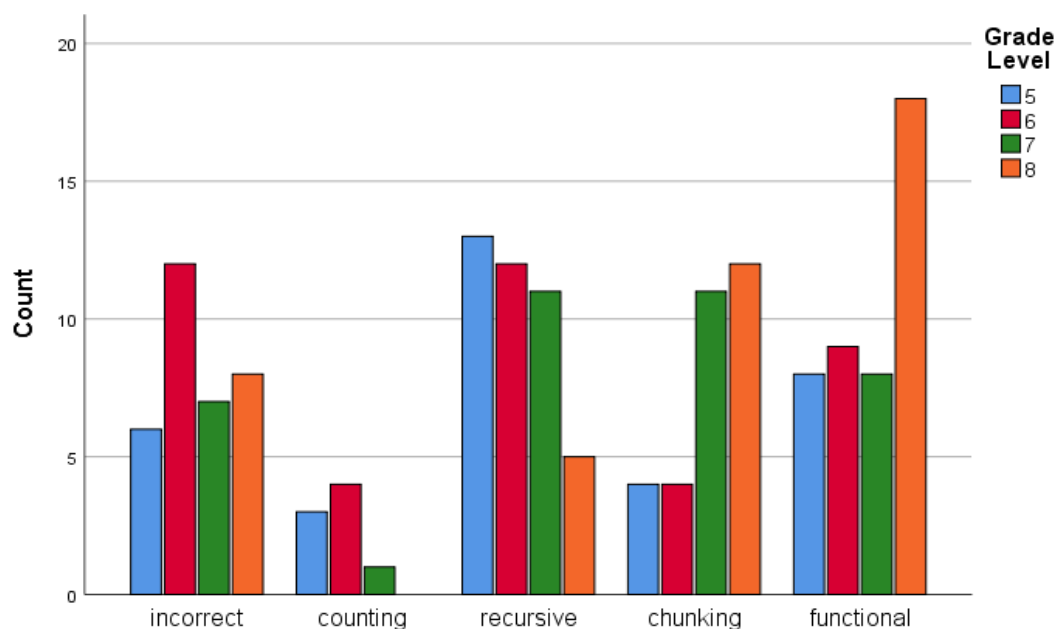


Figure 2. Trends of variation of the strategies across grades 5-8 for problems 1.

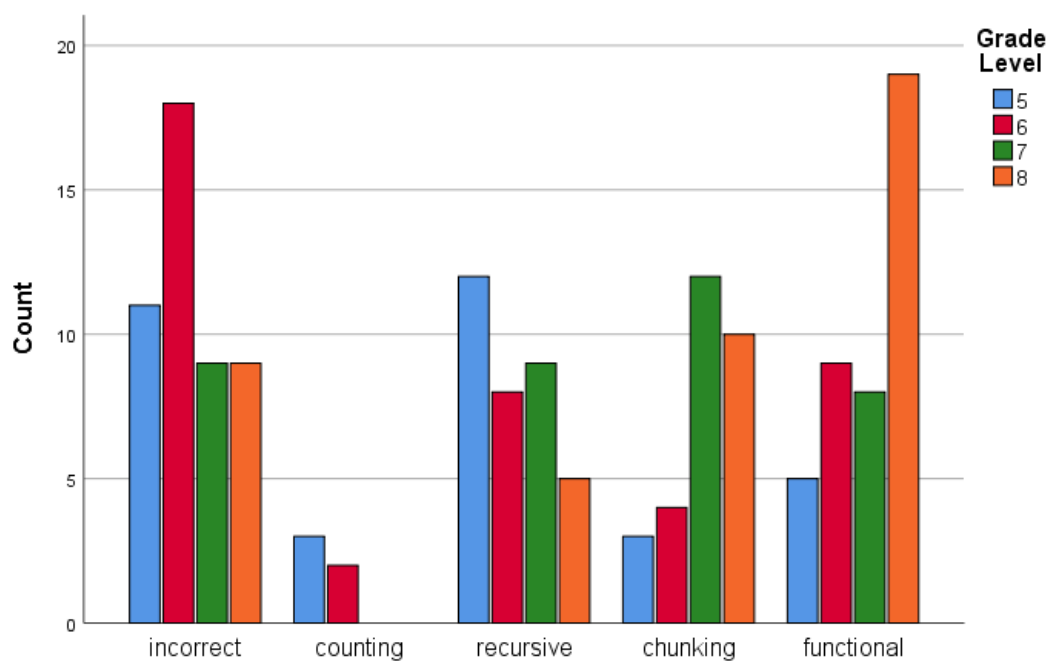


Figure 3. Trends of variation of the strategies across grades 5-8 for the problems 2.

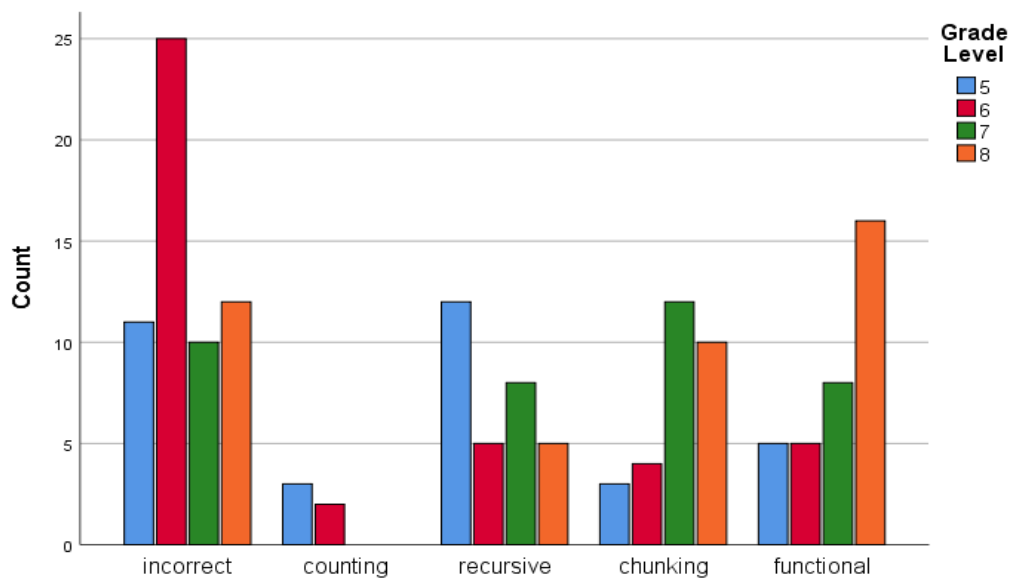


Figure 4. Trends of variation of the strategies across grades 5-8 for problems 3

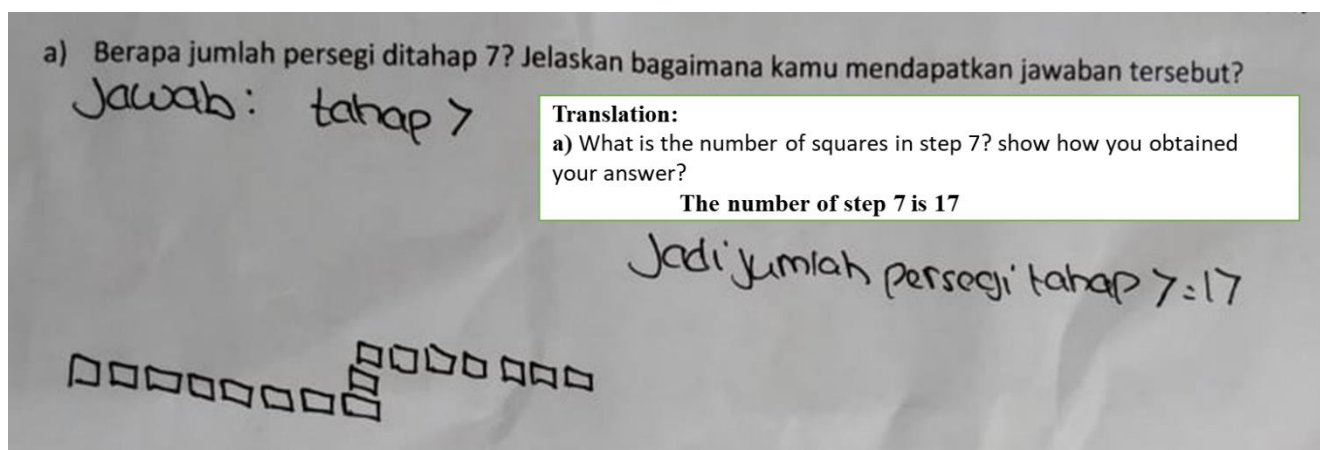


Figure 5. Fina used counting from drawing strategy to solving part an of the task

Diagram showing the progression of squares in stages (Tahap 1 to Tahap 5):

- Tahap 1: 5 squares
- Tahap 2: 7 squares
- Tahap 3: 9 squares
- Tahap 4: 11 squares
- Tahap 5: 13 squares

a) Berapa jumlah persegi ditahap 7? Jelaskan bagaimana kamu mendapatkan jawaban tersebut?

17 persegi

Tahap 6: $13 + 2 = 15$
Tahap 7: $15 + 2 = 17$

Translation:
a) What is the number of squares in step 7? show how you obtained your answer? **17 squares**
Step 6: $13 + 2 = 15$
Step 7: $15 + 2 = 17$

b) Berapa jumlah persegi ditahap 50? Jelaskan bagaimana kamu mendapatkan jawaban tersebut?

103 persegi

8: $17 + 2 = 19$	12: $25 + 2 = 27$	16: $33 + 2 = 35$	20: $41 + 2 = 43$	24: $49 + 2 = 51$	28: $57 + 2 = 59$	32: $65 + 2 = 67$	36: $73 + 2 = 75$	40: $81 + 2 = 83$	44: $89 + 2 = 91$	48: $97 + 2 = 99$	50: $99 + 2 = 101$
------------------	-------------------	-------------------	-------------------	-------------------	-------------------	-------------------	-------------------	-------------------	-------------------	-------------------	--------------------

Translation:
b) What is the number of squares in step 50? show how you obtained your answer? **103 squares.**

Figure 6. Andi used recursive strategy to solve part a and b of the task

a) Berapa jumlah persegi ditahap 7? Jelaskan bagaimana kamu mendapatkan jawaban tersebut?

Jawab: $2 \times 3 = 6$ $6 + 1 = 7$

Saya kalikan jumlah Tahap dengan 2 dan kemudian menambahkan dengan Tahap 4

Translation:
a) What is the number of squares in step 5? show how you obtained your answer?
I multiply the number step by 2 and I add by the number of step 4.

b) Berapa jumlah persegi ditahap 50? Jelaskan bagaimana kamu mendapatkan jawaban tersebut?

Jawab: $2 \times 46 = 92$ $92 + 11 = 103$

UNTUK mendapatkan jumlah persegi ke-50, saya kalikan dengan jumlah Tahap 2 dan menambahkan dengan Tahap 4

Translation:
b) What is the number of squares in step 5? show how you obtained your answer?
To get the number of step 50, I multiply the number of step by 2 and I add by the number of 4.

c) Jika ditanya tahap sembarang, jelaskan bagaimana kamu menemukan jumlah persegi ditahap tersebut? jawab: Untuk mendapatkan jumlah persegi ditahap sembarang, saya kalikan jumlah Tahap 2 dan menambahkan dengan Tahap 4

Translation:
c) If someone gives any step number, finding the number of squares on that step and explain how to obtain the answer.
To get the number of any steps, I multiply the number of step by 2 and I add by the number of 4.

Figure 7. Lia used a chunking strategy to solve part a, b, and c of the task

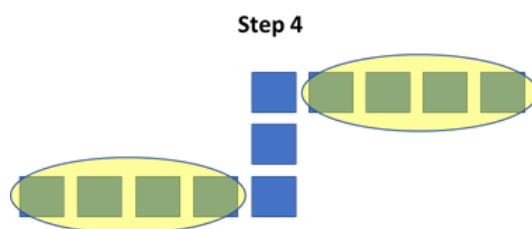


Figure 8. *The illustration of Ziki's invisible marks in step 4.*

OTIMIZAÇÃO DE UMA TECNOLOGIA DE PRODUÇÃO DE NP-FERTILIZANTES

OPTIMIZATION OF AN NP-FERTILIZER PRODUCTION TECHNOLOGY

ОПТИМИЗАЦИЯ ТЕХНОЛОГИИ ПОЛУЧЕНИЯ NP – УДОБРЕНИЯ

KYDYRALIYEVA, Aziza Dossymbekkyzy^{1*}; BESTEREKOV, Uilesbek²; NAZARBEEK, Ulzhalgas Bakytkyzy³; BOLYSBEK, Aidar Alibekuly⁴; URAKOV, Kinis Nurmagambetovich⁵;

^{1,2,3,4,5} M. Auezov South Kazakhstan State University, Department of Chemical Technology of Inorganic Substances, Shymkent, Republic of Kazakhstan.

* Corresponding author
e-mail: yesmm12@mail.ru

Received 25 December 2019; received in revised form 29 July 2020; accepted 18 August 2020

RESUMO

O nitrato de amônio é o fertilizante de nitrogênio mais comum e eficaz no mundo e sua demanda diminuiu significativamente devido ao risco de incêndio e explosão. Para a indústria agrícola, os fertilizantes compostos são os mais preferíveis. Portanto, o desenvolvimento da tecnologia otimizada é uma tarefa urgente. Este estudo teve como objetivo desenvolver a tecnologia de fertilizantes NP com base na mistura da solução do primeiro estágio da evaporação da produção atual de nitrato de amônio e rocha fosfática moída para obter o produto alvo com propriedades aprimoradas para o consumidor e agroquímicas. Foram estabelecidos parâmetros operacionais ótimos da tecnologia para consumo específico de nitrato de amônio e rocha fosfática moída. Os resultados mostraram a regulação da razão dos elementos nutrientes N / P₂O₅ em formulações de fertilizantes como 23/5%; 21/6%; 19/7%; 13/10% e 11/11%. O método de modelagem de segunda ordem de planejamento rotativo Box-Hunter foi usado para obter os dados. A influência das variáveis independentes - o consumo específico de nitrato de amônio e rocha fosfática moída sobre o teor de nutrientes nos produtos-alvo - foi determinado. Foi estabelecido que sua mudança é acompanhada de dois processos opostos, ou seja, aumenta por um aumento no consumo específico de nitrato de amônio com uma diminuição simultânea no consumo específico de rocha fosfática moída e vice-versa; e diminui com uma diminuição no teor específico consumo de nitrato de amônio com um aumento simultâneo no consumo específico de rocha fosfática moída na mistura inicial. Uma equação de regressão adequada foi encontrada para a influência das variáveis independentes na proporção de nutrientes nos produtos. Foi demonstrado que, com as alterações correspondentes na mistura inicial de 0,36 t para 0,67t, e 0,54 t para 0,29 t nos produtos, as relações N / P₂O₅ aumentaram de 2,51 para 4,68. Além disso, é possível obter um conjunto completo de fertilizantes NP com propriedades agroquímicas e de consumo aprimoradas com um teor total de NP de 25% a 28% em sua composição.

Palavras-chave: nitrato de amônio, rocha fosfática moída, nutrientes, nitrogênio, pentóxido de fósforo.

ABSTRACT

Ammonium nitrate is the most common and useful nitrogen fertilizer globally, and its demand has decreased significantly due to its fire and explosion hazard. For the agricultural industry, compound fertilizers are most preferable. So, optimized technology's development is an urgent task. This study aimed to develop NP-fertilizers technology based on the solution mixture of the evaporation's first stage of the current production of ammonium nitrate and ground phosphate rock to obtain the target product with improved consumer and agrochemical properties. It was established optimal operating parameters of the technology for specific consumption of ammonium nitrate and ground phosphate rock. The results showed the ratio regulation of nutrient elements N/P₂O₅ in fertilizer formulations as 23/5%; 21/6%; 19/7%; 13/10%, and 11/11%. The method of rotatable planning-Box-Hunter second-order modeling was used to achieve the data. The independent variables' influence – specific consumption of ammonium nitrate and ground phosphate rock on the nutrients' content in the target products were determined. It has been established that two opposite processes accompany their change, that is, it increases by an increase in the specific consumption of ammonium nitrate with a simultaneous decrease in the specific consumption of ground phosphate rock, and vice versa; and it decreases with a decrease in the specific consumption of ammonium nitrate with a simultaneous increase in the particular consumption of ground phosphate rock in the initial mixture. An adequate regression equation was found for the independent variables' influence on the nutrients' ratios in products. It was shown that, with corresponding changes in the initial mixture

from 0.36 t to 0.67t and 0.54t to 0.29t in the products, the N/ P₂O₅ ratios increased from 2.51 to 4.68. Moreover, it is possible to obtain a whole set of NP-fertilizers with improved agrochemical and consumer properties, with a total NP content of 25% to 28% in their composition.

Keywords: ammonium nitrate, ground phosphate rock, nutrients, nitrogen, phosphorus pentoxide

АННОТАЦИЯ

В настоящее время, к аммиачной селитре спрос существенно снизился из – за ее огне и взрывоопасности, для сельскохозяйственной отрасли наиболее предпочтительными считаются сложные удобрения. Поэтому, разработка оптимизированной технологии получения таких удобрительных композиций представляет собой актуальную задачу. Целевые задачи исследований заключались: в разработке технологии NP – удобрений на основе смеси раствора первой ступени выпарки действующего производства аммиачной селитры и фосфоритной муки с получением целевого продукта с улучшенными потребительскими и агрохимическими свойствами, в установлении оптимальных режимных показателей технологии по удельным расходам аммиачной селитры и фосфоритной муки. Приведены результаты по регулированию соотношений питательных элементов N/P₂O₅ в удобрениях составов в % 23/5; 21/6; 19/7; 13/10; 11/11. Результаты лабораторно-опытно-производственных исследований обобщены с использованием метода рототабельного планирования - моделирования второго порядка Бокса-Хантера. Определено влияние независимых переменных - удельных расходов аммиачной селитры и фосфоритной муки на содержания питательных элементов в целевых продуктах. Установлено, что их изменение сопровождается двумя противоположными процессами: возрастает с увеличением удельного расхода аммиачной селитры при одновременном уменьшении удельного расхода фосфоритной муки, и наоборот, снижается с уменьшением удельного расхода аммиачной селитры при одновременном увеличении удельного расхода фосфоритной муки в исходной смеси. Найдено адекватное уравнение регрессии влияния независимых переменных на отношения питательных элементов в продуктах. Показано, что при соответствующих изменениях последних в исходной смеси от 0,36т до 0,67т и 0,54т до 0,29т в продуктах отношения N/P₂O₅ возрастают от 2,51 до 4,68. При этом возможно получение целого набора NP - удобрений с улучшенными агрохимическими и потребительскими свойствами, с суммарным содержанием NP в их составе от 25% до 28%.

Ключевые слова: аммиачная селитра, фосфоритная мука, питательные вещества, азот, пятиокись фосфора

1. INTRODUCTION:

Ammonium nitrate is the most common and effective nitrogen fertilizer globally (Chernyshev A.K. *et al.*, 2009; V. M. Olevskiy, 1978; Besterekov U. *et al.*, 2019; Besterekov U. *et al.*, 2018). It is used in agriculture for all types of crops and on any kind of soil.

However, in recent years, both consumers and producers of ammonium nitrate have encountered some difficulties and limitations due to its severe consumer shortcoming - fire and explosion hazard [J. Oxley *et al.*, 2002; N. Dechy *et al.*, 2004; Lavrov V.V. and Shvedov K.K., 2004; Taran A.L. *et al.*, 1991; Usmonov K.P. 2011]. Therefore, to obtain high and high-quality yields, it is necessary to apply balanced fertilizers, so-called complex fertilizers characterized by the optimal ratio of nitrogen, phosphorus, and other fertilizing elements, and have a high agrochemical value (K. Gorbovskiy *et al.*, 2017; Ilin V.A., 2006; Pavlova G.S., 2007; Madenov B.D. *et al.*, 2012; Ghiga R. *et al.*, 2008; Kurbaniyazov R.K. *et al.*, 2007; Levin B.V. and Sokolov A.N., 2004; Sagdullayev U.Kh., *et al.* 2007; Belova N.P. and

Ryabtseval. Yu. 2007; Dmitriyeva O.A. and Ovchinnikov V.M., 2007; Artemenko V.G. and Gunin V.V., 2010; Kurbaniyazov R.K., 2011; Abramov O.B. *et al.*, 2010; Rakcheyeva L.V. *et al.*, 2010; Sharipov T.V. *et al.*, 2011; Obrestad T. and Oksvik A., 2012; Ilyin V.A. *et al.*, 2014; Reimov A.M., 2012; Pak D.G. *et al.*, 2017; Alimov U.K. *et al.*, 2016; Madenov B.D. *et al.*, 2015; Madenov B.D. *et al.*, 2015).

Because of this, in recent years, there has been a great demand for fertilizers containing nitrogen and phosphorus. Therefore, numerous studies are being conducted on the addition of phosphorus-containing components into the composition of ammonium nitrate melt, which are natural minerals, as well as products or the technogenic phosphorus-containing wastes produced based on their industrial processing (Botirov B.B. and Beglov B.M., 2008; Usmonov K.P., 2013; Taran Yu.A. and Taran A.V., 2016; Namazov Sh.S., 2008; Kurbaniyazov R.K., 2008; Vorobeveva T.A. *et al.*, 2013; A.M. Reymov *et al.*, 2013; Bolysbek A.A. *et al.*, 2018; Madenov B.D. *et al.*, 2015; Madenov B.D. *et al.*, 2012; Taran A.L. *et al.*, 2016; Gorbovskiy K.G. *et al.*, 2019). The

purpose of this work was to investigate the possibility of obtaining NP-fertilizers of improved agrochemical properties with an adjustable nutrient ratio N/P_2O_5 based on a solution of ammonium nitrate and ground phosphate rock.

In the Republic of Kazakhstan, the only producer of ammonium nitrate with fertilizing purpose is "KazAzot" JSC (Aktau, Republic of Kazakhstan). Concerning solving those mentioned above especially urgent tasks for this production to improve agrochemical value and increase consumer qualities of ammonium nitrate, own raw material reserves of phosphate ores of the Republic of Kazakhstan can be successfully used (Directory of Kazakhstan deposits). Following the requirements specification of "KazAzot" JSC (Aktau, Kazakhstan) for establishing new opportunities for improving the agrochemical and consumer properties of ammonium nitrate the scientific team of the Department "Chemical Technology of Inorganic Substances" of M. Auezov South Kazakhstan State University (Shymkent, Kazakhstan) carried out a research. The research purpose was to obtain new NP-fertilizers considering a comprehensive analysis of their composition and properties. The initial components were the ammonium nitrate solution produced by "KazAzot" JSC according to GOST-2-2013 (This GOST 2-2013 applies to ammonium nitrate intended for agriculture, industry and export.), and Chilisay ground phosphorite rock (GPR-2 grade TS 930640000252-01-2011) containing 17% of P_2O_5 ("Temir-Service" LLP, Aktyubinsk, Kazakhstan). The initial solution contained 64-71% of ammonium nitrate and was obtained according to the traditional ammonium nitrate production technology on the first evaporation stage. The customer also agreed on the limiting contents of nitrogen and phosphorus pentoxide in the final target products, respectively, in the range of $11 \pm 23\%$ and $5 \pm 11\%$.

This study aimed to investigate the possibility of obtaining NP-fertilizers of improved agrochemical properties with an adjustable nutrient ratio N/P_2O_5 based on a solution of ammonium nitrate and ground phosphate rock.

2. MATERIALS AND METHODS:

The research was conducted in the laboratories of M. Auezov SKSU. Their results were tested in the trial plot of "KazAzot" JSC, which is currently producing the ammonium nitrate. Ammonium nitrate solution with a concentration of 64-71% of the known volume and temperature of 110-130 ° C was mixed with the

calculated mass of ground phosphate rock. A modifying mineral additive was also added to the mixture in small quantities. The obtained suspension mixture was thoroughly mixed and fed to sprayers at the temperature of 120-130°C, and from there, it was sprayed into a granulator-drum, where it was dried by a drying agent in a direct-flow mode and granulated in compliance with the traditional technological operating parameters of the current production of ammonium nitrate (V. M. Olevskiy, 1978; Regulations of "KazAzot", 2012).

The analysis of composition and properties of the initial mixture and obtained samples NP-fertilizers were conducted according to the methods given in the normative documentation for fertilizer:

- the total nitrogen content in NP-fertilizer – according to GOST 30181.6-94 (Determination of total nitrogen in saltpeter and the resulting products was carried out by the titrimetric method GOST 30181.4-94. This method is based on the reduction of nitrate nitrogen to ammonium nitrogen by Devard's alloy in the presence of sodium hydroxide, followed by distillation of ammonia from the alkaline solution into a sulfuric acid solution and back titration of the excess acid with sodium hydroxide solution in the presence of a mixed indicator. The technique is designed to measure the amount of nitrogen in the range from 8% to 35%.);
- the P_2O_5 content of NP-fertilizer – according to GOST 20851.2-75 (The determination of the total P_2O_5 in the obtained products was carried out by the photocolormetric method according to the GOST 20851.2-75. The technique is designed to measure the amount of P_2O_5 in the range from 3% to 50%. The method is based on a photometric change in phosphates with vanadium and molybdenum salts, which form compounds colored yellow. The optical density of the resulting compound is measured on a photocolormeter.);
- the moisture content of the product – according to GOST 20851.4-75 (Determination of total moisture in ammonium nitrate, ground phosphate rock, and the resulting products was carried out by the drying method GOST 20851.4-75. This method is based on drying at a temperature of 105 - 110 ° C to constant weight and subsequent weighing. The moisture content is calculated from the difference in sample weight before and after drying. The technique is intended for measuring hygroscopic and total moisture in terms of H_2O from 0.1% to 12% by drying in a drying oven.), using hydrometer Mettler Toledo;
- the strength of NP-fertilizer's granules – on the

device IPG-1M;

- pH of 10% solution of NP-fertilizer – on the device I-160 MI.

3. RESULTS AND DISCUSSION:

The results of experimental studies conducted under the laboratory-test-industrial conditions are presented in tables 1 and 2. Specific consumptions of the ammonium nitrate and ground phosphate rock were calculated in terms of 1 ton of the target product. At the initial stage of the research, the influence of the specific consumption of ammonium nitrate and ground phosphate rock and the nutrients contained in them – N and P_2O_5 on their ratio in the target products were studied. The results of these studies are shown in Figures 1 and 2.

As follows from the results obtained, the increase in the ratio of nutrient elements N/ P_2O_5 in the target products is accompanied by two different processes: the increase in the specific consumption of ammonium nitrate with the simultaneous decrease in the specific consumption of ground phosphate rock in them. In this regard, further studies were carried out by the method of rotatable design of second-order experiment (Box-Hunter method) (Akhnazarova S.A. and Kafarov B.V., 1985). As independent variables, the specific consumption of ammonium nitrate and ground phosphate rock was used. The optimization parameter was the ratio N/ P_2O_5 in the product. Table 3 shows the information on the variation areas of the independent variables, compiled based on the data from Table 1. Table 4 shows the matrix of experimental design and its results.

Based on the data of table 4 and (Inkov A.M. *et al.*, 2000) we obtained the regression equation of influence of ammonium nitrate and ground phosphate rock consumption in the initial mixture on the N/ P_2O_5 ratio both in coded and natural forms:

$$N/P_2O_5_{\text{cod}} = 1,758Z_1^2 - 9,951Z_1Z_2 + 7,615Z_1 + 10,688Z_2^2 - 10,227Z_2 + 2,683 \quad (1)$$

$$N/P_2O_5_{\text{nat}} = 2,683 + 7,615AN - 10,227GPR + 1,758AN^2 + 10,688GPR^2 - 9,951AN \cdot GPR \quad (2)$$

Assessment of the significance of the regression equations (1-2) was determined using the Student's test, but the adequacy of the equation by the Fisher criterion. Table 5 shows the experimental and calculated according to the equation (2) values of the nutrients' ratios in the samples of the obtained target NP-fertilizers were

compared.

The table value of Fisher's criterion is 6.59, and the calculated is 0.188 taking into account 5% of the experiment's errors. In this regard, $F_{\text{tabl}} > F_{\text{calc}}$ regression equation obtained is adequate. Based on equation (2) using the MathCAD program (Ochkov V.F., 2007) a volumetric image of response surface $N/P_2O_5_{\text{nat}} = f(AN, GPR)$ and its horizontal sections were constructed.

Figure 3 shows that by increasing the consumption of ammonium nitrate and the decrease in ground phosphate rock consumption, the ratio of nutrients in the target product increases. N/ P_2O_5 in the target product reaches its maximum level (4.68) with a consumption of ammonium nitrate of 0.67t and ground phosphate rock of 0.29t. Table 6 shows the values of technological parameters in the abc areas, in which the N/ P_2O_5 ratios vary from 2.5 to 4.68. From Figure 3 and Table 6 it follows that the optimal consumption parameters of ammonium nitrate and ground phosphate rock for the N/ P_2O_5 ratio in the target NP-fertilizer from 0.25 to 4.68 are located along with the lines ac (for AN) and cb (for GPR), i.e. AN can vary from 0.36t to 0.67t and GPR from 0.29t to 0.54t.

4. CONCLUSIONS:

Based on the results obtained by modeling the process of the influence of specific consumption of ammonium nitrate and ground phosphate rock on the ratios of nutrients (N/ P_2O_5) in target NP-products, the following conclusions can be made:

1. the specific consumption of ammonium nitrate and ground phosphate rock on the ratio of nutrients in the target product has the opposite influence: the increase in the particular use of ammonium nitrate and the corresponding decrease in the specific consumption of ground phosphate rock results the growth of the N/ P_2O_5 ratio in the target product, and vice versa, the reduction in the particular consumption of ammonium nitrate and the corresponding increase in the specific use of ground phosphate rock leads to the decrease of the N/ P_2O_5 ratio in the target product;
2. by the rise in the consumption of ammonium nitrate in the system under consideration from 0.36 t to 0.67 t with the corresponding decrease in the specific consumption of phosphate rock, the ratio of nutrients N/ P_2O_5 in the target NP-fertilizers increases from 2.51

to 4.68;

3. by the increase in the consumption of ground phosphate rock in the system under consideration from 0.29 t to 0.54 t with the corresponding decrease in the specific consumption of ammonium nitrate, the ratio of nutrients N/P₂O₅ in the target NP-fertilizers decreases from 4.68 to 2.51;
4. for the production of target N/P - fertilizers based on a mixture of a solution of ammonium nitrate of GOST 2-2013, the concentration of 64-71% and Chilisay ground phosphate rock of FM-2 grade TS 930640000252-01-2011 with a 17% content of P₂O₅, consumption of ammonium nitrate and ground phosphate rock in their mixture should be supported by ammonium nitrate in the range of 0.36t and 0.67t and in-ground phosphate rock – 0.54t and 0.29t. Moreover, in the composition of possible assortments of N/P-fertilizers obtained, the total content of nutrients will be: 28%; 27%; 26%; 25% or, respectively, in mass % N/P₂O₅ – 23/5; 21/6; 19/7; 18/7, which is quite convincing evidence of their high agrochemical value.

5. REFERENCES:

1. Reymov, A.M., Namazov, Sh.S., Beglov, B.M. (2013). Effect of phosphate additives on physical-chemical properties of ammonium nitrate. *Journal of Chemical Technology and Metallurgy*, 48, 4, 391-395.
2. Abramov O.B., Boikov S.V., Zakharova O.M., Kiselevich P.V., Laverzhentseva I.V., Medyantseva D.G., Nechyayev V.N., Ponomarev N.P., Yuzhanin G.A. (2010). A complex nitrogen-phosphorus mineral fertilizer production way. *Patent of the Russian Federation* № 2378232 Cl. C05C 1/00. 01. 10.
3. Akhnazarova S.A., Kafarov B.V. (1985). Experiment optimization methods in chemical technology. *Vysshaya Shkola*, 327.
4. Alimov, U.K., Namazov, Sh.S., Seitnazarov, R. (2016). Nitrogen-phosphorus-calcium fertilizers produced by means of phosphoric acid processing of an off-balance Central Kyzyl Kum phosphorite ore. *Chemical industry today*. No.11 – P. 13-21.
5. Artemenko, V.G., Gunin, V.V. (2010). Development of a method for producing complex nitrogen-phosphorus fertilizer. *Khimicheskaya Tekhnologiya*. No.7, p. 400-403.
6. Belova, N.P., Ryabtseval, Yu. (2007). Obtaining complex fertilizer based on ammonium nitrate. *North-Caucasian State Technical University*, p. 61-62
7. Besterekov, U., Kydyralieva, A.D., Petropavlovskiy, I.A., Yeskendirova M.M., Urakov K.N., Pochitalkina I.A., Bolysbek A.A. (2019). Mass balance calculations of processes of ammonia saltpeter thermal decomposition and nitric acid absorption of ammonia. *Bulletin of the Karaganda university, Chemistry Series*. Karaganda, No.4(96), P:92-97 DOI 10.31489/2019Ch4/92-97
8. Kydyralieva, A.D., Besterekov, U., Petropavlivskiy, I.A. (2018). The results of studies of the processes of thermal decomposition of ammonium nitrate and acid absorption of ammonia. *Proceedings of the International science project*. Finland. Turku. 20, 56-58.
9. Bolysbek, A.A., Kydyraliyeva, A.D., Orazbayeva, K.U., Kulmyrzayev, A.M., Nazarbek, U.B. (2018). Research results on the possibility of using ground phosphate rock of Chilisay field to obtain complex fertilizer. *Transactions of M. Auezov SKSU*. ISSN 2522-4026 – Shymkent, No.4 (45). –p. 57-60.
10. Botirov, B.B., Beglov, B.M. (2008). Ways to improve the quality of ammonium nitrate. (*IONKhANRUz*). *Khimicheskaya tekhnologiya. Kontroliupravlenie*. No.6, P.12-24.
11. Chernyshev, A.K., Levin, B.V., Tugolukov, A.V., Ogarkov, A.A., Ilyin, V.A. (2009). Ammonium nitrate: Properties, Production, and Application. *Eds., Moscow: INFOKHIM*.
12. Directory of Kazakhstan deposits. The official website of the Ministry of Investment and Development of the Republic of Kazakhstan. Committee of Geology and Subsoil Use. www.geology.mid.gov.kz/ru/pages/spravochnik-mestorozhdeniy-kazahstana
13. Dmitriyeva, O.A., Ovchinnikov, V.M. (2007). New technologies of ammonia saltpeter based fertilizers manufacture at IChC "EuroChim" of PC "NevinnomysskAzot". *Collected papers of 2nd All-Russian scientific theoretical conference*, Stavropol', Northern Caucasus State Technical University. P. 62-64.

14. Ghiga, R., Iovi A., Negrea, P. (2008). Study of optimal conditions of an NP micronutrient-containing fertilizer production process. *Chim j ing med* 53:276-278.
15. Gorbovskiy, K.G., Norov, A.M., Kochetova, I.M., sokolov, V.V., Mikhaylichenko, A.I. (2019). Study of structural and mechanical properties of mineral fertilizer granules. THEORETICAL FOUNDATIONS OF CHEMICAL ENGINEERING. 53:620–625.
16. Ilyin, V.A. (2006). Development of a technology of complex nitrogen-phosphate fertilizer based on ammonium nitrate smelt. Dissertation thesis of Cand.Tech.Sci.: 05.17.01 Ivanovo, 113 p. RSL DD, 61:06-5/2994
17. Ilyin, V.A., Patokhin, O.I., Glagolev, O.L., Selin, Ye.N., Levin, B.V., Sokolov, A.N., Sokolov, A.Yu., Samsonov, V.P., Rezen'kov, M.I., Ansheles, V.R., Simbireva, Z.P., Zhavoronkova, N.Ye., Vasil'kova, O.Ye. (2014). A complex nitrogen-phosphoric fertilizers production way. *Patent of the Russian Federation* № 2223932 Cl. C05B 7/00, C05C 1/00. 10.01.2014.
18. Inkov, A.M., Tapalov, T., Umbetov, U.U., Hu Ven-Tsen, B., Akhmetova, K.T., Dyakova, Ye.T. (2000). Optimization techniques: *electronic book. M. Auezov South Kazakhstan State University*
19. Oxley, J., Smith, J., Rogers, E., Yu, M. (2002). Ammonium nitrate: Thermal stability and explosivity modifiers. *ThermochimActa*, No.384, 1, 23-45.
20. Gorbovskiy, K., Kazakov, A., Norov, A., Malyavin, A., Mikhaylichenko, A. (2017). Properties of complex ammonium nitrate-based fertilizers depending on the degree of phosphoric acid ammoniation. *Int J Ind Chem*. 8:315–327 DOI 10.1007/s40090-017-0121-4
21. Kurbaniyazov, R.K. (2011). Technology of a complex nitrogen-phosphorus fertilizers on the basis of an ammonia saltpeter melt and Central Kyzyl Kum phosphorite. *Abstract of a Cand. Tech. Sci. thesis*. Institute of general and inorganic chemistry of Academy of Sciences of the Republic of Uzbekistan, Tashkent. – 28 p.
22. Kurbaniyazov, R.K., Reimov, A.M., Dadakhodzhayev, A.T., Namazov, Sh.S., Beglov, B.M. (2007). Nitrogen-phosphorus fertilizers obtained by introducing phosphate raw material from the Central Kyzylkum into the smelt of ammonium nitrate. *Khimicheskaya promyshlennost*. Vol.84, No.5, p. 242-248.
23. Kurbaniyazov, R.K., Reimov, A.M., Namazov, Sh.S., Beglov, B.M. (2008). Nitrogen-phosphorus fertilizers obtained by the interaction of concentrated solutions of ammonium nitrate with ordinary phosphate rock of Central Kyzylkum. *Khimicheskaya promyshlennost. Kontroliupravlenie*. No.3, p.5-8.
24. Lavrov, V.V., Shvedov, K.K. (2004). On explosion hazard of ammonia saltpetre and fertilizers on its base. *Scientific and technical news: "INFOKHIM", special issue*, No.2. P.44-49.
25. Levin, B.V., Sokolov, A.N. (2004). Problems and technical solutions and production of complex fertilizers based on ammonium nitrate. *Mir. Series N, P and K*, No.2. p. 13-21
26. Madenov, B.D., Namazov, Sh.S., Reimov, A.M., Beglov, B.M. (2015). Phosphatized ammonium nitrate on the basis of its melt and the Nazarkhanskiy deposit phosphorites of Karakalpakstan. *Chemical technology. Control and management*. No.2. – P. 5-10.
27. Madenov, B.D., Namazov, Sh.S., Reimov, A.M., Seitnazarov, R. (2015). Nitrogen-phosphorus fertilizers on the basis of ammonium nitrate melt and ground phosphate rock of Hodzhakulskoye and Hodzheilinskoye deposits of Karakalpakstan. *Uzbekistan Chemical Journal*. No.1 – P. 68-73.
28. Madenov, B.D., Seitpazarov, R., Beglov, B.M. (2012). Nitrogen-phosphorus fertilizers obtained by introducing ground phosphate rock of the Chilisay deposit into the smelt of ammonium nitrate. *Khimicheskaya promyshlennost*. Vol.89, No.7, p. 327-332.
29. Madenov, B.D., Namazov, Sh.S., Ortikova, S.S., Reimov, A.M. (2015). Strength of granules of phosphatized ammonia saltpeter with the Karakalpakstan phosphorite additive. *Kazakhstan chemical journal*. – P. 110-114. www.chemjournal.kz
30. Madenov, B.D., Reimov, A.M. (2012). Rheological properties of ammonium nitrate melt with the Chilisay deposit ground phosphate rock additive. *Chemical technology. Control and management*. No.5, – P. 34-37.
31. Mining company "Temir-Servis" LLP <https://temir-servis.satu.kz/>.

32. Dechy, N., Bourdeaux, T., Ayrault, N., Kordek, M., Le Coze, J. (2004). First lessons of the Toulouse ammonium nitrate disaster, 21st September 2001, AZF plant, France, J. Hazard Mater, 111, 1-3, , 131-138.
33. Namazov, Sh.S., Kurbaniyazov, R.K., Reimov, A.M., Beglov, B.M. (2008). Strength of ammonium nitrate granules with phosphorite additives in Central Kyzylkum. *Khimicheskaya promyshlennost'*, Vol.85, No.2, p. 65-80.
34. Obrestad, T., Oksvik, A. Manufacture of nitrogen-phosphorus-potassium or nitrogen-phosphorus materials containing polyphosphates. Patent of the Russian Federation № 2439039 Cl. C05B 11/06. 10.01.2012.
35. Ochkov, V.F. (2007). Mathcad 14 for students, engineers and constructors. St. Petersburg: BKhV-Peterburg. 368 p.
36. Pak, D.G., Mamataliyev, A.A., Namazov, Sh.S. (2017). Nitrogen-phosphorus-potassium containing fertilizers on the basis of ammonia saltpeter, Central Kyzyl Kum ground phosphate rock, local potassium chloride and their physicochemical and commodity properties. *Uzbekistan Chemical Journal*, no. 1. P. 59-66.
37. Pavlova, G.S. (2007). Agrochemical servicing of agricultural production. *Tekhnika i oborudovaniye dlya sela*. no. 2. P. 6-10.
38. Rakcheyeva, L.V., Klados, D.K., Kochetkova, V.V., Kuzmicheva, T.N., Zlobina, Ye.P., Bogach, Ye.V., Klassen, P.V. (2010). A complex nitrogen-phosphoric fertilizers production way. Patent of the Russian Federation № 2407720 Cl. C05B 7/00. 27.12.2010.
39. Regulations of "KazAzot", 2012
40. Reimov, A.M. (2012). Studying modification transformations of the nitrogen-phosphorus fertilizer produced on the basis of ammonia saltpeter. *Chemical technology. Control and management*. no. 5. P. 19-23.
41. Sagdullayev, U.Kh. (2007). Complex nitrogen-phosphorus fertilizer based on ammonium nitrate. Vol. 5. Moscow: LENAND, p. 91-93.
42. Sharipov T.V., Mustafin A.G., Usmanov R.T., Volodin P.N., Kamaletdinova L.Sh., Galiyanov A.X. A complex nitrogen-phosphoric fertilizers production way. Patent of the Russian Federation № 2404149 Cl. C05B 7/00, C05C 1/00. 10.09.2011.
43. Taran, A.L., Ostanina, O.I., Taran, A.V. and Bepalova, V.O. (2016). Analysis of the National and Foreign Quality Requirements for Basic Mineral Nitrogenous Fertilizers, and Technical Solutions for Improving Their Quality. *Chemical and Petroleum Engineering*, volume 52, pages 10–14.
44. Taran, A.L., Shmelev, S.L., Olevskiy, V.M., et al. (1991). Study of the possibility of granulation in ammonium nitrate towers with ammonium sulfate additives. *Chemical Industry*, No. 12, 743–749.
45. Taran, Yu.A., Taran, A.V. Basic nitrogen-containing mineral fertilizers and technical solutions to improve their quality. *Izvestiya vuzov. Khimiyai khimicheskaya tekhnologiya*, Vol.59, No.3, P. 49-54.
46. The official webpage of "KazAzot" LLP <http://kazazot.kz>
47. Usmonov, K.P., Mamatkulov, A.V., Kondakov, D.F. (2011). Polymorphic transformations and properties of samples of the ammonia saltpeter modified by inorganic additives. *Successes of chemistry and chemical technology*. Vol. 25, no. 8, P. 61-64.
48. Usmonov, K.P. (2013). Modification of ammonium nitrate with inorganic silicon compounds: *dissertation of Cand.Tech.Sci.: 05.17.01 [Defense place: D.I. Mendelyev Russian Chemical Technological University]*. – Moscow. 136 p.: RSL DD, 61 14-5/386
49. Technology of ammonium nitrate/ Edited by Olevskiy, V.M. Moscow: Khimiya, 1978. 311p. (Production and use of mineral fertilizers). (Code 661/T38-525168)
50. Vorob'eva, T.A., Kostina, N.V. et al. (2013). Investigation of the physical and mechanical properties of fertilizers based on ammonium nitrate with inorganic additives. *Izvestiya vuzov. Khimiya i khimicheskaya tekhnologiya*, Vol. 56, No.11, p. 100-103.

Table 1. Specific consumptions of the initial components, contents, and ratios of nutrients in the target products

Samples of products obtained	Specific consumption, tonne		Content of the nutrients in the target product	The ratio of the nutrients in the target product
	Ammonium nitrate	Ground phosphate rock	N/ P ₂ O ₅ (%/%)	N/ P ₂ O ₅ (%/%)
1	0,320	0,647	11/11	1/1
2	0,378	0,588	13/10	1,3/1
3	0,552	0,412	19/7	2,71/1
4	0,610	0,353	21/6	3,5/1
5	0,668	0,294	23/5	4,6/1

Table 2. The basic physical and chemical properties of target products

Samples of products obtained	pH of 10% solution	The moisture of product (%)	Strength of product granules (N/g)	The ratio of nutrients in the product (N:P ₂ O ₅)	Granulometric composition of the target product, mass %	
					1-4 mm	2-4 mm
1	6,42	0,28	66,84	1/1	80-92	79-81
2	6,40	0,28	8,70	1,3/1	90-93	80-85
3	6,27	0,27	8,06	2,71/1	94-98	86-90
4	6,30	0,27	8,06	3,5/1	94-98	90-95
5	6,47	0,28	12,15	4,6/1	94-98	92-97

Table 3. Variation intervals of variables

Variation areas of the variables	Variables		
	In coded form	In natural form	
	X _i	Specific consumption of ammonium nitrate, t (AN)	Specific consumption of ground phosphate rock, t (GPR)
Basic level	0	0,494	0,470
Variation interval	Δ	0,123	0,125
Upper level	+1	0,617	0,595
Lower level	-1	0,371	0,345
Upper "stellar" arm	+1,414	0,668	0,647
Lower "stellar" arm	-1,414	0,320	0,294

Table 4. Planning matrix and research results on the impact of ammonium nitrate and ground phosphate rock in the initial mixture on the ratio of nutrients in the target products

No.	Variables				The ratio of N/ P ₂ O ₅ in fertilizer
	In coded form		In natural form		
	X ₁	X ₂	AN, t	GPR, t	
1	+1	+1	0,617	0,595	2,09
2	+1	-1	0,617	0,345	3,62
3	-1	+1	0,371	0,595	1,26
4	-1	-1	0,371	0,345	2,18
5	+1,414	0	0,668	0,470	3,02
6	-1,414	0	0,320	0,470	1,37
7	0	+1,414	0,494	0,647	1,54
8	0	-1,414	0,494	0,294	3,41
9	0	0	0,494	0,470	2,13
10	0	0	0,494	0,470	2,13
11	0	0	0,494	0,470	2,13
12	0	0	0,494	0,470	2,13
13	0	0	0,494	0,470	2,13

Table 5. Comparative information on the results of experimental and calculated values of the nutrients' ratios in samples of target NP – fertilizers

No.	N/P ₂ O ₅ experimental	N/P ₂ O ₅ calculated	% of errors
1	2,18	2,22	-1,84
2	3,62	3,67	-1,55
3	1,26	1,25	0,67
4	2,09	2,09	-0,35
5	3,02	2,98	1,16
6	1,37	1,35	0,91
7	1,54	1,55	-0,69
8	3,41	3,35	1,70
9	2,13	2,12	0,56
10	2,31	2,12	8,31
11	1,96	2,12	-8,06
12	2,04	2,12	-3,82
13	2,15	2,12	1,49

Table 6. Technological parameters in the abc areas boundary (according to Figure3)

Points in Figure 3	Specific consumption of ammonium nitrate, t	Specific consumption of ground phosphate rock, t	N/ P ₂ O ₅ ratio in the target product
a	0,36	0,29	2,51/1
b	0,67	0,54	2,51/1
c	0,67	0,29	4,68/1

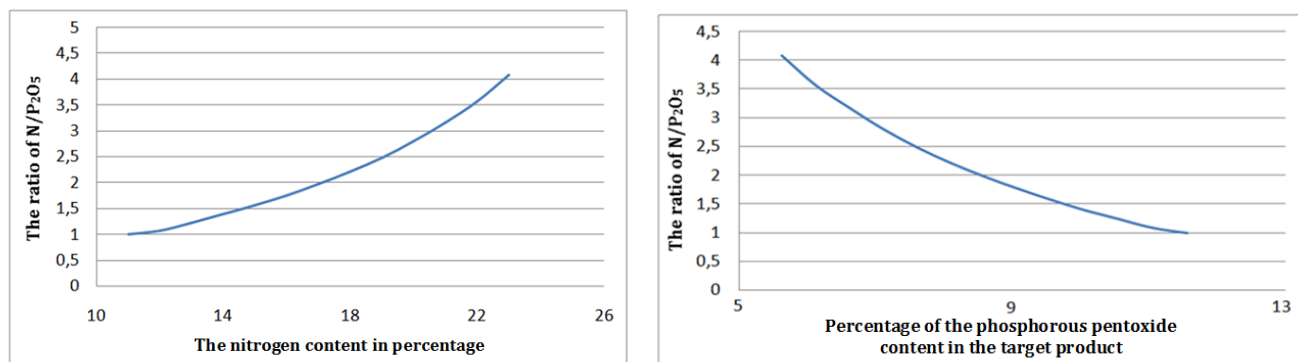


Figure 1. The change in the ratio of nutrients depending on the content of nitrogen and phosphorus pentoxide in the target product

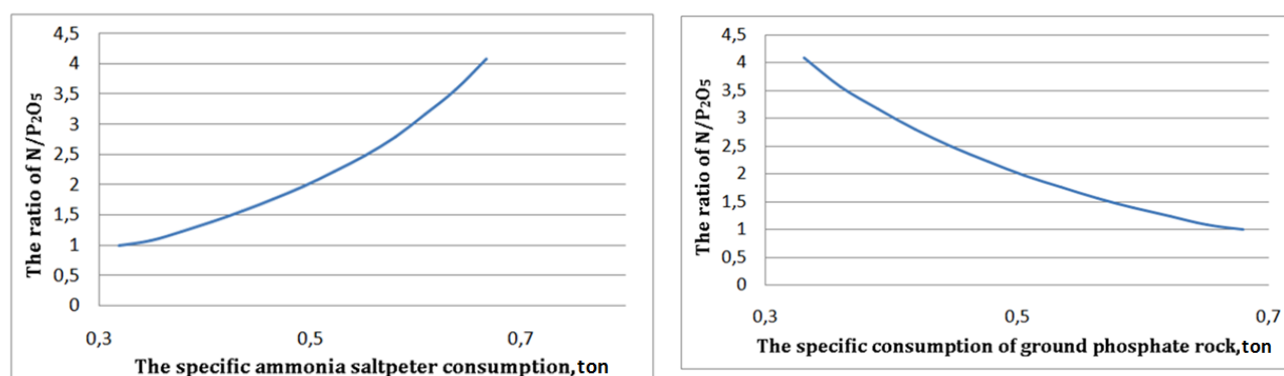


Figure 2. The change in the ratio of nutrients depending on the specific consumption of ammonium nitrate and ground phosphate rock in the target product

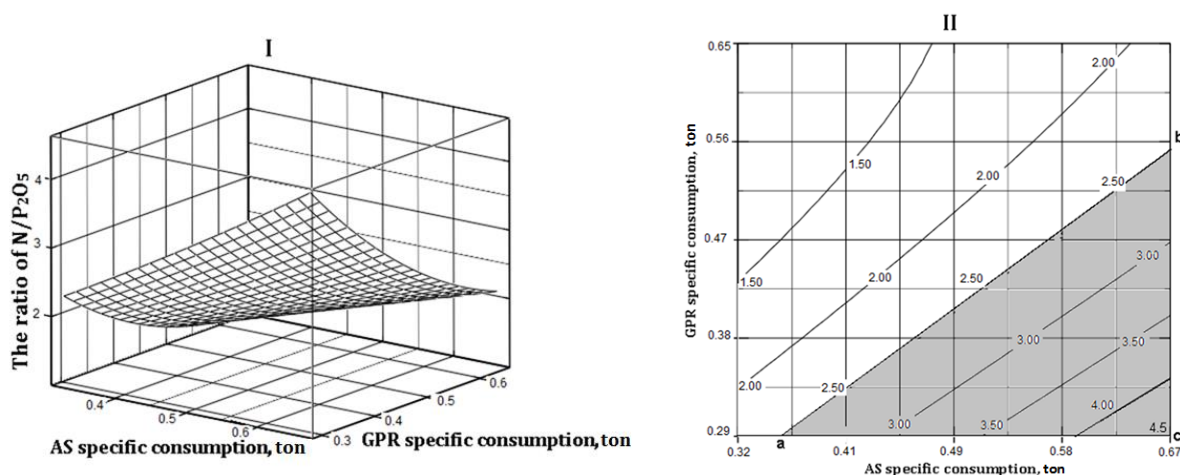


Figure 3. The influence of specific consumption of ammonium nitrate and ground phosphate rock on the ratio of nutrients (N/P₂O₅) in the target product. I – Volumetric image, II – Horizontal sections.

USANDO O ENSAIO DIAGNÓSTICO EM TRÊS NÍVEIS PARA AVALIAR CONCEPÇÕES DE ENERGIA DE IONIZAÇÃO

USING ONLINE THREE-TIER DIAGNOSTIC TEST TO ASSESS CONCEPTIONS OF IONIZATION ENERGY

PENGGUNAAN TES DIAGNOSTIK *ONLINE* TIGA TINGKAT UNTUK MENGASES KONSEPSI TERKAIT ENERGI IONISASI

SUPRAPTO, Nadi^{1*}; ABIDAH, Azmil²

¹Universitas Negeri Surabaya, Faculty of Mathematics and Natural Sciences, Department of Physics, Surabaya, Indonesia.

²Pharmacy Vocational High School of Sekesal, Surabaya, Indonesia

** Corresponding author*
e-mail: nadisuprpto@unesa.ac.id

Received 20 June 2020; received in revised form 20 October 2020; accepted 23 October 2020

RESUMO

O termo que descreve as noções dos alunos de conceitos científicos diferentes dos cientificamente aceitáveis pelo cientista ainda é debatido. Este estudo explora como conceitos científicos realizados por alunos do ensino médio (HSSs), professores em formação (PSTs) e professores em serviço (ISTs) simultaneamente para tornar claro entre sua concepção vs. concepção dos cientistas, principalmente no conceito de energia de ionização. Portanto, é fundamental levantar a posição da concepção científica e do equívoco. Para diagnosticar os equívocos, alguns métodos podem ser usados: mapas conceituais, entrevistas, testes de múltipla escolha (uma camada), testes de várias camadas (duas camadas, três camadas, quatro camadas), testes abertos e outras. Este estudo usou testes de várias camadas com três camadas. No total, 326 participantes da Indonésia, incluindo 118 HSSs, 165 PSTs e 43 ISTs com especialização em química, foram convidados a concluir um teste on-line de Diagnóstico-Modificação de Energia de Ionização (IEDI * M). O teste consistiu em 12 itens de diagnóstico de três níveis. O estudo indicou que quatro conceitos alternativos substanciais foram reconhecidos: conservação de energia, sub-camadas preenchidas pela metade ou totalmente preenchidas estáveis, estrutura de regras do octeto e raciocínio baseado em relações. Os ISTs tiveram um desempenho melhor do que os HSSs e PSTs no entendimento da energia de ionização. O estudo também especificou a distribuição das concepções de energia de ionização do Grupo 1 e 2, e Período 2 e 3 no sistema periódico. Ao utilizar o IEDI * M, as porcentagens de conceitos alternativos diminuíram de um nível para dois níveis e de dois para três níveis. Este estudo oferece algumas implicações para o governo, formuladores de políticas, professores de química, professores em formação e membros do corpo docente universitário.

Palavras-chave: teste de diagnóstico, energia de ionização, teste de três níveis.

ABSTRACT

The term describing the students' notions of scientific concepts dissimilar from scientifically acceptable by the scientist is still debated. This study explores of how scientific concepts performed by high school students (HSSs), pre-service teachers (PSTs), and in-service teachers (ISTs) simultaneously to make clear between their conception vs. scientists' conception, especially in the ionization energy concept. Therefore, it is crucial to raise the position of scientific conception and misconception. For diagnosing the misconceptions, some methods can be used: concept maps, interviews, multiple-choice tests (one-tier), multiple-tier tests (two-tier, three-tier, four-tiers), open-ended tests, and others. This study utilized multiple-tier tests with three-tier. Totally, 326 participants from Indonesia, including 118 HSSs, 165 PSTs, and 43 ISTs majoring in chemistry, were invited to complete an online -Ionization Energy Diagnostic-Modification (IEDI*M) test. The test consisted of 12 three-tier diagnostic items. The study indicated four substantial alternative conceptions were acknowledged: conservation of energy, half-filled sub-shells or stable fully-filled, octet rule framework, and relation-based reasoning. ISTs performed better than HSSs and PSTs on the understanding of ionization energy. The study has also specified the distribution of ionization energy conceptions of Group 1 and 2, and Period 2 and 3 on the periodic system. By

utilizing the IEDI*M, the percentages of alternative concepts decreased from one-tier to two-tier and from two-tier to three-tier. This study gives some implications for the government, policy-makers, chemistry teachers, pre-service teachers, and university faculty members.

Keywords: diagnostic test, ionization energy, three-tier test.

ABSTRAK

Istilah mendeskripsikan pemahaman siswa tentang konsep-konsep ilmiah yang berbeda dengan yang diterima secara ilmiah oleh ilmuwan masih menjadi perdebatan. Penelitian ini mengeksplor bagaimana konsep ilmiah yang ditunjukkan oleh siswa sekolah menengah atas (HSS), guru pra-jabatan (PST), dan guru dalam jabatan (IST) secara bersamaan untuk memperjelas antara konsepsi mereka vs konsepsi ilmuwan terutama atas konsep energi ionisasi. Oleh karena itu, penting untuk mengangkat posisi konsepsi ilmiah dan miskonsepsi. Untuk mendiagnosis kesalahpahaman, beberapa metode dapat digunakan: peta konsep, wawancara, tes pilihan ganda (satu tingkat), tes beberapa tingkat (dua tingkat, tiga tingkat, empat tingkat), tes terbuka, dan lainnya. Penelitian ini menggunakan tes tiga tingkat. Penelitian ini mengeksplorasi pemahaman konsep energi ionisasi antara siswa sekolah menengah (HSS), guru pra-jabatan (PST), dan guru dalam jabatan (IST) secara bersamaan. Sebanyak 326 peserta dari Indonesia, termasuk 118 HSS, 165 PST, dan 43 IST bidang kimia diundang untuk mengikuti tes online -Ionization Energy Diagnostic-Modification (IEDI * M). Tes terdiri dari 12 butir tes diagnostik tiga tingkat. Riset ini menunjukkan empat konsepsi alternatif substansial: konservasi energi, subkulit terisi setengah atau terisi penuh stabil, kerangka aturan oktet, dan penalaran berbasis hubungan. IST berkinerja lebih baik daripada HSS dan PST dalam pemahaman energi ionisasi. Riset ini juga telah menentukan distribusi konsepsi energi ionisasi dari Golongan 1 dan 2, dan Periode 2 dan 3 pada sistem periodik. Dengan memanfaatkan IEDI * M, persentase konsepsi alternatif menurun dari satu tingkat ke dua tingkat serta dari dua tingkat ke tiga tingkat. Penelitian ini memberikan beberapa implikasi bagi pemerintah, pembuat kebijakan, guru kimia, guru pra-jabatan, dan staf pengajar di universitas.

Kata-kata kunci: tes diagnostik, energi ionisasi, tes tiga tingkat.

1. INTRODUCTION:

There are some terms in describing the students' notions of scientific concepts. Previous scholars have used different words to represent the students' conception, such as "children's science ideas" (Osborne, Black, Meadows, and Smith, 1993), "alternative framework" (Klammer, 1998), "mental models" (Greca and Moreire, 2002), "misconceptions" (Suprpto, Abidah, Dwiningsih, Jauhariyah, and Saputra, 2018), and so forth. However, the terms of "alternative conception" and "misconceptions" more popular than others. Therefore these terms are frequently used in previous studies. However, both of them are used in this study.

For diagnosing the misconceptions, some methods can be used: concept maps, interviews, multiple-choice tests (one-tier), multiple-tier tests (two-tier, three-tier, four-tiers), open-ended tests, and others. Each method has pros and cons. Interviews and open-ended tests require a large amount of time to attain and analyze the data (Gurel, Eryilmaz, and McDermott, 2015; Suprpto *et al.*, 2018). In contrast, standard multiple-choice tests (MCT) don't afford an in-depth investigation into the students' ideas. Two-

tier multiple-choice tests can solve MCT's problem; however, they can't determine the proportion of the misconceptions since their lack of knowledge. Then, three-tier MCT will hold the strengths provided by two-tier and select the answers given to the first two-tier is due to false-negative (FN), false positive (FP), misconception (MSC), or a lack of knowledge (LK).

The major problem for using conventional MCT is to reduce FP and FN. "Students could provide correct answers with wrong reasoning as FP and wrong answers with correct reasoning as FN" (Suprpto *et al.*, 2018). Minimizing FP and FN offers a more valid test. Even though a two-tier test eliminates those drawbacks of a conventional MCT, it has a limitation: It cannot distinguish misconceptions (MSC) from a lack of knowledge (LK). The assumption that if more than 10% of the respondents picked a wrong combination of options across the two-tiers, that combination could be regarded as reflecting an MSC's presence. Three-tier tests enable researchers to address the drawback mentioned earlier by "adding tier that entails students to state whether or not they are sure about their answers to the first two-tiers" (Caleon and Subramaniam, 2010; Pesman and Eryilmaz, 2010; Suprpto *et al.*, 2018).

There were a few studies in science education on the development and application of three-tier tests, such as atmosphere-related environmental problems diagnostic test-AREPDit (Arslan, Cigdemoglu and Moseley, 2012), heat and temperature test (Eryilmaz, 2010), three-tier circular motion test (Kizilcik and Gunes, 2011), the wave diagnostic instrument-WADI (Pesman and Eryilmaz, 2010). Specifically, there are two popular three-tier conceptual tests in chemistry: a diagnostic test of states of matter (Kirbulut and Geban, 2014) and acids and bases three-tier test (Cetin-Dindar and Geban, 2011). Additionally, there are two-tier tests in chemistry: chemical concept tests (Chiu, 2007), ionization energy diagnostic instrument-IEDI (Tan, Taber, Goh, and Chia, 2005), etc. This study endeavors the IEDI with a three-tier conceptual test. The test is based on the work of Tan *et al.* (2005).

Four years ago, Chiu, Lin, and Chou (2016) found that chemistry in the third rank among the four science disciplines is studied by researchers after physics and biology in international journals. Therefore, study about chemistry content has also become the main attraction among researchers. Ionization energy is one of the essential topics in the ten-grade Indonesian curriculum. It discusses the basic concept of physical atomic properties and relates to electron affinity, atomic radius, and electronegativity, which are conceptually helpful in understanding each atom's characteristics. Research on this concept has concerned many researchers in the last 20 years (e.g., Taber, 2003; Lang and Smith, 2003; Tan *et al.*, 2005; Tan, Taber, Liu, Coll, Lorenzo, Li, Goh, and Chia (2008); Tan and Taber, 2011). Taber (2003) investigated college-level chemistry students in the UK. In Tan *et al.* (2005)' study, the investigation focused on A-level students (Grade 11 and 12) in Singapore and explored their understanding of the trend of ionization energies across Period 3.

However, no study investigated the understanding of ionization energy among high school students (HSSs), pre-service teachers (PSTs), and in-service teachers (ISTs) simultaneously. Therefore, this study describes the implementation of a three-tier diagnostic test to assess those participants' understanding of ionization energy either after their first time were taught (high school students) or appertained that subject (pre-service and in-service teachers).

Investigating the conception of ionization energy among HSSs, PSTs, and ISTs simultaneously explains the primary sources of misconception because the three levels are highly

correlated. PSTs will become ISTs and then transfer their knowledge to HSSs. Thus, this study assesses the conception of ionization energy and the main misconception which happens in this concept. The research questions (RQs) that directed this study were:

1. To what extent do the HSSs', PSTs', and ISTs' understanding and confidences in answering questions of ionization energy?
2. To what extent do HSSs, PSTs, and ISTs performing misconceptions of ionization energy?

Therefore, this study aimed to explore the HSSs', PSTs', and ISTs' understanding and confidences in answering ionization energy questions. It was also aimed at analyzing the HSSs', PSTs', and ISTs' misconceptions of ionization energy.

2. MATERIALS AND METHODS:

2.1. The modification of Ionization Energy Diagnostic -IEDI instrument

The development of the modification of the Ionization Energy Diagnostic -IEDI*M diagnostic instrument of ionization energy tangled a modified version from Suprpto *et al.* (2018); Tan *et al.* (2005); Taber and Tan (2011). Initially, the instrument consisted of 10 two-tier items with each tier (see Table 1 and Appendix) and explored participants' understanding of the trend of ionization energies across Period 3. After getting permission for research purposes, the authors modified and translated into the Indonesian language. The modification and addition were executed due to forgetting the whole picture of the conception of ionization energy across Period 2, Period 3, Group 1, and Group 2. Finally, 12 three-tier items were used in the study (see Appendix).

2.2. Participants

The study presented the responses of 326 participants: 118 HSSs, 165 PSTs, and 43 ISTs to the IEDI*M from East Java in Indonesia. The participants comprised 134 (41%) males and 192 (59%) females (Table 2). The researchers distributed a letter of permission in researching all participants as a form of ethical academic consent. Besides, the researchers have also got approval from the university committee in conducting data collection. IEDI*M was administered to the participants after experiencing at least three months (spread over 3 to 4 weeks) of formal instruction on the ionization energy. HSSs have already got subject matter knowledge in grade 10,

and PSTs have reviewed this content from the general chemistry course.

2.3 Procedure

Through an online survey (see Appendix) with an online-test facility in Google Form, participants could express themselves with more originality and enthusiasm, and it considers a real-time feature (Lina, Chang, Hou, and Wu, 2015).

2.4 Data Analysis

The IEDI*M responses of participants were input into an MS Excel datasheet. Variables were written in the columns, and participants' codes were written in the Excel datasheet rows. Six categories were produced (Table 3): i) Scientific Conception (SC), ii) False Positive (FP), iii) False Negative (FN), iv) Misconception (MSC), v) Lack of Knowledge because of Guessing (LKg), vi) Lack of Knowledge because of Deficiency (LKd). Among the six categories were simplified into four general categories: truly understanding (t), alternative conception (a), guessing (g), and deficient knowledge (d). This study follows the rule by Peterson, Treagust, and Gannett (1989): "the percentage of student responses >20% for the non-scientific options be defined as typical alternative responses".

3. RESULTS AND DISCUSSIONS:

3.1. The distribution of understanding about ionization energy among HSSs, PSTs, and ISTs

Table 4 demonstrates the percentages of SC, FP, FN, MSC, LKg, and LKd among HSSs, PSTs, and ISTs. When the items were checked for SC, it was found that the majority percentages above 20%, except for item 6 (all levels), item 7 and 12 (PSTs), and item 9 and 11 (HSSs and PSTs). Item 6 is related to the comparison of the first ionization energy between magnesium (Group 2) and aluminum (Group 3). While the items were cross-checked for FP, it was found that all participants performed the percentages above 20% for items 4, 6, 7, 8, and 11. Meanwhile, HSSs also indicated FP for items 2, 5, and 9, as well as for item 5 and item 12. Hereinafter, for FN, it was found that all the items, except for item 6 (HSSs and ISTs), were below 20%.

Turning to the MSC, it was found that the performance of participants to all items above 20%, except for items 2, 4, and 5. When items 9 and 12 were examined, it was seen that all levels

performed MSC. Item 9 assessed the comparison of the first ionization energy between phosphorus and sulfur (period 3). The true answer of the first-tier is "the first ionization energy of phosphorus is greater than that of sulfur" since "the effect of an increase in nuclear charge in sulfur is less than the repulsion between its 3p electrons" (2nd tier). Considering for item 9, it was seen that the most participants chose one of the wrong alternatives – "the first ionization energy of P is less than that of S" for the 1st-tier and "the effect of an increase in nuclear charge in sulfur is greater than the repulsion between its 3p electrons" for the 2nd tier. In addition, some participants chose either "more energy is required to overcome the attraction between the paired 3p electrons in sulfur" or "3p electrons of sulfur are further away from the nucleus compared to that of phosphorus" for their reasoning in the 2nd tier.

Item 12 assessed the comparison of the first ionization energy between beryllium and boron (Period 2). The true answer of the 1st-tier is "the first ionization energy of beryllium is greater than that of boron" since "the 2p electron of boron has a lower penetrating power than the 2s electrons. Therefore, it outweighing the increase in nuclear charge" (2nd-tier). Turning to item 12, it was seen that most of the participants chose one alternative conception – "the first ionization energy of beryllium is less than that of boron" since "the 2s electron of beryllium has lower penetrating power than the 1s electrons; therefore it was outweighing the increase in nuclear charge". Additionally, some participants chose either "the 2p electrons of boron are further away from the nucleus compared to that of beryllium" or "the effect of an increase in nuclear charge in boron is less than the repulsion between its 2p electrons" for their reasoning. Meanwhile, items 1, 3, 6, 7, and 10 indicated a partial misconception (HSSs and ISTs). At the same time, for items 8 and 11, only HSSs denoted misconceptions.

In terms of lack of knowledge (LK), it was indicated that all percentages were below 20%, except item numbers 2 and 10 for PSTs that achieved 30.30% LKg for item 2 and 24.24% for item 10. This result reinforced the pros of using three-tier tests rather than conventional MCT. Kirbulut and Geban (2014) corroborated that three-tier tests provide more accurate results for students' misconceptions by differentiating MSC from LKg and LKd.

The HSSs', PSTs', and ISTs' responses and their confidence in completing IEDI*M are concise in Table 5. Both the phenomena and reason tiers were illustrated to distinguish among

truly understanding (t), guessing (g), alternative conceptions (a), or deficient knowledge (d) (Lin, 2016).

3.2 The ionization process of the Sodium atom to form Sodium ion (item 1-4)

The MCT requires the participants to infer which reason of the sodium ion will combine with an electron to reform the sodium atom (Na) for item 1; the attraction of the nucleus for the 'lost' electron when an electron is removed from Na for item 2; the comparison of stability among Na(g) atom, Na^+ (g) ion, and a free electron for item 3; and the comparison between the second and the first ionization energy when Na is ionized for item 4.

For the category *truly understanding* in the context of phenomena 1 (P1) (Table 5), the participants performed that "the sodium ion will combine with an electron to reform the sodium atom since the Na^+ can appeal a negatively-charged electron" with the confidence level (40.68%, 31.52%, 72.09%) for HSSs, PSTs, and ISTs, respectively. However, some HSSs and PSTs have two *alternative conceptions* that "Sodium is strongly electropositive, so it only loses electrons," and "the sodium ion has a stable octet configuration, so it will not gain an electron to lose its stability".

In Phenomena 2, the participants performed that "the pull of the nucleus for the 'lost' electron will be redistributed among the remaining electrons in the Na^+ when an electron is removed from the Na atom", with the confidence level (61.02%, 42.42%, 69.77%) for HSSs, PSTs, and ISTs, respectively.

In the case of phenomena 3 (P3) for the category *truly understanding*, the participants performed that "the Na atom is more stable than the Na ion and a free electron" since "the sodium atom is neutral, and energy is required to ionize the sodium atom to form the sodium ion", with the confidence level (58.48%, 33.33%, 69.77%) for HSSs, PSTs, and ISTs, respectively. However, about 21.19% of HSSs and 24.24% of PSTs have an alternative conception that the outermost shell of sodium ion has achieved a stable octet configuration.

For the category *truly understanding* in the phenomena 4 (P4), HSSs and ISTs felt confidence that since "the second electron is removed from a paired 2p orbital and it experiences repulsion from the other electron in the same orbital," then "more

energy is required to remove a second electron when the Na is ionized", with the confidence level 26.27% and 62.79%, respectively. However, PSTs have some alternative conceptions in their reasoning: "the same number of protons in Na^+ attracts one less electron." In-lined with Tan *et al.* (2005), some alternative conceptions, as indicated from item 1-4 are related to two headings as *octet rule framework*, such as (P1R2, P3R4, and P4A1) and *conservation of energy (force thinking)*, such as (P2R3 and P4R2). (Note: P1R2 indicated phenomena number 1 - reasoning number 2; P3R4 was phenomena number 3 - reasoning number 4, and so on.

3.3 The comparison of the first ionization energy between Sodium and Magnesium (item 5)

For the category *truly understanding* of the phenomena 5 (P5), the participants performed that "the first ionization energy of Na is less than that of Mg" since "the paired electrons in the 3s orbital of Mg experience repulsion from each other, and this effect is greater than the increase in the nuclear charge in Mg", with the confidence level (42.37%, 25.46%, and 62.79%) for HSSs, PSTs, and ISTs, respectively. However, there were about 26.68% of PSTs argued that magnesium has a fully-filled 3s sub-shell, which gives it stability in their reasoning. This situation in-lined with an *et al.* (2005). This alternative conception relates to the problem of *stable fully-filled or half-filled sub-shells* (P5R1).

3.4 The comparison of the first ionization energy among sodium, magnesium, and aluminum (item 6 and item 7)

All participants' levels performed below 20% of the correct understanding of phenomena 6 (P6). The most alternative conception among them is the combination of phenomena: "The first ionization energy of Mg is greater than that of Al" with the reasoning "the 3p electron of Al is further from the nucleus compared to the 3s electrons of Mg" (22.03% for HSSs and 38.79% for PSTs). Also, there was a combination of alternative conceptions of HSSs (34.75%) and ISTs (32.56%): "the first ionization energy of Mg is less than that of Al".

For item 7 (P7), HSSs and ISTs showed above 20% of truly understanding. The correct answer for the first tier is "the first ionization energy of sodium is less than that of aluminum." The second-tier reasoning is "the effect of an increase in nuclear charge in aluminum is greater than the shielding of the 3p electron by the 3s electrons". The most alternative conception among them is

“the first ionization energy of sodium is less than that of aluminum” due to “the 3p electron of aluminum is further away from the nucleus compared to the 3s electron of sodium” (28.81% for HSSs, 43.63% for PSTs, and 23.25% for ISTs). However, HSSs have also varied in their reasoning, such as “aluminum will attain a fully-filled 3s sub-shell if an electron is removed” (20.34%), and “sodium will achieve a stable octet configuration if an electron is removed” (22.03%). Some alternative conceptions aforementioned were called relation-based reasoning (P6R2 and P7R3). This result corroborated the studies conducted by Tan *et al.* (2011).

3.5 The comparison of the first ionization energy among silicon, phosphorus, and sulfur (item 8, 9, and 10)

In P8, all participants expressed that “the first ionization energy of silicon is less than that of phosphorus” due to “the effect of an increase in nuclear charge in phosphorus is greater than the repulsion between its 3p electrons”, with the percentage of *truly understanding*: 24.58%, 20.61%, and 44.19%, respectively. However, some PSTs have *alternative conceptions*: either “the first ionization energy of silicon is greater than that of phosphorus” or “the first ionization energy of silicon is less than that of phosphorus”. Their reasoning varied either due to the problem of “*stable fully-filled or half-filled sub-shells*” (P8R2). The participant indicated that “the 3p sub-shell of P is half-filled. Hence it is stable” (21.21%) or due to “the 3p electrons of P are further away from the nucleus compared to that of Si” (23.03%).

For the category *truly understanding* in the context of P9, only ISTs performed that “the first ionization energy of phosphorus is greater than that of sulfur” due to “the effect of an increase in nuclear charge in sulfur is less than the repulsion between its 3p electrons”, with the confidence level 7.91%. Even though PSTs showed less understanding in P9, however, their alternative conceptions are below 20% among four options. Meanwhile, HSSs indicated some alternative concepts: “more energy is required to overcome the attraction between the paired 3p electrons in sulfur” and “the effect of an increase in nuclear charge in sulfur is greater than the repulsion between its 3p electrons”.

In P10, all participants performed above 20% of *truly understanding*: 27.97%, 23.64%, and 74.42, respectively. The scientific answer for the first-tier is “the first ionization energy of silicon is less than that of sulfur”. The reasoning for the

second-tier is, “The effect of an increase in nuclear charge in sulfur is greater than the repulsion between its 3p electrons”. Nevertheless, some HSSs also have *alternative reasoning*: “sulfur will have its 3p sub-shell half-filled if an electron is removed”, about 22.58%.

3.6 The comparison of the first ionization energy between lithium and sodium (item 11)

Phenomena 11 presented only ISTs with a proper understanding of comparing the first ionization energy between lithium and sodium (37.21%). There were some alternative conceptions among levels either “the first ionization energy of lithium is greater than that of sodium” due to “more energy is required to overcome the attraction between the paired 2s electrons in lithium” or “the 3s electrons of sodium are further away from the nucleus compared to that 2s of lithium”. Additionally, some participants understood that “the first ionization energy of lithium is less than that of sodium” due to “more energy is required to overcome the attraction between the paired 2s electrons in lithium”.

3.7 The comparison of the first ionization energy between beryllium and boron (item 12)

This phenomenon is similar to the phenomenon 6. It is noted that beryllium and boron in period 2, meanwhile magnesium and aluminum in period 3. However, both of the phenomena represent the comparison of the first ionization energy of Group 2 and 3. The best explanation in this context is “the first ionization energy of beryllium is greater than that of boron” due to “the 2p electron of boron has lower penetrating power than the 2s electrons. Therefore, it outweighing the increase in nuclear charge”. HSSs and ISTs performed *truly understanding* about 22% and 23.26%, respectively. In addition, each level has a different of the most alternative conception, such as: “the 2s electron of beryllium has lower penetrating power than the 1s electrons. Therefore, it outweighing the increase in the nuclear charge for HSSs”, “the 2p electrons of boron are further away from the nucleus compared to that of beryllium” for PSTs, and “the effect of an increase in nuclear charge in boron is less than the repulsion between its 2p electrons” for ISTs.

3.8 The misconceptions probed by the IEDI among HSSs, PSTs, and ISTs

Table 6 lists the misconceptions probed by the IEDI*M. Meanwhile, Table 7 depicts the

percentages of misconceptions for all-tiers. Accordingly, three-tier calculates participants' MSC more precisely compared to two-tier and traditional MCT since they include two-tier and confidence tier together. The trend of MSC decline from one-tier to three-tier. This result confirmed the study of Kirbulut and Geban (2014) and Pesman and Eryilmaz (2010). Most MSC has been experienced by HSSs, except item 2. PSTs performed a moderate MSC, except item 4 and 8. In contrast, ISTs indicated less misconception than others, except items 9 and 12. However, these two items become a serious problem for all participant levels because they have misconceptions of all tiers.

Figure 1 also indicates the part of misconceptions about ionization energy, especially for Group 1, 2, period 2, and period 3. For instance, many participants have a problem with the ionization energy of beryllium versus boron and magnesium versus aluminum and silicon versus phosphorus and phosphorus versus sulfur. It is noted that beryllium and boron in period 2, meanwhile magnesium and aluminum in period 3. Generally, a significant number of HSSs and PSTs and some of ISTs did not adequately comprehend the trend of ionization energy across periods 2 and 3 and the factors influencing ionization energy. Then, if we compare between the three-tier test and two-tier test of ionization energy, the trend of misconceptions declines from one-tier to three-tier.

4. CONCLUSIONS:

The study sees the sights of HSSs', PSTs', and ISTs' understanding and confidence in answering questions about ionization energy. There were four significant common alternative conceptions were identified: 'conservation of force thinking', 'octet rule framework', half-filled sub-shells' or 'stable fully-filled, and 'relation-based reasoning'.

There are some implications derived from this study. First, ISTs should be aware of their alternative conceptions. Second, chemistry teachers should be mindful of their students, especially in this expression: 'even though we get success on conventional MCT, it does not necessarily reflect our conceptual understanding of chemistry'. Therefore, teachers should consider using assessment tools that provide opportunities to probe students' reasoning and perform confidently. Third, the government should be

aware of the chemistry textbook since the most alternative conception and misconception either from books or the cycle of PSTs→ISTs→HSSs. Fourth, the government and university professors need to review the content knowledge and not assume that a university degree (PSTs) assures adequate teaching topics.

5. ACKNOWLEDGMENTS:

Thanks to the HSSs, PSTs, and ISTs who participated in the completion of the online survey.

6. REFERENCES:

1. Arslan, H.O., Cigdemoglu, C., and Moseley, C. (2012). A three-tier diagnostic test to assess pre-service teachers' misconceptions about global warming, greenhouse effect, ozone layer depletion, and acid rain. *International Journal of Science Education*, 34(11), 1667-1686.
2. Caleon, I.S., and Subramaniam, R. (2010). Development and application of a three-tier diagnostic test to assess secondary students' understanding of waves. *International Journal of Science Education*, 32(7), 939-961.
3. Cetin-Dindar, A. and Geban, Ö. (2011). Development of a three-tier test to assess high school students' understanding of acids and bases. *Procedia Social and Behavioral Sciences*, 15, 600-604.
4. Chiu, M. H. (2007). A national survey of students' conceptions of chemistry in Taiwan. *International Journal of Science Education*, 29(4), 421-452.
5. Chiu, M.-H., Lin, J.-W., and Chou, C.-C. (2016). Content analysis of conceptual change research and practice in science education: From localization to globalization. In M.-H. Chiu (Ed.), *Science education research and practices in Taiwan: Challenges and opportunities* (pp. 89-131). Singapore: Springer.
6. Eryilmaz, A. (2010). Development and application of three-tier heat and temperature test: Sample of bachelor and graduate students. *Eurasian Journal of Educational Research*, 40, 53-76.

7. Greca, I.M., and Moreire, M.A. (2002). Mental, physical and mathematical models in the teaching and learning of physics. *Science Education*, 86 (1), 106-121.
8. Gurel, Eryilmas, and McDermott. (2015). A review and comparison of diagnostic instruments to identify students' misconceptions in science. *Eurasia Journal of Mathematics, Science and Technology Education*, 11(5), 989-1008.
9. Kirbulut, Z.D., and Geban, O. (2014). Using three-tier diagnostic test to assess students' misconceptions of states of matter. *Eurasia Journal of Mathematics, Science and Technology Education*, 10(5), 509-521.
10. Kızılcık, H.S., and Güneş, B. (2011). Developing three-tier misconception test about regular circular motion. *Hacettepe University Journal of Education*, 41, 278-292.
11. Klammer, J. (1998). *An overview of techniques for identifying, acknowledging, and overcoming alternative conceptions in physics education*. (Report no: ED423121). Columbia University.
12. Lang, P.F., and Smith, B.C. (2003). Ionization energies of atoms and atomic ions. *Journal of Chemical Education*, 80(8), 938-946.
13. Lin, J.-W. (2016). Development and evaluation of the diagnostic power for a computer-based two-tier assessment. *Journal of Science Education and Technology*, 25, 497-511.
14. Lina, Y-T, Chang, C-H, Hou, H-T., and Wu, K-C. (2015). Exploring the effects of employing Google Docs in collaborative concept mapping on achievement, concept representation, and attitudes. *Interactive Learning Environments*, 24(7), 1552-1573.
15. Osborne, J.F., Black, P., Meadows, J., and Smith, M. (1993). Young children's (7-11) ideas about light and their development. *International Journal of Science Education*, 15(1), 83-93.
16. Peşman, H., and Eryılmaz, A. (2010). Development of a three-tier test to assess misconceptions about simple electric circuits. *The Journal of Educational Research*, 103, 208-222.
17. Peterson, R.F., Treagust, D.F., and Garnett, P.J. (1989). Development and application of a diagnostic instrument to evaluate grade 11 and 12 students' concepts of covalent bonding and structure following a course of instruction. *Journal of Research in Science Teaching*, 26(4), 301-314.
18. Suprpto, N., Abidah, A., Dwiningsih, K., Jauhariyah, M.N.R., and Saputra, A. (2018). Minimizing misconception of ionization energy through three-tier diagnostic test. *Periodico Tchê Química*, 15(30), 387-396.
19. Taber, K.S. (2003). Understanding ionization energy: Physical, chemical, and alternative conceptions. *Chemistry Education Research and Practice*, 4(2), 149-169.
20. Tan, K-C.D., Taber, K.S., Goh, N-G., and Chia, L-S. (2005). The ionization energy diagnostic instrument: a two-tier multiple-choice instrument to determine high school students' understanding of ionization energy. *Chemistry Education Research and Practice*, 6(4), 180-197.
21. Tan, K-C.D., Taber, K.S., Liu, X., Coll, R. K., Lorenzo, M., Li, J., Goh, N-G., and Chia, L-S. (2008). Students' conceptions of ionization energy: A cross-cultural study. *International Journal of Science Education*, 30(2), 263-283.
22. Tan, K-C.D., and Taber, K.S. (2011). The insidious nature of 'hard-core' alternative conceptions: Implications for the constructivist research programme of patterns in high school students' and pre-service teachers' thinking about ionization energy. *International Journal of Science Education*, 33(2), 259-297.

Appendix

Table 1. The key stages in the development of the instrument

Original study with two-tier items (Tan et al., 2005; Taber and Tan, 2011)		This study	
Two-tier		Three-tier	
1 st -tier	MCT (3 options): item 1-3; item 5-10 MCT (4 options): item 4	1 st -tier	MCT (2 options): item 1-12
2 nd -tier	MCT (3 options): item 1 and 2 MCT (4 options): item 3, 4, 8, and 10 MCT (5 options): item 5, 6, 7, and 9 -	2 nd -tier	MCT (3 options): item 1 and 2 MCT (4 options): item 3 - 12
		3 rd -tier	Level of confidence (sure or unsure): all items

Table 2. Participants' background and demographic data

Demographics		% Senior High School Students (n=118)	% Pre-service teachers (n=165)	% In-service teachers (n=43)
Gender	Male	69.49	19.39	46.51
	Female	30.51	80.61	53.49
Grade	10	33.90	-	-
	11	31.36	-	-
	12	34.74	-	-
Level	1	-	29.09	-
	2	-	18.18	-
	3	-	36.36	-
	4	-	16.36	-
Experience in teaching	<5 years	-	-	18.60
	5-10 years	-	-	20.93
	10-15 years	-	-	20.93
	15-20 years	-	-	18.60
	> 20 years	-	-	20.93

Table 3. Categories of Conception

Phenomena (P)	Reasoning (R)	Confidence	Category	
1 st -tier	2 nd -tier	3 rd -tier		
T	T	S	SC	t
T	F	S	FP	
F	T	S	FN	a
F	F	S	FN	
T	T	US		
T	F	US	LKg	g
F	T	US		
F	F	US	LKd	d

Note: T=True; F=False; S=Sure; US= Unsure; SC=Scientific Conception; FP=False Positive; FN=False Negative; LKg=Lack of Knowledge–Guessing; LKd= Lack of Knowledge–Deficiency of knowledge; t=truly understanding; a=alternative conception; g=guessing; and d=deficient knowledge

Table 4. The percentages of the conception of ionization energy among HSSs, PSTs, and ISTs

Conception level	Item 1			Item 2			Item 3			Item 4		
	HSSs	PSTs	ISTs	HSSs	PSTs	ISTs	HSSs	PSTs	ISTs	HSSs	PSTs	ISTs
SC	40.68	31.52	72.09	61.02	42.42	69.77	58.47	33.33	69.77	26.27	16.97	62.79
FP	17.80	11.52	13.95	23.73	10.91	6.98	9.32	12.73	18.60	41.52	58.18	23.26
FN	7.63	6.67	2.32	5.08	5.45	9.30	3.39	1.82	0	1.69	0.61	4.65
MSC	29.66	40.61	6.98	3.39	7.27	4.65	23.73	34.54	4.65	18.64	4.24	2.32
LK-g	3.39	7.88	0	5.3	30.30	9.30	3.39	9.70	4.65	7.63	16.97	6.98
LK-d	0.85	1.82	4.65	0.85	3.64	0	1.69	7.88	2.32	4.24	3.03	0
	Item 5			Item 6			Item 7			Item 8		
	HSSs	PSTs	ISTs	HSSs	PSTs	ISTs	HSSs	PSTs	ISTs	HSSs	PSTs	ISTs
SC	42.37	25.45	62.79	3.39	2.42	16.28	21.19	16.36	53.49	24.58	20.61	44.19
FP	23.73	44.24	13.95	18.64	30.91	25.58	41.52	34.54	27.91	28.81	46.06	32.56
FN	6.78	2.42	2.32	34.74	19.39	32.56	0	0.61	0	1.69	0.61	2.32
MSC	16.10	12.73	4.65	27.12	24.24	6.98	29.66	23.03	9.30	27.12	10.91	9.30
LK-g	8.47	10.30	11.63	11.86	15.15	13.95	4.24	17.58	4.65	12.71	16.36	0
LK-d	2.54	4.85	4.65	4.24	7.88	4.65	3.29	7.88	4.65	5.08	5.45	11.63
	Item 9			Item 10			Item 11			Item 12		
	HSSs	PSTs	ISTs	HSSs	PSTs	ISTs	HSSs	PSTs	ISTs	HSSs	PSTs	ISTs
SC	11.86	15.76	27.91	27.97	23.64	74.42	8.47	2.42	37.21	22.03	12.12	23.26
FP	22.88	16.97	4.65	20.34	22.42	4.65	45.76	58.18	46.51	16.95	28.48	23.26
FN	1.69	1.82	4.65	4.24	1.21	2.32	5.08	1.21	0	4.24	4.85	6.98
MSC	44.07	36.36	44.19	25.42	20.61	11.63	27.12	15.15	11.63	38.47	27.27	34.88
LK-g	8.47	18.79	13.95	16.95	24.24	2.32	9.32	12.73	4.65	10.17	10.91	4.65
LK-d	11.02	10.30	4.65	5.08	7.88	4.65	4.24	10.30	0	8.47	16.36	6.98

Note: The **bold- italics** means the percentage of this response > 20%, (typical response)¹; SC=Scientific Conception; FP=False Positive; FN=False Negative; LK-g=Lack of Knowledge–Guessing; LK-d= Lack of Knowledge–Deficiency of knowledge; HSSs= high school students; PSTs= pre-service teachers; ISTs= pre-service teachers

Table 5. The HSSs', PSTs', and ISTs' performance and confidence in answering IEDI*M

	HSSs			PSTs			ISTs		
P1	60.17^t	-	-	50.91^t	-	-	86.05^t	-	-
R1	25.42^a	0.85 ^g	0	27.87^a	1.21 ^g	1.82 ^d	0	11.64 ^a	2.32 ^d
R2	22.03^a	0.85 ^g	0.85 ^d	24.24^a	1.21 ^g	0	0	9.30 ^a	2.32 ^d
R3	40.68^t	1.69 ^g	7.63 ^a	31.52^t	5.45 ^g	6.67 ^a	72.09^t	2.32 ^a	0
P2	89.98^t	-	-	79.18^t	-	-	86.05^t	-	-
R1	61.02^t	4.23 ^g	5.08 ^a	42.42^t	18.19 ^g	5.46 ^a	69.77^t	6.98 ^g	9.30 ^a
R2	21.18^a	0.85 ^g	0.85 ^d	3.64 ^a	4.85 ^g	1.82 ^d	0	0	0
R3	5.93 ^a	0.85 ^g	0	14.54 ^a	7.27 ^g	1.82 ^d	11.63 ^a	2.32 ^g	0
P3	71.18^t	-	-	53.94^t	-	-	93.07^t	-	-
R1	58.48^t	2.54 ^g	3.39 ^a	33.33^t	4.85 ^g	1.82 ^a	69.77^t	0	0
R2	4.23 ^a	0	0.85 ^d	8.48 ^a	1.21 ^g	1.82 ^d	9.30 ^a	2.33 ^g	0
R3	7.63 ^a	0.85 ^g	0.85 ^d	14.54 ^a	3.64 ^g	1.21 ^d	2.33 ^a	2.33 ^g	0
R4	21.19^a	0	0	24.24^a	0	4.85 ^d	11.63 ^a	0	2.32 ^d
P4	75.42^t	-	-	89.09^t	-	-	93.07^t	-	-
R1	30.51^a	2.54 ^g	4.23 ^d	16.36 ^a	4.85 ^g	0	6.98 ^a	0	0
R2	19.49 ^a	2.54 ^g	0	22.42^a	4.85 ^g	1.21 ^d	0	0	0
R3	10.16 ^a	0	0	23.63^a	1.82 ^g	1.82 ^d	18.60 ^a	0	0
R4	26.27^t	2.54 ^g	1.69 ^a	16.97 ^t	5.45 ^g	0.61 ^a	62.79^t	6.98 ^g	4.65 ^a
P5	73.73^t	-	-	79.39^t	-	-	89.37^t	-	-
R1	12.71 ^a	3.39 ^g	1.69 ^d	26.68^a	3.64 ^g	1.21 ^d	6.98 ^a	4.65 ^g	4.65 ^d
R2	16.95 ^a	0.85 ^g	0	11.52 ^a	1.82 ^g	3.64 ^d	4.64 ^a	4.65 ^g	0
R3	42.37^t	3.39 ^g	6.78 ^a	25.46^t	4.25 ^g	2.42 ^a	62.79^t	2.32 ^g	2.32 ^g
R4	10.17 ^a	0.85 ^g	0.85 ^d	18.79 ^a	0.61 ^g	0	6.97 ^a	0	0

	HSSs			PSTs			ISTs		
P6	28.81^t	-	-	44.85^t	-	-	48.84^t	-	-
R1	13.56 ^a	2.54 ^g	0.85 ^d	9.69 ^a	3.64 ^g	1.21 ^d	13.96 ^a	0	0
R2	22.03^a	1.70 ^g	2.54 ^d	38.79^a	4.85 ^g	4.85 ^d	9.30 ^a	0	2.32 ^d
R3	3.39 ^t	6.77 ^g	34.75^a	2.42 ^t	4.85 ^g	19.39 ^a	16.28 ^t	6.98 ^g	32.56^a
R4	9.87 ^a	0.85 ^g	2.54 ^a	6.66 ^a	1.82 ^g	1.82 ^d	9.30 ^a	6.98 ^g	2.33 ^d
P7	66.95^t	-	-	66.67^t	-	-	86.05^t	-	-
R1	20.34^a	1.69 ^g	1.69 ^d	6.06 ^a	2.42 ^g	1.21 ^d	6.97 ^a	0	2.32 ^d
R2	22.03^a	0	0	7.88 ^a	1.21 ^g	3.03 ^d	6.97 ^a	0	2.32 ^d
R3	28.81^a	2.54 ^g	1.69 ^d	43.63^a	7.27 ^g	3.64 ^d	23.25^a	4.65 ^g	0
R4	21.19^t	0	0	16.36 ^t	6.67 ^g	0.61 ^a	53.49^t	0	0
P8	64.41^t	-	-	80.61^t	-	-	76.74^t	-	-
R1	27.96^a	5.93 ^g	2.54 ^d	12.72 ^a	2.42 ^g	1.82 ^d	16.28 ^a	0	4.65 ^d
R2	10.17 ^a	1.69 ^g	0.85 ^d	21.21^a	3.64 ^g	1.21 ^d	6.98 ^a	0	4.65 ^d
R3	17.79 ^a	1.69 ^g	1.69 ^d	23.03^a	2.42 ^g	2.42 ^d	18.60 ^a	0	2.32 ^d
R4	24.58^t	3.38 ^g	1.69 ^a	20.61^t	7.87 ^g	0.61 ^a	44.19^t	0	2.32 ^a
P9	43.22^t	-	-	47.88^t	-	-	44.19^t	-	-
R1	22.88^a	4.24 ^g	1.69 ^d	19.40 ^a	3.64 ^g	4.85 ^d	9.30 ^a	0	2.32 ^d
R2	12.71 ^a	1.69 ^g	5.08 ^d	19.39 ^a	4.85 ^g	2.42 ^d	0	0	0
R3	31.36^a	1.69 ^g	4.24 ^d	14.54 ^a	2.42 ^g	3.03 ^d	39.53^a	4.65 ^g	2.32 ^d
R4	11.86 ^t	0.85 ^g	1.69 ^a	15.76 ^t	7.88 ^g	1.82 ^a	27.91^t	9.30 ^g	4.65 ^a
P10	64.41^t	-	-	67.88^t	-	-	81.40^t	-	-
R1	22.58^a	4.24 ^g	1.69 ^d	11.52 ^a	3.03 ^g	3.64 ^d	9.30 ^a	0	0
R2	8.47 ^a	5.93 ^g	0.85 ^d	18.79 ^a	6.67 ^g	3.03 ^d	2.32 ^a	0	4.65 ^d
R3	27.97^t	6.61 ^g	4.24 ^a	23.64^t	11.51 ^g	1.21 ^a	74.42^t	0	2.32 ^a
R4	14.40 ^a	0.85 ^g	2.54 ^d	12.73 ^a	3.03 ^g	1.21 ^d	4.65 ^a	2.32 ^g	0
P11	61.02^t	-	-	72.73^t	-	-	89.37^t	-	-
R1	32.20^a	0.85 ^g	0.85 ^d	18.79 ^a	3.64 ^g	2.42 ^d	20.93^a	2.32 ^g	0
R2	21.19^a	2.54 ^g	2.54 ^d	36.97^a	5.45 ^g	4.85 ^d	23.25^a	0	0
R3	19.49 ^a	2.54 ^g	0.85 ^d	17.58 ^a	1.21 ^g	3.03 ^d	13.95 ^a	0	0
R4	8.47 ^t	3.39 ^g	5.08 ^a	2.42 ^t	2.42 ^g	1.21 ^a	37.21^t	2.32 ^g	0
P12	49.15^t	-	-	51.52^t	-	-	48.86^t	-	-
R1	22.03^t	3.39 ^g	4.24 ^a	12.12 ^t	5.45 ^g	4.85 ^a	23.26^t	4.64 ^g	6.98 ^a
R2	29.66^a	2.54 ^g	3.39 ^d	13.94 ^a	3.03 ^g	9.09 ^d	16.27 ^a	0	4.65 ^d
R3	8.48 ^a	0.85 ^g	4.24 ^d	29.70^a	2.42 ^g	3.64 ^d	18.60 ^a	0	2.32 ^d
R4	16.95 ^a	3.39 ^g	0.85 ^d	12.12 ^a	0	3.64 ^d	23.25^a	0	0

Note

1: "P" = phenomena (1st tier); "R" =reasoning (2nd tier), i.e P1R1 = phenomena 1 reasoning 1; P12R4 = phenomena 12 reasoning 4, and so on.

2: * = correct answer

3: The **bold-italics** means the percentage of this response > 20%, (typical response)

4: "t"=truly understanding; "g"=guessing; "a"=alternative response; "d"= deficient

Table 6. The misconceptions probed by the IEDI*M

No	Item Choices	Subjects
1	1A1, 1A2	PSTs, HSSs
2	2B2, 2B3	-
3	3B2, 3B3, 3B4	PSTs, HSSs
4	4B1, 4B2, 4B3	HSSs
5	5A1, 5A2, 5A4	HSSs
6	6B1, 6B2, 6B4	PSTs, HSSs
7	7A1, 7A2, 7A3	PSTs, HSSs
8	8A1, 8A2, 8A3	HSSs
9	9B1, 9B2, 9B3	ISTs, PSTs, HSSs
10	10A1, 10A2, 10A4	PSTs, HSSs
11	11B1, 11B2, 11B3	HSSs
12	12B2, 12B3, 12B4	ISTs, PSTs, HSSs

<i>Alternative conceptions</i>	vs	<i>Truly understanding</i>
Na < Mg < Al	vs	Na < Mg, Mg > Al, and Na < Al
Be < B	vs	Be > B
Si < P < S	vs	Si < P, P > S, and Si < S

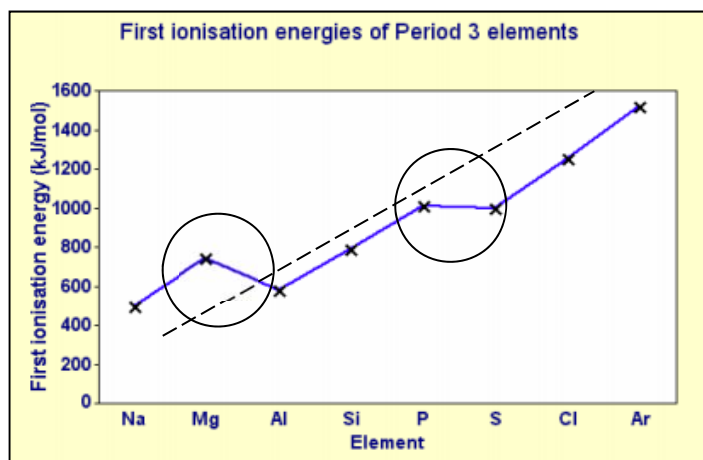
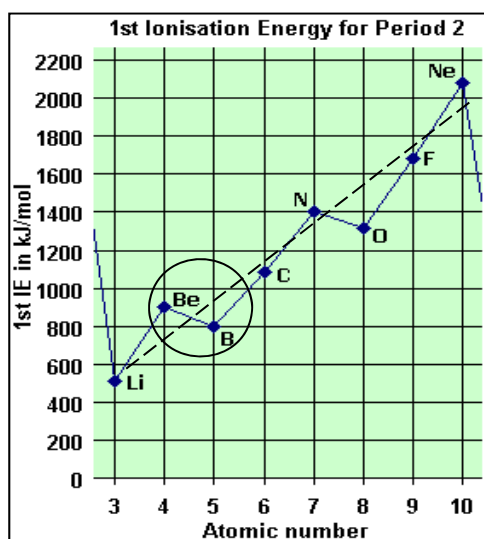


Figure 1. The first ionization energy of period 2 and 3 and the common parts of misconceptions.

Table 7. The trends of misconceptions for all-tiers

Misconception (MSC)	Percentages of Misconceptions								
	HSSs			PSTs			ISTs		
	one-tier	two-tier	three-tier	one-tier	two-tier	three-tier	one-tier	two-tier	three-tier
MSC 1	39.83*	30.51*	29.66*	49.09*	42.42*	40.61*	13.95	11.63	6.98
MSC 2	11.02	4.24	3.39	21.82*	10.91	7.27	13.95	4.65	4.65
MSC 3	28.82*	25.42*	23.73*	46.06*	42.42*	34.54*	6.98	6.98	4.65
MSC 4	24.58*	22.88*	18.64	10.91	7.27	4.24	6.98	2.32	2.32
MSC 5	26.27*	18.64	16.10	20.61*	17.58	12.73	11.63	9.30	4.65
MSC 6	71.19*	31.36*	27.12*	55.15*	32.12*	24.24*	51.16*	11.63	6.98
MSC 7	33.05*	33.05*	29.66*	33.33*	30.91*	23.03*	13.95	13.95	9.30
MSC 8	35.59*	32.20*	27.12*	19.39	16.36	10.91	23.26*	20.93*	9.30
MSC 9 **)	56.78*	55.08*	44.07*	52.12*	46.67*	36.36*	55.81*	48.84*	44.19*
MSC 10	35.59*	30.51*	25.42*	32.12*	28.48*	20.61*	18.60	16.28	11.63
MSC 11	38.98*	31.36*	27.12*	27.27*	25.45*	15.15	11.63	11.63	11.63
MSC 12 **)	50.85*	46.61*	38.14*	48.48*	43.64*	27.27*	51.16*	41.86*	34.88*

Note: * = the percentages of misconceptions > 20%

** = ISTs, PSTs, and HSSs have misconceptions of all-tiers

Sample of online test survey (Google forms with Indonesian version)

docs.google.com/forms/d/e/1FAIpQLScLFyYy4AGU6_UKwCPFPp4zAnk8HdzzbJeeMW4g6DG1D08qTQ/formResponse

The Ionization Energy Diagnostic Instrument (IED)

Pilihlah pilihan dan alasan yang paling cocok untuk jawaban di setiap pertanyaan

11. Lithium dan Natrium berada pada Golongan 1A. Bagaimana anda memprediksi energi ionisasi pertama dari Lithium (1s2 2s1) dibandingkan dengan Natrium (1s2 2s2 2p6 3s1)? *

☐ A. Energi ionisasi pertama dari Lithium lebih besar dari Natrium.

☐ B. Energi ionisasi pertama dari Lithium lebih kecil dari Natrium.

Alasan *

☐ (1) Lebih banyak energi yang diperlukan untuk mengatasi gaya tarik menarik antar pasangan 2s elektron dalam Lithium.

☐ (2) Jarak subkulit 3s pada Natrium lebih besar dari pada subkulit 2s pada Lithium.

☐ (3) Efek peningkatan muatan inti Lithium lebih besar daripada gaya tolak di antara elektron- elektron pada orbital 2s tersebut.

☐ (4) Efek melindungi elektron pada subkulit yang lebih dalam pada Lithium yang lebih besar dari pada efek peningkatan pemuatan inti.

Keyakinan *

☐ Yakin

☐ Tidak Yakin

The Ionization Energy Diagnostic * Modification (IEDI*M) Instrument

Instructions

Choose the most suitable option and the reason for your choice in each question by filling the appropriate circles in the answer sheet. **If you feel that all options given are inappropriate**, indicate the question number and write down what you think the correct answer should be behind the answer sheet.

For Questions 1 to 4, please refer to the statement below.

Sodium atoms are ionised to form sodium ions as follows:



1. Once the outermost electron is removed from the sodium atom forming the sodium ion (Na^+), the sodium ion will not combine with an electron to reform the sodium atom.

A True.

B False.

Reason:

(1) Sodium is strongly electropositive, so it only loses electrons.

(2) The Na^+ ion has a stable/noble gas configuration, so it will not gain an electron to lose its stability.

(3) The positively-charged Na^+ ion can attract a negatively-charged electron.

Confidence: (a) Sure (b) Unsure

2. When an electron is removed from the sodium atom, the attraction of the nucleus for the 'lost' electron will be redistributed among the remaining electrons in the sodium ion (Na^+).

A True.

B False.

Reason:

(1) The amount of attraction between an electron and the nucleus depends on the number of protons present in the nucleus and the distance of the electron from the nucleus. It does not depend on how many other electrons are present, although electrons do repel each other (and can shield one another from the nucleus)

(2) The electron which is removed will take away the attraction of the nucleus with it when it leaves the atom.

(3) The number of protons in the nucleus is the same but there is one less electron to attract, so the remaining 10 electrons will experience greater attraction by the nucleus.

Confidence: (a) Sure (b) Unsure

3. The Na(g) atom is a more stable system than the $\text{Na}^+(\text{g})$ ion and a free electron.

A True.

B False.

Reason:

(1) The Na(g) atom is neutral and energy is required to ionise the Na(g) atom to form the $\text{Na}^+(\text{g})$ ion.

(2) Average force of attraction by the nucleus on each electron of $\text{Na}^+(\text{g})$ ion is greater than that of Na(g) atom.

(3) The $\text{Na}^+(\text{g})$ ion has a vacant shell which can be filled by electrons from other atoms to form a compound.

(4) The outermost shell of $\text{Na}^+(\text{g})$ ion has achieved a stable octet/noble gas configuration.

Confidence: (a) Sure (b) Unsure

4. After the sodium atom is ionised (i.e. forms Na^+ ion), more energy is required to remove a second electron (i.e. the second ionisation energy is greater than the first ionisation energy) from the Na^+ ion.

A True.

B False.

Reason:

- (1) Removal of the second electron disrupts the stable octet structure of Na^+ ion.
- (2) The same number of protons in Na^+ attracts one less electron, so the attraction
- (3) The second electron is located in a shell which is closer to the nucleus.
- (4) The second electron is removed from a paired 2p orbital and it experiences repulsion from the other electron in the same orbital.

Confidence: (a) Sure (b) Unsure

5. Sodium, magnesium and aluminium are in Period 3. How would you expect the first ionisation energy of sodium ($1s^2 2s^2 2p^6 3s^1$) to compare to that of magnesium ($1s^2 2s^2 2p^6 3s^2$)?

A. The first ionisation energy of sodium is greater than that of magnesium.

B. The first ionisation energy of sodium is less than that of magnesium.

Reason:

- (1) Magnesium has a fully-filled 3s sub-shell which gives it stability.
- (2) Sodium will achieve a stable octet configuration if an electron is removed.
- (3) The paired electrons in the 3s orbital of magnesium experience repulsion from each other, and this effect is greater than the increase in the nuclear charge in magnesium.
- (4) The 3s electrons of magnesium are further from the nucleus compared to those of sodium.

Confidence: (a) Sure (b) Unsure

6. How do you expect the first ionisation energy of magnesium ($1s^2 2s^2 2p^6 3s^2$) to compare to that of aluminium ($1s^2 2s^2 2p^6 3s^2 3p^1$)?

A. The first ionisation energy of magnesium is greater than that of aluminium.

B. The first ionisation energy of magnesium is less than that of aluminium.

Reason:

- (1) Removal of an electron will disrupt the stable completely-filled 3s sub-shell of magnesium.
- (2) The 3p electron of aluminium is further from the nucleus compared to the 3s electrons of magnesium.
- (3) The effect of an increase in nuclear charge in aluminium is greater than the repulsion between the electrons in its outermost shell.
- (4) The effect of an increase in nuclear charge in aluminium is less than the repulsion between the electrons in its outermost shell.

Confidence: (a) Sure (b) Unsure

7. How do you expect the first ionisation energy of sodium ($1s^2 2s^2 2p^6 3s^1$) to compare to that of aluminium ($1s^2 2s^2 2p^6 3s^2 3p^1$)?

A. The first ionisation energy of sodium is greater than that of aluminium.

B. The first ionisation energy of sodium is less than that of aluminium.

Reason

(1) Aluminium will attain a fully-filled 3s sub-shell if an electron is removed.

(2) Sodium will achieve a stable octet configuration if an electron is removed.

(3) The 3p electron of aluminium is further away from the nucleus compared to the 3s electron of sodium.

(4) The effect of an increase in nuclear charge in aluminium is greater than the shielding of the 3p electron by the 3s electrons.

Confidence: (a) Sure (b) Unsure

8. Silicon, phosphorus and sulphur are in Period 3. How would you expect the first ionisation energy of silicon ($1s^2 2s^2 2p^6 3s^2 3p^2$) to compare to that of phosphorus ($1s^2 2s^2 2p^6 3s^2 3p^3$)?

A. The first ionisation energy of silicon is greater than that of phosphorus.

B. The first ionisation energy of silicon is less than that of phosphorus.

Reason:

(1) Silicon has less electrons than phosphorus, thus its 3p electrons face less shielding.

(2) The 3p sub-shell of phosphorus is half-filled, hence it is stable.

(3) The 3p electrons of phosphorus are further away from the nucleus compared to that of silicon.

(4) The effect of an increase in nuclear charge in phosphorus is greater than the repulsion between its 3p electrons.

Confidence: (a) Sure (b) Unsure

9. How would you expect the first ionisation energy of phosphorus ($1s^2 2s^2 2p^6 3s^2 3p^3$) to compare to that of sulphur ($1s^2 2s^2 2p^6 3s^2 3p^4$)?

A. The first ionisation energy of phosphorus is greater than that of sulphur.

B. The first ionisation energy of phosphorus is less than that of sulphur.

Reason

(1) More energy is required to overcome the attraction between the paired 3p electrons in sulphur.

(2) 3p electrons of sulphur are further away from the nucleus compared to that of phosphorus.

(3) The effect of an increase in nuclear charge in sulphur is greater than the repulsion between its 3p electrons.

(4) The effect of an increase in nuclear charge in sulphur is less than the repulsion between its 3p electrons.

Confidence: (a) Sure (b) Unsure

10. How would you expect the first ionisation energy of silicon ($1s^2 2s^2 2p^6 3s^2 3p^2$) to compare to that of sulphur ($1s^2 2s^2 2p^6 3s^2 3p^4$)?

A The first ionisation energy of silicon is greater than that of sulphur.

B The first ionisation energy of silicon is less than that of sulphur.

Reason

(1) Sulphur will have its 3p sub-shell half-filled if an electron is removed.

(2) The 3p electrons of sulphur are further away from the nucleus compared to that of silicon.

(3) The effect of an increase in nuclear charge in sulphur is greater than the repulsion between its 3p electrons.

(4) The effect of an increase in nuclear charge in sulphur is less than the repulsion between its 3p electrons.

Confidence: (a) Sure (b) Unsure

11. Lithium and Sodium are in the group 1A. How would you expect the first ionisation energy of Lithium ($1s^2 2s^1$) to compare to that of Sodium ($1s^2 2s^2 2p^6 3s^1$)?

A The first ionisation energy of Lithium is greater than that of Sodium.

B The first ionisation energy of Lithium is less than that of Sodium.

Reason :

(1) More energy is required to overcome the attraction between the paired 2s electrons in Lithium.

(2) The 3s electrons of Sodium are further away from the nucleus compared to that 2s of Lithium.

(3) The effect of an increase in nuclear charge in Lithium is greater than the repulsion between its 2s electrons.

(4) The shielding effect of the inner shells of electrons are greater than the effect of increasing nuclear charge.

Confidence: (a) Sure (b) Unsure

12. How would you expect the first ionisation energy of Beryllium ($1s^2 2s^2$) to compare to that of Boron ($1s^2 2s^2 2p^1$)?

A The first ionisation energy of Beryllium is greater than that of Boron.

B The first ionisation energy of Beryllium is less than that of Boron.

Reason :

(1) The 2p electron of Boron has a lower penetrating power than the 2s electrons therefore it outweighs the increase in nuclear charge.

(2) The 2s electron of Beryllium has a lower penetrating power than the 1s electrons therefore it outweighs the increase in nuclear charge.

(3) The 2p electrons of Boron are further away from the nucleus compared to that of Beryllium.

(4) The effect of an increase in nuclear charge in Boron is less than the repulsion between its 2p electrons.

Confidence: (a) Sure (b) Unsure

ESTIMATIVA DE ERRO DO ALGORITMO PARA A DEFINIÇÃO DO DESLOCAMENTO DE FASE DOS SINAIS HARMÔNICOS NO TEMPO MENOR QUE O PERÍODO DO SINAL UTILIZANDO AMOSTRAGEM ESTOCÁSTICA**ERROR ESTIMATION OF THE ALGORITHM FOR THE PHASE SHIFT DEFINITION OF HARMONIC SIGNALS IN THE TIMELESS THAN THE SIGNAL PERIOD USING STOCHASTIC SAMPLING****ОЦЕНКА ПОГРЕШНОСТЕЙ АЛГОРИТМА ОПРЕДЕЛЕНИЯ СДВИГА ФАЗ ГАРМОНИЧЕСКИХ СИГНАЛОВ ЗА ВРЕМЯ, МЕНЬШЕЕ ПЕРИОДА, С ИСПОЛЬЗОВАНИЕМ СТОХАСТИЧЕСКОЙ ДИСКРЕТИЗАЦИИ**ZAITSEVA, Irina N.^{1*}¹ Bunin Yelets State University, Department of Physics, Radio Engineering and Electronics, Russia.

** Corresponding author*
e-mail: irina.n.zaitseva@yandex.ru

Received 23 June 2020; received in revised form 27 July 2020; accepted 07 August 2020

RESUMO

A determinação dos parâmetros de um sinal harmônico é um dos tipos mais comuns de medições em engenharia de rádio, engenharia de comunicação, eletrônica e sistemas de automação. A pesquisa e o desenvolvimento de novos métodos para medir os parâmetros dos sinais harmônicos são relevantes. Este trabalho estudou os erros de algoritmo para determinar a mudança de fase dos sinais harmônicos utilizando amostragem estocástica. A relevância deste estudo é ditada pelo aumento dos requisitos de precisão e velocidade dos equipamentos de medição, a redução do tempo necessário para decidir sobre a presença de um sinal enquanto se procura por ele e o que torna necessário utilizar métodos estatisticamente ótimos para medir os parâmetros de sinais. O objetivo do trabalho foi desenvolver um algoritmo e estimar seus erros para a possibilidade de implementação prática do algoritmo para o processamento de sinais de rádio de frequência infra baixa durante a amostragem estocástica. Os valores instantâneos em cada amostra dos sinais sob investigação são baseados na amostragem estocástica no tempo, de acordo com a lei de distribuição uniforme. A modelagem matemática dos erros do algoritmo para determinar o deslocamento de fase dos sinais com harmônicas e, dependendo das harmônicas em comparação com a primeira (principal) harmônica do sinal sob investigação durante a amostragem por conversores analógico-digitais reais, foram realizados. Os valores obtidos dos erros do algoritmo para determinar o deslocamento de fase do harmônico principal estão dentro de uma faixa aceitável (<30%); em amplitudes harmônicas (até o 3º harmônico), dentro de 20%. Os resultados do experimento de computação para estimar os erros do algoritmo confirmam a possibilidade de obter alta precisão na determinação do deslocamento de fase dos sinais harmônicos. Este algoritmo pode ser usado para processar sinais de rádio de frequência infrabaixa com precisão suficiente em acústica, hidroacústica, acústica sísmica, comunicação subaquática e subterrânea.

Palavras-chave: tempo de acesso, modelagem computadorizada, sinal de rádio de frequência infrabaixa, conversor analógico-digital.

ABSTRACT

Determining the parameters of a harmonic signal is one of the most common types of measurements in radio engineering, communication engineering, electronics and automation systems. The research and development of new methods for measuring the harmonic signal parameters are relevant. This work studied algorithm errors for determining the phase shift of harmonic signals using stochastic sampling. The relevance of this study is dictated by increasing requirements for the accuracy and speed of measuring equipment, the reduction of time it takes to decide on the presence of a signal while searching for it, that make it necessary to use statistically optimal methods for measuring signal parameters. The work aimed to develop an algorithm and estimate its errors for the possibility of practical implementation of the algorithm for processing infra-low-frequency radio signals during stochastic sampling. According to the uniform distribution law, the instantaneous values in each sample of the signals under investigation are based on stochastic sampling in time.

Mathematical modeling of algorithm errors for determining the phase shift of signals with harmonics, and depending on harmonics compared to the first (main) harmonic of the signal under investigation during the sampling by real analog-to-digital converters have been carried out. The obtained values of the algorithm errors for determining the phase shift of the main harmonic are within an acceptable range (<30%); at harmonics amplitudes (up to the 3rd harmonic) within 20%. The computing experiment results for estimating the algorithm errors confirm the possibility of obtaining high accuracy in determining the phase shift of harmonic signals. This algorithm can be used for processing infra-low-frequency radio signals with sufficient accuracy in acoustics, hydroacoustics, seismic acoustics, underwater, and underground communication.

Keywords: *access time, computer modeling, infra-low frequency radio signal, analog-to-digital converter.*

АННОТАЦИЯ

Определение параметров гармонического сигнала является одним из самых распространенных видов измерений в радиотехнике, технике связи, электронике и системах автоматики. Исследование и разработка новых методов измерения параметров гармонического сигнала являются актуальными. Настоящая работа посвящена исследованию погрешностей алгоритма определения сдвига фаз гармонических сигналов, с использованием стохастической дискретизации. Актуальность данного исследования продиктована возрастающими требованиями к точности и быстроте действия измерительной аппаратуры, сокращению времени принятия решения о наличии сигнала при его поиске, делают необходимым использование статистически оптимальных методов измерения параметров сигнала. Цель работы заключается в разработке алгоритма и оценке его погрешностей для возможности практической реализации алгоритма для обработки инфранизкочастотных радиосигналов при стохастической дискретизации. Мгновенные значения в каждой выборке из исследуемых сигналов основываются на стохастической дискретизации во времени по равномерному закону распределения. Проведено метаматематическое моделирование погрешностей алгоритма определения сдвига фаз сигналов с гармониками и в зависимости от гармоник относительно первой (основной) гармоники исследуемого сигнала при дискретизации реальными аналого-цифровыми преобразователями. Полученные значения погрешностей алгоритма определения сдвига фаз основной гармоники находятся в приемлемом диапазоне (<30%); при амплитудах гармоник (не далее 3-й гармоники) – до 20%. Результаты вычислительного эксперимента оценки погрешностей алгоритма подтверждают возможность получения высокой точности определения сдвига фаз гармонических сигналов. Настоящий алгоритм может найти применение при обработке инфранизкочастотных радиосигналов с достаточной точностью в акустике, гидроакустике, сейсмоакустике, подводной и подземной связи.

Ключевые слова: *время обращения, математическое моделирование, инфранизкочастотный радиосигнал, аналого-цифровой преобразователь.*

1. INTRODUCTION:

The radio signals currently used in radio engineering systems have a wide variety of shapes and types. For example, signals with complex modulation are used in satellite and ground-based navigation and communications systems. More straightforward signals are used, for instance, in radiolocation, acoustics, and medicine. However, a harmonic signal is most often the basis of their carrier signal. The presence of the harmonic signal makes it possible to build high-precision measuring systems using one of the parameters of this signal – its phase (Shakhov and Ugol'kov, 1986; Ugol'kov, 2003, 2004; Zaitseva, 2019).

Therefore the research and development of new methods for measuring harmonic signal parameters are relevant. It is also appropriate for developing high-precision radio engineering

systems, measuring equipment, and the simpler systems that use harmonic signal parameters as information ones (geodesy, acoustics, and medicine) Marmarelis and Marmarelis, 1978; Levin, 1989; Bilinsky and Mikelson, 1983).

One of the main criteria for the quality of the radio system is the time of the measurement result issue from the moment when the signal is received at its input. This time depends, among other factors, also on the measurement (estimation) time of the parameters of the carrier harmonic signal. This is especially important for systems and devices that use sufficiently low-frequency radio signals, pulsed signals with harmonic filling. Also, for devices that output low-frequency signals during the processing of high-frequency signals (for example, signals containing Doppler frequency shift, in radiolocation, and the receiving and measuring equipment of satellite navigation systems). Reduction of the time for the definition of the

main parameters of harmonic signals such as amplitude, frequency, phase (phase shift) and spectrum based on various basic functions to the minimum values of access time to physical signals (at least much shorter than their period of existence by dozens of times and more), as well as the development of fundamental analog-digital algorithms corresponding to this goal, is a very relevant problem, according to paper (Zaitseva, 2019; Meshkov and Ugol'kov, 1984; Shakhov and Ugol'kov 1986).

It is necessary to reduce the access time to the signals understudy to less than one signal period to measure the parameters of signals in acoustics, hydroacoustics, and seismic acoustics. This is because the periods of infra-low-frequency signals can be equal to days, months, years or more. This raises the question of determining the minimum access time to the signal (minimum instantaneous counts) and determining the parameters of harmonic signals for a time significantly less than their period. In scientific works (Shakhov and Ugol'kov, 1986; Ugol'kov, 2003, 2004; Meshkov and Ugol'kov, 1984; Zaitseva, 2019), the issues of determining the main parameters of harmonic signals by the minimum of instantaneous readings for a time less than their period are considered.

Algorithms for defining the parameters of harmonic signals for the timeless than their period, using "classical" methods of uniform time sampling of these signals are considered in papers (Shakhov and Ugol'kov, 1986; Ugol'kov, 2003, 2004). Of particular interest are the studies (Zaitseva, 2019; Porschnev and Kussaikin, 2016) of the application in such algorithms of stochastic sampling for optimizing the algorithms under conditions of the definition of the real signals parameters with distortions, external noise, and self-noise.

Fundamental interest in such signal processing appears in the analysis of transmission lines, in which signals modulated by phase, frequency, or amplitude are encoded by conversion to "solitons." A soliton is a structurally stable solitary wave propagating in the nonlinear medium. Solitons behave like particles (wave-particle duality), and when interacting with each other or with some other disturbances, they are not destroyed but continue to move, keeping their structure. This transmission line usually consists of a large number of nonlinear chains. It can be described by a partial differential system that is transformed into the Korteweg-de Vries equation.

Therefore, the development and analysis of analog-to-digital algorithms for the definition of the parameters of harmonic low-frequency signals in the time much less of their period to both reduce the time for detecting processes and objects, and to predict critical phenomena in hydroacoustics, acoustics and thermal (wave) processes is a very relevant problem (Gorbunov, 2014; Amelin and Granichin, 2011; Marmarelis and Marmarelis, 1978; Porschnev and Kussaikin, 2016; Boashash, 2015; Rajan, 2017; Taylor, 2017; Ermolaeva, Goncharenko, and Gordienko, 2011; Chaparro, 2015; Chapman, 2017).

Thus, the study aimed to estimate the algorithm errors for determining the phase shift of harmonic signals in the time shorter than the period for a possible practical implementation of the algorithm in real conditions at underwater objects.

2. MATERIALS AND METHODS:

The problem of reducing the access time to signals to determine their parameters has always been considered in the form of a statement since the emergence of the theory of signal processing in electrical engineering, measurement technology, radio engineering, and numerous practical applications of this branch of science and technology. Since the early nineties, these studies have been further stimulated and developed with the advent of high-speed and small-size computing technology, new software, and the possibility of accessing it by a wide range of scientists and engineers.

Studies of digital methods for determining the parameters of harmonic signals by measuring their instantaneous values in a timeless than a period using analog-to-digital processing and high-speed ADCs are of great interest. Currently, various methods of digital processing of radio signals are used. Some examples are the orthogonal transformations, modeling, and digital filtering methods, an analytical apparatus for describing signals and noise, numerical methods of solving problems and systems of equations. (Bilinsky and Mikelson, 1983; Wentzel, 1969; Meshkov and Ugol'kov, 1984; Gorbunov, Kulikov, and Shpak, 2016).

In (Zaitseva, 2019), based on solving the system of equations, an algorithm for determining the phase shift of harmonic signals

was developed. The error estimation of the developed phase-shift algorithm for harmonic signals was studied with the probabilistic and statistical method using stochastic sampling in this work.

The basic relations will be presented for the algorithm for the phase shift definition of harmonic signals in access time less than one signal period.

It will be assumed that the reference $x(t)$ and the investigated $y(t)$ signals, along with the harmonic component, have constant components C_{0x} and C_{0y} , respectively. Equations 1-6 show their instantaneous sample values and finite differences:

$$\begin{cases} x_0 = A_{mx} \cdot \sin(\omega \cdot t) + C_{0x}; \\ x_1 = A_{mx} \cdot \sin(\omega \cdot t + h) + C_{0x}; \\ x_2 = A_{mx} \cdot \sin(\omega \cdot t + 2 \cdot h) + C_{0x}; \end{cases} \quad (\text{Eq. 1})$$

$$\begin{cases} \Delta_{1x} = x_1 - x_0 = 2 \cdot \sin(h/2) \cdot \cos(\omega \cdot t + h/2); \\ \Delta_{2x} = x_2 - x_1 = 2 \cdot \sin(h/2) \cdot \cos(\omega \cdot t + h \cdot 3/2); \end{cases} \quad (\text{Eq. 2})$$

$$\Delta_{ix} = x_{i+1} - x_i = 2 \cdot \sin(h/2) \cdot \cos(\omega \cdot t + i \cdot h/2); \quad (\text{Eq. 3})$$

$$\begin{cases} y_0 = A_{my} \cdot \sin(\omega \cdot t + \varphi) + C_{0y}; \\ y_1 = A_{my} \cdot \sin(\omega \cdot t + \varphi + h) + C_{0y}; \\ y_2 = A_{my} \cdot \sin(\omega \cdot t + \varphi + 2 \cdot h) + C_{0y}; \end{cases} \quad (\text{Eq. 4})$$

$$\begin{cases} \Delta_{1y} = y_1 - y_0 = 2 \cdot \sin(h/2) \cdot \cos(\omega \cdot t + \varphi + h/2); \\ \Delta_{2y} = y_2 - y_1 = 2 \cdot \sin(h/2) \cdot \cos(\omega \cdot t + \varphi + h \cdot 3/2); \end{cases} \quad (\text{Eq. 5})$$

$$\Delta_{iy} = y_{i+1} - y_i = 2 \cdot \sin(h/2) \cdot \cos(\omega \cdot t + \varphi + i \cdot h/2), \quad (\text{Eq. 6})$$

where: ω is the frequency of the harmonic components of signals $x(t)$ and $y(t)$; φ is the phase shift between the harmonic components of signals $x(t)$ and $y(t)$; $h = \omega \cdot \Delta t$ is the sampling step in angular measurement; Δt is the sampling interval of signals $x(t)$ and $y(t)$ over time; $i = 0, 1, 2, \dots, n$.

Having found the relations

$$J_1 = \frac{\Delta_{1x}}{\Delta_{2x}} = \frac{\cos(h/2) - \text{tg}(\alpha_0) \cdot \sin(h/2)}{\cos(h \cdot 3/2) - \text{tg}(\alpha_0) \cdot \sin(h \cdot 3/2)}; \quad (\text{Eq. 7})$$

$$J_2 = \frac{\Delta_{1y}}{\Delta_{2x}} = \frac{\cos(h/2) - \text{tg}(\varphi) \cdot \sin(\alpha_0 + h/2)}{\cos(\alpha_0 + h \cdot 3/2) - \text{tg}(\varphi) \cdot \sin(\alpha_0 + h \cdot 3/2)}, \quad (\text{Eq. 8})$$

and having solved Equations 7 and 8 for φ and α_0 , it is obtained the expression for the definition of the phase shift φ along the curve of instantaneous values of the first order finite differences Δ_{ix} и Δ_{iy} :

$$\varphi = \text{arctg} \frac{J_2 \cos(\alpha_0 + h \cdot 3/2) - \cos(\alpha_0 + h/2)}{J_2 \sin(\alpha_0 + h \cdot 3/2) - \sin(\alpha_0 + h/2)}, \quad (\text{Eq. 9})$$

where

$$\alpha_0 = \text{arctg} \frac{J_1 \cos(h \cdot 3/2) - \cos(h/2)}{J_1 \sin(h \cdot 3/2) - \sin(h/2)}.$$

The phase shift value φ obtained by the algorithm (9) does not depend on the constant components C_{0x} and C_{0y} and the amplitudes A_{m1} and A_{m2} of $x(t)$ and $y(t)$ signals.

The algorithm (9) allows for the definition of the phase shift with minimum access time to signals τ equal to $\tau = 2 \cdot \Delta t$ in the angular measure $2h$.

Stochastic processing of harmonic signals (1) and (4) to define the phase shift is that the random law carries out the sampling of instantaneous values from the signal. The sampling interval of signals (1) and (4) overtime is selected from uniformly distributed linearly transformed random values, arranged as an ordered series, according to papers (Boashash, 2015; Rajan, 2017; Taylor, 2017).

It is assumed that the uniform law distributes samples from signals (1) and (4). The expression describes the density of time intervals distribution for discrete samples:

$$p(t_i) = 1/T_m \text{ at } t_1 \leq t_i \leq t_n,$$

where $T_m = t_n - t_1$ is the measurement time or access time to the signal, and

$$p(t_i) = 0 \text{ in case of other } t_i. \quad (\text{Eq. 10})$$

It is determined the distribution density for $x(t_i)$ at t_i uniformly distributed in the range from t_1 до t_n , as a function of x according to papers (Wentzel, 1969; Levin, 1989):

$$p(x, t_i) = \frac{1}{\omega \cdot t_m}.$$

To define the phase shift of harmonic signals according to the algorithm (9), it was used the formula for the statistical expectation of values of the signals under consideration with stochastic sampling over time as a stochastic process. The constant components of the signals may not be taken into account, because they are reduced when finite differences of the first order are found (1)-(8). Taking into account Equations 10 and 11, the statistical expectation for the signal (1) is expressed by the formula:

$$m_{1x}(x, t_i) = \int_{x_1}^{x_n} x \cdot p(x, t_i) \cdot dx = \frac{2 \cdot A \cdot \sin(\omega \cdot T_m / 2)}{\omega^2 \cdot T_m} \cdot \sin(2 \cdot \alpha_0 + \omega \cdot T_m / 2),$$

where

$$x_1 = A \cdot \sin(\alpha_0);$$

$$x_n = A \cdot \sin(\alpha_0 + \omega \cdot T_m).$$

For the second sample from the signal (1), the statistical expectation, according to paper (Wentzel, 1969) is:

$$m_{2x}(x, t_i) = \int_{x_n}^{x_{n+1}} x \cdot p(x, t_i) \cdot dx = \frac{2 \cdot A \cdot \sin(\omega \cdot T_m / 2)}{\omega^2 \cdot T_m} \cdot \sin(2 \cdot \alpha_0 + 3 \cdot \omega \cdot T_m / 2),$$

where

$$x_{n+1} = A \cdot \sin(\alpha_0 + 2 \cdot \omega \cdot T_m).$$

For the third sample from the signal (1), the statistical expectation is:

$$m_{3x}(x, t_i) = \int_{x_{n+1}}^{x_{n+2}} x \cdot p(x, t_i) \cdot dx = \frac{2 \cdot A \cdot \sin(\omega \cdot T_m / 2)}{\omega^2 \cdot T_m} \cdot \sin(2 \cdot \alpha_0 + 5 \cdot \omega \cdot T_m / 2),$$

where

$$x_{n+1} = A \cdot \sin(\alpha_0 + 3 \cdot \omega \cdot T_m).$$

Using similar Equations 10 and 11, the expression for the signal (4) is:

$$m_{1y}(y, t_i) = \int_{y_1}^{y_n} y \cdot p(y, t_i) \cdot dy = \frac{2 \cdot A \cdot \sin(\omega \cdot T_m / 2)}{\omega^2 \cdot T_m} \cdot \sin(\varphi + 2 \cdot \alpha_0 + \omega \cdot T_m / 2)$$

where

$$y_1 = A \cdot \sin(\varphi + \alpha_0);$$

$$y_n = A \cdot \sin(\varphi + \alpha_0 + \omega \cdot T_m).$$

Calculating the statistical expectation for the second sample from the signal (4), according to paper (Wentzel, 1969):

$$m_{2y}(y, t_i) = \int_{y_n}^{y_{n+1}} y \cdot p(y, t_i) \cdot dy = \frac{2 \cdot A \cdot \sin(\omega \cdot T_m / 2)}{\omega^2 \cdot T_m} \cdot \sin(\varphi + 2 \cdot \alpha_0 + 3 \cdot \omega \cdot T_m / 2),$$

where

$$y_{n+1} = A \cdot \sin(\varphi + \alpha_0 + 2 \cdot \omega \cdot T_m).$$

The expression describes the statistical expectation for the second sample from the signal (4):

$$m_{3y}(y, t_i) = \int_{y_{n+1}}^{y_{n+2}} y \cdot p(y, t_i) \cdot dy = \frac{2 \cdot A \cdot \sin(\omega \cdot T_m / 2)}{\omega^2 \cdot T_m} \cdot \sin(\varphi + 2 \cdot \alpha_0 + 5 \cdot \omega \cdot T_m / 2),$$

where

$$y_{n+1} = A \cdot \sin(\varphi + \alpha_0 + 3 \cdot \omega \cdot T_m).$$

To find the finite differences of the first order from these samples:

$$\Delta_{1x} = m_{2x} - m_{1x} = k \cdot 2 \cdot \sin(\omega \cdot T_m / 2) \cdot \cos(\alpha_0 + \omega \cdot T_m);$$

$$\Delta_{2x} = m_{3x} - m_{2x} = k \cdot 2 \cdot \sin(\omega \cdot T_m / 2) \cdot \cos(\alpha_0 + 2 \cdot \omega \cdot T_m);$$

$$\Delta_{1y} = m_{2y} - m_{1y} = k \cdot 2 \cdot \sin(\omega \cdot T_m / 2) \cdot \cos(\varphi + 2 \cdot \alpha_0 + \omega \cdot T_m);$$

$$\Delta_{2y} = m_{3y} - m_{2y} = k \cdot 2 \cdot \sin(\omega \cdot T_m / 2) \cdot \cos(\varphi + 2 \cdot \alpha_0 + 2 \cdot \omega \cdot T_m),$$

where

$$k = \frac{2 \cdot A \cdot \sin(\omega \cdot T_m / 2)}{\omega^2 \cdot T_m}.$$

Having found the relations

$$J_1 = \frac{\Delta_{1x}}{\Delta_{2x}} = \frac{\cos(2 \cdot \omega \cdot T_m) - \operatorname{tg}(\alpha_0) \cdot \sin(2 \cdot \omega \cdot T_m)}{\cos(2 \cdot \omega \cdot T_m) - \operatorname{tg}(\alpha_0) \cdot \sin(2 \cdot \omega \cdot T_m)}; \text{ (Eq. 12)}$$

$$J_2 = \frac{\Delta_{1y}}{\Delta_{2y}} = \frac{\cos(2 \cdot \alpha_0 + \omega \cdot T_m) - \operatorname{tg}(\varphi) \cdot \sin(2 \cdot \alpha_0 + \omega \cdot T_m)}{\cos(2 \cdot \alpha_0 + 2 \cdot \omega \cdot T_m) - \operatorname{tg}(\varphi) \cdot \sin(2 \cdot \alpha_0 + 2 \cdot \omega \cdot T_m)}, \quad (\text{Eq. 13})$$

and having solved Equations 12 and 13 for φ and α_0 , it was obtained the expression for the definition of the phase shift φ along the curve of instantaneous values of the first order finite differences Δ_{ix} and Δ_{iy} :

$$\varphi = \operatorname{arctg} \frac{J_2 \cos(2 \cdot \alpha_0 + 2 \cdot \omega \cdot T_m) - \cos(2 \cdot \alpha_0 + \omega \cdot T_m)}{J_2 \sin(2 \cdot \alpha_0 + 2 \cdot \omega \cdot T_m) - \sin(2 \cdot \alpha_0 + \omega \cdot T_m)}, \quad (\text{Eq. 14})$$

where

$$\alpha_0 = (\operatorname{arctg} \frac{J_1 \cos(2 \cdot \omega \cdot T_m) - \cos(\omega \cdot T_m)}{J_1 \sin(2 \cdot \omega \cdot T_m) - \sin(\omega \cdot T_m)}) / 2.$$

The phase shift value φ obtained by the algorithm (14) does not depend on the constant components C_{0x} and C_{0y} and the amplitudes A_{m1} and A_{m2} of $x(t)$ and $y(t)$ signals.

The relative error of the phase shift definition φ in this case is equal to:

$$\gamma_\varphi = \frac{\varphi' - \varphi}{\varphi} \cdot 100\% \quad (\text{Eq. 15})$$

This algorithm can also be used for analyzing the effects of interference, even not a multiple of the frequency ω , on the error of the phase shift definition. For this purpose, it is necessary to select the corresponding k by limiting, for example, the signal (4) to the sum of any number of harmonic aliquant and multiple frequencies.

3. RESULTS AND DISCUSSION:

To estimate the errors of the presented algorithm for the phase shift definition of harmonic signals, harmonic signals in the form of an infra-low frequency sinusoidal wave with the frequency of the first harmonic $f = 20$ Hz and amplitude $A = 10$ B were studied, presented by the function:

$$x(t_i) = 10 \cdot \sin(\omega \cdot t_i); \quad (\text{Eq. 16})$$

$$y(t_i) = 10 \cdot \sin(\omega \cdot t_i + \varphi) + \frac{10}{g} \cdot \sin(2 \cdot \omega \cdot t_i + \varphi) + \frac{10}{g} \cdot \sin(3 \cdot \omega \cdot t_i + \varphi), \quad (\text{Eq. 17})$$

where: Δt_i are the time intervals of the discrete sample and signal, distributed according to the uniform law;

ω is the circular frequency of the signal, rad/s;

$\varphi = 0.5$ rad is the phase shift;

$g = 10 \dots 500$ is the coefficient.

The total number of discrete samples with uniform distribution is equal to 2000 for the signal period. The number of three discrete samples during the access time to the signal with access time less than its period arbitrarily is equal to 300. Then, the access time to the period of signals under investigation will be less than the first harmonic period.

The numerical modeling was performed in *MathCAD* software package. Using the built-in statistical function *rnd*, it was generated 2000 numbers with a uniform distribution law. Further, it was arranged the obtained values in the form of an ordered series in ascending order and calculate the values of discrete samples from sinusoidal signals without harmonics and with two harmonics (even and odd). The uniformly distributed harmonic amplitude values from 1% to 20% of the amplitude of the main (first) harmonic are of interest. The modeling results are illustrated in Figures 1 and 2.

Figure 1 represents the reconstructed period of the signals under investigation in the form of sinusoid $x(t)$ without harmonics and $y(t)$ with two harmonics with stochastic sampling over time and with the uniform distribution law. The harmonics are distributed with the uniform amplitude equal to 20% of the amplitude of the main (first) harmonic. It can be observed that the signal $y(t)$ is significantly distorted.

Figure 2 represents a diagram calculated compared to the phase shift error of harmonic signals where the signal $y(t)$ has harmonics with an amplitude between 1% and 20% of the amplitude of the main (first) harmonic. The errors have been calculated for three samples in the form of statistical expectation of three samples with 300 samples each, synchronously from both signals with time sampling in the form of samples with uniform distribution law.

Table 1 represents the computational results of the phase shift errors of harmonic signals with harmonics in time less than one signal period with stochastic sampling over time.

At the moment, there are some works focused on the development and research of analog-digital algorithms for determining the parameters of infra-low-frequency radio signals for a shorter period both for special cases and for individual signal parameters. However, such developments are important to reduce the time of identification and detection of processes and objects and study high-speed objects and forecast critical phenomena in hydroacoustics, acoustics, and thermal (wave) processes.

Of particular interest are studies on applying stochastic sampling in such algorithms for the optimization of algorithms' operation under conditions of organized interference and noise. The obtained results can be used in solving the following problems of science and exclusive equipment:

- In experimental investigations of the infra-low frequency hydroacoustic and meteorological properties of the processes taking place in the seas and oceans (especially in the coastal areas), using installed underwater hydroacoustic antennas and presence of fields of thermal sensors;

- In the development of devices with accelerated hydroacoustic and thermal detection and identification of high-speed (slow-moving or motionless) and low-noise underwater objects;

- In the development of methods and devices for short-term and long-term forecasting of catastrophic wave events such as seismic sea waves, earthquakes and atmospheric phenomena (hurricanes and global wind vortices) since their emergence;

- For the metrological certification of hydroacoustic antennas and fields of thermal sensors;

- For the development of methods and devices for non-destructive control of the state of large facilities and structures such as bridges, large sports facilities, tunnels, pipelines to accelerate the critical (short-term), and long-range forecasting of their standard operating condition.

4. CONCLUSIONS:

The developed algorithm for determining the phase shift of harmonic signals uses the minimum number of instantaneous readings of the measured signals (three). It can be used when measuring infra-low-frequency radio signals. Instantaneous values in each sample of

the signals under study are based on stochastic sampling in time according to a uniform distribution law with a signal access time of a shorter period.

The phase shift definition errors by the developed algorithm are fractions of a percent in the signal $y(t)$ when the harmonic content is less than 1%. Further, the phase shift errors (accuracy) increase almost linearly from -2% to -27% when the amplitude (total) of the harmonics increases from 2% to 20% of the amplitude of the first harmonic. The phase shift errors of the algorithm under investigation with stochastic sampling are in an acceptable range of <30 % at the amplitude of harmonics (up to the third harmonic) within 20%.

The error in determining the phase shift of the investigated harmonic signals by the developed algorithm with stochastic sampling is hundredths of a percent and depends little on the signal sampling accuracy by level. The obtained error values correspond to the sampling accuracy when converting the analog-to-digital converters (ADCs) of 12-bit ADCs into the accepted values.

Thus, in the broad sense, the proposed research is one of the parties to the further development of this and other algorithms of similar signals and analysis of their errors.

5. REFERENCES:

1. Amelin, K.S. and Granichin, O.N. (2011). Randomization possibilities in prediction algorithms of the Kalman type for arbitrary external interferences in tracking. *Gyroscopy and Navigation*, 2(73), 38-50.
2. Bilinsky, I.Y. and Mikelson, A.K. (1983). *Stochastic digital processing of continuous signals*. Riga, Latvia: Zinatne.
3. Boashash, B. (2015). *Time-frequency signal analysis and processing: A comprehensive reference*. Elsevier.
4. Chaparro, L. (2015). Fourier analysis of discrete-time signals and systems. In *Signals and systems using MATLAB* (pp. 683-768). Elsevier.
5. Chapman, N.R. (2017). Inverse methods in underwater acoustics. In T.H. Neighbors, III and D. Bradley (Eds.), *Applied*

- underwater acoustics* (pp. 553-585). Elsevier.
6. Ermolaeva, E.O., Goncharenko, B.I. and Gordienko, V.A. (2011). Vector-phase methods as the basis for creation of new generation of measuring hydroacoustic systems. *Proceedings of Forum Acusticus*, 2819-2824.
 7. Gorbunov, Yu.N. (2014). Stochastic radiolocation: conditions for the problem solving of detection, estimation and filtration. *Journal of Radio Electronics*, 11, 1-23.
 8. Gorbunov, Yu.N., Kulikov, G.V. and Shpak, A.V. (2016). *Radiolocation: stochastic approach*. Moscow, Russia: Scientific and Technical Publishing House "Hot Line Telecom".
 9. Levin, B.R. (1989). *Theoretical foundations of statistical radio engineering*. Moscow, Russia: Radio and Communication.
 10. Marmarelis, P.Z. and Marmarelis, V.Z. (1978). *Analysis of physiological systems: The white-noise approach*. Boston, MA: Springer.
 11. Meshkov, V.P. and Ugol'kov, V.N. (1984). *Definition of harmonic signal parameters with a minimum of instantaneous samples*. Krasnoyarsk, Russia: Publishing House of the L.V. Kirensky Institute of Physics of the Academy of Sciences of the USSR.
 12. Porschnev, S.V. and Kussaikin, D.V. (2016). About the accuracy of extraction of the periodic discrete signal of the finite-duration by means of the Kotel'nikov series. *T-Comm: Telecommunications and Transportation*, 10(11), 4-8.
 13. Rajan, D. (2017). Probability, random variables, and stochastic processes. In E. Serpedin, T. Chen and D. Rajan (Eds.), *Mathematical foundations for signal processing, communications, and networking* (pp. 205-244). Boca Raton, FL: CRC Press.
 14. Shakhov, E.K. and Ugol'kov, V.N. (1986). *The question of determining the phase shift of harmonic signals in the time less than the signal period in the presence of the constant component*. Krasnoyarsk, Russia: Publishing House of the L.V. Kirensky Institute of Physics of the Academy of Sciences of the USSR.
 15. Taylor, F.J. (2017). Digital signal processing. In V.G. Oklobdzija (Ed.), *Digital systems and applications*. Boca Raton, FL: CRC Press.
 16. Ugol'kov, V.N. (2003). Methods of measuring the phase shift and amplitude of harmonic signals using integral samples. *Measurement Techniques*, 46, 495-501.
 17. Ugol'kov, V.N. (2004). Some problems of the digital analysis of signal spectra. *Measurement Techniques*, 47(6), 601-606.
 18. Wentzel, E.S. (1969). *Probability theory*. Moscow, Russia: Science.
 19. Zaitseva, I.N. (2019, 1-3 July). *Some problems of discretization and determination of basic parameters of harmonic signals*. Paper presented at the Conference "Systems of Signal Synchronization, Generating and Processing in Telecommunications (SYNCHROINFO)". doi: 10.1109/SYNCHROINFO.2019.8814150

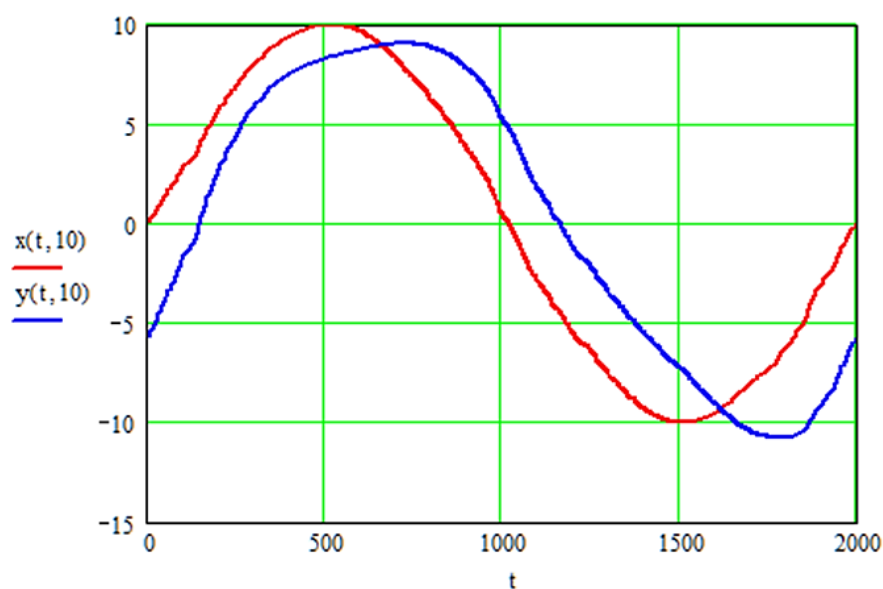


Figure 1. The reconstructed period of the signals under investigation $x(t)$ and $y(t)$ with the harmonics' amplitude equal to 20%. Source: the author

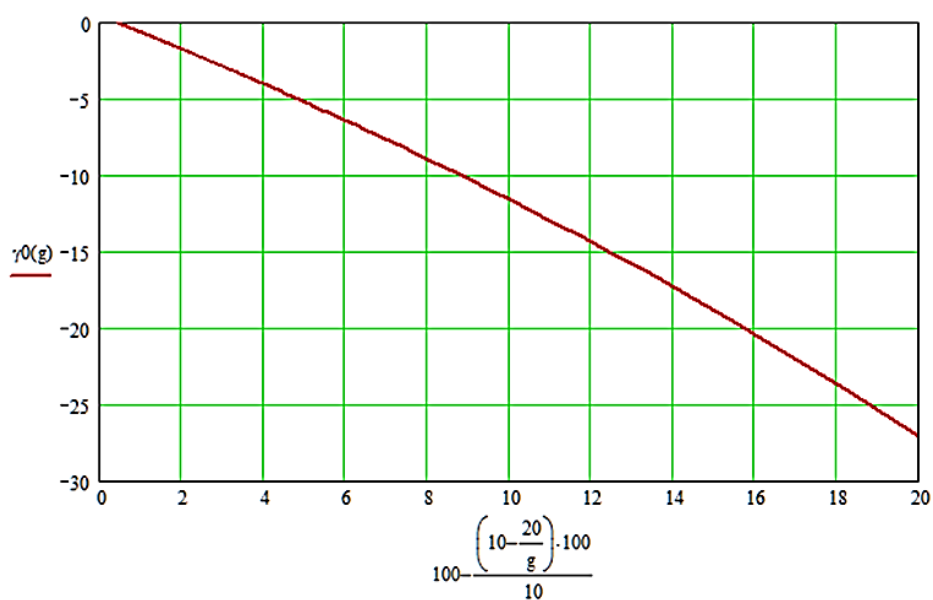


Figure 2. Errors of defining the phase shift of the signals under investigation (X-axis, %) compared to the harmonics in the signal $y(t)$ (Y-axis, %). Source: the author

Table 1. Computational results of the phase shift errors

Harmonic percentage (two harmonics), %	The relative error of phase shift detection using stochastic sampling on instantaneous samples with uniform distribution, %
1	0
2	-2
5	-5
10	-12
14	-17
18	-24
20	-27

DETERMINAÇÃO DO EFEITO DA SOBRECARGA DE FERRO NA VITAMINA D E DA PERCENTAGEM DE CADA GRUPO SANGUÍNEO EM PACIENTES COM TALASSEMIA

DETERMINATION THE EFFECT OF IRON OVERLOAD ON VITAMIN D AND THE PERCENTAGE OF EACH BLOOD GROUPS IN PATIENTS WITH THALASSEMIA

تحديد تأثير الحديد الزائد على فيتامين د ونسبة كل فصيلة دم لدى مرضى الثلاسيميا

AL-MASAOODI, Rusul Ali^{1*}; ALWAID, Shumoos H¹; Al-SHEMERY, Maryam Kadhim¹

¹ Department of Medical Laboratory Technique, College of Medical and Technique, Islamic University, 54001 Najaf, Iraq.

* Corresponding author
e-mail: rusulali.k@gmail.com

Received 12 June 2020; received in revised form 22 August 2020; accepted 09 September 2020

RESUMO

A talassemia pode ser caracterizada como anormalidades eritrocitárias hereditárias resultantes do defeito na síntese da cadeia de globina da hemoglobina que leva à anemia hipocrômica microcítica. Este estudo teve como objetivo encontrar alguma relação entre o sistema ABO e a doença talassêmica e determinar a relação entre ferritina e vitamina D em pacientes com talassemia. Este estudo estimou o nível de Hb, ferritina e vitamina D e também calculou a percentagem dos tipos sanguíneos ABO em pacientes talassêmicos e não-talassêmicos (grupo controle). Este estudo foi conduzido com 60 amostras sendo 20 para grupo controle e 40 de pacientes com talassemia. A idade dos pacientes com talassemia e controles variou de 2 a 29 anos. Este estudo encontrou a correlação entre ferritina e vitamina D. Os resultados demonstraram uma redução significativa ($p < 0,05$) de Hb e vitamina D, mas um aumento significativo ($p < 0,05$) na concentração de ferritina. O estudo encontrou ainda uma relação negativa não-significativa ($p < 0,05$) entre o nível de ferritina e vitamina D. Foi demonstrado que o grupo sanguíneo O está mais presente em pacientes talassêmicos (40%) ao passo que os grupos A, B e AB, estão, respectivamente, presentes em 23%, 28%, 10% dos pacientes. Pode-se concluir que os pacientes com talassemia são mais frequentes com o sangue tipo O seguido do tipo B e, menos frequente, no tipo sanguíneo AB.

Palavras-chave: *Talassemia; vitamina D; Ferritina; Sistema de grupo sanguíneo ABO.*

ABSTRACT

Thalassemia can be characterized as hereditary erythrocyte abnormalities resulting from the defect in the synthesis of the hemoglobin globin chain that leads to microcytic hypochromic anemia. This study aimed to find some relationship between the ABO system and thalassemia disease and to determine the relationship between ferritin and vitamin D in patients with thalassemia. This study estimated the level of Hb, ferritin, and vitamin D and also calculated the percentage of ABO blood types in thalassemia and non-thalassemia patients (control group). This study was conducted with 60 samples, 20 for the control group, and 40 for patients with thalassemia. The age of patients with thalassemia and controls ranged from 2 to 29 years. This study found a correlation between ferritin and vitamin D. The results demonstrated a significant reduction ($p < 0.05$) of Hb and vitamin D, but a significant increase ($p < 0.05$) in the concentration of ferritin. The study also found a non-significant negative relationship ($p < 0.05$) between the level of ferritin and vitamin D. It was demonstrated that blood group O is more present in thalassemia patients (40%) whereas groups A, B, and AB, respectively, are present in 23%, 28%, 10% of patients. It can be concluded that patients with thalassemia are more frequent with blood type O followed by type B and, less frequently, blood type AB.

Keywords: *Thalassemia; vitamin D; Ferritin; ABO blood group system.*

المخلص

مرض الثلاسيميا يمكن أن يُعرف على أنه تشوهات وراثية في كريات الدم الحمراء ناتجة عن خلل في تصنيع سلسلة غلوبين الهيموجلوبين يؤدي إلى فقر الدم الناقص الصبغ. هدفت هذه الدراسة إلى إيجاد علاقة بين نظام زمر الدم ABO ومرض الثلاسيميا وتحديد العلاقة بين الفيريتين وفيتامين د في مرضى الثلاسيميا. قدرت هذه الدراسة مستوى الهيموجلوبين والفيريتين وفيتامين د أيضًا حسب النسبة المئوية لأنواع ABO في مرضى الثلاسيميا وير المصابين

بالتلاسيميا (المجموعة الضابطة). أجريت هذه الدراسة على (60) عينة، (20) عينة للمجموعة الضابطة، 40 عينة لمرضى التلاسيميا. تراوحت اعمار مرضى التلاسيميا والمجموعة الضابطة بين (2-29) سنة. وجدت هذه الدراسة علاقة بين الفيريتين وفيتامين د. وأظهرت النتائج انخفاضاً معنوياً ($p < 0.05$) في الهيموغلوبين وفيتامين د، ولكن زيادة معنوية ($p < 0.05$) في تركيز الفيريتين. كما وجدت الدراسة وجود علاقة سلبية غير معنوية ($p < 0.05$) بين مستوى الفيريتين وفيتامين د. من النتائج تبين أن فصيلة الدم O هي الأكثر وجوداً في مرضى التلاسيميا (40%) بينما مجموعات الدم الأخرى من النوع A ، B ، و AB موجودة بنسبة (23%، 28%، 10%) على التوالي من المرضى. يمكن الاستنتاج أن مرضى التلاسيميا يكونون أكثر تكراراً مع فصيلة الدم O يليها فصيلة B ، والأقل تكراراً ، فصيلة الدم AB.

الكلمات المفتاحية: التلاسيميا، فيتامين د، الفيريتين، نظام زمر الدم ABO.

1. INTRODUCTION:

The thalassemia is an inherited disease of the blood that causes your body to have less hemoglobin than normal. Hemoglobin allows red blood cells to carry oxygen. Thalassemia accounts for about 3% of the world population, which has β -thalassemia, being the most common of congenital diseases in the world (Gregg *et al.*, 2019). Thalassemia results from a reduction in the synthesis of one or more of the polypeptide chains to hemoglobin (Hb), leading to interference in erythroid maturation, function, and ineffective erythropoiesis (Chaudhari, 2011). Two major factors related to the squeal of thalassemia: decrease the synthesis of the beta-globin chain leading to a reduced level of HbA, unbalanced alpha, and beta-globin chain synthesis (Be-Baun *et al.*, 2011).

Thalassemia was found with high commonness in Mediterranean countries, the Middle East, and Southeast Asia (Wong *et al.*, 2016), data from the World Health Organization (WHO) in 201. There are two major types of thalassemia (Galanello and Origa, 2010): i) α -thalassemia (α -T) – persons with alpha thalassemia, which inadequate synthesis of alpha-globin and ii) β -thalassemia (β -T) – persons with β -T, which inadequate synthesis of a beta-globin chain.

Alpha-Thalassemia is a congenital autosomal recessive disorder produced from mutations, includes deletion within the α -globin gene cluster, including two of alpha 1 ($\alpha 1$) and alpha 2 ($\alpha 2$) globin genes that are found on chromosome 16p13. More than 750 different variants in α -globin genes have been identified, leading to α -thalassemia worldwide (Giardine *et al.*, 2014). The α -thalassemia is most commonly found in the Mediterranean regions, sub-Saharan Africa, Middle East, Indian Subcontinent, East, Southeast Asia, and immigrants to these areas (Weatherall, 2011). The intensity of α -thalassemia relies on the type of mutation (deletional or non-deletional), and copies numbers of affected α - gene (Miri-Moghaddam *et al.*, 2015). The Hb Bart's hydrops fetalis (four defective α -globin genes) or Hb H disease (three

defective α -globin genes) can be diagnosed during prenatal (Zamani *et al.*, 2017).

Beta-thalassemia is considered a prevalent congenital disorder in the world, the cause of this disease is due to reducing or the absence of β -polypeptide chain synthesis. There are 200 mutations linked with a β -thalassemia phenotype that affect the expression phases of the β -globin gene, leading to decrease (β^+) or complete absence (β^0) of β -globin chain production (Bilgen *et al.*, 2013). β -thalassemia includes three main forms (Al-Mosawy, 2017):

i) β -thalassemia minor (trait) – is a heterozygous disorder that single mutation in the β -globin chain, leading to a reduction in synthesis of the β -polypeptide chain, and resulting in mild to moderate microcytic anemia called β -thalassemia trait (Sinha *et al.*, 2017). Thus, the patient with a β -thalassemia trait is clinically asymptomatic, without hepatosplenomegaly or jaundice present, with normal or close to normal hemoglobin levels (Al Raeesi *et al.*, 2017);

ii) β -thalassemia intermedia – can be defined as a heterogenetic disorder. The β -globin chain production is often mild when two genes are defective (Al Raeesi *et al.*, 2017). Beta-thalassemia intermedia is a less severe anemia in adolescence or early adulthood (Taher *et al.*, 2011). In this type of thalassemia, blood transfusions are not necessary or required frequently, but the patient continues to suffer the effects of the anomaly (Galanello and Origa, 2010).

iii) β -thalassemia major – is homozygous or compound heterozygous for more severe beta chain mutations (Jha and Jha, 2014). Beta-thalassemia is a major referred to sever anemia and medical attention, usually demanding in the first two years of life and depending on blood transfusions (Galanello and Origa, 2010). In β -thalassemia, major patients required iron chelation therapy to regulate iron overload. Blood transfusions are recommended, as they are caused by inefficiency in the production of β protein. Excessive α protein causes hemolytic anemia, reduced red blood cell survival, and

bone marrow over-stimulation (Rund and Rachmilewitz, 2005).

The unbalanced in α -globin and β -globin protein synthesis were to appear excess in alpha-globin chain production, which is the major pathophysiology of β -thalassemia (Leecharoenkiat *et al.*, 2016). Alpha-globin chains are different from β -globin chains when incapable of forming stable tetramers. So, the free excess of α -globin chains causes insoluble aggregates, accumulating in the erythroid cell (Mathias *et al.*, 2000). The free α -globin chains in β -thalassemia interfere with red cell maturation, and erythrocytes are ineffective and cause marrow expansion (Taher *et al.*, 2010). In the small percentage of erythroid cells that can be developed to mature cells, the precipitate of free α -globin chains produced reactive oxygen species and oxidative stress. Leading to red blood cell membrane destruction and hemolytic increase (Schrier, 2002).

Therapy of thalassemia is a chronic blood transfusion to improves the quality of life. Transfusion causes complications to include hemosiderosis and hemosiderosis. Induces morbidity can be prevented by adequate iron chelation therapy (Be-Baun *et al.*, 2011). Repeated blood transfusion causes progressive iron overload, a major complication of treatment (Suman *et al.*, 2016). The major complication of iron toxicity is the damage of organs and stunted growth. Iron is primarily deposited in the liver, then in the endocrine system, and then in the cardiac muscle. This leads to iron-induced liver injury, hypothyroidism (Be-Baun *et al.*, 2011).

The mortality in patients with thalassemia that are dependent on blood transfusion is iron overload-related to cardiomyopathy (Aboul-Enein *et al.*, 2015). Free iron is toxic to cells because free iron is the catalysis of free radicals' formation from Reactive Oxygen Species (ROS) through the Fenton reaction (Ezzat *et al.*, 2015). When erythrocytes die, phagocytosis occurs where hemoglobin is digested, and iron is eliminated (Al-Mosawy, 2017). Diagnosis of β -thalassemia can be performed by laboratory tests such as complete blood count (CBC), Hb electrophoresis, genetic testing (Tahir *et al.*, 2011).

The possible diagnoses for this anomaly are:

i) Clinical diagnosis: Usually, TM is diagnosed in an infant younger than two years of age with jaundice, severe microcytic anemia, and hepatosplenomegaly (Jha and Jha, 2014);

ii) Hematologic diagnosis: Is characterized by decrease in Hb concentration (< 7 g/dl), mean cell volume (MCV) $> 50 < 70$ fl (femtoliters) and mean cell Hb (MCH) $> 12 < 20$ pg (Al-Mosawy, 2017). Peripheral blood smear: The blood film of a patient with beta-thalassemia shows RBC microcytosis, hypochromic, anisocytosis, poikilocytosis (elongated cells and tear-drop), and nucleated RBC (erythroblasts) (Cao and Galanello, 2010).

iii) HPLC/electrophoresis: Hemoglobin electrophoresis is next step for patients with MCV < 80 fL or MCH < 27 pg, (Old, 2003). Separation of hemoglobin by different electrophoretic techniques is a mainstay of diagnosing hemoglobin disorders (Borbely *et al.*, 2013). However, several methods of HPLC high-performance liquid chromatography (HPLC) analysis are observed from different manufacturers, that are separated from hemoglobin dependent on cation exchange chromatography (Rhea and Molinaro, 2014). Also, an increase in hemoglobin A2 associated with β -T and an increase in HBB protein associated with HbH disorder are diagnosed by isoelectric focusing (Sabath, 2017).

iv) Molecular Genetic Analysis: Until recently, allele-specific oligonucleotide hybridization was a primary test for the detection of β -T mutations in the laboratory, which performed by using several mutation-specific probes (Vrettou *et al.*, 2003). Nowadays, the polymerase chain reaction (PCR) is a well-known technique for mutation detection, and the commonly used for detection of thalassemia mutation is Amplification Refractory Mutation (ARMS) (Rosatelli *et al.*, 2009).

The treatments of thalassemia are regular blood transfusions, iron chelating therapy, treatment of complications such as endocrine disorder, osteoporosis, and heart failure (Petrou *et al.*, 2010). The regular blood transfusions in TM were important to correct the anemia, inhibit erythropoiesis, and decrease in iron absorption (Cao and Galanello, 2010). The blood transfusions are based on several factors, such as weight, hemoglobin concentration, and PCV of blood (Rachmilewitz and Giardina, 2015). Chelation therapy iron overload is one of the serious complications of blood transfusion. (Zafeiriou *et al.*, 2006). The only approach to eliminate excess iron is the usage of iron chelators because the body has notability for removing iron (Glickstein *et al.*, 2006).

Therefore, there are three main iron-

chelating therapy: i) desferrioxamine (DFO); ii) deferiprone (DFP) and iii) deferasirox (DFX), that reducing the toxicity in cardiac, endocrine and hepatic which caused by excess iron in the body (Prus and Fibach, 2010). Bone marrow transplantation: In patients with thalassemia, the transplantation of bone marrow is a good therapy during childhood (Lawson *et al.*, 2003). Gene therapy is a genetic treatment in thalassemia, includes the replacement of nonfunctional globin genes with cloned beta-globin genes, while numerous factors of problems have hurdled this therapy due to the vectors, to the complex controlled of globin gene expression, as well as the very high level an expression which was required for the correction of genetic defects (Genovese *et al.*, 2014). Ferritin is an intracellular protein that storage and liberation of iron in a controlled fashion.

The protein is synthesis by nearly all organisms (Casiday and Frey, 2000). Ferritin is present in almost tissues as a cytosolic protein, but it excreted minor quantity into the bloodstream, and it acts as an iron carrier. The ferritin present in the plasma can act as indirect markers of the total iron storage quantity in the body. Thus, serum ferritin is used as a diagnostic test for iron-deficiency anemia (Wang and Knovich, 2010). Ferritin is a globular protein complex consisting of 24 protein subunits, forming a nanocage with multiple metal-protein interactions (Theil, 2012). The entry of ferritin in lysosomes is high when the cell needs iron for cellular use. On the other hand, when iron levels are high, the entry of ferritin into the lysosome decreases (Mancias *et al.*, 2015).

The ABO blood group system has an important role in human blood transfusions. The ABO system contains A antigens, B antigens, and antibodies against these antigens. The ABO system was exposed by Landsteiner in 1900. Additionally, in the ABO system Rh system was found, and this system has "naturally occurring" antibodies against A and B antigens. Those who do not express these antigens (Landsteiner's Law) it causes negative and sometimes fatal results in the first mismatched transfusion (Koeppen, 2010).

The presence of ABO and Rhesus (Rh) antigens is clinically important, as it plays a fundamental role in blood transfusions and organ transplants. Although all humans have these systems and blood groups, the frequency of ABO and Rh antigens varies between populations (Avent, 2000).

The vitamin is a steroid hormone, well known for its important role in regulating body levels of calcium and phosphorus in bone mineralization (Morris, 2014). This vitamin is synthesized in the skin after exposure to sunlight (Vanlint *et al.*, 2011). Vitamin D is found in two forms: D3 (cholecalciferol) and D2 (ergocalciferol). Vitamin D3 is synthesized in human skin from 7-dehydrocholesterol after exposure to sunlight and through nutritional sources (Chen *et al.*, 2009). The first hydroxylation site of vitamin D occurs in the liver and is converted to 25-hydroxyvitamin D[25(OH)D], and this structure is characterized by low biological activity. The second site that produces biologically active vitamin D is in the kidneys (Man *et al.*, 2016; Aloia *et al.*, 2006). Hydroxylation in the kidneys is stimulated by parathyroid hormone (PTH) and suppressed by phosphate (Weaver and Fleet, 2004).

The key function of vitamin D is regulated of phosphorus and calcium by that VD increases intestinal and tubular absorption of calcium. Additionally, vitamin D reduces the physiological activity of parathyroid hormone (PTH) in two ways: i) directly (by influenced parathyroid glands) and ii) indirectly by hyperkalemia (Aloia *et al.*, 2006). Vitamin D plays an important role in bone formation and resorption (Morris, 2014).

The role of vitamin D on the bone formation is by the affecting of vitamin D on osteoblasts via vitamin D receptors (VDR), increases the synthesis of osteocalcin, alkaline phosphatase (ALP), and the collagen type, whereas the vitamin D has an effect on osteoclasts it is doubled; indirect via osteoblasts (RANKL/RANK/osteoprotegerin system), and directly – by inhibition of differentiation from promyelocytes to monocytes, that are the precursors of osteoclasts (Boyle *et al.*, 2003).

Vitamin D is essential for maintaining calcium balance in the skeleton. Absorbed in the intestines, calcium promotes an increase in the number of osteoclasts, allowing the parathyroid hormone (Boyle *et al.*, 2003).

The influence of vitamin D on muscle cells is by regulating calcium metabolism in muscle cells that are vital for the process of contraction and relaxation of muscle fibers (Janssen *et al.*, 2002). The active form of vitamin D (1,25-(OH)₂) acts through the vitamin D receptor (VDR) that is found in the kidney, bone, intestine, and parathyroid gland, also found in tissues and organs that are not directly involved in the maintenance of calcium homeostasis, such as

the brain, breast, immune cells, muscle tissue (Holick, 2009). The biologically active form of vitamin D is 1,25-dihydroxy vitamin D ($1,25(\text{OH})_2\text{D}$). This molecule acts by means of VDR found in the kidneys, bone, intestine, and parathyroid gland. It is also found in tissues and organs that are not directly involved in maintaining calcium homeostasis, such as the brain, breast, immune cells, and muscle tissue (Holick, 2009; Holick, 2004).

2. MATERIALS AND METHODS:

This study was conducted at the Thalassemia Center in Al-Zahraa Teaching Hospital in Al-Najaf governorate, Iraq. A serum sample was collected from thalassemia transfusion patients in addition to a control group (healthy). The samples tested were (60) samples that were divided the control group, (20) samples were beginning from the (2-29) years, (40) samples are from thalassemia patients. The age of thalassemia patients was a range from the (2) year to (29) year. The study cases can be divided according to blood transfusion duration to < 1 year, 1-5 years, and > 5 years.

This study was conducted at the Thalassemia Center at Al - Zahraa University Hospital under the governorship of Al - Najaf, Iraq. A serum sample was collected from patients transfused with thalassemia, in addition to a control group (healthy). The samples were tested on 60 patients and divided into groups: i) 20 control patients aged 2 to 29 years and ii) 40 patients aged 2 to 29 years with thalassemia. The study is still divided according to the blood transfusion period (ranging from < 1 year, 1-5 years, and > 5 years).

2.1. Collection of samples

A blood sample was obtained from the elbow vein by sterilized synergies. The sample was placed in two tubes. The first tube contains EDTA as anticoagulants to prevent blood clotting for used in physiological studies. The second gel tube was used to allow clotting the blood at room temperature to prepare a serum after using the serum for biochemical biomarkers studies.

2.2. Hemoglobin Estimation

Hematological parameters have been used in the Hematology Laboratory at al-Zahraa Teaching Hospital with Mythic 18 (RINGELISA N CO., Turkey). This equipment provides an EDTA

anticoagulated blood count (Wasmuth, 2010) through a fully automated analyzer. Hemoglobin analysis is performed directly by 555 nm spectrophotometry. The formation of chromogenic cyanmethemoglobin detects hemoglobin (cyanide lytic solution) and oxyhemoglobin (cyanide-free lytic solution). Blank hemoglobin is measured for each analytical process and during the rinse phase.

2.3. Determination of Ferritin

The level of ferritin in serum was examined by using enzyme-linked immunosorbent assay (ELISA), according to a prepared processed from the Manufacturing company (E-EL-H0168).

2.3.1 Preparation of the reagent

i) Hold all reagents until they are used at room temperature ($18 \sim 25^\circ\text{C}$). Follow the Microplate Setup Reader Manual and preheat it to OD for 15 minutes.

ii) Wash buffers: dilute 30 mL of concentrated wash buffer with 720 mL of deionized or distilled water to make 750 mL of wash buffer. Note: if the crystals are concentrated, heat in a 40°C water bath and blend gently until the crystals are completely dissolved.

iii) Standard working solution: a standard centrifuge of 10,000 kilograms every 1 minute. Add 1.0 mL of regular reference and sample thinner, allow 10 minutes to stand, and reverse several times. All in all, combine it with a pipette until it is dissolved. This reconstitution results in a working solution of 10 ng/mL. Make serial dilutions as needed. The dilution gradient suggested is as follows: 10, 5, 2.5, 1.25, 0.63, 0.31, 0.16, 0 ng/mL. Take 7 EP tubes and add 500 μL of normal reference and diluent to each tube. 10 ng/mL working solution pipette 500 μL on the first tube and blend to produce a working solution of 5 ng/mL. The pipette 500 μL of the solution in the latter according to these steps of the former pipeline. The following example is for reference purposes. Note: the last tube is empty. Don't pipe the water in the old tube.

iv) Biotinylated Detection Working solution: calculate the quantity required before the experiment (100 μL /well). In preparation, a little more than estimated should be prepared. Until use, center the stock tube, dilute 100% bis, Concentrating Detection Biotinylated Ab to 1

using Biotinylated Detection Ab Diluent Working Solution.

v) Concentrated HRP Working solution: Measure the quantity required before the experiment (100 μ L/well). In preparation, a little more than estimated should be prepared. Dilute 100, Concentrate HRP, mix with 1 concentrated HRP, and conjugate dilute working solution.

2.3.2 Procedure

- i) Prepare the sample and the reagent:
- ii) Add 100 μ L standards, blanks, and samples to specific wells;
- iii) Cover the plate by a sealer that we have supplied. Incubate for 90 minutes at 37 minutes;
- iv) Remove the liquid well, do not wash it. Immediately apply 100 μ L of biotinylated detection;
- v) Incubate at 37 °C for 1 hour, then vacuum and wash each well;
- vi) Add 100 μ L of HRP. Join the work solution for each well;
- vii) Incubate at 37 °C for 30 minutes and then repeat the washing cycle five times.
- viii) Add 90 μ L of substrate solution to each well. Incubate at 37 °C for approximately 15 minutes;
- ix) Apply 50 μ L of stop solution to each well of water and read at 450 nm within 10 minutes.

2.4. Estimation of human vitamin D

25(OH) Vitamin D concentrations in the serum were examined by using enzyme-linked. Immunosorbent assay (ELISA), according to prepare processed from CALBIOTECH, China. All reagents and specimens must be approved for use at room temperature, and both reagents must be commonly combined without spraying. All procedures should be completed immediately after the start of the process.

2.4.1 Procedure

- i) Deposit 10 μ L of 25-OH Vitamin D levels, controls, and samples in each well, if necessary.
- ii) Distribute 200 μ L of biotinylated 25(OH)D reagent solution into each well.

iii) Mix the contents carefully in the wells for 20 seconds using a 200 to 400 RPM shaker (or similar movements). Remove the shaker and cover the plate with the adhesive plate seal to ensure that each well is completely screened.

iv) Incubate the sealed plate for 90 minutes at room temperature.

v) Carefully remove the plate seal.

vi) Shake the contents of the wells quickly into a waste reservoir.

vii) Dispense 300 μ L of 1X wash buffer in each well and shake it quickly into a waste storage tank. Shake the wells on the paper towel vigorously to extract the remaining droplets. Repeat two more times in all for three washes.

viii) Dispense 200 μ L (Streptavidin-HRP) of the conjugate enzyme in each well.

ix) Incubate at room temperature for 30 minutes.

x) Shake the contents of the wells in the waste container quickly.

xi) Dispense a 300 μ L 1X wash buffer in each well and shake it quickly into a reservoir. Shake the wells on the paper towel vigorously to extract the remaining droplets. Repeat two more times in all for three washes.

xii) Use a multichannel pipette to dispense 200 μ L of TMB Substrate into each well.

xiii) Incubate at room temperature, preferably in the dark, for 30 minutes.

xiv) Dispense 50 μ L of Stop Solution in each well to stop the enzyme response. Mix the contents of the plate carefully for 20-30 seconds.

xv) Write the ELISA Reader for absorption at 450 nm within 10 minutes of the stop solution applied.

xvi) Standard Curve: Seven standard rates are included for each run.

2.5. Statistical analysis

The results were analyzed using the GraphPad Prism software, which allows non-linear regression, understandable statistics, and data organization. The data is displayed as mean \pm standard error (SE). The T-test analyzed the comparison between patients and control groups. The value of $p < 0.05$ was considered significant.

3. RESULTS AND DISCUSSION:

3.1. Hematological characteristic

The result showed a significant ($p < 0.05$) decrease in the level of Hb in patients with thalassemia compared with the control group. The Hb value in patients with thalassemia (7.458 ± 0.2406) and the Hb value in control patients (12.60 ± 0.1748) are shown in Figure 1.

The results are following the studies by Shanthi *et al.* (2013), who observed a decrease in the level of Hb due to the early and continuous degradation of red blood cells. This anomaly leads to the destruction of red blood cells before maturation. Bhuiyan *et al.* (2020) studied 40 patients, and their results showed that 97.5% had a Hb level below 10 gm/dL, and only 2.5% of the patients reached high Hb levels, allowing to conclude that it is an adequate and accurate implementation in the regimen transfusion. The correct transfusion practice can guarantee normal growth without increasing the expansion of erythropoiesis and effective iron overload prevention.

The result in Figure 2 shows the percentage of ABO types in thalassemic patients. This result demonstrates the O blood group is most in thalassemic patients (40%), but other blood groups type A, B, and AB have a percentage (23%, 28%, 10%), respectively.

In Figure 3 revealed the patients with Rh-positive more than patients with Rh-negative. This result agrees with the study of Marbut *et al.* (2018). Another study shown the blood group O+ is most blood group in thalassemic patients, also shown the people with blood group O is most chance of family history diseases (Abbas, 2013; Sinha *et al.*, 2017).

According to the above studies, which demonstrations with the ABO types have related to thalassemia disorder, because thalassemia is one of the genetic diseases, and O blood groups were related to a family history disease.

3.2. Biomarker

Figure 4 shows a significant increase ($p < 0.05$) in serum levels of ferritin in a patient with thalassemia ($2,984 \pm 321.3$) compared with a control group (97.50 ± 0.7159), this study agrees with the study of Eissa and El-Gamal (2014). The increase in the concentration of ferritin in thalassemia patients is related to frequent blood transfusions and an ineffective red blood cell production process (Pasricha *et al.*, 2013).

The early organs affected by iron overload

are the liver, leading to damage in the tissue of the liver from direct toxic of iron on liver cells. This study found the relationship between serum ferritin and liver enzymes (Suman *et al.*, 2016). In thalassemia, the patients suffer from chronic anemia. Hypoxia causes an increase in iron absorption from the gastrointestinal tract and blood transfusions. This leads to a gradual accumulation of iron due to insufficient excretory pathways, when serum transferrin exceeds saturation 70% and high of ferritin, free iron species, that plays a role in generating reactive oxygen species with ultimate damage of tissue, dysfunction of organs, and death (Rachmilewitz and Giardina, 2011).

Figure 5 shows a decrease ($p < 0.05$) in serum vitamin D levels in patients with thalassemia ($8,390 \pm 1,081$). On the other hand, control groups have $29.44 \pm 2,771$ of vitamin D. These results are in agreement with the studies by Ezzat *et al.* (2015), where they concluded that high levels of iron in the liver interrupts the production of 25-hydroxyvitamin D. Soliman *et al.* (2013) identified a decrease in vitamin D levels in children with thalassemia. This behavior may be related to low mineral absorption in the bone matrix (Shaykhbaygloo *et al.*, 2020).

The decrease in vitamin D in patients with thalassemia causes an accumulation of iron in the liver and skin. A serious achievement of this anomaly is related to the synthesis of hydroxyl, a fundamental molecule in the structure of vitamin D (Pirinçcioğlu *et al.*, 2011). Al-Shemery and Al-Dujaili, (2019), in this study, indicated a high level of Procollagen type III peptide in patients with thalassemia that showed liver damage.

Figure 6 reveals discrepancies in serum ferritin levels according to the time of blood transfusion (<1 year, 1-5 years, and > 5 years). Significant amounts are evident between transfusions in the <1 year and > 5 year period. On the other hand, the duration of 1-5 years is of little significance, which is in accordance with the study by Bhuiyan *et al.* (2020). The researchers say that high levels of iron in the blood are a direct result of blood transfusions for patients with thalassemia. High levels of iron are due to the absence of a biological mechanism capable of eliminating excess iron in the body (Pasricha *et al.*, 2013).

Figure 7 again shows the discrepancies in the serum vitamin D concentration according to the duration of the blood transfusion (<1 year, 1-5 years, and > 5 years).

3.3. Relationship between biomarkers

The results of the linear regression (Figure 8) between the concentrations of ferritin and vitamin D in patients with thalassemia revealed a non-significant negative relationship ($r = -0.09$).

Gombar *et al.* (2018) demonstrated that the increase in serum ferritin in patients with thalassemia, resulting from multiple blood transfusions, led to the accumulation of iron in the liver. Thus, low levels of vitamin D decrease the synthesis of hydroxyl and, consequently, decrease serum levels. Shaykhbaygloo *et al.* (2020) report the same trend in the behavior of patients with thalassemia in diseases of the endocrine system due to the accumulation of iron.

4. CONCLUSIONS:

In view of the results obtained in this study, we can conclude that patients with thalassemia are more susceptible to blood type O+. The increase in ferritin in the liver and skin due to the accumulation of iron has the direct effect of decreasing vitamin D levels. Another factor that induces the increase in ferritin is the frequent blood transfusions in patients with thalassemia. Thus, the research carried out shows us a significant contribution to the scientific community, leading to conclusions on the concern and care for patients with thalassemia in the search for understanding and effective treatments. The data discussed in the Results and Discussion showing the relevance of the work and how different it is from other researches. Also, point out the benefits and improvements that can be observed to develop new science standards that can change something in the related.

5. ACKNOWLEDGMENTS:

The authors offer their thanks and great appreciation to the central thalassemia for their facilities to accomplish this research.

6. REFERENCES:

1. Gregg, X; Agarwal, A; Prchal, J. T. (2019). Congenital Hemolytic Anemias. Concise Guide to Hematology. Springer: 59–66.
2. Chaudhari, C. N. (2011). Red cell alloantibodies in multiple transfused thalassaemia patients. *Medical Journal Armed Forces India*, 67(1), 34-37.
3. Be-Baun, M. R; Frei-Jones, M; Vichinsky, E. (2011). Thalassemia Syndromes. In: Kliegman, R. M; Stanton, B; St. Geme, J; Schor, N. F; Behrman R. E. eds. *Nelson Textbook of Pediatrics*. 19th ed. Philadelphia, PA: Elsevier Saunders:1674-1677.
4. Wong, P; Fuller, P. J; Gillespie, M. T; Milat, F. (2016). Bone disease in thalassemia: a molecular and clinical overview. *Endocrine Reviews*, 37(4), 320-346.
5. Galanello, R; Origa, R. (2010). Beta-thalassemia. *Orphanet Journal of Rare Diseases*, 5(1), 11.
6. Giardine, B; Borg, J; Viennas, E; Pavlidis, C; Moradkhani, K; Joly, P; Wajcman, H. (2014). Updates of the HbVar database of human hemoglobin variants and thalassemia mutations. *Nucleic Acids Research*, 42(D1), D1063-D1069.
7. Weatherall, D. (2011). The inherited disorders of haemoglobin: an increasingly neglected global health burden. *The Indian Journal of Medical Research*, 134(4), 493.
8. Miri-Moghaddam, E; Nikraves, A; Gasemzadeh, N; Badaksh, M; Rakhshi, N. (2015). Spectrum of alpha-globin gene mutations among premarital Baluch couples in southeastern Iran. *International Journal of Hematology-Oncology and Stem Cell Research*, 9(3), 138.
9. Zamani, S; Borhan Haghighi, A; Haghighanah, S; Karimi, M; Bordbar, M. R. (2017). Transcranial Doppler screening in 50 patients with sickle cell hemoglobinopathies in Iran. *Journal of Pediatric Hematology/Oncology*, 39(7), 506-512.
10. Bilgen, T; Clark, O. A; Ozturk, Z; Akif Yesilipek, M; Keser, I. (2013). Two novel mutations in the 3' untranslated region of the betaglobin gene that are associated with the mild phenotype of beta-

- thalassemia. *International Journal of Laboratory Hematology*, 35(1), 26-30.
11. Al Raeesi, S; Alhashmi, H; Al Halabi, M. (2017). Oral health of children with special health care needs (SHCN). *JSM*, 5(2), 1091.
 12. Taher, A. T; Musallam, K. M; Cappellini, M. D; Weatherall, D. J. (2011). Optimal management of β thalassaemia intermedia. *British Journal of Haematology*, 152(5), 512-523.
 13. Jha, R; Jha, S. (2014). Beta thalassemia- a review. *Journal of Pathology of Nepal*, 4(8), 663-671.
 14. Rund, D; Rachmilewitz, E. (2005). β -Thalassemia. *New England Journal of Medicine*, 353(11), 1135-1146.
 15. Leecharoenkiat, K; Lithanatudom, P; Sornjai, W.; Smith, D. R. (2016). Iron dysregulation in beta-thalassemia. *Asian Pacific Journal of Tropical Medicine*, 9(11), 1035-1043.
 16. Mathias, L. A; Fisher, T. C; Zeng, L; Meiselman, H. J; Weinberg, K. I; Hiti, A. L; Malik, P. (2000). Ineffective erythropoiesis in β -thalassemia major is due to apoptosis at the polychromatophilic normoblast stage. *Experimental Hematology*, 28(12), 1343-1353.
 17. Schrier, S. L. (2002). Pathophysiology of thalassemia. *Current Opinion in Hematology*, 9(2), 123-126.
 18. Suman, R. L; Sanadhya, A; Meena, P; Goyal, S. (2016). Correlation of liver enzymes with serum ferritin levels in β -thalassemia major. *International Journal of Research in Medical Sciences*, 4(8), 3271-3274.
 19. Aboul-Enein, A; Amal, E. B; Hamdy, M; Shaheen, I; El-Saadany, Z; Samir, A; El-Samie, H. A. (2015). Peripheral expression of hepcidin gene in Egyptian β -thalassemia major. *Gene*, 564(2), 206-209.
 20. Ezzat, H. M; Wu, J; McCartney, H; Leitch, H. A. (2015). Vitamin D Insufficiency and Liver Iron Concentration in Transfusion Dependent Hemoglobinopathies in British Columbia. *Open Journal of Hematology*, 6(1).
 21. Al-Mosawy, W. F. (2017). The Beta-thalassemia. *Scientific Journal of Medical Research*, 1(1), 24-30.
 22. Tahir, H; Shahid, S. A; Mahmood, K. T. (2011). Complications in thalassaemia patients receiving blood transfusion. *Journal of Biomedical Science and Research*, 3, 339-46.
 23. Cao, A; Galanello, R. (2010). Beta-thalassemia. *Genetics in Medicine*, 12 (2), 61-76.
 24. Old, J. M. (2003). Screening and genetic diagnosis of hemoglobin disorders. *Blood Reviews*, 17, 43-53.
 25. Borbely, N; Phelan, L; Szydlo, R; Bain, B. (2013). Capillary zone electrophoresis for haemoglobinopathy diagnosis. *Journal of Clinical Pathology*, 66(1), 29-39.
 26. Rhea, J. M; Molinaro, R. (2014). Pathology consultation on HbA1c methods and interferences. *American Journal of Clinical Pathology*, 141(1), 5-16.
 27. Sabath, D. E. (2017). Molecular diagnosis of thalassemias and hemoglobinopathies, an ACLPS critical review. *American Journal of Clinical Pathology*, 148(1), 6-15.
 28. Vrettou, C; Traeger-Synodinos, J; Tzetzis, M; Malamis, G; Kanavakis, E. (2003). Rapid screening of multiple β -globin gene mutations by real-time PCR on the LightCycler, application to carrier screening and prenatal diagnosis of thalassemia syndromes. *Clinical Chemistry*, 49(5), 769-776.
 29. Rosatelli, M. C; Saba, L. (2009). Prenatal Diagnosis of β -Thalassemias and Hemoglobinopathies. *Mediterranean Journal of Hematology And Infectious Diseases*, 1(1).
 30. Petrou, M. (2010). Screening for beta thalassaemia. *Indian Journal of Human Genetics*, 16, 1-5.

31. Rachmilewitz, E. A; Giardina, P. J. (2015). How I treat thalassemia. *Blood*, 118, 3479-3489.
32. Zafeiriou, D. I; Economou, M; Athanasiou-Metaxa, M. (2006). Neurological complications in β -thalassemia. *Brain and Development*, 28(8), 477-481.
33. Glickstein, H; El, R. B; Link, G; Breuer, W; Konijn, A. M; Hershko, C; Cabantchik, Z. I. (2006). Action of chelators in iron-loaded cardiac cells, accessibility to intracellular labile iron and functional consequences. *Blood*, 108(9), 3195-3203.
34. Prus, E; Fibach, E. (2010). Effect of iron chelators on labile iron and oxidative status of thalassaemic erythroid cells. *Acta Haematologica*, 123(1), 14-20.
35. Lawson, S. E; Roberts, I. A; Amrolia, P; Dokal, I; Szydlo, R; Darbyshire, P. J. (2003). Bone marrow transplantation for β -thalassaemia major, the UK experience in two paediatric centres. *British Journal of Haematology*, 120(2), 289-295.
36. Genovese, F; Manresa, A. A; Leeming, D. J; Karsdal, M. A; Boor, P. (2014). The extracellular matrix in the kidney, a source of novel non-invasive biomarkers of kidney fibrosis. *Fibrogenesis & Tissue Repair*, 7(1), 4.
37. Casiday, R; Frey, R. (2000). Iron use and storage in the body: ferritin and molecular representations. Department of Chemistry, Washington University, St. Louis. USA.
38. Wang, W; Knovich, M. A; Coffman, L. G; Torti, F. M; Torti, S. V. (2010). Serum ferritin: past, present and future. *Biochimica et Biophysica Acta (BBA)-General Subjects*, 1800(8), 760-769.
39. Theil, E. C. (2012). Ferritin protein nanocages—the story. *Nanotechnology Perceptions*, 8(1), 7.
40. Mancias, J. D; Pontano, V. L; Nissim, S. (2015). Ferritinophagy via NCOA4 is required for erythropoiesis and is regulated by iron dependent HERC2-mediated proteolysis. *Elife*, 4, e10308.
41. Koeppen, B. M; SB, B. R. (2010). Berne and Levy Physiology. Updated ed. Philadelphia: Mosby.
42. Avent, N. D; Reid, M. E. (2000). The Rh blood group system: a review. *Blood, The Journal of the American Society of Hematology*, 95(2), 375-387.
43. Morris, H. A. (2014). Vitamin D activities for health outcomes. *Annals of Laboratory Medicine*, 34(3), 181-186.
44. Vanlint, S. J; Morris, H. A; Newbury, J. W; Crockett, A. J. (2011). Vitamin D insufficiency in aboriginal Australians. *Women*, 100, 120.
45. Chen, J. Q; Cammarata, P. R; Baines, C. P; Yager, J. D. (2009). Regulation of mitochondrial respiratory chain biogenesis by estrogens/estrogen receptors and physiological, pathological and pharmacological implications. *Biochimica et Biophysica Acta (BBA)-Molecular Cell Research*, 1793(10), 1540-1570.
46. Man, P. W; van der Meer, I. M; Lips, P. B; Middelkoop, J. C. (2016). Vitamin D status and bone mineral density in the Chinese population: a review. *Arch Osteoporos*, 11(1), 14.
47. Weaver, C. M; Fleet, J. C. (2004). Vitamin D requirements: current and future. *The American Journal of Clinical Nutrition*, 80(6), 1735S-1739S.
48. Aloia, J. F; Talwar, S. A; Pollack, S; Feuerman, M; Yeh, J. K. (2006). Optimal vitamin D status and serum parathyroid hormone concentrations in African American women. *The American Journal of Clinical Nutrition*, 84(3), 602-609.
49. Boyle, W. J; Simonet, W. S; Lacey, D. L. (2003). Osteoclast differentiation and activation. *Nature*, 423(6937), 337-342.
50. Janssen, H. C; Samson, M. M; Verhaar, H. J. (2002). Vitamin D deficiency, muscle function, and falls in elderly people. *The American Journal of Clinical Nutrition*, 75(4):611-615.

51. Holick, M. F. (2009). Vitamin D status: measurement, interpretation, and clinical application. *Annals of Epidemiology*, 19(2), 73-78.
52. Holick, M. F. (2004). Sunlight and vitamin D for bone health and prevention of autoimmune diseases, cancers, and cardiovascular disease. *The American Journal of Clinical Nutrition*, 80(6), 1678S-1688S.
53. Wasmuth A. K. (2010). Evaluation of the Mythic 18, hematology analyzer for its use in dogs, cats and horses. Inaugural-Dissertation. Faculty of Veterinary Medicine, University of Zurich.
54. Shanthi, G; Balasubramanyam, D; Srinivasan R. (2013). Studies on the Haematological Aspects of Beta β -Thalassemia in Tamilnadu. *Research Journal of Pharmaceutical, Biological and Chemical Sciences*, 4(3), 784-790.
55. Bhuiyan, M. N; Giti, S; Akhter, M; Naznin, L; Urmi, S. F. H; Hasan, R. (2020). Haematological and Biochemical status of Adolescent and Young Adults with Transfusion dependent thalassaemia—A study of 40 cases. *Bioresearch Communications-(BRC)*, 6(1), 782-790.
56. Marbut, S. M. M; Hamdi, M. A; Jumaa, A. M; Salman, B. A. (2018). Distribution of ABO blood groups in beta thalassemia patients dependent on blood transfusion In Bagdad city. *Journal of Madenat Alelem College*, 10(2), 1-11.
57. Abbas, A. M. (2013). Iron overload in thalassemia and its effect on gonads. M. Sc Thesis submitted to College of Medicine, Tikrit University.
58. Sinha, P. A; Mulkutkar, S. H; Bhavani, J. B. (2017). Study of distribution of ABO blood groups in β -thalassemia patients. *International Journal of Research in Medical Sciences*, 5(8), 3479-3483.
59. Eissa, D. S; El-Gamal, R. A. (2014). Iron overload in transfusiondependent β -thalassemia patients, defining parameters of comorbidities. *The Egyptian Journal of Haematology*, 39(3),164-70.
60. Pasricha, S. R; Frazer, D. M; Bowden, D. K. (2013). Transfusion suppresses erythropoiesis and increases hepcidin in adult patients with beta-thalassemia major, A longitudinal study. *Blood*, 122,124–133.
61. Rachmilewitz, E. A; Giardina, P. J. (2011). How I treat thalassemia. *Blood*, 118(13), 3479–3488.
62. Ezzat, H. M; Wu, J; McCartney, H; Leitch, H. A. (2015). Vitamin D Insufficiency and Liver Iron Concentration in Transfusion Dependent Hemoglobinopathies in British Columbia. *Open Journal of Hematology*, 6(1).
63. Soliman, A; De Sanctis, V; Yassin, M. (2013). Vitamin D status in thalassemia major: an update. *Mediterranean Journal of Hematology and Infectious Diseases*, 5(1).
64. Shaykhbaygloo, R; Moradabadi, A; Taherahmadi, H; Rafiei, M; Lotfi, F; Eghbali, A. (2020). Correlation of Cardiac and Liver Iron Level with T2* MRI and Vitamin D3 Serum Level in Patients with Thalassemia Major. *Journal of Blood Medicine*, 11, 83.
65. Piriñçioğlu, A. G; Akpolat, V; Köksal, O; Haspolat, K.; Söker, M. (2011). Bone mineral density in children with beta-thalassemia major in Diyarbakir. *Bone*, 49(4), 819-823.
66. Al-Shemery, M. K; Al-Dujaili, A. N. (2019). Estimation of Procollagen Type III Peptide (PIIIP) Level in β -Thalassemia Patients. *Indian Journal of Public Health Research & Development*, 10(7), 636-642.
67. Gombar, S; Parihar, K; Choudhary, M. (2018). Comparative study of serum ferritin and vitamin D in thalassemia patients with healthy controls. *International Journal of Research in Medical Sciences*, 6(2),693.

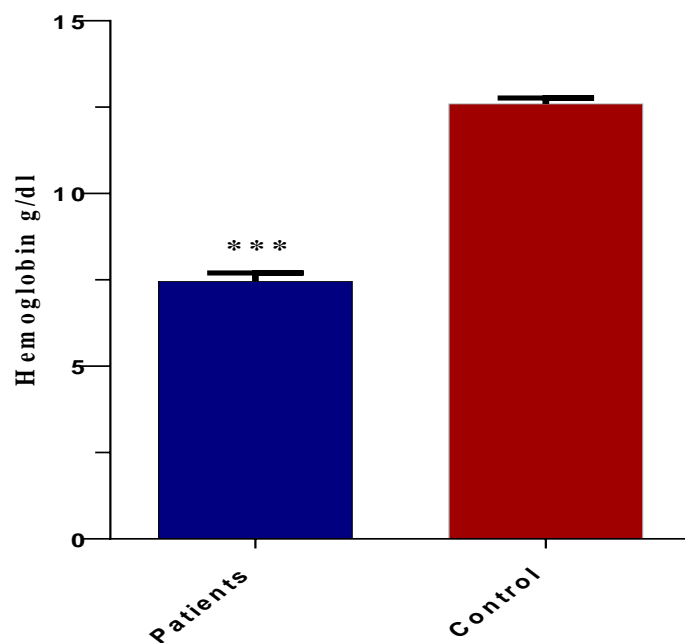


Figure 1. Level of hemoglobin in thalassemic patients and control group.

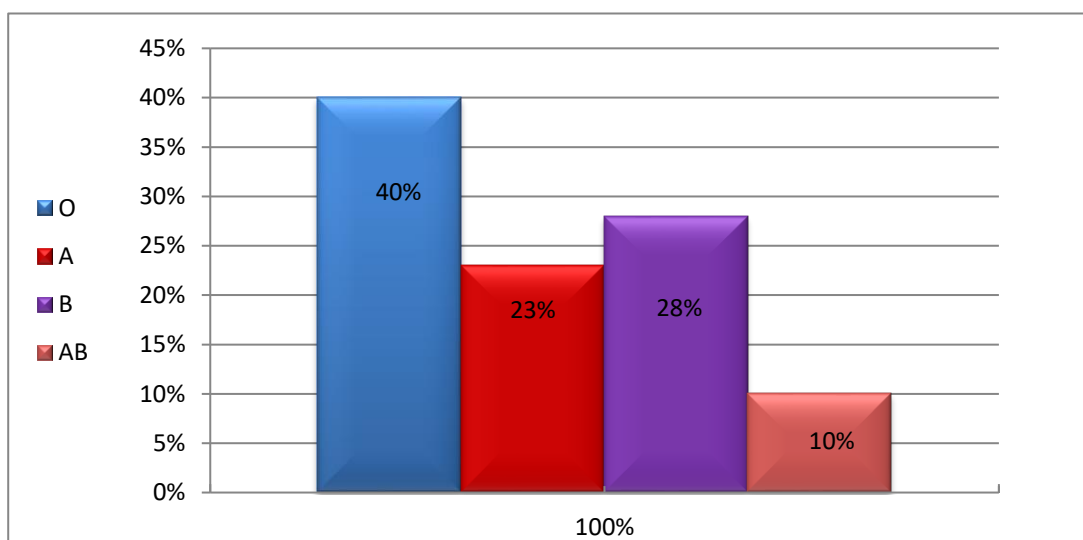


Figure 2. Percentage of ABO Types in patients with thalassemia.

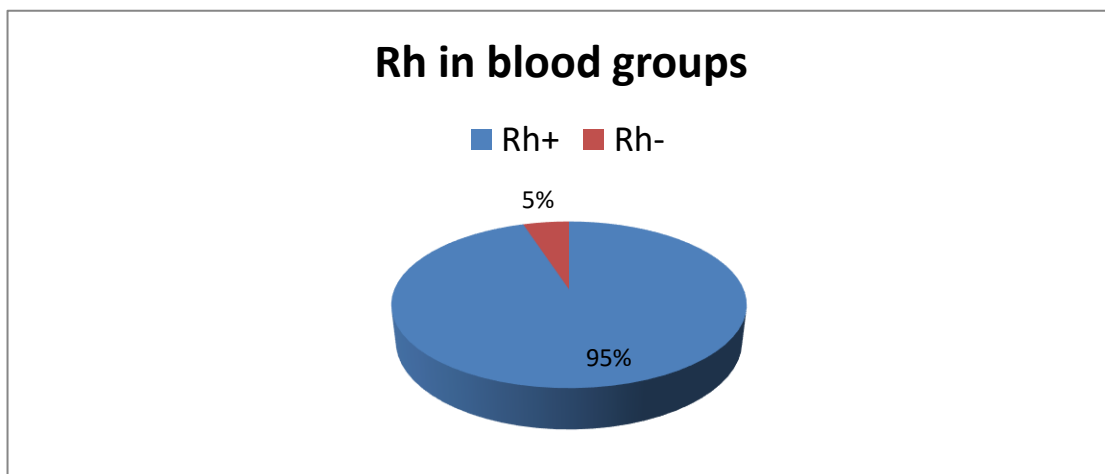


Figure 3. Percentage of Rh of ABO types in patients with thalassemia.

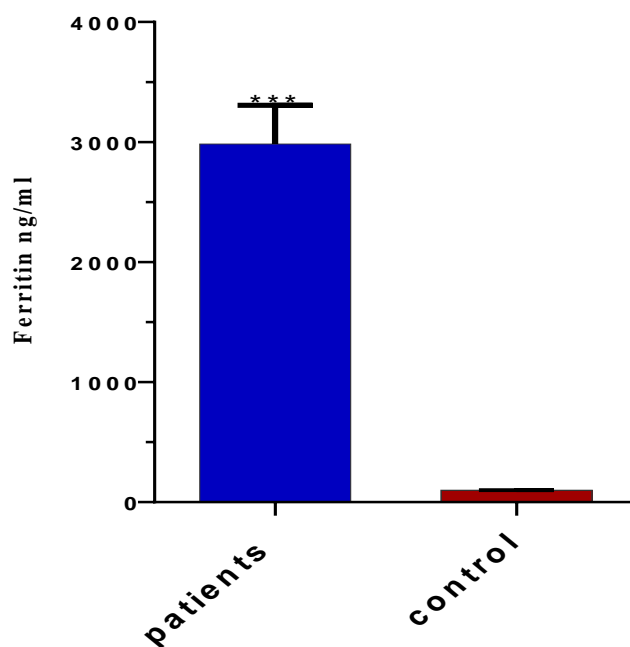


Figure 4. Concentration of the ferritin in the thalassemic and control group.

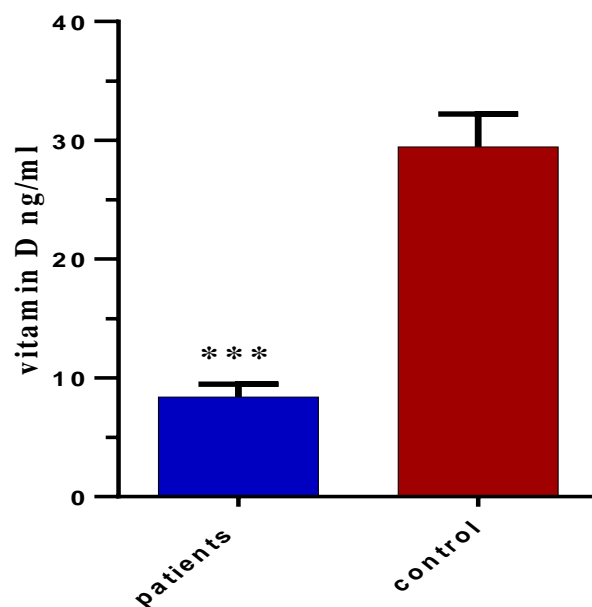


Figure 5. Concentration of the vitamin D in the thalassemic patients and control group.

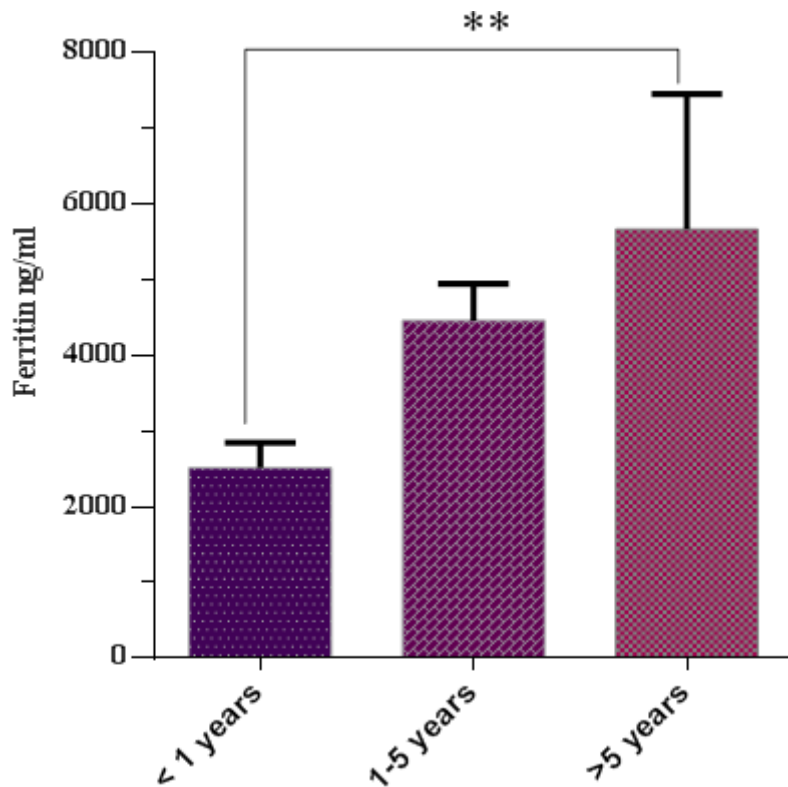


Figure 6. Concentration of ferritin according to the duration of blood transfusion in thalassemic patients.

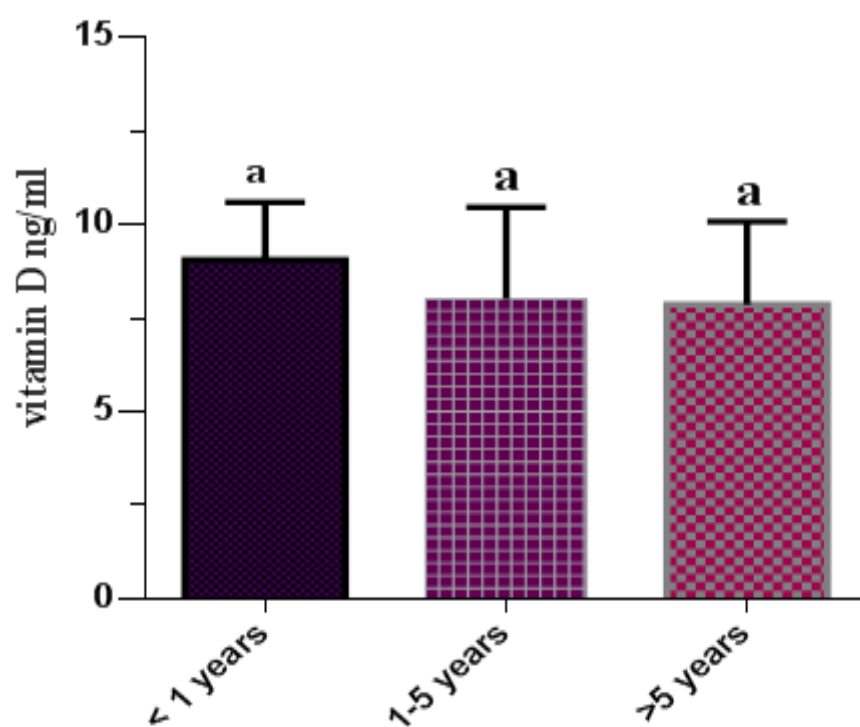


Figure 7. Concentration of vitamin D according to the duration of blood transfusion in patients with thalassemia.

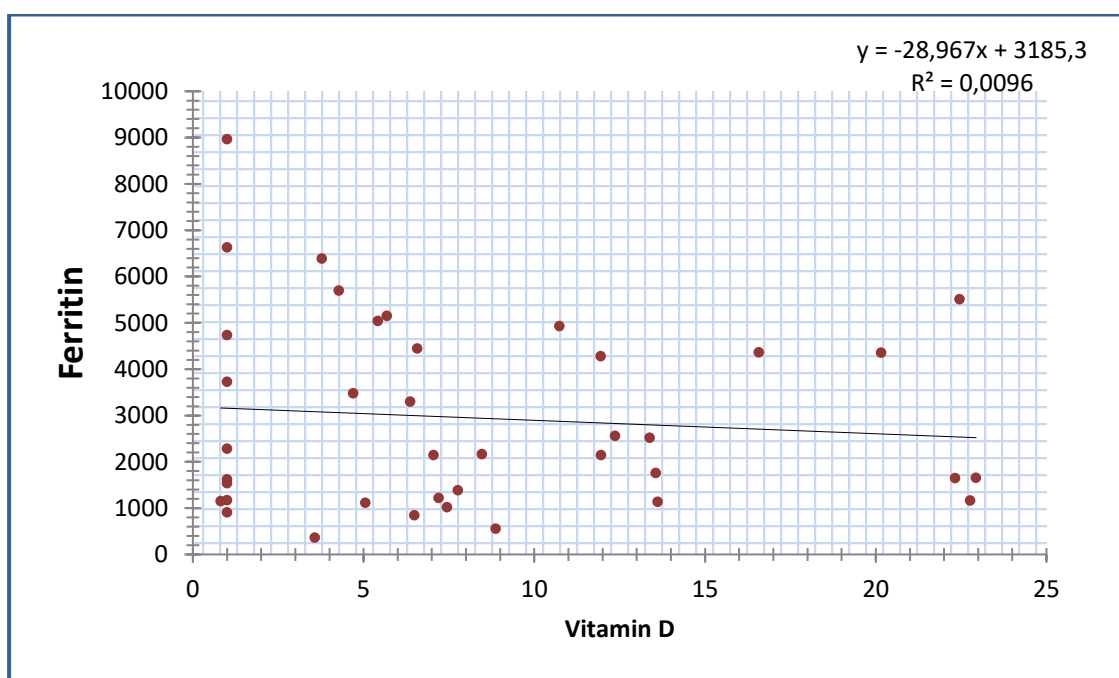


Figure 8. Relationship between ferritin and vitamin D.

A UTILIZAÇÃO DE SIMULADORES DE FINS ESPECIAIS COMO UMA FERRAMENTA DE TREINAMENTO PROFISSIONAL AVANÇADO SOB CONDIÇÕES DE E-LEARNING

THE USE OF SPECIAL-PURPOSE SIMULATORS AS AN ADVANCED PROFESSIONAL TRAINING TOOL UNDER E-LEARNING CONDITIONS

LA UTILIZACIÓN DE SIMULADORES PARA FINES ESPECIALES COMO INSTRUMENTO DE CAPACITACIÓN PROFESIONAL AVANZADA EN CONDICIONES DE ENSEÑANZA A DISTANCIA

MARTINEZ, Fredy^{1*}; MARTINEZ, Fernando¹; MONTIEL, Holman¹;

¹ Universidad Distrital Francisco José de Caldas, Facultad Tecnológica, Bogotá DC. Colombia.

* Corresponding author

e-mail: fhmartinezs@udistrital.edu.co

Received 14 August 2020; received in revised form 16 October 2020; accepted 27 October 2020

RESUMO

Tradicionalmente, a eletrônica de potência tem sido um campo de treinamento complexo para alunos de graduação na área elétrica da Universidade Distrital Francisco José de Caldas. Neste curso, múltiplas teorias e conceitos são difíceis de assimilar devido ao distanciamento de outros cursos do programa e à complexidade de conceituar elementos abstratos. Uma ferramenta fundamental de aprendizagem corresponde às práticas laboratoriais, que permitem visualizar conceitos, facilitando a sua compreensão e assimilação. No entanto, as restrições de mobilidade impostas em nível global têm impedido o acesso a esses espaços de aprendizagem, restringindo elementos fundamentais do processo, como a interação direta com circuitos e equipamentos de força e a socialização crítica entre os alunos. A eficácia do processo de aprendizagem está ligada aos recursos disponíveis, hoje esses recursos foram reduzidos em decorrência do isolamento social que se espera que continue nos próximos meses. Para reduzir este impacto, foi iniciado o desenvolvimento de uma ferramenta informática, capaz de substituir o trabalho dos alunos em laboratório em termos de interação direta com os circuitos, análise de comportamento e desenho de aplicações. A ferramenta é um simulador de circuitos especificamente orientado para a área da eletrônica de potência, pelo que é preferível para treino específico em comparação com os simuladores tradicionais, uma vez que permite simplificar o comportamento dos elementos ao nível do switch, eliminando a sua análise parasitária, e portanto reduzindo as demandas de capacidade de processamento, memória de armazenamento e tempo de simulação. O primeiro circuito implementado corresponde a um corretor de fator de potência ativo em um conversor do tipo *Boost*, aplicação que por si só justifica o uso da ferramenta. Como resultados preliminares, os educadores observaram um maior comprometimento e motivação dos alunos em seu trabalho autônomo.

Palavras-chave: *Simulador de circuitos, COVID-19, eletrônica de potência, corretor de fator de potência.*

ABSTRACT

Traditionally, power electronics has been a complex training field for undergraduate students in the electrical area of the Universidad Distrital Francisco José de Caldas. In this course, multiple theories and concepts are difficult to assimilate due to the distance from other program courses and the complexity of conceptualizing abstract elements. A fundamental learning tool corresponds to the laboratory practices, which allow visualizing concepts, facilitating their understanding and assimilation. However, the mobility restrictions imposed at a global level have prevented access to these learning spaces, restricting fundamental elements of the process, such as direct interaction with circuits and power equipment and critical socialization among students. The effectiveness of the learning process is linked to the resources available, today these resources have been reduced as a result of the social isolation that is expected to continue in the coming months. To reduce this impact, the development of a computer tool has been initiated, capable of replacing the work of students in the laboratory in terms of direct interaction with the circuits, analysis of behavior, and design of applications. The tool is a circuit simulator specifically oriented to the area of power electronics, which is why it is preferable for specific training compared to traditional simulators, since it allows simplifying the behavior of the elements at the switch level, eliminating their parasitic analysis, and therefore reducing the demands on processing capacity, storage memory and simulation time. The first circuit implemented corresponds to an active power factor corrector on a *Boost* type

converter, an application that in itself justifies the use of the tool. As preliminary results, educators have observed increased commitment and motivation of students in their autonomous work.

Keywords: *Circuit simulator, power electronics, power factor corrector.*

RESUMEN

Tradicionalmente, la electrónica de potencia ha sido un campo de entrenamiento complejo para los estudiantes de pregrado del área eléctrica de la Universidad Distrital Francisco José de Caldas. En este curso se aplican múltiples teorías y conceptos que son difíciles de asimilar debido a la distancia que existe con otros cursos del programa y a la complejidad de conceptualizar elementos abstractos. Una herramienta fundamental de aprendizaje es la práctica de laboratorio, que permite visualizar los conceptos, facilitando su comprensión y asimilación. Sin embargo, las restricciones de movilidad impuestas a nivel mundial han impedido el acceso a estos espacios de aprendizaje, restringiendo también elementos fundamentales del proceso como la interacción directa con los circuitos y equipos de potencia, y la socialización crítica entre los estudiantes. La eficacia del proceso de aprendizaje está vinculada a los recursos disponibles, que hoy en día se han reducido como resultado del aislamiento social que se prevé que continúe en los próximos meses. Para reducir este impacto, se ha iniciado el desarrollo de una herramienta informática capaz de sustituir el trabajo de los estudiantes en el laboratorio en cuanto a la interacción directa con los circuitos, el análisis del comportamiento y el diseño de aplicaciones. La herramienta es un simulador de circuitos orientado específicamente al área de la electrónica de potencia, por lo que es preferible para la formación específica en comparación con los simuladores tradicionales, ya que permite simplificar el comportamiento de los elementos a nivel de conmutador, eliminando su análisis parásito, y por lo tanto reduciendo las exigencias en cuanto a capacidad de procesamiento, memoria de almacenamiento y tiempo de simulación. El primer circuito implementado corresponde a un corrector del factor de potencia activo en un convertidor de tipo Boost, aplicación que por sí misma justifica el uso de la herramienta. Como resultados preliminares, los educadores han observado un aumento del compromiso y la motivación de los estudiantes en su trabajo autónomo.

Palabras clave: *Simulador de circuitos, electrónica de potencia, corrector del factor de potencia.*

1. INTRODUCTION:

As a consequence of COVID-19, governments in most countries have been quick to impose norms of social isolation and restrictions on activities involving groupings and meetings, which has directly impacted the dynamics of educational institutions, particularly those of higher education, with young people of working age and with emotional ties strongly linked to social interaction (Favale, Soro, Trevisan, Drago, and Mellia, 2020; Garcia, Corell, Abella, and Grande, 2020; Winarso, Yuliana, Muniroh, Halin, and Tyas, 2020). In Colombia, this occurs when higher education is making a strong commitment to technical and technological training as an alternative to traditional engineering training (Ospina and Galvis, 2017). This commitment has materialized in a staged training called propaedeutic cycles. In its basic design, the propaedeutic cycles are made up of three stages, a first technical stage, a second technological stage, and a final engineering stage. The first stages make a strong emphasis on the training for the work looking for fast labor bonding through specific professional qualifications in each cycle (Cuadros, Cáceres, and Lucena, 2018; Garzón, Silvera, and Garcés, 2018).

Colombian universities have had to implement very short time distance learning strategies that guarantee access to students while complying with national standards of isolation and guaranteeing the quality of their training processes (Bezerra, 2020). E-learning has become a generalized strategy that has helped in a short time to make the transition to a new training model that has resulted in greater interaction with concepts, more student dedication, a higher level of commitment, and better assimilation (Mystakidis, Berki, and Valtanen, 2019). However, it is also true that it has produced deficiencies at an emotional level in terms of social interaction between individuals and has neglected the practical aspects of laboratory and on-site training that are fundamental to technical and technological training courses (Baki, Birgoren, and Aktepe, 2018; You and Robert, 2018; Yue *et al.*, 2019). From these weaknesses of the new model arises the need for rapid update and improvement that allows the level of interaction of laboratories while strengthening the positive elements of E-learning and observing the rules of social isolation (Flor, Belmonte, and Fabregat, 2018; Lin, Wang, Wu, and Chen, 2019). Under this perspective, the research group has initiated specific application simulators as fundamental learning software tools in this new training scheme.

To develop the professional skills of the technologists, the traditional face-to-face scheme made a strong effort to have students interact directly with real-world situations involving the course concepts (Chorazy and Klinedinst, 2019). In the specific case of students in the Electrical Technology program, access was offered to specialized laboratories for electrical circuits, electronics, electrical machines, electronic instrumentation, electric drives, lighting, and electrical insulation. In these academic spaces, students developed practical work designed to put into practice theoretical concepts of design and manipulation, directly observing the effect of their actions in a controlled and safe environment (Mansor *et al.*, 2018; Oliveira, DAmore, Pinto, Urbina, and Souza, 2019). These conditions can hardly be replicated through audiovisual content on a screen. However, a specific design simulator can replicate many of the laboratory experiences under the current social restrictions. Furthermore, in the hands of the students, it can even increase their interaction and motivation.

When integrated into the learning process, these new software tools complement and enrich it, which occurs even under normal face-to-face operating conditions (Sanchez and Rios, 2015). The integration of digital environments in the learning and education processes has demonstrated strengths in comparison with the traditional scheme, particularly in what is related to encouraging self-critical thinking in the students' formation process, the creation of self-regulating structures, and the increase in motivational levels (Schwendimann, Kappeler, Mauroux, and Gurtner, 2018). Also, although the traditional social interaction between students is reduced, the truth is that another type of interaction is stimulated that is more focused on the process both between students and between students and educators (Alonso, Prieto, García, and Corchado, 2019; Sergeeva *et al.*, 2019).

The area of electrical energy is a discipline that cuts across all commercial enterprises and is a strong indicator of a society's level of industrial development. It is not the engineering field that most attracts young students, but it is one of the most complex in terms of concepts and content. On the other hand, the strong relationship between electrical engineering and computer science is becoming increasingly evident (Martínez, Marínez, and Jacinto, 2019; Wu, 2018), making it more dependent on computational tools for the design and operation of energy transformation systems and the provision of energy services within a circular economic system fed by

information (Martínez, Rendon, and Guevara, 2017). Therefore, the training process of future professionals must also be concerned with the development of computer skills and stress, particularly important if these stresses help to visualize concepts to facilitate learning (Jesiek and Jamieson, 2017).

The use of specialized software as a support tool in the training process of various disciplines has been widely documented by researchers in various disciplines 2018; (Stacey, Cheeseman, Glen, Moore, and Thomas, Suárez *et al.*, 2019). In the electrical area, it has a strong incidence, given the characteristic of electrical energy teaching. As such, concepts are difficult to visualize; asking a student to imagine an electron moving inside a conductor is a great act of faith that does not exist in other disciplines such as civil engineering or mechanical engineering. This is of great relevance since the importance of the principle of visualization in the learning process has been demonstrated (Chatzimpampas *et al.*, 2020; Roberts, Ritsos, Jackson, and Headleand, 2018; Wang, Yuan, Kirschner, Kushniruk, and Peng, 2018). Consistent with this principle, the interactive visualization of signals in an electrical circuit facilitates understanding concepts and the development of tasks. The ability to visually represent behaviors is key to developing analysis and design skills and encourages students' critical and imaginative thinking. Therefore, the objective of this study was the development of a simulator for the power electronics area that helps to consolidate the concepts as well as to strengthen the students' critical thinking, the formation of self-regulatory structures in the training process, and increase their motivation levels.

2. MATERIALS AND METHODS:

2.1 Research Design

The research design that formulated the simulator profile was supported by a qualitative analysis developed with fourth and fifth-semester students of the Technology in Electricity program under face-to-face classroom conditions at the Universidad Distrital's Faculty of Technology. At first, the simulator was projected as a tool to support traditional training, so that the process shortcomings were investigated. Surveys were applied to the students to identify weaknesses in power electronics concepts at the end of the course according to the training criteria defined and validated by the research group. The instrument consists of 20 elements designed

around the following questions:

- Did the student understand the overall picture of the course?
- What did the student learn?
- What aspects are still unclear to the student?
- What developmental problems does the student identify within the course?

From the analysis of the data, three problem topics were identified, organized by priority:

- Active power factor correction.
- Vector control of electrical machines.
- Average modeling of switched circuits.

Although the first two topics are developed with the support of the laboratories, it was observed that it is difficult for the students to understand the functional and theoretical details. Insufficient time was also identified in the student's dedication to the course outside the classroom. Therefore, it was outlined the design of a set of support tools capable of promoting self-training and critical processes focused initially on these topics, which also stimulate the student, and make the learning process more meaningful.

2.2 Tool Development

Based on the design profile defined from the analysis of the survey results, a methodological design was established that contemplated as a first step the definition of the competencies to be developed in the students. The curricular design of each one of the courses of the Electrical Technology program (as well as the other academic courses of the university) starts from the definition of the work competences to be developed in the student, and the necessary academic credits as a measure of dedication. Consequently, the first step corresponded to the definition of the levels of achievement expected in each competence. Later this definition was used to evaluate the performance of the tool. For the development of this definition, an environment was established for the implementation of different integrated tasks oriented to the practical application of these competencies in the specific field of action.

The first of the simulators were developed in the power electronics course, specifically in active power factor correction through a resistive emulator circuit. This problem was chosen as an initial prototype due to the theoretical complexity involved in the analysis and understanding of the

concept and the historical difficulty of the students during its development in the classroom, fact that was identified in the previous research. A particular feature of the concepts involved in this topic is the use of average models to analyze the behavior of non-linear circuits switching at high frequency (much higher than the frequency of the power grid). This strategy facilitates the analysis and development of the simulator. Each circuit setting is presented visually and interactively using waves of behavior concerning time to prioritize the stationary behavior of the circuit.

This methodological strategy aims to achieve cognitive activity through interactive visual stimulation about the operational parameters of the circuit. This strategy also focuses on the average behavior of the circuit, a key element in the design of DC/DC converters and many other inverter and rectifier circuits. The simulator algorithm was implemented in MathWorks' MatLab (MATrix LABoratory). The tool has a GUI (Graphical User Interface) developed for parameter capture and signal presentation (Figure 1). The entire application was compiled into binaries for both Windows and Linux operating systems. The circuit design corresponds to a single-phase medium-power converter; these design parameters are fixed as an analysis reference. This GUI is made up of several windows that allow to obtain usage information, configure the simulation parameters, and observe the detail of the circuit's behavior.



Figure 1. The initial window of the Boost Simulator

The simulator structure is based on three basic topology configurations, which characterize the operation of the circuit (Figure 2). These configurations are continuous or discontinuous conduction mode (CCM/DCM), activation or not the active power factor correction algorithm, and detailed display of switching diode and output

capacitor current curves. These three options can be combined to choose different circuit behavior and diversify current and voltage curves. For example, a single-phase rectifier without output factor correction but with a large inductive input filter (passive filtering), or a circuit with power factor correction in discontinuous mode, all for the same input and output load conditions, can be obtained as an alternative to the classic power factor correction.

3. RESULTS AND DISCUSSION:

The main window of the simulator presents most of the fields for parameter configuration and display of behavior curves (Figure 3). On the upper left side is the simplified schematic of the Boost converter, power topology used in the simulator. It is a DC/DC booster converter fed directly from the public single-phase grid through a full bridge rectifier. The Boost converter has a choke L for energy storage during switching, a controlled switch Q , and an uncontrolled switch D . The output is filtered with a capacitor. The load is resistive, and the control unit is responsible for keeping a constant output power of 250 W. The choke inductance can be adjusted with the slide control at the top of the circuit, allowing CCM and DCM.

In the upper-right part, the input signals for the selected simulation condition are displayed (input current in blue and mains voltage in red, Figure 4). Even without activating the power factor correction, it is possible to observe the behavior of the input current against variations in the inductance of the choke (Figure 5). The calculated values for each condition are shown in the GUI table at the bottom right of the window. This table is updated interactively for the new operating conditions of the circuit.

In the lower-left part of the window, it is possible to see the curves of the average behavior of the converter (Figure 6). These curves are activated by selecting the average current option at the bottom right of the window, to the right of the value table. The detail of the Q transistor duty cycle is shown in red, and the average value of the input current in the choke is shown in blue.

This option must be selected in the lower right part of the window to activate the active input current correction (the power factor correction) (Figure 7). When doing so, the input current curve automatically changes to a sinusoidal behavior. However, the behavior of this current signal depends on the inductance values in the choke and the output power of the converter (which is

kept constant by the control unit). Since both the input current and voltage behave more or less sinusoidally and in phase, this control circuit is a resistive emulator, even though what is connected to the single-phase network is not a resistor (in fact, it is a non-linear circuit). By moving the selection pointer over the input current curve, it is possible to change the point for which the useful cycle detail and the average current of the circuit are displayed (Figures 8 and 9).

Finally, the last two options at the bottom right of the window allow new windows to be opened with specific details of the current at the D diode and C capacitor (Figure 10), as well as the ripple in the output voltage (Figure 11). These parameters help evaluate the quality and performance of each converter configuration. The simulator allows us to quickly compare the behavior of all the curves of the regulator for CCM and DCM operations (Figure 12).

The development of the required skill in the design of these circuits and their integration to the concepts of the power electronics course, requires coordination and development of different specific training strategies. This simulator becomes a key tool since it is conceived from the training needs of the students, and it is designed, taking into account the objectives of the process and with the functional restrictions of the moment. Similar tools can close the gap not only of access to knowledge but also to specialized training laboratories.

4. CONCLUSIONS:

This technical note presents a software tool developed as a complement to professional training at the level of technologies in the area of power electronics in an undergraduate course in electrical engineering. The initial objective of the study was to develop a tool that would function as a temporary substitute for the course laboratories during the mandatory confinement due to the COVID-19 virus. This tool is a simulator of specific use related to the active correction of the power factor in a voltage regulator circuit. In addition to replacing the practical laboratories, it was intended to exploit the possible interactivity of the platform through visual stimulation, increase students' critical thinking, encourage self-training as well as motivational levels. This strategy has proven successful in previous cases and is expected to contribute to a deeper understanding of concepts and behaviors. Besides, it has been observed that this type of learning tool encourages self-study and motivation of the student and

promotes self-regulation (the student learns to control the duration, time, and place of his academic activities autonomously). To stimulate the use of computer tools familiar to the student and facilitate the implementation of algorithms, we implemented the simulator in MatLab, creating platform-independent executable binaries to facilitate their distribution. This research supports the demand for specialized tools in professional training in electrical engineering and raises the need for a study focused on evaluating the real effects of these tools on the training process and the effects on students.

5. ACKNOWLEDGMENTS:

This work was supported by the Universidad Distrital Francisco José de Caldas, partly through CIDC, and partly by the Facultad Tecnológica. Universidad Distrital does not necessarily endorse the views expressed in this technical note. The authors thank the research group ARMOS for supporting the development of the code.

6. REFERENCES:

1. Alonso, R., Prieto, J., García, O., and Corchado, J. (2019). Collaborative learning via social computing. *Frontiers of Information Technology and Electronic Engineering*, 20(2), 265-282.
2. Baki, R., Birgoren, B., and Aktepe, A. (2018). A meta analysis of factors affecting perceived usefulness and perceived ease of use in the adoption of e-learning systems. *Turkish Online Journal of Distance Education*, 19(4), 4-42.
3. Bezerra, I. (2020). State of the art of nursing education and the challenges to use remote technologies in the time of corona virus pandemic. *Journal of Human Growth and Development*, 30(1), 141-147.
4. Chatzimpampas, A., Martins, R., Jusufi, I., Kucher, K., Rossi, F., and Kerren, A. (2020). The state of the art in enhancing trust in machine learning models with the use of visualizations. *Computer Graphics Forum*, 39(3), 713-756.
5. Chorazy, M., and Klinedinst, K. (2019). Learn by doing: A model for incorporating high-impact experiential learning into an undergraduate public health curriculum. *Frontiers in Public Health*, 7(FEB).
6. Cuadros, M., Cáceres, M., and Lucena, F. (2018). Analysis of leadership styles developed by teachers and administrators in technical-technological programs: the case of the Cooperative University of Colombia. *International Journal of Leadership in Education*, 21(1), 1-16.
7. Favale, T., Soro, F., Trevisan, M., Drago, I., and Mellia, M. (2020). Campus traffic and e-learning during COVID-19 pandemic. *Computer Networks*, 176(1), 107290.
8. Flor, S., Belmonte, A., and Fabregat, A. (2018). Improving students' engagement and performance through new e-learning tools in laboratory subjects in mechanical engineering. *International Journal of Engineering Education*, 34(4), 1273-1284.
9. Garcia, F., Corell, A., Abella, V., and Grande, M. (2020). Online assessment in higher education in the time of covid-19. *Education in the Knowledge Society*, 21(1), 12.
10. Garzón, C., Silvera, A., and Garcés, L. (2018). The institutional accreditation. a step towards quality in technical and technological institutions in Colombia. *Espacios*, 39(51), 1-11.
11. Jesiek, B., and Jamieson, L. (2017). The expansive (dis)integration of electrical engineering education. *IEEE Access*, 5, 4561-4573.
12. Lin, Y., Wang, S., Wu, Q., and Chen, L. (2019). Key technologies and solutions of remote distributed virtual laboratory for e-learning and e-education. *Mobile Networks and Applications*, 24(1), 18-24.
13. Mansor, W., Sheikh, B., Taib, M., Mohamad, N., Abdul, M., and Mahmud, A. (2018). Effective sampling-based assessment method for evaluating electrical engineering programme performance. *Indonesian Journal of Electrical Engineering and Computer Science*, 9(2), 417-423.
14. Martínez, F., Marínez, F., and Jacinto, E. (2019). Strategy for the selection of reactive power in an industrial installation using k-means clustering. *Communications in Computer and Information Science*, 1(1071), 146-153.
15. Martinez, F., Rendon, A., and Guevara, P. (2017). A framework for knowledge creation based on m2m systems for the creation of flexible training environments for specific concepts in control. *Advances in Smart Systems Research*, 6(1), 36-43.
16. Mystakidis, S., Berki, E., and Valtanen, J. (2019). The patras blended strategy model for deep and meaningful learning in quality

- life-long distance education. *Electronic Journal of e-Learning*, 17(2), 66-78.
17. Oliveira, N., DAmore, R., Pinto, T., Urbina, L., and Souza, W. (2019). Interdisciplinary learning: An electronic and computer engineering case study to solve environmental problems. *International Journal of Engineering Education*, 35(4), 1206-1214.
 18. Ospina, Y., and Galvis, J. (2017). A novel design of an e-learning digital ecosystem. *Tekhnê*, 14(1), 55-60.
 19. Roberts, J., Ritsos, P., Jackson, J., and Headleand, C. (2018). The explanatory visualization framework: An active learning framework for teaching creative computing using explanatory visualizations. *IEEE Transactions on Visualization and Computer Graphics*, 24(1), 791-801.
 20. Sanchez, A., and Rios, J. (2015). Educational software for teaching of colors used in children under the age of five years. *Tekhnê*, 12(2), 65-74.
 21. Schwendimann, B., Kappeler, G., Mauroux, L., and Gurtner, J. (2018). What makes an online learning journal powerful for vet? distinguishing productive usage patterns and effective learning strategies. *Empirical Research in Vocational Education and Training*, 10(1).
 22. Sergeeva, M., Skvortsov, V., Sokolova, A., Rachek, S., Poyarkov, N., Konysheva, E., *et al.* (2019). Planning individual educational trajectory in continuing education. *International Journal of Recent Technology and Engineering*, 8(3), 654-658.
 23. Stacey, A., Cheeseman, E., Glen, K., Moore, R., and Thomas, R. (2018). Experimentally integrated dynamic modelling for intuitive optimisation of cell based processes and manufacture. *Biochemical Engineering Journal*, 132, 130-138.
 24. Suárez, M., Espina, R., Pacheco, V., Manso, A., Blanco, E., and Álvarez, E. (2019). A review of software tools to study the energetic potential of tidal currents. *Energies*, 12(9).
 25. Wang, M., Yuan, B., Kirschner, P., Kushniruk, A., and Peng, J. (2018). Reflective learning with complex problems in a visualization-based learning environment with expert support. *Computers in Human Behavior*, 87, 406-415.
 26. Winarso, W., Yuliana, Y., Muniroh, L., Halin, H., and Tyas, D. (2020). Changes in learning patterns during the pandemic covid-19; the case at university x in bekasi, west java, indonesia. *International Journal of Advanced Science and Technology*, 29(6), 8535-8539.
 27. Wu, T. (2018). Exploration and practice of talent training mode of mechanical and electrical specialty under the background of engineering education. *IPPTA: Quarterly Journal of Indian Pulp and Paper Technical Association*, 30(4), 444-450.
 28. You, S., and Robert, L. (2018). Emotional attachment, performance, and viability in teams collaborating with embodied physical action (epa) robots. *Journal of the Association for Information Systems*, 19(5), 377-407.
 29. Yue, J., Tian, F., Chao, K., Shah, N., Li, L., Chen, Y., *et al.* (2019). Recognizing multidimensional engagement of e-learners based on multi-channel data in e-learning environment. *IEEE Access*, 7, 149554-149567.

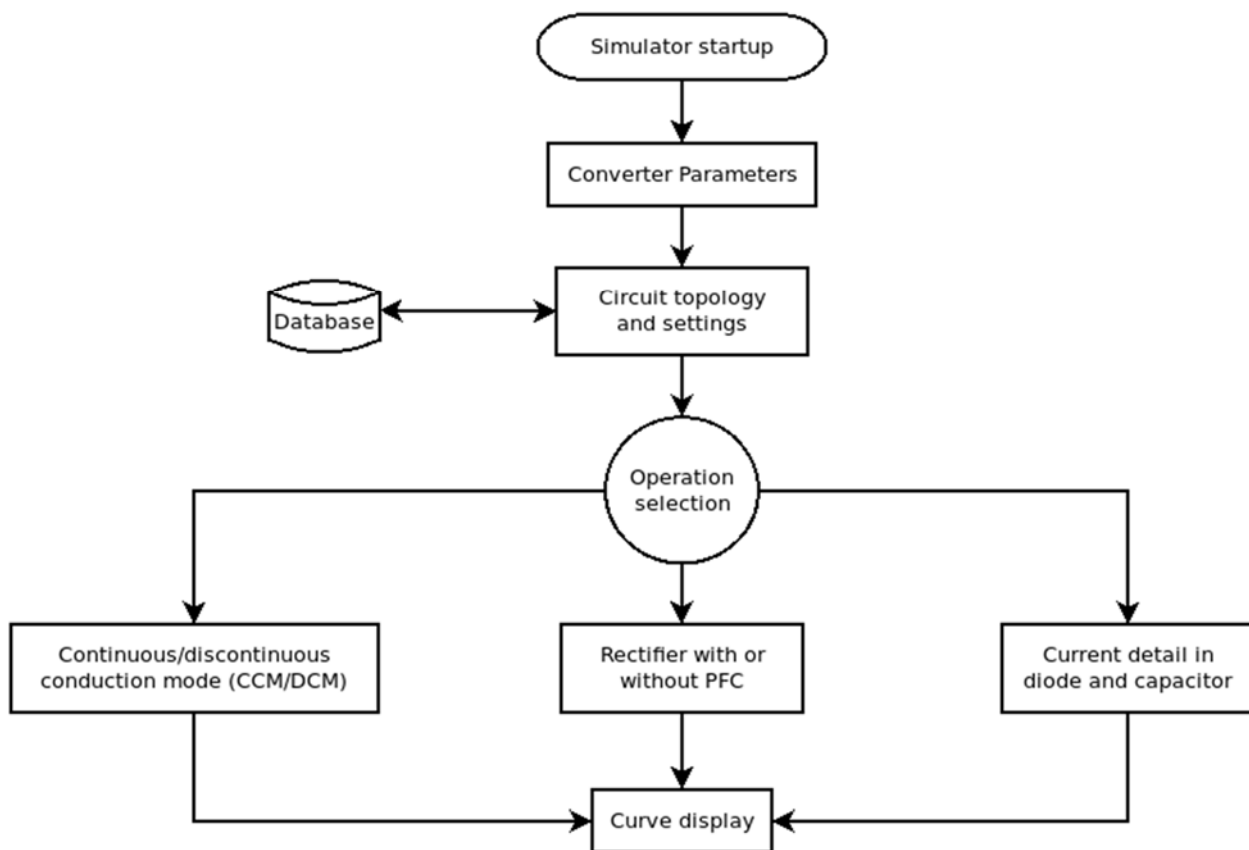


Figure 2. Simulator architecture. Source: the author

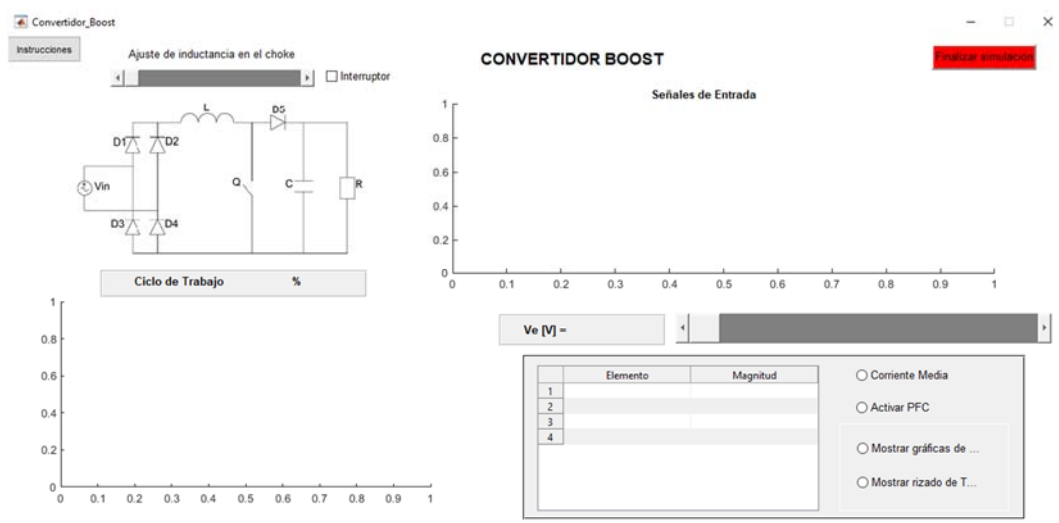


Figure 3. The main window of the simulator. Source: the author

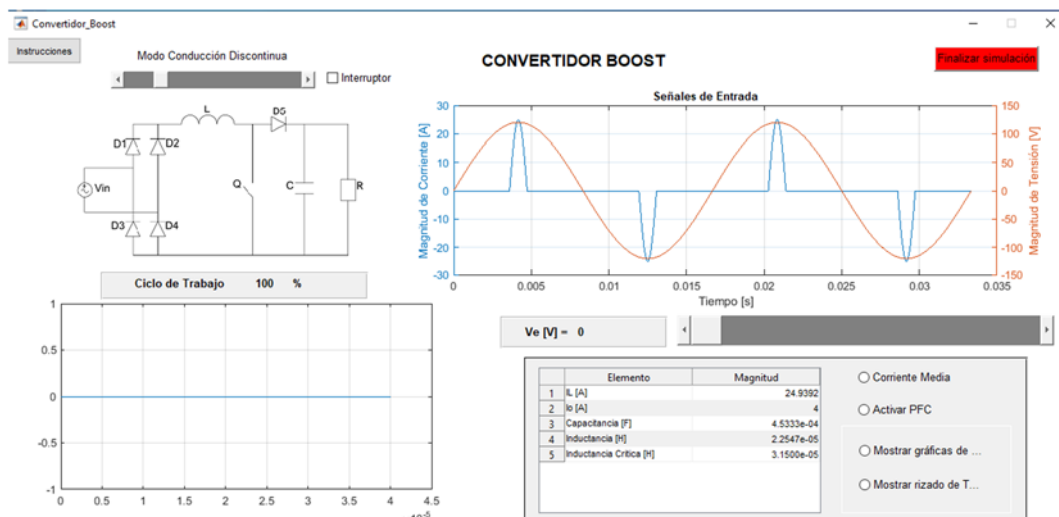


Figure 4. Operation as a rectifier without power factor correction with low inductance in the choke.
Source: the author

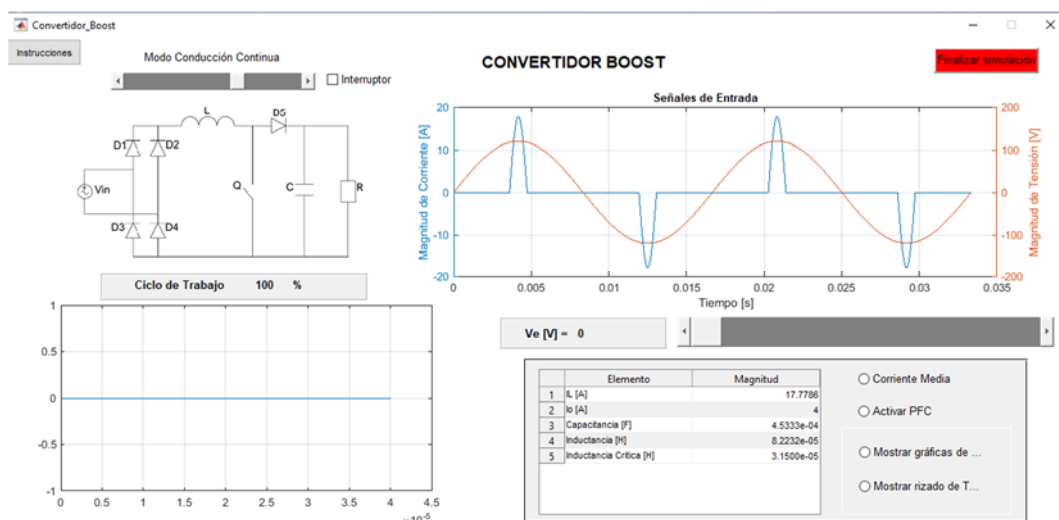


Figure 5. Operation as a rectifier without power factor correction with high inductance in the choke.
Source: the author

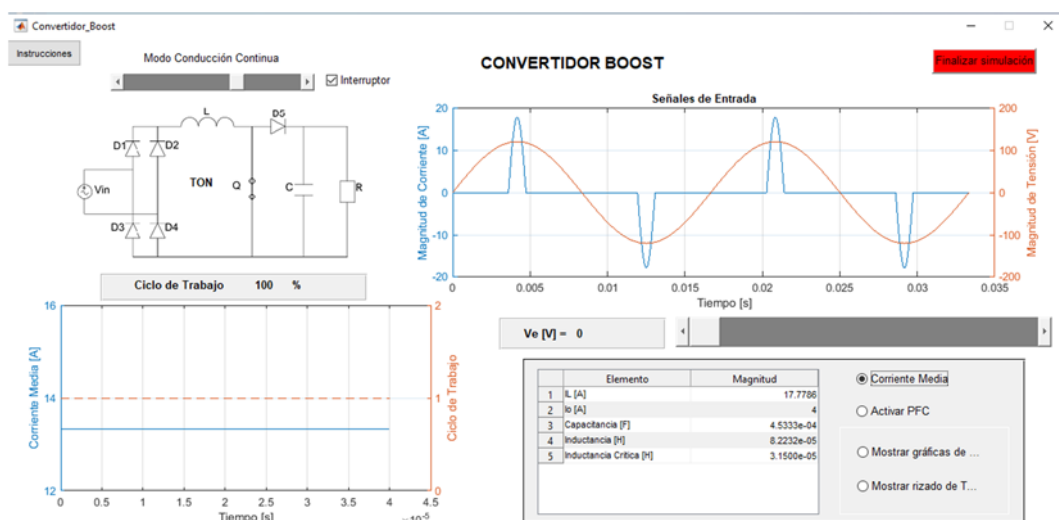


Figure 6. Activation of circuit average curves (input current and duty cycle). Source: the author

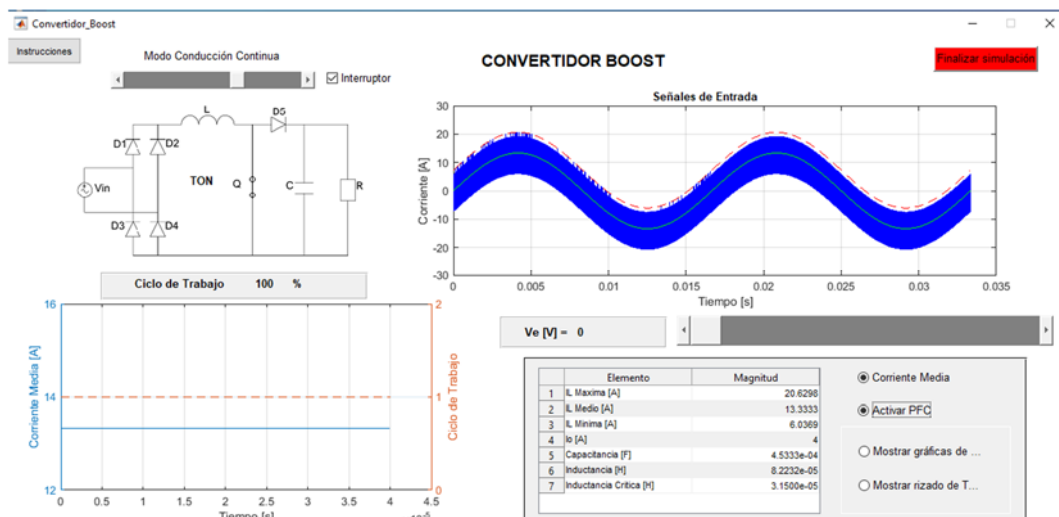


Figure 7. Operation as a rectifier with power factor correction. Source: the author

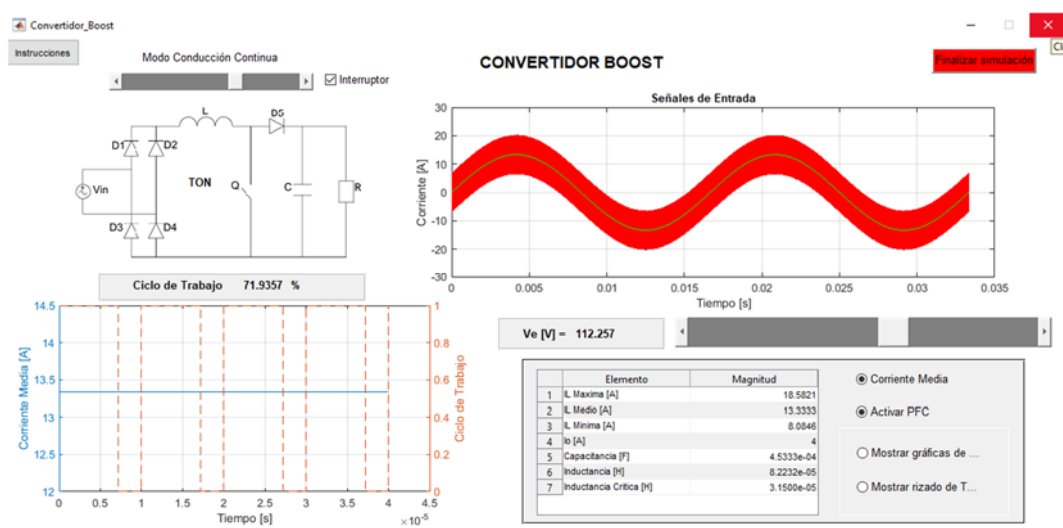


Figure 8. Operation as a rectifier with power factor correction and duty cycle detail 1. Source: the author

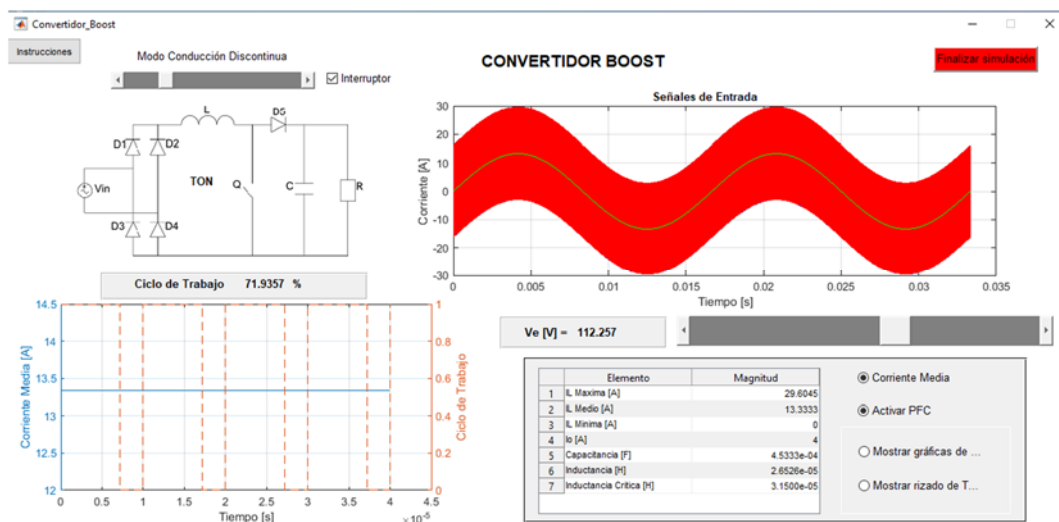


Figure 9. Operation as a rectifier with power factor correction and duty cycle detail 2. Source: the author

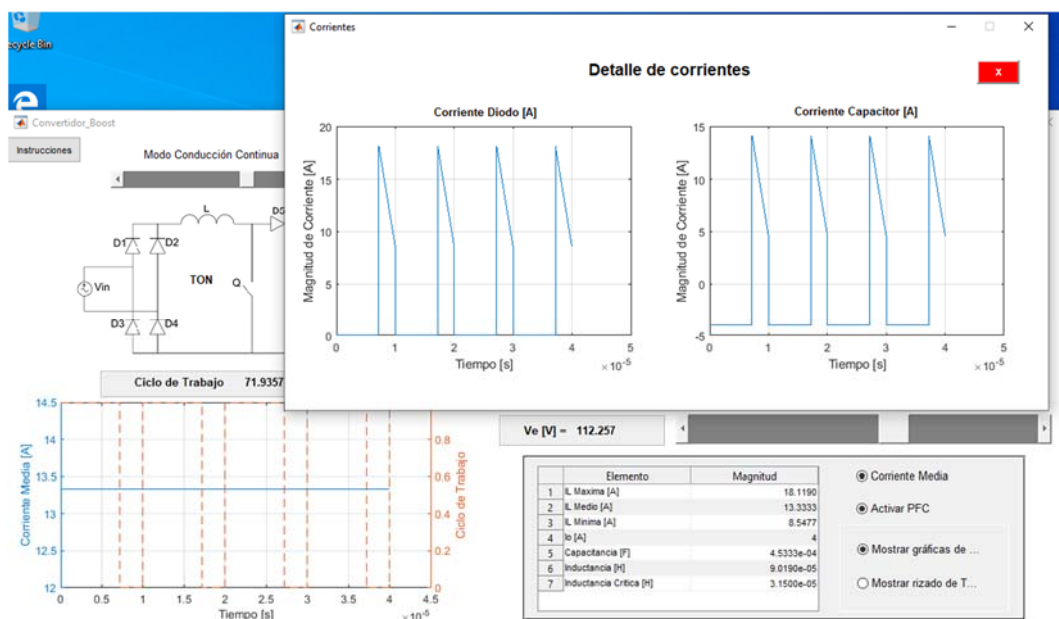


Figure 10. Operation as a rectifier with power factor correction and current detail. Source: the author

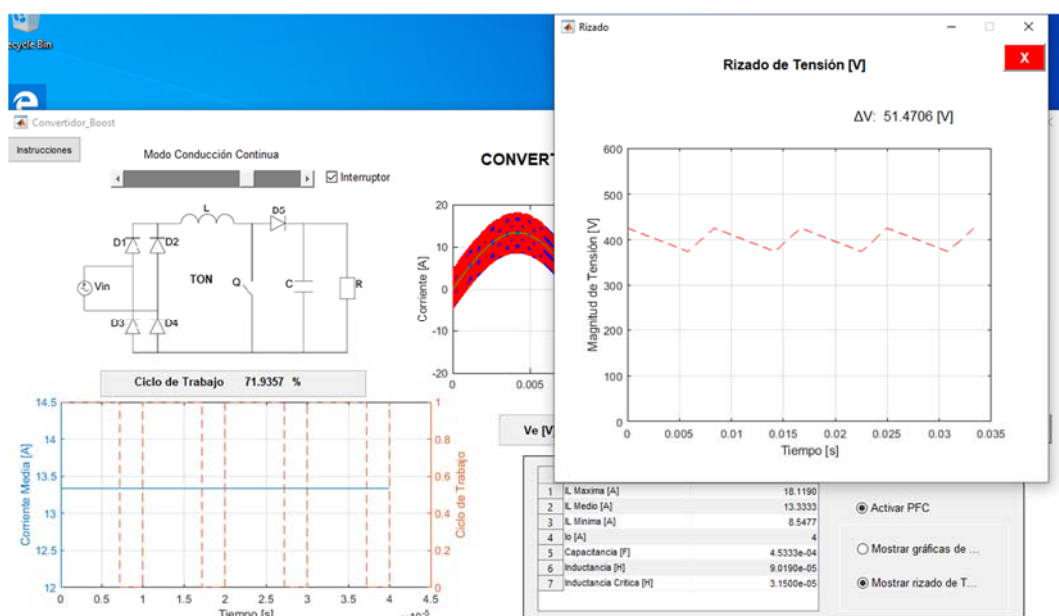


Figure 11. Operation as a rectifier with power factor correction and output voltage ripple detail. Source: the author

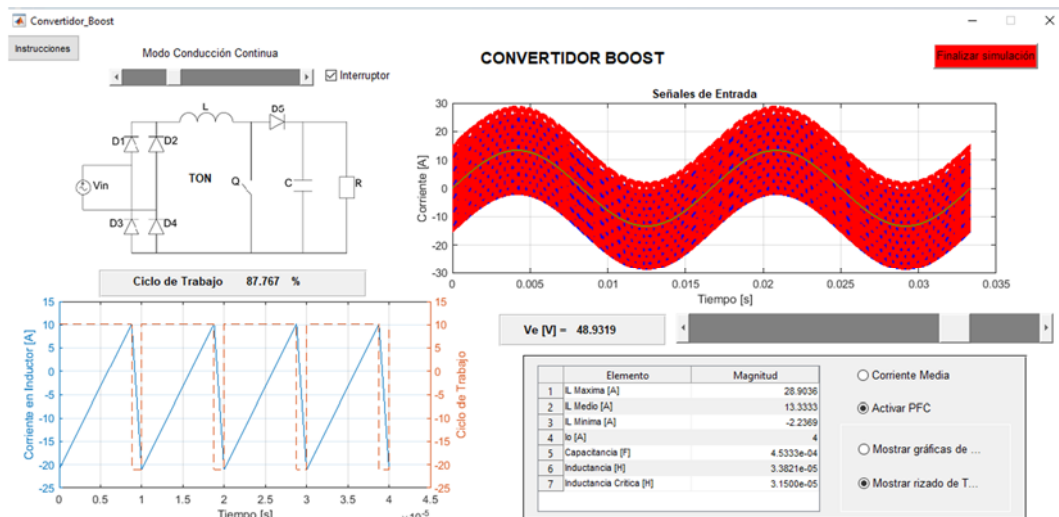


Figure 12. Operation as a rectifier with power factor correction in DCM. Source: the author

SÍNTESE, CARACTERIZAÇÃO E AVALIAÇÃO DA TOXICIDADE FRENTE A ARTEMIA SALINA DE GLICOSÍDEOS 2,3-INSATURADOS

SYNTHESIS, CHARACTERIZATION, AND EVALUATION OF TOXICITY AGAINST SALINE ARTEMIA OF 2,3-UNSATURATED GLYCOSIDES

DA SILVA, Edilma Elayne¹; BARBOSA, Maria Verônica de Sales¹; DE FREITAS, Jucleiton José Rufino³; FREITAS, Jucarlos Rufino², DE FREITAS FILHO, João Rufino^{1*}.

¹ Departamento de Química, Universidade Federal de Rural de Pernambuco. Brasil.

² Programa de Biometria e Estatística Aplicada, Universidade Federal de Rural de Pernambuco. Brasil.

³ Unidade Acadêmica do Cabo de Santo Agostinho (UACSA)/UFRPE. Brasil

* Autor correspondente

e-mail: joaoveronice@yahoo.com.br

Received 16 September 2020; received in revised form 29 October 2020; accepted 11 November 2020

RESUMO

Na química dos carboidratos, o O-glicosídeo 2,3-insaturados é uma molécula orgânica na qual a unidade sacarídica está ligado a outro grupo funcional por meio de uma ligação glicosídica. Derivados de carboidratos insaturados são intermediários úteis em transformações sintéticas que levam a uma variedade de compostos. O uso de glicosídeos 2,3-insaturados na glicosilação cresceu exponencialmente durante a última década. Por outro lado, existe pouco trabalho na literatura que descreve a síntese e atividade biológica de O-glicosídeo 2,3-insaturado contendo os 1,2,4-oxadiazóis como aglicona. Mediante o exposto, o objetivo do trabalho é sintetizar, caracterizar e avaliar a sua toxicidade utilizando *Artemia salina* Leach. Inicialmente preparou-se os precursores, o tri-O-acetil-D-glicol (7) e os 1,2,4-oxadiazóis racêmicos (6a/b). Em seguida, a reação entre o tri-O-acetil-D-glicol (7) e os álcoois (R,S)-3-aryl-[1,2,4-oxadiazol-5-yl]-propan-2-ol (6a/b) foi realizada utilizando como catalisador a montmorillonita K-10 em diclorometano seco, sob refluxo na temperatura de 45°C, fornecendo os compostos (8a/b) em excelente rendimentos (96% composto 8a e 93% composto 8b). Os compostos (8a/b) sintetizados foram caracterizados com base nas análises dos dados espectroscópicos de IV e RMN ¹H e ¹³C e posteriormente submetidos a bioensaios de toxicidade frente ao microcrustáceo *Artemia salina* Leach. Com as atividades citotóxicas constataram-se que o percentual de mortalidade variou de 75-100% em todas as concentrações, o que demonstra que os compostos apresentam potenciais para testes em outros bioensaios. A DL₅₀ é observada em 77,21 (composto 8a) e 74,09 (composto 8b). Esses resultados podem contribuir para o aprofundamento do conhecimento sobre os potenciais farmacológicos e podem ser utilizados em estudos de modificação estrutural por serem possíveis pró-drogas.

Palavras-chave: Carboidratos, Glicol, Citotoxicidade, 1,2,4-Oxidazol, Bioensaio.

ABSTRACT

In the chemistry of carbohydrates, the 2,3-unsaturated O-glycoside is an organic molecule in which the saccharide unit is linked to another functional group through a glycosidic bond. Unsaturated carbohydrate derivatives are useful intermediates in synthetic transformations leading to a variety of compounds. The use of 2,3-unsaturated glycosides in glycosylation has grown exponentially during the last decade. On the other hand, there is little work in the literature that describes the synthesis and biological activity of 2,3-unsaturated O-glycoside containing the 1,2,4-oxadiazoles as aglycone. Therefore, the objective of the work is to synthesize, characterize, and evaluate its toxicity using *Artemia salina*. Initially, precursors, tri-O-acetyl-D-glicol (7), and racemic 1,2,4-oxadiazoles (6a/b) were prepared. Then, the reaction between the tri-O-acetyl-D-glicol (7) and the alcohols (R, S)-3-aryl-[1,2,4-oxadiazol-5-yl]-propan-2-ol (6a/b) was carried out using montmorillonite K-10 in dry dichloromethane as a catalyst, under reflux at a temperature of 45 °C, providing the compounds (8a/b) in excellent yields (96% compound 8a and 93% compound 8b). Compounds 8a/b synthesized were characterized based on their IR, ¹H NMR, and ¹³C, and subsequently subjected to toxicity bioassays against the microcrustacean *Artemia salina* Leach. With cytotoxic activities, it was found that the mortality rate varied from 75-100% in all

concentrations, which demonstrates that the compounds have potential for testing in other bioassays. The LD₅₀ is observed at 77.21 (compound **8a**) and 74.09 (compound **8b**). These results can contribute to the deepening of knowledge about potential pharmacological and may be used in studies of structural modification studies to be possible pro-drugs.

Keywords: Carbohydrates, Glical, Cytotoxicity, 1,2,4-Oxidazole, Bioassay.

1. INTRODUÇÃO:

Os carboidratos, também denominados de açúcares, constituem um grupo dos mais abundante de compostos encontrados em fontes naturais, estando presentes desde os mais complexos organismos, tais como, as plantas e animais (Ferreira; Rocha; Silva, 2009), até organismos mais simples, como os animais marinhos e as bactérias de acordo com Bandera *et al.*, (2014). Na química dos carboidratos o glicosídeo é uma molécula orgânica na qual a porção sacarídica está ligado a outro grupo funcional por meio de uma ligação glicosídica. Por outro lado, os açúcares insaturados constituem uma importante categoria de precursores de carboidratos utilizados em síntese. Especificamente, os glicosídeos 1,2- e 2,3-insaturados são excelentes intermediários para derivatizar monossacarídeos e usado como blocos de construção na síntese orgânica.

Glicosídeos 2,3-insaturados, também conhecidos como pseudo-glicosídeos ou enosídeos, são uma classe importante de produtos naturais com muitas atividades biológicas e capacidade de servir como substratos para reações posteriores (Domon *et al.*, 2005; Meng *et al.*, 2007). A literatura descreve uma série de derivados de açúcar *N*-ftalimidometil 2,3-didesoxi- e 2,3-insaturados que apresentaram potente atividade antiinflamatória, por apresentar redução do edema induzido pela carragenina (Durham e Miller, 2002).

De acordo com Mohammad *et al.*, (2019) na literatura é relatado um grande número de glicosídeos (O-, N-, S e C-) com importantes atividades biológicas, a saber: atividade anti-inflamatória, antibiótica, anestésico, antitumoral, antioxidante e antitrombica. Por outro lado, para que a utilização dos glicosídeos 2,3-insaturados, para os mais diversos fins, seja colocada em prática é necessário que os mesmos possuam a ausência de efeitos tóxicos. Daí a necessidade de conhecer as condições de uso seguro dos glicosídeos 2,3-insaturados para a saúde humana e ambiental, assegurando a segurança de seu uso (Barros e Davino, 2008).

Todavia, os O-glicosídeos 2,3-insaturados são intermediários sintéticos utilizados como blocos de construção de diferentes estruturas complexas, como constituintes de diversos produtos naturais e moléculas de interesse biológico (Wang *et al.*, 2000; Popiołkiewicz *et al.*, 2005). Os glicosídeos 2,3 insaturados são obtidos pela reação de glicosidação de açúcares 1,2-insaturados com diversos aceptores, tais como, álcool, tiol, aminas, em presença de um ácido de Lewis moderado, como catalisador, promovendo um deslocamento alílico no glical (Ferrier, 2001; Gómez *et al.*, 2013).

Este tipo de reação fornece uma variedade de glicosídeos como potenciais blocos de construção para a síntese de produtos naturais com atividades biológicas promissoras (Panarese e Waters, 2009). Nos últimos anos, diversas condições foram utilizadas para facilitar este tipo de síntese em alto rendimentos e alta estereoseletividade em favor do α -anômeros. Por exemplo, o uso de diferentes catalisadores, a saber montmorilonita K-10 (Toshima *et al.*, 1995), montmorilonita K-10 dopada com FeCl₃·6H₂O (Melo *et al.*, 2015); ou mesmo diferentes procedimentos de síntese, tais como irradiação de micro-ondas sob condições sem solvente (de Oliveira, 2002), reação de Mitsunobu (Michigami e Hayashi, 2012) e outros protocolos relatados fornecendo os produtos desejados com resultados satisfatórios (Zhang *et al.*, 2008; Mukherjee e Jayaraman, 2011, Drew, Wall, Kim, 2012).

Na literatura é relatada a existência de muitos C-glicosídeo e poucos O-glicosídeos contendo o anel 1,2,4-oxadiazol na parte aglicônica, sendo eles (ribo, glico, alofuranose e 1',3'-dioxolano) (Brasileiro *et al.*, 2006; Magalhães *et al.*, 2007, Costa *et al.*, 2009). Srivastava e colaboradores relataram três trabalhos de glicosídeos 2,3-insaturados com ligação do tipo O-glicosídica (Srivastava *et al.*, 2015, dos Anjos *et al.*, 2007, Freitas Filho *et al.* 2007), no trabalho de 2004 e 2015 o monossacarídeo está ligado diretamente a porção do 1,2,4-oxadiazol, já no de 2007 apresenta um espaçador triazol entre o anel piranose e o 1,2,4-oxadiazol. Dos glico-heterocíclicos sintetizados, contendo os 1,2,4-

oxadiazóis como aglicona, alguns C-glicosídeos tiveram suas atividades biológicas testadas, como exemplo podemos citar o 5-(β -D-ribofuranozil) 1,2,4-oxadiazol-3-carboxamida. Este composto, mostrou inibição da leucemia L 1210 e P 388 em cultura celular, como também atividade antiviral dando um "Vírus Rating (V.R)" de 0,33 e 0,51 contra a Vaccinia e HSV-2, respectivamente, com muito pouco oxidase celular (Costa *et al.*, 2009).

James e colaboradores (2000), destaca que a realização de estudos toxicológicos possibilita a identificação dos riscos associados de um determinado composto e determina em quais condições de exposição esses riscos são induzidos. Anda segundo Hodgson (2004), estudos viabilizam a elaboração de medidas que protejam os seres vivos e o ambiente dos efeitos deletérios causados por esses compostos, bem como facilitam o desenvolvimento de agentes químicos nocivos mais seletivos, tais como drogas clínicas e pesticidas.

A *Artemia salina* Leach, um pequeno organismo zooplânctônico, que pertence ao filo dos artrópodes, mais especificamente ao subfilo crustáceo, que pode ser encontrado em ambientes marinhos (salinas). Devido ao fato de possuir elevada adaptabilidade e uma imensa distribuição geográfica é comumente utilizada na alimentação de diversos seres aquáticos (Ates *et al.*, 2016). A avaliação da toxicidade utilizando *A. salina* também permite a não utilização de ratos e camundongos em testes *in vivo* e pode ser utilizado como parâmetro para analisar diversas atividades biológicas, a citar a atividade antioxidante (Saraiva *et al.*, 2011), atividade fototóxica (Ojala *et al.*, 1999), atividade larvívora (Luna *et al.*, 2005), atividade citotóxica (Chohan *et al.*, 2010), entre outras, relevantes (Bagheri *et al.*, 2010; Nino; Correa e Mosquera, 2006). Então, avaliação da atividade citotóxica utilizando *Artemia salina* Leach, destaca-se no meio científico pela eficiência e eficácia trazendo a vantagem de ser um procedimento prático, de fácil e rápida execução associado ao baixo custo (Meyer *et al.*, 1982), sendo, portanto, uma excelente ferramenta para a análise preliminar da toxicidade geral (Luna *et al.*, 2005).

Mediante o exposto, este trabalho tem como objetivo a síntese, caracterização estrutural de O-glicosídeos 2,3-insaturados, e avaliar a sua toxicidade frente a larvas da *Artemia salina* Leach. Convém destacar que os compostos a partir da reação de Ferrier entre o tri-O-acetil-D-glicol **1** e os álcoois **2a/b** em presença de montmorillonita

como catalisador. As estruturas dos compostos obtidos foram determinadas através das técnicas espectroscópicas de infravermelho e Ressonância Magnética Nuclear de ^1H e ^{13}C .

2. PARTE EXPERIMENTAL:

2.1. Solventes e reagentes

Em geral utilizou reagentes e solventes na sua forma comercial, P.A., dos fornecedores Merck, Aldrich, Vetec e Cinética, sem nenhuma purificação adicional (só quando mencionado), como foi o caso dos solventes hexano e acetato de etila que indicavam presença de agentes contaminantes, entretanto os mesmos foram purificados através da destilação em sistema com coluna de Vigreux

O acompanhamento das reações foi feito através de cromatografia em camada delgada (CCD), onde utilizamos cromatofolhas de sílica-gel, contendo indicador fluorescente F_{254} , da Macherey/Nagel (Düren, Alemanha). Para revelação dos compostos foi utilizada luz ultravioleta, cuba contendo sistema de $\text{H}_2\text{SO}_4/\text{EtOH}$ e/ou vapores de iodo. Para cromatografia em coluna foi utilizada sílica gel 60 (Merck, 70-230 mesh).

2.2. Instrumentação

Os espectros de infravermelho com transformada de Fourier foram obtidos com o equipamento Varian modelo 640 FTIR. Os espectros de RMN de ^1H e de ^{13}C foram obtidos nos equipamentos da Varian modelos Unity Plus (300 MHz para hidrogênio e 75 MHz para carbono) e VNMRs (400 MHz para hidrogênio e 100 MHz para carbono), usando CDCl_3 como solvente ou o sinal residual do solvente como padrão interno de referência. Os valores de deslocamento químico (δ) estão expressos em partes por milhão (ppm) e as constantes de acoplamento (J) em Hertz (Hz). Os pontos de fusão dos compostos foram realizados no aparelho PFM II da BioSan.

2.3. Procedimentos experimentais

2.3.1. Síntese das amidoximas

Em um balão de 25 mL a nitrila (1 mmol) foi dissolvida em 5 mL de álcool etílico. Separadamente, em outro balão de 25 mL, foi dissolvido em 5 mL de água 3 mmol de cloridrato de hidroxilamina e 1,5 mmol de carbonato de sódio. Essa solução foi adicionada à primeira e o meio reacional foi levado a agitação por

aproximadamente 24 horas, até o consumo total da nitrila, acompanhado através de cromatografia em camada delgada (CCD), em sistema CH₂Cl₂:AcOEt (9:1). Após o término da reação, o etanol foi evaporado e duas fases são formadas: a fase aquosa e o produto insolúvel em água, podendo ser um óleo ou um sólido. Quando sólido, o precipitado foi filtrado e recristalizado em clorofórmio e/ou etanol. Quando o produto formado teve característica de um óleo, foi realizada uma extração com acetato de etila (2 x 10mL), à fase orgânica é adicionado Na₂SO₄. Após uma filtração, o solvente foi removido sob pressão reduzida e o produto purificado por cristalização em clorofórmio. Os produtos **3a/b** foram obtidos em bons rendimentos (90 e 85%). Os dados de IV, RMN ¹H e ¹³C, corroboram com os descritos na literatura (Andrade; Freitas Filho e Freitas, 2016).

2.3.2. Síntese dos 1,2,4-oxadiazóis

Em um frasco de vidro de 10 mL adicionou o acetatoacetato de etila (1,5 mmol) e arilamidoxima (1,0 mmol), estes foram misturados e levados para o banho de óleo em temperatura entre 100-110°C. O recipiente foi deixado em aquecimento durante 4 horas. O término da reação foi comprovada cromatografia em camada delgada (CCD), em sistema CH₂Cl₂:AcOEt (9:1). Os compostos **5a/b** foram purificados por cromatografia em coluna, utilizando um sistema eluente de hexano:AcOEt (9:1).

Composto **5a**: Sólido amarelado obtido com 88% de rendimento, R_f: 0,80 (CH₂Cl₂:AcOEt 9:1); IV (KBr): 2926, 1714, 1363, 1164 cm⁻¹; RMN¹H (300 MHz, CDCl₃): δ 8,10-8,04 (m, 2H, H7e H-8II, Ph-H), 7,53-7,47 (m, 3H, H-9, H-4 e H-5, Ph-H), 4,10 (s, 2H, CH₂), 2,33(s, 3H, CH₃); RMN¹³ C (75 MHz, CDCl₃): δ 198,93(C-2); 172,97(C-5); 168,56(C-4); 131,27(C-9) 128,82(C-8); 127,36(C-7); 126,35(C-6); 41,51(C-3); 29,84(C-1).

Composto **5b**: Sólido amarelado obtido com 74% de rendimento; R_f: 0,72 R_f: 0,80 (CH₂Cl₂:AcOEt 9:1); IV (KBr): 2924, 1720, 1592, 1361, 1169 cm⁻¹; RMN¹H (300 MHz, CDCl₃): δ 8,00-7,78 (d, 2H, J=8,1 Hz H7,); 7,21-7,18 (d, 2H, J=8,1 Hz H8); 4,10 (s, 2H, CH₂), 2,32(s, 3H, CH₃); 2,25(s, 3H, CH₃). RMN¹³ C (75 MHz, CDCl₃): δ 199,01(C-2); 172,79(C-5); 168,54(C-4); 141,63(C-6); 129,48(C-7); 127,27(C-8); 123,50(C-9); 41,50(C-3); 29,82(C-10); 21,34(C-1).

2.3.3. Síntese de 3-aryl-[1,2,4-oxadiazol-5-il]-propan-2-ol

Em um balão de fundo redondo de 100 mL

foi dissolvido o composto **5a/b** (1 mmol) em Metanol (15mL), em seguida foi adicionado o agente redutor boridreto de sódio à 0°C, deixando agitar por 30 minutos. Após o término da reação o solvente evaporado sob pressão reduzida. Em seguida a reação foi tratada com água (40 ml) e acetato de etila (40 mL) A fase orgânica foi adicionado sulfato de sódio anidro. O solvente foi removido sob pressão reduzida e material bruto foi cromatografia em coluna. Os produtos **6a/b** obtidos apresentaram rendimentos bons (88 e 74%).

Composto **6a**: óleo amarelado obtido com 88% de rendimento. R_f: 0,55(CH₂Cl₂:AcOEt 9:1); IV (KBr): 3406, 2973, 1595, 1367, 1117 cm⁻¹; RMN¹H(300 MHz, CDCl₃): δ 8,03-7,99 (m, 2H, H7e H-8II, Ph-H), 7,48-7,39 (m, 3H, H-9II, H-4 e H-5, Ph-H), 4,40 (m, 1H, CH), 3,41(Banda larga referente ao H do por OH), 3,08-2,95(m, 2H, CH₂); 1,32(S, 3H, CH₃); 1,30(S, 3H, CH₃); RMN¹³ C (75 MHz, CDCl₃): δ 178,12(C-5); 168,24(C-4); 131,56(C-9); 129,13(C-8); 127,67(C-7); 126,65(C-6); 65,36(C-2); 36,05(C-3); 23,07(C-1).

Composto **6b**: óleo amarelado obtido com 80% de rendimento, R_f: 0,42(CH₂Cl₂:AcOEt 9:1); IV (KBr): 3406, 2973, 1580, 1363, 1114 cm⁻¹; RMN¹H(300 MHz, CDCl₃): δ 7,84-7,82 (d, 2H, J=8,1Hz), 7,18-7,15 (d, 2H, J=8,1), 4,40 (m, 1H, CH), 3,2(Banda larga referente ao H do grupo OH), 3,08-2,95(m, 2H, CH₂); 1,32(S, 3H, CH₃); 1,30(S, 3H, CH₃); RMN¹³ C (75 MHz, CDCl₃): δ 177,11(C-5); 167,42(C-4); 141,09(C-9); 129,13(C-8); 129,02(C-7); 126,76(C-6); 64,52(C-2); 35,19(C-3); 22,79(C-10); 21,57(C-1).

2.3.4. Síntese de glicosídeos 2,3-insaturados

A um balão de fundo redondo (125 mL) foi adicionado o tri-O-acetil-D-glicol **7** (1 mmol), e os álcoois **6a/b** (1,5 mmol) e 30 mL de CH₂Cl₂ anidro. O meio reacional foi adicionado a temperatura de 0 °C a Montmorilonita K-10 (30%). A mistura foi deixada em refluxo por 3 horas, sendo a reação acompanhada por CCD em sistema CH₂Cl₂:AcOEt (9:1). Após a reação a mistura foi filtrada e o solvente removido sob pressão reduzida. Os produtos **8a/b** foram purificados por cromatografia em coluna de sílica gel, utilizando um sistema eluente de hexano:AcOEt (9:1).

Composto **8a**: óleo amarelado, rendimento 96%, R_f: 0,61 (CH₂Cl₂:AcOEt 9:1); IV (KBr): 2926, 1743, 1368, 1231, 1032, 722 cm⁻¹; RMN ¹H (300 MHz, CDCl₃), sinais em ppm, δ 8,1 (m, 3H, J=6,0Hz), 7,5(m, 4H, J=6,0Hz); 5,8(d, 1H, H2 e H3 J=9,5Hz);

5,2 (m, 1H, H-4), 5,1(s, 1H, H-1); 4,5(m, 1H, H-5); 4,2(dd, 2H, H6 e H6', J=1,74); 4,0 (m, 1H, H-7); 3,2(ddd, 1H, H-8); 2,1(s, 3H, OAc); 1,3 (d, 3H, CH₃ da aglicona, J=6,0Hz); RMN ¹³C (75 MHz, CDCl₃, sinais em ppm, δ 177,24 (C=O, OAc); 170,75(C-10); 168,27(C9); 131,29(C-3); 129,34(C-14); 128,84(C-13); 127,64(C11); 127,42(C12); 126,46(C-2); 95,05 e 92,32 (C1); 73,12(C5); 67,00(C-4); 65,26(C-6); 63,11(C-7); 34,45(C-8); 20,86 (CH₃ e OAc).

Composto **8b**: : óleo amarelado, rendimento 93%, R_f=0,59 (CH₂Cl₂:AcOEt 9:1); IV (KBr): 2926, 1743, 1368, 1231, 1032, 722 cm⁻¹; RMN ¹H (300 MHz, CDCl₃), sinais em ppm, δ 7,9 (d, 2H, J=8,1Hz); 7,3(d, 2H, J=8,10Hz); 5,8(d, 1H, H2 e H3, J=10 Hz); 5,3 (m, 1H, H-4); 5,1(s, 1H, H-1); 4,2(m, 1H, H-5); 4,2(dd, 2H, H6 e H6', J=1,4); 3,9 (m, 1H, H-7); 3,2(ddd, 1H, H-8); 2,4 (s, 3H, CH₃ da aglicona, J=6,0Hz); RMN ¹³C (75 MHz, CDCl₃), sinais em ppm, δ 177,01(C=O, OAc); 170,74(C-10); 168,27(C9); 141,51(C-3); 129,57(C-14); 128,99(C-13); 127,55(C11); 127,30(C12); 123,85(C-2); 95,05 e 92,32(C1); 73,15(C5); 66,99(C-4); 65,26(C-6); 63,11(C-7); 34,45(C-8); 20,86 (CH₃ e OAc).

2.4. Avaliação da toxicidade frente a *Artemia salina* Leach

Os ovos de *Artemia salina* foram colocados para eclodirem em solução de sal marinho e iluminação artificial. Decorridas 24 horas de eclosão, 10 larvas foram adicionadas em tubos de ensaio contendo soluções dos glicosídeos 2,3-insaturados de concentrações que variaram de 100-25 µg/mL em DMSO, todas estando em triplicatas. Para grupo controle uma triplicata de solução de sal marinho e DMSO foi preparada. Após 24 horas de exposição, foi feita a contagem de artêmia vivos e mortos, sendo considerados vivos todos aqueles que apresentassem qualquer tipo de movimento quando observados próximos a uma fonte luminosa. Só foram considerados válidos os testes nos quais o controle apresentou uma mortalidade igual ou inferior a 10 % da população.

2.5. Delineamento estatístico experimental

Para análise estatística, utilizou-se o software TEAM R CORE, para obtenção das CL₅₀ e respectivos intervalos de confiança (Team, 2013).

3. RESULTADOS E DISCUSSÃO:

O Esquema 1 descreve as etapas de síntese dos precursores para reação de glicosilação. Inicialmente, em uma primeira etapa foram sintetizadas duas arilamidoximas **3a/b**. O método utilizado para obtenção das arilamidoximas, foi o clássico, ou seja, agitação em temperatura ambiente por 24 horas. As diferentes arilamidoximas **3a/b** foram sintetizadas a partir de arilnitrilas **1a-c** com o cloridrato de hidroxilamina (NH₂OH. HCl) e carbonato de sódio (Na₂CO₃), numa solução hidroalcoólica, em bons rendimentos. Posteriormente, na segunda etapa, foi realizada a síntese dos 1-(3-aril-1,2,4-oxadiazol-5-il) propano-2-ona (**5a/b**), através da reação entre as arilamidoximas (**3a/b**) e acetoacetato de etila (**4**) sob aquecimento e sem utilização de solvente, fornecendo os compostos em bons rendimentos, ou seja, variando de 88 e 80%. Finalmente na última etapa ocorreu a reação de redução dos compostos **5a/b** com borohidreto de sódio em metanol a 0 °C, que resultou na formação dos compostos **6a/b**, em bons rendimentos (90-85%).

Os 3-aril-(1,2,4-oxadiazol-5-il) propano-2-ona (**5a/b**), foram obtidos na forma de um óleo amarelado. Os dados espectroscópicos de IV, RMN ¹H e RMN ¹³C corroboram com os valores encontrados na literatura para o 1-(3-aril-1,2,4-oxadiazol-5-il) butan-2-ona descrito por Freitas *et al.*, (2007). Por outro lado, a determinação estrutural dos 3-aril-(1,2,4-oxadiazol-5-il) propan-2-ol foram realizadas através de técnicas espectroscópicas de infravermelho e RMN ¹H e RMN ¹³C. No espectro de IV é possível observar o aparecimento da banda larga de estiramento característica de álcool em 3.406 cm⁻¹ e o desaparecimento da banda característica carbonila em 1.700 cm⁻¹ dos compostos (**6a/b**). Os valores dos deslocamento e constantes de acoplamento do espectro de RMN ¹H e RMN ¹³C são sumariadas na parte experimental.

De posse dos precursores e confirmadas suas estruturas por técnicas espectroscópicas, a quarta etapa reacional consistiu na síntese dos a síntese O-glicosídeos 2,3-insaturados através do rearranjo de Ferrier. Os autores empregaram a metodologia descrita por Toshima *et al.*, (1995), Melo *et al.*, (2017), e de Freitas Filho *et al.*, (2015), devido sua eficácia, baixo custo, fácil manipulação dos reagentes e por ser realizada em condições brandas de temperatura. Sendo assim, a reação de glicosilação entre o tri-O-acetil-D-glicol (**7**) e os álcoois (*R,S*)-3-aril-[1,2,4-oxadiazol-5-il]-propan-2-ol (**6a/b**) foi realizada utilizando como catalisador a montmorillonita K-10 em

diclorometano seco, sob refluxo na temperatura de 45°C, de acordo com o Esquema 2, fornecendo os compostos (**8a/b**) em excelentes rendimentos (96% composto **8a** e 93% composto **8b**) e alta estereosseletividade em favor do anômero α .

A partir da análise da mistura reacional, através de cromatografia gasosa, foi observado uma razão diastereomérica (r.d.) de 87:13 que demonstra a alta estereosseletividade da reação em favor do α -anômero. A mistura foi então submetida a cromatografia em coluna e isolado o isômero α de traços de isômeros β . Em seguida, a confirmação do α -anômero majoritário e o assinalamento completo dos núcleos de H e C foi realizado empregando diferentes técnicas espectroscópicas, tais como, IV e RMN ^1H e ^{13}C .

O espectro de RMN ^1H a 300 MHz do composto **8a** para a mistura de dois produtos (Figura 1) foi possível verificar em δ 2,0 e 2,1 ppm dois simpletos referentes aos hidrogênios das metilas do grupo OAc do anel piranosídeo. O simpleto largo em δ 5,1 ppm corresponde ao hidrogênio anomérico H-1. Em δ 5,82 ppm um par de dupletos referente ao acoplamento de H-3 com H-2, por sua vez em δ 5,73 ppm outro dupletos referente ao acoplamento de H-2 com H-3. A constante de acoplamento $J=9,5\text{Hz}$. Em δ 8,1 e 7,5 podemos observar os prótons aromáticos apresentando multipletos com integração para 3 hidrogênio e 4 hidrogênios respectivamente. Por sua vez o δ 5,27 referentes a H-4 possui uma constante de acoplamento com H-5 de $J=6,7$. Em δ 4,22 os prótons H6 e H-6' com esperado dupletos de dupletos com acoplamento germinal de $^2J=1,74$. O próton H-8 com δ 3,95 apresenta um par de duplos dupletos com $^2J_{ab}=14$ e $^3J_{ac}=5,9\text{Hz}$ referente ao acoplamento com H-7 característico de um acoplamento germinal diastereotópicos em sistemas alifáticos acíclicos. Na região de δ 1,30-1,45 ppm observa-se o grupo metila da aglicona que aparece na forma de dupletos, um em 1,35 ppm com $J=6\text{Hz}$ e outro em 1,45 ppm também com $J=6\text{Hz}$ na proporção 5:5 este dado ratifica o fato dos compostos ser diastereoisoméricos.

Por outro lado, o espectro de RMN ^{13}C do composto **8a** apresentou duplicidade de sinais devido à mistura diastereoisomérica (Figura 2). Em campo alto, observa-se o sinal do carbono das carbonilas dos grupos OAc bem como os carbonos do anel oxadiazólico C9 e C10 em δ 170,4 e 168,3 ppm. Sinais característicos de carbonos aromáticos C11, C12, C13, C14 aparecem entre δ 127,0 – δ 129,0 ppm. Os carbonos vinílicos do anel piranosídico C2 e C3

aparecem na faixa de δ 123,8 ppm, δ 141,5 ppm. Com dois sinais na região de δ 95,0 e 92,3 ppm encontra-se o carbono anomérico C1, fato este justificado pela presença do anômero β . Por sua vez em campo baixo ao carbono do anel piranosídico C5 com δ 73,1 ppm e δ 70,8 ppm. Os carbonos do anel piranosídico C4, C6 e C7 aparecem em δ 66,99 ppm, δ 65,2 ppm e δ 63,11 ppm respectivamente. Por fim o C8 aparece na região δ 34,6 ppm, típica de carbono sp^2 .

Uma vez sintetizado e caracterizado o (*R*-S) 3-*aril*-[1,2,4-oxadiazol-5-il]-propan-2,3-didesoxi- α -D-*eritro*-hex-2-enopiranosídeos (**8a/b**), a etapa seguinte do trabalho foi realizar o bioensaio toxicológico. Analisando o padrão de letalidade frente às larvas de *Artemia salina* Leach do composto, foi observado um bom desempenho por parte dos padrões positivos e negativos, assegurando assim a viabilidade do teste. A Tabela 1 mostra, para os compostos **8a** e **8b** os valores de DL_{50} e os limites de confiança obtidos da média das triplicatas para cada ensaio de toxicidade, assim como, a média dos valores de DL_{50} , o desvio padrão, a covariância (%) obtidos para cada composto. Conforme demonstrado na Tabela, observa-se que tanto o composto **8a** quanto **8b** apresentou $\text{DL}_{50}<100\text{ }\mu\text{g/mL}$.

Observa-se que, em geral, não houve grandes variações nos valores de DL_{50} entre as triplicadas de um mesmo composto. Os coeficientes de variação entre as triplicadas variaram entre 58,25 e 58,70%.

Segundo Nguta *et al.*, (2012) os ensaios com *A. Salina* são classificados seguindo os seguintes parâmetros: CL_{50} menor que 100 $\mu\text{g/mL}$ alta atividade toxicológica, entre 100 e 500 $\mu\text{g/mL}$ moderada atividade toxicológica, 500 a 1000 $\mu\text{g/mL}$ fraca atividade toxicológica e acima de 1000 $\mu\text{g/mL}$ não tóxicos.

Todavia, o teste de citotoxicidade avaliou o efeito de diferentes concentrações dos compostos **8a** e **8b** nos tempos de 24 horas. Os resultados do referido ensaio podem ser visualizados na Figura 3, onde a DL_{50} é observada em 77,21 (composto **8a**) e 74,09 (composto **8b**). A concentração letal média (CL_{50}) foi calculada com base na equação da reta obtida pela regressão linear, considerando a correlação das concentrações e a porcentagem de mortalidade. Ao valor de y (ordenadas) foi atribuído o número de mortes, ao resultado de x obtido (abscissas), onde foi aplicado o valor final da CL_{50} .

Finalizando, segundo Cavalcante *et al.*, (2000) a avaliação da bioatividade de compostos orgânicos, sejam eles provenientes de plantas ou de síntese, tem sido pouco viável em laboratórios tradicionais de química. Como descrito na literatura (Colegate e Molyneux, 1993), o ensaio de letalidade permite a avaliação da toxicidade geral e, portanto, é considerado essencial como bioensaio preliminar no estudo de compostos com potencial atividade biológica. Por outro lado, o bioensaio com *Artemia salina* é considerado um teste preliminar para avaliar substâncias tóxicas e possível ação antitumoral das mesmas (Carballo *et al.*, 2002).

4. CONCLUSÕES:

Neste trabalho, foi realizada a síntese dos materiais de partidas e de glicosídeos 2,3-insaturados contendo como aglicona os 1,2,4-oxadiazóis, em excelentes rendimentos (93% e 96%) e alta estereosseletividade em favor do α -anômero.

Os glicosídeos 2,3-insaturados obtidos foram purificados por cromatografia em coluna, fornecendo o anômero α e traços do anômero β . As estruturas dos compostos foram determinadas por técnicas de IV e RMN ^1H e ^{13}C . Convém destacar que para análise da atividade citotóxica foi realizada com a mistura diastereoisomérica (*R* e *S*).

As atividades citotóxicas foram realizadas frente a *Artemia salina* onde constatou que o percentual de mortalidade variou de 75-100% em todas as concentrações, o que demonstra que os compostos apresentam potenciais para testes em outros bioensaios. A DL_{50} é observada em 77,21 (composto **8a**) e 74,09 (composto **8b**).

5. AGRADECIMENTOS:

Os autores deste trabalho agradecem a todas as agências de fomento que financiaram a nossa pesquisa: CAPES, CNPq e FACEPE pelas bolsas concedidas aos estudantes de Pós-Graduação.

6. REFERÊNCIAS:

1. Ferreira, V. F.; Rocha, D. R.; Silva, F. C. (2009). Potencialidade e oportunidades na química da sacarose e outros açúcares. *Química Nova*, 32(3), 623- 638.
2. Bandera, D.; Sapkota, J.; Josset, S.;

- Weder, C.; Gao, X.; Foster, E. J.; Zimmermann, T. (2014). Influence of mechanical treatments on the properties of cellulose nanofibers isolated from microcrystalline cellulose. *Reactive and Functional Polymers*, 85, 134-141
3. Domon, D.; Fujiwara, K.; Ohtaniuchi, Y.; Takezawa, A.; Takeda, S.; Kawasaki, H.; Murai, A.; Kawai, H.; Suzuki, T. (2005). Synthesis of the C42-C52 part of ciguatoxin CTX3C. *Tetrahedron Letters*, 46, 8279–8283.
4. Meng, X. B.; Han, D.; Zhang, S. N.; Guo, W.; Cui, J. R.; Li, Z. J. (2007). Synthesis and anti-inflammatory activity os N-phthalimidomethyl 2,3-dideoxy- and 2,3-unsaturated glycosides. *Carbohydrate Research*, 342(9), 1169-1174.
5. Durham, T. B.; Miller, M. J. (2002). Conversion of glucuronic acid glycosides to novel bicyclic beta-lactams. *Organic Letters*, 4, 135-138.
6. Hossain, M. T.; Asadujjaman, M.; Manik, M. I. N.; Matin, M. A.; Chowdhury, R. Z.; Rashid, M. H. (2019). A study on the pharmacological effects and mechanism of action of alkaloids, glycosides and saponins. *The Pharmaceutical and Chemical Journal*, 6(2), 112-122.
7. Barros, S. B. M.; Davino, S. C. Avaliação da toxicidade. In: Oga, S.; Camargo, M. M. A.; Batistuzzo, J. A. O. Fundamentos de toxicologia. 3ª ed., São Paulo: Atheneu Editora, 2008.
8. Wang, Z. G.; Zhang, X. F.; Live, D.; Danishefsky, S. J. (2000). Toward fully synthetic homogeneous glycoproteins: A high mannose core containing glycopeptide carrying full H-type 2 human blood group specificity. *Angewandte Chemie International Edition*. 39, 3652.
9. Popiołkiewicz, J., Polkowski, K., Skierski, J.S, Mazurek A. P. (2005). In vitro toxicity evaluation in the development of new anticancer drugs-genistein glucosides. *Cancer Letters*, 229, 67-75.
10. Ferrier, R. J. (2001). Substitution-with-Allylic-Rearrangemetn reactions of glycal derivatives. *Topics in Current*

11. Gómez, A. M.; Lobo, F.; Uriel, C.; López, J. C. (2013). Recent Developments in the Ferrier Rearrangement. *European Journal of Organic Chemistry*, 32, 7221-7267.
12. Panarese, J. D.; Waters, S. P. (2009). Enantioselective formal total synthesis of (+)-aspergillide C. *Organic Letters*, 11(21), 5086-5088.
13. Toshima, K.; Ishizuka, T.; Matsuo, G.; Nakata, M. (1995). Practical glycosylation method using monmorillonite k-10 as an environmentally acceptable and inexpensive industrial catalyst. *Synlett*, 4, 306-308.
14. Melo, V. N.; Dantas, W. M.; Camara, C. A.; de Oliveira, R. N. (2015). Synthesis of 2,3-unsaturated alkynyl O-glucosides from tri-O-acetyl-D-glucal by using montmorillonite k-10/iron(III) chloride hexahydrate with subsequent copper (I)-catalyzed 1,3-dipolar cycloaddition. *Synthesis*, 47, 3529–3541.
15. De Oliveira, R. N.; De Freitas Filho, J. R.; Srivastava, R. M. (2002). Microwave-induced synthesis of 2,3-unsaturated O-glycosides under solvent-free conditions. *Tetrahedron Letters*, 64, 2141-2143.
16. Michigami, K.; Hayashi, M. (2012). O- and N-glycosylation of D-glycals using Ferrier rearrangement under Mitsunobu reaction conditions. *Tetrahedron*, 68, 1092-1096.
17. Zhang, G.; Liu, Q.; Shi, L.; Wang, J. (2008). Ferric sulfate hydrate-catalyzed O-glycosylation using glycals with or without microwave irradiation. *Tetrahedron*, 64, 339-344.
18. Mukherjee, A.; Jayaraman, N. (2011). Reactivity switching and selective activation of C-1 or C-3 in 2,3-unsaturated thioglycosides. *Carbohydrate Research*, 346, 1569-575.
19. Drew, M. D.; Wall, M. C.; Kim, J. T. (2012). Stereoselective propargylation of glycals with allenyltributyltin(IV) via a Ferrier type reaction. *Tetrahedron Letters*, 53, 2833-2836.
20. Brasileiro, B. G.; Pizziolo, V. R.; Raslan, D. S.; Jamal, C. M.; Silveira, D. (2006). Antimicrobial and cytotoxic activities screening of some Brazilian medicinal plants used in Governador Valadares district. *Revista Brasileira de Ciências Farmacêuticas*, 42, 195-202.
21. Magalhães, A. F.; Tozzi, A. M. G. A.; Santos, C. C.; Serrano, D. R.; Zanotti-Magalhães, E. M.; Magalhães, E. G.; Magalhães, L. A. (2007). Saponins from *Swartzia langsdorffii*: biological activities. *Memórias do Instituto Oswaldo Cruz*, 98, 713-718.
22. Costa, E.S.S.; Dolabella, M. F.; Póvoa, M. M.; Oliveira, D. S.; Muller, A. H. (2009). Estudos farmacognósticos, fitoquímicos, atividade antiplasmodica e toxicidade em *Artemia salina* de extrato etanólico de folhas de *Montrichardia linifera* (Arruda) Schott, Araceae. *Revista Brasileira de Farmacognosia*, 19(4), 834-838.
23. Dos Anjos, J. V.; Sinou, D.; Nascimento, S. C.; De Melo, S. J. (2007). Synthesis of some unusual (1,2,4-Oxadiazole)-linked hexenopyranosides and mannopyranosides. *Carbohydrate Research*, 342, 2440-2449.
24. Freitas, J. J. R.; de Freitas, J. C. R.; da Silva, L. P.; de Freitas Filho, J. R.; Kimura, G. Y.V.; Srivastava, R. M. (2007). Microwave-induced one-pot synthesis of 4-[3-(aryl)-1,2,4-oxadiazol-5-yl]-butan-2-ones under solvent free conditions. *Tetrahedron Letters*, 48, 6195-6198.
25. Freitas Filho, J. R.; Freitas, J. J. R.; Cottier, L.; Sinou, D.; Srivastava, R. M. (2015). Synthesis of 2,3-unsaturated O-glycosides from optically active alcohols via Ferrier rearrangement: configurational studies. *Journal of the Chilean Chemical Society*, 60, 2646-2549.
26. James, R. C.; Roberts, S. M.; Williams, P. L. *Principles of Toxicology: Environmental Industrial Applications*. 2^a ed., New York: John Wiley & Sons, 2000, cap. 1.
27. Hodgson, E. A. *Textbook of Modern Toxicology*. 3^a ed., New Jersey: John Wiley & Sons, 2004, cap. 1.

28. Ates, M.; Demir, V.; Arslan, Z.; Camas, M.; Celik, F. (2016). Toxicity of engineered nickel oxide and cobalt oxide nanoparticles to *Artemia salina* in seawater. *Water, Air, & Soil Pollution*, 227, 3, 70.
29. Saraiva, A.; Castro, R.; Cordeiro, R.; Sobrinho, T.; Castro, V.; Amorim, E.(2011). Antimicrobial activity and bioautographic study of antistaphylococcal componentes from *schinopsis brasiliensis* engl. *African Journal of Pharmacy and Pharmacology*, 5(14), 1724-1731.
30. Ojala, T.; Vuorela, P.; Kiviranta, J.; Vuorela, H.; Hiltunen, R. (1999). A bioassay using *Artemia salina* for detecting phototoxicity of plant coumarins. *Planta Medica*, 65(80), 715-718.
31. Luna, J.; Dos Santos, A.; De Lima, M.; De Omena, M.; De Mendonca, F.; Bieber, L. (2005). A study of the larvicidal and molluscicidal activities of some medicinal plants from northeast Brazil. *Journal of Ethnopharmacology*, 97, 199-206.
32. Chohan, Z.; Sumrra, S.; Youssoufi, M.; Hadda, T. (2010).Metal based biologically active compounds: Design, synthesis, and antibacterial/antifungal/cytotoxic properties of triazole-derived Schiff bases and their oxovanadium(IV) complexes. *European Journal of Medicinal Chemistry*, 45(7), 2739-2747.
33. Bagheri, S.; Sahebkar, A.; Gohari, A.; Saeidnia, S.; Malmir, M.; Iranshahi, M. (2010).Evaluation of cytotoxicity and anticonvulsant activity of some Iranian medicinal *Ferula* species. *Pharmaceutical Biology*, 48(3), 242-246.
34. Nino, J.; Correa, Y.; Mosquera, O. (2006). Antibacterial, Antifungal, and cytotoxic activities of 11 Solanaceae plants from Colombian biodiversity. *Pharmaceutical Biology*, 44(1), 14-18.
35. Meyer, B. N.; Ferrigni, N. R.; Putnam, J. E.; Jacobsen, L. B.; Nichols, D. E.; Mclaughlin, J. L. (1982). Brine shrimp: A convenient general bioassay for active plant constituents. *Planta Medica*, 45(5), 31-34.
36. Andrade, D.; Freitas Filho, J. R.; Freitas, J. C. R. (2016). Aplicação de amidoximas como catalisadores da reação de alilação por alitrifluoroborato de potássio em meio básico. *Química Nova*, 39(10), 1225-1235.
37. Team, R. C. R development core team. *RA Lang Environ Stat Comput*, 2013, 55, 275-286.
38. Melo, A. C. N.; Oliveira, R. N.; Freitas Filho, J. R.; Silva, T. G.; Srivastava, R M. (2017). Synthesis of anti-inflammatory 2,3-unsaturated O-glycosides using conventional and microwave heating techniques. *Heterocyclic Communications*, 23(3), 205-211.
39. Guta, J. M.; Mbariaa, J. M.; Gakuyab, D. W.; Gathumbic, P. K.; Kabasad, J. D.; Kiam, S. G. (2012). Evaluation of Acute toxicity of crude plant extracts from Kenyan Biodiversity using brine shrimp, *Artemia salina* L. (*Artemiidae*). *The Open Conference Proceedings Journal*, 3, 30-34.
40. Cavalcante, M. F.; Oliveira, M. C. C.; Velandia, J. R.; Echevarria, A. (2000). Síntese de 1,3,5-triazinas substituídas e avaliação da toxicidade frente a *Artemia salina* leach. *Química Nova*, 23(1), 20-22.
41. Colegate, S. M.; Molyneux, R. J. (1993). *Bioactive Natural Products: Detection, Isolation and Structural Determination*; Colegate, S. M., Ed.; CRC Press; London, 441.
42. Carballo, J. L.; Hernández-Inda, Z. L.; Pérez, P.; García-Gravalos, M. D. (2002). A comparison between two brine shrimp assays to detect in vitro cytotoxicity in marine natural products. *Bio Med Central Biotechnology*, 2,1-10.

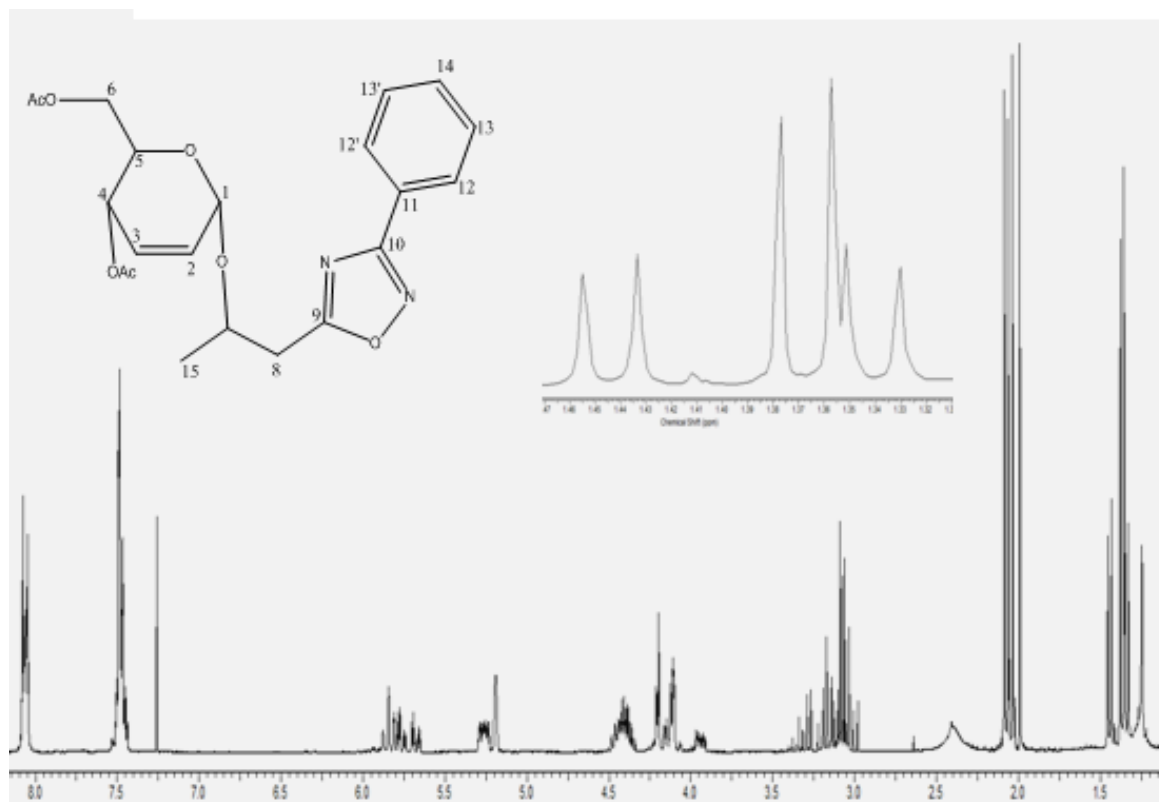


FIGURA 1. Espectro de RMN ^1H (300 MHz) em CDCl_3 do composto **8a**

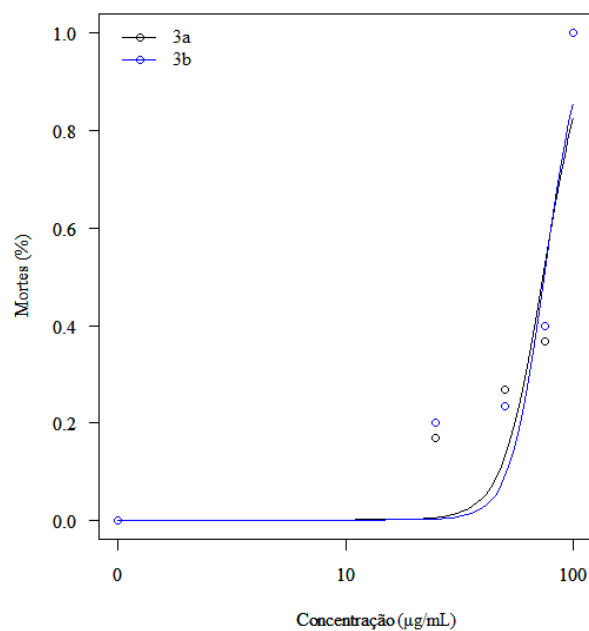


FIGURA 3. Porcentagem de *Artemia salina* mortas em relação ao aumento de concentração dos compostos **8a** e **8b**.

TABELA 1. Avaliação da toxicidade em *A. salina* Leach (DL_{50}) dos compostos **8a** e **8b** e seus respectivos limites do intervalo de confiança de 95%.

Compostos	DL_{50} ($\mu\text{g mL}^{-1}$)	Intervalo de confiança 95%	
		Limite inferior	Limite superior
8a	77,2130		
Média $DL_{50} \pm DP$	$77,2130 \pm 6,9673$	58,1609	88,2650
CV (%)	58,70		
8b	74,0989		
Média $DL_{50} \pm DP$	$74,0989 \pm 9,0474$	54,5531	93,6447
CV (%)	58,25		

DL_{50} = dose letal para 50% da população, DP= desvio padrão, CV= Coeficiente de variação

CHARACTERIZATION OF ZnO NANOFIBER ON DOUBLE-LAYER DYE-SENSITIZED SOLAR CELLS USING DIRECT DEPOSITION METHOD

CHARACTERIZATION OF ZnO NANOFIBER ON DOUBLE-LAYER DYE-SENSITIZED SOLAR CELLS USING DIRECT DEPOSITION METHOD

KARAKTERISASI ZnO NANOFIBER PADA SEL SURYA TERSENSITISASI PEWARNA DENGAN LAPISAN GANDA MENGGUNAKAN METODE *DIRECT DEPOSITION*

ARIFIN, Zainal^{1,*}, HADI, Syamsul¹, SUYITNO, Suyitno¹, PRABOWO, Aditya Rio¹,
PRASETYO, Singgih Dwi¹

¹ Department of Mechanical Engineering, Universitas Sebelas Maret, Jl. Ir. Sutami No.36A, Jebres, Surakarta 57126, Indonesia.

** Corresponding author*
e-mail: zainal_arifin@staff.uns.ac.id

Received 02 September 2020; received in revised form 19 October 2020; accepted 11 November 2020

ABSTRACT Characterization

Solar cells are capable of harvesting energy by converting solar heat into electrical energy through the photovoltaic process. A type of solar cell, namely dye-sensitized solar cells (DSSCs) which based on double-layer photoanode is attracting researchers and engineers considering its characteristics, e.g., high efficiency, low cost, and available mass-production. The TiO₂-ZnO double-layer semiconductor can be obtained from a nanofiber ZnO semiconductor which is deposited with a TiO₂ nanoparticle semiconductor. In this study, the direct deposition method was applied using an electrospinning machine. The intention is to directly capture the liquid of electro-jet spun from PVA/Zn(Ac)₂ solution onto fluorine-doped tin oxide (FTO) glass. The glass itself is coated with a TiO₂ nanoparticle semiconductor. The investigation was addressed to obtain the best tip distance to the collector and the best flow rate in the electrospinning process. The subject environment was designated on the manufacturing process of nanofiber ZnO semiconductors used as double-layer DSSC photoanodes. Variations in flow rates of 3, 4, 5, 6, 7, and 8 µL/minute were applied in the observation. Furthermore, collaboration with the tip to collector distances using a variation of 3, 4, 5, 6, 7, and 8 cm was also considered in this study. Based on these parameters, the effects of the electrospinning process on the morphology of the directly deposited ZnO nanofiber semiconductor were obtained. The results showed that a flow rate of 4 µL/minute and a tip distance to the collector of 8 cm produced a small diameter and uniform morphology. This morphology allowed ZnO nanofibers to have better color absorption and electron excitation. Thus, it was directly proportional to the high efficiency of double-layer DSSCs. The performance value for the 4 µL/min discharge was 2.39%, and the performance value for the 8 cm needle tip distance to the collector was 1.61%.

Keywords: *semiconductors, double layer, direct deposition, dye-sensitized solar cells (DSSCs)*

ABSTRACT

Solar cells are capable of harvesting energy by converting solar heat into electrical energy through the photovoltaic process. A type of solar cell, namely dye-sensitized solar cells (DSSCs) which based on double-layer photoanode is attracting researchers and engineers considering its characteristics, e.g., high efficiency, low cost, and available mass-production. The TiO₂-ZnO double-layer semiconductor can be obtained from a nanofiber ZnO semiconductor which is deposited with a TiO₂ nanoparticle semiconductor. In this study, the direct deposition method was applied using an electrospinning machine. The intention is to directly capture the liquid of electro-jet spun from PVA/Zn(Ac)₂ solution onto fluorine-doped tin oxide (FTO) glass. The glass itself is coated with a TiO₂ nanoparticle semiconductor. The investigation was addressed to obtain the best tip distance to the collector and the best flow rate in the electrospinning process. The subject environment was designated on the manufacturing process of nanofiber ZnO semiconductors used as double-layer DSSC photoanodes. Variations in flow rates of 3, 4, 5, 6, 7, and 8 µL/minute were applied in the observation. Furthermore, collaboration with the tip to collector distances using a variation of 3, 4, 5, 6, 7, and 8 cm was also considered in this study. Based on these parameters, the effects of the electrospinning process on the morphology of the directly deposited ZnO nanofiber semiconductor were obtained. The results showed that a flow rate of 4

$\mu\text{L}/\text{minute}$ and a tip distance to the collector of 8 cm produced a small diameter and uniform morphology. This morphology allowed ZnO nanofibers to have better color absorption and electron excitation. Thus, it was directly proportional to the high efficiency of double-layer DSSCs. The performance value for the 4 $\mu\text{L}/\text{min}$ discharge was 2.39%, and the performance value for the 8 cm needle tip distance to the collector was 1.61%.

Keywords: *semiconductors, double layer, direct deposition, dye-sensitized solar cells (DSSCs)*

ABSTRAK

Sel surya merupakan alat pemanen energi dengan mengubah panas matahari menjadi energi listrik melalui proses fotovoltaiik. Salah satu jenis sel surya, yaitu sel surya tersensitisasi pewarna (*dye-sensitized solar cells* atau DSSC). Fotoanoda DSSC dengan struktur lapisan ganda menarik para cendekiawan untuk melakukan observasi dan riset, karena memiliki efisiensi tinggi, biaya produksi rendah, dan kemampuan produksi secara massal. Semikonduktor dengan struktur lapisan ganda berupa $\text{TiO}_2\text{-ZnO}$ dapat diperoleh dari semikonduktor nanofiber ZnO yang dideposisikan dengan semikonduktor nanopartikel TiO_2 . Pendeposisian dapat dilakukan dengan metode *direct deposition* menggunakan bantuan mesin elektrospinning. Tujuannya adalah untuk secara langsung menangkap cairan elektro-jet yang dipintal dari larutan $\text{PVA}/\text{Zn}(\text{Ac})_2$ ke gelas oksida timah yang didoping fluor (FTO) yang terlapis semikonduktor nanopartikel TiO_2 . Studi ini ditujukan untuk mendapatkan jarak ujung jarum ke kolektor dan debit aliran terbaik dalam proses elektrospinning secara *direct deposition*. Eksperimen dilakukan pada proses pembuatan semikonduktor nanofiber ZnO yang digunakan sebagai fotoanoda DSSC dengan struktur lapisan ganda. Debit aliran dengan nilai 3, 4, 5, 6, 7, dan 8 $\mu\text{L}/\text{menit}$ diterapkan sebagai variasi parameter dalam eksperimen. Selain itu, jarak ujung ke kolektor juga divariasikan dengan nilai 3, 4, 5, 6, 7, dan 8 cm. Berdasarkan konfigurasi parameter yang ditetapkan, efek dari proses elektrospinning secara *direct deposition* yaitu pada perubahan morfologi semikonduktor nanofiber ZnO. Hasil penelitian menunjukkan bahwa debit aliran 4 $\mu\text{L}/\text{menit}$ dan jarak ujung ke kolektor 8 cm menghasilkan morfologi dengan diameter kecil dan seragam. Morfologi ini memungkinkan serat nano ZnO memiliki penyerapan warna dan eksitasi elektron yang lebih baik, dimana berbanding lurus dengan efisiensi tinggi DSSC dengan struktur lapisan ganda. Nilai kinerja untuk debit 4 $\mu\text{L}/\text{menit}$ adalah 2,39%, dan untuk jarak ujung jarum ke kolektor sejauh 8 cm adalah 1,61%.

Keywords: *semikonduktor, struktur lapisan ganda, metode direct deposition, sel surya tersensitisasi pewarna (dye-sensitized solar cells-DSSC)*

1. INTRODUCTION:

Solar cells harvest solar energy that is converted into electrical energy through the photovoltaic process (Grätzel, 2006; Valaski *et al.*, 2007). There have been three generations of solar cells, including silicon solar cells, thin layer type solar cells, and dye-sensitized solar cells (DSSCs) (Ali *et al.*, 2016). The DSSCs are easy to fabricate and have a lower cost than silicon solar cells or thin layer type solar cells (Qadir *et al.*, 2015). The performance of DSSCs, in general, can be characterized by several parameters, namely efficiency value, short-circuit photocurrent density (JSC), fill factor (FF), and open-circuit voltage (VOC). DSSCs are composed of two electrodes, a photoanode electrode and a photo inert counter electrode.

Photoanode electrodes are made of semiconductors that have absorbed dyes and are deposited on transparent conductive oxide. The photo inert counter electrodes are made of a platinum layer superimposed on transparent conductive oxide (Grätzel, 2003; Tobin *et al.*,

2011). Semiconductors in DSSCs' photoanodes function as converters of photon energy from solar radiation through the process of electron excitation based on the gap of material energy (bandgap) with an average of 1 to 5 eV. Some of the photoanode constituent semiconductor materials used for DSSCs are titanium oxide (TiO_2), zinc oxide (ZnO), and nickel (II) oxide

(NiO) (Grätzel, 2003; Tobin *et al.*, 2011). TiO_2 semiconductors have higher photovoltaic performance in the visible light region compared to ZnO semiconductors.

However, ZnO semiconductors have a lower electron charge recombination effect. In increasing electron mobility, nanomaterial engineering improves the properties of semiconductor materials with shapes such as nanoparticles, nanofibers, nanowires, nanorods, nanobelts, nanospirals, nanorings, and nanotubes, because nanomaterial engineering can increase chemical reactivity through the expansion of the relative area. ZnO and TiO_2 semiconductors have gone through a large amount of nanomaterial engineering because they have a better energy gap, i.e., 3.61 and 3.24

eV, respectively. These gaps can increase the semiconductor absorption of the dye and subsequently the excitation of electrons by photons (Bakr *et al.*, 2019; Khan *et al.*, 2019; Rani and Tripathi, 2015; Suprayogi *et al.*, 2019).

Engineering photoanode layers with TiO₂ nanoparticle semiconductors results in a higher surface area than other nanomaterial semiconductors because semiconductor nanoparticles can absorb dye molecules optimally (Chang and Lo, 2010; Seo *et al.*, 2007). However, the morphology of nanoparticles can reduce the mobility of electrons between particles and spread randomly (Mintcheva *et al.*, 2020). By contrast, the semiconductor ZnO nanofiber layer can bond directly with the substrate and dye to facilitate the mobility of excited electrons. Another advantage of fiber morphology is the effect of scattering photons in a photoanode, thereby increasing electron excitation (Saidin *et al.*, 2017; Sorayani Bafqi *et al.*, 2015). To increase the electron mobility of TiO₂ nanoparticle semiconductors, two layers of photoanodes can be engineered as follows: TiO₂ nanoparticle semiconductors are deposited with ZnO nanofiber semiconductors, where the first layer of semiconductor TiO₂ nanoparticles functions as a layer of dye loading (DL) and the second layer of semiconductor ZnO nanofibers functions as a layer of light scattering (LS). The use of a two-layer photoanode could increase the efficiency of DSSCs by up to 2.1 times that of using a single photoanode layer. This is also proportional to the bandgap value of 2.5–3 eV. The two-layer photoanode layer arranged to form a sandwich could strengthen the semiconductor bond with the substrate (adhesive properties), as shown in Figure 1 of Appendix (Cao *et al.*, 2017; Ghanbari Niaki *et al.*, 2014; Humayun *et al.*, 2019; Zhou *et al.*, 2019).

Manufacturing modification of the two layers of photoanode can consist of ZnO semiconductors deposited directly on TiO₂ semiconductors. Particulate TiO₂ semiconductors can be created using the doctor blade method (Dobrzański *et al.*, 2016), in which a TiO₂ paste is deposited on fluorine-doped tin oxide (FTO) glass and sintered. Subsequently, ZnO nanofiber semiconductors can be obtained from the direct deposition process on FTO glass that has been coated with a TiO₂ semiconductor using the electrospinning process. The use of direct deposition methods in the two-layer photoanode engineering is intended to reduce fabrication time and prevent damage to the nanoparticle and nanofiber structures, and can improve DSSCs'

performance (Yang *et al.*, 2017). However, the use of the electrospinning process depends on the distribution of molecular weight, the surface viscosity of the solution, and temperature (Panthi *et al.*, 2015; Sorayani Bafqi *et al.*, 2015).

The flow rate and the distance of the tip to the collector in the electrospinning process greatly affect the diameter size in nanofiber morphology. Therefore, this paper investigates the effect of variations in the distance of the tip to the collector and in the discharge of the direct deposition of ZnO semiconductors on the performance of DSSC double-layer photoanodes. The use of a flow rate of 4 µL/min and a distance of 8 cm in the electrospinning process were found to provide morphological results with a small and uniform diameter. Semiconductor morphology determines the dye loading value. The amount of dye loading value can affect the DSSC performance value (Alrikabi, 2017; Hekmati *et al.*, 2013; López-Covarrubias *et al.*, 2019). Therefore, flow rates of 3, 4, 5, 6, 7, and 8 µL/min and distances of 3, 4, 5, 6, 7, and 8 cm were examined.

2. MATERIALS AND METHODS:

2.1. Materials

In this study, the main reagents used were zinc acetate dihydrate ((CH₃COO)₂Zn·2H₂O, Merck) as the main material forming ZnO semiconductors; polyvinyl alcohol (PVA) (CH₂CH(OH)_n, MW = 72,000, Merck) as a carrier material in the electrospinning process; aquades as a solvent applied to the zinc acetate and PVA to form a homogeneous solution; a glass plate with 28 test working electrodes printed with TiO₂ opaque paste (160 mm x 80 mm x 3.2 mm); synthetic dyes—N719 ([RuL₂(NCS)₂]:2TBA (L = 2,2'-bipyridyl-4,4'-dicarboxylic acid; TBA = tetra-*n*-butylammonium)) and Iodide (I³⁻) EL-HPE electrolyte solution (Hongsih *et al.*, 2015).

2.2. Fabrication of ZnO Nanofibers

The addition of precursor solutions was used to produce the morphology of the nanofibers. The precursor solution was prepared using 2 g of PVA (Merck, MW = 72,000) mixed with 20 ml of H₂O (pH = 7). The homogenization process was carried out by stirring for 4 h at a 70 °C solution temperature. The Zn(Ac)₂ solution was synthesized using 2 g of zinc acetate dihydrate ((CH₃COO)₂Zn·2H₂O, Merck),

and 8 ml of H₂O, and then the homogenization process was carried out by stirring for 1 h while keeping the solution at 70 °C. Subsequently, the homogenization process between the PVA solution and Zn(Ac)₂ was carried out in a ratio of 4:1 wt% at 70 °C for 8 h. The entire solution was mixed in a closed container using a magnetic stirrer.

Following the above, the PVA/Zn(Ac)₂ solution was left in a closed room at room temperature for 24 h so that the foam formed could be lost. The result is a PVA/Zn(Ac)₂ solution, which is used to produce the ZnO nanofiber fibers using an electrospinning machine (Zhou *et al.*, 2019).

The PVA/Zn(Ac)₂ solution was used to form ZnO nanofibers on the TiO₂/ZnO double-layer DSSCs through an electrospinning process (Katoch *et al.*, 2014). As much as 1 mL of the solution was injected into a syringe pump and connected to the electrospinning machine at the Nanobioenergy Lab, Universitas Sebelas Maret Surakarta, as shown in Figure 2 of Appendix. Electrospinning machine specifications: collector; voltage power supply: 15 kV; injection pump tip distance to the collector: 10–200 mm; injection pump solution output: 2.237 ml/h. The tip on the syringe pump was connected to a high voltage positive terminal at varying distances (3, 4, 5, 6, 7, and 8 cm) located horizontally relative to the collector plate of the fluorine-doped tin oxide glass deposited with TiO₂ with negative terminals using the direct deposition method. The flow rate of the solution through the needle was varied (3, 4, 5, 6, 7, and 8 µL/min) based on the rate at the electrospinning machine. The fluorine-doped tin oxide glass deposited with TiO₂ nanoparticles and ZnO nanofibers was sintered at a temperature of 500 °C with a retention time of 1 h using a Digital Muffle Furnace model XD-1700M. The semiconductor deposition sintering results can be used as double-layer DSSC photoanodes (Hegazy *et al.*, 2016).

2.3 Assembling double-layer DSSCs

Double-layer DSSC photoanodes were soaked with synthetic dye N719 ([RuL₂(NCS)₂]: 2TBA (L = 2,2'-bipyridyl-4,4'-dicarboxylic acid; TBA = tetra-n-butylammonium) manufactured by Dyesol that was dissolved with a sensitizer solution. The sensitizer solution was prepared by dissolving 0.02 g N719 powder into 100 ml of ethanol. The resulting double-layer DSSC photoanodes were immersed in N719 dye for 24

h. The double-layered photoanode can absorb the solution completely (Sakai *et al.*, 2013). The results of the DSSC double-layer photoanode immersion were combined and bonded with a perforated counter electrode. Subsequently, EL-HPE Iodide (I³⁻) solution manufactured by Dyesol, which was used as an electrolyte, was injected through a hole in the counter electrode and covered with a Dyesol plaster. The FTO substrate components, colorants, electrolytes, and counter electrodes form unified DSSCs (Kouhestanian *et al.*, 2016; Wei and Hu, 2015).

2.4 Testing

DSSCs performance was examined using scanning electron microscopy (SEM) to determine the morphology and size of semiconductor nanofibers; absorbance testing with a UV 1800 UV-VIS spectrophotometer was used to measure the bandgap energy value using Tauc's plot method, as shown in Equation 1 (Alrikabi, 2017; Firdaus *et al.*, 2012). The bandgap energy function is the value of VOC, as shown in Equation 2 (Bakr *et al.*, 2019); the dye-loading ability of each sample was measured using the desorption method and the Lambert–Beer equation, which tests the solution's absorbance, as shown in Equation 3 (Asib *et al.*, 2018).

$$E = h\nu = \frac{h \cdot c}{\lambda} \quad (\text{Eq. 1})$$

$$V_{OC} = \frac{E_{CB}}{e} + \frac{k_B T}{e} \ln \left(\frac{n}{N_{CB}} \right) - E_{redox} \quad (\text{Eq. 2})$$

$$A = \varepsilon \cdot c \cdot l \quad (\text{Eq. 3})$$

The performance of the DSSCs was tested using a Solar Simulator Machine with a light intensity of 100 mW/cm² and a surface area of 1 cm². The DSSC performance was evaluated by measuring the following: open-circuit photovoltage (VOC), photocurrent voltage curve (IV curve), fill factor (FF), short-circuit photocurrent density (JSC), and efficiency (η). Voltage and current curves were obtained from measurements' results, as shown in Figure 3 of Appendix (Humayun *et al.*, 2019).

In the voltage–current curve (IV), was a maximum power point (P_{MAX}) could be observed, which is the product of the maximum current and voltage. The fill factor (FF) value arises from a comparison between maximum power (P_{max}) and the multiplication of ISC and VOC values, as shown in Equation 4. The

DSSCs' efficiency was obtained from the ratio between maximum power (P_{max}) and light emitted in the solar cell (P_{light}). Light emission produces power, which is the result of the multiplication of the intensity of sunlight with the area of the active region, so that solar cell efficiency was obtained as shown in Equation 5 (Chou *et al.*, 2007; Hongsih *et al.*, 2015; Junger *et al.*, 2018).

$$FF = \frac{V_{MAX} \times I_{MAX}}{I_{SC} \times V_{OC}} \quad (\text{Eq. 4})$$

$$\eta = \frac{P_{MAX}}{P_{light}} = \frac{P_{MAX}}{I \times A} = \frac{I_{SC} \times V_{OC} \times FF}{I \times A} \quad (\text{Eq. 5})$$

3. RESULTS AND DISCUSSION:

3.1. Analysis of Scanning Electron Microscope (SEM) Results

3.1.1. Variation of Flow Rate

Figure 4 in Appendix shows the morphological forms of ZnO nanofiber semiconductors on double-layer DSSCs fabricated with various flow rates using the electrospinning process. It can be seen that lower flow rates produced more uniform shapes and diameters of the nanofibers. This is due to the fact that the lower flow rate emitted smaller solution bubbles through the injection pump tip onto the electrospinning machine. The emitted bubbles showed better stretching characteristics for the same electrostatic field. Additionally, faster stretches make it easier to dry and form fibers in the collector (Benekohal and Demopoulos, 2012; Dissanayake *et al.*, 2016).

Solution which has flow rate of 4 $\mu\text{L}/\text{min}$ in the fabrication process, causes smaller and more uniform nanofiber diameter. This was influenced by operational conditions (solution rate, tip distance to the collector, potential difference, and syringe needle size) and the solution (viscosity, conductivity, and surface tension). Because in this study the flow rate was varied and all other conditions were equal, the differences in diameter can be attributed to changes in the flow rate in the electrospinning process. As can be seen in Table 1 of Appendix, the flow rates of 4 $\mu\text{L}/\text{min}$ produced an average diameter that was 118.335 nm smaller than the flow rates of 3, 5, 6, 7, and 8 $\mu\text{L}/\text{min}$. The smaller and more uniform the diameter of the nanofiber morphology, the more

active will the surface area be in the process of absorbing the dye, which will, in turn, increase the absorption of light (Firdaus *et al.*, 2012; Grätzel, 2003; López-Covarrubias *et al.*, 2019; Saidin *et al.*, 2017).

3.1.2. Variations in Tip Distance to Collectors

SEM images of the ZnO nanofiber semiconductors on double-layer DSSCs that resulted from varying the distance between the tip and the collector during the electrospinning process are shown in Figure 5 of Appendix. All of the conditions of the fabrication of the ZnO semiconductors using the electrospinning process were constant except for the tip distance to the collector, which was varied. The figure shows that the larger the distance between the tip and the collector was, the more uniform were the results' morphological shape and size. This is because a closer distance of the tip to the collector causes the jet/whip to accelerate while the solution bubbles stick to the collector and turn into fibers. The overlapping fibers then do not stretch and may evaporate. Therefore, with closer distances, the resultant nanofiber had an irregular size and shape (Firdaus *et al.*, 2012; Saidin *et al.*, 2017).

As shown in Table 2 of Appendix, using a tip-to-collector distance of 8 cm resulted in an average diameter that was smaller than the other variations by 92.70 nm. The small size of the nanofiber expanded the surface of the semiconductor, thus increasing the absorption of dyes. A high absorption value of the dye facilitates the entry of light and thus the electron flow, as observed from the performance of DSSCs (Sorayani Bafqi *et al.*, 2015).

3.2. Characterization of Light Absorbance and Transmittance

The absorbance value of the DSSCs was obtained using the desorption method by releasing the bonds between the semiconductor and the absorbed dye using a base solvent. In this study, the double-layer DSSC photoanode was soaked in 8 ml alkaline solution (0.1 M NaOH) for 1 h. The bond between the semiconductor surface and the carboxylic acid could thus be broken, then the OH^- ions bonded to the dye molecules. Hence, the dye was separated from the semiconductor entirely. The released dye solution was tested for its absorbance value using UV-VIS (Asib *et al.*, 2018; Marimuthu *et al.*, 2018).

3.2.1. Flow Rate Variation

Figure 6a of Appendix shows the magnitude of the absorbance value for each flow rate variation in the electrospinning process. It can be seen that based on the trend of the N719 dye, at a wavelengths of 450–550 nm, the use of 4 $\mu\text{L}/\text{min}$ discharge had a higher absorbance value compared to other flow rate variations (Alrikabi, 2017). This is related to the shape and size of the morphology that resulted from the flow rate of 4 $\mu\text{L}/\text{min}$, which was uniform and had a smaller average diameter compared to other flow rates. As a result, it had a better dye loading ability, which was $1.25 \times 10^{-7} \text{ mol}/\text{cm}^2$. A high absorbance value increases the current density (JSC), which affects the efficiency of the DSSCs (Lee *et al.*, 2015). As the dye trend we used is at a wavelengths of 450–550 nm, the transmittance value is inversely proportional to the absorbance value (Marimuthu *et al.*, 2017). As shown in Figure 6b of Appendix, the use of 4 $\mu\text{L}/\text{min}$ discharge resulted in the lowest transmittance value. This is because of the large absorption ability of the dye using a discharge variation of 4 $\mu\text{L}/\text{min}$.

3.2.2. Tip Distance to Collector Variations

Regarding tip-to-collector distance variations, the usage of a distance of 8 cm resulted in the double-layer DSSCs with the highest absorbance values at wavelengths of 450–550 nm. As shown in Figure 7a of Appendix, the farther the tip's distance to the collector, the higher the absorbance value that was obtained. Based on the double-layer photoanode's characteristics, a high absorbance value indicated a higher light absorption ability. This was also corroborated by the large value of dye loading calculated according to the Lambert–Beer equation. The usage of an 8 cm tip-to-collector distance resulted in a dye loading value of $1.25 \times 10^{-7} \text{ mol}/\text{cm}^2$, thus increasing the amount of electric current received from the DSSCs (Kabir *et al.*, 2019; Marimuthu *et al.*, 2017). The light transmitted from or exited by the photoanode was identified through the results of the transmittance test. The lower the transmittance value, the less light which came out. As can be seen in Figure 7b of Appendix, the use of an 8 cm tip-to-collector distance resulted in the lowest transmittance value at the 450–550 nm wavelengths. This indicates that the ZnO semiconductor nanofiber produced by direct deposition using the electrospinning process helped the dye loading by blocking the amount of light that came out.

3.3. Band Gap Testing

The bandgap energy value was determined through absorbance spectrum testing in ultraviolet rays and visible light, i.e., the wavelengths of 200 to 800 nm. Through the graph derived by Tauc plot method, the value of the bandgap was obtained by extrapolating the linear line of the curve formed by $(\alpha \cdot hv)^{1/r}$ to hv , where α is the absorbance coefficient and hv is the photon energy. Figures 8a and 8b of Appendix show the bandgap values for each variation. The results show that the larger the tip-to-collector distance and the smaller the flow rate, the lower the obtained bandgap value. A decrease in the value of the bandgap is an indication of a shrinking semiconductor size. This allows for easier electron excitation when obtaining energy from outside (Bakr *et al.*, 2019; Ghanbari Niaki *et al.*, 2014).

3.4. Performance of DSSCs

3.4.1. Flow Rate Variation

The curve in Figure 9a of Appendix indicates the photocurrent vs. photovoltage (IV) density for each DSSCs variation of discharge with an intensity of 100 mW/cm^2 . Table 3 of Appendix illustrates the performance of DSSCs according to VOC, JSC, FF, and efficiency values for the discharge variations. The results show that the morphological changes to the ZnO nanofiber semiconductors had a large influence on JSC and a small effect on the VOC of DSSCs. This shows that the 4 $\mu\text{L}/\text{min}$ precursor discharge in the nanofiber electrospinning process produced a small nanofiber size and the maximum electrical conductivity. Higher conductivity values were found to reduce electrical resistance in DSSCs (Seo *et al.*, 2007). With a greater dye loading ability for light absorption and optimal electrical conductivity, the variation of the 4 $\mu\text{L}/\text{min}$ precursor discharge had the maximum value of DSSCs efficiency among the variations examined. It can be seen that the discharge of 4 $\mu\text{L}/\text{min}$ had the highest efficiency of DSSCs at 2.39%. VOC, JSC, and FF values were 0.58 V, 9.14 mA/cm^2 , and 45.18%, respectively.

3.4.2. Tip Distance to Collector Variations

The performance characteristics of the double-layer photoanodes as a function of variation of tip-to-collector distance can be seen in Figure 9b and Table 4 of Appendix. DSSCs with direct deposition of ZnO nanofibers with a distance of 8 cm from tip to the collector had the highest photovoltaic conversion efficiency. As

seen from the SEM test results, the 8 cm tip-to-collector distance resulted in the smallest nanofiber size. The small ZnO nanofiber semiconductor diameter increased the DSSCs' photovoltaic performance due to the higher surface area for absorbing dye molecules (dye loading), resulting in higher light absorption (Hekmati *et al.*, 2013; Ramli *et al.*, 2019; Sorayani Bafqi *et al.*, 2015). It can be seen that the 8 cm tip-to-collector distance resulted in the highest efficiency of DSSCs at 1.61%. VOC, JSC, and FF values were 0.56 V, 6.41 mA/cm², and 44.920%, respectively.

4. CONCLUSIONS:

Double-layer TiO₂-ZnO DSSCs were obtained using nanofiber ZnO semiconductors deposited directly on fluorine-doped tin oxide (FTO) glass coated with a TiO₂ nanoparticle semiconductor using an electrospinning machine. The use of a solution flow rate of 4 µL/min and a distance of 8 cm from the tip of the needle to the collector in the direct deposition process using an electrospinning machine produced better nanofibers than other variations, whose morphology had a small and uniform diameter of 118.35 and 85.6 nm, with a dye loading value of 1.25×10^{-7} mol/cm². The performance value for the discharge of 4 µL/min was 2.39%, and for the 8 cm tip-to-collector distance the value was 1.61%.

5. ACKNOWLEDGMENTS:

This work was partially supported by a PDUPT grant from the Ministry of Research, Technology, and Higher Education, the Republic of Indonesia, with contract number 112/UN27.21/HK/2020 for FY 2020.

6. REFERENCES:

1. Ali, N., Hussain, A., Ahmed, R., Wang, M. K., Zhao, C., Haq, B. U., and Fu, Y. Q. (2016). Advances in nanostructured thin-film materials for solar cell applications. *Renewable and Sustainable Energy Reviews*, 59, 726–737. <https://doi.org/10.1016/j.rser.2015.12.268>
2. Alrikabi, A. (2017). Theoretical study of the design dye-sensitivity for usage in the solar cell device. *Results in Physics*, 7(July), 4359–4363. <https://doi.org/10.1016/j.rinp.2017.07.022>
3. Asib, N. A. M., Aadila, A., Afaah, A. N., Rusop, M., and Khusaimi, Z. (2018). Low-temperature growth of ZnO nanorods array via solution-immersion on TiO₂ seed layer. *AIP Conference Proceedings*, 1963. <https://doi.org/10.1063/1.5036904>
4. Bakr, Z. H., Wali, Q., Yang, S., Yousefsadeh, M., Padmasree, K. P., Ismail, J., Ab Rahim, M. H., Yusoff, M. M., and Jose, R. (2019). Characteristics of ZnO-SnO₂ Composite Nanofibers as a Photoanode in Dye-Sensitized Solar Cells. *Industrial and Engineering Chemistry Research*, 58(2), 643–653. <https://doi.org/10.1021/acs.iecr.8b03882>
5. Benekohal, N. P., and Demopoulos, G. P. (2012). Green Preparation of TiO₂-ZnO Nanocomposite Photoanodes by Aqueous Electrophoretic Deposition. 159(5), 602–610. <https://doi.org/10.1149/2.016206jes>
6. Cao, F., Tian, W., Gu, B., Ma, Y., Lu, H., and Li, L. (2017). High-performance UV-vis photodetectors based on electrospun ZnO nanofiber-solution processed perovskite hybrid structures. *Nano Research*, 10(7), 2244–2256. <https://doi.org/10.1007/s12274-016-1413-2>
7. Chang, H., and Lo, Y. J. (2010). Pomegranate leaves and mulberry fruit as natural sensitizers for dye-sensitized solar cells. *Solar Energy*, 84(10), 1833–1837. <https://doi.org/10.1016/j.solener.2010.07.009>
8. Chou, T. P., Zhang, Q., Fryxell, G. E., and Cao, G. (2007). Hierarchically structured ZnO film for dye-sensitized solar cells with enhanced energy conversion efficiency. *Advanced Materials*, 19(18), 2588–2592. <https://doi.org/10.1002/adma.200602927>
9. Dissanayake, S. S., Dissanayake, M. A. K. L., Seneviratne, V. A., Senadeera, G. K. R., and Thotawattage, C. A. (2016). Performance of Dye-Sensitized Solar Cells Fabricated with Electrospun Polymer Nanofiber Based Electrolyte. *Materials Today: Proceedings*, 3(Icfdm 2015), S104–S111. <https://doi.org/10.1016/j.matpr.2016.01.014>
10. Dobrzański, L. A., Mucha, A., Prokopowicz, M. P., Szindler, M., Drygała, A., and Lukaszewicz, K. (2016). Characteristics of dye-sensitized solar cells with carbon

- nanomaterials. *Materiali in Tehnologije*, 50(5), 649–654. <https://doi.org/10.17222/mit.2014.134>
11. Firdaus, C. M., Shah Rizam, M. S. B., Rusop, M., and Rahmatul Hidayah, S. (2012). Characterization of ZnO and ZnO: TiO₂ thin films prepared by sol-gel spray-spin coating technique. *Procedia Engineering*, 41(Iris), 1367–1373. <https://doi.org/10.1016/j.proeng.2012.07.323>
 12. Ghanbari Niaki, A. H., Bakhshayesh, A. M., and Mohammadi, M. R. (2014). Double-layer dye-sensitized solar cells based on Zn-doped TiO₂ transparent and light scattering layers: Improving electron injection and light scattering effect. *Solar Energy*, 103, 210–222. <https://doi.org/10.1016/j.solener.2014.01.041>
 13. Grätzel, M. (2003). Dye-sensitized solar cells. *Journal of Photochemistry and Photobiology C: Photochemistry Reviews*, 4(2), 145–153. [https://doi.org/10.1016/S1389-5567\(03\)00026-1](https://doi.org/10.1016/S1389-5567(03)00026-1)
 14. Grätzel, M. (2006). Photovoltaic performance and long-term stability of dye-sensitized mesoscopic solar cells. *Comptes Rendus Chimie*, 9(5–6), 578–583. <https://doi.org/10.1016/j.crci.2005.06.037>
 15. Hegazy, A., Kinadjian, N., Sadeghimakki, B., Sivorththaman, S., Allam, N. K., and Prouzet, E. (2016). TiO₂ nanoparticles optimized for photoanodes tested in large area Dye-sensitized solar cells (DSSC). *Solar Energy Materials and Solar Cells*, 153, 108–116. <https://doi.org/10.1016/j.solmat.2016.04.004>
 16. Hekmati, A. H., Rashidi, A., Ghazisaeidi, R., and Drean, J. Y. (2013). Effect of needle length, electrospinning distance, and solution concentration on morphological properties of polyamide-6 electrospun nanowebs. *Textile Research Journal*, 83(14), 1452–1466. <https://doi.org/10.1177/0040517512471746>
 17. Hongsith, K., Hongsith, N., Wongrataphisan, D., Gardchareon, A., Phadungthitidhada, S., and Choopun, S. (2015). Efficiency Enhancement of ZnO Dye-sensitized Solar Cells by Modifying Photoelectrode and Counterelectrode. In *Energy Procedia* (Vol. 79). Elsevier B.V. <https://doi.org/10.1016/j.egypro.2015.11.503>
 18. Humayun, M., Zheng, Z., Fu, Q., and Luo, W. (2019). Photodegradation of 2,4-dichlorophenol and rhodamine B over n-type ZnO/p-type BiFeO₃ heterojunctions: detailed reaction pathway and mechanism. *Environmental Science and Pollution Research*, 26(17), 17696–17706. <https://doi.org/10.1007/s11356-019-05079-0>
 19. Junger, I. J., Wehlage, D., Böttjer, R., Grothe, T., Juhász, L., Grassmann, C., Blachowicz, T., and Ehrmann, A. (2018). Dye-sensitized solar cells with electrospun nanofiber mat-based counter electrodes. *Materials*, 11(9). <https://doi.org/10.3390/ma11091604>
 20. Kabir, F., Bhuiyan, M. M. H., Hossain, M. R., Bashar, H., Rahaman, M. S., Manir, M. S., Ullah, S. M., Uddin, S. S., Mollah, M. Z. I., Khan, R. A., Huque, S., and Khan, M. A. (2019). Improvement of efficiency of Dye-Sensitized Solar Cells by optimizing the combination ratio of Natural Red and Yellow dyes. *Optik*, 179(October 2018), 252–258. <https://doi.org/10.1016/j.ijleo.2018.10.150>
 21. Katoch, A., Kim, J. H., and Kim, S. S. (2014). TiO₂/ZnO inner/outer double-layer hollow fibers for improved detection of reducing gases. *ACS Applied Materials and Interfaces*, 6(23), 21494–21499. <https://doi.org/10.1021/am506499e>
 22. Khan, M. I., Saleem, M., Rehman, S. U., Ali, S. S., Qadri, M. U., Ahmed, N., Javed, M. S., and Iqbal, J. (2019). Stacked Layer Effect of ZnO/TiO₂ on the Efficiency of Dye-Sensitized Solar Cells. *Journal of Nanoelectronics and Optoelectronics*, 14(2), 291–296. <https://doi.org/10.1166/jno.2019.2493>
 23. Kouhestanian, E., Mozaffari, S. A., Ranjbar, M., SalarAmoli, H., and Armanmehr, M. H. (2016). Electrodeposited ZnO thin film as an efficient alternative blocking layer for TiCl₄ pre-treatment in TiO₂-based dye-sensitized solar cells. *Superlattices and Microstructures*, 96, 82–94. <https://doi.org/10.1016/j.spmi.2016.05.012>
 24. Lee, J. S., Kim, K. H., Kim, C. S., and Choi, H. W. (2015). Synergistic effect of TiCl₄-ZnO treated TiO₂ nanotubes in dye-sensitized solar cell. *Japanese Journal of Applied Physics*, 54(6). <https://doi.org/10.7567/JJAP.54.06FK02>

25. López-Covarrubias, J. G., Soto-Muñoz, L., Iglesias, A. L., and Villarreal-Gómez, L. J. (2019). Electrospun nanofibers applied to dye solar sensitive cells: A review. *Materials*, 12(19), 1–18. <https://doi.org/10.3390/ma12193190>
26. Marimuthu, T., Anandhan, N., and Thangamuthu, R. (2018). Electrochemical synthesis of one-dimensional ZnO nanostructures on ZnO seed layer for DSSC applications. *Applied Surface Science*, 428, 385–394. <https://doi.org/10.1016/j.apsusc.2017.09.116>
27. Marimuthu, T., Anandhan, N., Thangamuthu, R., and Surya, S. (2017). Facile growth of ZnO nanowire arrays and nanoneedle arrays with flower structure on ZnO-TiO₂ seed layer for DSSC applications. *Journal of Alloys and Compounds*, 693, 1011–1019. <https://doi.org/10.1016/j.jallcom.2016.09.260>
28. Mintcheva, N., Yamaguchi, S., and Kulinich, S. A. (2020). Hybrid TiO₂-ZnO nanomaterials prepared using laser ablation in liquid. *Materials*, 13(3), 11–15. <https://doi.org/10.3390/ma13030719>
29. Panthi, G., Park, M., Kim, H. Y., Lee, S. Y., and Park, S. J. (2015). Electrospun ZnO hybrid nanofibers for photodegradation of wastewater containing organic dyes: A review. *Journal of Industrial and Engineering Chemistry*, 21, 26–35. <https://doi.org/10.1016/j.jiec.2014.03.044>
30. Qadir, M. B., Sun, K. C., Sahito, I. A., Arbab, A. A., Choi, B. J., Yi, S. C., and Jeong, S. H. (2015). Composite multi-functional over layer: A novel design to improve the photovoltaic performance of DSSC. *Solar Energy Materials and Solar Cells*, 140, 141–149. <https://doi.org/10.1016/j.solmat.2015.04.011>
31. Ramli, N. F., Fahsyar, P. N. A., Ludin, N. A., Teridi, M. A. M., Ibrahim, M. A., Zaidi, S. H., and Sepeai, S. (2019). Compatibility between compact and mesoporous TiO₂ layers on the optimization of photocurrent density in photoelectrochemical cells. *Surfaces and Interfaces*, 17(March), 100341. <https://doi.org/10.1016/j.surfin.2019.100341>
32. Rani, M., and Tripathi, S. K. (2015). A Comparative Study of Nanostructured TiO₂, ZnO and Bilayer TiO₂/ZnO Dye-Sensitized Solar Cells. *Journal of Electronic Materials*, 44(4), 1151–1159. <https://doi.org/10.1007/s11664-015-3636-5>
33. Saidin, N. U., Choo, T. F., Kok, K. Y., Yusof, M. R., and Ng, I. K. (2017). Fabrication and characterization of ZnO nanofibers by electrospinning. *Materials Science Forum*, 888 MSF, 309–313. <https://doi.org/10.4028/www.scientific.net/MSF.888.309>
34. Sakai, N., Miyasaka, T., and Murakami, T. N. (2013). Efficiency enhancement of ZnO-based dye-sensitized solar cells by low-temperature TiCl₄ treatment and dye optimization. In *Journal of Physical Chemistry C* (Vol. 117, Issue 21, pp. 10949–10956). <https://doi.org/10.1021/jp401106u>
35. Seo, J. W., Chung, H., Kim, M. Y., Lee, J., Choi, I. H., and Cheon, J. (2007). Development of water-soluble single-crystalline TiO₂ nanoparticles for photocatalytic cancer-cell treatment. In *Small* (Vol. 3, Issue 5, pp. 850–853). <https://doi.org/10.1002/sml.200600488>
36. Sorayani Bafqi, M. S., Bagherzadeh, R., and Latifi, M. (2015). Fabrication of composite PVDF-ZnO nanofiber mats by electrospinning for energy scavenging application with enhanced efficiency. *Journal of Polymer Research*, 22(7), 1–9. <https://doi.org/10.1007/s10965-015-0765-8>
37. Suprayogi, T., Masrul, M. Z., Diantoro, M., Taufiq, A., Fuad, A., and Hidayat, A. (2019). The Effect of Annealing Temperature of ZnO Compact Layer and TiO₂ Mesoporous on Photo-Supercapacitor Performance. *IOP Conference Series: Materials Science and Engineering*, 515(1). <https://doi.org/10.1088/1757-899X/515/1/012006>
38. Tobin, L. L., O'Reilly, T., Zerulla, D., and Sheridan, J. T. (2011). Characterising dye-sensitised solar cells. *Optik*, 122(14), 1225–1230. <https://doi.org/10.1016/j.ijleo.2010.07.028>
39. Valaski, R., Canestraro, C. D., Micaroni, L., Mello, R. M. Q., and Roman, L. S. (2007). Organic photovoltaic devices based on polythiophene films electrodeposited on FTO substrates. *Solar Energy Materials and Solar Cells*, 91(8), 684–688.

<https://doi.org/10.1016/j.solmat.2006.12.005>

40. Wei, W., and Hu, Y. H. (2015). Synthesis of carbon nanomaterials for dye-sensitized solar cells. In *International Journal of Energy Research* (Vol. 39, Issue 6, pp. 842–850). <https://doi.org/10.1002/er.3312>
41. Yang, M., Dong, B., Yang, X., Xiang, W., Ye, Z., Wang, E., Wan, L., Zhao, L., and Wang, S. (2017). TiO₂ nanoparticle/nanofiber-ZnO photoanode for the enhancement of the

efficiency of dye-sensitized solar cells. *RSC Advances*, 7(66), 41738–41744. <https://doi.org/10.1039/c7ra07644d>

42. Zhou, C., Wang, H., Huang, T., Zhang, X., Shi, Z., Zhou, L., Lan, Y., and Tang, G. (2019). High-Performance TiO₂/ZnO Photoanodes for CdS Quantum Dot-Sensitized Solar Cells. *Journal of Electronic Materials*, 48(11), 7320–7327. <https://doi.org/10.1007/s11664-019-07536-5>

APPENDIX

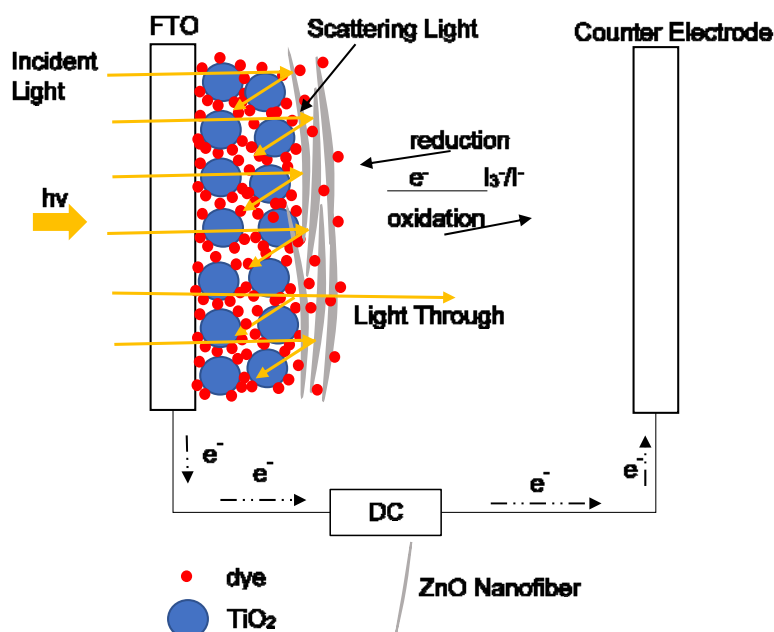
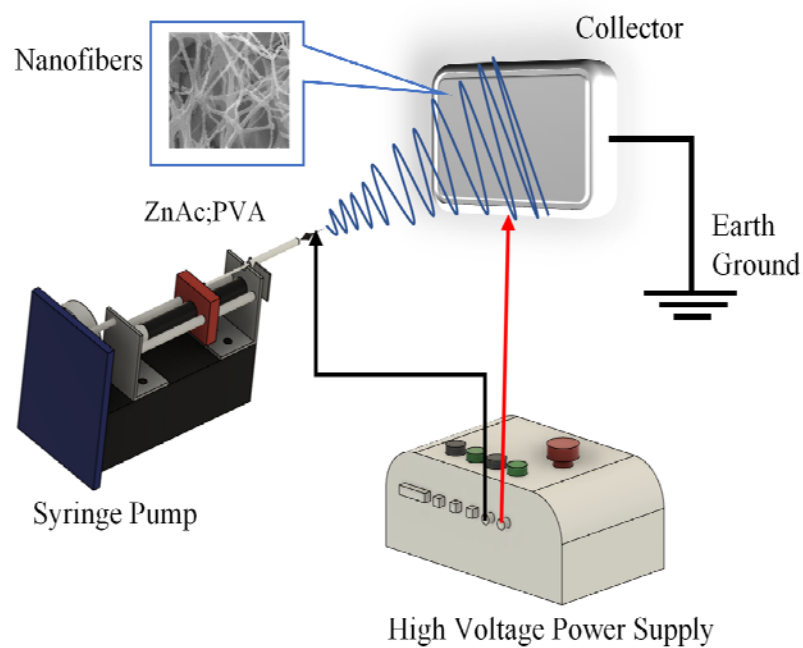
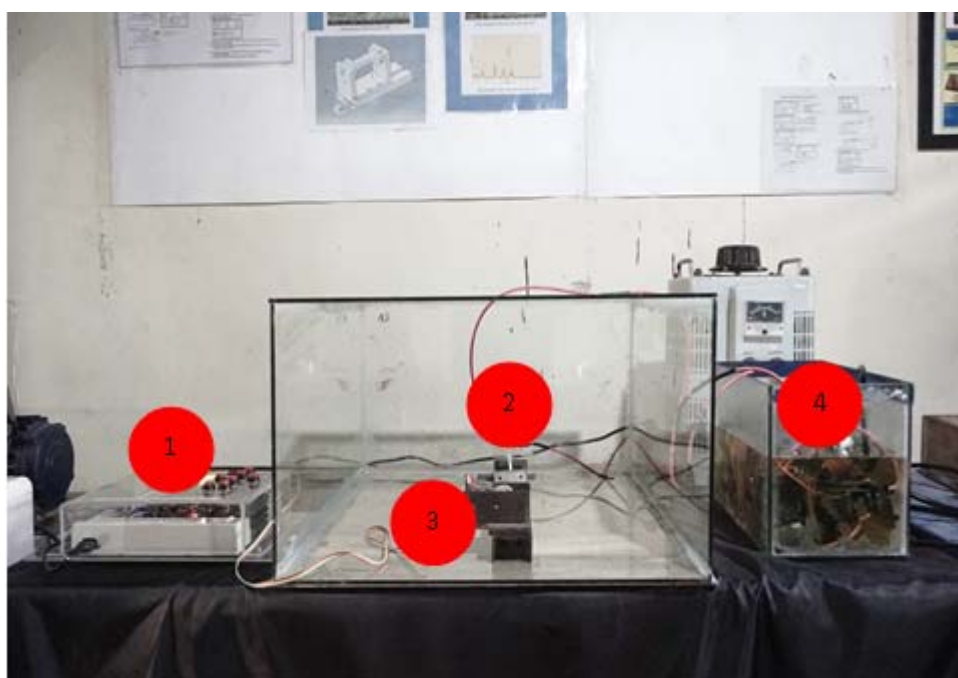


Figure 1. DSSCs double-layer photoanode structure.



(a)



(b)

Figure 2. (a) Scheme process (b) electrospinning machine.

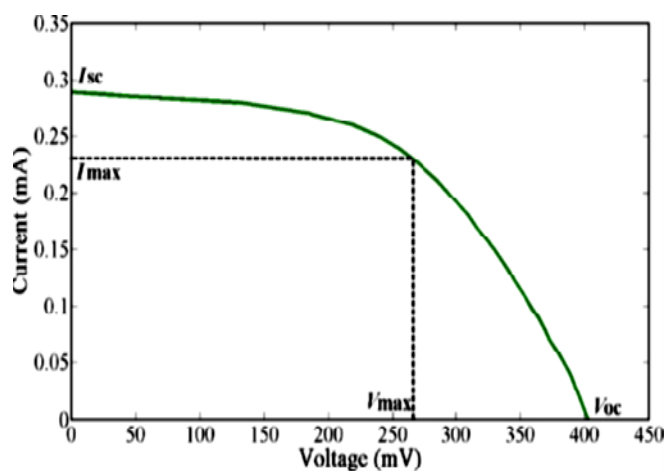
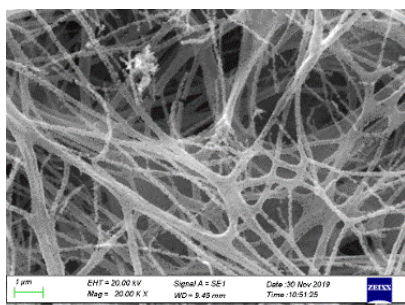
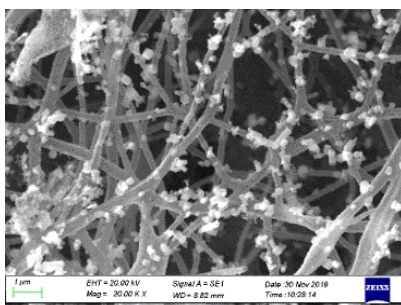


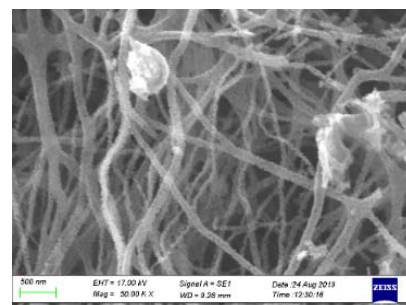
Figure 3. Voltage–current curves (IV curves) found on DSSCs (Tobin et al., 2011)



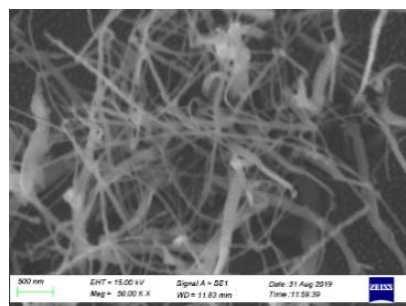
(a)



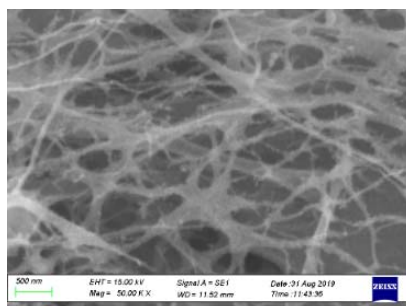
(b)



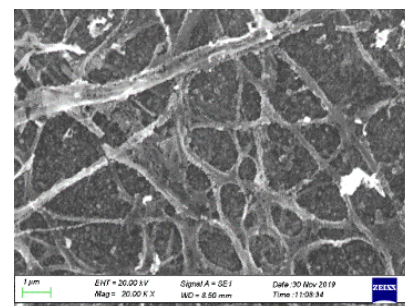
(c)



(d)



(e)



(f)

Figure 4. Semiconductor SEM photo results for variations of (a) 3 $\mu\text{L}/\text{min}$ (b) 4 $\mu\text{L}/\text{min}$ (c) 5 $\mu\text{L}/\text{min}$ (d) 6 $\mu\text{L}/\text{min}$ (e) 7 $\mu\text{L}/\text{min}$ (f) 8 $\mu\text{L}/\text{min}$.

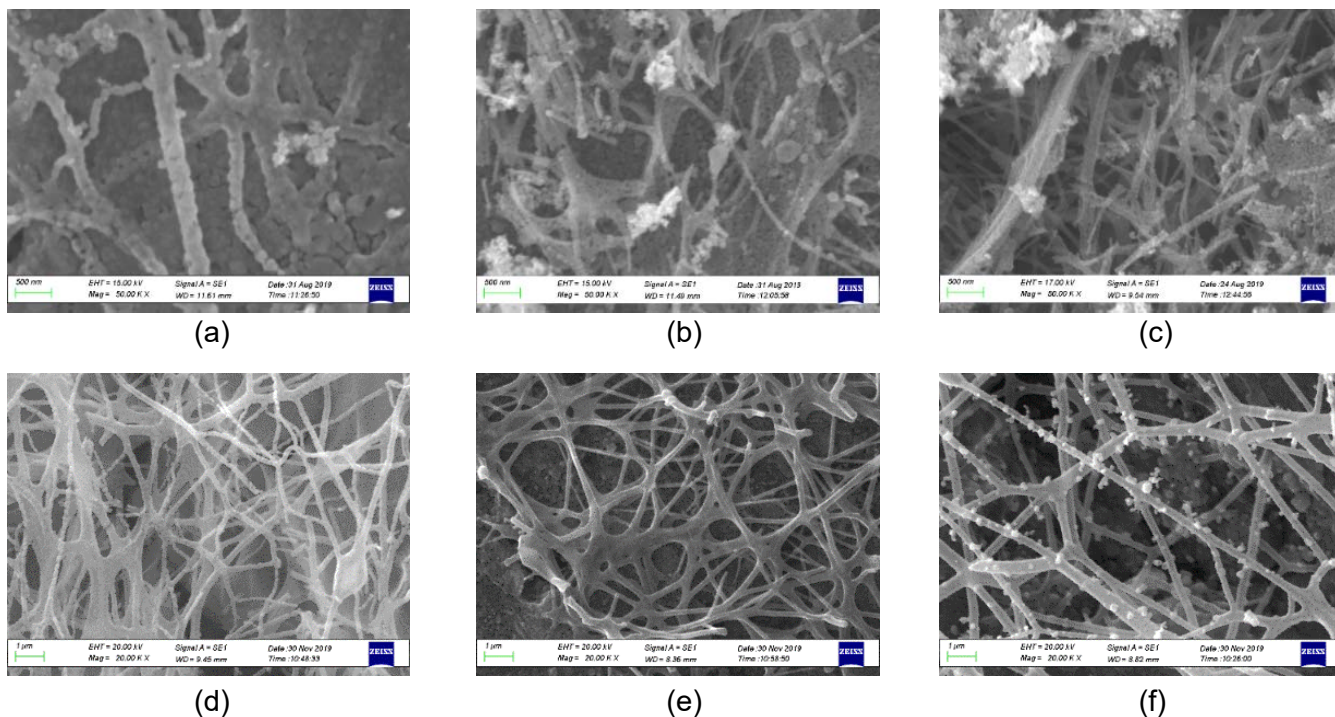


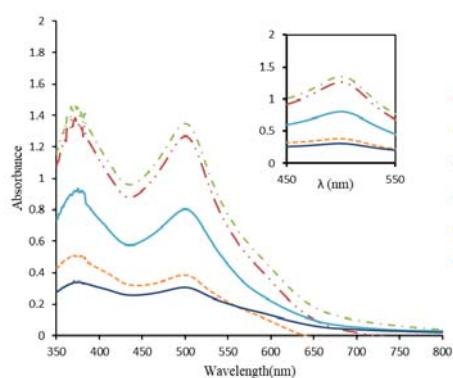
Figure 5 ZnO semiconductor SEM photo results for variations of (a) 3 cm (b) 4 cm (c) 5 cm (d) 6 cm (e) 7 cm (f) 8 cm.

Table 1. ZnO semiconductor diameter size for variations in flow rate.

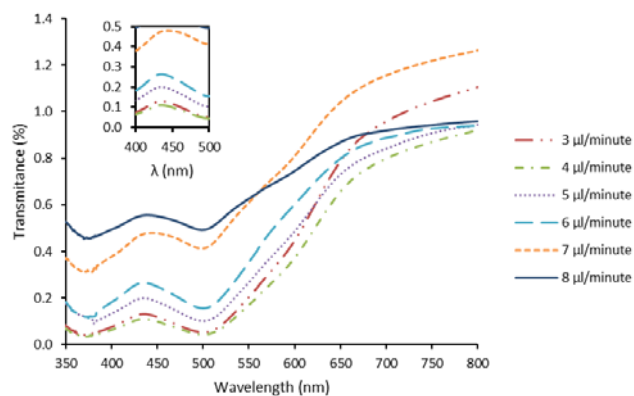
Flow Rate Variation ($\mu\text{L}/\text{minute}$)	Average diameter (nm)	Maximum diameter (nm)	Minimum Diameter (nm)	Standard deviation (nm)
3	122.18	150.15	94.33	16.25
4	118.35	158.82	80.88	17.24
5	125.43	175.52	100.23	15.16
6	129.37	176.47	107.94	18.85
7	134.45	175.50	95.45	16.20
8	141.39	169.11	98.76	16.18

Table 2. ZnO semiconductor diameter size for variations in distance.

Tip to collector distance (cm)	Average diameter (nm)	Maximum diameter (nm)	Minimum Diameter (nm)	Standard deviation (nm)
3	140.4	170.21	97.80	16.28
4	115.3	155.83	79.88	17.24
5	107.3	141.49	67.59	17.52
6	96.7	140.57	63.29	15.33
7	92.7	126.20	49.45	16.12
8	85.6	114.57	62.17	14.33

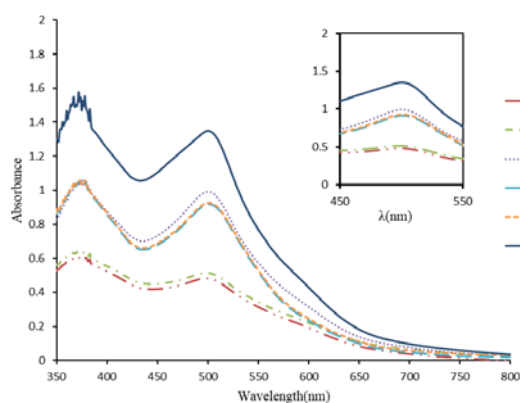


(a)

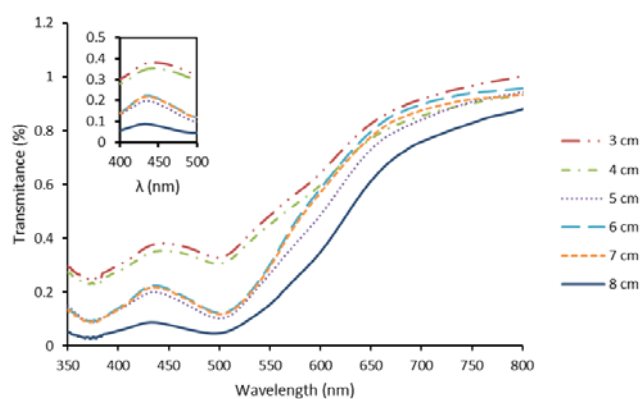


(b)

Figure 6. (a) The results of ZnO semiconductor absorbance tests for flow rate variations; (b) the results of ZnO semiconductor transmittance tests for flow rate variations.

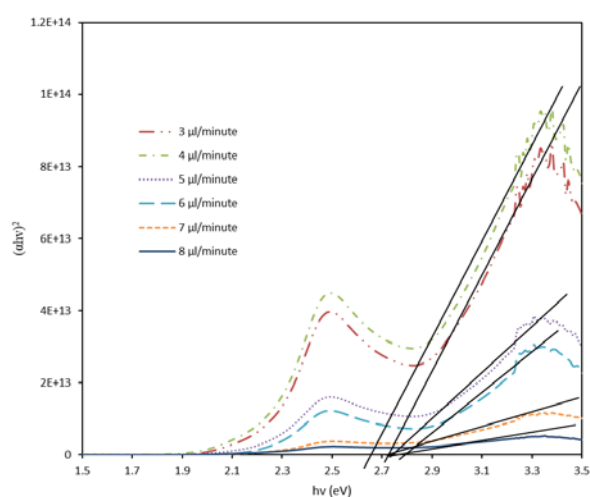


(a)

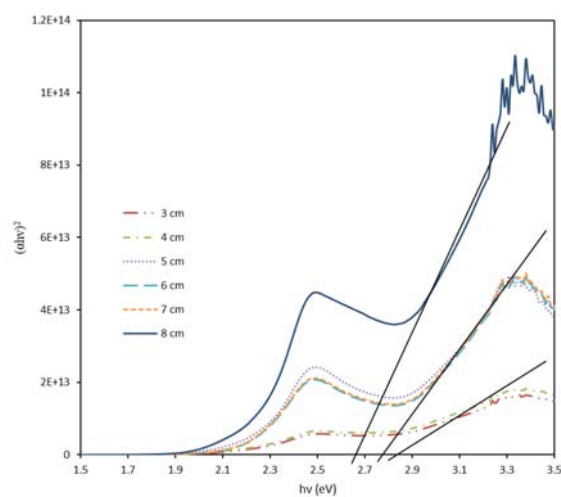


(b)

Figure 7. (a) ZnO semiconductor absorbance test results for distance variations; (b) ZnO semiconductor transmittance test results of distance variations.



(a)



(b)

Figure 8. (a) Tauc's plot method used in determining the ZnO semiconductor band gap for variations in flow rate; (b) Tauc's plot method used in determining the ZnO semiconductor band gap for distance variations.

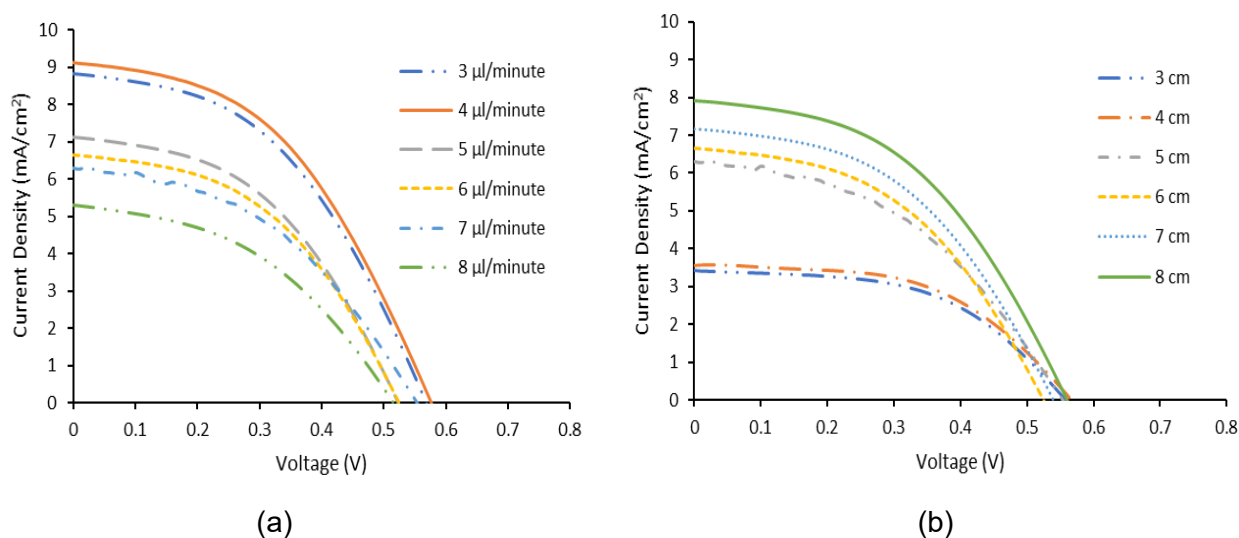


Figure 9. (a) IV curve of each flow rate variation; (b) IV curve of each tip-to-collector distance variation.

Table 3. DSSCs characteristics for flow rate variations.

Flow Rate Variation (µl/minute)	VOC (V)	JSC (mA/cm ²)	Fill Factor (%)	Efficiency (%)	Dye Loading (x 10 ⁻⁷ mol/cm ²)
3	0.56	8.84	45.80	2.27	1.17
4	0.58	9.14	45.18	2.39	1.25
5	0.53	7.14	45.09	1.71	0.74
6	0.53	6.65	45.72	1.61	0.65
7	0.55	6.29	44.13	1.53	0.35
8	0.52	5.31	42.97	1.19	0.28

Table 4. DSSCs characteristics for tip-to-collector distance variations.

Distance Variation (cm)	VOC (V)	JSC (mA/cm ²)	Fill Factor (%)	Efficiency (%)	Dye Loading (x 10 ⁻⁷ mol/cm ²)
3	0.56	2.71	52.02	0.79	0.44
4	0.56	2.85	52.09	0.85	0.47
5	0.55	4.49	44.13	1.09	0.81
6	0.53	4.89	45.72	1.18	0.85
7	0.54	5.66	45.45	1.39	0.86
8	0.56	6.41	44.92	1.61	1.25

PRODUTIVIDADE LEITEIRA E PROPRIEDADES TECNOLÓGICAS DO LEITE DAS VACAS HOLSTEIN E BLACK-MOTLEY**MILK PRODUCTIVITY AND TECHNOLOGICAL PROPERTIES OF THE MILK FROM THE HOLSTEIN AND BLACK-MOTLEY COWS****МОЛОЧНАЯ ПРОДУКТИВНОСТЬ И ТЕХНОЛОГИЧЕСКИЕ СВОЙСТВА МОЛОКА КОРОВ ГОЛШТИНСКОЙ И ЧЁРНО-ПЁСТРОЙ ПОРОД**

BABICH, Elena Anatolyevna^{1*}; OVCHINNIKOVA, Lyudmila Yuryevna²; OVCHINNIKOV, Aleksandr Aleksandrovich³; ZHAKSUMBAY, Zhanara Serikovna⁴

^{1,4} Kostanay Research Institute of Agriculture. Kazakhstan.

^{2,3} South Ural State Agrarian University, Institute of Veterinary Medicine. Russian Federation.

* Correspondence author
e-mail: elena._76@mail.ru

Received 12 June 2020; received in revised form 30 September 2020; accepted 28 October 2020

RESUMO

Ao avaliar vacas leiteiras, tanto as propriedades quantitativas quanto tecnológicas do leite são essenciais. Os conteúdos de matéria seca e de sólidos não gordurosos do leite determinam o valor nutricional do leite e do seu consumo para obter produtos lácteos. O artigo apresenta um estudo das características do leite de vacas das raças Holstein e black-motley. O estudo buscou determinar a adequação do leite para a produção de queijo. No experimento científico e econômico, as propriedades tecnológicas do leite das vacas Holstein e black-motley, com vários níveis de produtividade leiteira, foram comparativamente analisadas. Com base nos resultados dos estudos, descobriu-se que, com um alto nível de produtividade leiteira, o leite das vacas Holstein continha 12.4% menos matéria seca e que o leite das vacas black-motley continha 10.9% menos matéria seca. O aumento do conteúdo de matéria seca resultou em um aumento geral do conteúdo de gordura e de proteína para 93.0% e 87.1%, respectivamente. Uma correlação predominantemente positiva entre os componentes do leite foi encontrada. Para a produção de queijo, o leite de vaca com uma concentração maior de matéria seca é o mais valioso. A venda do leite com base no seu conteúdo de matéria seca permite que uma economia obtenha uma receita US\$ 3.07 maior para a raça Holstein e US\$ 1.90 maior para a raça black-motley.

Palavras-chave: *proteína, lactose, caseína, proteínas do soro, eficiência econômica.*

ABSTRACT

In assessing dairy cows, both quantitative and technological milk properties are essential. The contents of dry matter and nonfat milk solids determine the nutritional value of milk and its consumption for obtaining dairy products. The article presents a study of the characteristics of milk from cows of Holstein and black-motley breeds. The study aimed to determine the suitability of milk for cheese making. In the scientific and economic experiment, the technological properties of the milk from the Holstein and black-motley cows with various levels of milk productivity were comparatively analyzed. By the results of the studies, it has been found that with a high level of milk productivity, the milk of the Holstein cows contained less dry matter by 12.4 %, and the milk of black-motley cows contained less dry matter by 10.9 %. Increasing the content of dry matter has resulted in overall increasing fat and protein content to 93.0 % and 87.1 %, respectively. A predominantly positive correlation between the milk components has been found. For cheese-making, cow milk with a higher concentration of dry matter is the most valuable. The milk sale by its dry matter content allows an economy to obtain more revenue by USD 3.07 for the Holstein breed and by USD 1.90 for the black-motley breed.

Keywords: *protein, lactose, casein, whey proteins, economic efficiency.*

АННОТАЦИЯ

При оценке коров молочных пород важное значение имеют не только количественные, но и

технологические показатели молока. Показатели сухого вещества и СОМО обуславливают питательную ценность молока, его расход при производстве молочных продуктов. В статье приведены результаты исследования характеристик молока коров голштинской и чёрно-пёстрой породы. Целью исследования было определение пригодности молока для сыроделия. В научно-хозяйственном опыте проведен сравнительный анализ технологических свойств молока коров голштинской и чёрно-пёстрой породы разного уровня молочной продуктивности. По результатам исследований установлено, что при высоком уровне молочной продуктивности в молоке коров обеих пород содержалось меньше сухого вещества на 12,4% по голштинской и 10,9% по чёрно-пёстрой породе. Увеличение сухого вещества обусловило суммарное повышение содержания жира и белка 93,0% и 87,1% соответственно. Определена преимущественно положительная корреляционная связь между составными частями молока. Наиболее ценным для сыроделия является молоко коров с большей концентрацией сухого вещества. Реализация молока по содержанию сухого вещества позволяет хозяйству получать больше выручки на 3.07 доллара по голштинской породе и 1.90 доллара по черно-пестрой породе.

Ключевые слова: белок, лактоза, казеин, сывороточные белки, экономическая эффективность.

1. INTRODUCTION:

In all countries of the world, 652 breeds of cattle are currently bred, including about 30 breeds of various productivity orientations in Kazakhstan. Breeding so many breeds is explained by the fact that one or two breeds will not completely and optimally use various forage and climatic conditions in individual zones of this vast country. Among the indicators that characterize the biological, breeding, and productive qualities of breed or crossbred cattle, milk productivity and milk composition are important features. Depending on the main components in milk, cattle breeds differ against each other and are divided into rich-milking and so-called curd breeds, the milk of which is the richest in protein. Along with the task of increasing milk productivity, modern cattle breeding is facing the task of substantially improving milk quality, which means a combination of various properties, depending on the purpose (Babich, Kikebaev, Raketskiy, and Baysakalov, 2019; Katmakov, Gavrilenko, Bushov, and Prokofiev, 2019). The prospects of the development of dairy cattle breeding and the future of the dairy industry in Kazakhstan are mainly associated with the production of high-quality raw milk and its further processing into high-quality dairy products. In particular, ensuring the nutritional value of foodstuffs requires increasing the share of animal proteins, where a significant role is played by the milk protein, which has high biological value (Safronova, Babich, Ovchinnikova, Ovchinnikov, 2017; Babich, Nugmanov, Ovchinnikova, and Ovchinnikov, 2016). Milk proteins enter the human organism with milk, dairy products, and cheese. This causes redistribution in the structure of milk, namely, the share of the milk consumed fresh and the one processed into butter, and condensed milk reduces, while the share of the milk processed into cheese increases. This has brought forward new

demands to the milk quality and to increasing the content of all the components of dry matter, especially protein (Cole, Bickhart, Waurich, Wensch-Dorendorf, and Swalve, 2014 Adamczyk, Makulska, Jagusiakand, and Węglarz, 2017; Holroyd et al., 2002).

Milk, being the most proper food product, contains a set of all essential nutrients in an easily digestible and balanced form. Milk composition determines its biological and nutritional value and the yield and quality of dairy products. In this regard, knowledge of changes in the chemical composition of the milk from cows of various breeds during production and processing is of great importance. Milk has a complex chemical composition: the moisture content is within 87.5 %, the dry matter content is about 12.5 %. Dry matter includes fat (3.6 %), protein (3.2 %), lactose (4.7 %), minerals (0.7 %), and about 250 more components.

In the breeding work with dairy cattle, mainly the milk yield and the fat content in the milk have been taken into account for a long time. However, given the modern requirements for product quality, such an approach does not allow a comprehensive, in-depth assessment of milk productivity. The most valuable milk is the dry matter, which consists of fat, proteins, milk sugar, minerals, vitamins, pigments, hormones, enzymes, and immune bodies with high biological activity. Nonfat milk solids and lactose should also be taken into account. In the human organism, lactose plays an energetic role and creates a favorable environment for developing beneficial microflora.

Improving the quality and composition of produced raw milk remains relevant since making any type of dairy products requires raw materials compliance with several indicators. Therefore, the traditional traits of dairy cattle breeding have been

recently supplemented with the content of milk, protein, lactose, nonfat milk solids (NFMS), dry matter, and the total content of fat and protein (De Jong, 2000; Bastin, Loker, Gengler, Sewalem, and Miglior, 2010; Pimentel, Erbe, Knig, and Simianer, 2011; Wang, Segelke, Emmerling, Bennewitz, and Wellman, 2017). The purchase price for milk is also set by processing enterprises with consideration of the indicators set above.

1.2. Literature Review:

When the economic and social conditions in agricultural production have fundamentally changed, real opportunities have opened up for the accelerated intensification of dairy cattle breeding.

The basis for increasing the efficiency of dairy cattle breeding and improving the productive qualities is improving the breeding work. The analysis of the previous stages of work showed the gradually increasing intensification pace, which had been primarily caused by introducing the new biotechnological methods, the population genetics, and the use of the world's best gene pool of the dairy breeds.

In the leading countries, the intensification of dairy cattle breeding is ensured by increasing highly productive breeds, especially the Holstein one. Conditions are created for the maximum possible introduction and long-term use of the genotype. The high productivity of the cows and improving their reproductive abilities and long-term economic use are achieved only through the full-fledged feeding and balancing of the diets in terms of the content of all the necessary nutrition elements, creating comfortable conditions for animals, and high-productive work of the personnel. As a rule, on average, highly productive animals give better offsprings characterized by the growth and development energy, and, finally, valuable dairy traits. Some authors note that the most important factor affecting milk composition and quality is the breed features of the animals.

In assessing the productive qualities of the dairy cows, the following features were used: the milk yield obtained over 305 days of lactation, the peak daily milk yield, the uniformity of lactation, the milk flow intensity, the completeness of milking, and the content of fat, protein, and NFMS (Yesbolova and Maciejczak, 2012; Samusenko and Khimicheva, 2018).

The main task in dairy farming is intensifying the industry by accelerating the growth of the genetic potential of domestic cattle and the degree of its implementation. To increase the milk

productivity of motley-black cows, several commercial farms throughout the country engaged in breeding use the Holstein breed gene pool, which gives a powerful impetus to the development of the entire dairy cattle breeding. This breed occupies one of the leading places in terms of the milk productivity ratio to the operation of industrial complexes.

A high level of lactation causes a restructuring of the entire organism of the animal and changes the correlations between various indicators. First of all, milk productivity increases demand for qualitative milk composition (Faizullin and Kharlan, 2019; Khromova and Manzhurin, 2018; Nemtseva and Ignatieva, 2020).

A comparative assessment of the productivity and quality of the milk obtained from purebred motley-black cows showed that their origin influenced milk process parameters. For instance, cows of the Ues Ideal line were characterized by better rennet coagulation, high content of casein (2.65 – 2.70 %), and milk sugar (4.86 %) (Gagloev, Negreeva, Gagloeva, and Skobeev, 2017).

The quality of milk is not stable and depends on several factors, one of which is targeted breeding aimed at increasing the hereditary potential in the context of the modern breed composition and interbreed groups bred in specific keeping and feeding conditions, and breeding aimed at improving the composition of the milk as an important criterion for selecting animals of specialized dairy breeds.

In the conditions of breeding farms in the Russian Federation, the Holstein breed plays a leading role. The studies of N. I. Morozova, F. A. Musaeva, O. A. Morozova (2016) performed at the breeding plant of the Avangard LLC enterprise in the Ryazan region showed that milk productivity of individual cows of the Holstein breed was higher than that of black-motley cows with year-round stall keeping in terms of milk yield by 1,140 kg, or 16.1 %, the amount of milk fat — by 48.4 kg, or 21.2 %.

Holstein cows are genetically related to black-motley cows but differ in their pronounced milk type, high milk productivity, and better adaptability to the machine milking technology (Tumov, 2018). They use bulky coarse fodder well and are characterized by the absence of a tendency to obesity in abundant feeding with a high share of concentrated fodder in the diet (Kuznetsov and Ireykina, 2017; Brel-Kisseleva and Safronova, 2017).

Y. K. Tomilin, P. I. Zelenkov and V. K. Tomilin (2012) in the conditions of Imeni Ilyicha JSC in the Leningradsky district of the Krasnodar Krai found that cows belonging to the USA V.B. Ideal and M. Chieftain lines were superior to their peers in the milk yield by 1,194 kg, or 22.6 % and 1,079 kg, or 20.4 %, respectively; the cows of the Canadian R. Sovering line — by 1,204 kg or 22.8 %.

In the conditions of Udmurtia, Holstein cows were superior to their peers of the Ayrshire breed in terms of the milk yield over 305 days of the first lactation by 10.72 %, and over the second lactation — by 14.30 %, but were inferior to the Ayrshire breed in terms of the mass fraction of fat and protein by 8.27 % and 5.45 % due to the breed features (Izhboldina and Nikolaeva, 2013).

The duration of Holstein animals economic use at the breeding farms in the Northern Trans-Urals is 2.8 lactations, and the milk productivity is 8,452 kg of milk with the milk fat content of 4.4 %, or 370 kg of milk fat, protein — 3.2 %, or 268 kg of milk protein (Tatarkina and Belenkaya, 2017).

Scientists believe that the effectiveness of crossing is always higher when this breed, which is characterized by stable heredity and high genetic productivity potential, is used (as the paternal breed) (Paderina, 2020).

The selection of animals by their origin is of great importance for improving the productive qualities. Many authors, in particular A. S. Karamaeva, N. V. Soboleva, S. V. Karamaev (2016; 2018), L. V. Efimova, O. A. Frolova, and T. V. Zaznobina (2018), after studying and comparing the data in the scientific literature about milk productivity of motley-black breeds in various countries in dynamics, have found that at present no breed can compete with Holstein in terms of this indicator. Therefore, in improving domestic motley-black cattle and purebred breeding, it is widely crossed with the Holstein breed (Erofeev, 2018).

V. G. Kakhikalo and O. S. Chechenikhina (2009) stated that an increase in milk productivity was preserved in the animals with increased blood relationship with the improving breed. Blood relationship management in animal breeding and acceleration of the new population's consolidation remain urgent tasks in dairy cattle breeding.

The inheritance of milk productivity and milk composition (butter-fat yielding capacity and protein yielding capacity) is independent, while milk composition is mostly determined genetically. The maximum productivity of an animal depends

on certain important conditions: favorable keeping conditions, i.e., avoidance of behavior deviations; sufficient amount of milk "predecessors", i.e., complete and balanced diet; regular and fairly complete emptying of milk from the lacteous gland, i.e., complete high-quality milking (Pavlov, 2019; Pustotina and Pustotina, 2016).

A comparative assessment of the quality of the milk obtained from Holstein and black-motley cows with various milk productivity determines the relevance and the scientific and practical significance of the studies. Each breed has its characteristic features of milk composition and properties (Mkrtychyan, Bakai, and Bakai, 2020). According to most authors, the mass fraction of fat and protein in the milk from the most productive Holstein cows is rather low. For instance, with the 5,239 kg milk yield of full-aged cows, the content of fat and protein in the milk from Holstein cows is 3.73 % and 2.95 %, respectively. Simultaneously, several authors provide information about a rather high mass fraction of fat in the milk from Holstein cows. In turn, milk productivity of the German Holstein heifers breed was 5,022 kg over 305 days of lactation with fat content in the milk of 3.96 %, and protein — of 3.33 %. Over the period from 2007 to 2017, the average milk yield of the Holstein black-motley breed had increased by 2,477 kg, and in 2017, it amounted to 8,567 kg of milk, and the fat content was 3.86 %. The highest productive longevity of Holstein black-motley cows was noted in the North-West, the Far East, and the Volga Federal Districts. The average age of retirement there was 3.20; 3.18; 2.85 calvings, respectively. In 36.2 % of the monitored cows, the fat content in the milk ranged from 3.91 to 4.23 %, while in 21.8 % of the cows, the fat content in the milk exceeded 4 % (Firsova and Kartashova, 2019; Dunin, Tyapugin, Meshcherov, Khodykov, Mescherov, and Nikulkin, 2020; Dolgosheva, Korosteleva, and Romanova, 2018; Shushpanova and Tatarkina, 2020).

In the favorable environmental conditions, milk composition and properties depend on the genotypic characteristics of the organism, and the heritability estimates between the main milk components allow breeding following these characteristics.

In crossbreeding, it is important to preserve the high quality of the milk from improved breeds and adjust it in the proper direction by maximizing the use of the prepotent animals in this respect. Holstein cattle have the highest genetic potential in milk production and a set of qualities that ensure the best adaptability to the industrial milk production technology, which has made it a leader

in improving domestic cattle breeds. An important direction in dairy cattle breeding is the productive longevity of cows, which is directly related to milk productivity and the process indicators of the milk, which is becoming more and more relevant (Shishkina, Nikishova, and Naumov, 2017).

Scientific and practical experience shows that the yield of the dairy products made from milk and their quality are determined by the properties of milk and depend on the breed and the animals feeding and keeping conditions. In the studies of the authors, the suitability of the milk from Holstein and black-motley cows for making cheese was studied as the process property in the comparative aspect.

2. MATERIALS AND METHODS:

The objects of the studies were Holstein and black-motley breeds.

Four groups of cows were formed for the studies: the first and the second groups each contained 10 Holstein cows, and the third and the fourth groups each contained 10 black-motley cows. A total of 40 cows were used in the experiment. The groups were formed regarding the milk productivity of cows over 305 days of lactation and the dry matter content in the milk. In the first group with Holstein cows, the milk yield was 5,000 – 5,500 kg over 305 days of lactation, and the dry matter content in the milk was 12.5 – 13.0 %; in the second group, the milk yield was 5,500 – 6,000 kg, and the dry matter content was 12.0 – 12.5 %. In the third group with black-motley cows, the milk yield was 4,000 – 4,500 kg over 305 days of lactation, and the dry matter content in the milk was 13.0 – 13.5 %; in the fourth group, the milk yield was 4,600 – 5,100 kg, and the dry content matter was 12.5 – 13.0 %.

The milk productivity was accounted individually for each cow through monthly milk checks. For determining the milk yield per month, the milk yield for the reference days of months I, III, V, VII, IX was multiplied by 30, and that for months II, IV, VI, VIII, X — by 31. The milk yield over 305 days of lactation was determined by summing the milk yields for 10 months of lactation. The content of dry matter, fat, protein, lactose, and NFMS was determined using the Infra Milk automated measuring complex for milk quality analysis made by the Profi Company (manufactured in Novosibirsk, Russia, by Sibagropribor LLC). This device was also used for determining the composition of milk proteins — casein and whey proteins. The analyses were

performed monthly at an accredited laboratory (Accreditation Certificate No. KZ.T.11.2311) using the average milk sample taken during milk checks. The milk yield of each month was multiplied by the dry matter index of the month, and then the summed products were divided by the actual milk yield over 305 days of lactation. The quotient is the average dry matter content over 305 days of lactation. The mean values of fat, protein, lactose, and NFMS content were also determined. The content of fat + protein was found by summing fat and protein (Bezenko, 1983).

The data of the average values of milk yield, dry matter, fat, protein, lactose, fat + protein, and NFMS, $M \pm m_x$ by groups, presented in Table 1, were calculated using the Equations 1, 2, and 3 proposed by G.F. Lakin (1990) :

$$M = \frac{M_1 + M_2 + M_3 + M_4 + \dots + M_{10}}{n - 1}, \quad (\text{Eq. 1})$$

where M was the average value of the indicator (milk yield, dry matter, fat, protein, lactose, fat + protein, and NFMS),

$M_1, M_2, M_3 \dots M_{10}$ were the individual values of the indicator,

n was the number of indicator units (the number of animals in the group).

The m value was determined by Equations 2 and 3:

$$\sigma = \sqrt{\frac{\sum (M_i - M)^2}{n - 1}}, \quad (\text{Eq. 2})$$

where σ was the standard deviation,

M_i was each observed value of the indicator,

M was the arithmetic mean,

n was the number of animals in the group.

And the m value was determined by Equation 3:

$$m = \frac{\sigma}{\sqrt{n}}, \quad (\text{Eq. 3})$$

where m was the statistical error of the average value of the indicator,

σ was the standard deviation,

n was the number of animals in the group.

For determining the correlation dependence, the average values for each group were calculated for the 305 days of lactation: the milk yield and the dry matter, fat, protein, lactose, fat + protein, and NFMS. The correlation coefficient was expressed as a decimal fraction.

The + or - signs indicate the direction of the correlation. In the case of positive or direct correlation, when larger values of one trait correspond to larger values of another trait, the correlation coefficient is positive and ranges from 0 to +1; in the case of negative or reverse correlation, when larger values of one trait correspond to smaller values of another trait, the correlation coefficient is negative and ranges from 0 to -1.

Equation 4 was proposed by Lakin (1990) it was used to calculate the correlation coefficient (r):

$$r = \frac{\sum xy - \frac{\sum x \cdot \sum y}{n}}{\sqrt{ax \cdot ay}}, \quad (\text{Eq. 4})$$

where $ax = \sum x^2 - \frac{(\sum x)^2}{n}$ and $ay = \sum y^2 - \frac{(\sum y)^2}{n}$;

x was the variants of the first trait;

y was the variants of the second trait; and

n was the number of observations in the sample.

A simple correlation (r) was determined between two traits: milk yield and dry matter content, fat and dry matter content, protein and dry matter content, lactose and dry matter content, fat + protein and dry matter content, NFMS and dry matter content, milk yield and fat content, protein and fat content, lactose and fat content, fat + protein and fat content, NFMS and fat content, milk yield and protein content, lactose and protein content, fat + protein and protein content, NFMS and protein content, milk yield and lactose content, fat + protein and lactose content, NFMS, and lactose content, milk yield, and fat + protein content, NFMS and fat + protein content, milk yield and NFMS content.

The Equation 5 was used to calculate the veracious value of the correlation coefficient (Td):

$$Td = \frac{r - \sqrt{n-2}}{\sqrt{1-r^2}}, \quad (\text{Eq. 5})$$

where

r was the correlation coefficient;

n was the number of observations in the sample; and

Td was the standard value of the criterion determined according to the Student's table (Lakin, 1990).

All the experimental animals were kept in

the same conditions consistent with the zoohygienic and zootechnical requirements.

3. RESULTS AND DISCUSSION:

With the overall high milk productivity (4,469 – 5,901 kg), the Holstein and black-motley cows, the milk of which contained less dry matter (groups II and IV), were characterized by higher milk yields, compared to their peers in groups I and III (12.4 % for the Holstein breed, and 10.9 % for the black-motley breed, respectively), Table 1.

The compared groups of cows of the same breed differed in the content of dry matter: the Holstein breed — by 0.57 % ($P > 0.95$), the black-motley breed — by 0.7 % ($P > 0.99$). Higher milk saturation with the dry matter was accompanied by a higher content of the other components, namely, fat, protein, and lactose. The highest differences in the milk composition within the same breed were noted in terms of protein, fat, and the total content of fat and protein ($P > 0.95 - 0.99$), lower and unreliable differences — in terms of NFMS, and the minimum differences — in terms of lactose. However, in the total increase of the dry matter content in the milk (100 %), the share of fat was 64.9 % (the Holstein cows) and 71.4 % (the black-motley cows), the share of protein was 28.1 % and 15.7 %, the share of lactose — 5.3 % and 2.8 %, the share of total fat and protein — 93.0 % and 87.1 %, and the share of NFMS — 35.1 % and 28.6 %, respectively. The above data showed that increasing the share of dry matter was mainly due to the total increase in fat and protein content. This was also confirmed by the established relationship between the studied productivity values of milk (Table 2).

A negative relationship was found between the milk yield and the content of the main milk components, although this relationship differed in the magnitude and the level of reliability.

The analysis of the correlations between the milk components showed that they had a predominantly positive value. Naturally, the most veracious relationship existed between the content of dry matter and other milk components, mainly the content of fat and protein. There were different levels of relationship between the content of fat and protein: it was reliable in group I, moderate in group II, virtually absent in group III, and weakly positive in group IV. The correlation between the content of fat and protein was significantly inferior to the positive relationship between each of them (fat or protein) and the content of dry matter in the milk. The relationship

between the fat content and NFMS in the milk, although it differed in the cows in the experimental groups by both the sign and the value, was not veracious. A weak negative or positive correlation existed between the content of fat and that of protein with lactose.

Based on the observed nature of the relationship between the milk yield and the main milk components, studying their total content in the milk yield per lactation is of great interest (Table 3).

Table 3: The total content of the main milk components, kg

Indicator	The Holstein breed		The black-motley breed	
	Group			
	I	II	III	IV
Dry matter	667.4	728.8	596.8	634.8
Fat	210.8	218.8	197.0	196.1
Protein	174.9	190.7	153.3	166.4
Lactose	236.9	268.3	204.5	229.1
Fat + protein	385.7	409.5	350.3	362.5
NFMS	456.7	510.0	399.8	438.8

The experimental data showed that increasing the percentage of the studied milk components in the milk from the cows in groups I and III did not decrease their total amount. This was explained by the lower yield from these cows, compared to the cows in groups II and IV. However, the difference between the cows in the experimental groups reduced significantly. For instance, while the difference in the milk yield values from the Holstein cows was 12.4 %, the total content of dry matter decreased to 8.4 %, of fat — to 3.7 %, of protein — to 8.3 %, and the total content of fat and protein — to 5.8 %. For the black-motley cows, these values were 10.9 %, 6.0 %, 0.5 %, 7.9 %, and 3.4 %, respectively. This suggested that the absolute content of the nutrients in the lactation milk yield was the most objective set of the productive quality indicators of cows. Along with that, the crossbreed analysis showed that in the absence of a significant difference between the milk yields and the milk composition, the advantage in terms of all the milk productivity parameters was with the Holstein breed.

However, the milk characteristic as a food product and the raw material for processing may not be only limited to its composition. This requires a more in-depth assessment of its qualities, including the technological ones. In the study, the protein share increased in the milk with a high

content of dry matter due to increased content of casein (Table 4). For instance, the share of casein in the total content of protein in the milk from the cows in groups I and III was 81.3 % and 83.9 %, respectively, compared to their peers in groups II and IV — 77.5 % and 81.9 %, the milk of which contained more whey proteins. This allowed considering the milk from the cows in groups I and III more fit for cheese-making, confirmed by the shares of casein and whey proteins (Table 4).

The milk from the cows of both breeds with a higher concentration of dry matter was characterized by an increased content of the α - and β -fractions of casein, which are the most valuable for cheese-making. Due to these fractions, the casein content increased in the milk from the cows in groups I and III. For cheese-making, the composition of milk whey proteins is important, mainly the content of α -lactoalbumin and β -lactoglobulin, the increased content noted in cow milk a higher content of dry matter. With the statistical insignificance of the differences between these milk protein composition values, some advantage stayed with the black-motley breed.

The analysis of the technological characteristics of milk, such as the size and the weight of casein micelles, the content and the composition of amino acids, and the physicochemical properties of the milk (the duration of rennet clotting, the density and elasticity of the rennet clot, and the Ca and P levels) allowed considering the milk from the cows in groups I and III with the increased content of dry matter to be the most biologically complete and suitable for cheese-making. Upon comparison of the breeds, the advantage stayed with the black-motley breed. Better technological properties of such milk predetermined the higher relative yield of cheese and lower consumption for obtaining a unit of its weight.

The results obtained after the comparative analysis of the economic efficiency of the production and sales of the milk with various compositions are shown in Table 5.

For instance, for the Holstein breed, the payment for the milk-based on the amount of milk fat per a single cow from group II would be greater by USD 13.13, compared to group I; based on the amount of dry matter, the calculated difference would be USD 3.08; for the black-motley breed, these values would be USD 0.14 and USD 1.9, respectively. With that, the milk from the cows with a high absolute yield of dry matter (group II of the Holstein cows and group IV of the black-motley

cows) would be estimated by USD 1.76 and USD 2.05 higher than if paid for by the content of fat alone. As a result, the payment for the milk sold by its dry matter content would allow an economy to get higher profits, and the state would not overpay for a product inferior in the nutritional and technological qualities.

4. CONCLUSION:

Based on the studies, it has been found that the Holstein and black-motley breeds are characterized by high milk quality, the composition of which varies depending on the milk production. For instance, in the Holstein cows with low productivity of the herd, the dry matter, fat, protein, lactose, and dry skim milk residue were higher by 4.6 %, 9.9 %, 4.9 %, 0.7 %, and 2.3 %, respectively, than in the cows with higher productivity. A positive correlation has been found between the milk components. Based on the data obtained during the studies, a conclusion can be made that the milk from the cows with high dry matter content is the most suitable for making cheese. In terms of dry matter content, milk sales will allow a farm to increase revenues by USD 1.9 – 3.1.

5. ACKNOWLEDGMENTS:

The scientific research was performed with financial support from the Ministry of Agriculture of the Republic of Kazakhstan. The authors express their gratitude to Shagmanov Serik Zakiryanovich, the Olzha Ak Kuduk LLC farm head, who assisted in the research.

6. ETHICAL CLEARANCE:

Ethical permission was obtained from and agreed upon with the Academic Councils at the Kazakh Scientific Research Institute of Animal Husbandry and Forage Production (Almaty, Kazakhstan) and the Institute of Veterinary Medicine (Troitsk, Russia).

The source of funding: The research was funded by the Ministry of Agriculture of the Republic of Kazakhstan within budget program 267 "Increasing the Availability of Knowledge and Scientific Research", subprogram 101 "Program-oriented Funding of Research Studies and Measures".

7. REFERENCES:

1. Adamczyk, K., Makulska, J., Jagusiakand, W., and Węglarz, A. (2017). Associations between strain, herd size, age at first calving, culling reason, and lifetime performance characteristics in Holstein-Friesian cows. *Animal*, 11(2), 327–334.
2. Babich, E. A., Kikebaev, N. A., Raketskiy, V. A., and Baysakalov, A. A. (2019). Dependence of Growth and Development of Rearing Stock in Northern Kazakhstan on the Origin of Servicing Bulls. *Annals of Agri-Bio Research*, 24(1), 134–138.
3. Babich, E., Nugmanov, A., Ovchinnikova, L., and Ovchinnikov, A. (2016). The efficiency of dairy herds created based on first-calf heifers of Karatomar black-and-white interbreed cattle on northern Kazakhstan. *Research Journal of Pharmaceutical, Biological, and Chemical Sciences*, 7(4), 2376 – 2381.
4. Bastin, C., Loker, S., Gengler, N., Sewalem, A., and Miglior, F. (2010). Genetic relationships between body condition score and reproduction traits for Canadian Holstein and Ayrshire first-parity cows. *Journal of Dairy Science*, 93, 2215–2228.
5. Bezenko, T. I. (1983). *Metodicheskie rekomendatsii po tekhnike analiza moloka i molochnykh produktov [Methodical recommendations for the milk and dairy products analysis technique]*. Dubrovitsy, Russia: VIZ, 68 p.
6. Brel-Kisseleva, I. M., and Safronova, O. S. (2017). The reserves of increasing of domestic horses breeds use efficiency in the Republic of Kazakhstan. *Ecology, Environment and Conservation*, 23(2), 833–838.
7. Cole, J. B., Bickhart, D. M., Waurich, B., Wensch-Dorendorf, M., and Swalve, H. H. (2014). A genome-wide association study of calf birth weight in Holstein cattle using single nucleotide polymorphisms and phenotypes predicted from auxiliary traits. *Journal of dairy science*, 97(5), 3156–3172.
8. De Jong, G. (2000). *Type classification in the Netherlands*. Veeopro Holland, pp. 20–21.

9. Dolgosheva, E. V., Korosteleva, L. A., and Romanova, T. N. (2018). Molochnaya produktivnost i pokazateli kachestva moloka korov raznykh porod v MK OOO "Radna" [Milk productivity and quality of the milk from cows of various breeds at Radna Milk Plant LLC]. In *Collection of scientific papers for International Scientific-Practical Conference: Innovative achievements in science and technology of the AIC* (pp. 42-45). Kinel, Russia: RIO SGSKHA.
10. Dunin, I. M., Tyapugin, S. E., Meshcherov, R. K., Khodykov, V. P., Mescherov, S. R., and Nikulkin, N. S. (2020). Razvedenie skota golshtinskoi porody na territorii Rossiiskoi Federatsii [Breeding Holstein cattle on the territory of the Russian Federation]. *Zootechny*, 2, 5–8.
11. Efimova, L. V., Frolova, O. A., and Zaznobina, T. V. (2018). Vliyanie bykov-proizvoditelei golshtinskoi porody na fiziko-khimicheskie i tekhnologicheskie svoistva moloka docherei [The effect of Holstein stud bulls on the physicochemical and process properties of the milk of the daughters]. *News of the Ulyanovsk State Agricultural Academy*, 4(44), 154–157.
12. Erofeev, V. I. (2018). Molochnaya produktivnost vysokoproduktivnykh korov cherno-pestroi porody v zavisimosti ot nasledstvennykh faktorov [Milk productivity of highly productive black-motley cows depending on the hereditary factors]. In *Materials of the International Scientific-Practical Conference: Increasing the competitiveness of livestock breeding and the tasks of staffing* (pp. 67-73). Podolsk, Russia: Russian Academy of Management in Livestock.
13. Faizullin, P. V., and Kharlan, S. Y. (2019). Tekhnologicheskie svoistva moloka korov raznykh porod [Process properties of the milk from cows of various breeds]. *Youth and Science*, 5–6, 59.
14. Firsova, E. V., and Kartashova, A. P. (2019). Golshtinskaya poroda v Rossiiskoi Federatsii, sovremennoe sostoyanie i perspektivy razvitiya [The Holstein breed in the Russian Federation, its current state and development prospects]. *Genetics and animal breeding*, 1, 62–69.
15. Gagloev, A. C., Negreeva, A. N., Gagloeva, T. N., and Skobeev, A.D. (2017). Sostav i svoistva moloka korov cherno-pestroi porody razlichnogo proiskhozhdeniya [Composition and properties of the milk from black-motley cows of various origin]. In: V.A. Solopov (Ed.), *Modern technologies in animal husbandry: issues and solutions. Materials of the International Scientific-Practical Conference* (pp. 132-136). Michurinsk, Russia: Michurinsk State Agrarian University.
16. Holroyd, R.G., Doogan, V.J., De Faveri, J., Fordyce, G., McGowan, M.R., Bertram, J.D., Vankan, D.M., Fitzpatrick, L.A., Jayawardhana, G.A., Miller, R.G. (2002). Bull selection and use in northern Australia. 4. Calf output and predictors of fertility of bulls in multiple-sire herds. *Animal Reproduction Science*, 71, 67–79.
17. Izhboldina, S. N., and Nikolaeva, S. V. (2013). Molochnaya produktivnost korov airshirskoi, golshtinskoi porod v usloviyakh Udmurtskoi respubliki [Milk productivity of the Ayrshire and Holstein cows in the conditions of the Udmurt Republic]. *Scientific notes of the Bauman Kazan State Academy of Veterinary Medicine*, 213, 100–103.
18. Kakhikalo, V. G. (Ed.). (2009). *Seleksionnye i tekhnologicheskie metody povysheniya produktivnosti cherno-pestrogo skota Zauralya [Breeding and technological methods of increasing the productivity of black-motley cattle in the Trans-Urals]*. Kurgan, Russia: The Kurgan State Agricultural Academy, 275 p.
19. Karamaev, S. V., Karamaeva, A. S., and Soboleva, N. V. (2016). *Tekhnologicheskie svoistva moloka korov molochnykh porod v zavisimosti ot sezona otela [Process properties of the milk from dairy cows depending on the calving season]*. Kinel, Russia: Samara State Agricultural Academy, 181 p.
20. Karamaeva, A. S., Soboleva, N. V., and Karamaev, S. V. (2018). Vliyanie porody na syroprigodnost moloka i kachestvo syra [The effect of the breed on milk suitability for making cheese and cheese quality]. *Dairy and beef cattle breeding*, 5, 34–38.
21. Katmakov, P. S., Gavrilenko, V. P., Bushov, A. V., and Prokofiev, A. N. (2019). *Seleksionno-plemennaya rabota v molochnom skotovodstve [Breeding work in dairy cattle breeding]*. Ul'yanovsk,

Russia: Stolypin Ulyanovsk State Agrarian University, 167 p.

22. Khromova, L. G., and Manzhurin, O. A. (2018). *Produktivnye i biologicheskie osobennosti korov molochnykh porod v usloviyakh intensivnoi tekhnologii* [Productive and biological characteristics of dairy cows in the conditions of intensive technology]. Voronezh, Russia: Emperor Peter I Voronezh SAU, 153 p.
23. Kuznetsov, V. M., and Irekina, R. P. (2017). Osobennosti zagotovki kormov i sposoby uluchsheniya kormovykh ratsionov dlya laktiruyushchikh korov sakhalinskoj populyatsii golshtinskoj porody [Peculiarities of fodder preparation and the methods of improving diets for lactating cows of the Sakhalin Holstein population]. In: V.A. Chuvilina (Ed.), *Collection of scientific articles: Scientific support, features and perspectives of agriculture development in the Far East region* (pp. 60-72). Yuzhno-Sakhalinsk, Russia: Poligraficheskaya kompaniya "Kano".
24. Lakin, G. F. (1990). *Biometriya [Biometrics]: Textbook. A guide for biological specialities in higher education institutions*. 4th ed., revised and amended. Moscow, Russia: Vysshaya Shkola, 352 p.
25. Mkrtchyan, G. V., Bakai, A. V., and Bakai, I. R. (2020). Nasledovanie belkovomolochnosti u krupnogo rogatogo skota raznoi selektsii [The inheritance of protein milk in cattle of various breeding origins]. *Agricultural science*, 2, 36–38.
26. Morozova, N. I., Musaeva, F. A., and Morozova, O. A. (2016). Sravnitel'naya otsenka molochnoi produktivnosti korov golshtinskoj porody i cherno-pestroi pri kruglogodovom stoilovom soderzhanii [A comparative assessment of Holstein and black-motley cows' milk productivity with year-round keeping in stalls]. *News of the Michurinsky State Agrarian University*, 3, 66–69.
27. Nemtseva, E. Y., and Ignatieva, N. L. (2020). Planirovanie selektsionno-plemennoi raboty v molochnom skotovodstve [Planning of breeding work in dairy cattle breeding]. In *Materials of the All-Russian scientific-practical conference with international participants, held at Cheboksary, February 20, 2020* (pp. 73–80).
28. Paderina, R. V. (2020). Lineinaya otsenka eksterera i ee svyaz s molochnoi produktivnostyu [Linear assessment of the exterior and its relationship with the milk productivity]. In: L.P. Blinkova (Ed.), *Innovative paradigm in the development of natural sciences* (pp. 26-37). Petrozavodsk, Russia: International Center for Scientific Partnership "New Science".
29. Pavlov, S. D. (2019). Molochnaya produktivnost korov golshtinirovannoi cherno-pestroi porody [Milk productivity of cows of the Holsteinized black-motley breed]. In: A.B. Kudzaev (Resp. Ed.), *Scientific works of students of the Gorsky State Agrarian University* (pp. 181-183). Vladikavkaz, Russia: Gorsk State Agrarian University.
30. Pimentel, E. C. G., Erbe, M., Knig, S., and Simianer, H. (2011). Genome partitioning of genetic variation for milk production and composition traits in Holstein cattle. *Front. Livest. Genomics.*, 2, 19.
31. Pustotina, G. F., and Pustotina, N. V. (2016). Proizvodstvo moloka pri ratsionalnom ispolzovanii geneticheskikh resursov otechestvennykh porod skota [Milk production with the rational use of the genetic resources of domestic cattle breeds]. *News of the Orenburg State Agrarian University*, 3(59), 133–135.
32. Safronova, O. S., Babich, E. A., Ovchinnikova, L. Y., and Ovchinnikov, A. A. (2017). Polymorphism of Kappa-Casein, Somatotropin, Beta-Lactoglobulin, Prolactin, and Thyreoglobulin Genes of Black and White Cattle of North Kazakhstan. *Journal of Pharmaceutical Sciences and Research, India*, 9(5), 568–573.
33. Samusenko, L. D., and Khimicheva, S. N. (2018). Kachestvo i bezopasnost moloka: osnova prodovolstvennoi bezopasnosti [Milk quality and safety: the bases of food safety]. *News of Agrarian Science*, 1(70), 46–51.
34. Shishkina, T. V., Nikishova, N. V., and Naumov, A. A. (2017). Vliyanie krovnosti po golshtinskoj porode na molochnuyu produktivnost i prodolzhitel'nost khozyaistvennogo ispolzovaniya korov

- cherno-pestroi porody [The effect of blood relationship to the Holstein breed on the milk productivity and the duration of economic use of black-motley cows]. *Chief zootechnician*, 12, 22–26.
35. Shushpanova, K. A., and Tatarkina, N. I. (2020). Produktivnost korov golshtinskoi porody [Productivity of Holstein cows]. *News of the Kurgan State Agricultural Academy*, 2(34), 44–47.
 36. Tatarkina, N. I., and Belenkaya, A. E. (2017). Prodolzhitel'nost produktivnogo ispolzovaniya korov golshtinskoi porody v usloviyakh Severnogo Zauralya [The duration of productive use of Holstein cows in the conditions of the Northern Trans-Urals]. *Bulletin of the State Agrarian University of the Northern Trans-Urals*, 1, 73–77.
 37. Tomilin, Y. K., Zelenkov, P. I., and Tomilin, V. K. (2012). Produktivnost i perspektiva ispolzovaniya germanskikh golshtino-frizov dlya uluchsheniya golshtinizirovannogo cherno-pestrogo skota otechestvennoi selektsii [Productivity and the prospects of using German Holstein Friesian cattle for improving Holsteinized black-motley cattle of domestic breeding]. *Scientific Journal of the KubSAU*, 76, 742–753.
 38. Tumov, A. A. (2018). Produktivnye osobennosti korov golshtinskoi porody raznoi selektsii [Productive features of Holstein cows of various breeding origin]. *Bulletin of the Altai SAU*, 3(161), 101–105.
 39. Wang, Y., Segelke, D., Emmerling, R., Bennewitz, J., and Wellman, R. (2017). Long – Term Impact of Optimum Contribution Selection Strategies on Local Livestock Breeds with Historical Introgression Using the Example of German Angler Cattle. *G3: Genes, Genomes, Genetics*, 7(12), 4009–4018.
 40. Yesbolova, A., and Maciejczak, M. (2012). Livestock production in Kazakhstan: situation, problems, and possible solutions. In: P. Bórawski (Ed.), *Multifunctional development of rural areas. International experience*, Vol. 2 (pp. 43–50). Ostrołęka, Poland: Publishing House of the University of Economics and Social Sciences in Ostrołęka.

Table 1. Milk productivity and composition

Indicator	The Holstein breed		The black-motley breed	
	Group			
	I	II	III	IV
The milk yield, kg	5,167 ± 112	5,901 ± 154	4,469 ± 143	5,018 ± 128
Dry matter, %	12.92 ± 0.84	12.35 ± 0.77	13.35 ± 0.73	12.65 ± 0.62
Fat, %	4.08 ± 0.02	3.71 ± 0.01	4.41 ± 0.03	3.91 ± 0.02
Protein, %	3.39 ± 0.03	3.23 ± 0.01	3.43 ± 0.04	3.32 ± 0.02
Lactose, %	4.58 ± 0.82	4.55 ± 0.58	4.58 ± 0.68	4.56 ± 0.71
Fat + protein, %	7.47 ± 0.23	6.94 ± 0.25	7.84 ± 0.32	7.23 ± 0.28
NFMS, %	8.84 ± 0.62	8.64 ± 0.53	8.94 ± 0.64	8.74 ± 0.50

Table 2. The correlation between the milk yield and milk composition

Indicator	Group			
	I	II	III	IV
Milk yield vs. dry matter	-0.42	-0.74*	-0.30	-0.51
Fat vs. dry matter	+0.86	+0.90***	+0.84**	+0.84**
Protein vs. dry matter	+0.99***	+0.84**	+0.32	+0.65*
Lactose vs. dry matter	+0.20	+0.50	+0.17	+0.66**
Fat + protein vs. dry matter	+0.96***	+0.97***	+0.90***	+0.96***
NFMS vs. dry matter	+0.85**	+0.79**	+0.40	+0.82**
Milk yield vs. fat	-0.30	-0.63*	-0.43	-0.13
Protein vs. fat	+0.80**	+0.59	-0.02	+0.23
Lactose vs. fat	-0.24	+0.14	-0.19	+0.40
Fat + protein vs. fat	+0.96***	+0.96***	+0.95***	+0.87***
NFMS vs fat	+0.46	+0.45	-0.17	+0.37
Milk yield vs. protein	-0.36	-0.64	-0.12	-0.79**
Lactose vs. protein	+0.22	+0.53	-0.12	+0.24
Fat + protein vs. protein	+0.94***	+0.79**	+0.29	+0.68*
NFMS vs. protein	+0.88***	+0.91***	+0.62	+0.86**
Milk yield vs. lactose	-0.15	-0.45	-	-0.26
Fat + protein vs. lactose	-0.04	+0.29	-0.18	+0.42
NFMS vs. lactose	+0.59	+0.83**	+0.63*	+0.70*
Milk yield vs. fat + protein	-0.34	-0.70*	-0.45	-0.50
NFMS vs. fat + protein	+0.69	+0.65*	+0.03	+0.71*
Milk yield vs. NFMS	-0.42	-0.63*	+0.18	-0.72*

* — $P < 0.05$; ** — $P < 0.01$; *** — $P < 0.001$

Table 4: The composition of protein in the milk from the Holstein and black-motley cows, %

Indicator	The Holstein breed		The black-motley breed	
	Group			
	I	II	III	IV
Total protein, total	3.27	3.25	3.35	3.31
Including:				
casein	2.66	2.52	2.81	2.71
whey proteins	0.61	0.73	0.54	0.60
% of total protein:				
casein	81.3	77.5	83.9	81.9
whey proteins	18.7	22.5	16.1	18.1
Casein:				
α-	44.38	44.03	44.89	44.62
β-	50.51	50.34	51.51	50.97
γ-	5.11	5.63	3.60	4.41
Whey proteins:				
Immune globulins	19.91	22.45	19.59	21.27
α-lactoalbumin	20.45	18.74	18.30	17.33
β-lactoglobulin	57.35	56.11	59.19	57.67
serum albumin	2.29	2.70	2.92	3.73

Table 5: *The economic efficiency of milk production and sales*

Indicator	The Holstein breed		The black-motley breed	
	Group			
	I	II	III	IV
Cost of milk per lactation, USD	19.23	21.96	18.63	20.92
Sales cost of milk with the basic fat content, USD	31.93	31.79	31.93	31.78
Profit from milk sales in terms of fat, USD	14.93	13.51	13.30	10.87
Sales cost of milk in terms of nonfat solids, USD	33.39	36.46	29.85	31.76
Profit from milk sales in terms of nonfat solids, USD	14.15	14.49	11.23	10.84

AVALIAÇÃO DA DOSE EFETIVA COMPROMETIDA DE GÁS RADÔNIO EM ÁGUA POTÁVEL NA PROVÍNCIA DE AL-QADISIYAH, IRAQUE

EVALUATION OF COMMITTED EFFECTIVE DOSE OF RADON GAS IN DRINKING WATER IN AL-QADISIYAH PROVINCE, IRAQ

تقييم الجرعة الفعالة من غاز الرادون في مياه الشرب في محافظة القادسية، العراق

ASWOOD, Murtadha S.^{1*}; ALMUSAWI, Mustafa S.^{2*}; MAHDI, Naser K. W.³; SHOWARD, Ansam F.¹

¹ Department of Physics, College of Education, University of Al-Qadisiyah, Al-Diwaniyah, Iraq.

² Department of Physiology, College of Medicine, Mustansiriyah University, Iraq.

³ Directorate of Diwaniyah Education, Iraq.

* Corresponding author

e-mail: dr.mustafa.salih@uomustansiriyah.edu.iq

Received 07 September 2020; received in revised form 20 October 2020; accepted 02 November 2020

RESUMO

A pesquisa científica está dando interesse em determinar as concentrações de Radônio na água potável e em sedimentos, devido à ocorrência de doenças graves relacionadas a este elemento químico. A solubilidade do Radônio em água (potável e subterrânea) permite a percolação em solos e rochas. As concentrações de radioatividade natural do Radônio foram medidas na água potável e sedimentos na estação de tratamento (Al-Diwaniyah, Iraque) usando detector de traços RAD7 e CR-39 (câmara de difusão, Landauer). A amostragem foi realizada em 20 amostras (10 de água potável e 10 de sedimento). Os resultados de radioatividade mostraram que a concentração de ²²²Rn na água potável variam de 0,05 a 0,47 Bq/L com média de 0,24 Bq/L. No entanto, as concentrações de ²²²Rn no sedimento variam de 29,16 a 60,52 Bq/m³ com uma média de 42,43 Bq/m³. A partir dos resultados foi possível calcular a contribuição do Radônio na água potável associado a idade. As doses anuais ficaram abaixo dos limites recomendados. As concentrações de Radônio na água potável e no sedimento apresentaram altos níveis de radioatividade quando comparadas ao limite natural. No entanto, os mesmos resultados indicaram baixos níveis de radioatividade quando comparados ao Comitê Científico das Nações Unidas sobre o Efeito da Radiação Atômica e à Organização Mundial da Saúde. Desta forma, toda a água potável nessa estação é segura para uso.

Palavras-chave: Água potável; radônio; RAD7, sedimento; CR-39; dose efetiva comprometida.

ABSTRACT

Scientific research is giving interest in determining the concentrations of Radon in drinking water and sediments due to the occurrence of serious diseases related to this chemical element. The solubility of Radon in water (potable and underground) allows percolation in soils and rocks. The concentrations of Radon natural radioactivity were measured in drinking water and sediment at a wastewater treatment plant (Al-Diwaniyah, Iraq) using trace detector RAD7 and CR-39 (diffusion chamber, Landauer). Sampling was carried out at 20 samples (10 of drinking water and 10 of sediment). The results of radioactivity showed that the concentration of ²²²Rn in drinking water varies from 0.05 to 0.47 Bq/L, with an average of 0.24 Bq/L. However, the ²²²Rn concentrations in the sediment vary from 29.16 to 60.52 Bq/m³, with an average of 42.43 Bq/m³. From the results, it was possible to calculate the contribution of Radon to drinking water associated with age. The effective annual doses were found below the recommended limit. Radon concentrations in drinking water and sediment showed high levels of radioactivity compared to the natural limit. However, the same results indicated low radioactivity levels compared to the United Nations Scientific Committee on the Effects of Atomic Radiation and the World Health Organization. In this way, all drinking water at these stations is safe to use.

Keywords: Drinking water; Radon; RAD7, sediment; CR-39; committed effective dose.

يهدف البحث العلمي بتحديد تراكيز غاز الرادون في مياه الشرب والرواسب نتيجة الإصابة بأمراض خطيرة مرتبطة بهذا العنصر الكيميائي. تسمح قابلية ذوبان الرادون في المياه (الصالحة للشرب وتحت الأرض) بالتسرب في التربة والصخور. تم قياس تراكيز النشاط الإشعاعي الطبيعي للرادون في مياه الشرب والرواسب في محطة معالجة مياه الصرف الصحي (الديوانية، العراق) باستخدام كاشف التتبع RAD7 و CR-39 (غرفة الانتشار، لاندوار). العينات المأخوذة للدراسة 20 عينة (10 من مياه الشرب و 10 من الرواسب). أظهرت نتائج النشاط الإشعاعي أن تركيز ^{222}Rn في مياه الشرب يتراوح بين 0.05 و 0.47 بيكريل / لتر بمتوسط 0.24 بيكريل / لتر. ومع ذلك، فإن تراكيز ^{222}Rn في الرواسب تتراوح من 29.16 إلى 60.52 بيكريل / م³ بمتوسط 42.43 بيكريل / م³. من النتائج، كان من الممكن حساب مساهمة الرادون في مياه الشرب المرتبطة بالعمر. تم العثور على الجرعات السنوية الفعالة أقل من الحد الموصى به. أظهرت تراكيز الرادون في مياه الشرب والرواسب مستويات عالية من النشاط الإشعاعي مقارنة بالحد الطبيعي. ومع ذلك، أشارت النتائج نفسها إلى انخفاض مستويات النشاط الإشعاعي مقارنة بلجنة الأمم المتحدة العلمية المعنية بآثار الإشعاع الذري ومنظمة الصحة العالمية. بهذه الطريقة، تكون جميع مياه الشرب في هذه المحطات آمنة للاستخدام.

الكلمات المفتاحية: مياه الشرب؛ رادون RAD7؛ الرواسب؛ CR-39؛ جرعة فعالة المترسبة.

1. INTRODUCTION

The aquatic environment is the final destination of many potentially toxic and radioactive industrial residues that hinder the growth of biota, causing irreversible ecological damage (Shannoun, 2015; Cho *et al.*, 2019). The determination of radionuclide concentrations in aquatic systems is fundamental mainly in two aspects: i) protection of human health (drinking water consumption) and ii) control of environmental pollution. Thus, Radon determination has become a public health concern due to its dangerous nature regarding its exposure (Al-Fifi *et al.*, 2012; Alshahri *et al.*, 2019). Radon is a product of the disintegration of radium (atomic number 88), a highly radioactive element, as well as thorium (atomic number 90), where the name of one of its isotopes, toron, with a half-life ($t_{1/2}$) of 55 seconds and atomic mass 220. The ^{219}Rn isotope is called actinon, it is a product of the disintegration of actin and has a half-life of 4 seconds. In addition to these, Radon has 22 artificial isotopes, produced in nuclear reactions by artificial transmutation in a cyclotron and linear accelerators (AS-Subaihi *et al.*, 2020; Binesh *et al.*, 2012). The most stable isotope is ^{222}Rn , the most abundant, with a half-life of 3.8 days and a disintegration of ^{226}Ra . When emitting alpha particles, it becomes an isotope of the polonium element (Shannoun, 2015; Somlai *et al.*, 2007; Al-Nafiey *et al.*, 2014).

Radionuclides are naturally present in all environmental elements. They are found in atmospheric air, water, sand, plants, animals, soils, rocks, and in the human body itself in varying amounts (Shannoun, 2015; Al-Alawy *et al.*, 2018). The presence of radionuclides in the environment is responsible for significant exposure to radiation for humanity (Shannoun, 2015). Radionuclides can emit alpha or beta particles and can be ingested or inhaled by the body. ^{222}Rn gas is one of the most dangerous

nuclides for humans (Gruber *et al.*, 2009).

Inhalation and ingestion of ^{222}Rn correspond to 54% of registered deaths, and about 10% is due to exposure in closed rooms or caves causing lung cancer (Al-Mosuwai and Subber, 2013; Chanyotha *et al.*, 2016; Atallah *et al.*, 2001). Radon is present in rocks that make up the earth's crust, and for this reason, there is a percolation of this chemical element through porous cavities reaching the groundwater. This phenomenon also occurs in sediments by physical and biological processes through leaching of sediment and water (Shannoun, 2015; Showard and Aswood, 2019; Todorovic *et al.*, 2012; Jobbágy *et al.*, 2017). Radon is a radioactive gaseous element belonging to the group of noble gases. (Appleton, 2007; Divya *et al.*, 2019; Martins *et al.*, 2020). The risk of Radon being ingested is generally small when compared to inhaled Radon (Gruber *et al.*, 2009).

Radon is a completely inert, tasteless, and odorless gas. Within the radionuclides descending from ^{238}U , ^{226}Ra stands out, which has a half-life of 1600 years and which, by alpha emission, forms ^{222}Rn , Radon, with a half-life of 3.82 days (Fares, 2017). Their descendants are ^{218}Po , ^{214}Pb , ^{214}Bi , and ^{214}Po , all with a very short half-life. ^{222}Rn is an inert gas with accumulated property in closed environments such as homes, caves, mines, and tunnels (Nikolopoulos and Louizi, 2008; Subber *et al.*, 2011). Therefore, together with their parents ^{218}Po and ^{214}Po , they are responsible for approximately 50% of the equivalent effective dose produced by natural ionizing radiation (Subber *et al.*, 2017). In the ^{232}Th series, a similar process occurs with ^{220}Rn , also called toron, with a half-life of 55 seconds and with its descendants ^{216}Po , ^{212}Pb , ^{212}Bi , ^{208}Tl , and ^{212}Po (Jaber *et al.*, 2015; Kiat *et al.*, 2008).

Radon consists of several isotopes; however, only three are naturally occurring: Radon (^{222}Rn), actinon (^{219}Rn), and toron (^{220}Rn).

These radionuclides come from the series of decay originated from ^{238}U , ^{235}U , and ^{232}Th , respectively. Despite being produced continuously in rocks and minerals by the α decay of ^{226}Ra , ^{224}Ra and ^{223}Ra , these radionuclides do not form chemical compounds (Henshaw *et al.*, 1993; Kurnaz and Çetiner, 2016). In practice, only ^{222}Rn and ^{220}Rn isotopes are relevant from the point of view of radiological protection or environmental and geological interest (Lopes, 2005). ^{219}Rn is rarely found in nature due to its very short half-life of 4 seconds and the isotopic abundance of its parent ^{235}U of only 0.72%. ^{222}Rn has a half-life of 3.83 days, which allows its mobility significant to escape the rock on which it was generated (Nasir and Shah, 2012; Wallner and Steininger, 2007). ^{220}Rn is of concern from the point of view of radiological protection only if high concentrations of ^{232}Th are present in the minerals. The emission of ionizing radiation by rocks and soils depends on their content of U, Th, and K; Radon contents will depend mainly on the concentration of uranium.

A widely used device to detect the presence of Radon in water is RAD7 (DurrIDGE Company Inc.) (Al-Nafiey *et al.*, 2014; Zalewski *et al.*, 2001; Fard *et al.*, 2020). RAD7 is a solid-state detector composed of a semiconductor material (usually silicon) that converts alpha radiation directly into an electrical signal. During the Radon decay, the alpha particle is 50 percent likely to penetrate the detector and produce an electrical signal (Wang *et al.*, 2011; Wong *et al.*, 1992). Therefore, to detect the concentrations of Radon in sediments, the widely used equipment is the CR-39 (Columbia Resin-39) composed of a polymer with optical properties similar to that of optical glass (Al-Nafiey *et al.*, 2014; Mustapha *et al.*, 2002; Xinwei, 2006; Muhammad *et al.*, 2012). This research aims to examine Radon exposure in drinking water and sediments, establishing an adequate intake.

2. MATERIALS AND METHODS

2.1. Samples collection

Samples of drinking water and sediment were obtained at drinking water stations in the city of Al-Diwaniya, in southern Iraq. Ten samples of drinking water were obtained and stored in polyethylene bottles. Based on the International Atomic Energy Agency (IAEA) requirements, the polyethylene bottles were rinsed with double distilled water at least five times with 1:1 $\text{HNO}_3\text{:H}_2\text{O}$. To avoid accumulating organic materials and minimizing radioactive material

loss, hydrochloric acid (HCl) was used. Ten samples of sediment were collected to determine the availability of radionuclides based on the International Atomic Energy Agency standards. The samples were removed by dredging stainless steel. From each location, 250 g of sediment were collected and deposited in polyethylene bags. The samples were identified and labeled with time, place, and date (Al-Alawy *et al.*, 2018).

2.2. Experimental method

After the collection process, the samples were taken to the laboratory (Department of Physics, Faculty of Education), where the preparation process began. In this step, the RAD-7 and CR-39 techniques were used to measure the Radon concentration in the samples, as shown in Figure 1. The Radon concentration in drinking water were calculated according to the EPA protocol. The RAD7 detector (model 2890 - DurrIDGE Company) was exposed to a known concentration of Radon (or Thoron) during calibration. The detector was set up to perform counts of five minutes in five minutes, with four cycles for each sample (Divya *et al.*, 2019).

Therefore, for the sediment samples (250 g) were heated in an oven at 110 °C for about 24 hours to remove moisture and ground to obtain a homogeneous powder. To measure the Radon concentrations in the sediments, 10 g of the powder was stored inside the PVC tubes (Showard and Aswood, 2019). CR-39 detectors were installed on the bottom of the tube and stored for 60 days to ensure that the radionuclide reaches a steady-state, as shown in Figure 2 (Al-Alawy *et al.*, 2018). When the ionizing particle travels through the solid, an unseen latent path appears with the naked eye. The physical-chemical changes at the damage site depend on the chemical composition of the detection material and the atmosphere (temperature and pressure).

The CR-39 detector was then chemically attacked in a standard 6.25 N NaOH solution for 6 h at 70 °C. The tracks were captured with an Olympus optical microscope with 400 X magnification, as shown in Figure 3.

2.3. Calculation

The annual effective dose due to ingestion of ^{222}Rn in drinking water were calculated according to Equation 1 (Somlai *et al.*, 2007; Singh *et al.*, 2010):

$$E = K \cdot C_{W222Rn} \cdot KM \cdot t \quad \text{Eq. 1}$$

where:

E represents the effective ingestion dose (Sv - Sievert is the unit used to give an assessment of the impact of ionizing radiation on humans); K is the ingesting dose conversion factor of ^{222}Rn (1×10^{-8} Sv/Bq for adults and 2×10^{-8} Sv/Bq for children); C_{W222Rn} represent the Radon concentration in drinking water (Bq/L); KM is the water intake, and t is the duration of intake.

The indoor Radon was calculated in drinking water using Equation 2 (Zalewski *et al.*, 2001):

$$C_{A222Rn} = C_{W222Rn} \cdot W \cdot \frac{e}{V \cdot \lambda_c} \quad \text{Eq. 2}$$

where:

C_{A222Rn} is the indoor Radon; $C_{WRn-222}$ represent the Radon concentration in drinking water (Bq/L), W is the intake of water; V is the bulk of indoor room; e is the ratio of Radon transfer from indoor (water to air); λ_c is the air exchange (0.7/h) (Xinwei, 2006). On the other hand, Radon concentrations in sediment were calculated using Equation 3 (Showard and Aswood, 2019):

$$C_{S222Rn} = \frac{\rho}{K \cdot T} \quad \text{Eq. 3}$$

where:

C_{S222Rn} is the Radon concentrations in sediment (Bq/m³); K represents the calibration factor of the detector (0.024); T is the exposure time; ρ is the density of track that particle appears on the surface of detector CR-39. The density was determined using Equation 4 (Showard and Aswood, 2019).

$$\rho = \frac{N_t}{A} \quad \text{Eq. 4}$$

where:

N_t is the average of tracks number in grids area (8×8), and A is the visible area under the microscope.

3. RESULTS AND DISCUSSION

The average Radon concentrations are expressed in Bq/L (for drinking water) and Bq/m³ for sediments. The samples were collected at the water treatment plant in different areas in Al-Diwaniyah, Iraq. Table 1 shows that the

concentrations of ^{222}Rn in drinking water vary from 0.05 Bq/L (sample W07) to 0.47 Bq/L (sample W05). In turn, the contribution of indoor Radon varied from 0.02 Bq/L (sample W07) to 0.19 Bq/L (sample W05). Therefore, for the sediment samples, the concentrations of ^{222}Rn varied from 29.16 Bq/m³ (sample S08) to 60.52 Bq/m³ (sample S05). The highest concentrations of ^{222}Rn were found in the Il-Hemad area due to the high levels of uranium in the region due to the Gulf War (a conflict that involved Kuwait, Iraq, and the United States in 1991).

Figure 4 shows the ratio between the average concentrations of Radon in samples of drinking water and sediments. We identified the highest proportion in Al-Shamiya (16%), while the lowest proportion was found in Al-Jazzier I (2%). This discrepancy in the ratio depends on the sorption potential of the sediments. The partition coefficient of ^{222}Rn in sediments decreases according to the pores of water entering the rock. Consequently, sediment irrigation rates change ^{222}Rn levels. Also, the sorption/desorption kinetics, taking into account the contact time in the water-sediment interaction, can impact the determination of the concentration of this radionuclide. A slow percolation between water and sediment can interfere with the determination of ^{222}Rn .

In turn, the results of the concentration of Radon in the sediment vary considerably due to the presence of uranium and radium. The amount of Radon in sediments and in the air changes over time. Other factors that need to be considered are atmospheric pressure, temperature, wind speed, and relative humidity. The granulometry and morphology of the sediments control the emanation of Radon in solid samples.

The United Nations Security and Energy Commission for Sustainable Development reports that the relationship between grain size and emanation of ^{222}Rn is inversely proportional. The uranium content in the samples led to the discrepancies observed in the concentrations of ^{222}Rn in the sediments. In any case, the levels of ^{222}Rn are below the limits recommended by the International Commission for Radiological Protection (200 to 600 Bq/m³).

The measures taken in this study are following environmental protection standards. The results indicate that the areas under study did not represent a risk to public health, thus allowing the reuse of these sediments in civil construction. The results obtained for the

effective dose of Radon intake in drinking water (Table 2), depending on the population's age group. Among children, there is a variation of 0.001×10^{-10} to 0.007×10^{-10} Sv/Bq and for the adult population from 0.001×10^{-10} to 0.004×10^{-10} Sv/Bq. When we compare the concentrations of ^{222}Rn in drinking water and sediments, we can identify a much greater tendency for particulate matter. This is due to the water filtration process, geological structure of the regions, and high rainfall. Thus, we can conclude that the Radon concentration in the samples, in general, is lower than the level reported by the Environmental Protection Agency (11.1 Bq/L (Khattak *et al.*, 2011)).

Considering the World Health Organization indicators, the safety limit for the concentration of ^{222}Rn is 100 Bq/L, being lower than the average concentrations observed in this study (0.24 Bq/L). The result clearly shows that the drinking water samples in the research areas are healthy and free from radiation. Generally, Radon levels in groundwater are higher than in drinking water samples due to high concentrations of uranium and radio (Mustapha *et al.*, 2002; Ahmad *et al.*, 2018). As for the effective dose of drinking water intake for children equal to twice the dose for adults (Figure 5). Tables 3 and 4 show the concentrations of ^{222}Rn in drinking water and sediments in other countries.

The values obtained in the present study were lower than the levels found in Pakistan, United Kingdom, Iran, Portugal, Malaysia, India, Austria, Giro, and Greece, except Iraq and Turkey. The same behavior is seen for the regions of Yemen, Iraq (Basra), Saudi Arabia (Jazan), Iraq (Arabian Gulf), Saudi Arabia (Arabian Gulf), and Jordan, except Egypt, Thailand, and China.

4. CONCLUSIONS

In the present work, ^{222}Rn levels were determined in a water treatment plant located in the city of Al-Diwaniya/Iraq. In a total of 20 samples (10 of drinking water and 10 of sediment), the RAD7 and CR-39 equipment were used in order to measure the concentrations of ^{222}Rn . With the aid of the RAD7 detector, the results for drinking water reveal that it can be used safely from the radiological point of view. Likewise, the sediments analyzed with the CR-39 detector proved to be below the levels recommended by health and environmental organizations and can be reused in civil

construction without causing damage. The low concentration of ^{222}Rn in drinking water is due to the filtration process of the treatment plant and the geological nature of the rocks through which the water percolates. On the other hand, the concentrations of radionuclide in sediments are high when compared to samples of drinking water. This is due to the granulometry and morphology of the material that directly influences the sorption/desorption of ^{222}Rn . According to the results of this research, the population of the city of Al-Diwaniya/Iraq is safe regarding drinking water because the concentration of ^{222}Rn is below the acceptable limits in the environmental protection and public health agencies.

5. ACKNOWLEDGMENTS

The authors acknowledge the staff of drinking water treatment stations and the staff department of the environment in Al-Diwaniyahgovernorate, for their cooperation and outmost help to complete this work. I would like to thank the Department of Physics, College of Education staff, for assisting the authors throughout conducting this research. A special thank goes to the professional editor, Dr. Ghyath K. Al Shabani, for his valuable academic comments and editing.

6. REFERENCES

1. Shannoun, F. (2015). Medical exposure assessment: the global approach of the United Nations scientific committee on the effects of atomic radiation. *Radiation Protection Dosimetry*, 165(1-4), 125–128.
2. Cho, B. W; Kim, H. K; Kim, M. S; Hwang, J. H; Yoon, U; Cho, S. Y; Choo, C. O. (2019). Radon concentrations in the community groundwater system of South Korea. *Environmental monitoring and assessment*, 191(3), 189.
3. Al-Fifi, Z; El-Araby, E. H; Elhaes, H. (2012). Monitoring of Radon concentrations in Jazan beach soil. *Journal of Applied Sciences Research*, 823–827.
4. Alshahri, F; El-Taher, A; Elzain, A. E. A. (2019). Measurement of Radon exhalation rate and annual effective dose from marine sediments, Ras Tanura, Saudi Arabia, using CR-39 detectors. *Romanian Journal of Physics*, 64, 811– 823.
5. AS-Subaihi, F. A; Salem, T. A; Aisa, M; Alnakeeb, F. (2020). Measurement of Radon exhalation rate, annual effective

- dose, and radium activity from marine sediment samples collected from Abian beach, Aden Gulf, Yemen. *Science and Technology*, 6(2), 19–26.
6. Binesh, A; Mowlavi, A. A; Mohammadi, S. (2012). Estimation of the effective dose from Radon ingestion and inhalation in drinking water sources of Mashhad, Iran. *International Journal of Radiation Research*, 10 (1), 37–41.
 7. Somlai, K; Tokonami, S; Ishikawa, T; Vancsura, P; Gáspár, M; Jobbágy, V; Somlai, J; Kovács, T. (2007). ^{222}Rn concentrations of water in the Balaton Highland and in the southern part of Hungary, and the assessment of the resulting dose. *Radiation Measurements*, 42(3), 491–495.
 8. Al-Nafiey, M. S; Jaafar, M. S; Bauk, S. (2014). Measuring Radon concentration and toxic elements in the irrigation water of the agricultural areas in Cameron Highlands, Malaysia. *Sains Malaysiana*, 43(2), 227–231.
 9. Al-Alawy, I. T; Mohammed, R. S; Fadhil, H. R; Hasan, A. A. (2018). Determination of radioactivity levels, hazard, cancer risk, and Radon concentrations of water and sediment samples in the Al-Husseiniya River (Karbala, Iraq). *Journal Physics: Conference Series*, 1(1032), 1–18.
 10. Gruber, V; Maringer, F. J; Landstetter, C. (2009). Radon and other natural radionuclides in drinking water in Austria: measurement and assessment. *Applied Radiation and Isotopes*, 67(5), 913–917.
 11. Al-Mosawi, W. H; Subber, A. R. H. (2013). Radon Concentration: The cases of study are Shut-Al-Basra, riverbanks, and Basra Sports City, Basra, Iraq. *Archives of Physics Research*, 4(6), 16–23.
 12. Chanyotha, S; Kranrod, C; Kritsanuwat, R; Lane-Smith, D; Burnett, W. C. (2016). Optimizing laboratory-based Radon flux measurements for sediments. *Journal of environmental radioactivity*, 158, 47–55.
 13. Atallah, M; Al-Bataina, B; Mustafa, H. (2001). Radon emanation, along with the dead sea transform (rift) in Jordan. *Environmental Geology*, 40(11-12), 1440–1446.
 14. Showard, A. F; Aswood, M. S. (2019). Measuring of Alpha particles in Blood samples of Leukemia patients in Babylon governorate, Iraq. *Journal of Physics: Conference Series*, 1234(1), 012062).
 15. Todorovic, N; Nikolov, J; Forkapic, S; Bikit, I; Mrdja, D; Krmar, M; Veskovic, M. (2012). Public exposure to Radon in drinking water in Serbia. *Applied Radiation and Isotopes*, 70(3), 543–549.
 16. Jobbágy, V; Altitzoglou, T; Malo, P; Tanner, V; Hult, M. (2017). A brief overview on Radon measurements in drinking water. *Journal of Environmental Radioactivity*, 173, 18–24.
 17. Appleton, J. D. (2007). Radon: sources, health risks, and hazard mapping. *Ambio*, 85–89.
 18. Divya, P. V; Prakash, V. (2019). Investigation on Radon concentration in drinking water to assess the whole-body dose and excess lifetime cancer risk along with coastal Kerala, India. *Journal of Radioanalytical and Nuclear Chemistry*, 322(1), 37–42.
 19. Martins, L. M. O; Pereira, A. J. S. C; Oliveira, A. S; Fernandes, L. S; Pacheco, F. A. L. (2020). A new Radon prediction approach for an assessment of radiological potential in drinking water. *Science of The Total Environment*, 712, 136427.
 20. Duggal, V; Sharma, S; Mehra, R. (2020). Risk assessment of Radon in drinking water in Khetri Copper Belt of Rajasthan, India. *Chemosphere*, 239, 124782.
 21. Fares, S. (2017). Measurements of natural radioactivity level in black sand and sediment samples of the Tamsah Lake beach in Suez Canal region in Egypt. *Journal of radiation research and applied sciences*, 10(3), 194–203.
 22. Nikolopoulos, D; Louizi, A. (2008). Study of indoor Radon and Radon in drinking water in Greece and Cyprus: implications to exposure and dose. *Radiation Measurements*, 43(7), 1305–1314.
 23. Subber, A. R. H; Ali, M. A; Al-Asadi, T. M. (2011). The determination of Radon exhalation rate from water using active and passive techniques. *Advances in Applied Science Research*, 2(6), 336–346.
 24. Subber, A. R. H; Al-Hashimi, N. H. N; Jaber, M. Q. (2017). The concentrations of Radon in the marine sediments of Ra's Al-Besha, Northern west of the Arabian Gulf. *Mesopotamian Journal of Marine Science*, 32(1), 1–8.
 25. Jaber, M. Q; Subber, A. R; Al-Hashimi, N. H. (2015). Radon concentrations in the marine sediments of Khor-Abdulla Northern West of the Arabian Gulf.

- International Journal of Physics*, 3(6), 239–243.
26. Kiat, C. C; Ab Ghani, A; Abdullah, R; Zakaria, N. A. (2008). Sediment transport modeling for Kulim River—A case study. *Journal of Hydro-environment Research*, 2(1), 47–59.
 27. Henshaw, D. L; Perryman, J; Keitch, P. A; Allen, J. E; Camplin, G. C. (1993). Radon in domestic water supplies in the UK. *Radiation Protection Dosimetry*, 46(4), 285–289.
 28. Kurnaz, A. S. I. L; Çetiner, M. A. (2016). Exposure assessment of the Radon in residential tap water in Kastamonu. *International Journal of Radiation Research*, 14(3), 245–250.
 29. Lopes, I; Madruga, M. J; Carvalho, F. P. (2005). Application of liquid scintillation counting techniques to gross alpha, gross beta, Radon and radium measurement in Portuguese waters. *Naturally occurring radioactive materials (NORM IV)*, 357–367.
 30. Nasir, T; Shah, M. (2012). Measurement of annual effective doses of Radon from drinking water and dwellings by CR-39 track detectors in Kulachi City of Pakistan. *Journal of Basic & Applied Sciences*, 8, 528–536.
 31. Wallner, G; Steininger, G. (2007). Radium isotopes and Rn-222 in Austrian drinking waters. *Journal of Radioanalytical and Nuclear Chemistry*, 274(3), 511–516.
 32. Zalewski, M; Mnich, Z; Karpi_ska, M; Kapala, J; Zalewski, P. (2001). Indoor Radon concentrations in Poland as determined in short-term (two-day) measurements. *Radiation Protection Dosimetry*, 95(2), 157–163.
 33. Fard, Z. D; Rahimi, M; Malakootian, M; Javid, N. (2020). Studying Radon concentration in drinking water resources in Zarand city (Iran) and its villages. *Journal of Radioanalytical and Nuclear Chemistry*, 39, 1–7.
 34. Wang, N; Xiao, L; Li, C; Liu, S; Huang, Y; Liu, D; Peng, M. (2011). Distribution and characteristics of Radon gas in soil from a high-background-radiation city in China. *Journal of Nuclear Science and Technology*, 48(5), 751–758.
 35. Wong, C. S; Chin, Y. P; Gschwend, P. M. (1992). Sorption of Radon-222 to natural sediments. *Geochimica et cosmochimica acta*, 56(11), 3923–3932.
 36. Mustapha, A. O; Patel, J. P; Rathore, I. V. S. (2002). Preliminary report on Radon concentration in drinking water and indoor air in Kenya. *Environmental Geochemistry and Health*, 24(4), 387–396.
 37. Xinwei, L. (2006). Analysis of Radon concentration in drinking water in Baoji (China) and the associated health effects. *Radiation Protection Dosimetry*, 121(4), 452–455.
 38. Muhammad, B. G; Jaafar, M. S; Azhar, A. R; Akpa, T. C. (2012). Measurements of ²²²Rn activity concentration in domestic water sources in Penang, Northern Peninsular Malaysia. *Radiation protection dosimetry*, 149(3), 340–346.
 39. Singh, S; Kumar, A; Bajwa, B. S; Mahajan, S; Kumar, V; Dhar, S. (2010). Radon monitoring in soil gas and groundwater for earthquake prediction studies in northwest Himalayas, India. *Terrestrial, Atmospheric and Oceanic Sciences*, 21(4), 6.
 40. Khattak, N; Khan, M; Shah, M; Javed, M. (2011). Radon concentration in drinking water sources of the Main Campus of the University of Peshawar and surrounding areas, Khyber Pakhtunkhwa, Pakistan. *Journal of Radioanalytical and Nuclear Chemistry*, 290(2), 493–505.
 41. Ahmad, N; Jaafar, M. S; Nasir, T; Rafique, M. (2018). Determination of Radon concentration and heavy metals (Ni, Pb, Cd, As, Cr) in drinking and irrigated water sampled from Kulim, Malaysia. *International Journal of Radiation Research*, 16(3), 341–349.

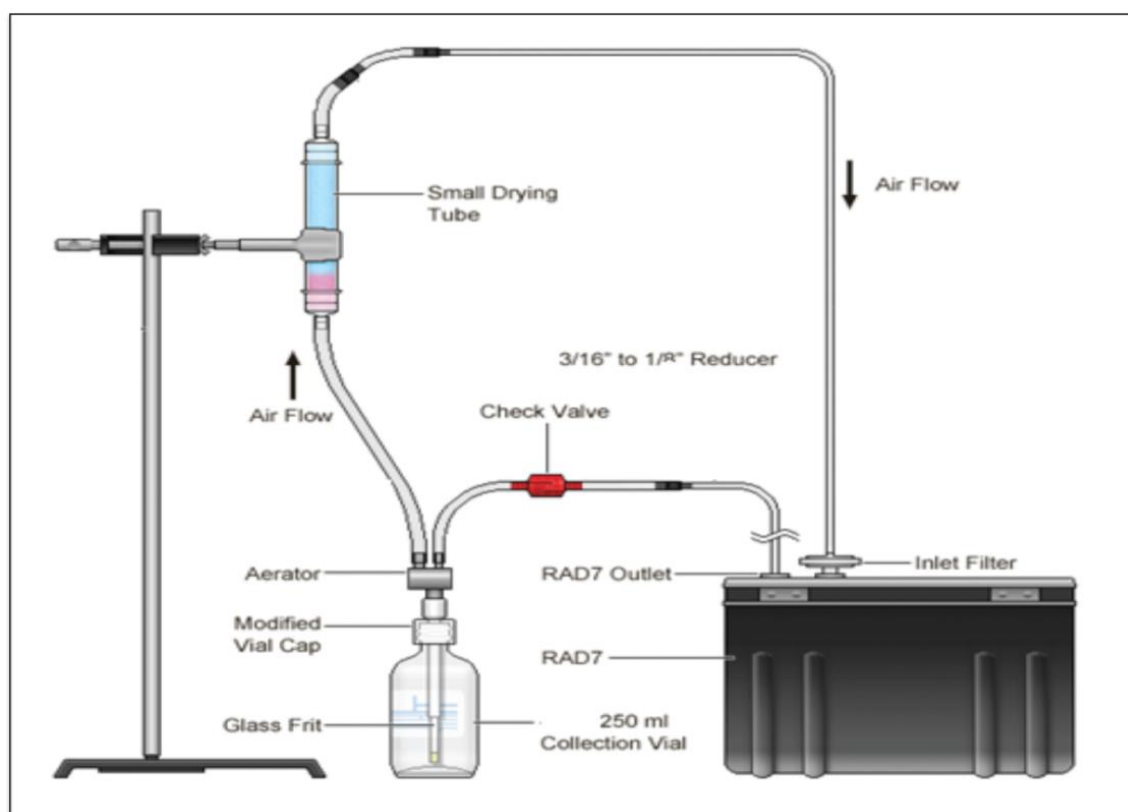


Figure 1. Diagram of RAD7 instrument for active Radon measurement.

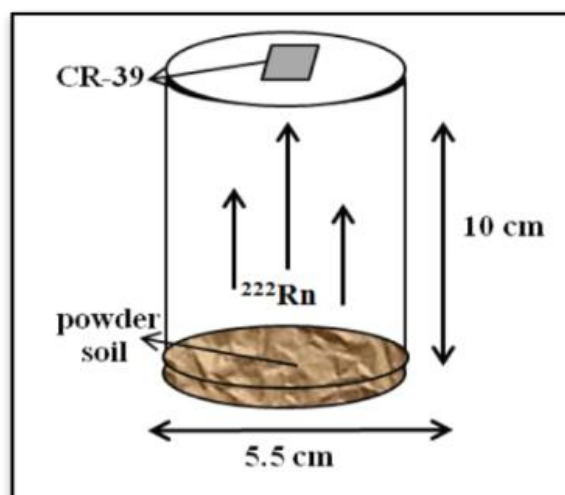


Figure 2. Apparatus for measurements of Radon in sediments.

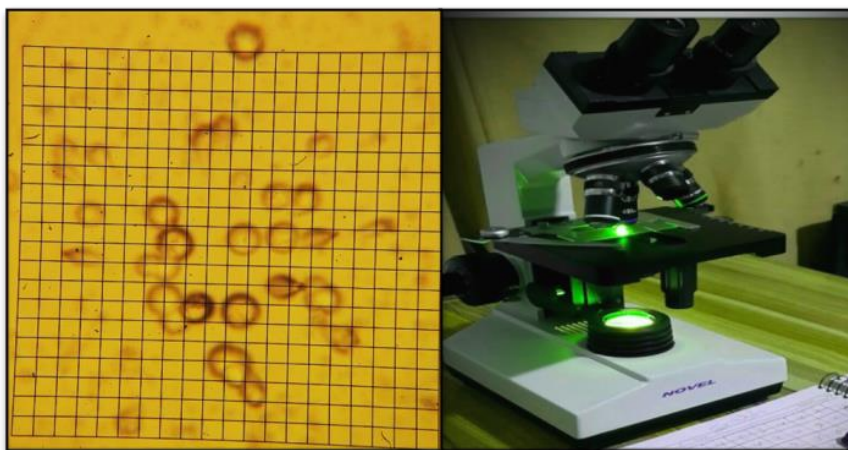


Figure 3. Optical microscope and track on CR-39 detector.

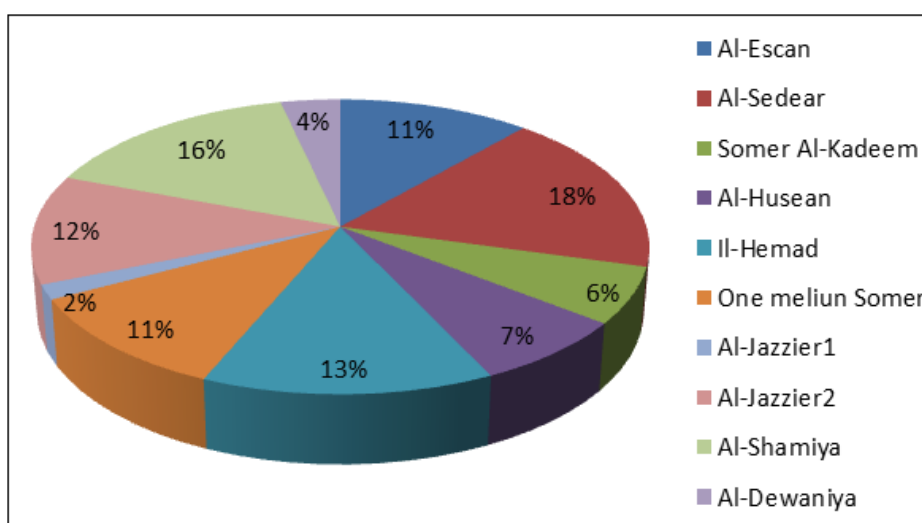


Figure 4. Ratio of average concentrations of Radon in drinking water and sediments.

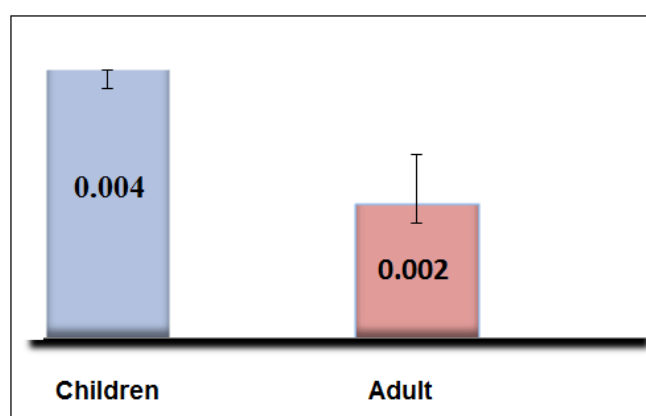


Figure 5. Comparison of Radon ingestion to children and adults (Sv 10^{-10}).

Table 1. The concentration of indoor Radon in drinking water and sediment from the water treatment plant (Al-Diwaniya, Iraq).

Site	Code	Concentration of Radon in water	Contribution of Radon to indoor	code	Concentration of Radon in sediment C_{S222Rn}
		C_{W222Rn} (Bq/L)	C_{A222Rn} (mBq/L)		(Bq/m ³)
Al-Ilskan	W01	0.27 ± 0.09	0.11 ± 0.03	S01	40.70 ± 2.16
Al-Sdyr	W02	0.40 ± 0.10	0.16 ± 0.04	S02	39.25 ± 1.90
Sumir Al-Qadim	W03	0.13 ± 0.06	0.05 ± 0.02	S03	37.80 ± 1.77
Al-Husain	W04	0.20 ± 0.06	0.08 ± 0.02	S04	47.25 ± 2.63
Il-Hemad	W05	0.47 ± 0.20	0.19 ± 0.08	S05	60.52 ± 4.33
1 Million Sumir	W06	0.27 ± 0.08	0.11 ± 0.03	S06	43.15 ± 2.28
Al-Jazayir 1	W07	0.05 ± 0.02	0.02 ± 0.01	S07	48.97 ± 2.76
Al-Jazayir 2	W08	0.20 ± 0.07	0.08 ± 0.02	S08	29.16 ± 0.93
Al-Shamiya	W09	0.40 ± 0.20	0.16 ± 0.08	S09	44.70 ± 2.35
Al-Diwaniyah	W10	0.07 ± 0.03	0.03 ± 0.01	S10	32.80 ± 1.28
Average		0.24 ± 0.11	0.10 ± 0.03		42.43 ± 2.24

Table 2. Effective doses of ingestion of drinking water samples from the water treatment plant (Al-Diwaniya, Iraq)

Site	Code	Committed effective doses from ingestion E_d (Sv 10 ⁻¹⁰)	
		For children	For adults
Al-Ilskan	W01	0.004 ± 0.005	0.002 ± 0.002
Al-Sdyr	W02	0.006 ± 0.001	0.003 ± 0.001
Sumir Al-Qadim	W03	0.002 ± 0.003	0.002 ± 0.001
Al-Husain	W04	0.003 ± 0.003	0.002 ± 0.001
Il-Hemad	W05	0.007 ± 0.001	0.004 ± 0.001
1 Million Sumir	W06	0.004 ± 0.004	0.002 ± 0.002
Al-Jazayir 1	W07	0.001 ± 0.002	0.001 ± 0.003
Al-Jazayir 2	W08	0.003 ± 0.004	0.002 ± 0.002
Al-Shamiya	W09	0.006 ± 0.001	0.003 ± 0.001
Al-Diwaniyah	W10	0.002 ± 0.001	0.002 ± 0.001
Average		0.004 ± 0.002	0.002 ± 0.001

Table 3. Comparison of Radon concentrations in drinking water in the world.

Country	²²² Rn concentration (Bq/L)	Reference
Pakistan	0.602 ± 0.005	Nasir and Shah, 2012
Iraq	0.174 ± 0.001	Subber <i>et al.</i> , 2011
UK	0.19 ± 0.001 – 71.1 ± 0.023	Henshaw <i>et al.</i> , 1993
Iran	11.44 ± 0.023	Binesh <i>et al.</i> , 2012
Turkey	0.025 ± 0.001 – 0.128 ± 0.001	Kiat <i>et al.</i> 2008
Portugal	1.9 ± 0.002 – 112.77 ± 0.89	Lopes <i>et al.</i> , 2005
Iran	1.23 ± 0.002 – 11.94 ± 0.046	Kurnaz and Cetiner, 2016
Malaysia(a)	2.64 ± 0.003	Ahmad <i>et al.</i> , 2018
Austria	1.46 ± 0.005 – 644 ± 2.86	Wallner and Steininger, 2007
Cyprus and Greece	0.3 ± 0.002 – 24 ± 0.29	Nikolopoulos and Louizi, 2008
India	12.5 ± 1.5 – 862 ± 38	Fares, 2017
Malaysia(b)	5.37 ± 0.008	Ahmad <i>et al.</i> , 2018
Iraq, Al-Diwaniyah	0.05 ± 0.02 – 0.47 ± 0.20	Present study

Table 4. Comparison of Radon concentrations in sediment in the world.

Country	²²² Rn concentration (Bq/m ³)	References
Yemen	103.88 ± 8.80	AS-Subaihi <i>et al.</i> , 2020
Iraq (Basra)	304.3 ± 79.4	Subber <i>et al.</i> , 2011
Iraq (Arabian Gulf)	400.7 ± 198	Jaber <i>et al.</i> , 2015
Saudi Arabia (Jazan)	88.17 ± 0. 5.6	Nasir and Shah, 2012
Saudi Arabia (Arabian Gulf)	33 ± 2.10	Alshahri <i>et al.</i> , 2019
Egypt	29.40 ± 4.08	Fares, 2017
Thailand	4.5 ± 0.6	Chanyotha <i>et al.</i> , 2016
Jordan	918 ± 214	Atallah <i>et al.</i> , 2001
China	37.64 ± 3.89	Wang <i>et al.</i> , 2011
Iraq (Al-Diwaniyah)	42.43 ± 2.24	Present study

COMPLEXAÇÃO DE PRAZIQUANTEL COM α -, β - E γ -CICLODEXTRINAS EM SOLUÇÕES HIDROALCOÓLICAS

COMPLEXATION OF PRAZIQUANTEL WITH α -, β - AND γ -CYCLODEXTRINS IN AQUEOUS-ALCOHOLIC SOLUTIONS

КОМПЛЕКСООБРАЗОВАНИЕ ПРАЗИКВАНТЕЛА С α -, β - И γ -ЦИКЛОДЕКСТРИНАМИ В ВОДНО-СПИРТОВЫХ РАСТВОРАХ

IBRAKOVA, Nurgiza F.^{1*}; KUTLUGILDINA, Galiya G.²; ZIMIN, Yuriy S.³;

^{1,2,3} Bashkir State University, Department of Physical Chemistry and Chemical Ecology, 450076, 32 Zaki Validi Str., Ufa – Russian Federation

* *Corresponding author*

e-mail: n.ibrakova95@mail.ru

Received 12 September 2020; received in revised form 30 October 2020; accepted 02 November 2020

RESUMO

Hoje, a percentagem de infecções por doenças invasivas (parasitárias) é bastante grande, portanto, o tratamento das helmintíases é um problema urgente em medicina veterinária. Os vermes parasitas infligem danos significativos ao gado, levando à morte de animais, escassez de carne, produtos lácteos e lã. O objetivo deste trabalho foi estudar a complexação do praziquantel com α -, β - e γ -ciclodextrinas em soluções hidroalcoólicas. A interação de um medicamento anti-helmíntico, praziquantel, com α -, β - e γ -ciclodextrinas em soluções hidroalcoólicas foi estudada pelo método de espectroscopia ultravioleta. Verificou-se que a adição de ciclodextrinas às soluções hidroalcoólicas de praziquantel leva a alterações espectrais, indicando a presença de interações intermoleculares e complexação. O método da série isomolar mostrou que em soluções diluídas o praziquantel forma compostos complexos com as ciclodextrinas de composição 1:1, ou seja, há uma molécula de praziquantel por uma molécula de α -, β - ou γ -ciclodextrina. As constantes de estabilidade dos complexos resultantes foram calculadas usando o método da razão molar. É mostrado que na faixa de 296-316 K a composição dos compostos complexos permanece inalterada (1:1), e sua estabilidade diminui com o aumento da temperatura. O estudo das dependências das constantes de estabilidade com a temperatura possibilitou determinar os valores padrão das variações da energia de Gibbs, entalpia e entropia de complexação.

Palavras-chave: *medicamentos anti-helmínticos, praziquantel, doenças parasitárias, substâncias contendo nitrogênio, lei de Beer-Lambert-Bouguer.*

ABSTRACT

Currently, the percentage of infections with invasive (parasitic) diseases is quite large; therefore, the treatment of helminthiasis is an urgent problem in veterinary medicine. Parasitic worms inflict significant damage on animal husbandry, leading to the death of animals, shortage of meat, dairy products, and wool. The most common active ingredient in anthelmintics is praziquantel, which is well known as an effective broad-spectrum anthelmintic. At the same time, praziquantel has low solubility in water and a pronounced bitter taste, which represents a significant obstacle in developing liquid forms of drugs that are convenient for administration to animals. One way to solve these problems is the complexation of medicinal substances with various (natural and synthetic) compounds. In this regard, this paper aims to study the complexation of praziquantel with α -, β -, and γ -cyclodextrins in aqueous-alcoholic solutions. The studies were carried out by the method of ultraviolet spectroscopy. It was found that the addition of cyclodextrins to aqueous-alcoholic solutions of praziquantel leads to spectral changes indicating the presence of intermolecular interactions and complexation. The isomolar series method showed that in dilute solutions, praziquantel forms complex compounds with cyclodextrins 1:1, that is, one molecule of praziquantel falls on one molecule of α -, β - or γ -cyclodextrin. The stability constants of the resulting complexes were calculated using the molar ratio method. It is shown that in the range of 296-316 K, the composition of complex compounds remains unchanged (1:1), and their stability decreases with increasing temperature. The study of the temperature dependences of the

stability constants made it possible to determine the standard values of changes in the Gibbs energy, enthalpy, and complexation entropy.

Keywords: *anthelmintic drugs, praziquantel, parasitic diseases, nitrogen-containing substances, Bouguer-Lambert-Beer law.*

АННОТАЦИЯ

На сегодняшний день процент заболевания инвазионными (паразитарными) болезнями достаточно велик, поэтому лечение гельминтозов является актуальной проблемой ветеринарии. Значительный ущерб паразитические черви наносят животноводству, приводя к гибели животных, недополучению мясной и молочной продукции, шерсти. Целью настоящей работы явилось изучение комплексообразования празиквантела с α -, β - и γ -циклодекстринами в водно-спиртовых растворах. Методом ультрафиолетовой спектроскопии исследовано взаимодействие антигельминтного препарата – празиквантела – с α -, β - и γ -циклодекстринами в водно-спиртовых растворах. Установлено, что добавление циклодекстринов к водно-спиртовым растворам празиквантела приводит к спектральным изменениям, свидетельствующим о наличии межмолекулярных взаимодействий и комплексообразования. Методом изомольных серий показано, что в разбавленных растворах празиквантел образует с циклодекстринами комплексные соединения состава 1:1, то есть на одну молекулу α -, β - или γ -циклодекстрина приходится одна молекула празиквантела. С помощью метода молярных отношений рассчитаны константы устойчивости образующихся комплексов. Показано, что в интервале 296-316 К состав комплексных соединений остается неизменным (1:1), а их устойчивость с ростом температуры падает. Изучение температурных зависимостей констант устойчивости позволило определить стандартные значения изменений энергии Гиббса, энтальпии и энтропии комплексообразования.

Ключевые слова: *антигельминтные препараты, празиквантел, паразитарные болезни, азотсодержащие вещества, закон Бугера-Ламберта-Бера.*

1. INTRODUCTION:

Currently, the percentage of infections with invasive (parasitic) diseases is quite large; therefore, the treatment of helminthiasis is an urgent problem in veterinary medicine. Unlike microorganisms such as unicellular, fungi, viruses, and bacteria, which have a rather delicate and soft cover, most helminths, especially nematodes, have a multi-layered muscle cuticle that sufficiently protects the organs of the parasite. Great economic damage is inflicted on animal husbandry due to the widespread of nematodes, leading to the death of animals, shortage of meat and dairy products, and wool. Lack of treatment for invasive diseases can lead to severe damage to internal organs up to death. Also, some helminthiasis are dangerous to humans. It should be noted that annually in the Russian Federation alone, more than 20 million people fall ill with parasitic diseases, and most often, they are residents of rural areas (Butko *et al.*, 2018). In this regard, invasive (parasitic) diseases are of great importance today, which leads to an increase in demand for veterinary drugs used to treat them.

Praziquantel-2-(cyclohexylcarbonyl)-1,2,3,6,7,11b-hexahydro-4H-pyrazino[2,1-a]isoquinolin-4-one is often used as an active component of antihelmintics. This drug is known as an effective broad-spectrum anthelmintic agent (Subbotin *et al.*, 2000). It is a broad-spectrum drug used to treat many parasitic infections, including cysticercosis, tapeworm disease, and clonorchiasis (Zhang *et al.*, 2020). Praziquantel is considered a relatively low-toxic drug that does not possess embryotoxic, mutagenic, and teratogenic properties and does not affect the postnatal development of the body (Demidov, 1982; Engasheva, 2011; Garcia *et al.*, 2011; Zolotareva and Zeynalov, 2015; Harvie *et al.*, 2019; Liu *et al.*, 2019; Nono *et al.*, 2020). At the same time, with all the listed advantages, praziquantel has several disadvantages: 1) low solubility in water and, as a result, limited bioavailability of this substance in liquid compositions; 2) lack of the necessary activity concerning the roundworms; 3) the lack of complete clearance of praziquantel from the body, which, with prolonged use, can lead to increased toxicity to animals; 4) pronounced bitter taste, which is a significant obstacle in the development of medicinal products for oral administration and, in particular, their liquid

forms intended for dogs and cats (Subbotin *et al.*, 2000; Xu *et al.*, 2009; Sousa-Figueiredo *et al.*, 2012; Zolotareva and Zeynalov, 2015).

One way to solve these problems is the complexation of medicinal substances with various (natural and synthetic) compounds. The prospects of this approach are confirmed by data on the study of the complexation of some nitrogen-containing, including medicinal, substances (derivatives of uracil, 4- and 5-aminosalicylic acids) with polyfunctional acids (see, for example, (Baltina *et al.*, 2001; Chernyshenko, 2008; Myshkin *et al.*, 2009; Borisova *et al.*, 2013; Gimadieva *et al.*, 2014; Wangchuk *et al.*, 2016a; Zimin *et al.*, 2017), and the sources cited there). It should be borne in mind that complexation can eliminate some of the disadvantages of medicinal substances and introduce new beneficial properties. In recent years, biologically degradable, non-toxic, and relatively cheap cyclodextrins are built from glucose residues, which have a hydrophilic outer surface and a volumetric hydrophobic inner cavity comparable to many substrates (organic and inorganic), are often used as a complexing agent (Szejtli, 1998; Crini *et al.*, 2018). Due to their structure, cyclodextrins can form "host-guest" complexes with various types of molecules (Uekama *et al.*, 1998; Pandey *et al.*, 2010; Crini *et al.*, 2018). The formation of such complexes can significantly change the physicochemical and biological properties of the "guest" molecule, which determined their relevance as an object and tool of the modern chemical and pharmaceutical technologies (Fedorova *et al.*, 2011). Complexation with cyclodextrins makes it possible to increase the selectivity and, therefore, the dose efficiency of pharmacologically active substances; stabilize compounds sensitive to the action of light, heat, and oxygen in the air; multiply the solubility of substances hardly soluble in water and increase their bioavailability; prolong the effects of drugs, ensure their targeted transport in the body; prevent the irritating effect of drugs on mucous membranes; reduce toxicity; mask unpleasant tastes and smells (Uekama *et al.*, 1998; Pandey *et al.*, 2010; Fedorova *et al.*, 2011). In connection with the above, the purpose of this paper is to study the complexation of praziquantel with α -, β - and γ -cyclodextrins in aqueous-alcoholic solutions.

2. MATERIALS AND METHODS:

The complexing agents were natural

cyclic oligosaccharides, cyclodextrins produced by the company "AppliChem" (Darmstadt, Germany). Of the huge family of cyclodextrins, this study was used three main, most studied and widespread products: α -cyclodextrin (α -CD), β -cyclodextrin (β -CD), and γ -cyclodextrin (γ -CD), the macrorings of which consist of 6, 7, and 8 glucopyranose residues, respectively. These cyclodextrins have the following empirical formulas: α -CD - $C_{36}H_{60}O_{30}$, β -CD - $C_{42}H_{70}O_{35}$, and γ -CD - $C_{48}H_{80}O_{40}$. Praziquantel (PR) was provided by the research and production company "Ecohimtech" (Ufa), where a unique scheme for the synthesis of this drug was developed. The solvent was a water-alcohol mixture with a volume ratio of water and alcohol 1:1.

The complexation of praziquantel with α -, β - and γ -cyclodextrins was studied by UV spectroscopy in the temperature range from 296 to 316 K. Since cyclodextrins, when transmitted by UV light, do not give absorption peaks in the wavelength range of 190-360 nm. Therefore, all studies were carried out at the maximum absorption wavelength of praziquantel. Complex compounds were obtained under equilibrium conditions at low concentrations of the starting reagents (10^{-4} – 10^{-3} mol/L) in aqueous-alcoholic solutions. UV spectra of praziquantel and complex compounds were recorded on a UV-2401 PC spectrophotometer (Shimadzu, Japan) in temperature-controlled quartz cells 1 cm thick relative to the solvent - aqueous-alcoholic mixture.

To determine the composition of the resulting complexes, the isomolar series method was used (Bulatov and Kalinkin, 1986; Beck and Nadpal, 1989). This method is based on determining the ratio of isomolar concentrations of the interacting substances, which corresponds to the maximum yield of the resulting complex compound. In this case, the curve of the dependence of the yield of the complex and the change in optical density on the composition of the solution should be characterized by an extremum point. Such a point will indicate the maximum possible concentration of the complex, and its position on the abscissa axis will correspond to the stoichiometric ratio of the reactants. Based on the above, experiments were prepared and carried out, the essence of which was as follows. Aqueous-alcoholic solutions of praziquantel and α -, β - or γ -cyclodextrin of the same molar concentration ($1 \cdot 10^{-3}$ mol/L) were mixed in inverse relation (from 1:9 to 9:1) while

maintaining the total volume of the solution unchanged. In this case, the total number of moles of both components in the solution also remained constant. After 1 hour, the optical densities of the solutions were measured. The comparison cuvette was filled with a solvent, a water-alcohol mixture (1:1 by volume). By measuring the optical densities of the prepared solutions of the isomolar series, a graph of the dependence of the change in optical density on the ratio of the concentrations of the components were plotted, and the position of the absorption maximum on the isomolar curve was determined. The maximum light absorption is possessed by a solution in which the content of the resulting complex compound is biggest. The extreme point on the isomolar diagram was used to determine the composition of the resulting complex (Bulatov and Kalinkin, 1986; Beck and Nadpal, 1989).

To determine the stability constants (K) of complex compounds, molar ratios were used (Bulatov and Kalinkin, 1986; Beck and Nadpal, 1989). This method is based on establishing the dependence of the change in optical density (ΔA) on the concentration of one of the components at a constant concentration of the second component, and vice versa. The experiments were carried out as follows. Aqueous-alcoholic solutions of praziquantel (PR) and cyclodextrin (CD) (α -, β -, or γ -) with the same molar concentration of $1 \cdot 10^{-3}$ mol/L were prepared. In 10 volumetric flasks, 2 ml of PR solution and from 0.5 to 8 ml of CD solution were poured. Then the total volume of each flask was brought up to 10 ml with a water-alcohol mixture. The resulting solutions were thoroughly mixed and left for 1 hour at room temperature, after which the optical densities were measured at the maxima of the absorption wavelength of praziquantel. To find the stability constants, graphs of $[PR]/\Delta A$ versus $1/[CD]$ were built, from which the K values were calculated from the ratio of cut-offs to the slope tangents

3. RESULTS AND DISCUSSION:

The UV spectrum of praziquantel has three characteristic absorption bands at 193 nm, 263 nm, and 271 nm. Studies have shown that the most convenient were the last two absorption bands (at wavelengths $\lambda = 263, 271$ nm), used for further study. At the first stage of research, the range of working concentrations of praziquantel was determined. For this, was

applied the Bouguer-Lambert-Beer law (Equation 1). Where A – optical density of aqueous-alcoholic solutions of praziquantel; ϵ_λ – extinction coefficient of praziquantel at wavelength λ ($\text{mol/L}^{-1} \text{ cm}^{-1}$); $[PR]$ – concentration of praziquantel (mol/L); l – sample cell thickness ($l = 1 \text{ cm}$).

It was found that the linear relationship between the optical density of praziquantel and its concentration in a water-alcohol solution is fulfilled up to $[PR] = 1 \cdot 10^{-3}$ mol/L. Thus, for further studies, praziquantel concentrations not exceeding $1 \cdot 10^{-3}$ mol/L were used. The extinction coefficient of praziquantel in an aqueous-alcoholic solution was calculated from the slope of the dependence (Equation 2).

In this study, it was found that the addition of cyclodextrins (α -CD, β -CD, or γ -CD) to aqueous-alcoholic solutions of praziquantel leads to the following changes in its UV spectra: a shift of the absorption band maxima to shorter wavelengths and a decrease in the intensities of the absorption peaks. The observed changes are due to intermolecular interactions that take place in the reaction systems “ α -CD+PR”, “ β -CD+PR” or “ γ -CD+PR”, and lead to the formation of complex compounds (most likely, inclusion complexes (Uekama *et al.*, 1998; Wangchuk *et al.*, 2016b; Pandey *et al.*, 2010; Fedorova, 2011; Crini *et al.*, 2018; Park *et al.*, 2019; Cunha *et al.*, 2020)). Figure 1 shows the UV spectra of aqueous-alcoholic solutions of praziquantel and its complex with α -cyclodextrin.

The complexation of praziquantel with α -, β - and γ -cyclodextrins is also evidenced by isomolar diagrams obtained by the method of isomolar series (Bulatov and Kalinkin, 1986; Beck and Nadpal, 1989). So, Figure 2 shows the isomolar diagram for the complex compound formed by praziquantel and α -cyclodextrin.

An analysis of this diagram suggests that the dependence (Equation 3) passes through a maximum with an increase in the concentration of the optically active substance (PR). This fact confirms the existence of interactions between praziquantel and α -cyclodextrin, otherwise, a different (not extreme) character of the dependence would be observed.

The isomolar diagram (Figure 2) was used to determine the composition of the complex formed in the reaction system “ α -CD +

PR". The maximum change in optical density (ΔA) observed at a ratio of isomolar solutions equal to 0.5 indicates the formation of a 1:1 complex compound in dilute aqueous-alcoholic solutions. It should be noted that in the reaction systems " β -CD + PR" and " γ -CD + PR", similar dependences were obtained, indicating a ratio of components in the complexes equal to 1:1. Thus, in the considered complex compounds, one molecule of α -, β - or γ -cyclodextrin accounts for one molecule of praziquantel.

The stability constants of complex compounds were calculated according to the studies of Bulatov and Kalinkin (1986), Beck and Nadpal (1989). According to this method, spectral changes in the investigated reaction systems " α -CD + PR", " β -CD + PR" and " γ -CD + PR" are described by the Equation 4. Where [PR] – concentration of praziquantel in an aqueous-alcoholic solution (mol/L); A and A_0 – optical densities of praziquantel solutions in the presence and absence of cyclodextrins ($A - A_0 = \Delta A$); ε and ε^0 – molar extinction coefficients of the complexes and praziquantel, respectively (mol/L⁻¹ cm⁻¹); K is the stability constant of the complex compound (mol/L); [CD] – concentration of cyclodextrins (α -, β - or γ -). To find the stability constants, a dependency diagram of [PR]/ ΔA versus 1/[CD] was built (Figure 3), from which the K values were calculated from the ratio of cut-offs to the slope ratio.

Studies were carried out on the temperature effect on the composition and stability of the resulting complexes. It was found that in the studied temperature range of 296-316 K, the complex compounds retain their composition (1:1), i.e., there is always one praziquantel molecule for every single α -, β - or γ -cyclodextrin molecule. Simultaneously, the stability of the resulting complexes decreases with increasing temperature (Table 1).

Having processed the data of the dependences (Equation 5) in the coordinates of the equation (Equation 6) (Poltorak, 1991). Standard thermodynamic parameters (changes in entropies ΔS° and enthalpies ΔH°) of the reactions of formation of praziquantel with α -, β - and γ -cyclodextrins in aqueous-alcoholic solutions were calculated (Table 2). The standard values of changes in Gibbs energies ΔG° at a certain temperature were found according to (Equations 7, 8) (Poltorak, 1991). Table 2 shows that the values of all thermodynamic parameters have a negative

sign. A negative value of ΔS° indicates a decrease in entropy, which is associated with restrictions on the freedom of vibrational and rotational motions of molecules that arise during complexes formation. Negative values of ΔH° and ΔS° indicate, respectively, the exothermicity and spontaneity of complexation processes in the investigated temperature range (296-316 K).

Based on the data obtained on the composition, stability, and thermal stability of the studied complex compounds, a procedure was developed for the synthesis of an individual complex (a complex of α -cyclodextrin with praziquantel), a prototype of this compound was developed, and its solubility in water was studied. In addition, the complex of α -cyclodextrin with praziquantel was transferred to the research and production company "Ecochimtech" (Ufa) for biological tests.

The complex compound α -CD...PR was synthesised by mixing equimolar amounts of the starting reagents (α -cyclodextrin and praziquantel) in a water-alcohol solution. The reaction mixture was stirred for eight days at a temperature of 297 K, after which the water was removed by evaporation under reduced pressure. As a result, the complex compound was obtained in quantitative yield. Below are the spectral characteristics of the α -CD...PR complex in aqueous solution (Equation 9).

In this study, the extinction coefficient of the complex formed by α -cyclodextrin and praziquantel was determined. Using the Bouguer-Lambert-Beer formula (Equation 1), the authors studied the dependence of the optical density of aqueous solutions of complex compound (A) on its initial concentration. The extinction coefficient of the investigated complex in an aqueous solution (Equation 10) was calculated from the tangent of the slope of the dependence (Equation 11).

To confirm the formation of the inclusion complex of praziquantel with α -cyclodextrin and to reveal the nature of the bonds formed in it, the method of IR spectroscopy was used. In the IR spectrum of the initial substrate, praziquantel (Figure 4), the most informative are the regions 1700 - 1600 cm⁻¹, where vibrations of the R-CN-R group (1650 and 1627 cm⁻¹) and stretching vibrations of the carbonyl group C=O (1668 cm⁻¹). The absorption bands at 2900-2800 cm⁻¹ belong to the stretching vibrations of CH groups.

A characteristic functional group inherent in α -cyclodextrin is a hydroxyl group. Therefore, in its IR spectrum (Figure 5), it is possible to observe a band of O-H bond vibrations, which manifests itself in a wide range of wave numbers 3537-3265 cm^{-1} and is quite intense. The absorption bands at 2900-2800 cm^{-1} belong to the stretching vibrations of C-H groups. In the IR spectrum of the complex compound (Figure 6), absorption maxima at 1668, 1650, and 1627 cm^{-1} disappear and one band appears at 1635 cm^{-1} , and a broadened band at 863 cm^{-1} is formed, which is characteristic of plane bending N-H vibrations bonds. At the same time, it should be noted that the complex is characterised by a decrease in the intensity of the bands of the hydroxyl group. This data indicates the participation of the O-H groups of praziquantel in the formation of the inclusion complex. Based on the IR spectroscopy data, it can be concluded that the complexation of α -cyclodextrin and praziquantel occurs due to the formation of intermolecular bonds, in which participate the C=O and CN groups of praziquantel and the O-H groups of cyclodextrin.

At the final stage, studies were carried out to determine the solubility of the complex of α -cyclodextrin with praziquantel synthesised by the authors. The solubility of the complex compound was determined by a visual method. For this, a weighed portion of the synthesised complex was dissolved in 50 ml of a solvent (double-distilled water), after which the resulting mixture was shaken for 1-2 minutes at room temperature (297 K). Then the solubility was checked against a white sheet of paper and under additional lighting. If suspended particles of a substance were found in the solution, another 50 ml of water was added, the solution was shaken and checked again for solubility. Thus, this procedure was repeated until suspended particles of the α -cyclodextrin complex with praziquantel were found in the solution. The complex compound was considered dissolved in the absence of substance particles.

Studies have shown that for the complete solubility of praziquantel with a mass of 0.0016 g, 2100 ml of double-distilled water is required, while a complex compound of the same mass is completely dissolved in 100 ml of water. Thus, the solubility of praziquantel was $2.38 \cdot 10^{-6}$ mol/L, and the solubility of the compound was $5 \cdot 10^{-5}$ mol/L, i.e., it increased 21 times. In addition, it was found that the

synthesised complex compound α -CD...PR is characterised by the absence of odour and a significant decrease in bitterness.

Thus, the complexation of praziquantel with cyclodextrins allows to get rid of a number of disadvantages inherent in PR (see the introduction). So, for example, the solubility of praziquantel in the composition of the complex compound α -CD...PR increased more than 20 times, which opens up possibilities for creating a drug in liquid compositions. In addition, the absence of odour and a significant reduction in bitterness found for the α -CD...PR compound will remove the obstacle to the creation of a medicinal product for oral administration and, in particular, its liquid form intended for pets (dogs and cats).

4. CONCLUSIONS:

In this study, using the method of ultraviolet spectroscopy, the possibility of complexation of an anthelmintic drug, praziquantel, with natural oligosaccharides (α -, β -, and γ - cyclodextrins) in aqueous-alcoholic solutions was investigated. The choice of solvent is due to the extremely low solubility of praziquantel in water. According to the Bouguer – Lambert-Beer law, the extinction coefficient of praziquantel in a water-alcohol mixture was determined at an equal ratio of the volumes of H_2O and $\text{C}_2\text{H}_5\text{OH}$. It was found that the addition of cyclodextrins (α -, β - or γ -) to aqueous-alcoholic solutions of praziquantel leads to the following changes in its UV spectra: a shift of the absorption band maxima to shorter wavelengths and a decrease in the intensities of the absorption peaks. The observed changes are caused by intermolecular interactions in the reaction systems under study and lead to the formation of complex compounds (most likely, inclusion complexes).

By the method of isomolar series, it was shown that in dilute aqueous-alcoholic solutions, praziquantel forms complex compounds with cyclodextrins 1:1, that is, one molecule of praziquantel falls on one molecule of α -, β - or γ - cyclodextrin. Using the method of molar ratios in the temperature range 296-316 K, the stability constants of the resulting complex compounds are calculated. The findings indicated that praziquantel forms relatively unstable complexes with the studied cyclodextrins: the values of the stability constants in the studied temperature range vary

within $(1 \div 7) \cdot 10^2$ mol/L. It was found that an increase in temperature does not affect the composition of complex compounds, while the stability of the complexes decreases with increasing temperature. The study of the temperature dependencies of the stability constants made it possible to determine the standard values of changes in the Gibbs energy (ΔG°), enthalpy (ΔH°), and entropy (ΔS°) of complexation.

It follows from the results obtained that the values of all thermodynamic parameters have a negative sign. The negative value of ΔG° indicates the spontaneous occurrence of complexation processes in the studied temperature range (296-316 K). A negative value of ΔH° indicates exothermicity of the complex compounds' formation processes. The negative value of ΔS° indicates a decrease in entropy during complexation, which is associated with the restrictions on the freedom of vibrational and rotational motions of molecules that arise during the complexation.

5. ACKNOWLEDGMENTS:

The study was supported by a grant from the Russian Science Foundation (project No. 19-73-20073).

6. REFERENCES:

1. Baltina, L. A., Murinov, Yu. I., Ismagilova, A. F., Davydova, V. A., Zarudii, F. S., and Tolstikov, G. A. (2001). Synthesis and Antitumor Activity of Complex Compounds of β -Glycyrrhizic Acid with Antitumor Drugs. *Pharmaceutical Chemistry Journal*, 35, 11, 585-587.
2. Beck, M., and Nadpal, I. (1989). *Research of complexation by the latest methods*. Moscow: Mir.
3. Borisova, N. S., Koroleva, I. P., Zimin, Yu. S., Gimadieva, A. R., and Mustafin, A. G. (2013). Spectrophotometric study of the interaction of uracils with apple pectin and its oxidation products. *Bulletin of Higher Educational Institutions. Chemistry and Chemical Technology*, 56(3), 46-50.
4. Bulatov, M. I., and Kalinkin, I. P. (1986). *A practical guide to photometric methods of analysis*. Leningrad: Chemistry.
5. Butko, M. P., Popov, P. A., Osipova, I. S., Semenova, E.A., and Lavina, S.A. (2018). Invasive diseases of farm animals, dangerous to human health. *Russian Journal "Problems of Veterinary Sanitation, Hygiene and Ecology"*, 2(26), 18-24.
6. Chernyshenko, Yu. N. (2008). *Synthesis of new derivatives of 6-methyluracil with pharmacological activity: thesis of the candidate of chemical sciences*. Ufa: Institute of Organic Chemistry, Ufa Scientific Center, Russian Academy of Sciences.
7. Crini, G., Fourmentin, S., Fenyvesi, É., Torri, G., Fourmentin, M., and Morin-Crini, N. (2018). Fundamentals and Applications of Cyclodextrins, in S. Fourmentin, G. Crini, E. Lichtfouse, *Cyclodextrin Fundamentals, Reactivity, and Analysis. Environmental Chemistry for a Sustainable World*. Cham: Springer.
8. Cunha, F. C., de Holanda, R. C., Secchi, A. R., de Souza Jr, M. B., and Barreto Jr, A. G. (2020). Simultaneous absorption of UV-vis and circular dichroism to measure enantiomeric concentrations of praziquantel under nonlinear conditions. *Spectrochimica Acta Part A: Molecular and Biomolecular Spectroscopy*, 241, Article number 118645.
9. Demidov, N. V. (1982). *Anthelmintics in veterinary medicine*. Moscow: Kolos.
10. Engasheva, E. S. (2011). The timing of elimination of residual amounts of praziquantel and ivermectin from organs and tissues of ducks treated with monizen and the kinetics of these drugs. *Problems of Veterinary Sanitation, Hygiene and Ecology*, 2(6), 98-101.
11. Fedorova, P. Yu., Andreson, R. K., Alekhin, E. K., and Usanov, N. G. (2011). Natural cyclic oligosaccharides – cyclodextrins in drug delivery systems. *Medical Bulletin of Bashkortostan*, 6(4), 125-131.
12. Garcia, H., Lescano, A., Lanchote, V., Pretell, E., Gonzales, I., Bustos, J., Takayanagui, O., Bonato, P., Horton, J., Saavedra, H., Gonzalez, A., and Gilman, R. (2011). Cysticercosis Working Group in Peru.

- Pharmacokinetics of combined treatment with praziquantel and albendazole in neurocysticercosis. *British Journal of Clinical Pharmacology*, 72, 77-84.
13. Gimadieva, A. R., Myshkin, V. A., Mustafin, A. G., Chernyschenko, Yu. N., Borisova, N. S., Zimin, Yu. S., and Abdrakhmanov, I. B. (2014). Preparation and Antihypoxic Activity of Complexes of Uracil Derivatives with Dicarboxylic Acids. *Pharmaceutical Chemistry Journal*, 48(2), 93-96.
 14. Harvie, M., McManus, D., You, H., Rivera, V., Nawaratna, S., MacDonald, K., Ramm, G., and Gobert, G. (2019). Live imaging of collagen deposition during experimental hepatic schistosomiasis and recovery: a view on a dynamic process. *Lab Invest*, 99, 231–243.
 15. Liu, J., Kong, D., Qiu, J., Xie, Y., Lu, Z., Zhou, C., Liu, X., Zhang, R., and Wang, Y. (2019). Praziquantel ameliorates CCl₄ -induced liver fibrosis in mice by inhibiting TGF-beta/smad signalling via upregulating Smad7 in hepatic stellate cells. *British Journal of Clinical Pharmacology*, 176, 4666–4680.
 16. Myshkin, V., Srubilin, D., and Enikeev, D. (2009). Antioxidant properties of pyrimidine derivatives and their molecular complexes with biologically active substances in a variety of oxidative systems. *Medical Bulletin of Bashkortostan*, 4(2), 151-154.
 17. Nono, J. K., Fu, K., Mpotje, T., Varrone, G., Aziz, N. A., Mosala, P., Hlaka, L., Kamdem, S. D., Xu, D., Spangenberg, T., and Brombacher, F. (2020). Investigating the antifibrotic effect of the antiparasitic drug Praziquantel in in vitro and in vivo preclinical models. *Scientific Reports*, 10, 10638.
 18. Pandey, S., Kumar, B., Vijayendra Swamy, S.M., and Gupta, A. (2010). A Review on Pharmaceutical Application of Cyclodextrins. *International Journal of Pharmacy and Technology*, 2(3), 281-319.
 19. Park, S., Gunaratne, G., Chulkov, E., Moehring, F., McCusker, P., Dosa, P., Chan, J., Stucky, C., and Marchant, J. (2019). The anthelmintic drug praziquantel activates a schistosome transient receptor potential channel. *Journal of Biological Chemistry*, 294, 18873–18880.
 20. Poltorak, O. M. (1991). *Thermodynamics in Physical Chemistry*. Moscow: Vysshaya shkola.
 21. Sousa-Figueiredo, J. C., Betson, M., Atuhaire, A., Arinaitwe, M., Navaratnam, A. M., Kabatereine, N. B., Bickle, Q., and Stothard, J. R. (2012). Performance and safety of praziquantel for treatment of intestinal schistosomiasis in infants and preschool children. *PLOS Neglected Tropical Diseases*, 6, Article number e1864.
 22. Subbotin, V. M., Subbotina, S. G., and Alexandrov, I. D. (2000). *Modern medicines in veterinary medicine*. Rostov-on-Don: Feniks.
 23. Szejtli, J. (1998). Introduction and General Overview of Cyclodextrin Chemistry. *Chemical Reviews*, 98(5), 1743-1754.
 24. Uekama, K., Hirayama, F., and Irie, T. (1998). Cyclodextrin Drug Carrier Systems. *Chemical Reviews*, 98(5), 2045-2076.
 25. Wangchuk, P., Giacomini, P., Pearson, M., and Loukas, A. (2016a). Identification of lead chemotherapeutic agents from medicinal plants against blood flukes and whipworms. *Scientific Reports*, 6, Article number 32101.
 26. Wangchuk, P., Pearson, M., Giacomini, P., Becker, L., Sotillo, J., Pickering, D., Smout, M., Loukas, A. (2016b). Compounds Derived from the Bhutanese Daisy, *Ajania nubigena*, Demonstrate Dual Anthelmintic Activity against *Schistosoma mansoni* and *Trichuris muris*. *PLOS Neglected Tropical Diseases*, 10(8), Article number e0004908.
 27. Xu, J., Guo, J. G., Wu, X. H., Zeng, X. J., Yang, W. P., Yang, G. B., Zheng, J., and Zhou, X. N. (2009). Efficacy and adverse effects of film coated praziquantel for treatment of schistosomiasis japonica. *Zhonghua Yufang Yixue Zazhi*, 43, 718-722.

28. Zhang, Y., Fu, Y., Deng, H., Li, Q., and Lai, J. (2020). Acute pancytopenia due to praziquantel treatment for cerebral cysticercosis: A rare case report. *Journal of Infection and Chemotherapy*, 26(10), 1082-1085.
29. Zimin, Yu. S., Borisova, N. S., Gimadieva, A. R., and Mustafin, A. G. (2017). Composition, stability, toxicity, and anti-inflammatory activity of the complex of 5-hydroxy-6-methyluracil with 5-aminosalicylic acid. *Butlerov Communications*, 49(3), 12-21.
30. Zolotareva, V. A., and Zeynalov, O. A. (2015). Composition based on r (-) – praziquantel for the treatment and prevention of helminthiasis in warm-blooded animals: Patent of the Russian Federation No. 2613490. Appl. 27.01.2015. Publ. 03/16/2017.

$$A = \varepsilon_{\lambda} \cdot [\text{PR}] \cdot l, \quad (\text{Eq. 1})$$

$$A = f([\text{PR}]): \varepsilon_{\lambda} = (2.6 \pm 0.2) \cdot 10^3 \text{ mol/L}^{-1} \text{ cm}^{-1} (\lambda = 263 \text{ nm}) \quad (\text{Eq. 2})$$

$$\Delta A = f([\text{PR}] / ([\text{PR}] + [\alpha\text{-CD}])) \quad (\text{Eq. 3})$$

$$\frac{[\text{PR}]}{(A-A_0)} = \frac{1}{(\varepsilon-\varepsilon_0)} + \frac{1}{((\varepsilon-\varepsilon_0) \cdot K \cdot [\text{CD}])}, \quad (\text{Eq. 4})$$

$$K = f(T) \quad (\text{Eq. 5})$$

$$\ln K = \frac{\Delta S^\circ}{R} - \frac{\Delta H^\circ}{R} \cdot \frac{1}{T}, \quad (\text{Eq. 6})$$

$$\Delta G^\circ = \Delta H^\circ - T\Delta S^\circ. \quad (\text{Eq. 7})$$

$$\varepsilon_{\lambda} = (2.6 \pm 0.2) \cdot 10^3 \text{ mol/L}^{-1} \text{ cm}^{-1} (\lambda = 263 \text{ nm}) \quad (\text{Eq. 8})$$

$$\text{UV spectrum (H}_2\text{O)} (\lambda, \text{ nm}): \max^1 = 197, \max^2 = 264, \max^3 = 271 \quad (\text{Eq. 9})$$

$$A = f([\alpha\text{-CD} \cdots \text{PR}]) \quad (\text{Eq. 10})$$

$$\varepsilon_{\lambda} = (5.5 \pm 0.1) \cdot 10^3 \text{ L mol}^{-1} \text{ cm}^{-1} (\lambda = 264 \text{ nm}) \quad (\text{Eq. 11})$$

Table 1. Temperature dependences of the stability constants of complex compounds formed by praziquantel and α -, β -, and γ -cyclodextrins

T, K	$K \cdot 10^{-2}$, mol/L		
	α -CD...PR	β -CD...PR	γ -CD...PR
296	7.1 ± 0.8	5.7 ± 0.7	4.6 ± 0.6
301	5.6 ± 0.7	4.6 ± 0.6	3.9 ± 0.5
306	4.0 ± 0.5	3.8 ± 0.5	3.1 ± 0.4
311	2.7 ± 0.3	3.0 ± 0.4	2.0 ± 0.2
316	1.1 ± 0.1	2.1 ± 0.2	1.8 ± 0.2

Table 2. Thermodynamic parameters of the complexation reactions of praziquantel with α -, β - and γ -cyclodextrins

Reaction systems	ΔS° , kJ/mol $^{-1}$ K $^{-1}$	ΔH° , kJ/mol	ΔG° (298 K), kJ/mol
α -CD + PR	-180 ± 20	-70 ± 8	-16 ± 2
β -CD + PR	-70 ± 8	-35 ± 4	-14 ± 2
γ -CD + PR	-80 ± 9	$-40 \pm$	-16 ± 2

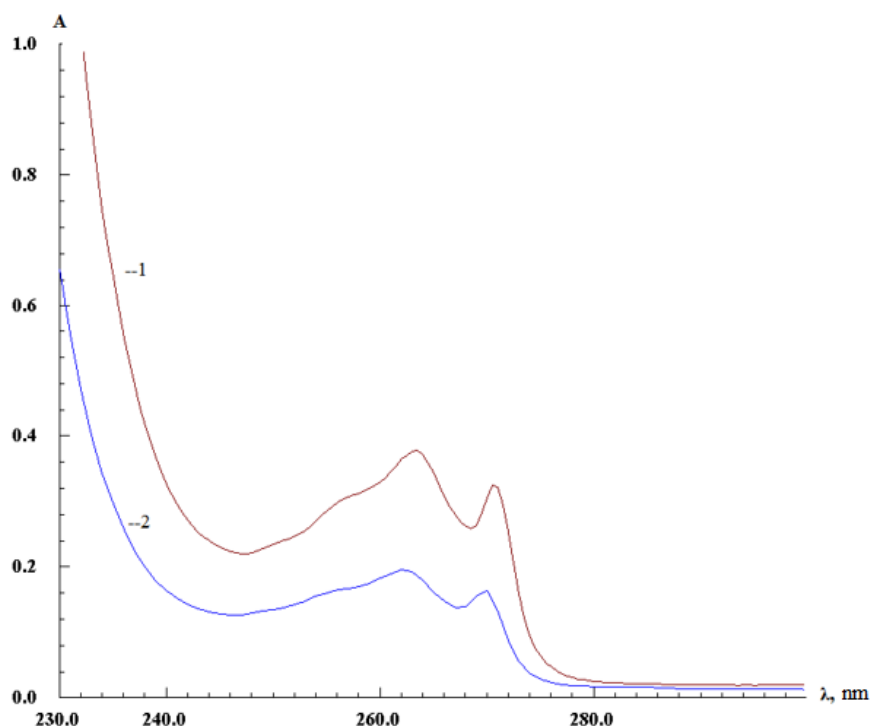


Figure 1. UV spectra of aqueous-alcoholic solutions of praziquantel (1) and its complex with α -cyclodextrin (2), 296 K, $[PR] = [\alpha\text{-CD}] = 5 \cdot 10^{-4}$ mol/L

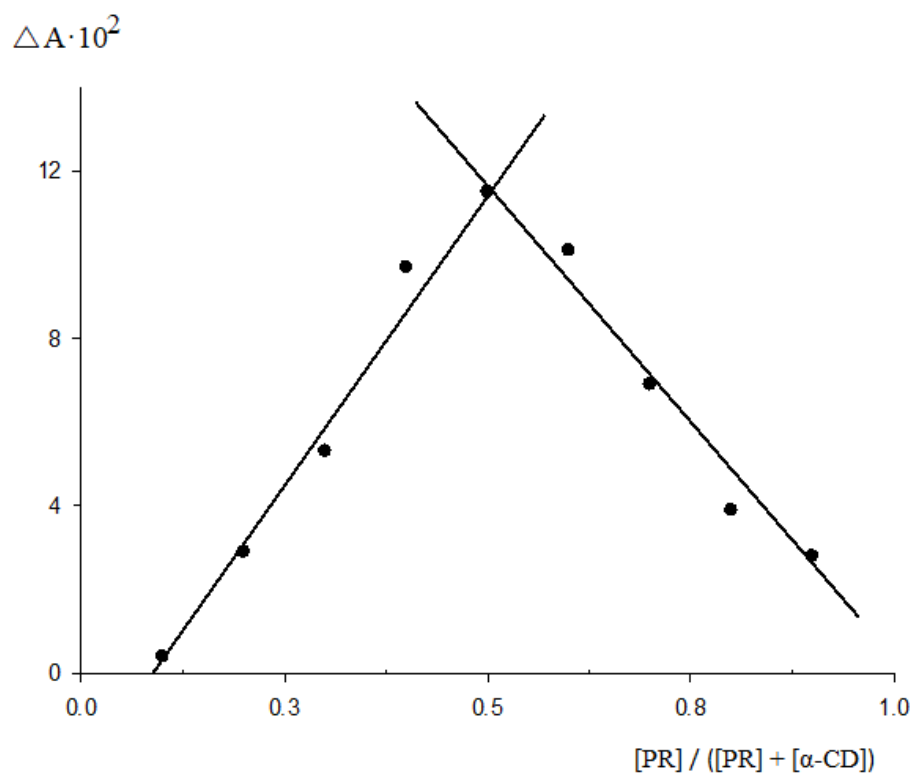


Figure 2. Isomolar diagram for the complex of praziquantel with α -cyclodextrin; 296 K, $[PR] + [\alpha-CD] = 1 \cdot 10^{-3}$ mol/L

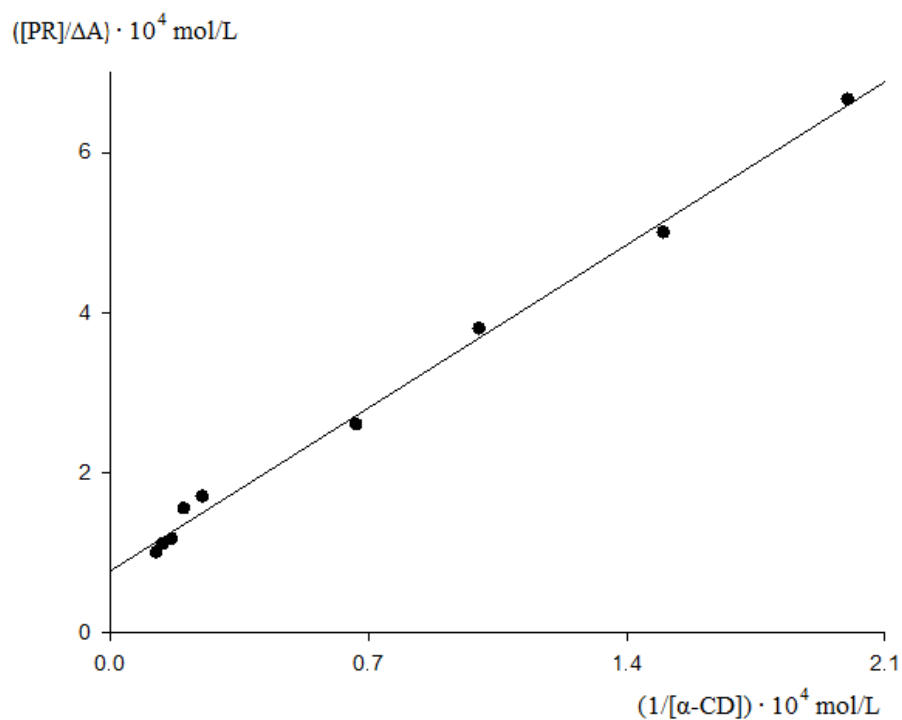


Figure 3. Dependency diagram of $[PR]/\Delta A$ versus $1/[\alpha-CD]$ for a complex formed by praziquantel and α -cyclodextrin; 296 K, $[PR] = 2.0 \cdot 10^{-4}$ mol/L, $[\alpha-CD] = (0.5 \div 8.0) \cdot 10^{-4}$ mol/L

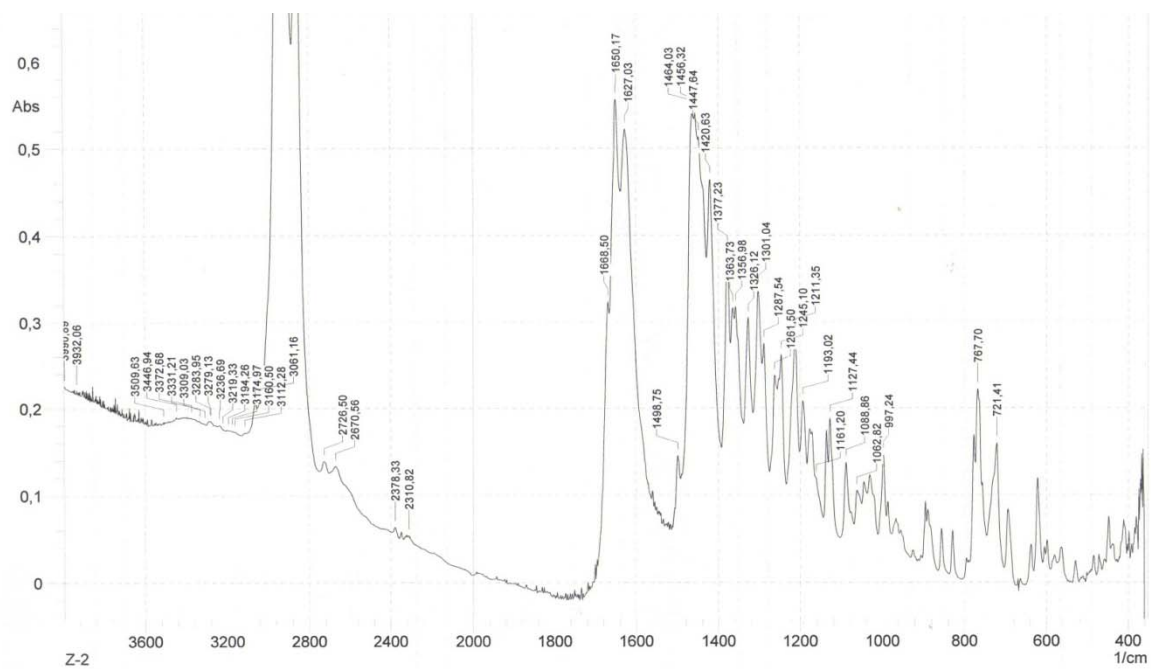


Figure 4. IR spectrum of praziquantel

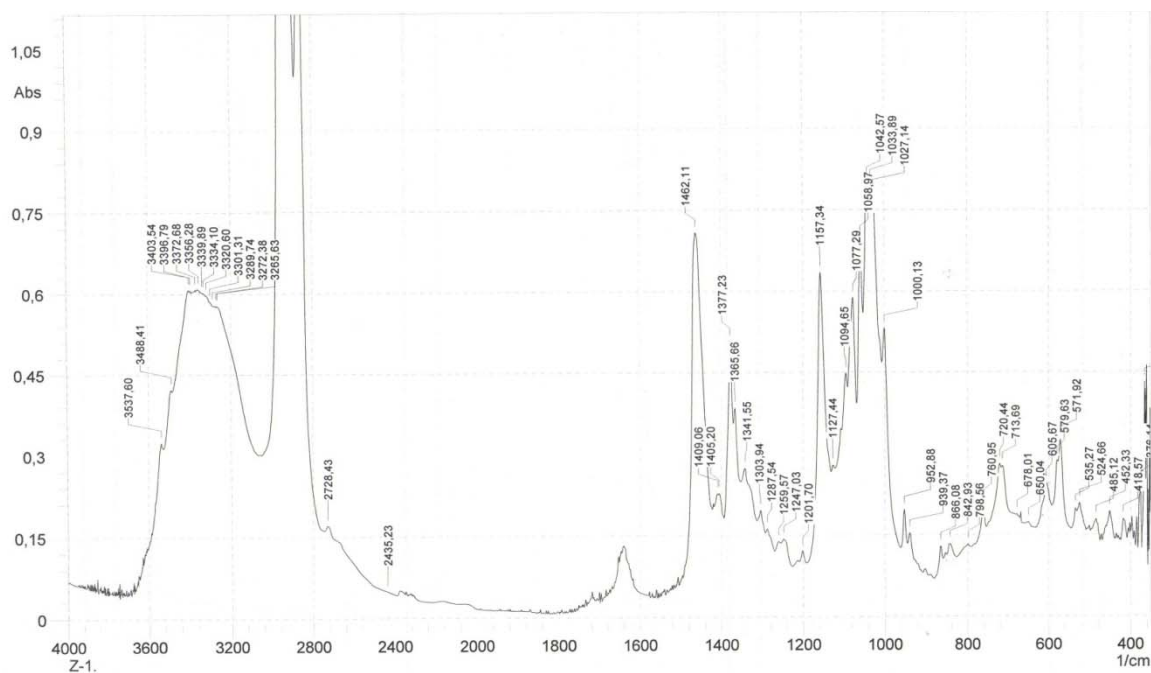


Figure 5. IR spectrum of α -cyclodextrin

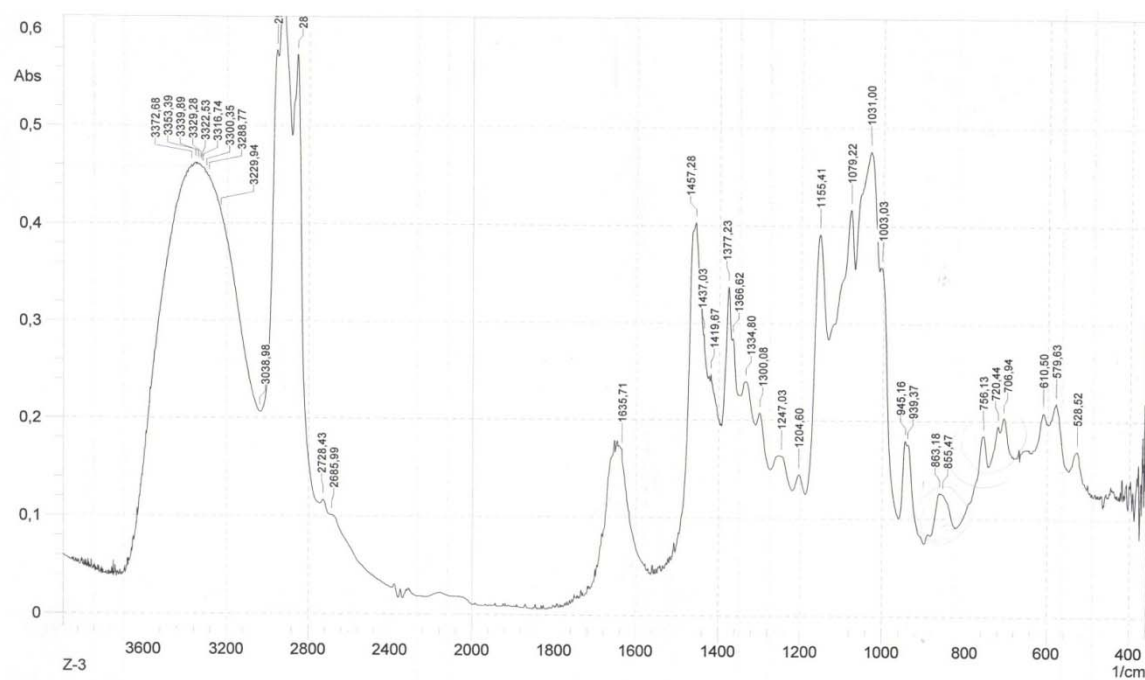


Figure 6. IR spectrum of the complex of α -cyclodextrin with praziquantel

CRIAÇÃO E IMPLEMENTAÇÃO DE UM NOVO REGULADOR DE CRESCIMENTO ALTAMENTE EFICAZ PARA RESTAURAR A FERTILIDADE DO SOLO NAS REGIÕES ÁRIDAS DO CAZAQUISTÃO**DEVELOPMENT AND INTRODUCTION OF NEW HIGH-POTENCY GROWTH REGULATOR FOR RESTORING SOIL FERTILITY IN ARID AREAS OF KAZAKHSTAN****СОЗДАНИЕ И ВНЕДРЕНИЕ НОВОГО ВЫСОКОЭФФЕКТИВНОГО РЕГУЛЯТОРА РОСТА ДЛЯ ВОССТАНОВЛЕНИЯ ПЛОДОРОДИЯ ПОЧВ В АРИДНЫХ ОБЛАСТЯХ КАЗАХСТАНА**

ARYNOV, Kazhimukhan T.^{1*}; ZHUBATOV, Zhailaubay²; AUESHOV, Abdirazah P.³; SARUAROVA, Gulnur M.⁴; NURTAZA, Nazgul M.⁵;

^{1,2,4,5} "AspanTau LTD" LLP; Department of Science; 6 Gabdul Slanov Str.; zip code 050062; Almaty – Republic of Kazakhstan

³ M. Auezov South Kazakhstan State University; Laboratory of Physical and Chemical Research Methods; 5 Tauke Khan Ave.; zip code 160012; Shymkent – Republic of Kazakhstan

* Corresponding author
e-mail: tau_aspan@mail.ru

Received 20 September 2020; received in revised form 30 October 2020; accepted 02 November 2020

RESUMO

O objeto da pesquisa são os fertilizantes minerais orgânicos obtidos a partir da hulha castanha e do vermicomposto para aumentar a produtividade das culturas de grãos e hortaliças, além de diversas variedades de árvores. O objetivo do trabalho é criar e introduzir um novo fertilizante orgânico-mineral para restaurar a fertilidade do solo e das florestas, reduzir os processos de desertificação e aumentar o rendimento das culturas agrícolas. Nesse processo, foram realizados os estudos para selecionar as condições ideais de obtenção dos fertilizantes minerais orgânicos, determinar sua composição e estrutura, bem como estabelecer a concentração de ação do produto. Como resultado do trabalho realizado, vários fertilizantes minerais orgânicos com efeito de estimulação do crescimento foram sintetizados a partir de uma matéria-prima complexa: hulha castanha e vermicomposto, contendo enzimas, aminoácidos, vitaminas, ácidos orgânicos, fitohormônios, bem como um complexo de minerais e microelementos. Foram realizados os testes de laboratório e de campo sobre o efeito do novo fertilizante mineral orgânico em vegetais, grãos e algumas variedades de árvores. Foi estabelecido que o uso do novo fertilizante aumenta o rendimento das culturas de grãos em 4,2-4,7 c/ha (*c – cem quilogramas*), e das hortaliças em 2,4-3,2 t/ha. O uso desse produto no cultivo agrotécnico de árvores coníferas proporciona um acréscimo de 4,0-4,7 cm em comparação com o caso base. No viveiro de mudas de instituição pública "Bakanasskoe lesnoye khozyaystvo" ("Silvicultura de Bakanas"), os testes do efeito da fertilização orgânico-mineral nas sementes do saxaul preto são realizados em uma área de 1,0 hectares. O grau de implementação – foram apresentados os pedidos de patentes da República do Cazaquistão e do Escritório de Patentes da Eurásia (EAPO). Com base nos resultados do trabalho realizado, prevê-se o desenvolvimento e introdução de 1 produto na prática do cultivo de plantas. Os resultados da investigação podem ter aplicação nas seguintes áreas: agricultura e silvicultura, ecologia de solos e agroquímica, biotecnologia. Eficiência – simplicidade de tecnologia de produção, complexidade (de vários componentes), boa solubilidade em água, baixa dose de aplicação – 0,01% do ingrediente ativo (0,1 g por 100 l de água) ou longa vida de prateleira, segurança, ampla gama de culturas abrangidas.

Palavras-chave: *hulha castanha, biohumus, agricultura, culturas de grãos e hortaliças, variedades de árvores coníferas.*

ABSTRACT

The object of the study is organic mineral fertilizers obtained from brown coal and vermicompost to increase the yield of grain and vegetable crops, as well as various tree varieties. The purpose of the study is the development and implementation of a new organomineral fertilizer to restore the fertility of soil and forests, reduce

desertification, and increase the yield of agricultural crops. In the process, studies were carried out to select the optimal conditions for obtaining organomineral fertilizers, determine their composition and structure, and establish the optimal concentration of the compound. As a result of the work carried out, several organomineral fertilizers with the effect of growth stimulation have been synthesized from a complex feedstock: brown coal and vermicompost, containing enzymes, amino acids, vitamins, organic acids, phytohormones, as well as a complex of minerals and trace elements. Laboratory and field experiments on the effect of the new organomineral fertilizer on vegetables, grain crops, and some trees were carried out. It has been discovered that the use of the new fertilizer increases the yield of grain crops by 4.2-4.7 dt/ha and vegetable crops by 2.4-3.2 t/ha. The use of this compound in the agrotechnical cultivation of coniferous trees increases 4.0-4.7 cm compared to the basic version of fertilizer. At the forest nursery of MPI "Bakanasskoe Forestry", experiments on the effect of organic fertilization on the seeds of black saxaul are carried out on the territory of 1.0 hectares. Degree of implementation - applications for patents of the Republic of Kazakhstan and the Eurasian Patent Office have been submitted. Based on the research results, it is planned to develop and introduce 1 compound into the practice of plant growth. The research results can find application in the following areas: agriculture and forestry, soil ecology and agrochemistry, biotechnology. Efficiency – the simplicity of production technology, multicomponent, good solubility in water, a low dose of application – 0.01% of the active ingredient (0.1 g per 100 l of water) or long shelf life, safety, a wide range of crops covered.

Keywords: *brown coal, biohumus, agriculture, grain and vegetable crops, coniferous tree varieties.*

АННОТАЦИЯ

Объектом исследования является органоминеральные удобрения, полученные из бурого угля и вермикомпоста для повышения урожайности зерновых и овощных культур, а также различных сортов деревьев. Цель работы – создание и внедрение нового органоминерального удобрения для восстановления плодородия почвы, лесов, снижения процессов опустынивания земель и повышения урожая сельскохозяйственных культур. В процессе проводились исследования по выбору оптимальных условий получения органоминерального удобрения, по определению их состава и структуры, а также по установлению оптимальной концентрации действия препарата. В результате проведенных работ синтезированы ряд органоминеральных удобрений с эффектом ростстимулирования из комплексного исходного сырья: бурого угля и вермикомпоста, содержащий ферменты, аминокислоты, витамины, органические кислоты, фитогормоны, а также комплекс минералов и микроэлементов. Были проведены лабораторные и полевые испытания действия нового органоминерального удобрения на овощные, зерновые культуры и некоторые сорта деревьев. Установлено, что применение нового удобрения повышает урожайность зерновых культур на 4.2-4.7 ц/га, а овощных культур 2.4-3.2 т/га. Применение данного препарата в агротехнической культуре обработки хвойных пород деревьев обеспечивает прирост на 4.0-4.7 см по сравнению с базовым вариантом. На лесном питомнике КГУ «Баканасское лесное хозяйство» проводятся испытания влияния органоминерального удобрения на семена черного саксаула на территории 1.0 га. Степень внедрения – поданы заявки на патенты РК и Евразийского патентного ведомства. По результатам проведенных работ планируется разработать и внедрить в практику растениеводства 1 препарат. Результаты исследований могут найти применение в следующих областях: сельское и лесное хозяйство, экология почв и агрохимия, биотехнология. Эффективность – простота технологии производства, многокомпонентность, хорошая растворимость в воде, низкая доза применения – 0.01% по действующему веществу (0.1 г на 100 л воды) или длительные сроки хранения, безопасность, широкий спектр охватываемых культур.

Ключевые слова: *бурый уголь, биогумус, сельское хозяйство, зерновые и овощные культуры, хвойные сорта деревьев.*

1. INTRODUCTION:

New conditions for the interaction of living and non-living matter have developed in the surrounding world – as a result of human interaction with the technosphere, the technosphere with the biosphere (nature), and other elements. It is appropriate to talk about the emergence of a new field of knowledge – “Ecology of the technosphere”, where the main “actors” are – man, the technosphere created by man, and the

natural environment (Stevenson, 1994). There have been significant changes in the human environment. The biosphere is gradually losing its dominant position, and in the regions of the Earth inhabited by people, it is increasingly turning into a technosphere. In the modern world, environmental problems in their social significance have come to one of the first places, pushing aside even the danger of a nuclear war (Lavrukov, 2012). The rapid development of human economic activity has led to an intensive, often destructive

impact on the environment. Human influence on nature occurs both through the transformation of natural systems that have developed over millennia and as a result of pollution of soil, water, and air, which led to a sharp deterioration in the state of nature, and often with irreversible consequences (Shchetkin, 2004; Golovkov *et al.*, 2017). Ecological problems that take on a global character and lead to a deterioration in the conditions for the development of mankind threaten its existence. This is manifested in a shortage of energy, loss of biodiversity and stability of ecosystems, deforestation and soil degradation, dehumidification, imbalance in the biogeochemical cycles of carbon and nitrogen (Dobrovolskiy, 2002; Semenov and Kogut, 2013).

For the south-east of the Trans-Baikal Territory, as well as for the territory of Central Asia as a whole, advance desertification is characteristic, associated both with global warming and with the phase of reduced moisture in the regional climatic cycle ongoing since the early 2000s (Budantsev, 1987; Shchetkin, 2004). Climate aridification through changes in soil properties and hydrological conditions leads to a permanent loss of ecosystem services and poses a serious threat to the sustainable development of agricultural production.

The rapid development of human economic activity has led to an intensive, often destructive impact on the environment. Human influence on nature occurs both through the transformation of natural systems that have developed over millennia and pollution of soil, water, and air, which led to a sharp deterioration in the state of nature, and often with irreversible consequences (Solovev, 2013). The ecological crisis poses a real danger since there is a rapid development of crisis situations in each region. Many modern methods of industrial, agricultural production are anti-ecological. The presence of monoculture causes them overgrazing of livestock, large-scale use of pesticides with excessively high doses of mineral fertilizers, continuous plowing of the soil. They lead to disruption of the normal functioning of ecosystems, simplification of their structure, instability, and catastrophic changes in nature. The most advanced direction of modern agriculture is the transition from the principles of confrontation with nature to cooperation with it (Shchetkin, 2004; Popov, 2004). This means maximum adherence to environmental laws in agricultural practice. The noted is directly related to animal husbandry in general, and in particular, to poultry farming, the most intensively developing

and functioning branch of agricultural production. Waste from poultry farms is practically not processed, so the land, water bodies, and air closest to the poultry farms are polluted (Review of the market..., 2018).

Efforts are being made both by governments of different countries and numerous scientists to solve these complex environmental problems (Zherebtsov, 1998). One of the promising ways to combat these phenomena is developing green chemistry technologies based on the use of substances obtained from biomass. In particular, compounds based on humic substances, a complex mixture of high molecular weight organic compounds of natural origin, resistant to biodegradation, which are formed during the decomposition of plant and animal residues, are widely used (Orlov, 1990; Savicheva and Inisheva, 2003). At present, there is an increased interest in humic substances all over the world, which is explained by their use in crop production as a safe, in terms of environmental impact, an alternative to fertilizers and, in some cases, pesticides (Romanchuk, 2008). Production technologies are being improved; the raw material base is expanding, which involves all new types of coal, peat, shale, peloids, production wastes (Orlov, 1997). Based on humic substances, active humic compounds are obtained, which find various applications (Timoshina, 2003).

Based on the variety of humic substances in the biosphere, humic compounds have found wide application in agriculture and issues of reclamation and detoxification of territories. Humic compounds can be divided into 3 groups: fertilizers, growth stimulants; land-improving (soil structure-formers, stimulators of microbiological activity); detoxifying agents (Oil industries..., 2018). Numerous studies have established a stimulating effect of humic substances, especially humic acids and their salts, on the growth and development of plants, increasing their resistance to unfavorable environmental factors, stimulating seed germination, increasing the productivity of cattle and poultry (Androkhanov *et al.*, 2004; Shchadov, 2007; Androkhanov and Kurachev, 2010).

2. THEORETICAL OVERVIEW:

Rashid (1985) devoted to developing methods for the chemical modification of peat humic acids (HA), the identification of the nature of the effect of modification on the structural parameters of HA. To enrich the soil with organic and mineral substances and restore the fertility of

degraded lands, a complex organic fertilizer has been created (Proydaikov *et al.*, 2005). Chitosan in the fertilizer has high growth-stimulating efficiency, combined with the antibacterial and antifungal activity of a systemic nature, which manifests itself in a prolonged manner and without harm to the environment (Prihodko *et al.*, 1980).

Fertilizer increases the bioproductivity of low-productive arid and permafrost soils, accelerates biochemical processes, and increases the number and activity of microbial communities, increasing the yield of forage crops, and sown grasses accelerate their ripening, and improves their qualitative composition (Klein *et al.*, 2007). To increase the level of growth-stimulating activity of humates, it is proposed to hydroxylate humified lignin – ligno-humate with reagents, which are aqueous solutions of iron sulfate and hydrogen peroxide (Radchevsky *et al.*, 2010). Tripoli treated with a solution of $K_3[Al(OH)_6]$ is used as an adsorption additive (Yarkova, 2007). Selenium-containing peat-zeolite fertilizers can increase the yield of corn, intensify biochemical and microbiological processes, increase efficiency, and solve environmental protection problems from pollution with chemical fertilizers.

A mixture of an organic nitrogen-containing fraction with a complex sorbent increases the efficiency of the fertilizer effect on soil fertility while simultaneously absorbing toxic components and radioactive elements from the soil with high selectivity. The complex sorbent is a solution of a hydroxo complex of aluminum with potassium $K_3[Al(OH)_6]$ with tripoli, neutralized with phosphoric acid. The organic nitrogen-containing fraction is peat treated with 50% potassium hydroxide solution and 30.7% H_3PO_4 solution. The following ingredients are introduced into the mixture: crushed dry peat, ammonium nitrate NH_4NO_3 , and trace elements, in the form of boric acid H_3BO_3 , magnesium sulfate $MgSO_4$ and acid ammonium molybdate, $(NH_4)_6Mo_7O_{24} \cdot 4H_2O$ (Efimov, 1986). Slow-release fertilizer, environmentally friendly, can restore and improve soil structure (Inisheva, 2006).

A mixture of mineral components selected from the variety of carbamide, diammonium phosphate, ammonium nitrate, superphosphate, double superphosphate, ammonium sulfate, potassium chloride, potassium sulfate, potash, phosphate rock; mineral components containing trace elements: Mg, B, Mn, Zn, Cu, Ni, Co, Cr, Mo, and an organic component from several humic substances (HS) allows the formation of nanoscale complexes of HS with mineral components. Grained organomineral nanofertilizer

s have the properties of growth stimulants, prolonged action, and increased biological activity (Alekseeva *et al.*, 1999).

As an organomineral, the nutrient filler can be used humus, peat, biocompost, sapropel, clay, if necessary, balanced by the content of NPK mineral fertilizers and trace elements, and by the content of soluble humic substances with potassium humate and sodium. The moisture-accumulating compound ensures vegetation cultivation on sandy soils in the semi-desert zone to fix the sands (Sorokin *et al.*, 2007). As a result of intensive dispersion and homogenization of vermicompost in water, a homogeneous mixture with fine particles is formed, enriched with NPK nutrients, humic substances, and beneficial soil microflora in the form of a stable compound (Hoffmann and Hoffmann, 2007). Fertilizer provides an increase in soil fertility and environmental sustainability and increases yields (Gondek, 2009). The use of the bio-organomineral complex as a fertilizer provides an increase in soil fertility without damage due to the elimination of synthetic mineral fertilizers, as well as a decrease in yield losses from drought and an increase in the resistance of stress factors (Gladkowska and Kielbowicz, 2011). In this case, a decrease in the size of particles occurs, accompanied by a change in their chemical properties, an increase in reactivity, and an increase in solubility (Gao *et al.*, 2017).

Thus, in the work of Klein *et al.* (2007), the possibility of obtaining physiologically active humic substances from secondary coal raw materials using basidiomycetes was considered. In the study, G.V. Pirogovskaya *et al.* (1993) revealed the effectiveness of using such a combination of fertilizers. The tests were carried out on potatoes and root crops, i.e., with the crops in the first group by their responsiveness to mineral fertilizers (Naumova *et al.*, 2007; Panov *et al.*, 2010; Sorokin, 2015). In addition to the direct effect of KOH, the use of humic acids as a “matrix” for the introduction of microelements into the soil is of interest (Sorkina *et al.*, 2007; Sorokina *et al.*, 2008). All this can complicate the predictability of the effect of the compound used (Yakimenko, 2004).

3. MATERIALS AND METHODS:

More and more new humic organomineral fertilizers (NOF) have been registered for use in agriculture every year. While NOF from coal has its positive properties (high concentration), liquid fertilizers obtained from peat or biohumus

(vermicompost) have other valuable properties, such as biologically active substances: enzymes, amino acids, vitamins, organic acids, phytohormones. This study aimed to obtain liquid NOF from a combined raw material while preserving all the positive properties of its components. For this, two separate liquid NOFs were obtained from brown coal and vermicompost and mixed to obtain relatively high concentrations of humic acids and the presence of biologically active substances of vermicompost. Since vermicompost is produced in Kazakhstan by many companies, it was a local raw material, and peat was imported mainly from the Russian Federation. Prototypes of the compound were accumulated by combining vermicompost and brown coal.

Two solutions were prepared to obtain the proposed organomineral fertilizer: A – concentrated solution of coal sodium humate and B – extract of biohumus (vermicompost). To obtain solution A, 15 liters of tap water and 5 kg of crushed (hydromodule 1:3) brown coal powder with a particle size of less than 0.2 mm were loaded into a laboratory reactor with a stirrer, and the water was heated to a temperature of 70 °C with stirring. Then 300 g of NaOH, 100 g of carbamide, and 50 g of Trilon B were added, and the temperature was brought to 90 °C. With constant stirring, the extraction process is carried out for 2 hours at a temperature of 80-90 °C. The solution was filtered through a cloth, and a concentrate was obtained with a dry matter content of at least 25% in a volume of 15-16 liters of the first component of the liquid fertilizer. The compound was left overnight to cool and stabilize (Figure 1).

To obtain solution B (vermicompost extract), 15 liters of tap water were poured into a reactor with a stirrer, 5 kg of vermicompost was added and heated to 35-38 °C and stirred for 2 hours, infused for 10-12 hours for fermentation at a temperature of 20-30 °C. After fermentation, coarse filtration was carried out, as a result, 14-15 liters of the second component of liquid fertilizer are obtained (Figure 2). The first and second components were mixed (A + B) in a ratio of 1:1 to ensure a dry matter content of at least 10% in the final compound. The resulting mixture was aged for 3 days to complete the biochemical processes, then packed in containers for shipment to consumers. The resulting product contained dry matter 12-15%, ash content 3-5%, humic acid content not less 2.5%.

The obtained samples were studied with the use of a JSM-6490LV scanning electron microscope with INCA Energy dispersive

microanalysis and HKL-Basic structural analysis systems and IR spectroscopy on a Shimadzu IR Prestige-21 FTIR spectrometer with an attached Miracle total internal reflection (ATR) by Pike Technologies. The samples were pre-dried, the data on the dry residue are presented in Table 1. A field experiment to determine the effectiveness of NOF for grain and vegetable crops was carried out in the fields of the experimental farm "Svetlana" in the Zhambyl district of the Almaty region.

1. Cultivar: "Kazakhstanskaya 10" spring wheat. The new synthesized humic organomineral fertilizer of the following composition was used: nitrogen – 2.156 mg/l, phosphorus – 300 mg/l, potassium – 400 mg/l, dry residue – 8.65%. Soil type – grey earth. Precipitation in mm during the growing season (May-August): long-term average – 314 mm, in the year of testing – 459 mm. Air temperature for the growing season (May-August): long-term average – 18.86 °C, in the test year – 23.52 °C. Area: experimental plot 21 m², replication – 4 times. Plot location: randomized. Experimental design: 1) control without fertilizer s; 2) NOF 0.01%. Fertilizer consumption rate: NOF – 0.2 l/ha, spray material consumption – 200 l/ha. Fertilizer application method: soaking seeds before sowing, two-fold foliage spraying. Sprayer Type: backpack sprayer.

2. Cultivar: "Svetlanka" spring barley. The new synthesized humic organomineral fertilizer was used with the following composition: nitrogen – 2.5 mg/l, phosphorus – 309 mg/l, potassium – 410 mg/l, dry residue – 8.7%. Soil type – grey earth. Precipitation in mm during the growing season (May-August): long-term average – 314 mm, in the year of testing – 459 mm. Air temperature for the growing season (May-August): long-term average – 18.86 °C, in the test year – 23.52 °C. Area: experimental plot 21 m², replication – 4 times. Plot location: randomized. Experimental design: 1) control without fertilizer s; 2) NOF 0.01%. Fertilizer consumption rate: NOF – 0.2 l/ha, spray material consumption – 200 l/ha. Fertilizer application method: soaking seeds before sowing, two-fold foliage spraying. Sprayer Type: backpack sprayer.

3. Cultivar: "Red Giant" carrot. The new synthesized humic organomineral fertilizer of the following composition was used: nitrogen – 2.23 mg/l, phosphorus – 298 mg/l, potassium – 405 mg/l, dry residue – 9.0%. Soil type – grey earth. Precipitation in mm during the growing season (May-August): long-term average – 314 mm, in the year of testing – 459 mm. Air temperature for the growing season (May-August): long-term average

– 18.86°C, in the test year – 23.52 °C. Predecessor: cucumber. Soil preparation: in the fall, after harvesting the predecessor, disking, plowing to a depth of 20-22 cm. In the spring, cultivation was carried out to cover moisture and pre-sowing soil cultivation with AKSH-3.6 tillthmaker. Sowing seeds: the first decade of May with a combined sowing unit AKP-4, sowing pattern 62+8 cm. On ridges 18 cm high. Seeding rate: 2.5 kg/ha. Registration plot area: 14 m², replication - 4 times, the location of the variants was randomized. Experimental design: 1) control without fertilizers (water); 2) NOF 0.01%. Consumption rate: NOF – 0.25-0.3 l/ha, spray material consumption – 250 l/ha. Phases of development of cultivated plants during the period of application of the compound: in the phase of 4-5 leaves of the culture and again 20 days after the first spraying. Method of application: spraying plants. Sprayer type: backpack sprayer. Accounting: accounting and observation of the growth and development of plants, the formation of the yield, and plant productivity were carried out according to generally accepted methods (Belik, 1992). Carrots yield accounting was carried out by weighing separately standard and non-standard products according to (GOST 1721-85, 1986). Tests to assess the effectiveness of the new organomineral fertilizer (NOF) on carrots ("Red Giant" cultivar) were carried out on the experimental field of the farm "Svetlana", Zhambyl district, Almaty region. The compound was applied twice: spraying of carrot plants in the phase of 4-5 leaves of the culture (06/15/2019) and again 20 days after the first treatment (05/07/2019).

4. Vegetable cultivar: white cabbage. The new synthesized humic organomineral fertilizer of the following composition was used: nitrogen – 2.054 mg/l, phosphorus – 302 mg / l, potassium – 410 mg/l, dry residue – 8.05%. Soil type – grey earth. Precipitation in mm during the growing season (May-August): long-term average – 314 mm, in the year of testing – 459 mm. Air temperature for the growing season (May-August): long-term average – 18.86 °C, in the test year – 23.52 °C. Soil and soil type: light-brown. Seedlings were grown in plastic cassettes with a cell volume of 65 cm³. Sowing cabbage seeds was carried out on April 25, 2019, to a depth of 1-1.5 cm. The cassettes were then placed in heated greenhouses on wooden blocks and covered with a translucent polyethylene film. When seedlings appeared, the film was removed. A week before planting, the seedlings were hardened by taking the cassettes with seedlings into the open ground. A day later, the seedlings were watered abundantly. Predecessor: cucumber. Soil

preparation: in the fall, after harvesting the predecessor, disking, plowing to a depth of 20-22 cm was carried out. In the spring, cultivation was carried out to cover moisture and pre-sowing soil cultivation with AKSH-3.6 tillthmaker. Registration plot area: 14 m², replication – 4-times, the location of the variants was randomized. Experimental design: 1) control without fertilizers (water); 2) NOF 0.01%. Consumption rate: NOF – 0.25-0.3 l/ha, spray material consumption – 250 l/ha. Phases of development of cultivated plants during the period of application of the compound: the first treatment was spraying after the seedlings were fully established (10-15 days after planting), the second treatment was spraying 15-20 days after the first treatment, the third treatment was spraying in the phase of the mass setting of heads. Method of application: spraying plants. Sprayer type: backpack sprayer. Accounting: accounting and observation of the growth and development of plants, the formation of the yield, and plant productivity were carried out according to generally accepted methods (Belik, 1992). Accounting for cabbage yield was carried out by a continuous method, dividing it into standard and non-standard parts. Tests to assess the effectiveness of the new organomineral fertilizer (NOF) on cabbage crops were carried out on the experimental field of the "Svetlana" farm in the Zhambyl district of the Almaty region. The compound was applied three times: processing of cabbage seedlings (06/12/2019), in the phase of 6-7 true leaves of the culture (06/27/2019), and the phase of the mass setting of heads (21.07.2019).

5. Conifers: Scots pine, Tien Shan spruce. The new synthesized humic organomineral fertilizer was used with the following composition: nitrogen – 2.51 mg/l, phosphorus – 299 mg/l, potassium – 402 mg/l, dry residue – 8.8%. Soil type – grey earth. Precipitation in mm during the growing season (May-August): long-term average – 314 mm, in the year of testing – 459 mm. Air temperature for the growing season (May-August): long-term average – 18.86 °C, in the test year – 23.52 °C. Soil: grey earth. Planting time: May 2019. Agrometeorological indicators: air temperature – 30-32 °C, air humidity – 25-30%. Area: plants were planted on 10 acres (Figure 3)

Experimental design. Compound – NOF: 1) concentration – 0.01%, consumption rate of the compound – 0.5 l/ha; kg/ha, method of application – root feeding (watering of plants), number of treatments – 1; 2) concentration – 0.01%, consumption rate of the compound – 0.24 l/ha; kg/ha, method of application – top foliar dressing (spraying of plants), number of treatments – 2.

Terms of application of the compound: the first treatment was carried out – in the phase of active growth – June, the second – July, the third – August. Phases of plant development at the time of application of the compound: the phase of active plant growth. Method of application: watering and spraying of plants with the working solution of the compound. Surveys carried out: observations of seedlings during the experiments from May to September 2019; measurements of plant height before treatment and two weeks after the last treatment. Determination of the plant growth during the experiment. In the tested plots, the effectiveness of fertilization was tested – on 20 pine and spruce seedlings. The height of the plants was measured before applying the fertilizer. It was done with a ruler. After the treatments, 15 days later, the height of the plants was re-measured, and the growth of pine and spruce seedlings in height was calculated (by the addition method).

4. RESULTS AND DISCUSSION:

Chemical analysis was carried out, and the IR spectrum of the presented brown coal sample was taken. The results are presented under the code "1D" (code). A liquid suspension of coal sodium humate, the presented sample was filtered, then the residue and filtrate were analyzed separately. Before analysis, the filtrate was dried (100-105 °C), code "2A-F", residue under the code "2A-R". The initial coal sodium humate was separately dried (100-105 °C). The results are designated with the code "2A-ini." The rest of the samples, vermicompost extract (3), organomineral fertilizers (4), were studied according to Figure 4 above.

The chemical analysis results of the content of the main nutrients in the new liquid fertilizer and its components are presented in Table 2. The results of chemical analysis (elemental analysis) of the initial brown coal powder and after the processes of their separation on the Scanning electron microscope JSM-6490LV with energy dispersive microanalysis systems INCA Energy and HKL-Basic structural analysis are presented in Table 3. SEM data shows the contents of several useful macronutrients. However, given that the data are obtained only for a local point, we cannot extend this data to the weight of the sample having a colloidal system.

Figures 5-10 show the IR spectra of all obtained samples and components of the liquid fertilizer. The observed absorption bands at 1446

and 1389 cm⁻¹, caused by in-plane bending vibrations of the O-H group, interacting with the fan-shaped vibrations of C-H in the primary and secondary alcohol groups, and absorption bands in the so-called "polysaccharide" region (1170-950 cm⁻¹). The obtained data in terms of a unit of dry residue, we can expect a more active manifestation of the nutritional and stimulating properties of the combined liquid humic NOF. Fieldwork on the application of NOF on cereals, vegetables, forage crops, and seedlings (conifers and saxaul):

1. Cultivar: "Kazakhstanskaya 10" spring wheat. The results indicated that soaking of seeds before sowing and foliar feeding of wheat crops with a new organomineral fertilizer contributed to an increase in grain yield (Table 4). Two-fold foliar feeding of wheat with organic fertilizer s increased grain yield by 4.2 dt/ha. Fertilizer compatibility with pesticides: not studied. At the same time, there were no side effects from the studied fertilizer on vegetative wheat plants.

2. Cultivar: "Svetlanka" spring barley. According to the results, it was found that soaking seeds before sowing and foliar feeding of barley crops with a new organomineral fertilizer contributed to an increase in grain yield (Table 5). Two-fold foliar feeding of barley with organomineral fertilizer s increased the grain yield by 4.7 c/ha. Fertilizer compatibility with pesticides: not studied. Side effects of the fertilizer on vegetative barley plants: not observed.

3. Vegetable cultivar: "Red Giant" carrot. Biometric studies revealed that under the conditions of 2019 (in arid areas of Kazakhstan), as a result of the treatment of carrot crops with organic fertilizer, the length of the leaves in relation to the control variant increased by 7.4%, and the weight increased by 5.3%. The length of the root crop exceeded this indicator by 9.6%. Foliar treatments of carrot crops with NOF made it possible to obtain the highest yield – 47.6 t/ha. The yield increase relative to the control variant was 2.4 t/ha or 5.4%. Compatibility data: not available. Observed side effects: NOF does not have a phytotoxic effect on the culture, provided that the consumption rate of the compound and the concentration of the compound's working fluid are observed.

4. Vegetable cultivar: white cabbage. Biometric studies indicated that under the conditions of 2019, as a result of the treatment of cabbage crops with organic fertilizer, the number of leaves was 14 pieces, which exceeded the control specimen. The height of the plant was

38.9, the diameter of the head (18.7 cm) exceeded the control by 8.7%, and the rosette of leaves also exceeded the control by 5.3%. According to the results of field tests, it was found that foliar treatment of cabbage crops with organomineral fertilizer after complete survival of seedlings (10-15 days after planting) at a dose of 0.25-0.3 l/ha, 15-20 days after the first treatment (0.25-0.3 l/ha) and in the phase of the mass setting of heads of cabbage (0.25-0.3 l/ha) can significantly increase the yield of cabbage by 3.2 t/ha or 5.4% compared to the control. Compatibility data: not available. Observed side effects: NOF does not have a phytotoxic effect on the culture, provided that the consumption rate of the compound and the concentration of the compound's working fluid are observed.

5. Conifers: Scots pine, Tien Shan spruce. Table 6 shows data on the effectiveness of fertilization on pine and spruce seedlings used in spraying and watering plants.

It has been established that NOF is a highly effective fertilizer for the growth and development of seedlings of pine and spruce. A good growth effect was obtained with watering and spraying. This fertilization (application – watering the soil) stimulated the growth of spruce seedlings in comparison with the control by 152.2%, pine seedlings – 155.6%; in the variant with spruce – by 140.3% on average, in the variant with pine spraying – by 134.5% (Figures 11-12).

Combination with other compounds: not performed. No side effects in the form of phytotoxicity were observed. As a result of vegetation experiments, a high stimulating effect of NOF on the growth of pine and spruce seedlings was noted. The application of fertilizer (watering or spraying) provided an increase in plant height from 30 to 55% compared to the control. Based on the data obtained, the authors consider it possible to recommend NOF with a consumption rate of 0.5 kg/ha (irrigation with 0.001% solution), 0.24 kg/ha (spraying with 0.001% solution).

6. Tests of NOF efficiency on black saxaul (*Haloxylon aphyllum*). An agreement was concluded with the MPI "Bakanasskoe Forestry" to determine the effectiveness of the NOF on black saxaul. 1.0 hectares of land were allocated, seed consumption is about 80.0 kg, seed soaking method (duration: 3, 5, 7, 9 days). Sowing time October 2019; compound concentration 1.0 g per 10 l of solution (Figures 13-14).

5. CONCLUSIONS:

1. Based on the study of literature data on humic organomineral fertilizers, their high efficiency has been revealed for modern technologies to restore soil fertility and forests and reduce land degradation in arid, semi-arid, and desert regions increase crop yields. The prospects and high efficiency of brown coal, peat, and biohumus (vermicompost) for the production of humic organomineral fertilizers and their interconnection are shown.

2. The main methods (fertilizer application method; method of application; continuous method et al.) of physical and chemical analysis of humic compounds for studying their composition and structure were presented. The main methods of spectral analysis for establishing the structure of humic substances are presented; the most informative methods for studying the structure of target substances are nuclear magnetic resonance (NMR) methods on atomic nuclei of hydrogen (protium, ^1H) and carbon ^{13}C , as well as methods of IR spectroscopy.

3. A method for obtaining a new humic organomineral fertilizer from a combined raw material was developed: brown coal and vermicompost or peat. It was shown that the proposed method for obtaining liquid humic fertilizer allows combining in one compound the positive qualities of coal humates and liquid humic fertilizers based on biohumus or peat.

4. Laboratory and field tests of the effect of the new organomineral fertilizer on vegetables, grain crops, and some varieties of trees were carried out. It has been established that the use of the new fertilizer increases the yield of grain crops by 4.2-4.7 dt/ha and vegetable crops by 2.4-3.2 t/ha. It has been revealed that the use of this compound in the agrotechnical cultivation of coniferous trees provides an increase of 4.0-4.7 cm in comparison with the baseline variant.

6. REFERENCES:

1. Alekseeva, T. P., Perfiliev, V. D., and Krinitsyn, G. G. (1999). Complex organo-mineral fertilizers of prolonged action based on peat. *Chemistry of Vegetable Raw Materials*, 4, 53-59.
2. Androkhanov, V. A., Kulyapin, E. D., and Kurachev, V. M. (2004). *Soils of technogenic landscapes: Genesis and evolution*. Novosibirsk, Russian Federation: Publishing house of the SB RAS.

3. Androkhanov, V. A., and Kurachev, V. M. (2010). *Soil-ecological state of technogenic landscapes: Dynamics and assessment*. Novosibirsk, Russian Federation: Publishing house of the SB RAS.
4. Belik, B. F. (Ed.). (1992). *Methodology of experimental business in vegetable growing and melon growing*. Moscow, Russian Federation: Agropromizdat.
5. Budantsev, I. A. (1987). System of the genus *Dracocephalum* (Lamiaceae). *Botanical Journal*, 72(2), 260-267.
6. Dobrovolskiy, V. G. (Ed.). (2002). *Degradation and protection of soils*. Moscow, Russian Federation: Publishing house of Moscow State University.
7. Efimov, V. N. (1986). *Peat soils and their fertility*. Leningrad, Russian Federation: Agropromizdat.
8. Gaoa, Y., Heb, J., and Hea, Z. (2017). Effects of fulvic acid on growth performance and intestinal health of juvenile loach *Paramisgurnus dabryanus* (Sauvage). *Fish & Shellfish Immunology*, 62, 47-56.
9. Gladkowskaia, W., and Kielbowicza, G. (2011). Fatty acid composition of egg yolk phospholipid fractions following feed supplementation of Lohmann Brown hens with humic-fat preparations. *Food Chemistry*, 126(3), 1013-1018.
10. Golovkov, V. F., Koshelev, A. V., Afanasyev, V. V., Kozlov, G. V., and Eleev, Yu. A. (2017). Application of salts of humic acids in the reclamation of contaminated areas. *Chemistry and Technology of Organic Substances*, 2, 64-69.
11. Gondek, K. (2009). Zinc in Maize (*Zea mays* L.) and soils fertilized with sewage sludge and sewage sludge mixed with peat. *Polish Journal of Environmental Studies*, 18(3), 359-368.
12. GOST 1721-85. (1986). Fresh food garden carrot for supply and delivery. Specifications. Retrieved from: <http://docs.cntd.ru/document/gost-1721-85>.
13. Hoffmann, K., and Hoffmann, J. (2007). The utilization of peat, lignite and industrial wastes in the production of mineral-organic fertilizers. *American Journal of Agrocultural and Biological Sciences*, 2, 254-259.
14. Inisheva, L. I. (2006). Peat soils: their genesis and classification. *Soil Science*, 6, 781-786.
15. Klein, O. I., Stepanova, E. V., Kulikova, N. A., Landesman, E. O., Suprenok, V. V., and Koroleva, O. V. (2007). New approaches to the processing of industrial slimes using basidiomycetes: obtaining physiologically active humic-like substances. In: *Proceedings of the 4th All-Russian Conference – Humic substances in the biosphere*. Moscow, Russian Federation: Russian Academy of Sciences.
16. Lavrukov, M. Yu. (2012). *Influence of the organic-mineral fertilizer "Stimulife" and sodium humate on the growth and development of specimens of the snakehead (Dracocephalum L.) in the conditions of the Leningrad region*. St. Petersburg, Russian Federation: St. Petersburg State Agrarian University.
17. Naumova, G. V., Zhmakova, N. A., Ovchinnikova, T. F., and Makarova, N. L. (2007). New humic preparations of fungicidal and bactericidal action based on peat. In: *Proceedings of the 4th All-Russian Conference – Humic Substances in the Biosphere*. Moscow, Russian Federation: Russian Academy of Sciences.
18. Oil industries: Results of 2017 and short-term prospects (2018). Retrieved from: <https://nangs.org/analytics/analiticheskij-tsentr-pri-pravitelstve-rf-neftyanaya-otrasl-itogi-2017-goda-i-kratkosrochnye-perspektivy-yanvar-2018-pdf>.
19. Orlov, D. S. (1990). *Humus acids of soils and general theory of humification*. Moscow, Russian Federation: Publishing house of Moscow State University.
20. Orlov, D. S. (1997). Humic substances in the biosphere. *Soros Educational Journal*, 2, 56-63.
21. Panov, A. N., Lycheva, T. V., and Belousov, N. M. (2010). Absorption capacity of high-moor peat for water, mineral and organic components of effluents. *Bulletin of the Samara Scientific Center of the Russian Academy of Sciences*, 12(1(4)), 1020-1022.
22. Pirogovskaya, G. V., Bogomaz, I. A., Shagieva, E. I., Kovalenok, M. F., Kuleshova, S. I., Naumova, G. V., and Raitsina, G. I. (1993). The use of humic preparations in the production of mineral fertilizers. In: *Collection of works "Humic substances in the biosphere" (pp. 166-174)*. Moscow, Russian Federation: Nauka.
23. Popov, A. I. (2004). *Humic substances*:

- properties, structure, education. St. Petersburg, Russian Federation: Publishing house of St. Petersburg. University.
24. Prikhodko, L. A., Gorovaya, A. I., Globa, M. P., and Kulik, A. F. (1980). The effectiveness of humic and mineral fertilizers in the cultivation of crops against the background of increased doses of atrazine. In: *Humic fertilizers. Theory and practice of their application* (pp. 243-253). Dnepropetrovsk, Ukraine: Publishing House of the Agricultural Institute.
 25. Proydakov, A. G., Polubentsev, A. V., and Kuznetsova, L. A. (2005). Humic acids from brown coal, mechanically processed in the presence of air. *Chemistry for Sustainable Development*, 13, 641-647.
 26. Radchevsky, P. P., Moroz, N. B., and Troshin, L. P. (2010). Innovations of viticulture in Russia. Application of biologically active substances of humate in the cultivation of grape planting material. *Scientific Journal of KubSAU*, 60, 1-17.
 27. Rashid, M. (1985). *Geochemistry of marine humic compounds*. Oxford, UK: Springer-Verlag.
 28. Review of the market for humic fertilizers in Russia and the world. (2018). Retrieved from: <https://www.infomine.ru>.
 29. Romanchuk, N. I. (2008). *Influence of organomineral fertilisation based on hydrolytic ligin on the fertility of sod-podzolic soils and the productivity of the main agrocenochs of the Middle taiga*. Barnaul, Russian Federation: Syktyvkar State University.
 30. Savicheva, O. G., and Inisheva, L. I. (2003). Biochemical activity of peats of different botanical composition. *Chemistry of Vegetable Raw Materials*, 3, 41-50.
 31. Semenov, V. M., and Kogut, B. M. (2013). I. V. Tyurin and current trends in the development of the theory of soil organic matter in the 21st century. In: *Materials of the International Scientific Conference* (pp. 9-15). Kazan, Russian Federation: Publishing house "Otechestvo".
 32. Shchadov, V. M. (2007). *Complex processing of coals and increasing the efficiency of their use*. Moscow, Russian Federation: NTK "Track".
 33. Shchetkin, B. N. (2004). *Methodology of ecological safe processing of poultry manure into organic fertilizers and creation of devices for assessing the quality of their introduction into the soil during the cultivation of agricultural crops*. St. Petersburg, Russian Federation: St. Petersburg State Agrarian University.
 34. Solovev, M. A. (2013). *Influence of organomineral fertilizers and growth regulators on the productivity of spring barley varieties in the zone of insufficient moisturization of the Rostov region*. Stavropol, Russian Federation: Azov-Black Sea State Agroengineering Academy.
 35. Sorkina, T. A., Kulikova, N. A., Filippova, O. I., Lebedeva, G. F., and Perminova, I. V. (2007). Biological activity of iron humate in relation to wheat seedlings. In: *Proceedings of the 4th All-Russian Conference – Humic Substances in the Biosphere*. Moscow, Russian Federation: Russian Academy of Sciences.
 36. Sorokin, I. B., Titov, E. V., and Glagoliev, V. P. (2007). Long aftereffect of lowland peat. *Bulletin of the Tomsk State University*, 3, 235-236.
 37. Sorokin, N. T. (2015). On the development of scientific and practical cooperation at the international level in the field of agriculture. *Section I Materials of the 9th International Scientific Conference of Central and Eastern Europe (CEEAgEng): Collection of Scientific Papers*, 87, 11-17.
 38. Sorokina, T., Kulikova, N., Necvetay, A., Fillipova, O., Lebedeva, G., and Perminova, I. (2008). Synthesis and use of iron humates for correction of iron deficiency chlorosis in higher plants. In: *From Molecular Understanding to Innovative Applications of Humic Substances; Proceedings of the 14th International Meeting of the International Humic Substances Society*. Moscow, Russian Federation: Nauka.
 39. Stevenson, F. J. (1994). *Humus chemistry: genesis, composition, reactions*. New York, USA: John Wiley & Sons.
 40. Timoshina, N. A. (2003). *Influence of new organomineral fertilizers on the growth and development, productivity and quality of potatoes in sod-podzolic sandy loam soil*. Moscow, Russian Federation: All-Russian Scientific Research Institute of Potato Economy named after A. G. Lorkh.
 41. Yakimenko, O. S. (2004). Industrial humic preparations: prospects and limitations of use. In: *Materials of the 2nd International Scientific and Practical Conference "Earthworms and*

Soil Fertility” (pp. 249-252). Vladimir, Russian Federation: Russian Academy of Agricultural Sciences.

42. Yarkova, T. A. (2007). *Chemical modification of the structure of peat humic acids with the purpose of increasing their biological and sorption activity*. Moscow, Russian Federation: Novomoskovsk Institute of the Russian University of Chemical Technology

named after D.I. Mendeleev.

43. Zharebtsov, S. I. (1998). Non-fuel use of Itatsky brown coal. In: *Experience and prospects of science-intensive technologies in the coal industry of Kuzbass: Materials of a scientific and technical conference* (pp. 258-262). Kemerovo, Russian Federation: Institute of Coal and Coal Chemistry SB RAS.

Table 1. Dry residues of liquid samples of components and final NOF compound

No.	Liquid fertilizer and its components	Dry residue, %
1	Coal sodium humate	35.1
2	Vermicompost extract	1.1
3	Organomineral fertilizer	8.65

Table 2. Analysis of the content of the main nutrients in the NOF and in its components

No.	Specimens	Nitrogen, mg/l	Phosphorus, mg/l	Potassium, mg/l
1	Brown coal	0.616	0.040	-
2	Coal sodium humate	5.628	850	500
3	Vermicompost extract	1.960	1000	1500
4	Organomineral fertilizer	2.156	300	400

Table 3. Results of chem. analysis (elemental analysis) of the initial brown coal powder and after the processes of their separation on the device “Scanning electron microscope JSM-6490LV” with the systems of energy-dispersive microanalysis INCA Energy and structural analysis HKL-Basic

Code	% by weight									
	1D	2A-ini.	2A-R	2A-F	3B-ini.	3B-R	3B-F	4S-ini.	4C-R	4C-F
C	53.30	49.52	48.5	49.3	32.95	40.76	27.05	47.82	52.10	28.60
O	33.22	35.23	35.6	36.2	38.83	42.46	35.67	35.66	33.83	42.13
Mg	0.06	2.44	2.79	5.96	1.81	0.43	4.15	3.72	1.31	17.79
Al	2.86	0.05	0.04	1.59	1.05	1.14	0.66	0.08	0.12	0.08
Si	9.76	2.75	2.90	5.37	1.08	1.59	0.39	2.25	2.99	1.47
S	0.14	9.20	9.29	0.04	4.62	5.79	0.22	8.92	8.70	3.82
Cl	0.06	0.15	0.16	0.22	1.07	1.18	2.50	0.25	0.10	0.34
K	0.12	0.03	0.05	0.29	1.46	0.34	6.02	0.15	0.30	0.97
Ca	0.13	0.09	0.12	0.10	1.90	1.48	22.29	0.47	0.16	1.27
Ti	0.29	0.12	0.14	0.50	10.83	3.73	-	0.34	0.29	1.63
Fe	0.06	0.29	0.30	0.16	3.53	0.06	-	0.22	0.09	1.57

Note: 1D – initial brown coal powder; 2A-ini. – initial coal sodium humate (100-105 °C); 2A-R – coal sodium humate residue; 2A-F – coal sodium humate filtrate; 3B-ini. – initial extract of vermicompost (100-105 °C); 3B-R – vermicompost extract residue; 3B-F – vermicompost extract filtrate; 4C-ini. – initial organomineral fertilizer (100-105 °C); 4C-R – organomineral fertilizer residue; 4C-F – organomineral fertilizer filtrate.

Table 4. Influence of NOF foliar dressing on grain yield

Variants	Yield, dt/ha	Gain, dt/ha
1. Control without fertilization	32.0	-
2. New organomineral fertilizer (NOF)	36.2	4.2

Table 5. Influence of NOF foliar dressing on grain yield

Variants	Yield, dt/ha	Gain, dt/ha
1. Control without fertilizati	29.4	-
2. New ganomineral fertilizer (NOF)	34.1	4.7

Table 6. The efficiency of NOF on spruce seedlings

Variant	Method of application	Consumption rate of the compound, l/ha; kg/ha	Multiplicity of processing	Replication	Height gain	Increase in height gain relative to control, %
NOF	watering		3	1	4.7	151.6
				2	4.6	148.4
				3	4.7	151.6



Brown coal



Concentrated coal sodium humate solution

Figure 1. Component A



Vermicompost



Vermicompost extract

Figure 2. Component B



Figure 3. General view of the nursery garden

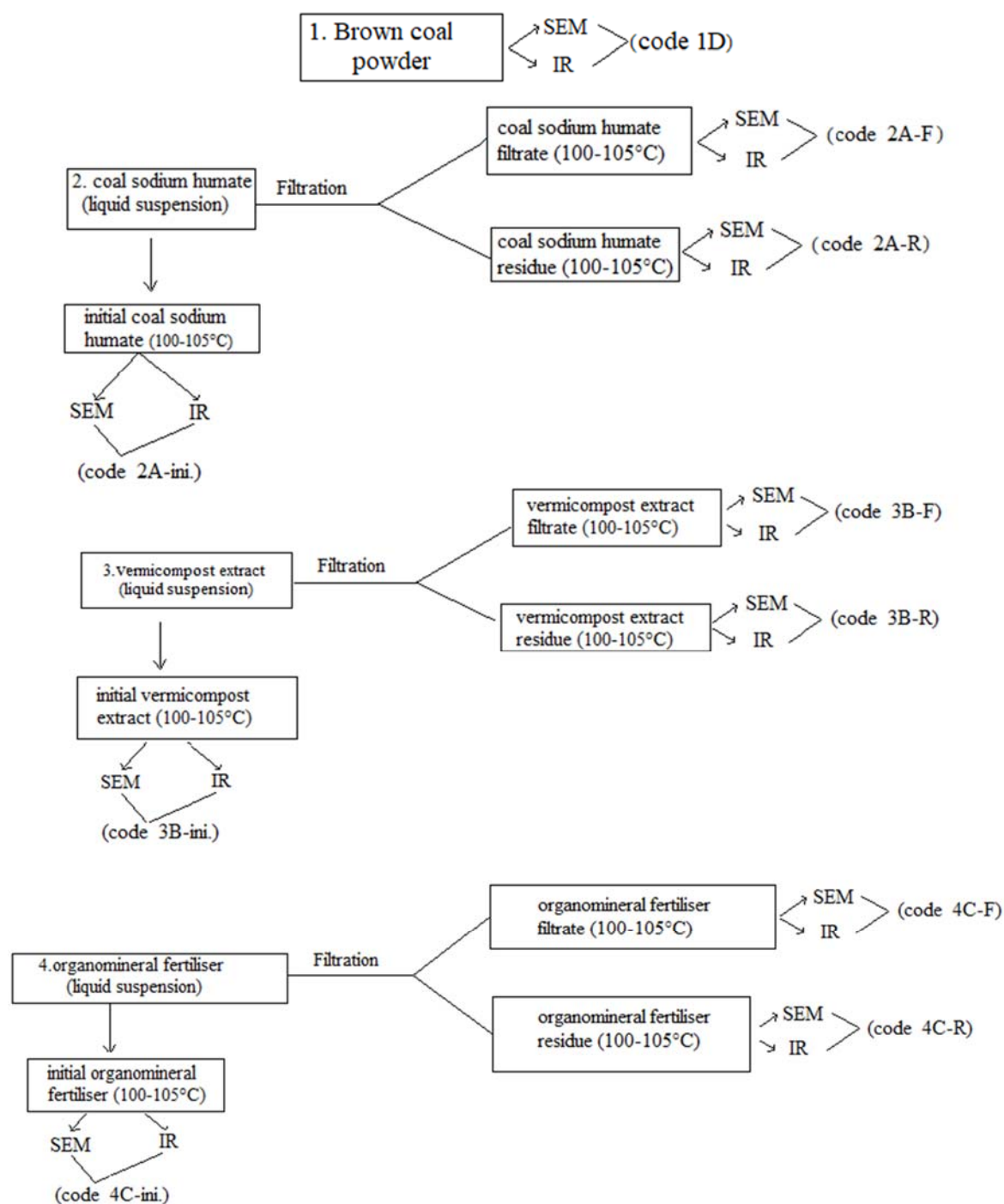


Figure 4. Methodology of processes and results of chemical analysis

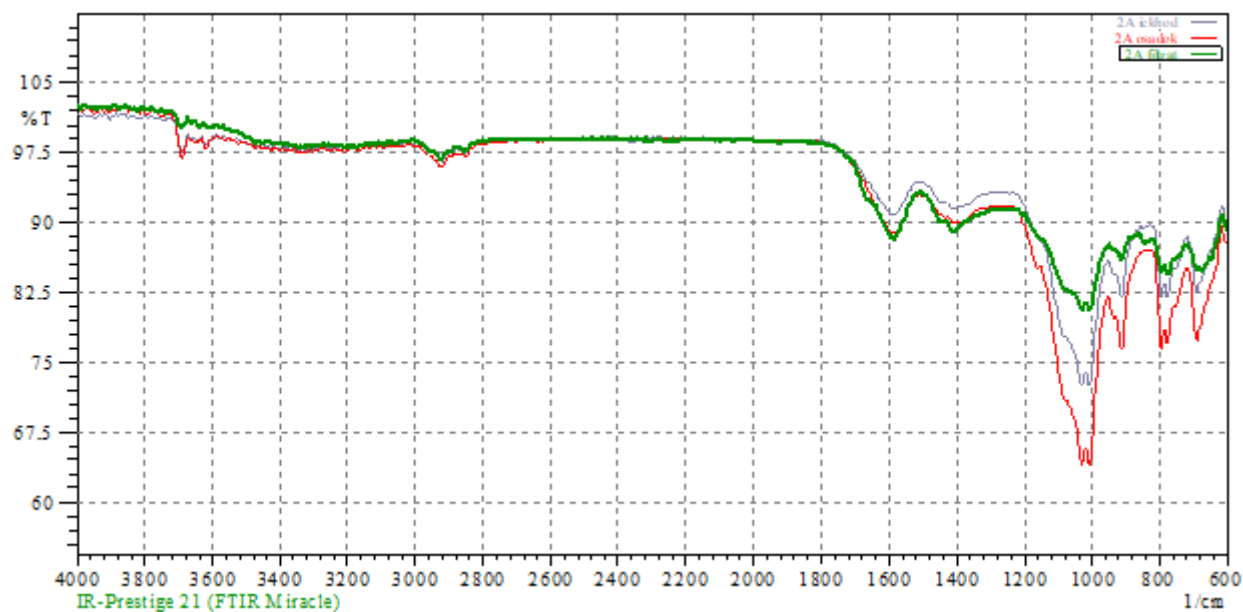


Figure 5. Overlay of IR spectra of coal sodium humate samples (2A - ini., residue, filtrate)

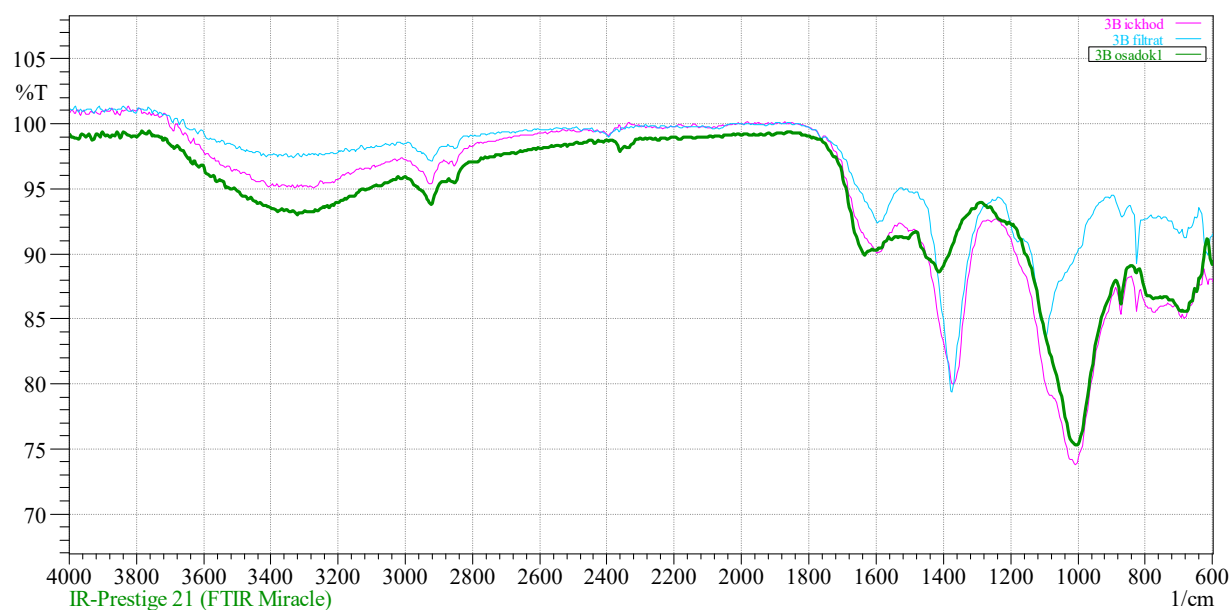


Figure 6. Overlay of IR spectra of vermicompost extract samples (3B - ini., residue, filtrate)

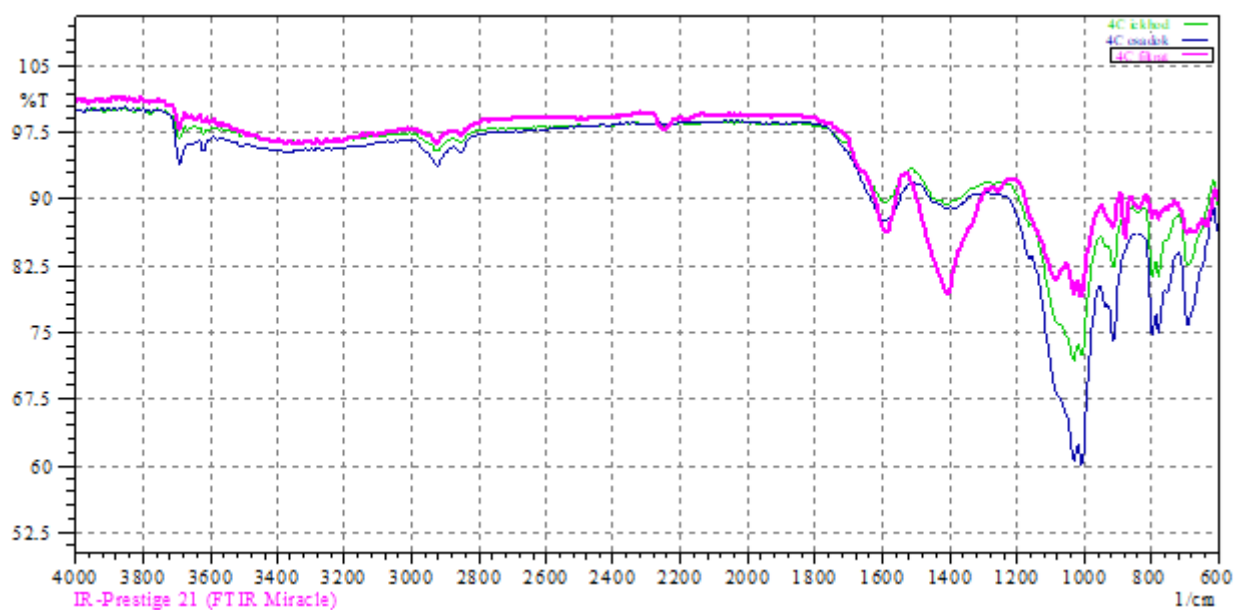


Figure 7. Overlay of IR spectra of organomineral fertilizer samples (4C - ini., residue, filtrate)

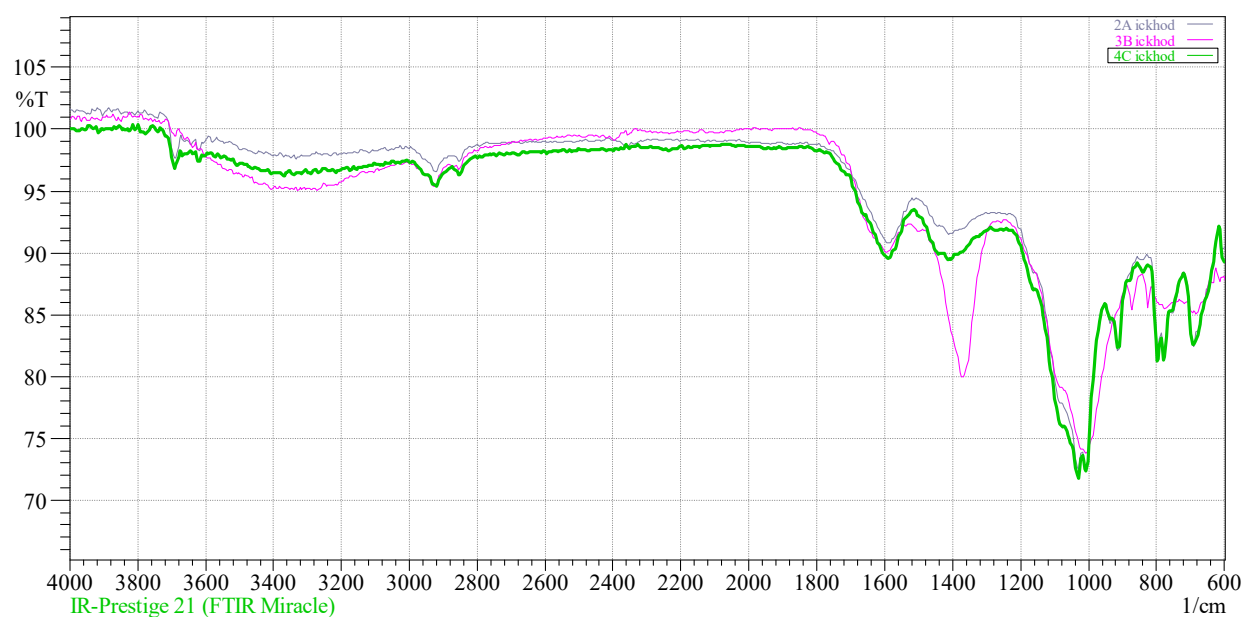


Figure 8. Overlay of IR spectra of samples (2A, 3B, 4C - initial)

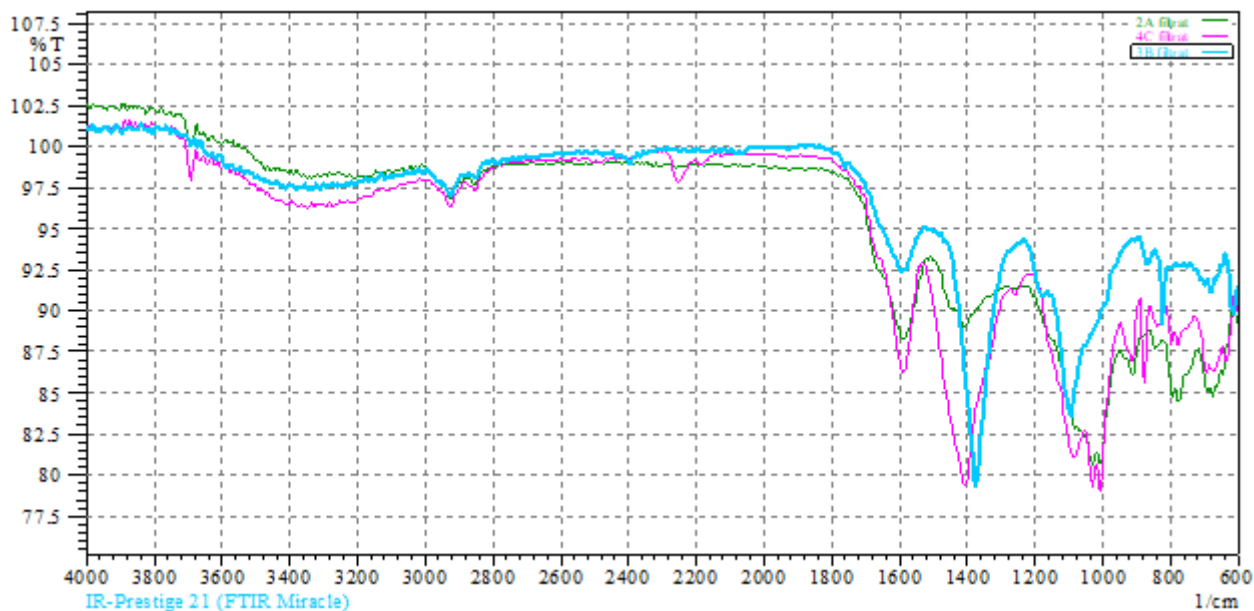


Figure 9. Overlay of IR spectra of samples (2A, 3B, 4C - filtrate)

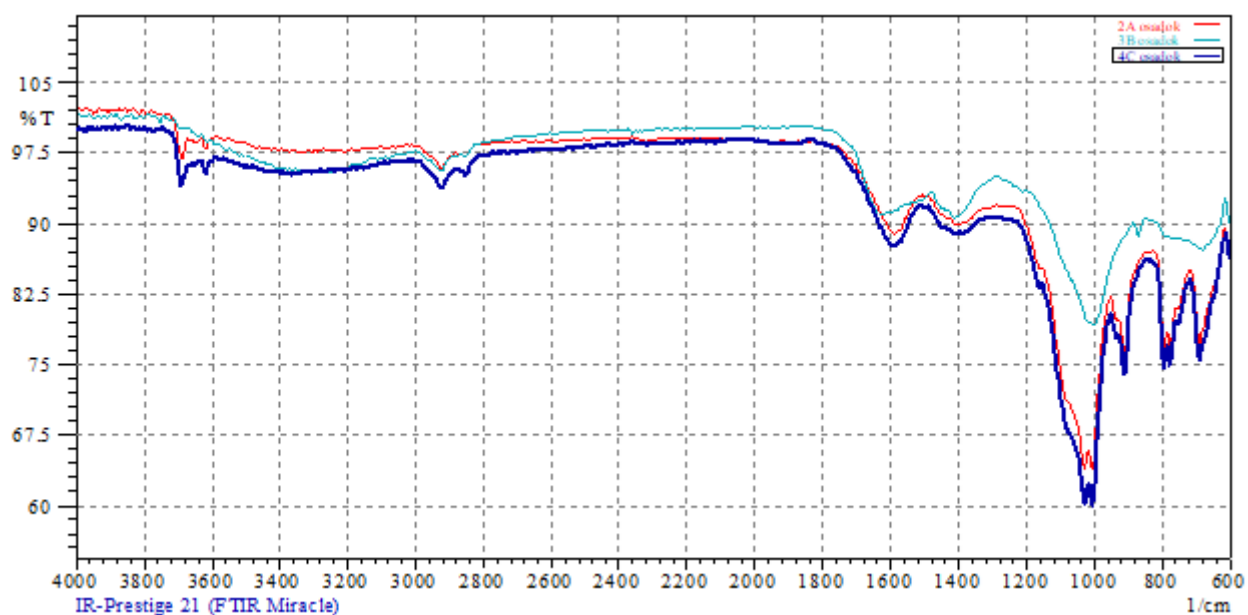


Figure 10. Overlay of IR spectra of samples (2A, 3B, 4C - residue)



NOF Control

NOF Control

Figure 11. NOF testing on conifers of FE "Green Helper & Carg "



NOF Control



NOF Control

Figure 12. NOF testing on conifers of FE “Green Helper & Cargo”



Figure 13. Sowing saxaul in the fields of MPI “Bakanasskoe Forestry”



Figure 14. Laying of LEU-treated saxaul (*Haloxylon aphyllum*) seeds

CARACTERÍSTICAS BIOLÓGICAS DA PLANTA MEDICINAL *ELAEAGNUS RHAMNOIDES* CULTIVADA NO SUDESTE DO CAZAQUISTÃO

BIOLOGICAL FEATURES OF MEDICINAL PLANT *ELAEAGNUS RHAMNOIDES* GROWING AT SOUTH-EAST OF KAZAKHSTAN

БИОЛОГИЧЕСКИЕ ОСОБЕННОСТИ ОБЛЕПИХИ (*ELAEAGNUS RHAMNOIDES*), ПРОИЗРАСТАЮЩЕЙ В ЮГО-ВОСТОЧНОМ КАЗАХСТАНЕ

KASSIMBEKOVA, Mereke¹; KALIYEVA, Anar^{1*}; KASSYMBAYEV, Bekbossyn²; MEDEUOVA, Galiya¹, MAMYTOVA, Nurgul³

¹ Kazakh National Women's Teacher Training University, Faculty of Natural Science, Department of Biology. The Republic of Kazakhstan.

² Kazakh National Agrarian University, Faculty IT - technology, Automation, and Mechanization of Agro-Industrial Complex. The Republic of Kazakhstan.

³ Al-Farabi Kazakh National University, Faculty of Biology and Biotechnology. The Republic of Kazakhstan.

* Corresponding author:

email: anar.kaliyeva28@gmail.com

Received 18 May 2020; received in revised form 03 August 2020; accepted 18 August 2020

RESUMO

As bagas de *Elaeagnus rhamnoides* contêm quantidades significativas de vitaminas bioativas, lipídios, carotenóides, compostos fenólicos. São amplamente utilizadas como ingrediente em produtos funcionais, cosméticos e formulações farmacêuticas para a prevenção e tratamento de doenças cardiovasculares, estomacais, cutâneas e hepáticas. As populações naturais de espinheiro marítimo são comuns no Cazaquistão. Os dados sobre indicadores fitoquímicos e de diagnóstico estão ausentes para *E. rhamnoides* cultivados no Cazaquistão. Neste trabalho, as bagas do mar do Cazaquistão foram pesquisadas quanto a indicadores de diagnóstico, compostos lipofílicos e hidrofílicos. As análises foram conduzidas para os principais indicadores diagnósticos de folhas e frutos por microtécnicas padrão; perfis de ácidos graxos por cromatografia em fase gasosa; β -caroteno por HPLC-PDA; vitamina C e B por eletroforese capilar e substâncias de pectina por titulação. Os principais indicadores diagnósticos das folhas foram o complexo anômocítico estomático; pêlos corimbósicos e estrelados; feixe condutor - colateral fechada; frutas - passagens secretoras e feixes condutores do tipo espiral no parênquima pulpar e grande quantidade de óleo graxo e grãos de aleuron no embrião. No óleo de polpa / casca de baga, os ácidos graxos dominantes foram os ácidos palmitoléico e palmítico (28,53 e 30,03%, respectivamente). O óleo de semente de espinheiro marítimo, com seus altos níveis de α -linolênico juntamente com uma proporção próxima de 1: 1 de ácidos graxos ω -6: ω -3, representou uma fonte muito equilibrada de ácidos graxos poliinsaturados para a saúde e nutrição humana. O conteúdo de β -caroteno foi de 7,75 mg por kg, substâncias de pectina - 3,27%. Além disso, as bagas eram ricas em vitaminas do complexo B (0,0035-0,014 mg/100g) e vitamina C (0,21 mg/100g). Este trabalho constitui a primeira abordagem do conhecimento sobre o perfil fitoquímico de frutas de *E. rhamnoides* do Cazaquistão e fornece argumentos para o uso múltiplo de *Elaeagnus rhamnoides* tanto para consumo fresco quanto para preparações industriais na forma de compotas e produtos relacionados (alimentos multivitamínicos funcionais) assim como subprodutos (sementes) como matéria-prima para a produção de óleos adequados para serem comercializados pelas indústrias farmacêutica, cosmética e alimentícia.

Palavras-chave: *Elaeagnus rhamnoides*, Plantas medicinais, Fitoquímica, Anatomia, ácidos graxos poliinsaturados.

ABSTRACT

Elaeagnus rhamnoides berries contain significant amounts of bioactive vitamins, lipids, carotenoids, and phenolic compounds. They are widely used as an ingredient in functional products, cosmetics, and pharmaceutical formulations to prevent and treat cardiovascular, stomach, skin, and liver diseases. Natural sea buckthorn populations are widespread in Kazakhstan. Data on phytochemical and diagnostic indicators are absent

for *E. rhamnoides* growing in Kazakhstan. In this work, seaberry from Kazakhstan was surveyed for diagnostic indicators, lipophilic and hydrophilic compounds. Analyses were conducted for main diagnostic indicators of leaves and fruits by standard microtechniques; fatty acid profiles by gas-chromatography; β -carotene by HPLC-PDA; vitamin C and B by capillary electrophoresis, and pectin substances by titration. The main diagnostic indicators of leaves were stomatal anomocytic complex; corymbose and stellate hairs; conductive bundle - closed collateral; fruits - secretory passages and conducting bundles of a spiral type in the pulp parenchyma, and a large amount of fatty oil and aleuron grains in the embryo. In the oil from berry pulp/peel, the dominating fatty acids were palmitoleic and palmitic (28.53 and 30.03 %, respectively). Sea buckthorn seed oil, with its high α -linolenic levels and a near 1:1 ratio of ω -6: ω -3 fatty acids, represented a very balanced source of polyunsaturated fatty acids for human health and nutrition. β -Carotene content was 7.75 mg per kg, pectin substances – 3.27 %. In addition, the berries were rich in vitamins B complex (0.0035-0.014 mg/100g) and vitamin C (0.21 mg/100g). This work constitutes the first approach on knowledge about the phytochemical profile of *Elaeagnus rhamnoides* fruits from Kazakhstan and provides arguments multiple using of *E. rhamnoides*, both for fresh consumption and for industrial preparations in the form of jams and related products (functional multivitamin food) as well as byproducts (seeds) as raw materials for the production of oils suitable to be marketed by the pharmaceutical, cosmetic and food industries.

Keywords: *Elaeagnus rhamnoides*, Medicinal plants, Phytochemistry, Anatomy, polyunsaturated fatty acids.

АННОТАЦИЯ

Ягоды облепихи *Elaeagnus rhamnoides* содержат значительные количества биологически активных веществ - витаминов, липидов, каротиноидов, фенольных соединений и широко используются в функциональных продуктах, косметических средствах и фармацевтических составах для профилактики и лечения заболеваний сердечно-сосудистой системы, желудочно-кишечного тракта, кожи и печени. Естественные популяции облепихи широко распространены в Казахстане. Данные о фитохимических и диагностических показателях для *E. rhamnoides* в Казахстане отсутствуют. В данной работе изучены диагностические показатели, липофильные и гидрофильные соединения облепихи, произрастающей в Казахстане. Основные диагностические показатели листьев и плодов определяли по стандартной микротехнике; профили жирных кислот - методом газовой хроматографии; β -каротин с помощью ВЭЖХ-КПК; витамин С и В - методом капиллярного электрофореза и пектиновые вещества с помощью титрования. Основными диагностическими показателями листьев были: устьичный аппарат аномоцитного типа; щитковидные и звездчатые волоски; закрытый проводящий пучок; плодов - проводящие пучки спирального типа в паренхиме пульпы, а также большое количество жирного масла и алейроновых зерен в зародыше. В масле из мякоти / кожуры доминирующими жирными кислотами были пальмитолеиновая и пальмитиновая (28,53 и 30,03% соответственно). Масло облепихи с высоким содержанием α -линоленовой кислоты и соотношением жирных кислот ω -6: ω -3 около 1: 1 представляет собой очень сбалансированный источник полиненасыщенных жирных кислот для здоровья и питания человека. Содержание β -каротина составило 7,75 мг на кг, пектиновых веществ - 3,27%. Кроме того, ягоды были богаты комплексом витаминов группы В (0,0035-0,014 мг / 100 г) и витамином С (0,21 мг / 100 г). В этой работе впервые изложены данные о фитохимическом профиле плодов *Elaeagnus rhamnoides* из Казахстана и приведены аргументы в пользу их комплексного использования, как для потребления в свежем виде, так и в виде джемов и сопутствующих продуктов (функциональных поливитаминных продуктов питания), а также возможности использования побочных продуктов (семян) в качестве источника масел для фармацевтической, косметической и пищевой промышленности.

Ключевые слова: *Elaeagnus rhamnoides*, облепиха, фитохимия, анатомия, полиненасыщенные жирные кислоты

1. INTRODUCTION:

The properties of *Elaeagnus rhamnoides* L. (Elaeagnaceae) known as sea buckthorn, or Siberian pineapple as a medicinal plant were known even since ancient times, and in 1977 the species received the status of pharmacopeia in China (The State of Pharmacopoeia Commission of People's Republic of China, 1997). The first clinical studies on the medicinal use of *E. rhamnoides* were initiated in Russia during the 1950s (Ding *et al.*, 2016). Now fruits and other

organs of *E. rhamnoides* have been used in traditional medicine, especially in Tibet, Mongolia, China, and Central Asia Luchowski, Pecio, Marciniak, Kontek, and Stochmal, 2019). Sea buckthorn is grown almost worldwide, but in the most significant volumes in Russia and in China (Olas, Skalski, and Ulanowska, 2018).

The popularity of sea buckthorn has been growing, mainly because of the high nutritional value and medicinal properties of its fruit. Sea buckthorn is reported to be a natural reservoir of

many nutrients including vitamins, essential polyunsaturated fatty acids, carotenoids, phytosterols, essential volatiles, flavonoids, phenolics, organic acids (e.g., hydroxybenzoic acid derivatives), and amino acids. Sea buckthorn berries, known as seaberry, or Siberian pineapple have a range of bioactive chemicals (elements and vitamins (especially A, C, and E), lipids, carotenoids, amino acids, unsaturated fatty acids, and phenolic compounds). These compounds exhibit a wide range of anti-inflammatory, anticancer, antioxidant, and anti-atherosclerotic activities. Nowadays, extracts from *Elaeagnus rhamnoides* different parts use as cosmetics, functional food, and pharmaceutical formulation for diseases of the gastrointestinal tract, heart, liver, and skin (Olas *et al.*, 2018).

Simultaneously, raw fruits exhibit biological activity and jams, tinctures, marmalades, liquors, and other food products prepared from them. This makes sea buckthorn an indispensable component of a healthy diet and an ingredient in functional products.

E. rhamnoides in ecological respect to a very ductile appearance grows on different types of soil, drought-resistant, and salt-tolerant withstanding both high and low temperatures (vibration amplitude - 90 ... 95 ° C), which makes it well adapted to growth in different climatic zones, such as Kazakhstan. It is common in floodplains and along river banks, on sandy stony-crushed mountain soils. Natural sea buckthorn populations in Kazakhstan occupy about 680 hectares in the Eastern Shallow Hills, Zaysan, Balkhash, Altai, the Alatau Mountains, Karatau, and the Western Tien Shan. As a result of the work of a group of Kazakhstani botanists, various varieties and promising forms placed in leshozes of Almaty, Taldy-Kurgan and Dzhambul regions: "Gift of Katun", "News of Altai", "Golden Ear", "Vitamin", "Scherbinka-1", "Chuyskaya", "Golden Siberia", "Orange" *et al.*

Despite the widespread use of sea buckthorn in Kazakhstan, scientific research is limited by ecology and fruit processing technology. Research works showed that almost the spectrum of vital microelements is contained in the vegetative organs of sea buckthorn, which is growing in the Zailiysk Alatau. In contrast, the primary accumulation of microelements occurs not in the stem, but in the sea, buckthorn leaves. This circumstance highlights the value to the local sea buckthorn as a medicinal plant and raw material for the manufacture of medicines and biologically active supplements (Kumar, Kumar, Chaurasia, and Bala Singh, 2011).

Considering the bioactive and unusual fatty acid composition of sea buckthorn berry, and its potential as a health product, this study aimed to analyze lipophilic and hydrophilic bioactive compounds in sea buckthorn (*Hippophae rhamnoides* L.) berries collected from the south-east side of Kazakhstan.

2. MATERIALS AND METHODS:

2.1. Plants materials

E. rhamnoides was collected from Mountains Alatau, Almaty Region South-East side of Kazakhstan, ca 950 m 30 Sep 2018 (43°10'13" N, 76°41'53" E). The herbarium materials have been deposited at the Herbarium of the Department of Biology, Kazakh National Women's Teacher Training University. Manual harvesting fruits were picked, rinsed, and were brought to the laboratory in polythene bags. The powdered samples were stored in a refrigerator at 4°C until further analysis.

2.2. Methods of anatomical and morphological study

The plants were identified according to Flora of Kazakhstan and illustrated the keys to the plants of Kazakhstan. Morphological characters were compared from five randomly-selected plants (in triplicate for each population), and mean values were taken for analysis using the ANOVA method. The results of the analysis were expressed as a mean of three determinations \pm SD. The material was fixed in a mixture of alcohol, water, and glycerol with ratio 1:1:1, according to Strasburger and Flemming. Anatomical and morphological studies were conducted according to the methods of M.N. Prozina (1960).

The anatomic slices were made by microtome MZP-01 "Technom" (Ekaterinburg, Russia). The temporary preparations were immersed in glycerol. The thickness of the anatomic slices ranged from 10 to 15 micrometers. For microscopic analysis of fruits, dried ground fruits were placed in a container with hexane for a day, then treated with a solution of chloral hydrate—over 1000 temporary and permanent preparations made for microphotography and morphometric analysis. For quantitative analysis, morphometric indicators were measured by MCX 100 Micros microscope (Austria) with camera adapter (with lens4x/0.10, and multiplication ratio EW 10x/20). The statistical analysis of

morphometric indicators performed according to the methods of Lakin (1990).

2.3. Lipophilic compounds analysis

2.3.1 Determination of β -Carotene

β -Carotene extraction and HPLC-PDA analysis were carried out according to Biehler, Mayer, Hoffmann, Krause, and Bohn (2010) with modifications. Samples were extracted (0.1 g/ml) with ice-cold hexane: acetone (1:1, v/v). The mixture was centrifuged at 2000 rpm for 2 min after vortexing for 2 min. The organic phase was decanted into a tube with a saturated sodium chloride solution and placed on ice. The residue was extracted until the extract was discolored, and the organic phase was combined in a test tube with a saturated solution of sodium chloride. Then, the obtained organic phase was filtered through a 0.45-mm membrane filter. β -Carotene was analyzed using a Prominence-i HPLC-PDA model system equipped with sample cooler LC-2030C (Shimadzu, Japan) and a C18 Luna® column (150 \times 4.6 mm, 5 μ). The column temperature was set at 35 °C, and the injection volume was 20 μ L. The compound was analyzed with an isocratic mobile phase using acetonitrile: dichloromethane: methanol (7:2:1) as eluents at ambient temperature. A flow rate of 1.0 mL/min was set. Peaks were monitored at 450 nm and identified by congruent retention times compared with pure β -carotene standard. Quantification of the compound was made using calibration curves obtained from pure standards in the HPLC system.

2.3.2 Method for determination of the fatty acid composition

A Soxhlet apparatus extracted the oil for four hours using petroleum ether as a solvent. This was evaporated under reduced pressure, using a rotary evaporator at 50 °C, and then were hydrolyzed by 10% KOH in methanol at 60°C for 30 minutes. The product of hydrolysis was extracted with chloroform. Methyl esters were prepared via methylation using diazomethane (Fieser and Fieser, 1967).

The fatty acid composition was analyzed by GC (Crystallux-4000M "Meta-Chrom", Russia) equipped with a flame ionization detector (FID) and a capillary column DB-5ms (5% diphenyl and 95% dimethylpolysiloxane, phase thickness 0.25 μ m) with a size of 30 m \times 0.25 mm. The initial temperature of the thermostat is 40 °C; holding at initial temperature - 1 min; temperature programming - from 40 to 210 °C with a speed of

15 °C / min, from 210 to 280 °C with a speed of 5 °C / min. Holding at the final temperature - 20 min. Carrier gas-helium, 1 cm / min. Sample 0.2 μ L, the evaporator - 280 °C. The temperature of the evaporator is 280 °C.

2.4. Hydrophilic compounds analysis

2.4.1 Method for determination of vitamin C and B

Vitamin C and B were determined by method M 04-41-2005 "Determination of the mass fraction of free forms of water-soluble vitamins in samples of premixes, vitamin supplements, concentrates and mixtures by the method of capillary electrophoresis using the system of capillary electrophoresis "Drop-105" (Certificate on certification of measurement procedure No. 224.04.17.035/2006).

2.4.2 Pectin substances determination

The carbazole test carried out substantially, as described by Filipov and Vlasieva (1973). The sample sizes were 20-25 g fresh weight of fruits. Per 10ml of solution or suspension, 1-2 ml of 1 N NaOH was added and thoroughly mixed. De-esterification occurred for 20 min at 20-25°C. Subsequently, the suspension was acidified by the addition of 1 N HCl, 1-5 x the volume of 1 N NaOH added before, and mixed thoroughly. To precipitate the pectin, 50 ml of 0.1 N HCl added. The suspension stirred and kept for 5 min at room temperature to equilibrate the medium and pectin flakes concentrations. The final volume or weight of each sample was measured. The mixture filtered through a wide pore filter (Whatman). 10-20ml of this filtrate pipetted into a 250 ml volumetric flask. The residue of the filter was pooled with the remaining filtrate. Funnel and vial washed twice with distilled water and the wash solutions added to the residue filtrate mixture and thoroughly stirred. The filtrate in the flask and the mixture were separately titrated with 0.1 N NaOH using Hinton's indicator. From the result of the titration of the 10-20ml filtrate, the HCl content of the original volume was calculated.

2.5. Statistical analysis

All determinations were obtained from triplicate measurements, and results were expressed as means \pm standard deviations. The data were analyzed using a one-way analysis of variance (ANOVA) for mean differences.

3. RESULTS AND DISCUSSION:

3.1. Morphological and microscopic characterization of *E. rhamnoides*

3.1.1 Macroscopic characters

E. rhamnoides is a small tree 2m tall with black bark, have strong spines, 2-7 cm in length. Shoots of different ages create a rounded, pyramidal crown. The sea buckthorn root system develops close to the surface, no deeper than 40 cm, spreading over a wide area. The root system consists of skeletal, semi-skeletal, weakly branching roots, on which are formed nodules that contain nitrogen-fixing bacteria.

Sea buckthorn is a dioecious plant; on some bushes grow female flowers, from which developed fruits; on other bushes grow male flowers, which pollinate female flowers with wind help. The flowers are regular, with a simple perianth cup-shaped.

Leaves are alternate, simple, linear-lanceolate 4-8 cm long. Above of leaves grayish-green, below side grayish-white and have stellate hairs. The smell is weak, peculiar, taste slightly bitter. Fruits are oval or round 0,5-1 cm long, smooth pitted yellowish-golden, red or orange, with one bone, shiny, juicy, with a peculiar taste and smell, reminiscent the scent of pineapple (Figure 1).

3.1.2. Microscopic study

In the cross-section of the leaf on both sides, have epidermis, columnar and spongy mesophyll in a single row. In the center of a leaf, there is collateral, larger conductive fascicle with well-developed xylem vessels (Figure 2).

The transverse section of a leaf of sea buckthorn shows dorsal ventral characters. The mesophyll is divided into two layers: the upper, palisade layer, and the lower spongy layer. Palisade parenchyma consists of 2-3 elongated rows of cells, located under the cuticle and the upper epidermis on the inner side of the leaf. Isodiametric cells of the spongy parenchyma are located under the epidermal tissue of the outer side of the leaf plate. The chlorophyll-bearing cells of the palisade parenchyma are oriented perpendicular to the leaf; they differ in size from chlorenchyma cells of the spongy parenchyma. There are rather large intercellular cavities in the spongy mesophyll, which connect and stomata of the dorsal side of the leaf. The cuticle is even but wrinkled in the region of vein on the underside of

the leaf. On the ventral side of the leaf, stomata are not available, and the lower part is densely covered with gray, multicellular stellate hairs. There is collantern on the center of the leaf and a larger conducting bundle with well-developed xylem and phloem (Figure 2).

Thickness of lamina 528 microns length. Cells of the upper epidermis have straight walls. The length is 20, 33 microns. Cells of the lower epidermis more thin-walled than cells of the upper epidermis; walls are straight—length 18.33 microns. The stomata are found only on the lower epidermis, an anomocytic type (4-8 cells), with a frequency of 345-603 per 1 mm. The leaf mesophyll is protected on both sides by a single layer of rounded epidermal cells. The epidermal cells of the upper side of the leaf are cutinized with a waxy fat-like substance. The length of the xylem is 69.41 microns; the length of the phloem is 56.66 microns (Table 1).

3.1.3 Sea buckthorn fruits diagnostic indicators

Macroscopic characters. Fruits (Figure 3) are 6–10 mm long, 4–8 mm in diameter, oblong, highly wrinkled, oval, soaked, with one bone, with a peduncle. The pulp of the fetus is formed from the receptacle. The stone in outline is elongated obovate, dark brown, the surface is smooth shiny, with a clearly visible longitudinal line, up to 5 mm long. Fruits are yellow with a characteristic odor; the taste is sour.



Figure 3. Fruits of *E. rhamnoides*

Trichomes with a diameter of 197.8 - 291.8 microns were found. The cells of the epidermis are polygonal in shape, 18–48 μm long, 3–40 μm wide irregular stony cells with a length of 8.98 μm and a width of 2.87 μm (Figure 4a). In the pulp parenchyma, secretory passages and conducting bundles of a spiral type are found. Seabuckthorn seed consists of palisade cells. Behind it, there is a perisperm and many cells of the aleuron layer

and an embryo composed of tight-fitting cells, a large amount of fatty oil, and aleuron grains (Figure 4b, c, d).

3.2. Analysis of lipophilic bioactive compounds

3.2.1 Fatty acid composition

Both seeds and flesh (pulp) of sea buckthorn berries are rich in lipids (Table 2). Oil can be extracted from the seeds and the pulp (Zeb and Ullah, 2015). The seeds contain 22.5% oil, the fruit pulp - about 24.32%, the berries—27.89%, which is consistent with data from other researchers (Kumar *et al.*, 2011). The fatty acid profiles in pulp oil and seed oil were different. The predominant fatty acids in seed oil were linoleic acid (C18:2 ω -6, 35.34%) and α -linolenic acid (C18:3 ω -3, 25.46%), in the oil from berry pulp/peel – palmitoleic (C16:1 ω -7, 30.03%) and palmitic acids (28.53%). The saturated fatty acids (SFA) fraction ranged between 11.13 and 32.45% of the total FA. The main SFA in all samples investigated was palmitic acid (PA, hexadecanoic acid, 16:0), which is the most common SFA found in animals and plants.

Seed oil was richer in total polyunsaturated fatty acids (PUFA), because of higher linoleic and linolenic acids (the major fatty acid components of the PUFA fraction). Linoleic acid was found in the greatest proportion of PUFA in the seed and soft parts oils. α -linolenic acid content was at the highest level in the seed oil (25.46%) but was found to be at the lowest level in pulp/peel oil (3.82 %). It should be noted, that the seed oil contains linoleic acid (18:2cisD9,12) (35.34 %) and α -linolenic acid (18:3cisD9,12,15) (25.46%) in close to 1:1 ratio. This ratio is unique to plant lipids (Ursin, 2003).

Because the whole fruit oil is mostly made up of pulp oil, the features of these two oil kinds were very similar. Pulp and whole fruit oils were richer in individual monounsaturated fatty acids (both in palmitoleic acid, and berries in oleic acid), as well as in total monounsaturated fatty acids (MUFA). The analyzed oil is attracting attention because of the increasing interest in the physiological role of the monounsaturated fatty acids (Ranalli *et al.*, 2002) and given the fact that a high level of palmitoleic acid is not common in the plant kingdom. High levels of palmitoleic acid are present in only a few plants, for example, in Nuez Australiana (*Macadamia integrifolia* Maiden and Betcher). *Macadamia* oil contains ~17% palmitoleic acid (Parveez *et al.*, 2012). Palmitoleic acid is low in seed oils but is characteristic of the fruit pulp (Saeidi, Alirezalu, and Akbari, 2016). The

monounsaturated fatty acid palmitoleate (palmitoleic acid) is one of the most abundant fatty acids in serum and tissues, particularly adipose tissue and liver (Frigolet and Gutiérrez-Aguilar, 2017). Palmitoleic acid is an omega-7 monounsaturated fatty acid essential for pharmaceutical applications. Palmitoleic acid has been reported to have anti-thrombotic effects, favorable effects on insulin sensitivity, cholesterol metabolism, and hemostasis and averts beta-cell apoptosis persuaded by glucose or saturated fatty acids (Hernandez, 2016). This fatty acid is less susceptible to oxidation than polyunsaturated fatty acids, which is especially important when used in the food industry with frying and baking processes. Also, palmitoleic acid is widely used in cosmetics.

LA and ALA obtained from foods furnished by the diet is the starting point for synthesizing a variety of other unsaturated fatty acids. After ingestion, ALA is converted to very-long-chain PUFAs, i.e., readily to eicosapentaenoic acid, 20:5 ω -3, and more slowly to docosahexaenoic acid, 22:6 ω -3. Using the same pathways (the same enzymes) and in competition with ALA, LA is converted into arachidonic acid, 20:4 ω -6, which is, in a competition (again) with eicosapentaenoic acid, the starting point for the synthesis of eicosanoids and prostaglandins that are important mediators in many inflammatory diseases and in particular in cardiovascular diseases (de Lorgeril, Salen, Laporte, and de Leiris, 2001).

It has been previously found that a diet rich in fish and seafood significantly reduces the risk of heart disease due to the high eicosapentaenoic acid (EPA) and docosahexaenoic acid [DHA] content of these foods (Blondeau *et al.*, 2015). With growing concerns regarding the accumulation of environmental pollutants in fish oil as well as the sustainability of marine fish stocks, plants rich in n-3 fatty acids may offer a sustainable source of these beneficial fatty acids.

Except for flaxseed oil, which contains 50% α -linolenic acid, such high levels of n-3 fatty acids are different in seed oils. Research is currently underway to find and produce n-3 fatty acid-enriched products, both for human consumption and use as animal feed. Sea buckthorn seed oil, growing at South-East of Kazakhstan, with its high α -linolenic acid content and 1:1 ratio of ω -6: ω -3 fatty acids may be a new balanced source of polyunsaturated fatty acids.

3.2.2 Carotenoids content

The orange-yellow color of sea buckthorn berry reflects the existence of carotenoids.

Typically, carotenoids content is much lower in seeds than in pulp (Yang and Kallio, 2002). Therefore, the carotene content was determined in the fruit (7.75 mg/kg, Table 3).

Table 3. β -Carotene content

Name	Result, mg/kg
β -Carotene	7.75 \pm 0.84

Note: Values are means of triplicate determinations ($n = 3$) \pm standard deviations.

Even though some authors showed a significantly higher content of β -carotene (between 4 and 7.5 mg/100 g) (Pop *et al.*, 2014), our results are consistent with the results of Yang's (2002). They showed the concentration of β -carotene ranged between 0.2 and 17 mg/100 g and that of total carotenoids from 1 to 120 mg/100 g of sea buckthorn berries (Teleszko, Wojdyło, Rudzińska, Oszmiański, and Golis, 2015). Among biologically active substances, β -carotene is a member of the carotene family with no polar functional groups and can be cleaved in the liver into two vitamins A molecules. β -Carotene can be supplemented in many individuals with a reduced concern of toxicity (Hammond and Renzi, 2013). Carotenoids receive much interest, as they have multiple activities such as antioxidant, anti-mutagenic, and anti-tumour (Pop *et al.*, 2014).

Carotenoids are biologically active compounds in residual pomace after juice extraction from sea buckthorn berries consisting of pulp, seed, and skin. Interestingly, Corbu *et al.* concluded that the carotenoids from dried sea buckthorn byproducts might be safely used as a source of natural carotenoids for the enrichment of vegetable oils for their coloring effect and for the appeal to enhance the acceptability and valorization of the edible oils (Corbu, Rotaru, and Nour, 2019). The β -carotene is served as a quality checkpoint for sea buckthorn oil in some countries (Suryakumar and Gupta, 2011).

3.2.3 Analysis of hydrophilic bioactive compounds

The berries of sea buckthorn were rich in vitamins B complex (content ranged from 0.0035 to 0.014 mg/100g), vitamin C (0.21 mg/100g) and pectin (3.27 %) (Table 4). These compounds have high biological activity.

So, pectins are the polysaccharides found in plant cell walls and the outer skin and rind of fruits and vegetables. They are soluble in hot water and then form gels on cooling, hence gelling

and thickening agents in various food products such as jams and jellies. Cholesterol-lowering effects of pectin is due to its gel-forming capacity too. Pectin lowers cholesterol by binding the cholesterol and bile acids in the gut and promoting their excretion (Mudgil and Barak, 2013).

Vitamin C has antioxidant, immunomodulatory, anti-infectious, antimicrobial, antibacterial, antiviral, antiparasitic, and antifungal effects (Mousavi, Bereswill, and Heimesaat, 2019). Vitamin C content in analyzed sea buckthorn berries samples was lower than showed (27.8 mg/100 g). However, vitamin C content depends on the geographical location and related environmental parameters. For example, fresh sea buckthorn fruits from coastal dunes of Europe contain 120–315 mg% of vitamin C, while from Alps – 405– 1100 mg% (Zielińska and Nowak, 2017). Besides, in sea buckthorn, extensive chemical composition variations have been revealed among populations, subspecies, or cultivars. For example, seven wild berries of *subsp. sinensis*, native to China, contained 5–10 times more vitamin C in the juice fraction than the berries of *subsp. rhamnoides* from Europe and of *subsp. mongolica* from Russia. The content of ascorbic acid among Russian cultivars (*subsp. mongolica*) may range from 0.5 to 3.3 g/kg, whereas in berries of *subsp. turkistanica* ranged from 2.52 to 4.19 g/kg (Teleszko *et al.*, 2015). The lower vitamin C concentration in our samples could be due to the specific geographical nature of the area where the short growing season prevails (Shi, Ho, and Shahidi, 2010).

As for vitamin B, other researches also showed the vitamin B complex group in sea buckthorn berries (B1 (0.035 mg%), B2 (up to 0.056 mg%), and B6 (Zielińska and Nowak, 2017). The B vitamins are cofactors for many enzymes for biosynthetic processes in mammalian cells, including the de novo production of RNA and DNA (Lai, 2013).

4. CONCLUSIONS:

In short, sea buckthorn growing in Kazakhstan is a unique plant with high medical and nutritional value. *Hippophae* fruits are appreciated due to their multiple-use, both for fresh consumption and for industrial preparations in jams and related products (functional multivitamin food), and may use to obtain MUFAs-rich functional oils from industrial byproducts; i.e., the seeds. Juice extraction from sea buckthorn berries leads to a residual pomace consisting of pulp, seed, and skin, rich in biologically active

compounds with antioxidant properties, such as vitamins C, B, pectin, β -carotene, and unsaturated fatty acids. A diet rich in MUFAs may be a choice to a low-fat diet, which may lower blood cholesterol levels, modulate immune function, decrease susceptibility of oxidation of low-density lipoprotein and improve the fluidity of high-density lipoprotein. The PUFAs enriched diet may also be necessary for the structure and function of many membrane proteins, including receptors, enzymes, and active transport molecules. Thus, sea buckthorn from Kazakhstan can be widely used for the production of functional foods and in the pharmaceutical industry due to the rich composition of biologically active compounds with a broad spectrum of biological activity.

5. CONFLICT OF INTEREST STATEMENT:

The authors declare that they have no conflicts of interest.

6. REFERENCES:

1. Biehler, E., Mayer, F., Hoffmann, L., Krause, E., and Bohn, T. (2010). Comparison of 3 Spectrophotometric Methods for Carotenoid Determination in Frequently Consumed Fruits and Vegetables. *Journal of Food Science*, 75(1), C55-C61. <https://doi.org/10.1111/j.1750-3841.2009.01417.x>
2. Blondeau, N., Lipsky, R. H., Bourourou, M., Duncan, M. W., Gorelick, P. B., and Marini, A. M. (2015). Alpha-Linolenic Acid: An Omega-3 Fatty Acid with Neuroprotective Properties—Ready for Use in the Stroke Clinic? *BioMed Research International*, 2015, 1-8. <https://doi.org/10.1155/2015/519830>
3. Corbu, A. R., Rotaru, A., and Nour, V. (2019). Edible vegetable oils enriched with carotenoids extracted from by-products of sea buckthorn (*Hippophae rhamnoides* ssp. *sinensis*): The investigation of some characteristic properties, oxidative stability and the effect on thermal behaviour. *Journal of Thermal Analysis and Calorimetry*, 1-8. <https://doi.org/10.1007/s10973-019-08875-5>
4. de Lorgeril, M., Salen, P., Laporte, F., and de Leiris, J. (2001). Alpha-linolenic acid in the prevention and treatment of coronary heart disease. *European Heart Journal Supplements*, 3(suppl_D), D26-D32. [https://doi.org/10.1016/S1520-765X\(01\)90115-4](https://doi.org/10.1016/S1520-765X(01)90115-4)
5. Ding, J., Ruan, C. J., Guan, Y., Shan, J. Y., Li, H., and Bao, Y. H. (2016). Characterization and identification of ISSR markers associated with oil content in sea buckthorn berries. *Genetics and Molecular Research*, 15(3), gmr.15038278. <https://doi.org/10.4238/gmr.15038278>
6. Fieser, L. F., and Fieser, M. (Eds.). (1967). *Reagents for organic synthesis* (Vol. 1). New York: Wiley.
7. Filipov, M. P., and Vlasyeva, T. V. (1973). Photometric measurement of the uronide moiety in pectins. *Applied Biochemistry and Microbiology*, 9, 134–137.
8. Frigolet, M. E., and Gutiérrez-Aguilar, R. (2017). The Role of the Novel Lipokine Palmitoleic Acid in Health and Disease. *Advances in Nutrition: An International Review Journal*, 8(1), 173S-181S. <https://doi.org/10.3945/an.115.011130>
9. Hammond, B. R., and Renzi, L. M. (2013). Carotenoids. *Advances in Nutrition*, 4(4), 474-476. <https://doi.org/10.3945/an.113.004028>
10. Hernandez, E. M. (2016). Specialty Oils. In *Functional Dietary Lipids* (pp. 69–101). <https://doi.org/10.1016/B978-1-78242-247-1.00004-1>
11. Kumar, R., Kumar, G. P., Chaurasia, O., and Bala Singh, S. (2011). Phytochemical and Pharmacological Profile of Seabuckthorn Oil: A Review. *Research Journal of Medicinal Plant*, 5(5), 491–499. <https://doi.org/10.3923/rjmp.2011.491.499>
12. Lai, Y. (2013). Membrane transporters and the diseases corresponding to functional defects. In *Transporters in Drug Discovery and Development* (pp. 1–146). <https://doi.org/10.1533/9781908818287.1>
13. Lakin, G. F. (1990). *Biometriya [Biometrics]*. Moscow: Higher School.
14. Mousavi, S., Bereswill, S., and Heimesaat, M. M. (2019). Immunomodulatory and antimicrobial effects of vitamin C. *European Journal of Microbiology and Immunology*, 9(3), 73–79. <https://doi.org/10.1556/1886.2019.00016>
15. Mudgil, D., and Barak, S. (2013). Composition, properties and health

- benefits of indigestible carbohydrate polymers as dietary fiber: A review. *International Journal of Biological Macromolecules*, 61, 1-6. <https://doi.org/10.1016/j.ijbiomac.2013.06.044>
16. Olas, B., Skalski, B., and Ulanowska, K. (2018). The anticancer activity of sea buckthorn (*Elaeagnus rhamnoides* (L.) A. Nelson). *Frontiers in Pharmacology*, 9, 232. <https://doi.org/10.3389/fphar.2018.00232>
 17. Parveez, G. K. A., Rasid, O. A., Hashim, A. T., Ishak, Z., Rosli, S. K., and Sambanthamurthi, R. (2012). Tissue Culture and Genetic Engineering of Oil Palm. In *Palm Oil* (pp. 87–135). <https://doi.org/10.1016/B978-0-9818936-9-3.50007-1>
 18. Pop, R. M., Weesepeol, Y., Socaciu, C., Pinte, A., Vincken, J.-P., and Gruppen, H. (2014). Carotenoid composition of berries and leaves from six Romanian sea buckthorn (*Hippophae rhamnoides* L.) varieties. *Food Chemistry*, 147, 1–9. <https://doi.org/10.1016/j.foodchem.2013.09.083>
 19. Prozina, M. N. (1960). *Botanicheskaya mikrotekhnik* [Botanical microtechnique. Moscow: Higher School.
 20. Ranalli, A., Pollastri, L., Contento, S., Di Loreto, G., Iannucci, E., Lucera, L., and Russi, F. (2002). Acylglycerol and Fatty Acid Components of Pulp, Seed, and Whole Olive Fruit Oils. Their Use to Characterize Fruit Variety by Chemometrics. *Journal of Agricultural and Food Chemistry*, 50(13), 3775–3779. <https://doi.org/10.1021/jf011506j>
 21. Saeidi, K., Alirezalu, A., and Akbari, Z. (2016). Evaluation of chemical constitute, fatty acids and antioxidant activity of the fruit and seed of sea buckthorn (*Hippophae rhamnoides* L.) grown wild in Iran. *Natural Product Research*, 30(3), 366-368. <https://doi.org/10.1080/14786419.2015.1057728>
 22. Shi, J., Ho, C.-T., and Shahidi, F. (Eds.). (2010). *Functional Foods of the East*. <https://doi.org/10.1201/b10264>
 23. Suryakumar, G., and Gupta, A. (2011). Medicinal and therapeutic potential of Sea buckthorn (*Hippophae rhamnoides* L.). *Journal of Ethnopharmacology*, 138(2), 268-278. <https://doi.org/10.1016/j.jep.2011.09.024>
 24. Teleszko, M., Wojdyło, A., Rudzińska, M., Oszmiański, J., and Golis, T. (2015). Analysis of Lipophilic and Hydrophilic Bioactive Compounds Content in Sea Buckthorn (*Hippophae rhamnoides* L.) Berries. *Journal of Agricultural and Food Chemistry*, 63(16), 4120-4129. <https://doi.org/10.1021/acs.jafc.5b00564>
 25. The State of Pharmacopoeia Commission of People's Republic of China. (1997). *Pharmacopoeia of the People's Republic of China*. Beijing: People's Medical Publishing House.
 26. Ursin, V. M. (2003). Modification of Plant Lipids for Human Health: Development of Functional Land-Based Omega-3 Fatty Acids. *The Journal of Nutrition*, 133(12), 4271-4274. <https://doi.org/10.1093/jn/133.12.4271>
 27. Yang, B., and Kallio, H. (2002). Composition and physiological effects of sea buckthorn (*Hippophae*) lipids. *Trends in Food Science and Technology*, 13(5), 160-167. [https://doi.org/10.1016/S0924-2244\(02\)00136-X](https://doi.org/10.1016/S0924-2244(02)00136-X)
 28. Zeb, A., and Ullah, S. (2015). Sea buckthorn seed oil protects against the oxidative stress produced by thermally oxidized lipids. *Food Chemistry*, 186, 6-12. <https://doi.org/10.1016/j.foodchem.2015.03.053>
 29. Zielińska, A., and Nowak, I. (2017). Abundance of active ingredients in sea-buckthorn oil. *Lipids in Health and Disease*, 16(1), 95. <https://doi.org/10.1186/s12944-017-0469-7>

Table 1. Morphometric indicators of the anatomical structure of leaf *E. rhamnoides*

Thickness of lamina, μm	Upper Epidermis thickness, μm	Lower Epidermis thickness, μm	Columnar mesophyll thickness, μm	Spongy mesophyll thickness, μm	Xylem, μm	Phloem, μm
528 \pm 0.04	20.33 \pm 0.58	18.33 \pm 0.89	127.75 \pm 0.35	115,83 \pm 0.75	69.41 \pm 1.66	56.66 \pm 2.07

Table 2. Oil content and fatty acid composition of oils from seeds, whole berries and pulp/peel of sea buckthorn berries

Indicator	Seeds	Soft parts (pulp/peel)	Berries
Oil content, %	22.55 \pm 1.31	24.32 \pm 0.54	27.89 \pm 2.41
16:0	8.80 \pm 0.32	28.53 \pm 0.44	32.45 \pm 1.32
16:1	1.49 \pm 0.02	30.03 \pm 2.51	33.05 \pm 4.21
18:0	2.33 \pm 0.01	2.28 \pm 0.34	-
18:1 ω 9	14.97 \pm 0.87	6.45 \pm 0.98	28.65 \pm 2.2
18:1 ω 7	1.41 \pm 0.03	5.76 \pm 0.31	9.63 \pm 0.34
18:2 ω 6	35.34 \pm 1.31	10.01 \pm 0.02	3.48 \pm 0.01
18:3 ω 3	25.46 \pm 1.23	3.82 \pm 0.04	13.62 \pm 1.78
SFA	11.13	30.81	32.45
MUFA	17.87	42.24	71.33
PUFA	60.80	13.83	17.10
ω-6 / ω -3 ratio	1.39	2.62	0.26

Table 4. Hydrophilic compounds contents

No.	Compound	Content
1	B ₂ , mg/100g	0.0035 \pm 0.0015
2	B ₃ , mg/100g	0.033 \pm 0.007
3	B ₅ , mg/100g	0.037 \pm 0.007
4	B ₆ , mg/100g	0.014 \pm 0.003
5	B _c , mg/100g	0.0077 \pm 0.0015
6	C, mg/100g	0.21 \pm 0.07
7	Pectin substances, %	3.27 \pm 0.43

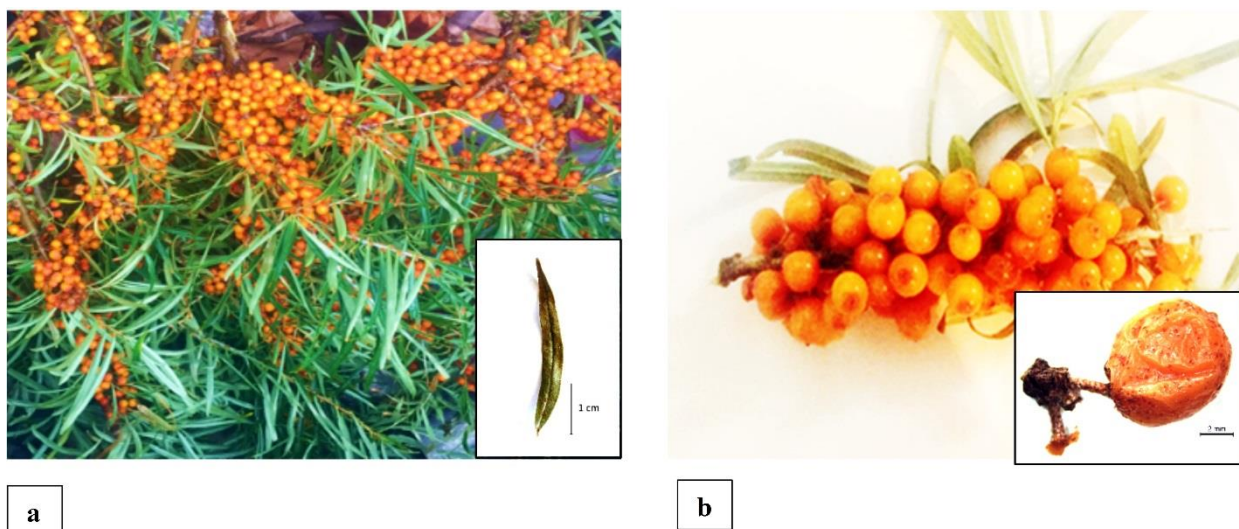


Figure 1. Leaves (a) and fruits (b) shape of *E. rhamnoides*

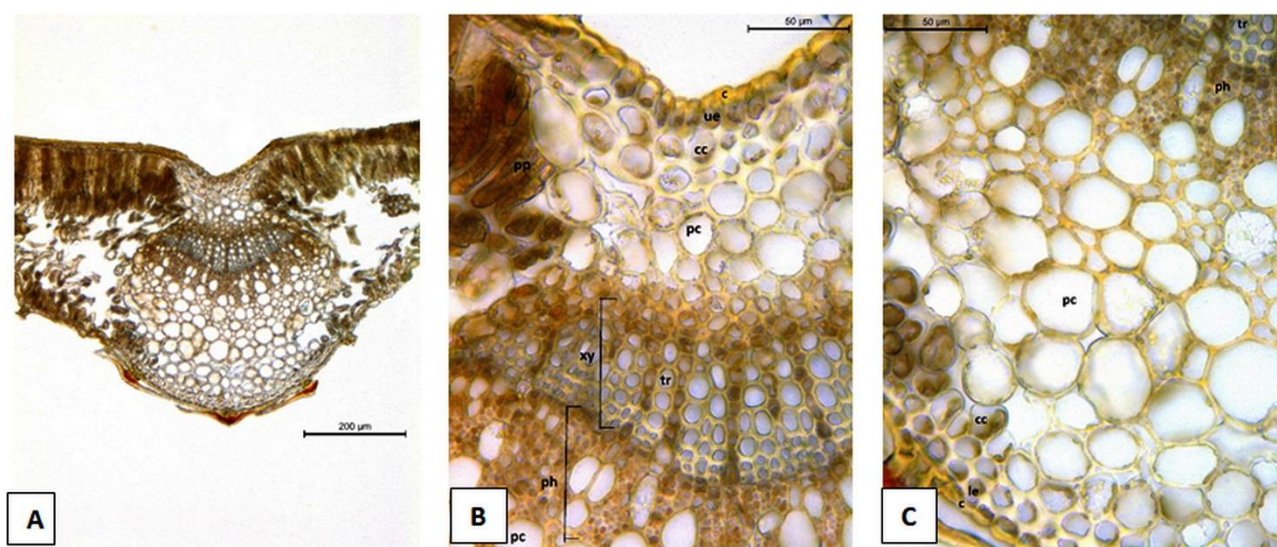


Figure 2. A: General anatomical view of *H. rhamnoides*, B and C: Cross-section of leaf from upper to lower (c: cuticle, ue: upper epiderma, cc: chlorenchymal cell, pc: parenchyma cell, pp: palisade parenchyma, xy: xylem, tr: trachae, ph: phloem, le: lower epiderma)

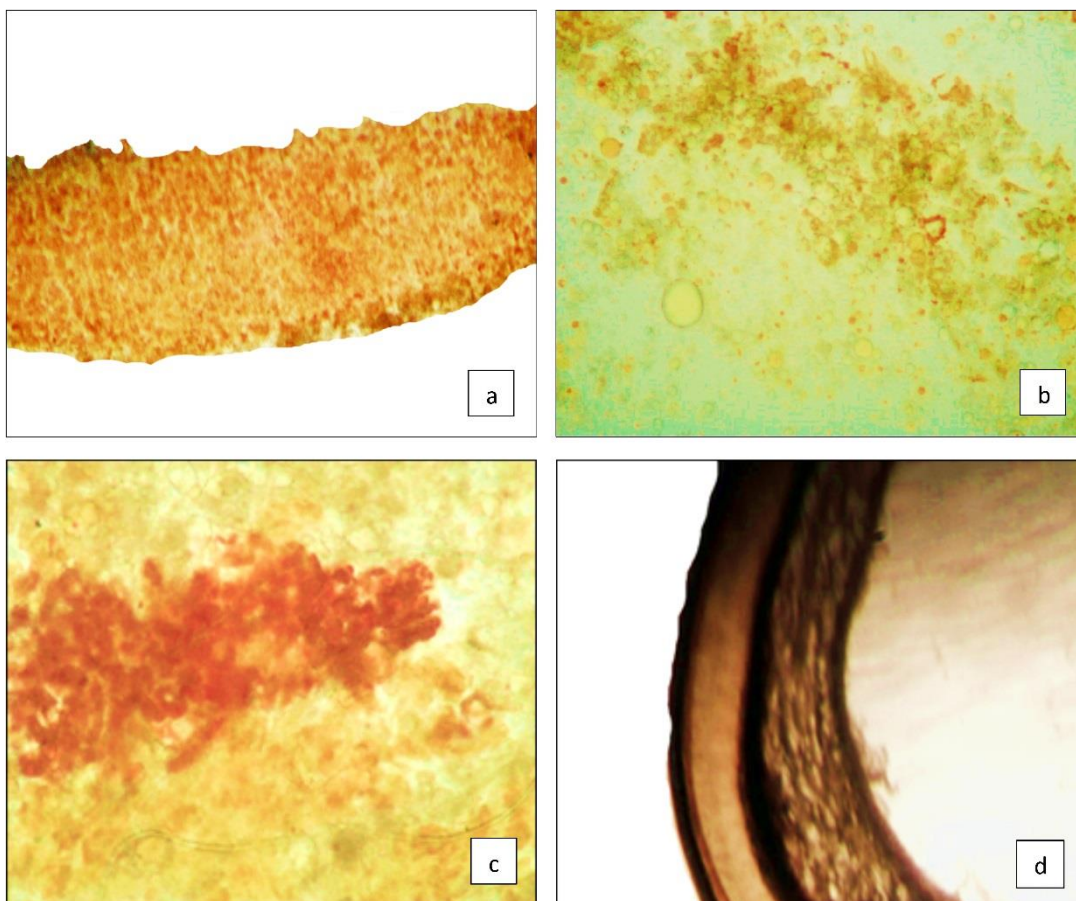


Figure 4. The fruits of *E. rhamnoides* (a: the epidermis of the fetus; b: drops of sea buckthorn fruit oil; c: inner layer - the pulp of the fetus; d: cross section of the peel of the seed)
[with 10x / 0.25 lens and EW factor 10x / 20]

EFEITO DO ESTRESSE INDUZIDO POR HORMÔNIOS NO COAGULOGRAMA DE CARPA (*CYPRINUS CARPIO*)**EFFECT OF HORMONE-INDUCED STRESS ON CARP (*CYPRINUS CARPIO*) COAGULOGRAM****ВЛИЯНИЕ ГОРМОНИНДУЦИРОВАННОГО СТРЕССА НА КОАГУЛОГРАММУ КАРПА (*CYPRINUS CARPIO*)**BEREZINA, Daria I.^{1*}; FOMINA, Lyubov L.²¹ Vologda State Dairy Farming Academy named after N.V. Vereshchagin, "Aquabiocenter", Department of Veterinary Medicine and Biotechnology. Russia.² Vologda State Dairy Farming Academy named after N.V. Vereshchagin, Department of Veterinary Medicine and Biotechnology. Russia.

* Corresponding author

e-mail: berezina.daria@inbox.ru

Received 16 June 2020; received in revised form 10 August 2020; accepted 18 August 2020

RESUMO

A carpa (*Cyprinidae*) é uma das espécies de peixes dominantes e mais valiosas em termos de piscicultura. Em condições de cultivo de alta intensidade, os peixes são sistematicamente expostos a fatores extremos que causam reações de estresse que são acompanhadas por mudanças no estado funcional dos sistemas de defesa do organismo e exercem impacto principalmente nos parâmetros hematológicos. O sistema hemostático é um desses sistemas de defesa, que neutraliza o sangramento por meio de um mecanismo de coagulação. A hemocoagulação segue o mesmo padrão em todos os vertebrados, de peixes sem mandíbula a mamíferos, e representa uma adaptação ancestral dos animais a condições estressantes, frequentemente associada à perda de sangue na natureza. O objetivo desta pesquisa foi estudar o efeito do estresse induzido por hormônios na hemostasia plasmática (secundária) em peixes. Dada a fragmentação dos dados e diferenças na metodologia e condições, a falta de padronização no estudo da hemostasia em peixes, especialmente em condições críticas, esse problema permanece não totalmente divulgado na ciência global. O artigo apresenta os resultados do estudo dos parâmetros do coagulograma da carpa (*Cyprinus carpio*) sob a influência de respostas de estresse agudo e crônico simulados por injeções de análogos de cortisol sintético (dexametasona para estresse de curto prazo e betametasona para estresse crônico) durante 21 dias. A dinâmica desses indicadores foi analisada em comparação com peixes intactos. Foi estabelecido que, ao acelerar o tempo de tromboplastina parcial ativada, tempo de protrombina e ao aumentar a quantidade de fibrinogênio no sangue de peixes, os processos de coagulação do sangue foram claramente acelerados em todos os grupos de animais testados até o último dia do experimento. A dinâmica de outros parâmetros, como o conteúdo dos complexos monoméricos de fibrina solúveis ou o conteúdo da antitrombina III, indicou o desenvolvimento simultâneo de processos de hipercoagulação em alguns grupos. Suposições foram feitas para explicar o padrão de mudanças observadas não apenas em peixes tratados, mas também em animais de controle.

Palavras-chave: coagulação, hemostasia, cortisol.**ABSTRACT**

Carp (*Cyprinidae*) is one of the dominating and most valuable fish species in fish farming. Under conditions of high-intensity cultivation, fish are systematically exposed to extreme factors that cause stress reactions, accompanied by changes in the functional state of the defense of the body systems and exert impact, primarily, on hematological parameters. The hemostatic system is one such defense systems, which counteracts bleeding through a coagulation mechanism. Hemocoagulation follows the same pattern in all vertebrates, from jawless fish to mammals, and represents an ancient adaptation of animals to stressful conditions, often associated with blood loss in nature. This research aimed to study the effect of hormone-induced stress on plasma (secondary) hemostasis in fish. Given the data fragmentation and differences in methodology and conditions, the lack of standardization in studying hemostasis in fish, especially in critical conditions, this problem remains not fully disclosed in global science. The article presents the results of studying carp (*Cyprinus carpio*) coagulogram parameters under the influence of acute and chronic stress responses, simulated by injections of synthetic cortisol

analogues (dexamethasone for short-term stress, and betamethasone for chronic stress) during 21 days. The dynamics of these indicators were analyzed in comparison to intact fish. It has been established that by accelerating the activated partial thromboplastin time, prothrombin time, and increasing the amount of fibrinogen in the blood of fish, blood coagulation processes were clearly accelerated in all groups of animals tested by the last day of the experiment. The dynamics of other parameters, such as the content of soluble fibrin monomer complexes or antithrombin III content, indicated the simultaneous development of hypercoagulation processes in some groups. Assumptions have been made to explain the pattern of changes observed not only in treated fish but also in control animals.

Keywords: *coagulation, hemostasis, cortisol.*

АННОТАЦИЯ

Карп (*Cyprinidae*) является одним из доминирующих и наиболее ценных видов рыб с точки зрения рыбоводства. В условиях высокоинтенсивного выращивания рыба систематически подвергается воздействию экстремальных факторов, вызывающих стрессовые реакции, которые сопровождаются изменением функционального состояния систем защиты организма и оказывают влияние, прежде всего, на гематологические параметры. Одной из таких систем защиты является гемостатическая система, противодействующая кровотечениям через механизм коагуляции. Гемокоагуляция проходит по одной и той же схеме у всех позвоночных животных, от безчелюстных рыб до млекопитающих, и представляет собой древнюю адаптацию животных к стрессовым условиям, часто связанным с кровопотерей в природе. Целью данного исследования было изучение влияния гормонального стресса на плазменный (вторичный) гемостаз у рыб. Учитывая фрагментацию данных и различия в методологии и условиях, отсутствие стандартизации при изучении гемостаза у рыб, особенно в критических условиях, эта проблема остается не до конца раскрытой в мировой науке. В статье представлены результаты исследования параметров коагулограммы карпа (*Cyprinus carpio*) под влиянием острой и хронической стрессовых реакций, симитированные синтетическими аналогами кортизола в течение 21 дня. Проанализирована динамика этих показателей в сравнении с интактными рыбами. Установлено, что за счет ускорения активированного частичного тромбопластинового времени, протромбинового времени и увеличения количества фибриногена в крови рыб к последнему дню эксперимента процессы свертывания крови явно ускоряются у всех групп животных, участвующих в опыте. Динамика других параметров, таких, как содержание растворимых фибрин-мономерных комплексов или содержание антитромбина III, говорят об одновременном развитии гипокоагуляционных процессов у некоторых групп. Были высказаны предположения, призванные объяснить картину изменений, наблюдаемую не только у обработанных рыб, но и у контрольных животных.

Ключевые слова: *коагуляции, гемостаз, кортизол.*

1. INTRODUCTION:

As one of the dominant *Cyprinidae* species, *C. carpio* (common carp) is cultivated in more than 100 countries around the world and accounts for up to 10% of the world's annual freshwater aquaculture production (Xu *et al.*, 2014). *C. carpio* is also an important species of ornamental fish; they are an object of contemporary veterinary medicine, which has recently entered a new stage in the development of surgical care for these animals. These fish are readily available and suitable for carrying out hemostasiological studies, in contrast to species of more value or smaller size, since such studies involve sampling large volumes of biomaterial. Routine hematological examinations in fish require 0.5-1 ml of blood with preservation of the fish life (Blaxhall and Daisley, 1973), while for the coagulogram studies (without conducting morphological and biochemical blood tests), 5-9

ml are required according to medical techniques (Momot, 2006). Carp contains 5.08 ml circulating blood per 100 g of body weight (Itazawa, Takeda, Yamamoto, and Azuma, 1983). In contrast, this amount varies in some other cultured fish: 2.8-3.5 ml/100 g in trout, 1.8 ml/100 g in catfish (Conte, Wagner, and Harris, 1963).

The hemostatic system that coagulates the blood and regulates its aggregation state in the bloodstream is of considerable interest from the veterinary, medical, and evolutionary viewpoints. The hemostatic system is designed to ensure the integrity of the internal environment of the body and stop bleeding in case of damage to the vascular wall, its permeability and resistance, and to maintain the liquid state of the blood in the vascular bed. Studies conducted on Teleostei indicate that the coagulation process is fundamentally similar to other vertebrates, particularly mammals (Kudryashov, 1975; Jagadeeswaran, Gregory, Day, Cykowski, and

Thattaliyath, 2005), the only difference is in its being adapted to lower temperatures. And the enzymes involved in coagulation can work on a broader temperature range than in hematothermal species (Botyazhova, 2000).

The dynamics and influence of endogenous cortisol in stress responses resulting from hypoxia (Prychepa, 2015), intoxication (Gluth and Hanke, 1984, 1985; Romanenko, Potrokhov, and Zinkovsky, 2010), temperature disturbances (Chen, Sun, Tsai, Song, and Chang, 2002; Strange, Schreck, and Golden, 1977), catching (Pottinger, 1998; Ruane, Huisman, and Komen, 2001), increased stocking density (Ruane, Carballo, and Komen, 2002) and even transportation (Möck and Peters, 1990) have been well studied in fish. As is known, an enhanced content of this hormone causes destabilization in the state of cellular and humoral factors of immunity, and depletion of the immune system (Mikryakov, 2004; Tort, 2011). Besides, it was noted that hemostatic mechanisms were triggered in fish exposed to endogenous cortisol impact induced by acute and chronic hypoxia (Berezina, 2020). This effect was previously confirmed by other authors who studied the coagulation time, platelet count, fibrinogen level (Bouck and Ball, 1966; Hattingh and Van Pletzen, 1974) and activated partial thromboplastin time (APTT) (Fujikata and Ikeda, 1985) in stressed fish. Some of them noted that the clotting time is advantageous as an indicator of stress (Tavares-Dias and Oliveira, 2009; Casillas and Smith, 1977; Barton and Iwama, 1991), although they concluded that hypercoagulation is likely to be associated with increased platelet count in the blood (Casillas and Smith, 1977; Wedemeyer *et al.*, 1976; Hunn *et al.*, 1992) and activation of the vascular- thrombocytic link of hemostasis caused by the production of catecholamines and corticosteroids during stress.

It is assumed that interspecies differences in blood coagulation in captured fish might well be the result of differences in the stress resistance of these fish (Ivanov, 2011). An experience was obtained in simulating stress responses with dexamethasone phosphate in carps (Balabanova, Mikryakov, and Mikryakov, 2009), as well as other synthetic corticosteroids (Houghton and Matthews, 1986; Roth, 1972) in freshwater fish, which resulted in marked processes of immune depression comparable to the endogenous cortisol effect. Information on the influence of synthetic corticosteroid analogs on fish blood coagulation is currently not available in the literature. Therefore, it seems relevant to compare

the exogenous and endogenous cortisol effects on the plasma-coagulation hemostasis unit.

Therefore, this study aimed to assess changes in the functional state of secondary hemostasis in fish under the impact of hormone-induced stress.

2. MATERIALS AND METHODS:

2.1. Ethics

The research was conducted in strict accordance with ethical principles established by the European Convention on the protection of the Vertebrata used for experimental and other scientific purposes (adopted in Strasbourg on March 18, 1986, and confirmed in Strasbourg in June 15, 2006) and approved by the local Ethics Committee of the Vologda State Dairy Farming Academy named after N.V. Vereshchagin (Record No. 12 dated December 3, 2015).

2.2. Animals and groups of study

The research was carried out in the Aquabiocenter, aquaculture development center, the Vologda State Dairy Farming Academy. The experiment involved 24 *Cyprinus carpio* L., grown in the Diana fishery (Kaduy village, the Vologda Region), which were previously divided into three groups (n=8 to each group): the first experimental group that underwent hormonal induction of acute stress; the second experimental group with the induced chronic stress, and the control group, which remained intact (Table 1).

According to Mead's resource equation (Van Zutphen, Baumans, and Beynen, 2001), and the local "Guidelines for the development of water quality standards for water bodies of fishery importance" (Registered in the Ministry of Justice of Russia on 03.09.2009 under N 14702), this number of animals (n=8) was considered appropriate for the research (6-10 individuals) and statistically relevant.

2.3. Procedures

Dexamethasone phosphate (4 mg/ml) was used as a hormonal drug simulating acute stress (Balabanova *et al.*, 2009) and metabolizing within four hours. This synthetic hormone is an analog of natural cortisone. Betamethasone suspension (2.63 mg of betamethasone sodium phosphate + 6.43 mg of betamethasone dipropionate/ml) was used as a hormonal drug simulating chronic stress; its run-out period took more than ten days.

Fish of the first experimental group were treated with dexamethasone phosphate (Ellara, Russia) by parenteral injection at a dose of 0.2 ml or 0.8 mg of the dexamethasone phosphate active substance per individual. Fish of the second experimental group were injected with Diprospan (Schering-Plow Labo N.V., Belgium) at a dose of 0.5 ml per individual, which corresponded to 3.5 mg of the active substance.

The fish were kept in an experimental setup providing continuous water circulation between the aquariums and forced aeration at a water temperature of 18–20°C; feeding schedule implied feeding fish once a day with granulated feed. Before blood collection, the fish were anesthetized by adding clove oil to the water at a dose of 0.033 ml/l (Hamackova, Kouril, Kozak, and Stupka, 2006), followed by holding for 15 minutes. Blood was collected with a syringe from the caudal artery into glass tubes containing 3.8% sodium citrate solution, and into glass tubes with a coagulation activator. Blood sampling in animals participating in the experiment was performed immediately after acclimatization, and then 7, 14 and 21 days after injection of drugs (Balabanova *et al.*, 2009).

The plasma coagulation hemostasis parameters were determined on a Thrombostat coagulometer manufactured by Behnk Elektronik (Germany). To assess the state of plasma coagulation hemostasis, the following parameters were determined: APTT, prothrombin time (PT), and TT (thrombin time) using human thrombin, and quantitative analysis of fibrinogen (Fomina, Kulakova, and Berezina, 2017). The anticoagulant properties of blood were evaluated by the content of Antithrombin III in plasma. Plasma fibrinolytic activity was measured by detecting soluble fibrin monomer complexes (SFMC) in O-phenanthroline test (plate version).

2.4. Statistics

The obtained results are presented in the form of the mean value and the standard error of the mean ($M \pm m$). The statistical significance of carp coagulogram indicators for multiple independent samples was determined using the Kruskal-Wallis test, and the Wilcoxon test was used for paired dependent samples. The research results with a value of the alpha error probability being equal to or less than 5% ($p < 0.05$) were considered statistically significant. The difference between the two indicators was considered significant if it was equal to or exceeded its average error of difference by two or more times.

Also, the statistical criteria (the Kruskal–Wallis H test, which is a generalization of the Mann-Whitney U-test, and the Wilcoxon test) used in this research allowed the authors to conduct statistical analysis on small ($n \geq 3$) samples.

3. RESULTS AND DISCUSSION:

The coagulogram data presented in Tables 2-4. APTT characterizes the first phase of blood clotting (prothrombinase formation) and is responsible for the internal path of hemocoagulation. The research results show that the APTT changed significantly in all groups: synchronously and unidirectionally toward the decrease compared to baseline (Figures 1-3). No differences between the control and experimental groups were marked at the beginning of the experiment. Thus, the degree of influence of coagulation factors on thrombus formation increased with the experiment days, which indicates the acceleration of blood coagulation (hypercoagulation).

The intensity of the external coagulation pathway, which is predominant for fish (Berezina *et al.*, 2017, Doolittle and Surgenor, 1962), is indicated by the PT that characterizes the first and second phases of coagulation. After analyzing the data obtained, we should note a gradual reduction of this time by the last day of exposure to hormone-induced stress in all fish groups. While the nature of changes in each group was different: in the control (significantly) and the second experimental groups, the changes had a stepped shape (Figures 1 and 3) in fish with simulated acute stress, the changes were smoother (Figure 2). The PT shortening also indicates the activation of the external link of hemostasis and hypercoagulation, which may be conditioned by corticosteroid effects. For example, it was shown in the experiments on the effects of stress on hemocoagulation involving mice (Polidanov, Skorokhod, and Babichenko, 2020).

In the same publication, the authors noted a stress-induced increase in plasma fibrinogen levels, this also proved to be true for fish as we showed earlier (Berezina and Fomina, 2018). Quantitative characteristics of fibrinogen, together with TT, characterize the third phase of blood coagulation (fibrin formation). The amount of this protein in the blood plasma increased in animals of all groups during the experiment, as stated above. The curve of changes in the first and second experimental groups of animals (Figures 2 and 3) treated with hormones has a similar shape, in contrast to the control group (Figure 1).

Fibrinogen is an important functional indicator of the plasma hemostasis system, providing the formation of a clot, and its increase indicates the activation of coagulation.

The TT is an equally significant indicator that reflects the rate of fibrinogen conversion to fibrin. Its analysis in dynamics indicates that in the control group (Figure 1) and the first experimental group (Figure 2) the TT underwent a peak increase in its duration on the 14th day of the research, and by the 21st day it showed a similar sharp decrease. In the 2nd experimental group of fish exposed to long-acting hormones, on the contrary, the TT sharply decreased by the 14th day and then remained at a level below the initial one (Figure 3). A sharp increase in the TT means a high risk of developing coagulopathies toward hypocoagulation, while its reduction indicates a tendency toward hypercoagulation and thrombosis. Both processes undoubtedly lead to disturbances in the body homeostasis.

Antithrombin III exerts a major depressant (anticoagulant) effect on blood clotting processes. The level of this anticoagulant factor changed significantly: more sharply in the fish of the control group (Figure 1), more smoothly toward the decrease in the 1st experimental group (Figure 2), which may be associated with blood sampling or with increased demand in compensatory processes of hemostasis because of hypercoagulation. The content of AT III in fish of the second experimental group also changed significantly over time, but eventually exceeded the initial level (Figure 3). Excess of antithrombin III in blood plasma indicates hypocoagulation processes in the plasma coagulation unit.

The amount of SFMCs, which are thrombinemia markers in intravascular coagulation in humans, still remains quite high in fish compared to most mammals, which is consistent with previous studies (Berezina *et al.*, 2017). In the experiment, the same significant fluctuations of fibrin-monomer complexes with a tendency to decrease could be observed in the control and experimental groups. The SFMC concentration decreased more smoothly in the second experimental group (Figure 3). The mechanism for increasing the number of fibrin monomer complexes implied creating a large amount of SFMC during the activation of coagulation processes and increased thrombin content. And if the coagulation processes accelerated by the end of the experiment, it can be assumed that this indicator should increase. However, the quantitative characterization of SFMCs in the blood of fish and their role in the

physiology of aquatic organisms has not yet been described in the literature. Therefore, any conclusions in this regard should be made with caution.

4. CONCLUSIONS:

It should be noted that changes in the coagulogram, such as APTT reduction, increased fibrinogen level, shortened PT and TT, indicate a change in the tendency for blood to clot toward its acceleration during the experiment, not only in treated fish, but also in the control group. At the same time, a reduced concentration of SFMC may theoretically indicate hypocoagulable state. Other parameters did not change similarly in all groups, for example, AT III increased in 2nd experimental group. However, it should be highlighted that the form of the above changes between groups often differed greatly from each other.

While considering the results of the data analysis from control animals, not subjected to artificial hormonal exposure, the hypercoagulation effect may be associated with the strong short-term stress caused by handling, even in anesthetized fish. In any case, at this stage the coagulogram response to the acute and chronic action of exogenous cortisol during the days of the experiment was similar in its vector to that of intact fish. As a result, it can be concluded about a weak effect of synthetic hormones, and either insignificant or missing plasma coagulation factors to hormone-induced stress.

However, these findings require refinement and further research to describe the impact of corticosteroid treatment on plasma endogenous cortisol levels and related effects and investigate the response force of synthetic cortisol analogs on the hemostasis system compared to natural stress responses.

5. ACKNOWLEDGMENTS:

The reported study was funded by RFBR, Project Number 19-34-90109.

6. REFERENCES:

1. Balabanova, L.V., Mikryakov, D.V. and Mikryakov, V.R. (2009). Cyprinus carpio leukocyte response to hormone-induced stress. *Biology of Inland Waters*, 1, 91-93.
2. Barton, B.A. and Iwama, G.K. (1991). Physiological changes in fish from stress in aquaculture with emphasis on the

- response and effects of corticosteroids. *Annual Review of Fish Diseases*, 1, 3-26.
3. Berezina, D.I. (2020). The effect of stress on the coagulation and immunological functions of the blood in carps. In *Achievements of young scientists in the development of organic agriculture: Proceedings of the international scientific-practical conference* (pp. 8-11). Horki, Belarus: Belarusian State Agricultural Academy Press.
 4. Berezina, D.I. and Fomina, L.L. (2018). Dynamics of the level of stress-induced fibrinogen in the blood of fish. *Dairy Farming Bulletin*, 3(31), 8-15.
 5. Berezina, D.I., Vaitzel, L.L. and Fomina, L.L. (2017). Comparative physiological aspects of the hemostatic system in fish. Evolutionary and environmental aspects of the study of living matter. In *Proceedings of the 1st All-Russian Scientific Conference* (pp. 38-43). Cherepovets, Russia: Cherepovets State University Press.
 6. Blaxhall, P.C. and Daisley, K.W. (1973). Routine haematological methods for use with fish blood. *Journal of Fish Biology*, 5(6), 771-781.
 7. Botyazhova, O.A. (2000). *Physiology of the blood system: comparative, ecological and evolutionary aspects*. Yaroslavl, Russia: Yaroslavl State University Press.
 8. Bouck, G. R., and Ball, R. C. (1966). Influence of capture methods on blood characteristics and mortality in the rainbow trout (*Salmo gairdneri*). *Transactions of the American Fisheries Society*, 95(2), 170-176.
 9. Casillas, E., and Smith, L. S. (1977). Effect of stress on blood coagulation and haematology in rainbow trout (*Salmo gairdneri*). *Journal of Fish Biology*, 10(5), 481-491.
 10. Chen, W.H., Sun, L.T., Tsai, C.L., Song, Y.L. and Chang, C.F. (2002). Cold-stress induced the modulation of catecholamines, cortisol, immunoglobulin M, and leukocyte phagocytosis in tilapia. *General and Comparative Endocrinology*, 126(1), 90-100.
 11. Conte, F.P., Wagner, H.H. and Harris, T.O. (1963). Measurement of blood volume in the fish (*Salmo gairdneri gairdneri*). *American Journal of Physiology-Legacy Content*, 205(3), 533-540.
 12. Doolittle, R.F. and Surgenor, D.M. (1962). Blood coagulation in fish. *American Journal of Physiology*, 203(5), 964-970.
 13. Fomina, L.L., Kulakova, T.S. and Berezina, D.I. (2017). Determination of plasma-coagulation unit activity of fish hemostasis system by clotting methods using the coagulometer. *Actual Questions of Veterinary Biology*, 3(35), 54-58.
 14. Fujikata, A. and Ikeda, Y. (1985). Effect of handling on blood coagulation in carp. *Nippon Suisan Gakkaishi*, 51(7), 1093-1096.
 15. Gluth, G. and Hanke, W. (1984). A comparison of physiological changes in carp, *Cyprinus carpio*, induced by several pollutants at sublethal concentration—II. The dependency on the temperature. *Comparative Biochemistry and Physiology - Part C: Comparative Pharmacology*, 79(1), 39-45.
 16. Gluth, G. and Hanke, W. (1985). A comparison of physiological changes in carp, *Cyprinus carpio*, induced by several pollutants at sublethal concentrations: I. The dependency on exposure time. *Ecotoxicology and Environmental Safety*, 9(2), 179-188.
 17. Hamackova, J., Kouril, J., Kozak, P. and Stupka, Z. (2006). Clove oil as an anaesthetic for different freshwater fish species. *Bulgarian Journal of Agricultural Science*, 12(2), 185-194.
 18. Hattingh, J., and Van Pletzen, A. J. J. (1974). The influence of capture and transportation on some blood parameters of fresh water fish. *Comparative Biochemistry and Physiology Part A: Physiology*, 49(3), 607-609.
 19. Houghton, G. and Matthews, R.A. (1986). Immunosuppression of carp (*Cyprinus*

- carpio L.) to ichthyophthiriasis using the corticosteroid triamcinolone acetonide. *Veterinary Immunology and Immunopathology*, 12(1-4), 413-419.
20. Hunn, J.B., Wiedmeyer, R.H., Greer, I.E. and Grady, A.W. (1992). Communications: blood chemistry of laboratory-reared golden trout. *Journal of Aquatic Animal Health*, 4(3), 218-222.
 21. Itazawa, Y., Takeda, T., Yamamoto, K.I. and Azuma, T. (1983). Determination of circulating blood volume in three teleosts, carp, yellowtail and porgy. *Japanese Journal of Ichthyology*, 30(1), 94-101.
 22. Ivanov, A.A. (2011). *Fish physiology*. St. Petersburg, Russia: Lan.
 23. Jagadeeswaran, P., Gregory, M., Day, K., Cykowski, M. and Thattaliyath, B. (2005). Zebrafish: a genetic model for hemostasis and thrombosis. *Thrombosis and Haemostasis*, 3(1), 46-53.
 24. Kudryashov, B.A. (1975). *Biological problems of regulation of the blood liquid state and coagulation*. Moscow, Russia: Medicine.
 25. Mikryakov, D.V. (2004). *The effect of certain corticosteroid hormones on the structure and function of the immune system of fish*. Moscow, Russia.
 26. Momot, A.P. (2006). *Pathology of hemostasis: principles and algorithms for clinical laboratory diagnostics*. St. Petersburg, Russia: Format.
 27. Möck, A. and Peters, G. (1990). Lysozyme activity in rainbow trout, *Oncorhynchus mykiss* (Walbaum), stressed by handling, transport and water pollution. *Journal of Fish Biology*, 37(6), 873-885.
 28. Polidanov, M.A., Skorokhod, A.A. and Babichenko, N.E. (2020). Reactivity and stress: hemostatic reactivity of a body under stress. Investigation of the effect of stress on hemocoagulation. *Modern Science*, 3-1, 308-312.
 29. Pottinger, T.G. (1998). Changes in blood cortisol, glucose and lactate in carp retained in anglers' keepnets. *Journal of Fish Biology*, 53(4), 728-742.
 30. Prychepa, M.V. (2015). Cortisol content in the tissues of ruff and pike perch under different wintering conditions. *Scientific Notes of Ternopil National Pedagogical University named after Volodymyr Hnatyuk. Series: Biology*, 3/4(64), 547-550.
 31. Romanenko, V.D., Potrokhov, A.S. and Zinkovsky, O.G. (2010). The hormonal mechanism for energy supply of fish adaptation to the effects of mineral nitrogen. *Hydrobiological Journal*, 46(6), 58-66.
 32. Roth, R.R. (1972). Some factors contributing to the development of fungus infection in freshwater fish. *Journal of Wildlife Diseases*, 8(1), 24-28.
 33. Ruane, N.M., Carballo, E.C. and Komen, J. (2002). Increased stocking density influences the acute physiological stress response of common carp *Cyprinus carpio* (L.). *Aquaculture Research*, 33(10), 777-784.
 34. Ruane, N.M., Huisman, E.A. and Komen, J. (2001). Plasma cortisol and metabolite level profiles in two isogenic strains of common carp during confinement. *Journal of Fish Biology*, 59(1), 1-12.
 35. Strange, R.J., Schreck, C.B. and Golden, J.T. (1977). Corticoid stress responses to handling and temperature in salmonids. *Transactions of the American Fisheries Society*, 106(3), 213-218.
 36. Tavares-Dias, M. and Oliveira, S.R. (2009). A review of the blood coagulation system of fish. *Revista Brasileira de Biociências*, 7, 205-224.
 37. Tort, L. (2011). Stress and immune modulation in fish. *Developmental and Comparative Immunology*, 35(12), 1366-1375.
 38. Van Zutphen, L.F., Baumans, V. and Beynen, A.C. (2001). *Principles of laboratory animal science*. Amsterdam, Netherlands: Elsevier.
 39. Wedemeyer, G.A., Meyer, F.P. and Smith,

L. (1976). *Environmental stress and fish diseases*. Neptune City, NJ: T.F.H. Publications.

40. Xu, P., Zhang, X., Wang, X., Li, J., Liu, G., Kuang, Y., Xu, J., Zheng, X., Ren, L., Wang, G., Zhang, Y., Huo, L., Zhao, Z., Cao, D., Lu, C., Li, C., Zhou, Y., Liu, Z., Fan, Z., Shan, G., Li, X., Wu, S., Song, L., Hou, G., Jiang, Y., Jeney, Z., Yu, D., Wang, L., Shao, C., Song, L., Sun, J., Ji, P., Wang, J., Li, Q., Xu, L., Sun, F., Feng, J., Wang, C., Wang, S., Wang, B., Li, Y., Zhu, Y., Xue, W., Zhao, L., Wang, J., Gu, Y., Lv, W., Wu, K., Xiao, J., Wu, J., Zhang, Z., Yu, J. and Sun, X. (2014). Genome sequence and genetic diversity of the common carp, *Cyprinus carpio*. *Nature Genetics*, 46(11), 1212-1219.

Table 1. Distribution of the experimental groups.

Group	Description	Number of animals
Control group	Intact fish	8
1 st experimental group	Hormonal induction of acute stress	8
2 nd experimental group	Induced chronic stress	8
Total		24

Table 2. Coagulogram dynamics in fish after the 7th day. Source: the authors

Indicator	Prior to treatment			7 th day		
	Control group (n=8)	1 st experimental group (n=8)	2 nd experimental group (n=8)	Control group (n=8)	1 st experimental group (n=8)	2 nd experimental group (n=8)
1	2	3	4	5	6	7
TT, sec	128,43±10,38*	157,85±24,17 ^a	221,29±33,37 ^{bc}	144,9±20,4 ^c	128,75±19,98 ^b	184,58±39,30 ^b
PT, sec	296,88±101,59 ^{abc}	211,93±60,56	249,5±116,93	160,75±16,45 ^c	157,18±18,59*	257,10±69,11 ^{bc}
APTT, sec	27,05±1,06 ^{abc}	20,85±2,63 ^{abc}	25,35±4,93 ^{abc}	8,90±0,23 ^{bc}	8,13±0,38* ^b	10,30±0,53 ^{bc}
Fibrinogen, g/l	0,86±0,03 ^{ac}	0,69±0,20 ^{abc}	0,60±0,17 ^{abc}	0,77±0,05* ^{bc}	0,97±0,01	1,06±0,01 ^{bc}
SFMC, mg/100 ml	29,00±0,41 ^{bc}	28,00±0,71* ^{bc}	30,00±0,71 ^{abc}	28,50±0,29 ^{bc}	29,00±0,58 ^{bc}	27,75±1,31
AT III, %	95,54±1,99 ^{abc}	101,38±4,63 ^{abc}	90,57±13,52	65,17±3,91 ^{#b}	78,21±2,91 ^{bc}	76,69±9,08 ^c

The difference from the indicator of the first experimental group on the same day of the experiment is significant (p≤0.05)

*The difference from the indicator of the second experimental group on the same day of the experiment is significant (p≤0.05)

^a The difference from a similar indicator of a similar group on the 7th day of the experiment is significant (p≤0.05)

^b The difference from a similar indicator of a similar group on the 14th day of the experiment is significant (p≤0.05)

^c The difference from a similar indicator of a similar group on the 21st day of the experiment is significant (p≤0.05)

Notes: TT, sec – thrombin time; PT, sec - prothrombin time; APTT, sec - activated partial thromboplastin time; Fibrinogen, g/l – fibrinogen level, SFMC, mg/100 ml – soluble fibrin-monomeric complexes level; AT III, % - antithrombin III level

Table 3. Coagulogram dynamics in fish after the 14th day. Source: the authors

Indicator	Prior to treatment			14 th day		
	Control group (n=8)	1 st experimental group (n=8)	2 nd experimental group (n=8)	Control group (n=8)	1 st experimental group (n=8)	2 nd experimental group (n=8)
1	2	3	4	5	6	7
TT, sec	128,43±10,38*	157,85±24,17 ^a	221,29±33,37 ^{bc}	177,20±27,99 ^c	217,65± 35,54* ^c	107,63± 16,92
PT, sec	296,88±101,59 ^{abc}	211,93±60,56	249,5±116,93	175,10±19,76 ^c	139,03± 13,39	129,60± 7,39
APTT, sec	27,05±1,06 ^{abc}	20,85±2,63 ^{abc}	25,35±4,93 ^{abc}	7,28± 0,24 ^c	6,95± 0,30	7,33± 0,13 ^c
Fibrinogen, g/l	0,86±0,03 ^{ac}	0,69±0,20 ^{abc}	0,60±0,17 ^{abc}	0,85± 0,05* ^c	0,98± 0,02*	1,17± 0,03
SFMC, mg/100 ml	29,00±0,41 ^{bc}	28,00±0,71* ^{bc}	30,00±0,71 ^{abc}	24,25± 2,25	23,25± 1,49*	28,00± 0,00
AT III, %	95,54±1,99 ^{abc}	101,38±4,63 ^{abc}	90,57±13,52	47,66±12,55* ^{bc}	87,80± 2,75	85,01± 4,99 ^c

The difference from the indicator of the first experimental group on the same day of the experiment is significant (p≤0.05)

*The difference from the indicator of the second experimental group on the same day of the experiment is significant (p≤0.05)

^a The difference from a similar indicator of a similar group on the 7th day of the experiment is significant (p≤0.05)

^b The difference from a similar indicator of a similar group on the 14th day of the experiment is significant (p≤0.05)

^c The difference from a similar indicator of a similar group on the 21st day of the experiment is significant (p≤0.05)

Notes: TT, sec – thrombin time; PT, sec - prothrombin time; APTT, sec - activated partial thromboplastin time; Fibrinogen, g/l – fibrinogen level, SFMC, mg/100 ml – soluble fibrin-monomeric complexes level; AT III, % - antithrombin III level

Table 4. Coagulogram dynamics in fish after the 21st day. Source: the authors

Indicator	Prior to treatment			21 st day		
	Control group (n=8)	1 st experimental group (n=8)	2 nd experimental group (n=8)	Control group (n=8)	1 st experimental group (n=8)	2 nd experimental group (n=8)
1	2	3	4	5	6	7
TT, sec	128,43±10,38*	157,85±24,17 ^a	221,29±33,37 ^{bc}	119,70± 25,50	132,23± 30,92	130,33± 14,39
PT, sec	296,88±101,59 ^{abc}	211,93±60,56	249,5±116,93	110,90± 14,81	137,90± 26,45	134,88± 10,24
APTT, sec	27,05±1,06 ^{abc}	20,85±2,63 ^{abc}	25,35±4,93 ^{abc}	7,98± 0,35	7,58± 0,33	8,28± 0,52
Fibrinogen, g/l	0,86±0,03 ^{ac}	0,69±0,20 ^{abc}	0,60±0,17 ^{abc}	0,97± 0,05*	0,99± 0,02*	1,22± 0,03
SFMC, mg/100 ml	29,00±0,41 ^{bc}	28,00±0,71* ^{bc}	30,00±0,71 ^{abc}	25,50± 1,26*	24,25± 1,18*	28,00± 0,00
AT III, %	95,54±1,99 ^{abc}	101,38±4,63 ^{abc}	90,57±13,52	75,64± 10,41*	95,15± 2,83	107,04± 3,67

The difference from the indicator of the first experimental group on the same day of the experiment is significant (p≤0.05)

*The difference from the indicator of the second experimental group on the same day of the experiment is significant (p≤0.05)

^a The difference from a similar indicator of a similar group on the 7th day of the experiment is significant (p≤0.05)

^b The difference from a similar indicator of a similar group on the 14th day of the experiment is significant (p≤0.05)

^c The difference from a similar indicator of a similar group on the 21st day of the experiment is significant (p≤0.05)

Notes: TT, sec – thrombin time; PT, sec - prothrombin time; APTT, sec - activated partial thromboplastin time; Fibrinogen, g/l – fibrinogen level, SFMC, mg/100 ml – soluble fibrin-monomeric complexes level; AT III, % - antithrombin III level

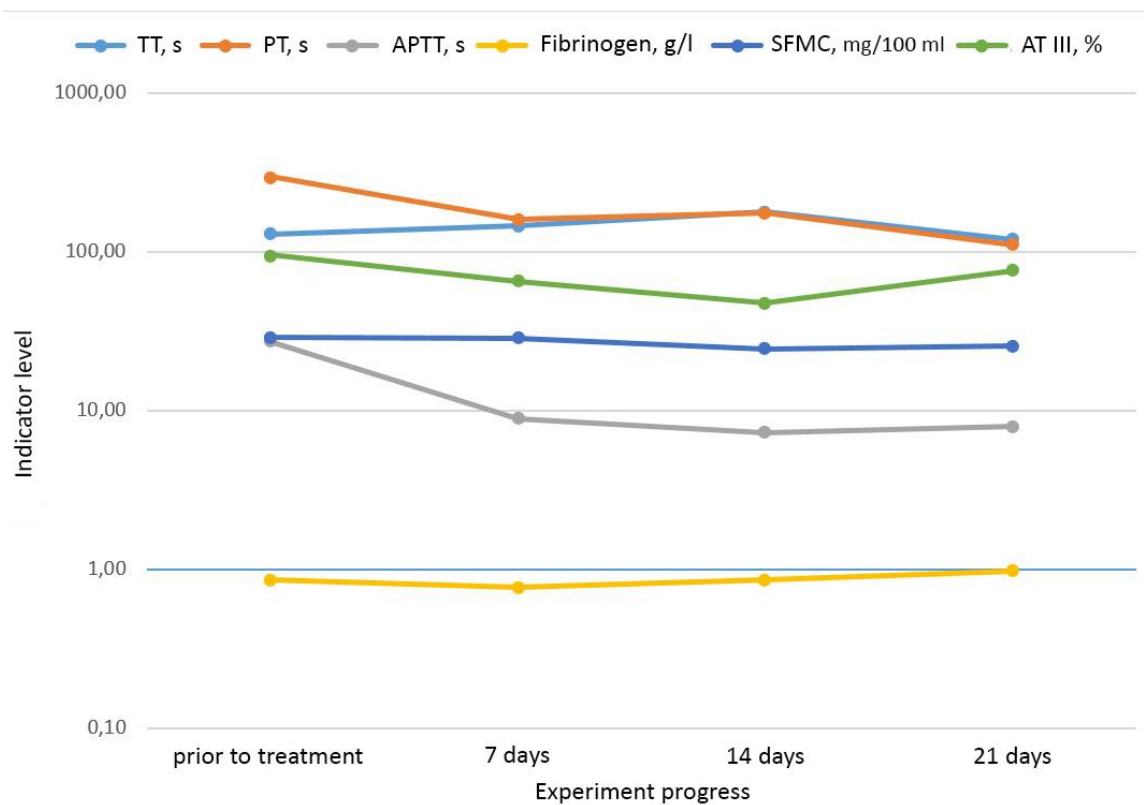


Figure 1. Dynamics of coagulogram indicators in fish of the control group during the experiment. Source: the authors

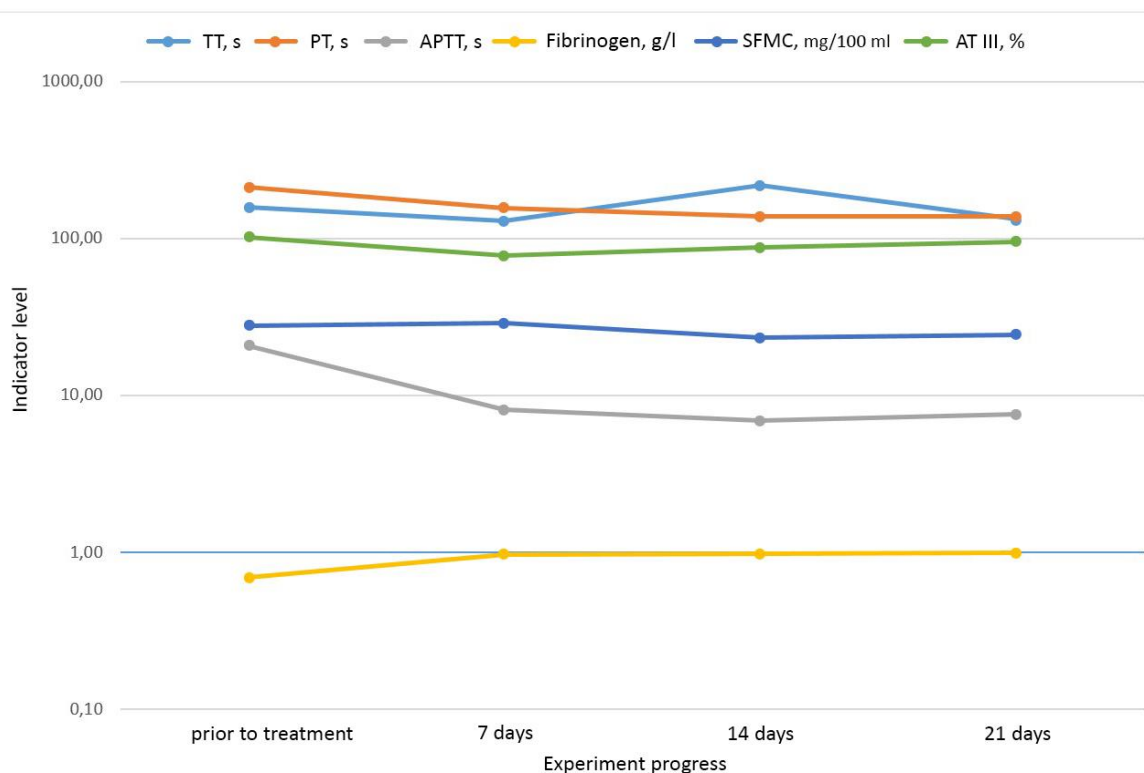


Figure 2. Dynamics of coagulogram indicators in fish of the first experimental group during the experiment. Source: the authors

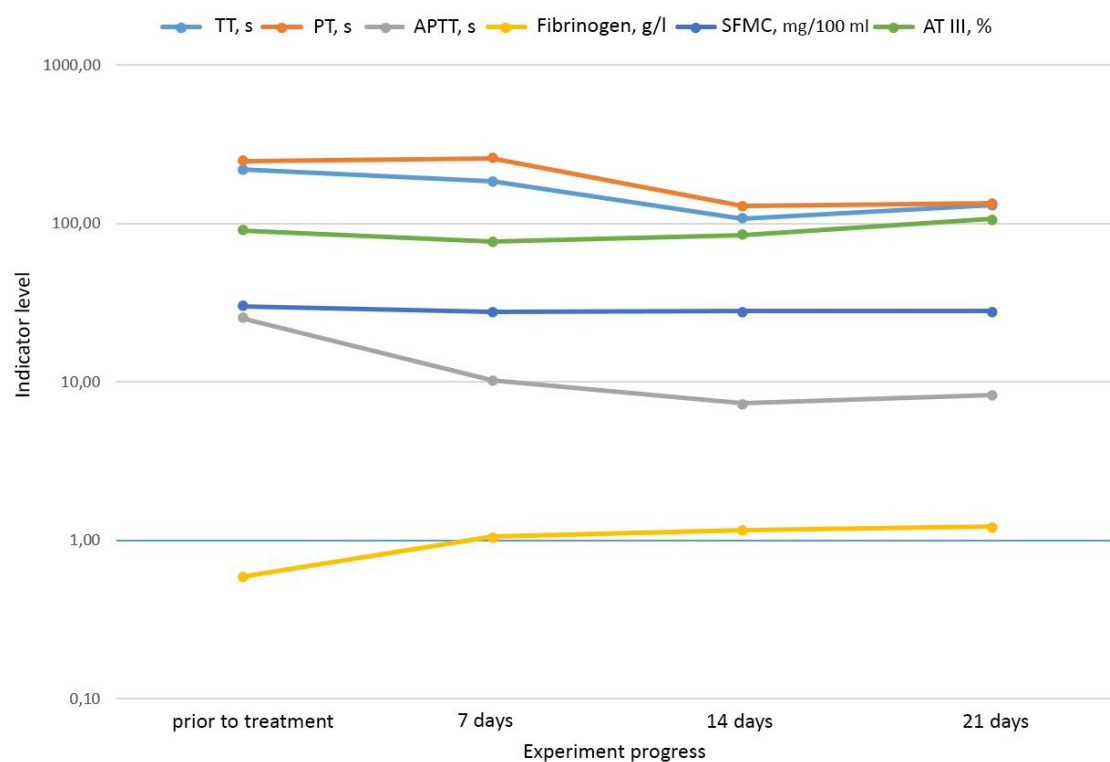


Figure 3. Dynamics of coagulogram indicators in fish of the second experimental group during the experiment. Source: the authors

MONITORAMENTO E CÁLCULO DAS EMISSÕES DE DIÓXIDO DE CARBONO EM BAGDÁ E SEU EFEITO NO AUMENTO DAS TEMPERATURAS DE 2003-2018 USANDO DADOS DE SENSORIAMENTO REMOTO

MONITORING AND CALCULATING THE CARBON DIOXIDE EMISSIONS IN BAGHDAD AND ITS EFFECT ON INCREASING TEMPERATURES FROM 2003-2018 USING REMOTE SENSING DATA

مراقبة وحساب انبعاث غاز الكربون في مدينة بغداد واثره في ارتفاع درجات الحرارة من الفترة 2003-2018 باستخدام بيانات التحسس النائي

JASIM, Mazin Shakir^{1*}; MASHEE, Fouad Kadhum²

¹ Computer Science Department, Almamoon University College, Baghdad, Iraq.

² Remote Sensing Unit, College of Science, College of Science, University of Baghdad, Baghdad, Iraq

* Corresponding author

e-mail: mazin.s.jasim@almamonuc.edu.iq

Received 22 June 2020; received in revised form 09 August 2020; accepted 18 August 2020

RESUMO

A cidade de Bagdá testemunhou uma expansão urbana e industrial com aumento da população, especialmente a partir de 2003. As fontes de poluição do ar se multiplicaram pelo aumento do número de veículos e geradores de energia elétrica causando a emissão de grandes quantidades de gases de hidrocarbonetos, incluindo o dióxido de carbono, CO₂. A emissão desses gases na atmosfera, e em grandes quantidades, certamente terá um papel em contribuir para o aquecimento global. Portanto, terá efeitos negativos proeminentes em influenciar a elevação das temperaturas na cidade. A pesquisa teve como objetivo mostrar o aspecto aplicado das técnicas de sensoriamento remoto e sistemas de informação geográfica na estimativa do CO₂ e sua relação com o balanço térmico para a cidade de Bagdá por meio de quinze estações distribuídas pela cidade. Dados de sensoriamento remoto adotados do *US Geological* e do *European Center*, além de dados de CO₂ para a sonda atmosférica infravermelha (AIRS) de Giovanni para o período prolongado (2003-2018) foram usados. Processamento e análise estatística foram realizados nos dados usando o software GIS 10.6 e Origin 2018. As taxas mensais de CO₂ apresentaram oscilações sazonais entre inverno e verão, sendo o maior valor de CO₂ em julho e o menor valor em fevereiro. A tecnologia *Inverse Distance Weighting* (IDW) foi usada para representar a distribuição espacial das concentrações de CO₂ na cidade. As regiões residenciais e industriais experimentaram concentrações mais altas se comparadas às regiões agrícolas. O coeficiente de correlação de Pearson foi usado para descobrir a relação entre o dióxido de carbono e as temperaturas. O coeficiente de correlação mostrou uma alta relação positiva entre concentrações aumentadas de gás e altas temperaturas para todas as estações de estudo durante todo o período de estudo. Pode-se concluir que a concentração de dióxido de carbono difere localmente nas regiões de Bagdá, como residenciais, comerciais, de trânsito, industriais e rurais, bem como durante os meses do ano.

Palavras-chave: AIRS, ECMWF, concentração de CO₂, Técnicas de Sensoriamento Remoto.

ABSTRACT

The city of Baghdad has witnessed an urban and industrial expansion with an increase in population, especially since 2003. Air pollution sources have multiplied by the increase in the number of vehicles and electricity generators, causing the emission of large quantities of hydrocarbon gases, including carbon dioxide, CO₂. The discharge of such gases into the atmosphere and large amounts, will surely have a role in contributing to global warming. Therefore, it will have prominent adverse effects in influencing the rise in temperatures in the city. The research aimed to show the applied aspect of remote sensing and geographic information systems techniques in estimating the CO₂ and its relationship to thermal balance for Baghdad city through fifteen stations distributed throughout the city. Remote sensing data adopted from US Geological and the European Centre, in addition to CO₂ data for the Atmospheric Infrared sounder (AIRS) from Giovanni for the extended period (2003-2018), were used. Processing and statistical analysis were performed on data using GIS 10.6 and Origin 2018.

software. The monthly rates of CO₂ showed seasonal fluctuations between winter and summer, where the highest value of CO₂ in July and the lowest value in February. Inverse Distance Weighting (IDW) technology was used to represent the spatial distribution of CO₂ concentrations in the city. Residential and industrial regions experienced higher levels compared to agricultural areas. Pearson correlation coefficient was used to find out the relationship between carbon dioxide and temperatures. The correlation coefficient showed a high positive relationship between increased gas concentrations and high temperatures for all study stations over the entire study period. It can be concluded the concentration of carbon dioxide differs locally in regions of Baghdad, such as residential, commercial, traffic, industrial, and rural areas, as well as during the months of the year.

Keywords: AIRS, ECMWF, CO₂ concentrations, Remote Sensing Techniques.

المخلص

شهدت مدينة بغداد توسعاً حضرياً وصناعياً مع زيادة في عدد السكان خاصة منذ عام 2003. حيث تضاعفت مصادر تلوث الهواء بزيادة عدد المركبات ومولدات الكهرباء، مما تسبب في انبعاث كميات كبيرة من الغازات الهيدروكربونية بما في ذلك الكربون ثاني أكسيد، CO₂. إن انبعاث مثل هذه الغازات في الغلاف الجوي، وبكميات كبيرة، سيكون له بالتأكيد دور هام في المساهمة في الاحتباس الحراري. وبالتالي سيكون لها آثار سلبية بارزة في التأثير على ارتفاع درجات الحرارة في المدينة. يهدف البحث الى اظهار الجانب التطبيقي لتقنيات الاستشعار عن بعد ونظم المعلومات الجغرافية في تقدير غاز ثاني اكسيد الكربون وعلاقته بالتوازن الحراري لمدينة بغداد من خلال خمس عشرة محطة موزعة في عموم المدينة. تم استخدام بيانات الاستشعار عن بعد ممثلة بالمركز الجيولوجي الأمريكي والمركز الأوروبي، بالإضافة إلى بيانات CO₂ لمسبار الأشعة تحت الحمراء للغلاف الجوي (AIRS) من جيوفاني للفترة الممتدة (2003-2018). تم إجراء المعالجة والتحليل الإحصائي للبيانات باستخدام برنامج GIS 10.6 و Origin 2018. أظهرت المعدلات الشهرية لثاني أكسيد الكربون تقلبات موسمية بين الشتاء والصيف، حيث بلغت أعلى قيمة لثاني أكسيد الكربون في يوليو وأدنى قيمة في فبراير. تم استخدام تقنية معكوس المسافة الموزون (IDW) لتمثيل التوزيع المكاني لتراكيز ثاني أكسيد الكربون في المدينة. شهدت المناطق السكنية والصناعية مستويات أعلى مقارنة بالمناطق الزراعية. تم استخدام معامل ارتباط بيرسون لمعرفة العلاقة بين ثاني أكسيد الكربون ودرجات الحرارة. أظهر معامل الارتباط علاقة موجبة عالية بين زيادة تركيزات الغاز وارتفاع درجات الحرارة لجميع محطات الدراسة خلال فترة الدراسة بأكملها. وعليه يمكن الاستنتاج ان تركيز ثاني اكسيد الكربون يختلف محليا في مناطق بغداد مثل المناطق السكنية والتجارية والمرورية والصناعية والريفية وكذلك خلال اشهر السنة.

الكلمات المفتاحية: متحسس AIRS، المركز الاوربي للتنبؤات الجوية، تراكيز غاز ثاني اوكسيد الكربون، تقنيات الاستشعار عن بعد

1. INTRODUCTION:

The role of carbon dioxide in the atmosphere and its effect on global temperature is central to the contemporary debate on global warming caused by human activities. Carbon dioxide is a colorless and tasteless gas. It is formed naturally through breathing processes and the natural decomposition of dead bodies and the earth's crust rocks. Also, it can be found in volcanoes. About 40% of the gas released from the volcanoes during the eruption is carbon dioxide; that is, the volcanoes release between 130 and 230 million tons of carbon dioxide into the atmosphere every year (Al-jaf and Al-Taai, 2019).

The seas and oceans contain large amounts of it, as the total of exchanges with the atmosphere annually, up to 100 billion. It also created due to human activities through the burning of fossil fuels, burning, and deforestation and changes in the land-use patterns and other industrial processes. However, carbon dioxide emissions from human activities are about 135 times higher than volcanic emissions (Falkowski *et al.*, 2000). The presence of carbon dioxide in the atmosphere and at high concentrations works to trap heat and prevent it from penetrating through the absorption of infrared radiation. The higher concentration, the higher in temperature, and more climatic and environmental changes, this

phenomenon is known as global warming (Al-Bayati and Al-Salihi, 2019).

Global warming is a natural phenomenon that occurs in any region. However, when there is an exacerbation of this phenomenon from its natural limits, it becomes an environmental problem. The increase in the proportions of some gases in the atmosphere, where the most important of which is carbon dioxide, leads to the temperature rise. The global temperature has increased by about 0.7°C over the past century due to an increase in carbon dioxide (Weinbauer *et al.*, 2011).

Recent readings show a 30% increase in the concentration of carbon dioxide in the atmosphere since the readings began in 1958. The level of this gas in its first measurement reached 315 parts per million, while its concentration exceeded the barrier of 400 parts per million for the first time in 2013. In contrast, the carbon dioxide rate in the atmosphere was about 280 parts per million before the year 1800 (Hashim and Sultan, 2010). Global warming has affected the climate of Iraq, especially in Baghdad, with a significant and noticeable effect on the temperature; according to Iraq meteorological organization, the temperatures in Baghdad have increased significantly in their rates. As a result of the change in the rates of greenhouse gases

resulting from industrial activities, means of transportation, the widespread prevalence and use of diesel generators, and an increase in the population (Al-ramahi, 2020). This increase in temperature affected various natural and environmental phenomena in Iraq by increasing the amount of evaporation from the Tigris and Euphrates water, and this leads to serious ecological problems including drought, desertification and the problem of sand dune encroachment (Hassoon, 2015; AL-Hassany and Hindi, 2016)

This study aimed to monitor carbon dioxide emissions in Baghdad and its impact on increasing temperatures seeking to control it and contribute to reducing global warming by using the Inverse Distance Weighting (IDW) technology provided by the GIS program (Al Nageeb *et al.*, 2020).

2. MATERIALS AND METHODS:

2.1. Study area

Baghdad is the administrative capital of Iraq, and it is considered the largest city in terms of population. According to 2015 statistics, its population reached 8.405.172 million people with a population density of 11614 people per km². The Tigris River divides it into two parts: Karkh and Rusafa, including 288 residential areas. It is located between latitudes (33.10°N) and (32.04°N) and longitude (44.77°E) and (43.29°E), at an altitude of 34 meters above sea level (Jasim *et al.*, 2020).

Baghdad is one of the urban areas with explicit human activity and, after 2003, witnessed significant changes in the areas of land use, random population density, urban and industrial expansion. Also, the increased vehicles and electricity generators led to a diversity of pollution sources, which enhances the increase in carbon dioxide. The climate of Baghdad is characterized by the continental characteristic of being hot dry in summer and cold rainy in winter, according to the Köppen classification, where the highest temperatures in the world were recorded in recent years. Temperatures vary between summer and winter, as the highest monthly average was in July when it reached (36.2) °C. It also recorded the lowest decrease in January, where the monthly average was (10.7) °C (AL-Hassany and Hindi, 2016).

The current study included estimating carbon dioxide gas through fifteen selected stations throughout Baghdad, and these stations

were represented by some residential, traffic, and industrial areas, including two stations in the agricultural areas for comparison, as shown in Figure 1 and Table 1.

2.2. Data collected

This study used remote sensing data, represented by the United States Geological Survey (USGS). One satellite image of the Sentinel-2 satellite was used (acquisition time: 13 April 2019 approximately CCT 10:37 a.m.) with spectral beams (MID IR NER-IR, GREEN) to help to implement returns and projections according to the World Geodetic System 1984. This was done for the study area maps and to positioning the spatial locations of the stations chosen on them.

Besides, data from the European Centre for Medium-Range Weather Forecasts (ECMWF) represented by the monthly average of temperature were used. Also, data of a monthly average of carbon dioxide taken from the atmospheric infrared sounder (AIRS) from Giovanni of NASA with an accuracy of $2^{\circ} \times 2.5^{\circ}$, where the spectral coverage of AIRS sensor at (3.74 μm to 4.61 μm), (6.20 μm to 8.22 μm), and (8.8 μm to 15.4 μm) were taken (Thomas *et al.*, 2011).

The annual, monthly rates for February and July were used for the period from (2003-2018) and for each station depending on the GPS locations of these stations and in the form of coordinates (x, y). The Pearson test was chosen from several statistical tests for regression analysis and knowledge of the relationship between temperature variables and carbon dioxide concentrations using the Origin 2018 statistical program. The study area was divided into residential, industrial, and agricultural. Spatial distribution maps of carbon dioxide concentration with temperature were performed using a GIS program. The inverse distance weighted method was used to plot the spatial differences of carbon dioxide and temperature according to the selected areas.

2.3. Spatial and statistical analysis

Spatial analysis is one of the necessary techniques to represent the spatial distribution of carbon dioxide concentrations and its relationship to temperature changes to know spatial differences between one part and another in the selected areas, among the geostatistical techniques (Muthanna *et al.*, 2018).

The Inverse Distance Weighting (IDW)

technology provided by the ArcGIS 10.6 program was used to produce spatial distribution maps of carbon dioxide concentrations and temperature in the city. This method depends on the spatial correlation of the data measured at specific points in the region to calculate the required data at points where measurements are not available (Al Ramahi and Al Bahadly, 2020; Ghazal *et al.*, 2012).

The data of each known point affects more whenever it is close to the unknown points or does not contain measurements. Its effect decreases whenever you move away from it so that each known location has a specific weight included in the calculation. It expects or predicts unknown values depending on their proximity or distance from the source. This technique is characterized by accurate estimates such that the Mean error, Mean Prediction Error, Root-mean-square error. The standard average mistake is close to zero. There are many statistical measures that can be used to find the correlation relationship between two variables (AL Naqeeb *et al.*, 2020; Hadi and Mashee, 2017).

The Pearson correlation coefficient provided by Origin 2018 was used to detect the relationship between gas concentration and temperature. It is a statistical measure to measure the strength of the relationship between two variables and is expressed as a value between (+1 and -1). The number (+1) indicates a strong positive correlation between the two variables, which means that a positive change will follow any positive change in one of the variables in the other variable. The number (-1) indicates a robust negative correlation between the two variables, which means that a negative change will follow any positive change in one of the variables in the other variable. While zero indicates no relationship between the two variables or that there is no clear relationship between the changes (Gelfand *et al.*, 2010).

3. RESULTS AND DISCUSSION:

3.1. Spatial distribution and temporal trends of carbon dioxide means

Figure 2 illustrates the Time Series, Area-Averaged of Carbon Dioxide in PPM, 2 x 2.5 deg. [AIRS AIRX3C2M v005] over 2003-Jan - 2018-Dec, Region (43.4762 °E, 32.9919 °N, 44.3221 °E, 33.783 °N) plotting by Origin 2018. Figures 3 and 4 illustrate the spatial distribution of the monthly average of carbon dioxide concentrations in Baghdad for the period (2003-2018) and for

February and July months using the Inverse Distance Weighting (IDW) technology provided by ArcGIS (Chen and Liu, 2012). The monthly rates of carbon dioxide concentrations showed a spatial difference in most parts of a region with variations in the spatial area patterns for each season. They depend on different seasonal fluctuations and weather conditions.

The increase of the population and the significant emissions of fuel burned from many vehicles and electric power generators are one of the factors to the growth of carbon dioxide levels. The agricultural degradation and the change of thousands of dunums of agricultural and open areas to residential, industrial, and commercial areas have also contributed to this increase in the CO₂ levels.

The highest values of carbon dioxide concentrations were found in July, where the average gas concentration was 379.80 ppm in 2003, with a continuous increase to 406.35 ppm in 2018. In contrast, in February, the lowest values were where the average gas concentration was 376.35 ppm in 2003, with a continuous increase to 410.79 ppm in 2018 (Al-Timimi and Al-Jiboori, 2013). These differences between July and February are due to several reasons. The most important is the low consumption of gas from plants in the summer, where photosynthesis is less in the summer than the spring months, and, thus, the use of carbon dioxide decreases. Also, increasing electrical energy consumption for cooling leads to an increase in the quantities of fuel burned, so the percentage of gas in the atmosphere also increases. While the growing season of plants and trees begins in Baghdad in February, photosynthesis in the plant is at its highest value, thus increasing the consumption of carbon dioxide and reducing the amount of gas in the atmosphere (Al Jiboori *et al.*, 2016). The concentration of carbon dioxide differs in residential, commercial, traffic, industrial, and rural areas. It can be observed a significant increase in the concentration of carbon dioxide in industrial and traffic-congested areas with cars compared to stations in agricultural and open areas. The rate of concentration of carbon dioxide in regions of Al-Taji and Al-Rashid was relatively low compared to the stations of Al-Shu'ala, New Baghdad, Karrada, and Sadr City. These cities witnessed a relatively high value due to industrial activity, as these areas are considered industrial and traffic-related areas, with cars and high population density. Dora station recorded the most elevated concentrations over time due to the presence of an electric power station that

consumes large quantities of fuel for energy production apart from the bulldozing of agricultural lands, especially during recent years, where turned these areas to residential lands or factories. Due to the proliferation of brick production plants in the Al-Bawi region, east of Baghdad, high carbon dioxide concentrations have also been seen (Worrell *et al.*, 2001). An increase in the levels of carbon dioxide will lead to negative consequences to the atmosphere, as it affects various natural and environmental phenomena of the city of Baghdad. The most important of which is the high temperatures, where Baghdad recorded the most elevated temperatures in the world during recent years. Other negative consequences are drought, desertification, and an imbalance in precipitation, as the city has suffered from persistent floods due to torrential rains (Solomon *et al.*, 2009).

3.2. Spatial distribution and temporal trends of temperature means

Figure 5 illustrates the Time Series, Area-Averaged of temperature in °C, 0.125 x 0.125 deg. [ERA-interim] over 2003-Jan - 2018-Dec, Region (43.4762 °E, 32.9919°N, 44.3221°E, 33.783°N) plotting by Origin 2018. Figures 6 and 7 illustrate the spatial distribution of the monthly average of carbon dioxide concentrations in Baghdad for the period (2003-2018) and for February and July months using the Inverse Distance Weighting (IDW) technology provided by ArcGIS (Chen and Liu, 2012). It can be observed that the spatial distribution of the monthly average temperatures showed a spatial difference in most parts of the region. The highest monthly average temperature was during July, while the lowest monthly rate was in February.

By analyzing trends for the entire period, the increase was apparent, as the average temperature of the city of Baghdad increased by (1.73) degrees Celsius since the monthly average for July was 36.4°C from the year 2003 with a continuous increase to 38.45° C in 2018. At the same time, the monthly rate was in February 13.2°C from 2003, with a constant rise to 15.27 °C in 2018 (Fenner *et al.*, 2014). This increase is due to several reasons, the most important of which is the increase in the area of land use according to the urban expansion in terms of built areas or those that entered into human activity, especially after 2003, where many green and agricultural fields were subjected to significant deterioration. Hence, the urban character became prevalent in the city, especially in recent years, in addition to increasing the concentrations of carbon dioxide

gas as the molecules of this gas have a great ability to absorb infrared radiation and thus work to trap heat in the lower layers and prevent them from penetrating into outer space, which leads to an increase in temperature (Salman *et al.*, 2018).

The lowest temperature was found along the Tigris River from the far north of the study area to the far south and southwest. This was due to the nature of the wet soil and the presence of agricultural lands at the Al-Taji and Al-Rashid regions. The highest temperature was in the center of Baghdad because of the low vegetation cover in urban areas at the Karrada and New Baghdad and Sadr City once these areas are considered to be of high population density, with vehicles and generators widespread. Dora and Al-Bawi region stations recorded the most elevated temperatures, as they are deemed industrial areas. Accordingly, there are multiple sources of pollution, which enhances the carbon level in them (Al-Timimi and Al-Khudhairy 2018).

3.3. Carbon dioxide concentrations and temperature: the assumed correlation

By studying the spatial distribution of carbon dioxide, it could be seen that carbon dioxide is continuously increasing due to the increased combustion of fossil fuels, oil, gas, transportation, aviation, and electricity generation. Another factor that plays a vital role in this increase is the increase in population density. The stations of the study area were divided into three types of residential, industrial, and agricultural, according to the presence of these stations in the Baghdad regions. Pearson correlation coefficient was used to find out the relationship between carbon dioxide concentrations and temperatures by taking annual averages of February and July along the study period (Shakun *et al.*, 2012).

The correlation coefficient showed a high positive relationship between increased gas concentrations and high temperatures for all study stations over entire study period. The highest value of the correlation coefficient between gas concentrations and temperatures in residential areas of Baghdad, as it reached (0.92) in July while it was (0.89) in February. As for the stations in the industrial regions was (0.83) in July and (0.82) in February, especially in Dora region, and this is due to the bulldozing of its agricultural lands and its transformation into factories and residential lands (French *et al.*, 2009). Al-Bawi region has witnessed high correlation values over time, especially in recent years. The proliferation of factories causes this, mainly since those plants

emit a lot of gas, including carbon dioxide, which affects raising gas levels in the neighboring regions like New Baghdad, Karrada and Sadr City.

Stations in the agricultural areas at Al-Taji and Al-Rashid have witnessed different correlation values where dioxide decreases during the winter and the beginning of the plant growth season as plants withdraw carbon dioxide from the atmosphere through photosynthesis. Therefore the value of carbon dioxide in the cold months is less than the warm summer months were (0.80) in February and (0.91) in July (Rehan and Nehdi, 2005). Fig (8) shows a scatter plot of correlation coefficients between temperature and carbon dioxide concentrations for February and July over the period (2003-2018). Table 2 shows the values of Pearson's r coefficient correlation, Adj. R-Square, Standard Error, and T-Value between carbon dioxide concentrations and temperature and for the same period.

4. CONCLUSIONS:

1. The concentration of carbon dioxide differs locally based on Baghdad areas such as residential, commercial, traffic, industrial, and rural areas, as well as changes during the months of the year.
2. Stations in agricultural regions at Al-Taji and Al-Rashid have witnessed different correlation values where dioxide decreases during the winter and the beginning of the plant growth season as plants withdraw carbon dioxide from the atmosphere through photosynthesis. Therefore the value of carbon dioxide in the cold months is less than the warm summer months were (0.80) in February and (0.91) in July.
3. Human activity increases carbon dioxide concentrations - which is estimated at 38.7 parts per million -. This is a relatively significant increase related to other ground cover changes, such as agricultural land, abandonment land, and arid land. During the winter, the water level increased due to rainfall leading to low nutrients concentrations.
4. The continuous increase in the concentration of carbon dioxide has negative results about the atmosphere as it affects the several natural and environmental phenomena of the city of Baghdad. The most important of which are high temperatures, drought, desertification, and the imbalance in the amount of precipitation, as the city has

suffered from continuous flooding, especially in recent years.

5. The correlation coefficient showed a high positive relationship between increased gas concentrations and high temperatures for all study stations over the entire study period. The highest value of the correlation coefficient between gas concentrations and temperatures in residential areas of Baghdad, as it reached (0.92) in July while it was (0.89) in February.

5. REFERENCES:

1. AIRS (Atmospheric Infrared Sounder). onboard NASA's Aqua Satellite . [Online] Available at: <https://giovanni.gsfc.nasa.gov>
2. Al Jiboori, M. H., Hassan, A. S., and Hashim, B. M. (2016). Evaluation of Industrial CO₂ Emissions from Cement Production and Transportation Sector in Iraq Using IPCC Methods. *Diyala Journal for pure science*, 12(4-part 2), 58-69.
3. Al Naqeeb, N.A., Mashee, F.K. and Al Hassany, J. S. (2020). Estimation the factors affecting on growth of algae in um el-naaj lake by using remote sensing techniques. *Periódico Tchê Química*, 17 (35), 227-238.
4. Al Ramahi, F. K. M., and Al Bahadly, Z. K. I. (2020). The Spatial Analysis for Bassia eriophora (Schrad.) Asch. Plant Distributed in all IRAQ by Using RS and GIS Techniques. *Baghdad Science Journal*, 17(1), 126-135.
5. Al-Bayati, R. M., and Al-Salihi, A. M. (2019). Monitoring carbon dioxide from (AIRS) over Iraq during 2003-2016. In *AIP Conference Proceedings* (Vol. 2144, No. 1, p. 030007). AIP Publishing LLC.
6. AL-Hassany, J. S., and Hindi, M. T. (2016). A Study of Epiphytic and Epipellic Algae in Al-Dora Site/Tigris River in Bagdad Province-Iraq. *Baghdad Science Journal*, 13(4), 721-733.
7. Al-jaf, S. J., and Al-Taai, O. T. (2019). Impact of carbon dioxide concentrations on atmospheric temperature changes over Iraq and some neighboring countries. *Plant Archives*, 19(2), 1450-1456.
8. Al-ramahi, F.K.M. (2020). Spatial analysis

- of radon concentration distrusted at Baghdad city using remote sensing techniques and geographic information systems. *Iraqi Journal of Agricultural Sciences*, 51(Special Issue), 21-32.
9. Al-Timimi, Y. K., and Al-Jiboori, M. H. (2013). Assessment of spatial and temporal drought in Iraq during the period 1980-2010. *Int. J. Energ. Environ*, 4(2), 291-302.
 10. Al-Timimi, Y. K., and Al-Khudhairi, A. A. (2018). Spatial and Temporal Analysis of Maximum Temperature over Iraq. *Al-Mustansiriyah Journal of Science*, 29(1), 1-8.
 11. Chen, F. W., and Liu, C. W. (2012). Estimation of the spatial rainfall distribution using inverse distance weighting (IDW) in the middle of Taiwan. *Paddy and Water Environment*, 10(3), 209-222..
 12. ECMWF (European Centre for Medium-Range Weather Forecasts). ERA-interim model. [Online] Available at: <http://apps.ecmwf.int>
 13. Falkowski, P., Scholes, R. J., Boyle, E. E. A., Canadell, J., Canfield, D., Elser, J., Gruber, N., Hibbard, K., Högberg, P. , Linder, S., Mackenzie, F. T., Moore III, B., Pedersen, T. , Rosenthal, Y. , Seitzinger, S., Smetacek, V., and Steffen, W. (2000). The global carbon cycle: a test of our knowledge of earth as a system. *science*, 290(5490), 291-296.
 14. Fenner, D., Meier, F., Scherer, D., and Polze, A. (2014). Spatial and temporal air temperature variability in Berlin, Germany, during the years 2001–2010. *Urban Climate*, 10, 308-331.
 15. French, S., Levy-Booth, D., Samarajeewa, A., Shannon, K. E., Smith, J., and Trevors, J. T. (2009). Elevated temperatures and carbon dioxide concentrations: effects on selected microbial activities in temperate agricultural soils. *World Journal of Microbiology and Biotechnology*, 25(11), 1887-1900.
 16. Gelfand, A. E., Diggle, P., Guttorp, P., and Fuentes, M. (Eds.). (2010). *Handbook of spatial statistics* (pp12-23). CRC press.
 17. Ghazal, N. K., Shaban, A. H., Mashi, F. K., and Raihan, A. M. (2012). Change Detection Study Of Al Razaza Lake Region Utilizing Remote Sensing And GIS Technique. *Iraqi Journal of Science*, 53(5), 950-957.
 18. Hadi, G. S., and Mashee, F. K. (2017). Study the Wet Region in Anbar Province by Use Remote Sensing (RS) and Geographic Information System (GIS) Techniques. *Iraqi Journal of Science*, 58(3A), 1333-1344.
 19. Hashim, M.B., and Sultan, M. A. (2010). Using remote sensing data and GIS to evaluate air pollution and their relationship with land cover and land use in Baghdad City. *Iranian Journal of Earth Sciences*, 2(1), 20-24.
 20. Hassoon, A. F. (2015). Assessment of air pollution elements concentrations in Baghdad city from periods (May-December) 2010. *International journal of energy and environment*, 6(2), 191
 21. Jasim, O., Ali, A. R. B., and Hashim Hamed, N. (2020). Urban expansion of Baghdad city and its impact on the formation of Thermal Island based upon Multi-Temporal Analysis of satellite images. *MSandE*, 737(1), 012215.
 22. Muthanna, M. A., Mashee, F. K., and Fadhil, M. (2018). Assessment of Irrigation Water Quality for Dabdaba for Mation by Using GIS Techniques in Karbala Province. *Indian Journal of Natural Sciences*, 19(50), 14677-14684.
 23. Rehan, R., and Nehdi, M. (2005). Carbon dioxide emissions and climate change: policy implications for the cement industry. *Environmental Science and Policy*, 8(2), 105-114.
 24. Salman, S. A., Shahid, S., Ismail, T., Ahmed, K., and Wang, X. J. (2018). Selection of climate models for projection of spatiotemporal changes in temperature of Iraq with uncertainties. *Atmospheric Research*, 213, 509-522.
 25. Shakun, J. D., Clark, P. U., He, F., Marcott, S. A., Mix, A. C., Liu, Z., ... and Bard, E. (2012). Global warming preceded by increasing carbon dioxide concentrations during the last deglaciation. *Nature*, 484(7392), 49-54.
 26. Solomon, S., Plattner, G. K., Knutti, R., and Friedlingstein, P. (2009). Irreversible climate change due to carbon dioxide emissions. *Proceedings of the national academy of sciences*, 106(6), 1704-1709.

27. Thomas, H. E., Watson, I. M., Carn, S. A., Prata, A. J., and Realmuto, V. J. (2011). A comparison of AIRS, MODIS and OMI sulphur dioxide retrievals in volcanic clouds. *Geomatics, Natural Hazards and Risk*, 2(3), 217-232.
28. USGS (United States Geological Survey), (2017). Landsat — A Global Land-Imaging Mission.[Online] Available at: <http://glovis.usgs.gov>
29. Weinbauer, M. G., Mari, X., and Gattuso, J. P. (2011). Effect of ocean acidification on the diversity and activity of heterotrophic marine microorganisms. *Ocean acidification. Oxford University Press, Oxford*, 83-98.
30. Worrell, E., Price, L., Martin, N., Hendriks, C., and Meida, L. O. (2001). Carbon dioxide emissions from the global cement industry. *Annual review of energy and the environment*, 26(1), 303-329.

Table 1. Location of study area stations and its types, names, global coordinate system (λ , φ), and Universal Transverse Mercator (UTM) coordinate (x , y).

Stations	Longitude (E°)	Latitude (N°)	UTM Easting	UTM Northing	Station type
Adhamiyah	33.368	44.358	440276.74	3692268.71	Residential (Re)
Al-Taji	33.428	44.309	435762.50	3698950.10	Agricultural (Ag)
Al-Shu'ala	33.368	44.259	431066.89	3692329.84	Residential, Traffic (Re, Tr)
Al-A'amiriya	33.295	44.288	433709.47	3684217.56	Residential (Re)
Baghdad airport	33.29	44.215	426908.49	3683711.96	Residential, Traffic (Re, Tr)
Sha'ab	33.422	44.402	444404.38	3698231.30	Residential (Re)
Sadr City	33.398	44.466	450340.83	3695538.06	Residential (Re)
Karrada	33.342	44.4	444167.33	3689362.82	Residential (Re)
Al-Jadriya	33.282	44.393	443477.24	3682714.50	Residential, Agricultural (Re, Ag)
Mansour	33.329	44.342	438760.99	3687954.09	Residential (Re)
Al-Bawi region	33.401	44.536	456852.00	3695839.46	Industrial (In)
New Baghdad	33.32	44.486	452158.08	3686880.97	Residential, Industrial (Re, In)
Dora	33.255	44.48	451563.72	3679677.38	Residential, Industrial (Re, In)
Al-Rashid	33.214	44.389	443060.68	3675177.72	Agricultural (Ag)
Hayy Al-Jihad	33.253	44.321	436751.70	3679540.62	Residential (Re)

Table 2. Statistical summary of the study area stations.

	Stations types	Pearson's r	Adj. R-Square	Standard Error	T-Value
February	agricultural	0.80914	0.79551	0.00384	2.14449
	industrial	0.82321	0.81058	0.00388	2.33883
	residential	0.89663	0.78995	0.00447	1.09056
July	agricultural	0.90031	0.90461	0.00694	1.03030
	industrial	0.83841	0.82687	0.00951	1.68395
	residential	0.92738	0.9222	0.00662	1.58674

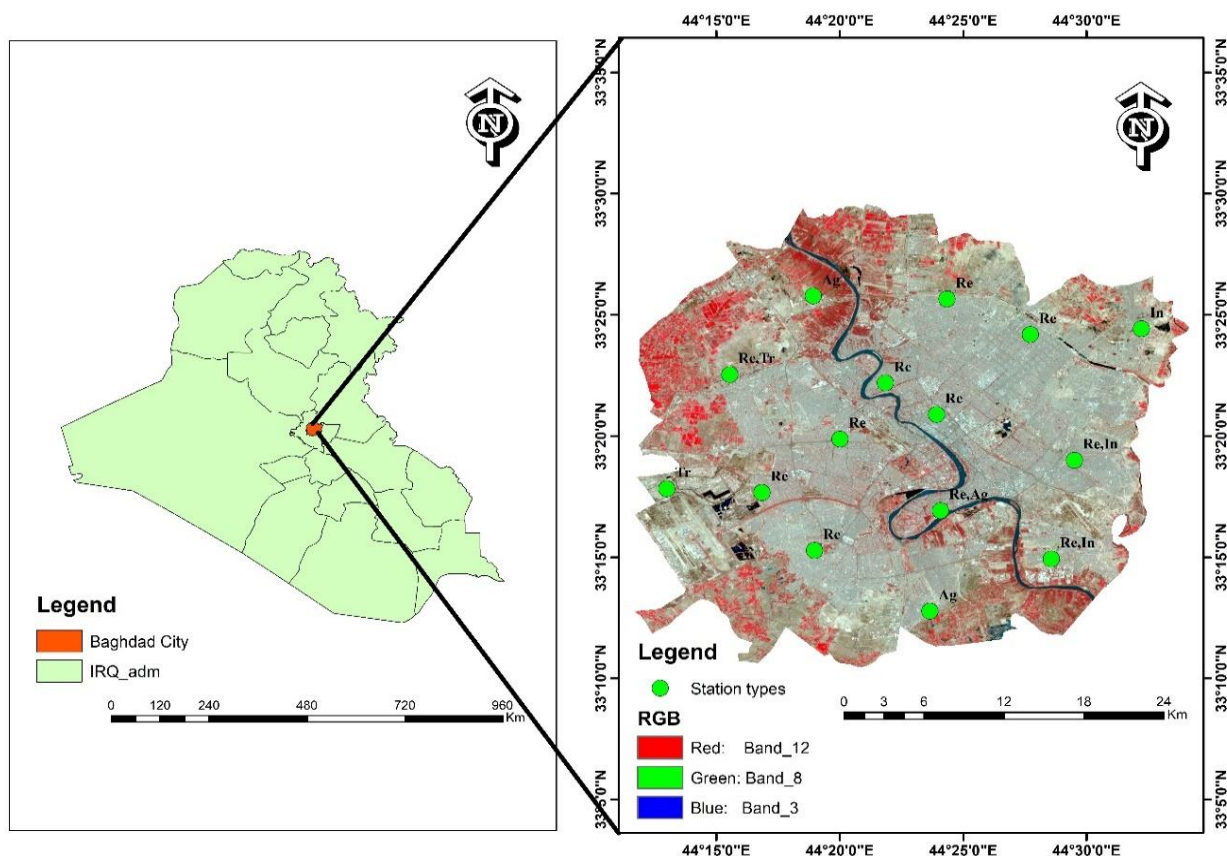


Figure 1. Boundaries of study area of Sentinel-2 satellite with spectral beams (MID IR, GREEN) and distribution of stations, include fifteen stations (●) plotting by ArcGIS.

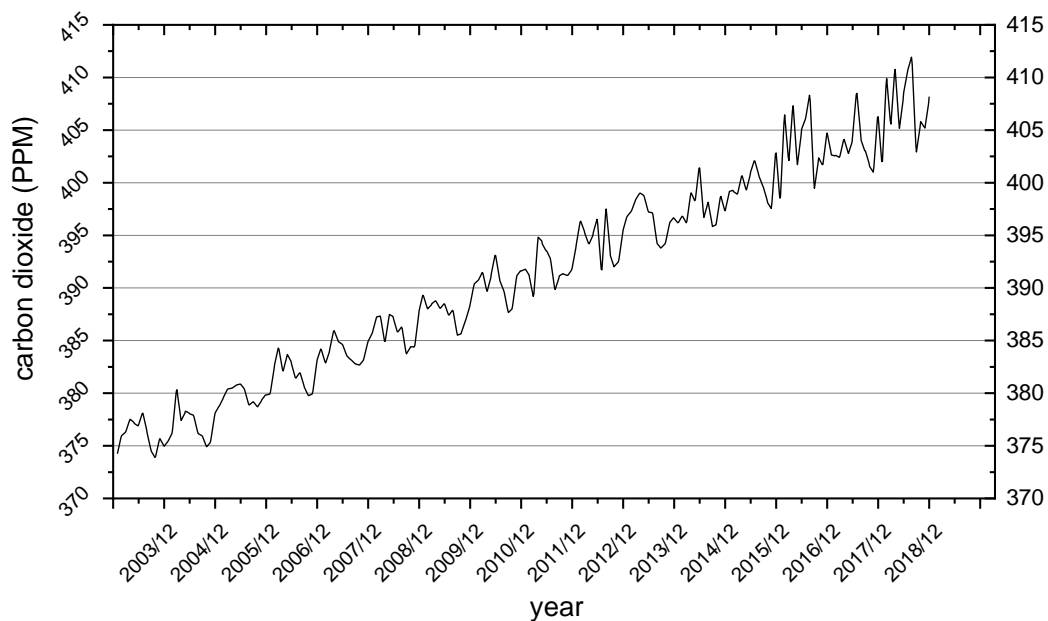


Figure 2. Analyzing trends of the monthly average of Carbon Dioxide over 2003-Jan - 2018-Dec for Baghdad city

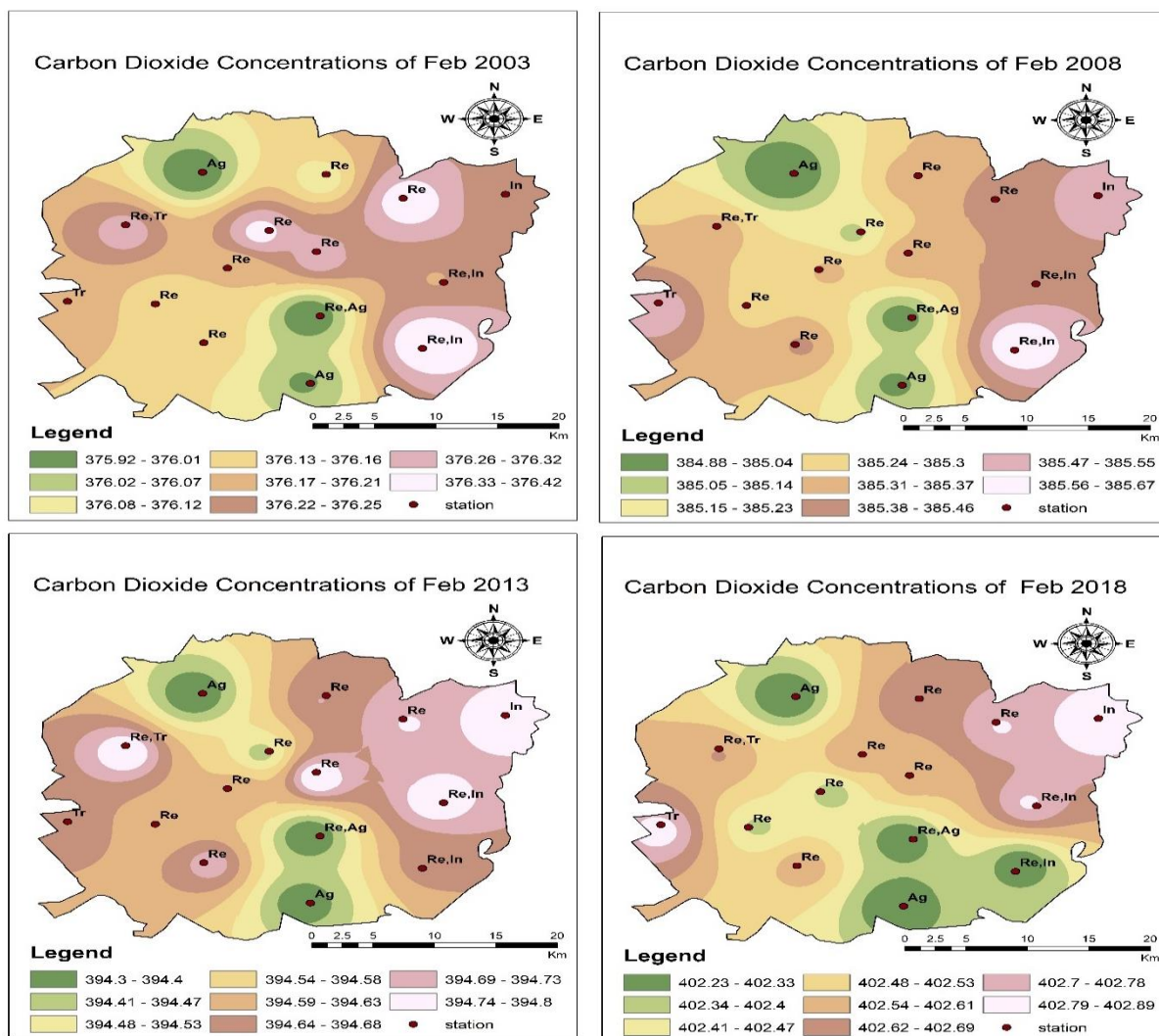


Figure 3. Spatial analysis map of monthly average carbon dioxide concentrations in (PPM) for the February (2003, 2008, 2013 and 2018) years representation by Inverse Distance Weighting (IDW) technology

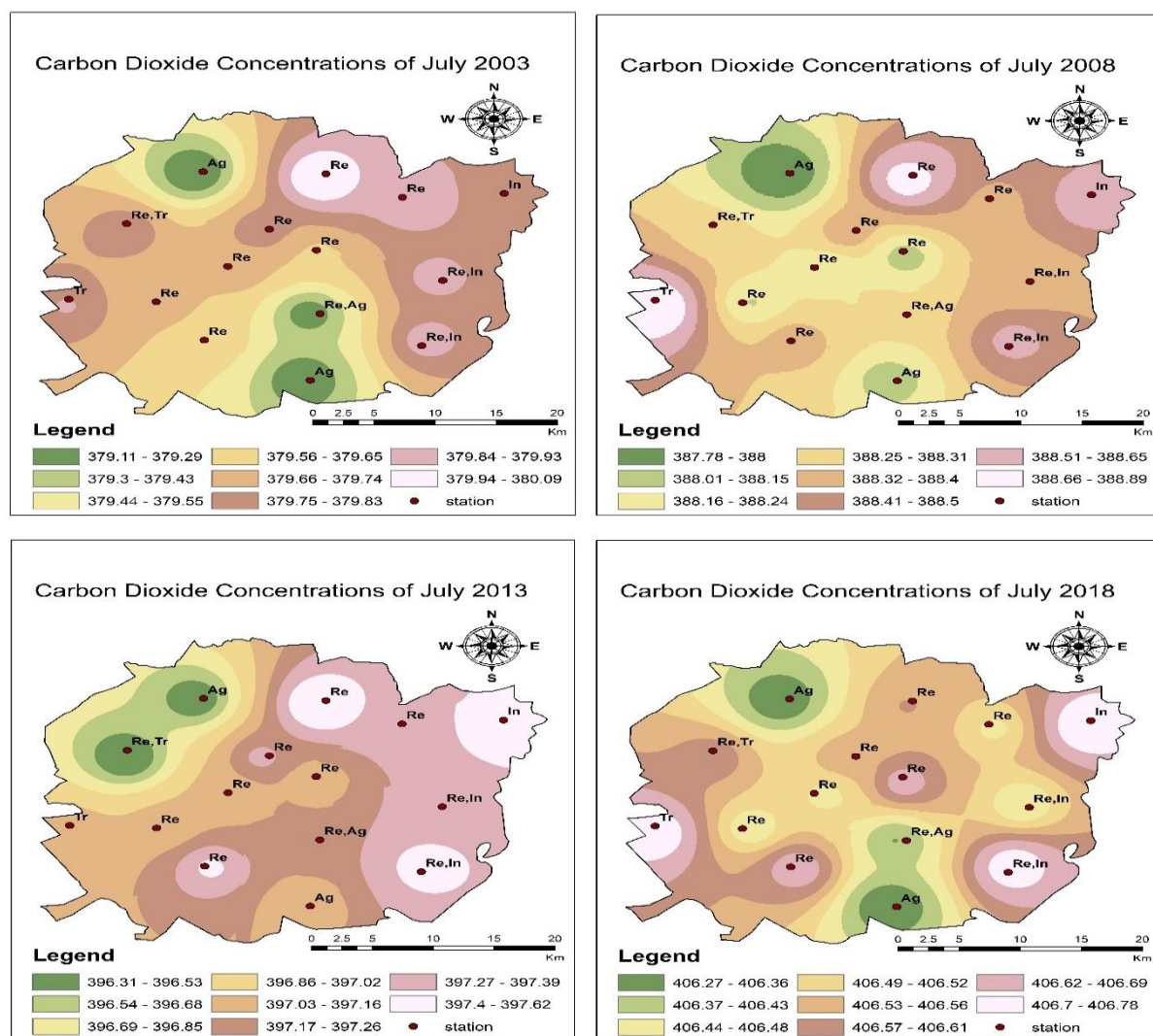


Figure 4. Spatial analysis map of monthly average carbon dioxide concentrations in (PPM) for the July (2003, 2008, 2013 and 2018) years representation by Inverse Distance Weighting (IDW) technology

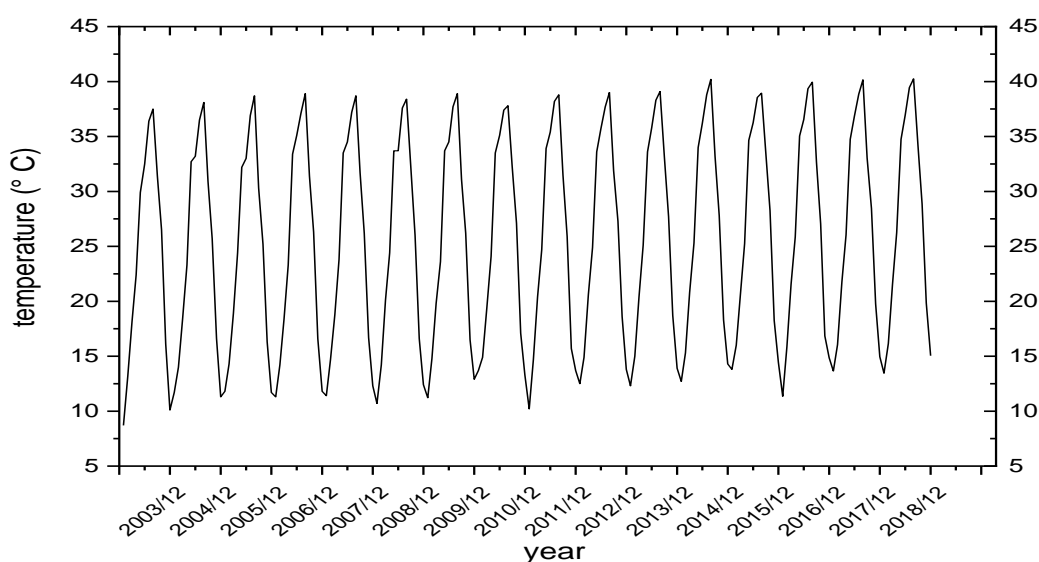


Figure 5. Analyzing trends of the monthly average of Carbon Dioxide over 2003-Jan - 2018-Dec for Baghdad city

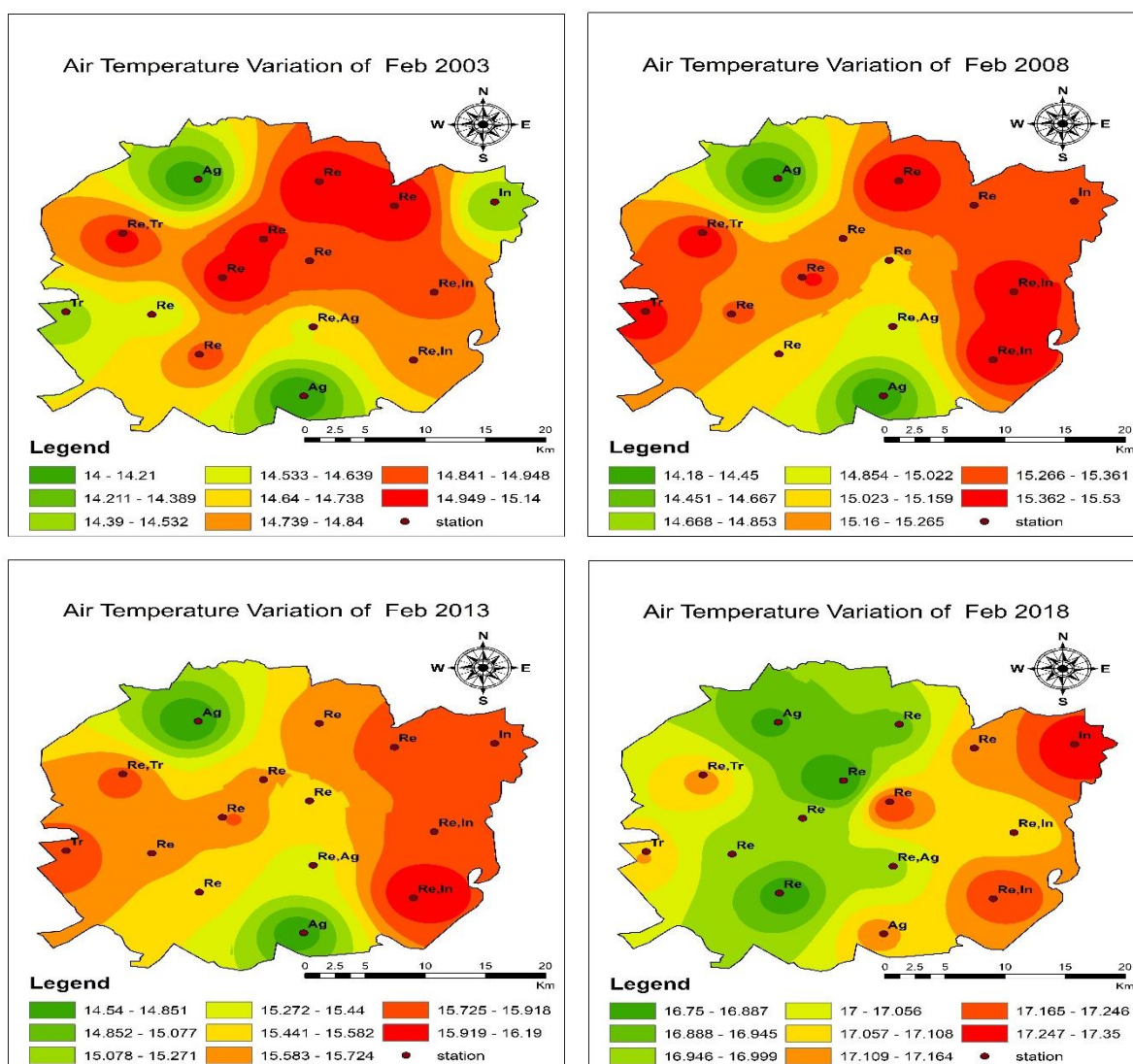


Figure 6. Spatial analysis map of monthly average temperature in ($^{\circ}\text{C}$) for the February (2003, 2008, 2013 and 2018) years representation by Inverse Distance Weighting (IDW) technology.

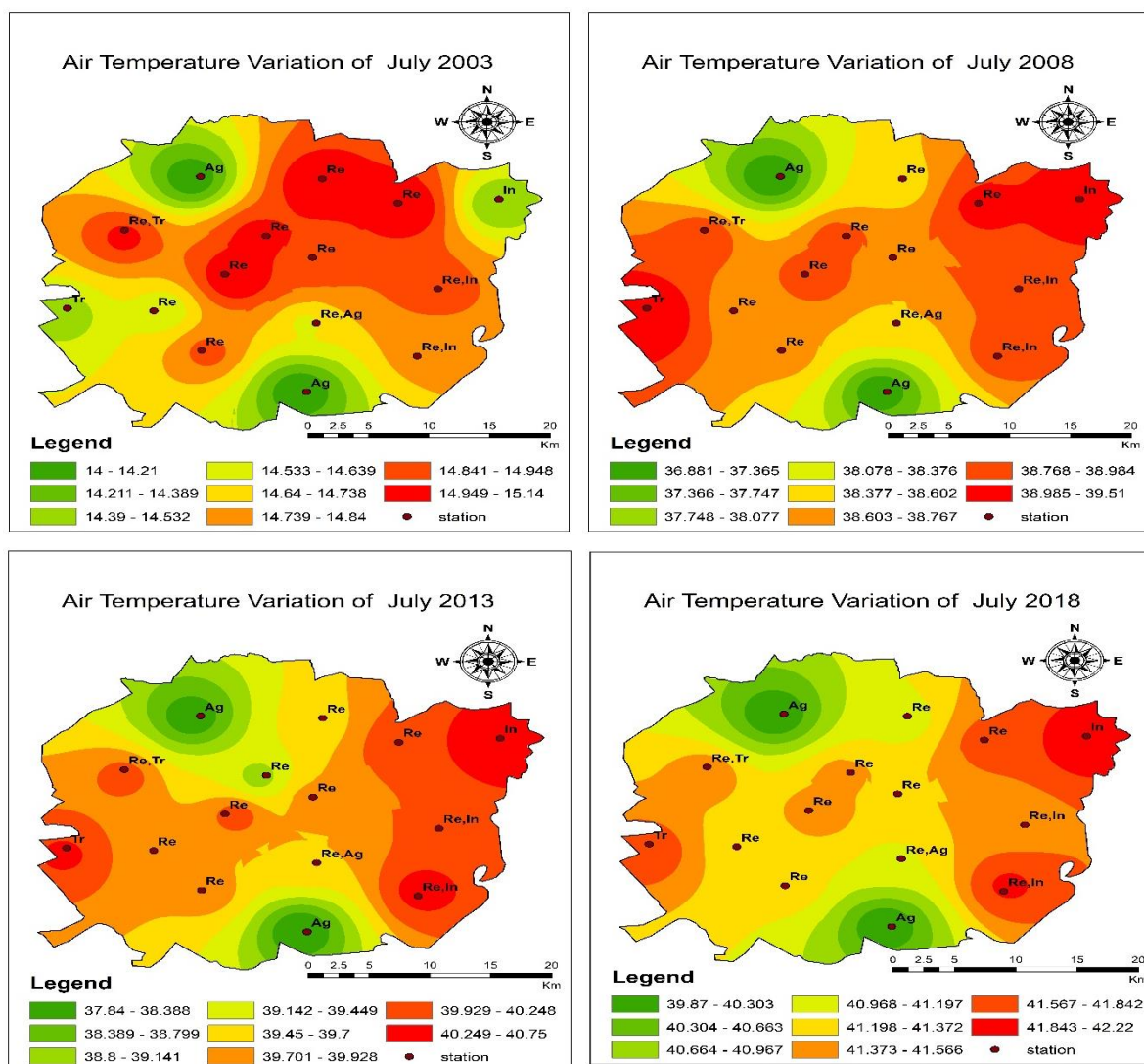


Figure 7. Spatial analysis map of monthly average temperature in ($^{\circ}\text{C}$) for the July (2003, 2008, 2013 and 2018) years representation by Inverse Distance Weighting (IDW) technology.

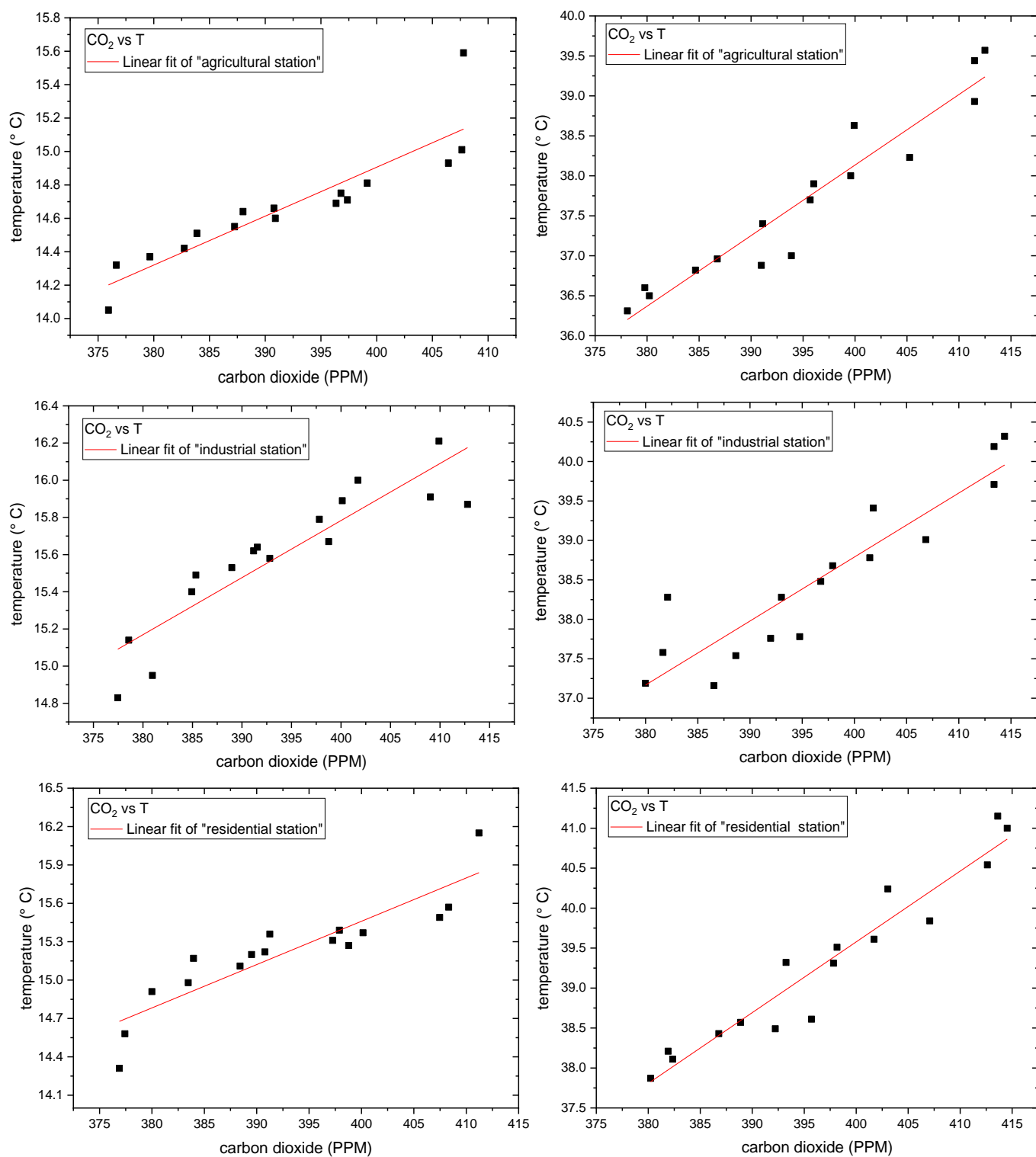


Figure 8. Correlation of carbon dioxide concentrations vs. temperature, February (left) and July (right).

AVALIAÇÃO DOS PARÂMETROS DA SUPERFÍCIE DE CONTATO NA SUPERFÍCIE DE TROCADOR DE CALOR COM ALETAS SERRILHADAS POR SERRILHAS EM AROS VAZIOS**EVALUATION OF THE CONTACT SURFACE PARAMETERS AT KNURLING FINNED HEAT-EXCHANGING SURFACE BY KNURLS AT RING BLANKS****ОЦЕНКА ПАРАМЕТРОВ КОНТАКТНОЙ ПОВЕРХНОСТИ ПРИ НАКАТЫВАНИИ ОРЕБРЕННОЙ ТЕПЛООБМЕННОЙ ПОВЕРХНОСТИ РОЛИКАМИ НА КОЛЬЦЕВЫХ ЗАГОТОВКАХ**

TATARKANOV, Aslan Adal'bievich¹; ALEXANDROV, Islam Alexandrovich¹; OLEJNIK, Andrej Vladimirovich^{2*}

¹ IDTI RAS, Russia.

² MSUT "STANKIN", Department of Management and Informatics in Technical Systems. Russia.

* *Corresponding author*
e-mail: olejnikandrejv@yandex.ru

Received 06 August 2020; received in revised form 24 August 2020; accepted 04 September 2020

RESUMO

As peças tubulares com uma superfície externa com troca de calor aletada são geralmente produzidas pelo laborioso método de corte em tornos. Além disso, existe um método para a fabricação de aletas de alto desempenho por serrilhado a frio com serrilhados em anel o que, comparado com o corte, reduz a intensidade de trabalho de duas a seis vezes com um aumento significativo nas propriedades operacionais do produto. A desvantagem do método de serrilhado a frio com serrilhas de corte em anel pode ser defeitos de superfície indesejados e deformações de todo o produto. A obtenção de superfícies com alhetas em blanks de anel com alta qualidade superficial durante a serrilhagem requer um cálculo preciso da proporção de deformações longitudinais e transversais. Os fatores mais importantes que determinam a relação entre as deformações longitudinais e transversais (*rolling-out e rolling-off*) são o comprimento e a largura da superfície de contato. A necessidade de uma avaliação quantitativa dos parâmetros das deformações longitudinais e transversais determinou a finalidade deste manuscrito. O objetivo desse estudo foi desenvolver uma metodologia para calcular a superfície de contato de uma serrilha com um anel em branco (tubo) ao serrilhar com serrilhas de corte em anel. A metodologia proposta para calcular a superfície de contato da serra com um tubo ao serrilhar com serrilhas de corte em anel permite estimar a gama recomendada de tamanhos de tubos para serrilhar. Com base nas dependências mencionadas no manuscrito, os tamanhos-limite para tubos vazios foram calculados para garantir uma alheta de alta qualidade. Experimentos com o uso de aletas a frio em tubos com diferentes proporções de comprimento e diâmetro foram realizados, confirmando a possibilidade de utilizar a metodologia proposta para calcular a superfície de contato da serrilha com um tubo ao serrilhar aletas de troca de calor com serrilhas de corte em anel.

Palavras-chave: *alheta externas, tubos vazios, zona de deformação.*

ABSTRACT

Tubular parts with an external finned heat-exchanging surface are usually produced by the laborious method of cutting on lathes. Besides, there is a method for the high-performance manufacturing of fins by cold knurling with ring-cut knurls, which, compared with cutting, reduces labor intensity by two to six times with a significant increase in the operational properties of the product. The disadvantage of the cold knurling method with ring-cut knurls can be unwanted surface defects and deformations of the entire product. Obtaining finned surfaces on ring blanks with high surface quality during knurling requires accurate calculation of the ratio of longitudinal and transverse strains. The most important factors determining the ratio of longitudinal and transverse strains (*rolling-out and rolling-off*) are the length and width of the contact surface. The need for a quantitative assessment of the parameters of longitudinal and transverse strains determined the purpose of this manuscript. This study aimed to develop a methodology for calculating the contact surface of a knurl with

a ring blank (pipe) when knurling with ring-cut knurls. The proposed method for calculating the knurl's contact surface with a tube when knurling with ring-cut knurls allows for estimating the recommended range of pipe sizes for knurling. Based on the dependencies mentioned in the manuscript, the limiting sizes for blank pipes were calculated to ensure high-quality finning. Experiments on cold rolling of ribbing on pipes with different lengths and diameter ratios were carried out, confirming the possibility of using the proposed methodology for calculating the knurl's contact surface with a pipe when knurling heat-exchanging finning with ring-cut knurls.

Keywords: *external finning, blank pipes, deformation zone.*

АННОТАЦИЯ

Трубчатые детали с наружной оребренной теплообменной поверхностью обычно изготавливают трудоёмким методом резания на токарных станках. Помимо этого, существует способ высокопроизводительного изготовления оребрения путем холодного накатывания роликами с кольцевой нарезкой, который по сравнению с резанием позволяет снизить трудоемкость в два-шесть раз при значительном повышении эксплуатационных свойств изделия. Недостатком метода холодного накатывания роликами с кольцевой нарезкой могут являться нежелательные дефекты поверхности и деформации всего изделия. Для получения на кольцевых заготовках оребрения с высоким качеством поверхности в процессе накатывания требуется точно рассчитывать соотношение продольной и поперечной деформаций. Важнейшими факторами, определяющими при этом соотношение продольной и поперечной деформаций (вытяжки и раскатки) являются длина и ширина контактной поверхности. Необходимость количественной оценки параметров продольной и поперечной деформаций определила цель настоящей работы. Целью данного исследования являлась разработка методики расчета параметров контактной поверхности ролика с кольцевой заготовкой (трубой) при накатывании оребрения роликами с кольцевой нарезкой. Предложенная в работе методика расчета контактной поверхности ролика с трубой при накатывании оребрения роликами с кольцевой нарезкой позволяет оценить рекомендуемый диапазон размеров трубы под накатывание оребрения. Используя полученные в работе зависимости выполнен расчет предельных размеров гладких труб, обеспечивающих качественное накатывание на них оребрения. Проведены эксперименты по холодной прокатке оребрения на трубах с различным соотношением длины и диаметра, подтверждающие возможность использования предложенной методики расчета контактной поверхности ролика с трубой при накатывании теплообменного оребрения роликами с кольцевой нарезкой.

Ключевые слова: *наружное оребрение, гладкие трубы, очаг деформации.*

1. INTRODUCTION:

Pipes with the external finned heat-exchanging surfaces (Figure 1) are used in many industries (Čarija *et al.*, 2014; Kuzma-Kichta *et al.*, 2007; Galushchak, 2017; Filippov, Cherepennikov and Leshchenko, 2010; Kim and Lee, 2013). The main areas of application for finned tubes are the machine-building industry uses them in refrigeration units, oil coolers, and compressors; chemical, oil refining, and petrochemical - in condensers, gas heaters and gas coolers; nuclear power - in gas coolers, intermediate refrigerators, steam air heaters, drying towers; in technology for air conditioning and in heat exchangers.

Finned tubes are monometallic or bimetallic structures consisting of two elements: an inner tube and outer ribs. The inner tube is a supporting element, through the inner cavity of which the working medium moves. It is made from metal, most often from steel. Cast iron and non-ferrous metals are used much less

frequently. The material from which the inner part of the structure is made is resistant to temperature extremes and high pressure and has anti-corrosion properties (Sawicki and Dyja, 2010). The outer ribs can be made of steel, cast iron, and non-ferrous metals. The outer ribs efficiently transfer heat from the carrier.

To achieve the desired performance properties of the finned tube, appropriate materials are used. Ribbed tube heating elements are made of the following metals: cast iron (with magnesium and cerium); stainless steel, copper, brass, aluminum. In the manufacture of a bimetallic tube for heat exchangers, the layout of materials can be as follows (support tube + ribs): steel + aluminum; aluminum + aluminum; brass + aluminum (Wang *et al.*, 2013). The fins are often covered with a heat-resistant coating, which makes it possible to increase the heat transfer rate up to 55%. The previously degreased finned tube is coated with magnesium oxide, and subsequent annealing ensures heat resistance. Finned

bimetallic pipes are often coated with copper to prevent corrosion (Paquet, 1993).

There are several options for producing ribbed pipes (Kocurek and Adamiec, 2013). Depending on the method, the purpose of the products also differs. Ribbed tube heating elements are carried out in three main ways: rolling, winding, welding. Also, pipes with the external finned heat-exchanging surfaces are often obtained by cutting on screw-cutting machines and lathes. However, the complexity of finning, in this case, as a rule, is high.

Meanwhile, a known method of high-performance finning is cold knurling by ring-cut knurls. Compared with cutting, this method allows for reducing the complexity in two to six times with a significant increase in the operational properties of the product (Olejnik *et al.*, 2020). External finning of thin-walled products is usually done by ring-cut knurls. The process is based on the principle of self-tightening (screwing knurls into the turns). In this case, the billet or tool moves along with its axis at a constant distance between the axes of freely rotating knurls. The axes of the knurls are located at an angle corresponding to the elevation angle of the finning. Depending on the diameter of the billet, knurling can be done with a different number of knurls; their number increases with the increasing diameter of the billet. The first two to three turns of the knurling head are made with forced axial feed to ensure capturing the billet with -the knurls—further, billet self-tightens. Plastic deformation is done mainly by the tapered lead (conical) and partially calibrating (cylindrical) part of the knurl.

However, in the process of cold knurling, the finning itself can be deformed, its dimensions can change (Figure 2), as well as the diameter of the part's hole. This can be avoided by selecting the proper design of the hollow parts and using rigid mandrels inserted into the holes of the knurled part along with the sliding fit. Mandrels cause an increase in auxiliary time and often lead to their "being bit" during knurling. Also, difficulties often arise when removing mandrels.

Thin-walled hollow parts (pipes) can be finned by increasing the diameter of the billet, then the diameter of the billet is approximately taken equal to the average finning diameter. However, finning ring blanks with minimal ovality and high surface quality require accurate calculating the ratio of longitudinal and transverse strains at knurling. The most

important factors determining the ratio of longitudinal and transverse strains (rolling-out and rolling-off) are the length and width of the contact surface. This problem has defined the purpose of this manuscript.

This study aimed to develop a methodology for calculating the contact surface of a knurl with a ring blank (pipe) when knurling with ring-cut knurls.

2. LITERATURE REVIEW:

An important mechanical engineering task is to reduce the amount of machining by cutting upon getting a billet approaching in shape and size to the finished product (Hakansson, 2015; Hitomi, 2017; Zheng, 2014; Semenov *et al.*, 2019b). As a result, there is the development of additive and hybrid shaping technologies, including pressure processing methods (Semenov *et al.*, 2019; Kopp, 1996; Kulikov *et al.*, 2016; Kulikov *et al.*, 2017). Simultaneously, engineers and technologists face tasks of increasing the efficiency of new technologies and reducing their implementation cost. The choice of a particular technology is determined by the design features of the manufactured product and economic feasibility and productivity (Alexandrov, Sheptunov, and Sannikov, 2019; Cherkashina, 2019).

Various technological methods can be used for external finning (Kulikov *et al.*, 2017). One of the external finning methods is the plastic deformation of metal in a hot or cold state (Sakai *et al.*, 2014). Using the plastic deformation method reduces processing waste, tool consumption, and labor costs. Thus, in most cases, the net cost of technological operations of external finning by cold knurling is much lower than cutting (Jiang, 2011). The reason for this is higher productivity of the method, a higher utilization rate of the processed material, lower costs for equipment depreciation, and replacement of the processing tool (Strycharska, 2019). If various defects often arise on the working surface during hot knurling as a result of heating and cooling the billet (scales, cracks, etc.), these defects are absent during cold knurling (Johnson, 2000; Liu, Tang, and Gu, 2014). Besides, cold plastic shaping has several significant technical advantages compared to cutting methods (Olejnik *et al.*, 2020).

Under pressure exceeding the stress value of the plastic flow of the processed material (Jiang, 2011), plastic deformation

(Johnson, 2000) occurs in it at room temperature, thus resulting in not only shaping but also a significant change in the material properties of the billet (McDowell and Moyer, 1991). A change in the properties of a deformed material is associated with changes in its structure that occur at various scale levels during the shaping of the final product (Kar'kina, Zubkova, and Yakovleva, 2013; Yakovleva, Kar'kina, and Zubkova, 2011; Qiao, Gao, and Starink, 2012). Peening at cold knurling helps in achieving an increase in the hardness and strength of the surface layer of the metal (Bower and Johnson, 1989; Yoshimi *et al.*, 2009). This greatly increases the wear resistance of the finning (Merkulov, 2008). The wear resistance of products obtained by plastic deformation is 30–40% higher than that obtained by cutting, and the strength characteristics are 10–20% higher (Song, Liu, and Tang, 2014). In addition to a significant change in the processed material properties under the influence of a smooth and practically non-deformable tool, the roughness of the processed surface decreases (Li, 2018).

External finning by cold knurling is not associated with heavy loads but is accompanied by a deformation of the metal. The maximum allowable deformation during cold knurling is determined by the plastic properties of the billet's material (Johnson, 2000). The metal extruded by the knurling tool flows upward. At the same time, as a result of feeding the knurls or the billet, the deformed metal flows axially in both directions, forming a wave in front of itself. Thus, manufacturing products with a finned heat-exchanging surface have the geometry of the knurled profile, which depends not only on the geometry of the knurling tool, but also on the laws of the metal flow process, which makes it necessary to analyze the processes occurring in the deformation zone during cold knurling (Salunke *et al.*, 2016).

3. MATERIALS AND METHODS:

This study seeks to solve the problem of determining the shape and area of the knurl's contact surface with a ring blank in the following formulation. The model approximation assumes that the elastic deformations of the tool and part are small. The knurl's contact surface with a ring blank is formed in the deformation zone from the cylindrical and conical parts of the tool. The generatrix of the contact surface of the ring blank and the knurl with ring turns is a broken line in longitudinal section $a_1, a_2, a_3 \dots a_i$ (Figure 3).

The generatrix of the knurl's contact surface with the billet for its taper lead (conical) part is denoted by a straight line AB , located at an angle α to the billet's axis. The generatrix of the knurl's contact surface with the billet for its calibrating (cylindrical) part is denoted by a straight line BC parallel to the billet's axis.

The actual length of the contact surface along the finning surface exceeds the nominal length of the contact surface of the cylindrical and conical sections. To account for this difference, it is relevant to introduce two proportionality coefficients that separately consider the excess of the contact surface length for the conical η_{CON} and cylindrical η_{CYL} parts of the knurl, respectively. The length excess coefficient for the contact surface on the conical part of the knurl η_{CON} is defined by Eq. 1:

$$\eta_{CON} = L'_{1CON} / L_{1CON} \quad (\text{Eq. 1})$$

where L'_{1CON} is the length of the actual contact finned surface along with the knurl's taper lead in the longitudinal section; L_{1CON} is the length of the straight conical section along with the apices of the forming tool in the longitudinal section.

The full application of the screw profile in the billet's metal is possible when its outer diameter is equal to or slightly less than the nominal diameter D_{CON1} of the conical part mouth of the tool along with the cutting dents. The actual length of the contact surface, in this case, is determined by Eq. 2:

$$L'_{1CON} = a_1 a_2 + n_{CON} (a_2 a_3 + a_3 a_4) \quad (\text{Eq. 2})$$

where n_{CON} is the number of turns of the conical section; η_{CYL} coefficient considering the excess the contact length of the cylindrical section on the knurl's calibrating part is determined by Eq. 3:

$$\eta_{CYL} = L'_{CYL} / L_{CYL} \quad (\text{Eq. 3})$$

where L'_{CYL} is the actual length of the contact finned surface along with the cylindrical part of the knurl; L_{CYL} is the length of the cylindrical part of the knurl and the finning apices of the tool.

Provided that the screw profile of the tool is completely filled with the billet's metal, the length of the actual contact surface in the longitudinal section L'_{CYL} is determined by Eq. 4:

$$L_{\text{CYL}} = n_{\text{CYL}} (Bb_1 + b_1b_2) \quad (\text{Eq. 4})$$

where n_{CYL} is the number of turns at the cylindrical (calibrating) part of the tool.

Next, it is relevant to determine the contact surface of the billet with a smooth roller (i.e., to a first approximation, without ring cutting). In the process of continuous longitudinal movement of the billet, the generatrix of the contacting conical section AB (Figure 4), before meeting the next knurl, will take the position $A'B'$. With a sufficient degree of accuracy, then it can be assumed that the generatrix of the billet's conical section, $A'B'$, is a straight line. Accordingly, AA' is the axial feed of the billet S_Z to one knurl, and BB' is the total linear displacement of the metal equal to the product of $S_Z \mu_\Sigma$, where μ_Σ is the total rolling-out of the tubular billet in the longitudinal section, determined by Eq. 5:

$$\mu_\Sigma = D_{\text{BM}} t_P / D_{\text{PM}} t_P \quad (\text{Eq. 5})$$

where D_{BM} is the mean diameter of a billet to be knurled; D_{PM} is the mean diameter of a knurled part t_B is the wall thickness of the billet; t_P is the wall thickness of the processed part.

The contact surface of the smooth roller and the ring blank is formed by the intersection of the following surfaces: billet's cylinder/cone of the smooth roller; ring blank cone/knurl cone; ring blank cone/knurl cylinder. Accordingly, the contact surface is divided into sections L_1 , L_2 and L_3 , each of which is determined according to Eqs. 6a-c:

$$L_1 = S_Z \quad (\text{Eq. 6a})$$

$$L_2 = \frac{D_B - D_O - D_P}{2 \tan \alpha} - S_Z = \frac{t_B - t_P + \Delta}{\tan \alpha} - S_Z \quad (\text{Eq. 6b})$$

$$L_3 = S_Z \mu_\Sigma \quad (\text{Eq. 6c})$$

where L_1 is the length of the smooth knurl's contact with the ring blank at the AA' section; L_2 is the length of the smooth knurl's contact with the ring blank at the $A'B$ section; L_3 is the length of the smooth knurl's contact with the ring blank at the BB' section.

The total length of the contact surface L is obtained by summing L_1 , L_2 and L_3 :

$$L = \frac{(D_O - D_T)(t_B - t_P + 1)}{2 \tan \alpha} + S_Z \mu_\Sigma = \frac{\Delta(t_\Sigma + 1)}{\tan \alpha} + S_Z \mu_\Sigma \quad (\text{Eq. 7})$$

where $\Delta t_\Sigma = t_B - t_P$; $\Delta = (D_O - D_P)/2$.

The expression of the total length of the contact surface is valid for the case when the generatrix of the conical and cylindrical sections of the contact surface in a longitudinal section are straight lines. In this case, the generators of the conical and cylindrical sections have the form of broken lines corresponding to the cross-section of the profile of the turns of the knurls. In particular, the profile of the knurl (Figure 3) can serve for finning in the form of an isosceles triangle with an angle between the sides of 55° and with rounded peaks of radius r and spacing S .

To determine the contact surface of the ring blank with a ring cut knurl, it turns to Figure 4, which shows a longitudinal section of the deformation zone and a vertical projection of the longitudinal section of the contacting sections. In the process of continuous longitudinal movement of the billet, the generatrix of the contacting conical part of the knurl, before meeting the next knurl, will assume a position similar to processing with a smooth roller. The only difference is that the generatrix of the conical and cylindrical sections of the knurl is a broken line.

Thus, the total rolling-out of the tubular billet in the longitudinal direction can be determined by Eq. 8, which is similar to Eq. 1, but has different values of some parameters included in it:

$$\mu'_\Sigma = \frac{D'_{\text{BM}} t_B}{D'_{\text{PM}} t'_P} \quad (\text{Eq. 8})$$

where μ'_Σ is total rolling-out of ring blank in the longitudinal direction at knurling finning by the ring-cut knurls; D'_{BM} is the mean diameter of a ring blank; D'_{PM} is the mean diameter of a knurled heat-exchanging part, determined by Eq. 9:

$$D'_{\text{PM}} = D_{\text{PM}} + t_2 / 4 \quad (\text{Eq. 9})$$

where D_{PM} is the mean radius of the pipe without threading; t_2 is the finning height.

Since the midline of the profile is approximately symmetrical to its height, the value of t'_P is determined by Eq. 10, where t_P

denotes the minimum wall thickness of the ring blank at the finning:

$$t'_p = t_p + t_2 / 4$$

(Eq. 10)

Using the above formulas, the final dependence for determining the total rolling-out of the rolling-out in the process of finning on it is obtained (Eq. 11):

$$\mu'_\Sigma = \frac{D'_{BM} t_B}{\left(D_{PM} + \frac{t_2}{2}\right) \left(t_p + \frac{t_2}{2}\right)} \quad (\text{Eq. 11})$$

The contact surface of a roller having an annular cut with a tubular billet is formed by the intersection of the surfaces of the cylindrical part of the billet and the conical part of the knurl; the conical part of the ring blank and the conical part of the knurl; the conical part of the ring blank and the cylindrical part of the knurl. Therefore, by analogy with (6), the contact surface can be conditionally divided into sections L'_1 , L'_2 and L'_3 , the length of each of which is determined in accordance with Eqs. 12a-c:

$$L'_1 = S / z \quad (\text{Eq. 12a})$$

$$L'_2 = \frac{D_B - D_0 - D_M}{2 \tan \alpha} - \frac{S}{z} = \frac{t_B - t_M + \Delta}{\tan \alpha} = \frac{\Delta t_\Sigma + \Delta}{\tan \alpha} - \frac{S}{z} \quad (\text{Eq. 12b})$$

$$L'_3 = S \mu_\Sigma / z \quad (\text{Eq. 12c})$$

where S is the finning spacing; z is the number of knurls in the knurling head.

After adding the lengths of the sections L'_1 , L'_2 and L'_3 , it is obtained the total length of the contact surface (Eq. 13):

$$L' = \frac{\Delta t_\Sigma + \Delta}{\tan \alpha} + \frac{S}{z} \mu_\Sigma \quad (\text{Eq. 13})$$

Considering the coefficients of exceeding the lengths of the contact surface, Eqs. 12a-c can be rewritten in the following form (Eqs. 14a-c):

$$L'_1 = S \eta_{\text{CON}} / z \quad (\text{Eq. 14a})$$

$$L'_2 = \eta_{\text{CON}} \left(\frac{\Delta t_\Sigma + \Delta}{\tan \alpha} - \frac{S}{z} \right) \quad (\text{Eq. 14b})$$

$$L'_3 = \mu_\Sigma \eta_{\text{CYL}} S / z \quad (\text{Eq. 14c})$$

After substitution and transformations, Eq. 13 for determining the total length L' takes the form of Eq. 15:

$$L = \eta_{\text{CON}} \frac{\Delta t_\Sigma + \Delta}{\tan \alpha} + \frac{S \mu_\Sigma \eta_{\text{CYL}}}{z} \quad (\text{Eq. 15})$$

Final determination of the contact surface length of the knurl with a thin-walled ring blank requires expressing the unknown coefficients η_{CON} and η_{CYL} in terms of the known parameters of the knurl, i.e. through r , ε , H , S (Figure 5).

Determining the contact length of the cylindrical section in the longitudinal section does not present significant difficulties if one singles out the profile of one turn, designating its elements in the most general form (Figure 5a). This requires determining archs $\cup BM$, $\cup EB_1F$ and $\cup NB_2$, and segments ME and FN . Following Figure 5, one can write the geometric dependences (Eqs. 16a-c), which ultimately allow for obtaining the dependence (Eq. 16d):

$$OG = EG \sin \varepsilon / 2 = r \sin \varepsilon / 2 \quad (\text{Eq. 16a})$$

$$GG = \frac{H}{n} + r \quad (\text{Eq. 16b})$$

$$CO = GG - OG \quad (\text{Eq. 16c})$$

$$CO = H / n + r (1 - \sin \varepsilon / 2) \quad (\text{Eq. 16d})$$

where n defines CB_1 distance.

Knowing CO , it is easy to find that $EC = AM = ND$ can be expressed by Eq. 17:

$$EC = \frac{CO}{\cos(\varepsilon/2)} = \frac{(H/n) + r [1 - \sin(\varepsilon/2)]}{\cos(\varepsilon/2)} \quad (\text{Eq. 17})$$

Since the segment $ME = AC - 2EC$, then EM is expressed by Eq. 18:

$$EM = \frac{S}{2 \sin(\varepsilon/2)} - 2 \frac{(H/n) + r [1 - \sin(\varepsilon/2)]}{\cos(\varepsilon/2)} \quad (\text{Eq. 18})$$

Figure 5a shows that $\cup BN = \cup EB_1F / 2 = \cup NB_2$, i.e. it is sufficient to determine only one of these values (Eq. 19):

$$LEGF = 2(90^\circ - \varepsilon/2) = 180^\circ - \varepsilon \quad (\text{Eq. 19})$$

Thus, Eq. 20 is obtained, and the contact length of one turn in the cylindrical section, respectively, is expressed by Eq. 21:

$$\cup EB_1F = \frac{2\pi r(180^\circ - \varepsilon)}{360^\circ} = \frac{\pi r(180^\circ - \varepsilon)}{180^\circ} \quad (\text{Eq. 20})$$

$$L'_{\text{CYL}} = 2(ME + EB_1F) \quad (\text{Eq. 21})$$

Substituting the previously found values (Eq. 18) and (Eq. 20) into Eq. 21, it is obtained the dependence (Eq. 22):

$$L'_{\text{CYL}} = \frac{S}{\sin(\varepsilon/2)} + \frac{(2H/n) + 2r[1 - \sin(\varepsilon/2)]}{\cos(\varepsilon/2)} + \frac{\pi r(180^\circ - \varepsilon)}{90^\circ} \quad (\text{Eq. 22})$$

After substituting the L'_{CYL} value in Eq. 3, taking into account the number of turns of the profile on the cylindrical part, it is found the excess coefficient of the contact length of the cylindrical section in the deformation zone (Eq. 23):

$$\eta_{\text{CYL}} = \frac{L'_{\text{CYL}}}{L_{\text{CYL}}} n_{\text{CYL}} \quad (\text{Eq. 23})$$

where n_{CYL} is the number of turns at the cylindrical section of the knurl.

$$L'_{\text{CYL}} = S n_{\text{CYL}} \quad (\text{Eq. 24})$$

By substituting the found values into Eq. 23, and the following is obtained (Eq. 25) after the transformations:

$$\eta_{\text{CYL}} = \frac{1}{\sin(\varepsilon/2)} - \frac{2H + 2rh[1 - \sin(\varepsilon/2)]}{Sh \cos(\varepsilon/2)} + \frac{\pi r(180^\circ - \varepsilon)}{90^\circ} \quad (\text{Eq. 25})$$

It is often more convenient, without setting the parameters r and H , to find the η_{CYL} value through the parameters S and ε . In this case, Eq. 25 will take the following form (Eq. 26):

$$\eta_{\text{CYL}} = \frac{1}{\sin(\varepsilon/2)} - \frac{2[S - \cos(\varepsilon/2)]}{n \cos(\varepsilon/2) \text{ctg}(\varepsilon/2)} + \frac{\pi(180^\circ - \varepsilon)}{90^\circ} \frac{S - 2\cos(\varepsilon/2)}{2Sn[\text{ctg}(\varepsilon/2) - \cos(\varepsilon/2)]} \quad (\text{Eq. 26})$$

The final values of the parameters H and r are determined in S and ε , since the transformations are simple and cumbersome, the intermediate derivation of Eqs. 27a and 27b is not presented:

$$H = S / 2 \text{ctg}(\varepsilon/2) \quad (\text{Eq. 27a})$$

$$r = \frac{S - 2\cos(\varepsilon/2)}{2n \text{ctg}(\varepsilon/2)[1 - \sin(\varepsilon/2)]} \quad (\text{Eq. 27b})$$

When determining the contact length of one turn of the profile on the conical section of the contact surface in the deformation zone, it should be remembered that the generatrix of the conical section, having an angle α with the knurl's axis, somewhat distorts the profile of the turn. It has to be determined the maximum value of the contact length of one turn of finning, taking into account the distortion of the latter in the conical section. Consider the profile of a single turn (Figure 5b-c) for this. Since the turns profile on the knurl's conical part is inclined relative to the profile of the turn of the cylindrical part, provided that the finning spacing S and the rounding radius of the vertices r and dents on both parts of the knurl are maintained, the sides of the profile of the turn at the finned heat transfer strand will have different tilt angles relative to the centerline CC' : $\varepsilon_{1/2}$ and $\varepsilon_{2/2}$. It is known that the angle between the tangent and the chord is measured by half of the arc enclosed inside the central angle. Therefore, the straight line E_1F_1 , resting at the tangency points on two chords located symmetrically to the chord EF intersects each chord at the point of tangency at an angle of $\alpha/2$. If one assumes that $E_1\sigma_2 \approx EO$ and considering that the intersection angle equals to $\alpha/2$, then the equation $\sigma_2O \approx EO \cdot \text{tg}(\alpha/2)$ can be written like that, but since $EO \approx r \cdot \text{tg}(\alpha/2)$, then $\sigma_2O \approx r \cdot \cos(\varepsilon/2) \cdot \text{tg}(\alpha/2)$. The value $E_1\sigma_2$ can be specified in the following way: $E_1\sigma_2 \approx EO - EE'' = r(\cos(\varepsilon/2) - \sin(\varepsilon/2) \cdot \text{tg}(\alpha/2))$. At that, $EE'' \approx \sigma_2O \cdot \text{tg}(\varepsilon/2)$. Accordingly, the unknown angle $\angle \sigma_2E_1i_2$ (Figure 5c) one defines by equality (Eq. 28a), and the analytical value of the angle is expressed through the inverse trigonometric function (Eq. 28b):

$$\cos(\varepsilon_1/2) \equiv \sigma_2 \varepsilon/2 = \cos(\varepsilon/2) - \sin(\varepsilon/2) \operatorname{tg}(\alpha/2) \quad (\text{Eq. 28a})$$

$$\varepsilon_1 = 2 \arccos[\cos(\varepsilon/2) - \sin(\varepsilon/2) \operatorname{tg}(\alpha/2)] \quad (\text{Eq. 28b})$$

The unknown angle $\angle \sigma_2 E_1 i_2$ will be defined in the same way, with the purpose of what one preliminary defines $K_2 F_1$:

$$K_2 F_1 = FO + F'F_1 = r[\cos(\varepsilon/2) + \sin(\varepsilon/2) \operatorname{tg}(\alpha/2)] \quad (\text{Eq. 29})$$

Since $FO = r \cdot \cos(\varepsilon/2)$, a
 $F'F_1 = E'E_1 = r \cdot \cos(\varepsilon/2) \cdot \operatorname{tg}(\alpha/2)$, then the
 analytical value of the ε_2 angle will be expressed
 as the inversed trigonometric function (Eq. 30):

$$\varepsilon_2 = 2 \arccos[\cos(\varepsilon/2) - \sin(\varepsilon/2) \operatorname{tg}(\alpha/2)] \quad (\text{Eq. 30})$$

The obtained expressions (Eq. 28b) and (Eq. 30) allow for determining the length of the contact arcs of the profile turn on the conical part of the knurl (Eq. 31a) and (Eq. 31b):

$$\cup E_1 a_3 \equiv \cup N_1 a_4 = \frac{\pi r \varepsilon_1}{360^\circ} \quad (\text{Eq. 31a})$$

$$\cup F_1 a_3 \equiv \cup N_1 a_4 = \frac{\pi r \varepsilon_2}{360^\circ} \quad (\text{Eq. 31b})$$

The lengths of the contact lengths are expressed in terms of known values by Eqs. 32a and 32b:

$$M_1 E_1 = \frac{Stg\alpha + 2H(1 - 2/n) - 4r[1 - \sin(\varepsilon_1/2)]}{2\cos(\varepsilon_1/2)} \quad (\text{Eq. 32a})$$

$$F_1 N_1 = \frac{Stg\alpha + 2H(1 - 2/n) - 4r[1 - \sin(\varepsilon_2/2)]}{2\cos(\varepsilon_2/2)} \quad (\text{Eq. 32b})$$

The maximum contact length of one turn of the profile on the conical section $L'_{\text{CON}1}$ can be determined by Eq. 33a. After substitution in Eq. 33a of values $M_1 E_1$ и $F_1 N_1$, Eq. 33b is obtained:

$$L'_{\text{CON}1} = 2 \cup E_1 a_3 + 2 \cup F_1 a_3 + F_1 N_1 + E_1 M_1 \quad (\text{Eq. 33a})$$

After that, taking into account the number of turns on the conical part of the knurl, one finds the value of the coefficient of the contact length excess of the conical section in the deformation zone (Eq. 34):

$$\eta_{\text{CON}} = \frac{L'_{\text{CON}} n_{\text{CON}}}{L_{\text{CON}}} = \frac{L'_{\text{CON}} n_{\text{CON}} \cos \alpha}{S n_{\text{CON}}} \quad (\text{Eq. 34})$$

where n_{CON} is the number of turns at the conical section of $L_{\text{CON}} = S \cdot n_{\text{CON}}$. In the end, Eq. 34 will take the form shown in the appendix (Eq. 35).

The width of the contact surface b_x can be determined using the following formula (Eq. 36):

$$b_x = \sqrt{\delta t_x \frac{Dd}{D+d}} \quad (\text{Eq. 36})$$

where D is the knurl's engagement diameter, calculated according to the formula $D = D_1 - \xi(D_H - d_1)$; d is the engagement diameter of the finning, which is equal to $d = d_1 - \xi(D_H - d_1)$; δt_x is the reduction in the section; ξ is the engagement coefficient depending on the profile; D_H is outer diameter along with the vertices; D_1 is the knurl's outer

diameter; d_1 is the inner diameter along with the dents.

It is known that the rotation from the knurks to the deformable part during the knurling is transmitted without slipping only in section along the height of the profile. The diameters of the knurls and parts corresponding to this section are the engagement radii. Suppose one assumes that the specific forces during plastic deformation on the contact surfaces are equal along the entire profile. In that case, the magnitude of the engagement diameter is determined from the condition of equality of sliding friction over sections of the profile that lie above and below the engagement radius. Therefore, calculation of the width of the contact surface uses the engagement diameters presented in the formula D и d .

Reduction size at the borders of the sections L_1 and L_2 (Figure 4), respectively, will be determined by Eq. 37a, and at the borders of the sections L_2 and L_3 – by Eq. 37b.

$$\delta t_1 = m \eta_{\text{CON}} \operatorname{tg} \alpha \quad (\text{Eq. 37a})$$

$$\delta t_2 = \frac{m \mu_{\Sigma} \eta_{\text{CON}} \eta_{\text{CYL}} (\Delta t_{\Sigma} + \Delta) \operatorname{tg} \alpha}{\eta_{\text{CON}} (\Delta t_{\Sigma} + \Delta) + m (\mu_{\Sigma} \eta_{\text{CYL}} - \eta_{\text{CON}}) \operatorname{tg} \alpha} \quad (\text{Eq. 37b})$$

Further, analyzing the ratio (Eq. 38)

$$\frac{\delta t_2}{\delta t_1} = \frac{\mu_\Sigma (\Delta t_\Sigma + \Delta)}{(\Delta t_\Sigma + \Delta) + m(\mu_\Sigma - 1) \text{tg}\alpha} \quad (\text{Eq. 38})$$

At $\Delta = 0$ and $D_B = D_P$, $\mu_\Sigma = t_B/t_P$. Then $\delta t_2/\delta t_1 = t_B / (t_P + m \text{tg}\alpha)$.

At $(m \text{tg}\alpha) < \Delta t_\Sigma$ the ratio is $(\delta t_2 / \delta t_1) > 1$, i.e. the minimum reduction corresponds to the section limits L_2 and L_1 . The width of the deformation zone at the border of each section (Eq. 39a) and (Eq. 39b):

$$b_1 = \sqrt{\frac{m\eta_{\text{CON}} D_{\text{LIM}} \text{tg}\alpha}{2}} \quad (\text{Eq. 39a})$$

$$b_2 = \frac{mD_{\text{LIM}}\mu_\Sigma\eta_{\text{CON}}\eta_{\text{CYL}}(\Delta t_\Sigma + \Delta)\text{tg}\alpha}{2\eta_{\text{CON}}(\Delta t_\Sigma + \Delta) + m(\mu_\Sigma\eta_{\text{CYL}} - \eta_{\text{CON}})\text{tg}\alpha} \quad (\text{Eq. 39b})$$

Thus, Eqs. 1-39 determine all the characteristic dimensions of the metal contact surface of ring blank with knurls, the horizontal projection of which resembles a curved trapezoid in shape.

4. RESULTS AND DISCUSSION:

The main task when introducing the process of rolling ribs is to achieve the required accuracy of the workpiece. The main reason for the formation of defects during the technological process of rolling is associated with the conditions for forming rib profiles. Extrusion of the profile is carried out due to the redistribution of elementary volumes of metal, displaced by the working turns of the forming tool. In the process of extrusion of the profile, both symmetric and asymmetric deformation may occur. The nature of the deformation depends on the path of the working turns of the rolling tool along the surface of the formed rib. The formation of defects at the top of the rib profile is possible due to symmetric deformation. However, defects on the rib profile can have a different location, depending on the amount of displacement of the tool profile in the deformation cycle. Controlling deformed metal flow is an important condition for the rolling process (Jiang *et al.*, 2010; Feng and Wang, 2004; Zhang *et al.*, 2014; Aljabri, Jiang and Wei, 2014).

The experimental studies of the imprints of the contact surface of the knurled billet confirmed the correctness of the proposed

methodology and formulas for calculating the contact surface of metal with the knurl. Since in practice $m\eta_{\text{CON}} \ll \eta_{\text{CON}}(\Delta t_\Sigma + \Delta)/\text{tg}\alpha$, i.e. $L_1 \ll L_2 + L_1$, then, without a large error, the sides of the trapezoid can be straightened, and then the vertical and horizontal projections of the contact surface of the billet's metal with the knurl are determined by Eqs. 40a and 40b:

$$F_{\text{VERT}} = \frac{\delta t_1 b_1 + b_2 \delta t_2 + (b_1 + b_2)(\Delta t_\Sigma + \Delta \delta t_2 - \delta t_2)}{2} \quad (\text{Eq. 40a})$$

$$F_{\text{HOR}} = \frac{(L_1 b_1 + L_3 b_2) + L_2 (b_1 + b_2) / 2}{2} \quad (\text{Eq. 40b})$$

As it can be seen from Figure 5, filling strands in the deformation zone depends on the billet's diameter: the larger its diameter, the larger the filling strands is, and the more contact has the billet with the knurl, and the larger the billet coverage perimeter of the knurl is. and the higher the η_{CON} and η_{CYL} coefficients are. Accordingly, for certain ratios of diameter to wall thickness, the diameter of a thin-walled pipe should vary from D'_{BMIN} to D'_{BMAX} (Figure 6), where D'_{BMIN} is the minimum outer diameter of the blank pipe to be knurled; D'_{BMAX} is the maximum outer diameter of the blank pipe to be knurled. In this case, the minimum diameter of the pipe D'_{BMIN} should, accordingly, be in the range from the minimum outer finning diameter d'_{OMIN} to the maximum finning diameter d'_{OMAX} . If the minimum outer diameter of the pipe is determined by the outer largest mouth diameter of the working solution D_{CON1} of the knurl's conical part during their installation (Figure 6), then $D_{\text{BMAX}} \leq D_{\text{CON1}}$. Thus, the larger the billet's diameter, the greater the η_{CON} and η_{CYL} values in Eqs. 12a-c, and since $\eta_{\text{CON}} > 1$ and $\eta_{\text{CYL}} > 1$, the contact surface length L increases with increasing billet's diameter.

Analysis of Eqs. 37a, b allows for stating that with an increase in the billet's diameter, the amount of compression at the boundary of the sections L_1 and L_2 , as well as L_2 and L_3 also increases. Thus, the length of the contact surface with a certain ratio of diameter to wall thickness increases with increasing billet's diameter from minimum to maximum. Similarly, with an increase in the length of the contact surface, the number of compression increases. The reduction, according to Eqs. 37a, b increases with increasing billet's diameter from minimum to maximum. It is known that the knurling force P_{ROL} directly depends on the width

and length of the contact surface, i.e. $P_{ROL} = \rho F_C$, where ρ are specific pressing forces at knurling; F_C is the contact area. Respectively, at $\rho = \text{const}$ there are the following ratios of the forces: $P_{ROL} > P_{ROL}$ at $F > F_C$; $P_{ROL} < P_{ROL}$ at $F < F_C$. Thus, the knurling force will increase with increasing length of the contact surface, which is ultimately proportional to the billet's diameter (in a wide range of diameter to wall thickness ratios).

Cold plastic deformation has a significant effect on the physical and mechanical properties, macro- and microstructure of the processed metal. As a result of cold deformation, the initial metal, which had properties approximately the same in different directions and a chaotically oriented structure, receives a directionally oriented fibrous structure and increased anisotropic mechanical characteristics. The change in metal properties depends on the degree of plastic deformation, with an increase in which all characteristics of the metal's resistance to deformation increase, namely, the strength of the metal increases, and the hardness and fluidity increase. At the same time, the values of plasticity decrease: the relative elongation and impact strength decrease. The effect of cold plastic deformation on the surface quality of parts is especially significant.

5. CONCLUSIONS:

Method for the high-performance manufacturing of fins by cold knurling, compared with cutting, reduces labor intensity by two to six times with a significant increase in the operational properties of the product. The disadvantage of the cold knurling method with ring-cut knurls can be unwanted surface defects and deformations of the entire product. Obtaining finned surfaces on ring blanks with high surface quality during knurling requires for accurate calculation of the ratio of longitudinal and transverse strains.

The manuscript proposed a method for calculating the knurl's contact surface with a pipe when knurling with ring-cut knurls, which allows for estimating the recommended range of pipe sizes for knurling. Based on the above-listed dependencies, the limiting sizes for blank pipes were calculated to ensure high-quality finning. The authors experimented with cold finning on pipes with different length and diameter ratios, confirming the possibility of using the proposed methodology for calculating the knurl's contact surface with a pipe when finning with ring-cut

knurls. The main reason for the formation of defects during the technological process of rolling is associated with the conditions for the formation of rib profiles. Extrusion of the profile is carried out due to the redistribution of elementary volumes of metal, displaced by the working turns of the forming tool. It should be noted that the most important factors determining the ratio of longitudinal and transverse strains (rolling-out and rolling-off) are the length and width of the contact surface. No defects are observed at the ribs under the recommended rolling conditions.

6. ACKNOWLEDGEMENTS:

Some results of this manuscript were obtained as part of the work under the Agreement on the provision of subsidies under date of 13 December 2019 No. 075-15-2019-1941 (the agreement internal number 05.607.21.0321) on the topic: "Development of design and technological solutions for modular prefabricated transmission line towers with integrated systems for continuous digital monitoring of the condition and thermal stabilization of the soil to meet the needs of the Arctic regions and the Far North" with the Ministry of Science and Higher Education of the Russian Federation. The unique identifier of the applied research (project) is RFMEFI60719X0321.

7. REFERENCES:

1. Alexandrov, I.A., Sheptunov, S.A. and Sannikov, A.S. (2019, 23-27 September). *Some approaches to the formalization principles of achieving the target properties of products in the automation of technological processes in mechanical engineering*. Paper presented at the International Conference "Quality Management, Transport and Information Security, Information Technologies". doi:10.1109/itqmis.2019.8928338
2. Aljabri, A., Jiang, Z.Y., and Wei, D.B. (2014). Analysis of Thin Strip Profile during Asymmetrical Cold Rolling with Roll Crossing and Shifting Mill. *Advanced Materials Research*, 894, 212–216. doi: 10.4028/www.scientific.net/amr.894.212
3. Bower, A.F. and Johnson, K.L. (1989). The influence of strain hardening on

- cumulative plastic deformation in rolling and sliding line contact. *Journal of the Mechanics and Physics of Solids*, 37(4), 471-493. doi:10.1016/0022-5096(89)90025-2
4. Čarija Z., Franković B., Perčić M., and Čavrak M. (2014). Heat transfer analysis of fin-and-tube heat exchangers with flat and louvered fin geometries. *International Journal of Refrigeration*, 45, 160–167. doi:10.1016/j.ijrefrig.2014.05.026
 5. Cherkashina, O. (2019). Management of quality of technological processes in mechanical engineering using three-parameter modeling. *Engineering*, 23, 159–165. doi:10.32820/2079-1747-2019-23-159-165
 6. Feng, C.-X.J., and Wang X.-F. (2004). *Data mining techniques applied to predictive modeling of the knurling process*. IIE Transactions, 36(3), 253–263. doi: 10.1080/07408170490274214
 7. Filippov, E.B., Cherepennikov, G.B., and Leshchenko, T.G. (2010). A numerical study of the thermal efficiency of a tubular heating surface with split spiral-tape finning. *Thermal Engineering*, 57(7), 598–602. doi:10.1134/s0040601510070116
 8. Galushchak, I. (2017). Experimental investigation of heat transfer in interfin channels of punched spiral tube finning. *Technology Transfer: Fundamental Principles and Innovative Technical Solutions*, 12–14. doi:10.21303/2585-6847.2017.00473
 9. Hakansson, H. (2015). *Industrial technological development (Routledge revivals): A network approach*. London, United Kingdom: Routledge. doi:10.4324/9781315724935
 10. Hitomi, K. (2017). *Manufacturing systems engineering*. London, United Kingdom: Routledge. doi:10.1201/9780203748145
 11. Jiang, Z.Y. (2011). Mechanics of cold rolling of thin strip. In J. Awrejcewicz (Ed.). *Numerical analysis: Theory and application*. IntechOpen. doi:10.5772/23344
 12. Jiang, Z.Y., Du, X.Z., Du, Y.B., Wei, D.B., and Hay, M. (2010). Strip Shape Analysis of Asymmetrical Cold Rolling of Thin Strip. *Advanced Materials Research*, 97-101, 81–84. doi:10.4028/www.scientific.net/amr.97-101.81
 13. Johnson, K.L. (2000). Plastic deformation in rolling contact. In B. Jacobson and J.J. Kalker (Eds.), *Rolling contact phenomena* (Vol. 411, pp. 163-201). Vienna, Austria: Springer. doi:10.1007/978-3-7091-2782-7_3
 14. Kar'kina, L.E., Zubkova, T.A. and Yakovleva, I.L. (2013). Dislocation structure of cementite in granular pearlite after cold plastic deformation. *The Physics of Metals and Metallography*, 114(3), 234-241. doi:10.1134/s0031918x13030095
 15. Kim, K., and Lee, K.-S. (2013). Frosting and defrosting characteristics of surface-treated louvered-fin heat exchangers: Effects of fin pitch and experimental conditions. *International Journal of Heat and Mass Transfer*, 60, 505–511. doi:10.1016/j.ijheatmasstransfer.2013.01.036
 16. Kocurek, R., and Adamiec, J. (2013). Manufacturing Technologies of Finned Tubes. *Advances in Materials Sciences*, 13(3). doi:10.2478/adms-2013-0009
 17. Kopp, R. (1996). Some current development trends in metal-forming technology. *Journal of Materials Processing Technology*, 60(1-4), 1-9. doi:10.1016/0924-0136(96)02301-1
 18. Kulikov, M.Y., Larionov, M.A., Sheptunov, S.A. and Gusev, D.V. (2016, 4-11 October). *The influence of pre-settings of the automated system rapid prototyping on the qualitative characteristics of formation*. Paper presented at the IEEE Conference on Quality Management, Transport and Information Security, Information Technologies. doi:10.1109/itmqs.2016.7751916
 19. Kulikov, M.Y., Sheptunov, S.A., Larionov, M.A. and Gusev, D.V. (2017, 24-30 September). *Manufacturing of highquality products to the method of DLP RP — Technology*. Paper presented at the International Conference “Quality

- Management, Transport and Information Security, Information Technologies". doi:10.1109/itmqls.2017.8085932
20. Kulikov, M.Y., Yagodkin, M.V., Larionov, M.A. and Sheptunov, S.A. (2017, 24-30 September). *The anodic mechanical machining application for thread cutting of small diameters*. Paper presented at the International Conference "Quality Management, Transport and Information Security, Information Technologies". doi:10.1109/itmqls.2017.8085931
 21. Kuzma-Kichta, Y.A., Savel'ev, P.A., Koryakin, S.A., and Dobrovol'skii, A.K. (2007). Studying of heat-transfer enhancement in tubes with screw knurling. *Thermal Engineering*, 54(5), 407–409. doi:10.1134/s0040601507050138
 22. Li, Z. (2018). Elastic deformation of surface topography under line contact and sliding-rolling conditions. *Journal of Mechanical Engineering*, 54(5), 142-148. doi:10.3901/jme.2018.05.142
 23. Liu, B., Tang, C.L. and Gu, T.Q. (2014). A method to avoid strip breakage for thin strip steel in cold rolling. *Advanced Materials Research*, 1004-1005, 1211-1215. doi:10.4028/www.scientific.net/amr.1004-1005.1211
 24. McDowell, D.L. and Moyer, G.J. (1991). Effects of non-linear kinematic hardening on plastic deformation and residual stresses in rolling line contact. *Wear*, 144, 19-37. doi:10.1016/b978-0-444-88774-0.50006-7
 25. Merkulov, D.V. (2008). Pipe rolling in helical-rolling mills without a guide system. *Steel in Translation*, 38(7), 580–584. doi:10.3103/s096709120807022x
 26. Olejnik, A.V., Kapitanov, A.V., Alexandrov, I.A. and Tatarkanov, A.A. (2020a). Calculation methodology for geometrical characteristics of the forming tool for rib cold rolling. *Journal of Applied Engineering Science*, 18(2), 292-300. doi:10.5937/jaes18-25211
 27. Qiao, X.G., Gao, N. and Starink, M.J. (2012). A model of grain refinement and strengthening of Al alloys due to cold severe plastic deformation. *Philosophical Magazine*, 92(4), 446-470. doi:10.1080/14786435.2011.616865
 28. Paquet, A. (1993). Comparison of Brazing Processes for Aluminum Heat Exchanger Manufacturing. *SAE Technical Paper Series*. doi:10.4271/931093
 29. Sakai, T., Belyakov, A., Kaibyshev, R. and Miura, H. (2014). Dynamic and post-dynamic recrystallization under hot, cold and severe plastic deformation conditions. *Progress in Materials Science*, 60, 130-207. doi:10.1016/j.pmatsci.2013.09.002
 30. Salunke, K.A., Lambhate, V., Jadhav, U., and Kumbhar, S. (2016). Optimization of Pipe Finning Process with Engineering Principles. *International Journal of Science and Research (IJSR)*, 5(3), 270–272. doi:10.21275/v5i3.nov161849
 31. Sawicki, S., and Dyja, H. (2010). Theoretical and Experimental Analysis of the Bimetallic Ribbed Bars Steel - Steel Resistant to Corrosion Rolling Process. *Archives of Metallurgy and Materials*, 57(1). doi:10.2478/v10172-011-0153-2
 32. Song, M., Liu, X.H., and Tang, D.L. (2014). Texture Evolution of Commercially Pure Copper during Ultra-Thin Strip Rolling. *Advanced Materials Research*, 941-944, 1532–1536. doi:10.4028/www.scientific.net/amr.941-944.1532
 33. Semenov, A.B., Fomina, O.N., Muranov, A.N., Kutsbakh, A.A. and Semenov, B.I. (2019a). The modern market of blank productions in mechanical engineering and the problem of standardization of new materials and technological processes. *Advanced Materials and Technologies*, 1, 3-11. doi:10.17277/amt.2019.01.pp.003-011
 34. Semenov, A.B., Kutsbakh, A.A., Muranov, A.N. and Semenov, B.I. (2019b). Metallurgy of thixotropic materials: the experience of organizing the processing of structural materials in engineering Thixo and MIM methods. *IOP Conference Series: Materials Science and Engineering*, 683, 012056. doi:10.1088/1757-899x/683/1/012056
 35. Strycharska, D. (2019). Analysis of roll wear costs during multi-strand rolling of

- ribbed bars using new slitting pass system. *New Trends in Production Engineering*, 2(2), 267-278. doi:10.2478/ntpe-2019-0091
36. Wang, S., Cheng, S., Yu, H., Rao, Z., and Liu, Z. (2013). Experimental investigation of Al–Cu composed tube–fin heat exchangers for air conditioner. *Experimental Thermal and Fluid Science*, 51, 264–270. doi: 10.1016/j.expthermflusci.2013.08.007
 37. Yakovleva, I.L., Kar’kina, L.E. and Zubkova, T.A. (2011). Effect of cold plastic deformation on the structure of granular pearlite in carbon steels. *The Physics of Metals and Metallography*, 112(1), 101-108. doi:10.1134/s0031918x11010388
 38. Yoshimi, T., Matsumoto, S., Tozaki, Y., Yoshida, T., Sonobe, H. and Nishide, T. (2009). Work hardening and change in contact condition of rolling contact surface with plastic deformation. *Tribology Online*, 4(1), 1-5. doi:10.2474/trol.4.1
 39. Zhang, P., Kou, S., Lin, B., and Wang, Y. (2014). Optimization for radial knurling connection process of assembled camshaft using response surface method. *The International Journal of Advanced Manufacturing Technology*, 77(1-4), 653–661. doi:10.1007/s00170-014-6486-z
 40. Zheng, D. (2014, 10-11 July). *Industrial engineering and manufacturing technology*. Paper presented at the International Conference on Industrial Engineering and Manufacturing Technology. doi:10.1201/b18144

$$L'_{\text{CON1}} = \frac{\pi r (\varepsilon_1 + \varepsilon_2)}{180^\circ} + \frac{2H(1-2/n) - \text{Stg}\alpha - 4r[1 - \sin(\varepsilon_1/2)]}{2\cos(\varepsilon_1/2)} + \frac{2H(1-2/n) + \text{Stg}\alpha + 4r[1 - \sin(\varepsilon_2/2)]}{2\cos(\varepsilon_2/2)} \quad (\text{Eq. 33b})$$

$$\eta_{\text{CON}} = \frac{\pi r (\varepsilon_1 + \varepsilon_2) \cos(\alpha/S)}{180^\circ} + \psi;$$

$$\psi = \frac{\cos \alpha}{2S} \left[\frac{2H(1-2/n) - \text{Stg}\alpha - 4r[1 - \sin(\varepsilon_1/2)]}{\cos(\varepsilon_1/2)} + \frac{2H(1-2/n) + \text{Stg}\alpha + 4r[1 - \sin(\varepsilon_2/2)]}{\cos(\varepsilon_2/2)} \right] \quad (\text{Eq. 35})$$



Figure 1. Finned tube heat exchanger

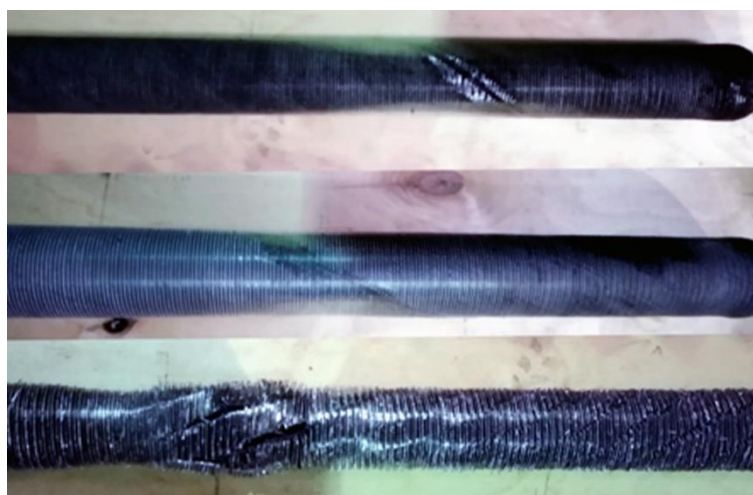


Figure 2. Possible unacceptable defects at cold knurling

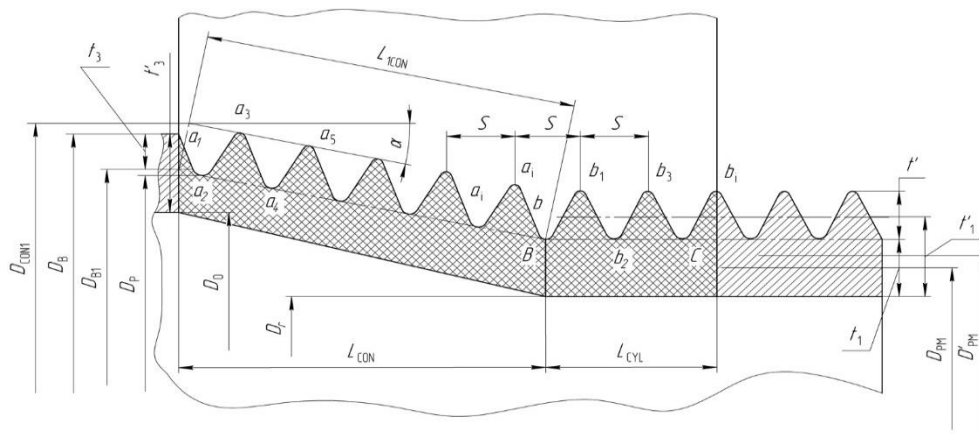


Figure 3. Frontal section of the deformation zone and projection of the contact surface

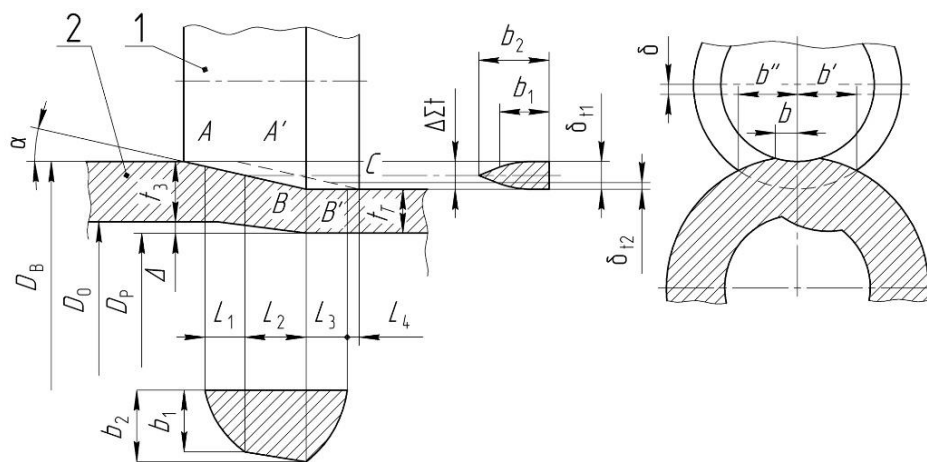


Figure 4. Frontal and profile sections of the deformation zone and projection of the contact surface: 1 - knurl; 2 - ring blank

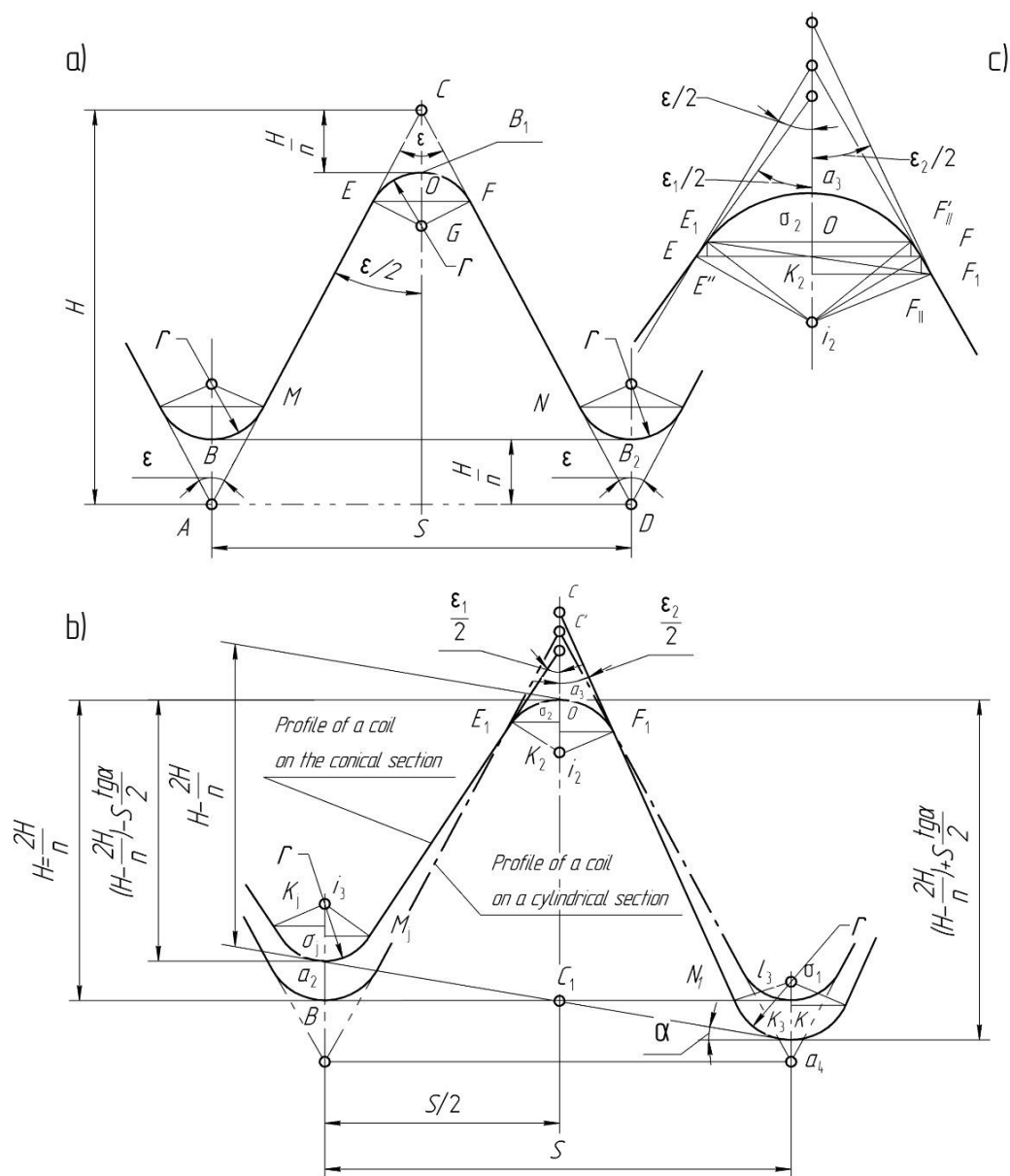


Figure 5. Profile of a turn of a ring-cut knurl: a) in a cylindrical section; b), c) - on the cylindrical and conical sections (diagrams of the relations of the geometric dimensions of the profile of the turn)

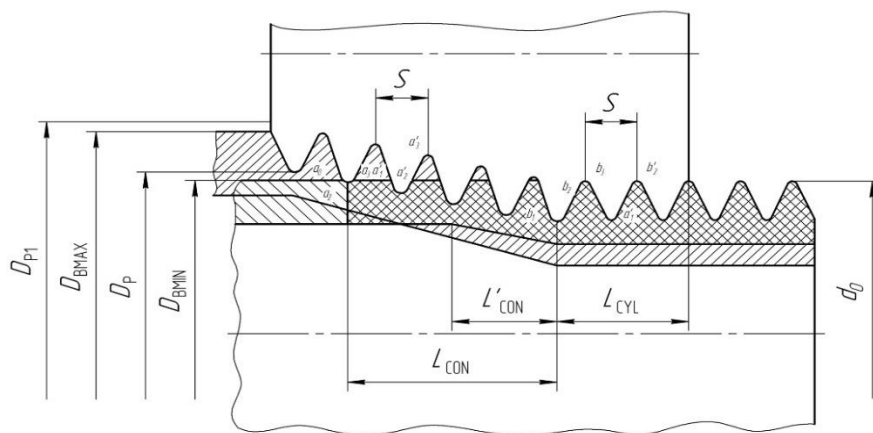


Figure 6. Dimensions of the deformation zone depending on the billet's diameter

8. APPENDIX:

THE LEGEND OF ABBREVIATIONS:

b_x – the width of the contact surface;
 b_1 – deformation zone width at the border of the 1st section;
 b_2 – deformation zone width at the border of the 2nd section;
 d – engagement diameter of the finned surface;
 d_1 – inner diameter of the finned surface along with the dents;
 d'_{0MIN} – minimum outer diameter of the finned surface;
 d'_{0MAX} – maximum outer diameter of the finned surface;
 D – the knurl's engagement diameter;
 D_1 – the knurl's outer diameter;
 D_{BM} – the mean diameter of a billet to be knurled;
 D_{BMAX} – maximum diameter of a billet to be knurled;
 D_{BM} – the mean diameter of a ring blank;
 D'_{BMIN} – minimum outer diameter of a blank pipe to be knurled;
 D'_{BMAX} – maximum outer diameter of a blank pipe to be knurled;
 D_H – outer diameter of the finned surface along with the vertices;
 D_{PM} – the mean diameter of a knurled part;
 D'_{PM} – the mean diameter of a knurled finned part;
 D_{CON1} – nominal mouth diameter of the conical portion of the tool along with the dents;
 F_C – contact area at knurling;
 F_{HOR} – horizontal plan of the billet metal contact surface with the knurl;
 F_{VERT} – vertical plan of the billet metal contact surface with the knurl;
 H – theoretical height of the initial triangular profile of the forming tool;

L – the total length of the smooth knurl's contact surface and the ring blank;

L_1 – the length of the smooth knurl's contact with the ring blank at the AA' section;

L_2 – the length of the smooth knurl's contact with the ring blank at the $A'B$ section;

L_3 – the length of the smooth knurl's contact with the ring blank at the BB' section;

L – total length of the pipe billet and the ring-cut knurl;

L'_i – length of the pipe billet's contact surface and the ring-cut knurl;

L_{1CON} – the length of the straight conical section along with the apices of the forming tool;

L_{CYL} – the length of the cylindrical part of the knurl along with the apices of the forming tool;

L'_{1CON} – the length of the actual contact finned surface along with the knurl's taper lead;

L'_{CYL} – the actual length of the contact finned surface along with the cylindrical part of the knurl;

n_{CON} – the number of turns of the conical section;

n_{CYL} – the number of turns at the cylindrical (calibrating) part of the tool;

P_{ROL} – the knurling force;

r – the rounding radius at the finning apices at the processing knurl;

S_z – spacing equal to the length of the L_1 section of the contact surface of the smooth roller and the ring blank;

S – fin spacing at the processing knurl;

t_i – finning height;

t_B – the wall thickness of the billet;

t_P – minimum wall thickness of the billet;

z – the amount of knurls in the processing head;

Δt_z – the difference between t_B and t_P ;

Δ – half of the difference between D_0 and D_P ;

δt_x – reduction;

α – the angle between the billet's axis and billet's forming surface contacting the knurl;

ε – the pressure angle at the apex of the initially finning triangle at the process tool;

ξ – the engagement coefficient depending on the finning characteristics;

η_{CON} – the proportionality coefficient, considering the excess length of the contact surface for the conical part of the knurl;

η_{CYL} – the proportionality coefficient, considering the excess length of the contact surface for the cylindrical part of the knurl;

μ_{Σ} – total rolling-out of the pipe billet in longitudinal section;

μ'_{Σ} – total rolling-out of ring blank in the longitudinal direction at knurling finning by the ring-cut knurls;

ρ – specific pressing forces at knurling.

APLICAÇÃO DE TECNOLOGIAS DE GEOINFORMAÇÃO E SENSORIAMENTO REMOTO PARA DETECTAR O USO DA TERRA E MUDANÇAS NA COBERTURA DO SOLO CAUSADA PELA SECAGEM DO MAR DE ARAL**APPLICATION OF GEOINFORMATION TECHNOLOGIES AND REMOTE SENSING TO DETECT LAND USE AND CHANGES IN THE SOIL COVER CAUSED BY THE DRYING OF THE ARAL SEA****ПРИМЕНЕНИЕ ГЕОИНФОРМАЦИОННЫХ ТЕХНОЛОГИЙ И ДИСТАНЦИОННОГО ЗОНДИРОВАНИЯ, ДЛЯ ОБНАРУЖЕНИЯ ЗЕМЛЕПОЛЬЗОВАНИЯ И ИЗМЕНЕНИЙ В ЗЕМНОМ ПОКРОВЕ, ВЫЗВАННЫХ ВЫСЫХАНИЕМ АРАЛЬСКОГО МОРЯ**

SAFAROV, Eshkabil¹; PRENOV, Shavkat^{2*}; BEKANOV, Kuatbay³;
SALOKHITDINOVA, Sevar⁴; UVRAYIMOV, Sunnatilla⁵

^{1,2,3,4,5} National University of Uzbekistan named after Mirzo Ulugbek, Department of Cartography. Uzbekistan.

* *Corresponding author*
e-mail: shavkat04@mail.ru

Received 01 June 2020; received in revised form 16 August 2020; accepted 2 September 2020

RESUMO

Está estabelecido que o problema do Mar de Aral, devido ao impacto negativo da atividade humana ao longo do tempo, levou à degradação ambiental na região do Mar de Aral, bem como a mudanças na cobertura do solo. A extensão deste problema ambiental pode ser detectada usando tecnologias de geoinformação e métodos de sensoriamento remoto. Neste estudo, o algoritmo de classificação de máxima verossimilhança foi aplicado na apresentação das imagens do Landsat para detectar alterações na cobertura do solo com base em dados de satélite multiespectrais obtidos do Landsat 7 e Landsat 8 para 2008 e 2018, respectivamente. Os mapas de uso da terra resultantes indicam um aumento significativo de áreas salinas de 18% para 22% durante o período estudado. Essas transformações de terras representam uma séria ameaça aos recursos terrestres da área. Consequentemente, é necessária uma gestão adequada dos recursos da terra para preservá-los e garantir que eles continuem a desempenhar seu papel no desenvolvimento socioeconômico da região.

Palavras-chave: *Terra, Mudança no uso da terra, Classificação, Sensoriamento remoto, Sistema de informação geográfica.*

ABSTRACT

It is established that the Aral Sea problem, which is due to the negative impact of human activity over time, has led to environmental degradation in the Aral Sea region and changes in the soil cover. The extent of this ecological problem can be detected using geoinformation technologies and remote sensing methods. In this study, the maximum likelihood classification algorithm was applied in the presentation of Landsat images to detect changes in the soil cover based on multispectral satellite data obtained from Landsat 7 and Landsat 8 for 2008 and 2018, respectively. The resulting land-use maps indicate a significant increase in saline land from 18% to 22% during the period under study. These land transformations pose a severe threat to the land resources of the area. Consequently, proper management of the land resources is required to preserve them and to ensure that they continue to play their part in the socio-economic development of the region.

Keywords: *Land, Land use change, Classification, Remote sensing, Geographic information system.*

АННОТАЦИЯ

Как известно, проблема Аральского моря, вызванная негативным воздействием деятельности человека в течение прошедшего периода, привела к деградации окружающей среды в районе Аральского моря и изменениям в земном покрове, и выявить такую экологическую проблему можно обнаружение на основе геоинформационных технологий и методов дистанционного зондирования является эффективным решением. В исследовании был применен алгоритм классификации максимального правдоподобия в

представлении снимков Landsat для обнаружения изменений почвенного покрова, по многоспектральным спутниковым данным, полученным с Landsat 7 и Landsat 8 за 2008 и 2018 годы соответственно. Результирующие карты землепользования, созданные в ArcGIS 10.1, указывают на значительный рост засоленных земель с 18% до 22% соответственно. Эти преобразования земель представляют серьезную угрозу для земельных ресурсов района. Следовательно, требуется надлежащее управление земельными ресурсами района, иначе эти ресурсы вскоре будут потеряны и больше не смогут играть свою роль в социально-экономическом развитии района.

Keywords: *Земельные угодья, изменение землепользования, классификация, дистанционное зондирование, геоинформационная система.*

1. INTRODUCTION:

The world is currently undergoing significant changes due to the negative impact of human activities. Climate change and its consequent various natural disasters are being felt globally, while changes in the human environment due to the strong anthropogenic implications for living and non-living components are causing environmental problems on the local, regional, and global scales. Among others, these issues have led to the emergence of the Aral Sea problem, which is one of the most dangerous environmental crises in the region (Golubov, 2018; Karakus, Cerit, and Kavak, 2015; Rafihov, Ergashev, and Khaidarov, 1997).

Over the past 40-45 years, the water level in the Aral Sea has decreased by 22 meters, the water area has decreased more than 4-fold, the volume of water has reduced 10-fold (from 1064 km³ to 70 km³), and the salt content in the water is 112 g / l. Because of the above, the Aral Sea is now practically a "dead" sea. The drying area of the sea encompasses 4.2 million hectares and has become a source of dust, sand, and salt aerosols, which have spread to the surrounding areas. It is estimated that between 80 and 100 million tons of dust have been produced. As a result, the environmental situation in the Aral Sea region is deteriorating, leading to significant environmental changes, whereby the environmental problems are primarily associated with land use and changes in land cover (Aidarov and Pankova, 2007; Degife, Zabel, and Mauser, 2018; Jazouli, Barakat, Khellouk, Rais, and Baghdadi, 2019; Micklin, 2014; Safari and Sohrabi, 2019; Tang, Zhang, Jing, and Gao, 2018; White, 2013).

In studying changes in earth's crust, global changes play a significant role. Data on land use and land cover change represent a crucial source of information for environmental monitoring, land-use planning, and the prediction of future land conditions. Determining land use potential, including soil capabilities and other characteristics, is key to conducting regional

planning studies (Karakus *et al.*, 2015; Reis, 2008; Srivastava, Singh, Gupta, Thakur, and Mukherjee, 2013).

Remote sensing and geographic information technologies (GIS) provide accurate, reliable data on current and emerging changes in land use and land cover (Alam, Bhat, and Maheen, 2019; Jovanovic *et al.*, 2015; Lambin, Geist, and Lepers, 2003; Schaefer and Thinh, 2019). Meanwhile, research conducted by organizations and academic institutions worldwide is mainly focused on studying the changes in land use and land cover (Degife *et al.*, 2018; Schaefer and Thinh, 2019). Over the past 15 years, remote sensing data have been widely used to determine land-use changes and land cover changes. The usefulness of remote sensing data is also recognized globally (Gadrani, Lominadze, and Tsitsagi, 2018; Xian *et al.*, 2020).

High-resolution aerial photography, aerial photography, and drones are the best way to detect changes in any given region. However, due to the high cost of obtaining such data, Landsat satellite imagery can also be used to study large areas. The use of the Landsat data is almost free (Gadrani *et al.*, 2018), and the Landsat archive contains information on land management from 1970 to the present (Gadrani *et al.*, 2018).

The object of the study is the Chimbay district of the Republic of Karakalpakstan, about 150 km from the dry Aral Sea in the Republic of Uzbekistan. This area was chosen for the study as it has the most significant number of irrigated lands in the Aral Sea region (Bekchanov, Ringler, Bhaduri, and Jeuland, 2016; Breckle, Wucherer, Dimeyeva, and Ogar, 2012). Quantitative data show that in recent years there has been an increase in soil salinization, a decrease in productivity, an increase in the incidence of the population, and a significant increase in soil erosion, as well as a substantial reduction in agricultural production. It is observed that the local conditions in this area have deteriorated significantly (Abdullaev, 2018).

This study aimed to use GIS and remote sensing to identify land use and land cover changes in the Chimbay district of the Republic of Karakalpakstan.

2. MATERIALS AND METHODS:

2.1. Area of research

The Chimbay region of the Republic of Karakalpakstan was chosen as the object of study. Chimbay district was formed in 1927 and borders the districts of Kegeyli in the west and south, Muynak to the north, and Karauzyak to the east. The district area encompasses 217557.6 hectares and contains one city (Chimbay) and eleven makhallas, namely Tazadzhol, Koksuy, Bakhtli, Kosterek, Tazgara, Kamsarik, Kyzyluzyak, Kenes, Mayap, Pashentov, Marked. The center is the city of Chimbay. The population of the district is 109,500 people (as of January 1, 2015). Of these, 53.8 thousand live in urban areas and 55.7 thousand comprise the rural population. The distance from Chimbay to Nukus is 56 km. Chimbay district is located in the north of the Republic of Karakalpakstan along the Kegaili canal. The climate is very variable, the groundwater is located close to the earth's surface, the summers are hot and dry, and the winters are short but cold (Aidarov and Pankova, 2007).

The total irrigated area in the district is 46910.0 ha, of which 41576.8 ha (88.6%) are saline soils, and 5333.2 (11.4%) are non-saline soils. Of the saline soils, 15 365.3 ha are weak saline (32.8%), 13390.4 ha (28.5%) moderately saline, 3871.5 ha (8.4%) are highly saline, and 8949.6 ha (19.1%) are very highly saline (Abdullaev, 2018). There are salt marshes with slightly saline soils, chloride-sulfate soils, and sulfate soils (Haque and Basak, 2017). The geographic location and satellite image of the object under study are shown in Figure 1.

2.2. Collection of the data

Pictures of Landsat 7 ETM dated 07/27/2008 and Landsat 8 OLI / TIRS dated 07/07/2018 were used to determine the land area changes in the Chimbay district. ArcGIS 10.1 software was used to detect land-use changes, and topographic maps and portable "field-type" GPS were used to determine the ground control points. The types of satellite image data used in the study are shown in Table 1.

2.3. Research methodology

The use of geographic information technologies and remote sensing methods in determining changes in land use and land cover are shown in Figure 2. The general function of the classification process is to classify all image pixels according to surface classes automatically. As a rule, multispectral data are used to classify images and as a digital basis for categorizing the spectrogram for each pixel in the database. Different forms are a combination of various numerical indicators based on their spectral reflective and dispersion properties (Spruce, Bolten, Mohammed, Srinivasan, and Lakshmi, 2020).

In the first stage, satellite images of Landsat 7 ETM 2008 and Landsat 8 OLI / TIRS 2018 from USGS (US Geological Survey) relevant to the research area were downloaded (Chen, 2014; Liu, Luo, and Zheng, 2018; Trisakti, Nugroho, and Zubaidah, 2016). Landsat 7 ETM satellite imagery consists of 7 groups (Pereira *et al.*, 1999), and Landsat 8 OLI / TIRS satellite imagery consists of 11 groups (Hawbaker *et al.*, 2017; Miranda, Alves, Pozza, and Santos Neto, 2020). Then, for the decryption, a combination of pictures by groups was selected. The main reason for choosing a combination of groups for decryption was to obtain a color image that was natural and close to the color of the image of the land.

Next, land type indicators were identified according to five classes (vegetation, disturbed land, water surface, saline land, and barren land). A topographic map of the studied lands was analyzed using high-resolution images obtained from GPS and Google Earth. Then, the method of land classification (maximum likelihood classification) was selected (Abino, Kim, Jang, Lee, and Chung, 2015; Cabral, Silva, Silva, Vanneschi, and Vasconcelos, 2018). A feature of image classification is the process of extracting classes of information from a multi-channel raster image. The raster obtained as a result of the image classification was then used to create various thematic maps. In the classification of maximum likelihood, the algorithm is based on probability and it assumes that the statistics of the studied data are distributed over each spectral range and class. The pixels were calculated based on the probability that each *m* class is defined, and then the pixel probability was assigned according to the highest class (Juliev, Pulatov, Fuchs, and Hübl, 2019).

In the next stage, the compliance of land types with indicators and classification methods was checked. If the obtained results of the decryption of the land types by years met the established requirements and allowed classification, the land types were determined, and the results were interpreted.

3. RESULTS AND DISCUSSION:

The cartographic map, satellite imagery, and statistical data presented in the study were analyzed by refining them by pixels and differentiating the area into five classes based on the value of the specific digital differences of the landscape elements. A description of the land-use classes in the area is given in Table 2. Samples were taken from each specific land-use type by delimiting polygons around representative sites. The spectral brightness of the signature for the corresponding types of land cover obtained from the satellite images was recorded using the pixels enclosed in these polygons. A satisfactory spectral signature ensures that there is "minimal confusion" between the land-use classes. After that, the maximum likelihood algorithm was used for the controlled classification of the images. This image classification is mainly controlled by the analyst, as the analyst selects pixels that represent the desired classes.

The maps of the land-use classes of Chimbay district in 2008 and 2018 are presented in Figure 3. The overall classification accuracy achieved was 95.32% and 95.13%, respectively, and the overall statistics were 0.9237 and 0.9070, respectively, for the classification of images in 2008 and 2018. According to Lea and Curtis (2010), accuracy assessment reports require an overall classification accuracy of over 90% and κ statistics above 0.9, which were successfully achieved in this study. The land classification results for 2008 and 2018 are shown in Table 3. The percentage of classes based on these results reflects compliance with land-use practices in the area during 2008 and 2018 (Figure 4). The resulting land-use maps and overlays created in ArcGIS 10.1 indicate a significant shift in land classes: vegetation from 28% to 22%, water surface from 15% to 14%, disturbed land from 22% to 24%, saline land from 18% to 22%, and barren land from 17% to 18%.

Based on the Strategy for the Further Development of Uzbekistan, approved by Decree of the President of the Republic of Uzbekistan dated February 7, 2017, No. UP-4947, approved by Decree of the President of the Republic of

Uzbekistan dated January 18, 2017 No. PP-2731 "On the State Program for the Development of the Aral Sea Region for 2017–2021" "Effective use of land and water resources in agriculture", approved by Decree of the President of the Republic of Uzbekistan dated June 17, 2019 No. R-5742, this study will contribute to the implementation of the goals set forth in other rules.

One of the prerequisites for sustainable land use is the timely monitoring of irrigated arable land and the systematic management of land resources (Zhao, Lin, and Warner, 2004). As part of the topic, the work carried out by scientists on the study of land use in this area using geoinformation techniques and remote zoning methods was investigated. In particular, Scientists studied the province of Guangzhou, China, from 1998 to 2003 concerning changes in land use and land cover based on Landsat TM / ETM + images. They showed that changes in land use and its topography and global environmental changes, are important in the fastest growing countries in the world (Fan, Weng, and Wang, 2007), based on remote sensing methods.

The above-mentioned studies mainly used GIS and remote sensing methods to detect changes in land use and land cover due to urban expansion. In the current study, the differences in the land use and land cover as a result of the negative impact of the dry Aral Sea on the Republic of Uzbekistan as well as the impact of anthropogenic factors on the health of the population in this area and their arable land is explored using GIS and remote sensing methods (Shen, Abuduwalli, Ma, and Samat, 2018).

When mapping some natural areas in many developing countries, it was found that some of the study areas were weakly associated with changes in land use and land cover. Such situations require individual research in the field of environmental protection and environmental studies. Accordingly, remote sensing and GIS technology are practical tools for mapping the nature of changes (Haque and Basak, 2017; Schaefer and Tinh, 2019). The study of land use and land cover change has been one of the most popular and widely used methods in the last decade. Based on the data obtained using remote sensing methods, it has been shown that various analytical studies are useful and effective in monitoring land use and targeted land management (Tarawally, Wenbo, Weiming, Mushore, and Kursah, 2019). Using the methods used by previous scientists, we also examined the factors that led to the drying of the Aral Sea, which ultimately became a global problem, by studying

land use and changes in the land cover in this region (Micklin, 2014; Reimov and Fayzieva, 2014; Umarov, 2011).

Besides, GIS technologies, including remote sensing, were used to map land-use programs in Chimbay district in the Republic of Karakalpakstan, and these were subjected to environmental analysis. They were also revised to collect data from existing data that are consistent with mapping, classification schemes, and mapping methods (Jazouli *et al.*, 2019). This was followed by the use of Landsat satellite imagery using the geographic information from the US Geological Survey (USGS) of the Chimbay area associated with the object under study and a map of the Chimbay area based on ArcGIS. Landsat photos are free and easy to work with, and they have an extensive historical archive and extensive space-based coverage (10).

The map shows the geographical location of the study area. In contrast to previous work done on this topic, the work that we present is based on four parameters and characteristics of the data on the accuracy of satellite images. This study is aimed at determining the total amount of soil salinization and its degradation using the RGB model in a GIS environment (Kidane, Bezie, Kesete, and Tolessa, 2019). It is hereby intended to achieve a more accurate result of the studied object. In determining the variation of land types in Chimbay district, the network was divided into five classes. A description of each class is provided separately. Using the analysis results based on ArcGIS 10.1, the land-use map in the Chimbay region in western Uzbekistan was scaled to 1: 500 000. The map shows changes in the environmental situation in the region during 2008-2018.

Land and its field classes (Table 3) and annual indicators of land use and land use loss and percentage of land lost were used to provide more accurate GIS and remote sensing information. In short, the relationship between humans and the environment is based on certain rules and regulations. It is known that environmental conditions can deteriorate if a partial violation of these occurs (Prenov and Safarov, 2015). Given this, we hope that the use of the proposed methods will aid in the further investigation of the Aral Sea problem using geoinformatics and remote sensing methods as this is a global problem, not only in Uzbekistan but also in the CIS.

4. CONCLUSION:

The practice of land use in the research area has changed significantly over ten years. The land occupied by vegetation decreased from 60916.13 ha to 47862.67 ha, water surface declined from 32633.64 ha to 30458.06 ha, disturbed land increased from 47862.67 ha to 52213.82 ha, the area of saline land increased from 39160.37 ha to 47862.67 ha, and barren land increased from 36984.79 ha to 39160.37 ha. The expansion of barren land in the area was mainly due to the lack of proper land use management and planning and the lack of continuous satellite monitoring. It is recommended that (1) the use of water resources and the location of types of crops in the area should be properly regulated under consideration of the environmental situation; (2) it is necessary to create a land information system (LIS) for the district, based on remote sensing data; and (3) there should be an organization of the monitoring of optimal land use and its mapping based on GIS technologies.

5. REFERENCES:

1. Abdullaev, A. K. (2018). Improvement and land reclamation of irrigated lands in Uzbekistan. In *Scientific and practical recommendations on the reclamation state and improvement of irrigated lands in Uzbekistan*. Tashkent: University.
2. Abino, A. C., Kim, S. Y., Jang, M. N., Lee, Y. J., and Chung, J. S. (2015). Assessing land use and land cover of the Marikina sub-watershed, Philippines. *Forest Science and Technology*, 11(2), 65–75. <https://doi.org/10.1080/21580103.2014.957353>
3. Aidarov, I. P., and Pankova, E. I. (2007). Salt accumulation and its control on the plains of Central Asia. *Eurasian Soil Science*, 40(6), 608–615. <https://doi.org/10.1134/S1064229307060026>
4. Alam, A., Bhat, M. S., and Maheen, M. (2019). Using Landsat satellite data for assessing the land use and land cover change in Kashmir valley. *GeoJournal*. <https://doi.org/10.1007/s10708-019-10037-x>
5. Bekchanov, M., Ringler, C., Bhaduri, A., and Jeuland, M. (2016). Optimizing irrigation efficiency improvements in the

- Aral Sea Basin. *Water Resources and Economics*, 13, 30–45. <https://doi.org/10.1016/j.wre.2015.08.003>
6. Breckle, S.-W., Wucherer, W., Dimeyeva, L. A., and Ogar, N. P. (Eds.). (2012). *Aralkum - a man-made desert: The desiccated floor of the Aral Sea (Central Asia)*. Springer Science and Business Media.
 7. Cabral, A. I. R., Silva, S., Silva, P. C., Vanneschi, L., and Vasconcelos, M. J. (2018). Burned area estimations derived from landsat ETM+ and OLI data: Comparing genetic programming with maximum likelihood and classification and regression trees. *ISPRS Journal of Photogrammetry and Remote Sensing*, 142, 94–105. <https://doi.org/10.1016/j.isprsjprs.2018.05.007>
 8. Chen, H. (2014). Chemical composition and structure of natural lignocellulose. In H. Chen, *Biotechnology of Lignocellulose* (pp. 25–71). https://doi.org/10.1007/978-94-007-6898-7_2
 9. Degife, A. W., Zabel, F., and Mauser, W. (2018). Assessing land use and land cover changes and agricultural farmland expansions in Gambella Region, Ethiopia, using Landsat 5 and Sentinel 2a multispectral data. *Heliyon*, 4(11), e00919. <https://doi.org/10.1016/j.heliyon.2018.e00919>
 10. Fan, F., Weng, Q., and Wang, Y. (2007). Land Use and Land Cover Change in Guangzhou, China, from 1998 to 2003, Based on Landsat TM /ETM+ Imagery. *Sensors*, 7(7), 1323–1342. <https://doi.org/10.3390/s7071323>
 11. Gadrani, L., Lominadze, G., and Tsitsagi, M. (2018). F assessment of landuse/landcover (LULC) change of Tbilisi and surrounding area using remote sensing (RS) and GIS. *Annals of Agrarian Science*, 16(2), 163–169. <https://doi.org/10.1016/j.aasci.2018.02.005>
 12. Golubov, B. N. (2018). Anomal'nyy pod'yom urovnya Kaspiyskogo morya i katastroficheskoye obmeleniye Aral'skogo morya kak rezul'tat drenirovaniya Arala pod plato Ustyurt i v Kaspiy vsledstviye tekhnogennykh vozmushcheniy nedr [An abnormal rise in the level of the Caspian Sea and a catastrophic shallowing of the Aral Sea as a result of drainage of the Aral Sea under the Ustyurt plateau and into the Caspian Sea due to anthropogenic disturbances of the bowels]. *Electronic Scientific Edition Almanac Space and Time*, 16(1–2), 1–18. <https://doi.org/10.24411/2227-9490-2018-11072>
 13. Haque, Md. I., and Basak, R. (2017). Land cover change detection using GIS and remote sensing techniques: A spatio-temporal study on Tanguar Haor, Sunamganj, Bangladesh. *The Egyptian Journal of Remote Sensing and Space Science*, 20(2), 251–263. <https://doi.org/10.1016/j.ejrs.2016.12.003>
 14. Hawbaker, T. J., Vanderhoof, M. K., Beal, Y.-J., Takacs, J. D., Schmidt, G. L., Falgout, J. T., ... Dwyer, J. L. (2017). Mapping burned areas using dense time-series of Landsat data. *Remote Sensing of Environment*, 198, 504–522. <https://doi.org/10.1016/j.rse.2017.06.027>
 15. Jazouli, A. E., Barakat, A., Khellouk, R., Rais, J., and Baghdadi, M. E. (2019). Remote sensing and GIS techniques for prediction of land use land cover change effects on soil erosion in the high basin of the Oum Er Rbia River (Morocco). *Remote Sensing Applications: Society and Environment*, 13, 361–374. <https://doi.org/10.1016/j.rsase.2018.12.004>
 16. Jovanovic, D., Govedarica, M., Sabo, F., Bugarinovic, Z., Novovic, O., Beker, T., and Lauter, M. (2015). Land cover change detection by using remote sensing: A case study of Zlatibor (Serbia). *Geographica Pannonica*, 19(4), 162–173. <https://doi.org/10.5937/GeoPan1504162J>
 17. Juliev, M., Pulatov, A., Fuchs, S., and Hübl, J. (2019). Analysis of land use land cover changedetection of Bostanlik district, Uzbekistan. *Polish Journal of Environmental Studies*, 28(5), 3235–3242. <https://doi.org/10.15244/pjoes/94216>
 18. Karakus, C. B., Cerit, O., and Kavak, K. S. (2015). Determination of Land Use/Cover Changes and Land Use Potentials of Sivas City and its Surroundings Using Geographical Information Systems (GIS) and Remote Sensing (RS). *Procedia Earth and Planetary Science*, 15, 454–

461. <https://doi.org/10.1016/j.proeps.2015.08.040>
19. Kidane, M., Bezie, A., Kesete, N., and Tolessa, T. (2019). The impact of land use and land cover (LULC) dynamics on soil erosion and sediment yield in Ethiopia. *Heliyon*, 5(12), e02981. <https://doi.org/10.1016/j.heliyon.2019.e02981>
20. Lambin, E. F., Geist, H. J., and Lepers, E. (2003). Dynamics of land-use and land-cover change in tropical regions. *Annual Review of Environment and Resources*, 28(1), 205–241. <https://doi.org/10.1146/annurev.energy.28.050302.105459>
21. Liu, Q., Luo, L., and Zheng, L. (2018). Lignins: Biosynthesis and Biological Functions in Plants. *International Journal of Molecular Sciences*, 19(2), 335. <https://doi.org/10.3390/ijms19020335>
22. Micklin, P. (2014). Aral Sea Basin Water Resources and the Changing Aral Water Balance. In P. Micklin, N. V. Aladin, and I. Plotnikov (Eds.), *The Aral Sea* (pp. 111–135). https://doi.org/10.1007/978-3-642-02356-9_5
23. Miranda, J. da R., Alves, M. de C., Pozza, E. A., and Santos Neto, H. (2020). Detection of coffee berry necrosis by digital image processing of landsat 8 oli satellite imagery. *International Journal of Applied Earth Observation and Geoinformation*, 85, 101983. <https://doi.org/10.1016/j.jag.2019.101983>
24. Pereira, J. M. C., Sá, A. C. L., Sousa, A. M. O., Silva, J. M. N., Santos, T. N., and Carreiras, J. M. B. (1999). Spectral characterisation and discrimination of burnt areas. In E. Chuvieco (Ed.), *Remote Sensing of Large Wildfires* (pp. 123–138). https://doi.org/10.1007/978-3-642-60164-4_7
25. Prenov, S. M., and Safarov, E. Y. (2015). Analysis of eco-meliorative condition for soil of Southern Aral Sea region, and about its mapping. *European Science Review*, 15–17. <https://doi.org/10.20534/ESR-15-9.10-15-17>
26. Rafihov, A. A., Ergashev, Sh. E., and Khaidarov, E. (1997). *Desertification processes in the South Aral Sea region*. Tashkent: University.
27. Reimov, P., and Fayzieva, D. (2014). The Present State of the South Aral Sea Area. In P. Micklin, N. V. Aladin, and I. Plotnikov (Eds.), *The Aral Sea* (pp. 171–206). https://doi.org/10.1007/978-3-642-02356-9_7
28. Reis, S. (2008). Analyzing land use/Land cover changes using remote sensing and GIS in Rize, Aorth-East Turkey. *Sensors*, 8(10), 6188–6202. <https://doi.org/10.3390/s8106188>
29. Safari, A., and Sohrabi, H. (2019). Effect of climate change and local management on aboveground carbon dynamics (1987–2015) in Zagros oak forests using Landsat time-series imagery. *Applied Geography*, 110, 102048. <https://doi.org/10.1016/j.apgeog.2019.102048>
30. Schaefer, M., and Thinh, N. X. (2019). Evaluation of land cover change and agricultural protection sites: A GIS and remote sensing approach for ho Chi Minh City, Vietnam. *Heliyon*, 5(5), e01773. <https://doi.org/10.1016/j.heliyon.2019.e01773>
31. Shen, H., Abuduwaili, J., Ma, L., and Samat, A. (2018). Remote sensing-based land surface change identification and prediction in the Aral Sea bed, Central Asia. *International Journal of Environmental Science and Technology*, 16(4), 2031–2046. <https://doi.org/10.1007/s13762-018-1801-0>
32. Spruce, J., Bolten, J., Mohammed, I. N., Srinivasan, R., and Lakshmi, V. (2020). Mapping land use land cover change in the Lower Mekong Basin from 1997 to 2010. *Frontiers in Environmental Science*, 8, 21. <https://doi.org/10.3389/fenvs.2020.00021>
33. Srivastava, P., Singh, S., Gupta, M., Thakur, J. K., and Mukherjee, S. (2013). Modeling impact of land use change trajectories on groundwater quality using remote sensing and GIS. *Environmental Engineering and Management Journal*, 12(12), 2343–2355. <https://doi.org/10.30638/eemj.2013.287>
34. Tang, Y., Zhang, J., Jing, L., and Gao, H. (2018). Geostatistical modelling of spatial dependence in area-class occurrences for improved object-based classifications of remote-sensing images. *ISPRS Journal of*

- Photogrammetry and Remote Sensing*, 141, 219-236. <https://doi.org/10.1016/j.isprsjprs.2018.05.003>
35. Tarawally, M., Wenbo, X., Weiming, H., Mushore, T. D., and Kursah, M. B. (2019). Land use/land cover change evaluation using land change modeller: A comparative analysis between two main cities in Sierra Leone. *Remote Sensing Applications: Society and Environment*, 16, 100262. <https://doi.org/10.1016/j.rsase.2019.100262>
 36. Trisakti, B., Nugroho, U., and Zubaidah, A. (2016). Technique for identifying burned vegetation area using landsat 8 data. *International Journal of Remote Sensing and Earth Sciences (IJReSES)*, 13(2), 121. <https://doi.org/10.30536/j.ijreses.2016.v13.a2447>
 37. Umarov, E. K. (2011). Economic and social geography of Karakalpakstan. Nukus: Karakalpakstan.
 38. White, K. D. (2013). Nature-society linkages in the Aral Sea region. *Journal of Eurasian Studies*, 4(1), 18–33. <https://doi.org/10.1016/j.euras.2012.10.003>
 39. Xian, G. Z., Loveland, T., Munson, S. M., Vogelmann, J. E., Zeng, X., and Homer, C. J. (2020). Climate sensitivity to decadal land cover and land use change across the conterminous United States. *Global and Planetary Change*, 192, 103262. <https://doi.org/10.1016/j.gloplacha.2020.103262>
 40. Zhao, G. X., Lin, G., and Warner, T. (2004). Using Thematic Mapper data for change detection and sustainable use of cultivated land: A case study in the Yellow River delta, China. *International Journal of Remote Sensing*, 25(13), 2509–2522. <https://doi.org/10.1080/01431160310001619571>

Table 1. Data types and satellite image properties

Data types	Data characteristics	
	2008	2018
Type of satellite	Landsat 7 ETM	Landsat 8 OLI/TIRS
Spatial resolution	30 m	15 m
Radiometric resolution properties	8 bit	16 bit
Coordinate system	WGS84	WGS84

Table 2. Description of the land-use classes

Class name	Class description
Vegetation	Fields, fallow lands, and mixed forest lands
Disturbed land	Pastures, industrial lands, and settlements
Water surface	Creeks, canals, lakes, reservoirs, and irrigated lands at the time of observation
Saline land	Land of high, medium, and low salinity
Barren land	Non-farm land and desert

Table 3. Land classes and their area (in ha)

Land use classes	2008		2018		Increase		Loss	
	Square (ha)	(%)	Square (ha)	(%)	Square (ha)	(%)	Square (ha)	(%)
Vegetation	60916.13	28	47862.67	22			13053.46	6
Disturbed land	47862.67	22	52213.82	24	4351.15	2		
Water surface	32633.64	15	30458.06	14			2175.58	1
Saline land	39160.37	18	47862.67	22	8702.30	4		
Barren land	36984.79	17	39160.37	18	2175.58	1		

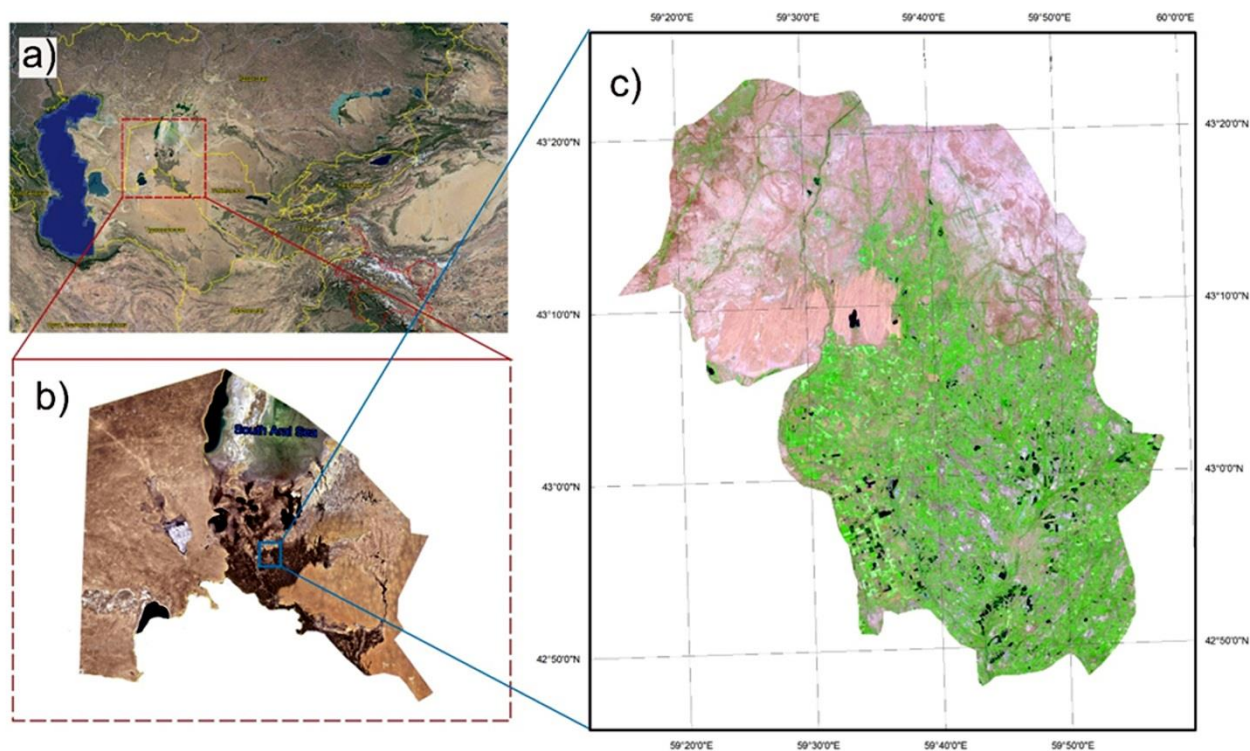


Figure 1. Location of the object of study: a) the Republic of Uzbekistan; b) the Republic of Karakalpakstan as part of the Republic of Uzbekistan; c) the combination of satellite images from Landsat 8 of Chimbay district of the Republic of Karakalpakstan in groups 7: 5: 2 displayed as RGB

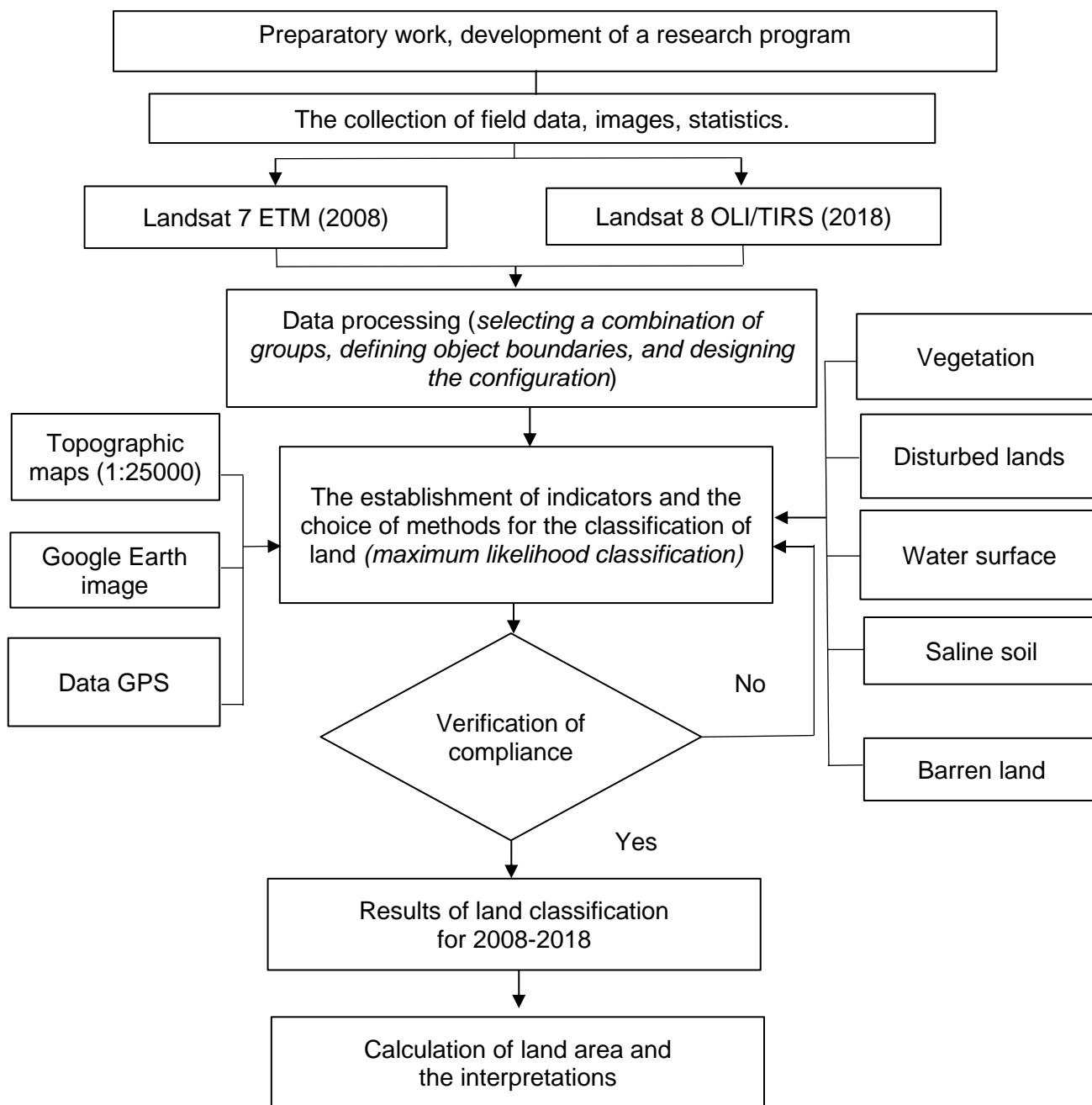


Figure 2. Flowchart of the research methodology

LAND-USE MAPS OF CHIMBAY DISTRICT (REPUBLIC OF UZBEKISTAN (2008 AND 2018)).

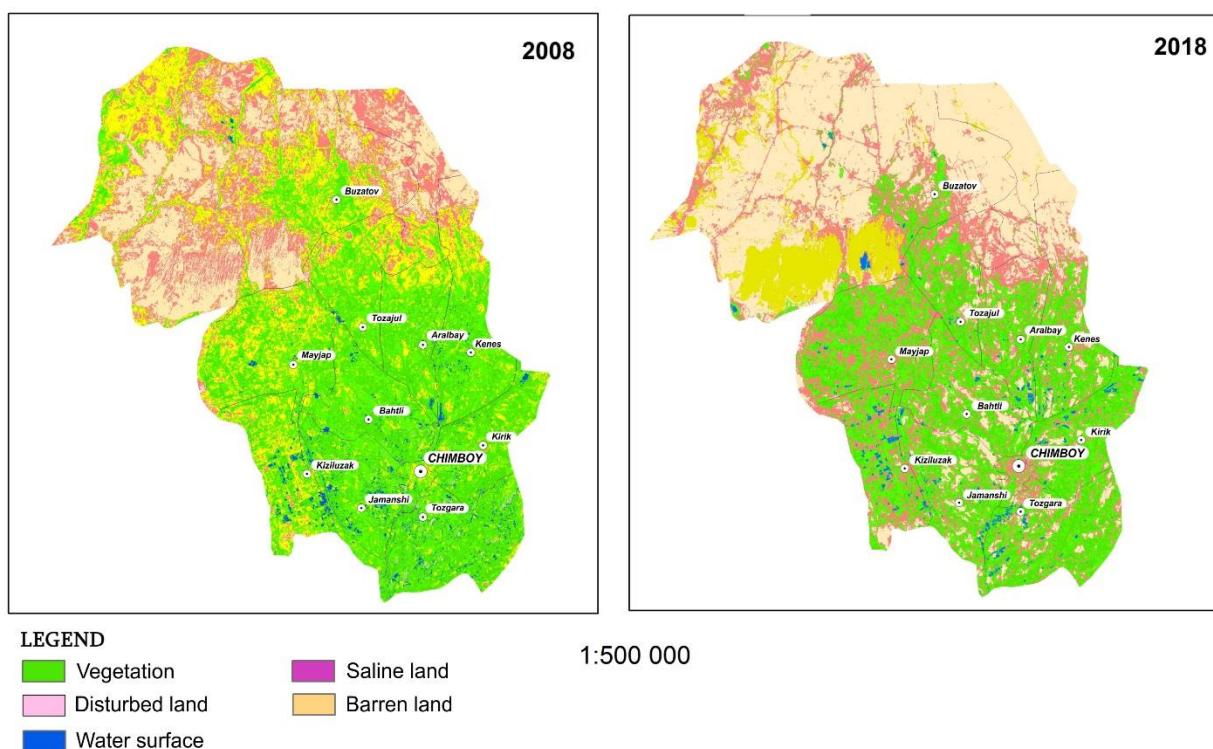


Figure 3. Land-use maps of Chimbay district (Republic of Uzbekistan) (2008 and 2018)

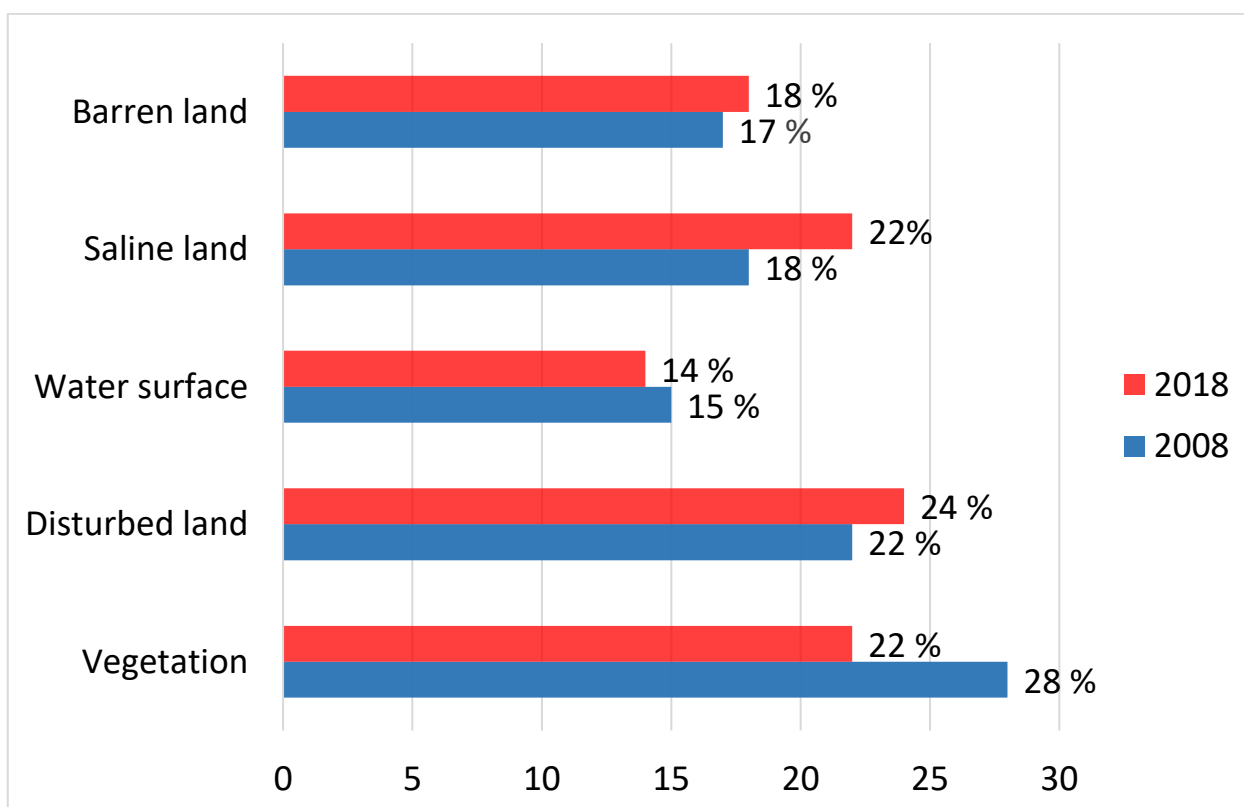


Figure 4. Diagram of classes and areas of land use and land cover changes in Chimbay district (2008 and 2018)

IMPLEMENTAÇÃO DE WEBINARS EM MODELOS DE APRENDIZAGEM COMBINADA PARA MELHORAR A MOTIVAÇÃO E RESULTADOS NA APRENDIZAGEM DO ESTUDO DO SISTEMA ESQUELETAL HUMANO**IMPLEMENTATION OF WEBINARS IN BLENDED LEARNING MODELS TO IMPROVE MOTIVATION AND LEARNING OUTCOMES OF THE STUDY OF HUMAN SKELETAL SYSTEM****PENGARUH MODEL BLENDED LEARNING MELALUI APLIKASI WEBINAR DAN MOTIVASI TEHADAP HASIL BELAJAR SISWA PADA MATERI SISTEM RANGKA MANUSIA**ANDRINI, Vera Septi¹; MATSUN²; MADURETNO, Tri Wahyuni³^{1,3}STKIP PGRI Nganjuk, East Java, Indonesia²IKIP PGRI Pontianak, Indonesia

* Corresponding author

e-mail: vera@stkipnganjuk.ac.id

Received 08 June 2020; received in revised form 31 July 2020; accepted 10 September 2020

RESUMO

A existência da pandemia de Covid-19 em 2020 teve um impacto devastador na educação. A interação entre professores e alunos normalmente não pode ser feita. Com base nisso, as inovações na educação devem continuar sendo realizadas para melhorar a qualidade da aprendizagem. Esse estudo objetivou descobrir modelos de aprendizagem combinada por meio de aplicativos de webinar e motivação sobre os resultados da aprendizagem do aluno no curso Sistema Esquelético Humano. O estudo foi realizado na Associação de Professores do Ensino Médio da República da Indonésia 2 Nganjuk Regency, Java Oriental, Indonésia, na classe 1 do ano acadêmico 2019/2020, em disciplinas de ciências com material no Sistema de Ordem Humana. O número de amostras foi de 83 alunos, divididos em 42 alunos da turma experimental e 41 da classe controle. A classe experimental usa o modelo de aprendizado combinado utilizando um aplicativo de webinar, enquanto a classe de controle usa a ajuda dos módulos eletrônicos. Os métodos de coleta de dados a serem utilizados são observação, questionários e testes. As técnicas de análise de dados utilizaram o Two Way Anova. Os resultados mostraram que (1) houve diferenças nos resultados da aprendizagem dos alunos no curso do Sistema Esquelético Humano com base no modelo de aprendizagem combinada por meio de aplicativos de webinar, (2) houve diferentes resultados na aprendizagem dos alunos no curso do Sistema Esquelético Humano com base na alta motivação para a aprendizagem e baixa motivação para o aprendizado, (3) há interação entre os modelos de aprendizagem combinada por meio de aplicativos de webinar e motivação nos resultados de aprendizagem dos alunos no curso Sistema Esquelético Humano. A novidade deste resultado é a aplicação de webinar no processo de aprendizagem e resultados na forma de produtos de mídia de aprendizagem holográficos desenvolvidos no sistema esquelético humano. Através da mídia holográfica, o material parece mais real e se assemelha à sua forma original. Os alunos podem aprender sistemas esqueléticos através de imagens holográficas de uma variedade de perspectivas diferentes. Os alunos são mais motivados por projetos apresentados pelos professores, porque os projetos fornecidos são interessantes e capazes de melhorar as habilidades. Os alunos podem estudar material tanto em termos de ciências físicas quanto biológicas.

Palavras-chave: *aprendizagem combinada, motivação, seminários on-line, resultados de aprendizagem, módulos eletrônicos, hologramas*

ABSTRACT

The existence of the Covid-19 pandemic in 2020 has had a devastating impact on education. Interaction between teachers and students typically cannot be done. Based on this, innovations in education must continue to be done to improve the quality of learning. This study aimed to find out blended learning models through webinar applications and motivation on student learning outcomes in the Human Skeletal System course. The study was conducted at the Vocational High School Teachers Association of the Republic of Indonesia 2 Nganjuk Regency, East Java, Indonesia, and held in class 1 of the academic year 2019/2020 on science subjects with material on

the Human Order System. The number of samples was 83 students divided into 42 experimental class students and 41 control class students. The experimental class uses the blended learning model by utilizing a webinar application, while the control class uses the help of e-modules. Data collection methods that be used are observation, questionnaires, and tests. Data analysis techniques used Two Way Anova. The results showed that (1) there were differences in student learning outcomes in the Human Skeletal System course based on the blended learning model through webinar applications, (2) there were different student learning outcomes in the Human Skeletal System course based on high learning motivation and low learning motivation, (3) there is an interaction between blended learning models through webinar applications and motivation on students' learning outcomes in the Human Skeletal System course. The novelty of this result is the application of webinars in the learning process and outcomes in the form of the holographic learning media products developed on the human skeletal system. Through holographic media, the material looks more real and resembles its original form. Students can learn skeletal systems through holographic images from a variety of different perspectives. Students are more motivated through projects given by teachers because the projects provided are engaging and able to improve skills. Students can study material both in terms of physical and biological sciences.

Keywords: *blended learning, motivation, webinars, learning outcomes, e-modules, holograms*

ABSTRAK

Adanya pandemi Covid-19 pada tahun 2020 ini memberikan dampak yang buruk khususnya dalam bidang pendidikan. Interaksi antara guru dan siswa secara normal tidak bisa dilakukan. Berdasarkan hal tersebut, inovasi dalam pendidikan harus terus dilakukan agar mampu meningkatkan kualitas pembelajaran. Tujuan penelitian ini adalah mengetahui model blended learning melalui aplikasi webinar dan motivasi terhadap hasil belajar siswa pada mata kuliah Sistem Rangka Manusia. Penelitian dilaksanakan di Sekolah Menengah Kejuruan Persatuan Guru Republik Indonesia 2 Kabupaten Nganjuk Jawa Timur Indonesia. Dilaksanakan pada kelas 1 tahun akademik 2019/2020 pada mata pelajaran IPA dengan materi Sistem Rangka Manusia. Jumlah sampel sebesar 83 siswa terbagi menjadi 42 siswa kelas eksperimen dan 41 siswa kelas kontrol. Kelas eksperimen menggunakan model pembelajaran blended learning dengan memanfaatkan aplikasi webinar sedangkan kelas kontrol menggunakan bantuan e-module. Metode pengumpulan data menggunakan observasi, angket, dan tes. Teknik analisis data menggunakan Two Way Anova. Hasil penelitian menunjukkan bahwa (1) ada perbedaan hasil belajar siswa pada mata kuliah Sistem Rangka Manusia berdasarkan model blended learning melalui aplikasi webinar, (2) ada perbedaan hasil belajar siswa pada mata kuliah Sistem Rangka Manusia berdasarkan motivasi belajar tinggi dan motivasi belajar rendah, (3) ada interaksi antara model blended learning melalui aplikasi webinar dan motivasi terhadap hasil belajar siswa pada mata kuliah Sistem Rangka Manusia. Kebaharuan dalam penelitian ini adalah penerapan webinar dalam proses pembelajaran dan luaran berupa produk media pembelajaran hologram yang dikembangkan pada materi Sistem Rangka Manusia. Melalui media hologram, materi terlihat lebih riil dan menyerupai bentuk aslinya. Siswa dapat belajar sistem rangka melalui gambar hologram dari berbagai perspektif yang berbeda. Siswa lebih termotivasi melalui proyek yang diberikan guru karena proyek yang diberikan menarik dan mampu meningkatkan keterampilan. Siswa bisa mengkaji materi baik ditinjau dari keilmuan fisika maupun biologi.

Kata kunci: *blended learning, motivasi, webinar, hasil belajar, e-module, hologram*

1. INTRODUCTION:

Coronavirus outbreak or Covid-19 that struck in this part of the world changed the order of people's lives. Among the main changes that occur is the involvement of technology in the world of education. The impact of COVID-19 on technology for teaching and learning is felt, especially now that distance learning systems are an option so that teachers and students can reduce the spread of the virus. The Indonesian Minister of Education said, with software tools were various types that had been partitioned because they were constrained with classrooms and others, now they could innovate because they could be more personalized, more segmented learning with multimedia. So it is not just the

teacher sitting in front of students but with a variety of other tools, digital video chalkboard, and others (Lia, 2020). Therefore, the need for innovation and always actively follows existing developments both from teachers, students, and parents so that the learning process continues to run smoothly and quality.

Other problems in education in Indonesia, when viewed from the learning outcomes, the value of the National Examination (UN) for the SMA / SMK level in 2018 has decreased significantly. National Education Standards Agency, the decline in grades occurs in students in 50% of Indonesia schools. Specifically for the East Java Education Office, the UN level for SMA / SMK / MA equivalent with scores below 55 in

2018 reached 78.88% while in 2017 it was only 55.41% ((BNSP), 2018).

Based on data from the Ministry of Education and Culture, two factors cause a decline in the average UN score. First, the change in norms. In 2018, the standard of questions is made higher than in 2017. The question leads to the type of reasoning (HOTS). Second, it changed the exam mode from the Paper and Pencil-based National Examination (UNKP) to the Computer-Based National Examination (UNBK). The implementation of UNBK is not evenly distributed throughout Indonesia due to infrastructure problems, internet network problems, and teachers and students are not accustomed to using computers.

Based on data from interviews with teachers at the Republic of Indonesia 2 Nganjuk Vocational Teachers Middle School (SMK PGRI 2 Nganjuk), East Java Indonesia, the decline in UN scores inseparable from the application of the learning process that lacks integrating technology. The learning process generally uses lectures, discussions, practices, and presentations. Learning models that are still teacher-centered impact the lack of increased ability of the High Order Thinking Skill. The survey results show that only 40% of teachers can apply Information and Communication Technology (ICT). The percentage of teachers who have not yet used ICT is dominated by senior teachers over the age of 50 years (Henny, R. 2019)

Based on the problems outlined above, it is the need to improve the learning process for teachers and the application of innovative technology-based learning. The blended learning model accommodates innovative learning concepts based on online and offline (Shih, 2010). Blended learning is learning that is conventionally done in the classroom, combined with online learning both independently and collaboratively, using the information and the communication technology infrastructure (Quevedo, 2011). The model commonly used in blended learning is Web-Centric Course. It is the use of the internet that combines distance learning and face-to-face (conventional). Some materials are delivered via the internet and some through face-to-face. In this model, educators can provide instructions for the students to learn subject matter through the web that has been made. Students are also given directions to look for other sources from relevant websites. In face to face, students and educators more discussion about the findings of material that have been learned through the internet (Quevedo, 2011).

The advantage of this model is that it allows freedom of learning to be done anytime and anywhere, increases mastery of digital literacy, and teachers can control learning outside of school hours (Dangwal and Lata, 2017; Kim and Yoon, 2014). In the implementation of blended learning, electronic media is supported, such as websites, smartphones, video streaming, synchronous, and asynchronous audio communication.

Thus, there is a need to improve the quality and learning outcomes by applying more innovative learning models and the need to increase student motivation. This study aimed to determine the effect of blended learning and motivation learning models on learning outcomes. The use of blended learning in this study was accompanied by the use of webinar applications.

2. MATERIALS AND METHODS:

The research design used in the study was quasi-experimental. The study was intended to determine the effect of the blended learning model through webinar applications and motivation on student learning outcomes in the Human Framework System course. The study used an experimental class and a control class. An experimental class is a class that is treated using a blended learning model through a webinar application, and a control class is a class that is treated using an e-module. Independent variables in this study are blended learning models through webinar applications and the students' learning motivation, while the dependent variable in this study is the students' learning outcomes.

In this study, the blended learning model was combined with a web-based application, a webinar. Webinars are face-to-face meetings conducted online through the internet media, which can be attended by many people from different locations and on agreed-upon actions via video or chat (Mohamad *et al.*, 2017). The reason for using webinars is that teachers can interact and do tutoring outside school hours (Amhag, 2017). When at home, if there are students who have difficulty learning, it can be done online guidance through the webinar application.

The study was conducted at SMK PGRI 2 Nganjuk, East Java, Indonesia, with a sample of 83 students divided into 42 experimental class students and 41 control class students taking science subjects. All students who agreed to be the sample in this study were grade 1 students with an average age of 16 years, consisting of 34 male and 49 female students. Data collection

methods used observation, questionnaires, and tests (APPENDIX 1). Data analysis techniques used Two Way Anova. This analysis is used to compare the average difference between groups that have been divided into two variables. The research hypotheses proposed are: (1) there are differences in student learning outcomes in the Human Skeletal System course based on the blended learning model through the webinar application, (2) there are different students' learning outcomes in the Human Skeletal System course based on the high learning motivation and the low learning motivation, and (3) there is an interaction between blended learning models through webinar applications and motivation on students' learning outcomes in the Human Skeletal System course.

3. RESULTS AND DISCUSSION:

The impact of motivation on student learning outcomes was also examined. The students who have high interest and motivation to learn are usually characterized by good academic grades, have structured learning habits, have a good understanding of each reading (Black and Allen, 2017), have high self-efficacy, and have high learning performance (Howard, Tang, and Austin, 2015). Students who have low interest and motivation to learn usually have a tendency to withdraw, not go to school, drop out of school, have relatively high anxiety and have low academic results (Sturges, Maurer, Allen, Gatch, and Shankar, 2016). The motivation of students of SMK PGRI 2 Nganjuk, East Java, Indonesia, is relatively low, which can be seen from the number of students who do not attend subjects, especially science.

Empirical data based on Table 1 shows that the number of students who were absent in a period of two consecutive academic years is quite high. This indicates that the interest and motivation of students for learning are still low because attendance is one form of student participation in the classroom's learning process (Sha, Schunn, Bathgate, and Ben-Eliah, 2016). The results of the influence test between variables can be seen in Table 2.

3.1. First Hypothesis: The Effect of Learning Models on Learning Outcomes in the Human Skeletal System Course

The first research objective was to test for the differences in learning outcomes courses Human Skeletal System, taught using a model

blended learning through webinar applications and e-module learning. The first hypothesis proposed is there are differences in student learning outcomes in the Human Skeletal System course based on the blended learning model through a webinar application.

Based on the Two Way Anova analysis results in Table 2, the calculated F value of 25.109 with Sig. 0.040. It is less than the significance level of 0.05. Thus it can be concluded that hologram was rejected. This matter means there are differences in student learning outcomes in the Human Skeletal System course based on the blended learning model through a webinar application. Webinars provide a student-centered approach to learning with technology and can improve communication. The results show a positive increase in students' knowledge and skills in the learning process (Lieser, Taf, and Murphy-Hagan, 2018).

Based on Table 3, the learning process is categorized into 2, namely using a blended learning model through webinars and the learning process using e-modules. The model of blended learning through a webinar called Synchronous E-Learning is a learning process through direct communication carried out through computer mediation and online services (in a network). Through webinar media, the students and the teachers can carry out the learning process in real-time and on a scheduled basis. This method is very familiar to students and teachers because they can be face to face (virtually) in the classroom so that communication can take place more effectively. If students have difficulty learning, they can directly ask the teacher. Through the blended learning model, some materials are delivered via the internet and some through face-to-face. In this model, the educators can provide instructions to students to learn subject matter through the web that has been made. The students are also given directions to look for other sources from relevant websites. In face to face, the students and the educators are more discussions about the findings of material that has been learned through the internet (Albhnsawy and Aliweh, 2016).

In the learning process, webinars help communication between the teachers and the students. The analysis shows that the webinar is able (1) the effective cost because it does not need transportation to the seminar venue, (2) is very flexible, can be done anywhere and anytime, (3) can interact with many people without face to face. The use of e-learning based on webinars greatly supports the implementation of learning, students' skills in using computer technology in learning

increases, and supports the concept of online lectures (Purwandini, 2017). The utilization of ICT such as LMS and webinars, effectively improves the teachers skills and students skills. Both teachers and students can discuss and communicate online and provide teachers with convenience in giving feedback (Polanco-Bueno, 2013).

It contrasts with the learning process through the E-Module, or it can be called Asynchronous E-Learning. In its implementation, communication occurs indirectly and unscheduled. The students can choose reference material from the various sources or according to what the teacher prepares. Because the teachers and the students cannot face to face directly, the communication process becomes slower. Even the evaluation process cannot be done directly like Synchronous E-Learning (Perveen, 2016).

Figure 1 shows an example of a simple hologram application project by converting 2D images into 3D. In this project, students can learn two materials in terms of biological and physical scientific aspects.

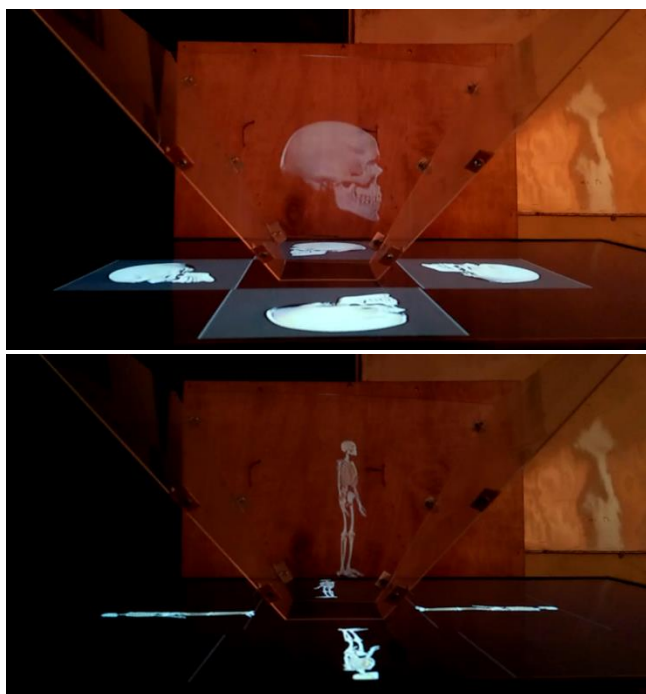


Figure 1. Example of a Hologram Making Project on Material for Human Skeleton Systems (Source: The Author)

In the concept of physics, a hologram is a photography technology that records the light scattered from an object and presents it in a 3-dimensional form. This hologram is formed from a combination of 2 coherent rays of light in microscopic form. In the physical concept, the

hologram applies the diffraction principle and the interference that is a wave phenomenon (Figure 2).

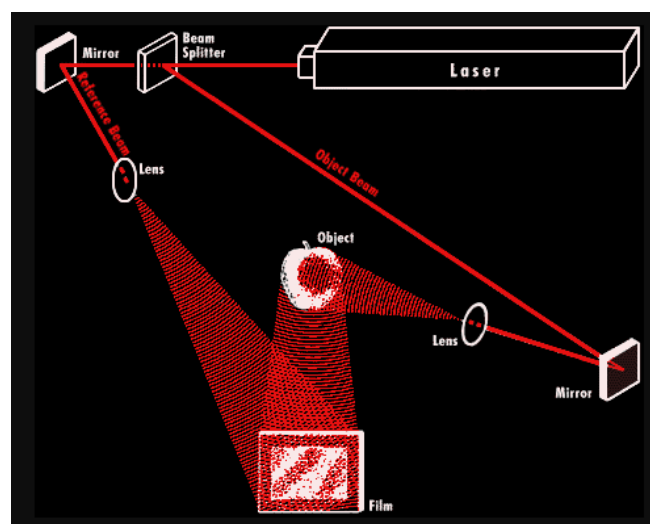


Figure 2. Illustration of Hologram Transmission Working Principle (Source: web.mit.edu)

Based on Figure 2, the hologram is formed due to the collision between the reference beam and the object beam on the holographic surface. In principle, the beam splitter is a glass that is half mirror and half lens that functions to separate the beam into two, namely the reference beam and object. The reference beam is directed towards the holographic surface, while the object beam is directed towards the object and reflected toward the holographic surface. Mixing the reference beam and the object beam on the holographic surface can produce reconstructed images that can be seen on the holographic side that is not exposed to light or the opposite side of the holographic surface exposed to light. After processing, the appearance of objects will look different from various angles (3600) (Capuno, 2016; Husain, 2015).

Biologically, the material of the Human Skeleton System can be studied to be more interesting because the appearance of the image resembles its original and more real form. The light reaching the eye of the observer, which comes from the image reconstructed from a hologram, is the same as the original object. The observer can see the holographic image both by parallax, see depth, and see from various perspectives (giving the observer a 360° view of the object). Holograms can present items virtually to effectively support the distance learning process (Kalansooriya, Marasinghe, and Bandara, 2015). Utilization of 3D holographic technology by utilizing the working principle of Holographic reflection makes the learning process more exciting and can increase

the students' motivation (Listyorini and Riadi, 2016).

3.2. Second Hypothesis: The effect of the high learning motivation and the low learning motivation on students' learning outcomes in the Human Skeletal System course

The second research objective is to examine the differences in learning outcomes of courses Human Skeletal System in the students who have high learning motivation and have low learning motivation. The hypothesis is that there are different students' learning outcomes in the Human Skeletal System course based on high learning motivation and low learning motivation.

Based on the Two Way Anova analysis results in Table 2, the calculated F value was 4.364 with the Sig. of 0,000. Sig value This is less than the significance level of 0.05. Thus it can be concluded that hologram was rejected. This matter means there are different student learning outcomes in the Human Skeletal System course based on high learning motivation and low learning motivation.

Based on Figure 3, students who have the motivation to learn to tend to pay attention to the duration of learning activities, frequency of study, persistence, grit, tenacity, and ability to face obstacles and difficulties, devotion and sacrifice, the level of aspiration, the level of achievement/product qualifications (outputs), and the direction of learning attitude. The students who have high learning motivation tend to be involved in all learning activities intensively, focused, and diligently during the learning process. Learning motivation is one factor that can distinguish students who maximize their learning potential from students who lack academic achievement. Also, from being one of the factors that determine the direction of attitude, the amount of willingness, and perseverance of student behavior (Keller, 2016), learning motivation refers to expectations and values. The expectation shows that the students be able to do the assignment that be given, and the value shows the students' conviction strongly to successful in the study (Maduretno, Sarwanto, and Sunarno, 2016; Riconscente, 2014).

The duration aspect has an average class score of 2.87 (good category). The duration is the period of the learning process carried out. During the process, the students show a tendency to pay attention to the material provided. In the aspect of learning frequency, it has a score of 3.11 (very good category). The frequency shows the intensity

of the students in learning. The more activities that are given, the more active the students are in following them. Even at this stage, it does not indicate boredom. In the aspect of persistence, it has a score of 2.9 (good category). This persistence is an act of the students who volunteer to achieve maximum results despite experiencing failures and difficulties.

In the aspect of the devotion is 2.79 (good category). Devotion is a sacrifice made by the students in achieving goals. Actively and voluntarily, the students make various efforts to solve the problems given by the teacher. It is starting from finding references, doing projects, and doing an independent practicum. In the aspect of the tenacity is 2.85 (good category). Students tenacity can be seen from their ability and patience in facing the challenges and difficulties that are given. In the aspect of the aspirations' level is 3.24 (very good category). Aspirations of the students showed significant results and were marked by the enthusiasm in participating in the learning process and the benefits obtained from these activities. In the aspect of the qualification level is 3.05 (very good category). This level of qualification is measured from the products achieved by students through a given project. The product shows the quality and is following the learning objectives. In the aspect of attitude towards 2,75 (good category). Students who have high learning motivation tend to be involved in all learning activities intensively, focused, and diligently during the learning process. So in this stage, the direction of student attitudes shows positive results (Ricardo and Meilani, 2017). The importance of learning motivation as a psychological aspect of students that has a positive and significant influence on learning outcomes. In increasing the students' aspirations, the teachers and the parents need to recognize the aspirations/ideals that students have and develop programs or various activities to facilitate students aspirations (Suardi, 2018).

3.3. Third Hypothesis: The interaction between blended learning models through webinar applications and motivation on students' learning outcomes in the Human Skeletal System course

The third research objective was to examine the interaction between learning models with learning motivation towards learning outcomes of courses Human Skeletal System. The hypothesis put forward was there is an interaction between blended learning models through webinar applications and motivation on

students' learning outcomes in the Human Skeletal System course.

Based on the Two Way Anova analysis results in Table 2, the calculated F value was 4.710 with the Sig. 0.033. Sig value. This is less than the significance level of 0.05. Thus, it can be concluded that the hologram was rejected. This matter means there is an interaction between blended learning models through webinar applications and motivation on students' learning outcomes in the Human Skeletal System material. Figure 4 shows the misalignment of lines between variables. This means there is an interaction between learning models and motivation on learning outcomes.

Table 4 shows that the mean value of learning outcomes with blended learning through a webinar (Synchronous E-Learning) is higher than the learning process using E-Module (Asynchronous E-Learning). The mean learning outcomes using webinars on aspects of high motivation ability is 89.36 higher than learning outcomes using E-Module on aspects of the high motivation of 78.85. This applies to aspects of webinars and E-modules on aspects of low motivation. The application of webinars in descriptive synchronous learning effectively promotes students' knowledge than asynchronous learning. Descriptively, it seems that the students' satisfaction in synchronous webinars is higher than asynchronous online instruction (Ebner and Gegenfurtner, 2019).

4. CONCLUSIONS:

The blended learning model through webinar applications proved to be effective in improving learning outcomes in the material of the Human Framework System. The results of the research hypothesis test showed that (1) First Hypothesis: there are differences in student learning outcomes in the Human Skills System course based on blended learning models through webinar applications. This is evidenced by the Sig value of 0.040; (1) Second Hypothesis: there are different student learning outcomes in the course of the Human Framework System based on high learning motivation and low learning motivation. This is evidenced by the value of Sig. amounting to 0,000; (3) there is an interaction between blended learning models through webinar applications and motivation on student learning outcomes in the Human Skills System course. This is evidenced by the value of Sig. in the amount of 0.033. Mean learning outcomes using webinars on the aspect of high motivation ability is 89.36 higher

than on learning outcomes using the E-Module on the high motivation aspect of 78.85. Students who have high learning motivation are more active than students who have low learning motivation. As a result, highly motivated students have better learning outcomes. Motivation aspects are measured based on eight indicators, namely aspects of the duration of learning activities, frequency of activities, persistence, fortitude, tenacity, and ability to deal with obstacles and difficulties, devotion and sacrifice, the level of aspiration, the level of achievement/product qualifications (output), and the direction of learning attitudes. The novelty in this research was the product output in making holograms as learning media in the material of the Human Order System. This project can make students more active. Students find learning more engaging and can apply concepts both physically and biologically through the holographic media. In further research, teachers, students, and even parents need to adapt to all forms of change in education, especially those related to technology. So that in the future, it will be better prepared and able to keep up with developments.

5. REFERENCES:

1. (BNSP), N. E. S. A. (2018). National Examination (UN) Results for Improving Education Quality. Retrieved May 8, 2018, from <https://www.kemdikbud.go.id/main/blog/2018/05/hasil-un-for-represent-quality-ducation>
2. Albhnsawy, A. A., and Aliweh, A. M. (2016). Enhancing Student Teachers' Teaching Skills through a Blended Learning Approach. *International Journal of Higher Education*, 5(3), 131–136.
3. Amhag, L. (2017). Mobile-Assisted seamless learning activities in higher distance education. *International Journal of Higher Education*; 3, 6.
4. Capuno, F. T. (2016). The use of alternative animation and 3-d model in teaching photosynthesis. *International Journal Of Biology Education*, 5(1).
5. Dangwal, K. L., and Lata, K. (2017). Blended learning: An innovative approach. *Universal Journal of Educational Research*, 5(1), 129–136.
6. Ebner, C., and Gegenfurtner, A. (2019). Learning and satisfaction in webinar, online, and face-to-face instruction: a meta-analysis. *Frontiers in Education*, 4, 92.

Frontiers.

7. Husain, A. N. (2015). Holographic Principle of Work. Retrieved May 29, 2020, from <https://www.insinyoer.com/principles-work-holograms/>
8. Kalansooriya, P., Marasinghe, A., and Bandara, K. (2015). Assessing the Applicability of 3D Holographic Technology as an Enhanced Technology for Distance Learning. *IAFOR Journal of Education*.
9. Keller, J. M. (2016). Motivation, learning, and technology: Applying the ARCS-V motivation model. *Participatory Educational Research*, 3(2), 1–15.
10. Kim, H., and Yoon, M. (2014). Adopting smartphone-based blended learning: An Experimental study of the implementation of Kakao-Talk and Mocafe. *Multimedia-Assisted Language Learning*, 17(2), 86–111.
11. Lia, H. (2020). No Title. Retrieved May 30, 2020, from IDN TIMES website: <https://www.idntimes.com/news/indonesia/li-a-hutasoit-1/mendikbud-ada-3-per-change-education-kibat-pandemik-virus-corona/3>
12. Lieser, P., Taf, S. D., and Murphy-Hagan, A. (2018). The Webinar Integration Tool: A Framework for Promoting Active Learning in Blended Environments. *Journal of Interactive Media in Education*, 2018(1).
13. Listyorini, T., and Riadi, A. A. (2016). 3d Hologram as Interactive Media Introduction to Dinosaur Antiquities. *SNATIVE Proceedings*, 25–32.
14. Maduretno, T. W., Sarwanto, S., and Sunarno, W. (2016). Pembelajaran IPA Dengan Pendekatan Saintifik Menggunakan Model Learning Cycle Dan Discovery Learning Ditinjau Dari Aktivitas Dan Motivasi Belajar Siswa Terhadap Prestasi Belajar. *Jurnal Pendidikan Fisika Dan Keilmuan (JPFK)*, 2(1), 1–11.
15. Mohamad, A. M., Jaafar, M. Z., Ishar, N. I. M., Adnan, A., Aziz, N. A., Ramli, M. Z., ... Azman, J. J. (2017). Using Integrated Technologies for Lifelong Learning: Case Study of Doctorate Support Group Webinars. *Advanced Science Letters*, 23(8), 7809–7812.
16. Perveen, A. (2016). Synchronous and asynchronous e-language learning: A case study of virtual university of Pakistan. *Open Praxis*, 8(1), 21–39.
17. Polanco-Bueno, R. (2013). Blogs, Webinars and Significant Learning: A Case Report on a Teacher Training Program for College Teachers. *Higher Learning Research Communications*, 3(1), 56–67.
18. Pratama, H., and Prastyaningrum, I. (2019). Effectiveness of the use of Integrated Project Based Learning model, Telegram messenger, and plagiarism checker on learning outcomes. *Journal of Physics: Conference Series*, 1171(1), 12033. IOP Publishing.
19. Purwandini, I. (2017). Organizing Elearning Using Wiziq in Learning Parenting in the Community of Professional Mother Institute. *Journal of Computer Science and Technology*, 2(2), 102–107.
20. Quevedo, A. (2011). Blended-learning Implementation in Undergraduate Teacher's Formation Courses: Difficulties from the Students' Point of View. *International Journal of Technology, Knowledge and Society*, 7(2).
21. Ricardo, R., and Meilani, R. I. (2017). Impak minat dan motivasi belajar terhadap hasil belajar siswa. *Jurnal Pendidikan Manajemen Perkantoran (JPManper)*, 2(2), 188–201.
22. Riconscente, M. M. (2014). Effects of perceived teacher practices on Latino high school students' interest, self-efficacy, and achievement in mathematics. *The Journal of Experimental Education*, 82(1), 51–73.
23. Shih, R.-C. (2010). Blended learning using video-based blogs: Public speaking for English as a second language students. *Australasian Journal of Educational Technology*, 26(6).
24. Suardi, M. (2018). *Belajar and pembelajaran*. Deepublish.

Table 1. Number of Students Not Attending Teaching and Learning Activities in 2 Academic Years

Class	School year	Total students	Average Number of Students Absent	Percentage
X-1	2018/2019	42	13	31%
X-2	2019/2020	41	16	29%

Table 2. Variable Influence Test Results (Tests of Between-Subjects Effect - Dependent variable: Learning Outcome)

Source	df	Mean Square	F	Sig
Corrected Model	3	1471,778	11,675	,000
Intercept	1	503278,789	3992,366	,000
Learning Model	1	550,173	4,364	,040
Learning Motivation	1	3165,202	25,109	,000
Learning Model *Learning Motivation	1	593,706	4,710	,033
Total	83			
Corrected Total	82			

a. R squared = ,307 (Adjusted R Square = ,281);
dF=Degrees of freedom, F= one way analysis of co-variance, Sig=significance SS

Table 3. Learning Process Using Blended Learning Models through Webinars and Using E-Modules

Model	Media	Characteristic	Advantages	Weakness
Synchronous E-Learning	Live Webinar	<ul style="list-style-type: none"> • Real-time • Scheduled • Collective and can be a collaborative learning • Presenting virtual learning • Content requires instructors • The need for direct communication between the educators and the students 	<ul style="list-style-type: none"> • Familiar with students because learning is carried out directly on a virtual basis • The presence of instructors is significant in the learning process • Communication between the educators and the students becomes faster • The evaluation process can be done directly 	<ul style="list-style-type: none"> • Additional costs required • Requires adequate infrastructure such as internet access speed and bandwidth
Asynchronous E-Learning	E-Module and Email	<ul style="list-style-type: none"> • Interaction cannot occur continuously • Unscheduled • Self-learning (sometimes collaborative) • Content stands alone 	<ul style="list-style-type: none"> • Students can determine their own learning needs and the desired reference • Having an instructor can guarantee the quality of the learning process 	<ul style="list-style-type: none"> • Communication between the students is slower • The evaluation process cannot be done directly

Table 4. Mean values in the interaction of Learning Models * Learning Motivation

Dependent Variable	Learning model	Model_Learning * Motivation_Learning	
		Motivation to learn	The mean (%)
Learning outcomes	Webinar	High	89.36
		Low	71.65
	E-Module	High	78.85
		Low	71.86

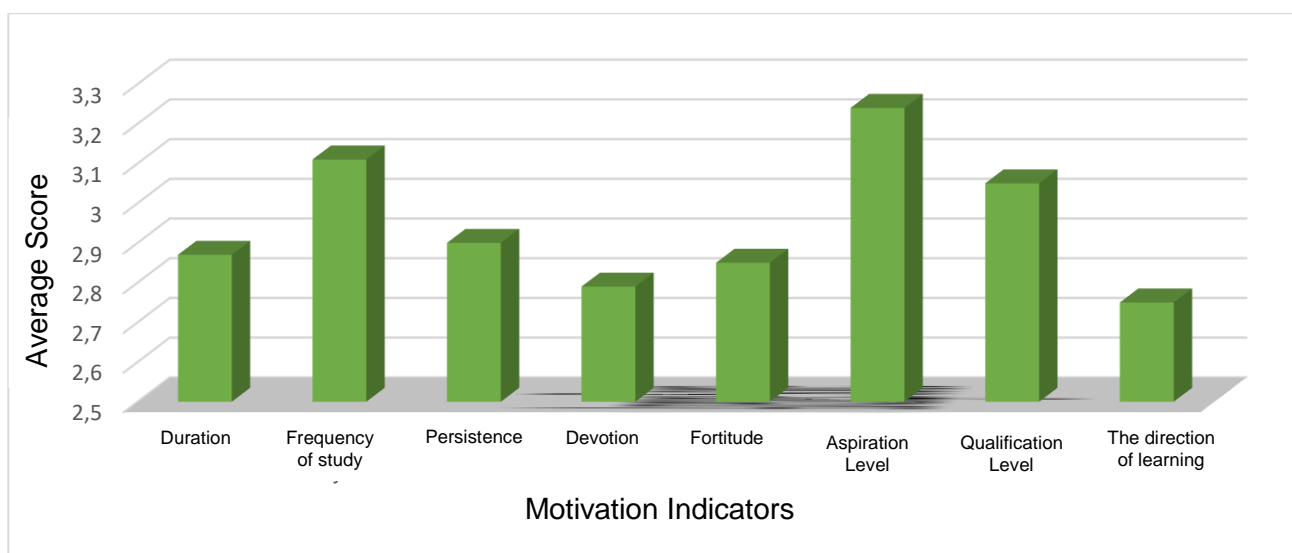


Figure 3. Average Score of Learning Motivation Indicators

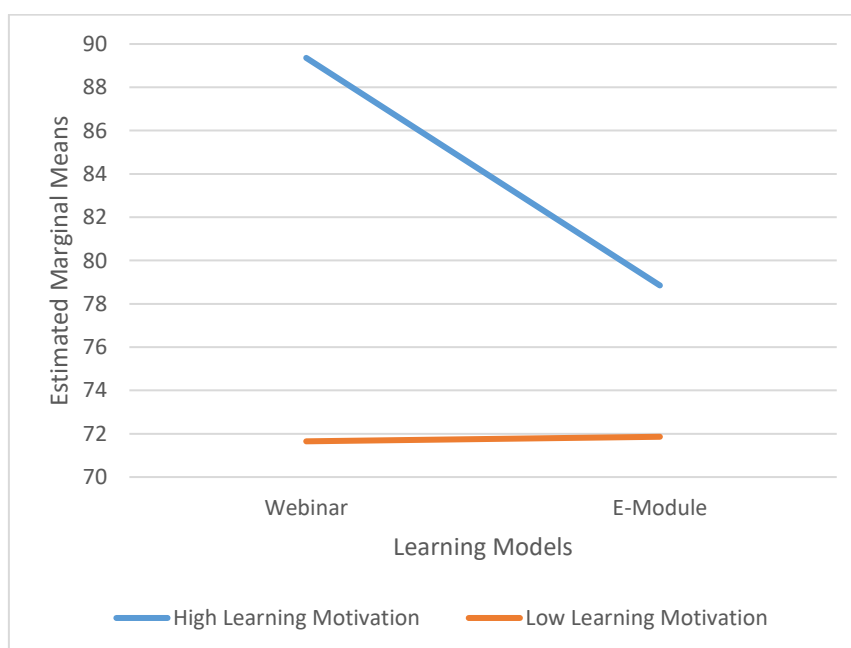


Figure 4. Model Interaction Learning with Learning Motivation Against Learning Outcomes Human Skeletal System

APPENDIX 1

LEARNING MOTIVATION TO LEARN

Instructions for Questionnaire Filling

Select the assessment score using the checklist (✓) on a Likert scale (Strongly Agree (SS) = 5, Agree (S) = 4, Less Agree (KS), Disagree (KS) TS) = 2 and Strongly Disagree (STS) = 1).

No.	Statement of	Alternative Answers				
		SS	S	KS	TS	STS
1	You pay attention to the material delivered by the lecturer from beginning to end.					
2	You always delay doing the assignment given by the lecturer					
3	You are eager to take part in the learning activities.					
4	You always want the learning to be completed quickly by the lecturer					
5	You are serious about participating in the learning activities					
6	You know the rules explained by the lecturer regarding the rules and regulations during the learning activities					
7	You try to understand the material delivered by the lecturer					
8	You don't understand the material delivered by the lecturer					
9	The material delivered by the lecturer, with you understand					
10	You need repetition of the material from the lecturer so you can understand the material					
11	You get the benefits of participating in learning the subject of natural science concepts					
12	You feel that you don't understand the benefits of participating in the learning activities of the basic science course subjects					
13	You can concentrate during the learning activities of the course basic concepts of science					
14	when exam, you attempt to answer with your abilities					
15	you need to open the notebook when the task					
16	civil bold expression class in front of					
17	you feel embarrassed when I express an opinion in front of the class					
18	I feel discussing with friends exciting					
19	You feel less confident to discuss with friends					
20	In doing competitive tasks, you try to be superior to friends					
21	Feel learning activities of basic science concepts are useful later on					
22	Feel the learning activities of basic science concepts courses can answer my curiosity					
23	Participate in learning activities from beginning to end					
24	You do not like it if there are friends who help with your assignments					
25	lecture weight encourages to get the best value					
26	I feel equipment during the activity learning of basic science concepts courses are met					

EXAMPLE OF PRE-TEST FORMATIVE TEST

Formative Tests Pre Test

Put a Cross (X) on the Answer That You Think Is Right!

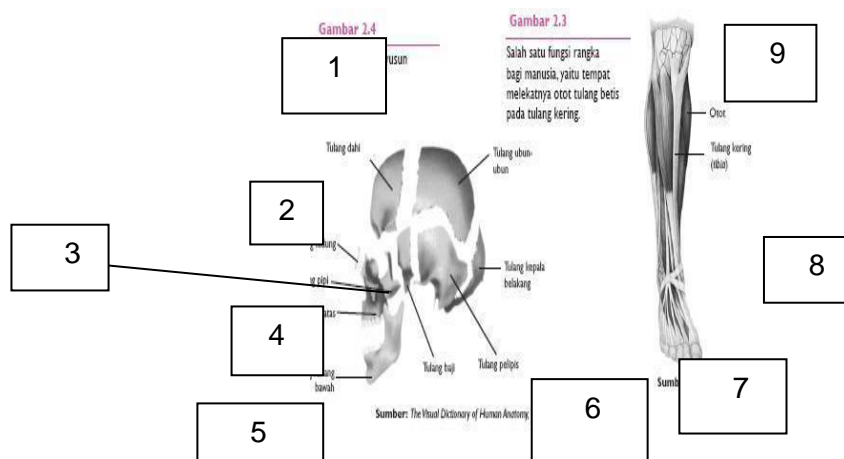
1. Among the bones with each other bones connected by...
 - a. Muscle
 - b. Framework of
 - c. collagen
 - d. joints
2. Function bone to our bodies, among others ...
 - a. Giving shape
 - b. circulatory Points
 - c. muscles forming
 - d. Points attach organs in
3. For example, organs are composed of cartilage is .. .
 - a. The nose and earlobe
 - b. mouth and nose
 - c. cheeks and mouth
 - d. and cheekauricle
4. boneloud composed of ...
 - a. calcium and ligaments
 - b. calcium and joints
 - c. ligaments and collagen
 - d. collagen and calcium
5. Here are forms of bone are:

1) The thigh bone	4) bone shank
2) bone soles of the feet	5) Arm
3) bones Chest bones	6) Palm bones

Which are included in the pipe bones are indicated by numbers

- a. 1, 4, and 5
- b. 1, 2, and 3
- c. 4, 5, and 6
- d. 1, 5, and 2

6. Pay attention to the draw a skull bone below.



Cheekbones, temples, and wedge bones are shown by numbers ...

- a. 3, 9, and 1
- b. 6, 7, and 3
- c. 3, 6, and 7
- d. 3, 7, and 6

MELHORANDO A TOLERÂNCIA DE ESTRESSE A FRIO EM *CORYLUS AVELLANA* L. USANDO VÁRIOS COMPOSTOS QUÍMICOS

IMPROVING COLD STRESS TOLERANCE IN *CORYLUS AVELLANA* L. USING VARIOUS CHEMICAL COMPOUNDS

بهبود مقاومت به تنش سرما در *CORYLUS AVELLANA* L. با استفاده از ترکیبات شیمیایی مختلف

BAHRAMI, Saeed¹; SAADATMAND, Sara^{2*}; HAJIVAND Shokrollah³; FATH Mojtaba^{4,5};

^{1,2} Islamic Azad University, Science and Research Branch, Faculty of Basic Science, Department of Biology. Iran.

³ Agricultural Research, Education and Extension Organization (AREEO), Horticultural Science Research Institute, Department of Genetics and Breeding, Temperae Fruits Research Center. Iran.

⁴Zanjan University of Medical Sciences, School of Medicine, Department of Clinical Biochemistry. Iran.

⁵Zanjan University of Medical Sciences, Cancer Gene Therapy Research Center. Iran.

* Corresponding author

e-mail: saadatmand.srbiau@gmail.com

Received 13 July 2020; received in revised form 18 August 2020; accepted 10 September 2020

RESUMO

Corylus avellana L., avelã comum, é uma árvore de nozes cultivada globalmente e economicamente valiosa que tem uma sensibilidade a estresses abióticos, especialmente a baixas temperaturas, cuja intensidade varia com base no crescimento e estágio de desenvolvimento. As consequências comerciais do estresse pelo frio na definição de nozes de avelãs são significativas e abordagens práticas para resolver o problema são altamente exigidas. Para enfrentar a questão da intolerância ao estresse pelo frio em *C. avellana* e fornecer aos produtores soluções práticas, este estudo teve como objetivo investigar os efeitos de várias substâncias químicas em árvores de *C. avellana* com dez anos de idade sob estresse pelo frio e suas respostas nos níveis fisiológico e bioquímico em folhas e flores femininas e masculinas. As avelãs foram tratadas com ácido salicílico (3 mg L⁻¹), potássio (2 mg L⁻¹), tiofer (5 mg L⁻¹), biobloom (66 mg L⁻¹) e aminoácido (0,5 mg L⁻¹) em tratamentos separados utilizando a pulverização foliar sob temperatura média de 4,13°C. Pôde-se observar que a aplicação exógena dos compostos afetou a regulação osmótica (aumento do teor de proteína e prolina) e enzimas antioxidantes (superóxido dismutase, catalase, ascorbato peroxidase e glutathione peroxidase). No caso da antocianina e dos pigmentos fotossintéticos, o teor de clorofila a, b, e total nas folhas das árvores tratadas com potássio com 217,38 ± 6,13, 66,23 ± 6,21, 150,66 ± 4,32 e 19,01 ± 2,20 mg g⁻¹ de peso fresco, apresentou as maiores quantidades. As folhas tratadas com ácido salicílico apresentaram o maior teor de carotenóides (289,62 ± 2,41). O mesmo padrão quase pode ser aplicado à gama dessas substâncias em flores masculinas e femininas. Embora todos os cinco usados ajudem as plantas de *C. avellana* a superar melhor o estresse causado pelo frio, o ácido salicílico e o potássio foram os mais eficazes. Pode-se concluir que a ampla aplicação comercial desses compostos químicos para conferir resistência ao frio às avelãs é altamente recomendável.

Palavras-chave: Enzimas antioxidantes, H₂O₂, Prolina, Proteína, Resistência à baixa temperatura

ABSTRACT

Corylus avellana L., common hazelnut, is a globally cultivated economically valuable nut crop tree with a sensitivity to abiotic stresses remarkably low temperature. Its intensity varies based on the growth and developmental stage. The commercial consequences of cold stress on nut setting of hazelnuts are significant and practical approaches to address the problem are highly demanded. To tackle the issue of cold stress intolerance in *C. avellana* and provide producers with practical solutions, this study aimed to investigate the effects of various chemical substances on ten years old *C. avellana* trees under cold stress and its responses at the physiological and biochemical levels in leaves and female and male flowers. Hazelnut trees were treated with salicylic acid (3 mg L⁻¹), potassium (2 mg L⁻¹), thiofer (5 mg L⁻¹), biobloom (66 mg L⁻¹), and amino acid (0.5 mg L⁻¹) in different

treatments using the foliar spray under an average temperature of 4.13°C. It could be observed that the exogenous application of the compounds affected osmotic regulation (enhancement of protein and proline content) and antioxidant enzymes (superoxide dismutase, catalase, ascorbate peroxidase, and glutathione peroxidase). In the case of the anthocyanin and photosynthetic pigments, the content of chlorophyll a, b, and total in leaves of trees treated by potassium with 217.38 ± 6.13 , 66.23 ± 6.21 , 150.66 ± 4.32 , and 19.01 ± 2.20 mg g⁻¹ fresh weight, showed the highest quantities. The leaves treated by salicylic acid had the highest content of carotenoid (289.62 ± 2.41). The same pattern can almost be applied to the range of these substances in male and female flowers. Although all five used helps *C. avellana* plants to overcome cold stress better, salicylic acid and potassium were the most effective. It can be concluded that the widespread commercial application of these chemical compounds to confer cold resistance to hazelnut trees is highly recommended.

Keywords: Antioxidative enzymes, H₂O₂, Proline, Protein, Resistance to low temperature

چکیده

Corylus avellana L., فندق معمولی یک درخت آجیلی با ارزش اقتصادی بالا و سطح کشت و کار جهانی بوده که دارای حساسیت به تنش‌های محیطی بخصوص تنش دمای پایین می‌باشد که شدت آن وابسته به رشدی متفاوت است. اثرات اقتصادی تنش سرما به درخت فندق قابل توجه است و ارائه راهکارهای عملی برای رفع این مشکل بسیار مورد توجه و تقاضا قرار دارند. در جهت مقابله با عدم تحمل سرما در *C. avellana* و ارائه تولید کنندگان با راهکارهای عملی، در این مطالعه سعی بر بررسی اثرات ترکیبات شیمیایی مختلف رو درختان ده ساله *C. avellana* تحت تنش سرما داشته و واکنش‌های آن را در سطح فیزیولوژیکی و بیوشیمیایی در برگ، گل‌های نر و ماده را مورد مطالعه قرار گرفت. درختان بطور جداگانه با سالیسیلیک اسید (3 mg L^{-1})، پتاسیم (2 mg L^{-1})، تیوفر (5 mg L^{-1})، بیوبلوم (66 mg L^{-1})، و آمینو اسید (0.5 mg L^{-1}) با اسپری روی برگ تیمار گردیدند. قابل مشاهده است که اعمال خارجی پنج ترکیب تنظیم اسمز (افزایش محتوای پروتئین و پرولین) و آنزیم‌های آنتی‌اکسیدانی (سوپر اکسید دیسموتاز، کاتالاز، آسکوربات پروکسیداز، گلاپکول پروکسیداز) را تحت تاثیر قرار داد. در مورد محتوای آنتوسیانین رنگ‌دانه‌های فتوسنتزی، محتوای کلروفیل a, b و کل در برگ درختان تیمار شده با پتاسیم به ترتیب با 217.38 ± 6.13 , 66.23 ± 6.21 , 150.66 ± 4.32 و 19.01 ± 2.20 mg g⁻¹ وزن تر، از بیشترین میزان ممکن برخوردار بودند. برگ‌های تیمار شده با سالیسیلیک اسید از بیشترین محتوای کارتنوئید (289.62 ± 2.41) برخوردار بودند. الگوی مشابهی را تقریباً می‌توان نسبت به محتوای این ترکیبات در گل‌های نر و ماده درختان تیمار شده اعمال نمود. اگرچه همه ترکیبات اعمال شده رو درختان فندق به آن‌ها در غلبه بر تنش سرما کمک نمود، سالیسیلیک اسید و پتاسیم به‌عنوان موثرترین ترکیبات مشاهده شدند. نتایج به دست آمده از این آزمایش اطلاعات تازه‌ای را در مورد نقش فیزیولوژیکی و بیوشیمیایی این ترکیبات در ایجاد مقاومت به سرما ارائه می‌دهند. می‌توان نتیجه گرفت که استفاده گسترده تجاری این ترکیبات برای ایجاد مقاومت به سرما در درختان فندق به شدت توصیه می‌گردد.

کلیدواژه‌ها: آنزیم‌های آنتی‌اکسیدانی، H₂O₂، پرولین، پروتئین، مقاومت به دمای پایین

1. INTRODUCTION:

Low-temperature stress is one of the principal limiting environmental stresses that can reduce the productivity of crops. Low-temperature stress is classified into chilling (temperatures above 0°C) and freezing (temperatures under 0°C). Chilling stress causes cellular membrane injury, oxidative stress, and a decrease in plant growth. Freezing stress leads to creating ice crystals in the cells (Xin and Browse, 2000; Huang *et al.*, 2014). Cold stress disturbs cellular metabolism in plants. Membrane damage is one of the adverse impacts of cold stress in plants that eventually reduces germination, aging of leaves, and a decrease in crops' growth (Suzuki *et al.*, 2008). Plants have enzymatic and non-enzymatic antioxidant mechanisms to deal with ROS's oxidative stress. These solutes contribute to enzymes, membranes, and other cell constituents' stability, adjust cellular water content, and reduce cellular desiccation (Farooq *et al.*, 2009).

Generally, environmental stresses such as drought, salinity, heavy metals, and high or low-temperature more often than not impose their negative effect by increasing the generation of reactive oxygen species (ROS). Moreover, an imbalance between primary and secondary photosynthesis reactions leads to ROS accumulation in chloroplast and mitochondria under cold stress (Li *et al.*, 2009). These products can directly degrade proteins, amino acids, nucleic acids, and lipids' peroxidation in membranes (Gwozdz *et al.*, 1997). By transferring an electron to oxygen molecular radical superoxide (O²), with the transfer of two electrons to molecular H₂O₂, and by moving three electrons to oxygen, radical hydroxyl oxygen (OH⁻) is generated. Plants have enzymatic and non-enzymatic antioxidant mechanisms to deal with ROS's oxidative stress (Malecka *et al.*, 2012). Examples of the antioxidant enzymes are superoxide dismutase (SOD), catalase (CAT), and peroxidase (POX) that involve in the defense system and maintain cells from oxidative damage (Mittler, 2002). In plants,

SOD plays a significant role in defending against oxidative stress. This enzyme belongs to metalloenzymes that convert superoxide radicals into oxygen and hydrogen peroxide. GPX is also a protein that preferentially oxidizes electron-giving aromatic compounds in exchange for hydrogen peroxide (Jebara *et al.*, 2005; Sharma *et al.*, 2012). The critical role of CAT in eradicating ROS, in particular, H_2O_2 in mitochondria that are produced during electron transport, β -oxidation of the fatty acids, and, most importantly, photorespiratory oxidation, has been proven by numerous reports (Li *et al.*, 2009; Malecka *et al.*, 2012).

Corylus avellana L. is a monoecious and wind-pollinated broadleaf species that belongs to Betulaceae, which comprises 25 species that 9 are economically cultivated and essential for breeding. Mostly in the form of shrubs and rarely seen as a tree (Qaderi *et al.*, 2012). Hazelnut is one of the most important nut products globally, which is used as a fruit and has various applications in the food industry and benefits health. Hazelnut fruit is an essential source of vitamin B6 and oleic acid (83 %). It's a rich source of other critical components, including protein, carbohydrates, fiber, vitamins (vitamin E), minerals, phytosterols, mainly cytosterols and antioxidant phenols that can protect the body against diseases (Seyhan *et al.*, 2007; Oliveira *et al.*, 2008; Alasalvar *et al.*, 2012;). Traditionally, the public often views hazelnuts as an unhealthy food because of their high-fat content. However, recent epidemiological and clinical studies have shown that nuts' consumption leads to optimal plasmid lipid levels (Gürcan *et al.*, 2010).

As in the ancient Chinese scripts, the history of its cultivation has shown it goes back to 8000-5000 years ago. In Europe, hazelnut is of the predominant species; however, its exact origin is not clear. This species has a wide distribution range from Portugal's coast to Ireland, and its northern extension goes from Norway to Russia. Still, the main areas of cultivation are proximity to large water bodies with mild winters and cool summers. The main areas of cultivation are Turkey, which is under the influence of the Black Sea, Italy, and Spain due to being close to the Mediterranean Sea and the United States under the Pacific Ocean's influence, owing to geographical features. The countries mentioned above are significant producers of hazelnut (Lunde *et al.*, 2006; Mehlenbacher and Smith 2006; Boccacci and Botta 2009; Gürcan *et al.*, 2010), and Iran, with 14,000 tons production from 18,000 hectares, ranked eighth in the world.

Because *C. avellana* has a low tolerance to heat, cold, drought, and wind stress (Larcher, 2003; Salimi and Hoseinova *et al.*, 2012; Arzanlou *et al.*, 2018). To date, studies on reducing the effect of abiotic stress, particularly cold stress, as one of the critical limiting factors, can increase the yield per hectare.

Plants respond to environmental and biotic stresses by synthesizing signaling molecules. These signal molecules activate the signaling pathways. Several signals or signaling molecules have been identified in plants, including calcium, jasmonic acid, ethylene, salicylic acid (SA), and hydrogen peroxide (H_2O_2). The application of several compounds, such as SA or Potassium (K) is an essential tool for increasing crop production under abiotic stress. Numerous works exhibited that utilizing various compounds reduced the negative impacts of the abiotic stresses in plants (Kaczmarek *et al.*, 2017; Shaki *et al.*, 2017; Rezayian *et al.*, 2018). The role of SA as a defense signal in plants is now proven. SA has also been introduced as a plant hormone due to its substantial roles in the plant (Wilson 1996; Zhang *et al.*, 2007). Over the past 20 years, researchers have paid particular attention to the ability of SA to induce protective substances in plants under environmental stress. There are reports of the role of SA in increasing salinity resistance in wheat, rice, and cucumber, heat and cold in tomatoes and beans, and heavy metals in rice (Zhang *et al.*, 2007; Taşgîn *et al.*, 2003). SA regulates the development and expression of senescence genes in Arabidopsis (Morris *et al.*, 2000). The impact of SA in resistance to cold stress and possibly through its effect on enzymatic antioxidants and metabolism of H_2O_2 , reducing cold stress damage and increasing plant tolerance to cold stress. Efficacy of SA in induction stress tolerance, depending on plant type or concentration of SA. exogenous application of SA, increases low-temperature tolerance (Khan *et al.*, 2012; Miura and Tada, 2014).

Potassium (K) has a significant effect on plant responses and tolerance to environmental stresses (Hasanuzzaman *et al.*, 2018). Zhang *et al.* (2014) showed that exogenous K application reduced the adverse effects of stress in *Zea mays* L. Proline application diminished stress-induced inhibitory impact on wheat growth (Bekka *et al.*, 2018). Proline, as an essential osmolyte, plays a crucial role in modulating the osmotic pressure of cells under stresses such as soil salinity, drought, low temperatures, nutrient deficiencies, heavy metal exposure, and high acidity. High production of proline inhibits cold stress damage on the

normal cellular process by increasing intracellular osmotic pressure. This increase in proline levels persists for about a month, even after the stress conditions have been resolved. The positive role of proline in modulating osmotic pressure relative to low-temperature, drought, and salinity has been reported by researchers in various plants such as maize (Chen and Li 1979), alfalfa (Liu *et al.*, 2009), and Arabidopsis (Khavari-Nejad *et al.*, 2013). Proline influenced cryoprotectant under chilling stress (Gleeson *et al.*, 2004). α -aminobutyric acid treatment mitigated the injury induced by chilling stress in *Lycopersicon esculentum* L. (Shang *et al.*, 2011). Given K's significant effect on protecting plants against cold stress, there is fertilizer so-called Bio bloom contains more than 85% of organic matter, high amounts of phosphorus, and potassium. In addition to affecting the rate of metabolism and the structure of living membranes, organic Bio bloom regulates the membrane's fluidity by creating stability and balance of certain types of fatty acids so that proteins and enzymes can function correctly. Potassium is involved in the regulation of osmosis and the prevention of ice formation that can damage energy-carrying molecules (Rezayian *et al.*, 2018).

One of the essential organic antifreeze is called Thiofer. It contains various Thiobacillus bacteria, minerals, and proteins and can increase the resistance of plants to stress such as heat, cold, and frost (Stipešević *et al.*, 2014). The application of this substance at the right time causes the plant to produce antifreeze protein (AFP) and antifreeze amino acids (AAA). It increases the plant's resistance to cold and frost. This substance is systemic and penetrates plant tissues and prevents ice formation (Balesini *et al.*, 2013).

Therefore, this study aimed to evaluate the ameliorating influence of K, SA, thiofer, amino acids, and Bio Bloom on the physiological and biochemical responses of hazelnut trees. The primary purpose was to provide a practical solution to a very limiting environmental condition that jeopardizes the hazelnut orchards of Iran located in mountainous areas. Considering the extent of this study, this is the first comprehensive research on improving low-temperature tolerance in hazelnut to the best of our knowledge.

2. MATERIALS AND METHODS:

2.1. Plant materials

This research was conducted at the Agricultural and Natural Resources Research

Center of Qazvin Province (East of Alamut) in 2016 (October)-2017 (March). The average temperature in this area was 4.13 °C. Various compounds [SA (3 mg L⁻¹), potassium (2 mg L⁻¹), thiofer (5 mg L⁻¹), biobloom (66 mg L⁻¹), and amino acid (0.5 mg L⁻¹)] were sprayed uniformly on 10 years old hazelnut trees using an atomizer four times for 18 months (Figure 1). After treatments, the leaves were harvested and stored at -70 °C and analyzed the following parameters (Figure 2).

2.2. Antioxidant enzymes assay

For the measurement of enzymes activities, fresh material was extracted at 4 °C in 1 M Tris-HCl (pH 6.8) and centrifuged at 13000 rpm for 30 min. Supernatants were kept at -70 °C and used for enzymes assay. The content of protein was measured by Bradford (1976) using bovine serum albumin as the standard.

SOD activity was assayed based on the Giannopolitis and Ries (1977) method. Reaction solution comprised sodium phosphate buffer (50 mM), 0.1 mM EDTA, 13 mM methionine, 75 μ M nitroblue tetrazolium (NBT), 75 μ M riboflavin and 100 μ L of enzyme extract. The reaction solution was placed in front of the light for 18 minutes, and then absorbance was measured at 560 nm.

CAT activity was determined by the method of Aebi (1984). Assay mixture contained 50 mM phosphate buffer (pH 7.0), H₂O₂; 3% and 10 μ L enzyme extract. The decline in absorption was followed for 180s, and CAT activity was expressed as units per mg of protein.

Ascorbate peroxidase (APX) activity was determined by Jebara *et al.*, (2005) method. Reaction mixture comprised ascorbic acid (0.5 mM), 50 mM potassium phosphate buffer (pH 7.0), H₂O₂ (0.1 mM) and 10 μ L of enzyme extract. In this reaction, ascorbate was oxidized and the concentration of oxidized ascorbate was determined by the decrease in absorbance at 290 nm. One unit of APX was defined as 1 μ M oxidized ascorbate per min per mg protein.

Glutathione peroxidase (GPX) activity was assayed using the method of Lin and Kao (1999). Reaction mixture (1.0 mL) comprised 50 mM sodium phosphate buffer (pH 7.0), 9 mM glutathione, 19 mM H₂O₂ and protein extract. After the addition of protein extract, the increase in absorbance at 470 nm was recorded for 1 min.

2.3. Hydrogen peroxide

The H₂O₂ content was estimated via Velikova *et al.* (2000) method. Leaf tissue (0.3 g)

was homogenized in 0.1% Trichloroacetic acid (TCA) then was centrifuged at 12000 rpm for 15 min. The supernatant (0.5 mL) was added to 0.5 ml potassium phosphate buffer (pH 7.0) and 1 ml potassium iodide (1 M), and absorbance was recorded by spectrophotometer at 390 nm.

2.4. Determination of Proline

Proline content was measured, according to Bates *et al.* (1973). Fresh tissues were homogenized in 5 mL sulfosalicylic acid (3%) and then centrifuged at 13000 rpm for 20 min. Two mL of supernatant was mixed with acid ninhydrin (2 mL) and glacial acetic acid (2 mL) and then was boiled at 100°C for one hour. The reaction mixture was extracted with 4 mL toluene, and the absorbance was recorded at 520 nm.

2.5. Measurement of anthocyanin and pigments content

Anthocyanin content was determined in 0.3% HCl in methanol at 25°C using the extinction coefficient ($33 \text{ cm}^2 \text{ mol}^{-1}$) at 550 nm (Wagner, 1979). Chlorophyll a (Chl a), chlorophyll b (Chl b) chlorophyll total (Chl T), and carotenoids were extracted by 80 % acetone and quantified spectrophotometrically (UNFCO-2100 model) according to Lichtenthaler and Wellburn (1983) and calculated based on the following formula:

$$\text{Chl. a } (\mu\text{g/g}) = 12.25 A_{663} - 2.79 A_{646} \times V/W \quad (1)$$

$$\text{Chl. b } (\mu\text{g/g}) = 21.50 A_{646} - 5.1 A_{663} \times V/W \quad (2)$$

$$\text{Chl. T. } (\mu\text{g/g}) = \text{Chl. a} + \text{Chl. b} \quad (3)$$

$$\text{Carotenoid } (\mu\text{g/g}) = (1000A_{470} - 1.82\text{Chl.a} - 85.02\text{Chl.b})/198 \times V/W \quad (4)$$

Where A_{663} , A_{646} , A_{470} are absorptions at wavelengths of 663, 646, and 470 nm. The final results were expressed as mg g^{-1} fresh weight (FW).

2.6. Protein extraction and 2-DE

Proteins were extracted using the method described by Damerval *et al.* (1986). 500 mg of fresh material was homogenized in liquid nitrogen using a mortar and pestle. The resulting powder was placed in a 2-mL microtube, and 1 mL of extraction buffer [10% TCA in acetone] was added. The samples were incubated for 60 min at 4°C and then centrifuged at 16000 rpm for 30 min. The supernatant was discarded, and the pellet was washed three times in cold acetone with 20 mM DTT. Subsequently, the pellets were resuspended in 1 mL of buffer containing 7M urea, 2M thiourea, 1% DTT, 2% Triton-100, and 1mM

phenylmethanesulfonyl fluoride and stirred for 60 min at 4°C until the samples were resuspended entirely. The samples were incubated on ice for 30 min and then centrifuged at 16000 rpm for 10 min. Gels were visualized by Coomassie Brilliant Blue G-25. The gels were scanned using a GS-800 densitometer (BioRad) and analyzed using Melanie 7 software (GeneBio).

2.7. Statistical analysis

The experiment was designed in a six-factorial complete randomized experiment with three replications per treatment. The experimental data were subjected to one-way ANOVA, and significant differences between means were determined by Duncan multiple rang ($P < 0.05$).

3. RESULTS AND DISCUSSION:

Plants need to an optimum temperature for appropriate growth and development. Low temperature is one of the environmental stresses that lead to a reduction in yield (Bray *et al.*, 2000). Various physiological parameters were measured in male and female flowers and leaves. SA and potassium treatment increased protein content in leaf, but the other four treatments declined these parameters. While treatments enhanced protein content in male and female flowers (Table 1).

Proteomics analysis was carried out for leaf and two types of flowers under SA treatment which the results of this analysis indicated a fluctuation in protein in trees treated by SA. Foliar application of SA enhanced the proteins 122, 147, 117, 34, 113, 31, 114, 16 and 89 in leaf, but reduced the proteins 38, 4, 74, 3, 58, 71, 57, 64, 102, 46, 110, 137 and 177. The proteins 103, 47, 75, 32, 180, 25, 115 and 37 showed a significant increase in female flowers under SA treatment, whereas the proteins 157, 38, 3, 4, 41, 30, 73, 106, 46, 71, 65, 62, 63 and 179 declined. SA treatment-induced protein 32 and decreased in proteins 41 and 62 (Figures 3 to 8). One of the key responses in increasing freezing tolerance during cold acclimation is the synthesis of particular proteins (Antikainen *et al.*, 1996). Our results showed that SA and potassium application improved the protein content of *C. avellana* and enabled the possibility of overcoming cold stress. SA prevents protein destruction by neutralizing free radicals and leads to an increase in protein content (Mellouk *et al.*, 2016). These findings are in agreement with Tasgin *et al.* (2003) and Farooq *et al.* (2008). By its involvements in osmoregulation, energy source, osmoprotectant, and ROS scavenger, proline plays an important role in

tolerance to abiotic stresses (Trovato *et al.*, 2008). Proline accumulation is a response in plants under cold stress that maintains plants from dryness, causing cold stress by decreasing plant cells' water potential (Szekely *et al.*, 2008). Liu *et al.* (2008) showed that proline content increased in *Avena nuda* L. under cold stress. In our study, all treatments enhanced proline accumulation in *C. avellana* plants. This compound is a compatible osmolyte that causes osmotic regulation and osmoprotectants under stress. These data show that these compounds help to *C. avellana* to overcome stress via osmolytes accumulation better. These results are in agreement with Misra and Saxena (2009), Ali *et al.* (2014), and Bekka *et al.* (2018). Apoplastic water losses in plants due to freezing under freezing stress lead to dehydration, and an appropriate K amount regulates the osmotic potential and declines dehydration under freezing (Wang *et al.*, 2013).

The alteration in the activities of antioxidant enzymes, including SOD, CAT, APX, and GPX, showed different trends under various treatments. SOD activity was not changed in the treated three tissues. Potassium, SA, and biobloom application improved CAT activity in leaf; however, the effect of SA was more prominent (3-fold). Five types of treatments induced CAT activity in female flowers, but potassium, thiofer, and amino acid increased this enzyme activity in male flowers. Biobloom treatment only enhanced (1.23-fold) APX activity in leaf. Exogenous application of thiofer, biobloom, and amino acid promoted APX activity in male flowers, whereas potassium caused its reduction. All treatments decreased or did not affect APX activity in female flowers. GPX activity remarkably increased in leaf by SA, potassium, and amino acid treatments. Exogenously applied all chemical compounds induced GPX activity in male flowers, and this increase by amino acid was more than other treatments. In contrast to male flowers, most treatments declined GPX activity in female flowers (Table 1).

Potassium, thiofer, and amino acid application lessened H₂O₂ content in leaf. A relatively higher accumulation of H₂O₂ occurred in the plants exposed to biobloom. SA, potassium, and biobloom declined H₂O₂ content in male flowers by 12.4, 30.7, and 30.71%, respectively. All treatments significantly affected the content of H₂O₂ in female flowers (Table 1).

Proline showed a sharp increase in the leaf of trees received the foliar application of chemical compounds. SA and biobloom application induced the accumulation of proline (58.33%) when compared to control. Proline content significantly

increased by SA, thiofer, and amino acid treatments in female flowers, but other treatments had little effect on this parameter. All treatment, except potassium, caused proline accumulation in male flowers (Table 2). Abiotic stresses increase the ROS production in plants, comprising superoxide anion radicals, hydroxyl radicals, H₂O₂, alkoxy radicals, and singlet oxygen. ROS causes adverse effects on proteins, lipids, and DNA, thus disrupts cell function (Foyer and Fletcher, 2001; Munné-Bosch and Penuelas, 2003). The enzymatic antioxidant defense system leads to ROS degradation and has a primary role in maintaining cell homeostasis. SOD leads to the dismutation of superoxide radicals to oxygen and H₂O₂. APX is an enzyme that plays a prominent role in the alteration of H₂O₂ into H₂O by ascorbate, such as an electron donor (Rosa *et al.*, 2010). Cold stress boosted CAT activity in some wheat cultivars (Javadian *et al.*, 2010). Fahimirad *et al.* (2013) indicated that antioxidative enzymes enhanced in canola under cold stress. High activities of antioxidant enzymes are essential for abiotic stress tolerance. The treatments caused a reduction of H₂O₂ and an increase of antioxidant enzymes in *C. avellana*; however, the oxidative injury was increased by the application of compounds simultaneously. According to our results, these treatments' enhancement of antioxidant enzymes may play an important role in cold tolerance. Similar results have been published in barley (Mutlu *et al.*, 2013), Lettuce (Shams *et al.*, 2016), and *Triticum aestivum* L. (Jan *et al.*, 2017).

Anthocyanin content substantially enhanced using potassium, thiofer, and amino acid treatments in leaf. The highest anthocyanin content in leaf was observed in potassium treated plants, of which 31.92% higher as compared to the control. Anthocyanin content was not shown a significant change in male and female flowers under different treatments (Table 2).

Carotenoid content notably increased by 36.9% in leaves exposed to SA, but it did not change in treated leaves with other treatments. All five compounds applied in this study affect carotenoid content in male flowers, and the highest increase was (81%) in SA-treated plants (Table 2).

The exogenous application of thiofer, K, SA, and amino acid enhanced Chl a, Chl b, and Chl T contents in leaf. Chl content was much higher in SA-treated plants than the plants exposed to other treatments. SA application only triggered a significant increase (1.23%) in Chl content in female flowers. In contrast to Chl a, Chl b and Chl

T contents improved by five treatments, and the thiofer was more effective than the other compounds. Chl a and Chl T content were not induced in male flowers under all treatments, whereas Chl b enhanced by potassium and biobloom (Table 2). Anthocyanins are types of water-soluble pigments derived from flavonoids that synthesis of the shikimic acid pathway. Plants generate anthocyanins under stress for cell defense (Chutipaijit *et al.*, 2009). Potassium, amino acid, and thiofer induced accumulation of anthocyanin in *C. avellana*, which was positively related to antioxidant capacity. So, these treatments can help this plant to better cope with cold stress. Our results are in agreement with other previous reports (Amira *et al.*, 2017; Kocira, 2019).

Low temperature leads to disruption in the photosynthetic apparatus by photo-inhibition (Huang *et al.*, 2014). Li *et al.* (2018) displayed that cold stress declined Chl content in zoysiagrass genotypes. Tewari and Tripathy (1998) described that a decline in Chl biosynthesis in plants under cold stress is due to 5-aminolevulinic acid biosynthesis inhibition. The applied compounds mainly enhanced the Chl content in *C. avellana*. An increase in Chl content as the critical photosynthetic pigment in plants could improve photosynthetic activity. The present research data were in agreement with the results of previous studies (Hussein *et al.*, 2014; Fayez and Bazaid, 2014; Shaki *et al.*, 2018). Carotenoids are the first line of defense against $^1\text{O}_2$ toxicity and can stabilize membranes and preventing lipid peroxidation by their antioxidant activity (Niyogi, 1999). SA treatment alleviated the effect of cold tolerance in *C. avellana* by the increase of carotenoid content.

4. CONCLUSIONS:

Mitigating compounds can alleviate the adverse effects of cold stress on *C. avellana* by improving antioxidant capacity, accumulating proline, and increasing the content of photosynthetic pigments. Although all five applied compounds in this study have the potential to be stress protectants, SA and potassium were the most effective in which spraying K markedly enhanced the content of protein, proline, antioxidant enzymes (SOD, CAT, APX, and GPX). While SA was found to have the highest positive impact on increasing the content of anthocyanin, chlorophyll a, b, and total in leaves and male and female flowers. Additionally, 2-D gel results for the influence of SA on the protein profile of leaves, and male and female flowers indicated enhancing

some specific proteins while caused a decrease in some others. This study revealed applicable critical results to protect hazelnut trees against cold stress. However, give the complicated biological mechanisms involved, further research using a broad spectrum of low-temperature stress treatments are highly recommended to uncover the physiological responses of *C. avellana*.

5. REFERENCES:

1. Aebi H. (1984). Catalase *in vitro*. *Methods Enzymology*, 105:121-126.
2. Ali, M; Bakht, J; Khan, G. D. (2014). Effect of water deficiency and potassium application on plant growth, osmolytes, and grain yield of Brassica napus cultivars. *Acta Botanica Croatica*, 73(2), 299-314.
3. Alasalvar, C; Pelvan, E; Bahar, B; Korel, F; Ölmez, H. (2012). Flavour of natural and roasted Turkish hazelnut varieties (*Corylus avellana* L.) by descriptive sensory analysis, electronic nose and chemometrics. *International journal of food science and technology*, 47(1), 122-131.
4. Antikainen, M; Griffith, M; Zhang, J; Hon, W. C; Yang, D. S; Pihakaski-Maunsbach, K. (1996). Immunolocalization of antifreeze proteins in winter rye leaves, crowns, and roots by tissue printing. *Plant Physiology*, 110(3), 845-857.
5. Arzanlou, M; Torbati, M; Golmohammadi, H. (2018). Powdery mildew on hazelnut (*Corylus avellana*) caused by Erysiphe corylacearum in Iran. *Forest Pathology*, 48(5), e12450.
6. Bates, L. S; Waldren, R. P; Teare, I. D. (1973). Rapid determination of free proline for water-stress studies. *Plant and soil*, 39, 205-207.
7. Bekka, S; Abrous-Belbachir, O; Djebbar, R. (2018). Effects of exogenous proline on the physiological characteristics of Triticum aestivum L. and Lens culinaris Medik. under drought stress. *Acta agriculturae Slovenica*, 111(2), 477-491.
8. Bray, E. A. (2000). Response to abiotic stress. *Biochemistry and molecular biology of plants*, 1158-1203.
9. Boccacci, P; Botta, R. (2009). Investigating the origin of hazelnut (*Corylus avellana* L.) cultivars using chloroplast microsatellites. *Genetic Resources and Crop Evolution*, 56(6), 851-859.
10. Bradford, M. M. (1976). A rapid and sensitive method for the quantitation of microgram

- quantities of protein utilizing the principle of protein-dye binding. *Analytical biochemistry*, 72(1-2), 248-254.
11. Chen, W. P., and Li, P. H. (2002). Membrane stabilization by abscisic acid under cold aids proline in alleviating chilling injury in maize (*Zea mays* L.) cultured cells. *Plant, Cell and Environment*, 25(8), 955-962.
 12. Chutipaijit, S; Cha-Um, S; Sompornpailin, K. (2009). Differential accumulations of proline and flavonoids in indica rice varieties against salinity. *Pakistan Journal of Botany*, 41(5), 2497-2506.
 13. Damerval, C; De Vienne, D; Zivy, M; Thiellement, H. (1986). Technical improvements in two-dimensional electrophoresis increase the level of genetic variation detected in wheat-seedling proteins. *Electrophoresis*, 7(1), 52-54.
 14. Farooq, M; Basra, S. M. A; Rehman, H; Saleem, B. A. (2008). Seed priming enhances the performance of late sown wheat (*Triticum aestivum* L.) by improving chilling tolerance. *Journal of Agronomy and Crop Science*, 194(1), 55-60.
 15. Farooq, M; Wahid, A; Kobayashi, N; Fujita, D. B. S. M. A; Basra, S. M. A. (2009). Plant drought stress: effects, mechanisms and management. In *Sustainable agriculture* (pp. 153-188). Springer, Dordrecht.
 16. Fayez, K. A; Bazaid, S. A. (2014). Improving drought and salinity tolerance in barley by application of salicylic acid and potassium nitrate. *Journal of the Saudi Society of Agricultural Sciences*, 13(1), 45-55.
 17. Foyer, C. H; Fletcher, J. M. (2001). Plant antioxidants: colour me healthy. *Biologist (London, England)*, 48(3), 115.
 18. Giannopolitis, C. N; Ries, S. K. (1977). Superoxide dismutases: II. Purification and quantitative relationship with water-soluble protein in seedlings. *Plant physiology*, 59(2), 315-318.
 19. Gürcan, K; Mehlenbacher, SA; Botta, R; Boccacci, P. (2010). Development, characterization, segregation, and mapping of microsatellite markers for European hazelnut (*Corylus avellana* L.) from enriched genomic libraries and usefulness in genetic diversity studies. *Tree Genetics and Genomes*, 6(4), 513-531.
 20. Gwóźdz, EA; Przymusiński, R; Rucińska, R; Deckert, J. (1997). Plant cell responses to heavy metals: molecular and physiological aspects. *Acta Physiologiae Plantarum*, 19: 459-465.
 21. Hasanuzzaman, M; Bhuyan, M. H. M; Nahar, K; Hossain, M; Mahmud, J. A; Hossen, M; Fujita, M. (2018). Potassium: A vital regulator of plant responses and tolerance to abiotic stresses. *Agronomy*, 8(3), 31.
 22. Hegazi A. M; El-Shraiy, A. M (2017). Stimulation of Photosynthetic Pigments, Anthocyanin, Antioxidant Enzymes in Salt Stressed Red Cabbage Plants by Ascorbic Acid and Potassium Silicate. *Middle East Journal*, 6:553-68.
 23. Huang, B; DaCosta, M; Jiang, Y. (2014). Research advances in mechanisms of turfgrass tolerance to abiotic stresses: from physiology to molecular biology. *Critical reviews in plant sciences*, 33(2-3), 141-189.
 24. Hussein, M. M; Mehanna, H; Zaki, S. N; Nagwan, F. A. H. (2014). Influences of salt stress and foliar fertilizers on growth, chlorophyll and carotenoids of jojoba plants. *Middle East Journal of Agricultural Research*, 3, 221-226.
 25. Hughes, M. A; Dunn, M. A. (1996). The molecular biology of plant acclimation to low temperature. *Journal of Experimental Botany*, 47(3), 291-305.
 26. Javadian, N; Karimzadeh, G; Mahfoozi, S; Ghanati, F. (2010). Cold-induced changes of enzymes, proline, carbohydrates, and chlorophyll in wheat. *Russian Journal of Plant Physiology*, 57(4), 540-547.
 27. Jan A. U; Hadi, F; Nawaz, M. A; Rahman, K. (2017). Potassium and zinc increase tolerance to salt stress in wheat (*Triticum aestivum* L.). *Plant Physiology and Biochemistry*, 116:139-149.
 28. Jebara, S; Jebara, M; Limam, F; Aouani, M. E. (2005). Changes in ascorbate peroxidase, catalase, guaiacol peroxidase and superoxide dismutase activities in common bean (*Phaseolus vulgaris*) nodules under salt stress. *Journal of plant physiology*, 162(8), 929-936.
 29. Kaczmarek, M; Fedorowicz-Strońska, O; Głowacka, K; Waśkiewicz, A; Sadowski, J. (2017). CaCl₂ treatment improves drought stress tolerance in barley (*Hordeum vulgare* L.). *Acta Physiologiae Plantarum*, 39(1), 41.
 30. Kang, G; Li, G; Xu, W; Peng, X; Han, Q; Zhu, Y; Guo, T. (2012). Proteomics reveals the effects of salicylic acid on growth and

- tolerance to subsequent drought stress in wheat. *Journal of Proteome Research*, 11(12), 6066-6079.
31. Khavari-Nejad, RA; Band, RS; Najafi, F; Nabiuni, M; Gharari, Z. (2013). The role of Pro-P5C Cycle in chs mutants of Arabidopsis under cold stress. *Russian journal of plant physiology*, 60(3), 375-382.
 32. Kocira, S. (2019). Effect of amino acid biostimulant on the yield and nutraceutical potential of soybean. *Chilean journal of agricultural research*, 79(1), 17-25.
 33. Larcher, W. (2003). *Physiological plant ecology: ecophysiology and stress physiology of functional groups*. Springer Science and Business Media.
 34. Li, Z; Wakao, S; Fischer, B. B; Niyogi, K. K. (2009). Sensing and responding to Excess light. *Annual review of plant biology*, 60, 239-260.
 35. Li, S; Yang, Y; Zhang, Q; Liu, N; Xu, Q; Hu, L. (2018). Differential physiological and metabolic response to low temperature in two zoysiagrass genotypes native to high and low latitude. *PLoS One*, 13(6), e0198885.
 36. Lichtenthaler, H. K; Wellburn, A. R. (1983). Determinations of total carotenoids and chlorophylls a and b of leaf extracts in different solvents. *Biochemical Society Transactions*, 603, 591-593.
 37. Lin, C. C; Kao, C. H. (1999). NaCl induced changes in ionically bound peroxidase activity in roots of rice seedlings. *Plant and Soil*, 216(1-2), 147.
 38. Liu, W; Yu, K; He, T; Li, F; Zhang, D; Liu, J. (2013). The low temperature induced physiological responses of *Avena nuda* L., a cold-tolerant plant species. *The Scientific World Journal*, 12, 451-457.
 39. Liu, L; Chen, LB; Li, ZY; Wang, MZ; Guo, SJ. (2009). Effect of temperature in late autumn on free proline, soluble sugar and POD in alfalfa. *Pratacultural Science*, 10: 326-335.
 40. Mehlenbacher, SA; Smith, DC. (2006). Self-compatible seedlings of the cutleaf hazelnut. *HortScience*, 41(9), 482-483.
 41. Malecka, A; Piechalak, A; Mensinger, A; Hanć, A; Baralkiewicz, D; Tomaszewska, B. (2012). Antioxidative defense system in *Pisum sativum* roots exposed to heavy metals (Pb, Cu, Cd, Zn). *Polish Journal of Environmental Studies*, 21, 16-25.
 42. Mellouk, Z; Benammar, I; Hernandez, Y. (2016). Effects of foliar application with salicylic acid on the biochemical parameters and redox status in two canola plant varieties exposed to cold stress. *International Journal of Agronomy and Agricultural Research*, 8, 77-87.
 43. Mittler, R. (2002). Oxidative stress, antioxidants and stress tolerance. *Trends in plant science*, 7(9), 405-410.
 44. Misra, N; Saxena, P. (2009). Effect of salicylic acid on proline metabolism in lentil grown under salinity stress. *Plant Science*, 177(3), 181-189.
 45. Miura, K; Tada, Y. (2014). Regulation of water, salinity, and cold stress responses by salicylic acid. *Frontiers in plant science*, 5, 4.
 46. Morris, K; Mackerness, SAH; Page, T; John, CF; Murphy, AM; Carr, JP; Buchanan-Wollaston, V. (2000). Salicylic acid has a role in regulating gene expression during leaf senescence. *The Plant Journal*, 23: 677-685.
 47. Munne-Bosch, S; Penuelas, J. (2003). Photo- and antioxidative protection, and a role for salicylic acid during drought and recovery in field-grown *Phillyrea angustifolia* plants. *Planta*, 217(5), 758-766.
 48. Mutlu, S; Karadağoglu, Ö; Atici, Ö; Nalbantoğlu, B. (2013). Protective role of salicylic acid applied before cold stress on antioxidative system and protein patterns in barley apoplast. *Biologia Plantarum*, 57(3), 507-513.
 49. Niyogi, K. K. (1999). Photoprotection revisited: genetic and molecular approaches. *Annual review of plant biology*, 50(1), 333-359.
 50. Oliveira, I; Sousa, A; Morais, JS; Ferreira, IC; Bento, A; Estevinho, L; Pereira, J. A. (2008). Chemical composition, and antioxidant and antimicrobial activities of three hazelnut (*Corylus avellana* L.) cultivars. *Food and Chemical Toxicology*, 46(5), 1801-1807.
 51. Rezayian, M; Niknam, V; Ebrahimzadeh, H. (2018). Improving tolerance against drought in canola by penconazole and calcium. *Pesticide biochemistry and physiology*, 149, 123-136.
 52. Rosa, S. B; Caverzan, A; Teixeira, F. K; Lazzarotto, F; Silveira, J. A; Ferreira-Silva, S. L; Margis-Pinheiro, M. (2010). Cytosolic APx knockdown indicates an ambiguous redox responses in rice. *Phytochemistry*, 71(5-6), 548-558.

53. Seyhan, F; Ozay, G; Saklar, S; Ertaş, E; Satır, G; Alasalvar, C. (2007). Chemical changes of three native Turkish hazelnut varieties (*Corylus avellana* L.) during fruit development. *Food Chemistry*, 105(2), 590-596.
54. Shaki, F; Ebrahimzadeh Maboud, H; Niknam, V. (2017). Central role of salicylic acid in resistance of safflower (*Carthamus tinctorius* L.) against salinity. *Journal of plant interactions*, 12(1), 414-420.
55. Salimi, S; Hoseinova, S. (2012). Selecting hazelnut (*Corylus avellana* L.) rootstocks for different climatic conditions of Iran. *Crop Breeding Journal*. 2(2), 139-144
56. Shang, H; Cao, S; Yang, Z; Cai, Y; Zheng, Y. (2011). Effect of exogenous γ -aminobutyric acid treatment on proline accumulation and chilling injury in peach fruit after long-term cold storage. *Journal of agricultural and food chemistry*, 59(4), 1264-1268.
57. Shams, M; Yildirim, E; Ekinçi, M; Turan, M; Dursun, A; Parlakova, F; Kul, R. (2016). Exogenously applied glycine betaine regulates some chemical characteristics and antioxidative defence systems in lettuce under salt stress. *Horticulture, Environment, and Biotechnology*, 57(3), 225-231.
58. Sharma, P; Jha, A. B; Dubey, R. S; Pessarakli, M. (2012). Reactive oxygen species, oxidative damage, and antioxidative defense mechanism in plants under stressful conditions. *Journal of Botany*.
59. Stipešević, B; Brozović, B; Jug, D; Jug, I; Ranogajec, L; Šego, D. (2014). Economic comparison of different cropping systems for niger (*Guizotia abyssinica*) in Croatia. In *Proceedings of TEAM 2014 6 th International Scientific and Expert Conference of the International TEAM Society 10–11 th November 2014, Kecskemét, Hungary* (p. 81).
60. Suzuki, K; Nagasuga, K; Okada, M. (2008). The chilling injury induced by high root temperature in the leaves of rice seedlings. *Plant and Cell Physiology*, 49(3), 433-442.
61. Szekely, G; Abrahám, E; Cséplő, A., Rigó, G; Zsigmond, L; Csiszár, J; Strizhov, N. J; ásik, J; Schmelzer, E; Koncz, C; Szabados, L. (2008). Duplicated P5CS genes of *Arabidopsis* play distinct roles in stress regulation and developmental control of proline biosynthesis. *Plant Journal* 53, 11-28.
62. Taşgín, E; Atıcı, Ö; Nalbantoğlu, B. (2003). Effects of salicylic acid and cold on freezing tolerance in winter wheat leaves. *Plant Growth Regulation*, 41(3), 231-236.
63. Trovato, M; Mattioli, R; Costantino, P. (2008). Multiple roles of proline in plant stress tolerance and development. *Rendiconti Lincei*, 19(4), 325-346.
64. Qaderi, A; Omid, M; Etminan, A; Oladza, A; Ebrahimi, C; Dehghani, M. M; Mehrafarin, A. (2012). Hazel (*Corylus avellana* L.) as a new source of taxol and taxanes. *Journal of Medicinal Plants* 1:66-77.
65. Velikova, V; Yordanov, I; Edreva, A. (2000). Oxidative stress and some antioxidant systems in acid rain-treated bean plants: protective role of exogenous polyamines. *Plant science*, 151(1), 59-66.
66. Wang, M; Zheng, Q; Shen, Q; Guo, S. (2013). The critical role of potassium in plant stress response. *International journal of molecular sciences*, 14(4), 7370-7390.
67. Wilson, JM. (1996). The Mechanism of chill and drought hardiness. *New Physiologist*, 97: 257-270.
68. Xin, Z; Browse, J. (2000). Cold comfort farm: the acclimation of plants to freezing temperatures. *Plant, Cell, and Environment*, 23(9), 893-902.
69. Zhang, L; Gao, M; Li, S; Alva, A. K; Ashraf, M. (2014). Potassium fertilization mitigates the adverse effects of drought on selected *Zea mays* cultivars. *Turkish Journal of Botany*, 38(4), 713-723.
70. Zhang, HQ; Zou, YB; Xiao, GC; Xiong, YF. (2007). Effect and Mechanism of Cold Tolerant Seed-Coating Agents on the Cold Tolerance of Early *Indica* Rice Seedlings. *Agricultural Sciences in China*, 6: 792-801.



Figure 1. The emergence of male (long catkins) and female (small reddish-purple florets) flowers of treated *Corylus avellana* tree.



Figure 2. Assays for the content of enzymatic antioxidants after bain-marie.

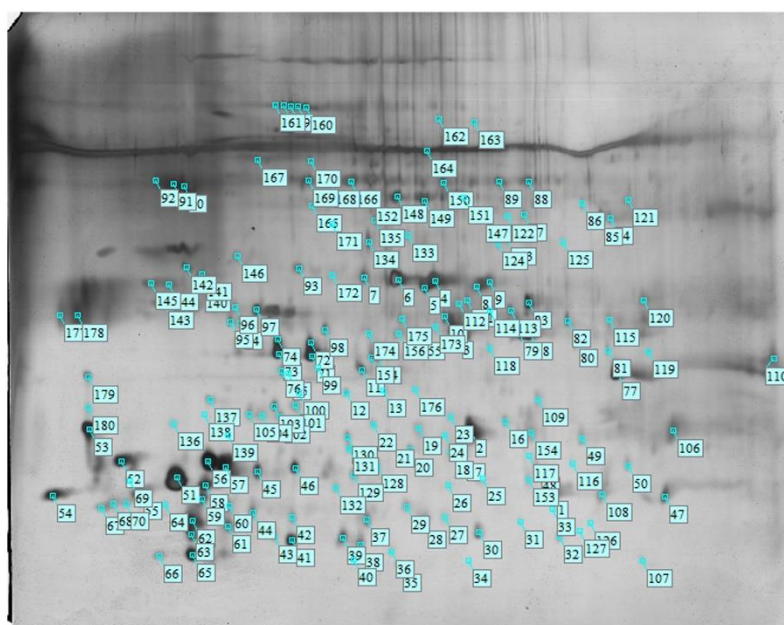


Figure 3. 2-D gel of proteins extracted from the leaf in the control condition.

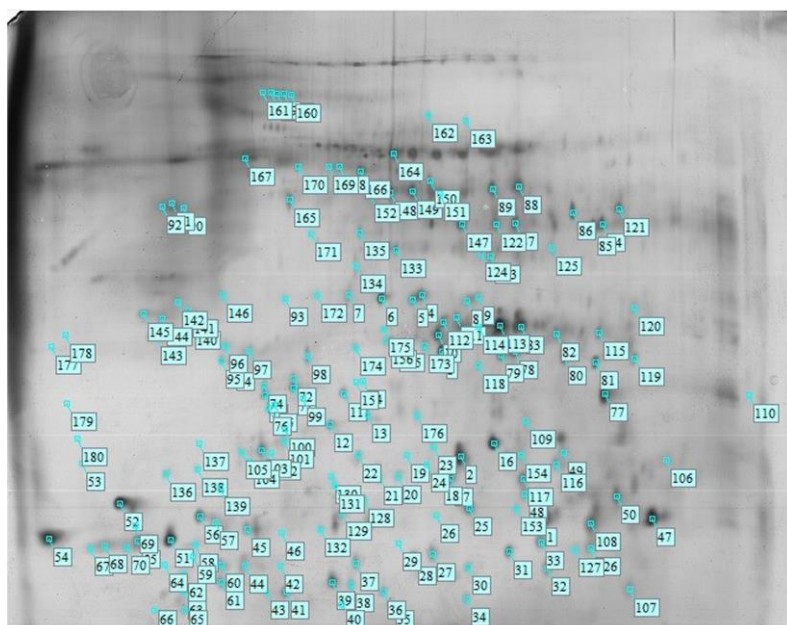


Figure 4. 2-D gel of proteins extracted from leaf under salicylic acid (SA) treatment.

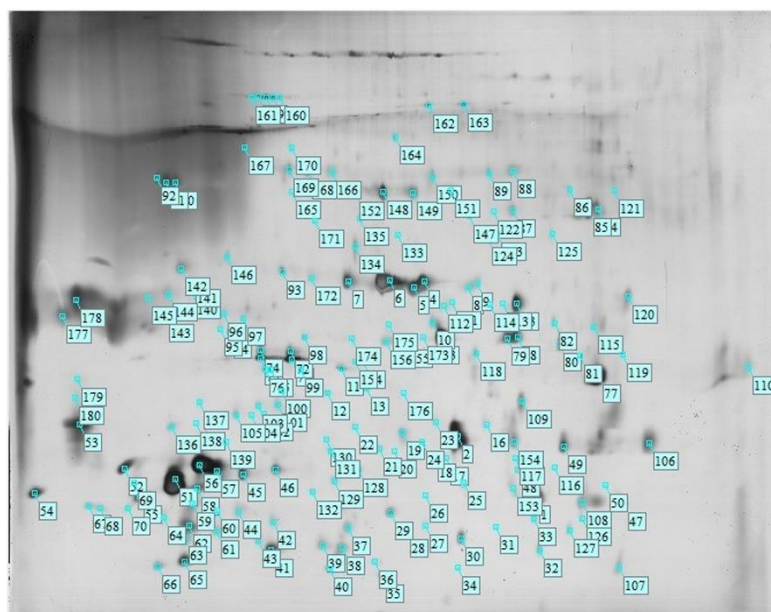


Figure 5. 2-D gel of proteins extracted from male flowers in the control condition.

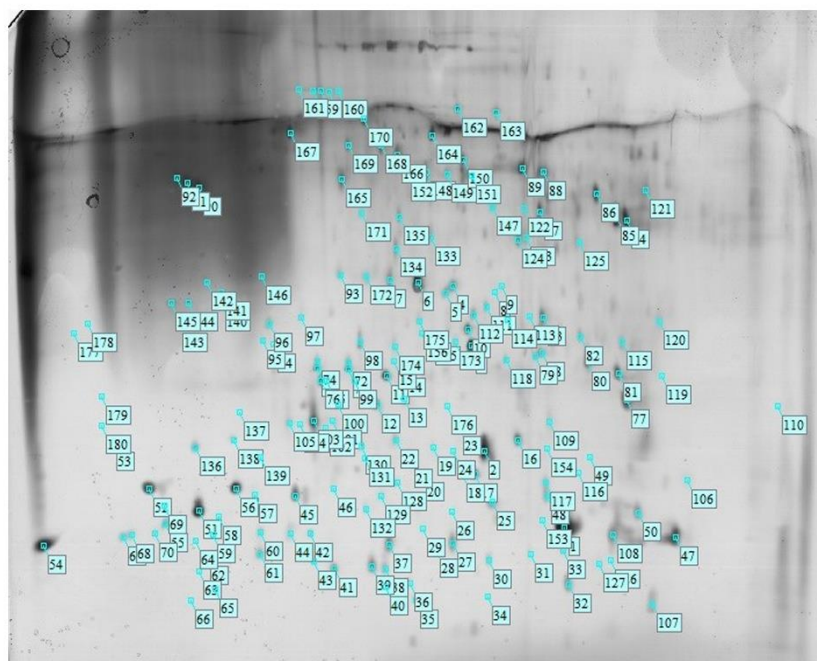


Figure 6. 2-D gel of proteins extracted from male flowers under salicylic acid (SA) treatment.

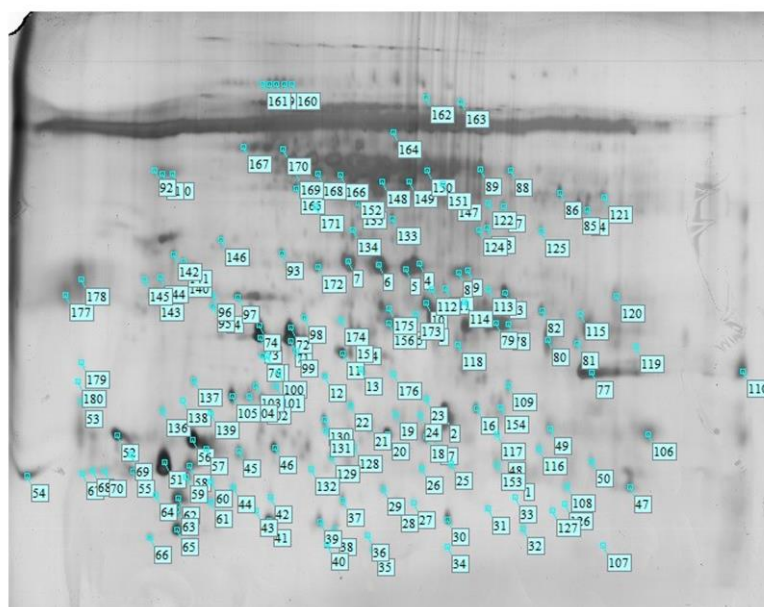


Figure 7. 2-D gel of proteins extracted from female flowers in the control condition.

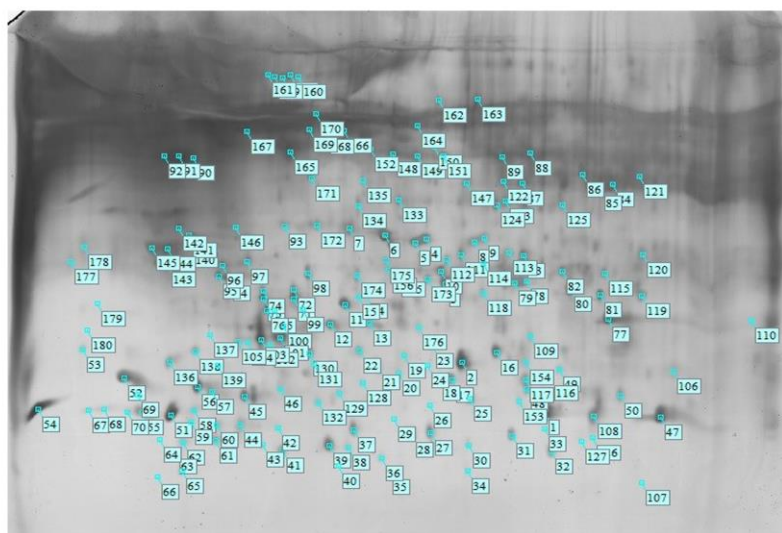


Figure 8. 2-D gel of proteins extracted from female flowers under salicylic acid (SA) treatment.

Table 1. Effects of different treatments on protein, H₂O₂, and antioxidative enzymes in *Corylus avellana*.

Treatment	Tissue	Protein	H ₂ O ₂	SOD	CAT	APX	GPX
Control	Leaf	1±0.02 b	0.58±0.23 b	98.29±2.12 a	0.01±0.00 c	1.85±0.1 bc	0.82±0.09 d
Potassium		1.10±0.01 a	0.30±0.022 e	98.26±4.32 a	0.01±0.00 c	1.75±0.1 cd	1.66±0.11 a
Thiofer		0.92±0.11 d	0.53±0.056 c	98.36±2.13 a	0.01±0.00 c	1.65±0.02 d	0.67±0.30 e
Biobloom		0.98±0.04 c	0.96±0.02 a	98.38±2.11 a	0.03±0.00 b	2.28±0.14 a	0.44±0.01 f
Amino acid		0.97±0.04 c	0.47±0.036 d	98.34±1.12 a	0.009±0.001d	1.43±0.11 e	1.12±0.30 b
Salicylic acid		1.10±0.05 a	0.60±0.04 b	98.53±2.21 a	0.04±0.01 a	1.91±0.14 b	1.02±0.40 c
Control	Male flowers	1.17±0.01 c	0.50±0.02 b	98.51±2.22 a	0.14±0.01 b	1.54±0.3 bc	0.96±0.6 1d
Potassium		1.38±0.11 b	0.35±0.021 d	98.56±1.14 a	0.16±0.01 a	1.32±0.45 c	1.66±0.10 a
Thiofer		1.44±0.13 ab	0.61±0.034 a	98.54±3.46 a	0.17±0.07 a	2.02±0.06 a	1.66±0.20 a
Biobloom		1.40±0.04 b	0.35±0.012 d	98.59±4.90 a	0.12±0.06 c	1.69±0.09 b	1.20±0.30 c
Amino acid		1.53±0.05 a	0.51±0.06 b	98.93±2.56 a	0.18±0.05 a	1.76±0.12 ab	1.73±0.21 a
Salicylic acid		1.42±0.06 b	0.44±0.045 c	98.57±2.13 a	0.13±0.01 b	1.62±0.03 bc	1.41±0.22 b
Control	Female flowers	0.94±0.13 b	0.15±0.08 a	98.35±3.23 a	0.03±0.01 d	0.97±0.09 a	1.05±0.09 c
Potassium		0.97±0.24 b	0.01±0.08 a	98.30±2.78 a	0.04±0.01 c	0.92±0.02 a	2.14±0.12 a
Thiofer		1.02±0.06 ab	0.93±0.09 b	98.38±2.67 a	0.05±0.01 c	0.43±0.09 ab	1.83±0.14 b
Biobloom		1.08±0.45 a	0.01±0.01 a	98.46±4.86 a	0.09±0.05 a	0.62±0.08 ab	1.88±0.32 b
Amino acid		1.08±0.09 a	0.01±0.02 a	98.30±3.213 a	0.06±0.01 b	0.31±0.021 b	2.32±0.43 a
Salicylic acid		1.10±0.08 a	0.04±0.01 a	98.47±2.124 a	0.09±0.08 a	0.34±0.05 b	1.05±0.32 d

Notes: Values are means ± SE of three replicates. Different letters indicated significant (P<0.05) differences. Protein (mg g⁻¹ FW), Hydrogen peroxide (H₂O₂ μM g⁻¹ FW), superoxide dismutase (SOD U mg⁻¹ protein), catalase (CAT U mg⁻¹ protein), peroxidase (POX U mg⁻¹ protein) and Glutathione peroxidase (GPX U mg⁻¹ protein).

Table 2. Effects of different treatments on proline, anthocyanin, chlorophyll (Chl a, Chl b, and Chl T) and carotenoid (mg g⁻¹ FW) in *Corylus avellana*.

Treatment	Tissue	Proline	Anthocyanin	Chl a	Chl b	Chl T	Carotenoid
Control	Leaf	0.04±0.01 c	14.41±2.31 d	127.41±2.12 d	41.50±3.10 e	168.70±5.80 e	192.07±6.09 c
Potassium		0.07±0.01 ab	19.01±2.20 a	150.66±4.32 a	66.23±6.21 a	217.38±6.13 a	195.33±8.12 c
Thiofer		0.06±0.01 b	16.26.60 b	135.29±2.13 c	56.52±1.31 d	192.80±4.32 d	287.41±3.33 a
Biobloom		0.07±0.01 a	10.63±2.11 e	98.54±2.11 e	40.44±1.51 f	138.64±3.14 f	268.83±4.01 b
Amino acid		0.07±0.04 a	15.69±3.61 bc	145.35±1.12 b	59.57±1.81 c	204.58±5.11 c	258.27±3.39 b
Salicylic acid		0.07±0.05 a	15.05±4.11 cd	144.48±2.21 b	63.66±3.70 b	208.42±3.14 b	289.62±2.41 a
Control	Male flowers	0.06±0.01 d	9.09±2.07 a	35.34±2.22 a	37.62±2.11 c	72.96±4.38 a	24.98±1.61 c
Potassium		0.07±0.01 d	8.15±1.32 a	3.63±0.14 a	60.58±3.11 a	64.21±1.45 b	40.02±2.11 b
Thiofer		0.32±0.01 b	8.69±2.11 a	8.74±1.46 a	12.67±0.98 e	21.41±4.06 d	62.02±1.21 a
Biobloom		0.11±0.03 c	7.19±1.21 a	30.97±2.90 a	44.64±0.06 b	75.61±2.09 a	44.10±1.33 b
Amino acid		0.12±0.045 c	7.26±2.61 a	17.81±1.56 a	22.423±2.55 d	40.23±1.12 c	47.84±4.21 b
Salicylic acid		0.39±0.06 a	8.57±0.52 a	24.76±3.13 a	22.6±2.19 d	47.36±5.03 c	63.34±2.22 a
Control	Female flowers	0.06±0.01 d	6.32±0.11 a	127.79±3.93 b	103.71±7.12 c	232.48±7.11 d	80.76±2.41 a
Potassium		0.06±0.04 d	5.14±0.80 a	94.63±1.78 f	224.54±5.80 a	319.81±5.02 ab	77.67±2.12 a
Thiofer		0.07±0.06 c	4.73± 1.01 a	120.51±3.67 e	231.17±4.40 a	350.65±3.19 a	89.64±2.15 a
Biobloom		0.06±0.00 cd	4.30±0.90 a	124.38±4.86 d	174.35±5.55 b	298.37±5.89 bc	83.25±3.32 a
Amino acid		0.08±0.01 b	5.16±0.20 a	126.54±3.21 c	151.58±6.78 b	277.59±6.02 c	85.34±5.13 a
Salicylic acid		0.09±0.02 a	6.08±1.09 a	158.29±2.40 a	152.50±2.80 b	311.42±3. 54 bc	85.35±1. 21 a

Notes: Values are means ± SE of three replicates. Different letters indicated significant (P<0.05) differences.

CONFIGURAÇÃO TRIDIMENSIONAL DE MATERIAIS COMPÓSITOS COMO FORMA DE ALCANÇAR ALTAS PROPRIEDADES MECÂNICAS**THREE-DIMENSIONAL SETUP OF COMPOSITE MATERIALS AS A WAY TO ACHIEVE HIGH MECHANICAL PROPERTIES****ТРЁХМЕРНАЯ ОРГАНИЗАЦИЯ КОМПОЗИТНЫХ МАТЕРИАЛОВ КАК СПОСОБ ДОСТИЖЕНИЯ ВЫСОКИХ МЕХАНИЧЕСКИХ ПОКАЗАТЕЛЕЙ**AMANKULOV, Yerdos^{1*}; PETUNINA, Irina²; LOBANOVA, Nadezhda³¹ Al-Farabi Kazakh National University, Department of Theoretical and Nuclear Physics. Kazakhstan² Federal State Budgetary Educational Institution of Higher Education "Kuban State Agrarian University named after I.T. Trubilin", Department of Higher Mathematics. Russian Federation³ MIREA - Russian Technological University, Department of Chemistry and Technology of High-Molecular Compounds named after Medvedev S. S. Russian Federation

* Corresponding author
e-mail: ayerdos@rambler.ru

Received 07 August 2020; received in revised form 03 September 2020; accepted 23 September 2020

RESUMO

As resinas de polímero são lubrificantes secos populares e revestimentos protetores para produtos metálicos. No entanto, seu coeficiente de atrito é alto e isso leva a taxas de desgaste aumentadas e vida útil limitada. O reforço com cargas em nanoescala, devido à sua grande área superficial e sua distribuição uniforme dentro do volume da matriz polimérica, pode ajudar a reduzir o atrito e o desgaste. O objetivo deste trabalho foi estudar o efeito da organização tridimensional de nanopartículas de dióxido de silício com concentração de 1, 3 e 5% nas propriedades mecânicas de uma resina epóxi. A dispersão das nanopartículas foi realizada usando tecnologia de campo ultrassônico. O coeficiente de atrito foi medido usando um tribômetro de pêndulo. Resultados empíricos mostraram que a redução na concentração de nanopartículas de 5% para 1% resultou em uma redução de duas vezes nos valores do coeficiente de atrito. Além disso, verificou-se que o prolongamento do tempo de teste em experimentos com concentração de nanopartículas de 3 e 1% praticamente não afetou os valores do coeficiente de atrito. Este comportamento está associado à regulação da mobilidade da interface do polímero devido à baixa concentração de nanoinclusões e à organização tridimensional uniforme da matriz polimérica pelo campo ultrassônico, o que contribuiu para uma redistribuição uniforme das cargas aplicadas. A técnica desenvolvida pode ser aplicada a outros tipos de nanocompósitos poliméricos para estudar o efeito da organização tridimensional de cargas em nanoescala na resistência ao desgaste, resistência à flexão e resistência ao impacto.

Palavras-chave: *Nanopartículas de óxido de silício; configuração tridimensional; propriedades tribológicas, nanocompósitos.*

ABSTRACT

Polymer resins are popular dry lubricants and protective coatings for metal products. However, their friction coefficient is high, which leads to increased wear rates and limited service life. Reinforcement with nanoscale fillers, due to their large surface area and their uniform distribution within the polymer matrix volume, can help reduce friction and wear. This paper aimed to study the effect of three-dimensional organization of silicon dioxide nanoparticles with a concentration of 1, 3, and 5% on the mechanical properties of an epoxy resin. The dispersion of nanoparticles was carried out using ultrasonic field technology. The friction coefficient was measured using a pendulum tribometer. Empirical results have shown that reduction in the concentration of nanoparticles from 5% to 1% resulted in a two-fold decrease in the values of the friction coefficient. Also, it was found that prolongation of test time in experiments with a nanoparticle concentration of 3 and 1% had practically no effect on the friction coefficient values. This behavior is associated with the polymer interface mobility regulation due to the low concentration of nano inclusions and uniform three-dimensional organization in the polymer matrix by the ultrasonic field, which contributed to a uniform redistribution of applied loads. The developed technique can be

used to other types of polymer nanocomposites to study the effect of the three-dimensional organization of nanoscale fillers on wear resistance, bending strength, and impact resistance.

Keywords: *Silicon oxide nanoparticles; three-dimensional setup; tribological properties, nanocomposites.*

Аннотация

Полимерные смолы - популярные сухие смазочные материалы и защитные покрытия для металлических изделий. Однако их высокий коэффициент трения приводит к повышенному износу и ограниченному сроку службы. Упрочнение наноразмерными наполнителями из-за их большой площади поверхности и их равномерного распределения в объеме полимерной матрицы может помочь снизить трение и износ. Целью данной работы было изучение влияния трехмерной организации наночастиц диоксида кремния с концентрацией 1, 3 и 5% на механические свойства эпоксидной смолы. Диспергирование наночастиц осуществлялось с помощью ультразвуковой обработки. Коэффициент трения измеряли с помощью маятникового трибометра. Результаты эксперимента показали, что снижение концентрации наночастиц с 5% до 1% привело к двукратному снижению значений коэффициента трения. Кроме того, было обнаружено, что продление времени испытаний в экспериментах с концентрацией наночастиц 3 и 1% практически не повлияло на значения коэффициента трения. Такое поведение связано с регулированием подвижности границы раздела полимеров из-за низкой концентрации нановключений и однородной трехмерной организации в полимерной матрице ультразвуковым полем, что способствовало равномерному перераспределению приложенных нагрузок. Разработанная методика может быть использована для других типов полимерных нанокомпозитов с целью изучения влияния трехмерной организации наноразмерных наполнителей на износостойкость, прочность на изгиб и ударопрочность.

Ключевые слова: *наночастицы оксида кремния; трехмерная организация; трибологические свойства, нанокомпозит*

1. INTRODUCTION:

In widespread use of various mechanical systems such as parts of friction units (e.g., bearings, compressor cylinders) (Lampaert *et al.*, 2018; Xiang and Gao, 2017), metal forming and cutting tools (Flegler *et al.*, 2020; Idusuyi and Olayinka, 2019), transport mechanisms, and technological machines for various industries (Cho and Bhushan, 2016; Holmberg *et al.*, 2017), constant monitoring of friction and wear of structural parts is required. As the main binder component that enhances tribological properties, various liquid, dry lubricants are used (Mushtaq and Wani, 2017; Zhu *et al.*, 2019) or polymer coatings applied to parts.

Due to the limited use conditions for an extended period under challenging conditions, the various physical and chemical properties of different types of lubricants significantly reduce their effectiveness and durability (Busch *et al.*, 2016; Singh *et al.*, 2020). If due to restrictions on the use, liquid lubricants cannot be used, then polymer coatings are considered the best option for controlling friction and wear. However, polymeric materials must meet certain requirements for practical application in various mechanisms, such as high mechanical strength and durability, the required stiffness, the corresponding coefficient of thermal expansion (Zalaznik *et al.*, 2016). For example, for some

polymer composite coatings, low values of both the coefficient of friction (<0.2) and the wear rate ($<10^{-6}$ mm³/Nm) were achieved; additional lubrication was not required in the contact zone (Rodriguez *et al.*, 2016).

However, under conditions of high loads and mechanism speeds, polymer composites should have both high wear-resistant properties and self-lubrication characteristics. To solve the first condition, various types of polymer matrix fillers are usually introduced, which can vary in shape and size, such as particles and fibers (Gad *et al.*, 2017). As for the second condition, based on numerous previous studies, it was found that the peeling of the upper layers of the coatings followed by the transfer of thin lubricating films with wear residues significantly improved the tribological characteristics of polymer composites (Cui *et al.*, 2020; Pham *et al.*, 2019; Saravanan *et al.*, 2017; Zhang *et al.*, 2017).

Despite the significant advantages, polymer composites have several disadvantages, such as the loss of inherent mechanical properties when exposed to a liquid medium. For example, in contact with seawater, which includes a set of different salts, the surface layer enters into a chemical reaction with salt, which leads to a decrease in the efficiency and durability of the polymer coating.

Polymer nanocomposites are a class of

composite materials. The polymeric material matrix is reinforced with one or more types of nanoobjects smaller than 100 nm (Li *et al.*, 2016) to improve performance. The most common materials used as a matrix for polymer nanocomposites are various epoxies, nylon, polyepoxide, polyetherimide, and others. Unlike traditional polymer composites with a high filler density (about 60%) of different kinds of micrometer size particles, a lower density (less than 5%) of fillers is used in polymer nanocomposites. Recently, many new polymer nanocomposites have appeared, which have some unique properties and provide an opportunity for further implementation in the industry. For example, transparent conductive nanocomposites reinforced with nanotubes have been developed for use as electrodes of solar cells. Amorphous polymers with nanoparticles have been introduced into production due to the high scratch resistance of various transparent coatings in cell phones and CD technology (Wang and Alexandridis, 2016). In general, the use of nanoparticles to reinforce the matrix of traditional polymer composites increases mechanical, optical, or conductive properties.

The advantage of nanosized fillers is that, due to their size, they prevent cracks on the surface, which characterizes the increased ductility and strength of the polymer coating. As shown in the work of Roy *et al.* (2007), the introduction of nanoparticles into the polymer matrix contributes to an increase in the electric tensile strength and endurance. Also, it provides insignificant optical scattering on existing defects (Hanemann *et al.*, 2009). Because of the large surface area of the fillers, nanocomposites have a large volume of interphase boundaries, which differ significantly from the properties of a pure polymer. Depending on the volume of the interphase boundaries and its uniform distribution in the polymer matrix, the composite properties can differ significantly from each other. For example, to improve the tribological properties of composite coatings, it is necessary to observe the following rules, called the mixture rule. Namely, the strength modules of polymer nanocomposites should be directly proportional to the volume ratio of nanosized fillers when both phases are aligned to bear the same amount of load (Rivière *et al.*, 2016). Still, this optimal mechanical state is usually challenging to achieve due to aggregation and uneven distribution of the nanofiller. Surface optimization often helps to improve the dispersion of nano inclusions. Even with a concentration of up to 5%, it does not provide uniform load distribution, and friction coefficients remain high enough

(Domun *et al.*, 2015). The layer-by-layer application of polymer and nanofiller layers provides a structure with a more uniform dispersion of fillers (Li *et al.*, 2017). However, a layered structure containing a continuous interface between the phase components, due to the anisotropy in the layers, also limits the uniform distribution of the applied load, which leads to rapid wear of the coating.

The development of the design of continuous composite materials consisting of a network of physically separated two phases is a promising technique for overcoming the dispersion limitation of nanofillers in a matrix. The basis of this method is a phased preparation, consisting of the preparation of a porous matrix (template) and infiltration of the nanofiller into the pores. Three-dimensional matrix formation using PnP technology, which includes single-stage exposure through an appropriate phase mask, is the most effective method for constructing a matrix with a nanoscale step (less than 100 nm) (Park *et al.*, 2010). This method is effective, but very energy-consuming and expensive, and such low availability leads to a decrease in its application possibilities.

Among the most used reinforcing fillers, carbon fibers, short glass fibers, carbon nanotubes, or carbon nanofibers are used to improve the tribological properties of nanocomposite coatings (Yan *et al.*, 2013). However, various types of fillers have several disadvantages. For example, increasing the volume of carbon nanotubes to 1% usually greatly simplifies manufacturing a composite due to its porous structure. Still, often nanotubes scratch the surface, which damages the coating. The most effective way is a combination of reinforcing elements (carbon fibers with nanoparticles), which can significantly improve the tribological characteristics of polymers (Visco *et al.*, 2016). However, the selected objects are more difficult to distribute evenly due to their intricate design, unlike spherical nanoparticles. Besides, there is not enough research on the influence of nanoparticles' organization on improving the tribological properties of polymer composites.

The purpose of this research was to study the silicon dioxide nanoparticles' ultrasonic dispersion effect on the uniform distribution of the composite in the volume of the polymer matrix to improve tribological properties. Abrasion resistance tests under cyclic loading were carried out on three series of samples of polymer nanocomposites with different volume contents of nanoparticles.

2. MATERIALS AND METHODS:

2.1. Preparation of materials and samples

Three series of samples were obtained using standard technology. Colloidal quartz nanoparticles (Aerosil R8200) with average particle sizes of 15 nm with 1, 3, and 5 %, respectively, were dispersed in epoxy resin (DER331, DOW). Samples of series 1 contained 1% of nanoparticles, series 2, and 3 had 3 and 5% of nanoparticles, respectively. A cycloaliphatic amine hardener was used (HY 2954; Huntsman). Volume fractions of fillers were calculated, taking into account their weight and density. Densities of pure epoxide and nanoparticles SiO₂ were 1.14 and 2.00 g/cm³, respectively.

2.2. Ultrasonic dispersion technique for three-dimensional structure of nanoparticles

The use of an ultrasonic field for dispersion in a liquid medium has many significant advantages compared to other methods, such as low energy consumption, high productivity, and the ability to obtain ultrafine particles with a repeatable result (Ma *et al.*, 2018).

The main characteristics describing the propagation of a sound field in a liquid medium are the pressure and sound speed in the medium. Propagating in a liquid, sound creates compression and rarefaction areas in which pressure changes occur for the average external statistical pressure (Herzfeld and Litovitz, 2013). Sound pressure is the main quantitative characteristic of sound and the main parameter of acoustic measurements.

The amount of energy of the wave motion, which is transferred in one second through the unit area, placed perpendicularly to the direction of wave propagation, is called the sound intensity and is expressed through the following formula:

$$I = \frac{1}{2} \frac{p_0^2}{R_a} \quad (1)$$

where, p_0 - sound pressure amplitude, R_a – acoustic impedance.

Acoustic impedance depends only on the properties of the medium, and sound pressure depends on the characteristics of the medium, such as the density and speed of sound propagation in the medium and on the amplitude and cyclic frequency of the ultrasonic wave.

The dependence of the acoustic velocity U in a liquid medium on sound pressure is expressed through the following formula:

$$\Delta p = R_a U \quad (2)$$

In a liquid medium, the main mechanism of ultrasonic dispersion of powder materials is the occurrence of the cavitation effect (Gaynutdinova *et al.*, 2016), the essence of which is the formation of cavities or bubbles with a local decrease in pressure in the liquid to the pressure of saturated vapor. To stimulate cavitation in a liquid, it is necessary to stimulate a sound wave of a certain intensity, associated with other parameters from the formulas (1-2). Knowing one of them, one can find other characteristics when calculating an acoustic reactor to stimulate cavitation.

It is known that cavitation nuclei in a liquid can be randomly distributed. As a result of the oscillations, the bubbles reach a larger size, and the accumulations of bubbles under the action of the arising sound flows move at a sufficiently high speed in the volume of the liquid. The scattering and reflection of ultrasonic waves depending on changes in the time and space of the cavitation region lead to a significant averaging of the field, and the interference pattern is smoothed out, and the field acquires a fairly clear small-scale diffuse character. This diffuse nature, which is necessary for research, depends on the intensity of sound, which is governed by the clarity of the interference pattern. The basis of this technique includes the following - the application of an ultrasonic field leads to the acceleration of nanoparticles in volume of the polymer. The acceleration intensity can be adjusted to provide the most necessary conditions for a uniform distribution of particles by adjusting the sound intensity.

A series of samples was tested on an ultrasonic unit UP200St with a wide frequency range (up to 20 kHz). In a flat glass bath, two emitters were installed opposite each other to smooth the interference pattern. The intensity of the ultrasonic wave was adjusted by leveling the interference pattern on the surface of the liquid, an example of which is shown in Figure 1.

The dispersion of nanoparticles in the resin of each series of samples was carried out for 30 minutes. Then, the parts were coated with mixtures for tribological studies, and for curing were placed in an oven at 70 °C for 8 hours, then for 8 hours at 120 °C.

2.3. The methodology of tribological studies

Tribological tests were carried out on a pendulum tribometer with microprocessor processing of experimental data. In tests on a pendulum tribometer, the components of a friction

pair from a titanium sample with a surface hardness of 12.63 GPa were used, coated with previously obtained polymers of series 1, 2, and 3, respectively. The installation parameters were as follows: the length of the pendulum - 0.51 m, the weight of the load - 35.8 N, and the initial deflection angle - 20°.

The formula calculated the coefficient of friction:

$$f = \frac{\Delta A}{4(n-1)r} \quad (3)$$

where f – coefficient of friction; ΔA – decrease in the amplitude of the pendulum over the period (m); r – radius of the roller of the friction support unit (m); n – number of oscillation cycles.

3. RESULTS AND DISCUSSION:

The results of the experimental measurements of tribological properties are presented in Figure 2.

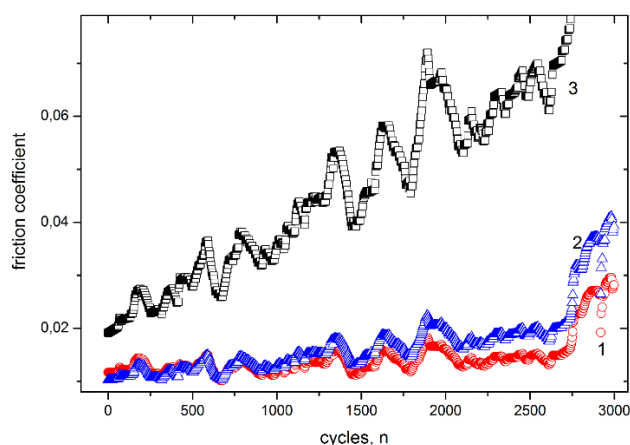


Figure 2. Time dependences of a friction coefficient f for a series of samples with different content of nanoparticles SiO_2 in the polymer matrix: 1 – series 1, 2 – series 2, 3 – series 3, respectively

As can be seen from Figure 2, a sample of series 3 with a maximum amount of introduced filler (in a volume of 5%) shows high values of the coefficient of friction f . Also, the sawtooth shape of the curve indicates the occurrence of defects in the test, such as cracks or tearing of the films. Large jumps in values and a sharp increase in f values over time indicate (1) a large volume fraction of nanofiller can adversely affect the structure and properties of the polymer coating or (2) there are agglomerates of nanoparticles, for breaking which ultrasonic frequency is not enough.

In recent works (Bittmann *et al.*, 2009; Kumar *et al.*, 2016; Ma *et al.*, 2018) similar results were obtained, according to which the optimal

dispersion process of nanoparticles in epoxy resin was achieved due to a systematic change in the parameters of the ultrasonic dispersion process. The effectiveness of applying the ultrasonic dispersion technique consists of using the maximum allowable amplitude of the ultrasonic device and the dispersion time in proportion to the volume of the material processed by ultrasound. However, some shortcomings of the chosen method were also found, such as the presence of residual agglomerates of nanoparticles. This explains the result obtained in sample 3.

However, samples with a smaller amount of reinforcing filler (series 1 and 2) demonstrate a significant improvement in the strength properties of nanocomposite coatings. As can be seen from Figure 2, the values of friction coefficient f for the samples of series 1 and 2 are almost two times less than for samples of series 3. Besides, there are smaller deviations in f values frequency and a slower growth rate over time (up to 2700 oscillation cycles of the pendulum). The results obtained in this work are in good agreement with the work of Zhang *et al.* (2011), where it has been shown that the increase in the volume fraction of the filler to 5 % leads to a decrease in tensile strength, and, consequently, the deterioration of tribological properties. In this work, the authors used a different approach to the uniform distribution of particles in the polymer matrix. Zare (2016) proposed a methodology for studying the effect of agglomeration of spherical nanoparticles in polymer nanocomposites. This methodology showed reliable results for determining the volume fraction of agglomerated nanoparticles in nanocomposite samples. According to the results of calculations by this technique for various samples, it was shown that the degree of agglomeration increased with an increase in the content of nanofiller and a decrease in particle size. In addition, it was found that agglomeration reduced the efficiency of nanoparticles in the polymer matrix, which led to a decrease in the mechanical properties of composite samples. The results of theoretical modeling are in excellent agreement with the experimental results obtained in this paper.

There were other studies of the effect of SiO_2 nanoparticles on the formation of a transfer film and the tribological properties of epoxy composites reinforced with different types of fillers (Zhang *et al.*, 2016). These studies showed that the presence of silicon dioxide nanoparticles at the interface gave rise to a transfer film with different structures and functional properties. The inclusion of different nanofillers of the same or different type

in the epoxide matrix improves the tribological properties. However, as shown above, it is not entirely effective. There was also a study of the dynamics of silicon dioxide nanoparticles at the interface between the polymer and the nanoparticle (Holt *et al.*, 2014) using various research methods.

The findings showed that the mobility of the interfacial polymer layer on the surface of nanoparticles with a lower concentration of nanoparticles is two orders lower than that of a bulk polymer. Analysis of small-angle X-ray scattering data showed that the interfacial layer has a thickness of 4–6 nm regardless of the concentration of nanoparticles. From these works, the authors conclude that due to the mobility of the interfacial polymer layer, depending on the degree of nanoparticle content, the necessary mechanical properties of the composite can be adjusted. Besides, uniform distribution can also contribute to a uniform redistribution of the applied loads throughout the polymer volume. Since the goal of this work has been to study the influence of the organization of nanoparticles in a polymer matrix in a three-dimensional setup, the results of the chosen technique demonstrate entirely new results. Thus, the following assumptions describing the results obtained can be made.

Due to the action of an ultrasonic field with a stable cavitation region, the nanoparticles are accelerated at a certain speed throughout the polymer volume, which is controlled by the sound intensity and interference pattern. The distributed nanoparticles in the polymer matrix of the composite are not static, or rather, the interface boundary is mobile. When a load is applied, this layer can compensate for large stress gradients due to its mobility (tension or compression), which leads to a uniform distribution of stresses arising in the volume, which significantly reduces the occurrence of cracks and breaks in the coatings. This explains the low values of the coefficient of friction, and its small changes over time at constant load. To confirm the above assumptions, it is necessary to carry out many additional tests, which expands the possibilities of this work for further studies.

Various approaches to the three-dimensional setup of nanofillers to improve the mechanical properties of nanocomposites have also been used. For example, Ahn *et al.* (2018, 2019), in their works, used the technique of constructing a three-dimensional template through a phase mask and filling the pores by electrolysis of particles. As the results show, the chosen method is very effective; however, it requires the

accuracy of the phased procedures and the cost of materials, which significantly complicates the process of obtaining the composite. A different approach was applied in the work of Zhao *et al.* (2018), where the authors pursued the goal of constructing a sponge structure from carbon nanotubes, which, depending on the morphology of the structure, significantly improved mechanical stiffness and allowed controlling viscoelastic characteristics. This review shows the importance of choosing a methodology for organizing nano inclusions. According to the results of this work, ultrasonic technology and a small volume of nanoscale inclusions (up to 3%) provide a significant improvement in mechanical properties and require further research in this direction. For example, this technology can be applied to other types of polymers and nanofillers to study the optical, electrical, and photoelectric properties, which significantly expands the field of experimental research.

4. CONCLUSIONS:

This paper reports on the empirical results obtained through investigating the effect of the three-dimensional organization of composite polymers, reinforced by silicon dioxide nanoparticles, on their mechanical properties. The silicon dioxide content was 1, 3, and 5%. It was found that the use of ultrasound and a smaller concentration of nanoparticles (1-3%) promote a uniform distribution of particles within the volume of the polymer matrix. The tribological analysis results revealed that a reduction in the concentration of nanoparticles from 5% to 1% resulted in a two-fold decrease in the values of the friction coefficient. The friction parameter for samples with 1 and 3% of silicon dioxide nanoparticles slightly increased over time under cyclic loading. The literature explains this behavior by referring to the regulation of the polymer interface mobility, which contributes to a uniform redistribution of applied loads across the composite volume. This slows down the coating wear. The proposed technique for organizing nano inclusions in the polymer matrix can be applied to other types of polymer nanocomposites with various properties such as wear resistance, bending strength, and impact resistance. It is expected that this proposal will help improve the mechanical properties of polymer nanocomposites.

5. REFERENCES:

- Ahn, C., Kim, S. M., Jung, J. W., Park, J., Kim, T., Lee, S. E., and Jeon, S. (2018). Multifunctional polymer nanocomposites reinforced by 3D continuous ceramic nanofillers. *ACS nano*, 12(9), 9126-9133.
- Ahn, C., Park, J., Cho, D., Hyun, G., Ham, Y., Kim, K., ... and Ang, J. N. S. (2019). High-performance functional nanocomposites using 3D ordered and continuous nanostructures generated from proximity-field nano Patterning. *Functional Composites and Structures*, 1(3), 032002.
- Bittmann, B., Hauptert, F., and Schlarb, A. K. (2009). Ultrasonic dispersion of inorganic nanoparticles in epoxy resin. *Ultrasonics sonochemistry*, 16(5), 622-628.
- Busch, K., Hochmuth, C., Pause, B., Stoll, A., and Wertheim, R. (2016). Investigation of cooling and lubrication strategies for machining high-temperature alloys. *Procedia CIRP*, 41, 835-840.
- Cho, D. H., and Bhushan, B. (2016). Friction and wear of various polymer pairs used for label and wiper in labeling machine. *Tribology International*, 98, 10-19.
- Cui, W., Raza, K., Zhao, Z., Yu, C., Tao, L., Zhao, W., ... and Hu, Y. (2020). Role of transfer film formation on the tribological properties of polymeric composite materials and spherical plain bearing at low temperatures. *Tribology International*, 1526 106569.
- Domun, N., Hadavinia, H., Zhang, T., Sainsbury, T., Liaghat, G. H., and Vahid, S. (2015). Improving the fracture toughness and the strength of epoxy using nanomaterials—a review of the current status. *Nanoscale*, 7(23), 10294-10329.
- Flegler, F., Neuhauser, S., and Groche, P. (2020). Influence of sheet metal texture on the adhesive wear and friction behaviour of EN AW-5083 aluminum under dry and starved lubrication. *Tribology International*, 141, 105956.
- Gad, M. M., Fouda, S. M., Al-Harbi, F. A., Năpănkangas, R., and Raustia, A. (2017). PMMA denture base material enhancement: a review of fiber, filler, and nanofiller addition. *International journal of nanomedicine*, 12, 3801.
- Gaynutdinova, D. F., Modorskii, V. Y., and Shevelev, N. A. (2016). Experimental modeling of cavitation occurring at vibration. In *AIP Conference Proceedings* (Vol. 1770, No. 1, p. 030111). AIP Publishing LLC.
- Hanemann, T., Haußelt, J., and Ritzhaupt-Kleissl, E. (2009). Compounding, micro injection moulding and characterisation of polycarbonate-nanosized alumina-composites for application in microoptics. *Microsystem technologies*, 15(3), 421-427.
- Herzfeld, K. F., and Litovitz, T. A. (2013). *Absorption and dispersion of ultrasonic waves* (Vol. 7). Academic Press.
- Holmberg, K., Kivikytö-Reponen, P., Härkisaari, P., Valtonen, K., and Erdemir, A. (2017). Global energy consumption due to friction and wear in the mining industry. *Tribology International*, 115, 116-139.
- Holt, A. P., Griffin, P. J., Bocharova, V., Agapov, A. L., Imel, A. E., Dadmun, M. D., and Sokolov, A. P. (2014). Dynamics at the polymer/nanoparticle interface in poly (2-vinylpyridine)/silica nanocomposites. *Macromolecules*, 47(5), 1837-1843.
- Idusuyi, N., and Olayinka, J. I. (2019). Dry sliding wear characteristics of aluminium metal matrix composites: a brief overview. *Journal of Materials Research and Technology*, 8(3), 3338-3346.
- Kumar, K., Ghosh, P. K., and Kumar, A. (2016). Improving mechanical and thermal properties of TiO₂-epoxy nanocomposite. *Composites Part B: Engineering*, 97, 353-360.
- Lampaert, S. G. E., Fellingner, B. J., Spronck, J. W., and Van Ostayen, R. A. J. (2018). In-plane friction behaviour of a ferrofluid bearing. *Precision Engineering*, 54, 163-170.
- Li, Y., Huang, Y., Krentz, T., Natarajan, B., Neely, T., and Schadler, L. S. (2016). Polymer Nanocomposite Interfaces: The Hidden Lever for Optimizing Performance in Spherical Nanofilled Polymers. In *Interface/Interphase in Polymer Nanocomposites* (pp. 1-69). Hoboken, NJ, USA: John Wiley and Sons, Inc.

19. Li, Y., Wang, S., and Wang, Q. (2017). A molecular dynamics simulation study on enhancement of mechanical and tribological properties of polymer composites by introduction of graphene. *Carbon*, 111, 538-545.
20. Ma, X., Peng, C., Zhou, D., Wu, Z., Li, S., Wang, J., and Sun, N. (2018). Synthesis and mechanical properties of the epoxy resin composites filled with sol-gel derived ZrO₂ nanoparticles. *Journal of Sol-Gel Science and Technology*, 88(2), 442-453.
21. Mushtaq, S., and Wani, M. F. (2017). Self-lubricating tribological characterization of lead free Fe-Cu based plain bearing material. *Jurnal Tribologi*, 12, 18-37.
22. Park, J., Yoon, S., Kang, K., and Jeon, S. (2010). Antireflection Behavior of Multidimensional Nanostructures Patterned Using a Conformable Elastomeric Phase Mask in a Single Exposure Step. *Small*, 6(18), 1981-1985.
23. Pham, S. T., Wan, S., Tieu, K. A., Ma, M., Zhu, H., Nguyen, H. H., ... and Nancarrow, M. J. (2019). Unusual Competitive and Synergistic Effects of Graphite Nanoplates in Engine Oil on the Tribofilm Formation. *Advanced Materials Interfaces*, 6(19), 1901081.
24. Rivière, L., Lonjon, A., Dantras, E., Lacabanne, C., Olivier, P., and Gleizes, N. R. (2016). Silver fillers aspect ratio influence on electrical and thermal conductivity in PEEK/Ag nanocomposites. *European Polymer Journal*, 85, 115-125.
25. Rodriguez, V., Sukumaran, J., Schlarb, A. K., and De Baets, P. (2016). Influence of solid lubricants on tribological properties of polyetheretherketone (PEEK). *Tribology International*, 103, 45-57.
26. Roy, M., Nelson, J. K., MacCrone, R. K., and Schadler, L. S. (2007). Candidate mechanisms controlling the electrical characteristics of silica/XLPE nanodielectrics. *Journal of Materials Science*, 42(11), 3789-3799.
27. Saravanan, P., Selyanchyn, R., Tanaka, H., Fujikawa, S., Lyth, S. M., and Sugimura, J. (2017). Ultra-low friction between polymers and graphene oxide multilayers in nitrogen atmosphere, mediated by stable transfer film formation. *Carbon*, 122, 395-403.
28. Singh, A., Chauhan, P., and Mamatha, T. G. (2020). A review on tribological performance of lubricants with nanoparticles additives. *Materials Today: Proceedings*, 25, 586-591.
29. Visco, A. M., Pistone, A., Brancato, V., Iannazzo, D., and Fazio, M. (2016). Mechanical and physical properties of epoxy resin based nanocomposites reinforced with polyamine functionalized carbon nanotubes. *Polymer Composites*, 37(4), 1007-1015.
30. Wang, W., and Alexandridis, P. (2016). Composite polymer electrolytes: Nanoparticles affect structure and properties. *Polymers*, 8(11), 387.
31. Xiang, L., and Gao, N. (2017). Coupled torsion-bending dynamic analysis of gear-rotor-bearing system with eccentricity fluctuation. *Applied Mathematical Modelling*, 50, 569-584.
32. Yan, L., Wang, H., Wang, C., Sun, L., Liu, D., and Zhu, Y. (2013). Friction and wear properties of aligned carbon nanotubes reinforced epoxy composites under water lubricated condition. *Wear*, 308(1-2), 105-112.
33. Zalaznik, M., Kalin, M., Novak, S., and Jakša, G. (2016). Effect of the type, size and concentration of solid lubricants on the tribological properties of the polymer PEEK. *Wear*, 364, 31-39.
34. Zare, Y. (2016). Study of nanoparticles aggregation/agglomeration in polymer particulate nanocomposites by mechanical properties. *Composites Part A: Applied Science and Manufacturing*, 84, 158-164.
35. Zhang, G., Rasheva, Z., Karger-Kocsis, J., and Burkhart, T. (2011). Synergetic role of nanoparticles and micro-scale short carbon fibers on the mechanical profiles of epoxy resin. *Express Polymer Letters*, 5(10), 859-872.
36. Zhang, L., Qi, H., Li, G., Zhang, G., Wang, T., and Wang, Q. (2017). Impact of reinforcing fillers' properties on transfer film structure and tribological performance of POM-based materials. *Tribology International*, 109, 58-68.
37. Zhang, L., Zhang, G., Chang, L., Wetzel, B., Jim, B., and Wang, Q. (2016). Distinct tribological mechanisms of silica nanoparticles in epoxy composites

reinforced with carbon nanotubes, carbon fibers and glass fibers. *Tribology International*, 104, 225-236.

38. Zhao, W., Li, T., Li, Y., O'Brien, D. J., Terrones, M., Wei, B., and Lu, X. L. (2018). Mechanical properties of nanocomposites reinforced by carbon nanotube sponges. *Journal of Materiomics*, 4(2), 157-164.
39. Zhu, S., Yu, Y., Cheng, J., Qiao, Z., Yang, J., and Liu, W. (2019). Solid/liquid lubrication behavior of nickel aluminum-silver alloy under seawater condition. *Wear*, 420, 9-16.

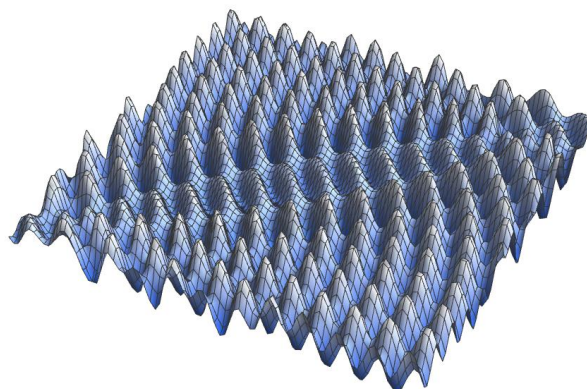


Figure 1. 3D model of the interference pattern on the surface of a liquid while equalizing the ultrasound intensity of two emitters.

PREFERÊNCIAS SENSORIAIS VARK DE ALUNOS DE ENSINO MÉDIO NA APRENDIZAGEM DE CIÊNCIAS: ELES SÃO CONFIÁVEIS?

SECONDARY STUDENTS' VARK SENSORY PREFERENCES IN SCIENCE LEARNING: ARE THEY RELIABLE?

PREFERENCIAS SENSORIALES VARK DEL ALUMNADO DE SECUNDARIA EN EL ESTUDIO DE CIENCIAS: ¿SON FIABLES?

ORTEGA-TORRES, Enric¹; SOLAZ-PORTOLÉS, Joan-Josep^{2*}; SANJOSE LÓPEZ, Vicente²;¹ Science Education, Florida Universitària / Universitat de València, Spain² Science Education and CDC research group, Universitat de València

* Corresponding author

e-mail: Joan.Solaz@uv.es

Received 21 August 2020; received in revised form 12 September 2020; accepted 28 September 2020

RESUMO

As preferências sensoriais dos alunos (SP), ou seja, as formas ou canais pelos quais preferem receber informações, têm sido propostas como um fator pessoal que influencia a aprendizagem de ciências. Existem estudos que relacionam a melhoria do aprendizado com a adaptação dos recursos instrucionais às SP individuais. Um instrumento amplamente utilizado para determinar SP é o questionário VARK. No entanto, os SP individuais devem ser confiáveis para serem considerados úteis para melhorar o ensino. Não há estudos suficientes sobre a confiabilidade deste questionário. O objetivo desta pesquisa foi avaliar a confiabilidade (estabilidade temporal) da SP, medida pelo instrumento VARK. Além disso, foi avaliada a confiabilidade da percepção subjetiva dos alunos sobre suas SP pessoais. Foi utilizada uma metodologia mista, quantitativa e qualitativa. A amostra foi composta por 582 alunos, do 1º ano do ESO ao 1º do ensino médio (7º ao 11º ano). O questionário foi aplicado duas vezes a uma subamostra de alunos, com diferença de aplicação de alguns meses. Um pequeno grupo de alunos também foi entrevistado. Na análise dos resultados por meio dos testes do qui-quadrado (X^2) e da MANCOVA de medidas repetidas, não foram encontradas mudanças permanentes na distribuição dos grupos de PS ao longo do ensino médio. Essa estabilidade permitiria aos professores adaptar materiais a essa distribuição. Os SP individuais permaneceram estáveis ao longo do tempo sob um critério permissivo, mas não quando um critério mais rígido foi usado. Além disso, a confiabilidade da percepção subjetiva do PS encontrada foi baixa.

Palavras-chave: *Aprendizagem, Preferências sensoriais, questionário VARK, Confiabilidade, Ensino médio*

ABSTRACT

Students' sensory preferences (SP), that is, the ways or channels they prefer to receive the information, have been proposed as personal factors influencing science learning. Some studies relate improvement in learning to the adequacy of instructional resources to individual SP. A widely used instrument to determine SP is the VARK questionnaire. However, the individual SP has to be reliable to be considered useful to improve instruction. There are not enough studies on the reliability of this questionnaire. This study aimed to assess the reliability (temporal stability) of SP, as measured by the VARK instrument. Also, the reliability of the student's subjective perception of his/her personal SP was evaluated. A mixed methodology was used, combining techniques for obtaining both quantitative and qualitative information. The sample was made of 582 male and female students, from 7th to 11th grades. The questionnaire was administered twice to a subsample of students, with a few months' delay. Besides, a small group of students was interviewed. In the analysis of the results, using chi-square tests (X^2) and a repeated measure MANCOVA, no massive permanent changes in the group distribution of SP were found along with secondary education. This would be useful for teachers to adapt learning materials to their students' preferences. The individual SP was stable enough under a permissive criterion, but not when a stricter standard was used. Besides, the reliability of students' self-perception of SP was low.

Keywords: *Learning, Sensory Preferences, VARK questionnaire, Reliability, Secondary Education*

RESUMEN

Las preferencias sensoriales de los estudiantes (SP), es decir, las formas o canales mediante los cuales prefieren recibir la información, se han propuesto como un factor personal que influye en el aprendizaje de las ciencias. Hay estudios que relacionan una mejora en el aprendizaje con la adecuación de recursos instruccionales a las SP individuales. Un instrumento muy utilizado para determinar las SP es el cuestionario VARK. Sin embargo, las SP individuales deben ser fiables para poder considerarse útiles con el fin de mejorar la enseñanza. No hay estudios suficientes sobre la fiabilidad de este cuestionario. El objetivo de esta investigación fue evaluar la fiabilidad (estabilidad temporal) de las SP, medida mediante el instrumento VARK. Además, se evaluó la fiabilidad de la percepción subjetiva del alumnado sobre su SP personal. Se ha empleado una metodología mixta, cuantitativa y cualitativa. La muestra se compuso de 582 estudiantes, de 1º de ESO hasta 1º de bachillerato (7º a 11º grado). El cuestionario se aplicó dos veces a una submuestra de estudiantes, con una diferencia de aplicación de algunos meses. También se entrevistó a un pequeño grupo de estudiantes. En el análisis de los resultados mediante pruebas chi cuadrado (χ^2) y un MANCOVA de medidas repetidas, no se encontraron cambios permanentes en la distribución grupal de SP a lo largo de la educación secundaria. Esta estabilidad permitiría al profesorado adaptar materiales a dicha distribución. Las SP individuales fueron estables en el tiempo bajo un criterio permisivo, pero no cuando se utilizó un criterio más estricto. Además, la fiabilidad de la percepción subjetiva de la SP encontrada fue baja.

Palabras clave: *aprendizaje, cuestionario VARK, educación secundaria, fiabilidad, preferencias sensoriales*

1. INTRODUCTION:

Knowing students' preferences and individual difficulties dealing with instructional materials could help teachers improve their proposals and help students select resources, activities, and procedures to enhance their effectiveness (then, their self-efficacy) when studying science. Adapting the curriculum to students' differences has been suggested as a possible solution to learning difficulties (Bovill and Bulley, 2011; Rose, Meyer and Hitchcock, 2005; Tomlinson, 1999) instead of lowering the required levels in evaluation (Linnenbrink and Pintrich, 2002). Curriculum adaptations involve designing learning materials, activities, and teaching methodologies to meet individual students' capabilities and preferences (Snow, 1986; Triantafyllou, Pomportsis, Demetriadis, and Georgiadou, 2004). These adaptations have to be made not only for disabled students (Bryant, Bryant, and Smith, 2015) but for any student. Students' learning styles (Cassidy, 2010) focused on many studies addressed to determine individual differences and concomitances in learning activities and to develop the curricular adaptations in a better way to students' characteristics and preferences.

Throughout the last 40 years, the number of models and instruments about learning styles has been growing up in an almost exponential way (Geake 2008). Still, most of them have proved to be not reliable enough (Coffield, Moseley, Hall, and Ecclestone, 2004). Several reviews that span decades have revised these instruments (Arter and Jenkins, 1979; Kampwirth and Bates, 1980;

Kavale and Forness, 1987; Kavale, Hirshoren, and Forness, 1998), and most of them suggested that there is not enough statistical evidence to support their outcomes. In his complete overview, Cassidy (2010) pointed out that it is necessary to provide evidence about the validity of the models underlying these instruments.

This criticism began a long time ago with the research conducted by Stumpf and Freedman (1981). Different researchers focused on the lack of accuracy of the instruments or inventories used to assess students' learning styles (Curry, 1990; Newstead, 1992), and some of them insisted on the importance of validating these inventories: this validation becomes a necessary step to adapt the instructional approach to students' learning styles in a significant way (Willingham, Hughes, and Dobolyi, 2015).

This is also the case of the VARK instrument. Fleming and Mills (1992) created this questionnaire (Appendix 1) to have a tool to classify people's sensory preferences (SP) about the learning resources. The basis of this SP today can be related to the research studies undertaken by Gilmore, McCarthy, and Spelke (2007), and Dekker, Lee, Howard-Jones, and Jolles (2012). These researchers obtained results that validate that visual, auditory, and kinaesthetic information is processed in different parts of the human brain.

The concept of Sensory Preferences (SP onwards), the kind of personal quality assessed by the VARK questionnaire, refers to a quite permanent individual factor created by a brain pattern, and not to a student's temporary whim. If SP were relatively stable over time, they could be

understood as a part of the students' individual differences influencing learning. Then SP would deserve specific attention in instructional design. Conversely, if SP were not steady for every student (at least in continuous, long enough intervals compared to the typical times needed to achieve educational goals), this construct wouldn't be useful to improve instructional effectiveness.

Even though the VARK questionnaire has been validated in its four-factor structural design (Leite, Svinicki, and Shi, 2009), up to our knowledge, there is no evidence of its reliability (understood as constancy or steadiness) in secondary school students. Most of the studies conducted using the VARK questionnaire involved university students. Therefore, this work focuses on the reliability of the sensory preferences of secondary school students, obtained as outcomes of the VARK questionnaire.

1.1. VARK Sensory Preferences

Fleming and Mills (1992; Fleming, 2001) elaborated on the concept of students' Sensory Preference when they found that many students pointed out as a learning obstacle the way (the channel through) teachers presented their learning material. The reason seemed to be associated with a particular sensory preference of each student. According to Fleming and Mills' (1992) idea, if a student's choice was not in tune with the sensory inputs needed to process the learning materials properly, some learning obstacles could appear associated with inappropriate attitudes towards the tasks or with low use of cognitive-metacognitive skills. These two types of factors, low motivation, indifference, and displeasure, or the perception of low self-efficacy (Koballa and Glynn, 2007; Osborne, Simon, and Collins, 2003), and the unproductive management of cognitive and metacognitive resources (Phan, 2009; Miñano, Castejón, and Gilar, 2012) had been pointed out as essential causes of learning obstacles in science education.

A student's SP is understood as the individual sensitivity to the specific format of the information presented by the science teacher through a prominent, specific sensory channel. This is not a rigid or immovable preference in each student and discipline, and it does not exclude the possibility of learning through other sensory channels.

In the present paper, the VARK questionnaire was used (Fleming and Mills (1992; Fleming, 2001), assuming the particular way this instrument defines students' sensory preferences. The VARK questionnaire is an adaptation of the previous one

designed by Stirling (1987) where only three categories were established: Visual, Aural, and Kinesthetic. Fleming and Mills (1992) considered these three categories insufficient. They decided to divide the Visual preference selected by Stirling (1987) into two different preferences that they called Visual and Reading/Writing because although the eyes are used to taking all the visual information, this information is different in itself. The presentation of the information given by the teacher was put on one side. It is based on visual representations of concepts through diagrammatic materials, graphics, symbols, hierarchy schemes, drawings, etc. On the other side, there were the materials, the information of which is mediated by texts. Then, reading is necessary to take benefit of them. These different materials were considered enough to differentiate the modes Visual, for the first type of material preference, and Reading/Writing, for the second.

Therefore, the VARK questionnaire considers four necessary preferences or "pure" modes: (V) Visual; (A) Aural; (R) Reading/Writing; (K) Kinesthetic. It is also considered any combination of these "pure" modes (i.e. VK, AR, ARK, etc.). These four "pure" modes can be related to different types of learning materials as follows (Fleming, 2001; Fleming and Mills, 1992):

- Visual (V): Visual students like to learn by representing information in tables, graphs, diagrams, drawings, and all the visual possibilities offered by new technologies.
- Aural (A): Aural students benefit from the information that is "heard". Students with this preference learn better through lectures, explanations from the teacher, devices that reproduce the information in a resonant way, and speaking with other students.
- Reading / Writing (R): The favorite learning materials for these students are notes, books, magazines, websites that offer written information, and the information supplied mainly as a text.
- Kinesthetic (K): Kinesthetic students prefer to learn through corporal experience (simulated or real). They like to manipulate any mechanism, device, or machine, and carry out tests and trials with them. They consider that practice is paramount for learning.

Two different versions of the VARK questionnaire have been proposed and used in educational research. The first one is made of 13 items. Still, a few years later, Fleming (2006)

added three extra items to balance the main pure preferences (V, A, R, K) in the questionnaire (4 situations X 4 pure preferences = 16 items). This second version was used to validate the 4-factor structure of the VARK model and to check the reliability of the four scales, which was considered good enough (Leite *et al.*, 2009). However, Leite *et al.* (2009) found that the factor loadings of these three additional items in the four theoretical factors (V, A, R, and K) were of similar size, meaning that any of them especially contribute to any factor.

Each item in the questionnaire has multiple choice answer questions. Thus the participant can choose one option, two, or all of them to find the optimal match with their unique position in the proposed situation. Each option is associated with one of the four different modes considered: Visual (V), Aural (A), Reading (R), and Kinesthetic (K). Four different V, A, R, and K-type responses are obtained (the number of options chosen in all items corresponding to each sensory mode). The final type of SP is assigned to each participant by composing the different scores according to a (complicated) specific procedure.

Different daily-life situations are portrayed in VARK items: information-receiving situations, information sending circumstances, and contexts in which information has to be used to decide. These situations are easy to understand for students of different ages. In that way, possible erroneous individual interpretations are prevented. They invite participants to think-and-answer from their own daily life experience and not from purely hypothetical or unreal situations.

This questionnaire has been used in some studies aimed at characterizing student's sensorial preferences or at adapting instructional activities to students' characteristics. The samples were usually made up of university students (Dobson, 2009; El Tantawi, 2009; Kharb, Samanta, Jindal and Singh, 2013; Leasa and Batlolona, 2016; Slater, Lujan, and DiCarlo, 2007). VARK preferences have also been related to academic achievement, but usually in university students samples again (Dobson, 2009; El Tantawi 2009; Kharb *et al.* 2013; Awang, Samad, Faiz, Roddin, and Kankia, 2017; Horton, Wiederman, and Saint 2012).

In summary, the VARK-questionnaire administration has produced different outcomes in samples usually made of university students. However, if VARK was not reliable, conclusions could not be elaborated from these previous studies.

1.2. Aims, objectives, and rationale

First, the present study aimed at analysing the reliability of secondary school students' SP as assessed by the VARK questionnaire. The existence of SP as a real individual psychological factor influencing learning requires its stability in long periods. The stability of students' preferences can be assessed following synchronous or asynchronous procedures. Both procedures were used, and then data was analyzed to find whether they were convergent and showed a coherent picture or not.

The first objective was to obtain the distribution of students' SP throughout the years comprised in the compulsory secondary school education and then analyze whether massive changes occur in classroom groups of students (not in individuals). Group constancy (associated with prevalence) of the SP distribution could be important in educational contexts. Here, the stability of the VARK-assigned SP will be analyzed by conducting a cross-sectional synchronous study. The degree of stability will be obtained by comparing the outcomes of groups of students with different ages, but equivalent to other relevant factors.

The second objective was to assess the reliability of the VARK-assigned SP of each student by looking at their constancy in time. If the questionnaire provided reliable information, then two different administrations would give similar results for the same student. In this analysis, an asynchronous study was conducted as the VARK questionnaire was administered twice to the same (sub)sample at different times.

Second, this study also aimed at assessing the students' accuracy when they self-assigned a particular SP. This student's self-assignment was done independently from the VARK-assigned SP, and then both results could diverge.

If VARK-assigned SP were not reliable or continuously changed over time (as an effect of the students' development, for instance), then the SP construct would not be handy for teachers to improve instructional materials. Also, if students' subjective perceptions of their SP were not reliable, they should not attribute learning obstacles to their subjective feelings. In this case, teachers would help students to be aware of their real SP to use them properly.

The third objective was to test the reliability of student's self-perceived SP by comparing the self-assigned sensory preference with the VARK instrument (VARK-assigned SP). However, this

comparison implies considering the VARK questionnaire as reliable, and then, the possibility of meeting this third objective depends on the result of the previous purposes.

In most analyses, students' gender was considered a possible factor causing differences in students' preferences. Provide sufficient details to permit repetition of the experimental work. The technical description of methods should be given when such practices are new.

2. METHODOLOGY:

2.1. Participants

A total of 582 Spanish male and female students from the 7th year (1st of ESO in Spain)-to 11th year (1st of Baccalaureate in Spain)-completed the VARK questionnaire this study. They belonged to several intact groups in eight secondary schools of three different ownerships (public, private arranged-cooperative, private arranged-religious). All high-schools are located in a big Spanish city. There was not a sampling procedure, so participants were chosen according to their availability. However, biasing criteria in selecting participants - such as assigning students with high academic performance, poorer general aptitude - were avoided. The distribution of students in the different school years was not the same but ranged from 24 percent (2nd ESO-8th year) to 15 percent (3rd ESO-9th year) of the total sample. Table 1 provides the amount and percentage of students according to gender and grade level.

Table 1. Distribution of the sample according to gender and academic year.

	7th	8th	9th	10th	11th	Total
Average Age (y.o.)	12,7	13,4	14,2	15,1	16,5	
Boys. N=	74	78	46	74	54	326
Percent=	55%	56%	54%	54%	63%	56%
Girls. N=	61	61	39	63	32	256
Percent=	45%	44%	46%	46%	37%	44%
Total N	135	139	85	137	86	582

Incomplete data was from some participants (experimental mortality), so in some analyses, the sample size was smaller. To analyze the stability of the VARK-questionnaire, this instrument was administered again to a sub-sample of 128 participants. This sub-sample was obtained by selecting at random 20-30 boys and

girls from every academic year.

To increase the reliability of students' comprehension of the VARK items and researchers' interpretations, a group of 10 students was selected for individual interviews after the first administration of the questionnaire. The selection of this sub-set of participants followed two criteria: (a) the most frequent SP resulting from the first administration of the questionnaire had to be represented; (b) the number of girls and boys had to be balanced according to their distribution in each academic year (see Table 1).

2.2. Variables, Instruments, and Measures

The shorter, 13-item version of the VARK questionnaire (Fleming and Mills, 1992) was used in the present study. This version was chosen, instead of the longer ones, for different reasons: a) As it was stated before, when participants are younger students, a shorter version implies a lower risk of random responses due to boredom; (b) This more concise version of the questionnaire does not need specific permissions, and it is available and free, and (c) According to the results obtained by Leite *et al.* (2009), there was not expected singular contributions from the three additional items included in the more extended version of the questionnaire.

The 13-item VARK questionnaire was used to (a) obtain the five scores for pure or elemental modes V, A, R, K, and for the total amount of options chosen by each student; and (b) to assign one of the 15 different types of SP to each participant:

- Unimodal: V, A, R, or K. In these cases, the student has a clearly defined preference for learning through only one of the sensory channels considered.
- Bimodal: AV, AR, VK, AR, AK, or RK. In these cases, the student benefits from materials given in any of two different channels or their combination.
- Trimodal: VAR, VAK, ARK, or ARK. Students having these sensory preferences benefit from any of the sensory channels except for one. Hence, VAR also means that the student does not prefer (or avoid) materials using the K channel, and so on.
- Tetramodal: VARK. This is the "neutral" preference, as any sensory channel is good for learning identically.

To obtain independent evidence of the

students' self-assigned SP, before administering the VARK questionnaire, students were asked to self-assign the most relevant sensory preference, under their own criteria. An explanation preceded this question about the meaning of Fleming and Mills' SP, and of each of the V, A, R, and K main sensory preferences. The possible answers to this question were only the four pure modes V, or A, or R or K, and only one of them could be chosen.

The interviews were performed by one of the researchers after the first administration. The structure was based on the following stages:

1. Connecting the interview with the VARK questionnaire fulfilled some weeks ago. The meaning of each sensory preference V, A, R, K was explained again.
2. Asking the interviewees to self-assign the main unimodal preference again, to verify the students' constancy in this self-evaluation.
3. Finding out the student's interpretation and justification of the self-assigned SP. Participant's understanding of the real meaning of each unimodal SP and its coherence with the self-assignment was verified by using different examples.
4. Using some VARK items to ask for the meaning the student gave to each item and option, and also to compare the answers given in the interview and in the questionnaire administration.

2.3. Data collection procedure

The first administration of the VARK questionnaire to the whole sample took place in the last third of the academic year. The individual interviews were conducted two to four months later. The second administration to a subsample was done from three to six months after the first administration.

The questionnaire was translated from English into Spanish and Catalan. The science teacher in each school was instructed in the VARK model and in the correct administration of the questionnaire. Permissions were obtained and then, sessions were scheduled for data collection.

The science teacher conducted the data collection session in each school. Written instructions were read aloud to explain the objectives and possible benefits of the study to the participants. First, the teacher explained the meaning of SP, solved out students' doubts, and then, students were asked to self-assign a

unimodal SP. Second, the VARK questionnaire was administered. Particular emphasis was put on: (a) centering attention to science learning only; and (b) the possibility of choosing more than one option in each VARK item. Afterward, students' doubts and worries were met. Students individually fulfilled the questionnaire in a typical time of 45-55 min.

The completed questionnaires were evaluated by one of the researchers, according to the particular procedure established for the VARK instrument (a description of the course can be found at Appendix 1). The SPSS 22.0 TM program was used for all data analyses.

For the individual interviews, one of the researchers visited the schools and asked some additional collaboration participants. The interviews took place in a small meeting room. In the introduction, the researcher referred to the VARK questionnaire previously completed by the students and explained the objectives of the interview: to clarify students' answers and to assure the comprehension of items. The interviews lasted approximately 20 minutes per student.

3. RESULTS AND DISCUSSION

3.1. Distribution of SP in the Secondary School

In the whole sample, the Type of School did not produce significant differences in the distribution of VARK scores, V, A, R, K, and Total responses (Pillai's trace: $F(6,1136) = 1.578$; $p > .10$). The distribution of the VARK-assigned SP, obtained by compounding these scores in a specific way, was not significantly associated with the Type of School (Chi-square: $\chi^2(28) = 30.312$; $p = .348$). Thus, the type of school was collapsed in further analyses. Figure 1 shows the distribution of the VARK-assigned SP in the sample after the first administration.

There were less unimodal (35 percent) than multimodal students (bimodal: 33 percent; trimodal: 24 percent; tetramodal: 8 percent). This distribution was not different from the expected at random (unimodal: 27 percent, bimodal: 40 percent; trimodal: 27 percent and tetramodal: 7 percent) according to χ^2 test ($\chi^2(3) = 4.07$; $p > .05$). The "pure", unimodal SP appeared in frequencies significantly different from the expected at random ($\chi^2(3) = 29.89$; $p > 0.001$): 22 percent of K, 9 percent of A, 3 percent of R and only 1 percent of V ($\chi^2(3) = 29.89$; $p > 0.001$). The K preference was clearly more frequent, and R and V were less

frequent than expected at random. Only 10 percent of students showed strong unimodal sensory preferences.

Six types of SP accumulated 80 percent of the sample. These “most frequent SP” were: K, AK, ARK, A, VARK, and VAK. The remaining “less frequent SP” (each under 5 percent of the sample) were RK, AR, R, VK, VRK, V, VA, VAR, VR, and together made 20 percent of the participants. As the pure modes concern, there appeared a significant predominance of SPs containing the K mode (81 percent of participants) in the unimodal SP or the different multimodal combinations (as AK or ARK, for instance). Conversely, the V mode was the least frequent in unimodal or multimodal combinations (22 percent).

3.2. Changes in the group distribution of Sensory Preferences along with Secondary School

To test SP stability along with Secondary School, the data of the initial period was compared with the data of the final one in these academic years. Two years were considered together (so their data were collapsed) for a period to guarantee a period long enough in academic terms. In this way, the influence of minor and not permanent changes due to maturation adjustments would be minimized. The “Initial Stage” or period was defined as 7th and 8th years; and the “Final Stage” as 10th and 11th years.

First, the set of more or less frequent SP was the same in both academic stages. The academic stage was not significantly associated to the percentage of students in the set of more or in the set of less frequent SP (Initial stage: 80.7 percent; Final stage: 80.3 percent; $\chi^2(1) < 1$). Selecting only the most frequent SP (K, AK, ARK, A, VARK, VAK) there was not a significant association between academic stage and SP ($\chi^2(5) = 6.04$; $p = .303$), neither for girls ($\chi^2(5) = 4.093$; $p = .536$) nor for boys ($\chi^2(5) = 8.36$; $p = .137$). Thus, the most frequent SP distribution was similar in the first two years and the two last years. The same applied when only the less frequent SP were selected and associated with the academic stage ($\chi^2(8) = 8.03$; $p = .430$). As the “pure” SP concerns (V, A, R, K), their distributions did not vary with the stage either (Global: $\chi^2(3) = 2.95$; $p = .399$; Girls only: $\chi^2(3) < 1$; Boys only: $\chi^2(3) = 3.42$; $p = .332$). Figure 2 shows the relevant data for the initial to final stage comparison.

The possible impact of gender on VARK sensory preferences was also analyzed. There was not a significant association between SP and gender ($\chi^2(14) = 16.07$; $p = .309$). Independent χ^2 tests were performed for each academic year, and

none of them showed a significant association SP-gender ($p > 0.10$ in any year). These data suggest that the distributions of SP for girls or for boys were statistically similar.

3.3. Reliability VARK-assigned sensory preference

Different outcomes from two different administrations in a subsample ($N = 128$), were used to analyze the stability of VARK-assigned SP. The analysis focused on the four scores, but also on the compounded SP.

3.3.1 Score Analysis

When the four scores were taken into account, constancy analyses followed standard procedures, as the test-retest method. Usually, two conditions are required when comparing two different administrations of a particular instrument to be considered stable enough: a) there will not be significant differences; b) a significant correlation is expected to appear.

A repeated measure MANCOVA was performed with two within-subjects factors: Administration (first/second) and type of Score (V/A/R/K). The main effect of the type of Score was significant with a large effect size (Pillai's trace: $F(3,124) = 142.55$; $p < 0.001$; $\eta^2 = .78$), but there was not a significant effect of the Administration factor ($F < 1$), and there was not a significant interaction Administration X type of Score ($F(3,124) = 2.46$; $p = .066$). Therefore, globally, there were no significant differences between the first and the second administration of the VARK-questionnaire when the four scores were taken into account. Post-hoc pre-post comparisons for every type of score were performed. After the Bonferroni correction (i.e. stating $0.05/4 = .0125$ as the limit of significance), none of them were significant.

The correlation between the first and the second administration were significant for V ($r = 0.30$; $p = 0.001$), R ($r = 0.34$; $p < 0.001$) and K ($r = 0.24$; $p = 0.006$) scores, and also for the Total responses score ($r = 0.30$; $p = 0.001$), but reached only marginal significance for the A score ($r = 0.17$; $p = 0.06$).

3.3.2 VARK-assigned SP analysis

Next, the VARK-assigned SP, obtained by compounding the scores, was analyzed. Due to the different possible pure-mode combinations in the assigned SP (uni, bi, tri, and tetra-modal), comparisons to assess the stability can be made using strict or more permissive criteria. In the stricter case, if the SP assigned to the same

student were not exactly the same combination of pure modes in both administrations, it would be considered that both VARK-assigned SP differs each other. Using the more permissive criterion, if the first and second SP for the same student shared at least one pure mode, it would be considered that both assignments do not differ.

According to the stricter criterion, only 17 percent of participants obtained precisely the same assignation from both VARK administrations. Nonetheless, when the permissive criterion was adopted, 89 percent of students shared at least one pure mode in both administrations, i.e., only 11 percent of students completely changed their combination of pure modes from the first to the second administration. Each administration was considered a "judgement" made by the VARK-questionnaire on every participant. Then, it computed the Cohen's Kappa to obtain a quantitative indicator for the agreement between both administrations keeping apart random effects. The value was $K = 0.78$, meaning a good agreement between both administrations (under the more permissive criterion).

3.4. Reliability of students' self-assigned Sensory Preferences

When the more permissive criterion expressed before was assumed, the VARK instrument could be considered as reliable enough to determine students' sensory preferences. Thus, these (reliable) assigned SP can be compared to the self-assigned students' preferences. Remember that the self-assigned SP was necessary unimodal SP (i.e. V, or A, or R, or K).

The self-assigned SP was considered coherent when this (pure) mode was included in the VARK-assigned SP (usually, a combination of pure modes). Otherwise, the self-assigned preference was considered incoherent. For instance, if a participant considered him/herself as K but the instrument assigned him/her the (bimodal) type VA, the student's self-perception was considered as incoherent because VA does not contain the mode K.

In this way, the self-assigned SP and the VARK-assigned SP were coherent only in 61 percent of the participants in the first administration ($N = 582$). The percentages of incoherent self-assignments ranged from 72 percent of those students' self-considered V, to 14 percent of those self-considered K. Figure 3 shows the proportions of participants with coherent or incoherent self-assignments.

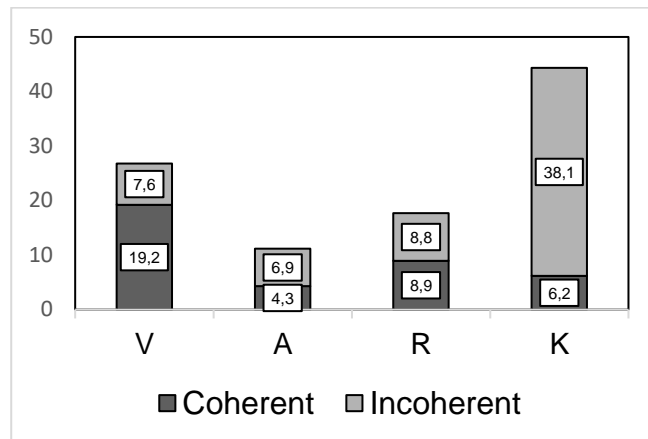


Figure 3. Students' proportions with a self-assigned sensory preference, which is coherent or incoherent with the VARK-assigned sensory preference. The height of the bars represents the percentage concerning the total number of participants.

Therefore, even using the most permissive criterion, 39 percent of students in the sample self-assigned a sensory preference in full disagreement with the VARK-assigned SP. This percentage of disagreement reached 49 percent when the same agreement was computed for the second administration of the questionnaire in the subsample.

If the questionnaire was considered reliable, then the students' self-perceptions wouldn't be considered reliable enough. Opposite, if the reliability of the VARK questionnaire was considered low (for example, assuming the stricter criterion exposed before), then independent evidence would be required to assess the reliability of students' self-assignments.

The stability of the self-assigned SP in the subsample ($N = 128$) was also assessed comparing their first and second self-assignments. As students could self-assign just a pure mode, the probability of concordance diminished (only a strict criterion is possible). The obtained Cohen's Kappa was $K = 0.30$. Therefore, the students' self-assignments appeared to have low reliability, at least when periods of few months were considered.

3.5. Participants' Interviews

The interviewed students had correct interpretations of the VARK SP. They seemed to understand the meaning of their preference and clearly explain the differences with other preferences. These few passages seem to support these conclusions:

S96 [1:00] (...) in my case, when I see an image of science I can understand it better. For example, when the teacher tells us about an animal, about a special feature it has, when she shows a picture, I can see better this quality in the image than when it is explained by the teacher using her own words (#96 student explaining his Visual preference)

S3 [12:56] I like auditory classes, auditory explanations because I have this auditory memory. When I listen to something, later on, when I have to study it, I can remember that (#S3 student explaining their Auditory preference)

Half of the interviewed students changed their self-assignment from the first administration of the questionnaire (the added question) in the interview. Among the students who maintain their first self-assignment, half of them differed from the VARK-assigned SP according to the more permissive criterion. Therefore, the researcher formulated some VARK items again to these “coherent” students, and, surprisingly, no one repeated the same answer given in the first administration.

However, all the students interviewed, except for one, showed a high coherence to justify their present self-assignments, even when this self-assignment differs from the previous self-assigned ones. It suggested that in brief periods (a few minutes), students did not change their criteria, concepts, and feelings about themselves. Opposite, in a few months, most students changed their perceptions, feelings, and conceptions about themselves.

3.6. Discussion

VARK model was developed by Fleming and Mills (1992) after a perception: the mismatch between students' sensory preferences (SP) and the type of instructional materials offered by teachers seem to cause students' learning obstacles. This mismatch may be objective or subjective. In the first case, it is assumed that real individual sensory preferences influence the effectiveness of students' harnessing of particular instructional materials. These real individual sensory preferences are supposed to be obtained from the VARK questionnaire. In the second case, subjective perception of a mismatch can occur when a student feels that he/she learns better using particular formats that imply sensory channels that are different from the ones implied in the instructional materials offered by the teacher. In this subjective case, the mismatch is

based on a student's self-assessment, not on an objective assessment.

From an educational perspective, the study of the causal relationship between the aforementioned mismatch and students' learning difficulties is welcomed (Awang *et al.*, 2017; Dobson, 2009; El Tantawi 2009; Kharb *et al.* 2013). However, the reliability of the sensory preference understood as a personal construct influencing learning is a pre-requisite to take educational advantage of these studies.

The present work aimed at analyzing the reliability (understood as stability over time) of both, the objective and the subjective assessment of the students' sensory preferences. The objectives in the present work were: (a) to obtain the distribution of VARK sensory preferences in Secondary education; (b) to assess the reliability, understood as stability over time, of the VARK sensory preferences assigned by the VARK questionnaire (objective assessment); (c) to assess the reliability of the students' (subjective) self-perceived sensory preferences.

VARK questionnaire was analyzed by Leite *et al.* (2009), and the supposed 4-factor structure (V, A, R, K) was confirmed. However, stability over time is also necessary for the reliable use of the questionnaire. Results in the sample made up of secondary school students from 7th to 11th academic years are not conclusive, as different conclusions can be elaborated from others, but sensible, criteria.

First, in a cross-section study, group distribution of SP was not different at the beginning or the final stages in secondary school, and this was true for girls or for boys. Second, the distribution of the VARK scores was statistically similar in both the different administrations of the questionnaire using the same subsample of students. Third, when the VARK-assigned SP after the first administration of the questionnaire were compared with the SP assigned after the second administration (with a few months of the interval between them), only 17 percent of participants obtained exactly the same SP. However, in 89 percent of students, both assignments shared at least one pure mode (V, or A, or R or K).

The reliability of the subjective students' self-assigned sensory preferences was also analyzed. These self-assignments were first compared to the VARK-assignments. The obtained percentages of share were not high: 61 percent and 51 percent of participants, in the 1st and 2nd administrations, self-assigned a unimodal SP that was included in

their VARK-assigned SP. Next, it was compared to the first and second self-assigned SP in the subsample of participants who asked twice the specific question. Again the match was not good ($Kappa = 0.30$).

4. CONCLUSIONS:

To conclude, data from this study suggested that, although secondary school students seem to be coherent in their feelings along with a personal interview (lasting 20 min), their perceptions about their sensory preferences when studying science were not reliable enough, at least when relatively large periods (months) are considered. The results obtained in the present study did not facilitate knowing whether or not the personal sensory preference can be considered as a real construct. Nevertheless, based on the results of this study, it cannot be concluded that VARK-assigned SP is not reliable. Simply, the SP obtained after two different applications of the VARK questionnaire were not as convergent as desired. Conclusions strongly depended on the criterion used to assess the convergence, and then the results did not show an explicit scene. Therefore, additional studies are needed to conclude on the reliability of students' sensory preferences as personal constructs. On the other side, and despite the SP were real individual characteristics or not, results suggest that students' group distributions of SP are stable enough. The group distribution of students' SPs did not significantly change from the initial to the final two-years stages of Secondary school, and this was true when distributions for girls or boys were considered apart. Thus, science teachers could still benefit from instructional changes addressed to meet secondary students' SP, especially the most frequent ones (in this study, K, AK, ARK, A, VARK, VAK).

5. REFERENCES:

- Arter, J. A., and Jenkins, J. R. (1979). Differential diagnosis—prescriptive teaching: A critical appraisal. *Review of Educational Research*, 49(4), 517-555. <https://doi.org/10.3102/00346543049004517>
- Awang, H., Samad, N. A., Faiz, N. M., Roddin, R., and Kankia, J. D. (2017, August). Relationship between Learning Styles Preferences and Academic Achievement. In IOP Conference Series: Materials Science and Engineering (Vol. 226, No. 1, p. 012193). Bristol, UK: IOP Publishing. <https://doi.org/10.1088/1757-899X/226/1/012193>
- Bovill, C. and Bulley, C.J. (2011). A model of active student participation in curriculum design: exploring desirability and possibility. In C. Rust (Ed.), *Improving Student Learning (ISL) 18. Global Theories and Local Practices: Institutional, Disciplinary and Cultural Variations* (pp. 176-188). Oxford: Oxford Brookes University.
- Bryant, D. P., Bryant, B. R., and Smith, D. D. (2015). *Teaching students with special needs in inclusive classrooms*. Thousand Oaks, California: Sage Publications.
- Cassidy, S. (2010). Learning styles: An overview of theories, models, and measures. *Educational Psychology*, 24(4), 419-444. <https://doi.org/10.1080/0144341042000228834>
- Coffield, F., Moseley, D., Hall, E., and Ecclestone, K. (2004). *Learning styles and pedagogy in post-16 learning: A systematic and critical review*. London: Learning and Skills Research Centre. Retrieved March 5, 2015, from <http://www.leerbeleving.nl/wp-content/uploads/2011/09/learning-styles.pdf>
- Curry, L. (1990). A critique of the research on learning styles. *Educational Leadership*, 48(2), 50-56. Retrieved January 5, 2015, from http://www.ascd.org/ASCD/pdf/journals/ed_lead/el_199010_curry.pdf
- Dekker, S., Lee, N. C., Howard-Jones, P., and Jolles, J. (2012). Neuromyths in education: Prevalence and predictors of misconceptions among teachers. *Frontiers in Psychology*, 3, 429. <https://doi.org/10.3389/fpsyg.2012.00429>
- Dobson, J. L. (2009). Learning style preferences and course performance in an undergraduate physiology class. *Advances in Physiology Education*, 33(4), 308-314. <https://doi.org/10.1152/advan.00048.2009>
- El Tantawi, M.M. (2009). Factors affecting postgraduate dental students' performance in a biostatistics and research design course. *Journal of Dental Education*, 73(5), 614-623. Retrieved January 25, 2015, from <http://www.jdentaled.org/content/jde/73/5/614.full.pdf>
- Fleming, N.D. (2001). *Teaching and learning styles: VARK strategies*. Christchurch, New Zealand: N.D. Fleming
- Fleming, N. D. (2006). *VARK: A guide to learning styles*. Retrieved March 21, 2015, from <http://www.vark->

13. Fleming, N. D., and Mills, C. (1992). Not another inventory, rather a catalyst for reflection. *To Improve the Academy*, 11(1), 137-155. <https://doi.org/10.1002/j.2334-4822.1992.tb00213.x>
14. Geake, J. (2008). Neuromythologies in education. *Educational Research*, 50(2), 123-133. <https://doi.org/10.1080/00131880802082518>
15. Gilmore, C. K., McCarthy, S. E., and Spelke, E. S. (2007). Symbolic arithmetic knowledge without instruction. *Nature*, 447, 589-592. <https://doi.org/10.1038/nature05850>
16. Horton, D. M., Wiederman, S. D., and Saint, D. A. (2012). Assessment outcome is weakly correlated with lecture attendance: influence of learning style and use of alternative materials. *Advances in Physiology Education*, 36(2), 108-115. <https://doi.org/10.1152/advan.00111.2011>
17. Kampwirth, T. J., and Bates, M. (1980). Modality preference and teaching method: A review of the research. *Academic Therapy*, 15(5), 597-605.
18. Kavale, K. A., and Forness, S. R. (1987). Substance over style: Assessing the efficacy of modality testing and teaching. *Exceptional Children*, 54(3), 228-239.
19. Kavale, K. A., Hirshoren, A., and Forness, S. R. (1998). Meta-Analytic Validation of the Dunn and Dunn Model of Learning-Style Preferences: A Critique of What Was Dunn. *Learning Disabilities Research and Practice*, 13(2), 75-80.
20. Kharb, P., Samanta, P. P., Jindal, M., and Singh, V. (2013). The learning styles and the preferred teaching—learning strategies of first year medical students. *Journal of clinical and diagnostic research JCDR*, 7(6), 1089-1092. <https://doi.org/10.7860/JCDR/2013/5809.3090>
21. Koballa, T. R. and Glynn, S. M. (2007). Attitudinal and Motivational Constructs in Science Learning. In S. K. Abell and N. G. Lederman (Eds.), *Handbook of Research in Science Education*, Volume 1 (75-102). Mahwah, N. J.: Lawrence Erlbaum Associates.
22. Leasa, M., Talakua, M., and Batlolona, J. R. (2016). the Development of a thematic Module based on Numbered Heads together (NHT) Cooperative Learning Model for elementary students in Ambon, Moluccas-indonesia. *The New Educational Review*, 46(4), 174-185. <https://doi.org/10.15804/tner.2016.46.4.15>
23. Leite, W. L., Svinicki, M., and Shi, Y. (2009). Attempted Validation of the Scores of the VARK. Learning Styles Inventory With Multitrait–Multimethod Confirmatory Factor Analysis Models. *Educational and Psychological Measurement*, 70(2), 323-339. <https://doi.org/10.1177/0013164409344507>
24. Linnenbrink, E. A., and Pintrich, P. R. (2002). Achievement goal theory and affect: An asymmetrical bidirectional model. *Educational Psychologist*, 37(2), 69-78. https://doi.org/10.1207/S15326985EP3702_2
25. Miñano, P., Castejón, J. L., and Gilar, R. (2012). An explanatory model of academic achievement based on aptitudes, goal orientations, self-concept and learning strategies. *The Spanish Journal of Psychology*, 15(1), 48-60. https://doi.org/10.5209/rev_SJOP.2012.v15.n1.37283
26. Newstead, S. E. (1992). A study of two “quick-and-easy” methods of assessing individual differences in student learning. *British Journal of Educational Psychology*, 62(3), 299-312. <https://doi.org/10.1111/j.2044-8279.1992.tb01024>
27. Osborne, J., Simon, S., and Collins, S. (2003). Attitudes towards science: A review of the literature and its implications. *International Journal of Science Education*, 25(9), 1049-1079. <https://doi.org/10.1080/0950069032000032199>
28. Phan, H. P. (2009). Exploring students’ reflective thinking practice, deep processing strategies, effort, and achievement goal orientations. *Educational Psychology*, 29(3), 297-313. <https://doi.org/10.1080/01443410902877988>
29. Rose, D. H., Meyer, A., and Hitchcock, C. (2005). *The Universally Designed Classroom: Accessible Curriculum and Digital Technologies*. Cambridge, MA: Harvard Education Press.
30. Slater, J. A., Lujan, H. L., and DiCarlo, S. E. (2007). Does gender influence learning style preferences of first-year medical students? *Advances in Physiology Education*, 31(4), 336-342. <https://doi.org/10.1152/advan.00010.2007>
31. Snow, R. E. (1986). Individual differences and the design of educational programs. *American*

Psychologist, 41 (10), 1029-1039.
<http://dx.doi.org/10.1037/0003-066X.41.10.1029>

32. Stirling, P. (1987, June 20). Power lines. *NZ Listener*, 13-15.
33. Stumpf, S. A., and Freedman, R. D. (1981). The Learning Style Inventory: still less than meets the eye. *Academy of Management Review*, 6(2), 297-299.
34. Tomlinson, J. (1999). *Globalization and culture*. Chicago: University of Chicago Press.
35. Triantafillou, E., Pomportsis, A., Demetriadis, S., and Georgiadou, E. (2004). The value of adaptivity based on cognitive style: an empirical study. *British Journal of Educational Technology*, 35(1), 95-106.
<https://doi.org/10.1111/j.1467-8535.2004.00371.x>
36. Willingham, D. T., Hughes, E. M., and Dobolyi, D. G. (2015). The scientific status of learning styles theories. *Teaching of Psychology*, 42(3), 266-271.
<https://doi.org/10.1177/0098628315589505>

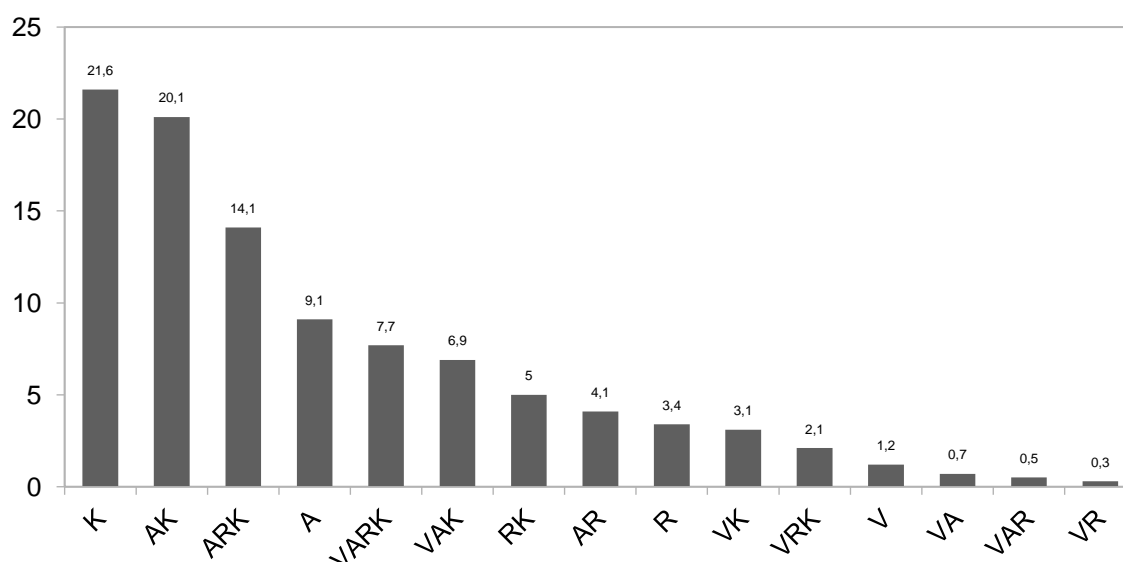


Figure 1. Percentage of participants having different sensory preferences according to the VARK questionnaire.

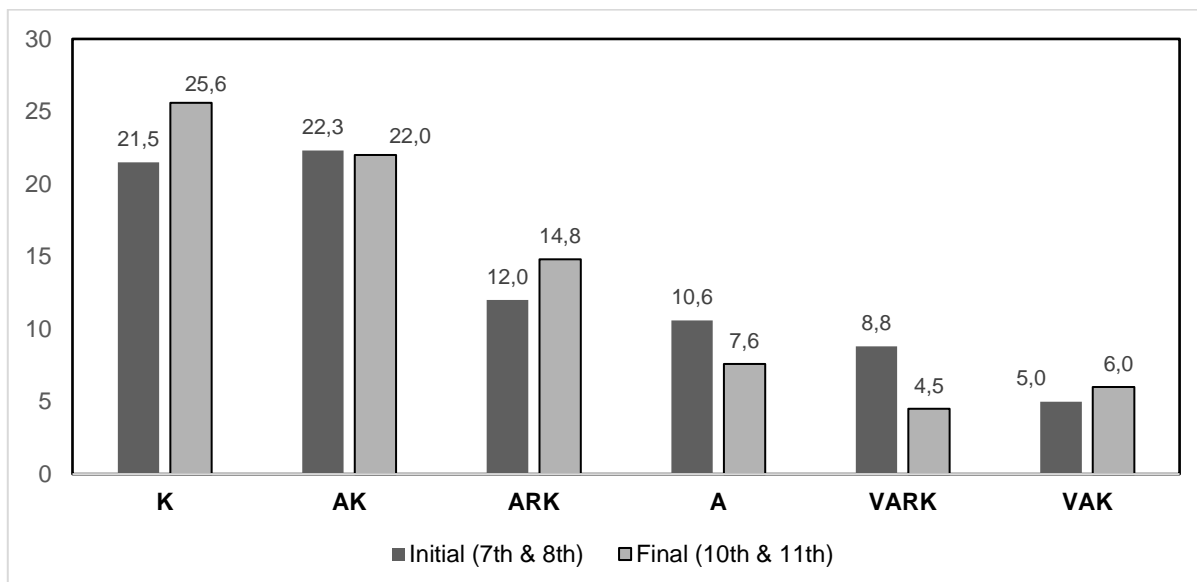


Figure 2. Percentages of students with the most frequent VARK-assigned sensory preferences in the initial of final academic stages.

APPENDIX 1

All information of the Appendix 1 has been taken from <http://mercury.educ.kent.edu/database/eureka/documents/LearningStylesInventory.pdf>

The VARK Questionnaire: How Do I Learn Best?

This questionnaire aims to find out something about your preferences for the way you work with information. You will have a preferred learning style and one part of that learning style is your preference for the intake and output of ideas and information.

Choose the answer which best explains your preference and circle the letter next to it. Please circle more than one if a single answer does not match your perception.

Leave blank any question which does not apply, but try to give an answer for at least 10 of the 13 questions. When you have completed the questionnaire, use the marking guide to find your score for each of the categories, Visual, Aural, Read/Write and Kinesthetic. Then, to calculate your preference, use the Scoring sheet.

1. You are about to give directions to a person who is standing with you. She is staying in a hotel in town and wants to visit your house later. She has a rental car. I would:

- draw a map on paper
- tell her the directions
- write down the directions (without a map)
- collect her from the hotel in my car

2. You are not sure whether a word should be spelled 'dependent' or 'dependant'. I would:

- look it up in the dictionary.
- see the word in my mind and choose by the way it looks
- sound it out in my mind.
- write both versions down on paper and choose one.

3. You have just received a copy of your itinerary for a world trip. This is of interest to a friend. I would:

- phone her immediately and tell her about it.

- b. send her a copy of the printed itinerary.
 - c. show her on a map of the world.
 - d. share what I plan to do at each place I visit.
4. You are going to cook something as a special treat for your family. I would:
- a. cook something familiar without the need for instructions.
 - b. thumb through the cookbook looking for ideas from the pictures.
 - c. refer to a specific cookbook where there is a good recipe.
5. A group of tourists has been assigned to you to find out about wildlife reserves or parks. I would:
- a. drive them to a wildlife reserve or park.
 - b. show them slides and photographs
 - c. give them pamphlets or a book on wildlife reserves or parks.
 - d. give them a talk on wildlife reserves or parks.
6. You are about to purchase a new stereo. Other than price, what would most influence your decision?
- a. the salesperson telling you what you want to know.
 - b. reading the details about it.
 - c. playing with the controls and listening to it.
 - d. it looks really smart and fashionable.
7. Recall a time in your life when you learned how to do something like playing a new board game. Try to avoid choosing a very physical skill, e.g. riding a bike. I learnt best by:
- a. visual clues -- pictures, diagrams, charts
 - b. written instructions.
 - c. listening to somebody explaining it.
 - d. doing it or trying it.
8. You have an eye problem. I would prefer the doctor to:
- a. tell me what is wrong.
 - b. show me a diagram of what is wrong.
 - c. use a model to show me what is wrong.
9. You are about to learn to use a new program on a computer. I would:
- a. sit down at the keyboard and begin to experiment with the program's features.
 - b. read the manual which comes with the program.
 - c. telephone a friend and ask questions about it.
10. You are staying in a hotel and have a rental car. You would like to visit friends whose address/location you do not know. I would like them to:
- a. draw me a map on paper.
 - b. tell me the directions.
 - c. write down the directions (without a map).
 - d. collect me from the hotel in their car.
11. Apart from the price, what would most influence your decision to buy a particular textbook:?:
- a. I have used a copy before.
 - b. a friend talking about it.
 - c. quickly reading parts of it.
 - d. the way it looks is appealing.
12. A new movie has arrived in town. What would most influence your decision to go (or not go)?
- a. I heard a radio review about it

- b. I read a review about it.
- c. I saw a preview of it.

13. Do you prefer a lecturer or teacher who likes to use:?

- a. a textbook, handouts, readings
- b. flow diagrams, charts, graphs.
- c. field trips, labs, practical sessions.
- d. discussion, guest speakers.

• The VARK Questionnaire Scoring Chart

Use the following scoring chart to find the VARK category that each of your answers corresponds to.

Circle the letters that correspond to your answers

e.g. If you answered b and c for question 3, circle R and V in the question 3 row.

Scoring Chart

Question	A	B	C	D
1	V	A	R	K
2	R	V	A	K
3	A	R	V	K
4	K	V	R	-
5	K	V	R	A
6	A	R	K	V
7	V	R	A	K
8	A	V	K	-
9	K	R	A	-
10	V	A	R	K
11	K	A	R	V
12	A	R	V	-
13	R	V	K	A

• Calculating your scores

Count the number of each of the VARK letters you have circled to get your score for each VARK category.

Total number of **Vs** circled =

Total number of **As** circled =

Total number of **Rs** circled =

Total number of **Ks** circled =

• Calculating your preferences

Use the "Scoring Instructions" sheet to work out your VARK learning preferences.

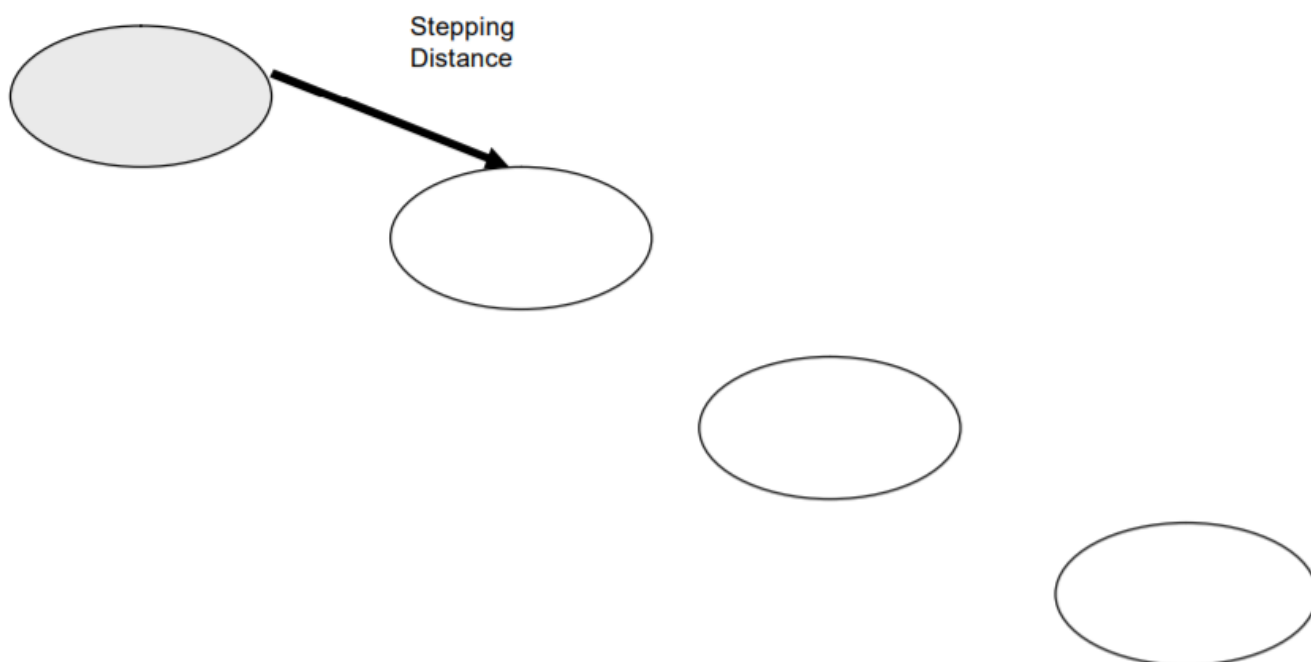
Copyright for this version of VARK is held by Neil D. Fleming, Christchurch, New Zealand and Charles C. Bonwell, Green Mountain, Colorado, USA

• Scoring Instructions

Because respondents can choose more than one answer for each question the scoring is complex. It can be likened to a set of four stepping-stones across

water.

1. Add up your scores, **V + A + R + K =**
2. Enter your scores from highest to lowest on the stones below, with their V, A, R, and K labels.



3. Your stepping distance comes from this table.

Total of my four VARK scores is	My stepping distance is
10-16	1
17-22	2
23-26	3
More than 26	4

3. Your first preference is your highest score so check the first stone as one of your preferences and enter its label on the stone.
4. If you can reach the next stone with a step equal to or less than your stepping distance then check that one too.

Once you cannot reach the next stone you have finished defining your set of preferences.

Administering the questionnaire

When you are instructing others to fill in the questionnaire they should be verbally advised to make a selection (a, b, c or d) for each question, but they may omit a question or choose two or three options if appropriate. Some may contest the meaning of words in the questionnaire and others may ask for additional contextual or situational information before they choose their answers. Avoid giving further information, as it may prejudice responses to the questions. Encourage them to choose more than one response if they think the context is not clear. Some may want to discuss the purpose of the questionnaire or its validity or reliability. Ask them to hold such questions till later when they can be more appropriately answered.

Stress, in whatever ways you can, that the results indicate their preferences but are not necessarily their strengths. This reduces the anxiety for respondents who may express the view

that the questionnaire says they are not good readers or not visually strong.

You should make the point that some strong preferences may lessen as individuals mature. Work experiences and life experiences will blur differences between preferences as people learn to use aural, visual, read/write and kinesthetic modes equally well. Preferences may also be masked by experiences.

No one mode is superior and there is no superior profile. Although our academic institutions may be strongly read/write, life is much more varied. And you can be successful with almost any combination. You may be different but you are not dumb. Students and teachers can investigate the preferences shown and explore their own views about whether the preference fits. For example, a student with a strong visual (V) preference could be asked: "How important is colour in your life?" "Do you consider yourself a visual person?" "Are there aspects of your life where your visual preference is obvious?" "Do you think you have a strong sense of space or shape or position or location?" "Do the study strategies fit with what you do now?"

Finally, some may ask questions about output preferences rather than input preferences. "How is it that I like reading but I hate writing?" Research indicates that those who have a strong preference for "taking in the world" in any particular mode (V, A, R, or K) will want to output in the same mode.

ESTUDO COMPARATIVO DAS ESTRUTURAS HISTOMORFOLÓGICAS E HISTOQUÍMICAS NO ESÔFAGO DE OVELHAS (*Ovis aries*) E COELHOS (*Oryctolagus Cuniculus*)**COMPARATIVE HISTOCHEMICAL AND HISTOMORPHOMETRICAL STUDY OF ESOPHAGUS STRUCTURES IN SHEEP (*Ovis aries*) AND RABBITS (*Oryctolagus Cuniculus*)****دراسة مقارنة كيميائية ونسجية وقياسات نسيجية لتركيب المريء في الأغنام (*Ovis aries*) والارانب (*Oryctolagus Cuniculus*)**MOHAMMAD, Hawraa Jabbar¹, ALI, Ali Khalaf^{1*} and AL-ALI, Zainab Abdul Jabbar Ridha¹¹ Department of Biology, College of Science, University of Misan, Maysan, Iraq.

* Corresponding author

e-mail: Dr.AliKhalaf@uomisan.edu.iq

Received 16 July 2020; received in revised form 20 September 2020; accepted 29 September 2020

RESUMO

A evolução entre os animais provoca muitas mudanças para que eles possam se adaptar ao seu ambiente. Cada espécie possui características únicas que os ajudam a sobreviver e podem consumir diferentes tipos de alimentos. Ovelhas e coelhos são animais economicamente importantes e usados em muitos aspectos da medicina veterinária. Este estudo teve como objetivo comparar as características histomorfométricas e histoquímicas do esôfago de vinte machos adultos de Ovelhas (n = 10) e Coelhos (n = 10). As amostras foram coletadas no abatedouro e mercado de Misan e foram usadas para estudos histológicos de dois tipos de coloração, hematoxilina e eosina, e colorações especiais (coloração de ácido periódico + reativo de Schiff). O estudo histológico mostrou diferenças no tipo de epitélio da mucosa que reveste o esôfago entre ovelhas e coelhos. O revestimento do epitélio era composto por um epitélio escamoso estratificado queratinizado em ovelhas, enquanto no coelho era composto por um epitélio escamoso estratificado não-queratinizado. Em ambos os animais, a camada submucosa não possui glândulas. A camada muscular de ambos era composta por músculo estriado nas partes cervical, torácica e abdômen do esôfago. Ambos os animais continham camada externa de tecido conjuntivo frouxo chamada adventícia. Todas as camadas em ovelhas mostraram mais espessura do que em coelhos. O estudo histoquímico mostrou que a reação à coloração de Schiff com ácido periódico foi semelhante entre os animais e em locais diferentes. Apenas células do estrato córneo de ovelhas da mucosa e células escamosas da mucosa de coelho demonstraram forte reação a essa coloração. Em contraste, o resto das células da mucosa e das camadas musculares foram reações moderadas com a coloração de Schiff com ácido periódico em todas as regiões do esôfago de ovelhas e coelhos. A submucosa e a adventícia mostraram reação fraca com a coloração de Schiff com ácido periódico em ambos os animais. Em conclusão, este estudo mostrou que ovelhas e coelhos apresentam semelhanças e diferenças no esôfago, ou seja, as camadas deste órgão têm espessuras diferentes e respondem de forma diferente à coloração de Schiff com ácido periódico.

Palavras-chave: Esôfago; Coelho; Ovelhas; Histomorfologia; Histoquímica.**ABSTRACT**

Evolution between animals causes many changes so that it can adapt to its environments. Each species has unique features that help them survive and can consume different types of food. Sheep and rabbits are economically important animals and used in many aspects of veterinary medicine. This study aimed to compare the histomorphometric and histochemical features of the esophagus of twenty sheep (n=10) and rabbit (n=10) adult males. The samples were collected from slaughterhouse and market Misan and were used for histological studies of two types of stains, hematoxylin and eosin, and special stains (Periodic acid Schiff stains). Histological study showed differences in the type epithelium of mucosa lining the esophagus between sheep and rabbits. The epithelium lining was composed of a keratinized stratified squamous epithelium in sheep while in rabbit was composed of a non-keratinized stratified squamous. In both animals, the submucosa layer does not possess glands. The muscular layer of both was composed of striated muscle in the cervical, thoracic, and abdomen parts

of the esophagus. Both animals contained an outer layer of loose connective tissue called the adventitia. All layers in sheep showed more thickness than in rabbits. The histochemical study showed that the reaction to Periodic acid Schiff stain was similar between the animals and in different places. Only stratum corneum cells of the sheep mucosa and squamous cells of the rabbit mucosa demonstrated a strong reaction to this stain. In contrast, the rest of the cells of the mucosa and muscular layers were moderate reactions with Periodic acid Schiff stain in all regions sheep and rabbit esophagus. Submucosa and adventitia showed weakly reaction with Periodic acid Schiff's stain in both animals. In conclusion, this study showed that sheep and rabbits have similarities and differences in the esophagus; that is, the layers of this organ has different thicknesses and respond differently to Periodic acid Schiff stain.

Keywords: *Esophagus; Rabbit; Sheep; Histomorphology; Histochemical.*

المخلص

يسبب التطور بين الحيوانات العديد من التغييرات حتى تتمكن من التكيف مع بيئاتها. لكل نوع ميزات فريدة تساعده على البقاء ويستهلك أنواعاً مختلفة من الطعام. تعتبر الأغنام والأرانب حيوانات مهمة اقتصادياً وتستخدم في العديد من جوانب الطب البيطري. هدفت هذه الدراسة إلى مقارنة الخصائص القياسية النسيجية والكيمياء النسيجية لمريء عشرين حيواناً (الأغنام = العدد = 10) والأرانب (العدد = 10) ذكور بالغين. جمعت العينات من مسلخ والأسواق ميسان واستخدمت في الدراسات النسيجية نوعين من الصبغات، الهيماتوكسيلين والأيوزين، والصبغة الخاصة (صبغة حمض شيفف الدورية). أظهرت الدراسة النسيجية وجود اختلافات في نوع ظهارة الغشاء المخاطي المبطن للمريء بين الأغنام والأرانب. تتكون بطانة الظهارة من ظهارة حرشفية طبقية مقترنة في الأغنام بينما في الأرانب تتكون من طبقة حرشفية طبقية غير مقترنة. في كلا الحيوانين، لا تمتلك الطبقة تحت المخاطية غدة. تتكون الطبقة العضلية لكليهما من عضلات مخططة في لأجزاء العنقية والصدرية والبطنية من المريء. كان كلا الحيوانين يحتويان على طبقة خارجية من النسيج الضام الرخو تسمى البرانية. أظهرت جميع طبقات الأغنام سماكة أكبر من تلك الموجودة في الأرانب. أظهرت الدراسة الكيميائية النسيجية أن التفاعل مع صبغة دورية حامض شيفف كان متشابهاً بين الحيوانات وفي أماكن مختلفة. أظهرت خلايا الطبقة القرنية فقط من الغشاء المخاطي للأغنام والخلايا الحرشفية من الغشاء المخاطي للأرانب تفاعلاً قوياً لهذه الصبغة. في المقابل، كانت بقية خلايا الغشاء المخاطي والطبقات العضلية تفاعلات معتدلة مع صبغة حمض شيفف الدورية في جميع مناطق مريء الأغنام والأرانب. أظهرت الطبقة تحت المخاطية والبرانية تفاعلاً ضعيفاً مع صبغة حمض شيفف الدورية في كلا الحيوانين. في الختام، أظهرت هذه الدراسة أن الأغنام والأرانب لها أوجه تشابه واختلاف في المريء؛ أي أن طبقات هذا العضو لها سمك مختلف وتستجيب بشكل مختلف لصبغة شيفف الدورية.

الكلمات المفتاحية: المريء، الأرنب، الأغنام، القياسات النسيجية، الكيمياء النسيجية.

1. INTRODUCTION:

Evolution between animals causes many changes so that it can adapt to its environments. Each species has unique characters that help them survive and can consume different types of food. Rabbits are considered economically significant animals as they have the advantage of their meat and furring, are used as pets, and they are substantial at scientific and medical experiences (Hristov *et al.*, 2006). On the other hand, sheep have been able to use lignocellulosic materials and convert them to animal products of high nutritional value, such as meat, milk, wool/fur, hide, and manure. In the same vein, sheep intestine may be used to make catguts, which are still used for internal human surgical sutures and strings for musical instruments (Agrawal *et al.*, 2014). They are herbivorous mammals, but rumen and hindgut represent two different fermentation organs (Mi *et al.*, 2018). They depend on a symbiotic relationship with a community of microbes, primarily bacteria with fibrinolytic ability in either their foregut (which the rumen of ruminants and the pseudo-ruminants) or their

hindgut (which the cecum and colon of non-ruminant herbivores), for fiber digestion (Crowley *et al.*, 2017; Furness *et al.*, 2015; Kingston-Smith *et al.*, 2013).

Besides, there are phenotypic and dramatic physiological differences found between ruminant and non-ruminant mammalian species. For example, volatile fatty acids produced as by-products of the microbial fermentation in the rumen are used as the primary source of energy in ruminants, as oppose to glucose absorbed from the small intestine in non-ruminants because of this difference in nutrient usage (Bao *et al.*, 2013). Furthermore, one of the most original features of the rabbit feeding behavior is the caecotrophy, which involves an excretion and immediate consumption of specific feces named soft feces or (caecotrophes). Consequently, the daily intake behavior of the rabbit is constituted of two meals, caecotrophes, and feeds (Bels, 2006).

Animals are classified into various types based on their habitats. Land Animals, such as sheep, cattle, and camel, live in homes and dairy farms. The second type of land animals is called

wild animals. They are called wild because human beings do not domesticate them as a rabbit, for instance (Qureshi *et al.*, 2012).

Generally, the esophagus is one of the first parts of the digestive system. In terms of function, the primary function of the esophagus is to transfer food and fluid from the oral cavity to the stomach. It is the only part of the digestive system which does not have metabolic, digest, and absorb functions. Kumar *et al.* (2009), reported that the esophagus is divided into cervical, thoracic, and abdominal. Histologically, it has four tunics layers (mucosa, submucosa, muscular, and adventitia), as seen in the digestive system (Aughey and Fry, 2001). The mucosa layer consists of three layers; the epithelium, the lamina propria, and the muscularis mucosa. The epithelium and lamina propria are separate by the basal lamina (Hussein *et al.*, 2016). However, the degree of keratinization of the esophagus depends on the animal's food (Alsafy and El-Gendy, 2012). Previously, Ahmed *et al.* (2009), observed that the epithelium of the esophagus of *Varanus niloticus* cover by ciliated columnar epithelium and mucous secreting goblet. Whereas, the submucosa is a thick layer of loose connective tissue containing collagen fibers, fibroblasts, and numerous blood vessels with large lumens (capillaries, arterioles, and venules) (Calamar *et al.*, 2014).

The esophageal muscular consists of two layers of muscle; in ruminants and dogs, the entire muscular tunic consists of skeletal muscles (Eurell and Frappier, 2006). The adventitia locates at the outer layer of the cervical and thoracic region. It was composed of loose connective tissue (Cui *et al.*, 2011). Gastrointestinal secretion in vertebrates contains several mucous substances that can vary according to cell type, functional status, anatomical region, pathological condition, sex, age, and species mucosubstances detect by many techniques (Choi *et al.*, 2003; Schumacher *et al.*, 2004). Many researchers have also been publishing about the microscopic structure for the esophagus in different species (Gupta and Sharma, 1991; Ali *et al.*, 2008; Islam *et al.*, 2008; Hameed *et al.*, 2018).

This study aimed to compare the histomorphometric and histochemical similarities of the esophagus of sheep (herbivorous ruminant) and rabbit (herbivorous and coprophagous).

2. MATERIALS AND METHODS:

2.1. Surgical Procedures

This study was carried out in the department of biology Sciences at the University of Misan. A total of ten sheep, adult males, were collected from local slaughterhouses. The esophageal samples were taken from different regions (the cervical, thoracic, and abdomen). A total of ten three months old, adult males rabbits weighting 1.5 - 2.5 kg were collected from Misan city. The experiments on rabbits followed the guidelines provided by the University's Animal Ethics Committee. The rabbits were raised under standard procedures and euthanized following the animal euthanization protocol. A physical examination was performed to all animals to guarantee they are all in the right health conditions before euthanasia. The euthanizing procedures were done by placing 2 mL of chloroform (CHCl₃) on cotton and then set on the nose of the animal, according to Blackshaw *et al.*, 1988. By using appropriate tools like scissors, tweezers, and scalpels, regional gross dissection was performed of each specimen. The abdomen of the rabbits was incised, and the esophagus extracted. After, segments of 1 cm from each esophagus were taken and from different parts (cervical, thoracic, and abdominal).

2.2. Histological examination

All esophagus samples of rabbits and sheep were fixed in 10% neutral buffered formalin promptly. After fixation for 72 hours, all samples were processed with a series of ascending ethanol concentrations (70% for 2h, 80% for 30min, 96% for 2h repeat three times, and the absolute 99% for 9h) then finally put them in absolute ethanol 99% for one hour to dehydrate. All samples were then cleared with xylene for one hour and embedded in paraffin wax to make paraffin blocks. Finally, sections were cut at the 7-micrometer thickness and processed with two stains (Luna, 1968). Hematoxylin and Eosin and Periodic Acid-Schiff (PAS) stains were used to stain all tissue sections for histomorphometry identification and carbohydrates determinations, respectively (Luna, 1968).

2.3. Micromorphometric measurements

Ten slides were made for each part of the esophagus (cervical, thoracic, and abdominal). To detect mucosa, submucosa, muscular, and serosa thickness, an optical microscope was employed with the exact ophthalmic scale (ocular micrometer) after the exact ophthalmic scale was matched with the theatrical scale using the magnification force (Galigher and Kozloff, 1964).

2.4. Statistical analysis

The values were expressed as mean \pm SD (standard deviation). The statistical analysis of the data was performed to know the significant differences using the t-test at $P < 0.05$ of probability (Al-Rawi and Khalaf Allah, 2000).

3. RESULTS AND DISCUSSION:

3.1. Histological study

In sheep and rabbits, all esophagus regions (cervical, thoracic, and abdominal) were their walls composed of four layers (Tunics): Mucosa, submucosa, muscular, and adventitia layer or serosa (Figures 1 and 2). Mucosa contains epithelium, lamina propria, and muscular mucosa; the findings showed variations in the form of mucosa epithelium lining the esophagus between sheep and rabbits. The epithelium lining consisted of a keratinized stratified squamous epithelium in sheep (Figure 3), while a non-keratinized stratified squamous epithelium was present in rabbit (Figure 4).

The epithelium layer of the ovine esophagus consisted of four cells. Stratum basale has a cuboidal or low columnar form and basophilic cytoplasm, while the last three strata (spinosum, stratum granulosum, and stratum corneum) have varied forms and are full of keratin (Figure 3). On the other hand, the epithelium of the esophagus of the rabbit is formed of three cells. Stratum basal are cuboidal or low columnar and are located below the stratified epithelium; cells in the intermediate layers of the epithelium are polyhedral and surface flattened; squamous cells lack keratin. The presence of keratin in the sheep that covers the stratified squamous epithelium may also be because these animals consume raw food. The presence of keratin on the surface of the epithelium supports its protection and this agreement with the Meyer and Schnapper study (2014), who suggest that keratinization of the epithelium plays an essential role in mechanical stabilization.

Malik and his team (2018) reported that lamina epithelium in sheep esophagus consists of keratinized stratified squamous epithelium with four regions, stratum corneum, stratum granulosum, stratum spinosum, and stratum basale. Besides, Mahmood *et al.* (2017) and (Boonzaier, 2012) reported that the epithelium lining of the esophagus is the non-keratinized stratified squamous epithelium. Eroschenko (2008) stated that the non-keratinized stratified

squamous epithelium layer of the esophagus consisted of three cells, squamous cells, polyhedral cells, and stratum basale. Furthermore, Ranjan and Das (2016) observed that the epithelium lining of the rabbit esophagus consists of keratinized stratified squamous epithelium. In both animals, the lamina propria formed from loose connective tissue contain elastic and collagen fibers, fibrocytes, and blood vessels. Many of dermal papillae appeared as finger-like extensions. The lamina propria was identified and was thicker in sheep than the rabbit (Figures 5 and 6).

The muscular mucosa consisted of smooth muscle fiber arranged longitudinally, and it was more thickness in sheep than in the rabbit (Figures 1 and 2). The muscular mucosa was located between lamina propria and submucosa, and it was identifiable along the length of the esophagus. This finding disagrees with the study of Selim *et al.* (2017), which observed that in the lactating rabbit, the muscular mucosa layer was absent, and this difference may be due age.

In both sheep and rabbits, the submucosa layer has loose connective tissue composed of interwoven collagen fiber, elastic fiber, fibrocytes, lymphocytes, and blood vessels with the adipose connective tissue in sheep denser of the rabbit. Also, no submucosal glands were observed throughout the length of the esophagus for both animals. These results are similar to the study of Hameed *et al.* (2018). According to Pawan *et al.*, 2009, the presence or absence of esophageal glands was dependent on gruff feed, especially vegetable fodder (Pawan *et al.*, 2009). On the other hand, this study disagrees with the results of Naghani and Andi (2012), which reported the presence of great submucosal glands throughout the length of the esophagus in a one-humped camel, and this difference in results might be due type food and species. However, Gupta and Sharma (1991) detected a seromucous tubuloalveolar gland in the initial portion of the esophagus in buffalo calves. Mahmood *et al.* (2017) observed glands in rabbits' esophagus. Regarding the information about the absence or presence of glands at the esophagus, the literature is contradictory and scarce. The glands are more numerous in certain animal species such as dogs and pigs and less abundant at humans (Shiina *et al.*, 2005).

The muscular layer was composed of two layers in both animals: the outer longitudinal layer and inner circular layer. Collagen and reticular fibers separated the two muscle layers from each other. Moreover, both sheep and rabbit tunica

muscular was composed of striated muscle throughout the cervical, thoracic, and abdominal region. Banks (1986) suggested that striated skeletal muscle might allow regurgitation to chew and also allow to push any foreign body toward the rumen faster. However, complete striated muscles had been reported in buffalo calves esophagus (Gupta and Sharma, 1991) and ruminants (Banks, 1986). Ranjan and Das (2016) wrote that tunic muscular in all rabbit esophagus regions are formed of striated muscle, and this finding matches with the results of this study. In the abdominal area, the adventitia layer consisted of loose connective tissue (Figures 9 and 10) slowly transformed into tunica serosa, which consists of loose connective tissue and a mesothelium layer. It matches with the study of Hussein *et al.* (2016).

3.2. Histomorphometric study

The thickness of sheep mucosa in the cervical ($629.91 \pm 109.97 \mu\text{m}$), thoracic ($657.90 \pm 56.93 \mu\text{m}$), and abdominal ($657.90 \pm 56.93 \mu\text{m}$) sections were significantly ($p < 0.05$) larger in comparison to the cervical, thoracic, and abdominal sections of the rabbits' esophagus where the values found were ($289.29 \pm 110.63 \mu\text{m}$), ($251.96 \pm 21.44 \mu\text{m}$) and ($312.62 \pm 45.61 \mu\text{m}$), respectively (Table 1). This finding might be related to the fact that the rabbit has epithelium of type non-keratinized stratified squamous epithelium.

The thickness of sheep submucosa in the cervical ($891.20 \pm 269.11 \mu\text{m}$), thoracic ($639.23 \pm 121.06 \mu\text{m}$), and abdominal ($513.26 \pm 83.75 \mu\text{m}$) sections were significantly ($p < 0.05$) larger in comparison to the same sections of the rabbits' esophagus ($429.27 \pm 227.84 \mu\text{m}$), ($319.62 \pm 85.22 \mu\text{m}$) and ($228.63 \pm 47.68 \mu\text{m}$), respectively (Figures 11, 12 and 17). This finding might be related to the physiological situation related to the blood supply, nervous and lymphatic system and the difference of species or back submucosa thickness of sheep once it has a great amount of adipose tissue.

In sheep, the submucosa thickness in the thoracic region was ($639.32 \pm 121.06 \mu\text{m}$) (Table 1). This result agrees with Malik *et al.* (2018), which observed that submucosa thickness in the thoracic region was ($645.5 \pm 46.93 \mu\text{m}$). In the same context, the thickness of the submucosa of the rabbit in the thoracic region was ($319.62 \pm 85.22 \mu\text{m}$) (Table 1). This finding, however, disagrees with the study of Kadhim (2019), which observed that the thick submucosa in this region of (*Herpestidae edwardsii*) was ($131 \pm 17.7 \mu\text{m}$). This difference might be related to the nature of

the nutrition intake of the animals.

The thickness of the muscular sheep layer in the cervical ($1572.41 \pm 97.27 \mu\text{m}$), thoracic ($1530.42 \pm 117.00 \mu\text{m}$), and abdominal ($1250.45 \pm 255.39 \mu\text{m}$) sections were significantly ($p < 0.05$) larger in comparison to the same sections of the rabbits' esophagus ($552.92 \pm 59.27 \mu\text{m}$), ($613.57 \pm 60.28 \mu\text{m}$) and ($424.60 \pm 70.24 \mu\text{m}$), respectively (Figures 7, 8 and Table 1). This finding might be related to a difference in the use of esophageal muscles; that is, to swallow food from the mouth to the top and again to return food from rumen to the mouth for rumination; and a third time to push food from the mouth to the stomach. There were non-significant ($p > 0.05$) differences between the thickness of the serosa in sheep and rabbit in the cervical and thoracic part. On the other hand, the thickness of the sheep abdominal part was significantly ($p < 0.05$) larger ($163.31 \pm 19.04 \mu\text{m}$) in comparison to the same section in the rabbits ($65.32 \pm 18.40 \mu\text{m}$) (Table 1).

3.3. Histochemical study

The results showed that the stratum corneum cells of stratified squamous keratinized of the mucosa layer had a strong reaction with PAS (Figure 13). In contrast, the rest of the mucosa layer cells had a moderate response with PAS in all regions of the sheep esophagus (Figures 15, 17, and 19). In the rabbit, it showed a strong reaction with PAS of the squamous cells of the mucosa layer (Figure 14). The rest of the mucosa layer cells had a moderate response with PAS in all regions of the rabbit esophagus (Figures 16, 18, and 20). This finding indicates that the presence of carbohydrates includes cytoplasm in these cells.

The results of this study are in agreement with Malik *et al.* (2018), which stated that the stratum corneum cells in sheep esophagus showed a strong reaction with PAS. Selim *et al.* (2017) observed that the response with PAS was a strong reaction with the inner layer of mucosa and moderate reaction with lamina propria in the esophagus rabbit. Ranjan and Das (2016) observed in rabbit esophageal that the epithelium and basement membrane performed a moderate PAS reaction. Igboke and Obinna (2016) observed in rope squirrel esophagus that the mucosal layer reacted moderately with PAS. In both animals, the submucosa showed weakly reaction with PAS in each region's esophagus in the cervical (Figures 15 and 16), thoracic (Figures 17 and 18), and abdominal (Figures 19 and 20).

This might be because of the absence of glands. In the same context, Nzalak *et al.* (2010) reported the esophagus of the African giant rat does not have glands in the submucosa layer. The mucous produced by the salivary glands might help protect the mucosal surface of the esophagus from sharp objects since the mucous barrier was also an essential factor in the protection of the esophagus from damage.

In sheep and rabbits, the muscular external layer reacted moderately with PAS in cervical, thoracic, and abdominal esophagus regions (Figures 19 and 20). This might be because of the presence of glycogen in the muscle-skeletal but in quantities not high. Listrat and his team (2016) detected that muscle-skeletal contain 1% of glycogen. The results of this study disagree with Selim *et al.* (2017) which observed a low reaction with PAS of the muscular layer. However, the serosa showed a weak reaction with PAS in the cervical, thoracic, and abdominal regions in both sheep and rabbits.

4. CONCLUSIONS:

In sheep and rabbits, the esophagus is composed of four layers: mucosa, submucosa, muscular, and adventitia layer or serosa. The epithelium layer of the ovine esophagus consisted of four cells, and the epithelium lining consisted of a keratinized stratified squamous epithelium. In comparison, the epithelium of the rabbit esophagus is formed of three cells, and a non-keratinized stratified squamous epithelium was present. In both animals, no submucosal glands were observed throughout the length of the esophagus. The mucosa, submucosa, and the muscular layer thickness were significantly larger for sheep than rabbits. There were non-significant differences between the thickness of serosa in sheep and rabbit. The stratum corneum cells showed a strong reaction with PAS. A strong response with PAS was also observed in the squamous cells of the mucosa layer in rabbits. The rest of the mucosa layer cells showed a moderate reaction with PAS in all regions, both to the rabbit and sheep esophagus.

5. ACKNOWLEDGMENTS:

The authors want to thank the head of the Department of Biology at the College of Science for his cooperation.

6. REFERENCES:

1. Agrawal, A. R., Karim, S. A., Kumar, R., Sahoo, A., and John, P. (2014). Sheep and goat production: basic differences, impact on climate and molecular tools for rumen microbiome study. *International Journal of Current Microbiology and Applied Sciences*, 3(1), 684-706.
2. Ahmed, Y. A., El-Hafez, A. A. E., and Zayed, A. E. (2009). Histological and histochemical studies on the esophagus, stomach and small intestines of *Varanus niloticus*. *Journal of veterinary anatomy*, 2(1), 35-48.
3. Ali, M. N., Byanet, O., Salami, S. O., Imam, J., Maidawa, S. M., Umosen, A. D., Alphonsus, C., and Nzalak, J. O. (2008). Gross anatomical aspects of the gastrointestinal tract of the wild African giant pouched rat (*Cricetomys gambianus*). *Scientific Research and Essays*, 3(10), 518-520.
4. Al-Rawi, K. M., and Khalaf Allah, A. M. (2000). Design and Analysis of Agricultural Experiments. University of Mosul. Ministry of Higher Education and Scientific Research. Dar Al Kuttab for printing and publishing. *Mosul. Iraq*.
5. Alsafy, M. A. M., and El-Gendy, S. A. A. (2012). Gastroesophageal junction of Anatolian shepherd dog; a study by topographic anatomy, scanning electron and light microscopy. *Veterinary research communications*, 36(1), 63-69.
6. Aughey, E., and Frye, F. L. (2001). *Comparative veterinary histology with clinical correlates*. CRC Press.
7. Banks, w.J. (1986). *Applied Veterinary Histology*. (3rded.), Mosby Year Book, Baltimore.
8. Bao, H., Kommadath, A., Sun, X., Meng, Y., Arantes, A. S., Plastow, G. S., and Stothard, P. (2013). Expansion of ruminant-specific microRNAs shapes target gene expression divergence between ruminant and non-ruminant species. *BioMed Center genomics*, 14(1), 609.
9. Bels, V. L. (Ed.). (2006). *Feeding in domestic vertebrates: from structure to behaviour*. Cabi.

10. Blackshaw, J. K., Fenwick, D. C., Beattie, A. W., and Allan, D. J. (1988). The behaviour of chickens, mice and rats during euthanasia with chloroform, carbon dioxide and ether. *Laboratory Animals*, 22(1), 67-75.
11. Boonzaier, J. (2012). *Morphology and mucin histochemistry of the gastrointestinal tracts of three insectivorous mammals: Acomys spinosissimus, Crocidura cyanea and Amblysomus hottentotus* (Doctoral dissertation, Stellenbosch: Stellenbosch University).
12. Calamar, C. D., Patruica, S., Dumitrescu, G., Bura, M., Dunea, I. B., and Nicula, M. (2014). Morpho-histological study of the digestive tract and the annex glands of Chinchilla laniger. *Scientific Papers Animal Science and Biotechnologies*, 47(1), 269-274.
13. Choi, B. Y., Sohn, Y. S., Choi, C., and Chae, C. (2003). Lectin histochemistry for glycoconjugates in the small intestines of piglets naturally infected with *Isospora suis*. *Journal of veterinary medical science*, 65(3), 389-392.
14. Crowley, E. J., King, J. M., Wilkinson, T., Worgan, H. J., Huson, K. M., Rose, M. T., and McEwan, N. R. (2017). Comparison of the microbial population in rabbits and guinea pigs by next-generation sequencing. *PloS one*, 12(2), e0165779.
15. Cui, D., Daley, W. P., Fratkin, J. D., Haines, D. E., Lynch, J. C., Naftel, J. P., and Yang, G. (2011). *Atlas of histology: with functional and clinical correlations*. Wolters Kluwer/Lippincott Williams & Wilkins.
16. Eroschenko, V. P. (2008). *DiFiore's atlas of histology with functional correlations*. Lippincott Williams & Wilkins.
17. Eurell, J.A. and Frappier, B.L. (2006). *Dellmann's Textbook of Veterinary Histology*. 3rd ed, Black well Publishing Limited. pp 190.
18. Furness, J. B., Cottrell, J. J., and Bravo, D. M. (2015). Comparative gut physiology symposium: comparative physiology of digestion. *Journal of animal science*, 93(2), 485-491.
19. Galigher, A. E., and Kozloff, E. N. (1964): *Essentials of practical microtechnique*. 1st ed. lea and febiger. Philadelphia, pp:40-45.
20. Gupta, S.K. and Sharma, D.N. (1991). Regional histology of the oesophagus of buffalo calves. *Indian Journal. Animals. Science*. 61:722-724.
21. Hameed, B. K., Ebraheem, A. H., and Hussein, F. A. (2018). Histological structure of the cervical segment oesophagus in goats and sheep (Comparison study). *Tikrit Journal of Pure Science*, 23(1), 55-60.
22. Hristov, H., Kostov, D., and Vladova, D. (2006). Topographical anatomy of some abdominal organs in rabbits. *Trakia Journal of Sciences*, 4(3), 7-10.
23. Hussein, A. J., Cani, M. M., and Hussein, D. M. (2016). Anatomical and histological studies of esophagus of one-humped camel (*Camelus dromedarius*). *Mirror of Research in Veterinary Sciences and Animals*, 5, 11-8.
24. Igbokwe, C. O., and Obinna, S. J. (2016). Oesophageal and gastric morphology of the African Rope Squirrel *Funisciurus anerythrus* (Thomas, 1890). *Journal of Applied Life Sciences International*, 1-9.
25. Islam, M.S., Awal, M.A., Quasem, M.A., Asaduzzaman, M. and Das, S.K. (2008). Histology of esophagus of Black Bengal goat. Bangladesh. *Journal. Veterinary. Medicine.*, 3(2): 152-154.
26. Kadhim, K. K. (2019). Histomorphology and Histochemical Study of Esophagus and Stomach in Grey MongOOSE (*Herpestes edwardsii*) In Iraq. *Indian Journal of Natural Sciences*, 9(52): 16458-16475.
27. Kingston-Smith, A. H., Marshall, A. H., and Moorby, J. M. (2013). Breeding for genetic improvement of forage plants in relation to increasing animal production with reduced environmental footprint. *Animal: an international journal of animal bioscience*, 7 Suppl 1, 79–88.
28. Kumar, P., Mahesh, R and Kumar, P. (2009). Histological architecture of esophagus of goat (*Capra hircus*). *Haryana veterinary.*, 48: 29-32.
29. Listrat, A., Lebre, B., Louveau, I., Astruc, T., Bonnet, M., Lefaucheur, L., and Bugeon, J. (2016). How muscle structure and composition influence meat and flesh quality. *The Scientific World Journal*, 2016.

30. Luna, L.G. (1968). *Manual of Histologic Staining Methods of the Armed Forces Institute of Pathology*. 3rd ed., McGraw Hill Book Co., New York, pp. 368.
31. Mahmood, H. B., Al-aameli, M. H., and Obead, W. F. (2017). Histological study of esophagus in dogs and rabbits. *Journal of Kerbala University*, 15(3), 55-62.
32. Malik, S. A., Rajput, R., Rafiq, M., Farooq, U. B., and Gori, H. (2018). Histomorphological and Histochemical Studies on Esophagus in Gaddi Sheep (*Ovis aries*). *The Indian Journal Of Veterinary Science And Biotechnology*, 14(2), 22-27.
33. Meyer, W. and Schnapper, A. (2014). Keratinization of the esophageal epithelium of domesticated mammals. *Acta Histochemica*, 116(1): 235-242.
34. Mi, L., Yang, B., Hu, X., Luo, Y., Liu, J., Yu, Z., and Wang, J. (2018). Comparative analysis of the microbiota between sheep rumen and rabbit cecum provides new insight into their differential methane production. *Frontiers in microbiology*, 9, 575.
35. Naghani, S.E. and Andi, A.M. (2012). Some histological and histochemical study of the esophagus in one-humped camel. *Global. Veterinary*, 8(2): 124-127.
36. Nzalak, J. O., Onyeanus, B., Samuel, A. O., Voh, A. A., and Ibe, C. S. (2010). Gross Anatomical, Histological and Histochemical Studies of the Esophagus of the African Giant Rat (AGR) (*Cricetomys gambianus*-Waterhouse, 1840). *Journal of Veterinary Anatomy*, 3(2), 55-64.
37. Pawan, K., Mahesh, R., and Kumar, P. (2009). Histological architecture of esophagus of goat (*Capra hircus*). *Haryana Veterinarian*, 48, 29-32.
38. Qureshi, S. S., Jamal, M., Qureshi, M. S., Rauf, M., Syed, B. H., Zulfiqar, M., and Chand, N. (2012). A review of halal food with special reference to meat and its trade potential. *Journal Animal Plant Sciences*, 22 (2 Suppl), 79-83.
39. Ranjan, R and Das, P (2016). Gross Morphology and HistoArchitecture of Rabbit Esophagus. *The Indian Veterinary Journal*, (05) : 40 – 44.
40. Schumacher, U., Duku, M., Katoh, M., Jörns, J., and Krause, W. J. (2004). Histochemical similarities of mucins produced by Brunner's glands and pyloric glands: A comparative study. *The Anatomical Record Part A: Discoveries in Molecular, Cellular, and Evolutionary Biology: An Official Publication of the American Association of Anatomists*, 278(2), 540-550.
41. Selim, A., Hazaa, E., and Goda, W. (2017). Comparative histological studies of the esophagus wall of *Oryctolagus cuniculus* rabbit adult, young and lactating using light microscope. *Journal of Cytology and Histology*, 8, 456.
42. Shiina, T., Shimizu, Y., Izumi, N., Suzuki, Y., Asano, M., Atoji, Y., Nikami, H., and Takewaki, T. (2005). A comparative histological study on the distribution of striated and smooth muscles and glands in the esophagus of wild birds and mammals. *Journal of veterinary medical science*, 67(1), 115-117.

Table 1. Mean thickness of mucosa, submucosa, muscularis, and adventitia in Cervical, Thoracic, and Abdominal regions of the esophagus of the sheep and rabbit.

Thickness	Thick mucosa		Thick submucosa		Thick muscularis		Thick serosa	
Esophagus	Sheep Mean ±SD	Rabbit Mean ±SD	Sheep Mean ±SD	Rabbit Mean ±SD	Sheep Mean ±SD	Rabbit Mean ±SD	Sheep Mean ±SD	Rabbit Mean ±SD
Cervical region	629.91 ^a ± 109.97	289.29 ^b ± 110.63	891.20 ^a ± 269.11	429.27 ^b ± 227.84	1572.41 ^a ± 97.27	552.92 ^b ± 59.27	100.29 ^a ± 15.72	93.32 ^a ± 26.93
Thoracic region	657.90 ^a ± 56.93	251.96 ^b ± 21.44	639.23 ^a ± 121.06	319.62 ^b ± 85.22	1530.42 ^a ± 117.00	613.57 ^b ± 60.28	100.29 ^a ± 15.72	83.98 ^a ± 25.07
Abdominal region	657.90 ^a ± 56.93	312.62 ^b ± 45.61	513.26 ^a ± 83.75	228.63 ^b ± 47.68	1250.45 ^a ± 255.39	424.60 ^b ± 70.24	163.31 ^a ± 19.04	65.32 ^b ± 18.40

Notes: *value represent (mean± SD); *different letters refer to (p<0.05) significant difference between values;
*the similar letters refer to non-significant (p>0.05) difference between values.

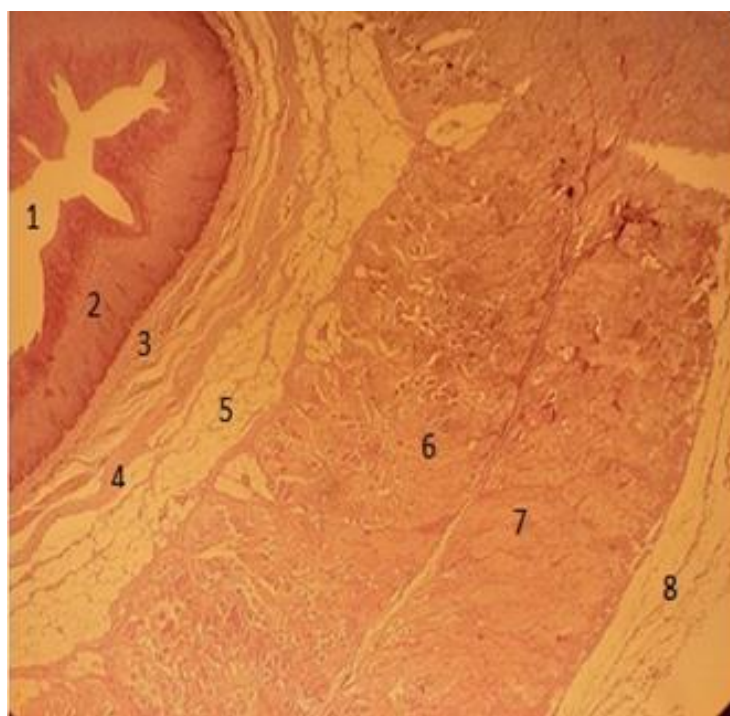


Figure 1. The esophagus of the sheep. (1) lumen, (2) stratified squamous epithelium layer (keratinized), (3) lamina propria, (4) muscularis mucosa, (5) submucosa, (6) circular muscularis layer, (7) longitudinal, (8) serosa. H&E.40X.

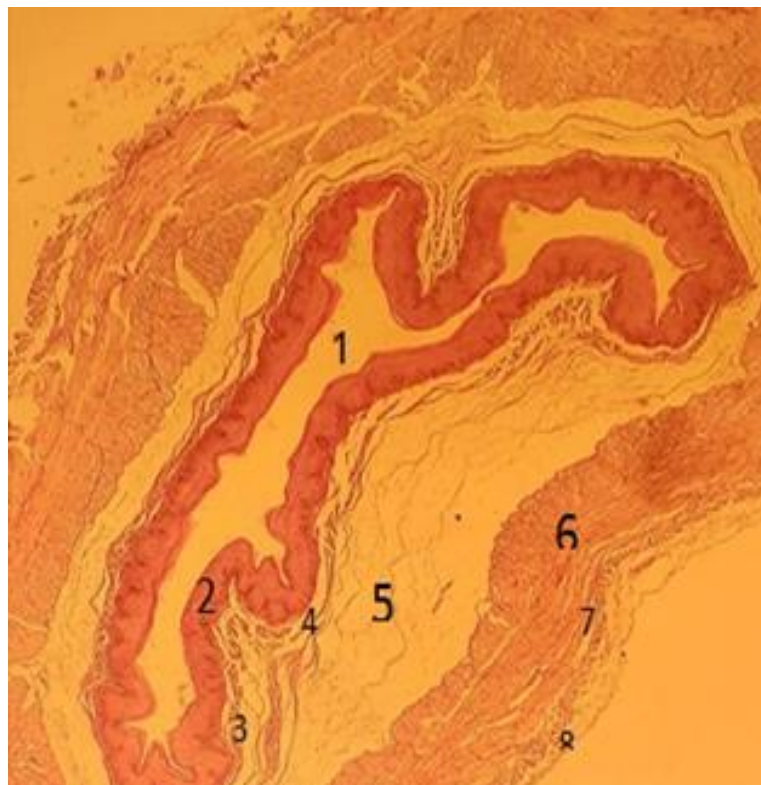


Figure 2. The esophagus of the rabbit. (1) leumin, (2) stratified squamous epithelium layer (non-keratinized), (3) lamina propria, (4) muscularis mucosa. (5) submucosa muscularis layer (6) circular muscularis (7) longitudinal, (8) serosa. H&E.40X

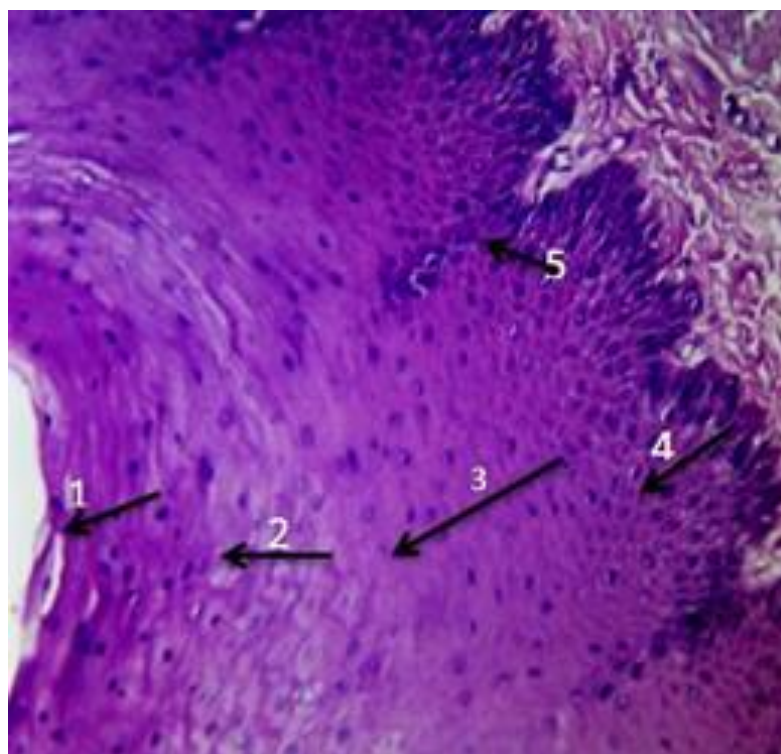


Figure 3. The esophagus of the sheep showing a stratified squamous epithelium layer (keratinized), including four cells (1) Stratum corneum full keratin, (2) Stratum granulosum, (3) Stratum spinosum, (4) stratum basale, and the (5) dermal papillae. H&E .100X

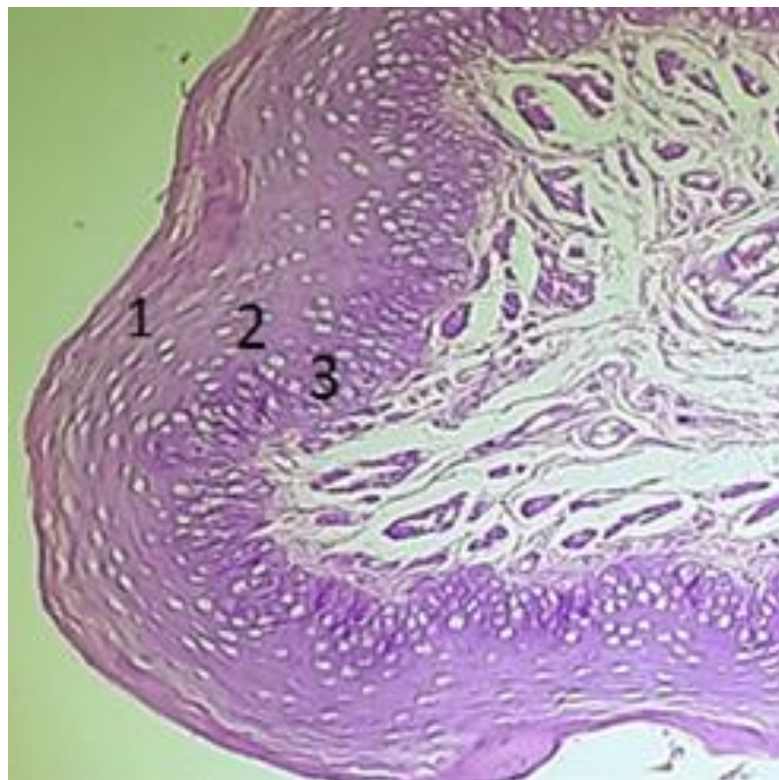


Figure 4. The esophagus of the rabbit showing a stratified squamous epithelium layer (non-keratinized) consisting of three cells (1) Squamous cells, (2) polyhedral cells and, (3) stratum basale. H&E. 100X

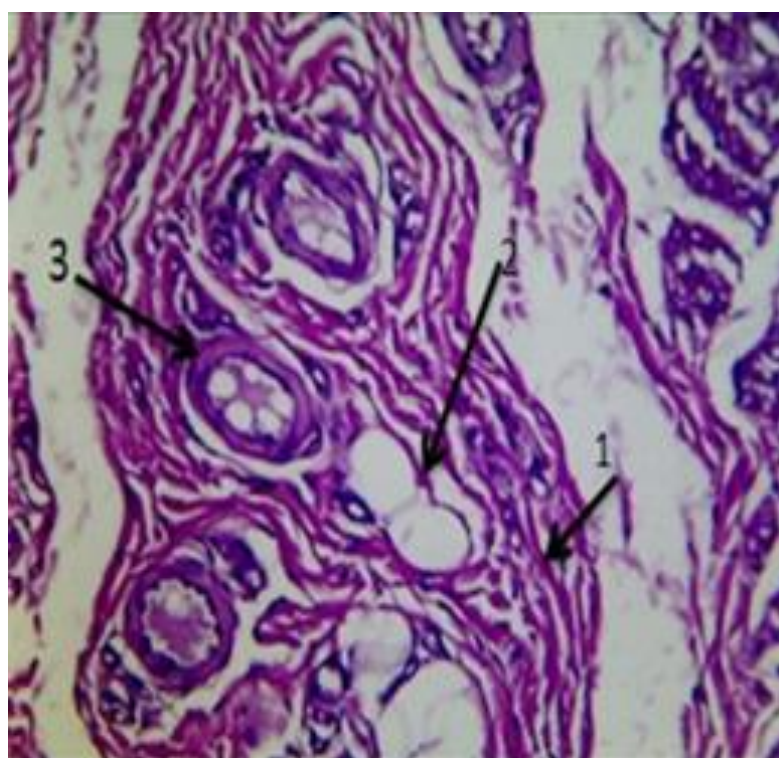


Figure 5. The esophagus of the sheep showing lamina propria consisting of loose connective tissue contains (1) fiber, (2) fat cells and, (3) blood vessels. H&E 100X.

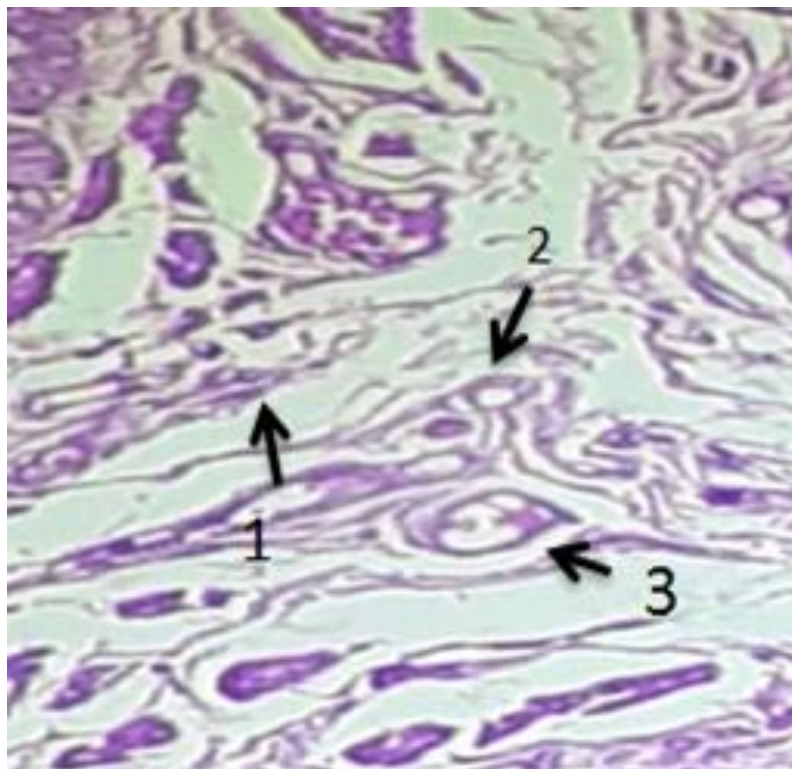


Figure 6. The esophagus of the rabbit showing lamina propria consist of loose connective tissue containing (1) fiber, (2) fat cells and, (3) blood vessels. H&E 100X.

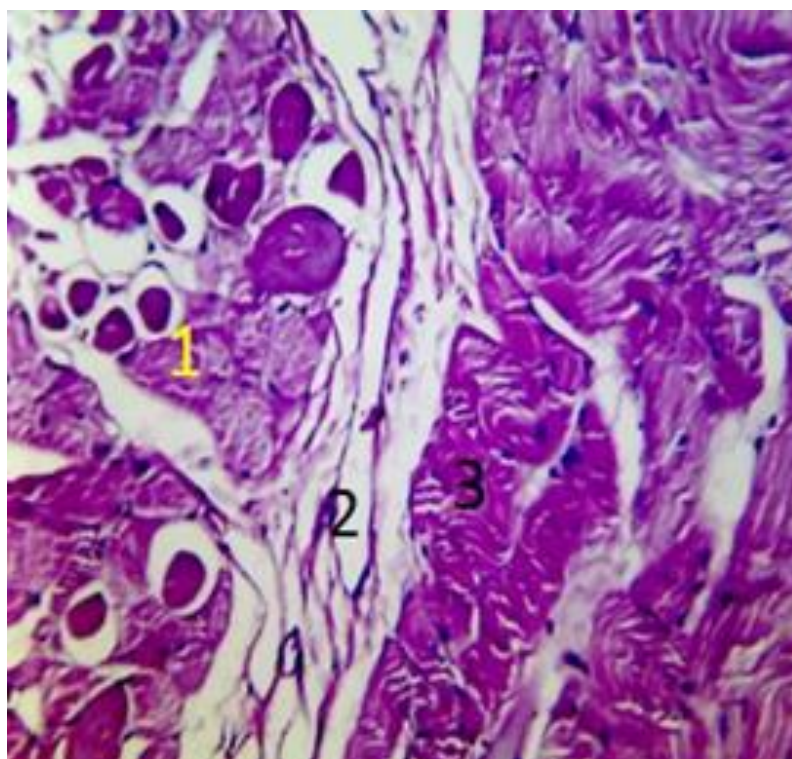


Figure 7. The cervical esophagus region of the sheep showing (skeletal muscle) (1) circular muscularis, (2) connective tissue, and (3) longitudinal muscularis. H&E.100x

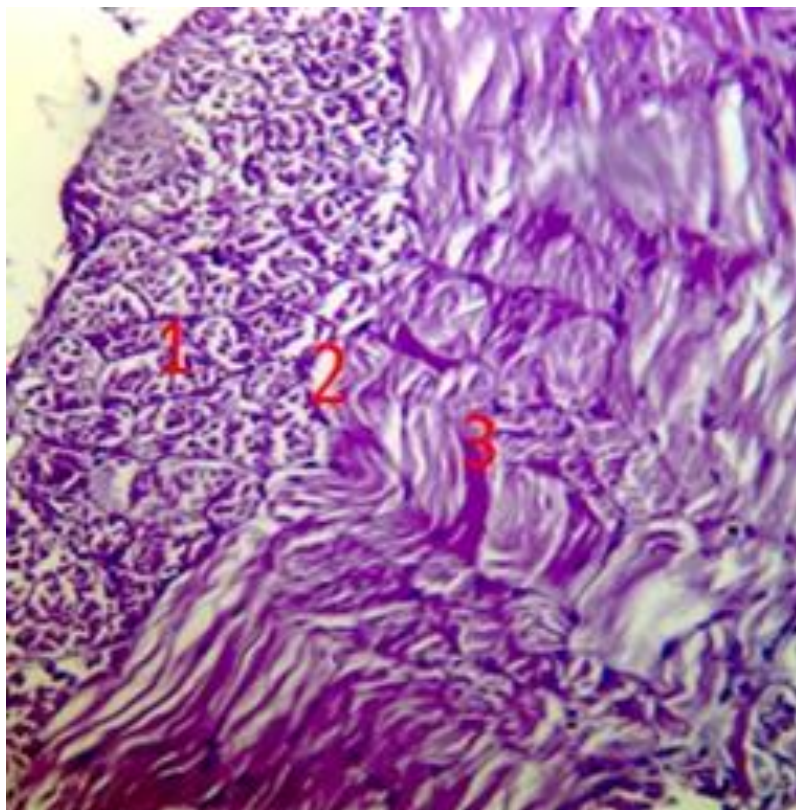


Figure 8. The cervical esophagus region of the rabbit showing (skeletal muscle). (1) circular muscularis, (2) connective tissue and, (3) longitudinal muscularis. H&E.100x

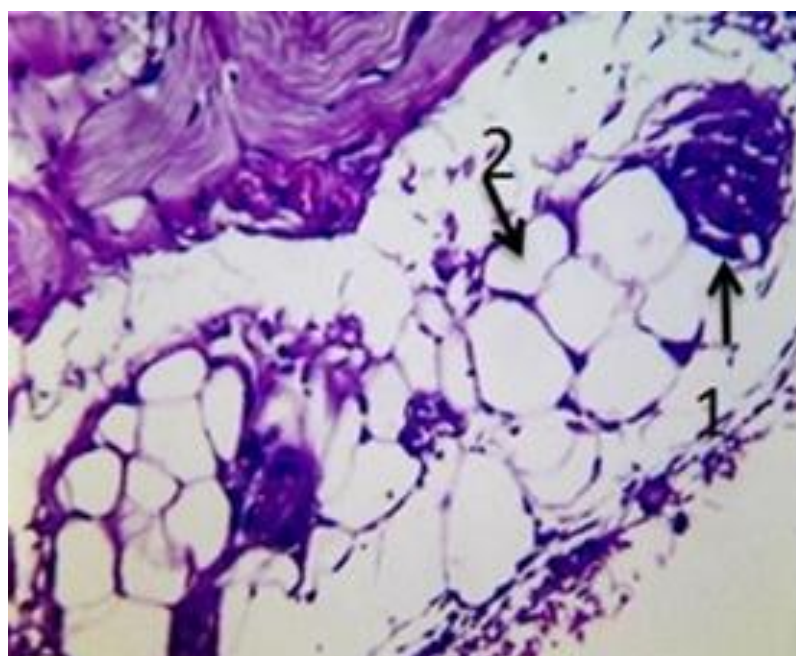


Figure 9. The esophagus of the sheep showing serosa consisting of (loose connective tissue) and containing (1) blood vessels and (2) fat cells. H&E 100X

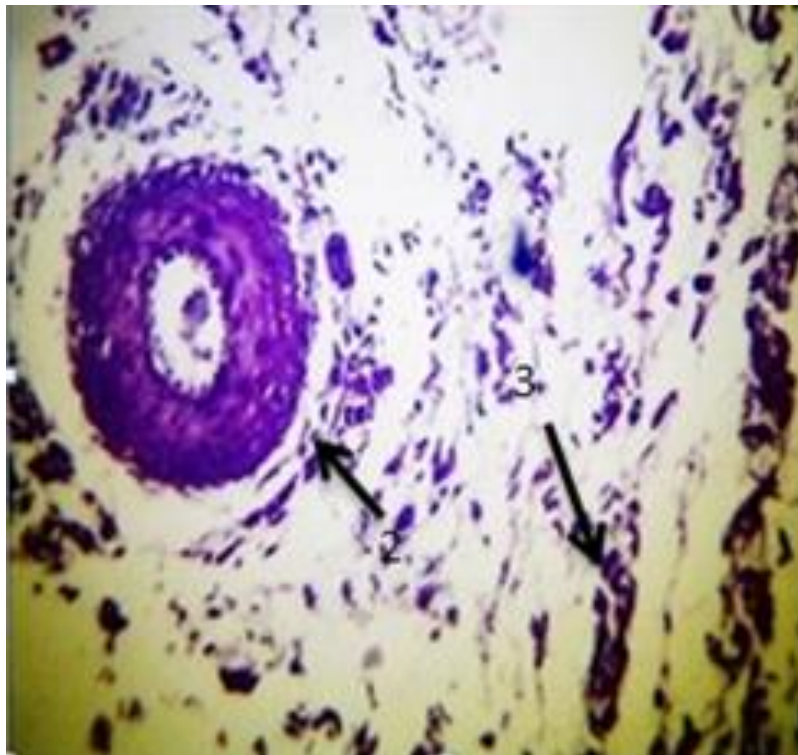


Figure 10. The esophagus of the rabbit showing serosa consisting of (loose connective tissue) and containing (1) blood vessels and (2) fibers. H&E 100X

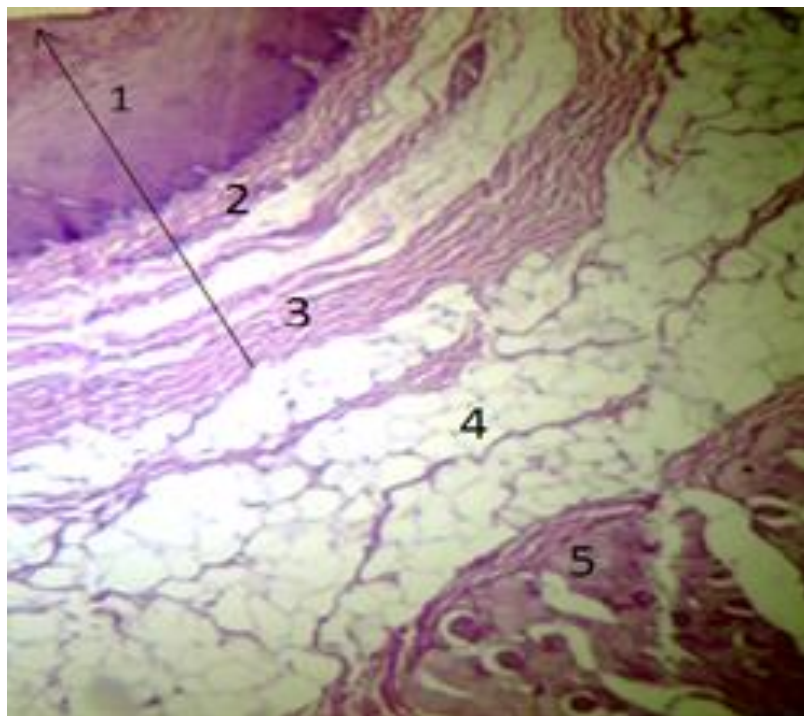


Figure 11. The abdominal esophagus region of the sheep showing (1) stratified squamous epithelium layer (keratinized layer), (2) lamina propria, (3) muscularis mucosa, (4) submucosa and (5) muscularis .H&E 100X

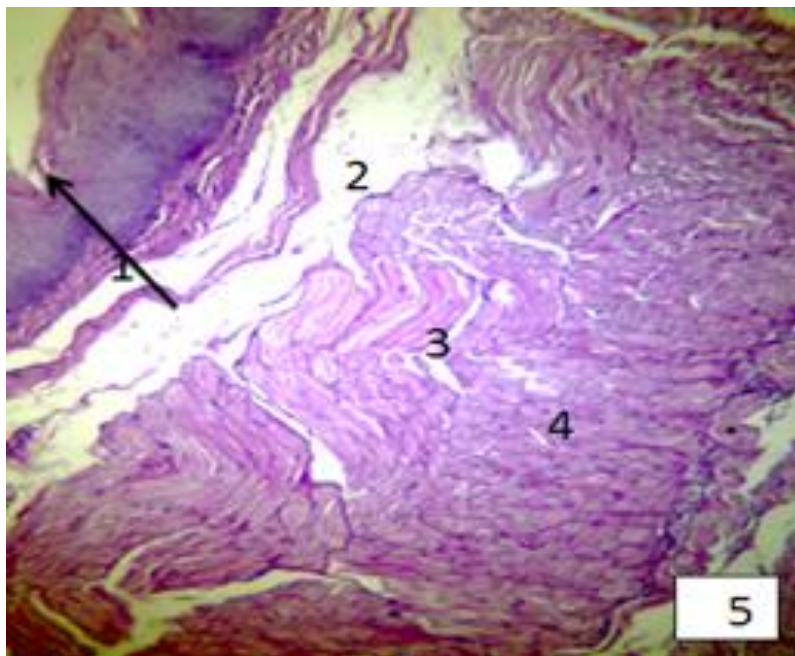


Figure 12. The abdominal esophagus region of the rabbit showing (1) mucosa, (2) submucosa skeletal muscle including (3) circular muscularis, (4) longitudinal muscularis and (5) serosa. H&E100X

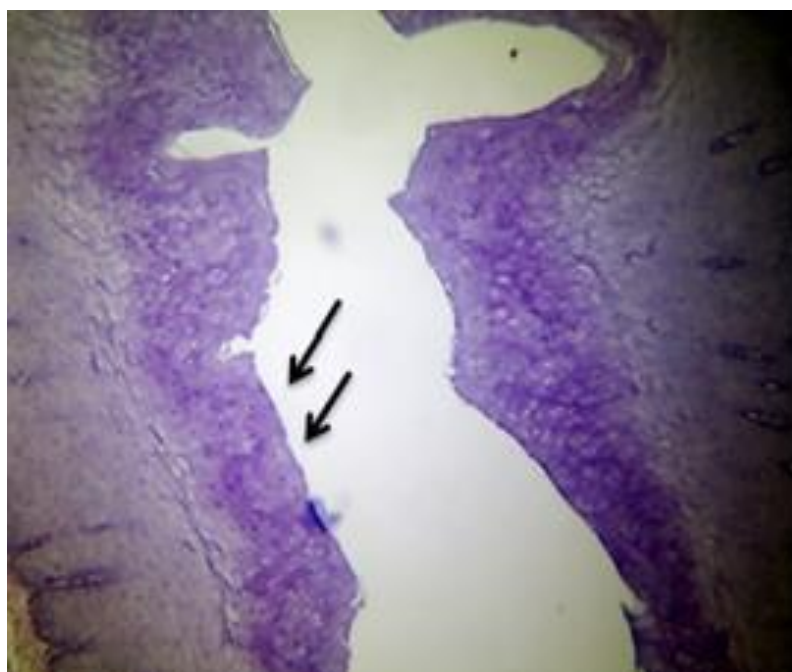


Figure 13. The esophagus of the sheep showing Stratum corneum cells of keratinized stratified squamous epithelium layer with a strong reaction with PAS 100X.

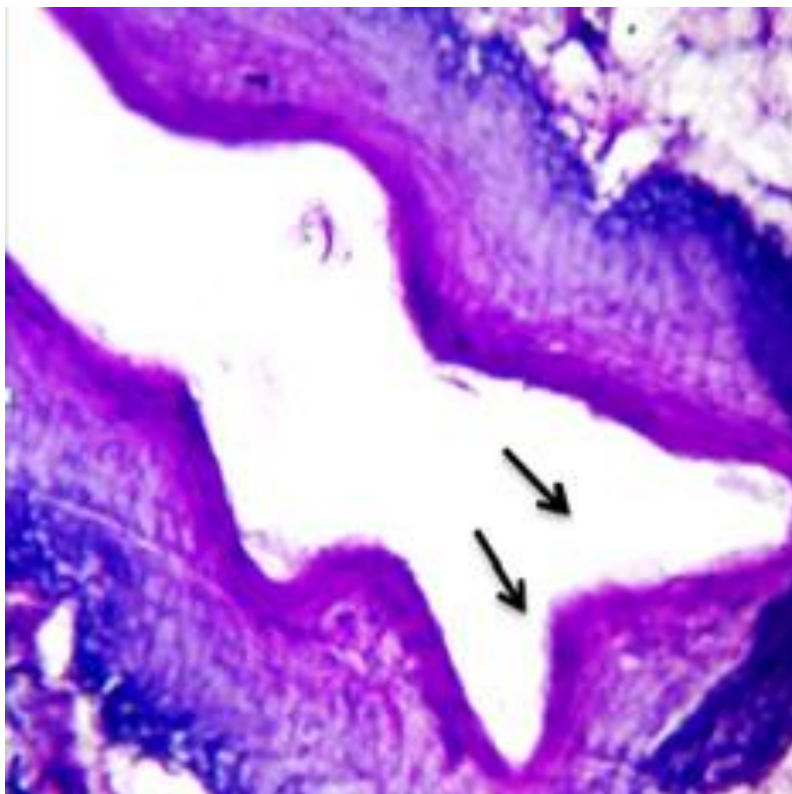


Figure 14. The esophagus of the rabbit showing Squamous cells of non- keratinized stratified squamous epithelium layer with strong reaction with PAS 100X.

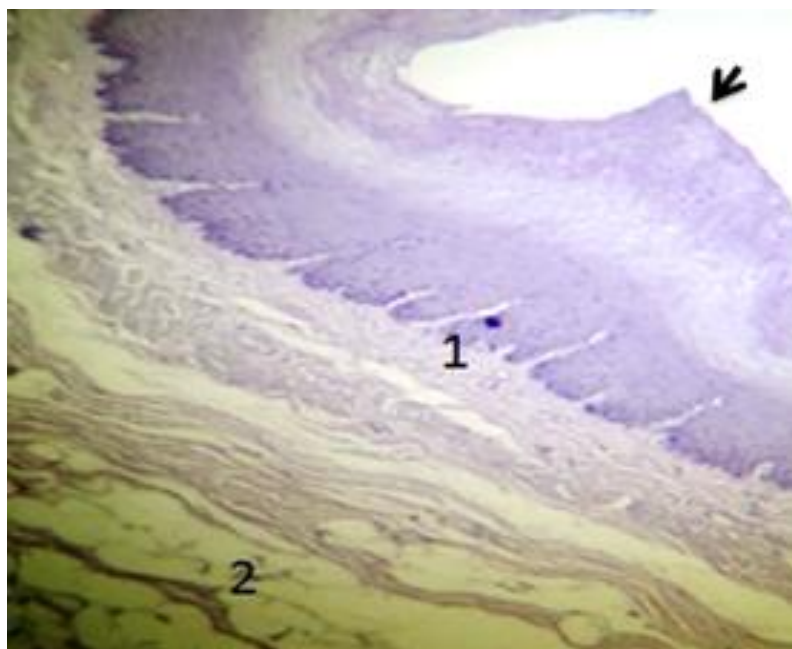


Figure 15. The cervical esophagus region of the sheep showing (arrow black) corneum cells with a strong reaction with PAS. (1) mucosa cells (except for corneum cells) with a moderate reaction with PAS and (2) submucosa with a weak reaction with PAS 100X.

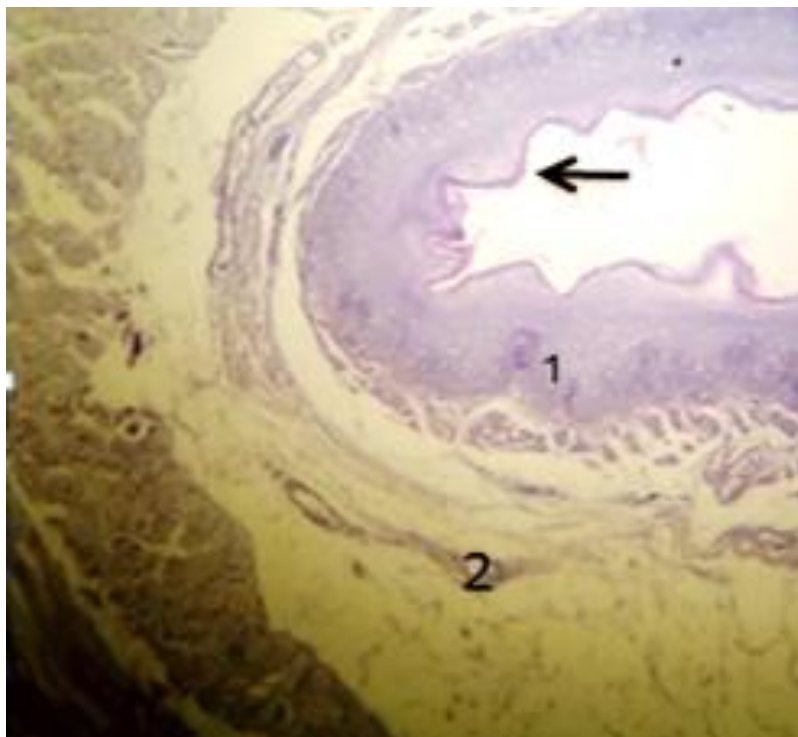


Figure 16. The cervical esophagus region of the rabbit showing (arrow black) squamous cells with a strong reaction with PAS, (1) mucosa cells layer (except for squamous cells) with a moderate reaction with PAS and (2) submucosa layer with a weak reaction with PAS 100X.

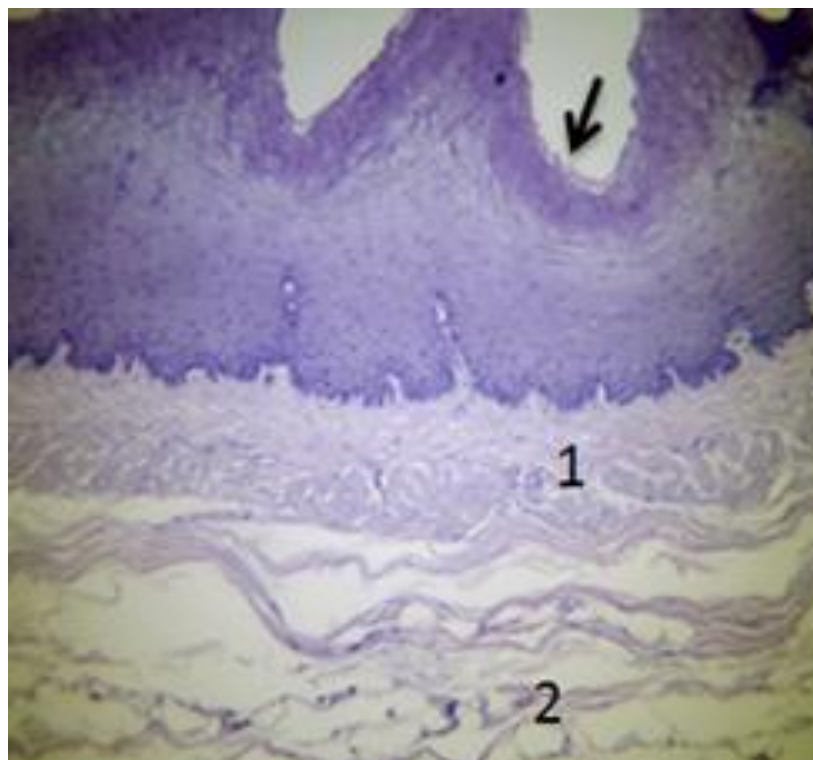


Figure 17. The thoracic esophagus region of the sheep showing (arrow black) corneum cells with a strong reaction with PAS, (1) mucosa cells (except for corneum cells) with a moderate reaction with PAS, (2) submucosa with a weak reaction with PAS 100X.

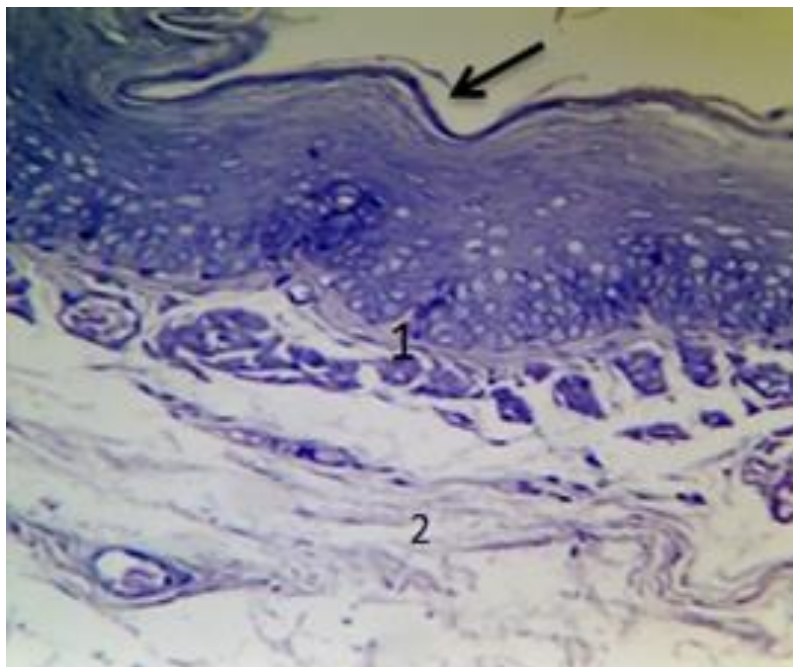


Figure 18. The thoracic esophagus region of the rabbit showing (arrow black) squamous cells with a strong reaction with PAS, (1) mucosa cells (except for squamous cells) with a moderate reaction with PAS, (2) submucosa with a weak reaction with PAS 100X.

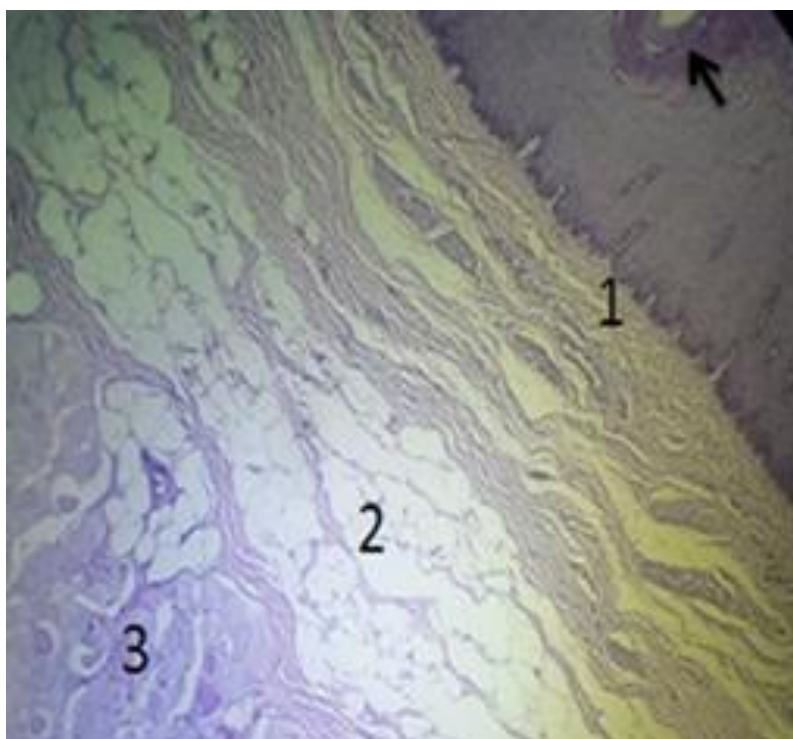


Figure 19. The abdominal esophagus region of the sheep showing (arrow black) corneum cells with a strong reaction with PAS, (1) mucosa cells (except for corneum cells) with a moderate reaction and (2) submucosa with a weak reaction with PAS, (3) muscularis with a moderate reaction with PAS 100X.

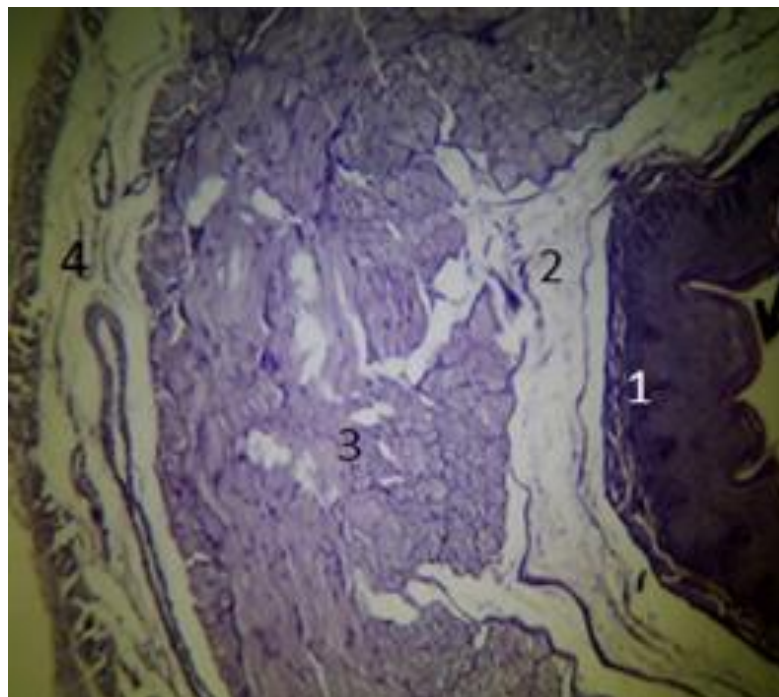


Figure 20. The abdominal esophagus region of the rabbit showing (arrow black) squamous cells with a strong reaction with PAS, (1) mucosa cells (except for squamous cells) with a moderate reaction, (2) submucosa and serosa with a weak reaction with PAS, (3) muscularis with a moderate reaction with PAS 100X.

AVALIAÇÃO DOS NÍVEIS DE VITAMINA D3 E DE ZINCO EM CRIANÇAS IRAQUIANAS COM DEFICIÊNCIA DO HORMÔNIO DE CRESCIMENTO E SUA RELAÇÃO COM OUTROS PARÂMETROS BIOQUÍMICOS**EVALUATION OF VITAMIN D3 AND ZINC LEVELS IN IRAQI CHILDREN WITH GROWTH HORMONE DEFICIENCY AND THEIR RELATION WITH OTHER BIOCHEMICAL PARAMETERS****تقييم مستوى فيتامين D3 والزنك لدى الأطفال العراقيين المصابين بنقص هرمون النمو وعلاقتها بالمتغيرات الحيوية الكيميائية**FALIH, Israa Qusay^{1*}; TAHIR, Noor Thair²; AL-JEDDA, Walaa Ahmed³¹ Department of Chemistry, College of Science, University of Misan, Maysan, Iraq.² National Diabetic Center, University of Mustansiriyah, Baghdad, Iraq.³ Department of Clinical Biochemistry, College of Medicine, University of Mustansiriyah, Baghdad, Iraq.

* Corresponding author

e-mail: israaqusai@uomisan.edu.iq

Received 31 August 2020; received in revised form 18 September 2020; accepted 11 October 2020

RESUMO

Há suspeita de deficiência de hormônio do crescimento (GHD) em indivíduos com baixa estatura (SS) e velocidade de crescimento diminuída, nos quais outras causas de baixo crescimento foram excluídas. O próprio hormônio do crescimento tem ação estimuladora direta sobre a produção de vitamina D3. O metabolismo da vitamina D e do hormônio do crescimento influencia um ao outro. O nível de zinco também desempenha um regulador essencial do crescimento ósseo e da via de crescimento potencial. Um total de 50 crianças com idades entre 4 e 12 anos com deficiência de hormônio do crescimento participaram deste estudo. Elas foram comparadas com 38 crianças saudáveis como grupo controle. Este estudo foi realizado durante o período de setembro de 2019 a junho de 2020. Os pacientes frequentavam o Centro Nacional de Diabéticos / Universidade AL-Mustansiriyyah, Bagdá, Iraque. Hormônio do crescimento, fator de crescimento semelhante à insulina-1, teste de função tireoidiana, nível de cortisol, vitamina D3, nível de zinco, açúcar no sangue em jejum e perfil lipídico foram medidos em crianças com deficiência de hormônio do crescimento. Uma diferença não significativa foi encontrada no hormônio do crescimento basal entre os pacientes com deficiência e controle do hormônio do crescimento. Houve uma diminuição altamente significativa no nível do hormônio do crescimento após 1 hora (provocação com clonidina) ($p < 0,001$) e uma diminuição significativa no nível do hormônio do crescimento após 1:30 horas (provocação com clonidina) ($p < 0,01$) em pacientes com deficiência de crescimento hormonal em comparação com o grupo controle. Além disso, foi observada uma diminuição altamente significativa ($p < 0,001$) dos níveis de fator de crescimento semelhante à insulina-1 em pacientes com deficiência de hormônio do crescimento quando comparados ao controle. Foi observado ainda que houve uma diminuição significativa ($p < 0,001$) nos níveis de Zn e vitamina D em pacientes com deficiência de hormônio do crescimento em comparação com o controle além de a distribuição dos níveis de vitamina D e zinco ter aumentado mais nas mulheres do que nos homens. Pode-se concluir que houve uma diminuição altamente significativa nos níveis de vitamina D e Zn em pacientes com deficiência de hormônio do crescimento em comparação com o grupo controle. A deficiência dos níveis de vitamina D e zinco pode desempenhar um papel importante na patogênese de crianças em crescimento com distúrbio do hormônio do crescimento

Palavras-chave: *Hormônio do crescimento, IGF-1, teste de função tireoidiana, cortisol.***ABSTRACT**

Growth hormone deficiency (GHD) is suspected in subjects with short stature (SS) and decreased growth velocity in whom other causes of low growth have been excluded. The growth hormone itself has a direct stimulatory action on the production of vitamin D3. Both vitamin D and growth hormone metabolism influences each other. Zinc level also plays an essential regulator of bone growth and potential growth pathway. A total of 50 children aging 4-12 years old with growth hormone deficiency have participated in this study. They were

compared with 38 healthy children as a control group. This study was conducted during the period from September 2019 to June 2020. The patients were attending the National Diabetic Center/ AL-Mustansiriyah University, Baghdad, Iraq. Growth hormone, insulin-like growth factor-1, thyroid function test, cortisol level, vitamin D3, zinc level, fasting blood sugar, and lipid profile were measured in children with growth hormone deficiency. A non-significant difference was found in basal growth hormone between patients of growth hormone deficiency and control. There was a highly significant decrease in growth hormone level after 1 hour (provocation with clonidine) ($p < 0.001$) and a significant decreased in growth hormone level after 1:30 hours (provocation with clonidine) ($p < 0.01$) in patients of growth hormone deficiency compared to the control group. Also, it was observed a highly significant decrease ($p < 0.001$) of insulin-like growth factor-1 levels in growth hormone deficiency patients when compared to control. It was also observed that there was a significant decrease ($p < 0.001$) in the levels of Zn and vitamin D in patients with growth hormone deficiency compared to the control in addition to the distribution of the levels of vitamin D and Zinc have increased more in women than in men. It can be concluded that there was a highly significant decrease in vitamin D and Zn levels in patients with growth hormone deficiency compared to the control group. The deficiency of vitamin D and zinc levels may play an essential role in the pathogenesis of growing children with a growth hormone disorder.

Keywords: Growth hormone, IGF-1, thyroid function test, cortisol.

الملخص:

الأشخاص ذوي القامة القصيرة يشتبه لديهم نقصان في هرمون النمو وانخفاض سرعه النمو المتمثل بضعف النمو لديهم. يمتلك هرمون النمو نفسه تأثير مباشر وتحفيزي على إنتاج فيتامين D3، حيث يؤثر كل منها على الآخر. يلعب مستوى الزنك أيضا دورا تنظيميا مهم لنمو العظام ومسار النمو. شارك في هذه الدراسة خمسون طفلا يعانون من نقص هرمون النمو، حيث تراوحت أعمارهم بين (الأربع – اثني عشر) سنة مع ثمانية وثلاثين طفلا من الأصحاء كمجموعة ضابطة لأجل المقارنة. أجريت هذه الدراسة خلال الفترة من أيلول ٢٠١٩ الى حزيران ٢٠٢٠ وكان المرضى يترددون على المركز الوطني للسكري والغدد الصماء الجامعة المستنصرية في بغداد العراق. تم قياس هرمون النمو وهرمون النمو الشبيه بالانسولين 1 واختبار وظائف الغدة الدرقية ومستوى الكورتيزول وفيتامين D3 ومستوى الزنك، سكر الدم الصائم وصور الدهون عند الأطفال الذين يعانون من نقص هرمون النمو. أظهرت الدلالة ان هناك نقصان عالي في الدلالة المعنوية لتحليل هرمون النمو بعد مرور ساعه من التحفيز بدواء الكلوندين (0,001) ونقصان في الدلالة المعنوية لتحليل هرمون النمو بعد مرور ساعه ونصف من التحفيز بدواء الكلوندين (0,01) لدى المرضى المصابين بنقص هرمون النمو مقارنة مع الأطفال الأصحاء. كذلك نقصان عالي في الدلالة المعنوية (0,001) في هرمون النمو الشبيه بالانسولين 1 لدى المرضى المصابين بنقص هرمون النمو مقارنة مع الأطفال الأصحاء. وجد أيضا انخفاض معنوي ($p < 0.001$) بمستويات الزنك وفيتامين D3 لدى الأطفال المصابين بنقص هرمون النمو مقارنة بالأصحاء وان توزيع مستويات الزنك وفيتامين D3 ظهرت لدى الاناث أكثر تركيزا من الذكور. بالإمكان الاستنتاج ان هنالك انخفاض كبير في مستويات فيتامين D3 ومستوى الزنك لدى الأطفال الذين يعانون من نقص هرمون النمو مقارنة مع الأصحاء وان فيتامين D3 ومستوى الزنك يمكن ان يلعبوا دورا رئيسيا ومهم في نسبة اضطراب هرمون النمو لدى الأطفال المصابين بنقص النمو.

الكلمات المفتاحية: هرمون النمو، هرمون النمو الشبيه بالانسولين-1، اختبار وظائف الغدة الدرقية، مستوى الكورتيزول.

1. INTRODUCTION:

The human growth rate depends on genetic, environmental, and nutritional factors; complex processes are calculated about this rate by diagnostic bone tissue accretion (Nilsson *et al.*, 2005). The first computational steps of growth rates begin in fetal life and end in adolescence (Frank, 2003). The main hormone that contributes to growth at every stage of growth is growth hormone (GH). Some children have what is known as a constitutional delay of growth and puberty (CDGP). This is the most common cause of short stature and pubertal delay in males. Typically they have slowed linear growth within the first three years of life (Carani *et al.*, 1997). The assessment in children with short stature is to identify the subgroup of children with pathologies (such as Turner syndrome, inflammatory bowel disease, other primary systemic diseases, or growth hormone deficiency) (Grote, 2007). Growth hormone deficiency (GHD) is a medical condition that occurs when missing or reducing for growth hormone, created in the pituitary gland to excite

the body to grow (Rikken *et al.*, 1995). Perhaps, a diminishing in growth hormone gets by genetic mutations, abnormalities on the hypothalamus or pituitary gland during evolution, or destructive the pituitary (Parkin *et al.*, 2020). Therefore, children wounded many symptoms, mostly short stature. Other abnormal growth hormone deficiency situations may be occurred during infancy or later in childhood (Stanley, 2012). GHD may be isolated or combined with other anterior and/or posterior hormonal deficiencies. GHD is a rare but important cause of short stature in children (Dattani and Malhotra, 2019).

The incidence of congenital GHD with male predominance is 1 out of 4000 to 1 out of 10,000 live births (Kautsar *et al.*, 2019). The most important effect of growth hormone administration in humans is a marked increase in free fatty acids that influence stimulating lipolysis and ketogenesis after 1-2 hours. This stimulation constitutes a major physiological adaptation of stress and fasting (Møller *et al.*, 2003). Children with GHD reveal a tendency towards a lipid disturbance. Also, growth hormone (GH) levels are inversely

correlated with abdominal fat mass. Therefore, GHD causes increased abdominal fat, unusual carbohydrate, and lipid metabolism (Al-hindawi *et al.*, 2020).

The direct effects of growth hormone on protein metabolism are demonstrated by the stimulation of insulin-like growth factor 1 (IGF-1). This hormone focuses on tissue anabolism. When growth hormone deficiency occurs during fasting or any other catabolic conditions, it increases protein loss and urea production rates by 50% with a corresponding increase in muscle protein separation (Moller *et al.*, 2009). Vitamin D3 is a fat-soluble vitamin. The major vitamin D source is exposure to sunlight that can be endo synthesized under the skin during the irradiation ergosterol and 7-dehydro cholesterol compounds by ultraviolet-B (UVB) ray coming from the sun (Nair and Maseeh, 2012). It is possible to raise the level of vitamin D in the body by consuming some foods or nutritional supplements (Silva and Furlanetto, 2018). The association between vitamin D level and IGF is very complicated. The regular value of vitamin D is essential to the growing bone well.

Meanwhile, increases or decreases in growth hormone affect the expected growth process (Esposito *et al.*, 2019). Many present biological studies focused on the biochemical interaction between vitamin D and the GH/IGF-1 axis in humans (Wei, *et al.*, 1998). Vitamin D's effect with GH metabolism relates together and increases IGF-1 levels through taken vitamin D supplementation orally. IGF-1 updates the action of the 1 α -hydroxylase enzyme responsible for regulating vitamin D 1,25(OH)₂D or cholesterol yields from the kidney (Henry, 2011). Further, GH itself has a direct stimulatory action on the production of 1,25(OH)₂D (Esposito *et al.*, 2019).

Research showed an increase in malnutrition, an autoimmune disorder, and fatalities among children who had zinc deficiency. Thus, the metal's decrement value had been essentially related to the impairment of growth, anorexia, delay in wound healing, immunosuppressive, memory, and testicular functions (El-Shazly *et al.*, 2015). The metabolism of thyroid hormones, androgens, and growth hormone are inversely related to the lack of zinc (Esposito *et al.*, 2019). It looks that the zinc levels in the body critically control bone growth, restoration, and bone formation outside the womb through uncertain mechanisms (Şıklar *et al.*, 2003).

The evaluation also assesses the severity of short stature and potential growth pathway to

facilitate decision-making about the intervention, if appropriate. The growth hormone is the first cause, but several hormones indirectly lead to the same situation (Yuen *et al.*, 2019). Growth hormone is manufactured in the pituitary gland under the influence of growth hormone-releasing hormone (GHRH), which is the main hormone for growth sanitary. Because of its action, all body tissue is affected by stimulating the hepatocytes to release the protein IGF-1 (Romero *et al.*, 2012), which, in turn, affects the bone ends, helping them to grow. Other hormones have a dyscrasia in their levels of blood. The growth retardation is caused indirectly by the thyroid-stimulating hormone (TSH). This hormone is manufactured in the pituitary gland. It stimulates the thyroid gland to produce its hormones that regulate the body's metabolism processes, while the Adrenocorticotrophic hormone (ACTH) stimulates the adrenal gland to produce cortisol.

The growth hormone employs adipose tissue to increase lipolysis and perform a high release of free fatty acids into the blood (Vottero *et al.*, 2013). Children with GHD bring out a disposition towards a lipid disturbance. On the other hand, GH levels are inversely correlated with abdominal fat mass (Zhang *et al.*, 2016). As a result, GHD causes increased abdominal fat, unusual carbohydrate, and lipid metabolism (Bengtsson, 1997). GH has a known effect on lipid conditions. A single dose of external GH will increase the amount of Free Fatty Acids (FFA) and ketone bodies in the circulatory system (Moller *et al.*, 1990). Also, its most prominent role was by stimulated lipolysis in the adipose tissue primarily by promoting hormone-sensitive lipase (HSL) (Vijayakumar *et al.*, 2010; Dietz and Schwartz, 1991). However, it has been shown that the effect on lipoprotein lipase (LPL) is either suppressive or non-existent, indicating that GH plays a minor role in lipid uptake of adipose tissue (Vijayakumar *et al.*, 2011).

On the other hand, LPL expression is regulated by GH in the skeletal muscles, which leads to the absorption of free fatty acids and enhances the use of fats as fuel (Oscarsson *et al.*, 1999a). The same mechanism also appears in the liver where growth hormone also enhances its (HL) activity (Hoogerbrugge *et al.*, 1993; Oscarsson *et al.*, 1999b). The increasing cortisol level in the blood leads to a developmental disorder in children (Kojima and Kangawa, 2005; Walter *et al.*, 2012).

This study aimed to assess vitamin D3 and zinc levels in Iraqi children with growth hormone

deficiency and its relation with other biochemical parameters.

2. MATERIALS AND METHODS:

A total of 88 serum sample participants (50 children for basal measurements of GH and IGF-1 with growth hormone deficiency compared with 38 children as healthy control) were selected from the outpatient department of the National Diabetes center/ AL- Mustansirya University, Baghdad, Iraq. The patients were diagnosed by an endocrinology specialist as a short stature with a growth hormone deficiency, with age ranged between (4-12) years, from September 2019 to June 2020.

2.1. Ethical approval

All patients and their families were informed about the aim and the suspected benefit of the study before obtaining their agreements for participation according to the medical research and ethical regulation. Oral consent was taken from all enrolled participants and their families.

2.2. Exclusion Criteria:

All information was obtained directly by medical history in a private interview by the authors, including family history. All subjects were not receiving GH or any medications that interfere with IGF-1 analyses. Also, participants with renal diseases, liver diseases, malignant disorders, diabetes mellitus, and other diseases.

2.3. Measurement

2.3.1 Sample collection

5 ml of blood was drawn from each child through a vein puncture using disposable syringes and collected in a gel tube. Blood samples were collected from each participant between 8:30-11 a.m. after overnight fasting. Then, the blood samples were centrifuged at 3000 rpm for 10 minutes. The resulting serum was stored at -20 °C until the time of analysis. Samples were analyzed at the National Center for Diabetes and Endocrinology at Al- Mustansiriya University. Orally clonidine was chosen to stimulate GH secretion (Topper *et al.*, 1984).

2.3.2 Anthropometric Measurements:

The body mass index was calculated from the subjects studied by the following (Eq. 1)

(Simon *et al.*, 2005).

$$\text{BMI} = \text{weight (kg)} / \text{length (m}^2\text{)} \quad \text{Eq. 1}$$

2.3.3 Biochemical Assessment:

All biochemical assessment was estimated enzymatically using the colorimetric following the protocol of the available kits supplied by BIOLABO/France.

2.3.3.1 Determination of Fasting Blood Sugar (FBS):

Serum FBS was measured according to Trinder method (Trinder, 1969).

Reagents of the test

Components	Quantity
R1: REAGENT Phosphate Buffer	150 mmol/L
Glucose oxidase (GOD)	> 20 000 UI/L
Peroxidase (POD)	> 1000 UI/L
4-Amino-antipyrine (PAP)	0.8 mmol/L
Chloro-4-phenol	2 mmol/L
R2: STANDARD Glucose	100 mg/dL = 5.55 mmol/L

Procedure

	Automated analyzer	Manual procedure
Reagent	300 µL	1000 µL
Standard, Controls, Samples	3 µL	10 L

After mixing well, the tubes were incubated for 10 minutes at 37°C and performed a read absorbance at 500 nm against reagent blank.

Normal values: Children 60-100mg/dL

2.3.3.2 Determination of Serum Total Cholesterol (TC)

The method for the measurement of total cholesterol in serum involves the use of three enzymes; cholesterol esterase (CE), cholesterol oxidase (CO), and peroxidase (POD). In the serum sample, cholesterol concentration is estimated according to the formation of a quinone imine colored complex. The quantity of this pink dye Quinonimine complex is proportional to the cholesterol concentration (Allain *et al.*, 1974; Richmond, 1973).

Reagents of the test

Components	Quantity
R1: BUFFER	
Phosphate buffer	100 mmol/L
Chloro-4-phenol	5 mmol/L
Sodium Cholate	2.3 mmol/L
Triton x 100	1.5 mmol/L
R2: ENZYMES	
Cholesterol oxidase (CO)	> 100 IU/L
Cholesterol esterase (CE)	> 170 IU/L
Peroxidase (POD)	> 1200 IU/L
4 - Amino – antipyrine (PAP)	0.25 mmol/L
PEG 6000	167 µmol/L
R3: STANDARD	
Cholesterol	200 mg/dL (5.17 mmol/L)

Procedure

	Blank	Standard	Assay
Reagent	1 mL	1 mL	1 mL
Demineralized water	10 µL		
Standard		10 µL	
Specimen			10 µL

The above mixtures were well mixed for 5 minutes at 37°C, and then the sample absorption (test) was displayed at 500 nm against the reagent blank.

Normal values: <200 mg/dL

2.3.3.3 Determination of Serum Triacylglycerol (TG)

The method is based on serum triglyceride's enzymatic hydrolysis to glycerol and free fatty acids (FFA) by lipoprotein lipase (LPL).

Reagents of the test

Components	Quantity
R1: BUFFER	
PIPES	100 mmol/L
Magnesium chloride	9.8 mmol/L
Chloro-4-phenol	3.5 mmol/L
R2: ENZYMES	
Lipase	> 1000 IU/L
Peroxidase (POD)	> 1700 IU/L
Glycerol 3 phosphate oxidase (GPO)	> 3000 IU/L

Glycerol Kinase (GK)	> 660 IU/L
4 - Amino – antipyrine (PAP)	0.5 mmol/L
Adenosine triphosphate Na (ATP)	1.3 mmol/L
R3: STANDARD	
Glycerol	mmol/L
Equivalent to triolein or triglycerides	200mg/dL (2.28mmol/L)

Procedure

	Blank	Standard	Assay
Reagent	1 mL	1 mL	1 mL
Demineralized water	10 µL		
Standard		10 µL	
Specimen			10µL

The above mixtures were well mixed for 5 minutes at 37°C, and then the sample absorption (test) was displayed at 500 nm against the reagent blank.

Normal values: Reference range 35 - 160 mg/dL

2.3.3.4 Determination of Serum High-Density Lipoprotein-Cholesterol (HDL-C)

Serum HDL is directly measured using the accelerator selective detergent methodology. In this method, during the first stage, the LDL, VLDL, and chylomicrons generate free cholesterol, which produces hydrogen peroxide through an enzymatic reaction. The resulting peroxide is consumed by the reaction of peroxidase with the DSBmT, yielding a colorless product. In the second phase, specific detergent solubilizes HDL-Cholesterol. In conjunction with CO and CE action, POD + 4-AAP develops a colored reaction proportional to HDL-Cholesterol concentration.

2.3.3.5 Determination of Serum Low-Density Lipoprotein-Cholesterol (LDL-C)

LDL was calculated indirectly by using the Friedewald's equation (Friedewald *et al.*, 1972).

$$\text{LDL-C} = \text{TC} - [\text{HDL-C} + \text{TAG}/5].$$

This equation is only accurate when TG levels are below 400 mg/dl.

2.3.3.6 Determination of blood urea (B. Urea)

Urea is hydrolyzed in the presence of water

and urease to produce ammonia and carbon dioxide. The ammonia formed in the first reaction combines with a oxoglutarate and NADH to form glutamate and NAD⁺ (Mayo *et al.*, 1995).

Reagents of the test

Components	Quantity
R1: TRIS BUFFER Tris pH 7.9 + 0.1 at 30°C	80 mmol/L
Oxoglutarate	5 mmol/L
R2: ENZYME/COENZYME NADH Urease GLDH	≥ 0,2 mmol/L 20000 IU/L ≥ 1200 IU/L
R3: STANDARD Urea	40 mg/dL (6.66 mmol/L)

Procedure

	Standard	Assay
Reagent	1 mL	1 mL
Standard	5 µL	
Specimen		5 µL

Mix and after 30 seconds record absorbance A1 at 340 nm and then absorbance A2 after 90 seconds.

Normal values: 11-39 mg/dL.

2.3.3.7 Determination of serum creatinine concentration

Creatinine in an alkaline solution reacts with picric acid to form a colored complex. The complex formed amount is directly proportional to the creatinine concentration (Bernard *et al.*, 2015).

Reagents of the test

Components	Quantity
R1: BASE Disodium Phosphate Sodium hydroxide	6.4 mmol/L 150 mmol/L
R2: DYE Sodium dodecyl sulfate Picric acid	0.75 mmol/L 4.0 mmol/L pH 4.0
R3: STANDARD	177 µmol/L (2 mg/dL)

Procedure

	Blank	Standard	Assay
Working reagent (R1 + R2)	1 mL	1 mL	1 mL

Demineralized water	100 µL		
Standard		100 µL	
Specimen			100 µL

After mixing well for 30 seconds, the absorbance A1 at 490 nm against reagent blank was recorded.

2.3.3.8 Determination of serum Zinc concentration

Reagents of the test

Components	Quantity
Standard (St.)	200 mg/dl (30.6 mmol/l)
Reagent (R)	5-Br-PAPS (0.02 mmol/L) Bicarbonate buffer pH (9.8 200 mmol/L) Sodium Citrate (170 mmol/L) Dimethylglyoxime (4 mmol/L) Detergent (1 %)

Procedure

	Blank	Slandered	Sample
Reagent	1 ml	1 ml	1 ml
Slandered		50 ml	
Sample			50 ml

Normal values: Children: 90 - 160 µg/dl

2.3.4 Hormonal Assessment

Mini Vidas device was used to do the thyroid profile assay (bioMérieux / France) Kit

2.3.4.1 Determination of triiodothyronine (TT3)

Procedure

1. The required reagents were removed from the refrigerator and allowed for at least 30 minutes to reach the room temperature.
2. For each sample to be tested, one T3 strip and one T3 SPR were used. After removing the requirement of SPRs, the storage pouch was thoroughly released.
3. A volume of 100 µl from calibrator control with samples was mixed and samples by using a vortex type mixer
4. T3 SPRs and T3 strips were inserted into VIDAS instrument, then the color labels with assay code were matched. All assay steps were done by VIDAS instrument automatically.

5. The test was finished in about 40 minutes, then, SPRs and strips were removed from the VIDAS instrument and disposed into an appropriate recipient.
6. Once the test was finished, findings automatically evaluated by the computer and expressed in nmol/l or µg/dl.

Normal values:

1-5 years (1.54-11.40) nmol/L
 5-10 years (1.62-4.14) nmol/L
 10-15 years (1.45-3.71) nmol/L

2.3.4.2 Determination of tetraiodothyronine (TT4):

Procedure

1. The required reagents were taken out from the refrigerator and allowed for at least 30 minutes to reach room temperature.
2. For each sample to be tested, one T4 strip and one T4 SPR were used. The storage pouch was carefully released after removing the required
3. A volume of 100 µl from calibrator control and samples were mixed using a vortex type mixer.
4. T4 SPRs and T4 strips were inserted into VIDAS instrument, then the color of the labels with assay code on the SPRs reagent strip were matched and all assay steps were done automatically by VIDAS instrument.
5. The test was completed in about 40 minutes, then the SPRS and strips were removed from the VIDAS instrument and placed in the appropriate recipient.
6. Once test was finished, the findings were automatically evaluated by the computer and expressed in nmol/l or µg/dl.

Normal values:

1-5 years (94-194) nmol/L
 5-10 years (83-172) nmol/L
 >10 years (60-160) nmol/L

2.3.4.3 Determination of Thyroid Stimulation Hormone (TSH)

Procedure

1. The necessary reagents were taken out of the refrigerator and allowed for at least 30 minutes to arrive at room temperature.

2. For each sample to be tested, one TSH strip and one TSHSPR were used. The storage pouch was carefully released after the required SPRs were removed.
3. A volume of 100 µl of a calibrator control and samples were mixed using a vortex type mixer.
4. TSH SPRs and TSHs trips were inserted into VIDAS instrument, then the color labels with assay code on the SPRs and the reagent strips were matched. All assay steps were done automatically by VIDAS instrument.
5. The assay was completed within approximately 40 min; then, the SPRs and strips were removed from the VIDAS instrument and disposed into the appropriate recipient.
6. Once the test was finished, the findings were automatically evaluated by the computer and expressed in µIU/ml.

Normal values:

- Euthyroid: 0.25 - 5 µIU/ml
 - Hyperthyroid: < 0.15 µIU/ml
 - Hypothyroid: > 7 µIU/ml

2.3.4.4 Determination of Cortisol:

Procedure

1. The necessary reagents were taken away from the refrigerator and allowed for at least 30 minutes to arrive at room temperature.
2. For each sample to be tested, one cortisol strip and one cortisol SPR were used. The storage pouch was released after the required SPRs have been removed.
3. A volume of 100 µl of a calibrator control and samples were mixed using a vortex type mixer.
4. Cortisol SPRs and cortisol strips were inserted into VIDAS instrument, then the color labels with assay code on the SPRs and the reagent strips were matched. All assay steps were done automatically by VIDAS instrument.
5. The assay was completed within approximately 40 min; then, the SPRs and strips were removed from the VIDAS

instrument and disposed into the appropriate recipient.

6. Once the test finished, the findings were automatically evaluated by the computer and expressed in ng/mL or nmol/L.

Normal values:

- Morning (8-10 a.m.): 54.94 – 287.56 ng/mL.
- Afternoon (4-7 p.m.): 24.61 – 171.52 ng/mL.

2.3.4.5 Determination of Human Growth Hormone (Hgh)

Human growth hormone (hGH) is determined using a sandwich chemiluminescence immunoassay technique supplied by Liaison/DiaSorin/ Italy Kit.

Procedure:

Liaison/ DiaSorin Analyzer is used to the quantitative determination of hGH. The operations of the assay are as follows:

1. The response module was provided with calibrators, control, or samples.
2. Covered magnetic elements were dispensed.
3. The conjugate was dispensed into the reaction module.
4. The tubes were incubated.
5. The washing step of the tubes was done with wash –system liquid.
6. Starter kit was added, and the light emitted was measured.
7. Once the test was finished, the results automatically calculated and hGH concentration were determined in ng/ml.

Normal values (<7 ng/ml) after clonidine stimulation tests are considered as indicative of GHD (Lowe and Anderson, 2015).

2.3.4.6 Determination of Insulin-Like Growth Factor-1(IGF-1)

The method for the quantitative determination of IGF-1 is based on a one-step sandwich chemiluminescence immunoassay technique supplied by Liaison/DiaSorin/ Italy Kit (Cole and Kramer, 2016).

Procedure:

Liaison/ DiaSorin Analyzer is used to the quantitative determination of IGF-1. The operations of the assay are as follows:

1. Samples or controls were dispensed into the reaction module.
2. The acidification solution was dispensed.
3. Diluted samples, diluted controls or calibrator were dispensed into the reaction Module.
4. Coated magnetic particles (Solid Phase), neutralization buffer, and conjugate were dispensed.
5. Samples were incubated.
6. Washing was done with wash/system Liquid.
7. The starter reagent was added, and the light emitted was measured.
8. The analyzer automatically calculates IGF-1 concentrations for the unknown samples in ng/ml.

Normal values: < 5 years (30-160) ng/ml, 5-10 years (135-385) ng/ml 10-18 years (165-620) ng/ml

2.3.5 Determination of Vitamin D3

The Mini VIDAS 25-OH Vitamin D Total Assay design is based on a 2-step competitive immunoassay.

1. Serum or plasma 25(OH)D is dissociated from its protein carrier (DBP) then added to alkaline-phosphatase (ALP)conjugated Vitamin D-specific antibody.
2. Unbound ALP-antibody is then exposed to the vitamin D analog coated-solid phase receptor. Solid-phase is then washed, and substrate reagent is added to initiate the fluorescent reaction. An inverse relationship exists between the amount of 25(OH)D in the sample and the amount of relative fluorescence units detected by the system.

Normal value: 30-57 ng/dl

2.4. Statistical analysis

All the statistical work and registration of obtained data were carried out by using Microsoft Office Excel 2010 Worksheet. Differences considered of statistical significance according to

the t-test at P-value < 0.05

3. RESULTS AND DISCUSSION:

All anthropometric data obtained from patients with growth hormone deficiency and the control group are summarized. Table 1 shows the distribution of the studied subjects according to sex. Most of the patients (60%) were males, while (40%) were females. The control group also showed the same distribution as the patients (60.5%) were males, and (39.5%) were females, indicating the age matching between the patients and control groups. The present results in Table-1 show that there were no significant differences between males and females with short stature. This is similar to a study done at (AlZubaidi *et al.*, 2017). The anthropometric measurements of GH deficient patients and control (Table 2) about weight, length, and BMI are in agreement with those of an earlier work (Saja *et al.*, 2020), that showed a highly significant decrease ($p < 0.05$) in the mean values of patients' weight, length and BMI compared to the control values.

According to Table 3, a non-significant difference was found in basal GH between patients of GHD and control. GH levels after 1 hour and 1:30 hours (provocation with clonidine) decreased high significantly ($p < 0.01$) in patients of GHD compared to control values. The results revealed that IGF-1 levels high significant ($p < 0.001$) in patients of GHD compared to control. Regarding IGF-1 and D levels, the current results are consistent with a previous study (Ameri *et al.*, 2013; Matilainen *et al.*, 2005). Many data manifest the turn of thyroid hormones in regulating body growth (Smyczynska *et al.*, 2010). Table 4 shows a non-significant difference between TT3, TT4, and Cortisol levels in patients of GHD and control regarding the thyroid profile findings. At the same time, there was a significant increase ($p < 0.05$) in TSH level of patients compared to the control group. These data are in agreement with those from other authors (Witkowska-Sędek *et al.*, 2018).

Collective results describing the total values of the study groups' measured parameters are summarized in Table 5. The results confirmed no significant differences in the FBS, HDL, LDL, cholesterol, urea, and creatinine of GHD patients compared with the control group, and there was a significant increase ($p < 0.05$) in the triglyceride level of patients compared to the control group. Also, there was a significant decrease ($p < 0.001$) in Zn and Vitamin D levels at patients compared to the control group. These results are consistent

with a previous study (Stawerska *et al.*, 2017) that showed non-significant differences in cholesterol, HDL, and LDL levels and a significant increase in patients' triglyceride levels growth hormone deficiency compared to the control group.

At the childhood, a negative effect occurs during bone mineralization caused of incompetence D vitamin (Goltzman, 2018). The growth skeletal depended mainly on vitamin D and the GH/IGF-1 axis, nonetheless, the interplay between them is indistinct, particularly when dysfunction in one agitated the other (Esposito *et al.*, 2019). There is an initial view that explains the interaction between vitamin D functions and those of GH during GHD patient's observation who used GH replacement therapy. Subsequently, according to scientific information that has been obtained about the matter, there is increasing in calcium gut absorption and urinary calcium excretion and a decrease in urinary phosphorus excretion; identical to the normal work induced by vitamin D (Henneman *et al.*, 1960). Many present biological studies focused on the biochemical interaction between vitamin D and the GH/IGF-1 axis in humans. Also, Zinc plays an essential role in regulating nutrition, and its deficiency in the human lead to decreased appetite and decreased body mass (El-Shazly *et al.*, 2015). So, Zinc had a great affected in protein synthesis and IGF-1 synthesis can be impaired by zinc deficiency. A reduction in circulating IGF-1 concentrations has been proposed as a potential mechanism for growth retardation induced by zinc deficiency (Nishi, 1996). An important observation was the significant elevation in the IGF-1 level after zinc supplementation (Nakamura *et al.*, 1993). Lifshitz and Nishi reported that zinc supplementation improved the growth in patients who had abnormal growth patterns without any other abnormality except hypozincemia; hence all information above were consistent with the results showed in Table 5 (Lifshitz and Nishi, 1980).

Figures 1 and 2 explain the distribution of vitamin D3 and zinc levels between males and females in growth hormone deficiency patients. A previous study (Hong *et al.*, 2017) showed that vitamin D3 is a potent regulator of sex steroid hormone, which agrees with Figure 1. Increased growth velocity associated with increased plasma IGF-I concentrations during zinc supplementation of undernourished children has also been demonstrated (Imamoglu *et al.*, 2005; Ninh *et al.*, 1996). Regarding the results of Zn levels (Figure 2), they agree with those (Hamza *et al.*, 2012), who reported a significant decrease in zinc levels for males and females in GH deficient.

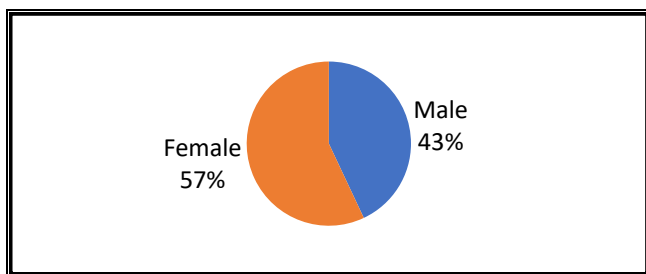


Figure 1. Distribution of vitamin D3 between male and female with growth hormone deficiency

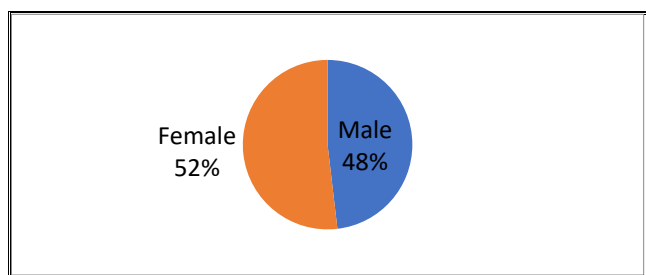


Figure 2. Distribution of zinc level between male and female with growth hormone deficiency

Other factors, such as sex hormones, thyroxine, and IGF-1 are also relevant about regulating growth in children. In the survey of (Wit *et al.*,1996), which is oriented on final height, the role of sex hormones is of Special interest. Testosterone develops to exert its full growth-promoting action only in normal endogenous GH secretion or with sufficient GH replacement (Daniel Jr *et al.*,1976). From clinical observations by the authors (Wit *et al.*,1996) in patients with hypogonadism and precocious puberty, it can be concluded that an early presence of sex steroids accelerates epiphyseal maturation in the long bones. In contrast, in the absence of sex steroids, epiphyseal maturation is delayed, which allows the legs more time to grow. On the other hand, the sex steroids (especially estrogens) stimulate bone maturation, leading to the closure of epiphyses, practically terminating longitudinal bone growth (Péter, 2003).

4. CONCLUSIONS:

There was a highly significant decrease in Vitamin D and Zinc levels in growth hormone deficiency patients than the control group. Vitamin D and zinc levels deficiency can play an essential role in developing growth for children with a growth hormone disorder.

5. REFERENCES:

1. Al-hindawi, G. K., Al-Lami, M. Q., and Al-Samarraie, A. Y. (2020). Assessment of Levels of Metabolic Hormones and Lipid Profile in Growth Hormone Deficient Patients. *Iraqi Journal of Science*, 61(4), 732-741.
2. Allain, C. C., Poon, L. S., Chan, C. S., Richmond, W. F. P. C., and Fu, P. C. (1974). Enzymatic determination of total serum cholesterol. *Clinical chemistry*, 20(4), 470-475.
3. AlZubaidi, M. A., Saleh, M. M., and Jawad, Z. M. (2017). Causes of short stature in Iraqi hospital based study patients. *Journal of the Faculty of Medicine*, 59(3), 221-225.
4. Ameri, P., Giusti, A., Boschetti, M., Bovio, M., Teti, C., Leoncini, G., Diego Ferone, D., Murialdo, G., and Minuto, F. (2013). Vitamin D increases circulating IGF1 in adults: potential implication for the treatment of GH deficiency. *European journal of endocrinology*, 169(6), 767-772.
5. Bengtsson, B. Å., Christiansen, J. S., Cuneo, R. C., and Sacca, L. (1997). Cardiovascular effects of GH. *Journal of endocrinology*, 152(1), 1-3.
6. Bernard, V., Young, J., Chanson, P., and Binart, N. (2015). New insights in prolactin: pathological implications. *Nature Reviews Endocrinology*, 11(5), 265-275.
7. Carani, C., Qin, K., Simoni, M., Faustini-Fustini, M., Serpente, S., Boyd, J., Korach, K. S., and Simpson, E. R. (1997). Effect of testosterone and estradiol in a man with aromatase deficiency. *New England Journal of Medicine*, 337(2), 91-95.
8. Cole, L. A., and Kramer, P. R. (2016). *Human physiology, biochemistry and basic medicine*. Academic Press.pp 69-77.
9. Dattani, M. T., and Malhotra, N. (2019). A review of growth hormone deficiency. *Paediatrics and Child Health*, 29(7), 285-292.
10. Daniel Jr, W. A., Aynsley-Green, A., Zachmann, M., and Prader, A. (1976). Interrelation of the therapeutic effects of growth hormone and testosterone on growth in hypopituitarism. *The Journal of pediatrics*, 89(6), 992-999.

1. Al-hindawi, G. K., Al-Lami, M. Q., and

11. Dietz, J., and Schwartz, J. (1991). Growth hormone alters lipolysis and hormone-sensitive lipase activity in 3T3-F442A adipocytes. *Metabolism*, 40(8), 800-806.
12. El-Shazly, A. N., Ibrahim, S. A. E. H., El-Mashad, G. M., Sabry, J. H., and Sherbini, N. S. (2015). Effect of zinc supplementation on body mass index and serum levels of Zinc and leptin in pediatric hemodialysis patients. *International Journal of Nephrology and Renovascular Disease*, 8, 159-163.
13. Esposito, S., Leonardi, A., Lanciotti, L., Cofini, M., Muzi, G., and Penta, L. (2019). Vitamin D and growth hormone in children: a review of the current scientific knowledge. *Journal of translational medicine*, 17(1), 87.
14. Péter, F. (2003). Sex steroid replacement during and after the induction of puberty. *Growth hormone and IGF research*, 13, S136-S142.
15. Frank, G. R. (2003). Constitutional delay of growth and puberty. *The Endocrinologist*, 13(4), 341-346.
16. Friedewald, W. T., Levy, R. I., and Fredrickson, D. S. (1972). Estimation of the concentration of low-density lipoprotein cholesterol in plasma, without use of the preparative ultracentrifuge. *Clinical chemistry*, 18(6), 499-502.
17. Goltzman, D. (2018). Functions of vitamin D in bone. *Histochemistry and cell biology*, 149(4), 305-312.
18. Grote, F. K. (2007). Assessment of short stature in children: auxological screening and diagnostic work-up. [Doctoral dissertation, Universiteit Leiden]. ISBN: 978-90-6464-083-4, Netherlands.
19. Hamza, R. T., Hamed, A. I., and Sallam, M. T. (2012). Effect of zinc supplementation on growth hormone insulin growth factor axis in short Egyptian children with zinc deficiency. *Italian journal of pediatrics*, 38(1), 21.
20. Henneman, P. H., Forbes, A. P., Moldawer, M., Dempsey, E. F., and Carroll, E. L. (1960). Effects of human growth hormone in man. *The Journal of clinical investigation*, 39(8), 1223-1238.
21. Henry, H. L. (2011). Regulation of vitamin D metabolism. *Best practice and research Clinical endocrinology and metabolism*, 25(4), 531-541.
22. Hoogerbrugge, N., Jansen, H., Staels, B., Seip, M. J., and Birkenhäger, J. C. (1993). Growth hormone normalizes hepatic lipase in hypothyroid rat liver. *Metabolism*, 42(6), 669-671.
23. Hong, S. H., Lee, J. E., An, S. M., Shin, Y. Y., Hwang, D. Y., Yang, S. Y., Cho, S. K., and An, B. S. (2017). Effect of vitamin D3 on biosynthesis of estrogen in porcine granulosa cells via modulation of steroidogenic enzymes. *Toxicological research*, 33(1), 49-54.
24. Imamoglu, S., Bereket, A., Turan, S., Taga, Y., and Haklar, G. (2005). Effect of zinc supplementation on growth hormone secretion, IGF-I, IGFBP-3, somatomedin generation, alkaline phosphatase, osteocalcin and growth in prepubertal children with idiopathic short stature. *Journal of Pediatric Endocrinology and Metabolism*, 18(1), 69-74.
25. Kojima, M., and Kangawa, K. (2005). Ghrelin: structure and function. *Physiological reviews*, 85(2), 495-522.
26. Kautsar, A., Wit, J. M., and Pulungan, A. (2019). Isolated Growth Hormone Deficiency Type 2 due to a novel GH1 Mutation: A Case Report. *Journal of clinical research in pediatric endocrinology*, 11(4), 426-431.
27. Lifshitz, F., and Nishi, Y. (1980). Mineral deficiencies during growth. *Anast C and De Luca H. Pediatric Diseases Related to Calcium New York, Elsevier*, 305-21.
28. Lowe, J. S., and Anderson, P. G. (2015). Chapter 14-Endocrine System. *Stevens and Lowe's Human Histology (Fourth Edition)*. Philadelphia: Mosby, 263-285.
29. Matilainen, M., Malinen, M., Saavalainen, K., and Carlberg, C. (2005). Regulation of multiple insulin-like growth factor binding protein genes by 1 α , 25-dihydroxyvitamin D3. *Nucleic acids research*, 33(17), 5521-5532.

30. Mayo, K. E., Godfrey, P. A., Suhr, S. T., Kulik, D. J., and Rahal, J. O. (1995, January). Growth hormone-releasing hormone: synthesis and signaling. In *Proceedings of the 1993 Laurentian Hormone Conference* (pp. 35-73). Academic Press.
31. Møller, N., Jorgensen, J. O., Schmitz, O., Møller, J., Christiansen, J., Alberti, K. G., and Orskov, H. (1990). Effects of a growth hormone pulse on total and forearm substrate fluxes in humans. *American Journal of Physiology-Endocrinology And Metabolism*, 258(1), E86-E91.
32. Møller, N., Gjedsted, J., Gormsen, L., Fuglsang, J., and Djurhuus, C. (2003). Effects of growth hormone on lipid metabolism in humans. *Growth hormone and IGF research*, 13, S18-S21.
33. Møller, N., Vendelbo, M. H., Kampmann, U., Christensen, B., Madsen, M., Norrelund, H., and Jorgensen, J. O. (2009). Growth hormone and protein metabolism. *Clinical Nutrition*, 28(6), 597-603.
34. Nakamura, T., Nishiyama, S., Futagoishi-Suginohara, Y., Matsuda, I., and Higashi, A. (1993). Mild to moderate zinc deficiency in short children: effect of zinc supplementation on linear growth velocity. *The Journal of pediatrics*, 123(1), 65-69.
35. Nilsson, O., Marino, R., De Luca, F., Phillip, M., and Baron, J. (2005). Endocrine regulation of the growth plate. *Hormone research in paediatrics*, 64(4), 157-165.
36. Ninh, N. X., Thissen, J. P., Collette, L., Gerard, G., Khoi, H. H., and Ketelslegers, J. M. (1996). Zinc supplementation increases growth and circulating insulin-like growth factor I (IGF-I) in growth-retarded Vietnamese children. *The American journal of clinical nutrition*, 63(4), 514-519.
37. Oscarsson, J., Ottosson, M., and Eden, S. (1999a). Effects of growth hormone on lipoprotein lipase and hepatic lipase. *Journal of endocrinological investigation*, 22(5 Suppl), 2-9.
38. Oscarsson, J., Ottosson, M., Vikman-Adolfsson, K., Frick, F., Enerback, S., Lithell, H., and Edén, S. (1999b). GH but not IGF-I or insulin increases lipoprotein lipase activity in muscle tissues of hypophysectomised rats. *Journal of Endocrinology*, 160(2), 247-256.
39. Nishi, Y. (1996). Zinc and growth. *Journal of the American College of Nutrition*, 15(4), 340-344.
40. Nair, R., and Maseeh, A. (2012). Vitamin D: The "sunshine" vitamin. *Journal of pharmacology and pharmacotherapeutics*, 3(2), 118-126.
41. Parkin, K., Kapoor, R., Bhat, R., and Greenough, A. (2020). Genetic causes of hypopituitarism. *Archives of Medical Science: AMS*, 16(1), 27-33.
42. Richmond, W. (1973). Preparation and properties of a cholesterol oxidase from *Nocardia* sp. and its application to the enzymatic assay of total cholesterol in serum. *Clinical chemistry*, 19(12), 1350-1356.
43. Rikken, B., van Busschbach, J., le Cessle, S., Mantenaf, W., Spermon, T., Grobbee, R., Wit, J. M., and Dutch Growth Hormone Working Group. (1995). Impaired social status of growth hormone deficient adults as compared to controls with short or normal stature. *Clinical Endocrinology*, 43(2), 205-211.
44. Romero, C. J., Pine-Twaddell, E., Sima, D. I., Miller, R. S., He, L., Wondisford, F., and Radovick, S. (2012). Insulin-like growth factor 1 mediates negative feedback to somatotroph GH expression via POU1F1/CREB binding protein interactions. *Molecular and cellular biology*, 32(21), 4258-4269.
45. Saja S. Fali, Falah S. Al-Fartusie, and Noor T. Tahir. (2020). Association between lipid profile and other biochemical parameters with growth hormone in children and adolescents with short stature. *International Journal of Research in Pharmaceutical Sciences*, 11(3), 4295-4302.
46. Şıklar, Z., Tuna, C., Dallar, Y., and Tanyer, G. (2003). Zinc deficiency: a contributing factor of short stature in growth hormone deficient children. *Journal of tropical pediatrics*, 49(3), 187-188.
38. Oscarsson, J., Ottosson, M., Vikman-

47. Simon, C., Everitt, H., and Kendrick, T. (2005). *Oxford Handbook of General Practice* (2nd ed.). Oxford, New York: Oxford University Press.
48. Smyczynska, J., Hilczer, M., Stawerska, R., and Lewinski, A. (2010). Thyroid function in children with growth hormone (GH) deficiency during the initial phase of GH replacement therapy-clinical implications. *Thyroid research*, 3(1), 1-11.
49. Stanley, T. (2012). Diagnosis of growth hormone deficiency in childhood. *Current opinion in endocrinology, diabetes, and obesity*, 19(1), 47.
50. Stawerska, R., Smyczyńska, J., Hilczer, M., and Lewiński, A. (2017). Relationship between IGF-I concentration and metabolic profile in children with growth hormone deficiency: the influence of children's nutritional state as well as the ghrelin, leptin, adiponectin, and resistin serum concentrations. *International journal of endocrinology*, 2017.
51. Silva, M. C., and Furlanetto, T. W. (2018). Intestinal absorption of vitamin D: a systematic review. *Nutrition reviews*, 76(1), 60-76.
52. Trinder, P. (1969). Determination of glucose in blood using glucose oxidase with an alternative oxygen acceptor. *Annals of clinical Biochemistry*, 6(1), 24-27.
53. Topper, E., Gil-Ad, I., Bauman, B., Josefsberg, Z., and Laron, Z. (1984). Plasma growth hormone response to oral clonidine as compared to insulin hypoglycemia in obese children and adolescents. *Hormone and Metabolic Research*, 16(S 1), 127-130.
54. Vijayakumar, A., Novosyadlyy, R., Wu, Y., Yakar, S., and LeRoith, D. (2010). Biological effects of growth hormone on carbohydrate and lipid metabolism. *Growth Hormone and IGF Research*, 20(1), 1-7.
55. Vijayakumar, A., Yakar, S., and LeRoith, D. (2011). The intricate role of growth hormone in metabolism. *Frontiers in endocrinology*, 2, 32.
56. Vottero, A., Guzzetti, C., and Loche, S. (2013). New aspects of the physiology of the GH-IGF-1 axis. In *Hormone Resistance and Hypersensitivity* (Vol. 24, pp. 96-105). Karger Publishers.
57. Wei, S., Tanaka, H., and Seino, Y. (1998). Local action of exogenous growth hormone and insulin-like growth factor-I on dihydroxyvitamin D production in LLC-PK1 cells. *European journal of endocrinology*, 139(4), 454-460.
58. Walter, K. N., Corwin, E. J., Ulbrecht, J., Demers, L. M., Bennett, J. M., Whetzel, C. A., and Klein, L. C. (2012). Elevated thyroid stimulating hormone is associated with elevated cortisol in healthy young men and women. *Thyroid research*, 5(1), 13.
59. Wit, J. M., Kamp, G. A., and Rikken, B. (1996). Spontaneous growth and response to growth hormone treatment in children with growth hormone deficiency and idiopathic short stature. *Pediatric research*, 39(2), 295-302.
60. Witkowska-Sędek, E., Borowiec, A., Majcher, A., Sobol, M., Rumińska, M., and Pyrżak, B. (2018). Thyroid function in children with growth hormone deficiency during long-term growth hormone replacement therapy. *Central-European Journal of Immunology*, 43(3), 255-261.
61. Yuen, K. C., Biller, B. M., Radovick, S., Carmichael, J. D., Jasim, S., Pantalone, K. M., and Hoffman, A. R. (2019). American association of clinical endocrinologists and american college of endocrinology guidelines for management of growth hormone deficiency in adults and patients transitioning from pediatric to adult care: 2019 aace growth hormone task force. *Endocrine Practice*, 25(11), 1191-1232.
62. Zhang, Y., Yu, H., Gao, P., Chen, J., Yu, C., Zong, Lu S., Li X., Ma X., Liu Y. and Wang, X. (2016). The effect of growth hormone on lipid accumulation or maturation in adipocytes. *Cellular Physiology and Biochemistry*, 39(6), 2135-2148.

Table 1. Distribution of the studied subjects according to sex

Study group	Sex				P-value
	Male		Female		
	No.	%	No.	%	
growth hormone deficiency (GHD)	30	60	20	40	0.413 NS
Control	23	60.5	15	39.5	0.123 NS

NS: Non-Significant.

Table 2. Anthropometric Measurements between GHD and Control

Anthropometric Measurements	Mean \pm SD		P-value
	GHD (n=50)	Control (n=38)	
Age (years)	9.93 \pm 1.450	10.079 \pm 3.750	0. 668 NS
Weight(kg)	19.676 \pm 3.764	25.816 \pm 4.21	0.05*
High(cm)	102.73 \pm 6.986	122.763 \pm 13.288	0.05*
BMI (kg/m2)	15.8 \pm 3.3	20.9 \pm 2.0	0.05*

NS: Non-Significant, * (p<0.05) Significant.

Table 3. Mean \pm SD of GH before and after stimulation, with IGF-1 in Child GHD and Control

Parameters (ng/ml)	GHD (n=50)	Control (n=38)	P-value
GH (basal)	0.398 \pm 0.423	0.587 \pm 0.497	0.063 NS
GH after(1hr.)	3.292 \pm 1.20	15.718 \pm 5.212	0.001**
GH after (1:30 hr.)	2.0342 \pm 0.928	7.142 \pm 3.693	0.01**
IGF-1	82.282 \pm 12.43	153.513 \pm 45.326	0.001**

NS: Non-Significant, ** (p<0.01) and (p<0.001) high significant

Table 4. Mean \pm SD of triiodothyronine (TT3), tetraiodothyronine (TT4) thyroid stimulation hormone (TSH), and cortisol in Child GHD and Control

Parameters	GHD (n=50)	Control (n=38)	P-value
TT3 (mmol/L)	1.662 \pm 0.604	2.411 \pm 1.204	0.118 NS
TT4 (mmol/L)	92.6 \pm 29.3	102.842 \pm 29.8	0.549 NS
TSH (IU/L)	6.628 \pm 8.630	2.197 \pm 2.727	0.05*
Cortisol (ng/dl)	85.66 \pm 10.174	88.382 \pm 11.833	0.365 NS

NS: Non-Significant, * (p<0.05) Significant.

Table 5. *Characteristic of some Biochemical Parameters in Child of GHD and Control*

Parameters	GHD (n=50)	Control (n=38)	P-value
FBS (mg/dl)	75.16±4.302	81.763±5.355	0.357 NS
TC (mg/dl)	161.16±19.514	154.816±28.879	0.448 NS
TG (mg/dl)	112.14±16.297	93.553±9.934	0.05*
HDL-C (mg/dl)	52.3±5.12	53.184±5.579	0.875 NS
LDL-C (mg/dl)	86.432±11.135	83.032±21.313	0.217 NS
Urea (mg/dl)	25.959±5.96	25.553±4.7	0.866 NS
Creatinine (mg/dl)	0.71±0.218	0.734±0.243	0.422 NS
Zn (µg/dl)	64.56±10.490	142.868±25.434	0.001**
Vitamin D3(ng/dl)	8.204±1.580	31.23684±2.476203	0.01**

NS: Non-Significant, * (p<0.05) Significant, ** (p<0.01) and (p<0.001) high significant.

DEBATE DA ABORDAGEM STEM: HABILIDADE DE PENSAMENTO CRÍTICO E CRIATIVO EM MATERIAL DE FLUIDO ESTÁTICO**STEM-INQUIRY BRAINSTORMING: CRITICAL AND CREATIVE THINKING SKILLS IN STATIC FLUID MATERIAL****STEM-INQUIRY BRAINSTORMING: KEMAMPUAN BERPIKIR KRITIS DAN KREATIF PADA MATERI FLUIDA STATIS**

SAREGAR, Antomi^{1*}; LATIFAH, Sri²; HUDHA, Muhammad Nur³; SUSANTI, Fina⁴; SUSILOWATI, Nur Endah⁵

^{1, 2, 4, 5} Universitas Islam Negeri Raden Intan Lampung, Department of Physics Education. Indonesia.

³ Universitas Kanjuruhan Malang, Department of Physics Education. Indonesia.

* Corresponding author

E-mail: antomisaregar@radenintan.ac.id

Received 15 July 2020; received in revised form 11 August 2020; accepted 30 October 2020

RESUMO

A abordagem de Ciência, Tecnologia, Engenharia e Matemática (STEM) tornou-se um objeto de pesquisa interessante. Vários estudos provaram que a abordagem STEM superou vários problemas de aprendizagem. Envolve muitos aspectos de ensino e aprendizagem, sejam os domínios cognitivo, afetivo ou psicomotor, que afetarão positivamente os resultados de aprendizagem dos alunos. Este estudo teve como objetivo descrever o efeito da abordagem STEM com o método Brainstorming nas habilidades de pensamento crítico e pensamento criativo de alunos na aprendizagem de física. Este estudo empregou pesquisa quase experimental com um desenho de grupo de controle não equivalente. A amostragem foi realizada por meio da técnica de amostragem aleatória simples com uma amostra total de 60 alunos do ensino médio. O instrumento usado neste estudo foi um instrumento de teste de ensaio para medir o pensamento crítico e as habilidades de pensamento criativo. A Análise Multivariada de Variância (MANOVA) foi utilizada como técnica de teste de hipóteses de pesquisa. Os resultados mostraram que a pontuação de significância das habilidades de pensamento crítico foi de 0,001 e a pontuação de significância das habilidades de pensamento criativo foi de 0,019. Assim, pode-se concluir que a aplicação da abordagem STEM com o método de Brainstorming é eficaz para melhorar o pensamento crítico e as habilidades de pensamento criativo dos alunos na aprendizagem de física, tanto por meio de testes multivariados quanto separados..

Palavras-Chave: *brainstorming, habilidades de pensamento criativo, habilidades de pensamento crítico, abordagem STEM.*

ABSTRACT

The Science, Technology, Engineering, and Mathematics (STEM) approach has become an interesting research object. Several studies have proven that the STEM approach has overcome various learning problems. It involves many teaching and learning aspects, either the cognitive, affective, or psychomotor domains, positively affecting the students' learning outcomes. This study aimed to describe the effect of the STEM approach with the Brainstorming method on critical thinking and creative thinking skills of students in physics learning. This study employed quasi-experimental research with a non-equivalent control group design. The sampling was done through the simple random sampling technique with a total sample of 60 high school students. The instrument used in this study was an essay test instrument to measure critical thinking and creative thinking skills. The Multivariate Analysis of Variance (MANOVA) was used as the research hypothesis testing technique. The results showed that the significance score of critical thinking skills was 0.001, and the significance score of creative thinking skills was 0.019. So, it can be concluded that the application of the STEM approach with the Brainstorming method is effective in improving students' critical thinking and creative thinking skills in learning physics, both through multivariate tests and separate tests.

Keywords: *brainstorming, creative thinking skills, critical thinking skills, STEM approach.*

ABSTRAK

Pendekatan Science, Technology, Engineering, and Mathematics (STEM) menjadi objek penelitian yang menarik. Beberapa penelitian membuktikan bahwa pendekatan STEM mampu mengatasi berbagai permasalahan dalam pembelajaran karena pembelajaran STEM melibatkan banyak aspek dalam kegiatan belajar baik dalam aspek kognitif, afektif maupun psikomotorik yang berdampak positif terhadap hasil belajar anak. Penelitian ini bertujuan untuk membuktikan pengaruh pendekatan STEM dengan metode Brainstorming terhadap kemampuan berpikir kritis dan kreatif siswa dalam pembelajaran fisika. Penelitian ini menggunakan jenis penelitian eksperimen semu (quasi experiment) dengan non-equivalent control group design. Pengambilan sampel dilakukan dengan teknik simple random sampling dengan jumlah sampel 60 siswa SMA. Instrumen yang digunakan dalam penelitian ini adalah instrumen tes essay untuk mengukur kemampuan berpikir kritis dan kreatif siswa. Pengujian hipotesis penelitian menggunakan Multivariate Analysis of Variance (MANOVA). Hasil penelitian menunjukkan untuk kemampuan berfikir kritis diperoleh nilai sig. 0,001 dan nilai sig. 0,019 untuk kemampuan berfikir kreatif, sehingga dapat disimpulkan bahwa penerapan pendekatan STEM dengan metode Brainstorming efektif dalam meningkatkan kemampuan berpikir kritis dan berpikir kreatif siswa dalam pembelajaran fisika, baik melalui tes multivariat maupun tes terpisah

Kata Kunci: *brainstorming, kemampuan berfikir kreatif, kemampuan berfikir kritis, pendekatan STEM*

1. INTRODUCTION:

Global competition in education is one of the challenges that must be overcome quickly and responsively (Wurianto, 2018; Wijaya *et al.*, 2016). This competition requires teachers to develop good lesson plans in the learning process (Harjono *et al.*, 2019; Sukoco *et al.*, 2019). Not only teachers but also students are required to be able to overcome their problems and the problems around them (Farida *et al.*, 2018; Yulia, 2015). Some issues often identify in science learning (Nuangchalerm *et al.*, 2019; Perdana *et al.*, 2019; Pratiwi *et al.*, 2019; Sari *et al.*, 2019; Wartono *et al.*, 2019) such as the low level of students' creative and critical thinking skills (Ekosari, 2018; Siswanto, 2018; Ismayani, 2016; Syukri *et al.*, 2013), the low level of students' problem-solving skills (Amanah *et al.*, 2017), and the low level of students' scientific literacy skills (Sari *et al.*, 2019; El Islami *et al.*, 2019).

Science learning covers various branches where physics is one of them. Learning physics is not only about memorizing theories and formulae, but students must also be able to understand the concepts well (Sari and Swistoro, 2018; Rivai and Yuliati, 2018). Students will understand the physics concept in a higher context based on scientific findings (Hanna *et al.*, 2016; Indri, 2017). Thus, physics learning considers as a means to develop thinking and problem-solving skills for students (Rivai and Yuliati, 2018) because the concept of physics is closely related to the phenomenon in everyday life, one of which is in the static fluid subject (Rizalul, 2019; Sukma, 2018).

The data obtained through interviews with

the eleventh-grade mathematics and science teachers during the pre-research on several public high schools in Lampung Province, Indonesia, revealed that students' critical thinking and creative thinking skills were relatively low. The results of pre-research tests supported the results of the interviews. These results were also strengthened by observations that showed that students' thinking skills in physics were lacking. However, in the industrial revolution 4.0 era, the skills to search, analyze, and connect the information to solve problems is needed. (Boonjeam *et al.*, 2017).

Based on the creative and critical thinking of the students, whether from pre-research or research results throughout the world, it could be overcome by using the Science, Technology, Engineering, and Mathematics (STEM) learning approach. STEM approach applies the knowledge and skills at the same time to solve a problem because it requires students to use their skills in understanding, calculating, and analyzing empirical data (Syafei *et al.*, 2020). The purpose of STEM learning is to upgrade the mindsets quality of the people in understanding and use science and innovation in technology products to compete globally (Indri, 2017; Kelley and Knowles, 2016).

STEM approach can integrate with any learning model that can train the knowledge of the students (Sagala *et al.*, 2019). Among the models that can incorporate are problem-based learning, project-based learning, and cooperative learning combined with STEM to improve students' creative and critical thinking (Fathoni *et al.*, 2020; Mu'minah and Aripin, 2019; Satriani, 2017). The STEM approach also makes students accustomed to finding solutions to solve any problems and

becomes the key to creating a globally competitive generation to become a reference for the future of education (Sagala *et al.*, 2019). Besides, the STEM approach can also increase the effectiveness of learning and can support future careers.

The use of the STEM approach in the learning process aims to train students to have hard skills and soft skills (Sunarno, 2018; Thahir *et al.*, 2020). In its application, STEM can collaborate with various learning methods (Ariani *et al.*, 2019). The learning method allows students to upgrade the skills they need to face competition in education. The learning method applied in this study was the brainstorming method. The brainstorming method chooses because this method is effective in training students to get used to thinking of good ideas and turning those ideas into results (Sunandar and Effendi, 2018; Seeber *et al.*, 2017). So, the use of the brainstorming method expects to support the application of the STEM approach.

Based on previous research, STEM has proved to train students to think critically (Sagala *et al.*, 2019; Syukri *et al.*, 2013; Ekosari, 2018) and creatively (Sagala *et al.*, 2019; Ismayani, 2016; Siswanto, 2018). Then, brainstorming has also been proven effective in improving students' critical and creative thinking skills (Widiana and Hernadi, 2018), increasing students' activity and learning outcomes (Yuni, 2017), and can improve students' problem-solving skills (Liani *et al.*, 2018).

There have been many studies that applied the STEM approach and the brainstorming method in the learning process. However, there has been no research that collaborated on the STEM approach with the six steps of the inquiry model from the National Research Council (NRC) and the brainstorming method. Thus, it was deemed essential to research to determine the effect of the STEM approach, collaborated with the brainstorming method, and see its impact on students' critical and creative thinking skills in physics learning.

Therefore, this study aimed to describe the STEM approach effect collaborated with the brainstorming method on the students critical and creative thinking skills in physics learning.

2. MATERIALS AND METHODS:

This research employed quasi-experimental research with a non-equivalent control group design (Dasgupta *et al.*, 2019). This study population was all students of class XI-MIPA

(eleventh-grade of natural science class) at SMA Negeri 1 Sukoharjo (Sukoharjo 1 Public Senior High School) in Indonesia. Using the random sampling technique, selected grade XI-MIPA 1 as the experimental class and XI-MIPA 4 chosen as the control class. The total sample was 60 students 16-17 years, precisely 26 male students and 34 female students. The school and the students have agreed to participate in the study.

The instrument used in this research was a test instrument in the form of essay questions to measure students' critical (Appendix 2) and creative thinking skills (Appendix 1). Appendix 1 shows the critical thinking test, and Appendix 2 shows the creative thinking test. Before the treatments were given, pre-tests were administered to students to find out their initial knowledge. After that, the treatments were given to the sample classes, which then continued by administering post-tests. The post-tests were conducted to determine students' critical thinking and creative thinking skills after implementing the STEM approach and brainstorming methods. The STEM approach application with the six inquiry steps and the brainstorming method on static fluid material (only for the experimental class) is presented in table 1 in the form of a storyboard. The static fluid material chose because this material could easily find in everyday life.

In this study, the brainstorming method can increase the activeness and learning outcomes (Karim, 2017; Wardani, 2016; Yuni Tri Astuti, 2017), and presentation skills (Amin, 2017) of the students. The stages of the brainstorming method are (1) teacher orientation stage (teacher introduces new problems or situations to students); (2) analysis stage (the students identify relevant materials and problems or in other words, they identify the issues); (3) hypothesis stage (the students are allowed to express their opinions related to the issues); (4) incubation stage (the students work individually in their groups to establish their frame of thinking); (5) synthesis stage (the teacher opens a class discussion where the students asked to express and write their opinions as well as to decide which is the best); and (6) verification stage (the teacher chooses the best argument as to the best solution).

The research data were analyzed using prerequisite and hypothesis tests. The prerequisite tests consisted of the normality and the homogeneity test. Then, the hypothesis tested using a Multivariate Analysis of Variance (MANOVA). The students' critical and creative thinking skills data obtain after the treatment given to the sample class. The statistical tests performed

using the SPSS 20.00 program with a significance level of 5%. Before the data used in the hypothesis test, it must pass the Multivariate Analysis of Variance (MANOVA) test. The data required to pass the MANOVA test is the data must normally distribute and pass the homogeneity test.

3. RESULTS AND DISCUSSION:

The data of this study were the students' critical and creative thinking skills data. The data obtained from the experimental class, which consisted of 30 students, and the control class, which consisted of 30 students. The average pre-test and post-test scores can be seen in table 2.

Table 2 showed that the average score of students pre-tests on critical thinking in the experimental class was higher than the control class average pre-test score. The average score of students pre-tests on creative thinking in the experimental class was lower than the control class average score. After the treatment had been applied and then followed by the post-tests, the average score of students' critical thinking and creative thinking skills in the experimental class was higher than the average post-test score in the control class. However, the post-test score difference between the experimental class and the control class was not significant.

3.1 Prerequisite Test

The hypothesis testing was done by performing the Multivariate Analysis of Variance (MANOVA). Data on critical and creative thinking skills were obtained after the treatment had been given. The statistical calculation was assisted by SPSS 20.00 program with a significance level of 5%. Before the data used for hypothesis testing, it must pass the prerequisite tests because MANOVA requires the data to be normally distributed and homogeneously.

3.2 Normality Test

The normality of the data tested using the Kolmogorov Smirnov test assisted by the SPSS 20.00 program. The normality test results from the post-test of critical and creative thinking skills presented in table 3.

3.3 Homogeneity Test

After the data had been declared normal distributed, the next step was to find the homogeneity values. In this study, the

homogeneity value calculated using the SPSS 20.00 program. The homogeneity test results are shown in Table 4. Table 4 shows the significant value of the group homogeneity test results, which is greater than 0,05. It concluded that the post-test scores were taken from homogeneous populations or the variance of each sample was the same. The homogeneity test results of the post-test are in table 5. Table 5 shows the significance values of the homogeneity test results separately. Based on table 5, it can be seen that the significance value was more than 0,05 based on the results of the post-test of critical thinking skills and creative thinking skills. It can be concluded that the post-test scores were taken from homogeneous populations or the variance of each sample was the same.

3.4 Multivariate Test

The hypothesis tested using the MANOVA (Multivariate Analysis of Variance) test assisted by the SPSS 20.00 program. MANOVA test results using multivariate test numbers in table 6. Table 6 shows that the significant value results using multivariate test numbers were less than 0,05 (H_0 rejected). So, applying the STEM approach to collaboration with the brainstorming method affected both variables (critical thinking skills and creative thinking skills). The tests of between-subjects effect can be seen in table 7. Table 7 shows the significant value of the MANOVA test between-subjects effect was smaller than 0,05 (H_0 rejected). It concluded that the STEM Approach that collaborated with the brainstorming method affected students' critical and creative thinking skills. This research results in line with the findings revealed by previous researchers, where the application of the STEM approach collaborated with the brainstorming method can improve critical thinking and creative thinking skills. Previous research stated that the STEM approach could enhance critical thinking and creative thinking skills (Ismayani, 2016; Siswanto, 2018). Other research related to the brainstorming method has proven that this method can improve critical thinking skills (Ardiansyah, 2018) and creative thinking skills (Widiana and Hernadi, 2018). It is because STEM learning requires students to integrate the four aspects of the STEM approach in learning. The four aspects of the STEM approach can encourage students to improve their thinking skills (Thahir *et al.*, 2020). Besides, applying the STEM approach in learning can encourage students to understand natural phenomena based on science concepts, utilize technology, design tools or technology, and

interpret solutions from data and calculated results (Thahir *et al.*, 2020).

STEM approach realizes student-centered learning, so students can play an active role in the learning process (see Table 1). It makes students accustomed to finding solutions to a problem to continue to be actively involved in learning (Khoiriyah *et al.*, 2018). STEM learning trains students to develop critical thinking skills and problem-solving skills in the learning process. It can be seen from students' activity in group works and individual projects (Lutfi *et al.*, 2017). Through the STEM learning approach, which is a learning process that links science processes with science, engineering, and technology, can be presented in the learning to trigger students' learning interest and, at the same time, develop their skills.

The application of the STEM approach in this study cannot separate from the brainstorming method support. The brainstorming method in learning can increase spontaneous ideas, imagination, creativity, and flexibility (Zuhdi and Maulidyana, 2018). This method can also make the learning atmosphere more active and fun. In learning with the brainstorming method, students gather and have discussions or exchange ideas and express opinions with one another. The collaboration between STEM, 6-steps Inquiry, and brainstorming method is done to make students feel free and have to explore all spontaneous ideas and imaginations to understand science phenomena, utilize technology, and design and interpret solutions from data and calculated results (Thahir *et al.*, 2020).

The learning process that collaborates with the STEM approach and brainstorming method is student-centered. The teacher role is only as a facilitator and supervisor for students during the learning process. So, the teacher can encourage passive students to be active. The application of this approach and method makes students accustomed to discussing and expressing all ideas. It also can train student cooperation in group learning. It is the best answer to the post-test of students' critical and creative thinking skills to see the difference in students' responses after the STEM approach collaborated with the brainstorming method. Based on table 8, we can see the difference in students' answers between the experimental and control classes in completing the tests. The students from the control class were mostly incorrect in analyzing and evaluating the problems of the questions. In contrast, the students in the experimental class solved the problems by analyzing, evaluating, and creating. Even though most experimental class students

answered correctly, the post-test average scores between the two classes were not different.

When answering the post-test questions, all students from both classes could answer satisfactorily. Furthermore, based on their answers in the post-tests, the level of students' critical thinking and creative thinking skills could be determined. If students can answer the questions well, it can be said that they have good critical thinking and creative thinking skills. The questions used in the post-test had been adjusted to the indicators of critical thinking and creative thinking. Since the experimental class students' answers were better than the answers of students in the control class, it can be concluded that the critical thinking and creative thinking skills of the experimental class students were higher than the control class students.

Before starting learning, the teachers must consider the vital thing: the teachers must prepare a lesson plan and learn media correctly. Thus, teachers will be required to think more critically and creatively to produce good and interesting learning so that learning goals can be more easily achieved.

4. CONCLUSIONS:

The use of the Science, Technology, Engineering, and Mathematics (STEM) approach collaborated with the brainstorming method was increasing students' critical thinking and creative thinking skills in physics learning effectively. On the other hand, learning by using the STEM approach collaborated with the brainstorming method can explore students' spontaneous ideas and imagination and trigger passive students to be more active. In this research, it could be seen that the STEM approach collaborated with the brainstorming method can be used as an alternative to teaching static fluid materials.

5. REFERENCES:

1. Amanah, P. D., Harjono, A., and Gunada, I. W. (2017). Kemampuan pemecahan masalah dalam fisika dengan pembelajaran generatif berbantuan scaffolding dan advance organizer. *Jurnal Pendidikan Fisika Dan Teknologi*, 3(1), 84–91.
2. Amin, D. N. F. (2017). Penerapan metode curah gagasan (brainstorming) untuk meningkatkan kemampuan mengemukakan pendapat siswa. *Jurnal Pendidikan Sejarah*, 5 (2), 1. <https://doi.org/10.21009/jps.052.01>

3. Ardiansyah, H. (2018). Pengaruh metode pembelajaran brainstorming terhadap kemampuan berpikir kritis berdasarkan kemampuan awal peserta didik. *Indonesian Journal of Economics Education*, 1 (1), 31–42. <https://doi.org/10.17509/jurnalijee>
4. Astuti, Y. T., and Haryono, A. (2017). Implementasi metode brainstorming dalam model group investigation pada mata pelajaran ekonomi untuk meningkatkan keaktifan dan hasil belajar siswa kelas X IPS 3 SMAN 1 Batu. *Jurnal Pendidikan Ekonomi*, 10 (2), 109–117. <https://doi.org/10.17977/um014v10i22017p109>
5. Boonjeam, W., Tesaputa, K., and Sri-ampai, A. (2017). *Program development for primary school teachers' critical thinking*. 10(2), 131–138. <https://doi.org/10.5539/ies.v10n2p131>
6. Dasgupta, C., Magana, A. J., and Vieira, C. (2019). Investigating the affordances of a CAD enabled learning environment for promoting integrated STEM learning. *Computers and Education*, 129, 122–142. <https://doi.org/10.1016/j.compedu.2018.10.014>
7. Ekosari, F. . (2018). The effect of STEM-PBL on critical thinking And Cognitive Outcome. *E-Journal Pendidikan IPA*, 7 (5), 239–244.
8. El Islami, R. A. Z., Sari, I. J., Sjaifuddin, S., Nurtanto, M., Ramli, M., and Siregar, A. (2019). An assessment of pre-service biology teachers on student worksheets based on scientific literacy. *Journal of Physics: Conference Series*, 1155 (1), 1–5. <https://doi.org/10.1088/1742-6596/1155/1/012068>
9. Farida, L., Rosidin, U., Herlina, K., and Hasnunidah, N. (2018). Pengaruh penerapan model pembelajaran Argument-Driven Inquiry (ADI) terhadap keterampilan argumentasi siswa smp berdasarkan perbedaan jenis kelamin. *Journal of Physics and Science Learning*, 02, 15–26.
10. Farwati, R., Permanasari, A., Firman, H., and Suhery, T. (2017). Integrasi problem based learning dalam STEM education berorientasi pada aktualisasi literasi lingkungan dan kreativitas. *Prosiding Seminar Nasional Pendidikan IPA*, 198–206.
11. Fathoni, A., Muslim, S., Ismayati, E., Rijanto, T., and Nurlaela, L. (2020). STEM: Inovasi dalam pembelajaran bookcase. *Jurnal Pendidikan Teknologi Dan Kejuruan*, 17(1), 33–42.
12. Hanna, D., Sutarto, S., and Harijanto, A. (2016). Model pembelajaran tema konsep disertai media gambar pada pembelajaran fisika di SMA. *Jurnal Pembelajaran Fisika Universitas Jember*, 5(1), 23–29.
13. Harjono, A., Makhrus, M., Savalas, L. R. T., and Rasmi, D. A. C. (2019). Pelatihan pengembangan perangkat pembelajaran IPA untuk mendukung kesiapan guru sebagai role model keterampilan abad 21. *Jurnal Pendidikan dan Pengabdian Masyarakat*, 2(3), 343–347.
14. Hartati, R., and Asyhari, A. (2015). Profil peningkatan kemampuan literasi sains siswa melalui pembelajaran saintifik. *Pendidikan Fisika Al-Biruni*, 4(1), h.3.
15. Indri, S. F, R. dkk. (2017). Pengembangan STEM-A (Science, Technology, Engineering, Mathematics and Animation) berbasis kearifan lokal dalam pembelajaran fisika. *Jurnal Ilmiah Pendidikan Fisika Al-BiRuNi*, 06(April), 67–73. <https://doi.org/10.24042/jipf>
16. Ismayani, A. (2016). Pengaruh penerapan STEM project based learning terhadap kreativitas mathematics siswa SMK. *Indonesian Digital Journal of Mathematic and Education*, 3, 264–272.
17. Kallesta, K. S., and Erfan, M. (2018). Analisis faktor penyebab kesulitan belajar IPA fisika pada materi bunyi. *QUARK: Jurnal Inovasi Pembelajaran Fisika Dan Teknologi*, 1(1), 46–50.
18. Karim, A. (2017). Penerapan metode brainstorming pada matapelajaran IPS untuk meningkatkan hasil belajar kelas VIII di SMPN 4 Rumbio Jaya. *Jurnal Pendidikan Ekonomi Akuntansi FKIP UIR*, 5(1), 1–12
19. Kelley, T. R., and Knowles, J. G. (2016). A conceptual framework for integrated STEM education. *International Journal of STEM Education*. <https://doi.org/10.1186/s40594->

20. Khoiriyah, N., Wahyudi, I., Fisika, P., Keguruan, F., Lampung, U., Prof, J., ... Lampung, G. B. (2018). *Implementasi pendekatan pembelajaran STEM untuk meningkatkan kemampuan berpikir kritis siswa SMA pada materi gelombang bunyi*. 5(1), 53–62.
21. Liani, E., Hamdani, D., and Risdianto, E. (2018). Penerapan model problem based learning dengan metode brainstorming untuk meningkatkan kemampuan pemecahan masalah siswa. *Jurnal Kumparan Fisika*, 1, 20–24.
22. Lutfi, Ismail, and Azis, A. A. (2017). Pengaruh project-based learning terintegrasi stem terhadap literasi sains, kreativitas dan hasil belajar peserta didik effect of project-based learning integrated stem against science literacy, creativity and learning outcomes on environmental pollution. *Prosiding Seminar Nasional Biologi Dan Pembelajarannya*, 189–194.
23. Mu'minah, I. H., and Aripin, I. (2019). Implementasi pembelajaran IPA berbasis STEM berbantuan ICT untuk meningkatkan keterampilan abad 21. *Journal Sainsmat*, 8 (2), 28–35.
24. Nuangchalerm, P., Sagala, R., Saregar, A., and Ellslami, R. A. Z. (2019). Environment-friendly education as a solution to against global warming: A case study at Sekolah Alam Lampung, Indonesia. *Journal for the Education of Gifted Young Scientists*, 7 (2), 85–97.
<https://doi.org/10.17478/jegys.565454>
25. Pareken, M., Patandean, A. J., and Palloan, P. (2015). *Penerapan model pembelajaran berbasis fenomena terhadap keterampilan berpikir kritis dan hasil belajar fisika peserta didik kelas X SMA Negeri 2 Rantepao Kabupaten Toraja Utara*. 2015, 214–221.
26. Perdana, R., Riwayani, R., Jumadi, J., Rosana, D., and Soeharto, S. (2019). Specific open-ended assessment: Assessing students' critical thinking skills on the kinetic theory of gases. *Jurnal Ilmiah Pendidikan Fisika Al-Biruni*, 8(2), 127–140.
<https://doi.org/10.24042/jipfalbiruni.v0i0.395>
27. Pratiwi, R. D., Ashadi, Sukarmin, and Harjunowibowo, D. (2019). Students' creative thinking skills on heat phenomena using pogil learning model. *Jurnal Ilmiah Pendidikan Fisika Al-BiRuNi*, 08(2), 221–231.
<https://doi.org/10.24042/jipfalbiruni.v0i0.4629>
28. Rivai, H. P., and Yuliati, L. (2018). Penguasaan konsep dengan pembelajaran STEM berbasis masalah materi fluida dinamis pada siswa SMA. *Jurnal Pendidikan*, 3, 1080–1088.
29. Rizalul.M, M. dkk. (2019). Upaya meningkatkan kreativitas siswa dalam membuat karya fisika melalui model pembelajaran berbasis STEM pada materi fluida statis. *Jurnal Wahana Pendidikan Fisika*, 4.
30. Sagala, R., Umam, R., Thahir, A., Saregar, A., and Wardani, I. (2019). The effectiveness of stem-based on gender differences: The impact of physics concept understanding. *European Journal of Educational Research*, 8 (3), 753–761. <https://doi.org/10.12973/euler.8.3.753>
31. Sari, B. S. K., Jufri, A. W., and Santoso, D. (2019). Pengembangan bahan ajar IPA berbasis inkuiri terbimbing untuk meningkatkan literasi sains. *Jurnal Penelitian Pendidikan IPA*, 5(2).
<https://doi.org/10.29303/jppipa.v5i2.279>
32. Sari, V. J., and Swistoro, E. (2018). Upaya peningkatan kemampuan pemecahan masalah dan hasil belajar peserta didik melalui penerapan metode cooperative problem solving. *Jurnal Kumparan Fisika*, 1(1), 70–77.
33. Satriani, A. (2017). Meningkatkan kemampuan berpikir kritis siswa dalam pembelajaran kimia dengan mengintegrasikan pendekatan STEM dalam pembelajaran berbasis masalah. *Prosiding Seminar Nasional Pendidikan IPA: STEM Untuk Pembelajaran SAINS Abad 21*, 207–213.
34. Seeber, I., de Vreede, G. J., Maier, R., and Weber, B. (2017). Beyond brainstorming:

- Exploring convergence in teams. *Journal of Management Information Systems*, 34(4), 939–969.
<https://doi.org/10.1080/07421222.2017.1393303>
35. Siswanto, J. (2018). Keefektifan pembelajaran fisika dengan pendekatan STEM untuk meningkatkan kreativitas mahasiswa. *Jurnal Penelitian Pembelajaran Fisika*, 9(2), 133–137.
<https://doi.org/10.26877/jp2f.v9i2.3183>
 36. Sukma, M. (2018). Pengaruh pendekatan STEM terhadap pengetahuan sikap dan kepercayaan. *Prosiding Seminar Nasional MIPA IV*. Aceh.
 37. Sukoco, Ibrahim, M., and Sukartiningsi, W. (2019). Pengembangan perangkat pembelajaran berbasis pendekatan saintifik untuk melatih keterampilan berpikir dan pemahaman konsep siswa pada materi sifat cahaya kelas V SD. *Jurnal Kajian Pendidikan Dan Hasil Penelitian*, 5(2).
 38. Sulistyaningrum, A., Prihandono, T., and Subiki. (2015). Penerapan model pembelajaran jurisprudensial inquiry disertai media audio visual pada pembelajaran fisika di SMA. *Jurnal Pembelajaran Fisika*, 4(1), 21–25.
 39. Sunandar, D., and Effendi, E. (2018). Penerapan metode brainstorming pada pembelajaran fisika materi wujud zat. *JIPFRI (Jurnal Inovasi Pendidikan Fisika Dan Riset Ilmiah)*, 2(1), 38–42.
<https://doi.org/10.30599/jipfri.v2i1.209>
 40. Sunarno, W. (2018). Pembelajaran IPA di era revolusi Industri 4.0 Widha. *Seminar Nasional Pendidikan Fisika IV*, 1–8.
 41. Syafei, I., Saregar, A., Hairul, Hahir, A., Sari, P. M., and Anugrah, A. (2020). E-learning with STEM-based Schoology on static fluid material. *Journal of Physics Conferences Series*, 1457 (1), 1–9.
<https://doi.org/10.1088/1742-6596/1467/1/012052>
 42. Syukri, M., Lilia, H., and Subahan, M. M. T. (2013). Pendidikan STEM dalam entrepreneurial science thinking “ESciT”: Satu Perkongsian Pengalaman dari UKM untuk Aceh. *Aceh Development International Conference*, (26-28 MARCH), 105–112.
 43. Thahir, A., Anwar, C., Saregar, A., Choiriah, L., Susanti, F., and Pricilia, A. (2020). The effectiveness of STEM learning: Scientific attitudes and students’ conceptual understanding. *Journal of Physics: Conference Series*, 1467 (1).
<https://doi.org/10.1088/1742-6596/1467/1/012008>
 44. Wardani, N. T. (2016). Penerapan metode brainstorming dalam rangka peningkatan aktivitas dan hasil belajar pada mata pelajaran ekonomi siswa kelas XI IPS 1 SMA Negeri 1 Sukasada tahun ajaran 2016/2017. *Journal Program Studi Pendidikan Ekonomi*, 8 (3), 1–10.
<https://ejournal.undiksha.ac.id/index.php/JJPE/article/view/8663/5647>
 45. Wartono, W., Alfroni, Y. F., Batlolona, J. R., and Mahapoonyanont, N. (2019). Inquiry-scaffolding learning model: Its effect on critical thinking skills and conceptual understanding. *Jurnal Ilmiah Pendidikan Fisika Al-Biruni*, 8(2), 245–255.
<https://doi.org/10.24042/jipfalbiruni.v8i2.4214>
 46. Widiana, Z. R. W., and Hernadi, J. (2018). Analisis penerapan brainstorming terhadap kemampuan berfikir kreatif dan berfikir kritis siswa pada pembelajaran matematika. *Jurnal Mahasiswa Universitas Muhammadiyah Ponorogo*, 2, 113–122.
 47. Wijaya, E. Y., Sudjimat, D. A., Nyoto, A., and Yulianti, E. (2016). Transformasi pendidikan abad 21 sebagai tuntutan pengembangan sumber daya manusia di era global. *Prosiding Seminar Nasional Pendidikan Matematika*, 1, 263–278.
 48. Wuriyanto, A. B. (2018). Pengembangan pendidikan vokasi bidang sosio-humaniora menghadapi revolusi industri era 4 . 0. *Prosiding Seminar Nasional Vokasi Indonesia*, 1, 89.
 49. Yulia Evaliana. (2015). Pengaruh efikasi diri dan lingkungan keluarga terhadap minat berwirausaha siswa. *Jurnal Pendidikan Bisnis Dan Manajemen*, 1(1), 70.
 50. Yuni Tri Astuti, A. H. (2017). Implementasi

metode brainstorming dalam model group investigation pada mata pelajaran ekonomi untuk meningkatkan keaktifan dan hasil belajar siswa kelas x ips 3 sman 1 batu. *Jurnal Pendidikan Ekonomi*, 10(2), 96–103. <https://doi.org/https://dx.doi.org/10.17977/U M014v10i22017p096>

51. Zuhdi, U., and Maulidyana, M. (2018). The effect of the brainstorming method on problem-solving in our best friend environment theme. *2nd International Conference on Education Innovation (ICEI 2018)*, 212, 489–495. <https://doi.org/10.2991/icei-18.2018.105>

Table 1. Storyboard of the Application of STEM-based Inquiry Model with Brainstorming Method

Inquiry steps	STEM	Teacher role	Students role
Problem orientation and present questions	<ul style="list-style-type: none"> - Science: The theory presented is static fluid - Technology: Showing a video about how a hydraulic pump works and showing a video of a car being lifted by a hydraulic jack. 	- The teacher stimulates students' thinking activities by asking questions about events related to static fluid theory.	- Students try to answer some questions from the teacher.
		- The teacher displays videos about several phenomena/events in daily life related to static fluid theory using LCD.	- Students observe several events related to static fluid displayed by the teacher.
Making a hypothesis	<ul style="list-style-type: none"> - Science: The theory presented is static fluid - Technology: Showing a video about how a hydraulic pump works and showing a video of a car being lifted by a hydraulic jack. 	- The teacher directs the students to understand the static fluid theory by making a hypothesis from their videos.	- Students construct a hypothesis from the results of their brief observation.
Planning and doing an investigation	<ul style="list-style-type: none"> - Science: The theory presented is static fluid - Technology: Making a simple hydraulic pump - Mathematics: Make a simple hydraulic pump formula from the application of static fluid theory 	- The teacher divides students into groups and asks students to gather with groups.	- Students gather with their groups.
		- The teacher directs each group to plan a simple hydraulic pump by creating a simple hydraulic pump scheme.	- Each group plans the process of making a simple hydraulic pump according to the teacher's direction.
		- The teacher directs each group to make a simple hydraulic pump.	- Each group makes a simple hydraulic pump according to the teacher's direction.
		- The teacher gives instructions to students to conduct observations and retrieve data by comparing the difference between the pressure on the small injections with the massive injections.	- Each group observes and analyzes the concept of static fluid in a simple hydraulic pump they made.
Analysis and data	- Science: The theory presented is static fluid	- The teacher instructs each group to discuss	- Each group analyzes and

Inquiry steps	STEM	Teacher role	Students role
interpretation	Technology: Simple water rocket Engineering: Make a water rocket design Mathematics: Write the formula for making water rockets based on the application of static fluid	brainstorming to analyze and interpret the data from the observations. - The teacher directs and guides students in discussions with brainstorming .	interprets the data by comparing the small injections' pressure with the massive injections. - Students discuss with group mates by following the teacher's directions and guidance.
Making arguments	Science: The theory presented is static fluid Technology: PowerPoint, simple hydraulic pump	- The teacher instructs each group to have another discussion with brainstorming. This step is aimed to make students dare to come up with arguments about the results of their observations and strengthen their arguments by comparing them with static fluid theory.	- Students express all their arguments and thoughts about the observations and strengthen their thoughts with static fluid theory.
Concluding and presenting results	Science: The theory presented is static fluid Technology: PowerPoint, simple hydraulic pump Mathematics: Write the formula of a simple hydraulic pump based on the application of static fluid theory.	- The teacher instructs each group to make a PowerPoint presentation and conclude all learning activities about static fluid theory.	- Each group makes a presentation and concludes the lesson.

Table 2. Results of the Students Critical and Creative Thinking Skills

Class		Critical Thinking	Creative Thinking
Experimental	Pre-test	43,4	40,7
	Post-test	68,5	70,5
Control	Pre-test	41,7	42,5
	Post-test	63,3	65,5

Table 3. Normality Test

Class		Sig.	Conclusion
Critical Thinking	Experimental	0,200	Normal
	Control	0,112	Normal
Creative Thinking	Experimental	0,133	Normal
	Control	0,200	Normal

Table 4. Box Test of Equality of Covariance Matrices

Box's M	0,381
F	0.122
df1	3
df2	605520.00
Sig.	0,947

Notes: Box's M = box's test of equality of covariance matrices; F = the approximate F statistic for the given effect and test statistic; df1 = the number one of degrees of freedom in the model; df2 = the number two of degrees of freedom in the model; Sig. = the p-value associated with the F statistic and the hypothesis and error degrees of freedom of a given effect and test statistic.

Table 5. Levene Test of Equality of Error Variances

Thinking Skills	F	df1	df2	Sig.
Critical thinking	0.004	1	58	0,949
Creative thinking	0,018	1	58	0,892

Notes: F = The approximate F statistic for the given effect and test statistic; df1 = The number one of degrees of freedom in the model; df2 = The number two of degrees of freedom in the model; Sig. = The p-value associated with the F statistic, the hypothesis, and error degrees of freedom of a given effect and test statistic.

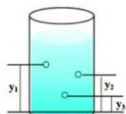
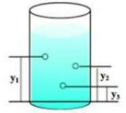
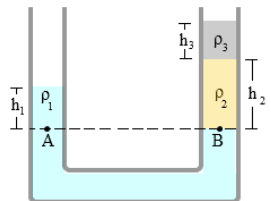
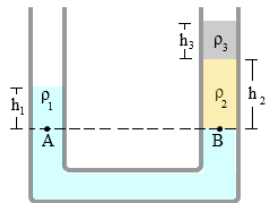
Table 6. Multivariate Tests

Effect		Sig.
Class	<i>Pillai's Trace</i>	0,002
	<i>Wilk's Lambda</i>	0,002
	<i>Hotelling's Trace</i>	0,002
	<i>Roy's Largest Root</i>	0,002

Table 7. Tests of Between-Subjects Effects

Source	Dependent Variable	Sig.
Class	Critical Thinking Skills	0,001
	Creative Thinking Skills	0,019

Table 8. The Examples of Students' Answers on the Experimental class and the Control Class

	Critical Thinking	
Experimental Class	<p>Question:</p> <p>Look at the picture below!</p>  <p>Which hole has the most pressure? Why? Write a conclusion!</p>	<p>Answer:</p> <p>Y_3 has the most pressure because the Y_3 hole is closest to the bottom of the glass. The deeper the position of an object in the fluid, the greater the pressure.</p>
Control Class	<p>Question:</p> <p>Look at the picture below!</p>  <p>Which hole has the most pressure? Why? Write a conclusion!</p>	<p>Answer:</p> <p>Y_3, because it is closest to the bottom of the glass.</p>
	Creative Thinking	
Experimental Class	<p>Question:</p> <p>Look at the picture below!</p>  <p>Based on the picture, formulate the equation to determine the density of the third liquid!</p>	<p>Answer:</p> <p>Based on hydrostatic law, so:</p> $P_A = P_B$ $P_1 = P_2 + P_3$ $\rho_1 g h_1 = \rho_2 g h_2 + \rho_3 g h_3$ $\rho_1 h_1 = \rho_2 h_2 + \rho_3 h_3$ $\rho_3 h_3 = \rho_1 h_1 - \rho_2 h_2$ <p>So, to find the density of the third liquid, we can use:</p> $\rho_3 h_3 = \rho_1 h_1 - \rho_2 h_2$ <p>or</p> $\rho_2 = \frac{\rho_1 h_1 - \rho_3 h_3}{h_2}$
Control Class	<p>Question:</p> <p>Look at the picture below!</p>  <p>Based on the picture, formulate the equation to determine the density of the third liquid!</p>	<p>Answer:</p> $P_A = P_B$ $P_1 = P_2 + P_3$ $h_1 \rho_1 = h_2 \rho_2 + h_3 \rho_3$

QUESTION SHEET

Material: Static Fluid

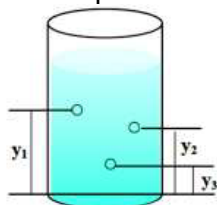


Direction:

- Pray before working on the question, then write your name and class on the answer sheet.
- Please answer the questions that are considered easy first.
- Write down the order of solving the problem, starting from writing down the known quantity and the questioned quantity. Provide a sketch (if possible) and then continue with the process of answering the questions.
- Believe in your abilities.

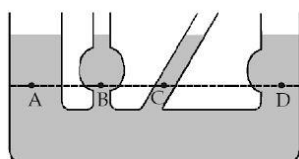
1. Bima places a clip on the surface of the water in the glass. However, Bima saw that the clip did not sink to the bottom of the glass. Consider the following statements:
 1. Boil the water
 2. Freeze the water
 3. Pour soap into the water
 4. Dye the water
 To make the clip sinks, what must Bima do? Explain why!

2. Look at the picture below.



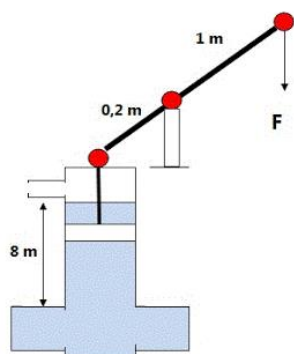
Which hole has the most significant hydrostatic pressure? Why is that? Write your conclusion!

3. Look at the picture below.



Analyze the image to determine whether one of the vessel's points has the most significant hydrostatic pressure? Explain based on the knowledge you have!

4. A metal C, which is a mixture of metal A and metal B, has a mass of 200 grams when weighed in air, whereas if it is weighed in water, the mass of the metal is 185 grams. With the density of metal A 20 gram/cm^3 and the density of metal B 10 gram/cm^3 , calculate the mass of metal A is?
5. A water pump with a cross-sectional pipe area of 75 cm^2 is used to pump water from a depth of 8 m (see picture).



Analyze the image to determine the minimum force required to pump If it is known that the acceleration due to gravity is 10 cm^2 , and when pumping, there is a friction force on the suction of 20 N while other friction is ignored.

6. A hydraulic jack with pipes 1 cm and 7 cm in diameter. How much force is required to lift an object with a mass of 1500kg?
7. Read the following illustration.
Dina experimented by putting egg A into a glass A filled with water mixed with salt. After being observed, it turned out that the egg was floating. Then Dina puts egg B into a glass B filled with water without any mixture. Once observed, the eggs are either at the bottom of the liquid or sink.



Glass A



Glass B

After reading and understanding the illustration above, determine what causes the conditions of glass A and glass B to be different?

8. A ship made of weighty metal can float on the seawater's surface, but a small rock, when thrown into the sea, will sink. Why is that?

QUESTION SHEET

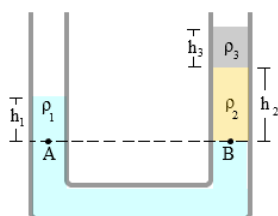
Material: Static Fluid



Direction:

- Pray before working on the question, then write your name and class on the answer sheet.
- Please answer the questions that are considered easy first.
- Write down the order of solving the problem, starting from writing down the known quantity and the questioned quantity. Provide a sketch (if possible) and then continue with the process of answering the questions.
- Believe in your abilities.

1. In a tub filled with water, an ice floe with a density of 0.9g/cm^3 . Explain the buoyancy force and formulate an equation to determine the total volume of ice if the volume of ice that appears on the water's surface is 50 cm^3 .
2. Draw a picture of a block-shaped object in a vessel filled with water and oil. 50% of the volume of the block is in water, and 30% is in oil. The water density is 1 g / cm^3 , and the density of oil is 0.8 g / cm^2 . Based on the drawing that has been made, make a picture from the forces acting on the block and determine the block's density!
3. Draw a picture of the hydraulic jack where the left cylinder P has a cross-sectional area of 600 cm^2 and is given an $M\text{ kg}$ load. The right suction Q has a cross-sectional area of 20 cm^2 , while its weight is negligible. Liquid filled the system with a density of 900kg/m^3 . If F balanced system is 25 N , then analyze the image to find the Mass M ($g = 10\text{m/s}^2$).
4. Look at the picture below.



Based on the picture above, formulate an equation to determine the ρ of the third liquid (ρ_3).

5. A glass is full of water. There is an ice float so that some of the ice is above the surface of the water. If the ice melts, will the water spill? Draw a picture and associate it with Archimedes' Law.

FONTE DE MATÉRIA PRIMA DE HIDROCARBONETOS DA ZONA ÁRTICA DA RÚSSIA

RAW MATERIAL SOURCE OF HYDROCARBONS OF THE ARCTIC ZONE OF RUSSIA

СЫРЬЕВАЯ БАЗА УГЛЕВОДОРОДОВ АРКТИЧЕСКОЙ ЗОНЫ РОССИИ

PRISCHEPA, Oleg M.¹; NEFEDOV, Yuri V.^{2*}; IBATULLIN, Aydar Kh³^{1,2,3} St. Petersburg Mining University, St. Petersburg, Russian Federation.

* Corresponding author

e-mail: yurijnefedov@yandex.ru

Received 15 June 2020; received in revised form 18 September 2020; accepted 15 October 2020

RESUMO

O estudo do potencial de hidrocarbonetos do Ártico está sendo considerado na Rússia como a direção mais importante na preparação de uma nova base de matérias-primas de petróleo e gás, que substituirá as reservas extraídas nas áreas tradicionais de desenvolvimento durante o segundo trimestre desse século. A queda acentuada nos preços globais de hidrocarbonetos levou a uma redução nos custos de pesquisa e exploração, especialmente em áreas de difícil acesso e reservas de difícil recuperação, bem como na necessidade de determinar a contribuição para o equilíbrio de combustível e energia do país a partir do desenvolvimento da zona do Ártico, incluindo a superfície, sem a qual é impossível planejar e desenvolver novos projetos caros. Uma avaliação justa do potencial de petróleo e gás com base em um conjunto de ideias sobre os processos de formação de bacias sedimentares e processos de geração de petróleo e gás contribuiu para a obtenção de novas informações geofísicas sobre os resultados do trabalho sísmico executado na zona ártica da Federação Russa entre 2010 e 2020. Foi realizada uma avaliação quantitativa dos recursos de petróleo e gás, utilizando o método de analogias geológicas (para áreas geológicas e geofísicas bem estudadas) e o método genético-volume (para bacias menos estudadas). Foram verificadas diferenças significativas em relação às avaliações mais conhecidas do Ártico, tanto em termos do volume total de hidrocarbonetos quanto de sua composição de fases. Concluiu-se que existe ambiguidade na avaliação do potencial das zonas de águas profundas dos mares do Ártico e, por isso, é importante estudar áreas costeiras e rasas, especialmente o teor de óleo.

Palavras-chave: *potencial de hidrocarbonetos do Ártico russo, métodos de avaliação de recursos, método de analogias geológicas, método de avaliação de sistemas de hidrocarbonetos, composição de fases de hidrocarbonetos.*

ABSTRACT

The study of the hydrocarbon potential of the Arctic is being considered in Russia as the most crucial direction of preparing a new raw material base of oil and gas, which will replace the extracted reserves in traditional areas of development during the second third of this century. The sharp fall in global hydrocarbon prices has led to a reduction in research and exploration costs, especially in hard-to-reach areas and hard-to-recover reserves as well as the need to determine the contribution to the country's fuel and energy balance from the hydrocarbons development of the Arctic zone, including the shelf, without which it is impossible to plan and develop new expensive projects. A fair assessment of oil and gas potential, based on a set of ideas about the processes of formation of sedimentary basins and oil and gas generation processes, contributed to obtaining new geophysical information on the results of seismic work executed in the Arctic zone of the Russian Federation between 2010 and 2020. A quantitative assessment of oil and gas resources was performed using geological analogies (for well-studied geological and geophysical areas) and the volume-genetic method (for less studied basins). It showed significant differences from the most well-known assessments of the Arctic, both in terms of the total volume of hydrocarbons and their phase composition. It was concluded that there is ambiguity in assessing the potential of deepwater zones of the Arctic seas. Because of that, it is important to study coastal and shallow areas, especially oil content.

Keywords: *hydrocarbon potential of the Russian Arctic, methods of resource assessment, method of geological analogies, the evaluation method of hydrocarbon systems, phase composition of hydrocarbons.*

АННОТАЦИЯ

Изучение и подготовка к освоению углеводородного потенциала Арктики рассматривается в России как важнейшее направление развития новой сырьевой базы нефти и газа, которая заменит добываемые запасы нефти и газа в традиционных районах освоения во второй трети текущего столетия. Резкое снижение мировых цен на углеводороды привело к сокращению затрат на исследования и разведку, особенно в труднодоступных районах и применительно к трудноизвлекаемым запасам, а также к необходимости более внимательного определения возможного вклада в топливно-энергетический баланс страны от освоения углеводородов Арктической зоны, в том числе Арктического шельфа, без чего невозможно планирование и подготовка к реализации новых дорогостоящих инвестиционных проектов. Адекватной оценке перспектив нефтегазоносности, основанной на совокупности представлений о процессах формирования осадочных бассейнов и процессах нефтегазообразования, способствовало получение новой геофизической информации по результатам сейсморазведочных работ, выполненных в Арктической зоне Российской Федерации в период с 2010 по 2020 годы. Проведена количественная оценка ресурсов нефти и газа с использованием метода геологических аналогий (для хорошо изученных геолого-геофизическими методами районов) и объемно-генетического метода (для менее изученных частей бассейнов). Она показала существенные отличия от наиболее известных оценок ресурсов Арктики как по общему объему углеводородов, так и по их фазовому составу. Сделан вывод о наличии неоднозначности в оценке потенциала глубоководных зон арктических морей и, в связи с этим, о важности изучения прибрежных и мелководных районов на продолжении в акваторию осадочных бассейнов, преимущественно нефтеносных и содержащих скопления газоконденсата.

Ключевые слова: углеводородный потенциал Арктики России, методы оценки ресурсов, метод геологических аналогий, метод оценки углеводородных систем, фазовый состав углеводородов.

1. INTRODUCTION:

The increased interest in the development of the Arctic region, shown in recent years by the international community, is caused by energies and economic and geopolitical factors. The development of the Arctic for Russia is not only a matter of national and energy security in the long term but also one of the most potent drivers for the development of innovation, science, high-tech production, and technology, comparable to the ambitious project for space exploration in the USSR (a comparison of academicians E.P. Velikhov and A.E. Kontorovich) (Kontorovich, 2015).

By its synergistic effect, is likely to be on a par with such events that provided a breakthrough in the country's economy in the last century, such as the space program mentioned above, the creation of the science campus, which determined scaling up scientific research, that led to tremendous progress in technology and the industrial development of the oil and gas potential of Western Siberia (Prischepa *et al.*, 2019), which allowed making the country one of the leading economies in the world. Despite the wide variety of oil and gas basins in Russia, the generally accepted perspective is that the most significant part of the territories and water areas promising for gas is located in the Arctic zone. Its oil potential remains somewhat uncertain.

The Arctic territories provide more than 80% of gas production in Russia and about 12% of the production of liquid hydrocarbons (HC) (Table 1) (Pavlenko, 2013; Prischepa *et al.*, 2019; Prischepa *et al.*, 2020; Carayannis *et al.*, 2019; Cherepovitsyn *et al.*, 2018). In official government documents of the Russian Federation (Strategy of social and economic development, 2013; Bases of public policy, 2020; Draft of strategy, 2020, Research of the Analytical Centre, 2015) it is designated as an essential element for the implementation of the Arctic projects such as "intensification of geological exploration for oil and gas".

The implementation of the strategic plans of development of the Russian Arctic is only possible if the adequacy of the oil and gas potential of the Arctic and the task of creating conditions and mechanisms ensuring the development of the Arctic regions and the favorable market of hydrocarbons and transportation, which directed the efforts of the state support (Kontorovich, 2015).

2. LITERATURE REVIEW:

2.1. State of the Arctic zone resource base

The basis for the quantitative assessment of the oil and gas potential is the geological understanding of the development of sedimentary basins, the characteristics of the strata, the

reserves of already identified deposits, seismic data determining both regional, zonal and local features of the region, and a whole series of oil and gas potential criteria (Bogoyavlensky *et al.*, 2019; Carayannis *et al.*, 2019; Tcvetkov *et al.*, 2020). The official result of the oil and gas potential is assessing the total in-situ resources (TIR) of oil and gas, carried out and approved by the state authority of the Russian Federation - the Federal Agency for Subsoil Use. It covers all promising and gas-bearing basins and, accordingly, includes the Russian Federation (Kaminsky *et al.*, 2018; Prischepa *et al.*, 2019, 2020).

Numerous land-based companies and two state-owned companies - Gazprom PJSC and Rosneft PJSC - which have exclusive rights to work on the Arctic shelf, are conducting their hydrocarbon potential studies. However, they often relate exclusively to existing licenses or promising licensed areas, which companies consider a priority for their development. The results of the official quantitative assessment of the resources of the Arctic waters and territories have been published more than once (Kontorovich, 2015; Vorotnikov *et al.*, 2019; Kaminsky *et al.*, 2016; Kaminsky *et al.*, 2017; Suprunenko *et al.*, 2016; Suprunenko *et al.*, 2012; Kaminsky *et al.*, 2018; Prischepa *et al.*, 2019, 2020) and in this report an attempt is made to compare them with the most well-known independent estimates and those of Western experts.

There are serious concerns that the official estimate of resources to a significant extent, reflects current trends indicated by the official point of view about the Arctic's considerable potential. First of all, this conclusion is based on the fact that a comparison of the potential estimates of the least studied part of the Arctic shelf indicates a steady increase, often not confirmed by an increase in exploration, new significant discoveries or the identification of fundamentally new directions for increasing the raw CHC material base (Kontorovich, 2015; Kaminsky *et al.*, 2018; Prischepa *et al.*, 2019).

For example, the total hydrocarbon resources of the richest West-Arctic shelf as of 01.01.1993 were estimated at 75.3 billion tons of fuel equivalent. The next assessment (as of 01.01.2002) showed their increase (by 256 million tons of standard fuel equivalent in Pechorsky, by 1,860 million tons of technical equivalent in the Barents and 5,096 million standard tons in the Kara Sea) in the amount of 7.2 billion tons of standard fuel equivalent. The next assessment (as of 01.01.2009) showed an additional increase in

resources (17.5 billion tons of standard fuel) and the achievement of a total resource estimate of more than 100 billion tons of fuel equivalent, and a preliminary (state) estimate (as of 01.01.2019) also showed a slight increase in the amount of up to 103 billion tons of fuel equivalent. It led to a paradoxical situation of a significant decrease in the indicator of exploration of oil and gas reserves against the background of an increase in geological and geophysical knowledge (Varlamov, 2018; Skorobogatov *et al.*, 2019, 2020).

This is especially surprising in the Pechora Sea water area. The discovery of new deposits dates back to the period between 1993 and 2002. A significant increase in the resource estimate occurred when there was practically no increase in reserves in 2002-2009. These discrepancies make us more attentive to the estimates obtained later (Chanysheva *et al.*, 2019).

The oil and gas potential of the Russian sector of the Arctic is unique both in volume and in composition diversity. It is proved by numerous discoveries of unique, giant, and large oil and gas deposits on its mainland (more than 50 giant and large deposits have been identified) and gas reserves in the waters of the seas of the Arctic Ocean (Prischepa *et al.*, 2019). Below, the author considers the most famous assessments and their potential of the Arctic performed by the following organizations and researchers: U.S. Geological Survey (USGS), Arctic Council, Mackenzi, UN; Gazprom VNIIGAZ LLC, VNIGNI, VNIGRI, VNIIOkeangeologiya, Russian Academy of Sciences, Kenneth J. Bird, Ronald R. Charpentier, Donald L. Gautier, David W. Houseknecht, Timothy R. Klett, Janet K. Pitman, Thomas E. Moore, Christopher J. Schenk, Marilyn E. Tennyson, Craig R. Wandrey (Neville, 2017; Durbano *et al.*, 2015, Energy Futures, 2013; Mulrooney *et al.*, 2017; Llopart *et al.*, 2019; Lerch *et al.*, 2016; Houseknecht *et al.*, 2018; Harada, 2020; Galloway *et al.*, 2018; Dewing, 2019; Kontorovich, Kaminsky *et al.*, Suprunenko *et al.*, 2016; Yurchenko, 2018; Blumenberg, 2016; Sobolev, 2016; Skorobogatov, Prischepa *et al.*, 2020; Otmas *et al.*, 2017; Tolstikov, 2018).

The international community of experts (Geological Survey of the USA (USGS) in 2008; Wood Mackenzie, 2006; Resources to Reserves, 2013; Research and Development, 2010) in the oil and gas industry is making attempts to assess the hydrocarbon potential of the Arctic, including its international and Russian segments.

2.2 State of the Arctic zone resource base

The best-known estimates were made by the consulting companies Wood Mackenzie and Fugro Robertson in 2006 and the Geological Survey of the USA (USGS) in 2008. They conducted two individual studies of the Arctic hydrocarbon potential (Schenk, 2012; Houseknecht *et al.*, 2012).

Before discussing and comparing the results of these assessments, it should be noted that the research areas, according to USGS, were limited to those located north of the Arctic Circle. Suppose for water areas, and this approach is not entirely different from that used in Russia for the Arctic shelf, then for land areas (territories). In that case, the Arctic regions' assignment is regulated in Russia by specific documents. These territories differ significantly from those estimated in USGS's work (Decree of the President of the Russian Federation of May 2, 2014). Therefore, the assessment's given comparison must be adjusted, taking into account this condition (Ivanitskaya *et al.*, 2019). Simultaneously, all Arctic water areas are unambiguously comparable with international experts' assessment areas (Figures 1 and 2). (Arctic Environmental Protection Strategy, 1991; Oil and gas exploration in the Arctic; Fundamentals of the state policy of the Russian Federation in the Arctic, 2020; Research of the Analytical Centre under the Government of the Russian Federation, 2015)

USGS estimates include 6 Arctic land areas of Russia - the northern part of the Timan-Pechora and West Siberian sedimentary basins, the Yenisei-Khatanga, and Leno-Anabarsky basins, the extreme North-Eastern fragment of the Lena-Vilyui basin and the Zyryan basin. At the same time, the Northern part of the Lenno-Tunguska NGP, including areas north of the Arctic Circle, was not evaluated. Since some subjects, for example, Yamal-Nenets Autonomous Okrug are completely included in the ADR, the borders of the ADR are expanded to areas south of the Arctic Circle. It does not coincide with the areas of USGS, 2008, Mackenzie (Ivanova *et al.*, 2019; Shemin, 2019; Proceedings of the All-Russian Scientific-Practical Conference, 2013).

The report of Wood Mackenzie and Fugro Robertson was based on a detailed analysis of geophysical and seismic data in various Arctic basins. According to a Future of the Arctic - A New Dawn for Exploration (Geological Survey, 2008) study, new oil and gas resources in the Arctic are estimated at 233 billion barrels of oil equivalent, or more than 30 billion tons (conversion factor of 5.35 trillion cubic feet to 1 billion barrels of oil equivalent

was used). At the same time, 85% of explored reserves and 74% of expected (resources) are gas. In 2008, USGS US Geological Survey prepared a report, Assessment of the Unexplored Oil and Gas Reserves of the Arctic North of the Arctic Circle (Wood Mackenzie, 2006).

In USGS study, the main emphasis was made on probabilistic geological analysis and identification of those areas that have a chance to contain relatively large reserves of oil or gas (more than 50 million tons of oil equivalent). According to USGS study, the total unexplored oil and gas resources of the entire Arctic is about 413 billion BOE (barrel of oil equivalent), or about 22% of the total unexplored reserves of traditional hydrocarbons in the world (which is about twice as high as the estimates made by Wood Mackenzie/Fugro Robertson). Novel oil resources are estimated at approximately 90 billion barrels (or 13 billion tons of about 7% of global resources), gas - 1,700 trillion cube feet of gas (about 47 trillion m³), and 44 billion barrels of natural gas condensate (about 5.5 billion tons). The total assessment of the Arctic hydrocarbons is about 65 billion tons (USGS, 2008).

At the same time, the share of traditional oil (including liquid fractions of natural gas, NGL) accounts for about 134 billion barrels or about 18 billion tons, which corresponds to 13-15% of its global resources, and for traditional natural gas - the remaining 279 billion BOE, or slightly less than 30% of the total gas resources in the world (USGS, 2008). About 80% of the Arctic's resources are located in the subsoil beneath the waters (offshore area); however, a significant part is concentrated in relatively shallow water (shelf) - at sea depths of less than 200-500 m. Moreover, according to USGS estimates, the probability of detection of any significant hydrocarbon reserves in the central part of the Arctic Ocean, as well as in the areas adjacent to them, are close to zero (USGS, 2008; Hansen *et al.*, 2020; Research and Development in the Energy Sector, 2010).

Russia possesses approximately 70% of the total unexplored Arctic gas resources with the West Siberian basin (18.5 trillion m³). It includes the southern part of the Kara Sea and the East Barents Sea basin (8.1 trillion m³), located entirely in the eastern part of the Barents Sea, in the Yenisei-Khatanga basin (2.5 trillion m³), the Laptev Sea (0.83 trillion m³) and in the deeper part of the Barents (0.67 trillion m³) and the Kara seas (0.38 trillion m³) (Figures 3 and 4) (Kontorovich, 2015; Kaminsky, 2018; Prischepa, 2019). It is interesting to estimate that, in general, in the Arctic, more than 80% of oil resources are

concentrated on the shelf. For Russia, this share is determined at 70%, while the Norwegian and Greenland oil-bearing regions of the Arctic are almost entirely located in the seas (Pak *et al.*, 2019).

According to USGS, about 65% of non-NGL oil resources, concentrated in the North American sector of the Arctic zone: approximately 30 billion BOE (barrels of oil equivalent) accounts for Arctic Alaska (the USA), almost 10 billion BOE - to the so-called Amerasian basin (north of the coast of Canada) and another 9 billion BOE - on the shelf of Greenland (mainly on its eastern rift zone).

Russia, according to USGS (USGS, 2008) has about 30 billion BOE (33% of Arctic oil resources) with a distribution of 7.4 billion BOE - in the southeastern part of the Barents Sea, 5.6 billion BOE - in the Yenisei-Khatanga basin, 3.7 billion BOE - in the West Siberian NGB, 3.1 billion BOE - in the Laptev Sea NGB, 2.0 and 1.8 billion BOE - in the deepwater part of the Barents and the Kara seas and another 1.9 billion BOE - in Leno-Anabar and 1.6 billion BOE - in the Timan-Pechora oil-and-gas bearing basin. With the addition of NGL resources (3.7 billion tons), the share of liquid hydrocarbons in the Russian Arctic is growing significantly - up to 41% of the total Arctic resources (Zharov, 2019).

Thus, the total recoverable resources of the Russian sector of the Arctic are estimated by USGS at about 40 billion tons of oil equivalent tons, of which about 4.3 billion tons are oil, more than 32 trillion m³ is gas and about 3.7 billion tons is condensate (USGS, 2008; UN Convention on the Law of Sea, 1982). The potential of hydrocarbons in the Russian Arctic is estimated even more modestly and less optimistically by experts from the International Energy Agency (IEA) that believes that geological resources amount to about 76.3 billion tons BOE. Simultaneously, the recoverable part (probably it is a question of technical availability) of oil in the Russian sector does not exceed 9.6 billion, and gas resources in the Arctic region of Russia are estimated at a modest 21.4 trillion m³. The total estimate of recoverable resources for the Russian Arctic (without condensate) is 31 billion tons.

In the same study, data are presented that a total of 61 large oil and gas fields have already been discovered north of the Arctic Circle, and of these, 43 – in Russia (today here are already more than 50), 11 – in Canada, 6 – in Alaska and 1 – in Norway.

According to researches of UN (UN

Convention on the Law of Sea, 1982) the geological oil resources of the Arctic regions are estimated at 140-180 billion tons, of which almost 40% are in the eastern part of the area, and about a third lie between the North Pole and the American continent. UN experts stated that given the enormous technical difficulties that companies will have to face in the industrial development of these resources, projects' economic feasibility raises great doubts (UN Convention on the Law of Sea, 1982).

The noted imbalances in the structure of real discoveries and assessing the potential of the Arctic indicate the insecurity of the experts themselves, probably caused by the lack of experience in such work with shallow exploration degrees (Prischepa, 2019).

3. MATERIALS AND METHODS:

An adequate assessment of the Arctic region oil and gas potential is necessary for long-term planning and expansion of research projects and appropriate management decisions.

One of the existing contradictions and disagreements when choosing promising areas and objects of exploration is that official estimates accepted for approval by state structures in the Russian Federation are based on regulatory and methodological documents that are based on principles that allow comparing the potential of poorly studied areas with fairly well-studied ones. Companies primarily use basin modeling technology or compare many criteria for oil and gas content on the weakest link principle. Comparison of such approaches leads to paradoxical results, when areas with a significant amount of estimated forecast resources are unclaimed by companies when placing the corresponding sites for licensing, and when, on the contrary, companies show interest in small areas that have significant prospects in their opinion (Zharov, V. and Zharov, N., 2019; Kleshchev *et al.*, 2000, Tcvetkov *et al.*, 2020; Sobota *et al.*, 2020).

3.1. Methods of the quantitative forecast of oil and gas potential

Methods of the quantitative forecast of oil and gas content meet the purpose of determining the total value and distribution of hydrocarbon resources (by phase composition, the content of associated components, size, depth, timing to prospective complexes).

These tasks are solved based on projects by setting dependencies between the concentration

of reserves and geological, geophysical, geochemical, and other parameters; and establishing dependencies between the indicators of the discoveries dynamic and the reserves movement and the volume indicators of geological exploration. Analogy methods provide for establishing dependencies and quantitative measures of similarity between reference and calculated areas. They are combined in two ways - the technique of comparative geological analogies and the volume genetic method.

The application of the method of comparative geological analogies in "pure form" (by average specific densities per unit area or volume of a sedimentary complex or its prospective part), consists in comparing the calculated area with the reference one based on a set of oil and gas content criteria, which primarily include accumulative and conservation characteristics. The volume genetic method of assessment is based on the results of the separate counting of the hydrocarbon fluids generated and emigrated from oil and gas bearing strata (OGBS) and the number of scattered on the migration routes and in the areas of accumulation in rocks and waters.

The assessment of the total oil and gas potential of sedimentary strata is based (Larchenko *et al.*, 2020) on the statement of the universality of the processes of oil and gas formation in the sedimentary shell of the Earth. Thus, to determine the quantitative value of forecast resources, a complex calculation of the main parameters of sedimentary strata is carried out using the volume genetic method: the conditions for accumulation of organic matter and sediment (Kruk *et al.*, 2020; Grigorev *et al.*, 2020; Sabukevich *et al.*, 2020).

In the first group of sedimentation basins associated mainly with large platform areas formed by powerful strata of Paleozoic, Mesozoic and Cenozoic age, with a high volume rate of sedimentation (> 14 thousand $\text{km}^3/\text{million years}$), the value of specific reserves of HC contained in 1 km^3 of sedimentary rocks is more than 14 thousand tons/ km^3 . In the second group of relatively large basins, where the rate of sedimentation is characterized by a volume rate of 4 to 14 thousand $\text{km}^3/\text{million years}$ and the value of specific hydrocarbon reserves contained in 1 km^3 is 8-14 thousand tons/ km^3 . The third group consists of basins with an average volume rate of sedimentation: 1.5-4 thousand $\text{km}^3/\text{million years}$ and with the value of specific hydrocarbon reserves in the range of 3-8 thousand tons/ km^3 . The fourth group includes small basins with an

average sedimentation rate of less than 1.5 thousand $\text{km}^3/\text{million years}$, with the value of specific hydrocarbon reserves: less than 3 thousand tons/ km^3 (Egorov, 2018).

The maps of the thermal clay of maternal thicknesses and the cards equal to the content of bitumoids in rocks are designed to perform the calculation. The method is to identify oil and gas bearing strata, to study the history of its development (the structure of organic matter, the degree of metamorphism, thermal history), to determine the most optimal for oil and gas generation areas (centers of oil and gas generation), assessment of track losses from centres of generation to areas of accumulation (dissipation, the restoration of the forms of iron and sulfur), and most importantly – in the assessment of the possible generated quantities of oil and gas in a particular center (emigration rates) and quantities in the areas of accumulation (accumulation coefficient). Up to this main stage, all the indicators used for calculating resources are quite correct, although not very accurate. However, the emigration coefficient's determination, especially for gas and the accumulation coefficient for gas and oil (the desired forecast resources), introduces significant uncertainty in the calculations.

Changes in the volume and density of resources on the reference standards caused by new discoveries and deposits both on land and in the water area and a significant refinement of the strata of the main oil and gas complexes in the water area due to regional seismic surveys are the basis for refining resource assessment for poorly studied Arctic territories and water areas.

In connection with the above, it is useful to compare the results of refining the quantitative assessment of oil and gas resources using the method of geological analogies with the approach to assessing the potential of oil and gas accumulation zones as elements of oil and gas systems. It allows to an evaluation of both approaches critically, differentiates heterogeneous promising objects by significance. It offers subsurface users previously unclaimed objects for further study and entire exploration areas that were not yet involved in the geological study. The analysis of oil and gas systems is applied, which determines the possibility of accumulation of generated hydrocarbons in the zones of oil and gas accumulation of individual complexes dissected by regional fluid traps.

One of the important aspects of the quantitative assessment of the present study of

resources in neglected areas is the comparison of the reference to the investigated area with more or less similar geological conditions with the unexplored – valued (for the method of geological analogy), and volumetric-genetic recoverability of the history of diving and paleotemperature in the presence of oil and gas source strata, based on the thermal and geochemical data.

In general, the quantitative prediction methods of oil and gas content meet the goal of determining the total amount and distribution of hydrocarbon resources (by phase composition, the content of associated components, size, depth, confined to prospective complexes). These tasks can be solved based on establishing relationships between the concentration of reserves and geological, geophysical, geochemical parameters, establishing dependencies between the dynamics of discoveries and movement of resources, and the volume indicators of geological exploration, and expert evaluation.

The essence of the geological analogies used in this study consists of successive steps compared to the geological parameters of reference well-studied by geophysical methods and drilling sites with identified accumulations of hydrocarbons estimated areas with forecast potential. Crucial when using the geological analogy method becomes correctness (adequacy) indicators of oil potential backed by relatively homogeneous oil and gas formation conditions, which is possible only within single complexes and areas of similar geological structure.

An alternative assessment was made considering the modeling of oil and gas formation processes performed in the Temis software package of Baicifranlab (Petroleum System Analysis and Basin Modeling) based on the geochemical data of VNIGRI (Prischepa, Bazhenov) and VNIIOkeangeologiya. The main stages of assessment and creation of geological models were (1) creation of a structural framework (construction of structural maps for the main seismostratigraphic horizons based on the results of regional seismic surveys); (2) creating maps of the strata of seismic facies complexes with their transformation into lithic facies complexes (based on the dismemberment of seismic sections and linking them with good data); (3) creation of maps of the total organic matter content of Sorg and the hydrocarbon potential of rocks HI; (4) creating maps of temperature and paleotemperature conditions (creating maps of paleo depths and paleotemperature of the water environment and maps of thermal flows using trends in changes in

these parameters in geological time); and (5) restoration of the history of the sinking of selected oil and gas-bearing strata, determination of the time and possibility of generation of hydrocarbons, their migration and accumulation in natural reservoirs.

As the geological framework, the maps built-in VNIGRI over the North of the Timan-Pechora sedimentary basin and its offshore continuation, as well as over the waters of the Chukotka and the Bering seas, the maps of VNIIOkeangeologia in the Barents and the Kara seas, the maps SNIIGGIMS over the waters of the Laptev Sea, and the works of INGG of A.Trofimuk of Russian Academy of Sciences over the North of Western Siberia and the southern part of the Kara sea are used.

A team made assessments by the method of geological analogies of authors with the participation of employees of VNIGRI, VNIIOkeangeologia and VNIGNI. The most significant and comparable geological characteristics are (1) the thickness of the oil and gas complex or its part corresponding to the natural reservoir (the proportion of reservoir rocks-sandiness); (2) lithological-facies uniformity (variability); (3) reservoir properties of rocks; (4) area of accumulation of hydrocarbons (regional and zonal – structural factor or structure – bearing, specific area of traps); (5) depth of the complex; (6) quality of the layer (thickness, lithology); and (7) connection with the focus of oil and gas formation (distance, regional inclines).

Based on comparing these indicators on the calculated area and a well-studied standard, correction coefficients are introduced. The analogy coefficients were determined based on a comparison of the values of certain specific geological parameters (total thickness of complexes, the area occupied by positive structures (shafts, elevations, bridges, local objects), the proportion of possible reservoirs in the section (terrigenous and carbonate), and a qualitative assessment when comparing such parameters as the quality of fluid pores, the quality of connection with oil and gas formation and their potential. The total coefficient of analogy is defined as the product of the partial coefficients of analogy based on the fact that the range of values of these partial coefficients can vary from 0.5 to 2. (Methodological recommendations for quantitative assessment of VNIGNI resources, 2000).

Based on these indicators, a summary coefficient of analogy is derived, obtained as the product of all correction coefficients and reflects

the ratio of resource density in the calculated area and the standard. The specific densities of reserves and resources on the standard can be represented by values per unit area, per unit volume, or per averaged structure. The estimated area's resources are defined as the product of the specific density of reserves on the standard by the summary coefficient of analogy.

The sequence of steps for conducting an assessment using comparative geological analogies for large forecasted oil and gas accumulation zones: 1. Clarification of oil and gas-geological zoning. 2. Dividing of the section into oil-and-gas-bearing and oil-and-gas-prospective complexes. 3. The mapping criteria of oil potential: – thickness systems; – structural maps in RH close to the surface of OGC; – lithofacies maps; – maps for collectors forecast; maps of layers development; – the maps of natural reservoirs; - maps of oil and gas-bearing zones; – maps of oil and gas generation areas; – maps of hydrogeological criteria of oil potential; – maps of the fund of local objects; – maps of identified oil and gas fields; - maps of geological and geophysical studies (seismic exploration and drilling); – maps of objects removed from drilling with negative results. 4. Allocation of well-studied areas within oil and gas complexes, where positive (identified deposits) and negative results of exploration (reference areas) were obtained. 5. Calculation of resource densities obtained at reference sites resulting from the addition of reserves and resources of local undeveloped structures with confidence coefficients divided by the area of the contoured reference site. 6. Allocation of calculated areas characterized by a common geological structure (most often parts of oil and gas-bearing areas) and small variations in the criteria of oil and gas content. 7. Sequential comparison of all parameters on the calculated and reference sections within the considered complex. 8. Receipt of partial coefficients of analogy to compare all the criteria (thickness, structure only, the share of collectors, quality of layers, the distance from the source of generation, strata availability providing a migration, the presence of tectonic dislocations). 9. The calculation of the consolidated ratio of analogies by partial coefficients analogy. 10. Calculation of resource densities on the calculated plots obtained by multiplying the resource densities on the standard and the summary coefficient of analogy. 11. Calculation of the initial total resources obtained by multiplying the resource densities on the calculated plot and the calculated plot area.

4. RESULTS AND DISCUSSION:

The geological and geophysical exploration of the Arctic is extremely uneven. There are 13 large, medium, and small sedimentary basins prospective for oil and gas in the Russian Arctic, and only six of them have oil and gas deposits, five basins on land and two in the water area. The largest sedimentary basins in the Arctic are on land (or partially located on land, and partially in the water area) the Timan-Pechora, Western Siberia, Leno-Tunguska, Yenisei-Khatanga, Leno-Vilyuisky and Zyryansky (prospective); in the water area - the West Barents Sea, the East Barents, the South Kara, the North Kara, the Laptev, the East Siberian and the Chukotka (Zharkov, 2017; Matveeva, 2017; Vasiltssov, 2018).

The oil and gas potential of the Arctic shelf remains poorly explored. All discoveries (except the Pobeda deposit) were made more than 20 years ago. In recent years, geological exploration on the Arctic shelf for oil and gas has been reduced mainly to seismic exploration, which does not allow us to identify new or to explore previously discovered deposits. Although within the northern ends of the Timan-Pechora (Nenets Autonomous District - NAD) and West Siberian (Yamalo-Nenets Autonomous district - YNAD) provinces, the geological and geophysical exploration is significantly inferior to the exploration of the central and southern regions of these provinces. It can be called satisfactory and allowed to identify many oil and gas fields and have reliable estimates of resource potential (Prischepa, 2016).

The exploration of the Yenisei-Khatanga basin has grown significantly in terms of regional studies in recent years. Still, it remains extremely low, which also applies to the territories of the Lena-Vilyui and Zyryansk prospective basins. Both in the Yenisei-Khatanga and Leno-Vilyui basins, positive results of geological studies were obtained, which cannot be said about the Zyryan basin, the prospects of which remain extremely ambiguous. In the water area, the Barents and the Kara Seas' southern parts are relatively well studied. The water areas of the northern part of the Barents and Kara Seas, the Laptev Sea, the East Siberian and Chukotka Seas have not been sufficiently studied. The prospects for their oil and gas potential are not clear and not substantiated.

In total, about 750 thousand km of 2D seismic surveys of the 2D MOGT CDP 90 deep wells were drilled in the Arctic shelf (Suprunenko *et al.*, 2012; Kaminsky *et al.*, 2018). At the same time, the main volumes of seismic exploration

(over 630 thousand km) fall on the West Arctic seas, where the average density of seismic exploration reaches 0.5 km/km² in the Barents Sea (together with the southern part of the Pechora Sea) and 0.2 km/km² in the Kara Sea. Seismic density does not even provide a regional study level in the East Arctic seas and varies from 0.02 to 0.06 km/km². In recent years, the study has been reduced to regional seismic surveys, concentrated mainly within the shallow water transit zones and areal seismic surveys (including 3D), performed at Gazprom and Rosneft's licensed sites.

Within the land of the Russian Arctic, more than 350 oil and gas deposits have been identified (Figure 5), of which oil reserves were accounted for in 265 deposits (mainly oil or mixed), and gas reserves - in 189 (from purely gas, gas condensate to mixed oil and gas condensate). The most significant number of oil and gas deposits were identified within Yamalo-Nenets Autonomous Area the territory of which belongs to the West Siberian oil and gas production. It also revealed the largest land deposits in the Republic of Azerbaijan (Larchenko *et al.*, 2020).

The next entity in the Republic of Azerbaijan in terms of the number of discovered fields is NAD, where oil fields are predominantly established, and they are significantly inferior to them in terms of the number of deposits in the north of Krasnoyarsk Territory, north of the Republic of Sakha (Yakutia) and Chukotka Autonomous District. Within the Arctic waters, mainly gas-bearing basins are widely developed. The oil-bearing regions gravitate towards the southern parts of the seas - the territorial extensions of the land basins, where a significant part of Russia's oil potential is concentrated.

In the Arctic, oil and gas deposits have been identified within the Barents and the Kara Seas (Weniger, 2019). The identified oil reserves are concentrated mainly on the shelves of the Barents and the Kara Seas' southern parts. Oil reserves were recorded in 8 fields, gas – in 18. In the Barents and the Pechora Seas 8 fields were identified: 1 - oil (Prirazlomnoe) 1 - OGR (North-Gulyaevskoe), 3 - gas (Murmansk, North-Kildinskoe and Ludlovskoe) 3 - gas condensate (Pomeranian, Shtokman and Ledovoe). 13 deposits have been identified in the Kara Sea, partially or marine extensions of onshore fields: 1 - gas and oil (Pobeda), 1 oil and gas condensate - Yurkharovskoe, 4 gas (Kamennomyskoe-sea, Semakovskoe, Antipayutinskoe and Toto-Yakhinskoe) and 7 gas-condensate (Kruzenshternskoe, North-Kamennomyskoe,

Rusanovskoe, Kharasaveyskoe, South Tambeyskoe, Leningrad and Chugoryakhinskoe).

In the mainly gas-bearing Western Arctic basins, a significant amount of condensate is predicted. According to the results of the estimates, the volume of forecast hydrocarbon resources (oil, free gas, condensate, and dissolved gas) of the Russian Arctic is estimated at about 250 billion tons of o. e. tons, including about 43 billion tons of oil and condensate (17% of all resources) and about 206 trillion m³ of natural gas (Prischepa *et al.*, 2019). The distribution of hydrocarbon resources within the oil and gas prospective territories and water areas of the Russian Arctic is very uneven (Figure 5). The former account for about 136 billion tons BOE (almost 55% of the total volume). The vast majority are gas-containing facilities located administratively in YNAD (120 billion tons BOE, including 97 trillion m³ of gas). The remaining 42% are also predominantly gas dispersed within the Arctic shelf (Figure 6).

Note that in the estimates of the US Geological Survey, the share of land resources was estimated much more modestly (Nefedov, 2018). Simultaneously, the forecast of the hydrocarbon potential, as a whole, differ by more than six times (250 billion tons BOE and 40 billion tons BOE). Liquid - by more than five times (43 billion tons and 8 billion tons), gas - more than 6 times (206 trillion m³ and 32 trillion m³) Of course, even taking into account the fact that the southern regions of YNAD (West Siberian oil and gas field) and the north of the Lenno-Tunguska gas field were not included in the assessment of the geological service, the discrepancy between the estimates is more than obvious.

On land, the territory of YNAD is the most significant in terms of liquid hydrocarbons' potential. In the water area – the continuation of the Timan-Pechora and West Siberian provinces (Figures 7 and 8).

The most fundamental question concerns the prospects of the remote Arctic shelf (Figures 9 and 10). Judging by the cited and very ambiguous estimates (but extremely low), this region is estimated as promising solely out of geopolitical interest for Russia and is unlikely to be vital (economically) important even with a wide spread of work in the Arctic (Figures 11 and 12).

5. CONCLUSIONS:

Today, the Russian Arctic region's hydrocarbon potential is defined, in-demand and

on its basis, the new production will be created in the long term. There are no technical or technological limitations for its development, which is proved by successful experience in commissioning such fields as Vankorskoe, Bovanenkovskoe and North-Kamennomyskoe. The involvement rate in development will depend solely on demand for hydrocarbon raw materials and companies' investment opportunities.

The development of the Arctic shelf will require fundamentally new technologies both in research and development. Today's technology allows for large-scale seismic exploration on land in transit strata and even in remote areas of the Arctic shelf. It is essential to understand that no matter how much the seismic equipment studies the Arctic waters, an idea of the real oil and gas potential can only be obtained if the wells are drilled and tested completely. The concessions to drilling exploration and justification of the categories of reserves provided for in recent methodological documents when calculating the reserves of the Arctic shelf, unfortunately, will not allow the formation of full-fledged and design documents that can become the basis for the active development of these fields.

The cost of exploratory drilling (an order of magnitude higher than on land) and the complexity of technology today make exploratory drilling in offshore regions of the Arctic economically practically prohibitive. Oil and gas potential is not fully studied. However, it is significantly studied by the Western expert community. The main uncertainty is the proportion of liquid hydrocarbons on the Arctic seas (Prischepa *et al.*, 2019). The oil and gas potential of the Arctic shelf has not been fully studied. It is significantly lower according to the estimates of the international expert community than the official estimates of Russian estimations (Kontorovich, 2015; Vorotnikov *et al.*, 2019; Kaminsky *et al.*, 2016; Kaminsky *et al.*, 2017; Suprunenko *et al.*, 2016; Suprunenko *et al.*, 2012; Kaminsky *et al.*, 2018; Skorobogatov, Prischepa *et al.*, 2020). The author's approach to assessing the Western Arctic's raw material base in this study shows that it is much higher than international estimates for liquid hydrocarbons but significantly inferior to official estimates for gas. The main uncertainty is the estimation of the share of liquid hydrocarbons on the Arctic seas' shelf.

The most viable strategy that has proven effective in Norway is a radial or creeping strategy for promoting projects as technology evolves from the southern latitudes to the more northern and from coastal to the more remote deep-sea.

The study and development of the Arctic's hydrocarbon potential may become one of Russia's main challenges in the second quarter of the 21st century, determining its innovative and scientific development.

6. ACKNOWLEDGEMENTS:

The publication has been prepared in the context of a government order of Russia on «Development of interdisciplinary trends in the complex development of the Earth's interior and nature preservation» № 075-03-2020-127\1.

7. REFERENCES:

1. Arctic Environmental Protection Strategy (1991). Rovaniemi, Finland, Available at: http://library.arcticportal.org/1542/1/article_environment.pdf
2. Blumenberg, M., Lutz, R., Schlömer, S., Krüger, M., Scheeder, G., Berglar, K., and Weniger, P. (2016). Hydrocarbons from near-surface sediments of the Barents sea north of Svalbard - indication of subsurface hydrocarbon generation. *Marine and Petroleum Geology*, 76, 432-443. DOI:10.1016/j.marpetgeo.2016.05.031
3. Bogoyavlensky, V.I., Kazanin, G.S., and Kishankov, A.V. (2019). Gas saturation of shallow deposits of the Arctic and subarctic seas. *Marine Technologies*, Gelendzhik.
4. Carayannis, E.G., Cherepovitsyn, A.E., Ilinova, A.A. (2017). Sustainable Development of the Russian Arctic zone energy shelf: The Role of the Quintuple Innovation Helix Model. *Journal of the Knowledge Economy*. 8, 456–470, DOI: 10.1007/s13132-017-0478-9
5. Carayannis, Ilinova, A., Chanyшева, A. (2019). Arctic Offshore Oil and Gas Projects: Methodological Framework for Evaluating Their Prospects. *Journal of the Knowledge Economy*, 2019, DOI: 10.1007/s13132-019-00602-7
6. Chanyшева, A. F., Ilinova, A. A., Solovyova, V. M., and Cherepovitsyn, A. E. (2019). Long-term forecasts of the oil and gas arctic shelf development: The existing methodical approaches and assessment of a possibility of their

- application. *Paper presented at the IOP Conference Series: Earth and Environmental Science*, 302(1) doi:10.1088/1755-1315/302/1/012068
7. Cherepovitsyn, A.E., Lipina, S.A., Evseeva O.O. (2018). Innovative approach to the development of mineral raw materials of the Arctic zone of the Russian Federation. *Journal of Mining Institute*, 232, 438-444. <https://doi.org/10.31897/pmi.2018.4.438>
 8. Decree of the President of the Russian Federation of May 2, 2014 "On land territories of the Arctic zone of the Russian Federation".
 9. Proceedings of the All-Russian Scientific-Practical Conference. Development of the North and the Arctic: Challenges and Prospects. Apatity, November, 2013. *Kolsk Scientific Center of RAS*. Available at: <http://www.iep.kolasc.net.ru/tezis2013.pdf>
 10. Dewing, K., Hadlari, T., Pearson, D. G., and Matthews, W. (2019). Early ordovician to early devonian tectonic development of the northern margin of laurentia, Canadian Arctic islands. *Bulletin of the Geological Society of America*, 131(7-8), 1075-1094. DOI:10.1130/B35017.1
 11. Draft strategy for the development of the Arctic up to 2035 on the Basis of the state policy of the Russian Federation in the Arctic for the period up to 2035, 2020. Available at: <http://www.azrf.labourmarket.ru/docs/проект%20Стратегии%20АЗРФ-2035.pdf>
 12. Durbano, A. M., Pratt, B. R., Hadlari, T., and Dewing, K. (2015). Sedimentology of an early Cambrian tide-dominated embayment: Quyuq formation, Victoria island, arctic Canada. *Sedimentary Geology*, 320, 1-18. DOI:10.1016/j.sedgeo.2015.02.004
 13. Egorov, A.S., Vinokurov, I.Yu., and Telegin, A.N. (2018). Scientific and methodical approaches to increase prospecting efficiency of the Russian Arctic shelf state geological mapping. *Journal of Mining Institute*. 2018, 233, 447-458. DOI: 10.31897/PMI.2018.5.447
 14. Energy Futures. (2013). The role of research and technological development. European Commission. Brussels. *The World Petroleum Council Guide to Arctic Oil and Gas*. Research WPC. Available at: <http://www.world-petroleum.org/resources/education-guides/290-guide-oil-sp-233579939>
 15. Fundamentals of the state policy of the Russian Federation in the Arctic for the period up to 2035, approved by decree of the President of Russia on March 5, 2020 (Decree of the President of the Russian Federation of March 5, 2020, 164 "On the Basics of the state policy of the Russian Federation in the Arctic for the period up to 2035"). Available at: <http://publication.pravo.gov.ru/Document/View/0001202003050019>.
 16. Future of the Arctic, a new dawn for exploration (2006). Research by Wood Mackenzie. Available at: <http://www.woodmacresearch.com>
 17. Galloway, B. J., Dewing, K., and Beauchamp, B. (2018). Upper Paleozoic hydrocarbon systems in the Sverdrup basin, Canadian arctic islands. *Marine and Petroleum Geology*, 92, 809-821. DOI:10.1016/j.marpetgeo.2017.12.013
 18. Grigorev, M.B., Tananykhin, D.S., and Poroshin, M.A. (2020). Sand management approach for a field with high viscosity oil. *Journal of Applied Engineering Science*, 18(1), 64-69. doi:10.5937/jaes18-24541
 19. Geological Survey (2008). Circum – the Arctic resource appraisal: estimates of undiscovered oil and gas in North of the Arctic circle, CARA, U.S. Available at: <http://energy.usgs.gov/RegionalStudies/Arctic.aspx>.
 20. Hansen, J. A., Mondol, N. H., Jähren, J., and Tsikalas, F. (2020). Reservoir assessment of middle Jurassic sandstone-dominated formations in the egersund basin and ling depression, eastern central North sea. *Marine and Petroleum Geology*, 111, 529-543.
 21. Harada, D. (2020). Behind the recent acceleration of the arctic oil and gas

- development in Russia: Potential, ongoing projects and challenges. *Polar Record*. DOI:10.1017/S0032247420000091
22. Houseknecht, D. W. (2018). Petroleum systems framework of significant new oil discoveries in a giant Cretaceous (Aptian–Cenomanian) clinothem in the Arctic Alaska. Preliminary version published online, Ahead of Print. *AAPG Bulletin*, DOI: 10.1306/08151817281.
 23. Houseknecht, D.W., Bird, K.J., and Garrity, C.P. (2012). Assessment of undiscovered petroleum resources of the Amerasia basin petroleum province, U.S. *Geological survey scientific investigations report*, 5146, 36.
 24. Ivanitskaya, E. V., Buinovskiy, S. N., Nikonorov, S. M., and Sitkina, K. S. (2019). Industrial safety as the main element of the sustainable development of the Russian arctic zone. *Work safety in industry*, 3, 34-44.
 25. Ivanova, I. Y., Korneev, A. G., and Tuguzova, T. F. (2019). Assessment of feasible power supply options for new projects in the Arctic zone of the Republic of Sakha (Yakutia). International multi-conference on industrial engineering and modern technologies, *FarEastCon*.
 26. Kaminsky V.D., Suprunenko O.I., and Chernykh A.A. (2017). Big oil of the Arctic. Not only a dream, but also a real perspective. *Oil and Gas Vertical*, 5, 54-58.
 27. Kaminsky V.D., Suprunenko O.I., Smirnov A.N., Medvedeva T.Yu., Chernykh A.A., and Aleksandrova A.G. (2016). Current resource status and prospects for the development of small and medium-sized enterprises in the shelf region of the Russian Arctic. *Exploration and protection of mineral resources*. 136-142.
 28. Kaminsky, V.D., Suprunenko, O.I., Medvedeva, T.Yu., and Chernykh, A.A. (2016). The Arctic shelf of Russia. *Oil and gas vertical*, 6, 25-29.
 29. Kaminsky, V.D., Zuykova, O.N., Medvedeva, T.Yu., and Suprunenko, O.I. (2018). The hydrocarbon potential of the continental shelf of Russia: the state of knowledge and development prospects. *Mineral resources of Russia, Economics and Management*, 4-9.
 30. Kleshchev, K. A., Kontorovich, A. E., Krylov, N. A., and Mironov, Yu.P. (2000). Methodological guide to the quantitative and economic assessment of oil, gas and condensate resources in Russia. Moscow, 189.
 31. Kontorovich, A.E. (2015). Ways of developing oil and gas resources of the Russian sector of the Arctic, INIGG SB RAS named after A.A. Trofimuk. *Report at the scientific session of the general meeting of the RAS, Bulletin of the RAS*, 85, 5-6, pp. 420-430.
 32. Kruk M.N., Alabyev V.R., and Semenov A.S. (2020). Economic efficiency of application of artificial air cooling for normalization of thermal conditions in oil mines. *Scientia Iranika*, № 27, Vol. 3, Pp 1606 - 1615 .
 33. Larchenko, L. V., Kolesnikov, R. A., and Mukhametova, L. (2020). Russian oil and gas industry as a sphere of international interests and economic cooperation. *E3S Web of Conferences*, 161.
 34. Lerch, B., Karlsen, D. A., Abay, T. B., Duggan, D., Seland, R., Backer-Owe, K. (2016). Regional petroleum alteration trends in Barents sea oils and condensates as a clue to migration regimes and processes. *AAPG Bulletin*, 100, 2, 165-190. DOI:10.1306/08101514152
 35. Llopart, J., Urgeles, R., Forsberg, C. F., Camerlenghi, A., Vanneste, M., Rebesco, M., and Lantzsch, H. (2019). Fluid flow and pore pressure development throughout the evolution of a trough mouth fan, the western Barents sea. *Basin Research*, 31, 3, 487-513. DOI:10.1111/bre.12331
 36. Matveeva, T.V., Semenova, A.A., Shchur, N.A., Logvina, E.A., and Nazarova, O.V. (2017). Prospects of gas hydrate presence in the Chukotka Sea. *Notes of the Mining Institute*, 226, 387-396. DOI: 10.25515/PMI.2017.4.387
 37. Mulrooney, M. J., Leutscher, J., Braathen, A. (2017). 3D structural analysis of the Goliat field, the Barents sea, Norway. *Marine and Petroleum*

- Geology*, 86, 192-212. DOI:10.1016/j.marpetgeo.2017.05.038
38. Neville, L. A., McNeil, D. H., Grasby, S. E., Ardakani, O. H., and Sanei, H. (2017). Late Paleocene-middle Eocene hydrocarbon source rock potential in the arctic Beaufort-Mackenzie basin. *Marine and Petroleum Geology*, 86, 1082-1091. DOI:10.1016/j.marpetgeo.2017.06.042
 39. Otmas, A. A., Grokhotov, E. I., and Grigoriev, G. A. (2017). Shale strata of Kaliningrad region - geology, modelling, resource potential and prospects of development. *Paper presented at the EAGE/SPE Joint Workshop on Shale Science 2017*.
 40. Pak, A. A., Sukhorukova, R. N., and Nikolaev, A. I. (2019). Energy efficient polystyrene aerated concrete composite products and condition monitoring for building structures and facilities in the arctic regions. *IOP Conference Series: Earth and Environmental Science*, 2019, 302, 1.
 41. Pavlenko, V. (2013). Arctic zone of the Russian Federation in the national security system of the interests of the country. *The Arctic: ecology and economy*, 2013, 4, 12.
 42. Prischepa, O.M. (2016). Problems of reproduction of hydrocarbon reserves: the Arctic shelf and (or) hard-to-recover reserves. *Mineral resources of Russia, Economics and Management*, 1-2, 18-34.
 43. Prischepa, O.M., Metkin D.M., and Borovikov I.S. (2019). Hydrocarbon potential of the arctic zone of Russia and prospects for its development. *Mineral resources of Russia, Economics and Management*, 2019, 3-166, 14-28.
 44. Prischepa, O.M., Nefedov Y.V., and Grigiriev G.A. (2019). Prospects for further study and development of the hydrocarbon potential of the Arctic shelf of the Pechora-Barents sea region. *Scientific journal of the Russian gas society*, 3-4, 5-20.
 45. Research and Development in the Energy Sector. (2010). Solna, Vattenfall AB (Sweden).
 46. Research of the Analytical Centre under the Government of the Russian Federation, (2015). *Energy Bulletin*, 20 Issue.
 47. Resources to Reserves. (2013). Oil, Gas and Coal Technologies for the Energy Markets of the Future. *Research IEA*. Available at: <https://www.iea.org/w/bookshop/add.aspx?id=447>
 48. Sabukevich, V.S., Podoprigora, D.G., and Shagiakhmetov, A.M. (2020). Rationale for selection of an oil field optimal development system in the eastern part of the pechora sea and its calculation. *Periodico Tchê Química*, 17(34), 634-655.
 49. Schenk, C.J. (2012). An estimate of undiscovered conventional oil and gas resources of the world, U.S. *Geological Survey Fact Sheet*, 3042, 6.
 50. Shemin, G., Deev, E., Vernikovskiy, V. A., Drachev, S. S., Moskvina, V., Vakulenko, L., Sapyanik, V. (2019). Jurassic paleogeography and sedimentation in the northern West Siberia and the South Kara sea, Russian arctic and subarctic. *Marine and Petroleum Geology*, 104, 286-312. DOI:10.1016/j.marpetgeo.2019.03.030
 51. Skorobogatov, V. A., and Kabalin M. Yu. (2019). The Western Arctic shelf of Northern Eurasia: reserves, resources and production of hydrocarbons until 2040 and 2050. *Neftegaz.RU*.
 52. Skorobogatov, V. A., Pyatnitskaya, G. R., Soin, D. A., and Skorobogatko, A. N. (2018). Experience of estimates of potential free gas resources of sedimentary basins of Russia and their confirmability during prospecting and exploration. *Geology of oil and gas. Gazprom VNIIGAZ-70 years*, 59-65.
 53. Sobota Jerzy, Malarev V.I., Kopteva A.V. (2019). Calculation of Oil-saturated Sand Soils' Heat Conductivity. *Journal of Mining Institute. Zapiski Gornogo Instituta*. Vol. 238. Pp. 443-449. Doi: 10.31897/pmi.2019.4.443
 54. Sobolev, P., Franke, D., Gaedicke, C., Kus, J., Scheeder, G., Piepjohn, K., and Mouly, B. (2016). Reconnaissance study of organic geochemistry and petrology of Paleozoic-Cenozoic

- potential hydrocarbon source rocks from the New Siberian Islands, arctic Russia. *Marine and Petroleum Geology*, 78, 30-47. DOI:10.1016/j.marpetgeo.2016.09.005
55. Strategy of social and economic development of the Arctic zone of the Russian Federation until 2020 and ensuring national safety standards. Approved in 2013 <http://government.ru/static/viewer/index.html#files/2RpSA3sctElhAGn4RN9dHrtzk0A3wZm8.pdf>
 56. Suprunenko, O., Suslova, V.V., and Medvedeva, T.Yu. (2012). The state of the study and development of oil and gas resources of the Arctic shelf of Russia. *Geology of oil and gas*, 99-107.
 57. Tsvetkov, P., Cherepovitsyn, A., and Makhovikov, A. (2020). Economic assessment of heat and power generation from small-scale liquefied natural gas in Russia. *Energy Reports*, Volume. 6, Pages 391-402, DOI: 10.1016/j.egyr.2019.11.093
 58. Tolstikov, A.V. (2018). Reserves and resources of hydrocarbons, prospects for studying and industrial development of the subsoil of the Russian seas in the XXI century. *Geology of oil and gas*. 4, 73-85.
 59. UN Convention on the Law of Sea, 1982. The official website of the United Nations. Available at: https://www.un.org/depts/los/convention_agreements/texts/unclos/unclos_e.pdf
 60. Varlamov, A. I. (2017). Gas future of Russia: the Arctic. World resources and gas reserves and promising technologies for their development (WGRR-2017): abstracts of the IV International Conference. *scientific-practical.conferences*, Moscow, Gazprom VNIIGAZ, 2017, 9-10.
 61. Vasiltsov, V.S., and Vasiltsova, V.M. (2018). Strategic Planning of Arctic Shelf Development Using Fractal Theory Tools. *Journal of Mining Institute*, 234, 663-672. DOI: 10.31897/PMI.2018.6.663
 62. Vorotnikov, A. M., and Tarasov, B. A. (2019). Public-private partnership as a mechanism of the russian arctic zone's sustainable development. *IOP Conference Series: Earth and Environmental Science*, 302, 1.
 63. Weniger, P., Blumenberg, M., Berglar, K., Ehrhardt, A., Klitzke, P., Krüger, M., and Lutz, R. (2019). Origin of near-surface hydrocarbon gases bound in northern barents sea sediments. *Marine and Petroleum Geology*, 102, 455-476. DOI:10.1016/j.marpetgeo.2018.12.036
 64. Wood Mackenzie. Future of the Arctic - A New Dawn for Exploration, 2006. Available at: <http://www.woodmacresearch.com>
 65. Yurchenko, I. A., Moldowan, J. M., Peters, K. E., Magoon, L. B., and Graham, S. A. (2018). Source rock heterogeneity and migrated hydrocarbons in the Triassic shublik formation and their implication for unconventional resource evaluation in arctic Alaska. *Marine and Petroleum Geology*, 92, 932-952. DOI:10.1016/j.marpetgeo.2018.03.033
 66. Zharkov, A.M. (2017). The conceptual model for the formation and evaluation of hydrocarbon resources in the most significant "shale" formations of Russia, *EAGE/SPE Joint Workshop on Shale Science: Prospecting and Development*.
 67. Zharov, V. (2019). Conceptual framework for effective management of mining operations and fuel-and-energy development in the arctic. *IOP Conference Series: Earth and Environmental Science*, 263, 1.
 68. Zharov, V., and Zharov, N. (2019). Targeting innovation activities of arctic enterprises in developing mineral and energy resources. *IOP Conference Series: Earth and Environmental Science*, 302, 1.

Table 1. Assessment of hydrocarbon resources of the Arctic seas as of 01/01/2017 (Prischepa et al., 2020).

Subject of the Federation	Stocks	Undiscovered resources, million tons of equivalent fuel equivalent	Total potential Geological / recoverable
Barents Sea	<u>4777</u> 4769	<u>48881</u> 41012	<u>53658</u> 45781
Pechora Sea	<u>1637</u> 548	<u>19963</u> 9468	<u>21600</u> 10017
Kara Sea	<u>3392</u> 2497	<u>52433</u> 45357	<u>55824</u> 47854
Kara Sea (southern part + North Pole)	<u>3392</u>	<u>45652</u>	<u>49043</u>
	2497	40636	43133
Kara Sea (northern part)	<u>0</u> 0	<u>6781</u> 4721	<u>6781</u> 4721
Laptevih sea	<u>0</u> 0	<u>13468</u> 8839	<u>13468</u> 8839
ChukotkaSea	<u>0</u> 0	<u>16160</u> 0	<u>16160</u> 0
East-SiberianSea	<u>0</u> 0	<u>19060</u> 0	<u>19060</u> 0



Figure 1. Major oil and gas provinces in the Arctic according to the US Geological Survey (Geological Survey, 2008)



1. Murmansk oblast,
2. Republic of Karelia (part of Louhsky, Kemsy and Belomorsky municipal Murmansk oblast, Republic of Karelia (part of Louhsky, Kemsy and Belomorsky municipal districts),
3. Arkhangelsk oblast (part of the Onega, Primorsky and Mezensky municipal districts and urban districts of Arkhangelsk, Severodvinsk and Novodvinsk, and administrative owned Arctic Islands),
4. Nenets Autonomous Okrug,
5. Yamalo-Nenets Autonomous Okrug,
6. Krasnodar Krai (part of the Taimyr (Dolgano-Nenets) municipal district, municipal district of Norilsk, a municipal formation of the town of Igarka Turukhansk municipal district,
7. Republic of Sokha (Yakutia) (as part of Abyisky, Allaikhovsky, Anabarsky, Bulunsky, Verkhoyansky, Zhigansky, Oleneksky, Nizhnekolymsky, Srednekolymsky, Ust-Yansky and Eveno-Bytantaysky uluses),
8. Chukotka Autonomous district,
9. Komi Republic (as part of the city district of Vorkuta)

Figure 2. Arctic regions of the Russian Federation (Decree of the President of the Russian Federation of May 2, 2014).

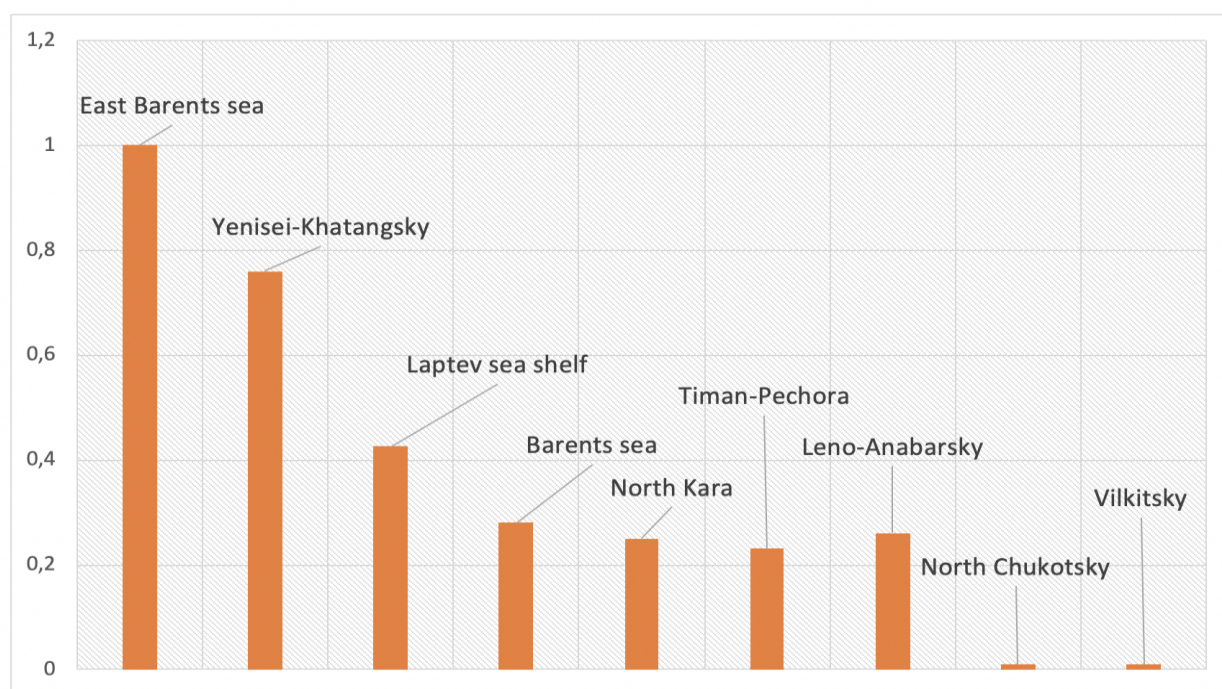


Figure 3. Distribution of oil resources in Russia's Arctic basins (according to the US Geological survey), billion tons (Geological Survey, 2008).

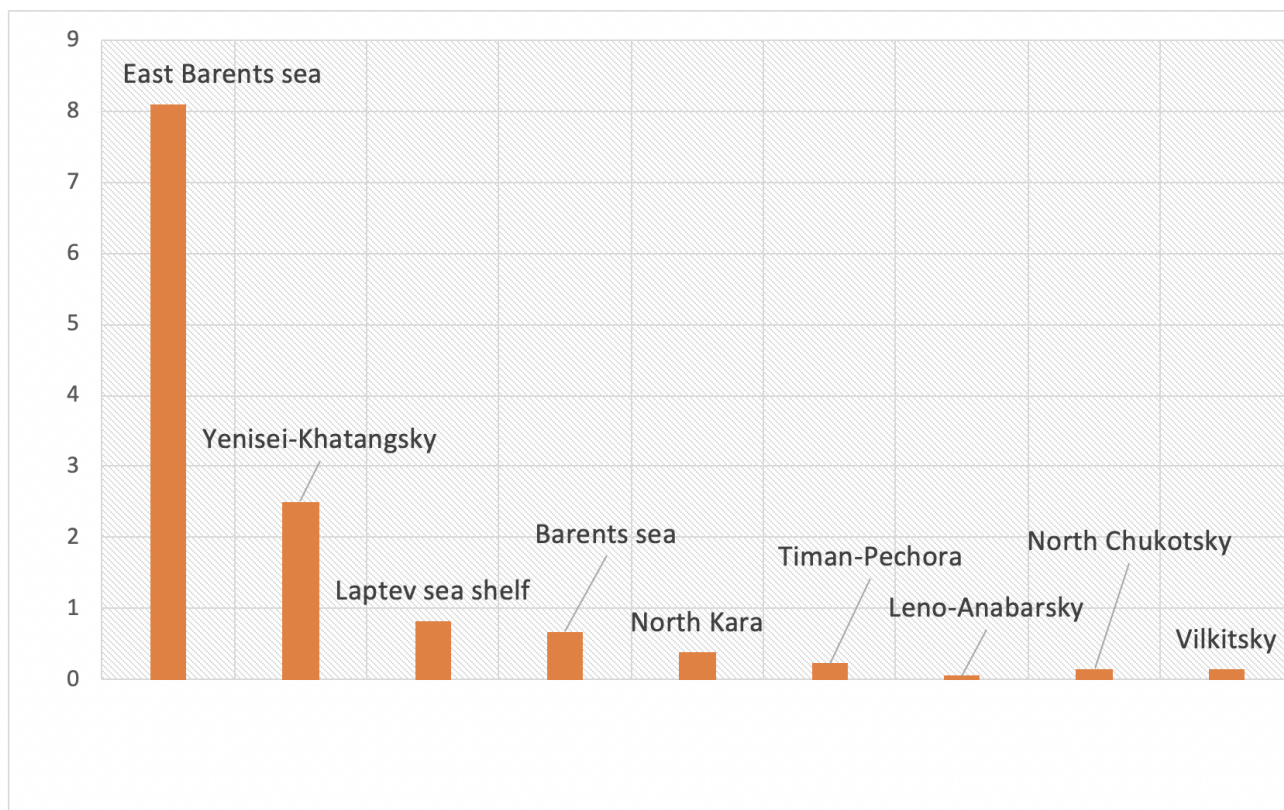


Figure 4. Distribution of gas resources in Russia's Arctic basins (according to the US geological survey), trillion cubic meters (Geological Survey, 2008).

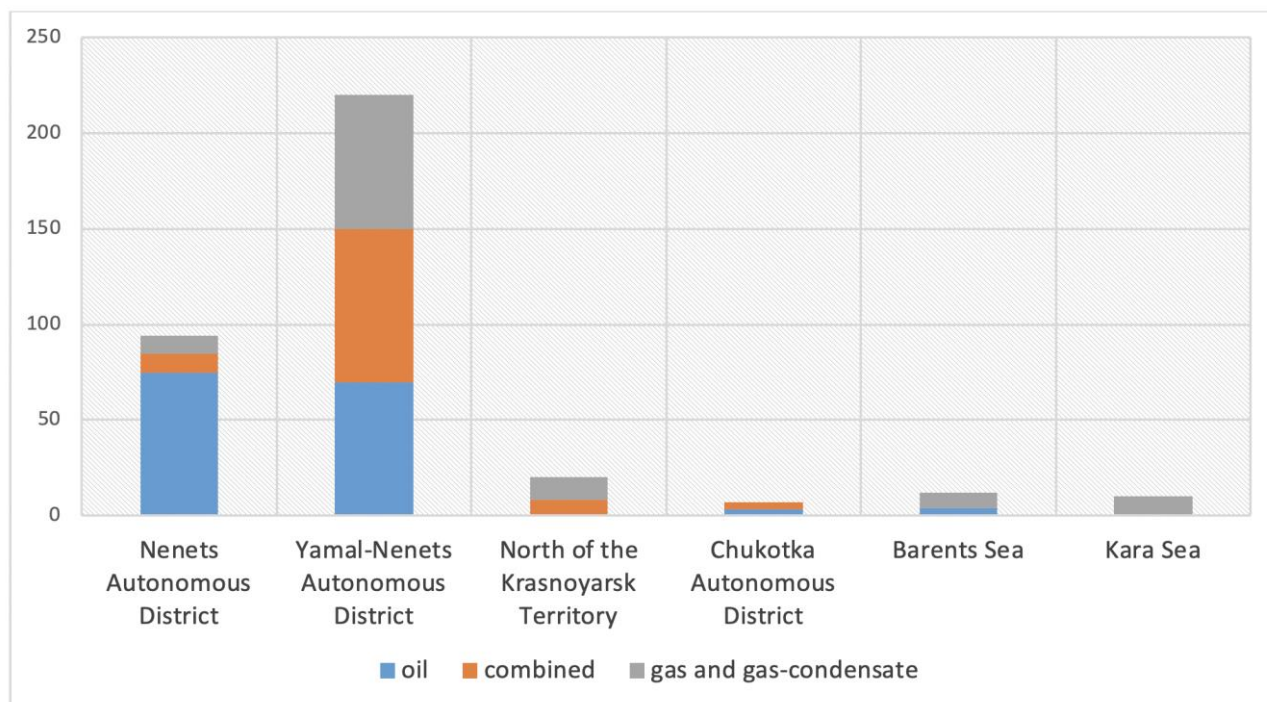


Figure 5. Distribution of identified oil and gas fields in the Russian Federation's Arctic zone by subjects (Geological Survey, 2008).

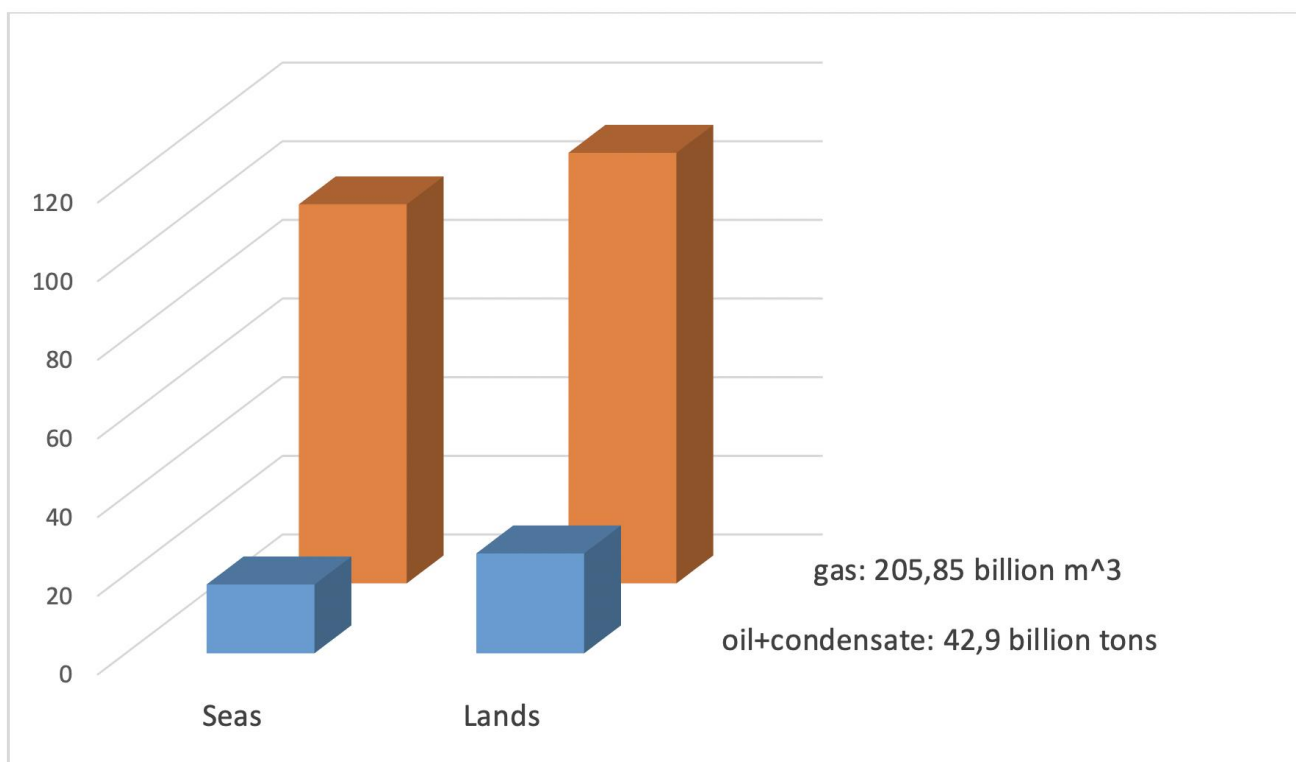


Figure 6. Distribution of oil and gas resources in Russia's Arctic zone (according to the quantitative assessment as of 01.01.2018). Source: the author.

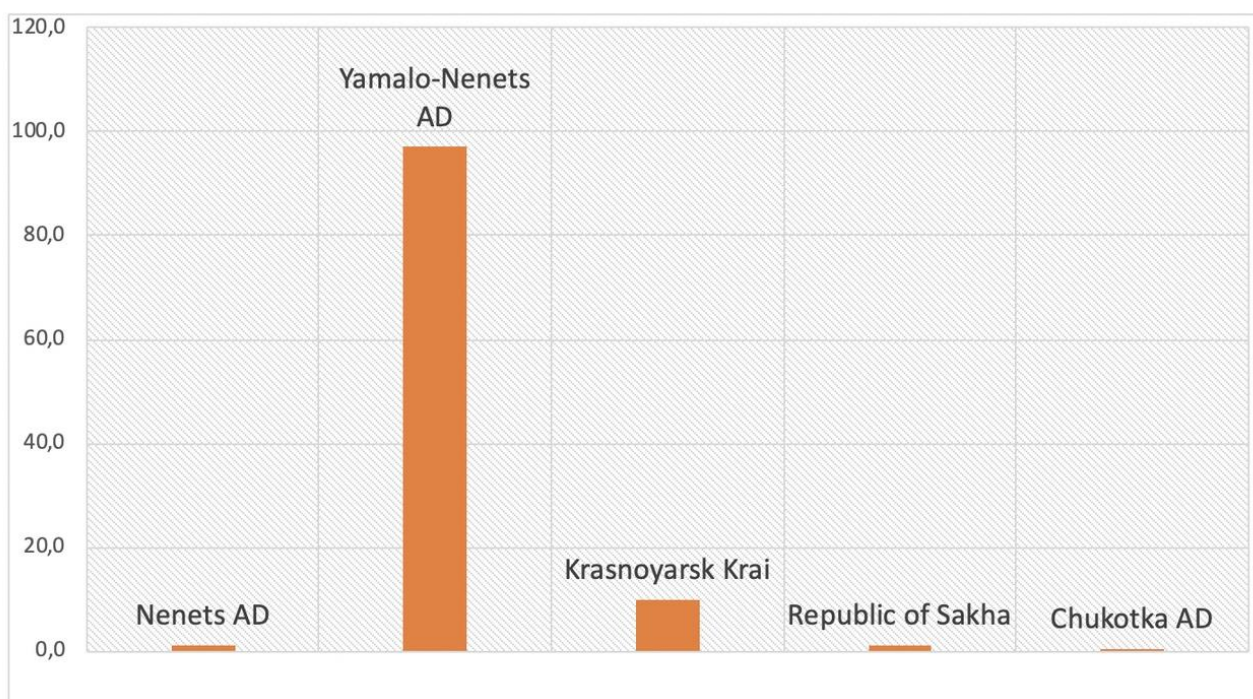


Figure 7. Distribution of gas resources on land in the Arctic of the Russian Federation, trillion cubic meters. (Source: the author).

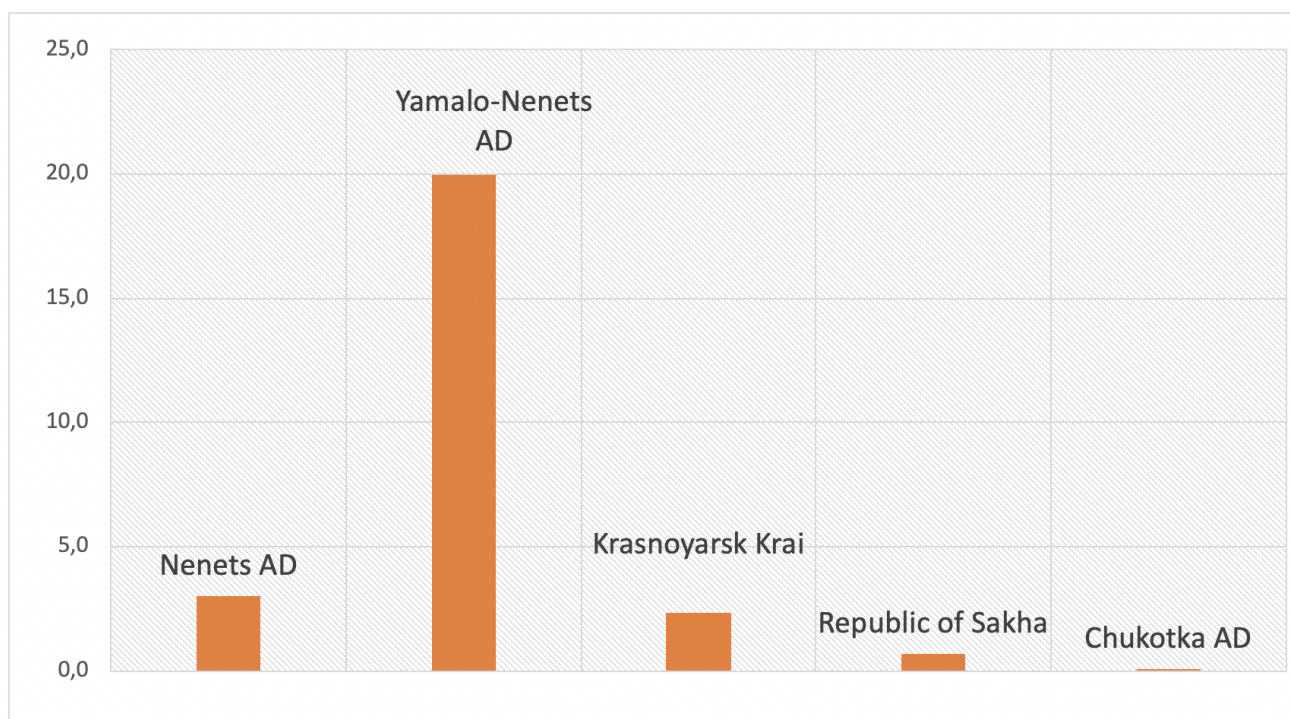


Figure 8. Distribution of liquid hydrocarbon resources on land in the Arctic of the Russian Federation, billion tons. (Source: the author).

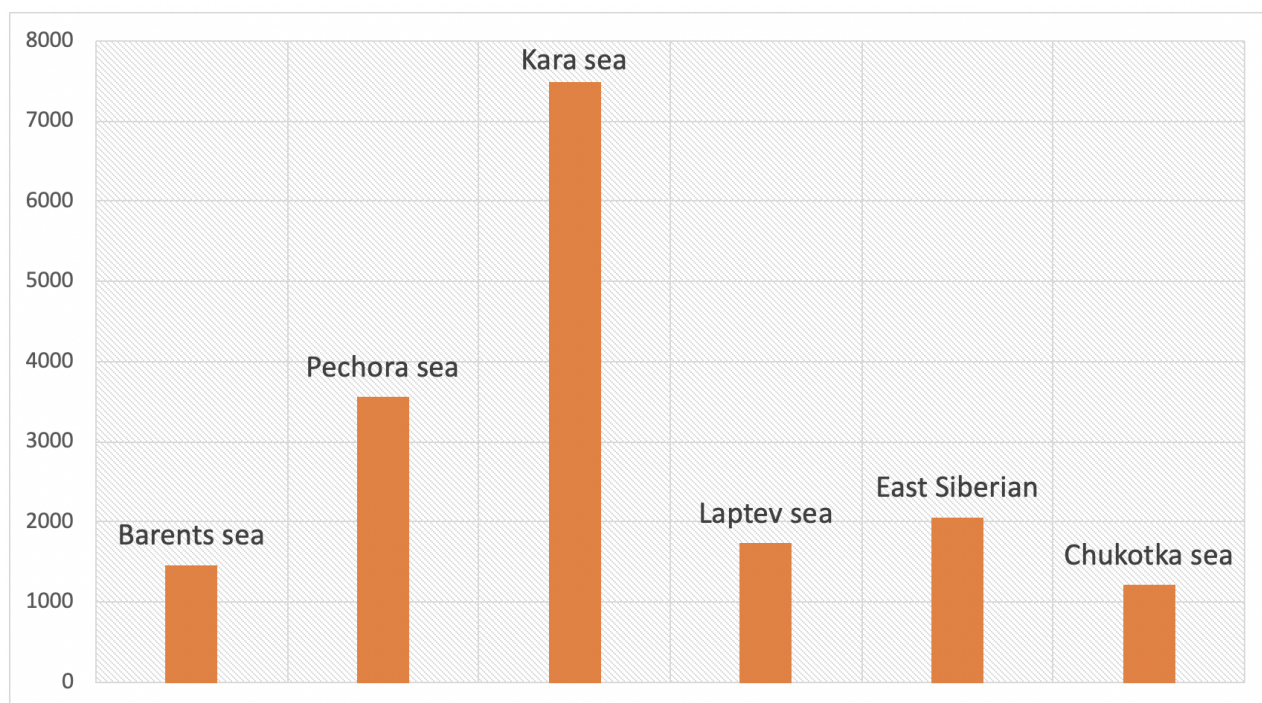


Figure 9. Distribution of initial total resources oil+condensate of the Arctic seas of Russia (Source: the author).

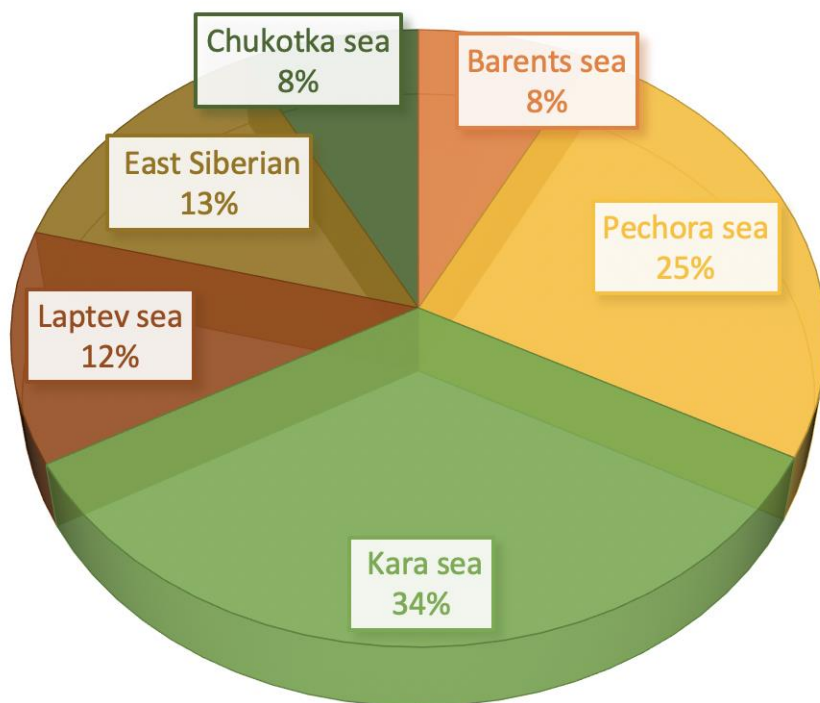


Figure10. Distribution of initial total resources of the Arctic seas of Russia (Source: the author).

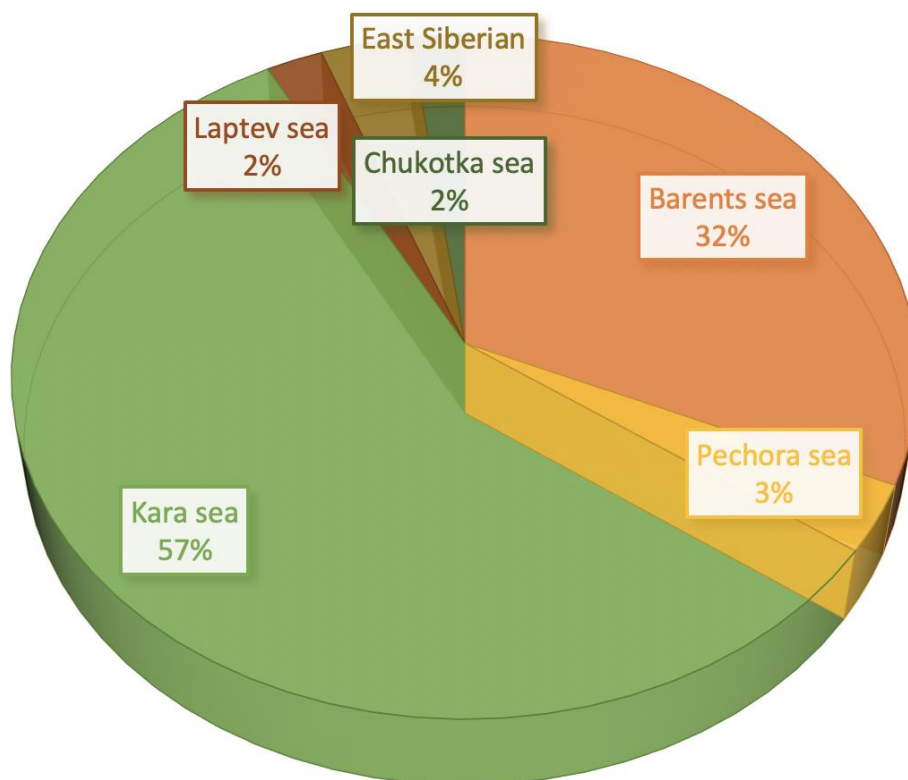


Figure 11. Distribution of initial total free gas resources of Russia's Arctic seas, billion m^3 (Source: the author).

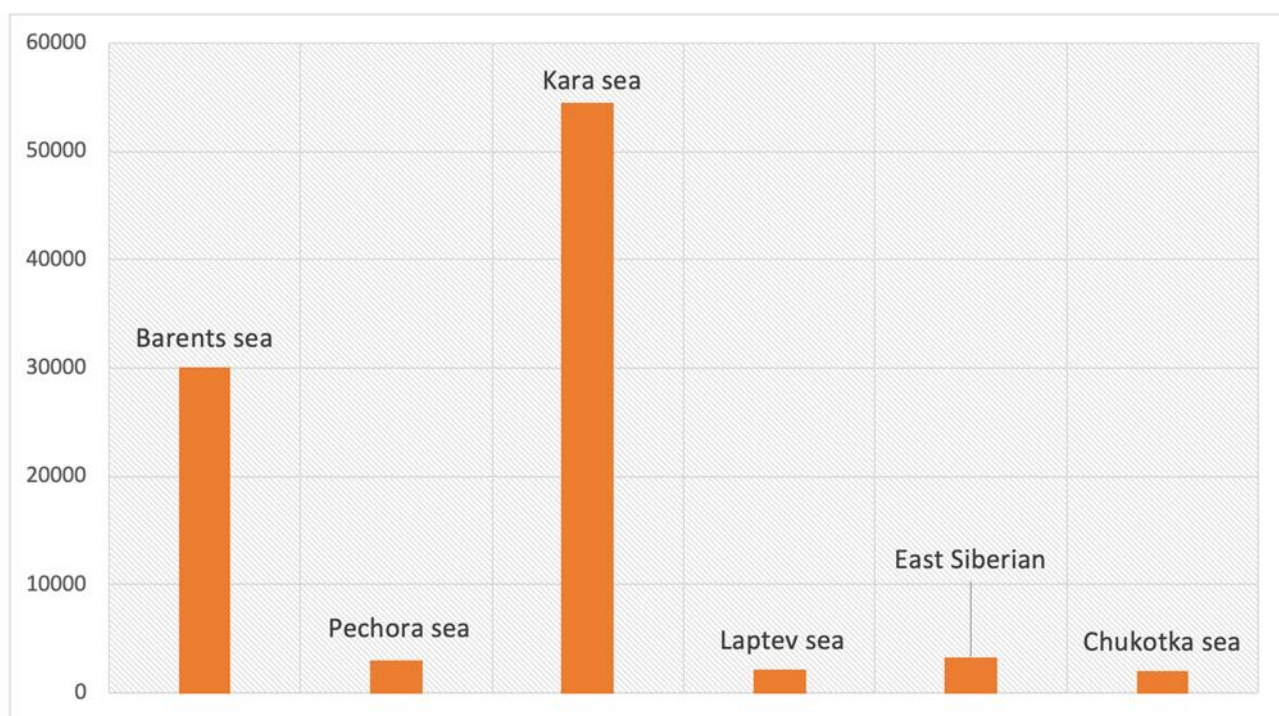


Figure 12. Distribution of initial total free gas resources of Russia's Arctic seas, billion m³ (Source: the author).

**ESTUDO DO PROCESSO DE EROÇÃO DE TURBINAS DE UMA MICRO USINA
HIDRELÉTRICA (UHE) NA FORMA DE UM HIDROCICLONE**

**STUDY OF THE PROCESS OF EROSION OF A MICRO HYDROELECTRIC POWER
PLANT (HPP) TURBINES IN THE FORM OF A HYDROCYCLONE**

**ИССЛЕДОВАНИЕ ПРОЦЕССА ЭРОЗИИ ТУРБИН МИКРОГИДРОЭЛЕКТРОСТАНЦИИ
(ГЭС) В ФОРМЕ ГИДРОЦИКЛОНА**

ZHUZBAY, Kassymbekov^{1*}, KULYASH, Alimova², GALIMZHAN, Kassymbekov³

^{1,2} Satbayev University, Republic of Kazakhstan.

³ Kasgidro Almaty, Republic of Kazakhstan.

* Corresponding author

e-mail: jkk2004@mail.ru

Received 22 July 2020; received in revised form 28 September 2020; accepted 15 October 2020

RESUMO

Um dos graves problemas de uma usina hidrelétrica (UHE) é abastecer uma unidade hidrelétrica com água purificada com a pressão necessária. Caso contrário, os corpos de trabalho centrais - turbinas hidráulicas - estão sujeitos a desgaste abrasivo e falham rapidamente. O desgaste abrasivo não apenas reduz a eficiência e a vida útil da turbina, mas também causa problemas na operação e manutenção. Esta pesquisa teve como objetivo estudar o grau de desgaste abrasivo (taxa de erosão) da superfície de uma turbina hidráulica de pás de uma micro UHE durante a purificação da água por meio de um hidrociclone e garantir seu layout racional com base nos estudos. A investigação de danos à superfície da turbina com o impacto dinâmico foi realizada por modelagem computacional do processo usando o programa Autodesk Simulation CFD, com diferentes versões do corpo do hidrociclone e teste de uma amostra experimental. O software adicional SolidWorks (simulação de fluxo) foi usado para verificar os cálculos. Verificou-se que as formas de dureza das partículas na água afetam significativamente a taxa e a magnitude da erosão, e um projeto diferente do corpo de tratamento na forma de um hidrociclone de maneiras diferentes garante a separação do fluxo em fases. Foi selecionado um esquema racional para a instalação de uma turbina hidráulica dentro de um hidrociclone, que fornece a característica de potência necessária de uma mini central hidrelétrica e outros parâmetros necessários. O maior grau de purificação de água de impurezas sólidas (94%) foi alcançado usando a opção de configuração em um design cilíndrico-cônico com uma entrada de água rotativa no hidrociclone. A localização da turbina hidráulica dentro de um hidrociclone de determinado desenho e o fornecimento tangencial de água às lâminas da turbina hidráulica protegem significativamente a superfície da unidade dos efeitos das partículas sólidas. Sua vida útil pode ser aumentada sem investimento adicional na restauração da unidade.

Palavras-chave: *Micro HPP, hidrociclone, hidroturbina, desgaste abrasivo, grau de purificação da água.*

ABSTRACT

One of the severe problems of a hydroelectric power plant (HPP) is providing a hydroelectric unit with purified water with the required pressure. Otherwise, the central working bodies - hydraulic turbines - are subjected to abrasive wear and quickly fail. Abrasive wear reduces the efficiency and life of the turbine and causes problems in operation and maintenance. This research aimed to study the degree of abrasive wear (erosion rate) of the surface of a blade hydraulic turbine of a micro HPP during water purification using a hydrocyclone and to ensure its rational layout based on the studies. Investigation of damage to the turbine surface from the dynamic impact was carried out by computer modeling of the process using the Autodesk Simulation CFD program, with different versions of the hydrocyclone body and testing of an experimental sample. Additional software SolidWorks (flow simulation) was used to check the calculations. It was found that the forms of particle hardness in water significantly affect the rate and magnitude of erosion, and a different design of the treatment body in the form of a hydrocyclone in different ways ensures the separation of the flow into phases. A rational scheme for installing a hydraulic turbine inside a hydrocyclone was selected, which provides the required power characteristic of a mini hydroelectric power station and other necessary parameters. The highest degree of water purification from solid impurities (94%) was achieved using the configuration option in a cylindrical-conical design with a rotational water

inlet into the hydrocyclone. The location of the hydraulic turbine inside a hydrocyclone of a certain design and the tangential supply of water to the blades of the hydraulic turbine significantly protects the surface of the unit from the effects of solid particles. Their service life can be increased without additional investment in the restoration of the unit.

Keywords: *micro HPP, hydrocyclone, hydro turbine, abrasive wear, degree of water purification.*

АННОТАЦИЯ

Одна из серьезных проблем гидроэлектростанции (ГЭС) - обеспечение гидроагрегата очищенной водой с необходимым давлением. В ином случае основные рабочие органы - гидротурбины подвергаются абразивному износу и быстро выходят из строя. Абразивный износ не только уменьшает эффективность и срок службы турбины, но также вызывает проблемы в эксплуатации и техническом обслуживании. Целью данного исследования было изучение степени абразивного износа (скорости эрозии) поверхности лопастной гидротурбины микроГЭС при очистке воды с помощью гидроциклона и обеспечение ее рациональной компоновки на основе проведенных исследований. Исследование повреждений поверхности турбины от динамического воздействия проводилось путем компьютерного моделирования процесса с использованием программы Autodesk Simulation CFD с различными вариантами корпуса гидроциклона и испытания экспериментального образца. Для проверки расчетов был использовано дополнительное программное обеспечение SolidWorks (flow simulation). Установлено, что формы твердости частиц в воде, существенно влияют на скорость и величину эрозии, а также различное исполнение очистного корпуса в виде гидроциклона по разному обеспечивает разделения потока по фазам. Выбрана рациональная схема установки гидротурбины внутри гидроциклона, которая обеспечивает требуемую энергетическую характеристику мини ГЭС и другие необходимые параметры. Наибольшая степень очистки воды от твердых примесей (94%) было достигнута при использовании варианта компоновки в виде цилиндрико-конического исполнения с вращательным входом воды в гидроциклон. Расположение гидротурбины внутри гидроциклона определенной конструкции и тангенциальная подача воды в лопасти гидротурбины значительно защищает поверхность агрегата от воздействия твердых частиц. Срок их службы можно увеличить без дополнительных вложений в восстановление агрегата.

Ключевые слова: *микроГЭС, гидроциклон, гидротурбина, абразивный износ, степень очистки воды*

1. INTRODUCTION:

The global hydropower capacity worldwide amounted to almost 1,292 GW of which more than a quarter are located in China (352 GW), followed by Brazil (104 GW), USA (103 GW), and Canada (81 GW). In 2018, the global hydropower generated approximately 4,200 TWh of electricity (Hydropower Status Report, 2019). In recent years, small hydropower has received notable development, i.e., constructing mini and micro-hydroelectric power plants (Ghumman *et al.*, 2020). This is because they have some advantages. They do not require the construction of dams and large flooded areas, proximity to consumers, the absence of expensive transporting power lines, the prostate in regulating operating modes, and ecological balance maintenance. It has been established that when compared with other unconventional energy sources, the minimum level of pollution occurs when using mini hydroelectric power plants (Yumaev, 2018).

One of the disadvantages of small and mini hydroelectric power plants is that they require additional construction of outstanding facilities for

preliminary treatment (purification) of water in the form of sedimentation tanks, which lead to an increase in construction costs and operating costs up to 25-30% (Oliver Peysh, 2002). Deterioration of the working bodies' performance due to wear by mechanical impurities sharply reduces the HPP's technological and energy parameters. Therefore, many scientific and practical works are devoted to studying the erosion of hydraulic turbines and technology development for their protection (Padhy, 2008; Kumar, 2015). They noted that the wear of the surface of the turbine blades by solid particles is directly proportional to the duration of exposure, the concentration of impurities, and the granulometric composition of river sediments.

It is indicated that only those particles whose hardness exceeds the hardness of the manufacture material represent a real danger to a hydraulic turbine, i.e., erosion resistance of structural material (Bhola and Hermod, 2004). Two areas are used to study the processes of abrasive wear of various materials — the theoretical and experimental modeling of processes in laboratory conditions (Tkhabisimov, 2019). Erosion analysis of Francis turbine sediments provides insight into the relative intensity of erosion and critical areas of erosion

damage to turbine components (Neopane, 2010). Simultaneously, the highest speeds and accelerations were achieved at the exit from the runner blade and had significant erosion. Besides, unexpected sludge erosion was found on the suction side of the guide vane, where the concept of critical diameter can be used.

To improve the study of the process, a computer 3D model has been developed to describe the movement of solid particles in the flow paths of axial and radial-axial turbomachines (Tabakoff, 1990). The proposed model can be used to visualize the expected nature of the movement of solid particles. A discrete computer simulation of the motion of one particle can be performed using instantaneous values of velocities versus time (Tsuji, 2000). Further computer simulation of moving spherical particles was developed in the works of Joseph (Joseph, 2001). However, this model, like the previous one, does not take into account the real shapes of particles, which are random.

Overall, the review of the study shows that current knowledge and research results are not enough to address this problem entirely. The work performed primarily examines the erosion of operating hydraulic turbines based on the actual technical condition and issues recommendations for their elimination. Practically few studies are studying the abrasive wear of the surfaces of hydraulic turbine blades when working together with a hydrocyclone water treatment device.

Consequently, this research aimed to study the degree of abrasive wear (erosion rate) of the surface of a blade hydro-turbine of a micro HPP during water purification using a hydrocyclone and to ensure its rational layout based on the studies performed.

2. MATERIALS AND METHODS:

The designs of micro-hydroelectric power plants developed differing from the existing ones to protect them from abrasive wear, the hydro-turbines are located inside the cylindrical part of the hydro-cyclone and rotate due to the centrifugal force of the water flow formed at the tangential entrance to the hydro-cyclone body (Petrov, 2013). This ensures the separation of the water composition into liquid and solid phases, i.e., water purification before it reaches the flow part of the hydro turbine (Pezzini, 2016). This arrangement is associated with the need to simplify the construction of the device, downsize the loss of capacity and power generation, and, most notably

to preserve the efficiency and increase the service life of the hydro turbine. For a comparative analysis of the spread of the erosion rate on the blades of the hydro turbine, the following four configuration options of micro-hydroelectric power plants of the hydro-cyclone type were considered (Figures 1 and 2).

The first version (Figure 1a) is made in the form of a classic cylindrical-conical hydro-cyclone. Here the water supply is tangent to the cylindrical part, along a straight pipe. Therefore, the impact of the jet from the pipe with the turbine blade is carried out along its upper part directly, i.e., until the solid particles are entirely separated from the water. The second variant (Figure 1b) differs from the first in the form of the final branch pipe of the water supply pipe in a bent shape. And, the end of the pipe is provided with a flat nozzle, which allows the initial free passage of the jet through the space between the wall of the hydro-cyclone and the turbine blade. Thus, the impact of the jet with the blade occurs after water purification, i.e., from the second approach of the twist. The third variant (Figure 2a) is made in the form of a shortened cylindrical hydro-cyclone. The water supply is made as in the second variant using a pipe with a curved end. For removing captured particles to the dump, a relatively located pipe is provided in the lower part of the unit. The fourth option (Figure 2b) is a structurally inappropriate connection of the bent pipe branch with an uneven surface of the cone. Otherwise, this option is not remarkably different from the others.

To predict the degree of separation of a two-phase liquid in a hydro-cyclone during combined operation with a hydraulic turbine in various versions and study surface damage due to abrasive wear, the processes were subjected to computer modeling (Buldygerov, 2004; Evtyushkin, 2007). A computer simulation was carried out using the Autodesk Simulation CFD program using the Computational Fluid Dynamics model based on the Reynolds Navier-Stokes equation (Autodesk Simulation CFD, 2019). To check the calculations, the additional software "SolidWorks (flow simulation)" was used (Rakhimzhanova, I.B. *et al.*, 2019). When comparing these programs, errors were allowed within 10-12%. The advantage of studying using computer modeling is that the main factors affecting wear can be reduced to a single equivalent (Klunk, M. A. *et al.*, 2019; Buldygerov D.S. 2004). The granulometric composition of the used sediments entering the inlet of the hydrocyclone body is almost half (44.6%) of dusty particles, and 34.4% of particles with diameters of

0.05-0.50 mm (Table 1).

The reduced composition of sediments in water during field tests was determined by hourly taking water samples from the drain and sand pipes of the hydrocyclone. Then they were dried and passed through calibrated meshes to establish the division gradation and analysis according to GOST 12536-2014 (Russia). In this case, sieves with 10 holes were used; five; 2; 1; 0.5; 0.25; 0.1 mm; technical scales with a relative weighing error of no more than 0.1% and a drying cabinet. Separation of soil into fractions without washing with water (size from 10 to 0.5 mm), according to the specified standard, was carried. The sieves of the appropriate dimensions were installed in the column in order of increasing hole sizes. The selected sample was transferred to the top sieve, and it was closed with a lid. Sifting of the soil until complete sorting was carried out by light side blows of the palm of the hand. Fractions of grain, which lingered on the sieves, poured into the dishes, starting from the upper sieve. The completeness of the sieve was checked by shaking each sieve over a sheet of paper. If some particles fall on the sheet, then sieving was repeated until the particles stop falling on the paper. Then the sieve fractions were weighed on a balance.

When separating the soil into fractions with rinsing with water (with a particle size of up to 0.1 mm), the initially moistened sample was thoroughly ground with a pestle. The weighed portion was transferred in parts onto a sieve with a hole diameter of 0.1 mm and elutriated under a stream of water until the sieve flows out clear water. The fractions were dried in an oven at 105 °C, and the dish with soil was weighed. The analysis results were recorded. Since tiny particles do not pose a particular risk of wear, a more in-depth study was mainly subjected to particles with a size of 0.25-0.5 mm. The hardness of the metal of the carbon steel hydraulic turbine on the Mohs scale was 5.0 - 5.5. Some results of a qualitative and quantitative assessment of the abrasive ability of particles entrained with water and predicting abrasive wear for various layouts of mini hydroelectric power plants are presented in the modeling graphs using the above-described method (Figures 3-11).

Bearing in mind that the abrasive wear of the turbine is proportional to the cube of the relative velocity of the mixture of water and solid particles, when modeling the process, the main initial parameters were the velocity heads at the inlet and outlet of the hydrocyclone body. Here, the discharge pipe of the hydrocyclone, through which

the purified water is discharged, plays the role of a suction pipe of a mini HPP. The relative input speed is described by the following formulas:

$$V_1 = k_1 \sqrt{2gH_1}, \text{ m/s} \quad (1)$$

and at the exit

$$V_2 = k_2 \sqrt{2gH_2}, \text{ m/s} \quad (2)$$

where k_1 and k_2 are the speed coefficients, depending on the shape of the turbine blades; H_1 - working head of the turbine, m; g is the acceleration of gravity. Based on existing experience, if $V_2 > V_1$, the greatest abrasive wear should occur at the outlet of the turbine in the direction of the water discharge pipe. As can be seen from Figure 4, this position is confirmed by the results of the simulation.

Preliminary analytical assessment of technological parameters of the adopted mini hydroelectric power plant designs was carried out using the following formulas:

1. Water flow rate at the inlet or in the discharge branch pipe of the hydrocyclone, m^3/s .

$$Q = V * F, \text{ m}^3/\text{s} \quad (3)$$

where V is the speed of water supplied to the hydrocyclone through the pipe from the river, m/s
 F - area cross-section of the inlet or drain pipe, m^2 .

2. Power of the hydraulic unit

$$N = Q * g * H * \eta_g, \text{ W} \quad (4)$$

where $\eta_g = 0.65$ is the efficiency for double (Crossfair) and simple active hydro turbines.

3. Torque, $\text{N} * \text{m}$

$$M = 9550 * N / n, \text{ N} * \text{m} \quad (5)$$

4. Hydroelectric power plant efficiency

$$\eta_g = N / P_{gQH}, 100\% \quad (6)$$

5. Hydraulic unit efficiency

$$P = N * \eta_g - \text{electric power of the hydraulic unit, kW} \quad (7)$$

6. The degree of water purification in a

hydrocyclone

$$S_v = 100 - q_p \quad (8)$$

where q_p - is the percentage of sand through the drain pipe, m^3/s

Thus, it is possible to select (for the considered pressure range at the inlet H) the correct inter-position of the turbine and the hydro-cyclone, ensuring normal functioning with a given water saturation with solid particles.

3. RESULTS AND DISCUSSION:

Initial materials for modeling the process and analyzing the studied parameters were the following data: the diameters of solid fractions of 0.25-0.50 mm, the head of the supplied water $H = 1.5$ m, the flow rate of the supplied water $Q = 0.266$ m^3/s and the concentration of the hydro mixture 5-10%. As shown in Figures 3 and 4, when mechanical impurities enter the hydro-cyclone with water, their main effect occurs along the upper edges of the blades. Then these particles scatter randomly over the areas of contact (red) surfaces. Simultaneously, the maximum rate of erosion is in the range of 8-10 mm/year. Suppose a graphical characteristic based on these indicators $n = f(t)$ is constructed. In that case, the dependence of the rotation frequency (n) on the acceleration time (T) of the hydraulic unit is presented in the following form (Figure 5). It follows that in all versions of the micro HPP operation mode, the hydraulic unit acceleration is set when $t = 3$ s is reached.

It was found that 58 of the 100 particles received directly contact the surface of the hydro-turbine, and the rest (42) are removed through the sand hole and the drain pipe to the outside without touching the blades. In the second variant, as can be seen from Figure 6, the area of erosion on the surface of the blades is much smaller. This shows that with such water supply with mechanical impurities, the flow has time to be cleaned of particles at the first twist, and therefore wear of the surface is insignificant. This is confirmed by the high percentage of particles carried out through the sand hole into the dump (94%). The erosion rate is only 0-1.1 mm/year.

The speed characteristic along the perimeter of the hydro turbine after entering (Figure 7) is improved due to centrifugal forces (up to 6-7 m/s) and in the areas of discharge openings (sand hole and drain pipe) are reduced to 2-3 m/s, which is quite enough for the removal of particles and purified water to the outside. In this mode of

operation, the speed of the turbine shaft was 234 rpm. With a cylindrical design of the micro hydroelectric power station housing of the hydro-cyclone type (3rd variant, Figure 8) with a rotational water outlet, it turned out that the wear area of the blade surface does not change much. This indicates that the absence of the cone part in this case does not negatively affect the cleaning capacity of the unit.

A characteristic feature is that most of the turbine blades are not subject to wear. This is probably due to an increase in the gap between the blades of the hydro turbine and the inner surface of the hydro-cyclone. The speed of the shaft is slightly reduced (up to 170 rpm) in comparison with the second option. During purification, 88% of particles fall into the sand hole of the hydro-cyclone, which shows the permissible degree of water purification with abrasives solid impurities (88%). The trajectory of the swirling jet (stream) in a cylindrical hydro-cyclone with a turbine, due to the limited height of the hydro-cyclone, has a more compressed form. The values of the speeds at the inlet, inside the device, do not differ much (within 4-5 m/s) from each other, and on the drain pipe slightly decreases to 2.5-3.0 m/s (Figure 9). Isolines of the propagation of the flow velocity and pressure inside the cylindrical hydrocyclone fully correspond to the parameters of the established flow path.

Calculations have shown that an average of 15-20 particles out of 100 come into contact with the turbine, which shows the normal cleaning capacity of such a technical design. With a head at the inlet of 1.51 m, the head at the drain pipe was 1.25 m. These losses are considered insignificant and do not adversely affect the required operating mode. The volume flow rate at the drain is 0.206 m^3/s , and at the outlet of the sand hole – 0.06 m^3/s .

The fourth version of the design of a hydro-cyclone with a turbine in the form of a cone (Figure 11) was not the best technical solution to protect the surface of the blades from abrasive wear. This is seen from the Figure and therefore requires a separate particular study in the future. As can be seen from the Figure, the technological feature of wear from others is that the erosion process occurs mainly on the end of the blades, especially on the side of the drain pipe. There is a negative effect of the too-close location of the conical hydro-cyclone (only 4-5 mm) to the end part of the blades. This restricts the free removal of particles through the drainpipe, as in other variants. During the modeling of the process, it turned out that 53 particles out of 100 come into contact with the

turbine, and 74 particles get into the sand trap. The pressure loss at the drain is 10-15%.

The trajectory of the flow with particles, with a diameter of 0.25 mm, in a cone-shaped hydro-cyclone does not differ much from the trajectory of the second option. In order to assess the technological capability of the cylinder-conical version of the micro-hydroelectric power plant layout with the least abrasive wear, an experimental sample was tested in natural conditions at $H = 1.5 - 3.0$ m (Figure 11). The obtained technological parameters are shown in Table 2.

In general, the results of the tests carried out show that the developed design is quite workable, and it allows you to achieve the set goal. As shown in Table 2, with an increase in the water pressure at the inlet - H_B , the supplied water flow rate - Q_B increases. The maximum flow rate for testing is provided at a head of $H_B = 2.5 - 3.0$ m. In this case, the front chamber shutter was opened to the full section. It is also possible to note the efficiency of directed water supply to the surface of the hydro-turbine blades using a pipe (nozzles), rather than using for this purpose 4-carbon branch pipes located tangentially to the outer surface of the hydrocyclone.

4. CONCLUSIONS:

It was found that the value of erosion damage to the surface of the turbine blades in the cases under consideration depends on the degree of water purification from solid impurities in the hydrocyclone body and the dynamic effect of the swirling flow. Simultaneously, the highest degree of water purification from solid impurities (94%) is achieved when using the cylindrical-conical version of the hydrocyclone, and the erosion rate is the lowest and is only 0-1.1 mm/year. It is revealed that the modeling of erosive wear processes using modern software systems makes it possible to predict the rate of possible burial at the stage of designing a hydraulic unit. The effectiveness of this technical solution is confirmed by the achieved capacity of the hydroelectric unit within the range of $N_a = 2.5 - 3.4$ kW, which is quite a good indicator for the individual use of energy at the selected test object, characterized by a low head of water flow due to the small drop in the river bed. This means that the mini hydroelectric power station under consideration has additional opportunities for increasing the power characteristics when using it on areas with a significant slope.

5. ACKNOWLEDGEMENTS:

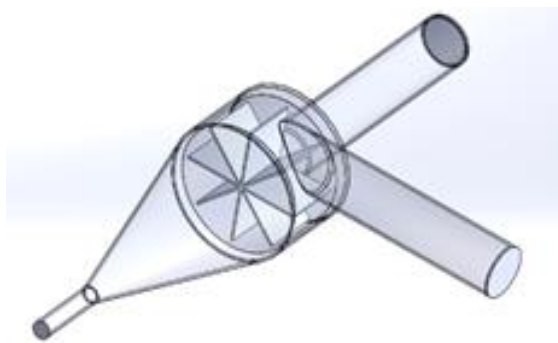
We are thankful for the target program of the Ministry of Education and Science of the Republic of Kazakhstan, "Creation of a base for serial production of world-class Kazakhstani renewable energy sources" (BR 05236263, NAS RK), which made it possible to carry out this work

6. REFERENCES:

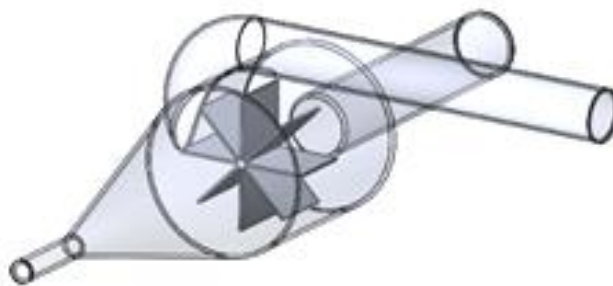
1. Autodesk Simulation CFD (2019). https://www.tadviser.ru/index.php%D0%9F%D1%80%D0%BE%D0%B4%D1%83%D0%BA%D1%82:Autodesk_Simulation_CFD
2. Belash I.G. (2010). Problems of Reliability and Efficiency of Hydraulic Turbine Equipment of Hydroelectric Power Stations. *Proceedings of the Conference "Improving Reliability and Efficiency of Operation of Power Stations and Power Systems"*, MEI [online]. www.energy2010.mpei.ru
3. Bukhtoyarov, V. V., Tynchenko, V. S., Petrovskiy, E. A.; Buryukin, F. A. (2019). Comparative analysis of modeling methods well operation using a submersible electric pump. *Periódico Tchê Química*, Vol. 16 N. 32: 621-632.
4. Buldygerov, D.S. (2004). Computer simulation: methods of statistical modeling.-M.
5. Brekke Hermod. (2002). Design of hydraulic machinery working in sand laden water. *Abrasive erosion and corrosion of hydraulic machinery*, London.
6. Experimental stand for studying the abrasive resistance of structural materials and protective coatings (2013)./ Tkhabisimov A.B., Kachalin G.V., Mednikov A.F. S.V. Sidorov // *Natural and technical sciences*. - No. 5 (67) : 234-238.
7. ETSAP (2010). Energy Technologies Systems Analysis Program. IEA ETSAP - *Technology Bulletin E12*. Available at www.etsap.org
8. European Renewable Energy Institute (2012). Renewable energy sources REN21. *Global Status Report* ". European Focus, Paris, France.

9. Evtushkin, E.V., Matvienko, O.V. (2004). Mathematical modeling of turbulent transfer of a dispersed phase in a turbulent flow. *Vestnik Tomsk State University*, 6 (43): 50 -53.
10. Ghuman, A.R, Haider, H., Yousuf, I (2020). Sustainable Development of Small Hydropower Plants: Multilevel decision making from site selection to optimal design. *Arab Science and Technology Journal*, 45: 4141 – 4159.
11. Global hydropower: development results in (2018).
<https://eenergy.media/2019/05/16/mirovaya-gidroenergetika-itogi-razvitiya-v-2018-godu/16.05.2019> - by Energy.media 451
12. GOST 12536 — 2014 (2015). SOILS. Methods for laboratory determination of particle size (grain) and micro-aggregate composition. M., *Standartinform*.
13. Grigorash, O.V., Kvitko, A.V., Popuchieva, M.A.(2015). Prospects of small hydropower Plants in the piedmont and mountain Streams/ *Scientific journal KubSAU*, 112 (08): 1-13.
14. Herbut, P., Rzepczyński, M., Angrecka, S. (2018). The Analysis of Efficiency and Investment Profitability of a Solar Water Heating System in a Multi-Family Building. *J. Ecol. Eng.*; 19(6):75– 80.
15. International Network on Small Hydro Power (IN-SHP) (2010), World Expo Special Edition Newsletter, *IN-SHP*, Vol. 1, issue 3.
16. Joseph, D.D (2001). Lift correlations from direct numerical simulation of solid-liquid flow. *Proc. Fourth International Conference on Multiphase Flow*. No. 385:1-11.
17. Kassymbekov, Zh.K., Ni, N.P., Botantseva, B.S. (2014). Testing of the water-pipe centrifugal vent valve-pressure damper in laboratory conditions, *Water and Ecology*. 2(58). Sankt – Peterburg: 39-44.
18. Klunk, M. A., Dasgupta, S., Das, M., Wander, P. R. (2019). Computer codes of geochemical modeling used to water-rock interaction simple and complex Systems. *Periódico Tchê Química*, Vol. 16 N. 32: 108 -118.
19. Lagerev, A. (2006). Probabilistic Forecast of Erosion of Steam Turbines, *Moscow. Mechanical engineering*.
20. Lipkin, V.I., Bogombaev, E.S. (2007). Microhydroelectric power plants: a guide to application: Bishkek. LLC "M Maxima".
21. Mini hydropower plants for water supply systems and sewage (2019). [online] .Available at: <http://www.alterenergy.info/hydropower/28-notes/343-mini-hydro-water-supply-sewerage-drains>
22. Neopane, H.P. (2010). Erosion of sediments in hydroturbines. *Dissertation. Norwegian University of Science and Technology*: 201-223.
23. Neopane, H.P., Cervantes, M., Dahlhaug, O. G.(2012). The effect of sediment characteristics for predicting erosion on Francis turbines blades. *Article in International Journal on Hydropower and Dams* 19(1):79-83 .
24. Neopane, H. P., Ole G. Dahlhaug, and Thapa Bhola. (2009). Experimental examination of the effect of particle size and shape in hydraulic turbines. *Waterpower XVI, Spokane, Washington, USA*.
25. Oliver Paish (2002). Small hydro power: Technology and current status. *Article in Renewable and Sustainable Energy Reviews* 6(6):537-556 . DOI: 10.1016/S1364-0321(02)00006-0
26. Ole G. Dahlhaug and Thapa Bhola (2004). Sand erosion in a Franciscan turbine: a case study at a power plant in Yimruk, Nepal. *22nd IAHR Symposium on Hydraulic Machinery and Systems*, Stockholm, Sweden.
27. Ovchinnikov, V.V., Uchevatkina N.V., Kurbatova I.A., Lukyanenko E.V., Yakutina S.V (2019). Titanium alloy wearability increase via implantation of copper and aluminum ions. *Periódico Tchê Química*, Vol. 16 N. 32.: 945-966.
28. Padhy, M. K. and Saini, R. P. (2008). A review on silt erosion in hydro turbines. *Renewable and Sustainable Energy Reviews* 12(7): 1974 - 1987.
29. Pezzini, Alessandra; Briao, Vandré B.; De Boni, Luis A. B.(2016). Preliminary study for a cleaning and water reuse System. *Tchê Química*, Vol. 13 – No. 26: 127 – 132.

30. Petrov, V.I., Sizov, A.G., Fatikhov, I.F. (2013). Analysis of the efficiency of hydrocyclones *KNITU*, 16 (22):255-257.
31. Rakhimzhanova, I.B., Issabaeva, S. N., Zhumartov M.; Nazarbekova, K..T; Turganbay,K.(2019). Modeling in studying computer graphics in the fundamentalization of computer science. *Periódico Tchê Química*, Vol. 16 N. 32: 755-767.
32. Sandeep Kumar, Brajesh Varshney (2015). Estimation of Silt Erosion in Hydro Turbine. *International Journal of Engineering Research & Technology (IJERT)*, Vol. 4.
33. Stakhoviyak, G.V., Batchelor, A.V. (2006). Abrasive, erosional and cavitation wear. *Tribology Engineering*, 3., Burlington, Butterworth-Heinemann: 501–551.
34. Shuyushbayeva, N. N., Sagimbaeva, S. Zh., Mussenova, E.K., Bizhanova, K.B., Zhanturina, N.N.(2020). Reduction of defective conditions of the wind power plant operation at reserving the operation modes of alternative energy. *Periódico Tchê Química*, Vol.17 N. 34: 976-997
35. Tabakoff, W. (1990). Effect of environmental particles on a radial compressor proc. on corrosion-erosion-wear of materials at elevated temperatures / Berkeley. : 261–268.
36. Thapa Bhola. (2007). Erosion Coatings for Hydraulic Turbines and Measurement of Erosion Resistance of Selected Coating Materials. *Journal of the Physical Society of Nepal*, 23 (1):1-6.
37. The current state and prospects for the development of small hydropower in the CIS countries / *Eurasian Development Bank (EDB)*. - Almaty, 2011.: 21-25.
38. Tsuji, Y. (2000). Activities in discrete particle simulation in Japan/*Powder Technology*. - No 113: 278–286.
39. Vinicius de Freitas, Trevisan Lisiane, Reguly Afonso. (2016). Tool steel wear resistance evaluation produced By powder metallurgy, heat treated vacuum. *Tchê Química*, Vol. 13 – N. 26: 97-104.
40. Wang, G. (2013). Current state and development of the research on solid particle erosion and repair of turbomachine. *20th CIRP International conference on life cycle engineering, No room*: 633-638.
41. Yumaev, N.R.(2018). Environmental aspects of the use of renewable energy sources / *Modern trends in technical sciences. Materials of the International Conference* (Kazan): 16-21.
42. Zhurinov, M., Kassymbekov, Zh.K., Kassymbekov, G. Zh. (2019). Mastering and development hydropower in Kazakhstan // *Of the national academy of sciences of the republic of Kazakhstan series of geology and technical sciences*. 3 (435): 219 – 224.

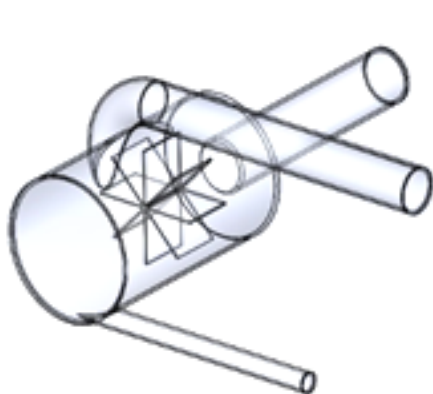


(a)

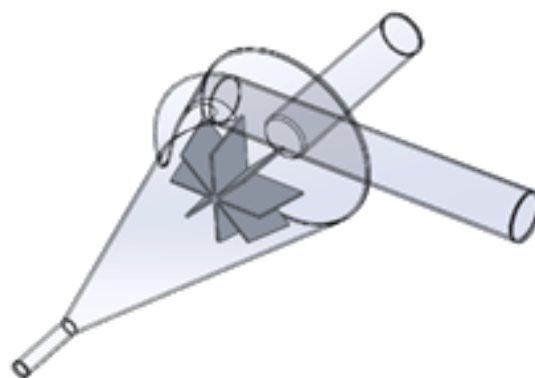


(b)

Figure 1. Layout diagrams of micro-hydroelectric power plants in the form of a cylindrical-conical (a) and hydro-cyclone (b).



(a)



(b)

Figure 2. Layout diagrams of micro electric power plants in the form of a cylindrical (a) and conical (b) hydro-cyclone.

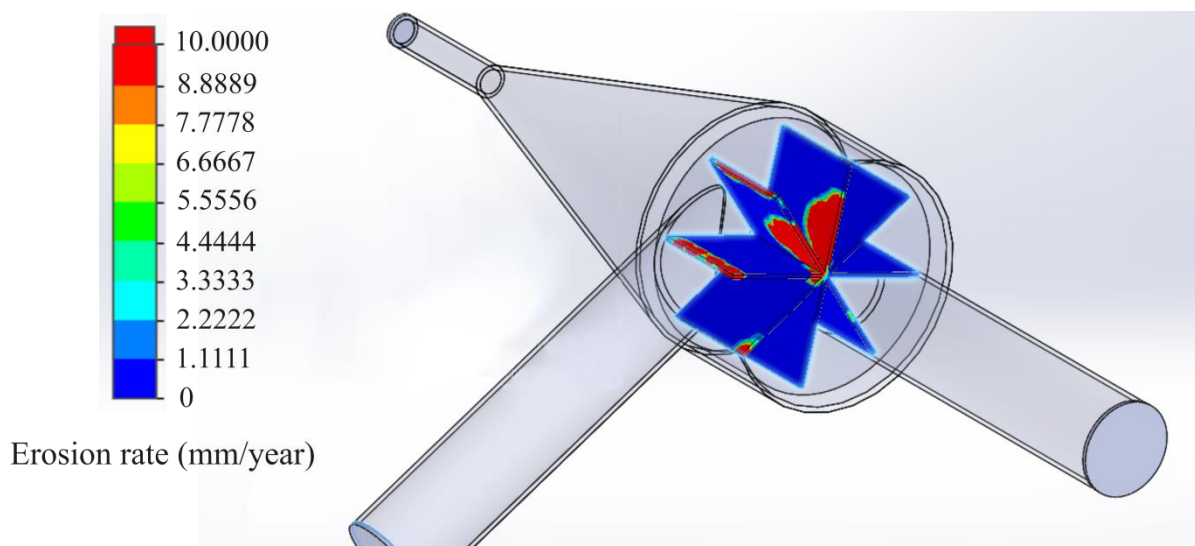


Figure 3. A general picture of hydro turbine blade erosion with the direct flow of water from mechanical admixtures (1st version).

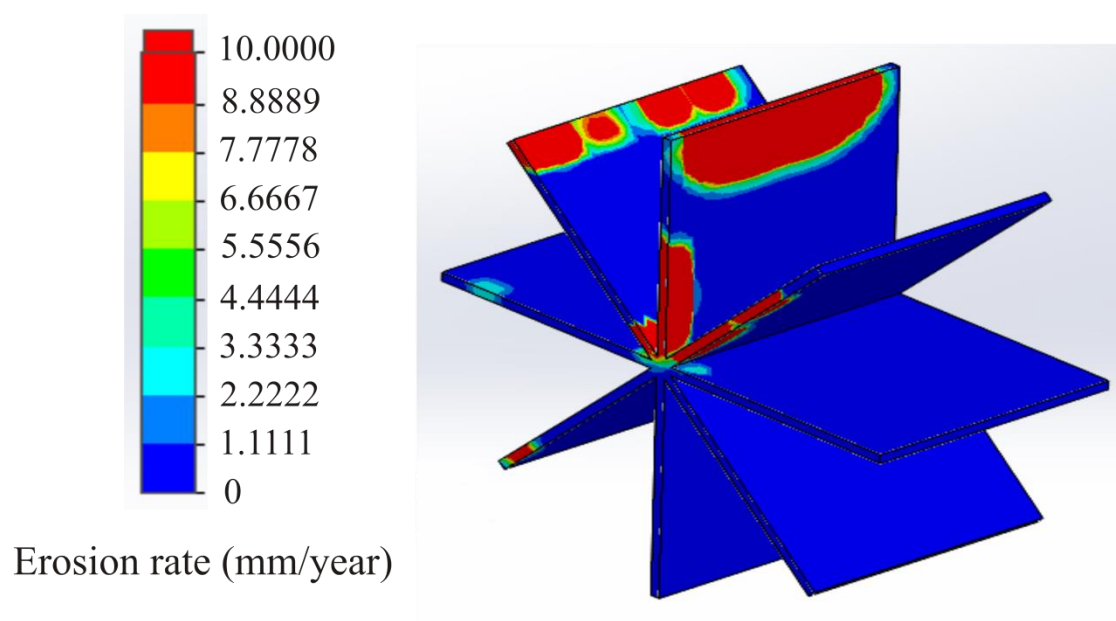


Figure 4. Areas of impact and spread of erosion along with the blades of a hydro turbine

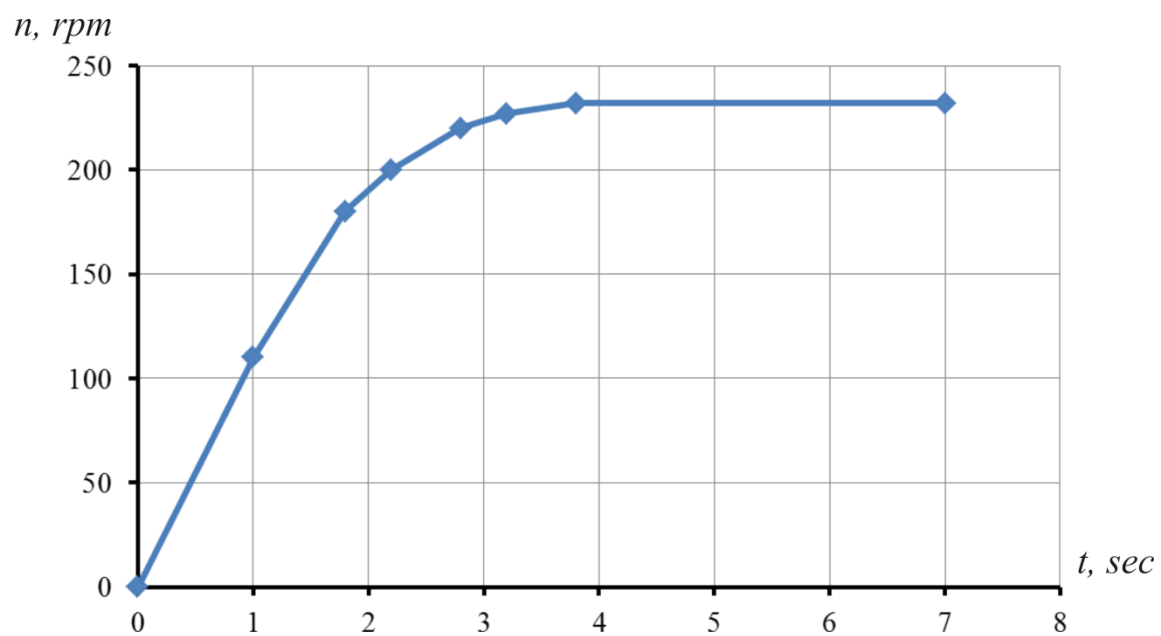


Figure 5. Graphical dependence of the speed (n) on the acceleration time (t).

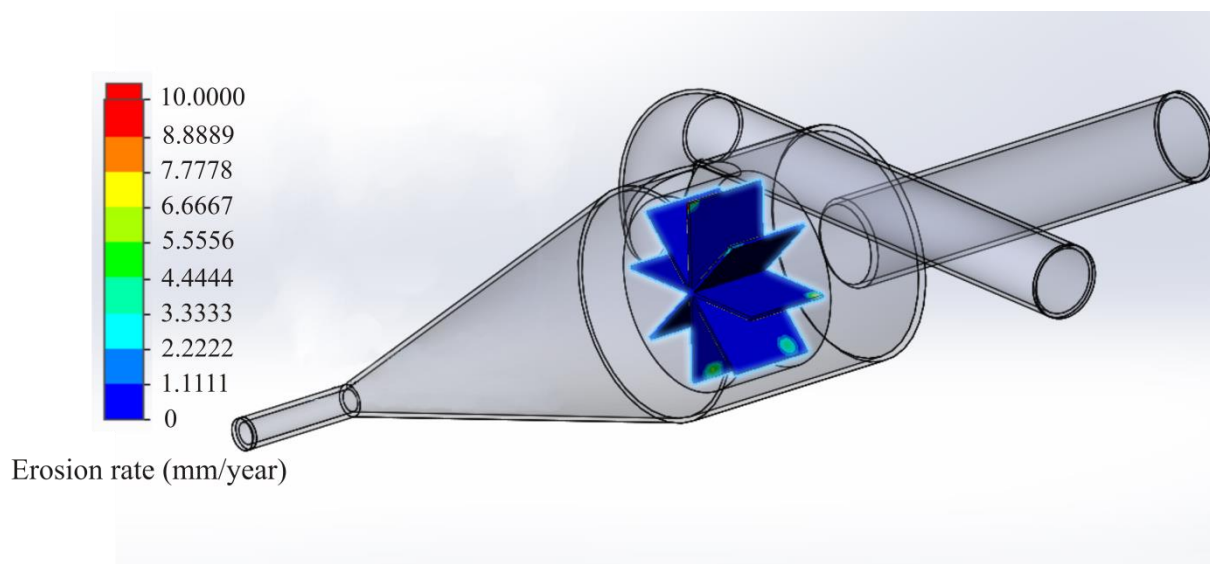


Figure 6. Picture of hydro turbine blade erosion when rotating water supply with mechanical mixtures (2nd option).

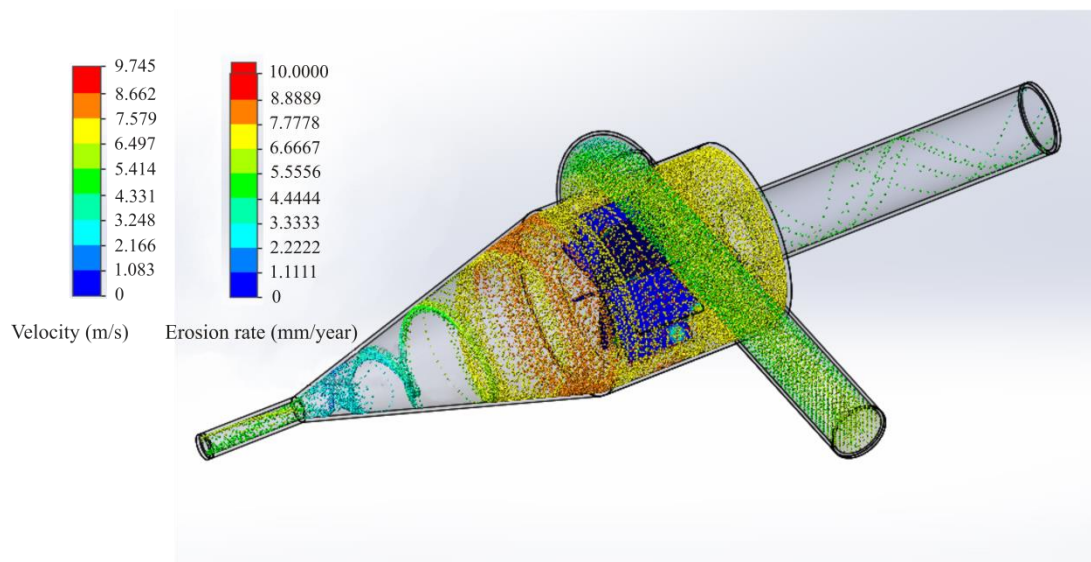


Figure 7. Trajectory and flow rates in a hydro-cyclone with a turbine.

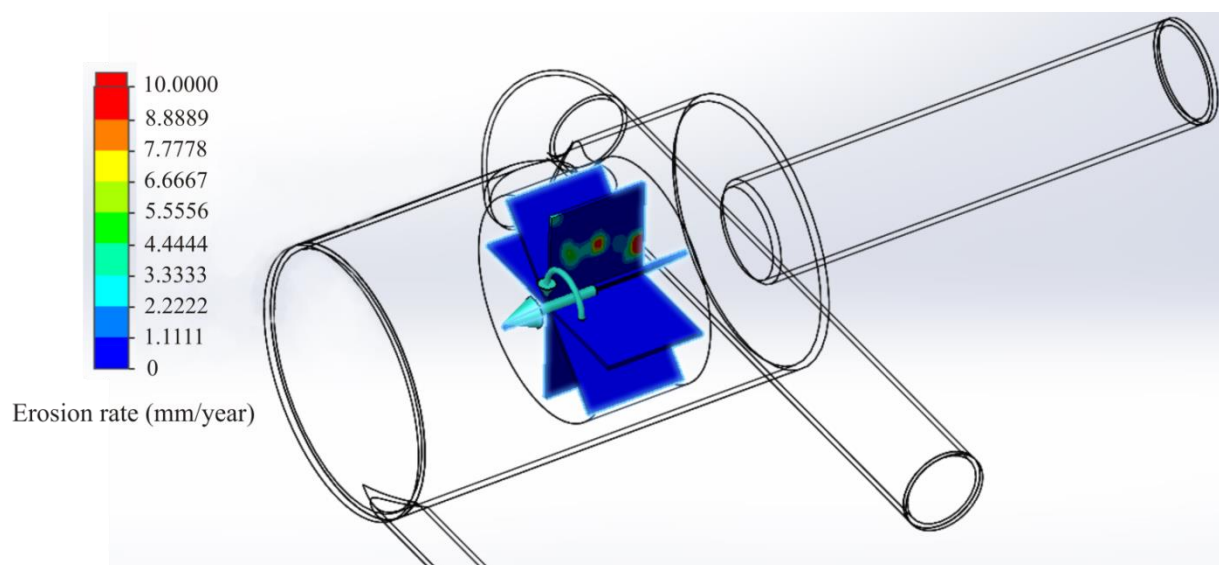


Figure 8. Picture of erosion of the turbine blades in the cylindrical form of the micro-hydroelectric power station (3rd version).

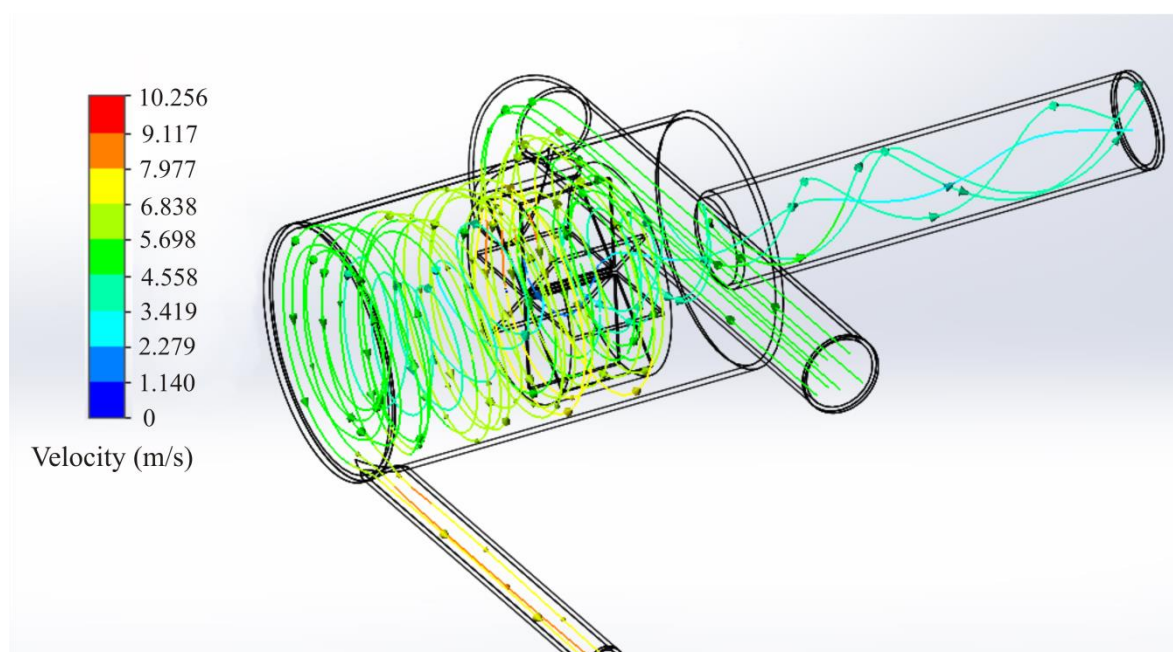
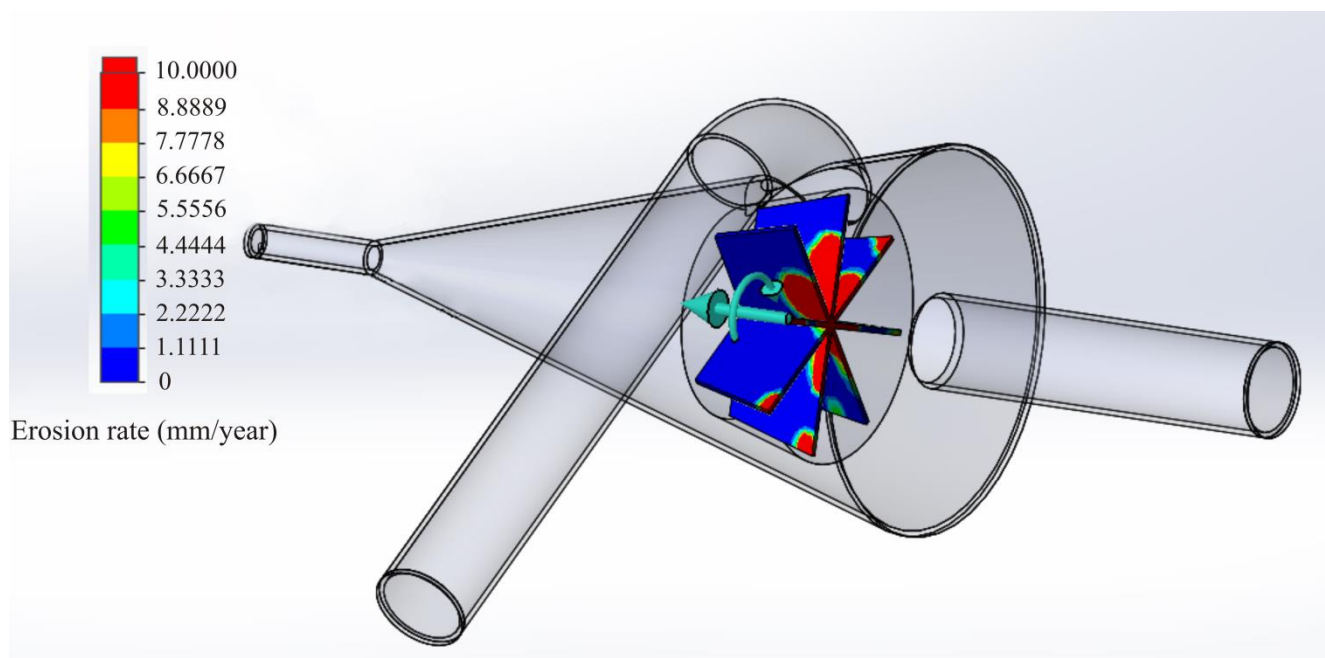


Figure 9. Trajectory and flow rates in a cylindrical hydro-cyclone with a turbine.



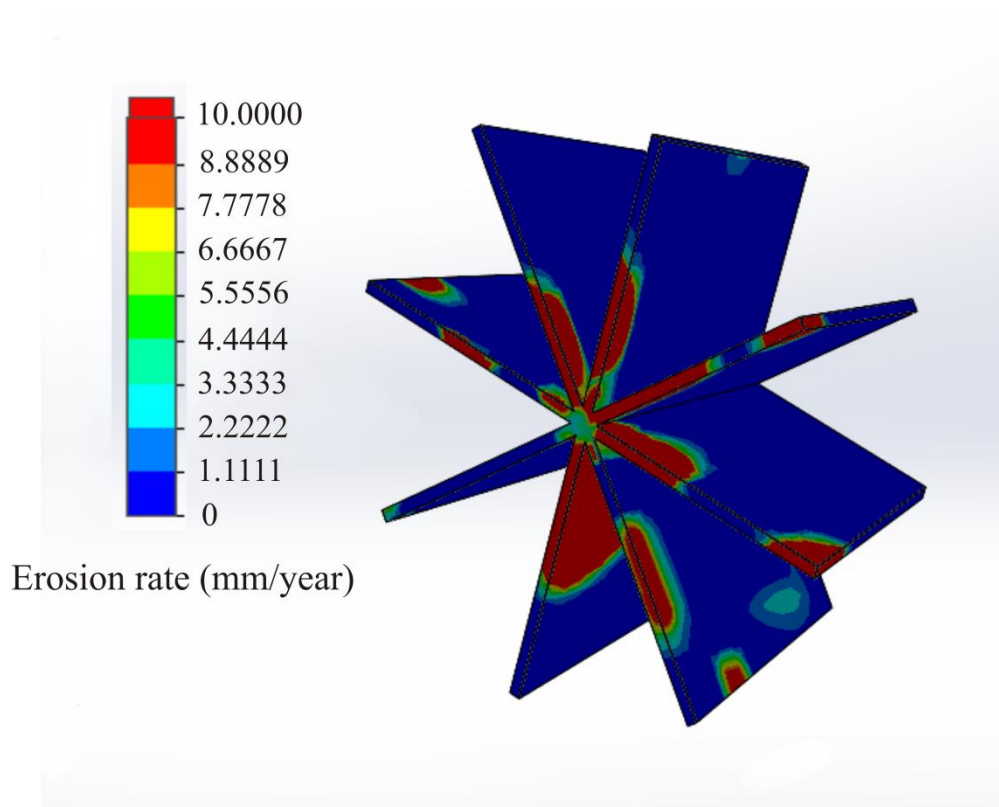


Figure 10. Area of the spread of erosion on the blades of a hydro turbine.



Figure 11. Types of an experimental model of a cylinder-conical version of a hydrocyclone of a micro HPP. a) type of test piece; b) the type of work of the sample in the river.

Table 1. *Granulometric composition of sediments.*

Name of water source	Fraction of sediment, mm						
	< 0,01	0,01-0,05	0,05 -0,10	0,10-0,25	0,25-0,50	> 0,50	Dcp (mm)
The Torgen river	44,6	16,54	16,3	18,1	3,3	1,1	0,06

Table 2. *Technological parameters of an experimental model of a mini hydrocyclone hydroelectric power station*

Area inlet, F, m ²	Heads water at the inlet and in the drain pipe, H1 / H2, m	Speed water on entrance, V1, m / s	Flow rates water through the inlet and drain pipe, Q1 / Q2, m ³ / s	Frequenc y rotation, rp/min	Torque moment, M, N * m	Power hydro-regatta, Na, kW
0,03	1,5/1,34	5,42	0,17/0,14	210	54,1	1,19
0,03	2,0/1,78	6,26	0,19/0,17	243	75,8	1,93
0,03	3,0/2,66	7,67	0,24/0,20	293	110,5	3,39

CÁTODO DE EMISSÃO DE CAMPO MULTIPONTO COMO GERADOR DE OSCILAÇÕES DE ALTA FREQUÊNCIA

MULTI-POINTED FIELD-EMISSION CATHODE AS A GENERATOR OF HIGH-FREQUENCY OSCILLATIONS

МНОГООСТРИЙНЫЙ ПОЛЕВОЙ КАТОД КАК ИСТОЧНИК ВЫСОКОЧАСТОТНЫХ КОЛЕБАНИЙ

BRATANOVSKII, Sergei^{1,2}; AMANKULOV, Yerdos^{3*}; MEDVEDEV, Ilya⁴;

¹ Institute of the State and Right of RAS, The Sector of Administrative Law. Russia

² Economic University of G.V. Plekhanov, Department of State and Legal Disciplines. Russia

³ Eurasian Technological University, Department of Engineering. Kazakhstan

⁴ Russian State Social University, Department of Adaptive Physical Education and Recreation. Russia

* Corresponding author

e-mail: yerdosamankulov@rambler.ru

Received 31 August 2020; received in revised form 16 September 2020; accepted 28 October 2020

RESUMO

Os cátodos de emissão de campo de semicondutores ganharam grande popularidade na moderna rádio-eletrônica e ótica eletrônica devido à alta potência de geração do feixe de elétrons no campo elétrico externo em temperaturas próximas às ambiente. No entanto, sua ampla aplicação é restringida pela alta dependência da corrente de emissão de elétrons com o valor do campo aplicado e parâmetros geométricos do cátodo. O objetivo deste estudo foi examinar o efeito dos processos de ressonância na amplificação da emissão de campo do cátodo semiconductor multiponto. A modelagem do comportamento do tunelamento ressonante de elétrons de semicondutores para o vácuo foi simulada resolvendo a equação de Schrodinger unidimensional e a amplificação devido a processos ressonantes foi estimada. Os resultados da modelagem mostraram que conforme o campo elétrico aumenta, as condições de ressonância mudam para níveis de energia baixos. Com o aumento da largura da barreira para o elétron dentro do corpo sólido, as condições de ressonância mudam para energias mais altas. Foi estabelecido que em semicondutores unidimensionais com elétrons de largura de baixa condutividade, a energia ressonante coincide com o nível de Fermi. Essas propriedades do cátodo são ideais para amplificar a corrente de emissão e reduzir as falhas de dispositivos eletrônicos de vácuo baseados em cátodos de campo semicondutores. A técnica proposta pode ser utilizada para estudar as regularidades de amplificação de emissão devido a processos ressonantes em cátodos semicondutores multiponto com estrutura multicamadas e com pontas metálicas.

Palavras-chave: *emissão de campo, equações de Fowler-Nordheim, oscilações de corrente, cátodo de campo, amplificação de campo geométrico.*

ABSTRACT

Semiconductor field-emission cathodes have gained considerable popularity in modern radio electronics and electronic optics due to the high-power generation of the electron beam in the external electric field at temperatures close to the room ones. However, their wide application is restricted by the high dependence of the electron emission current on the value of the applied field and geometrical parameters of the cathode. This study aimed to examine the effect of resonance processes on amplifying the field emission of the multi-pointed semiconductor cathode. Modeling the behavior of resonant tunneling of electrons from semiconductors to vacuum was simulated by solving the one-dimensional Schrodinger's equation, and the amplification due to resonant processes was estimated. The modeling results showed that as the electric field increases, the resonance conditions shift towards low energy levels. With the increase in the width of the barrier for the electron inside the solid body, the resonance conditions shift towards higher energies. It has been established that in one-dimensional semiconductors with electrons of low conductivity width, the resonant energy coincides with the Fermi level. These cathode properties are optimal for amplifying the emission current and reducing failures of vacuum

electronic devices based on semiconductive field cathodes. The proposed technique can be used to study the regularities of emission amplification due to resonant processes in multipoint semiconductor cathodes with multilayered structure and with metal tips.

Keywords: field emission, Fowler-Nordheim equations, resonant processes, semiconductive cathode

АННОТАЦИЯ

Полупроводниковые полевые катоды пользуются большой популярностью в современной радиоэлектронике и электронной оптике благодаря высокой мощности генерации электронного пучка во внешнем электрическом поле при температурах близких к комнатной. Однако их широкое использование ограничено большой зависимостью эмиссионного тока электронном от величины приложенного поля и геометрических параметров катода. Целью данного исследования являлось изучить влияние резонансных процессов на усиление полевой эмиссии многоострийного полупроводникового катода. Моделирование поведения резонансного туннелирования электронов из полупроводника в вакуум осуществлялось путем решения одномерного уравнения Шредингера и оценивалось усиление, обусловленное резонансными процессами. Результаты моделирования показали, что по мере увеличения величины электрического поля резонансные состояния смещаются в сторону низких уровней энергии. С увеличением ширины барьера для электрона внутри твердого тела наблюдается смещение резонансных состояний в сторону больших энергий. Установлено, что в одномерных полупроводниках с электронами малой полуширины проводимости резонансная энергия совпадает с уровнем Ферми. Данные свойства катода являются оптимальными для усиления эмиссионного тока и меньших сбоев в работе вакуумноэлектронных приборов на базе полупроводниковых полевых катодов. Предложенная методика может быть использована для изучения закономерностей усиления эмиссии за счет резонансных процессов в многоострийных полупроводниковых катодах с многослойной структурой и с металлическими наконечниками.

Ключевые слова: автоэлектронная эмиссия, уравнения Фаулера-Нордгейма, резонансные процессы, полупроводниковый катод

1. INTRODUCTION:

The history of vacuum electronics began with vacuum tubes used in electron microscopes, radio frequency power amplifiers, and thermionic energy conversion devices such as X-ray and microwave vacuum electronic devices (Eichmeier and Thumm, 2008; Parker *et al.*, 2002). In the past, vacuum tubes could only be manufactured in relatively large sizes. Furthermore, they were energy-intensive because electron beam generation from metals required the use of thermionic electron emitters at temperatures over 1000 °C to overcome the work function of the material (Machin, 1950) (Figure 1a).

Other disadvantages of thermionic emission include the broad energy spectrum of emitted electrons and material degradation due to the high operating temperature. One of the solutions to the above challenges was creating small electron sources based on the already known "cold" emission effect. The cold field electron emission, which was first described by Fowler and Nordheim, is suitable for low-temperature emission regimes (Fowler and Nordheim, 1928). In cold or field emission (FE), electrons are emitted from the surface of a metal or semiconductor under the influence of a strong

electric field (Figure 1b). This is called the quantum mechanical tunneling effect. In these conditions, field emission properties such as high current density and narrow energy spectrum are achieved using a high electric field (up to 110 V/cm) (Radauscher *et al.*, 2016; Yamamoto, 2005). Other advantages of cold cathodes are small size, stable emission over time, and high-frequency operability. In one of the first works on miniature vacuum field emission devices (Shoulders, 1961; Spindt, 1968), the authors suggest that electron emission sources that are below micron size are practically insensitive to heating in a broad temperature range (up to 1000 °C), unaffected by ionizing radiation, and with long lifetime, because a nonlinear function relates current and voltage characteristics of the field emission device, a small change in voltage can result in the exponential growth of emission current (Utsumi, 1991; Harris *et al.*, 2015). Due to the above advantages, cold cathodes have a wide range of applications such as in flat field emission displays (FEDs), miniature microwave and X-ray emitters, parallel electron beam microscopy, high-power accelerators, and more (Bachmann *et al.*, 2015; Garven and Parker, 2020). Often, field-emission cathodes are made of monocrystalline silicon and shaped into needle-like or pyramid-like tips (Egorov and Sheshin, 2017) (Figure 2).

In spite of their unique and desired properties, FE devices have a few drawbacks that hinder their wide-scale application, such as their ultra-high vacuum requirement ($10^{-5} - 10^{-9}$ Torr) and instability of the field emission current during the long-term and short-term emission operations (Swanson and Schwind, 2009). Another limitation is that CFE sources can experience a significant emission current decay (70–90% of the initial value) within the first hours of use, increasing energy consumption needed for heating to high temperatures. Studies on FE cathodes over the past decades focused on the use of tungsten nanowires (Chen and Yang, 2017), carbon nanotubes, and coatings (Jiang *et al.*, 2011), have found many limitations. For example, tungsten nanowires are only suitable for emission under the vacuum of less than 10^{-10} Torr since operation at higher vacuum pressure can be accompanied by significant current fluctuations (Yeong and Thong, 2006).

Recent studies (Liem and Choy, 2013) of various tip coatings have shown that nanoscale graphene coatings have several advantages over other types of coatings. Graphene, a single layer of carbon atoms arranged in a hexagonal lattice, has excellent thermal, mechanical, and electrical properties (Ang *et al.*, 2017; Balandin *et al.*, 2008). It can be used to create nanotip coatings to localize and enhance the applied electric field. This was the case of metallic and semiconducting nanotips (Huang *et al.*, 2016), which were coated with graphene-based thin films. However, none of the above methods is suitable for the electron device applications because the deposition of graphene creates multiple emission sites on the cathode plane (Santandrea *et al.*, 2011), rather than a single virtual source point at the gun exit. Various attempts to overlay an ultrathin (~ 1 nm) graphene flake onto a blunted tungsten probe (Tsai *et al.*, 2012) or a graphene ring (Shao *et al.*, 2016) have also failed because coatings of this thick were found to be easily detachable. The consequences of such damage to the coating are malfunctions and poor radiation control.

It is essential to study field emission specifics from nanostructured and composite cathodes to employ the nano-sized cold cathodes. These aspects are usually less pronounced in most reviews today and share relatively little attention, and may have some potential for significant technological progress. The methodological structure of such a comparative review is important for convenient and useful reading. Still, this task involves working with the huge diversity and complexity of the field of study.

This work presents the theoretical modeling of multi-tip cathode architecture and microwave oscillation patterns. For this, electron emission devices obtained by nanostructuring surfaces were discussed. The study focuses on theories describing the qualitatively new operational characteristics of multi-line field cathodes.

Therefore, this study aimed at establishing patterns and mechanisms to amplify field emission of semiconductor cathodes through resonant processes. For this purpose, the behavior of resonant tunneling of electrons is simulated using the theory of field emission. The effect of emission current gain due to resonant processes was estimated by solving the one-dimensional Schrodinger's equation for electrons tunneling from semiconductor to vacuum.

2. MATERIALS AND METHODS:

2.1. Field emission theory

Basic equations from the theory of field emission are applied to simulate resonance tunneling processes by electron from the surface of the semiconductor cathode.

Field emission refers to the emission of electrons from a solid surface into vacuum by tunneling through a surface potential barrier under the influence of an electrostatic field. The emission current density obtained by field emission depends on the intensity of electric field F and the work function Φ . Figure 1b shows that the effective work function Φ_{eff} for FE is dependent upon the strength of the electric field, and the emission current variation is determined by the field dependence of the barrier shape. For FE to occur, the electric field must be at $\sim 10^9$ V/m, and to create such strong fields, cathodes must have a cone shape or a tip shape (Figure 2), with a radius of less than a micron (Shoulders, 1961). The strong electric field concentrated at the tip of the emitter will thus narrow the potential barrier at the metal-vacuum interface to several nanometers. The result is a higher probability of tunneling.

Electron field emission is usually described by the Fowler-Nordheim equation (FNE) (Fowler and Nordheim, 1928). The general theory of field emission from semiconductors was described in fairly early publications (Morgulis, 1947; Stratton, 1964). It is based on statistics of degenerate carriers and takes into account different masses of electrons in a semiconductor and in vacuum. In addition, quantum-mechanical tunneling processes are an important mechanism for the transfer of current through thin barriers that are

present in metal-semiconductor transitions on highly doped semiconductors. According to the classical theory of field emission, the system is simplified to a one-dimensional structure along the direction of the external electric field. The emission tip is modeled as a semi-infinite quantum well with a work function Φ , and a linear potential approximates the applied electric field F . The FNE equation for the emission current density J would be:

$$J = A \frac{(\beta F)^2}{\Phi} \exp \left(-B \frac{\Phi^{3/2}}{\beta F} \right) \quad (\text{Eq. 1})$$

where: A and B are constants equal to $1.54 \cdot 10^{-6} \text{ AeV/V}^2$ and $6.83 \cdot 10^7 \text{ V/eV}^{2/3}\text{m}$, respectively; β is the field enhancement factor, which is the ratio between the local and the applied field. Normally, the local field potential exceeds the value of the applied field. Therefore, the field enhancement factor β can range between hundreds and thousands.

The equation (1) shows that the dependence of the emitted current on the local electric field and the work function is exponential-like. Thus, variation of the shape or surrounding of the emitter has a strong impact on the emitted current. The equation (1) can be re-arranged as follows:

$$\ln \left(\frac{J}{F^2} \right) = \ln \left(A \frac{\beta^2}{\Phi} \right) - B \frac{\Phi^{3/2}}{\beta F} \quad (\text{Eq. 2})$$

The plot of the equation (2) as a function of $1/F$ is called the F-N plot. Here, the field enhancement factor β can be calculated from the slope of the F-N plot if the work function of the emitter is already known (Fursey, 2007). The top of the triangular barrier used in our semiconductor-vacuum interface model was lowered by the electric polarization, as expected for the devices under study.

2.2. Emitters: architecture and properties

According to equation (2), the emission current density J depends on two factors: work function Φ and field enhancement factor β . Therefore, the emission current density at a low electric field will be high if the emitter exhibits a low work function or a high enhancement factor. Since the work function depends upon the intrinsic electronic properties and the surface state of the emitter, materials were chosen to create a tip or a

coating normally exhibit a lower work function. However, the lower work function is not the main factor of higher current density because not all materials have high stability and durability (Biswas, 2018). Therefore, another way to improve J is to increase β . The field enhancement factor represents amplification of the electric field at the emitter surface, determined by the geometrical shape of the emitter. The local electric field at the emitter surface can be defined as:

$$F_{loc} = \beta F \quad (\text{Eq. 3})$$

Based on the equation above, it can be noted that when the field enhancement factor β is higher, the enhancement over the local field is stronger. The value of field enhancement factor β depends upon the geometric parameters of the emitter, such as height (h) and radius of the curvature on its tip (r), as shown in:

$$\beta \propto \frac{h}{r} \quad (\text{Eq. 4})$$

Thus, the higher and the sharper the emitting center, the higher the value of the field enhancement factor. It should also be noted that the above expression (4) does not include a screening effect introduced by nearby emitters, which reduces the field enhancement factor. Therefore, it is only suitable for single emitters.

Devices using field emission and having a nanostructured cathode surface can usually be described as having a vacuum/specific material interface. The cathode material is deformed on a nanometer scale. Tunnel emission of electrons from flat surfaces can be created only in very high electric fields (or at high applied voltages), even if the cathode material is a metal. On the other hand, the creation of large fields in large volumes greatly increases the possibility of device failure due to electrical discharges. For this reason, the creation of localized deposits with a high degree of recovery is naturally preferable. This local field enhancement is most often achieved by the concentration of the radiation region in the very sharp tips of the cathodes/emitting surfaces.

The first cathodes proposed by Spindt (1968) were points with radii in the range of several tens of nanometers, etched from solid material using photolithography technologies to obtain a nanostructured surface (Figure 2). However, this development was quickly followed

by many developments: a wide variety of materials for field emission were investigated and many methods of nanostructuring of surfaces appeared. As a first obvious step, many research groups initially investigated field emission from silicon tips. This was a natural question, since the possibility of integrating field emission devices into existing silicon-based microelectronic technologies was a very attractive concept (Kleps *et al.*, 2009) further enhance the local extraction field, processes designed to convert a flat silicon surface into a porous material were performed by electrochemical etching. The obtained nanoresonators were localized near the surface and separated by nanometer-sized amorphous silicon fibrils, which became excellent field emission sites (Lee *et al.*, 2018).

In the present work, multipoint structures like multiblade silicon cathode in Figure 2 will be used to model resonance processes. The density of the homogeneous structure on the 0.5 mm diameter surface section was 200-300 points.

2.3. Tunneling probability

The probability of electron tunneling from a semiconductor to a vacuum from a stationary - time-independent Schrödinger equation is derived as:

$$-\frac{\hbar^2}{2m_e} \times \frac{d^2\Psi}{dx^2} + V(x)\Psi = E\Psi \quad (\text{Eq. 5})$$

Which can be rewritten as

$$\frac{d^2\Psi}{dx^2} = \frac{2m_e(V-E)}{\hbar^2} \Psi, \quad (\text{Eq. 6})$$

where \hbar is the Planck constant, Ψ is the wave function, m_e is the effective electron mass, $V(x)$ is the potential relief on the path of the electron, E is the electron energy and x is the coordinate along which tunneling occurs (direction from the solid to the vacuum).

Assuming that the potential relief changes quite smoothly, i.e. it can be written the condition: $V(x) - E$ varies slightly on the interval $x+dx$, this is the so-called WKB-approximation (Wentzel – Kramers – Brillouin), the second equation can be represented as:

$$\Psi(x + dx) = \Psi(x) \times e^{-kdx}, \quad (\text{Eq. 7})$$

$$\text{where } k = \frac{\sqrt{2m_e[V(x)-E]}}{\hbar}$$

The minus sign is chosen because it is assumed that the particles move from left to right. For a slowly changing potential, the amplitude of the wave function at $x = L$ can be related to the wave function at $x = 0$ using the following equation:

$$\Psi(L) = \Psi(0)e^{\left(-\int_0^L \sqrt{2m_e[V(x)-E]}/\hbar dx\right)}, \quad (\text{Eq. 8})$$

where L is the classical turning point and the outer boundary of the barrier, which is the last point where the electron is inside the barrier potential. Equation 8 also relates to the WKB approximation. The general case assumes that the triangular barrier is a good approximation to describe the semiconductor-vacuum interface. The tunneling probability Ξ can be calculated in the case of approaching a triangular barrier using the following equation:

$$\Xi = [\Psi(L)\Psi^*(L)/\Psi(0)\Psi^*(0)] = e^{-\left\{2\int_0^L \left(\frac{\sqrt{2m_e}}{\hbar}\right) \sqrt{q\chi_0\left[1-\left(\frac{x}{L}\right)^2}\right] dx\right\}}, \quad (\text{Eq. 9})$$

where χ_0 is the height of the barrier at the cathode-vacuum interface. The parameter Ξ can be estimated as a function of the electric field F :

$$\Xi_{\Delta}(F, E) = C \times e^{\left[\left(-\frac{4}{3}\hbar F\right) \times \sqrt{2m_e(\chi_0-E)^3}\right]}, \quad (\text{Eq. 10})$$

where Ξ_{Δ} is the probability of tunneling through the triangular barrier. The tunneling current can be represented as the electron velocity product and the probability of tunneling and the density of available electrons. The latter can be represented as the product of the density of states and electron distribution (Fermi statistics). The electron velocity referred to here may be somewhat different from the usually determined volume drift velocity due to the effect of scattering on the barrier. However, it is hypothesized that the barrier does not significantly violate the field dependence of the drift velocity, which in any case is a much weaker function compared to another factor. The velocity corresponds to the average velocity of carriers approaching the barrier. The current density is equal to the density of available electrons to the barrier, multiplied by the probability of tunneling and the drift velocity. So, the following expression for the density of the tunneling current can be written as:

$$J_C(F) = A_C \int_{E_C}^{\infty} N(F, E) \times \Xi_{\Delta}(F, E) \times V_D(F, E) dE, \quad (\text{Eq. 11})$$

Therefore, the tunneling current shows an exponential dependence of degree 3/2 on the barrier height if all other factors N , V_D , and A_C are constant or slightly different. In the well-developed Fowler-Nordheim approximation, the tunnel current has exactly this dependence:

$$J_{FN}(F) = C_{FN} \times \frac{F^2}{\varphi} e^{-B\varphi^{3/2}/F} \quad (\text{Eq. 12})$$

Therefore, the tunneling current shows an exponential dependence on 3/2 of the power of the barrier height if all other factors N , V_D , and A_C are constant or slightly different. In this approximation, the concentration of charge carriers depends on many quantities:

$$N_{3D}(F, E) = \frac{\sqrt{2}m_e^{3/2}}{\pi^2\hbar^3} \times \frac{\sqrt{E}}{1 + e^{\frac{E-\mu}{kT_e(F)}}} \quad (\text{Eq. 13})$$

This quantity describes the density of charge carriers for a bulk semiconductor, but moreover, in the case of a sufficiently thin semiconductor tip, a quantum-dimensional constraint should be expected. In this case the one-dimensional density of states will have a dramatic effect on the form of the function of the number density of carriers:

$$N_{1D}(F, E) = \frac{m_e^{1/2}}{\sqrt{2}\pi\hbar d^2} \times \frac{1}{1 + e^{\frac{E-\mu}{kT_e(F)}}} \times \sum \frac{1}{\sqrt{E-E_{ql}}} \quad (\text{Eq. 14})$$

2.4. Analysis conditions

The motion of electrons to the surface of a silicon pole with Fermi energy of 1.12 eV and 4.60-4.85 eV output is considered. The applied field F changes in the range from 0.1 V / nm to 5 V / nm. The cathode temperature is 300K. The energy of the electrons ranged from 0 to 12 eV in increments of 0.0012 eV. The width of the energy barrier varied from 1 to 5 nm. Calculations and graphs of dependence were performed through the software package in MathLab.

3. RESULTS AND DISCUSSION:

The results of modeling different

resonance states under variable conditions of the energy barrier width for the electron and the value of the applied field for multipoint silicone cathodes showed that both resonance and non-resonance effects influence the amplification of the emission current.

Figure 3 shows a diagram of dependence between tunneling probability and factors, such as variation in the applied electric field F (on the left) and energy barrier width L (on the right). As can be seen in Figure 3, the tunneling probability of electrons with $L=1$ nm increases with the applied field. Also, there is a clear resonance curve peaking. The observed shift of resonance towards lower energies with increasing F is typical for band bending in quantum tunnel systems. At the applied field of 1 V/nm, the probability of tunneling increased when the L decreased, and the resonance shifted towards higher energies. This can be explained as follows. The tunneling probability of electrons approaching the cathode surface increases due to a decrease in the potential barrier height.

The latter is the main result of this work and the axial meaning of the proposal. In the case of a one-dimensional semiconductor and a one-dimensional carrier spectrum, the shape of this spectrum is very different from the wide spectrum typical of a bulk semiconductor and will show an extremely small half-width. This has interesting consequences, see Figure 4. Having a small half-width, the electrons tunneled into the vacuum will have approximately the same speed. It means they will react uniformly to control influences and the anode will also be reached uniformly. This means high quality factor, low stray currents and a low level of distortion in the operation of vacuum-electronic devices based on such field cathodes.

However, due to the integrated contribution to the emission current from several electronic states (which is typical for multi-band semiconductors), the increase in current near the resonances is usually rougher, but should also be high enough and sharp so that it can be attributed to such (Filip *et al.*, 2016; She *et al.*, 2004). There are situations where facilities designed to detect the effects of resonant field emission do not show relevant salient features (Gu *et al.*, 2012; Sarker *et al.*, 2014). In most cases, the absence of resonance behavior in the current-voltage diagrams is associated with the loss of coherence of the electron wave function when crossing the region with a high probability of scattering by defects (including free interlayer boundaries). Although experimentally quite difficult to investigate, the emission of resonant current

through an electron field from the so-called “quantum cathodes” has long been of particular interest because of its high potential for use. For example, the areas of negative conductivity of the current–voltage characteristics near resonances can allow the vibrational behavior of the field emission structure (Mukherjee and Paul, 2018).

Theoretical approaches are mainly based on the solution of the one-electron Schrödinger equation with intrinsic constraints of the envelope of the electron wave function at various interfaces, modeled as finite discontinuities in potential energy, which allows one to calculate the electron transfer coefficient (Tan *et al.*, 2016). To calculate the field emission current, the old statistical/kinetic argument is used (Murphy and Good, 1956): the contributions of all states in the substrate are taken into account using the so-called power function, weighted by the probability of transmission for each state. The feed function from the volume includes the statistical distribution of electrons (which are usually assumed in local thermodynamic equilibrium). This is a general outline that allows for many improvements. For example, when it comes to the emission of an electron field from silicon through a thin layer of diamond-like carbon, one can take into account defects in this layer, modeling them as randomly located delta potentials between which there is tunnel transport under the applied field (Xu and Huq, 2005). Without obtaining a large resonant signature, the result of this coherent model is an oscillatory current – voltage characteristic with qualitative similarity to many experimental results. No less interesting is the study of the effect of two or more layers deposited on a base substrate (Chang and Pao, 2019; Wang *et al.*, 2005).

If the uppermost layer is conductive, it represents a potential well between the previous layer and the vacuum barrier. It is interesting how the possible accumulation of electrons in this well can affect the radiation (Wang *et al.*, 2017), because the accumulated space charge changes the profile of potential energy. Therefore, to obtain the emission current in this case, a self-consistent approach of the coupled Schrödinger and Poisson equations is necessary. Besides, the very electronic structure of the substrate can also significantly affect the radiation current obtained from quantum cathodes. A thorough analysis of this aspect can explain the specific behavior of such emitters. For example, sudden changes in the slope of the current-voltage characteristics in the Fowler–Nordheim representation and the effect of substrate illumination on the field emission current (Nahhas, 2018).

It is also worth adding that no matter how promising the phenomenon of resonant tunneling through an electric field from quantum cathodes is, it should be recognized that this phenomenon can rarely be identified in its pure form in practice. When a complex emitting structure has a potential well in front of the vacuum barrier, the accumulation of electrons in this region is inevitable. Therefore, an additional type of electron transfer into vacuum should always be taken into account. This is the so-called sequential tunneling mechanism, which, unlike resonant tunneling, is necessarily inelastic and occurs in two or more “steps”. The electron breaks from one potential well to another, and as a result, to vacuum. Both resonant and sequential transfer processes must occur simultaneously from the same batch of incoming electrons from the bulk substrate. One interesting question will concern the relative share of these two mechanisms in the same field emission process. It is equally important to know the relationship (if any) between these two different processes. To answer these questions, a simple type of quantum cathode has recently been reviewed (Filip and Wong, 2016).

The individual contributions of the resonant and sequential tunneling processes to the total radiation current are estimated (Huttner *et al.*, 2017). It was assumed that the electrons undergoing sequential transfer are among those that deviate from resonance states due to various inelastic interactions within different material layers. Besides, accumulating in the structure, these electrons cause changes in the potential energy profile, directly affecting the local energy spectrum and, therefore, the resonant transfer. Thanks to this basic hypothesis, the two transfer mechanisms are closely intertwined. Both of them are directly affected by the constraints imposed by the quantum constraint in the narrow potential wells of the structure (Karlewski *et al.*, 2016). As a result, on separate volt-ampere diagrams of both current components, features can be related both to the conditions of transverse confinement and the balance of the electron flow through different layers.

4. CONCLUSIONS:

This paper applied a one-dimensional field emission model to estimate the impact of resonance processes on the probability of tunneling electrons from the surface of a semiconductor cathode with a multipoint structure. It has been shown that the emission current is amplified at a small width of the energy barrier due to resonance and non-resonance effects. In

contrast, the resonance process prevailed at increasing the external field. Such amplification is achieved through the local emission current density. It has been established that at the shift of resonance energies, the maximum increase of emission current density is reached at the coincidence of values of resonance energy with Fermi energy of semiconductor cathode. The current emission gain can be adjusted by resonance effects when calculating the design and material selection parameters for multipoint field cathodes. In the future, the proposed technique can be used to optimize the field emission current by matching the resonance processes for multipoint semiconductor cathodes with multilayer structures and metal tips.

5. REFERENCES:

1. Ang, Y. S., Liang, S. J., and Ang, L. K. (2017). Theoretical modeling of electron emission from graphene. *Mrs Bulletin*, 42(7), 505-510.
2. Bachmann, M., Dams, F., Düsberg, F., Hofmann, M., Pahlke, A., Langer, C., ... and Schreiner, R. (2015). Stability investigation of high aspect ratio n-type silicon field emitter arrays. In 2015 28th International Vacuum Nanoelectronics Conference (IVNC) (pp. 204-205). IEEE.
3. Balandin, A. A., Ghosh, S., Bao, W., Calizo, I., Teweldebrhan, D., Miao, F., and Lau, C. N. (2008). Superior thermal conductivity of single-layer graphene. *Nano letters*, 8(3), 902-907.
4. Biswas, D. (2018). A universal formula for the field enhancement factor. *Physics of Plasmas*, 25(4), 043113.
5. Chang, W. T., and Pao, P. H. (2019). Field Electrons Intercepted by Coplanar Gates in Nanoscale Air Channel. *IEEE Transactions on Electron Devices*, 66(9), 3961-3966.
6. Chen, S., and Yang, W. (2017). Flexible low-dimensional semiconductor field emission cathodes: fabrication, properties and applications. *Journal of Materials Chemistry C*, 5(41), 10682-10700.
7. Egorov, N., and Sheshin, E. (2017). *Field emission electronics*. Springer International Publishing.
8. Eichmeier, J. A., and Thumm, M. (2008). *Vacuum electronics: components and devices*. Springer Science and Business Media.
9. Filip, V., and Wong, H. (2016). Comparative study of resonant and sequential features in electron field emission from composite surfaces. *Thin Solid Films*, 608, 26-33.
10. Filip, V., Wong, H., Tam, W. S., and Kok, C. W. (2016). Study of composite cathodes in electron field emission devices: Relative contributions of resonant and sequential tunneling. In 2016 5th International Symposium on Next-Generation Electronics (ISNE) (pp. 1-2). IEEE.
11. Fowler, R. H., and Nordheim, L. (1928). Electron emission in intense electric fields. *Proceedings of the Royal Society of London. Series A, Containing Papers of a Mathematical and Physical Character*, 119(781), 173-181.
12. Fursey, G. N. (2007). *Field emission in vacuum microelectronics*. Springer Science and Business Media.
13. Garven, M., and Parker, R. K. (2020). Vacuum Microelectronics for Microwave Power Amplifiers. In *Generation and Application of High Power Microwaves* (pp. 109-119). CRC Press.
14. Gu, C., Jiang, X., Lu, W., Li, J., and Mantl, S. (2012). Field electron emission based on resonant tunneling in diamond/CoSi₂/Si quantum well nanostructures. *Scientific reports*, 2, 746.
15. Harris, J. R., Jensen, K. L., and Shiffler, D. A. (2015). Modelling field emitter arrays using line charge distributions. *Journal of Physics D: Applied Physics*, 48(38), 385203.
16. Huang, B. R., Chan, H. W., Jou, S., Chen, G. Y., Kuo, H. A., and Song, W. J. (2016). Structure and field emission of graphene layers on top of silicon nanowire arrays. *Applied Surface Science*, 362, 250-256.
17. Huttner, U., Kira, M., and Koch, S. W. (2017). Ultrahigh off-resonant field effects in semiconductors. *Laser and Photonics Reviews*, 11(4), 1700049.
18. Jiang, K., Wang, J., Li, Q., Liu, L., Liu, C., and Fan, S. (2011). Superaligned carbon nanotube arrays, films, and yarns: a road to applications. *Advanced Materials*, 23(9), 1154-1161.
19. Karlewski, C., Heimes, A., and Schön, G. (2016). Lasing and transport in a multilevel double quantum dot system coupled to a microwave oscillator. *Physical Review B*, 93(4), 045314.

20. Kleps, I., Miu, M., Simion, M., Ignat, T., Bragaru, A., Craciunoiu, F., and Danila, M. (2009). Study of the micro-and nanostructured silicon for biosensing and medical applications. *Journal of biomedical nanotechnology*, 5(3), 300-309.
21. Lee, S., Kang, J., and Kim, D. (2018). A mini review: Recent advances in surface modification of porous silicon. *Materials*, 11(12), 2557.
22. Liem, H., and Choy, H. S. (2013). Superior thermal conductivity of polymer nanocomposites by using graphene and boron nitride as fillers. *Solid State Communications*, 163, 41-45.
23. Machin, K. E. (1950). *Components Handbook*. MIT Radiation Laboratory Series, vol. 17. McGraw-Hill, New York.
24. Morgulis, N. (1947). About field emission composite semiconductor cathodes. *Journal of Technical Physics*, 17, 983.
25. Mukherjee, T., and Paul, A. (2018). Dielectric breakdown-based microsensor for on-chip ambient pressure monitoring. *IEEE Transactions on Electron Devices*, 65(5), 1946-1955.
26. Murphy, E. L., and Good, Jr. R. H. (1956). Thermionic emission, field emission, and the transition region. *Physical review*, 102(6), 1464.
27. Nahhas, A. M. (2018). Review of GaN/ZnO Hybrid Structures Based Materials and Devices. *American Journal of Nano Research and Applications*, 6(2), 34.
28. Parker, R. K., Abrams, R. H., Danly, B. G., and Levush, B. (2002). Vacuum electronics. *IEEE transactions on microwave theory and techniques*, 50(3), 835-845.
29. Radauscher, E. J., Gilchrist, K. H., Di Dona, S. T., Russell, Z. E., Piascik, J. R., Amsden, J. J., ... and Glass, J. T. (2016). Improved Performance of Field Emission Vacuum Microelectronic Devices for Integrated Circuits. *IEEE Transactions on Electron Devices*, 63(9), 3753-3760.
30. Santandrea, S., Giubileo, F., Grossi, V., Santucci, S., Passacantando, M., Schroeder, T., ... and Di Bartolomeo, A. (2011). Field emission from single and few-layer graphene flakes. *Applied Physics Letters*, 98(16), 163109.
31. Sarker, D., Kumar, H., Patra, R., Kabiraj, D., Avasthi, D. K., Vayalil, S. K., ... and Ghosh, S. (2014). Enhancement in field emission current density of Ni nanoparticles embedded in thin silica matrix by swift heavy ion irradiation. *Journal of Applied Physics*, 115(17), 174304.
32. Shao, X., Srinivasan, A., Zhao, Y., and Khursheed, A. (2016). A few-layer graphene ring-cathode field emitter for focused electron/ion beam applications. *Carbon*, 110, 378-383.
33. She, J. C., Xu, N. S., Deng, S. Z., Chen, J., Li, Z. B., Huq, S. E., and Wang, L. (2004). Experimental evidence of resonant field emission from ultrathin amorphous diamond thin film. *Surface and Interface Analysis*, 36(5-6), 461-464.
34. Shoulders, K. R. (1961). Microelectronics using electron-beam-activated machining techniques. *Advances in Computers*. Elsevier, Amsterdam, 2, 135-293.
35. Spindt, C. A. (1968). A thin-film field-emission cathode. *Journal of Applied Physics*, 39(7), 3504-3505.
36. Stratton, R. (1964). Energy distributions of field emitted electrons. *Physical Review*, 135(3A), A794.
37. Swanson, L. W., and Schwind, G. A. (2009). A review of the cold-field electron cathode. *Advances in imaging and electron physics*, 159, 63-100.
38. Tan, X., Rumbach, P., Griggs, N., Jensen, K. L., and Go, D. B. (2016). Theoretical analysis of 1D resonant tunneling behavior in ion-enhanced cold field and thermo-field emission. *Journal of Applied Physics*, 120(21), 213301.
39. Tsai, J. T., Chu, T. Y., Shiu, J. Y., and Yang, C. S. (2012). Field emission from an individual freestanding graphene edge. *Small*, 8(24), 3739-3745.
40. Utsumi, T. (1991). Vacuum microelectronics: what's new and exciting. *IEEE Transactions on Electron Devices*, 38(10), 2276-2283.
41. Wang, R. Z., Ding, X. M., Wang, B., Xue, K., Xu, J. B., Yan, H., and Hou, X. Y. (2005). Structural enhancement mechanism of field emission from multilayer semiconductor films. *Physical Review B*, 72(12), 125310.
42. Wang, R. Z., Zhao, W., and Yan, H. (2017). Generalized Mechanism of Field Emission

from Nanostructured Semiconductor Film Cathodes. Scientific reports, 7, 43625.

43. Xu, N. S., and Huq, S. E. (2005). Novel cold cathode materials and applications. Materials Science and Engineering: R: Reports, 48(2-5), 47-189.
44. Yamamoto, S. (2005). Fundamental physics of vacuum electron sources. Reports on Progress in Physics, 69(1), 181.
45. Yeong, K. S., and Thong, J. T. L. (2006). Field-emission properties of ultrathin 5 nm tungsten nanowire. Journal of applied physics, 100(11), 114325.

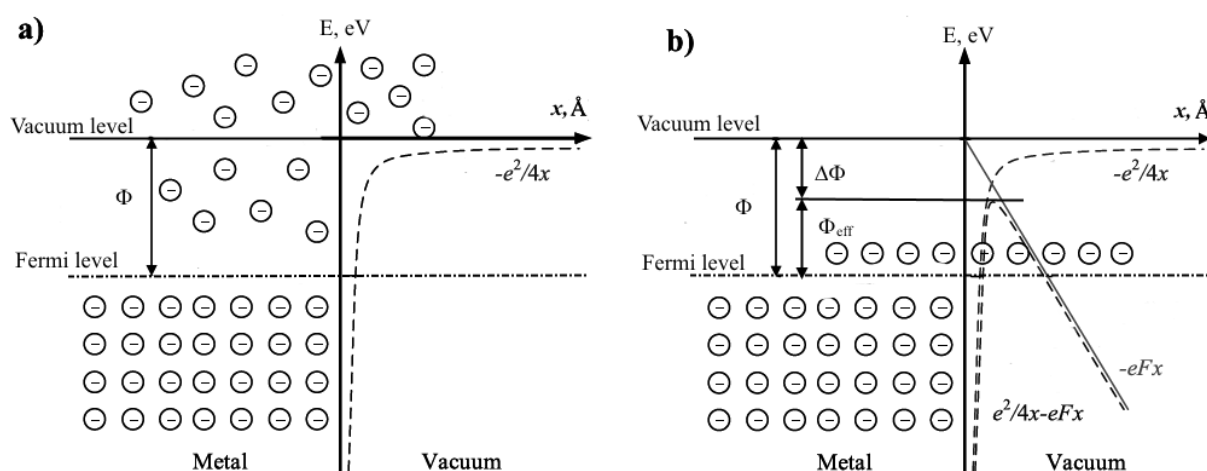


Figure 1. Schematic diagram showing how electrons overcome potential barriers in the metal-vacuum system via thermionic (a) and cold field electron (b) emission. Designations: x represents distance from the metal surface; $-e^2/4x$ is the potential barrier; Φ is the work function; $-eFx$ is the electric field potential with intensity F ; $e^2/4x - eFx$ is the potential barrier in an external field with an effective work function (Φ_{eff}).

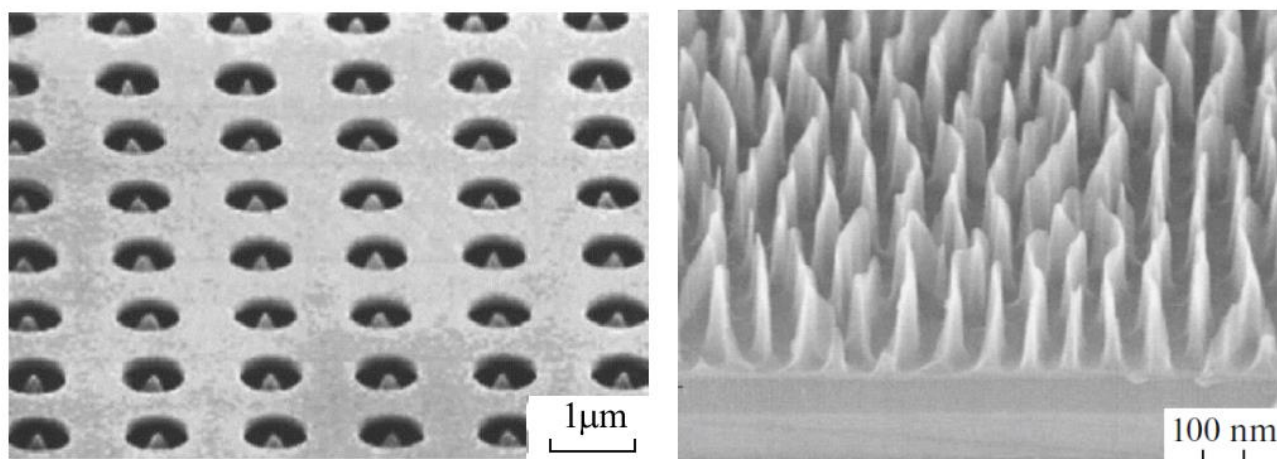


Figure 2. SEM images of multitip and multiblade silicon field-emission cathodes

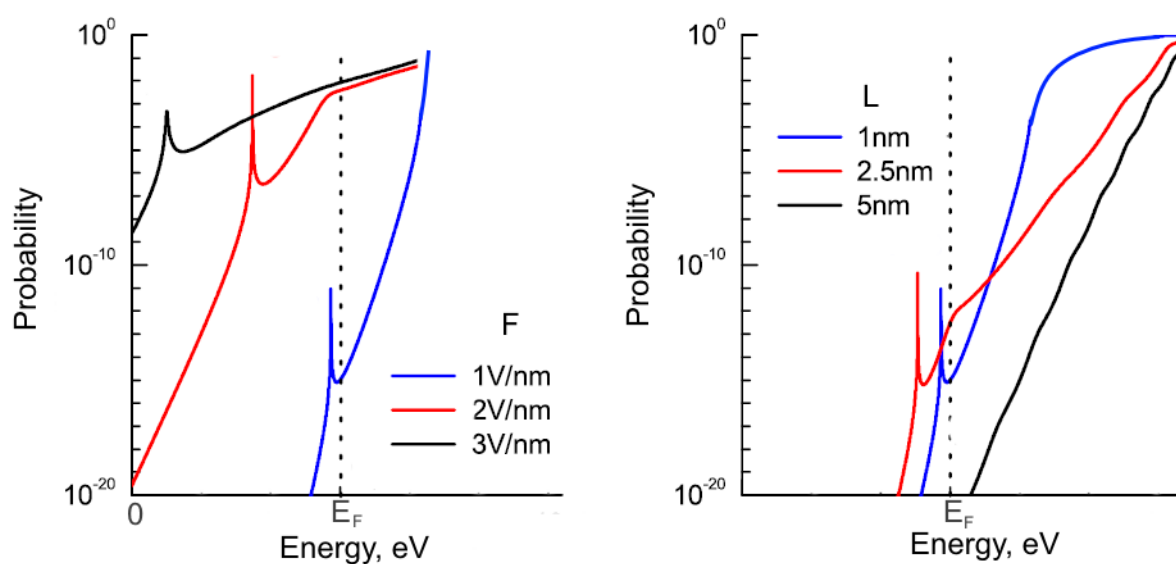


Figure 3. A schematic representation of dependence between tunneling probability and conduction electron energy relative to the Fermi energy level (E_F). The figure on the left shows dependence data for electrons, which are energy barrier width $L = 1$ nm, at varying applied fields. The figure on the right shows dependence data for electrons with varying energy barrier width at $F = 1$ V/nm.

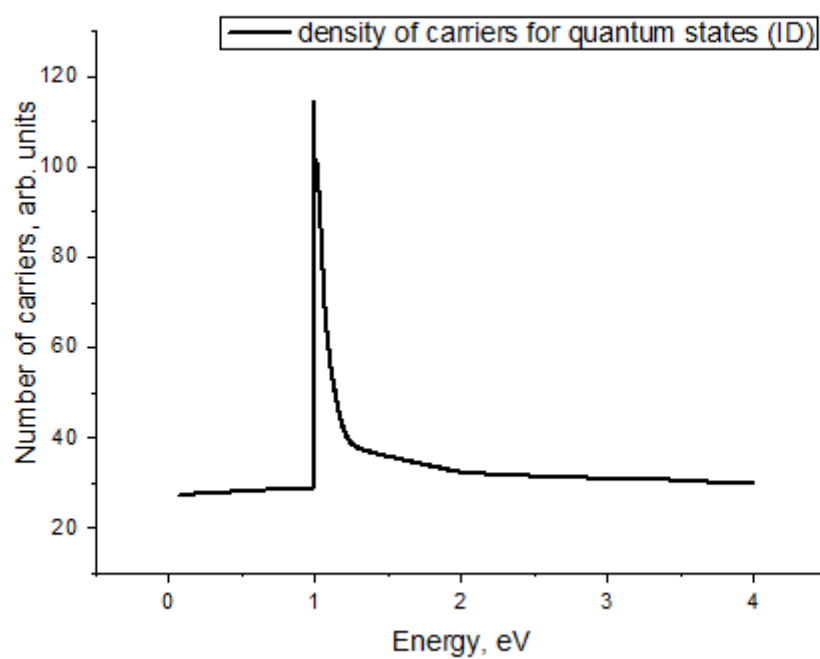


Figure 4. Type of energy distribution of the density of current carriers in the emitted current in the case of a one-dimensional cathode experiencing a quantum-size constraint.

ESTIMAÇÃO SIMULTÂNEA DE CLONAZEPAM E METRONIDAZOL EM COMPRIMIDOS FARMACÊUTICOS PELO MODO DE CROMATOGRRAFIA LÍQUIDA DE ALTA EFICIÊNCIA DE FASE REVERSA COM DETECÇÃO UV

SIMULTANEOUS ESTIMATION OF CLONAZEPAM AND METRONIDAZOLE IN PHARMACEUTICAL TABLETS BY REVERSED-PHASE HIGH-PERFORMANCE LIQUID CHROMATOGRAPHY MODE WITH UV DETECTION

التقدير التلقائي لكلونازيبام وميترونيدازول في الأقراص الصيدلانية بطريقة كروماتوغرافيا السائل عالي الأداء باستخدام مكشاف الأشعة فوق البنفسجية

ABED, Sadeem Subhi¹; RASHEED, Ashraf Saad^{1*}

¹ Department of Chemistry, College of Science, University of Baghdad, Al-Jadriya campus, 10071 Baghdad, Iraq.

* Corresponding author

e-mail: ashraf_analytical@yahoo.com

Received 31 July 2020; received in revised form 13 September 2020; accepted 22 October 2020

RESUMO

O clonazepam (CLO) desempenha um papel significativo no tratamento de convulsões, convulsões mioclônicas e outras infecções clínicas, enquanto o metronidazol (MTZ) é um medicamento antiprotózoário e antibacteriano. A técnica de cromatografia líquida de alta eficiência em fase reversa (RP-HPLC) tem proporcionado maior precisão e sensibilidade em relação a outros métodos, principalmente o colorimétrico e espectrofotométrico. O objetivo deste estudo foi implementar um método simples em comprimidos puros e farmacêuticos para a determinação simultânea de CLO e MTZ. O desenvolvimento e otimização do método RP-HPLC para validar um método de separação para a estimativa simultânea de ambos os fármacos na formulação farmacêutica envolveu o estudo da fase móvel ideal, concentração do tampão e valor de pH. Sob as condições cromatográficas, o sistema RP-HPLC obteve excelente separação em um Phenomenex HyperClone BDS (250 x 4,60 mm, 130A e 5μ) a uma temperatura de 45 °C e nas seguintes condições: 65:35% de acetonitrila: ácido acético e solução tampão de acetato de sódio (NaOAc / HAc) como fase móvel (pH 3,5); volume de injeção de 20 μL a uma taxa de fluxo de 0,75 mL / min e comprimento de onda de detecção de 310 nm. O procedimento de RP-HPLC proposto demonstrou alta precisão (RSD% <1%), bem como a boa relação linear do gráfico de calibração nas faixas de concentração de 50-160, 35-100 ppb com um coeficiente de determinação (r^2) do linha de regressão de 0,9996 e 0,9997 para metronidazol e clonazepam, respectivamente. O método proposto ofereceu excelentes valores validados tanto para LOD (4,24 e 3,06 ppb) e LOQ (14,15–10,21 ppb) para metronidazol e clonazepam, respectivamente. O método RP-HPLC foi aplicado com sucesso para estimar metronidazol e clonazepam nos conhecidos comprimidos farmacêuticos comerciais e deu uma recuperação excelente (> 98%) para ambos os medicamentos. Os resultados do método foram comparados com o método farmacopéico padrão para ambas as drogas por meio de testes estatísticos, que não indicaram diferença na precisão entre os métodos

Palavras-chave: Clonazepam, metronidazol, fase reversa, HPLC, preparações farmacêuticas.

ABSTRACT

Clonazepam (CLO) plays a significant role in treating seizures, myoclonic seizures, and other clinical infections, while metronidazole (MTZ) is an antiprotzoal, antibacterial drug. The reversed-phase high performance liquid chromatographic (RP-HPLC) technique has provided greater precision and sensitivity over other methods, especially the colorimetric and spectrophotometric. This study aimed to implement a simple method in pure and pharmaceutical tablets for the simultaneous determination of CLO and MTZ. The RP-HPLC method's development and optimization for validating a separation method for the simultaneous estimation of both drugs in pharmaceutical formulation involved studying the optimum mobile phase, buffer concentration, and the pH value. Under the chromatographic conditions, RP-HPLC system achieved excellent separation on a Phenomenex HyperClone BDS (250 x 4.60 mm, 130A, and 5μ) at a temperature of 45°C and the following conditions: 65:35% acetonitrile:acetic acid and sodium acetate buffer solution (NaOAc/HAc) as

mobile phase (pH 3.5); 20 μ L injection volume at a flow rate of 0.75 mL/min and detection wavelength of 310 nm. The proposed RP-HPLC procedure demonstrated high precision (RSD% < 1%), as well as the good linear relationship of the calibration graph at concentration ranges of 50-160, 35-100 ppb with a coefficient of determination (r^2) of the regression line of 0.9996 and 0.9997 for metronidazole and clonazepam respectively. The proposed method offered excellent validated values for both LOD (4.24 and 3.06 ppb) and LOQ (14.15–10.21 ppb) for both metronidazole and clonazepam drugs, respectively. The RP-HPLC method has been successfully applied to estimate metronidazole and clonazepam in the well-known commercial pharmaceutical tablets and gave an excellent recovery > 98% for both drugs. The results of the method was compared with the standard pharmacopeial method for both drugs using statistical tests, which indicated no difference in accuracy between the methods.

Keywords: *Clonazepam, metronidazole, reversed-phase, HPLC, pharmaceutical preparations*

المخلص:

ان التأثير الفعال للكلونازيبام هوفي علاج النوبات المصحوبة بغيوبة ونوبات الرمع العضلي وغيرها من المؤشرات السريرية. في حين أن الميترونيدازول هو دواء مضاد للجراثيم. قدمت تقنية الكروماتوغرافيا السائلة ذات الطور العكسي (RP-HPLC) قدرًا أكبر من التوافقية والحساسية على الطرق الأخرى وخاصة طرق القياس اللوني والطيف الضوئي. تشرح المقالة كيفية تطوير طريقة RP-HPLC الحساسة التي يمكن تطبيقها للتقدير التلقائي للميترونيدازول والكلونازيبام في المستحضرات الصيدلانية. تم دراسة الظروف المثلى لطريقة RP-HPLC للتحقق من صحة طريقة الفصل لتقدير لكلا العقارين في المستحضر الصيدلاني، ودراسة الطور المتحرك الأمثل وتركيز البفر ودرجة الحموضة. في ظل الظروف الكروماتوغرافية، حقق نظام RP-HPLC فصلًا ممتازًا على Phenomenex HyperClone BDS (250 x 4.60mm,) بابعاد 130 انكستروم، و 5 مايكرون) عند درجة حرارة 45 درجة مئوية، باستخدام (35:65) % أسيتونيتريل: محلول بفر (حمض الأسيتيك وأسيات الصوديوم (NaOAc / HAc)) كطور متحرك (درجة الحموضة 3.5)، حجم حقن 20 ميكرو لتر بمعدل سريان 0.75 مل / دقيقة، بينما كان الطول الموجي للكشف 310 نانومتر. أظهرت طريقة RP-HPLC المقترحة دقة عالية (RSD% > 1)، بالإضافة إلى العلاقة الخطية الجيدة لمنحني المعايرة عند التركيز من (50-160) و (35-100) جزء في البليون مع معامل ارتباط (r^2) ذو قيمة 0.9996 و 0.9997 للميترونيدازول والكلونازيبام على التوالي. قدمت الطريقة المقترحة قيمًا ممتازة لحد الكشف مقدار 4.24 و 3.06 جزء في البليون) وحد الكمية فكانت القيم (14.15 و 10.21 جزء في البليون) لكل من أدوية الميترونيدازول وكلونازيبام على التوالي. تم تطبيق طريقة RP-HPLC بنجاح لتقدير الميترونيدازول والكلونازيبام في الأقراص الصيدلانية التجارية المعروفة وأعطت قيم استرداد ممتازة < 98% لكلا العقارين على التوالي. تم مقارنة نتائج الطريقتين مع طرق دستور الأدوية القياسية بواسطة الاختبارات الاحصائية التي بينت عدم وجود فرق بالدقة بين هذه الطرق.

الكلمات المفتاحية: الكلونازيبام، الميترونيدازول، الطور العكس، كروماتوغرافيا السائل العالي الاداء، المستحضرات الصيدلانية

1. INTRODUCTION:

Clonazepam (CLO) (Figure 1) chemically known as 5-(2-chlorophenyl)-7-nitro-1H-*enzo* [e] [1,4]diazepin-2(3H)-one. CLO is a benzodiazepine medication used to relax the brain and nerves with anticonvulsants for many epilepsy, anxiety, and schizophrenia (Hart, Gourley, and Herfindal, 1992; Sweetman, 2009). CLO activity contributes to enhanced GAMMA receptor responses to aminobutyric acid (Lehoullier and Ticku, 1987; Riss, Cloyd, Gates, and Collins, 2008; Seubert and Saad Rasheed, 2017; Skerritt and Johnston, 1983).

The CLO half-life in plasma has varied from 19 to 60 h, where the mean value is 40 hr (Steentoft and Linnet, 2009). CLO has a variety of clinical indications, including sedative, anti-anxiety, anticonvulsant, and muscle relaxant. However, it is one of the Benzodiazepine with high potency and potentially addictive.

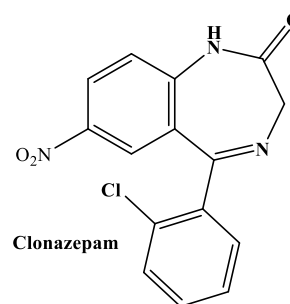


Figure 1. Structures formal of CLO

Therefore, the delicate balance between using and misusing is always a concern in medical uses (Al-Phalahy, Muhamad, and Rasheed, 2016; Longo and Johnson, 2000). CLO oral tablet may cause drowsiness, addictive, and it can cause other side effects as well. This medication will slow the movement, thought, and reaction time of the brain. Clonazepam oral tablet may have a more severe side effect: drowsiness, walking and balance difficulties, dizziness, insomnia, exhaustion, and memory issues (Lee-Chiong, 2008; Sorel, Mechler, and Harmant, 1981; Wollman, Lavie,

and Peled, 1985).

Due to the therapeutic significance of CLO, several techniques for determining it in pharmaceutical and/or biological forms have been developed. HPLC technique is extensively used for the assay of drugs and other compounds. The literature involved several HPLC methods for estimation of CLO, and most of these methods use the C18 column (Bares, Pehourcq, and Jarry, 2004; El Mahjoub and Staub, 2000; Ibrahim, El-Enany, Shalan, and Elsharawy, 2016; Meghana, Lahari, Kumari, and Prakash, 2012; Patil, Wankhede, and Chaudhari, 2015), with different mobile phase such as acetonitrile:0.01M sodium acetate (Bares *et al.*, 2004), acetonitrile: phosphate buffer (El Mahjoub and Staub, 2000; Meghana *et al.*, 2012), acetonitrile: methanol (60:40 v/v) (Patil *et al.*, 2015), and sodium dodecyl sulfate: 12% n-propanol in phosphoric acid (Ibrahim *et al.*, 2016).

Reversed-phase high-performance liquid chromatography (RP-HPLC) (reversed to normal HPLC) involved non-polar or hydrophobic stationary and polar mobile phases. As a result, the high polarity compounds are eluted earlier than non-polarity or low polarity, which retained for a longer time. The columns most widely used for reversed-HPLC separations are octyl (C₈), octadecyl (C₁₈), phenyl, Octadecyl silane (ODS), or cyanopropyl chemically bonded to microporous silica particles (Hodges and Mant, 1991; Mant, Cepenine, and Hodges, 2010). On the other hand, various mixtures of solvents are used as mobile phases such as acetonitrile, water, and methanol, thus playing an essential role in the efficient separation process (Henry, 2009; Unger and Liapis, 2012). RP-HPLC provides many advantages, such as high speed (analysis process can be done in a few minutes), good sensitivity (various detectors can be used), and reusable columns (Dong, 2013).

Metronidazole (MTZ) (Figure 2) is chemically known as 2-(2-methyl-5-nitro-1H-imidazole-1-yl) ethanol (Naveed, Waheed, and Nazeer, 2014) and extensively used in clinical treatment. The discovery of the antitrichomonal properties of antibiotic azomycin led to the investigation of nitroimidazoles as antiparasitic agents (Edwards, 1993; Pharmacopoeia, 2016). MTZ is a medicine for amebiasis (liver and colon), giardiasis (small bowel), and trichomoniasis that can be used as a treatment option (Katzung and Trevor, 2015; Reynolds and Parfitt, 1993).

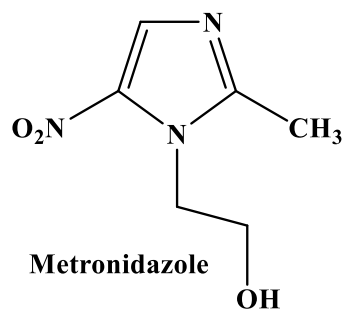


Figure 2. Structures formal of MTZ

MTZ was used against anaerobic organisms, anaerobic bacteria, amoebozoa infections, and antiprotozoal (Peyghan, Powell, and Zadkarami, 2008; Wilson, Gisvold, Block, and Beale, 2004). The initial clinical tests of MTZ indicated that it was capable of curing *Helicobacter pylori* (peptic ulcer diseases) and treating invasive amoebic dysentery (Rossi, 2013). MTZ antimicrobial activity is due to the presence of a nitrogen group that has been decreased chemically by bacterial inhibition due to anaerobic bacteria and protozoans and resulting in bacterial cell death (Chrystal, Koch, McLafferty, and Goldman, 1980). The resulting product is responsible for the MTZ antimicrobial activity and the parasite DNA interaction of the MTZ (Eisenstein and Schaechter, 2007). The toxicity of the central nervous system can be pancreatitis and serious. MTZ is a little well tolerated but can produce a spectrum from peripheral neuropathy, cerebellopathy, encephalopathy, and epilepsy to adverse neurological effects. The use of alcohol for MTZ therapy can lead to nausea and vomiting (Hwang *et al.*, 2012; Kim *et al.*, 2004; Kuriyama, Jackson, Doi, and Kamiya, 2011).

Several HPLC methods for evaluating MTZ in pharmaceutical forms have been developed. These methods involved use Hypersil BDS C18, 150x4.6, 5μ as stationary phase with phosphate buffer and acetonitrile : (90:10 %v/v) as a mobile phase, while the other method used C₁₈ column (250x 4.6 mm, 5μm) with Acetonitrile: 0.5 M potassium dihydrogen orthophosphate buffer pH 4.5 with triethylamine 30:70 (v/v) as mobile phase, with a wavelength of 289 nm (Al-Abachi, Abed, and Alamri, 2020; Ghante, Pannu, Loni, and Shivsharan, 2012). No analysis of the retention characteristics of CLO and MTZ on a Phenomenex HyperClone BDS (250 x 4.60 mm, 130A, and 5μ), has been conducted, given the availability of numerous works of separation CLO and MTZ on HPLC.

This study aimed to implement a simple method in pure and pharmaceutical tablets for the simultaneous determination of CLO and MTZ.

2. MATERIALS AND METHODS:

2.1. Chemicals

Metronidazole and clonazepam and as standards were donations from SDI, Samara, Iraq. Acetonitrile (ACN), sodium acetate, acetic acid were HPLC grade and were obtained from Sigma-Aldrich. For applications, pharmaceutical tablets were obtained from a pharmacy to different companies (Julphar-UAE, SDI-Iraq, Hoffman-LaRoche-Switzerland, and Roche Farma-Spain).

2.2. HPLC apparatus

The chromatographic system Merck-Hitachi was equipped with a flow pump Model L-6200, a Model L-4200 UV/Vis detector, and an N2000 Photographic Data Workstation Module Integrator. The chromatographic separation was performed with an RP-C8 stationary phase Phenomenex HyperClone BDS 250 x 4.60 mm, 130A, and 5 μ). The mobile phase, acetonitrile–10 mM sodium acetate buffer (pH = 3.5)–(35: 65, v/v) was controlled at a flow rate of 0.75 mL/min at 45 °C. A 310 nm UV detector tracked the column effluent.

2.3. Preparation of standard solutions

A stock solution of CLO or MTZ (1000 μ g mL⁻¹) was prepared by dissolving 0.100 g in 100 mL of acetonitrile. More working standard solutions were prepared by dilution of the stock solution with the same solvent to the desired concentration. From the stock solutions of clonazepam and metronidazole, a working solution (200 ppb) was made-up in millipore water in a brown flask. The calibration standards were prepared freshly from this working solution. The calibration standards of clonazepam used were 35, 52, 68, 85, and 100 ppb whereas for the metronidazole the final concentrations were 50, 78, 105, 130, and 160 ppb.

2.3.1 Preparation of CLO and MTZ tables

A total of twenty-five of CLO tablets containing 2 mg of commercial drugs were weighed. The average weight was calculated and powdered. After shaking well and pouring into a 50 mL volumetric flask, an equal quantity of 50 mg

CLO was dissolved in 30 mL of ACN for waste. The residue has been ACN washed, and the amount with ACN has gradually been raised to 50 mL. Twenty-five MTZ tablets containing 500 mg of the commercial drug were weighed, and the average weight was calculated. Then, the tablets were powdered. After well-filtering and residue disposal, the quantity equivalent to 100 mg MTZ was dissolved in 10 mL. The residue was washed with ACN, and the amount with ACN eventually reached 20 mL. Subsequently, the solution was filtered by filters (0.45 μ m).

2.5. Method development

The sensitive and straightforward RP-HPLC method using C₈ stationary phase Phenomenex HyperClone BDS (250 x 4.60 mm, 130A, and 5 μ) and 0.75 mL/min as a flow rate in addition to acetic acid and sodium acetate buffer solution as mobile phase-ACN(NaOAc/HAc) was developed and validated for the simultaneous determination MTZ and CLO. To achieve an effective RP-HPLC method with high resolution and efficient separation, significant factors were optimized. In addition to the MTZ and CLO retention behavior, various acetonitrile containing, buffer levels, and pH eluent have been examined. The detection was carried at 310 nm. And the conditions were adjusted for the construction of calibration curves to estimate both drugs MTZ and CLO.

3. RESULTS AND DISCUSSION:

3.1. Separation of clonazepam and metronidazole

In RP-HPLC system development and quantitative estimation, the separation process is a preliminary stage. The main objective of this project was to select a clear approach that ensures that MTZ and CLO are goodly separated. A mobile NaOAc / HAc buffer phase with a varying ACN content on the RP column was chosen as test pharmaceuticals by the CLO and MTZ for a study on their retention mechanism in RP-mode. Figure 3 displays the chromatogram. The chromatogram was obtained in a NaOAc / HAc buffer with 35% ACN and 10 mM (pH 3.5).

3.2. The effect of ACN percent on retention of MTZ and CLO

Mobile phase compositions are changed systemically by variation of the ACN content from 35% to 95% (v/v) with constant the concentration of the buffer 10 mM at pH 3.5 (Figure 4). The

pharmaceutical CLO shows behavior hydrophobic interaction with increasing ACN content in the mobile phase. Otherwise, MTZ shows behavior hydrophilic (HILIC). The hydrophilicity of the drug compounds is responsible for this difference in behavior. The values of the pharmaceuticals are evident from the $\log P_{ow}$. This is explained in $\log P_{ow}$ MTZ and CLO values, respectively (-0.46, 3.15) (Sangster, 2010).

3.3. The effect of buffer pH on retention of MTZ and CLO

The buffer pH was varied from 3.5-5.5 with constant the concentration of the buffer 10 mM at ACN content 35% (Figure 5). The retention factor of CLO and MTZ decreased with increasing pH buffer from 3.5 to 5.5. The source of this behavioral difference is the isoelectric point (9.22, 6.77) values of MTZ and CLO, respectively.

3.4. The effect of buffer concentration on retention of MTZ and CLO

At the end of optimization conditions, the buffer concentration was changed from 10 to 30 mM with constant the ACN content 35% at pH 3.5, and therefore, we found no significantly altered (Figure 6).

3.5. Calibration graph

MTZ and CLO calibration graphs have been developed in optimal conditions (eluent: 10 mM sodium acetate, pH 3.5, 35% acetonitrile), 310 nm UV detection, 20 μ L injection volume, flow rate 0.75 mL/min, 45°C temperature) by plotting area versus to CLO and MTZ concentrations and display the 50 -160 and 35-100 ppb range concentration of MTZ and CLO, respectively (Figure 7).

3.6. Statistical data analysis

The direct calibration graphs were constructed, and the statistical results are shown under Table 1 for the direct determination of CLO and MTZ in RP-Mode. The approach has been ICH-validated (Guideline, 2005) for two concentrations covering the range. Each concentration was repeated (n=3) and five consecutive days of calibration samples analyzed. The accuracy and the precision of RSD and recovery measurements were measured in one run (intra-day) and in between (inter-day) assays (Table 2).

3.7. Determination of CLO and MTZ in pharmaceutical tablets

Two of the pharmaceutical preparations containing the target drugs (tablet) with the stated concentration of 2 and 500 mg respectively per unit are successfully used in MTZ and CLO determinations, and the obtained results are described in Table 3. The data obtained using the RP-mode (Table 3) was compared with the standard method (Pharmacopeia, 2009) using the 95% confidence student t-test test and variance F-test. The t- and F-values (Tables 4) calculated did not exceed the theoretical values which indicate that the accuracy and precision method for determining MTZ and CLO in pharmaceutical formulations did not differ significantly.

4. CONCLUSIONS:

The proposed method was validated for precision, accuracy, specificity, reproducibility, and robustness for simultaneous quantitative estimation of MTZ and CLO in dosage forms. The chromatographic conditions were investigated to achieve good separation efficiency. Retention times of approximately 3 and 6 minutes for MTZ and CLO, respectively, were recorded on the C_8 stationary phase Phenomenex HyperClone BDS (250 x 4.60 mm and 5 μ) column. The proposed RP-HPLC method was applied for the determination of the mentioned drugs (MTZ and CLO) in pharmaceutical formulations with high accuracy and precision. Therefore the proposed RP-HPLC method can be used for routine extermination of MTZ and CLO in pharmaceutical dosages.

5. REFERENCES:

1. Al-Abachi, M. Q., Abed, S. S., and Alamri, M. H. A. (2020). Charge Transfer Spectrophotometric Determination of Metronidazole in Pharmaceutical Formulations by Normal and Reverse Flow Injection Analysis Coupled with Solid-Phase Reactor Containing Immobilized FePO₄. *Iraqi Journal of Science*, 1541-1554.
2. Al-Phalahy, B. A., Muhamad, Y. H., and Rasheed, A. S. (2016). Zwitterionic Ion Chromatography of Dansyl Amino Acids with 4-Vinylbenzyl Dimethyl Ammonio Pentanesulfonate as Stationary Phase.

- Asian Journal of Chemistry*, 28, 2411-2414.
- Bares, I. F., Pehourcq, F., and Jarry, C. (2004). Development of a rapid RP-HPLC method for the determination of clonazepam in human plasma. *Journal of pharmaceutical and biomedical analysis*, 36(4), 865-869.
 - Chrystal, E., Koch, R. L., McLAFFERTY, M. A., and Goldman, P. (1980). Relationship between metronidazole metabolism and bactericidal activity. *Antimicrobial agents and chemotherapy*, 18(4), 566-573.
 - Dong, M. W. (2013). The essence of modern HPLC: advantages, limitations, fundamentals, and opportunities.
 - Edwards, D. I. (1993). Nitroimidazole drugs-action and resistance mechanisms I. Mechanism of action. *Journal of Antimicrobial Chemotherapy*, 31(1), 9-20.
 - Eisenstein, B., and Schaechter, M. (2007). DNA and chromosome mechanics. *Schaechter's mechanisms of microbial disease* (ed. NC Engleberg, et al.), 28.
 - El Mahjoub, A., and Staub, C. (2000). High-performance liquid chromatographic method for the determination of benzodiazepines in plasma or serum using the column-switching technique. *Journal of Chromatography B: Biomedical Sciences and Applications*, 742(2), 381-390.
 - Ghante, M. R., Pannu, H. K., Loni, A., and Shivsharan, T. (2012). Development and validation of a RP-HPLC method for simultaneous estimation of metronidazole and norfloxacin in bulk and tablet dosage form. *International Journal of Pharmacy and Pharmaceutical Sciences*, 4, 241-245.
 - Guideline, I. H. T. (2005). *Validation of analytical procedures: text and methodology Q2 (R1)*. Paper presented at the International conference on harmonization, Geneva, Switzerland.
 - Hart, L. L., Gourley, D., and Herfindal, E. T. (1992). *Workbook for Clinical Pharmacy and Therapeutics*: Williams and Wilkins.
 - Henry, R. A. (2009). The early days of HPLC at DuPont.
 - Hodges, R., and Mant, C. (1991). Standard chromatographic conditions for size exclusion, ion-exchange, reversed phase and hydrophobic interaction chromatography. In (pp. 11-22): CRC Press, Boca Raton.
 - Hwang, G. H., Sim, Y.-J., Jeong, H. J., Kim, G. C., Sin, B. W., and Jung, J. H. (2012). Metronidazole induced encephalopathy with peripheral polyneuropathy in patient with spinal cord injury. *Korean Journal of Spine*, 9(1), 44-48.
 - Ibrahim, F., El-Enany, N., Shalan, S., and Elsharawy, R. (2016). Micellar high performance liquid chromatographic method for simultaneous determination of clonazepam and paroxetine HCl in pharmaceutical preparations using monolithic column. *J. Chromatogr. Sep. Tech.*, 7(4), 331-339.
 - Katzung, B. G., and Trevor, A. J. (2015). *Basic and clinical pharmacology*: McGraw-Hill Education New York.
 - Kim, D. W., Park, J.-M., Yoon, B.-W., Baek, M. J., Kim, J. E., and Kim, S. (2004). Metronidazole-induced encephalopathy. *Journal of the neurological sciences*, 224(1-2), 107-111.
 - Kuriyama, A., Jackson, J. L., Doi, A., and Kamiya, T. (2011). Metronidazole-induced central nervous system toxicity: a systematic review. *Clinical neuropharmacology*, 34(6), 241-247.
 - Lee-Chiong, T. (2008). *Sleep medicine: Essentials and review*. Oxford University Press.
 - Lehoullier, P. F., and Ticku, M. K. (1987). Benzodiazepine and β -carboline modulation of GABA-stimulated $^{36}\text{Cl}^-$ influx in cultured spinal cord neurons. *European journal of pharmacology*, 135(2), 235-238.
 - Longo, L. P., and Johnson, B. (2000). Addiction: Part I. Benzodiazepines-side effects, abuse risk and alternatives. *American family physician*, 61(7), 2121-2128.
 - Mant, C. T., Cepeniene, D., and Hodges, R. S. (2010). Reversed-phase HPLC of peptides: Assessing column and solvent selectivity on standard, polar-embedded

- and polar endcapped columns. *Journal of separation science*, 33(19), 3005-3021.
23. Meghana, D., Lahari, K., Kumari, K. S., and Prakash, K. (2012). Development and validation of RP-HPLC method for simultaneous estimation of clonazepam and propranolol hydrochloride in bulk and pharmaceutical dosage forms. *Inventi Rapid: Pharm Analysis and Quality Assurance*, 2, 1-4.
 24. Naveed, S., Waheed, N., and Nazeer, S. (2014). Degradation study of metronidazole in active and different formulation by UV spectroscopy. *J Bioequiv Availab*, 6(4), 124-127.
 25. Patil, P., Wankhede, S., and Chaudhari, P. (2015). A validated stability-indicating HPLC method estimation of clonazepam in the bulk drug and pharmaceutical dosage form. *Pharm Anal Acta*, 6(2), 332-337.
 26. Peyghan, R., Powell, M., and Zadkarami, M. (2008). In vitro effect of garlic extract and metronidazole against *Neoparamoeba pemaquidensis*, page 1987 and isolated amoebae from Atlantic salmon. *Pak. J. Biol. Sci.*, 11(1), 41-47.
 27. Pharmacopeia, B. (2009). by system simulation ltd., the stationary office, London. In: CD-ROM.
 28. Pharmacopoeia, B. (2016). British pharmacopoeia.
 29. Reynolds, J. E., and Parfitt, K. (1993). Martindale; Extra pharmacopoeia.
 30. Riss, J., Cloyd, J., Gates, J., and Collins, S. (2008). Benzodiazepines in epilepsy: pharmacology and pharmacokinetics. *Acta neurologica scandinavica*, 118(2), 69-86.
 31. Rossi, S. (2013). Adelaide: The Australian Medicines Handbook Unit Trust. *Antimycotic imidazoles. part, 4*.
 32. Sangster, J. (2010). LOGKOW: A databank of evaluated octanol-water partition coefficients (LogP). *Sangster Research Laboratories*, pp <http://logkow.cisti.nrc.ca/logkow>.
 33. Seubert, A., and Saad Rasheed, A. (2017). Separation of Metal-Trifluoperazine Hydrochloride Complexes Using Zwitterionic Ion Chromatography (ZIC) Coupled Online with ICP-AES. *Current Pharmaceutical Analysis*, 13(4), 328-333.
 34. Skerritt, J. H., and Johnston, G. A. (1983). Enhancement of GABA binding by benzodiazepines and related anxiolytics. *European journal of pharmacology*, 89(3-4), 193-198.
 35. Sorel, L., Mechler, L., and Harmant, J. (1981). Comparative trial of intravenous lorazepam and clonazepam im status epilepticus. *Clinical therapeutics*, 4(4), 326-336.
 36. Steentoft, A., and Linnet, K. (2009). Blood concentrations of clonazepam and 7-aminoclonazepam in forensic cases in Denmark for the period 2002–2007. *Forensic science international*, 184(1-3), 74-79.
 37. Sweetman, S. C. (2009). *Martindale: the complete drug reference* (Vol. 3709): Pharmaceutical press London.
 38. Unger, K. K., and Liapis, A. I. (2012). Adsorbents and columns in analytical high-performance liquid chromatography: A perspective with regard to development and understanding. *Journal of separation science*, 35(10-11), 1201-1212.
 39. Wilson, C. O., Gisvold, O., Block, J. H., and Beale, J. M. (2004). *Wilson and Gisvold's textbook of organic medicinal and pharmaceutical chemistry/edited by John H. Block, John M. Beale Jr.* Philadelphia: Lippincott Williams and Wilkins.
 40. Wollman, M., Lavie, P., and Peled, R. (1985). A hypernycthemeral sleep-wake syndrome: a treatment attempt. *Chronobiology international*, 2(4), 277-280.

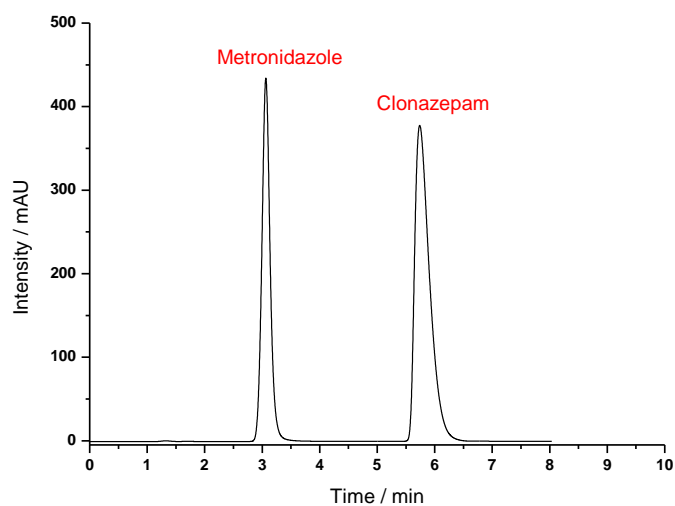


Figure 3. Chromatogram for MTZ and CLO

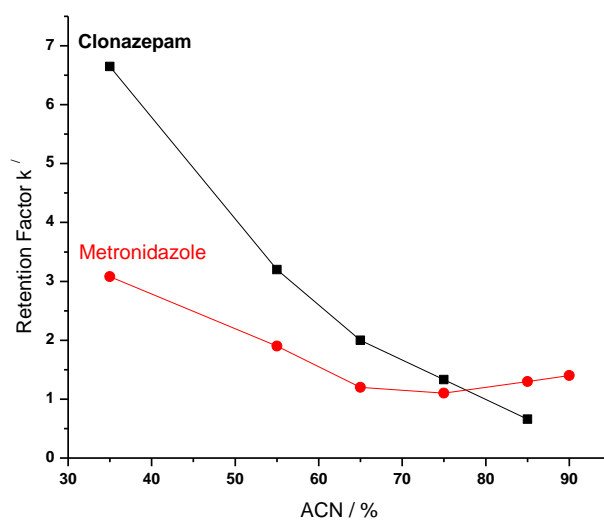


Figure 4. Effect of ACN ratio on retention factor for MTZ and CLO.

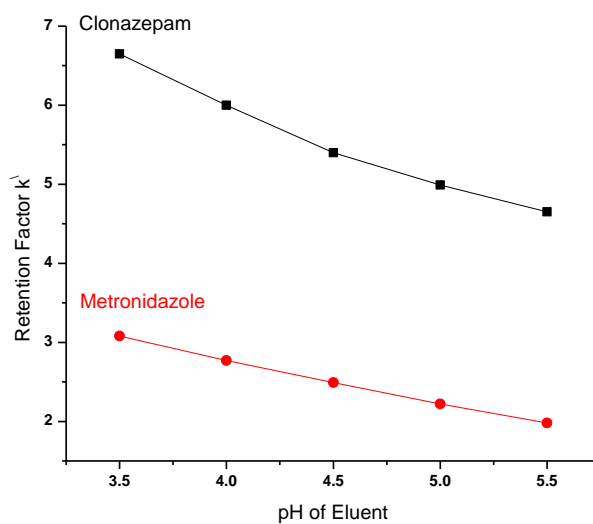


Figure 5. The buffer pH effect on retention factor for MTZ and CLO.

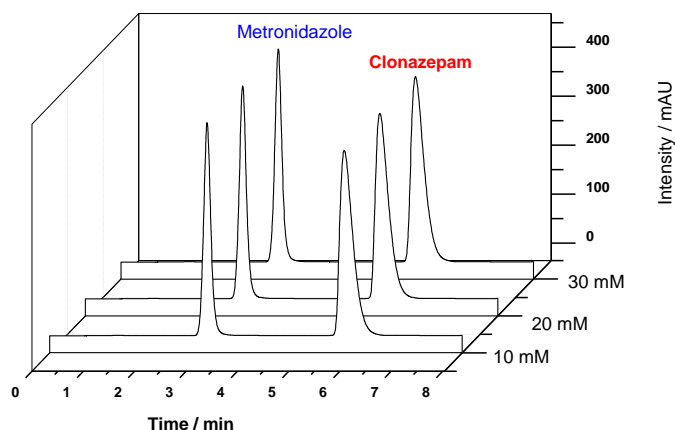


Figure 6. Influence of buffer concentration on the chromatogram

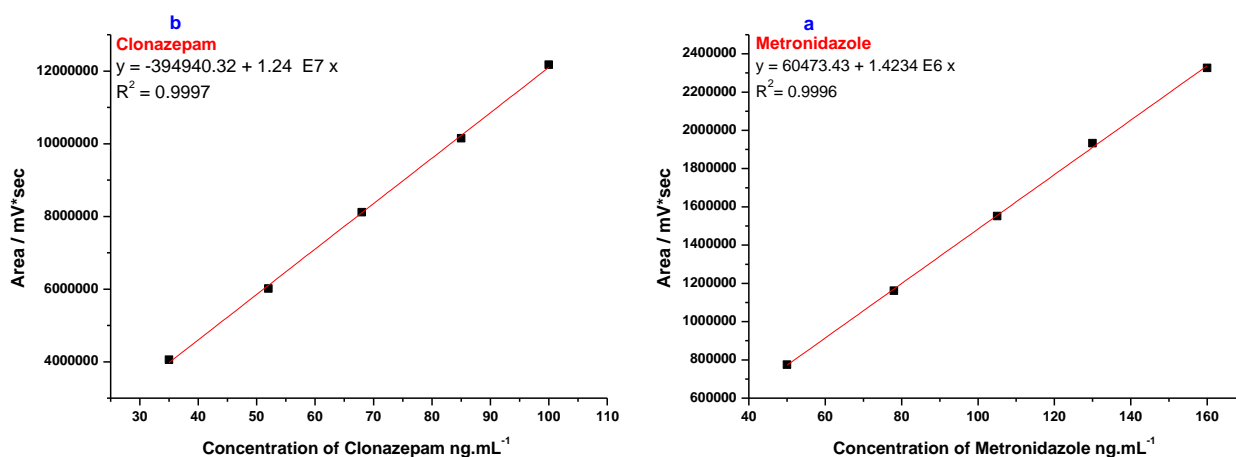


Figure 7. Calibration graphs for CLO and MTZ.

Table 1. Analytical values of statistical treatments for determination of CLO and MTZ from the calibration graph

Parameter	MTZ	CLO
Linear range (ppb)	50-160	35-100
Regression equation	$y = 60473.43 + 1.4234 \text{ E}6 \text{ x}$	$y = -394940.32 + 1.24 \text{ E}7 \text{ x}$
Coefficient of determination (r^2)	0.9996	0.9997
LOD (ppb)	4.24	3.06
LOQ (ppb)	14.15	10.21

Table 2. The accuracy and precision of the proposed method for the determination of CLO and MTZ

		intra-day n=5			inter-day n=5			
MTZ								
Present (ppb)	Found (ppb)	%Rec.	% Erel.	%RSD	Found (ppb)	% Rec.	% Erel.	%RSD
70	70.22	100.31	0.31	0.73	70.49	100.70	0.70	0.76
80	80.55	100.68	0.68	0.78	80.62	100.77	0.77	0.81
CLO								
70	69.5	99.28	- 0.72	0.44	70.05	100.07	0.03	0.55
80	79.86	99.82	- 0.18	0.50	79.97	99.96	- 0.04	0.59

Notes: %Rec.= Recovery percentage; % Erel. = Relative error percentage; %RSD=Relative Standard Deviation; Found (ppb)= The concentration found from the direct calibration graph

Table 3. Implementation of the method of determination proposed of MTZ and CLO in pharmaceutical preparations

Name of pharmaceutical	Manufacturer	Present conc. (mg)	Found direct calb. (mg)	Rec %	RSD % n=5	RE %
MTZ						
Negazole	Julphar, UAE	500	498.22	99.64	0.51	- 0.36
MEDAZOLE	SDI, Iraq	500	497.73	99.54	0.67	- 0.46
CLO						
Rivotril Hoffman-LaRoche	Hoffman-LaRoche, Switzerland	2.00	1.98	99.00	0.73	- 1.00
Rivotril Roche Farma, S.A	Roche Farma, Spain	2.00	1.97	98.50	0.33	- 1.50

Notes: Present conc. (mg)= The concentration of drug taken; Found direct calb. (mg)= The concentration found from the direct calibration graph.

Table 4. The comparison of the suggested RP-HPLC method with conventional methods for MTZ and CLO measurements using t-test and F-statistical measures.

Name of pharmaceutical	Proposed method Rec%	Standard method Rec% (Pharmacopeia, 2009)	t _{cal}	F _{cal}
MTZ				
Pure	100.495	99.87	0.97	1.67
Negazole	99.64	98.633		
MEDAZOLE	99.54	99.733		
CLO				
Pure	99.55	100.59	-0.42	4.47
Rivotril (2mg) Hoffman-LaRoche	99.00	98.55		
Rivotril (2mg) Roche Farma, S.A	98.50	98.81	*t _{tab} = 2.77	**F _{tab} =19.0

Theoretical values at 95% confidence limit, $n_1 = n_2 = 3$.

* $t = 2.776$, where t has degrees of freedom $= (n_1 + n_2 - 2) = 4$

** $F = 19.0$, where F has degrees of freedom $= (n_1 - 1) = 2, (n_2 - 1) = 2$

ANÁLISE DAS FUNÇÕES DE ENERGIA E ONDA E DAS PROPRIEDADES TERMODINÂMICAS DA EQUAÇÃO DE SCHRODINGER 6-DIMENSIONAL SOB DUPLO OSCILADOR EM FORMA DE ANEL (DRSO) E POTENCIAIS MANNING-ROSEN USANDO MÉTODO SUSY QM

ANALYSIS OF ENERGY AND WAVE FUNCTIONS AND THE THERMODYNAMICS PROPERTIES OF THE 6-DIMENSIONAL SCHRODINGER EQUATION UNDER DOUBLE RING-SHAPE OSCILLATOR (DRSO) AND MANNING-ROSEN POTENTIALS USING SUSY QM METHOD

ANALISIS ENERGY DAN FUNGSI GELOMBANG DAN SIFAT TERMODINAMIS DARI PERSAMAAN SCHRODINGER 6-DIMENSI DIBAWAH PENGARUH POTENSIAL DOUBLE RING-SHAPE OSCILLATOR (DRSO) DAN POTENSIAL MANNING-ROSEN MENGGUNAKAN METODE SUSY QM.

BILAUT, Dedy Adrianus ²; SUPARMI, A ^{1*}; CARI, C ¹; FANIANDARI, Suci ²;

¹ Sebelas Maret University, Physics Department, Faculty of Mathematics and Natural Sciences. Indonesia.

² Sebelas Maret University, Physics Department, Graduate Program. Indonesia.

* Corresponding author
e-mail: soeparmi@staff.uns.ac.id

Received 17 July 2020; received in revised form 18 August 2020; accepted 25 October 2020

RESUMO

As soluções exatas das equações de Schrodinger (SE) no sistema de coordenadas D-dimensional têm atraído a atenção de muitos pesquisadores teóricos nos ramos da física quântica e química quântica. Os autovalores de energia e a função de onda são as soluções da equação de Schrodinger que implicitamente representam o comportamento de um sistema mecânico quântico. O estudo teve como objetivo obter os autovalores, funções de onda e propriedades termodinâmicas da equação de Schrodinger 6-Dimensional sob duplo oscilador em forma de anel (DRSO) e potencial de Manning-Rosen. O método de separação variável foi aplicado para reduzir a única equação de Schrodinger 6-Dimensional dependente do potencial radial e angular não central em cinco equações de Schrodinger unidimensionais: uma equação de Schrodinger radial e cinco equações de Schrodinger angulares. Cada uma dessas equações de Schrodinger unidimensionais foi resolvida usando o método SUSY QM para obter um autovalor e uma função de onda da parte radial, cinco autovalores e cinco funções de onda angular da parte angular. Algumas propriedades termodinâmicas, tais como energia vibracional média U , calor específico vibracional C , energia livre vibracional F e entropia vibracional S , foram obtidas por meio das equações de energia radial. Os resultados mostraram que, exceto o n_{l1} , todo incremento do número quântico angular diminui os valores de energia. Incrementos de todos os parâmetros potenciais aumentam os valores de energia. O incremento do número quântico angular e do parâmetro de potenciais aumenta a amplitude e desloca as funções de onda para a esquerda. Entretanto, o incremento de n_{l1} , α , σ e ρ diminui a amplitude e muda as funções de onda para a direita. Além disso, a energia média vibracional U e a energia livre F aumentaram com o aumento do valor dos parâmetros dos potenciais, onde o parâmetro ω tem o efeito dominante do que os outros parâmetros. O calor vibracional específico C e a entropia S são afetados apenas pelo parâmetro ω , onde C e S diminuem com o aumento de ω .

Palavras-chave: Sistema D-dimensional, potencial não central, potencial de forma de anel, supersimetria, mecânica quântica, quantidades termodinâmicas.

ABSTRACT

The exact solutions of the Schrodinger equations (SE) in the D-dimensional coordinate system have attracted the attention of many theoretical researchers in branches of quantum physics and quantum chemistry. The energy eigenvalues and the wave function are the solutions of the Schrodinger equation that implicitly represents the behavior of a quantum mechanical system. This study aimed to obtain the eigenvalues, wave functions, and thermodynamic properties of the 6-Dimensional Schrodinger equation under Double Ring-Shaped Oscillator (DRSO) and Manning-Rosen potential. The variable separation method was applied to reduce the one

6-Dimensional Schrodinger equation depending on radial and angular non-central potential into five one-dimensional Schrodinger equations: one radial and five angular Schrodinger equations. Each of these one-dimensional Schrodinger equations was solved using the SUSY QM method to obtain one eigenvalue and one wave function of the radial part, five eigenvalues, and five angular wave functions angular part. Some thermodynamic properties such, the vibrational mean energy U , vibrational specific heat C , vibrational free energy F , and vibrational entropy S , were obtained using the radial energy equations. The results showed that except the n_{l1} , all increment of angular quantum number decreases the energy values. Increments of all potential parameter increase the energy values. Increment of angular quantum number and potentials parameter increases the amplitude and shifts the wave functions to the left. However, the increment of n_{l1} , α , σ , and ρ decrease the amplitude and shift wavefunctions to the right. Moreover, the vibrational mean energy U and free energy F increased as the increasing value of potentials parameters, where the ω parameter has the dominant effect than the other parameters. The vibrational specific heat C and entropy S affected only by the ω parameter, where C and S decreased as the increase of ω .

Keywords: *D-dimensional system, non-central potential, ring shape potential, supersymmetry quantum mechanics, thermodynamics quantities.*

ABSTRAK

Solusi eksak dari persamaan Schrodinger (SE) dalam sistem koordinat D-dimensi telah menarik banyak perhatian peneliti-peneliti fisika teori dalam cabang fisika dan kimia kuantum. Nilai eigen energi dan fungsi gelombang merupakan solusi dari persamaan Schrodinger, yang secara implisit merepresentasikan perilaku suatu sistem kuantum. Penelitian ini bertujuan untuk mendapatkan nilai eigen, fungsi gelombang, dan sifat termodinamika dari persamaan Schrodinger 6 Dimensi dengan potensial *Double Ring-Shaped Oscillator* (DRSO) dan Manning-Rosen. Metode pemisahan variabel diterapkan untuk mereduksi satu persamaan Schrodinger 6-Dimensi yang bergantung pada potensial non-sentral fungsi radial dan sudut menjadi lima persamaan Schrodinger satu dimensi: satu persamaan Schrodinger bagian radial, dan lima persamaan Schrodinger bagian sudut. Masing-masing persamaan Schrodinger satu dimensi ini diselesaikan menggunakan metode SUSY QM untuk mendapatkan: satu nilai eigen dan satu fungsi gelombang dari bagian radial, lima nilai eigen dan lima fungsi gelombang sudut dari bagian sudut. Beberapa sifat termodinamika seperti vibrasi energi rata-rata U , vibrasi panas spesifik C , vibrasi energi bebas F , dan vibrasi entropi S diperoleh dengan menggunakan persamaan energi radial. Hasil penelitian menunjukkan bahwa, selain n_{l1} , semua kenaikan bilangan kuantum sudut menurunkan nilai energi. Kenaikan semua parameter potensial meningkatkan nilai energi. Penambahan bilangan kuantum sudut dan parameter potensial meningkatkan amplitudo dan menggeser fungsi gelombang ke kiri. Namun, kenaikan n_{l1} , α , σ , dan ρ menurunkan amplitudo dan menggeser fungsi gelombang ke kanan. Selain itu, nilai vibrasi mean energi U dan energi bebas F semakin meningkat seiring dengan meningkatnya nilai parameter potensial, dimana parameter ω memiliki pengaruh yang dominan dibandingkan dengan parameter lainnya. vibrasi panas jenis C dan entropi S hanya dipengaruhi oleh parameter ω , di mana C dan S menurun seiring bertambahnya ω .

Kata Kunci: *Sistem D-Dimensi, potensial non sentral, potensial cincin ganda, mekanika kuantum super simetri, kuantitas termodinamika.*

1. INTRODUCTION:

The solution of the Schrodinger equation (SE), Klein Gordon (KGE) and Dirac equations (DE) have been attracted the attention of many researchers in theoretical physics area (Durmus and Yasuk, 2007; Karayer, 2019; Yahya and Oyewumi, 2016) because these equations contain all information on the quantum mechanics system. The SE is used to analyze the quantities of nonrelativistic systems, while the KGE and DE are used in relativistic systems to analyze the spin-0 and spin- $\frac{1}{2}$ particles, respectively (Arda and Sever, 2009; Candemir, 2016; Zarrinkamar *et al.*, 2010). The solution of SE, KGE, and DE with some potentials have a great rule in atomic and particles physics, plasma and solid-state (Ebomwonyi, *et*

al., 2017; Zhang, 2000), scattering cross-section, tunneling, and decay rate (Antia *et al.*, 2017). However, to get analytic solutions from these equations requires special methods and approaches. Various methods are still being developed in the interest of looking for nonrelativistic wave solutions. The Nikiforov-Uvarov (NU) method has been used to solve the Dirac Equation, which is influenced by hyperbolic potential (Karayer, 2019), Klein Gordon Equation (KGE) with multi-parameter q-deformed Wood Saxon potential (Lütfüoğlu, *et al.*, 2018). Asymptotic Iteration Method (AIM) has been used to solve several problems. For instance, this method has been used to investigate Dirac Equation with Morse potential with tensor interaction (Alsadi, 2015), and Klein Gordon Equation with exponential scalar and vector

potential (Ikhdair and Falaye, 2013), relativistic and nonrelativistic wave equation under Poschl-Teller potential and its thermodynamic properties (Taşkın, *et al.*, 2008). Romanovski polynomial method has been used to investigate a quantum mechanical system of Dirac with the effect of Scarf plus new tensor coupling potential (Suparmi, *et al.*, 2014). The quantization rule approach has been used to solve the Schrodinger Equations problem with hyperbolic plus second Poschl-Teller potential (Dong and Gonzalez-Cisneros, 2008). Supersymmetry Quantum Mechanics (SUSY QM) method to analyze the Schrodinger equation with heavy-quarkonia potential (Abu-Shady and Ikot, 2019) and Dirac equation under hyperbolic and Coulomb potential (Hassanabadi, *et al.*, 2011).

$$V(r, \theta) = \frac{1}{2}\mu\omega^2 r^2 + \frac{\hbar^2}{2\mu} \left(\frac{\alpha}{r^2 \sin^2 \theta} + \frac{\sigma}{r^2 \cos^2 \theta} \right) \quad (\text{Eq. 1})$$

The Double Ring-Shape Oscillator (DRSO) potential (1) is a type of ring-shaped potential with its mathematical interests and its physics and chemistry quantum applications. The ring-shaped type potential is one of non-central potential with a highly symmetrical system because of its invariance under reflection and axial symmetry (Carpio-Bernido and Chrisopher, 1989). This ring-shape type potential is generally a combination of Coulomb, oscillator, or Hartman potential which involves $\left(\frac{1}{r^2 \sin^2 \theta}\right)$ on a ring-shaped type of single-ring-shaped and $\left(\frac{1}{\sin^2 \theta} + \frac{1}{\cos^2 \theta}\right)$ in the double ring-shaped type (You, *et al.*, 2018). This potential type in recent times has been an interesting topic of researchers in physics and quantum chemistry because of its importance when applied to describe the structure of benzene molecules in quantum chemistry and deformed nuclei in nuclear physics. Ring-shaped harmonic oscillators are also used to study the spin symmetry of an antinucleon embedded in nucleus and the linear and nonlinear optical effects of moving electrons in the non-central field (Chang-Yuan, *et al.*, 2013; Fa-Lin, Lu and Chang-Yuan, 2010; Hassanabadi, *et al.*, 2014; Ikot, A. N., *et al.*, 2016; Sun, *et al.*, 2014; Yasuk and Durmus, 2007; You *et al.*, 2018).

Improvement to solve the Schrodinger equation in a higher dimensional system still necessary to carry out because it is important under the field of quantum physics (André, *et al.*, 2019; Falaye and Oyewumi, 2011; Onate, *et al.*, 2018; Wang, *et al.*, 2002). One of the motivations that attracted the attention of scientists to continually identify D-dimensional systems is the pretentious unified theory 20th century between the Relativity and Quantum theory. Another

reason is to obtain clarity from one of the products from string and supergravity theory, the Klauza-Klein theory if its additional dimensions are the spatial dimension (Dong, 2011).

Therefore, to obtain more advancement information on the D-dimensional quantum mechanical system, it should not be restricted to four or five-dimensional spaces. The investigation needs to be made for higher dimensional spaces and various potential systems to get more general solutions. So, this study tried to analyze the 6-dimensional quantum mechanical system, both for radial and each of its angular parts.

$$V(\theta) = \frac{\hbar^2 v(v+1)}{2\mu \sin \theta} - \frac{\hbar^2 2\rho}{2\mu v} \cot \theta \quad (\text{Eq. 2})$$

DRSO (1) plus Manning Rosen potential (2) could be extended into a 6-Dimensional separable non-central potential written as follows

$$V(r, \theta_1, \theta_2, \theta_3, \theta_4, \theta_5) = V(r) + \frac{1}{r^2} \left\{ \frac{V_1(\theta_1)}{\sin^2 \theta_2 \sin^2 \theta_3 \sin^2 \theta_4 \sin^2 \theta_5} + \frac{V_2(\theta_2)}{\sin^2 \theta_3 \sin^2 \theta_4 \sin^2 \theta_5} + \frac{V_3(\theta_3)}{\sin^2 \theta_4 \sin^2 \theta_5} + \frac{V_4(\theta_4)}{\sin^2 \theta_5} + V_5(\theta_5) \right\} \quad (\text{Eq. 3})$$

with

$$V(r) = \frac{1}{2}\mu\omega^2 r^2 \quad (\text{Eq. 4})$$

$$V_1(\theta_1) = \frac{\hbar^2}{2\mu} \left(\frac{\alpha}{\sin^2 \theta_1} + \frac{\sigma}{\cos^2 \theta_1} \right) \quad (\text{Eq. 5})$$

$$V_2(\theta_2) = \frac{\hbar^2}{2\mu} \left(\frac{v_2(v_2+1)}{\sin^2 \theta_2} - 2\rho_2 \cot \theta_2 \right) \quad (\text{Eq. 6})$$

$$V_3(\theta_3) = \frac{\hbar^2}{2\mu} \left(\frac{v_3(v_3+1)}{\sin^2 \theta_2} - 2\rho_3 \cot \theta_3 \right) \quad (\text{Eq. 7})$$

$$V_4(\theta_4) = \frac{\hbar^2}{2\mu} \left(\frac{v_4(v_4+1)}{\sin^2 \theta_4} - 2\rho_4 \cot \theta_4 \right) \quad (\text{Eq. 8})$$

$$V_5(\theta_5) = \frac{\hbar^2}{2\mu} \left(\frac{v_5(v_5+1)}{\sin^2 \theta_5} - 2\rho_5 \cot \theta_5 \right) \quad (\text{Eq. 9})$$

Where equation (3) is a special form of equation (25) for the 6-dimensional system. With $0 \leq \theta_1 \leq 2\pi$, and $0 \leq \theta_2, \theta_3, \theta_4, \theta_5 \leq \pi$. \hbar , μ , and ω are Planck constant, mass, and frequency of a particle. α , σ , v_i , and ρ_i are the potential

parameters, respectively.

The thermodynamics properties for quantum mechanical systems are an interesting problem to consider because of their interactions with the energy spectrum that contains the physical properties of the quantum system itself. There are many studies of thermodynamic properties. Some of them are the thermodynamical properties for systems with double ring-shaped quantum dot type potential (Khordad and Sedehi, 2018), thermodynamical properties from Klein Gordon equation with DFPEP potential D-dimensional spaces (A N Ikot *et al.*, 2016). For example, thermodynamical properties from Schrodinger Equation and Klein Gordon equation with Poshcl-Teller potential (Yahya and Oyewumi, 2016), thermodynamical properties of Schrodinger equation with an anharmonic oscillator in cosmic string framework (Sobhani, *et al.*, 2018), thermodynamical properties of diatomic molecules using general molecular potential (A N Ikot *et al.*, 2018).

The vibrational mean energy U , the vibrational specific heat C , the vibrational free energy F , and the vibrational entropy S can be solved using some following order. Starting by solving the Shrodinger equation in the D-dimensional system to get the energy level equations and eigenfunctions for the angular and radial parts, respectively. The energy equation is then employed to determine the partition function, which is the principal element for defining the thermodynamics properties.

The research of thermodynamics properties in a D-dimensional system with ring shape type potentials is still an interesting topic in the quantum mechanics. Generally, ring-shaped type potential in D-dimensional space is analyzed without being extended to study thermodynamic properties. The complexity of the theory and application in quantum mechanical systems analyzed the thermodynamics properties of the Schrodinger equation in 6-dimensional spaces with DRSO plus Manning Rosen potential using the SUSY QM technique.

This study aimed to find the nonrelativistic energy spectra equation, radial wave function and angular wave functions, and also the corresponding thermodynamics properties such as the vibrational mean energy, vibrational free energy, vibrational specific heat and vibrational entropy of six-dimensional Schrodinger equation for Double Ring-Shape Oscillator (DRSO) and Manning Rosen potential.

2. MATERIALS AND METHODS:

2.1. Supersymmetry Quantum Mechanic (SUSY QM) Method

One of the powerful techniques to solve Schrodinger-like equations is Supersymmetry Quantum Mechanics (SUSY QM) method. The method proposed by Witten is principally developed based on the existence of fermionic operators which are commute with the Hamiltonian (Witten, 1981) Concerning the supersymmetry system in general, the Hamiltonian H is composed of the square of supersymmetry charges and can be expressed as a multiplication between a pair of supersymmetry operators as

$$H_{\mp}(x) = A^{\pm} A^{\mp} \quad (\text{Eq. 10})$$

with

$$A^{\pm} = \mp \frac{\hbar}{\sqrt{2\mu}} \frac{d}{dx} + W(x) \quad (\text{Eq. 11})$$

where A^{+} and A^{-} are rising and lowering operators, and a pair of SUSY QM partner potentials $V_{\mp}(x)$ gave as

$$V_{\mp}(x) = W^2(x) \mp \frac{\hbar}{\sqrt{2\mu}} \frac{dW(x)}{dx} \quad (\text{Eq. 12})$$

The general Hamiltonian can be factored into

$$H = H_{-} + E_0 = -\frac{\hbar^2}{2\mu} \frac{d^2}{dx^2} + V_{-}(x; a_0) + E_0 \quad (\text{Eq. 13})$$

Therefore, using equations (12) and (13) it has got the equation 14

$$\begin{aligned} V(x) &= V_{-}(x; a_0) + E_0 \\ &= W^2(x) - \frac{\hbar}{\sqrt{2\mu}} \frac{dW(x)}{dx} + E_0 \end{aligned} \quad (\text{Eq. 14})$$

where $V(x)$ is an effective potential and E_0 is the groundstate energy. Superpotential $W(x)$ is hypothetically determined by considering the effective potential equation form of the related system expressed in equation (14).

The supersymmetry solely presents the relationship between the eigenvalues and eigenfunctions between two Hamiltonian partners but does not provide the actual spectrum. Consequently, one has to consider shape invariance condition. The potential is said to shape invariance if its supersymmetry partner potential has similar shapes but not for the parameters. More specifically, if $V_-(x; a_j)$ is a potential with its partner superpotential $V_+(x; a_j)$ have to satisfy the equation

$$V_+(x; a_j) = V_-(x; a_{j+1}) + R(a_{j+1}) \quad (\text{Eq. 15})$$

with

$$V_+(x; a_j) = W^2(x; a_j) + \frac{\hbar}{\sqrt{2m}} \frac{dW(x; a_j)}{dx};$$

$$V_-(x; a_{j+1}) = W^2(x; a_{j+1}) - \frac{\hbar}{\sqrt{2m}} \frac{dW(x; a_{j+1})}{dx} \quad (\text{Eq. 16})$$

where $j = 0, 1, 2, \dots$ and a is a parameter of the potential V_- when its ground state energy is zero, $a_j = f_j(a_0)$ for f_j is a function that is applied j times, $R(a_j)$ is an independent Constanta towards x . Furthermore, the Hamiltonian eigenvalue can be written as (Dutt, *et al.*, 1988; Khare and Bhaduri, 1993).

$$E_n^{(-)} = \sum_{k=1}^n R(a_k) \quad (\text{Eq. 17})$$

Thus, from equation (13) and (17), it is possible to get the energy spectrum of the system

$$E_n = E_n^{(-)} + E_0 \quad (\text{Eq. 18})$$

Ground state wave function of H_- which the energy is zero could be obtained by

$$A^-\psi_0^{(-)} = 0 \quad (\text{Eq. 19})$$

The excited wave function $\psi_1^{(-)}(x; a_0), \dots, \psi_n^{(-)}(x; a_0)$ from H_- can be determined by applying raising operator on the lower wave function

$$\psi_n^{(-)}(x; a_0) \approx A^+(x; a_0)A^+(x; a_1) \cdots A^+(x; a_{n-1}), \psi_0^{(-)}(x; a_n) \quad (\text{Eq. 20})$$

2.2. Schrodinger Equation in 6-Dimensional Coordinates

The time-independent Schrodinger equation with potential in D-dimensional is given by (Hassanabadi, *et al.*, 2011; Wang, *et al.*, 2002)

$$\left(\nabla_D^2 - \frac{2\mu}{\hbar^2}V\right)\psi_{l_1, \dots, l_{D-1}}^{(l_D-1=l)}(\hat{X}) = -\frac{2\mu}{\hbar^2}E\psi_{l_1, \dots, l_{D-1}}^{(l_D-1=l)}(\hat{X}) \quad (\text{Eq. 21})$$

with E is the energy of the particle. $\psi_{l_1, \dots, l_{D-1}}^{(l_D-1=l)}(\hat{X})$ is the Laplace operator for D-dimensional space, ∇_D^2 and D-dimensional position vector are given as

$$\nabla_D^2 = \frac{1}{h} \sum_{j=0}^{D-1} \frac{d}{d\theta_j} \left(\frac{\hbar}{h_j^2} \frac{\partial}{\partial \theta_j} \right) \quad (\text{Eq. 22})$$

$$\theta_0 = r; h = \prod_{j=0}^{D-1} h_j; h_j^2 = \sum_{i=0}^D \left(\frac{\partial X_i}{\partial \theta_j} \right)^2 \quad (\text{Eq. 23})$$

The relevance between D-dimensional position vector $\hat{X} = (r, \theta_i)$, and hyperspherical Cartesian coordinates x_1 can be written as follows:

$$x_1 = r \cos \theta_1 \sin \theta_2, \dots, \sin \theta_{D-1}$$

$$x_2 = r \sin \theta_1 \sin \theta_2, \dots, \sin \theta_{D-1}$$

$$x_b = r \cos \theta_{b-1} \sin \theta_b, \dots, \sin \theta_{D-1}$$

$$\vdots$$

$$x_{D-1} = r \cos \theta_{D-2} \sin \theta_{D-1}$$

$$x_D = r \cos \theta_{D-1} \quad (\text{Eq. 24})$$

where $r \in [0, \infty]$, $\theta_1 \in [0, 2\pi]$, $\theta_b \in [0, \pi]$, $D = 2, 3, \dots$, and $b = 3, 4, \dots, (D-1)$ (Dong, 2011). Specifically, for the case when $D = 3$, the hyperspherical coordinate system reduced into spherical coordinates (r, θ, φ) .

The separable D dimensional non-central potential hypothetically proposed as

$$\begin{aligned}
V(r, \theta_1, \theta_2, \dots, \theta_{D-1}) \\
= V(r) + \frac{1}{r^2} \sum_{j=1}^{D-1} \frac{V_j(\theta_j)}{\sin^2 \theta_{j+1} \dots \sin^2 \theta_{D-1}} \\
+ \dots + \frac{V_{D-2}(\theta_{D-2})}{\sin^2 \theta_{D-1}} + V_{D-1}(\theta_{D-1})
\end{aligned}
\quad (\text{Eq. 25})$$

For 6 dimensional quantum system with a separable 6 dimensional non central potential it has got the D dimensional coordinate system obtained from equation (24) as

$$\begin{aligned}
x_1 &= r \cos \theta_1 \sin \theta_2 \sin \theta_3 \sin \theta_4 \sin \theta_5 \\
x_2 &= r \sin \theta_1 \sin \theta_2 \sin \theta_3 \sin \theta_4 \sin \theta_5 \\
x_3 &= r \cos \theta_2 \sin \theta_3 \sin \theta_4 \sin \theta_5 \\
x_4 &= r \cos \theta_3 \sin \theta_4 \sin \theta_5 \\
x_5 &= r \cos \theta_4 \sin \theta_5 \\
x_6 &= r \cos \theta_5
\end{aligned}
\quad (\text{Eq. 26})$$

with the coordinate scale obtained from equation (23) as

$$\begin{aligned}
h_1 &= r \sin \theta_2 \sin \theta_3 \sin \theta_4 \sin \theta_5 \\
h_2 &= r \sin \theta_3 \sin \theta_4 \sin \theta_5 \\
h_3 &= r \sin \theta_4 \sin \theta_5 \\
h_4 &= r \sin \theta_5 \\
h_5 &= r \\
h_0 &= h_r = 1
\end{aligned}
\quad (\text{Eq. 27})$$

Apply equations (26) and (27) on equation (22), it has got the Laplacian operator for the 6-Dimensional system as

$$\begin{aligned}
\nabla_6^2 \\
= \frac{1}{r^5} \frac{\partial}{\partial r} \left(r^5 \frac{\partial}{\partial r} \right) \\
+ \frac{1}{r^2} \left\{ \frac{1}{\sin^2 \theta_2 \sin^2 \theta_3 \sin^2 \theta_4 \sin^2 \theta_5} \left(\frac{\partial^2}{\partial \theta_1^2} \right) \right. \\
+ \frac{1}{\sin^2 \theta_3 \sin^2 \theta_4 \sin^2 \theta_5} \left[\frac{1}{\sin \theta_2} \frac{\partial}{\partial \theta_2} \left(\sin \theta_2 \frac{\partial}{\partial \theta_2} \right) \right] \Bigg\} \\
+ \frac{1}{r^2} \left\{ \frac{1}{\sin^2 \theta_4 \sin^2 \theta_5} \left[\frac{1}{\sin^2 \theta_3} \frac{\partial}{\partial \theta_3} \left(\sin^2 \theta_3 \frac{\partial}{\partial \theta_3} \right) \right] \right. \\
+ \frac{1}{\sin^2 \theta_5} \left[\frac{1}{\sin^3 \theta_4} \frac{\partial}{\partial \theta_4} \left(\sin^3 \theta_4 \frac{\partial}{\partial \theta_4} \right) \right] \\
+ \left. \frac{1}{\sin^4 \theta_5} \frac{\partial}{\partial \theta_5} \left(\sin^4 \theta_5 \frac{\partial}{\partial \theta_5} \right) \right\}
\end{aligned}
\quad (\text{Eq. 28})$$

The potential form that allows the variable separation in 6-dimensional system obtained from equation (25) have been given in equations (3-9).

By setting up

$$\psi_{l_1, \dots, l_{D-1}}^{(l_{D-1}=l)}(\hat{X}) = R(r) P_i(\theta_i) ; \quad i = 1, 2, 3, 4, 5
\quad (\text{Eq. 29})$$

then it is possible to make the separation of variables by applying equations (27) - (29) into (21). Using simple mathematical procedures, it can be obtained wave equations of the 6-dimensional system for radial r and angular θ_i functions, respectively.

$$\begin{aligned}
r^2 \frac{1}{r^5} \frac{d}{dr} \left(r^5 \frac{dR(r)}{dr} \right) + \frac{2\mu}{\hbar^2} (Er^2 - V_1(r)r^2) R(r) \\
- \lambda_5 R(r) = 0
\end{aligned}
\quad (\text{Eq. 30})$$

$$\left\{ \frac{d^2}{d\theta_1^2} - \frac{2\mu}{\hbar^2} V_1(\theta_1) + \lambda_1 \right\} P_1 = 0
\quad (\text{Eq. 31})$$

$$\begin{aligned}
\frac{1}{\sin \theta_2} \frac{d}{d\theta_2} \left(\sin \theta_2 \frac{dP_2}{d\theta_2} \right) \\
- \left\{ \frac{2\mu}{\hbar^2} V_2(\theta_2) + \frac{\lambda_1}{\sin^2 \theta_2} - \lambda_2 \right\} P_2 = 0
\end{aligned}
\quad (\text{Eq. 32})$$

$$\begin{aligned}
\frac{1}{\sin^2 \theta_3} \frac{d}{d\theta_3} \left(\sin^2 \theta_3 \frac{dP_3}{d\theta_3} \right) \\
- \left\{ \frac{2\mu}{\hbar^2} V_3(\theta_3) + \frac{\lambda_2}{\sin^2 \theta_3} - \lambda_3 \right\} P_3 = 0
\end{aligned}
\quad (\text{Eq. 33})$$

$$\begin{aligned}
\frac{1}{\sin^3 \theta_4} \frac{d}{d\theta_4} \left(\sin^3 \theta_4 \frac{dP_4}{d\theta_4} \right) \\
- \left\{ \frac{2\mu}{\hbar^2} V_4(\theta_4) + \frac{\lambda_3}{\sin^2 \theta_4} - \lambda_4 \right\} P_4 = 0
\end{aligned}
\quad (\text{Eq. 34})$$

$$\begin{aligned}
\frac{1}{\sin^4 \theta_5} \frac{d}{d\theta_5} \left(\sin^4 \theta_5 \frac{dP_5}{d\theta_5} \right) \\
- \left\{ \frac{2\mu}{\hbar^2} V_5(\theta_5) + \frac{\lambda_4}{\sin^2 \theta_5} - \lambda_5 \right\} P_5 = 0
\end{aligned}
\quad (\text{Eq. 35})$$

with $\lambda_1 - \lambda_5$ are the variable separation constants.

Each of these equations (30), (32) – (35) has both first and second derivative forms, so we need to reduce these equations to the form of a Schrodinger-like equation with the second derivative form only. Therefore, we set $R(r) = r^{-\left(\frac{D-1}{2}\right)} \chi(r)$ and $P_i = \sin^{-\left(\frac{i-1}{2}\right)} \theta_i Q(\theta_i)$, $i = 2-5$ then using simple mathematic operations, it can be obtained

$$\left\{ \frac{d^2}{dr^2} - \frac{2\mu}{\hbar^2} V_r(r) - \frac{\lambda_5 + \frac{15}{4}}{r^2} + \frac{2\mu}{\hbar^2} E \right\} \chi(r) = 0$$

(Eq. 36)

$$\left\{ \frac{d^2}{d\theta_1^2} - \frac{2\mu}{\hbar^2} V_1(\theta_1) + \lambda_1 \right\} Q_1(\theta_1) = 0$$

(Eq. 37)

$$\left\{ \frac{d^2}{d\theta_2^2} - \frac{2\mu}{\hbar^2} V_2(\theta_2) - \frac{\lambda_1 - \frac{1}{4}}{\sin^2 \theta_2} + \left(\frac{1}{4} + \lambda_2 \right) \right\} Q_2(\theta_2) = 0$$

(Eq. 38)

$$\left\{ \frac{d^2}{d\theta_3^2} - \frac{2\mu}{\hbar^2} V_3(\theta_3) - \frac{\lambda_2}{\sin^2 \theta_3} + (1 + \lambda_3) \right\} Q_3(\theta_3) = 0$$

(Eq. 39)

$$\left\{ \frac{d^2}{d\theta_4^2} - \frac{2\mu}{\hbar^2} V_4(\theta_4) - \frac{\lambda_3 + \frac{3}{4}}{\sin^2 \theta_4} + \left(\frac{9}{4} + \lambda_4 \right) \right\} Q_4(\theta_4) = 0$$

(Eq. 40)

$$\left\{ \frac{d^2}{d\theta_5^2} - \frac{2\mu}{\hbar^2} V_5(\theta_5) - \frac{\lambda_4 + 2}{\sin^2 \theta_5} + (4 + \lambda_5) \right\} Q_5(\theta_5) = 0$$

(Eq. 41)

the radial Schrodinger-like wave equation (36) and angular Schrodinger-like wave equations (37) – (41) are solvable using the SUSY QM method.

3. RESULTS AND DISCUSSION:

3.1. The solution of the Schrodinger Equation in 6-Dimensional System

3.1.1 Solution of angular θ_1

Substitute the angular θ_1 potential in equations (3) and (5) into equation (37)

$$\left\{ -\frac{\hbar^2}{2\mu} \frac{d^2}{d\theta_1^2} + \frac{\hbar^2}{2\mu} \left(\frac{\alpha}{\sin^2 \theta_1} + \frac{\sigma}{\cos^2 \theta_1} \right) \right\} Q_1(\theta_1) = \frac{\hbar^2}{2\mu} \lambda_1 Q_1(\theta_1)$$

(Eq. 42)

then it has got its effective potential as,

$$V_{\text{eff}}(\theta_1) = \frac{\hbar^2}{2\mu} \left(\frac{\alpha'(\alpha' - 1)}{\sin^2 \theta_1} + \frac{\sigma'(\sigma' - 1)}{\cos^2 \theta_1} \right)$$

(Eq. 43)

where $\alpha' = \sqrt{\alpha + \frac{1}{4}} + \frac{1}{2}$, $\sigma' = \sqrt{\sigma + \frac{1}{4}} + \frac{1}{2}$ and $E_{\theta_1} = \frac{\hbar^2}{2\mu} \lambda_1$.

Using the following hypothetical superpotential for the effective potential in equation (43),

$$W(\theta_1) = \frac{\hbar}{\sqrt{2\mu}} (M \cot \theta_1 + N \tan \theta_1)$$

(Eq. 44)

then inserting equations (43) and (44) into equation (14) it is possible to obtain

$$\begin{aligned} \frac{\hbar^2}{2\mu} \left(\frac{\alpha'(\alpha' - 1)}{\sin^2 \theta_1} + \frac{\sigma'(\sigma' - 1)}{\cos^2 \theta_1} \right) - E_0 \\ = \frac{\hbar^2}{2\mu} \left(\frac{M^2 + M}{\sin^2 \theta_1} + \frac{N^2 - N}{\cos^2 \theta_1} \right) \\ - \frac{\hbar^2}{2\mu} (M - N)^2 \end{aligned}$$

(Eq. 45)

It has got several parameter relations as follows

$$M(M + 1) = \alpha'(\alpha' - 1) \rightarrow M = -\alpha'$$

(Eq. 46)

$$N(N - 1) = \sigma'(\sigma' - 1) \rightarrow N = \sigma'$$

(Eq. 47)

$$E_0(\theta_1) = (M - N)^2 = (\alpha' + \sigma')^2$$

(Eq. 48)

The superpartner potential for angular θ_1 is obtained by substituting equation (44) and (46) - (48) into (12)

$$V_-(\theta_1; a_0) = \frac{\hbar^2}{2\mu} \left(\frac{\alpha'(\alpha' - 1)}{\sin^2 \theta_1} + \frac{\sigma'(\sigma' - 1)}{\cos^2 \theta_1} \right) - \frac{\hbar^2}{2\mu} (\alpha' + \sigma')^2$$

(Eq. 49)

$$V_+(\theta_1; a_0) = \frac{\hbar^2}{2\mu} \left(\frac{\alpha'(\alpha' + 1)}{\sin^2 \theta_1} + \frac{\sigma'(\sigma' + 1)}{\cos^2 \theta_1} \right) - \frac{\hbar^2}{2\mu} (\alpha' + \sigma')^2$$

(Eq. 50)

These superpartner potential are similar and differ only in their parameters. Consequently, to obtain $V_{\mp}(\theta_1; a_{1,2,\dots}, a_n)$ it is necessary to shift these parameters $\alpha' \rightarrow \alpha' + 1$ and $\sigma' \rightarrow \sigma' + 1$.

By generalization using a characteristic of shape invariance (15), it is obtained

$$R(\theta_1; a_n) = -\frac{\hbar^2}{2\mu} ((\alpha' + \sigma' + 2(n - 1))^2 + (\alpha' + \sigma' + 2n)^2)$$

(Eq. 51)

Therefore, by using equation (17) and (18), the eigenvalue for angular part θ_1 can be easily obtained as

$$E_{n_l}(\theta_1) = \frac{\hbar^2}{2\mu} (\alpha' + \sigma' + 2n_{l1})^2 \quad (\text{Eq. 52})$$

hence, it has got

$$\lambda_1 = (\alpha' + \sigma' + 2n_{l1})^2 \quad (\text{Eq. 53})$$

where n_l is the orbital quantum number.

Applying the superpotential (44) on equation (11) has raised and lowered operator, respectively.

$$A^+(\theta_1) = -\frac{\hbar}{\sqrt{2\mu}} \frac{d}{d\theta_1} + \frac{\hbar}{\sqrt{2\mu}} (-\alpha' \cot\theta_1 + \sigma' \tan\theta_1) \quad (\text{Eq. 54})$$

$$A^-(\theta_1) = \frac{\hbar}{\sqrt{2\mu}} \frac{d}{d\theta_1} + \frac{\hbar}{\sqrt{2\mu}} (-\alpha' \cot\theta_1 + \sigma' \tan\theta_1) \quad (\text{Eq. 55})$$

Thus, using equation (55) and (19) it is obtained the ground-state angular θ_1 wave function as

$$\psi_0^{(-)}(\theta_1) = \aleph_{\theta_1} (\sin\theta_1)^{\alpha'} (\cos\theta_1)^{\sigma'} \quad (\text{Eq. 56})$$

with \aleph_{θ_1} is the normalization constant of angular θ_1 wave function.

3.1.2 Solution of angular θ_2

Substitute the angular θ_1 potential in equations (3) and (6) into equation (38)

$$\begin{aligned} & -\frac{\hbar^2}{2\mu} \frac{d^2 Q_2(\theta_2)}{d\theta_2^2} \\ & + \frac{\hbar^2}{2\mu} \left(\frac{v_2(v_2+1) + \left(\lambda_1 - \frac{1}{4}\right)}{\sin^2\theta_2} - 2\rho_2 \cot\theta_2 \right) Q_2(\theta_2) \\ & = \frac{\hbar^2}{2\mu} \left(\frac{1}{4} + \lambda_2 \right) Q_2(\theta_2) \end{aligned} \quad (\text{Eq. 57})$$

thus it is obtained its effective potential as,

$$V_{\text{eff}}(\theta_2) = \frac{\hbar^2}{2\mu} \left(\frac{v'_2(v'_2+1)}{\sin^2\theta_2} - 2\rho_2 \cot\theta_2 \right) \quad (\text{Eq. 58})$$

where $v'_2 = \sqrt{v_2(v_2+1) + \lambda_1} - \frac{1}{2}$ and $E_{\theta_2} = \frac{\hbar^2}{2\mu} \left(\frac{1}{4} + \lambda_2 \right)$.

By using following hypothetical superpotential for the effective potential (58),

$$W(\theta_2) = \frac{\hbar}{\sqrt{2\mu}} \left(B_2 \cot\theta_2 + \frac{C}{B_2} \right) \quad (\text{Eq. 59})$$

And inserting (58) and (59) into equation (14)

$$\begin{aligned} & \frac{\hbar^2}{2\mu} \left(\frac{v'_2(v'_2+1)}{\sin^2\theta_2} - 2\rho_2 \cot\theta_2 \right) - E_0(\theta_2) \\ & = \frac{\hbar^2}{2\mu} \left(\frac{B_2^2 + B_2}{\sin^2\theta_1} - 2\rho_2 \cot\theta_2 \right) + \frac{\hbar^2}{2\mu} \left(\frac{C^2}{B_2} - B_2^2 \right) \end{aligned} \quad (\text{Eq. 60})$$

It is got several parameter relations as follows

$$B_2 = v'_2 \quad (\text{Eq. 61})$$

$$C_2 = \rho_2 \quad (\text{Eq. 62})$$

$$E_0(\theta_2) = -\frac{\hbar^2}{2\mu} \left(\frac{C^2}{B_2} - B_2^2 \right) \quad (\text{Eq. 63})$$

The superpartner potential for the angular θ_2 part is obtained by substituting equation (59) and (61) – (63) into (12).

$$\begin{aligned} V_-(\theta_2; a_0) &= \frac{\hbar^2}{2\mu} \left(\frac{v'_2(v'_2+1)}{\sin^2\theta_2} - 2\rho_2 \cot\theta_2 \right) \\ &+ \frac{\hbar^2}{2\mu} \left(\frac{C^2}{v'_2} - v'^2_2 \right) \end{aligned} \quad (\text{Eq. 64})$$

$$\begin{aligned} V_+(\theta_2; a_0) &= \frac{\hbar^2}{2\mu} \left(\frac{v'_2(v'_2-1)}{\sin^2\theta_2} - 2\rho_2 \cot\theta_2 \right) \\ &+ \frac{\hbar^2}{2\mu} \left(\frac{C^2}{v'_2} - v'^2_2 \right) \end{aligned} \quad (\text{Eq. 65})$$

These superpartner potential (64) and (66) are similar and differ only on their parameters. Consequently, to obtain $V_{\mp}(\theta_2; a_{1,2}, \dots, a_n)$ it is necessary to shift these parameters $v' \rightarrow v' - 1$.

By generalization using a characteristic of shape invariance (15), it is obtained

$$\begin{aligned} R(\theta_2; a_n) &= \frac{\hbar^2}{2\mu} \left(\frac{\rho_2^2}{v'^2_2} - v'^2_2 \right) \\ &- \frac{\hbar^2}{2\mu} \left(\frac{\rho_2^2}{(v'_2 - n)^2} - (v'_2 - n)^2 \right) \end{aligned} \quad (\text{Eq. 66})$$

Therefore, by using equation (17), (18) and (63), the eigenvalue for angular θ_2 can be obtained easily as

$$E_{n_l}(\theta_2) = -\frac{\hbar^2}{2\mu} \left(\frac{\rho_2^2}{(v'_2 - n_{l2})^2} - (v'_2 - n_{l2})^2 \right) \quad (\text{Eq. 67})$$

hence, it is got

$$\lambda_2 = -\frac{\rho_2^2}{\left(\sqrt{v_2(v_2+1)} + \lambda_1 - n_{l2}\right)^2} + \left(\sqrt{v_2(v_2+1)} + \lambda_1 - n_{l2}\right)^2 - \frac{1}{4} \quad (\text{Eq. 68})$$

Apply the superpotential (59) on equation (11), then it has got raising and lowering operator, respectively.

$$A^+(\theta_2; a_0) = -\frac{\hbar}{\sqrt{2\mu}} \frac{d}{d\theta_2} + \frac{\hbar}{\sqrt{2\mu}} \left(v'_2 \tan \theta_2 + \frac{\rho_2}{v'_2} \right) \quad (\text{Eq. 69})$$

$$A^-(\theta_2; a_0) = \frac{\hbar}{\sqrt{2\mu}} \frac{d}{d\theta_2} + \frac{\hbar}{\sqrt{2\mu}} \left(v'_2 \tan \theta_2 + \frac{\rho_2}{v'_2} \right) \quad (\text{Eq. 70})$$

Thus, using equation (70) and (19) it is obtained the ground-state angular θ_2 wave function as

$$P_0^{(-)}(\theta_2) = \aleph_{\theta_2} (\sin \theta_2)^{v'_2} e^{-\frac{\rho_2}{v'_2} \theta_2} \quad (\text{Eq. 71})$$

with \aleph_{θ_2} is the normalization constant of angular θ_2 wave function.

3.1.3 Solution of angular θ_3 , θ_4 , and θ_5

Using similar steps as well as the solution for θ_2 it is obtained the λ_3 , λ_4 , and λ_5 , respectively.

$$\lambda_3 = \left(-\frac{\rho_3^2}{(v'_3 - n_{l3})^2} + (v'_3 - n_{l3})^2 \right) - 1 \quad (\text{Eq. 72})$$

$$\lambda_4 = \left(-\frac{\rho_4^2}{(v'_4 - n_{l4})^2} + (v'_4 - n_{l4})^2 \right) - \frac{9}{4} \quad (\text{Eq. 73})$$

$$\lambda_5 = \left(-\frac{\rho_5^2}{(v'_5 - n_{l5})^2} + (v'_5 - n_{l5})^2 \right) - 4 \quad (\text{Eq. 74})$$

where,

$$v'_3 = \sqrt{v_3(v_3+1) + \lambda_2 + \frac{1}{4}} - \frac{1}{2} \quad (\text{Eq. 75})$$

$$v'_4 = \sqrt{v_4(v_4+1) + \lambda_3 + 1} - \frac{1}{2} \quad (\text{Eq. 76})$$

$$v'_5 = \sqrt{v_5(v_5+1) + \lambda_4 + \frac{9}{4}} - \frac{1}{2} \quad (\text{Eq. 77})$$

Furthermore, the groundstate wave

function for angular θ_3 , θ_4 , and θ_5 are

$$P_0^{(-)}(\theta_3) = \aleph_{\theta_3} (\sin \theta_3)^{v'_3} e^{-\frac{\rho_3}{v'_3} \theta_3} \quad (\text{Eq. 78})$$

$$P_0^{(-)}(\theta_4) = \aleph_{\theta_4} (\sin \theta_4)^{v'_4} e^{-\frac{\rho_4}{v'_4} \theta_4} \quad (\text{Eq. 79})$$

$$P_0^{(-)}(\theta_5) = \aleph_{\theta_5} (\sin \theta_5)^{v'_5} e^{-\frac{\rho_5}{v'_5} \theta_5} \quad (\text{Eq. 80})$$

with \aleph_{θ_3} , \aleph_{θ_4} , and \aleph_{θ_5} are the normalization constant.

3.1.4 Solution of radial part

The radial Schrodinger equation (36) with DRSO plus Manning Rosen potential (9) in D-dimensional space

$$\left\{ -\frac{\hbar^2}{2\mu} \frac{d^2}{dr^2} + \frac{1}{2} \mu \omega^2 r^2 + \frac{\hbar^2 \lambda_5 + \frac{15}{4}}{2\mu r^2} - E \right\} \chi(r) = 0 \quad (\text{Eq. 81})$$

has the following effective potential

$$V_{\text{eff}}(r) = \frac{1}{2} \mu \omega^2 r^2 + \frac{\hbar^2 m(m+1)}{2\mu r^2} \quad (\text{Eq. 82})$$

where $m(m+1) = \lambda_5 + \frac{15}{4}$, or

$$m = \sqrt{\lambda_5 + \frac{15}{4} + \frac{1}{4}} - \frac{1}{2} \quad (\text{Eq. 83})$$

Further, substituting this radial effective potential (82) with its hypothetical superpotential (84)

$$W(r) = Kr + \frac{V}{r} \quad (\text{Eq. 84})$$

into equation (14)

$$\begin{aligned} \frac{1}{2} \mu \omega^2 r^2 + \frac{\hbar^2 m(m+1)}{2\mu r^2} - E_0(r) \\ = \left(K^2 r^2 + \frac{V(V+1)}{r^2} \right) \\ + 2K \left(V - \frac{1}{2} \right) \end{aligned} \quad (\text{Eq. 85})$$

then it has got some following relation

$$K = \omega \sqrt{\frac{\mu}{2}} \quad (\text{Eq. 86})$$

$$V = -\frac{\hbar}{\sqrt{2\mu}}(m+1) \quad (\text{Eq. 87})$$

$$E_0(r) = \omega\hbar\left(m + \frac{3}{2}\right) \quad (\text{Eq. 88})$$

As well as previous work on the angular part, now it is possible to determine the superpotential of the radial part by applying equations (44), (46) – (48) into equation (12).

$$V_-(r; a_0) = \frac{\mu\omega^2}{2}r^2 + \frac{\hbar^2}{2\mu}\frac{m(m+1)}{r^2} - \omega\hbar\left(m + \frac{3}{2}\right) \quad (\text{Eq. 89})$$

$$V_+(r; a_0) = \frac{\mu\omega^2}{2}r^2 + \frac{\hbar^2}{2\mu}\frac{(m+1)(m+2)}{r^2} - \omega\hbar\left(m + \frac{1}{2}\right) \quad (\text{Eq. 90})$$

Via a mapping parameter $m \rightarrow m+1$ on equation (89) and (90), it has got $V_{\mp}(r; a_1, a_2, \dots, a_n)$. Further, using the characteristic of shape invariance (15) and (17) it is obtained

$$R(r; a_n) = 2\omega\hbar \quad (\text{Eq. 91})$$

and $E_n^{(-)} = 2n\omega\hbar$. Therefore, using equation (18) it has got the energy eigenvalue for the radial part as

$$E_{n_r}(r) = \omega\hbar\left(\left(\sqrt{\lambda_5 + \frac{15}{4} + \frac{1}{4} - \frac{1}{2}}\right) + \frac{3}{2} + 2n_r\right) \quad (\text{Eq. 92})$$

The raising and lowering operators are obtained using superpotential $W(r)$ (84) and equation (11)

$$A^+(r) = -\frac{\hbar}{\sqrt{2\mu}}\frac{d}{dr} + \sqrt{\frac{\mu}{2}}\omega r - \frac{\hbar}{\sqrt{2\mu}}\frac{(m+1)}{r} \quad (\text{Eq. 93})$$

$$A^-(r) = \frac{\hbar}{\sqrt{2\mu}}\frac{d}{dr} + \sqrt{\frac{\mu}{2}}\omega r - \frac{\hbar}{\sqrt{2\mu}}\frac{(m+1)}{r} \quad (\text{Eq. 94})$$

Finally, applying equation (94) on (19) and continue with equation (93) and (20) it is obtained the ground-state and first excited radial r wave function, respectively,

$$R_0^{(-)}(r) = \aleph_r r^{\left(\left(\sqrt{\lambda_5 - \frac{15}{4} + \frac{1}{4} - \frac{1}{2}}\right) + 1\right)} e^{-\left(\frac{\mu}{2\hbar}\omega r^2\right)} \quad (\text{Eq. 95})$$

$$R_1^{(-)}(r) = \aleph_r \left(\sqrt{2\mu}\omega r - \frac{\hbar}{\sqrt{2\mu}}\frac{2\left(m + \frac{3}{2}\right)}{r} \right) (r^{(m+2)}) e^{-\left(\frac{\mu}{2\hbar}\omega r^2\right)} \quad (\text{Eq. 96})$$

with \aleph_r is the normalization constant of the radial r wave function. Since the $\int_{-\infty}^{\infty} |\aleph_x \psi_0|^2 dx = 1$, then it has got

$$\aleph_r = \frac{\left(\frac{\mu\omega}{2\hbar}\right)^{\left(\frac{2m+3}{2}\right)}}{\Gamma\left(\frac{2m+3}{2}\right)} \quad (\text{Eq. 97})$$

3.2. Thermodynamics Properties

To obtain some thermodynamics properties such as the vibrational mean energy U , specific heat C , vibrational free energy F , and vibrational entropy S it is necessary to derive the partition function Z equation first. This function is also known as the distribution function and its existence is important since someone wants to study the thermodynamical properties. Furthermore, this function can be derived using the energy equation from the considered system (Akpan N Ikot et al., 2018; Suparmi, Cari, and Pratiwi, 2016). The partition function for the 6-dimensional system with DRSO plus Manning Rosen potentials can be written as

$$Z(\zeta, \beta) = \sum_{n=0}^{\zeta} e^{-\beta E_n}, \beta = \frac{1}{k_B T} \quad (\text{Eq. 98})$$

with k_B and T are Boltzmann constant and temperature, E_n is the nonrelativistic energy from the system. Rewrite the energy equation (92)

$$E_{n_r} = \omega\hbar\left(m + \frac{1}{2} + 2n_r + 1\right) \quad (\text{Eq. 99})$$

with $m = \lambda_5 + \frac{15}{4} + \frac{1}{4} - \frac{1}{2}$.

Therefore it is obtained the vibrational partition function Z as follow

$$Z(\beta) = \sum_{n=0}^{\infty} e^{-\beta\omega\hbar\left(m + \frac{1}{2} + 2n_r + 1\right)} = e^{-\beta\omega\hbar\left(m + \frac{1}{2}\right)} \frac{1}{2 \sinh(\beta\omega\hbar)} \quad (\text{Eq. 100})$$

3.2.1 Vibrational Mean Energy

The vibrational mean energy U for DRSO

plus Manning Rosen potential in 6-dimensional space is

$$\begin{aligned} U(\beta) &= -\frac{\partial}{\partial \beta} \ln(Z) \\ &= -\frac{\partial}{\partial \beta} \ln\left(e^{-\beta\omega\hbar\left(m+\frac{1}{2}\right)} \frac{1}{2 \sinh(\beta\omega\hbar)}\right) \\ &= \omega\hbar\left(m+\frac{1}{2}\right) + \omega\hbar \coth(\beta\omega\hbar) \end{aligned} \quad (\text{Eq. 101})$$

3.2.2 Vibrational Specific Heat

The vibrational mean energy C for DRSO plus Manning Rosen potential in 6-dimensional space is

$$\begin{aligned} C(\beta) &= -\frac{\partial U}{\partial T} = -k_B\beta^2 \left(\frac{\partial U}{\partial \beta}\right) \\ &= k_B(\omega\hbar\beta)^2 \text{csch}^2(\beta\omega\hbar) \end{aligned} \quad (\text{Eq. 102})$$

3.2.3 Vibrational Free Energy

The vibrational free energy F for the DRSO plus Manning Rosen potential in D-dimensional system is solved as follows

$$F = -\frac{1}{\beta} \ln Z = \omega\hbar\left(m+\frac{1}{2}\right) + \frac{\ln(2 \sinh(\beta\omega\hbar))}{\beta} \quad (\text{Eq. 103})$$

3.2.4 Vibrational Entropy

The vibrational entropy S for the DRSO plus Manning Rosen potential in D-dimensional system is solved as follows

$$\begin{aligned} S(\beta) &= k \ln Z + kT \left(\frac{\partial \ln Z}{\partial T}\right) \\ S(\beta) &= k\beta\omega\hbar \coth(\beta\omega\hbar) - k \ln(2 \sinh(\beta\omega\hbar)) \end{aligned} \quad (\text{Eq. 104})$$

3.3. Discussion

The analysis of the energy values, wave functions, and thermodynamics properties are explained by graphical representation. To obtain the graphics of energy versus radial quantum number n_r , equation (92) was used by substituting the separable constants λ_5 (74), λ_4 (73), λ_3 (72), λ_2 (68), and λ_1 (53).

From Figure 1, the energy versus radial quantum number n_r was plotted for various orbital quantum number n_l by set the $\hbar = \mu = 1$, $\omega = \alpha = \sigma = \nu_i = \rho_i = 5$. The graphic shows that every increment of the orbital quantum number tends to decrease energy, with the increment of n_{l5} causes

more decrement than other orbital quantum numbers. Exceptionally for the n_{l1} , when its increase caused a decrease at energy. From Figure 2, the energy versus radial quantum number n_r was plotted for various values of the potential parameters. It shows that in general, the increment of potentials parameters made an increase in energy values, with the increment of ω causes more increment than others. Exceptions for ρ_i enhancement, it decreases the energy values, although the effect is insignificant.

The behavior of radially DRSO plus Manning Rosen's potentials wave function in 6-dimensional system as a function of r are presented from Figures 3 and 4. Figure 3 presents the effect of orbital quantum numbers n_l against radial ground state wave functions. The graphic shows that in general, the increases of n_l cause the amplitude to become large, together with the wave functions move to the left. The angular quantum number n_{l5} has more influence than others. Exceptional for the increment of n_{l1} it causes the wave amplitude to becomes lower, and the wave function moves to the right. Figure 4 presents the potential parameters against the radial ground state wave functions. The graphic shows that the amplitude of wave function becomes large and move to the left caused by the increase of ω and ρ_i , but becomes lower and move to the right cause by the increase of α , σ , and ν_i .

For Figure 5 – Figure 9 it was set $\hbar = \mu = 1$, $n_r = n_{li} = 1$. It was plotted the partition function $Z(\beta)$ and some thermodynamical properties such as $U(\beta)$, $C(\beta)$, $F(\beta)$ and $S(\beta)$ for various values of frequencies ω and parameters of angular potentials.

It could be observed from Figure 5 that the partition function Z decreases monotonically with increasing of β and some potential parameters ω , α , σ , and ν_i . With, the frequency ω from DRSO plus Manning Rosen Potential leads more dominant than some angular parameters α , σ , ν_i . Unlike other, increasing of all ρ_i escalates the Z becoming more increase, although it is too small compared to the ω . From Figure 6, for every value of DRSO plus Manning Rosen potential parameters ω , α , σ , ν_i and ρ_i it is offered, the vibrational mean energy U decreases monotonically as the increasing of β . Moreover, U is increased when the frequency and other angular parameters α , σ , ν_i enlarged. With, the ω parameter leads more dominant than some angular parameters α , σ , ν_i . Exceptional for ρ_i , increasing of all ρ_i decreases the Z , although it is too small compared to the ω . Based on Figure 7,

the specific heat C decreases monotonically as increasing of β and frequencies ω . Meanwhile, this is unique because other angular parameters α , σ , ν_i , and ρ_i are not affecting C . Figure 8 shows that for every value of ω , α , σ , ν_i , and ρ_i it is offered, the vibrational free energy F of the system with DRSO plus Manning-Rosen potential increases monotonically as the increasing of β and some potentials parameters. With, ν_i , and ω lead more dominant than α and σ . Meanwhile, the increase in all ρ_i decreases the F , although it is too small compared to other parameters. From Figure 9, it can be observed that for every value of potential parameters it is offered, the vibrational entropy S of the system decreases monotonically as the increasing of β and ω . It appears that variations on angular parameters α , σ , ν_i and ρ_i does not effect on S .

4. CONCLUSION:

The energy spectrum and ground-state wave function of the 6-dimensional Schrodinger equation governed by the Double Ring-Shape Oscillator (DRSO) plus Manning Rosen potential have been obtained using SUSY QM method. In general, the increment of orbital quantum numbers decreases the energy, but specifically for the increment of n_{l1} cause increases at energy values. Overall, the increment of the potential parameters increases the energy values, with the increment of ω causes more enhancement in energy values compares to the other potentials parameters. The angular quantum numbers and potential parameters have also influence on wave functions. In general, the increment of orbital quantum numbers and the potential parameters causes the wave amplitude to become high, and the wave functions move to the left. Specifically, for the increment at n_{l1} , α , σ , and ρ cause the wave amplitude to become low, and the wave functions move to the right. The energy spectrum equation was used to derive the partition function. This partition function was employed to obtain the thermodynamics properties such as vibrational and vibrational mean energy U , vibrational specific heat C , vibrational free energy F and vibrational entropy energy S . The vibrational mean energy U and free energy F were increasing as the increased of all potentials parameters, with the ω is more dominant compare to the others. Vibrational specific heat C and vibrational entropy S only affected by the ω , where C and S decreasing as the increment of the ω .

5. ACKNOWLEDGEMENTS:

This research was partly supported by the Mandatory Research Grant of Sebelas Maret University with contract number 452/UN27.21/PN/2020.

6. REFERENCES:

1. Abu-Shady, M., and Ikot, A. N. (2019). Analytic solution of multi-dimensional Schrödinger equation in hot and dense QCD media using the SUSYQM method. *Eur. Phys. J. Plus*, 134(7).
2. Alsadi, K. S. (2015). Analytical Solution of Dirac-Morse Problem with Tensor Potential by Asymptotic Iteration Method. *Applied Mathematics and Information Sciences*, 9(4), 1931–1936.
3. André, R., Lemos, J. P. S., and Quinta, G. M. (2019). Thermodynamics and entropy of self-gravitating matter shells and black holes in d dimensions. *Physical Review D*, 99(12), 125013.
4. Antia, A. D., Isonguyo, C. N., Ikot, A. N., Hassanabadi, H., Obong, H. P., and Maghsoodi, E. (2017). Solution of Schrödinger Equation with Shifted Deng-Fan Potential by NU method. *The African Review of Physics*, 12(003).
5. Arda, A., and Sever, R. (2009). Exact solutions of effective mass dirac equation with non-pt-symmetric and non-hermitian exponential-type potentials. *Chinese Physics Letters*, 26(9), 2–5.
6. Candemir, N. (2016). Klein-Gordon particles in symmetrical well potential. *Applied Mathematics and Computation*, 274, 531–538.
7. Carpio-Bernido, and Chrisopher. (1989). Algebraic Treatment of a Double Ring-shaped Oscillator. *Physics Letters A*, 137(1), 1–3.
8. Chang-Yuan, C., Fa-Lin, L., Dong-Sheng, S., and Shi-Hai, D. (2013). Analytic solutions of the double ring-shaped Coulomb potential in quantum mechanics. *Chinese Physics B*, 22(10), 100302.
9. Dong, S. (2011). *Wave Equations in Higher*

Dimensions. New York: Springer Dordrecht Heidelberg.

10. Dong, S., and Gonzalez-Cisneros, A. (2008). Energy spectra of the hyperbolic and second Pöschl-Teller like potentials solved by new exact quantization rule. *Annals of Physics*, 323, 1136–1149.
11. Durmus, A., and Yasuk, F. (2007). Relativistic and nonrelativistic solutions for diatomic molecules in the presence of double ring-shaped Kratzer potential. *Journal of Chemical Physics*, 126(7), 074108.
12. Dutt, R., Khare, A., and Sukhatme, U. P. (1988). Supersymmetry, shape invariance, and exactly solvable potentials. *American Journal of Physics*, 56(2), 163–168.
13. Ebomwonyi, O., Onate, C. A., Onyeaju, M. C., and Ikot, A. N. (2017). Any l -states solutions of the Schrödinger equation interacting with Hellmann-generalized Morse potential model. *Karbala International Journal of Modern Science*, 3(1), 59–68.
14. Fa-Lin, Lu and Chang-Yuan, C. (2010). Bound states of the Schrodinger equation for the Poschl—Teller double-ring-shaped Coulomb potential. *Chinese Phys. B*, 19, 100309.
15. Falaye, B. J., and Oyewumi, K. J. (2011). Solutions of the Dirac equation with spin and pseudospin symmetry for trigonometric Scarf potential in D-dimensions. *ArXiv Preprint ArXiv:1111.6501*.
16. Hassanabadi, H., Ikot, A. N., and Zarrinkamar, S. (2014). Exact solution of Klein-Gordon with the Pöschl-Teller double-ring-shaped Coulomb potential. *Acta Physica Polonica A*, 126(3), 647–651.
17. Hassanabadi, H., Maghsoodi, E., Zarrinkamar, S., and Rahimov, H. (2011). An approximate solution of the Dirac equation for hyperbolic scalar and vector potentials and a Coulomb tensor interaction by susyqm. *Modern Physics Letters A*, 26(36), 2703–2718.
18. Hassanabadi, H., Zarrinkamar, S., and Rahimov, H. (2011). Approximate solution of D-Dimensional Klein—Gordon equation with Hulthén-Type potential via SUSYQM. *Communications in Theoretical Physics*, 56(3), 423.
19. Ikhdair, S. M., and Falaye, B. J. (2013). Approximate analytical solutions to relativistic and nonrelativistic Pöschl--Teller potential with its thermodynamic properties. *Chemical Physics*, 421, 84–95.
20. Ikot, A N, Lutfuoglu, B. C., Ngwueke, M. I., Udoh, M. E., Zare, S., and Hassanabadi, H. (2016). Klein-Gordon equation particles in exponential-type molecule potentials and their thermodynamic properties in D dimensions. *The European Physical Journal Plus*, 131(12), 1–17.
21. Ikot, Akpan N, Chukwuocha, E. O., Onyeaju, M. C., Onate, C. A., Ita, B. I., and Udoh, M. E. (2018). Thermodynamics properties of diatomic molecules with general molecular potential. *Pramana*, 90(2), 22.
22. Ikot, Akpan Ndem, Akpan, I. O., Abbey, T. M., and Hassanabadi, H. (2016). Exact Solutions of Schrödinger Equation with Improved Ring-Shaped Non-Spherical Harmonic Oscillator and Coulomb Potential. *Commun. Theor. Phys.*, 65(5), 569–574.
23. Karayer, H. (2019). Analytical solution of the Dirac equation for the hyperbolic potential by the extended Nikiforov-Uvarov method. *European Physical Journal Plus*, 134(9), 2–7.
24. Khare, A., and Bhaduri, R. K. (1993). Supersymmetry, shape invariance and exactly solvable noncentral potentials. *ArXiv Preprint Hep-Th/9310104*.
25. Khordad, R., and Sedehi, H. R. R. (2018). Thermodynamic Properties of a Double Ring-Shaped quantum dot at low and high temperatures. *Journal of Low Temperature Physics*, 190(3–4), 200–212.
26. Lütfüoğlu, B. C., Ikot, A. N., Chukwocha, E. O., and Bazuaye, F. E. (2018). Analytical solution of the Klein Gordon equation with a multi-parameter q-deformed Woods-Saxon type potential. *European Physical*

27. Onate, C. A., Ebomwonyi, O., Dopamu, K. O., Okoro, J. O., and Oluwayemi, M. O. (2018). Eigen solutions of the D-dimensional Schrödinger equation with inverse trigonometry scarf potential and Coulomb potential. *Chinese Journal of Physics*, 56(5), 2538–2546.
28. Sobhani, H., Hassanabadi, H., and Chung, W. S. (2018). Effects of cosmic-string framework on the thermodynamical properties of anharmonic oscillator using the ordinary statistics and the q-deformed superstatistics approaches. *The European Physical Journal C*, 78(2), 106.
29. Sun, D.-S., You, Y., Lu, F.-L., Chen, C.-Y., and Dong, S.-H. (2014). The quantum characteristics of a class of complicated double ring-shaped non-central potential. *Physica Scripta*, 89(4), 45002.
30. Suparmi, A., Cari, C., and Deta, U. A. (2014). Exact solution of Dirac equation for Scarf potential with new tensor coupling potential for spin and pseudospin symmetries using Romanovski polynomials. *Chinese Physics B*, 23(9), 90304.
31. Suparmi, A., Cari, C., and Pratiwi, B. N. (2016). Thermodynamics properties study of diatomic molecules with q-deformed modified Poschl-Teller plus Manning Rosen non-central potential in D dimensions using SUSYQM approach. *J. Phys.: Conf. Ser.*
32. Taşkın, F., Boztosun, I., and Bayrak, O. (2008). Exact solutions of Klein-Gordon equation with exponential scalar and vector potentials. *International Journal of Theoretical Physics*, 47, 1612–1617.
33. Wang, L.-Y., Gu, X.-Y., Ma, Z.-Q., and Dong, S.-H. (2002). Exact Solutions to D-Dimensional Shrodinger Equation with a Pseudoharmonic Oscillator. *Physics Letters*, 15(6), 569–576.
34. Witten, E. (1981). Dynamical Breaking of supersymmetry. *Nuclear Physics B*, 185, 513–554.
35. Yahya, W. A., and Oyewumi, K. J. (2016). Thermodynamic properties and approximate solution of the l-state Poschl-Teller-type potential. *Journal of the Association of Arab Universities for Basic and Applied Sciences*, 21, 53–58.
36. Yasuk, F., and Durmus, A. (2007). Relativistic solutions for double ring-shaped oscillator potential via asymptotic iteration method. *Physica Scripta*, 77(1).
37. You, Y., Lu, F.-L., Sun, D.-S., Chen, C.-Y., and Dong, S.-H. (2018). The visualization of the space probability distribution for a particle moving in a double ring-shaped Coulomb potential. *Advances in High Energy Physics*, 2018, 1–26.
38. Zarrinkamar, S., Rajabi, A. A., and Hassanabadi, H. (2010). Dirac equation for the harmonic scalar and vector potentials and linear plus coulomb-like tensor potential; The SUSY approach. *Annals of Physics*, 325(11), 2522–2528.
39. Zhang, J. (2000). Spectrum of q -deformed Schrodinger equation ". *Physics Letters B*, 477, 361–366.

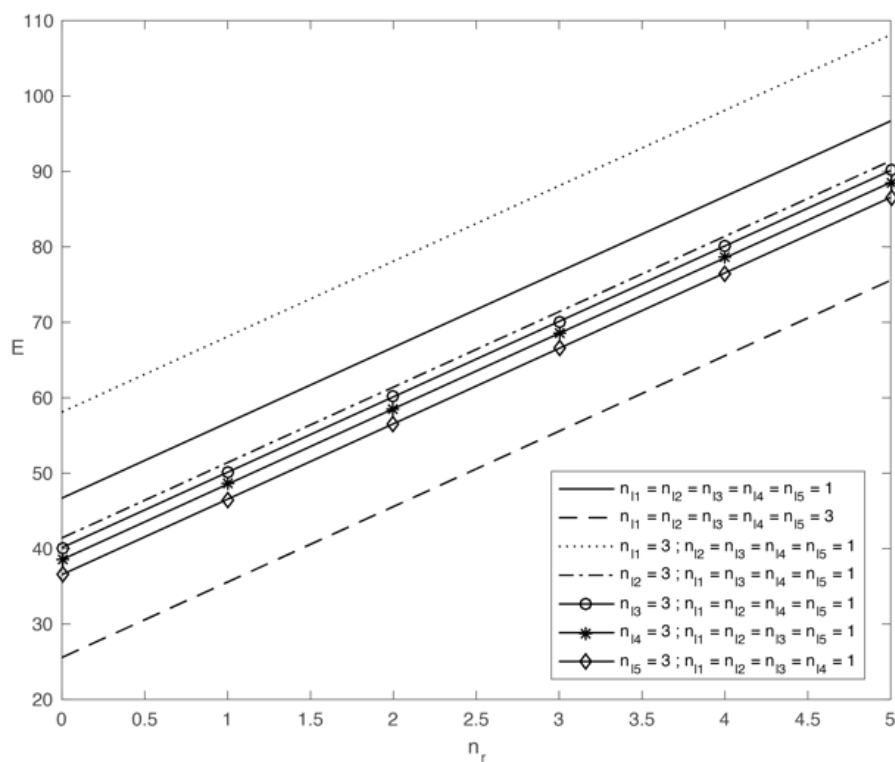


Figure 1. The plot of energy for various n_l
 $\hbar = \mu = 1, \omega = \alpha = \sigma = v_i = \rho_i = 5$

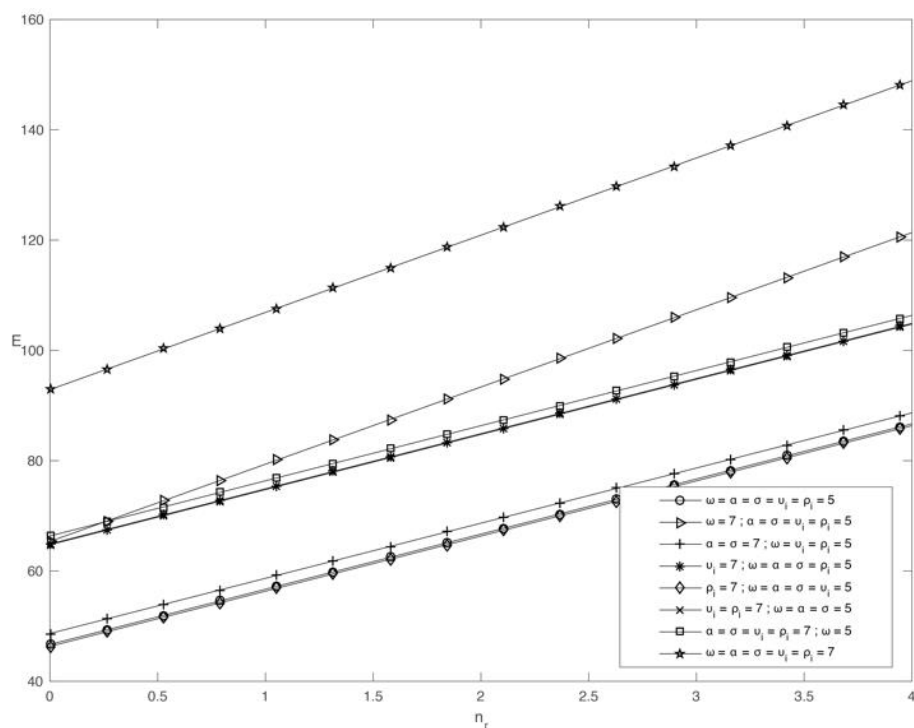


Figure 2. The plot of energy for various potentials parameter
 $\hbar = \mu = 1, n_{li} = 1$

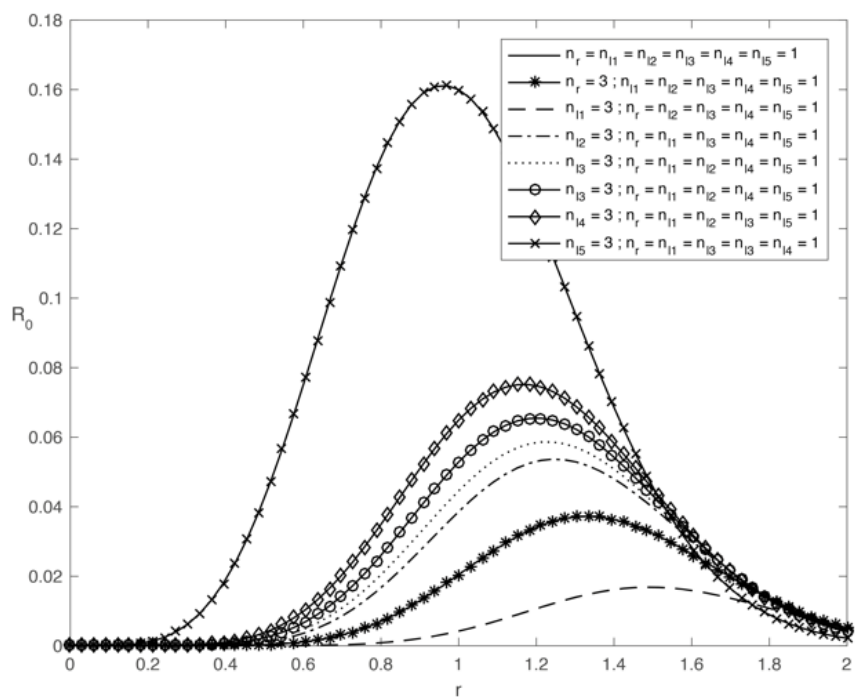


Figure 3. The plot of the groundstate radial wave function R_0 vs r for various n_l
 $\hbar = \mu = 1, \omega = \alpha = \sigma = v_i = \rho_i = 5$

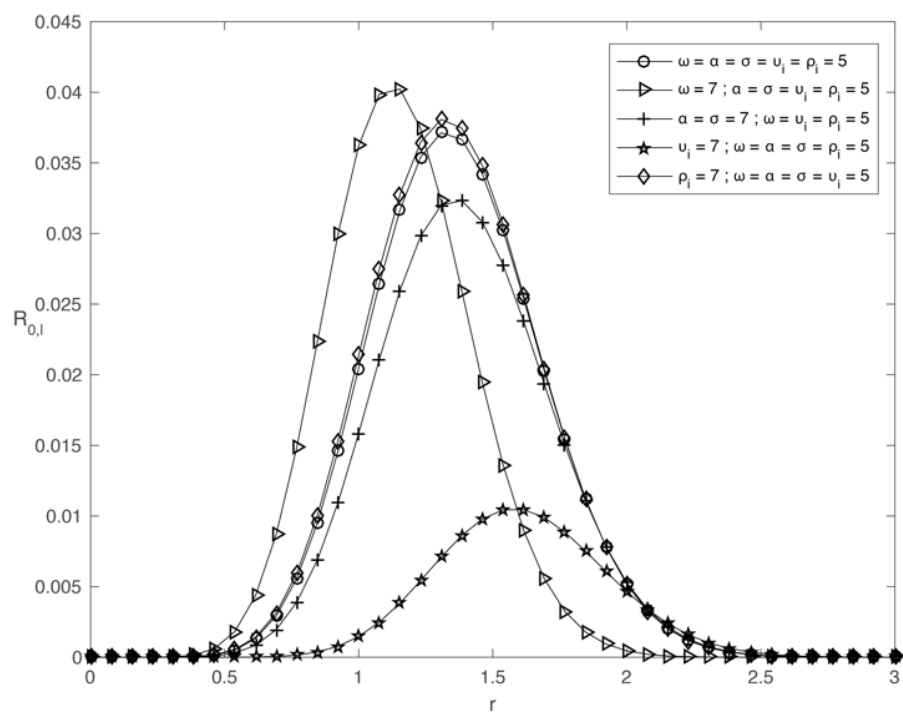


Figure 4. The plot of the groundstate radial wave function R_0 vs r for various potentials parameters
 $\hbar = \mu = 1, n_r = n_{li} = 1$

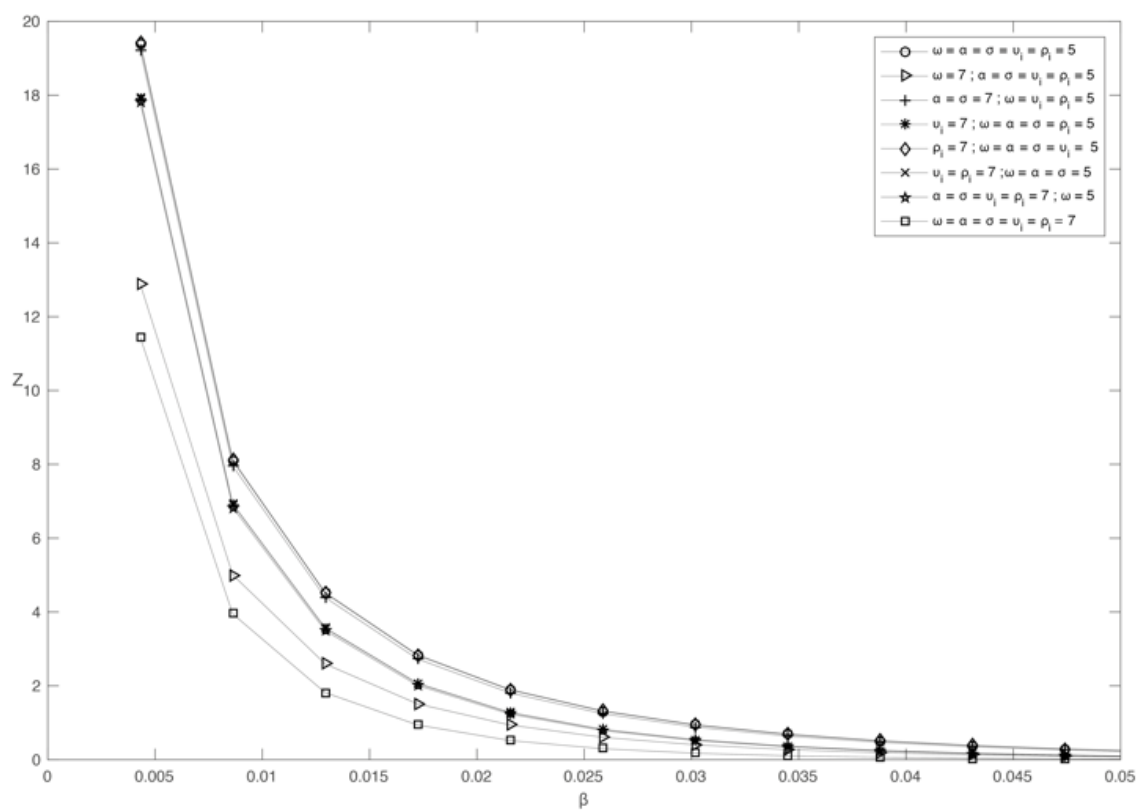


Figure 5. Partition function Z vs β
 $\hbar = \mu = 1, n_r = n_{li} = 1$

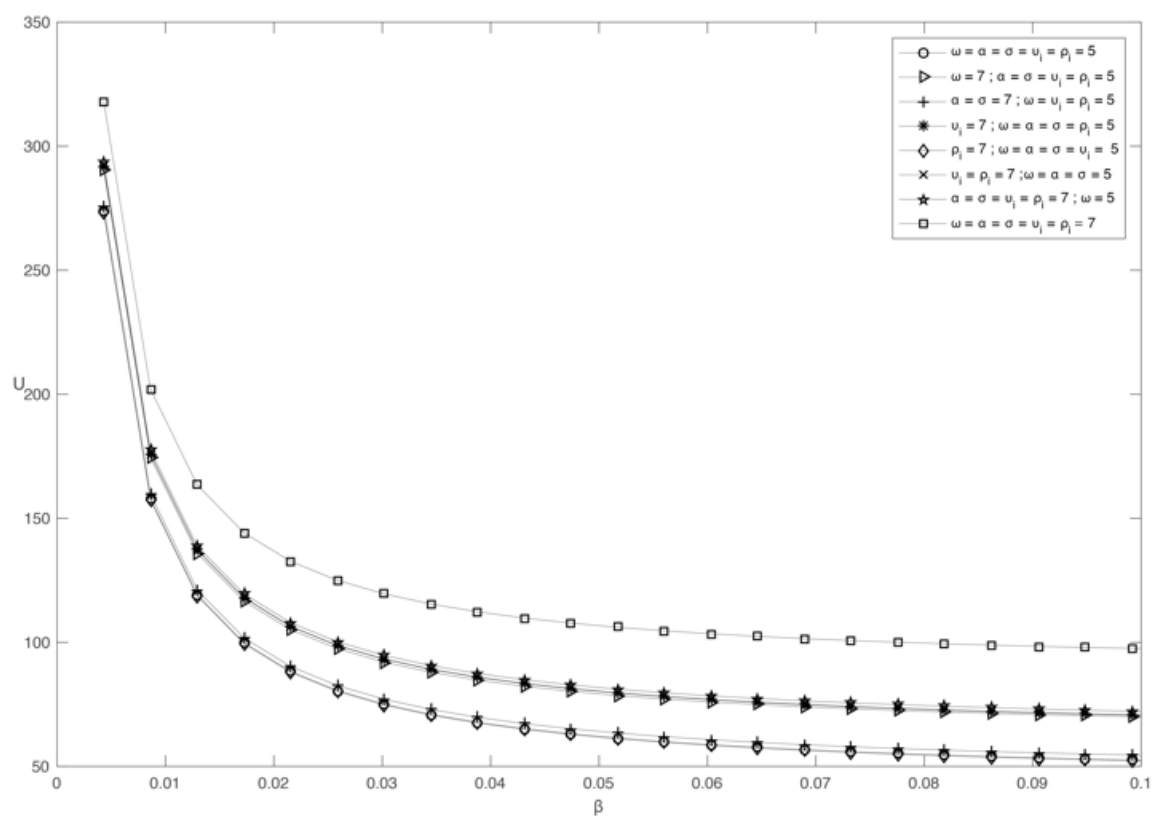


Figure 6. Vibrational mean energy U vs β
 $\hbar = \mu = 1, n_r = n_{li} = 1$

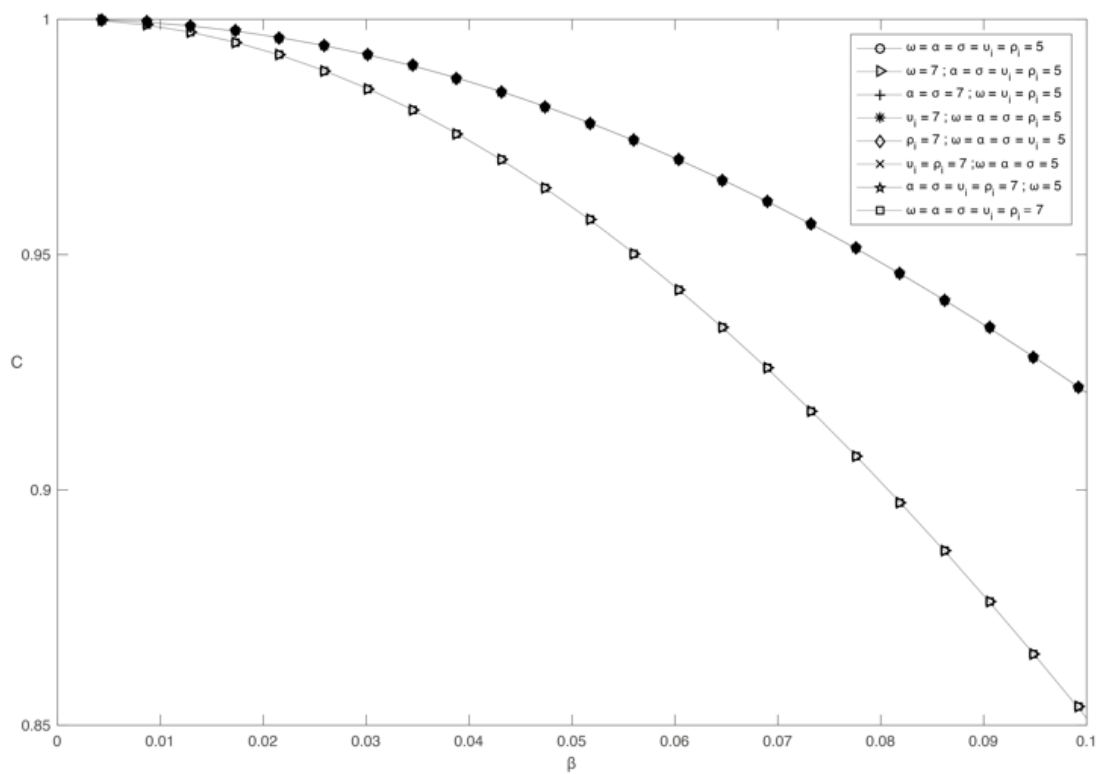


Figure 7. Vibrational specific heat C vs β
 $\hbar = \mu = 1, n_r = n_{li} = 1$

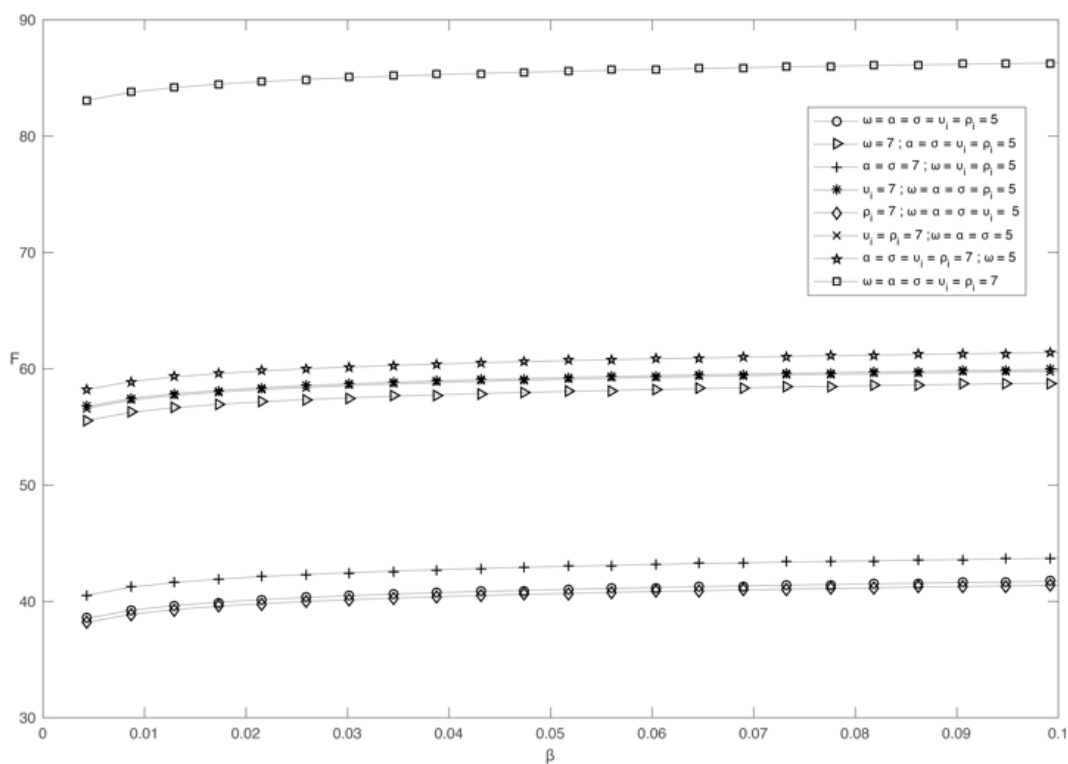


Figure 8. Vibrational free energy F vs β
 $\hbar = \mu = 1, n_r = n_{li} = 1$

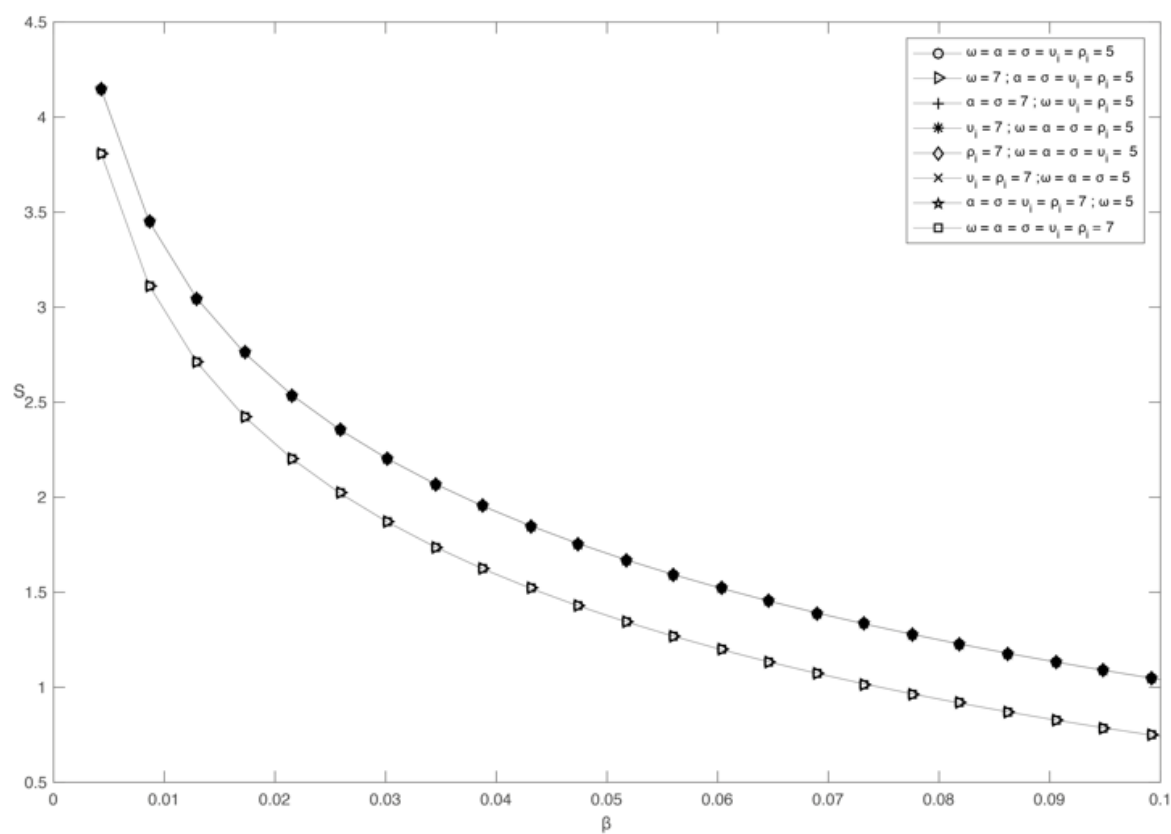


Figure 9. Vibrational entropy S vs β
 $\hbar = \mu = 1, n_r = n_{li} = 1$

ESTUDO DE ESPECTROSCOPIA DE CLUSTER $MCl_2(H_2O)_n$ USANDO CÁLCULOS
AB INITIO

SPECTROSCOPY STUDY OF $MCl_2(H_2O)_n$ CLUSTER USING AB INITIO CALCULATIONS

AB INITIO دراسة طيفية لمعقدات $MCl_2(H_2O)_n$ باستخدام حسابات

SADOON, Ahmed M.^{1*}; SHEEJ AHMAD, Omar^{1,2}

¹ Department of Chemistry, College of Education for Pure Sciences, University of Mosul, Mosul, Iraq

² Department of Chemistry, University of Leicester, University Road, Leicester LE1 7RH, United Kingdom

* Corresponding author

e-mail: ams95@uomosul.edu.iq

Received 13 August 2020; received in revised form 27 September 2020; accepted 15 October 2020

RESUMO

A espectroscopia de infravermelho (IV) de complexos de sal de haleto alcalino-terroso (MX_2) com poucos números de moléculas de água foi investigada pela primeira vez neste trabalho. $BeCl_2$ e $MgCl_2$ são sais divalentes e foram incorporados com água como solvente polar para formar complexos do tipo $MX_2(H_2O)_n$. O efeito do tamanho do íon desempenha uma regra crítica nas interações entre solvente e soluto. Portanto, os sais de berílio e magnésio com cloreto foram escolhidos para explorar essa diferença. A importância do $BeCl_2$ e do $MgCl_2$ vem de suas diversas aplicações na indústria e farmácia. Por exemplo, $BeCl_2$ é amplamente utilizado na indústria como catálise de reações de Friedel-Craft, enquanto a principal aplicação de $MgCl_2$ em farmácia é como fluidos de hemodiálise e diálise peritoneal. Três complexos de cada $BeCl_2$ e $MgCl_2$ com água, $MX_2(H_2O)_n$ ($n = 1-3$) foram estudados e as estruturas químicas desses complexos foram realizadas usando cálculos ab initio. Cálculos ab initio foram usados para prever estruturas possíveis, isômeros e seus espectros de IV correspondentes usando a teoria de perturbação de Møller-Plesset de segunda ordem (MP2) com 6-311 ++ G como conjuntos de base. As avaliações de geometria, buscas de energia, cálculos de frequência vibracional e a energia de ligação de cada complexo também foram extraídos teoricamente. As energias mínimas das estruturas complexas foram calculadas e diferentes isômeros foram registrados. As ligações iônicas de hidrogênio (IHBs) entre o OH em cada molécula de água e o íon cloreto no MCl_2 foram propostas como sendo a principal contribuição prevalente para a ligação entre o sal e a água. O comprimento da ligação entre o metal alcalino e o cloro mostrou um aumento significativo com o aumento da molécula de água ligada como resultado da formação do IHB. Além disso, as bandas vibracionais infravermelhas da região de alongamento OH foram registradas para as estruturas mínimas e redshift dramático foi executado. A formação de estruturas de pares de íons de contato nas quais cada molécula de solvente forma uma ligação de hidrogênio iônica (IHB) ao par de íons de sal ($X-M + X^-$) foi confirmada pelos espectros infravermelhos previstos.

Palavras-chave: Espectroscopia, cálculos Ab initio, Complexos metal alcalino-terrosos-água.

ABSTRACT

The Infrared (IR) spectroscopy of alkali earth halide salt (MX_2) complexes with few numbers of water molecules have been investigated for the first time in this work. $BeCl_2$ and $MgCl_2$ are divalent salts and have been incorporated with water as a polar solvent to form complexes of type $MX_2(H_2O)_n$. The effect of ion size plays a critical rule in the interactions between solvent and solute. Therefore, Beryllium and Magnesium salts with chloride were chosen to explore this difference. The importance of $BeCl_2$ and $MgCl_2$ comes from their several applications in the industry and pharmacy. For instance, $BeCl_2$ is widely used in the industry as a catalysis of Friede-Craft reactions, while the main application of $MgCl_2$ in pharmacy is as hemodialysis and peritoneal dialysis fluids. Three complexes of each $BeCl_2$ and $MgCl_2$ with water, $MX_2(H_2O)_n$ ($n=1-3$), were studied, and the chemical structures of these complexes have been performed using *ab initio* calculations. *Ab initio* calculations were used to predict possible structures, isomers, and their corresponding IR spectra using Second-order Møller-Plesset perturbation theory (MP2) with 6-311++G as a basis sets. The Geometry evaluations, energy searches, vibrational frequency calculations, and the binding energy of each complex were also extracted theoretically. The minimum energy of complexes structures was calculated, and different isomers have been recorded. Ionic hydrogen bonds (IHBs) between the OH in each water molecule and the chloride ion in the MCl_2 was proposed to be the main prevalent contribution to the binding between the salt and water. The bond length between the alkaline metal and chlorine

showed a significant increase with increasing the attached water molecule as a result of forming the IHB. Also, the infrared vibrational bands of the OH stretching region were recorded for the minimum structures, and dramatic redshift was performed. The formation of contact-ion pair structures in which each solvent molecule forms an ionic hydrogen bond (IHB) to the salt ion-pair ($X^+M^+X^-$) has been confirmed by the predicted infrared spectra.

Keywords: Spectroscopy, *Ab initio* calculations, Alkaline earth metal-water complexes.

المخلص

تمت دراسة وتسجيل طيف الأشعة تحت الحمراء (IR) لمعقدات تتكون من أملاح الهاليدات القلوية (MX_2) مع الماء لأول مرة في هذا البحث. تعتبر أملاح كلوريد البريليوم وكلوريد المغنيسيوم من الأملاح الرئيسية والمعروفة والتي تم استخدامها مع الماء كمذيب قطبي لتكوين معقدات من النوع $MX_2(H_2O)_n$. إن تأثير حجم الأيونات يلعب دوراً رئيسياً في التداخلات بين المذيب والمذاب. لذلك تم اختيار أملاح البريليوم والمغنيسيوم مع الكلوريد لاستكشاف هذا الاختلاف. إن أهمية أملاح كلوريد البريليوم والمغنيسيوم تأتي من التطبيقات العديدة لهذه الأملاح في الصناعة والتطبيقات الصيدلانية. على سبيل المثال، يستخدم ملح كلوريد في الصناعة لحفاز في تفاعل فيدل كرافت بينما يستخدم كلوريد المغنيسيوم في الصناعات الصيدلانية في محاليل غسيل الكلى. كل هذه التطبيقات تجعل هذه الدراسة ذات فائدة وأهمية كبيرة. تمت دراسة ثلاثة معقدات من كل من $BeCl_2$ و $MgCl_2$ مع الماء تحمل الصيغة العامة التالية، $MX_2(H_2O)_n$ ($n=1-3$)، وتم إجراء حساب التراكيب الكيميائية لهذه المعقدات باستخدام حسابات *ab initio*. تم استخدام هذه الحسابات لاستكشاف التراكيب الممكنة والأيزومرات وأطياف الأشعة تحت الحمراء المقابلة لها باستخدام نظرية اضطراب Møller-Plesset من الدرجة الثانية (MP2) مع 311-6 $G++$ كمجموعات أساسية. كما تم استخلاص الحسابات التركيبية الهندسية، الطاقة الاوطأ، وحسابات التردد الاهتزازي وطاقة الارتباط لكل معقد نظرياً في هذه الدراسة.

تم حساب الحد الأدنى من الطاقة لتراكيب المعقدات المدروسة وتم تسجيل أيزومرات مختلفة. أوضحت النتائج أن الارتباط بين الملح والماء من يأتي من خلال روابط الهيدروجين الأيونية (IHBS) بين مجموعة الهيدروكسيل في كل جزيء ماء وأيون الكلوريد في جزيئة الملح MCl_2 . يظهر طول الاصرة بين الفلز القلوي والكلور زيادة كبيرة مع كل إضافة لجزيء الماء نتيجة لتكوين الاواصر الهيدروجينية. أيضاً، تم تسجيل طيف الأشعة تحت الحمراء للحزم الاهتزازية لمجموعة الهيدروكسيل للمعقدات ذات للحد الأدنى من الطاقة وتم ملاحظة انزياح أحمر كبير لهذه الحزم. تتوافق الأطياف المسجلة مع تكوين الأزواج الأيونية المترابطة حيث يشكل كل جزيء مذيب رابطة هيدروجين أيونية مع الزوج الأيوني $X^+M^+X^-$.

الكلمات المفتاحية: دراسة طيفية، حسابات *Ab initio*، معقدات الماء- فلزات الارترية القلوية

1. INTRODUCTION:

Over many decades, the behavior of ions in solutions has been in the spotlight of many studies (Burgess, 1999; Conway; Weller, 1988). Understanding the behavior of the ion in solution became necessary as a result of their critical role in the chemical solutions, in addition to their applications in specific areas such as environmental chemistry and electrochemistry (Grossfield, Ren, and Ponder, 2003).

kosmotropic or *chaotropic* ions behavior is usually used to express the salt and water interaction as a solvent. Kosmotropic ions have a relatively high charge density, which increases the stability of the hydrogen bonding grid and then increases the water-water interactions, and, for this aspect, it is called (order-makers). However, chaotropic ions (disorder-makers) reduce the stability of the hydrogen bonding grid and thus destabilize the structures of water clusters due to their large size with low charge density that disrupts the water-water structure. (Marcus, 2010; Moelbert, Normand, and De Los Rios, 2004).

It is well known that alkaline earth halides behave as divalent salts. These salts are dissolved in water after distributing the crystalline structure of the solid salt by water to form separated ions in dilute solutions. The size and charge density of the cation and anion are

expected to be the main factor that gives the ability of a single alkaline earth halide molecule to dissolve in a small number of water molecules. $BeCl_2$ and $MgCl_2$ were chosen for this study as an example of salt with a positively charged ion coupled with Cl^- as an anion.

The importance of $BeCl_2$ and $MgCl_2$ comes from their applications in industry and pharmacy. The primary usage of $BeCl_2$ in the industry is a raw material for the electrolysis of beryllium, and as catalysis of Friedel-Craft reactions (Lide, 2004; Raiz, Noor, Rasheed, and Mohammad, 2017). On the other hand, Magnesium chloride is used in several medical applications, especially related to skin. Also, $MgCl_2$ is widely used in pharmaceutical requirements as hemodialysis and peritoneal dialysis fluids (Coşofre and Buck, 1993; Luzzi and Palmieri, 1984).

The comparison between the Alkaline halide (MX) and Alkaline earth halide (MX_2) complexes with water looks useful because of the close behavior between these two kinds of salts in the aqueous solution. Several early researches (Li *et al.*, 2013; Mizoguchi, Ohshima, and Endo, 2003, 2011; Sadoon *et al.*, 2016; Tandy *et al.*, 2016) were concentrated on studying the structure and behavior of Alkaline halide (MX) complexes with water focusing on their geometry structures by recording the infrared (IR) and Mass spectrum using Helium nanodroplet apparatus. These

studies proved that the ionic hydrogen bonds (IHBs) perform a critical role in the formed structures.

Few recent pieces of research deal with MX_2 water complexes. Keshri and Tembe (2017) focused on studying the dynamical and structural properties of MCl_2 in the bulk solution using Molecular dynamics (MD) simulations. The binding energies of $\text{M}^{+2}(\text{H}_2\text{O})_n$ ($n=4,6$) complexes were performed by Ariyaratna and Miliordos (Ariyaratna and Miliordos, 2019). The electronic structures of these complexes are studied using quantum chemical calculations. Naleem *et al.* proposed the force field simulation of alkaline earth halide salts in an aqueous solution (Naleem, Benteritis, and Smith, 2018).

The structures, energetics of alkaline earth metal anion-water clusters $\text{M}-(\text{H}_2\text{O})_n$ ($n=3-6$) were performed by Bajaj and *et al.*, (Bajaj *et al.*, 2019) using Molecular dynamics MD simulations and vibrational spectroscopy calculations. This study suggested the formation of three hydrogen-bond in the metal-legend clusters for the $\text{M}-(\text{H}_2\text{O})_3$ cluster and this number of ionic hydrogen bonds (IHBs) were increased with increasing the number of attached waters. Another *ab initio* calculations study (Glendening and Feller, 1996) was performed in the gas phase and reported the structures, enthalpies, and binding energies for alkaline earth cation M^{+2} clusters with water $\text{M}^{+2}(\text{H}_2\text{O})_n$ ($n=1-6$). The formation of Contact ion pair structures has been suggested in this study by attaching water molecules to MCl_2 via IHBs between the water H atom and the chloride ion. These structures are similar to the salt-water structures mentioned in the previous researches (Sadoon *et al.*, 2016; Tandy *et al.*, 2016) for Alkaline halide salt (NaCl) complexes with water and methanol.

The theoretical calculation of chemical reactions has been widely used in many recent studies (Mattje, Pinheiro, and Pereira, 2019; Rodrigues, Assis, and Bruni, 2019). The formation of salt-water complexes are usually prepared and studied in bulk solutions (Nancollas, 1970; Turq, Barthel, and Chemla, 2012). Even in the diluted solutions, the separation of $\text{MX}_2(\text{H}_2\text{O})_n$ complexes, where n has a small value, is difficult because of the strong ionic hydrogen network (Meot-Ner, 2012). Unfortunately, an accurate simulation of the properties is still tricky to record even in simple electrolytic solutions (Eisenberg, 2013). Considering this limited experimental evidence, the *ab initio* calculations study of these complexes looks useful and provides a unique tool to explore the chemistry of these complexes.

Therefore, this work aimed to study the interaction of Alkaline earth halides (MX_2) with water in the gas phase theoretically using *ab initio* calculations.

2. MATERIALS AND METHODS:

2.1. $\text{MX}_2(\text{H}_2\text{O})_n$ complexes

The complexes of (MCl_2) salts in the existence of a small number of water molecules ($\text{H}_2\text{O})_n$ where $n=1-3$ were drawn using Chemcraft software package (Zhurko and Zhurko, 2016). Several premier structures were generated with different places and randomly rotating of MCl_2 and water molecules to explore a wide range of potential geometries and possible isomers of $\text{MCl}_2(\text{H}_2\text{O})_n$ complexes. The matrix of geometry was then utilized to find the minima structures of each complex using *ab initio* calculations.

2.2. *Ab initio* calculations

Ab initio calculations were performed using Second-order Møller-Plesset perturbation theory (MP2) (Møller and Plesset, 1934) within the gaussian 03 software package (Frisch, Trucks, and Schlegel, 2009). The basis set (6-311++G) obtained from the EMSL basis set exchange library (Schuchardt *et al.*, 2007) was then used to extract the isomer's geometry, energy, and the infrared (IR) spectra, (vibrational frequency values). To reduce the calculation time, Hartree-Fock (HF) level of theory was first used with (6-311++G) bases set to evaluate the optimized structures. The optimized structures at the HF level were then re-optimized using MP2 level of theory at the same bases set. The vibrational frequencies of the final optimized structures were scaled by 0.950 to gain the correct final values of vibrational frequencies. This scaling factor is suggested by the National Institute of Standards and Technology (NIST) for MP2 level of theory (Johnson III, 2005).

2.3. Geometry and structure data

The final results of the infrared (IR) spectra, frequencies of the OH stretching bands, the minimum energy of isomers, bond length, angles, and the Binding Energy (BE) were extracted later using Chemcraft software.

3. RESULTS AND DISCUSSION:

3.1. Predicted structures of $\text{MCl}_2(\text{H}_2\text{O})_n$

3.1.1 $\text{BeCl}_2(\text{H}_2\text{O})_n$ structures

Two structures of $\text{BeCl}_2(\text{H}_2\text{O})$ were found in the MP2 calculations, shown in Figure 1, for the $\text{BeCl}_2(\text{H}_2\text{O})$ complex corresponding to distinct minima. The global minimum structure shows that the BeCl_2 ions take the position so that the chloride ion can form an IHB with the Hydrogen atom of water. Another IHB is formed between the other chloride of BeCl_2 with the other water molecule. Additional stabilization comes from the Be^{+2} ion to the O^- atom. The next energy minimum structure has an energy 105.64 kJ/mol higher than the global minimum.

As shown in Figure 2, three minima structures were noticed for $\text{BeCl}_2(\text{CH}_2\text{O})_2$. The global minimum structure is similar to the $n = 1$ complex but now has four IHBs bonding the chloride ion and the H atoms of water. The next minimum structure has 20.4 kJ/mol higher than the global minimum structure and has only two IHB. One with water attached to the BeCl_2 via an IHB. The other water molecule in this structure takes the position to allow partial interaction with the other water molecule and another interaction with the chloride atom by IHB. The bond length of these two structures was 1.93 and 1.8 Å, respectively. The last minimum structure was raised in energy above the global minimum structure in about 58.28 kJ/mol. The two water molecules in this structure inserted between the Be^+ ion and one of the Cl^- ions forming two IHBs and increase the bond length between these two atoms to 3.423 Å compared with 1.838 Å for the other Be-Cl bond length.

For $n = 3$, Five minima structures were found (Figure 3). The global minimum for $\text{BeCl}_2(\text{H}_2\text{O})_3$ is different from those found for $\text{BeCl}_2(\text{H}_2\text{O})$ and $\text{BeCl}_2(\text{H}_2\text{O})_2$. Two water molecules were bonded by IHB and then interacted with BeCl_2 with one IHB. The other water molecule is oriented far from the two water molecules and interact with BeCl_2 separately by IHB. However, other minima structures have higher energy from the global minimum structure in about 12.04, 21.004, 24.47, 26.255 kJ/mol, respectively. These structures have different water positions and interact with BeCl_2 via IHBs (Figure 3).

3.1.2 $\text{MgCl}_2(\text{H}_2\text{O})_n$ structures

The predicted calculations for $\text{MgCl}_2(\text{H}_2\text{O})_n$ ($n=1-3$) were found and seen in Figures 4, 5, and 6, respectively. No significant changes were observed in these structures for $\text{MgCl}_2(\text{H}_2\text{O})$ and $\text{MgCl}_2(\text{H}_2\text{O})_2$ compared with the $\text{BeCl}_2(\text{H}_2\text{O})_n$ ($n=1$ and 2) predicted structures. For $n=3$, The minimum structure is different from

$\text{BeCl}_2(\text{H}_2\text{O})_3$ and similar to the minimum structures for $\text{MgCl}_2(\text{H}_2\text{O})$ and $\text{MgCl}_2(\text{H}_2\text{O})_2$ were three water molecules bonded to chloride atom by IHBs. The other minima structures for $\text{MgCl}_2(\text{H}_2\text{O})_n$ complexes illustrated different isomers with higher energy than the minimum structure (Figures 4, 5 and 6).

3.2. IR Spectra Analysis in OH Stretching Region for $\text{MCl}_2(\text{H}_2\text{O})_n$ Complexes

The assignment of IR spectra of $\text{BeCl}_2(\text{H}_2\text{O})_n$ $n=1-3$ were recorded theoretically using MP2 level of theory concentrating on the OH stretching region to evaluate the effect of IHBs on the OH bands frequencies. The global minimum structures of $\text{BeCl}_2(\text{H}_2\text{O})_n$, $n=1-3$ were chosen for this IR analysis, and the OH stretching frequencies are summarized in Table 1. The prediction of MP2 calculations shows a significant decrease in the OH frequency from 3651 cm^{-1} in the $\text{BeCl}_2(\text{H}_2\text{O})$ complex to 3625 cm^{-1} and 3575 cm^{-1} for the $\text{BeCl}_2(\text{H}_2\text{O})_2$ and $\text{BeCl}_2(\text{H}_2\text{O})_3$, respectively. This redshift can be assigned to the OH band which bonded to the chloride ion via ionic hydrogen bond (IHB). Relative to the free OH frequency band, the predictive OH stretching frequency is strongly red-shifted in about 146 cm^{-1} compared to the OH frequency of $\text{BeCl}_2(\text{H}_2\text{O})$ complex. This redshift can be assigned to the IHB that weakens the OH bond and so the OH stretching frequency. This trend of OH stretching redshift has been recorded previously in several studies (Cabarcos, Weinheimer, Martínez, and Lisy, 1999; Tandy *et al.*, 2016).

The OH stretching frequency for the minimum structures of $\text{MgCl}_2(\text{H}_2\text{O})_n$ complexes are seen in Table 2. Similar behavior of OH stretching bands was seen in $\text{MgCl}_2(\text{H}_2\text{O})$ and $\text{MgCl}_2(\text{H}_2\text{O})_2$ complexes compared to $\text{BeCl}_2(\text{H}_2\text{O})_n$ $n=1-2$ complexes. Redshifts for OH stretching bands are also seen in these complexes due to the IHBs effect compared to the free OH frequency band. For $\text{MgCl}_2(\text{H}_2\text{O})_3$, only two bands at 3671 and 3790 cm^{-1} were observed and assigned to the OH stretching, which bonded to the chloride atom via IHBs.

3.3. Binding energy calculations for $\text{MCl}_2(\text{H}_2\text{O})_n$ ($n = 1-3$) complexes

The Binding energy (BE) of the global minimum complexes was extracted from the MP2 calculations and summarized in Table 3 for $\text{BeCl}_2(\text{H}_2\text{O})_n$ and in Table 4 for $\text{MgCl}_2(\text{H}_2\text{O})_n$ complexes. The BE were calculated using the following equation:

$$BE = \Delta E = E(\text{BeCl}_2(\text{H}_2\text{O})_n) - (E(\text{BeCl}_2) + E(\text{H}_2\text{O})_n)$$

In both $\text{MCl}_2(\text{H}_2\text{O})_n$ ($n=1-3$) complexes, a gradual increase was seen in the value of BE with increasing n value. The high values of BE in $\text{MCl}_2(\text{H}_2\text{O})$ complex come from the IHB and the proximity of M^+ ion to O atom. The addition of water molecule in the $\text{BeCl}_2(\text{H}_2\text{O})_n$ $n=1-2$ complexes raised the BE in about 176 and 149 kJ/mol, respectively. For $\text{MgCl}_2(\text{H}_2\text{O})_n$ complexes, BE were increased in about 189 kJ/mol for $\text{MgCl}_2(\text{H}_2\text{O})_2$ and 163 kJ/mol for $\text{MgCl}_2(\text{H}_2\text{O})_3$. As can be seen, there is a pronounced reduction in the BE value with adding water molecule to form $\text{M}^{+2}\text{Cl}_2(\text{H}_2\text{O})_3$ complexes compared with adding Water molecule in $\text{M}^{+2}\text{Cl}_2(\text{H}_2\text{O})$ to form $\text{M}^{+2}\text{Cl}_2(\text{H}_2\text{O})_2$. This decrease in the BE value with increasing (n) value may result from dividing the Be^+ ion charge between the water molecules. Furthermore, the increase of IHBs number will weaken the chloride ion charge and reduce the BE value.

4. CONCLUSIONS:

Infrared spectra (IR), structure parameters, Binding Energy of $\text{M}^{+2}\text{Cl}_2(\text{H}_2\text{O})_n$, $n=1-3$ complexes have been performed in this work theoretically for the first time. The results were performed using *Ab initio* calculations. Vibrational bands in OH stretching regions for the minimum structures and other isomers were recorded for the complexes. A Redshift in the positions of the OH stretching bands was seen and this consistent with the formation of the IHBs between the chloride ions and the H atom of each water molecule. Also, a significant increase in the Binding energy (BE) was seen with increasing n value of water. This increase indicated that the IHB and the proximity of M^+ ion to O atom play an essential role in $\text{MX}_2(\text{H}_2\text{O})_n$ complexes. A significant observation was seen for $\text{MCl}_2(\text{H}_2\text{O})_3$ complexes that show a dramatic increase in the M-Cl bond length, which increased by 30% compared with $\text{MCl}_2(\text{H}_2\text{O})$ complex. This increment comes from the effect of water molecules that insert between M and Cl atoms.

5. ACKNOWLEDGMENTS:

This work was supported and funded by the University of Mosul and the Chemistry department at the College of Education for pure sciences. The authors thank the University of Leicester for access to its High-Performance Computer facility.

6. REFERENCES:

1. Ariyaratna, I. R., and Miliordos, E. (2019). Superatomic nature of alkaline earth metal–water complexes: the cases of Be (H_2O)_{0,+4} and Mg (H_2O)_{0,+6}. *Physical Chemistry Chemical Physics*, 21(28), 15861-15870.
2. Bajaj, P., Riera, M., Lin, J. K., Mendoza Montijo, Y. E., Gazca, J., and Paesani, F. (2019). Halide Ion Microhydration: Structure, Energetics, and Spectroscopy of Small Halide–Water Clusters. *The Journal of Physical Chemistry A*, 123(13), 2843-2852.
3. Burgess, J. (1999). *Ions in solution: basic principles of chemical interactions*: Elsevier.
4. Cabarcos, O. M., Weinheimer, C. J., Martínez, T. J., and Lisy, J. M. (1999). The solvation of chloride by methanol—surface versus interior cluster ion states. *The Journal of chemical physics*, 110(19), 9516-9526.
5. Conway, B. Ionic hydration in chemistry and biophysics. 1981. *Studies in Physical and Theoretical Chemistry*, 12.
6. Coşofre, V. V., and Buck, R. P. (1993). Recent advances in pharmaceutical analysis with potentiometric membrane sensors. *Critical Reviews in Analytical Chemistry*, 24(1), 1-58.
7. Eisenberg, B. (2013). Ionic interactions are everywhere. *Physiology*, 28(1), 28-38.
8. Frisch, M., Trucks, G., and Schlegel, H. (2009). Gaussian 03 package software, Gaussian Inc. Wallington CT USA.
9. Glendening, E. D., and Feller, D. (1996). Dication–Water Interactions: $\text{M}^{2+}(\text{H}_2\text{O})_n$ Clusters for Alkaline Earth Metals $\text{M} = \text{Mg}, \text{Ca}, \text{Sr}, \text{Ba}, \text{and Ra}$. *The Journal of Physical Chemistry*, 100(12), 4790-4797.
10. Grossfield, A., Ren, P., and Ponder, J. W. (2003). Ion solvation thermodynamics from simulation with a polarizable force field. *Journal of the American Chemical Society*, 125(50), 15671-15682.
11. Johnson III, R. D. (2005). NIST Computational Chemistry Comparison and Benchmark Database, NIST Standard Reference Database Number 101, Release 15b. 2011. *cccbdb.nist.gov*.
12. Keshri, S., and Tembe, B. (2017). Structural and Dynamical Properties of Alkaline Earth Metal Halides in Supercritical Water: Effect of Ion Size and Concentration. *The Journal of Physical Chemistry B*, 121(46), 10543-10555.

13. Li, R.-Z., Liu, C.-W., Gao, Y. Q., Jiang, H., Xu, H.-G., and Zheng, W.-J. (2013). Microsolvation of LiI and CsI in water: Anion photoelectron spectroscopy and ab initio calculations. *Journal of the American Chemical Society*, 135(13), 5190-5199.
14. Lide, D. R. (2004). *CRC handbook of chemistry and physics* (Vol. 85): CRC press.
15. Luzzi, L., and Palmieri, A. (1984). An overview of pharmaceutical applications. In *Biomedical Applications of Microencapsulation* (pp. 1-18): CRC Press Boca Raton, FL.
16. Marcus, Y. (2010). Effect of ions on the structure of water. *Pure and Applied Chemistry*, 82(10), 1889-1899.
17. Mattje, V. M., Pinheiro, A. R., and Pereira, D. H. (2019). Theoretical study of structural geometry and electronic properties of magnesium diboreth (MgB₂). *Periodico tche quimica*, 16(31), 301-307.
18. Meot-Ner, M. (2012). Update 1 of: Strong Ionic Hydrogen Bonds. *Chemical reviews*, 112(10), PR22-PR103. doi:10.1021/cr200430n
19. Mizoguchi, A., Ohshima, Y., and Endo, Y. (2003). Microscopic hydration of the sodium chloride ion pair. *Journal of the American Chemical Society*, 125(7), 1716-1717.
20. Mizoguchi, A., Ohshima, Y., and Endo, Y. (2011). The study for the incipient solvation process of NaCl in water: The observation of the NaCl-(H₂O)_n (n= 1, 2, and 3) complexes using Fourier-transform microwave spectroscopy. *The Journal of chemical physics*, 135(6), 064307.
21. Moelbert, S., Normand, B., and De Los Rios, P. (2004). Kosmotropes and chaotropes: modelling preferential exclusion, binding and aggregate stability. *Biophysical chemistry*, 112(1), 45-57.
22. Møller, C., and Plesset, M. S. (1934). Note on an approximation treatment for many-electron systems. *Physical Review*, 46(7), 618.
23. Naleem, N., Benteinitis, N., and Smith, P. E. (2018). A Kirkwood-Buff derived force field for alkaline earth halide salts. *The Journal of chemical physics*, 148(22), 222828.
24. Nancollas, G. H. (1970). The thermodynamics of metal-complex and ion-pair formation. *Coordination Chemistry Reviews*, 5(4), 379-415.
25. Raiz, S., Noor, S. H., Rasheed, N., and Mohammad, A. S. (2017). Conceptual Importance of Electrolytic Replenishers: A Review. *Asian Journal of Research in Pharmaceutical Science*, 7(2), 77-80.
26. Rodrigues, C. H. P., Assis, V. O., and Bruni, A. T. (2019). y theoretical spectroscopy in the infrared region: a didactic approach. *Periodico tche quimica*, 16(31), 398-407.
27. Sadoon, A. M., Sarma, G., Cunningham, E. M., Tandy, J., Hanson-Heine, M. W., Besley, N. A., . . . Ellis, A. M. (2016). Infrared spectroscopy of NaCl (CH₃OH)_n complexes in helium nanodroplets. *The Journal of Physical Chemistry A*, 120(41), 8085-8092.
28. Schuchardt, K. L., Didier, B. T., Elsethagen, T., Sun, L., Gurumoorthi, V., Chase, J., Windus, T. L. (2007). Basis set exchange: a community database for computational sciences. *Journal of chemical information and modeling*, 47(3), 1045-1052.
29. Tandy, J., Feng, C., Boatwright, A., Sarma, G., Sadoon, A. M., Shirley, A., Ellis, A. M. (2016). Communication: Infrared spectroscopy of salt-water complexes. In: AIP Publishing LLC.
30. Turq, P., Barthel, J. M., and Chemla, M. (2012). *Transport, relaxation, and kinetic processes in electrolyte solutions* (Vol. 57): Springer Science and Business Media.
31. Weller, K. (1988). *Ion Solvation*: Y. Marcus. Wiley, Chichester, New York, Brisbane, Toronto, Singapore, 1985, ISBN 0-471-90756-1, viii+ 306 pp., £ 42.00. In: Elsevier.
32. Zhurko, G., and Zhurko, D. (2016). Chemcraft-graphical software for visualization of quantum chemistry computations. In.

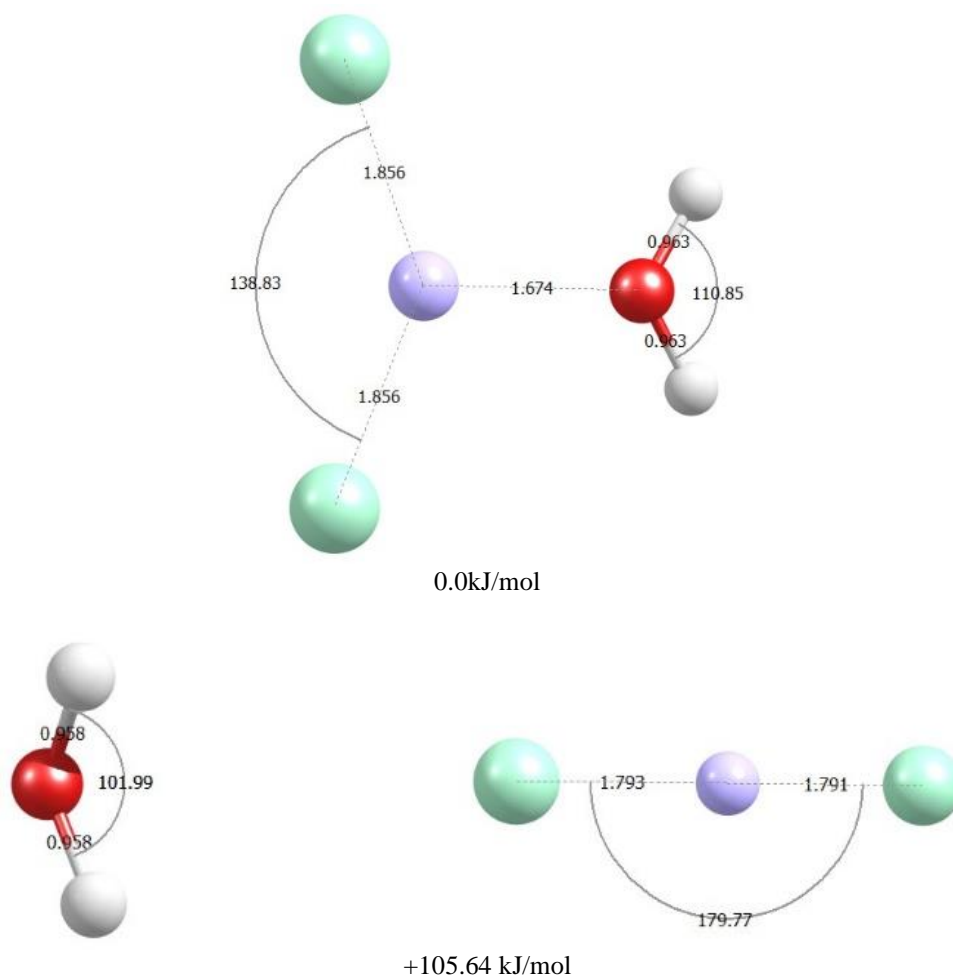


Figure 1. The calculated structures for $\text{BeCl}_2(\text{H}_2\text{O})$ with their energies in kJ/mol

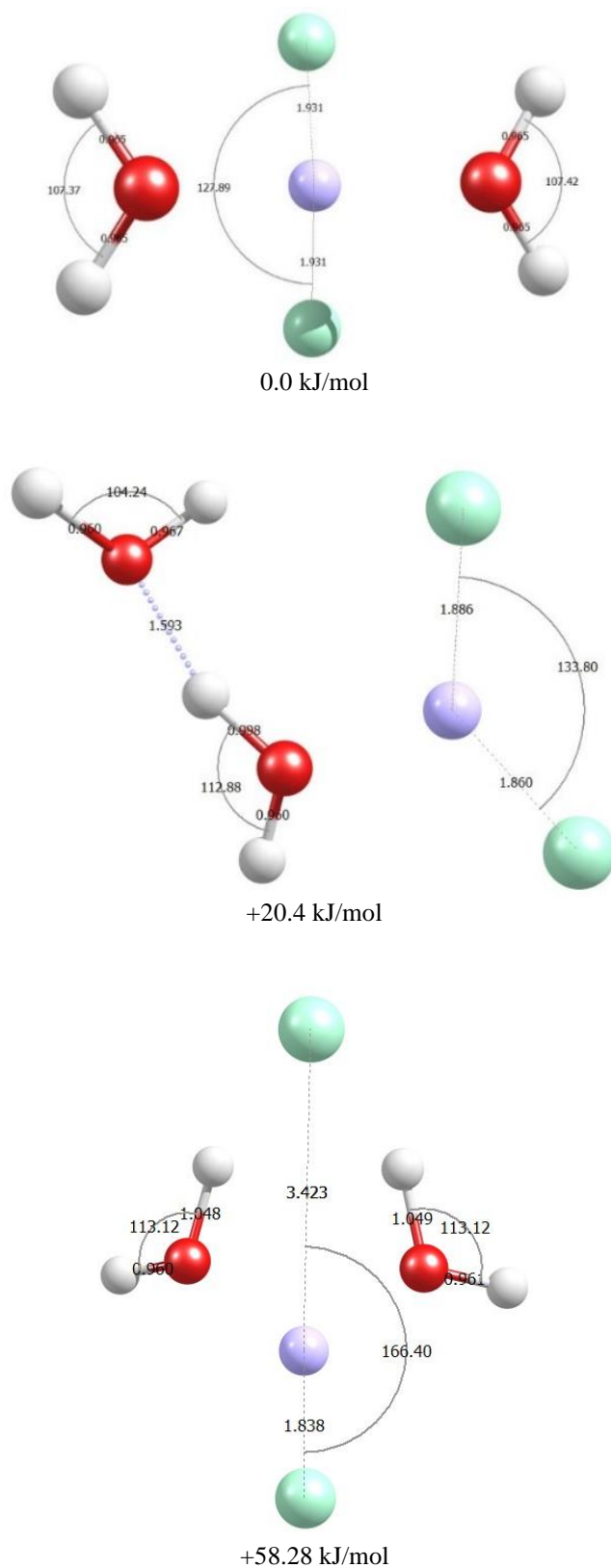


Figure 2. The calculated structures for $\text{BeCl}_2(\text{H}_2\text{O})_2$ with their energies in kJ/mol

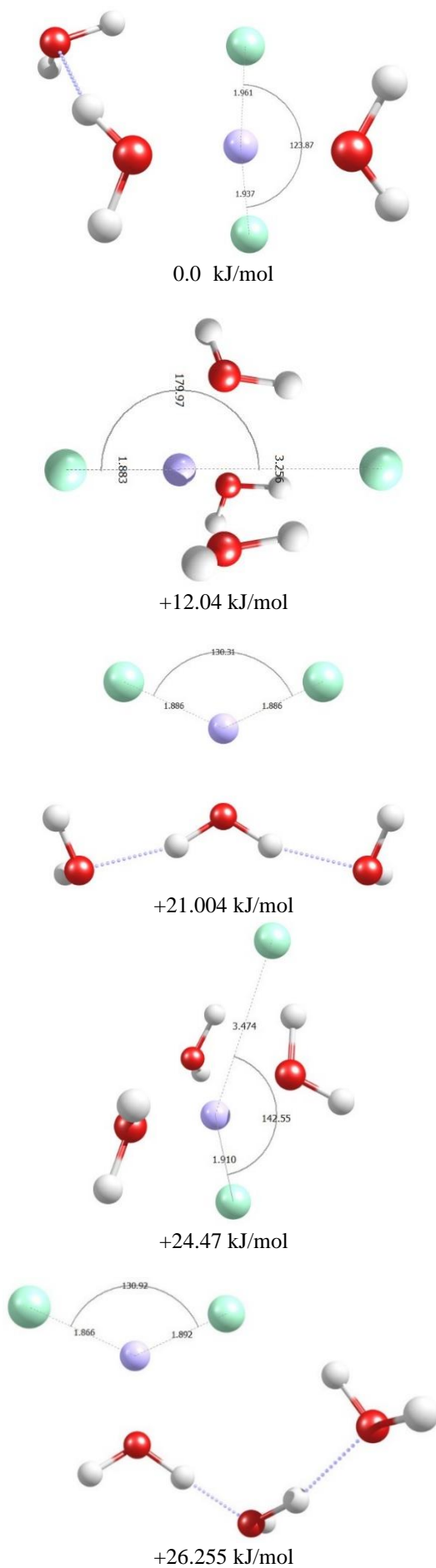


Figure 3. The calculated structures for $\text{BeCl}_2(\text{H}_2\text{O})_3$

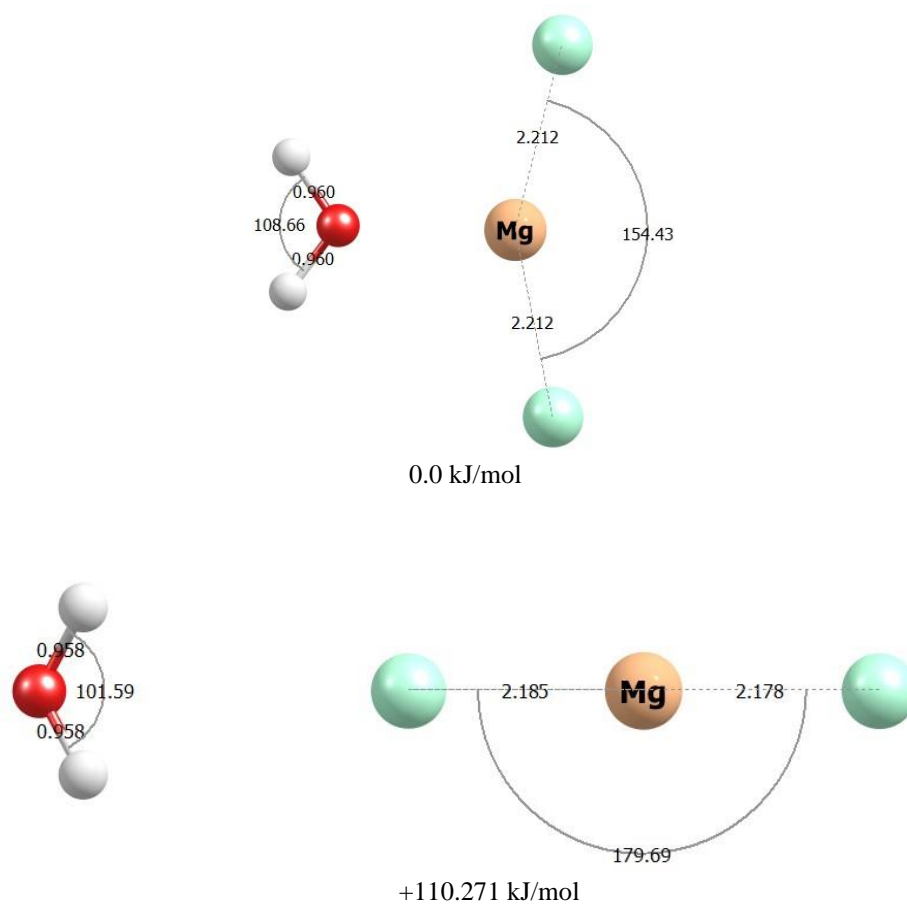


Figure 4. The calculated structures for $\text{MgCl}_2(\text{H}_2\text{O})$ with their energies in kJ/mol

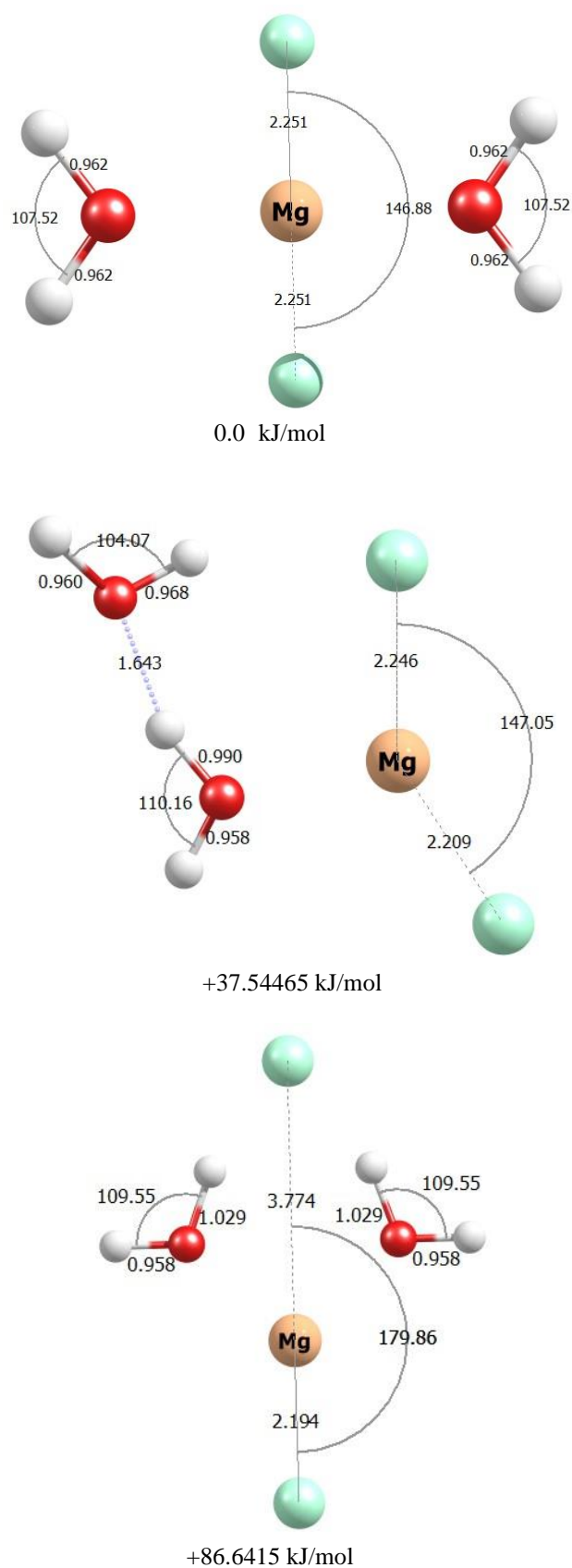
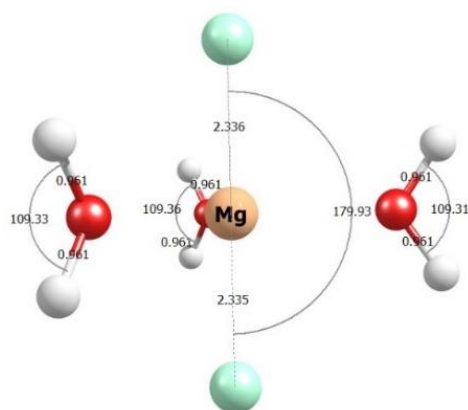
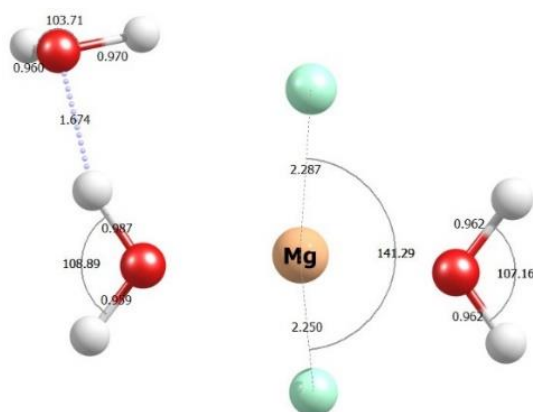


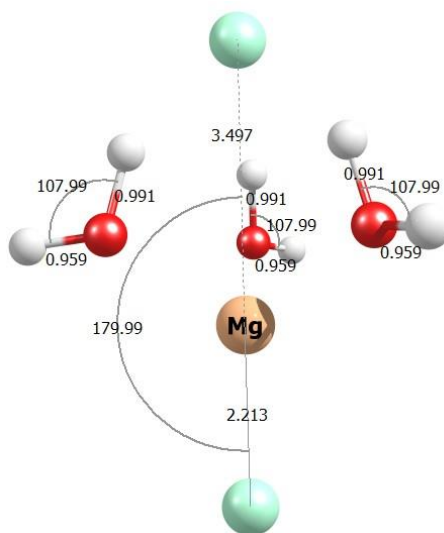
Figure 5. The calculated structures for $\text{MgCl}_2(\text{H}_2\text{O})_2$ with their energies in kJ/mol



0.0 kJ/mol



+13.91515 kJ/mol



+30.166997 kJ/mol

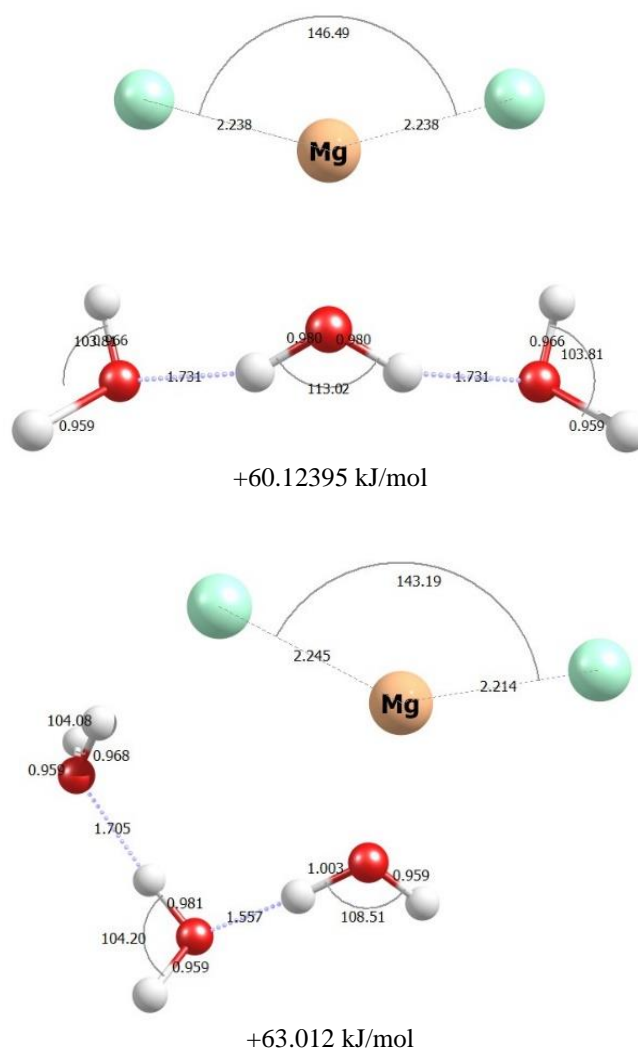


Figure 6. The calculated structures for $\text{MgCl}_2(\text{H}_2\text{O})_3$ with their energies in kJ/mol

Table 1. The OH Stretching frequencies for the minimum structures of $\text{BeCl}_2(\text{H}_2\text{O})_n$ ($n=1-3$) Complexes at MP2 Level of Theory

OH Band position cm^{-1}	Assigned Complex
3651	$\text{BeCl}_2(\text{H}_2\text{O})$
3625 3727	$\text{BeCl}_2(\text{H}_2\text{O})_2$
3575 3625 3701	$\text{BeCl}_2(\text{H}_2\text{O})_3$

Table 2. The OH Stretching frequencies for the minimum structures of $\text{MgCl}_2(\text{H}_2\text{O})_n$ ($n= 1-3$) Complexes at MP2 Level of Theory

OH Band position cm^{-1}	Assigned Complex
3792	$\text{MgCl}_2(\text{H}_2\text{O})$
3669 3775	$\text{MgCl}_2(\text{H}_2\text{O})_2$
3671 3790	$\text{MgCl}_2(\text{H}_2\text{O})_3$

Table 3. The Binding Energy (BE) for $\text{BeCl}_2(\text{H}_2\text{O})_n$ ($n = 1-3$) Complexes at MP2 Level of Theory

BE kJ/mol	Assigned Complex
194.287	$\text{BeCl}_2(\text{H}_2\text{O})$
370.196	$\text{BeCl}_2(\text{H}_2\text{O})_2$
519.849	$\text{BeCl}_2(\text{H}_2\text{O})_3$

Table 4. The Binding Energy (BE) for $\text{MgCl}_2(\text{H}_2\text{O})_n$ for $n = 1-3$ Complexes at MP2 Level of Theory

BE kJ/mol	Assigned Complex
199.538	$\text{MgCl}_2(\text{H}_2\text{O})$
388.574	$\text{MgCl}_2(\text{H}_2\text{O})_2$
551.355	$\text{MgCl}_2(\text{H}_2\text{O})_3$

MEDIÇÃO DA CONCENTRAÇÃO DE CHUMBO NO SANGUE DE MOTORISTAS DE TRANSPORTE PÚBLICO NO DOMÍNIO DE BANDUNG, WEST JAVA, INDONÉSIA**MEASUREMENT OF LEAD CONCENTRATION IN THE BLOOD OF PUBLIC TRANSPORT DRIVERS IN BANDUNG REGENCY, WEST JAVA, INDONESIA****PENGUKURAN KONSENTRASI TIMBAL DALAM DARAH PENGEMUDI ANGKUTAN UMUM DI KABUPATEN BANDUNG, JAWA BARAT, INDONESIA**

BAEHAKI, Farhan^{1*}; FAJRIANI, Gita Nur^{2*}; HAERANI, Ani³; AENI, Suci Rizki Nurul⁴; SARI, Ayu Yunita⁵,

^{1,2,3,4,5} Medical Laboratory Technology, Institut Kesehatan Rajawali, Bandung, West Java, Indonesia

** Corresponding author*

e-mail: farhanbaehaki71@gmail.com

Received 18 June 2020; received in revised form 18 August 2020; Accepted 20 October 2020

RESUMO

Como as atividades industriais e de transporte em Bandung Regency estão crescendo rapidamente, a Indonésia pode correr o risco de aumentar os níveis de poluição do ar. Um dos poluentes atmosféricos muito prejudiciais ao organismo é o chumbo (Pb), que pode ser gerado em atividades industriais, mineração, gases de escapamento de veículos e poeira do solo. O chumbo é um metal pesado muito perigoso para o organismo, pois é cancerígeno com seu caráter de atividade como inibidor do metabolismo celular. Este estudo teve como objetivo analisar a concentração de chumbo no sangue de motoristas de transporte público que trafegam diariamente nas rodovias e apresentam maior risco de exposição ao Pb. A medição da concentração de Pb foi realizada em Espectrofotômetro de Absorção Atômica (AAS). Amostras de sangue foram coletadas de motoristas de transporte público no Terminal Soreang, Bandung Regency, West Java, Indonésia. Os resultados da análise mostraram que o teor médio de chumbo no sangue dos motoristas de transporte público foi 1.032 mg/L. O nível mais baixo foi 0,889 mg/L e o mais alto foi 1.200 mg/L. Isso mostra que o teor de chumbo no sangue de motoristas de transporte público já está em níveis excessivos (valores de faixa 0,800-1,200 mg/L) quando comparado com o limite de chumbo no sangue com base no Regulamento do Ministério da Saúde da República da Indonésia (0,10 - 0,25 mg/L) e o valor limite estabelecido pela Organização Mundial da Saúde, que é 0,4 mg/L.

Palavras-chave: *Espectrofotômetro de Absorção Atômica, Metais Pesados, Chumbo.*

ABSTRACT

As industrial and transportation activities in Bandung Regency are growing rapidly, Indonesia could be at risk of increasing air pollution levels. One of the air pollutants that are very harmful to the body is lead (Pb) generated from industrial activities, mining, vehicle exhaust gas, and dust from the ground. Lead is a heavy metal that is very dangerous for the body because it is carcinogenic with its activity character as an inhibitor in cell metabolism. This study aimed to analyze the concentration of lead in the blood of public transport drivers who are active on the highway every day and are most at risk of being exposed to Pb. Measurement of Pb concentration was carried out using an Atomic Absorption Spectrophotometer (AAS). Blood samples were taken from public transport drivers at Soreang Terminal, Bandung Regency, West Java, Indonesia. The analysis results showed that the average blood lead content of public transport drivers was 1,032 mg/L. The lowest level was 0.889 mg/L, and the highest was 1,200 mg/L. This shows that the lead content in the blood of public transport drivers is already in excess levels (range numbers 0.800-1.200 mg/L) when compared with the threshold for lead in the blood based on the Regulation of the Ministry of Health of the Republic of Indonesia (0.10 - 0.25 mg/L) and the threshold value set by the World Health Organization, which is 0.4 mg/L.

Keywords: *Atomic Absorption Spectrophotometer, Heavy Metals, Lead.*

ABSTRAK

Aktivitas industri dan transportasi di wilayah Kabupaten Bandung yang semakin berkembang dengan pesat dapat beresiko untuk meningkatkan tingkat pencemaran udara. Salah satu pencemar udara yang sangat

berbahaya bagi tubuh adalah timbal (Pb) yang dapat dihasilkan dari aktivitas industri, pertambangan, gas buangan kendaraan, dan debu yang berasal dari permukaan tanah. Timbal merupakan logam berat yang sangat berbahaya bagi tubuh karena bersifat karsinogenik dengan sifat aktivitasnya sebagai penghambat metabolisme sel. Penelitian ini bertujuan untuk menganalisis kandungan timbal di dalam darah sopir angkutan umum yang setiap hari beraktivitas di jalan raya dan beresiko paling tinggi untuk terpapar Pb. Pemeriksaan kadar Pb dilakukan dengan menggunakan *Atomic Absorption Spectrophotometer* (AAS). Sampel darah diambil dari sopir angkutan umum di wilayah Terminal Soreang, Kabupaten Bandung. Hasil analisis menunjukkan bahwa rata-rata kadar timbal yang terdapat di dalam darah sopir angkutan umum sebesar 1.032 mg/L. Kadar terendah berada pada angka 0.889 mg/L dan kadar tertinggi berada pada angka 1.200 mg/L. Hal ini menunjukkan kandungan timbal dalam darah pengemudi angkutan umum sudah melebihi kadar (kisaran angka 0.800-1.200 mg/L) jika dibandingkan dengan ambang batas timbal dalam darah berdasarkan Peraturan Kementerian Kesehatan Republik Indonesia (0,10 - 0,25 mg/L) dan nilai ambang batas yang ditetapkan oleh Organisasi Kesehatan Dunia, yaitu 0,4 mg/L.

Keywords: *Atomic Absorption Spectrophotometer, Logam Berat, Timbal*

1. INTRODUCTION:

In the development of increasingly modern times, air quality has experienced a lot of declines. Air is a basic human need for breathing. Good air quality can support human life (Chertok, Voukelatos, Sheppard, and Rissel, 2004). The decrease in air quality is caused by an increase in industrial activity and traffic. Based on The World Bank data, in 2020, it is estimated that half of Indonesia's population will experience air pollution problems (Gunawan, 2015; Suksmerri, 2008). One city that has a high level of air pollution is the City of Bandung. This is directly proportional to the increase in the number of vehicles and industries. Andriyawan (2018) revealed that the number of vehicles in Bandung increases by 11% per year. Data in 2018 showed there were 1,251,080 units of two-wheeled vehicles and 536,973 units of four-wheeled vehicles. Also, the development of the number of industries in the city of Bandung also continues to increase. Research conducted by Gunawan (2015) shows that the level of air pollution in Padalarang, Bandung Regency Suspended Particulate Matter (TSP/dust) is very high, around 255.58 $\mu\text{g}/\text{Nm}^3$. From 2010 to 2015, the average Pb pollutant air pollution level has been above 1 $\mu\text{g}/\text{Nm}^3$ (annual national ambient quality standard). Only in the first semester of 2011, the Pb pollution level was below 1 $\mu\text{g}/\text{Nm}^3$ and the highest in the second semester of 2010, which was around 1.96 $\mu\text{g}/\text{Nm}^3$, occurred at the location of the Padalarang toll gate.

One of the pollutants produced from industrial activities and traffic is lead (Pb) (Abdi and Kazemi, 2015; Loukidou, Zouboulis, Karapantsios, and Matis, 2004; Lichtfouse and Schwarzbauer, 2012; Kiziloz, 2019; Ordouee and Hazheminezhad, 2019; Suksmerri, 2008). Lead is usually added to the fuel to increase the octane value (Ismail, 2004; Intani, 2010). Traffic activity is

the largest source of lead, which is 60% (Ardillah, 2016). Aside from traffic activities, lead can also be produced from industrial waste, burning coal, rocks, soil, and plants (Olukanni, Agunwamba, and Ugwu, 2014; Rodríguez, Cárdenas-González, Juárez, Pérez, Zarate, and Castillo, 2018; Acar and Malkoc, 2004). Sources classified as large are coal combustion, smoke from factories that process alkyl-Pb compounds, Pb-Oxides, Pb ore smelting, and motor vehicle fuel transfer alkyl-Pb compounds contained in these fuels are very volatile (Palar, 2012). The problem that arises from lead is its very small size, 0.02-1.00 μm , with a period of stay in the air for 4 - 40 days (Naria, 2005). This causes the risk of lead inhaled by humans to be higher.

The traffic sector is becoming more concerned with air pollution by Pb metal, especially for residents who work as public transport drivers. This profession has a very high risk because the working area is on the highway. Especially if the traffic conditions are very congested. Air quality on high traffic with high road density contains a higher lead than air on road with low traffic density (Ardillah, 2016).

The entry of lead into the body will be hazardous because it has no biological function so that it can disrupt the health of the body (Rodríguez, Cárdenas-González, Juárez, Pérez, Zarate, and Castillo, 2018). Lead metal can enter the body in three ways: the skin, respiratory tract, and digestive tract (Palar, 2012; Nasir, 2018). Of the several forms of the lead entering the body, the respiratory pathway is the most common lead (Patrick, 2006). When the lead enters through breathing, the absorption process takes place in the inner lungs. Lead absorption through respiration can reach 30% of the total amount entered, while it is only 5-10% in the digestive track. When absorbed, the lead will enter the circulatory system and bound in red blood cells by

90% and 15% stored in body tissues and excreted mainly through the kidneys and digestive tract (Palar, 2012). Lead absorbed by blood is distributed to soft tissues (liver, lungs, kidneys, spleen, heart, brain) and to hard tissues (bones, hair, teeth) (Palar, 2012; Wittmers Jr., 2010; Rabinowitz, 1991; Kosnett *et al.*, 2007).

When the lead enters the body and spreads in the body, the excretion or excretion process does not occur as a whole. This is because the half-life of lead in the blood is ± 25 days, in the soft tissue for ± 40 days, while in the bones for ± 25 years (Nordberg, 1998). This prolonged excretion process can cause lead to accumulate quickly in the body. The toxic effects of lead can cause symptoms of sleep disorders, weakness, headaches, muscle and bone pain, abdominal pain, nausea and vomiting, weight loss, and reduced appetite (Naria 2005, Gusnita, 2012; Rosita, and Sosmira, 2017; Papanikolaou *et al.*, 2005; Anies, 2005). Meanwhile, chronic diseases can be caused, namely epilepsy, hallucinations, anemia, and even cancer (Nasir, 2018; Ardillah, 2016; Patrick, 2006; Etiang *et al.*, 2018; Schober *et al.*, 2006). Pb can cause anemia because it interferes with the process of hemoglobin formation (Needleman, 2004). Of the various toxic effects caused, the nervous system is the most sensitive part of Pb. Besides, Pb can also attack brain tissue.

Needleman (2004), Richard, Phillips, and Kushner (2006), and Dwilestari (2012) explained that lead could inhibit the formation of hemoglobin by inhibiting the activity of the delta-aminolevulinic acid dehydratase enzyme (delta-ALAD and ALAD). When the total lead level in the blood exceeds 0.20 mg / L, ALAD activity will be inhibited by 50 percent. This inhibition is characterized by an increase in the level of aminolevulinic acid (ALA) in the urine, a substrate that accumulates due to a decrease in ALAD. Delta-ALAD inhibition will also prevent ALA from being converted into porphobilinogen to inhibit the incorporation of iron into the protoporphyrin ring. Thus, heme synthesis will be reduced, both for hemoglobin and for cellular respiration.

Toxic effects can be caused because Pb is an inhibitor. This means that Pb can inhibit the performance of certain enzymes in the body. Toxic effects begin when lead buildup occurs in the body. Febrianti and Azizah (2015) and the World Health Organization (1995) divided the threshold value for male workers by 0.4 mg / L and for female workers by 0.3 mg / L. Meanwhile, according to the Decree of the Minister of Health of the Republic of Indonesia Number 1406 / MENKES / SK / IX /

2002, the threshold value of lead levels in blood specimens in normal adults is 0.10 - 0.25 mg / L. Pb concentrations in the blood that exceed this threshold value can cause symptoms of poisoning. The amount of lead in the blood will continue to increase as the air quality gets worse. Measurement of Pb levels in the blood is very important because it can be used as an index of exposure and level of danger (Ardillah, 2016; Gunawan, 2015). Based on the threshold value determined by the Government of Indonesia and the World Health Organization, Palar (2012) categorizes the level of Pb exposure in the blood in Table 1.

To measure the concentration of Pb in the blood, an Atomic Absorption Spectrophotometer (AAS) can be used. Using AAS, the measurement method is a quantitative analysis method whose measurement is based on light absorption with certain wavelengths by metal atoms in the free state in the gas phase (Aprilia and Rahayu, 2015; Anshori, 2005; Slavin, 1978). Measurement of metal concentrations with AAS is considered more accurate because it has high accuracy and selectivity (Dewi, Mahmudah, Kumalawati, and Amalullia, 2019; Slavin, 1978).

The research method used is descriptive. Based on Saryono and Anggraeni (2013) and Notoatmodjo (2012), this study aimed to analyze the concentration of lead in the blood of public transport drivers who are active every day on the highway and are most at risk for exposure to Pb. The value of the content obtained can provide information about the description of the level of air pollution by the presence of Pb. The test results obtained were then compared with the threshold value of lead exposure in the blood.

2. MATERIALS AND METHODS:

The research was carried out at the Laboratory of Applied Chemistry and Toxicology, Rajawali Institute of Health, and the Central Laboratory of Padjadjaran University. Samples were taken in the form of venous blood obtained from public transport drivers in the Soreang Terminal area, Bandung Regency, West Java, Indonesia. Before the venous blood was drawn, participants were asked about their willingness to take blood as a sample. They were also given a general description of the research and its benefits to them. After they agree, they were required to fill out the informed consent (IC) as written consent.

Participants were determined randomly using accidental sampling technique from public transport drivers operating at Soreang Terminal.

All participants were male. The selected participants were determined based on their tenure, namely being a public transport driver for 5 years and working a minimum of 8 hours a day. Consideration of this criterion was carried out to see the relationship between the time of exposure and the Pb level in the blood. Driver's age data was also collected to see how age affects Pb levels in the blood. Based on these criteria, there were as many as 10 public transport drivers who could fulfill this. Also, to obtain more in-depth data, interview sessions were also conducted with the ten participants covering their daily activities, residence location, and work length per day.

Then the blood sample was taken to the laboratory for measurements. Research in the laboratory was carried out in several stages, namely sample preparation, destruction, standard curve creation, and measure of blood lead levels (Ardillah, 2016; Baehaki, Rudibyani, Aeni, Perdana, and Aqmarina, 2020; Batool, Ahmad, Zahidqureshi, Mahboob, and Nimra, 2018; Takwa, Bujawati, and Mallapiang, 2017).

2.1. Sample Preparation

Of the ten public transport drivers who meet the criteria, 3 mL of blood each was obtained using a pipette into a cup and added 500 mg of potassium citrate. Next, 5 ml of concentrated nitric acid is added until the color turns blackish brown to destroy the organic compounds.

2.2. Sample Destruction

Blood samples that have been prepared are then destructed to damage organic compounds. Destruction was carried out for 6 hours at 400 °C until it turns to ashes. The resulting ash was dissolved using sufficient 0.5 M nitric acid solution. The solution was then filtered using filter paper to obtain 10 mL of filtrate using a measuring flask.

2.3. Making Standard Curve

Making a standard curve is done by making a series of standard solutions $\text{Pb}(\text{NO}_3)_2$ with a concentration of 1 mg/L, 2 mg/L, 3 mg/L, 4 mg/L, 5 mg/L. The solution was made by diluting a 100 mg/L standard $\text{Pb}(\text{NO}_3)_2$ solution. The solution was made using dilution formula, which are:

$$V_1 \cdot C_1 = V_2 \cdot C_2$$

where V_1 is the volume of the stock solution to be diluted, C_1 is the concentration of the stock

solution (100 mg/L), V_2 is the final volume of the dilute solution, and C_2 is the final concentration (in this case 1 mg/L, 2 mg/L, 3 mg/L, 4 mg/L, and 5 mg/L).

The calculations for making standard solutions can be seen below.

- Standard solution 1 mg / L
 $100 \text{ mg/L} \times V_1 = 1 \text{ mg/L} \times 100 \text{ mL}$
 $V_1 = \frac{1 \times 100}{100} = 1 \text{ mL}$
- Standard solution 2 mg / L
 $100 \text{ mg/L} \times V_1 = 2 \text{ mg/L} \times 100 \text{ mL}$
 $V_1 = \frac{2 \times 100}{100} = 2 \text{ mL}$
- Standard solution 3 mg / L
 $100 \text{ mg/L} \times V_1 = 3 \text{ mg/L} \times 100 \text{ mL}$
 $V_1 = \frac{3 \times 100}{100} = 3 \text{ mL}$
- Standard solution 4 mg / L
 $100 \text{ mg/L} \times V_1 = 4 \text{ mg/L} \times 100 \text{ mL}$
 $V_1 = \frac{4 \times 100}{100} = 4 \text{ mL}$
- Standard solution 5 mg / L
 $100 \text{ mg/L} \times V_1 = 5 \text{ mg/L} \times 100 \text{ mL}$
 $V_1 = \frac{5 \times 100}{100} = 5 \text{ mL}$

To each solution, 0.5 mL of nitric acid solution was added to the mark on the 100 mL volumetric flask. Absorbance measurements were performed at a wavelength of 283 nm. The curve is created by plotting the concentration value (x axis) and absorbance value (y axis). Making this curve is used to calibrate the instrument and calculate the Pb concentration in the sample.

2.4. Measurement of Lead Concentration in Blood Samples

The blood sample that has been degraded is dissolved into 0.5 mL of concentrated nitric acid and diluted in a 10 mL volumetric flask. The dilution solution was pipetted and put into a cuvette measured using AAS at 283 nm wavelength.

3. RESULTS AND DISCUSSION:

3.1 Standard Curve $\text{Pb}(\text{NO}_2)_3$ Solution

A standard curve was done to obtain a straight line equation that can be used to calculate Pb concentration in a sample. This method is a standard way of measuring using AAS. Generally,

the greater the concentration, the higher the absorbance value (Table 2). The data in Table 2 were then plotted into the x axis (concentration) and the y axis (absorbance). Plots of these values can form a straight line with the equation $y = mx + c$.

Based on the data plotted in Table 2, a straight line is obtained with the equation $y = 0.0095x + 0.0007$ with an R^2 value of 0.9991 (see Figure 1). The ideal linear relationship is achieved if $R^2 = 1$ or $R^2 = -1$ (Harmita, 2004). If the value of R^2 is getting closer to the value of 1 or -1, then the value of R^2 is getting closer to the ideal. Therefore, the R^2 value obtained in this study shows that the resulting line equation can be used to determine the Pb content in the sample.

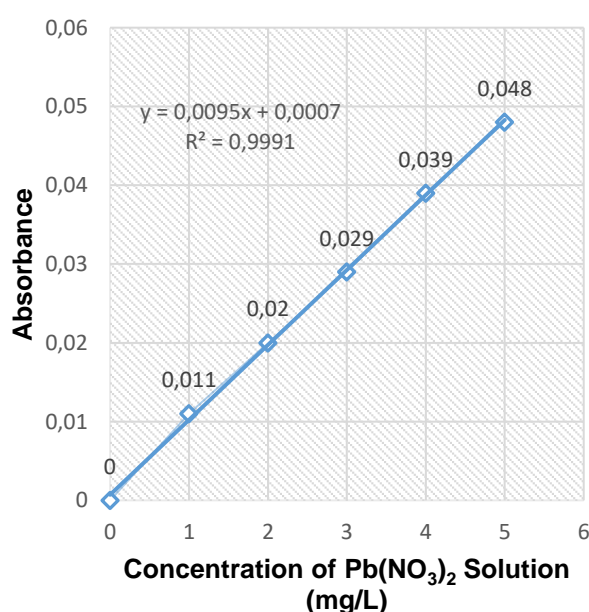


Figure 1. Standard Curve of Pb (NO₃)₂ Solution

3.2. Sample Measurement Results

The measurement results show a high Pb concentration value in the blood of public transport drivers (see Table 3). The average Pb concentration measured was 1.032 mg / L. Even the lowest Pb concentration was found in sample S4 with a value of 0.889 mg / L. This concentration value has exceeded the threshold for Pb concentration in the blood based on the Regulation of the Minister of Health of the Republic of Indonesia Number 1406 / MENKES / SK / IX / 2002, namely 0.10 - 0.25 mg / L blood. This value also has exceeded the threshold value determined by the World Health Organization, namely 0.4 mg / L (Febrianti and Azizah, 2015; The World Health Organization, 1995). If we look at the classification of Pb concentrations in the blood by Palar (2012) (see Table 1), the mean Pb concentration is in the

excessive category and is close to the dangerous level. These data indicate that the level of Pb exposure in the sample work area is very high (Zolaly *et al.*, 2012). Even the average value is in the range of values with an over-classification and begins to show poisoning (Palar, 2012). Symptoms commonly felt by all participants were easy fatigue and reduced concentration. The high Pb level in the blood is following the results of a survey conducted by Mujahidin (2019) in the Soreang area, Bandung Regency, West Java, Indonesia, which shows traffic density and industrial activity. According to Ardillah (2016), the higher the traffic activity, the higher the air pollution by the lead.

The relationship between driver's age and Pb levels is also analyzed from Table 3. This is because age is one factor that can affect Pb levels in the body (Suciani, 2007). The older a person is, the higher their Pb level. Based on the data in Table 3, the pattern of this relationship is not visible, so further research is needed to examine in more depth about this problem. This is possible due to the influence of other factors, namely the length of exposure (working hours per day) and lifestyle. The duration of exposure has a close relationship with the amount of Pb levels in the body (Frank, 1995).

The relationship between length of work and blood levels of Pb can be seen in Figure 2. In general, Figure 2 shows the increase in Pb levels with increasing work hours. But graphic patterns only show trends. For example, the interesting thing is in the S3 sample data, the sample has been working as a public transport driver for ± 23 years, but the measured Pb concentration is 0.996 mg/L. This Pb concentration value is smaller than the S1 sample that has only been working as a public transport driver for ± 10 years with a measured Pb concentration value of 1.010 mg/L. The existence of this phenomenon requires the deepening of extracting information.

The results of the interview provide more in-depth information. Sample S3 and sample S1 have the same average working hours for 8 hours per day (see Table 3). Their activities are almost the same at work. However, they reside in different areas. Sample S1 resides right on the edge of the highway, while the sample residence S3 is far from the highway. This could explain the phenomenon in the graph of the relationship of work duration with the concentration of Pb in the blood (Figure 2). This is quite influential because it means that the S1 sample takes longer to interact in the Pb exposure area than the S3 sample. Residence right on the side of the road has a higher risk of

exposure due to traffic activities. This is under Frank (1995) statement, who said that the duration of exposure is one of the factors that determine the level of Pb in the blood. Other factors are also found, such as daily habits like smoking, not washing your hands before eating and taking supplements. According to Hasan (2012), the habit of drinking supplement drinks can reduce Pb levels in the blood. Supplements that contain calcium and intake of magnesium, phosphate, alcohol, and fat can reduce the absorption of Pb in the body (Bogden *et al.*, 1992; Mahaffey, Gartside, Glueck, 1986; Barltrop and Meek, 1979; Barltrop and Khoo, 1975). However, there are no substantial data on the influence of these factors on Pb exposure, so further research is needed to do this.

4. CONCLUSIONS:

Lead levels (Pb) in the blood of public transport drivers in Soreang Terminal are in the excess category. Where the average concentration of Pb in the blood is 1.032 mg/L. Levels of this category have led to symptoms of mild poisoning. Generally, the public transport driver used as a sample feels his body easily tired and reduced concentration. This data can be used as a basis for the government or public transport facility managers to minimize exposure to public transport drivers. One simple effort that can be done is the use of masks when working, familiarizing clean life (washing hands before eating), reducing smoking habits, and so on. Also, there is a need for policies in handling traffic activities by setting vehicle rules that must reduce the levels of smoke produced by exhaust, urge to use public transportation rather than private vehicles, and limit road access for large vehicles (trucks and buses) so on. So that traffic activity can be minimized or at least can be reduced.

5. ACKNOWLEDGMENTS:

The authors are grateful to The Institut Kesehatan Rajawali and Central Laboratory, Padjajaran University, who were willing to cooperate in completing this research. The authors also want to thank all those who have helped both material and moral so that this research can be carried out well.

6. REFERENCES:

1. Chertok, M., Voukelatos, A., Sheppeard, V., and Rissel, C. (2004). Comparison Of Air Pollutan Exposure For Five Commuting

- Modes In Sydney-Car, Train, Bus, Bicycle And Walking. *Health promotion journal of Australia: official journal of Australian Association of Health Promotion Professionals*, 15(1).
2. Gunawan, G. (2015). Tingkat Pencemaran Udara Debu Dan Timbal Di Lingkungan Gerbang Tol. *Jurnal Jalan Jembatan*, 32(2).
3. Suksmerri (2008). Dampak Pencemaran Logam Timah Hitam (Pb) Terhadap Kesehatan. *Jurnal Kesehatan Masyarakat*, 2(2).
4. Andriyawan, D. (2018). Pertumbuhan Kendaraan di Bandung 11% Tiap Tahunnya, *Car Pooling Dinilai Efektif*. (Online), <https://bandung.bisnis.com/read/20181002/549/1114194/pertumbuhan-kendaraan-di-bandung-11-per-tahun>, accessed on July 3 2019.
5. Abdi, O., Kazemi, M. (2015). A Review Study of Biosorption of Heavy Metals And Comparison Between Different Biosorbents. *J. Mater. Environ. Sci.*, 6(5), 1386-1399.
6. Loukidou, M. X., Zouboulis, A.I., Karapantsios, T.D., and Matis, K.A. (2004). Equilibrium and kinetic modeling of chromium(VI) biosorption by *Aeromonas caviae*. *Colloids and Surfaces A: Physicochem. Eng. Aspects*, 242, 93-104. doi:10.1016/j.colsurfa.2004.03.030
7. Lichtfouse, E., Schwarzbauer, J., and D. Robert. (2012). *Environmental Chemistry For A Sustainable World Volume 1: Nanotechnology And Health Risk*, New York: Springer.
8. Kiziloğlu, B. (2019). Investigation Of Some Hazardous Agents And Trace Elements In Drinking Water Of Kocaeli Region. *Periodico Tchê Química*, 16(31), 381–389.
9. Ordouee, B., Hazheminezhad, H. (2019). Measurement And Adsorption Of Heavy Metals Ion From Water Using Porous Nano-Adsorbents By Atomic Absorption Method. *Periodico Tchê Química*, 16(32), 228–238.
10. Ismail F. (2004). *Hubungan antara penggunaan masker hidung karbon aktif dengan kadar timbal urin petugas parkir yang terpajan emisi timbal pada sebuah perusahaan disebuah basement mall di Jakarta*. Jakarta: Universitas Indonesia.

11. Intani Y.C. (2010). *Pengaruh Timbal (Pb) pada Udara Jalan Tol Terhadap Gambaran Mikroskopis Testis dan Kadar Timbal (Pb) dalam Darah Mencit Balb/c Jantan*. Semarang: Universitas Diponegoro.
12. Zolaly M.A., et al. (2012). Association between blood lead levels and environmental exposure among Saudi schoolchildren in certain districts of Al-Madinah. *International Journal of General Medicine*, 5:355–364. <http://doi.org/10.2147/ijgm.s28403>
13. Ardillah, Y. (2016). Faktor Resiko Kandungan Timbal Di Dalam Darah. *Jurnal Ilmu Kesehatan Masyarakat*, 7(3), 150-153. <https://doi.org/10.26553/jikm.2016.7.3.150-155>
14. Olukanni, D. O., Agunwamba, J. C., and Ugwu, E. C. (2014). Biosorption of Heavy Metals In Industrial Wastewater Using Microorganisms (*Pseudomonas Aeruginosa*). *American Journal Of Scientific And Industrial Research*, 5(2), 81 – 87.
15. Rodríguez, I. A., Cárdenas-González, J. F., Juárez, V. M. M., Pérez, A. R., Zarate, M. G. M., Castillo, N. C. P. (2018). Biosorption of Heavy Metals by *Candida albicans*. *Advances in Bioremediation and Phytoremediation*, 43–62. <http://dx.doi.org/10.5772/intechopen.72454>
16. Acar, F. N. And Malkoc, E. (2004). The Removal Of Cr(VI) From Aqueous Solutions By *Fagus Orientalis* L. *Bioresource Technology*, 94, 13–15.
17. Palar, H. (2012) *Pencemaran Dan Toksikologi Logam Berat 5th Edition*. Jakarta: PT. Rineka Cita.
18. Naria, E. (2005). Mewaspadai Dampak Bahan Pencemaran Timbal (Pb) Di Lingkungan Terhadap Kesehatan. *Repositori Institusi Universitas Sumatera Utara*, 17(4).
19. Nasir, M. (2018). Analisis Perbandingan Kadar Timbal (Pb) dan Besi (Fe) Dalam Darah Petugas Parkir Ruang Terbuka Dengan Ruang Tertutup. *Jurnal Media Analis Kesehatan*, 9(1), 69 – 71.
20. Patrick L. (2006). Lead toxicity, a review of the literature. Part 1: Exposure, evaluation, and treatment. *Altern Med Rev*, 11(1): 2-22.
21. Wittmers Jr., et al. (2010). Lead in Bone. IV. Distribution of Lead in the Human Skeleton. *Archives of Environmental Health: An International Journal*. 43(6): 381-391. <https://doi.org/10.1080/00039896.1988.9935855>
22. Rabinowitz MB. (1991). Toxicokinetics of bone lead. *Environ Health Perspect*, 91:33-37. <https://doi.org/10.1289/ehp.919133>
23. Kosnett M.J. et al. (2007). Recommendations for Medical Management of Adult Lead Exposure. *Environ Health Perspect*. 115(3): 463–471. <https://dx.doi.org/10.1289%2Fehp.9784>
24. Nordberg G. 1998. *Metal: Chemical Properties and Toxicity*. In: *Stellman Jm (ed); Encyclopedia of Occupational Health and Safety (4 ed)*. Geneva: ILO.
25. Gusnita, D. (2012). Pencemaran Logama Berat Timbal (Pb) Di Udara Dan Upaya Penghapusan Bensin Bertimbal. *Berita Dirgantara*, 13(3), 95-98.
26. Rosita, B. (2017). Verifikasi Analisa Kadar Logam Timbal (Pb) Dalam Darah Dan Gambaran Hematologi Darah Pada Petugas Tambang Batu Bara. Sosmira, E. *Journal of Sainstek*, 9(1), 68 – 75.
27. Papanikolaou N.C., et al. (2005). Lead toxicity update. A brief review. *Med Sci Monit*, 11:RA329-RA336.
28. Anies (2005). *Penyakit Akibat Kerja*. Jakarta: PT. Elex Media Komputindo.
29. Etiang N.A. et al. (2018). Environmental Assessment and Blood Lead Levels of Children in Owino Uhuru and Bangladesh Settlements in Kenya. *Journal of Health & Pollution*, 8(18):180605. <http://doi.org/10.5696/2156-9614-8.18.180605>
30. Schober S.E. et al. (2006). Blood Lead Levels and Death from All Causes, Cardiovascular Disease, and Cancer: Results from the NHANES III Mortality Study. *Environ Health Perspect*. 114(10): 1538–1541. <https://dx.doi.org/10.1289%2Fehp.9123>
31. Needleman H. (2004). Lead poisoning. *Annu Rev Med*, 55:208-222.

32. Richard S.A., Phillips, J. D., and Kushner, J.P. (2006). Biosynthesis of heme in mammals. *Biochemistry and Biophysics Actual*, 17(63):723–36.
33. Dwilestari K.O.H. (2012). *Analisis Hematologi Dampak Paparan Timbal pada Pekerja Pengecatan (studi Kasus: Industri Pengecatan Mobil Informal di Karasak, Bandung)*. Bandung: Institut Teknologi Bandung.
34. Febrianti, L. D. dan Azizah, R. (2015). Karakteristik Kadar Timbal (Pb) Dalam Darah, Dan Hipertensi Pekerja *Home Industry* Aki Bekas Di Desa Talun Kecamatan Sukodadi Kabupaten Lamongan. *Jurnal Kesehatan Lingkungan*, 8(1), 92-94.
35. The Decree of the Minister of Health of the Republic of Indonesia Number 1406 / MENKES / SK / IX / 2002 Regarding the standard for checking lead levels in human biomarker specimens, the measurement of lead levels in the human body can be done through blood, urine, and hair specimens.
36. Aprilia, D., Rahayu, D., dan Ayu, D. R. (2015). Spektropotometer serapan atom. (online), https://www.academia.edu/13867003/Spektrofotometri_Serapan_Atom_AAS_, accessed on July 3, 2019.
37. Anshori, J. (2005). *Materi Ajar Spektrofotometer Serapan Atom*. Bandung : UNPAD Press.
38. Slavin (1978). *Atomic Absorption Spectroscopy*. New York: Willey.
39. Dewi, D. C., Mahmudah, R., Kumalawati, O. R., dan Amalullia, D. (2019). Analisis Kadar Logam Timbal (Pb) Pada Bedak Tabur Dengan Variasi Zat Pengoksidasi Dan Metode Destruksi Basah Menggunakan Spektroskopis Serapan Atom (AAS). *Alchemy Journal of Chemistry*, 7(1). <http://dx.doi.org/10.18860/al.v7i1.7016>
40. Saryono dan Anggraeni, D. M. (2013). *Metodologi Penelitian Kualitatif Dan Kuantitatif Dalam Bidang Kesehatan*. Yogyakarta: Nuha Medika.
41. Notoatmodjo, S. (2012) *Metodologi Penelitian Kesehatan*. Jakarta: Rineka Cipta.
42. Baehaki, F., Rudibyani, R. B., Aeni, S. R. N., Perdana, R., and Aqmarina, S. N. (2020). Utilization Of *Salacca Zalacca* Seeds As Chromium(VI) Adsorbents. *Periodico Tchê Química*, 17(34), 381–389.
43. Batool, M., Ahmad, K. S., Zahidqureshi, Mahboob, N., and Nimra. (2018). Determination Of Heavy Metal Toxicity In Blood And Health Effect By AAS (Detection Of Heavy Metals And Its Toxicity In Human Blood). *Lupine Publisher*, 1(2). <http://dx.doi.org/10.32474/ANOAJ.2018.01.000107>
44. Takwa, A., Bujawati, E., dan Mallapiang, F. (2017). Gambaran Kadar Timbal Dalam Urine Dan Kejadian *Gingival Lead Line* Pada Gusi Anak Jalanan Di Flyover Jl. Ap. Pettarani Makassar. *Higiene Jurnal Kesehatan Lingkungan*, 3(2), 114 – 123.
45. Mujahidin, M. (2019) *Jalur Wisata Bandung Selatan Ke Ciwidey Mulai Dipadati Kendaraan, Ada Beberapa Titik Kemacetan Metro Bandung*, Jawa Barat: Tribunnews. <https://jabar.tribunnews.com/2019/06/07/jalur-wisata-bandung-selatan-ke-ciwidey-mulai-dipadati-kendaraan-ada-beberapa-titik-kemacetan>), accessed on July 8 2019.
46. Suciani S. (2007). Kadar Timbal Dalam Darah Polisi Lalu Lintas dan Hubungannya dengan Kadar Hemoglobin (Studi pada Polisi Lalu Lintas yang Bertugas di Jalan Raya Kota Semarang). Semarang: Universitas Diponegoro.
47. Frank, C. (1995) *Toksikologi Dasar : Asas, Organ, Sasara Dan Penilaian Resiko*. Jakarta : UI-Press.
48. Hasan, W. (2012). Pencegahan Keracunan Timbal Kronis Pada Pekerja Dewasa Dengan Suplemen Kalsium. *Makara Kesehatan*, 16(1), 1 – 8.
49. Bogden J.D., et al. (1992). Dietary calcium modifies concentrations of lead and other metals and renal calbindin in rats. *J Nutr*, 122:1351-1360.
50. Mahaffey K.R., Gartside P.S., Glueck C.J. (1986). Blood lead levels and dietary calcium intake in 1- to 11-year old children: the Second National Health and Nutrition Examination Survey, 1976 to 1980. *Pediatrics*, 78:257-262.
51. Barltrop D. and Meek F. (1979). Effect of particle size on lead absorption from the gut. *Arch Environ Health*, 34:280-285.
52. Barltrop D. and Khoo H.E. (1975). The

influence of nutritional factors on lead absorption. *Postgrad Med J.*, 51:795-800.

Table 1. Classification of Lead Blood Exposure

Category	mg Pb/L bloods	Description
A (normal)	< 0,40	Normal exposure level
B (can be tolerated)	0,40 – 0,80	Increased absorption from exposure but can still be tolerated
C (excessive level)	0,80 – 1,20	Increased absorption from large exposures and begins to show signs of poisoning
D (danger level)	> 1,20	Absorption reaches danger level with signs of mild to severe poisoning

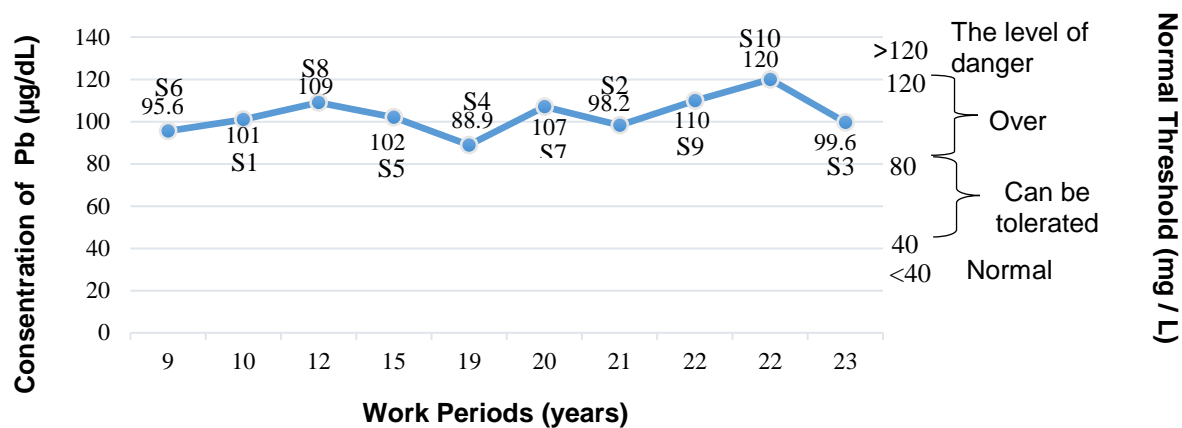
Table 2. Results of absorbance measurements on $Pb(NO_3)_2$ standard solution

Concentration (mg/L)	Absorbance
0	0
1	0,011
2	0,020
3	0,029
4	0,039
5	0,048

The data in Table 2 is plotted into a standard curve (Figure 1) so that it produces a straight-line equation.

Table 3. Results of examination of lead concentration in blood transport general transport in soreang terminal, bandung regency

Sample	Age (years)	Work Periods (years)	Average Length of Work per day (hours)	Concentration of Pb ($\mu\text{g/mL}$)
S1	39	10	8	101,0
S2	56	21	8	98,2
S3	54	23	8	99,6
S4	69	19	8	88,9
S5	46	15	8	102,0
S6	39	9	8	95,6
S7	46	20	8	107,0
S8	52	12	8	109,0
S9	37	22	8	110,0
S10	45	22	8	120,0
Average				103,2
Maximum				120,0
Minimum				88,9



Note:

S1: Sample from participants 1
 S2: Sample from participants 2
 S3: Sample from participants 3
 S4: Sample from participants 4
 S5: Sample from participants 5

S6: Sample from participants 6
 S7: Sample from participants 7
 S8: Sample from participants 8
 S9: Sample from participants 9
 S10: Sample from participants 10

Figure 2. Relationship between a work period and Pb level in the blood of public transportation driver.

MULTIMÍDIA INTERATIVA PARA MELHORAR A COMPREENSÃO DOS CONCEITOS DOS ESTUDANTES NO CURSO DE ENGENHARIA**INTERACTIVE MULTIMEDIA TO ENHANCE STUDENTS' UNDERSTANDING OF CONCEPTS IN ENGINEERING DRAWING COURSE****MULTIMEDIA INTERAKTIF UNTUK MENINGKATKAN PEMAHAMAN KONSEP MAHASISWA PADA MATAKULIAH GAMBAR TEKNIK**WIDAYANA, Gede^{1*}; RATNAWATI, Dianna²; ROHMAN, Mojibur³; SURYAMAN, Suryaman⁴¹ Mechanical Engineering Education, Universitas Pendidikan Ganesha, Bali, Indonesia.² Mechanical Engineering Education, Universitas Sarjanawiyata Tamansiswa, Yogyakarta, Indonesia.³ Mechanical Engineering, Universitas Islam Raden Rahmat, Malang, Indonesia.⁴ Primary Teacher Education, Universitas Islam Raden Rahmat, Malang, Indonesia.

* Corresponding author
e-mail: gede.widayana@undiksha.ac.id

Received 24 June 2020; received in revised form 10 August 2020; accepted 24 September 2020

RESUMO

O Desenho Técnico é uma das disciplinas obrigatórias ensinadas no Departamento de Engenharia Mecânica da Indonésia. Este curso visa dotar os alunos de conhecimentos e habilidades básicas em desenho. Esse estudo objetivou desenvolver mídia de aprendizagem na forma de multimídia interativa, determinar o nível de viabilidade da multimídia resultante e testar a eficácia da multimídia para melhorar a compreensão dos alunos sobre os conceitos básicos do desenho técnico. Por esse motivo, esta pesquisa utilizou um projeto de P&D com um modelo 4D para produzir e testar a eficácia de produtos multimídia. O teste de validade do produto foi realizado por 2 especialistas, um em material e outro em mídia. Quanto ao teste de efetividade, foi realizado o projeto de pesquisa pré-teste pós-teste de um grupo, envolvendo 28 alunos do Programa de Estudos em Educação em Engenharia Mecânica da Universidade de Educação Ganesha, em Bali, Indonésia. Os resultados mostraram que os especialistas em materiais e os especialistas em mídia concordaram que os resultados multimídia desse desenvolvimento eram apropriados para serem usados como materiais de ensino no processo da aula. Além disso, o teste de eficácia também mostrou que a multimídia desenvolvida foi eficaz para aumentar a compreensão dos alunos sobre os conceitos básicos do desenho técnico. O uso de multimídia interativa pode aumentar a motivação e a independência dos alunos na aprendizagem, aumentando assim a compreensão dos conceitos ensinados no curso de Desenho de Engenharia.

Palavras-chave: desenvolvimento, multimídia interativa, compreensão de conceitos, Desenhos de engenharia.

ABSTRACT

Engineering Drawing is one of the compulsory courses in the Department of Mechanical Engineering in Indonesia. This course aims to equip students with basic understanding and skills in drawing. In this case, this study aimed to develop learning media in the form of interactive multimedia determining the level of eligibility of the developed multimedia, and testing the effectiveness of the developed multimedia in enhancing students' understanding of the basic concepts of engineering drawings. For this reason, this study used an R&D design with the 4D model to produce and test the effectiveness of the developed multimedia. The product validity test was carried out by two experts, namely one material expert and one media expert. The effectiveness test, one-group pretest-posttest design was carried out by involving 28 students of the Mechanical Engineering Education study program at Universitas Pendidikan Ganesha, Bali, Indonesia. The results showed that both material and media experts agreed that the developed multimedia was suitable for teaching equipment in the lecture process. The effectiveness test also showed that multimedia developed effectively increased students' understanding of the basic concepts of engineering drawings. The use of interactive multimedia could improve students' motivation and independence in learning, thus increasing their understanding of the Engineering Drawing course concepts.

Keywords: *development, interactive multimedia, understanding of concept, engineering drawings.*

ABSTRAK

Gambar Teknik merupakan salah satu matakuliah wajib yang diajarkan dalam jurusan Teknik Mesin di Indonesia. Matakuliah ini bertujuan untuk membekali mahasiswa dengan pemahaman dan keterampilan dasar dalam menggambar. Tujuan penelitian ini adalah mengembangkan media pembelajaran dalam bentuk multimedia interaktif mengetahui tingkat kelayakan multimedia yang dihasilkan, dan menguji efektivitas multimedia dalam meningkatkan pemahaman konsep dasar mahasiswa tentang gambar teknik. Untuk itu, penelitian ini menggunakan desain R&D dengan model 4D untuk menghasilkan dan menguji efektivitas produk multimedia. Uji validitas produk dilakukan oleh 2 orang ahli masing-masing sebagai ahli materi dan ahli media. Sedangkan untuk uji efektivitas, desain penelitian One group pretes-posttest dilakukan dengan melibatkan 28 orang mahasiswa program studi Pendidikan Teknik Mesin di Universitas Pendidikan Ganesha Bali, Indonesia. Hasil penelitian menunjukkan bahwa ahli materi dan ahli media setuju bahwa multimedia hasil pengembangan ini layak digunakan sebagai bahan ajar dalam proses perkuliahan. Selain itu, uji efektivitas juga menunjukkan bahwa multimedia ini efektif dalam meningkatkan pemahaman konsep dasar mahasiswa tentang gambar teknik. Penggunaan multimedia yang interaktif dapat meningkatkan motivasi dan kemandirian belajar mahasiswa, dengan begitu pemahaman konsep mereka terhadap suatu materi juga akan meningkat.

Kata kunci: *pengembangan; multimedia interaktif; pemahaman konsep; gambar teknik.*

1. INTRODUCTION:

Engineering Drawing is a compulsory course in the mechanical engineering study program in Indonesia. In general, it discusses the procedures for drawings under the ISO standards, including basic rules in drawing, reading, and interpreting images (Narayana *et al.*, 2006). For engineering graduates, the ability to read engineering drawings is the most important requirement in any profession (Reddy, 2008). This is because such a kind of drawing serves as a communication language to express ideas in the form of images to be easily understood even though the real objects have not been existed or have never been made yet.

Engineering Drawing course that is commonly applied generally gives students less opportunity to understand and master the basic engineering drawing concepts. In this course, students' understanding of the concept of engineering drawing is one of the essential aspects they must master to have good skills in drawing (Narayana, 2006; Rohman *et al.*, 2019; Białkiewicz, 2019; Żychowska, 2019). Learning patterns with project-based approaches require them to have more psychomotor than cognitive skills (Prasetya, *et al.*, 2019). As a result, students will experience difficulties developing basic thinking patterns towards the higher ones in engineering images.

The constructivist approach is widely applied in the current learning process (Juanda, 2011). In constructivist theory, learning is the result of students' construction and interaction with

their learning environment. Direct experience can provide higher memory effectiveness, compared to what is provided by indirect experience (Khaidir, 2016). Thus, the more concrete the lesson material the students learn, the more the experience they get; the more abstract what they study, the less the background they get.

Success in the learning process significantly determines the same in achieving educational goals (Setiawan *et al.*, 2018). Engaging learning can give an impression and direct experience to students and motivate them to learn specific material. Miarso (2004), Sulistianingsih, and Carina (2019) also stated that a way to support the success of the learning process is developing multimedia utilizable to support learning activities in the classroom.

Practical and innovative learning media can be one of the main factors in successfully achieving learning goals (Nopriyanti and Sudira, 2015; Setiawan *et al.*, 2018; Diner *et al.*, 2020; Yulianti *et al.*, 2020; Widodo, *et al.*, 2020). Entering the digital era and the rapid development of information and communication technology (ICT) as it is today, the use of instructional media in the form of multimedia is becoming more innovative (Mayer, 2001; Prasetya, *et al.*, 2018; Sukenda, *et al.*, 2019). Simply put, multimedia can be interpreted as a combination of several medium such as texts, images, videos, and audio presented in an integrated way (Zhen, 2016). Rohman *et al.* (2019) and Samat and Aziz (2020) stated that multimedia learning is a combination of texts, images, graphics, sound, and video in an integrated way to improve the quality of learning in

the classroom.

Various studies showed that interactive multimedia used effectively could improve the quality of learning and student learning outcomes (Juanda, 2011; Husein *et al.*, 2015; Ramli *et al.*, 2019; Gunawan *et al.*, 2020; Samat and Aziz, 2020). It also allows students to improve their ability to think, problem-solving, create, and construct the knowledge they have (Zheng and Zou, 2006; Rohman *et al.*, 2019). In general, the benefits that can be obtained through the use of interactive multimedia are the learning process can run more interesting, more interactive, and more efficient in term of time spending (Husein *et al.*, 2015; Zhen, 2016; Saprudin and Hamid, 2018; Rohman 2020; Imansari *et al.*, 2020).

Research conducted by Sutarno and Desi (2012); Zainuddin *et al.*, (2018); Adhitama *et al.*, (2018); Ayob and Adnan (2019) found that the increase in mastery of the concept of students who took part in interactive multimedia-aided learning was significantly higher compared to students who took part in learning with conventional media. Furthermore, research conducted by Zheng and Zou (2006) and Gunawan (2011) also shows that the utilization of interactive multimedia has also been shown to increase the ability of students to draw conclusions and solve problems.

Observations made by researchers on the implementation of engineering drawing learning gained several results, including (1) student learning outcomes in engineering drawing subjects had not yet optimal; (2) most of the students still had difficulty in understanding basic concepts and material of engineering drawing; (3) the learning methods used were less appropriate and tended to use the assignment- or project-centered learning approach; (4) the way on which the material delivered still used the teacher-centered learning approach; and (5) no interactive multimedia was available in engineering drawing learning process.

The description above indicates that the limitations in the delivery of the material, less appropriate learning methods and less exciting learning media caused the students to lack understanding of the concepts and the material being studied. Therefore, this research aimed to (1) develop learning multimedia for engineering drawing course; (2) determine the feasibility of the multimedia products produced; and (3) test the effectiveness of the product in improving the students' ability to understand concepts in the Engineering Drawing course.

2. MATERIALS AND METHODS:

This research took place in the Mechanical Engineering Education study program, Faculty of Engineering and Vocations, Ganesha University of Education, Bali, Indonesia, as an R&D study with the 4D model (Thiagarajan *et al.*, 1974). It was chosen the 4D development model for being widely used in learning media for educational purposes. This research aimed to develop interactive multimedia to be more feasible and sufficient to support Engineering Drawing lectures. There are 4 main stages in the 4D development model, namely Define, Design, Develop, and Disseminate. Figure 1 shows the development flow using the 4D model.

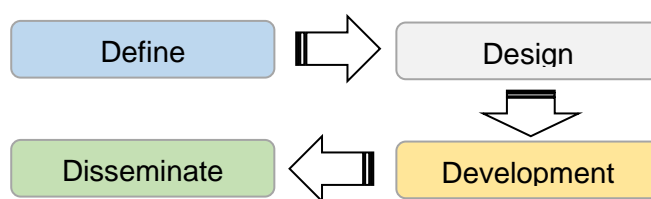


Figure 1. Flowchart of the 4D Model Development

The first stage, Define, aims to identify problems and analyze curriculum, student characteristics, concepts/ learning materials, and media. The second stage, Design, is for making learning designs and multimedia designs to be developed. The third stage, namely development, aims to arrange the initial form (prototype) of products. Researchers in this third stage also need to conduct validation tests, trials, and product revisions. The fourth stage, the last, namely Disseminate, means the distribution and implementation of multimedia products in groups of students to support learning in the Engineering Drawing course.

The instruments used to collect data were questionnaires and tests. The questionnaires were used to determine the feasibility level of the resulting multimedia. In this study, the questionnaires consisted of 2 types: a questionnaire filled out by a material expert and the other by a media expert. The test instrument is used to test the effectiveness of using multimedia in improving student understanding of concepts. This test consisted of 20 multiple choice questions and 2 essay questions that must be done by students (Appendix 1).

The data obtained were then analyzed in the form of descriptive and inferential analyses. Descriptive analysis is used to describe the results

of the validation of the feasibility of multimedia products by a material expert and a media expert so that it can be seen as the eligibility level of the resulting multimedia. A material expert is someone who is an expert in the field of engineering drawing. The material expert in this study acted as a validator regarding the learning media content being developed. A media expert is someone who is an expert and has experience in the field of learning media. The media expert in this study acted as a validator of the media being developed. The two experts who worked as multimedia validators in this study were senior lecturers at Universitas Pendidikan Ganesha, Bali, Indonesia. Meanwhile, the inferential analysis was used to determine the effectiveness of using multimedia in improving students' understanding of concepts in the engineering drawing course before and after using multimedia (pretest-posttest).

Table 1 shows the eligibility criteria of multimedia, as determined by the material expert and the media expert:

Table 1. Product Eligibility Criteria

Average	Category
3.26 – 4.00	Eligible
2.51 – 3.25	Somewhat eligible
1.76 – 2.50	Less eligible
1.00 – 1.75	Not eligible

Adapted from Arikunto (2002)

The students involved in this research were those from the Department of Mechanical Engineering Education, Universitas Pendidikan Ganesha, Bali, Indonesia. A total of 28 students, all male with ages ranging from 19 to 21 years and currently taking Engineering Drawing courses, were taken as the study sample. The involvement of these students was through their consent to be involved in research and data collection as scientific purposes. Besides, researchers have also obtained permission from teaching lecturers and the Department of Mechanical Engineering Education at Universitas Pendidikan Ganesha, Bali, Indonesia. The involvement of the 28 students in this study was conducted to test the effectiveness of the multimedia products being developed. Therefore, after knowing the feasibility level of the product, a pretest-posttest one-group research design was carried out.

A one-group pretest-posttest design was conducted to determine the effectiveness of multimedia in improving students' understanding of the Engineering Drawing course concept.

O ₁	X	O ₂
----------------	---	----------------

(Source: Sugiyono, 2011)

Notes:

O₁: Pretest (before using interactive multimedia)

X: Interactive multimedia utilization

O₂: Posttest (after using interactive multimedia).

3. RESULTS AND DISCUSSION:

The process of developing multimedia products is carried out in 4 stages according to the 4 D development model, namely: Define, Design, Development, and Disseminate as follows:

3.1 Define

The defined step aims to analyze the needs in the engineering drawing course. The results of the needs analysis conducted in this study indicate that there were problems in learning Engineering Drawing, including 1) this course was quite challenging to understand by most students. This difficulty could be seen from (1) the low level of their understanding; (2) the use of learning media was still rare and also less uniform between one student and another, and; (3) students' low interest in reading or student motivation. Some of these problems, of course, caused the learning process could not be optimized. Thus, the development of learning media in interactive multimedia became one solution to the problem.

3.2 Design

The Design stage is carried out to design the development of textbooks that will be developed. Therefore, this stage is carried out by formulating the main ideas and designs in multimedia development for the engineering drawing course. The multimedia design that will be developed in this study can be seen in Figure 2.

3.3 Development

The product generated in this research was multimedia, in the form of interactive digital books. It was created in .exe format using the help of Flipbook Maker software. It was then packaged into a digital book that combined various kinds of contents such as texts, images, graphics, animations, audios, and videos. This digital book could be opened or run on a computer or laptop. It was quite easy to use by students without having special training. Its presence could increase students' interest in reading or motivate them to learn the Engineering Drawing course.

As an illustration, Figure 3 shows the

resulting multimedia display. This multimedia was more interesting because of the flip effect on the e-book when moving between pages. On the other hand, interactive effects could be seen with audios and videos in the e-book to support the delivery of material to students. The use of multimedia was not too difficult because of the navigation buttons provided, such as bookmarks, zoom-in, zoom-out, search, and others that could facilitate the readers.

This developed multimedia also goes through a validation test conducted by the material expert and the media expert in its development. This was done to determine the eligibility of multimedia before used as a learning medium by students. Table 2 and Table 3 below show the results of validation tests by material experts as well as media experts.

Table 2. Validation by material expert

Scoring aspects	Score	Category
Content completeness	3.65	Eligible
Conformity between material and learning objectives	3.47	Eligible
Systematic delivery of material	3.56	Eligible
Average	3,56	Eligible

Table 3. Validation by media expert

Scoring aspect	Score	Category
Multimedia display	3,78	Eligible
Use of language	3,60	Eligible
Interactive effect	3,66	Eligible
Average	3,68	Eligible

Validation conducted by the material expert showed that the developed multimedia was categorized as eligible with an average score of 3.56 (see Table 2). However, there were also some notes to improve the product. The material expert, to improve the product, suggested the addition of material to various lines, question exercises at the end of the chapter, and discussion on the chapter of Intersection.

Based on the assessment, the media expert said that multimedia was in the category of eligible with an average score of 3.68 (see Table 3). However, the video content was found to be

incomplete, and some texts were overly large, thus need the addition of more content and the adjustment of the text size.

The development of interactive multimedia is an effort to optimize the role and function of information and computer technology (ICT) in the learning process (Elfeky and Masadeh, 2016; Rohman *et al.*, 2019; Syawaludin, *et al.*, 2019). In ICT-based learning, the learning process carried out by lecturers and students can be more accessible, more practical, and also efficient. Therefore, students can maximize their learning outcomes.

The step next to the validation test and the product revision tested the effectiveness of the multimedia to improve students' conceptualization of engineering drawings. For this reason, a one-group pretest-posttest design with a *t*-test analysis was carried out. Table 4 and Figure 4 shows the results of the pretest and posttest conducted on 28 students.

The pretest and posttest scores above provide some descriptions, as shown in Table 5:

Table 5. Data description

Score	Range	Min.	Max.	Mean	SD
Pretest	30	40	70	54.54	6.9
Posttest	12	76	88	82.75	3.1

Notes: Range: Difference between the maximum and the minimum scores; Min: Minimum score; Max: Maximum score; Mean: Mean score; SD: Standard Deviation

Furthermore, before *t*-test analysis, a normality test was needed to see whether the pretest and posttest scores were normally distributed. The data normality test in this study was carried out by Shapiro-Wilk analysis. Table 6 shows the results of the test with the help of SPSS 22.0.

Based on Table 6, the pretest and posttest data obtained Shapiro-Wilk values of 0.934 and 0.938, respectively, with sig. values of 0.077 and 0.099, respectively. Because the two sig values were greater than 0.05, it could be concluded that the data of the two data were normally distributed.

After the data was normally distributed, hypothesis testing was performed to see whether there was a significant difference between the pretest and posttest scores (before and after the use of interactive multimedia). In this study, hypothesis testing was done using the paired sample *t*-test, the results of which can be seen in

Table 7.

Table 7 shows that the value of sig. was 0.00, lower than 0.05. Thus, it could be observed that there was a significant difference between the pretest and posttest scores, indicating that the use of interactive multimedia in the learning process of Engineering Drawing could improve students' understanding of the concepts of the lecture materials.

This developed multimedia was in an interactive digital form used in the Engineering drawing course. It was made using Flipbook Maker software and packaged in soft files that could be run on computers or laptops. This interactive multimedia development followed the 4D model development path consisting of four main steps: Define, Design, Development, and Disseminate.

The resulting multimedia has been tested through a validation test and a trial to determine its eligibility and effectiveness. Based on the results, both material and media experts declared that it was categorized as eligible and offered some notes or revisions for its improvement. Besides, to determine its effectiveness in improving students' understanding of concepts, one-group pretest-posttest design was conducted on 28 students. The results showed a sig value of 0.000, less than 0.05, meaning that interactive multimedia was effective or had a significant effect on the student test scores (*pretest-posttest*).

There is an increase in student learning outcomes after using interactive multimedia, indicating that the use of interactive multimedia has a significant effect on student understanding of concepts in engineering drawing courses. The use of interactive multimedia allows students to study independently and adequately, the material they need both at home and on campus (Mayer, 2001; McLain, 2018; Adhitama, *et al.*, 2018; Imansari, *et al.*, 2020).

The use of interactive multimedia helps students to receive or understand the material presented (Munir, 2013; Sudarman *et al.*, 2019; Rohman *et al.*, 2019; Samat and Aziz, 2020; Widodo, *et al.*, 2020). Interactive learning media supported by a variety of contents such as images, graphics, audio, and videos will make abstract materials clearer (Hwang, *et al.*, 2018; Ramli *et al.*, 2019; Diner *et al.*, 2020, Imansari *et al.*, 2020), thus increasing students' interest in reading and learning independently. The learning process with the help of interactive multimedia will enhance students' understanding of the materials being studied.

3.4 Disseminate

Based on the feasibility and effectiveness test, it is known that the multimedia product developed has a decent category and is also useful in improving students' conceptual understanding in the engineering drawing course. Thus, this interactive multimedia can be disseminated for broader use among students, especially in the Department of Mechanical Engineering Education, Ganesha University of Education, Bali, Indonesia.

4. CONCLUSIONS:

1. The results of validation tests by the material expert and the media expert showed that the resulting multimedia products were categorized as feasible. From the material aspect, the product feasibility level got a value of 3.56, and from the media, aspect got 3.68.
2. The effectiveness test, involving 28 students, showed that interactive multimedia effectively improved students' understanding of concepts in engineering drawing courses. This can be seen from the *t*-test analysis (paired sample *t*-test) with the Sig. 0.000 which indicated that there was a significant increase in student pretest and posttest scores before and after the use of interactive multimedia.
3. The findings in this study indicated that information and communication technology could help the learning process become easier. The use of multimedia in learning provides students with opportunities to play a more active role and provide more meaningful learning experiences. Therefore, as educators, lecturers are required to be able to provide innovative learning media for students.

5. ACKNOWLEDGMENTS:

This publication was dedicated to the Education Fund Management Institution (LPDP) from the Ministry of Finance of Indonesia for the policy, information, and funding supports to complete this article.

6. REFERENCES:

1. Adhitama, Sujadi and Pramudya. (2018). Discover the pythagorean theorem using interactive multimedia learning. *Journal of*

Physics: Conf. Series 1008, 1-8.

2. Arikunto, S. (2002). *Prosedur Penelitian: Suatu Pendekatan Praktik*. Jakarta: Rineka Cipta.
3. Ayob, A. and Adnan, N.S. (2019). The Effects of Virtual Text and Graphic Integration Based on Interactive Multimedia Towards Students' Achievement in Summary Writing. *International Journal of Innovation, Creativity and Change*, 8(4), 328-338.
4. Białkiewicz, A. (2019). Propaedeutics of teaching drawing to architects. *Global Journal of Engineering Education*, 21(2), 115-120.
5. Diner, L., Utami, S. E., Kurniati, E., and Widayanti, M. J. A. (2020). Efforts to Increase Listening Ability Through Interactive Multimedia on Dokkai Learning in Japanese Language Education Program of UNNES. *International Journal of Innovation, Creativity and Change*, 10(12), 69-84.
6. Elfeky, A.I.M. and Masadeh, T.S.Y. (2016). The effect of mobile learning on student's achievement and conversational skills. *International Journal of Higher Education*, 5, 20-31.
7. Gunawan, Mashami, R. A., and Herayanti, L. (2020). Gender Description on Problem-Solving Skills in Chemistry Learning Using Interactive Multimedia. *Journal for the Education of Gifted Young*, 8(1), 571-589.
8. Gunawan. (2012). Penggunaan Simulasi Interaktif untuk Meningkatkan Penguasaan Konsep Mahasiswa pada Konsep Mekanika. *Jurnal Kependidikan*, 2(1), 25-30.
9. Husein, S., Herayanti, L., Gunawan. (2015). Pengaruh Penggunaan Multimedia Interaktif Terhadap Penguasaan Konsep dan Keterampilan Berpikir Kritis Siswa pada Materi Suhu dan Kalor. *Jurnal Pendidikan Fisika dan Teknologi*, 1(3), 221-225.
10. Hwang, G.-J., Tu, N.-T., and Wang, X.-M. (2018). Creating Interactive E-Books through Learning by Design: The Impacts of Guided Peer-Feedback on Students' Learning Achievements and Project Outcomes in Science Courses. *Educational Technology and Society*, 21 (1), 25–36.
11. Imansari, N., Dalu, Z. C. A., Sulistianingsih and Ratnawati, D. (2020). Multimedia-Based Teaching Materials at College Level: Expert and Student Assessment. *Talent Development and Excellence*, 12(2s), 3660-3669.
12. Juanda, E. A. (2011). Media Pembelajaran Berbasis Multimedia Interaktif Untuk Meningkatkan Pemahaman Dasar-Dasar Mikrokontroler. *Jurnal Ilmu Pendidikan*, 17, (6), 439-444.
13. Khaidir, C. (2016). Development of Constructivism-Based Numerical Method Textbook at IAIN Batusangkar. *Ta'dib*, 19(1), 67-82.
14. Mayer, R. E. (2001). *Multimedia learning*. New York: Cambridge University Press.
15. McLain, T. R. (2018). Integration of the Video Response App Flip Grid in the Business Writing Classroom. *International Journal of Educational Technology and Learning*, 4(2), 68-75.
16. Miarso, Y. (2004). *Menyemai Benih Teknologi Pendidikan*. Kencana.
17. Munir. (2013). *Multimedia: Konsep dan Aplikasi dalam Pendidikan*. Bandung: Alfabeta.
18. Narayana, K.L., Kannaiah, P., Reddy, K.V. (2006). *Machine Drawing: Third Edition*. New Delhi: New Age International (P) Ltd.
19. Nopriyanti and Sudira, P. (2015). Pengembangan Multimedia Pembelajaran Interaktif Kompetensi Dasar Pemasangan Sistem Penerangan dan Wiring Kelistrikan di SMK. *Jurnal Pendidikan Vokasi*, 5(2), 222-235.
20. Prasetya, D.Y., Suparmin and Johan, A.B. (2019). Application of project based learning models to improve student learning results techniques of manufacturing images of vocational school students. *Jurnal Taman Vokasi*, 7(1), 82-84.
21. Prasetya, D.D., Wibawa, A.P. and Hirashima, T. (2018). An Interactive Digital Book for Engineering Education Students. *World Transactions on Engineering and Technology Education*, 16 (1), 54-59.
22. Ramli, H., Said, T. S., Hazman, M. N. B., Malek, S. N. A. and Hussin, R. (2019). The Development and Evaluation of an Interactive Multimedia Module for the Topic of Art Elements of the Visual Art Education Subject. *International Journal of Innovation, Creativity and Change*, 10(6), 246-258.
23. Reddy, K. V. (2008). *Textbook of Engineering Drawing: Second Edition*. BS Publications.
24. Rohman, M. (2020). Analisis Motivasi Belajar Mahasiswa pada Pembelajaran Gambar

- Teknik Berbasis Multimedia. *Jupiter (Jurnal Pendidikan Teknik Elektro)*, 5 (1), 8-13.
25. Rohman, M., Sudjimat, D.A., Sugandi, M. and Nurhadi, D. (2019). Developing an Interactive Digital Book to Improve the Technical Drawing Abilities of Mechanical Engineering Students. *Global Journal of Engineering Education*, 21(3), 239-244.
 26. Samat, M.S. and Aziz, A.b.A. (2020). Indigenous Student's Perception of Multimedia Learning as an Approach for Enhancing Reading Comprehension Skills. *Open Journal of Science and Technology*, 3(1), 8-16.
 27. Saprudin and Hamid, F. (2018). Efektivitas Penggunaan Multimedia Interaktif Materi Kalor Berorientasi Peta Kompetensi Siswa Sekolah Menengah Atas. *Titian Ilmu: Jurnal Ilmiah Multi Sciences*, 10(1), 29-38.
 28. Setiawan, D. A., Wahjoedi and Towaf, S. M. (2018). Multimedia Interaktif Buku Digital 3D pada Materi IPS Kelas IV Sekolah Dasar. *Jurnal Pendidikan: Teori, Penelitian dan Pengembangan*, 3(9), 1133-1141.
 29. Sudarman, Riyadi, R. and Astuti, R. F. (2019). Development of Interactive Learning Multimedia to Increase Understanding of Basic Skills Teaching Procedures. *Advances in Social Science, Education and Humanities Research*, vol. 432, 132-136.
 30. Sugiyono. (2011). *Metode Penelitian Kualitatif Kuantitatif dan R&D*. Bandung: Alfabeta.
 31. Sukenda, Anjani, M. and Yustim, B. (2019). Learning Media for Biology Subject Based on Multimedia in Junior High School Level. *Universal Journal of Educational Research* 7(4A), 43-51.
 32. Sulistianingsih, A.S. and Carina, A. (2019). Developing Interactive E-book as Material Technology Coursebook by Flipbook Maker Software. *Journal of Education and Practice*, 10(24), 11-17.
 33. Sutarno and Desi. (2011). The Use of Interactive Multimedia in Magnetic Field Learning to Improve Students' Generic Science Thinking Skills. *Journal Exacta*, 9(1), 60- 66.
 34. Syawaludin, A., Gunarhadi and Rintayanti, P. (2019). Enhancing Elementary School Students' Abstract Reasoning In Science Learning Through Augmented Reality-Based Interactive Multimedia. *Jurnal Pendidikan IPA Indonesia*, 8(2), 289-298.
 35. Thiagarajan, S., Semmel, D.S and Semmel, M.I. (1974). *Instructional Development for Training Teachers of Exceptional Children: a Sourcebook*. Washington D.C.: National Center for Improvement of Educational System.
 36. Widodo, W., Sudibyo, E., Suryanti, Sari, D.A.P., Inzanah and Setiawan, B. (2020). The Effectiveness of Gadget-Based Interactive Multimedia in Improving Generation Z's Scientific Literacy. *Jurnal Pendidikan IPA Indonesia*, 9(2), 248-256.
 37. Yulianti, D., Wiyanto, Rusilowati, A. and Nugroho, S. E. (2020). Development of Physics Learning Teaching Materials Based on Science Technology Engineering and Mathematics to Develop 21st Century Learning Skills, *Periódico Tchê Química*, vol. 34, 711-717.
 38. Zainuddin, Hasanah, A.R., Salam, M. A., Misbah and Mahtari, S. (2019). Developing the interactive multimedia in physics learning. *Journal of Physics: Conf. Series* 1171, 1-5.
 39. Zhen, Z. (2016). The Use of Multimedia in English Teaching. *US-China Foreign Language*, 14(3), 182-189.
 40. Zheng, R. and Zhou, B. (2006). Recency Effect on Problem Solving in Interactive
 41. Multimedia Learning. *Educational Technology and Society*, 9 (2), 107-118.
 42. Żychowska, M.J. (2019). Teaching Drawing to a New Generation of Engineers Architects. *World Transactions on Engineering and Technology Education*, 17 (1), 60-65.

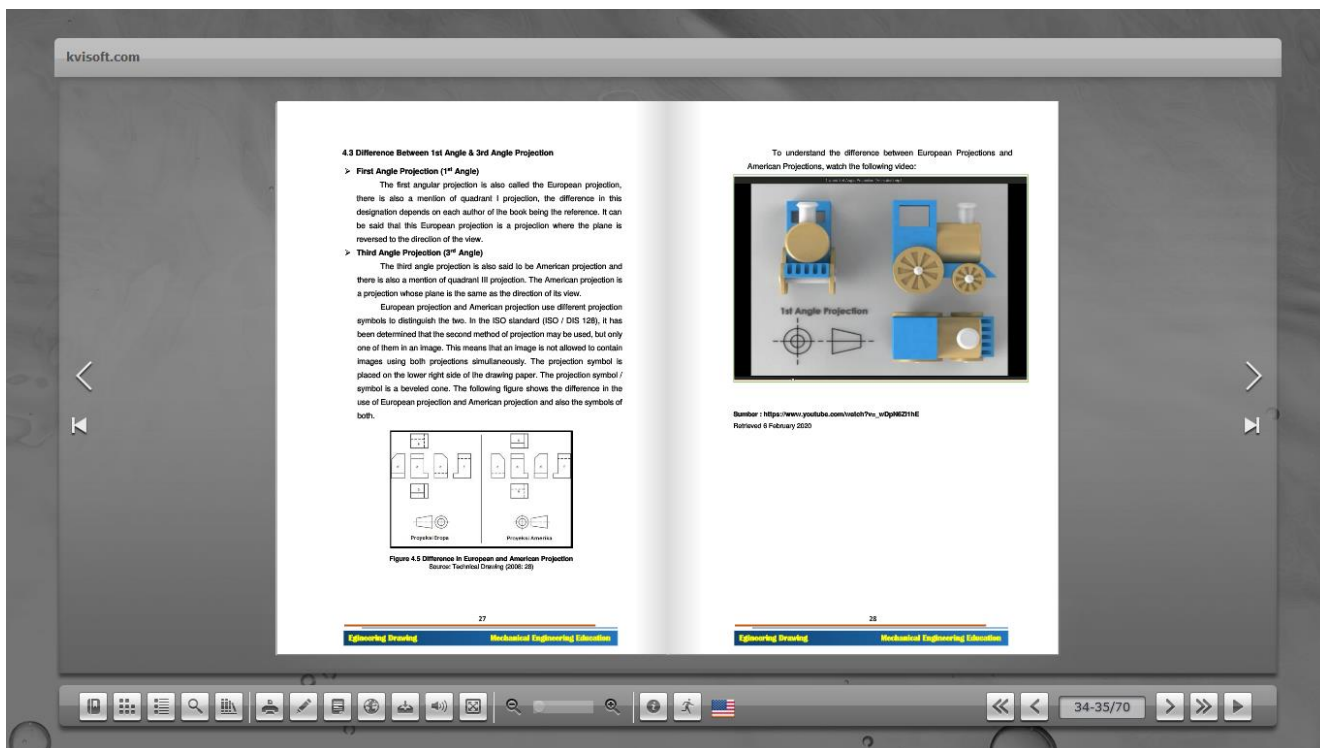


Figure 3. The developed multimedia displays.

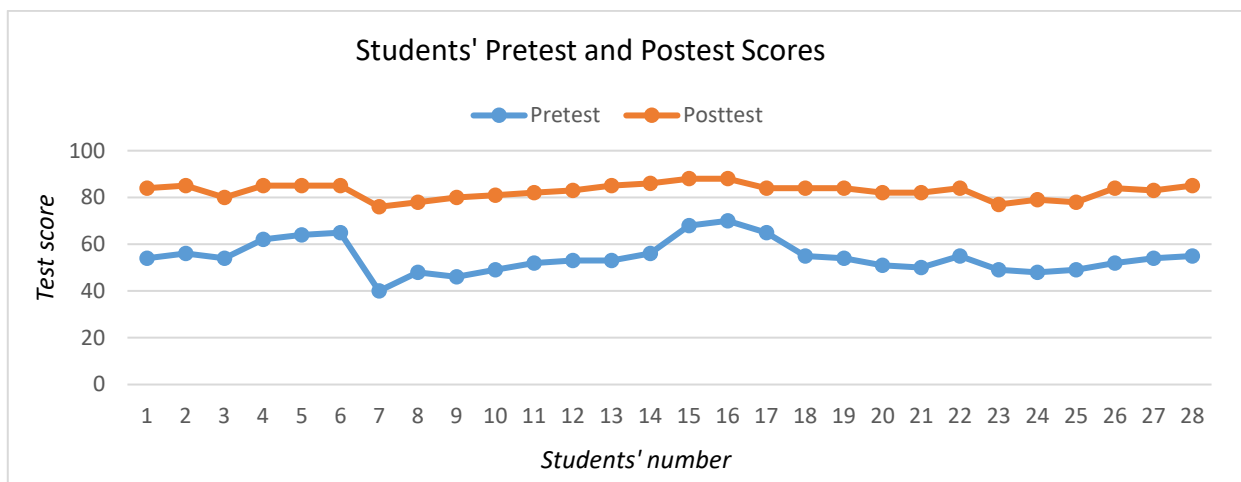


Figure 4. Chart of students' pretest and posttest scores

Table 4. Students' pretest and posttest results

No	Pretest	Posttest	No	Pretest	Posttest
1	54	84	15	68	88
2	56	85	16	70	88
3	54	80	17	65	84
4	62	85	18	55	84
5	64	85	19	54	84
6	65	85	20	51	82
7	40	76	21	50	82
8	48	78	22	55	84
9	46	80	23	49	77
10	49	81	24	48	79
11	52	82	25	49	78
12	53	83	26	52	84
13	53	85	27	54	83
14	56	86	28	55	85

Table 6. Results of the normality test of pretest and posttest data

Test of Normality							
	Score	Kolmogorov-Smirnov ^a			Shapiro-Wilk		
		Statistic	df	Sig.	Statistic	df	Sig.
Learning_outcome	Pretest	.202	28	.005	.934	28	.077
	Posttest	.191	28	.010	.938	28	.099

Notes: df: the degree of freedom; Sig.: Significance; a. Lilliefors Significance Correction

Table 7. Results of the paired sample t-test

Paired Samples Test									
		Paired Differences					t	df	Sig. (2-tailed)
		Mean	Std. Deviation	Std. Error Mean	95% Confidence Interval of the Difference				
					Lower	Upper			
Pair 1	Pretest - Posttest	-28.214	4.717	.891	-30.043	-26.385	-31.652	27	.000

Notes: Std. Deviation: Standard Deviation; df: the degree of freedom; Sig.: Significance

Validating questionnaire

No.	Assessment Aspects	Scoring scale			
		4	3	2	1
A. Content completeness					
1.	The depth level of discussion of material in multimedia has met the demands of the curriculum				
2.	The completeness of the material is following the level of student development				
3.	The content of the material has presented the competencies that students must master				
B. Conformity between material and learning objectives					
4.	The packaging of material in multimedia has been following the scientific approach in the field of mechanical engineering				
5.	The material in the multimedia has been presented coherently and correctly				
6.	The contents of the material in multimedia can help students achieve learning goals				
C. Systematic delivery of material					
7.	The development of material in multimedia has referred to the mechanical engineering study program curriculum				
8.	Presentation of material has been carried out systematically to achieve learning objectives				
9.	Presentation of the material has been done in a way that is easy for students to understand				
	TOTAL SCORE				

[illegible]

()

VALIDATION SHEET FOR MEDIA EXPERT

No.	Assessment Aspects	Scoring scale			
		4	3	2	1
A. Multimedia display					
1.	The use of fonts and colors in multimedia has attracted the attention of students				
2.	The media design is following the material in the engineering field				
3.	Images in multimedia can be seen clearly				
B. Use of language					
4.	The use of language in multimedia is clear and easily understood by students				
5.	The language used is following the student's level of thinking				
6.	The language used has stimulated student curiosity and motivation to learn the content				
C. Interactive effect					
7.	Multimedia is easy to operate by students				
8.	The interactive effect of the flip on multimedia can attract students' attention and increase their learning motivation				
9.	Additional audio and video in multimedia is presented in good quality				
	TOTAL SCORE				

Suggestions for Improvement and Conclusions

.....

.....

.....

.....

.....

.....

.....

.....

.....

.....

.....

Bali, 2019
Media expert

(_____)

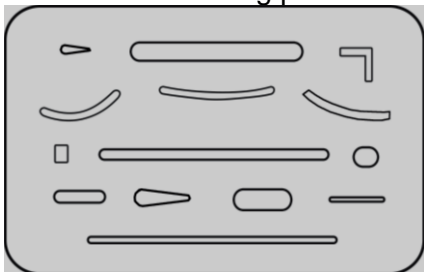
Student Test Instruments

Choose the correct answer!

1. Conveying the intentions of the designer appropriately to other parties in terms of process planning, manufacturing, inspection, and product / component assembly, is a function of engineering drawings as
- A. storage
 - B. delivery of idea
 - C. delivery of information
 - D. development

2. A uniformity that has been mutually agreed with the aim of avoiding misunderstanding in technical communication is called
- A. image size
 - B. standardization of engineering drawings
 - C. Image etiquette
 - D. engineering drawing projection

3. Look at the following picture!



The function of the drawing equipment is

- A. to make a curved line or semicircle
 - B. to make a straight line on the drawing paper
 - C. to create work symbols on working drawings
 - D. to make the image to be deleted precisely and not to remove another image
4. The A4 drawing paper size according to the ISO system is
- A. 297 x 210 mm
 - B. 277 x 210 mm
 - C. 397 x 210 mm
 - D. 420 x 297 mm
5. The A3 drawing paper size according to the ISO system is
- A. 287 x 210 mm
 - B. 277 x 210 mm
 - C. 594 x 420 mm
 - D. 420 x 297 mm

6. The left side of the border for all sizes of drawing papers according to the ISO system is
- A. 10 mm
 - B. 15 mm
 - C. 20 mm
 - D. 30 mm

7. Look at the following picture!



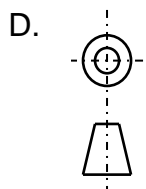
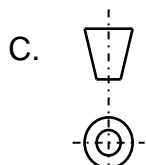
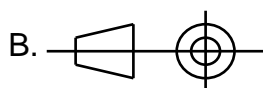
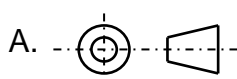
The function of the drawing equipment above is

- A. to make straight lines on the drawing paper
 - B. to create curved lines that couldn't be drawn with a compass
 - C. to create work symbols on working drawings
 - D. to make the image to be deleted precisely and not to remove another image
8. The number before the letter on a 2B pencil indicates the level of
- A. hardness
 - B. accuracy
 - C. softness
 - D. thickness
9. The number before the letter on a 2H pencil indicates the level of
- A. accuracy
 - B. coloring
 - C. hardness
 - D. thickness
10. To describe the workpiece axis, the line type used is.....
- A. thick line
 - B. real/continuous line
 - C. thin etched lines
 - D. double etched line
11. To describe the measuring line of an object, the type of line used is.....
- A. thick line
 - B. real/continuous line
 - C. continuous thin line
 - D. double etched line

12. Image headers or etiquettes are usually placed on
- bottom right side
 - bottom left side
 - upper left side
 - center right side

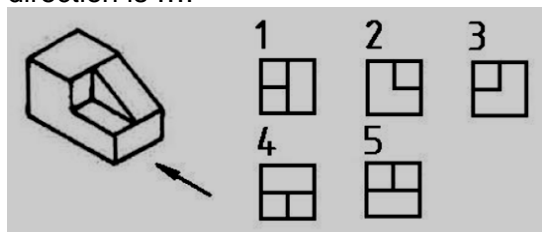
13. The following are included in the etiquette, except....
- the name of the drawer
 - line thickness
 - image title
 - the name of institution

14. The European projection symbol is indicated by the following figure



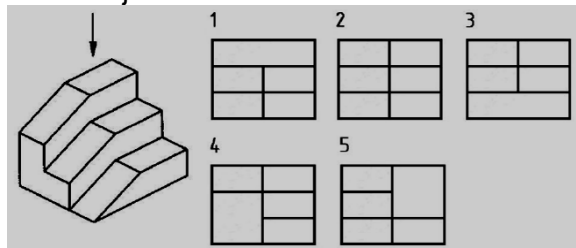
15. If A4 paper size is 210 x 297 mm, then A2 paper size is
- 297 x 420 mm
 - 420 x 594 mm
 - 420 x 841 mm
 - 595 x 841 mm

16. Look at the following picture! The correct front view of the object from the arrow direction is



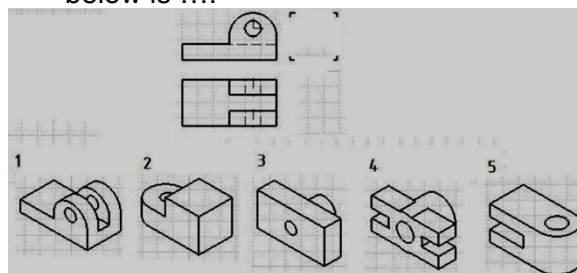
- 1
- 2
- 4
- 5

17. Look at the following picture. The top view of the object below is



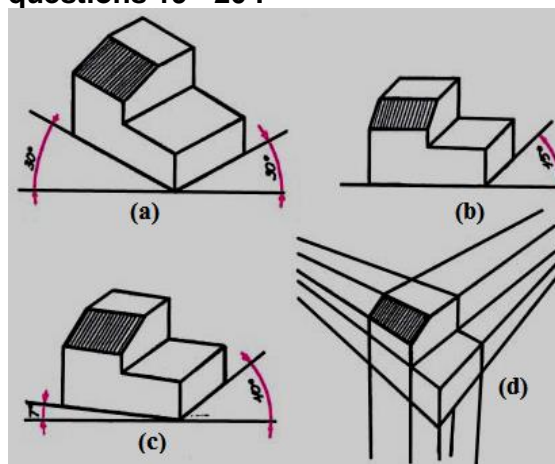
- 1
- 2
- 3
- 4

18. The correct 3D image from the 2D image below is



- 1
- 2
- 3
- 4

Look at the picture below to answer the questions 19 - 20 !



19. Figure (a) is a type of projection, namely....

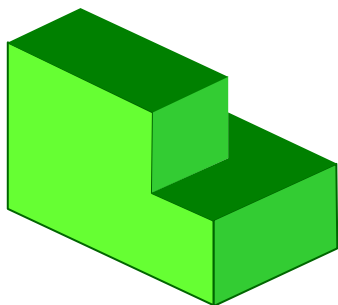
- perspective
- isometric
- dimetric
- oblique

20. Figure (b) is a type of projection, namely....

- perspective
- isometric
- oblique
- orthogonal

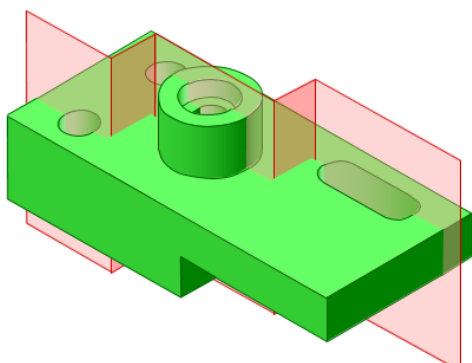
Student worksheets:

1. Look at the following 3-dimensional object!



Make a projection image of the object that shows top, front, and side views!

2. Look at the following object!



Make a projected image of the cut object above, showing the top-front views!

AVALIAÇÃO CITOTÓXICA BASEADA EM MTT DE SEIVA DO TRONCO DE BANANA AMBONESE (*Musa paradisiaca* var. *sapientum* (L.) Kuntze) EM FIBROBLASTOS

MTT-BASED CYTOTOXIC EVALUATION OF AMBONESE BANANA STEM SAP (*Musa paradisiaca* var. *sapientum* (L.) Kuntze) ON FIBROBLAST CELLS

UJI SITOTOKSISITAS GETAH BATANG PISANG AMBON PADA KULTUR SEL FIBROBLAS BERBASIS MTT

BUDI, Hendrik Setia^{1*}; JULIASTUTI, Wisnu Setyari¹; ARIANI, Winda²

¹ Universitas Airlangga, Faculty of Dental Medicine, Department of Oral Biology. Indonesia.

² Universitas Airlangga, Faculty of Dental Medicine, Undergraduate Program. Indonesia.

* Corresponding author

e-mail: hendrik-s-b@fkg.unair.ac.id

Received 26 July 2020; received in revised form 26 August 2020; accepted 12 October 2020

RESUMO

Os remédios fitoterápicos tradicionais são substâncias derivadas de plantas de ocorrência natural, sem processamento químico ou limitado, e têm sido usados nas tradições locais ou nacionais de cura para tratar doenças. Nos debates globais sobre saúde, os medicamentos fitoterápicos tradicionais estão recebendo considerável atenção. Muitos esperam que novas pesquisas em fitoterapia tenham um papel vital na saúde global. Países como China, Índia, Nigéria, EUA e também a Organização Mundial da Saúde (OMS) fizeram grandes investimentos em medicamentos fitoterápicos antigos. Atualmente, o uso de plantas da Indonésia melhorou dramaticamente o campo da medicina e odontologia. Os cuidados dentários e bucais muitas vezes estão relacionados a feridas e o caule de banana ambonense tem se mostrado um tratamento eficaz para essas lesões. Este estudo teve como objetivo avaliar a eficácia e segurança da seiva do caule da banana ambonense por meio de testes de citotoxicidade em cultura de fibroblastos de Baby Hamster Kidney-21 (BHK-21). Este estudo foi realizado em três culturas de fibroblastos BHK-21, a saber, o meio e o controle celular, e a seiva do caule da banana Ambonense com uma concentração de 10%, 20%, 30%, 40%, 50%, 60%, 70 %, 80%, 90% e 100% incubados por 24 horas a 37°C e 5% CO₂. Em seguida, o MTT foi disperso uniformemente no meio a fim de obter o valor de densidade óptica preciso. Todos os dados quantitativos foram analisados estatisticamente por meio de ANOVA de uma via e do Teste HSD de Tukey. O resultado mostrou diferenças significativas nos valores de densidade óptica entre os grupos com $p = 0,000$ ($p < 0,05$). Não houve diferença significativa entre o controle celular e o grupo de seiva do caule de banana ambonense com concentrações de 90%, 80%, 70%, 60%, 50%, 30%, 20% e 10%. Observou-se também que a seiva do caule da banana ambonense não é tóxica para os fibroblastos, pois seu valor de viabilidade foi superior a 60%.

Palavras-chave: fitoterapia, biocompatibilidade, BHK-21, cultura de células de fibroblastos, densidade óptica

ABSTRACT

Traditional herbal remedies are naturally occurring, plant-derived substances with limited to no chemical processing and have been used in local or national healing traditions to treat illness. In global health debates, traditional herbal medicines are gaining considerable attention. Many hope new research into herbal medicine will play a vital role in global health. Countries like China, India, Nigeria, USA, and also the World Health Organization (WHO) made large investments in ancient herbal medicines. Currently, the use of the Indonesian plant has dramatically improved the medical and dentistry field. The dental and oral care is often related to wounds, and the Ambonense banana stem has been proven as an effective treatment for these injuries. This study aimed to evaluate the effectiveness and safety of the Ambonense banana stem sap through cytotoxicity tests on the fibroblast cell culture of *Baby Hamster Kidney-21* (BHK-21). This study was carried out on three BHK-21 fibroblast cell culture, namely, the media and cell control, and the Ambonense banana stem sap with a concentration of 10%, 20%, 30%, 40%, 50%, 60 %, 70%, 80%, 90%, and 100% incubated for 24 hours at 37°C and 5% CO₂. Then, MTT was evenly dispersed on the media to obtain accurate optical density value. All quantitative data were statistically analyzed using one-way ANOVA and Tukey's HSD Test. The result showed significant differences in optical density values between groups with $p = 0.000$ ($p < 0.05$). There was no significant difference between the cell

control and the Ambonese banana stem sap group with concentrations of 90%, 80%, 70%, 60%, 50%, 30%, 20%, and 10%. It was also observed that the Ambonese banana stem sap is nontoxic to fibroblast cells since its viability value was more than 60%.

Keywords: *herbal medicine, biocompatibility, BHK-21, fibroblast cell culture, optical density*

ABSTRAK

Pengobatan tradisional menggunakan herbal merupakan pengobatan alami, zat yang terkandung dari tumbuhan dengan tanpa pemrosesan kimiawi telah digunakan dalam tradisi penyembuhan secara lokal atau nasional untuk mengobati suatu penyakit. Dalam perdebatan kesehatan global, obat-obatan herbal tradisional mendapatkan perhatian yang cukup besar. Banyak yang berharap penelitian baru tentang herbal akan memainkan peran penting dalam kesehatan global. Cina, India, Nigeria, AS, dan WHO semuanya melakukan investasi besar dalam obat-obatan herbal tradisional. Saat ini pemanfaatan tumbuhan Indonesia telah meningkat pesat dalam bidang kedokteran dan kedokteran gigi. Perawatan gigi dan mulut sering dikaitkan dengan luka, bahkan batang pisang ambon terbukti efektif mengobati luka tersebut. Penelitian ini bertujuan untuk membuktikan efektivitas dan keamanan getah batang pisang ambon melalui uji sitotoksitas pada kultur sel fibroblas *Baby Hamster Kidney-21* (BHK-21). Penelitian ini dilakukan pada tiga kultur sel fibroblas BHK-21 yaitu media dan kontrol sel, serta getah batang pisang ambon dengan konsentrasi 10%, 20%, 30%, 40%, 50%, 60%, 70 %, 80%, 90%, dan 100% diinkubasi selama 24 jam pada suhu 37°C dan 5% CO₂. Kemudian MTT diberikan secara merata pada media untuk mendapatkan nilai optical density yang akurat. Semua data kuantitatif dianalisis secara statistik menggunakan ANOVA satu arah dan Uji HSD Tukey. Hasil penelitian menunjukkan bahwa terdapat perbedaan yang signifikan nilai densitas optik antar kelompok dengan $p = 0,000$ ($p < 0,05$). Tidak ada perbedaan yang nyata antara kontrol sel dan kelompok getah batang pisang ambon dengan konsentrasi 90%, 80%, 70%, 60%, 50%, 30%, 20% dan 10%. Getah batang pisang ambon tidak toksik bagi sel fibroblas, karena nilai viabilitasnya lebih dari 60%.

Kata kunci: *tanaman obat, biokompatibilitas, BHK-21, kultur sel fibroblast, densitas optik*

1. INTRODUCTION:

Traditional herbal medicine has yielded a vast archive of treatments against many health conditions of complex chemical structures and bioactivities throughout history. A typical herbal medicine issue is restricting information about their pharmacological activities and their active constituents. Countries like China, India, Nigeria, the USA, and the World Health Organization (WHO) made large investments in ancient herbal medicines (Tilburt and Kaptchuk, 2008). Using herbal medicine has historically been based on scientific diagnosis and passed. Plant materials have been consistently used in the health sector for preventive, curative, and rehabilitative purposes (Sofowora *et al.*, 2013). Therefore, the use of medicinal plants for treatments has dramatically improved both the medicine and dentistry field (Ekor, 2014; Martínez *et al.*, 2017).

Dental disease is also regarded as a chronic public health problem and a significant drain on health care systems around the world (Hollist, 2004). In people with diabetes, periodontal disease impairs glycemic regulation, and poorly regulated diabetes may worsen periodontal disease (Preshaw *et al.*, 2012). Acacia catechu, Aloe vera, Azadirachta indica, Glycyrrhiza glabra, Cinnamomum

zeylanicum, Allium sativum, Propolis, Mikania laevigata, Mikania glomerata, Drosera peltata, Helichrysum italicum, Coptidis rhizome, Piper cubeba, Azadirachta indica, Syzygium aromaticum, and Tea tree oil are the frequently tested herbs used for the treatment of periodontitis. Many other herbal products are also undergoing clinical trials in addition to the aforementioned herbal remedies (Shama *et al.*, 2014).

Moreover, plant utilization for treatments needs more in-depth exploration, especially on Indonesian vegetative resources. Indonesia is one of ten member states of the Association of Southeast Asian Nations (ASEAN)'s economically and politically diverse national organization. Southeast Asia contains four of the world's 25 biodiversity hotspots, three of the 17 regional megadiverse countries (Indonesia, Malaysia, and the Philippines), and the world's most abundant coral reefs. Biodiversity, e.g., importance in traditional medicine and Indonesian society agriculture, is deep-rooted. In addition to environmental policies, modern biodiversity pathways provide new applications in technology, pharmacy, and the economy (Von Rintelen *et al.*, 2017). Correct identification of source plant species and selecting appropriate parts for use in herbal medicines are necessary and essential

steps for ensuring herbal medicines' safety, quality, and efficacy. Hence, herbal medicines' safety and quality at every stage of the production process have become a significant concern to health authorities, health care providers, the herbal industries, and the public (Kunle *et al.*, 2012). Currently, dentistry utilizes natural compounds as clinical and laboratory materials (Palombo, 2011; Kumar *et al.*, 2013). The bone grafting procedure is a technique often used to repair either bone defects or ridge augmentation. However, the failure of the process has been reported with different results. Graft materials used should have an osteoconductive ability that can potentially stimulate the growth of new bone. The development of new material is necessary to promote or accelerate bone growth activity. *Aloe vera* and *Musa paradisiaca* are natural materials known as a biogenic stimulator and hormonal activity modulator during wound healing (Kresnadi *et al.*, 2017; Kapadia *et al.*, 2015). Furthermore, dental and oral health care is often related to injuries that cause infection when not appropriately handled. Therefore, drugs are needed to prevent this occurrence.

One of the natural ingredients known to be efficacious in healing wounds is banana stem sap (*Musa paradisiaca*). Its extract is characterized by increased hydroxyproline levels, hexuronic acid, hexosamine, superoxide dismutase, and decreased glutathione in granulation tissue. Also, lipid peroxidation has been proven to be useful for ulcer treatment (Agarwal *et al.*, 2009). Ambonese banana stem sap has also been used to accelerate wound healing (Budi *et al.*, 2009), due to the presence of saponins (antibiotics), anthraquinones (painkiller), and the lectin content for stimulating skin cells growth (Priosoeryanto *et al.*, 2007).

Banana sap advantages include providing aesthetic effects by improving damaged skin structure, accelerating the re-epithelialization of epidermal tissue, forming new blood vessels (neocapilerization), and generating connective tissue infiltrating of inflammatory cells in the wound area (Budi *et al.*, 2017). Banana stem sap is known to be a wound medicine (Prasetyo, 2007) since it accelerates the healing process and increases connective tissue growth (Amutha and Selvakumari, 2016).

However, treatment using natural ingredients should be scientifically justified, both in terms of benefits and safety (Peacock *et al.*, 2019). Drug safety test is carried out using cell culture, while BHK-21 cells from kidney fibroblasts are more widely used in testing the cytotoxicity of

materials and drugs (Freshney, 2000; Stefanowicz and Ochocka, 2020). Fibroblast cells are the most essential and largest component of the pulp, periodontal ligament, and gingiva used in a culture system with various advantages such as the ability to control the environmental (pH, temperature, osmotic pressure, O₂, and CO₂), and physiological conditions (Huang *et al.*, 2009; Mitry and Hughes, 2012; Han *et al.*, 2014).

The MTT (3- (4-5-dymethylthiazol-2-yl) - 2,5-diphenyl tetrazolium bromide), is used in microplate analysis for measuring cell proliferation and cytotoxicity. This test is based on cells' ability to reduce yellow and soluble MTT salts to blue-purple and insoluble formazan (Mosmann, 1983). Furthermore, tetrazolium salts reduction occurs intracellularly involving the succinic enzyme dehydrogenase from the mitochondria and endoplasmic reticulum (Berridge and Tan, 1993; Marshall *et al.*, 1995; Berridge *et al.*, 1996).

Therefore, this study aimed to evaluate the effectiveness and safety of the Ambonese banana stem sap through cytotoxicity tests on the fibroblast cell culture of *Baby Hamster Kidney-21* (BHK-21).

2. MATERIALS AND METHODS:

2.1. Sample preparation

This study was carried out at the Farma Veterinaria Center in Surabaya, Indonesia, using the BHK-21 Clone-13 (BHK-21/C13) fibroblast cell culture (ECACC-85011433, Sigma), while the number of samples was obtained using a sample size of the Lemeshow's formulation (1990) :

$$n = 2\sigma^2 \times \frac{(Z(1 - \alpha) + Z(1 - \beta))^2}{\mu_0 - \mu_1}$$

Description :

n: sample size

σ : standard deviation

Z: value of Z table

α : significance level of 95%

β : power of test (80-90%)

2.2. Preparation of Ambonese banana (*Musa paradisiaca* var. *sapientum* (L.) Kuntze) stem sap concentration

Banana plants were obtained from the Purwodadi Botanical Garden Plant Conservation Center and the Indonesian Institute of Sciences (LIPI). The features of the banana plants used were age 12-13 months, the height of 2.5-3 m,

stem diameter of 17.3-18.9 cm, and were obtained shortly after fruiting. Ambonese banana sap was extracted by cutting the lower end of the stem and washed to remove dirt. The determination was made to prove that the banana tree species were Ambonese banana (Figure 1). Stems cut and made into small pieces of 200 grams were added into 200 mL of sterile distilled water and blended until it forms a smooth substance. The mixture was filtered using a Buchner funnel connected with a vacuum pump (Gast, USA) and placed into Whatman filter paper number 1. The resulting 375 mL filtrate was stored in a dark bottle, closed to reduce oxidation, and dried with a freeze dryer.

For the standard solution preparation, 1000 mg of Ambonese banana stem extract was dissolved with 1 L of sterile distilled water. The 100% concentration was prepared by taking 1 mL of the standard solution and adding sterile distilled water to 10 mL. Meanwhile, 90% concentration was obtained by taking 0.9 mL of standard solution, then adding sterile distilled water to 10 mL. The same preparation methods to obtained 80%, 70%, 60%, 50%, 40%, 30%, 20% and 10% concentration.

2.3. Preparation of BHK-21 fibroblast cell culture

Seed cell culture frozen in sterile distilled water at 37°C was thawed and centrifuged at 500 RPM for 5 mins. The cells were suspended into 36 mL Eagles media and 4 mL fetal bovine serum; therefore, the resulting 40 mL suspension was deposited in a sterile Roux bottle and incubated at 37°C and 5% CO₂ until a monolayer cell was formed (\pm two days, seen under a microscope). The large Roux bottle containing the BHK-21 cells was then discarded and washed with PBS 15 mL for 3-5 times, and filled with 1 mL of versene trypsin. The result showed that the cells were clustered and homogenized with Eagles media. The homogeneous cells were placed in a microplate of the density of 2×10^5 cells/mL, then incubated for 24 hours at 37°C and 5% CO₂ (Freshney, 2000).

2.4. Cytotoxicity test of Ambonese banana stem sap through MTT method

The microplate containing fibroblasts was observed under a light microscope to ensure the cells confluent in 96 wells plate, divided into 12 groups. A total of 10 of 12 groups were treatment groups containing Ambonese banana stem sap with concentrations of 10%, 20%, 30%, 40%, 50%, 60%, 70%, 80%, 90% and 100%. Two of 12 were control groups as control media and control cells.

Therefore, 25 μ L media was deposited in each dish and incubated for 24 hours at 37°C and 5% CO₂; after this, the media was replaced with 10 μ L MTT (M2003, Sigma), covered with aluminum foil paper, and incubated again for 4 hours. Lastly, each dish was deposited with 50 μ L DMSO, shook vigorously, and inserted into the Elisa Reader at a wavelength of 620 nm, and then the absorbance level was measured (Freshney, 2000).

3. RESULTS AND DISCUSSION:

The cytotoxicity test results of Ambonese banana stem sap deposited in a BHK-21 fibroblast cell culture showed differences in the formazan formed in each group. Purplish crystal formation was observed in the reaction of MTT with succinic dehydrogenase enzyme found in mitochondria (Figure 2). Formazan formed in each dish was observed using Elisa Reader at a wavelength of 650 nm.

There was a significant difference in optical density values between groups with $p = 0.000$ ($p < 0.05$). The results of the one-way ANOVA and HSD test showed that there were significant differences between the media and the cell control group. The optical density value showed a significant difference in the cell control group with $p = 0.044$ and $p = 0.034$ ($p < 0.05$). However, there was no significant difference between the cell control groups with the concentration of 90%, 80%, 70%, 60%, 50%, 30%, 20% and 10% (Table 1).

Ambonese banana stem sap is widely used for accelerating wound healing. However, drug safety level needs to be considered before administration, which is carried out on BHK-21 fibroblast cell culture before using experimental animals and humans (NRC, 2004; Greaves, 2011). According to Freshney (2000), safety testing is conducted using the cell culture system. The basic principle for growing cells is to design in vitro culture system similar to their initial medium. The cells to be investigated are removed from their original tissue and placed in the in vitro culture system to obtain adequate growth and nutrition at 37°C, pH 7.4-7.7, and a gas environment of 95% CO₂/ 95% air.

This research used BHK-21 cell culture from hamster kidney fibroblasts since it was widely used to test the cytotoxicity of materials and drugs in dentistry (Basuony *et al.*, 2018). The cytotoxicity testing method adopted the MTT assay (3-(4,5-dimethylthiazol-2-yl) -2,5-diphenyl tetrazolium bromide), for measuring cell proliferation and cytotoxicity. This was based on the living cells'

ability to reduce yellow and soluble MTT salts to blue-purple and insoluble formazene. In contrast, the tetrazolium salts reduction occurred intracellularly by involving a small amount of succinic dehydrogenase enzyme from mitochondria and endoplasmic reticulum enzyme. The MTT test was used due to its accurate measurement, sensitivity, ability to detect changes in cell metabolism, equipment availability, ability to save time and energy, and radioisotope disuse (Riss *et al.*, 2004). Spectrophotometric tool was used to test for absorbance level. Therefore, the more concentrated the color produced, the higher the absorbance value, and the more the number of cells (Mohler *et al.*, 1996; Santos-Ballardo *et al.*, 2015).

Previous studies had shown that the content of Ambonese banana stem sap, such as lectins, saponins, flavonoids, saponins, and tannins, played roles in the wound healing process (Atun *et al.*, 2010; Amutha and Selvakumari, 2016; Budi *et al.*, 2017). Meanwhile, saponins and lectins caused hemostatic and antibacterial effects. Saponins and lectins in banana stem sap modulated the immune response by increasing T cell lymphocytes with CD3 + CD4 + CD8 and the hematopoietic system to minimize infection (Swanson, 2010). Therefore, the T cells activated the B cell lymphocytes, NK cells, and macrophages in the presence of antigens (Alberts *et al.*, 2002; Uzhachenko and Shanker, 2019). The tannin content acted as the hemostatic (Song *et al.*, 2019) and antibacterial through the mechanism of protein precipitation in blood cells and bacteria, which resulted in coagulation (Budi and Astuti, 2019). Furthermore, tannins and anthraquinones also acted as donors of free radicals and Reactive Oxygen Species (ROS). Free radicals triggered lipid peroxidation and malondialdehyde (MDA) compound, which caused damages to protein and DNA cells (Kaimal *et al.*, 2010; Benmehdi *et al.*, 2017). The flavonoid contents such as leucocyanidin and anthocyanin acted as anti-inflammatory enzymes by inhibiting cyclooxygenase enzyme and prostaglandin synthesis (Sumathy and Vijayakumar, 2015; Pandey *et al.*, 2016).

Hydroxyproline is an amino acid which acts to improve the stability of collagen. One aspect of the wound healing process is the measurement of rates of hydroxyproline. The higher the hydroxyproline level, it means an improvement in collagen synthesis, which is closely linked to the acceleration of the wound healing process (Shoulders and Raines, 2009, Agarwal *et al.*,

2009). The glycosaminoglycans are known to stabilize the collagen fibers and likely regulate their ultimate orientation and characteristic size by improving electrostatic and ionic interactions with it. Concentrations of hexuronic acid and hexosamine, which are glycosaminoglycans' components, have risen dramatically in wound healing (Shetty *et al.*, 2008). Superoxide is dismutated by superoxide dismutase (SOD) into hydrogen peroxide (H_2O_2) and an oxygen atom, thus preventing extremely deleterious ROS, such as peroxynitrite ($ONOO^-$) or hydroxyl radicals (*OH). Low H_2O_2 levels can act as a signaling molecule that modulates specific signaling pathways that control blood coagulation, thrombosis, replication, proliferation, fibrosis, angiogenesis, and so on, in the process of hemostasis, proliferation, maturation and remodeling (Kurahashi and Fujii, 2015).

Cytotoxicity testing showed that the Ambonese banana stem sap was not toxic to fibroblast cells; the most connective tissue cell in a cell body. The use of 10%-100% concentration of the Ambonese banana stem sap showed the presence of more than 60% fibroblasts (Figure 3). Therefore, the higher the concentration used, the less the number of living cells, while the higher the active compounds in the banana stem sap, the more the effect of fibroblast cell death. The drug was considered safe when it has a broad therapeutic index or small effective dose and large toxic doses.

The result indicated that the Ambonese banana stem sap with a 10% concentration to 100% did not cause a toxic effect on fibroblast cells. This was evidenced by the fact that the percentage of living cells was more than 60% at all concentrations. However, when less than 60%, the material became toxic.

4. CONCLUSIONS:

Medicinal plants are beneficial in fulfilling human life's needs. Medicinal plants in the pharmaceutical world are a source of raw materials for both modern and traditional medicines. Nowadays, there is a trend for people to consume conventional drugs, owing to improvements in lifestyle returning to nature and the high cost of modern medicines that have raised the demand for medicinal plants, not just in Indonesia but also worldwide. If this medicinal plant can be developed as the Herbal Medicine Standard (OHT) and Fitofarmaka would have a higher sales value and greater competition in both domestic and foreign markets. This study has

proven that the use of Ambonese banana stem sap from a 10% concentration to 100% does not cause a toxic effect on fibroblast cells using the MTT assay method. This work was intended to offer additional scientific information about the advantages and disadvantages of using the Ambonese banana plant, which could help make decisions for the industry and government world and guide community medicinal plants.

5. ACKNOWLEDGMENTS:

The authors gratefully acknowledge the financial support provided by the Rector for Research Funding of Airlangga University, Indonesia ministry of research technology, and higher education.

6. REFERENCES:

1. Agarwal, P. K, Singh, A., Gaurav, K., Goel, S., Khanna, H., Goel, R. (2009). Evaluation of wound healing activity of extracts of plantain banana (*Musa sapientum* var. *paradisiaca*) in rats. *Indian Journal of Experimental Biology*, 47, 32-40.
2. Alberts, B., Johnson, A., Lewis, J., Morgan, D., Raff, M., Roberts, K., Walter, P. (2002). *Molecular biology of the cell* (6th ed.). New York, Garland Science.
3. Amutha, K., and Selvakumari, U. (2016). Wound healing activity of methanolic stem extract of *Musa paradisiaca* Linn. (Banana) in Wistar albino rats. *International wound journal*, 13(5), 763–767.
4. Atun, S., Arianingrum, R., Handayani, S., Rudyansah, R., Garson, M. (2010). Identification and antioxidant activity test of some compounds from methanol extract peel of banana (*Musa paradisiaca* Linn.). *Indonesian Journal of Chemistry*, 7(1), 83-87
5. Basuony, A. E., Hossary, E. N., Amin, R. N. (2018). Apoptosis inducing effects of chlorhexidine and essential oil mouthwashes on BHK-21 fibroblast cell line: An in vitro study. *F1000 Research*, 7, 1703.
6. Benmehdi, H., Behilil, A., Memmou, F., Amrouche, A. (2017). Free radical scavenging activity, kinetic behaviour and phytochemical constituents of *Aristolochia clematitis* L. roots. *Arabian Journal of Chemistry*, 10(Suppl 1), S1402-S1408.
7. Berridge, M., Tan, A., McCoy, K., Wang, R. (1996). The biochemical and cellular basis of cell proliferation assays that use tetrazolium salts. *Biochemical Journal*, 4, 14–19.
8. Berridge, M. V., and Tan, A. S. (1993). Characterization of the cellular reduction of 3-(4,5-dimethylthiazol-2-yl)-2,5-diphenyltetrazolium bromide (MTT): Subcellular localization, substrate dependence, and involvement of mitochondrial electron transport in MTT reduction. *Archives of Biochemistry and Biophysics*, 303(2), 474–482.
9. Budi, H. S, Kriswandini, I. L, Sudjarwo, S. A. (2016). Ambonese banana stem sap (*Musa paradisiaca* var. *sapientum*) effect on PDGF-BB expressions and fibroblast proliferation in socket wound healing. *International Journal of ChemTech Research*, 9(12), 558-564.
10. Budi, H. S, Soesilowati, P, Imanina, Z. (2017). Gambaran histopatologi penyembuhan luka pencabutan gigi pada makrofag dan neovaskular dengan pemberian getah batang pisang ambon. *Majalah Kedokteran Gigi Indonesia*, 3(3), 3-9.
11. Budi, H. S., and Astuti, E. R. (2019). The MMP-2, MMP-9 expression and collagen density of the ambonese banana stem sap administration on wound healing. *Journal of International Dental and Medical Research*, 12(2), 492-449.
12. Ekor, M. (2014). The growing use of herbal medicines: Issues relating to adverse reactions and challenges in monitoring safety. *Frontiers in Pharmacology*, 4,177.
13. Freshney, R. I. 2000. *Culture of animals cell: a manual of basic technique* (4th ed.) Newyork, Wiley.
14. Greaves, P. (2011). Preclinical testing. In: Schwab M. (eds) *Encyclopedia of Cancer*. Springer, Berlin, Heidelberg.
15. Han, J., Menicanin, D., Gronthos, S., Bartold, P. M. (2014). Stem cells, tissue

- engineering and periodontal regeneration. *Australian Dental Journal*, 59(1 Suppl), 117–130.
16. Hollist, N. A. (2004). *Collection of traditional Yoruba oral and dental medicaments*. Nigeria, Olubena Printers. Ibadan.
 17. Huang, G. T., Gronthos, S, Shi, S. (2009). Mesenchymal stem cells derived from dental tissues vs. those from other sources: Their biology and role in regenerative medicine. *Journal of Dental Research*, 88(9), 792-806.
 18. Kaimal, S., Sujatha, K. S., George, S. (2010). Hypoglycemic and antioxidant effect of fruits of musa AAA (chenkadali) in alloxan induced diabetic rats. *Indian Journal of Experimental Biology*, 48, 165-173.
 19. Kapadia, S. P., Pudakalkatti, P. S., Shivanaikar, S. (2015). Detection of antimicrobial activity of banana peel (*Musa paradisiaca* L.) on *Porphyromonas gingivalis* and *Aggregatibacter actinomycetemcomitans*: An in vitro study. *Contemporary Clinical Dentistry*, 6(4), 496–499.
 20. Kresnoadi, U., Rahayu, R. P., Rubianto, M., Sudarmo, S. M. Budi, H. S. (2017). TLR2 signaling pathway in alveolar bone osteogenesis induced by Aloe vera and xenograft (XCB). *Brazilian Dental Journal*, 28(3), 281-286.
 21. Kumar, G., Jalaluddin, M., Rout, P., Mohanty, R., Dileep, C. L. (2013). Emerging trends of herbal care in dentistry. *Journal of Clinical and Diagnostic Research*, 7(8), 1827-1829.
 22. Kunle, O. F., Egharevba, H. O., Ahmadu, P. O. (2012). Standardization of herbal medicines - A review. *International Journal of Biodiversity and Conservation*, 4(3), 101-112.
 23. Kurahashi, T., and Fujii, J. (2015). Roles of antioxidative enzymes in wound healing. *Journal of Developmental Biology*, 3, 57-70.
 24. Lemeshow, S., Hosmer, D. W., Klar, J., Lwanga, S. K., World Health Organization. (1990). *Adequacy of sample size in health studies*. Chichester, Wiley.
 25. Marshall, N. J., Goodwin, C. J., Holt, S. J. (1995). A critical assessment of the use of microculture tetrazolium assays to measure cell growth and function. *Growth Regulation*, 5(2), 69–84.
 26. Martínez, C. C., Gómez, M. D., Sook Oh, M. (2017). Use of traditional herbal medicine as an alternative in dental treatment in Mexican dentistry: A review. *Pharmaceutical Biology*, 55(1), 1992-1998.
 27. Mitry, R. R., and Hughes, R. D. (2012). Introduction to cell culture. In C. Philippeos, R. D. Hughes, A. Dhawan, R. R. Mitry (eds), *Human cell culture protocols, methods in molecular biology* (3rd ed.) (pp. 1-13). London, UK, Humana.
 28. Mohler, W. A., Charlton, C. A., Blau, H. M. (1996). Spectrophotometric quantitation of tissue culture cell number in any medium. *Biotechniques*, 21, 260-266.
 29. Mosmann, T. (1983). Rapid colorimetric assay for cellular growth and survival: Application to proliferation and cytotoxicity assays. *Journal of Immunological Methods*, 65, 55–63.
 30. National Research Council (US) Committee to Update Science, Medicine, and Animals. Science, Medicine, and Animals. (2004). *Safety Testing*. Washington (DC), National Academies Press (US).
 31. Palombo, E. A. (2011). Traditional medicinal plant extracts and natural products with activity against oral bacteria: Potential application in the prevention and treatment of oral diseases. *Evidence-Based Complementary and Alternative Medicine*, 2011, 680354.
 32. Pandey, A., Alok, A., Lakhwani, D., Singh, J., Asif, M. H., Trivedi, P. K. (2016). Genome-wide expression analysis and metabolite profiling elucidate transcriptional regulation of flavonoid biosynthesis and modulation under abiotic stresses in banana. *Scientific Reports*, 6, 31361.

33. Peacock, M., Badea, M., Bruno, F, Timotijevic, L, Laccisaglia, M, Hodgkins, C, Raats, M, Egan, B. (2019). Herbal supplements in the print media: communicating benefits and risks. *BMC Complementary Medicine and Therapies*, 19, 196.
34. Preshaw, P. M., Alba, A. L., Herrera, D., Jepsen, S., Konstantinidis, A., Makrilakis, K., Taylor, R. (2012). Periodontitis and diabetes: a two-way relationship. *Diabetologia*, 55(1), 21–31.
35. Priosoeryanto, B. P, Putriyanda, N, Listyanti, A. R, Juniantito, V, Wientarsih, I, Prasetyo, B. F, Tiuria, R. (2007). The effect of ambon banana stem sap (*Musa paradisiaca sapientum* L.) on the acceleration of wound healing process in mice (*Mus musculus albinus*). *Journal of Agriculture and Rural Development in the Tropics and Subtropics*, 35-49.
36. Riss, T. L., Moravec, R. A., Niles, A. L., Duellman, S., Benink, H. A., Worzella, T. J. (2004). Cell viability assays. In: Markossian, S., Sittampalam, G. S., Grossman, A., Brimacombe, K., Arkin, M., Auld, D., Austin, C. P., et al. *Assay Guidance Manual*. Bethesda (MD), Eli Lilly and Company and the National Center for Advancing Translational Sciences.
37. Santos-Ballardo, D. U., Rossi, R., Hernández, V., Gómez, R. V., Rendón-Unceta, M. C., Caro-Corrales, J., Valdez-Ortiz, A. (2015). A simple spectrophotometric method for biomass measurement of important microalgae species in aquaculture. *Aquaculture*, 448, 87-92.
38. Shama, N. S., Prasanna, K. R., Joshna, A., Lakshmi, S. T. (2014). Effect of herbs on periodontitis – a serious gum infection. *International Journal of Pharmacological Research*, 4(1), 17–22.
39. Shetty, S., Udupa, S., Udupa, L. (2008) Evaluation of antioxidant and wound healing effects of alcoholic and aqueous extract of *Ocimum sanctum* Linn in rats. *Evidence-Based Complementary and Alternative Medicine*, 5(1), 95–101.
40. Shoulders, M. D. and Raines, R. T. (2009). Collagen structure and stability. *Annual Review of Biochemistry*, 78, 929–958.
41. Sofowora, A., Ogunbodede, E., Onayade, A. (2013). The role and place of medicinal plants in the strategies for disease prevention. *African Journal of Traditional Complementary and Alternative Medicines*, 10(5), 210-229.
42. Song, B., Yang, L., Han, L., Jia, L. (2019). Metal ion-chelated tannic acid coating for hemostatic dressing. *Materials*, 12(11), 1803.
43. Stefanowicz-Hajduk, J., and Ochocka, J. R. (2020). Real-time cell analysis system in cytotoxicity applications: Usefulness and comparison with tetrazolium salt assays. *Toxicol Reports*, 7, 335-344.
44. Sumathy, C., and Vijayakumar, N. (2015). Review on antiulcerogenic activity of *Musa sapientum* on experimental peptic ulcers in rats. *World Journal of Pharmaceutical Research*, 4(5), 832-846.
45. Swanson, M. D. (2010). Molecular engineering of a banana lectin that inhibits hiv-1 replication. *The University of Michigan, Dissertation*, p. 16.
46. Tilburt, J. C., and Kaptchuk, T. J. (2008). Herbal medicine research and global health: an ethical analysis. *Bulletin of the World Health Organization*. 86(8), 577-656.
47. Uzhachenko, R. V., and Anil, S. (2019). CD8+ T lymphocyte and NK cell network: Circuitry in the cytotoxic domain of immunity. *Frontiers in Immunology*, 10, 1906.
48. Von Rintelen, K., Arida, E., Hauser, C. (2017). A review of biodiversity-related issues and challenges in megadiverse Indonesia and other Southeast Asian countries. *Research Ideas and Outcomes*, 3, e20860.

Table 1. The average optical density of BHK-21 fibroblast cells in Elisa Reader and the percentage of living cells

Groups	Optical Density $\bar{X} \pm SD$	Living cells (%)	P-value
Media control	0.099 \pm 0.012	0*	
Cell control	0.295 \pm 0.077	100	
K 100	0.225 \pm 0.051	82.23*	P = 0.000
K 90	0.241 \pm 0.017	83.29	
K 80	0.254 \pm 0.024	85.59	
K 70	0.234 \pm 0.029	84.52	
K 60	0.230 \pm 0.032	83.5	
K 50	0.231 \pm 0.026	83.76	
K 40	0.223 \pm 0.021	81.73*	
K 30	0.263 \pm 0.039	91.88	
K 20	0.309 \pm 0.039	103.55	
K 10	0.269 \pm 0.032	93.40	

*: Significant p-value<0.05. One-way Anova compare to control cell.



Figure 1. Freeze drying process of Ambonese banana stem sap.

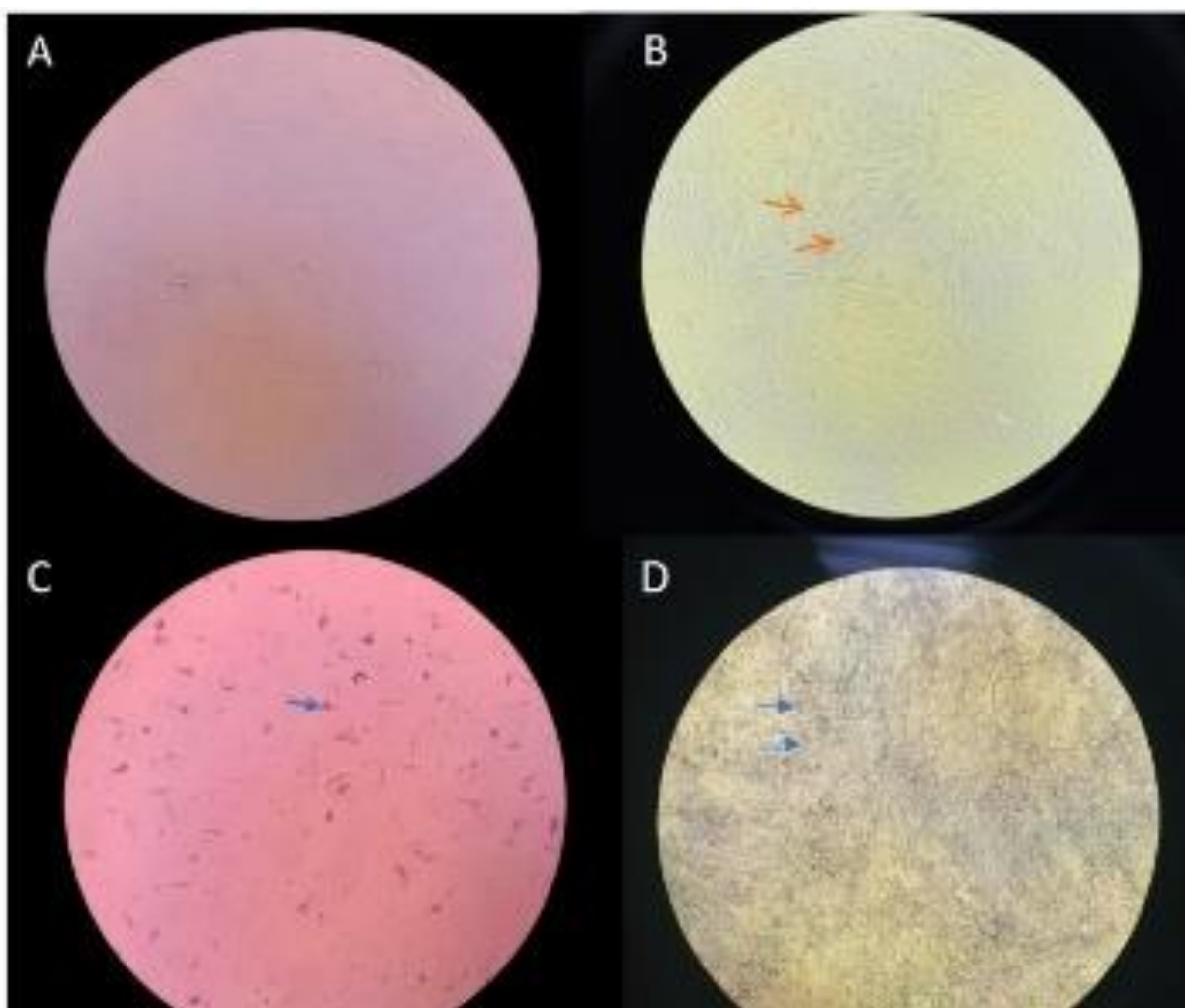


Figure 2. BHK-21 fibroblast cells at 40X magnification microscope observation. A) Media control, B) Cell control, C) Media control after MTT, D) Cell control after MTT. Red arrows were fibroblasts, while the blues were formazan.

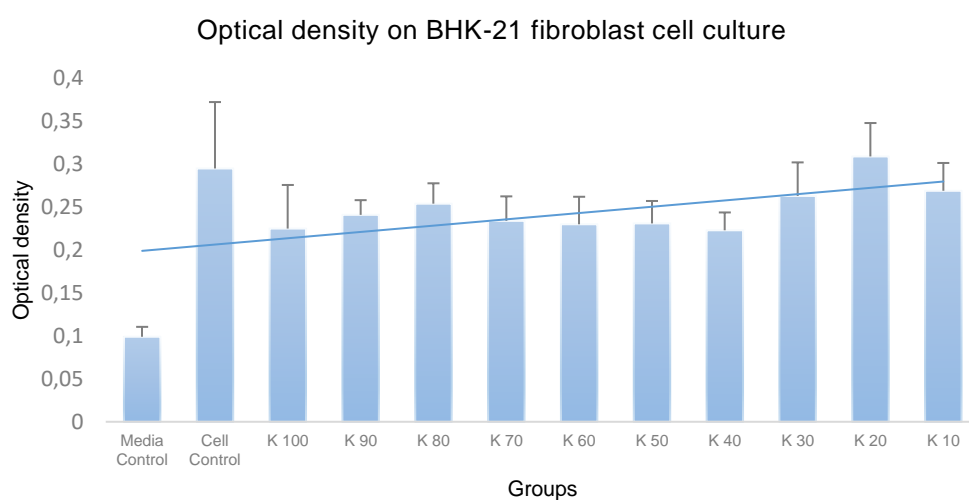


Figure 3. The relationship between the concentration of Ambonese banana stem sap and living cells percentage

UM SISTEMA DE LABORATÓRIO PARA INVESTIGAÇÃO DA CAPACIDADE DE FLUXO DE FLUIDOS ATRAVÉS DE AMOSTRAS DE AREIA NÃO CONSOLIDADAS**A LABORATORY SYSTEM FOR INVESTIGATING OF FLUIDS FLOW CAPACITY THROUGH UNCONSOLIDATED SAND SAMPLES****تصميم منظومة مختبرية لفحص كفاءة جريان السائل خلال نماذج رملية غير متماسكة**SULAIMAN, Izzat Niazi¹, TAWFEEQ, Yahya Jirjees^{2*}^{1,2} Department of Petroleum Engineering, Kirkuk University, Kirkuk, Iraq.

* Corresponding author

e-mail: yahyapetroleum@uokirkuk.edu.iq

Received 06 August 2020; received in revised form 26 September 2020; accepted 15 October 2020

RESUMO

Praticamente todos os estudos de engenharia de reservatório envolvem conhecimento detalhado das características do fluxo de fluido. O desempenho do fluxo de fluido em meios porosos é afetado pela pressão, taxa de fluxo e volume de fases de fluido único. A permeabilidade é uma medida de quão bem um meio poroso permite o fluxo de fluidos através dele. A permeabilidade e a porosidade formam as duas características significativas das rochas de reservatório. Esta pesquisa teve como objetivo apresentar o projeto de equipamentos de laboratório para testar a capacidade de escoamento de fluidos em diferentes amostras de arenito. Duas amostras de areia (amostra de areia grossa e amostra de areia fina) foram testadas. As medidas laboratoriais de porosidade, saturação, permeabilidade total, permeabilidade efetiva e permeabilidade relativa foram avaliadas. Os testes de laboratório foram realizados em areia de núcleo não consolidada parcialmente saturada para escoamento de fluido bifásico. O trabalho experimental foi desenvolvido para medir a capacidade de fluxo alcançada pelo método de condições de estado estacionário. Vários tamanhos de grãos de areia foram selecionados como um meio poroso para determinar as propriedades petrofísicas e a capacidade de fluxo de fluido da amostra de rocha. Nitrogênio e ar foram utilizados como fases gasosas e, para fases líquidas, a água foi escolhida como fluido de injeção. O método de processo em estado estacionário foi usado para determinar a permeabilidade e a permeabilidade relativa de areias não consolidadas ao fluxo de água. Taxas de fluxo diferentes foram medidas para gradientes de pressão diferentes em um fluxo viscoso. À medida que a taxa de fluxo aumenta, a diferença de pressão também aumenta. Pode-se observar que existe uma correlação e relação direta entre a vazão e a diferença de pressão. A permeabilidade absoluta do plug do núcleo foi medida usando a equação de Darcy. A permeabilidade absoluta não depende das características do fluido, mas apenas das propriedades do meio. O recipiente de amostra que contém uma quantidade mais significativa de areia, diminui a permeabilidade e, portanto, requer alta pressão para o fluido escoar dentro da amostra.

Palavras-chave: *fluxo de fluido; permeabilidade; permeabilidade efetiva; permeabilidade relativa; meio de poros.***ABSTRACT**

Practically all studies of reservoir engineering involve detailed knowledge of fluid flow characteristics. The fluid flow performance in porous media is affected by pressure, flow rate, and volume of single fluid phases. Permeability is a measure of how well a porous media allows the flow of fluids through it. Permeability and porosity form the two significant characteristics of reservoir rocks. This research aimed to present the design of laboratory equipment to test the ability of fluid flow through different sandstone samples. Two sand core samples (coarse sand sample and fine sand sample) were tested. The laboratory findings measurements of porosity, saturation, total permeability, effective permeability, and relative permeability were evaluated. The laboratory tests were performed on partially saturated, unconsolidated core sand for two-phase fluid flow. The experimental work was developed for measuring the flow capacity achieved under the steady-state conditions method. Various grain sizes sands were selected as a porous medium to determine petrophysical properties and fluid flow capacity of the rock sample. Nitrogen and air were utilized as gas-phases, and, for liquid-phases, water was chosen as an injection fluid. The steady-state process method was used to determine the permeability and relative permeability of unconsolidated sands to water flow. Different flow rates were measured for different pressure gradients in a viscous flow. As the flow rate increases, the pressure difference also increased. It can be observed that there are a direct correlation and relationship between the flow rate and the pressure difference. The core plug's absolute

permeability was measured using Darcy Equation. Absolute permeability does not depend on fluid characteristics but only on media properties. The sample container contains a more significant amount of sand, decrease the permeability, and therefore requires high pressure for fluid flowing within the sample.

Keywords: fluid flow; permeability; effective permeability; relative permeability; pores media.

المخلص

عملية جميع دراسات هندسة المكامن تتضمن معرفة تفصيلية لخصائص تدفق السوائل. يتأثر أداء تدفق السوائل في الوسط المسامي بالضغط ومعدل التدفق وحجم الطور السائل الاحادي. النفاذية هي مقياس لمدى سماح الوسائط المسامية بتدفق السوائل من خلالها. تشكل النفاذية والمسامية خاصيتين مهمتين لصخور المكمن. يهدف هذا البحث إلى تصميم منظومة مختبرية لفحص كفاءة تدفق السوائل عبر عينات مختلفة من الحجر الرملي. حيث تم اختبار عينتين من عينات الحجر الرملي في هذه الدراسة، احدهما الحجر الرملي الخشن والاخر الحجر الرملي الناعم. تم استحصا على النتائج المختبرية مثل قياسات المسامية والتشبع والنفاذية الكلية والنفاذية الفعالة والنفاذية النسبية من خلال اجراء التجارب العملية لتدفق السوائل ثنائية الطور على الحجر الرملي الغير المتماسك والمشبّع جزئيًا. عند تصميم وبناء المنظومة المختبرية تم الاخذ بنظر الاعتبار ان قياس وحساب سعة التدفق يكون تحت الظروف الحالة المستقرة. تم اختيار احجام مختلفة من الحجر الرملي كوسط مسامي لقياس الخواص البتروفيزيائية وقابلية جريان السوائل للنماذج الصخرية. من الجدير بالذكر تم استخدام النيتروجين والهواء كطور غازي، وبالنسبة للطور السائل، تم اختيار الماء كسائل حقن. تم الاعتماد على جريان الحالة المستقرة لإيجاد النفاذية والنفاذية النسبية للحجر الرملي الغير المتماسك لجريان الماء في الوسط المسامي. عند الجريان اللزج تم قياس معدلات تدفق مختلفة لتدرجات هبوط ضغوط مختلفة. وتبين ان الزيادة الحاصلة في معدل جريان السائل يقابله زيادة في فرق الضغط أيضًا. مما نلاحظ من الاستنتاجات أعلاه ان هناك علاقة طردية بين معدل التدفق وفرق الضغط. تم قياس النفاذية المطلقة للعيينة باستخدام معادلة دارسي. النفاذية المطلقة تعتمد على خصائص الوسط المسامي ولا تعتمد على خصائص سائل الجريان. إن وعاء العينة الذي يحتوي على كمية أكبر من الحجر الرملي تكون فيه النفاذية اقل مايمكن، لذلك يتطلب ضغطًا أعلى لجريان السوائل داخل العينة.

الكلمات المفتاحية: جريان الموائع; النفاذية; النفاذية الفعالة; النفاذية النسبية; الوسط المسامي

1. INTRODUCTION:

Fluid flow through porous media is an issue that has been addressed in many branches of engineering and science, e.g., soil water hydrology, reservoirs engineering, chemical engineering, soil science, and soil mechanics (Jacob Bear, 2013). Porous media fluid flow is a significant phenomenon in a wide variety of applications, including landslides risk assessment, groundwater hydrology, and biophysical systems (Rahimi-Gorji *et al.*, 2016).

A better understanding of the fluid flow fundamental through petroleum-reservoir rock is key to improving petroleum production methods (Vafai, Kambiz, 2015). Fluid flow is a complicated transportation process through porous media. The porous médium of material comprises a solid matrix with interconnected voids (pores). The interconnectedness of the pores permits the flow of one or more fluids through the material (D. B. Ingham *et al.*, 2012). In the simplest case, that is to say, 'single-phase flow,' the pores are saturated by a single fluid, while in 'two-phase flow' the void space shared with two fluids. Examples of porous media are sandstone and limestone rocks (D. B. Ingham *et al.*, 2012). The single-phase flow mathematical equations describe the physical processes which represent the relationship between porous medium rocks and fluids to the conditions of the flow (Yahya J. Tawfeeq, 2020). The movement of single-phase liquids across porous media is controlled by Darcy's law (Monicard, 1980; Amyx, 1960), which applies to

incompressible fluids. A calculation of capacity to move fluids of permeable material is specified by the transport coefficient called permeability (Tiab and Donaldson, 2012; Ekwere, 2012). This coefficient of transport is called the absolute permeability in the single-phase flow equation. However, where more than one fluid is in the porous medium, an effective permeability must be defined for each fluid phase. Two laboratory measurement methods are commonly used to evaluate the fluid flow capacity, steady-state method, and unsteady-state method (S. Abaci *et al.*, 1992).

In steady-state methods, constant flow rate and pressure are used to drive a fixed volume ratio of two phases simultaneously through the porous medium until stable saturation and differential pressure. On the other hand, unsteady-state technique includes displacing the saturated fluid phase by injecting another fluid phase, such as displacing oil by water. Also, the saturation equilibrium is not reached in this method. Steady – State techniques for calculating permeability more commonly used, arising from the consistency of mathematical study based on Darcy's Equation and the assumption that saturation is directly calculated. The steady-state approaches provide accurate permeability results for two or three fluids that are simultaneously injected at constant pressure and rates. For these reasons, the course of the steady-state was used in this study.

Darcy's law is the fundamental law of fluid movement in porous media. The mathematical

definition established in 1856 states that "the velocity of a homogeneous fluid in a porous medium is proportional to the gradient of the pressure and inversely proportional to the viscosity of the fluid" (Tarek and McKinney, 2005). Darcy equation was established in 1856 by Henry Darcy (Frick, 1962; Engler, 2003) for incompressible single-phase fluids flow (water) and expressed as shown in Eq. 1 (Olivier, 2005; Martin, 2011; Tarek, 2010):

$$v = \frac{q}{A} = \frac{k}{\mu} \left(\frac{dp}{dl} \right) \quad (1)$$

Where:

v = fluid flow superficial velocity (cm/sec)

q = flow rate (cm³/s)

k = permeability (Darcy)

A = cross-sectional area of sample (cm²)

ΔP = pressure differences (atm)

μ = fluid viscosity (cp)

L = sample length (cm)

For the permeability 'K', Eq. 1 could be transposed as Eq. 2:

$$K = \mu \frac{q}{A} \frac{L}{\Delta P} \quad (2)$$

The permeability dimensions are defined by substituting " μ , q , L , A , and ΔP " units in the above Equation. The Darcy unit derives from the selecting of "cgs" system units as shown Eq. 3.

$$\text{darcy } [D] = \frac{q \left[\frac{\text{cm}^3}{\text{s}} \right] \mu [\text{cp}] L [\text{cm}]}{\Delta P [\text{atm}] A [\text{cm}^2]} \quad (3)$$

In the early 1900s (Chalmers *et al.*, 1932; Muskat, 1937; Botset, 1940; Tiab and Donaldson, 2012), theoretical aspects and measuring methods relevant to the permeability studied. Muskat *et al.* (1937) showed that "the volumetric flow rate can be written individually for each fluid/phase flowing into the pore" (Olivier, 2005) as follows (Eq. 4):

$$Q_i = \left(\frac{K_n}{\mu_n} \right) \frac{A}{L} \Delta P \quad (4)$$

Where:

Q_n = flow rate of phase n (cm³/s)

K_n = phase " n " effective permeability (Darcy)

μ_n = fluid " n " viscosity (cP)

ΔP = pressure differences (atm)

L = core length (cm)

A = cross sectional area (cm²)

Muskat *et al.* (1937), suppose that the law of Darcy applies to any fluid when the fluids are liquid and gas, and showed that ' q ' could be written as a volumetric flow rate (Eq. 5 and 6):

$$Q_g = \left(\frac{K K_{rg}}{\mu_g} \right) \frac{A}{L} \Delta P_g \quad (5)$$

$$Q_l = \left(\frac{K K_{rl}}{\mu_l} \right) \frac{A}{L} \Delta P_l \quad (6)$$

where ' g ' refers to a gas phase, ' l ' refers to a liquid phase and the pressure drop along denotes by ' ΔP '. The value ' k_{rg} ' is gas effective permeability, and ' k_{rl} ' is effective liquid permeability. Every phase of the fluid is analogous to a homogenous system. The flow rate is proportional to the differential pressures and effective permeability and inversely proportional to the fluid phases' viscosity. The terms ' k_{rg} ' and ' k_{rl} ' are referred to as relative permeability.

Effective and relative permeabilities are functions of fluids that exist in a porous medium and porosity. Porosity can be measured directly or be calculated indirectly. The porous medium's flow characteristics are characterized by effective and relative permeability when saturated with an immiscible fluid phase. Therefore, the relative permeability of a porous medium depends on the saturation, so that relative permeability measurements require a precise saturation determination. By the presence of other phases, the flow of each phase is hindered. Therefore, the number of relative permeabilities is less than 1 (Bravo and Araujo, 2008). Theoretical aspects and measuring techniques of the relative permeability of sedimentary rocks were studied at the beginning of 1900s (Chalmers, J. Et.al, 1932; Muskat, M., 1937; Botset, H.G., 1940; Muskat, M., 1949; Wyckoff, R.D., and Botset, H.G., 1936).

Later, Wyckoff and Leverett (Wyckoff, R.D., and Botset, H.G., 1936; Leverett, M.C., 1939) discussed the gas-liquid mixtures flow through unconsolidated sands. Further experimental experiments were carried out, and laboratory measuring techniques were developed for the flow of two fluids through reservoir rocks by Richardson, Hafford, and other investigators (Osoba, J.S. *et al.*, 1951; Ceffen *et al.*, 1951; Caudle, B.H. *et al.*, 1951; Corey, A.T., 1957; Corey, A. T., 1954). There has been a growing interest in permeability testing on materials found near waste disposal sites, and research findings on relative permeability measurements have been reported to study the movement of typical pollutants (Faust, C. R., 1985).

This study aimed to design and build up a laboratory apparatus rig to determine the fluid flow capacity for two unconsolidated sand samples, using the Darcy equation. This test was essential since the understanding of flow capability can demonstrate how a porous medium makes fluids to flow through it and how effectively hydrocarbons would flow into the wellbore

2. MATERIALS AND METHODS:

2.1. Experimental Equipment Design

In the steady-state method, fluid flows at constant pressure and flow rate through the porous media until the differential pressure and saturation become constant. In the start-up of the research project during the apparatus's initiation process, equipment was not available in the research laboratory. Thus, tremendous effort and engineering thinking were made to build up the held equipment for the construction and building.

For limited cases, the sample of both fine sandstone and coarse sandstone were prepared by placing an amount of sandstone with different densities in a sieve shaker with different Mesh, used to separate sand granules according to its density, then the samples withdrawn from the sieve and placed after measuring in the 3" O.D. pipe core holder made from galvanized metal with 30 cm length. The core holder's ends are closed by glass wool to ensure no clarity of sands, and the filled sample is entirely squeezed to prevent the channeling phenomenon at high pressure. Water was injected into the core holder gradually, and it observed that the clay came out from the exiting side of the core holder due to its density less than the density of sand. A once through-flow system was designed and constructed to ensure studying flow capacity by water injection and

permeability under steady-state condition.

The flow system (Figure 1) consists of an air compressor with 16 maximum bar pressure as an air feeder, vacuum pump supplied from Kohler company removes gas molecules from a sealed volume. Pressure Regulator used to control the compressor pressure, core holder, water tank of 9-liter capacity. Valves and fittings are used to control fluid flowing inside the rig, different gauge pressure types, and float flow meter for measuring the exiting fluid.

2.2. Experimental Measurement Technique

In this research, the steady-state process method is used to determine the permeability and relative permeability of unconsolidated sands to water flow. Steady – State techniques for calculating permeability more commonly used, arising from the consistency of mathematical study based on Darcy's Equation and the assumption that saturation is directly calculated. The steady-state approaches provide accurate permeability results for two or three fluids simultaneously injected at constant pressure and rates. For these reasons, the course of the steady-state was used in this study. A standardized method includes the following determinations; liquid flow rate, gas flow rate, pressure gradient, and sample saturation. The fluid flow rate was calculated using the pressure gauges connected to the sample holder by measuring the pressure differences along with the core sample (Honarpour *et al.*, 1986; Honarpour *et al.*, 1988). The material saturation amounts can be calculated by dividing the volume of collected water in a cylinder by the core sample's total pore volume.

3. RESULTS AND DISCUSSION:

3.1. Core Sample Porosity Calculation

A rock's porosity is the proportion of the amount of space between the material's solid particles to the rock's total volume. Porosity measured as the rock's pore volume divided by its bulk volume as shown in Eq. 7 (Ghassan H. Ali *et al.*, 2019; Mohammed Y. Najmuldeen *et al.*, 2020):

$$\phi = \frac{V_p}{V_b} \quad (7)$$

The two cylindrical core samples' length and diameter are measured in inches using a Vernier caliper (Figure 2). The measurements were translated to centimeters (cm) [1 inch = 2.54 cm]. Core sample volume can be measured using

the cylinder volume by Eq. 8:

$$\text{Bulk Volume} = \frac{\pi}{4} D^2 L \quad (8)$$

Where:

D = diameter of the core sample

L = length of the core sample

$\pi = 3.14$

The core sample's pore volume was evaluated from subtracting the amount of water in (remaining water in the tank, valves, pipes, and amount of water out) from the original water inside to the tank. Finally, each core sample's porosity was calculated from the rock pore volume divided by its amount of bulk using Equation (7). The core specifications and porosity results are tabulated in Table 1.

3.2. Absolute Permeability Determination

The permeability measuring technique consisted of injecting gas or a liquid into the unconsolidated sand core sample at a steady rate (Yahya J. Tawfeeq *et al.*, 2020). Figure 1 displays the schematic diagram of the designed equipment. A known weight of the selected grain size of unconsolidated sand was filled in the sample container, which is known as a core holder. Each part of the volume of sand was tamped carefully by a rod. The laboratory procedure started with operating the vacuum pressure to empty the system from the air. During the evacuation, the system from air the two end valves must close, while inside valves opened. The pressure level will be achieved by changing the pressure control valve that wanted to supply to the system. Turn the valve gradually such that the pressure provided is directed into the cell-containing water and a sufficient flow produced into the core. We wait until the cylinder was filled to a readable level with liquid, the cylinder removed, and the timer stopped simultaneously. Read the amount of water that collects and record all data: volume, the time elapsed, and inlet pressure. Different flow rates measured for different pressure gradient, at viscose flow, the results for core sample #1 one, and sample #2 are shown in Tables 2 and 3.

As the flow rate increases, the pressure difference also increased. There was a direct correlation and relationship between the flow rate and the pressure difference. This relationship can be seen from Tables 3 and 4 when the flow rate

was 0.271 cm³/sec, and the pressure gradient was 1.283 atm. Also, when the flow rate increased to 0.469 cm³/s, the pressure gradient increased to 1.703 atm, resulting in a straight-line plot of pressure gradient against the flow, as shown in Figures 3 and 4. Darcy Equation could be used for measuring the core plug's absolute permeability through Eq. 9 and 10:

$$q = \frac{A K \Delta p}{\mu L} \quad (9)$$

and

$$q = \frac{Q}{\Delta t} \quad (10)$$

Where: "q" is the water flow rate cm³/sec; "Q" is the collected water volume during a specific time (sec); "ΔP" is the pressure differential (atm); "A" is cross-section area cm²; "L" is core sample length cm.

First, we find (ΔP/L), where L is the core length in cm, and q/A, where A= cross-sectional area of the core in cm²; the results are given in Table 4. Then plot ΔP/L versus (q/A) will provide a straight line with slope (Eq. 11);

$$\text{slope} = \frac{K}{\mu} \quad (11)$$

Figures 3 and 4 show that the linear best fit through all experimental data-points will give a slope, from which the permeability (K) calculated. The results of computed slope and absolute permeability are given in Table 5.

3.3. Effective / Relative Permeability and Fluid Saturation Determination

There are three primary types of permeability: absolute, relative, and effective. Phase (i) relative permeability could be expressed by Eq. 12:

$$K_{ri} = \frac{K_i}{K} \quad (12)$$

Where:

K_{ri} is the relative permeability of phase i (i = oil, water, and gas)

K_i is the effective permeability of phase i (i = oil, water, and gas)

k is the permeability of the porous medium in single-phase flow, i.e., the absolute permeability.

Muskat *et al.* (1937) (Olivier Darrigol, 2005), based on Darcy's law showed that "the volumetric flow rate can be written individually for each fluid/phase flowing into the pore" as shown in Eq 13:

$$Q_i = K k_{ri} \left(\frac{A}{\mu i} \right) \frac{\Delta P_i}{L} \quad (13)$$

The laboratory technique started applied to the sample one fluid phase (water) and changed this phase's flow rate until the sample was 100 percent filled with water. Regulators and pressure gauges attached to the system were responsible for assessing and changing water flow rates. A second phase injection, which was gas, began at a low rate, and the first phase flow significantly decreased. This technique maintained the differential pressure constant in the system. We wait until the cylinder filled up to a readable level with the water, remove the cylinder and simultaneously stop the timer. Read the amount of water that collects and record all of the data: distance, the time elapsed, and inlet pressure. The differential pressure was measured using the pressure gauges attached to the system. The effective permeability of water is calculated by Darcy equation using Equation (14) while the relative permeability of water computed using Equation (16) as;

$$K_w = \frac{q_w \mu_w L}{A \Delta P} \quad (14)$$

With

$$q_w = \frac{Q_w}{\Delta t} \quad (15)$$

$$K_{rw} = \frac{K_w}{K} \quad (16)$$

Where: "q_w" is the water flow rate cm³/sec; "Q_w" is the water volume collected in water graduated cylinder during a specific time (sec); "ΔP" is the pressure differential across the core (atm); "A" is cross-section área (cm²); "L" is core sample length cm; "μ_w" is the viscosity of water cp; "K_{rw}" is the relative permeability of water; "K_w" is the effective permeability of water; "k" is the absolute or total permeability of core sample

The results of the effective and relative permeability of water tabulated in Table 6. Relative permeability measurements require accurate determination of the saturation (Honarpour and Mahmud, 1988). The fluid saturation is given by Eq. 17:

$$S_f = \frac{V_f}{V_p} \quad (17)$$

Where: "S_f" is fluid saturation; "V_f" is fluid volume, and "V_p" is total pore volume. Saturation is a concept used to describe relative fluid concentrations in a porous medium; as the saturation varies over time, the total saturation value for two fluids is equal to one. Saturation and permeability are both affected by the porosity of the rock sample. Water saturation calculated by dividing the collected water volume in a cylinder by total core sample pore volume as shown in Eq. 18:

$$S_w = \frac{V_w}{V_p} \quad (18)$$

Where S_w is the water saturation, V_w is the volume of water accumulated in the graduated cylinder in cm³ and V_p is the total pore volume in cm³. The results of water saturation are tabulated in Table 6.

3.4. Present Study Limitations

In this experiment, the following errors may have arisen. The packed sand layer may not characterize the rock reservoir as reservoir rocks are not homogeneous, but heterogeneous. There could be a willingness to examine the best portions of sand medium and an inability to read the gages correctly. The sand medium's permeability altered whether it was collected from the original sample or if it was washed and packed.

4. CONCLUSIONS:

When preparing the sample, if the sample container is filled with a more significant amount of sand, the permeability will decrease, requiring high pressure for fluid flowing within the sample. The PVC plastic pipes used to prepare some equipment parts cannot withstand high pressure greater than 10 bar. A metallic material was used for the sample cover to withstand high pressure during the test. Distilled water is preferable to use during the experiment to avoid sample damage, leading to an error in calculations. The medium relative permeability depends on the saturation of the various phases. A proportional relationship exists between flow rate and pressure gradient during fluid flow through a porous medium. The relation between the flow rate, viscosity, sample length of rock bed, permeability, the sample size of the cross-sectional bed of rock, and pressure

gradient are proportional. To assess absolute permeability, the pores media must be 100% saturated with the specific fluid type. Absolute permeability does not depend on fluid characteristics but only on media properties.

5. REFERENCES:

1. Amyx, J.W., (1960). Bass, D.M., and Whiting R.L., Petroleum Reservoir Engineering, McGraw-Hill, New York, NY (1960).
2. Botset, H. G. (1940). Flow of Gas-Liquid Mixtures Through Consolidated Sand. Trans., AIME, 136, 91.
3. Bravo, M.C., Araujo, M. (2008). "Analysis of the Unconventional Behavior of Oil Relative Permeability during Depletion Tests of Gas-Saturated Heavy Oils". International Journal of Multiphase Flow. 34 (5): 447–460.
4. Caudle, B.H., Slobod, R.L. and Brownscornbe, E.R., (1951). Further Developments in the Laboratory Determination of Relative Permeability. Trans. of AIME. Petroleum Branch. Vol. 192: 145 - 150.
5. Chalmers, J., Taliaferro, D.B., Rawlins, E.L and Okla, B., (1932). Flow of Air and Gas Through Porous Media. Trans. Am. Inst. Min. Met Eng. (Petroleum Develop. and Techn.). Vol. 98: 375 - 400.
6. Corey, A.T., (1957). Measurement of Water and Air Permeability in Unsaturated Soil. Soil Science Society of America, Proceedings. Vol. 21 : 7 -11.
7. Corey, A. T., (1954). The Interrelation Between Gas and Oil Relative Permeabilities, Producers Monthly, Vol. 19 (1) : 38 - 41.
8. D. B. Ingham, Derek B. Ingham, Adrian Bejan, Eden Mamut, Ioan Pop., (2012). Emerging Technologies and Techniques in Porous Media, 2nd edition, Springer, NATO Science Series 134, Netherlands.
9. Ekwere, J.P, (2012). Advanced petrophysics; geology, porosity, absolute permeability, Heterogeneity and geo-statistics. Vol 3 1st ed. Live Oak Book Company. Chapter three.
10. Engler, T.W., (2003). Fluid Flow in Porous Media – Notes of Class Petroleum Engineering 524 – Fall 2003.
11. Faust, C. R., (1985). Transport of Immiscible Fluids Within and Below the Unsaturated Zone: A numerical Model. Water Resources Research, 21 (4): 587-596.
12. Frick T.C., (1962). Petroleum Production Handbook, Vol II; Society of Petroleum Engineers, Dallas, TX.
13. Ceffen, T.M., Qwens, W.W., Parrish, D.R. and Morse, R.A., (1951). Experimental Investigation of Factors Affecting Laboratory Relative Permeability Measurements. Trans. of AIME. Petroleum Branch. Vol. 192: 99 -110.
14. Ghassan H. Ali, Yahya J. Tawfeeq, and Mohammed Y. Najmuldeen, (2019). Comparative estimation of water saturation in a carbonate reservoir: A case study of northern Iraq. Periodicals of Engineering and Natural Sciences, Vol. 7, No. 4, December 2019, pp.1743-1754.
15. Honarpour, M. and Mahmud, S. M., (1988). Relative Permeability Measurements: An Overview, Soc.of Pet. Eng. (SPE), Journal of Petroleum Technology, Today Series, 963 - 966.
16. Jacob Bear, (2013). Dynamics of fluids in Porous Media, Dover Publications, ISBN 9780486131801.
17. Leverett, M.C., (1939). Flow of Oil - Water Mixtures Through Unconsolidated Sands. Trans. of AIME. Vol. 132 :149 - 171.
18. Honarpour, M., Koederitz, L. and Harvey, A.H., (1986). Relative Permeability of Petroleum Reservoirs, CRC Press, Inc. Boca Raton, Florida.
19. Honarpour, M. and Mahmud, S. M., (1988).Relative Permeability Measurements: An Overview, Soc.of Pet. Eng.(SPE), Journal of Petroleum Technology, Today Series, 963 - 966.
20. Martin Zerner, (2011). The origins of Darcy's law (1856), Documents pour l'histoire des techniques, p. 29-40.
21. Mohammed Y. Najmuldeen, Ali A. Fadhil, and Yahya J. Tawfeeq, (2020). Petrophysical Characterization of The Tertiary Oil Reservoir, Northern Iraq. Periodicals of Engineering and Natural Sciences, Vol. 8, No. 2.
22. Monicard, R. P., (1980). Properties of Reservoir Rocks: Core Analysis. Gulf Publishing Co., Houston, TX (1980).

23. Muskat, M., (1937). The Flow of Homogeneous Fluids Through Porous Media McGraw - Hill. New York.
24. Muskat, M., (1949). Physical Principles of Oil Production, McGraw – Hill Book Co. Inc., New York.
25. Olivier Darrigol, (2005). A History of Hydrodynamics from the Berboullis to Prandtl, Oxford University Press, ISBN 978-0-19-856843-8, lire en ligne.
26. Osoba, J.S., Richardson, J.G., Kerver, J.K., Hafford, J.A. and Blair, P.M., (1951). Laboratory Measurements of Relative Permeability. Trans. of the AIME. Petroleum Branch. Vol. 192 : 47 - 46.
27. S. Abaci, J. S. Edwards and B. N. Whittaker, (1992). Relative Permeability Measurements for Two-Phase Flow in Unconsolidated Sands, Mine Water and The Environment, Vol. 21, No. 2, June 1992, pp 12-26.
28. Rahimi-Gorji, M., Gorji, T.B., Gorji-Bandpy, M., (2016). Details of regional particle deposition and airflow structures in a realistic model of human tracheobronchial airways: two-phase flow simulation. Comput. Biol. Med. 74, 1–17.
29. Tarek, A., (2010). Reservoir Engineering Handbook. 4th ed. Oxford: Elsevier, Inc. Chapter 4 and 5.
30. Tarek, A., and McKinney, P.D., (2005). Advanced Reservoir Engineering. Burlington, Massachusetts: Elsevier, 2005.
31. Tiab, D and Donaldson, E.C., (2012). Petrophysics: theory and practice of measuring reservoir rock and fluid transport properties. 3rd ed. Oxford: Gulf Professional Publishing. Chapter 3.
32. Vafai, Kambiz, (2015). Handbook of porous media, Third edition, CRC Press.
33. Wyckoff, R.D., and Botset, H.G., 1936. The Flow of Gas-Liquid Mixtures Through Unconsolidated Sands. Physics, Vol. 7: 325 - 345.
34. Yahya J. Tawfeeq, Mohammed Y. Najmuldeen and Ghassan H. Ali, (2020). Optimal statistical method to predict subsurface formation permeability depending on open hole wireline logging data: A comparative study. Periodicals of Engineering and Natural Sciences, , Vol. 8, No. 2.
35. Yahya J. Tawfeeq, (2020). Mathematical modeling and numerical simulation of porous media single-phase fluid flow problem: a scientific review. International Research Journal of Engineering, IT & Scientific Research, 6(4), 15-28.

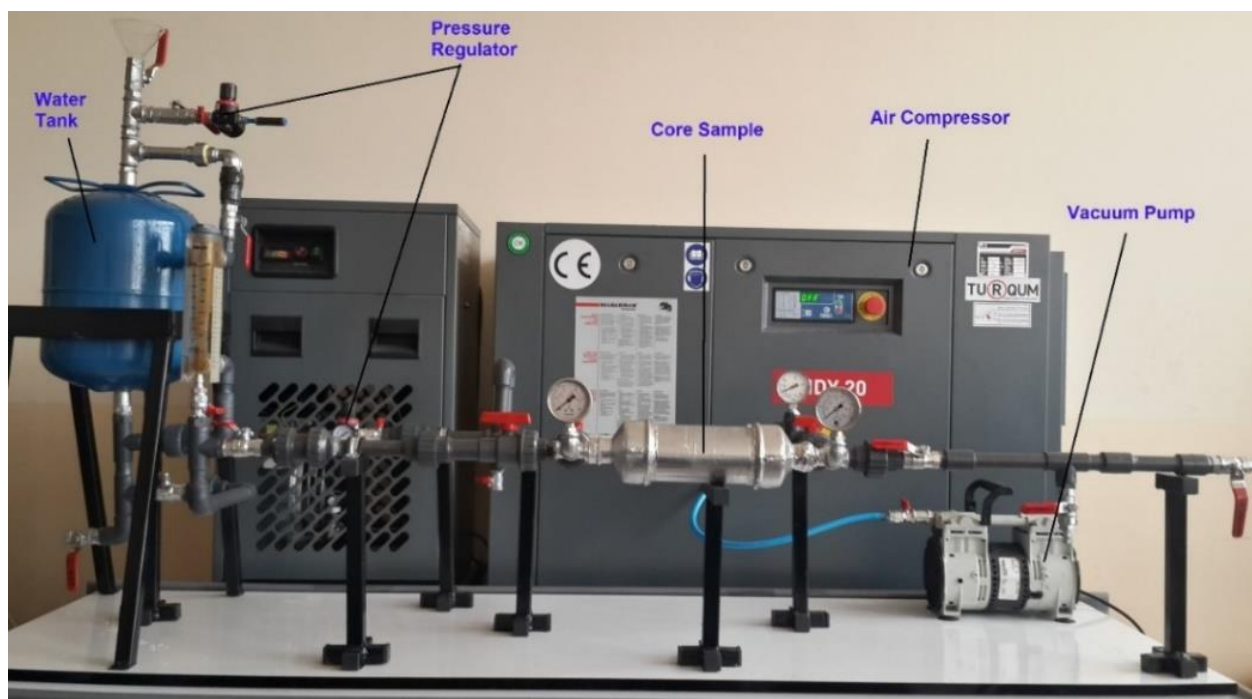
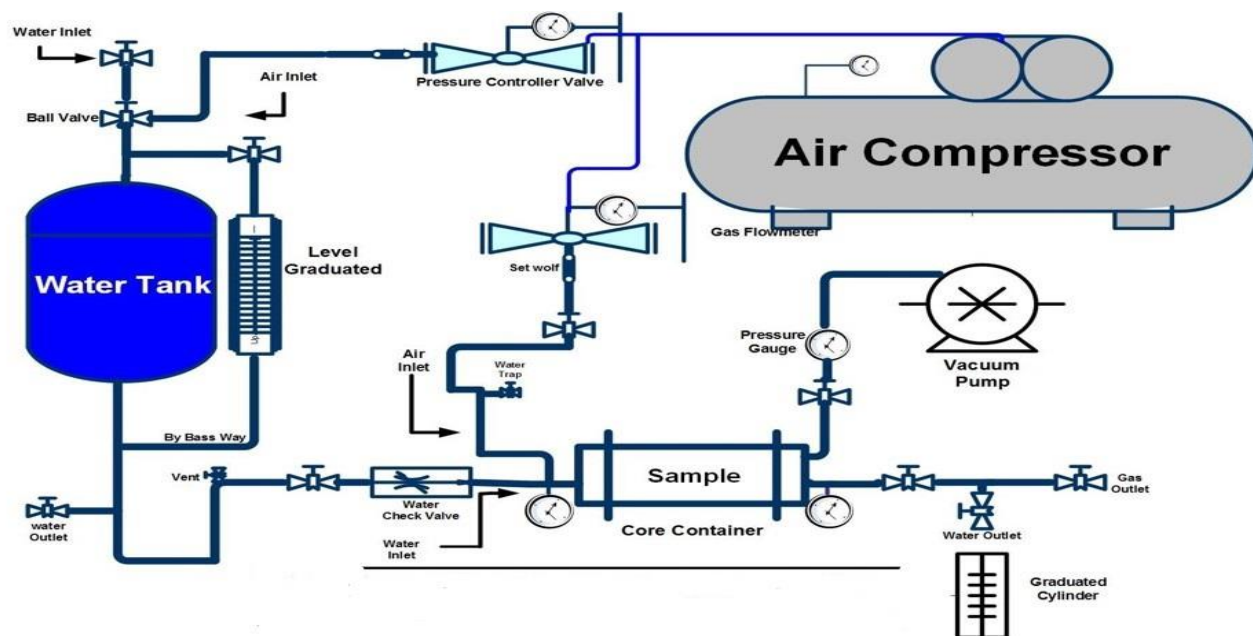


Figure 1. The schematic diagram of the designed apparatus.

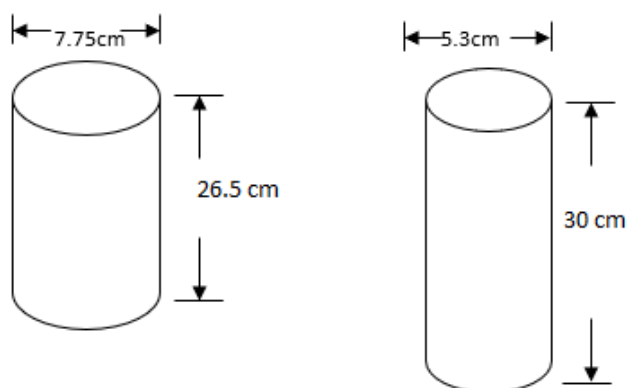


Figure 2. Sketch of Core Sample

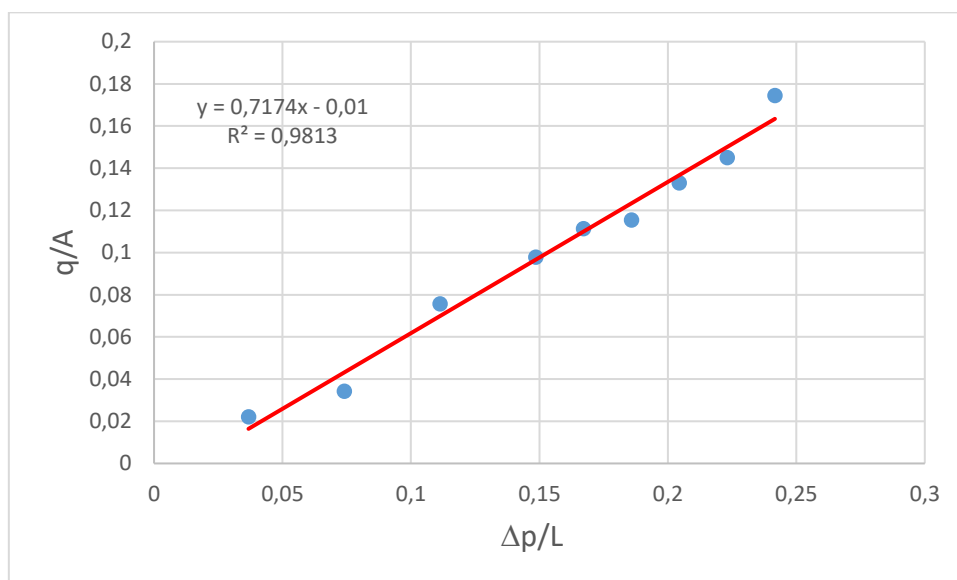


Figure 3. Pressure Gradient Vs. Flow Rate for Sample # 1

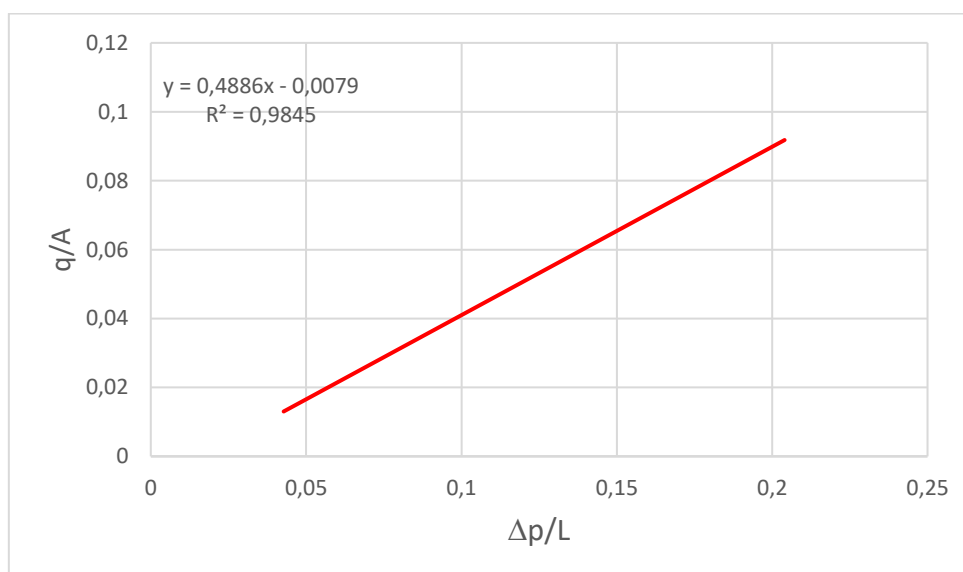


Figure 4. Pressure Gradient Against Flow Rate for Sample # 2

Table 1. Core Samples Dimensions and Calculated Porosity Results

	Core Sample # 1	Core Sample # 2
Lithology	Coarse sand	Fine sand
Grain Size (μm)	500	125
Core Diameter (cm)	7.75	5.3
Cross Section Area (cm^2)	47.173	22.062
Core Length (cm)	26.5	30
Pore Volume (cm^3)	359	102
Bulk Volume (cm^3)	1250	661.855
Core Porosity %	28.72	15.41

Table 2. Results of Flow rate vs. Pressure for Core Sample # 1

Test N°.	Δp (atm)	Volume of Liquid collected Q (cm^3)	Duration, Δt (sec)	Flow rate q (cm^3/sec)
1	0.9743	250	239.43	1.044
2	1.9615	250	154.63	1.616
3	2.9487	250	70.1	3.571
4	3.9358	250	54.14	4.617
5	4.4294	250	47.58	5.254
6	4.923	250	45.91	5.445
7	5.4166	250	39.82	6.278
8	5.9102	250	36.55	6.839
9	6.4038	250	30.36	8.234

Table 3. Results of Flow rate vs. Pressure for Core Sample # 2

Test N°.	Δp (atm)	Volume of Liquid collected Q (cm^3)	Duration, Δt (sec)	Flow rate q (cm^3/sec)
1	1.283	150	553.71	0.271
2	1.703	150	320.03	0.469
3	2.124	150	228.72	0.656
4	4.235	150	125.32	1.197
5	4.836	150	97.65	1.536
6	6.12	150	70.63	2.124

Table 4. Pressure Gradient Per core length and Flow Rate Per Core Area Results for Two Samples

Test N°.	Sample # 1		Sample # 2	
	q/A	$\Delta p/L$	q/A	$\Delta p/L$
1	0.022131	0.036766	0.01228	0.042767
2	0.034257	0.074019	0.021247	0.056767
3	0.0757	0.111272	0.029728	0.0708
4	0.097874	0.148521	0.054257	0.141167
5	0.111377	0.167147	0.069628	0.1612
6	0.115426	0.185774	0.096265	0.204
7	0.133085	0.2044		
8	0.144977	0.223026		
9	0.174549	0.241653		

Table 5. Determined Slope and Absolute Permeability Results for Two Samples

Core	Fluid Viscosity cp	Calculated Slope	Absolute Permeability Darcy
Core Sample # 1	1	0.7174	0.7174
Core Sample # 1	1	0.4886	0.4886

Table 6. Effective Permeability, Relative Permeability and Water Saturation Results for Two Samples

Test N°.	Core Sample # 1			Core Sample # 2		
	K _{eff} (Darcy)	K _{rw}	Sw%	K _{eff} (Darcy)	K _{rw}	Sw%
1	0.6351	1	100	0.01486	1	100
2	0.6034	0.9501	95	0.01373	0.924	91.23
3	0.5349	0.8422	90	0.01064	0.716	72.07
4	0.4048	0.6374	80.45	0.00814	0.548	57.36
5	0.1959	0.3085	75.98	0.005734	0.3858	41.57
6	0.1287	0.2026	69.83	0.003477	0.2339	27.21
7	0.0486	0.0765	65.36			
8	0.0382	0.0601	56.797			
9	0.0156	0.0246	49.91			
10	0.0044	0.0069	45.44			
11	0.0011	0.0017	43.57			
12	0.0005	0.0008	34.26			

EFEITO DE UMA BARREIRA NO AUTOVALOR ENERGÉTICO DA EQUAÇÃO DE SCHRÖDINGER NÃO RELATIVISTA E ALGUNS VALORES DE EXPECTATIVA DE POTENCIAIS COMBINADOS

EFFECT OF A BARRIER ON ENERGY EIGENVALUE OF THE NONRELATIVISTIC (SCHRÖDINGER EQUATION) AND SOME EXPECTATION VALUES OF COMBINED POTENTIALS

ONATE, Clement Atachegbe^{1*}; ONYEAJU, Michael Chukwudi²; ABOLARINWA, Abimbola³; OKORO, Joshua Otonritse⁴

¹ Physics Programme, Department of Physical Sciences, Landmark University, Omu-Aran, Nigeria.

² Department of Physics, Theoretical Physics Group, University of Port Harcourt, Choba, Nigeria

³ Department of Mathematics, University of Lagos, Akoka Lagos, Nigeria.

⁴ Mathematics Programme, Department of Physical Sciences, Landmark University Omu-Aran, Nigeria,

* Corresponding author
e-mail: onate.clement@lmu.edu.ng

Received 30 June 2020; received in revised form 18 August 2020; Accepted 25 October 2020

RESUMO

A equação de Schrödinger foi proposta na física teórica para fornecer informações e o comportamento do sistema de partículas. A equação de Schrödinger foi recentemente resolvida para uma combinação de diferentes potenciais usando diferentes metodologias tradicionais. Os estudos não consideram o efeito de uma barreira entre os potenciais. Na realidade, a barreira entre os potenciais tem efeito sobre os autovalores de energia. No presente trabalho, um potencial do tipo Kratzer-Mie, que é uma combinação dos potenciais constantes do tipo Kratzer e Mie, foi proposto como o potencial de interação. As soluções da equação de Schrödinger radial foram obtidas na presença da combinação de potenciais considerando uma barreira entre os potenciais. A equação de energia e as funções de onda correspondentes foram calculadas explicitamente. Os cálculos foram realizados utilizando a metodologia da mecânica quântica supersimétrica. Este método envolve a proposição da função superpotencial como uma solução para sua equação diferencial de Riccati. Resultados numéricos foram gerados para algumas moléculas diatômicas usando a equação de energia e os parâmetros do modelo diatômico. Alguns valores esperados para o potencial combinado foram calculados usando o teorema de Hellmann Feynman e o efeito da barreira sobre os valores esperados foram estudados numericamente. Pode-se observar que, quando uma partícula se move da extremidade inferior para a extremidade superior de uma barreira, ela absorve energia do sistema por alguns momentos. Esse mesmo comportamento também foi observado quando a partícula penetra por uma barreira. Assim, sua vibração dependerá apenas da energia inicial que absorveu. É igualmente visto que à medida que a largura da barreira se torna maior do que a altura, a energia do sistema diminui drasticamente.

Palavras-chave: *Eigen-soluções, equações de onda, potencial tipo Kratzer-Mie, moléculas diatômicas.*

ABSTRACT

Schrödinger equation was proposed in theoretical physics to provide information and the behavior of a system of particles. The Schrödinger equation was recently solved for a combination of different potentials using different traditional methodologies. The studies do not consider the effect of a barrier between the potentials. In reality, the barrier between the potentials has an effect on the energy eigenvalues. In the present work, a Kratzer-Mie-type potential, a combination of Kratzer and Mie-type-constant potentials, was proposed as the interacting potential. The solutions of the radial Schrödinger equation was obtained in the presence of the combined potentials by considering a barrier between the potentials. The energy equation and the corresponding wave functions were explicitly calculated. The calculations were performed by using the methodology of supersymmetric quantum mechanics. This method involves the proposition of superpotential function as a solution to its Riccati differential equation. Numerical results were generated for some diatomic molecules using the energy equation and the diatomic model parameters. Some expectation values for the combined potential were calculated using

Hellmann Feynman Theorem, and the effect of the barrier on the expectation values were numerically studied. It was observed that when a particle moves from the lower end to a higher end of a barrier, it absorbs energy from the system for some time. This same behavior was also noted when the particle penetrates through a barrier. Thus, its vibration will only depend on the initial energy, which is absorbed. It was equally seen that as the width of the barrier becomes larger than the height, the energy of the system decreases drastically.

Keywords: *Eigensolutions, Wave equations, Kratzer-Mie-type potential, diatomic molecules.*

1. INTRODUCTION:

The exact solutions of both the relativistic and nonrelativistic wave equations with some physical potential models are of great interest because the analysis of the solution makes a conceptual understanding of the state of the quantum and physical systems, such as the wave functions and eigenvalues. These solutions provide means to improve certain models and numerical methods for solving complicated physical systems (Flügge, 1974; Schiff, 1995) like Fisher information, Shannon entropy, and even some thermodynamic properties (mean energy, free energy, heat capacity, and entropy). The exact solutions of the wave equations are limited to a few numbers of physical potentials such as Harmonic oscillator, Coulomb potential, pseudoharmonic potential (Landau and Lifshitz, 1977; Ikhdair and Sever, 2007).

However, to make other potential models such as Frost-Musulin, Hellman, Yukawa, Inversely Quadratic Yukawa potentials relevant in the computation of Fisher information, Shannon entropy and thermodynamic properties, various traditional methods (analytic tools) have been developed by different authors to solve the wave equations in the presence of any physical potential models of interest. The traditional methods include supersymmetry quantum mechanics (Witten, 1981; Cooper *et al.*, 1995; Onate *et al.*, 2019), which involves the proposition of superpotential function based on the interacting potential. The superpotential function then relates to a Riccati equation where two partner potentials can be written. With some algebraic simplification and considering the negative partner potential, the energy equation can be obtained. The formula method for bound state problems (Falaye *et al.*, 2015) is another traditional method. This method involves a transformation of a variable for mathematical simplicity. The factorization method (Dong, 2007; Rahbar and Sadegh, 2016; Hoseein *et al.*, 2019) uses the formulation of independent variables. Nikiforov-Uvarov method (Nikiforov and Uvarov, 1988; Tezcan and Sever, 2009; Oluwadare *et al.*, 2012; Onate and Idiodi, 2016; Onyeaju *et al.*, 2017; Ikot *et al.*, 2018) involves the

reduction of a second-order linear differential equation to the generalized equation of the hypergeometric type. Asymptotic iteration method (Bayrak and Boztosun, 2007; Falaye, 2012; Falaye *et al.*, 2013; Oyewumi *et al.*, 2014), proposes variables that are sufficiently differentiable, which later leads to a recurrence relation where energy eigenvalues are obtained from the root of a quantized condition. The mathematical details of each of the methods can be found in the cited references and references therein. The most popular wave equations solved by these methods are Schrödinger equation, Dirac equation for spin and pseudospin symmetries, and Klein-Gordon equation. Under the Dirac equation, the solutions of both spin and pseudospin symmetries have been obtained in the presence of tensor interaction that brings about atomic stability as reported by Onate *et al.* (2017b; 2019), Ikot (2012), Hassanabadi *et al.* (2013) and others.

In bound state solutions of the Schrödinger equation, these methods have different approaches to the solutions but give each physical potential model an agreeable result. The energy equation obtained in most cases are used to generate energy eigenvalues (energy spectra) for some molecules. The generated eigenvalues are used to study the behaviour of different molecules with respect to the potential parameters under consideration. Different potential models have been combined and studied in terms of bound states. For instance, Edet *et al.* (2020) combined modified Kratzer potential and screened Coulomb potential and obtained bound state solutions in the domain of the nonrelativistic regime. Similarly, Okorie *et al.* (2020), combined Hyperbolic and Pöschl-Teller potentials to study the thermodynamic properties of a system. Other combinations of potentials were also reported. However, to the best of our knowledge, the effect of the boundary between these potentials on the bound state has not been investigated and reported yet. Motivated by this, the present study intends to investigate a one-dimensional radial Schrödinger equation with a combination of two different potentials. The two potential models to be considered in this work are the generalized Kratzer potential-type $V_1(r)$ and the Mie-type potential

$V_2(r)$. The Kratzer potential has played an important role in the history of quantum mechanics. So far, Kratzer potential has been used extensively to describe the molecular structure and interactions in the quantum domain.

As part of its applications, Bayrak *et al.* (2007), calculated the nonzero angular momentum solutions of the Schrödinger equation for the Kratzer potential and obtained the exact eigenvalues for different diatomic molecules, Ikot *et al.* (2019), obtained eigensolution, expectation values and thermodynamic properties of the screen Kratzer potential. Edet *et al.* (2020), in their own study, obtained bound state solutions of the Schrödinger equation for the modified Kratzer potential plus screened Coulomb potential. The generalized Kratzer potential and the Mie-type potentials are respectively given as

$$V_1(r) = D_e \left(\frac{r-r_e}{r} \right)^2 + \eta \quad (1)$$

$$V_2(r) = D_e \left[\frac{k}{j-k} \left(\frac{r_e}{r} \right)^j - \frac{j}{j-k} \left(\frac{r_e}{r} \right)^k \right], \quad (2)$$

The choice of potential in the present work is the interaction of Eq. (1) and Eq. (2) which is given as

$$V(r) = V_1(r) + V_2(r) = D_e \left(\frac{r-r_e}{r} \right)^2 + D_e \left[\frac{k}{j-k} \left(\frac{r_e}{r} \right)^j - \frac{j}{j-k} \left(\frac{r_e}{r} \right)^k \right] + \eta \quad (3)$$

In the above equation, D_e is a dissociation energy, r_e is the equilibrium bond length, r is the internuclear separation while j and k are potential parameters whose values are define later. The parameter η is a potential constant which can takes either negative or positive value. The potential can yield many results due to its subsets as will be seen later.

Thus, this study aimed to determine the effect of a barrier between two potential models on the energy eigenvalues.

2. MATERIALS AND METHODS:

2.1. Bound State Solutions

To obtain a one-dimensional Schrödinger equation, the original Schrödinger equation of the form is first considered as (Landau and Lifshitz, 1977; Schiff, 1995; Onate, 2016; Onate *et al.*, 2017a)

$$-\frac{\hbar^2}{2m} \left[\frac{1}{r^2} \frac{\partial}{\partial r} r^2 \frac{\partial}{\partial r} + \frac{1}{r^2 \sin \theta} \frac{\partial}{\partial \theta} \left(\sin \theta \frac{\partial}{\partial \theta} \right) + \frac{1}{r^2 \sin^2 \theta} \frac{\partial^2}{\partial \phi^2} \right] \psi(r, \phi, \theta) = (E_{nl} - V(r)) \psi(r, \phi, \theta). \quad (4)$$

To solve the radial part of the Schrödinger equation above, the wave function is set as

$$\psi_{n,\ell}(r, \phi, \theta) = \frac{R_{n,\ell}(r) Y_{m,\ell}(\phi, \theta)}{r}, \quad (4a)$$

and therefore, Eq. (4) becomes

$$\left[-\frac{\hbar^2}{2m} \frac{d^2}{dr^2} + V_1(r) + V_2(r) - \frac{\hbar^2 B_p}{2mr} + \frac{\hbar^2 \ell(\ell+1)}{2m r^2} \right] R_{n\ell}(r) = E_{n\ell} R_{n\ell}(r), \quad (5)$$

where \hbar is the reduced Planck's constant, m is the mass of the particle, $E_{n\ell}$ is the nonrelativistic energy of the system and $R_{n\ell}(r)$ is the wave function. In Eq. (5), the centrifugal term $\frac{\ell(\ell+1)}{r^2}$

and a barrier system $\frac{B_p}{r}$ have been introduced.

Substituting Eq. (3) into Eq. (5), we have a second order differential equation of the form

$$\frac{d^2 R_{n\ell}(r)}{dr^2} - \frac{2m(D_e + \eta - E_{n\ell})}{\hbar^2} = \left[\frac{4mD_e r_e^2 - 8mrD_e r_e - B_p r + \ell(\ell+1)}{\hbar^2 r^2} + \frac{2m(D_e + \eta - E_{n\ell})}{\hbar^2} \right] R_{n\ell}(r), \quad (6)$$

where $j = 2k$ and $k = 1$. To obtain energy equation of Eq. (6), the methodology of

supersymmetric quantum mechanics formalism and shape invariance technique is adopted (Gendenshtein, 1983; Cooper and Freedman, 1983; Comtet *et al.*, 1985; Jia *et al.*, 2007; Hassanabadi *et al.*, 2012a; Onate *et al.*, 2017b), to solve the calculations. Following the theory of calculations via supersymmetric approach for a state when $n = 0$, Eq. (6) can first be written as

$$R_{0,\ell}(r) = \exp\left(-\int W(r)dr\right), \quad (7)$$

where $W(r)$ is regarded as a superpotential function in supersymmetric quantum mechanics, which enables us to propose a solution to the differential equation of Eq. (6). Considering the potential function under consideration in Eq. (3), a superpotential function is given as

$$W(r) = \rho_0 - \frac{\rho_1}{r}. \quad (8)$$

The parameters ρ_0 and ρ_1 are two constants of the superpotential function whose values will be determine later. Substituting Eq. (7) into Eq. (6) results to a Riccati equation of the form

$$W^2(r) - \frac{dW(r)}{dr} = \frac{4mD_e r_e^2 - 8mrD_e r_e - \frac{ar}{w} + \ell(\ell+1)}{\hbar^2 r^2} + \frac{2m(D_e + \eta - E_{n\ell})}{\hbar^2}. \quad (9)$$

By substituting Eq. (8) into Eq. (9), the two parameters ρ_0 and ρ_1 in Eq. (8) can be determine as

$$\rho_0^2 = \frac{2m(D_e + \eta - E_{n\ell})}{\hbar^2}, \quad (10)$$

$$\rho_1 = -\frac{1}{2} \pm \sqrt{\left(\frac{1}{2} + \ell\right)^2 + \frac{4mD_e r_e^2}{\hbar^2}}, \quad (11)$$

$$\rho_0 = \frac{4mD_e r_e}{\hbar^2} \left(\frac{1}{\rho_1}\right), \quad (12)$$

$$B_p = \frac{a}{w}, \quad (13)$$

where a is the height of the barrier and w is the width of the barrier. In this work, the consideration of the bound state is ideal when the radial part of the wave function $\psi(r)$ clearly satisfies the boundary conditions that $R_{n,\ell}(r)/r$ becomes zero

as r tends to infinity and $R_{n,\ell}(r)/r$ is finite as r is zero. In order to make $R_{n,\ell}(r)/r$ satisfy the regularity conditions in this work, the value $\rho_0 > 0$ is obtained.

This is manifested in the energy equation. To achieve every desirable result, a pair of partner potentials is constructed (Witten, 1981; Cooper *et al.*, 1995; Wei and Dong, 2010; Hassanabadi *et al.*, 2011a; Onate, 2014) using the superpotential function of Eq. (8).

$$V_+(r) = \rho_0^2 - \frac{2\rho_0\rho_1}{r} + \frac{\rho_1(\rho_0+1)}{r^2}, \quad (14)$$

$$V_-(r) = \rho_0^2 - \frac{2\rho_0\rho_1}{r} + \frac{\rho_1(\rho_0-1)}{r^2}. \quad (15)$$

Comparing Eqs. (14) and (15), it reveals that the partner potentials satisfied the shape invariance potential and therefore, the shape invariance holds after a mapping of the form $\rho_1 \rightarrow \rho_1 - n$ as the following recurrence relations have been observed: $a_1 = a_0 - 1$, $a_2 = a_0 - 2$, $a_3 = a_0 - 3$. Therefore, the two partner potentials connect with a simple formula of the form:

$$R(a_1) = \frac{4mD_e r_e}{\hbar^2} \left(\frac{1}{a_0} - \frac{1}{a_1}\right), \quad (16)$$

$$R(a_2) = \frac{4mD_e r_e}{\hbar^2} \left(\frac{1}{a_1} - \frac{1}{a_2}\right), \quad (17)$$

$$R(a_3) = \frac{4mD_e r_e}{\hbar^2} \left(\frac{1}{a_2} - \frac{1}{a_3}\right), \quad (18)$$

$$R(a_n) = \frac{4mD_e r_e}{\hbar^2} \left(\frac{1}{a_{n-1}} - \frac{1}{a_n}\right). \quad (19)$$

In the above equations, a_1 is a new set of parameters uniquely determined from an old set of parameters a_0 (Wei and Dong, 2009; Oyewumi and Akoshile, 2010; Hassanabadi *et al.*, 2011b; Jia *et al.*, 2013). Considering the negative partner potential, the deduction of the energy equation begins as

$$E_{n\ell} = \sum_{k=1}^n R(a_k) = \frac{4mD_e r_e}{\hbar^2} \left(\frac{1}{a_0} - \frac{1}{a_1} \right), \quad (20)$$

which can fully be written as

$$E_{n\ell} = D_e + \eta - \frac{\hbar^2}{2m} \left(\frac{4mr_e D_e}{\hbar^2} + \frac{a}{2w} \right)^2 \times \left[n + \frac{1}{2} + \sqrt{\left(\frac{1}{2} + \ell \right)^2 + \frac{4mD_e r_e^2}{\hbar^2}} \right]^{-2}. \quad (21)$$

The corresponding wave function is given as

$$R(s) = N_{n,\ell} s^{\sqrt{\ell(\ell+1) + \frac{4mD_e r_e^2}{\hbar^2}}} e^{\frac{1}{\hbar} \sqrt{2m(D_e + \eta - E_{n,\ell})} s} \times L_n^{2\sqrt{\ell(\ell+1) + \frac{4mD_e r_e^2}{\hbar^2}} - 1} \left(\frac{2}{\hbar} \sqrt{2m(D_e + \eta - E_{n,\ell})} s \right), \quad (22)$$

where a simple transformation of the form $s = r$ was made.

2.1.1. Special Cases

2.1.1.1. Generalized Kratzer Potential

When $j = \eta = 0$, the interacting potential given in Eq. (3) results to a generalized Kratzer potential as

$$V_{GK}(r) = D_e \left(\frac{r - r_e}{r} \right)^2, \quad (23)$$

The energy equation for the generalized Kratzer potential is obtained as

$$E_{n\ell} = D_e - \frac{2mr_e^2 D_e^2}{\hbar^2} [n + \delta_T]^{-2} \quad (24)$$

$$\delta_T = \frac{1}{2} + \sqrt{\left(\frac{1}{2} + \ell \right)^2 + \frac{2mD_e r_e^2}{\hbar^2}}. \quad (24a)$$

2.1.1.2. The Kratzer-Fues potential

The Kratzer-Fues potential. The Kratzer-Fues potential is obtain when $r - r_e = \eta = 0$, $j = 1$ and $k = 2$. Thus, potential (3) turns to

$$V_{KF}(r) = D_e \left(\frac{r_e^2}{r^2} - \frac{2r_e}{r} \right). \quad (25)$$

The energy equation is given as

$$E_{n\ell} = -\frac{2mr_e^2 D_e^2}{\hbar^2} [n + \delta_T]^{-2}. \quad (26)$$

2.1.1.3. The Constant potential

The constant potential is obtained when $D_e = 0$. Thus,

$$V_C(r) = \eta. \quad (27)$$

This potential has energy equation as

$$E_{n\ell} = \eta - \frac{\hbar^2 (1 + n + \ell)}{2m}. \quad (28)$$

2.2. Expectation Values

In this section, some expectation values V , p^2 and r^{-2} of the interacting potential are calculated via the Hellmann Feynman Theorem (Feynman, 1939; Dong *et al.*, 2005; Hassanabadi *et al.*, 2012b; Falaye *et al.*, 2014). The Hellmann Feynman Theorem states that if a non-degenerate or degenerate energy eigenvalue and the corresponding eigenfunction of a Hamiltonian depends on a certain parameter, then the energy eigenvalue varies with respect to that parameter according to the following formula

$$\frac{\partial E_{n,\ell}(v)}{\partial v} = \left\langle R_{n\ell}(v) \left| \frac{\partial H(v)}{\partial v} \right| R_{n\ell}(v) \right\rangle, \quad (29)$$

provided that the associated normalized eigenfunction is continuous with respect to the parameter v . The effective Hamiltonian for our interacting potential radial wave function is given by

$$H = -\frac{\hbar^2}{2\mu} \frac{d^2}{dr^2} + \frac{\hbar^2}{2\mu} \frac{\ell(\ell+1)}{r^2} + \frac{A - Be^{-\alpha(r-r_e)}}{(1 - qe^{-\alpha(r-r_e)})} + \frac{k(C - De^{-\alpha(r-r_e)})^2}{(1 - qe^{-\alpha(r-r_e)})}. \quad (30)$$

According to the theorem, once the spatial distribution of the electrons has been determined by solving the Schrödinger equation, all forces in

the system can be calculated using classical electrostatics. This theorem finds some of its applications in the calculation of intramolecular forces in molecules. Having determined the effective Hamiltonian, the expectation values of the stated parameters can be calculated. The expectation value of V , p^2 and r^{-2} respectively can be obtain by setting $q = D_e$, $q = \mu$ and $q = \ell$.

(i): For V , then,

$$\langle V \rangle_{n,\ell} = D_e - \frac{\left[\frac{4\mu r_e^2 D_e^2}{\hbar^2} - \frac{2a r_e D_e \hbar^2}{w} \right]}{\left(n + \frac{1}{2} + \sqrt{\left(\ell + \frac{1}{2} \right)^2 + \frac{4\mu D_e r_e^2}{\hbar^2}} \right)^2} + \frac{\left[\frac{8\mu r_e^2 D_e^2}{\hbar^2} + \frac{a^2 \hbar^2}{8\mu w^2} - \frac{2a D_e r_e^2 \hbar^2}{w} \right] \left[\frac{4\mu D_e r_e^2}{\hbar^2} + \delta \right]}{\left(n + \frac{1}{2} + \sqrt{\left(\ell + \frac{1}{2} \right)^2 + \frac{4\mu D_e r_e^2}{\hbar^2}} \right)^4} \quad (31)$$

$$\delta = \frac{\frac{2\mu D_e r_e^2}{\hbar^2} (2n+1)}{\sqrt{\left(\ell + \frac{1}{2} \right)^2 + \frac{4\mu D_e r_e^2}{\hbar^2}}} \quad (32)$$

(ii): For p^2 , then,

$$\langle p^2 \rangle_{n,\ell} = \frac{\left[\frac{8\mu r_e^2 D_e^2}{\hbar^2} + \frac{a^2 \hbar^2}{8\mu w^2} - \frac{2a D_e r_e^2 \hbar^2}{w} \right] \left[\frac{4D_e r_e^2}{\hbar^2} + \delta_1 \right]}{\delta_p^4} - \frac{\left[\frac{8r_e^2 D_e^2}{\hbar^2} - \frac{a^2 \hbar^2}{8\mu^2 w^2} \right] \delta_p^2}{\delta_p^4} \quad (33)$$

$$\delta_p = n + \frac{1}{2} + \sqrt{\left(\ell + \frac{1}{2} \right)^2 + \frac{4\mu D_e r_e^2}{\hbar^2}} \quad (33a)$$

$$\delta_1 = \frac{\frac{2D_e r_e^2}{\hbar^2} (2n+1)}{\sqrt{\left(\ell + \frac{1}{2} \right)^2 + \frac{4\mu D_e r_e^2}{\hbar^2}}} \quad (34)$$

(iii): For r^{-2} , then,

$$\langle r^{-2} \rangle = \frac{\frac{2\mu}{\hbar^2 (2\ell+1)} \left[\frac{8\mu r_e^2 D_e^2}{\hbar^2} + \frac{a^2 \hbar^2}{8\mu w^2} - \frac{2a D_e r_e \hbar^2}{w} \right]}{\left(n + \frac{1}{2} + \sqrt{\left(\ell + \frac{1}{2} \right)^2 + \frac{4\mu D_e r_e^2}{\hbar^2}} \right)^2} \times \frac{\left[2\ell+1 + \frac{2\ell+1}{2\sqrt{\left(\ell + \frac{1}{2} \right)^2 + \frac{4\mu D_e r_e^2}{\hbar^2}}} (2n+1) \right]}{\left(n + \frac{1}{2} + \sqrt{\left(\ell + \frac{1}{2} \right)^2 + \frac{4\mu D_e r_e^2}{\hbar^2}} \right)^2} \quad (35)$$

3. RESULTS AND DISCUSSION:

Figure 1 shows the shape of generalized-Mie-type-constant potential. In Figure 2, the variation of the ground state energy $E_{0\ell}$ with the equilibrium bond length r_e for five values of ℓ was shown. The variation was studied with the length of the barrier greater than the width of the barrier. For all five values of the angular momentum quantum number, the ground state energy decreases as the equilibrium bond length increases. In Figure 3, the behaviour of the energy with respect to the dissociation energy was examined. In the observations, the energy of the system increases as the dissociation energy increases.

The energies for $\ell=1,2,3$ tends to decrease as $D_e > 100$. In Figure 4, the plot of energy against the height a of the barrier was shown. At the beginning of the height of the barrier (0 to 10), there is a sharp increase in the energy of the system. This energy tends to be constant as the height of the barrier increases above 10. This shows that a particle moving from the lower end of a barrier to the higher end of the barrier requires more energy at the beginning of its movement as it goes up until the particle is fully energized at a particular point, then, little or no additional energy is requires to get to the top.

In Figure 5, the plot of energy against the width of the barrier was shown. It can be observed that as the width of the barrier increases, the energy of the system initially decreases, and at a point, it remains constant. This indicates that the particle requires energy at the initial stage for a

particle to penetrate the barrier. After some times, the particle gains sufficient energy to penetrate the barrier without further consuming the energy of the system. The variation of the energy of each potential against the equilibrium bond length for the ground state and the first two excited states are shown in Figures 6 and 7 using equations (24) and (26) respectively. In each case, the energy of the system goes down as the equilibrium bond length increases. The energy, however, increases as the quantum number increases. Though the Figures have the same pattern, but the energy of the generalized kratzer potential are higher than that of the kratzer-Fues potential at every value of the equilibrium bond length. It was also noted that the energies of the kratzer-Fues potential were bounded.

Table 1 presented the model parameters (constants) for six diatomic molecules. In Tables 2 and 3, the numerical results of the energy eigenvalues for some diatomic molecules were presented. It is seen that the energy decreases as the quantum number n increases for the whole molecules considered. Similarly, the energy increases as the angular momentum quantum number ℓ increases. The numerical values of the calculated expectation values in Eqs. (31), (33) and (35) are presented in Tables 4(a) and 4(b) for various values of the height and width of the barrier. It was noted that an increase in the height of the barrier leads to an increase in each of the calculated expectation value while an increase in the width of the barrier decreases each of the calculated expectation value.

4. CONCLUSIONS:

The solutions of the one-dimensional Schrödinger equation obtained in the presence of a potential barrier for a combination of generalized Kratzer potential and Mie-type potentials revealed that the energy for the generalized Kratzer potential has the same behavior as the energy of the Kratzer-Fues potential. It was observed that the presence of a potential barrier affects the energy of a system. The energy eigenvalues in the presence of the potential barrier reduces as the width of the barrier increases but increases as the height of the barrier goes up. A particle moving up in this system absorbed more energy from the system at the beginning of its movement. The absorption of energy reduces as the particle goes up, and before it gets to the top, the particle requires little or no energy.

5. REFERENCES:

- 1 Bayrak, O. and Boztosun, I. (2007). Bound state solutions of the Hulthén potential by using the asymptotic iteration method. *Physical Scripta*, 76, 92-96.
- 2 Bayrak, O., Boztosun, I. and Ciftci, H. (2007). Exact analytical solutions to the Kratzer potential by the asymptotic iteration method. *International Journal Quantum Chemistry*, 107, 540-544.
- 3 Cooper, F., Khare, A. and Sukhatme, U. (1995). Supersymmetry and Quantum mechanics. *Physical Reports*, 251, 267-385.
- 4 Comtet, A., Bandrauk, A.D. and Campbell, D.K. (1985). Exactness of semiclassical bound state energies for supersymmetric quantum mechanics. *Physics Letters B*, 150, 159-162.
- 5 Dong, S. H. (2007). Factorization Method in Quantum Mechanics" (Springer, The Netherlands)
- 6 Dong, S.H., Chen, C.Y. and Lozada-Cassou, M. (2005). Generalized hypervirial and Blanchard's recurrence relations for radial matrix elements. *Journal of Physics B*, 38, 211-2220.
- 7 Edet, C. O., Okorie, U. S., Ngiangia, A. T. and Ikot, A. N. (2020). Bound state solutions of the Schrödinger equation for the modified Kratzer potential plus screened Coulomb potential. *Indian Journal of Physics*, 94, 425-433.
- 8 Falaye, B. J., Ikhdair, S. M. and Hamzavi, M. (2015). Formula method for bound state problems. *Few-Body System*, 56(1), 63-78.
- 9 Falaye, B. J., Oyewumi, K. J., Ibahim, T. T., Punyasena, M. A. and Onate, C. A. (2013). Bound state solutions of the Manning-Rosen potential. *Canadian Journal of Physics* 91: 97-104.
- 10 Falaye, B. J., Oyewumi, K. J., Ikhdair, S. M. and Hamzavi, M. (2014). Eigensolution techniques, their applications and Fisher's information entropy of the Tietz-Wei diatomic molecular model. *Physica Scripta*, 89, 115204.
- 11 Falaye, B. J. (2012). Any l-state solutions of the Eckart potential via asymptotic

- iteration method. *Central European Journal of Physics*, 10(4), 960-965.
- 12 Feynman, R. P. (1939). Forces in Molecules. *Physical Review* 56, 340.
- 13 Flügge, S. (1974). *Practical Quantum Mechanics* (Berlin: Springer)
- 14 Gendenshtein, L. E. (1983). Derivation of exact spectra of the Schrödinger equation by means of supersymmetry. *JETP Letters*, 38(6): 356-359.
- 15 Hassanabadi, H., Maghsoodi, E. and Zarrinkamar, S. (2012a). Relativistic Symmetries of Dirac equation and the Tietz potential. *European Physical Journal Plus*, 127, 31.
- 16 Hassanabadi, H., Maghsoodi, E., Zarrinkamar, S. and Rahimov, H. (2011a). An approximate solution of the Dirac equation for hyperbolic scalar and vector potentials and a Coulomb tensor interaction by SUSYQM. *Modern Physics Letters A*, 26(36), 2703-2718.
- 17 Hassanabadi, H., Zarrinkamar, S. and Maghsoodi, E. (2011b). Approximate solution of D-Dimensional Klein-Gordon equation with Hulthén-type potential. *Communications in Theoretical Physics*, 56(3), 423-428.
- 18 Hassanabadi, H., Yazarloo, B. H. and Lu, L. L. (2012b). Approximate solutions of Klein-Gordon equation with improved Manning-Rosen potential in D-dimensions using SUSYQM. *Chinese Letters*, 29, 020303.
- 19 Hassanabadi, H., Yazarloo, H. B., Mahmoudieh, M. and Zarrinkamar, S. (2013). Dirac equation under the Deng-Fan potential and the Hulthén potential as a tensor interaction via SUSYQM. *European Physical Journal Plus*, 128, 111
- 20 Hoseein, J., Jafar, S. and Farzaneh, S. (2019). Factorization method for fractional Schrödinger equation in D-dimensional fractional space and homogeneous manifold. *Computational Methods for Differential Equations*, 7(2), 199-205
- 21 Ikhdair, S. M. and Sever, R. (2007). Exact polynomial eigensolutions of the Schrödinger equation for pseudoharmonic potential. *Journal of Molecular Structure*, 806, 155-158.
- 22 Ikot, A. N., Chukwuocha, E. O., Onyeaju, M. C., Onate, C. A., Ita, B. I. and Udoh, M. E. (2018). Thermodynamics properties of diatomic molecules with general molecular potential. *Pramana Journal of Physics*, 90, 22.
- 23 Ikot, A. N., Okorie, U. S., Sever, R. and Rampho, G. R. (2019). Eigensolution, expectation values and thermodynamic properties of the screen Kratzer potential. *European Physical Journal Plus*, 134, 386.
- 24 Ikot, A. N. (2012). Solutions of Dirac equation for generalized hyperbolic potential including Coulomb-like tensor potential with spin symmetry. *Few-Body Systems*, 53, 549-555.
- 25 Jia, C. S., Guo, P., Diao, Y. F., Yi, L. Z. and Xie, X. J. (2007). Solutions of Dirac equations with the Pöschl-Teller potential. *European Physical Journal A*, 34, 41-48.
- 26 Jia, C. S., Chen, T. and He, S. (2013). Bound state solutions of the Klein-Gordon equation with the improved expression of the Manning-Rosen potential energy model. *Physics Letters A*, 377(9), 682-686.
- 27 Landau, L. D. and Lifshitz, E. M. (1977). *Quantum Mechanics: Nonrelativistic Theory*, 3rd Ed. (New York: Pergamon)
- 28 Nikiforov, A. F. and Uvarov, V. B. (1988). *Special Functions of Mathematical Physics*. (Birkhauser, Basel).
- 29 Okorie, U. S., Ikot, A. N., Chukwuocha, E.O., Onyeaju, M.C., Amadi, P.O., Sitholes M. J. and Rampho, G. J. (2020). Energies spectra and thermodynamic properties of hyperbolic Pöschl-Teller potential model. *International Journal of Thermophysics*, 41, 1-15.
- 30 Oluwadare, O. J., K J Oyewumi, K. J., Akoshile, C. O. and Babalola, A. O. (2012). Approximate analytical solutions of the relativistic equations with the Deng-Fan molecular potential including a Pekeris-type approximation to the (pseudo or) centrifugal term. *Physica Scripta*, 86, 035002.
- 31 Onate, C. A., Adebimpe, O., Lukman, A. F., Okoro, J. O. and Oluwayemi, M. O. (2019). Analytical Solutions of the Dirac Equation with Effective Tensor Potential. *Journal of the Korean Physical Society*, 74(3), 205-214.

- 32 Onate, C. A. and Idiodi, J. O. A. (2016). Fisher Information and Complexity Measure of Generalized Morse Potential Model. *Communications in Theoretical Physics*, 66(3), 275-279.
- 33 Onate, C.A. (2016). Bound state solutions of the Schrödinger equation with Second Pöschl-Teller like potential model and vibrational partition function, mean energy and mean free energy. *Chinese Journal of Physics*, 54(2), 165-174.
- 34 Onate, C. A., Onyeaju, M. C., Ikot, A. N., Idiodi, J. O. A. and Ojonubah, J. O. (2017a). Eigen solutions, Shannon entropy and Fisher information under Eckart Manning Rosen potential model. *Journal of the Korean Physical Society*, 70(4), 339-347.
- 35 Onate, C. A., Onyeaju, M. C., Ikot, A. N. and Ebomwonyi, O. (2017b). Eigen solutions and entropic system for Hellmann potential in the presence of the Schrödinger equation. *European Physical Journal Plus*, 132, 462.
- 36 Onate, C.A. (2014). Bound State Solutions of Duffin-Kemmer-Petiau Equation with Yukawa potential. *African Review of Physics* 9(0033), 259-264.
- 37 Onate, C. A., Adebimpe, O., Lukman, A. F., Okoro, J. O. and Olowayemi, M.O. (2019). Solutions of the Dirac Equation with Effective Tensor Potential. *Journal of the Korean Physical Society*, 74(3), 205-214.
- 38 Onyeaju, M. C., Ikot, A. N., Onate, C. A., Ebomwonyi, O., Udoh, M. E. and Idiodi, J. O. A. (2017). Approximate bound-states solution of the Dirac equation with some thermodynamic properties for the deformed Hylleraas plus deformed Woods-Saxon potential. *European Physical Journal Plus*, 132, 302.
- 39 Oyewumi, K. J., Falaye, B. J., Onate, C. A., Oluwadare, O. J. and Yahya, W. A. (2014). k state for the fermionic massive spin-1/2 particles interacting with double ring-shape Kratzer and oscillator potentials. *International Journal of Modern Physics E*, 23, 1450005.
- 40 Oyewumi, K. J. and Akoshile, C.O. (2010). Bound-state solutions of the Dirac-Rosen-Morse potential with spin and pseudospin symmetry. *European Physical Journal A*, 45, 311-318.
- 41 Rahbar, H. and Sadegh, J. (2016). Solving the Schrödinger Equation with Hartmann Potential by Factorization method and Supersymmetry. *Theoretical Physics*, 1(1), 7-13.
- 42 Schiff, L. I. (1995). *Quantum Mechanics 3rd Ed*". (New York: McGraw-Hill)
- 43 Tezcan, C. and Sever, R. (2009). A General Approach for the Exact Solution of the Schrödinger Equation. *International Journal of Theoretical Physics*, 48, 337-350.
- 44 Witten, E. (1981). Dynamical Breaking of Supersymmetry. *Nuclear Physics B*, 188, 513-554.
- 45 Wei, G.-F. and Dong, S.-H. (2010). A novel algebraic approach to spin symmetry for Dirac equation with scalar and vector Second Pöschl-Teller potentials. *European Physical Journal A*, 43, 185-190.
- 46 Wei, G.-F. and Dong, S.-H. (2009). Algebraic approach to pseudospin symmetry for the Dirac equation with scalar and vector modified Pöschl-Teller potentials. *Europhysics Letters*, 87, 40004.

Table 1. Spectroscopic parameters used in this work for the diatomic molecules taken from the paper of Falaye et al. (2014).

Molecules	$\mu/10^{-23}(g)$	$r_e(\text{\AA})$	$D_e(\text{cm}^{-1})$
$O_2(X^3\Sigma_g^+)$	1.337	1.207	42041
$I_2(X(O_g^+))$	10.612	2.666	12547
$H_2(X^1\Sigma_g^+)$	0.084	0.741	38318
$N_2(X^1\Sigma_g^+)$	1.171	1.097	79885
$NO^+(X^1\Sigma^+)$	1.239	1.063	88694
$CO(X^1\Sigma^+)$	1.146	1.128	90531

Table 2. Bound state eigenvalues of diatomic molecules for various n and ℓ with $\hbar c = 1973.29\text{eV}$.

n	ℓ	$O_2(X^3\Sigma_g^+)$	$I_2(X(O_g^+))$	$H_2(X^1\Sigma_g^+)$
0	0	1.359716716	1.030965494	1.381798095
1	0	1.404079134	1.089610643	1.382833900
	1	1.412718834	1.103060691	1.383025962
2	0	1.412967209	1.106749164	1.383026085
	1	1.416063865	1.112282505	1.383093345
	2	1.417608584	1.116431061	1.383124532
3	0	1.416170011	1.113998241	1.383093397
	1	1.417620807	1.116793887	1.383124537
	2	1.418462410	1.119116908	1.383141480
	3	1.418976038	1.120694311	1.383151698
4	0	1.417675579	1.117727020	1.383124564
	1	1.418469499	1.119331756	1.383141483
	2	1.418977981	1.120761888	1.383151699
	3	1.419311654	1.121796155	1.383158331
	4	1.419541372	1.122537576	1.383162879
5	0	1.418501361	1.119894384	1.383141498
	1	1.418982452	1.120899440	1.383151701
	2	1.419312957	1.121841810	1.383158332
	3	1.419541883	1.122556411	1.383162879
	4	1.419706266	1.123089175	1.383166132
	5	1.419828125	1.123491837	1.383168538
6	0	1.419002592	1.121264431	1.383151710
	1	1.419315956	1.121935114	1.383158333
	2	1.419542799	1.122588688	1.383162879
	3	1.419706639	1.123102961	1.383166132
	4	1.419828304	1.123498604	1.383168538
	5	1.419921007	1.123805607	1.383170369
	6	1.419993228	1.124047354	1.383171794

Table 3. Bound state eigenvalues of diatomic molecules for various n and ℓ with $\hbar c = 1973.29 \text{ eV}$.

n	ℓ	$N_2(X^1\Sigma_g^+)$	$NO^+(X^1\Sigma^+)$	$CO(X^1\Sigma^+)$
0	0	1.647845814	1.705229227	1.710414495
1	0	1.757261120	1.836475239	1.850885506
	1	1.778894376	1.862562517	1.878903057
2	0	1.779739343	1.863681707	1.880177315
	1	1.787554530	1.873132958	1.890347181
	2	1.791550260	1.878008462	1.895624478
3	0	1.787917231	1.873614143	1.890895625
	1	1.791593650	1.878066823	1.895691605
	2	1.793773007	1.880727120	1.898571934
	3	1.795108957	1.882360591	1.900342482
4	0	1.791781305	1.878316024	1.895975823
	1	1.793798193	1.880761006	1.898610918
	2	1.795115900	1.882369953	1.900353267
	3	1.795984086	1.883431626	1.901504134
	4	1.796582713	1.884164090	1.902298444
5	0	1.793907552	1.880906328	1.898776733
	1	1.795131795	1.882391344	1.900377879
	2	1.795988743	1.883437905	1.901511368
	3	1.796584543	1.884166559	1.902301291
	4	1.797012976	1.884690809	1.902869828
	5	1.797330806	1.885079824	1.903291784
6	0	1.795201009	1.882483362	1.900482907
	1	1.795999408	1.883452261	1.901527888
	2	1.796587816	1.884170973	1.902306376
	3	1.797014311	1.884692610	1.902871904
	4	1.797331446	1.885080688	1.903292780
	5	1.797573252	1.885376662	1.903613822
	6	1.797761705	1.885607365	1.903864090

Table 4 (a). Expectation values for various values of the barrier height with $n = \ell = \mu = \hbar = w = 1$, $r_e = 0.2$ and $D_e = 0.55$.

a	$\langle V \rangle_{n,\ell}$	$\langle p^2 \rangle_{n,\ell}$	$\langle r^{-2} \rangle_{n,\ell}$
0.2	0.549713029	-0.002356946	0.004376939
0.4	0.554521427	-0.001927517	0.004668735
0.6	0.559350533	-0.001199653	0.005431170
0.8	0.564200347	-0.000173354	0.006664243
1.0	0.569070869	0.001151379	0.008367955
1.2	0.573962100	0.002774547	0.010542305
1.4	0.578874038	0.004696151	0.013187294
1.6	0.583806684	0.006916188	0.016302922
1.8	0.588760039	0.009434660	0.019889188
2.0	0.593734101	0.012251568	0.023946093

Table 4 (b). Expectation values for various values of the barrier width with $n = \ell = \mu = \hbar = a = 1$, $r_e = 0.2$ and $D_e = 0.55$.

w	$\langle V \rangle_{n,\ell}$	$\langle p^2 \rangle_{n,\ell}$	$\langle r^{-2} \rangle_{n,\ell}$
0.2	0.670830012	0.090317349	0.141276299
0.4	0.606259856	0.020599488	0.036147399
0.6	0.585455502	0.007722519	0.017446051
0.8	0.575188143	0.003226970	0.011159430
1.0	0.569070869	0.001151379	0.008367955
1.2	0.565010663	0.000026710	0.006915512
1.4	0.562119320	-0.000649739	0.006078154
1.6	0.559955627	-0.001087686	0.005559566
1.8	0.558275609	-0.001387191	0.005221067
2.0	0.556933392	-0.001600889	0.004991123

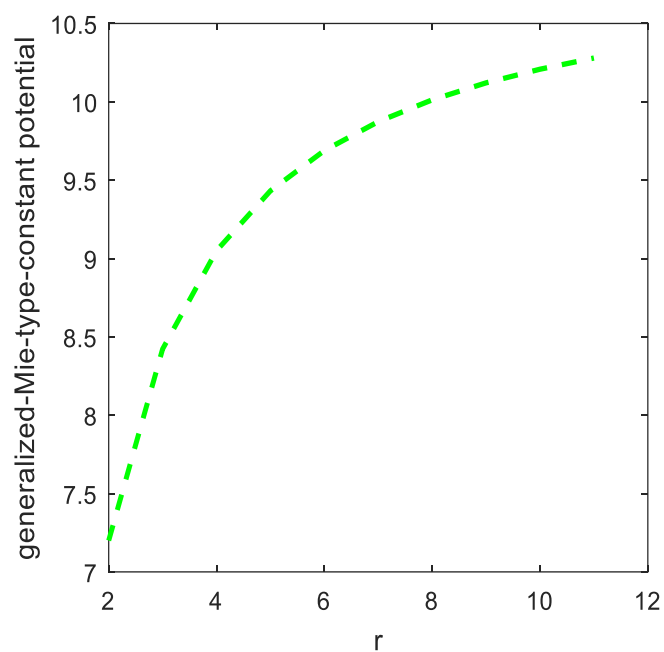


Figure 1. Generalized-Mie-type constant potential. This is the shape of the interacting potential given in Eq. (3)

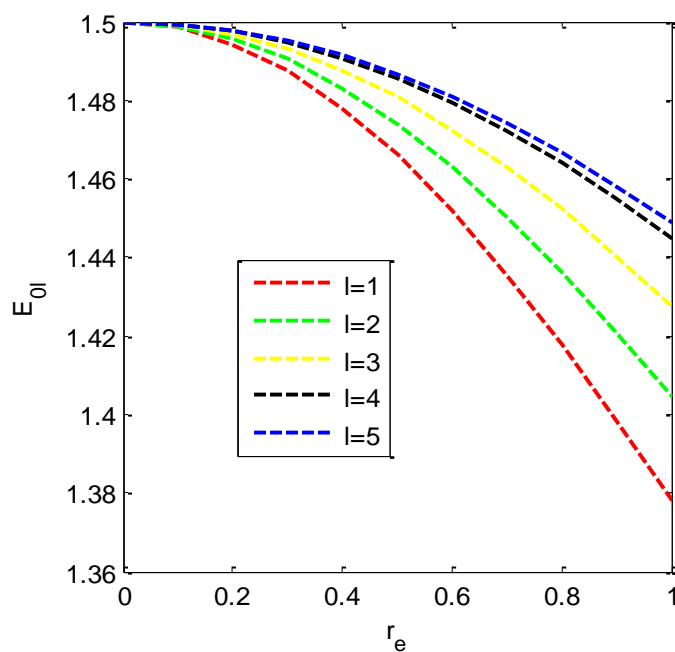


Figure 2. Ground state energy against the equilibrium bond length in the presence of a barrier with $m = \hbar = \ell = \eta = 1$, $a = 2.5$, $w = 0.1$ and $D_e = 0.5$.

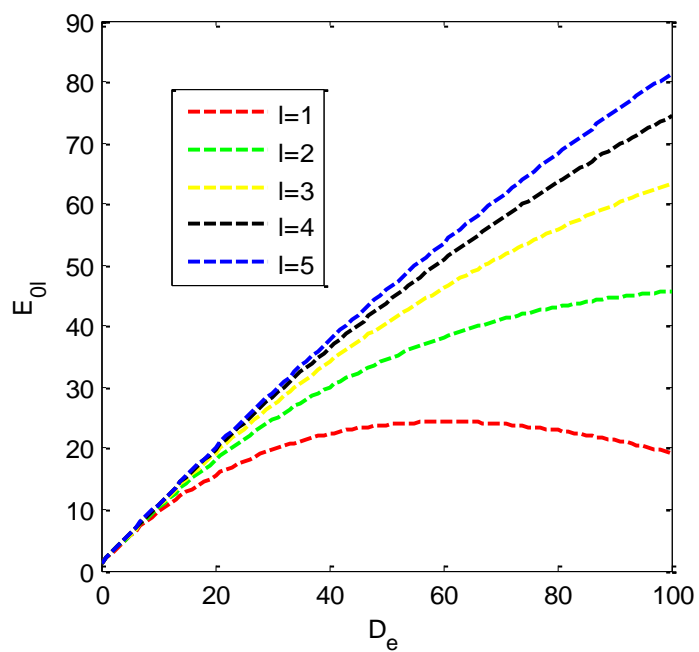


Figure 3. Ground state energy against the dissociation energy in the presence of a barrier with $m = \hbar = \ell = \eta = 1$, $a = 2.5$, $w = 0.1$.

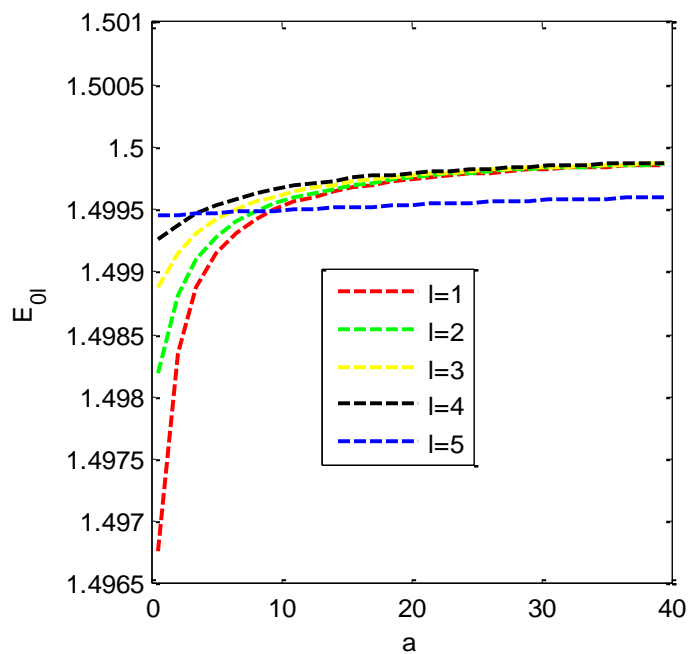


Figure 4. Ground state energy against the height of the barrier with $m = \hbar = \ell = \eta = 1$, $w = 0.1$ and $D_e = 0.5$.

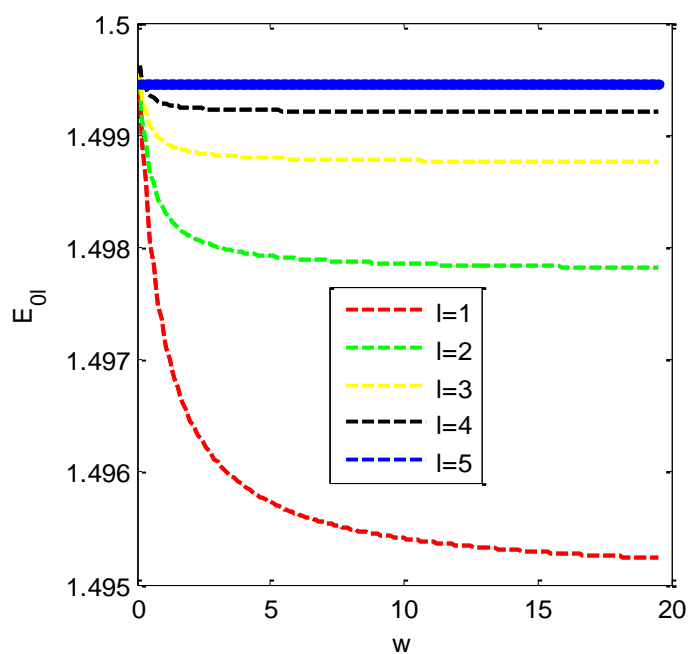


Figure 5. Ground state energy against the width of the barrier with $m = \hbar = \ell = \eta = 1$, $a = 2.5$ and $D_e = 0.5$.

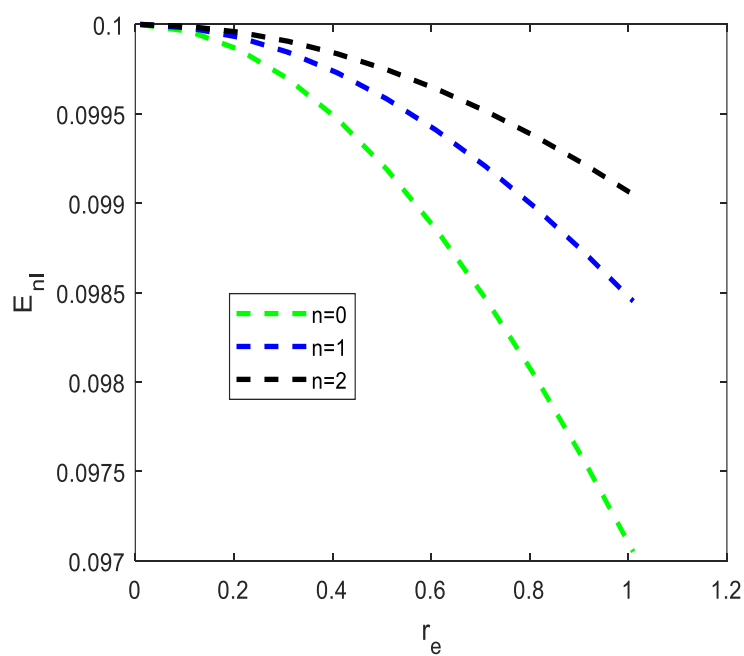


Figure 6. Energy against the equilibrium bond length for Generalized kratzer potential with $m = \hbar = \ell = 1$, and $D_e = 0.1$.

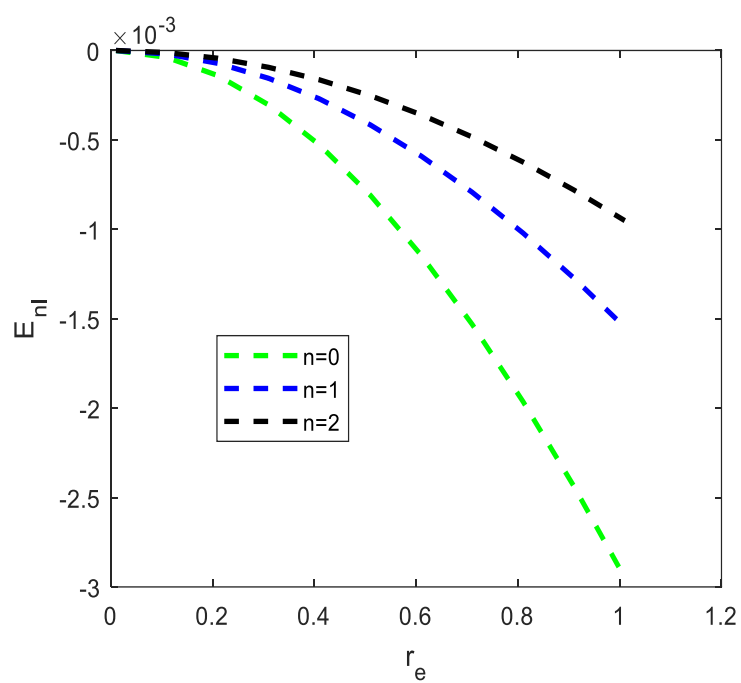


Figure 7. Energy against the equilibrium bond length for kratzer-Fues potential with $m = \hbar = \ell = 1$, and $D_e = 0.1$.

MEDIDA DA TAXA DE DOSE DE RADIAÇÃO PARA PROGRAMAS DE PROTEÇÃO NO AMBIENTE DE TRABALHO PARA OS TRABALHADORES DE SAÚDE: UM ESTUDO EXPERIMENTAL**RADIATION DOSE RATE MEASUREMENT FOR PROTECTION PROGRAMS IN THE WORK ENVIRONMENT FOR THE HEALTH WORKERS: AN EXPERIMENTAL STUDY****PENGUKURAN LAJU DOSIS RADIASI UNTUK PROGRAM PROTEKSI RADIASI DI LINGKUNGAN KERJA BAGI PEKERJA KESEHATAN: KAJIAN EKSPERIMENTAL**FARDELA, Ramacos^{1,3}; SUPARTA, Gede Bayu^{1*}; ASHARI, Ahmad²; TRIYANA, Kuwat¹¹ Universitas Gadjah Mada, Faculty of Mathematics and Natural Sciences, Department of Physics. Indonesia.² Universitas Gadjah Mada, Faculty of Mathematics and Natural Sciences, Department of Computer Science and Electronics. Indonesia.³ Technology Academy of Payakumbuh, Computer Engineering. Indonesia.

* Corresponding author
e-mail: gbsuparta@ugm.ac.id

Received 22 July 2020; received in revised form 27 August 2020; accepted 05 October 2020

RESUMO

A radiação é a energia emitida pelos elétrons na forma de partículas ou fótons (ondas), sendo classificada em não ionizada e ionizada. A radiação ionizante demonstra a capacidade de desintegrar a matéria ao longo de seu caminho e tem se mostrado benéfica na medicina. A exposição a essa energia tende a instigar efeitos adversos na saúde humana e na hereditariedade (genética). No entanto, a radiação não é medida diretamente, mas requer detector nuclear para servir como um dispositivo de monitoramento. A consciência dos trabalhadores de radiação sobre os níveis de radiação ionizante no ambiente de trabalho é um dos fatores mais importantes na prevenção dos efeitos negativos da radioatividade. Isso é possivelmente identificado por meio de vários tipos de detectores. O objetivo deste experimento foi fornecer uma visão geral sobre a medição da taxa de dose de radiação em duas condições. O primeiro é o caso de contaminação no ambiente de trabalho e o segundo envolve o uso de detector para determinar apenas a taxa de dose de uma única fonte, por exemplo, radiação gama. Portanto, a taxa de dose de radiação foi avaliada maximizando o uso de detectores equipados com uma GUI como um medidor de pesquisa de contaminação. A maior taxa (261,42 $\mu\text{Sv} / \text{h}$) foi observada na distância de 5 mm, enquanto a menor (69,21 $\mu\text{Sv} / \text{h}$) foi registrada a 50 mm. Além disso, uma taxa de dose de 5,4 $\mu\text{Sv} / \text{h}$ e 1,32 $\mu\text{Sv} / \text{h}$ foi obtida a uma distância de 5 mm e 50 mm da fonte de radiação, respectivamente, seguindo a operação como medidor de gama. Este resultado mostra a presença de forte linearidade entre as duas medições e é estimado para determinar com precisão o nível de contaminação dos elementos radioativos, juntamente com a taxa de dosagem dos elementos emissores de radiação gama.

Palavras-Chave: *Detector de radiação, taxa de dose de radiação, proteção contra radiação e radiação ionizante***ABSTRACT**

Radiation is the energy emitted from electrons in particles or photons (waves) and is classified into non-ionized and ionized. Ionizing radiation demonstrates the ability to disintegrate matter along its path and has proven beneficial in medicine. Exposure to this energy tends to instigate adverse effects on human health and heredity (genetics). However, the radiation is not directly measured but requires a nuclear detector to serve as a monitoring device. Radiation workers' awareness of ionizing radiation levels in the work environment is one of the most important factors in preventing the negative effects of radioactivity. This is possibly identified using various types of detectors. This experiment aimed to provide an overview of radiation dose rate measurement under two conditions. First is the event of contamination in the work environment. The second involves using a detector to solely determine the dose rate from a single source, e.g., gamma radiation. Therefore, the radiation dose rate was evaluated by maximizing the use of detectors with a GUI as a survey meter for contamination. The highest rate (261.42 $\mu\text{Sv} / \text{h}$) was observed at a distance of 5 mm, while the least (69.21 $\mu\text{Sv} / \text{h}$) was recorded at 50 mm. Also, a dose rate of 5.4 $\mu\text{Sv} / \text{h}$ and 1.32 $\mu\text{Sv} / \text{h}$ was obtained at a 5 mm and 50 mm distance from the radiation

source, respectively, following the operation as a gamma survey meter. This result shows strong linearity between both measurements and is estimated to accurately determine the contamination level of radioactive elements, alongside the doses rate of the gamma radiation emitting elements.

Keywords: *Radiation Detector, Radiation Dose Rate, Radiation Protection, and Ionizing Radiation*

ABSTRAK

Radiasi adalah pancaran energi yang berasal dari partikel atau foton. Berdasarkan kemampuan mengionkan materi, radiasi dapat dikelompokkan menjadi radiasi non-pengion dan radiasi pengion. Radiasi pengion adalah radiasi yang dapat mengionkan materi yang dilaluinya. Radiasi pengion telah terbukti bermanfaat dalam bidang kedokteran. Namun, paparan radiasi pengion potensial dapat menyebabkan efek negatif bagi kesehatan dan keturunan (genetik). Radiasi pengion juga tidak dapat diamati secara langsung sehingga diperlukan suatu detektor nuklir sebagai alat pemantau radiasi. Kesadaran akan tingkat radiasi pengion di sekitar lingkungan pekerja radiasi adalah salah satu faktor terpenting untuk mencegah dampak negatif penggunaan radiasi pengion. Hal ini dapat diketahui melalui penggunaan detektor radiasi dari berbagai jenis. Artikel ini melaporkan tentang teknik pengujian laju dosis radiasi dengan memaksimalkan penggunaan detektor radasi yang telah dilengkapi dengan GUI. Penelitian ini dilakukan dengan pendekatan eksperimental guna untuk memberikan gambaran proses pengukuran laju dosis radiasi ketika terjadi kontaminasi pada daerah kerja dan ketika detektor difungsikan hanya untuk mengetahui laju dosis radiasi yang berasal dari sumber tunggal yaitu radiasi gamma. Pada saat detektor difungsikan sebagai survey meter kontaminasi, didapatkan laju dosis radiasi tertinggi pada jarak 5 mm yaitu 261.42 $\mu\text{Sv/h}$ dan terendah pada jarak 50 mm sebesar 69.21 $\mu\text{Sv/h}$. Pada saat detektor sebagai survey meter gamma didapatkan laju dosis radiasi 5.4 $\mu\text{Sv/h}$ pada posisi 5 mm dan 1.32 $\mu\text{Sv/jam}$ pada posisi detektor 50 mm dari sumber radiasi. Hasil menunjukkan linearitas antara kedua pengukuran sangat kuat. Teknik pengukuran ini akurat untuk menentukan kontaminasi dari unsur radioaktif dan menentukan laju dosis radiasi dari unsur yang memancarkan radiasi gamma.

Kata kunci: *Detektor Radiasi, Laju Dosis Radiasi, Proteksi Radiasi, dan Radiasi Pengion*

1. INTRODUCTION:

Radiation is generally defined as the radiant energy generated from particles or photons. The source materials are classified by Stabin (2007) into (1) ionizing radiation, capable of ionizing the matter in its path, including photons, with wavelengths <1 nm or equivalent to 12 eV energy, as well as alpha, neutron, and beta (Ryan *et al.*, 2012). (2) the non-ionizing group comprises photons with wavelengths > 1 nm, as observed with radio waves and sunlight (Rosenberg, 2008). Based on this analysis, all the radiation terms used subsequently in this article refer to the ionizing type.

Radiation confers positive effects, as shown in various fields, including medical practice, radiodiagnostics, radiotherapy, and nuclear medicine. Radiation is applied in diagnostic radiology to detect potential diseases, bone abnormalities, and cancer (Krhovska *et al.*, 2019). The energy is also employed in radiotherapy as a treatment technique, particularly in eliminating cancer cells in organs or tissues. This is achieved by maximizing radiation dose in the cancerous tissue and minimizing the healthy peer (Benedict *et al.*, 2010). Meanwhile, radioactivity is fast gaining broader recognition in nuclear medicine and is characterized by radiopharmaceuticals known as radiopharmaceuticals for diagnostic and

radiotherapy purposes. (Missailidis *et al.*, 2007).

Furthermore, CT (computed tomography) scans are among significant utility instances applied to detect abnormalities or diseases (Kusminarto, 2015), (Fitousi, 2017). Also, cobalt-60 machines and medical linear accelerators are widely used for radiotherapy from external sources (Healy *et al.*, 2017). However, radiopharmaceuticals have been widely reported as a means for diagnosing bone metastasis (Hsia *et al.*, 2002), (Saeed *et al.*, 2017), and cancer therapy in nuclear medicine (Luster *et al.*, 2008). Recent studies have shown radiopharmaceuticals' development as a carrier of pain medicines or cancer cells' treatment in targeted organs (Kazakov *et al.*, 2020).

The application of ionizing radiation has witnessed a drastic upsurge due to rapid development in medical technology. However, the risk to health, both in patients and medical professionals, has also increased due to steady exposure to these radiations as modern evolution continues. Furthermore, ionizing radiation has become a major energy source from non-natural sources (Teles *et al.*, 2020). The adverse effects of radiation are grouped according to latency into direct (deterministic) and stochastic (delayed) (Santos, 2020). Remarkably, the deterministic impact is reported at doses more significant than

a certain threshold (Tubiana, 1998), and is generally observed immediately after exposure. Meanwhile, stochastic effects possibly occur in any predisposed individual (Richardson, 2015) and are characterized by (1) no threshold dose, (2) effect probability rises at higher levels, and (3) ascertained effect concerning the exposure (Radford, 1980). Furthermore, cancer is one of the diseases included in this category (Nambiar, 2011), (Mohan *et al.*, 2003), (Paunesku *et al.*, 2017), (Averbeck *et al.*, 2007).

The five human senses cannot directly detect nuclear radiation due to the absence of any biological sensors (Fardela *et al.*, 2019). Therefore, the risks or unwanted impacts are reduced by using a device or dosimeter to determine the presence of radiation. This instrumentation system is applied to measure and evaluate exposure values, kerma, and absorbed or equivalent doses associated with ionizing radiation, both directly and indirectly (Podgorsak, 2005).

The radiation dosimeters are divided into two groups, in the aspect of reading, including (1) the passive types, comprising measurement results, which is difficult to read directly. Hence, there is a need for initial special processing (Knoll, 2007), including film badge and thermoluminescent dosimeter (TLD) (Magalotti *et al.*, 2014). Medical personnel within the area of interventional radiology (IVR) are at risk of exposure to high doses of scattered radiation emitted from the patient (Fujibuchi *et al.*, 2019). For instance, the cardiologist site doses are spread out in the range from 1-14 mSv/hour during fluoroscopy. Workers in planned exposure situations are advised an equivalent dose limit of 20 mSv / year for eye lenses (Miller, 2018), averaged over five years with one-year exposure restricted to 50 mSv, based on ICPR recommendation (Fujibuchi, *et al.*, 2019) (Revised Law on the prevention of radiation hazards due to radioisotopes). This condition tends to increase the cataract risk for IVR personnel known to exceed the annual dose limit. Therefore, the management of additional occupational exposure is necessary. Medical personnel must always wear protective clothing (Apron) and use a passive type of personal dosimeters, including glass or quixel badge. This kind of device is shared among clinical practitioners. However, the inability to directly measure the radiation dose presents a disadvantage (Fujibuchi *et al.*, 2019).

The active dosimeters (2) generate results to be read directly, encompassing surveillance meters, pocket dosimeters, or the recently known

personal electronic dosimeters (EPD) or Active Person Dosimeters (APD) (Tsoulfanidis, 2010). Besides, the active device instantly displays the radiation dose, and exposure received compared to passive dosimeters (Benevides *et al.*, 2014). This provides a picture and a signal for exceeding the threshold (Fujibuchi *et al.* (2019).

Research on radiation dose rate measurements at facilities with nuclear techniques has been widely conducted. Mustofa *et al.*, 2019 reported on the desirable features of commercial EPD to be applied in radiation protection. Therefore several tests were performed, including reproducibility, dose linearity, dose rate, and angular dependence using a Cs-137 radiation source. Moreover, EPD has been used to monitor the radiation dose rate for workers' radiation protection (Taleb, 2013), (Fardela, 2018). Furthermore, Suliman *et al.* (2020) reported on the application to scrutinize the level received by some staff, doctors, and workers in the field of nuclear medicine. Therefore, the lack of radiation control programs and the use of occupational exposure control devices were of significant concern (Suliman, 2019).

One of the most important factors to be considered by workers in this field is the awareness of radiation level; therefore, various types of detectors are being adopted in the identification process. However, a basic understanding of the respective action mechanism is assumed to help make the best selection and maximize operational benefits. Currently, an active radiation detector shows the results of real-time radiation dose rate measurements (Donowsky, 2013). This helps the medical workers to maximize protection in an exposed work environment. However, not every employee is acquainted with detailed procedures despite being relatively expensive.

Therefore, this study aimed to provide an overview of the radiation dose rate measurement in a contaminated work environment and the use of a detector to exclusively determine the radiation dose from a single source (gamma radiation). The novelty of this study lies in the methodology and communication systems applied in the retrieval process using an active dosimeter, which is directly connected to a centralized real-time data acquisition system.

2. MATERIALS AND METHODS:

This article reports the radiation dose rate testing technique, using a radiation dosimeter equipped with a GUI (Graphical User Interface).

Furthermore, the unit was serially connected to a computer, and the respective placements and utilization techniques were substantially considered. These placements influence the measure of radiation dose rate. However, incorrect application hinders the possibility of describing the investigated condition, thus leading to errors in understanding the monitoring data results obtained from the work area. Therefore, this study focuses on measuring the radiation dose rate from various emission sources, including alpha particles, beta, and gamma radiation. Besides, this approach is expected to serve as a guide towards the rate determination for other elements. The study outcome is anticipated to be the basis for maximizing the use of radiation detector, and also to develop protection in ionized environments. The study was conducted at the Atomic and Nuclear Physics Laboratory, Department of Physics, Faculty of Mathematics and Natural Sciences, Universitas Gadjah Mada.

2.1. Materials and Tools

The material used included radioactive Cesium 137 (Cs-137) with activity (72483.97 ± 3%) Bq, characterized by an energy peak of 661 keV (Kefalidis *et al.*, 2017), and emits beta as well as gamma radiation. The radiation source activity (Cs-137) was calculated using equation 1 (Mann, 2012).

$$\frac{A_t}{A_0} = \left(\frac{1}{2}\right)^{\frac{t}{T}} \quad (1)$$

Where A_t is the activity of the radioactive elements over t time in Bq units. A_0 is the initial elemental activity in Bq units, T is the half-life in years, and t is the present time in years. Using available data i.e., $A_0 = 80426$ Bq, $T = 30,05$ years, and $t = 4,5$ years, A_t is determined by equation 2:

$$\begin{aligned} \frac{A_t}{80426 \text{ Bq}} &= \left(\frac{1}{2}\right)^{\frac{4,5}{30,05}} \\ A_t &= 72483,97 \text{ Bq} \end{aligned} \quad (2)$$

Therefore, the activity of the element radioactive at the time of data collection is evaluated at (72483.97 ± 3%) Bq.

The following tools were used: (a) Commercial radiation dosimeter, termed "Radiation Alert Ranger Radiation Detector". This is assumed sensitive to alpha, beta, and gamma

radiation, and is possibly connected serially to the computer with the help of a USB cable. The calibration factor is specified at 0.94, which is multiplied by the value of the measurement results. This value observes an operating range, including (0.001-100) mR / hr, (0-350000) cpm, (0.01-1000) μSv / hr, (0-5000) cps, and a total counts of 1 - 9999000. (b) The PC used to install the GUI program was provided by the "Radiation Alert Detector" and can save and display the radiation exposure rate monitoring process. (c) Lead (Pb) is used as a shield from radiation sources during the data collection process. (d) The detector is equipped with a real to vary the distance from the radiation source. The software used in this study was accessed at the following link <https://seintl.com/radiation-detectors/radiation-alert-software/>.

2.2. Method

Radiation exposure rate data was captured using a "radiation alert detector." This involved placing Cs-137 in a box already blocked by lead to prevent radioactive contamination around the study site. The background radiation rate was first determined before the radioactive element is removed from storage. Therefore, the measurements obtained were reduced by background radiation and multiplied by the detector correction factor.

A total of two data collection processes were performed, including (1) Determination of exposure rate, originating from the gamma energy emitted from Cs-137, as follow:

- This requires setting the detector rear window in a closed condition to allow for specific recognition and measurement.
- Figure 1 shows the test box was designed using available lead (Pb) at the Atomic and Core Physics Laboratory.
- The temperature and background radiation in the work environment is determined and recorded.
- The radioactive element (Cs-137) is situated in a box designed and coated with lead (Pb).
- The detector rail is placed in the box, where the radiation detector is placed at the detector rail position, as shown in Figure 1.
- The distance between the radiation detector and the source is specified at 10 mm.

- g. A set of detectors employed has been confirmed fit to communicate serially with the computer.
- h. Furthermore, radiation exposure is measured around the work environment by the Atomic and Core Laboratory Radiation Protection Officers to prevent contamination from the system (Box).
- i. On the computer connected to the detector, the data storage time is determined every 5 seconds.
- j. Measurements were performed repeatedly for each distance between dosimeters and radiation sources, termed 5 mm, 10 mm, 15 mm, up to 50 mm.
- k. The data obtained is in the form of radiation dose in units of $\mu\text{Sv} / \text{h}$.
- l. At the end of the process, click stop on the GUI screen available on the PC (computer).

And (2) Determination of exposure from beta particles and gamma radiation. This involved opening the detector rear window lid to measure all emission types (beta, gamma, and alpha) from Cs-137. Steps (a) to (i) were repeated by varying the distance of the detector to the radiation source by 5, 10 to 50 mm. Furthermore, the radiation exposure rate results were sent to the computer through serial communications, using a USB cable, subsequently displayed in graphics, TXT, and saved in a memory device.

2.3. Analysis

The experimental results are in the form of research data. This data was then processed using the origin data processing program to determine the standard deviation and graph plot. The linearity between the measurement results of the contamination detector dose rate and the gamma detector were also evaluated. To ascertain the linearity, a graph of the relationship between the contamination detector dose rate ($\mu\text{Sv} / \text{hour}$) (x_i) and the gamma detector output (y_i) was plotted. Furthermore, the linear function involves the standard deviation of the repeated measurement results by equation 3.

$$y(x) = a + bx \quad (3)$$

The least-squares fitting procedure minimizes X^2 with the associated coefficient, as shown in equation (4) (Bevington, 1969).

Chi-square (χ^2) (equation 4):

$$\chi^2 = \sum \left[\frac{1}{\sigma_i^2} (y_i - a - bx_i)^2 \right] \quad (4)$$

The a is the intercept to the y -axis, which is the offset value, as shown in equation (5), or the output signal when the input signal is zero. Meanwhile, b represents the line slope, representing the sensitivity of the detector, as shown in equation (6).

$$a = \frac{1}{\Delta} \left(\sum \frac{x_i^2}{\sigma_i^2} \sum \frac{y_i}{\sigma_i^2} - \sum \frac{x_i}{\sigma_i^2} \sum \frac{x_i y_i}{\sigma_i^2} \right) \quad (5)$$

$$b = \frac{1}{\Delta} \left(\sum \frac{1}{\sigma_i^2} \sum \frac{x_i y_i}{\sigma_i^2} - \sum \frac{x_i}{\sigma_i^2} \sum \frac{y_i}{\sigma_i^2} \right) \quad (6)$$

where Δ was calculated using equation (7).

$$\Delta = \sum \frac{1}{\sigma_i^2} \sum \frac{x_i^2}{\sigma_i^2} - \left(\sum \frac{x_i}{\sigma_i^2} \right)^2 \quad (7)$$

The estimated variance s^2 was showed by equation (8).

$$\sigma^2 \cong s^2 = \frac{1}{N-2} \sum (y_i - a - bx_i)^2 \quad (8)$$

$\sigma^2 \cong x_i$ for radiation dose rate data (Bevington, 1969), the uncertainty values of the coefficients a and b are shown in equations (9) and (10).

$$\sigma_a^2 \cong \frac{1}{\Delta} \sum \frac{x_i^2}{\sigma_i^2} \quad (9)$$

$$\sigma_b^2 \cong \frac{1}{\Delta} \sum \frac{1}{\sigma_i^2} \quad (10)$$

where σ_a^2 is uncertainty values of a and σ_b^2 is uncertainty values of b .

3. RESULTS AND DISCUSSION:

The radiation detector used in this research was equipped with a GUI to monitor the average dose rate. This was performed in a distance of 1 meter, or as long as the USB available. Therefore, the data obtained with this interface is automatically saved on a computer to reduce potential errors in reading the average dose rate values. Also, it was possible to reduce the observer's acceptance of the determinations at a specific time by 98%. This required the manual process of recording results, for output received to

be relatively large. The GUI to be equipped with several choices on units, capable of being changed according to the user's preferences. These include $\mu\text{Sv} / \text{h}$, CPM, or others.

Furthermore, the timing of data retrieval is known as a whole, and most importantly, it was possible to save the measurement results on a computer for evaluation. Figure 2 shows a variation in the data obtained, according to the distances for monitoring Cs-137 radiation contamination. Furthermore, the intensity was determined to be identical with the dose rate, which is inversely influenced by the square of the distance between the point and radiation source (Kang *et al.*, 2016), as in equation 11.

$$\dot{D}_1 : \dot{D}_2 = \frac{1}{(R_1)^2} : \frac{1}{(R_2)^2} \quad (11)$$

where \dot{D} is the radiation dose rate in $\mu\text{Sv}/\text{h}$, and R is the distance in meters. Figure 2 shows a decline in the radiation dose rate with increasing distance between the detector and source. Also, the intensity produced radiates in all directions, thus facilitating the rate determination at a point.

Figure 2 shows the capture of all radiation types from element Cs-137, including beta and gamma. This prompted a greater rate of $261.42 \mu\text{Sv} / \text{h}$ at the 5 mm distance, while $69.21 \mu\text{Sv} / \text{h}$ was the least at 50 mm. The decay results of Cs-137 evidence the detector function as a survey meter for contamination. This was perceived by the entry of Beta particles into the detector window, thus prompting more ionization power than gamma radiation. Furthermore, the detector was used to measure the dose rate of gamma radiation emitted by Cs-137 by closing the collimator window on the device's back.

The results (Figure 3) indicate a simultaneous decline in the resulting radiation dose rate at other positions. The value recorded in Figure 3 was smaller than Figure 2, because only gamma radiation was increased, while the beta and alpha particles were not measurable. Therefore, a reduction in the ionization power was observed, marked by a lower radiation dose rate, ranging from $1,32 \mu\text{Sv} / \text{h}$ at the detector position 50 mm to $5.4 \mu\text{Sv} / \text{h}$, at 5 mm from the radiation source. Furthermore, precise measurements were ascertained by plotting a linear relationship between the contamination dose rates and the gamma detector, as presented in Figure 4.

Therefore, the equation of the line obtained was $y = -0.081 + 0.021 * X$, with a solid correlation value of $R^2 = 0.99$. The slope and

intercept were determined as 0.021 and -0.081, respectively. Figure 4 shows accuracy in this measurement technique, following the application in deciding radioactive element contamination and doses rate responsible for gamma radiation emission. Besides, maximizing the detector function helps in improving protection. This result is expected to reduce the negative effects caused by ionizing radiations on workers. Also, it is necessary for handlers to understand the working principle of the operating detector to precisely and accurately determine the radiation dose rate.

4. CONCLUSIONS:

An experimental study of ionizing radiation dose rate measurement techniques designed to improve field workers' protection was completed. This assessment technique significantly influenced the outcome. Furthermore, application as a contamination detector showed a ratio value 50 times greater than the records obtained from measuring the gamma radiation dose rate. The method represents the accuracy of radiation dose rate measurement, both in detector as a contamination survey meter and as a gamma radiation sensor. Also, an active radiation dosimeter provided great assistance to radiation workers to directly determine radioactive elements' contamination. Moreover, direct, precise, and documented picture of the dose rate using a computer device is possible to achieve.

The following potential developments for this research area are proposed: 1) assessing the use of wireless systems with detectors from increased acquisition systems, during the collection of data related to radiation exposure rates, 2) It is necessary to obtain measurements from sources often utilized in the field of nuclear medicine, including Tc-99m, I-131, and others. This aims to maximize the use of radiation dosimeters, and ensure protection in nuclear medicine.

5. ACKNOWLEDGMENTS:

Mr. Ramacos Fardela would like to thank the Ministry of Research, Technology, and High Education of the Republic of Indonesia that granted a full Ph.D. scholarship, through Skema Beasiswa BUDI DN 2016, funded by Lembaga Pengelola Dana Pendidikan (LPDP) under contract number PRJ-1366/LPDP.4/2019. Thanks to Mr. Cipto Driyo as the protection against radiation staff at the Laboratorium Fisika Atom dan Inti Department of Physics Universitas Gadjah Mada that had provided assistance during the data

collection process and guaranteed working procedures in the nuclear field. Thanks to Mr. M. Zikri Hudaya, S.Si. and Mr. Trisna Julian, S.Si., who assisted in the hardware and software preparation process. Thanks to Ms. Sri Oktamuliani (Ph.D. students at Tohoku University, Japan), who helped during the radiation sensor acquisition process.

6. REFERENCES:

1. Averbeck, D., Salomaa, S., Bouffler, S., Ottolenghi, A., Smyth, V., and Sabatier, L. (2018). Progress in low dose health risk research: Novel effects and new concepts in low dose radiobiology. *Mutation Research/Reviews in Mutation Research*, 776, 46-69.
2. Benedict, S. H., Yenice, K. M., Followill, D., Galvin, J. M., Hinson, W., Kavanagh, B., and Purdie, T. (2010). Stereotactic body radiation therapy: the report of AAPM Task Group 101. *Medical physics*, 37(8), 4078-4101.
3. Benevides, L. A., Piper, R. K., and Romanyukha, A. (2014). A performance comparison of Thermo Fisher EPD-MK2 and TLD (LiF: Mg, Cu, P) as part of accreditation proficiency testing. *Radiation measurements*, 71, 183-186.
4. Bevington, P., 1969, *Data Reduction and Error Analysis for The Physical Sciences*, McGraw-Hill Book Company, United States of America.
5. Donowsky, M. (2013). *U.S. Patent Application No. 13/488,850*.
6. Fardela, R., and Ashari, A. (2018, October). Study of Wireless Sensor Network Application for Dosimeter Personal Real Time. In *2018 International Conference on Orange Technologies (ICOT)* (pp. 1-4). IEEE.
7. Fardela, R., Suparta, G. B., Ashari, A., and Triyana, K. (2019). Multi Sensor Data Acquisition System Design for Monitoring the Radiation Dose Based on Wireless Sensor Network. *International Journal of Engineering Research and Technology*. Vol.12, Number 6, pp. 848-853.
8. Fitousi, N. (2017). Patient dose monitoring systems: a new way of managing patient dose and quality in the radiology department. *Physica Medica*, 44, 212-221.
9. Fujibuchi, T., Inoue, A., Ishigaki, Y., and Matsumoto, Y. (2019). Development of a wireless multisensor active personal dosimeter-tablet system (The 9th International Symposium on Radiation Safety and Detection Technology (ISORD-9)). *Progress in nuclear science and technology*, 6, 73-76.
10. Healy, B. J., van der Merwe, D., Christaki, K. E., and Meghzifene, A. (2017). Cobalt-60 machines and medical linear accelerators: competing technologies for external beam radiotherapy. *Clinical Oncology*, 29(2), 110-115.
11. Hsia, T. C., Shen, Y. Y., Yen, R. F., Kao, C. H., and Changlai, S. P. (2002). Comparing whole body 18F-2-deoxyglucose positron emission tomography and technetium-99m methylene diophosphate bone scan to detect bone metastases in patients with non-small cell lung cancer. *Neoplasma*, 49(4), 267-271.
12. Kang, H. G., Song, J. J., Lee, K., Nam, K. C., Hong, S. J., dan Kim, H. C. (2016). An investigation of medical radiation detection using CMOS image sensors in smartphones. *Nuclear Instruments and Methods in Physics Research Section A: Accelerators, Spectrometers, Detectors and Associated Equipment*, 823, 126-134.
13. Kefalidis, E., Kandarakis, I., and David, S. (2017). Performance characteristics of a personal gamma spectrometer based on a SiPM array for radiation monitoring applications. *JPhCS*, 931(1), 012019.
14. Kazakov, A. G., Garashchenko, B. L., Yakovlev, R. Y., Vinokurov, S. E., Kalmykov, S. N., and Myasoedov, B. F. (2020). An experimental study of sorption/desorption of selected radionuclides on carbon nanomaterials: a quest for possible applications in future nuclear medicine. *Diamond and Related Materials*, 104, 107752.
15. Knoll, G. F. (2010). *Radiation detection and measurement*. John Wiley and Sons.

16. Krhovska, P., Minarik, J., Pika, T., Bacovsky, J., and Proskova, J. (2019). Comparison of Radiodiagnostic Methods (Conventional Radiography, Low-Dose Computed Tomography and Magnetic Resonance Imaging) With Selected Markers of Bone Metabolism and Bone Marrow Microenvironment. *Clinical Lymphoma, Myeloma and Leukemia*, 19 (10), e191.
17. Kusminarto, and Fadela, R. (2015). An X-Ray Detector Using a Fluorescent Material ZnS:Ag Attached on a Phototransistor in Darlington Configuration. *Applied Mechanics and Materials*, 771, 21–24. <https://doi.org/10.4028/www.scientific.net/amm.771.21>
18. Luster, M., Clarke, S. E., Dietlein, M., Lassmann, M., Lind, P., Oyen, W. J. G., and Bombardieri, E. (2008). Guidelines for radioiodine therapy of differentiated thyroid cancer. *European journal of nuclear medicine and molecular imaging*, 35(10), 1941.
19. Magalotti, D., Bissi, L., Conti, E., Paolucci, M., Placidi, P., Scorzoni, A., and Servoli, L. (2014). Performance of CMOS imager as sensing element for a real-time active pixel dosimeter for interventional radiology procedures. *Journal of Instrumentation*, 9(01), C01036.
20. Mann, W. B., Rytz, A., and Spornol, A. (Eds.). (2012). *Radioactivity measurements: principles and practice*. Elsevier.
21. Miller, D. L. (2018). Make radiation protection a habit. *Techniques in vascular and interventional radiology*, 21(1), 37-42.
22. Missailidis, S., and Perkins, A. (2007). Update: aptamers as novel radiopharmaceuticals: their applications and future prospects in diagnosis and therapy. *Cancer biotherapy and radiopharmaceuticals*, 22(4), 453-468.
23. Mohan, A. K., Hauptmann, M., Freedman, D. M., Ron, E., Matanoski, G. M., Lubin, J. H., ... and Linet, M. S. (2003). Cancer and other causes of mortality among radiologic technologists in the United States. *International journal of cancer*, 103(2), 259-267.
24. Musto, E., Assenmacher, F., Hofstetter-Boillat, B., Mayer, S., and Yukihara, E. G. (2019). Use of the D-Shuttle dosimeter for radiation protection of members of the public: Characterization and feasibility study. *Radiation Measurements*, 129, 106208.
25. Nambiar, D., Rajamani, P., and Singh, R. P. (2011). Effects of phytochemicals on ionization radiation-mediated carcinogenesis and cancer therapy. *Mutation Research/Reviews in Mutation Research*, 728(3), 139-157.
26. Paunesku, T., Haley, B., Brooks, A., and Woloschak, G. E. (2017). Biological basis of radiation protection needs rejuvenation. *International Journal of Radiation Biology*, 93(10), 1056-1063.
27. Podgorsak, E. B. (2005). Radiation oncology physics. Vienna: *International Atomic Energy Agency*, 123-271.
28. Radford, E. P. (1980). Human health effects of low doses of ionizing radiation: the BEIR III controversy. *Radiation Research*, 84(3), 369-394.
29. Richardson, D. B., Cardis, E., Daniels, R. D., Gillies, M., O'Hagan, J. A., Hamra, G. B. and Schubauer-Berigan, M. K. (2015). Risk of cancer from occupational exposure to ionizing radiation: retrospective cohort study of workers in France, the United Kingdom, and the United States (INWORKS). *Bmj*, 351.
30. Rosenberg, I. (2008). Radiation oncology physics: a handbook for teachers and students. *British journal of cancer*, 98(5), 1020.
31. Ryan, J. L. (2012). Ionizing radiation: the good, the bad, and the ugly. *Journal of Investigative Dermatology*, 132(3), 985-993.
32. Saeed, S., ul Haq, S., Sohaib, M., and Khan, A. N. (2017). Utility of Tc-99m MDP bone SPECT in evaluation of osseous involvement in craniofacial malignancies. *Journal of Cranio-*

Maxillofacial Surgery, 45(11), 1815-1819.

French Academy of Science: Problems associated with the effects of low doses of ionizing radiation'. *Journal of Radiological Protection*, 18(4), 243.

33. Santos, J. S., Uusi-Simola, J., Kaasalainen, T., Aho, P., and Venermo, M. (2020). Radiation Doses to Staff in a Hybrid Operating Room: An Anthropomorphic Phantom Study with Active Electronic Dosimeters. *European Journal of Vascular and Endovascular Surgery*.
34. Stabin, M. G. (2007). *Radiation protection and dosimetry: an introduction to health physics*. Springer Science and Business Media.
35. Suliman, I. I., Salih, L. H., Ali, D. M., Alaamer, A. S., Al-Rajhi, M. A., Alkhorayef, M., and Bradley, D. A. (2019). Occupational exposure in nuclear medicine and interventional cardiology departments in Sudan: Are they following radiation protection standards?. *Radiation Physics and Chemistry*, 160, 100-104.
36. Suliman, I. I., Salih, L. H., Ali, D. M., Alaamer, A. S., Al-Rajhi, M. A., Alkhorayef, M., and Bradley, D. A. (2020). Reprint of "Occupational exposure in nuclear medicine and interventional cardiology departments in Sudan: Are they following radiation protection standards?". *Radiation Physics and Chemistry*, 167, 108556.
37. Taleb, J., Janier, M., Bonazza, P., Roux, P., Miladi, I., Goutain-Majorel, C., ... and Kryza, D. (2013). Radiation dose measurements for staff members involved in holmium-166 preclinical trial. *Radiation measurements*, 58, 75-78.
38. Teles, P., Trincão, M., Alves, F., Antunes, V., Calado, D., Cantinho, G., and Isidoro, J. (2020). Evaluation of the Portuguese population exposure to ionizing radiation due to x-ray and nuclear medicine procedures from 2013 to 2017. *Radiation Physics and Chemistry*, 172, 108762.
39. Tsoulfanidis, N. (2010). *Measurement and detection of radiation*. CRC press.
40. Tubiana, M. (1998). The report of the

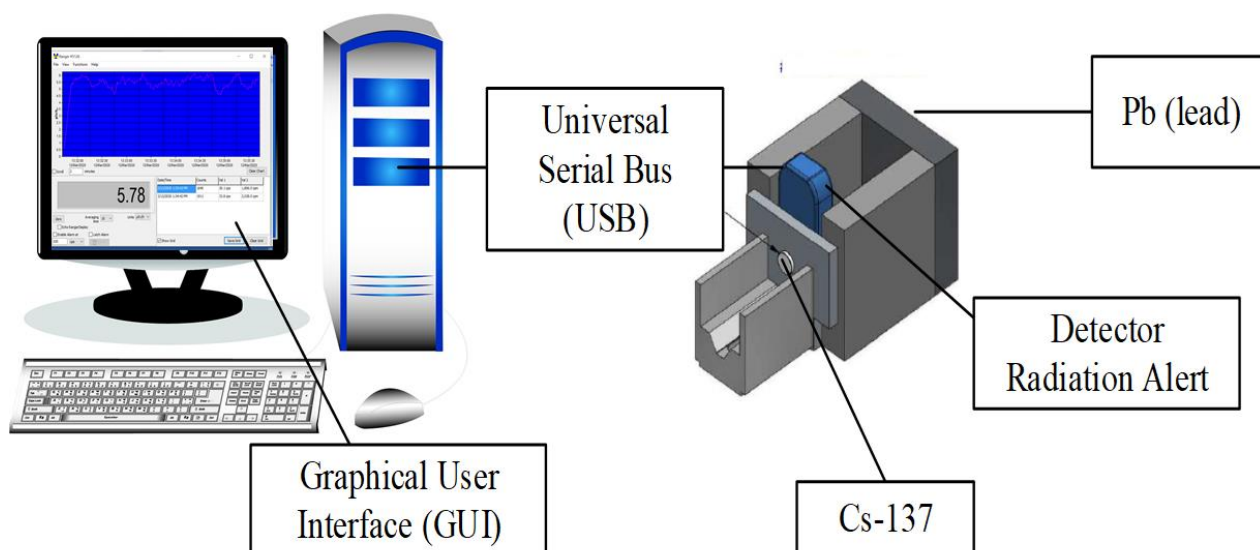


Figure 1. The scheme of exposure rate collecting data process using “radiation alert detector”.

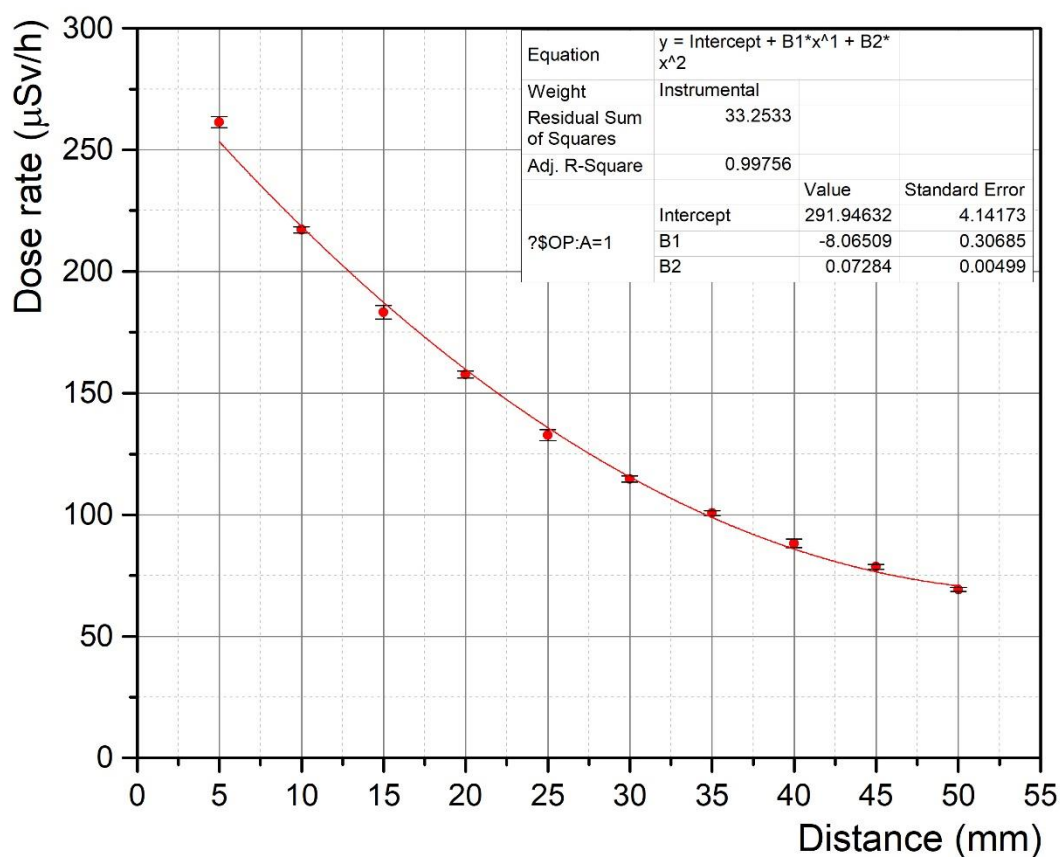


Figure 2. Radiation dose rate curves ($\mu\text{Sv} / \text{hr}$) against detector distance variations (mm) for Cs-137 radioactive contamination measurement

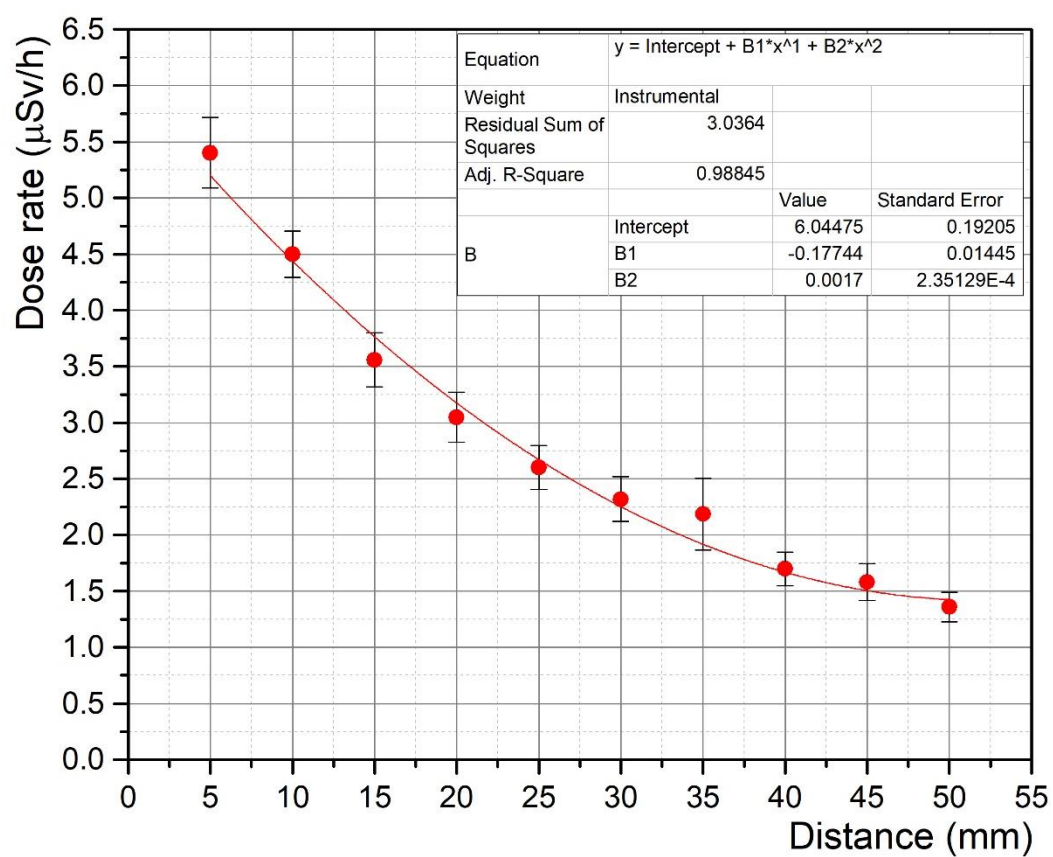


Figure 3. Radiation dose rate curves ($\mu\text{Sv} / \text{hr}$) against distance variations (mm) for Cs-137 radioactive gamma measurement

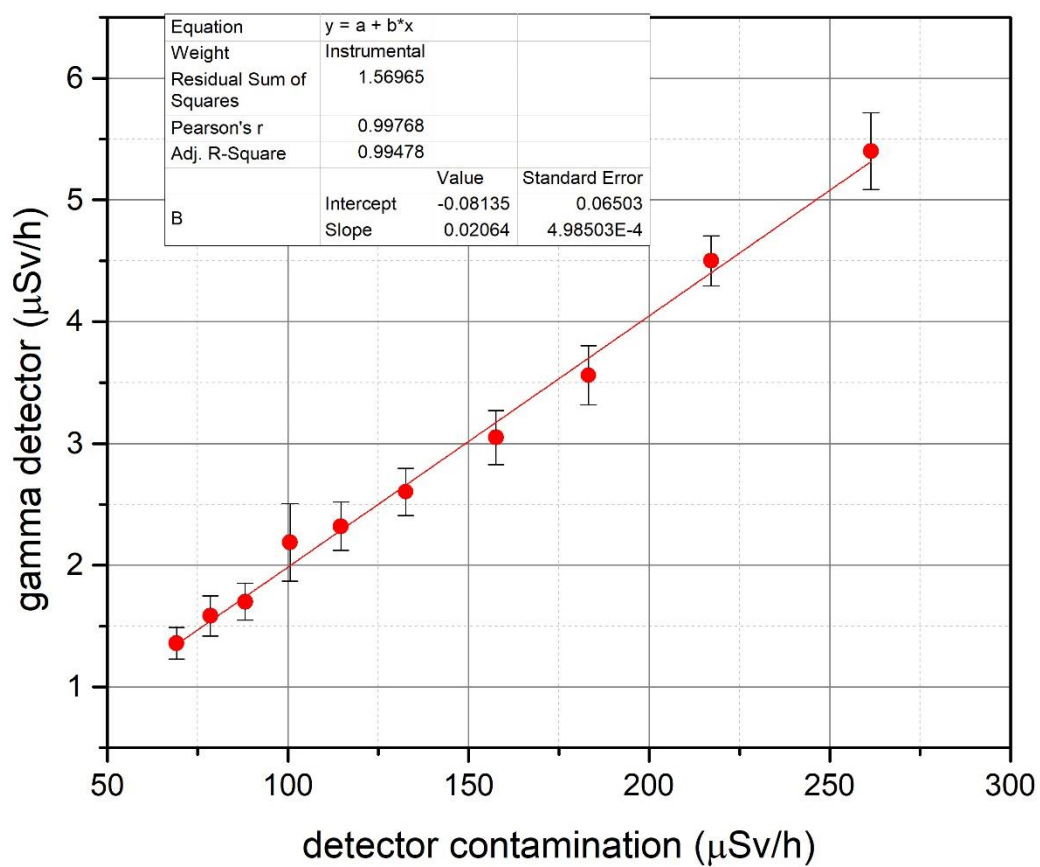


Figure 4. Graph of the relationship between the contamination detector dose rate with the experimental gamma detector

DESENVOLVIMENTO DE MISTURAS DE GÁS DE CALIBRAÇÃO (DIÓXIDO DE CARBONO E OXIGÊNIO EM MATRIZ DE NITROGÊNIO) EM UMA FAIXA DE CONCENTRAÇÃO TÍPICA DE EMBALAGEM DE ATMOSFERA MODIFICADA**DEVELOPMENT OF CALIBRATION GAS MIXTURES (CARBON DIOXIDE AND OXYGEN IN NITROGEN MATRIX) AT A TYPICAL CONCENTRATION RANGE OF MODIFIED ATMOSPHERE PACKAGING****PENGEMBANGAN CAMPURAN GAS KALIBRASI (KARBON DIOKSIDA DAN OKSIGEN DALAM MATRIKS NITROGEN) PADA KISARAN KONSENTRASI TIPIKAL UNTUK PENGEMASAN ATMOSFER TERMODIFIKASI**

HINDAYANI, Ayu¹; MULYANA, Muhammad Rizky²; BUDIMAN, Harry³; DARMAYANTI, Nur Tjahyo Eka⁴; ZUAS, Oman^{5*}

^{1,2,3,4,5} Center for Research and Human Resources Development (PUSRISBANG-SDM), National Standardization Agency of Indonesia (BSN), Kawasan PUSPIPTEK Building 420, Serpong 15314, Tangerang Selatan - Banten, Indonesia

* Corresponding author
e-mail: oman@bsn.go.id

Received 30 July 2020; received in revised form 27 August 2020; accepted 22 October 2020

RESUMO

A medição da concentração de dióxido de carbono (CO₂), oxigênio (O₂) e nitrogênio (N₂) em alimentos embalados em atmosfera modificada (MAP) é crítica para ser realizada pela indústria de alimentos. Uma ligeira variação nas concentrações de CO₂, O₂ e N₂ nas embalagens de alimentos pode ter um impacto significativo na qualidade do produto e na segurança para a saúde humana. A medição precisa e confiável das concentrações de CO₂, O₂ e N₂ em embalagens de alimentos é crucial e só pode ser obtida calibrando o analisador de gás. Este estudo teve como objetivo desenvolver misturas de gases para calibração de analisadores de gás CO₂, O₂ e N₂ em uma faixa de concentração típica de embalagens com atmosfera modificada. As misturas de gás de calibração foram preparadas gravimetricamente seguindo ISO 6142. A faixa de concentração de CO₂, O₂ e N₂ para misturas de gás de calibração foi definida em 9-19% mol/mol, 1-5% mol/mol e 74-88% mol/mol, respectivamente. Cada gás original foi identificado por suas impurezas usando cromatografia gasosa com um detector de ionização de hélio de descarga pulsada (GC-PDHID). As composições de CO₂, O₂ e N₂ nas misturas foram verificadas por meio da avaliação da consistência interna das misturas gasosas preparadas por meio de cromatografia gasosa com detector de condutividade térmica (GC-TCD). A estabilidade a curto prazo das misturas de gases preparadas foi avaliada usando um método de divisão igual. O resultado mostrou que foi obtida boa consistência interna entre os valores gravimétricos e de verificação do GC, havendo regressão do coeficiente linear (R²) ≥ 0,999. O resultado do teste t mostrou que o CO₂ tem melhor estabilidade de curto prazo do que O₂ e N₂. Em conclusão, as misturas de gases de calibração desenvolvidas em uma faixa de concentração típica de embalagens de atmosfera modificada têm mostrado resultados satisfatórios para o componente CO₂. No entanto, avaliações adicionais ainda são necessárias para minimizar a instabilidade dos componentes O₂ e N₂.

Palavras-Chave: *calibração de misturas de gás padrão, embalagem de atmosfera modificada, analisador de gás*

ABSTRACT

Measurement of carbon dioxide (CO₂), oxygen (O₂), and nitrogen (N₂) concentration in modified atmosphere packaging (MAP) food is critical to be carried out by the food industry. A slight variation in concentrations of CO₂, O₂, and N₂ in food packaging may have a significant impact on product quality and safety for human health. Accurate and reliable measurement of CO₂, O₂, and N₂ concentrations in food packaging is crucial, and it can only be achieved by calibrating the gas analyzer. This study aimed to develop gas mixtures for the calibration of CO₂, O₂, and N₂ gas analyzers at a typical concentration range of modified atmosphere packaging. The calibration gas mixtures were prepared gravimetrically by following ISO 6142. The concentration ranges of CO₂, O₂, and N₂ for calibration gas mixtures were set at 9-19% mol/mol, 1-5% mol/mol, and 74-88%

mol/mol, respectively. Each parent gas was identified for its impurities using gas chromatography with a pulsed discharge helium ionization detector (GC-PDHID). The compositions of CO₂, O₂, and N₂ in the mixtures were verified by evaluating the internal consistency within the prepared gas mixtures using gas chromatography with a thermal conductivity detector (GC-TCD). The short term stability of the prepared gas mixtures was evaluated using an equal division method. The result showed that good internal consistency was achieved between the gravimetric and GC's verification values, having linear regression coefficient ($R^2 \geq 0.999$). The t-test result has shown that CO₂ has better short term stability than O₂ and N₂. In conclusion, the developed calibration gas mixtures at a typical concentration range of modified atmosphere packaging have shown satisfying results for CO₂ component. However, further evaluation is still required to minimize the instability of O₂ and N₂ components.

Keywords: *calibration standard gas mixtures, modified atmosphere packaging, gas analyzer*

ABSTRAK

Pengukuran konsentrasi karbon dioksida (CO₂), oksigen (O₂), dan nitrogen (N₂) untuk pengemasan pangan atmosfer termodifikasi (MAP) sangat penting dilakukan oleh industri pangan. Sedikit perubahan konsentrasi CO₂, O₂, dan N₂ dalam pengemasan makanan dapat berdampak signifikan terhadap kualitas dan keamanan produk bagi kesehatan manusia. Pengukuran konsentrasi CO₂, O₂ dan N₂ yang akurat dan handal dalam pengemasan makanan menjadi sangat penting dan hanya dapat dicapai dengan mengkalibrasi peralatan analisa gas tersebut. Studi ini bertujuan untuk mengembangkan campuran gas untuk kalibrasi alat analisa gas CO₂, O₂ dan N₂ pada kisaran konsentrasi tipikal dari pengemasan atmosfer termodifikasi. Campuran gas kalibrasi dibuat secara gravimetri sesuai dengan ISO 6142. Kisaran konsentrasi CO₂, O₂, dan N₂ untuk campuran gas kalibrasi ditentukan masing-masing pada 9-19% mol/mol, 1-5% mol/mol, dan 74-88% mol/mol. Tiap gas induk diidentifikasi pengotornya menggunakan kromatografi gas dengan detektor *pulsed discharge helium ionization* (GC-PDHID). Komposisi CO₂, O₂, dan N₂ dalam campuran gas diverifikasi dengan mengevaluasi konsistensi internal menggunakan kromatografi gas dengan detektor keterhantaran panas (GC-TCD). Kestabilan campuran gas jangka pendek dievaluasi dengan menggunakan metode pembagian setara. Hasil studi menunjukkan bahwa terdapat konsistensi internal yang baik antara nilai gravimetri dan nilai verifikasi GC, dengan koefisien regresi linier ($R^2 \geq 0,999$). Hasil uji-t menunjukkan bahwa CO₂ memiliki stabilitas jangka pendek yang lebih baik dari pada O₂ dan N₂. Sebagai kesimpulan, campuran gas kalibrasi yang dikembangkan pada kisaran konsentrasi tipikal dari pengemasan atmosfer termodifikasi telah menunjukkan hasil yang memuaskan untuk komponen CO₂, namun diperlukan penanganan lebih lanjut untuk meminimalkan ketidakstabilan komponen O₂ dan N₂.

Kata Kunci: *campuran gas standar kalibrasi, pengemasan atmosfer termodifikasi, penganalisa gas*

1. INTRODUCTION:

Food is an essential element in the human body besides air and water (De and De, 2019; Aversa *et al.*, 2016). In general, food consists of essential nutrients, such as carbohydrates (Marinangeli *et al.*, 2020), proteins (Beals *et al.*, 2017), fats (Utyanov *et al.*, 2018), minerals, and vitamins (Kodentsova and Vrzhesinskaya, 2018) for human on providing energy, developing and maintaining life and stimulating growth (Millward, 2017; Dorgan *et al.*, 2019). Most of these nutritious foods are originated from natural products, such as vegetables, fruit, fish, and meat. However, the self-life of natural products is limited because of spoilage. Food spoilage is defined as a change in food quality, such as objectionable odor, texture, and appearance. Therefore, this food is unfit for consumption (Odeyemi *et al.*, 2020; Amit *et al.*, 2017). Storage temperature, pH, moisture loss, the action of enzymes, microorganism (molds, yeasts, and bacteria) contamination, processing operation, transportation, and food handlers influence the rate of spoilage (Franceschini *et al.*,

2020; Wagner *et al.*, 2020; Shwaiki *et al.*, 2019; Tsang *et al.*, 2018). Food spoilage can affect economic loss, such as in Australia. The cost of food losses related to spoilage was estimated at \$10,000,000 annually (Pitt and Hocking, 2009). Other than that, spoiled food contributes to food waste, in which approximately 1.3 billion tons of food is wasted every year (Odeyemi *et al.*, 2020; Rawat, 2015; Ishangulyyev *et al.*, 2019). Consequently, food preservation is needed to resolve the spoilage.

There are some possible ways to slow down the spoilage processes and to keep food edible as long as possible. It may include drying, refrigeration, fermentation, chilling, irradiation, pasteurization, canning, and the addition of synthetic chemicals (Vaclavik and Christian, 2008). However, this method has a limitation, such as significant loss of flavor, aroma, and nutrients, a decrease of some vitamin and mineral availability, crispiness reduction of selected food items, the deformation of the original color, and the formation of undesirable taste and appearance

(Cachon and Alwazeer, 2019; Kharobe, 2018; Amit *et al.*, 2017). Certain synthetic chemicals are used as a food preservative because they are the most effective longer shelf life (Linke *et al.*, 2018; Sharma, 2015). However, several synthetic chemicals have negative and potentially life-threatening side effects. Nitrates can cause loss of consciousness and death, especially in an infant; sulfite can cause severe allergic reactions and asthma; benzoates can cause skin rashes, and sorbates can contact dermatitis (Sharma, 2015; Anand and Sati, 2013; Mirza *et al.*, 2017; Dwivedi *et al.*, 2017).

A good packaging system for storage, transportation, and end-use of food is another preferable way to keep the quality of natural products. Practically, the good packaging system could prevent deterioration of the food quality because the environment may influence and contribute to the efficiency of distribution, sales, and consumption (Regattieri and Santarelli, 2013; Han *et al.*, 2018). Nowadays, the application of food packaging systems has been proven as an effective method for reducing food waste and spoilage (Opara and Mditshwa, 2013; Verghese, *et al.*, 2015). The food packaging systems have several advantages, including reducing the costs of preservation, extend the shelf life of foods, provide safe and convenient foods to consumers, maintain the quality of the food product, and contribute to sales and marketing efforts, as well as the address to environmental issues (Han *et al.*, 2018; Han, 2014; Montero-Calderón, *et al.*, 2010). Several factors of the package itself should be carefully tested because of the possible migration of harmful content into food products reported by previous studies (Gavriil, *et al.*, 2018; Lin, Q-B., *et al.*, 2017).

One of the most interesting food packaging systems is the modified atmosphere packaging (MAP). It is an effective preservation method for maintaining quality and extending the shelf-life of various foods (Hyun and Lee, 2017). The MAP can maintain the visual, textural, and nutritional appeal of natural products (Sandhya, 2010). It can provide an extended shelf life without the addition of chemical preservatives or stabilizers by slowing chemical and biochemical deteriorative reactions and inhibiting spoilage organisms (Abdulummeen, *et al.*, 2012; Sandhya, 2010; Mullan and McDowell, 2003).

The MAP is defined as the packaging of a perishable product in an atmosphere by which its composition is other than air (Mullan and McDowell, 2003). Normal air has a composition of 78 % nitrogen (N₂), 21 % oxygen (O₂) and 1 %

argon (Ar). In a MAP, the food packaging is flushed with a gas or a mixture of gases. The most common gases used are N₂, O₂, and CO₂. The choice of gas or mixture of gases is dependent on the food product being packed (Sandhya, 2010). An N₂ is an inert gas with a primary function as a filler gas to avoid the collapse when CO₂ dissolves in the food product and minimize the respiration rate in fruit and vegetables. An O₂ with a concentration below normal air (<21%) can inhibit the growth of aerobic microorganisms (Meredith *et al.*, 2014). A CO₂ with a high concentration (20% or greater) effectively inhibits spoilage bacteria and molds (Kotsianis *et al.*, 2002; Devlieghere *et al.*, 2003; Embleni, 2013).

Even though the MAP is the best available technology for food packaging, a failure such as leaks of packaging is inevitable, resulting in a severe effect from the loss of nutrients, taste, color, or structure to a foul smell and also risk to the consumer health (Wen *et al.*, 2018; Smolander *et al.*, 1997). Therefore, comprehensive quality assurance activities are essential to be carried out during and after the packaging process. It is required to monitor the correct composition gas mixture of the modified atmosphere and the leaks of packaging because variations of N₂, O₂, and CO₂ composition can significantly impact food product quality (Pu *et al.*, 2020; Javanmard, 2017).

In this regard, gas analyzers are used for quality control of MAP process to measure the modified atmosphere gas levels inside product packages (Ali *et al.*, 2019; Ozturk *et al.*, 2019; Scarabottolo, 2020). They can detect the leaks of the package to keep the quality of the product. The accurate and reliable result of measured gas levels can be achieved by calibrating the gas analyzer regularly using a calibration standard gas mixture (Budiman and Zuas, 2015). Besides, the calibration of the gas analyzer is required by ISO 17025 to establish the traceability of the measurement results (Jacksier and Weterings, 2017; Brown *et al.*, 2017; ISO, 2017b).

The availability of calibration gas mixtures in Indonesia, especially for the calibration of the gas analyzer in food packaging, is imported from overseas. This process is relatively costly and time-consuming, leading to an increase in production cost. Related to this issue, the National Institute of Standards and Technology (NIST) has studied the economic impact of their Gas Mixture NIST-Traceable Reference Materials Program on the local industry in the U.S. They have reported several financial benefits that could be gained from their calibration gas standards (Gallaher *et al.*, 2002).

Therefore, this study aimed to provide an insight into the development of calibration gas mixtures which are required as quality control in modified atmosphere packaging. In this article, relevant contributing factors involved in the preparation of calibration gas mixtures (CO₂ and O₂ in N₂ matrix) using the gravimetric method following ISO 6142 were discussed. It is expected that this study can be of help to potential stakeholders who need to develop their gas reference material for MAP of food products.

2. MATERIALS AND METHODS:

A preparation of calibration gas mixtures (CO₂ and O₂ in N₂ matrix) using the gravimetric method following ISO 6142 has been conducted. In the gravimetric method, the parent gases (target gases: CO₂ and O₂) were diluted by the high purity gases (matrix gas: N₂) in high pressurized cylinders. The composition of calibration gas mixtures was calculated from the weighing amount of parent and matrix gases, the amount fraction, and the molar mass of each component gases according to equation 1.

$$x_i = \frac{\sum_{A=1}^P \left(\frac{x_{i,A} \cdot m_A}{\sum_{i=1}^n x_{i,A} \cdot M_i} \right)}{\sum_{A=1}^P \left(\frac{m_A}{\sum_{i=1}^n x_{i,A} \cdot M_i} \right)} \quad (\text{Eq.1})$$

where x_i is the mole fraction of component i in the final mixtures. P is the total number of parent gases. n is the total number of the component in the final mixture. m_A is the mass of parent gas A determined by weighing. M_i is the molar mass of component i . $x_{i,A}$ is the mole fraction of component i , in parent gas A (ISO, 2001).

The brief preparation of calibration gas mixtures was taken from our previous work (Budiman *et al.*, 2017) and described as follows. Firstly, 4 L of the empty aluminum cylinder was cleaned by evacuating until 10⁻⁷ mbar and heating at 60 °C for 24 hours. After that, a specified amount of the parent gases (CO₂, O₂) were filled into the cleaned cylinders and diluted with high purity N₂ as matrix gas. Subsequently, the exact amount of parent gases and matrix gas were precisely weighed by a mass comparator located at a room with controlled temperature (22 ± 1 °C) and humidity (50 ± 5%). The weighing process was performed by weighing the mass of the sample and reference cylinder. The amounts of parent gases and matrix gas-filled were calculated by the difference between the sample and

reference cylinder mass. This calibration gas mixture is used for assuring the traceability of the measurement results. During the preparation process, the CO₂, O₂, and N₂ as parent gases were assessed for their impurities. For short term stability of the calibration, gas mixtures was evaluated using an equal division method.

2.1. Materials

Ultra-high purity grade of gases, such as CO₂ (Grade Alphagaz 2, claimed by the manufacturer as 99.9995% mol/mol of purity) and O₂ (Grade Alphagaz 2, claimed by the manufacturer as 99.9995% mol/mol of purity) from Air Liquide, Indonesia, and N₂ gas (Grade UHP, claimed by the manufacturer as 99.9995% mol/mol of purity) from Surya Indotim Imex-Indonesia, was used as the parent gases for each target of calibration standard gas mixtures concentration. The impurities of each gas were analyzed using GC-PDHID (Agilent Technologies, USA). The NET company, China, supplied the aluminum gas cylinders (capacity 4 Liter, 12 cm in diameter) equipped with stainless steel valve. All gas cylinders were checked for possible leakage by filling the gas cylinder with N₂ gas until its pressure reached 100 bar. The leakage test was conducted for 1 month. The gas cylinder is free from leakage if there is no difference in pressure between the initial and final tests. Subsequently, the gas cylinder was evacuated using a vacuum system until a pressure of 10⁻⁷ mbar while heated for 24 hours at 60 °C by using a heating mantle.

2.2. Equipment

A GC (7890B, Agilent Technologies, USA) equipped with Thermal Conductivity Detector (TCD) was used for the verification composition of the calibration gas mixtures. Analysis of the gas sample was conducted under optimum operating conditions (Table 1). Mass comparator XP10003S (Mettler Toledo, Switzerland) was used for the gravimetric preparation of the calibration gas mixture.

2.3. Procedure

2.3.1 Determination of Impurities in Parent Gas

The impurities in the parent gases have a significant effect on the composition of the calibration gas mixtures, because the impurities may react with other component gases in the gas mixtures (Mulyana *et al.*, 2019; ISO, 2001). Gas Chromatography can determine the impurities, such as CO₂, Argon (Ar), O₂, N₂, methane (CH₄)

and carbon monoxide (CO) at trace level - Pulsed Discharged Helium Ionization Detector (GC-PDHID) under the optimum operating condition as described in our previous work (Hindayani *et al.*, 2019, Mulyana *et al.*, 2019).

The optimum operating conditions of GC-PDHID were described as follows: the parent gas samples with flow 40 mL/min were maintained by a thermal mass flow controller and introduced to 1 mL of the GC-system loop. The gas samples were injected with a split ratio 1:1 to the column of GC-system. Two capillary columns were used to separate the gas component such as Pora PLOT Q column (50 m length, 530 μ m OD, 20 μ m film thickness) and Molsieve 5A column (50 m length, 530 μ m OD, 20 μ m film thickness). The getter instrument initially purified the helium carrier gas before it was flown to the GC-system. The programmed flow rate of helium carrier gas was performed with the following condition: initial 10 mL/min (hold for 11.5 min), ramp down 60 mL/min by each minute to 5 mL/min (hold for 3.4 min), ramped up 60 mL/min by each minute to 10 mL/min (hold for 0 min). The oven column was set to programmed temperature as follows: Initial 40 °C (hold for 6.5 min), first ramp down 100 °C/min to 30 °C (hold for 8.4 min), second ramp up 6 °C/min to 75 °C (hold for 0 min), third ramp up 12 °C/min to 160 °C (hold for 0 min). The gas sampling box and detector temperature were set to 100 °C and 250 °C, respectively.

2.3.2 Preparation of Calibration Standard Gas Mixtures of CO₂ and O₂ in N₂ Matrix

Firstly, a pre-mixture gas containing 10.042% mol/mol O₂ in N₂ balance (89.958% mol/mol) was gravimetrically prepared. After that, the calibration gas mixtures for MAP measurement were prepared by mixing the pre-mixture gas and pure CO₂ gas, followed by diluting the mixture with pure N₂ gas as a gas matrix. Three different calibration gas mixtures were prepared, and each calibration gas mixtures were having a composition, as shown in Table 2. The gravimetric concentration of the prepared gas mixtures was calculated according to ISO 6142. The transferring process of the gases was carried out using the gas filling station, as described in the previous report (Budiman *et al.*, 2017). Then, the filled gases in the cylinder were homogenized by rotating the cylinder using a cylinder homogenization system for 12 hours.

Table 2. Three cylinders of the calibration gas mixtures and their composition

Code of Cylinder	Gravimetric concentration (%mol/mol)		
	CO ₂	O ₂	N ₂
ADK 004	9.949	1.089	88.962
ADK 009	16.852	3.115	80.033
ADK 005	19.885	5.206	74.908

2.3.3 Verification of Internal Consistency between Calibration Standard Gas Mixtures

The prepared calibration gas mixtures were verified for their composition using GC-TCD. The linear regression curves were generated for each component gases (CO₂, O₂, and N₂) in calibration gas mixtures to investigate the consistency among the prepared calibration gas mixtures. The detail of the analysis procedure using GC-TCD is briefly explained in the following experimental condition (Budiman and Zuas, 2015).

The 30 mL/min of a constant flow of calibration gas mixtures samples were introduced to the 500 μ L loop of the GC-system using thermal mass flow controller. In the GC-system, the injector and detector temperature were set to 100 °C and 250 °C, respectively. The target gas components (CO₂, O₂, and N₂) were separated from their mixtures using two packed columns stainless steel, such as Porapak Q column (1/8 inch OD, 6 feet, 80-100 mesh) and Molsieve 5A (1/8 inch OD, 9 feet, 80-100 mesh) that were connected in series. The elution of gas components from the column was performed using the helium carrier gas 28 mL/min and isothermal condition (40 °C). This procedure aims to determine the consistency of the composition between calibration standard gas mixtures in each cylinder.

2.3.4 Short Term Stability of Calibration Standard Gas Mixtures

The short term stability of the prepared calibration gas mixtures was investigated and evaluated by the equal division method. The amount of gas from the ADK009 cylinder was equally divided into the AH06004 cylinder, and the concentration of each gas component was checked using GC-TCD. After that, a significant difference between the concentration of calibration gas mixtures in AH06004 and ADK009 were statistically tested using *t-test* (two-sample

assuming equal variances, two-tailed) method. If t_{stat} is less than $t_{critical}$, the concentration of each component in the two cylinders is not significantly different and can be categorized as a stable gas mixture (Minitab, 2019).

3. RESULTS AND DISCUSSION:

A calibration gas mixture can be defined as a mixture containing multiple gases with well-established and certified composition for measurement calibration, including gas measurement (ISO, 2017a). Establishing the response of a gas analyzer to a known concentration of a gas component through a calibration process is necessary (Shaw, 2020). In this regards, a certified standard gas mixture having traceability to the International Standard unit (SI) with precisely defined composition is required. In this work, a set of calibration gas mixtures was prepared by a gravimetric method following ISO 6142. The ISO 6142 specifies a gravimetric method to prepare calibration gas mixtures in cylinders with traceable values for the amount fraction of one or more components (ISO, 2015). The gravimetric method is one of the most precise and accurate methods for preparing a traceable calibration gas mixture through the mass unit (Shimosaka *et al.*, 2011).

3.1. Purity analysis of parent gas

The accuracy of the calibration gas mixtures composition depends significantly on the purity of parent gases (CO_2 , O_2 and N_2) used. The purity analysis of parent gases can be obtained by identifying and quantifying of the impurities in parent gases.

Table 3. The purity analysis data of CO_2 parent gas

Components	Concentration ($\mu\text{mol/mol}$)
Ar	0.49
O_2	0.85
N_2	2.25
CH_4	0.31
CO	0.85
CO_2	999994.25

The purity analysis data of the parent gases of CO_2 , O_2 , and N_2 were obtained by using GC-PDHID. For purity analysis of N_2 has been

conducted in the previous study (Mulyana *et al.*, 2019). The results are shown in Tables 3, 4, and 5, respectively.

Table 4. The purity analysis data of O_2 parent gas

Components	Concentration ($\mu\text{mol/mol}$)
CO_2	0.75
Ar	n.d.*
N_2	9.10
CH_4	n.d.*
CO	2.39
O_2	999987.77

note: n.d.* = not detected

Table 5. The purity analysis data of N_2 parent gas

Components	Concentration ($\mu\text{mol/mol}$)
CO_2	0.02
Ar	0.99
O_2	5.82
CH_4	3.16
CO	1.29
N_2	999987.0

Table 6. The comparison of the concentration of calibration standard gas mixtures from GC measurement and gravimetric calculation

Code of Cylinder	Gas	Concentration (%mol/mol)	
		GC-TCD	Gravimetric
ADK 004	CO_2	9.960	9.949
	O_2	0.523	1.089
	N_2	89.515	88.962
ADK 009	CO_2	17.012	16.852
	O_2	1.505	3.115
	N_2	81.491	80.033
ADK 005	CO_2	20.086	19.885
	O_2	2.525	5.206
	N_2	77.393	74.908

All impurities data above were used in calculating the composition of the prepared calibration gas mixtures. The concentrations of the

composition of prepared calibration standard gas mixtures are listed in Table 6. These values were obtained by calculating the mass of each transferred gas in the cylinders based on ISO 6142. The concentration from gravimetric, however, can be occasionally incorrect because of accidents in the preparation. The errors could be contamination from air, faulty of weighing, adsorption or desorption of gases like O₂ and N₂ from air to the inner wall of the cylinder, or other unknown factors (Shimosaka *et al.*, 2011). Therefore, this concentration needs to be verified further.

3.2. Verification of calibration standard gas mixtures

The composition of a calibration gas mixture must be verified experimentally by using GC. This verification is used to check the consistency of mixture composition between GC measured value and calculated value from the gravimetric preparation process (ISO, 2015). The peak areas of each component (O₂, CO₂, and N₂) from the GC were plotted as a function of the mole fraction of the calibration gas mixtures.

The results show that linear regression coefficients (R^2) were found to be ≥ 0.999 were generated for each component in the gas mixtures, as depicted in Figures 1, 2, and 3. These findings indicate a good consistency in the concentration of the prepared calibration standard gas mixtures for all mixture cylinders.

3.3. Short term stability of calibration standard gas mixtures

The short term stability was carried out by transferring the calibration gas mixture in ADK009 into another empty cylinder (AH06004) until the equilibrium of gas pressure in both cylinders was achieved. The concentrations of gases in the mixture from both cylinders were determined using GC-TCD. The significant difference in concentrations between the two cylinders was statistically evaluated using *t*-test: two-sample assuming equal variances two-tailed. If t_{stat} is less than $t_{critical}$, the concentration of two cylinders is not significantly different, and it can be categorized as stable gas mixtures (Minitab, 2019). The *t*-test results for CO₂ concentration in ADK009 and AH06004 are listed in Table 7.

From Table 7, it can be seen that t_{stat} (1.33) is less than $t_{critical}$ (2.18), indicating that the CO₂ in two cylinders is not significantly different. Thus, the CO₂ component in the calibration gas mixture is categorized as stable.

Besides, the *t*-test of O₂ and N₂ concentration are listed in Tables 8 and 9, respectively. It can be evaluated that t_{stat} of O₂ and N₂ values are higher than $t_{critical}$ indicating that the concentrations of O₂ and N₂ in ADK009 are different significantly compared to that of AH06004. Therefore, it can be concluded that O₂ and N₂ components are categorized as unstable components in the gas mixtures.

4. CONCLUSIONS:

1. The calibration gas mixtures prepared using the raw materials have shown satisfying results in general, judging from the good internal consistency and a high linear regression coefficient.
2. The purity of the parent gases used as raw materials is sufficient to prepare calibration gas mixtures in the typical concentration range of the modified atmosphere food package.
3. The good consistency also indicated that the concentration values from the gravimetric method were in good agreement with the concentration value verified by GC-TCD.
4. The stability of the gas mixture, however, shows a rather unsatisfying result for O₂ and N₂ components. Both are the major components in our ambient air with some probability to enter the systems during analysis or the equal division process. This might be considered as a possible cause of instability in the mixture composition.

Further treatment shall be taken into consideration to minimize the instability of the O₂ and N₂ components of the mixtures. Therefore, in further study, it is recommended to minimize ambient air effect by using very tight tubing system and gas cylinders that ensure no components could enter or escape the system.

5. ACKNOWLEDGMENTS:

The authors would like to express their acknowledgment to the Ministry of Research and Technology-BRIN for their support through the project INSINAS and Research Centre for Metrology - Indonesian Institute of Sciences (RCM - LIPI). Thanks to the Centre for Research and Human Resources and Development- National Standardization Agency of Indonesia (PUSRISBANG-BSN) for partial support of this study through a DIPA-BSN 2020 Project.

6. REFERENCES:

1. Abdulmumeen, H. A., Risikat, A. N., Sururah, A. R. (2012). Food: Its preservatives, additives and applications. *International Journal of Chemical and Biochemical Sciences*, 1, 36-47. <https://doi.org/10.13140/2.1.1623.5208>
2. Ali, S., Khan, A. S., Malik, A. U., Anjum, M. A., Nawaz, A., and Shah, H. M. S. (2019). Modified atmosphere packaging delays enzymatic browning and maintains the quality of harvested litchi fruit during low-temperature storage. *Scientia Horticulturae*, 254, 14-20. <https://doi.org/10.1016/j.scienta.2019.04.065>
3. Amit, S.K.; Uddin, M.M.; Rahma, R.; Islam, S.M.R.; Khan, M.S. (2017). A Review on Mechanism and Commercial Aspect of Food Preservation and Processing. *Agric and Food Security*, 6, 1-22. <https://doi.org/10.1186/s40066-017-0130-8>
4. Anand, S. P., and Sati, N. (2013). Artificial preservatives and their harmful effects: looking toward nature for safer alternatives. *International journal of pharmaceutical sciences and research*, 4(7), 2496. [https://doi.org/10.13040/IJPSR.0975-8232.4\(7\).2496-01](https://doi.org/10.13040/IJPSR.0975-8232.4(7).2496-01)
5. Aversa, R., Petrescu, R. V., Apicella, A., and Petrescu, F. I. (2016). The basic elements of life's. *American Journal of Engineering and Applied Sciences*, 9(4), 1189-1197. <https://doi.org/10.3844/ajeassp.2016.1189.1197>
6. Beals, J. W., Mackenzie, R. W., Van Vliet, S., Skinner, S. K., Pagni, B. A., Niemiro, G. M., ... and De Lisio, M. (2017). Protein-rich food ingestion stimulates mitochondrial protein synthesis in sedentary young adults of different BMIs. *The Journal of Clinical Endocrinology and Metabolism*, 102(9), 3415-3424. <https://doi.org/10.1210/jc.2017-00360>
7. Blackburn, C. D. W. (2006). Managing microbial food spoilage: an overview. In *Food spoilage microorganisms* (pp. 147-170). Woodhead Publishing.
8. Brown, R. J., Brewer, P. J., Harris, P. M., Davidson, S., van der Veen, A. M., and Ent, H. (2017). On the traceability of gaseous reference materials. *Metrologia*, 54(3), L11. <https://doi.org/10.1088/1681-7575/aa6ede>
9. Budiman, H., Mulyana, M. R., and Zuas, O. (2017, January). Gravimetric dilution of calibration gas mixtures (CO₂, CO, and CH₄ in He balance): toward their uncertainty estimation. In *AIP Conference Proceedings* (Vol. 1803, No. 1, p. 020056). AIP Publishing LLC. <https://doi.org/10.1063/1.4973183>
10. Budiman, H., and Zuas, O. (2015). Validation of analytical method for determination of high level carbon dioxide (CO₂) in nitrogen gas (N₂) matrix using gas chromatography thermal conductivity detector. *Periódico Tchê Química*, 12, 7-16.
11. Cachon, R.; Alwazeer, D. (2019). Quality Performance Assessment of Gas Injection During Juice Processing and Conventional Preservation Technologies. *The Science of Beverages*, 14, 465-485. <https://doi.org/10.1016/B978-0-12-816687-1.00014-X>
12. Conte, A., Angiolillo, L., Mastromatteo, M., and Del Nobile, M. A. (2013). *Technological options of packaging to control food quality* (pp. 354-379). InTech.
13. De, L. C., and De, T. (2019). Healthy Food For Healthy Life. *Journal of Global Biosciences*, 8(9), 6453-6468..
14. Devlieghere, F., Debevere, J., and Gil, M. I. (2003). MAP, product safety and nutritional quality. *Novel food packaging techniques*, 208e230.
15. Dorgan, V., Prodan, D., and Nastas, N. (2019). Food principles providing muscular activity energy in the sports training of students practicing powerlifting. *Physical Education, Sport and Kinetotherapy Journal*, 63-69. <https://doi.org/10.35189/iphm.icpesk.2019.10>
16. Embleni, A. (2013). Modified atmosphere packaging and other active packaging systems for food, beverages and other fast-moving consumer goods. In *Trends in Packaging of Food, Beverages and Other Fast-Moving Consumer Goods (FMCG)* (pp. 22-34). Woodhead

17. Fiori, R., Pizzolato, T. M., Noreña, C. P., and Brandelli, A. (2009). Investigation of Pentachlorophenol in edible gelatin and its paperboard packaging in southern Brazil. *Electronic Journal of Environmental, Agricultural and Food Chemistry*, 8(7), 492-499.
18. Franceschini, B., Previdi, M. P., and Schianchi, I. (2020). Food Spoilage by Bacilli: Combined Effects of pH, aw and Storage Temperature on Spore Germination and Growth in Cultural Broth Added with Solutes and Organic Acids. *Journal of Advances in Microbiology*, 49-55. <https://doi.org/10.9734/jamb/2020/v20i330227>.
19. Gallaher, M.P., O'Connor, A.C., White, W.W., Wright, R.S. (2002). The Economic Impact of the GasMixture NIST-Traceable Reference Materials Program. *Economic Analysis*. National Institute of Standards and Technology.
20. Gavril, G., Kanavouras, A., and Coutelieris, F. A. (2018). Food-packaging migration models: A critical discussion. *Critical Reviews in Food Science and Nutrition*, 58(13), 2262-2272. <https://doi.org/10.1080/10408398.2017.1317630>.
21. Han, J-W., Luis, R-G., Qian, J-P., and Yang, X-T., (2018). Jia-Wei Food Packaging: A Comprehensive Review and Future Trends. *Comprehensive Reviews in Food Science and Food Safety*, 17(4), 860-877. <https://doi.org/10.1111/1541-4337.12343>
22. Han, J. H. (2014). A review of food packaging technologies and innovations. In *Innovations in food packaging* (pp. 3-12). Academic Press.
23. Hindayani, A., Zuas, O., Mulyana, M. R., Budiman, H., Styarini, D., Krismastuti, F. S. H., and Sirenden, B. H. (2019, February). Validated method for trace impurities analysis in bulk gas using Gas Chromatography with Pulse Discharge Helium Ionization Detection. In *Journal of Physics: Conference Series* (Vol. 1153, No. 1, p. 012033). IOP Publishing. <https://doi.org/10.1088/1742-6596/1153/1/012033>.
24. Hyun, J. E.; Lee, S.Y. (2017). Preservation Method for Extending The Shelf-Life of Various Foods. *J.Food.Saf.* 38, 1-9. <https://doi.org/10.1111/jfs.12376>.
25. International Organization for Standardization. (2017). ISO 16664:2017: Gas analysis - Handling of Calibration Gases and Gas Mixtures - Guidelines. Switzerland.
26. International Organization for Standardization. (2017). ISO/IEC 17025:2017: General Requirements for the Competence of Testing and Calibration Laboratories. Switzerland.
27. International Organization for Standardization. (2001). ISO 6142:2001: Gas Analysis - Preparation of Calibration Gas Mixtures - Gravimetric method. Switzerland.
28. International Organization for Standardization. (2015). ISO 6142-1:2015: Gas analysis - Preparation of Calibration Gas Mixtures - Part 1: Gravimetric Method for Class I Mixtures. Switzerland.
29. Ishangulyyev, R., Kim, S., and Lee, S. H. (2019). Understanding Food Loss and Waste-Why Are We Losing and Wasting Food. *Foods (Basel, Switzerland)*, 8(8), 297. <https://doi.org/10.3390/foods8080297>.
30. Jacksier, A. T., and Weterings, W. (2017). Gaseous Calibration Standards: Manufacturing, Stability, Traceability and Uncertainty. In *Offshore Technology Conference*. Offshore Technology Conference. <https://doi.org/10.4043/27614-MS>.
31. Javanmard, M. (2017). Effect of Modified Atmosphere Packaging and Storage Temperatures on Quality of Shelled Raw Walnuts. *International Journal of Nutrition and Food Engineering*, 11(7), 510-514. <http://doi.org/10.5281/zenodo.1131405>.
32. Kharobe, V.B. (2018). Advantages and Disadvantages of Traditional Fermentation of Dairy Products. *International Journal of Recent Trends in Science And Technology*, Special issue. 52-55.
33. Kodentsova, V. M., and Vrzhesinskaya, O. A. (2018). Vitamin-mineral complexes: forms and application. *AV Skalny, MD, Prof.(Moscow, Russia)*, 21.

34. Kotsianis, I. S., Giannou, V., and Tzia, C. (2002). Production and packaging of bakery products using MAP technology. *Trends in Food Science and Technology*, 13(9-10), 319-324. [https://doi.org/10.1016/S0924-2244\(02\)00162-0](https://doi.org/10.1016/S0924-2244(02)00162-0).
35. Lin, Q-B., Song, X-c, Fang, H., Wu, Y-M., Wang, Z-W. (2017). Migration of styrene and ethylbenzene from virgin and recycled expanded polystyrene containers and discrimination of these two kinds of polystyrene by principal component analysis. *Food Additives and Contaminants: Part A*, 34(1), 126-132. <https://doi.org/10.1080/19440049.2016.1253875>.
36. Linke, B.G.O.; Casagrande, T.A.C.; Cardos, L.A.C. (2018). Food Additives and Their Health Effects: A Review On Preservative Sodium Benzoate. *Afr. J. Biotechnol.* 17, 306-310. <https://doi.org/10.5897/AJB2017.16321>
37. Marinangeli, C. P., Harding, S. V., Glenn, A. J., Chiavaroli, L., Zurbau, A., Jenkins, D. J., ... and Sievenpiper, J. L. (2020). Destigmatizing Carbohydrate with Food Labeling: The Use of Non-Mandatory Labelling to Highlight Quality Carbohydrate Foods. *Nutrients*, 12(6), 1725. <https://doi.org/10.3390/nu12061725>.
38. Meredith, H., Valdramidis, V., Rotabakk, B. T., Sivertsvik, M., McDowell, D., and Bolton, D. J. (2014). Effect of different modified atmospheric packaging (MAP) gaseous combinations on *Campylobacter* and the shelf-life of chilled poultry fillets. *Food microbiology*, 44, 196-203. <https://doi.org/10.1016/j.fm.2014.06.005>.
39. Millward, D. J. (2017). Nutrition, infection and stunting: the roles of deficiencies of individual nutrients and foods, and of inflammation, as determinants of reduced linear growth of children. *Nutrition research reviews*, 30(1), 50. <https://doi.org/10.1017/S0954422416000238>.
40. Minitab. (2019). Using The t-value to Determine Whether to Reject The Null Hypothesis. Minitab. Retrieved 18/03/2020 from <https://support.minitab.com/en-us/minitab-express/1/help-and-how-to/modeling-statistics/regression/supporting-topics/regression-models/using-the-t-value-to-determine-whether-to-reject-the-null-hypothesis/>.
41. Mirza, S. K., Asema, U. K., and Kasim, S. S. (2017). To study the harmful effects of food preservatives on human health. *J Medicinal Chemist Drug Discovery*, 2(2), 610-616.
42. Montero-Calderón, M., Rojas-Graü, M. A., Aguiló-Aguay, I., Martín-Belloso, O. (2010). Influence of Modified Atmosphere Packaging on Volatile Compounds and Physicochemical and Antioxidant Attributes of Fresh-Cut Pineapple (*Ananas comosus*). *Agriculture and Food Chemistry*, 58(8), 5042–5049. <https://doi.org/10.1021/jf904585h>.
43. Mullan, M., McDowell, D. (2003). Modified Atmosphere Packaging in Food Packaging Technology. *Food and Beverages Packaging Technology*. 303-339.
44. Mulyana, M. R., Budiman, H., Zuas, O., and Hindayani, A. (2019, February). Trace impurities measurement in ultra-high purity gases and their uncertainties: case study on permanent gas impurities in pure nitrogen. In *Journal of Physics: Conference Series* (Vol. 1153, No. 1, p. 012035). IOP Publishing. <https://doi.org/10.1088/1742-6596/1153/1/012035>.
45. Odeyemi, O. A., Alegbeleye, O. O., Strateva, M., and Stratev, D. (2020). Understanding spoilage microbial community and spoilage mechanisms in foods of animal origin. *Comprehensive Reviews in Food Science and Food Safety*, 19(2), 311-331. <https://doi.org/10.1111/1541-4337.12526>.
46. Opara, U. L., and Mditshwa, A. (2013). A review on the role of packaging in securing food system: Adding value to food products and reducing losses and waste. *African Journal of Agricultural Research*, 8(22), 2621-2630, <https://doi.org/10.5897/AJAR2013.6931>.
47. Ozturk, A., Yildiz, K., Ozturk, B., Karakaya, O., Gun, S., Uzun, S., and Gundogdu, M. (2019). Maintaining postharvest quality of medlar (*Mespilus germanica*) fruit using modified atmosphere packaging and methyl jasmonate. *LWT-Food Science and Technology*, 111, 117-124..
48. Pitt, J. I., and Hocking, A. D. (2009). Fungi

- and food spoilage (Vol. 519). New York: Springer.
49. Pu, Y., Zhou, Q., Yu, L., Li, C., Dong, Y., Yu, N., and Chen, X. (2020). Longitudinal analyses of lignin deposition in green asparagus by microscopy during high oxygen modified atmosphere packaging. *Food Packaging and Shelf Life*, 25, 100536. <https://doi.org/10.1016/j.fpsl.2020.100536>.
 50. Rawat, S. (2015). Food Spoilage: Microorganisms and their prevention. *Asian Journal of Plant Science and Research*, 5, 47-56.
 51. Sandhya. (2010). Modified atmosphere packaging of fresh produce: Current status and future needs. *LWT-Food Science and Technology*, 43(3), 381-392.
 52. Scarabottolo, N., Fedel, M., Cocola, L., and Poletto, L. (2020, April). In-line inspecting device for leak detection from gas-filled food packages. In *Sensing for Agriculture and Food Quality and Safety XII* (Vol. 11421, p. 1142103). International Society for Optics and Photonics. <https://doi.org/10.1117/12.2557784>.
 53. Sharma, S. (2015). Food Preservatives and their harmful effects. *International journal of scientific and research publications*, 5(4), 1-2.
 54. Shaw, M. (2020). Introduction to Calibration Gases. CAC Gas and Instrumentation. Retrieved 18/03/2020 from <https://www.cacgas.com.au/introduction-to-calibration-gases>.
 55. Shimosaka, T., Matsumoto, N., and Kato, K. (2011). High-precision GC-TCD for verification of gravimetrically prepared primary gas standards of oxygen in nitrogen. *Analytical Methods*, 3(2), 280-287. <https://doi.org/10.1039/C0AY00397B>.
 56. Shwaiki, L. N., Arendt, E. K., Lynch, K. M., and Thery, T. L. (2019). Inhibitory effect of four novel synthetic peptides on food spoilage yeasts. *International journal of food microbiology*, 300, 43-52. <https://doi.org/10.1016/j.ijfoodmicro.2019.04.005>.
 57. Smolander, M.; Hurme, E.; Ahvenainen, R. (1997). Leak indicators for modified-atmosphere packages. *Trends in Food Science and Technology*, 8, 101-106
 58. Tsang, Y. P., Choy, K. L., Wu, C. H., Ho, G. T. S., Lam, H. Y., and Tang, V. (2018). An intelligent model for assuring food quality in managing a multi-temperature food distribution centre. *Food Control*, 90, 81-97. <https://doi.org/10.1016/j.foodcont.2018.02.030>.
 59. Utyanov, D. A., Kulikovskii, A. V., Vostrikova, N. L., and Ivankin, A. N. (2018). Determination of Vegetable Fats in Food Products. *Food systems*, 1(4), 27-41. <https://doi.org/10.21323/2618-9771-2018-1-4-27-41>
 60. Vaclavik, V. A., and Christian, E. W. (2008). Food preservation and processing. In *Essentials of food science* (pp. 425-446). Springer, New York.
 61. Verghese, K., Lewis, H., Lockrey, S., and Williams, H. (2015). Packaging's Role in Minimizing Food Loss and Waste Across the Supply Chain: Packaging's Role in Minimizing Food Waste Across the Supply Chain. *Packaging Technology and Science*, 28(7), 603-620. <https://doi.org/10.1002/pts.2127>.
 62. Wagner, E. M., Pracser, N., Thalgueter, S., Fischel, K., Rammer, N., Pospíšilová, L., Alispahic, M., Wagner, M., and Rychli, K. (2020). Identification of biofilm hotspots in a meat processing environment: Detection of spoilage bacteria in multi-species biofilms. *International Journal of Food Microbiology*, 328, 108668. <https://doi.org/10.1016/j.ijfoodmicro.2020.108668>.
 63. Wen, J., Huang, S., Sun, Y., Chen, Z., Wang, Y., Li, H., and Liu, X. (2018). Titanium Dioxide Nanotube-Based Oxygen Indicator for Modified Atmosphere Packaging: Efficiency and Accuracy. *Materials*, 11(12), 2410. <https://doi.org/10.3390/ma11122410>.

Table 1. The optimum operating condition of GC-TCD

Parameters		Optimum condition
Injection	Flow rate sample	30 mL/min
	Loop	500 μ L
	Valve box temp	100°C
	Valve 1	on (0.1 min), off (1 min)
Column	Column	Porapak Q column (1/8 inch OD, 6 feet, 80-100 mesh) and Molsieve 5A (1/8 inch OD, 9 feet, 80-100 mesh)
	Oven temp	isothermal, 40 °C
	Carrier gas	He, 41 psi (28 mL/min)
Detector	Detector	TCD
	Temp	250 °C
	Reference flow	He, 20 mL/min
	Make-up flow	He, 7 mL min
	Negative pol	On

Table 7. The *t*-test result of CO₂ concentration in ADK009 and AH06004

	ADK009	AH06004
Mean	17.01	16.99
Variance	1.30E-03	3.60E-04
Observations	7	7
Pooled Variance	8.32E-04	
Hypothesized Mean Differ.	0	
df	12	
t_{stat}	1.33	
$t_{critical}$	2.18	

Table 8. The *t*-test result of O₂ concentration in ADK009 and AH06004

	ADK009	AH06004
Mean	1.51	1.50
Variance	3.68E-05	5.49E-05
Observations	6	6
Pooled Variance	4.59E-05	
Hypothesized Mean Differ.	0	
df	10	
t_{stat}	2.57	
$t_{critical}$	2.23	

Table 9. The *t*-test result of N₂ concentration in ADK009 and AH06004

	ADK009	AH06004
Mean	81.49	81.22
Variance	0.01	0.01
Observations	7	7
Pooled Variance	0.01	
Hypothesized Mean Difference	0	
df	12	
t_{stat}	5.41	
$t_{critical}$	2.18	

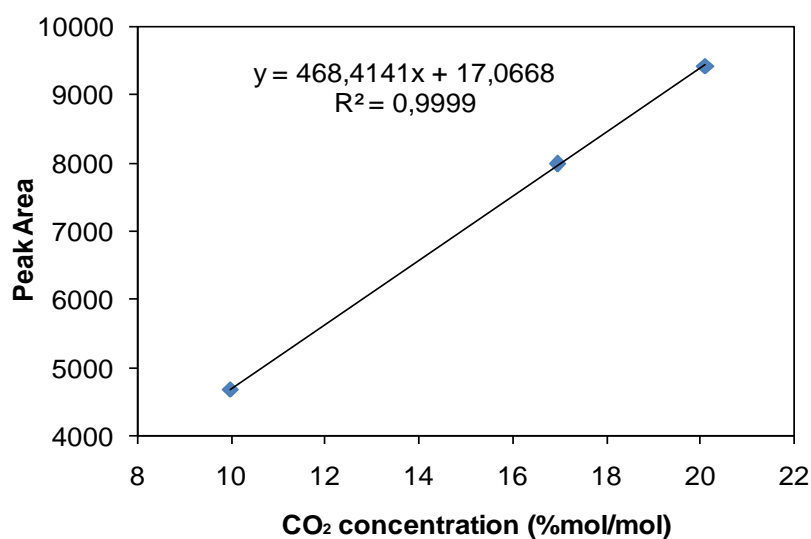


Figure 1. Linear regression curve of CO₂

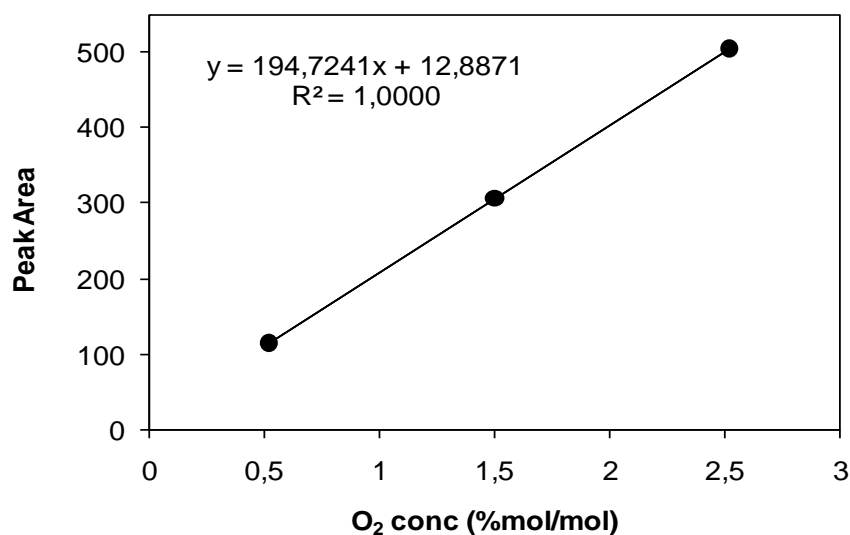


Figure 2. Linear regression curve of O₂

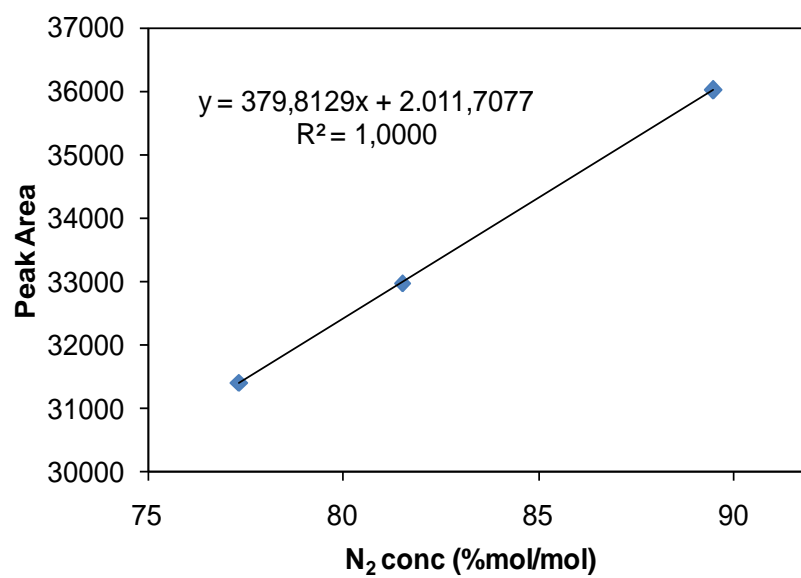


Figure 3. Linear regression curve of N₂

CAPTURA MELHORADA DE DIÓXIDO DE CARBONO POR NANOFLUIDOS CONTENDO NANOPARTICULAS INORGÂNICAS E LÍQUIDO ORGÂNICO DE LIGAÇÃO

IMPROVED CARBON DIOXIDE CAPTURE BY NANOFLUIDS CONTAINING INORGANIC NANOPARTICLES AND BINDING ORGANIC LIQUID

تحسين امتصاص ثاني أكسيد الكربون بواسطة السوائل النانوية التي تحتوي على جزيئات نانوية غير عضوية وسائل عضوي
رابط

SHAKIR, Safa Waleed¹; WIHEEB, Ahmed Daham^{2*}; KHALAF, Zainab abdulmajeed³; OTHMAN, Mohd Roslee⁴

¹Tikrit University, College of Engineering, Chemical Engineering Department. Iraq.

²University of Diyala, College of Engineering, Chemical Engineering Department. Iraq.

³Samarra University, College of Archaeology, Iraq.

⁴Universiti Sains Malaysia, School of Chemical Engineering. Malaysia.

* Corresponding author

e-mail: ahmed_chem76@uodiyala.edu.iq

Received 27 August 2020; received in revised form 21 September 2020; accepted 05 October 2020

RESUMO

A captura de dióxido de carbono (CO₂) tem sido a questão de pesquisa mais importante devido ao perigoso impacto das emissões de dióxido de carbono no aquecimento global e nas mudanças climáticas. Nas últimas décadas, uma nova tecnologia de absorção foi usada para se livrar do dióxido de carbono. Este procedimento está recebendo grande atenção sendo aplicado para melhorar a absorção de CO₂ usando nanofluidos. No entanto, outros estudos são necessários para melhorar a taxa de absorção / dessorção dos nanofluidos e diminuir as necessidades de energia através do processo de dessorção. Essa pesquisa objetivou estudar a influência da adição de nanopartículas por meio da determinação do fator de aumento da taxa de absorção / dessorção do dióxido de carbono. Todos os nanofluidos usados neste estudo foram preparados pela adição de nanopartículas com tratamento de ultrassom sem surfactantes. A influência da adição de nanopartículas à ligação de líquidos orgânicos (BOL) de mono etanolamina (MEA) e etanol na absorção / dessorção de CO₂ foi estudada experimentalmente em reator de agitação. Foram selecionadas as nanopartículas de Al₂O₃, Fe₂O₃ e SiO₂ que apresentaram diferentes propriedades para a investigação. Foram estudados o efeito da porcentagem de volume de nanopartículas, tipo de nanopartículas e velocidade de agitação na taxa de absorção de CO₂, bem como o efeito da porcentagem de volume de nanopartículas e tipo de nanopartículas na taxa de dessorção de CO₂. Foi descoberto que as nanopartículas suspensas em BOL são um absorvente promissor na infraestrutura MEA atual devido à sua natureza menos corrosiva e menores requisitos de energia para regeneração do que o MEA atual. Neste trabalho, a absorção de dióxido de carbono foi melhorada em 11% e a absorção de dióxido de carbono aumentou em 8,5% apenas com o BOL. O nanofluido de alumina a uma concentração de 0,05 absorveu o dióxido de carbono mais alto em 0,061 g/s. Por outro lado, o nanofluido de óxido de ferro concentração de 0,01% em volume absorveu o dióxido de carbono mais alto de 0,0077 g/s.

Palavras-chave: Captura de CO₂, absorção, ligação de líquido orgânico, nanopartículas, fator de aumento de CO₂.

ABSTRACT

Carbon dioxide (CO₂) capture has been the most crucial research issue due to the dangerous impact of carbon dioxide emissions on global warming and climate change. In recent decades, a new absorption technology has been used to get rid of carbon dioxide. This procedure is getting tremendous attention being applied to improve CO₂ uptake by using nanofluids. However, other studies are needed to enhance the nanofluid absorption/desorption rate and decrease the requirements of energy through the desorption process. This research aimed to study the influence of addition nanoparticles by determining the enhancement factor of the absorption/desorption rate of carbon dioxide. All nanofluids used in this study prepared by adding nanoparticles

with ultrasound treatment without surfactants. The influence of adding nanoparticles to the binding organic liquids (BOL) of monoethanolamine (MEA) and ethanol on the absorption/desorption of CO₂ was studied experimentally in a stirring reactor. The nanoparticles of Al₂O₃, Fe₂O₃, and SiO₂ were selected, which showed different properties for the investigation. The effect of volume percentage of nanoparticles, type of nanoparticles, and stirring speed on the rate of CO₂ absorption and the impact of volume percentage of nanoparticles and type of nanoparticles on the CO₂ desorption rate were studied. It has been found that nanoparticles suspended in BOL are a good absorbent in the current MEA infrastructure due to their less corrosive nature and lower energy requirements for regeneration than the current MEA. In this work, carbon dioxide absorption was improved by 11% and carbon dioxide absorption increased by 8.5% from BOL alone. The alumina nanofluid at a concentration of 0.05 absorbed the highest carbon dioxide by 0.061 g/s. In contrast, the iron oxide nano particles at a concentration of 0.01 volume% absorbed the most elevated carbon dioxide of 0.0077 g/s.

Keywords: CO₂ capture, absorption, binding organic liquid, nanoparticles, enhancement factor.

المخلص

كان احتجاز ثاني أكسيد الكربون (CO₂) هو أهم قضية بحثية بسبب التأثير الخطير لانبعاثات ثاني أكسيد الكربون على الاحتباس الحراري وتغير المناخ. في العقود الأخيرة، تم استخدام تقنية امتصاص جديدة للتخلص من ثاني أكسيد الكربون. يُحظى هذا الإجراء باهتمام كبير يتم تطبيقه لتحسين امتصاص ثاني أكسيد الكربون باستخدام السوائل النانوية. ومع ذلك، هناك حاجة لدراسات أخرى لتحسين معدل امتصاص / امتصاص سائل النانو وتقليل متطلبات الطاقة من خلال عملية الامتصاص. الهدف الأساسي من هذا البحث هو دراسة تأثير إضافة جزيئات النانو من خلال تحديد عامل التعزيز لمعدل امتصاص / امتصاص ثاني أكسيد الكربون. تم تحضير جميع سائل النانو المستخدمة في هذه الدراسة عن طريق إضافة جزيئات النانو مع العلاج بالموجات فوق الصوتية بدون مواد خافضة للتوتر السطحي. تمت دراسة تأثير إضافة جزيئات النانو إلى السوائل العضوية الرابطة (BOL) للإيثانول الأحادي (MEA) والإيثانول على امتصاص / امتصاص ثاني أكسيد الكربون بشكل تجريبي في مفاعل التحريك. تم اختيار الجسيمات النانوية من Al₂O₃ و Fe₂O₃ و SiO₂ والتي أظهرت خصائص مختلفة للتحقيق. تمت دراسة تأثير النسبة المئوية للحجم من الجسيمات النانوية ونوع الجسيمات النانوية وسرعة التحريك على معدل امتصاص ثاني أكسيد الكربون وكذلك تأثير النسبة المئوية للحجم من الجسيمات النانوية ونوع الجسيمات النانوية على معدل امتصاص ثاني أكسيد الكربون. لقد وجد أن الجسيمات النانوية المعلقة في BOL هي مادة ماصة واحدة، نظرًا لطبيعتها الأقل تآكلًا وانخفاض متطلبات الطاقة اللازمة للتجديد مقارنة بالـ MEA. في هذا العمل، تم تحسين امتصاص ثاني أكسيد الكربون بنسبة 11% وزيادة امتصاص ثاني أكسيد الكربون بنسبة 8.5% من BOL وحده. امتص سائل الألومينا النانوي بتركيز 0.05 أعلى ثاني أكسيد الكربون بمقدار 0.061 جم / ثانية، بينما امتص أكسيد الحديد النانوي بتركيز 0.01 حجم% أعلى ثاني أكسيد كربون قدره 0.0077 جم / ثانية.

الكلمات المفتاحية: التقاط ثاني أكسيد الكربون، الامتصاص، السائل العضوي الملزم، الجسيمات النانوية، عامل التحسين.

1. INTRODUCTION:

Nowadays, air pollution is considered the biggest curses facing the planet due to its impact on climate change and public and individual health that causes an increase in disease and death. Several pollutants are among the main factors that cause disease in humans (Manisalidis *et al.*, 2020). These pollutants include particulate, which are particles of very small in diameter that enter the inhalation system through breathing, causing diseases in respiratory and vascular, cancer, and dysfunction in the generative and nervous system. Also, sulfur dioxide, nitrogen oxide, dioxins, volatile organic compounds, and polycyclic aromatic hydrocarbons are considered harmful air pollutants.

Furthermore, Carbon monoxide can also cause direct poisoning when inhaled at high levels. The geographical distribution of many infectious diseases is affected by climate change caused by environmental pollution and natural disasters. The public consciousness, combined with an interdisciplinary team of scientific specialists, considers the only way to remedy this problem (Manisalidis *et al.*, 2020).

Without the slightest doubt, all declared above

is so associated with climate change, and if the danger does occur, the consequences can be dire for humanity (Radu *et al.*, 2016). The warming of the globe and the climate change affects the planet seriously affect many ecosystems, causing problems with food safety issues, melting ice and glaciers, animal extinction, and damage to plants (Munang, 2013).

The increase of greenhouse gases (GHGs) in the atmosphere raises the average global temperature and causes climate change. The growth of these gases lets the short sunlight wave's energy move into the atmosphere reaching the ground without being limited. When the wave energy reaches the earth's surface, some of the longer wave energy is emitted as heat to the atmosphere again. The heat traps in the atmosphere (lower layer) by GHGs (Carpenter *et al.*, 2013). The GHGs in the atmosphere involves 81% of carbon dioxide (CO₂), 6% nitrous oxide (N₂O), 11% methane (CH₄), and 3% fluorinate gases. The atmospheric composition is severely influenced by the growth of the GHGs, causing a reduction of the stratospheric ozone layer. During the 20th century, the first CO₂ analyzer had been finished, and this indicated that the CO₂ concentration in the atmosphere had improved significantly. Since the commencement of the

industrial's age, the CO₂ anthropogenic emissions have increased dramatically as a result of the burning of vast quantities of fossil fuels, such as coal, natural gas, petroleum, and diesel, used to generate electricity and transportation (Mondal *et al.*, 2012)

However, CO₂ emission has been the main subject in research concerning global issues. The normal concentration of CO₂ in the air has been hastily growing and, at present, is about 418 ppm (Scripps Institution of Oceanography 2020). This growth made a terrible problem for humans and many species of animals, for a sum of reasons. The most exposed concern is climate change. The association of increased CO₂ to global warming was well understood that the increase of atmospheric energy would raise the atmospheric temperatures and weather. However, climate change may not be a big concern for many people because it does not appear disastrous.

In this century, it may be possible to overlook the effects of the 5°C temperature increase by relocating to a more relaxed and safer geographical location. Alternatively, it is conceivable that humans have ignored the direct and instantaneous deadly feature of CO₂ increasing in the atmosphere. The CO₂ concentration levels in the third atmosphere of the Earth have already been outside the range of humans breathes during their evolution. As all know, when carbon dioxide levels are high, inhalation of carbon dioxide becomes toxic to humans, with many deaths reported based on working exposure. Based on comparatively instant clarifications of fitting and healthy, the limit of CO₂ exposure was set as 5000 ppm (part per million) for an eight hours exposure in the workday (Zhang *et al.*, 2017). So, the harmless limit of CO₂ concentration for lifetime exposure will be considerably lower than this limit. Moreover, with the increase in human CO₂ emissions, several researchers expect that there will be toxic effects shortly (McNeill and SAS 2016; Augusto *et al.*, 2018).

For all the above, reducing carbon dioxide from its emissions is a global concern that needs a robust and swift solution to slow the growing risk affecting climate change and global warming (Mondal *et al.* 2012). The industry accounts for almost 40% of worldwide CO₂ emissions, an essential point of concern (Marlon *et al.*, 2019). Several plans have been accounted for to decrease emissions of CO₂: post-combustion, pre-combustion, oxy-fuel combustion, and electrochemical separation. Capturing CO₂ from post-combustion is the most direct strategy for

application in existing processes. However, it is the most challenging application because of the deficient CO₂ concentration and pressure (about 12–15 mol. %) of the flue gas, and the low rate of the carbon recovered compounds (Fujimoto *et al.*, 2016; Wiheeb *et al.*, 2018).

Nonetheless, the increase of carbon dioxide produced from flue gas pretenses a real danger of global warming. Therefore, the removal of carbon dioxide is critical and has received increasing interest from energy researchers worldwide. Several approaches can be useful to reduce carbon dioxide production, such as using renewable fuels instead of fossil fuels and trying to seize carbon dioxide from its large emissions (Rocha *et al.*, 2016). The separation is a promising technique to control the CO₂ emissions from its source (Mondal *et al.*, 2012; Wiheeb *et al.*, 2018). Many technologies are used to remove CO₂ such: absorption, adsorption and gas-separation membranes. However, the membrane method is still in the lab research stage, and too much energy is needed for the adsorption method in the process of desorption (Araújo and de Medeiros, 2017). The chemical or physical absorption process is the standard method used to remove CO₂. The absorption process is one of the best established and mature procedures for CO₂ removal from large emission sources is through chemical absorption utilizing alkanolamine solvents. This technology has been proven to work successfully to separate CO₂ for decades (Yuan and Rochelle, 2019).

However, the treatment cost of fixed emission sources using this method is high due to increased energy consumption. The leading energy expended in alkanolamine solvents is about 80% of the total cost consumed through solvent regeneration. In contrast, the rest of the energy required comes from the pumps, refrigeration system, and compressor. In this technique, the solvent selection is an essential factor in designing the absorption process because this will improve equipment size while reducing operating costs. The choice of the absorbent depends on its turnover rate, and the heat of regeneration and corrosion problems can have an essential influence on the reactant absorption process as a result of its impact on the total costs (Wiheeb *et al.*, 2018; Conway *et al.*, 2014). Alkanolamines are the most used solvents to capture the acid gas commercially. These solvents include Monoethanolamine (MEA), Diethanolamine (DEA), and Triethanolamine (TEA) (Olajire, 2010; Meldon *et al.*, 2011; Budiman *et al.*, 2015; Hemmati *et al.*, 2019; Yuan and

Rochelle 2019). MEA has been the most common solvent used industrially because of its high ability to absorb CO₂, simplicity in use, low cost, and availability. However, the MEA performance is limited by numerous factors, including the high energy requirements for the regeneration, oxidative degradation, and corrosion concerns (Yuan and Rochelle 2019). Research for alternative solvents with improved absorption/desorption of CO₂ is thus needed to cope with the MEA unsustainability.

A new class of binding organic liquid (BOL) has been presented as solvents for CO₂ capture (Mathias *et al.*, 2015). The use of binding organic liquids for CO₂ capture (CO₂-BOLs) had been recommended in the previous work involved organic bases with alcohol (Zhang *et al.*, 2013). This kind of solvent uses alcohol instead of water to decrease energy consumption used for regeneration and solve the corrosion problems. Results from their experiment revealed that CO₂-BOLs solvent was superior to alkanolamine in terms of the former's higher CO₂ loading capacities, less corrosiveness, successful absorption of other acid gases such as SO₂, COS, with decreasing the regeneration energy requirement (Liu *et al.*, 2017; Dejan *et al.* 2018).

The chemical and physical absorption of CO₂ occurred when the CO₂ gas transfer from the gas phase to the liquid phase due to the difference in concentration. This transport phenomenon can be described well by the theory of the two films, as shown in Figure 1. The solute diffused from the bulk of the gas phase, through the gas-film and across the interface. The solute in the liquid film can be reacting chemically with solvent (Wang *et al.*, 2018).

The reaction mechanism was planned according to the interaction of amines with CO₂. The researches attempted to apply the theory of amine interaction with CO₂ to become relevant for the novel solvent system. There are several studies show that the final product of the CO₂ reaction with the alcohol solution is alkylcarbonate salts similar to bicarbonate and carbamate salts when the aqueous solutions of the amine interact with CO₂ (Barzagli *et al.*, 2013).

Recent studies applied the nanotechnology in the absorption process to enhance the performance of solvent. The nanoscale solid's dispersion in the solvent to enhance both mass and heat transfer has been a new attractive research field that has recently applied in some research. It has been found that the very high thermal conductivity of the nanoparticles plus the

nanoscale convection induced by the Brownian motion leads to enhance heat transfer (Kim *et al.*, 2012). According to the similarities between mass and heat transfer phenomena, it was expected that nanofluids would have the same effect on enhancing mass transfer. It has been shown that nanofluids increase the mass transfer also compared to the primary fluids before adding the nanomaterials (Kim *et al.*, 2012; Ashrafmansouri *et al.*, 2014). Therefore great attention has been given to nanofluids to enhance heat and mass transfer as next-generation working fluids.

In another development, it was discovered that the use of nanofluid containing nanoparticles and solvent (Bahmanyar *et al.*, 2011) could increase the CO₂ absorption rate (Ashrafmansouri *et al.*, 2014) more effectively than the solvent alone (Keshishian *et al.*, 2013). Nanofluid was formed by adding nanoparticles of 80 nm in diameter into a water-free solvent such as alcohol, and the particles were maintained in suspension in the fluid. The nanofluids' research is gaining momentum recently due to its less corrosiveness and lower temperature requirement for regeneration than its MEA counterpart. Nanofluids are a promising candidate to replace the MEA in the future.

In addition to its favorable characteristics in CO₂ capture, nanofluids can also use the existing MEA infrastructure, eliminating the need for an expensive capital upfront if nanofluid was used to replace MEA. However, before nanofluid can make its way into the industry to replace MEA, there are fundamental issues that need to be resolved first. The most vital issues revolve around the nano-particles interaction and the gas-liquid mass transfer that need explanation (Zhang *et al.*, 2013; Mathias *et al.*, 2015). Additional research to explain the effect of micro-scale interaction and types of nanoparticles and sizes on the CO₂ absorption is also imperative. This research aimed to study the effect of different types of nanoparticles, namely SiO₂, Fe₂O₃, and Al₂O₃, on the CO₂ absorption/desorption by water-free nanofluids.

The CO₂ absorption and desorption rate of the solvent is determined by the difference in CO₂ gas rate between the inlet and outlet of the absorber from the gas phase by using a CO₂ gas analyzer (Liu *et al.*, 2017) as in the following equations.

$$r = \frac{Q_{in} - Q_{out}}{m * 22.4 * 1000} \quad (\text{Eq. 1})$$

Where r : the solvent absorption rate (mol /kg. min). Q_{in} : Inlet gas flow rate (ml/min). Q_{out} : Outlet gas flow rate (ml/min). m : Quality of the solvent (kg).

Then, the influence of nanoparticles' presence on the CO_2 absorption rate, E_a , was quantified by a CO_2 absorption enhancement factor, which is defined in (Eq. 2) (Jiang, *et al.*, 2014).

$$E_a = \frac{\text{CO}_2 \text{ absorption rate in the presence of nanoparticles}}{\text{CO}_2 \text{ absorption rate in the absence of nanoparticles}} \quad (\text{Eq. 2})$$

The effect of nanofluids on the CO_2 desorption rate, E_d , was determined by CO_2 desorption enhancement factor, which is defined in (Eq. 3):

$$E_d = \frac{\text{CO}_2 \text{ desorption rate in the presence of nanoparticles}}{\text{CO}_2 \text{ desorption rate in the absence of nanoparticles}} \quad (\text{Eq. 3})$$

2. MATERIALS AND METHODS:

2.1. Preparation of nanofluids

The nanofluids used in the absorption experiments were prepared following a two-step method. The first step was the preparation of BOL solvent by mixing 1:1 molar ratio of MEA (C_2H_7NO , 98%, Merck) with ethanol (C_2H_5OH , 99.8%, sigma-Aldrich) and then stirring for 15 minutes at room temperature to obtain a homogeneous solution. The second step was the addition of nanoparticles with 80 nm in diameter of SiO_2 , Fe_2O_3 and Al_2O_3 (with a purity of 99% acquired from 99%, sigma-Aldrich) to the homogeneous BOL solvent at different concentration (0.5-0.15) vol.%. After each addition, the nanoparticles dispersed in the solution by ultrasonic wave to ensure uniform dispersion throughout the solution medium (BOL solvent). The prepared BOLs nanofluids with high nanoparticles vol. % containing SiO_2 , Al_2O_3 , and Fe_2O_3 nanoparticles had been visualized for 24 hours, as shown in Figure 2.

2.2. Experimental procedure of CO_2 absorption

The absorption of CO_2 was performed at a room temperature of 298 K and atmospheric pressure. A glass cell reactor of 100 mL containing the BOL nanofluid stirred and fixed on certain

stirring speed (1-4) rotation per second (rpm). CO_2 (99.99%, SDI Samarra, Iraq) and N_2 (99.99%, acquired from SDI Samarra, Iraq) were used as received and supplied at the preferred volume percentage of 15 vol. % CO_2 and 85 vol. % N_2 using calibrated flow meters gas and mixed to produce 200 L/h gas mixture replaced and flowed into the nanofluid cell reactor to make direct contact with the solvent. The gas bubbled out from the solution was analyzed with a CO_2 analyzer every one minute until the solvent reaches the saturation limit (no more CO_2 was absorbed). Then, the absorption rate was determined by (Eq.1). The schematic of the experimental setup for the CO_2 absorption process is presented in Figure 3.

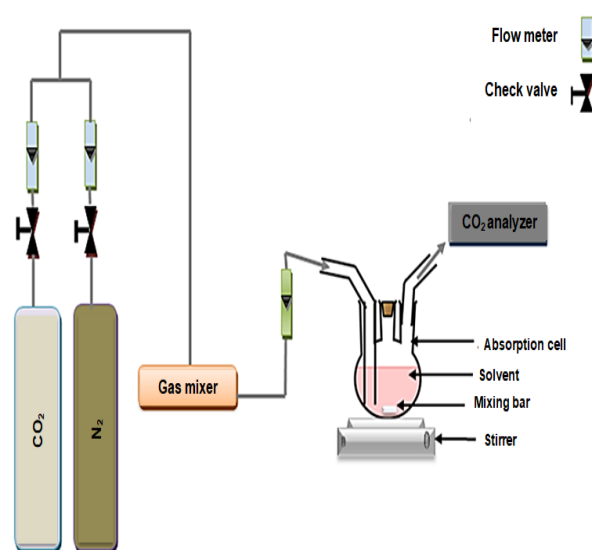


Figure 3. Schematic diagram of the CO_2 absorption process.

2.3. Experimental procedure of CO_2 desorption

The desorption rate of CO_2 , the solvent, and nanofluids were performed following the previous work (Nwaoha *et al.*, 2016; Wiheeb *et al.*, 2018; Yuan *et al.*, 2019). The experimental device consisted of a heating plate that provides the desorption energy requirement to the insulated oil bath. The 40 mL of the saturation solvent was placed into a 100 mL desorption reactor and immersed into an oil bath to reduce the heat losses which is fixed at the needed desorption temperature. The desorption reactor dipped in the oil bath until the desorption reactor's neck to lessen the heat losses. During the process, cold water runs into the condenser to decrease solvent loss due to evaporation. More than one thermometer was located to monitor the required temperature of 393 K. The first thermometer was located in the desorption reactor.

In contrast, the second was located in an oil bath. Also, The sample of the solvent saturated with CO₂ was agitated for 60 minutes at 393 K. The outlet gas from the top of the condenser was analyzed with a CO₂ analyzer until no more CO₂ was liberated. Then, the desorption rate was determined by (Eq.1). Figure 4 shows the schematic diagram of the desorption process setup.

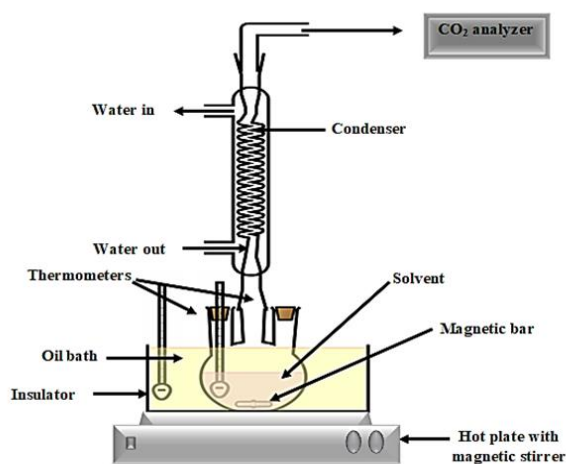


Figure 4. Schematic diagram of the CO₂ desorption

Also, for more checking the weight difference before and after the absorption/desorption process after reach the max. The limit of CO₂ absorbed/desorbed was measured using an analytical balance with a readability of 0.0001g following the previous method (Kim *et al.*, 2017).

Then, nanofluids' effect on the CO₂ absorption rate was determined by CO₂ absorption enhancement factor E_a , which is defined in (Eq. 2).

Also, the effect of nanofluids on the CO₂ desorption rate, E_d , was determined by the CO₂ desorption enhancement factor, which is defined in (Eq. 3)

3. RESULTS AND DISCUSSION

3.1 CO₂ absorption rate of nanofluids

The effect of adding SiO₂, Fe₂O₃, and Al₂O₃ nanoparticles at the predetermined volume percent of 0.005, 0.01, 0.05, 0.1, and 0.15vol.% to the BOL solvent on the CO₂ absorption rate at room temperature is presented in Figure 5.

The CO₂ absorption rate for BOL solvent without adding any nanoparticle was 0.0055 g/s, such as shown by the dotted horizontal line. The added nanoparticles provided marked

improvement of the CO₂ absorption rate. The highest CO₂ absorption rate of 0.0061 g/s was obtained when 0.05 vol.% of alumina nanoparticle was added in the BOL solvent. Fe₂O₃ and SiO₂ nanoparticles at the same level of the nanoparticle concentration in the solution improved the CO₂ absorption to some extent but were generally inferior to Al₂O₃ nanoparticles. The nanofluids' increased absorption could be explained by the affinitive effect of the dispersed nanoparticles for the CO₂ gas in the BOL medium. The nanoparticles behaved like a magnet that attracted more CO₂ onto the solid's micropores and successfully held the gas molecules on their micropores for some time until the gas molecules were desorbed. The affinitive characters of silica (Othman *et al.*, 2009) and alumina (Helwani *et al.*, 2012) for CO₂ gas molecules were also reported in the previous work.

Figure 6 shows the effect SiO₂, Fe₂O₃, and Al₂O₃ nanoparticles on the CO₂ absorption enhancement factor. An enhancement factor of greater than 1 suggests favorability of CO₂ absorption by the nanoparticles over the BOL solvent. The CO₂ absorption by alumina nanoparticles at 0.05 vol.% concentration in the nanofluid was enhanced by a factor of 1.09, which constituted the experiment's maximum enhancement factor. Although silica nanoparticles could achieve the same factor as that of alumina nanoparticles, the former nanofluid was not an acceptable choice since it required a lot more volume (0.1 vol. %) of silica nanoparticles to effect the same affinity as that of 0.05 vol.% alumina nanoparticles. In this respect, silica nanofluid would be a more costly alternative. The result also implies that alumina nanoparticles exhibited the highest affinitive character for CO₂ molecules, followed by silica and iron oxide nanoparticles.

In addition to the nanoparticles' affinitive characteristic, the enhanced CO₂ absorption of alumina nanofluid can also be explained by the Brownian motion of the convective flowing gas molecules that heightened the gas-liquid mass transfer as described previously (Jiang *et al.*, 2013). However, the addition of more than 0.05 vol.% nanoparticles caused the Brownian flow to cripple due to the narrower and more constricted space (high viscosity) when more nanoparticles were present in the fluid medium (Kim *et al.*, 2008). The other mechanisms for the enhanced absorption performance are summarized in Figure 7. The first mechanism is the bubble breaking by the suspended nanoparticles that actively split the interface between the gas bubbles and liquid to form smaller bubbles for more effective absorption

by the nanofluid (Veilleux, and Coulombe, 2011). The second mechanism is associated with the hydrodynamic effect upon collision of the nanoparticles at the gas-liquid interface that led to local turbulence. The turbulence caused a new boundary layer between the gas and liquid to develop, eventually inducing the gas molecules to blend into the bulk liquid (Pashaei *et al.*, 2018). The third mechanism is the shuttle effect because of an additional quantity of gas adsorbed by the nanoparticles in the gas-liquid diffusion layer, and then the adsorbed gas was desorbed into the bulk liquid.

Figure 8 shows the speed effect of stirring on the enhancement factor of CO₂ absorption using different nanofluids. The concentration of the nanoparticles in the fluid medium was maintained at 0.05 vol.%. An increase of stirring speed would increase the broken gas bubbles' contact area with the bulk liquid and nanoparticles and the growth in the Brownian motion, increasing CO₂ absorption. The CO₂ absorption improvement factor increased with the increasing stirring speed for all the three types of nanoparticles. However, the enhancement factor did not improve for Al₂O₃ nanofluid despite increasing the stirring speed from 3 to 4 rps, possibly due to the shuttle effect's reduction. The alumina nanoparticles could not hold the adsorbed CO₂ under turbulence caused by the stirring for long. The gas was immediately desorbed into the bulk liquid as soon as the nanoparticles adsorbed the gas. Hence, the incremental rise in CO₂ absorption at the increasing stirring speed was not observed.

3.2 CO₂ desorption rate from the CO₂ rich nanofluids

Figure 9 shows the CO₂ desorption rate from the rich nanofluids. CO₂ desorption rate for BOL solvent without nanoparticles was 0.0071 g/s (indicated by the dotted line). The CO₂ desorption rate was generally low in this work due to the difficulty of maintaining the CO₂ in the liquid at the ambient temperature. The application of heat during the process of desorption exacerbated the condition. Heat is known to provide the energy to CO₂ to liberate itself from the absorbate and absorbent. The application of heat to desorb CO₂ effectively in a pressure swing adsorption (PSA) was reviewed quite extensively in the past (Wiheeb *et al.*, 2016).

It was observed that the desorption rate of CO₂ increased with the increase of the nanoparticles' concentration up to a certain level and then decreased. The highest CO₂ desorption was observed for iron oxide nanofluid at 0.0077 g/s, followed by Al₂O₃ and SiO₂ nanofluids. The

different trends on the CO₂ desorption capacity by the three nanofluids could be due to the different thickness of the diffusion boundary layer (Ma *et al.*, 2009; Yang *et al.*, 2011) and the bulk viscosity of the fluid medium (Jung *et al.*, 2012). The different trends might also be induced by the different specific heat of the nanoparticles in the fluid. The trend seemed to follow the particular heat of the nanoparticles in the order of iron oxide (104 J.kg⁻¹.K⁻¹), alumina (451 J.kg⁻¹.K⁻¹), and silica (703 J.kg⁻¹.K⁻¹) that promoted the self-diffusion in the nanofluids (Turanov *et al.*, 2009).

Self-diffusion increased when there was an increase in the contact between the gas and liquid (Kwark *et al.*, 2010). Generally, the stability of the nanoparticles declined with the increasing amount of the absorbed CO₂. Figure 10 shows the effect of nanoparticle addition on the CO₂ desorption enhancement factor. The highest CO₂ desorption enhancement factor of 1.09 was observed for the low concentration of iron oxide nanofluid at 0.01 vol.% (which is precisely similar to the CO₂ absorption enhancement factor of 1.09 by alumina nanofluid at a concentration of 0.05 vol.%), followed by 0.05 vol.% Al₂O₃ with a desorption enhancement factor of 1.07 and 0.05 vol.% SiO₂ nanofluids with a desorption enhancement factor of 1.04. The addition of nanoparticles in BOL solvent improved the CO₂ desorption enhancement factor significantly due to the heat transfer mechanism discussed earlier in the previous reports (Kebinski *et al.*, 2002; Fan, and Wang, 2011; Pang *et al.*, 2012).

Figure 11 summarizes the CO₂ desorption mechanisms from nanofluids. The first mechanism described the CO₂ desorption process as a boiling process. The fluid phase changed as the fluid temperature increased, and CO₂ started to bubble out (desorb from the liquid) due to solubility differences. When there was nanoparticle in the fluid, nanoparticles' presence affects the heat transfer by way of gravity and natural convection. The suspended nanoparticles improved the heat transfer by continuously falling-down and moving-up in the fluid medium as the nanoparticles released and received the heat energy (a second mechanism) from the heater surface. The thermal conductivity of the nanoparticles could ascribe the third CO₂ desorption mechanism. The thermal conductivity of alumina, iron oxide and silica nanoparticles are 30 W.m⁻¹.K⁻¹, 2.2 W.m⁻¹.K⁻¹, and 1.38 W.m⁻¹.K⁻¹, respectively. The order of CO₂ desorption enhancement factor was observed to strictly follow the order of the nanoparticles' thermal conductivity if the concentration of the nanoparticles was to be maintained at 0.05 vol.%.

For example, at 0.05 vol.% concentration, the enhancement factor for alumina, iron oxide, and silica nanofluids was 1.07, 1.05, and 1.04 (refer to Figure 10). To recapitulate, the higher the thermal conductivity, the better the heat energy was dissipated to the entire nanofluid medium and transferred to CO₂ molecule for the gas molecule to liberate itself (desorb) from the fluid.

4. CONCLUSIONS:

There was an 11% increase in CO₂ absorption and an 8.5% increase in CO₂ desorption when nanofluids were used. Al₂O₃ nanofluid at 0.05 vol.% concentration was capable of absorbing CO₂ the highest (0.061 g/s) followed by silica nanofluid at 0.1 vol.% concentration (0.060 g/s) and iron oxide nanofluid at 0.05 vol.% concentration (0.059 g/s). Whereas, iron oxide nanofluid at 0.01 vol.% concentration desorbed CO₂ the highest (0.0077 g/s), followed by alumina nanofluid at 0.05 vol.% (0.0075 g/s) and silica nanofluid at 0.05 vol.% (0.0072 g/s). The nanofluids' three absorption mechanisms were identified, namely the bubble breaking, the hydrodynamic effect, and the shuttle effect. Three mechanisms of desorption by the nanofluids were known to prevail in the experiment. They were solubility difference, nanoparticles energy, and their thermal conductivity. From the perspective of CO₂ absorption and desorption enhancement factor, alumina nanofluid appeared to be a promising candidate for alternative solvent in the existing MEA infra-structure due to its high reversibility absorption-desorption effectiveness in acid gas removal without the corrosive and high energy requirement issues.

5. ACKNOWLEDGMENTS:

The authors appreciate acknowledging the Department of Chemical Engineering, College of Engineering, Tikrit University.

6. REFERENCES:

- Manisalidis, I ; Stavropoulou, E ; Stavropoulos, A; and Bezirtzoglou, E. (2020). Environmental and health impacts of air pollution: A review. *Frontiers in public health*, 8.
- Radu, O. B; van den Berg, M; Klimont, Z; Deetman, S; Janssens-Maenhout, G., Muntean, M., ... and van Vuuren, D. P. (2016). Exploring synergies between climate and air quality policies using long-term global and regional emission scenarios. *Atmospheric Environment*, 140, 577-591.
- Munang, R; Thiaw, I; Alverson, K., Mumba, M; Liu, J; and Rivington, M. (2013). Climate change and Ecosystem-based Adaptation: a new pragmatic approach to buffering climate change impacts. *Current Opinion in Environmental Sustainability*, 5(1), 67-71.
- Carpenter, A; Hotchkiss, E. and Kandt, A. (2013). An Interagency Pilot of Greenhouse Gas Accounting Tools: Lessons Learned. *National Renewable Energy Laboratory (NREL)*, Golden, CO. U.S.A.
- Mondal, M. K; Balsora, H. K; and Varshney, P. (2012). Progress and trends in CO₂ capture/separation technologies: a review. *Energy*, 46(1), 431-441.
- Scripps Institution of Oceanography. (2020). A daily record of global atmospheric carbon dioxide concentration. UC San Diego. <https://scripps.ucsd.edu/programs/keelingcurve/>
- Zhang, X; Wargocki, P; Lian, Z; and Thyregod, C. (2017). Effects of exposure to carbon dioxide and bioeffluents on perceived air quality, self-assessed acute health symptoms, and cognitive performance. *Indoor air*, 27(1), 47-64.
- McNeil, B. I; and Sasse, T. P. (2016). Future ocean hypercapnia driven by anthropogenic amplification of the natural CO₂ cycle. *Nature*, 529(7586), 383-386.
- Augusto, A; Ramaglia, A. C; and Mantoan, P. V. (2018). Effect of carbon dioxide-induced water acidification and seasonality on the physiology of the sea-bob shrimp *Xiphopenaeus kroyeri* (Decapoda, Penaeidae). *Crustaceana*, 91(8), 947-960.
- Marlon, J. R; Bloodhart, B; Ballew, M. T; Rolfe-Redding, J; Roser-Renouf, C; Leiserowitz, A; and Maibach, E. (2019). How hope and doubt affect climate change mobilization. *Frontiers in Communication*, 4, 20.
- Fujimoto, N., Hattori, K., and Yamaguchi, F. (2016). *U.S. Patent No. 9,399,192*. Washington, DC: U.S. Patent and Trademark Office.
- Rocha, J. A., Royo, V. D. A., and Menezes, E. V. (2016). Biodiesel production and paper chromatography in organic chemistry teaching. *Periodico Tchê Química*, 13(26), 52-58.
- Wiheeb, A. D; Shakir, S. W; Ahmed, M. A; and

- Rajab, E. A. (2018, January). Experimental investigation of carbon dioxide capturing into aqueous carbonate solution promoted by alkanolamine in a packed absorber. In *2018 1st International Scientific Conference of Engineering Sciences-3rd Scientific Conference of Engineering Science (ISCES)* (pp. 152-156). IEEE.
14. Araújo, O. D. Q. F; and de Medeiros, J. L. (2017). Carbon capture and storage technologies: present scenario and drivers of innovation. *Current Opinion in Chemical Engineering*, 17, 22-34.
 15. Conway, W; Yang, Q., James, S; Wei, C. C; Bown, M., Feron, P; and Puxty, G. (2014). Designer amines for post combustion CO₂ capture processes. *Energy Procedia*, 63, 1827-1834.
 16. Meldon, J. H; Morales-Cabrera, M. A. (2011). Analysis of carbon dioxide absorption in and stripping from aqueous monoethanolamine. *Chemical engineering journal*, 171(3), 753-759.
 17. Budiman, H; Zuas, O. (2015). Validation of analytical method for determination of high level carbon dioxide (CO₂) in nitrogen gas (N₂) matrix using gas chromatography thermal conductivity detector. *Periódico Tchê Química*, 12, 7-16
 18. Hemmati, A; Farahzad, R; Surendar, A; Aminahmadi, B. (2019). Validation of mass transfer and liquid holdup correlations for CO₂ absorption process with methyldiethanolamine solvent and piperazine as an activator. *Process Safety and Environmental Protection*, 126, 214-222.
 19. Olajire, A. A; (2010). CO₂ capture and separation technologies for end-of-pipe applications—a review. *Energy*, 35(6), 2610-2628.
 20. Zhang, J; Kutnyakov, I; Koech, P. K; Zwoster, A; Howard, C; Zheng, F; ... and Heldebrant, D. J. (2013). CO₂-binding-organic-liquids-enhanced CO₂ capture using polarity-swing-assisted regeneration. *Energy Procedia*, 37, 285-291.
 21. Liu, F; Jing, G; Lv, B; and Zhou, Z. (2017). High regeneration efficiency and low viscosity of CO₂ capture in a switchable ionic liquid activated by 2-amino-2-methyl-1-propanol. *International Journal of Greenhouse Gas Control*, 60, 162-171.
 22. Dejan, R. Y., Alkhatib, N., Quang, D. V; and Abu Zahra, M. (2018, October). Post-Combustion CO₂ Capture Using Diethanolamine in 1-Propanol. In *14th Greenhouse Gas Control Technologies Conference Melbourne* (pp. 21-26).
 23. Wang, C; Xu, Z; Lai, C; and Sun, X. (2018). Beyond the standard two-film theory: Computational fluid dynamics simulations for carbon dioxide capture in a wetted wall column. *Chemical Engineering Science*, 184, 103-110.
 24. Barzagli, F; Mani, F; and Peruzzini, M. (2013). Efficient CO₂ absorption and low temperature desorption with non-aqueous solvents based on 2-amino-2-methyl-1-propanol (AMP). *International Journal of Greenhouse Gas Control*, 16, 217-223.
 25. Kim, H ; Jeong, J ; and Kang, Y. T. (2012). Heat and mass transfer enhancement for falling film absorption process by SiO₂ binary nanofluids. *International journal of refrigeration*, 35(3), 645-651.
 26. Ashrafmansouri, S. S; and Esfahany, M. N. (2014). Mass transfer in nanofluids: A review. *International Journal of Thermal Sciences*, 82, 84-99.
 27. Mathias, P. M; Zheng, F; Heldebrant, D. J., Zwoster, A; Whyatt, G., Freeman, C. M; ... and Koech, P. (2015). Measuring the Absorption Rate of CO₂ in Nonaqueous CO₂-Binding Organic Liquid Solvents with a Wetted-Wall Apparatus. *ChemSusChem*, 8(21), 3617-3625.
 28. Bahmanyar, A; Khoobi, N; Mozdianfard, M. R; Bahmanyar, H. (2011). The influence of nanoparticles on hydrodynamic characteristics and mass transfer performance in a pulsed liquid-liquid extraction column. *Chemical Engineering and Processing: Process Intensification*, 50(11-12), 1198-1206.
 29. Keshishian, N; Esfahany, M. N; Etesami, N. (2013). Experimental investigation of mass transfer of active ions in silica nanofluids. *International communications in heat and mass transfer*, 46, 148-153.
 30. Jiang, J., Zhao, B., Zhuo, Y., and Wang, S. (2014). Experimental study of CO₂ absorption in aqueous MEA and MDEA solutions enhanced by nanoparticles. *International Journal of greenhouse gas control*, 29, 135-141.
 31. Nwaoha, C; Saiwan, C; Supap, T; Idem, R; Tontiwachwuthikul, P; Rongwong, W; ... and

- Benamor, A. (2016). Carbon dioxide (CO₂) capture performance of aqueous tri-solvent blends containing 2-amino-2-methyl-1-propanol (AMP) and methyldiethanolamine (MDEA) promoted by diethylenetriamine (DETA). *International Journal of Greenhouse Gas Control*, 53, 292-304.
32. Kim, H; Rajamanickam, R; and Park, J. W. (2017). Carbonation and decarbonation of non-aqueous solutions with different compositions of ethylene glycol and various amidines. *International Journal of Greenhouse Gas Control*, 59, 91-98.
 33. Jiang, J., Zhao, B., Cao, M., Wang, S., and Zhuo, Y. (2013). Chemical absorption kinetics in MEA solution with nano-particles. *Energy Procedia*, 37, 518-524.
 34. Kim, W. G., Kang, H. U., Jung, K. M., and Kim, S. H. (2008). Synthesis of silica nanofluid and application to CO₂ absorption. *Separation Science and Technology*, 43(11-12), 3036-3055.
 35. Othman, M. R; Tan, S. C; and Bhatia, S. (2009). Separability of carbon dioxide from methane using MFI zeolite-silica film deposited on gamma-alumina support. *Microporous and mesoporous materials*, 121(1-3), 138-144.
 36. Helwani, Z; Wiheeb, A. D; Kim, J; Othman, M. R. (2012). A flow through behavior of gas across meso-porous membranes. *Microporous and mesoporous materials*, 163, 115-121.
 37. Veilleux, J., and Coulombe, S. (2011). A dispersion model of enhanced mass diffusion in nanofluids. *Chemical engineering science*, 66(11), 2377-2384.
 38. Pashaei, H., Ghaemi, A., Nasiri, M., and Heydarifard, M. (2018). Experimental investigation of the effect of nano heavy metal oxide particles in Piperazine solution on CO₂ absorption using a stirrer bubble column. *Energy and Fuels*, 32(2), 2037-2052.
 39. Wiheeb, A. D., Helwani, Z., Kim, J., and Othman, M. R. (2016). Pressure swing adsorption technologies for carbon dioxide capture. *Separation and Purification Reviews*, 45(2), 108-121.
 40. Ma, X; Su, F; Chen, J; Bai, T; and Han, Z. (2009). Enhancement of bubble absorption process using a CNTs-ammonia binary nanofluid. *International Communications in Heat and Mass Transfer*, 36(7), 657-660.
 41. Yang, L; Du, K; Niu, X. F; Cheng, B; Jiang, Y. F. (2011). Experimental study on enhancement of ammonia-water falling film absorption by adding nano-particles. *International journal of refrigeration*, 34(3), 640-647.
 42. Jung, J. Y; Lee, J. W; Kang, Y. T. (2012). CO₂ absorption characteristics of nanoparticle suspensions in methanol. *Journal of mechanical science and technology*, 26(8), 2285-2290.
 43. Turanov, A. N., and Tolmachev, Y. V. (2009). Heat-and mass-transport in aqueous silica nanofluids. *Heat and mass transfer*, 45(12), 1583-1588.
 44. Kwark, S. M., Kumar, R., Moreno, G., Yoo, J., and You, S. M. (2010). Pool boiling characteristics of low concentration nanofluids. *International Journal of Heat and Mass Transfer*, 53(5-6), 972-981.
 45. Fan, J., and Wang, L. (2011). Review of heat conduction in nanofluids. *Journal of heat transfer*, 133(4).
 46. Koblinski, P., Phillpot, S. R., Choi, S. U. S., and Eastman, J. A. (2002). Mechanisms of heat flow in suspensions of nano-sized particles (nanofluids). *International journal of heat and mass transfer*, 45(4), 855-863.
 47. Pang, C., Jung, J. Y., Lee, J. W., and Kang, Y. T. (2012). Thermal conductivity measurement of methanol-based nanofluids with Al₂O₃ and SiO₂ nanoparticles. *International Journal of Heat and Mass Transfer*, 55(21-22), 5597-5602.

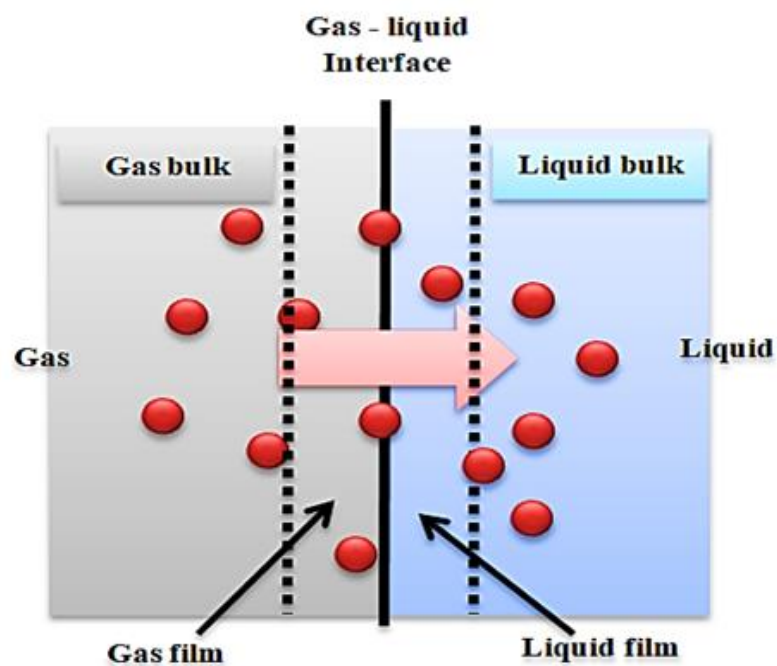
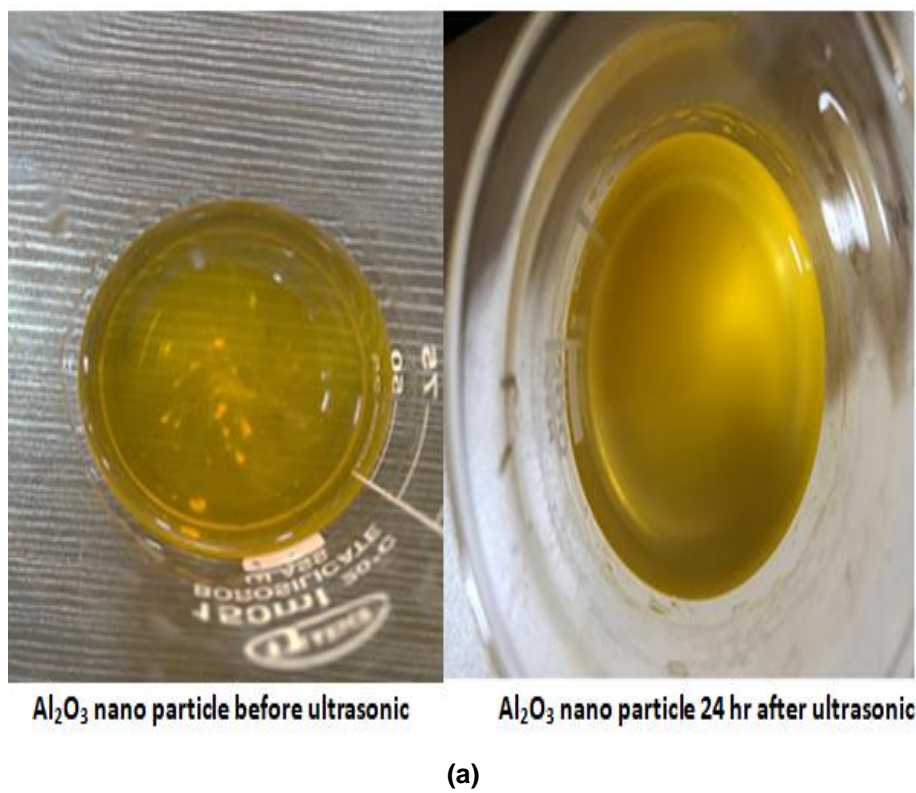


Figure 1. The absorption transport phenomena



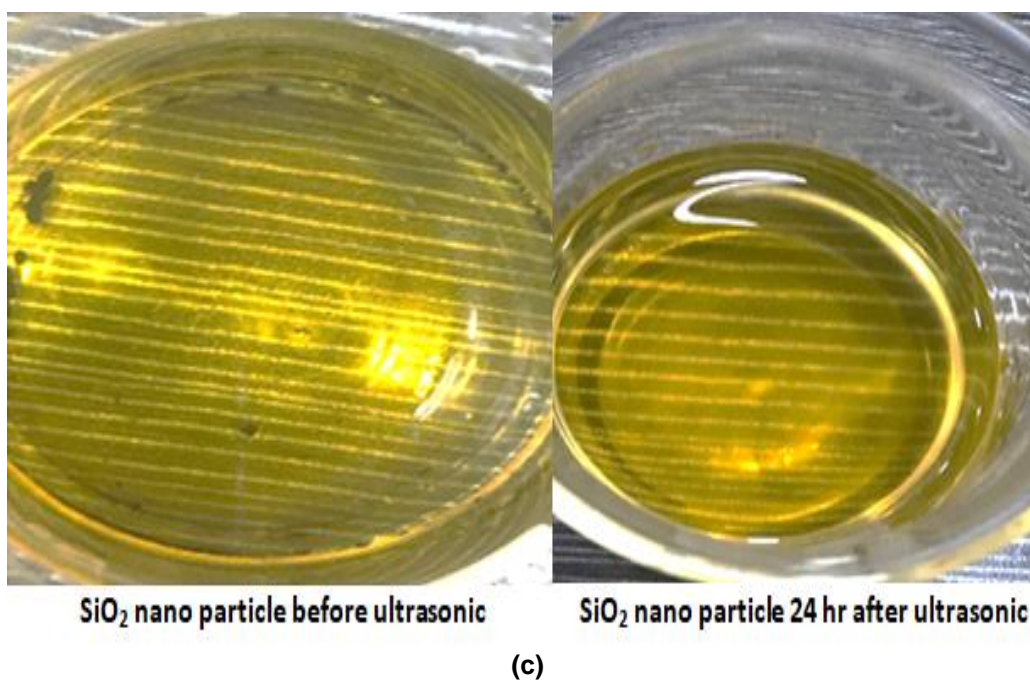
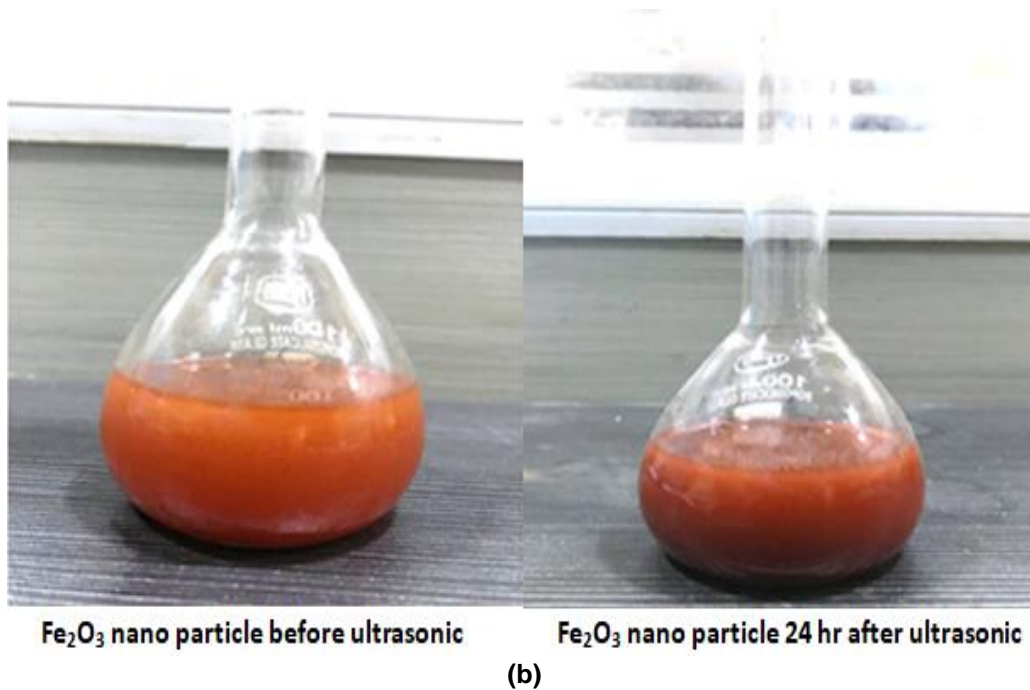


Figure 2. Nanofluids containing (a) Al_2O_3 (b) Fe_2O_3 and (c) SiO_2 nanoparticles

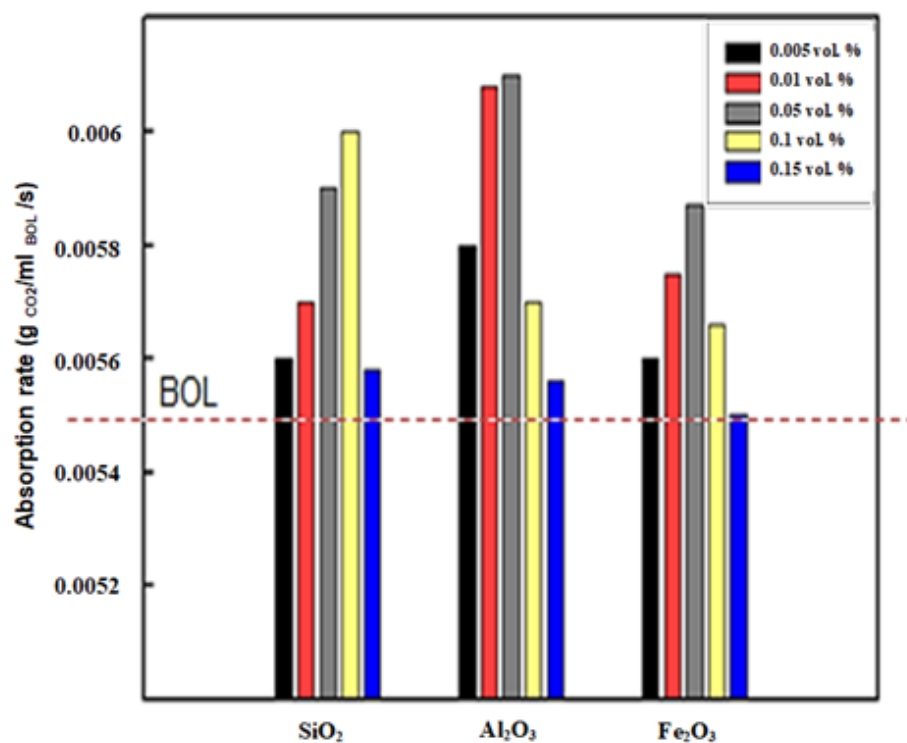


Figure 5. CO₂ absorption by nanofluids at different vol.% of the nanoparticles

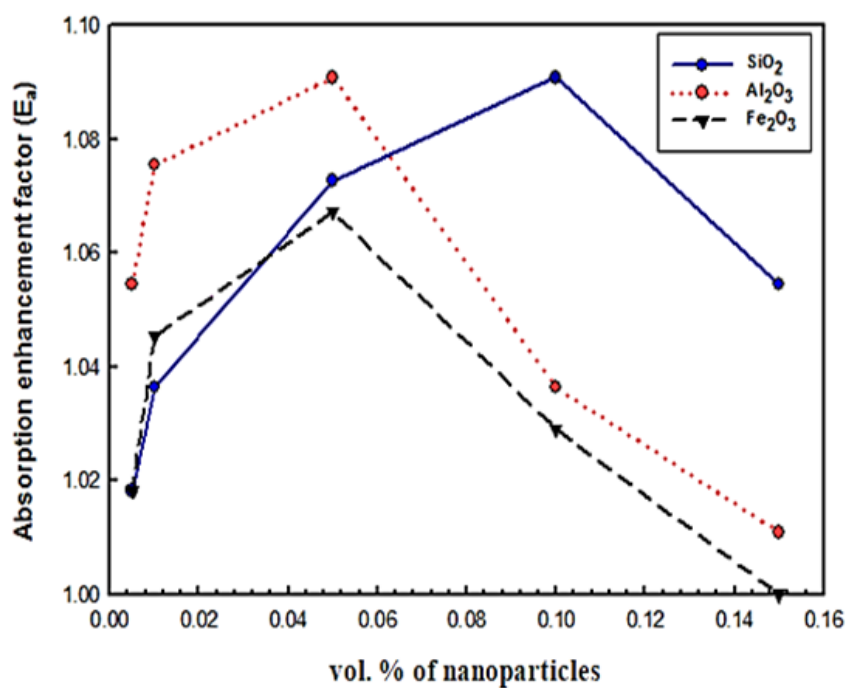
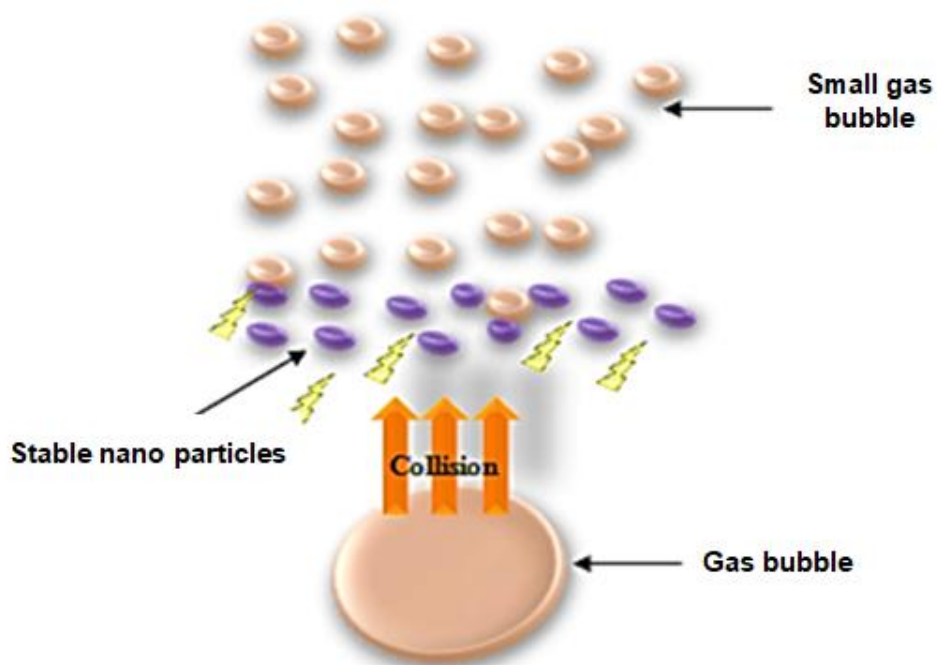
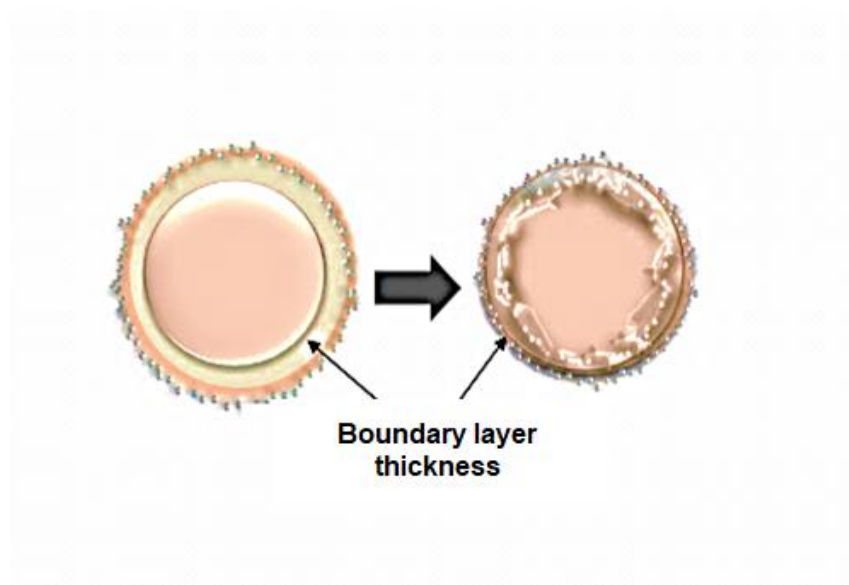


Figure 6. An enhancement factor of CO₂ absorption rate in the BOL with different types of nanoparticles and different vol. %.



(a)



(b)

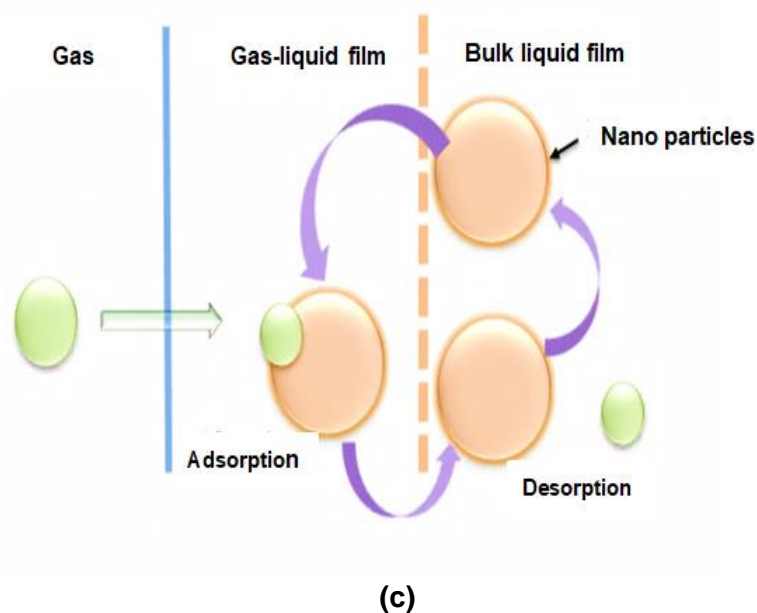


Figure 7. Schematic diagram of nanofluid mechanisms: (a) bubble breaking, (b) hydrodynamic, and (c) shuttle effects

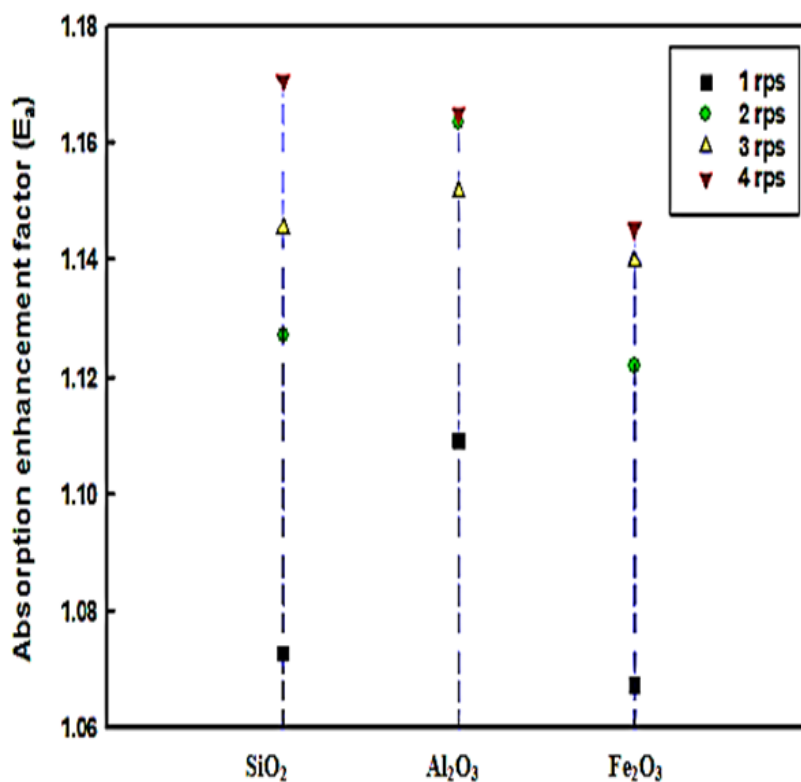


Figure 8. The influence of stirring speed on the enhancement factor of CO₂ absorption rate in the BOL solvent with different nanoparticles at 0.05 vol. %.

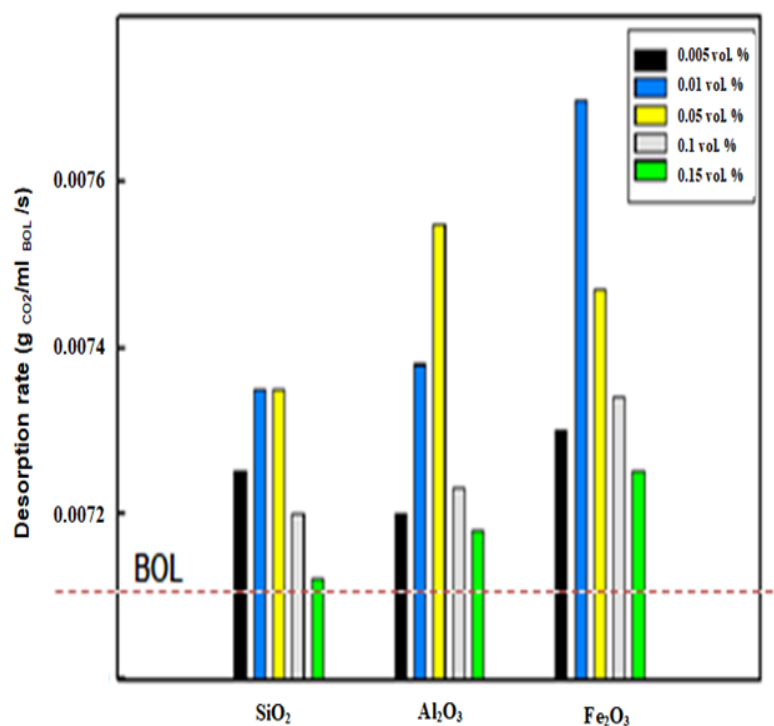


Figure 9. Desorption rate of the BOL and nanofluids.

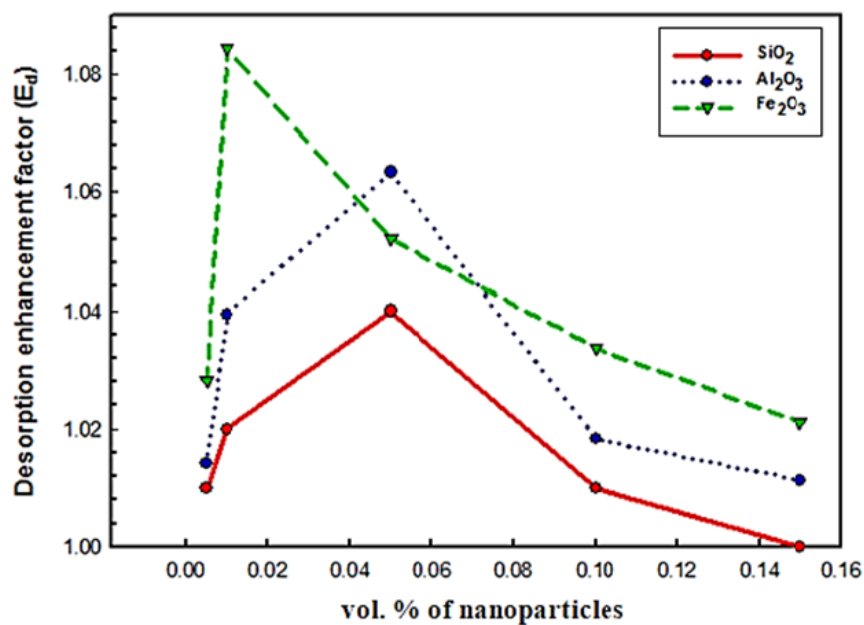
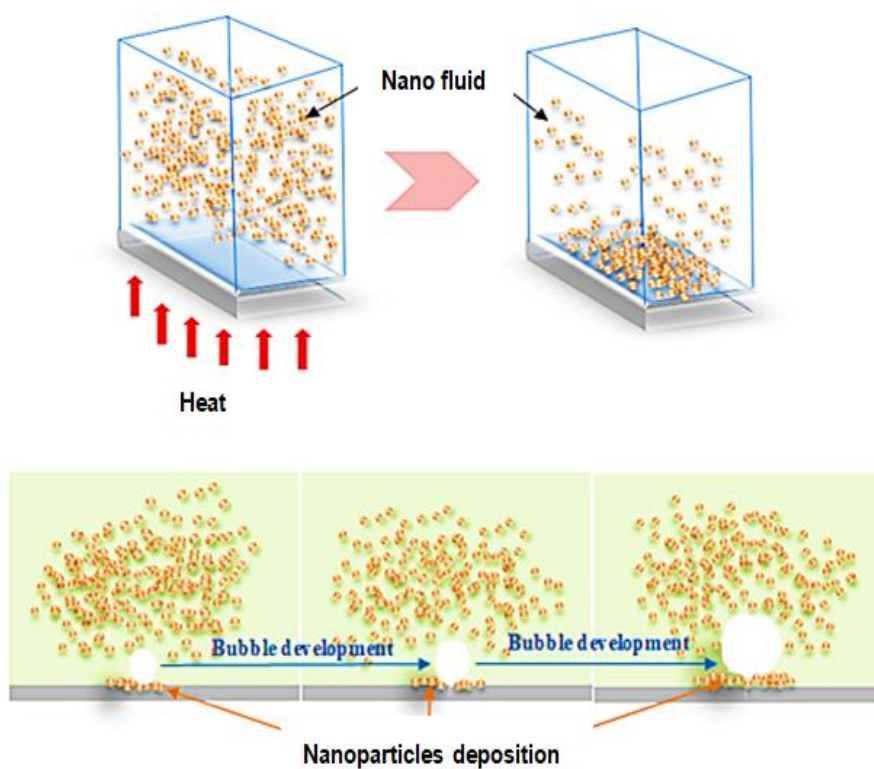
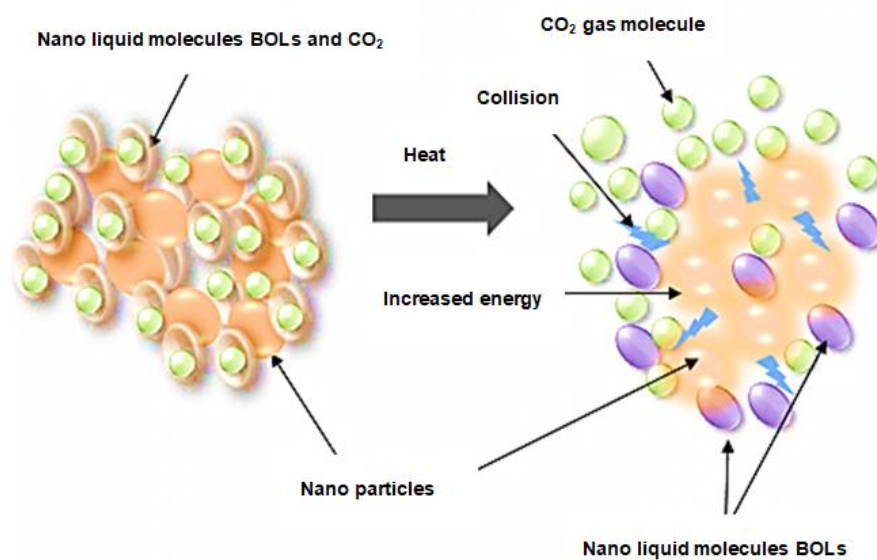


Figure 10. An enhancement factor of the CO₂ desorption by the nanofluids



(a)



(b)

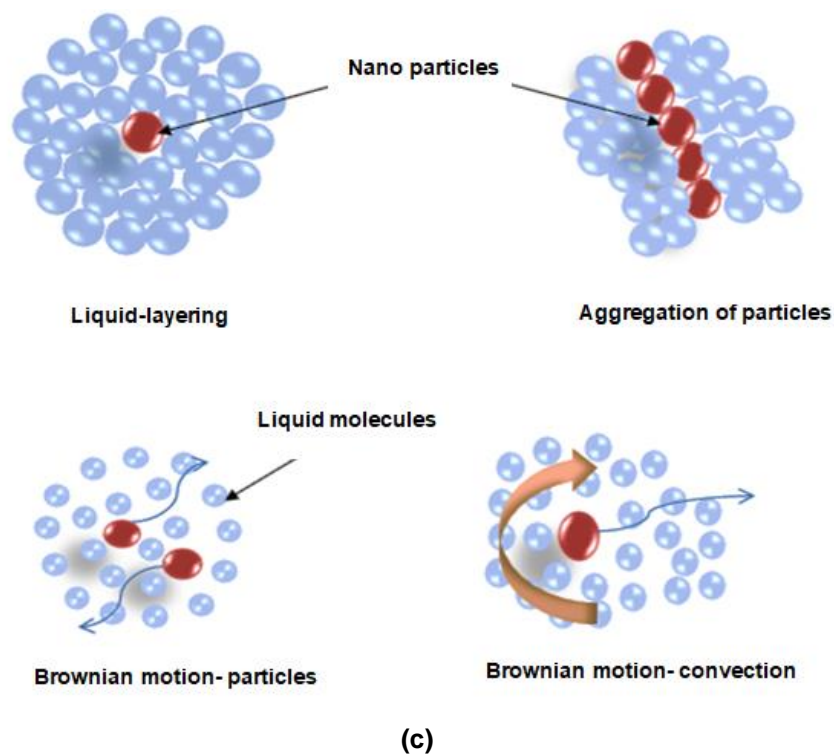


Figure 11. Schematic diagram of nanofluid desorption mechanisms: (a) solubility difference, (b) nanoparticles energy, (c) thermal conductivity

O EFEITO DE CEPAS DE *Agrobacterium tumefaciens* EM CALOS INDUZIDAS PELOS BROTOS DE GENGIBRE (*Zingiber officinale* var. Roscoe) NA PRODUÇÃO DE ALGUNS COMPOSTOS ATIVOS MEDICINAIS ESTIMADOS POR RP-HPLC

THE EFFECT OF *Agrobacterium tumefaciens* STRAINS ON CALLUS INDUCED FROM THE SHOOT TIPS OF GINGER (*Zingiber Officinale* var. Roscoe) IN THE PRODUCTION OF SOME MEDICINAL ACTIVE COMPOUNDS ESTIMATED BY RP-HPLC

تأثير سلالات من بكتريا *Agrobacterium tumefaciens* على الكالس المستحث من البراعم الطرفية لنبات الزنجبيل *Zingiber officinale* var. Roscoe في إنتاج بعض المركبات الفعالة الطبية وتقديرها بتقنية HPLC

AL-MAYAH, Abdulelah Abdulhussain¹; AL-TAHA, Huda Abdulkreem²; AL-BEHADILI, Widad Ali Abd^{3*}

¹ Department of Clinical Laboratory Sciences, College of Pharmacy, University of Basrah, Iraq.

² Department of Horticulture and Landscape Design, College of Agriculture, University of Basrah, Iraq.

³ Department of Pharmacognosy and Medicinal Plants, College of Pharmacy, University of Misan, Iraq.

* Corresponding author

e-mail: widad84ss@uomisan.edu.iq

Received 15 September 2020; received in revised form 10 October 2020; accepted 29 October 2020

RESUMO

O gengibre (*Zingiber officinale* var. Roscoe) é uma planta medicinal bem conhecida por suas propriedades farmacológicas. Esta pesquisa teve como objetivo estudar o efeito de diferentes concentrações da bactéria *Agrobacterium tumefaciens* sobre calos induzidos das pontas dos brotos do gengibre na produção de alguns compostos medicinais ativos. Calos foram induzidos a partir do cultivo de meias gemas em MS com 2,4-D na concentração de 1 mg/L com BA na concentração de 0,5 mg/L + 500 mg/L PVP. Foi o melhor meio para indução do calo. Um total de 100 mg de calo em desenvolvimento foi coletado e, após cultivo no mesmo meio, com duas semanas de idade, o calo foi tratado com duas cepas de *Agrobacterium* LBA4404 e C58 e três concentrações de 10¹, 10³ e 10⁵ bactérias/mL a cada tentativa. A análise do RP-HPLC mostrou que, quando tratado com a cepa LBA4404, que estava na concentração de 10⁵ bactérias/mL, o maior aumento na quantidade de Zingerone atingiu 0,278 mg/g, seguido de uma concentração de 10¹ bactérias/mL e que deu a maior concentração de Zingerone, 6-gingerol e 6-Shogaol que foram 0,199, 0,099 e 0,069 mg/g, respectivamente. Quanto à cepa C58, o tratamento registrou 10¹ bactérias/mL, a maior concentração de Zingerone 0,240 mg/g, seguida por uma concentração de 10³ bactérias/mL, que foi significativamente superior em fornecer a maior concentração de 6-gingerol e 6-Shogaol, que atingiu 0,053 e 0,027 mg/g, respectivamente. A partir dos resultados do experimento, pode-se considerar que os compostos médicos ativos produzidos pelo tecido caloso induzido *in vitro* podem aumentar quando expostos a estímulos biológicos, uma vez que os compostos medicinalmente ativos podem ser separados, purificados e usados na forma pura, pois são uma fonte natural para a preparação de medicamentos.

Palavras-chave: *zingiber officinale*, Calos, *Agrobacterium tumefaciens*, compostos ativos secundários medicinais, RP-HPLC

ABSTRACT

Ginger (*Zingiber officinale* var. Roscoe) is a medicinal plant well known for its pharmacological properties. This research aimed to study the effect of different concentrations of *Agrobacterium tumefaciens* bacteria on callus induced from the shoot tips of ginger in the production of some active medicinal compounds. Callus was induced from the cultivation of half-buds in MS with 2,4-D at a concentration of 1 mg/L with BA at a concentration of 0.5 mg/L + 500 mg/L PVP. It was the best medium for induced callus. A total of 100 mg of developing callus was taken, and, after cultivation on the same medium, at two weeks of age, the callus was treated with two strains of *Agrobacterium* LBA4404 and C58 and three concentrations of 10¹, 10³, and 10⁵ bacteria/mL each trial. The analysis of RP-HPLC showed that when treated with LBA4404 strain, which was at the concentration of 10⁵

bacteria/mL, the highest increase in the amount of Zingerone reached 0.278 mg/g, followed by a concentration of 10^1 bacteria/mL and which gave the highest concentration of Zingerone, 6-gingerol, and 6-Shogaol which were 0.199, 0.099 and 0.069 mg/g respectively. As for the C58 strain, the treatment recorded 10^1 bacteria /mL, the highest concentration of Zingerone 0.240 mg/g, followed by a concentration of 10^3 bacteria /mL, which was significantly superior in giving the highest concentration of 6-gingerol and 6-Shogaol, which reached 0.053 and 0.027 mg/g respectively. From the results of the experiment, it can be considered that the active medical compounds produced by the induced callus tissue *in vitro* can increase when exposed to biological stimuli, as the medicinally active compounds can be separated, purified and used in a pure form as they are a natural source for drug preparation.

Keywords: *Zingiber officinale*, callus, *agrobacterium tumefaciens*, medicinal secondary active compounds, RP-HPLC

الملخص

الزنجبيل (*Zingiber officinale* var. Roscoe) هو نبات طبي معروف جيداً بخصائصه الدوائية. هدفت الدراسة الحالية إلى تأثير تراكيز مختلفة من بكتريا الأجرعية المورمة *Agrobacterium tumefaciens* على الكالس المستحث من البراعم الطرفية لنبات الزنجبيل في إنتاج بعض المركبات الطبية الفعالة. تم تحفيز الكالس من زراعة انصاف براعم في وسط MS مع وجود 2,4-D بتركيز 1 ملغم / لتر مع BA بتركيز 0.5 ملغم / لتر + 500 ملغم / لتر PVP حيث كان الوسط الافضل لاستحثاث الكالس. تم أخذ 100 ملغم من الكالس النامي، وتمت زراعته على نفس الوسط، وفي عمر أسبوعين، تمت معاملة الكالس بسلالتين من بكتريا *Agrobacterium* وهما LBA4404 و C58 وبثلاثة تراكيز 10^1 و 10^3 و 10^5 خلية بكتيرية/مل، كل تجربة كانت على حدة. أظهر تحليل HPLC للنتائج عند المعاملة بسلالة LBA4404 بتركيز 10^5 بكتيريا/مل بلغت أعلى زيادة في كمية Zingerone 0.278 ملغم/غم يليها تركيز 10^1 بكتيريا/مل والذي أعطى أعلى تركيز من Zingerone و 6-gingerol و 6-Shogaol والذي كان 0.199 و 0.099 و 0.069 ملغم/غم على التوالي. أما بالنسبة لسلالة C58، فقد سجلت المعاملة 10^1 بكتيريا / مل أعلى تركيز من Zingerone 0.240 ملغم / غم، يليه تركيز 10^3 بكتيريا / مل والذي كان أعلى بكثير في إعطاء أعلى تركيز من 6-gingerol و 6-Shogaol التي بلغت 0.053 و 0.027 ملغم / غم على التوالي. من نتائج التجربة يتضح أن المركبات الثانوية الطبية التي ينتجها نسيج الكالس المستحث في المختبر يمكن أن تزداد عند تعرضها للمحفزات البيولوجية، حيث يمكن فصل هذه المركبات الطبية الفعالة وتنقيتها واستعمالها بشكل نقي إذ تعتبر مصدر طبيعى لتصنيع الدواء.

الكلمات المفتاحية: الزنجبيل، الكالس، بكتريا الأجرعية المورمة، المركبات الثانوية الطبية الفعالة، تقنية HPLC

1. INTRODUCTION:

Medicinal plants consider from ingredients that can be used in the development and synthesis of drugs. Also, these plants play a critical role in the growth of human cultures around the world, and after the World Health Organization announced the need to return to natural herbal treatment and reduce the intake of chemically manufactured treatments as their negative side effects (Mekuriya and Mekibib, 2018; Rasool Hassan, 2012). Among these plants is the ginger plant, which belongs to the family of Zingiberaceae, one of the largest monocotyledon families, which includes many medicinal plants, including *Curcuma longa* L. and *Elettaria cardamomum* (L.) Maton (Hartati *et al.*, 2014).

Zingiber officinale (ginger) is called the home pharmacy. Ginger produces rhizomes used for medicinal and food purposes (Dhanik *et al.*, 2017). It is one known plant for its frequent use as an alternative medicine since ancient times (Akoachere, 2002). It has been included among medicinal plants for its wide range of therapeutic uses (Sacchetti *et al.*, 2005; FAO, 2013). The chemical analyzes indicate that the *Z. Officinale* plant rhizomes contain 12.3% carbohydrates, 2-3% protein, 2.4% crude fiber, 2-3%, 0.9% fatty oil, and moisture 80.9%. It also contains many

vitamins, such as Riboflavin, Thiamine, Niacin, vitamin B6, vitamin E, and Ascorbic acid. Besides, it contains many essential minerals such as Copper, Zinc, Iron, Calcium, Nickel, Magnesium, Manganese, sodium and potassium, and many chemical active compounds that have therapeutic reasons against many diseases. These active compounds include volatile oils, alkaloids, phenols, flavonoids, glycosides, terpenes, tannins, saponins, and steroids, as main plant materials (Ghasemzadeh *et al.*, 2010; Pilerood and Prakash, 2011; Shahi and Hussain, 2012; Olubunmi *et al.*, 2013; Bijaya, 2018). It is used in Greek medicine to treat colds, stomach disorders, rheumatism, nerve diseases, gingivitis, dental pain, asthma, traumas, constipation, diabetes, vomiting, nausea, and seasickness (Wang and Wang, 2005; Tapsell *et al.*, 2006) as well as a tonic for blood circulation (Shoji *et al.*, 1982).

Many bioactive compounds in fresh ginger, including phenolic and terpene compounds, have been identified, such as gingerols, shogaols, paradols and zingerone (Figure 1), responsible for different ginger bioactivities (Gupta *et al.*, 2016). Ginger has been used in traditional medicines for the treatment of gastric issues. Ginger's distinctive pungency is caused by the so-called active components Shogaols, Zingerone, and Gingerols (Stoner, 2013). Gingerols can be transformed into

corresponding Shogaols with heat treatment or long term storage. Shogaols can be transformed into Paradols after hydrogenation (Gopi *et al.*, 2016). Gingerols mainly contribute to the pungency of the raw material of the ginger. In the ginger raw material, there is mainly 6-,8-,10-gingerol, 6-, 8- Shogaol (Semwal *et al.*, 2015). The most common chemical constituent found in ginger is 6-gingerol, which provides much of the desired flavor and aroma and many medicinal properties found in ginger. Also known as 5-hydroxy-1-(4-hydroxy-3-methoxyphenyl) decan-3-one, 6-gingerol has a $C_{17}H_{26}O_4$ chemical formula and a molecular weight of 294.3859 (Rahmani *et al.*, 2014). 6-Shogaol, the dehydrated form of gingerol, has many precious pharmacological properties as well. Shogaol is known as (E)-1-(4-Hydroxy-3-methoxyphenyl) dec-4-en-3-one and has a $C_{17}H_{24}O_3$ molecular formula and a molecular weight of 276.388 (Jung *et al.*, 2018). Zingerone is present in ginger in a significant quantity of about 9.25%. It is a member of the family of Methoxyphenols and their related derivatives. They have a basic phenolic ring attached to the benzene ring with a methoxy group. It is known that Zingerone has potent pharmacological activities (Zhang *et al.*, 2012). Zingerone is mainly present in dry ginger, but the retro-aldol reaction also converts gingerol (another component in ginger) into zingerone by cooking or drying. The use of high-profile liquid chromatography has shown that the 6-gingerol, 8-gingerol, and 10-gingerol content is generally low in fresh ginger while the amount of zingerone increases significantly when drying and roasting (Ahmad *et al.*, 2015).

Studies have developed in introducing tissue culture technology to increase the production of secondary active compounds from some medicinal plants compared to the quantities extracted from the whole plant (Oomah, 2003). Biotechnology is used in the agricultural, industrial and medical fields and in the production of useful compounds under controlled conditions and the extraction of effective substances with medicinal uses from the calculus of plants throughout the year without being bound by the growing season (Park *et al.*, 2008). These active compounds can be increased in callus induced from plant parts separated and cultivated *in vitro* when subjected to biotic and abiotic stimulation. These active compounds can be separated, purified, and used in a pure manner (Collin, 2001; Bisset, 2007).

This study aimed to increase the secondary active compounds in the ginger plant through treatment with *Agrobacterium*

tumefaciens.

2. MATERIALS AND METHODS:

This study was carried out in the laboratory of plant tissue culture in the College of Agriculture and the laboratories of the College of Pharmacy University of Basrah, Iraq.

2.1. Callus induced

Callus was induced from planting half-buds of the ginger plant (Figure 2) in MS (Murashige and Skoog) medium provided with 2,4-D (2,4-Dichlorophenoxy acetic acid) at a concentration of 1 mg/L with BA (Benzyl Adenine) and 0.5 mg/L + 500 mg/L with PVP (Polyvinyl Pyrrolidone) as it was the best medium for callus induction (Al-Taha *et al.*, 2020). A total of 100 mg of developing callus was taken and implanted on the same medium after two weeks of inoculation of the wounded callus with bacterial suspensions of *A. tumefaciens* of the strains LBA 4404 and C58 (Figure 3).

2.2. Preparing bacterial isolates

A. tumefaciens of the strains LBA4404 and C58 were activated on solid medium (Luria Bertani-LB), and after sterilizing the medium with an autoclave, the antibiotic Rifampicin was added at a concentration of 0.025 μ L. The plates were then incubated in a refrigerated incubator at 28°C for 48 hours (Figure 4) (Morgan *et al.*, 1987). The bacterial suspensions were made using the Nutrient Broth (NB) medium. The bacterial suspensions were selected at a concentration of 0, 10¹, 10³, 10⁵ bacteria /mL with the knowledge of the bacterial density shown in table 1.

2.3. Secondary active compounds estimation by HPLC

A total of 20 mg of the standard active compounds of ginger Zingerone, 6-gingerol, and 6-Shogaol were obtained from the Chinese company Shyuanyi yuanye Bio-tognologe with 98% purity. For the RP-HPLC Analysis, it was diluted with 500 μ L of pure ethanol 99.5% per active compound and mixed well using a Vortex mixer to get 0.13, 0.14, and 0.20 Molar respectively, then was kept in the refrigerator at 4°C to the next step. Plant extracts were prepared following the standard method (Ketel, 1986). Fresh weight (10 g) was taken from the resulting callus, washed well with distilled water, dried with filter paper, and cut well. The samples were

crushed well, placed in Petri dishes, and stored at -4°C for 48 hours. Then they were lyophilized by freeze dryer for 24 hours. 1 g of dried sample was dissolved in 5 mL ethanol and kept in the dark for 12 hours at 20±3°C. The next step was shaking the samples well using the Vortex mixing to ensure its dissolution. The dissolved samples were centrifuged, filtered then placed in the refrigerator in the dark until the secondary active compounds 6-gingerol, 6-Shogaol and Zingerone were measured in plant extracts by HPLC. A total of 30 µL of the three standard solutions 6-gingerol, 6-shogaol and Zingerone (10 µL per active compound) were withdrawn and injected together into HPLC.

2.4. HPLC analysis

HPLC type 100 LC-UV 100 Plus Angstrom determines the retention time and sample pack height of the standard solutions (Zhang *et al.*, 2013). The following conditions were set:

- Stationary phase: Nuceosil 100-S
- Column: Arcus type (4.6 × 250 mm)
- Temperature for Column: 30°C
- Mobile Phase: Acetonitrile and Water HPLC in a 50:50 V: V ratio.
- Flow rate: 1 mL / min.
- Wavelength: 282 nm.

The concentrations of secondary active compounds were quantified using a comparison between the standard active compound and the sample under the same laboratory conditions using equation 1 (Almukhtar, 2017).

3. RESULTS AND DISCUSSION:

Figure 5 shows the retention time and the peak area of the standard Zingerone and 6-gingerol and 6-Shogaol active compounds. The retention time of the three active compounds was 4.61, 9.26, and 11.42 min, respectively, while the peaks area of the active compounds above was 1238074.1, 1891032.8 and 2006960.1, respectively.

3.1. Effect of *A. tumefaciens* strain LBA4404

The results of Table 2 and Figure 6- A, B, C, D and E show that the concentrations of *Agrobacterium tumefaciens* from the LBA4404 strain has a significant effect on the callus content of the secondary three compounds active compounds Zingerone, 6-gingerol and 6-Shogaol.

The treatment of 10⁵ bacteria /mL was significantly superior, resulting in the highest concentration of Zingerone, (0.278) mg/g, followed by a concentration of 10¹ bacteria /mL, which showed the highest concentration of the three active compounds, (0.199, 0.099, 0.069) mg/g dry weight respectively.

3.2. Effect of *A. tumefaciens* strain C58

The results of Table 3 and Figures 7- A-C show that the concentrations of *Agrobacterium tumefaciens* from the C58 strain has a significant effect on the callus content of the three secondary compounds active Zingerone, 6-gingerol, and 6-Shogaol. The treatment of 10¹ bacteria/mL was significantly superior, resulting in the highest concentration of Zingerone, (0.240) mg/g, followed by a concentration of 10³ bacteria/mL, which showed the highest concentration of 6-gingerol and 6-Shogaol (0.053 and 0.027) mg/g dry weight, respectively.

The reason for the superiority of *Agrobacterium tumefaciens* increase the secondary of metabolism in callus tissue that was treated with bacterial suspensions of LBA4404 and C58 may be attributed to the dominance of stable genes in differentiated tissues over the region coding for enzymes needed for biosynthesis and providing the necessary vectors (Akramian *et al.*, 2008). Genetic transformation in wounded callus begins when the bacteria stick to the wounds due to the area to edit tissue cells callus materials phenolic (Acetosyringone) is necessary to stimulate a group of genes *Vir* genes in stable Ti plasmid (Bensaddek *et al.*, 2008). The transfer of a piece of T-DNA from the Ti plasmid and its association with the cell genome randomly results in the addition or deletion of the sequence of base pairs in the DNA of the transformed cells. In this way, the transferred T-DNA segment and depending on the site of its association may cause activation or suppression of some genes in the pathway of secondary metabolite (Alvarez, 2011).

Among the most important genes in T-DNA are Oncogenes carrying the gene group *roIA*, *roIB*, and *roIC* known to be responsible for the growth and differentiation of cells that work either alone or in combination in stimulating the construction of secondary metabolites in the transgenic cells (Bulgakov, 2008). The reason for using *Agrobacterium* rely on the fact it is considered a natural vector because it has a unique ability to confer one or both right RT-DNA or left LT-DNA or both from Ti plasmids and include them in the plant cell genome, causing a change in the metabolism

of auxin and cytokinin in the transgenic callus tissue (Zambryski *et al.*, 1989). Their genetic stability characterizes these transformed plants as they have high growth and are thus an effective means for forming and producing secondary medicinal metabolites (Hu and Du, 2006). That finding is consistent with his findings Rao *et al.* (2012), Singh *et al.* (2014), Tusevski *et al.* (2015), Sajjalaguddam and Paladugu (2016) and Nhut *et al.* (2017) in their studies on *Alpinia galangal*, *Hypericum perforatum*, *Hypericum perforatum*, *Abrus precatorius* L., and *Tagetes* spp. Sequentially, when exposing callus to *A. tumefaciens* and *A. rhizogenes*, they found there was an increase in stimulation of the callus tissue to produce secondary active compounds. This is the first study to observe *A. tumefaciens* on ginger callus in stimulating medicinal secondary active compounds.

4. CONCLUSIONS:

The ginger callus treatment with biotic elicitors (*Agrobacterium tumefaciens*) led to a significant increase in the number of medicinal compounds Zingerone, 6-gingerol and 6-Shogaol compared to the control treatment (untreated callus and fresh ginger). It can be seen that the LBA4404 strain (10^5 bacteria/mL) gives the highest concentration of the Zingerone content, followed by a concentration of 10^1 bacteria/mL that gave the highest concentration of the three active compounds Zingerone, 6-gingerol, and 6-Shogaol. Further, the treatment of 10^1 bacteria/mL of the strain C58 was significantly superior in giving Zingerone the highest concentration, followed by a 10^3 bacteria/mL concentration, which gave the highest concentration 6-gingerol and 6-Shogaol compared with fresh ginger and 0 treatments complement with the control.

5. REFERENCES:

1. Ahmad, B., Rehman, M. U., Amin, I., Arif, A., Rasool, S., Bhat, S. A., Afzal, I., Hussain, I., Bilal, S. and Rahman, M. M. (2015). A Review on Pharmacological Properties of Zingerone (4-(4-Hydroxy-3-methoxyphenyl)-2-butanone). *Sci. World J.*, 27(3): 1-6.
2. Akoachere, J. F., Ndip, R. N., Chenwi, E. B., Ndip, L. M., Njock, T. E. and Anong, D. N. (2002). Antibacterial effect of *Zingiber officinale* and *Garcinia kola* on respiratory tract pathogens. *East African Med. J.*, 79(11): 588-592.
3. Akramian, M., Tabatabaei, S. M. F. and Mirmasoumi, M. (2008). Virulence of different strains of *Agrobacterium rhizogenes* on genetic transformation of four *Hyoscyamus* species. *American-Eurasian J. Agric. Envir. Sci.*, 3(5): 759-763.
4. Al-Taha, H. A., Al-Mayah, A. A. and Al-Behadili, W. A. A. (2020). Effect of Auxin 2,4-D and NAA on Induction Callus and Adventitious Shoots and Roots regeneration from half Shoot Tips Culture of *Zingiber officinale* var. Roscoe White. *Journal of University of Babylon for Pure and Applied Sciences*, 28(2): 160-171.
5. Almukhtar, S. A. (2017). Effect of growth regulators and sucrose on the induction and production of flavonoids in callus of *Vitis Vinifera* (L) *In Vitro*. *Pak. J. Biotechnol.* 14 (4) 803-809.
6. Alvarez, M. A. (2011). Genetic Transformation. First ed., Dragana Manestar, Croatia.
7. Bensaddek, L., Villarreal, M. L. and Fliniaux, M. A. (2008). Induction and growth of hairy roots for the production of medicinal compounds. *Electronic J. Integrative Bio. Sci.*, 3(1): 1-11.
8. Bisset, N. G. (2007). Herbal Drug and Phytopharmaceuticals. Boca Raton, EL, CRC Press, 118-125.
9. Bijaya, B. B. (2018). Ginger Processing in India (*Zingiber officinale*): A Review. *Int. J. Curr. Microbiol. App. Sci.*, 7(4): 1639-1651.
10. Bulgakov, V. P. (2008). Functions of Rol genes in plant secondary metabolism. *Biotechnol. Adv.*, 26(4): 318-324.
11. Collin, H.A. (2001). Secondary production formation in plant tissue cultures. *Plant growth Regu.* 34: 119-134.
12. Dhanik, J., Arya, N. and Nand, V. (2017). A Review on *Zingiber officinale*. *Journal of Pharmacognosy and Phytochemistry*, 6(3): 174-184.
13. Food and Agricultural Organization of United Nations (FAO) (2013). Economic and Social department: The statistical division.
14. Ghasemzadeh, A., Jaafar, H. Z. E. and Rahmat, A. (2010). Synthesis of Phenolics and Flavonoids in Ginger

- (*Zingiber officinale* Roscoe) and Their Effects on Photosynthesis Rate. *Int. J. Mol. Sci.* 11 (2): 4539-4555.
15. Gopi, S., Varma, K. and Jude, S. (2016). Study on temperature dependent conversion of active components of ginger. *International Journal of Pharma Sciences*, 6(1): 1344-1347
 16. Gupta, R., Singh, P. K., Singh, R. and Singh, R. L. (2016). Pharmacological activities of *Zingiber officinale* (ginger) and its active ingredients: a review. *International Journal of Scientific and Innovative Research*, 4(1):1-18.
 17. Hartati, R.; Suganda, A. G. and Fidrianny, I. (2014). Botanical, Phytochemical and Pharmacological Properties of *Hedychium* (Zingiberaceae) - A Review. *Procedia Chemistry*, 13(4): 150-163.
 18. Hu, Z. and Du, M. (2006). Hairy root and its application in plant genetic engineering. *J. Integrative Plant Biol.*, 48(2): 121-127.
 19. Jung, M. Y., Lee, M. K., Park, H. J., Oh, E. B., Shin, J. Y., Park, J. S., Jung, S. Y., Oh, J. H., and Choi, D. S. (2018). Heat-induced conversion of gingerols to shogaols in ginger as affected by heat type (dry or moist heat), sample type (fresh or dried), temperature and time. *Food science and biotechnology*, 27(3), 687-693.
 20. Ketel, D. H. (1986). Morphological differentiation and occurrence of thiophenes in leaf callus cultures from *Tagetes* species: Relation to the growth medium of the plants. *Physiol. Plant.* 66 (1): 392-396.
 21. Mekuriya, W. and Mekibib, B. (2018). Review on the Medicinal Values of Ginger for Human and Animal Ailments. *J. Vet. Sci. Techno.*, 9(2): 1-5.
 22. Morgan, A. J., Cox, P. N., Turner, D. A., Peel, E., Davey, M. R., Garthand, K. M. A. and Mulligan, B. J. (1987). Transformation of tomato using an Ri-plasmid vector. *Plant Sci.*, 49:37-49.
 23. Nhut, D. T., Huy, N. P., Huong, T. T., Luan, V. Q., Hien, V. T., Tung, H. T., Cuong, D. M., Phuong, C. T. B., Ngoc, P. B., Trong, N. D., Hung, N. K. and Ha, C. H. (2017). *Agrobacterium*-mediated transformation of *Panax vietnamensis* ha et grushv. *Journal of Biotechnology* 15(4): 641-650.
 24. Olubunmi, B., Seun, F. A. and Funmilayo, T. A. (2013). Food value of Two Varieties of Ginger (*Zingiber officinale*) commonly consumed in Nigeria. *ISRN Nutrition*, 35(9): 72-75.
 25. Oomah, B. D. (2003). Isolation characterization and assessment of secondary metabolites from plants for use in human. *J. plant physio.* 2 (1): 81-98.
 26. Pilerood, S. A. and Prakash, J. (2011). Chemical composition and antioxidant properties of ginger root (*Zingiber officinale*). *J. of Medic.*, 4(24): 2674-2679.
 27. Park, S. V., Uddian, M. R., Xu, H., Kim, Y. K. and lee, S. Y. (2008). Biotechnological applications for rosmarinic acid production in plant. *Afr. J. of Biot.*, 7(25): 4954-4965.
 28. Rahmani, A. H., Al-Shabrimi, F. M. and Aly, S. M. (2014). Active ingredients of ginger as potential candidates in the prevention and treatment of diseases via modulation of biological activities. *Int. J. Physiol. Pathophysiol. Pharmacol.*, 6(2): 125-136.
 29. Rao, K., Chodiseti, B., Mangamoori, L. N. and Giri, A. (2012). *Agrobacterium*-Mediated Transformation in *Alpinia galanga* (Linn.) Willd. for Enhanced Acetoxychavicol Acetate Production. *Appl. Biochem. Biotechnol*, 168 (11): 339-347.
 30. Rasool Hassan, B. A. (2012). Medicinal Plants (Importance and Uses). *Pharmaceut. Anal. Acta.*, 3 (10): e139.
 31. Sacchetti, G., Maietti, S., Muzzoli, M., Scaglianti, M., Manfredini, S. and Radice, M. (2005). Comparative evaluation of 11 essential oils of different origin as functional antioxidants, antiradicals and antimicrobials in foods. *Food Chemistry*. 91(4):621-632.
 32. Sajjalaguddam, R. R. and Paladugu, A. (2016). Influence of *Agrobacterium rhizogenes* strains and elicitation on hairy root induction and Glycyrrhizin production from *Abrus precatorius*. *J. Pharm. Sci. and Res.* 8(12): 1353-1357.
 33. Semwal, R. B., Semwal, D. K., Combrinck, S. and Viljoen, A. M. (2015). Gingerols and Shogaols: Important

- nutraceutical principles from ginger. *Phytochemistry*, 117 (1): 554-568.
34. Shoji, A.; Iwasa, T. and Takemoto, Y. (1982). Cardiogenic principles of ginger (*Zingiber officinale* Roscoe). *J. Pharmac. Sci.*, 71: 1174-1175.
 35. Shahi, M. and Hussain, F. (2012). Chemical composition and mineral contents of *Zingiber officinale* and *Alpinia allughas* (Zingiberaceae) Rhizomes. *Int. J. Chem. Biochemical Sci.*, 2(2012): 101-104.
 36. Singh, R. K., Hou, W., Marslin, G., Dias, A. C. P. and Franklin, G. (2014). Lignin and flavonoid content increases in *Hypericum perforatum* cell wall after *Agrobacterium tumefaciens* co-cultivation. *Planta Med* 80: 1388.
 37. Stoner, G. D. (2013). Ginger: Is it ready for prime time. *Cancer Prev. Res.*, 6: 257-262.
 38. Tapsell, L. C., Hemphill, I., Cobiac, L., Patch, C. S., Sullivan, D. R., Fenech, M., Roodenrys, S., Keogh, J. B., Clifton, P. M., Williams, P. G., Fazio, V. A. and Inge, K. E. (2006). Health benefits of herbs and spices. The past, the present, the future, *Med. J. Aust.*, 185 (4). 4-24.
 39. Tusevski, O., Stanoeva, J. P., Stefova, M. and Simic, S. G. (2015). *Agrobacterium* enhances xanthone production in *Hypericum perforatum* cell suspensions. *Plant Growth Regul.* 76(2): 199-210.
 40. Wang, W. H. and Wang, Z. M. (2005). Studies of commonly used traditional medicine. Ginger. *Zhongguo zhong Yao Za Zhi.*, 30: 1569-1573.
 41. Zambryski, P., Tempe J. and Schell, J. (1989). Transfer and function of T-DNA gene from *Agrobacterium* Ti and Ri plasmids in plants. *Cell*, 56 (5): 193-201.
 42. Zhang, Y. X., Li, J. S., Chen, L. H., Peng, W. and Cai, B. (2012). Simultaneous determination of five gingerols in raw and processed ginger by HPLC. *Chinese Pharmaceutical Journal.* 47(6): 471-474.
 43. Zhang, A., Wan, L., Wu, C., Fang, Y., Han, G., Li, H., Zhang, Z. and Wang, H. (2013). Simultaneous Determination of 14 Phenolic Compounds in Grape Canes by HPLC-DAD-UV Using Wavelength Switching Detection. *Molecules*, 18 (8): 14241-1425.

$$\text{Sample con. (mg. gm}^{-1}\text{)} = \frac{\text{sample area}}{\text{standard area}} \times \text{standard solution con.} \times \text{dilution factor} \quad (\text{Eq. 1})$$

Table 1. Bacterial densities of *Agrobacterium* strains used in the study

Inoculate (bacteria /mL)	LBA4404	C58
10 ¹	2 × 10 ³	1 × 10 ³
10 ³	15 × 10 ⁵	25 × 10 ⁴
10 ⁵	2 × 10 ⁷	1 × 10 ⁷

Table 2. Effect of different concentrations of *A. tumefaciens* LBA4404 on ginger plant callus content from secondary active compounds.

Inoculate (bacteria /mL)	Zingerone (mg/g)	6-gingerol (mg/g)	6-Shogaol (mg/g)
fresh ginger	0.014	0.006	0.013
0	0.018	0.009	0.017
10 ¹	0.199	0.099	0.069
10 ³	0.177	0.091	0.064
10 ⁵	0.278	0.066	0.036
L.S.D _{0.01}	0.0025	0.0025	0.0025

Table 3. Effect of different concentrations of *A. tumefaciens* C58 on ginger plant callus content from secondary active compounds.

Inoculate (bacteria /mL)	Zingerone (mg/g)	6-gingerol (mg/g)	6-Shogaol (mg/g)
fresh ginger	0.014	0.006	0.013
0	0.018	0.009	0.017
10 ¹	0.240	0.002	0.003
10 ³	0.015	0.053	0.027
10 ⁵	0.055	0.039	0.002
L.S.D _{0.01}	0.0025	0.0025	0.0025

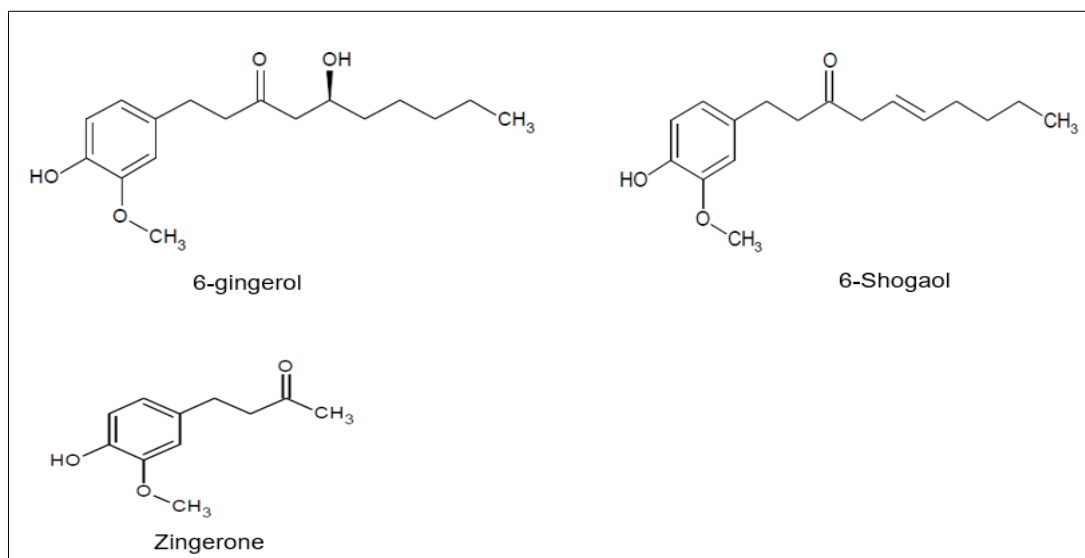


Figure 1. Major ginger active ingredients and their analogs



Figure 2. Callus induced from planting half-buds of the ginger plant in MS medium provided with 2,4-D at a concentration of 1 mg/L with BA at a concentration of 0.5 mg/L + 500 mg/L PVP

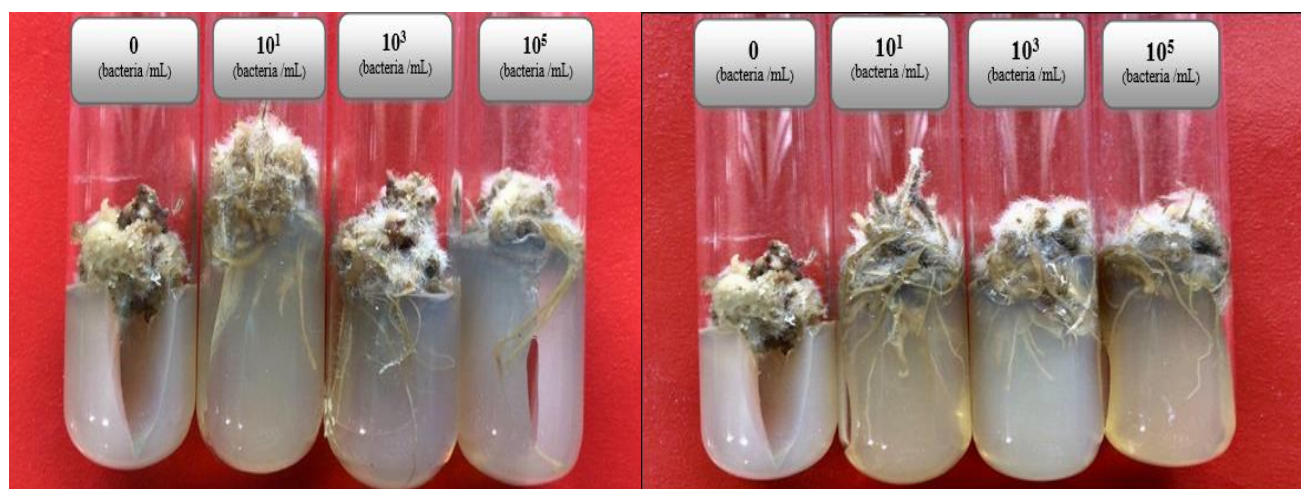


Figure 3. Effect of different levels of *A. tumefaciens*, LBA4404, and C58 in the ginger callus

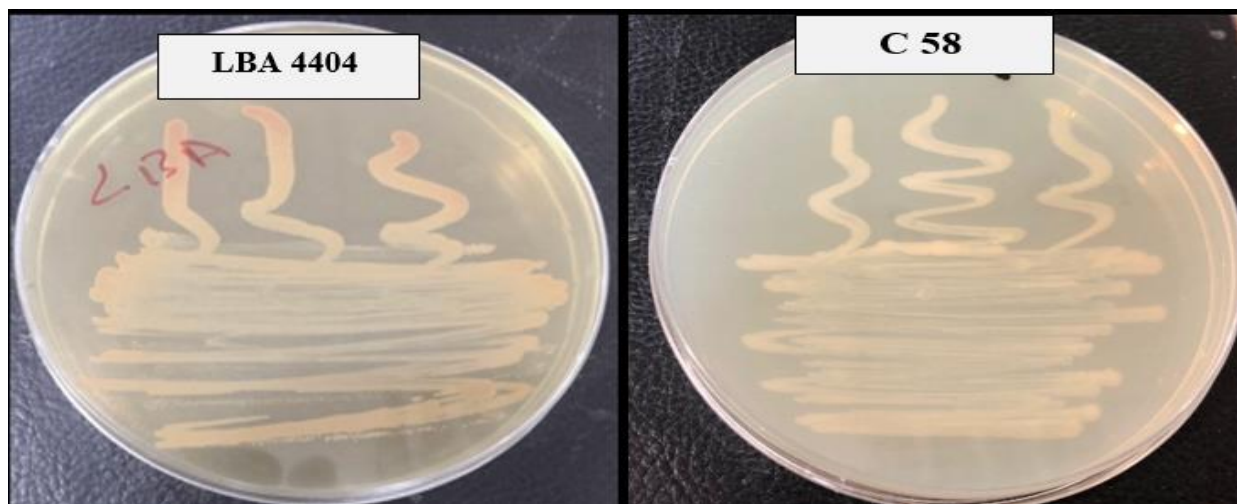


Figure 4. Bacterial isolates used in the study

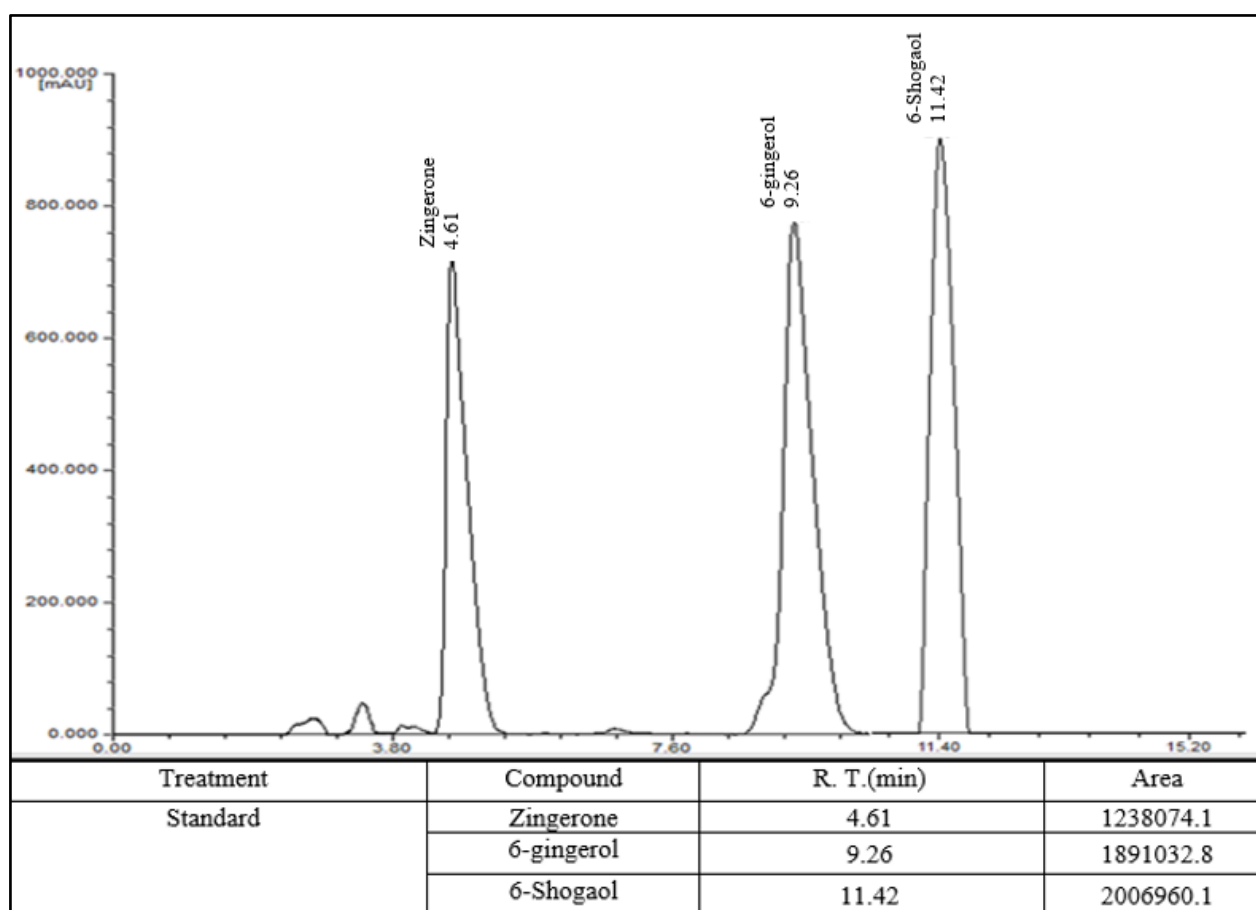


Figure 5. Curve chart, retention time, and peak area of standard solutions (Zingerone, 6-gingerol, and 6-Shogaol).

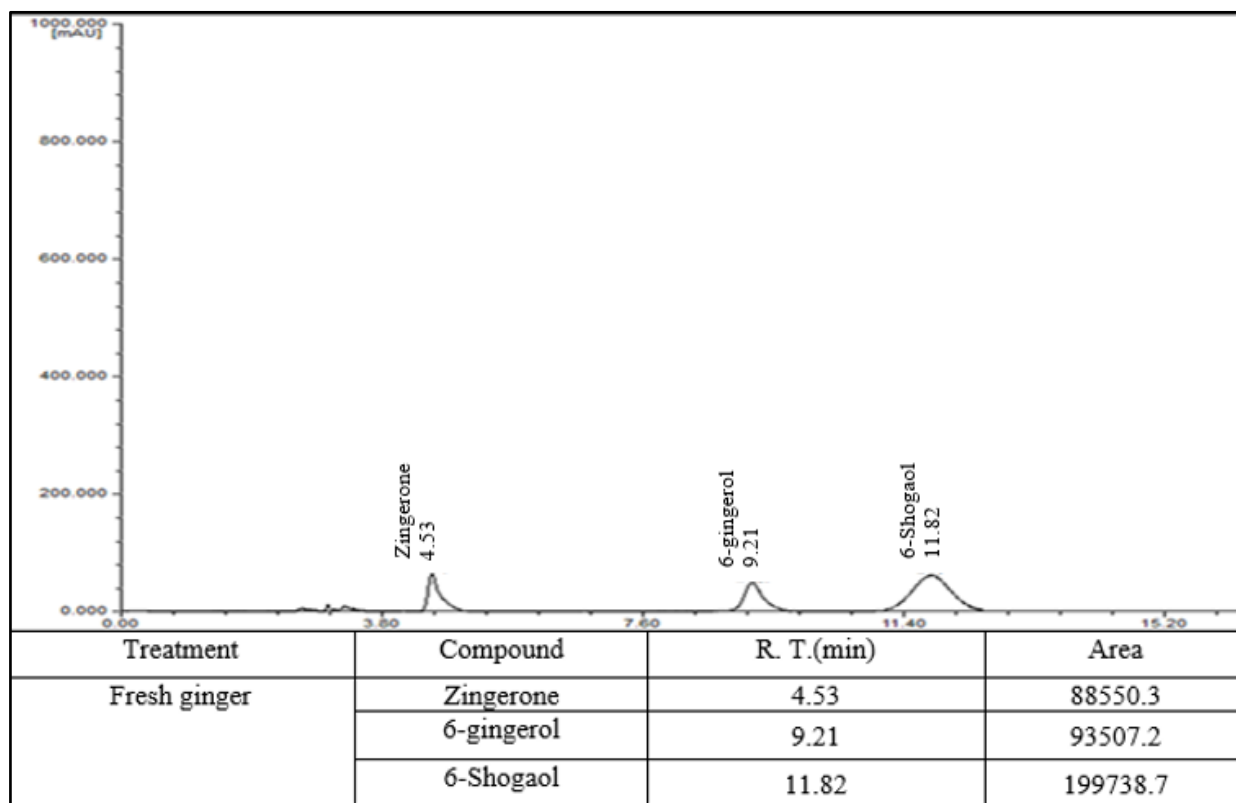


Figure 6-A. Curve chart, retention time, and peak area of fresh ginger and content of secondary active compounds.

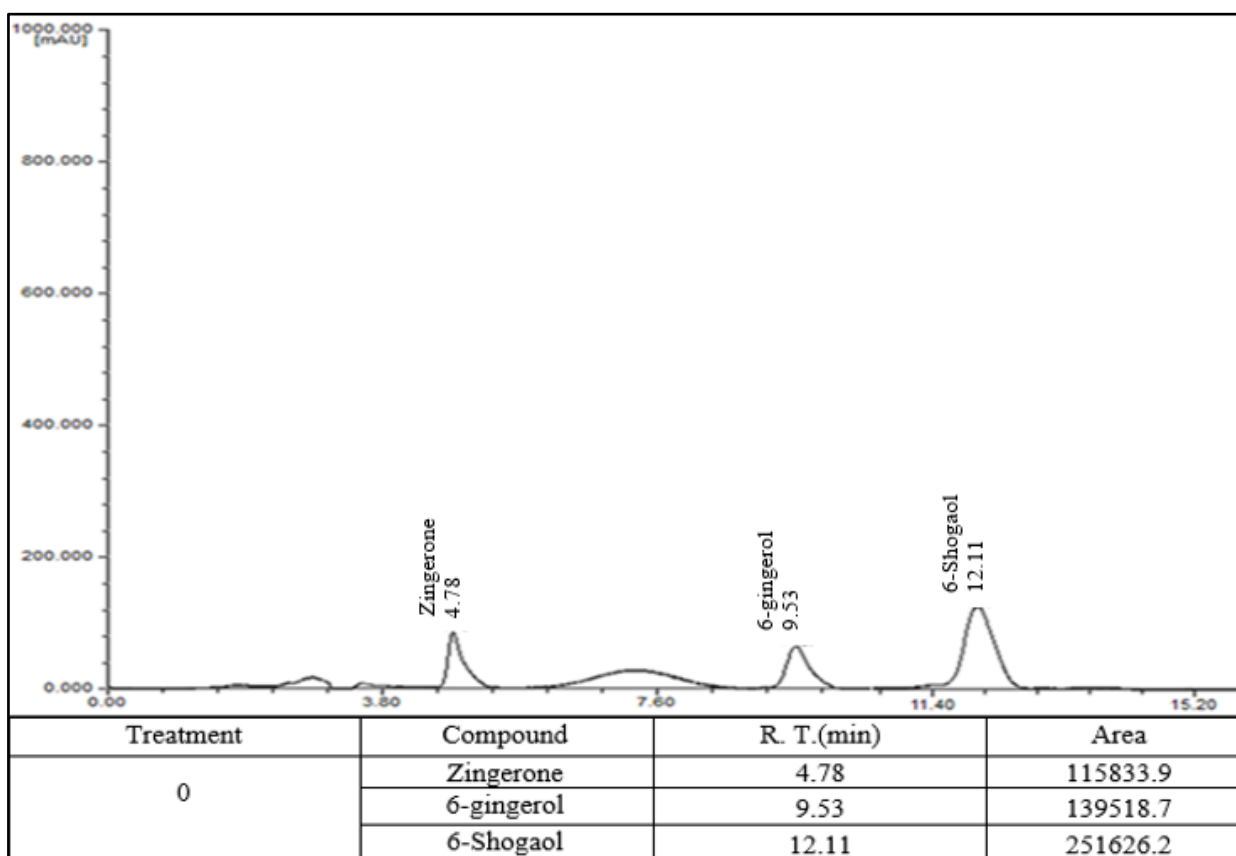


Figure 6-B. Curve chart, retention time, and peak area at a concentration of 0 and its effect on the production of secondary active compounds in callus.

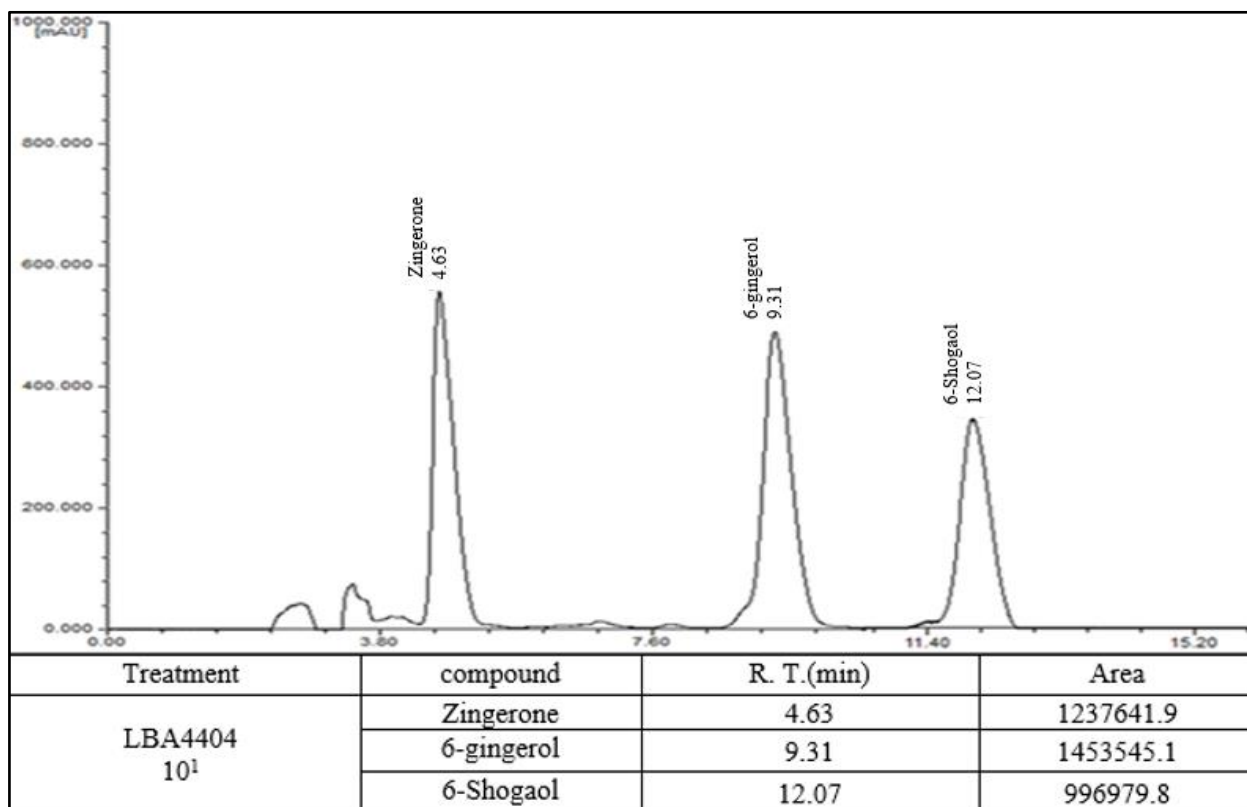


Figure 6-C. Curve chart, retention time, and peak area of *A. tumefaciens* LBA4404 strain at a concentration of 10^1 and its effect on producing secondary active compounds in callus.

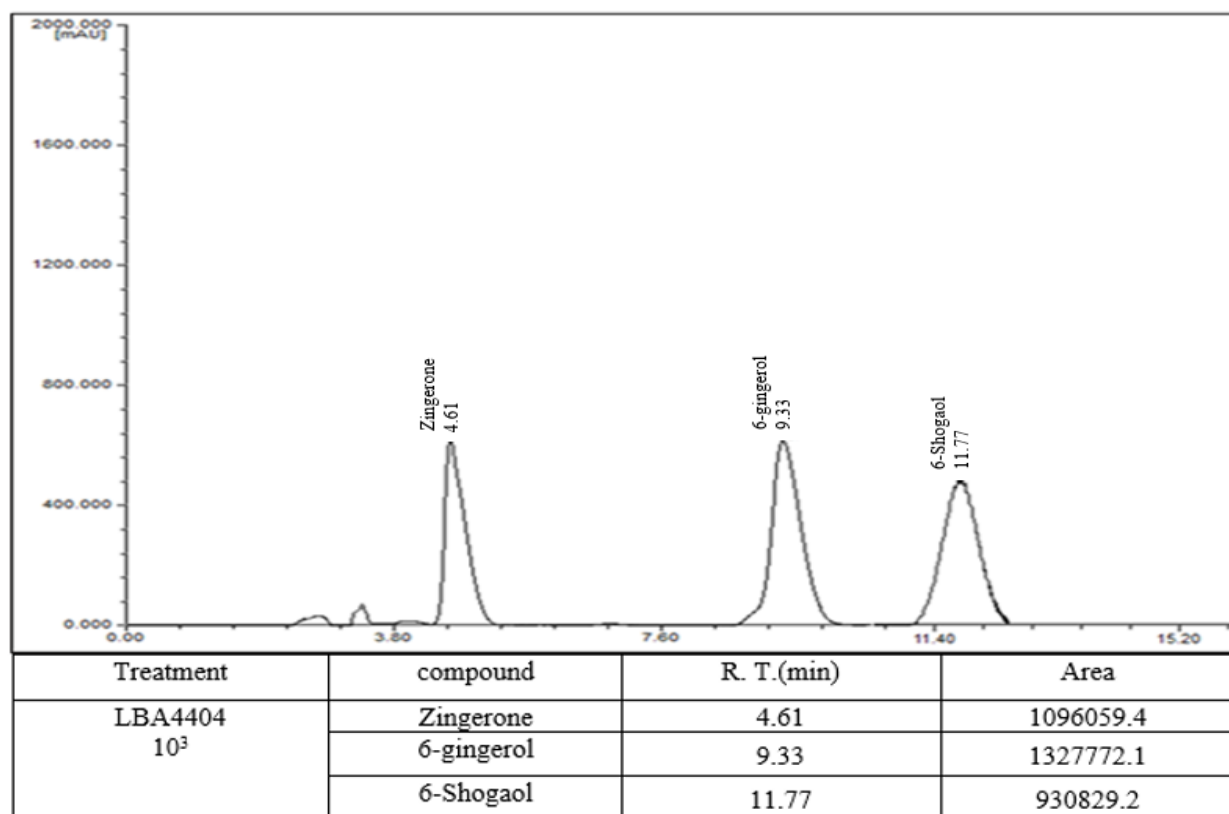


Figure 6-D: Curve chart, retention time, and peak area of *A. tumefaciens* LBA4404 strain at a concentration of 10^3 and its effect on the production of secondary active compounds in callus.

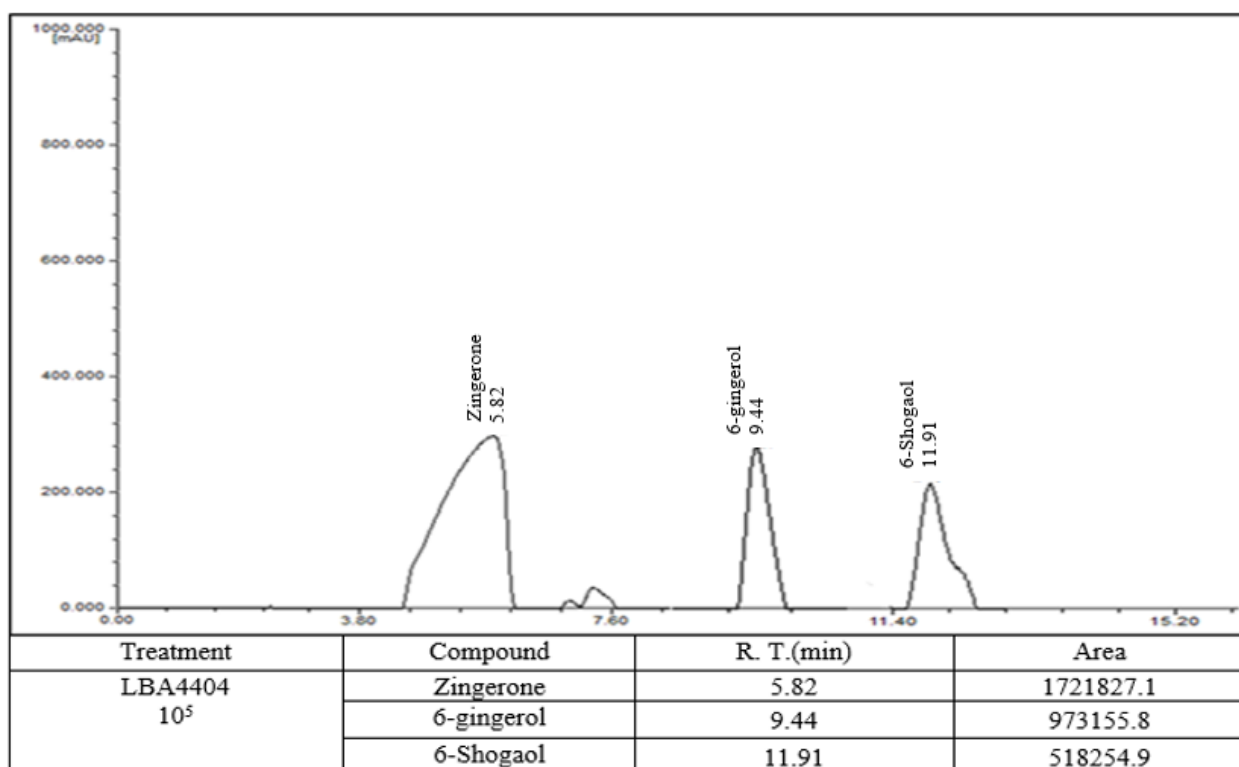


Figure 6-E: Curve chart, retention time, and peak area of *A. tumefaciens* LBA4404 strain at a concentration of 10^5 and its effect on the production of secondary active compounds in callus

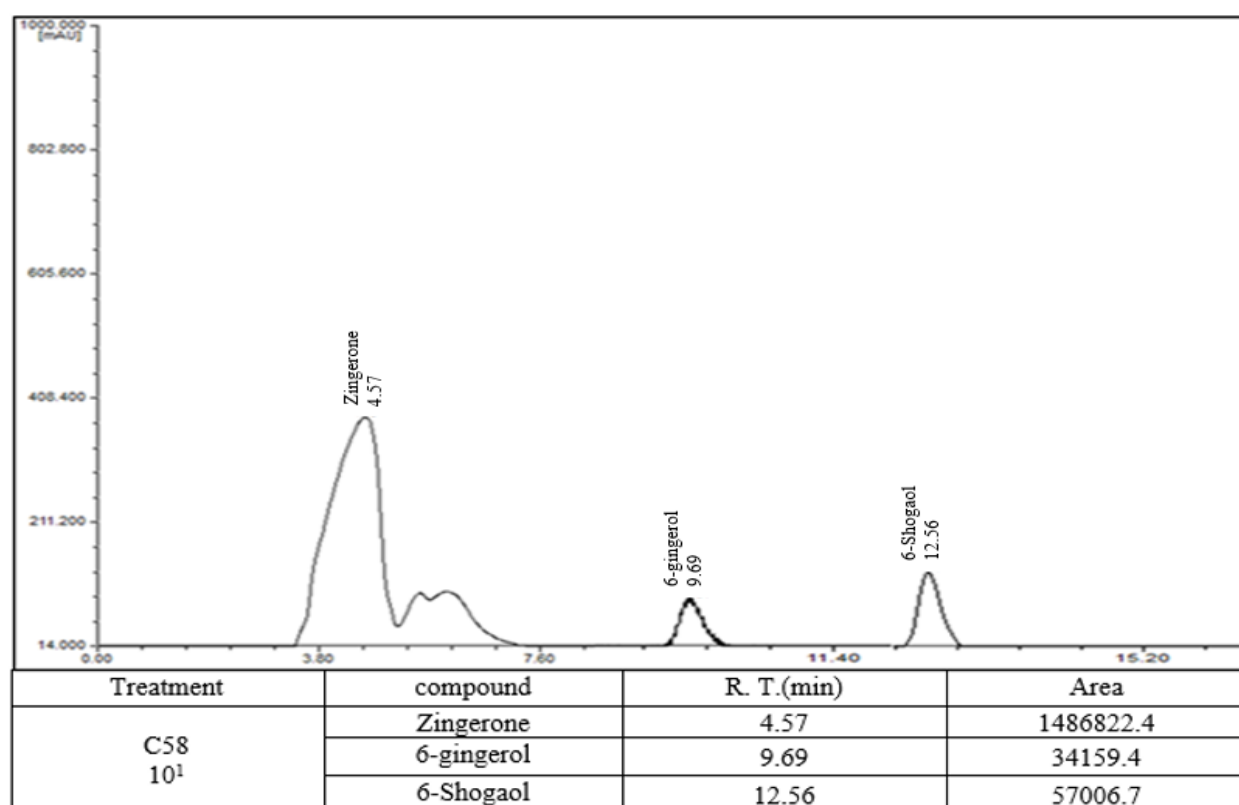


Figure 7-A: Curve chart, retention time, and peak area of *A. tumefaciens* C58 strain at a concentration of 10^1 and its effect on the production of secondary active compounds in callus

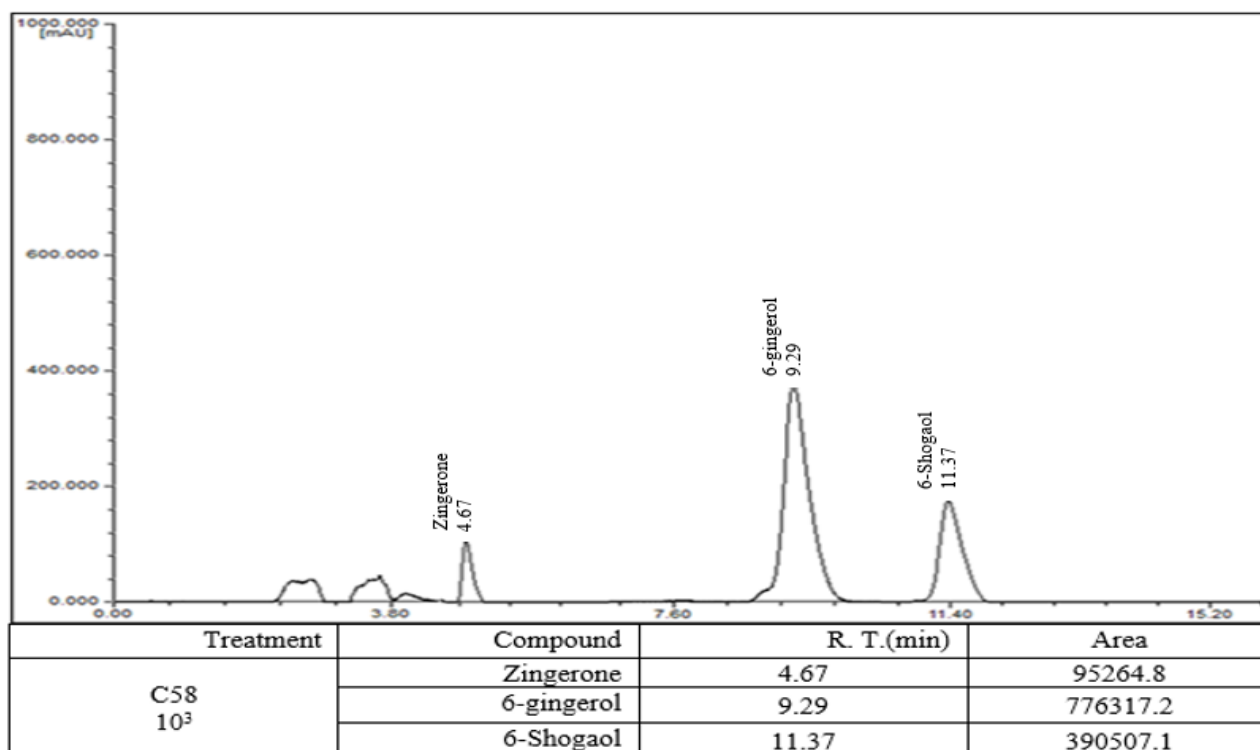


Figure 7-B: Curve chart, retention time, and peak area of *A. tumefaciens* C58 strain at a concentration of 10^3 and its effect on the production of secondary active compounds in callus

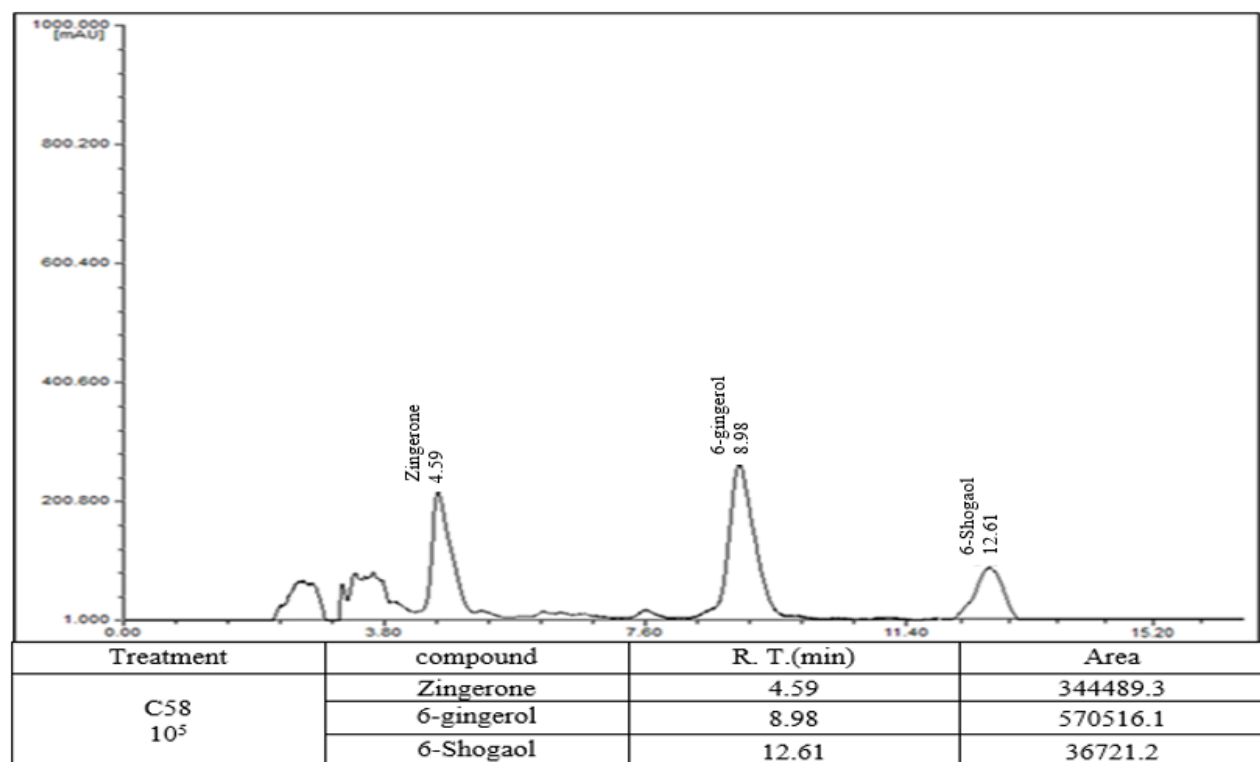


Figure 7-C: Curve chart, retention time, and peak area of *A. tumefaciens* C58 strain at a concentration of 10^5 and its effect on the production of secondary active compounds in callus.

AVALIAÇÃO DE IMPACTO DE CORRETORES BIOLÓGICOS ALIMENTARES NA EFICIÊNCIA ENERGÉTICA DO ESTADO NUTRICIONAL**IMPACT ASSESSMENT OF ALIMENTARY BIOLOGICAL CORRECTORS ON THE ENERGY EFFICIENCY OF NUTRITIONAL STATUS****ОЦЕНКА ВЛИЯНИЯ АЛИМЕНТАРНЫХ БИОКОРРЕКТОРОВ НА ЭНЕРГОЭФФЕКТИВНОСТЬ ПИЩЕВОГО СТАТУСА**

RODIONOVA, Natalia Sergeevna¹; POPOV, Evgeny Sergeevich^{2*}; KHITROV, Anatoly Anatolievich³; RODIONOVA, Natalia Alekseevna⁴; EGOROVA, Elena Ivanovna⁵

^{1,2,3,4,5} Voronezh State University of Engineering Technologies, Faculty of Economics and Management, Department of Service and Restaurant Business. Russia

** Corresponding author*

e-mail: evgeny.s.popov2@gmail.com

Received 07 September 2020; received in revised form 30 September 2020; accepted 30 October 2020

RESUMO

O funcionamento eficaz de todos os sistemas do corpo é amplamente determinado por uma série de substâncias essenciais que atuam como ativadores de reações metabólicas. Sua deficiência na dieta leva a violações da homeostase da natureza alimentar, que é exacerbada por fatores ambientais, sociais e econômicos. O presente estudo teve como objetivo comparar as propriedades anti-hipoxêmicas de nutrientes de origem vegetal e animal, seu impacto nos parâmetros respiratórios e de transporte das trocas gasosas, como critérios para o balanço energético do organismo, bem como a avaliação do fator probiótico na melhoria das propriedades anti-hipoxêmicas das substâncias biologicamente ativas direcionadas. O aumento na eficiência das trocas gasosas foi avaliado a partir do exemplo de alunos e professores de uma universidade de engenharia com idades de 16 a 65 anos no consumo diário de produtos alimentícios com propriedades biocorretivas conhecidas: óleo de gérmen de trigo (WGO), farelo de óleo de gérmen de trigo (WGOM), óleo de peixe de tecido concentrado (CTFO) e suas combinações com a biomassa do consórcio de bactérias lacto e bífidas. A mudança da eficiência energética do estado nutricional foi avaliada a partir da análise da concentração de dióxido de carbono (CO₂) e oxigênio (O₂) na mistura ar exalada e do nível de hemoglobina (SpO₂). Seus valores foram registrados antes e após o consumo diário dos produtos testados por 30 dias. A avaliação dos valores médios dos parâmetros em todas as faixas etárias demonstrou que o anti-hipoxêmico mais eficaz foi a farinha de óleo de gérmen de trigo. A combinação de biocorretores sob investigação com formas ativas de microrganismos probióticos fornece um efeito anti-hipoxêmico mais ativo para todos os produtos sob investigação em todas as idades. Os dados obtidos permitem afirmar a possibilidade de um efeito alimentar ativo sobre a eficiência das trocas gasosas, comprovar as propriedades anti-hipoxia do WGO, WGOM e CTFO, bem como o efeito sinérgico de sua combinação com microrganismos probióticos na forma ativa.

Palavras-chave: *biocorretores, metabolismo energético, oxigenação, hemoglobina, microrganismos probióticos*

ABSTRACT

The effective functioning of all body systems is mostly determined by many essential substances that act as activators of metabolic reactions. Their diet deficiency leads to violations of alimentary nature homeostasis, exacerbated by environmental, social, and economic factors. This study aimed to compare antihypoxant properties nutrients of the vegetable and animal origin, their impact on respiratory and transport parameters of gas exchange, as criteria for the energy balance of the body, and the assessment of probiotic factor in improving the antihypoxant properties of targeted biologically active substances. The increase in the efficiency of gas exchange was evaluated on the example of students and teachers of an engineering university at ages from 16 to 65 in daily consumption of food products with known biocorrective properties: wheat germ oil (WGO), wheat germ oil meal (WGOM), concentrated tissue fish oil (CTFO) and their combinations with the biomass of the lacto- and Bifidus bacteria consortium. The change of energy efficiency of the nutritional status was assessed based on the analysis of the carbon dioxide (CO₂) and oxygen (O₂) concentration in the exhaled gas-air mixture and the level of hemoglobin (SpO₂). Their values were recorded before and after the daily

consumption of the tested products for 30 days. The average values of parameters in all age groups have demonstrated that the most effective antihypoxant is the wheat germ oil meal. A combination of biocorrectors under investigation with active forms of probiotic microorganisms provides a more active antihypoxant effect for all products under investigation in all age groups. The obtained data make it possible to state the possibility of an operational alimentary impact on gas exchange efficiency and prove the antihypoxant properties of WGO, WGOM, CTFO, and the synergetic effect of their combination with probiotic microorganisms in the active form.

Keywords: *biocorrectors, energy metabolism, oxygenation, hemoglobin, probiotic microorganisms*

АННОТАЦИЯ

Эффективное функционирование всех систем организма во многом определяется рядом эссенциальных веществ, выполняющих роль активаторов обменных реакций. Их недостаток в рационе питания приводит к нарушениям гомеостаза алиментарной природы, что усугубляется экологическими, социальными и экономическими факторами. Целью работы является сравнительное исследование антигипоксанта нутриентов растительного и животного происхождения и их влияния на респираторные и транспортные показатели газообмена на примере студентов и преподавателей ВУЗа, как критерии энергетического баланса организма, а также оценка пробиотического фактора в повышении антигипоксанта свойств целевых биологически активных веществ. Оценку повышения эффективности газообмена проводили на примере студентов и преподавателей инженерного ВУЗа в возрасте от 16 до 65 лет при ежедневном употреблении пищевых продуктов с известными биокорректирующими свойствами: масла из зародышей пшеницы (МЗП), муки из жмыха зародышей пшеницы (МЖЗП), концентрированного тканевого рыбного жира (КТРЖ) и их комбинаций с биомассой консорциума лакто- и бифидобактерий. Изменение энергоэффективности пищевого статуса оценивали на основе анализа концентрации углекислого газа (CO_2) и кислорода (O_2) в выдыхаемой газовой смеси и уровня оксигенации гемоглобина (SpO_2). Значения данных показателей фиксировали до и после ежедневного употребления исследуемых продуктов в течение 30 дней. Оценка средних значений показателей во всех возрастных группах показала, что наиболее эффективным антигипоксантом является мука из жмыха зародышей пшеницы. Совмещение употребления исследуемых биокорректоров с пробиотическими микроорганизмами в активной форме обеспечивает более значимый антигипоксанта эффект во всех возрастных группах. Полученные данные позволяют констатировать возможность активного алиментарного воздействия на эффективность газообмена, доказывают антигипоксанта свойства МЗП, ЖЗП, КТРЖ, а также синергетический эффект их комбинирования с пробиотическими микроорганизмами в активной форме.

Ключевые слова: *биокорректоры, энергетический обмен, оксигенация, гемоглобин, пробиотические микроорганизмы*

1. INTRODUCTION:

Alimentary technologies of biocorrection of the nutritional status and pathophysiological states of the human body require fundamental and applied research of medical and biological assessment of new sources of food and ingredients. The introduction of innovative physical-chemical, bio- and nanotechnologies for producing highly effective food products of the biocorrective action is needed (Eamonn, 2019; Vernerey *et al.*, 2019; Rodionova *et al.*, 2019d; Fujimura *et al.*, 2010).

In the function of alimentary biocorrectors, dietary supplements have been investigated such as "Vitazar" wheat germ oil (WGO), "Vitazar" wheat germ oil meal (WGOM), "Econol" cryo-concentrated tissue fish oil (CTFO), and "Biomatrix" activated consortium of lacto and bifidus bacteria, which has a composition of *Str.*

thermophilus, *L. Casei* subsp. *Rhamnosus*, *L. acidophilus*, *L. plantarum*, *L. fermentum*, *B. bifidum*, *B. longum*, *B. adolescentis* in the concentration of milk-based active cells of at least 10^9 CFU/g (Rodionova *et al.*, 2019; Daliri and Lee, 2015).

Biocorrective properties of WGO are contingent upon the high content of vitamins A, D, E, polyunsaturated fatty acids, octacosanol and are confirmed by extensive clinical investigations of therapy for various diseases such as cardiovascular, gastroenterological, diabetes, hepatitis, infertility, burn, and wound injuries (Shpagina, 2008a; Shpagina, 2007; Poljsak, 2011); (Shpagina, 2008b); (Akool, 2019); (Juárez-López *et al.*, 2013); (Lepretti *et al.*, 2018); (Simopoulos, 2002); (Safarinejad *et al.*, 2010); (Ferreira *et al.*, 2012); (Dong, 2018); (Harris, 2008).

A by-product of WGO manufacturing is a

protein-carbohydrate component of the germ (mill cake) with a residual oil content of 6-8%, as determined in the monograph (Vishnyakov and Vlasov, 2011), registered as flour "Vitazar" biologically active dietary supplement (Vishnyakov and Vlasov, 2011). The residual lipid fraction in wheat germ oil meal (WGOM) is identical in chemical composition to the pressed oil and hypothetically preserves its active biological properties (Vishnyakov *et al.*, 2018; Rodionova and Alekseeva, 2015). Besides, WGOM contains up to 30% of the full-value protein in amino acid composition, up to 30% of carbohydrates represented by pentosans, mono-, di-, oligo polysaccharides. WGOM contains significant amounts of vitamins B1, B2, B6, PP, E, K, macro- and micronutrient elements such as Zn, Mn, Mg, Ca, K, Fe, Se, P, as has been demonstrated in previous papers (Shpagina, 2008b).

Biologically active dietary supplement "Econol" represents cryo- concentrated tissue fish oil (CTFO). It is a valuable active bioregulator of metabolic processes. It is obtained because of physical-chemical actions on the fish raw material, making it possible to destroy the cell membrane with subsequent mechanical separation of the lipid fraction from the rest of the processed raw materials. CTFO is a source of polyunsaturated fatty acids (PUFAs) such as ω -3 eicosapentaenoic and docosahexaenoic acids, vitamins A, D, and E. Clinical investigations conducted in many countries have indicated that lipids of marine organisms are an effective remedy for lipid metabolism disorders in the human body, which prevent cardiovascular diseases, hypercoagulability, as has been demonstrated in papers (Isaev and Simonenko, 2016; Isaev *et al.*, 2015; Isaev *et al.*, 2000; Kerry *et al.*, 2018).

Bio-correcting properties of probiotic microorganisms include trophic and energy supply of the macroorganism, energy supply of the epithelium, immune system stimulation, formation of immunoglobulins, regulation of intestinal peristalsis, participation in regulation, differentiation, and regeneration of the intestinal epithelium, provision of cytoprotection, detoxication, excretion of endo and exogenous toxic compounds, mutagen destruction, activation of drug compounds, the formation of signal molecules (neuro and transmitters), maintenance of ionic, physical and chemical parameters of homeostasis of the juxta-epithelial zone, the supply of substrates for lipo and glucogenesis (Kerry *et al.*, 2018; Banan-Mwine *et al.*, 2015;

Valdovinos-Garcia *et al.*, 2018; Guo *et al.*, 2011; Lee *et al.*, 2009; Bluher *et al.*, 2001).

This study aimed to compare antihypoxant properties nutrients of the vegetable (WGO, WGOM) and animal (CTFO) origin, their impact on respiratory and transport parameters of gas exchange on the example of university students and teachers, as criteria for the energy balance of the body, as well as the assessment of probiotic factor in improving the antihypoxant properties of targeted biologically active substances.

2. MATERIALS AND METHODS:

2.1. Samples

The experimental research objects were WGO contained 180-200 mg/100 g of vitamin E, 1.5-8.0 mg/100 g of polycosanol, and 60 g/100 g of PUFA (produced by PULAT LTD, the Russian Federation). WGOM contained 30-35 g/100 g of protein, 3-4 g/100 g of PUFA, 45-47 g/100 g of digestible carbohydrates, 18-26 g/100 g of dietary fibers 25-30 mg/100 g of vitamin E (produced by PULAT LTD, the Russian Federation). CTFO contained 6.60 mg/100 g of vitamin A, 100 mg/100 g of vitamin D, 100 mg/100 g of vitamin E; PUFA content was not less than 25 g/100 g (production of TRINITA LTD academic research and production enterprise, the Russian Federation). The concentration of active cells has characterized the biomass of "Biomatrix" consortium of lacto- and bifidobacteria (*Streptococcus thermophilus*, *Casei subspecies Rhamnosus*, *L. acidophilus*, *L. plantarum*, *L. fermentum*, *B. bifidum*, *B. longum*, *B. adolescentis*), not less than 109 CFU/ml (production of Lactinal LTD, the Russian Federation).

2.2. Analysis

In the function of recorded parameters – indicators of changes in energy metabolism efficiency at the time of nutritional intervention of the abovementioned biocorrectors and their combinations with probiotics - changes in the concentration of oxygen (O₂) and carbon dioxide (CO₂) in the exhaled gas-air mixture and the level of oxygenation of blood hemoglobin (SpO₂) have been investigated. To investigate the concentration of O₂ and CO₂ in the exhaled gas-air mixture, we used the TESTO-310 gas analyzer of TESTO RUS LTD production. The sensitivity of the device for O₂ was characterized by the concentration range of 0-21 % vol.,

resolution of 0.01 vol. %, error of ± 0.2 vol. %. The sensitivity of the device for CO₂ was characterized by the concentration range of 0-100 vol. %, resolution of 0.01 vol. %, and error of ± 0.2 vol. %. As well as MDG-1201capnograph was used with the measurement range for CO₂ concentration of 0-13 vol. % and error of ± 0.3 %.

2.3. Setting up an experiment

There was no forced ventilation and air conditioning in the room (laboratory and lecture hall), the room was not aerated; factors that significantly affect the initial oxygen content in the room have been minimized. The concentration of O₂ and CO₂ in the exhaled gas-air mixture was determined immediately after 90 minutes of classroom sessions. The motion activity of all students and teachers was the same and minimal. Before the experimental investigation, the patient was at rest for 10 minutes. To obtain stable and more significant results in terms of CO₂ content, the air intake into the lungs was accompanied by exhalation delay for at least 15-20 seconds, until stabilization of parameters of O₂ and CO₂ concentrations on the device display (Vishnyakov *et al.*, 2020).

Measurement of O₂ content in blood was carried out non-invasively, using ChoiseMmedMD 300C21C pulse oximeter. The saturation level was calculated as a ratio of the amount of HbO₂ to the total amount of hemoglobin, expressed as a percentage by the formula:

$$SpO_2 = \frac{HbO_2}{(HbO_2 + Hb)} \times 100\%$$

The respiratory quotient (RQ) was calculated as the ratio of concentrations of CO₂ excreted from the body to O₂ absorbed at the same time. Measurement of each of the investigated parameters was carried out in a three-fold repetition for all students and teachers under investigation with the subsequent obtaining of arithmetic mean values (Davis *et al.*, 2019; Rattaray *et al.*, 2014; Lawal *et al.*, 2017; Zaric *et al.*, 2014). The reliability assessment of the obtained arithmetic mean values of the investigated parameters was carried out by the non-parametric Mann-Whitney U-test (Nakagawa and Cuthill, 2007), according to the monograph (Grachev and Plaksin, 2005).

2.4. Experimental groups

In the course of the research, the volunteer patients were divided into four groups.

The first group consumed 3.5 g of WGO, the second group consumed WGOM in an amount that provided delivery of 3.5 g of oil in the form of a culinary product, which corresponded to 50 g of mill cake. The third and fourth groups consumed probiotic emulsion containing 3.5 g of WGO or 6.5 g of CTFO in combination with 10 g of lacto and bifidobacteria biomass. The stability of the emulsions was at least 70-75%, due to the high exo polysaccharide activity of probiotic biomass. These food forms were consumed by volunteers regardless of meals, without correction of the main diet. The duration of the experimental investigation was 30 days. At the beginning and the end of the biocorrectors intake, the parameters under investigation were monitored. On the day of sampling, the biocorrectors under investigation were not given to the research subjects; the time interval between the intake of the tested products and sampling was at least 24 hours.

Four experimental groups of research subjects voluntarily included men and women at the ages of 16 to 65 years old. They were students and teachers of Voronezh State University of Engineering Technologies, who spend at least 6 hours daily in the same conditions in the university's premises. The exclusion criteria were smoking, pregnancy, and chronic illnesses; these have been applied in the monograph (Vishnyakov *et al.*, 2020). All research subjects had not previously consumed the biocorrectors under study. To exclude changes related to the seasonality of nutrition and physical activity, the study was conducted in the fall period. Before starting the experimental studies, each volunteer has documented his consent to be included in the experimental group.

The number of experimental groups was 70, 36, 58, and 51 people respectively; the number of control groups that did not consume the products under investigation was the same (Table 1) as has been described in the monograph (Vishnyakov *et al.*, 2020).

3. RESULTS AND DISCUSSION:

Assessment of O₂ and CO₂ concentrations in the exhaled gas-air mixture in all age groups has demonstrated that the most effective antihypoxant is WGOM. The increase of the SpO₂ level by 0.83%, the increase of CO₂ level by 0.44%, and the decrease of O₂ concentrations by 0.36% in the exhaled gas-air mixture have been found on average all age groups. When taking WGO, the increase of the

SpO₂ level amounted to 0.77%, the increase of CO₂ level in the exhaled gas-air mixture amounted to 0.17%, the decrease of O₂ concentration in the exhaled gas-air mixture amounted to 0.21% also on the average for all age groups. The results are presented in Figures 1-6.

When comparing the results obtained with the age of patients, it has been found that in the first age group, the increase of SpO₂ level amounted to 0.91%, the increase of CO₂ concentration and the decrease of O₂ concentration in the exhaled gas-air mixture amounted to 0.38% and 0.29% respectively. In the second age group, the SpO₂ level increased by 0.82%, the concentration of CO₂ in the exhaled gas-air mixture increased by 0.27%, the decrease of O₂ concentration amounted to 0.25%. In the third age group, the SpO₂ level increased by 0.59%; simultaneously, the concentration of CO₂ increased by 0.39%, and the O₂ level decreased by 0.31% in the exhaled gas-air mixture (Figures 2, 3).

It is known that a 1% decrease in SpO₂ level is observed when the partial oxygen pressure decreases by 20% or corresponds to the research subject's rise to the height of 1000 m above sea level (Anderson and Hlastala, 2007). The increase of SpO₂ level within prescribed limits testifies to the rise of blood transport function, which is essential in ensuring the body performance as a whole (Popovsky and Korot'ko, 2003; Nikolic and Vranic, 2006; Akhem *et al.*, 1989). Found changes of the investigated parameters testify to the shift of the active reaction of blood to the alkaline side, which occurs in the pulmonary capillaries because of the transition of CO₂ in alveolar air (Cornack *et al.*, 1957). The higher the concentration of CO₂ in exhaled air, the more significant the shift of reaction to the alkaline side, the lower the probability of forming "strand coins" of red blood cells, and higher efficiency of O₂ transport (Birben *et al.*, 2012). The reliability of the presented data is confirmed by Mann-Whitney U-test values (Table 2). RQ's value was increased by 1.8% when WGO was taken and by 2.4% when WGOM was taken within 30 days. The increase in this parameter's values in the 1st, 2nd, and 3rd age groups when taking the biocorrectors under investigation amounted to 1.8%, 2.0%, and 1.7%, respectively.

The conducted analysis of the effect of WGO and WGOM, containing the same amount of target biologically active substance (BAS) such as the lipid fraction of wheat germ, demonstrated

that these food products can be attributed to the alimentary factors of biocorrective action, providing restoration of the equilibrium state of the body systems responsible for energy metabolism for age groups from 18 to 65 years. By the example of the biocorrectors under investigation which have, along with the identical concentration of target BAS the different composition of accompanying substances, possibly also having biocorrective properties (Cui *et al.*, 2014), the possibility of a fundamentally new integral approach to the assessment of biological activity of food objects of different nature and complex composition has been proved. WGOM biocorrector, containing a wider range of potentially useful nutrients such as water-soluble vitamins, prebiotics, proteins, and mineral elements, has also demonstrated the higher effectiveness.

The hypothesis of the possibility of increasing the efficiency of target biologically active substances by their combination with probiotic microorganisms made it possible to proceed to the next stage of the investigation described in papers (Isaev and Simonenko, 2015; Isaev *et al.*, 2015; Isaev *et al.*, 2000) – the comparative assessment of biocorrective effect of probiotic emulsions with WGO and CTFO inclusion.

It has been experimentally demonstrated that the combination of consumption of biocorrectors under investigation with the inclusion of probiotic microorganisms is specific for each biocorrector under investigation (Figure 4). Probiotic emulsion with CTFO inclusion demonstrated a more pronounced effect on the increase of CO₂ concentration in the exhaled gas-air mixture and increase of SpO₂ in comparison with the emulsion containing WGO. When probiotic emulsion with WGO and CTFO was taken, the SpO₂ level has increased by 0.85% and 0.90%, respectively, and the concentration of CO₂ in exhaled air has decreased by 0.33% and 0.35%, respectively.

The results illustrate the dependence between the age of patients and the antihypoxant effect achieved by consuming the considered probiotic forms. In the first age group, an increase of SpO₂ level by 0.96% and CO₂ concentration in the exhaled gas-air mixture by 0.29% have been found. In the second group, the SpO₂ level has increased by 0.90%, and the value of CO₂ concentration in the exhaled gas-air mixture has increased by 0.34%. In the third group, the SpO₂ level has increased by 0.69%, and in the exhaled gas-air mixture, the CO₂ level has increased by

0.28% (Figures 5, 6).

The results of experimental investigations on the intake of probiotic emulsion with WGO inclusion make it possible to state a more pronounced increase of SpO₂ level by 0.08% and decrease of CO₂ concentration in exhaled air by 0.16% in comparison with effect from WGO intake. Following the calculated Mann-Whitney U-test values, it has been found that the revealed differences in the arithmetic mean of the investigated parameters are reliable (Table 3).

When comparing the medical and biological indications for WGO, WGOM, and CTFO application in therapy for various diseases and experimentally proved positive correction of the food status energy efficiency, a stable correlation is observed according to works (Shpagina, 2008a; Shpagina, 2007; Shpagina, 2008b; Vishnyakov and Vlasov, 2011; Isaev and Simonenko, 2016; Isaev *et al.*, 2015; Isaev *et al.*, 2000; Vishnyakov *et al.*, 2020; Nikolic *et al.*, 2004; Szebeni and Toth, 1986; Rifkind *et al.*, 2003).

4. CONCLUSIONS:

It can be concluded that there was increase in the level of oxygenation of hemoglobin in the blood, an increase in the level of carbon dioxide, and a decrease in the concentration of oxygen in the exhaled gas mixture in all age groups when adding WGO, WGOM, and CTFO to the main diet. The most effective antihypoxant was WGOM. Less pronounced changes in the investigated parameters have been registered when taking WGO. Determined that a combination of the consumption of biocorrectors under investigation with probiotic microorganisms in active form provides a more significant antihypoxant effect in all age groups. The role of alimentary factors in increasing the efficiency of the most important energy functions of the organism regardless of sex and age, which naturally leads to an increase of the organism resistance to external and internal effects, is salient. This is especially relevant for students and teachers of a technical university in closed premises with low mobility and mental stress.

5. ACKNOWLEDGMENTS:

The work was supported by the Russian Science Foundation under agreement No. 19-76-10023.

6. REFERENCES:

1. Akhem, A.A., Andreyuk, G.M., Kisel, M.A., Kiselev, P.A. (1989). Hemoglobin conversion to hemichrome under the influence of fatty acids. *Biochimica et Biophysica Acta (BBA) – General Subjects*, 992(2), 191-194.
2. Akool, El-S. (2019) Molecular mechanisms of the protective role of wheat germ oil against oxidative stress-induced liver disease. *In book: Dietary Interventions in Liver Disease. Foods, Nutrients and Dietary Supplements*, ch. 19, 233-238.
3. Anderson, J.C., Hlastala, M.P. (2007). Breath tests and airway gas exchange. *Pulmonary Pharmacology & Therapeutics*, 20, 112-117.
4. Banan-Mwine, E., Byong, D., Lee, H. (2015). New perspectives on probiotics in health and disease. *Food Science and Human Wellness*, 4(2), 56–65.
5. Birben, E., Sahiner, U.M., Sackesen, C., Erzurum, S., Kalayci, O. (2012). Oxidative stress and antioxidant defense. *World Allergy Organ J.*, 5, 9-19.
6. Bluher, M., Hentschel, B., Rassoul, F., Richter, V. (2001). Influence of dietary intake and physical activity on annual rhythm of human blood cholesterol concentrations. *Chronobiology International*, 18, 541-557.
7. Cormack, R.S., Cunningham, D.J.C., Gee, J.B.L. (1957). The effect of carbon dioxide on the respiratory response to want of oxygen in man. *Quarterly Journal of Experimental Physiology and Cognate Medical Sciences*, 42, 323-334.
8. Cui, L., Morris, A., Huang, L., Beck, J.M., Twigg, H.L., von Mutius, E. (2014). The microbiome and the lung. *Ann Am Thorac Soc*, 11, 227-232.
9. Daliri, E.B.-M., Lee, B.H. (2015). New perspectives on probiotics in health and disease. *Food Science and Human Wellness*. 4, 56-65.
10. Davis, M.D., Fowler, S.J., Montpetit, A.J. (2019). Exhaled breath testing – A tool for the clinician and researcher. *Paediatric Respiratory Reviews*, 29, 37-41.

11. Dong, D.W. (2018) Dietary n-6 polyunsaturated fatty acids and cardiovascular disease: Epidemiologic evidence. *Prostaglandins, Leukotrienes and Essential Fatty Acids*, 135, 5-9.
12. Eamonn, M.M. (2019). Prebiotics and Probiotics in Digestive Health. *Clinical Gastroenterology and Hepatology*, 17(2), 333-344.
13. Ferreira, A.M., de Souza, B.M.V., Rigotti, M.A., Loureiro, M.R.D. (2012) The use of fatty acids in wound care: an integrative review of the Brazilian literature. *Rev Esc Enferm USP*, 46(3), 745-53.
14. Fujimura, K., Slusher, N., Cabana, M., Lynch, S. (2010). Role of the gut microbiota in defining human health. *Expert Review of Anti-infective Therapy*, 8(4), 435-454.
15. Grachev, Yu.P., Plaksin, Yu.M. (2005). *Mathematical methods of experiment planning*. Moscow: DeLiPrint.
16. Guo, Z., Liu, X.M., Zhang, Q.X., Shen, Z., Tian, F.W., Zhang, H., Sun, Z.H., Zhang, H.P., Chen, W. (2011). Influence of consumption of probiotics on the plasma lipid profile: A meta-analysis of randomized controlled trials. *Nutrition, Metabolism & Cardiovascular Diseases*, 21, 844-850.
17. Harris, W.S. (2008) Linoleic acid and coronary heart disease. *Prostaglandins, Leukotrienes and Essential Fatty Acids*, 79, 169-171.
18. Isaev, V.A., Kaplan, A.Y., Kochetova, A.G., Platonova, R.D., Ashmarin, I.P. (200). "Econol", a complex of PUFA optimizing human cognitive activity. *Human Physiology*, 26, 99-104.
19. Isaev, V.A., Simonenko, S.V. (2016). Influence of life style and "Econol" on physiological adaptation of blood fat component in case of arterial hypertension. *Problems of Nutrition*, 85(5), 120-127.
20. Isaev, V.A., Simonenko, S.V., Khlustov, V.N. (2015). Seafood in complex therapy of inflammatory processes. *Food Industry*, 1, 30-31.
21. Juárez-López, C., Klünder-Klünder, M., Madrigal-Azcárate, A., Flores-Huerta, S. (2013). Omega-3 polyunsaturated fatty acids reduce insulin resistance and triglycerides in obese children and adolescents. *Pediatric Diabetes*, 14, 377-383.
22. Kerry, R.G., Patra, J.K., Gouda, S., Park, Y., Shin, H.-S., Das, G. (2018). Benefaction of probiotics for human health: A review. *Journal of Food and Drug Analysis*, 26(3), 927-939.
23. Lawal, O., Ahmed, W.M., Nijssen, T.M.E., Goodacre, R., Fowler, S.J. (2017). Exhaled breath analysis: a review of 'breath-taking' methods for off-line analysis. *Metabolomics*, 13(10), 110.
24. Lee, D.K., Jang, S., Baek, E.H. (2009). Lactic acid bacteria affect serum cholesterol levels, harmful fecal enzyme activity, and fecal water content. *Lipids in Health and Disease*, 8, 1-8.
25. Lepretti, M., Martucciello, S., Aceves, M.A.B., Putti, R., Lionetti, L. (2018). Omega-3 fatty acids and insulin resistance: focus on the regulation of mitochondria and endoplasmic reticulum stress. *Nutrients*, 10 (3), E350.
26. Nakagawa, S., Cuthill, I.C. (2007). Effect size, confidence interval and statistical significance: a practical guide for biologists. *Biological Reviews of the Cambridge Philosophical Society*, 82(4), 591-605.
27. Nikolic, M., Vranic, D. (2006). Could cholesterol bound to haemoglobin be a missing link for the occasional inverse relationship between superoxide dismutase and glutathione peroxidase activities? *Biochemical and Biophysical Research Communications*, 348, 265-270.
28. Nikolic, M., Stanic, D., Antonijevic, N., Niketic, V. (2004). Cholesterol bound to hemoglobin in normal human erythrocytes: a new form of cholesterol in circulation? *Clinical Biochemistry*, 37, 22-26.
29. Pokrovsky, V.M., Korot'ko, G.F. (2003). *Human Physiology*. Moscow: Medicine.
30. Poljsak, B. (2011). Strategies for reducing or preventing the generation of oxidative stress. *Oxidative Medicine and Cellular Longevity*, 2011, 1-16.
31. Rattray, N.J., Hamrang, Z., Trivedi, D.K., Goodacre, F., Rowler, S.J. (2014). Taking your breath away: metabolomics

- breathes life into personalized medicine. *Trends Biotechnol*, 32(10), 538-548.
32. Rifkind, J.M., Nagababu, E., Ramasamy, S., Ravi, L.B. (2003). Hemoglobin redox reactions and oxidative stress. *Redox Report*, 8, 234-237.
 33. Rodionova, N.S., Alekseeva, T.V. (2015). *Food technology of balanced PUFA composition: monograph*. Voronezh: Voronezh State University of Engineering Technologies.
 34. Safarinejad, M.R., Hosseini, S.Y., Dadkhah, F., Asgari, M.A. (2010) Relationship of omega-3 and omega-6 fatty acids with semen characteristics, and anti-oxidant status of seminal plasma: A comparison between fertile and infertile men. *Clinical Nutrition*, 29 (20), 100-105.
 35. Shpagina, L.A. (2007). *A methodological guidance for doctors "Use of wheat germ oil and "Vitazar" meal in treatment of internal diseases"*. Novosibirsk: Novosibirsk State Medical Academy.
 36. Shpagina, L.A. (2008a). *Use of wheat germ oil and "Vitazar" in treatment of internal diseases: a methodological guidance for doctors*. Novosibirsk: Novosibirsk Book Publishing House.
 37. Shpagina, L.A. (2008b). *Modern aspects of functional nutrition. Clinical efficiency of wheat germ oil: a methodical manual for nutrition specialists*. Novosibirsk: Novosibirsk State University.
 38. Simopoulos, A.P., (2002). Omega-3 fatty acids in inflammation and autoimmune diseases. *Journal of the American College of Nutrition*, 21, 495-505.
 39. Szebeni, J., Toth, K. (1986). Lipid peroxidation in hemoglobin-containing liposomes. Effects of membrane phospholipid composition and cholesterol content. *Biochimica et Biophysica Acta (BBA)*, 857, 139-145.
 40. Valdovinos-García, L.R., Abreu, A.T., Valdovinos-Díaz, M.A. (2018). Uso de probióticos en la práctica clínica: resultados de una encuesta nacional a gastroenterólogos y nutriólogos. *Revista de Gastroenterología de México*, 1–7.
 41. Vernerey, F.J., Benet, E., Blue, L.A., Fajrial, K., Borden, M.A. (2019). Biological active matter aggregates: inspiration for smart colloidal materials. *Advances in Colloid and Interface Science*, 263, 38–51.
 42. Vernia, P., Cesarini, M., de Carolis, A. (2020). Early hydrogen excretion peaks during breath tests. Small intestinal bacterial overgrowth or accelerated transit? *Digestive and Liver Disease*.
 43. Vishnyakov, A.B., Rodionova, N.S., Isayev, A.V., Popov, E.S., Belokurova, E.V., Rodionova, N.A., Interesova, E.A. (2020). *Nutrition. Energy. Entropy: monograph*. Voronezh: Voronezh State University of Engineering Technologies.
 44. Vishnyakov, A.B., Vlasov, V.N. (2011). *Health Germ*. Moscow: Kolos.
 45. Vishnyakov, A.B., Vlasov, V.N., Rodionova, N.S., Alekseeva, T.V., Popov, E.S., Dyakov, A.A. (2018). *Health Germ: monograph. 2nd ed., revised and supplemented*. Voronezh: Voronezh State University of Engineering Technologies.
 46. Zaric, B., Petrovic, S. (2014). Analysis of human exhaled breath in a population of young volunteers. *Arch. Biol. Sci.*, 66, 1529-1538.

Table 1. Composition and size of experimental groups

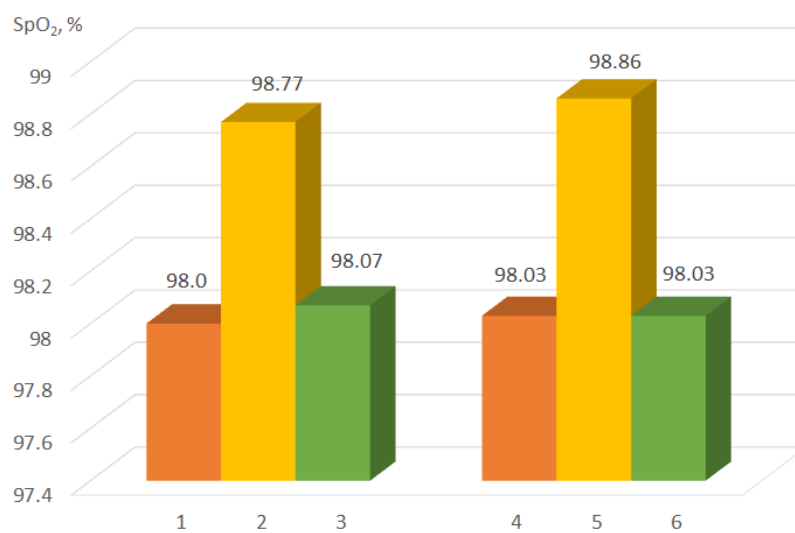
Name of biocorrector	Age of patients, years old			Total
	16-24	25-44	45-65	
WGO	35	18	17	70
WGOM	24	5	7	36
Probiotic emulsion with WGO inclusion	28	20	10	58
Probiotic emulsion with CTFO inclusion	21	20	10	51

Table 2. Calculated Mann-Whitney U-test values

After the course of WGO administration		After the course of WGOM administration	
SpO ₂ , %	O ₂ /CO ₂ , %	SpO ₂ , %	O ₂ /CO ₂ , %
1st group, Ucr=113.0 (30.0)			
92.5	94.0/97.5	19.5	22.5/23.5
2nd group, Ucr=99.0 (5.0)			
71.5	78.5/73.5	2.5	3.0/4.0
3rd group, Ucr=87.0 (8.0)			
72.0	64.0/68.0	4.5	6.0/3.5

Table 3. Calculated Mann-Whitney U-test values

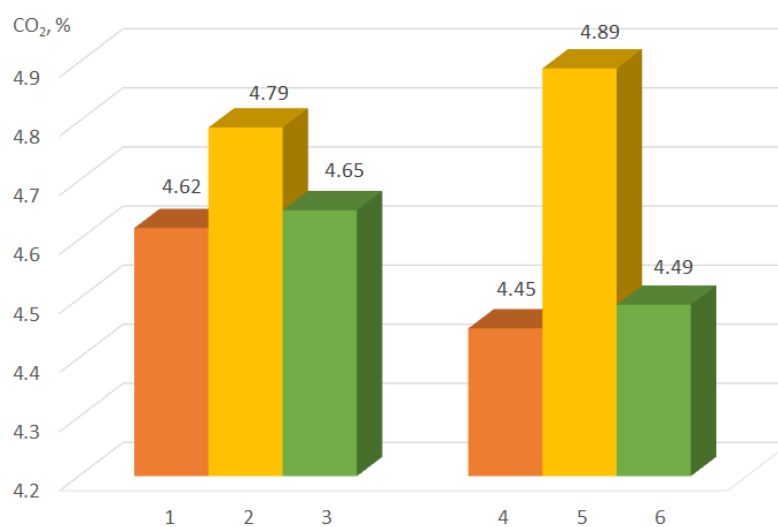
After the course of probiotic emulsion with WGO inclusion administration		After the course of probiotic emulsion with CTFO inclusion administration	
SpO ₂ , %	CO ₂ , %	SpO ₂ , %	CO ₂ , %
1st group. Ucr=23.0 (23.0)			
16.5	14.0	17.5	16.0
2nd group. Ucr=23.0 (23.0)			
15.0	16.5	19.7	18.0
3rd group. Ucr=23.0 (23.0)			
17.0	18.5	18.0	17.5



a

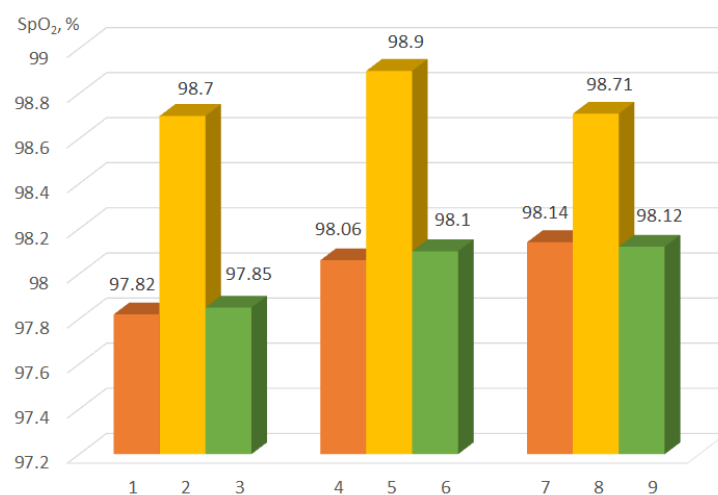


b

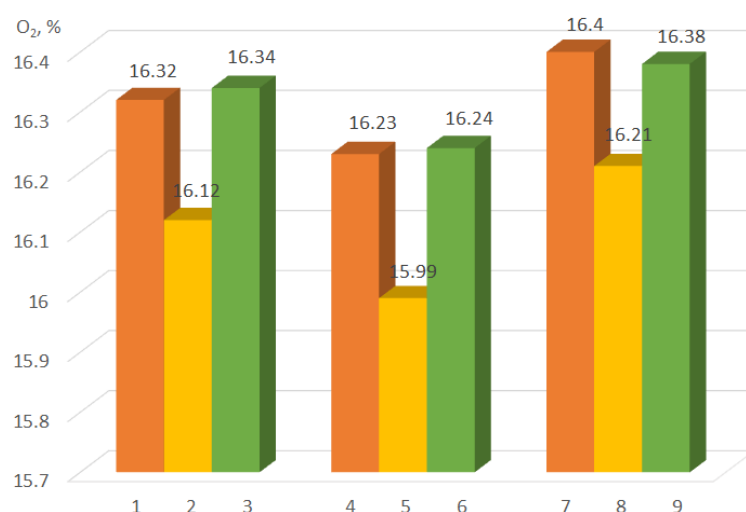


c

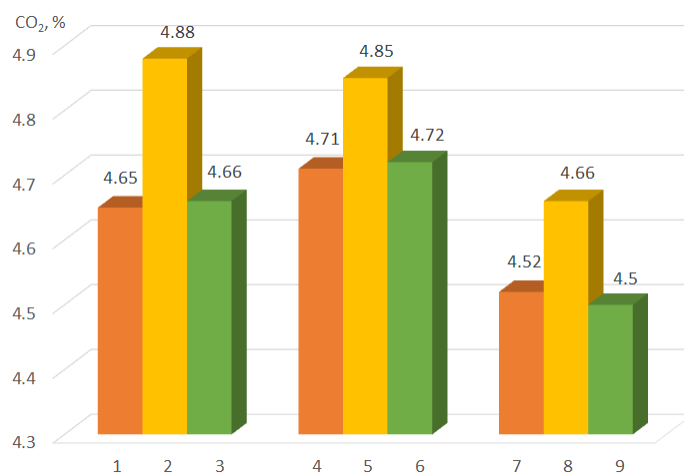
Figure 1. Concentration of SpO₂, % in blood (a); concentration O₂, % (b) and CO₂, % (c) in exhaled gas-air mixture. 1 – before WGO intake; 2 – after 30 days of WGO intake; 3 – the control group (during the whole period); 4 – before WGOM intake; 5 – after 30 days of WGOM intake; 6 – the control group (during the whole period)



a

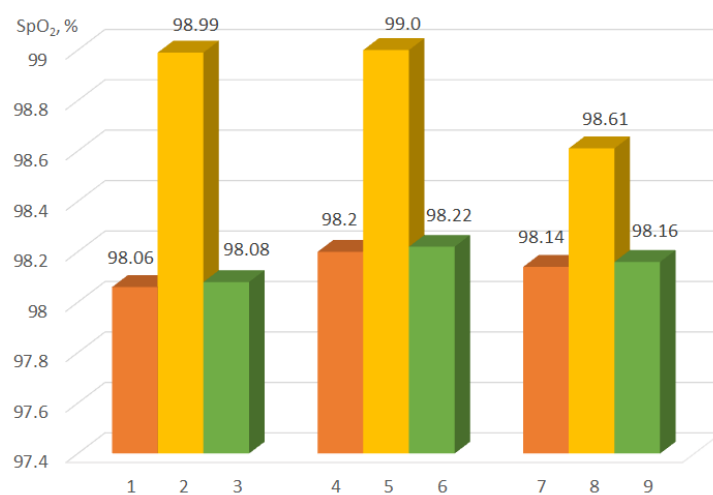


b

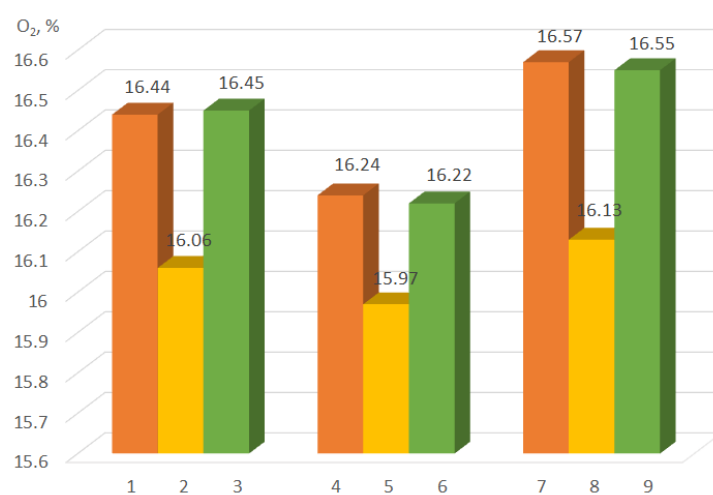


c

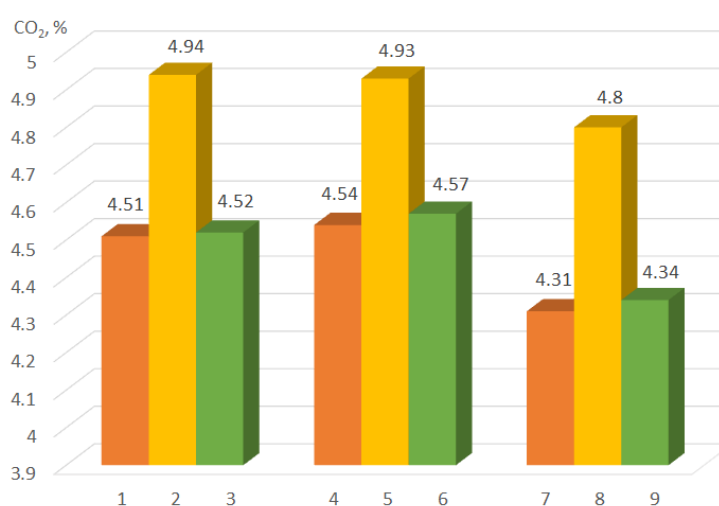
Figure 2. Concentration of SpO₂, % in the blood (a); concentration O₂, % (b) and CO₂, % (c) in the exhaled gas-air mixture. 1, 4, 7– before WGO intake in the 1st, 2nd, and 3rd age groups; 2, 5, 8– after 30 days of WGO intake in the 1st, 2nd, and 3rd age groups; 3, 6, 9 – the control group (during the whole period)



a

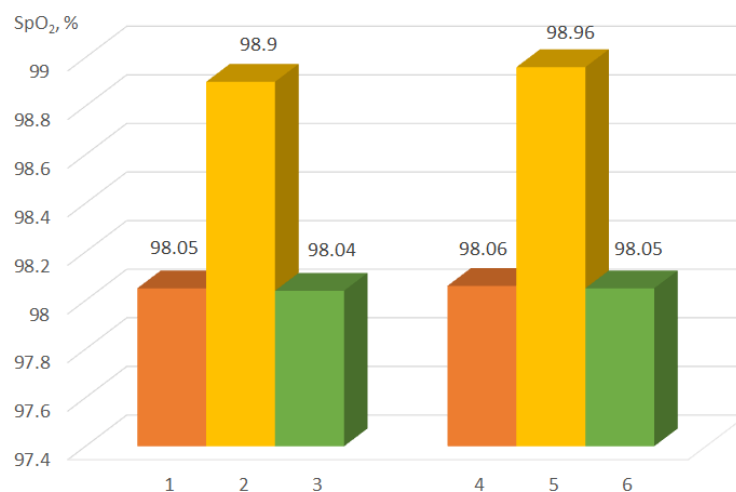


b



c

Figure 3. Concentration of SpO₂, % in the blood (a); concentration O₂, % (b) and CO₂, % (c) in the exhaled gas-air mixture. 1, 4, 7– before WGOM intake in the 1st, 2nd, and 3rd age groups; 2, 5, 8– after 30 days of WGOM intake in the 1st, 2nd, and 3rd age groups; 3, 6, 9 – the control group (during the whole period)

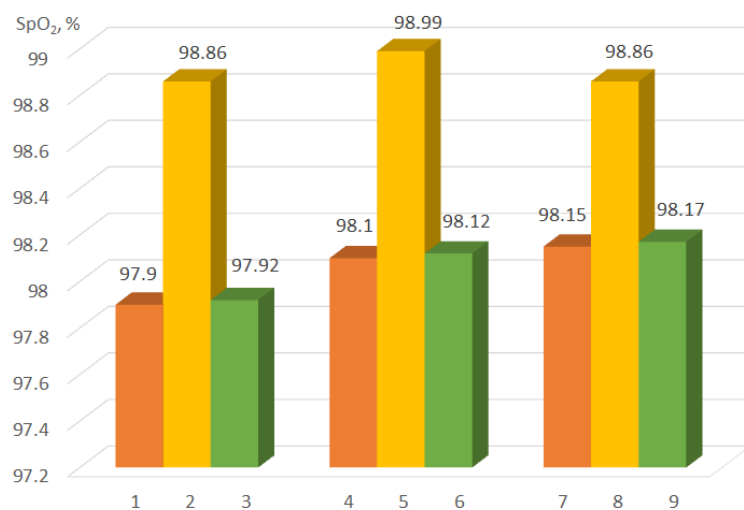


a

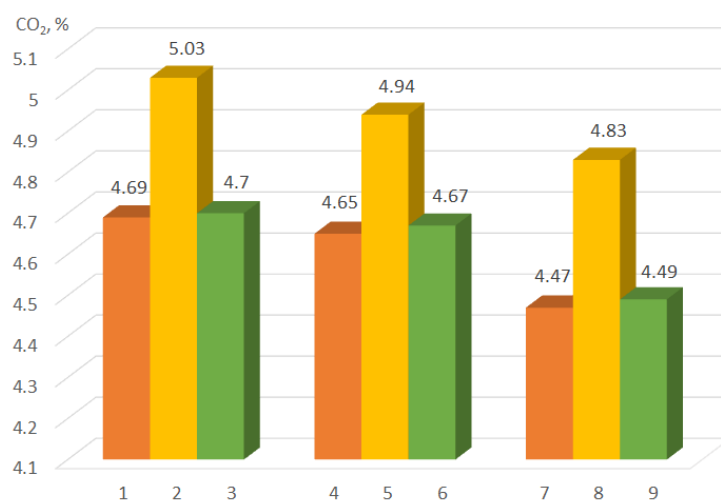


b

Figure 4. Concentration of SpO₂, % in the blood (a) and CO₂, % in the exhaled gas-air mixture (b)
 1 – before intake of probiotic emulsion with WGO inclusion; 2 – after 30 days of intake of probiotic emulsion with WGO inclusion; 3 – the control group; 4 – before intake of probiotic emulsion with CTFO inclusion; 5 – after 30 days of intake of probiotic emulsion with CTFO inclusion; 6 – the control group (during the whole period)



a



b

Figure 5. Concentration of SpO₂, % in the blood (a) and CO₂, % in the exhaled gas-air mixture (b) 1, 4, 7– before intake of probiotic emulsion with WGO inclusion in the 1st, 2nd and 3rd age groups; 2, 5, 8– after 30 days of intake of probiotic emulsion with WGO inclusion in the 1st, 2nd, and 3rd age groups; 3, 6, 9– the control group (during the whole period)

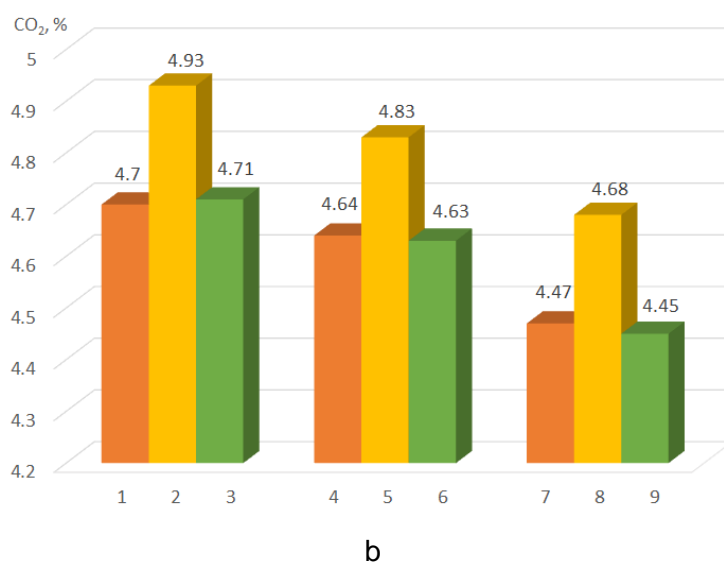
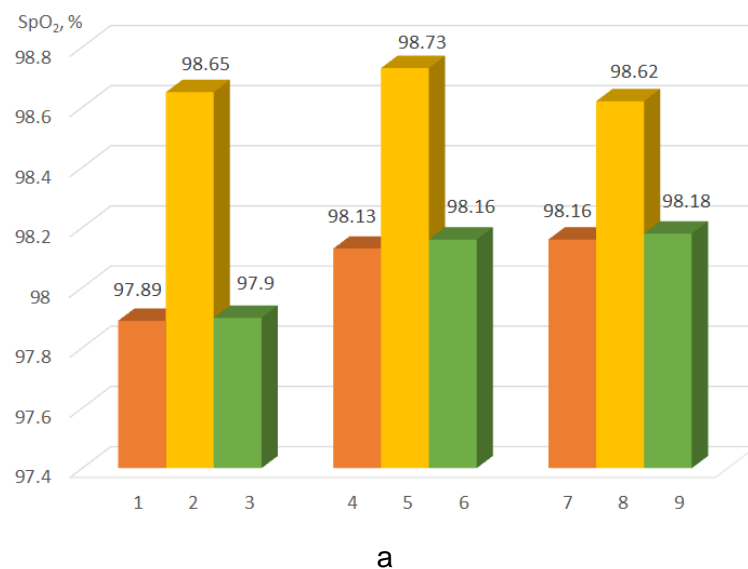


Figure 6. Concentration of SpO_2 , % in the blood (a) and CO_2 , % in the exhaled gas-air mixture (b) 1, 4, 7– before intake of probiotic emulsion with CTFO inclusion in the 1st, 2nd and 3rd age groups; 2, 5, 8– after 30 days of intake of probiotic emulsion with CTFO inclusion in the 1st, 2nd, and 3rd age groups; 3, 6, 9– the control group (during the whole period)

DETERMINAÇÃO AMPEROMÉTRICA DE CÉRIO (III) USANDO SOLUÇÃO DE ÁCIDO 2,7-DINITROZO-1,8-DI-HIDROXINAFTALENO-3,6-DISSULFÔNICO

AMPEROMETRIC DETERMINATION OF CERIUM (III) USING 2,7-DINITROZO-1,8-DIHYDROXYNAPHTHALENE-3,6-DISULFONIC ACID SOLUTION

АМПЕРОМЕТРИЧЕСКОЕ ОПРЕДЕЛЕНИЕ ЦЕРИЯ(III) РАСТВОРОМ 2,7-ДИНИТРОЗО-1,8-ДИГИДРОКСИНАФТАЛИН-3,6-ДИСУЛЬФОКИСЛОТЫ

QUTLIMUROTOVA, Nigora^{1*}; MAHMADOLIEV, Salohiddin²; SMANOVA, Zulayho³; YAKHSHIYEVA, Zuhra⁴; TURSUNKULOV, Zhasur⁵

^{1,2,3,5} National University of Uzbekistan named after Mirzo Ulugbek, Department of Analytical Chemistry, Uzbekistan.

⁴ Jizzakh State Pedagogical Institute named after Abdullah Kadiri, Department of Chemistry Teaching Methods, Uzbekistan.

* Corresponding author
e-mail: n.kutlimurotova@nuu.uz

Received 21 July 2020; received in revised form 27 September 2020; accepted 28 October 2020

RESUMO

O cério e seus compostos são amplamente utilizados na produção de dispositivos eletrônicos e semicondutores, razão pela qual essas substâncias entrarão no meio ambiente com mais frequência no futuro. Há uma necessidade de métodos expressos eficazes que sejam capazes de determinar as quantidades residuais de cério e outros elementos de terras raras com alta precisão para controlar e estudar o possível impacto negativo dos compostos de cério nos ecossistemas. O objetivo deste trabalho de pesquisa foi elaborar um método expresso capaz de produzir resultados precisos e confiáveis sobre o teor de cério em águas residuais na presença de outros elementos de terras raras. A elaboração do método expresso foi realizada com base no método de titulação amperométrica estudando o efeito de várias soluções tampão na determinação de cério. Além disso, o efeito dos íons estrôncio, lutécio, ferro, ítrio, samário, nióbio, hólmio, praseodímio, gadolínio e érbio na precisão de aquisição dos íons cério (III) em amostras de água de processo foi estudado. Com base nos resultados da pesquisa, foi apresentado um método para a determinação amperométrica de cério (III) aplicando ácido 2,7-dinitroso-1,8-di-hidroxinaftaleno-3,6-dissulfônico em um microeletrodo de disco de platina rotativo. O método de análise extração-amperométrica foi proposto para a análise de água de processo. As concentrações ideais de eletrólitos de fundo e misturas de tampão, bem como os valores de voltagem, foram determinados; a constante de estabilidade do complexo foi calculada; foi definido o limite inferior do teor de cério determinado. Nenhuma influência de interferência de íons estranhos na determinação de íons de cério (III) foi observada. O método desenvolvido para a determinação de cério (III) tem um design de hardware mais simples do que o método descrito anteriormente de espectrometria de massa de descarga luminescente de corrente contínua pulsada, mas tem um limite de detecção mais alto.

Palavras-chave: Titulação amperométrica, ácido 2,7-dinitroso-1,8-di-hidroxinaftaleno-3,6-dissulfônico, potencial de meia onda, eletrólitos de fundo, extração.

ABSTRACT

Cerium and its compounds are widely used in the production of electronic devices and semiconductors, which is why these substances will enter the environment more often in the future. There is a need for effective express methods that can determine the trace amounts of cerium and other rare earth elements with high accuracy to control and study the possible negative impact of cerium compounds on the ecosystems. The objective of this research paper was to elaborate on an express method capable of producing accurate and reliable results on the content of cerium in wastewaters in the presence of other rare earth elements. The elaboration of the express method was carried out based on the amperometric titration method studying the effect of various buffer solutions on cerium determination. Moreover, the effect of strontium, lutetium, iron, yttrium, samarium, niobium, holmium, praseodymium, gadolinium, and erbium ions on acquisition accuracy of the cerium (III) ions in samples of process water was studied. The research results presented a method for the amperometric

determination of cerium (III) applying 2,7-dinitroso-1,8-dihydroxynaphthalene-3,6-disulfonic acid on a rotating platinum disk microelectrode. The extraction-ampereometric method of analysis was proposed for the analysis of process water. The optimal concentrations of background electrolytes and buffer mixtures and the voltage values, were determined; the stability constant of the complex was calculated; the lower limit of the determined cerium content was defined. No interfering influence of foreign ions on the determination of cerium (III) ions was observed. The developed method for determining cerium (III) has a simpler hardware design than the previously described method of pulsed direct current glow discharge mass spectrometry but has a higher detection limit.

Keywords: *ampereometric titration, 2,7-dinitroso-1,8-dihydroxynaphthalene-3,6-disulfonic acid, half-wave potential; background electrolytes, extraction.*

АННОТАЦИЯ

Церий и его соединения широко применяются при производстве электронных устройств, и полупроводников, из-за чего данные вещества в дальнейшем будут всё чаще попадать в окружающую среду. Для контроля и изучения возможного негативного влияния соединений церия на экосистемы требуются эффективные экспресс-методы, способные с высокой точностью определять микроколичества церия и других редкоземельных элементов. Цель работы заключалась в разработке экспресс-метода, способного давать надежные и достоверные результаты по содержанию церия в сточных водах в присутствии других редкоземельных элементов. Разработку экспресс-метода проводили на основе метода амперометрического титрования с исследованием влияния различных буферных растворов на определение церия. Кроме того, исследовали влияние ионов стронция, лантана, железа, иттрия, самария, ниобия, гольмия, празеодима, гадолиния и эрбия на точность обнаружения ионов церия(III) в образцах технологических сточных вод. По результатам исследований представлена методика амперометрического определения церия(III) с использованием 2,7-динитрозо-1,8-дигидроксинафталин-3,6-дисульфокислоты на вращающемся платиновом дисковом микроэлектродом. Для анализа технологических сточных вод предложен экстракционно – амперометрический метод анализа. Установлены оптимальные концентрации фоновых электролитов и буферных смесей, а также значения напряжения, рассчитана константа устойчивости комплекса и определена нижняя граница определяемого содержания церия. Мешающее влияние посторонних ионов на определение ионов церия(III) не наблюдалось. Разработанный метод определения церия (III) отличается более простым аппаратным оформлением, чем описанный ранее метод импульсной постоянной токовой масс-спектрометрии с тлеющим разрядом, но обладает более высоким пределом обнаружения.

Ключевые слова: *амперометрическое титрование, 2,7-динитрозо-1,8-дигидроксинафталин-3,6-дисульфокислота, потенциал полуволны, фоновые электролиты, экстракция.*

1. INTRODUCTION:

The chemical industry, medicine, and the electric power industry are currently developing rapidly, increasing the need to develop express methods for determining the micro concentrations of rare and rare earth metals. The development of new technologies for the processing of sludge containing rare earth metals (REM) and materials based on them is especially relevant as global consumption of these elements increases with the growth in the production of electronics and microelectronics (Gwenzi *et al.*, 2018; Romero-Freire *et al.*, 2019). Cerium and its compounds are used to manufacture electronic devices, semiconductors, luminophores, heat-resistant ceramics and optical glasses, catalysts, pigments, batteries, superconductors, and UV filters, neutron accelerators (Zefirov and Knunjan, 1995). Besides, the use of cerium can be mentioned in the corrosion protection of aluminum in marine environment (H. Allachi *et al.*, 2010; M.A.

Osipenko *et al.*, 2019), in batteries (Lianbang Wang *et al.*, 2020), for purification of various gases (Ye Shan *et al.*, 2020), for detecting phosphates in water (Meng Liu *et al.*, 2020). Cerium compounds are used in medicine (S. Rajeshkumar and Poonam Naik, 2018) and to treat cancer (Fatemeh Kadivar *et al.*, 2020).

Thereby, the microgram quantities of cerium will increasingly frequently be released into the environment; and to prevent that, various treatment methods are under development (Ebrahim Allahkarami *et al.*, 2019; James McNeice *et al.*, 2020; A.G. Morozova *et al.*, 2020; Xin-jun Bao *et al.*, 2020). The need for purification is justified by a negative impact from cerium onto the plants, including the food crops (Sanghamitra Majumdar *et al.*, 2014; Sanghamitra Majumdar *et al.*, 2016; Wei Zhang *et al.*, 2016; Anuja Koul *et al.*, 2018; Yu Wu *et al.*, 2019; Jiu-Qiang Xiong *et al.*, 2020; Cyren M. *et al.*, 2020).

One of the main problems is that determining cerium in complex biological objects at environmentally significant concentrations is rather complicated in hardware terms. For example, trace amounts of cerium were previously studied in the shoots of four plant species, including cucumber, tomato, soy, and pumpkin (Dan *et al.*, 2016). In this study, we used the method of single-particle inductively coupled plasma mass spectrometry (SP-ICP-MS), which requires expensive and sophisticated equipment to implement. Together with that, in the study of Dan Y. *et al.* (2016), the size and distribution of particles, the concentration of particles, and dissolved cerium by size are determined. This study is the first one that reports and demonstrates dissolved cerium in the shoots of plant seedlings. The degree of absorption and accumulation by plants depends on the type of plants, which requires further systematic study of these mechanisms, which, in turn, requires a long analysis period (Stowers *et al.*, 2018). In the study of Singh, Hussain, Singh, and Singh (2019), it is shown that the effect of cerium oxide nanoparticles ranging in size from 30 to 75 nm in concentrations of 20 and 100 mg/l on plants may be more favorable for the growth and metabolism of tomato plants than the effect of CeO₂ in equivalent concentrations.

The study of Wang Y., *et al.* (Wang *et al.*, 2019) shows that CeO₂ nanoparticles can activate plant (in this case, rice) antioxidant defense systems to counteract oxidative stress caused by such pollutants as NaCl and CdCl₂. This leads us to the conclusion that, despite the ambiguous effect of cerium on plants, control over the distribution of cerium in natural objects and the development of methods for its detection are relevant nowadays.

Studies are being conducted worldwide based on the use of specific analytical reagents for the development of sensitive and selective methods for the determination of trace amounts of rare and rare earth metals in ores, sludges, and technological wastes. There is a method that allows determining trace amount of cerium by the potentiometric method with Schiff base N,N bis-(Furan-2-ylmethylene)-1,4-phenylene diamine (BFMPDA) (Moustafa and Abd-Allah, 2011a) and with 1,4-bis(2'-carboxyphenylazomethine)phenylene (Moustafa and Abd-Allah, 2011b) in dioxane medium and also to calculate the stability constants of the resulting complexes.

There is also a spectrofluorimetry method to study the content of cerium with N-acetyl-4-

aminophenol (paracetamol) at the ultra-trace level (Jamaluddin, Prosenjit, and Tazul, 2019). This method is based on the oxidation of paracetamol in the presence of a slightly acidic (0.05 – 0.15M H₂SO₄) water solution with fast oxidizing agent cerium (IV) for direct spectrofluorimetric determination of paracetamol. As well there is a method for determining cerium (III) and manganese (II) by the spectrophotometric method using iodine-based on Dushman reactions (Ungureanu, Duca, Humelnicu, and Bourceanu, 2018). Reactions are based on redox processes; the solution potential depends on the concentration of the determined element.

The extraction method using extragent DX-510A of β -diketones class which was studied by the electroflotation method, was previously developed for extraction and separation of cerium (III), (IV) and copper (II) ions from the water solutions (Meduntseva *et al.*, 2015; Volkova, Gaydukova, Brodskiy, and Kolesnikov, 2015). The maximum degree of extraction of cerium (III) ions is achieved by separating cerium (III) from lanthanum (III) in an extraction system using nitric acid solutions at pH 4.0, and lanthanum (III) at pH 7.0 (Gayfullina *et al.*, 2015). To increase extraction, the extraction process is carried out several times.

The method of pulsed direct current glow discharge mass spectrometry is described in the literature. Using this method (PGD-TOF-MS) 24 elements (As, B, Ce, Co, Dy, Fe, K, La, Lu, Mg, Mn, Na, Nb, Nd, P, Pr, Rb, S, Sb, Si, Sm, Th, Ti, and U) in ore samples were studied (Ganeev *et al.*, 2019; Jaison, Kumar, Telmore, and Aggarwal, 2009; Jaison *et al.*, 2009). The samples were prepared by pressing powdered samples into aluminum tablets with 10 mm diameter to determine cerium. The detection limits of the developed method were within the range $2-4 \cdot 10^{-6}$ mass % depending on the element. Some elements prevent the determination of cerium.

The literature data shows that the development of a technique with high sensitivity, accuracy, and a wide range of determined concentrations is required. Thus, the amperometric method stands out by simplicity of hardware and methodological implementation, comparative rapidity of analysis (Shaydarova, Chelnokova, Ilina, Gedmina, and Budnikov, 2017).

This study aimed to develop a new express and highly sensitive amperometric methods for determining the mass concentrations of cerium (III) with a synthesized reagent 2,7-dinitrozo-1,8-dihydroxynaphthalene-3,6-disulfonic acid in

objects various in nature at the level of micro quantities with improved metrological characteristics (accuracy, reproducibility, expansion of the range of determined contents, selectivity).

2. MATERIALS AND METHODS:

The influence of the potential supplied to the indicator electrodes (0.25-1.0 V) on the shape of the curves, and the results of amperometric titration (AT) of cerium (III) using 2,7-dinitrozo-1,8-dihydroxynaphthalene-3,6-disulfonic acid solution was examined.

As a rule, the concentration of reagents must significantly exceed the number of metals to be determined. The titrant was added in small portions 30 μ l with a precision piston microburette, so dilution of the test solution could be neglected (Lurye, 2012). Standard cerium (III) solutions were made by dissolving precise salt samples $\text{CeCl}_3 \cdot 6\text{H}_2\text{O}$ (99% of basic substance) by known methods: 0,35461 grams of the $\text{CeCl}_3 \cdot 6\text{H}_2\text{O}$ salt samples were weighed up using the analytic scales, and brought up to the mark by bidistilled water in the 1 l measuring flask. The concentration of the resulting solution amounted to 0,001 M or 141 μ g/ml of cerium (Geyrovskiy, Kuta, Geyrovskiy, and Kuta, 1965).

The solutions of 2,7-dinitrozo-1,8-dihydroxynaphthalene-3,6-disulfonic acid were made by dissolving the sample 0,1 g in bidistilled water 100 ml with a concentration equal to 0.1%. Solutions of buffer mixtures and metals were prepared from the relevant salts and acids. The universal buffer mixture was prepared in the 1 l measuring flask from phosphoric, acetic and boric acids, with 0,04 M of each by the procedure as follows: 2,33 ml of acetic acid of 1,05 g/ml density, 2,48 g of boric acid and 2,45 ml of phosphoric acid of 1,755 g/ml density was poured into the measuring flask, and was adjusted upto the mark by bidistilled water. pH of the universal buffer mixture amounted to 1,81.

The solutions of background electrolytes as below were also used in the study: 0,2 M solution of potassium phthalic acid (40,846 g of salt was dissolved in a 1 l measuring flask, with pH 2,20; (content of the main substance being 99,8 %)), 0,1 M solution of potassium citrate (21,014 g of citric acid monohydrate was added to 200 ml of 1 n. potassium hydroxide solution and brought upto the mark in the 1 l measuring flask (citric acid monohydrate, basic substance content being 99,5%)); 0,1 n. of aminoacetic acid solution (7,507

g of aminoacetic acid was added to 5,85 g sodium chloride and brought up to the mark in the 1 l measuring flask (aminoacetic acid, content of the main solution being 98,5%)).

The bidistilled water obtained using the distiller Heal Force CR-RO30 (China) was used for the experiment. The electrical conductivity of bidistilled water was 0.475 mSm/m. The piston microburette of 2.0 ml allowing to dose the titrant with an accuracy up to 0.001 ml was used for titration with 2,7-dinitrozo-1,8-dihydroxynaphthalene-3,6-disulfonic acid solution. The manual ammeter "Expert – 001 A" pH-meter pH/mV/TEMP Meter P25 EcoMet (Korea) was used for AT.

Britton-Robinson universal buffer mixture was prepared using Lurye method (Lurye, 2012): a solution of the mixture of acetic, boric, and phosphoric acids (0.04M in respect of each) was prepared in a 1 L measuring flask. Then it was brought to the mark by bidistilled water. The remaining buffer solutions were prepared according to known methods. The solutions of potassium phthalate (99.8% of basic substance), potassium citrate (potassium citrate monohydrate, 99.5% of basic substance), and aminoacetic acid (98.5% of basic substance) were used in the study as background electrolytes.

To determine the effect of other ions on the determination of cerium (III) ions, the substances shown in Table 1 were used. For bringing ions in, 0.01 M salt solutions were prepared. A sample of the required mass was weighed on an analytical balance and dissolved in a 250 ml measuring flask. The weighing error was $\pm 0,00001$ g. All the substances used were produced by Merck company (Germany). Technical waters used in the study were previously analyzed by the atomic absorption method using an AA spectrometer Shimadzu 6200.

Method for determination of cerium was: 2 ml of a standard solution of cerium was added to a measuring cup, 1 ml of a Britton-Robinson universal buffer mixture with pH 3.55 was added, and distilled water was added to reach 10 ml of volume. Then it was titrated with a 0.1 % solution of 2,7-dinitrozo-1,8-dihydroxynaphthalene-3,6-disulfonic acid and the cerium concentration was determined by the equivalence point.

For statistical estimation of the accuracy of the developed method for cerium (III) determination using 2,7-dinitrozo-1,8-dihydroxynaphthalene-3,6-disulfonic acid solution with two platinum indicator electrodes, AT of its various amounts was carried out with multiple (at

least 4 times) repetition of each determination under the following optimal conditions: 2.0 ml of 0.04 M universal buffer solution (pH 3.55), the potential difference $\Delta E = 0.75$ V, the total volume of the examined solution was 10 ml.

2.1. Influence of voltage

The development of AT methods should start with taking polarogram of the corresponding ion. The polarogram is taken on the electrode which is supposed to be titrated in the future, and in the same medium. The potential of the indicator electrode should be set more negative (on 0.1-0.3). The composition and acidity of the examined solution at a selected potential value can lead to the release of impurities present in the solution or hydrogen recovery. The correctness of the choice of potential can be easily checked as follows: a solution which should serve as the background for the proposed titration is placed in the titration cup; a solution containing the ion which should give an electrode reaction is placed in the burette. The selected potential is set on the indicator electrode. The polarogram is usually taken on the background on which the titration will take place. Amperometric indication of the titration endpoint (TEP) of ions of various metals with two indicator electrodes must be carried out at a voltage of 0.30-1.10 V. The current-voltage curves of 2,7-dinitrozo-1,8-dihydroxynaphthalene-3,6-disulfonic acid on a platinum disk microanode in the presence of various background electrolytes in an aqueous solution indicate the optimal voltage for the complex formation of cerium ions should be (ΔE) 0.75 V (Spiridonov, Lopatkin, Spiridonov, and Lopatkin, 1970).

2.2. Logarithmic analysis

The number of electrons emitted during cerium electrooxidation was determined from the slope of the line chart showing dependence on E when studying the mechanism of the electrode complex formation process of cerium with 2,7-dinitrozo-1,8-dihydroxynaphthalene-3,6-disulfonic acid. The half-wave potential of the obtained complex compounds was determined at different concentrations of the reagent in the optimal value of the buffer mixtures by adding surfactants, and the values of current-voltage curves of the ABC polarographs (made in Russia) and the three-electrode cell were taken.

2.3. Statistical processing

Statistical processing of the obtained results was carried out by calculating the standard

deviation and relative standard deviation. The standard deviation was determined by the equation:

$$S = \sqrt{\frac{\sum_{i=1}^n (x_i - \bar{x})^2}{n - 1}} \quad (1)$$

Where S is standard deviation,

\bar{x} – arithmetic mean of n measurements

x_i – measurement result

n – number of measurements

The relative standard deviation was determined by the equation:

$$S_r = \frac{S}{\bar{x}} \quad (2)$$

where S_r is relative standard deviation.

3. RESULTS AND DISCUSSION:

The results obtained from cerium (III) AT using 2,7-dinitrozo-1,8-dihydroxynaphthalene-3,6-disulfonic acid solution with various buffers are shown in Figure 1. For a statistical assessment of the method's accuracy, amperometric titration of various amounts of cerium was conducted under optimized conditions. The titration results are shown in Table 2. The developed method was also tested by the analysis of process water. Extraction with TBF was used to separate cerium from other metals (Bukin and Igumnov, 2002; Simonova, 2019). The results of cerium (III) extraction-amperometric determination using 2,7-dinitrozo-1,8-dihydroxynaphthalene-3,6-disulfonic acid solution with the presence of foreign ions are shown in Table 3.

When developing AT techniques with one or two solid indicator electrodes in any (aqueous, non-aqueous and mixed) medium, it is necessary to know the peculiarities of the voltammetric behavior in it on the corresponding electrode of not only the detected ions, but also the reagent used and its metal complexes. This is necessary in order to correctly select the optimal titration conditions and the potential difference applied to the indicator electrodes. $E_{1/2}$ becomes more negative with increasing pH for electrode recovery processes involving hydrogen ions in the potential-determining stage. Conversely, the effect of pH on $E_{1/2}$ unambiguously indicates the participation of hydrogen ions in the potential-determining stage.

In the case of reversible processes, the hydrogen concentration is found by the Nernst equation. Kinks are often observed on the curves of the dependence of $E_{1/2}$ on pH. If the recovered form is protonated, then the incline of the almost rectilinear section after the kink is greater than before it with an increase in pH, and the pH of the kink corresponds to the pK_a of the recovered form. If, on the contrary, the oxidized form is protonated, the $E_{1/2}$ – pH curve consists of line segments, the incline of which decreases with increasing pH, and the kink corresponds to the pK_a of the oxidized form. If both the oxidized and reduced forms are able to protonate or if one or both forms are polybasic acids (bases), then the dependence of $E_{1/2}$ on pH is a polyline, each kink of which corresponds to one of the pK_a values. In a wide range of pH changes, the dependence of $E_{1/2}$ on pH is expressed by an S-shaped curve: in a strongly acidic medium, $E_{1/2}$ ceases to depend on pH, since the entire depolarizer is in protonated form. In an alkaline medium, $E_{1/2}$ usually does not depend on pH; in this case, the recovery process takes place with the participation of only one proton donor – water. The vast majority of the electrochemical transformations of organic compounds on a platinum electrode in protogenic media involve adding or removing protons. Most often, the source of protons is the hydroxonium ions present in the solution, but any other proton donors can function as such a source. Proton transfer can take place either before electron transfer, or after it. Before the actual electrochemical stage, the addition of protons affects the $E_{1/2}$ value of both a reversible and an irreversible process.

Electrooxidation of 2,7-dinitrozo-1,8-dihydroxynaphthalene-3,6-disulfonic acid in different media is studied while determining metals in AT. Half-wave potential of 2,7-dinitrozo-1,8-dihydroxynaphthalene-3,6-disulfonic acid in acidic medium equals ($E_{1/2}$) 0.72 V. Chemical mechanism of reagent electrooxidation is shown in Figure 2.

Nernst equation shows that the half-wave potential of the solution is directly proportional to the concentration of the titrant being determined. Therefore, a straight line is observed up to the equivalence point during amperometric titration as a result of complex formation of the studied metal with an organic reagent, and a curve grows after the equivalence point, confirming the electrooxidation of the organic reagent.

The background electrolyte affects the complex formation reaction; therefore, we studied the effect of the nature and concentration of

background electrolytes and buffer mixtures in this work. We studied the effect of the nature and concentration of background electrolyte and buffer mixture on the results of cerium (III) AT using 2,7-dinitrozo-1,8-dihydroxynaphthalene-3,6-disulfonic acid solution. Results of titration using universal buffers with pH 1.12 showed that cerium (III) is titrated well enough in strongly acidic environments (pH 1.18-4.2), and in neutral and basic ones it forms low-strength complex compounds with the used reagent and, accordingly, is not titrated well enough (Figure 1).

Based on the polarogram curves, the half-wave potential and the dependence of the logarithmic value of the reagent were found, the composition of the complex was found, and the conclusion was made about the complex formation of cerium with a solution of 2,7-dinitrozo-1,8-dihydroxynaphthalene-3,6-disulfonic acid. The obtained data is shown in Table 4 and in Figure 3.

Figure 3 shows that complexes of Me:Reagent=2:1 compound are obtained by AT of cerium (III) ions with 2,7-dinitrozo-1,8-dihydroxynaphthalene-3,6-disulfonic acid. The graph showing their dependence is given in Figure 4. The dependence of the half-wave potential on the concentration of the complexing reagent can be calculated by the stability constant of the complex and its compound by the Lingane method (Lurye, 2012):

$$(E_{1/2})_{comp} - (E_{1/2})_{reagent} = \frac{RT}{nF} \ln \sqrt{\frac{D}{D^*}} - \frac{RT}{nF} \ln K - \frac{RT}{nF} \ln [X^{m-}]^p \quad (3)$$

The calculated value of the complex stability constant equals $1.6 \cdot 10^4$.

The mechanism of cerium and reagent complex formation shows that there is the complex and after the equivalence point up to the equivalence point 2,7-dinitrozo-1,8-dihydroxynaphthalene-3,6-disulfonic acid electrooxidizes.

3.1. Statistical evaluation of the accuracy

Table 2 and Figure 5 show different amounts of cerium (III) with 2,7-dinitrozo-1,8-dihydroxynaphthalene-3,6-disulfonic acid solution titration, processed following the rules and procedures known in the literature of mathematical statistics (Kutlimurotova, Mahmadiyev, and Smanova, 2018). As Table 3 and Figure 5 show,

the found amounts of Ce (III) correspond to its introduced contents and do not go beyond the confidence interval. This once again confirms the high accuracy of the developed amperometric method for determining cerium (III) with a relative standard deviation (S_r) not exceeding 0.014 and a lower limit of the determined contents equal to 0.7 mcg/ml. Complex characteristics are shown in Table 5.

3.2. Process water analysis

Cerium is found in process water together with scandium, yttrium, uranium, thorium, and lanthanides. As mentioned above, cerium was separated from other metals by extraction with TBF. Due to the large separation coefficient (> 1000), extraction of cerium (IV) can be single. The best results in the separation of cerium from REE are shown with extraction of 40% TBF in kerosene from 4M HNO_3 . The separation of REE into groups using TBF can be conducted at a relatively low acidity of the solution (7 - 9M HNO_3), at which the separation and distribution coefficients are quite high. It is possible to divide the REE of the yttrium subgroup into separate groups and individual elements from more acidic solutions (12 – 13M HNO_3). The results are shown in Table 3. In the extraction-amperometric determination of cerium (III), the interfering effect of samarium, holmium, lutetium, and neodymium was not observed.

3.3. Comparison with the methods used

The detection limit of the proposed method is $70 \cdot 10^{-6}$ mass %, which is inferior to the method of pulsed direct current glow discharge mass spectrometry with a detection limit of $2-4 \cdot 10^{-6}$ mass % depending on the determined REE (Ganeev *et al.*, 2019; Jaison *et al.*, 2009; Kumar *et al.*, 2013). However, unlike the latter method, the method of amperometric titration requires less hardware implementation and allows us to determine the content of cerium (III) ions in the process water.

4. CONCLUSIONS:

The developed method for the determination of cerium (III) can be used in metallurgical and chemical production, as well as for environmental monitoring of industrial facilities. The method allows determining the cerium (III) content in samples of ores and alloys, controlling the concentration of cerium in process water during production, and wastewater before and after treatment. The simple hardware

implementation of the method and the relative simplicity of the analysis do not require serious retraining of laboratory personnel when introducing this method to industrial enterprises.

5. REFERENCES:

1. Bukin, V. I., and Igumnov, M. S. (2002). *Pererabotka proizvodstvennykh othodov i vtorichnykh syirevykh resursov, soderzhaschikh redki, blagorodnykh i tsvetnyye metally* [Processing of industrial waste and secondary raw materials containing rare, noble and non-ferrous metals]. Moscow: Business Capital.
2. Dan, Y., Ma, X., Zhang, W., Liu, K., Stephan, C., and Shi, H. (2016). Single particle ICP-MS method development for the determination of plant uptake and accumulation of CeO_2 nanoparticles. *Analytical and Bioanalytical Chemistry*, 408(19), 5157-5167. <https://doi.org/10.1007/s00216-016-9565-1>
3. Ganeev, A., Titova, A., Korotetski, B., Gubal, A., Solovyev, N., Vyacheslavov, A., ... Sillanpää, M. (2019). Direct Quantification of Major and Trace Elements in Geological Samples by Time-of-Flight Mass Spectrometry with a Pulsed Glow Discharge. *Analytical Letters*, 52(4), 671-684. <https://doi.org/10.1080/00032719.2018.1485025>
4. Gayfullina, D. I., Kondrateva, E. S., Gubin, A. F., Kolesnikov, V. A., Gayfullina, D. I., Kondrateva, E. S., ... Kolesnikov, V. A. (2015). Ekstraktsiya ionov Ce (III) i La (III) iz azotnokislykh rastvorov β -diketonov DH-510A [Extraction of Ce (III) and La (III) ions from nitric acid solutions with β -diketone DX-510A]. *Advances in Chemistry and Chemical Technology Magazine*, 29(3), 26-27.
5. Geyrovskiy, Y., Kuta, Y., Geyrovskiy, Y., and Kuta, Y. (1965). *Osnovy poliarografii* [The basics of polarography]. Moscow.
6. Gwenzi, W., Mangori, L., Danha, C., Chaukura, N., Dunjana, N., and Sanganyado, E. (2018). Sources, behaviour, and environmental and human health risks of high-technology rare earth elements as emerging contaminants. *Science of the Total Environment*, 636, 299-313. <https://doi.org/10.1016/j.scitotenv.2018.04.235>

7. Jaison, P. G., Kumar, P., Telmore, V. M., and Aggarwal, S. K. (2009). Comparative Study of Ion Interaction Reagents for the Separation of Lanthanides by Reversed-Phase High Performance Liquid Chromatography (RP-HPLC). *Journal of Liquid Chromatography and Related Technologies*, 32(15), 2146–2163. <https://doi.org/10.1080/10826070903163230>
8. Jamaluddin, A. M., Prosenjit, R. M., and Tazul, I. A. (2019). A Highly Selective and Sensitive Spectrofluorimetric Method for the Determination of N-acetyl-4-aminophenol at Nano-trace Levels in Pharmaceuticals and Biological Fluids Using Cerium (IV) | Pakistan Journal of Analytical and Environmental Chemistry. *Pakistan Journal of Analytical and Environmental Chemistry*, 20(1), 17–31. Retrieved from <http://www.pjaec.pk/index.php/pjaec/article/view/535>
9. Kumar, P., Jaison, P. G., Rao, D. R. M., Telmore, V. M., Sarkar, A., and Aggarwal, S. K. (2013). Determination of lanthanides and yttrium in high purity dysprosium by rp-hplc using α -hydroxyisobutyric acid as an eluent. *Journal of Liquid Chromatography and Related Technologies*, 36(11), 1513–1527. <https://doi.org/10.1080/10826076.2012.692148>
10. Kutlimurotova, N. H., Mahmadiyev, S. B., and Smanova, Z. A. (2018). Konduktometricheskoe titrovaniye tseriya rastvorom 2,7-Dinitrozo-1,8-digidroksinaftalin-3,6-disulfokisloty [Conductivity titration of cerium with a solution of 2,7-Dinitrozo-1,8-dihydroxynaphthalene-3,6-disulfonic acid]. *Bulletin of SamSU*, 3, 118–122.
11. Lurye, Yu. Yu. (2012). *Spravochnik po analiticheskoy himii [Handbook of Analytical Chemistry]*. Moscow: Book on Request.
12. Meduntseva, E. V., Gaydukova, A. M., Kolesnikov, V. A., Meduntseva, E. V., Gaydukova, A. M., and Kolesnikov, V. A. (2015). Razdelenie ionov tseriya (III) i tseriya (IV) elektroflotatsionnyim metodom [Separation of cerium (III) and cerium (IV) ions by the electroflotation method]. *Advances in Chemistry and Chemical Technology Magazine*, 29(3), 21–22.
13. Moustafa, M. H., and Abd-Allah, M. T. (2011a). Synthesis and Characterization of Some New Coordination Polymers of Schiff Base Derived from Furfural. *Egyptian Journal of Chemistry*, 54(3), 333–347. <https://doi.org/10.21608/ejchem.2011.1399>
14. Moustafa, M. H., and Abd-Allah, M. T. (2011b). Synthesis, characterization and stability of the polymeric complexes of zinc (II), cadmium (II) and cerium (III) with 1,4-bis (2'-carboxyphenyl)-zomethine) phenylene. *Egyptian Journal of Chemistry*, 54(5), 533–548.
15. Romero-Freire, Turlin, André-Mayer, Pelletier, Cayer, and Giamberini. (2019). Biogeochemical Cycle of Lanthanides in a Light Rare Earth Element-Enriched Geological Area (Quebec, Canada). *Minerals*, 9(10), 573. <https://doi.org/10.3390/min9100573>
16. Shaydarova, L. G., Chelnokova, I. A., Iliina, M. A., Gedmina, A. V., and Budnikov, G. K. (2017). Amperometricheskoe detektirovaniye gidroksipurinov na elektrode, modifitsirovannom kompozitom na osnove smeshanovaleantnykh oksidov ruteniya i kobalta, v usloviyakh protochno-inzhetsionnogo analiza [Amperometric detection of hydroxypurines on an electrode modified by a composite based on mixed valent ruthenium and cobalt oxides under flow-injection analysis]. *Journal of Analytical Chemistry*, 72(1), 91–96.
17. Simonova, I. (2019). Learning English Grammar in the Smart Learning Environment. In V. L. Uskov, R. J. Howlett, L. C. Jain, and L. Vlasic (Eds.), *Smart Education and e-Learning 2018* (pp. 142–150). https://doi.org/10.1007/978-3-319-92363-5_13
18. Singh, A., Hussain, I., Singh, N. B., and Singh, H. (2019). Uptake, translocation and impact of green synthesized nanoceria on growth and antioxidant enzymes activity of Solanum lycopersicum L. *Ecotoxicology and Environmental Safety*, 182, 109410. <https://doi.org/10.1016/j.ecoenv.2019.109410>
19. Spiridonov, V. P., Lopatkin, A. A., Spiridonov, V. P., and Lopatkin, A. A. (1970). *Matematicheskaya obrabotka fiziko-himicheskikh dannykh [Mathematical processing of physicochemical data]*. Moscow: MSU.

20. Stowers, C., King, M., Rossi, L., Zhang, W., Arya, A., and Ma, X. (2018). Initial Sterilization of Soil Affected Interactions of Cerium Oxide Nanoparticles and Soybean Seedlings (*Glycine max* (L.) Merr.) in a Greenhouse Study. *ACS Sustainable Chemistry and Engineering*, 6(8), 10307–10314. <https://doi.org/10.1021/acssuschemeng.8b01654>
21. Ungureanu, I., Duca, G., Humelnicu, I., and Bourceanu, G. (2018). The Possibility of Ce³⁺ and Mn²⁺ Complex Ions Formation With Iodine Species in a Dushman Reaction. *Chemistry Journal of Moldova*, 13(1), 103-110. <https://doi.org/10.19261/cjm.2017.464>
22. Volkova, V. V., Gaydukova, A. M., Brodskiy, V. A., and Kolesnikov, V. A. (2015). Elektroflotatsionnoe izvlechenie i razdelenie ionov tseriya (III, IV) i medi (II) iz vodnyih rastvorov [Electroflotation extraction and separation of cerium (III, IV) and copper (II) ions from aqueous solutions]. *Advances in Chemistry and Chemical Technology Magazine*, 29(3), 19–20.
23. Wang, Y., Wang, L., Ma, C., Wang, K., Hao, Y., Chen, Q., ... Rui, Y. (2019). Effects of cerium oxide on rice seedlings as affected by co-exposure of cadmium and salt. *Environmental Pollution*, 252, 1087-1096. <https://doi.org/10.1016/j.envpol.2019.06.007>
24. Zefirov, N. S., and Knunjanc, I. L. (Eds.). (1995). *Khimicheskaya entsiklopediya: [Chemical Encyclopedia]*, Vol. 4.. Moscow: Great Soviet Encyclopedia.
25. James McNeice, Rina Kim, Ahmad Ghahrema Oxidative precipitation of cerium in acidic chloride solutions: Part II – oxidation in a mixed REE system. *Hydrometallurgy*. Volume 194, June 2020, <https://doi.org/10.1016/j.hydromet.2020.105331>
26. A.G. Morozova, T.M. Lonzingier, V.A. Skotnikov, J.N. Sahu, G.G. Mikhailov, J.L. Schenk, A. Bhattacharyya, Y. Kapelyushin Utilization of metallurgical slag with presence of novel CaO-MgO-SiO₂-Al₂O₃ as a composite sorbent for wastewater treatment contaminated by cerium. *Journal of Cleaner Production*. Volume 255, 10 May 2020 <https://doi.org/10.1016/j.jclepro.2020.120286>
27. Ebrahim Allahkarami, Bahram Rezai. Removal of cerium from different aqueous solutions using different adsorbents: A review. *Process Safety and Environmental Protection*. Volume 124, April 2019, Pages 345-362 <https://doi.org/10.1016/j.psep.2019.03.002>
28. H. Allachi, F. Chaouket, K. Draoui. Protection against corrosion in marine environments of AA6060 aluminium alloy by cerium chlorides. *Journal of Alloys and Compounds*. Volume 491, Issues 1–2, 18 February 2010, Pages 223-229. <https://doi.org/10.1016/j.jallcom.2009.11.042>
29. Jiu-Qiang Xiong, Shaoguo Ru, Qing Zhang, Min Jang, Mayur B. Kurade, Sang-Hyoun Kim, Byong-Hun Jeon. Insights into the effect of cerium oxide nanoparticle on microalgal degradation of sulfonamides. *Bioresource Technology*. Volume 309, August 2020. <https://doi.org/10.1016/j.biortech.2020.123452>
30. Meng Liu, Shengjian Li, Nian Tang, Yating Wang, Xiangjun Yang, Shixiong Wang. Highly efficient capture of phosphate from water via cerium-doped metal-organic frameworks. *Journal of Cleaner Production*. Volume 265, 20 August 2020. <https://doi.org/10.1016/j.jclepro.2020.121782>
31. Wei Zhang, Zhichao Pu, Songyan Du, Yongsheng Chen, Lin Jiang. Fate of engineered cerium oxide nanoparticles in an aquatic environment and their toxicity toward 14 ciliated protist species. *Environmental Pollution*. Volume 212, May 2016, Pages 584-591. <https://doi.org/10.1016/j.envpol.2016.03.011>
32. M.A. Osipenko, V.I. Yanushevskii, D.S. Kharitonov, I.V. Makarova, I.I. Kurilo. Corrosion Inhibition of AD31 Alloy by Cerium Nitrate (III) and Sodium Metavanadate. *Materials Today: Proceedings*. Volume 6, Part 2, 2019, Pages 164-170. <https://doi.org/10.1016/j.matpr.2018.10.090>
33. Fatemeh Kadivar, Gholamhassan Haddadi, Mohammad Amin Mosleh-

- Shirazi, Fatemeh Khajeh, Alireza Tavasoli. Protection effect of cerium oxide nanoparticles against radiation-induced acute lung injuries in rats. *Reports of Practical Oncology & Radiotherapy*. Volume 25, Issue 2, March–April 2020, Pages 206–211. <https://doi.org/10.1016/j.rpor.2019.12.023>
34. Xin-jun Bao, Ze-jie Zhang, Tian-zhong Luo, Xi-tao Wu, Zhen-shan Xie, Shi-kun Lan, Sheng-zhong Xie, De-bi Zhou. Conversion of cerium and lanthanum from rare earth polishing powder wastes to CeO₂ and La_{0.6}Ca_{0.4}CoO₃. *Hydrometallurgy*. Volume 193, May 2020. <https://doi.org/10.1016/j.hydromet.2020.105317>
 35. Yu Wu, Xiaoqiao Tang, Wenxiang Yang, Jun Fan, Lijun Tang, Chunhong Wang, Zhou Yu, Xu-Dong Jia, Bolin Fan. Subchronic toxicity of cerium nitrate by 90-day oral exposure in wistar rats. *Regulatory Toxicology and Pharmacology*. Volume 108, November 2019. <https://doi.org/10.1016/j.yrtph.2019.104474>
 36. Lianbang Wang, Siyuan Chen, Jinpei Hei, Rui Gao, Liu Liu, Liwei Su, Gaoran Li, Zhongwei Chen. Ultrafine, high-loading and oxygen-deficient cerium oxide embedded on mesoporous carbon nanosheets for superior lithium–oxygen batteries. *Nano Energy*. Volume 71, May 2020. <https://doi.org/10.1016/j.nanoen.2020.104570>
 37. Sanghamitra Majumdar, Jose R. Peralta-Videa, Jesica Trujillo-Reyes, Youping Sun, Ana C. Barrios, Genhua Niu, Juan P. Flores-Margez, Jorge L. Gardea-Torresdey. Soil organic matter influences cerium translocation and physiological processes in kidney bean plants exposed to cerium oxide nanoparticles. *Science of The Total Environment*. Volumes 569–570, 1 November 2016, Pages 201–211. <https://doi.org/10.1016/j.scitotenv.2016.06.087>
 38. Sanghamitra Majumdar, Jose R. Peralta-Videa, Susmita Bandyopadhyay, Hiram Castillo-Michel, Jose-Angel Hernandez-Viezcas, Shivendra Sahi, Jorge L. Gardea-Torresdey. Exposure of cerium oxide nanoparticles to kidney bean shows disturbance in the plant defense mechanisms. *Journal of Hazardous Materials*. Volume 278, 15 August 2014, Pages 279–287. <https://doi.org/10.1016/j.jhazmat.2014.06.009>
 39. Ye Shan, Yangxian Liu, Ying Li, Wei Yang. A review on application of cerium-based oxides in gaseous pollutant purification. *Separation and Purification Technology*. Volume 250, 1 November 2020. <https://doi.org/10.1016/j.seppur.2020.117181>
 40. Anuja Koul, Anil Kumar, Vivek K. Singh, Durgesh K. Tripathi, Sharada Mallubhotla. Chapter 8 Exploring Plant-Mediated Copper, Iron, Titanium, and Cerium Oxide Nanoparticles and Their Impacts. *Nanomaterials in Plants, Algae, and Microorganisms Concepts and Controversies: Volume 1*, 2018, Pages 175–194. <https://doi.org/10.1016/B978-0-12-811487-2.00008-6>
 41. S. Rajeshkumar, Poonam Naik. Synthesis and biomedical applications of Cerium oxide nanoparticles – A Review. *Biotechnology Reports*. Volume 17, March 2018, Pages 1–5. <https://doi.org/10.1016/j.btre.2017.11.008>
 42. Cyren M. Rico, Oluwasegun M. Abolade, Dane Wagner, Brett Lottes, Justin Rodriguez, Richard Biagioni, Christian P. Andersen. Wheat exposure to cerium oxide nanoparticles over three generations reveals transmissible changes in nutrition, biochemical pools, and response to soil N. *Journal of Hazardous Materials*. Volume 384, 15 February 2020. <https://doi.org/10.1016/j.jhazmat.2019.121364>

Table 1. Substances for studying the influence of other ions.

Substance	The content of the main component/purity qualification
ScCl ₃	99%
FeCl ₃	98%
YCl ₃ ·6H ₂ O	99%
NdCl ₃	99.99%
HoCl ₃	99%
PrCl ₃	99%
ErCl ₃ ·6H ₂ O	99.999%
Lu(NO ₃) ₃ ·6H ₂ O	99.9%
Sm(NO ₃) ₃ ·6H ₂ O	99.99%
Gd(NO ₃) ₃ ·6H ₂ O	99.9%

Table 2. Results of amperometric titration of different amounts of cerium (III) with 2,7-dinitrozo-1,8-dihydroxynaphthalene-3,6-disulfonic acid solution under optimized conditions

No.	Added Ce(III), µg	Found Ce(III), µg ($\bar{X} \pm \Delta X$; P=0,95)	S	S _r
1	1.40	1.49±0.02	0.021	0.014
2	14.00	14.22±0.05	0.043	0.003
3	28.00	28.38±0.06	0.052	0.002
4	42.00	42.31±0.06	0.048	0.001
5	56.00	56.36±0.08	0.069	0.001

Note: S – standard deviation, S_r – relative standard deviation

Table 3. Results of 14 mcg of cerium (III) extraction-conductometric determination ($D=0.8$) ($P = 0.95$; $n=5$)

Extractant	Titrant	Foreign cation [x]	Added [x], μg	$\frac{[x]}{[Ce]}$	Found Ce(III), μg ($\bar{X} \pm \Delta X$)	S	Sr
40 % TBF kerosene 4M HNO_3	2,7-dinitrozo-1,8-dihydroxy naphthalene-3,6-disulfonic acid	Sc(III)	2.5	0.17	14.12 \pm 0.19	0.17	0.012
		Lu(III)	3.8	0.27	14.06 \pm 0.16	0.14	0.010
		Fe(III)	5.7	0.40	14.08 \pm 0.22	0.19	0.013
		Y(III)	6.8	0.48	14.07 \pm 0.14	0.12	0.008
		Sm(III)	8.2	0.58	14.04 \pm 0.08	0.07	0.005
		Nd(III)	9.8	0.70	14.06 \pm 0.12	0.11	0.008
		Ho(III)	10.5	0.75	14.07 \pm 0.15	0.13	0.009
		Pr(III)	18.0	1.28	14.09 \pm 0.17	0.15	0.011
		Gd(III)	22.4	1.60	14.08 \pm 0.10	0.09	0.006
		Er(III)	28.0	2.00	14.05 \pm 0.09	0.08	0.005

Note: S – standard deviation, S_r – relative standard deviation

Table 4. The calculated data of the stability constant of the cerium with 2,7-dinitrozo-1,8-dihydroxynaphthalene-3,6-disulfonic acid solution complex

Cation	HR	C_{HR} , mole fraction	$\lg C_{HR}$	$E_{1/2}$ of the complex, V	K	P number of reagents
Cerium(III)	2,7-dinitrozo-1,8-dihydroxynaphthalene-3,6-disulfonic acid	0.001	-3	-0.29	$1.6 \cdot 10^4$	0.5
		0.01	-2	-0.22		
		0.1	-1.3	-0.15		
		0.2	-1	-0.14		
		0.5	-0.69	-0.16		

Note: HR – titration reagent; C_{HR} – reagent concentration; $\lg C_{HR}$ – logarithm of concentration; $E_{1/2}$ of the complex – half-wave potential of the complex, B; K – complex stability constant; P number of reagents – see Figure 3.

Table 5. Certain characteristics of the complex Ce (III) with 2,7-dinitrozo-1,8-dihydroxynaphthalene-3,6-disulfonic acid

Cation	HR	C_{HR} , mole fraction	Contents of the complex	K	Ionic strength, mol/L
Ce^{3+}	2,7-dinitrozo-1,8-dihydroxynaphthalene-3,6-disulfonic acid	0.01	2:1	$1.6 \cdot 10^4$	0.1

Note: HR – titration reagent; C_{HR} – reagent concentration; contents of the complex – the ratio of the determined metal and reagent in the complex; K – complex stability constant; Ionic strength – ionic strength of solution.

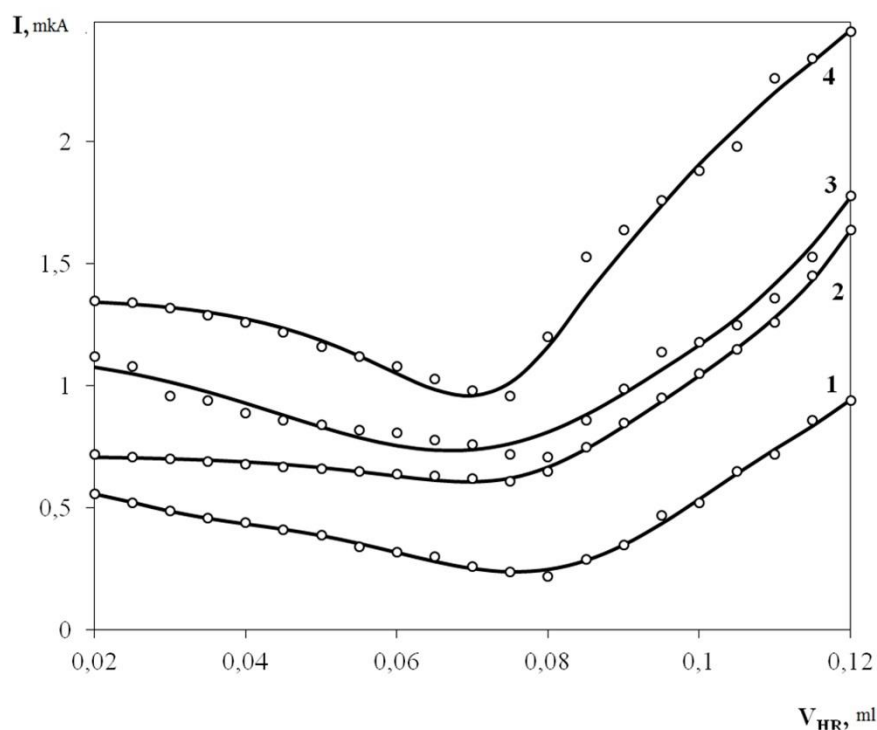


Figure 1. The impact of different in nature background electrolytes on the shape of curves of cerium (III) amperometric titration with 2,7-dinitrozo-1,8-dihydroxynaphthalene-3,6-disulfonic acid solution: 1 – potassium phthalate (pH 2.20); 2 – potassium citrate (pH 1.68); 3 – aminoacetic acid (pH 1.50); 4 – universal buffer (pH 1.81).

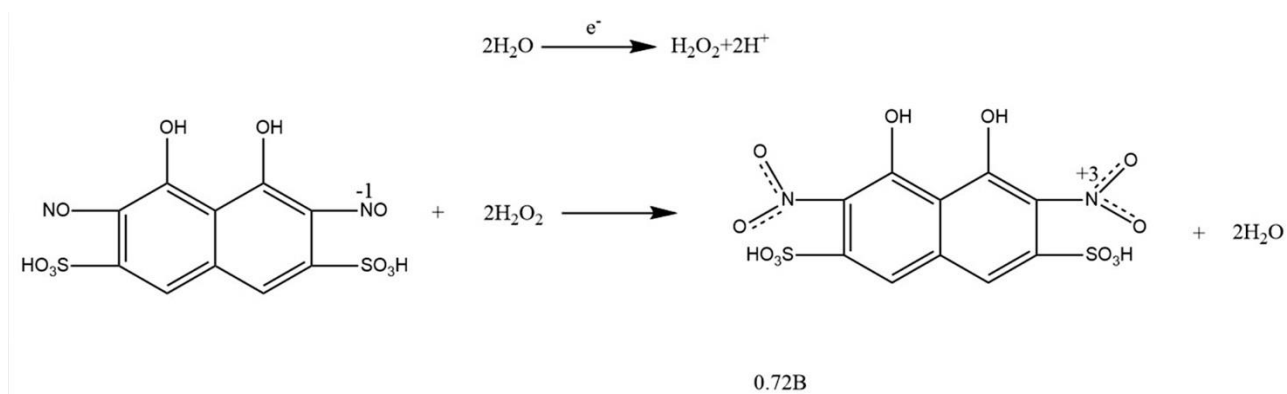


Figure 2. Chemical mechanism of 2,7-dinitrozo-1,8-dihydroxynaphthalene-3,6-disulfonic acid electrooxidation

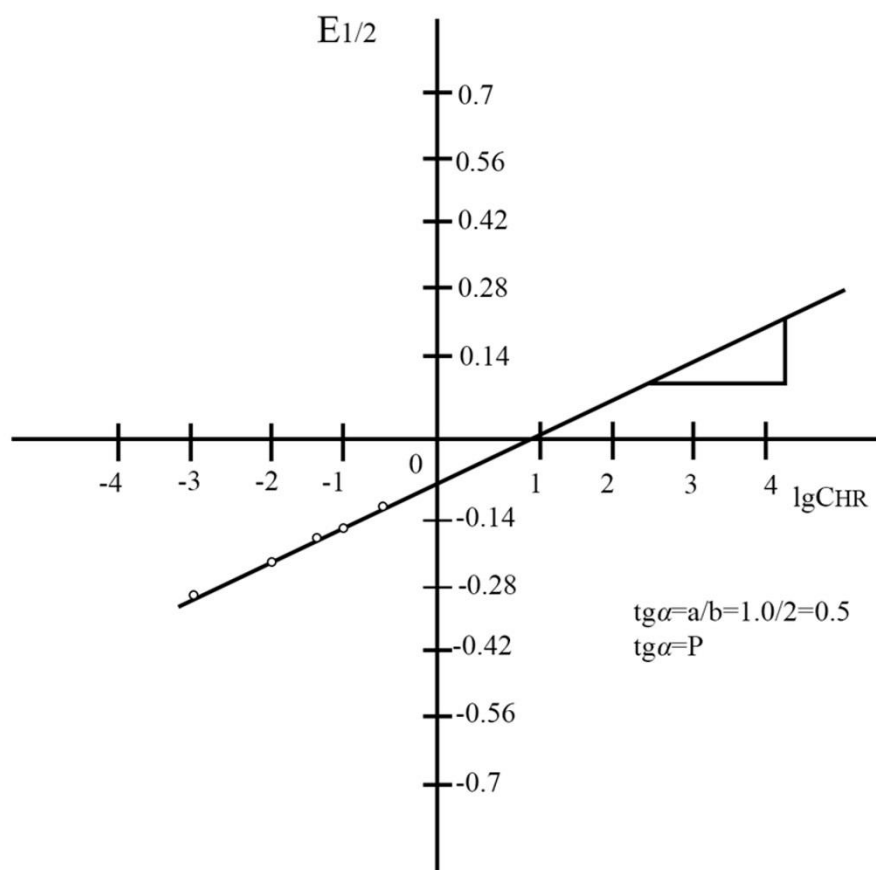


Figure 3. Finding the stability constant value of the cerium (III) with 2,7-dinitrozo-1,8-dihydroxynaphthalene-3,6-disulfonic acid solution

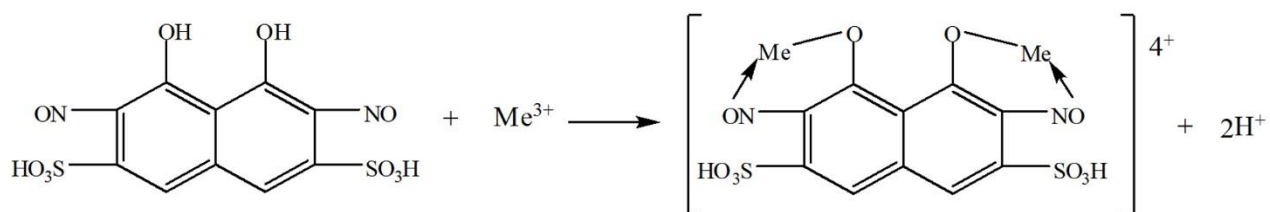


Figure 4. Scheme of the interaction of metal ions with 2,7-dinitrozo-1,8-dihydroxynaphthalene-3,6-disulfonic acid

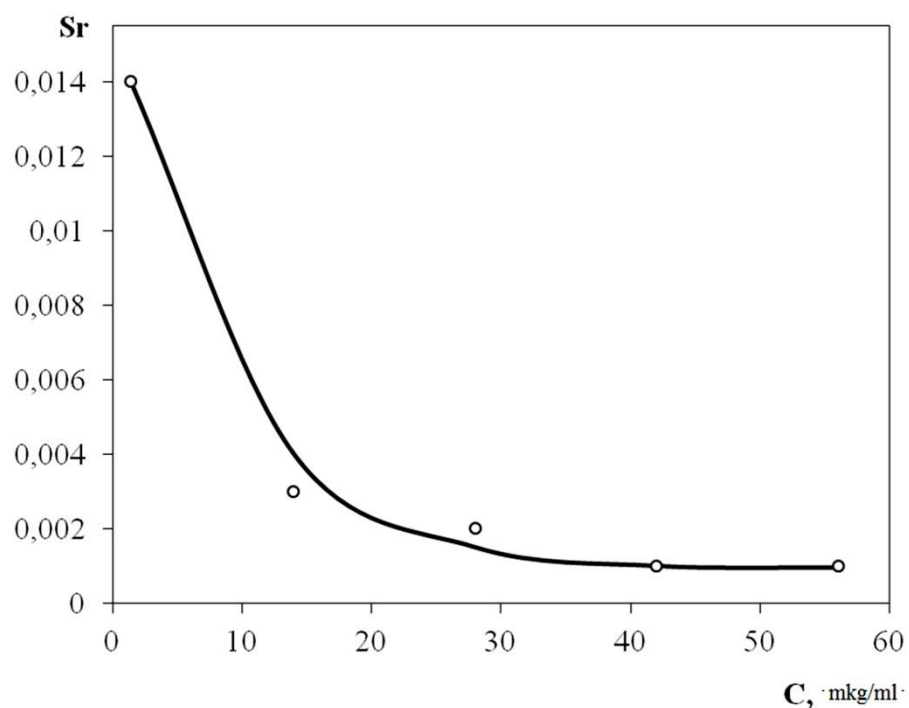


Figure 5. Curves of the dependence of the relevant standard deviation (S_r) values on the determined element contents (C_{Ce}) using the reagent 2,7-dinitrozo-1,8-dihydroxynaphthalene-3,6-disulfonic acid

AVALIAÇÃO DE EFICIÊNCIA DA DESPARAFINIZAÇÃO DE CALOR DO POÇO DE PRODUÇÃO EQUIPADA POR SUBBOMBA COM HASTES OCAS

EFFICIENCY EVALUATION OF THE HEAT DEPARAFINIZATION OF PRODUCING WELL EQUIPPED BY SUB PUMP WITH HOLLOW RODS

ОЦЕНКА ЭФФЕКТИВНОСТИ ПРОЦЕССА ТЕПЛОВОЙ ДЕПАРАФИНИЗАЦИИ СКВАЖИНЫ, ОБОРУДОВАННОЙ ГЛУБИННЫМ НАСОСОМ С ПОЛЫМИ ШТАНГАМИ

LEKOMTSEV, Alexander Viktorovich^{1*}, KANG, Wanli², GALKIN, Sergey Vladislavovich³, KETOVA, Yulia Anatolievna⁴

^{1,3,4} Perm National Research Polytechnic University, Perm, Russian Federation

² School of Petroleum Engineering, China University of Petroleum (East China), Qingdao, China

**Corresponding author
e-mail: alex.lekومتsev@mail.ru*

Received 24 August 2020; received in revised form 18 September 2020; accepted 22 October 2020

RESUMO

Uma das principais complicações da produção de petróleo é que os depósitos de asfalto-resina-parafina (ARPD) são formados durante a operação dos poços de produção. Este é um problema urgente na indústria de petróleo e gás, especialmente nos campos da região de Ural-Volga (Rússia). Este estudo teve como objetivo desenvolver uma solução tecnológica para o tratamento térmico eficaz de depósitos a partir do cálculo do estado térmico dos poços durante o funcionamento de uma bomba de haste de sucção. Na prática, o efeito térmico no ARPD é realizado por lavagem com um agente quente (água, óleo). Tradicionalmente, as descargas são realizadas através do anular do revestimento. Porém, este método é ineficaz devido às grandes perdas de calor e à impossibilidade de aquecer de forma suficiente a parte interna da tubulação, onde o ARPD é depositado. A modelagem dinâmica do processo foi realizada no produto de software ANSYS Fluent. O problema do calor foi resolvido com base na equação de transferência média de calor e massa de Navier-Stokes Reynolds. Observou-se que a temperatura do agente injetado (óleo quente ou água) afeta a temperatura da parede interna da tubulação em menor grau do que a vazão do refrigerante. Foi estabelecido que é impossível atingir o ponto de fusão da cera no nível da bomba submersível. A taxa de fluxo do refrigerante afeta este parâmetro mais intensamente. Ao lavar com óleo quente a 120°C com vazão de 300 m³/dia, a temperatura acima da bomba será igual à temperatura de derretimento da cera. Os cálculos indicam que é mais aconselhável usar óleo aquecido a 120°C como refrigerante para a lavagem de poços do que água com temperatura de 90°C. A implementação do método proposto pode ser usado em qualquer poço equipado com uma bomba de haste de sucção

Palavras-chave: *complications at oil-producing, hollow rods, flushing-out of well.*

ABSTRACT

One of the main oil production complications is that asphaltene-resin-paraffin deposits (ARPD) are formed during production wells' operation. This is an urgent problem in the oil and gas industry, especially in the fields of the Ural-Volga region (Russia). This study aimed to develop a technological solution for the effective thermal treatment of deposits based on the wells' thermal state calculation during a sucker rod pump operation. In practice, the thermal effect on ARPD is carried out by flushing-out with a hot agent (water, oil). Traditionally, flushes are carried out through the casing annulus. However, this method is ineffective due to large heat losses and the impossibility of heating the inner part of the tubing in a sufficient way, where ARPD is deposited. Dynamic modeling of the process was performed in the ANSYS Fluent software product. The heat problem was solved on the basis of the Navier-Stokes Reynolds-averaged heat and mass transfer equation. It was noted that the temperature of the injected agent (hot oil or water) affects the temperature of the tubing's inner wall to a lesser extent than the coolant flow rate. It has been established that it is impossible to reach the melting point of wax at the submersible pump level. The flow rate of the coolant affects this parameter more intensively. When flushing with hot oil 120°C with a flow rate of 300 m³/day, the temperature above the pump will be equal to the wax melting temperature. Calculations indicate that it is most advisable to use oil heated to 120°C as a coolant for flushing

wells than water with a 90°C temperature. The implementation of the methods proposed can be used on any well equipped with a sucker rod pump.

Keywords: *complications at oil-producing, hollow rods, flushing-out of well.*

АННОТАЦИЯ

Одним из основных осложнений при добыче нефти является образование асфальтеносмолопарафинистых отложений (АСПО) при эксплуатации добывающих скважин. Это актуальная проблема в нефтегазовой отрасли, особенно на месторождениях Урало-Поволжья (Россия). Целью данной работы являлась разработка технологического решения для эффективного воздействия термическим методом на отложения на основе расчета теплового состояния скважин во время работы штангового глубинного насоса. На практике термическое воздействие на АСПО осуществляется путем промывки горячим агентом (вода, нефть). Традиционно промывки проводят через затрубное пространство. Однако такой способ неэффективен за счет больших потерь тепла и невозможности прогрева внутренней части насосно-компрессорных труб (НКТ), где откладывается АСПО, достаточным образом. Динамическое моделирование процесса проводилось в программном продукте ANSYS Fluent. Тепловая задача решалась на основе уравнения теплопереноса, усредненного по Навье-Стоксу и Рейнольдсу. Было отмечено, что температура нагнетаемого агента (горячей нефти или воды) влияет на температуру внутренней стенки НКТ в меньшей степени, чем скорость потока теплоносителя. Установлено, что достичь точки плавления АСПО на уровне погружного насоса невозможно. Расход теплоносителя сильнее влияет на этот параметр. При промывке горячей нефтью при 120°C с расходом 300 м³/сут температура над насосом будет равна температуре плавления парафина. Расчеты показывают, что в качестве теплоносителя для промывки скважин целесообразнее использовать нагретую до 120°C нефть, чем воду с температурой 90°C. Предложенный метод может быть использован на любой скважине, оборудованной штанговым насосом.

Ключевые слова: *осложнения при добыче нефти, полые штанги, промывки скважин*

1. INTRODUCTION:

Within the territory of the Perm region, the main problem arising during the operation of wells is asphaltene-resin-paraffin deposits (ARPD), establishing onto the surface of deep-pumping equipment (Figure 1) (Khizhnyak, 2014). Wherein, there are premature failures of pumping equipment and well shutdowns, accompanied by shortages in oil production (Eskin, 2014). Known methods for paraffin deposition prognostication are divided into two main groups – methods aimed to determine the depth of the beginning of ARPD establishing (the beginning of paraffin crystallization) and methods determining the intensity (velocity) of ARPD establishing (Johansen, 1991; Newberry, 1999; Turbakov, 2009; Escobedo, 2010; Aiyejina, 2011; Al-Yaari, 2011).

The basis for determining the depth of the beginning of the formation of paraffin deposits are the physical and chemical properties of oil and thermodynamic conditions of its production (Korobov, 2018; Movchan *et al.*, 2019). As the oil lifts through the pipe, the flow's temperature and pressure decrease to the paraffin-formation point (Rehan, 2016; Sullivan, 2020; Abramovich *et al.*, 2019). Above this deep, ARPD is sedimented on the pipe surfaces and equipment plugging free

space. The interval of intensive deposits is 300-800 m for the Ural-Volga fields.

There are thermal, chemical, and mechanical ways among different methods of ARPD removing from well (Huang, 2016; Wang, 2015). The simple-to-apply method is mechanical, but there is a risk of jamming rods and equipment failure when the process of paraffin deposition is quite intensive. The chemical method is expensive when chemicals are required in a lot rate (Hassan, 2019). The thermal method has industrial limitations about heating agents and transporting it to wells (Zhao, 2015). But the choice of technological and economic effective method depends on the content of paraffin, resin and asphaltene (Buenrostro-Gonzalez, 2004; Bemani, 2019). In practice, the intensity of precipitation of solid organic substances is estimated using the inter-cleaning period (ICP) of the well (Moradi, 2019), which means the interval between cleaning. The ICP is evaluated practically and set in such a way when producing wells work without failures connected with ARPD. Flushing of wells is the most economically and technologically method in condition with low ICP and intensive organic deposits (Barker, 1999; Ustkachintsev, 2016; Mahmoud, 2019). It has current interest when deposits have stable surface crust from asphaltene-wax complexes (Rogel, 2015), which leads to a decrease in their solubility by chemical

(Zlobin, 2015; Hashemi, 2016; Guzman, 2017; Khalaf, 2019; Behnous, 2020).

Hot oil and freshwater are considered to be coolant (agent). These are traditional agents, which are found in the oil treatment plant and easy to get at any time. Typically, such an agent can be delivered to the well site within 1 or 2 hours by special trucks.

Therefore, this study aimed to develop a technological solution for the effective thermal treatment of deposits based on the calculation of the wells' thermal state during a sucker rod pump operation.

2. MATERIALS AND METHODS:

In this study, there were considered wells equipped with sucker rod pumps (SRP), artificial-lift pumping systems. The system has a surface power source to drive a downhole pump assembly. A beam and crank assembly create reciprocating motion in a sucker-rod string that connects to the downhole pump assembly. The pump contains a plunger and valve assembly to convert the reciprocating motion to vertical fluid movement. The authors deal with a topical issue of conducting thermal treatment throughout the SRP's hollow rods without shutting a well-operating down. Currently, the theoretical material and field experience of wells backwash with coolant supply into the annular space (Ramey, 2013) have been accumulated, but systematic ideas concerning the effectiveness of flushing throughout hollow rods have not been represented (Garcia, 2001; Soulgani, 2010; Khaleel, 2020; Kovalev, 2018; Yemelyanov *et al.*, 2019).

The issue regarding estimation of a thermal condition of a well under the heat treatment throughout hollow rods and the definition of the most optimal conditions concerning effective removal of ARPD was considered.

2.1. Problem Statement and Solution

The geometric model of a well is shown in Figure 2. SRP is lowered onto the tubing into the well. The movement of the pump plunger is performed throughout the hollow rods. A coupling is installed to bypass the coolant from the rod column into the tubing at a given depth. During the well's operation, the coolant is fed into the hollow rods, passing through which, the agent heats the flow of downhole products, leaves through the coupling, then are mixed with the main flow and rise to the wellhead. An essential advantage of this

technology before flushing the well throughout the annular space is reducing heat losses into the environment, thereby increasing heat flow density into the ARPD removal area.

The main tasks were to determine the coolant's temperature at which the complete melting of paraffin occurs and assess the impact of operational characteristics of the well regarding the washing efficiency.

2.2. Method of Solving Problem

The stated problems were solved numerically by the finite element method. The finite element method is a systematic way to convert the functions in an infinite-dimensional function space to the first function in finite-dimensional function space. Finally, ordinary vectors (in a vector space) tractable with numerical methods. It used the realizable k-epsilon (k- ϵ) model as a model of turbulent heat-and-mass transfer Reynolds-Averaged Navier-Stokes (RANS) (Launder, 1972; Wilcox, 1998; Sumer, 2007). The traditional RANS equations are directly applied for turbulent flow and heat transfer of the fluid, ignoring the thermal physical properties' turbulent effect due to the intense nonlinearity.

This model was relatively recently developed. It differs from the standard k- ϵ model by (Shih, 1995; Dobek, 2012) (1) improving notation for turbulent viscosity; and (2) the new transport equation for the dissipation rate is obtained from the exact transport equation for the mean-square pulsating vortex. The realizable k- ϵ model was tested for the case of a single rotating coordinate system. The results showed a more accurate solution than in the case of the standard k- ϵ turbulence model. Used in the article model describes well sufficiently for a round section modeling pipe.

The interaction of well production and coolant was described by the convection-diffusion equation (Jia, 2014). The natural convection was considered within the paper. The issue was solved as stationary (Lei, 2016). The thermophysical properties of solid materials did not depend on temperature. A limited area replaced the infinite array of the earth. The oil liquid was considered a single-phase medium (Ghasemi, 2020). The axisymmetric formulation of the issue was used to save computing resources (Table 1). The ICEM CFD processor was used to construct a geometric model. It divided the model into a finite element mesh (Figure 3). Engineering calculations were performed in the software product ANSYS Fluent.

2.3. Numerical experiment

The mathematical model of motion and heat transfer within an oil well is based on the rules of conservation of mass, amount of motion, and energy (Shirani, 2012; Al-Safran, 2018). Taking into account the assumptions made, the system of differential equations has got the form (1)-(9). Transfer equations (Navier-Stokes equations averaged by Reynolds):

$$\begin{aligned} \rho_i (\bar{v}_{ir} \frac{\partial \bar{v}_{ir}}{\partial r} + \bar{v}_{iz} \frac{\partial \bar{v}_{ir}}{\partial z}) = \\ = -\frac{\partial \bar{P}_i}{\partial r} + \mu_i \left(\frac{\partial^2 \bar{v}_{ir}}{\partial r^2} + \frac{1}{r} \frac{\partial \bar{v}_{ir}}{\partial r} + \frac{\partial^2 \bar{v}_{ir}}{\partial z^2} - \frac{\bar{v}_{ir}}{r^2} \right) + \\ + \frac{1}{r} \frac{\partial}{\partial r} \left(-r \rho_i \overline{v_{ir}'^2} \right) + \frac{\partial}{\partial z} \left(-\rho_i \overline{v_{ir}' v_{iz}'} \right), \quad (1) \end{aligned}$$

$$\begin{aligned} \rho_i (\bar{v}_{ir} \frac{\partial \bar{v}_{iz}}{\partial r} + \bar{v}_{iz} \frac{\partial \bar{v}_{iz}}{\partial z}) = \\ = -\frac{\partial \bar{P}_i}{\partial z} + \mu_i \left(\frac{\partial^2 \bar{v}_{iz}}{\partial r^2} + \frac{1}{r} \frac{\partial \bar{v}_{iz}}{\partial r} + \frac{\partial^2 \bar{v}_{iz}}{\partial z^2} \right) + \\ + \frac{1}{r} \frac{\partial}{\partial r} \left(-r \rho_i \overline{v_{ir}' v_{iz}'} \right) + \frac{\partial}{\partial z} \left(-\rho_i \overline{v_{iz}'^2} \right), \quad (2) \end{aligned}$$

Transporting equation for the kinetic energy of turbulence k :

$$\begin{aligned} \left(\frac{\partial \rho_i k \bar{v}_{ir}}{\partial r} + \frac{\partial \rho_i k \bar{v}_{iz}}{\partial z} \right) = \frac{\partial}{\partial r} \left[\left(\mu_i + \frac{\mu_t}{\sigma_k} \right) \frac{\partial k}{\partial r} \right] + \\ + \frac{\partial}{\partial z} \left[\left(\mu_i + \frac{\mu_t}{\sigma_k} \right) \frac{\partial k}{\partial z} \right] + G_k + G_b - \rho_i \varepsilon - Y_M \quad (3) \end{aligned}$$

Transfer equation for the rate of dissipation of the kinetic energy of turbulence:

$$\begin{aligned} \left(\frac{\partial \rho_i \varepsilon \bar{v}_{ir}}{\partial r} + \frac{\partial \rho_i \varepsilon \bar{v}_{iz}}{\partial z} \right) = \frac{\partial}{\partial r} \left[\left(\mu_i + \frac{\mu_t}{\sigma_\varepsilon} \right) \frac{\partial \varepsilon}{\partial r} \right] + \\ + \frac{\partial}{\partial z} \left[\left(\mu_i + \frac{\mu_t}{\sigma_\varepsilon} \right) \frac{\partial \varepsilon}{\partial z} \right] + \rho_i C_1 S \varepsilon - \\ - \rho_i C_2 \frac{\varepsilon^2}{k + \sqrt{v_i \varepsilon}} + C_{1\varepsilon} \frac{\varepsilon}{k} C_{3\varepsilon} G_b \quad (4) \end{aligned}$$

Turbulent viscosity μ_t :

$$\mu_t = \rho_i C_\mu \frac{k^2}{\varepsilon} \quad (5)$$

Continuity equation:

$$\begin{aligned} -\rho_i \left(\frac{\partial (r \bar{v}_{iz})}{\partial z} + \frac{\partial (r \bar{v}_{ir})}{\partial r} \right) = \\ = \left(\bar{v}_{iz} \frac{\partial (r \rho_i)}{\partial z} + \bar{v}_{ir} \frac{\partial (r \rho_i)}{\partial r} \right) \quad (6) \end{aligned}$$

Energy equation:

$$\begin{aligned} \frac{\partial}{\partial r} [\bar{v}_{ir} (\rho_i E + p)] + \frac{\partial}{\partial z} [\bar{v}_{iz} (\rho_i E + p)] = \\ = \frac{\partial}{\partial r} \left(k_{eff} \frac{\partial T}{\partial r} + \bar{v}_{ir} (\tau)_{eff} \right) + \\ + \frac{\partial}{\partial z} \left(k_{eff} \frac{\partial T}{\partial z} + \bar{v}_{iz} (\tau)_{eff} \right) + S_h \quad (7) \end{aligned}$$

Convection-diffusion equation:

$$\begin{aligned} \frac{\partial (\rho_i \vec{v} Y_i)}{\partial r} + \frac{\partial (\rho_i \vec{v} Y_i)}{\partial z} = \\ = - \left(\frac{\partial \vec{J}_i}{\partial r} + \frac{\partial \vec{J}_i}{\partial z} \right) + R_i + S_i \quad (8) \end{aligned}$$

where \vec{J}_i - is the diffusion flow, which is as:

$$\begin{aligned} \vec{J}_i = - \left(\rho_i D_{i,m} + \frac{\mu_t}{S c_t} \right) \left(\frac{\partial Y_i}{\partial r} + \frac{\partial Y_i}{\partial z} \right) - \\ - D_{T,i} \frac{\nabla T}{T} \quad (9) \end{aligned}$$

where r, z - cylindrical coordinates; i - index of areas studied, $i=1$ - oil, $i=2$ -associated petroleum gas, $i=3$ - pump - compressor- pipe, $i=4$ - casing

string, $i=5$ -hollow rods, $i=6$ - soil; $i=7$ - water;
 $\bar{v}_{ir}, \bar{v}_{iz}$ - time - averaged velocity components;
 $v'_{ir}v'_{iz}$ - pulsation velocity components;
 $\overline{v'_{ir}v'_{iz}}$ - turbulent stresses;
 T -temperature; \bar{p}_t - time-averaged pressure; ρ_i - medium density; μ_i - dynamic viscosity of the medium; k -kinetic energy of turbulence; ε -velocity turbulence energy dissipation; σ_k and σ_ε - turbulent Prandtl numbers for k and ε , respectively; G_k -kinetic energy of turbulence due to mean velocity gradients; G_b - kinetic energy of turbulence due to buoyancy; μ_t -turbulent viscosity; C_μ -variable determining turbulent viscosity; ν_i -kinematic viscosity; Y_M -dilation dissipation taking into account the effect of compressibility under turbulence; $C_2, C_{1\varepsilon}, C_{3\varepsilon}$ - constants; E -total energy; $(\tau)_{eff}$ -deviator stress tensor; k_{eff} -effective thermal conductivity; S_h -volumetric heat sources; Y_i -mass fraction of substance; \vec{j}_i -diffusion flux; R_i -reaction rate; S_i -mixing rate with dispersed phase; $D_{i,m}$ -mass diffusion coefficient; Sc_t -Schmidt turbulent number; $D_{T,i}$ -turbulent diffusion, - author defined source; $\bar{\nu}$ - molecular kinetic viscosity; p - pressure.

During the numerical experiment, the following characteristics of the deep-pumping equipment were taken as initial data: the diameter and wall thickness of casing – 146 mm and 8 mm; the tubing diameter and wall thickness – 73 and 5.5 mm; the length, diameter, and wall thickness of the 1st stage rod string is 500 m, and 4 37 mm; the length, diameter and wall thickness of the 2nd stage rod string – 300 m, 34th and 3.5 mm; the installation depth of the by-pass coupling (H_{coup}) – 800 m; the temperature of the downhole production installation depth of clutch – 15 °C; geothermal gradient is 0.02 deg/m; the melting point of the paraffin – 52 °C (at the wellhead), 60 °C (level of coupling) (Turbakov, 2011); the production rate of oil of 20 m³/day. Thermophysical characteristics of materials and media are provided in Table 2.

2.4. Practical Substantiation

To assess the possibility of ARPD removing (melting) within the tubing under heat treatment throughout hollow rods, a temperature distribution (onto the tubing inner wall (products extracted within the wellbore) is defined depending on the flow rate and the temperature of the coolant of 120, 200, 300°C. The temperature of 200 and 300°C is adopted to perform theoretical calculations and evaluate heat treatment

possibilities.

To confirm the applicability of the results, the hydraulic resistance was evaluated during the organization of heat treatments through hollow rods. Further calculations were carried out, considering the volume and duration of time, based on flushing wells' practical experience. The results of such operations onto wells within the Ural-Volga region indicate the practical applicability and definite success of the operation with a flow rate of 12-16 m³ / h (288-384 m³/day) using a well dewaxing unit (ADP, ADPM type) without additional pumping equipment.

Besides, upon injecting the coolant into the well throughout the hollow rods, the inevitable pressure loss to overcome the hydrodynamic resistances occurs. The estimation of the pressure loss onto the resistances during the motion of the coolant was performed according to the Darcy-Weisbach equation:

$$P_r = \lambda \frac{L}{d} \frac{V^2}{2} \rho \quad (10)$$

where λ – the coefficient of hydraulic resistance based onto the flow mode (turbulent and laminar), and the value of the Reynolds number per this high-speed flow regime, $Re=f(V, d, \nu)$; L – characteristic length; d – characteristic outer diameter, V – the linear flow velocity; ρ , ν – the density and kinematic viscosity of the coolant.

3. RESULTS AND DISCUSSION:

The calculations for oil and water washing for the flow rate of 300 m³/day and the problem's conditions are shown in Tables 3 and 4. Using the equivalent roughness value within the range of 0.15-0.3 mm, which corresponds to the values for pipes past several years of operation, the total pressure loss according to The Altschul formula $\lambda=0.11 (\Delta/d)^{0.25}$ was 13.2-15.7 MPa (Δ - equivalent absolute roughness). The estimated calculations regarding the determination of hydraulic resistances associated with the loss of pressure due to friction forces along the rod column's length also confirm the applicability under specified conditions, only within the range of costs up to 300m³/day with the involvement of ADP without additional equipment. The pressure loss during the agent's delivery into the coupling inlet to a depth of 800 m does not exceed 16 MPa within this flow range.

Figure 4 displays that even at the injected hot oil temperature equal to 300°C (curve 1), the temperature at the coupling level falls below the

paraffin's melting point and is 47°C. While at a coolant temperature equal to 120°C, the coupling inlet's temperature is 36°C (curve 3). According to the calculation results, it may be noted that the coolant's temperature has got its little effect on the temperature of the inner wall of the tubing at a depth of 800 meters. By changing this parameter within the technical capabilities of oilfield equipment (not above 150°C), it is not possible to achieve effective well heating.

The agent's thermal power injected for warming up the well is determined by its temperature and thermophysical properties and the flow rate. Therefore, to assess this parameter's influence, the problems for the coolant injection conditions of 150, 250, and 300 m³/day, respectively, are solved. The results are shown in Figure 5. Upon increasing the coolant flow rate, the tubing's inner wall's temperature at the coupling level increases more significantly compared to the increase in the coolant temperature (Figure 5). When oil heated up to 120°C is pumped at a flow rate of 300 m³ / day, the temperature at the coupling level is 59-60°C, which corresponds to the melting point of paraffin (Figure 5). Therefore, within the entire considered area, the wax will melt. At the same flow rates, when the water plays the role of the coolant being heated up to 90°C, the temperature equal to the melting temperature of paraffin is not reached at the level of the coupling (Figure 6).

Under these technological parameters of production, changing the coolant's temperature, it is not possible to achieve the temperature at the level of the coupling equal to the melting temperature of paraffin. Technologically, it is more efficient to change the flow rate of the coolant. Thus, under the oil temperature equal to 120°C and a flow rate of 300 m³/day, the temperature at the coupling inlet is equal to paraffin's melting temperature.

The degree of heating of downhole products during thermal washing throughout hollow rods depends on the well's technological mode of operation. The value of the dynamic liquid level within the annular space (H_{dyn}) has got its significant impact. Upon increasing the H_{dyn} , the petroleum-associated gas column height increases, removing the heat to the surrounding rocks less intensively than the liquid column. For operating conditions of wells within the Perm region, the dynamic level is maintained at 150-300 m above the depth of the rod pump descent, which is, on average, 900-1200 m (Kamentschikov, 2005).

The well model can also be divided into zones reflecting the dewaxing process stages performed by pumping coolant within the volume of 150 m³/day into hollow rods located in the tubing (Jorg Oschrmann, 2002). In zone I the temperature onto the tubing wall does not fall below 52°C; therefore, it may be argued that there is a complete melting of paraffin within this area. In zone II the exfoliation of paraffin deposits is most likely. This zone's lower boundary is determined by the temperature at which the paraffin mass shift is observed (30-32°C) (Zlobin, 2015). In zone III, the zone of weakened adhesion of paraffin to the surface of the pipe is very small and is assumed to be 50 m; and in zone IV is practically inaccessible for the method of thermal dewaxing of wells.

Figure 7 depicts an example of the calculations' results regarding the area of probable (I-III) ARPD washing out. The calculations of the probable depth of the ARPD washing out were made regarding the conditions of washing with hot water and oil under different dynamic liquid levels within the annular space. The results are shown in Table 5. In this theoretical research, the effectiveness evaluation method is used to study the effect of ARPD removal and application study results to the real industry (Kamentschikov, 2005; Rahman, 2017). This section discusses the interpretation of modeling results during the process of flushing out of wells.

4. CONCLUSIONS:

It can be concluded that, as the coolant for flushing-out of well, it is most expedient to use oil heated up to 120°C than water with its temperature of 90 ° C. The best indicators of the technological efficiency of the flushing-out of well with the coolant are observed provided that $H_{dyn} > H_{coup}$, and with the increase in the dynamic level in the well, the thermal efficiency washing throughout the hollow rods is increased. It was established that, given the technological production parameters and the increase of the coolant temperature, it is not possible to reach the melting point of the paraffin at the depth of the coupling level. The flow rate of the coolant affects this parameter more intensively. Thus, under the oil temperature equal to 120°C and a flow rate of 300 m³/day, the temperature at the coupling inlet is equal to paraffin's melting temperature. Improving the technological efficiency of the technology of washing wells throughout hollow rods may enhance the design of the rod column and its coating with thermal insulation materials.

5. ACKNOWLEDGMENTS:

The article was prepared based on research conducted with financial support from the Russian Ministry of Education and Science within the framework of the Federal Target Program "Research and Development in Priority Directions for the Development of the Russian Science and Technology Complex for 2014–2020" (Unique project identifier RFMEFI62120X0038.)

6. REFERENCES:

1. Aiyejina, A, Chakrabarti, D.P., Pilgrim, A., and Sastry, Mk. S. (2011). Wax formation in oil pipelines: A critical review. *International journal of multiphase flow*, 7, 671-694.
<https://doi.org/10.1016/j.ijmultiphaseflow.2011.02.007>
2. Abramovich, B. N., Sychev, Y. A., and Zimin, R. Y. (2019). Efficiency estimation of hybrid electrical complex for voltage and current waveform correction in power systems of oil enterprises. Paper presented at the *Proceedings of the 2019 IEEE Conference of Russian Young Researchers in Electrical and Electronic Engineering, EIConRus 2019*, 401-406.
<https://doi.org/10.1109/EIConRus.2019.8657081>
3. Al-Safran, E., (2018). Prediction of asphaltene precipitation risk in oil wells using coupled thermohydraulics model. *Journal of Petroleum Science and Engineering*, 167, 329-342.
<https://doi.org/10.1016/j.petrol.2018.04.024>
4. Al-Yaari, M. (2011). Paraffin wax deposition: Mitigation and removal techniques. *Proceedings of the SPE Saudi Arabia Section Young Professionals Technical Symposium*, 14-16. <https://doi.org/10.2118/155412-MS>
5. Barker, K.M., Sharum, D.B, and Brewer, D. (1999). Paraffin damage in high temperature formations, removal and inhibition. SPE 52156-MS. *The 1999 SPE Mid-Continent Operations Symposium, Oklahoma City, Oklahoma*, 28 – 31.
6. Behnous, D., Palma, A., Zeraibi, N., and Coutinho, J.A. (2020). Modeling asphaltene precipitation in Algerian oilfields with the CPA EoS. *Journal of Petroleum Science and Engineering*, 190, 107-115.
<https://doi.org/10.1016/j.petrol.2020.107115>
7. Bemani, A., Poozesh, A., Bahrami M., and Ashoori, S., (2019). Experimental study of asphaltene deposition: Focus on critical size and temperature effect. *Journal of Petroleum Science and Engineering*, 181, 106-186
<https://doi.org/10.1016/j.petrol.2019.106186>
8. Buenrostro-Gonzalez, E., Lira-Galeana, C., Gil-Villegas, A. Wu J. (2004). Asphaltene precipitation in crude oils: Theory and experiments. *AIChE Journal*, 50 (10), 2552-2570.
<https://doi.org/10.1002/aic.10243>
9. Dobek, S. (2012). Fluid dynamics and the Navier – Stokes Equation, available at: http://www.cs.umd.edu/~mount/Indep/Steven_Dobek/dobek-stable-fluid-final-2012.pdf
10. Garcia, M., and Carbognani, L. (2001). Asphaltene-paraffin structural interactions. Effect on crude oil stability. *Energy and Fuels*, 15 (05), 1021–1027.
<https://doi.org/10.1021/ef0100303>
11. Ghasemi, M., and Al-Safran E. (2020). Integrated reservoir/wellbore production model for oil field asphaltene deposition management. *Journal of Petroleum Science and Engineering*, 192, 107-213.
<https://doi.org/10.2523/IPTC-19936-MS>
12. Guzman, R, Ancheyta, J, Trejo, F, and Rodriguez, S. (2017). Methods for determining asphaltene stability in crude oils. *Fuel*, 188, 530–543.
<https://doi.org/10.1016/j.fuel.2016.10.012>
13. Escobedo, J., and Mansoori, G. A. (2010). Heavy-organic particle deposition from petroleum fluid flow in oil wells and pipelines. *Pet. Sci.*, 7, 502–508.
<https://doi.org/10.1007/s12182-010-0099-4>
14. Eskin, D, Ratulowski, J., and Akbarzadeh, K. (2014). Modelling wax deposition in oil transport pipelines. *The Canadian Journal of Chemical Engineering* 92(6).
<https://doi.org/10.1002/cjce.21991>
15. Hassan, A. Alade, O. Mahmoud, and M. Al-Majed, A. (2019). A Novel Technique for Removing Wax Deposition in the Production System Using

- Thermochemical Fluids. *Abu Dhabi International Petroleum Exhibition and Conference*, 11-14 November, Abu Dhabi, UAE. <https://doi.org/10.2118/197323-MS>
16. Hashemi, R., Kshirsagar, L.K., Jadhav, P.B., Nandi, S., and Ghaleh, E. (2016). An overview on asphaltene precipitation phenomena from crude oil. *International Journal of Chemical Studies*, 4 (02), 46–50.
 17. Huang, Q., Wang, W., Li, W., Ren Y., and Zhu F., (2016) A Pigging Model for Wax Removal in Pipes, *SPE Annual Technical Conference and Exhibition*, 26-28 September, Dubai, UAE. <https://doi.org/10.2118/181560-MS>
 18. Jia, R., Wang, Y., Xiong, J., and Shi, H. (2014). Experimental and numerical study on the self-balancing heating performance of a thermosyphon during the process of oil production. *Applied Thermal Engineering*, 73 (1), 1270-1278. <https://doi.org/10.1016/j.applthermaleng.2014.09.027>
 19. Johansen, S T. (1991). The deposition of particles on vertical walls. *International Journal of Multiphase flow*, 3, 355–362. [https://doi.org/10.1016/0301-9322\(91\)90005-N](https://doi.org/10.1016/0301-9322(91)90005-N)
 20. Jorg Oschrmann, H., (2002). New methods for the selection of asphaltene inhibitors in the field. *Chemistry in the oil industry*, 254-255. <https://doi.org/10.1039/9781847550460-00254>
 21. Kamentschikov, F. A. (2005). The Thermal Dewaxing of Wells. *M. Izhevsk: SRC "Regular and Chaotic Dynamics"*, 253.
 22. Khalaf, M. H., Mansoori G. A., Yong, and Ch. W. (2019). Magnetic treatment of petroleum and its relation with asphaltene aggregation onset (an atomistic investigation). *Journal of Petroleum Science and Engineering*, 176, 926-933. <https://doi.org/10.1016/j.petrol.2019.01.059>
 23. Khaleel, A.T., Abutaiya, M.I.L., Sisco, C.J., and Vargasa, F.M. (2020). Mitigation of asphaltene deposition by re-injection of dead oil. *Fluid Phase Equilibria*, 514, 112-143. <https://doi.org/10.1016/j.fluid.2020.112552>
 24. Khizhnyak, G. P., Usenkov, A.V., and Ustkachintsev, E. N. (2014). Complicating Factors in the Development of the Nozhov Group of Deposits of "LUKOIL-PERM" LLC. *Vestnik permskogo natsional'nogo issledovatel'skogo politekhnicheskogo universiteta. Geologiya. neftegazovoe i gornoe delo (the Bulletin of Perm National Research Polytechnic University. Geology. Oil, Gas and Mining)*, 13, 59-68. (in Russ).
 25. Korobov, G., and Podoprighora, D. (2018). Depth computation for the onset of organic sedimentation formation in the oil producing well as exemplified by the Sibirskeye oil field. *Acta Technica CSAV (Ceskoslovensk Akademie Ved)* 63(3), 481-492. [http://www.actatechnica.com/63\(2018\)-3/Complete%20Issue%2063\(2018\)-3.pdf](http://www.actatechnica.com/63(2018)-3/Complete%20Issue%2063(2018)-3.pdf)
 26. Kovalev, A.V. Miftakhov, R. T. Ryakhin, M. S. and Kolyvanov, A. V. (2018). Equipment for flushing of wells complicated by asphaltene-resin-paraffin deposits using hollow sucker rods. *Oil Industry Journal*, (07). <https://doi.org/10.24887/0028-2448-2018-7-110-112>
 27. Launder B.E., and Spalding D.B. (1972). Lectures in Mathematical Models of Turbulence. *London, Academic Press*, 169. [https://doi.org/10.1016/0307-904X\(86\)90045-4](https://doi.org/10.1016/0307-904X(86)90045-4)
 28. Lei, Y., Han, Sh., and Zhang, J., (2016). Effect of the dispersion degree of asphaltene on wax deposition in crude oil under static conditions. *Fuel Processing Technology*, 146, 20-28. <https://doi.org/10.1016/j.fuproc.2016.02.005>
 29. Mahmoud, M., (2019). Well Clean-Up Using a Combined Thermochemical /Chelating Agent Fluids. *Journal of Energy Resources Technology*, 141(10), p.102905. <https://doi.org/10.1115/1.4043612>
 30. Moradi, S., Amirjahadi S., Danaee I., and Soltanic B., (2019). Experimental investigation on application of industrial coatings for prevention of asphaltene deposition in the well-string. *Journal of Petroleum Science and Engineering*, 181, 106-195.

<https://doi.org/10.1021/acs.energyfuels.5b01237>

31. Movchan, I. B., Yakovleva, A. A., and Daniliev, S. M. (2019). Parametric decoding and approximated estimations in engineering geophysics with the localization of seismic risk zones on the example of northern part of kola peninsula. *Paper presented at the 15th Conference and Exhibition Engineering and Mining Geophysics 2019*, Gelendzhik 2019, 188-198. <https://doi.org/10.3997/2214-4609.201901705>
32. Newberry, M. E., Barker, K. M., and Flynn, K. P. (1999). Identification and remediation of organic skin damage. *The 1999 AIChE Spring National Meeting, Houston, Texas. International Conference on Petroleum and Gas Phase Behavior and Fouling*, 14 – 18.
33. Rahman, P. A. (2017). Analysis of the mean time to data loss of nested disk arrays RAID-01 on basis of a specialized mathematical model. *IOP Conference Series: Materials Science and Engineering*, 177(1). <https://doi.org/10.1088/1757-899X/177/1/012088>
34. Ramey, H.J. (2013). Jr. Wellbore heat transmission. *Journal of Petroleum Technology* 14 (4), 872-875 <https://doi.org/10.2118/96-PA>
35. Rehan, M., Nizami, A.S., Taylan, O., Al-Sasi, B.O. and Demirbas, A., (2016). *Determination of wax content in crude oil. Petroleum Science and Technology*, 34 (9), 799–804. <https://doi.org/10.1080/10916466.2016.1169287>
36. Rogel, E., Roye, M., Vien, J., and Miao, T. (2015). Characterization of Asphaltene Fractions: Distribution, Chemical Characteristics, and Solubility Behavior. *March. Energy and Fuels*, 29(4), 2143-2152. <https://doi.org/10.1021/ef5026455>
37. Sumer, B.M. Lecture notes on turbulence (2007). *Technical University of Denmark*, available at: http://www.external.mek.dtu.dk/personal/bms/turb_bo-ok_update_30_6_04.pdf
38. Shirani, B., Nikazar, M., and Mousavi-Dehghani S. A. (2012). Prediction of asphaltene phase behavior in live oil with CPA equation of state. *Fuel*, 97, 89-96. <https://doi.org/10.1016/j.fuel.2012.02.016>
39. Shih, T.-H., Liou, W.W., Shabbir, A., Yang, Z., and Zhu J. (1995). A new k– eddy-viscosity model for high Reynolds number turbulent flows. Model development and validation. *Computers fluids*, № 24 (3), 227–238. [https://doi.org/10.1016/0045-7930\(94\)00032-T](https://doi.org/10.1016/0045-7930(94)00032-T)
40. Soulgani, B. S., Rashtchian, D., Tohidi, B., and Jamialahmadi, M. (2010). A Novel Method for Mitigation of Asphaltene Deposition in the Wellstring. *Iranian Journal of Chemistry and Chemical Engineering*, 29 (2), 131-142. available at: http://www.ijcce.ac.ir/article_6709_9640cbd1410f6a223f64dbaba5cb9f0f.pdf
41. Sullivan, M., Smythe, E.J., Fukagawa, S., Hadrien Dumant., and Borman C., A (2020). Fast Measurement of Asphaltene Onset Pressure. *SPE Reservoir Evaluation and Engineering*. 23(3). <https://doi.org/10.2118/199900-PA>
42. Turbakov, M. S., Erofeev, A. A., and Lekomtsev, A.V. (2009). The Determination of Depth of the Beginning of Establishing of Asphaltene-Resin-Paraffin Deposits upon Operating the Oil-Producing Wells. *Geologiya, geofizika i razrabotka neftnyanykh i gazovykh mestorozhdenij (Geology, Geophysics and Development of Oil and Gas Fields)*, 10, 62-65.
43. Turbakov, M. S., Lekomtsev, A.V., and Erofeev, A. A. (2011). The Saturation Temperature of Oil with Paraffin for the Fields of the Upper Kama Region. *Neftyanoe khozyajstvo (Oil Industry)*, 8, 123-125.
44. Ustkachkintsev, E. N., and Melekhin, S. V. (2016). The Determination of Efficiency of Methods to Prevention of Asphaltene-Resin-Paraffin Deposits. *Geologiya, geofizika i razrabotka neftnyanykh i gazovykh mestorozhdenij (Geology, Geophysics and Development of Oil and Gas Fields)*, 15 (18), 61-70.
45. Wang, W.D., Huang, Q.Y., Liu, Y.J., and Kamy Sepehrnoori. (2015). Experimental Study on Mechanisms of Wax Removal During Pipeline Pigging. *Presented at the SPE Annual Technical Conference and Exhibition, Houston, Texas*, 28-30

September.

<https://doi.org/10.2118/174827-MS>

46. Wilcox, David C (1998). Turbulence Modeling for CFD. *Second edition*, Anaheim: DCW Industries, 1998, pp. 174.
47. Yemelyanov, V. A., Yemelyanova, N. Y., Nedelkin, A. A., Glebov, N. B., and Tyapkin, D. A. (2019). Information system to determine the transported liquid iron weight. Paper presented at the *Proceedings of the 2019 IEEE Conference of Russian Young Researchers in Electrical and Electronic Engineering*, ElConRus 2019, 377-380. <https://doi.org/10.1109/ElConRus.2019.8656693>
48. Zhao, Y., Limb, D., and Zhu, X., (2017) A study of wax deposition in pipeline using thermal hydraulic model. *18th International Conference on Multiphase Production Technology*, 7-9 June, Cannes, France.
49. Zlobin, A. A. (2015). Experimental Studies of the Processes of Aggregation and Self-Assembly of Nanoparticles within Oil Disperse Systems. *Vestnik permskogo natsional'nogo issledovatel'skogo politekhnicheskogo universiteta. Geologiya. neftegazovoe i gornoe delo (The Bulletin of Perm National Research Polytechnic University. Geology. Oil, Gas and Mining)*, 14 (15), 57-72.



(a)



(b)

Figure 1. Picture of ARPD Establishing onto the Surface of Deep-Pumping Equipment: (a) ARPD in Pipes; (b) Deposits onto Pump and Rods

Source: the author

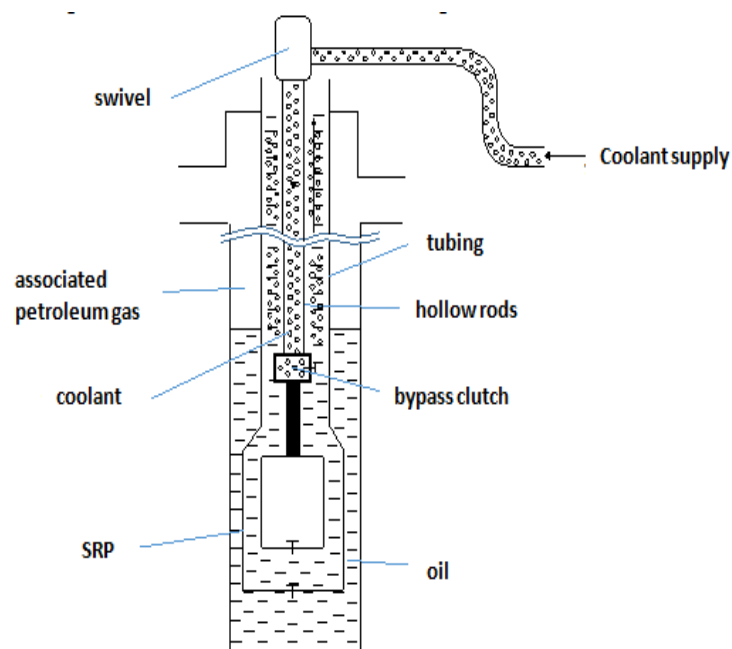


Figure 2. Geometric Model of a Well Equipped with SRP with Hollow Rods. Source: The author.

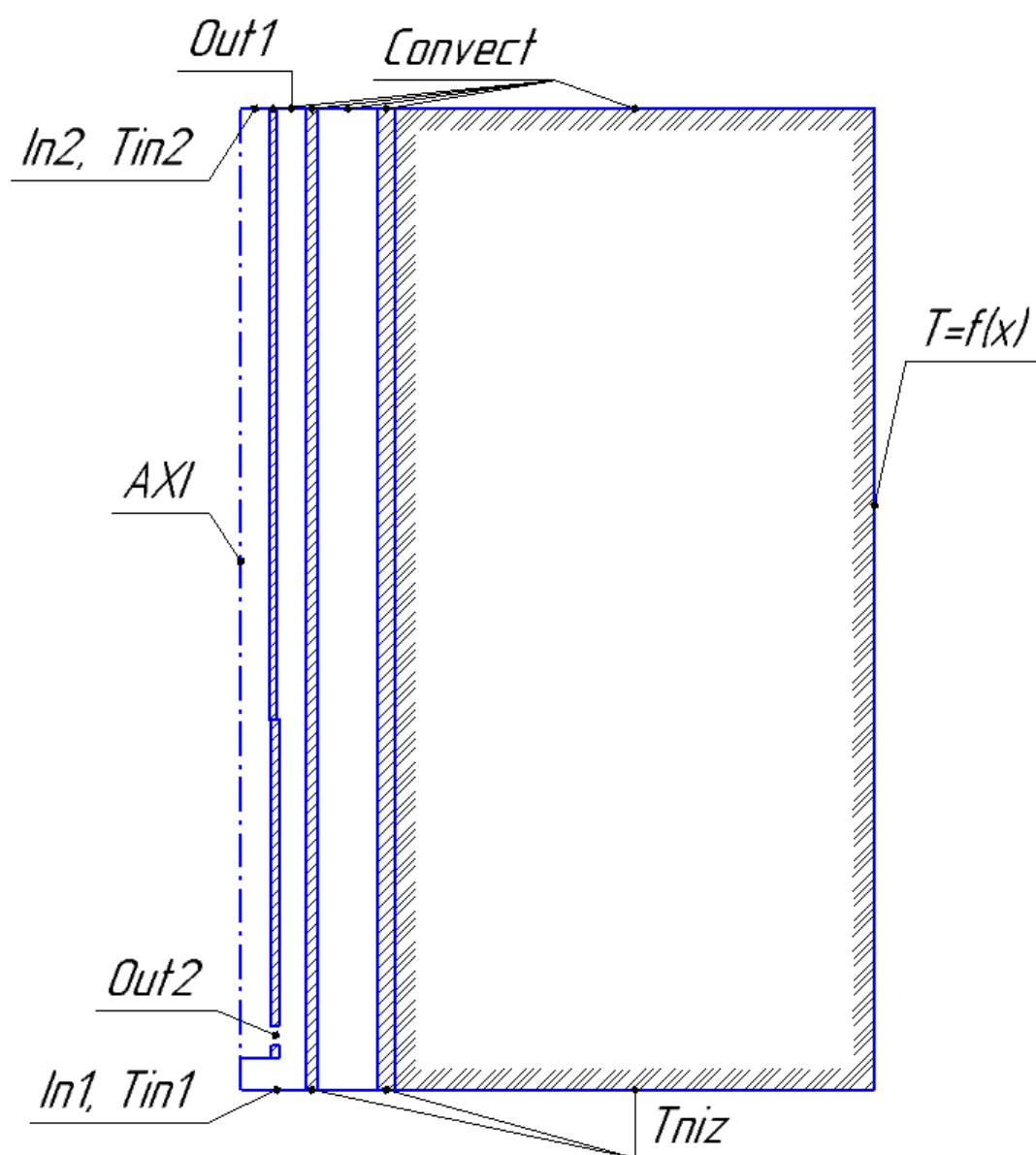


Figure 3. Computational Domain with Boundary Conditions. Source: The author.

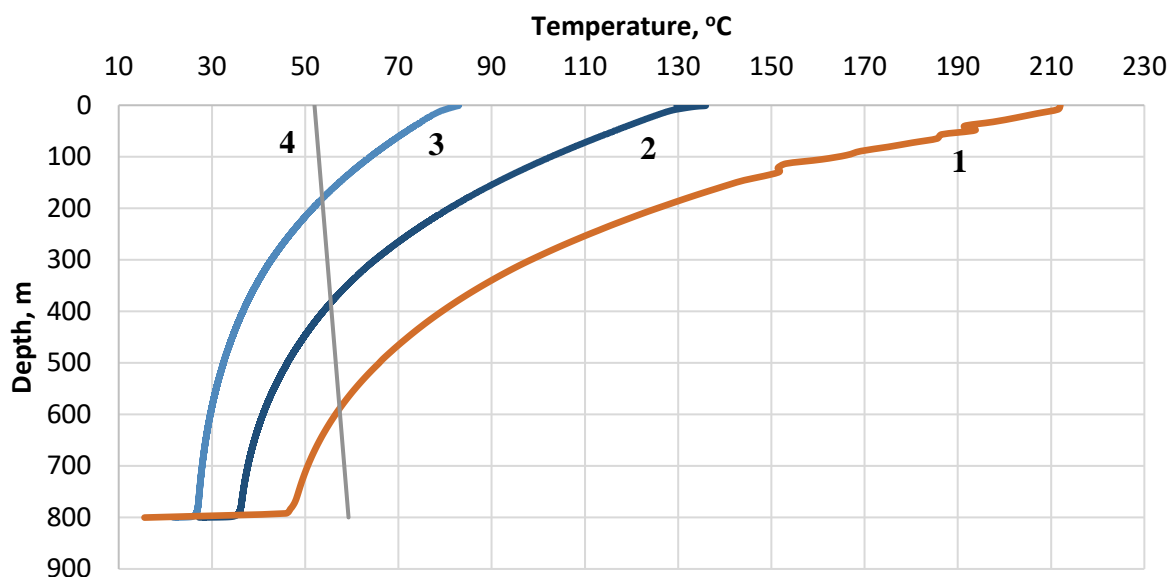


Figure 4. The Temperature Distribution onto the Inner Wall of the Tubing from the Depth under Different Temperatures of the Coolant. Dynamic Level – 0 m. Coolant - oil supplied with a flow rate of $150 \text{ m}^3 / \text{day}$ and temperature: 1 – 300°C ; 2 – 200°C ; 3 – 120°C ; 4 -the temperature of paraffin melting. Source: The author.

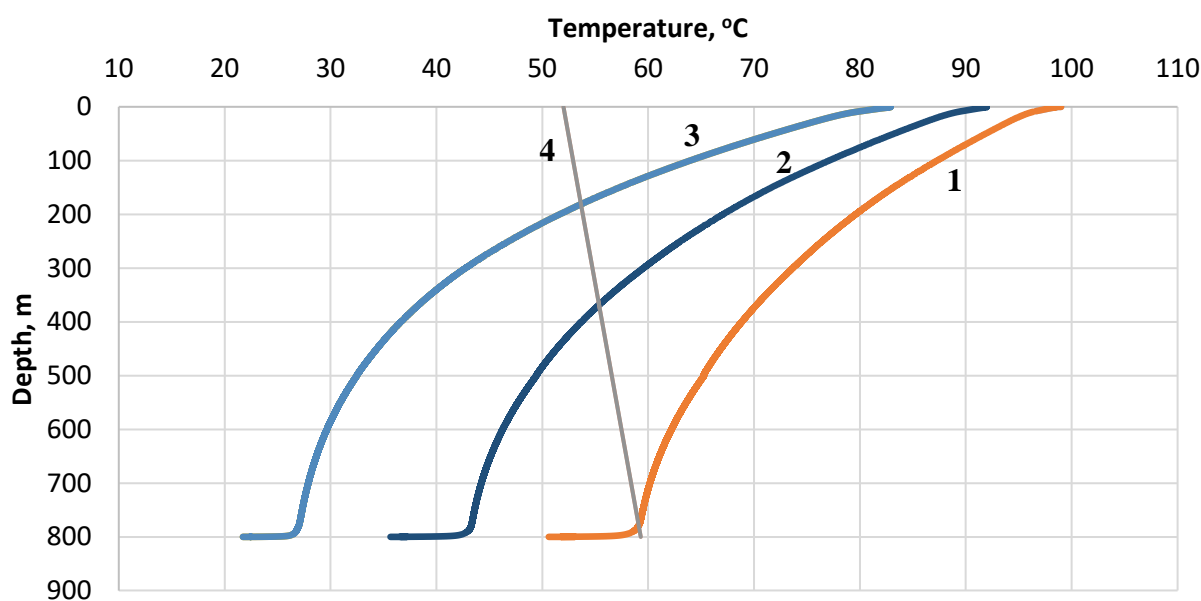


Figure 5. The temperature distribution onto the inner wall of the tubing from the depth under different coolant flow. Dynamic Level – 0 m. Coolant oil heated up to 120°C during injection consumption: 1- $300 \text{ m}^3 / \text{day}$; 2- $250 \text{ m}^3 / \text{day}$; 3- $150 \text{ m}^3 / \text{day}$; 4-the melting temperature of paraffin. Source: the author

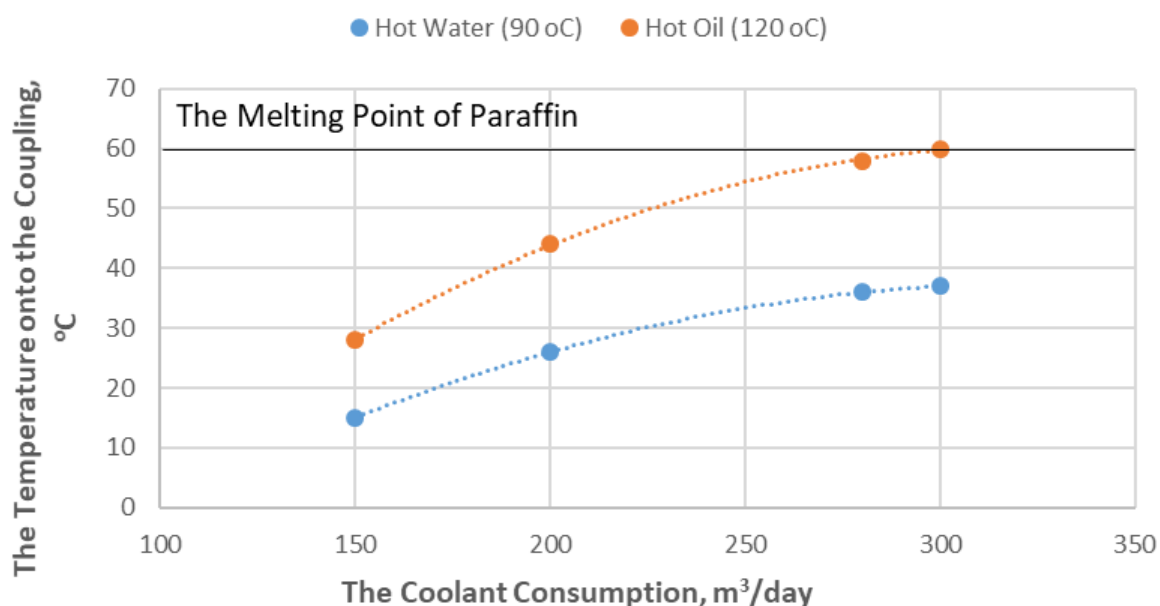


Figure 6. The Dependence of the Downhole Production Temperature at the Coupling Level onto the Flow Rate and the Coolant Type. Source: the author

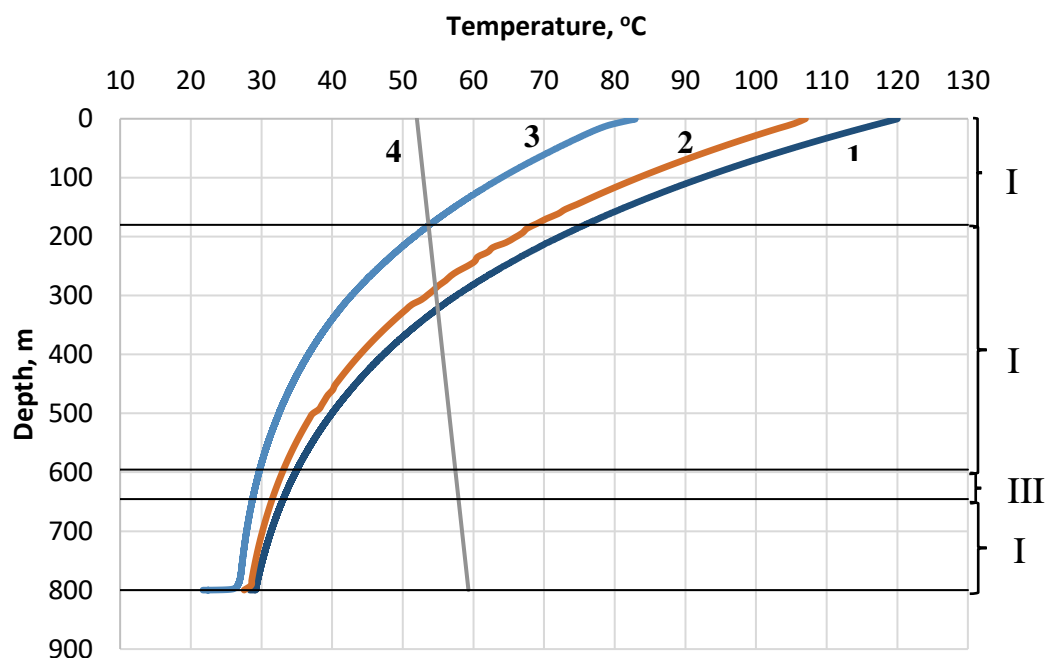


Figure 7. The Temperature Distribution within the Well Depth. Coolant is the oil with its flow rate of 150 m³/day; within the annulus - oil, $H_{dyn}=0$: 1 - is oil flow temperature in a hollow rod; 2 - is hollow rod wall temperature; 3 - is tubing wall temperature; 4 - is paraffin melting point. Source: the author

Table 1. Boundary conditions

No.	Boundary condition	Specified parameter
1	AXI	Axis of symmetry
2	In1, Tin1	Plot of oil flow rates corresponding to the well production rate. Oil temperature at the coupling level equal to 15 °C
3	Out1	The boundary condition for the liquid outlet at the wellhead
4	In2, Tin2	Plot of coolant flow rates corresponding to a given flow rate. Heat carrier temperature equal to 90 °C for water and 120 °C for oil
5	Out2	The boundary condition for the release of the coolant from the coupling
6	Tniz	Temperature at the coupling level equal to 15 °C
7	Convect	Condition of natural convection on the surface
8	T=f(x)	Geothermal gradient equal to 0.2 °C / 10 m

Table 2. The Properties of Materials and Media

Material	Density ρ , kg / m ³	Heat capacity C, j/(kg·K)	Thermal Conductivity λ , W/(m·K)	Viscosity μ , MPa·s
Soil	1,900	1,680	1.82	-
Steel	8,030	502	16.27	-
Water	998.2	4,200	0.6	1
Oil	761.5	2,000	0.15	10
Associated Petroleum Gas	1.225	1,006	0.0242	0.0018

Table 3. The Results of Calculation of Hydraulic Pressure Losses During Hot Water Washing

No.	Characteristic	Hot Water onto the Rods Flow	
1	Rod Length, m	500	300
2	Inner Diametre of the Rod, mm	29	27
3	Consumption, m ³ / day	300	300
4	Kinematic Viscosity, mm ² / s	0.326	0.326
Result of Calculation			
1	Flow Rate, m / s	6.1	5.3
2	Reynolds number, un.	502,524	467,867
3	The Coefficient of Hydraulic Resistance, un.	0.0295	0.0290
4	Head Loss due to Friction, m	604	692
5	Friction Pressure Loss, MPa	6.0	6.9
6	Total Pressure Loss, MPa	12.9	

Table 4. The Results of Calculation of Hydraulic Pressure Losses during Hot Oil Washing

No.	Characteristic	Hot Oil onto the Rods Flow	
1	Rod Length, m	500	300
2	Inner Diametre of the Rod, mm	29	27
3	Consumption, m ³ / day	300	300
4	Kinematic Viscosity, mm ² / s	1.71	1.71
Result of Calculation			
1	Flow Rate, m / s	6.1	5.3
2	Reynolds number, un.	95,803	89,196
3	The Coefficient of Hydraulic Resistance, un.	0.0303	0.0299
4	Head Loss due to Friction, m	620	714
5	Friction Pressure Loss, MPa	6.2	7.1
6	Total Pressure Loss, MPa	13.3	

Table 5. Probable Depth of ARPD Washing under Different H_{dyn} and a Type of the Heat Carrier

Dynamic Level, m	Hot Oil (120°C)	Hot water (90°C)
0	645	360
300	698	427
500	above 800	500
800	above 800	596

Note: * Technological efficiency and probable depth of washing are provided at productivity of the unit (ADP, ADPM type) operated not below the second speed.

A EFICÁCIA DO TEXTO DE REFUTAÇÃO PARA MELHORAR A COMPREENSÃO DOS CONCEITOS DE ÁCIDO-BASE PARA ESTUDANTES DO ENSINO MÉDIO**THE EFFECTIVENESS OF THE REFUTATION TEXT TO IMPROVE UNDERSTANDING OF THE ACID-BASE CONCEPTS FOR HIGH SCHOOL STUDENTS****ANALISIS HASIL REMEDIASI PEMAHAMAN KONSEP MENGGUNAKAN BAHAN BACAAN REFUTATION TEXT PADA MATERI ASAM BASA**HARYANI, Sri^{1*}; DEWI, Siti Herlina²; HARJITO³.^{1,2,3} Semarang State University, Mathematics and Sains Faculty, Chemistry Department. Indonesia

* Corresponding author

e-mail: haryanikimia83@mail.unnes.ac.id

Received 15 June 2020; received in revised form 23 September 2020; accepted 25 October 2020

RESUMO

Ácido-base é um assunto difícil de aprender. Inclui palavras conceitualmente complicadas para os alunos. O assunto também é considerado difícil pelos professores e futuros professores, tanto em termos de ensino quanto em termos de avaliação do domínio do aluno. O não entendimento em tópicos de química é um dos maiores desafios para o professor. Isso faz com que muitos alunos não atinjam o objetivo de aprendizado. O tópico ácido-base é considerado um dos assuntos mais difíceis e existem muitos conceitos mal compreendidos acerca desse tema. A falta de compreensão pode ser reduzida ao fornecer uma fonte de aprendizado simples e fácil de entender, como texto de refutação. O objetivo deste estudo foi determinar a eficácia do texto de refutação para melhorar a compreensão dos conceitos e reduzir o mal entendimento na aprendizagem corretiva no tópico ácido-base para o ensino médio. Existem seis subtópicos sobre o conteúdo de ácido-base para o ensino médio. O método de teste utilizado foi o pré e pós-projeto de um grupo, com um número limitado de sujeitos. O instrumento de teste usado foi composto por três camadas de várias opções para material ácido-base (teste de entendimento do conceito). O resultado da análise mostrou que 17 dos 19 alunos estavam aumentando a compreensão de conceitos e diminuindo os conceitos errôneos. A mudança de conceito foi significativa de acordo com o teste de Mc Nemar. O valor do tamanho do efeito (ES) baseado no teste Crochan-Q foi 4,12, que é uma categoria alta. Pode-se concluir que o texto de refutação é eficaz o suficiente para melhorar a compreensão dos conceitos dos alunos e aplicável à aprendizagem corretiva.

Palavras-chave: *texto de refutação; equívoco; materiais à base de ácido; aprendizagem corretiva.***ABSTRACT**

Acid-base is a difficult subject to learn. It includes conceptually tricky words for the students. The theme is also considered difficult by teachers and prospective teachers in teaching and assessing student mastery. A misconception in chemistry topics is one of the biggest challenges for the teacher. This means that many students do not reach the learning objective. The acid-base question is considered one of the most challenging subjects, and there are many misunderstood concepts on this topic. Lack of understanding can be reduced by providing a simple and natural source of learning, such as a refutation text. This study aimed to determine the effectiveness of the refutation text to improve understanding of concepts and reduce misunderstanding in corrective learning on the acid-base topic for high school. There are six subtopics on acid-base content for high school. The test method used was the pre and post-project of a group, with a limited number of subjects. The test instrument used was the three-tiers of multiple choices for acid-base material (concept understanding's test). The analysis result showed that 17 of 19 students had increased knowledge of concepts and decreased misconceptions. The concept change was significant, according to Mc Nemar Test. The value of effect size (ES) based on the Crochan-Q test was 4.12, a high category. It could be concluded that refutation text is effective enough to improve students' concepts and apply them to remedial learning.

Keywords: *refutation text; misconception; acid-base materials; remedial learning.*

ABSTRAK

Asam basa adalah mata pelajaran yang sulit dipelajari. Ini mencakup kata-kata yang secara konseptual rumit bagi siswa. Tema tersebut juga dianggap sulit oleh guru dan calon guru baik dalam hal pengajaran maupun dalam hal menilai penguasaan siswa. Kesalahpahaman dalam topik kimia adalah salah satu tantangan terbesar bagi guru. Artinya banyak siswa yang belum mencapai tujuan pembelajaran. Pertanyaan asam basa dianggap sebagai salah satu mata pelajaran yang paling menantang, dan ada banyak konsep yang disalahpahami tentang topik ini. Kurangnya pemahaman dapat dikurangi dengan menyediakan sumber belajar yang sederhana dan alami, seperti teks sanggahan. Tujuan penelitian ini adalah untuk mengetahui keefektifan teks sanggahan dalam meningkatkan pemahaman konsep dan mengurangi kesalahpahaman dalam pembelajaran korektif topik asam basa di SMA. Ada enam subtopik tentang kandungan asam basa untuk SMA. Metode tes yang digunakan adalah pra dan pasca proyek suatu kelompok, dengan jumlah mata pelajaran yang terbatas. Instrumen tes yang digunakan adalah tiga tingkatan pilihan ganda untuk bahan asam basa (tes pemahaman konsep). Hasil analisis menunjukkan bahwa 17 dari 19 siswa mengalami peningkatan pengetahuan konsep dan penurunan miskonsepsi. Perubahan konsep itu signifikan menurut Mc Nemar Test. Nilai effect size (ES) berdasarkan uji Crochran-Q sebesar 4.12 dan termasuk kategori tinggi. Dapat disimpulkan bahwa teks sanggahan cukup efektif untuk meningkatkan pemahaman konsep siswa dan dapat diterapkan pada pembelajaran remedial.

Kata kunci: *teks sanggahan/ refutation text; miskonsepsi; konsep asam-basa; pembelajaran remedial.*

1. INTRODUCTION:

Acid-base is a difficult subject to learn. It includes conceptually tricky words for the students. The subject is also considered difficult by teachers and prospective teachers in teaching and assessing student mastery (Haryani, T. P., and Saptarini, 2014). The students difficulties in learning the acid-base subject can be seen from the many misconceptions about it. The problems include delusions in the acid-base theory and acid-base examples (Mughtar, Sciences, and Iskandar, 2012), the nature of acids and bases (Demircioğlu, 2009; Effendi, 2012; Sesen, 2011), acid-base equilibrium, and the concept of pH (Halstead, 2009; Metin, 2011; Sheppard, 2006).

A misconception in the acid-base topic could affect student learning outcomes. The traditional passing grade value for the material ranges from 40-50%. Based on these data, the teacher should do remedial learning (Kemendikbud, 2019). Remedial learning can be interpreted as an improvement program directed at overcoming students' learning difficulties by changing, correcting, or clarifying students' frame of mind to achieve teaching goals to the maximum extent possible, effectively and efficiently (Buna'i, 2007). Besides, with the existence of this remedial program, the teacher can make improvements to his teaching mistakes or deliver learning material that is felt to be lacking and / or late (Dole, 2011; Hastuti, 2000; Margolis, McCabe, Margolis, and McCabe, 2016).

The implementation of remedial learning was only in the form of a re-test with the same or different questions. It is influenced by several factors, including limited learning time, the burden

of teaching the teacher, and the significant learning burden of students and other extracurricular activities. It is less possible to do re-learning to improve student understanding. Remedial misconception can be done by using conceptual change text (CCT) or meaningful learning involving reorganizing or replacing students' initial conception by accommodating ideas called conceptual change (Brix, 2017; Chambers and Andre, 1997; Chi, 2008). One type of remedial learning with CCT with a high effect size is an alternative reading by refutation text.

Refutation text is the text that generally consists of three components. The first component is a statement that is usually a misconception about a concept. The second component is a refutation statement, such as "*incorrect, it is not right...*". The third component is the correct and scientifically acceptable statement of misconception in the first component (Tippett, 2010). Some studies related to remedial in the form of reading material in the way of refutation text, among others, on the content of Light on Mirror (Physics), refutation text could reduce student errors by 42.92% with effect size 1.47 (Apeng, 2009). Refutation text for Vibration (Physics) material also shows effect size, a relatively large of 1,170 with a contribution of reducing student errors by 37.90% (Hardiansyah, 2009).

Refutation text can also improve understanding of concepts, and read refutation text is more pleasing than reading ordinary textbooks to overcome misconceptions (Danielson, Sinatra, and Kendeou, 2016; Kendeou, Walsh, Smith, and O'Brien, 2014; Tippett, 2010). A study with the solubility content

employing refutation text showed that the refutation text can reduce misconception up to 49.20% compared to ordinary textbooks (Figure 1) (Regita, Enawaty, Harun, and Text, 2015).

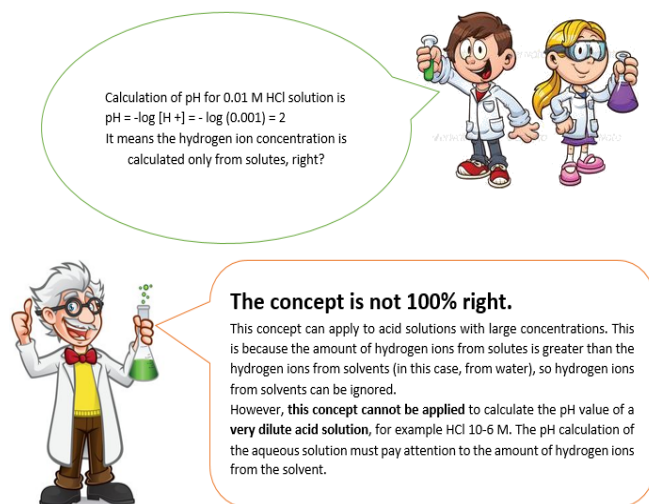


Figure 1. The refutation text (Regita, Enawaty, Harun, and Text, 2015).

This study aimed to determine the effectiveness of remedial teaching materials in refutation text in improving students' conceptual understanding, especially in acid-base content.

2. MATERIALS AND METHODS:

2.1. Method of the study

The method of this study was a descriptive experiment with one group pre-and-post-design. The purpose of the study was to analyze the effect of refutation text on acid-base remedial learning. The effect was known by measuring the student's understanding of the acid-base topic.

2.2. Sample and Ethics

The research sample were students of 11-grade science class who had not to pass at the acid-base topic. The sample was limited to one class because the refutation text is still in development research (limited test). There were 30 students between the ages of 15-16 who were involved, consisting of 9 boys and 21 girls. A total of 19 students did not pass on the topic of acid-base, then the analysis of remedial learning results only focused on these 19 students, consisting of 8 boys and 11 girls. There are no exceptions in the analysis process. All participants consciously and voluntarily agreed to be involved in the research. The research results can be published, but the identity of the participant was not explicitly

mentioned.

2.3. The study content

There are six subtopics in acid-based for senior high school in Indonesia. (1) development of the concept of acids and bases; (2) identification of acid-base; (3) acid strength (weak acid pH, weak base, and strong base acid pH strong); (4) calculation of pH; (5) the concept of pH in the environment; and (6) acid and base reactions or neutralizing reactions. The research samples were classified into three categories based on their daily test scores, namely the upper group (A), consisted of 7 students; the middle group (B), consists of 8 students, and the lowest group (C), consists of 4 students. The grouping aimed to facilitate the analysis of understanding concepts in students. The effectiveness of teaching materials can be known from the pretest and posttest (Appendix 1) (Creswell, 2015).

2.4. Instruments

The instruments used were in the form of conceptual understanding tests of three-tiers multiple choices (Appendix 1) that were adapted from other studies (Halstead, 2009; Ilmah, 2017; Milenković, Hrin, Segedinac, and Horvat, 2016; Modell, H., Michael, J., and Wenderoth, 2005; Muchtar *et al.*, 2012; Nurlialawati, 2017; Pohan, 2017; Treagust, 1988; Tuysuz, 2009). The concept of understanding test questions consists of 20 items. The detail of the test can be seen at Appendix 1.

2.5. Lessons

All participants took regular lessons on the topic of acid and base and took an exam at the end of the lesson. Based on exam results, classical passing grade rates have not yet been reached. Therefore, remedial learning is done by using refutation text. After remedial learning, all participants took a conceptual understanding test. Remedial learning consisted of two parts. Activities in the first part, beginning with conducting activities pretest. Then proceed with the provision of teaching materials part 1 in the form of refutation text. After that, continue to posttest. All the activities were done in one meeting (about 120 minutes). The second part is almost the same as the first part, by giving teaching materials part 2 and doing posttests with the same research subject. The different stages of implementation between the first and second part were in the second part, 1) the provision of teaching materials carried out with additional

discussion for 2 lesson hours (about 80 minutes); 2) students are also given a reading control card; 3) posttest is carried out 2 days after giving teaching materials so that there is more time to read refutation text than in first part.

2.6. Results presentation and statistics

The results of the pre and posttest answers were analyzed by grouping the answers of each student based on the categories in Table 1. The answer pattern analysis results was then converted into a percentage to determine the changes that occur. Mc Nemar Test and Cochran-Q Test were conducted to determine whether the data was significant or not (Yarnold, 2015). Recapitulation of results data is pre, and posttest frequency in the form of 2x2 tables is based on the categories in Table 2. In contrast, the determination of changes in the answer category is based on Table 3. The data analyzed are only data "a" and "d" (Table 2). The code in Table 3 was based on Table 1, e.g., U-LK has meant the answer in the pretest include in 'understanding (U)'. Then in the posttest, it changes into 'lack knowledge (LK)'. Then, it includes changing the concept from positive to negative categories.

The Mc-Nemar statistical test was conducted to determine whether the change in number was significant or not. The Mc-Nemar test selection was based on the fact that the study sample was less than 25, so nonparametric tests were used; besides that, the data were not normally distributed. The test can be used to test whether there are significant differences between 2 pairs of samples. The purpose of 2 paired samples can be 1 sample measured 2 times, for example, 1 person measured his understanding by giving pre and posttest. The paired sample in question can also be in the form of 2 samples measured together, i.e., 1 sample is treated, and the other is not treated. The statistical result using Mc-Nemar test (in metode) is given in terms of χ^2 . It is same with the t test, to determine the data signification but for nonparametric data (Creswell, 2015).

The Q-Cochran test is a non-parametric test, which is similar to repeated ANOVA measures and is used to detect differences in multiple sets of matching numerical responses. This procedure also calculates a two-sided pairwise multiple comparison test, making it possible to determine which groups of individuals differ if the null hypothesis in the Q-Cochran test is rejected. The Cochran's Q test is an extension of the McNemar test to situations where there are

more than two suitable samples (Creswell, 2015).

3. RESULTS AND DISCUSSION:

In general, in group A, six of seven students have an increased understanding of the concept and decrease misconceptions. Although there were students who have not concept change and have grown in misunderstanding. The result of group B was six of eight students has increased in the understanding of concepts and has decreased in misconceptions. A total of 4 students in group C have increased in understanding concepts and have decreased in misconceptions. The planned improvement was given a time lag between giving teaching materials and posttest. Besides, students are also given a reading control card to control students to read teaching materials seriously.

The results posttest in part 2 showed that all students (groups A, B, and C) have increased in understanding concepts. Although all students experienced an increase in understanding of concepts, some students also have increased in misconceptions. For group A, one of seven students experienced an increase in misunderstandings occurring in item number 16 (about the relationship between Ka's value and pH strength). Misunderstandings for the same number of questions in group B occurred in 4 of the 8 students who initially did not understand the concept as a misconception. In comparison, the other 4 students did not experience changes in conceptual understanding. Whereas in group C, misconceptions still occur in items number 12, 14, 17, and 18 of Appendix 1.

Question number 12 (Appendix 1) is related to the concept of acid strength. There were three of four students has a misconception about the degree of dissociation. They have not been able to distinguish strong acids and weak acids. Item number 14 deals with the use of the acid-base theory. As many as 1 in 4 students still answer Arrhenius's acid-base theory can explain all acid-base concepts. Items number 17 and 18 relate to the concept of pH calculation and neutralization reaction. As many as 1 out of 4 students (different people) who initially did not understand became a misconception. The misconception found is that students still think that the pH of weak acids and strong acids is always different, and the results of neutralization reactions are always neutral.

The second posttest result was combined with data first posttest to be analyzed with indicators of understanding concepts and learning

achievement indicators and the results pretest. In general, the number of students who understand the concept increases, and those who experience misconceptions decrease. This applies to the six sub-concepts in acid-base material. The complete change can be seen in Figures 2 and 3. Sub-concepts in acid-base material based on syllabus surgery namely (1) development of the concept of acids and bases, (2) identification of acid-base, (3) acid strength (weak acid pH, weak base, and strong base acid pH strong), (4) calculation of pH, (5) the concept of pH in the environment and (6) acid and base reactions or neutralizing reactions.

The 1st sub-conception is the development of the theory of acid-base. The theories discussed include the theory of acid-base Arrhenius, Brönsted-Lowry, and Lewis. One of the misconceptions in this sub-concept is that students cannot understand the use of acid-base theory. Most students think that using one of these theories can explain all acid-base reactions. Also, some students had difficulty understanding the theory of the Brönsted-Lowry acid-base. This difficulty is evidenced by some students still being wrong in answering the 9th question item.

The second sub-conception material includes a discussion of acid-base characteristics, various indicators, and how to identify acid bases with indicators. The misconception in this sub-concept is that students assume that acidic compounds are more dangerous than alkaline compounds. The pretest and posttest results also show that the number of students who understand this concept is quite high.

Acid-base strength (3rd sub-conception) is a reasonably tricky concept. This is evidenced by most students not yet understanding the difference between strong/weak acids/bases. As many as 6 out of 19 experienced misconceptions based on the results of the pretest. The misconception is that the pH shows the strength of the acid. The smaller the pH the stronger the acid. Another difficulty in this concept is that students do not understand the concept of acid/base constant. Based on the answers to item number 12, some students still answered that K_a 's value for acetic acid was equal to 1. The results of the posttest showed that there was an increase in understanding and a decrease in misconceptions. As many as 2 out of 19 people still experience misconceptions, especially regarding the concept of K_a / K_b . The two students understood that the value of K_a for weak acids was less than one, but they still did not understand the reason.

The fourth sub-concept, namely the

calculation of pH, is the most difficult, as evidenced by 11 of 19 students experiencing misconceptions based on the pretest results. A common misconception is that they think that the pH value of a strong and weak acid / base compound is different. They also still have difficulty understanding the calculation of weak and strong acid / base pH (difficulty in reducing equations).

The fifth sub-concept discusses the influence of pH in everyday life, one of which is on the environment. Many students still know that pH can affect river water quality, but they are still not right in answering the reason. Students think that acidic chemical plant wastes only cause the change in pH in river water without connecting whether the river water pH increases or decreases (4 out of 19 students). After conducted refutation text was, only 1 in 4 students still experienced misconceptions.

The final sub-conception in acid-base material is an acid-base reaction known as neutralization reaction. This sub-concept introduces students to writing and equalizing acid-base reactions. This sub-concept is very important because it relates to further materials such as hydrolysis and buffer solutions. The neutralization reaction in the concept of acid-base is the number of moles of acids and bases that react equally or both react precisely. Still, the pH of the resultant reaction is not necessarily neutral. There were 8 of the 19 students still did not understand, and 9 of them had misconceptions. They think that neutralization reactions always produce a neutral solution. After remedial learning, 7 of 19 students were had conceptual understanding while 6 students keep has misconceptions. The reason is probably that students are more focused on learning concepts related to calculations.

The recapitulation of the Mc-Nemar test can be seen in Figure 4. The value of the degree of freedom is equal to 1, and the alpha value is 5%, obtained χ^2_{standard} is 3.85. Based on this result, the results of 14 items experienced a significant change, while 6 items were not significant. The six items that are not significant changes are numbers 1, 2, 9, 12, 14 and 16. Items number 1, 2 and 14 are not significant because the students who already understand the pretest and posttest results are almost equal. For item number 9, 12, and 16, it occurs because the number of students who experience change from negative to positive is the same as from positive to negative.

Analysis of the results of further implementation to test the increase in understanding concepts in the first and second

parts was significantly or not, carried out by the Crochan-Q Test. Q value obtained is 18.32 for part 1 and 12.7 for part 2 with the value of x_{standard} 9.49. It means that the increased understanding of concepts occurs significantly. The effect size (ES) obtained at each part is 5.94 and 4.12. The ES value of part 1 is more significant than part 2, probably because the sub-concept on part 1 is more accessible than part 2.

The research results were appropriate with the opinions of other researchers that refutation text has effect size high enough in improving understanding of concepts (Broughton and Reynolds, 2010; Hardiansyah, 2009; Hardigaluh, B. and Djudin, n.d.; Regita *et al.*, 2015). Also, it can minimize the adverse effects of learning distortions (misconceptions) (Ariasi, Hyönä, Kaakinen, and Mason, 2017; Broughton and Reynolds, 2010; Diakidoy, Mouskounti, and Fella, 2016). Refutation text also requires less time to be understood than ordinary explanatory texts (Broughton and Reynolds, 2010; Van Boekel, Lasonde, O'Brien, and Kendeou, 2017). Other studies have also found that refutation text is more effective with the presentation of analogies and images. Refutation text can be modified and integrated with other media such as posters, comics (Lasonde, Kolquist, and Vergin, 2017; Modell, H., Michael, J., and Wenderoth, 2005).

The reader, refutation text, remembers more scientific facts than non-refutation text readers (Ariasi *et al.*, 2017). Refutation text is suitable for remedial programs as a corrective action. The refutation sentence in refutation text helps increase integrative processing at the end of the paragraph. The process helps readers connect the reading contents and the concept of faith more quickly (Kendeou *et al.*, 2014; Lasonde *et al.*, 2017; Van Boekel *et al.*, 2017).

The shortcomings of this study are the number of research subjects used is still very limited. Classical completeness was not achieved because only 11 were completed from 19 students who attended the remedial program. Classical completeness is said to have been achieved if at least 12 of the 19 students completed the re-test conducted at the end of this remedial study.

4. CONCLUSIONS:

There were improvements in the understanding of concepts even though there were some students who had increased in misconceptions. Some factors might have influenced them. The distance between the time of taking pretest and posttest which were very close;

the distance between the provision of teaching materials and the execution of the posttest which were also very close; students were still unfamiliar with the teaching material working time of questions; the lack of control of students' sincerity in learning the teaching materials given. It can be concluded that the use of refutation text can improve students' conceptual understanding of the acid-base topic. Nevertheless, there are still students who have an increase in misconceptions. Further research with a more significant sample must be done to gain more valid data.

5. ACKNOWLEDGMENTS:

Thank you so much to Dr. Sri Wardani, M.Sc., Sri Kadarwati, Ph.D., and Nunik Widiarti, M.Si, as validators of teaching material and to Yuniati Ida N., S.Pd. as a teacher of collaborators.

6. REFERENCES:

1. Apeng, B. (2009). Penyediaan bacaan berbentuk refutation text untuk meremidial kesalahan konsep siswa tentang pemantulan cahaya pada cermin di kelas VII SMP N 6 Pontianak. *Jurnal Penelitian Pendidikan*.
2. Ariasi, N., Hyönä, J., Kaakinen, J. K., and Mason, L. (2017). An eye-movement analysis of the refutation effect in reading science text. *Journal of Computer Assisted Learning*, 33(3), 202–221. doi: 10.1111/jcal.12151
3. Brix, J. (2017). Exploring knowledge creation processes as a source of organizational learning: A longitudinal case study of a public innovation project. *Scandinavian Journal of Management*, 33(2), 113–127. doi: 10.1016/j.scaman.2017.05.001
4. Broughton, S. H., and Reynolds, R. E. (2010). The nature of the refutation text effect: an investigation of attention allocation. *The Journal of Education Research*, 103, 407–423. doi: 10.1080/00220670903383101
5. Buna'i. (2007). Program remedial (solusi alternatif bagi siswa yang kesulitan belajar dalam UNAS) Buna'i. *Tadris*, 2(264–278).
6. Chambers, S. K., and Andre, T. (1997). *Gender, Prior Knowledge, Interest, and Experience in Electricity and Conceptual Change Text Manipulations in Learning about Direct Current*. 34(2), 107–123.

7. Chi, M. T. H. (2008). *Three Types of Conceptual Change: Belief Revision, Mental Model Transformation, and Categorical Shift*. 61–82.
8. Creswell, J. W. (2015). *Educational Research: Planning, Conducting, and Evaluating Quantitative and Qualitative Research* (4th ed.; P. A. Smith, Ed.). Boston: Pearson.
9. Danielson, R. W., Sinatra, G. M., and Kendeou, P. (2016). *Augmenting the refutation text effect with analogies and graphics augmenting the refutation text effect with analogies and graphics*. 6950(2). doi: 10.1080/0163853X.2016.1166334
10. Demirdoğlu, G. (2009). *Comparison of the effects of conceptual change texts implemented after and before instruction on secondary school students' understanding of acid-base concepts*. 10(2), 1–29.
11. Diakidoy, I., Mouskounti, T., and Fella, A. (2016). Comprehension processes and outcomes with refutation and expository texts and their contribution to learning. *Learning and Instruction*, 41, 60–69. doi: 10.1016/j.learninstruc.2015.10.002
12. Dole, J. A. (2011). Reading and Writing Quarterly: overcoming learning difficulties readers, texts and conceptual change learning. *Reading and Writing Quarterly*, 16(2), 99–118. doi: 10.1080/105735600277980
13. Effendi, A. (2012). *Pengembangan dan penggunaan instrument diagnostic two tier untuk mengidentifikasi miskonsepsi siswa tentang asam dan basa di SMA N 7 Malang*. Universitas Negeri Malang.
14. Halstead, S. E. (2009). *A critical analysis of research done to identify conceptual difficulties in acid-base chemistry* (University of KwaZulu-Natal). Retrieved from https://www.google.com/url?q=https://pdfs.semanticscholar.org/efad/74b887858eab63b65fe6ebf87437dd72807.pdf&sa=U&ved=2ahUKEwjsnJr_w6vqAhXbeisKHXbMCHYQFjABegQIBxABandusg=AOvVaw3mwcljgoGFFX5PMEoSnmMJ9
15. Hardiansyah. (2009). Efektifitas remediasi dengan bantuan bahan bacaan efutation text untuk mengurangi miskonsepsi siswa tentang konsep getaran. *Jurnal Penelitian Pendidikan. Jurnal Penelitian Pendidikan*.
16. Hardigaluh, B. and Djudin, T. (n.d.). Efektivitas penyediaan bacaan berbentuk refutation text untuk meremediasi kesalahan konsep suhu dan kalor pada siswa SLTP di Kodya Pontianak. *Jurnal Penelitian Pendidikan. FKIP UNTAN*.
17. Haryani, S., T.P., A., and Saptarini. (2014). Identifikasi materi kimia SMA sulit menurut pandanganguru dan calon guru kimia. *Seminar Nasional Kimia Dan Pedidikan Kimia 44*. Surakarta.
18. Hastuti, S. (2000). *Pengajaran Remedial*. Yogyakarta: PT. Mitra Gama Widya.
19. Kemendikbud. (2019). Laporan Hasil Ujian Nasional. Retrieved from Kemendikbud website: https://hasilun.puspendik.kemdikbud.go.id/#2019!smp!capaian_nasional!99and99and999!TandTandTandTand1and1!and
20. Kendeou, P., Walsh, E. K., Smith, E. R., and O'Brien, E. J. (2014). Knowledge Revision Processes in Refutation Texts. *Discourse Processes*, 51(5–6), 374–397. doi: 10.1016/j.jpcs.2018.10.009
21. Lassonde, K. A., Kolquist, M., and Vergin, M. (2017). Revising psychology misconceptions by integrating a refutation-style text framework into poster presentations. *Teaching of Psychology Journal*, 44(3), 255–262. doi: 10.1177/0098628317712754
22. Margolis, H., McCabe, P. P., Margolis, H., and McCabe, P. P. (2016). *Overcoming Resistance to a New Remedial Program*. 8655(April). doi: 10.1080/00098655.1988.10114028
23. Metin, M. (2011). Effect of teaching material based on 5E model removed preservice teacher misconception about acid base. *Bulgarian Journal of Science and Education Policy*, 5(2).
24. Modell, H., Michael, J., and Wenderoth, M. P. (2005). Helping the learner to learn: The role of uncovering misconceptions. *The American Biology Teacher*, 67, 20–27. Retrieved from <http://proquest.umi.com/pqdweb?index=1&did=786223161&SrchMode=1&sid=3&Fmt=4&VInst=PROD&VType=PQD&RQT=309&VName=PQD&TS=1185120158&clientId=68516>
25. Muchtar, Z., Sciences, N., and Iskandar,

- W. (2012). *Analyzing of Students' Misconceptions on Acid-Base Chemistry at Senior High Schools in Medan*. 3(15), 65–74.
26. Regita, I., Enawaty, E., Harun, A. I., and Text, R. (2015). Penyediaan refutation text untuk meremediasi kesalahan konsep siswa materi kelarutan dan hasil kali kelarutan. *Jurnal Pendidikan Matematika Dan Sains*, 1–10.
 27. Sesen, B. A. and T. L. (2011). Active learning versus teacher centered instruction for acid-base learning. *Research in Science and Techonolgical Educatin*, 29(2), 205–226.
 28. Sheppard, K. (2006). High school students' understanding of titrations and related acid-base phenomena. *Education in Chemistry*, 7(1), 32–45. doi: 10.1039/b5rp90014j
 29. Tippet, C. D. (2010). Refutation text in science education: a review of two decades of research. *Intenational Journal of Science and Mathematics Education*, 8(May 2009), 951–970. doi: 10.1007/s10763-010-9203-x
 30. Van Boekel, M., Lassonde, K. A., O'Brien, E. J., and Kendeou, P. (2017). Source credibility and the processing of refutation texts. *Memory and Cognition*, 45(1), 168–181. doi: 10.3758/s13421-016-0649-0

Table 1. Patterns of grouping to analyze the answers of the three-tiers test

Tier -1	Tier 2	Tier 3	Category
True	True	Sure	Understanding (U)
True	True	Not Sure	Less Understood (GL)
False	True	Not Sure	Guess (G)
True	False	Not sure	Guessing (G)
False	False	Not sure	Leak Knowledge (LK)
False	True	Sure	Misconception (M)
True	False	Sure	Misconception (M)
One	One	Sure	Misconception (M)

Table 2. The answer change's categories

Pretest	Posttest	
	Negative	Positive
Positive	a	b
Negative	c	d

Table 3. Pattern for Determining Changes to Answers

Pretest	Posttest	The Answer Change
Positive	Negative	U-LK; U-M; U-GL; U-G; GL-G; GL-M; GL-LK; G-M; G-LK; M-LK
Positive	Positive	U-U; GL-GL; G-G
Negative	Negative	LK-LK; M-M
Negative	Positive	LK-G; LK-GL; LK-U; M-G; M-GL; M-U; G-GL; G-U; GL-U

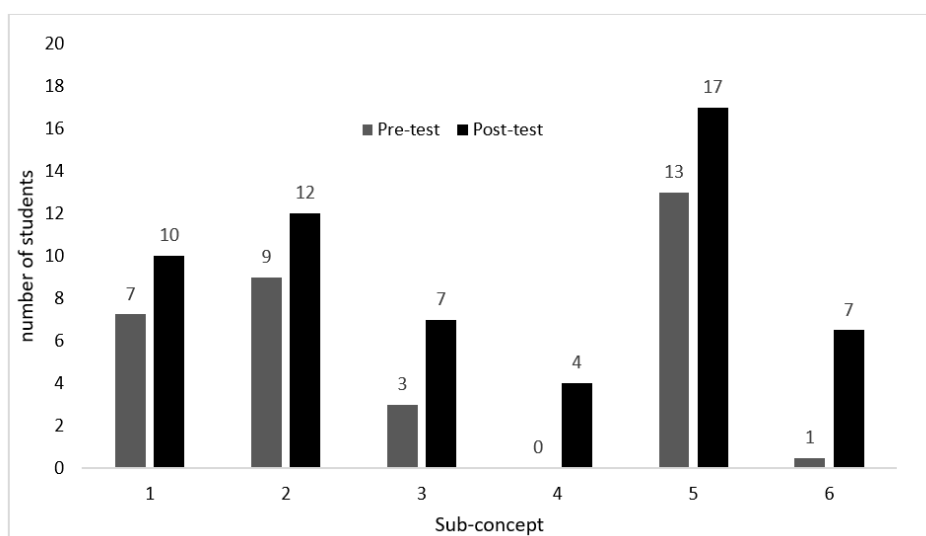


Figure 2. Changes in concept understanding

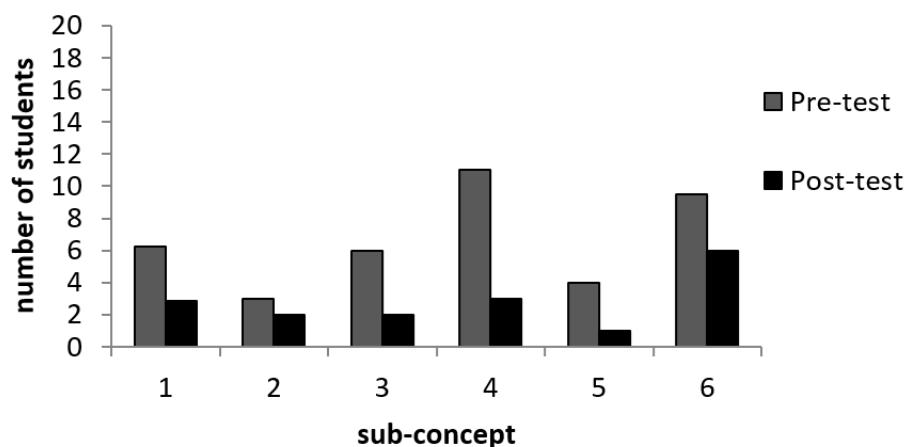


Figure 3. Changes in misconception

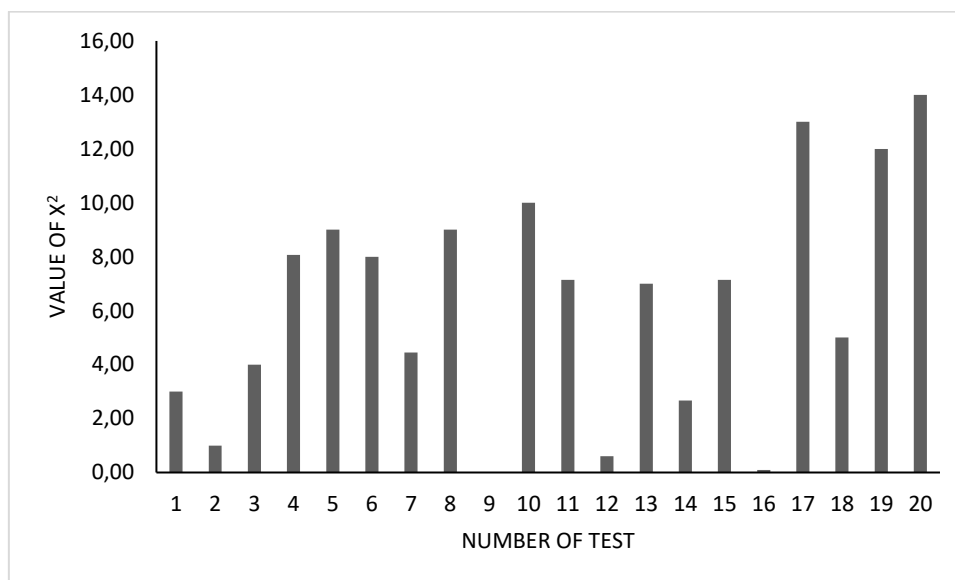


Figure 4. The Mc-Nemar Test's result

APPENDIX 1

• THREE-TIERS MULTIPLE CHOICES TESTS OF ACID-BASE TOPIC FOR SENIOR HIGH SCHOOL STUDENTS

WORK INSTRUCTIONS:

- Fill in the complete identity, including Name, No. Absent, and Class Name.
- The questions consist of 15 questions with three tiers of answers
 Tier 1: Answer
 Tier 2: Reason
 Tier 3: Confidence level
- Write your answer by crossing (X) on the answer sheet according to your answer
- Scoring rules
 - if level 1 and 2 are correct, and you are sure : 4
 - if level 1 and 2 are correct, and you are not sure : 3
 - if level 1 or 2 is wrong, and you're not sure : 2
 - if level 1 or 2 is wrong and you are sure : 1
 - if level 1 and 2 are wrong and you are not sure : 0
 - if level 1 and 2 are wrong and you are sure : -1
 - if not answer either part or all : -2
- It is permissible to bring periodic tables and calculators, but it is **forbidden** to use communication devices or computer

THREE-TIERS MULTIPLE CHOICES TESTS:

- The nature of pure water based on Arrhenius's theory is ...

Answer Choice:

- Neutral
- Weak acid
- Strong acid
- Weak base
- Strong bases

Choice of Reason:

1. Nonpolar
2. water is colorless
3. Is a universal solvent
4. Water molecules do not break down easily
5. The amount of H^+ and OH^- ions in pure water is equal.

Confidence Level

- I. Sure
- II. Not sure

2. Pay attention to Table 1!

Table 1. Definition of acids and bases

Acid	Base
1. Ionized acid in water produces H^+ ions	a. Bases are substances that can bind to H^+ ions
2. Acid is a substance that can donate H^+	b. The OH^- ion in water is a characteristic of bases
3. Acid is a compound that has an H atom	c. Bases are all compounds containing the $-OH$ group

The exact statement according to Arrhenius's acid-base theory is...

Answer choices:

- A. 1 and a
- B. 1 and b
- C. 2 and a
- D. 3 and b
- E. 3 and c

A. Choice of reasons:

1. According to Arrhenius, acids and bases will ionize into cation and anion
2. According to Arrhenius, the nature of acids or bases is based on the handover of protons (H^+)
3. According to Arrhenius the nature of acids or bases is based on the transfer of lone pairs
4. According to Arrhenius, acidic or basic compounds are electron and proton donors (H^+)
5. According to Arrhenius, the H^+ ion is the carrier of acidic properties, and the OH^- ion is the carrier of basic properties

Confidence level

- I. Sure
- II. Not sure

3. The following theory statement, which is following the Brönsted-Lowry acid-base theory, is ...

B. Answer choices:

- A. The acid in water releases H^+ ions
- B. Alkaline in water releases OH^- ions
- C. A base is a substance that can receive protons (H^+)
- D. Acids and bases in water can receive protons
- E. An acid is a substance that can be bound to a pair of free electrons in a base

C. Choice of reasons:

- 1) H^+ and OH^- ions as conjugate acid-base pairs
- 2) According to Brönsted-Lowry, the acidic or basic nature is based on electron handover
- 3) Brönsted-Lowry substances that are acidic or basic are only dissolved in water solvents
- 4) Substances which act as acids will form conjugate acids because they provide donor protons

- (H⁺)
- 5) Substances that act as bases will form into conjugate acids because they receive a donor proton (H⁺)

Confidence level

- I. Sure
II. Not sure

4. The following reaction is an acid-base reaction, except ...

Answer choices

- A. $\text{Al}(\text{OH})_3 (\text{aq}) + \text{OH}^- (\text{aq}) \rightleftharpoons \text{Al}(\text{OH})_4^+ (\text{aq})$
 B. $\text{H}_2\text{O} (\text{l}) + \text{H}_2\text{O} (\text{l}) \rightleftharpoons \text{H}_3\text{O}^+ (\text{aq}) + \text{OH}^- (\text{aq})$
 C. $\text{BF}_3 (\text{g}) + \text{NH}_3 (\text{g}) \rightleftharpoons \text{NH}_3\text{-BF}_3 (\text{s})$
 D. $2\text{NH}_3 (\text{l}) \rightleftharpoons \text{NH}_4^+ (\text{l}) + \text{NH}_2^- (\text{l})$
 E. $3\text{Ni}^{2+} (\text{aq}) + 2\text{Cr}(\text{OH})_3 (\text{aq}) + 10\text{OH}^- (\text{aq}) \rightleftharpoons 3\text{Ni} (\text{s}) + 2\text{CrO}_4^{2-} (\text{aq}) + 8\text{H}_2\text{O} (\text{l})$

Choice of reasons

- 1) Every acid-base reaction must involve OH⁻ and or H⁺ ions
 2) the phase of reagents not in water solvents
 3) is a reduction-oxidation reaction
 4) is a depositional reaction
 5) the product produced is not salt and water

Confidence level

- I. Sure
II. Not sure

5. The reactions in question number 4, which are acid-base reactions, according to Brønsted-Lowry, are ...

Answer choices:

- A. Reactions A and B
 B. Reactions A and C
 C. Reactions A and E
 D. Reactions B and C
 E. Reaction B and D

D. Choice of reasons:

- 1) The ions are ionized into cations and anions
 2) Acid and base compounds dissolved in water solvents
 3) Ionized acid compounds produce hydrogen ions
 4) Co-existence with a pair of free electron pairs
 5) Acid and base compounds undergo proton (H⁺) handover

Confidence level

- I. Sure
II. Not sure

6. The reactions in question number 4, which are acid-base reactions, according to Lewis, are ...

E. Answer choices:

- A. Reactions A and B
 B. Reactions A and C
 C. Reactions A and E
 D. Reactions B and C
 E. Reaction B and D

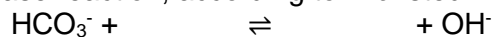
F. Choice of reasons:

- 1) Base compounds involve hydroxide ions in their reaction
- 2) Acid and base compounds do not depend on water solvents
- 3) Base compounds donate lone pairs to acidic compounds
- 4) Acid compounds donate lone pairs to base compounds
- 5) Base compounds provide free electron pairs for acid compounds to be used together

Confidence level

- I. Sure
- II. Not sure

7. Consider the following acid-base reaction, according to Brönsted-Lowry!



The right compound to complete the acid-base reaction in succession if HCO_3^- as a base and OH^- as a conjugate base is ...

G. Answer choices:

- A. OH^- and H_2O
- B. OH^- and CO_3^{2-}
- C. OH^- and H_2CO_3
- D. H_2O and CO_3^{2-}
- E. H_2O and H_2CO_3

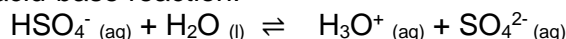
H. Choice of reasons:

- 1) H_2CO_3 accepts protons (H^+) from H_2O
- 2) OH^- gives protons (H^+) to HCO_3^-
- 3) H_2O gives protons (H^+) to HCO_3^-
- 4) H_2CO_3 gives protons (H^+) to HCO_3^-
- 5) HCO_3^- receives protons (H^+) from H_2O to CO_3^{2-}

Confidence level

- I. Sure
- II. Not sure

8. Consider the following acid-base reaction!



The conjugate acid-base pair, according to Brönsted-Lowry from the above reaction, is...

I. Answer choices:

- A. SO_4^{2-} and H_2O
- B. HSO_4^- and H_2O
- C. HSO_4^- and SO_4^{2-}
- D. H_3O^+ and SO_4^{2-}
- E. H_3O^+ and HSO_4^-

J. Choice of reasons:

- 1) H_2O accepts protons (H^+) from H_3O^+
- 2) H_2O gives protons (H^+) to HSO_4^-
- 3) H_3O^+ gives protons (H^+) to SO_4^{2-}
- 4) SO_4^{2-} acts as a conjugate acid and H_2O as a base
- 5) HSO_4^- acts as an acid and SO_4^{2-} as its conjugate base

Confidence level

- I. Sure
- II. Not sure

9. Sulfide acid solution (H_2S) has two ionization constant values namely $K_{a1} = 8.9 \times 10^{-8}$ and $K_{a2} = 1.2 \times 10^{-13}$. Species in sulfide acid (H_2S) solution are ...

Answer choices:

- A. H_2S , HS^- , S^{2-} , H^+ , OH^- , H_2O
- B. HS^- , H^+ , OH^- , H_2O
- C. S^{2-} , H^+ , OH^- , H_2O
- D. H_2S , S^{2-} , H^+ , OH^- , H_2O
- E. H_2S , HS^- , H^+ , S^{2-} , H_2O

Choice of reasons:

- A. H_2S solution is a strong polyprotic acid so that it will ionize completely in one stage
- B. H_2S solution is a polyprotic weak acid so that it will ionize completely in one step
- C. H_2S solution is a polyprotic weak acid so that it will ionize partially in one stage
- D. H_2S solution is a polyprotic weak acid so that it will ionize partially in 2 stages
- E. H_2S solution is a weak acid so it has no base species in the solution.

Confidence level

- I. Sure
- II. Not sure

10. A 0.1 grams of NaOH solids were dissolved in water to 100 mL at 25 ° C. The nature of the solution is

11.

K. Answer choices:

- A. neutral
- B. bases
- C. acid
- D. can be acidic or basic
- E. can be basic or neutral

L. Choice of reasons:

- 1) neutral because the solution has a $\text{pH} = 7$
- 2) acidic because the solution has a $\text{pH} > 7$
- 3) acidic because the solution has a $\text{pH} < 7$
- 4) alkaline because the solution has a $\text{pH} > 7$
- 5) alkaline because the solution has a $\text{pH} < 7$

Confidence level

- I. Sure
- II. Not sure

12. Valid acid solution with a concentration of 0.01 M turned out to have a pH value above 2. The degree of ionization (α) of the acid is.....

M. Answer choices:

- A. more than 1
- B. less than 1
- C. is equal to 1
- D. is less than equal to 1
- E. More than equal to 1

N. Choice of reasons:

- 1) is a monoprotic strong acid and completely dissociated
- 2) is a monoprotic strong acid and partially dissociated
- 3) is acidic weak monoprotic and fully dissociated

- 4) is acidic weak monoprotic and partially dissociated
- 5) is a strong but dilute acid, so the pH value of the solution is high

Confidence level

- I. Sure
- II. Not sure

13. Two 150 mL glass bottles, each containing 0.01 M HCl solution and 0.01 M CH₃COOH solution. Do the two solutions have different acid strengths?

O. Answer choices:

- A. Yes B. Not

P. Choice of reasons:

- 1) Both are acidic solutions with the same acid strength
- 2) The number of binding atoms affects the strength of acids
- 3) The ability to ionize in different waters affects the strength of the acid
- 4) The concentration of the same solution results in the same acid strength
- 5) Acetic acid has more hydrogen atoms compared to hydrochloric acid

Confidence level

- I. Sure
- II. Not sure

14. Is the theory of acid-base according to Arrhenius sufficient to explain all substances that are acidic or basic?

Q. Answer choices:

- A. Yes B. Not

R. Choice of reasons:

- 1) Not limited to solvents
- 2) Not to include the smallest things
- 3) Limited to free electron handover
- 4) Limited to the reaction of H⁺ and OH⁻ in water
- 5) Take and give H⁺ occurs in a water solvent

Confidence level

- I. Sure
- II. Not sure

15. The researchers found that the pH of mountain water was 6.8 - 7, while in the low region which is a downstream area of the river the pH value of the river was obtained to 9. Based on the illustration, does the change in pH affects the river's water quality?

S. Answer choices:

- A. Yes B. Not

T. Choice of reasons:

- 1) Changes in pH value experienced by the river water does not affect the quality of river water
- 2) Changes in the pH value of river water may be caused by acid rain, thereby reducing water quality
- 3) Changes in the pH value of river water may be caused by household soap waste, thereby reducing water quality
- 4) The change in pH value is due to the pH changing by itself due to differences in water level, thereby improving water quality

- 5) Changes in the pH value of river water may be caused by chemical plant waste containing hydrochloric acid compounds, which is high enough to reduce water quality

Confidence level

- I. Sure
II. Not sure

16. Sulfonic acid solution (H_2SO_3) and sulfuric acid (H_2SO_4) in concentrated conditions can cause serious injury if it affects the skin / other body parts. The K_{a2} values of each acid were 1.2×10^{-2} and 6.43×10^{-8} . A laboratory assistant makes a solution of sulphonic acid with a concentration of 0.1 M and 0.5 M sulfuric acid with the same volume. Is the sulfuric acid solution made by the laboratory assistant stronger than sulfonic acid?

Answer Choice:

- A. Yes B. No

Choice of Reason:

- 1) The strengths of sulfuric acid and sulfonic acid are the same or almost the same because they are strong acids.
- 2) Sulfuric acid is stronger than sulfonic acid because the value of K_a sulfuric acid is greater than sulfonic acid.
- 3) Sulfuric acid is stronger than sulfonic acid because there are more O atoms in sulfuric acid.
- 4) Sulfuric acid is stronger than sulfonic acid because of its greater concentration.
- 5) Sulfuric acid is stronger than sulfonic acid because the pH of sulfuric acid is greater than the pH of sulfonic acid.

Confidence level:

- I. Sure
II. Not sure

17. A total of 10 mL of 0.1 M cyanide acid (HCN) solution ($K_a = 4.9 \times 10^{-10}$) mixed with 10 mL of pyridine ($\text{C}_2\text{H}_5\text{N}$) 0.1 M ($K_b = 1.7 \times 10^{-9}$) produce saline solution. Is the pH of the salt solution equal to 7?

Answer Choice:

- A. Yes
B. Not

Choice of Reasons

- A. Both of these solutions react appropriately (both equivalent moles are the same)
- B. The salt solution comes from weak acids and weak bases
- C. K_a and K_b values do not affect the nature of the solution
- D. The salt solution is acidic because the value of K_a cyanide acid is smaller than the pyridine base
- E. The salt solution is basic because the value of K_a cyanide acid is smaller than the pyridine base

Confidence level:

- I. Sure
II. Not sure

18. There are two acid solutions, acetic acid (CH_3COOH) solution of 200 mL ($K_a = 1 \times 10^{-5}$) has a dissociation degree of 1% and 200 mL of 5×10^{-4} M sulfuric acid (H_2SO_4) solution. Are both of the solutions have the same pH value?

Answer choices

- A. Yes
- B. Not

Choice of reasons

- 1) both of these solutions have the same concentration
- 2) the concentration of acetic acid is greater than sulfuric acid
- 3) sulfuric acid is diprotic acid so that the acid pH value is lower
- 4) The pH of weak acids and strong acids is always different
- 5) the amount of H^+ and OH^- ions in the two solutions is the same

Confidence level:

- I. Sure
- II. Not sure

19. The following compounds in water that provide the most powerful alkaline properties are....

Answer choices

- A. CH_3CH_2CHO
- B. $CH_3CH_2CH_2OH$
- C. $CH_3CH_2CO_2H$
- D. $CH_3CH_2CH_2NH_2$
- E. CH_3COCH_3

Choice of reasons

- 1) Base compounds are compounds that have the -OH group
- 2) The less the number of H atoms the more alkaline
- 3) The -NH₂ group gives the basicity of nature stronger than the -OH group
- 4) The -NH₂ group gives basic properties weaker than the -OH group
- 5) Cluster =O gives a stronger nature than the -OH group

Confidence level:

- I. Sure
- II. Not sure

20. Hydrogen fluoride (HF) compounds in water are weak acids. A 0.1 mol of HF was dissolved in 500 mL of solution and the K_a value was 6.5×10^{-4} , was the pH of the solution less than 2?

Answer choices:

- A. Yes
- B. Not

Choice of reasons

- 1) K_a HF is more than 10^{-4} so the pH value of HF is always more than 2
- 2) The concentration of the solution is 0.1 M
- 3) The concentration of the solution is 0.2 M
- 4) The higher the pH the weaker an acid, and HF is a weak acid
- 5) Volume does not affect the pH value

Confidence level:

- I. Sure
- II. Not sure

21. A total of 100 mL of 0.1 M NaOH solution was reacted with 100 mL of 0.1 M H_2SO_4 solution, was the resulting solution neutral?

Answer choices

- A. Yes
- B. Not

Choice of reasons:

- 1) The reaction is an acid and base reaction which produces a neutral solution
- 2) The reaction is a reaction of strong acids and strong bases and produces a neutral solution
- 3) The concentrations of the two reactants are the same so the solution will be neutral
- 4) In this reaction, the number of moles of acid and base reacting is equivalent
- 5) In this reaction, the number of moles of acid and base that reacts is not equivalent

Confidence level:

- I. Sure
- II. Not sure

A PREVALÊNCIA DO PARASITA *TRICHOMONAS VAGINALIS* ENTRE MULHERES EM ALGUMAS REGIÕES DA PROVÍNCIA DE MAYSAN

THE PREVALENCE OF *TRICHOMONAS VAGINALIS* PARASITE AMONG WOMEN IN SOME REGIONS OF MAYSAN PROVINCE

معدل انتشار طفيلي المشعرات المهبليّة بين النساء في بعض مناطق محافظة ميسان

AL-MAJIDII, Noor K. Saad¹; ALSAADY, Hussain A. Mhouse^{1*}

¹ Department of Biology, College of Science, University of Misan, Maysan, Iraq.

* Corresponding author

e-mail: hussainsaady@uomisan.edu.iq

Received 20 September 2020; received in revised form 11 October 2020; accepted 29 October 2020

RESUMO

Trichomonas vaginalis é um protozoário parasita flagelado extracelular. Ele se adapta para viver em condições anaeróbicas da vagina da mulher e causa tricomoníase que é uma doença sexualmente transmissível (DST) não viral. Esse parasita se espalha em todas as regiões do mundo, e a taxa de prevalência global da tricomoníase vaginal em mulheres é maior do que em homens. No Iraque, é considerada uma doença negligenciada, pois há poucos estudos sobre esse parasita, principalmente na província de Maysan, onde os estudos são praticamente ausentes. Neste estudo, duzentos e vinte e seis esfregaços vaginais foram coletados de mulheres que visitaram hospitais, centros de saúde e clínicas médicas em algumas áreas do *governorate* de Maysan (distrito de Amara, distrito de Al-Kahla, distrito de Al-Maymouna, distrito de Al-Majar Al-Distrito de Kabir) durante o período de 10 de novembro de 2019 a 10 de fevereiro de 2020. Os resultados do exame microscópico de esfregaços vaginais mostraram que a taxa de infecção geral foi de 75,22% (170/226). O distrito de AL-Kahla teve a maior taxa de infecção (96,15%), enquanto a mais baixa foi no distrito de Maimouna (60,00%). A faixa etária de 34 a 40 anos apresentou a maior taxa de infecção (86,95%), enquanto a faixa etária <15 anos apresentou a menor taxa de infecção (37,50%). Mulheres casadas apresentaram maior taxa de infecção (80,92%) do que mulheres solteiras (40,62%). A taxa de infecção entre mulheres não grávidas foi alta (81,11%) do que entre mulheres grávidas (78,57%). Este estudo mostrou que o pH vaginal tem um papel significativo na proteção da vagina da mulher contra tricomoníase, sendo que a maior taxa de infecção (96,63%) foi registrada na vagina com pH 6, enquanto nenhuma infecção foi registrada em pH 4. De destes resultados podemos concluir que a tricomoníase é amplamente difundida entre as mulheres das comunidades de Maysan, verificou-se que a infecção foi afetada significativamente por alguns fatores demográficos como idade, ocupação, estado civil, marido polígamo, secreções vaginais e prurido e pH da vagina.

Palavras-chave: *Trichomonas vaginalis*, DST, Microscopia, pH, Iraque.

ABSTRACT

Trichomonas vaginalis is an extracellular flagellated parasitic protozoan. It adapts to live in anaerobic conditions of the women's vagina and causes Trichomoniasis, a non-viral, sexually transmitted disease (STD). This parasite spreads in all regions of the world, and the global prevalence rate of vaginal Trichomoniasis in women is higher than in men. It is considered a neglected disease in Iraq, as there are few studies about this parasite, especially in Maysan province, where researches are near absent. In this study, two hundred and twenty-six vaginal swabs were collected from women who visited hospitals, health centers, and medical clinics in some areas of Maysan province (Amara district, Al-Kahla district, Al-Maymouna district, Al-Majar Al-Kabir district) during the period from November 10, 2019 to February 10, 2020. The microscopic examination of vaginal smears showed that the overall infection rate was 75.22% (170/226). AL-Kahla district had the highest rate of infection (96.15%), while the lowest was in the Maimouna district (60.00%). The age group 34-40 years had the highest infection rate (86.95%), while the age group < 15 years had the lowest infection rate (37.50%). Married women had a higher infection (80.92%) than unmarried women (40.62%). The infection rate among nonpregnant women was high (81.11%) than with pregnant women (78.57%). This study showed that vaginal pH has a significant role in protecting the women vagina from Trichomoniasis, once the highest rate of infection (96.63%) was recorded in the vagina with a pH 6, while no infection was recorded at pH 4. It can be concluded that Trichomoniasis is widely spread among women of the Maysan communities, and the condition was affected significantly by some

demographic factors such as age, occupation, marital status, husband polygamous, vaginal secretions, and itching and pH of the vagina.

Keywords: *Trichomonas vaginalis*, STD, Microscopy, pH, Iraq.

المخلص:

المشعرات المهبليّة *Trichomonas vaginalis* هو طفيلي ابتدائي سوطي خارج خلوي. يتأقلم للعيش في الظروف اللاهوائية لمهبل المرأة ويسبب داء المشعرات وهو مرض غير فيروسي ينتقل جنسياً (STD). وينتشر هذا الطفيلي في جميع مناطق العالم، ويكون معدل الانتشار العالمي للمشعر المهبلي في النساء أعلى منه في الرجال. في العراق يعد داء المشعرات من الأمراض المهملة، إذ هناك القليل من الدراسات حول هذا الطفيلي، خاصة في محافظة ميسان حيث تكون الدراسات شبه معدومة. في هذه الدراسة تم جمع مائتين وست وعشرين مسحة مهبليّة من النساء الزائرات للمستشفيات والمراكز الصحية والعيادات الطبية في بعض مناطق محافظة ميسان (قضاء العمارة، قضاء الكحلاء، قضاء الميمونة، قضاء المجر الكبير) خلال الفترة من 10 تشرين الثاني 2019 إلى 10 شباط 2020. وأظهرت نتائج الفحص المجهرى للمسحات المهبليّة أن معدل الإصابة الكلية بلغ 75.22% (226\170). وأن قضاء الكحلاء سجل أعلى معدل للإصابة (96.15%) بينما كان أدناها في قضاء الميمونة (60.00%). وسجلت الفئة العمرية 40-34 سنة أعلى معدل للإصابة (86.95%)، في حين سجلت الفئة العمرية أقل من 15 سنة أدنى معدل للإصابة (37.50%). سجلت النساء المتزوجات أعلى معدل للإصابة (80.92%) من النساء غير المتزوجات (40.62%). بلغ معدل الإصابة بين النساء غير الحوامل 81.11% وفي النساء الحوامل بلغ 78.57%. أظهرت هذه الدراسة أن الرقم الهيدروجيني المهبلي له دور كبير في حماية مهبل المرأة من داء المشعرات، حيث تم تسجيل أعلى نسبة إصابة (96.63%) في المهبل برقم هيدروجيني 6، بينما لم تسجل أي إصابة عند الرقم الهيدروجيني 4. يمكن أن نستنتج أن داء المشعرات ينتشر على نطاق واسع بين نساء مجتمعات ميسان وقد تأثرت العدوى بشكل كبير ببعض العوامل الديموغرافية مثل العمر، المهنة، والحالة الاجتماعية، تعدد الزوجات، الإفرازات المهبليّة والحكة ودرجة الحموضة في المهبل.

الكلمات المفتاحية: المشعرات المهبليّة، الأمراض المتقلّة جنسياً، الفحص المجهرى، درجة الحموضة، العراق.

1. INTRODUCTION:

The human vagina has a balanced natural environment with an acidic environment, where the pH was ranging from 3.8 to 4.5. This is returning to the presence of bacteria normal flora of *Lactobacillus spp.* which has a positive role in protecting the vagina from pathogens like *Trichomonas vaginalis*, Donne 1836 (Trichomonadidae, Trichomonadida), and Vaginitis bacteria (Adnan and Marjani, 2020). It is an obligated parasite, and human is the only known host (Riestra *et al.*, 2019). This parasite takes an oval or pear shape, but sometimes amoeboid in form when it attached to the epithelial cells of the vagina (Mahmud *et al.*, 2018).

The *T. vaginalis* size is ranging from 7-32 x 5-12 um (long x wide), it has four free anterior flagella and the 5th flagellum return back along the edge of the undulating membrane and the ending posterior of 5th flagellum to the middle of the organism body (Roberts and Janovy, 2009). It has a simple life cycle, and it appears that *T. vaginalis* does not have a cyst stage and cannot survive well on the outside of the human body, but it can live in the external environment in a humid environment for more than three hours (Burch *et al.*, 1959). It contains only a trophozoite stage in its life cycle, where the trophozoite is the stage of infection and diagnosis (Beri *et al.*, 2020).

Trichomoniasis is a widespread non-viral, sexually transmitted disease (STD) (Trein *et al.*, 2019). It infected both males and females of all ages, adults, or children in all regions of the world, whether rich or poor (Morris *et al.*, 2019). *T. vaginalis* was the first species of the Genus

Trichomonas to be identified as causing Trichomoniasis in 1916 (Stephen and Richard, 2001). *T. vaginalis* lives in close association with the vagina, urethra, endocervix of the females and prostate tissues, seminal vesicles, and urethra of males. It is an important source of reproductive morbidity (Roberts and Janovy, 2009; Kissinger, 2015). It is transmitted between males and females via vaginal sexual intercourse by using contaminated fomites (Ferré *et al.*, 2019) and via water (Crucitti *et al.*, 2011). Several studies reported that the infection rate (IR) of *T. vaginalis* increased with the increase of IR of bacterial vaginitis. This may cause genital inflammation that may increase the risk of HIV or HSV-2 infection, thereby increasing the risk of transmission to the sexual partner (Deivam *et al.*, 2014; Rostami *et al.*, 2017; Shipitsyna *et al.*, 2020). Also, Trichomoniasis is related to a 1.9-times risk of cervical neoplasia (Zhang and Begg, 1994).

There were about 122 million new trichomoniasis cases in 2015 (Vos *et al.*, 2016). About 2 million women are affected by Trichomoniasis in the USA, and it occurs more often in women than in men (Adams and Fosnight, 2018). The global IR of *T. vaginalis* was estimated to be about 1.0 % and 8.1 % for males and females, respectively (WHO, 2001). According to the records of WHO in some countries, the IR among pregnant women is: in Brazil, 2.11%, Chile, 5-2.7%, Central Africa, 9.9%, and South Africa, 41.4% (Bolumburu *et al.*, 2020). In Iraq, Trichomoniasis was one of the neglected diseases. In Basra, in Southern Iraq, Al-Assadi *et al.* (2020) showed the IR was 5.7-8.5%.

The direct microscopic examination of the

vaginal wet amount is the most common method used to diagnose vaginal Trichomoniasis, which gives high specificity of fresh vaginal spacemen (Al-Mamoori *et al.*, 2020). The testing with a swab, culture media of vaginal secretions, or vaginal swabs has a sensitivity that reaches 63.0–98.2%, and high specificity that reaches 99.4 –100% (Smith *et al.*, 2005).

Metronidazole (Flagyl) is a choice treatment and an effective antibiotic for Trichomoniasis in all world regions, especially in the USA (Workowski and Berman, 2010). It was taken as a single dosage of 2gm/day or 500mg twice daily, for seven days (Workowski and Bolan, 2015). The Metronidazole cure rate was reached 97% (Sherrard, 2020). It estimated that 2.5–5% of all Trichomoniasis treated cases with metronidazole exhibit resistance to metronidazole (Tien *et al.*, 2020).

This study aimed to determine the infection rate of *T. vaginalis* parasite among Maysan province women by using direct microscopic of the wet amount of vaginal discharge and endocervical specimen and investigates infection relation with some sociodemographic factors.

2. MATERIALS AND METHODS:

2.1. The regions of the study

Maysan province is located in South-Eastern Iraq besides the border with Iran. It is located astronomically between two latitudes (31°15'-32° 56') and two longitudes (47° 50' - 46°15'). The province of Maysan extends over 16,072 km², and the population was about (1150000) Peoples. It consists of six districts (Ali-Algarbi, Al-Amara, Al-Maymouna, Al-Kahla, Qulat Saleh, and Al-Majar Al-Kabir). Maysan province has a dry climate and a high temperature. The annual average was 25° C with a range between 6.2 to 45.7° C, and the rainfall is concentrated in the winter months. The annual average of rainfall was 177.3 mm. A total of four districts Al-Amara center, Al-Kahla, Al-Maymouna, Al-Majar Al-Kabir (Figure 1) were randomly chosen for this study. Al-Amara City is the center of Maysan province, with an area of 6,287.07 Km² which consisted of 39.1% of the Maysan area and the population was about 420,000 people, and the area and population of Al-Maymouna, 2,081.49 Km² and 150,678 people; Al-Kahla, 1289.80 Km², and 85000 people and Al-Majar Al-Kabir 1434.92 Km² and 96338 people (Malinowski, 2002; Atiaa *et al.*, 2013; Jaber, 2014; Al-Abadi *et al.*, 2017).

2.2. The study population criteria

The region (Al-Amara, Al-Kahla, Al-Maymouna, and Al-Majar Al-Kabir); age (<15, 15-19, 20-26, 27-33, 34-40, 41-47, 48-54 and ≥55 years old); social status (married and unmarried); education level (illiteracy, primary, secondary and a graduate); occupation (housewife, employee, student, baby girl); marital status of the husband (monogamous, polygamous and not a husband); the number of birth (0, 1-3, 4-6, 7-9); residence (urban and rural); status of women (pregnant, not pregnant and single); pH values (4, 5.5, 6 and 6.5); secretions (yes or no) and itching (yes or no) were used as the parameters of the sample of this study.

2.3. Samples

This study was done under the agreement of the Maysan Health statement. All samples were taken under the direct supervision of the gynecologist physician in all hospitals, health care centers and medical clinics. The nature of the study was explained, and the participants consents were obtained before work began. Using the vaginal speculum, two specimens of the vaginal wet amount had been collected (the first for microscopic examination and the second for cultivation) from every 226 females of different ages of 5-60 years old, who visited hospitals, health care centers, and medical clinics from some regions of Maysan province distributed as Al-Amara city 161, Al-Kahla 26, Al-Maymouna 25 and Al-Majar Al-Kabir 14 women from the period November 10, 2019, to February 10, 2020.

2.4. pH measuring

The pH of the vagina of each participant had been measured by using peat moss paper strips (Merck, Darmstadt, Germany) by taking a drop of vaginal secretions (Sgibnev and Kremleva, 2020).

2.5. Microscopic examination of vaginal secretions samples

For microscopic examination, one drop of phosphate buffer saline pH 7.2 (PBS) was mixed with the vaginal wet amount specimen, and then six slides were prepared: three slides without stain and three for stained with Giemsa stain (mixed of eosin and azure B) (Solarbio, China) and then examined under a compound microscope with 40X magnification.

2.6. Cultivation of vaginal specimens

For cultivation, the 2nd vaginal secretion specimen that loaded in the cotton swap was mixed with three milliliters of PBS. The mixture was cultured with sterile Amies Transport Media (Biozek Medical, Netherlands) (Figure 2) and then incubated at 37°C for seven days. The cultivation specimens were examined periodically every two days to confirm the results.



Figure 2. Amies transport medium.

2.7. Statistical analysis

The data were statistically analysed with the Statistical Package for Social Science software (SPSS version 24) using the Chi-square (χ^2) test to determine the relations between the infection rate and some clinical and sociodemographic factors of the current study. The probability value ($p \leq 0.05$) was used as a criterion statistically significant.

2.8. Ethical clearance

Permission was issued to conduct this study by all health institutions in Maysan province and in the institute where this study was conducted.

3. RESULTS AND DISCUSSION:

The microscopic examination results depend on watching the *T. vaginalis* parasite (Figure 3) in the microscopic field. The results of the present study (Table 1) are shown a high overall IR of *T. vaginalis* among women of 75.22%, and the highest IR (96.15%) is recorded in Al-Kahla district, and the lowest (60.00%) is in Al-Maymouna district. There are significant differences between the IRs of Trichomoniasis among women in this study ($\chi^2=12.118$, $p=0.007$). These results in line with the finding of a previous study in Iraq, Bagdad, 85.50% (Saheb *et al.*, 2016). And higher than of earlier studies in

different regions of Iraq such as Al-Mosul, 25.86% (Al-Mallah, 1981), Baghdad, 22.60% (Al-Kaisi, 1994) Basra, 57.85% (Jarallah, 2013), Diyala, 24.60% (Al-Hussuny, 2015), Baghdad, 19.10% (Al-Muqdad *et al.*, 2017), Al-Najaf, 27.9% (Al-Abbas and Radhi, 2019), Al-Muthana, 26.00% (Al-Abodi *et al.*, 2019), and higher than that reported from other countries such as the USA, 38.0% (Schwebke and Burgess, 2004), Turkey, 3.2% (Kassem and Majoud, 2006), Saudi Arabia, 28.% (Madani, 2006), Iran, 1.7% (Matini *et al.*, 2012),

The high IR in this study may be returned to the lack of personal hygiene, low level of education, social status (Eshete *et al.*, 2013) or due to asymptomatic infection which may extend to six months, or to lack of female doctors in the primary health care center specialized in gynecology, or as a result of incorrect treatment.

Regarding age, it can be said (34-40) years age group had the highest IR (86.95%), and the lowest was (37.50%) at (<15) years age group, ($\chi^2 = 13.334$, $p=0.064$). These results agree with Fattah and Kadir (2010) and do not agree with Sutton *et al.* (2007), where the group (14-19) years was the most affected because the IR was increasing at ages with more significant sexual activity. This may be due to the high level of estrogen that makes the vaginal environment suitable for the growth of the *T. vaginalis* parasite (Nwokah *et al.*, 2019),

On the other hand, this study (Table 1) showed that the IR of Trichomoniasis among married women (80.92%) is higher than that of unmarried women (40.62%), ($\chi^2=23.938$, $p<0.001$). This result is similar to what Al-Kahfaji(2020) found that IR among married women was (81.90%). The higher IR among married women is attributed to sexual intercourse or contraceptive use, leading to increased trichomoniasis IR in married women (Paniker and Ghosh, 2017).

Regarding the education level, it showed that illiteracy women have the highest IR (77.67%) and the lowest (50.00%) is at women with the secondary level ($\chi^2=6.342$, $p=0.096$). This finding agrees with Jarallah (2013) and does not agree with Salman and Kareem (2013), who found the women with primary education levels had the highest IR. This result may be due to poor health care and a lack of women's awareness programs, in which women are at risk of infection (Yeh *et al.*, 2013).

Concerning the occupation, it was found the housewife has the highest IR (78.00%) than others ($\chi^2=10.598$, $p=0.014$). This finding agrees

with Nas *et al.* (2020), who found the highest IR was among unemployed women, which is not in agreement with Mahdi *et al.* (2001). The increasing of IR among non-working women (housewife) may be to some extent resulted from a poor economic level that will be caused malnutrition and thus decline in the body's immunity, which makes it is weak for facing invading of pathogens, including the *T. vaginalis* parasite, or due to lack of the awareness, and neglect of taking proper treatment (Wiesenfeld *et al.*, 2001),

The present study showed a significant relationship between Trichomoniasis and the marital status of the husband (polygamy or monogamy), ($\chi^2=5.734$, $p<0.017$). Women with polygamous husbands had a higher IR of 87.44% than women with monogamous husbands (85.33%). This result agrees with that reported by Adjei *et al.* (2019) and does not agree with Helms *et al.* (2008). This finding is in line with an early report that the IR of Trichomoniasis increases much with the increase in the chances of having vaginal sex (Thurman and Doncel, 2011), especially in populations with high-risk behaviors such as unhealthy sexual activity and having multiple sexual partners (Arbabi *et al.*, 2014).

Table 1 showed that women who had (4-6) births record presented the highest trichomoniasis IR (88.33%) in comparison to unique or other multiple births (but there is no significant, $\chi^2=4.867$, $p=0.182$). This result agrees with Al-Hussuny (2015) and disagrees with Nouraddin and Alsakee (2015). The high IR in women with multiple births may be due to the overwork of the immune system with multiple, repeated pregnancies for long periods (Poole and McClelland, 2013).

The outcomes also showed that women from the rural area had high IR (81.54%) compare with urban's women (72.67%). This finding is in line with the previous studies of Eshete *et al.* (2013) and Taher and shaker (2018), and disagrees with Ali *et al.* (2017). The reasons for the high infection rate in rural women may be due to poor awareness, lack of literacy level, low socioeconomic level, lack of personal hygiene, and most importantly, lack of treatment (Ray *et al.*, 2008)

Regarding pregnancy, it was found (Table 1) that nonpregnant women have a higher IR (81.11%) compared with pregnant women (78.57%). This IR is lower than the IR (89.0%) recorded in nonpregnant women from India

(Masand *et al.*, 2015) but higher than the IR (15.4%) obtained from women in Ethiopia (Mulu *et al.*, 2015). This finding agrees with Abdul-Aziz *et al.* (2019) and does not agree with Kadhum (2012). Vaginal Trichomoniasis is highly affected human fertility, such as sperm activity, and hinders their access to eggs, and thus results in failure to fertilize them (Al Saeed, 2011), which leads to the failure of the embryo implantation, and pregnancy did not occur (Lucena *et al.*, 2015)

This study showed that the pH of a woman's vagina has a very significant effect on the IR of vaginal Trichomoniasis ($\chi^2=185.276$, $p<0.001$). The current results show that the highest infection rate of 96.63% is recorded in the vagina of women with a pH 6. This result is in line with Hawel and Alasadiy (2017) findings, where they found that all infected women with Trichomoniasis were at pH 6. And also in agreement with Glehn *et al.* (2016). This is due to the ability of this parasite to change the pH of the vagina (Korosh *et al.*, 2017) towards alkalinity at a pH of 5 to 6 (Roberts and Janovy, 2009) in order to maintain its survival. And current results showed that no infection was recorded among women with a vagina have a pH 4.

Another clinical sign characteristic of the infection with this parasite is vaginal secretions. The present study (Table 2) shows the IR of 89.40% among women with vaginal secretions is high compared with IR of 46.66% among women without vaginal secretions. There is a highly significant association between *T. vaginalis* IR and the clinical sign of vaginal secretions ($\chi^2=49.105$, $p<0.001$). This finding is in agreement with Asiegbu *et al.* (2018) and does not agree with Ranjit *et al.* (2018), who found the highest IR was with light secretion.

Table 2 shows vaginal trichomoniasis infection is significantly related to the presence of vaginal itching ($\chi^2 = 4.428$, $p= 0.035$). The highest IR is recorded among women with vaginal itching (77.72%) than women without vaginal itching (60.60%). These results align with the finding of Ajayi *et al.* (2016) and disagree with Nzomo *et al.* (2013). Sometimes, the itching may be caused by other pathogenic microorganisms such as bacteria, fungi, and yeasts, which enhanced the infection of this parasite. It is attributed to the cause of the abundance of vaginal secretions and skin itching and accompanied by other clinical manifestations such as unpleasant odors that smell like fish (Al-Marsomy, 2020).

4. CONCLUSIONS:

Trichomoniasis is a prevalent and widespread disease in Maysan province, South of Iraq. The infection rate of women with *T. vaginalis* is affected by sociodemographic factors such as age, marital status, polygamy, and others. The IR is affecting by the pH of the vagina. It was also found that clinical signs such as vaginal secretions and itching are often associated with *T. vaginalis* infection. Significantly, a relationship was observed between IR and Region, social status, occupation, marital status of the husband, number of birth and pregnancy, And we did not notice a relationship between IR and education level, residence, and birth number. The clinical signs such as vaginal pH, secretions, and vulva itching are considered to be evidence of infection of the vagina with Trichomoniasis. Moreover, we show the direct microscopic examination of a wet amount of vaginal secretion spacemen has a high sensitivity for detecting the *T. vaginalis* parasite.

5. ACKNOWLEDGEMENTS:

We would like to thank the head of the Department of Biology, college of science, University of Misan for their assistance, and Hussein A. al-Quzweeni for their help.

6. REFERENCES:

1. Abdul-Aziz, M., Mahdy, M. A. K., Abdul-Ghani, R., Alhilali, N. A., Al-Mujahed, L. K. A., Alabsi, S. A., Al-Shawish, F. A. M., Alsarari, N. J. M., Bamashmos, W., Abdulwali, S. J. H., Al Karawani, M. and Almikhlafe, A. A. (2019). Bacterial vaginosis, vulvovaginal candidiasis and trichomonal vaginitis among reproductive-aged women seeking primary healthcare in Sana'a city, Yemen. *BMC infectious diseases*, 19(1), 879.
2. Adams, H. P., and Fosnight, A. R. (2018). *Women's Health, An Issue of Physician Assistant Clinics E-Book* (Vol. 3, No. 3). Elsevier Health Sciences.
3. Adjei, C., Boateng, R., Dompheh, A., Okyere, B., and Owiredo, E. W. (2019). Prevalence and the evaluation of culture, wet mount, and ELISA methods for the diagnosis of Trichomonas vaginalis infection among Ghanaian women using urine and vaginal specimens. *Tropical medicine and health*, 47(1), 33.
4. Adnan, Z., Dhaher, H., and Marjani, M. F. (2020). Prevalence of Aerobic Bacterial Vaginosis and Trichomonas Vaginalis Associated with Socioeconomic Factors among Women in Misan Governorate. *Indian Journal of Forensic Medicine and Toxicology*, 14(1), 745-752.
5. Ajayi, V. D., Sadauki, H. M., and Randawa, A. (2016). Bacterial vaginosis is a common vaginal infection among first-time antenatal clinic attendees: evidence from a tertiary health facility in North-West Nigeria. *J Prev Inf Cntrl*, 2, 2.
6. Al Saeed, W. M. (2011). Detection of Trichomonas vaginalis by different methods in women from Dohok province, Iraq. *EMHJ-Eastern Mediterranean Health Journal*, 17 (9), 706-709, 2011.
7. Al-Abadi, A. M., Al-Shamma'a, A. M., and Aljabbari, M. H. (2017). A GIS-based DRASTIC model for assessing intrinsic groundwater vulnerability in northeastern Missan governorate, southern Iraq. *Applied Water Science*, 7(1), 89-101.
8. Al-Abbas, W. D. S., and RADHI, O. A. (2019). Incidence of Chlamydia trachomatis and Trichomonas Vaginalis Genital Infections among Nonpregnant Women in Al-Najaf Province. *kufa Journal for Nursing sciences*, 9(1), 1-8.
9. Al-abodi, H. R. J., Al-Shaibani, K. T. M., and Shaker, E. M. (2019, July). Molecular investigation of Trichomoniasis in women in Al-Muthana province/Iraq. In *Journal of Physics: Conference Series* (Vol. 1234, No. 1, p. 012078). IOP Publishing.
10. Al-Assadi, A. F., Yassin, Z., and Abood, H. S. (2020). The Prevalence of Chlamydia Trachomatis Infection Among Gynecological Outpatients Attendees at Central Basra Hospitals Using One-Step Chlamydia Test. *J Obst Gynecol Surg*, 1(2), 1-6.
11. Al-Hussuny, E. M. (2015). An epidemiological study of Trichomonas vaginalis in among women living in Baquba City, Diyala Province, Iraq. *Diyala journal for pure sciences*, 11(3), 13-25.
12. Ali, M. K., HATHAL, H. D., and Almoayed, H. A. (2017). Prevalence and diagnosis of sexually transmitted pathogens in a

- sample of iraqi women: a molecular study. *Iraqi Journal of Medical Sciences*, 15(4), 364-376.
13. Al-Kahfaji, M. S. A. (2020). Infection Rate of Trichomoniasis among Women in AL Hilla City. *Indian Journal of Public Health Research and Development*, 11(2), 2358-2362.
 14. Al-Kaisi, A. A. R. (1994). *The incidence of Trichomonas vaginalis among females with vaginal discharge* (Doctoral dissertation, M. Sc. Thesis, Coll. Med., Univ. Baghdad: 85pp).
 15. Al-Mallah, O. A. R. (1981). *Studies on Trichomonas vaginalis infection in Mosul* (Doctoral dissertation, M. Sc. Thesis, Coll. Med., Univ. Mosul: 68pp).
 16. Al-Mamoori, Z. Z. M., Alhisnawi, A. A. A., and Yousif, J. J. (2020). Prediction of Trichomoniasis in women complaining vaginal discharge by different methods and determine some immunological markers. *Plant Archives*, 20(1), 3653-3658.
 17. Al-Marsomy, H. D. (2020). Association between Trichomonas vaginalis and vaginal bacterial community composition in Human vagina. *Research Journal of Pharmacy and Technology*, 13(6), 2925-2931.
 18. Al-Muqdad, S. F., Mhaisen, F. T., and Al-Tae, A. A. (2017). Distribution of the Infection with Trichomonas vaginalis and Associated Microorganisms in Women Attending Two Hospitals in Al-Sader City, Baghdad. *Ibn AL-Haitham Journal For Pure and Applied Science*, 23(1), 19-25.
 19. Arbabi, M., Fakhrieh, Z., Delavari, M., and Abdoli, A. (2014). Prevalence of Trichomonas vaginalis infection in Kashan city, Iran (2012-2013). *Iranian journal of reproductive medicine*, 12(7), 507.
 20. Asiegbu, O. G., Asiegbu, U. V., Onwe, B., and Iwe, A. B. C. (2018). Prevalence of bacterial vaginosis among antenatal patients at federal teaching hospital Abakaliki, South East Nigeria. *Open Journal of Obstetrics and Gynecology*, 8(1), 75-83.
 21. Atiaa, A. M., Al-Shamma'a, A. M., Aljabbari, M. A., and Al-Kaabi, F. K. (2013). Impact of Climate changes on the hydrological regime of Teeb River, Missan Governorate, South of Iraq. *Marsh Bulletin*, 8(2), 148-158.
 22. Beri, D., Yadav, P., Devi, H. R., Narayana, C., Gadara, D., and Tatu, U. (2020). Demonstration and Characterization of Cyst-Like Structures in the Life Cycle of Trichomonas vaginalis. *Frontiers in Cellular and Infection Microbiology*, 9, 430.
 23. Bolumburu, C., Zamora, V., Muñoz-Algarra, M., Portero-Azorín, F., Escario, J. A., and Ibáñez-Escribano, A. (2020). Trichomoniasis in a tertiary hospital of Madrid, Spain (2013–2017): prevalence and pregnancy rate, coinfections, metronidazole resistance, and endosymbiosis. *Parasitology Research*, 1-9.
 24. Burch, T. A., Rees, C. W., and Reardon, L. V. (1959). Epidemiological studies on human Trichomoniasis. *The American journal of tropical medicine and hygiene*, 8(3), 312-318.
 25. Crucitti, T., Jespers, V., Mulenga, C., Khondowe, S., Vandepitte, J., and Buvé, A. (2011). Non-sexual transmission of Trichomonas vaginalis in adolescent girls attending school in Ndola, Zambia. *PloS one*, 6(1), e16310.
 26. Deivam, S., Rajalakshmi, R., Priyadharshini, S., Seethalakshmi, R. S., Balasubramanian, N., Brindha, T., Lakshmi Priya, P. and Prabhu, N. (2014). Prevalence of Trichomonas vaginalis infection among patients that presented to rural tertiary care hospital in Tiruchirapalli, India in 2011 and 2013. *Int J Pharm Res Health Sci*, 2(3), 255-260.
 27. Eshete, A., Mekonnen, Z., and Zeynudin, A. (2013). Trichomonas vaginalis infection among pregnant women in Jimma university specialized hospital, southwest Ethiopia. *ISRN Infectious Diseases*, 2013.
 28. Fattah, C. O., and Kadir, M. A. (2010). Trichomonas vaginalis Among Women in Sulaimania Governorate-Iraq. *Tikret Journal of Pharmaceutical Sciences*, 6(1), 1-9.
 29. Ferré, V. M., Ekouevi, D. K., Gbeasor-Komlanvi, F. A., Collin, G., Le Hingrat, Q., Tchounga, B., Salou, M., Descamps, D., Charpentier, C., and Dagnra, A. C.

- (2019). Prevalence of human papillomavirus human immunodeficiency virus and other sexually transmitted infections among female sex workers in Togo: a national cross-sectional survey. *Clinical Microbiology and Infection*, 25(12), 1560-e1.
30. Glehn, M. D. P., Ferreira, L. C. E. S., Da Silva, H. D. F., and Machado, E. R. (2016). Prevalence of *Trichomonas vaginalis* and *Candida albicans* among Brazilian Women of reproductive age. *Journal of Clinical and Diagnostic Research: JCDR*, 10(11), LC24.
 31. Hawel, N. H., and Alasadiy, Y. D. K. (2017). Immunological Diagnosis for Trichomoniasis in Women in Al-Muthanna Province. *Almuthanna Journal of Pure Science (MJPS)*, 4(2).
 32. Helms, D. J., Mosure, D. J., Metcalf, C. A., Douglas Jr, J. M., Malotte, C. K., Paul, S. M., and Peterman, T. A. (2008). Risk factors for prevalent and incident *Trichomonas vaginalis* among women attending three sexually transmitted disease clinics. *Sexually transmitted diseases*, 35(5), 484-488.
 33. Jaber, Mohammad A. (2014). Map of Numerical Change for Maysan Governorate for the Period 1977-2010 Employing Geographic Information Systems (GIS). *Basic Education College Magazine For Educational and Humanities Sciences*, 15, 119-136.
 34. Jarallah, H. M. (2013). *Trichomonas vaginalis* infection among women in Basrah marshes villages south Iraq. *Egyptian Journal of Experimental Biology*, 9(1), 71-74.
 35. Kadhum, S. A. (2012). Epidemiological Study of *Trichomonas Vaginalis* in married females. *The Iraqi Journal of Veterinary Medicine (ISSN-P: 1609-5693 ISSN-E: 2410-7409)*, 36(0E), 293-298.
 36. Kassem, H. H., and Majoud, O. A. K. (2006). Trichomoniasis among women with vaginal discharge in Benghazi city, Libya. *Journal of the Egyptian Society of Parasitology*, 36(3), 1007-1016.
 37. Kissinger, P. (2015). *Trichomonas vaginalis*: a review of epidemiologic, clinical and treatment issues. *BMC infectious diseases*, 15(1), 1-8.
 38. Korosh, T., Bujans, E., Morada, M., Karaalioglu, C., Vanden Eynde, J. J., Mayence, A., Huang, T. L. and Yarlett, N. (2017). Potential of bisbenzimidazole-analogs toward metronidazole-resistant *Trichomonas vaginalis* isolates. *Chemical Biology and Drug Design*, 90(4), 489-495.
 39. Lucena, E., Moreno-Ortiz, H., Coral, L., Lombana, O., Moran, A., and Esteban-Pérez, C. I. (2015). Unexplained infertility caused by a latent but serious intruder: *Trichomonas vaginalis*. *JFIV Reprod Med Genet*, 3, 139.
 40. Madani, T. A. (2006). Sexually transmitted infections in Saudi Arabia. *BMC infectious diseases*, 6(1), 3.
 41. Mahdi, N. K., Gany, Z. H., and Sharief, M. (2001). Risk factors for vaginal Trichomoniasis among women in Basra, Iraq. *EMHJ-Eastern Mediterranean Health Journal*, 7 (6), 918-924, 2001.
 42. Mahmud, R., Lim, Y. A. L., and Amir, A. (2018). *Medical parasitology: a textbook*. Springer.
 43. Malinowski, J. C. (2002). Iraq: A Geography.
 44. Masand, D. L., Patel, J., and Gupta, S. (2015). Utility of microbiological profile of symptomatic vaginal discharge in rural women of reproductive age group. *Journal of clinical and diagnostic research: JCDR*, 9(3), QC04.
 45. Matini, M., Rezaie, S., Mohebbali, M., Maghsood, A. H., Rabiee, S., Fallah, M., and Rezaeian, M. (2012). Prevalence of *Trichomonas vaginalis* Infection in Hamadan City, Western Iran. *Iranian journal of parasitology*, 7(2), 67.
 46. Morris, B. J., Hankins, C. A., Banerjee, J., Lumbers, E. R., Mindel, A., Klausner, J. D., and Krieger, J. N. (2019). Does Male Circumcision Reduce Women's Risk of Sexually Transmitted Infections, Cervical Cancer, and Associated Conditions?. *Frontiers in public health*, 7, 4.
 47. Mulu, W., Yimer, M., Zenebe, Y., and Abera, B. (2015). Common causes of vaginal infections and antibiotic susceptibility of aerobic bacterial isolates in women of reproductive age attending at Felegehiwot referral Hospital, Ethiopia: a cross sectional study. *BMC women's*

health, 15(1), 42.

48. Nas, F. S., Yahaya, A., Muazu, L., Halliru, S. A. N., and Ali, M. (2020). Prevalence of *Trichomonas vaginalis* among pregnant women attending ante-natal care in Kano, Nigeria. *Eur. J. Med. Health Sci*, 2(2), 39-45.
49. Nouraddin, A. S., and Alsakee, H. M. (2015). Prevalence of *Trichomonas vaginalis* infection among women in Erbil governorate, Northern Iraq: An epidemiological approach. *European Scientific Journal*, 11(24).
50. Nwokah, E. G., Monday, Z. M., and Azike, C. A. (2019). Improving Detection of *Trichomonas vaginalis* Infection among Adult Females in a Resource-poor Setting in Ogoniland, Niger Delta, Nigeria. *Asian Journal of Research in Infectious Diseases*, 1-5.
51. Nzomo, J., Waiyaki, P., and Waihenya, R. (2013). Bacterial vaginosis and correlates in women of reproductive age in Thika, Kenya. *Advances in Microbiology*, 3(3):249-254.
52. Paniker, C. J., and Ghosh, S. (2017). *Paniker's textbook of medical parasitology*. JP Medical Ltd.
53. Poole, D. N., and McClelland, R. S. (2013). Global epidemiology of *Trichomonas vaginalis*. *Sexually transmitted infections*, 89(6), 418-422.
54. Ranjit, E., Raghubanshi, B. R., Maskey, S., and Parajuli, P. (2018). Prevalence of bacterial vaginosis and its association with risk factors among nonpregnant women: A hospital based study. *International journal of microbiology*, 2018.
55. Ray, K., Bala, M., Bhattacharya, M., Muralidhar, S., Kumari, M., and Salhan, S. (2008). Prevalence of RTI/STI agents and HIV infection in symptomatic and asymptomatic women attending peripheral health set-ups in Delhi, India. *Epidemiology and Infection*, 136(10), 1432-1440.
56. Riestra, A. M., Valderrama, J. A., Patras, K. A., Booth, S. D., Quek, X. Y., Tsai, C. M., and Nizet, V. (2019). *Trichomonas vaginalis* induces NLRP3 inflammasome activation and pyroptotic cell death in human macrophages. *Journal of innate immunity*, 11(1), 86-98.
57. Roberts, L. S., and Janovy, J. (2009). *Gerald D. Schmidt and Larry S. Roberts' Foundations of Parasitology* (No. 574.5249 R6/2009).
58. Rostami, M. N., Rashidi, B. H., Habibi, A., Nazari, R., and Dolati, M. (2017). Genital infections and reproductive complications associated with *Trichomonas vaginalis*, *Neisseria gonorrhoeae*, and *Streptococcus agalactiae* in women of Qom, central Iran. *International journal of reproductive biomedicine*, 15(6), 357.
59. Saheb, E. J., Kuba, R. H., Zghair, K. H., and Mosa, I. S. (2016). A comparison between trichomoniasis Infection and other vaginal infection among females in Baghdad governorate-Iraq. *Iraqi Journal of Science*, 57(1C), 545-551.
60. Salman, Y. J., and Kareem, E. A. (2013). Detection of *Trichomonas vaginalis* among females attending private gynaecological clinics in Kirkuk province using different laboratory methods. *J Kirkuk Med Coll*, 1(2), 1-8.
61. Schwebke, J. R., and Burgess, D. (2004). Trichomoniasis. *Clinical microbiology reviews*, 17(4), 794-803.
62. Sgibnev, A., and Kremleva, E. (2020). Probiotics in addition to metronidazole for treatment *Trichomonas vaginalis* in the presence of BV: a randomized, placebo-controlled, double-blind study. *European Journal of Clinical Microbiology and Infectious Diseases*, 39(2), 345-351.
63. Sherrard, J. (2020). How to diagnose and manage *Trichomonas vaginalis*. *Evaluation*, 14(47), 19.
64. Shipitsyna, E., Khusnutdinova, T., Budilovskaya, O., Krysanova, A., Shalepo, K., Savicheva, A., and Unemo, M. (2020). Bacterial vaginosis-associated vaginal microbiota is an age-independent risk factor for *Chlamydia trachomatis*, *Mycoplasma genitalium* and *Trichomonas vaginalis* infections in low-risk women, St. Petersburg, Russia. *European Journal of Clinical Microbiology and Infectious Diseases*, 1-10.
65. Smith, K. S., Tabrizi, S. N., Fethers, K. A., Knox, J. B., Pearce, C., and Garland, S. M. (2005). Comparison of conventional

- testing to polymerase chain reaction in detection of *Trichomonas vaginalis* in indigenous women living in remote areas. *International journal of STD and AIDS*, 16(12), 811-815.
66. Stephen, H. G., and Richard, D. (2001). Principles and practice of clinical parasitology. *John Willey and Sons, Ltd.*
 67. Sutton, M., Sternberg, M., Koumans, E. H., McQuillan, G., Berman, S., and Markowitz, L. (2007). The prevalence of *Trichomonas vaginalis* infection among reproductive-age women in the United States, 2001–2004. *Clinical infectious diseases*, 45(10), 1319-1326.
 68. Taher, J. H., and Shaker, M. A. (2018). Epidemiological Study of *Trichomonas vaginalis* and Other Microorganisms Isolated from Genital Tract of Women in Najaf Province–Iraq. *Al-Kufa University Journal for Biology*, 10(2), 1-9.
 69. Thurman, A. R., and Doncel, G. F. (2011). Innate immunity and inflammatory response to *Trichomonas vaginalis* and bacterial vaginosis: relationship to HIV acquisition. *American journal of reproductive immunology*, 65(2), 89-98.
 70. Tien, V., Punjabi, C., and Holubar, M. K. (2020). Antimicrobial resistance in sexually transmitted infections. *Journal of Travel Medicine*, 27(1), taz101.
 71. Trein, M. R., e Oliveira, L. R., Rigo, G. V., Garcia, M. A. R., Petro-Silveira, B., da Silva Trentin, D., Macedo, A. J., Regasini, L. O., and Tasca, T. (2019). Anti-*Trichomonas vaginalis* activity of chalcone and amino-analogues. *Parasitology Research*, 118(2), 607-615.
 72. Vos, T., Allen, C., Arora, M., Barber, R. M., Bhutta, Z. A., Brown, A. and Coggeshall, M. (2016). Global, regional, and national incidence, prevalence, and years lived with disability for 310 diseases and injuries, 1990–2015: a systematic analysis for the Global Burden of Disease Study 2015. *The lancet*, 388(10053), 1545-1602.
 73. Wiesenfeld, H. C., Lowry, D. L., Heine, R. P., Krohn, M. A., Bittner, H., Kellinger, K., Shultz, M., and Sweet, R. L. (2001). Self-collection of vaginal swabs for the detection of Chlamydia, gonorrhea, and Trichomoniasis: opportunity to encourage sexually transmitted disease testing among adolescents. *Sexually transmitted diseases*, 28(6), 321-325.
 74. Workowski, K. A., and Berman, S. M. (2010). Sexually transmitted diseases treatment guidelines, 2010. *CDC MMWR Morbidity and Mortality Weekly Report* December 17, 2010 / Vol. 59 / No. RR-12
 75. Workowski, K. A., and Bolan, G. A. (2015). Sexually transmitted diseases treatment guidelines, 2015. *MMWR. Recommendations and reports: Morbidity and mortality weekly report*, 64(RR-03), 1.
 76. World Health Organization. (2001). *Global prevalence and incidence of selected curable sexually transmitted infections: overview and estimates* (No. WHO/CDS/CSR/EDC/2001.10). World Health Organization.
 77. Yeh, Y. M., Huang, K. Y., Gan, R. C. R., Huang, H. D., Wang, T. C. V., and Tang, P. (2013). Phosphoproteome profiling of the sexually transmitted pathogen *Trichomonas vaginalis*. *Journal of Microbiology, Immunology and Infection*, 46(5), 366-373.
 78. Zhang, Z. F., and Begg, C. B. (1994). Is *Trichomonas vaginalis* a cause of cervical neoplasia? Results from a combined analysis of 24 studies. *International Journal of Epidemiology*, 23(4), 682-690.

Table 1. The *T. vaginalis* infection rate of women in Maysan province and their relation with some of the social characteristics of the study population.

Variable	Sections	No. Exam	No. Infection (%)	% of total	χ^2	p-value
Region	Al-Amara	161	117(72.67%)	51.80%	12.118	0.007**
	Al-Kahla	26	25(96.15%)	11.10%		
	Al-Maymouna	25	15(60.00%)	6.60%		
	Al-Majar Al-Kabir	14	13(92.85%)	5.80%		
	Total	226	170(75.22%)	100%		
Age	<15	8	3(37.5%)	1.30%	13.334	NS
	15-19	22	13(59.09%)	5.80%		
	20-26	49	38(77.55%)	16.80%		
	27-33	42	32(76.19%)	14.20%		
	34-40	46	40(86.95%)	17.70%		
	41-47	27	19(70.37%)	8.40%		
	48-54	26	20(76.92%)	8.80%		
	≥ 55	6	5(83.33%)	2.20%		
	Total	226	170(75.22%)	100%		
Social Status	Married	194	157(80.92%)	69.50%	23.938	<0.001***
	Unmarried	32	13(40.62%)	5.80%		
	Total	226	170(75.22%)	100%		
Education level	illiteracy	112	87(77.67%)	38.50%	6.342	NS
	Primary	85	66(77.64%)	29.20%		
	Secondary	16	8(50.00%)	3.50%		
	A graduate	13	9(69.23%)	4.00%		
	Total	226	170(75.22%)	100%		
Occupation	Housewife	200	156(78.00%)	69.00%	10.598	0.014*
	Employee	14	8(57.14%)	3.50%		
	Student	10	6(60.00%)	2.70%		
	Baby girl	2	0(0.00%)	0.00%		
	Total	226	170(75.22%)	100%		
Marital status of the husband	Monogamous	75	64(85.33%)	28.30%	24.431	<0.001***
	Polygamous	116	91(87.44%)	40.30%		

	Not a husband	35	15(42.85%)	6.60%		
	Total	226	170(75.22%)	100%		
No. Birth					27.812	<0.001***
	0	23	20(86.95%)	8.80%		
	1 – 3	77	58(75.32%)	25.70%		
	4 – 6	60	53(88.33%)	23.50%		
	7 – 9	34	26(76.47%)	11.50%		
	Single	32	13(40.62%)	5.80%		
	Total	226	170(75.22%)	100%		
Residence					1.954	NS
	Urban	161	117(72.67%)	51.80%		
	Rural	65	53(81.54%)	23.50%		
	Total	226	170(75.22%)	100%		
Status of women					23.983	<0.001***
	Pregnant	14	11(78.57%)	4.90%		
	Not pregnant	180	146(81.11%)	64.60%		
	Single	32	13(40.62%)	5.80%		
	Total	226	170(75.22%)	100%		

* P<0.05, ** P<0.01, *** P<0.005, NS= No Significance, P≤0.05

Table 2. The relation of Trichomoniasis IR among women in Maysan province with some of the clinical characteristics of the study population

Variable	Sections	No. exam	No. Infection (%)	% Of total	χ ²	P-value
pH values					185.276	<0.001***
	4	48	0(0.00%)	0.00%		
	5.5	26	24(92.30%)	10.60%		
	6	119	115(96.63%)	50.90%		
	6.5	33	31(93.93%)	13.70%		
	Total	226	170(75.22%)	100%		
Secretions					49.105	<0.001***
	Yes	151	135(89.40%)	59.70%		
	No	75	35(46.66%)	15.50%		
	Total	226	170(75.22%)	100%		
Itching					4.428	0.035*
	Yes	193	150(77.72%)	66.40%		
	No	33	20(60.60%)	8.80%		
	Total	226	170(75.22%)	100%		

* P<0.05, ** P<0.01, *** P<0.005, NS= No Significance, P≤0.05

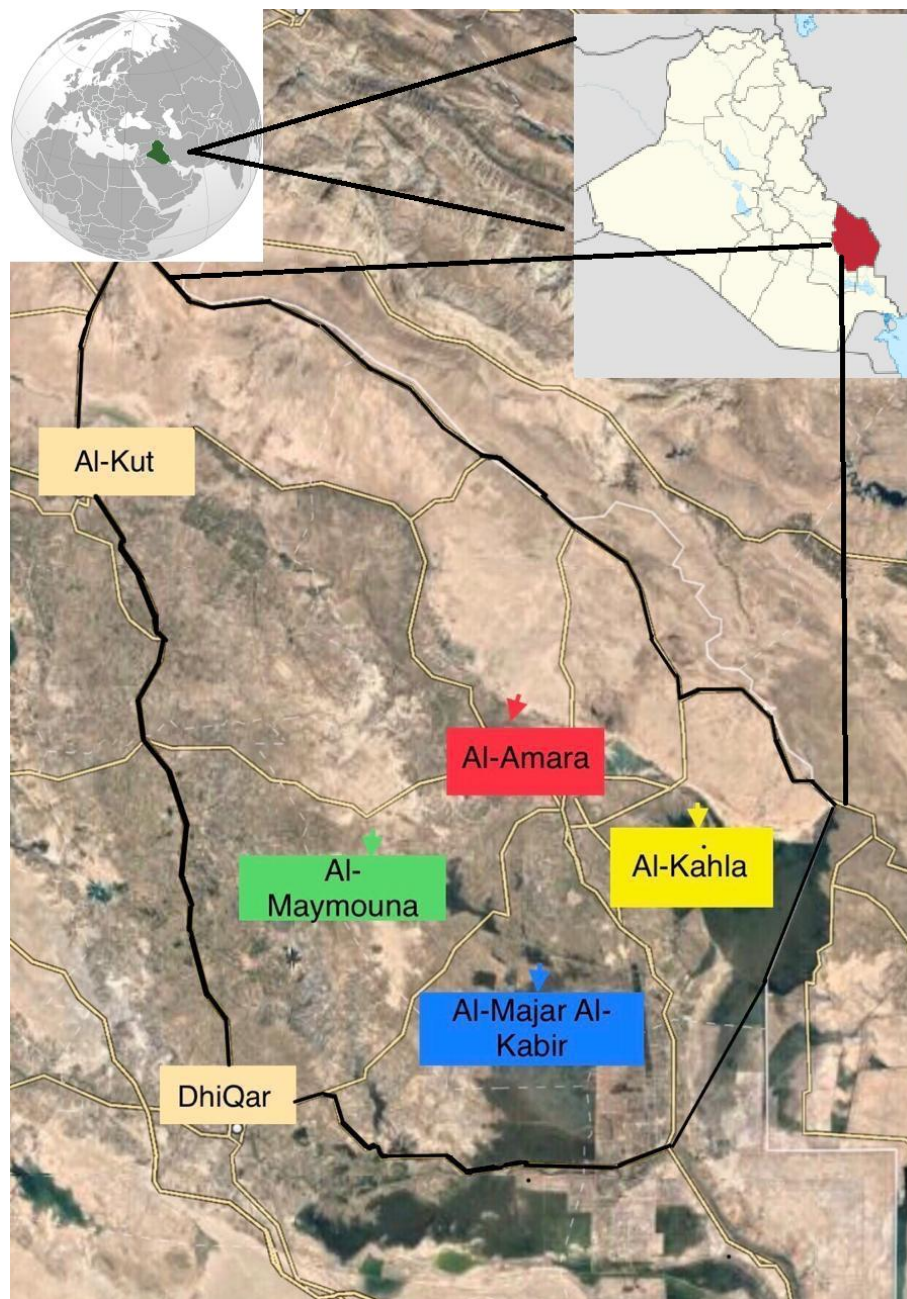
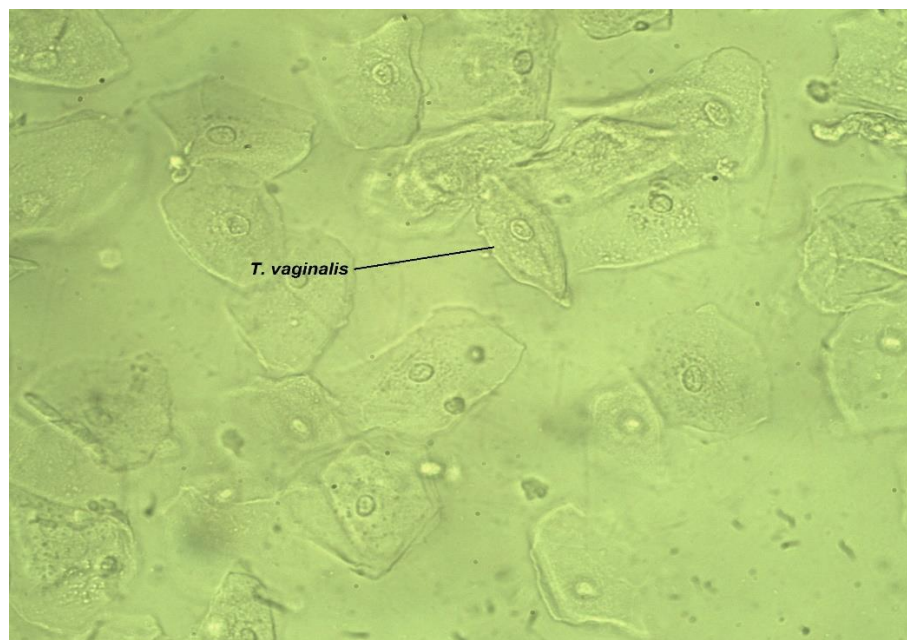
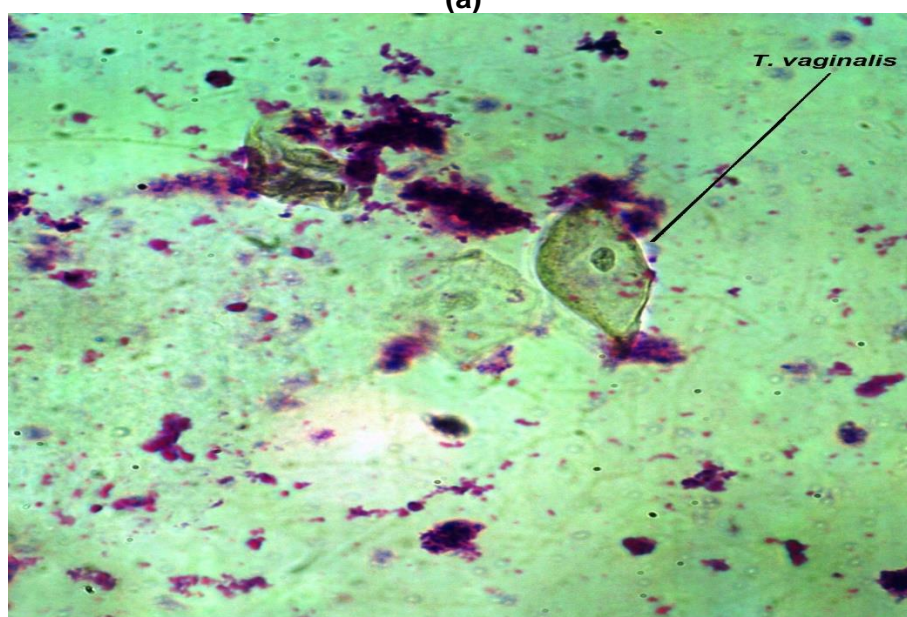


Figure 1. A map of the Maysan province showing the regions of the study.
 ▼ Al-Amara ▼ Al- Kahla ▼ Al- Majar Al-Kabir ▼ Al- Maymouna, Source: Al-Abadi et al., 2017
 (authors carried out some additions).



(a)



(b)

Figure 3. The *Trichomonas vaginalis* parasite under 40X magnification. **(a)** in a fresh smear of wet mount vaginal secretions; **(b)** after staining with Giemsa stain.

ESTRUTURA CONCEITUAL DE HABILIDADES CRÍTICAS DE PENSAMENTO PARA TESTES DE TRABALHO E ENERGIA APLICADOS AO ENSINO DE FÍSICA**CONCEPTUAL FRAMEWORK OF CRITICAL THINKING SKILLS FOR WORK AND ENERGY TESTS APPLIED TO PHYSICS LEARNING****IMPLEMENTASI KERANGKA KONSEPTUAL TES KETERAMPILAN BERPIKIR KRITIS USAHA DAN ENERGI PADA PEMBELAJARAN FISIKA**SAPUTRO, Sigit Dwi^{1,2*}; TUKIRAN³; SUPARDI, Zainul Arifin Imam⁴; JATMIKO, Budi⁴¹ Postgraduate Program, Universitas Negeri Surabaya, Surabaya Indonesia² Faculty of Education, University of Trunojoyo, Bangkalan, Indonesia.³ Postgraduate Program, Universitas Negeri Surabaya, Surabaya, Indonesia.⁴ Departement of Physics, Universitas Negeri Surabaya, Surabaya, Indonesia.

* Corresponding author

e-mail: sigit.19003@mhs.unesa.ac.id

Received 21 May 2020; received in revised form 26 July 2020; accepted 26 October 2020

RESUMO

Trabalho e energia são conteúdos tradicionalmente abordados no estudo de física e engenharia. Isso se deve ao fato desse tópico fazer parte da vida cotidiana das pessoas, ou seja, são habilidades de pensamento crítico incluídas nas realizações de aprendizagem do século XXI que devem ser dominadas pelos alunos. Este estudo teve como objetivo fazer uma formulação de avaliação apropriada para medir as habilidades de pensamento crítico dos alunos a respeito do tópico de trabalho e energia. O método sistemático de revisão foi realizado em três etapas. O primeiro passo foi procurar fontes relevantes de literatura por meio de um banco de dados e livros. O banco de dados utilizado incluiu Revistas SAGE, Biblioteca *Wiley Online*, *Science Direct* e *Google Scholar*. Foram examinados 115 periódicos ou procedimentos e selecionados 50 artigos de acordo com os critérios estabelecidos. O segundo estágio determinou a formulação de indicadores de desempenho, e o terceiro estágio desenvolveu testes conceituais de habilidades de pensamento crítico. Com base nesse estudo sobre a estrutura conceitual do estudo para medir as habilidades de pensamento crítico dos alunos em materiais didáticos para trabalho e energia, pôde-se concluir que (1) indicadores de habilidades de pensamento crítico sobre trabalho e energia incluem interpretação, análise, avaliação, inferência, explicação; (2) os princípios básicos da fabricação de instrumentos de teste do pensamento crítico incluem a apresentação de fenômenos, testes abertos e o teste da racionalidade das respostas; e (3) houve exemplos da aplicação do desenvolvimento do instrumento de teste de habilidades de pensamento crítico para análise de indicadores.

Palavras-chave: *habilidades de pensamento crítico, energia do trabalho, avaliação.***ABSTRACT**

Work and energy are contents traditionally addressed in the study of physics and engineering. This is because this topic is part of people's daily lives; that is, they are critical thinking skills included in 21st-century learning achievements that must be mastered by students. This study aimed to make an appropriate assessment formulation to measure students' critical thinking skills in work and energy. The systematic method of review was carried out through three stages. The first step was to search for relevant literature sources through a database and books. The database used included SAGE Journals, Wiley Online Library, Science Direct, and Google Scholar. There were 115 journals or proceedings that have been examined and then selected 50 articles following established criteria. The second stage determined formulating achievement indicators, and the third stage developed conceptual tests of critical thinking skills. Based on this study on the conceptual framework of the study to measure students' critical thinking skills in teaching materials for work and energy, it was concluded that (1) indicators of critical thinking skills on work and energy include interpretation, analysis, evaluation, inference, explanation; (2) the basic principles of making critical thinking test instruments include presenting phenomena, open-ended tests, and testing the rationality of answers; and (3) there were examples of the application of the development of the critical thinking skills test instrument for indicator analysis.

Keywords: *critical thinking skills, work, and energy, assessment.*

ABSTRAK

Usaha dan energi merupakan materi pokok yang dibahas dalam pelajaran fisika dan teknik. Materi ini berisi fakta dengan topik kehidupan sehari-hari yang dialami oleh masyarakat, dengan demikian, diperlukan keterampilan berpikir kritis sebagai bagian dari capaian pembelajaran abad ke-21 yang harus dikuasai oleh siswa. Penelitian ini bertujuan membuat formulasi penilaian yang tepat untuk mengukur keterampilan berpikir kritis siswa dalam materi usaha dan energi. Metode review sistematis dilakukan melalui tiga tahap. Tahap pertama adalah mencari sumber literatur yang relevan melalui basis data dan buku. Basis data yang digunakan meliputi SAGE Journals, Wiley Online Library, Science Direct, dan Google Scholar. Sejumlah 115 jurnal yang telah diperiksa kemudian dipilih 50 artikel sesuai dengan kriteria yang ditetapkan. Tahap kedua menentukan rumusan ketercapaian indikator, dan tahap ketiga mengembangkan tes konseptual keterampilan berpikir kritis. Berdasarkan penelitian ini kerangka kerja konseptual untuk mengukur keterampilan berpikir kritis siswa dalam materi usaha dan energi, disimpulkan bahwa (1) indikator keterampilan berpikir kritis pada usaha dan energi terdiri atas interpretasi, analisis, evaluasi, inferensi, penjelasan; (2) prinsip dasar pembuatan instrumen tes berpikir kritis meliputi penyajian fenomena, tes terbuka, menguji rasionalitas jawaban; dan (3) ada contoh penerapan pengembangan instrumen tes keterampilan berpikir kritis pada indikator analisis.

Kata kunci: *keterampilan berpikir kritis, usaha dan energi, penilaian.*

1. INTRODUCTION:

Mastery of physics is identical to Mastery of physical material, which is identical to systematic investigation and draws conclusions from applications based on theories and models developed in science. This is closely related to critical thinking skills (Holmes, Wieman, and Bonn, 2015; Arend, 2012). Work and energy Material became part of studying physics and engineering (Jeweet, 2010). The most crucial element in learning work and energy is the law of conservation of energy (Giancoli, 1997). This is because the work and energy are part of daily human life that cannot be separated by humans.

In science, energy is defined as the ability to do work. Even when you breathe, blink, or shift position in a chair, all the work requires energy. Energy can also be defined as the ability to cause change. Every change that occurs, big or small, involves energy (Hill, 2008). For example, when someone boils water, the initially cold water when it gets heat energy from the fire after 15 minutes turns the water into heat. Energy cannot be created and destroyed but can be changed from one form of energy to another form of energy known as the Law of Conservation of Energy. There are several examples of changes in the form of energy. A rock that falls at a certain height and a car that slides down on a hill are some. Both examples are a form of change in gravitational potential energy into kinetic energy (Giancoli, 1997).

Thus work, and energy materials become an essential part of the education curriculum in

Indonesia. Shiva must master the skills specified in the curriculum. One way to develop students' understanding of learning the material is to get students to think critically because critical thinking is the main asset in shaping one's intellect (Adey P, 1994). Critical thinking skills become an important recommendation in the 21st-century framework, which is parallel to the skills of creative thinking and innovation, problem-solving, collaboration, and communication (Trilling, n.d.). In survival skills, critical thinking skills are also included in an important part that must be considered (Wager, 2008). Critical thinking skills are essential in the context of student learning. Every decision students will consider rationality (Ennis, 1985; Facione, 2009; Mason, 2009; Wallace, 2001).

Besides, students will be more careful to provide stairs to any information that comes in (Dana S. Dunn, Jane S. Halonen, 2009; Mason, 2009). Every decision that is determined has a strong reason and can be justified (Crews-Anderson, 2007; Mason, 2009). So that someone will effectively achieve the desired goals (Halpern, 1999; Paul, Richard; Elder, 2014). Also, critical thinking skills are indicators of student success on an international level, such as TIMSS and PISA. This means that education in Indonesia must pay attention to critical thinking skills if you want to get good ranking results on an international scale. However, the fact the results of PISA in 2018 for Indonesian students is 396. This means that Indonesian students have not been able to solve complex problems or are only able to at a more superficial level. Solving complex problems requires students' thinking skills. The impact of the ability of our students who are still in the category

of simple problem solving is that Indonesian students are only ranked 70th out of 78 countries measured (OECD, 2019). In the context of educators, to know the development of critical thinking skills, an instrument that gives students to do argumentation is necessary. As Gutires's research results show, students' learning difficulties will be seen if the questions are given in essays, qualitative. So the instrument of thinking skills development becomes part of the research that is continuously being developed (Facione, N.C., Facione, P., Blohm, S.W., and Gittens, 2008)

The purpose of the paper was to make an appropriate assessment formulation to measure students' critical thinking skills on the work and energy subject.

2. MATERIALS AND METHODS:

The design of this research was an integrative review in three stages, namely: (1) searching for relevant literature, (2) the formulation of indicators of critical thinking skills on work and energy, and (3) developed conceptual tests critical thinking skills.

The first step was to search for relevant literature sources through a database and books. The database used included (1) SAGE Journals, (2) Wiley Online Library, (3) Science Direct and (4) Google Scholar. The selection of papers was made based on the inclusion of criteria (1) Journals and proceedings published in 1990-2020 written in English, (2) implementation of critical thinking skills in the world of education, and (3) the critical study scientific article about the level of science. Keywords used to search literature included critical thinking skills, critical thinking in science, critical thinking skills in physics, assessment of critical thinking skills. A total of 115 have been examined, but only 50 articles were selected that fit the established criteria. Thirty books written by experts under critical thinking skills, work, energy, learning theory using English, and Indonesian were also used to build critical thinking skills test concepts on work and energy materials.

The second stage was the formulation of indicators of critical thinking skills on work and energy. This stage was carried out by examining several concepts of critical thinking skills that have been written by experts in the critical field of the environment, such as Ennis, Halpern, Crew Andreson, Fasione, Paul, and Elder. This thinking is important to obtain an excellent concept to be set as an indicator of critical thinking skills on work and energy materials.

The third stage of developing conceptual tests was appropriate to measure these indicators by developing existing empirical questions and facts.

3. RESULTS AND DISCUSSIONS:

3.1. Literature review

3.1.1 Learning

The definition of learning, according to Mahmud, is a change in a person's behavior due to interactions with the environment (Mahmud, 2012). The environment in question in learning to start from learning resources, learning processes, and behaviors that support learning. If someone does the learning process to the maximum, this is the same as developing thinking skills (Jurfri, 2013). Thus people who are learning are practicing their thinking skills to be developed continuously. As a result, someone will have life skills. Learning is practicing one's cognitive skills, not just memorizing (Hamruni, 2011). This means that an educator must always evaluate whether during the learning process can facilitate students to train students' cognitive or just memorize information. As noted, learning is a complex student action and behavior (Dimiyati, 2011).

Learning is developed for the thought process and develops one's skills and attitudes (Nana Syaodih, 2011). The knowledge that has been possessed can also be applied in real life through good behavior. To achieve the ultimate goal in learning needed meaningful learning, which can master the concepts and linking science and analyzing other ideas to obtain optimal results (Suryabrata, 2008). Learning is a long process that has characteristics not only mastering the concept but also developing thinking skills, cognitive so that it can have a complete understanding that can link science and analyze concepts that enter a person's mind.

3.1.2 Critical Thinking skills

Critical thinking reflects one's understanding and reasoning with an element of creativity in making a decision. The decision type is based on formulating hypotheses, questions, alternatives, and activity plans (Ennis, 1996). Although the decision taken is still in one study of science, it does not involve analyzing other areas of science. The keyword in thinking about critical thinking skills is action based on the concept of rationality.

Critical thinking is the goal and directed

towards the goal (Halpern, 1999). This is a type of thinking with a specific purpose with a foundation of rationality. These goals include solving problems, formulating conclusions, calculating possibilities, and making decisions. This opinion also requires a person to have a rational decision base. Another view of critical thinking is thinking to process the knowledge possessed by someone in the form of analysis of understanding, existing synthesis, and ideas by considering aspects of a sense of accuracy and skills to provide solutions or anticipation of problems (Moon, 2007). Managing knowledge to become a synthesis also requires a process of rationality in thinking.

Opinions about critical thinking also relate to incoming information, namely, the ability of a person to give detailed responses to the strengths and weaknesses (Crews-Anderson, 2007). The opinion is analyzed in principle with a general view of truth, by arranging arguments in a structured way to facilitate information interpretation. Even though the opinions expressed must also be based on the ratio of our reason, namely general truth, meaning truth that is following common sense. Likewise, Mason thinks critically is the ability of someone based not only rooted in the dogma of reality at a particular perspective but also integrates various perspectives, information that has a reasonable rationale (Mason, 2009). Whatever knowledge comes in and can still be justified logically can be the basis in critical thinking skills. Reason and evidence are also important in critical thinking skills; critical thinking is not a set of skills that can be used at any time, in any context (Willingham, 2008). Critical thinking lies in the domain of knowledge mastery owned by someone and has an open attitude towards new ideas that have reasoned with evidence.

Other opinions concerned with critical thinking skills include the ability to recognize events with specific patterns (Dana S. Dunn, Jane S. Halonen, 2009). The ability to solve problems through scientific and practical ways to be used, involving reasoning and adapting different sense, is new. Critical reasoning includes (a) asking questions and being willing to ask questions, (b) defining the problem clearly, (c) examining evidence, (d) analyzing assumptions (e) avoiding emotional reasons, (f) avoiding oversimplification, (g) consider alternative interpretations, and (h) tolerate uncertainty.

In the critical perspective in testing one's thinking, it also puts forward rational thinking and the reflective thinking of evaluating thinking independently to get better results (Paul, Richard; Elder, 2014). The meditative process of thought

includes (1) asking essential questions and problems, (2) formulating them clearly and precisely, (3) collecting and assessing relevant information, (4) using abstract ideas to be interpreted effectively, (5) arriving at conclusions and reasonable solutions, (6) testing the relevant criteria and standards, (7) thinking openly in alternative thought systems, (8) recognizing and assessing, as needed, their assumptions, implications, and practical consequences; and (9) communicating effectively with others in finding solutions to complex problems.

Judge, Jones, and McCreery (2009) discussed the ability to think about how to evaluate the students' thoughts so that they will find strengths and weaknesses in their skills or knowledge. Based on these results, they will have a perspective on themselves as consideration for taking action to improve their abilities by not closing themselves to one's opinion or being open to the views of others. There are also opinions to respond to arguments (Wallace, 2001). His opinion is the skill used to identify, analyze, and evaluate statements and truth claims; to find and overcome personal problems of bias and bias; to formulate and present convincing reasons in support of conclusions, and to make sensible and intelligent decisions about what to believe and what to do.

Representations of critical thinking skills have self-thinking and respond to a phenomenon or object (Facione, 2009). Described in detail as a person's cognitive skills, including interpretation, analysis, evaluation, inference, explanations, and self-regulation, which have good, exact, logical, wise thinking properties, pay attention to facts, are open to alternatives. Based on some of these opinions, it can be concluded that critical thinking skills are students' skills in rational decision-making with facts learned through experience or experimental activities.

3.1.3 Thought Requiring Instrument Critical Thinking Skills

In the scenario of education, critical thinking skills are a part that is, actually, not an option that must be chosen but is a unity that cannot be released by the purpose of education itself (Norris, 1985). With critical thinking skills, this will help in the problem-solving process based on valid and relevant information (Paul, 1991; Gagne, 1988; Niu, Behar-Horenstein, and Garvan, 2013).

Critical thinking skills are important thinking skills and are needed by students to carry out learning activities ranging from assignments,

interpreting work, and engaging in creative assignments given by the teacher (Bailin., 2002).

Students who are not accustomed to thinking critically, if they get a different concept, feel themselves a failure, and cannot withstand feelings of sadness. The inculcation of critical thinking skills needs to start from elementary school to college to have an open habit of problems or criticism of differences (Sarigoz, 2012).

3.1.4 Existing instruments

Mastery of learning in science, including Physics, Biology, and chemistry, this in every material requires critical thinking skills. Each material must be reviewed in depth to prepare students' critical thinking skills (Holmes *et al.*, 2015; Arend, 2012)

The importance of thinking skills encourages experts to develop instruments to get valid results. The tools of students' critical thinking skills are still limited (Bassett, 2016; Sustekova, Kubiato, and Usak, 2019; Istiyono, Dwandaru, Lede, Rahayu, and Nadapdap, 2019). Examples include Watson-Glaser Critical Appraisal Appraisal (WGCTA) (Watson, 1980). This instrument continues to develop and undergo improvements (Watson, G., Glaser, E. M., and Rust, 2002). The Ennis-Weir Critical Thinking Essay Test (EWCTET) (Ennis, Robert H, 1985), Cornell Critical Thinking Test (CCTT) (Ennis, R.H., Millman, J., Tomko, 1985; Tomko, 1985), the California Critical Thinking Disposition (CCTDI) (Banning, 2006), the International Critical Thinking Essay Test (Paul, R., and Elder, 2007) the California Critical Thinking Skills test (CCTST) (Facione, N.C., Facione, P., Blohm, S.W., and Gittens, 2008), and Assessment Critical Thinking Halpern (Halpern, 2010).

The measurement of critical thinking skills will be maximized to be applied to a particular subject matter, so this impacts teachers to practice critical thinking skills in each subject (Nitco, 2011). The measurement results will also be more valid if critical thinking skills are developed to certain specifications (Tiruneh, De Cock, Weldeslassie, Elen, and Janssen, 2017; Kuhn and Kuhn, 1999). Research that measures critical thinking skills uses The California Critical Thinking Disposition Inventory (CCTDI-R), which Fasione has developed (Özsoy-Güneş, Güneş, Derelioğlu, and Kırbaşlar, 2015). It uses the basic principle of Halpern in the form of a Multi Response Format Test on heat material (Mahbubah, Rusdiana, Juanda, Hermita, and Hakim, 2018; Sya'Bandari,

Firman, and Rusyati, 2018). The material on momentum has been developed using essay tests (Negoro, Rusilowati, Aji, and Jaafar, 2020), electrical matter (April and Kuswanto, 2017), fluid matter (Wartono, Hudha, and Batlolona, 2018; Maknun, 2020; Rosidin, W Distrik, and Herlina, 2018; Yulianti, Wiyanto, Rusilowati, Nugroho, and Pangesti, 2019), photoelectric effect (Sutarno, Setiawan, Suhandi, Kaniawati, and Malik, 2019) and Hooke's law (Asmawati, Rosidin, and a, 2018).

The development of measurement of critical thinking skills allows continuing on any physics material due to the nature of the material (Holmes *et al.*, 2015). One of the materials used to measure students' critical thinking skills is work and energy. Energy material is still found basic mistakes in everyday life (Dega and Govender, 2016)

3.1.5 Work and Energy

The energy takes various forms. In general, all physical processes that occur in the universe require energy (Jeweet, 2010). Everyone cannot be avoided in the concept of energy. For example, the sun, needed by the leaves for photosynthesis, and there is a long process of the food chain, which also requires energy. The definition of the concept of energy is still considered a source that has the potential to drive an object (Bächtold, 2018). Students assume that energy is something needed to move, heat, or ignite. Or, the teacher can express the definition of energy by giving examples. Lights require energy to illuminate. When discussing energy that needs to be conveyed is the most important concept in energy, namely the law of energy (Jeweet, 2010). The law of conservation of energy and momentum is fundamental when dealing with the systems of every object. The concept of energy is not only useful in the study of motion but all fields in physics and science (Giancoli, 1997).

The subject of the study discussed energy, including gravitational potential energy, kinetic energy, and work, which is usually difficult to separate so that it is included in the law of conservation of mechanical energy. However, this energy conservation statement remains limited to the ideal system without mentioning energy degradation. In the classroom learning process, a teacher must be able to relate the energy context to the experience of students at the school level. Besides, in teaching scientific work, teachers must consider a language easily understood by students (Warren and Richmond, 2018). One of the difficulties of the students in learning energy is

building the relationship between work and energy. That an educator finds valid results in learning work and energy in the future can apply essay questions, so it will be easy to analyze the difficulty of what parts of the learning process. (Gutierrez-Berraondo, Guisasola, and Zuza, 2019).

Energy learning becomes more meaningful when students are asked to analyze concepts whose themes are still mastered with mapping concepts. For example, when studying the material work and energy, there is a relation to existing ideas in Newton's laws related to motion (Giancoli, 1997). It is even more interesting when the phenomenon is confronted with the events experienced. When learning energy, it is important to make students make predictions, so they can carry out scientific activities through experiments, further strengthened by linking it in daily life. By making predictions, students will find out the level of truth or concept errors predicted through scientific experimentation activities (Papadouris, Hadjigeorgiou, and Constantinou, 2014).

During this time, evaluating student understanding is placed mainly on the quantitative application of conservation (mechanical) energy in simple systems. This approach refrains from explicitly answering the fundamental question of what energy is, why is it needed in science, and how is it used? Although it might be enough to help students solve standard quantitative problems, it is certainly not enough to help them interpret the epistemology knowledge gained in learning. (Papadouris *et al.*, 2014). Therefore, it is necessary to develop tests that allow students to interpret the understanding obtained in work and energy learning.

3.2. Determination of Critical Thinking Skills Indicators on and Energy material

The number of studies related to critical thinking skills impacts the many different indicators of achievement of each expert thinker (Halpern, 2014a). This can cause no standard reference for the development of measuring instruments. Some use Facione (Özsoy-Güneş *et al.*, 2015), Helpers concept (Mahbubah *et al.*, 2018; Sutarno *et al.*, 2019), Ennis concept (Nisa, Jatmiko, and Koestiari, 2018; Wartono *et al.*, 2018), Watson concept (Folly Eldy and Sulaiman, 2013), Fasione concept (Ilfiandra Nurhudaya, 2019; Walsh, Quinn, Wieman, and Holmes, 2019; Aizikovitsh-Udi and Amit, 2011). Another form of determining indicators of critical thinking is one that summarizes the opinions of experts (Negoro *et al.*, 2020; April and Kuswanto, 2017;

Damayanti, Suyatna, Warsono, and Rosidin, 2017; Istiyono *et al.*, 2019; Suastra, Ristiati, Adnyana, and Kanca, 2019).

Therefore, it becomes crucial to analyze and determine critical thinking skills in business materials and energy. The determination of these indicators is based on the research conclusions conducted by one competent expert in education. Peter Facione was appointed by the *American Philosophical Association* (APA) to develop benchmarks for critical thinking skills with 46 experts from the fields of education, nursing philosophy, social science, and physics. This development research results concluded that the core cognitive skills of critical thinking are interpretation, analysis, evaluation, inference, explanations, and self-regulation (Nair and Stamler, 2013). The latest research-based on Fasione's review is developing critical thinking skills assessment for secondary school students (Aizikovitsh-Udi and Amit, 2011). Employing the six indicators of conclusions of the Fasione research results (Facione, 2009) above, it is possible to adjust to the characteristics of learning outcomes in the material work and energy.

The achievement of work and energy learning for the Physics learning curriculum in Indonesia includes (a) analyzing the concepts of energy, work, work relations (work) and energy changes, energy conservation laws, and their application in everyday events; and (b) propose ideas for solving motion problems in daily life by applying scientific methods, energy concepts, work, and energy conservation laws. Based on operational verbs as outlined in the learning curriculum at the high school level, namely analyzing and proposing problem-solving, the development of indicators of critical thinking skills chosen in the cognitive realm in work and energy material are interpretation, analysis, evaluation, inference, and explanations (Table 1). The self-regulation indicators are included in the affective domain (Paul, R., and Elder, 2007). It does not become a part that is measured for the achievement of critical thinking skills on the material work and energy.

Table 1 can be described as the process of determining indicators for work energy material by looking for a list of indicators that are often used as a benchmark that the indicators have in common with the opinions of other experts. The five indicators have a relationship with learning achievement in work and energy materials. So an operational definition needs to be made to facilitate the measurement standards.

The first indicator is related to the interpretation. It has the same thought in determining the interpretation indicators in critical thinking skills (Dana S. Dunn, Jane S. Halonen, 2009) and (Facione, 2009), which is relevant to learning achievement in point a. Interpretation in work and energy learners is a process of understanding and expressing meaning or a broad meaning, various experiences, situations, data, events related to work and energy phenomena into language that is easily understood by others (Maknun, 2020; Yulianti *et al.*, 2019; Reynders *et al.*, 2020).

The second indicator is related to determine analytical indicators in critical thinking skills. These indicators are the basic characteristics of thinking skills (Bassham and Wallace, 2013; Crews-Anderson, 2007; Dana S. Dunn, Jane S. Halonen, 2009; Facione, 2009; Moon, 2007) relevant to the indicators of learning achievement of learning in point a. In other words, it is an analysis in the application of work and energy learners to identify the desired and actual inferential relationships among questions, concepts, descriptions, or other forms in the work and energy frame (Negoro *et al.*, 2020; Yulianti *et al.*, 2019; Reynders, Lantz, Ruder, Stanford, and Cole, 2020).

The Third, evaluation indicator, some experts have the same thought in determining evaluation indicators in critical thinking skills (Facione, 2009; Wallace, 2001) relevant to learning achievement of learning in point b. The evaluation itself can be applied in work and energy learners as a process of assessing a statement or information related to concepts contained in work and energy (Yulianti *et al.*, 2019; Reynders *et al.*, 2020).

The fourth indicator is related to inference. Some experts have the same thought in determining indicators of formulating hypotheses in critical thinking skills (Ennis, 1996) and (Dana S. Dunn, Jane S. Halonen, 2009) relevant to learning achievement of learning in point b. Formulating one's hypothesis can be applied in work and energy learners, identifying a phenomenon related to work and energy implementation to draw conclusions that make sense to form guesses or assumptions (Maknun, 2020; Reynders *et al.*, 2020).

The fifth is related to explanations indicator. Some experts have the same thought in determining explanatory indicators in critical thinking skills (Moon, 2007) and (Facione, 2009), relevant to learning achievement in point a. This

causes explanations to be applied in work and energy learners, to state and explain by considering the conceptual evidence of work and energy agreed to convince someone (Reynders *et al.*, 2020).

3.3. The basic principle of making a Test Instrument Critical thinking

After the indicator of critical thinking skills is determined, the next step is how to make the test instrument. The instrument is said to be good if it can evaluate or assess something with results following the objectives of critical thinking skills (Facione, 2009).

Based on both theoretical and research findings related to critical thinking skills, there were three basic principles in making critical thinking test instruments, namely (1) presentation of phenomena, (2) open-ended approach, and (3) measure rationality answer (Özsoy-Güneş *et al.*, 2015; Halpern, 2014b; Lawson, 2004; Willingham, 2008; Etkina and Planinšič, 2015; Sya'Bandari *et al.*, 2018; (Franco, Costa, and Almeida, 2018) Tiruneh *et al.*, 2017; Asmawati *et al.*, 2018; Mahbubah *et al.*, 2018; Negoro *et al.*, 2020; Istiyono *et al.*, 2019; Abidin, Istiyono, Fadilah, and Dwandaru, 2019; Sutarno *et al.*, 2019).

The phenomena are related to making tests in critical thinking based on events or phenomena around students (Özsoy-Güneş *et al.*, 2015; Halpern, 2014b; Lawson, 2004), and also events that have been experienced by students (Willingham, 2008; Etkina and Planinšič, 2015). The test can be in pictures, graphics, daily life events, and information from a media (Sya'Bandari *et al.*, 2018).

Second, the type of test, the design, is made in the form of an open-ended. This is because it gives more opportunity to express students' thinking strategies. Open-ended test questions can stimulate essential aspects of critical thinking like analyzing, rethinking, or generating new ideas (Franco, Costa, and Almeida, 2018; Franco *et al.*, 2018; Tiruneh *et al.*, 2017; Asmawati *et al.*, 2018)

Third, measure rationality answer. Critical thinking means someone has a reasonable explanation (Mahbubah *et al.*, 2018; Negoro *et al.*, 2020; Istiyono *et al.*, 2019; Abidin, Istiyono, Fadilah, and Dwandaru, 2019). Reasonable means the ability to think that tries to connect known facts into a conclusion (Ennis, 1996; Sutarno *et al.*, 2019; Abidin, Istiyono, Fadilah, and Dwandaru, 2019).

3.4. Framework Critical Thinking Work and Energy Test

The test is the final part of the learning process to measure learning achievement goals and learning activities (McTighe and Wiggins, 2012). A good test must measure the learning objectives that have been set (Ennis, R.H., Millman, J., Tomko, 1985). The framework for the development of this test was determined by considering the achievement of learning objectives on work and energy in measuring critical thinking skills. Critical thinking skills include five indicators (interpretation, analysis, evaluation, inference, and explanation). Each of these indicators will be developed in the form of tests with basic principles, including (1) presentation of phenomena, (2) open-ended questions, and (3) measure the rationality of student answers. The design flow conceptual framework development is shown in Figure 1.

3.5. Examples of the application of the development of the critical thinking skills test instrument for indicator analysis

The example of the application presented was taken from appendix 1 (item number 2) to analyze critical thinking skills indicators. For instance: Description: Look at Figure 2, a pendulum is dropped from point P. Pay attention to the movement of the pendulum. The movement starts from point P, going to Q, R, S, and finally going to T.

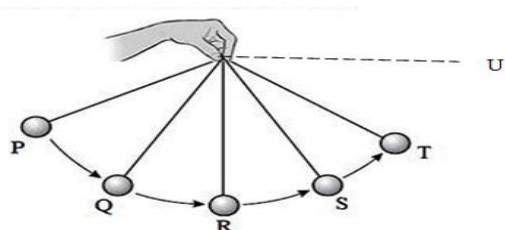


Figure 2. A pendulum is dropped from point P to T point

Question: Why do you think the pendulum never reaches the U-point?

Scoring guide: Grading Guide for item The following are the ideal complete answers that it was expected from the students:

- The difference in the height of the positions p and U affects the difference in potential energy. Or the potential energy at point U is greater than the potential energy at point P or vice versa. This is contrary to the law of

conservation of mechanical energy, namely the amount between potential energy and kinetic energy is always constant. (Substance score answer: 4 points)

- The potential energy at point U is greater than the potential energy at point P or vice versa. (Substance of the answer score: 3 points)
- There is a potential energy difference. (Substance of the answer score: 2 points)
- Altitude impacts potential energy. (Substance of the answer score: 1 point)
- Answering with a wrong concept or not responding. (Score: 0 points)

Information:

Analyze indicator, an indicator that explains the causal effect relationship in a particular phenomenon (Negoro *et al.*, 2020; Yulianti *et al.*, 2019; Reynders, Lantz, Ruder, Stanford, and Cole, 2020). The final goal in the problem presented is that students are asked to determine why the pendulum does not reach U-point.

Presentation of phenomena, providing information on the situation that has been experienced around students or experimental activities (Özsoy-Güneş *et al.*, 2015; Halpern, 2014b; Lawson, 2004; Willingham, 2008; Etkina and Planinšič, 2015). Presentation of the phenomenon in the example problem is the pendulum image that is given information P, Q, R, S, and T accompanied by the direction of the arrow

The open-ended approach gives students opportunities to express their ideas (Franco *et al.*, 2018; Franco *et al.*, 2018; Tiruneh *et al.*, 2017; Asmawati *et al.*, 2018). The form of the open-ended test in the example questions is the question sentence, "Why do you think the pendulum never reaches the U-point?"

Measure rationality answer, answers based on understanding concepts, in fact, to conclude (Mahbubah *et al.*, 2018; Negoro *et al.*, 2020; Istiyono *et al.*, 2019; Abidin, Istiyono, Fadilah, and Dwandaru, 2019; Sutarno *et al.*, 2019; Abidin, Istiyono, Fadilah, and Dwandaru, 2019). The form of rationality testing for each student's answer is a standard reference assessment guideline.

Five indicators of critical thinking skills that include interpretations, analyzes, evaluations, inferences, and explanations in the material business and energy in detail are explained in appendix 1.

4. CONCLUSIONS:

1. Indicators of critical thinking skills on work and energy include interpretation, analysis, evaluation, inference, explanation.
2. The basic principles of making critical thinking test instruments include presenting phenomena, open-ended tests, and testing the rationality of answers.
3. There was an example of applying the development of the critical thinking skills test instrument for indicator analysis.

5. REFERENCES:

1. Abidin, A. Z., Istiyono, E., Fadilah, N., and Dwandaru, W. S. B. (2019). A computerized adaptive test for measuring the physics critical thinking skills. *International Journal of Evaluation and Research in Education*, 8(3), 376–383. <https://doi.org/10.11591/ijere.v8i3.19642>
2. Adey P, S. M. (1994). *Really raising standards: Cognitive intervention and academic achievement*. Routledge.
3. Aizikovitsh-Udi, E., and Amit, M. (2011). Developing the skills of critical and creative thinking by probability teaching. *Procedia - Social and Behavioral Sciences*, 15, 1087–1091. <https://doi.org/10.1016/j.sbspro.2011.03.243>
4. April, F., and Kuswanto, H. (2017). Improving Critical Thinking through Research Based Learning Model for Pre-Service Teacher. *International Journal of Sciences: Basic and Applied Research (IJSBAR)*, 4531, 134–140.
5. Arend, R. (2012). *Learning to Teach 9th Edition*. McGraw-Hill.
6. Asmawati, E., Rosidin, U., and a, A. (2018). the Development of Assessment Instrument Towards the Students' Critical Thinking Ability on the High School Physics Lesson With the Creative Problem Solving Model. *International Journal of Advanced Research*, 6(6), 90–99. <https://doi.org/10.21474/ijar01/7191>
7. Bächtold, M. (2018). How Should Energy Be Defined Throughout Schooling? *Research in Science Education*, 48(2), 345–367. <https://doi.org/10.1007/s11165-016-9571-5>
8. Bailin., S. (2002). Critical Thinking and Science Education. *Science and Education*, 11(1), 361–375. <https://doi.org/10.5325/jgeneeduc.62.1.0028>
9. Banning, M. (2006). Nursing research: Perspectives on critical thinking. *British Journal of Nursing*, 15(1), 458–46.
10. Bassett, M. H. (2016). Teaching Critical Thinking without (Much) Writing: Multiple-Choice and Metacognition. *Teaching Theology and Religion*, 19(1), 20–40. <https://doi.org/10.1111/teth.12318>
11. Bassham, G., and Wallace, J. M. (2013). *Critical Thinking a Student ' S Introduction Fifth Edition*. 27.
12. Crews-Anderson, T. (2007). Critical thinking and informal logic. In *Encyclopedia of Creativity*. <https://doi.org/10.1016/B978-0-12-375038-9.00057-1>
13. Damayanti, R. S., Suyatna, A., Warsono, W., and Rosidin, U. (2017). Development of Authentic Assessment instruments for Critical Thinking skills in Global Warming with a Scientific Approach. *International Journal of Science and Applied Science: Conference Series*, 2(1), 289. <https://doi.org/10.20961/ijssascs.v2i1.16730>
14. Dana S. Dunn, Jane S. Halonen, and R. A. S. (2009). *Teaching Critical Thinking in Psychology: A Handbook of Best Practices*. <https://doi.org/10.1002/9781444305173.ch4>
15. Dega, B. G., and Govender, N. (2016). Assessment of students' scientific and alternative conceptions of energy and momentum using concentration analysis. *African Journal of Research in Mathematics, Science and Technology Education*, 20(3), 201–213. <https://doi.org/10.1080/18117295.2016.1218657>
16. Dimiyati, M. (2011). *Belajar dan Pembelajaran*. Rineka Cipta.
17. Ennis, R.H., Millman, J., Tomko, T. N. C. (1985). *Critical thinking Test level X and level Z: A manual (3rd ed.)*. Midwest Publications.

18. Ennis, Robert H, and W. (1985). *The Ennis-Weir Critical Thinking Essay Test*. Midwest Publications.
19. Ennis, R. H. (1985). A Logical Basis for Measuring Critical Thinking Skills. *Educational Leadership*, oktober, 44–48.
20. Ennis, R. H. (1996). Critical Thinking Dispositions: Their Nature and Assessability. *Informal Logic*, 18(2), 165–182.
<https://doi.org/10.22329/il.v18i2.2378>
21. Etkina, E., and Planinšič, G. (2015). Defining and Developing “Critical Thinking” Through Devising and Testing Multiple Explanations of the Same Phenomenon. *The Physics Teacher*, 53(7), 432–437.
<https://doi.org/10.1119/1.4931014>
22. Facione, N.C., Facione, P., Blohm, S.W., and Gittens, C. (2008). *California Critical Thinking Skills Test manual*. The California Academic Press.
23. Facione, P. A. (2009). *Facione, Peter A. Critical Thinking: What It Is and Why It Counts*. Measured Reasons LLC.
24. Folly Eldy, E., and Sulaiman, F. (2013). Integrated PBL Approach: Preliminary Findings towards Physics Students’ Critical Thinking and Creative-Critical Thinking. *International Journal of Humanities and Social Science Invention ISSN (Online)*, 2(3), 2319–7722.
25. Franco, A. R., Costa, P. S., and Almeida, L. da S. (2018). Traducción, adaptación y validación del halpern critical thinking assessment en Portugal: Efecto del área disciplinaria y nivel académico en el pensamiento crítico. *Anales de Psicología*, 34(2), 292–298.
<https://doi.org/10.6018/analesps.34.2.272401>
26. Gagne, R. (1988). Some Reflections on Thinking Skill. *Instructional Science*, 17(4), 387–390.
27. Giancoli, D. C. (1997). *Fisika Jilid 1 Edisi Keempat*. Alih bahasa oleh Cuk Imawan, dkk. 1997. Erlangga.
28. Gutierrez-Berraondo, J., Guisasola, J., and Zuza, K. (2019). Addressing undergraduate students’ difficulty in learning the Generalized Work-Energy Principle in introductory Mechanic. *Journal of Physics: Conference Series*, 1287(1). <https://doi.org/10.1088/1742-6596/1287/1/012024>
29. Halpern, D. F. (1999). Teaching for Critical Thinking: Helping College Students Develop the Skills and Dispositions of a Critical Thinker. *Education*, 80, 69–75.
30. Halpern, D. F. (2010). *The Halpern CT Assessment: Manual*. Schuhfried GmbH.
31. Halpern, D. F. (2014a). *Critical thinking across the curriculum: A brief edition of thought and knowledge (5th ed.)*. Routledge.
32. Halpern, D. F. (2014b). *Thought and knowledge: An introduction to critical thinking*. Psychology Press.
33. Hamruni. (2011). *Strategi Pembelajaran*. Insan Madani.
34. Hill, G. M. (2008). *Introduction to Physical Science*. Howel.
35. Holmes, N. G., Wieman, C. E., and Bonn, D. A. (2015). Teaching critical thinking. *Proceedings of the National Academy of Sciences of the United States of America*, 112(36), 11199–11204.
<https://doi.org/10.1073/pnas.1505329112>
36. Ilfiandra Nurhudaya, M. L. (2019). The analysis of critical thinking skills test in social-problems for physics education students with Rasch Model The analysis of critical thinking skills test in social-problems for physics education students with Rasch Model. *MSCEIS 2018*, 1–8.
<https://doi.org/10.1088/1742-6596/1280/5/052012>
37. Istiyono, E., Dwandaru, W. S. B., Lede, Y. A., Rahayu, F., and Nadapdap, A. (2019). Developing IRT-based physics critical thinking skill test: A CAT to answer 21st century challenge. *International Journal of Instruction*, 12(4), 267–280.
<https://doi.org/10.29333/iji.2019.12417a>
38. Jeweet, S. (2010). *Fisika Untuk Sains dan Teknik*. Salemba Teknika.
39. Judge, B., Jones, P., and McCreery, E. (2009). Study Skills in Education: Critical Thinking Skills for Education Students. *Learning Matters Ltd*.
<https://doi.org/10.1017/CBO9781107415324.004>

40. Jurfri, W. (2013). *Belajar dan Pembelajaran Sains*. Rineka Cipta.
41. Kuhn, D., and Kuhn, D. (1999). A Developmental Model of Critical Thinking. *Educational Researcher*, 28(16), 16–25. <https://doi.org/10.3102/0013189X028002016>
42. Lawson, A. E. (2004). The nature and development of scientific reasoning: A synthetic view. *International Journal of Science and Mathematics Education*, 2(3), 307–338. <https://doi.org/10.1007/s10763-004-3224-2>
43. Mahbubah, K., Rusdiana, D., Juanda, E. A., Hermita, N., and Hakim, I. R. (2018). *Constructing secondary students' critical thinking skill test on heat concept*. 3, 221–226.
44. Mahmud. (2012). *Metode Penelitian Pendidikan*. CV Pustaka Setia.
45. Maknun, J. (2020). Implementation of Guided Inquiry Learning Model to Improve Understanding Physics Concepts and Critical Thinking Skill of Vocational High School Students. *International Education Studies*, 13(6), 117. <https://doi.org/10.5539/ies.v13n6p117>
46. Mason, M. (2009). Critical Thinking and Learning. In *Critical Thinking and Learning*. <https://doi.org/10.1002/9781444306774>
47. McTighe, J., and Wiggins, G. (2012). Understanding By Design® Framework. Alexandria, VA: Association for Supervision ..., 1–13.
48. Moon, J. (2007). Critical thinking: An exploration of theory and practice. In *Critical Thinking: An Exploration of Theory and Practice*. <https://doi.org/10.4324/9780203944882>
49. Nair, G. G., and Stamler, L. L. (2013). A conceptual framework for developing a critical thinking self-assessment scale. *Journal of Nursing Education*, 52(3), 131–138. <https://doi.org/10.3928/01484834-20120215-01>
50. Nana Syaodih. (2011). *Landasan Psikologi Proses Pendidikan*. Remaja Rosdakarya.
51. Negoro, R. A., Rusilowati, A., Aji, M. P., and Jaafar, R. (2020). Critical Thinking in Physics: Momentum Critical Thinking Test for Pre- Service Teacher. *Jurnal Ilmiah Pendidikan Fisika Al-Biruni*, 9(1), 73–86. <https://doi.org/10.24042/jipfalbiruni.v9i1.4834>
52. Nisa, E. K., Jatmiko, B., and Koestiari, T. (2018). Development of Guided Inquiry-based Physics Teaching Materials to Increase Critical Thinking Skills of Highschool Students. *Jurnal Pendidikan Fisika Indonesia*, 14(1), 18–25. <https://doi.org/10.15294/jpfi.v14i1.9549>
53. Nitco, A. J. and B. S. M. (2011). *Educational assessment of students* (6th ed.). Pearson Education.
54. Niu, L., Behar-Horenstein, L. S., and Garvan, C. W. (2013). Do instructional interventions influence college students' critical thinking skills? A meta-analysis. *Educational Research Review*, 9, 114–128. <https://doi.org/10.1016/j.edurev.2012.12.002>
55. Norris, S. P. (1985). Synthesis of research on critical thinking. *Educational Leadership*, 42(8), 40–45.
56. OECD. (2019). *OECD programme for international student assessment 2018*. OECD Publishing.
57. Özsoy-Güneş, Z., Güneş, İ., Derelioğlu, Y., and Kırbaşlar, F. G. (2015). The Reflection of Critical Thinking Dispositions on Operational Chemistry and Physics Problems Solving of Engineering Faculty Students. *Procedia - Social and Behavioral Sciences*, 174, 448–456. <https://doi.org/10.1016/j.sbspro.2015.01.688>
58. Papadouris, N., Hadjigeorgiou, A., and Constantinou, C. P. (2014). Pre-service Elementary School Teachers' Ability to Account for the Operation of Simple Physical Systems Using the Energy Conservation Law. *Journal of Science Teacher Education*, 25(8), 911–933. <https://doi.org/10.1007/s10972-014-9407-y>
59. Paul, R., and Elder, L. (2007). *International Critical Thinking Essay Test*. Foundation for Critical Thinking.

60. Paul, Richard; Elder, L. (2014). Critical Thinking Concepts and Tools. *Radiologic Technology*, 85(6), 697.
61. Paul, R. W. (1991). *aching critical thinking in the strong sense*. In A. L. Costa (Ed.), *Developing minds: A resource book for teaching thinking*. Association For Supervision And Curriculum Development.
62. Reynders, G., Lantz, J., Ruder, S. M., Stanford, C. L., and Cole, R. S. (2020). Rubrics to assess critical thinking and information processing in undergraduate STEM courses. *International Journal of STEM Education*, 7(1). <https://doi.org/10.1186/s40594-020-00208-5>
63. Rosidin, U., W Distrik, I., and Herlina, K. (2018). *The Developmment of Assessment Instrument for Learning Science to Improve Student's Critical and Creative Thinking Skills*. 1, 61–67. <https://doi.org/10.26499/iceap.v1i1.74>
64. Sarigoz, O. (2012). Assessment of the High School Students' Critical Thinking Skills. *Procedia - Social and Behavioral Sciences*, 46, 5315–5319. <https://doi.org/10.1016/j.sbspro.2012.06.430>
65. Suastra, I. W., Ristiati, N. P., Adnyana, P. P. B., and Kanca, N. (2019). The effectiveness of Problem Based Learning - Physics module with authentic assessment for enhancing senior high school students' physics problem solving ability and critical thinking ability. *Journal of Physics: Conference Series*, 1171(1). <https://doi.org/10.1088/1742-6596/1171/1/012027>
66. Suryabrata. (2008). *Psikologi Kepribadian*. Raja Grafindo Persada.
67. Sustekova, E., Kubiato, M., and Usak, M. (2019). Validation of critical thinking test on Slovak conditions. *Eurasia Journal of Mathematics, Science and Technology Education*, 15(12). <https://doi.org/10.29333/ejmste/112295>
68. Sutarno, S., Setiawan, A., Suhandi, A., Kaniawati, I., and Malik, A. (2019). The development and validation of critical thinking skills test on photoelectric effect for pre-service physics teachers. *Journal of Physics: Conference Series*, 1157(3). <https://doi.org/10.1088/1742-6596/1157/3/032032>
69. Sya'Bandari, Y., Firman, H., and Rusyati, L. (2018). The validation of science virtual test to assess 7th grade students' critical thinking on matter and heat topic (SVT-MH). *Journal of Physics: Conference Series*, 1013(1). <https://doi.org/10.1088/1742-6596/1013/1/012067>
70. Tiruneh, D. T., De Cock, M., Weldelessie, A. G., Elen, J., and Janssen, R. (2017). Measuring Critical Thinking in Physics: Development and Validation of a Critical Thinking Test in Electricity and Magnetism. *International Journal of Science and Mathematics Education*, 15(4), 663–682. <https://doi.org/10.1007/s10763-016-9723-0>
71. Trilling, F. (n.d.). *21st Century skills: Learning for life in our times*. John Wiley and Sons, Ltd., The.
72. Wager, T. (2008). *The Global Achievement Gap*. Basic Books.
73. Wallace, G. B. W. I. H. N. J. M. (2001). *Critical Thinking A Student's Intruduction* (Fourth Edi). McGraw-Hill.
74. Walsh, C., Quinn, K. N., Wieman, C., and Holmes, N. G. (2019). Quantifying critical thinking: Development and validation of the physics lab inventory of critical thinking. *Physical Review Physics Education Research*, 15(1), 10135. <https://doi.org/10.1103/physrevphyseducres.15.010135>
75. Warren, J. W., and Richmond, P. E. (2018). Teaching about energy. *Physics Education*, 18(2), 55–56. <https://doi.org/10.1088/0031-9120/18/2/101>
76. Wartono, W., Hudha, M. N., and Batlolona, J. R. (2018). How are the physics critical thinking skills of the students taught by using inquiry-discovery through empirical and theoretical overview? *Eurasia Journal of Mathematics, Science and Technology Education*, 14(2), 691–697. <https://doi.org/10.12973/ejmste/80632>
77. Waston, G. and G. E. M. (1980). *Watson-Glaser Critical Thinking Appraisal manual*. Psychological Corp.
78. Watson, G., Glaser, E. M., and Rust, J.

(2002). *Manual of the Watson-Glaser Critical Thinking Appraisal (UK Edition)*. Psychological Corporation.

79. Willingham, D. T. (2008). Critical Thinking: Why Is It So Hard to Teach? *Arts Education Policy Review*, 109(4), 21–32.
<https://doi.org/10.3200/AEPR.109.4.21-32>
80. Yulianti, D., Wiyanto, Rusilowati, A., Nugroho, S. E., and Pangesti, K. I. (2019). Science, technology, engineering, and mathematics (STEM) based learning of physics to develop senior high school student's critical thinking. *Journal of Physics: Conference Series*, 1321(2).
<https://doi.org/10.1088/1742-6596/1321/2/022029>

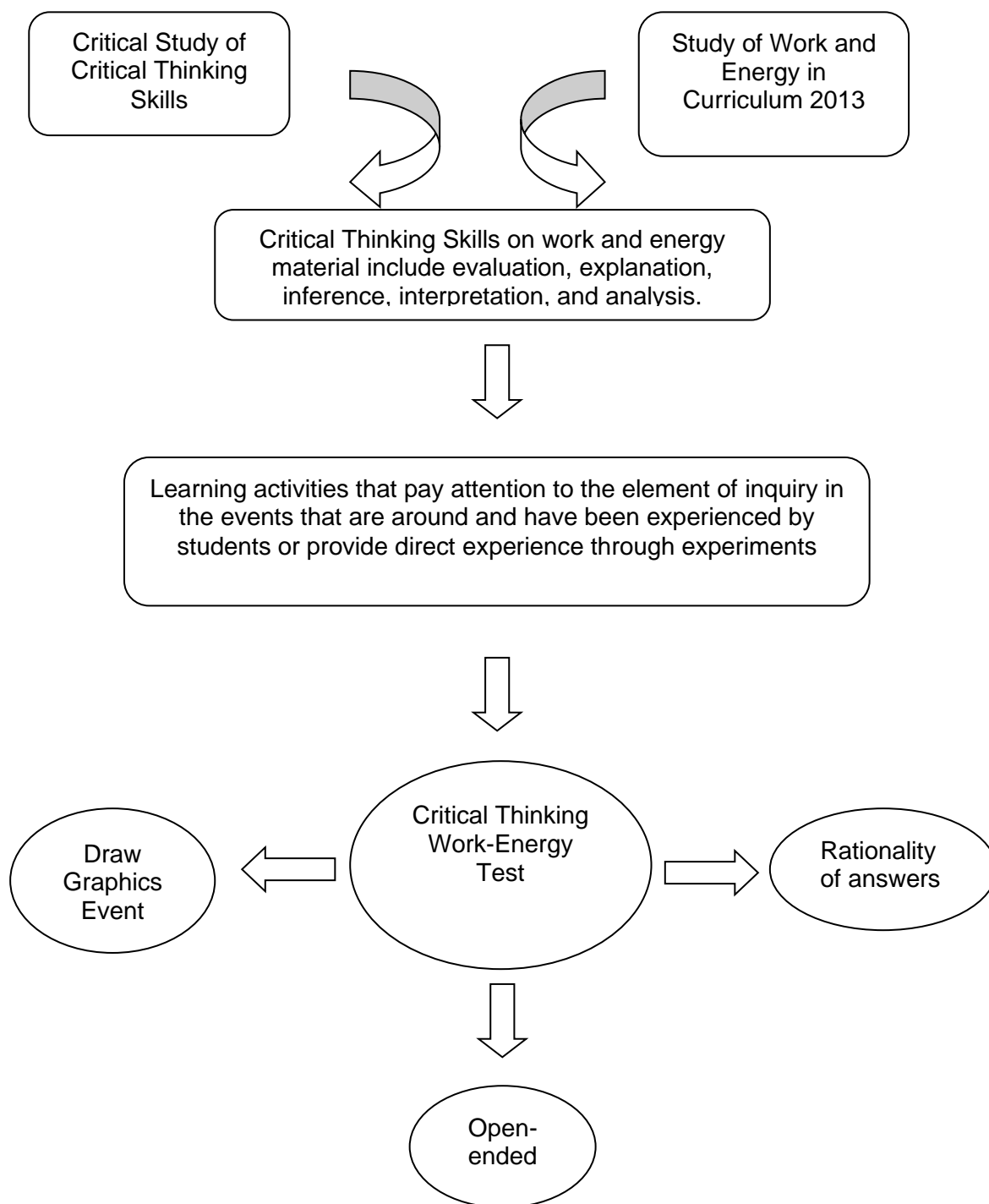


Figure 1. Conceptual Framework of Critical Thinking Work-Energy Test

Table 1. Determination of Critical Thinking Skills Indicators on Work and Energy Material

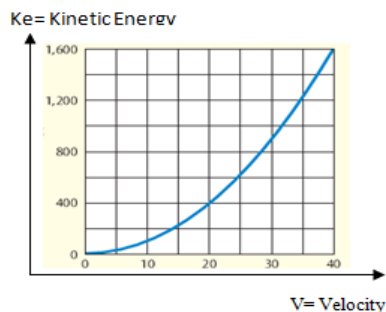
No	Literature	Indicator of Critical Thinking	Basic Competencies	Relevance Indicators
1.	Ennis, 1996	a. formulate a hypothesis b. question, c. alternative, d. and activity plan	3.9 Analyzing the concepts of energy, work, work relations (work) and energy changes, energy conservation laws, and their application in everyday events 4.9 Propose ideas for solving motion problems in daily life by applying scientific methods, energy concepts, work, and energy conservation laws	Interpretation (Dana S. Dunn, Jane S. Halonen, 2009; Facione, 2009)
2.	Dana S. Dunn, Jane S. Halonen, 2009	a. Formulate a hypothesis b. conclusion, c. calculating possibilities,		
3.	Moon 2007	a. understanding analysis b. explanation		
4.	Crews-Anderson, 2007	Analysis Interpretation		Analysis (Bassham and Wallace, 2013; Crews-Anderson, 2007; Dana S. Dunn, Jane S. Halonen, 2009; Facione, 2009; Moon, 2007)
5.	Mason, 2009	Analysis		Evaluation (Bassham and Wallace, 2013; Facione, 2009)
6.	Willingham, 2008	Analysis		
7.	Dana S. Dunn, Jane S. Halonen, 2009	a. asking question, b. examine the evidence, c. analyze assumptions d. avoid emotional reasons, e. avoid oversimplification, f. interpretation, and g. tolerate uncertainty		
8.	Bassham and Wallace, 2013	a. identify, b. analyze, and c. evaluate arguments, and d. truth claims;		Inference (Dana S. Dunn, Jane S. Halonen, 2009; Ennis, 1996)
9.	Facione, 2009	a. interpretation, b. analysis, c. evaluation, d. Inference, e. explanation f. self-regulation		Explanation(Facione, 2009; Moon, 2007)

APPENDIX 1

Example Assessment of Thinking Skills Tests on Work Materials and Energy

The application of making critical thinking tests of students in grade 11 high school students to provide an overview related to indicators, answer keys, and guiding guidelines which include indicators (1) Interpret the experimental data, (2) analyze kinetic energy, (3) evaluating work concept statements correctly, (4) making inference related to kinetic energy and (5) explaining the concept of kinetic energy.

A. Item number 1



Description of the problem

An object moving with a certain mass moves with a change in speed and then measured its energy value as a graph.

Question

What do you understand about the chart?

Information

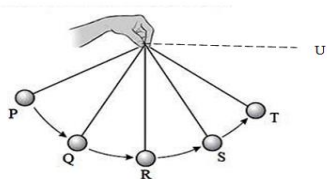
Item number 1 measures one sub-skill in the element of critical thinking skills, namely **interpretation indicator**: Students Interpret experimental data on the relationship of kinetic energy with speed

(see Table 1). The figure is the observational data related to the relationship between speed and the kinetic energy produced.

Scoring guide: Grading Guide for item problem number 1

- The following are the ideal complete answers that the authors expect from a student:
With the same period, kinetic energy is proportional to the speed quadrant. (Substance of answer, score: 4 Point)
- The greater the speed, the kinetic energy also increases. (Substance score answer: 3 points)
- Kinetic energy is related to the speed of forming a curve. (Substance score answer: 3 points)
- Kinetic energy is determined by speed (Substance answer score: 3 points)
- Answering with a wrong concept or not answering. (Score: 1 point)

B. Item number 2



Description of the problem

A pendulum is dropped from point P, pay attention to the movement of the pendulum. The movement starts from point P, going to Q, going to S, and finally going to T.

Question

Why do you think the pendulum never reaches the U-point?

Information

Item number 2 measures one sub-skill in the element of critical thinking skills, namely **analyze indicator**: Students explore the kinetic energy in a pendulum (see Table 1). The item requires that why the pendulum removed does not exceed the initial height when the object was removed, associate the phenomenon with the laws of conservation of mechanical energy.

Scoring guide: Grading Guide for item problem number 2

- The following are the ideal complete answers that the authors expect from a student:
The difference in the height of the positions p and U affects the difference in potential energy. Or the potential energy at point U is greater than the potential energy at point P or vice versa. This is contrary to the law of conservation of mechanical energy, namely the amount between potential energy and kinetic energy is always constant. (Substance score answer: 4 points)
- The potential energy at point U is greater than the potential energy at point P or vice versa. (Substance of the answer score: 3 points)
- There is a potential energy difference. (Substance of the answer score: 2 points)
- Altitude impacts potential energy. (Substance of the answer score: 1 point)
- Answering with a wrong concept or not responding. (Score: 0 points)

C. Item number 3



Description of the problem

An employee in a company always chooses a sloping area to put goods into a car that has a high body. According to him this is due to the work needed to move objects lighter than directly lifting up.

Question

Do you think that the employee statement is true or false?

Information

Item number 3 measures one sub-skill in critical thinking skills, **namely evaluate indicator**: Students consider work concept

statements correctly (see Table 1). The item requires that students criticize or evaluate the general statement that 'in the incline of the work required to move objects lighter than directly raised,' whether the principle is following the concept of work.

Scoring guide: Grading Guide for item number 3

- The following are the ideal complete answers that the authors expect from a student:
The statement of employees of works of lighter value compared to being directly lifted is not quite right. The work should be of the same amount. What is different is the style, the force required by the employee is lighter because the resultant force between the weight of the object and the normal force towards the back is lighter than the weight of the object. So the employee needs less force than the weight of the object. [Score: 4 points];
- The statement is not quite right. The right thing is the style is smaller because it forms an angle so that the style is smaller. (Substance of the answer score: 3 points)
- The statement is less precise, which is precisely the small force due to the length of the track. (Substance of the answer score: 2 points)
- The statement is incorrect. (Score: 1)
- Answering is not following the concept. Or not at all (Score: 0)

D. Item number 4

Description of the problem

Mirna has three marbles with size difference

- a. Large marbles
- b. Medium-sized marbles
- c. Small marbles

Of the three marbles dropped with a height of 2 meters on the floor prepared plasticine to measure the depth of the marbles.

Question

Which marbles do you think to have the deepest basins?

Information

Item number 4 measures one sub-skill in the element of critical thinking skills, namely **interference indicator**: Students make hypotheses related to kinetic energy (see Table 1). The item requires that the phenomenon when marbles with different mass sizes are dropped at the same height impacts the speed of the law of conservation of mechanical energy.

Scoring guide: Grading Guide for item problem number 4

- The following are the ideal complete answers that the authors expect from a student:
The kinetic energy of the object determines the depth of the plasticine basin. The greater the kinetic energy of the plastic depth, the deeper the plastic basin. The amount of mass and speed determine kinetic energy. Kinetic energy is proportional to the mass and the speed of the quadrants. Therefore the greater the mass, the greater the kinetic energy. So that the biggest number one marble has the deepest basin. (Substance of answer, score: 4 Point)
- Depth will be different; differences in kinetic energy cause this. So that the most significant number one marble has the deepest basin. (Substance answer score 3)
- The most significant number one marbles have the deepest basins because they have the most prominent time. (Substance score answer: 2 points)
- Marbles number one. (Score: 1 point)
- Answering with a different concept or not answering (Score 0)

E. Item number 5.

Description of the problem

When riding a bicycle, when going down the bridge without us, the speed of the bike decreases faster and faster.

Question

Why do you think so?

Information

Item number 5 measures one sub-skill in the element of critical thinking skills, namely **explanation indicator**: Students explain the concept of mechanical energy (see Table 1). The item requires that the phenomenon when traveling downhill the speed gets bigger 'relate the phenomenon to the law of conservation of mechanical energy.

Scoring guide: Grading Guide for item problem number 5

- The following are the ideal complete answers that the authors expect from a student:
This is caused by the existence of the law of conservation of energy. in that case, there are three main concepts, namely potential energy, work, and kinetic energy, the amount when the main component is equal to the value of the object at maximum height. If the bicycle decreases, the amount of gravitational potential energy decreases to impact the magnitude of kinetic energy and work. (Substance of answer, score: 4 Point)
- This is due to the law of conservation of energy so that in time decreases, potential energy decreases, and kinetic energy increases. (Substance score answer: 3 points)
- This is due to the law of conservation of energy (Substance answer score: 2 points)
- Gravitational potential energy decreases (Score: 1 point)
- Answering with a different concept or not answering (Score: 0)

CARACTERÍSTICAS ECOLÓGICAS E BIOLÓGICAS E COMPOSIÇÃO QUANTITATIVA DA FAUNA DE INFUSORIA EM DIFERENTES PARTES DO ESTÔMAGO DE ALCES EUROPEUS (*ALCES ALCES*) QUE VIVEM NAS REGIÕES DE OMSK E CHELYABINSK DA RÚSSIA**THE ECOLOGICAL AND BIOLOGICAL FEATURES AND QUANTITATIVE COMPOSITION OF INFUSORIA FAUNA IN DIFFERENT PARTS OF THE STOMACH OF EUROPEAN ELK (*ALCES ALCES*) LIVING IN THE OMSK AND CHELYABINSK REGIONS OF RUSSIA****ЭКОЛОГО-БИОЛОГИЧЕСКИЕ ОСОБЕННОСТИ И КОЛИЧЕСТВЕННЫЙ СОСТАВ ИНFUЗОРНОЙ ФАУНЫ РАЗЛИЧНЫХ ОТДЕЛОВ ЖЕЛУДКА ЛОСЯ ЕВРОПЕЙСКОГО (*ALCES ALCES*) ОМСКОЙ И ЧЕЛЯБИНСКОЙ ПОПУЛЯЦИЙ РОССИИ**KORCHAGINA, Tatyana^{1*}¹ Omsk State Pedagogical University, Department of Fundamentals of Health and Safety and Biology Teaching Methods. Russia.* Corresponding author
e-mail: korchagina.ospu@bk.ru

Received 25 May 2020; received in revised form 24 August 2020; accepted 30 September 2020

RESUMO

Os alces (*Alces alces* L.) são os maiores animais da família dos veados e um importante animal comercial e de caça na Rússia. Desde os tempos antigos, os alces oferecem carne nutritiva e peles valiosas. Por esta razão, existem repetidas tentativas de domesticar alces. No entanto, a domesticação dos alces e sua implementação nas fazendas não foi além das fazendas experimentais. Isso se deve em grande parte à fisiologia inexplorada da digestão do alce, incluindo o papel dos ciliados endobiontes. A dieta do alce é muito diversa e inclui brotos, folhas, a casca de várias espécies de árvores e arbustos, várias ervas, rizomas e folhas de plantas aquáticas e cogumelos. Esta pesquisa teve como objetivo realizar um estudo quantitativo e específico da composição do infusório do trato digestivo de alces europeus que vivem no território das regiões de Omsk e Chelyabinsk da Rússia em relação ao habitat, nutrição e clima. São apresentados os resultados de uma análise comparativa das espécies e da composição numérica de protozoários ciliados simbióticos em estômagos de alces europeus. O número médio de espécies individuais de cílios do estômago de alce dependendo do território de habitat do animal, bem como a composição qualitativa e quantitativa de várias partes do estômago é apresentada. O gênero dominante de cílios em alces é *Entodinium*, que inclui 10 espécies. O *Entodinium* representa 63% de todos os protozoários no rúmen dos alces na população de Chelyabinsk e 73% na população de Omsk. A participação da família ophrioscolecidae é responsável por 98% da composição total dos cílios no rúmen dos alces da população de Chelyabinsk e por 96% da população de Omsk. Nenhum cílio foi encontrado no coalho. Os resultados permitem avaliar as perspectivas para a domesticação dos alces europeus.

Palavras-chave: *Alce, Infusoria Fauna, Rúmen, Retículo, Omasum, Ração alimentar de animais comerciais.***ABSTRACT**

Elk (*Alces alces* L.) are the largest animals in the deer family and an important commercial and hunting animal in Russia. Since ancient times, elk have offered nutritious meat and valuable hides. For this reason, there are repeated attempts to domesticate elk. However, the domestication of elk and their implementation on farms has not gone beyond experimental farms. This is mostly due to the elk's digestion's unexplored physiology, including the role of endobiont ciliates. The elk's diet is very diverse and includes shoots, leaves, the bark of various tree species and shrubs, multiple herbs, rhizomes and the leaves of aquatic plants, and mushrooms. This research aimed to perform a quantitative and specific study of the infusory composition of the digestive tract of European elk, which lives on the territory of the Omsk and Chelyabinsk regions of Russia in connection with habitat, nutrition, and climate. A comparative analysis of the species and numerical composition of symbiotic ciliated protozoa in the stomachs of European elk are presented. The average number of individual species of elk stomach cilia depending on the territory of the animal's habitat and the qualitative and quantitative composition of various parts of the stomach are presented. The dominant genus of cilia in elk is *Entodinium*, which includes ten species. *Entodinium* makes up 63% of all protozoa in the rumen of moose in the Chelyabinsk population and 73%

in the Omsk population. The ophrioscolecidae family share accounts for 98% of the total composition of cilia in the moose rumen of the Chelyabinsk population and 96% of the Omsk population. No cilia were found in the rennet. The results allow us to assess the prospects for European elk domestication.

Keywords: *Elk, Infusoria fauna, Rumen, Reticulum, Omasum, Food ration of commercial animals.*

АННОТАЦИЯ

Лось (*Alces alces L.*) - крупнейшее животное семейства оленых и важное промысловое и охотничье животное в России. С давних времен лоси предлагали питательное мясо и ценные шкуры. По этой причине предпринимаются неоднократные попытки приручить лося. Однако приручение лосей и их внедрение на фермах не вышло за рамки экспериментальных хозяйств. В основном это связано с неизученной физиологией пищеварения лося, в том числе с ролью инфузорий эндобионта. Рацион лося очень разнообразен и включает в себя побеги, листья, кору различных древесных пород и кустарников, множество трав, корневища и листья водных растений, а также грибы. Цель данного исследования заключалась в количественном и качественном изучении инфузионного состава пищеварительного тракта европейского лося, обитающего на территории Омской и Челябинской областей России, в зависимости от среды обитания, питания и климата. Представлены результаты сравнительного анализа видового и численного состава симбиотических мерцательных простейших в желудках европейского лося. Приведено среднее количество отдельных видов инфузорий желудка лося в зависимости от территории ареала животного, а также качественный и количественный состав различных отделов желудка. Доминирующим родом инфузорий лося является *Entodinium*, который включает 10 видов. Энтодиниум составляет 63% всех простейших в рубце лося в челябинской популяции и 73% в омской популяции. На долю семейства *Ophrioscolecidae* приходится 98% от общего состава ресничек рубца лосей челябинской популяции и 96% омской популяции. Реснички у сычужного фермента не обнаружены. Полученные результаты позволяют оценить перспективы одомашнивания европейского лося.

Ключевые слова: *Лось, инфузориальная фауна, рубец, ретикулум, книжка, пищевой рацион промысловых животных.*

1. INTRODUCTION:

Elk (*Alces alces L.*, 1758) are the largest animals in the deer family and an important commercial and hunting animal in Russia. Since ancient times, elk have offered nutritious meat and valuable hides. The literature discusses repeated attempts to domesticate elk in various parts of its range (Skalon and Khoroshikh, 1958). It describes how, in Siberia, salmon farming already existed several thousand years ago, but then disappeared, becoming replaced by other, more promising animal husbandry (Kornilova, 2003). Since 1949, there has been an elk farm in the Pechora-Ilych reserve, where it was possible to domesticate European elk and study their biology, ecology, and diseases in detail. Studies on domestication have allowed for a deep analysis of elk ecology, behavior, physiological and morphological features, and diseases (Bełżęcki, Miltko, and Michalowski, 2004).

It is possible to discuss the prospects of domestication of elk connected with the mass introduction of mechanical modes of transport in the everyday life of the Northern taiga regions. Still, there is no denying the versatile significance of domestication experiments of this valuable animal and the need for further development. Also

important are considerations regarding the use of wild elk populations that make massive seasonal migrations in the wild. It is very fruitful for the development of science to properly combine its interests with the demands of the national economy (Khaziev, 2011).

However, the domestication of elk and their implementation on farms has not gone beyond experimental farms. This is mostly due to the elk's digestion's unexplored physiology, including the role of endobiont ciliates. The elk's diet is very diverse and includes shoots, leaves, the bark of various tree species and shrubs, multiple herbs, rhizomes and the leaves of aquatic plants, and mushrooms. Simultaneously, unlike most ungulates, elk needs a large amount of salt (Gorobtsova, Khezheva, Uligova, and Tembotov, 2015).

It is useless to undertake any wild animal's domestication without having a clear idea of its specific biological features. Many scientific articles on moose biology and physiology have been published in Russia and other countries. However, the information given in them is very contradictory in many respects. It is possible to clarify them only experimentally and use the data obtained about physiological processes in the future. And especially – the peculiarities of digestion - in the process of domestication of elk. There are data on

the study of the composition of protozoa's fauna living in the digestive tract of many wild and commercial animals specific geographical habitats (Korchagina, 2012; Likhachev, Baimakova, and Koplik, 2010; Likhachev, Korchagina, Seryodkin, and Maksimova, 2016). However, individual studies on the elk's gastrointestinal fauna's qualitative and quantitative composition do not create a complete picture of the digestion processes in these animals. This hinders from making scientific recommendations on the composition of feed for elk, which could simplify domesticating these valuable game animals.

The objective of this study was formulated based on the foregoing conditions and encompasses a study of the numerical and species composition of the ciliates that inhabit the digestive tract of European elk to select the diet in different seasons with the prospect of creating elk farms for growing elk and processing its meat and skins.

2. MATERIALS AND METHODS:

The studies were conducted from 2002 to 2015. The objects of study were male and female European elk, commercially caught in the taiga and subtaiga zones of Russia: 10 individuals from the territory of Bolsheukovskiy, Tevriz, Znamenskiy and Tarskiy Districts of the Omsk Region and 10 individuals from the territory of the Nizyapetrovskiy District of the Chelyabinsk Region (Figure 1).

The studies were carried out in the winter when the elk diet is dominated by branches from deciduous trees, spruce, pine and fir needles, bark, and the shoots of forest raspberries. In the southern parts of the range, elk feed on lichens growing on tree trunks, blueberry and lingonberry shrubs, and sedge where frequent thaws occur. In the winter, elk hardly drink or eat any snow, so as not to lose heat. The qualitative and quantitative composition of protozoa was coordinated with elk diet living in the Omsk and Chelyabinsk regions of Russia. To study the infusoria composition of the digestive tracts of the animals, samples were taken from the contents of the stomach and intestines of each individual immediately after slaughter and were fixed in a 4% formalin solution (Kornilova, 2004).

No more than 20 minutes passed after the elk were slaughtered until the samples were taken. During this time, the temperature of the stomach contents remained unchanged. Infusoria were fixed in the native state, without being affected by external environmental conditions. An incision was made in the wall of each part of the stomach and

samples of the food lump were taken directly near the stomach wall. The food lump was squeezed through a filter and divided into two fractions: large particles larger than 0.1 mm and small particles smaller than 0.1 mm. Small particles were placed in a vessel with a 4% formalin solution. Pressing the food lump continued until the jar's bottom formed a solution with a precipitate of 2-3 cm, which contains the infusoria. The obtained material was used to determine the species and study the external morphology of endobiont infusoria.

The research was carried out within the framework of the University's research plan in compliance with international standards on the ethics of animals' treatment. The collection of animal material was carried out by agreement with hunters who shot animals for commercial purposes under the Russian Federation's license. All the conditions for the social welfare of animals were met.

In the laboratory, all material was analyzed using cytochemical techniques (Likhachev, 2004). The Cytochemical methods used to identify the features of cell morphology of certain types of endobiont infusoria were performed as follows. Staining was performed only in vitro as the retainers used the liquid Karnovsky on ethanol (in the laboratory). Vital dyes were used in the study of cell morphology. A 0.001% aqueous solution of neutral red, methylene blue, and methylene green was used to contrast the organelles and cell contours. In the course of the study of General cell morphology, Romanovsky-Giemsa staining and Meyer hematoxylin were used. The cilia were stained with 1% alcohol solution of iodine. Cytostome was detected by adding 2-4% solution of baking soda. The skeletal elements were studied by staining with iodine and Lugol's liquid. To detect glycogen, Lugol's liquid (a solution of iodine in potassium iodide) was used. Identification of acidic mucopolysaccharides was performed using the Stidman method, with the color alcyon blue (Pierce, 1968; Krylenko, Levin, Samoilova, 1979). The action of Sudan-3 detected neutral lipids. Lysosomes and digestive vacuoles were detected by the action of a 0.1% aqueous solution of neutral red. To study the processes of intracellular digestion, a 0.1% solution of Congo red was applied. Macronucleus, and in some cases, micronucleus, was detected by the action of 0.1% solution of glacial acetic acid. The core was stained using the Giemsa method with hydrolysis, using the Felgen nucleal reaction (hydrolysis time of 10 min) and Mayer acid hemalaunum staining using the standard method.

The data presented in work were obtained using two brands of BioMed-2 and MBI-6 light microscopes with a phase-contrast device and microphoton attachment. In the field, an MBI-3 microscope was used. The number of ciliates was determined by the calibrated drop method of the Goryaev counting chamber (Baimakova, 2003). Fixed infusoria were counted in the fields of view and in the Goryaev counting chamber. Camera Goryaeva – optical device for counting the number of trophozoites in a given volume of liquid. It consists of a thick slide having a rectangular recess (chamber) with a microscopic grid applied and a thin cover glass. The Goryaev cell grid consists of 225 large squares, 25 divided into 16 small squares. Dimensions of the small square of the Goryaev chamber 0.05×0.05 mm. Dimensions of the large square of the Goryaev camera 0.2×0.2 mm. The camera depth is 0.1 mm. Volume of liquid under 1 small square 0.00025 mm³ (MKL) = 1/4000 mm³ (microliter). Volume of liquid under 1 large square 0.004 mm³ (MKL) = 1/250 mm³ (microliter). The volume of the Goryaev chamber is 0.9 mm³ (MKL). In a square, the infusoria that lies inside it and those that touch the left and upper borders, are considered. Infusoria related to the right and lower borders are not counted.

Infusoria were measured using an ocular micrometer on random samples. Moreover, no less than 100 specimens were measured, and for single species no less than 10-20 specimens were found. To determine the percentage of species, all infusoria in several total preparations from each sample were calculated. The number of infusoria was calculated using the "calibrated drop" method, i.e. all trophozoites of infusoria that fell into a drop of 0.1 ml when diluting the sample in a fixator in a strict ratio of 1:2 were counted. A drop from the sample was taken with a precisely measured pipette, placed on a slide under a cover glass, and organisms in several fields of view of the microscope were taken into account by visual examination. The number of organisms in a drop is determined by counting, and then by converting to 1 ml. After viewing 3-5 preparations (each preparation in 10 fields of view), i.e. in 30-50 fields of view, the arithmetic mean for 1 field of view is found and the formula determined the number of organisms in 1 ml:

$$D = Sd / r_2 p, \text{ where}$$

D - the number of organisms studied in ml of liquid;

d - the number of organisms in one field of view (the arithmetic mean of the number of viewed fields of view);

r₂ - the area of the lens field of view in mm (the ruler of the object-micrometer determines the radius r of the lens field of view);

S - cover glass area in mm (18×18 or 20×20).

p - volume of the drop.

Ofrioscolecid identification tables were used to assess ciliates' species composition (Belžecki *et al.*, 2004; Dogel, 1929). Variance analysis was used for statistical evaluation of the obtained indicators. These studies were carried out in triplicate; for statistical processing, the computer programs "Statistica for Windows V6.0" and "STATAN - 2006" were used.

3. RESULTS AND DISCUSSION:

It was found that all the species diversity of ciliates is concentrated only in the stomach of the animal, and protozoa were not found in the intestine (cecum, rectum). The distribution of endobionts in the stomach is heterogeneous. Their number and species diversity decrease from rumen to abomasum, which is associated with the medium's acidity in these sections of the stomach (Figure 2a, 2b and 2c). Ciliates in a slightly alkaline or neutral environment are in optimal conditions to thrive.

Representatives of the *Ophryoscolecidae* family with the genera *Entodinium*, *Diplodinium*, *Epidinium*, and the *Isotrichidae* family with one species *Dasytricha ruminantium*, form the basis of the infusoria fauna of the elk's stomach. Among the rumen's ciliate population, the leading genus of ofrioscolecid is the genus *Entodinium*, represented in the rumen by 10 species for elk in both populations (Figure 3).

In the rumens of elk in the Chelyabinsk population, the dominant abundant *Entodinium* ciliate is *E. simulans-dubardi* with a frequency of occurrence of 54.1 ind./ml, which is 17% of the total number of *Entodiniums* in the rumen. *E. nanellum* (51.9 ind./ml) and *E. exiguum* (49.2 ind./ml) make up 16% of the total number of representatives of this genus in the rumen, and *E. ovinum* (44.6 ind./ml) makes up 15% of all *Entodiniums* in the rumen. It was found the species *E. furca nanellum* only in the rumen with a total number of 38.1 ind./ml, which accounted for 11% of the total number of rumen *Entodiniums*. Representatives of the species *E. simplex* account for 10% (35.2 ind./ml) of the total representatives from this genus. The least represented species of the genus *Entodinium* in the rumen are *E. bursa*,

E. alces, *E. caudatum*, and *E. longinucleatum*, which together make up about 15%.

In the rumens of elk in the Omsk population, the dominant abundant *Entodinium* ciliate is *Entodinium furca nanellum* at 65.2 ind./ml, which is 26% of the total number of rumen *Entodiniums*. The subdominant species of the genus *Entodinium* include *E. exiguum* (56.3 ind./ml), *E. simulans-dubardi* (40.8 ind./ml) and *E. ovinum* (36.8 ind./ml), each of which make up 23%, 17% and 15%, respectively, of the total representatives of this genus in the rumen. The species *E. simplex* accounts for 11% (26.4 ind./ml) of the total, which is similar to this species' population among rumen *Entodinium* in the elk from the Chelyabinsk population. Low abundance in the rumen is noted for the species *E. bursa*, *E. alces*, *E. caudatum*, *E. nanellum*, *E. longinucleatum*, ranging from 1.1 to 7.4 ind./ml, which amounts to 7% of the total number of all *Entodiniums* in the rumen. Upon study of the infusoria population in the reticulum, there was a decrease in the number of *Entodiniums* to 139.8 ind./ml (Chelyabinsk population) and 109.5 ind./ml (Omsk population), as well as a decrease in the number of species of *Entodiniums* to seven in elk of the Chelyabinsk population and six in the Omsk population (Figure 4).

It should be noted that for the elk in the Chelyabinsk population, the dominant genus of ciliates, as in the rumen, is from the genus *Entodinium*, and the most numerous species of *Entodiniums* is *E. simulans-dubardi* with a frequency of occurrence of 43.2 ind./ml, which is 31% of the total number of reticulum *Entodiniums*. Subdominant species include *E. ovinum* (27.6 ind./ml), *E. nanellum* (22.5 ind./ml), and *E. simplex* (23.4 ind./ml). The abundance of *E. ovinum* is 20% of the total number of reticulum *Entodiniums*, and *E. nanellum* and *E. simplex* make up 16% each. The abundance of the species *E. longinucleatum* in the elk reticulum of the Chelyabinsk population only slightly decreased and amounted to 15.2 ind./ml or 11% of the total number of species of this genus in the reticulum. The least frequent species of the genus *Entodinium* in the reticulum are *E. bursa* and *E. alces* with a population of 5.7 ind./ml and 2.2 ind./ml, respectively, which makes up 6% of the total number of representatives of this genus in the reticulum.

In the reticulum of elk in the Omsk population, the dominant abundant *Entodinium* ciliate is *E. simulans-dubardi* with a frequency of 33.6 ind./ml is 31% of the total number of *Entodiniums* in the reticulum. *Entodinium furca nanellum* with a total number of 29.4 ind./ml is the

subdominant species, which makes up 27% of the total number of reticulum *Entodiniums*. The species *E. exiguum*, *E. ovinum*, and *E. simplex* have approximately the same numbers in the reticulum – from 12.6 to 18.5 ind./ml, which is 12%, 13%, and 16% of the total number of reticulum *Entodiniums* for each species, respectively. Meanwhile, the *Entodinium* species *E. furca nanellum* and *E. exiguum* were not observed in elk reticulum from the Chelyabinsk population.

In the omasum of elk in both populations, the number of *Entodiniums* is extremely small and the species diversity consists of four (for the Chelyabinsk elk population) and two species (for the Omsk elk population) of ciliates (Figure 5). *E. nanellum* is a subdominant species in this section of the stomach, numbering 9.3 ind./ml or 27% of the total number of omasum *Entodiniums*. The species *E. exiguum* (5.7 ind./ml) and *E. bursa* (1.4 ind./ml) are extremely infrequent in this section and together account for 11% of the total number of omasum *Entodiniums*. The omasum of elk in the Omsk population contain two species, out of which *E. simulans-dubardi* (11.8 ind./ml), as in the reticulum, is the dominant species and accounts for 86% of the total population of this genus. The species *E. furca nanellum* with 2.6 ind./ml makes up 14% of the total number of omasum *Entodiniums*. The genus *Diplodinium* also makes up infusoria fauna in the stomach of elk in both populations; it is only necessary to note that the number of species and the number of diplodiniums are significantly inferior to the leading genus of *Entodinium* (Figure 6).

Five species of diplodiniums were noted for the elk rumen of the Chelyabinsk population, the dominant of *D. monacanthum* with 56 ind./ml, which accounts for 48% of genus *Diplodinium* species in the rumen. *Diplodinium rangiferi* (29.2 ind./ml) in the rumen is a subdominant species and makes up 27% of the total number of rumen diplodiniums. The species *D. anisacanthum* (19.2 ind./ml), *D. bubalidis consors* (3.3 ind./ml) and *D. bubalidis bubalidis* (4.9 ind./ml) account for 17%, 5% and 3% of rumen diplodiniums, respectively.

In the reticulum of elk in the Chelyabinsk population, the species diversity of diplodiniums went down to three species with a total number of 19.8 ind./ml, however, the dominant and subdominant species are the same as in the rumen (Figure 7). The most numerous species of diplodiniums in the reticulum are *D. monacanthum* (10.1 ind./ml) or 53% of the total number. The subdominant species is *Diplodinium rangiferi* (7.1 ind./ml), which is 37% of the total number of diplodiniums in the reticulum. Representatives of

the species *D. bubalidis bubalidis* (2.6 ind./ml) make up 10% of the reticulum's total number. In the omasum of elk in the Chelyabinsk population, an extremely scarce amount of diplomonads is noted of only two species with a low number of ciliate species *D. monocanthum* (2.4 ind./ml) and *D. bubalidis bubalidis* (1.2 ind./ml).

Four species of diplomonads were found in the rumen of the Omsk population. The dominant species was *D. monocanthum* (33.2 ind./ml), accounting for 66% of the total number of rumen diplomonads (Figure 6). The species *Diplodinium rangiferi* in the rumen became subdominant with many 14.1 ind./ml, which amounts to 28% of the total number of diplomonads in the rumen. It should be noted that both species of diplomonads are identical to those of the elk in the Chelyabinsk population, but are significantly inferior in number.

The most infrequent rumen species consists of *D. bubalidis consors* (1.2 ind./ml) and *D. bubalidis bubalidis* (1.6 ind./ml), which together make up only 6% of the total number of rumen diplomonads. Diplomonads were not found in the reticulum and omasum of elk in the Omsk population. The genus *Epidinium* is represented in the stomach of elk in both populations by only one species – *Ep. ecaudatum ecaudatum*, and the abundance of this species in the rumen is much higher than in the reticulum, while it was not found at all in the omasum (Figure 8).

There are very few representatives of the genus *Dasytricha*: in the rumen, with the highest numbers, they make up from 9.6 to 14.2 ind./ml (2% and 5%, respectively), in the reticulum - from 5.2 to 9.1 ind./ml (4% and 3% of the total number of ciliates in the reticulum), in the omasum - from 1.2 to 1.4 ind./ml, which is about 1% of the total number of ciliates in the omasum for elk in both populations (Figure 9). Representatives of this species were found in all sections of the elk stomach of both populations.

Elk feed in the snowless times of year is unlimited, and the animals, as a rule, have it available to them almost any place. However, even in the summer, with an abundance of leaves, grassy and wetland vegetation, the basis of elk nutrition is branch feed. In severe frosts, the percentage of branches and needles from fir, spruce, and juniper in the total food mass of elk is 85%, 15%, and 8%, while in warming periods, it is 22%, 0%, and 0%. This diet sets the pace for a normal digestion cycle (Baimakova, 2003; Kornilova, 2003).

Animals that feed on plant foods face obtaining essential amino acids contained only in

animal proteins. In ruminants, this process is carried out in a complex stomach (which is why they are called “protist-eaters”). They use ciliates and other protozoa that breed in the rumen, reticulum and omasum to digest feed. Many researchers suggest that ciliates can serve as one source of nitrogen for the host, since the amount of nitrogen in a ciliate's body is very significant and, between the rumen to the abomasum, they are easily digested (Chornaya, 2015).

When studying the infusoria population of each European digestive tract of elk, it is found and described 17 species of ciliates in the Chelyabinsk population and 16 species in the animals of the Omsk population. The anatomical structure of and conditions in the rumen almost entirely meet the life requirements of microorganisms. The first three sections – the rumen, the reticulum, and the omasum – form the so-called stomach and are lined with a multilayer epithelium. The stomach is devoid of digestive glands and only bacterial fermentation occurs there, involving the symbionts inhabiting it, which can exist only in a slightly alkaline or neutral environment. The ciliates use the food fed into the rumen for their nutrition, building their own bodies, and digesting the fiber using bacteria living in symbiosis with them.

The feeding regimen affects the digestibility of feed, rumen function and ciliate populations. Food that decomposes relatively quickly in the rumen (fruits and herbaceous food) goes into the omasum more quickly. After processing in the rumen, solid foods (branches, shoots) get into the reticulum and require further decomposition to be digested. Any change in the composition of the feed disturbs the metabolic processes in the animal's body, leading to further changes in the normal functioning of other systems (Korchagina and Likhashev, 2005). Based on the analysis of the data obtained, it was found that the rumen is the most densely populated part of the stomach in elk from both populations, and is where the most species were found.

Utilization in the rumen of ruminant monosaccharides (glucose, fructose, xylose), coming from the feed, and mainly formed during the hydrolysis of polysaccharides, is carried out mainly by rumen microorganisms (Dehority, 1996). Ciliates inhabit the rumens of animals in huge quantities (Agatha, 2004). The population of endobiont ciliates consists of representatives of the *Ophrioscolecidae* family, and they dominate both in terms of species diversity and in numbers (Aesch, 2001).

The conditions existing in the rumen contribute to the development of abundant microflora there. Among them are a favorable and constant temperature, a rumen environment with near-neutral acidity, and an abundance and constant influx of nutrients. In addition to processes for the microbial decomposition of feed, very active synthesis processes occur in the rumen. Considering the qualitative and quantitative composition of stomach ciliates in the animals studied, it can be said that the rumen is a very important specialized chamber in a complex stomach, where protozoa develop. In this capacity, they use fiber as feed. The dominant species of the omasum's *Entodiniums*, as in the rumen and reticulum, of elk in the Chelyabinsk population is *E. simulans-dubardi* frequency of occurrence of 16.9 ind./ml, which is 52% of the total number of omasum *Entodiniums*. Rumen ciliates are actively involved in the metabolism of easily fermentable carbohydrates, proteins, and lipids (Bergen, 2004). Therefore, cooperation, or symbiosis, takes place. In the rumen, the feed is delayed long enough so that the components of plant fibers accessible to microorganisms can be broken down.

Ofrioscolecids absorb carbohydrates entering the rumen, mainly in the form of starch. All ciliates of this family can use starch grains for food. Endobiont ciliates can extract starch grains from the liquid fraction of the stomach contents, where the ciliates make the starch inaccessible to bacteria (Gocmen, Dehority, Talu, and Rastgeldy, 2001). As with most representatives of the deer family (*Cervidae*), in elk, the dominant genus of ciliates is *Entodinium*, which is made up of 10 species. The proportion of all *Entodiniums* in the rumen, in the most densely populated section of the stomach, is 63% among the elk in the Chelyabinsk population, and 73% of the total number of protozoa in the Omsk population. They turn food proteins and broken down fiber components into glycogen, which serves as a source of nutrition for both the ciliates and the ruminants. Ofrioscolecids account for 98% of the total infusoria composition in the stomachs of elk in the Chelyabinsk population and 96% in the Omsk population. Thus, ciliates' positive role is that they, by consuming an often inferior vegetable protein, turn it into a complete one for the animal's nutrition.

During the seasonal change of feed, microorganisms adapt to new feeds, and digestion is not impaired. The food processed by the ciliates rolls into balls in another part of the stomach - the reticulum - and from there returns to the mouth as

cud. Then the food goes to the third section - the omasum, then to the next section - the abomasum. Here, food is processed by digestive juices.

The diet of ofrioscolecids is quite diverse, and there are known specializations in different species. The smallest species of the genus *entodinia* feed on bacteria, starch grains, fungi and other small particles. Many medium and large ofrioscolecids absorb plant tissue particles, which make up the bulk of the contents in the rumen. The endoplasm of some species is clogged with plant particles.

4. CONCLUSION:

Thus, the species composition of the symbiotic fauna in European elk depends on their habitat, but namely on a diet. Whether this gives any advantages to the host remains unclear. All these questions are of great practical interest since it has been discussed about the digestion of ruminants – important objects of animal husbandry. The faunistic and ecological studies conducted make it possible to assess the infusoria fauna in the stomachs of elk to identify the distribution patterns of endobiont ciliates in different parts of the elk's stomach, and the nature of the spatial dynamics of the number and species diversity of ciliates in the host organism. This significantly expands the understanding of fauna, morphology, biology, and ecology of endobiont infusoria in European elk and commercial ungulates that live in other habitats that differ in the climate and composition of animals diet.

With the results obtained, it can be hypothesized that the features of infusoria fauna are determined by the species-related ties of the hosts and the natural and territorial conditions of their habitat. Further research prospects must assess the possible ways endobiont ciliates are exchanged between different hosts. A further study of the fauna, biology, and ecology of wild ruminant ciliates in different world regions should be carried out to expand the ideas about these unique and well-adapted protozoa.

5. CONFLICT OF INTEREST STATEMENT:

The authors declare that they have no conflict of interest.

6. REFERENCES:

1. Abramova, L. M. (2004). Synantropization vegetation: patterns and control to the

- process (on the example of Republic Bashkortostan). Abstract of the Doctor of Science Dissertation. Perm. 45 pp.
2. Abukenova, V. S. and Khanturin, M. R. (2010). Adaptive features of life forms in *Aporrectodea caliginosa*: (Oligochaeta: Lumbricidae). *Zoology in the Middle East* 2:59–65.
 3. Aescht, E. (2001). Catalogue of the Generic Names of Ciliates (*Protozoa, Ciliophora*). *Denisia*, 1, 1–350.
 4. Agatha, S. A. (2004). Cladistic approach for the classification of oligotrichid ciliates (*Ciliophora: Spirotricha*). *Acta Protozoologica*, 43, 201–217.
 5. Ananyeva, N. D. (2003). Microbiological aspects of self-purification and stability of soils. Moscow: Nauka Publishers. 223 pp.
 6. Ananyeva, N. D., Susyan, E. A., Chernova, O. V., and Wirth, S. (2008). Microbial respiration activities of soils from different climatic regions of European Russia. *European Journal of Soil Biology* 44(2):147–157.
 7. Anderson, T. H. and Domsch, K. H. (2010). Soil microbial biomass: the eco-physiological approach. *Soil Biology and Biochemistry* 42(12):2039–2043.
 8. Ashabokov, B. A., Bischokov, R. M., Zherukov, B. Kh., and Kalov, Kh. M. (2008). Analysis and forecast of climate changes of atmospheric precipitation and temperature regime in different climate belts of the North Caucasus. Nalchik. 182 pp.
 9. Baimakova, L. G. (2003). Nekotoryye ekologicheskiye osobennosti endobiontovykh infuzoriy sibirskoy kosuli [Some ecological features of endobiont ciliates of the Siberian roe deer]. In *Metodologiya i metody yestestvoznaniya [Methodology and methods of natural sciences]: Vol. Issue 9* (pp. 33–38). Omsk: "Om SPU" Publishing.
 10. Bastida, F., Moreno, J. L. A., Hernandez, T., and Garcia, C. (2008). Past, present and future of soil quality indices: a biological perspective. *Geoderma* 147:159–171.
 11. Belżęcki, G., Miltko, R., and Michalowski, T. (2004). Why does the establishment of the starch preferring *Entodinium caudatum* in the rumen decrease the numbers of the fibrolytic ciliate *Eudiplodinium maggii*? *Folia Microbiologica*, 49(2), 139–142. <https://doi.org/10.1007/BF02931388>
 12. Bergen, W. G. (2004). Quantitative Determination of Rumen Ciliate Protozoal Biomass with Real-Time PCR. *The Journal of Nutrition*, 134(12), 3223–3224. <https://doi.org/10.1093/jn/134.12.3223/>
 13. Caldwell, B. A. (2005). Enzymes as a component of soil biodiversity. *Pedobiologia* 49:637–644.
 14. Chornaya, L. V. (2015). Features of nutrition of endobiont ciliates. *International Journal of Applied and Basic Research*, 4, 233–237.
 15. Dehority, B. A. (1996). A New Family of Entodiniomorph Protozoa from the Marsupial Forestomach, with Descriptions of a New Genus and Five New Species. *The Journal of Eukaryotic Microbiology*, 43(4), 285–295. <https://doi.org/10.1111/j.1550-7408.1996.tb03991.x>
 16. Dogel, V. A. (1929). Protozoa and Oligotricha. Ophryoscolecidae. Keys to the fauna of the USSR. Leningrad: ZIN AN publishing, Retrieved from https://www.zin.ru/publ_e.htm
 17. Fernández, R., Novo, M., Gutiérrez, M., Almodóvar, A., and Díaz Cosín D. (2010). Life cycle and reproductive traits in *Aporrectodea trapezoids* (Dugès, 1828) (Oligochaeta, Lumbricidae) in laboratory cultures. *Pedobiologia* 53:295–299.
 18. Gedgafova, F. V., Uligova, T. S., Gorobtsova, O. N., and Tembotov, R. Kh. (2015). The biological activity of chernozems in the Central Caucasus Mountains (Terskiy variant of altitudinal zonality), Kabardino-Balkaria. *Eurasian Soil Sciences* 12:1341–1348.
 19. Gocmen, B., Dehority, B. A., Talu, G. H., and Rastgeldy, S. (2001). The Rumen Ciliate Fauna of Domestic Sheep (*Ovis ammon aires*) from the Turkish Republic of Northern Cyprus. *The Journal of Eukaryotic Microbiology*, 48(4), 455–459. <https://doi.org/10.1111/j.1550-7408.2001.tb00179.x>
 20. Gorobtsova, O. N., Khezheva, F. V., Uligova, T. S., and Tembotov, R. Kh. (2015). Ecological and geographical regularities of changes in the biological activity of automorphic soils on the foothills

- and adjacent plains the Central Caucasus Region (Kabardino-Balkarian Republic). *Eurasian Soil Sciences* 3:303–313. <https://doi.org/10.1134/S106422931501007X>
21. Kazeev, K. Sh., Kolesnikov, S. I., and Val'kov, V. F. (2004). Biology of soils of Southern Russia. Rostov-on-Don: Center of Valeology of Russian Higher Education Institutions. 350 pp.
 22. Khaziev, F. Kh. (2011). Soil and biodiversity. *Russian Journal of Ecology* 42(3):199–204. <https://doi.org/10.1134/S1067413611030088>
 23. Korchagina, T. A. (2012). Infuzornaya fauna podzheludochnoy zhelezy nekotorykh predstaviteley semeystva Bovidae i Deer (Cervidae) [The infusorian fauna of the pancreas of some representatives of the family Bovidae and Deer (Cervidae)]. *Actual Problems of Veterinary Biology*, 2(14), 30–33.
 24. Kornilova, O. A. (2003). Sluchaynost' i razryv v formirovaniy ekosistem endobiontov [Randomness and discontinuity in the formation of ecosystems of endobionts]. *Materials of Scientific and Practical Conference "Problems of Method Training Biology and Ecology in the Context of Modernized Image*, 80–82. Saint-Petersburg: TESSA.
 25. Kornilova, O. A. (2004). Metody kompleksnogo obsledovaniya fauny infuzoriy endobiontov [Methods for a comprehensive examination of the fauna of endobiont ciliates]. In *Scientific Zoology. Russian State Pedagogical University Named after A.I. Herzen: Vol. Issue 4. Funktsional'naya morfologiya, ekologiya i zhiznennyye tsikly zhivotnykh [Functional morphology, ecology and animal life cycles]* (pp. 75–77). Saint-Petersburg: TESSA.
 26. Likhachev, S. F. (2004). Polevyie issledovaniya bespozvonochnykh [Field studies of invertebrates]. Saint-Petersburg: TESSA.
 27. Likhachev, S. F., Baimakova, L. G., and Koplik, A. A. (2010). Morfofiziologicheskiye osobennosti infuzionnykh infuzoriy pishchevaritel'nogo trakta kosuli sibirskoy [Morphological and physiological features of the endobiont ciliates of the digestive tract of Siberian roe deer]. In *Bulletin of ChSPU* (Vols. 1–10, pp. 325–332). Chelyabinsk: ChSPU Publishing.
 28. Likhachev, S. F., Korchagina, T. A., Seryodkin, I. V., and Maksimova, D. A. (2016). Ciliate (Ciliata, Ciliophora) fauna of different stomach departments of sika deer (Cervus nippon Temminck, 1838). *Tyumen State University Herald. Natural Resource Use and Ecology*. <https://doi.org/10.21684/2411-7927-2016-2-2-96-106>
 29. Onipchenko, V. G. (2011). The role of soil in formation and conservation of plant diversity; pp. 86–155 in: The role of soil in formation and conservation of biological diversity. Moscow: KMK Scientific Press.
 30. Skalon, V. N., and Khoroshikh, P. P. (1958). Domashniy los' na petroglifakh Sibiri [Domestic elk on petroglyphs of Siberia]. *The Zoological Journal*, 37(3), 441–446.
 31. Striganova, B. R. (2005). Spatial variations of the functional structure of soil populations in the steppes of European Russia. *Povolzhskiy Journal of Ecology* (3):268–276.
 32. Tembotova, F. A. and Tsepkova, N. L. (2009). On the problem of steppe ecosystem conservation in the Central Caucasus. *Russian Journal of Ecology* 40(1):65–67
 33. Tsepkova, N. L. (2006). Diversity of phytocenoses on plains of the Kabardino-Balkarian Republic; pp. 151–154 in: Environmental problems of mountain territories. Moscow: KMK Scientific Press.
 34. Val'kov, V. F., Kolesnikov, S. I., and Kazeev, K. Sh. (2002). Soils of the South of Russia: Classification and Diagnostics. Rostov-on-Don: North Caucasus Scientific Center. 168 pp.
 35. Val'kov, V. F., Eliseeva, N. V., Imgrut, I. I., Kazeev, K. Sh., and Kolesnikov, S. I. (2004). Reference book of the soil assessment. Maikop: GURIPP "Adigeya". 236 pp.
 36. World reference base for soil resources. (2006). World soils resources reports. № 103. Rome: FAO. 145 pp.



Omsk Region



Chelyabinsk Region

Figure 1. European elk hunting areas in Russia. Source: The authors.

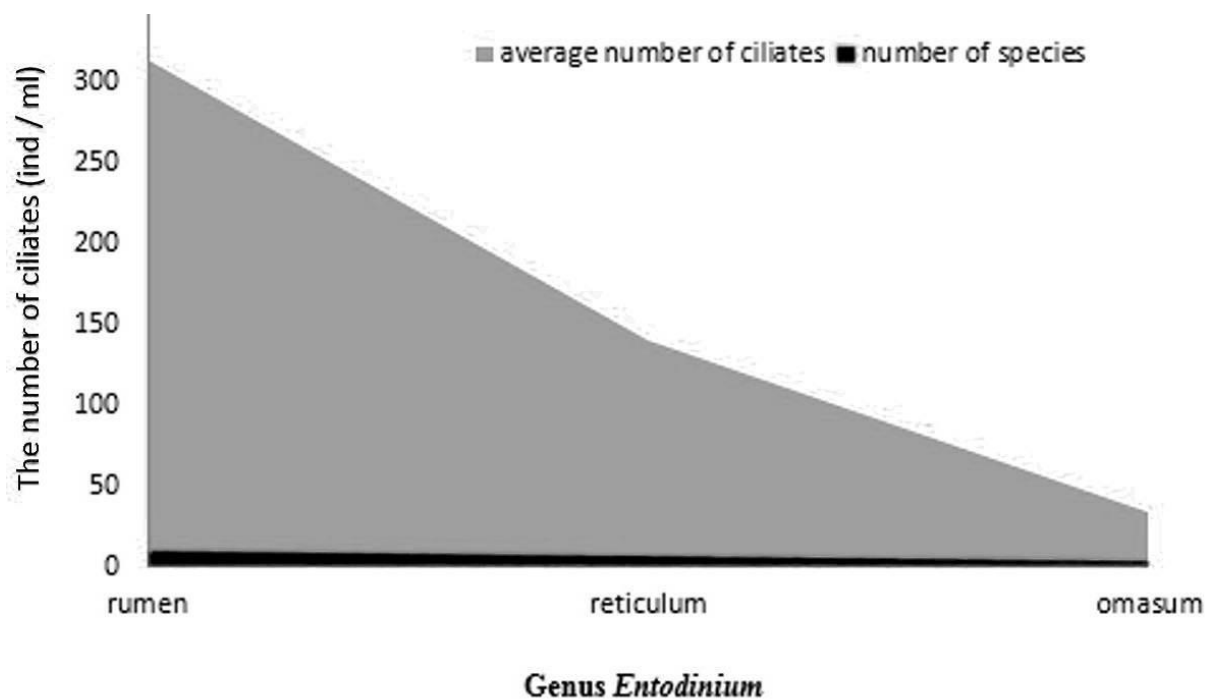


Figure 2a. The average number of ciliates, ind./ml (number of individuals per milliliter), and the number of species by stomach section (Genus *Entodinium*).

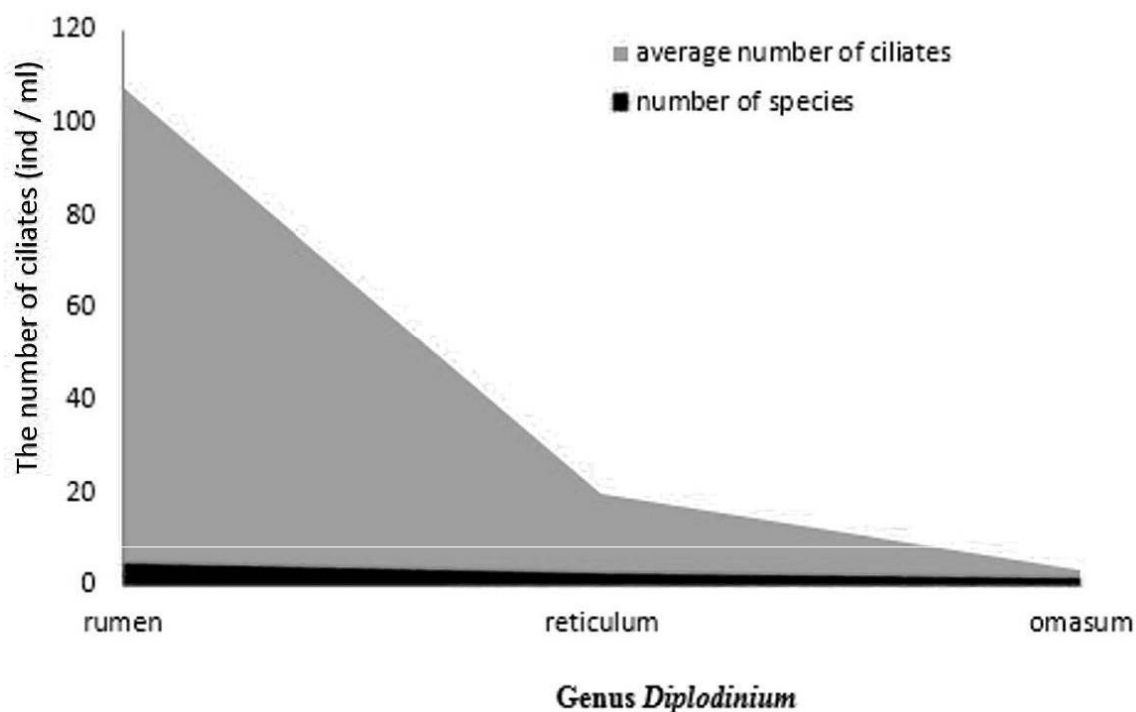


Figure 2b. The average number of ciliates, ind./ml (number of individuals per milliliter), and the number of species by stomach section (Genus *Diplodinium*).

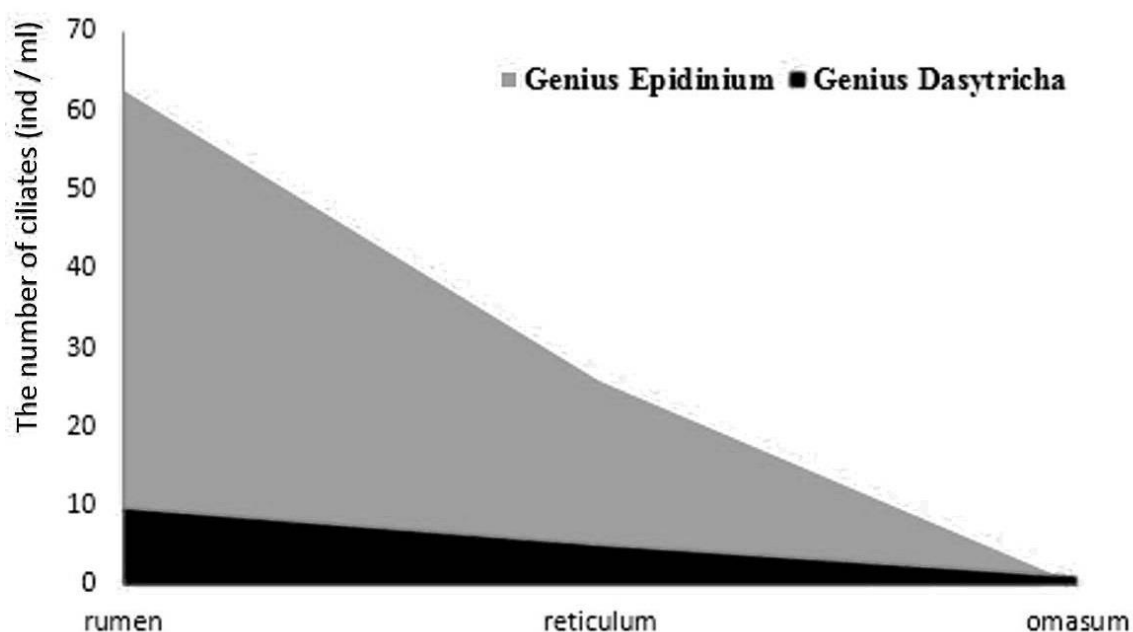


Figure 2c. The average number of ciliates, ind./ml (number of individuals per milliliter), and the number of species by stomach section (Genus Epidinium, Genus Dasytricha).

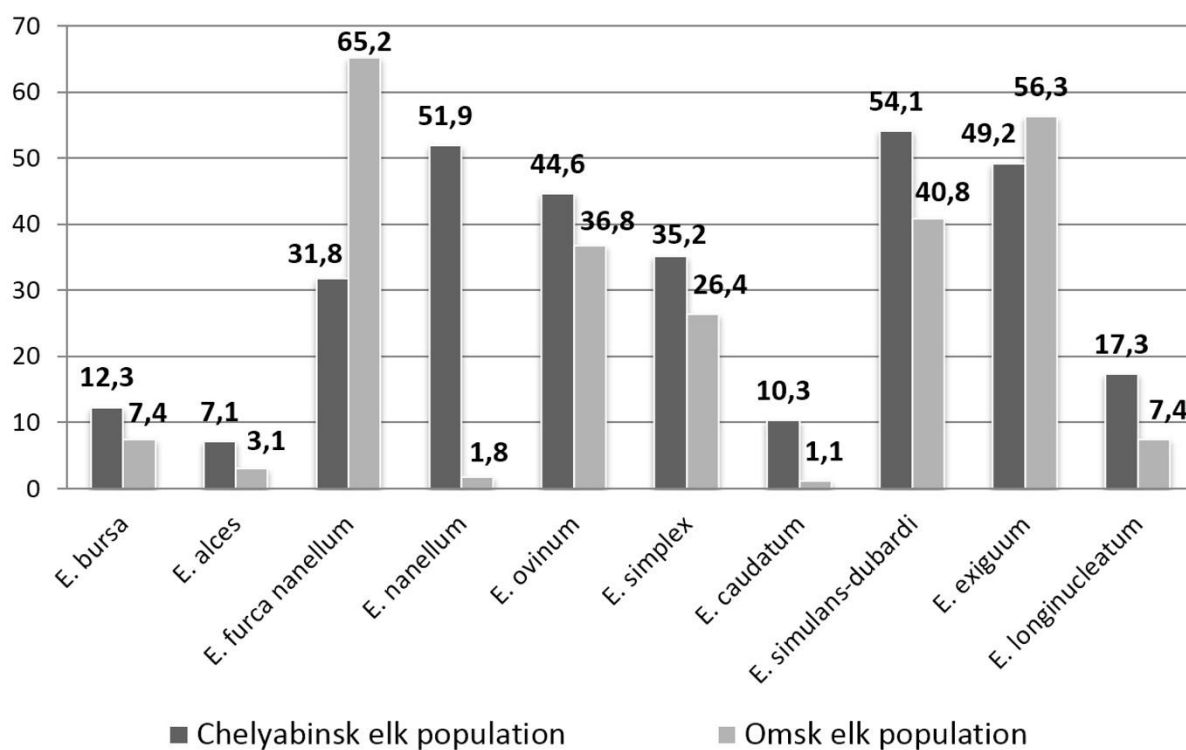


Figure 3. The number of ciliates of the genus *Entodinium* in the rumen of elk in the Chelyabinsk and Omsk populations, ind./ml (number of individuals per milliliter)

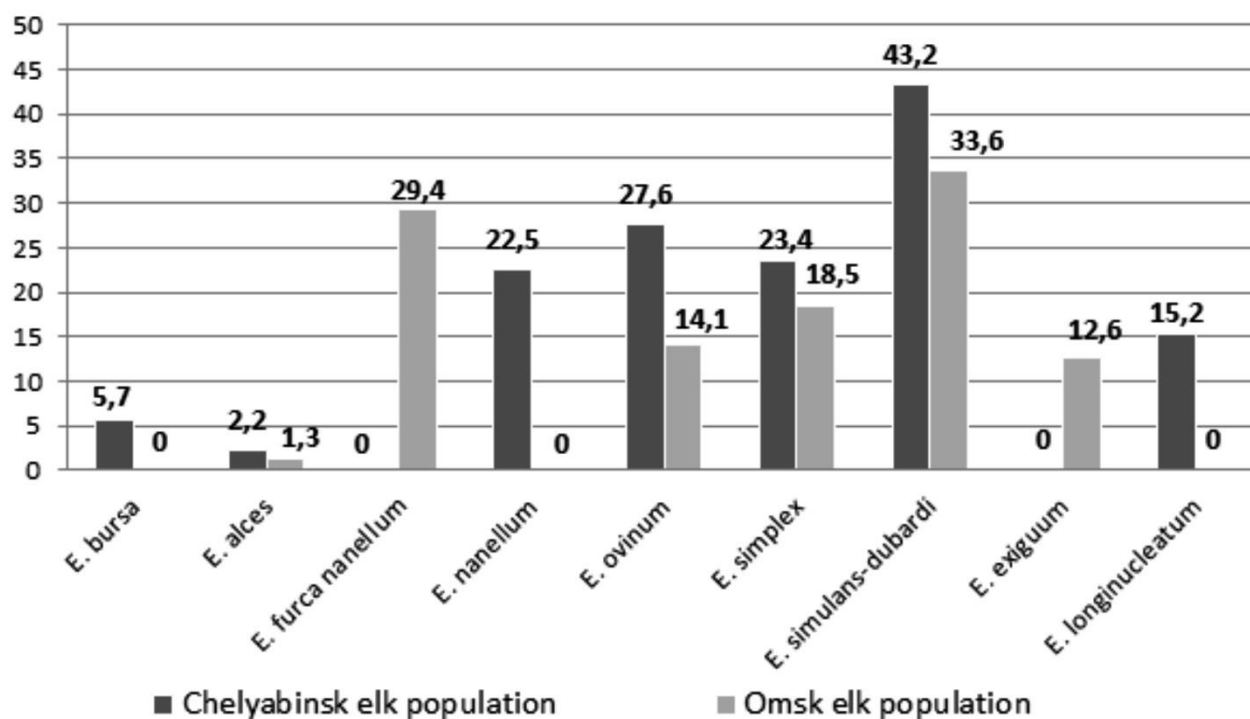


Figure 4. The number of ciliates of the genus *Entodinium* in the reticulum of elk in the Chelyabinsk and Omsk populations, ind./ml (number of individuals per milliliter)

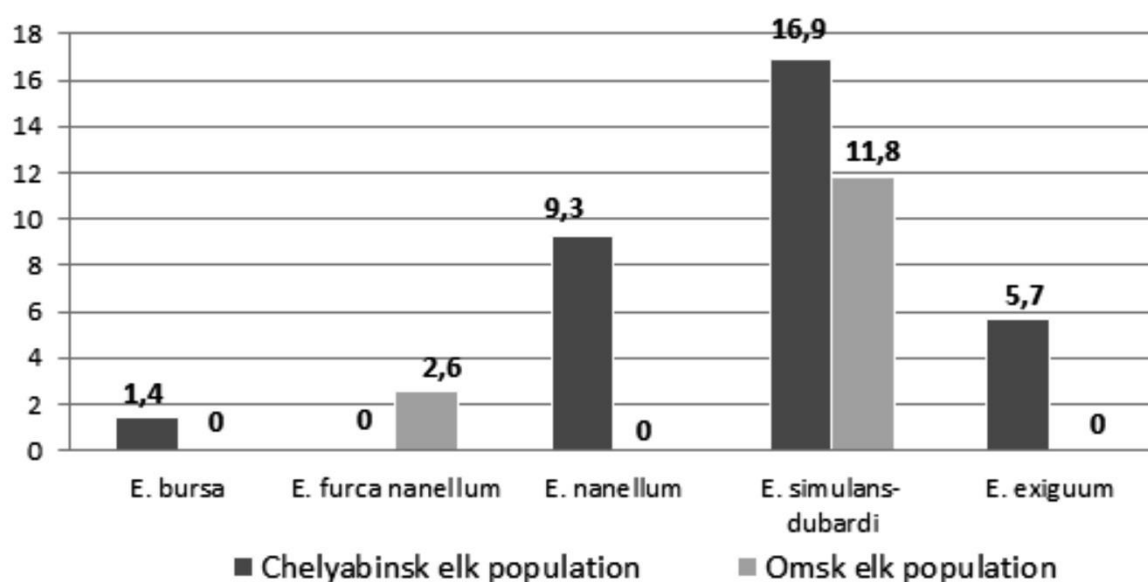


Figure 5. The number of ciliates of the genus *Entodinium* in the omasum of elk of the Chelyabinsk and Omsk populations, ind./ml (number of individuals per milliliter)

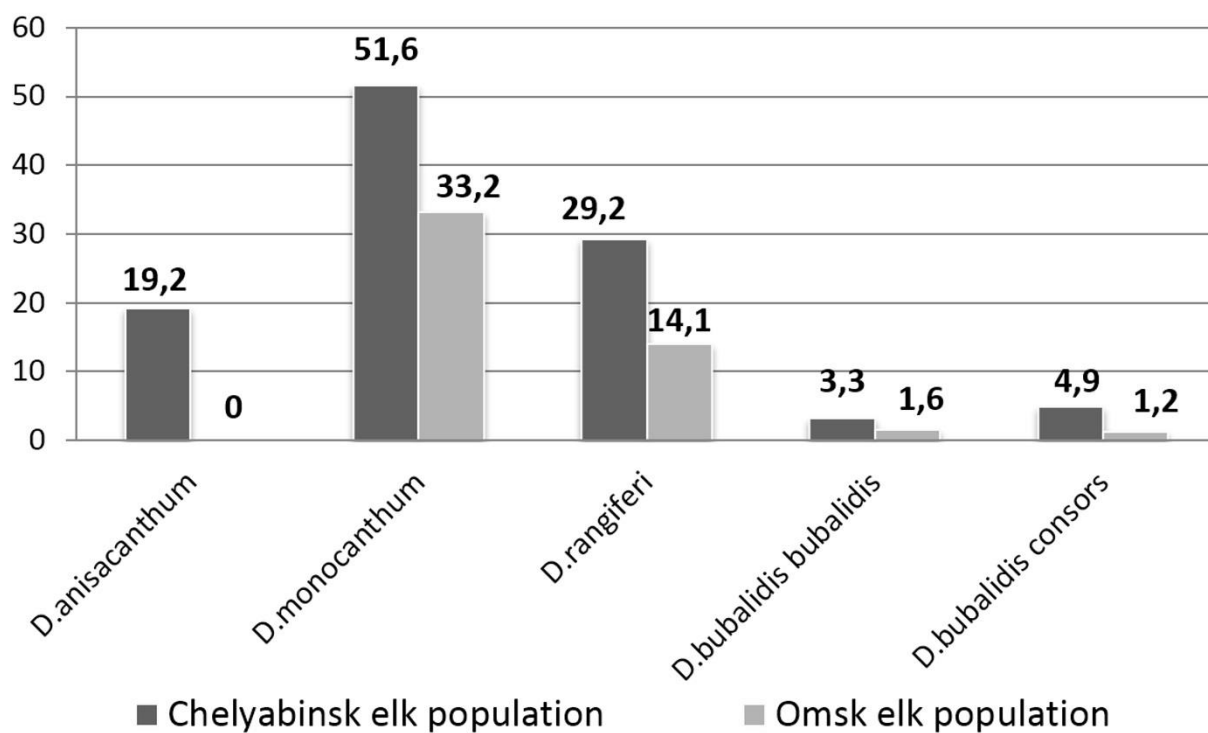


Figure 6. The number of ciliates of the genus *Diplodinium* in the rumen of elk in the Chelyabinsk and Omsk populations, ind./ml (number of individuals per milliliter)

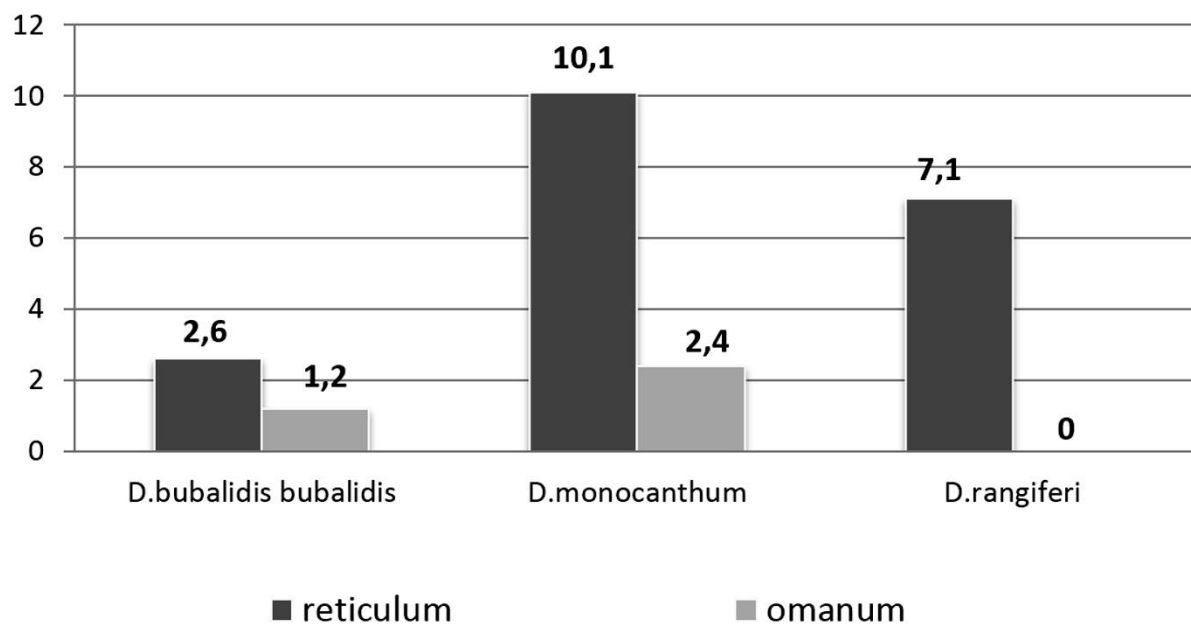


Figure 7. The number of ciliates of the genus *Diplodinium* in the reticulum and omasum of elk in the Chelyabinsk populations, ind./ml (number of individuals per milliliter)

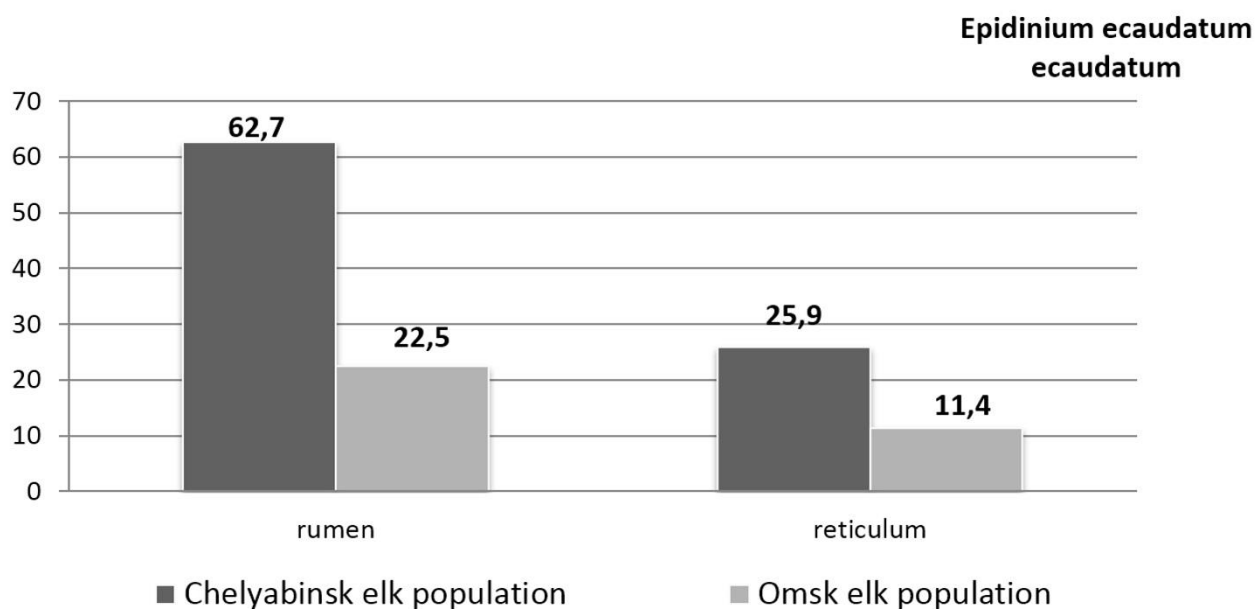


Figure 8. The number of ciliates of the genus *Epidinium ecaudatum ecaudatum* in the rumen and reticulum of elk in the Chelyabinsk and Omsk populations, ind./ml (number of individuals per milliliter)

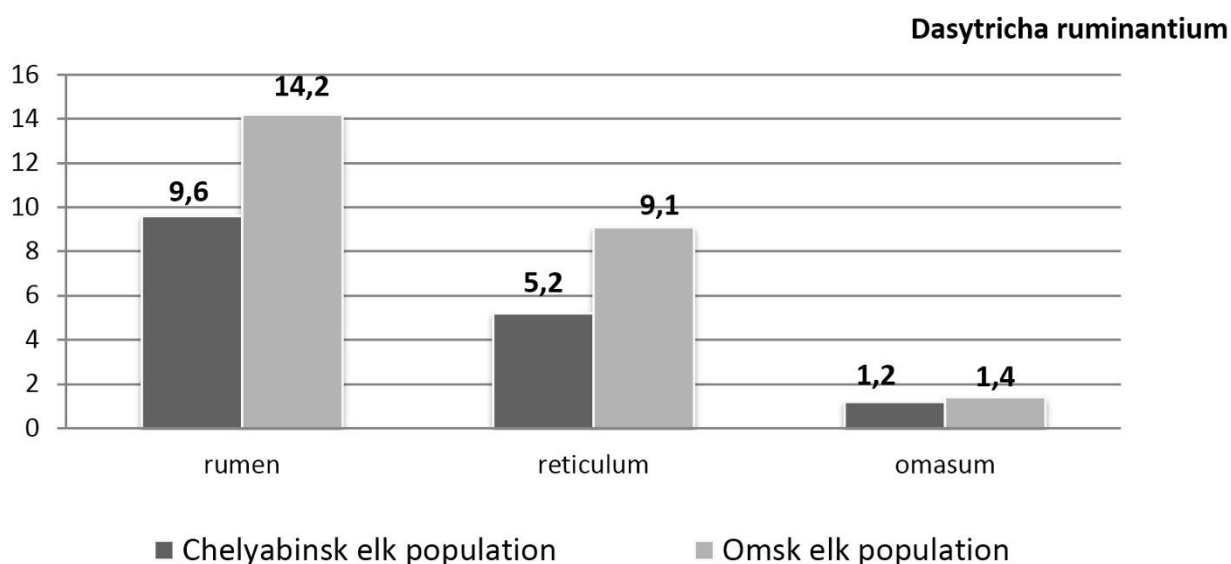


Figure 9. The number of ciliates of the *Dasytricha ruminantium* species in the stomachs of elk in the Chelyabinsk and Omsk populations, ind./ml (number of individuals per milliliter)

CARACTERIZAÇÃO BIOQUÍMICA DA PLANTA MEDICINAL DE *Ferula rutbaensis* NO DESERTO OCIDENTAL IRAQUIANO

BIOCHEMICAL CHARACTERIZATION OF *Ferula rutbaensis* MEDICINAL PLANT IN IRAQI WESTERN DESERT

التشخيص الكيموحيوي لنبات *Ferula rutbaensis* الطبي في صحراء العراق الغربية

DAWOOD, Kutayba Farhan^{1*}; ALFALAHI, Ayoob Obaid²; NEAMAH, Shamil Ismail³; DHANNOON, Omar Mahmood⁴

¹ University of Anbar, College of Education for Pure Sciences, Department of Chemistry. Iraq.

² University of Anbar, College of Agriculture, Department of Field Crops. Iraq.

³ University of Anbar, Center of Desert Studies. Iraq.

⁴ Ministry of Agriculture, Agricultural Research Office, Department of Maize and Sorghum. Iraq.

* Corresponding author

e-mail: eps.kutayba.farhan.dawood@uoanbar.edu.iq

Received 20 August 2020; received in revised form 11 September 2020; accepted 14 October 2020

RESUMO

As plantas usadas na medicina popular não apenas representam fontes ricas de materiais terapêuticos, mas também desempenham um papel crucial no desenvolvimento de novas drogas sintetizadas completa ou parcialmente. A planta Mharut (*Ferula rutbaensis*) é parte integrante das práticas terapêuticas beduínas no deserto ocidental da província de Anbar-Iraque, mas, até o momento, este é o primeiro estudo que descreve seus constituintes fitoquímicos. A planta está crescendo perto da fronteira do Iraque com a Arábia Saudita e bem adaptada a uma ampla variedade de solos. Tradicionalmente, *F. rutbaensis* tem sido amplamente utilizado para tratar acne, distúrbios estomacais e intestinais, intoxicações alimentares e problemas respiratórios. Amostras frescas de plantas foram coletadas e caracterizadas morfologicamente. Da mesma forma, a técnica de codificação de barras de DNA baseada em ITS foi usada de forma eficiente para aprovar a identificação morfológica de *F. rutbaensis*. O espectro GC-MS foi adotado na caracterização fitoquímica de extratos aquosos e metanólicos de partes frescas e secas de plantas. O extrato aquoso de raízes secas foi a fonte mais rica de compostos bioativos em comparação com raízes frescas ou extratos metanólicos de partes frescas ou secas de plantas. Em geral, os fitoquímicos detectados caem em ácidos graxos, terpenos, hidrocarbonetos alcanos e ésteres. Notavelmente, os ácidos graxos na forma de ácidos oléico e palmítico foram os dois compostos bioativos mais abundantes em extratos aquosos e metanólicos de raízes frescas e secas de plantas. Aparentemente, os ácidos graxos insaturados detectados e / ou outros componentes bioativos estão por trás das propriedades terapêuticas de *F. rutbaensis* que podem ser ingredientes úteis para preparar cosméticos à base de Mharut, como sabonetes médicos, loções corporais, condicionadores de pele e protetores solares. Além disso, alguns outros componentes possuem propriedades anti-inflamatórias, antioxidantes e antimicrobianas. Mais investigações serão necessárias para confirmar a atividade antimicrobiana dos extratos de *F. rutbaensis*.

Palavras-chave: Mharut, *Ferula rutbaensis*, DNA barcoding, ITS, espectro de GC-MS.

ABSTRACT

Plants used in folk medicine not only represent rich sources for therapeutic materials, but it also plays a crucial role in developing completely or partially novel synthesized drugs. Mharut plant (*Ferula rutbaensis*) is an integral part of Bedouin therapeutic practices in the western desert of Anbar province-Iraq. Still, to date, this is the first study describing its phytochemical constituents. The plant was growing near the Iraq-Saudi Arabia borders and adapted to a wide range of soils. Traditionally, *F. rutbaensis* has been widely used to treat acne, stomach and bowel disorders, food poisoning and respiratory problems. Fresh plant samples were collected and morphologically characterized. Likewise, the ITS-based DNA barcoding technique was efficiently used to approve the morphological identification of *F. rutbaensis*. The GC-MS spectrum was adopted in the phytochemical characterization of aqueous and methanol extracts of fresh and dry plant parts. The aqueous extract of dry roots

was the richest source for bioactive compounds than fresh or methanolic extracts of either fresh or dry plant parts. In general, the detected phytochemicals falling into fatty acids, terpenes, hydrocarbon alkanes, and esters. Notably, fatty acids in Oleic and Palmitic acids were the two most abundant bioactive compounds in both aqueous and methanolic extracts of plant fresh and dry roots. The detected unsaturated fatty acids and/or other bioactive components are laying behind the therapeutic properties of *F. rutbaensis* that can be useful ingredients to prepare Mharut-based cosmetics such as medical soaps, body lotions, skin conditioners and sunscreens. Additionally, some other components were found to have anti-inflammatory, antioxidants, and antimicrobial properties. Further investigations will be necessary to confirm the antimicrobial activity of *F. rutbaensis* extracts.

Keywords: Mharut, *Ferula rutbaensis*, DNA barcoding, ITS, GC-MS spectrum

المستخلص

لا تمثل النباتات التي تستخدم في الطب الشعبي مصادر غنية للمواد العلاجية فحسب، بل إنها تلعب دوراً مهماً في تطوير عقاقير مصنعة جديدة كلياً أو جزئياً. على الرغم من أن نبات المحروت (*Ferula rutbaensis*) جزء لا يتجزأ من الممارسات العلاجية البدوية في الصحراء الغربية لمحافظة الانبار-العراق، إلا أن هذه هي الدراسة الأولى التي تصف مكوناته الكيميائية. ينمو النبات بالقرب من الحدود العراقية مع العربية السعودية وهو متأقلم جيداً مع مدى واسع من التربة. تقليدياً، استخدم نبات *F. rutbaensis* بشكل واسع في علاج حب الشباب واضطرابات المعدة والإمعاء والتسمم الغذائي ومشاكل التنفس. تم جمع النماذج الطرية للنبات وتشخيصها مظهرياً. فضلاً عن ذلك، تم استخدام تقنية ترميز الحامض النووي المستندة إلى ITS بكفاءة في إثبات التشخيص المظهري لنبات *F. rutbaensis*. أعتمد تحليل GC-MS الطيفي في تشخيص المكونات النباتية الفعالة للمستخلص المائي والميثانولي للأجزاء النباتية الطرية والجافة. كان المستخلص المائي للجذور الجافة هو المصدر الأغنى للمركبات النشطة بيولوجياً، مقارنة بالجذور الطرية أو المستخلصات الميثانولية لأجزاء النبات الطرية أو الجافة. بشكل عام، فإن المواد الكيميائية النباتية المكتشفة تقع ضمن الأحماض الدهنية والتربينات والألكانات الهيدروكربونية والإسترات. تجدر الإشارة إلى أن الأحماض الدهنية بشكل حامضي الأوليك والبالمتيك، كانت أكثر المركبات النشطة بيولوجياً وفرة في المستخلصات المائية والميثانولية لجذور النبات الطرية والجافة. وعلى ما يبدو، فإن الأحماض الدهنية المكتشفة و / أو المكونات النشطة بيولوجياً الأخرى تكمن وراء الخصائص العلاجية لنبات *F. rutbaensis* التي يمكن أن تكون مكونات مفيدة في تصنيع مستحضرات التجميل المضادة لحب الشباب، كالصابون الطبي ومرطبات الجسم ومكيفات الجلد وواقى الشمس. بالإضافة إلى أن بعض المكونات الأخرى وجد أن لها خصائص مضادة للالتهابات وللأكسدة والأحياء المجهرية. هناك حاجة إلى مزيد من الفحوصات للتأكد من الفعالية المضادة للأحياء المجهرية لمستخلصات نبات *F. rutbaensis*.

الكلمات المفتاحية: المحروت، *Ferula rutbaensis*، ترميز الحامض النووي، ITS، تحليل GC-MS الطيفي

1. INTRODUCTION:

Plants are an integral part of human dietary and therapeutic habits, especially in Middle Eastern countries, whereby over 20000 different plant species habituate a wide geographical region (Othman *et al.*, 2019). Historically, wild plant species have been the first and perhaps the only choice available for medication, particularly for rural and Bedouin communities (Alencar *et al.*, 2010). More recently, wild plants have attracted extra attention to cope with the growing demands of the changing lifestyle towards natural resources, in which practicing green medicine become inherent (Ross, 2005; Ekor, 2014). About 80% of the developing countries residents are reliant on natural sources in their primary healthcare. On the other hand, there is a growing demand for natural drugs derived from wild plant species (Hamilton, 2004; Cole *et al.*, 2007).

In Iraq, desert climate prevails most of the country areas, mainly in the west part where Anbar, the largest province is located (32% of the total country area; 600 m above the sea level; 31° and 35° latitude; 39° and 44° longitude), (Figure 1). This wide geographical expansion provides unrivaled natural biodiversity, including plant genera. Unfortunately, due to different reasons, there are no concrete efforts to explore the nutritive, industrial, or pharmacological importance of wild plants that inhabiting and discriminating

these areas (Chen *et al.*, 2016).

Ferula is one of the three major genera in the Apiaceae family. However, more than 175 species belong to this widely distributed genus across Asia and the Mediterranean (Zhou *et al.*, 2017; Mohammadhosseini *et al.*, 2019). The genus members had proven numerous remedial properties making them eligible for treating many epidemics and diseases for centuries (Pavlovic *et al.*, 2015; Nguir *et al.*, 2016; Bagheri *et al.*, 2017; Upadhyay *et al.*, 2017). In addition to the pungent odor, most *Ferula* members are being characterized as gum-resin producers.

"Mharut" is the local name of *Ferula rutbaensis* C.C. Towns., the Bedouin food plant growing in the southwest part of the western desert near the Iraqi-Saudi Arabia borderlines. *F. rutbaensis* is described as a perennial herb growing to 50-60 cm high and has bleached green leaves covered with a white veil (Mandaville, 2011). The edible part is a thick taproot (5-7 cm diameter, Figure 2) that typically extends to 60 cm depth and can be easily characterized via peculiar odor (Ghazanfer and Edmondson, 2013). The species designation "*rutbaensis*" is originated from the name of "Rutba" city (310 km to the west of Ramadi city) where it grows nearby. Like most of *Ferula* members, *rutbaensis* has many therapeutic aspects served as antioxidant, antispasmodic digestive, antiseptic, anthelmintic, anti-

inflammatory, carminative, analgesic, expectorant, and laxative (Yaqoob and Ahmad, 2016), which enabled it to be widely practiced in folklore medicine (Mohammadhosseini *et al.*, 2019). Even though *Ferula* genus has received considerable attention and its extracts have been extensively studied, there is no available data describing the phytochemical composition of *F. rutbaensis*. Characterization of active pharmaceutical constituents of medically valuable species will create alternative sources for natural therapies and limit the irrational use of certain medicinal species that may result in their extinction (Chen *et al.*, 2016).

The environmental independency of molecular markers gives them an advantage over the morphological approaches that may reveal significant alterations in response to environmental effects (Dormontt *et al.*, 2018). Under this, a wild type may show minor phenotypic modifications (ecotypes) reflecting on a biased evaluation (Zhao *et al.*, 2018; Kevin *et al.*, 2019). Taxonomic identification of plant species is a very delicate and time-consuming process. It requires competent experts who are able to distinguish between even closely related species based on their complex phenotypic characteristics (Oliveira *et al.*, 2018). Unfortunately, like any other technique that relies on human skill, it may reflect in unreliable results.

DNA barcoding is a well-known molecular approach serving in biodiversity investigations (Costion *et al.*, 2016; Babychuk *et al.*, 2017). This technique is mainly depending on a short conservative DNA sequence adequate to identify inter- and intra-variations of plant species (Hebert *et al.*, 2003; Smith *et al.*, 2005; Desalle, 2006). Although Internal Transcribed Spacer (ITS) have some disadvantages hindered their extensive embracing in assessing the genetic diversity of plant populations (Fusco and Minelli, 2010; Timpano *et al.*, 2020), growing interest has been reported for applying the second internal transcribed spacer (ITS2) in DNA barcoding of various plant species (Sickel *et al.*, 2015; Fahner *et al.*, 2016; Moorhouse-Gann *et al.*, 2018; Timpano *et al.*, 2020). The ITS2 was found to be the most suitable molecular marker for standard DNA barcoding due to its high distinctive ability of intra- and/or inter-specific variation (Chiou *et al.*, 2007; Chen *et al.*, 2010).

Therefore, the present study aimed to characterize the *Ferula rutbaensis* species at phenotypic and molecular levels and the phytochemical constituents of aqueous and methanolic extracts of fresh and dry plant parts

that may have medicinal importance.

2. MATERIALS AND METHODS:

2.1. Collection of plant material

A fresh sample of naturally growing *F. rutbaensis* was collected at the blooming stage from the Western Desert, 160 km west of Ramadi (Figure 1). Whole plants were uprooted and transferred directly to the lab in polyethylene bags. The identification and authentication of the collected plant were made by Dr. Mohammed Othman Mosa/Center of Desert Studies/University of Anbar/Iraq and the Iraqi National Herbarium according to the deposited voucher specimen no. 51513 (Figure 2).

2.2. Genomic DNA Extraction

Fresh roots were used for DNA extraction with aid of Wizard® Genomic DNA Kit (Promega, Madison, WI, USA), and the supplier instructions were followed literally. A total of 100 mg of fresh root tissues was transferred to a 1.5 ml microfuge tube. Nuclei lysis solution of 600 µl volume was added and vortexed for 3 seconds. The mixture was then incubated at 65°C for 15 min. Then, 3 µl of RNase solution was added to the cell lysate, and incubated at 37°C for 15 min. Protein was precipitated by adding 200 µl of protein precipitation solution and vortex vigorously at high speed for 20 seconds, followed by centrifugation at 13,000 × g. Supernatant that contains the DNA (the protein pellet was left behind) was carefully removed and transferred to a clean 1.5 ml microcentrifuge tube containing 600 µl of room temperature isopropanol. The solution was mixed gently by inversion until thread-like strands of DNA form a visible mass. The centrifugation step was performed at 13,000 × g for 1 min. The supernatant was carefully decanted, subsequently, 600 µl of room temperature 70% ethanol was added and gently inverted the tube several times to wash the DNA, then centrifuged at 13,000 × g for 1 min. Ethanol was carefully aspirated by using a sequencing pipette tip. The tube was inverted onto clean absorbent paper and the pellet was air-dried for 15 min. DNA was rehydrated by adding 100 µl of DNA rehydration solution, then incubated at 65°C for 1 hour, then stored at 2–8°C till used.

According to Nanodrop reads, the final DNA concentration was adjusted to 50 ng/µl. Two previously designed plant-specific primers (5'-ATGCGATACTTGGTGTGAAT-3' as forward and 5'-GACGCTTCTCCAGACTACAAT-3' as

Reverse) were applied to amplify the ITS2 region of *F. rutbaensis* genome (Chiou *et al.*, 2007).

2.3. ITS amplification and Sequencing

A final volume of Polymerase Chain Reaction (PCR) was of 25 μ l (12.5 μ l of Green MasterMix (Promega, Madison, WI, USA), 1 μ l of each primer, 3 μ l of DNA template, and nuclease-free water was used to complete the volume) subjected to the following PCR thermal profile: Initial denaturation was at 94°C for 5 min, then subjected to 36 cycles of denaturation for 40 sec. at 94°, followed by annealing at 56°C for 45 sec. Extension and final extension steps were at 72°C for 1 and 7 min., respectively. The purified PCR product was sequenced following the Sanger sequencing technique on ABI 3730 Genetic Analyzer (Applied Biosystems, Foster City, CA, USA) in MacroGen Inc. (Seoul, South Korea).

2.4. Phytochemicals extraction

The aqueous and ethanol extraction procedures were adopted alternatively to extract the phytochemicals from each of the fresh and dried leaves and roots of *F. rutbaensis*. For aqueous extraction, 25 g of fresh parts (leaves and roots) were washed thoroughly and separately macerated in 100 ml of sterilized distilled water for one week, next placed on a shaker for 24 hours. Subsequently, the extract was filtered with Whatman filter paper (no.1). two times, then filtrates were concentrated and dried using a rotary evaporator (ISOLAB Laborgeräte GmbH, Germany) at 45° C under vacuum.

For dry extraction, leaves and roots were left to dry at room temperature until a constant weight is achieved. The dried plant materials were milled separately with an electric mill. A weight of 25 g from each of plant leaves and roots was separately soaked in 100 ml of sterilized distilled water and 10% ethanol (v/v), subsequently placed on a shaker for 72 hours. Then, the aqueous and ethanolic extracts were centrifuged for 10 min at 6000 rpm, filtered with Whatman filter paper (no.1). Finally, filtrates were concentrated with a rotary evaporator at 45° C under reduced pressure. The crud aqueous and ethanolic extracts were separately dissolved in DMSO at a rate of 100 mg 5 ml⁻¹ for GC-MS analysis.

2.4. GC-MS Conditions

The GC-MS profile was generated using GCMS-QP2010 plus instrument (Shimadzu, Kyoto, Japan) equipped with autoinjector and 5ms

capillary column of 30x0.25 mm dimension with 0.25 μ m film thickness. Helium served as the carrier gas at 1.15 ml/min. flow rate. Mass spectroscopic analysis was done with 70eV ionization system. The primary temperature was established at 80°C for 2 min. to be gradually elevated at a rate of 10°C per min. up to 280°C for 5 min. The sample injection was according to split mode at 250°C. Two mass spectral databases National Institute of Standards and Technology (NIST14), and Wiley 10th/NIST 2014 mass spectral library (W10N14) adopted in the characterization of the extracted components based on retention time and mass spectra.

3. RESULTS AND DISCUSSION:

3.1. ITS-based DNA barcoding

The used primers were successfully amplified the Internal Transcribed Spacer of *F. rutbaensis* was in roughly 600 bp (Figure 3). The resulted sequence was registered in the NCBI (National Center for Biotechnology Information) under the accession number LC570805.1 and that was identical in 452 out of 519 original hits with solitary previously registered *F. rutbaensis* (voucher Rechinger 12872) under the accession number of KJ660812.1 collected from Jordan by (Panahi *et al.*, 2018), (Figure 4).

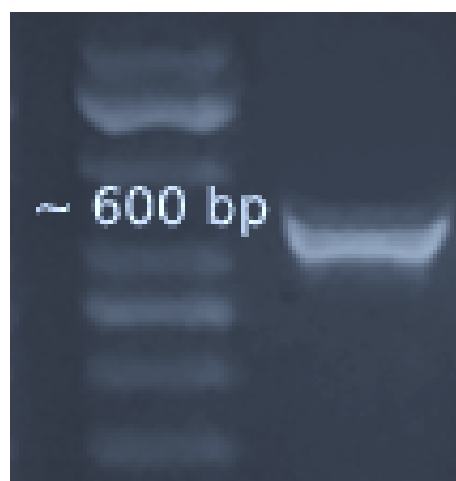


Figure 3. PCR product of ITS region of *F. rutbaensis* electrophoresed on 2% agarose gel at 5 volt/cm². 1x TBE buffer for 1:30 hours.

3.2. Gas Chromatography-Mass Spectrometry (GC-MS)

3.2.1 Aqueous Extract

The combination between GC and MS techniques has many advantages over other traditional methods adopted to identify plant

phytochemicals for many reasons, mainly to achieve reliable qualification and quantification. Traditionally, roots of *F. rutbaensis* are the edible and remedially important part that has been widely used for folklore medication in Bedouin communities.

The GC-MS chromatogram indicated the presence of 12 phytochemicals in the aqueous extract of *F. rutbaensis* fresh roots, namely Tetradecane; Pentadecane; Hexadecane; 2-Methylhexacosane; 1-Heneicosyl formate; Nonadecane; Carbonic acid, decyl hexadecyl ester; n-Hexadecanoic acid; Thiosulfuric acid ($\text{H}_2\text{S}_2\text{O}_3$), S-(2-aminoethyl) ester; Eicosyl nonyl ether; Oleic acid and Octadecenoic acid (Table 1). The characterized phytochemicals are categorized into terpenes, hydrocarbon alkanes, esters, and fatty acids.

Nevertheless, Oleic and Palmitic (n-Hexadecanoic) fatty acids were the two main components of the aqueous extract occupied a peak area of 32.64% and 26.35%, respectively (Table 1). Interestingly, both active compounds are fatty acids that have been characterized with anti-inflammatory (Aparna, 2012; Korbecki and Bajdak-Rusinek, 2019), anticancer (Ismail, 2020), antioxidant (Vaithiyanathan and Mirunalini, 2015), antibacterial and antifungal activities (Ogunlesi, 2009).

Nona- and Pentadecane existed in smaller amounts of 4.34% and 3.25%, and both characterized with antioxidant, anti-inflammatory (Ali *et al.*, 2015), and antimicrobial activity (Girija, 2014), respectively. From Table 1, the three alkanes, 2-methylhexacosane (2.52%), hexadecane (2.06%), and tetradecane (1.54%) were designated recently as effective inhibitors to microbial infections (Nair, 2019), decreasing blood cholesterol (Pandey *et al.*, 2016) and antimicrobial diuretic, anti-tuberculosis (Girija, 2014; Kavitha and Mohideen, 2017), respectively.

From GC-MS analysis, the aqueous extract of *F. rutbaensis* dry roots was the richest and the most diverse compared to other extracts, whereby 19 bioactive compounds of terpenes, hydrocarbon alkanes and fatty acids, in addition to individual compound of each of alcohol, acetate, alkene, alkyl halide, and sulfolane were recognized (Table 2). Depending on the retention time (min.), the detected compounds were (3R)-1-Phenyl-1-pentyn-3-ol; 5-Acetoxymethyl-2,6,10-trimethyl-2,9-undecadien-6-ol; Isolongifolen-5-one; 3H-Cyclodeca[b]furan-2-one, 4,9-dihydroxy-6-methyl-3,10-dimethylene-3a,4,7,8,9,10,11,11a-octahydro-; 11,13-Dimethyl-12-tetradecen-1-ol

acetate; Cyclopentane, 1,2-dimethyl-3-(1-methylethenyl)-; 1-Methylbicyclo[3.2.1]octane; 1-Tetracosene; Cyclotetracosane; Heptadecane; n-Hexadecanoic acid; Hexadecanoic acid; 2,6,10,14-Hexadecatetraen-1-ol, 3,7,11,15-tetramethyl-, acetate, (E,E,E)-; Triacotane, 1-bromo; Cyclopentanol, 1-(1-methylene-2-propenyl); 4-n-Hexylthiane, S,S-dioxide; trans-Verbenol; 9-Octadecenoic acid and Octadecanoic acid.

However, n-Hexadecanoic and 9-Octadecenoic acids were the two most abundant components of the dry roots aqueous extract with a peak area of 27.69% and 27.28%, respectively (Table 2). Recently, several reports pointed to the substantial potent of such fatty acids, particularly as an anti-inflammatory (Aparna, 2012; Korbecki and Bajdak-Rusinek, 2019), anticancer (Ismail, 2020), antioxidant (Vaithiyanathan and Mirunalini, 2015), antibacterial and antifungal properties (Ogunlesi, 2009).

Diterpenoid in the form of 2,6,10,14-Hexadecatetraen-1-ol, 3,7,11,15-tetramethyl-, acetate, (E,E,E), (4.37 %) was detected in the dry roots aqueous extract known with various pharmacological activities like antimicrobial, anti-inflammatory, anticancer and diuretic activities (Devi and Muthu, 2015). Heptadecane (4.11%) and less abundant components such as 4-n-Hexylthiane S,S-dioxide (2.13%), and trans-Verbenol (1.12%) distinguished with antimicrobial activity (Girija, 2014; Mathew and Retna, 2016; Utegenova, 2018).

By contrast, GC-MS data of dry leaves reveals the existence of only 5 phytochemicals categorized into two groups; the first consisted of three fatty acids (n-Hexadecanoic acid (41.81%), 9-Octadecenoic (30.11%) and acid Octadecanoic acid (23.72%), while the second group was hydrocarbon alkane in the form of Nonadecane (4.35%), (Table 2). Both groups have distinctive bioactivity, as previously addressed by several reports.

3.2.2 Methanolic Extract

According to the GC-MS profile, methanol-based extraction was less efficient in extracting plant chemical constituents from each of fresh and dry roots compared to water-based extraction, where the screened methanolic extract of fresh roots included only 6 bioactive compounds namely, Nonadecane; n-Hexadecanoic acid; Thiosulfuric acid ($\text{H}_2\text{S}_2\text{O}_3$), S-(2-aminoethyl) ester; Sulfurous acid, 2-propyl tetradecyl ester; Oleic Acid and Octadecanoic acid. These compounds

can be categorized into fatty acids, esters, and hydrocarbon alkane (Table 3).

Likewise, screening of phytochemicals in the dry roots of *F. rutbaensis* showed the presence of almost the same bioactive compounds recognized in the fresh roots methanolic extract (Nonadecane; n-Hexadecanoic acid; Thiosulfuric acid ($H_2S_2O_3$), S-(2-aminoethyl) ester; Carbonic acid, decyl undecyl ester; Octadec-9-enoic acid and Octadecanoic acid (Table 3). However, Sulfurous acid, 2-propyl tetradecyl ester (2.32%) in the fresh roots methanolic extract was replaced by Carbonic acid, decyl undecyl ester (0.66%) in the dry roots counterpart.

In terms of peak area, Oleic acid and n-Hexadecanoic acid still representing the identified major constituents in the methanolic extract of fresh and dry roots having the largest peak area (%) of 38.58 and 27.73 in fresh roots and 35.65 and 32.02 in dry roots, respectively. Following the methanol-based extraction procedure, the dried leaves were the poorest source in respect of extracted phytochemicals. However, it showed distinct phytochemical profile by expressing acyclic alkane in the form of Tetracosane (57.55%) and organosilicon compound in the form of Methyltris (trimethylsiloxy) silane (42.45%) (Table 3). The former is reported to have antibacterial, antimicrobial (Panicker *et al.*, 2019), and antioxidant properties (Boussaada, 2008).

4. CONCLUSIONS:

The wild plant types like *Ferula rutbaensis* are valuable sources for therapeutic and bioactive compounds, particularly as antioxidants, anti-inflammatory, antispasmodic digestive, and laxative. According to the GC-MS profile, a wide range of phytochemicals differed between plant parts. However, plant roots were the richest source for bioactive compounds. Under this, the aqueous extraction procedure exhibited a sophisticated ability to extract plant phytochemicals compared to methanolic extract, mainly from dry roots whereby nineteen biochemical constituents were recognized with remarkable bioactivities based on several reports.

5. ACKNOWLEDGMENTS:

We would like to thank Dr. Mohammed Othman Mosa, Center of Desert Studies, University of Anbar, and the Iraqi National Herbarium for identifying the collected plant sample. We also thank Dr. Ahmed A. Suleiman, Department of Biotechnology, University of Anbar

for helping in interpreting DNA sequencing data.

6. REFERENCES:

1. Alencar, L.A., N., de Sousa Araújo, T.A., de Amorim, E.L.C., de Albuquerque, U.P., (2010). The inclusion and selection of medicinal plants in traditional pharmacopoeias—evidence in support of the diversification hypothesis. *Economic Botany* 64, 68–79. <https://doi.org/10.1007/s12231-009-9104-5>
2. Ali, H.A.M., Imad, H.H., Salah, A.I., (2015). Analysis of bioactive chemical components of two medicinal plants (*Coriandrum sativum* and *Melia azedarach*) leaves using gas chromatography-mass spectrometry (GC-MS). *African Journal of Biotechnology* 14(40), 2812–2830. <https://doi.org/10.5897/ajb2015.14956>
3. Aparna, V., Dileep, K.V., Mandal, P.K., Karthe, P., Sadasivan, C., Haridas, M., (2012). Anti-Inflammatory property of n-Hexadecanoic acid: Structural evidence and kinetic assessment. *Chemical Biology and Drug Design* 80(3), 434–439. <https://doi.org/10.1111/j.1747-0285.2012.01418.x>
4. Babiychuk, E., Kushnir, S., Vasconcelos, S., Dias, M.C., Carvalho-Filho, N., Nunes, G.L., Dos Santos, J.F., Tyski, L., da Silva, D.F., Castilho, A., Fonseca, V.L.I., Oliveira, G., (2017). Natural history of the narrow endemics *Ipomoea cavalcantei* and *I. Marabaensis* from Amazon Canga savannahs. *Sci. Rep.* 7, 7493.
5. Bagheri, S.M., Abdian-Asl, A., Moghadam, M.T., Yadegari, M., Mirjalili, A., Zare-Mohazabieh, F., Momeni, H., (2017). Antitumor effect of *Ferula assa foetida* oleo gum resin against breast cancer induced by 4T1 cells in BALB/c mice. *J. Ayurveda Integr. Med.* 8, 152–158.
6. Boussaada, O., Ammar, S., Saidana, D., Chriaa, J., Chraif, I., Daami, M., Mighri, Z., (2008). Chemical composition and antimicrobial activity of volatile components from capitula and aerial parts of *Rhaponticum acaule* DC growing wild in Tunisia. *Microbiological Research* 163(1), 87–95. <https://doi.org/10.1016/j.micres.2007.02.010>
7. Chen, S., Yao, H., Han, J., Liu, C., Song, J., Shi L., (2010). Validation of the ITS2 region as a novel DNA barcode for identifying medicinal plant species. *PLoS ONE*. 2010; 5(1):e8613. <https://doi.org/10.1371>

8. Chen, S.L., Yu, H., Luo, H.M., Wu, Q., Li, C.F., Steinmetz, A., (2016). Conservation and sustainable use of medicinal plants: problems, progress, and prospects. *Chinese Medicine*, 11, 37. <https://doi.org/10.1186/s13020-016-0108-7>
9. Chiou, S.-J., Yen, J.-H., Fang, C.-L., Chen, H.-L., Lin, T.-Y., (2007). Authentication of medicinal herbs using PCR-amplified ITS2 with specific primers. *Planta Medica* 73(13), 1421–1426. <https://doi.org/10.1055/s-2007-990227>
10. Cole, I.B., Saxena, P.K., Murch, S.J., (2007). Medicinal biotechnology in the genus *scutellaria*. *In Vitro Cell Dev. Plant.* 43, 318–327. <https://doi.org/10.1007/s11627-007-9055-4>.
11. Costion, C., Lowe, A., Rossetto, M., Kooyman, R., Breed, M., Ford, A., Crayn, D., (2016). Building a plant DNA barcode reference library for a diverse tropical Flora: an example from Queensland, Australia. *Diversity* 8, 5.
12. Devi, J.A.I., Muthu, A.K., (2015). Gas chromatography-mass spectrometry analysis of phytocomponents in the ethanolic extract from whole plant of *lactuca runcinata* DC. *Asian Journal of Pharmaceutical and Clinical Research* 8(1), 202–206.
13. Desalle, R., (2006). Species discovery versus species identification in DNA barcoding efforts: response to Rubinoff. *Conserv. Biol.* 20, 1545–7.
14. Dormontt, E.E., van Dijk, K., Bell, K.L., Biffin, E., Breed M.F., Byrne, M., Caddy-Retalic, S., Encinas-Viso, F., Nevill, P.G., Shapcott, A., Young, J.M., Waycott, M., Lowe, A.J., (2018). Advancing DNA barcoding and metabarcoding applications for plants requires systematic analysis of herbarium collections—an Australian perspective. *Frontiers in Ecology and Evolution* 6, 134. <https://doi.org/10.3389/fevo.2018.00134>
15. Ekor, M., (2014). The growing use of herbal medicines: issues relating to adverse reactions and challenges in monitoring safety. *Frontiers in pharmacology*, 4, 177. <https://doi.org/10.3389/fphar.2013.00177>
16. Fahner, N.A., Shokralla, S., Baird, D.J., Hajibabaei, M., (2016). Large-scale monitoring of plants through environmental DNA metabarcoding of soil: recovery, resolution, and annotation of four DNA markers. *PLoS ONE* 11(6), e0157505. <https://doi.org/10.1371>
17. Fusco, G., Minelli, A., (2010). Phenotypic plasticity in development and evolution: facts and concepts. Introduction. *Philosophical transactions of the Royal Society of London. Series B, Biological Sciences*, 365(1540), 547–556. <https://doi.org/10.1098/rstb.2009.0267>
18. Ghazanfer, S.A., Edmondson, J.R., (2013). *Flora of Iraq*. Ministry of Agriculture and Royal Botanic Gardens, Kew. V.5, P.2; Pp, 221–222.
19. Girija, S., Duraipandiyar, V., Kuppusamy, P.S., Gajendran, H., Rajagopal, R., (2014). Chromatographic characterization and GC-MS evaluation of the bioactive constituents with antimicrobial potential from the pigmented ink of *Loligo duvauceli*. *International Scholarly Research Notices* 1–7. <https://doi.org/10.1155/2014/820745>
20. Hamilton, A.C., (2004). Medicinal plants, conservation and livelihoods. *Biodivers Conserv.* 13, 1477–1517. <https://doi.org/10.1023/B:BIOC.0000021333.23413.42>.
21. Hebert, P.D.N., Cywinska, A., Ball, S.L., de Waard, J.R., (2003). Biological identifications through DNA barcodes. *Proc. R. Soc. B. Biol. Sci.* 270, 313–21.
22. Ismail, N.Z., Toha, Z.M., Muhamad, M., Kamal, N.N., Zain, N.N., Arsad, H., (2020). Antioxidant effects, antiproliferative effects, and molecular docking of *Clinacanthus nutans* leaf extracts. *Molecules* 25(9), 2067. <https://doi.org/10.3390/molecules25092067>
23. Kavitha, R., Mohideen, A.M., (2017). Identification of bioactive components and its biological activities of *abelmoschas moschatus* flower extract-A Gc-MS study. *IOSR Journal of Applied Chemistry* 10(11), 19–22. <https://doi.org/10.9790/5736-1011011922>
24. Kevin, J.P., McWhinnie, K., Pilakouta, N., Walker, L., (2019). Does phenotypic plasticity initiate developmental bias? <https://doi.org/10.1111/ede.12304>
25. Korbecki, J., Bajdak-Rusinek, K., (2019). The effect of palmitic acid on inflammatory response in macrophages: an overview of molecular mechanisms. *Inflammation Research* 68(11), 915–932. <https://doi.org/10.1007/s00011-019-01273-5>
26. Mandaville, J.P., (2011). *Bedouin Ethnobotany; Plant concepts and uses in a desert pastoral world*. The University of Arizona Press, Tucson. Pp, 107–273

27. Mathew, A., Retna, A.M., (2016). Antilithiatic activity and pharmacognostic studies of *Scoparia dulcis*. *Green Chemistry & Technology Letters* 2(1), 01–10. <https://doi.org/10.18510/gctl.2016.211>
28. Mohammadhosseini, M., Venditti, A., Sarker, S.D., Nahar, L., Akbarzadeh, A., (2019). The genus *Ferula*: Ethnobotany, phytochemistry and bioactivities – A review. *Industrial Crops and Products* 129, 350–394. <https://doi.org/10.1016/j.indcrop.2018.12.012>
29. Moorhouse-Gann, R.J., Dunn, J.C., Symondson, W.O.C., (2018). New universal ITS2 primers for high-resolution herbivory analyses using DNA metabarcoding in both tropical and temperate zones. *Sci. Rep.* 8, 8542. <https://doi.org/10.1038/s41598-018-26648-2>
30. Nair, N.M., Kanthasamy, R., Mahesh, R., Selvam, S.I.K., Ramalakshmi, S., (2019). Production and characterization of antimicrobials from isolate *Pantoea agglomerans* of *Medicago sativa* plant rhizosphere soil. *Journal of Applied and Natural Science* 11(2), 267–272. <https://doi.org/10.31018/jans.v11i2.2031>
31. Ngair, A., Mabrouk, H., Douki, W., Ben Ismail, M., Ben Jannet, H., Flamini, G., Hamza, M.A., (2016). Chemical composition and bioactivities of the essential oil from different organs of *Ferula communis* L. growing in Tunisia. *Med. Chem. Res.* 25, 515–525.
32. Ogunlesi, M., Okiei, W., Ofor, E., Osibote, A.E., (2009). Analysis of the essential oil from the dried leaves of *Euphorbia hirta* L. (Euphorbiaceae), a potential medication for asthma. *African Journal of Biotechnology* 8(24), 7042–7050. <https://doi.org/10.5897/AJB09.1324>
33. Oliveira, R.R.M., Nunes, G.L., de Lima, T.G.L., Oliveira, G., Alves, R., (2018). PIPEBAR and OverlapPER: tools for a fast and accurate DNA barcoding analysis and paired-end assembly. *BMC Bioinformatics* 19, 297. <https://doi.org/10.1186/s12859-018-2307-y>
34. Othman, L., Sleiman, A., Abdel-Massih, R.M., (2019). Antimicrobial activity of polyphenols and alkaloids in middle eastern plants. *Front. Microbiol.* 10, 911. <https://doi.org/10.3389/fmicb.2019.00911>
35. Panahi, M., Banasiak, Ł., Piwczyński, M., Puchalka, R., Kanani, M.R., Oskolski, A.A., Modnicki, D., Miłobędzka, A., Spalik, K., (2018). Taxonomy of the traditional medicinal plant genus *Ferula* (Apiaceae) is confounded by incongruence between nuclear rDNA and plastid DNA. *Botanical Journal of the Linnean Society* 188(2), 173–189. <https://doi.org/10.1093/botlinnean/boy055>
36. Pandey, A., Biswas, S.J., Khatua, S., Surjyo, C., Biswas, J., (2016). Phytochemical evaluation and antimicrobial properties of *Trichosanthes dioica* root extract. *Journal of Pharmacognosy and Phytochemistry* 5(5), 410–413.
37. Panicker, R., Mohanan, A., Mishra, A.K., (2019). Physico-chemical analysis of *Darunakaroganashaka arka* (*Amrabeejadi Arka*). *Int. J. Ayu. Pharm. Chem.* 11(2), 260–265.
38. Pavlovic, I., Petrovic, S., Milenkovic, M., Stanojkovic, T., Nikolic, D., Krunić, A., Niketić, M., (2015). Antimicrobial and cytotoxic activity of extracts of *Ferula heuffelii* Griseb. Ex Heuff. and its metabolites. *Chem. Biodivers.* 12, 1585–1594.
39. Ross, I.A., (2005). Medicinal plants of the world (volume 3): chemical constituents, traditional and modern medicinal uses. New Jersey: Humana Press Inc. USA, pp.110–132.
40. Saeed, J.M., (2017). Ecology and geographical distribution of the genus *Ferula* L. Apiaceae (Umbelliferae) grown in Iraq. *Diyla Journal For Pure Science* 13(3), 30–39. <https://doi.org/10.24237/djps.1303.222A>
41. Sickel, W., Ankenbrand, M.J., Grimmer, G., Holzschuh, A., Lanzen J., (2015). Increased efficiency in identifying mixed pollen samples by meta-barcoding with a dual-indexing approach. *BMC Ecol.* 15(1), 20. <https://doi.org/10.1186>
42. Smith, M.A., Fisher, B.L., Hebert, P.D.N., (2005). DNA barcoding for effective biodiversity assessment of a hyperdiverse arthropod group: the ants of Madagascar. *Philos. Trans. R. Soc. Lond. Ser. B. Biol. Sci.* 360, 1825–34.
43. Timpano, E.K., Scheible, M.K.R., Meiklejohn, K.A., (2020). Optimization of the second internal transcribed spacer (ITS2) for characterizing land plants from soil. *PLOS ONE* 15(4), e0231436. <https://doi.org/10.1371/journal.pone.0231436>
44. Upadhyay, P.K., Singh, S., Agrawal, G., Vishwakarma, V.K., (2017). Pharmacological activities and therapeutic uses of resins

obtained from *Ferula asafoetida* Linn.: A review. Int. J. Green Pharm. 11, S240–S247.

45. Utegenova, G.A., Pallister, K.B., Kushnarenko, S.V., Özek, G., Özek, T., Abidkulova, K.T., Voyich, J.M., (2018). Chemical composition and antibacterial activity of essential oils from *Ferula* L. species against methicillin-resistant *Staphylococcus aureus*. *Molecules* 23(7), 1–18.
<https://doi.org/10.3390/molecules23071679>
46. Vaithiyanathan, V., Mirunalini, S., (2015). Quantitative variation of bioactive phyto compounds in ethyl acetate and methanol extracts of *Pergularia daemia* (Forsk.) Chiov. *Journal of Biomedical Research* 29(2), 169–172. <https://doi.org/10.7555/JBR.28.20140100>
47. Yaqoob, U., Ahmad, I., (2016). Nawchoo Distribution and taxonomy of *Ferula* L.: a review. *Research & Reviews: Journal of Botany* 5(3), 15-23.
48. Zhao, L.L., Feng, S.J., Tian, J.Y., Wei, A.Z., Yang, T.X., (2018). Internal transcribed spacer 2 (ITS2) barcodes: a useful tool for identifying Chinese *Zanthoxylum*. *Applications in plant sciences*, 6(6), e01157.
<https://doi.org/10.1002/aps3.1157>
49. Zhou, F.X., Zhang, G., H. Qu, Yang, D., Han, X., (2017). Recent advances on bioactive constituents in *Ferula*. *Drug Development Research* 78(7), 321-331.
<https://doi.org/10.1002/ddr.21402>

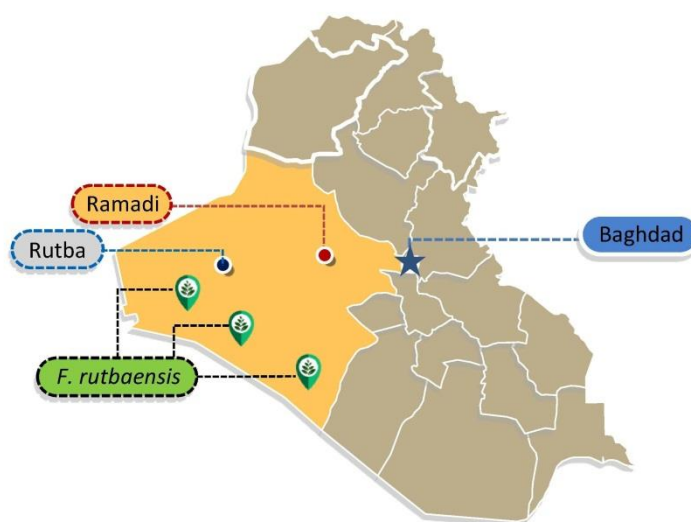


Figure 1. Geographical origin of *F. rutbaensis*. Source: the author

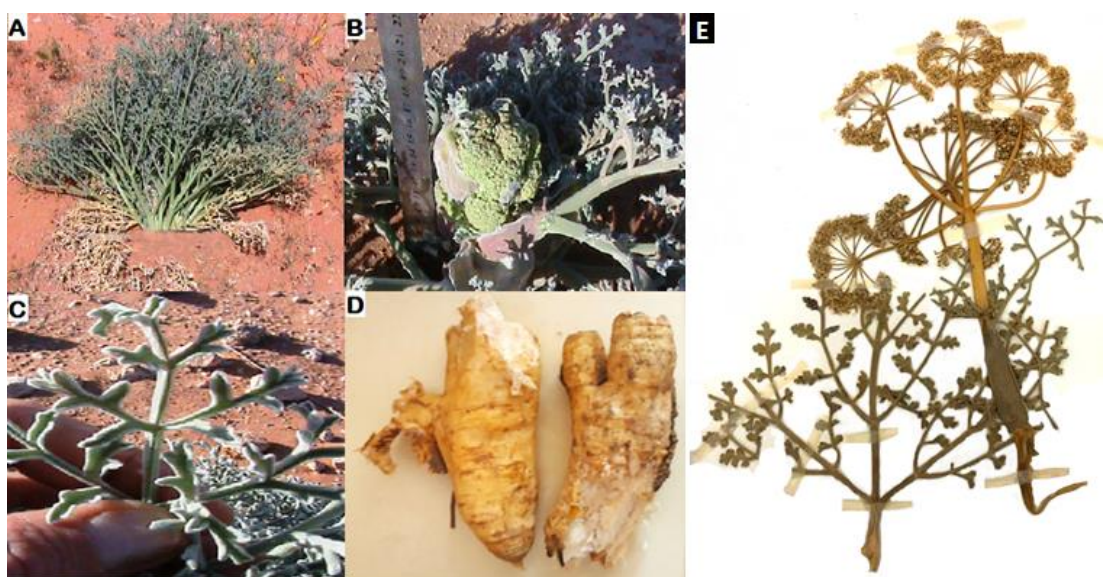


Figure 2. The *F. rutbaensis* plant, (A) Aerial shoot, (B) The emerged flower, (C) Leaf, (D) Root, (E) Deposited voucher specimen no. 51513. Source: the author

```

LC570805.1: 1   aaggaaattaatactgaattgttcgtcgttctcgttcgcgggcagcggcgtcagtc tga 60
               ||||||||||||||||||||||||||||||||||||||||||||||||||||
KJ660812.1: 153 aaggaaattaatactgaattgttcgtcgttctcgttcgcgggcagcggcgtcagtc tga 212

LC570805.1: 61   aacacaaacgactctcggcaacggatatcccggctctcgcatcgatgaagaacgtagcga 120
               ||||||||||||||||||||||||||||||||||||||||||||||||||||
KJ660812.1: 213 aacacaaacgactctcggcaacggatatcccggctctcgcatcgatgaagaacgtagcga 272

LC570805.1: 121  aatgcgatacttgggtgtgaattgcagaatcccgtgaaccatcgagtc tttgaacgcaagt 180
               ||||||||||||||||||||||||||||||||||||||||||||||||||||
KJ660812.1: 273 aatgcgatacttgggtgtgaattgcagaatcccgtgaaccatcgagtc tttgaacgcaagt 332

LC570805.1: 181  tgcgccgaagccattaggctgagggcacgtctgcctgggtgtcacgcatcggtgtgcc 240
               ||||||||||||||||||||||||||||||||||||||||||||||||||||
KJ660812.1: 333 tgcgccgaagccattaggctgagggcacgtctgcctgggtgtcacgcatcggtgtgcc 392

LC570805.1: 241  ctgaccaaacatccctctaggagatgttccggtttggggcggtatctggcctcccgtgc 300
               ||||||||||||||||||||||||||||||||||||||||||||||||||||
KJ660812.1: 393 ctgaccaaacatccctctaggagatgttccggtttggggcggtatctggcctcccgtgc 452

LC570805.1: 301  cttgttgtgcggctggcgcaaaaatgagtcctctggcgatggacgtcgcgacatcggtggt 360
               ||||||||||||||||||||||||||||||||||||||||||||||||||||
KJ660812.1: 453 cttgttgtgcggctggcgcaaaaatgagtcctctggcgatggacgtcgcgacatcggtggt 512

LC570805.1: 361  tgtaagaagaccttcttgtcttgtcgtgtatgcccgtcactttagtcagctcaaggaccc 420
               ||||||||||||||||||||||||||||||||||||||||||||||||||||
KJ660812.1: 513 tgtaagaagaccttcttgtcttgtcgtgtatgcccgtcactttagtcagctcaaggaccc 572

LC570805.1: 421  ttaggcgccacaaaatgtgtgatgcgcttcga 452
               ||||||||||||||||||||||||||||||||||||||||||||||||||||
KJ660812.1: 573 ttaggcgccacaaaatgtgtgatgcgcttcga 604

```

Figure 4. Sequence alignment of ITS (internal transcribed spacer 1, partial sequence; 5.8S ribosomal RNA gene, complete sequence; and internal transcribed spacer 2, partial sequence) of the studied *F. rutbaensis* (LC570805.1) and the previously registered voucher *Rechinger 12872 (E)* (KJ660812.1).
Source: the author

Table 1. GC-MS analysis of aqueous extract of *F. rutbaensis* fresh roots. Source: the author

Pea No.	RT (min)	Name of the compound	Molecular Formula	MW (g/mol)	Peak Area (%)	Nature of compound
1	14.13	Tetradecane	C ₁₄ H ₃₀	198.4	1.54	Acyclic alkane
2	15.91	Pentadecane	C ₁₅ H ₃₂	212.4	3.25	Acyclic alkane
3	17.61	Hexadecane	C ₁₆ H ₃₄	226.4	2.06	Acyclic alkane
4	19.22	2-Methylhexacosane	C ₂₇ H ₅₆	380.7	2.52	Branched alkane
5	21.91	1-Heneicosyl formate	C ₂₂ H ₄₄ O ₂	340.6	0.98	Monoterpene
6	22.24	Nonadecane	C ₁₉ H ₄₀	268.5	4.34	Acyclic alkane
7	22.51	Carbonic acid, decyl hexadecyl ester	C ₂₇ H ₅₄ O ₃	426.7	0.69	Carbonate ester
8	23.72	n-Hexadecanoic acid	C ₁₆ H ₃₂ O ₂	256.4	26.35	Saturated fatty acid
9	24.04	Thiosulfuric acid (H ₂ S ₂ O ₃), S-(2-aminoethyl) ester	C ₂ H ₇ NO ₃ S ₂	157.2	6.92	Thiosulfuric acid ester
10	25.01	Eicosyl nonyl ether	C ₂₉ H ₆₀ O	424.7	1.57	Dialkyl ether
11	26.14	Oleic Acid	C ₁₈ H ₃₄ O ₂	282.5	32.64	Unsaturated fatty acid
12	26.35	Octadecenoic acid	C ₁₈ H ₃₆ O ₂	284.5	17.14	Saturated fatty acid

(RT= Retention time) (MW= Molecular weight)

Table 2. GC-MS analysis of aqueous extract of *F. rutbaensis* dry roots and leaves. Source: the author

Plant part	Peak No.	RT (min)	Name of the compound	Molecular Formula	MW (g/mol)	Peak Area (%)	Nature of compound
Dry roots	1	10.57	(3R)-1-Phenyl-1-pentyn-3-ol	C ₁₁ H ₁₂ O	160.2	1.49	Propargylic alcohol
	2	18.29	5-Acetoxymethyl-2,6,10-trimethyl-2,9-undecadien-6-ol	C ₁₇ H ₃₀ O ₃	282.4	0.61	Monoterpene
	3	20.28	Isolongifolen-5-one	C ₁₅ H ₂₂ O	218.3	0.9	Sesquiterpene
	4	20.94	3H-Cyclodeca[b]furan-2-one, 4,9-dihydroxy-6-methyl-3,10-dimethylene-3a,4,7,8,9,10,11,11a-octahydro-	C ₁₅ H ₂₀ O ₄	264.3	1.76	Sesquiterpene
	5	21.12	11,13-Dimethyl-12-tetradecen-1-ol acetate	C ₁₈ H ₃₄ O ₂	282.5	1.84	Acetate compound
	6	21.42	Cyclopentane, 1,2-dimethyl-3-(1-methylethenyl)-1-	C ₁₀ H ₁₈	138.3	2.4	Monoterpene
	7	21.59	Methylbicyclo[3.2.1]octane	C ₉ H ₁₆	124.2	1.1	Cyclic hydrocarbon
	8	21.92	1-Tetracosene	C ₂₄ H ₄₈	336.6	2.02	Acyclic olefin
	9	22.06	Cyclotetracosane	C ₂₄ H ₄₈	336.6	1.41	Cyclic alkane
	10	22.24	Heptadecane	C ₁₇ H ₃₆	240.5	4.11	Acyclic Alkane
	11	23.72	n-Hexadecanoic acid	C ₁₆ H ₃₂ O ₂	256.4	27.69	Saturated fatty acid
	12	24.05	Hexadecanoic acid	C ₁₆ H ₃₂ O ₂	256.4	5.7	Saturated fatty acid
	13	24.82	2,6,10,14-Hexadecatetraen-1-ol, 3,7,11,15-tetramethyl-, acetate, (E,E,E)-	C ₁₆ H ₂₆ O	234.4	4.37	Diterpenoid
	14	25.01	Triacontane, 1-bromo	C ₃₀ H ₆₁ Br	501.7	7.07	Alkyl halide
	15	25.46	Cyclopentanol, 1-(1-methylene-2-propenyl)	C ₉ H ₁₄ O	138.2	1.26	Monoterpene
	16	25.59	4-n-Hexylthiane, S,S-dioxide	C ₁₁ H ₂₂ O ₂ S	218.4	2.13	Sulfolane
	17	25.8	trans-Verbenol	C ₁₀ H ₁₆ O	152.2	1.12	Monoterpene
	18	26.16	9-Octadecenoic acid	C ₁₈ H ₃₄ O ₂	282.5	27.28	Unsaturated fatty acid
	19	26.37	Octadecanoic acid	C ₁₈ H ₃₄ O ₂	282.5	5.74	Saturated fatty acid
Dry leaves	1	22.24	Nonadecane	C ₁₉ H ₄₀	268.5	4.35	Acyclic alkane
	2	23.72	n-Hexadecanoic acid	C ₁₆ H ₃₂ O ₂	256.4	33.07	Saturated fatty acid
	3	24.04	n-Hexadecanoic acid	C ₁₆ H ₃₂ O ₂	256.4	8.74	Saturated fatty acid
	4	26.14	9-Octadecenoic acid	C ₁₈ H ₃₄ O ₂	282.5	30.11	Unsaturated fatty acid
	5	26.35	Octadecanoic acid	C ₁₈ H ₃₆ O ₂	284.5	23.72	Saturated fatty acid

(RT= Retention time) (MW= Molecular weight)

Table 3. GC-MS analysis of methanol extract of dry and fresh roots of *F. rutbaensis*. Source: the author

Plant part	Peak No.	RT (min)	Name of the compound	Molecular Formula	MW (g/mol)	Peak Area(%)	Nature of compound
Fresh roots	1	22.24	Nonadecane	C ₁₉ H ₄₀	268.5	3.58	Acyclic alkane
	2	23.72	n-Hexadecanoic acid	C ₁₆ H ₃₂ O ₂	256.4	27.73	Saturated fatty acid
	3	24.05	Thiosulfuric acid (H ₂ S ₂ O ₃), S-(2-aminoethyl) ester	C ₂ H ₇ NO ₃ S ₂	157.2	10.38	Thiosulfuric acid ester
	4	25.01	Sulfurous acid, 2-propyl tridecyl ester	C ₁₆ H ₃₄ O ₃ S	306.5	2.32	Sulfurous acid ester
	5	26.14	Oleic Acid	C ₁₈ H ₃₄ O ₂	282.5	38.58	Unsaturated fatty acid
	6	26.35	Octadecanoic acid	C ₁₈ H ₃₆ O ₂	284.5	17.41	Saturated fatty acid
Dry roots	1	22.25	Nonadecane	C ₁₉ H ₄₀	268.5	7.06	Acyclic alkane
	2	23.72	n-Hexadecanoic acid	C ₁₆ H ₃₂ O ₂	256.4	32.02	Saturated fatty acid
	3	24.05	Thiosulfuric acid (H ₂ S ₂ O ₃), S-(2-aminoethyl) ester	C ₂ H ₇ NO ₃ S ₂	157.2	7.29	Thiosulfuric acid ester
	4	25.02	Carbonic acid, decyl undecyl ester	C ₂₂ H ₄₄ O ₃	356.6	0.66	Carbonate ester
	5	26.15	Octadec-9-enoic acid	C ₁₈ H ₃₄ O ₂	282.5	35.65	Unsaturated fatty acid
	6	26.35	Octadecanoic acid	C ₁₈ H ₃₆ O ₂	284.5	17.32	Saturated fatty acid
Dry leaves	1	10.05	Methyltris (trimethylsiloxy)silane	C ₁₀ H ₃₀ O ₃ Si ₄	310.7	42.45	Organosilicon compound
	2	22.75	Tetracosane	C ₂₄ H ₅₀	338.7	57.55	Acyclic alkane

(RT= Retention time) (MW= Molecular weight)

CARACTERÍSTICAS DE FORÇA DE COMPÓSITOS DE POLÍMERO BASEADOS EM POLIPROPILENO RECICLADO PREENCHIDO DE CASCA DE ARROZ NO PROCESSO DE ABSORÇÃO DE UMIDADE E ENVELHECIMENTO NATURAL**STRENGTH CHARACTERISTICS OF POLYMER COMPOSITES BASED ON RECYCLED POLYPROPYLENE FILLED WITH RICE HUSK DURING MOISTURE ABSORPTION AND NATURAL AGING****ПРОЧНОСТНЫЕ ХАРАКТЕРИСТИКИ ПОЛИМЕРНЫХ КОМПОЗИТОВ НА ОСНОВЕ ВТОРИЧНОГО ПОЛИПРОПИЛЕНА, НАПОЛНЕННОГО РИСОВОЙ ШЕЛУХОЙ, В ПРОЦЕССЕ ПОГЛОЩЕНИЯ ВЛАГИ И ЕСТЕСТВЕННОГО СТАРЕНИЯ**

SADRITDINOV, Aynur R.^{1*}; CHERNOVA, Valentina V.²; BAZUNOVA, Marina V.³; ZAKHAROVA, Elena M.⁴; ZAKHAROV, Vadim P.⁵;

^{1,2,3,5} Bashkir State University, Faculty of Chemistry, Department of Macromolecular Compounds and General Chemical Technology, 450076, 33 Zaki Validi Str., Ufa – Russian Federation

⁴ Ufa Federal Research Centre of the Russian Academy of Sciences, Department of Macromolecular Compounds, 450054, 71 October Ave., Ufa – Russian Federation

* Corresponding author
e-mail: aynur.sadritdinov@mail.ru

Received 20 September 2020; received in revised form 26 October 2020; accepted 05 November 2020

RESUMO

A relevância do problema em estudo deve-se ao aumento da carga ambiental sobre o meio ambiente devido ao contínuo crescimento dos resíduos plásticos, dos quais uma parcela significativa é de polipropileno. Uma das soluções para esse problema é o uso do polipropileno reciclado na reciclagem para obtenção de produtos plásticos à base de compósitos preenchidos com casca de arroz. Isso permite reduzir o custo original dos produtos acabados, regular suas propriedades físicas e mecânicas e reduzir o volume de polímero sintético de difícil decomposição que acaba em resíduos. A principal propriedade do polipropileno, que muda durante o seu enchimento com casca de arroz, é a absorção de umidade, que contribui para uma mudança nas características de resistência do compósito polimérico e acelera seu envelhecimento sob a influência de fatores ambientais. Nesse sentido, o objetivo deste artigo é identificar as regularidades da influência da umidade absorvida e do envelhecimento natural nas propriedades físicas e mecânicas de compósitos poliméricos à base de polipropileno reciclado preenchido com casca de arroz. A abordagem principal para o estudo deste problema são os testes de laboratório sobre a saturação de compósitos poliméricos com água com diferentes temperaturas e tempos de exposição, bem como os testes de materiais no processo de envelhecimento natural de longo prazo sob a influência de fatores ambientais. O fator chave que caracteriza a mudança nas propriedades físicas e mecânicas dos materiais, neste caso, é o módulo de elasticidade, alongamento e resistência à ruptura no processo de alongamento dos protótipos. Os materiais do artigo são de valor prático para o processamento de polímeros termoplásticos reciclados, bem como para a criação de compósitos poliméricos biodegradáveis.

Palavras-chave: *polipropileno reciclado, casca de arroz, absorção de umidade, envelhecimento natural, propriedades físicas e mecânicas.*

ABSTRACT

The relevance of the issue under investigation is conditioned by an increase of the ecological burden on the environment due to the continuous increase of plastic waste, a significant proportion of polypropylene. One solution to this problem is the involvement of recycled polypropylene to obtain plastic products based on composites filled with rice husk. It makes it possible to reduce the prime cost of finished products, regulate their physical and mechanical properties, and reduce the volume of difficult-to-decompose synthetic polymers that end up in waste. The key property of polypropylene, which changes during its filling with rice husk, is moisture absorption, which contributes to a change in the strength characteristics of the polymer composite and accelerates

its aging under the influence of environmental factors. In this regard, this research aims to identify the patterns of the influence of absorbed moisture and natural aging on the physical and mechanical properties of polymer composites based on recycled polypropylene filled with rice husk. The leading approach to the study of this issue is laboratory tests on the saturation of polymer composites with water of different temperatures and duration of exposure and testing materials during long-term natural aging under the influence of environmental factors. The key factor characterizing the change in the physical and mechanical properties of materials, in this case, is the elasticity modulus, elongation, and tensile stress at the break during stretching of the prototypes. The materials of the paper are of practical value for the processing of secondary thermoplastic polymers, as well as the development of biodegradable polymer composites.

Keywords: *recycled polypropylene, rice husk, moisture absorption, natural aging, physical and mechanical properties.*

АННОТАЦИЯ

Актуальность исследуемой проблемы обусловлена увеличением экологической нагрузки на окружающую среду за счет непрерывного роста пластиковых отходов, значительную долю которых составляет полипропилен. Одним из решений этой проблемы является вовлечение вторичного полипропилена в повторную переработку с получением пластмассовых изделий на основе композитов, наполненных рисовой шелухой. Это позволяет снизить себестоимость готовых изделий, регулировать их физико-механические свойства, снизить объем трудно разлагаемого синтетического полимера, попадающего в отходы. Ключевым свойством полипропилена, изменяющимся в процессе его наполнения рисовой шелухой, является поглощение влаги, что способствует изменению прочностных характеристик полимерного композита и ускорению его старения под действием факторов внешней среды. В связи с этим, данная статья направлена на выявление закономерностей влияния поглощенной влаги и естественного старения на физико-механические свойства полимерных композитов на основе вторичного полипропилена, наполненного рисовой шелухой. Ведущим подходом к исследованию данной проблемы являются лабораторные испытания по насыщению полимерных композитов водой с различной температурой и длительностью воздействия, а также проведение испытаний материалов в процессе длительного естественного старения под действием факторов внешней среды. Ключевым фактором, характеризующим изменение физико-механических свойств материалов в этом случае, является модуль упругости, удлинение и прочность при разрыве в процессе растяжения опытных образцов. Материалы статьи представляют практическую ценность для переработки вторичных термопластичных полимеров, а также создания биоразлагаемых полимерных композитов.

Ключевые слова: *вторичный полипропилен, рисовая шелуха, влагопоглощение, естественное старение, физико-механические свойства.*

1. INTRODUCTION:

Polypropylene is the most demanded thermoplastic for various polymeric products: medical materials, bottles, food containers, pipelines, chemical tanks. It is an affordable material that is easy to process and has good physical and mechanical properties. At the same time, out-of-service plastic products made of polypropylene, due to the long time required for their decomposition, cause serious harm to the environment (Asad *et al.*, 2011; Geyer *et al.*, 2017; Poletto, 2017; Herbort *et al.*, 2018; Salikhov *et al.*, 2018; Camargo and Saron, 2020). As a result, an urgent task is to develop plastic waste methods in recycling, including polymer composites based on multicomponent systems (Iwona *et al.*, 2017; Rahimi and García, 2017; Rhodes, 2018).

One of the ways to solve this problem is

to fill polypropylene with components of plant origin, which makes it possible to reduce the cost of the obtained polymer composites, improve the physical and mechanical properties of finished products and reduce the ecological burden by increasing the share of the biodegradable component in the plastic product and reducing the volume of plastic waste (Leja and Lewandowicz, 2010). For these purposes, the use of rice husks as a plant-based filler for recycled polypropylene has become widespread (Bondaletova and Bondaletov, 2013; Reza *et al.*, 2015; Aridi *et al.*, 2016; Chen *et al.*, 2016; Nwosu-Obieogu *et al.*, 2016; Arjmandi *et al.*, 2017; Bazunova *et al.*, 2018; Vasyukova and Bazunova, 2018; Oisik *et al.*, 2019).

One of the disadvantages of polymer composites based on a mixture of synthetic polymers and plant-based fillers is their weak resistance to water absorption (Ismail *et al.*, 2003; Espert *et al.*, 2004; Ares *et al.*, 2010; Yan

et al., 2016; Vaisanen *et al.*, 2017). Moisture absorption degrades the physical and mechanical properties of polymer composites and, consequently, affects the performance characteristics of plastic products. Also, moisture saturation of the plant component in the composition of the synthetic polymer matrix will affect the strength properties of the polymer composite during natural aging under the influence of environmental factors (Fujisawa *et al.*, 2019; Chiang *et al.*, 2020;).

This research aimed to study the effect of absorbed moisture and natural aging on the physical and mechanical properties of polymer composites based on recycled polypropylene filled with rice husk (Rogovina, 2016; Garcia and Robertson, 2017).

The paper indicates that filling hydrophobic secondary polypropylene with rice husk leads to an increase in the hydrophilicity of the polymer composite surface and an increase in the amount of absorbed moisture. Polymer composites achieve a high degree of water saturation in hot water (100 °C) in no more than 30 minutes, while the elasticity modulus and strength at break decrease and the change in these characteristics are determined not by the duration of exposure but by the amount of absorbed moisture (Wang *et al.*, 2020). In the process of natural aging under the influence of environmental factors for composites containing up to 15 parts per hundred rice husk, there is an increase in the elasticity modulus at the break, which decreases for recycled polypropylene filled with 30 parts per hundred of rice husk with a natural aging duration of more than 90 days. A method is proposed for predicting the effect on the strength characteristics of polymer composites based on recycled polypropylene filled with rice husks during long-term natural aging due to short-term (no more than 30 minutes) exposure to hot water (Zheng *et al.*, 2017; Zakharov *et al.*, 2018). This will make it possible to estimate the lower limit of the decrease in the elasticity modulus and tensile stress under the influence of environmental factors (Taynton *et al.*, 2016; Fakhretdinov *et al.*, 2017; Turku *et al.*, 2017; Yang *et al.*, 2017).

2. MATERIALS AND METHODS:

The leading approach to the study of this problem is laboratory tests on the saturation of polymer composites with water of different temperatures and duration of exposure and testing materials in the process of long-term

natural aging under the influence of environmental factors. The key factor characterizing the change in the physical and mechanical properties of materials, in this case, is the elasticity modulus, elongation, and strength at the break during stretching of the prototypes.

It was used recycled polypropylene in the study by crushing substandard plastic products produced in industrial conditions. Rice husks (cellulose 40-45%, lignin 20-25%, hemicellulose 15-17%, mineral substances 18-22%) were used as a plant-based filler, the fraction of which contained particles with a diameter of no more than 0.6 mm. The relation of the mass fraction (pph) of rice husks was calculated per 100 fractions of recycled polypropylene.

Homogenization of the initial components was carried out in a mixing cylinder of a "Plastograph EC" (Brabender) plastograph at a temperature of 180 °C, a screw speed of 30 rpm for 15 min at a load of 200 N. The prototypes for testing were prepared by injection molding using an automatic molding machine "Babyplast" horizontal type with injection volume up to 15 cm³. The dimensions of the test samples correspond to GOST 11262-2017 (Appendix B. Small test samples. Type 5), where the sample length is 80 mm, the width of the test sample is 5 ± 0.2 mm, the thickness of the test sample is 1-4 mm (in this study – 2 mm). The initial weight of the test samples was 1094 ± 0.3 mg. The surface finishing of the samples was not performed. The moisture content of rice husks was determined on a moisture analyzer MOC63u (Shimadzu, Japan) in a standard mode and was 6.8% (GOST 11262-2017..., 2018).

Testing of polymer composites for water absorption was carried out following GOST 4650-2014. Following GOST 4650-2014, two methods were applied. Method 1: the samples were dried for testing in an oven at a temperature of 50 ± 2 °C for at least 24 hours, then cooled to ambient temperature in a desiccator and weighed. Further, the weighing results were recorded in milligrams accurate to the first decimal place. This process is repeated until the mass of the samples is constant, i.e., two consecutive weighings will differ by no more than ± 0.1 mg. The test samples were then placed in a thermostat filled with distilled water at a temperature of 23.0 ± 1.0 °C. After holding in water for 24 ± 1 h, the test samples were removed from the water, the water was removed from the surface of the samples with a clean, dry cloth or filter paper, and within no more than 1

min after removing the samples from the water, they were weighed to the nearest 0.1 mg. Following method 2 pursuant to GOST 4650-2014, the test samples were dried in a drying oven at a temperature of 50.0 ± 2.0 °C for at least 24 hours. Then the samples were cooled to ambient temperature in a desiccator and weighed to the nearest 0.1 mg. This process is repeated until the mass of the samples is constant. Then the test samples were placed in a thermostat with boiling distilled water so that they rest on one edge and were completely immersed in water. (30 ± 2) min later, the test samples are removed from the boiling water and cooled in distilled water to ambient temperature. After cooling the samples for (15 ± 1) min, they are removed from the water one by one. Water is removed from the surface of the samples with a dry cloth, and the samples are immediately weighed to the nearest 0.1 mg (GOST 4650-2014..., 2015).

Mechanical uniaxial tensile tests were performed following GOST 11262-2017 on an AGS-X10kN universal testing machine (Shimadzu, Japan) at a temperature of 23 ± 2 °C and a moving gripper speed of 1 mm/min to determine the elasticity modulus and a speed of 5 mm/min to determine other characteristics (GOST 11262-2017..., 2018).

To analyze the wetting properties of the test samples surface, the contact angle of wetting was determined from the projection of a drop of distilled water applied to the surface of the material. The contact angle of wetting was calculated according to Equation 1:

$$\cos \theta = \frac{(d/2)^2 - h^2}{(d/2)^2 + h^2} \quad (\text{Eq. 1})$$

Where d – water drop diameter; h – drop height.

In order to study the patterns of changes in the physical and mechanical properties of polymer composites under the influence of environmental factors, the prepared samples were subjected to natural aging from September to February (including all months) following GOST 9.708-83 "Unified system of protection against corrosion and aging. Plastics aging test methods under the influence of natural and artificial climatic factors". The essence of the method lies in the fact that the samples are exposed to natural climatic factors (in this study, UV irradiation is at room temperature) for a given

test duration, and the resistance to the specified effect is determined by changing one or several property indicators (in this study, physical and mechanical) (GOST 9.708-83..., 1985).

3. RESULTS AND DISCUSSION:

Filling the hydrophobic polypropylene with rice husk with a hydrophilic surface leads to an improvement in the surface wetting properties of the polymer composite (Table 1), which is confirmed by a corresponding change in the contact angle of wetting. Recycled polypropylene is characterized by low values of the surface hydrophilicity (contact angle of wetting of 72 degrees), which is characteristic of polyolefins. The introduction of a hydrophilic filler consistently increases the surface wettability with water and a rice husk content of 30. the contact angle of wetting is reduced to 54 degrees. An increase in the hydrophilicity of the surface of the polymer composite when it is filled with rice husk will increase the moisture absorption of the plastic product and accelerate the biodegradation of the plant-based component in the polymer matrix under the influence of microorganisms.

Analysis of the data obtained on the effect of moisture on polymer composites during their exposure to hot water at 100 °C indicates that the maximum value of water absorption is achieved when the exposure time of the sample is no more than 30 min (Figure 1).

This is caused by the fact that the kinetic dependencies of the amount of absorbed moisture on holding the sample in hot water have the form of curves that reach a plateau upon water absorption for 30 min. Further exposure to hot water has practically no effect on the increase in the mass of the prototype. With an increase in rice husk content, the polymer composite increase in the degree of water absorption occurs. So, when the sample is kept in hot water for 3 hours, the moisture absorption of the composite containing 2 pph rice husks is 0.9% and increases 6 times with an increase in the degree of filling of polypropylene with plant filler by 15. A lower increase in the amount of absorbed water than an increase in the content of rice husks in the polymer sample indicates that water absorption mainly occurs in the outer layers of composite materials. This determines an insignificant increase in the mass of absorbed water when polymer samples are kept in hot water for more than 30 minutes.

A decrease in the temperature of polymer

composites in water to 23 °C does not fundamentally affect the form of water absorption curves (Figure 2). The moisture content also increases with an increase in the degree of filling of recycled polypropylene with rice husk. Simultaneously, a decrease in temperature leads to a decrease in the rate of saturation of the polymer sample with water. Thus, when immersed in water with a temperature of 23 °C, the composites, on average, only on the second day, reach the same values of the mass content of absorbed water as when the experiment is carried out in the water with a temperature of 100 °C for 30 minutes.

The results obtained indicate that an increase in the time of exposure of polymer samples, even with a decrease in water temperature from 100 °C to 23 °C determines the possibility of increasing the moisture content in the sample. In particular, a sample of recycled polypropylene filled with 30 pph rice husks, when exposed to hot water with a temperature of 100 °C, absorbs 5.7% moisture within 3 hours. A sample of the same composition at 23 °C for 8 days is saturated with 8% water. Moisture saturation of the polymer composite will contribute to a change in its deformation and strength characteristics. As a result, the study of the physical and mechanical properties of materials makes it possible not only to analyze their behavior during operation but also to predict the ability of materials to biodegrade after they are out of service. In this case, the determining factors of the bioavailability of composite materials are the structure of the composites (particularly their density), the hydrophilicity of the surface, and the ability to absorb water.

To simulate the effect of moisture absorption processes on the deformation and strength characteristics of polymer composites, for filled polymer samples exposed to hot water, their physical and mechanical properties were determined. As the studies have indicated, water absorption in hot water significantly affects the deformation and strength characteristics of polymer composites (Table 2).

Filling of recycled polypropylene with rice husk in an amount of 5 pph leads to an increase in the elasticity modulus from 1910 MPa to 1926 MPa. With a further increase in the content of rice husks, a decrease in the elasticity modulus is observed, down to 1489 MPa, when the polymer is filled with rice husks in an amount of 30 pph. Holding the polymer composite in hot water for 30 min leads to a decrease in the elasticity modulus. The minimum decrease in which is at

the level of 1% compared with the sample not exposed to moisture, is achieved for a composite containing 10 pph rice husk. Further increase in the content of rice husks to 15 and 30 pph leads to a decrease in the elasticity modulus by 9 and 36%, respectively, after 30 minutes of moisture absorption in hot water. It should be noted that a further increase of exposure time of the polymer compound to hot water to 60 and 90 min leads to a slight decrease in the elasticity modulus. This is because the change in the physical and mechanical parameters of polymer composites is determined not by the duration of exposure to hot water but by absorbed moisture content.

The tensile stress of recycled polypropylene increases from 25.4 MPa to 25.9 MPa with the addition of 5 pph rice husk. A further increase in the content of the plant-based filler leads to a decrease in the tensile strength, the value of which reaches 14.7 MPa for a composite with 30 pph rice husks. Exposure to hot water for 30 min of the sample with 2 pph rice husk reduces the tensile strength by 2.7%, and for polymer composites with 5 pph and 30 pph this decline is 12% and 36%, respectively. For the elasticity modulus, an increase in exposure to hot water for more than 30 min has practically no effect on the value of the stress at break of the polymer composite. In the process of water absorption by the polymer sample, the elongation at break decreases, while the maximum decrease in this indicator occurs for the sample containing 10 pph rice husks.

The absorption of water by polymer composites filled with plant-based components will affect the physical and mechanical properties of plastic products due to the destruction of the cellulose-containing filler under the action of microorganisms, as well as in the process of exposure to the polymer matrix from the water-saturated areas in the process of multiple freeze-thaw cycles. In order to study the effect of these factors on the physicochemical properties of polymer composites, the prototypes were exposed to the external environment, which makes it possible to take into account the influence of cyclic temperature changes and, to a lesser extent, biodegradation under the action of microorganisms on the water-saturated areas of the samples of recycled polypropylene filled with rice husk.

In the process of natural aging under the influence of environmental factors during the entire test period (up to 180 days) for polymer composites containing up to 15 pph rice husks, there is a higher elasticity modulus compared to

the original sample (Figure 3). The greatest increase in the elasticity modulus occurs when the samples are kept during the first 30 days. Further exposure to the external environment for 90 days and 180 days consistently reduces the elasticity modulus. A significant decrease in the elasticity modulus under the influence of environmental factors occurs for samples containing 30 pph rice husks. When holding such samples for 90 days and 180 days the elasticity modulus decreases to 1050 MPa and 926 MPa, respectively. It should be noted that for composites containing up to 10 pph the elasticity modulus of samples not subjected to natural aging differs slightly from the value achieved after exposure to hot water. Simultaneously, when filling recycled polypropylene with 30 pph rice husks, the elasticity modulus after treatment with hot water decreases to a value reached after natural aging for 180 days.

Long-term polymer composites exposure to environmental factors leads to a decrease in tensile stress (Figure 4). Before exposure to the external environment, the polymer composite has a maximum strength value at 5 pph rice husk content. In the process of natural aging for 30 days, 90 days, and 180 days tensile stress decreases by 8.2%, 13.6%, and 26.5%, respectively, compared to the sample not subjected to aging. It should be noted that, in comparison with natural aging, the effect of hot water on polymer composites containing rice husks of more than 10 pph has a greater effect on the decrease in strength characteristics. In the process of natural aging, a sequential decrease in tensile stress occurs, while the lower limit of this decrease can be modeled in the process of a short-term (no more than 30 minutes) exposure to hot water. Consequently, it is possible to propose a method for predicting the effect on the strength characteristics of polymer composites based on recycled polypropylene filled with rice husks during long-term natural aging due to short-term (no more than 30 minutes) exposure to hot water.

4. CONCLUSIONS:

Thus, filling hydrophobic recycled polypropylene (contact angle of wetting is 72 degrees) with rice husk in the amount of 30 pph allows increasing the hydrophilicity of the polymer composite surface (the contact angle of wetting is reduced to 54 degrees). This determines an increase in the amount of absorbed moisture with an increase in the

degree of filling the recycled polypropylene with rice husks. Highly filled (more than 10 pph) rice husk samples of recycled polypropylene achieve a high degree of moisture absorption in hot water in less than 30 minutes. A decrease in the water temperature from 100 °C to 23 °C reduces the rate of moisture absorption by almost 100 times, while the long-term presence of the sample in water with a temperature of 23 °C determines the possibility of achieving a higher degree of water saturation. Under the influence of hot water on polymer composites, the elasticity modulus and stress at break decrease, while the change in these characteristics is determined not by the duration of exposure but by the amount of absorbed moisture.

In the process of natural aging under the influence of environmental factors for composites containing up to 15 pph rice husks, there is an increase in the rigidity of materials expressed by an increase in the elasticity modulus at the break. A significant decrease in the elasticity modulus occurs for recycled polypropylene filled with 30 pph rice husks, with a natural aging duration of more than 90 days. It should be noted that the rigidity of the polymer composite under the influence of environmental factors for 180 days reaches the same value as when exposed to hot water. In the process of natural aging, a sequential decrease in tensile stress occurs, while the lower limit of this decrease can be modeled in the process of a short-term (no more than 30 minutes) exposure to the material with hot water.

5. ACKNOWLEDGMENTS:

This study was performed in the framework of state assignment FZWU-2020-0027.

6. REFERENCES:

1. Ares, A., Bouza, R., Pardo, S., Abad, M., and Barral, L. (2010). Rheological, Mechanical, and Thermal Behaviour of Wood Polymer Composites Based on Recycled Polypropylene. *Journal of Polymers and the Environment*, 18, 318–325.
2. Aridi, N. A. M., Sapuan, S. M., Zainudin, E. S., and AL-Oqla Faris, M. (2016). Mechanical and morphological properties of injection-molded rice husk polypropylene composites. *International*

- Journal of Polymer Analysis and Characterization*, 21(4), 305-313.
- Arjmandi, R., Hassan, A., and Zakaria, Z. (2017). Rice husk and kenaf fiber reinforced polypropylene biocomposites. In: M. Jawaid, P. Md Tahir, N. Saba (Eds.), *Lignocellulosic Fibre and Biomass-Based Composite Materials: Processing, Properties, and Applications. Woodhead Publishing Series in Composites Science and Engineering*. Cambridge: Woodhead Publishing.
 - Asad, N., Tariq, Y., and Atif, I. (2011). Thermo-oxidative degradation behavior of recycled polypropylene. *Journal of Applied Polymer Science*, 119 (6), 3315-3320.
 - Bazunova, M., Fakhretdinov, R., Galiev, L., Shurshina, A., Sadritdinov, A., Kulish, E., and Zakharov, V. (2018). Influence of biodestruction on the deformation-strength properties of polymer composites based on secondary polypropylene and natural plant components. *Perspective Materials*, 5, 50-59.
 - Bondaletova, L., and Bondaletov, V. (2013). *Polymer composite materials*. Tomsk: Tomsk Polytechnic University Publishing House.
 - Camargo, R. V., and Saron, C. (2020). Mechanical-chemical recycling of low-density polyethylene waste with polypropylene. *Journal of Polymers and the Environment*, 28(3), 794-802.
 - Chen, R. S., Ahmad, S., and Gan, A. (2016). Characterization of rice husk-incorporated recycled thermoplastic blend composites. *BioResources*, 11(4), 8470-8482.
 - Chiang, T., Liu, H., Tsai, L., Jiang, T., Ma, N., and Tsai, F. (2020). Improvement of the mechanical property and thermal stability of polypropylene/recycled rubber composite by chemical modification and physical blending. *Scientific Reports*, 10, 2432.
 - Espert, A., Vilaplana, F., and Karlsson, S. (2004). Comparison of water absorption in natural cellulosic fibres from wood and one-year crops in polypropylene composites and its influence on their mechanical properties. *Composites Part A: Applied Science and Manufacturing*, 35 (11), 1267-1276.
 - Fakhretdinov, R., Galiev, L., Mingazova, A., and Zakharov, V. (2017) Processing of polymer composites based on secondary polypropylene by injection casting. *Constructions from Composite Materials*, 3(147), 14-18.
 - Fujisawa, S., Togawa, E., Kuroda, K., Saito, T., and Isogai, A. (2019). Fabrication of ultrathin nanocellulose shells on tough microparticles: via an emulsion-templated colloidal assembly: towards versatile carrier materials. *Nanoscale*, 11, 15004-9.
 - Garcia, J., and Robertson, M. (2017). The future of plastics recycling chemical advances are increasing the production of polymer waste that can be recycled. *Science*, 358(6365), 870-872.
 - Geyer, R., Jambeck, J., and Law, K. (2017). Production, use, and fate of all plastics ever made. *Science Advances*, 3(7), e1700782.
 - GOST 11262-2017 "Plastics. Tensile test method". (2018). Retrieved from <http://docs.cntd.ru/document/1200158280>
 - GOST 4650-2014 "Plastics. Methods for the determination of water absorption". (2015). Retrieved from <http://docs.cntd.ru/document/1200110854>
 - GOST 9.708-83 "Unified system of corrosion and ageing protection plastics. Ageing test methods on exposure to natural and artificial climatic factors". (1985). Retrieved from <http://docs.cntd.ru/document/gost-9-708-83-eszks>
 - Herbort, A., Sturm, M., Fiedler, S., Abkai, G., and Schuhen, K. (2018). Alkoxy-silyl Induced Agglomeration: A New Approach for the Sustainable Removal of Microplastic from Aquatic Systems. *Journal of Polymers and the Environment*, 26(11), 4258-4270.
 - Ismail, H., Mohamad, Z., and Bakar, A. (2003). A comparative study of processing, mechanical properties, thermo-oxidative aging, water absorption and morphology of rice husk powder and silica fillers in polystyrene = styrene

- butadiene rubber blends. *Polymer-Plastics Technology and Engineering*, 42(1), 81-103.
20. Iwona, M., Tomasz, R., Piotr, M., Olga, S., and Vijay, K. (2017). A study on the thermodynamic changes in the mixture of polypropylene (PP) with varying contents of technological and post-user recyclates for sustainable nanocomposites. *Vacuum*, 146, 641–648.
 21. Leja, K., and Lewandowicz, G. (2010). Polymer biodegradation and biodegradable polymers – a review. *Polish Journal of Environmental Studies*, 19, 255-266.
 22. Nwosu-Obieogu, K., Chiemenem, L., and Adekunle, K. (2016). Utilization of rice husk as reinforcement in plastic composites fabrication – a review. *American Journal of Materials Synthesis and Processing*, 1(3), 32-36.
 23. Oisik, D., Mikael, S. H., Chaitra, P., and Richard, J. T. L. (2019). Nanoindentation and flammability characterisation of five rice husk biomasses for biocomposites applications. *Composites Part A: Applied Science and Manufacturing*, 125, Article number 105566.
 24. Poletto, M. (2017). Mechanical, dynamic mechanical and morphological properties of composites based on recycled polystyrene filled with wood flour wastes. *Maderas. Ciencia y tecnología*, 19(4). Retrieved from https://scielo.conicyt.cl/scielo.php?script=sci_arttext&pid=S0718-221X2017000400433#aff.
 25. Rahimi, A., and García, J. (2017). Chemical recycling of waste plastics for new materials production. *Nature Reviews Chemistry*, 1, 0046.
 26. Reza, A., Azman, H., Khaliq, M., and Zainoha, Z. (2015). Rice husk filled polymer composites: review article. *International Journal of Polymer Science*, 2015, Article number 501471.
 27. Rhodes, C. J. (2018). Plastic pollution and potential solutions. *Science Progress*, 101(3), 207-260.
 28. Rogovina, S. (2016). Polymer Science. *Series C*, 58, 62.
 29. Salikhov, R. B., Bazunova, M. V., Bazunova, A. A., Salikhov, T. R., and Zakharov, V. P. (2018). Study of thermal properties of biodegradable composite materials based on recycled polypropylene. *Letters on Materials*, 8(4), 512-515.
 30. Taynton, P., Ni, H., Zhu, C., Yu, K., Loob, S., Jin, Y., Qi, H., and Zhang, W. (2016). Repairable woven carbon fiber composites with full recyclability enabled by malleable polyimine networks. *Advanced Materials*, 28, 2904–2909.
 31. Turku, I., Keskiisaari, A., Kärki, T., Puurtinen, A., and Marttila, P. (2017). Characterization of wood plastic composites manufactured from recycled plastic blends. *Composite Structures*, 161, 469-476.
 32. Vaisanen, T., Das, O., and Tomppo, L. (2017). A review on new bio-based constituents for natural fiber-polymer composites. *Journal of Cleaner Production*, 149, 582-596.
 33. Vasyukova, A., and Bazunova, M. (2018). Influence of biodestruction on the deformation-strength properties of polymer composites based on secondary polypropylene and natural plant components. In: *Collection of the XVII International Scientific and Practical Student Conference*. Novosibirsk: Publishing Center “Golden Ear”.
 34. Wang, M., Wu, Y., Yang, B., Deng, P., Zhong, Y., Fu, C., Lu, Z., Zhang, P., Wang, J., and Qu, Y. (2020). Comparative study of the effect of rice husk-based powders used as physical conditioners on sludge dewatering. *Scientific Reports*, 10, 17230.
 35. Yan, Y., Herzele, S., Mahendran, A., Edler, M., Griesser, T., Saake, B., Li, J., and Gindl-Altmutter, W. (2016). Microfibrillated lignocellulose enables the suspension-polymerisation of unsaturated polyester resin for novel composite applications. *Polymers*, 8(7), 255.
 36. Yang, N., Zhang, Z., Ma, N., Liu, H., Zhan, X., Li, B., Gao, W., Tsai, F., Jiang, T., Chang, C., Chiang, T., and Shi, D. (2017). Effect of surface modified kaolin on properties of polypropylene grafted

maleic anhydride. *Results in Physics*, 7, 969–974.

37. Zakharov, V., Fakhretdinov, R., Galiev, L., and Mingazova, A. (2018). Influence of moisture on the physical and mechanical properties of wood-polymer composites based on recycled polypropylene. *Plastic Mass*, 5-6, 56-58.

38. Zheng, Y., Gu, F., Ren, Y., Hall, P., and

Miles, N. (2017). Improving Mechanical Properties of Recycled Polypropylene-based Composites Using TAGuchi and ANOVA Techniques. *Procedia CIRP*, 61, 287-292.

Table 1. Contact angle of wetting Θ of polymer composites at 23 °C

Rice husk content, pph	Θ , °C
0	72
2	68
5	63
10	62
15	57
30	54

Table 2. Deformation and strength characteristics of polymer composites after absorption of hot water

Water absorption time, h.	Rice husk content, pph	Elasticity modulus, MPa	Tensile stress at break, MPa	Elongation at break, %
0	2	1910	25.4	12.5
	5	1926	25.9	13.4
	10	1872	22.2	11.7
	15	1788	19.0	7.2
	30	1489	14.7	3.8
0.5	2	1876	23.1	11.2
	5	1907	22.8	10.8
	10	1855	18.9	8.1
	15	1625	14.3	5.9
	30	956	7.7	3.4
1	2	1861	23.0	11.1
	5	1900	22.6	10.7
	10	1847	18.3	8.0
	15	1611	14.0	5.6
	30	952	7.6	3.3
1.5	2	1855	23.1	10.9
	5	1882	22.4	10.4
	10	1827	18.1	7.8
	15	1599	14.1	5.4
	30	952	7.6	3.2

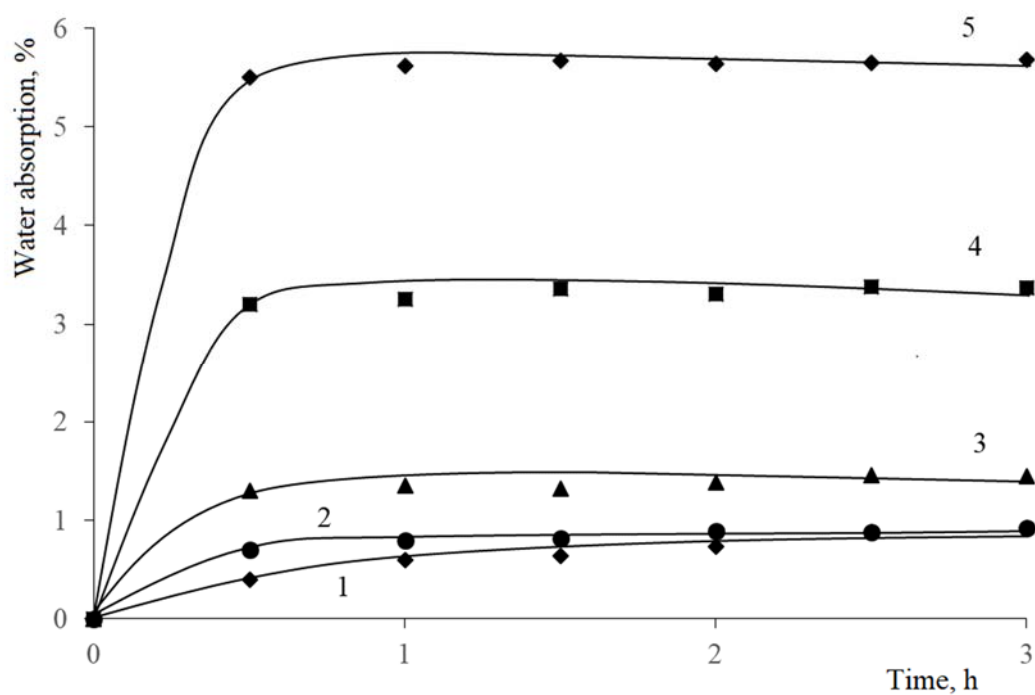


Figure 1. Water absorption of polymer composite samples at a temperature of 100 °C. Rice husk content 2 (1), 5 (2), 10 (3), 15 (4) and 30 (5) parts per hundred.

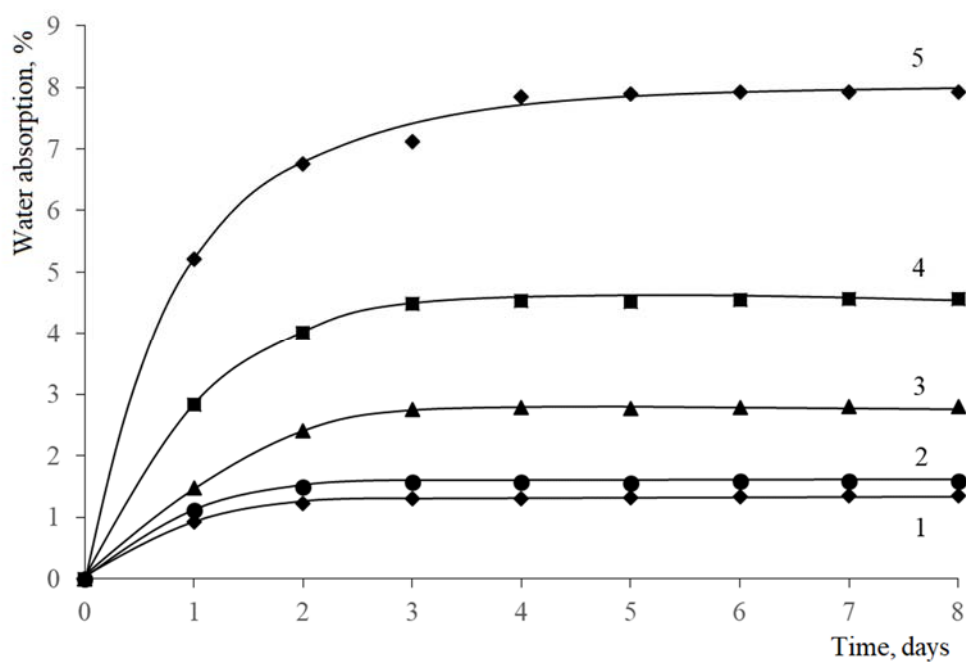


Figure 2. Water absorption of polymer composite samples at a temperature of 23 °C. Rice husk content 2 (1), 5 (2), 10 (3), 15 (4) and 30 (5) parts per hundred.

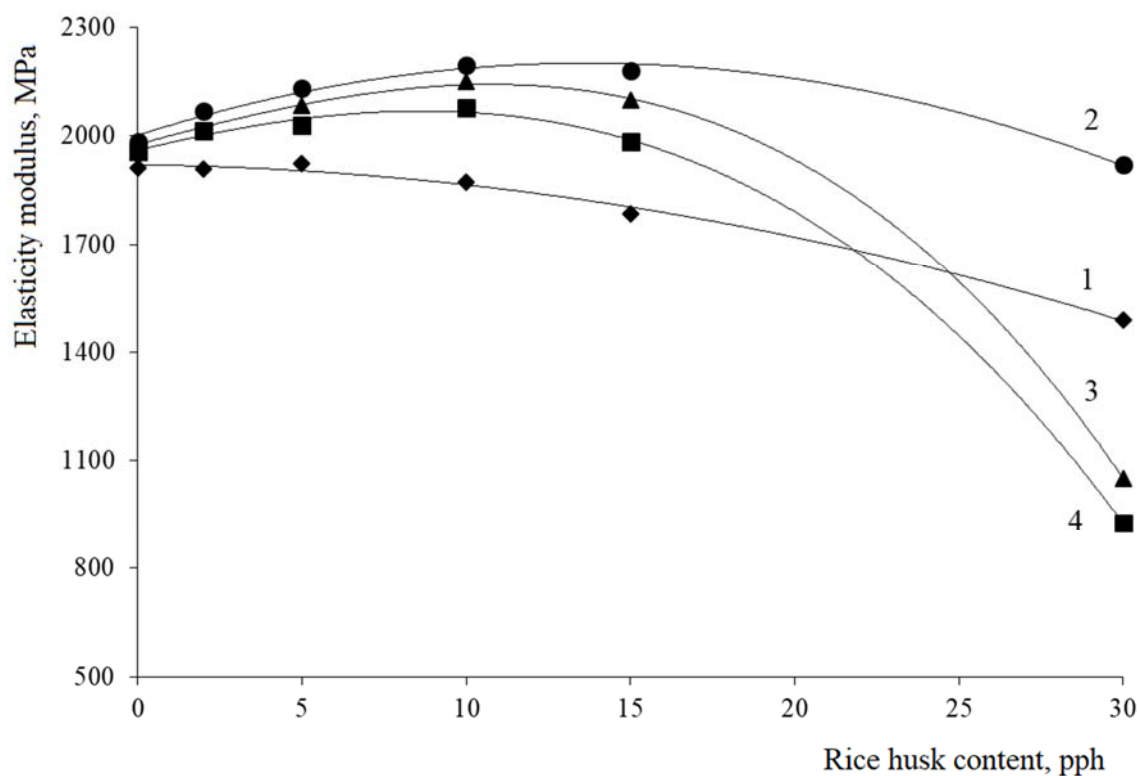


Figure 3. Dependence of the elasticity modulus of polymer composite on the content of rice husks. Original sample (1), natural aging for 30 (2), 90 (3), 180 (4) days.

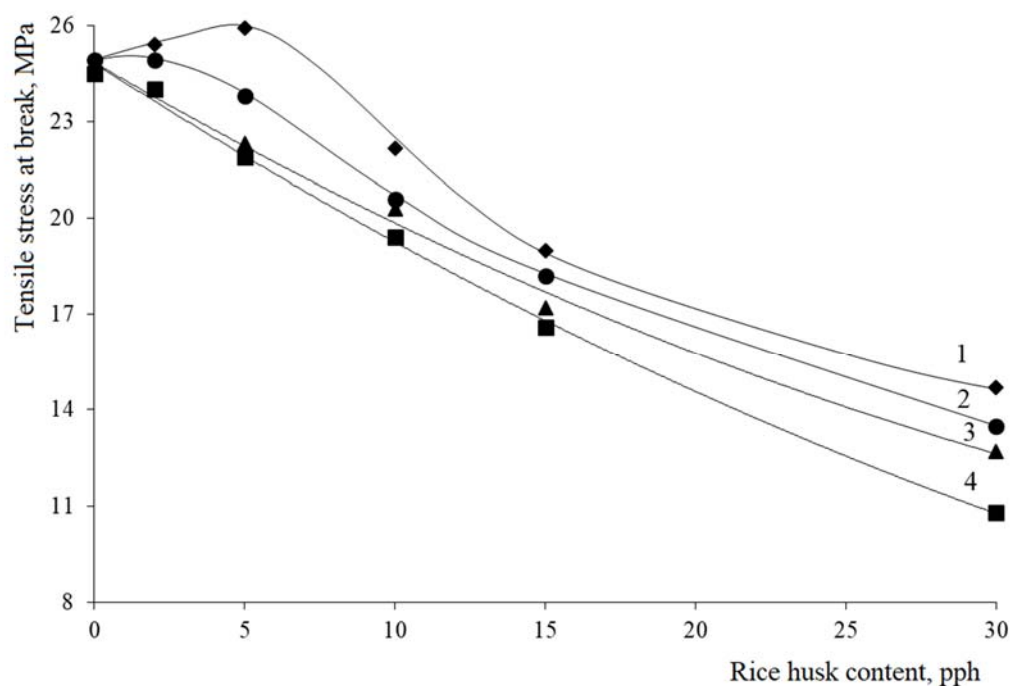


Figure 4. Dependence of tensile stress at break of a polymer composite versus rice husk content. Original sample (1), natural aging for 30 (2), 90 (3), 180 (4) days.

PESQUISA DOS MODOS DE COMBUSTÃO DURANTE A QUEIMA EM GRELHA DE CARVÃO DE SHUBARKOL NA GRELHA DE COMBUSTÃO COM FORNALHA MANUAL DA CALDEIRA DE ÁGUA QUENTE KSVR-0.43**RESEARCH OF COMBUSTION MODES DURING LAYER-BURNING OF SHUBARKUL COAL ON THE FIRE GRATE WITH THE HAND FURNACE OF THE KSVR-0.43 HOT WATER BOILER****ИССЛЕДОВАНИЕ РЕЖИМОВ ГОРЕНИЯ ПРИ СЛОЕВОМ СЖИГАНИИ ШУБАКУЛЬСКОГО УГЛЯ НА КОЛОСНИКОВОЙ РЕШЕТКЕ С РУЧНОЙ ТОПКОЙ ВОДОГРЕЙНОГО КОТЛА КСВР-0.43**

ORUMBAYEV, Rakhimzhan K.¹; KIBARIN, Andrey A.^{1*}; BAKHTIYAR, Balzhan T.¹; KASSIMOV, Arman S.¹; KOROBKOV, Maxim S.¹;

¹ Almaty University of Power Engineering and Telecommunications named after Gumarbek Daukeev, Institute of Heat Power Engineering and Control Systems, Department of Thermal Power Plants, 126/1 Baytursynuli Str., zip code 050013, Almaty – Republic of Kazakhstan

** Corresponding author
e-mail: a.kybaryn@aues.kz*

Received 01 October 2020; received in revised form 28 October 2020; accepted 05 November 2020

RESUMO

Como mostram os números, a tendência de usar combustíveis sólidos no setor de energia do Cazaquistão permanecerá por um longo tempo. Com isto, a tendência mundial passa a ser o endurecimento dos requisitos ambientais, que impõem a tarefa de continuar a melhorar a eficiência da combustão do carvão, de forma a minimizar as emissões de substâncias nocivas e gases com efeito de estufa na atmosfera. O objetivo do artigo é realizar testes complexos de engenharia térmica da caldeira de água quente KSVr-0.43. Para isso, foram utilizados tais instrumentos de medição e controle como dispositivos secundários padrão da sala da caldeira, analisador de gases industrial Testo-350, módulo de controle (leitura) Testo-454 com sondas de temperatura e o tubo de Pitot, medidor de número de fuligem Testo-308, medidor de temperatura 2TPM1, medidor de fluxo líquido Vzlet-PRC portáteis e cronômetro com certificados válidos de verificação e calibração. A análise da composição dos gases, parâmetros técnicos da caldeira de água quente KSVr-0.43 realizada no modo de operação investigado com carvão de Shubarkol durante o teste de longa duração, mostrou que é possível operar caldeiras desta série em modos de baixa carga sem forçar o ar e combustível, permitindo reduzir as emissões de óxidos de NOx tóxicos e gases de efeito estufa CO₂ na atmosfera. Ao mesmo tempo, a combustão do carvão de Shubarkol sem forçar o ar é caracterizada por emissões significativas de monóxido de carbono CO. Os óxidos de nitrogênio NOx formados se decompõem em reações com CO para formar nitrogênio molecular e oxigênio.

Palavras-chave: *combustão, resíduo de coque na camada, etapas da combustão do carvão, emissões de substâncias nocivas.*

ABSTRACT

Experience shows that the trend towards using solid fuels in the energy sector of Kazakhstan will be implemented for a rather long time. At the same time, the global trend is currently tightening environmental requirements. They set the task to continue improving coal combustion efficiency and minimize emissions of harmful substances and greenhouse gases into the atmosphere. This article aims to conduct complex thermal engineering tests of the KCVr-0.43 hot water boiler. For this, the following measurement and control tools were used: the standard boiler room secondary devices, an industrial gas analyzer Testo-350, a control (reading) module Testo-454 with temperature probes and a Pitot tube, a soot number meter Testo-308, a temperature meter 2TPM1, a portable liquid flow meter Vzlet-PRC and a stopwatch. All they had valid verification and calibration certificates. An analysis of the gas composition and technical parameters of the KCVr-0.43 hot water boiler in the investigated operation mode with Shubarkul coal during a long-term test showed that it seems possible to operate boilers of this series under low load conditions without boosting air and fuel. They can reduce emissions of toxic

NO_x and greenhouse gases CO₂ into the atmosphere. In this case, burning Shubarkul coal without forcing through the air is characterized by significant carbon monoxide CO emissions. The formed nitrogen oxides NO_x decompose in reactions with CO with the formation of molecular nitrogen and oxygen.

Keywords: *burning, coke residue in the layer, coal-burning stages, emissions of harmful substances.*

АННОТАЦИЯ

Как показывают цифры, тенденция с использованием твердого топлива в энергетическом секторе Казахстана будет реализовываться еще достаточно долгое время. При этом мировым трендом в настоящее время является ужесточение требований по экологии, которые ставят задачу продолжать совершенствовать эффективность сжигания угля, максимально снижать выбросы вредных веществ и парниковых газов в атмосферу. Целью статьи является проведение комплексных теплотехнических испытаний водогрейного котла КСВр-0.43. Для этого были использованы такие средства измерения и контроля, как штатные вторичные приборы котельной, газоанализатор промышленный Testo-350, управляющий (считывающий) модуль Testo-454 с температурными зондами и трубкой Пито, измеритель сажевого числа Testo-308, измеритель температуры 2ТРМ1, расходомер жидкости портативный Взлет-ПРЦ и секундомер, имеющие действующие сертификаты поверки и калибровки. Выполненный анализ по составу газов, техническим параметрам водогрейного котла КСВр-0.43 в исследованном режиме работы на Шубаркульском угле при длительном испытании показал, что представляется возможным эксплуатировать котлы этой серии в режимах малых нагрузок без форсировки по воздуху и топливу, позволяющих снизить выбросы токсичных окислов NO_x и парниковых газов CO₂ в атмосферу. При этом сжигание каменного Шубаркульского угля без форсировки по воздуху характеризуются значительными выбросами окиси углерода CO, и образовавшиеся окислы азота NO_x разлагаются в реакциях с CO с образованием молекулярного азота и кислорода.

Ключевые слова: *сжигание, коксовый остаток в слое, стадии горения каменного угля, выбросы вредных веществ.*

1. INTRODUCTION:

1.1. Problem statement

The current state of affairs shows that the use of solid fuels in the energy sector of Kazakhstan will be implemented for a rather long time (Decree of the Government..., 2014). Simultaneously, the global trend is currently tightening environmental requirements, which set the task to continue to improve the efficiency of coal-burning and minimize emissions of harmful substances and greenhouse gases into the atmosphere (Liu *et al.*, 2017a; Chen *et al.*, 2020). Therefore, at the Department of Thermal Power Plants of the Non-profit joint-stock Company "Almaty University of Energy and Communications named after Gumarbek Daukeev", research is actively ongoing to develop new designs of hot water and steam boilers, mechanical furnace and burner devices with high efficiency, to reduce both specific fuel consumption and harmful emissions. For small and medium-sized coal-fired boiler houses, bed burning is typical (Kang and Ding, 2020; Maznoy *et al.*, 2020). According to estimates, for a layered combustion process, there are significant opportunities to intensify the combustion of solid fuels (Ermakov, 2005; Kamenetsky, 2010). In this case, the intensity of combustion on the surface of coal particles in the

flare process approaches its limit physically (Braconnier *et al.*, 2020). Layer burning of coal allows maximum retention and capture of solid coarse and fine fractions of slag and ash particles within the boiler on a grate (Ermakov, 2005; Kamenetskii, 2006; Kamenetskii, 2013a; Bao *et al.*, 2020).

Another aspect is that many boiler houses with low-power hot water boilers are located near residential buildings. Their chimneys rarely exceed 15-20 m and are low sources of toxic emissions and greenhouse gases. The total number of hot-water and heating domestic solid fuel boilers operating in the territory of Kazakhstan is tens of thousands (Fuel and energy..., 2018). Such sources of harmful emissions must have more stringent requirements for the content of harmful substances released into the atmosphere (Zhang *et al.*, 2017; Liu *et al.*, 2017b; Kornilova and Trubaev, 2018). However, coal prismatic and cylindrical coal-fired boilers with heat pipes widespread in Kazakhstan have an efficiency of not higher than 55-65%. Often, the water volume in a cylindrical boiler is several times greater than in a water tube boiler of the same capacity. The presence of a large volume of water in the boiler (especially in emergencies with frequent interruptions in the supply of energy and the cessation of water circulation with unauthorized

coal burning in a furnace with a large layer of coal) can trigger vaporization processes in the boiler and an accident (Volynkina and Pryanichnikov, 2002; Bochkarev *et al.*, 2011).

Conventional traditional water-tube boilers of a classical profile in active heat transfer used only up to 84% of the pipe surface (except for cylindrical) (Zhang *et al.*, 2018; Van Kenhove *et al.*, 2019). Therefore, a new series of solid fuel hot water tube boilers were developed with the minimum possible volume of water in the boiler and with the maximum (up to 96%) use of the pipe surface in active heat transfer (Alekseenko *et al.*, 2019). When creating a new hot water boiler (Orumbaev and Airich, 2007), the authors solved the problem of ensuring reliable operation at water pressures corresponding to the operation of hot water boilers, both according to the open hot water supply scheme (when the water pressure decreased to values close to the boiling temperature) and the closed-circuit (Rajić *et al.*, 2018). The connection order of the screens in the new boiler allows you to work effectively in operating conditions both in the optimal mode (with a nominal water flow rate) and to reduce the heat load by up to 20% with minimum water pressure and stable operation (Labidi *et al.*, 2017).

This article aims to conduct complex thermal engineering tests of the KCVr-0.43 hot water boiler (Almaty, Republic of Kazakhstan).

1.2. Theoretical overview

Analysis of the results of tests performed in earlier works (Glazyrin *et al.*, 2010; Kamenetskii, 2013b) with small coal-fired boilers during layer-by-layer combustion showed a large unevenness in the content of CO₂ in the exhaust gases and the emission of nitrogen oxides NO_x. Measurements made at the time of the release and combustion of volatile components from coals with the content of a volatile component of V_{vol} = 35-37% showed that the concentration of NO_x in the exhaust gases behind the boiler with a fire grate and with manual maintenance is a maximum of 250-350 mg/m³, and the oxide carbon CO 15000-40000 mg/m³ (Kamenetskii, 2013c; Widziński *et al.*, 2019). In experiments with fuel boosting at a fire grate thermal stress of 300 kW/m², with coal burning in a layer, the maximum value of carbon monoxide emissions is 2.3%, at 454 kW/m² 3%, and at 715 kW/m², the maximum value of carbon monoxide is already 6.0%. The average values for a burning cycle of 10 minutes between casts, according to the test procedure, are 0.5%, 0.8%, and 1.3% with air excess factors of 1.32-1.44, respectively (Kamenetskii, 2006; Babenko *et al.*, 2017;

Jasinskas *et al.*, 2020).

Change in layer forcing (increase in air supply under the grates) in experiments (Kamenetskii, 2006; Kamenetskii, 2013b) showed that the nature of the gas composition curves does not change, but the length of successive burnout zones of coal is reduced. This is illustrated clearly in Figures 1a and 1b, which qualitatively and quantitatively illustrate the nature of Donetsk coal burning with a layer forced through the air from 875 m³/m²×h to 2430 m³/m²×h. This corresponds to the average airflow velocity $w_0 = 0.23$ m/s and $w_0 = 0.68$ m/s and the average thermal intensity of the furnace $q_{\text{furn}} = 0.76 \times 10^6$ kcal/m²×h and $q_{\text{furn}} = 2.2 \times 10^6$ kcal/m²×h, respectively. From the experimental data presented in (Ermakov, 2005; Kamenetskii, 2006; Kamenetskii, 2013a), an increase in air supply by 2.77 times increases the thermal stress of the layered furnace by 2.89 times. Simultaneously, the duration of CO formation is reduced by 2.66 times, and the absolute values of CO formation are reduced from 8% to 5%.

The experimental work by G.F. Knorre (1951) with a two- and three-row thin layer of spherical particles of solid fuel showed that after heating the layer and transition the layering process to the high-temperature coke burning mode, even such a thin layer is enough to consume all of the oxygen from the air passing upward through the thin layer of fuel (Barkan and Kornev, 2017; Król and Poskrobko, 2017; Nakamura *et al.*, 2019). Therefore, in the known and used in practice range of increasing airflow under a thin layer of burning coke (during forced combustion), chemical reactions in the high-temperature coke burning zone proceed at a much higher rate than oxygen supply, and the process proceeds in the diffusion region (Surawski *et al.*, 2020; Hampp and Lindstedt, 2020). At high temperatures developed in the layer, the reactions of reduction of CO₂ and H₂O on the heated surface of solid carbon begin to distill and displace the oxidation of solid carbon (Saha *et al.*, 2020).

2. MATERIALS AND METHODS:

In a boiler house preliminarily prepared for thermotechnical tests (Figure 2) with a KCVr-0.43 hot water solid fuel boiler with a fire grate area of 0.98 m² and a furnace volume of V_{furn} = 1.66 m³, the horizontal part of the flue behind the boiler was located in the boiler room. The boiler operates on such fuel as brown coal, hard coal. KSVR-0.43 (according to Figure 3) is structurally a solid-fuel hot-water boiler with a horizontal layout with a

layer furnace. The boiler consists of parallel pipes connected to collectors having partitions, external, ceiling and front screens, assembled in a furnace screen with the first and second collectors, a layer grid, herewith the water supply pipe is connected to the collector of the ceiling screen, and the front screen has a step collector connected through a rack to the bypass pipe connected to the first collector of the furnace screen, forming a loading opening for supplying solid fuel to the boiler. The ascending part of the flue behind the boiler is made with a three-fold increase in cross-section for collecting ash. In front of the chimney, a smoke exhaust was installed in parallel with a bypass to the main gas flue duct to ensure the reliable operation of the boiler and in natural draft mode (Nguyen and Sirignano, 2018). A chimney with a 325 mm diameter and a height of 12 m, preheated by the operation of the boiler in the nominal mode without a smoke exhaust, provided a vacuum of up to 100-150 Pa.

Complex thermotechnical tests were carried out, which consisted of a set of technical measures: instrumental gas analysis of the composition of exhaust gases in the furnace and in the boiler flue (by means of a portable industrial gas analyzer based on an electrochemical method for determining the concentrations of gas mixture components); instrument analysis of the heat transfer agent flow rate and assessment of the heat flow with standard and portable measuring devices (ultrasonic method using a portable ultrasonic flow meter with temperature sensors and using standard thermometers); technical analysis of the composition of coal fuel and furnace refuse (with sampling and analysis in a chemical laboratory using a calorimetric bomb). Complex thermotechnical tests of the KCVr-0.43 hot water boiler were carried out in an operating coal-fired boiler house and following the procedures (Kamenetskii, 2009; Kamenetskii, 2013c; Domestic heating..., 2016), with the authors repeatedly used in tests of other boiler units with tested measuring instruments. In particular, the following measurement and control tools were used: standard secondary equipment of the boiler room, industrial gas analyzer Testo-350, control (reading) module Testo-454 with temperature probes, and Pitot tube, soot number meter Testo-308, temperature meter 2TPM1, portable liquid flow meter Vzlet-PRC and stopwatch. All of them had valid verification and calibration certificates (Ruan *et al.*, 2020).

Technical characteristics of the presented batch of Shubarkul coal used in thermal engineering tests in an existing boiler house

(according to the data from the supplied fuel passport) were as follows: fuel carbon content of as-received basis $C_{\text{cont}} = (49.56 \div 51.81)\%$; total moisture of as-received basis $M_{\text{cont}} = (19.4 \div 19.7)\%$; ash content of as-received basis $A_{\text{cont}} = (13.6 \div 14.19)\%$; $V_{\text{furn}} = 44\%$; net calorific value of fuel $Q_{\text{ncv}} = (18.43 \div 23.11)$ MJ/kg or $(4409.8 \div 5530)$ kcal/kg; $N = (0.45 \div 0.51)\%$; fuel sulfur content of as-received basis $S_{\text{cont}} = 0.42\%$.

The first series of above mentioned measurements were carried out on 30.01.2020 in two modes. In the first mode – during the period after casting a portion of Shubarkul coal in the burning layer and when a stable combustion mode was reached, at a boiler heat power $N_{\text{bhp}} = 230$ kW and a thermal stress of the combustion mirror (firebed surface heat release rate) $q_{\text{fbs}} = 309.3$ kW/m². In the second mode – during the period after the complete separation and burning out of volatile components of Shubarkul coal with stable combustion of coke. The heat power N_{bhp} of the KCVr-0.43 boiler was 136 kW, with the thermal stress of the combustion mirror q_{fbs} was 204 kW/m².

The second series of heat engineering tests were carried out on 02.20.2020 on the same KCVr-0.43 boiler without cleaning the convective heating surfaces. The thermal performance of the boiler in the first mode with the start of loading a new portion of coal reached $N = 248$ kW with a thermal stress $q_{\text{fbsl}} = 328$ kW/m², and in the second mode, after reaching a stable coke burning mode, the thermal performance was $N = 226$ kW with thermal stress of the combustion mirror in layer $q_{\text{fbs}} = 283$ kW/m². The conditions for the release of the heat-transfer agent as far as possible the operation of the existing boiler room remained the same. According to standard devices, the water temperature at the boiler inlet is $t_1 = 35\text{--}39^\circ\text{C}$, the water temperature at the boiler outlet was in the first experiment $t_1 = 50\text{--}54^\circ\text{C}$ and $\Delta t = 15^\circ\text{C}$, the average constant water flow through the boiler $G = 2.17$ kg/s.

3. RESULTS AND DISCUSSION:

The results of the heat engineering tests (Table 1) in the first mode and in the second mode on coal from Shubarkul coalfield on a boiler with a manual layer grate made it possible to estimate emissions by the content of O_2 , CO , SO_2 , NO , NO_2 , NO_x , CO_2 in real operating conditions. Table 1 presents the measurement results for the periods 30.01.2020 and 02.20.2020. Each row displays the average values of the quantities in each experiment, divided by time. It should be

noted that the oxygen O_2 content is somewhat overestimated. Suction cups partially explain this through the loading door since it had to be ajar during measurements directly above the burning coal layer.

In the first part, the average values of the results of gas composition measurements in the furnace, at the height of 250-350 mm above the layer, and the boiler gas duct after 5-10 minutes from the moment of casting a portion of coal are given. For this regime, SO_2 and NO_2 , characteristic of the active phase of fuel combustion, are noted. In this case, the NO_x values reach their maximum values (up to 631.05 mg/m³), and the CO content decreases (up to 1982.83 mg/m³). The second part shows the average values of the results of the gas composition measurements during prolonged burning of the coke residue of coal with measurements at the height of 200-350 mm above a thin low-temperature layer of the grate. The second regime is characterized by the absence of SO_2 and NO_2 in the composition. The absence of NO_2 and the minimum values of NO_x (up to 48.07 mg/m³) are explained by the active, reducing medium with a high content of CO (up to 32739.45 mg/m³).

In the course of the experiment, the dependence of an increase in SO_2 , NO, NO_x , and exhaust gas temperature T_{eg} was observed as the distance from the front increased by 300 mm, 600 mm, and 1200 mm to the back wall of the furnace at the height of 200-210 mm above the layer of dying coke residue (uneven air intake with natural traction and the influence of cold air entering through front leaks). The total duration of the gas composition measurements continued in the active phase of combustion of about 40 minutes, and in the phase of the stabilized process of burning out of coke residue about 3-4 hours.

For the obtained data, calculation Tables 1-2 were compiled, and values were approximated with a confidence value of $R^2 = 0.63...0.91$. The lowest value was obtained for the curve of measurement values in the composition of O_2 , due to the technical impossibility of eliminating the suction of outside air into the furnace. Also, to preserve the properties of piecewise continuity, monotony, and limitation, values due to "misses" and a gross error in measurements were excluded. For data analysis, the most indicative time sections were taken from the data set of two test series 01/30/2020 and 02/20/2020. For each series, the average values and the obtained characteristic experimental data are presented in Table 2. Data analysis showed a clear separation of combustion modes. The first mode

characterizes the active phase of coal combustion with forced air supply. The beginning of the second mode occurs after the volatile components completely burn out, reduce the air supply by the blower fan and turn off the smoke exhaust, i.e., the transition to stable combustion of coke residue with a natural draft and without blowing.

Figure 4 shows the burn-up quality of Shubarkul coal with the smoke exhauster turned off and the airflow supplied by natural draft at a speed of up to 0.075 m/s under a thin layer of coal. The marked curves on the graph were obtained by approximation and smoothing by a polynomial (in this case, the approximation confidence value was $R^2 \geq 0.63$). Comparison with Figures 1a and 1b at an airflow velocity of $w_0 = 0.23$ m/s and $w_0 = 0.68$ m/s and an average thermal stress of the furnace $q_{furn} = 882$ kW/m² and $q_{furn} = 2552$ kW/m², respectively, shows that in Figure 4 with thermal stress of up to $q_{furn} = 193$ kW/m², the graph of coal burnout in a thin layer is more extended in time relative to Figures 1a and 1b, while the harmful emissions of NO_x and CO_2 are significantly reduced. As can be seen from Table 2 and Figure 4, immediately after loading coal onto the grid and heating a fresh portion of solid fuel, the output of volatile components and its active burning increases the thermal stress of the combustion mirror and the thermal stress of the boiler furnace volume. Similarly, the level of NO_x emissions varies depending on the operating mode of the manual layered furnace and depending on the loading time of fresh coal (Figure 5).

An increase in the temperature of the torch over a thin layer of coal in the furnace affects the increase in water temperature at the outlet of the boiler on visually fixed secondary devices. During this period, the maximum NO_x emission is observed and reaches 10-15 minutes after casting up to 630 mg/m³, while the growth of CO_2 output begins and is about 7-8%, and the CO emission is about 1840-3680 mg/m³ (Figure 6). After thirty minutes of burning coal in the layer after casting (the blower fan supply was reduced to a minimum, followed by switching off, and the smoke exhauster was turned off), NO_x emissions begin to decrease by more than a quarter from the maximum to 400-300 mg/m³, the percentage of CO_2 is reduced to 4%, CO content increases by order of magnitude to 5000 mg/m³. In the next twenty minutes after stabilizing the coke combustion processes without forced air supply and in natural draft mode, the oxides NO_x and CO_2 continue to decrease, the SO_2 content in the gases decreases to zero the percentage of CO rapidly increases.

An hour and a half after loading, the maximum burning of volatile components and the beginning of stable combustion of coke of Shubarkul coal with a continuing natural decrease in the layer thickness in the natural draft mode, NO_x emissions decrease to 232 mg/m^3 , CO_2 content to 2.1%, CO content increases to the level of 23000 mg/m^3 . Further, the combustion process completely switches to the second mode (burning a thin coke layer). Stable indicators note this after 90 minutes of the experiment and 7-8 hours after casting coal. In this mode, the minimum values of $\text{NO}_x = 48.07 \text{ mg/m}^3$ are noted, while the values of the carbon monoxide CO content in the gases are maintained at the level of $25000\text{-}27000 \text{ mg/m}^3$. The intense onset of the burning of volatile components does not immediately warm up the entire fresh portion of coal above the layer after it is loaded. However, this ensures a high-temperature level in the furnace volume (Figure 7).

The staged combustion (characteristic of the works by Knorre (1951)) was obtained (Figure 1). However, this test process took significantly less time (Figure 8) due to several factors. First of all, forcing combustion through the air with a maximum flow of the blower fan ensured a powerful uniform flow with high speed. This intensified the process of active heating and combustion of fuel as much as possible, with the maximum yield of volatile components. Secondly, the process took the shortest possible time due to the layer thinness and the lack of fuel boost (the experiment was conducted for one portion of coal).

According to the data presented, it is clear that the oxygen zone is quite short, and the reduction reaction with the repeated formation of CO ($\text{CO}_2 + \text{C} = 2\text{CO}$) occurs quickly and stretches over a long period, stabilizing after 90 minutes of the experiment. In the active stage of combustion, the reaction oxygen content above the layer is already insufficient due to its consumption in the lower coke layer. Therefore, the nitrogen of the "late" volatile components during coke combustion does not have time to react due to the carbon surface reduction reaction. Therefore, short-term maximum emissions of nitrogen oxides from 555 mg/m^3 to 760 mg/m^3 after casting a fresh portion of the fuel remain at the level of (limiting) average values of nitrogen oxide emissions with the flare method of burning coals. However, after completing the active phase of combustion and the maximum yield of volatile components upon completion of forcing, the coke combustion process stabilizes but is characterized by unevenness in the layer area. Due to the impossibility of a uniform air supply, separate

active combustion zones arise under the layer, where there is enough air for the process, and "smoldering" zones in places where there is either insufficient air or the temperature is already shifted from the optimal reaction zone.

In (Kamenetskii, 2006; Babenko *et al.*, 2017) studies of the formation of nitrogen oxides when burning coal in briquettes, nitrogen oxide emissions are reduced by six times. In this work, according to the experimental results shown in Tables 1 and 2 and in Figure 5, values of NO_x emissions of the order of $150\text{-}48 \text{ mg/m}^3$ are achieved, and in the active phase after complete burn-up, volatile components emissions were of the order of 300 mg/m^3 . However, the obtained coke combustion regime without blowing and at a natural draft should be further optimized. So, with natural traction and without forcing through the air, the unevenness of the process increases over time. After a long period (7-8 hours) without casting a new portion of coal and forcing combustion, the furnace cools down, the intensity of combustion reactions decreases, and insufficient burning increases. Therefore, the process in this stage should be further optimized. This question is the goal of further studies of coal combustion regime in the bed in boilers with a manual furnace. In the future, it is planned to carry out new heat engineering tests to clarify and confirm the following conclusions:

1. Reducing the supply of blow air to a minimum under the fire grate with a thin layer of coal, and the results of experiments should show that the nature of the curves O_2 , CO, CH_4 , CO_2 , and NO_x does not change qualitatively. However, at the same time, their duration increases significantly, along with the burnout zone of the coke residue of Shubarkul coal.

2. When burning Shubarkul coal in layered furnaces with manual maintenance, keep a small thickness of the layer recommended for working with long-flame coals of not more than 100 mm and optimize the forcing process by air.

3. To eliminate the dip and entrainment of coal fractions less than $8\text{-}10 \text{ mm}$, the coal fines should be sieved since this size corresponds to that of the groove on all grates (conventional in the practice of burning in the bed) in furnaces with manual maintenance.

4. CONCLUSIONS:

The results obtained in the form of practical data on the operation modes of a hot water boiler allowed authors to achieve the research goal and

show the constructive need for organizing a stable combustion process with air supply (primary and secondary) by forcing the air supply or changing the design of the grate (in tests in a hot-water boiler, the cross-section of the grate was 20% of the total surface area of the grate). According to the data obtained, the possibility of implementation and separation into two stages of the combustion process (to efficiently burn solid fuel in a thin layer on a fixed fire grate) has been experimentally shown, and the operation of a hot water boiler with manual maintenance has been confirmed by the example of long-term burning of Shubarkul coal. The obtained work experience makes it possible to conditionally divide the first stage of coal heating, emission, and active combustion of volatile components with a further variation in the supply of secondary air to scarce combustion zones by the oxidizing agent.

An analysis of the gas composition and technical parameters of the KCVr-0.43 boiler in the investigated operation mode at Shubarkul coal during a long-term test showed that it seems possible to operate the boilers of this series under low load conditions without forcing through air and fuel. This can reduce emissions of toxic NO_x and greenhouse gases CO_2 into the atmosphere. Moreover, burning of Shubarkul coal without forcing through the air is characterized by significant emissions of carbon monoxide CO , and the formed nitrogen oxides NO_x decompose in reactions with CO with the formation of molecular nitrogen and oxygen.

5. ACKNOWLEDGMENTS:

This research is funded by the Science Committee of the Ministry of Education and Science of the Republic of Kazakhstan (Grant No. AP05133388).

6. REFERENCES:

1. Alekseenko, S. V., Kuznetsov, V. A., Maltsev, L. I., Dekterev, A. A., and Chernetskii, M. Y. (2019). Analysis of combustion of coal-water fuel in low-power hot-water boiler via numerical modeling and experiments. *Journal of Engineering Thermophysics*, 28(2), 177-189.
2. Babenko, G. S., Zakharov, G. A., Sopova, V., and Tsygankova, K. V. (2017). Grate firing of low-grade coal having high moisture content in mechanised furnaces of low power hot-water boilers. *FEFU: School of Engineering Bulletin*, 4(33), 44-55. DOI: 10.5281/zenodo.1119159.
3. Bao, J., Wang, D., Liu, F., Qu, Z., and Xu, H. (2020). Transient evaporation simulation of the forced circulation hot water boiler. *IOP Conference Series: Materials Science and Engineering*, 721(1), article number 012068.
4. Barkan, M. S., and Kornev, A. V. (2017). Prospects for the use of associated gas of oil development as energy product. *International Journal of Energy Economics and Policy*, 7(2), 374-383.
5. Bochkarev, V. A., Frolov, A. G., and Morozov, K. A. (2011). Improving the burning efficiency of azeisky in the boiler KB-TCB-20. *Bulletin of National Research Irkutsk State Technical University*, 8(56), 186-192.
6. Braconnier, A., Gallier, S., Halter, F., and Chauveau, Ch. (2020). Aluminum combustion in CO_2 - CO - N_2 mixtures. *Proceedings of the Combustion Institute*. Retrieved from: <https://www.sciencedirect.com/science/article/abs/pii/S1540748920300547>.
7. Chen, L., Wang, W., Kong, Y., Yang, L., and Du, X. (2020). Hot air extraction to improve aerodynamic and heat transfer performances of natural draft dry cooling system. *International Journal of Heat and Mass Transfer*, 163, article number 120476.
8. Decree of the Government of the Republic of Kazakhstan No. 724 "On approval of the Concept of development of the fuel and energy complex of the Republic of Kazakhstan until 2030". (2014). Retrieved from: <http://adilet.zan.kz/rus/docs/P1400000724#z45>.
9. Domestic heating boilers fired by solid fuel nominal heat output up to 50 kW. Requirements and test methods. (2016). Retrieved from: <http://docs.cntd.ru/document/1200121803>.
10. Ermakov, M. V. (2005). *Justification of priority areas for improving heat sources of small capacity with layered burning of brown coal*: thesis of the candidate of technical sciences. Irkutsk, Russian Federation: Institute of Energy Systems named after L.A. Melentyev SB RAS.
11. Fuel and energy consumption in households in the Republic of Kazakhstan. (2018). Retrieved from: <https://stat.gov.kz/>.
12. Glazyrin, V. A., Nenichev, A. S., and Orumbaev, R. K. (2010). Comparative

- analysis of coal burning in boilers of a new modification. *News of higher educational institutions of the Black Earth Region. Metallurgy*, 1(19), 67-71.
13. Hampp, F., and Lindstedt, R. P. (2020). Quantification of fuel chemistry effects on burning modes in turbulent premixed flames. *Combustion and Flame*, 218, 134-149.
 14. Jasinskas, A., Domeika, R., Jotautiene, E., Masek, J., and Streikus, D. (2020). Investigation of reed and bulrush preparation and usage for energy purposes and determination of biofuel properties and harmful substance emissions. *Engineering for Rural Development*, 19, 1953-1958.
 15. Kamenetskii, B. Ya. (2006). Optimization of the air regime of stoker furnaces. *Thermal Engineering*, 53, 473-475. DOI: 10.1134/S0040601506060140.
 16. Kamenetskii, B. Ya. (2009). Stages through which polyfractional fuel burns in a bed. *Thermal Engineering*, 56, 469-472. DOI: 10.1134/S0040601509060044.
 17. Kamenetskii, B. Ya. (2013a). Burning rate of solid fuel in the layer. *Thermal Processes in Engineering*, 5(8), 339-342.
 18. Kamenetskii, B. Ya. (2013b). Engineering calculation of heat transfer in layer furnaces. *Thermal Processes in Engineering*, 5(2), 76-79.
 19. Kamenetskii, B. Ya. (2013c). Radiation heat transfer in layer furnaces. *Industrial Energy*, 10, 31-34.
 20. Kamenetsky, B. Ya. (2010). Features of heat transfer in layered furnaces. *Industrial Heat Power Engineering*, 7, 14-18.
 21. Kang, Zh., and Ding, X. (2020). Numerical analysis on combustion process and sodium transformation behavior in a 660 MW supercritical face-fired boiler purely burning high sodium content Zhundong coal. *Journal of the Energy Institute*, 93(2), 450-562.
 22. Knorre, G. F. (1951) *Furnace processes*. Moscow; Leningrad, Russian Federation: State Energy Publishing House.
 23. Kornilova, N. V., and Trubaev, P. A. (2018). Analysis of MSW combustion temperature in a hot water boiler with the low-capacity. *Journal of Physics: Conference Series*, 1066(1), article number 012003.
 24. Król, D., and Poskrobko, S. (2017). Combusting fuel formed from waste. reduction in emission of chromium, nickel and lead. *Environment Protection Engineering*, 43(1), 101-112.
 25. Labidi, M., Eynard, J., Faugeroux, O., and Grieu, S. (2017). A new strategy based on power demand forecasting to the management of multi-energy district boilers equipped with hot water tanks. *Applied Thermal Engineering*, 113, 1366-1380.
 26. Liu, X., Yang, D., Lu, J., Guan, J., and Qi, G. (2017a). Combustion characteristics and design of hot water boiler. *IOP Conference Series: Earth and Environmental Science*, 59(1), article number 012069.
 27. Liu, Z., Li, N., Zhou, Q., and Liu, T. (2017b). Study on the effects of external stress on hot corrosion behavior of steel T91 in the oxidizing atmosphere containing SO₂. *American Society of Mechanical Engineers, Power Division (Publication) POWER*, 1, article number 130327.
 28. Maznoy, A., Pichugin, N., Yakovlev, I., Fursenko, R., and Petrov, D. (2020). Fuel interchangeability for lean premixed combustion in cylindrical radiant burner operated in the internal combustion mode. *Applied Thermal Engineering*, article number 115997. Retrieved from: <https://www.sciencedirect.com/science/article/pii/S1359431120334797>.
 29. Nakamura, Yu., Yoshitome, H., Yamazaki, T., Matsuoka, T., and Gao, J. (2019). Combustion of activated carbon particles part 1: Experimental investigation of the two distinctive burning modes in a packed bed. *Energy Procedia*, 158, 2152-2157.
 30. Nguyen, T. M., and Sirignano, W. A. (2018). The impacts of three flamelet burning regimes in nonlinear combustion dynamics. *Combustion and Flame*, 195, article number 170-182.
 31. Orumbaev, R. K., and Airich, Yu. E. (2007). Patent for the invention of the Republic of Kazakhstan No. 18797. Hot water boiler. publ. bull. No 9.
 32. Rajić, M. N., Banić, M. S., Živković, D. S., Tomić, M. M., and Mančić, M. V. (2018). Construction optimization of hot water fire-tube boiler using thermomechanical finite element analysis. *Thermal Science*, 22, S1511-S1523.
 33. Ruan, J. L., Domingo, P., and Ribert, G. (2020). Analysis of combustion modes in a

cavity based scramjet. *Combustion and Flame*, 215, 238-251.

34. Saha, M., Gitto, G., and Dally, B. B. (2020). Burning characteristics of grape marc under mild combustion conditions. *Experimental Thermal and Fluid Science*, 114, article number 110059.
35. Surawski, N. C., Macdonald, L. M., Baldock, J. A., Sullivan, A. L., Roxburgh, S. H., and Polglase, P. J. (2020). Exploring how fire spread mode shapes the composition of pyrogenic carbon from burning forest litter fuels in a combustion wind tunnel. *Science of The Total Environment*, 698, article number 134306.
36. Van Kenhove, E., De Backer, L., Janssens, A., and Laverge, J. (2019). Simulation of Legionella concentration in domestic hot water: comparison of pipe and boiler models. *Journal of Building Performance Simulation*, 12(5), 595-619.
37. Volynkina, E. P., and Pryanichnikov, E. V. (2002). Reducing atmospheric emissions from coal-fired boiler houses with fuel-bed firing systems. *Thermal Engineering (English translation of Teploenergetika)*, 49, 122-130.
38. Widziński, M., Chaja, P., Andersen, A. N., Jaroszewska, M., Bykuć, S., and Sawicki, J. (2019). Simulation of an alternative energy system for district heating company in the light of changes in regulations of the emission of harmful substances into the atmosphere. *International Journal of Sustainable Energy Planning and Management*, 24, 43-56.
39. Zhang, L., Jiang, Y., Chen, W., Zhou, S., and Zhai, P. (2017). Experimental and numerical investigation for hot water boiler with inorganic heat pipes. *International Journal of Heat and Mass Transfer*, 114, 743-747.
40. Zhang, P., Liu, S., He, C., Tao, H., Qing, C., Li, P., and Li, D. (2018). Experimental and numerical study of the characteristics of biomass suspension combustion in a hot-water boiler. *Journal of Renewable and Sustainable Energy*, 10(3), article number 033103.

Table 1. The results of measurements of the gas composition in the furnace and gas collection chamber

Test No.	Measuring point	O ₂ , %	CO, mg/m ³	SO ₂ , mg/m ³	NO, mg/m ³	NO ₂ , mg/m ³	CO ₂ , %	NO _x , mg/m ³	CH ₄ , mg/m ³	T _{eg} , °C
In the 1st mode – active combustion (after 5-10 minutes from the moment of loading coal)										
1	10-20', in the furnace, above the layer, 30.01.2020	16.80	6833.9	14.45	203.65	29.16	4.01	340.51	642.51	200.03
2	20-30', in the furnace, above the layer, 30.01.2020	16.89	8386.3	41.60	255.23	2.22	3.90	392.60	557.92	207.52
3	30-40', in the furnace, above the layer, 30.01.2020	16.62	8702.1	74.84	263.60	0.08	4.15	403.26	539.89	208.69
4	5-15', in the flue, 20.02.2020	15.11	2217.71	571.99	412.45	0.0	6.05	631.05	897.24	277.93
5	15-30', in the flue, 20.02.2020	15.30	1982.83	431.59	366.41	0.0	5.53	560.55	764.16	365.06
6	30-40', in the flue, 20.02.2020	16.04	6837.94	159.53	346.91	0.0	4.73	530.70	1451.99	267.45
In the 2nd mode – afterburning (after 7-8 hours from the moment of the last coal loading)										
1	In the furnace, over a layer of 30 cm, 30.01.2020	19.60	32739.45	0.0	72.12	11.73	1.29	121.93	1497.26	60.33
2	In the furnace, over a layer of 30 cm, 30.01.2020	19.59	31691.24	0.0	79.69	9.68	1.22	131.59	781.36	91.58
3	In the furnace, over a layer of 30 cm, 30.01.2020	18.77	31015.96	0.0	58.30	12.06	1.95	101.26	1748.40	74.72
4	In the furnace, over a layer of 30 cm, 20.02.2020	18.97	28781.08	0.0	86.95	0.0	1.79	138.48	2080.18	85.85

Test No.	Measuring point	O ₂ , %	CO, mg/m ³	SO ₂ , mg/m ³	NO, mg/m ³	NO ₂ , mg/m ³	CO ₂ , %	NO _x , mg/m ³	CH ₄ , mg/m ³	T _{eg} , °C
5	In the furnace, over a layer of 30 cm, 20.02.2020	19.82	28128.35	0.0	30.27	0.0	1.05	48.07	4616.83	67.33
6	In the flue, 20.02.2020	19.37	28298.06	0.0	79.61	0.0	1.45	122.89	3995.82	76.09

Table 2. Experimental test data (average values) of the KCVr-0.43 hot water boiler and coal characteristics

Parameters of the boiler KCVr-0.43, coal characteristics	The 1st mode (from the moment of coal casting), 30.01.20	The 2nd mode (in the long coke burn out), 30.01.20	The 1st mode (from the moment of coal casting), 20.01.20	Exit to the 2nd mode (stabilization of the process), 20.02.20
Ash content on working weight A_{cont} , %	13.61	13.61	14.19	14.19
Humidity M_{cont} , %	19.48	19.48	19.73	19.73
Nitrogen content, %	0.41	0.41	0.51	0.51
Net calorific value of coal Q_{ncv} , kJ/kg	22743	22743	23154	23154
Boiler heat power B_{hp} , kW	230	136	248	226
Consumption of Shubarkul coal C_{fc} , kg/s	0.0133	0.0088	0.0139	0.012
Thermal stress of the combustion mirror q_{fbs} , kW/m ²	309.3	204.2	328	283
Thermal stress of the furnace volume q_{furn} , kW/m ³	182.2	120.5	193	167

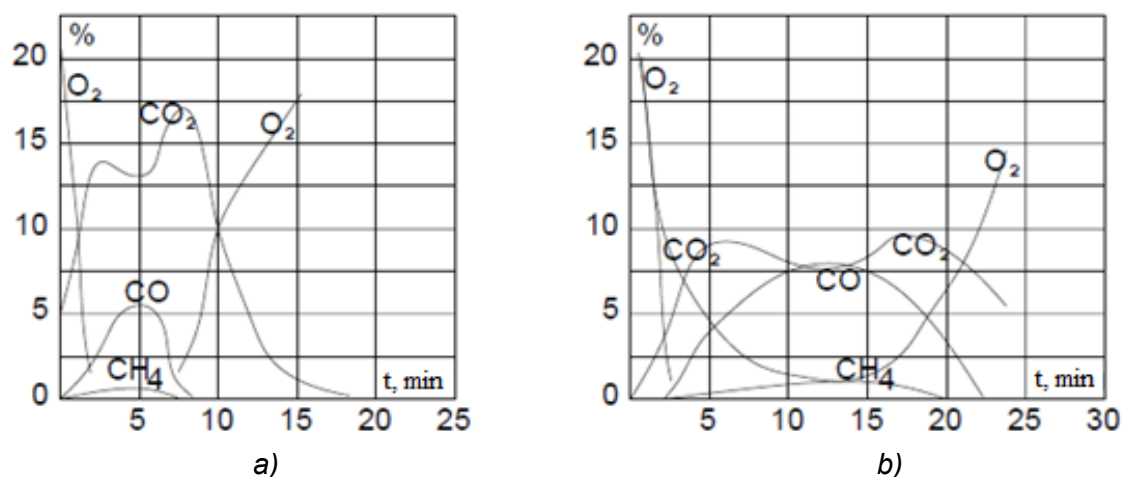


Figure 1. The composition of the gases over a thin layer of coal on a grate with a layer forced through the air when burning Donetsk coal at an air flow rate: a) $w_0 = 0.68$ m/s; b) $w_0 = 0.23$ m/s

Source: Knorre (1951), Kamenetskii (2006).

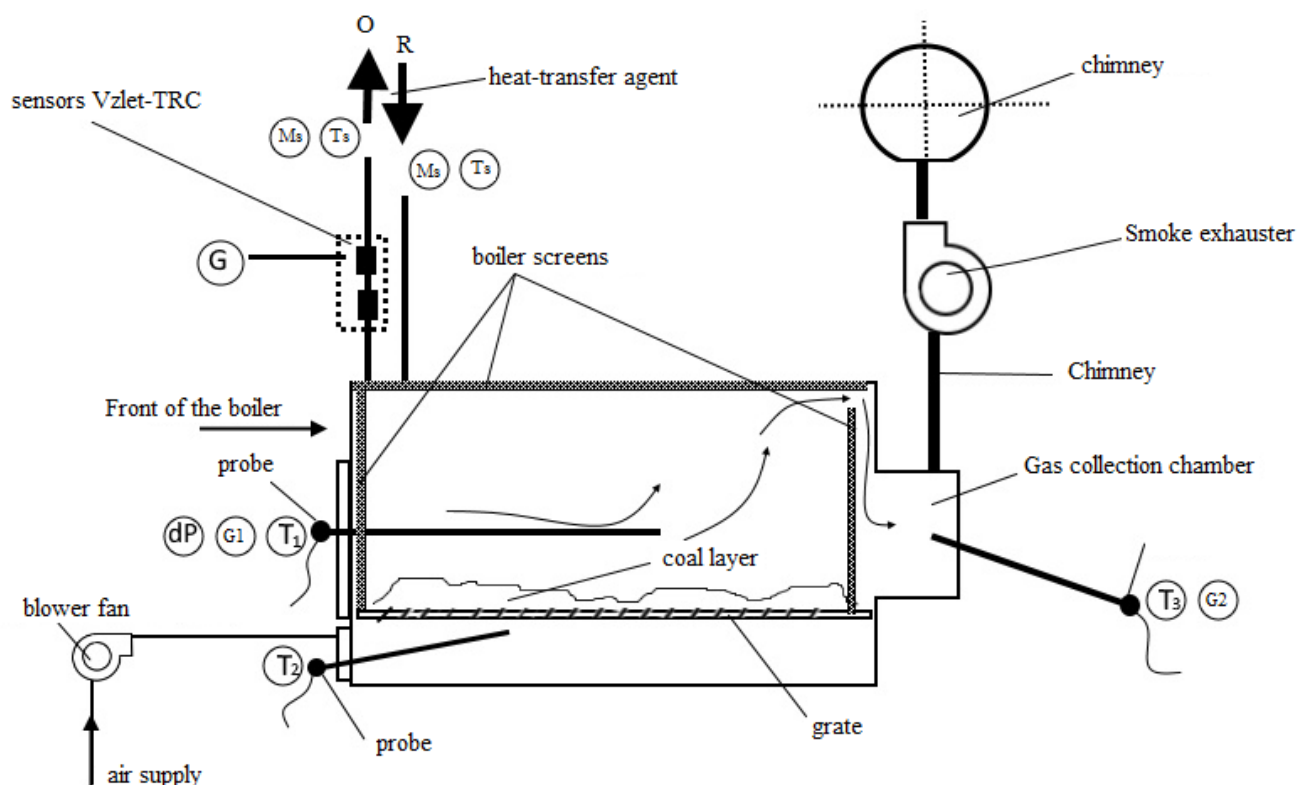


Figure 2. Diagram of the elements of the measuring system for thermotechnical testing of the boiler KSVr-0.43 (O and R – direct and return pipes of the heat-transfer agent; Ms, Ts – standard manometers and thermometers installed on the direct and return lines of the heat-transfer agent, dP – measurement of vacuum in a furnace with a Pitot tube probe, G1 – measuring the gas composition in a furnace with a gas analyzer probe, T1 – measuring the thermocouple Pitot tube temperature in the furnace, T2 – measuring the air temperature in the hearth under the grate with a thermocouple, T3 – measuring the temperature of the exhaust gases in the gas collection part (duct) with a thermocouple, G2 – measuring the temperature of the flue gases in the gas collection part (gas duct) with a gas analyzer probe)

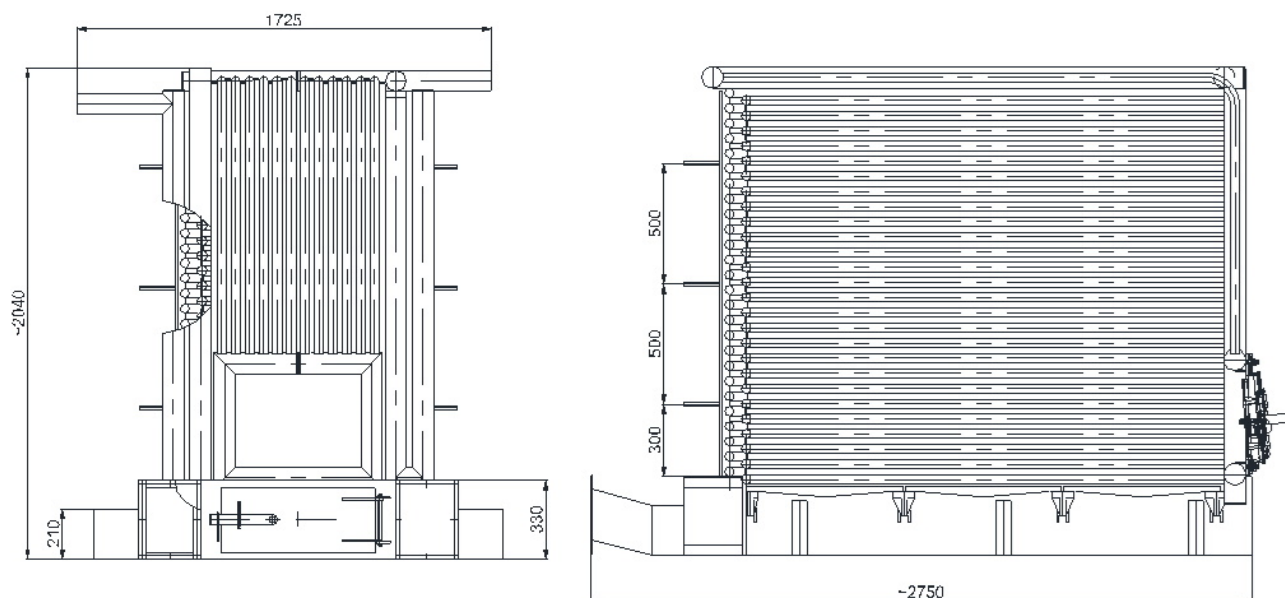


Figure 3. Front and side view of the hot water solid fuel boiler KSVR-0.43

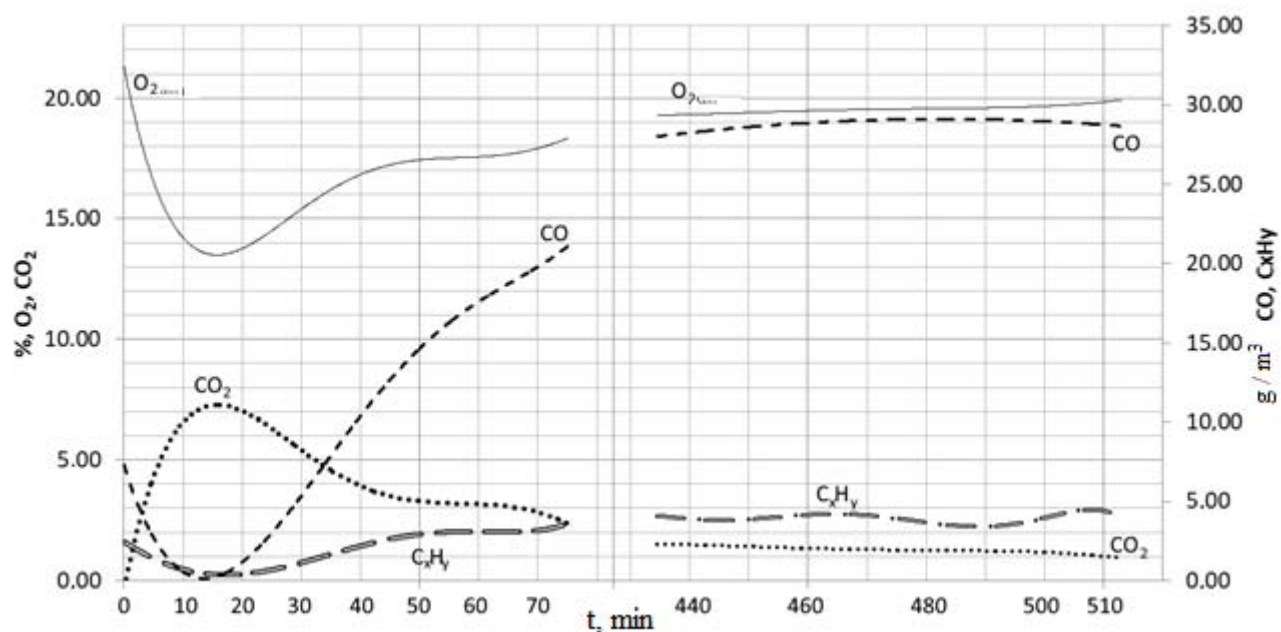


Figure 4. The composition of the gases over a thin coal layer on a grate with forced air over the layer and during natural draft at burning Shubarkul coal in a layer up to 70 mm at an airflow rate of $w_0 = 0.075 \text{ m/s}$ (with separation of the combustion regime time: 0-80 minutes – from the moment of coal loading; 430-520 minutes – during the stable process of coke burning out)

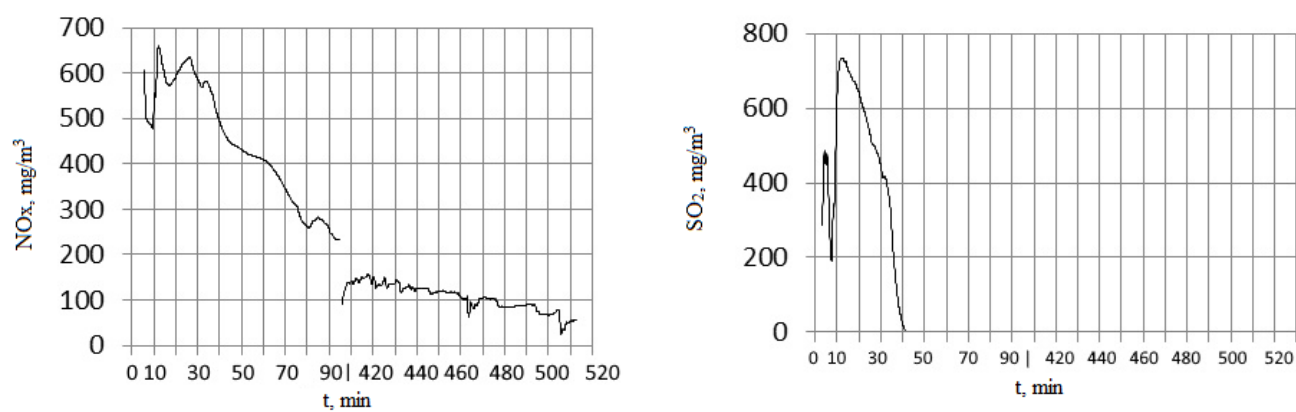


Figure 5. Approximate NO_x and SO₂ content measurement data for two combustion modes

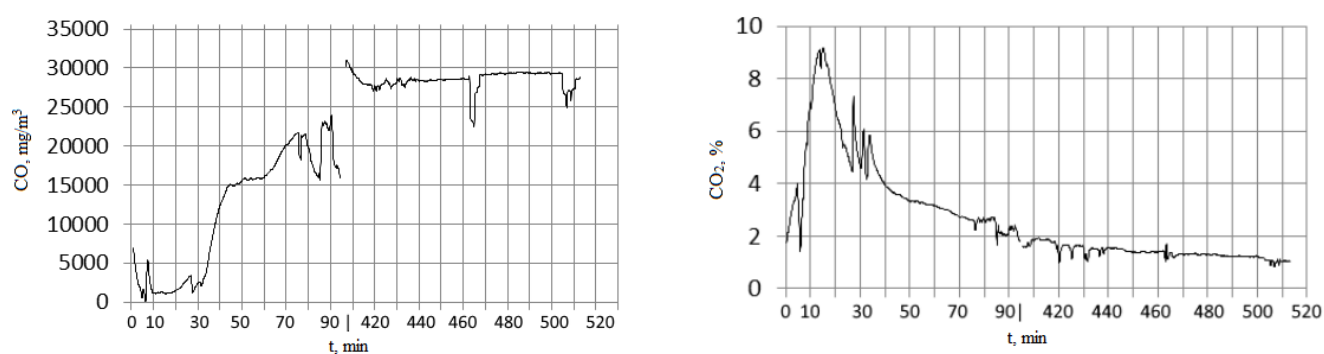


Figure 6. Approximate CO and CO₂ content measurements data for two combustion modes

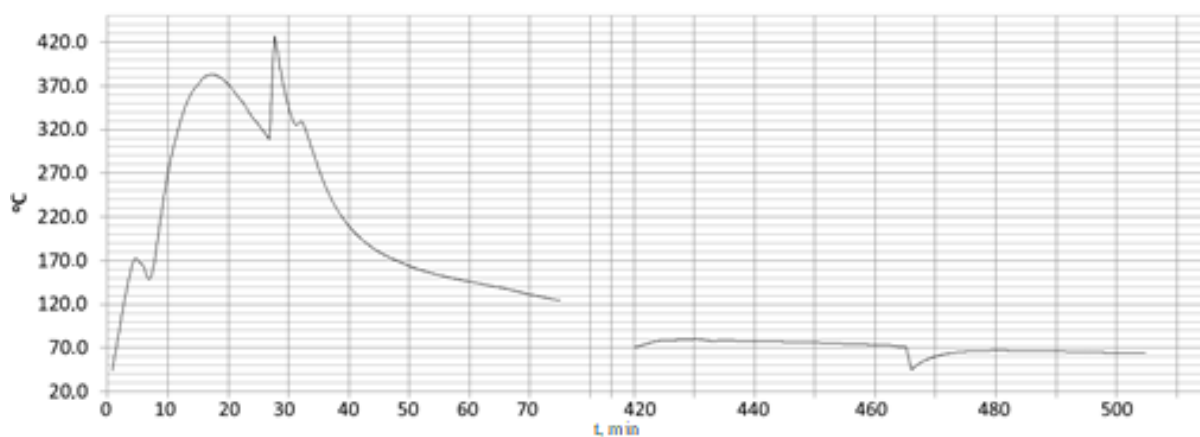


Figure 7. Approximate data of measurements of the temperature of gases in the furnace for two combustion modes

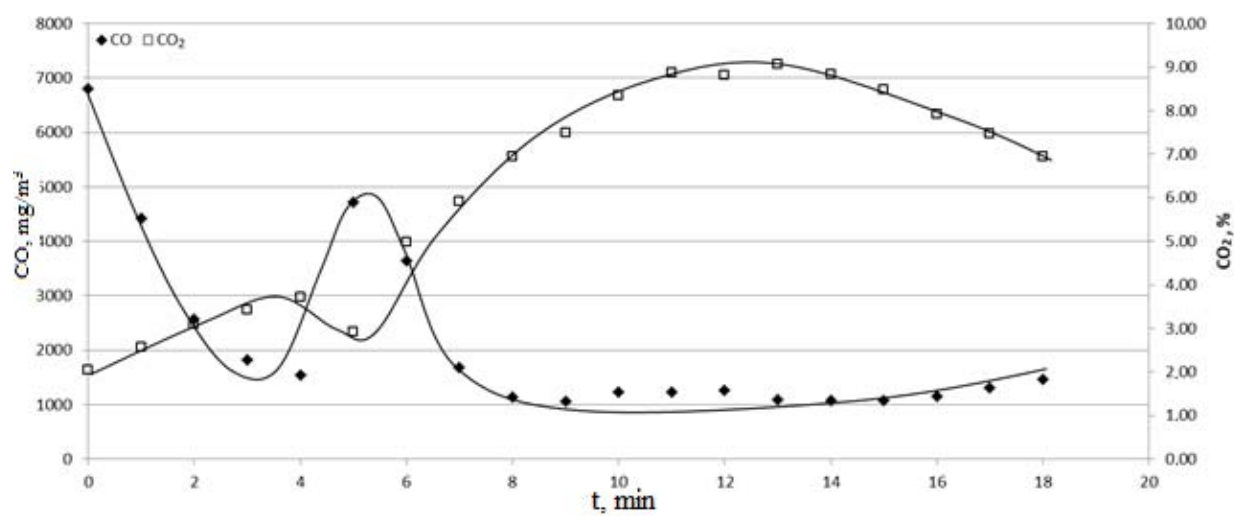


Figure 8. Measurement data of CO and CO₂ in the active stage of burning of Shubarkul coal with forced air

SÍNTESE E ATIVIDADE ANTITUMORAL DE NOVAS CUMARINAS MULTIFUNCIONAIS

SYNTHESIS AND ANTITUMOR ACTIVITY OF NEW MULTIFUNCTIONAL COUMARINS

تصنيع وفحص النشاط المضاد للورم لمركبات جديدة من الكومارينات المتعددة الوظائف

BASHIR, Moath Kahtan ¹; MUSTAFA, Yasser Fakri ^{2*}; OGLAH, Mahmood Khudhayer ³;

^{1, 2, 3} Pharmaceutical Chemistry Department, College of Pharmacy, Mosul University-41002, Nineveh, Iraq.

* Corresponding author

E-mail: Dr.yassermustafa@uomosul.edu.iq

Received 19 September 2020; received in revised form 27 October 2020; accepted 30 October 2020

RESUMO

O câncer constitui uma das mais graves ameaças à saúde pública em todo o mundo. É imperativo sintetizar novos compostos e explorar sua atividade antitumoral para encontrar uma resolução potencial para este problema de saúde. A síntese de novos scaffolds e a avaliação de sua atividade antitumoral é uma abordagem relevante para o combate ao desenvolvimento do câncer. As cumarinas podem apresentar diversas atividades biológicas, sendo uma delas a atividade antitumoral. Este estudo teve como objetivo sintetizar novas cumarinas enxertando seus precursores nas aminas aromáticas via formação de base de Schiff e avaliando sua atividade antitumoral introdutória. Novas cumarinas multifuncionais (MC1-MC9) foram preparadas integrando uma cumarina funcionalizada com diferentes derivados de toluidina por meio de uma ligação à base de Schiff. A caracterização espectral inspirada nas espectroscopias FTIR, ¹H- e ¹³C- NMR estabeleceu as estruturas químicas dos produtos sintetizados. A atividade antitumoral foi explorada *in vitro* contra quatro linhagens de câncer humano dominante, incluindo HeLa, SKG, MCF-7 e AMN3. Os resultados adquiridos do ensaio de viabilidade celular inspecionado pela aplicação de corante MTT revelaram que as cumarinas multifuncionais sintetizadas, particularmente MC3, têm uma atividade promissora. Pode-se concluir que para as cumarinas sintetizadas foi observada tendência semelhante de atividade contra as linhagens de células de teste, sendo a melhor ação contra MCF-7 e, pelo menos, uma contra AMN3. Este estudo não apenas fornece uma nova estrutura de uma atividade antitumoral significativa, mas também fornece alguns insights sobre sua relação estrutura-atividade.

Palavras-Chave: Base de Schiff, cumarina, atividade antitumoral, ensaio de MTT.

ABSTRACT

Cancer constitutes one of the most severe public health menaces worldwide. It is imperative to synthesize new compounds and explore their antitumor activity to find a potential resolution to this health problem. Synthesis of new scaffolds and evaluating their antitumor activity is a relevant approach for combating cancer development. Coumarins can exhibit diverse biological activities, and one of these is the antitumor activity. This study aimed to synthesize new coumarins by grafting their precursors to the aromatic amines via Schiff base formation and evaluating their introductory antitumor activity. New multifunctional coumarins (MC1-MC9) were prepared by integrating a functionalized coumarin with different toluidine derivatives via a Schiff-base linkage. Spectral characterization inspired by FTIR, ¹H- and ¹³C- NMR spectroscopies has established the chemical structures of the synthesized products. The antitumor activity was explored *in vitro* versus four dominant human cancer lines, including HeLa, SKG, MCF-7, and AMN3. The outcomes acquired from the cell viability assay inspected by applying MTT dye have revealed that the synthesized multifunctional coumarins, particularly MC3, have a hopeful activity. It can be concluded that a similar trend of activity against the test cell lines was observed for the synthesized coumarins, with the best action being versus MCF-7 and the least one versus AMN3. This study not only affords a new scaffold of a significant antitumor activity but also provides some insights into its structure-activity relationship.

Keywords: Schiff-base, coumarin, antitumor activity, MTT assay.

يشكل السرطان أحد أخطر تهديدات الصحة العامة في جميع أنحاء العالم. من الضروري تصنيع مركبات جديدة واستكشاف نشاطها المضاد للأورام لإيجاد حل محتمل لهذه المشكلة الصحية. يعد تركيب السقالات الجديدة وتقييم نشاطها المضاد للأورام نهجاً مناسباً لمكافحة تطور السرطان. يمكن أن تظهر الكومارينات أنشطة بيولوجية متنوعة ، وأحد هذه الأنشطة هو النشاط المضاد للأورام. هدفت هذه الدراسة إلى تصنيع كومارين جديدة عن طريق تطعيم سلائفها للأمينات العطرية عن طريق تكوين قاعدة شيف وتقييم نشاطها التمهيدي المضاد للأورام. تم تحضير الكومارينات الجديدة المتعددة الوظائف (MC1-MC9) من خلال دمج الكومارين الوظيفي مع مشتقات التولويدين المختلفة عبر ارتباطها بقاعدة شيف. إن التوصيف الطيفي المستوحى من مطياف الأشعة تحت الحمراء والرنين النووي المغناطيسي للبروتون وللكاربون المشع قد أنشأ الهياكل الكيميائية للمنتجات المركبة. تم استكشاف النشاط المضاد للورم في المختبر مقابل أربعة خطوط سرطانية بشرية سائدة ، بما في ذلك سرطان عنق الرحم و سرطان المريء و سرطان الثدي و سرطان الغدة الثديية الفئران. أظهرت النتائج المكتسبة من اختبار قابلية الخلية للفحص عن طريق تطبيق صبغة التسرطن أن الكومارينات المصنعة، وخاصة مركب MC3 ، له نشاط يبعث على الأمل. يمكن أن نستنتج أنه لوحظ وجود اتجاه مماثل للنشاط ضد خطوط خلايا الاختبار بالنسبة للكومارينات المصنعة، مع أفضلية لخلايا MCF-7 والأقل مقابل AMN3. لا توفر هذه الدراسة دعامة جديدة للنشاط المضاد للأورام المهمة فحسب ، بل توفر أيضاً بعض الأفكار حول علاقة الهيكل الكيميائي بالنشاط المضاد للسرطان.

الكلمات الافتتاحية: قاعدة شيف ، كومارين ، نشاط مضاد للورم ، صبغة فحص التسرطن

(2018; Teran *et al.*, 2019).

1. INTRODUCTION:

Cancer constitutes one of the most serious public health menaces worldwide. The rate of its incidence is highly elevated in almost all parts of the world since 1990 (Fitzmaurice *et al.*, 2015). The effective prevention and treatment of different kinds of cancer are hard to achieve despite discovering and developing many experimental antitumor agents from natural (Rahimi Khoigani *et al.*, 2017) or synthetic origins (Mustafa, 2019). Therefore, it is still a fundamental demand to synthesize new chemical entities and explore their antitumor activity to find a potential resolution to this mysterious health problem (Bashir *et al.*, 2020).

Coumarin is a charming chemical nucleus and alongside its natural and synthetic derivatives comprise an important oxygen-containing heterocycle class. Coumarins as bioactive agents can exhibit diverse biological activities, which include the antibacterial (Kumar *et al.*, 2015; Al Zoubi *et al.*, 2018; Gonelimali *et al.*, 2018), antifungal (Medimagh-Saidana *et al.*, 2015), anticholinesterase (Cakmak and Gülçin, 2019), antitumor (Jing Lia, Fei Yua, Yi Chena, 2015; Detsi *et al.*, 2017; Yao *et al.*, 2017; Haq *et al.*, 2019), anti-inflammatory (Srikrishna *et al.*, 2016), antioxidant (Chen, 2016; Pasciu *et al.*, 2019; Alfahad *et al.*, 2020), antidiabetic (Pisoschi and Pop, 2015; Li *et al.*, 2017; Forni *et al.*, 2019; Iheagwam *et al.*, 2019), and many other important effects (Stefanachi *et al.*, 2018). Although there are many synthetic routes for coumarins preparation, Pechmann condensation, and its recent improvements remain the most utilized technique (Dandriyal *et al.*, 2016; Jung *et al.*,

Schiff bases, or as named azomethines comprise the functional group that results from the direct condensation of a carbonyl compound with primary amine (Kajal *et al.*, 2013). In addition to its soft formation, Schiff base can be considered a versatile pharmacophore that exhibits various biological and medicinal activities. Example activities may include anti-inflammatory, anticancer, analgesic, antioxidant, antimicrobial, anticonvulsant, antidepressant, and antitubercular effects (Hameed *et al.*, 2017). In this context, Schiff bases of primary aromatic amine substituted with the electron-donation group have played an essential role in regulating and enhancing the activities mentioned above (Al Zoubi *et al.*, 2018).

This study aimed to synthesize new coumarins by grafting their precursors to the aromatic amines via Schiff base formation and evaluating their introductory antitumor activity utilizing MTT test versus four human cancer cells lines named HeLa, SKG, MCF-7, and AMN3.

2. MATERIALS AND METHODS:

2.1. Reagents and chemicals

Chemicals, solvents, and reagents applied in this study were obtained from Scharlau, Haihang, Sigma-Aldrich, Bio-World, and other documented international companies. These chemicals and reagents included concentrated H₂SO₄, citric acid, m-guaiacol, NaOH, lithium tri-*tert*-butoxyaluminum hydride, acetaldehyde, propionaldehyde, butyraldehyde, 2-methyltoluidine, 3-methyltoluidine, and 4-methyltoluidine.

2.2. Thin-layer chromatography (TLC)

The ascending TLC technique was used to establish the purity of the synthetic products using pre-coated silica gel plates (GF254 type 60, Merck, Germany). The spots were eluted on the chromatograms using CHCl_3 : methanol (5:1) as an eluent.

2.3. Melting point (mp)

The electrochemical CIA 9300 instrument was utilized for the examination of the melting points of synthesized products through an open-capillary method, and they are uncorrected.

2.4. Fourier transforms infrared (FTIR)

The FTIR spectra of the synthetic products were recorded by using Bruker-Alpha ATR-FTIR spectrophotometer (Germany). The sample (25 mg) was applied directly to the superficial mass detector of the instrument without the need to prepare KBr disk. The band positions in the FTIR spectrum are shown as Wavenumber (ν , cm^{-1}), whereas the band intensities are expressed as Transmittance %.

2.5. Ultraviolet (UV)

The UV/Visible spectra were recorded by using UVD-2950 (LABOMED, USA). The sample was prepared by mixing (10 μM) of the investigated product with 10 ml EtOH, and 2 ml of the resulted solution was placed in the instrument's cell for the investigation. The wavelength of maximum absorption (λ_{max}) was recorded in nm for the synthetic products.

2.6. Nuclear magnetic resonance (NMR)

The proton-nuclear magnetic resonance (^1H -NMR) and carbon-nuclear magnetic resonance (^{13}C -NMR) spectra of the synthetic products were scanned on Bruker Analytische Messtechnik GmbH (400 MHz). To prepare the ^1H -NMR sample, 5mg of the investigated product was mixed in a small vial with 0.7 ml $\text{DMSO}-d_6$ for 10 min, and the resulted solution was transferred into the NMR tube by a glass pipette. For the ^{13}C -NMR sample preparation, 55mg of the investigated product was mixed in a small vial with 0.7 ml $\text{DMSO}-d_6$ for 30 min, and the resulted solution was transferred to the NMR tube by a glass pipette. The chemical shifts (δ) of these spectra were expressed in part per million (ppm) downfield to the internal standard tetramethylsilane (TMS). In an explanation of ^1H -NMR spectrum, the following

terms were utilized to detect the spin-spin coupling: singlet (s), doublet (d), triplet (t) and multiplet (m).

2.7. Chemical synthesis

The designed steps adopted for the chemical synthesis of the target multifunctional coumarins (MC1-MC9) are depicted in Scheme 1.

2.7.1 Synthesis of 7-methoxycoumarin-4-acetic acid (MA1)

In a small conical flask immersed in a salt-ice bath, concentrated H_2SO_4 (10 ml) was added. As the acid temperature dropped to 0°C , citric acid (0.96 g, 5 mmol) was added in tiny portions over 2 hr. The frequency of addition was controlled by observing the temperature, which was maintained below 4°C . Subsequently, the reaction mixture was stirred at room temperature (RT) for 16 hr in a slow-motion style, poured on an ice-water mixture contained in a beaker, and filtered. The gray crystals of acetone dicarboxylic acid were washed with ethyl acetate (25 ml \times 3), dried by suction, weighted, and directly used in the next step (Swamy *et al.*, 2015).

A solution of acetone dicarboxylic acid (1.46 g, 10 mmol) in 10 ml concentrated H_2SO_4 was stirred in a salt-ice bath for 30 min. The stirring was continued at RT until the evolution of gas was arrested. m-Guaiacol (1.08 ml, 10 mmol) was added to the above solution very slowly over 2 hr, and the reaction mixture was stirred in an ice-water bath. Then, the mixture was stirred at RT for two days, poured on an ice-water mixture, and filtered. The crude was dissolved in NaOH (50 ml, 1N), filtered, acidified, and the solid product was recrystallized from ethanol (Swamy *et al.*, 2015).

MA1: mp= $184-186^\circ\text{C}$; λ_{max} (EtOH)=296 nm; % yield=49; R_f = 0.56; FTIR (ν , stretching, cm^{-1}) 3095 (C-H, alkene), 3005 (O-H, COOH), 2884 (C-H, alkane), 1725 (C=O, ester), 1706 (C=O, COOH), 1692 (C=C, alkene), 1581 (C=O, aromatic), 1252 and 1071 (C-O-C, ether).

2.7.2 Synthesis of 7-methoxycoumarin-4-carbaldehyde (MA2)

A precooled mixture of **MA1** (1.17 g, 5 mmol) in 25 ml dry ether was added dropwise to a stirred solution of lithium tri-*tert*-butoxyaluminum hydride ($\text{LiAlH}(\text{OtBu})_3$, 1.27 g, 5 mmol) in 75 ml dry ether at 0°C . As the addition ended, the reaction mixture was stirred for 1 hr in an ice-water bath. To this, HCl (1N) was added and the pH of the resulted mixture was justified at 5. The product

was extracted by ethyl acetate, washed with saturated NaCl solution, dried over sodium sulfate, and vaporized. The target product was recrystallized from CH₂Cl₂ (Fessler *et al.*, 2013).

MA2: mp=152-155°C; λ_{\max} (EtOH)=289 nm; % yield=51; R_f = 0.61; FTIR (v, stretching, cm⁻¹) 3062 (C-H, alkene), 2912 (C-H, alkane), 2724 (C-H, aldehyde), 1722 (C=O, ester), 1700 (C=O, aldehyde), 1690 (C=C, alkene), 1580 (C=O, aromatic), 1248 and 1063 (C-O-C, ether).

2.7.3 Acid-catalyzed synthesis of 7-methoxy-4-but-2-enal derivatives (MA3-MA5)

A solution of acetaldehyde derivative (5 mmol) in 20 ml concentrated H₂SO₄ was stirred at RT for 30 min. To this, a solution of **MA2** (1.09 g, 5 mmol) in 30 ml ether was added dropwise over 15 min. The reaction mixture was refluxed for 24 hr, poured on an ice-water mixture, filtered, and washed with water several times. The crude product was recrystallized from a mixture of ether: ethyl acetate (Amarasekara and Ha, 2018).

MA3: mp=136-139°C; λ_{\max} (EtOH)=311 nm; % yield=63; R_f = 0.63; FTIR (v, stretching, cm⁻¹) 3043 (C-H, alkene), 2916 (C-H, alkane), 2710 (C-H, aldehyde), 1727 (C=O, ester), 1691 (C=O, aldehyde), 1688, 1627 (C=C, alkene), 1582 (C=O, aromatic), 1247 and 1057 (C-O-C, ether).

MA4: mp=142-145°C; λ_{\max} (EtOH)=310 nm; % yield=57; R_f = 0.66; FTIR (v, stretching, cm⁻¹) 3046 (C-H, alkene), 2919 (C-H, alkane), 2709 (C-H, aldehyde), 1724 (C=O, ester), 1694 (C=O, aldehyde), 1690, 1625 (C=C, alkene), 1582 (C=O, aromatic), 1242 and 1057 (C-O-C, ether).

MA5: mp=140-143°C; λ_{\max} (EtOH)=321 nm; % yield=58; R_f = 0.67; FTIR (v, stretching, cm⁻¹) 3062 (C-H, alkene), 2953 (C-H, alkane), 2722 (C-H, aldehyde), 1720 (C=O, ester), 1686 (C=O, aldehyde), 1698, 1624 (C=C, alkene), 1589 (C=O, aromatic), 1240 and 1065 (C-O-C, ether).

2.7.4 Synthesis of multifunctional coumarins (MC1-MC9)

A mixture of 7-methoxy-4-but-2-enal derivative (2 mmol) and toluidine derivative (2 mmol) in 25 ml benzene was refluxed for 30 min. As its temperature dropped to RT, the reaction mixture was filtered and the solid was washed with cold benzene (10 ml \times 3) then with n-hexane (10 ml \times 3). The mother filtrate combined with the washings was concentrated under vacuum and the product was recrystallized from ethyl acetate (Sanap and Samant, 2015).

7-methoxy-4-((2*E*)-4-(*o*-tolylimino)but-2-en-1-yl)-2*H*-chromen-2-one (**MC1**): mp=150-153°C; λ_{\max} (EtOH)=346 nm; % yield=81; R_f = 0.74; FTIR (v, stretching, cm⁻¹): 3049 (C-H, alkene), 2910 (C-H, alkane), 1727 (C=O, ester), 1682, 1626 (C=C, alkene), 1639 (N=C), 1582 (C=O, aromatic), 1243 and 1052 (C-O-C, ether); ¹H-NMR (DMSO-d₆, 300 MHz): δ = 8.24 (1H, d, H-5), 8.12 (1H, d, H-14), 8.02 (1H, t, H-19), 7.60 (1H, d, H-17), 7.32 (1H, d, H-20), 7.06 (1H, s, H-8), 6.91 (1H, d, H-7), 6.83 (1H, t, H-18), 6.50 (1H, s, H-3), 6.12 (1H, t, J = 15 Hz, H-12), 5.65 (1H, t, J = 15 Hz, H-13), 4.24 (3H, s, OCH₃), 3.02 (2H, d, H-11), 2.85 (3H, s, H-21) ppm; ¹³C-NMR (DMSO-d₆, 75 MHz): δ = 165.8 (CH, C-14), 162.4 (C, C-2), 158.1 (C, C-7), 156.1 (C, C-4), 155.0 (C, C-9), 149.6 (C, C-15), 144.9 (C, C-4), 139.5 (CH, C-12), 132.9 (CH, C-17), 130.1 (C, C-16), 128.3 (CH, C-18), 127.0 (CH, C-19), 124.8 (CH, C-5), 124.0 (CH, C-13), 121.2 (CH, C-20), 115.2 (C, C-10), 113.5 (CH, C-3), 111.8 (CH, C-6), 103.8 (CH, C8), 57.7 (CH₃, OCH₃-C-7), 44.6 (CH₂, C-11), 22.7 (CH₃, C-21) ppm.

7-methoxy-4-((2*E*)-4-(*m*-tolylimino)but-2-en-1-yl)-2*H*-chromen-2-one (**MC2**): mp=159-162°C; λ_{\max} (EtOH)=345 nm; % yield=85; R_f = 0.76; FTIR (v, stretching, cm⁻¹): 3044 (C-H, alkene), 2916 (C-H, alkane), 1724 (C=O, ester), 1681, 1628 (C=C, alkene), 1642 (N=C), 1588 (C=O, aromatic), 1249 and 1060 (C-O-C, ether); ¹H-NMR (DMSO-d₆, 300 MHz): δ = 8.22 (1H, d, H-5), 8.15 (1H, d, H-14), 8.01 (1H, t, H-19), 7.36 (1H, s, H-16), 7.25 (1H, d, H-18), 7.17 (1H, d, H-20), 7.05 (1H, s, H-8), 6.90 (1H, d, H-7), 6.53 (1H, s, H-3), 6.11 (1H, t, J = 15 Hz, H-12), 5.67 (1H, t, J = 15 Hz, H-13), 4.27 (3H, s, OCH₃), 3.03 (2H, d, H-11), 2.86 (3H, s, H-21) ppm; ¹³C-NMR (DMSO-d₆, 75 MHz): δ = 165.5 (CH, C-14), 162.7 (C, C-2), 158.2 (C, C-7), 156.6 (C, C-4), 155.1 (C, C-9), 151.6 (C, C-15), 145.0 (C, C-4), 142.5 (C, C-17), 140.1 (CH, C-12), 129.9 (CH, C-19), 125.1 (CH, C-18), 124.9 (CH, C-5), 123.6 (CH, C-13), 122.4 (CH, C-16), 119.6 (CH, C-20), 115.4 (C, C-10), 113.1 (CH, C-3), 112.0 (CH, C-6), 104.1 (CH, C8), 57.8 (CH₃, OCH₃-C-7), 44.5 (CH₂, C-11), 25.2 (CH₃, C-21) ppm.

7-methoxy-4-((2*E*)-4-(*p*-tolylimino)but-2-en-1-yl)-2*H*-chromen-2-one (**MC3**): mp=144-147°C; λ_{\max} (EtOH)=342 nm; % yield=79; R_f = 0.76; FTIR (v, stretching, cm⁻¹): 3052 (C-H, alkene), 2892 (C-H, alkane), 1725 (C=O, ester), 1680, 1625 (C=C, alkene), 1640 (N=C), 1583 (C=O, aromatic), 1242 and 1058 (C-O-C, ether); ¹H-NMR (DMSO-d₆, 300 MHz): δ = 8.27 (1H, d, H-5), 8.14 (1H, d, H-14), 8.08 (1H, d, H-16), 7.84 (1H, d, H-19), 7.78 (1H, d, H-20), 7.08 (1H, s, H-8), 6.92 (1H, d, H-17), 6.87 (1H, d, H-7), 6.47 (1H, s, H-3), 6.06 (1H, t, J = 15 Hz, H-12), 5.66 (1H, t, J = 15 Hz, H-13), 4.24 (3H,

s, OCH₃), 3.08 (2H, d, H-11), 2.82 (3H, s, H-21) ppm; ¹³C-NMR (DMSO-d₆, 75 MHz): δ= 165.2 (CH, C-14), 162.9 (C, C-2), 159.0 (C, C-7), 155.9 (C, C-4), 153.7 (C, C-9), 150.2 (C, C-15), 145.2 (C, C-4), 141.5 (C, C-18), 141.3 (CH, C-12), 131.1 (CH, C-16), 127.4 (CH, C-19), 125.4 (CH, C-5), 124.1 (CH, C-20), 123.8 (CH, C-13), 123.5 (CH, C-17), 115.5 (C, C-10), 113.1 (CH, C-3), 112.1 (CH, C-6), 105.2 (CH, C-8), 57.7 (CH₃, OCH₃-C-7), 44.4 (CH₂, C-11), 22.1 (CH₃, C-21) ppm.

7-methoxy-4-((2*E*)-3-methyl-4-(*o*-tolylimino)but-2-en-1-yl)-2*H*-chromen-2-one (**MC4**): mp=154-156°C; λ_{max} (EtOH)=346 nm; % yield=82; R_f= 0.79; FTIR (v, stretching, cm⁻¹): 3051 (C-H, alkene), 2929 (C-H, alkane), 1722 (C=O, ester), 1680, 1621 (C=C, alkene), 1632 (N=C), 1589 (C=O, aromatic), 1252 and 1060 (C-O-C, ether); ¹H-NMR (DMSO-d₆, 300 MHz): δ= 8.20 (1H, d, H-5), 8.14 (1H, s, H-14), 8.00 (1H, t, H-19), 7.66 (1H, d, H-17), 7.37 (1H, d, H-20), 7.03 (1H, s, H-8), 6.96 (1H, d, H-7), 6.75 (1H, t, H-18), 6.47 (1H, s, H-3), 5.90 (1H, t, H-12), 4.26 (3H, s, OCH₃), 3.10 (2H, d, H-11), 2.86 (3H, s, H-21), 2.37 (3H, s, CH₃-13) ppm; ¹³C-NMR (DMSO-d₆, 75 MHz): δ= 165.2 (CH, C-14), 162.7 (C, C-2), 158.2 (C, C-7), 156.1 (C, C-4), 155.6 (C, C-9), 150.1 (C, C-15), 145.2 (C, C-4), 141.2 (CH, C-12), 133.4 (CH, C-17), 130.9 (C, C-16), 128.8 (CH, C-18), 126.7 (CH, C-19), 124.2 (CH, C-5), 121.5 (C, C-13), 118.4 (CH, C-20), 115.2 (C, C-10), 113.5 (CH, C-3), 110.1 (CH, C-6), 103.3 (CH, C-8), 57.1 (CH₃, OCH₃-C-7), 38.1 (CH₂, C-11), 22.8 (CH₃, C-21), 18.6 (CH₃, CH₃-C-13) ppm.

7-methoxy-4-((2*E*)-3-methyl-4-(*m*-tolylimino)but-2-en-1-yl)-2*H*-chromen-2-one (**MC5**): mp=167-170°C; λ_{max} (EtOH)=342 nm; % yield=78; R_f= 0.79; FTIR (v, stretching, cm⁻¹): 3064 (C-H, alkene), 2925 (C-H, alkane), 1727 (C=O, ester), 1680, 1628 (C=C, alkene), 1649 (N=C), 1583 (C=O, aromatic), 1255 and 1043 (C-O-C, ether); ¹H-NMR (DMSO-d₆, 300 MHz): δ= 8.30 (1H, d, H-5), 8.12 (1H, s, H-14), 8.00 (1H, t, H-19), 7.32 (1H, s, H-16), 7.26 (1H, d, H-18), 7.18 (1H, d, H-20), 7.07 (1H, s, H-8), 6.88 (1H, d, H-7), 6.50 (1H, s, H-3), 5.83 (1H, t, H-12), 4.28 (3H, s, OCH₃), 3.09 (2H, d, H-11), 2.88 (3H, s, H-21), 2.39 (3H, s, CH₃-13) ppm; ¹³C-NMR (DMSO-d₆, 75 MHz): δ= 166.4 (CH, C-14), 161.3 (C, C-2), 159.0 (C, C-7), 157.4 (C, C-4), 155.0 (C, C-9), 152.7 (C, C-15), 146.2 (C, C-4), 142.3 (C, C-17), 141.7 (CH, C-12), 130.2 (CH, C-19), 125.3 (CH, C-18), 124.6 (CH, C-5), 122.4 (CH, C-16), 121.4 (C, C-13), 119.1 (CH, C-20), 115.1 (C, C-10), 113.8 (CH, C-3), 112.2 (CH, C-6), 103.4 (CH, C-8), 58.2 (CH₃, OCH₃-C-7), 38.8 (CH₂, C-11), 25.0 (CH₃, C-21), 18.4 (CH₃, CH₃-C-13) ppm.

7-methoxy-4-((2*E*)-3-methyl-4-(*p*-tolylimino)but-2-en-1-yl)-2*H*-chromen-2-one (**MC6**): mp=153-155°C; λ_{max} (EtOH)=340 nm; % yield=76; R_f= 0.79; FTIR (v, stretching, cm⁻¹): 3062 (C-H, alkene), 2902 (C-H, alkane), 1727 (C=O, ester), 1677, 1623 (C=C, alkene), 1635 (N=C), 1585 (C=O, aromatic), 1249 and 1055 (C-O-C, ether); ¹H-NMR (DMSO-d₆, 300 MHz): δ= 8.22 (1H, d, H-5), 8.12 (1H, s, H-14), 8.02 (1H, d, H-16), 7.89 (1H, d, H-19), 7.76 (1H, d, H-20), 7.12 (1H, s, H-8), 6.90 (1H, d, H-17), 6.76 (1H, d, H-7), 6.44 (1H, s, H-3), 5.77 (1H, t, H-12), 4.28 (3H, s, OCH₃), 3.13 (2H, d, H-11), 2.86 (3H, s, H-21), 2.42 (3H, s, CH₃-13) ppm; ¹³C-NMR (DMSO-d₆, 75 MHz): δ= 167.3 (CH, C-14), 164.2 (C, C-2), 157.1 (C, C-7), 154.2 (C, C-4), 153.3 (C, C-9), 150.2 (C, C-15), 145.7 (C, C-4), 141.8 (C, C-18), 141.1 (CH, C-12), 131.8 (CH, C-16), 127.5 (CH, C-19), 125.5 (CH, C-5), 124.3 (CH, C-20), 123.8 (CH, C-17), 121.4 (CH, C-13), 116.2 (C, C-10), 114.3 (CH, C-3), 110.3 (CH, C-6), 105.5 (CH, C-8), 53.4 (CH₃, OCH₃-C-7), 37.6 (CH₂, C-11), 22.8 (CH₃, C-21), 19.1 (CH₃, CH₃-C-13) ppm.

7-methoxy-4-((2*E*)-3-((*o*-tolylimino)methyl)pent-2-en-1-yl)-2*H*-chromen-2-one (**MC7**): mp=160-163°C; λ_{max} (EtOH)=345 nm; % yield=76; R_f= 0.80; FTIR (v, stretching, cm⁻¹): 3066 (C-H, alkene), 2912 (C-H, alkane), 1727 (C=O, ester), 1678, 1620 (C=C, alkene), 1637 (N=C), 1588 (C=O, aromatic), 1250 and 1052 (C-O-C, ether); ¹H-NMR (DMSO-d₆, 300 MHz): δ= 8.21 (1H, d, H-5), 8.11 (1H, s, H-14), 8.00 (1H, t, H-19), 7.68 (1H, d, H-17), 7.36 (1H, d, H-20), 7.10 (1H, s, H-8), 6.92 (1H, d, H-7), 6.71 (1H, t, H-18), 6.45 (1H, s, H-3), 5.95 (1H, t, H-12), 4.22 (3H, s, OCH₃), 3.13 (2H, d, H-11), 2.84 (3H, s, H-21), 2.60 (2H, q, *J*= 9 Hz, CH₂CH₃-13), 1.86 (3H, t, *J*= 9 Hz, CH₂CH₃-13) ppm; ¹³C-NMR (DMSO-d₆, 75 MHz): δ= 165.2 (CH, C-14), 162.7 (C, C-2), 158.2 (C, C-7), 156.1 (C, C-4), 155.6 (C, C-9), 150.1 (C, C-15), 145.2 (C, C-4), 140.4 (CH, C-12), 133.4 (CH, C-17), 131.5 (C, C-13), 130.9 (C, C-16), 128.8 (CH, C-18), 126.7 (CH, C-19), 124.2 (CH, C-5), 118.4 (CH, C-20), 115.2 (C, C-10), 113.5 (CH, C-3), 110.1 (CH, C-6), 103.3 (CH, C-8), 57.1 (CH₃, OCH₃-C-7), 38.8 (CH₂, C-11), 22.8 (CH₃, C-21), 20.4 (CH₂, CH₂CH₃-C-13), 16.8 (CH₃, CH₂CH₃-C-13) ppm.

7-methoxy-4-((2*E*)-3-((*m*-tolylimino)methyl)pent-2-en-1-yl)-2*H*-chromen-2-one (**MC8**): mp=173-176°C; λ_{max} (EtOH)=347 nm; % yield=71; R_f= 0.80; FTIR (v, stretching, cm⁻¹): 3073 (C-H, alkene), 2908 (C-H, alkane), 1724 (C=O, ester), 1675, 1630 (C=C, alkene), 1640 (N=C), 1584 (C=O, aromatic), 1250 and 1042 (C-O-C, ether); ¹H-NMR (DMSO-d₆, 300 MHz): δ= 8.26 (1H, d, H-5), 8.15 (1H, s, H-14), 7.89 (1H, t, H-19), 7.41 (1H, s, H-

16), 7.33 (1H, d, H-18), 7.19 (1H, d, H-20), 7.02 (1H, s, H-8), 6.87 (1H, d, H-7), 6.46 (1H, s, H-3), 5.78 (1H, t, H-12), 4.30 (3H, s, OCH₃), 3.06 (2H, d, H-11), 2.90 (3H, s, H-21), 2.67 (2H, q, *J* = 9 Hz, CH₂CH₃-13), 1.82 (3H, t, *J* = 9 Hz, CH₂CH₃-13) ppm; ¹³C-NMR (DMSO-d₆, 75 MHz): δ = 164.2 (CH, C-14), 161.6 (C, C-2), 158.1 (C, C-7), 156.2 (C, C-4), 154.4 (C, C-9), 152.3 (C, C-15), 146.2 (C, C-4), 142.6 (C, C-17), 140.1 (CH, C-12), 130.9 (C, C-13), 128.1 (CH, C-19), 125.8 (CH, C-18), 124.0 (CH, C-5), 122.4 (CH, C-16), 119.5 (CH, C-20), 115.2 (C, C-10), 113.8 (CH, C-3), 110.9 (CH, C-6), 103.4 (CH, C-8), 58.5 (CH₃, OCH₃-C-7), 39.1 (CH₂, C-11), 24.6 (CH₃, C-21), 21.1 (CH₂, CH₂CH₃-C-13), 17.2 (CH₃, CH₂CH₃-C-13) ppm.

7-methoxy-4-((2*E*)-3-((p-tolylimino)methyl)pent-2-en-1-yl)-2H-chromen-2-one (**MC9**): mp = 168–171 °C; λ_{max} (EtOH) = 340 nm; % yield = 73; R_f = 0.81; FTIR (ν, stretching, cm⁻¹): 3055 (C-H, alkene), 2911 (C-H, alkane), 1726 (C=O, ester), 1680, 1620 (C=C, alkene), 1632 (N=C), 1586 (C=O, aromatic), 1243 and 1050 (C-O-C, ether); ¹H-NMR (DMSO-d₆, 300 MHz): δ = 8.20 (1H, d, H-5), 8.11 (1H, s, H-14), 8.01 (1H, d, H-16), 7.92 (1H, d, H-19), 7.72 (1H, d, H-20), 7.10 (1H, s, H-8), 6.94 (1H, d, H-17), 6.72 (1H, d, H-7), 6.46 (1H, s, H-3), 5.74 (1H, t, H-12), 4.31 (3H, s, OCH₃), 3.18 (2H, d, H-11), 2.84 (3H, s, H-21), 2.64 (2H, q, *J* = 9 Hz, CH₂CH₃-13), 1.80 (3H, t, *J* = 9 Hz, CH₂CH₃-13) ppm; ¹³C-NMR (DMSO-d₆, 75 MHz): δ = 165.1 (CH, C-14), 162.8 (C, C-2), 155.9 (C, C-7), 154.7 (C, C-4), 153.2 (C, C-9), 149.1 (C, C-15), 145.7 (C, C-4), 141.9 (CH, C-12), 139.2 (C, C-18), 133.2 (CH, C-16), 130.9 (CH, C-13), 128.3 (CH, C-19), 125.3 (CH, C-5), 124.7 (CH, C-20), 122.3 (CH, C-17), 116.9 (C, C-10), 114.0 (CH, C-3), 109.6 (CH, C-6), 103.9 (CH, C-8), 53.5 (CH₃, OCH₃-C-7), 37.9 (CH₂, C-11), 24.2 (CH₃, C-21), 20.5 (CH₂, CH₂CH₃-C-13), 17.8 (CH₃, CH₂CH₃-C-13) ppm.

2.8. Introductory antitumor activity

In a sheet of 96 holes, the cells (10.000) of the chosen cancer line were dispersed in each single hole and subsequently exposed in the next 24 hr to the screened products at a defined concentration. The applied concentrations that ranged from 200 µg/ml to 6.25 µg/ml were prepared from a stock DMSO solution (1 mM) in a double-dilution manner. The MTT test was initiated in the next 72 hr of exposure by detaching the medium, applying 26 µl of the MTT reagent (3.23 mM), and posteriorly incubating the exposed cells for 90 min at 37 °C. The cell viability was estimated via a multi-mode microplate reader adjusted at 492 nm by following the absorbances of the exposed hole (A_E) and unexposed hole (A_U).

The cytotoxic evaluation of the screened products was verified by calculating the growth inhibition (GI) percentage via the following mathematical rule: GI % = (A_U – A_E)/A_U × 100 (Borges *et al.*, 2005; Altemimi *et al.*, 2017; Nejres *et al.*, 2020).

3. RESULTS AND DISCUSSION:

3.1. Chemical approach

The synthetic plan for preparing the target products was depicted in Scheme 1. This plan commenced by utilizing the strong acidic feature of H₂SO₄ to transform citric acid to acetone dicarboxylic acid, which was condensed via a Pechmann reaction with m-guaiacol affording 7-methoxycoumarin-4-acetic acid (**MA1**) (Hari Krishna and Thriveni, 2016; Bouasla *et al.*, 2017; Jung *et al.*, 2018; Melita Lončarić, Dajana Gašo-Sokač, 2020). The carboxylic acid moiety of the aforementioned product was reduced to aldehyde group by using a mild reducing agent, LiAlH(OtBu)₃, which was selected to avoid the cleavage of the lactone ring (Liu *et al.*, 2017) yielding **MA2** product. In the next step, the aldol condensation reaction was designed to involve the nucleophilic attack of the enol form of **MA2** to the protonated aldehyde moiety of the employed acetaldehyde derivatives affording **MA3-MA5** products (Amarasekara and Ha, 2018). The aldehyde groups of these products were coupled with the primary amine groups of the utilized toluidine derivatives to generate Schiff-base containing products termed multifunctional coumarin derivatives (**MC1-MC9**) (Purkait *et al.*, 2016; Al Zoubi *et al.*, 2018; van Schijndel *et al.*, 2019). The design of the synthetic plan, as well as the characterization data, confirmed that the chemical structures represented in Figure 1 could be attributed to the target synthetic products.

3.2 Introductory antitumor activity

The cytotoxic estimation of the synthesized multifunctional coumarins (**MC1-MC9**) was inspected with MTT dye to determine the cell viability. The cancer lines utilized in this estimation included HeLa (cervix), SKG (esophageal), MCF-7 (breast), and AMN3 (murine mammary adenocarcinoma). In this study, six concentrations of the individual product were prepared via serial double-dilution and employed to calculate the IC₅₀ values. Also, the solvent DMSO and the standard cytotoxic agent 5-fluorouracil were employed as negative and positive leading reagents respectively (Saha *et al.*, 2017; Haq *et al.*, 2019; Stringlis *et al.*, 2019).

The outcomes illustrated in Table 1 and explained in Figure 2 reflect several interesting considerations. Firstly, IC_{50} values of the synthesized multifunctional coumarins are generally higher than that of the positive standard. Secondly, the position of R' group has a notable effect on the cytotoxicity; the order of increasing effect is $4-CH_3 > 2-CH_3 > 3-CH_3$. From this order, it is concluded that the cytotoxicity may be enhanced by substituting the aromatic ring with an electron-donating group in such a manner to increase the inductive effect toward the nitrogen portion of the Schiff-base (Purkait *et al.*, 2016; Dos Santos *et al.*, 2017; Teran *et al.*, 2019).

Thirdly, the steric factor exerted by the group substituted on the carbon next to the carbon bound to the Schiff-base nitrogen has an effect on the cytotoxicity (Purkait *et al.*, 2016). This can be clarified by observing the decline in the antitumor activity of the synthesized products as this substituted group becomes bulkier. In this context, compounds **MC1**, **MC2**, and **MC3** have a better antitumor activity versus the test cell lines than that of their corresponding compounds **MC4**, **MC5**, and **MC6** which in turn have a better activity than that of compounds **MC7**, **MC8**, and **MC9**.

Fourthly, the steric factor described in the third point exerts a higher impact on cytotoxicity than that of the inductive effect described in the second point (Fattuoni *et al.*, 2020). Fifthly, similar antitumor tendency of the synthesized multifunctional coumarins was predestined versus the test cell lines, with the best activity being against MCF-7 cells and the least effect being versus AMN3 cells.

Finally, it can be assumed that the nitrogen portion of the Schiff-base may play a significant role in the cytotoxicity of the synthesized coumarins by participating in the product-target interactions as a hydrogen-bond acceptor (Chow *et al.*, 2014).

4. CONCLUSIONS:

Based on the results acquired from the antitumor activity versus four prevalent human tumor lines, compound **MC3** showed the best activity. From that, it is concluded the nitrogen fraction of the Schiff-base linkage may play a significant role as a hydrogen-bond acceptor in the antitumor activity of the synthesized coumarins. This role may rely on the steric factor on the carbon next to that attached to nitrogen and on the inductive factor exerted by the moiety linked directly to this nitrogen. The position of R' group has a significant effect on the cytotoxicity of the

synthesized products; the order of increasing effect is $4-CH_3 > 2-CH_3 > 3-CH_3$. From this order, it is concluded that the cytotoxicity may be enhanced by substituting the aromatic ring with an electron-donating group in such a manner to increase the inductive effect toward the nitrogen portion of the Schiff-base. Also, the steric factor described above exerts a higher impact on cytotoxicity than that of the inductive effect. Accordingly, these coumarins may represent a novel template for the evolution of new antitumor agents.

5. ACKNOWLEDGEMENTS:

The authors thank the Mosul University/Faculty of Pharmacy for their support. The linguistic assistance provided by Dr. Mahmood H. Jasim is also gratefully acknowledged.

6. CONFLICT OF INTEREST:

There are no conflicts of interest.

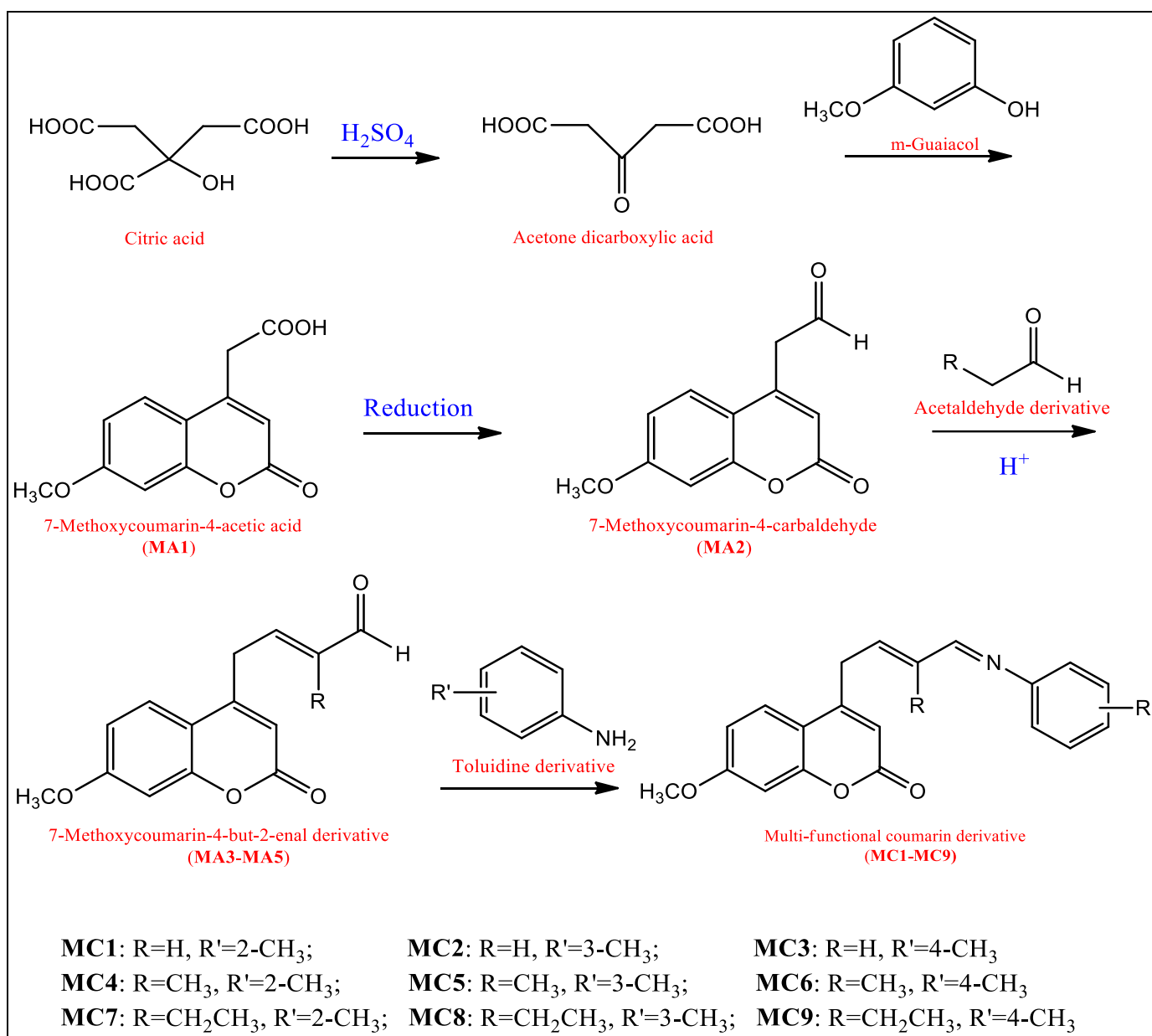
7. REFERENCES:

1. Alfahad, M., Qazzaz, M. E., Abed, M. N., Alassaf, F. A. and Jasim, M. H. M. (2020) 'Comparison of Antioxidant activity of different brands of esomeprazole available in Iraqi pharmacies', *Systematic Reviews in Pharmacy*, 11(5), pp. 330–334. doi: 10.31838/srp.2020.5.48.
2. Altemimi, A., Lakhssassi, N., Baharlouei, A., Watson, D. G. and Lightfoot, D. A. (2017) 'Phytochemicals: Extraction, isolation, and identification of bioactive compounds from plant extracts', *Plants*, 6(4). doi: 10.3390/plants6040042.
3. Amarasekara, A. S. and Ha, U. (2018) 'Acid catalyzed aldol condensations of ketones with glyoxylic acid: A simple single-step synthesis of 4-oxo-2,5-heptdienedioic acids', *Synthetic Communications*. Taylor & Francis, 48(19), pp. 2533–2538. doi: 10.1080/00397911.2018.1511998.
4. Bashir, M. K., Mustafa, Y. F. and Oglah, M. K. (2020) 'Antitumor, antioxidant, and antibacterial activities of glycosyl-conjugated compounds: A review', *Systematic Reviews in Pharmacy*, 11(4), pp. 175–187. doi: 10.31838/srp.2020.4.26.
5. Borges, F., Roleira, F., Milhazes, N.,

- Santana, L. and Uriarte, E. (2005) 'Simple Coumarins and Analogues in Medicinal Chemistry: Occurrence, Synthesis and Biological Activity', *Current Medicinal Chemistry*, 12(8), pp. 887–916. doi: 10.2174/0929867053507315.
6. Bouasla, S., Amaro-Gahete, J., Esquivel, D., López, M. I., Jiménez-Sanchidrián, C., Teguche, M. and Romero-Salguero, F. J. (2017) 'Coumarin derivatives solvent-free synthesis under microwave irradiation over heterogeneous solid catalysts', *Molecules*, 22(12). doi: 10.3390/molecules22122072.
 7. Cakmak, K. C. and Gülçin, İ. (2019) 'Anticholinergic and antioxidant activities of usnic acid-an activity-structure insight', *Toxicology Reports*, 6(October), pp. 1273–1280. doi: 10.1016/j.toxrep.2019.11.003.
 8. Chen, C. (2016) 'Sinapic acid and its derivatives as medicine in oxidative stress-induced diseases and aging', *Oxidative Medicine and Cellular Longevity*. Hindawi Publishing Corporation, 2016. doi: 10.1155/2016/3571614.
 9. Chow, M. J., Licon, C., Yuan Qiang Wong, D., Pastorin, G., Gaiddon, C. and Ang, W. H. (2014) 'Discovery and investigation of anticancer Ruthenium–Arene SchiffBase complexes via water-promoted combinatorial three component assembly', *Journal of Medicinal Chemistry*, 57(14), pp. 6043–6059. doi: 10.1021/jm500455p.
 10. Dandriyal, J., Singla, R., Kumar, M. and Jaitak, V. (2016) 'Recent developments of C-4 substituted coumarin derivatives as anticancer agents', *European Journal of Medicinal Chemistry*, pp. 141–168. doi: 10.1016/j.ejmech.2016.03.087.
 11. Detsi, A., Kontogiorgis, C. and Hadjipavlou-Litina, D. (2017) 'Coumarin derivatives: an updated patent review (2015-2016)', *Expert Opinion on Therapeutic Patents*. Taylor & Francis, 27(11), pp. 1201–1226. doi: 10.1080/13543776.2017.1360284.
 12. Fattuoni, C., Vascellari, S. and Pivetta, T. (2020) 'Synthesis, protonation constants and biological activity determination of amino acid–salicylaldehyde-derived Schiff bases', *Amino Acids*. Springer Vienna, 52(3), pp. 397–407. doi: 10.1007/s00726-019-02816-0.
 13. Fessler, M. B., Rudel, L. L. and Brown, M. (2013) 'Enantioselective synthesis of pactamycin, a complex antitumor antibiotic', *Science*, 340(6129), pp. 180–182. doi: 10.1038/jid.2014.371.
 14. Fitzmaurice, C., Dicker, D., Pain, A., Hamavid, H., Moradi-Lakeh, M., MacIntyre, M. F., Allen, C., Hansen, G., Woodbrook, R., Wolfe, C., Hamadeh, R. R., Moore, A., Werdecker, A., Gessner, B. D., Te Ao, B., McMahon, B., Karimkhani, C., Yu, C., Cooke, G. S., and others (2015) 'The global burden of cancer 2013', *JAMA Oncology*, 1(4), pp. 505–527. doi: 10.1001/jamaoncol.2015.0735.
 15. Forni, C., Facchiano, F., Bartoli, M., Pieretti, S., Facchiano, A., D'Arcangelo, D., Norelli, S., Valle, G., Nisini, R., Beninati, S., Tabolacci, C. and Jadeja, R. N. (2019) 'Beneficial role of phytochemicals on oxidative stress and age-related diseases', *BioMed Research International*. Hindawi, 2019(Figure 1). doi: 10.1155/2019/8748253.
 16. Gonelimali, F. D., Lin, J., Miao, W., Xuan, J., Charles, F., Chen, M. and Hatab, S. R. (2018) 'Antimicrobial properties and mechanism of action of some plant extracts against food pathogens and spoilage microorganisms', *Frontiers in Microbiology*, 9(JUL), pp. 1–9. doi: 10.3389/fmicb.2018.01639.
 17. Hameed, A., al-Rashida, M., Uroos, M., Abid Ali, S. and Khan, K. M. (2017) 'Schiff bases in medicinal chemistry: a patent review (2010-2015)', *Expert Opinion on Therapeutic Patents*. Taylor & Francis, 27(1), pp. 63–79. doi: 10.1080/13543776.2017.1252752.
 18. Haq, S. H., Al-Ruwaished, G., Al-Mutlaq, M. A., Naji, S. A., Al-Mogren, M., Al-Rashed, S., Ain, Q. T., Al-Amro, A. A. and Al-Mussallam, A. (2019) 'Antioxidant, Anticancer Activity and Phytochemical Analysis of Green Algae, Chaetomorpha Collected from the Arabian Gulf', *Scientific reports*. Springer US, 9(1), p. 18906. doi: 10.1038/s41598-019-55309-1.
 19. Hari Krishna, M. and Thriveni, P. (2016) 'Synthesis of coumarins via Pechmann reaction using Cr(NO₃)₃·9H₂O as a Catalyst under microwave irradiation', *Der Pharma Chemica*, 8(9), pp. 94–98.
 20. Iheagwam, F. N., Israel, E. N., Kayode, K. O., De Campos, O. C., Ogunlana, O. O.

- and Chinedu, S. N. (2019) 'GC-MS Analysis and Inhibitory Evaluation of Terminalia catappa Leaf Extracts on Major Enzymes Linked to Diabetes', *Evidence-based Complementary and Alternative Medicine*, 2019. doi: 10.1155/2019/6316231.
21. Jing Lia, Fei Yua, Yi Chena, and D. O. (2015) 'Polymeric drugs: Advances in the development of pharmacologically active polymers', *Journal of Controlled Release*, 219(1), pp. 139–148. doi: 10.1016/j.jconrel.2015.09.043.
 22. Jung, J. W., Kim, N. J., Yun, H. and Han, Y. T. (2018) 'Recent advances in synthesis of 4-arylcoumarins', *Molecules*. doi: 10.3390/molecules23102417.
 23. Kajal, A., Bala, S., Kamboj, S., Sharma, N. and Saini, V. (2013) 'Schiff Bases: A Versatile Pharmacophore', *Journal of Catalysts*, 2013(1), pp. 1–14. doi: 10.1155/2013/893512.
 24. Kumar, K. A., Nagamallu, R. and Govindappa, V. K. (2015) 'Comprehensive review on coumarins: Molecules of potential chemical and pharmacological interest Comprehensive review on coumarins: Molecules of potential chemical and pharmacological interest', *Journal of Chemical and Pharmaceutical Research*, 7(9), pp. 67–81.
 25. Li, H., Yao, Y. and Li, L. (2017) 'Coumarins as potential antidiabetic agents', *Journal of Pharmacy and Pharmacology*, pp. 1253–1264. doi: 10.1111/jphp.12774.
 26. Liu, J., Maisonia-Besset, A., Wenzel, B., Canitrot, D., Baufond, A., Chezal, J. M., Brust, P. and Moreau, E. (2017) 'Synthesis and in vitro evaluation of new fluorinated quinoline derivatives with high affinity for PDE5: Towards the development of new PET neuroimaging probes', *European Journal of Medicinal Chemistry*, 136(3), pp. 548–560. doi: 10.1016/j.ejmech.2017.03.091.
 27. Medimagh-Saidana, S., Romdhane, A., Daami-Remadi, M., Jabnoun-Khiareddine, H., Touboul, D., Jannet, H. Ben and Hamza, M. A. (2015) 'Synthesis and antimicrobial activity of novel coumarin derivatives from 4-methylumbelliferone', *Medicinal Chemistry Research*. Springer US, 24(8), pp. 3247–3257. doi: 10.1007/s00044-015-1368-y.
 28. Melita Lončarić, Dajana Gašo-Sokać, S. J. and M. M. (2020) 'Recent Advances in the Synthesis of Coumarin Derivatives from Different Starting Materials', *Biomolecules*, 10(151). doi: 10.3390/biom10010151.
 29. Mustafa, Y. F. (2019) 'Synthesis, characterization and preliminary cytotoxic study of sinapic acid and its analogues', *Journal of Global Pharma Technology*, 11(9), pp. 1–10.
 30. Nejres, A. M., Mustafa, Y. F. and Aldewachi, H. S. (2020) 'Evaluation of natural asphalt properties treated with egg shell waste and low density polyethylene', *International Journal of Pavement Engineering*. doi: 10.1080/10298436.2020.1728534.
 31. Pasciu, V., Baralla, E., Varoni, M. V. and Demontis, M. P. (2019) 'Evaluation of curcuma and ginger mixture ability to prevent ROS production induced by bisphenol S: an in vitro study', *Drug and Chemical Toxicology*. Taylor & Francis, 0(0), pp. 1–7. doi: 10.1080/01480545.2019.1690499.
 32. Pisoschi, A. M. and Pop, A. (2015) 'The role of antioxidants in the chemistry of oxidative stress: A review', *European Journal of Medicinal Chemistry*. Elsevier Masson SAS, 97, pp. 55–74. doi: 10.1016/j.ejmech.2015.04.040.
 33. Purkait, K., Chatterjee, S., Karmakar, S. and Mukherjee, A. (2016) 'Alteration of steric hindrance modulates glutathione resistance and cytotoxicity of three structurally related Ru(II)-P-cymene complexes', *Dalton Transactions*. Royal Society of Chemistry, 45(20), pp. 8541–8555. doi: 10.1039/c5dt04781a.
 34. Rahimi Khoigani, S., Rajaei, A. and Goli, S. A. H. (2017) 'Evaluation of antioxidant activity, total phenolics, total flavonoids and LC-MS/MS characterisation of phenolic constituents in *Stachys lavandulifolia*', *Natural Product Research*. doi: 10.1080/14786419.2016.1233410.
 35. Saha, S. K., Lee, S. Bin, Won, J., Choi, H. Y., Kim, K., Yang, G. M., Dayem, A. A. and Cho, S. G. (2017) 'Correlation between oxidative stress, nutrition, and cancer initiation', *International Journal of Molecular Sciences*, 18(7). doi: 10.3390/ijms18071544.

36. Sanap, K. K. and Samant, S. D. (2015) 'Regiospecific inverse electron demand Diels-Alder reactions of 7-methylcoumarin-4-azadienes', *RSC Advances*. Royal Society of Chemistry, 5(46), pp. 36696–36706. doi: 10.1039/c5ra06262d.
37. Dos Santos, A. G., Marquês, J. T., Carreira, A. C., Castro, I. R., Viana, A. S., Mingeot-Leclercq, M. P., De Almeida, R. F. M. and Silva, L. C. (2017) 'The molecular mechanism of Nystatin action is dependent on the membrane biophysical properties and lipid composition', *Physical Chemistry Chemical Physics*, 19(44), pp. 30078–30088. doi: 10.1039/c7cp05353c.
38. van Schijndel, J., Molendijk, D., Spakman, H., Knaven, E., Canalle, L. A. and Meuldijk, J. (2019) 'Mechanistic considerations and characterization of ammonia-based catalytic active intermediates of the green Knoevenagel reaction of various benzaldehydes*', *Green Chemistry Letters and Reviews*, 12(3), pp. 323–331. doi: 10.1080/17518253.2019.1643931.
39. Srikrishna, D., Godugu, C. and Dubey, P. K. (2016) 'A Review on Pharmacological Properties of Coumarins', *Mini-Reviews in Medicinal Chemistry*, 18(2). doi: 10.2174/1389557516666160801094919.
40. Stefanachi, A., Leonetti, F., Pisani, L., Catto, M. and Carotti, A. (2018) *Coumarin: A natural, privileged and versatile scaffold for bioactive compounds*, *Molecules*. doi: 10.3390/molecules23020250.
41. Stringlis, I. A., De Jonge, R. and Pieterse, C. M. J. (2019) 'The Age of Coumarins in Plant-Microbe Interactions', *Plant and Cell Physiology*, 60(7), pp. 1405–1419. doi: 10.1093/pcp/pcz076.
42. Swamy, R. R., Gowda, R., Gowda, K. V. A. and Basanagouda, M. (2015) 'Crystal structure of 7,8-benzocoumarin-4-acetic acid', *Acta Crystallographica Section E: Crystallographic Communications*. International Union of Crystallography, 71(1415), pp. o617–o618. doi: 10.1107/S2056989015014103.
43. Teran, R., Guevara, R., Mora, J., Dobronski, L., Barreiro-Costa, O., Beske, T., Pérez-Barrera, J., Araya-Maturana, R., Rojas-Silva, P., Poveda, A. and Heredia-Moya, J. (2019) 'Characterization of antimicrobial, antioxidant, and leishmanicidal activities of Schiff base derivatives of 4-aminoantipyrine', *Molecules*, 24(15). doi: 10.3390/molecules24152696.
44. Yao, H., Liu, J., Xu, S., Zhu, Z. and Xu, J. (2017) 'The structural modification of natural products for novel drug discovery', *Expert Opinion on Drug Discovery*. Taylor & Francis, 12(2), pp. 121–140. doi: 10.1080/17460441.2016.1272757.
45. Al Zoubi, W., Mohamed, S. G., Al-Hamdani, A. A. S., Mahendradhany, A. P. and Ko, Y. G. (2018) 'Acyclic and cyclic imines and their metal complexes: recent progress in biomaterials and corrosion applications', *RSC Advances*. Royal Society of Chemistry, 8(41), pp. 23294–23318. doi: 10.1039/C8RA01890A.



Scheme 1. The designed steps adopted for the chemical synthesis of the target multifunctional coumarins (MC1-MC9).

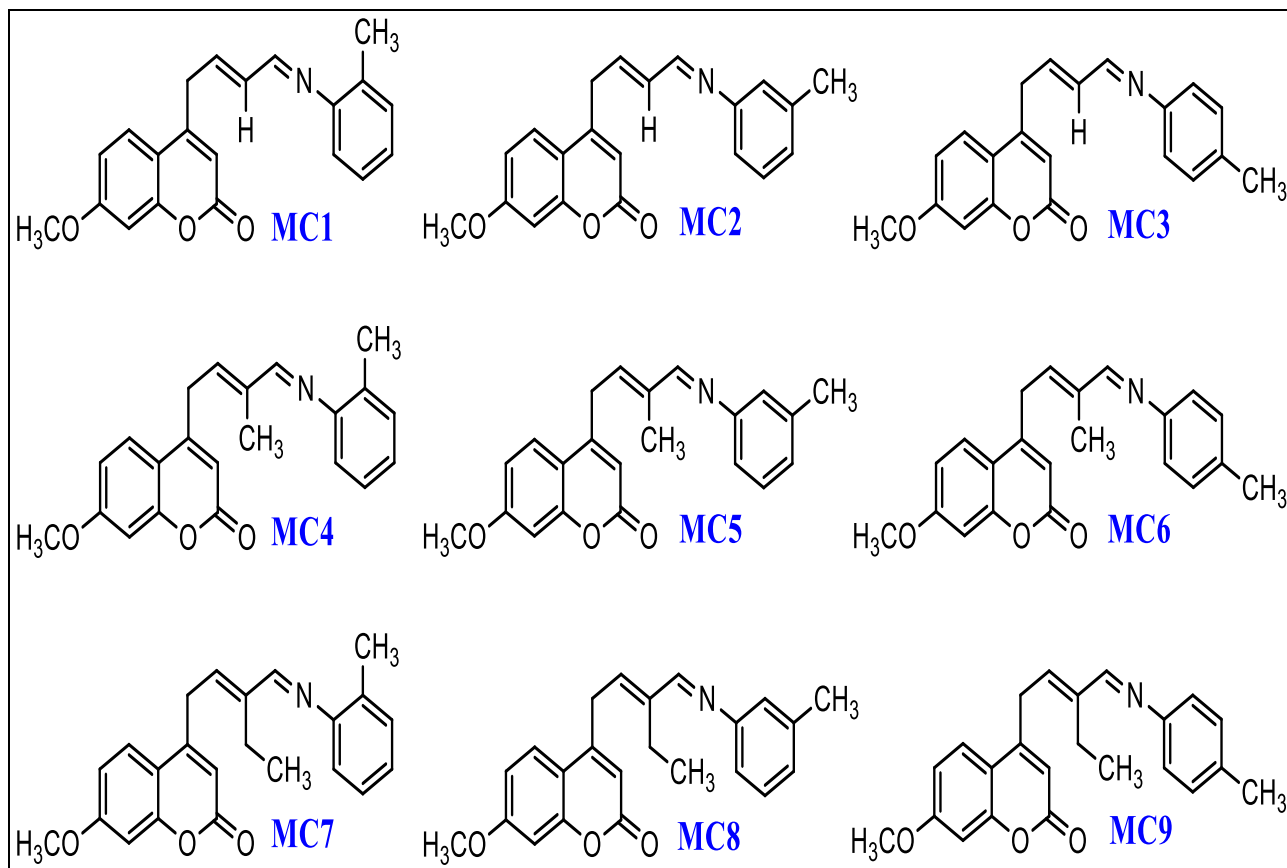


Figure 1. Chemical structures of the target multifunctional coumarins (MC1-MC9).

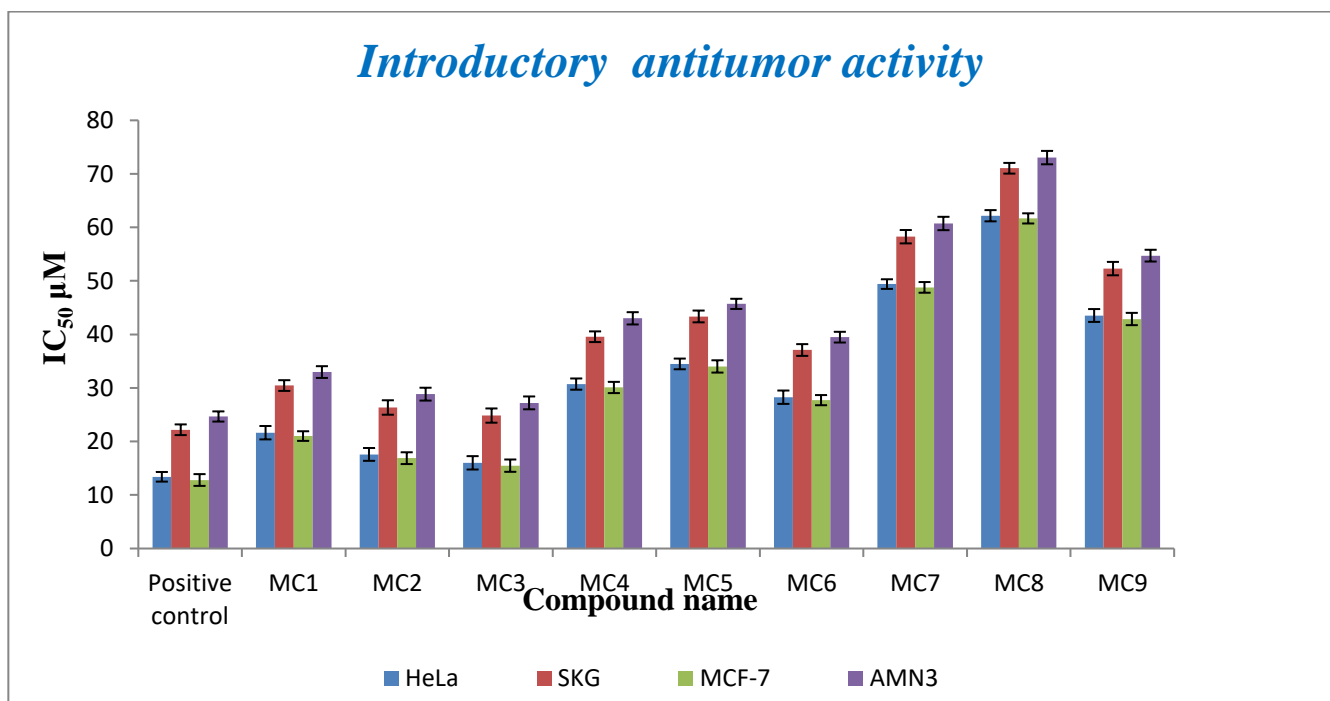


Figure 2. Graph representing the IC_{50} values of the synthesized multifunctional coumarins and the positive control versus the employed tumor cell lines.

Table 1. Outcomes assumed from assaying the *in vitro* antitumor activity of the positive control and synthesized multifunctional coumarins utilizing MTT test.

Compound Name	Introductory antitumor activity			
	IC ₅₀ ± SD			
	HeLa	SKG	MCF-7	AMN3
Positive control*	13.40 ± 0.90	22.19 ± 1.00	12.80 ± 1.10	24.67 ± 0.95
MC1	21.64 ± 1.25	30.45 ± 1.00	21.01 ± 0.90	32.97 ± 1.10
MC2	17.58 ± 1.20	26.35 ± 1.35	16.88 ± 1.10	28.84 ± 1.20
MC3	16.01 ± 1.25	24.84 ± 1.33	15.48 ± 1.15	27.21 ± 1.20
MC4	30.72 ± 1.05	39.57 ± 1.00	30.09 ± 1.05	43.01 ± 1.15
MC5	34.49 ± 1.00	43.36 ± 1.10	34.02 ± 1.15	45.71 ± 0.95
MC6	28.27 ± 1.25	37.09 ± 1.10	27.72 ± 0.95	39.49 ± 1.00
MC7	49.41 ± 0.90	58.26 ± 1.25	48.79 ± 1.00	60.73 ± 1.25
MC8	62.18 ± 1.05	71.05 ± 1.00	61.68 ± 0.95	73.04 ± 1.25
MC9	43.54 ± 1.20	52.30 ± 1.25	42.88 ± 1.15	54.72 ± 1.10

Notes: * The positive control is 5-fluorouracil. IC₅₀ are expressed in µM. SD is calculated from three independent experiments.

O EMPREGO DE UM JOGO DE PERGUNTAS E RESPOSTAS COMO UMA FORMA DE PROBLEMATIZAR E MOTIVAR O ENSINO DE FÍSICA NO ENSINO MÉDIO**EMPLOYMENT OF A SET OF QUESTIONS AND ANSWERS AS A WAY TO PROBLEMATIZE AND MOTIVATE THE TEACHING OF PHYSICS IN HIGH SCHOOL**RIATTO, Fabrizio Belli ^{1*};¹ Universidade Federal do Rio Grande do Sul, Departamento de Física. Brasil

* Autor correspondente

e-mail: fabrizio2305@hotmail.com

Received 17 July 2020; received in revised form 25 August 2020; accepted 23 October 2020

RESUMO

A Física, assim como o ensino de ciências naturais, é fundamental para o desenvolvimento científico e tecnológico. Embora de fundamental importância para a sociedade, observa-se um desinteresse muito grande por parte dos alunos de ensino médio. O objetivo desse trabalho foi desenvolver e aplicar uma estratégia que envolveu um “jogo de perguntas e respostas” para introduzir o estudo da mecânica de forma diferenciada e mais atraente para os alunos. Quando se fala em forças, por exemplo, o senso comum está muito enraizado e torna-se complexo promover a mudança conceitual nos jovens aprendizes. O jogo foi utilizado como problematização visando criar um ambiente de necessidade de busca de novos conhecimentos para enfrentar situações e responder questões. A proposta foi aplicada a uma turma de segundo ano do ensino médio de uma escola particular de Porto Alegre. A amostra consistiu de trinta e três alunos com idade entre quinze e dezessete anos, divididos entre dezoito meninas e quinze meninos. A aplicação foi feita em horário regular das aulas. O jogo nasceu da necessidade de criar nos alunos uma vontade e predisposição para buscar o conhecimento e transformar sua forma de pensar a física. A formulação das perguntas e respostas foram pensados com o objetivo de criar subsunçores mínimos para que os estudantes possam dar os passos iniciais em busca do novo conhecimento. Foi possível observar através das respostas dadas pelos alunos que o grau de satisfação foi bastante elevado e que eles gostaram não só do jogo em si, mas também da mudança na forma clássica e engessada que o conteúdo foi trabalhado.

Palavras-chave: *ensino de física; dinâmica; jogo de perguntas e respostas; aprendizagem significativa.***ABSTRACT**

Physics, like the teaching of natural sciences, is fundamental for scientific and technological development. Although of fundamental importance to society, there is a significant lack of interest in high school students. This study aimed to develop and apply a strategy that involved a “game of questions and answers” to introduce the study of mechanics in a differentiated and more attractive way for students. For example, when talking about strengths, common sense is very ingrained, and it becomes complex to promote conceptual change in young apprentices. The game was used as a problematization to create an environment of need to search for new knowledge to face situations and answer questions. The proposal was applied to a second-year high school class at a private school in Porto Alegre. The sample consisted of thirty-three students aged between fifteen and seventeen, divided between eighteen girls and fifteen boys. The application was made during regular classes. The game was born from the need to create students with a willingness and predisposition to seek knowledge and transform their thinking about physics. The formulation of questions and answers was designed to make minimal subunits to search for a new experience. Through the students' responses, it was possible to observe that the degree of satisfaction was relatively high and that they liked the game itself and the change in the classic and plastered form that the content was worked on.

Keywords: *physics teaching; dynamics; game of questions and answers; meaningful learning.*

1. INTRODUÇÃO:

O Brasil passa por um momento delicado, de mudanças e novas políticas públicas endereçadas à educação, em especial, na busca pela qualidade da educação. Ainda que não haja consenso sobre o conceito de “qualidade da educação”, entendida como uma construção histórica que assume diferentes significados em tempos e espaços diversos (BRASIL, 2012, p. 8, Parecer), a busca por novas estratégias que possam resultar em melhorias no processo de ensino e aprendizagem. Segundo Gadotti (2010, p. 15), “*o direito à educação não é o direito de se matricular na escola*”, mas sim, o de aprender na escola. O Brasil, a partir da última década do século XX, buscando melhorar seu IDH (Índice de Desenvolvimento Humano), optou por uma política de matrículas em massa, que gerou um aumento substancial do número de alunos que passaram a cursar os três níveis de Ensino (Fundamental, Médio e Superior). Embora essa não seja a única medida para mensurar o nível de educação de um país, tal manobra acarretou um aumento substancial nos índices medidos.

Por outro lado, não se pode deixar de reconhecer que esse movimento democratizou o acesso à educação, através da escolarização, que se consolidou como um direito social, oportunizando aos jovens da sociedade moderna a difusão do conhecimento científico construído pela humanidade no curso de sua história. (Oliveira, 2003). No entanto, não basta ofertar vagas na escola, é necessário que o Estado apresente políticas públicas eficazes de forma a garantir, não somente a entrada, mas a permanência desses jovens e a conclusão de seus cursos, pois, como destacam Nascimento & Abreu (2011), “*há um desejo da sociedade que essa educação seja ofertada com um ensino de qualidade*”.

O aumento do número de alunos matriculados nas escolas brasileiras não significa, necessariamente, uma melhora na educação brasileira. Para se ter um melhor aproveitamento em sala de aula é fundamental que tanto os alunos como os professores se sintam interessados e predispostos a uma interação frutífera. Mas não é, em geral, o que se observa dado que os problemas são muitos e de naturezas diversas (Lapo, 2003).

Segundo Lapo (2003):

O abandono da profissão docente tem sido crescente em todo o Brasil e com dados alarmantes em

ciudades como São Paulo. A falta de perspectiva do professor está amplamente relacionada à percepção de ausência de reconhecimento e valorização da atividade docente por parte dos alunos, pais e da sociedade em geral (ibid., p.65).

Observa-se assim um grave problema já anunciado, até mesmo por autoridades, do apagão de professores em várias disciplinas, entre elas a Física. Sem falar nas gravíssimas questões sociais, como violência e insegurança, que intimidam e ameaçam professores e estudantes nas escolas (Lapo, 2003).

Do ponto de vista da didática, em pleno século XXI, a despeito do uso no cotidiano massificado das tecnologias de comunicação e informação, ainda prevalece um modelo engessado, tradicional de aula, em que o professor fala e os alunos copiam. Um modelo ultrapassado que leva o aluno a se portar como um “aluno-objeto”, pois ele apenas escuta a aula e reproduz o mesmo na prova (Demo, 2007). Segundo esse autor, “*o aluno precisa ser motivado desde os primeiros passos imitativos e avançar na autonomia da expressão própria*” (ibid., p.29). Precisamente pensando em modificar os fatores pouco atrativos da sala de aula que, como já dito, afetam tanto professores como alunos, é que os jogos podem ser pensados como uma dinâmica capaz de oferecer nova perspectiva ao ensino (Melo; Sardinha, 2009).

Como referencial teórico, foi adotada a teoria de aprendizagem significativa de David Ausubel (Moreira, 2014) complementada pela teoria de Joseph Novak (Moreira, 2014). Essas teorias oferecem suporte à dinâmica do jogo dado que o que se busca é que o aluno aprenda a Física com significado, que não seja apenas uma memorização de fórmulas ou uma lista de exercícios padrão. Na perspectiva de Novak, segundo Moreira (2014), “*(...) os seres humanos fazem três coisas: pensam, sentem e atuam (fazem)*”. O uso do jogo em sala de aula busca justamente fazer com que o aluno se torne peça-chave em sua própria construção cognitiva, mas que também se envolva afetiva e ativamente. Ou seja, o estudante é incentivado a assumir um papel ativo, com a responsabilidade de criar, redigir, pesquisar, explicar, entre outras habilidades (Moreira, 2014).

Pode-se criar um ambiente social de sala de aula em que o aluno deixe de ser passivo, alvo somente de “cópias burocráticas”, e passe a ter

um papel ativo na construção do seu próprio conhecimento, na proposição e resolução de situações de aprendizagem. Por sua vez, o professor deixa de ser o centro das atenções, socializando o conhecimento de forma menos impositiva, criando situações capazes de incitar a curiosidade e a necessidade de busca pelo conhecimento, em um ambiente em que o aluno possa criar, planejar, montar materiais e, principalmente, compartilhar conhecimentos recém adquiridos com seus colegas (Freire, 1975).

O emprego de jogos em sala de aula apresenta potencial pedagógico tanto para questionar concepções intuitivas, quanto para facilitar a compreensão de explicações aceitas cientificamente. Sabe-se que o senso comum leva os alunos a construir inúmeras concepções alternativas e isso se torna um problema no ensino da Dinâmica porque os novos conteúdos se relacionam com esses conhecimentos pré-existentes na estrutura cognitiva dos alunos. Os conceitos aristotélicos, por exemplo, assim como os conhecimentos do dia a dia são muito intuitivos e convincentes, mas equivocados e podem representar um obstáculo epistemológico ao entendimento de conceitos mais abstratos. Associar, por exemplo, força à velocidade é quase que uma unanimidade entre os estudantes (Tezani, 2006).

Segundo Hestenes (1992), a visão massificada do aluno em relação ao seu senso comum é muito problemática no ensino de física e o professor deve sempre buscar identificar o que o aluno já sabe e investir em uma forma de ensiná-lo de adequadamente. Silveira (1992), através da validação de um teste sobre concepções alternativas sobre força e movimento, mostra como os alunos têm dificuldades em compreender certos conceitos físicos e é nesse ponto que o jogo pode se tornar um coadjuvante potencial. Fugir da aula tradicional – professor/quadro/giz – pode ser uma estratégia fundamental para que os próprios alunos se deem conta de seus equívocos, afinal, uma aula tradicional, em que o aluno somente copia e responde àquilo que o professor pergunta, engessa tanto quem leciona, quanto quem é lecionado. Trata-se de um modelo bastante ultrapassado que, muitas vezes, é fonte de desinteresse por parte do aluno.

O jogo aprimora o ato de pensar a Física, pois ao invés de apenas ouvir e copiar, os estudantes participam ativamente e desenvolvem uma nova percepção de como estudar. Espera-se também que os alunos tenham adquirido novas concepções e/ou transformado, pelo menos em

parte, suas concepções alternativas, que costumeiramente são percebidas no estudo da Dinâmica. Ideias aristotélicas são amplamente difundidas e facilmente entendidas entre os alunos, embora, como já referido, não sejam aceitas cientificamente. Mas quando o aluno tem oportunidades de pesquisar, escrever, ler, criar, ele começa a perceber que suas idealizações primeiras, embora muito interessantes de seu próprio ponto de vista, estão equivocadas. Isso é fundamental para permitir que sejam criados novos conceitos, novas ideias, novos subsunçores, não necessariamente em substituição aos conhecimentos que ele já possui, mas buscando transformá-los (Silveira, 1992).

Piaget (1998) introduziu a ideia de que quando há o conflito cognitivo o indivíduo “joga fora” suas ideias de senso comum e internaliza o novo conhecimento de forma substitutiva. Na mesma linha seguiu Kuhn (1978), para quem o aluno ao entrar em contato com o conhecimento científico passa a reconhecê-lo como uma explicação mais articulada, mais promissora e frutífera do mundo e substitui seu paradigma pessoal em favor do da ciência. Sucessivas pesquisas mostraram que isto, de fato, não ocorre, pois o aluno não abdica facilmente de suas crenças muito enraizadas em favor das novas ideias aprendidas na escola (Piaget, 1998).

Toulmin (1977) e Mortimer (1992) apresentaram visões mais adequadas sobre a mudança conceitual, no sentido de que as ideias novas e as antigas podem coexistir de forma pacífica na estrutura cognitiva do aprendiz. Toulmin descreve o processo de coexistência em termos de uma ecologia conceitual. Mortimer, em seu trabalho, acredita que as concepções alternativas não serão nem abandonadas e muito menos substituídas, elas passam a conviver com novas concepções aprendidas na escola. (Toulmin, 1977). Acredita-se que uma vez bem trabalhados os conceitos científicos, através de estratégias diversificadas, conflitos cognitivos, problematizações, discussões de lacunas, jogos, entre outras estratégias, o aluno pode, por um processo contínuo, lento e progressivo, transformar os conceitos alternativos em conceitos científicos, ou pelo menos minimizar a importância relativa de suas próprias concepções, à medida que percebe que a Física explica o mundo de forma mais coerente. Dessa forma, a convivência de distintas explicações ou paradigmas pode, ainda assim, permitir que os estudantes aprendam de forma significativa os conteúdos da Física e este projeto trabalhará nessa linha (Mortimer, 1992).

Esse estudo teve por objetivo desenvolver um módulo para introduzir o ensino de um tópico de Física, a dinâmica newtoniana, em que os alunos e o professor trabalhassem em sala de aula através de um jogo de perguntas e respostas.

2. METODOLOGIA:

2.1. Participantes e Instrumentos

A proposta foi aplicada a uma turma de segundo ano do ensino médio do colégio Província de São Pedro, uma escola da rede privada de Porto Alegre, Rio Grande do Sul. Nessa turma havia trinta e três alunos com idade entre quinze e dezessete anos, divididos entre dezoito meninas e quinze meninos. O trabalho foi supervisionado pela coordenação do colégio e todos os alunos estavam cientes que o jogo se tornaria a base para um trabalho acadêmico. Durante todo o processo, padrões éticos e comportamentais foram garantidos aos alunos. A participação dos alunos no jogo foi facultativa

A dinâmica baseou-se na utilização de um jogo de perguntas e respostas (Apêndice A), que envolveu leituras, pesquisas, preparação das perguntas e respostas do jogo, em si, para ensinar e discutir o tópico da Dinâmica no Ensino Médio. O Quadro 1 oferece uma visão mais detalhada de como o jogo se deu ao longo das aulas. Visando um melhor aproveitamento dos alunos, a dinâmica começou com uma aula inaugural, motivadora e dialogada, com o intuito de mapear o conhecimento prévio e definir qual o grau de concepções alternativas e/ou de conhecimentos de Física os alunos, em geral, possuíam. Segundo Ausubel (*apud* Moreira, 2014), o professor deve mapear os conhecimentos prévios, identificar quais os subsunçores são necessários para a aprendizagem do tópico que pretende ensinar e encaminhar sua aula de forma a maximizar a aprendizagem significativa.

2.2. Materiais e dinâmica do jogo

Um dos principais aspectos do jogo foi fazer com que o aprendiz assimilasse novos conceitos sobre Dinâmica em um processo progressivo de diferenciação dos subsunçores iniciais (conhecimentos prévios) e até de “desconstrução” lenta caso eles possuísem *subsunçores* alternativos, isto é, conceitos não aceitos cientificamente.

Esses conhecimentos prévios foram problematizados e à medida que avançava o jogo, podiam modificar-se interagindo com novos

conhecimentos, gerando assim, subsunçores modificados, mais ricos e mais elaborados. Neste viés, Ausubel mostra que o processo cognitivo pode avançar quando uma informação nova interage com os subsunçores da estrutura cognitiva. Mas independente da forma com que se dá a aprendizagem (se receptiva ou por descoberta), é fundamental que ela seja de fato significativa.

O jogo incluiu a apresentação de materiais previamente organizados e/ou selecionados (no presente trabalho um material inicial foi o Texto de Apoio aos Alunos, que é mostrado no Apêndice A, mas outros materiais foram organizados e oferecidos) permitindo que os alunos se aprofundassem através de pesquisas orientadas que faziam uso de outras fontes. Isto pode ser inicialmente tomado como um processo mecânico de aprendizagem, mas há a possibilidade de se transformar em uma aprendizagem substantiva, não arbitrária, com o avanço dos passos da dinâmica até o desenvolvimento final do jogo.

Durante o jogo, buscou-se incentivar fortemente a interação aluno-aluno, aluno-material instrucional e também aluno-professor. Neste último caso, o professor atuava principalmente como mediador dos diálogos, visando corrigir rumos, sempre que os estudantes se dispersavam ou apresentavam dificuldades para assimilar algum conceito que emergia das leituras e pesquisas. Quando se analisa essa interação social, é possível lançar um novo olhar epistemológico para a sala de aula, isto é, percebe-se que o aprendiz deixa de ser passivo e passa a participar do processo de construção do seu aprendizado.

O trabalho de leitura do Texto de Apoio (Apêndice A) e de outros materiais na fase da pesquisa foi feito em pequenos grupos de, no máximo, seis componentes. Cada grupo recebeu também um material escrito contendo as regras do jogo (Apêndice B), além do texto de apoio, contendo os conceitos iniciais da Dinâmica. Na fase de preparação das perguntas, os alunos foram incentivados a consultar diversos materiais de pesquisa, como: livros, revistas, artigos e *sítes* da internet. Isto é fortemente recomendado no caso de a escola disponibilizar esses meios eletrônicos durante os períodos de aula, mas caso a escola não disponha, por exemplo, de acesso à internet, é importante que o professor selecione o material e disponibilize na sua forma física aos alunos. Após a leitura e discussões no interior dos grupos deu-se início à construção de 15 perguntas e também das 15 respostas. As perguntas deveriam ser redigidas com a maior clareza

possível, evitando-se perguntas mal formuladas ou ambíguas. Deviam evitar também materiais copiados, ou seja, cópias simples de perguntas e respostas sem interpretação por parte dos alunos. Este é um dos papéis do professor, isto é, orientar no início da unidade didática sobre esses cuidados.

Durante o processo de construção das perguntas e respostas, pelas regras do jogo, o professor não podia ser consultado. O objetivo era fazer com que adquirissem certa autonomia e responsabilidade em suas produções. Somente ao final da pesquisa, os grupos puderam escolher três dúvidas (três perguntas) para serem discutidas, mas de forma restrita, isto é, apenas entre o grupo e o professor, sem que o grande grupo os ouvisse para evitar antecipar a resposta.

O início do jogo ocorreu mediante sorteio de um grupo, utilizando o envelope “perguntar”. Cada grupo escolheu uma letra que o identificava. Assim foram criados, por exemplo, os grupos A, B, C e D. No envelope “perguntar” havia cartões com as letras impressas (ou manuscritas) que identificam os grupos que estavam no jogo. Caso existissem quatro grupos participando do jogo, e como são 15 perguntas cada grupo, existiriam, dentro do envelope, 15 cartões com a letra A, 15 com a letra B, 15 com a letra C e 15 com a letra D. Dessa forma, todos os grupos perguntariam o mesmo número de vezes. Toda vez que uma letra fosse sorteada, ela representaria uma participação do respectivo grupo e essa letra não poderia voltar para o envelope.

Um grupo era sorteado (isto é, um cartão era retirado aleatoriamente de dentro do envelope “perguntar” pelo professor), e um integrante desse grupo era sorteado para fazer a pergunta utilizando-se um grande dado que era lançado no centro da sala de aula para que todos acompanhassem. O processo se repetia em relação ao sorteio do grupo e do aluno respondente, porém utilizando-se, nesse passo, o envelope “responder”. Novamente fazia-se uso do lançamento do dado para sortear o aluno respondente, que era o responsável pela escolha do número da pergunta de uma lista de 15 perguntas do grupo adversário, sendo que tal lista já fora previamente entregue e se encontrava de posse do professor.

Na sequência, os cartões sorteados, tanto do grupo que perguntou quanto do grupo que respondeu, eram retirados dos envelopes e não podiam ser recolocados até o final do jogo. Uma vez lida pelo aluno perguntante a primeira pergunta, o aluno sorteado para responder tinha

três escolhas possíveis:

1° POSSIBILIDADE: RESPONDER À PERGUNTA.

- Se a resposta fosse correta, o grupo ganharia 100 pontos;
- Se a resposta fosse incompleta, o grupo ganharia 40 pontos;
- Se a resposta fosse errada, o grupo perderia 20 pontos.

2° POSSIBILIDADE: ESCOLHER OUTRO INTEGRANTE DO SEU GRUPO PARA RESPONDER.

- Se a resposta fosse correta, o grupo ganharia 50 pontos;
- Se a resposta fosse incompleta, o grupo ganharia 20 pontos;
- Se a resposta fosse errada, o grupo perderia 60 pontos.

3° POSSIBILIDADE: REPASSAR A PERGUNTA PARA O GRUPO ORIGINÁRIO.

- Se a resposta fosse correta, o grupo ganharia 100 pontos;
- Se a resposta fosse incompleta, o grupo ganharia 20 pontos;
- Se a resposta fosse errada, o grupo perderia 50 pontos.

O objetivo era fazer com que todos os alunos estudassem e assumissem responsabilidades frente ao grupo e frente a sua aprendizagem, pois todos conheciam as regras do jogo que lhes tinham sido entregues no início do processo (Apêndice B).

O procedimento de sorteio através do lançamento do dado se repetiu continuamente até o término do jogo. As perguntas inconsistentes, ambíguas ou ininteligíveis faziam com que o grupo adversário ganhasse 100 pontos. Como já explicado, todos os grupos construíram durante a primeira etapa da dinâmica, 15 perguntas e também responderam, durante o jogo, a 15 perguntas, de forma que todos tiveram as mesmas oportunidades no decorrer do processo. Sempre que um grupo lia uma pergunta mal redigida, respondia erroneamente, ou mesmo de maneira incompleta o professor intervinha, no exato momento do jogo, e explicava qual era o erro cometido e como seria a explicação ou resposta adequada. Este era um esforço para minimizar a proliferação de ideias equivocadas fazendo com que, aos poucos, os estudantes

compreendessem melhor os conceitos e princípios físicos em estudo. O jogo terminou quando a última pergunta foi respondida e quem obteve a maior pontuação foi considerado vencedor.

Para a realização do jogo foram empregados alguns materiais que estão especificados no Quadro 2. Após o término do Jogo, foi enviado a todos os alunos, por meio da internet, ou alternativamente pode ser entregue em formato físico, caso a escola não disponha de acesso à rede, um questionário com perguntas sobre os assuntos tratados na sequência didática, da mesma forma como foi feito no início do jogo, para que se pudesse ter uma avaliação quantitativa e qualitativa, opiniões dos alunos e indícios sobre se o aprendizado foi significativo. Uma sugestão de perguntas que podem compor esse questionário é apresentada no Apêndice C.

2.3. Aplicação da proposta

Segundo a Teoria da Aprendizagem Significativa, o jogo cumpre duas funções muito importantes previstas que são (1) ser um organizador prévio, pois o processo de preparação das perguntas e respostas pelos grupos e a aplicação, em si, do jogo busca cumprir (ou funciona como) um importante papel que é o de construir subsunçores adequados que permitam dar significado aos novos conhecimentos da dinâmica newtoniana, como proposto por Ausubel (Moreira, 2014b). Neste sentido, assume a função de recurso instrucional apresentado (ou utilizado) em um nível mais elevado de generalidade e inclusividade, pois as perguntas e respostas podem ser construídas sobre quaisquer aspectos da dinâmica clássica em um nível de abstração possivelmente elevado e que serão abordados detalhadamente ao longo do curso e, além disso, precede a apresentação formal pelo professor que não pode ser dispensada; e (2) promover predisposição do aluno para aprender, pois o jogo busca movimentar conhecimentos e tornar os alunos mais ativos, envolvidos e predispostos a realizarem uma aprendizagem da Física com significado, superando a tradicional aprendizagem mecânica (geralmente baseada na memorização e aplicação de fórmulas). Esta segunda função está grandemente ligada à primeira, pois para que o aluno tenha predisposição para aprender ele precisa ter subsunçores adequados e o material de aprendizagem precisa ser potencialmente significativo, evidentemente, mediado pelo professor. Na prática o jogo é um problematizador

inicial que leva o aluno a “querer saber mais” para dar respostas mais adequadas a perguntas instigantes que podem ser colocadas pelos diferentes grupos na dinâmica do jogo.

Além dessas funções, a Mecânica é uma parte da Física que constitui um verdadeiro “campo conceitual”, na acepção de Gérard Vergnaud, e que para sua compreensão com significado são necessárias inúmeras situações, vivências, noções espaciais, temporais, causais e isto constitui um processo que pode ser grandemente facilitado por atitudes proativas, positivas dos alunos. Para oferecer uma visão geral do jogo e da configuração da sala de aula durante a dinâmica, foi construída uma representação (Figura 1).

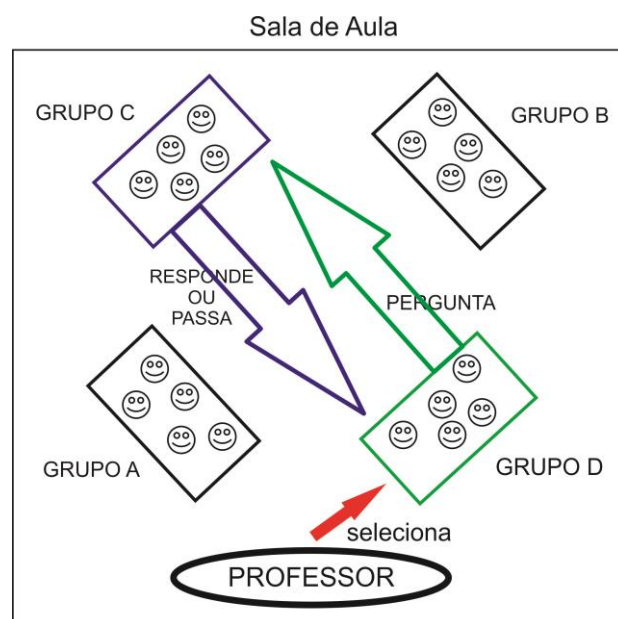


Figura 1. Esquema da sala de aula durante o jogo de perguntas e respostas. Fonte: O autor.

O jogo foi aplicado a três turmas de segundo ano do Ensino Médio. A aplicação durou aproximadamente dois meses e foi feita no horário regular de aula. O tempo de aplicação do jogo foi de quatorze horas e trinta minutos envolvendo treze (13) encontros.

3. RESULTADOS E DISCUSSÃO:

Após o término do jogo, foi feita uma atividade online em que os alunos foram solicitados a responder algumas perguntas para tentar averiguar e mapear aspectos positivos e/ou negativos do jogo, e conhecer opiniões dos estudantes sobre a dinâmica realizada para introduzir conceitos de Dinâmica. Conforme descrição anterior, o jogo foi aplicado a três

turmas, mas as respostas aqui compiladas referem-se à Turma 200, cuja proposta didática foi descrita neste trabalho. Destaca-se que, apesar de ser uma turma pequena, possuía a característica de ser bastante crítica, interessada e participativa, o que facilitava a coleta de dados.

Foram elaboradas nove perguntas e disponibilizadas na plataforma virtual para que os alunos pudessem responder ao questionário através do *Google For Education*, utilizando o *Google Forms*. Essa ferramenta mostrou-se excelente, pois além de permitir montar e editar as perguntas de forma rápida facilita a que os alunos respondam (também rapidamente), e ainda oferece graficamente os resultados de forma clara e fácil de interpretar.

Assim, de forma online, a partir do acesso de sua turma, puderam responder às perguntas tanto no colégio como em suas residências. Na sequência foi mostrado um “*print*” de como os alunos foram chamados a responder ao questionário através da plataforma *Google For Education*. Destaca-se que é possível usar o *Google Forms* mesmo sem auxílio desta plataforma. Na sequência foram apresentadas as nove perguntas que davam aos estudantes a possibilidade de responderem sim; não; indiferente; outros.

A Figura 2 ilustra a forma como as perguntas apareciam aos alunos na plataforma. A Figura 3 representa a primeira pergunta do questionário apresentado aos alunos. As respostas à primeira pergunta (Você gostou do jogo de perguntas e respostas?) estão representadas na Figura 4. Apesar do pequeno grupo amostral, o resultado indicou que a maioria dos estudantes gostou da dinâmica do jogo (93,3% respondeu “sim”).

A Figura 5 apresenta as respostas à segunda pergunta – Você acha que com o jogo ficou mais fácil de aprender os conceitos básicos de dinâmica? - apontando que os estudantes consideraram que a dinâmica do jogo (as leituras preparatórias, a construção de perguntas e respostas e o jogo em si) ajudou na compreensão de conceitos físicos. A Figura 6 apresenta as respostas à terceira pergunta – Se o professor tivesse adotado essa estratégia no início do estudo da cinemática você acredita que teria mais facilidade em aprender? - Apontando que mais da metade dos estudantes acha que a utilização do jogo é válida como ferramenta para que se possa estudar outros tópicos (por exemplo, Cinemática) o que nos leva a inferir que eles atribuíram ao jogo um papel positivo na sua aprendizagem.

A Figura 7 representa as respostas à quarta pergunta – Ao final do jogo você se sentiu mais confiante para continuar o estudo da dinâmica? - apontando que 80% dos alunos se sentiram mais confiantes no estudo da Dinâmica após o jogo. Como já comentado, embora a amostragem desse estudo seja pequena, esses resultados sugerem que a utilização do jogo em outras áreas pode ser uma ferramenta potencial para uma aprendizagem mais significativa, no sentido de ocorrer assimilação e uma subsequente diferenciação progressiva dos conceitos científicos.

A Figura 8 mostra as respostas à quinta pergunta – O jogo foi uma forma mais motivadora de aprender? - apontando que mais de 90% dos alunos se sentiram mais motivados a aprender física a partir do jogo. Isto, por si só, é um resultado positivo e bastante relacionado ao referencial teórico, que alerta para a importância de se pensar em formas de promover predisposição ao estudo.

A Figura 9 mostra as respostas à sexta pergunta – Se você pudesse escolher entre aprender a dinâmica com o jogo ou sem o jogo, o que escolheria? - apontando que mais de 70% dos alunos perguntados gostariam, se pudessem escolher, de aprender utilizando métodos mais lúdicos, como os jogos. A Figura 10 mostra as respostas dissertativas à sétima pergunta - Descreva em poucas palavras aspectos positivos do jogo - em que os alunos puderam descrever alguns aspectos positivos do jogo. A partir das respostas, foram selecionadas algumas palavras que resumem suas posições (divertido; eficiente; diferente; interação; instrutivo; esforço; trabalho em equipe; estudo dirigido; útil).

A Figura 11 mostra as respostas também descritivas à oitava pergunta – Descreva, com poucas palavras, aspectos negativos do jogo. A partir das respostas dadas, foram selecionadas algumas palavras que resumem suas escolhas: nenhum; nada; não tem; injustiças; perguntas repetitivas; falta de explicação antes do jogo; não existe. A Figura 12 mostra as respostas à nona pergunta – Em poucas palavras escreva suas sugestões para a melhoria do jogo - onde os alunos puderam sugerir alterações para melhorar a dinâmica do jogo utilizado. Da mesma forma, em relação às respostas foram selecionadas algumas palavras que resumem suas escolhas (nada; as respostas poderiam ser conjuntas; número de respostas deveria ser igualitárias por grupo, e não por sorteio).

Ao analisar as respostas das perguntas

feitas aos alunos fica-se bastante confiante e otimista em relação à aplicação do jogo. Observa-se que a maioria dos alunos da Turma 200 gostou do jogo; suas falas deixam claro, durante o questionário, que o jogo os motivou a estudar e que sua compreensão foi auxiliada pela estratégia utilizada. Relatos dos alunos durante e após o jogo também nos levam a acreditar que, mesmo sabendo que não é possível ensinar todos os conteúdos de física através de métodos lúdicos, sempre é interessante alterar os métodos didáticos para que a aula não se torne monótona e enfadonha, e nesse aspecto o jogo foi fundamental.

Em relação ao aspecto motivacional, também se vê um crescimento de alguns alunos que durante o ano eram desinteressados em sala de aula, mas que quando trabalhavam em equipe mostravam-se muito mais colaborativos e entusiasmados. O aspecto social que o jogo proporciona mostrou-se uma ótima ferramenta para agregar ainda mais a turma, pois aprender enquanto se brinca é uma forma divertida de estudar (ou, dito de outra forma, estudar brincando é mais atraente).

Nesse estudo, o jogo foi apenas uma introdução, uma problematização inicial, e ficou claro que depois do jogo era necessário voltar às aulas formais para que o conteúdo fosse ministrado com maior rigor. Não acredita-se que o jogo possa suprir o ensino formal e o rigor técnico do qual o professor não pode abrir mão, e nem se tem a pretensão disso, mas ao oferecer ao aluno uma forma diferenciada de estudar, uma forma diferente da que ele já está acostumado, isso modifica o ambiente social de sala de aula, pois as relações professor-aluno são alteradas e os próprios alunos passam a interagir entre si de maneira mais colaborativa.

Atitudes como alterar os lugares na sala de aula, trabalhar em grupos e também oferecer autonomia para criar, fazem despertar no aluno interesses diversos daqueles que ele tem na aula tradicional. O jovem de hoje tem muita informação nas mãos, mas nem sempre sabe usufruir dela. Foi possível observar que o jogo também auxiliou nesse aspecto, pois procurar artigos e incitar a que os alunos os leiam, fazendo com que eles tenham acesso a materiais de maior qualidade e rigor científico; incitar a que procurem sites confiáveis para a criação das perguntas e respostas, foi um norteamiento que resultou em aprendizado. Os alunos aprenderam a fazer buscas mais qualificadas, a fugir de artigos escritos em blogs ou do “*Yahoo resposta*”, por exemplo.

De forma geral, as críticas também foram bastante amenas, muitas delas em relação à discrepância entre o número de respostas para cada grupo, o que já havia sido corrigido durante o jogo e que também poderá servir de alerta para futuras aplicações. Um dos melhores indícios que o jogo surtiu efeitos positivos na Turma 200 foi o fato de que ao chegarem ao terceiro ano, agora como Turma 300, ao começar o conteúdo de magnetismo, alguns alunos quiseram saber se também no referido ano seria realizado o jogo. Infelizmente, com a atual cobrança conteudista dos vestibulares e exames de ingresso ao Ensino Superior, muitas vezes se torna impossível fazer trabalhos lúdicos com os alunos, pois há uma pressão dos colégios e pais para vencer os extensos conteúdos. De qualquer forma, o principal legado foi o de que os alunos se envolveram com o jogo e pareceram mais motivados ao estudo.

Os alunos também foram muito importantes durante a criação do jogo, mesmo que eles não se dessem conta disso. A troca entre professor-aluno foi fundamental para dar um norte ao desenvolvimento do trabalho e, aos poucos, adaptar o jogo a uma realidade mais próxima das suas vivências. Ao acompanhar de perto suas inseguranças e ansiedades iniciais, foi observado que é possível transformar o trabalho coletivo em um conjunto perguntas e respostas, um material que, embora bastante superficial, foi criado por eles mesmos, fruto de seus esforços.

Pode-se destacar também alguns aspectos desfavoráveis durante a aplicação do projeto. Por exemplo, durante o jogo alguns alunos reclamavam do sorteio, pois certos times respondiam mais seguidamente que outros. Esse fator de irregularidade foi solucionado durante o projeto, para que todos os times fizessem o mesmo número de perguntas e também respondessem o mesmo número de vezes. Outro fator citado foi que alguns alunos respondiam mais que outros no grupo, pois isso também é determinado por sorteio (utilizando o dado). Resolveu-se isso determinando que um aluno somente poderia responder pela segunda vez após todos os integrantes do grupo terem respondido ao menos uma vez. Esses ajustes foram se mostrando necessários e importantes à medida que o jogo foi sendo aplicado.

Alguns alunos acharam que o tempo dado para a confecção das perguntas e respostas fora muito reduzido (pequeno), visto que eles deveriam estudar e entender a matéria antes da criação, o que, segundo eles, causou certa insegurança. Um dos aspectos desfavoráveis foi

o tempo de duração do jogo, pois hoje existe uma quantidade muito grande de assuntos a serem trabalhados no Ensino Médio, visto que, em geral, há a expectativa de preparar os estudantes para vestibulares e Enem, que são exames que cobram grande variedade de assuntos. Embora acredite-se no potencial de jogos interativos em sala de aula, assim como quaisquer outros meios didáticos que tirem o aluno da passividade, da monotonia de uma aula expositiva clássica, sempre que opta-se por estratégias não tradicionais de ensino, é muito difícil finalizar todos os conteúdos que são “impostos” ao professor, especialmente pelos exames e provas de seleção aplicadas no nosso país.

4. CONCLUSÕES:

Foi possível observar que o grau de satisfação foi bastante elevado e os alunos gostaram não só do jogo em si, mas também da mudança na forma clássica e engessada que a matéria foi ministrada. Ficou claro que, para muitos, o jogo poderia ser ministrado também em outras disciplinas. Embora se esteja consciente de que não é possível ministrar aulas apenas desta forma, pois haveria muitas dificuldades para vencer a tradicional lista de conteúdos, o intuito de empregar o jogo foi mostrar ao aluno um outro lado da sala de aula, onde o aprendizado pode ser prazeroso, em que ele pode criar, pesquisar, aprender colaborativamente com os colegas. Em outras palavras, ele pode ser o protagonista do seu desenvolvimento cognitivo.

No geral, os alunos mostraram-se entusiasmados com a proposta e com a utilização de recursos didáticos diferentes, como, por exemplo, a internet, bem como as trocas de informações entre colegas. Dessa forma, gerou-se um clima bastante amigável e descontraído. O ambiente saudável criado pela interação durante o jogo foi um dos fatores cruciais para que alguns alunos, mesmo com muitas dificuldades em Física, tivessem uma ótima participação durante o processo de criação de perguntas e respostas e também durante o jogo, o que facilitou bastante a aplicação do projeto.

A dinâmica apresentada neste trabalho tanto pode ser aplicada no nível Médio como no Ensino Fundamental. Durante todo o processo passa-se a acreditar mais nos aspectos lúdicos como forma relevante e concreta de aprendizagem, o que auxilia a refletir e a compreender, uma vez mais, como os aprendizes vêm mudando de uns anos para cá. O mundo não é mais o mesmo, tudo ficou mais rápido e, assim

como a tecnologia, a informação e os meios de comunicação, os professores também devem atualizar-se para que não se tornem ultrapassados como profissionais. É relevante salientar que o trabalho com o jogo de perguntas e respostas, agora mais bem sistematizado, tem sido uma experiência extremamente gratificante e enriquecedora à medida que mudou as concepções sobre ensino e aprendizagem. Implica dizer que ensinar não é uma questão de vocação, mas sim uma profissão que pode, dia a dia, ser reaprendida, especialmente quando se busca aportes teóricos que servem para auxiliar, e aproximar professor-aluno.

5. REFERÊNCIAS:

1. Brasil. MEC. (2012). Diretrizes Curriculares Nacionais para o Ensino Médio. *Parecer CNE/CEB nº 5/2011 e Resolução CNE/CEB nº 2/12*.
2. Demo, P. (2007). *Educar pela pesquisa*, 8ª Edição, Editora Autores Associados, ISBN 978-85-85701-21-5,
3. Freire, P. (1975). *Pedagogia do oprimido*. Paz e Terra.
4. Gadotti, M. (2010). *Qualidade na Educação: uma nova abordagem*. Editora e Livraria Instituto Paulo Freire.
5. Hestenes, D.; Wells, M.; Swackhamer, G. (1992) Force Concept Inventory. *The Physics Teacher*, Vol. 30,141-158.
6. Kuhn, T. S. (1978) A estrutura das revoluções científicas. *Perspectiva*.
7. Lapo, F. R.; Bueno B. O. (2015) Professores, desencanto com a profissão e abandono do magistério. *Cadernos de Pesquisa*, n. 118, 65-67
8. Mazur, E. (2015) *Peerinstruction: A revolução da aprendizagem ativa*. Penso.
9. Melo, S. A; Sardinha, M. O. B. (2009) Jogos no Ensino Aprendizagem de Matemática: uma estratégia para aulas mais dinâmicas. *Revista F@P Ciência, Apucarana-PR*, v.4, n. 2, 5- 15.
10. Moreira, M. A. (2014). *Teorias de aprendizagem*. 2ª Edição, Editora E. P. U.

11. Moreira, M. A. (2014b). Aprendizagem Significativa, Organizadores Prévios, Mapas Conceituais, Diagramas V e Unidades de Ensino Potencialmente Significativas. *Material de apoio sobre Aprendizagem Significativa e Estratégias Facilitadoras*.
12. Mortimer, E. F. (1992) Pressupostos epistemológicos para uma metodologia de ensino de química: mudança conceitual e perfil epistemológico. *Química Nova*, 15 (3): 242-249.
13. Newton, I. (2012) PRINCIPIA: Princípios Matemáticos de Filosofia Natural, *Livro I – 2.ed., 2. Reinpr. Editora da Universidade de São Paulo*.
14. Oliveira, S. A. (2007). O lúdico como motivação nas aulas de matemática. *Jornal Mundo Jovem*, (377), 5-6. <http://www.mundojovem.com.br/projetos-pedagogicos/projeto-ludico-motivacao-aulas-matematica>. Acessado em 08/05/2014.
15. Piaget, J. (1998). Jean Piaget Sobre a Pedagogia. *Casa do Psicólogo*, 137-151.
16. Silveira, F.; Moreira, M. A.; Axt, R. (1992) Estrutura interna de testes de conhecimento em Física: um exemplo em Mecânica. *Enseñanza de las Ciencias*, 10 (2), 187-194.
17. Tezani, T. C. R. (2006) O jogo e os processos de aprendizagem e desenvolvimento: aspectos cognitivos e afetivos, *Educação em Revista*, (7) 1-16.
18. Toulmin, S. (1977) La comprensión humana –Volumen I: *El uso colectivo y la evolución de conceptos*. Alianza.



Figura 2. mensagem aos alunos através do Google Classroom, na plataforma Google For Education. Fonte: O autor.

Figura 3. Questionário aplicado aos alunos após o término do jogo – Primeira pergunta. Fonte: construído pelo autor a partir da plataforma Google For Education.

Você gostou do jogo de perguntas e respostas ? (15 respostas)

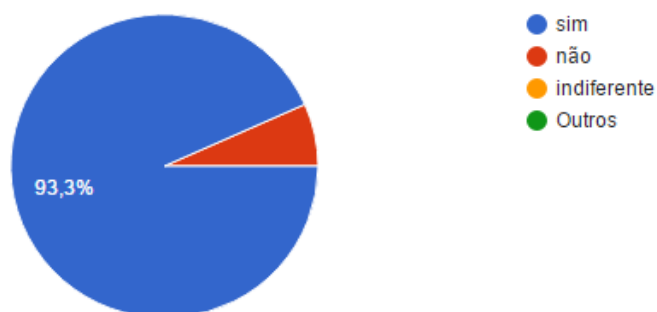


Figura 4. Respostas à primeira pergunta aplicada aos alunos após o término do jogo. Fonte: construído pelo autor a partir da plataforma Google For Education.

Você acha que com o jogo ficou mais fácil de aprender os conceitos básicos de dinâmica?

(15 respostas)

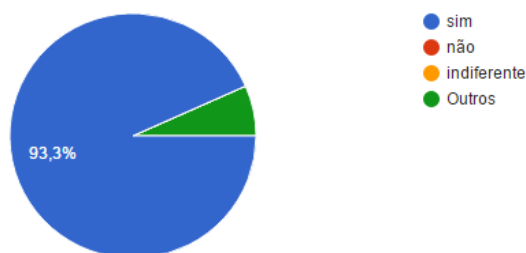


Figura 5. Respostas à segunda pergunta aplicada aos alunos após o término do jogo. Fonte: construído pelo autor a partir da plataforma Google For Education.

Se o professor tivesse adotado essa estratégia no início do estudo da Cinemática (MRU,MRUV,MCU...) você acredita que teria mais facilidade em aprender ?

(15 respostas)

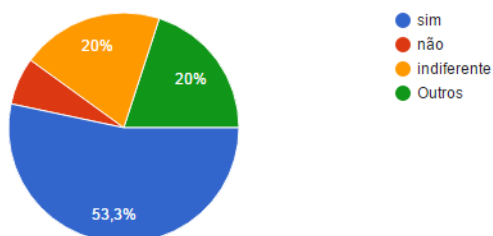


Figura 6. Respostas à terceira pergunta aplicada aos alunos após o término do jogo. Fonte: construído pelo autor a partir da plataforma Google For Education.

Ao final do Jogo você se sentiu mais confiante para continuar o estudo da dinâmica ?

(15 respostas)

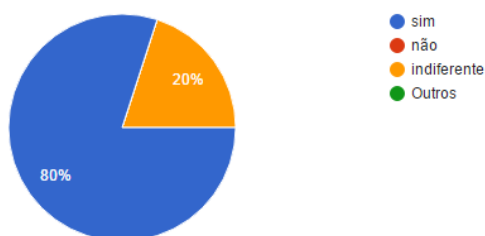


Figura 7. Respostas à quarta pergunta aplicada aos alunos após o término do jogo. Fonte: construído pelo autor a partir da plataforma Google For Education.

O jogo foi uma forma mais motivadora de aprender ? (15 respostas)

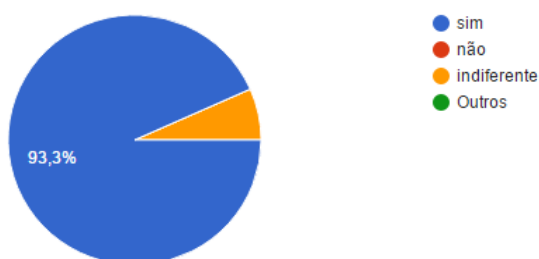


Figura 8. Respostas à quinta pergunta aplicada aos alunos após o término do jogo. Fonte: construído pelo autor a partir da plataforma Google For Education.

Se vc pudesse escolher entre aprender a dinâmica com o jogo e sem o jogo, o que escolheria ?
(15 respostas)

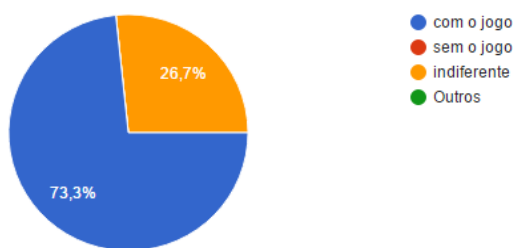


Figura 9. Respostas à sexta pergunta aplicada aos alunos após o término do jogo. Fonte: construído pelo autor a partir da plataforma Google For Education.

Descreva com poucas palavras aspectos positivos do jogo. (13 respostas)

Divertido e fácil para aprender
Maneira mais eficiente de aprendizado
Foi uma forma diferente de aprender
Modo diferente de aprender
Nos sentimos na obrigação de dominar o assunto pois os outros integrantes dependem de você
Interação e aprendizado com os colegas
Instrutivo
Me esforcei para ganhar o jogo dai tive que estudar bastante
Maneira divertida de estudar
Na minha opinião, o principal aspecto positivo do jogo foi conduzirmos um estudo dirigido no qual o professor nos apresentou uma base e a partir dela aprofundamos, em grupos, nossos conceitos na matéria. Essa experiência nos fez buscar o conteúdo de uma maneira diferenciada dos métodos normais de ensino, o que nos ajudou muito a criar mais confiança e responsabilidade ao estudar, não apenas física, outras matérias também.
O trabalho em equipe e a diversidade, um novo modo de aprender.
Util
Aprendizado mais divertido

Figura 10. Respostas à sétima pergunta aplicada aos alunos após o término do jogo. Fonte: construído pelo autor a partir da plataforma Google For Education.

Descreva com poucas palavras aspectos negativos do jogo. (8 respostas)

Nenhum
"injustiças" causadas pela sorte, que está sempre presente nos jogos, mas que faz parte
Nada que eu possa notar
Não tem
Nao teve pontos negativos
Perguntas um pouco repetitivas entre os grupos
Não creio que existam ao se aplicar esse método de ensino.
Não ter explicação antes

Figura 11. Respostas à oitava pergunta aplicada aos alunos após o término do jogo. Fonte: construído pelo autor a partir da plataforma Google For Education.

Em poucas palavras escreva suas sugestões para melhoria do jogo.

(8 respostas)

--
O grupo poderia responder às perguntas de maneira conjunta
Não tenho sugestões
se houvesse alguma maneira de distribuir melhor as perguntas entre os grupos, para que cada grupo respondesse o mesmo número de perguntas.
Melhor ciclo de perguntas
Bah nao sei, achei que ficou bem feito
Fazer com que cada grupo pergunte e responda o mesmo numero de vezes
Foi ótimo. Eu não mudaria nada.

Figura 12. Respostas à nona pergunta aplicada aos alunos após o término do jogo. Fonte: construído pelo autor a partir da plataforma Google For Education.

Quadro 1. mostra a sequência do módulo didático através de um jogo.

Aula		Atividade	Argumento/objetivos	CH
1ª Semana	1ª	Aula motivadora inicial. Haverá um diálogo com os alunos sobre o tema. Indicação de material introdutório para leitura (uso de plataforma virtual).	Aula problematizadora, motivacional; alterar a configuração da sala e apresentar sites, links para leitura.	1 h-a (40min)
	2ª	Aula introdutória sobre a Dinâmica Aristotélica e as Leis de Newton.	Apresentar uma visão da Dinâmica Aristotélica e confrontá-la a Newtoniana.	1.5 h-a (90min)
	3ª	Entrega de material complementar (texto construído pelo professor) e início da leitura do texto proposto.	Os alunos recebem um texto previamente construído para leitura e discussão.	1 h-a (40min)
2ª Semana	4ª	Leitura e discussão sobre os textos propostos.	Ler e discutir e interpretar os textos.	1.5 h-a (90min)
	5ª	Os alunos recebem as regras do jogo e dá-se início a formação dos grupos. O professor esclarece eventuais dúvidas relativas à construção das perguntas e respostas conforme as regras estabelecidas no jogo.	Evitar que muitas perguntas sejam mal formuladas ou formuladas de forma ambígua, equivocada, confusa.	1 h-a (40min)
	6ª	Trabalho em grupo pesquisando e formulando as perguntas e as respostas.	Trabalhar em grupos para construir perguntas, basicamente conceituais.	1.5 h-a (90min)
3ª Semana	7ª	Trabalho em grupo pesquisando e formulando as perguntas e as respostas.	Trabalhar em grupos	1 h-a (40min)
	8ª	Os grupos entregarão ao professor, por escrito, as 15 perguntas e respostas.	Revisão final e entrega das perguntas e respostas	1.5 h-a (90min)
	9ª	Início do jogo. Sorteio da ordem (quem pergunta/quem responde) com ajuda de um dado.	Dinâmica de perguntas e respostas entre os grupos, contagem de pontos, monitoramento pelo professor.	1 h-a (40min)
	10ª	Desenvolvimento do jogo.	Dinâmica de perguntas e respostas entre os grupos, contagem de pontos, monitoramento pelo professor.	1.5 h-a (90min)
5ª Semana	11ª	Sequência do jogo.	Dinâmica de perguntas e respostas entre os grupos, contagem de pontos, monitoramento pelo professor.	1 h-a (40min)
	12ª	Desenvolvimento do jogo.	Dinâmica de perguntas e respostas entre os grupos, contagem de pontos, monitoramento pelo professor.	1.5 h-a (90min)

	13ª	Finalização do jogo.	Finalização do jogo, quando se esgotam todas as perguntas de todos os grupos.	1.5 h-a (90min)
--	-----	----------------------	---	--------------------

Fonte: construído pelo autor.

Quadro 2. Lista de materiais empregados na dinâmica do “jogo de perguntas e respostas”.

Material	Aplicação
Um envelope com a inscrição “PERGUNTAR”	No interior do envelope deve haver 15 cartões com a letra que identifica cada grupo, sendo que cada cartão é usado para a escolha do grupo que irá perguntar. Exemplo: 15 cartões com a inscrição “grupo A”, 15 com a inscrição “grupo B” e assim sucessivamente.
Um grande DADO (de seis faces, conforme	O dado é construído pelos alunos e utilizado para: sorteio do grupo que inicia o jogo; do aluno integrante do grupo sorteado para perguntar; do grupo que responde; do aluno integrante do grupo sorteado para responder. Assim, a escolha é aleatória.
Um envelope com a inscrição “RESPONDER”	No interior do envelope deve haver 15 cartões com as letras que identificam os grupos. Exemplo: 15 cartões com a inscrição “grupo A”, 15 cartões com a inscrição “grupo B” e assim sucessivamente.
Material teórico	Esse material (Texto de Apoio aos Alunos – Apêndice A) é um guia inicial com conceitos básicos para a confecção das perguntas e das respostas, pelos grupos, além de outros materiais organizados, selecionados ou monitorados pelo professor.

Fonte: construído pelo autor.

APÊNDICE A

Simulação de um diálogo entre professor e alunos no início de uma aula em que o jogo de perguntas e respostas é introduzido

Professor: *Bom meninos e meninas vamos dar início ao jogo; aqui encontram-se um grande dado, um envelope para o sorteio dos grupos que irão perguntar, um segundo envelope com as letras dos grupos que irão responder; tenho em mãos as listas de perguntas e respostas que vocês já prepararam, corrigiram, imprimiram, ou seja, são quatro listas com 15 perguntas e 15 respostas.*

Aluno: *O que fazemos agora professor?*

Professor: *Organizem-se formando os grupos que vocês já selecionaram e se coloquem a certa distância um do outro, como se cada grupo estivesse em lados de um quadrado e eu fico no vértice. Cada integrante do grupo deverá conseguir enxergar todos os outros integrantes dos outros grupos como neste desenho que vou colocar no quadro (Figura 1), Também escolham um número para cada integrante do grupo, que deve ser de um a seis, esse número não será mais modificado até o final do jogo.*

(pausa).

Professor: *Agora que vocês já se arrumaram nos grupos, vamos dar início ao jogo. Sorteie um grupo para iniciarmos com as perguntas abrindo o envelope “perguntar” e selecionando um cartão com uma letra; o grupo escolhido foi o B, e o integrante que fará a pergunta é... (joga-se o dado) o número três. Quem é o número três? (João levanta a mão). Por favor, João levante-se para que você possa ler a pergunta. Agora vamos sortear o grupo que irá responder abrindo o envelope “responder” e selecionando um grupo... o grupo que irá responder é o grupo C, e o seu integrante é...(joga-se o dado) o componente “dois”. Quem é o número dois do grupo C? Maria levanta a mão. Por favor, Maria, levante-se e escolha qual das 15 perguntas formuladas pelo grupo B você deseja responder.*

Maria: *Profe, eu quero responder a pergunta quatro.*

É importante lembrar que as perguntas e as respostas ficarão sempre na mão do professor, pois uma vez entregues pelos grupos eles não terão mais acesso às mesmas. Nota-se também que é o aluno sorteado do grupo que responde quem decide, de forma aleatória, qual das perguntas do grupo adversário irá responder. Isso se faz necessário para evitar que o grupo que formulou as perguntas escolha entre perguntas mais fáceis ou mais difíceis, uma vez conhecido o aluno que irá responder. Assim, teremos uma imparcialidade em relação às perguntas e respostas.

Professor: *Ok Maria, ai vai... João e seu grupo fiquem atentos, pois existe a possibilidade de vocês responderem.* (pausa). *Pergunta quatro do grupo B, vamos lá...*

João: *Determine se a frase a seguir é verdadeira ou falsa, caso seja falsa, organize a se de forma a deixá-la correta: "Massa é uma medida de peso e deve ser medida em Newton",*

Professor: *Maria pense e caso você não queira responder, lembre-se das regras do jogo.*

Maria: *Não lembro professor... o que eu posso fazer?*

Professor: *Você pode responder, escolher outro integrante do grupo para responder por você, ou repassar a pergunta ao grupo B, e nesse caso, João obrigatoriamente terá que responder. Aproveite, olhe para o quadro, e veja a tabela de pontuação para cada escolha.*

Maria: *Tá bom Profe, não sei! Posso perguntar ao meu grupo?*

Professor: *Pode sim Maria, pode falar com seu grupo e decidir rapidamente qual decisão vocês irão tomar. Porém nada poderão comentar sobre a questão, absolutamente NADA! Caso isso ocorra vocês terão a resposta anulada e o grupo adversário ganhará a pontuação máxima da pergunta, isto é, 100 pontos.*

Maria: *Tá bom professor. Oh pessoal, me ajudem, eu não sei o que faço, acho que vou errar se responder, não tenho certeza.*

Pedro (integrante do grupo C e colega de Maria): *Vai Maria, a pergunta é fácil, você consegue, pensa um pouco!*

Maria: *Não sei não, tô na dúvida...*

Carlos (outro colega de Maria, integrante do C): *Tá, mas se você acha que vai errar é melhor me escolher, pois assim ganhamos pelo menos 50 pontos e eu tenho certeza da resposta...*

Maria: *É... pode ser... acho que vou... não sei...*

Professor: *Bem grupo C, vocês têm a partir de agora trinta segundos para tomar uma decisão ou passarei a pergunta ao grupo B e vocês perderão o direito de responder. O tempo está passando!*

Maria: *Tá bom, vou passar a pergunta para meu colega Carlos.*

Professor: *Ok Maria, decisão tomada. Carlos, agora é com você, pode responder.*

Carlos: *Professor, você se importa em ler a pergunta novamente para mim?*

Professor: *Pode ser sim, vou ler novamente. "Pergunta quatro do grupo B - Determine se a frase a seguir é verdadeira ou falsa, caso seja falsa, organize a frase de forma a deixá-la correta - Massa é uma medida de peso e deve ser medida em Newton".*

Carlos: *Ok, entendi, vou responder. A afirmação está errada, pois massa não é a medida do peso, e sim da inércia de um corpo e deve ser medida em kg ou em qualquer outra unidade de massa.*

Professor: *Muito bem Carlinhos, sua resposta está correta e o grupo C acaba de ganhar 50 pontos. Vamos ao sorteio novamente... (pega o envelope de perguntas e sorteia o cartão A e já retira do envelope). Atenção... grupo A, o integrante que irá perguntar é o de número... (joga o dado) quatro! Levante-se, por favor, número quatro do grupo A. Ah, é você Ricardo, então, fique de pé. Agora vamos sortear o grupo que responde (pega o envelope "responder" e retira um cartão). O grupo que irá responder é o grupo D e o integrante é... (joga o dado) o um. Quem é? Ah Clara, é você! Então, fique de pé e já me diga qual o número da questão você quer responder do grupo D!*

Clara: *Professor, eu quero responder a questão dez.*

Professor: *Ok, Clara, vamos lá (pega as folhas de perguntas e respostas do grupo D).*

Ricardo: Qual a terceira lei de Newton?

Clara: Essa eu sei professor, posso responder? A terceira lei de Newton é a lei da Inércia.

Professor: Clara, infelizmente sua resposta está errada, a terceira lei é a lei da "Ação e Reação" e o seu grupo acabou de perder 20 pontos. Vamos para a próxima...

Com essa sequência de diálogos, espera-se ter elucidado como a dinâmica ocorre dia a dia após o início do jogo, até que todas as perguntas se esgotem.

APÊNDICE B

Texto de apoio aos alunos: **A Dinâmica de Newton**

Isaac Newton (1642-1727), em sua obra *Princípios Matemáticos da Filosofia Natural*, publicados em 1687 unifica as conquistas de Galileu e a Astronomia de Kepler, além de colocar os princípios e as bases do que se passou a entender como metodologia da pesquisa científica. Newton utiliza um esquema metodológico semelhante ao da Geometria, partindo de definições e encadeando-as logicamente para chegar ao estabelecimento de axiomas, princípios e proposições. É no primeiro livro desta obra que se encontra enunciadas as três leis fundamentais da Mecânica: "Axiomas ou leis do Movimento".

Primeira lei: Todo corpo continua em seu estado de repouso ou movimento retilíneo uniforme em uma linha reta, a menos que ele seja obrigado a mudar aquele estado por forças imprimidas sobre ele.

Segunda lei: A mudança de movimento é proporcional à força motora imprimida, e é produzida na direção da linha reta na qual aquela força é imprimida.

Terceira lei: A toda ação há sempre uma reação igual ou, as ações mútuas de dois corpos um sobre o outro são sempre iguais e dirigidas a partes opostas. (NEWTON)

1. Os referenciais inerciais

Para que Newton pudesse explicar de forma mais satisfatória a dinâmica ele adotou um referencial denominado "referencial inercial". O referencial pode ser entendido como um ponto para a observação de um determinado experimento, é já sabido que dependendo do referencial adotado, as observações do mesmo fenômeno tornam-se diferentes. Newton definiu como referencial inercial o repouso ou o movimento retilíneo uniforme, dessa forma, ao analisar um experimento físico envolvendo a dinâmica newtoniana se deverá estar em repouso ou em movimento retilíneo uniforme (MRU) em relação ao experimento.

De forma menos acadêmica, é possível exemplificar as três leis de Newton:

A primeira lei de Newton é intitulada de Inércia, a Inércia é a propriedade comum a todos os corpos materiais, mediante a qual eles tendem a manter o seu estado de movimento retilíneo uniforme ou de repouso. Em outras palavras: um corpo livre da ação de forças externas permanece em repouso, se já estiver em repouso ou em movimento retilíneo uniforme, se já estiver em movimento.

Um bom exemplo é ônibus em MRU em relação ao solo, quando freado, as pessoas em seu interior tendem, por inércia, a serem "lançadas" para frente. Na verdade elas não foram lançadas, apenas continuaram em seu movimento de MRU em relação ao solo, foi o ônibus que freou. (Já que todo corpo em MRU tende a permanecer em MRU até que uma força externa atue sobre ele).

O sintoma de segurança é um dos exemplos diários do conhecimento da inércia, se ele não fosse utilizado, ao frear bruscamente o carro, por inércia, pode-se bater fortemente a cabeça, tanto no painel do veículo como no vidro. É por isso que o cinturo se tornou obrigatório, pois muitas vidas serão poupadas em caso de acidentes.

Analogamente, quando o ônibus inicia seu movimento, o motorista sente-se atirado para trás (comprimindo o banco) por inércia, pois tende a ficar em repouso. Da mesma forma os passageiros que estiverem em pé e sem se segurar, serão "lançados" para a traseira do ônibus, novamente eles não serão lançados, apenas estarão em repouso enquanto o ônibus foi quem acelerou.

Esse exemplo pode ser facilmente entendido com uma simples experiência: coloque uma moeda sobre uma folha de caderno apoiada sobre uma mesa, em seguida, com um movimento brusco e rápido puxe a folha e observe a moeda, ela basicamente não se moverá, ficando em repouso em relação à mesa, está aí a Inércia.

A segunda lei de Newton demonstra a relação entre a massa de um corpo, a força resultante aplicada e a aceleração que ele adquire graças a essa força. A aceleração produzida em um corpo por uma força resultante é diretamente proporcional à intensidade da força e inversamente proporcional à massa do corpo. Matematicamente o enunciado dessa lei é representado pela equação:

$$\boxed{\vec{F}_r = m \cdot \vec{a}} \quad \text{Eq. 1}$$

Onde as unidades serão [N] para força, [m/s²] para aceleração e [kg] para massa

A terceira lei de Newton é denominada "Ação e Reação" e descrita como: A toda ação corresponde uma reação, com a mesma intensidade, mesma direção e sentidos contrários, são simultâneas e nunca se anulam, pois estão em corpos diferentes. Um bom exemplo da terceira lei é o movimento de foguetes. Para que o foguete se movimente é necessário que expulse gases com alta velocidade de seu interior. Em outras palavras:

Ação: O foguete empurra os gases para fora.

Reação: Os gases empurram o foguete com a mesma força e em sentido oposto.

2. O conceito de força

Geralmente utiliza-se uma força com o objetivo de empurrar, puxar ou levantar objetos. Essa ideia está correta, mas incompleta. A ideia de puxar ou empurrar está quase sempre associada à ideia de contato, o que exclui uma característica importante da noção de força: a ação à distância.

A atração gravitacional entre a Lua e a Terra, por exemplo, é exercida a milhões de quilômetros de distância. A palavra força não possui uma definição única, expressa em palavras, mas uma forma habitual de defini-la é: Força é um agente capaz de variar a velocidade de um objeto ou deformá-lo.

A Física moderna admite a existência de quatro tipos de força na natureza, chamadas mais adequadamente de interações: gravitacional, eletromagnética, força nuclear forte e força nuclear fraca. Em relação aos movimentos e de suas causas, pode-se dizer que força é a ação capaz de modificar a velocidade de um corpo. Como várias outras grandezas em física, a força é uma grandeza vetorial, ou seja, possui módulo (valor numérico), direção (reta suporte ao vetor) e sentido (para onde o vetor aponta). Pode-se então, resumir a definição de força da seguinte forma: força é uma grandeza vetorial que caracteriza a ação de um corpo sobre outro e que tem como efeito a deformação ou a alteração de sua velocidade.

3. Tipos de forças:

3.1 A força peso

Newton observou que toda massa atrai outra massa, isto é, nesse exato momento você está sendo atraído pela folha de papel em que esse texto foi escrito. Mas por que essa força não é perceptível? A resposta mais adequada é porque as massas são muito pequenas. Observou-se que para que a força entre as massas (força gravitacional) não fosse desprezível, seria necessário que pelo menos uma das massas fosse muito grande (grande mesmo, como planetas), por isso que em nosso dia a dia não observa-se os objetos se atraindo, mas vê-se a Terra atraindo os objetos que estão próximo a ela. A força com que a Terra atrai os objetos é denominada Peso.

Mas não confunda peso com massa, erroneamente utiliza-se termos equivocados em nosso dia a dia: "Meu peso é 75 quilos"; "Por favor me pesa 600 gramas de queijo"...é comum ouvir essas frases, inclusive todos entendem muito bem o que se quer dizer. Mas, do ponto de vista da física, nessas frases há um equívoco entre essas duas grandezas, massa e peso. A massa está associada com a inércia do corpo e o peso, como já dito, é a força com que a terra atrai os corpos.

Ao dizer que o peso de um objeto é de três (3) kg, por exemplo, utiliza-se erroneamente a palavra peso ao invés de “massa” (veja-se que a unidade quilograma (kg) é de massa, não de força). A massa de um corpo não se altera se ele for levado da Terra para qualquer outro lugar. Mas, dependendo do lugar em que ele estiver seu peso poderá alterar, isso porque a gravidade poderá ser diferente. Como exemplo, pode-se analisar os primeiros astronautas que viajaram para a Lua, a massa de cada um deles não sofreu qualquer modificação pelo fato de terem saído da Terra e ido para a Lua, mas, ao chegarem à Lua, eles sentiram uma diferença em seus próprios pesos. A força peso é de natureza gravitacional e sua reação sempre estará no centro da Terra.

O peso de um corpo pode ser calculado a partir da equação abaixo;

$$\vec{P} = m \cdot \vec{g} \quad \text{Eq. 2}$$

Onde as unidades serão [N] para Peso, [m/s²] para aceleração e [kg] para massa

3.2 A força normal (N)

A força Normal é uma força de natureza eletromagnética, sua natureza pode ser melhor entendida quando se observa que os corpos são formados de átomos que contêm em sua eletrosfera elétrons com cargas negativas, tanto no interior de corpos sólidos como em sua superfície. Dessa forma, ao tentar penetrar com um corpo no outro, surge uma barreira coulombiana de repulsão. Interessante notar então que, quando se empurra ou toca-se em um corpo, a sensação do toque não é nada mais do que uma repulsão elétrica.

A força normal (Figura 13) está sempre associada ao contato existente entre os corpos. De forma minimalista é possível fazer uma analogia a uma “compressão” que um corpo exerce no outro. Abaixo encontra-se um exemplo de atuação da força normal. Ao desenhar seu vetor, deve-se ter o cuidado de iniciá-lo da superfície de contato, visto que é uma força de contato e sempre será perpendicular ao plano.

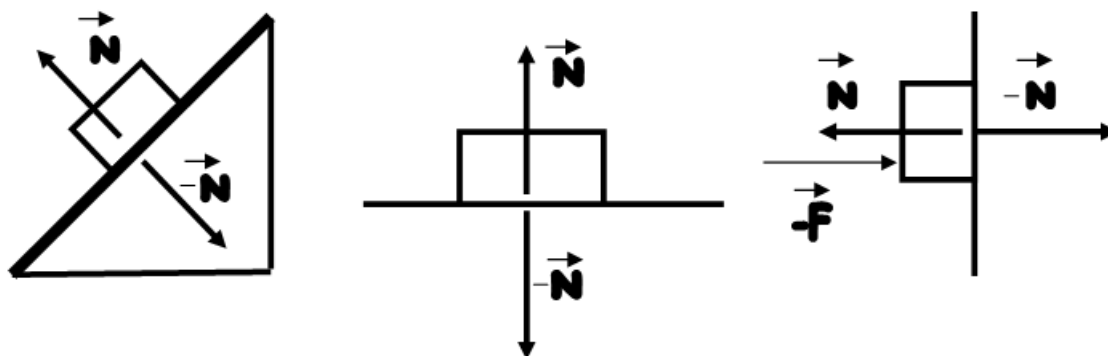


Figura 13. Aplicação da força de contato normal. Fonte: O autor

3.3 A força de atrito estático

Força de atrito estática (Figura 14) não é uma força trivial, mas é, em princípio, uma força de natureza eletromagnética que se opõe ao movimento relativo de escorregamento entre as superfícies. É importante notar que enquanto o atrito for estático não existe deslizamento.

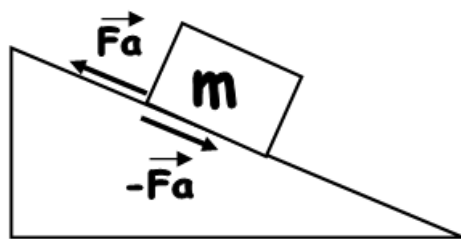


Figura 14. Aplicação da força de atrito estático. Fonte: O autor.

A medida em que se aumenta a força motriz “F”, a força de atrito “Fa” também aumenta, de modo a equilibrar a força motriz e impedir o movimento. Isto é, a força de atrito estática que atua no corpo quando não há movimento relativo entre as duas superfícies é sempre igual à força motora. Porém, ela não cresce indefinidamente, existindo um valor máximo conhecido como força de *atrito máximo ou limite*.

Quando a força motora ultrapassa esse valor limite o bloco entra em movimento e o atrito passa a ser denominado *atrito cinético* e, neste momento, ocorre deslizamento entre as superfícies. A força de atrito estático sempre será paralela à superfície e pode ser uma força motora, isto é, gera movimento.

3.4 A força de atrito cinético

É a força que surge durante o movimento relativo de escorregamento entre as superfícies dos corpos (Figura 15). Uma vez iniciado o movimento, a força de atrito estática deixa de existir, passando a atuar, como já dito, a força de atrito cinético. Ela é sempre contrária ao movimento relativo, e de intensidade inferior à da força de atrito estático. Tem como característica ser paralela à superfície e depender somente dos materiais dos corpos em contato (coeficiente de atrito) e da força normal. O atrito cinético, a contrário senso, não depende do peso e nem da área da superfície do corpo. Ela é dissipativa, isto é, transforma energia mecânica em energia térmica e deformação, sua natureza também é eletromagnética.

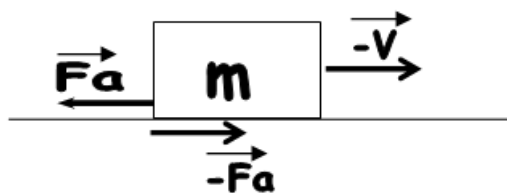


Figura 15. Aplicação da força de atrito cinético. Fonte: O autor.

O texto, embora bastante resumido, tem como objetivo oferecer aos alunos subsídios para a construção de alguns subsunçores para que eles possam iniciar os primeiros passos em busca de um novo conhecimento em relação à Dinâmica. De forma alguma se acredita que o presente texto possa sanar as dúvidas e resolver todos os problemas de compreensão dos alunos. Ele foi construído apenas como um material básico de apoio, com uma linguagem simples e direta, apostando que associado às suas pesquisas, o aluno possa compreender melhor alguns aspectos da física newtoniana.

- MATERIAL CONFECCIONADO PELOS ALUNOS

Perguntas, respostas e tipos de comentários

EXEMPLOS DE PERGUNTAS E RESPOSTAS QUE FORAM CONFECCIONADAS PARA O JOGO PELO GRUPO A (TURMA 200) DO COLÉGIO PARTICULAR EM QUE A DINÂMICA VEM SENDO APLICADA.

Grupo A; Integrantes: quatro (4) integrantes (Pedro, Maria, Roberto e Claudia - nomes fictícios)
Data: 03/11/2015. Turma: 200.

Abaixo, das 15 perguntas e respostas formuladas pelo grupo A, foram citadas apenas dez.

As Perguntas:

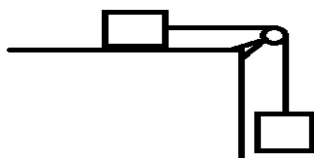
1. Em uma situação hipotética, se o planeta Terra parasse de rotar, praticamente tudo nele se alteraria. Uma dessas alterações seria a percepção de duração de um dia. Nessas condições, um dia (com a Terra rotando e transladando), seria equivalente a quantos anos se a Terra não estivesse rotando? Por quê?

2. Em um corpo extenso, quando o atrito deixa de ser estático e passa a ser cinético (dinâmico), sabemos que esse corpo entrou em movimento. Assim, sua força resultante é maior, menor ou igual a força de atrito estático máxima? Por quê?

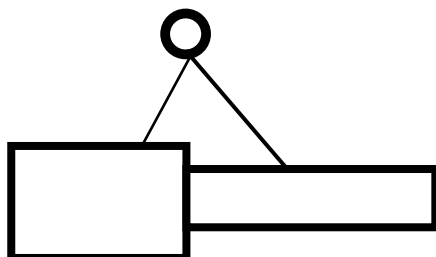
3. Pode-se afirmar que a massa é a medida da inércia de um corpo? Por quê?

Nas questões 4, 5, 6 e 7 desenhe corretamente as forças peso, tensão e normal levando em consideração polias ideais e fios inextensíveis de massas desprezíveis.

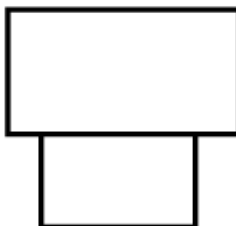
- 4.



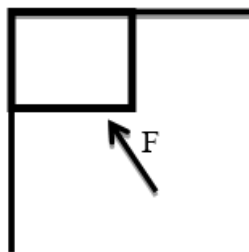
- 5.



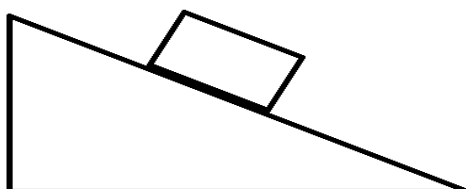
6. (Blocos apenas encostados, em queda livre, desprezando a resistência do ar)



7. (A força F não é uma força de contato)



8. De acordo com o Teorema das Três Forças, desenhe corretamente as forças peso, normal e atrito no bloco:

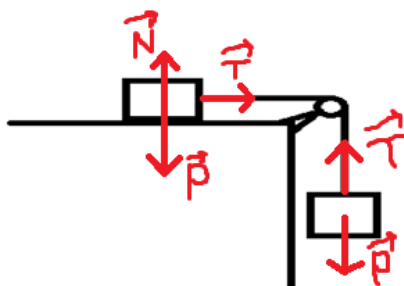


9. Segundo a terceira Lei de Newton: se uma aranha arranha um jarro, então?
10. Em cima de um copo está um papel e em cima do papel está um dado. Ao puxar o papel com determinada força, o dado, ao invés de seguir o mesmo movimento do papel, cai no interior do copo. Por que isso ocorre?

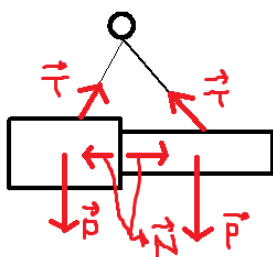
As Respostas:

- Um dia (com a Terra rotando e transladando) seria equivalente a um ano se ela não estivesse rotando, pois a Terra apenas faria o movimento de translação, deixando na metade de um ano a Terra iluminada e na outra metade, escura.
- Sua força resultante é maior, pois ela vence a força de atrito estático máximo e a partir disso se inicia o movimento.
- Sim, pois através do Princípio Fundamental da Dinâmica pode-se concluir que, se aplicarmos em corpos de massas diferentes a mesma força resultante, o corpo de maior massa adquirirá aceleração de menor módulo, isto é, ele resiste mais a variações em sua velocidade.

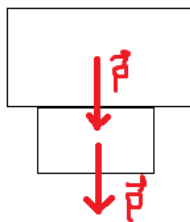
4.



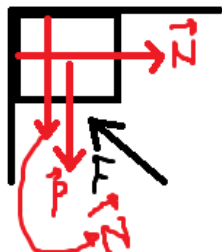
5.



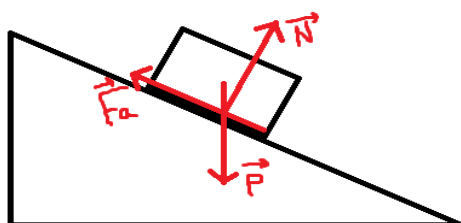
6.



7.



8.



9. O jarro arranha a aranha.

10. De acordo com a inércia, o dado tende a se manter em repouso, e com a retirada rápida do papel ele cai verticalmente.

ANOTAÇÕES DO PROFESSOR SOBRE AS PERGUNTAS E RESPOSTAS DO GRUPO A (TURMA 200) DURANTE A APLICAÇÃO DO JOGO

1) A primeira questão foi anulada, pois claramente o assunto tratado pela pergunta foge completamente do objetivo do trabalho e dos assuntos estudados pelos alunos.

2) Na pergunta 2 observa-se que o grupo confunde a força com que o bloco é puxado com a força resultante.

3) Nas questões 4, 5, 6 e 7, no enunciado, o grupo não mencionou nada sobre os blocos sofrerem ou não ação do atrito, isso gerou certo desconforto durante as respostas.

4) No desenho da questão 7 foi perguntado aos integrantes do grupo que força seria a do desenho (F), visto que o grupo afirma que essa força não seria uma força de contato. A resposta do grupo foi confusa e, ao final, acabamos por anular a questão pelo fato de não se entender que força seria a força F.

5) A questão 8 foi aceita, porém modificada pelo grupo na hora da pergunta, visto que o teorema das três forças é um teorema bastante particular e específico, saindo do contexto básico do jogo. Em vez do teorema, o grupo que vai responder deverá desenhar somente a força de atrito, a força normal e a força peso no bloco sobre o plano inclinado.

6) A questão 9 também foi anulada pois não se entendeu o que o grupo queria, embora a pergunta tenha sido bastante original, estava mal redigida e dessa forma não havia como respondê-la.

Estes são exemplos ou tipos de comentários que o professor pode ou deve fazer ao ser consultado pelos grupos, na medida em que as regras do Jogo de Perguntas e Respostas permitem que ao final da tarefa de construção das perguntas e das respostas os grupos podem eleger três (03) para discutir com o professor. Mas principalmente no próprio andamento do jogo o professor faz pequenas intervenções sempre que detecta problemas na própria construção das perguntas ou nas respostas dadas. Isto tem o objetivo de evitar que se propague entendimentos, conceitos ou princípios errôneos. Assume-se que errar não é um erro, ou seja, errar faz parte do processo de aquisição do conhecimento científico, mas é preciso ir corrigindo os erros para que o processo possa resultar em aprendizagem significativa para os alunos. Este é o principal papel do professor neste tipo de dinâmica, no sentido de garantir que o jogo avance com o máximo de aprendizagem dos conceitos, princípios e modos de pensar alinhados à visão da Física.

APÊNDICE C

Regras do Jogo de Perguntas e Respostas

Aluno: **Turma:**.....

O EMPREGO DE UM JOGO DE PERGUNTAS E RESPOSTAS COMO UMA FORMA DE PROBLEMATIZAR E MOTIVAR O ENSINO DE FÍSICA NO ENSINO MÉDIO

O trabalho é feito em pequenos grupos de, no máximo, seis componentes. Cada grupo recebe um material contendo as regras do jogo e outro, preparado pelo professor, contendo os conceitos iniciais da Dinâmica.

Na fase de preparação das perguntas, os alunos são incentivados a consultar diversos materiais de pesquisa, como livros, revistas e *sítes* da internet (caso a escola disponibilize esses meios aos alunos durante o período de aula). Após a leitura dos materiais dá-se início à confecção, em cada grupo, de 15 perguntas e também das 15 respostas. As perguntas são redigidas com a maior clareza possível, evitando perguntas mal formuladas e ambíguas. Deve-se evitar também materiais copiados, ou seja, simples cópias sem interpretação por parte dos alunos.

Durante o processo de formulação das perguntas e respostas o professor não pode ser consultado. Somente ao final da pesquisa o grupo poderá escolher cinco dúvidas para serem discutidas. Das cinco, três são compartilhadas somente entre o grupo e o professor, já as outras duas, são lidas em voz alta e na presença de toda a turma, para uma explicação coletiva.

O início do jogo dá-se com o sorteio de um grupo utilizando o envelope “PERGUNTAR”. Um integrante desse grupo, que também deve ser sorteado utilizando um dado, por exemplo, será o responsável pela leitura da primeira pergunta. Dando continuidade ao jogo, o mesmo processo se repetirá em relação ao sorteio do grupo que irá responder, porém agora utilizando o envelope “RESPONDER” e, novamente, o dado. Na sequência, o cartão sorteado tanto do grupo que perguntou como do grupo que respondeu será retirado do envelope e assim permanecerá até o final do jogo.

Uma vez lida a primeira pergunta, o aluno sorteado para responder terá três escolhas possíveis:

1º POSSIBILIDADE: RESPONDER À PERGUNTA

- Se a resposta estiver correta o grupo ganhará 100 pontos;
- Se a resposta estiver incompleta o grupo ganhará 40 pontos;
- Se a resposta estiver errada o grupo perderá 20 pontos.

2º POSSIBILIDADE: ESCOLHER OUTRO INTEGRANTE DO SEU GRUPO PARA RESPONDER

- Se a resposta estiver correta o grupo ganhará 50 pontos;

- Se a resposta estiver incompleta o grupo ganhará 20 pontos;
- Se a resposta estiver errada o grupo perderá 60 pontos.

3ºPOSSIBILIDADE: REPASSAR A PERGUNTA PARA O GRUPO ORIGINÁRIO:

- Se a resposta estiver correta o grupo ganhará 100 pontos;
- Se a resposta estiver incompleta o grupo ganhará 20 pontos;
- Se a resposta estiver errada o grupo perderá 50 pontos.

O objetivo, assim, é fazer com que todos os alunos estudem, participem e assumam responsabilidades frente ao grupo.

O processo de sorteio se repetirá continuamente até o término da atividade. As perguntas inconsistentes ou erradas farão com que o grupo adversário ganhe 100 pontos. Todos os grupos farão 15 perguntas e também responderão a 15 perguntas, de forma que todos terão as mesmas oportunidades no decorrer do jogo. Sempre que um grupo ler uma pergunta mal redigida, responder erroneamente, ou mesmo de maneira incompleta o professor intervirá, no exato momento do jogo e, de forma bastante sucinta, explicará qual foi o erro cometido e como seria a explicação ou resposta correta. Dessa forma irá minimizar fortemente a proliferação das ideias equivocadas. O jogo terminará quando a última pergunta for respondida e quem obtiver a maior pontuação será o vencedor. Para a realização do jogo serão empregados alguns materiais conforme a Quadro 3.

Quadro 3. *Lista de materiais empregados na dinâmica do jogo.*

Material	Aplicação
UM ENVELOPE com a inscrição "PERGUNTAR"	No interior do envelope haverá 15 cartões com os nomes dos grupos. Exemplo: 15 cartões escrito "grupo A", 15 cartões escrito "grupo B" e assim sucessivamente.
UM GRANDE DADO DE SEIS FACES	Será utilizado para sorteio dos alunos que irão perguntar e responder. Assim, a escolha é aleatória.
UM ENVELOPE com a inscrição "RESPONDER"	No interior do envelope haverá 15 cartões com os nomes dos grupos. Exemplo: 15 cartões escrito "grupo A", 15 cartões escrito "grupo B" e assim sucessivamente.
MATERIAL TEÓRICO	Esse material será um guia inicial para a confecção das perguntas e respostas
PERGUNTAS ON LINE	Será feito um teste interativo, antes e depois do jogo, sobre os assuntos tratados.

Após o Jogo, será enviado a todos os alunos, por meio da internet, um questionário com perguntas básicas sobre os assuntos tratados, da mesma forma como foi feito no início do jogo, para que se possa ter uma avaliação quantitativa e indícios de que o aprendizado foi significativo.

ESTIMATIVA DO NÍVEL DE ADROPINA PARA PACIENTES IRAQUIANOS COM DOENÇA CARDÍACA E ATHEROSCLEROSE E OS FATORES QUE AFETAM O SEU NÍVEL

ESTIMATION THE LEVEL OF ADROPIN FOR IRAQI PATIENTS WITH CARDIAC DISEASE AND ATHEROSCLEROSIS AND THE FACTORS AFFECTING ITS LEVEL

تقدير مستوى الأدرابين للمرضى العراقيين المصابين بأمراض القلب وتصلب الشرايين والعوامل المؤثرة على مستواه

HAMODAT, Zahraa Mohammed Ali^{1*}

¹ Assistant Professor, PhD, Biochemistry, University of Mosul, College of Science, Chemistry, Iraq.

* Corresponding author

e-mail: zahraahamodat@uomosul.edu.iq

Received 13 September 2020; received in revised form 29 September 2020; accepted 18 October 2020

RESUMO

Adropina é um biomarcador de doença cardíaca e aterosclerose. Descoberto em 2008, esse peptídeo está envolvido no controle do metabolismo de carboidratos e ácidos graxos. Um conhecimento detalhado dos mecanismos desses peptídeos e dos fatores que afetam sua liberação pode fornecer um novo diagnóstico e tratamento de distúrbios metabólicos, incluindo doença cardíaca e aterosclerose. Este estudo teve como objetivo estimar o nível de adropina para pacientes iraquianos com doença cardíaca e aterosclerose e os fatores que afetam seu nível, bem como sua relação com as variáveis estudadas. Este estudo foi realizado em 130 adultos, incluindo 90 pacientes com doença cardíaca e aterosclerose e 40 adultos não infectados foram considerados um grupo de controle. Nível sérico de adropina e perfil lipídico (HDL, LDL e TC) foram estimados. Os resultados do estudo mostraram uma diminuição significativa no nível de adropina ($p < 0,0001$) nos seguintes casos: geralmente em todos os pacientes afetados com doença cardíaca e aterosclerose ($4,3 \pm 1,5$ ng/ml) em comparação com indivíduos saudáveis ($10,2 \pm 2,3$ ng/ml); em pacientes obesos ($3,4 \pm 0,7$ ng/ml) em comparação com pacientes não-obesos ($5,2 \pm 1,2$ ng/ml); em pacientes que também apresentam diabetes mellitus tipo 2 ($3,2 \pm 0,8$ ng/ml) e pacientes que também afetam com hipertensão ($4,1 \pm 1,2$ ng/ml) quando comparados com pacientes que não têm outra doença ($5,7 \pm 1,5$ ng). Uma correlação negativa significativa entre o nível de adropina sérica e o nível de IMC ($r = 0,493$; $p = 0,0001$), LDL ($r = -0,628$; $p = 0,0001$) e nível de TC ($r = -0,249$, $p = 0,018$). Uma correlação positiva significativa ($r = 0,395$, $P = 0,0001$) apareceu do nível de adropina com o nível de HDL. Pode-se observar que um nível mais baixo de adropina pode desempenhar um papel vital na fisiopatologia cardíaca e aterosclerose. Além disso, a diminuição do nível de adropina pode ser considerada um fator de risco para esses pacientes. Portanto, a medição e a vigilância das alterações na adropina sérica podem ser consideradas como um novo diagnóstico e avaliação da progressão da doença.

Palavras-chave: Doença cardíaca, aterosclerose, obesidade, diabetes mellitus-2, hipertensão.

ABSTRACT

Adropin is a biomarker for cardiac disease and atherosclerosis. Discovered in 2008, this peptide is involved in controlling the metabolism of carbohydrates and fatty acids. Detailed knowledge of these peptides' mechanisms and the factors that affect their release can provide new diagnostic and treatment of metabolic disorders, including cardiac disease and atherosclerosis. This study aimed to estimate the level of adropin for Iraqi patients with cardiac disease and atherosclerosis and the factors affecting its level and its relationship with the studied variables. This study was conducted on 130 adults, including 90 patients suffering from cardiac disease and atherosclerosis, and 40 uninfected adults were considered a control group. Serum levels of adropin and lipid profile (HDL, LDL, and TC) were estimated. The results of the study showed a significant decrease in the level of adropin ($p < 0.0001$) in the following cases: generally in all patients who affected with cardiac disease and atherosclerosis (4.3 ± 1.5 ng/ml) compared with healthy subjects (10.2 ± 2.3 ng/ml); in obese patients (3.4 ± 0.7 ng/ml) compared to non-obese patients (5.2 ± 1.2 ng/ml); in patients who also affected with diabetes mellitus type 2 (3.2 ± 0.8 ng/ml) and patients who also affected with hypertension (4.1 ± 1.2 ng/ml) when compared with patients who do not have other diseases (5.7 ± 1.5 ng). A negative significant correlation between serum adropin level and BMI ($r = 0.493$; $p = 0.0001$), LDL ($r = -0.628$; $p = 0.0001$) level and TC ($r = -0.249$, $p = 0.018$) level. A positive significant ($r = 0.395$, $P = 0.0001$) appeared correlation of adropin level with HDL level. It was observed

that a lower adropin level could play a vital role in cardiac pathophysiology and atherosclerosis. Also, a decrease in the adropin level can be considered a risk factor for these patients. Therefore, measurement and surveillance of changes in serum adropin can consider as a new diagnosis and assessment of disease progression.

Keywords: Cardiac disease, atherosclerosis, obesity, diabetes mellitus-2, hypertension

الملخص

الأدروبين هو علامة بيولوجية لأمراض القلب وتصلب الشرايين. اكتشف هذا الببتيد في عام 2008، وهو يساهم في التحكم في عملية التمثيل الغذائي للكربوهيدرات والأحماض الدهنية. يمكن أن توفر المعرفة التفصيلية لآليات هذه الببتيدات والعوامل التي تؤثر على إطلاقها تشخيصًا جديدًا وعلاجًا لاضطرابات التمثيل الغذائي، بما في ذلك أمراض القلب وتصلب الشرايين. هدفت هذه الدراسة إلى تقدير مستوى الأدروبين للمرضى العراقيين المصابين بأمراض القلب وتصلب الشرايين والعوامل المؤثرة على مستواه وكذلك علاقته بالمتغيرات المدروسة. أجريت هذه الدراسة على 130 بالغًا، من بينهم 90 مريضًا يعانون من أمراض القلب وتصلب الشرايين، واعتبر 40 بالغًا غير مصاب مجموعة ضابطة. تم تقدير مستوى المصل من الأدروبين والدهون (HDL و LDL و TC). أظهرت نتائج الدراسة انخفاضًا معنويًا في مستوى الأدروبين ($p < 0.0001$) في الحالات التالية: عند كل المرضى المصابين بأمراض القلب وتصلب الشرايين (1.5 ± 4.3 نانوغرام / مل) مقارنة مع الأصحاء (2.3 ± 10.2 نانوغرام / مل)؛ في المرضى الذين يعانون من السمنة المفرطة (0.7 ± 3.4 نانوغرام / مل) مقارنة مع غير المصابين بالسمنة (5.2 ± 1.2 نانوغرام / مل)؛ في المرضى الذين أصيبوا أيضًا بداء السكري 2 (0.8 ± 3.2 نانوغرام / مل) والمرضى الذين أصيبوا أيضًا بارتفاع ضغط الدم (1.2 ± 4.1 نانوغرام / مل) عند مقارنتهم بالمرضى الذين ليس لديهم مرض آخر (1.5 ± 5.7 نانوغرام). ارتباط معنوي سلبي بين مستوى الأدروبين في الدم ومؤشر كتلة الجسم ($r = 0.493$; $p = 0.0001$)، ومستوى LDL ($r = -0.628$; $p = 0.0001$) ومستوى HDL. يمكن ملاحظة أن انخفاض مستوى الأدروبين يمكن أن يلعب دورًا حيويًا في الفيزيولوجيا المرضية للقلب وتصلب الشرايين. أيضًا، يمكن اعتبار انخفاض مستوى الأدروبين عامل خطر لهؤلاء المرضى. لذلك، يمكن اعتبار قياس ومراقبة التغيرات في أدروبين الدم بمثابة تشخيص وتقييم حديثين لتطور المرض.

الكلمات المفتاحية: الأدروبين، مرضى القلب، تصلب الشرايين، السمنة، مرض السكري 2، ارتفاع ضغط الدم.

1. INTRODUCTION:

A major global public health concern is Cardiac disease and atherosclerosis (Ambrosy *et al.*, 2014; Guo, Lip, and Banerjee, 2013; Lüscher, 2015; Sayago-Silva, García-López, and Segovia-Cubero, 2013). Atherosclerosis is the leading cause of the cardiac disease (Li, Xie, Zheng, Yin, and Tang, 2016; Tian *et al.*, 2012). The etiology of atherosclerosis includes multiple metabolic disorders, including obesity, diabetes, and hyperlipidemia (Li *et al.*, 2016; Markelic *et al.*, 2011). In recent years, scientists have identified new regulatory peptides called adropin, which control the metabolism of carbohydrates and fatty acids (Cao *et al.*, 2019; Li *et al.*, 2016). Various research on different fields of medical sciences tends to expose their unique properties. Detailed knowledge of the mechanisms of these peptides and the factors that affect their release can provide new diagnostic and treatment of metabolic disorders, including Cardiac disease and atherosclerosis (Li *et al.*, 2016)

Adropin was discovered in 2008 by Kumar while studying the expressing gene that affects obesity in rat liver (Kumar *et al.*, 2008; Li *et al.*, 2016; Marczyk, Cecerska-Heryć, Jesionowska, and Dołęgowska, 2016). The name adropin is derived from two Latin words, the first "duro" meaning to set fire, and the second word "pinquis"

meaning fat or oil (Marczyk *et al.*, 2016). It is a peptide hormone with a molecular weight of 45-59 kDa (Cao *et al.*, 2019; Chang, Chu, Lin, Hsu, and Chen, 2018; Li *et al.*, 2016; Marczyk *et al.*, 2016). Besides, it is formed by the Enho gene, which is mainly generated in the liver and brain (Chang *et al.*, 2018; Kumar *et al.*, 2008; Li *et al.*, 2016). Adropin is composed of 76 amino acids and is monomeric (Kuloglu and Aydin, 2014; Kumar *et al.*, 2008; Li *et al.*, 2016). The amino acid sequence of adropin is similar in humans, mice, and rats (Kumar *et al.*, 2008; Li *et al.*, 2016; Marczyk *et al.*, 2016): in pig, the amino acid sequence is similar to 98-99% of the amino acid sequence (Li *et al.*, 2016; Wang *et al.*, 2015). Adropin is a membrane-bound protein, the first 9 amino acids from the amino end are expressed within of cytoplasm region (Li *et al.*, 2016), and the 9-30 amino acids are expressed within the cytoplasmic membrane; these amino acids are characterized by being hydrophobic (Li *et al.*, 2016; Marczyk *et al.*, 2016; Wang *et al.*, 2015). The remainder of the amino acids from the carboxylic end of the 30-76 amino acid is outside the cytoplasmic membrane (Li *et al.*, 2016; Wang *et al.*, 2015). Adropin is essential in regulating glucose and fatty acid metabolism and energy balance (Cao *et al.*, 2019; Chang *et al.*, 2018; Kumar *et al.*, 2008; Marczyk *et al.*, 2016). And that obesity affects the level of adropin, where the level

of pathways decreases in obese people (Chang *et al.*, 2018; Marczuk *et al.*, 2016). Also, adropin is a regulator of cardiovascular function as it increases blood flow and has a protective role in protecting endothelial cells (Li *et al.*, 2016; Lovren *et al.*, 2010; Marczuk *et al.*, 2016).

The study aimed (1) to estimate the level of adropin for Iraqi cardiac disease and atherosclerosis patients, (2) the effect of the factor of obesity and other diseases (diabetes mellitus-type 2 (DM-2, and hypertension), age, and sex at the level of adropin and (3) the relationship of adropin with the studied variables such as obesity, affected with other diseases (diabetes-2 or hypertension) age and sex.

2. MATERIALS AND METHODS:

The current study evaluated the adropin hormone level in patients with heart disease and atherosclerosis in Mosul City in 2019 from 5 May to 10 December.

2.1 Patients and Methods

This study was performed with 130 adults, including 90 patients suffering from cardiac disease and atherosclerosis of both sexes (31 females, 59 males, ages ranging from 35 to 65). They were attending Al-Salam Teaching Hospital, Ibn Sina Teaching Hospital, and medical clinics for heart disease and atherosclerosis, which were licensed by the Ministry of Health in Mosul - Iraq. A total of 40 uninfected adults were considered a control group of both sexes (18 females, 22 males aged 35 to 55 years). Besides, the patient group was divided into two groups. The first was non-obese (BMI <30 kg/m²), and the second was obese (BMI > 30 kg/m²). Moreover, the patient group was also divided into three groups. The first of which the patients had no other disease (n = 33, 14 females, 19 males, 35 to 52 years of age); The second patients had diabetes-2 (n = 30, 12 females, 18 males, ages 48-65 years); And the third patients had hypertension (n = 27, 12 females, 15 males, aged 46-65 years). Excluded from the study were people who smoke and pregnant women, and those with other diseases such as kidney disease and cancer. The study protocol was reviewed by the ethics commission at Mosul University and the Nineveh Department of Health, and all subjects were informed written form of informed consent.

2.2 Sample Collection

Informed consent was obtained from all

participants. Five milliliters (5 ml) of venous blood were collected after overnight fasting; the serum obtained was kept under freezing -20°C (Hammodat and Mustafa, 2018) to analyze adropin lipid profile weekly.

2.3 Variables Assay

2.3.1 Serum adropin

It was measured using a commercial ELISA Kit (biosciences), an immunoassay for the quantitative in vitro diagnostic measurement of adropin in plasma, serum, and tissue. All serum samples were diluted 25 folds with diluting the sample. Also, the adropin level was expressed in terms of ng/ml.

2.3.2 Serum lipid profile

Lipid profiles, including high-density lipoprotein (HDL), low-density lipoprotein (LDL), and total cholesterol (TC), were measured by cobas c111 system that automatically calculated the level of each sample (Haritwal, Chourasia, and Ojha, 2015).

2.3.3 Body mass index (BMI)

BMI was estimated by dividing the weight (Kg) on height (m²) (Jacobsson *et al.*, 2009).

2.3. Statistical Analysis

The results were carried out using the statistical program package for social sciences (SPSS), version 25.0. The results were expressed as a mean ± SD (standard deviation). Correlation analysis is expressed by using Pearson's correlation coefficient. That p-value considers significant when it is less than 0.05 of a statistical significance (Beddo and Kreuter, 2004).

3. RESULTS AND DISCUSSION:

Adropin is a hormone peptide that plays an essential role in patients with cardiac disease and atherosclerosis. While research into the effects of adropin is still in the early stages. Nonetheless, our current awareness of the cardiovascular safety of adropin comes mainly from animal studies.

Table 1 shows the average age of patients was 52.7 ±11.1 years, and the average age of healthy people was 50.5 ±14.3 years. Moreover, a significant decrease (p<0.0001) in the level of adropin in cardiac and atherosclerosis patients is 4.3±1.5 ng/ml compared with serum controls

10.2±2.3 ng/ml. These results agree with (Celik *et al.*, 2013; Yu *et al.*, 2014; Zhang *et al.*, 2014). This result can be explained because of adropin is associated with nitric oxide synthase (eNOS). When eNOS level is full down in cardiac disease and atherosclerosis patients, the level of adropin also reduced (Li *et al.*, 2016; Lovren *et al.*, 2010). Kuloglu *et al.* had researched adropin variability and inducible expression of nitric oxide synthase (iNOS) in streptozotocin (STZ)-induced diabetic rats in the renal tissues. With the severity of diabetes, the intensities of adropin and iNOS immunoreactivities increase (Kuloglu and Aydin, 2014)

Patients with cardiac disease have a significant difference in lipid profile level (Table 1), where patients had a lower HDL level (40±8.4 mg/dl patients vs. 54.1 ±14.5 mg/dl control; $p<0.0001$), and higher level of LDL (111.7±34.6mg/dl patients vs. 82.9±25.4 mg/dl control; $p<0.0001$) and TC (195.6 ±57.3mg/dl patients vs. 155.8 ±43.4 mg/dl control; $p<0.0001$). And that's consistent with (Akçilar *et al.*, 2016; Cao *et al.*, 2019; Ghoshal *et al.*, 2018).

Moreover, various factors on the level of adropin, such as obesity, are affected by other diseases (diabetes-2 or hypertension), age, and sex (Table 2 and Figure 1). Serum adropin level significantly decreased ($p<0.0001$) in obese patients (3.4±0.7kg/m²) when compared to non-obese patients (5.4±1.2kg/m²); these results are in concordance with (Butler *et al.*, 2012; Ganesh-Kumar *et al.*, 2012; Sayın, Tokgöz, and Arslan, 2014). Lian *et al.*, 2016 showed that serum adropin level was not affected by obesity (Lian, Wu, Liu, Jiang, and Jiang, 2016). This may be because of adropin has a significant role in the regulation of fatty acid metabolism (Altamimi *et al.*, 2019; Cao *et al.*, 2019; Li *et al.*, 2016; Marczuk *et al.*, 2016)

Additionally, the adropin level decreased significantly ($p<0.0001$) in patients who were also affected with type 2 diabetes mellitus (DM-2) (3.2±0.8 ng/ml) when compared with patients who were non-affected with other diseases (5.7±1.5 ng/ml). These results were in agreement with (Kuloglu and Aydin, 2014). This may be because adropin has a significant role in regulating glucose metabolism (Altamimi *et al.*, 2019; Lin *et al.*, 2014; Marczuk *et al.*, 2016). Gao *et al.* (2015) showed that DM-2 affected adropin levels in mice (Gao *et al.*, 2015). Also, patients affected with hypertension had lower adropin levels (4.1±1.2 ng/ ml; $p<0.0001$) when compared with patients non-affected with other diseases (5.7±1.5 ng/ ml). This result agrees with (Chen, Ouyang, and Zhou, 2015) and may be due to the association of adropin with nitric oxide

synthase (eNOS) (Li *et al.*, 2016; Lovren *et al.*, 2010). Aydin *et al.*, 2015, revealed that adropin level effects on blood pressure by protective endothelial job (Aydin *et al.*, 2016), while Altincik *et al.*, 2015 showed no blood effects pressure on adropin level in obese children (Altincik and Sayın, 2015).

No significant difference was observed for sex ($p=0.7$) and age ($p=0.91$). The serum adropin in males and females was 4.9± 1.3 ng/ml, 4±1.2 ng/ml, respectively. These results are in concordance with (Butler *et al.*, 2012; Sayın *et al.*, 2014). Butler found that males have more adropin levels than females, but without significant differences (Butler *et al.*, 2012). Sex factors do not show a moral effect on the level of adropin. Moreover, serum adropin levels in age groups ≤45 years and ≥46 years, which were 4.7±1.4 ng/ml and 4±1.3 ng/ml respectively, had non-significant differences. These results are in concordance with (Butler *et al.*, 2012).

Table 3 and Figure 2 also showed that the level of serum adropin in patients is associated with a significant negative correlation with obesity ($r=-0.493$ ($p=0.0001$)), which means that obesity has a bad effect on the level of adropin and, therefore, negatively affects patients. These results are in concordance with (Ganesh-Kumar *et al.*, 2012). Besides, the adropin level in patients was associated with a significant positive correlation with HDL level ($r=0.395$, $p=0.0001$). In contrast, it was associated with a meaningful inverse relationship with both LDL ($r=-0.79$, $p=0.0001$) and TC ($r=-0.249$, $p=0.0001$). These results are in concordance with (Ghoshal *et al.*, 2018).

4. CONCLUSION:

Serum adropin levels in patients with cardiac disease and atherosclerosis significantly decreased. Also, adropin levels were affected by patients with obesity, type 2 diabetes mellitus, and hypertension. A lower adropin level could play a vital role in cardiac pathophysiology and atherosclerosis. Also, decreased adropin levels can be considered a risk factor for patients affected by cardiac disease and atherosclerosis, especially for patients affected by DM-2 or hypertension. Therefore, measurement and monitoring changes in serum adropin can be known as new disease diagnosis and progression assessment. Although research into the effects of adropin is still in its early stages, rising evidence has suggested that this hormone peptide plays a protective role in developing cardiovascular

diseases.

5. REFERENCES:

1. Akcılar, R., Koçak, F. E., Şimşek, H., Akcılar, A., Bayat, Z., Ece, E., and Kökdaşgil, H. (2016). The effect of adropin on lipid and glucose metabolism in rats with hyperlipidemia. *Iranian journal of basic medical sciences*, 19(3), 245.
2. Altamimi, T. R., Gao, S., Karwi, Q. G., Fukushima, A., Rawat, S., Wagg, C. S., . . . Lopaschuk, G. D. (2019). Adropin regulates cardiac energy metabolism and improves cardiac function and efficiency. *Metabolism*, 98, 37-48.
3. Altincik, A., and Sayin, O. (2015). Evaluation of the relationship between serum adropin levels and blood pressure in obese children. *Journal of Pediatric Endocrinology and Metabolism*, 28(9-10), 1095-1100.
4. Ambrosy, A. P., Fonarow, G. C., Butler, J., Chioncel, O., Greene, S. J., Vaduganathan, M., Shah, A. N. (2014). The global health and economic burden of hospitalizations for heart failure: lessons learned from hospitalized heart failure registries. *Journal of the American College of Cardiology*, 63(12), 1123-1133.
5. Aydin, H. I., Eser, A., Kaygusuz, I., Yildirim, S., Celik, T., Gunduz, S., and Kalman, S. (2016). Adipokine, adropin and endothelin-1 levels in intrauterine growth restricted neonates and their mothers. *Journal of Perinatal Medicine*, 44(6), 669-676.
6. Beddo, V. C., and Kreuter, F. (2004). *A Handbook of Statistical Analyses using SPSS*. Sabine Landau and Brian Everitt. Chapman and Hall/CRC, Boca Raton, Florida, 2004. ISBN 1-58488-369-3. vii+ 354 pp.
7. Rabe-Hesketh, S; and Everitt, B. *A Handbook of Statistical Analyses using Stata*. Chapman and Hall/CRC, Boca Raton, Florida, 2004. ISBN 1-58488-404-5. xiii+ 308 pp.
8. Butler, A. A., Tam, C. S., Stanhope, K. L., Wolfe, B. M., Ali, M. R., O'Keeffe, M., Havel, P. J. (2012). Low circulating adropin concentrations with obesity and aging correlate with risk factors for metabolic disease and increase after gastric bypass surgery in humans. *The Journal of Clinical Endocrinology and Metabolism*, 97(10), 3783-3791.
9. Cao, J.-F., Wang, M.-S., Bian, C.-Y., Tao, Y.-F., You, T., Xu, W.-T., and Gu, X.-S. (2019). Association between serum adropin and subclinical atherosclerosis in patients with hyperlipidemia. *International journal of clinical and experimental medicine*, 12(7), 9351-9358.
10. Celik, A., Balin, M., Kobat, M. A., Erdem, K., Baydas, A., Bulut, M., . . . Aydin, S. (2013). Deficiency of a new protein associated with cardiac syndrome X; called adropin. *Cardiovascular therapeutics*, 31(3), 174-178.
11. Chang, J.-B., Chu, N.-F., Lin, F.-H., Hsu, J.-T., and Chen, P.-Y. (2018). Relationship between plasma adropin levels and body composition and lipid characteristics amongst young adolescents in Taiwan. *Obesity research and clinical practice*, 12(1), 101-107.
12. Chen, M., Ouyang, F., and Zhou, S. (2015). Adropin as a novel energy factor likely has the ability to regulate blood pressure. *Medical hypotheses*, 85(2), 234.
13. Ganesh-Kumar, K., Zhang, J., Gao, S., Rossi, J., McGuinness, O. P., Halem, H. H., Butler, A. A. (2012). Adropin deficiency is associated with increased adiposity and insulin resistance. *Obesity*, 20(7), 1394-1402.
14. Gao, S., McMillan, R. P., Zhu, Q., Lopaschuk, G. D., Hulver, M. W., and Butler, A. A. (2015). Therapeutic effects of adropin on glucose tolerance and substrate utilization in diet-induced obese mice with insulin resistance. *Molecular metabolism*, 4(4), 310-324.
15. Ghoshal, S., Stevens, J. R., Billon, C., Girardet, C., Sitaula, S., Leon, A. S., . . . Bouchard, C. (2018). Adropin: An endocrine link between the biological clock and cholesterol homeostasis. *Molecular metabolism*, 8, 51-64.
16. Guo, Y., Lip, G. Y., and Banerjee, A. (2013). Heart failure in East Asia. *Current cardiology reviews*, 9(2), 112-122.
17. Hammodat, Z. M., and Mustafa, L. A. (2018). Biochemical Studies on Synovial Fluid and Serum from Rheumatoid Arthritis Patients. *Rafidain journal of science*, 27(4E), 37-46.

18. Haritwal, A. K., Chourasia, R. K., and Ojha, S. (2015). A comparative study of serum lipid profile and glucose level between breast cancer patients and controls at tertiary care hospital in India. *International Journal of Medical Science Research and Practice*, 2(1), 16-19.
19. Jacobsson, J. A., Risérus, U., Axelsson, T., Lannfelt, L., Schiöth, H. B., and Fredriksson, R. (2009). The common FTO variant rs9939609 is not associated with BMI in a longitudinal study on a cohort of Swedish men born 1920-1924. *BMC medical genetics*, 10(1), 131.
20. Kuloglu, T., and Aydin, S. (2014). Immunohistochemical expressions of adropin and inducible nitric oxide synthase in renal tissues of rats with streptozotocin-induced experimental diabetes. *Biotechnic and Histochemistry*, 89(2), 104-110.
21. Kumar, K. G., Trevaskis, J. L., Lam, D. D., Sutton, G. M., Koza, R. A., Chouljenko, V. N., . . . Thearle, M. (2008). Identification of adropin as a secreted factor linking dietary macronutrient intake with energy homeostasis and lipid metabolism. *Cell metabolism*, 8(6), 468-481. doi:<https://doi.org/10.1016/j.cmet.2008.10.011>
22. Li, L., Xie, W., Zheng, X.-L., Yin, W.-D., and Tang, C.-K. (2016). A novel peptide adropin in cardiovascular diseases. *Clinica chimica acta*, 453, 107-113. doi:<http://dx.doi.org/10.1016/j.cca.2015.12.010> 0009-8981/©
23. Lian, A., Wu, K., Liu, T., Jiang, N., and Jiang, Q. (2016). Adropin induction of lipoprotein lipase expression in tilapia hepatocytes. *Journal of molecular endocrinology*, 56(1), 11.
24. Lin, Y.-J., Kwok, C.-F., Juan, C.-C., Hsu, Y.-P., Shih, K.-C., Chen, C.-C., and Ho, L.-T. (2014). Angiotensin II enhances endothelin-1-induced vasoconstriction through upregulating endothelin type A receptor. *Biochemical and biophysical research communications*, 451(2), 263-269.
25. Lovren, F., Pan, Y., Quan, A., Singh, K. K., Shukla, P. C., Gupta, M., . . . Verma, S. (2010). Adropin is a novel regulator of endothelial function. *Circulation*, 122(11_suppl_1), S185-S192.
26. Lüscher, T. F. (2015). Heart failure: the cardiovascular epidemic of the 21st century. In: Oxford University Press.
27. Marczuk, N., Cecerska-Heryć, E., Jesionowska, A., and Dołęgowska, B. (2016). Adropin-physiological and pathophysiological role. *Advances in Hygiene and Experimental Medicine/Postepy Higieny i Medycyny Doswiadczalnej*, 70.
28. Markelic, M., Velickovic, K., Golic, I., Otasevic, V., Stancic, A., Jankovic, A., Korac, A. (2011). Endothelial cell apoptosis in brown adipose tissue of rats induced by hyperinsulinaemia: the possible role of TNF- α . *European journal of histochemistry: EJH*, 55(4).
29. Sayago-Silva, I., García-López, F., and Segovia-Cubero, J. (2013). Epidemiology of heart failure in Spain over the last 20 years. *Revista Española de Cardiología (English Edition)*, 66(8), 649-656.
30. Sayin, O., Tokgöz, Y., and Arslan, N. (2014). Investigation of adropin and leptin levels in pediatric obesity-related nonalcoholic fatty liver disease. *Journal of Pediatric Endocrinology and Metabolism*, 27(5-6), 479-484.
31. Tian, G.-P., Chen, W.-J., He, P.-P., Tang, S.-L., Zhao, G.-J., Lv, Y.-C., . . . Cheng, H. (2012). MicroRNA-467b targets LPL gene in RAW 264.7 macrophages and attenuates lipid accumulation and proinflammatory cytokine secretion. *Biochimie*, 94(12), 2749-2755.
32. Wang, S.-p., Gao, Y.-l., Liu, G., Deng, D., Chen, R.-j., Zhang, Y.-z., . . . Feng, Z.-m. (2015). Molecular cloning, characterization and expression of the energy homeostasis-associated gene in piglet. *Journal of Zhejiang University-SCIENCE B*, 16(6), 524-532.
33. Yu, X.-H., Qian, K., Jiang, N., Zheng, X.-L., Cayabyab, F. S., and Tang, C.-K. (2014). ABCG5/ABCG8 in cholesterol excretion and atherosclerosis. *Clinica Chimica Acta*, 428, 82-88.
34. Zhang, C., Zhao, L., Xu, W., Li, J., Wang, B., Gu, X., and Chen, J. (2014). Correlation of serum adropin level with coronary artery disease. *Zhonghua yi xue za zhi*, 94(16), 1255-1257.

Table 1. Clinical and biochemical characteristics of controls and patients with cardiac disease and atherosclerosis

Variables	Controls, n=40	Patients, n=90	p-value
Age (mean \pm SD) years, (range, years)	50.5 \pm 14.3, (35-55)	52.7 \pm 11.1, (35-65)	0.4 (NS)
Sex (F:M)	18:22	31:59	-
Adropin (ng/ml)	10.2 \pm 2.3	***4.3 \pm 1.5	0.0001
BMI (kg/m ²)	28.7 \pm 4.1	29.61 \pm 3.6	0.41 (NS)
HDL (mg/ dl)	54.1 \pm 14.5	***40 \pm 8.4	0.0001
LDL (mg/dl)	82.9 \pm 25.4	***111.7 \pm 34.6	0.0001
TC mg/dl)	155.8 \pm 43.4	***195.6 \pm 57.3	0.0001
Smoking/ non-smoking	9/14	39/27	--
patients			
Total Patients, n=90	Patients without affected any disease, n=33 (36.4%)	Patients affected with diabetes mellitus, n=30 (33.3%)	Patients affected with hypertension, n=27 (30.3%)
Age (mean \pm SD) years,(range, years)	52.7 \pm 11.1, (35-55)	49.3 \pm 11.1, (49-65)	65.2 \pm 12.4, (48-63)
Sex (F:M)	14:19	12:18	12:15

SD: Stander deviation; M: Male; F: Female; **significant when p–value equal at 0.001; while, ***significant whn p-value equal to 0.0001

Table 2. The effect of obesity, affected by other diseases (diabetes-2, hypertension) age, sex, and smoking on the level of adropin in patients with cardiac disease and atherosclerosis.

Obesity factor						
Adropin (ng/ml)/Obesity	BMI 20-29, 27.4±7.3 (kg/m ²), n= 33			BMI ≥ 30, 35.6±9.2 (kg/m ²), n=57		p-value
	5.2±1.2			***3.4±0.7		0.0001
Patients affected with other disease						
Adropin (ng/ml)/patients affected with other diseases (diabetes mellitus-2 or hypertension)	Diabetes mellitus-2 (DM-2)			Hypertension(HT)		
	Without-DM-2, n=33	With-DM-2, n=30	p-value	Without-HT, n=33	With-HT, n=27	p-value
	5.7±1.5	***3.2± 0.8	0.0001	5.3±1.5	***4.1± 1.2	0.0001
Age factor						
Adropin (ng/ml)/Age	≤ 45 years, n=28			≥ 46 years, n= 62		p-value
	4.7±1.4			4±1.3		0.091
Sex factor						
Adrropin (ng/ml)/Sex	Male, n=59			Female, n=31		p-value
	4.9±1.3			4± 1.2		0.07

SD: Stander deviation; M: Male; F: Female; ng: Nano gram; kg: kilogram; m: miter; ml: milliliter; mg: milligram; dl: Deciliter; n: number; HDL: High density lipoprotein; LDL: Low density lipoprotein; TC: Total cholesterol; BMI: Body mass index; *** significant when the level of p- value equal to 0.0001; **significant when the p-value equal to 0.001; Diabetes mellitus-2 (DM-2); Hypertension(HT); BMI; Body mass index; kg: kilogram; n: number; m: miter.

Table 3. The relationship of adropin level with the studied variables of patients with cardiac disease and atherosclerosis

Variables	Adropin (ng/ml), r =, (p, Pearson correlation), n= 90
BMI (kg/m ²)	** -0.628, (0.0001)
HDL (mg/dl)	** 0.395, (0.0001)
LDL (mg/dl)	** -0.698 (0.0001)
TC (mg/dl)	* -0.249 (0.018)

ng: nano gram; kg: kilogram; m: miter; mg: milligram; dl: Deciliter; n: number; LDL: Low density lipoprotein; HDL: High density lipoprotein; TC: Total cholesterol; BMI: Body mass index; ** correlation is significant when the level of p-value equal to 0.001; * correlation is significant when the level of p-value equal to 0.05.

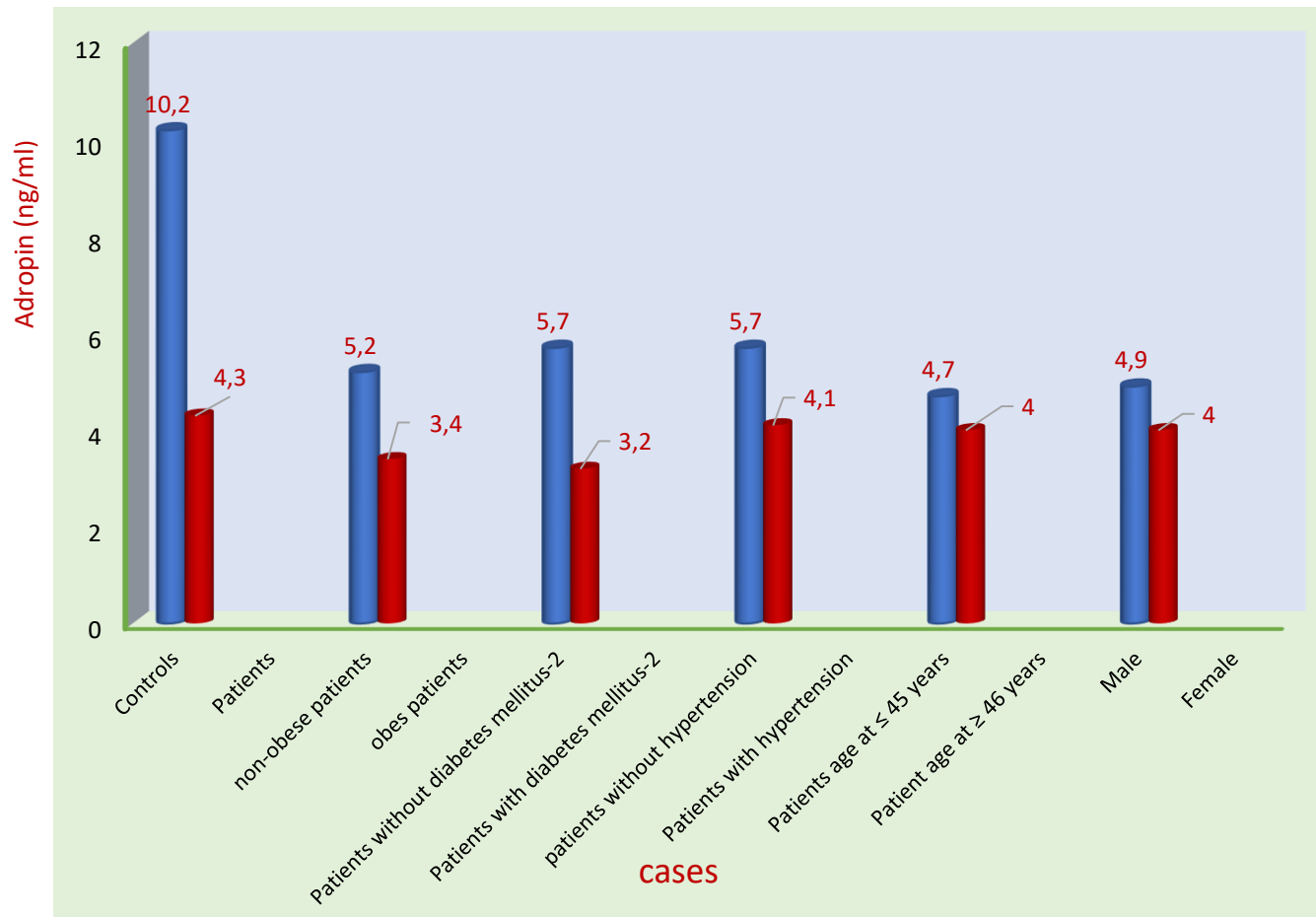


Figure 1. A comparison of serum adropin levels between healthy controls and patients; the effect of obesity factor and other diseases (diabetes-2, hypertension) age, sex, and smoking on the level of adropin in patients with heart disease and atherosclerosis

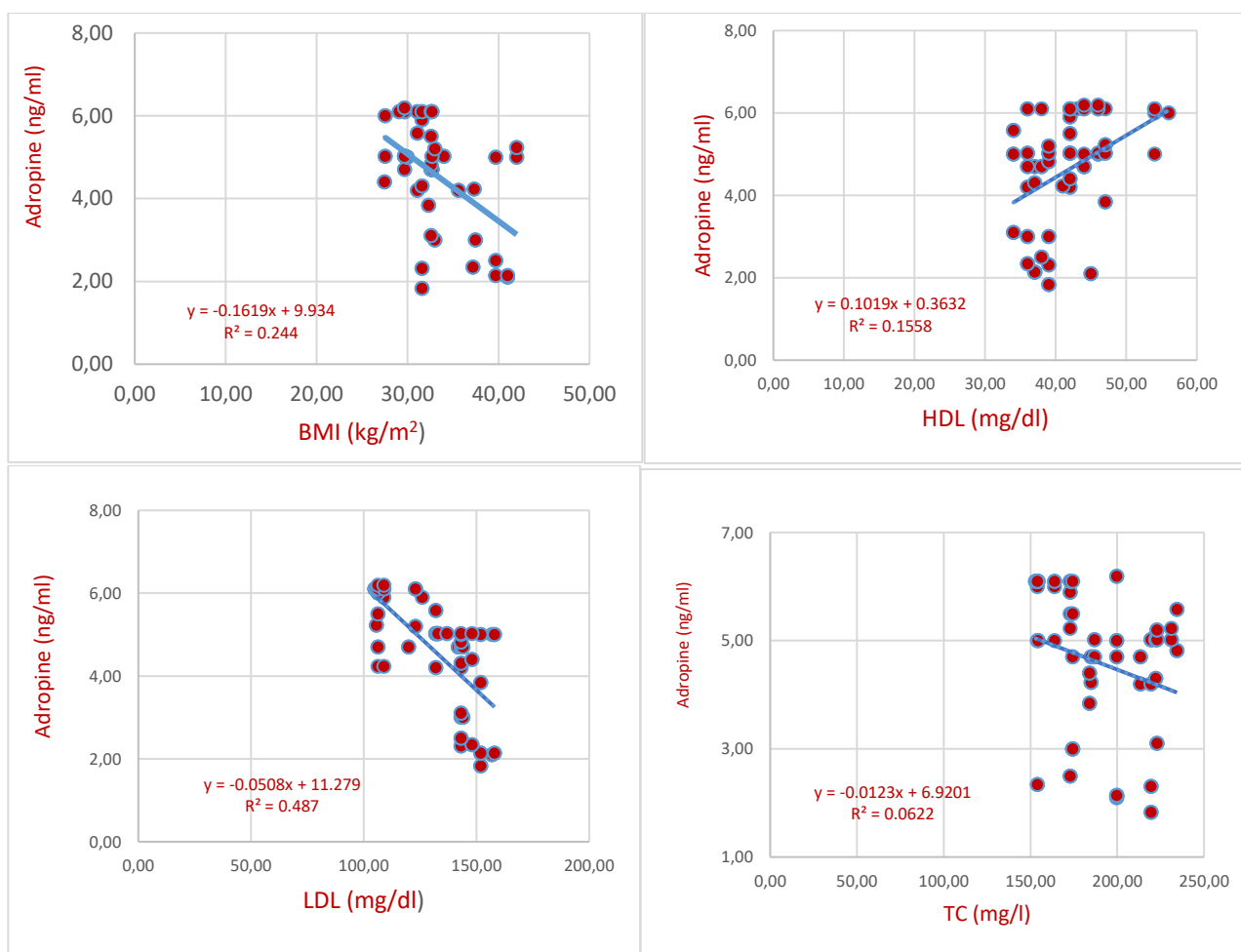


Figure 2. The relationship of serum adropin level and the variables studied for patients with cardiac disease and atherosclerosis. ng: Nano gram; ml: milliliter; kg: kilogram; m: meter; mg: milligram; dl: Deciliter; HDL: High density lipoprotein; LDL: Low density lipoprotein; TC: Total cholesterol; BMI: Body mass index.

**ESTADO DE MELHORAMENTO DOS CHERNOSSOLOS CLAROS IRRIGADOS DA
REGIÃO DO TURQUESTÃO****THE AMELIORATIVE CONDITION OF THE IRRIGATED LIGHT SEROZEM OF THE
TURKESTAN REGION****МЕЛИОРАТИВНОЕ СОСТОЯНИЕ ОРОШАЕМЫХ СВЕТЛЫХ ЧЕРНОЗЕМОВ
ТУРКЕСТАНСКОЙ ОБЛАСТИ**

TANIRBERGENOV, Samat I.^{1*}; SULEIMENOV, Beibut U.²; ÇAKMAK, Dragan³;
SALJNIKOV, Elmira⁴; SMANOV, Zhassulan⁵;

^{1,2} U.U. Uspanov Kazakh Research Institute of Soil Science and Agrochemistry, Department of Agrochemistry and Soil Ecology, 75 Al-Farabi Ave., zip code 050060, Almaty – Republic of Kazakhstan

³ University of Belgrade, Institute for Biological Research “Sinisa Stankovic”, Department of Ecology, 142 Despot Stefan Blvd, zip code 11060, Belgrade – Republic of Serbia

⁴ Institute of Soil Science, Department of Ecology, 7 Teodor Drajzer, zip code 11000, Belgrade – Republic of Serbia

⁵ U.U. Uspanov Kazakh Research Institute of Soil Science and Agrochemistry, Department of Reclamation of Saline Soils, 75 Al-Farabi Ave., zip code 050060, Almaty – Republic of Kazakhstan

** Corresponding author*

e-mail: samat.soil.kz@gmail.com

Received 15 September 2020; received in revised form 22 October 2020; accepted 07 November 2020

RESUMO

A relevância do estudo se deve ao fato de que a irrigação em grande escala de campos de algodão em regiões áridas e desérticas da região do Turquestão leva inevitavelmente a processos de salinização do solo. A salinização é um problema global para a humanidade. A salinização do solo está associada a problemas de drenagem, uso inadequado dos recursos hídricos; crescente demanda por produtos agrícolas, o que leva a um aumento da pressão sobre as terras agrícolas. A este respeito, o presente trabalho tem como objetivo estudar a salinidade do solo cinza claro (serozem) irrigado na indústria de algodão do Cazaquistão do Sul (agora região do Turquestão) sob condições de drenagem vertical, o que fornecerá o pano de fundo necessário para a reconstrução do sistema de drenagem coletor em toda a região, o que contribui para um aumento no rendimento líquido e na qualidade de algodão em linha e também evita a deterioração do solo. O método principal para estudar as questões do artigo é o método de dispersão, segundo o qual a salinidade do solo foi determinada de acordo com estações do ano. As principais tarefas eram estudar a dinâmica das mudanças sazonais e oportunas nos sais sob drenagem vertical e estudar a distribuição espacial dos sais nas fazendas de algodão. Os resultados mostraram que em 2014 houve uma dinâmica positiva de mudanças em comparação com 2012. Na primavera de 2014, a área sob solos moderadamente salinos na camada de 0-20 cm diminuiu de 79,5 para 57,7%; a área de solos levemente salinos aumentou de 20,5 para 34,6%. No período de outono-inverno, a área de solos altamente salinos diminuiu de 25,6 para 14,1%. A área de solos não salinos foi de 7,7%. Os resultados mostraram que a mudança no número de íons, tanto verticalmente quanto de acordo com a estação do ano, ocorre com a transferência de sais ao longo do perfil do solo sob a influência dos gradientes de temperatura e níveis de água subterrânea, ou seja, na primavera de baixo para cima, no outono e no inverno – vice-versa. O valor teórico e prático do estudo reside no facto de que o material para a melhoria, prevenção da salinização do solo levará a um aumento no nível geral de segurança ecológica da região e do país como um todo.

Palavras-chave: irrigação, solo cinza claro (serozem), salinidade do solo, distribuição espacial, distribuição sazonal, drenagem vertical.

ABSTRACT

The relevance of the study is conditioned by the fact that the large-scale irrigation of cotton fields in arid and desert areas of the Turkestan region inevitably leads to the processes of soil salinization. Salinity is a global problem for humanity. Soil salinization is associated with drainage problems, improper use of water resources, growing demand for agricultural products, which leads to increased pressure on agricultural land. In this regard, this paper is directed at investigating the soil salinity of the irrigated light serozem in a cotton farm of Southern Kazakhstan (now Turkestan region) under the vertical drainage, which would provide the necessary background for the reconstruction of the collection-drainage system of the whole region, thus contributing to the increasing the net yield and the quality of the row cotton, as well as preventing soil deterioration. The leading method for studying the issues of the article was the dispersion method, according to which the salinity of soils was determined by seasons. The main objectives were studying the dynamics of salts changes seasonally and timely under the vertical drainage and studying the spatial distribution of salts in the cotton-based farm. The results showed that in 2014 there was recorded a positive dynamic of changes compared to 2012. In spring 2014, the area under medium saline soil in the 0-20 cm layer decreased from 79.5 to 57.7 %; the weakly saline soil area increased from 20.5 to 34.6 %. In the autumn and winter periods, the area of strongly saline soils decreased from 25.6 to 14.1 %. The area of non-saline soils was recorded at 7.7 %. The results showed that changes in the amount of the ions, both vertically and seasonally, occur with the transport of salts along with soil profile under the influence of temperature gradients and the level of groundwater, i.e., in spring from up to down, and in autumn and winter, contrary from down to up. The theoretical and practical value of the study lies in the fact that the material for improving, preventing the salinization of soils will lead to an increase in the general level of ecological safety of the region and country in general.

Keywords: *irrigation, light serozem, soil salinity, spatial distribution, seasonal distribution, vertical drainage*

АННОТАЦИЯ

Актуальность исследования обусловлена тем, что масштабное орошение хлопковых полей в засушливых и пустынных районах Туркестанской области неизбежно приводит к процессам засоления почв. Засоление является глобальной проблемой человечества. Засоление почв связано с проблемами дренажа, неправильным использованием водных ресурсов; ростом спроса на сельскохозяйственную продукцию, что приводит к повышенной нагрузке на сельскохозяйственные земли. В связи с этим данная работа направлена на исследование засоленности почвы орошаемого светлого серозема в хлопковом хозяйстве Южного Казахстана (ныне Туркестанская область) в условиях вертикального дренажа, что обеспечит необходимый фон для реконструкции коллекторно-дренажной системы по всему региону, что способствует повышению чистой урожайности и качества пропашного хлопка, а также предотвращает ухудшение состояния почвы. Ведущим методом изучения вопросов статьи явился метод дисперсии, согласно которому засоленность почв определялась по сезонам года. Основными задачами были изучение динамики сезонных и своевременных изменений солей под вертикальным дренажем и изучение пространственного распределения солей в хлопководческих хозяйствах. Результаты показали, что в 2014 году зафиксирована положительная динамика изменений по сравнению с 2012 годом. Весной 2014 года площадь под средnezасоленными почвами в слое 0-20 см уменьшилась с 79.5 до 57.7 %; площадь слабозасоленных почв увеличилась с 20.5 до 34.6 %. В осенне-зимний период площадь сильнозасоленных почв уменьшилась с 25.6 до 14.1 %. Площадь незасоленных почв составила 7.7 %. Результаты показали, что изменение количества ионов, как по вертикали, так и по сезонам, происходит с переносом солей по профилю почвы под влиянием градиентов температуры и уровня грунтовых вод, то есть весной снизу вверх, осенью и зимой наоборот. Теоретическая и практическая ценность исследования заключается в том, что материал для улучшения, предотвращения засоления почв приведет к поднятию общего уровня экологической безопасности области и страны в целом.

Ключевые слова: *орошение, светлый серозем, засоление почвы, пространственное распределение, сезонное распределение, вертикальный дренаж.*

1. INTRODUCTION:

The large-scale irrigation of cotton fields in arid and desert areas of the Turkestan region inevitably leads to soil salinization processes. According to A. Singh and R. S. Sengar (2014),

the problems of salt-affected paddy soils might be due to inadequate water management in irrigated areas of Kazakhstan. Scientists Y. Sugimori *et al.* (2008), in his study of irrigated and low-salt soils, determined that due to improper irrigation practices, moderately or highly saline soils on

irrigated lands reached 42.1 %, and the yield decreased by 8.6 %. W.A.M. Abdel Kawy and Kh. M. Darwish (2019) reported that the salinization process is referred to as the most frequently occurring land degradation type in aridic regions. Soil salinization lasting for a longer period causes lower production potential of soil (Metternicht and Zinck, 2003; Farifteh et al., 2006; Adibah et al., 2020; Ahmed et al., 2017; Iqbal, 2018).

Turkestan region is the only region growing cotton on an area of 204.1 thousand hectares in 2005 (11.4 % of the territory), that was reduced to 99.3 thousand hectares in 2015 due to inappropriate agricultural management that resulted in a decrease of soil fertility and cotton yield (Umbetaev et al., 2015; Petrick et al., 2017; Murzabaev et al., 2019; Pachykyn et al., 2019; Pereira et al., 2019). Due to the deterioration in operating both irrigation and drainage systems, disorders in intensive cotton cultivation technology, reducing water supply both in the growing season and for soil washing, a sharp increase of the areas subject to secondary salinization was recorded (Bekbayev, 2016; Tanirbergenov et al., 2016; Hamidov et al., 2016; Issanova et al., 2017; Murzabaev et al., 2019; Suska-Malawska et al., 2019). The parent rocks of Golodnaya Steppe are ancient alluvial modified in the upper strata by the secondary processes of lessivage (Rukhovich et al., 2010). The mineralogical composition of these rocks is presented by weakly weathered and re-deposited calcite-quartz-feldspar, which is considered favorable in terms of mineral nutrition of plants (Schoups and Hopmans, 2002; Suleimenov, 2008; Rath et al., 2016).

In this respect, observation of salt movement and advanced geophysical survey, for detection and prediction of salt-affected areas, considered as promising tools for the evaluation and control of ameliorative soil state of irrigated agricultural lands (Kitamura et al., 2006; Weng and Gong, 2006; Mandal et al., 2009; Chernousenko et al., 2012; Bhat et al., 2015; Shrivastava and Kumar, 2015; Vyrahmanova et al., 2020). The repeated salt survey allows obtaining a quantitative characteristic of changes in the salt regime of the soil for a given period (Arunachalam et al., 2011; Allbed and Kumar, 2013). The spatial modeling of salt accumulation regime provides vital information on understanding the dynamic of salt movement regime laterally and vertically (Laiskhanov et al., 2016; Nuruzzaman Manik et al., 2019; Zhumadilova et al., 2019; Hu et al., 2020).

The research was conducted in the Golodnaya Steppe geological formation that is a

vast intermountain drainage basin, bounded on the south by Turkestan range and on the northeast by Kuramin and Chat Kal ranges (Mueller et al., 2014; Bekbayev et al., 2015; Micklin et al., 2016; Kaushal et al., 2018; Soltanaeva et al., 2018). The main goal of the research was establishing the soil salinity state of the irrigated light serozem soils in a cotton farm of Turkestan region (Maktaaral district) under the vertical drainage, which would provide the necessary background for the reconstruction of the collection-drainage system of the whole region, thus contributing to the increasing the net yield and the quality of the row cotton (Sugimori et al., 2008; Stoilova et al., 2014; Wang et al., 2019; Wichern et al., 2020), as well as preventing soil deterioration. The main objectives were studying the dynamics of salts changes seasonally and timely under the vertical drainage and studying the spatial distribution of salts under the vertical drainage in a cotton-based farm in the Turkestan region.

2. MATERIALS AND METHODS:

Soil and solution samples were collected in 2012 and 2014 from the cotton monoculture experimental station in Maktaaral district in Turkestan region (Dzhalankuzov et al., 2011) (40°49'58.03"N and 68° 30'3.07"E) on light serozem soil (Nabyeva, 2016). Soil samples were taken with a dedicated sampler tool. The mean annual precipitation is 262 mm; the average air temperature is 12.4°C. To study the effect of vertical drainage on soil amelioration state, the 78 ha of the experimental plot was divided into 15 basic sub-plots, with each subplot around 5 ha (Figure 1). Each subplot was sampled in three replications three times per year: in winter – before washing; in spring – after washing and before sowing; and in autumn – during cotton ripening from three soil depth: 0-20, 20-50, and 50-100 cm. The soil was washed with 5000 m³/ha in winter; the irrigation rate was 2000-3000 m³/ha in summer (2nd and 3rd parts of July). Water samples were taken from the irrigation canal, the vertical drainage, and the discharge canal. The level of groundwater was measured seasonally. Salt regime survey was conducted according to methodology to the E. Pankova, M. Gerasimova, and T. Korolyuk (Pankova et al., 2018). Soil salinity was determined based on the assessment of the “cumulative effect” impact of toxic ions according to the Equation 1: $1 \text{ Cl}^- = 0,1 \text{ CO}_3^{2-} = (2.75) \text{ HCO}_3^- = (5.5) \text{ SO}_4^{2-}$, where 1 mEq. of Cl⁻ for 10 times less toxic for plants than 1 mEq of CO₃²⁻; for 2.5-3 times, more toxic than HCO₃⁻, and for 5-6 times more toxic than SO₄²⁻. This experimental data was

obtained for 2012-2014 and mapped to build a soil salinity map (1: 10.000) by seasons (spring, autumn, winter) and vertically (0-20, 20-50, and 50-100 cm). Using MapInfo Professional software. Soil samples were air-dried and passed through a 1-mm mesh sieve for chemical analyses. Soil samples were analyzed for water-soluble salts by extractions at a ratio 1:5. Concentrations of HCO_3^- , CO_3^{2-} were calculated using their ratio determined by solution pH. The K^+ and Na^+ contents were determined by flame photometer FLAPHO 4 (Carl Zeiss Jena); Mg^{2+} , Ca^{2+} content by complexometric titration; Cl^- – by Mohr method with titration (AgNO_3 – 0.02N); SO_4^{2-} was calculated as ions (anions and cations) and content of carbonate CO_2 by gas calorimetry method.

It is also called the Scheibler method based on determining the carbonate content in the soil by the volumetric method. The carbonates in the sample are converted to CO_2 by adding hydrochloric acid to it. The Analysis of Variance (ANOVA) was done using IBM SPSS statistical analysis package. The Least Significant Difference (LSD) among different treatments was tested individually on triplicate data and collectively by considering the mean values of data for each year as a single replication (Equation 1), where, a – the sum of numbers, N – the amount of numbers. The overall significance/effectiveness of treatments (by considering the years and locations as fixed variables) was also evaluated by applying the LSD test on grand mean data at the 5 % level of probability ($p \leq 0.05$) based on the F-test of the analysis of variance. Correlations between some of the study parameters were also considered by using SPSS 12 for Windows (Equation 2), where t = t-distribution value; MSw = ANOVA root mean square; n = number of points used to calculate the average.

3. RESULTS AND DISCUSSION:

In 1964, the Resolution of the All-Union Scientific and Technical Conference was adopted on combating salination and improving the ameliorative condition of irrigated lands in Central Asia, based on the construction of drainage and irrigation leaching regime, recognized as the main measure to combat salination on irrigated lands. It was envisaged to create a leaching irrigation regime on the irrigated lands with an intensity of 20-30% of the net irrigation norm. This allowed to create downdraft flows of moisture in the aeration zone, which was supposed to ensure the desalination of the soil, and drainage was supposed to ensure the removal of the leaching

part of the irrigation norm and maintain the groundwater level at a depth of 2.5-3 m. However, this approach had a serious side effect: water intake from rivers for irrigation, considering filtration losses from canals (with efficiency <0.7), increased by 1.7-1.9 times. Discharge of drainage water into rivers by the end of the 20th century increased the salinity of river water, which also aggravated the situation. As a result of a decree adopted in 1964, by the second half of the 20th century, the area of irrigated land in the region considerably increased (Glazovsky, 1987). In addition to that, hydromorphic and semi-hydromorphic regimes were established and maintained on the irrigated lands, which contributed to the activation of secondary salination on the irrigated lands of the studied region. Thus, the foreseen leaching irrigation regime against the background of 2.5-3 m drainage did not lead to the expected positive effect: the area of saline soils on irrigated lands increased and reached 50% of the irrigated land area. In general, the area of saline irrigated soils in the Turkestan region territory is currently high and even increasing. There is no doubt that the cause of salt accumulation on irrigated lands is the hydromorphic regime, which is artificially maintained on the irrigated lands of the Central Asian region. The high salt content in the soil-forming and underlying rocks of the region, due to both the modern geochemical runoff and the high relict reserves of salts in the underlying rocks, including those associated with sea transgressions, allows to state that the drainage runoff carries not only salts from the soils of irrigated fields but also salts contained in rocks and groundwater, which significantly increases the total amount of salts carried out with drainage runoff. This conclusion is in good agreement with the calculations performed by I.P. Aydarov (Aydarov, 2006; Aydarov and Pankova, 2007) for individual irrigation tracts (Golodnaya Steppe), which indicated that despite the large removal of salts with drainage runoff on the irrigated tracts, a positive salt balance is maintained due to the input of salts from groundwater and underlying rocks. Thus, the reason for the widespread development of secondary salination on the irrigated lands of the Turkestan region is the hydromorphic irrigation regime, against the background of the high salinity of the parent rocks, as well as the arid climate, which contributes to the evaporative concentration of salts in hydromorphic conditions.

The solution to this issue requires new approaches to the development of irrigation in the region. First of all, it is necessary to make an inventory of irrigated lands based on modern

methods of remote sensing and modeling of salination-desalination processes for individual irrigation areas in order to establish the direction and intensity of the salt accumulation process. These data alone can help identify the most promising lands for irrigation. On these tracts, the new irrigation methods, which are currently widely used in the world, should be introduced.

Generally, the soil pH ranged from 8.38 to 8.58 (medium alkali), carbonate CO_2 is 7.02-8.11 % (Bhargavarami Reddy *et al.*, 2013). In spring, the medium saline groundwaters are located at 0.8-1.0 m depth, while in the autumn and winter, they went down to 2.0-3.0 m. Such groundwater depths ensure the constant moisture flow from the lower layers of soil and into the root zone. The up moving moisture transports water-soluble salts, which accumulated in upper horizons resulting in salt accumulation in all the experimental plots by the end of vegetation season (Bekbayev *et al.*, 2015; Yang *et al.*, 2019). The obtained results classified sampled soils according to Table 1.

Spring soil washing allowed a significant decrease in the salinity of soil profile simultaneously, increasing the salinity of groundwater up to 11.1 g/l (Table 2). The total salinity of groundwater by autumn was decreased to 3.6 g/l due to the capillary moving of salts up to the soil surface. The salinity of irrigation and drainage waters was not exceeding 1.1 and 1.4 g/l, respectively. During irrigation, the salts brought by irrigation water and the salts from groundwater and soil solution are all involved in re-distribution laterally and vertically. The vertical re-distribution of salts under irrigation started at the time when groundwaters were still deep. The essence of this process lies in the periodic desalination of flat and low areas. Simultaneously, less wet and more dry micro reliefs are subject to secondary salinization due to the salts migrating from the flat and low relief with film-capillary currents in the soil profile. As a result of such migration, the small spots of saline soils are formed on the irrigated fields.

Unlike other salt-affected soils, in which chloride or sulfate anions prevail, in this study, the Cl^- , HCO_3^- and SO_4^{2-} (the latter estimated by difference) ions along the soil depth (0-20, 20-50 and 50-100 cm) were balanced (Table 2). However, seasonally (spring, autumn, and winter), chlorides and sulfates tended to dominate. Na^+ dominated among the ions, and its amount increased from 0-20 cm to 1 m depth and from spring to winter, while K^+ decreases with depth during the whole season. Content of Mg^{++} and Ca^{++} generally increased downward the soil profile,

except in spring and winter at 20-50 cm where more Mg and Ca cations in upper and deeper layers were recorded. The prevalence of Mg^{++} explains this and Ca^{++} as cations and SO_4^{2-} as an anion in the composition of water-soluble salts in the soils.

The favorable physical characteristics of studied loess loam soils were good permeability, porosity, and relatively low conjunction. Negative properties of the parent rocks shown to be high water-lifting capacity (2.5-3.5 m), relatively low infiltration coefficient (an average of 0.003 mm/sec), which explains the rapid rise in groundwater under irrigation and the slow decline after the termination of irrigation. The secondary re-distribution of salts occurred slower in natural non-drained, and weakly drained areas. However, as time passed, the secondary re-distribution resulted in serious salinization. Also, in non-drained and weakly drained irrigated soils during the re-distribution of salts, some areas showed a relatively satisfactory reclamation state. In contrast, others had many hotspots of salt accumulation (Bekbayev *et al.*, 2015).

The secondary salinization in 2012 was strongly developed covering all the area. However, after the soil washing was undertaken, the salinization process has been reduced, and the gradual desalinization has been recorded. In spring 2012, in the upper layer, there were prevailing the medium and weakly saline soils, occupying respectively 79.5 and 20.5 % of the studied area after winter washing. In the autumn-winter period of 2012, there were recorded spots with salinization levels from weakly saline to strongly saline (weakly saline – 33.3 and 20.5 %; medium saline – 9.0 and 39.7 % and strongly saline – 57.7 and 39.7%, respectively). Our studies showed that the salinity of most of the studied soils significantly differs from spring to winter. In 2014 there was recorded a positive dynamic of changes comparing to 2012. In spring 2014, the area under medium saline soil in the 0-20 cm layer decreased from 79.5 to 57.7 %; the area of weakly saline soils increased from 20.5 to 34.6 %, and 7.7 % of non-saline soil area was recorded (Figures 2 and 3). The spatial distribution of the salt accumulation seasonally and annually is shown in Figures 3-5.

In the autumn-winter period of 2014, the area under strongly saline soils decreased from 25.6 to 14.1 %, respectively, in 0-20 cm comparing to 2012 (Figures 2, 4 and 5). The areas of medium saline soils increased to 24.3 % in autumn and to 6.5 % in winter, while areas of weakly saline soils decreased in autumn to 6.4 % and didn't change

in winter. The area of non-saline soils was 7.7 %. This studies showed that using the vertical drainage for three years transforms strongly saline soil recorded in 2012 into medium, weakly, and non-saline soils. So, the washing of soil in spring significantly reduces soil salinity due to the moving of salts downward, and on the contrary, in the autumn-winter period increases soil salinity.

Analysis of the vertical distribution of salts allows assuming that the reasons for soil salinity in light serozem soil of the Turkestan region could be one or a combination of the following circumstances: 1. Capillary rise of the saline groundwater table from shallow water tables to the soil surface. 2. Salt accumulations in the plow layer, where subsoil leaching is insufficient to remove the salt. 3. Poor water management and inadequate drainage system subjected to periodic flooding and high evaporation. The dynamic of ion content seasonally and vertically is presented in Table 3. In the period from 2012 to 2014, the amount of HCO_3^- decreased from 0.36 to 0.25 mEq (at significance 0.00), while the amount of SO_4^{2-} increased from 7.06 to 7.75 in 2012 and from 5.85 to 7.7 mEq in 2014 (sig. 0.032); the amount of Mg^{2+} increased from 3.1 to 3.31 mEq in 2012 and from 1.97 to 2.57 mEq in 2014 (sig. 0.001) in 1 meter soil layer from spring to winter.

In spring 2012, there was recorded increase of HCO_3^- (sig 0.001), Cl^- (sig 0.013), SO_4^{2-} (sig 0.016) and Na^+ (sig 0.002) and K^+ (sig 0.000) from upper to lower layers. In spring 2014 amount of Cl^- (sig 0.013) and Na^+ (sig 0.002) also increased, while amount of K^+ (sig 0.000) didn't change. In autumn and winter 2012 there was recorded decrease of HCO_3^- (sig. 0.013) and K^+ (sig 0.000) in 0-20, 20-50, 50-100 cm. In autumn 2014, the amount of HCO_3^- (sig 0.012) and K^+ (sig 0.000) also decreased with depth. In winter, the decrease was observed only for K^+ (sig 0.000). These results show that changes in the amounts of ions vertically and seasonally occur with the transport of salts along with soil profile under the influence of temperature gradients and the level of groundwater, i.e., in spring from up to down, and in autumn and winter, contrary from down to up. Obtained results assume that after winter washing (5000 m³/ha) in spring, the amount of salts in soil decreases, but the level of groundwater approaches the soil surface (to 0.8 m), and the salinity of groundwater increases (11.1 g/l). While in the autumn-winter period, due to evaporation and transpiration sharp decrease in groundwater level (to 2-3 m), a salinity of 3.6 g/l is recorded. These processes result in the enrichment of salt exchange between groundwater and soil.

4. CONCLUSIONS:

The reclamation state of studied soils primarily depends on soil physical properties and saline groundwater depth. Washing the soil in spring significantly reduces soil salinization due to migration of salts into deeper layers, while contrarily, in autumn and winter, an increase of salinization in upper soil layers occurs due to the high water-lifting capacity of studied light serozem soil. The research results indicated that reducing soil salinity using vertical drainage allows adjustment of groundwater level maintaining more optimal use of water (1.4 g/l) for washing in winter and spring periods and for watering crops. For the improvement of soil quality and management of irrigated light serozem soil in the Turkestan region and for maintaining higher cotton yield, it is necessary to not only ameliorative and agro-technical measures but also additional investments for the restoration of vertical drainage wells with systematic cleaning.

5. ACKNOWLEDGMENTS:

This research has was funded by the Ministry of Agriculture of the Republic of Kazakhstan (Grant No. BR06349612).

6. REFERENCES:

1. Abdel Kawy, W. A. M., and Darwish, Kh. M. (2019). Assessment of land degradation and implications on agricultural land in Qalyubia Governorate, Egypt. *Bulletin of the National Research Centre*, 43, Article number 70.
2. Adibah, F. S. F., Jahan, M. S., and Fatihah, H. N. N. (2020). Betaine-rich nano fertilizer improves growth parameters of zea mays var. saccharata and arabidopsis thaliana under salt stress. *Bulgarian Journal of Agricultural Science*, 26(1), 177-185.
3. Ahmed, K., Qadir, G., Jami, A. R., Saqib, A. I., and Qaisar, M. (2017). Comparative reclamation efficiency of gypsum and sulfur for improvement of salt-affected. *Bulgarian Journal of Agricultural Science*, 23(1), 126-133.
4. Allbed, A., and Kumar, L. (2013). Soil salinity mapping and monitoring in arid and semi-arid regions using remote sensing technology: a review. *Advances in Remote Sensing*, 2, 373-385.
5. Arunachalam, S., Maharani, K.,

- Chidambaram, S., Prasanna, M. V., Manivel, M., and Thivya, C. (2011). A study on the land use pattern change along the coastal region of Nagapattinam, Tamil Nadu. *International Journal of Geomatics and Geosciences*, 1(4), 700-720.
6. Aydarov, I.P. (2006). Essays on the history and development of irrigation in the USSR and Russia. Moscow: MGUP Publishing House.
 7. Aydarov, I.P., and Pankova, E.I. (2007). Salt accumulation in the plains of Central Asia and ways of its regulation. *Soil Science*, 6, 676-690.
 8. Bekbayev, R. K. (2016). Factors influencing on the degradation of water and land resources of mahtaaral irrigation massif. *Academia Journal of Agricultural Research*, 4(3), 118-122.
 9. Bekbayev, R., Balgabayev, N., Zhaparkulova, Y., Karlihanov, O., and Musin, Z. (2015). Factors that intensify soil degradation in the Kazakhstan part of the golodnostep sky irrigation massif. *Life Science Journal*, 12(1s), 1-4.
 10. Bhargavarami Reddy, C. H., Guldekar, V. D., and Balakrishnan, N. (2013). Influence of soil calcium carbonate on yield and quality of Nagpur mandarin. *African Journal of Agricultural Research*, 8(42), 5193-5196.
 11. Bhat, M. A., Sheoran, H. S., Dar, E. A., Dahiya, H. S., Wani, S. A., Singh, I., and Singh, S. (2015). Geoinformatics as a tool for appraisal of salt-affected soils – a review. *International Journal of Innovative Science, Engineering and Technology*, 2(10), 480-490.
 12. Chernousenko, G. I., Kalinina, N. V., Rukhovich, D. I., and Koroleva, P. V. (2012). Digital map of salt-affected soils of Khakassia. *Eurasian Soil Science*, 45(11), 997-1012.
 13. Dzhalankuzov, T. D., Suleimenov, B. U., and Seytmenbetova, A. T. (2011). History of development of the world's cotton production and particularly in Kazakhstan. *Soil Science and Agrochemistry*, 1, 92-98.
 14. Farifteha, T. A., Farshada, R., and George, J. (2006). Assessing salt-affected soils using remote sensing, solute modelling, and geophysics. *Geoderma*, 130, 191-206.
 15. Glazovsky, N.F. (1987). Modern salt accumulation in arid areas. Moscow: Nauka.
 16. Hamidov, A., Helming, K., and Balla, D. (2016). Impact of agricultural land use in Central Asia: a review. *Agronomy for Sustainable Development*, 36, Article number 6.
 17. Hu, Y., Han, Y., and Zhang, Y. (2020). Land desertification and its influencing factors in Kazakhstan. *Journal of Arid Environments*, 180, Article number 104203.
 18. Iqbal, T. (2018). Rice straw amendment ameliorates harmful effect of salinity and increases nitrogen availability in a saline paddy soil. *Journal of the Saudi Society of Agricultural Sciences*, 17, 445-453.
 19. Issanova, G., Abuduwaili, J., Mamutov, Zh., Kaldybaev, A., Saporov, G., and Bazarbaeva, T. (2017). Saline soils and identification of salt accumulation provinces in Kazakhstan. *Arid Ecosystems*, 7, 243-250.
 20. Kaushal, S. S., Likens, G. E., Pace, M. L., Utz, R. M., Haq, S., Gorman, J., and Grese, M. (2018). Freshwater salinization syndrome. *Proceedings of the National Academy of Sciences*, 115(4), E574-E583.
 21. Kitamura, Y., Yano, T., Honna, T., Yamamoto, S., and Inosako, K. (2006). Causes of farmland salinization and remedial measures in the Aral Sea basin – Research on water management to prevent secondary salinization in rice-based cropping system in arid land. *Agricultural Water Management*, 85(1-2), 1-14.
 22. Laishanov, S. U., Otarov, A., Savin, I. Y., Tanirbergenov, S. I., Mamutov, Z. U., Duisekov, S. N., and Zhogolev, A. (2016). Dynamics of soil salinity in irrigation areas in South Kazakhstan. *Polish Journal of Environmental Studies*, 25(6), 2469-2475.
 23. Mandal, A. K., Sharma, R. C., and Singh, G. (2009). Assessment of salt affected soils in India using GIS. *Geocarto International*, 24(6), 437-456.
 24. Metternicht, G. I. and Zinck, J. A. (2003). Remote sensing of soil salinity: Potentials and constraints. *Remote Sensing of Environment*, 85, 1-20.
 25. Micklin, P., Aladin, N. V., and Plotnikov, I. (2016). *Aral Sea*. Berlin: Springer-Verlag.

26. Mueller, L., Saparov, A., and Lischeid, G. (2014). *Novel measurement and assessment tools for monitoring and management of land and water resources in agricultural landscapes of Central Asia*. Heidelberg: Springer Science and Business Media.
27. Murzabaev, B., Ismail, R., Anselm, K., and Zhumabaev, A. R. (2019). Soil salinization in the old-irrigated zones under agriculture production in Makhtarl region, Kazakhstan. *Industrial Technology and Engineering*, 2(31), 66-70.
28. Nabyeva, H. M. (2016). Changes in soil properties and microbiological activity under pasture plants. *Biological Communications*, 2, 140-148.
29. Nuruzzaman Manik, S. M., Pengilley, G., Dean, G., Field, B., Shabala, S., and Zhou, M. (2019). Soil and crop management practices to minimize the impact of waterlogging on crop productivity. *Frontiers in Plant Science*, 10, Article number 140.
30. Pachykyn, K. M., Erokhyna, O.H., Saparov, A. S., Omyrzakova, A. N., and Sonhulov, E. E. (2019). Soil researches of irrigable and "worthless" in salt soils of Turkestan area. *Soil Science and Agrochemistry*, 4, 5-17.
31. Pankova, E., Gerasimova, M., and Korolyuk, T. (2018). Salt-affected soils in Russian, American, and international soil classification systems. *Eurasian Soil Science*, 51, 1297-1308.
32. Pereira, C. S., Lopes, I., Abrantes, I., Sousa, J. P., and Chelinho, S. (2019). Salinization effects on coastal ecosystems: a terrestrial model ecosystem approach. *Philosophical Transactions of the Royal Society B*, 374, Article number 20180251.
33. Petrick, M., Oshakbayev, D., Taitukova, R., and Djanibekov, N. (2017). The return of the regulator: Kazakhstan's cotton sector reforms since independence. *Central Asian Survey*, 36(4), 430-452.
34. Rath, K. M., Maheshwari, A., Bengtson, P., and Rousk, J. (2016). Comparative toxicities of salts on microbial processes in soil. *Applied and Environmental Microbiology*, 82, Article number 2012.
35. Rukhovich, D. I., Pankova, E. I., Chernousenko, G. I., and Koroleva, P. V. (2010). Long-term salinization dynamics in irrigated soils of the Golodnaya Steppe and methods of their assessment on the basis of remote sensing data. *Eurasian Soil Science*, 43(6), 682-692.
36. Schoups, G., and Hopmans, J. W. (2002). Analytical model for vadose zone solute transport with root water and solute uptake. *Vadose Zone Journal*, 1(1), 158-171.
37. Shrivastava, P., and Kumar, R. (2015). Soil salinity: a serious environmental issue and plant growth-promoting bacteria as one of the tools for its alleviation. *Saudi Journal of Biological Sciences*, 22(2), 123-131.
38. Singh, A., and Sengar, R. S. (2014). Salinity stress in rice : an overview. *Plant Archives*, 14(2), 643-648.
39. Soltanaeva, A., Suleimenov, B., Saparov, G., and Vassilina, T. (2018). Effect of sulfur-containing fertilizers on the chemical properties of soil and winter wheat yield. *Bulgarian Journal of Agricultural Science*, 24(4), 586-591.
40. Stoilova, A., Valkova, N., Spasova, D., Spasov, D., and Mihajlov, L. (2014). Agroecological assessment of new Bulgarian and Macedonian cotton varieties. *Bulgarian Journal of Agricultural Science*, 20(2), 122-131.
41. Sugimori, Y., Funakawa, S., Pachikin, K. M., Ishida, N., and Kosaki, T. (2008). Soil salinity dynamics in irrigated fields and its effects on paddy-based rotation systems in southern Kazakhstan. *Land Degradation and Development*, 19(3), 305-320.
42. Suleimenov, B.U. (2008). *Increase of fertility of irrigated Serozems in cotton growing areas of Southern Kazakhstan*. Almaty: U.U. Uspanov Kazakh Research Institute of Soil Science and Agrichemistry.
43. Suska-Malawska, M., Sulwiński, M., Wilk, M., Otarov, A., and Mętrak, M. (2019). Potential eolian dust contribution to accumulation of selected heavy metals and rare earth elements in the aboveground biomass of Tamarix spp. from saline soils in Kazakhstan. *Environ Monit Assess*, 191(2), Article number 57.
44. Tanirbergenov, S. I., Soltanayeva, A. M., Kabylbekova, B. Z., Suleimenov, B. U., and Saparov, A. S. (2016). The fertilizer system increasing the salt tolerance and

- productivity of cotton in the conditions of saline soils in southern Kazakhstan. *Research Journal of Pharmaceutical, Biological and Chemical Sciences*, 7(6), 147-155.
45. Umbetaev, I., Bigaraev, O., and Baimakhanov, K. (2015). Effect of soil salinity on the yield of cotton in Kazakhstan. *Russian Agricultural Sciences*, 41, 222-224.
 46. Vyrahmanova, A. S., Otarov, A., Saparov, A. S., Suska-Malavska, M., Duisikov, S. N., Poshanov, M. N., and Tanirbergenov, S. I. (2020). The ecological status of irrigated saline soils of the Shaulder massif of the Turkestan region. *Eurasian Journal of Biosciences*, 14(1), 347-354.
 47. Wang, Z., Fan, B., and Guo, L. (2019). Soil salinization after long-term mulched drip irrigation poses a potential risk to agricultural sustainability. *European Journal of Soil Science*, 70, 20-24.
 48. Weng, Y. L., and Gong, P. (2006). A review on remote sensing technique for salt-affected soils. *Scientia Geographica Sinica*, 26(6), Article number 375.
 49. Wichern, F., Islam, Md. R., Hemkemeyer, M., Watson, C., and Joergensen, R. G. (2020). Organic amendments alleviate salinity effects on soil microorganisms and mineralisation processes in aerobic and anaerobic paddy rice soils. *Frontiers in Sustainable Food Systems*, 4, Article number 30.
 50. Yang, H., Chen, Y., and Zhang, F. (2019). Evaluation of comprehensive improvement for mild and moderate soil salinization in arid zone. *Plos One*, 14(11), Article number e0224790.
 51. Zhumadilova, Zh. Sh., Tautenov, I. A., Abdieva, K. M., Shorabaev, Ye. Zh., and Sadanov, A. K. (2019). Bioproduction phytomelioration of the salted soils in rice field systems in the Aral Sea region of Kazakhstan. *Journal of Ecological Engineering*, 20(7), 98-102.

$$\bar{x} = \frac{a_1 + a_2 + a_N}{N} \quad (\text{Eq. 1})$$

$$LSD_{A,B} = t_{0.05/2DFW} \sqrt{MSW(1/n_A + 1/n_B)} \quad (\text{Eq. 2})$$

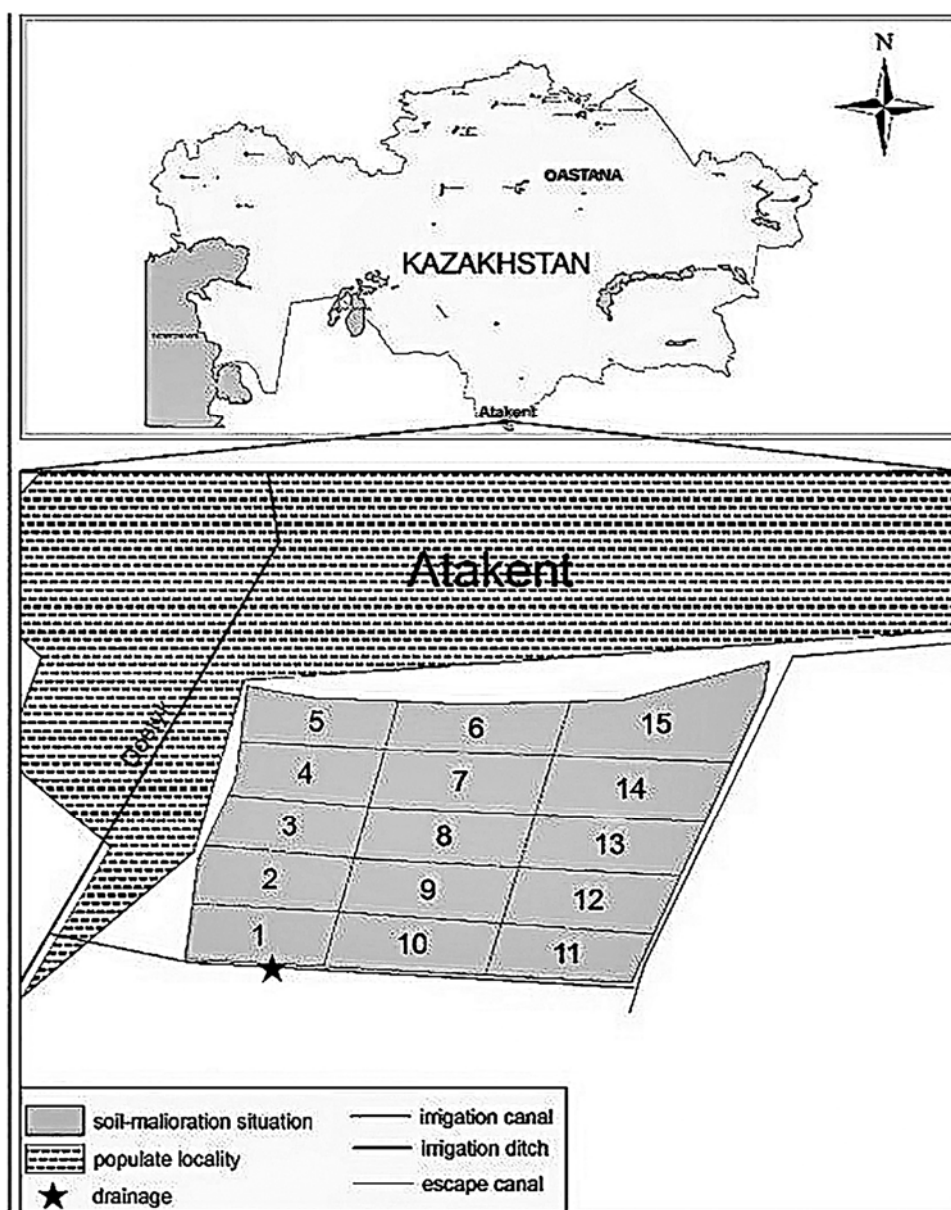


Figure 1. Location of the sampling site

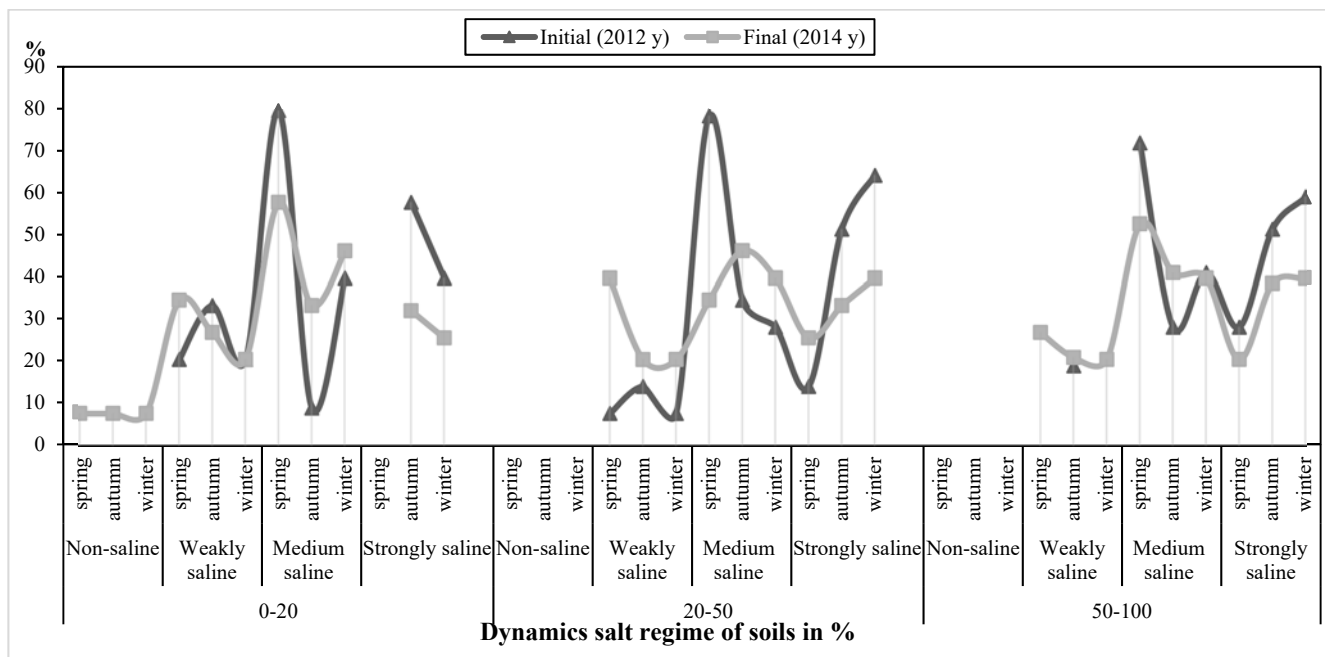


Figure 2. Dynamic of salt regime seasonally and vertically, %

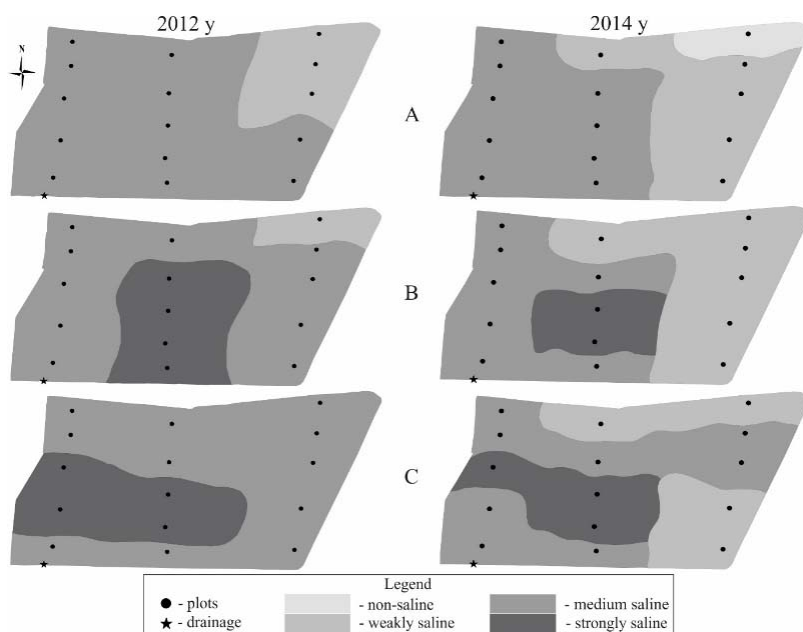


Figure 3. Map of soil salinity in spring (A – 0-20 cm; B – 20-50 cm; C – 50-100 cm)

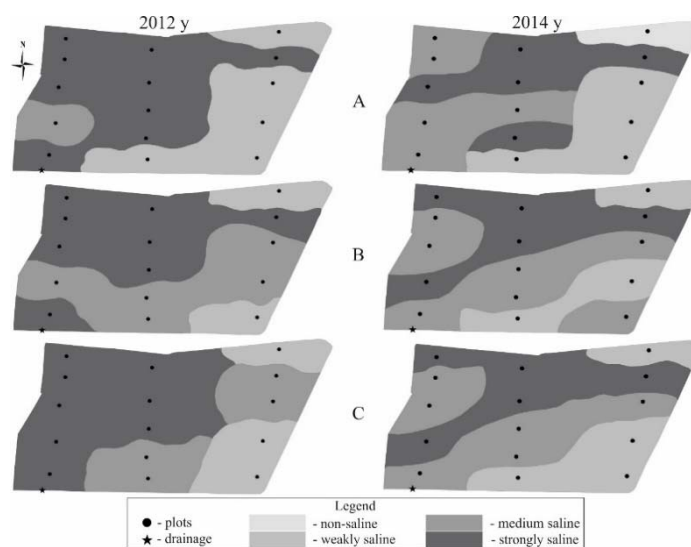


Figure 4. Map of soil salinity in autumn (A – 0-20 cm; B – 20-50 cm; C – 50-100 cm)

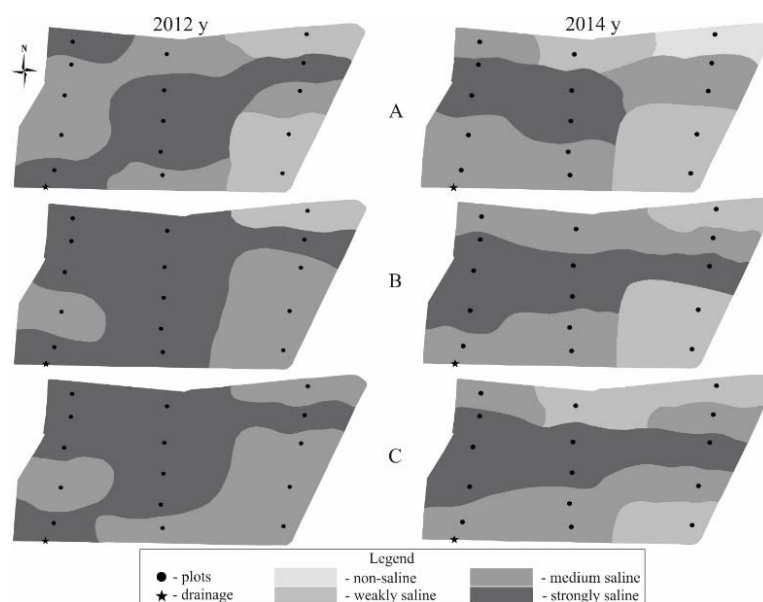


Figure 5. Map of soil salinity in winter (A – 0-20 cm; B – 20-50 cm; C – 50-100 cm).

Table 1. Soil classification on salinity level as “cumulative effect” of toxic ions (Pankova et al., 2018)

Salinity level	“Cumulative effect” of toxic ions (CO_3^{2-} , HCO_3^- , Cl^- , SO_4^{2-}), mEq Cl^-
Non-saline	<0.3
Weakly saline	0.31-1.0
Medium saline	1.1-3.0
Strongly saline	3.1-7.0
Extremely saline	>7.0

Table 2. Content of water-soluble salts seasonally and by depth, 2012-2014

Horizon, cm		Sum of salts, %	mEq								CO ₂ %	pH
			HCO ₃ ⁻	CO ₃ ²⁻	Cl ⁻	SO ₄ ²⁻	Ca ²⁺	Mg ²⁺ ₊	Na ⁺	K ⁺		
Spring												
0-20		0.374 a	0.36 a	-	0.35 a	4.91	2.31	1.95	1.24 a	0.11 a	7.02 a	8.4 6
20-50		0.538 ab	0.33 ab	-	0.53 ab	7.28	3.75	2.55	1.74 ab	0.09 ab	7.21 ab	8.4 0
50-100		0.513 c	0.29c	-	1.05c	6.67	3.00	2.54	2.45c	0.02c	8.11c	8.4 9
ground water	g/l	11.1	0.51	-	1.73	5.76	0.96	0.9	1.26	0.00 2	-	
	mEq q		8.39	-	48.8	120. 0	48.1 5	74.2 5	54.8	0.07	-	
Autumn												
0-20		0.588	0.34 a	-	1.46	7.15	3.61	2.35	2.76	0.16 a	7.03 a	8.5 2
20-50		0.620	0.30 ab	-	1.32	7.81	3.72	2.65	3.00	0.08 ab	7.57 ab	8.4 8
50-100		0.641	0.25c	-	1.54	8.03	3.78	2.72	3.27	0.04c	7.83c	8.5 8
ground water	g/l	3.56	0.24	0.02	0.18	2.12	0.37	0.19	0.43	0.00 6	-	7.6 6
	mEq q		3.96	0.63	5.21	44.3	18.6 7	15.7 9	18.8	0.16	-	
Winter												
0-20		0.570	0.35 a	-	1.10	7.31	2.83	3.32	2.49	0.12 a	7.55	8.3 8
20-50		0.711	0.31 ab	-	1.52	9.15	3.97	3.96	2.92	0.10 ab	7.42	8.3 8
50-100		0.654	0.27c	-	1.35	8.46	3.64	3.56	2.84	0.04c	-	8.4 6
irrigation water	g/l	1.05	0.15	0.00 6	0.08	0.52	0.13	0.05	0.09	0.00 6	-	8.4 4
	mEq q		2.47	0.2	2.44	10.8	6.87	4.72	4.02	0.15	-	
drainage water	g/l	1.35	0.17	0.00 5	0.09	0.72	0.14	0.09	0.12	0.00 6	-	8.4 8
	mEq q		2.79	0.17	2.66	15.0 1	7.25	7.94	5.13	0.15	-	

Table 3. Dynamic of ion content in soil seasonally and vertically, mEq

Ions	Season	2012	2014	depth, cm	Spring		Autumn		Winter	
					2012	2014	2012	2014	2012	2014
HCO_3^-	Spring	0.37	0.33	0-20	0.33	0.36	0.33	0.34	0.28	0.30
	Autumn	0.33	0.30	20-50	0.38	0.30	0.32	0.28	0.27	0.24
	Winter	0.29	0.25	50-100	0.39	0.32	0.33	0.30	0.32	0.22
Cl^-	Spring	1.04	0.90	0-20	0.29	0.40	0.45	0.61	1.04	1.06
	Autumn	1.14	1.11	20-50	1.67	1.24	1.53	1.12	1.48	1.61
	Winter	1.30	1.33	50-100	1.15	1.04	1.44	1.60	1.37	1.33
SO_4^{2-}	Spring	7.06	5.85	0-20	4.53	5.28	7.05	7.52	5.81	7.53
	Autumn	9.27	6.89	20-50	7.65	6.66	8.94	6.69	8.15	7.92
	Winter	7.75	7.70	50-100	9.01	5.61	11.82	6.47	9.28	7.64
Ca^{2+}	Spring	3.03	2.80	0-20	1.83	2.80	3.60	3.89	2.27	3.72
	Autumn	4.25	3.38	20-50	3.99	3.22	4.37	3.08	4.12	3.45
	Winter	3.24	3.70	50-100	3.28	2.38	4.78	3.16	3.35	3.93
Mg^{2+}	Spring	3.11	1.98	0-20	2.13	1.77	2.68	2.42	2.62	2.46
	Autumn	3.75	2.36	20-50	2.51	2.19	2.99	2.31	2.63	2.82
	Winter	3.31	2.57	50-100	4.68	1.97	5.57	2.35	4.68	2.44
Na^+	Spring	2.22	2.11	0-20	1.12	1.36	1.45	2.03	2.22	2.68
	Autumn	2.67	2.44	20-50	3.06	2.47	3.38	2.61	3.11	3.44
	Winter	2.75	2.97	50-100	2.47	2.52	3.16	2.68	2.91	2.77
K^+	Spring	0.14	0.12	0-20	0.10	0.12	0.10	0.09	0.02	0.03
	Autumn	0.09	0.10	20-50	0.19	0.14	0.09	0.08	0.04	0.03
	Winter	0.03	0.04	50-100	0.12	0.12	0.08	0.13	0.03	0.05

A EFICÁCIA DA UTILIZAÇÃO DE OFICINAS DE LABORATÓRIO VIRTUAL NA EDUCAÇÃO ON-LINE DE ALUNOS QUE ESTUDAM A DISCIPLINA “QUÍMICA INORGÂNICA”**THE EFFECTIVENESS OF USING VIRTUAL LABORATORY WORKSHOPS IN ONLINE EDUCATION OF STUDENTS STUDYING THE DISCIPLINE “INORGANIC CHEMISTRY”****ЭФФЕКТИВНОСТЬ ПРИМЕНЕНИЯ ВИРТУАЛЬНОГО ЛАБОРАТОРНОГО ПРАКТИКУМА В ONLINE ОБУЧЕНИИ СТУДЕНТОВ ИЗУЧАЮЩИХ ДИСЦИПЛИНУ «НЕОРГАНИЧЕСКАЯ ХИМИЯ»**

RAYISYAN, Maria G.^{1*}; BORODINA, Maria Anatolievna²; DENISOVA, Olga Igorevna³; BOGACHEV, Yuri Sergeevich⁴; SEKERIN, Vladimir Dmitriyevich⁵

¹ First Moscow State Medical University after I. M. Sechenov. Moscow, Russia.

² Peoples' Friendship University of Russia (RUDN University). Moscow, Russia.

³ Moscow Aviation Institute (National Research University), Russia.

⁴ Financial University under the Government of the Russian Federation. Moscow, Russia.

⁵ Moscow Polytechnic University. Moscow, Russia

* Correspondence author
e-mail: rayisyan.m.g@mail.ru

Received 18 August 2020; received in revised form 30 October 2020; accepted 07 November 2020

RESUMO

O ensino a distância já faz parte do processo educacional. Nesse sentido, surgem questionamentos quanto à sua organização e solução de problemas específicos. Incluem oficinas laboratoriais, parte integrante do processo educativo no ensino superior, uma vez que os trabalhos de laboratório permitem aos alunos adquirir conhecimentos e competências, um pré-requisito para a formação da sua competência de especialista. Os problemas de obtenção de informações educacionais durante o ensino à distância podem ser resolvidos com bastante sucesso. No entanto, a aquisição de habilidades experimentais continua sendo um problema educacional, científico e metodológico que requer uma solução. O artigo define as peculiaridades da utilização de oficinas de laboratório virtual na educação online de alunos da disciplina “Química Inorgânica”. A análise teórica das principais afirmações do problema de pesquisa foi apresentada no artigo. Os resultados do estudo experimental comprovaram que o uso da modelagem computacional e das ferramentas de um laboratório virtual no estudo das disciplinas de química aumenta o aproveitamento escolar dos alunos, independentemente do nível inicial de conhecimento. Um pré-requisito para a aquisição efetiva de habilidades pelos alunos é o uso sistemático de ferramentas de laboratório virtual. Com o uso ocasional de instrumentos de laboratório virtuais, as habilidades obtidas durante o experimento não foram aprendidas ou não foram aprendidas por um longo tempo. O uso de laboratórios virtuais proporciona treinamento independente para os alunos, aumenta a motivação para o domínio de novos materiais. Os alunos se concentram no processo experimental, não em equipamentos e ferramentas, como acontece em um laboratório real, o que pode se tornar tanto um aspecto positivo quanto negativo na aquisição de habilidades práticas de futuros engenheiros, médicos e farmacêuticos.

Palavras-chave: ensino à distância, laboratório virtual, oficina de laboratório virtual, oficina de laboratório à distância, alunos de química.

ABSTRACT

Distance learning has already become a part of the educational process. In this regard, questions appear concerning its organization and the solution of specific problems. They include laboratory workshops, which is an integral part of the educational process in higher education since laboratory works allow students to gain

knowledge and acquire skills, which is a prerequisite for the formation of their specialist competence. The problems of obtaining educational information during distance learning can be quite successfully solved. However, the acquisition of experimental skills remains an educational, scientific, and methodological problem that requires a solution. The article defines the peculiarities of using virtual laboratory workshops in the online education of students studying the discipline "Inorganic Chemistry". The theoretic analysis of the main statements of the research problem was presented in the article. The results of the experimental study have proved that the use of computer modeling and the tools of a virtual laboratory when studying chemistry disciplines increases the educational achievements of the students, regardless of the initial level of knowledge. A prerequisite for the effective acquisition of skills by students is the systematic use of virtual laboratory tools. With the occasional use of virtual laboratory instruments, the skills obtained during the experiment were not learned or were not learned for a long time. The use of virtual laboratories provides independent training for students, increases motivation to master new material. Students focus on the experimental process, not on equipment and tools, as it happens in a real laboratory, which can become both a positive and a negative aspect of acquiring practical skills of future engineers, doctors, and pharmacists.

Keywords: *distance learning, virtual laboratory, virtual laboratory workshop, distance laboratory workshop, chemistry students.*

АННОТАЦИЯ

Дистанционное обучение уже стало реальностью в образовании, в связи с этим возникают вопросы его организации и решение конкретных проблем. К ним относится лабораторный практикум, который является неотъемлемой составляющей учебного процесса в высшей школе, поскольку благодаря выполнению лабораторных работ студент не только получает знания, но и приобретает умения, что является обязательным условием формирования его компетентности как специалиста. Если проблемы получения учебной информации при дистанционном обучении достаточно успешно решаются, то приобретение экспериментальных умений остается не только учебной, но и научно-методической проблемой, которая требует своего решения. В статье определены особенности применения виртуального лабораторного практикума в online обучении студентов, изучающих дисциплину «Неорганическая химия». В статье представлен теоретический анализ основных положений проблемы исследования. На основании экспериментального исследования было доказано, что применение компьютерного моделирования при изучении химических дисциплин с использованием инструментария виртуальной лаборатории приводит к повышению учебных достижений студентов вне зависимости от начального уровня знаний. Обязательным условием для эффективного получения навыков студентами является систематичность использования инструментария виртуальной лаборатории. При эпизодическом использовании инструментов виртуальной лаборатории, навыки полученные в процессе эксперимента не усваивались или усваивались не на длительный период времени. Использование виртуальных лабораторий обеспечивает самостоятельную подготовку студентов, повышает мотивацию к освоению нового материала. Студенты сосредотачивают внимание на экспериментальном процессе, а не на оборудовании и инструментах, как это происходит в реальной лаборатории, что может стать как позитивным, так и негативным аспектом в ходе приобретения навыков практической деятельности будущих инженеров, врачей, фармацевтов.

Ключевые слова: дистанционное обучение, виртуальная лаборатория, виртуальный лабораторный практикум, дистанционный лабораторный практикум, студенты-химики.

1. INTRODUCTION:

Distance learning is interactive communication in work, providing students with the opportunity to master the studied material independently, and consulting support in the research activities. The purpose of distance learning is to provide educational services with modern information and communication technologies (ICT) in teaching certain educational or qualification levels following state educational standards (Golubeva, Kokhanovskaya, Golovneva, Fatykhova, and Terekhova, 2020). Distance learning is one of the most promising forms of education using modern ICT and

appropriate technical tools (Manning, Cohen, and DeMichiell, 2003).

New approaches are also needed in teaching natural sciences. One of these approaches is the use of ICT during the educational process. The use of ICT in teaching chemistry disciplines makes it possible to intensify the educational process, accelerate the transfer of knowledge and experience, and improve the quality of learning and education (Ardac and Akaygun, 2004). Modeling the studied processes and phenomena makes it possible to carry out computer experiments in those areas of human knowledge where real experiments are either labor-intensive or not possible at all (Lindgren,

Tscholl, Wang, and Johnson, 2016; Smetana and Bell, 2012). The use of ICT increases the information and communication competences of students. It forms the skills and abilities to use modern Internet technologies, particularly those used for distance learning and monitoring (Sergeeva et al., 2019; Nikiforov, Kokorina, Bagdasarian, Shishanova, and Beskorovaynaya, 2019).

One of the directions of using ICT in teaching chemistry disciplines is computer modeling of real-world objects, phenomena, and experiments, which are practically impossible to demonstrate, as well as the creation of simulation models (Rutten, Joolingen, and van der Veen, 2012; Trundle and Bell, 2010). However, it is important to remember that the introduction of information technologies in the educational process will be warranted only when they effectively complement the existing teaching technologies or have additional advantages over traditional education forms (Dadashev, Muskhanova, Batchaeva, and Yahyaeva, 2020; Dolzhenkov, Maltzagov, Makarova, Kamarova, and Kukhtin, 2020).

According to J.R. Brinson (2015), the main advantages of computer simulations are an intensification of the learning process; the ability to change the focus on the fragments of the model; the involvement of an unlimited number of students in the work at the same time (peer education); doing exercises at any time from any computer; reducing the cost of the experiment.

The special software: the so-called "virtual laboratories" (VL) aimed at creating and performing the imitation laboratory work. (Baran, Currie, and Kennepohl, 2004).

The issue of creating a laboratory workshop in distance learning is studied in different scientific and methodological works. In the literature, the concept of a VL is defined differently. In the simplest case, it can be a local computer with a pre-installed virtual simulator or some other program for modeling an experiment (Nico, van Joolingen, and van der Veen, 2012). A more precise definition can be found in the work (Jorda, 2013), where the term VL also includes information technology to create an interactive virtual environment, taking into account the needs of students and teachers.

According to R.K. Scheckler (2003), VL is a virtual learning environment that allows one to simulate the behavior of real-world objects in a computer environment and helps in mastering new knowledge and skills. Such a laboratory can act as

a means for researching various natural phenomena to construct their mathematical and physical models.

In H.M. Babateen's opinion (Babateen, 2011), VL is a program that allows one to simulate chemical processes on a computer, to change the conditions and parameters of their implementation. This program creates special opportunities for interactive learning. The implementation of laboratory work in a VL includes the emulation of the actions that the user should carry out in real conditions. This allows one to test one's theoretical knowledge in practice and get experimental work skills.

T. Wolf (2010) considers VL to be a software and hardware complex that allows experiments to be carried out without direct contact with a real facility or in its absence. According to D. Liu and others (2015), VL is a virtual software environment in which the possibility of researching objects' models, their populations, and derivatives, given at a certain level of detail concerning real objects, within a certain area of knowledge, is organized.

VL allows simulating objects and processes of the surrounding world and organizing computer access to real laboratory equipment (Shin, Yoon, Park, and Lee, 2000). The computer allows one to carry out experiments that are quite complex or unreal under standard conditions, to develop skills of handling hazardous substances or devices (Nicholson, Nicholson, and Valacich, 2008).

Software developers use different approaches to create VL (Figure 1).

D. Kennepohl (2001) believes that a variety of educational tasks can be solved while teaching chemistry disciplines with the help of VL, for example, familiarization with the experimental techniques and equipment before carrying out real laboratory work, as well as checking the level of preparation of the student (programs react instantly to incorrect steps); modeling experiments, which are dangerous or costly to carry out in a chemical laboratory; acquiring the skills of recording observations, compiling reports and interpreting data in a laboratory journal.

According to Y.J. Dori and J.W. Belcher (2005), the best of the software products provide the possibility of realizing the teacher's creative personality. They allow creating laboratory experiments, have a rather convenient and easy-to-use constructor of works. In that case, teachers

can correct all the shortcomings (or most of them) of the program on their own.

S. Chen (2010) believes that distance laboratory workshops of the university require the creation of a special laboratory, where the developed laboratory works are accumulated, and the methodological base is located. Links with distance learning participants are established from the laboratory. For this purpose, a separate website is created on a special university server linked to the learning management system. This site provides access to the VL server, and the schedule of students' research, consultations, and performance of tests are organized there. The use of Wi-Fi wireless data transmission technology facilitates the introduction and implementation of distance laboratory work.

The work (Dalgarno, Bishop, Adlong, and Bedgood, 2009) proposes the general structure of a VL as an interactive virtual space, which includes technological, pedagogical, and human (academic) resources for research, adapted to the needs of students and teachers in a virtual learning environment. Technical resources include virtual communication, remotely performed laboratory work, virtual simulators, an automatic assessment system, virtual computers, and software. Pedagogical resources include methodological supply, and academic resources include students and teachers.

Among the means mentioned above necessary for a distance laboratory workshop in modern higher education, the greatest difficulties, according to B.F. Woodfield (2004), are caused by the creation of remotely performed laboratory works and virtual simulators and the provision of the corresponding instruments and software products. To minimize the required time and labor costs, creating a workshop based on automated laboratory work or research facilities is the most reasonable (Pekdag, 2010). Such equipment makes it possible to accumulate experimental databases and upgrade the existing software to create a remotely performed laboratory work and virtual simulators. In the future, the developed programs and databases can be changed for the needs of different universities and transferred to other educational centers. This interchange significantly facilitates the workshop organization in universities that do not have an appropriate laboratory base. In this case, the distance workshop can contain only simulations, for the development and creation of which only the cooperation of the programmer and the teacher is required.

When creating remotely performed laboratory work and virtual simulators, it is important to consider the basic didactic rules and principles formulated based on the acquired pedagogical experience. In works (Huppert, Lomask, and Lazarowitz, 2002; Rajendran, Veilumuthu, and Divya, 2010), following the analysis of modern research, such basic and generally recognized principles are highlighted as the scientific character, consistency, systematicity, accessibility, visibility, consciousness, and activity, the connection between theory and practice, unity of the individual and collective.

The analysis of the VL peculiarities shows the possibility of observing these principles in e-learning, and in some cases, there are advantages over traditional forms of education. Thus, the requirements of scientific character, systematicity, and consistency depend mainly on the curriculum and their content and, to a lesser extent, on the form of education. The 24-hour functioning of the distance workshops servers makes it possible to access works convenient for students and ensures systematic and consistent education. The use of animation technologies makes it possible to demonstrate the course of processes with a high degree of similarity, the laboratory study associated with experimental difficulties. VL that use ideal models allows students to compare virtual measurements with a modern experiment conducted on expensive research equipment and expand the ability to explore and understand complex ideas and phenomena. Simultaneously, there is a transition to a higher degree of visualization of teaching, and students' interest and their activity in the study of educational material increases. A powerful stimulus for enhancing students' consciousness and activity is to independently test the achieved result. Such rapid self-control, which has an educational character, enables students to correct mistakes and stimulates their creative abilities, interest, and curiosity (Martinez-Jimenez, Pontes-Pedrajas, Polo, and Climent-Bellido, 2003).

Modern equipment used in scientific research, in many cases, is created with the help of computers. Measurement results, equipment condition, parameters, and results of the investigated processes are observed on the computer screen, and control commands are given with the help of the keyboard or manipulator. In this case, performing laboratory work with the help of VL does not physically differ from working with similar devices in a laboratory. In other cases, the use of multimedia demonstrations helps to visually show the course of the studied processes

and use them in practice, which is often impossible in a laboratory. Together, this facilitates the connection between theory and practice in the process of learning (Falvo, 2008).

The main feature of a students' work with VL is independence, and communication with the teacher is carried out using communication. Therefore, with the distant use of VL, there is a need for the broadest use of interactive modes, which can choose the parameters and the course of the experiment, operating modes of devices, and measurement ranges. This provides an independent study of the principles of devices operation and measurement techniques, research of statistical regularities based on the results obtained, an assessment of accuracy, the correlation between the random error of the measured value and the error of devices, the presence of noise. The configuration of VL works can be diversified, and new implementation options can be quickly created depending on the required educational level. Such approaches make it possible to make laboratory work similar to the real one and acquire the skills of research work (Tatli and Ayas, 2013). Together, this contributes to the fulfilment of the above didactic rules and principles.

The study (Logar and Ferk Savec, 2011) notes that remote performance of laboratory work is, to a certain extent, an imitation of laboratory work, despite the illusion of real execution. Therefore, to make a virtual experiment similar to real laboratory work and fully consider the principles of didactics in teaching, it is necessary to widely use all these tools that can be implemented using modern electronic technologies.

The study aims to prove the possibility of introducing VL into the distance learning process of future chemists.

Research hypothesis: the use of computer modeling when studying chemistry disciplines using the tools of a VL increases students' educational achievements, regardless of the initial level of knowledge.

According to the results of the study, it can be concluded that the aim was achieved.

2. MATERIALS AND METHODS:

In the study, a complex of modern methods of pedagogical research was used: theoretical (analysis, generalization, comparison, synthesis, review of scientific, educational, and methodical

literature to determine the current state of the examined problem); empirical (observation, conversation, interviewing, survey, testing); pedagogical experiment; methods of mathematical statistics.

The experiment aimed to describe the results of an experimental test of the distance learning effectiveness of the first-year students studying the discipline "Inorganic Chemistry" at the First Moscow State Medical University after I. M. Sechenov, 141 people in total. The experiment was carried out through a laboratory workshop using the ChemLab for Windows, a chemical laboratory simulation. It has several versions, one of which is adapted for use in Russian educational institutions.

The formative experiment was carried out during a real educational process. The use of ICT in teaching chemistry in the experimental group was not opposed to traditional distance learning. However, it was carried out systematically and in close combination with them, as the methodology required it of the experiment. As for organization, all conditions and content of education in the control and experimental groups were the same, except for using a simulation chemical laboratory ChemLab.

The initial and final check-ups and resorted to the element-by-element analysis of the experiment results were carried out. The effectiveness of the learning process was determined by several characteristics, such as the level of assimilation of knowledge in the field of chemistry, the pedagogical effect of experimental learning, motivation for learning. These criteria were used to evaluate the success of academic achievements and motivation.

The level of effectiveness was measured with the coefficient of knowledge assimilation (K_a), which is the correlation of the number of correctly reproduced elements of knowledge (correct answers) and the total number of questions of the input (output) test (20 questions): level I – $K_a \leq 0.5$; level II – $0.5 \leq K_a \leq 0.7$; level III – $0.7 \leq K_a \leq 0.9$; level IV – $K_a \geq 0.9$.

The results were processed with the help of methods of statistical analysis: the characteristics of the samples were compared, the reliability was determined, the significance of differences was estimated, and a correlation analysis was carried out.

The online laboratory workshop was chosen as a method that was well accepted by the majority of students, regardless of their

educational strengths. The ChemLab environment was used for its implementation, as it most closely matches the developed principles of effective chemistry teaching. The work in it makes it possible to visualize the connections between the microscopic level of data presentation, phenomena of the material world, and symbolic forms of description and study situations that develop in time. ChemLab has interface elements that allow students to adapt the process to their characteristics and allow teachers to manage the total cognitive load of students.

The didactically grounded course of actions in the educational and information environment of the virtual chemical laboratory consisted of the following stages: stage 1 – the theoretical material review; stage 2 – reflection and assimilation of knowledge during the preparation for self-control questions or solving test tasks (practical work); stage 3 – the acquisition and development of practical skills, the accumulation of professional experience using VL workshops; stage 4 – solving practical problems with the help of science-intensive specialized programs and software.

A short questionnaire survey of students after the completion of the pedagogical experiment included the following questions:

1. What is the reason for using virtual laboratory workshops in the study of chemistry?
2. Do you find useful virtual laboratory workshops in the study of chemistry? Why?
3. Would you like to continue using virtual laboratory workshops in the study of chemistry?

3. RESULTS AND DISCUSSIONS:

According to the results of the initial and final check-ups, we analyzed the changes in the levels of knowledge assimilation by students from the experimental and control groups (Figure 2-3).

In the experimental groups, there was a shift in the number of students from I and II levels of knowledge assimilation to III and IV levels. Accordingly, there is a decrease in the number of weak students (I and II levels of knowledge assimilation). In the control groups, the number of students with different levels of knowledge assimilation remains almost unchanged. The difference between the final and initial check-ups results for all levels does not exceed 1.5%. All the above mentioned allows us to conclude that the experimental methodology contributes to a

significant improvement in the learning process results.

Table 1 shows the coefficients of assimilation of knowledge in the field of chemistry of students from experimental and control groups.

The generally accepted indicator of the effectiveness of the learning process is $K \geq 0.7$. Therefore, the obtained result of the final check-up indicates a high level of knowledge assimilation in chemistry by students who were taught according to the experimental method. Table 1 shows that the pedagogical effect is 0.085 in the experimental groups and 0.014 in the control groups. The increase in knowledge, which is considered the difference in the coefficients of knowledge assimilation by students from the experimental and control groups, is positive, it is 0.065. This proves the pedagogical effectiveness of the proposed experimental method of teaching the discipline "Inorganic chemistry".

A normal distribution within both datasets makes it possible to compare the mean check-up results for both groups using the student's t-test for two independent samples. The results (Table 1) indicate a statistically significant difference between the coefficients of knowledge assimilation in the experimental groups and the control groups.

The results of the fulfillment of the tasks by students of the experimental groups were also analyzed qualitatively, basing on the changes in the assimilation of the elements of knowledge, which in the given experiment were identified as the most problematic. In comparison to the control group, the number of correct answers increased by more than 30% for the questions related to the periodic trends in the properties of chemical elements, the establishment of correspondences, "type of bond and substance", the prediction of the changes in reaction conditions, recognition of strong and weak electrolytes, writing ion-molecular and hydrolysis equations, understanding the theories of acids and bases. The answers to questions related to the temperature, pressure, and volume change have changed most of all. The number of correct answers for some of them increased by 50-65%.

Summing the obtained data up, the following was found out:

- the results of calculating the difference between the average points of the initial and final control using the t-test for two samples showed the presence of a statistically significant increase in

points for all groups of students, which indicated a significant knowledge improvement;

- the application of the online laboratory workshop allowed correcting some long-standing misconceptions. Their presence meant that for some initial test questions, the majority of students (more than 67%), who could not answer them correctly, chose the same wrong option. The results of the final testing showed that for most of the problematic tasks, the number of correct answers increased at least by 1.5-4 times;

- the most difficult tasks for students to solve were those containing interlevel transitions, which included three levels of representation of knowledge in the field of chemistry: macro-, microscopic, and symbolic. The use of computer modeling provided the best increase in knowledge for such tasks;

- independent work using the virtual chemical laboratory, ChemLab contributed to significant progress in students' ability to work with equations and graphs. The increase in points for such tasks during the final testing turned out to be higher than the increase in points for other tasks based on figurative or verbal representation;

- the results of testing the effectiveness of using the virtual chemical laboratory ChemLab to study various topics showed that in all groups, the number of learned elements of knowledge increased significantly: it almost doubled in the control groups and increased by 2.4-2.8 times in the experimental ones. The level of assimilation of elements of knowledge by students from the experimental groups exceeded the level in the control groups by 22-25%.

- when performing laboratory work using the ChemLab, students learned how to algorithmize the sequence of actions during laboratory work; to develop appropriate instructional materials; to carry out methodological processing and analysis of specific sections of the educational course independently; to find the necessary didactic material; to master the techniques and methods of chemical experiment and modern educational technologies; to plan study time; to model fragments of classes.

As a result, the comparative analysis of the findings of the initial and final testing of students from the control and experimental groups before and after the experimental form of education indicates that a statistically significant increase in the results was obtained. Therefore, the use of VL workshops in distance learning increased students' educational achievements, and the size

of the effect did not depend on the initial level of knowledge of the respondents.

Students' behavior observation during the online practical work made it possible to conclude the need for organizational changes to ensure favorable conditions for working with the ChemLab. For this purpose, it is necessary to minimize the impact of insufficient preparation of students in ICT by organizing educational classes in small groups. At least one student has the best basic chemical and computer training. These students can also help the group members in online co-working.

A survey of students about their evaluation of the importance of using VL during practical work in chemistry showed that an important difference in students' motivation was the desire to study not for the sake of erudition but practical works (76% of respondents). 83,5% of respondents noted the usefulness of VL workshops since this method provided them with the opportunity to master such activity, which is close to professional. Formulating their attitude to working with a VL, the overwhelming majority of students from the experimental group (92,5% of respondents) spoke in favor of continuing such educational activities.

The experiment carried out within the study showed that using VL in the learning process, even for independent work, creates a more favorable situation for the manifestation of individual motivation of the students. There is a transition to real personal motives. The use of VL provides students with adequate information about their progress in learning, maintains their competence and self-confidence, hence stimulates intrinsic motivation. The students themselves control the cognitive process. They feel responsible for their behavior and consider the reasons for their success to be not any external factors but their diligence. The survey conducted at the final stage of the experiment showed that most respondents believe that such work stimulates the desire to study the proposed educational material in more detail.

Let us discuss the capabilities of the VL ChemLab in more detail.

ChemLab is designed to demonstrate laboratory experiments and check the quality of students' preparation for their independent implementation.

The main window of ChemLab is a graphical drawing depicting a part of a chemical laboratory, which allows students to feel like they are in a real chemical laboratory.

The user is provided with: a pH-meter, an analytical balance, a titration burette, an electric oven, a thermometer. Openable drawers contain chemical reagents; on the shelves, there is a large range of titrimetry indicators. The program is controlled by choosing commands from the main menu and using hyperlinks. In the main menu of the program, one can specify the name of the laboratory work to be performed, choose the equipment, and design the workshop. So, during titration, it is possible to visualize the titration curve (Figure 5), the appearance of points on which is synchronized with the addition of titrant drops.

The laboratory is equipped with an additional room containing several gas cylinders and equipment necessary for working with them. The program has a section with videos of experiments (the clips are of low quality, but the reactions are interesting).

The program can be used in two modes. The first is a self-study mode for students, which provides them with demonstrations and reference materials. It can be used for the laboratory works, namely, for the familiarization with the purpose, the necessary reagents and equipment, safety precautions, and work procedures; for the performing interactive experiments, laboratory and practical work in a virtual environment; and finally, for the self-control with the help of tests.

The second mode is the mode of the lesson. It allows broadcasting the content of the educational program and reference materials; to demonstrate all the components of the work, namely the purpose, reagents and equipment, safety rules, the procedure for working in a VL; to develop experiments, practical laboratory work in the created environment; to do test tasks.

The advantage of the program is the ability to use both standard models and models created by the user. One can develop new works using the tools of Lab Wizard to build a graphical interface for performing a particular operation. Using Lab Wizard allows one to set a sequence of actions step by step and create a personalized laboratory.

During the working process, instructive materials for conducting practical exercises were prepared and tested to make it easier for students to master the method of conducting imitation laboratory experiments. There are two stages of student work. The first one is to get acquainted with the interface and the main functions of the program, and the second one is to perform ready-made laboratory work.

Also, students had the opportunity to change the conditions of the experiment and to draw appropriate conclusions. Students compared the results obtained with those displayed on the screen independently, corrected their mistakes, and reported completing tasks, and the teacher commented and corrected the answers.

For a more detailed study of key or specific issues during interactive learning, the teacher conducted consultations that complemented the material and drew students' attention to the key elements of the course.

The research results by different authors confirm the conclusions of the conducted experiment about the effectiveness of the use of VL in the learning process of future specialists. Generalized data on the effectiveness of the use of VL and information about the effects that caused the work with them are given in Table 2.

4. CONCLUSION:

In the article, we analyzed the problems of creating a distance laboratory workshop and discussed the requirements for remotely performed laboratory work. We also determined the ways of using a distance laboratory workshop in distance learning.

Literary sources review and the analysis of the results of our experimental research led to the following conclusions:

- VL software can be effectively used as an auxiliary tool for distance learning;

The use of a virtual chemical experiment allows students with a significant amount of knowledge. It develops their intellectual and creative abilities, acquiring new knowledge independently and working with various sources of information. Convenient software and sufficient computer literacy allow students to participate actively in the virtual work and to reduce the time for laboratory work;

- *the use of VL makes it possible to meet the following goals in the learning process of chemistry students: providing students with the possibility of self-preparation; increasing motivation to master new material;* students focus on the experimental process, not on equipment and tools, as they do in a real laboratory;

- the use of VL workshops is cost-effective since no materials are wasted, students work safely, and the exploitation of tools is more technological;

The experimental research results confirmed the hypothesis that the use of computer modeling when studying chemistry disciplines using the tools of a VL increases students' educational achievements, regardless of the initial level of knowledge.

In general, there is no doubt that using computer technology in teaching chemical disciplines is relevant. The effectiveness of the learning process increases significantly if they are used not occasionally but systematically during the whole course.

5. REFERENCES:

1. Ardac, D., and Akaygun, S. (2004). Effectiveness of multimedia-based instruction that emphasizes molecular representations on students' understanding of chemical change. *Journal of Research in Science Teaching*, 41(4), 317-337.
2. Babateen, H. M. (2011). The role of Virtual Laboratories in Science Education. *International Online Journal of Education Sciences*, 12, 100-104.
3. Baran, J., Currie, R., and Kennepohl, D. (2004). Remote Instrumentation for the Teaching Laboratory. *Journal of Chemical Education*, 81, 1814-1816.
4. Brinson, J. R. (2015). Learning outcome achievement in non-traditional (virtual and remote) versus traditional (hands-on) laboratories: a review of the empirical research. *Computers and Education*, 87, 218-237.
5. Bruck, L. B., Towns, M., and Bretz, S. L. (2010). Faculty perspectives of the undergraduate chemistry laboratory: goals and obstacles to success. *Journal of Chemical Education*, 87(12), 1416-1424.
6. Chen, S. (2010). The view of scientific inquiry conveyed by simulation-based virtual laboratories. *Computers and Education*, 55(3), 1123-1130.
7. Dadashev, R. Kh., Muskhanova, I. V., Batchaeva, H. H. – M., and Yahyaeva, A. H. (2020). The ethnic system of the chechens in the context of modern synergetics. *Revista Inclusiones*, 7(Sp), 701-715.
8. Dalgarno, B., Bishop, A. G., Adlong, W., and Bedgood, D. R. (2009). Effectiveness of a virtual laboratory as a preparatory for distance education chemistry students. *Computers and Education*, 53, 853-865.
9. DeKorver, B. K., and Towns, M. H. (2016). General chemistry students' goals for chemistry laboratory coursework. *Journal of Chemical Education*, 92(12), 2031-2037.
10. Dolzhenkov, V. N., Maltzagov, I. D., Makarova, A. I., Kamarova, N. S., and Kukhtin, P. V. (2020). Software Tools for Ontology Development. *International Journal of Advanced Trends in Computer Science and Engineering*, 9(2), 935-941.
11. Dori, Y. J., and Belcher, J. W. (2005). How does technology-enabled active learning affect students' understanding of scientific concepts? *The Journal of the Learning Sciences*, 14(2), 243-279.
12. Falvo, D. A. (2008). Animations and simulations for teaching and learning molecular chemistry. *International Journal of Technology in Teaching and Learning*, 4(1), 68-77.
13. Galloway, K. R., and Bretz, S. L. (2015). Measuring meaningful learning in the general chemistry and organic chemistry laboratories: a longitudinal study. *Journal of Chemical Education*, 92(12), 2019-2030.
14. Golubeva, T. I., Kokhanovskaya, I. I., Golovneva, E. V., Fatykhova, A. L., and Terekhova, N. V. (2020). Social networks and education: the increase in student learning efficiency and the search for means of control. *Revista Inclusiones*, 7(Sp), 48-60.
15. Grob, A. (2002). The virtual chemistry lab for reactions at surfaces: Is it possible? Will it be useful? *Surface Science*, 500, 347-367.
16. Hofstein, A., and Lunetta, V. (2004). The laboratory in science education: foundations for the twenty-first century. *Science Education*, 88(1), 28-54.
17. Huppert, J., Lomask, S. M., and Lazarowitz, R. (2002). Computer simulations in the high school: Students' cognitive stages, science process skills and academic achievement. *International Journal of Science Education*, 24, 803-821.
18. Jorda, M. (2013). Virtual Tools: Virtual Laboratories for Eksperimental Science -

- an Experience with VCL Tools. *Procedia - Social and Behavioral Sciences*, 106, 3355-3365.
19. Josephsen, J., and Kristensen, A. K. (2006). Simulation of laboratory assignments to support students' learning of introductory inorganic chemistry. *Chemistry Education Research and Practice*, 7, 266-279.
 20. Kennepohl, D. (2001). Using computer simulations to supplement teaching laboratories in chemistry for distance delivery, *Journal of Distance Education*, 16(2), 58-65.
 21. Kozma, R., Chin, E., Russell, J., and Marx, N. (2000). The roles representations and tool in the chemistry laboratory and their implications for chemistry learning. *The Journal of the Learning Sciences*, 9(2), 105-143.
 22. Lindgren, R., Tscholl, M., Wang, S., and Johnson, E. (2016). Enhancing learning and engagement through embodied interaction within a mixed reality simulation. *Computers and Education*, 95, 174-187.
 23. Liu, D., Díaz, P. V., Riofrio, G. S., and Barba, R. (2015). Integration of Virtual Labs into Science E-learning. *Procedia Computer Science*, 75, 95-102.
 24. Logar, A., and Ferik Savec, V. (2011). Students' hands-on experimental work vs lecture demonstration in teaching elementary school chemistry. *Acta Chimica Slovenica*, 58, 866-875.
 25. Manning, R. D., Cohen, M. S., and DeMichiell, R. L. (2003). Distance Learning: Step by Step. *Journal of Information Technology Education: Research*, 2, 115-130.
 26. Martinez-Jimenez, P., Pontes-Pedrajas, A., Polo, J., and Climent-Bellido, M. S. (2003). Learning in chemistry with virtual laboratories. *Journal of Chemical Education*, 80(3), 346-352.
 27. Nicholson, J., Nicholson, D., and Valacich, J. (2008). Examining the effects of technology attributes on learning: a contingency perspective. *Journal of Information Technology Education*, 7(11), 185-204.
 28. Nikiforov, A. I., Kokorina, O. R., Bagdasarian, A. S., Shishanova, E. I., and Beskorovaynaya, S. A. (2019). The evolution of environmental education as a driver for improving the technologies of managing the use of natural resources. *Humanities and Social Sciences Reviews*, 7(6), 1235-1240.
 29. Pekdag, B. (2010). Chemistry learning alternative routes: Animation, simulation, video, multimedia. *Journal of Turkish Science Education*, 7(2), 79-110.
 30. Rajendran, L., Veilumuthu, R., and Divya, J. (2010). A study on the effectiveness of virtual lab in E-learning. *International Journal on Computer Science and Engineering*, 2(6), 2173-2175.
 31. Rutten, N., Joolingen, W., and van der Veen, Jan, T. (2012). The Learning Effects of Computer Simulations in Science Education. *Computers and Education*, 58(1), 136-153.
 32. Scheckler, R. K. (2003). Virtual labs: a substitute for traditional labs. *The International Journal of Developmental Biology*, 47, 231-236.
 33. Sergeeva, M. G., Sirotova, A. A., Kolchina, V. V., Brega, G. V., Kaftan, V. V., Kulakova, N. N., and Luchina, E. V. (2019). Content and language integrated competence of students at non-linguistic universities, *Journal of Advanced Pharmacy Education and Research*, 9(2), 143-148.
 34. Shin, D., Yoon, E. S., Park, S. J., and Lee, E. S. (2000). Web-based interactive virtual laboratory system for unit operations and process systems engineering education. *Computers and Chemical Engineering*, 24, 1381-1385.
 35. Smetana, L. K., and Bell, R. K. (2012). Computer Simulations to Support Science Instruction and Learning: A critical review of the literature. *International Journal of Science Education*, 34(9), 1337-1370.
 36. Tatli, Z., and Ayas, A. (2013). Effect of a Virtual Chemistry Laboratory on Students' Achievement. *Educational Technology and Society*, 16(1), 159-170.
 37. Trundle, K. C., and Bell, R. L. (2010). The use of a computer simulation to promote

- conceptual change: a quasi-experimental study. *Computers and Education*, 54(4), 1078-1088.
38. Winberg, T. M., and Berg, A. R. (2007). Students' cognitive focus during a chemistry laboratory exercise: effects of a computer-simulated prelab. *Journal of Research in Science Teaching*, 44, 1108-1133.
 39. Wolf, T. (2010). Assessing Student Learning in a Virtual Laboratory Environment. *IEEE Transactions on Education*, 53(2), 216-222.
 40. Woodfield, B. F., Catlin, H. R., Waddoups, G. L., Moore, M. S., Swan, R., Allen, R., and Bodily, G. (2004). The virtual ChemLab Project: A Realistic and Sophisticated Simulation of Inorganic Qualitative Analysis. *Journal of Chemical Education*, 81, 1672-1678.

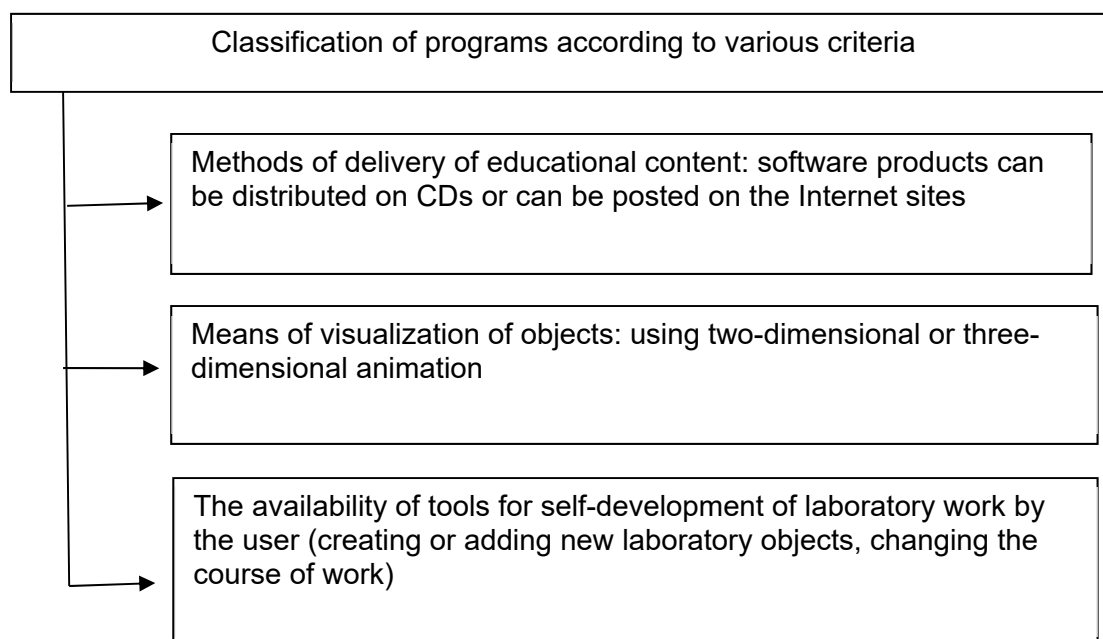


Figure 1. Main approaches to VL creation. Source: Compiled by the authors based on literature (Hofstein and Lunetta, 2004)

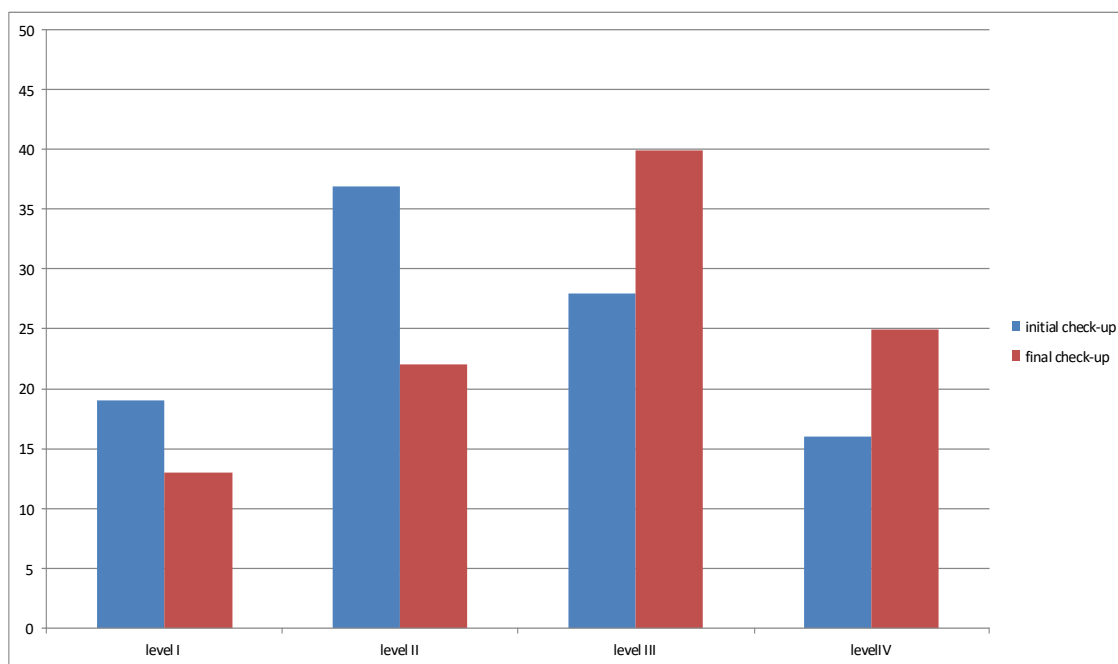


Figure 2. Dynamics of the levels of knowledge assimilation by students from the experimental group during experimental learning.

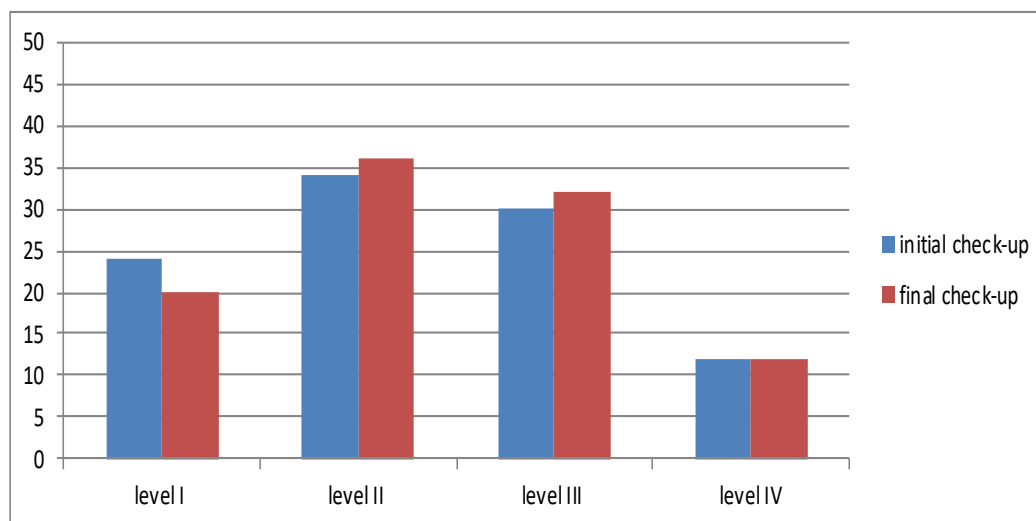


Figure 3. Dynamics of the levels of knowledge assimilation by students from the control group during experimental learning



Figure 4. Corel ChemLab 1.0 the main application window

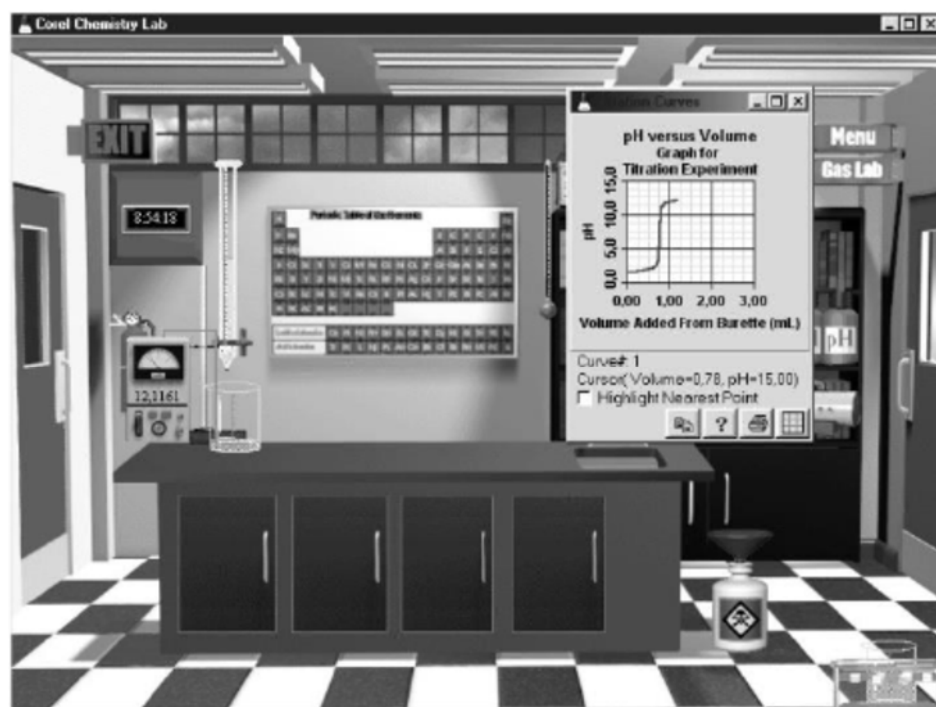


Figure 5. Corel ChemLab 1.0 software window during acid-base titration (the titration curve is on the right)

Table 1. Results of the pedagogical experiment

Number of students	Number of correctly reproduced elements of knowledge		coefficient of knowledge assimilation, Ka (mean and standard deviation)		Results of student's t-test for the final check-up		Pedagogical effect	
	Initial check-up	Final check-up	Initial check-up	Final check-up	t	Significance (2-sided)	Quantitative	Qualitative
Experimental group								
67	1013	1127	0.756±0.010	0.841±0.012	0.0567	0.001	0.085	+
Control group								
74	1128	1149	0.762±0.010	0.776±0.010	0.0627	0.001	0.014	+

Table 2. Generalized data on the effectiveness of the use of VL in teaching chemistry disciplines

The purpose of using VL	Sampling	Data collection tool	Findings	Reference
To evaluate the effectiveness of Vlab-Chem in learning chemistry disciplines	100 students and 14 teachers from the Faculty of Chemistry	Two achievement tests	Increases students' achievements. Teachers and students think that using Vlab-Chem is beneficial for planning, learning instructions, and education.	(Kozma, Russell, and Marx, 2000)
To analyze the consequences of the use of VL by students before performing real laboratory works	88 students from the Faculty of Chemistry	Achievement test	Increases students' achievements and their sense of mastery during the classes. Students feel more relaxed, less tired, and understand new material more easily.	(Grob, 2002)
To analyze the impact of virtual works on students in comparison with real works	72 first-year students who studied the basic course of general chemistry	Questionnaire for the assessment of laboratory work; achievement test	Increases students' achievements. The work takes less time (VL takes 24 minutes, while real laboratory work takes 36 minutes). Students favor VL and consider the experiments using software to be easier and clearer.	(Bruck, Towns, and Bretz, 2010)
To evaluate the effectiveness of VL developed to study the phase condition of water	70 students from the Faculty of Chemistry	Experimental tool, equipment recognition test, questionnaire	Students with a high level of spatial skills receive the highest level of conceptual learning.	(DeKorver and Towns, 2016)
To analyze virtual learning environments in dimensions of cognitive learning, skills, and attitudes	78 students from the Faculty of Chemistry	Interviews, observations, and working papers	Virtual environments increase productivity and lead to a higher learning level; students use VL programs and think that they are attractive and	(Galloway and Bretz, 2015)

To research into the impact of virtual chemistry laboratories on student success and attitudes towards learning	341 students	Achievement tests, observation	<p>enjoyable.</p> <p>The VL software (Winberg and Berg, 2007) positively affects the success and the motivation of students and makes it easier for students to understand the studied concepts. VL is an alternative to a real laboratory when experiments cannot be carried out in reality for some reason.</p>
To evaluate the impact of VL software on college students	464 students from 26 colleges	Achievement tests, observation	<p>Students who use (Josephsen and Kristensen, 2006) laboratory software answers to questions related to experimental methods more precisely, and they tend to use this software in learning chemistry (55%) (89% versus 26%). Due to the software, students can focus on the experimental process and understand the experiment fully.</p>

DETECÇÃO DE INTERLEUCINA PRÓ-INFLAMATÓRIA 17 EM PACIENTES COM *L. TROPICA* NA PROVÍNCIA THI-QAR, IRAQUE

DETECTION OF PRO- INFLAMMATORY INTERLEUKIN 17 IN PATIENTS WITH *L. TROPICA* IN THI-QAR PROVINCE, IRAQ

تحديد الانترلوكين 17 المحرض للالتهاب في المرضى المصابين بطفيلي *L. TROPICA* في محافظة ذي قار

FLAIH, Mohammed Hassan^{1*}; AL-ABADY, Fadhil Abbas²; HUSSEIN, Khwam Reissan¹

¹ University of Southern Technical, Institute of Al-Nasiriya Technical, Department of Medical Laboratory. Iraq.

² University of Thi-Qar, Faculty of Education for pure Sciences, Department of Biology. Iraq.

*Corresponding author

e-mail: moh.alqurayshi@stu.edu.iq

Received 03 August 2020; received in revised form 28 October 2020; accepted 09 November 2020

RESUMO

A leishmaniose cutânea (LC) é um grande problema de saúde e considerada uma das doenças endêmicas no Iraque. A lesão dérmica ocorre devido a um parasita intracelular obrigatório de *Leishmania* que transmite pela picada do flebotômíneo fêmea infectado. Este estudo tem como objetivo identificar espécies de *Leishmania* na província de Thi-Qar/sul do Iraque, bem como detectar o nível de IL-17 no soro de pacientes infectados com *L. tropica*. O estudo foi realizado em três locais, Al-Hussein Teaching, Al-Suq Al-Shyokh General e Al-Shatrah General Hospitals na província no período entre o início de novembro de 2018 e o final de outubro de 2019. Após o diagnóstico clínico, oitenta das duzentas e quarenta e sete amostras foram selecionadas para exame molecular pela técnica de nested-PCR, onde a borda da lesão foi injetada com soro fisiológico normal e novamente puxada para obter o DNA do parasita. Também é uma medida do nível de concentração de IL-17 no soro dos pacientes com ELISA. Os achados da eletroforese do gene do DNA do minicírculo do cinetoplasto mostraram que 65 amostras eram positivas para leishmaniose cutânea e observaram duas espécies de *Leishmania* spp. na área de estudo, 46 (57,5%) amostras foram *L. tropica* a 750 pb e 19 (23,75%) amostras foram *L. major*. A concentração sérica de IL-17 registrou um aumento significativo entre os pacientes infectados com *L. tropica* em diferentes estágios de infecção, em comparação com as amostras controle. Geralmente, a técnica Nested-PCR é um método preciso para o diagnóstico de amostras clínicas e a determinação molecular de parasitas de *Leishmania*. *L. tropica* é a principal espécie que causou CL na província de Thi-Qar, enquanto *L. major* registrou uma baixa incidência.

Palavras-chave: *Leishmania tropica*, IL-17, leishmaniose cutânea, Nested-PCR, kDNA

ABSTRACT

Cutaneous leishmaniasis (CL) is a widespread health problem and considered one of the endemic diseases in Iraq. The dermal lesion occurs due to an obligate intracellular *Leishmania* parasite, which transmits by the bite of the infected female sandfly. This study aims to identify *Leishmania* species in Thi-Qar province/ South of Iraq and detect IL-17 level in serum of infected patients with *L. tropica*. The study was conducted in three local locations, Al-Hussein Teaching, Al-Suq Al-Shyokh General, and Al-Shatrah General Hospitals in the province for the period from the beginning of November 2018 to the end of October 2019. After clinical diagnosis, eighty out of two hundred forty-seven samples were selected for molecular examination by nested-PCR technique, where the lesion edge was injected by normal saline and pulled again to obtain the parasite DNA. Also, a measure of the IL-17 concentration level in serum of the patients with ELISA. The findings of the electrophoresis of the kinetoplast minicircle DNA gene showed that 65 samples were positive for cutaneous leishmaniasis, and observed two species of *Leishmania* spp. in the study area, 46 (57.5%) samples were *L. tropica* at 750bp and 19 (23.75%) samples were *L. major*. Serum IL-17 concentration recorded a significant increase among patients infected with *L. tropica* at different infection stages than control samples. Generally, the Nested-PCR technique is an accurate method for diagnosing clinical samples and molecular determination of *Leishmania* parasites. *L. tropica* is the dominant specie that caused CL in Thi-Qar province, while *L. major* recorded a low incidence.

Keywords: *Leishmania tropica*, IL-17, cutaneous leishmaniasis, Nested-PCR, kDNA

يعتبر داء اللشمانيا مشكلة صحية واسعة النطاق ويعتبر أحد الأمراض المتوطنة في العراق. الافة الجلدية تحدث بسبب طفيلي اللشمانيا وهو اجباري داخل خلوي الذي يحدث بسبب عضه انثى ذبابة الرمل المصابة. هدفت هذه الدراسة الى تشخيص أنواع طفيلي اللشمانيا في محافظة ذي قار/ جنوب العراق، كذلك قياس مستوى تركيز الانترلوكين 17 في مصل المرضى المصابين بـ *L. tropica*. أجريت الدراسة في ثلاث مواقع هي مستشفى الحسين التعليمي، مستشفى سوق الشيوخ العام ومستشفى الشرطة العام في المحافظة للفترة من بداية شهر تشرين الثاني 2018 الى نهاية شهر تشرين الأول 2019. ثمانين من أصل 247 عينة اختيرت بعد تشخيصهم سريريا، لغرض الفحص الجزيئي بواسطة تقنية Nested-PCR حيث حققت الافة بواسطة المحلول الملحي وسحب مجدول لغرض الحصول على DNA الطفيلي. كذلك قيس مستوى تركيز IL-17 في مصل المرضى بواسطة جهاز الـ ELISA. أظهرت نتائج الترحيل الكهربائي لجين kDNA ان 65 عينة كانت موجبة لداء اللشمانيا الجلدي ولوحظ وجود نوعين من طفيلي اللشمانيا في منطقة الدراسة حيث كانت 46 عينة بنسبة (57.5%) لطفيلي *L. tropica* بطول 750bp و 19 عينة بنسبة (23.75%) كانت لـ *L. major*. سجل تركيز الـ IL-17 في المصل زيادة معنوية بين المرضى المصابين بطفيلي *L. tropica* على مراحل إصابة مختلفة مقارنة مع عينة السيطرة. عموما تقنية Nested-PCR هي طريقة مناسبة لتشخيص العينات السريرية والتشخيص الجزيئي لطفيليات اللشمانيا. *L. tropica* هو المسبب الرئيسي للشمانيا الجلدية في محافظة ذي قار، في حين *L. major* سجل حدوث منخفض.

الكلمات المفتاحية: طفيلي *L. tropica*، الانترلوكين 17، داء اللشمانيا الجلدي، تقنية Nested-PCR، kDNA.

1. INTRODUCTION:

Leishmaniasis is caused by flagellated *Leishmania* parasites, an obligate intracellular protozoan, and infects humans and other mammals (Ramírez *et al.*, 2016). It is a vector-borne disease transmits by an infected females sandfly bite, and the disease highly spreads in poor populations and tropical and subtropical countries (Dayakar *et al.*, 2019). However, *Leishmania* parasites can establish and survive inside host cells. They resist and circumvent anti-parasitic immune response pathways (Oghumu *et al.*, 2015). Indeed, the immunological status and the genetic background of the patient, also *Leishmania* species effects severely on the form and type of the CL dermal lesion (Maksouri *et al.*, 2017).

Leishmania spp. have different strategies to affect both innate and adaptive immunity for its survival (Rossi and Fasel, 2017). Generally, *Leishmania spp.* infect immune phagocytes, such as neutrophil, dendritic cell (DC), and especially macrophage. The immunological and cellular mechanisms associated with leishmaniasis infection are not completely clear, and most of the present knowledge about leishmaniasis is based on experimental models (Meira and Gedamu, 2019).

It is necessary to understand immune cell interactions and its secretion. Also, cytokines interplay in host defense or pathogenesis to determine appropriate immunotherapies of leishmaniasis (Dayakar *et al.*, 2019). However, Interleukin-17 has an instrumental role in the protection of the host against several pathogens, such as Gram-positive bacteria, fungi, and parasites (Banerjee *et al.*, 2016). The role of IL-17 in leishmaniasis infections remains poorly

understood, and more studies are required (Gonzalez-lombana *et al.*, 2013). IL-17 is mostly produced by Th17 cells (Andargie and Ejara, 2015). Several modern studies refer to elevated IL-17 with human inflammatory or autoimmune diseases (McGeachy *et al.*, 2019). However, it works on a broad range of cells. It induces other cytokine expression and activates and attracts and recruits neutrophils to inflammation sites (Banerjee *et al.*, 2016). IL-17 plays a vital role in the elimination of the intracellular parasite. Th17 cells are essential in the clearance of *Leishmania* parasites (Gonçalves-de-Albuquerque *et al.*, 2017). IL-17 stimulates other immune cells to produce inflammatory molecules. It affects the neutrophil function at the site of inflammation, reduces apoptosis, and induce the secretion of proinflammatory cytokines, also tissue-damaging molecules (Dayakar *et al.*, 2019). Gonzalez-lombana *et al.* (2013) were observed blocking IFN- γ results a significant high in neutrophil accumulation and IL-17 production in the lesions of mice.

PCR techniques are used to identify *Leishmania* in clinical samples and the detection of causative specie of dermal lesion (Mosleh *et al.*, 2015) (Rodríguez-Brito *et al.*, 2015). The nested-PCR technique is considered a suitable method, has high sensitivity and very resolution identification of *Leishmania* parasites in clinical samples (Al-Tamemy and Al-Qurashi, 2017) (Akhoundi *et al.*, 2017). Moreover, the kinetoplast DNA (kDNA) gene has shown high sensitivity and specificity in detecting (Ranasinghe *et al.*, 2015) (Naseri *et al.*, 2016).

According to the importance and plenty of cutaneous leishmaniasis infections in the province, this study aimed to identify the prevalence of *Leishmania* species and to measure

serum interleukin-17 concentration among infected patients.

2. MATERIALS AND METHODS:

2.1. Study area and patients

The study was conducted in Thi-Qar province, South of Iraq, it included three locations to the samples collection: Al-Hussein Teaching, Al-Suq Al-Shyokh General, and Al-Shatrah General Hospitals for the period from the beginning of November 2018 to the end of October 2019. The hospitals have received patients suffering from Cutaneous leishmaniasis (CL). A total of 247 patients were diagnosed clinically by dermatologists as cutaneous leishmaniasis and did not show any other cutaneous diseases. However, 80 samples were collected randomly from patients with CL (Figure 1). The lesions were injected using normal saline (0.2 ml) in the lesion edge, then pulled again. After that, the fluid was kept in a plain tube for molecular examination. Also, 3 ml of the venous blood was collected from patients before their take treatment, then separated by centrifuge 3000 rpm. The serum was put in a plain tube and stored at -20 °C until use for interleukin-17 level measuring using ELISA assay.

2.2. Ethical approval

Ethical approval was obtained from the Committee of the university. Participation in this study was voluntary, and all patients consented to participate in this study and were free to withdraw at any time from this research (Schroter *et al.*, 2006).

2.3. Genomic DNA extraction

The gSYAN DNA kit (Geneaid, Taiwan) was used for DNA extraction from lesion fluid, according to the protocol of the produced company. DNA concentration was examined using a Nanodrop spectrophotometer and then stored at -20°C until used in PCR amplification (Al-Difaie, 2013).

2.4. Nested-PCR amplification

The kinetoplast minicircle DNA was amplified for identification of *Leishmania* spp, using the Nested-PCR technique, with some modification of PCR assay, according to Izadi *et al.* (2016), which included two steps. DNA of parasite undergone the first run with external primers: CSB2XF 5'-CGA GTA GCA GAA ACT

CCC GTT CA-3' and CSB1XR 5'-ATT TTT CGC GAT TTT CGC AGA ACG-3', then first run product passed with the second run with internal specific primers: 13Z 5'-ACT GGG GGT TGG TGT AAA ATA G-3' and LiR 5'-TCG CAG AAC GCC CCT-3'. PCR-master mix was prepared by (AccuPower® PCR PreMix kit. Bioneer, Korea). Nested PCR primers were provided via the Macrogen Company, Korea. Nested PCR master mix was prepared 5µL of genomic DNA, 10 pmol of each external primer, and 13 µL of PCR water and placed in standard PCR tubes. Thermal conditions of the PCR reaction were included an initial denaturation at 95 °C for five min, followed by 30 cycles at 95 °C for 30 s., 55 °C for 30 s. and 72 °C for one min and finally, final extension 72 °C for five min. A nested PCR master mix of the second run was included 3 µL of first-run product, 10 pmol of each internal primer, and 15 µL of PCR water and placed in standard PCR tubes with thermal conditions for the PCR reaction. The PCR products were passed electrophoresis in 1% agarose gel with 3µL of ethidium bromide. PCR product (10 µl) was added into each comb well and 5 µl of (100bp ladder) in each well. The gel tray was fixed in the electrophoresis chamber and filled by a 1X TBE buffer. The electric current was connected at 100 volts and 80 mA for 1 hr. PCR products were visualized using an ultraviolet transilluminator.

2.5. Human Interleukin-17 level measure

For quantitative determination of IL-17 concentrations in the serum of patients, samples were performed according to company instruction (Elabscience, China). All kit reagents and samples were brought at room temperature before used (Al-Ubaydi, 2018). 100µL of standard, blank, or sample were added per micro ELISA plate well and covered the plate with sealer and incubated for 90 min at 37 °C. The liquid of each well was removed. Immediately 100 µL biotinylated detection Ab working solution was added to each well, covered with the plate sealer, and incubated for 1 hour at 37 °C. All plate wells were washed three times. 100 µL of HRP conjugate working solution was added to each well and covered with the plate sealer, then incubated for 30 minutes at 37 °C. After that, wells were washed five times. Next, 90 µL of substrate solution was added to each well and covered with a new plate sealer, then incubated for about 15 minutes at 37 °C. 50 µL of stop solution was added to each well. The color was turned to yellow immediately. Finally, to determine the optical density (OD value) of each well at once, a microplate reader set at 450 nm.

2.6. Statistical analysis

In the study, an Independent-Samples T test was used to analyze the data using SPSS statistical package software V.17. A significant level was set at ($P \leq 0.05$) (Al-Ubaydi, 2018).

3. RESULTS AND DISCUSSION:

The most common leishmaniasis form is CL and invades the skin epidermis to form a lesion that is usually chronic and painless (Aronson *et al.*, 2016). Currently, there is no vaccine available against leishmaniasis infections. Control of CL is challenging due to the variety of *Leishmania* spp., reservoir hosts, and biological factors (Aflatoonian *et al.*, 2019). CL is often left disfiguring scars, especially on visible body sites, causing also social, psychological, and economic problems (Bilgic-Temel *et al.*, 2019).

Indeed, it is necessary to distinguish between *Leishmania* species for identifying clinically different manifestations of the disease (VL, CL, or MCL) to correct diagnosis, administration of the appropriate treatment, and control of the disease (Mesa *et al.*, 2020). Molecular techniques, mainly PCR-based assays, are nowadays used to detect *Leishmania* spp. in the clinical samples, also to diagnose parasite species, strains, and genotypes (Albuquerque *et al.*, 2017), and they have high sensitivity and specificity for *Leishmania* identification (Izadi *et al.*, 2016) (Soleimanpoor *et al.*, 2016).

3.1. Molecular diagnosis

The Nested-PCR technique for targeting the kDNA gene to detect and characterize *Leishmania* parasites directly in clinical samples was used. Moreover, the kDNA gene has shown high sensitivity and specificity in detecting *Leishmania* (Ranasinghe *et al.*, 2015) (Naseri *et al.*, 2016). A high abundance of kDNA minicircles in each kinetoplast makes an ideal target for the diagnosis of *Leishmania* parasites (Abdolmajid *et al.*, 2015) (Kocher *et al.*, 2017).

The kDNA minicircle amplification results showed that 65 out of 80 were positive for CL and recorded two co-existing species in the local area. The most common species were *L. tropica*, which comprised 46 (57.5%) samples of the total positive samples, while *L. major* 19 (23.75%) showed at a low level. The electrophoresis of the Nested-PCR product of *L. tropica* was generated at 750 bp (Figure 2).

Geographical expansion and global increase of leishmaniasis are still associated with vector population expansion (Cunze *et al.*, 2019). An increase in migration, rapid urbanization, deforestation, and *Leishmania* adaptation with mammalian hosts and additional vectors (Galgamuwa *et al.*, 2018). However, it is necessary to identify and detect *L. major* and *L. tropica* infections because treatment is administered with different protocols (Salloum *et al.*, 2016). This finding is close to Mezher (2017) in Al-Muthanna province; Al-Fahdawi *et al.* (2018) in Al-Ramadi City, and Abdolmajid *et al.* (2015) in Khorasan-Razavi province, Iran. It was inconsistent with Jafer *et al.* (2015) in Kerbala province; Mohammad and Hmood (2018) in Al-Qadisiyah province, and Rahi *et al.* (2019) in Kut City.

3.2. Serum Interleukin-17 level

The results of IL-17 level recorded a significant increase ($P > 0.05$) in 46 infected patients by *L. tropica* compared to the (25) control sample, which was the mean kit values 280 ± 33 pg/ml. In contrast, IL-17 concentration level in the patients was high, where it reached mean values 405 ± 160 pg/ml, and t . The value was 3.83, whereas P Value was 0.00 (Figure 3).

Immunologically, cutaneous leishmaniasis infection accompanies a complex set of interactions, leading to a differentiation of the Th17 cell subset, which is characterized by producing IL-17 (Gabriel *et al.*, 2019). IL-17 induces different proinflammatory cytokines and other chemokines (Maspi *et al.*, 2016) (Khazaei *et al.*, 2019). Generally, the level of IL-17 is high in peripheral blood and tissue of leishmaniasis patients, also associated with the intensity of inflammatory cellular infiltration (Rasouli *et al.*, 2019). Although the role of IL-17 in leishmaniasis is still unclear and differs according to the *Leishmania* species, host, and stage of the infection, its participation in the protective response and disease-promoting during infection is unquestionable (Gonçalves-de-Albuquerque *et al.*, 2017). IL-17 stimulates iNOS activation and several cytokines and chemokines, which lead to the recruitment of leukocytes, especially neutrophils that migration, to create a robust inflammatory infiltrate (Teixeira *et al.*, 2018).

The significant increase of IL-17 level in patients' serums with *L. tropica* compared to the control sample is consistent with Pitta *et al.* (2009) showed that *L. donovani* stimulated differentiation of Th17 cells to produce IL-17, IL-22, and IFN- γ ,

also mention that IL-17 and IL-22 were independent and strongly associated with protection against Kala Azar; Katara *et al.* (2013) have observed significantly higher in plasma IL-17 level of CL samples compared to control sample. Andargie and Ejara (Andargie and Ejara, 2015) concluded that IL-17 contributed significantly to VL pathogenesis during inducing TNF- α and NO production. Teixeira *et al.* (2018) have mentioned that the presence of *L. infantum* leads to an increase of IL-17 production, that associated with neutrophils recruitment that plays an active role at the site of the infection.

4. CONCLUSIONS:

There is little information about identifying and detecting *Leishmania* species responsible for human CL in Thi-Qar province. The study has shown two species that co-existing in the province. The most common causes of dermal lesions have infected with *L. tropica*. The Nested-PCR is a sensitive and accurate method for direct diagnosis and molecular studies of *Leishmania* parasites. The increased level for IL-17 concentration in *L. tropica* patients showed an important role that it plays in the interactions between immune cells at the infections with this parasite.

5. ACKNOWLEDGMENTS:

This study is part of a Ph.D. thesis for Mohammed H. Flaih. The authors thank the staff of dermatology and laboratory departments in the above Hospitals for their kind assistance in the sample collection. This study did not support financially.

6. REFERENCES:

1. Abdolmajid, F., Ghodratollah, S. S., Hushang, R., Mojtaba, M. B., Ali, M. M., and Abdolghayoum, M. (2015). Identification of *Leishmania* species by kinetoplast DNA-polymerase chain reaction for the first time in Khaf district, Khorasan-e-Razavi province, Iran. *Tropical Parasitol.*, 5(1), 50–55. <https://doi.org/10.4103/2229-5070.145587>
2. Al-Difaie, R. S. (2013). Prevalence of Cutaneous Leishmaniasis in AL-Qadissia province and the evaluation of treatment response by pentostam with RT-PCR. *Wasit Uni. Coll. Sci.*
3. Al-Ubaydi, N. A. H. (2018). Epidemiological, Immunological and Physiological Study of type2 Diabetic Patients infected with Toxoplasmosis. *Coll. Edu. pure Sci. Uni. Thi-Qar.*
4. Aflatoonian, M. R., SharifilD, I., Aflatoonian, B., Bamorovat, M., Heshmatkhah, A., Babaei, Z., Almani, P. G. N., Mohammadi, M. A., Salarkia, E., Afshar, A. A., Sharifi, H., Sharifi, F., Khosravi, A., Khatami, M., Arefinia, N., Fekri, A., Farajzadeh, S., Khamesipour, A., Mohebbali, M., Gouya, M. M., Shirzadi, M. R., and Varma, R. S. (2019). Associated-risk determinants for anthroponotic cutaneous leishmaniasis treated with meglumine antimoniate : A cohort study in Iran. *PLoS Negl Trop Dis*, 13(6), 1–18.
5. Akhoundi, M., Downing, T., Votýpka, J., Kuhls, K., Lukes, J., Cannet, A., Ravel, C., Marty, P., Delaunay, P., Kasbari, M., Granouillac, B., Gradoni, L. and Sereno, D. (2017). *Leishmania* infections: Molecular targets and diagnosis. *Molecular Aspects of Medicine*, 57, 1–29. <https://doi.org/10.1016/j.mam.2016.11.012>
6. Al-Fahdawi, H. A., Al-Ani, S. F., and Al-Kubaisi, T. A. (2018). Detection of Cutaneous Leishmaniasis Based on ITS1 Gene by PCR-RFLP Technique. *Egypt. Acad. J. Biolog. Sci.*, 10(2), 1–13.
7. Al-Tamemy, A. K. A., and Al-Qurashi, N. N. S. (2017). Identification and Sequences of Two *Leishmania* Species Isolated From Human Cutaneous Lesion in Iraq. *IOSR-JPBS*, 12(4), 53–57. <https://doi.org/10.9790/3008-1204075357>
8. Albuquerque, A., Campino, L., Cardoso, L., and Cortes, S. (2017). Evaluation of four molecular methods to detect *Leishmania* infection in dogs. *Parasites and Vectors*, 10(57), 1–5. <https://doi.org/10.1186/s13071-017-2002-2>
9. Andargie, T. E., and Ejara, E. D. (2015). Pro- and Anti-inflammatory Cytokines in Visceral Leishmaniasis Journal of Cell Science and Therapy. *J Cell Scie and Ther*, 6(3). <https://doi.org/10.4172/2157-7013.1000206>
10. Aronson, N., Herwaldt, B. L., Libman, M., Pearson, R., Lopez-velez, R., Weina, P.,

- Carvalho, E. M., Ephros, M., Jeronimo, S. and Magill, A. (2016). Diagnosis and Treatment of Leishmaniasis: Clinical Practice Guidelines by the Infectious Diseases Society of America (IDSA) and the American Society of Tropical Medicine and Hygiene (ASTMH). *Clinic Infect Dis*, 63, 202–264. <https://doi.org/10.1093/cid/ciw670>
11. Banerjee, A., Bhattacharya, P., Joshi, A. B., Ismail, N., Dey, R., and Nakhasi, H. L. (2016). Role of proinflammatory cytokine IL-17 in *Leishmania* pathogenesis and in protective immunity by *Leishmania* vaccines. *Cell Immunol*, 309, 37–41. <https://doi.org/10.1016/j.cellimm.2016.07.004>
 12. Bilgic-Temel, A., Murrell, D. F., and Uzun, S. (2019). Cutaneous leishmaniasis: A neglected disfiguring disease for women. *Internat J Women's Dermatol*, 5(3), 158–165. <https://doi.org/10.1016/j.ijwd.2019.01.002>
 13. Cunze, S., Kochmann, J., Koch, L. K., Hasselmann, K. J. Q., and Klimpel, S. (2019). Leishmaniasis in Eurasia and Africa : geographical distribution of vector species and pathogens. *R. Soc. Open Sci.*, 6, 1–12. Retrieved from <http://dx.doi.org/10.1098/rsos.190334>
 14. Dayakar, A., Chandrasekaran, S., Kuchipudi, S. V., and Kalangi, S. K. (2019). Cytokines : Key Determinants of Resistance or Disease Progression in Visceral Leishmaniasis : Opportunities for Novel Diagnostics and Immunotherapy. *Fronti in Immunol*, 10(670), 1–23. <https://doi.org/10.3389/fimmu.2019.00670>
 15. Gabriel, A., Valério-Bolas, A., Palma-Marques, J., Mourata-Gonçalves, P., Ruas, P., Dias-Guerreiro, T., and Santos-Gomes, G. (2019). Cutaneous Leishmaniasis: The Complexity of Host's Effective Immune Response against a Polymorphic Parasitic Disease. *J Immunol. Res.*, 2019, 1–16. <https://doi.org/10.1155/2019/2603730>
 16. Galgamuwa, L. S., Dharmaratne, S. D., and Iddawela, D. (2018). Leishmaniasis in Sri Lanka : spatial distribution and seasonal variations from 2009 to 2016. *Parasites and Vectors*, 11(60), 1–10. <https://doi.org/10.1186/s13071-018-2647-5>
 17. Gonçalves-de-Albuquerque, S. C., Pessoa-e-Silva, R., Trajano-Silva, L. A. M., Goes, T. C., Moraes, R. C. S. , Oliveira, C. N. C., Lorena, V. M. B., and Paiva-Cavalcanti, M. (2017). The equivocal Role of Th17 Cells and Neutrophils on immunopathogenesis of Leishmaniasis. *Fronti in Immunol*, 8(1437), 1–11. <https://doi.org/10.3389/fimmu.2017.01437>
 18. Gonzalez-lombana, C., Gimblet, C., Bacellar, O., Oliveira, W. W., Passos, S., Carvalho, L. P., Goldschmidt, M., Carvalho, E. M., and Scott, P. (2013). IL-17 Mediates Immunopathology in the Absence of IL-10 Following *Leishmania major* Infection. *PLoS Pathogens*, 9(3), 1–14. <https://doi.org/10.1371/journal.ppat.1003243>
 19. Izadi, S., Mirhendi, H., Jalalizand, N., Khodadadi, H., Mohebbi, M., Nekoeian, S., Jamshidi, A., and Ghatte, M. A. (2016). Molecular Epidemiological Survey of Cutaneous Leishmaniasis in Two Highly Endemic Metropolises of Iran, Application of FTA Cards for DNA Extraction From Giemsa-Stained Slides. *Jundishapur J Microbiol.*, 9(2), 1–7. <https://doi.org/10.5812/jjm.32885>
 20. Jafer, A. M., Al-Kubessy, A. H., and Al-Amar, M. H. (2015). Molecular and Immunological study of Cutaneous *Leishmania* in Karbala city. *J. of Kerbala Univ.*, 13(2), 34–47.
 21. Katara, G. K., Raj, A., Kumar, R., Avishek, K., Kaushal, H., Ansari, N. A., Bumb, R. A., and Salotra, P. (2013). Analysis of localized immune responses reveals presence of Th17 and Treg cells in cutaneous leishmaniasis due to *Leishmania tropica*. *BMC Immunology*, 14(1), 1–9. <https://doi.org/10.1186/1471-2172-14-52>
 22. Khazaei, N., Moghaddas, E., Rezaee, S. A., and Shamsian, S. A. (2019). IL-8 and IL-23 Levels in Peripheral Blood Mononuclear Cells of Patients with Cutaneous Leishmaniasis Caused by *Leishmania major*: A Case-Control Study. *Iran Red Crescent Med J*, 21(6), 1–6. <https://doi.org/10.5812/ircmj.85441>. Research
 23. Kocher, A., Valière, S., Bañuls, A., and Murienne, J. (2017). High-throughput sequencing of kDNA amplicons for the

- analysis of *Leishmania* minicircles and identification of Neotropical species. *Parasitology*, 1–8
24. Maksouri, H., Dang, P. M., Rodrigues, V., Estaquier, J., Riyad, M., and Akarid, K. (2017). Moroccan strains of *Leishmania major* and *Leishmania tropica* differentially impact on nitric oxide production by macrophages. *Parasites and Vectors*, 10(1), 1–10. <https://doi.org/10.1186/s13071-017-2401-4>
 25. Maspi, N., Abdoli, A., and Ghaffarifar, F. (2016). Pro-and anti-inflammatory cytokines in cutaneous leishmaniasis: a review. *Pathogens and Global Health*, 110(6), 247–260. <https://doi.org/10.1080/20477724.2016.1232042>
 26. McGeachy, M. J., Cua, D. J., and Gaffen, S. L. (2019). The IL-17 Family of Cytokines in Health and Disease. *Immunity*, 50(4), 892–906. <https://doi.org/10.1016/j.immuni.2019.03.021>
 27. Meira, C. S., and Gedamu, L. (2019). Protective or Detrimental? Understanding the Role of Host Immunity in Leishmaniasis. *Microorganisms*, 7(695), 1–25.
 28. Mesa, L. E., Manrique, R., Muskus, C., and Robledo, S. M. (2020). Test accuracy of polymerase chain reaction methods against conventional diagnostic techniques for Cutaneous Leishmaniasis (CL) in patients with clinical or epidemiological suspicion of CL: Systematic review and meta-analysis. *PLoS Negl Trop Dis*, 41(1), 1–15
 29. Mezher, J. O. (2017). *Study of comparison between traditional methods and molecular diagnosis of cutaneous leishmaniasis in Al-Muthanna Province*. Coll. Sci. Uni. Muthanna.
 30. Mohammad, F. I., and Hmood, K. A. (2018). Detection of *Leishmania* species by Nested-PCR and virulence factors GPIPS, GP63 in *L. major* by conventional-PCR. *Biochem. Cell. Arch.*, 18(2), 2255–2259
 31. Mosleh, I. M., Schönian, G., Geith, E., Al-Jawabreh, A., and Natsheh, L. (2015). The Jordanian Mid Jordan Valley is a classic focus of *Leishmania major* as revealed by RFLP of 56 isolates and 173 ITS-1-PCR-positive clinical samples. *Exp. Parasitol.*, 148, 81–85
 32. Naseri, A., Fata, A., Rezai, A., Hedayatimoghadam, M., Berengi, F., Akbarzadeh, O., and Shamsian, S. A. (2016). Molecular identification of *Leishmania* species in Torbat-e Heydarieh, Khorasan Razavi province, Iran. *Int J Med Res and Hea Scie*, 5(6), 87–92
 33. Oghumu, S., Natarajan, G., and Satoskar, A. R. (2015). Pathogenesis of Leishmaniasis in Humans. *Human Emerging and Re-Emerging Infections*, 1, 337–348. <https://doi.org/10.1002/9781118644843.ch18>
 34. Pitta, M. G. R., Romano, A., Cabantous, S., Henri, S., Hammad, A., Kouriba, B., Argiro, L., Kheir, M., Bucheton, B., Mary, C., El-Safi, S. H., and Dessein, A. (2009). IL-17 and IL-22 are associated with protection against human kala-azar caused by *Leishmania donovani* Find the latest version: IL-17 and IL-22 are associated with protection against human kala-azar caused by *Leishmania donovani*. *J Clinic. Investig.*, 119(8), 2379–2387. <https://doi.org/10.1172/JCI38813>. Neutrophils
 35. Rahi, A. A., Jasim, S. E., and Abed, F. A. (2019). Clinical picture of cutaneous leishmaniasis in Wasit, Iraq. *EAS J Orthop Physiother*, 1(3), 29–32
 36. Ramírez, J. D., Hernández, C., León, C. M., Ayala, M. S., Flórez, C., and González, C. (2016). Taxonomy, diversity, temporal and geographical distribution of Cutaneous Leishmaniasis in Colombia: A retrospective study. *Nature Publishing Group*, 1–10. <https://doi.org/10.1038/srep28266>
 37. Ranasinghe, S., Wickremasinghe, R., Hulangamuwa, S., Sirimanna, G., Opathella, N., Maingon, R. D. C., and Chandrasekharan, V. (2015). Polymerase chain reaction detection of *Leishmania* DNA in skin biopsy samples in Sri Lanka where the causative agent of cutaneous leishmaniasis is *Leishmania donovani*. *Mem Inst Oswaldo Cruz*, 110(8), 1017–1023. <https://doi.org/10.1590/0074-02760150286>
 38. Rasouli, M., Moazamian, E., Nasiri, M.,

- Keshavarz, M., and Asaei, S. (2019). Interleukin-17A Genetic Polymorphisms as a Prognostic Markers for Resistance to Visceral Leishmaniasis in the Iranian Population. *Arch Clin Infect Dis*, 14(2). <https://doi.org/10.5812/archcid.57163>. Research
39. Rodríguez-Brito, S., Camacho, E., Mendoza, M., and Niño-Vega, G. A. (2015). Differential identification of *Sporothrix* spp and *Leishmania* spp by conventional PCR and qPCR in multiplex format. *Med. Mycol.*, 53, 22–27
 40. Rossi, M., and Fasel, N. (2017). How to master the host immune system? *Leishmania* parasites have the solutions! *Internat Immunol*, 30(3), 103–111. <https://doi.org/10.1093/intimm/dxx075>
 41. Salloum, T., Khalifeh, I., and Tokajian, S. (2016). Detection, molecular typing and phylogenetic analysis of *Leishmania* isolated from cases of leishmaniasis among Syrian refugees in Lebanon. *Para Epidemiol and Cont*, 1(2), 159–168. <https://doi.org/10.1016/j.parepi.2016.02.002>
 42. Schroter, S., Plowman, R., Hutchings, A., and Gonzalez, A. (2006). Reporting ethics committee approval and patient consent by study design in five general medical journals. *J Medical Ethics*, 32(12), 718–723. <https://doi.org/10.1136/jme.2005.015115>
 43. Soleimanpoor, H., Dabirzadeh, M., and Fooladi, B. (2016). Identification of Species Causing Cutaneous Leishmaniasis by PCR in Chahbahar, Iran. *Med Laborato J*, 10(2), 46–51.
 44. Teixeira, C. R., Santos, C. S., Prates, D. B., Santos, R. T., Araújo-Santos, T., Souza-Neto, S. M., Borges, V. M., Barral-Netto, M., and Brodskyn, C. I. (2018). *Lutzomyia longipalpis* Saliva Drives Interleukin-17-Induced Neutrophil Recruitment Favoring *Leishmania infantum* Infection. *Frontiers in Microbiology*, 9(881), 1–10. <https://doi.org/10.3389/fmicb.2018.00881>

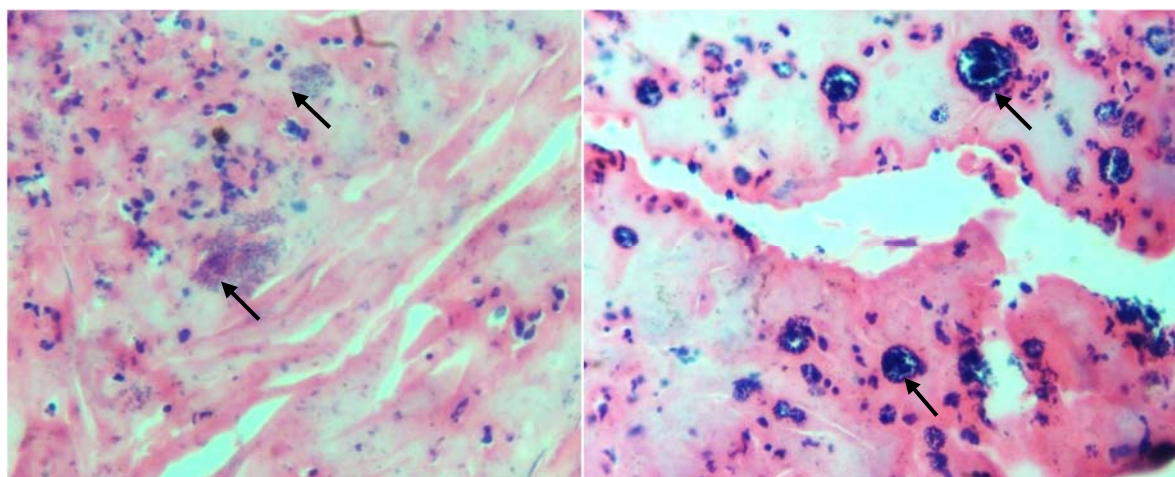


Figure 1: Cross-section of the dermal lesion showed amastigotes inside phagocytes (400X H&E).

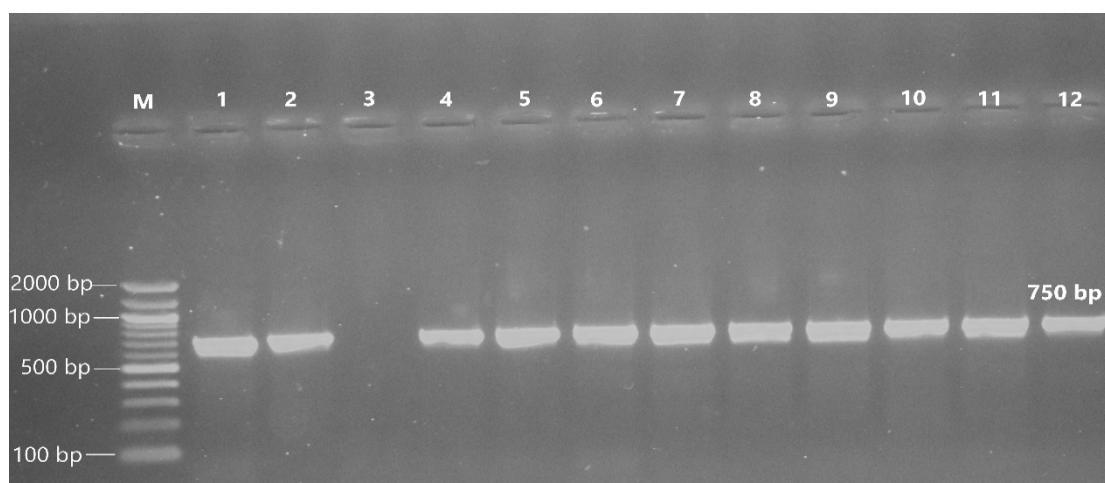


Figure 2: Agarose gel (1%) electrophoresis of *Leishmania* species using nested-PCR of kDNA in CL positive samples. Where M: marker (100-2000 bp), lanes 1, 2, and 4-12 show positive at product size 750 bp of *L. tropica* isolated from human skin lesions, while lane 3 shows a negative sample.

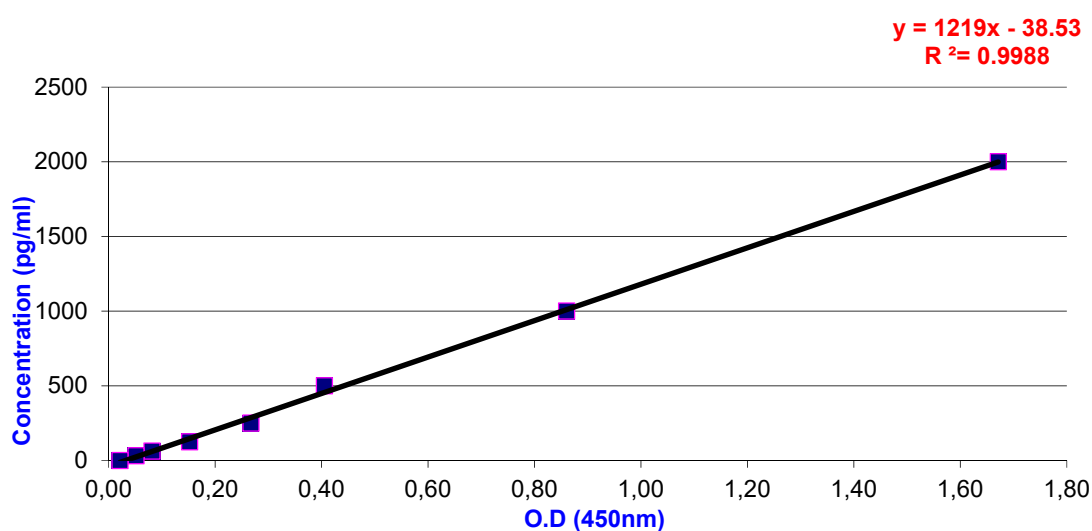


Figure 3: Human IL-17 ELISA standard curve

**HABILIDADES BIOLÓGICAS E ADAPTATIVAS DE BOVINOS JOVENS DAS RAÇAS
HEREFORD E ABERDEEN-ANGUS E SUAS CRUZAS EM REGIÕES ÁRIDAS DO
CAZAQUISTÃO OCIDENTAL****BIOLOGICAL AND ADAPTIVE ABILITIES OF YOUNG CATTLE OF HEREFORD AND
ABERDEEN-ANGUS BREEDS AND THEIR CROSS-BREEDS IN ARID TERRITORIES OF
WEST KAZAKHSTAN REGION****БИОЛОГИЧЕСКИЕ И АДАПТАЦИОННЫЕ СПОСОБНОСТИ МОЛОДНЯКА
ГЕРЕФОРДСКОЙ, АБЕРДИН-АНГУССКОЙ ПОРОД И ИХ ПОМЕСЕЙ В УСЛОВИЯХ
ЗАСУШЛИВЫХ ТЕРРИТОРИЙ ЗАПАДНО-КАЗАХСТАНСКОЙ ОБЛАСТИ**

AKHMETALIYEVA, Aliya^{1*}, NASSAMBAYEV, Yedige¹, BOZYMOV, Kazybay¹,
NUGMANOVA, Aruzhan¹

¹ Zhangir Khan West Kazakhstan Agrarian Technical University. Kazakhstan.

* Correspondence author

e-mail: aliya.akhmetalieva@mail.ru

Received 20 August 2020; received in revised form 20 October 2020; accepted 09 November 2020

RESUMO

Nos últimos anos, tem ocorrido um desenvolvimento anômalo persistente do clima, como resultado do qual as pastagens foram queimadas, a produção dos campos de feno diminuiu drasticamente e foram observadas quedas de temperatura. Nessas condições, a escolha da raça com embasamento científico e a criação de novos genótipos adaptados às condições locais e às exigências do mercado é um problema urgente. O objeto do estudo foram rebanhos jovens (bezerros-touros, bezerros) e bovinos adultos (vacas) das raças Hereford, Aberdeen-Angus e Cazaque de cabeça branca e bovinos jovens de cruzamentos de touros Hereford e Aberdeen-Angus com gado local. O artigo apresenta os resultados da análise e determinação dos recursos raciais de bovinos de corte para a obtenção de carne bovina ambientalmente segura. O estudo foi conduzido para estabelecer o grau de adaptação das raças de corte não-cazaques às condições naturais e climáticas da região do oeste do Cazaquistão. Animais mestiços apresentaram propriedades adaptativas mais pronunciadas em termos de cobertura e estrutura de pelos do 1º e 2º grupos de controle. Ao mesmo tempo, em termos de parâmetros principais de mudanças na cobertura e estrutura do cabelo, os animais de raça pura das raças Hereford e Aberdeen-Angus dos 1º e 2º grupos experimentais, em geral, foram caracterizados por propriedades adaptativas bastante boas dependendo das mudanças no ambiente externo. Os dados sobre a composição bioquímica do sangue indicaram o estado fisiológico normal dos animais de todos os grupos e mostraram boas capacidades adaptativas ao clima acentuadamente continental das estepes e semi-deserto do Cazaquistão Ocidental em animais de todos os grupos.

Palavras-chave: *bovinos jovens, habilidades biológicas e adaptativas, parâmetros clínicos e fisiológicos, cobertura de pêlo, bioquímica do sangue..*

ABSTRACT

In recent years, there has been a persistent anomalous development of the climate. As a result of which pastures have been scorched, the yield of hayfields has sharply decreased, and temperature drops have been observed. In these conditions, the scientifically grounded choice of the breed and the creation of new genotypes adapted to local conditions and market requirements is an urgent problem. The object of the study were young stock (bulls-calves, heifer calves) and adult cattle (cows) of the Hereford, Aberdeen-Angus, and Kazakh white-headed breeds and young cattle cross-breeds of Hereford and Aberdeen-Angus bulls with scrub cattle. The article presents the analysis and determination of the breed resources of beef cattle for obtaining environmentally-safe beef. The study was conducted to establish the degree of adaptation of non-Kazakhstani beef breeds to the natural and climatic conditions of the West Kazakhstan region. Cross-bred animals had more pronounced adaptive properties in terms of hair cover and hair structure of the 1st and 2nd control groups. Simultaneously, in terms of main parameters of changes in hair cover and hair structure, purebred animals of the Hereford and Aberdeen-Angus breeds of the 1st and 2nd experimental groups, in general, were characterized by rather good

adaptive properties depending on changes in the external environment. The data on the biochemical composition of blood indicated the normal physiological state of animals of all groups. They showed good adaptive capabilities to the sharply continental climate of the steppes and semidesert of West Kazakhstan in animals of all groups.

Keywords: *young cattle, biological and adaptive abilities, clinical and physiological parameters, hair cover, blood biochemistry.*

АННОТАЦИЯ

В последние годы и в настоящее время наблюдается стойкое аномальное проявление климата, результатом которого являются выгорание пастбищ, резкое снижение урожайности сенокосов, температурные перепады. В этих условиях актуальным вопросом является научно-обоснованный выбор породы и создание новых, приспособленных к местным условиям и требованиям рынка генотипов. Объектом исследования являлся молодняк (бычки, телочки) и взрослый скот (коровы) герефордской, абердин-ангусской и казахской белоголовой пород, а также помесный молодняк, полученный от использования в скрещивании герефордских и абердин-ангусских быков с беспородными коровами. В статье проанализированы и установлены породные ресурсы мясного скота для получения экологически чистой говядины, а также проведена исследования по установлению степени адаптации зарубежных мясных пород к природно-климатическим условиям Западно-Казахстанской области. По показателям волосяного покрова и строения волос более выраженными адаптационными свойствами отличались помесные животные. В то же время по основным параметрам изменения волосяного покрова, его структуры чистопородные животные герефордской и абердин-ангусской пород в целом характеризовались довольно хорошими приспособительными свойствами в зависимости от изменения внешней среды. Полученные данные биохимического состава крови свидетельствуют о нормальном физиологическом состоянии организма животных всех групп, а также указывают на хорошую адаптационную способность животных всех групп к резко-континентальному климату сухих степей и полупустыни Западного Казахстана.

Ключевые слова: *молодняк, биологические и адаптационные способности, клинико-физиологические показатели, волосяной покров, биохимия крови.*

1. INTRODUCTION:

Breeding beef cattle is a traditional industry for West Kazakhstan, and it is the leading region in the country in this field. At present, several farms are engaged in breeding the Hereford and Aberdeen-Angus breeds and providing scientific support for the selection process for these breeds. The relevance and scientific novelty of the project were also underlined by the need to select breeds of cattle characterized by high adaptability to changing natural and climatic conditions (Berman, 2011; Zinullin *et al.*, 2016).

In recent years and today, there has been a persistent anomalous development of the climate. As a result of which pastures have been scorched, the yield of hayfields has sharply decreased, and temperature drops have been observed (Dubovskova and Kuzin, 2005; Oraz *et al.*, 2019). In these conditions, the scientifically grounded choice of the breed and the creation of new genotypes adapted to local conditions and market requirements are an urgent problem (Sharafutdinova, Zhukov, and Rostova, 2016; Kosilov *et al.*, 2005; Wyatt *et al.*, 2013; Sahagun, Medina, and Ruiz, 2009; Pilvere, Proskina, and Nipers, 2016).

In developed countries, a special industry of specialized beef cattle breeding was created. Its role and importance as a source of high-quality meat production are steadily increasing (Kosilov *et al.*, 2015; Makaev, 2005; Aitzhanova *et al.*, 2017).

It should be noted that the further development of specialized beef cattle breeding in Kazakhstan can be successful if there is a good breeding base, including valuable breeding cattle with a high genetic potential for productivity (Zinullin and Nugmanova, 2016). Unfortunately, the breeding base in Kazakhstan does not provide farms with young breeding stock to achieve the indicators of the outlined program for cattle production development. To develop the breeding base and cattle production in Kazakhstan, it is necessary to expand and strengthen the existing multiplication farms for breeding animals and create new ones by importing limited livestock populations of the most valuable and promising breeds while focusing on traditional beef breeds from the CIS countries, in particular, the Hereford and Aberdeen-Angus breeds. However, the advantage should be given to the use of homegrown breeding resources (Belousov and Godzhiev, 1990; Bozymov, Nasambaev, Akhmetalieva, and Nugmanova, 2019; Kayumov,

2005; Dzhulamanov, 2006; Piccoli *et al.*, 2020; Wyatt *et al.*, 2014).

The social aspect of the need to breed and study animals of the Hereford and Aberdeen-Angus breeds and compare them with the Kazakh white-headed cattle is the need to factor in the specific natural and climatic zones of the Western region of Kazakhstan (Kayumov, Dubovskova, and Kuzin, 2005).

The study of the adaptive abilities of Hereford and Aberdeen-Angus breeds of animals in West Kazakhstan conditions compared with other genotypes is of scientific interest (Salikhov and Kosilov, 2008; Kosilov, Buravov, and Salikhov, 2006; Gabidullin, Belousov, and Tagirov, 2016). The Hereford and Aberdeen-Angus breeds were brought from far abroad to the "Musa" farm in the Zhangalinsky district of the West Kazakhstan region to increase beef production and expand the gene pool of beef cattle breeds.

Since these breeds were brought into this farm for the first time, comprehensive scientific and industrial research was conducted (concerning local natural and climatic conditions) to study their adaptive abilities to the new environment and determine economic and biological characteristics, and to compare the Hereford and Aberdeen-Angus cattle with the Kazakh white-headed breed from the "Khafiz" farm (Shevchenko, Kladova, and Chufeneva, 2008; Zelenkov, Drobot, and Zelenkov, 2009; Zhuzenov, Muskhanov, Umarov, Sadykova, and Seitmuratov, 2013; Meshcheryakov, 2004; Makaev, Kayumov, and Nasambaev, 2005).

The object of the study were young stock (bull-calves, heifer calves) and adult cattle (cows) of the Hereford, Aberdeen-Angus, and Kazakh white-headed breeds and young cattle cross-breeds of Hereford and Aberdeen-Angus bulls with scrub cattle. Biological and economically useful features of the Hereford and Aberdeen-Angus cattle imported from far abroad were studied for the first time in Kazakhstan.

The study aimed to analyze and determine breed resources for obtaining environmentally-safe beef and identifying the individual parameters of the degree of acclimatization of non-Kazakhstani beef breeds to the climatic conditions of the West Kazakhstan region by studying the biological characteristics of different genotypes.

2. MATERIALS AND METHODS:

2.1. Duration of the study and samples

The study was conducted in 2019-2020 in the Zhangalinsky district of the West Kazakhstan region at the "Musa" farm that breeds the Hereford and Aberdeen-Angus breeds and the "Khafiz" farm that breeds the Kazakh white-headed breed.

2.2. Experimental groups

Several groups of animals of various breeds were formed: 1st experimental (Hereford), 2nd experimental (Aberdeen-Angus), and control groups (Kazakh white-headed); 15 heads in each group in the age from birth to 15 months. Feeding and maintenance conditions of animals of all groups were the same and at the same level.

2.3. Ethics

Experimental studies and maintenance of animals were carried out taking into account the instructions and recommendations of Russian Regulations, 1987 (Order No. 755 on August 12, 1977, the USSR Ministry of Health) and "The Guide for Care and Use of Laboratory Animals (National Academy Press Washington, DC 1966)". In the research, everything possible was done to ensure a minimum of animal suffering and reduce the number of experimental prototypes (Aitzhanova *et al.*, 2017; Kazhgaliyev, Shaulyanov, Omarkozhauy, Shaikenova, and Shurkin, 2016).

2.4. Experimental procedures

The rations of experimental animals were made up of a set of feeds available on the farm. The limit of the feed set determined feed costs. Milk production of cows was determined by the live weight of young stock at 6 months of age.

The weighing was carried out to study the growth and development of young stock monthly before feeding. The weighing was carried out on electronic stationary scales "VPE-1000-S" (Farmer). Based on its results, live weight was determined at different ages, and the average daily increase in live weight in different age periods was calculated.

2.5. Blood collection

Blood was taken from three animals from each sex and age group during each season (autumn, winter, spring, summer) in the laboratory of the Zhangir khan West Kazakhstan Agrarian-Technical University.

2.6. Biochemical Paramaters

The study of the biochemical composition of blood was carried out using a ChemWell biochemical analyzer (manufactured by Awareness (USA)). In all groups of animals, the following parameters were determined: glucose (mmol/l), albumin (g/l), alanine aminotransferase (ALT) (units/l), aspartate aminotransferase (AST) (units/l), bilirubin (total, direct; $\mu\text{mol/l}$), cholesterol (mmol/l), triglycerides (mmol/l), urea (mmol/l), creatinine ($\mu\text{mol/l}$), alkaline phosphatase (ALP) (units/l), gamma-glutamyltransferase ($\gamma\text{-GT}$) (units/l), uric acid ($\mu\text{mol/l}$), iron (Fe) ($\mu\text{mol/l}$), pancreatic amylase (units/l), lactate dehydrogenase (LDH) (units/l). Sampling was carried out on a stainless steel sampler with a level sensor. The following biochemical stabilized liquid reagents were also used: calcium; magnesium; phosphorus; albumen; amylase; ALP; AST; ALT; total bilirubin; direct bilirubin; bilirubin direct and total; cholesterol; creatine kinase; creatine kinase MB-fraction; creatinine; glucose; $\gamma\text{-GT}$; high-density lipoproteins (HDL) direct; low-density lipoproteins (LDL) direct; LDH; total protein; triglycerides; uric acid; urea.

The total acid capacity of the blood was determined by Nevodov's titrimetric method. The mixture of 10 ml of 0.01 N HCL and 0.2 ml of blood was shaken and titrated with 0.1 N NaOH solution until turbidity and flakes appeared (protein precipitate), then 10 drops of indicator (1% phenolphthalein alcoholic solution) were added. The amount of alkali spent on titration was subtracted from unity (consumption of alkali in the control experiment); the resulting difference was multiplied by a factor of 20, an alkalinity index of 100 ml of blood was obtained (in mg%).

For each type of farm animals, there were average indicators of the biochemical composition of the blood, and there were also variations within different breeds. So, for cattle, the following average levels of biochemical parameters were determined: glucose: 2.3 - 4.1 $\mu\text{mol/l}$; albumin: 38 - 50%; ALT: 6.9 - 35 units/l; AST: 45 - 100 units/l; bilirubin: 0.7 - 14 $\mu\text{mol/l}$; cholesterol: 2.3 - 6.6 $\mu\text{mol/l}$; triglycerides: 0.0 - 0.2 $\mu\text{mol/l}$; urea: 2.8 - 8.8 $\mu\text{mol/l}$; ALP: 18 - 153 $\mu\text{mol/l}$.

2.7. Physiological indicators

The degree of development of the hair coat was studied on bulls of Kazakh white-headed and Hereford, and Aberdeen-Angus breeds in the arid steppe and semidesert zone of Western Kazakhstan by the seasons of the year according

to the method of E. A. Arzumanyan (1957) in the wool laboratory of the Higher School "Technology of production of animal products" West Kazakhstan Agrarian Technical University named after Zhangir khan.

In cows, the period from calving to the first heat, fertility, insemination index, duration of the service period, and fruiting was taken into account according to the data of the primary journal "Register of the breeding and calving of beef cows" (Form 3-meat). To determine the age of puberty by constant observation, the timing of the first manifestation of the sexual cycle and the established sexual cycle were recorded. The results of the pregnancy of heifers were clarified by rectal examination 3 months after mating.

Physiological indicators of young stock (body temperature, respiratory rate, pulse rate) were determined at the age of 9 and 15 months in winter (January) and summer (July) in the morning and at noon. According to the generally accepted method, physiological studies were conducted at the age of 9 to 15 months in the winter (January) and summer (July) periods in the morning and at noon in farm conditions. To study the clinical and physiological state of young stock, body temperature, pulse, and respiratory rate were measured, and three heads of young stock were selected for the study. The body temperature of young stock was measured with a special veterinary thermometer in the rectum (through the anus). The pulse rate was determined by placing a finger on the femoral artery, the respiratory rate – by the movement of the chest, by the tremors of exhaled air, felt by the palm of the hand placed near the nostrils.

2.8. Statistical Analysis

Digital materials were processed by biometric methods using the office software package "Microsoft Office" using the program "Excel" ("Microsoft", USA) with the determination of the reliability of the difference at three levels of probability according to Student-Fisher.

3. RESULTS AND DISCUSSION:

3.1 Breeding and production qualities of young stock of the Hereford and Aberdeen-Angus breeds

The object of studies of the breeding and productive qualities were the Kazakh white-headed animals in the "Khafiz" farm, and the Hereford and Aberdeen-Angus breed in the "Musa" farm of the Zhangalinsky region. The farms

are located on the same territory; natural and climatic conditions, soil and vegetation cover, botanical, the composition of the pasture and hayfields were the same.

The genealogical structure of foreign breeding cattle was based on the breeding certificates of servicing bulls.

The genealogical structure of the Aberdeen-Angus breed in the number of 383 heads was established from the records of breeding certificates for belonging to servicing bulls EG FRONTIER 678 OF107 – 28 heads, EG POUND MARKER 612 Of415 – 12 heads, S A V Premier 0096 – 67 heads, S A V Viper 0986 – 42 heads, EG POUND MARKER 612 OF 415 – 20 heads, BUFFALOS FINAL PRODUCT 12 – 22 heads, BUFFALOS MIDLANDER 143 – 9 heads, RANDY'S REACH OUT 112 – 10 heads, BUFFALOS KING EMPIRE 133 – 20 heads, BUFFALOS CC and 7 JR 118 – 20 heads, BUFFALOS SURTITLE 136 – 8 heads, BUFFALOS SIR CC and 7 18 – 13 heads, DF TOTAL 1729 – 8 heads, KAF N61 – 4 heads, SCHELKES K37 ABERDEEN 169 – 12 heads, SCHELKES IRONWOOD 1380A – 6 heads, SCHELKES K37 ABERDEEN 171 – 4 heads, SCHELKES EXPEDITION 1063M – 3 heads, SCHELKES K37 ABERDEEN 164 – 10 heads, Schelskes Expedition 1064M – 7 heads, SCHELKES 15 K37 – 15 heads SCHELKES K37 ABERDEEN 187 – 7 heads, SCHELKES ON TARGET 1067M – 4 heads, SCHELKES 747 LEGEND 134 – 5 heads, Connealy True Answer 892 – 27 heads.

The genealogical structure of the Hereford breed in the number of 120 heads: UPS DOMINO 3027 – 2 heads, E RIBSTONE STANDARD JR ET – 1 head, CJH HARLAND 408 – 1 head, UPS DOMINO 5216 – 2 heads, CHURCHILL NEON 626S – 2 heads, BLL DIAMOND 72S – 5 heads, CHURCHILL YANKEE ET – 1 head, KB L1 DOMINO 655 ET – 1 head, C 5131 DOMINO 7084 – 1 head, C 5131 DOMINO 7084 – 1 head, KT JOHN WAYNE 7167 – 2 head, UPS NAVARRO – 1 head, F REST EASY 847 – 1 head, BLL STANDARD 17U – 5 heads, BLL STANDARD 13U – 2 heads, H5 3027 DOMINO 957 – 2 heads, CD STANDARD C99 – 3 heads, CTY EASY 9904W – 1 head, HH ADVANCE 0184X ET – 4 heads, H W4 GRIZZLY 0146 ET – 1 head, BLL STANDARD TIME 743 7X – 5 heads, BIRD 157K ISSIAH 114 – 2 heads, HH ADVANCE 1173Y ET – 4 heads, CHURCHILL RED EYE 1107Y – 8 heads, BLL TRAVELER 9121W 185Y – 1 head, WSF LCR RCR ONSTAR 23NET – 1 head, THM DURANGO 4037 – 1 head, B REMITALL ANCHOR ET – 1

head, MSU TCF REVOLUTION 4R – 1 head, KCF BENNETT 9126J R294 – 1 head, HB LOADED 7822 – 6 heads, CRR ABOUT TIME 743 – 1 head, KJ HVH 33N REDEEM 485T ET – 1 head, RST P20 PROGRESS 7020 – 6 heads, NJW 98S DURANGO 44U – 2 heads, R LEGEND 2218 – 2 heads, TDP VINTAGE 402U ET – 1 head, LJR 023R WHITMORE 10W – 1 head, MOHICAN WARRENT 50W – 3 heads, H WCC / WB 668 WYARNO 9500 ET – 3 heads, RST R117 RIB EYE 9093 – 2 heads, B NORTHSTAR 951 – 8 heads, AW RIBSTONE 954 – 2 heads, MOHICAN XEROX 404X ET – 1 head, B RIBSTONE BRAXTON 072 – 1 head, BLL WARRIOR 309 26X – 4 heads, OHR BULLSEYE 110N 68X ET – 4 heads, LSW WCC ABOUT TIME X06 – 3 heads, TH 60W 719T VICTOR 43Y – 1 head, DD ANCHOR PRIDE 068 – 1 head, NJW 5M 100W TRUST 81Y ET – 1 head, TRICKY 'SVICTORW37-719T Y04 – 2 heads.

The qualitative composition of animals in the experimental and control groups is presented in Table 1. All animals were of pure breed. Table 1 shows that the servicing bulls of all genotypes belonged to the highest classes, while the breeding stock was of different quality. Animals of the highest classes occupied the highest proportion in the herd of Hereford and Aberdeen-Angus breeds – 79.2% and Aberdeen-Angus – 79.6%, respectively, and in the herd of the Kazakh white-headed breed – 40.0%. A similar trend was observed in the qualitative composition of young stock. Although the young stock of all genotypes corresponded to the complex class of the breed standard, the Hereford breed was noticeably dominated by animals of higher classes in bulls – 84.4% and heifers – 92.2% against peers of the Aberdeen-Angus breed, respectively – 89.9% and 85.1% and Kazakh white-headed breed – 60.9 % and 62.0%, respectively.

Indicators of age dynamics of the live weight of young stock of different genotypes are of particular interest (Table 2). The live weight of young stock of all genotypes met and exceeded the breed standard requirements for all age indicators, and in general, all age periods were marked by a rather high live weight of bulls heifers. The bulls of the 1st experimental group exceeded their peers of the Kazakh white-headed breed at birth by 2.1 kg (at $P > 0.95$), at 6 months of age by 49.0 kg (at $P > 0.999$), at 8 months of age by 53.6 kg (with $P > 0.99$), at 12 months of age by 21.5 kg (with $P > 0.95$), at 15 months of age by 25.5 kg (with $P > 0.95$). The bulls of the 2nd experimental group exceeded their peers of the Kazakh white-headed breed at birth by 0.1 kg (at $P < 0.95$), at 6

months of age by 39.2 kg (at $P > 0.99$), at 8 at the age of 57 kg (at $P > 0.99$), at the age of 12 months by 14.4 kg (at $P > 0.95$), at 15 months of age by 24.2 kg (at $P > 0.95$).

Comparison of bulls of the 1st and 2nd experimental groups showed that the superiority of Herefords over their peers of the Aberdeen-Angus breed was observed at 6 months of age by 9.8 kg (at $P > 0.95$) and 12 months – by 7.1 kg (at $P > 0.95$); at other ages, the differences in live weight were insignificant.

The heifers of the 1st experimental group exceeded their contemporaries in the control group (Kazakh white-headed breed) at birth by 3.1 kg (at $P > 0.99$), at 6 months of age by 20.9 kg (at $P > 0.99$), at 8 months of age by 20.9 kg (with $P > 0.99$), at 12 months of age by 15.7 kg (with $P > 0.95$), at 15 months of age by 19.9 kg (at $P > 0.95$). The heifers of the 2nd experimental group exceeded their peers in the control group (Kazakh white-headed breed) at 6 months of age by 16.36 kg (at $P > 0.95$), at 8 months of age by 17.7 kg (at $P > 0.95$), at 12 months of age by 20.7 kg (with $P > 0.99$), at 15 months of age by 11.9 kg (with $P > 0.95$). When comparing the 1st and 2nd experimental groups (Hereford and Aberdeen Angus heifers), a more noticeable difference in live weight in favor of the 1st experimental group is 8.0 kg (at $P > 0.95$). The main feature in selection and breeding work with beef cattle breeds is the growth rate of young stock in different age periods (Table 3).

The research results showed that a significant advantage in terms of the average daily increase in live weight was in the bulls of the control group (Kazakh white-headed breed) in 8-12 months and for the entire period of 8-15 months compared with the peers of the 1st experimental group by 267.22 g ($P > 0.95$) and 133.97 g ($P > 0.95$), for 2nd experimental group – by 354.44 g ($P > 0.95$) and 155.87 g ($P > 0.95$), respectively. The post-weaning adaptation of young Kazakh white-headed breeds was more successful with lower stress costs than peers of imported breeds. High indicators of average daily growth of young stock in 0-6 months of the 1st and 2nd experimental groups compared with the control group are associated with higher milk production of livestock. Thus, the average difference between bulls was 239.3 g ($P > 0.999$) and between heifers – 93.9 g ($P > 0.999$).

3.2 Reproductive qualities of young stock

The reproductive qualities of young stock were studied according to the following indicators: sexual reflexes, reaction to taking sperm products,

and seed quality (Table 4). It should be noted that the indicators of sexual activity of bulls of different genotypes were at a rather desirable level. Nevertheless, according to the locomotor reflex, more noticeable activity was observed in bulls of the control group, as it was in comparison with the 1st experimental group by 3 sec and the 2nd experimental group by 4 sec higher. The copulation reflex was also the most pronounced in the bulls of the control group. Bulls of the 2nd experimental group showed the most significant activity on the reflex of erections. Thus, the manifestation of sexual reflexes indicates a sufficiently high reproductive capacity of young stock of different genotypes.

Inbreeding work on the study of reproductive qualities of animals, especially on the selection of bulls for reproduction, the quality of sperm production is of particular importance (Table 5). The table shows that the bulls of the control group outperformed the peers of the 1st and 2nd experimental groups in sperm activity by 1 point with the same volume of ejaculate. In general, the quality of sperm production of young stock of different genotypes is quite suitable for artificial insemination in manual and free mating.

3.3 Reproductive qualities of cows

Successful reproduction of the herd is one of the main factors in the efficiency of the production of beef cattle products since the only marketable product in the industry is a calf. Moreover, the reproductive capacity of cows is determined, among other things, by the breed characteristics, as well as the natural and climatic conditions of their breeding place. Such indicators characterize the reproductive qualities of cows as the manifestation of sexual reflexes, the duration of pregnancy, the service period, the inter-body period, fertilization, insemination index, and the yield of calves. When organizing the reproduction of the herd, especially the need to obtain four calving or equalization of calving according to the season of the year, it is important to take into account the manifestation of sexual reflexes of cows.

Indicators of sexual reflexes of cows of different breeds are shown in Table 6. Table 6 shows that the longest duration of sexual excitement was observed in cows of the 1st and 2nd experimental groups, the 1st experimental group in particular – 0.7 hours and the 2nd experimental group – 2.4 hours higher than the control group. The duration of estrus was the lowest in cows of the control group; the duration of the immobility reflex in cows of different genotypes was in the range of 8.6-10.3 seconds. The interbody period is

a generalizing indicator, one of the key indicators among the characteristics of the reproductive abilities of cows. The length of the service period has the greatest impact on the variability of lactation duration. This indicator is determined to assess the state of the reproductive functions of cows. The value of the service period depends on the rate of involution of the uterus (restoration of its normal shape, size, and sexual cyclicity), which takes from 28 to 80 days (Diaz *et al.*, 2018; Kazhgaliyev *et al.*, 2016).

The main indicator that characterizes the reproductive capacity of meat cows is the interbody period, the average values of which are influenced by all cases of violation of the reproductive function (Table 7). It follows from the table that the cows of the control group did not have significant age-related differences in terms of the duration of the interbody period, service period, and pregnancy; they were within the physiological norms. It follows from Table 6 that the cows of the control group had the minimum calving period (344.4 days), the maximum – in cows of the 1st and 2nd experimental groups (348-351 days); the difference in comparison with the cows of the 1st experimental group was close to the reliability of the first level of probability with a large number of observations (1.61), and with the cows of the 2nd experimental group, the differences turned out to be significant ($P > 0.95$).

Due to the lack of artificial insemination of cows on farms, fertilization in cows of the 1st, 2nd experimental and control groups was determined by the number of fertilized cows during the breeding season. The fertilization rate of cows of the 1st and 2nd experimental and control groups averaged 96.56%, which has unjustified economic costs for beef cattle breeding. It should be noted that the indicators of the duration of the service period, as one of the important indicators of the reproductive properties of cows, in all genotypes were within the acceptable and desirable limits for normal reproduction of the herd (62.3-69.1 days).

The calf yield indicator reflects not only the economic value but also, to a certain extent, characterizes the reproductive qualities of cows. The highest rate of calf yield was observed in cows of the 1st experimental group, and the difference was in the range of 7.1-3.8% in comparison with the peers of the 2nd experimental and control groups, respectively. Cows of the Kazakh white-headed breed of 5-year-old age had an advantage in the yield of calves (by 2%), and cows of the Hereford breed had the highest yield of calves (89.1%).

An important practical value in the reproduction of the herd is taking into account the manifestation of sexual reflexes of cows. The results of the research showed that the shortest duration of sexual excitement was observed in cows of the 5-year-old control group compared to cows of 4 years old and was less by 0.6 hours. An insignificant difference in 4 and 5-year-old cows was observed in the duration of the immobility reflex and estrus at $P > 0.95$. Animals of all genotypes were generally characterized by quite good reproductive qualities, while Kazakh white-headed cows had minor advantages.

3.4 Reproductive abilities of animals of different sex and age groups

It was studied the indicators of sexual activity and the quality of sperm production in bull calves at 15 months of age. The results of studying the sexual activity of bulls of different genotypes are shown in Table 8. Table 8 shows that sexual reflexes were most pronounced in the control group of bulls. Simultaneously, the indicators of sexual reflexes of bulls of the 1st and 2nd experimental groups fully met the requirements of a high level of reproductive quality.

A more objective description of the reproductive properties of young stock can be obtained by indicators of the quality of sperm production (Table 9). Table 9 shows that the activity of sperms in comparison with the 1st and 2nd experimental groups was 1 point higher in the bulls of the control group.

3.5 Biological and adaptive abilities of young Hereford and Aberdeen-Angus breeds and their cross-breeds in the conditions of arid steppes of the West Kazakhstan region

For the use of classic imported beef breeds of cattle for industrial breeding or cross-breeding, it is important to study individual physiological and clinical indicators of both purebred and cross-bred animals (Table 10), where: 1st experimental (Hereford breed), 1st control (crosses from Herefords and outbred cattle), 2nd experimental (Aberdeen-Angus breed), 2nd control (Aberdeen-Angus and outbred cattle cross-breed).

Table 10 shows that body temperature indicators (38.1-38.6 °C) were practically at the same level in animals of different genotypes both during winter and during summer. Pulse and respiration rates were higher in winter in all animals of different genotypes. At the same time, fluctuations in pulse rate and respiration rate during the day over the seasons of the year were more adequate in crosses of animals of the 1st and 2nd control groups, which is associated with the

better adaptive ability of scrub cattle used in crossing.

It is important to determine the features of the structure of the hair cover during different seasons of the year to study the adaptive abilities of cattle of foreign selection and their cross-breeds with scrub animals (Table 11). Table 11 shows that the indicators of the amount of hair per 1 cm², hair length, and hair mass in summer are lower than in winter in animals of all genotypes, which naturally reflects their adaptive response to changes in environmental conditions. Simultaneously, animals of 1st and 2nd control groups (scrub cattle with the Hereford and Aberdeen-Angus breeds) adapted better in terms of the amount of hair per 1 cm², hair length, and hair mass both in winter and summer.

In winter, indicators of the amount of hair per 1 cm² animal of the 1st control group from animals of the 1st experimental group were 62.6 pcs higher than in the 2nd control group and 136.2 pcs higher than from animals of the 2nd experimental group of the same age. In the summer, on the contrary, the amount of hair per 1 cm² in animals of the 1st control group was 24.1 pcs lower than in the 1st experimental group, and animals of the 2nd control group had 23.4 pcs lower amount of hair than animals of the 2nd experimental group of the same age. No significant differences between animals of different genotypes for the rest of the hair cover parameters were observed in winter and summer, which, to a certain extent, characterized animals of all genotypes as sufficiently adapted to environmental conditions.

The structure of the hair characterizes biological characteristics and, to a certain extent, the adaptive abilities of the animal body (Table 12). Table 12 shows that fluff content was prevalent in the hair structure (63.8-71.8%) in animals of all genotypes in winter. In comparison, the content of awn was prevalent (42.1-46.1%) in summer, which naturally reflects the adaptive abilities of animals to changing environmental conditions. A comparison of the genotypic characteristics of the animals showed that animals of the 1st control group had 2.7% higher fluff content than animals of 1st experimental group, and animals of the 2nd control group had 2.5% lower fluff content than animals of the 2nd experimental group in winter. The fluff content was 1.3% lower in cross-bred Hereford animals and 0.9% lower in cross-bred Aberdeen-Angus animals compared to purebred animals, which also, to a certain extent, indicates higher adaptive abilities of cross-breed animals with scrub cattle

genetic material.

It can be concluded that more pronounced adaptive abilities characterized the cross-bred animals in terms of the hair cover and hair structure. Simultaneously, in terms of the main parameters of the change in the hair coat and its structure, purebred animals of the Hereford and Aberdeen-Angus breeds were generally characterized by good adaptive abilities, depending on changes in the external environment.

The biochemical composition of the blood of different genotypes was analyzed to reveal the adaptive qualities of the animal organism to the natural and climatic conditions of West Kazakhstan. (Table 13). The results showed that the indicators of the biochemical composition of the blood of animals of all genotypes were within the physiological norm. Simultaneously, in comparison with cross-bred animals, there was an increased level of activity of AST and ALT in the blood of young cattle of the 1st experimental group and an increased level of AST in animals of the 2nd experimental groups. It is possible to predict fattening and meat qualities by the level of enzyme activity. According to recent studies, the maximum activity of blood serum aminotransferases coincides with the maximum growth of muscle tissue in bulls. A significant positive correlation was established between the activity of serum aminotransferases and the live weight and growth energy of bulls at the age of four and twelve months. At the same time, Marutyan believed that the age of four months is optimal for prediction.

The alkaline phosphatase activity was the highest in the 1st experimental group, and the lowest activity was in the 2nd control group. The bulls of the 2nd control group were distinguished by higher blood creatinine and iron (Fe) levels, which makes it possible to expect higher live weight gains when rearing and fattening young cattle with this genotype. The level of albumin and GGT in the blood serum was slightly higher in bulls of the 1st control group. It can be taken into account when organizing the selection of individual genotypes for fattening.

The data on the biochemical parameters of blood indicated the normal physiological state of the organism of animals of all genotypes and good adaptive abilities to the sharply continental climate of West Kazakhstan in animals of all groups.

4. CONCLUSION:

The Hereford breed's genealogical structure is represented by the descendants of 6 servicing bulls and the Aberdeen-Angus – by the descendants of 15 servicing bulls. The live weight of young stock of all genotypes met and exceeded the breed standard requirements for all age indicators by an average of 41.8 kg, and in general, all age periods were marked by a rather high live weight of bull calves and heifers. High indicators of the average daily gain of young stock in 0-6 months of the 1st and 2nd experimental groups compared with animals of the 1st control group were associated with a higher milk yield of cattle. Indicators of the quality of sperm production of young stock of different genotypes were suitable for artificial insemination, manual, and free mating. Cows of all genotypes were characterized by good reproductive qualities, while cows of the control group had insignificant advantages. Indicators of the duration of the service period, as one of the important indicators of the reproductive properties of cows, in all genotypes were within the acceptable and desirable limits for normal reproduction of the herd (62.3-69.1 days).

Analysis of the research results showed that in terms of the hair coat and hair structure, animals of the 1st and 2nd control groups had more pronounced adaptive properties. Since the hair-covering is one of the signs of the adaptability of a living organism to environmental conditions, it serves as a heat insulator. In terms of the main parameters of the change in the hair coat and its structure, animals of the 1st and 2nd experimental groups were generally characterized by good adaptive abilities, depending on changes in the external environment, which are due to the same reaction of the organism of imported and local animals to changing environmental conditions. The data on the biochemical composition of blood showed the normal physiological state of the organism of animals of all groups. Also, they indicated good adaptive abilities to the sharply continental climate of the steppes and semidesert of West Kazakhstan in animals of all groups.

5. ACKNOWLEDGMENTS:

The study was performed in the Grant Funding framework of the Ministry of Education and Science of the Republic of Kazakhstan, project AP05134009 "Efficiency of the use of genetic resources of beef cattle for the production of environmentally-safe beef" of the Zhangir Khan West Kazakhstan Agrarian Technical University.

6. REFERENCES:

1. Aitzhanova, I., Naimanov, D. K., Miciński, B., Dzik, S., and Miciński, J. (2017). Fattening performance of bulls of three breeds fattened semi-intensively in the Kostanay Region. *OnLine Journal of Biological Sciences*, 17(3), 157-165.
2. Belousov, A. M., and Godzhiev, S. (1990). Otechestvennaya populyatsiya aberdin-angusskogo skota [Domestic population of Aberdeen Angus cattle]. *Molochnoe i myasnoe skotovodstvo [Dairy and beef cattle breeding]*, 6, 13-16.
3. Berman, A. (2011). Invited review: Are adaptations present to support dairy cattle productivity in warm climates? *Journal of Dairy Science*, 94(5), 2147-2158.
4. Bozymov, K. K., Nasambaev, E. G., Akhmetalieva, A. B., and Nugmanova, A. E. (2019). Exterior Features and Productive Qualities of Young Beef Cattle of Various Genotypes. *International Journal of Engineering and Advanced Technology*, 9(2), 745-750.
5. Diaz, D., Vander, P. M., Xiao, Y., Renquist, B., Wright, A., Collier, R., and Compart, D. (2018). Environmental chamber heat stress responses and adaptations in cross-bred Hereford steers. *Translational Animal Science*, 2, S185-S188.
6. Dubovskova, M. P., and Kuzin, A. V. (2005). Myasnaya produktivnost bychkov mestnoi populyatsii kazakhskoi belogolovoi porody i potomkov bykov Ankatinskogo i "Zavolzhskego" zavodskikh tipov [Meat productivity of bulls of the local population of the Kazakh white-headed breed and descendants of bulls "Ankatinsky" and "Zavolzhske" factory types]. *Beef cattle bulletin: Proceedings of international scientific and practical conference dedicated to the 75th anniversary of Mendeleev All-Russian Institute for Metrology*, 2(58), 195-196.
7. Dzhulamanov, K. M. (2006). Volosyanoi pokrov zhivotnykh kazakhskoi belogolovoi porody [Hair cover of animals of the Kazakh white-headed breed]. *Beef cattle bulletin: Proceedings of international scientific and practical conference dedicated to the 75th anniversary of*

Mendelev All-Russian Institute for Metrology, 2(59), 40-42.

8. Gabidullin, V. M., Belousov, A. A., and Tagirov, Kh. Kh. (2016). Opredelenie plemennoi tsennosti bykov-proizvoditelei v zavisimosti ot metoda otsenki determination of the breeding value of servicing bulls depending on the assessment method]. *Vestnik myasnogo skotovodstva*, 2(94), 22-26.
9. Kayumov, F. G. (2005). Znachenie myasnykh porod v intensivatsii proizvodstva govyadiny [The importance of beef breeds in the intensification of beef production]. *Beef cattle bulletin: Proceedings of international scientific and practical conference dedicated to the 75th anniversary of Mendelev All-Russian Institute for Metrology*, 1(58), 73-79.
10. Kayumov, F. G., Dubovskova, M. P., and Kuzin, A. V. (2005). Uluchshenie produktivnosti skota kazakhskoi belogolovoi porody metodom krossirovaniya v usloviyakh Yuzhnogo Urala [Improvement of the productivity of cattle of the Kazakh White-headed breed by the method of crossing in the conditions of the Southern Urals]. *Beef cattle bulletin: Proceedings of international scientific and practical conference dedicated to the 75th anniversary of Mendelev All-Russian Institute for Metrology*, 1(58), 165-168.
11. Kazhgaliyev, N. Z., Shauyenov, S. K., Omarkozhauy, N., Shaikenova, K. H., and Shurkin, A. I. (2016). Adaptability and productive qualities of imported beef cattle under the conditions of the northern region of Kazakhstan. *Biosciences Biotechnology Research Asia*, 13(1), 531-538.
12. Kosilov, V. I., Buravov, A. F., and Salikhov, A. A. (2006). Osobennosti formirovaniya myasnoi produktivnosti molodnyaka simmental'skoi i chernopestroj porod [Features of the formation of meat productivity of young simmental and black-spotted breeds]. Orenburg, Russia: Izdat. tsentr OGAU, 268 p.
13. Kosilov, V. I., Irgashev, T. A., Shabunova, B. K., and Akhmedov, D. (2015). Klinicheskie i gematologicheskie pokazateli cherno-pestrogo skota raznykh genotipov i yakov v gornykh usloviyakh Tadzhikistana [Clinical and hematological parameters of black-and-white cattle of different genotypes and yaks in the mountainous conditions of Tajikistan]. *Bulletin of Orenburg State Agrarian University*, 1(51), 112-115.
14. Kosilov, V. I., Kuvshinov, A. I., Mufazalov, E. F., Nurzhanova, S. S., and Mironenko, S. I. (2005). *Effektivnost ispolzovaniya simmental'skogo i limuzinskogo skota dlya proizvodstva govyadiny pri chistoporodnom razvedenii i skreshchivanii* [Efficiency of using simmental and limousine cattle for beef production in pure-bred breeding and crossbreeding]. Orenburg, Russia: Orenburg State Agrarian University, p. 246.
15. Makaev, Sh. A. (2005). Seleksionno-geneticheskaya otsenka i metody sovershenstvovaniya kazakhskoi belogolovoi porody selection and genetic assessment and methods of improving the Kazakh white-headed breed]. *Beef cattle bulletin: Proceedings of international scientific and practical conference dedicated to the 75th anniversary of Mendelev All-Russian Institute for Metrology*, 2(58), 65-71.
16. Makaev, Sh. A., Kayumov, F. G., and Nasambaev, E. G. (2005). Kazakhskii belogolovyi skot i ego sovershenstvovaniye. Nauchnoe izdanie [Kazakh White-headed cattle and their improvement. Scientific publication]. Moscow, Russia: All-Russian Scientific Research Institute of Beef Cattle Breeding, 336 p.
17. Meshcheryakov, V. S. (2004). *Myasnaya produktivnost krupnogo rogatogo skota yuga Zapadnoi Sibiri i metody ee povysheniya* [Meat productivity of cattle in the south of Western Siberia and methods of its increase]: abstract of a thesis of a Doctor of Agricultural Science. Siberian Research and Design Technological Institute of Livestock, Novosibirsk, Russia, 58 p.
18. Oraz, G. T., Ospanov, A. B., Chomanov, U. C., Kenenbay, G. S., and Tursunov, A. A. (2019). Study of beef nutritional value of meat breed cattle of Kazakhstan. *Journal of Hygienic Engineering and Design*, 29, 99-105.

19. Piccoli, M. L., Brito, L. F., Braccini, J., Oliveira, H. R., Cardoso, F. F., Roso, V. M., Schenkel, F. S. (2020). Comparison of genomic prediction methods for evaluation of adaptation and productive efficiency traits in Braford and Hereford cattle. *Livestock Science*, 231, 103864.
20. Pilvere, I., Proskina, L., and Nipers, A. (2016). Technological and economic aspects of meat cattle farming in Latvia. In *Engineering for Rural Development*. Paper presented at the 15th International Scientific Conference, held at Jelgava, Latvia, May 25-27, 2016 (pp. 473-480). Jelgava, Latvia: Latvia University of Agriculture, Faculty of Engineering.
21. Sahagun, R., Medina, J. H. V., and Ruiz, I. J. (2009). Estimates of genetic and environmental parameters in tropical areas that influence the growth beef bovine F₁. *Journal of Animal and Veterinary Advances*, 8(12), 2503-2507.
22. Salikhov, A. A., and Kosilov, V. I. (2008). Produktivnye kachestva molodnyaka cherno-pestroi porody [Productive qualities of young black-and-white breed]. *Izvestiya Orenburgskogo gosudarstvennogo agrarnogo universiteta*, 1(17), 64–65.
23. Sharafutdinova, E. B., Zhukov, A. P., and Rostova, N. Yu. (2016). Adaptinaya reaktsiya importnogo skota golshtinskoi porody na temperaturnye usloviya sredy [Adaptive response of imported Holstein cattle to ambient temperature conditions]. *Bulletin of Orenburg State Agrarian University*, 2(58), 156-159.
24. Shevchenko, N. I., Kladova, L. A., and Chufeneva, S. V. (2008). Vliyanie sezona rozhdeniya na intensivnost rosta molodnyaka gereforskoi porody [Influence of the season of birth on the growth rate of young Hereford breed]. *Vestnik Altaiskogo gosudarstvennogo agrarnogo universiteta*, 7(45), 56-58.
25. Wyatt, W. E., Collier, R. J., Blouin, D. C., Scaglia, G., and Collier, J. L. (2014). Growth and reproductive performances in F₁ cross-bred heifers from Hereford, Braford, and Bonsmara sires and Angus and Brangus dams. *Professional Animal Scientist*, 30(3), 342-353.
26. Wyatt, W. E., Lawrence, T. E., Collier, R. J., Blouin, D. C., Scaglia, G., Bidner, T. D., and Collier, J. L. (2013). Feedlot performance, carcass merit, and meat tenderness in cross-bred cattle from Hereford, Braford, and Bonsmara sires and Angus and Brangus dams. *Professional Animal Scientist*, 29(6), 632-644.
27. Zelenkov, P. I., Drobot, I. A., and Zelenkov, A.P. (2009). Otsenka bykov po vosproizvoditelnym kachestvam [Assessment of bulls by reproductive qualities]. In *Aktualnye problemy razvitiya zootszennoi nauki [Actual problems of the development of zooengineering science]*. Paper presented at the International scientific and practical conference, March 20-22, 2009 (pp. 66-69). Persianovsky village, Russia: DonGAU.
28. Zhuzenov, Sh. A., Muskhanov, Zh. V., Umarov, K. T., Sadykova, L. U., and Seitmuratov, A. E. (2013). *Selektsionnye i tekhnologicheskie osnovy povysheniya potentsiala produktivnosti myasnogo skota [Breeding and technological bases for increasing the productivity potential of beef cattle]*. Almaty, Kazakhstan: TOO "Izdatelstvo Bastau", 172 p.
29. Zinullin, A. Z., and Nugmanova, A. E. (2016). Selecting beef cows according to the selection index concerning their natural resistance in the conditions of the sands of the Naryn semidesert. *International Journal of Pharma and BioSciences*, 7(2), 68-75.
30. Zinullin, A. Z., Sadykov, R. S., Alimbekov, S. A., Akhmetalieva, A. B., and Nugmanova, A. E. (2016). The economic traits and adaptive capacity of bull-calves of the Kazakh white-headed breed to the conditions of the semidesert zone of the Naryn sands. *Biosciences Biotechnology Research Asia*, 13(1), 539-546.

Table 1. Breed and class composition of the cattle herd of the "Musa" and the "Khafiz" farms

Class	Youngstock											
	By herd		Cows		Servicing bulls		Heifers at the age of 18 months		Bulls at the age of 6-12 months		Heifers in the age of 6-12 months	
	Heads	%	Heads	%	Heads	%	Heads	%	Heads	%	Heads	%
	1	2	3	4	5	6	7	8	9	10	11	12
Groups												
1 st experimental												
Elite-record	141	64.1	86	71.7	-	-	-	-	24	53.3	31	60.8
Elite	43	19.5	9	7.5	6	100	-	-	14	31.1	16	31.4
1 st class	11	5	-	-	-	-	-	-	7	15.6	4	7.8
2 nd class	25	11.4	25	20.8	-	-	-	-	-	-	-	-
2 nd experimental												
Elite-record	228	32.9	86	22.4	4	26.6	-	-	83	49.4	55	39.0
Elite	363	52.4	219	57.2	11	73.4	-	-	68	40.5	65	46.1
1 st class	42	6.1	4	1.0	-	-	-	-	17	10.1	21	14.9
2 nd class	-	-	-	-	-	-	-	-	-	-	-	-
Control												
Elite-record	48	10.4	27	9.8	-	-	-	-	10	8.1	11	11.0
Elite	199	43.4	83	30.2	-	-	-	-	65	52.8	51	51.0
1 st class	200	43.6	154	56.0	-	-	-	-	48	39.1	38	38.0
2 nd class	11	2.4	11	4	-	-	-	-	-	-	-	-

Table 2. Age dynamics of live weight of young stock of different genotypes, kg

No.	Sex of animals	n	Groups					
			Experimental				Control	
			1 st		2 nd			
			x±Sx	C _v , %	x±Sx	C _v , %	x±Sx	C _v , %
At birth								
1	Bulls	15	27.2±0.59	8.24	25.2±0.64	9.50	25.1±0.66	9.96
2	Heifers		25.8±0.58	8.44	22.1±0.69	11.69	22.7±0.70	11.81
6 months								
1	Bulls	15	231.4±2.13	3.44	221.6±3.85	6.51	182.4±1.96	4.03
2	Heifers		195.2±3.38	6.48	190.66±3.58	7.03	174.3±2.02	4.33
8 months								
1	Bulls	15	271.4±1.93	2.67	274.8±3.21	4.37	217.8±2.87	4.93
2	Heifers		232.3±2.70	4.35	229.1 ±3.84	6.27	211.4±1.40	2.48
12 months								
1	Bulls	15	347.7±2.76	2.97	340.6±2.70	2.96	326.2±3.17	3.64
2	Heifers		292.1±2.82	3.62	297.1±4.20	5.29	276.4±2.76	3.74
15 months								
1	Bulls	15	403.8±3.28	3.04	402.5±3.45	3.21	378.3±4.72	4.67
2	Heifers		337.1±3.53	3.91	329.1±3.80	4.32	317.2±2.48	2.93

Table 3. Dynamics of average daily growth by age period (y)

Groups	Sex	Growth period, months				
		0-6	6-8	8-12	12-15	8-15
		x±Sx	x±Sx	x±Sx	x±Sx	x±Sx
1 st experimental	Bulls	1,134.4±12.4 5	667.77±52.4 4	635.55±19.14	622.96±26.6 1	630.15±13. 19
	Heifers	941.1±20.70	618.88±20.6 7	498.33±17.86	499.25±17.4 7	498.73±10. 68
2 nd experimental	Bulls	1,091.48±23. 25	885.55±37.2 6	548.33±22.27	688.14±32.3 4	608.25±13. 12
	Heifers	936.29±19.3 7	641.11±25.1 3	566.11±16.95	355.56±19.8 5	475.87±11. 56
Control	Bulls	873.70±10.9 1	591.11±48.2 3	902.77±37.96	579.25±61.7 7	764.12±21. 96
	Heifers	844.81±9.66	618.88±34.2 5	541.66±26.33	453.33±15.1 5	503.80±12. 89

Table 4. Indicators of sexual activity of bulls (13 months)

Groups	Reflexes, sec			
	locomotor	erections	hugging	copulatory
1 st experimental	17.0±0.7	15.0±2.5	11.2±1.2	11.0±1.8
2 nd experimental	18.0±2.5	12.0±1.8	13.0±3.7	14.0±2.1
Control	14.0±0.7	14.0±2.1	11.0±0.7	10.0±1.4

Table 5. Qualitative indicators of sperm production in bulls of different genotypes

Groups	Ejaculate volume	Activity of undiluted sperm, point	Density
1 st experimental	5.3±0.98	8.0±0.81	average
2 nd experimental	5.0±1.24	8.0±0.47	average
Control	5.0±0.74	9.0±0.47	average

Table 6. Manifestation of sexual reflexes in cows of different breeds

No.	Indicators	Groups		
		Experimental		Control
		1 st	2 nd	
		$\bar{x} \pm Sx$	$\bar{x} \pm Sx$	
1	Number of cows	120	383	275
2	Duration of the hunting period, hour	16.3±0.70	18.0±0.94	15.6±1.16
3	Duration of estrus, hours	37.3±1.62	35.2±1.03	34.7±1.44
4	Immobility reflex, sec	9.4±0.89	8.6±0.57	10.0±0.56

Table 7. Comparative indicators of the reproductive capacity of cows of different breeds

No.	Indicators	Groups		
		Experimental		Control
		1 st	2 nd	
		5 years	5 years	
1	Number of cows	120	383	187
2	Pregnancy	278.9±0.06	284.4±0.78	282.1±1.20
3	Service period	69.1±0.10	68.6±0.54	62.3±0.43
4	Calving interval	348.0±0.53	351±0.34	344.4±0.46
5	Breeding efficiency, %	96.1	95.4	98.2
6	The period of sexual excitement	16.3±0.70	18.0±0.94	15.6±1.16
7	Estrus	37.3±1.62	35.2±1.03	34.7±1.44
8	Immobility reflex	9.4±0.89	8.6±0.57	10.0±0.56
9	Output of calves per 100 heads, %	89.1	84.4	83.0

Table 8. Indicators of sexual activity of bulls of different genotypes (15 months)

Groups	Reflexes, sec			
	locomotor	erections	hugging	copulatory
1 st experimental	16.0±0.71	14.0±2.50	12.2±1.22	12.0±1.83
2 nd experimental	15.0±2.52	124.0±1.82	13.0±3.71	14.0±2.12
Control	14.0±0.71	15.0±2.11	11.0±0.72	11.0±1.41

Table 9. Indicators of the quality of sperm production of bulls of different genotypes (15 months)

Groups	Volume of ejaculate, ml	Activity of undiluted sperm score	Density
1 st experimental	5.3±0.98	8.0±0.81	average
2 nd experimental	5.0±1.24	8.0±0.47	average
Control	5.0±0.74	9.0±0.47	average

Table 10. Clinical and physiological parameters of young stock of different genotypes

Groups	Time of day, hour	Air temperature , °C	Clinical parameters		
			Body temperature	Respiratory rate	Pulse rate
Winter					
1 st experimental	8:00	-27.21	57.2±1.54	14.3±0.74	38.5±0.81
	12:00	-24.33	61.6±0.85	16.2±1.51	38.6±1.66
	18:00	-26.11	60.3±1.16	17.1±2.71	38.3±0.78
2 nd experimental	8:00	-27.21	59.3±2.74	15.4±0.58	38.2±1.04
	12:00	-24.33	61.3±2.55	17.9±1.34	38.4±1.54
	18:00	-26.11	61.7±0.47	17.5±2.08	38.2±0.55
1 st control	8:00	-27.21	56.3±2.35	13.2±0.71	38.1±0.53
	12:00	-24.33	57.2±0.06	14.2±1.34	38.3±0.65
	18:00	-26.11	55.4±1.19	12.3±0.07	38.3±0.27
2 nd control	8:00	-27.21	56.2±1.65	15.0±0.91	38.1±0.08
	12:00	-24.33	60.8±1.24	16.5±0.48	38.3±0.44
	18:00	-26.11	59.3±0.38	15.9±1.12	38.2±0.27
Summer					
1 st experimental	8:00	+23.2	68.1±1.77	29.6±1.41	38.1±0.52
	12:00	+28.1	72.2±0.69	39.1±1.65	38.4±2.34
	18:00	+25.4	69.3±3.56	37.7±2.56	38.3±1.09
2 nd experimental	8:00	+23.2	69.6±1.24	31.2±2.23	38.3±1.36
	12:00	+28.1	71.2±2.52	40.4±2.62	38.3±0.54
	18:00	+25.4	71.1±3.14	37.6±0.96	38.6±1.47
1 st control	8:00	+23.2	64.6±1.63	26.9±0.86	38.1±0.48
	12:00	+28.1	67.5±1.69	37.2±1.42	38.3±1.22
	18:00	+25.4	66.2±2.37	33.4±2.81	38.3±1.33
2 nd control	8:00	+23.2	68.5±0.44	31.0±1.05	38.2±1.06
	12:00	+28.1	70.6±1.22	38.2±0.67	38.2±0.13
	18:00	+25.4	68.2±0.14	36.3±0.04	38.1±1.02

Table 11. Hair cover indicators of bulls of different breeds

No.	Groups	Amount of hair per 1 cm ² , pcs	Hair length per 1 cm ² , mm	Hair mass, mg
Winter (n=5)				
1	1 st experimental	1,281.3 ±28.65	39.7±1.35	49.3±1.47
2	1 st control	1,344.1 ±21.24	40.7±2.21	50.2±2.55
3	2 nd experimental	1,155.8 ±29.41	40.3±0.81	46.1±2.43
4	2 nd control	1,292.0±18.26	39.2±1.56	46.8±1.72
Summer (n=5)				
1	1 st experimental	575.3 ±19.14	21.3±1.62	14.1±1.25
2	1 st control	551.2 ±17.14	21.1±0.95	13.5±0.47
3	2 nd experimental	512.6±18.77	23.1±1.39	13.3±1.65
4	2 nd control	489.2 ±12.71	22.7±1.44	13.0±0.32

Table 12. Indicators of the hair structure of animals of different genotypes

Hair fraction	Season	Groups			
		1st experimental	1st control	2nd experimental	2nd control
Awn, %	Winter	19.3± 0.54	18.7±0.66	20.5±1.15	19.2±1.15
	Summer	43.1± 1.08	42.1±0.17	43.2±1.65	46.1±1.25
Fluff, %	Winter	69.1±1.32	71.8±1.02	66.3±1.24	63.8±1.64
	Summer	17.7±0.71	16.4±0.65	15.5±0.39	14.6±0.39
Intermediate, %	Winter	11.6± 0.22	9.5±0.02	13.2±0.85	17.0±0.25
	Summer	39.2±0.58	41.5±1.22	41.3±1.80	39.3±0.56

Table 13. Biochemical parameters of the blood of animals of different genotypes

Breed	Glucose mmol/l	Albumin g/l	ALT units/l	AST units/l	Total bilirubin μmol/l	Direct bilirubin μmol/l	Cholest erol mmol/l	Triglyce rides mmol/l
1 st experimental	2.3±0.32	35.8±1.4 3	31.2±2.0 4	165.7±17 .28.	3.4±0.16	1.2±0.31	2.0±0.20	0.07±0.0 2
2 nd experimental	2.7±0.24	38.2±1.3 4	30.1±1.2 5	165.6±16 .32	4.4±0.70	1.5±0.30	1.7±0.21	0.09±0.0 2
1 st control	3.1±0.38	41.6±0.6 7	26.0±1.1 6	114.2±11 .35	4.5±0.47	1.3±0.24	2.3±0.21	00.9±0.0 2
2 nd control	2.6±0.30	38.1±1.4 2	26.6±1.2 7	150.1±18 .61	3.9±0.26	1.5±0.12	1.9±0.12	0.1±0.01
	AP units/l	GGT units/l	Uric acid μmol/l	Fe μmol/l	Pancrea tic amylase units/l	LDH units/l	Creatini ne μmol/l	BUN mmol/l
1 st experimental	193.2±27 .01	13.8±2.0 4	54.6±3.9 1	52.9±5.9 8	88.3±3.8 2	3600.2± 278.16	82.4±11. 94	8.4±0.45
2 nd experimental	161.8±3. 99	11.4±2.7 0	60.3±3.1 2	32.7±5.7 0	98.9±7.7 7	3588.8±1 37.02	80.6±13. 40	7.9±0.87
1 st control	181.4±50 .77	16.6±4.1 4	50.3±6.2 6	31.3±5.1 6	95.8±3.9 8	3230.0±2 98.45	65.2±5.5 5	6.8±0.90
2 nd control	152.8±12 .92	13.8±2.1 1	59.5±3.1 5	30.0±4.2 3	95.5±4.3 8	3239.1±3 09.54	79.7±5.0 6	7.4±0.69

Planning the publication in the journal

Please use Table 1 to plan the submission date of the manuscripts. Table 1 represents a prediction of when a newly submitted manuscript tends to be published.

Table 1. Calendar of publication until 2025.

The first issue (March)											
January	February	March	April	May	June	July	August	September	October	November	December
The second issue (July)											
January	February	March	April	May	June	July	August	September	October	November	December
The third issue (November)											
January	February	March	April	May	June	July	August	September	October	November	December

Definition of the colors:

Red: Editorial working time, usually no new manuscripts are accepted for this issue.

Yellow: There is a good possibility that the manuscript will be moved for the next issue.

Green: Open submission time

Tips to increase the evaluation speed:

- The only e-mail address of the journal is **journal.tq@gmail.com**. The journal does not use any other e-mail address.
- Include the complete cover letter in the first submitted message.
- Before the submission of the manuscript to **journal.tq@gmail.com**, review it. Check to see if it follows the common organizational structure of the journal (Introduction, Materials and Methods, Results and Discussion, Conclusion, References);
- Always reply to the original message that the manuscript was submitted. Do not create new messages to reply to an evaluation.
- If the original English translation quality is not good, consider hiring a professional translator and including a translation certificate.

Planejando a publicação na revista

Use a Tabela 1 para planejar a data de submissão dos manuscritos. A Tabela 1 representa uma previsão de quando um manuscrito recentemente submetido tende a ser publicado.

Tabela 1. Calendário de publicação até 2025.

Primeira edição (Março)											
Janeiro	Fevereiro	Março	Abril	Maio	Junho	Julho	Agosto	Setembro	Outubro	Novembro	Dezembro
Segunda edição (Julho)											
Janeiro	Fevereiro	Março	Abril	Maio	Junho	Julho	Agosto	Setembro	Outubro	Novembro	Dezembro
Terceira edição (Novembro)											
Janeiro	Fevereiro	Março	Abril	Maio	Junho	Julho	Agosto	Setembro	Outubro	Novembro	Dezembro

Definição das cores:

Vermelho: Tempo de trabalho editorial, geralmente nenhum manuscrito novo é aceito para esta edição.

Amarelo: Há uma boa possibilidade de que o manuscrito seja movido para a próxima edição.

Verde: Temporada de envio aberta.

Dicas para aumentar a velocidade de avaliação:

- O único endereço de e-mail da revista é **journal.tq@gmail.com**. A revista não usa nenhum outro endereço de e-mail.
- Inclua a carta de apresentação completa na primeira mensagem enviada.
- Antes do envio do manuscrito para **journal.tq@gmail.com**, revise-o. Verifique se segue a estrutura organizacional comum da revista (Introdução, Materiais e Métodos, Resultados e Discussão, Conclusão, Referências);
- Responder sempre à mensagem original de que o manuscrito foi submetido. Não crie novas mensagens para responder a uma avaliação.
- Se a qualidade da tradução original em inglês não for boa, considere contratar um tradutor profissional e incluir um certificado de tradução.

SOBRE AS PROPRIEDADES DISSIPATIVAS EFICAZES DA CAMADA WHISKERIZADA EM COMPÓSITOS DE FIBRA MODIFICADOS COM FIBRAS WHISKERIZADAS**EFFECTIVE DISSIPATIVE PROPERTIES OF A WHISKERED LAYER IN MODIFIED FIBROUS COMPOSITES WITH WHISKERED FIBRES****ОБ ЭФФЕКТИВНЫХ ДИССИПАТИВНЫХ СВОЙСТВАХ ВИСКЕРИЗОВАННОГО СЛОЯ В МОДИФИЦИРОВАННЫХ ВОЛОКНИСТЫХ КОМПОЗИТАХ С ВИСКЕРИЗОВАННЫМИ ВОЛОКНАМИ**

LURIE, Sergey A. ^{1,2}; RABINSKIY, Lev N. ^{3*}; KRIVEN, Galina I. ⁴; MAKOVSKII, Sergey. V. ⁵;

¹ Russian Academy of Sciences, Institute of Applied Mechanics, 7 Leningradsky Ave., zip code 125040, Moscow – Russian Federation

^{2,3,4} Moscow Aviation Institute (National Research University), Research Department of the Institute of General Engineering Training, 4 Volokolamskoe shosse, zip code 125993, Moscow – Russian Federation

⁵ Moscow Aviation Institute (National Research University), Research Department of the Institute of Aerospace, 4 Volokolamskoe shosse, zip code 125993, Moscow – Russian Federation

** Corresponding author*

e-mail: rabinskiy.lev@yandex.ru

Received 12 October 2020; received in revised form 30 October 2020; accepted 10 November 2020

RESUMO

Sabe-se que as propriedades mecânicas dos compósitos fibrosos são controladas pelas condições de contato entre a fibra e a matriz. Nesse sentido, grandes esforços dos engenheiros mecânicos são direcionados para o desenvolvimento de diversas técnicas para melhorar a qualidade da interface. Os mais comuns são: modificação da superfície da fibra, melhoria das interações químicas ou adição de uma terceira fase (camada interfacial) entre a fibra e a matriz. No presente trabalho, pretendemos examinar as propriedades dinâmicas efetivas da camada whiskerizada de fibras em compósitos modificados levando em consideração as características estruturais da camada interfacial – sua espessura – comprimento de whiskers, conteúdo volumétrico de whiskers e suas propriedades mecânicas. Avaliamos o desempenho dinâmico da camada whiskerizada ao redor da fibra base em compósitos modificados. A camada whiskerizada é considerada um compósito fibroso, que é formado por whiskers nanométricos crescidos na superfície e uma determinada matriz. Um aglutinante de epóxi ou um polímero viscoelástico é considerado a matriz. Foi utilizado um modelo aproximado, segundo o qual as características efetivas da camada whiskerizada foram modeladas e determinadas como as propriedades de um sistema fibroso isotrópico transversal com o eixo de isotropia coincidindo com os nanowiskers na camada whiskerizada. Uma característica da camada whiskerizada é que a densidade dos whiskers muda com a distância a partir da superfície da fibra e, portanto, depende do comprimento dos nanowiskers (espessura da camada interfacial). Acontece, neste caso, que o volume da matriz na camada whiskerizada é muito significativo mesmo na densidade máxima de nanowiskers crescidos na superfície da fibra e para camadas interfaciais suficientemente finas.

Palavras-chave: *compósito de fibra difusa, nanofibras, aglutinante de epóxi, propriedades de amortecimento.*

ABSTRACT

It is known that the mechanical properties of fiber-reinforced composites are controlled by the conditions of contact between the fiber and the matrix. In this regard, great efforts of mechanics are directed to developing various techniques to improve the quality of the interface. The most common are: modification of the fiber surface, improvement of chemical interactions, or the addition of a third phase (interfacial layer) between the fiber and the matrix. The most common are: modification of the fiber surface, improvement of chemical interactions, or a third phase (interfacial layer) between the fiber and the matrix. In this study, the authors aim to examine the effective dynamic properties of a whiskered layer of fibers in modified composites, taking into account the structural characteristics of the interfacial layer – its thickness – length of whiskers, volumetric content of whiskers, and their

mechanical properties. The dynamic performance of the whiskered layer surrounding the base fiber in modified composites was estimated. The whiskered layer is considered a fibrous composite formed by nanoscale whiskers grown on the surface and a matrix. An epoxy binder or a viscoelastic polymer is considered as a matrix. An approximate model was used. The effective characteristics of the whiskered layer were modeled and determined as the properties of a transversally isotropic fibrous system with the isotropy axis coinciding with nanowhiskers in the whiskered layer. A feature of the whiskered layer is that the density of whiskers varies with distance from the fiber surface. Therefore, it depends on the length of the nanowhiskers (the thickness of the interfacial layer). In this case, it turns out that the bulk for the matrix in the whiskered layer, even at the maximum density of nanowhiskers grown on the fiber surface and for sufficiently thin interfacial layers, is very significant.

Keywords: *fuzzy fiber composite, nanofibers, epoxy binder, damping properties.*

АННОТАЦИЯ

Известно, что механические свойства волокнистых композитов контролируются условиями контакта между волокном и матрицей. В связи с этим большие усилия механиков направляются на разработку различных методик для повышения качества интерфейса. Наиболее распространенными являются: модификация поверхности волокна, улучшение химических взаимодействий, либо добавление третьей фазы (межфазного слоя) между волокном и матрицей. В этой работе авторами были изучены эффективные динамические свойства вискеризованного слоя волокон в модифицированных композитах с учетом структурных характеристик межфазного слоя – его толщины – длины вискерсов, объемного содержания вискерсов, их механических свойств. Авторами были оценены динамические характеристики вискеризованного слоя, окружающего базовое волокно в модифицированных композитах. Вискеризованный слой рассматривается как волокнистый композит, который образован наноразмерными вискерсами, выращенными на поверхности и некоторой матрицей. В качестве матрицы рассматривалось эпоксидное связующее или вязкоупругий полимер. Использовалась приближенная модель, согласно которой эффективные характеристики вискеризованного слоя моделировались и определялись как свойства трансверсально изотропной волокнистой системы с осью изотропии, совпадающей с нановискерсами в вискеризованном слое. Особенностью вискеризованного слоя является то, что плотность вискерсов меняется с расстоянием от поверхности волокна, и, следовательно, зависит от длины нановискерсов (толщины межфазного слоя). Оказывается, при этом, что объемная часть для матрицы в вискеризованном слое даже при максимальной плотности нановискерсов, выращенных на поверхности волокна и для достаточно тонких межфазных слоев, весьма значительна.

Ключевые слова: *Фuzzy-волокнистый композит, нановолокна, эпоксидное связующее, демпфирующие свойства.*

1. INTRODUCTION:

1.1. The main features of fibrous composites

It is known that the mechanical properties of fiber composites are controlled by the conditions of contact between the fiber and the matrix. In this regard, great efforts of mechanics are directed to developing various techniques to improve the quality of the interface. The most common are: modification of the fiber surface, improvement of chemical interactions, or the addition of a third phase (interfacial layer) between the fiber and the matrix (Kim and Mai, 1998; Lin *et al.*, 2009). The ideas behind these techniques are to improve the interfacial adhesion properties and to increase the fiber surface area for more efficient transfer of loads between the fibers and the matrix, and further improve composite properties. At present, technologies for obtaining modern fiber composites are actively developed, in which

special microstructures containing nanofibers (whiskers) – nanowires are grown to increase the shear properties on the fiber surface (Lin *et al.*, 2009; Galan *et al.*, 2011) and carbon nanotubes (“fuzzy” fibers) (Garcia *et al.*, 2008; Sharma and Lakkad, 2010).

Among the many types of whisker-reinforced composites, it is possible to distinguish fiber composites, including CNT- whiskered structures (carbon fiber (T-650-5, whiskers-CNT, epoxy matrix), fiber composites including nanowires as whisker-reinforced systems (carbon fiber IM7, additional phase – zinc oxide). There are fibrous composites, based on aluminum, reinforced with continuous fibers Al_2O_3 , whiskered by Mullites. Nanowires of cadmium telluride (CdTe), whiskered by nanowires of silicon oxide (SiO_2), have been created (Wang *et al.*, 2004). This structure has three components (Sealy, 2004; Guz *et al.*, 2008): 1) solid CdTe nanowire; 2) SiO_2 coating, and 3) SiO_2 nanowire. Experimental

strength analysis has shown that for composite materials with whiskered fibers, higher ultimate strength and shear stiffness are manifested in comparison with standard composites that do not have an additional microstructure on the fiber surface (Goan and Prosen, 1969; Garcia *et al.*, 2008; Galan *et al.*, 2011; Agnihotri *et al.*, 2011), as well as significantly increases the compressive strength of the composite in the direction of growing nanotubes (Sharma and Lakkad, 2010). Tests show that by varying the diameter and length of the nanowire, the shearing strength of the interface can be increased up to 228%, while the average shear modulus increases by 37.5% (Lin *et al.*, 2009).

Depending on the thickness of the interfacial layer, the degree of its substitution for the epoxy matrix can be very significant. As shown by preliminary studies of composites, their dynamic characteristics significantly depend on the relative stiffness characteristics of the phases. Consequently, the influence of the interfacial layer on both the mechanical and dynamic properties can be significant, especially if to take into account that the stiffness characteristics of the microstructure of the interfacial layer can vary within wide limits.

In the present work, the authors aim to examine the effective dynamic properties of a whiskered layer of fibers in modified composites considering the structural characteristics of the interfacial layer – its thickness – length of whiskers, volumetric content of whiskers, and their mechanical properties.

1.2. Theoretical overview

Composite materials based on functional fibers (Galan *et al.*, 2011) are called combined composite materials. Different properties of composites can be simultaneously improved for them: strength, stiffness, damping, fatigue, and electrical and thermal conductivity (Gibson, 2010). Initially, to simulate such composites, a modified matrix model was used (Tarnopolskij *et al.*, 1987), which did not fundamentally differ from the calculated models of elastic characteristics of materials, and did not allow taking into account (except for the volume fraction of whiskers) the geometric characteristics (length and diameter) and density of whiskers in the composite. There are currently several analytical models to consider the effect of whiskers characteristics on the effective mechanical properties of fiber composites. In papers (Guz *et al.*, 2008; Guz *et al.*, 2009; Guz *et al.*, 2013), using the complex

potential method, the effect of the density of whiskers on the effective elastic properties of a carbon fiber composite with four layers – a base fiber, a coating, a whiskered interphase layer, and a matrix.

The Mori-Tanaka method was used to simulate the properties of a fuzzy fiber composite (Kundawal and Ray, 2011). The same composite system was investigated in (Chatzigeorgiou *et al.*, 2012) using methods of combining two phases and three phases. In (Lurie and Minhat, 2014), based on the three-phase method, a method was proposed for studying the effective properties of multifunctional composites, which simultaneously considers the effect of density, diameter, length, volume fraction, and properties of whiskers in the interphase layer. This method was investigated in studies where it was shown that depending on the type of loading, the strength of whisker-reinforced composites with an interfacial layer can be controlled either by the strength of the fiber or by the strength of the whiskered interfacial layer (Lurie *et al.*, 2018). Later in (Lurie *et al.*, 2019), an analytical method was proposed for assessing the strength of modified whisker-reinforced composites, which, depending on the type of loading, allows taking into account the geometric and physical characteristics of all elements of the composite structure (fibers, whiskers, matrices).

It was found that the whisker-reinforced interphase layer increases not only the transverse strength and rigidity but also the damping characteristics and electrical conductivity of composites (Garcia *et al.*, 2008). However, at the moment, there are practically no theoretical studies of the damping characteristics of multifunctional fiber composites, despite the intensive study of the dissipative properties of composites (Chandra *et al.*, 1999; Gusev and Lurie, 2009; Fisher and Brinson, 2011). In the aerospace industry, the requirement for high vibrational damping and high strength/stiffness materials now seems to be mandatory since more structural parts of aircraft are being designed with reinforced polymer-matrix composite materials. Several “traditional” design optimization concepts and materials were proposed to enhance the damping properties of composites at the micromechanical or macromechanical level (Finegan and Gibson, 1999; Chandra *et al.*, 2019). With this kind of optimization, a remarkable high loss amplification effect can be observed. A hybrid concept of viscoelastic and composite material to design composites with a good combination of high damping and high stiffness properties is elaborated in (Lakes, 2003; Wei and Huang, 2004;

Fisher and Brinson, 2011; Meaud *et al.*, 2013). Obtained results revealed that there is a trade-off between its stiffness and damping properties. Finding the optimal balance of properties in the work (Gusev and Lurie, 2009) examined the effect of thickness of the viscoelastic coating layer surrounding spherical inclusions embedded in the epoxy matrix system. It is found that at an extremely thin coating layer of lossy material, the effective shear loss modulus of the composite increases substantially. Based on the paper (Gusev and Lurie, 2009), it can be concluded that high damping and high stiffness composite structure might be attainable due to the presence of high shearing damping mechanism in lossy material (Gusev and Lurie, 2009; Meaud *et al.*, 2013).

In papers (Lurie *et al.*, 2018) for the first time, the dynamic properties of modified fiber composites containing fibers with a whiskered layer were investigated. It was assumed that the fiber microstructure of the whiskered layer is elastic, and the damping properties of the composite as a whole are related to the viscoelastic properties of the matrix. It is shown that the remarkable loss enhancement mechanism works in materials with particle morphology when the effective loss properties of the composite can exceed the loss modulus of the pure matrix by more than 20 times.

2. MATERIALS AND METHODS:

The study investigated the dissipative properties of a whiskerized layer in modified fiber composites with whiskerized fibers based on mathematical analysis, synthesis, assessment of dynamic composites, and modeling (Tarnopolskij *et al.*, 1987).

The case of an epoxy matrix corresponds to a modified fiber composite with whiskerized fibers, in which an epoxy matrix provides the solidity. In the future, the damping properties of the whiskerized layer are investigated depending on the volumetric content of the matrix in this layer V . In this case, the volumetric content of whiskers is equal to $(1-V)$. It was assumed that the minimum volumetric content of the matrix in the whiskerized layer, in reality, does not exceed 0.3. In this case, the epoxy binder has viscoelastic characteristics. Cases in which the viscoelastic layer and nanowhiskers form a whiskerized coating of the base fibers correspond to special modifications of the fiber composite, associated with an attempt to improve the dissipative properties of the modified composite. The idea of using a viscoelastic

polymer in a whiskerized layer to increase the modulus of losses in a modified composite is based on research (Gusev and Lurie, 2009), showing that ultra-thin viscoelastic fiber coatings make it possible to obtain fiber composites with extremely high damping properties while maintaining high stiffness characteristics.

To study a composite with inclusions containing viscoelastic coatings and with high parameter b/a , $b/a \gg 1$, it is necessary to go through a number of stages:

- 1 To estimate the optimal thickness of the viscoelastic layer providing the maximum effective damping properties of the composite, it is enough to consider a lamellar media with the volume content of a viscoelastic polymer V and find the volume content of a viscoelastic polymer corresponding to the maximum effective shear loss modulus. The authors consider Reuss formula discussed before for the effective complex shear modulus (Equation 1), where μ_1^* and μ_2^* are complex-valued shear moduli of the two layers respectively, and V is the volume fraction of the second layer. Suppose now that the first layer is stiff and nonlossy with a shear modulus of $\mu_1 = b$ while the second layer weak and lossy with Equation 2, where a , b , and η are real-valued parameters. It is easy to see that the effective shear modulus goes through a maximum, reaching values orders of magnitude larger than that of the lossy layer. By analyzing the asymptotic behavior for $a/b \rightarrow 0$, we can see that the volume fraction of the matrix which provides the optimal value of the thickness of the viscoelastic coating is given by Equation 3;

2. Direct numerical estimates indicate that this statement is also true for fibrous composites with fibers containing viscoelastic coatings (Lakes, 2003).

3. The amplitude of the effective loss modulus of the lamella composites is proportional to the value of the modulus of the elastic phase of the lamella-type two-phase composite, $\mu_1^* = b$ and proportional to viscosity characteristics η (Equation 4). Using Equation 1, it is possible to immediately find the equation for the maximum value of shear loss modulus (Equation 4). The amplitude of the effective loss modulus of the lamella composites (Equation 4) is proportional to the value of the modulus of the elastic phase of the lamella-type two-phase composite, $\mu_1^* = b$ and proportional to viscosity characteristics η .

4. The dynamic performance of the whiskered layer surrounding the base fiber in modified composites was evaluated. The

whiskered layer was considered to be a fibrous composite formed by nanoscale whiskers grown on the surface and some matrix. The properties of polymeric materials depend on the choice of the initial components and their ratio, the interaction between them, the method and technological conditions for manufacturing the product (pressure, temperature, time), additional treatment of the product, and a number of other factors. An epoxy binder or a viscoelastic polymer was considered as a matrix. An approximate model was used. The effective characteristics of the whiskered layer were modeled and determined as the properties of a transversely isotropic fibrous system with an isotropy axis coinciding with nanowhiskers in the whiskered layer.

5. The interfacial layer characteristics were investigated separately as a transversely isotropic fibrous material with an isotropic plane perpendicular to the nanofibers. The effective properties of the interfacial layer, determined from this preliminary consideration, were subsequently used to evaluate the effective properties of the modified fiber composite as a whole. In the general case, for all phases of the modified composite, a cylindrical coordinate system was used for an orthotropic material with constitutive relations connecting the stress vector (Equation 5) and the strain vector (Equation 6) through the tensor of elastic moduli of the sixth rank (Equations 7-9).

The lower indices of r, θ, z in the stiffness tensors were replaced by indices 1, 2, and 3, respectively. The upper bracketed right index represents the i -th layer, for example, for fiber $i = 1$, for coating layer $i = 2$, for matrix $i = 3$, and for the effective medium $i = 4$. For isotropic layers ($i = 1, 2, 3$), the stiffness constants in Equations 7-9 have these typical relations (Sealy, 2004). The effective properties of the viscous layer were found with the use of the generalized self-consistent (GSC) method for the representative volume element (RVE) of whiskered interphase layer. To implement the GSC method, it was required to determine the pre-stress-strain state of the basic solutions system for canonical cylindrical domains in analytical form.

The statement of the boundary problems for the bases strain-stress states solutions were formulated using the constitutive Equation 3, Cauchy's relations for deformations in the cylindrical coordinates, and the equilibrium equations and the specific boundary conditions. The solution used in the generalized self-consistent method was based on the fundamental original result of Eshelby (Eshelby, 1956) where for a two-phase composite, the difference in elastic

energy between medium with inclusion U^{RVE} and medium without the inclusion U^0 can be written as (Equation 10), where U' is the surface energy interaction between inclusion and matrix (Equation 11). However, this original approach was only applicable to a composite with a dilute concentration of inclusions. To solve for non-dilute solution and search for the correct estimation of transverse shear modulus that lies within the Hashin-Shtrikman bounds, the study (Christensen and Lo, 1979; Christensen, 2005) developed a self-consistent in which the initial two-phase composite was fictitiously embedded in an equivalent effective medium. As mentioned earlier, such a medium has its unknown properties the same as the unknown effective properties of the homogenized composite. This model assumed that the elastic energies of the medium with and without inclusions were identical. Mathematically this condition with the use of (Equation 10) was written as follows (Equation 12), where U' is the increment of energy in a unit cell of matrix material containing the inclusion; S is the contact surface between matrix and effective medium; σ_{ij}^1, u_i^1 are taken to be the stress tensor and displacement vector components at the contact surface that are found from the contact problem; and σ_{ij}^0, u_i^0 are the stress tensor and displacement. Eshelby's integral relation (Equation 12) always solves the problem of determining the effective modulus.

Vector components on the contact surface, which are related to the conditions of the problem at infinity. For example, to find an axial shear modulus, it was necessary to consider the fibers composite under shear homogeneous loading. For this case, at infinity, displacement $2\varepsilon_0 r \cos \theta$ was applied. It was easy to prove that the only admissible displacement field under this loading condition can be found by means of Equation 13, and admissible stress fields for every phase can be written as (Equations 14; 15). The coefficient $D_2^{(1)}$ is equal to zero to avoid singularity, while the coefficient $D_1^{(4)}$ is equal to $2\varepsilon_0$ in satisfying the boundary condition applied at infinity. All unknown coefficients and one unknown effective property $\mu_{23}^{(4)}$ in Equations 14, 15 can now be solved with the use of the displacement and stress continuity conditions at contact boundaries (Equation 16). According to the Eshelby integral equation (Equation 17): $D_2^{(4)}$ equals zero. Specifically, the axial shear modulus $\mu_{23}^{(4)} = \mu_{23}^{eff}$ was found by analyzing the stress continuity condition at R_3 , which leads to Equation 18.

The problem of determining the entire system of effective elastic moduli was solved similarly. The two-phase method based on the

polydisperse model (Christensen, 2005; Chatzigeorgiou *et al.*, 2012) provided virtually the same results as the self-consistent three-phase method developed in this study to determine the effective longitudinal Young's modulus, longitudinal shear modulus, bulk modulus of compression, and Poisson's ratio. Such a coincidence of the results in the methods of two and three phases was already noted earlier in (Hashin, 1990). On the other hand, the two-phase method provides only upper and lower limits for the effective transverse shear modulus. It is not suitable for obtaining refined estimates of this elastic modulus. Therefore, the three-phase method was used to solve the problem of determining the transverse shear modulus. Moreover, as demonstrated in (Lurie and Minhat, 2014), the self-consistent three-phase method estimates all elastic moduli of the considered systems for modified composites.

4. RESULTS AND DISCUSSION:

4.1. Approximate estimation of the effective damping properties of composites with interlayers of viscoelastic polymers

Christensen and Lo (1979) provide a detailed general procedure for the self-consistent method of many Eshelby phases in determining the effective properties of a multiphase composite – a whisker-reinforced fiber composite ($N \geq 3$), which has orthotropic phases corresponding to the base fiber, a whiskered interphase layer, an epoxy matrix. To estimate the five effective moduli of fiber composites in a cylindrical coordinate system, two statements are considered – in the isotropy plane (orthogonal to the fiber axis) and the plane perpendicular to it, i.e., in the direction of the fiber axis. The effective compression modulus and transverse shear modulus are determined, respectively, from solving uniform tension-compression problems across the fibers and pure shear in the transverse plane. The effective longitudinal modulus is determined by solving the problem of pure shear along the fibers. The effective longitudinal Young's modulus and Poisson's ratio in the direction of the fibers are determined by solving the problem of uniaxial tension.

In this work, the simple problem of the lamella-type composite was considered, where two types of loads can be implemented separately by shear stresses and normal transversal stresses. The effective complex shear and transverse Young's moduli can be determined using Reuss estimation with the viscoelastic

correspondence principle. Thus, their effective complex moduli can be written as follows (Equations 19; 20). Where V is the volume fraction of the second phase; μ_1^* and μ_2^* are the complex shear moduli of the first and second phase, respectively, and E_1^* and E_2^* are their transverse Young's moduli, respectively. For the shear case, the first phase is considered as an elastic material with $\mu_1^* = b$, and the second phase is a polymeric material with Equation 21. In what follows, composites containing thin layers of viscoelastic polymers will be considered, one of the features of which is greater than the value of the parameter b/a . The behavior of the considered composite material under external harmonic strain (Equation 22) is studied: in the infinity with a given angular frequency ω , ε_0 is the amplitude of harmonic strain applied to a viscoelastic continuum.

Then in the steady-state, the system stress is also harmonic (Equation 23). At specified cyclic frequency, the typical complex modulus is defined by the real part μ' representing the storage modulus and the imaginary part representing the loss modulus of the material. The effective complex modulus is defined as Equation 24 and the effective loss factor as Equation 25, related to the dampening of a material. The following statement has a place (Gusev and Lurie, 2009). The following features of the considered composites can be formulated (Gusev and Lurie, 2009). First, the shear and bulk moduli are a similar dependence, but with a different magnification factor at the maximum. Second, it is important that for the materials under consideration, the bulk modulus magnification factor is significantly lower than the shear modulus, and the maximum is implemented at higher than for shear volumetric contents of a viscous polymer. Third, it can be concluded that the abnormally high effective damping properties of a composite with simultaneously high effective mechanical properties are realized for the second peak corresponding to the shear mode.

Figure 1, demonstrates the benefit of viscoelastic polymers at T_g (viscous polymer (at T_g), $a_v = 0.01$ GPa and $\eta_v = 1$) when compared to solid polymer below T_g (solid polymer (below T_g), $a_m = 1$ GPa and $\eta_m = 0.02$) for the following parameters of elastic phases: the shear modulus of elastic phase, $b = 30$ GPa, on the figures (a), (b) and the shear modulus of elastic phase, $b = 51.85$ GPa, on the figures (c) and (d). It is easy to see that the curves are shown in Figures 1 (a), and 1 (c) fully correspond to the stated statement. The use of an epoxy matrix instead of a viscoelastic polymer leads to such low effective dissipative

properties of the system under consideration in the given figures 1 (a), 1 (c), on the accepted scales, the curves corresponding to them coincided with the abscissa axis.

It can be seen that the effective shear loss modulus at a very thin layer of viscoelastic material significantly exceeds the effective shear loss modulus of solid polymer-matrix ($\eta_m = 0.02$) almost by 300 times and its solid polymer composite by 30 times. For the composite with the epoxy matrix and with very small damping properties $\eta = 0.005$, the maximum of the effective shear loss modulus of composite realizes for thin enough layer of epoxy matrix $V=0.1$ and exceeds the effective shear loss modulus of an epoxy matrix ($\eta_m = 0.005$) almost by 5 times. On the other hand, using the solid polymer (below T_g) and the epoxy matrix leads to composites with higher effective storage modulus (Figure 1 (b)).

4.2. Modelling the effective dissipative properties of layered systems and fiber modified composites

The author consider two examples of fiber composites for which the effective properties were calculated using the self-consistent four-phase method (fiber, viscoelastic polymer coating, matrix, and effective medium). In the first case, a unidirectional lamina was considered, which consists of a typical epoxy matrix reinforced with glass fibers coated with a viscous polymer coating (Table 1). The results of the computations on the imaginary part of the effective axial (a) and transversal shear (b) moduli are given in Figure 2.

The curves presented in Figure 2 show that the maximum values corresponding to the maximum values of the loss moduli correspond to the approximate estimates given by Equations 3, and 4. For very thin viscoelastic coatings, a second peak is observed in the shear loss modulus, which is extremely attractive for obtaining composites with high mechanical and, at the same time, abnormally high damping properties. It was shown that this property is also transferred to layered composites obtained from monolayers of a fiber composite with viscoelastic coatings. In the second case, a unidirectional composite lamina of whiskered fiber was investigated that consists of IM7 carbon fibers coated with ZnO NWs embedded in typical epoxy polymer-matrix material. The properties of these materials are summarised in Table 2.

Here, first, the general dynamic behaviors of whiskered fiber composite based on a specific configuration of whiskered interphase layer were investigated. In this numerical example, the base

fiber of IM7 carbon fiber has a diameter of 5.2 μm , and the diameter and length of ZnO NW is 50 nm and 500 nm, respectively. The surface of the fiber is fully coated with NWs (100% density), and the volume fraction of NWs in whiskered interphase coating is 0.72. The authors investigated the effect of nanofiber's length on the effective dynamic properties of whiskered fiber composite with four values of fiber volume fraction V_f , which are 10%, 25%, 40%, and 50%. The diameter of base fiber and nanowires are 5.2 μm and 20 nm, respectively. The surfaces of fibers are fully coated with nanowires (100% density). The results of investigations of the axial and transversal shear moduli are illustrated in Figure 3. Curves in Figure 3 demonstrate the possibility of obtaining modified composites with sufficiently high damping properties. However, these properties are not so great in comparison with the case of viscoelastic polymer coatings. This result is quite understandable since the damping properties are associated exclusively with the viscous properties of the epoxy matrix. Even approximate estimates based on Equations 3, and 4 show that in the case of an epoxy matrix, the amplitude coefficient in Equation 4 is approximately two orders of magnitude lower than for the case of a viscoelastic polymer.

Note also that the properties of the second peak in the loss modulus for the effective transverse shear modulus are lost. Nevertheless, the curves shown in Figure 3 show that the effective damping properties of modified composites associated with longitudinal and transverse shears in the fiber system can be significant even if they are associated only with the viscous properties of the epoxy matrix. Figure 3 that all loss moduli are enhanced with increasing the length of the interphase layer for damping characteristics of whiskered fiber composite material. It is easy to see that the modified composite increases the loss moduli compared to the classical fiber composite. So, at 50% fiber volume fraction, the axial and transverse Young's loss moduli, axial, and transverse shear loss moduli are improved compared to classic fiber composites by 105%, 23%, respectively. The following question arises. Is it possible to significantly improve the dissipative properties of the modified composites if to consider the structural features of the interphase layer? In this regard, the authors will approximately estimate the effective characteristics of the interfacial layer damping and qualitatively its effect on the effective properties of the modified composite, since the previous estimates found in the literature were given without taking this factor into account. The

importance of this study is because, for modified composites, the volume fraction of the whiskered layer with its dissipative properties can be significant and may exceed the volume fraction of the epoxy binder, which ensures the solidity of the whiskered fibers.

4.3. Damping properties of the whiskered layer

Various advanced fibers are used to improve the quality of composite materials. Therefore, modified fiber composites constitute the object of this study. Tables 1 and 2 demonstrate the properties of fiber composites. Table 3 demonstrates the characteristics of the whiskered layer formed by ZnO nanowhiskers. Consider the whiskered layer due to the presence of nanostructures surrounding the surface of the fiber, a so-called whiskered interphase layer is formed between fiber and matrix when such a fiber system is embedded in the matrix material. Figure 4 shows that the whiskered interphase layer is a nanocomposite system, consisting of nanofibers and matrix material.

To estimate the effective properties of whiskered interphase layer, an approximate geometrical model was developed, which will be used in conjunction with a generalized self-consistent (GSC) method. The representative volume element has three concentric cylindrical phases. The first phase, which represents nanofiber with radius r_1 is assumed to be linear elastic isotropic material. In contrast, matrix material of the second phase with outer radius r_2 is linear viscoelastic isotropic material. An equivalent homogenized medium represents the third phase with an infinite outer radius, and its properties are unknown. According to GSC method, the unknown properties of this phase represent the unknown effective properties of whiskered interphase layer. Realistically, when nanofibers are fully wetted by matrix, together, they formed cylindrically orthotropic material around the fiber (radial type of structure (Hashin, 1990)), which has gradient properties along the length of its nanofibers. However, for the analytical study, the authors will assume that the properties of this layer are constant along the length of nanofibers. This simplification seems reasonable because the length of nanofibers is very small. As a result, the whiskered interphase layer can be treated as transversely isotropic material with an axis of symmetry parallel to the principal axis of nanofibers or r -axis. Consider a whiskered layer formed by ZnO nanowhiskers. The authors believe that an epoxy matrix, a viscoelastic polymer at a temperature below the glass transition, and a

viscoelastic polymer at a glass-transition temperature can be considered a matrix. The properties of nanowhiskers, epoxy matrix, and viscoelastic polymer are given in Table 3.

The evaluation of the specific dynamic properties of the whiskered layer for three types of such layers was carried out in the work. It is proposed to evaluate the specific dynamic properties of the whiskered layer for three types of such layers. Figure 5 shows the longitudinal shear loss modulus dependences obtained using the GSC Eshelby-Christensen's method. The same figures show more approximate estimates obtained using the Reis averaging. A comparison of the curves shown in Figure 5 indicates the effect of a significant increase (by about an order of magnitude) in the effective modulus of loss of the whiskered layer if a viscoelastic polymer below T_g is used instead of an epoxy matrix. Note that the use of carbon nanotubes (fuzzy fiber) as whiskers leads to a significant increase in damping properties or whiskered interphase layer (Figure 6).

However, note that these effects can be significant only for small volumetric contents of the matrix (Figure 6), i.e., for very thin whiskered layers. For the value of the volumetric contents greater than 0.3, the use of CNT NW leads to a slight increase in effective dynamic properties. A much more significant effect of increasing the effective loss modulus (more than 1000 times higher than that of an epoxy matrix) can be obtained if a viscoelastic polymer at T_g is used as a matrix in a whiskered layer. The same effect was previously found for inclusions with very thin viscoelastic coatings (Gusev and Lurie, 2009). However, this anomalous effect manifests itself for small volumetric contents of the matrix V , and in a very small range of V . This must be taken into account in qualitative assessments of the dynamic properties shown in Figure 5. Indeed, taking this circumstance into account, it will be necessary to exclude from consideration a very promising case (Gusev and Lurie, 2009), when a viscoelastic polymer at T_g is used as a matrix.

The author now consider an example of the thinnest whiskered layer with a viscoelastic polymer below T_g because it is, in this case, that the effective mechanical properties controlled by the base fibers of the modified fiber composite remain high. It was showed that in this case, very high damping properties can be realized in the composite. Note that for a qualitative assessment of the dynamic characteristics of the whiskered layer and the composite as a whole, the results obtained on the basis of the GSC Eshelby-

Christensen's method. However, according to curves in Figure 5, approximate analytical estimates obtained based on Reiss formulas or ratios (Equations 3, 4) can be used. The authors consider the modified fiber composite reinforced with IM7 carbon fibers of diameter $D = 5200$ nm with a layer of ZnO nanowires of thin whiskered interphase layer width $L = 500$ nm. Thin viscoelastic polymer below T_g . The average density c_0 of nanotubes/nanowires in the layer can be estimated by formula (Equation 26), where D is the diameter of the base fiber, d is the diameter of the nanofibers in the layer, L is the length of the whisker layer, $h \geq d$ is the distance between nanofibers on the surface of the base fiber, at the maximum density of nanofibers on the surface $h \approx \pi D/d$. For the considered case, the "whisker" layer with width $L = 500$ nm consists of ZnO nanowires with an average density $c_0 = 0.72$ and with following parameters: $E = 140$ GPa, $\nu = 0.35$. The matrix of the "whisker" layer is assumed to be the viscoelastic polymer at T_g with damping parameters $\mu_M = (1 + i0.02)$ GPa and loss modulus is shown in Figure 4 for volume fraction of matrix $V \geq 0.3$. Now consider a modified fiber composite with a double modification. Firstly, a composite is reinforced with IM7 carbon fibers, in which the base carbon fibers have a "whisker" layer with ZnO nanowires. Secondly, the "whisker" layer described above has a viscoelastic layer instead of an epoxy matrix. The solidity of the entire double modified composite as a whole is ensured by epoxy resin with damping parameters $\mu_M = 2.5 + i0.005$ GPa. For an approximate estimate of the effective dynamic properties under longitudinal shear, the Reuss procedure was used, generalized to a four-layer system, which leads to the following simple relations (Equations 27; 28). It is important to note that the proposed new procedure for modifying a fibrous composite leads to a significant increase in the effective loss modulus when the effective loss modulus can be significantly increased in comparison with modified composites obtained based on only an epoxy matrix and even in comparison with the loss modulus of the epoxy matrix itself (more than 40 times the loss modulus of an epoxy matrix (Figure 7)). Simultaneously, it is easy to verify that the effective mechanical properties change insignificantly, and all the useful characteristics and features of the modified fiber composites remain unchanged.

Using the example of longitudinal shear, it is shown that among the considered combinations of materials from which the main structural elements of the whiskered layer of the modified

fiber composite are made, the most promising is the interphase layer, in which carbon nanotubes (CNTs) play the role of whiskers, and a viscoelastic polymer acts as a binder at a temperature below the glass transition temperature. Other systems were considered, where an epoxy matrix or a viscoelastic polymer was considered a binder and ZnO nanofibers as whiskers. It is shown that even when an epoxy matrix is used as a binder, the effective loss modulus of the whiskered layer at minimum volumetric matrix contents significantly exceeds the loss modulus of the epoxy matrix itself. The paper also shows that most of the estimates, which are the basis for choosing the optimal structures, can be obtained based on analytical expressions found using the Reiss relations. It was found that such assessments are adequate not only from qualitative results but also give fairly accurate quantitative results. Using a more accurate procedure for estimating effective properties using the generalized Eshelby-Christensen's method confirms these conclusions. Quite simple analytical solutions are obviously of significant applied interest since they are very convenient in design calculations when determining the optimal characteristics of the structures under study.

5. CONCLUSIONS:

It has been established that the dissipative properties of modified composites with whiskered fibers largely depend on the dynamic characteristics of an inhomogeneous nanostructured layer of whiskers "grown" on fibers in such composites. The whiskered layer created on the surface of the base fibers can exhibit different physical and mechanical properties depending on the density of whiskers, their rigidity, and the thickness of the interfacial layer. The presence of whiskerising provides the technological possibilities of creating stable nanostructures with specified characteristics. It was shown that the loss modulus of a layer with nanosized whiskers can significantly exceed the loss modulus of a viscoelastic matrix, which is a source of damping effects. It was established that this characteristic is determined mainly by the shear nature of deformation in an inhomogeneous system, increases with an increase in the relative stiffness of whiskers, and decreases significantly with an increase in the volumetric content of the matrix. In the general case, shear deformations in the interphase layer are associated with a longitudinal shear in the direction of the whiskers

and a transverse shear in the perpendicular direction.

Finally, it was found that taking into account the high damping properties of whiskered layers with an optimal nanostructure around the base fibers makes it possible to significantly increase the damping properties of the modified fibrous composite without reducing its high mechanical stiffness characteristics due to the small thickness of the curved layers. The above estimates show that the value of the effective loss modulus of the modified composite can be tens of times higher than the matrix loss modulus.

6. ACKNOWLEDGMENTS:

This work was implemented with the support of the Russian Science Foundation (grant No. 20-19-00395).

7. REFERENCES:

1. Agnihotri, P., Basu, S., and Kar, K. K. (2011). Effect of carbon nanotube length and density on the properties of carbon nanotubes coated carbon fiber/polyester composites. *Carbon*, 49, 3098–3106.
2. Asthana, A., Momeni, K., Prasad, A., Yap, Y.K., and Yassar, R.S. (2011). In-situ observation of size-scale effects on the mechanical properties of ZnO nanowires. *Nanotechnology*, 22, 1–10.
3. Chandra, R., Singh, S. P., and Gupta, K. (1999). Damping studies in fiber-reinforced composites – a review. *Composite Structures*, 46, 41–51.
4. Chatzigeorgiou, G., Siedel, G. D., and Lagoudas, D. (2012). Effective mechanical of “fuzzy fiber” composites. *Composites B*, 43, 2577–2593.
5. Christensen, R. M. (2005). *Mechanics of composite materials*. New York: Dover.
6. Christensen, R. M., and Lo, K. H. (1979). Solutions of effective shear properties in three phase shears and cylinders models. *Journal of the Mechanics and Physics of Solids*, 27(4), 315–330.
7. Eshelby, J. D. (1956). The continuum theory of lattice defects. *Solid State Physics – Advances in Research and Applications*, 3, 79–144.
8. Finegan, I., and Gibson, R. (1999). Recent research on enhancement of damping in polymer composites. *Composite Structures*, 44, 89–98.
9. Fisher, F. T., and Brinson, L. C. (2011). Viscoelastic interphases in polymer-matrix composites: Theoretical models and finite element analysis. *Composites Science and Technology*, 61, 731–748.
10. Galan, U., Lin, Y., Ehlert, G. J., and Sodano, H. A. (2011). Effect of ZnO nanowire morphology on the interfacial strength of nanowire coated fibers. *Composites Science and Technology*, 71, 946–954.
11. Garcia, E. J., Wardle, B. L., Hart, A. J., and Yamamori, N. (2008). Fabrication and multifunctional properties of a hybrid laminate with aligned carbon nanotubes grown in situ. *Composites Science and Technology*, 68(9), 2034–2041.
12. Gibson, R. F. (2010). A review of recent research on mechanics of multifunctional composite materials and structures. *Composite Structures*, 92, 2793–2810.
13. Goan, J. C., and Prosen, S. P. (1969). Interfacial bonding in graphite fiber-resin composites, *Interfaces of composites. American Society of Testing*, 14, 3–26.
14. Gusev, A. A., and Lurie, S. A. (2009). Loss amplification effect in multiphase materials with viscoelastic interfaces. *Macromolecules*, 42(14), 5372–5377.
15. Guz, I. A., Guz, A. N., and Rushchitsky, J. J. (2009). Modelling properties of micro- and nanocomposites with brush-like reinforcement. *Materials Science and Engineering Technology*, 40(3), 154–160.
16. Guz, I. A., Rodger, A. A., Guz, A. N., and Rushchitsky, J. J. (2008). Predicting the properties of micro- and nanocomposites: From the microwhiskers to the whiskered nano-centipedes. *Philosophical Transactions of the Royal Society A*, 366, 1827–1833.
17. Guz, I. A., Rushchitsky, J. J., and Guz, A. N. (2013). Effect of a special reinforcement on the elastic properties of micro- and nanocomposites with polymer matrix. *The Aeronautical Journal*, 117(1196), 1019–1036.
18. Hashin, Z. (1990). Thermoelastic properties and conductivity of carbon/carbon fiber composites. *Mechanics of Materials*, 8, 293–308.

19. Kim, J. K., and Mai, Y. W. (1998). *Engineered interfaces in fiber reinforced composites*. Amsterdam: Elsevier Science Ltd.
20. Kumar, R.S., and Talreja, R. (2003). A continuum damage model for linear viscoelastic composite materials. *Mechanics of Materials*, 35, 463-480.
21. Kundawal, S. I., and Ray, M. C. (2011). Micromechanical analysis of fuzzy fiber reinforced composites. *International Journal of Mechanics and Materials in Design*, 7, 149-166
22. Lakes, R. S. (2003). High damping composite material. Effect of structural hierarchy. *Journal of Composite Materials*, 36(3), 287-297.
23. Lin, Y., Ehlert, G. J., and Sodano, H. A. (2009). Increase interface strength in carbon fiber composites through a ZnO nanowire interphase. *Advanced Functional Materials*, 19(16), 2654-2660.
24. Lurie, S. A., and Minhat, M. (2014). Application of generalized self-consistent method to predict effective elastic properties of whiskered fiber composites. *Composites B*, 61, 26-40.
25. Lurie, S. A., Kriven', G. I., and Rabinskij, L. N. (2019). On the strength of a modified composite with whiskerized fibers. *Composites and Nanostructures*, 11(1), 1-15.
26. Lurie, S. A., Rabinskij, L. N., Kriven', G. I., and Lykosova, E. D. (2018). Stress State in Structural Elements of Modified Fibrous Composite Materials with Whiskerized Fibers. *Mechanics of Composite Materials in Construction*, 24(1), 122-144.
27. Meaud, J., Sain, T., Hulbert, G. M., and Waas, A. M. (2013). Analysis and optimal design of layered composites with high stiffness and high damping. *International Journal of Solids and Structures*, 50, 1342-1353.
28. Sealy, C. (2004). Nanocentipedes could make strong composites. *Materials Today*, 17(2), 15-23.
29. Sharma, S. P., and Lakkad, S. C. (2010). Compressive strength of carbon nanotubes grown on carbon fiber reinforced epoxy matrix multi-scale hybrid composites. *Surface & Coatings Technology*, 205, 350-355.
30. Tarnopolskij, Yu. M., Zhigun, I. G., and Polyakov, V. A. (1987). *Spatially reinforced composite materials*. Moscow: Mashinostroyeniye.
31. Wang, Y., Tang, Z., Liang, X., Liz-Marzan, L. M., and Kotov, N. A. (2004). SiO₂-Coated CdTe nanowires: whiskered nano centipedes. *Nano Letters*, 4(2), 225-231.
32. Wei, P. J., and Huang, Z. P. (2004). Dynamic effective properties of the particle reinforced composites with viscoelastic interphase. *International Journal of Solids and Structures*, 41, 6993-7007.

$$1/\mu_{eff}^* = (1-V)/\mu_1^* + V/\mu_2^*, \quad (\text{Eq. 1})$$

$$\mu_2^* = a(1+i\eta) = \mu_2' + i\mu_2'' \quad (\text{Eq. 2})$$

$$V = (a/b) \sqrt{1 + \eta^2}, \Delta/R \approx V, \quad (\text{Eq. 3})$$

$$\mu'' \approx b(\sqrt{1 + \eta^2} - 1)/2\eta \approx b\eta + O(\eta^2) \quad (\text{Eq. 4})$$

$$[\sigma] = (\sigma_{rr}^{(i)}, \sigma_{\theta\theta}^{(i)}, \sigma_{zz}^{(i)}, \sigma_{rz}^{(i)}, \sigma_{\theta z}^{(i)}, \sigma_{r\theta}^{(i)})^T \quad (\text{Eq. 5})$$

$$[\varepsilon] = (\varepsilon_{rr}^{(i)}, \varepsilon_{\theta\theta}^{(i)}, \varepsilon_{zz}^{(i)}, \varepsilon_{rz}^{(i)}, \varepsilon_{\theta z}^{(i)}, \varepsilon_{r\theta}^{(i)})^T \quad (\text{Eq. 6})$$

$$[\sigma] = C[\varepsilon] \quad (\text{Eq. 7})$$

$$[\sigma] = (\sigma_{rr}^{(i)}, \sigma_{\theta\theta}^{(i)}, \sigma_{zz}^{(i)}, \sigma_{rz}^{(i)}, \sigma_{\theta z}^{(i)}, \sigma_{r\theta}^{(i)})^T, \quad (\text{Eq. 8})$$

$$[\varepsilon] = (\varepsilon_{rr}^{(i)}, \varepsilon_{\theta\theta}^{(i)}, \varepsilon_{zz}^{(i)}, \varepsilon_{rz}^{(i)}, \varepsilon_{\theta z}^{(i)}, \varepsilon_{r\theta}^{(i)})^T, \quad (\text{Eq. 9})$$

$$U^{RVE} = U^0 + U', \quad (\text{Eq. 10})$$

$$U' = \int_S (\sigma_{ij}^1 u_i^0 - \sigma_{ij}^0 u_i^1) dS, (i, j = 1, 2, 3). \quad (\text{Eq. 11})$$

$$U' = \int_S (\sigma_{ij}^1 u_i^0 - \sigma_{ij}^0 u_i^1) dS = 0, (i, j = 1, 2, 3) \quad (\text{Eq. 12})$$

$$u_z^{(i)}(r, \theta) = (D_1^{(i)} r + D_2^{(i)} r^{-1}) \cos \theta \quad (\text{Eq. 13})$$

$$\sigma_{rz}^{(i)}(r, \theta) = C_{44}^{(i)} (D_1^{(i)} - D_2^{(i)} r^{-2}) \cos \theta, \quad (\text{Eq. 14})$$

$$\sigma_{\theta z}^{(i)}(r, \theta) = -C_{55}^{(i)} (D_1^{(i)} + D_2^{(i)} r^{-2}) \sin \theta. \quad (\text{Eq. 15})$$

$$u_z^{(i)}(R_i, \theta) = u_z^{(i+1)}(R_i, \theta), \sigma_{rz}^{(i)}(R_i, \theta) = \sigma_{rz}^{(i+1)}(R_i, \theta), (i = 1, 2, 3). \quad (\text{Eq. 16})$$

$$\int_S (\sigma_{rz}^{N+1} u_z^{eff} - \sigma_{rz}^{eff} u_z^{N+1})_{r=r_N} dS = 0. \quad (\text{Eq. 17})$$

$$\mu_{23}^{eff} = \frac{1}{2\varepsilon_0} C_{55}^{(3)} (D_1^{(3)} - D_2^{(3)} R_3^{-2}). \quad (\text{Eq. 18})$$

$$1/\mu_{eff}^* = (1 - V)/\mu_1^* + V/\mu_2^*, \quad (\text{Eq. 19})$$

$$1/E_{eff}^* = (1 - V)/E_1^* + V/E_2^*, \quad (\text{Eq. 20})$$

$$\mu_2^* = a(1 + i\eta) = \mu_2' + i\mu_2''. \quad (\text{Eq. 21})$$

$$\varepsilon = \varepsilon_0 \sin \omega t, \quad (\text{Eq. 22})$$

$$\sigma = \sigma_0 \sin(\omega t + \delta). \quad (\text{Eq. 23})$$

$$\mu^* = \sigma_0/\varepsilon_0 \quad (\text{Eq. 24})$$

$$\tan \delta = \mu''/\mu', \quad (\text{Eq. 25})$$

$$c_0 = \frac{\pi D}{4(D+L)} \left(\frac{d}{h}\right)^2 \quad (\text{Eq. 26})$$

$$\frac{1}{\mu_{23}^{eff}} = V_1 \left(\frac{1}{\mu_{23}^{(1)}}\right) + V_1 \left(\frac{2\Delta}{d}\right) \left(\frac{1}{\mu_{23}^{(2)}}\right) + V_3 \left(\frac{1}{\mu_{23}^{(3)}}\right); \quad (\text{Eq. 27})$$

$$V_1 = (1 - V_3)/(1 + 2\Delta/d, V_3 \equiv V. \quad (\text{Eq. 28})$$

Table 1. The assumed phase properties for phases in a lamina (Gusev and Lurie, 2009).

Material	Bulk Modulus, K (GPa)	Shear Modulus, μ (GPa)
Glass fiber	50	30
Viscous polymer coating	3	0.02 + i 0.01
Epoxy matrix	2.5	2.5 + i 0.005

Table 2. Characteristics of a composite with whiskerized fibers

Fiber: IM7 carbon fiber:	Epoxy matrix:	ZnO NW
EL=256.76 GPa	K=2.5 GPa	E=140 GPa
ET=25.51 GPa	$\mu=2.3$	$\nu=0.35$
$\mu_L=22.06$ GPa		
$\mu_T=9.25$ GPa		
$\nu_L=0.289$		

Source: (Gusev and Lurie, 2009; Kumar and Talreja, 2003; Asthana et al., 2011).

Table 3. Material characteristics

Parameters	Binder			Inclusion	
	Epoxy matrix	Polymer at glass-transition temperature	Polymer below glass-transition temperature	ZnO	CNT
Shear modulus, GPa	2.5+0.005i	0.01(1+i)	1+0.02i		
Modulus of elasticity of the first kind, GPa				140	1100
Volume modulus of plane deformation, GPa	2.5	3.5(1+0.1i)	4		
Poisson's ratio				0.35	0.14

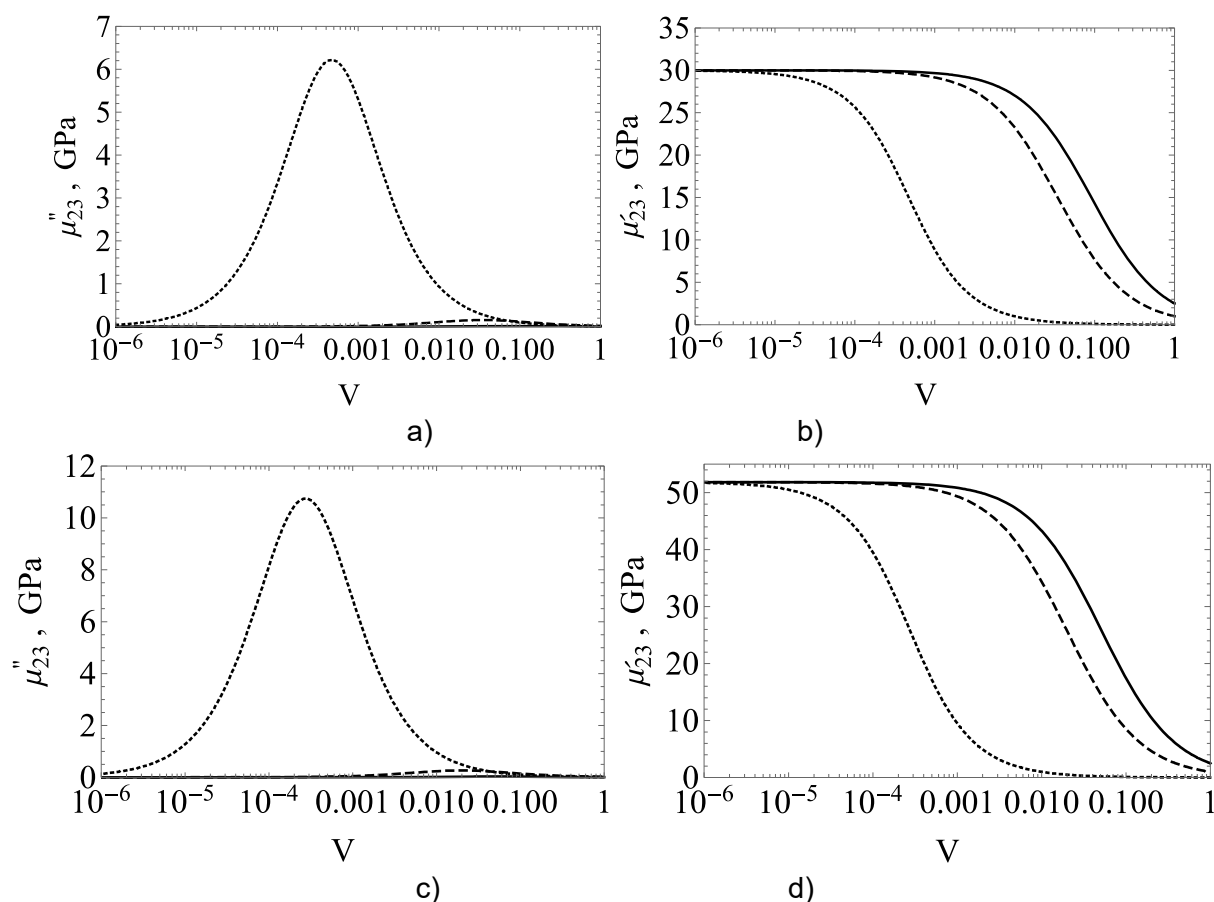


Figure 1. Effective shear complex modulus of lamella composite with different types of polymers: (a), (c) Loss modulus (dotted line – at T_g , dashed line – below T_g); (b), (d) – storage modulus (dotted line – at T_g , dashed line – below T_g , solid line – epoxy matrix)

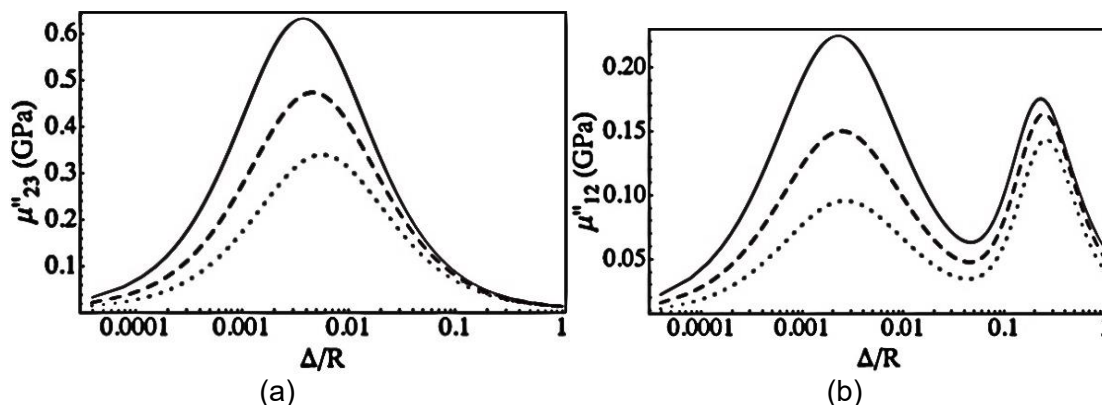


Figure 2. The dependence of effective shear complex moduli of unidirectional composite lamina on the coating thickness of viscoelastic polymer. The straight line represents 50% volume fraction, the dashed line represents 40%, and the dot-line represents 30% volume fraction. Symbol Δ represents thickness of coating layer ($\Delta = R_2 - R_1$) and R_1 is the radius of fiber, R_2 is the radius of fiber with coating: a) axial shear moduli, b) transverse shear moduli

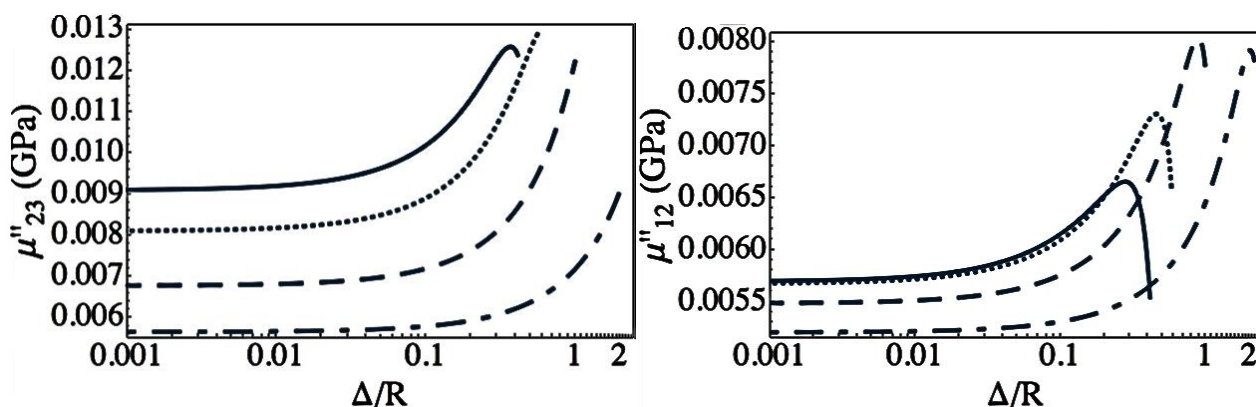


Figure 3. The dependence of effective dynamic properties of whiskered fiber composite lamina on the length of nanofibers for a) axial shear moduli; b) transverse shear moduli, $\Delta = R_2 - R_1$ is the length of nanowires and R is the radius of base fiber

Note: Continuous line: $V_f = 50\%$, dotted line: $V_f = 40\%$, dashed line: $V_f = 25\%$, dash-dotted line: $V_f = 10\%$.

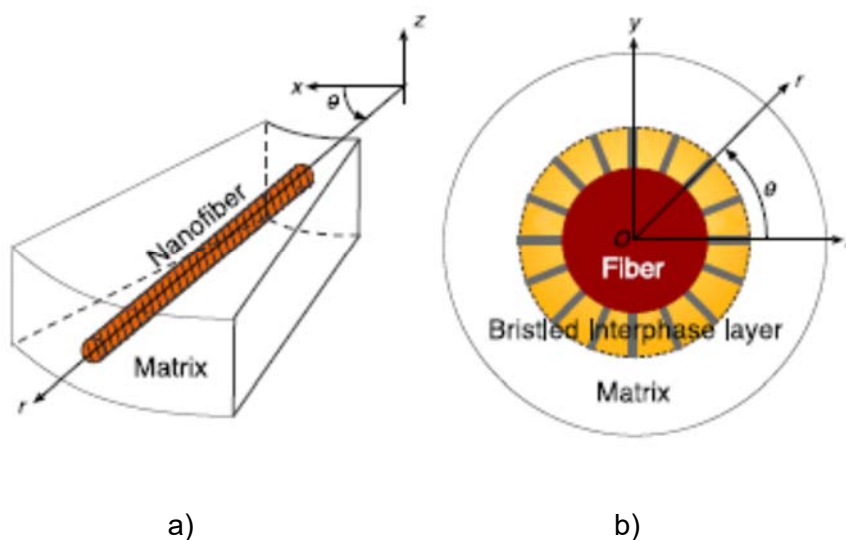


Figure 4. Unidirectional whiskered fiber composite (a) – a cell of a whiskered interfacial layer; (b) – a cell of a whiskered fiber composite

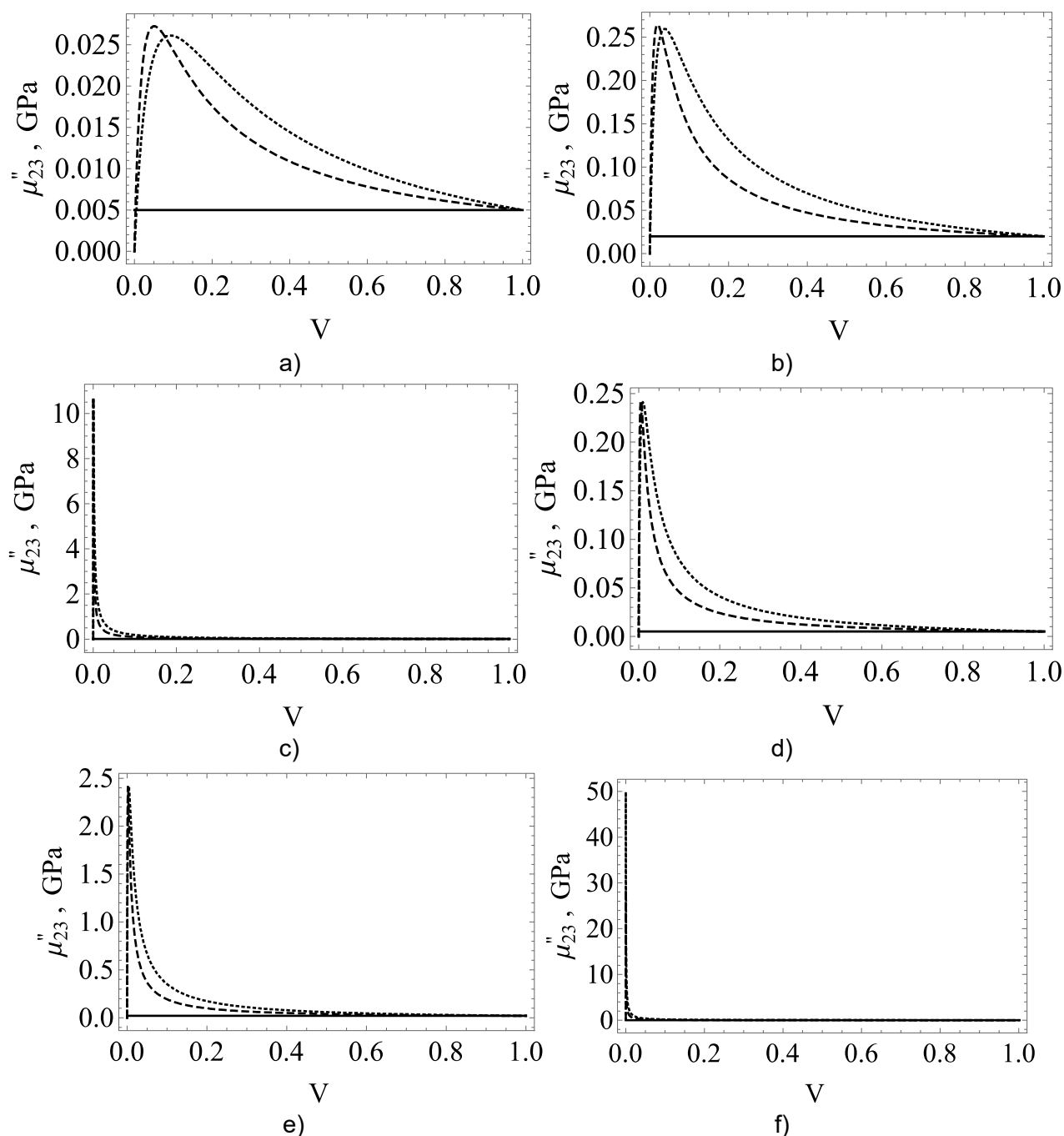


Figure 5. Dependences of the effective modulus of longitudinal shear loss, GSC method (dotted lines), Reiss method (dashed lines), (a) – whiskered layer with ZnO and epoxy matrix; pure epoxy matrix – solid lines; (b) – whiskered layer with ZnO and viscoelastic polymer below T_g , pure viscoelastic polymer below T_g – solid lines, (c) – whiskered layer with ZnO and viscoelastic polymer at T_g , solid line is the pure viscoelastic polymer at T_g , (d) – whiskered layer with CNT and epoxy matrix; pure epoxy matrix – solid lines; (e) – whiskered layer with CNTs and viscoelastic polymer below T_g , pure viscoelastic polymer below T_g – solid lines, (f) – whiskered layer with CNTs and viscoelastic polymer at T_g , solid line is the pure viscoelastic polymer at T_g

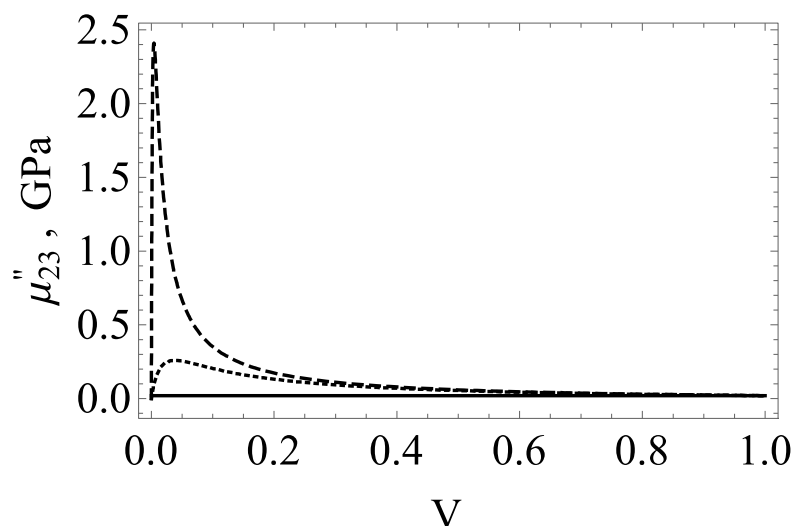


Figure 6. The dependence of effective dynamic axial shear moduli for whiskered interphase layer with viscoelastic polymer below T_g and with two different nanowires: CNT NW – dashed line, ZnO NW – dotted line, pure viscoelastic polymer below T_g – solid line

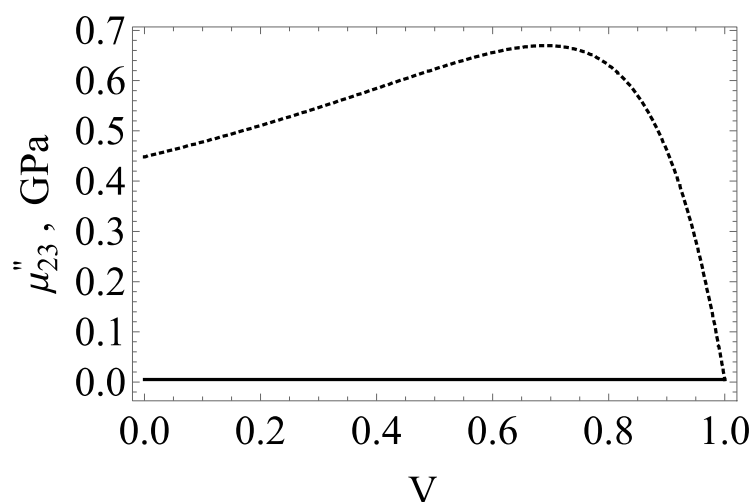


Figure 7. The dependence of effective dynamic axial shear moduli for double modified fibers composite with whiskered interphase viscoelastic polymer below T_g and with nanowires: ZnO NW – dotted line, pure epoxy matrix – solid line

CONTEÚDO DE CARBOIDRATOS ESTRUTURAIS E LIGNINA EM GRAMÍNEAS FORRAGEIRAS PERENES DEPENDENDO DA FASE DE CRESCIMENTO

ASSESSMENT OF CONTENTS OF STRUCTURAL CARBOHYDRATES AND LIGNIN OF PERENNIAL FODDER HERBAGES DEPENDING ON VEGETATIVE STAGE GROWTH

СОДЕРЖАНИЕ СТРУКТУРНЫХ УГЛЕВОДОВ И ЛИГНИНА В МНОГОЛЕТНИХ КОРМОВЫХ ТРАВАХ В ЗАВИСИМОСТИ ОТ ФАЗЫ РОСТА

KHUDYAKOVA, Hatima K.^{1*}; SHITIKOVA, Aleksandra V.²; ZARENKOVA, Nadezhda V.³; KUKHARENKOVA, Olga V.⁴; KONSTANTINOVICH, Anastasiia V.⁵;

¹ Federal Williams Research Center of Forage Production and Agroecology, Laboratory of Physical and Chemical Research Methods, 1 Nauchnyy Gorodok, zip code 141055, Lobnya – Russian Federation

^{2,3,4,5} Russian State Agrarian University – Moscow Timiryazev Agricultural Academy, Department of Crop Production and Meadow Ecosystems, 49 Timiryazevskaya Str., zip code 127550, Moscow – Russian Federation

* Correspondence author
e-mail: hatima40@mail.ru

Received 16 September 2020; received in revised form 12 October 2020; accepted 10 November 2020

RESUMO

O objetivo desses estudos é avaliar as gramíneas – *Bromus inermis*, *Festuca pratensis*, *Phleum pratense* e leguminosas – *Trifolium pratense* e *Medicago sativa* (alfafa) de acordo com o teor de fibra em detergente ácido (FDA), fibra em detergente neutro (FDN) e lignina em detergente ácido (LDA), hemicelulose (HC) e celulose (C), dependendo da fase da vegetação: gramíneas – no início da emergência do tubo, nas fases da emergência de cabeça e floração; leguminosas – nas fases da emergência de caule, início da emergência de botão e floração. Verificou-se que à medida que as gramíneas crescem, há um aumento em todas as frações das paredes celulares das leguminosas. As paredes celulares ocupam uma proporção menor de matéria seca do que nas gramíneas, devido ao seu menor conteúdo de HC – 10-12%, em comparação com 25-30% nas gramíneas. Os níveis de FDA, FDN e LDA (% em matéria seca) nelas são – na fase inicial – 25-28, 35-37, 6-7; no início da emergência de botão – 34-38, 41-46, 7-9; no início da floração – 38-41, 49-52, 10-12, respectivamente. Nas leguminosas, observa-se um maior conteúdo de LDA. Conforme a estação de crescimento de gramíneas, a proporção de FDA na FDN aumenta, mas nas gramíneas não excede 50%, enquanto nas leguminosas é de 70-80%, independentemente da fase de crescimento, o que explica a digestibilidade mais baixa das leguminosas em comparação com as gramíneas. Para poder avaliar os níveis de FDA e FDN em gramíneas quanto ao conteúdo de fibra bruta (FB), as equações de regressão correspondentes foram calculadas para gramíneas e forragens preparadas a partir delas. A relação entre FB e FDA foi mais próxima ($n = 64$, $s = 2,4\%$, $r = 0,93$) do que entre SC e FDN ($n = 64$, $s = 4,4\%$, $r = 0,87$). Com base na pesquisa conduzida e na generalização dos dados da literatura, as normas para o conteúdo de FDA e FDN no padrão para feno e silagem são recomendadas.

Palavras-chave: gramíneas e leguminosas, fases de crescimento, fibra bruta, fibra em detergente ácido, fibra em detergente neutro.

ABSTRACT

The purpose of this study is to evaluate cereal grasses – *Bromus inermis*, *Festuca pratensis*, *Phleum pratense*, and legumes: *Trifolium pratense*, *Medicago varia* in terms of their content of acid-detergent fibre (ADF), neutral detergent fibre (NDF), acid-detergent lignin (ADL) and hemicellulose (HC), cellulose depending on phases of vegetation – grasses: at vegetative, earing and flowering; legumes– vegetative. It was found that as the herbs grow, an increase in all fractions of the cell walls of leguminous herbs is observed, the cell walls occupy a smaller fraction of dry matter than in grasses, due to the lower HC content in them –10-12%, compared with 25-30% in grasses. The contents of ADF, NDF and ADL (% of dry matter) in grasses prior earing are 31-31, 50-55, 4-6: in earing – 32-37, 55-65, 5-6; in flowering – 40-45, 65-70 and 70-72, 7-9, respectively. Legumes have a higher content of ADL. As plants grow, the relative proportion of ADF in NDF increases, but it does not exceed 50% in grasses. In legumes – 70-80% regardless of the growth phase, explains the lower digestibility of legumes than grasses. To judge the levels of ADF and NDF in herbs, depending on the content of crude fibre (CF), the

corresponding regression equations were calculated for grasses and feed prepared from them. The relationship between CF and ADF was closer ($n = 64$, $s = 2.4\%$, $r = 0.93$) than between CF and ADL ($n = 64$, $s = 4.4\%$, $r = 0.87$). Based on these studies and generalisation of the literature data, ADF and NDF in hay and haylage standard are recommended.

Keywords: *perennial fodder, phase of growth, crude fibre, acid detergent fibre, neutral detergent fibre.*

АННОТАЦИЯ

Целью настоящих исследований является оценка злаковых трав – костреца безостого, овсяницы луговой, тимофеевки луговой и бобовых – клевера лугового и люцерны посевой по содержанию в них кислотно-детергентной клетчатки (КДК), нейтрально-детергентной клетчатки (НДК) и кислотно-детергентного лигнина (КДЛ), гемицеллюлоз (ГЦ) и целлюлозы (Ц) в зависимости от фазы вегетации: злаков – в начале выхода в трубку, в фазы колошения и цветения; бобовых – в фазы стеблевания, начала бутонизации и цветения. Установлено, что по мере роста трав наблюдается увеличение всех фракций клеточных стенок бобовых трав клеточные стенки занимают меньшую долю сухого вещества, чем в злаковых травах, за счет более низкого содержания в них ГЦ – 10-12%, по сравнению с 25-30% в злаковых. Уровни КДК, НДК и КДЛ (% в сухом веществе) в них составляют – в раннюю фазу – 25-28, 35-37, 6-7; в начале бутонизации – 34-38, 41-46, 7-9; в начале цветения – 38-41, 49-52, 10-12, соответственно. В бобовых отмечается более высокое содержание КДЛ. По мере вегетации злаковых трав, возрастает доля КДК в НДК, но у злаковых трав она не превышает 50%, в то время как у бобовых трав – 70-80% независимо от фазы роста, чем объясняют более низкую переваримость бобовых трав по сравнению со злаковыми. Чтобы иметь возможность судить об уровнях КДК и НДК в травах в зависимости содержания сырой клетчатки (СК) рассчитаны соответствующие уравнения регрессии для злаковых трав и кормов, приготовленных из них. Связь между СК и КДК была более тесной ($n=64$, $s=2.4\%$, $r=0.93$), чем между СК и НДК ($n=64$, $s=4.4\%$, $r=0.87$). На основании проведенных исследований и обобщения литературных данных рекомендованы нормы содержания КДК и НДК в стандарте на сено и сенаж.

Ключевые слова: *злаковые и бобовые, фазы роста, сырая клетчатка, кислотно-детергентная клетчатка, нейтрально-детергентная клетчатка.*

1. INTRODUCTION

Structural carbohydrates (SC) together with lignin make up the cell walls of plants. These include pectin, hemicellulose (HC) and cellulose (C) (Bailey, 1973). They are of interest due to their value as an energy source for ruminants, which can partially digest them with the help of the microflora of the gastrointestinal tract. It should also be noted the physiological role of structural substances, which consists in ensuring the normal functioning of the rumen and motor function of the gastrointestinal tract (White *et al.*, 2017). Structural carbohydrates together with lignin are combined under the general name “fibre” or “cellulose”. In this case, “cellulose” does not mean “cellular tissue”, but is a term adopted when evaluating feed by the content of structural (fibrous) substances (Kammoun *et al.*, 2020; Rocha-Meneses *et al.*, 2020).

Since the end of the last century, the evaluation of feed and rations for the content of detergent forms of fibre in them has become widespread throughout the world. In the Russian Federation, some forages and forage grasses were also studied by the level of ADF and NDF, for

example, in the conditions of the Moscow, Kaluga and Orenburg regions (Vorobyova, 2002; Kharitonov *et al.*, 2008; Levakhin *et al.*, 2015) and Tatarstan, studies have been conducted on digestion in bull calves and cows depending on the content of structural carbohydrates in the diet. The content of NDF in feed tables is also given (Kirilov, 2009). However, there is still insufficient information on acid-detergent fibre (ADF) levels and neutral detergent fibre (NDF) in different types of forage grasses depending on the growing phase and other conditions.

Currently, a routine evaluation of feed quality is carried out according to two schemes of zootechnical analysis. In both schemes, the feed is divided into crude nutrients (crude protein, crude fat) and crude ash (Kharitonov and Hotmirova, 2009). The differences in these schemes relate to estimates of the carbohydrate nutritional value of feed. Carbohydrates of feeds are usually divided into two main groups: non-structural carbohydrates (NSC), localised inside plant cells and carbohydrates of the cell walls, or structural carbohydrates (SC). From the role of these groups in the body of an animal, the carbohydrates of the first group — mono-, di-, and oligosaccharides, low

molecular weight fructosides and starch — are almost completely digestible, and they are also called easily hydrolysable or easily digestible carbohydrates (Bykova and Gibadullina, 2010; Levakhin *et al.*, 2007). According to the Weende scheme, which has been effectively used since the end of the 19th century, SC and lignin of feed are included in two groups – crude fibre (CF) and nitrogen-free extracts (NFE). However, their separation by species and digestibility of animals is not achieved. The second scheme, called the Van-Soest scheme, is devoid of these shortcomings, which explains its widespread use since the end of the 20th century (Bykova and Gibadullina, 2010; Pan *et al.*, 2017).

Structural carbohydrates and associated lignin are usually determined empirically during feed analyses. This is a widely used method for determining crude fibre and according to the Weende scheme, which was developed in the 19th century, but is still used in many countries, including the Russian Federation. Over the past decades, another group of empirical methods for analysing plant cell walls, based on the extraction of feed with detergent solutions, first proposed by Van-Soest, has also found widespread use. In both schemes, the feed is analysed for the content of raw nutrients: crude protein, crude fat, and crude ash, and structural carbohydrates along with lignin. They are called crude because they are determined by empirical methods under specified conditions and do not represent pure chemical compounds. Crude protein, determined by the method proposed by the founders of the analysis scheme and bearing the name of their surnames – Hanneberg and Shtoman, is an empirical residue obtained by sequential processing of feed with solutions of sulfuric acid and potassium hydroxide of a strictly defined concentration.

In the non-chernozem zone of Russia, in the crops of perennial grasses, such types of cereal grasses as *Bromus inermis*, *Festuca pratensis*, *Phleum pratense* are widely cultivated, and of legumes – *Trifolium pratense*, *Medicago varia*. These types of grasses and feed from them occupy a high proportion in the feed balance of ruminants (Chateigner-Boutin *et al.*, 2018). The research aims to evaluate the most widely cultivated cereal and legume forage grasses by the content of structural carbohydrates and lignin in them, depending on the vegetation phase (Bosworth and Hudson, 2011). The analysis of the content of structural carbohydrates in forage grasses and the linking of their amount to the phases of plant vegetation is necessary to determine the most rational terms of fodder

harvesting, since a balanced feed composition is one of the factors of sustainable development of livestock (Subaeva *et al.*, 2018).

The purpose of this work is to assess the amount of structural carbohydrates and lignin in perennial forage grasses depending on the growth phases.

2. MATERIALS AND METHODS

2.1. Samples

The research target was samples of forage grasses grown on soddy-podzolic soil of the Central experimental base of the V.R. Williams All-Russian Research Institute of Feed. *Bromus inermis* (Morshansky 760 cultivar), *Festuca pratensis* (VIK 5 cultivar), *Phleum pratense* (VIK 7 cultivar) were mown during the phases of leaf-tube formation, ear emergence (heading) and flowering; *Trifolium pratense* (VIK 7 cultivar) and *Medicago varia* (Lugovaya 67 cultivar) – during the shooting, flower-bud formation and flowering phases. Herbal growth phases were determined by visual estimation.

2.2. Determination of the content of structural carbohydrates

To determine the content of structural carbohydrates, empirical methods were used to ensure the separation of carbohydrates according to their digestibility in animal nutrition. Weende scheme assumes the use of empirical methods that imply the definition of not clearly defined chemical compounds, but groups of compounds: crude protein, crude fibre, crude ash, crude fat, neutral detergent fibre, acid detergent fibre. These groups are determined under strictly defined conditions. For example, crude fibre is determined by sequential processing of a sample with solutions of sulfuric acid and potassium hydroxide of specified concentrations. Crude fat is determined by an extract of organic solvents. Crude ash is empirically defined as the residue after combustion of a sample of feed in a muffle furnace. According to the Weende scheme, crude fibre is determined analytically, and nitrogen-free extract (NFE) is determined by a calculation method by the formula (Equation 1). According to Weende scheme, structural carbohydrates and lignin are included in two groups – (crude fibre) CF and nitrogen-free extracts.

In the framework of the analysis of feed by the Weende scheme, the level of structural substances is estimated by the content of crude fibre (CF). The sample is prepared in the following

way: samples of freshly cut plants are crushed on sample grinders, then dried at a temperature of 60°C in a drying cabinet with forced ventilation. The dry sample is ground in a mill until it passes through a 1 mm sieve, for this, the international standard "GOST 31675-2012. Stern. Methods for Determining Crude Fibre Content Using Intermediate Filtration". At the same time, the following equipment was used: laboratory scales of high accuracy class, a plant sample grinder, a laboratory mill, an electric drying cabinet with a temperature range in the working chamber from 0°C to 160°C, an electric muffle furnace, an electric vacuum pump, a water jet, an electric stove. However, CF does not represent the sum of indigestible substances, as well as the entire amount of structural carbohydrates, some of which, as well as part of lignin, are removed during its determination and enter, along with non-structural carbohydrates, in the group of NFE. Simultaneously, knowledge of the entire amount of structural carbohydrates and its components is necessary for more accurate feed intake and digestibility prediction.

In the 1960s Van-Soest proposed a method for analysing carbohydrates in cell walls of feed grass using detergents (Van-Soest, 1963a; 1963b). When processing a feed sample with a neutral detergent, the contents of the cell are removed. The resulting residue, called neutral detergent fibre (NDF), is the sum of cellulose (C), hemicellulose (HC) and acid-detergent lignin (ADL), and the acid detergent dissolves the HC, leaving C and ADL – acid-detergent fibre (ADF). NDF, representing the entire amount of SC and lignin, is one of the most important feed quality indicators. The feed intake (Mertens, 2010), its nutritional value (Weiss, 1998) and, ultimately, the productive effect, depend on its level and digestibility. Current models for determining the digestibility of organic matter. Consequently, the energy content in feeds is based on data on the NDF content and its digestion rate in animals. NDF is also necessary to calculate the content of carbohydrates soluble in a neutral detergent (Van-Soest *et al.*, 1991; Beth de Ondarza, 2000) normalised in the diet of cows. The content of ADF correlates with digestibility. On its basis a regression equation is proposed for determining the digestibility of nutrients (Rohweder *et al.*, 1978), which is used to evaluate the energy value of feed (Bogomolov and Malinin, 2008).

Samples of feed dried at a temperature of 60-65°C in an oven with forced ventilation were ground before passing through a sieve with 1 mm openings. Samples of fresh green grasses were

taken – *Bromus inermis*, *Festuca pratensis* and *Phleum pratense* on the Central experimental base of the V.R. Williams All-Russian Research Institute of Feed. For this, an area of 5 by 5 meters was allocated on the crops of each culture. After mowing the grass in this area, point samples were taken diagonally, which, after combining, amounted to a mass of 2 kg. The samples were transported to the laboratory within 30 min after taking, and were crushed on a plant grinder into sections of 1-3 cm. After thorough mixing, an average sample weighing 0.5 kg was isolated from the combined sample by dividing the sample by the diagonal, spread on a flat solid surface. The average sample was immediately dried in an oven with forced ventilation in trays with a perforated bottom with a layer of 2 cm at 60°C until constant weight. Then grinded on a mill until passing through a sieve with holes of 1 mm. Analyses for the content of NDF, ADF and ADL were carried out according to (Goering and Van-Soest, 1970). The results of analysis for the content of NDF, ADF and ADL are shown in Figure 1. ADF is the sum of cellulose and lignin, and NDF is the sum of ADF and hemicellulose. Both the ADF and NDF are higher in the flowering phase for all three analysed crops – *Bromus inermis*, *Festuca pratensis* and *Phleum pratense*. Using paper filters instead of glass filters (Vorobiev *et al.*, 1984), hemicelluloses (HC) – by the difference between NDF-ADF, cellulose (C) – ADF-ADL. ADF and NDF were determined in separate subsamples of the sample, ADL – treatment of ADF 72% sulfuric acid. In the samples, the content of NDF, ADF and ADF-lignin was determined. Since NDF is the sum of hemicellulose, cellulose, and lignin, and the ADL is the sum of only cellulose and lignin, hemicellulose was determined by calculation – by subtracting the ADL value from the ADF content. Similarly, the ADF is the sum of cellulose and lignin, so the cellulose content was found by subtracting lignin from the value of the ADL (Table 1). Statistical data processing was performed using the "Excel" program using "Statistica 6.0", (Stat Soft Inc.), USA.

3. RESULTS AND DISCUSSION:

As the herbs grow, the proportion of cell walls in all types of cereal grass increases (Figure 1), although they differ somewhat depending on the growth phase in the level of accumulation of structural substances. So, *Phleum pratense* already in the booting phase was characterised by a higher level of NDF, and in the *Bromus inermis* in the phases of heading and flowering, it remains lower than the other two grasses. In *Festuca*

pratensis and *Phleum pratense* NDF content to flowering reaches >70%. Types of grasses also differ in the dynamics of the accumulation of structural substances. During the period from shooting to flowering, the increase in NDF in the relatively early ripening *Festuca pratensis* occurred at a higher rate (0.8% per day) than in the *Bromus inermis* (0.45% per day) and the later ripe form – *Phleum pratense* (0.38% per day). In all phases of growth, *Phleum pratense* has a higher ADL content, but its accumulation rate was higher in *Festuca pratensis*.

In legumes, the accumulation of cell walls also increases with growth (Table 2). However, they occupy a smaller fraction of dry matter than in cereal grasses due to the lower hemicellulose (HC) content in them, which did not exceed 10-12%. The increase in the NDF level from the shooting phase to flowering occurs mainly due to cellulose, which is the main part of the ADF. Legumes are also characterised by a higher content of ADL. *Bromus inermis*, *Festuca pratensis*, and *Phleum pratense* in terms of lignification in the flowering phase to *Medicago varia*. By the time of flower-bud formation and flowering, there was a more intensive accumulation of cell walls in *Trifolium pratense* than in *Medicago varia*.

As the herbs grow simultaneously as the cell walls accumulate, their composition changes (Table 3). The increase in NDF is mainly due to cellulose and, to a lesser extent, lignin. In this regard, the share of ADF in the composition of the NDF increases, including C and ADL, while there is a significant decrease in the proportion of HC. So, the NDF of young grasses is composed of HC by half. In the future, the proportion of HC decreases, which is especially typical for *Festuca pratensis*.

In NDF of leguminous herbs in all phases of growth, cellulose prevails, and a higher proportion of ADL is noted than in NDF of cereals. In this regard, the proportion of ADF in the NDF in the budding and flowering phases of legumes exceeds 80%, while in cereal grasses, depending on the growth phase, it was in the range 44-64%. Lower digestibility of legume fibre may be associated with the composition of NDF compared to cereal. However, this is offset by a higher rate of legumes digestion, which contributes to an increase of their consumption (West, 1998).

The fact that structural carbohydrates accumulate as herbs grow has been reported in many studies. Such information is most fully contained in the tables on the composition of feeds

in the USA and Canada, later data refer to climatic conditions of the US states: North Dakota (Schroeder, 2008); Wisconsin (Mertens, 2002); Colorado (Stanton, 2010). There are results of studies conducted in several other countries, such as, for example, Finland (Rinne *et al.*, 2002), Serbia (Vasiljević *et al.*, 2009), Czech Republic (Homolka *et al.*, 2012), Romania (Leto *et al.*, 2013) and others.

The generalisation of this data is somewhat difficult because it was obtained under different soil, climatic and weather conditions. The phases of vegetation are often interpreted and fixed in different ways, mostly by visual estimation. For example, for different researchers, the shooting stage is referred to as the phase of “vegetative growth” or “early stage of growth”, or “before heading”, “before flower-bud formation”. At the same time, this phase in cereal grasses consists of 7 stages, depending on the length of the stem from the tillering node and can last 10-20 days (Zadoks *et al.*, 1974). As for the earing and flowering phases, each of them has the duration up to 7-10 days, so in some studies the beginning, middle and end of these phases are noted, and in other cases there is no such separation. At the same time, the composition of growing herbs changes daily. Nevertheless, it is possible to reveal a certain agreement between the data on the content of ADF and NDF, depending on the phase of growth of herbs with the given results.

Achieving optimal ADF and NDF in herbs cannot always be established by the growth phase, especially since the growth phases are somewhat stretched over time. Therefore, it is advisable to determine grass harvesting timing based on actual analysis data by daily sampling throughout the entire period of fodder harvesting, as suggested in (Instruction of the Ministry..., 2009). In the last decade, digital technologies, technologies for remote sensing of the state of crops, and the Internet (Khudyakova *et al.*, 2019), have been more active in collecting information on the content of nutrients in the grass. However, these methods require further improvement.

As already noted, in the analysis of feed according to the Weende scheme, the content of fibrous substances and the degree of digestibility of the feed are estimated by the level of crude fibre. To this day, a lot of data on the level of CF was accumulated. Therefore, it is of interest to study the relationship between CF and ADF and NDF to have some opportunity to assess the levels of detergent forms of fibre, based on the content of CF. Correlation analysis (the sample includes the results of the analysis of samples of five types

of cereal grasses in three growth phases each, as well as silage and haylage prepared from these herbs) showed a fairly close relationship between CF and ADF (Figure 2, Equation 1). Between CF and NDF, it was less close (Figure 3, Equation 2), which is related to the composition of these fibre types. CF and ADF consist of the same compounds – cellulose and lignin, although in quantitative terms differ from each other, while the NDF, in addition to them, includes hemicellulose (Equations 2-3).

As is known, the adequacy of the regression models depends on the size and composition of the sample; these models describe the relationship rather well for herbs of one family, although of different growth phases within the same soil and climatic zone, but worse for herbs of different families grown under different conditions. However, with a large sample size including samples of herbs obtained in a wide range of growing conditions, it becomes possible to develop more universal equations. For example, in (Pan *et al.*, 2017), it is possible to determine the concentration of ADF in herbs by the regression equations derived from a large sample: for cereal grass (Equation 4), for legumes (Equation 5).

4. CONCLUSIONS:

Based on the purpose of the article, the study evaluated the structural carbohydrates of cereals and legumes (alfalfa and meadow clover) depending on the growth phases. It was found that as the herbs grow, an increase in all fractions of the cell walls of legumes is observed, the cell walls form a smaller fraction of dry matter than in cereal herbs, due to the lower HC content of – 10-12%, compared with 25-30% in grasses. The ADF levels, NDF and ADL (% in dry matter) in them are – in the early phase – 25-28, 35-37.6-7; at the beginning of budding – 34-38, 41-46, 7-9; at the beginning of flowering – 38-41, 49-52, 10-12, respectively. In legumes, a higher content of ADL was noted. As the vegetation of cereal grasses, the proportion of ADF in the NDF increases, but in cereal grass it does not exceed 50%. In comparison, in leguminous grasses it is 70-80% regardless of the growth phase, explaining the lower digestibility of legumes compared to cereal grasses. To assess the levels of ADF and NDF in grasses, depending on the content of crude fibre (CF), the corresponding regression equations were calculated for cereal grasses and feed prepared from them. The relationship between CF and ADF turned out to be closer ($n=64$, $s=2.4\%$, $r=0.93$) than between CF and NDF ($n=64$, $s=4.4\%$,

$r=0.87$).

The results obtained will contribute to making optimal decisions regarding the timing of mowing herbs and their use in feeding livestock.

5. REFERENCES:

1. Bailey, R. W. (1973). Structural carbohydrates. In: *Chemistry and Biochemistry of Herbage* (pp. 157-211). New York, USA: Academic Press.
2. Beth de Ondarza, M. (2000). Non-fibre carbohydrates. Retrieved from <https://docs.cntd.ru/document/1200024343>.
3. Bogomolov, V. V., and Malinin, I. I. 2008. Why determine neutral and acid-detergent fibre. *Cattle Breeding*, 7, 26-29.
4. Bosworth, S., and Hudson, D. (2011). Sensory evaluation of hay for quality, UVM Extension. In: *The Vermont crops and soils home page, plant and soil science dept.* Burlington, USA: University of Vermont.
5. Bykova, M. Yu., and Gibadullina, F. S. (2010). The content of structural carbohydrates in the feed of Tatarstan and their optimization in the diets of young cattle. *Scientific Notes of the Kazan State Academy of Veterinary Medicine named after N.E. Bauman*, 202, 50-55.
6. Chateigner-Boutin, A.-L., Lapierre, C., Alvarado, C., Yoshinaga, A., Barron, C., Bouchet, B., Bakan, B., Saulnier, L., Devaux, M.-F., Girousse, Ch., and Guillon, F. (2018). Ferulate and lignin cross-links increase in cell walls of wheat grain outer layers during late development. *Plant Science*, 276, 199-207.
7. Goering, H. K., and Van-Soest, P. J. (1970). *Forage fiber analyses (Apparatus, reagents, procedure and some applications)*. Washington, USA: US Government Printing Office.
8. Homolka, P., Koukolova, V., Podsedniček, M., and Hlavačková, A. (2012). Nutritive value of red clover and lucerne forages for ruminants estimated by in vitro and in vivo digestibility methods. *Czech Journal of Animal Science*, 57, 454-468.
9. Instruction of the Ministry of Agriculture and Food of the Republic of Belarus "On Evaluation of the quality of feed during harvesting, storage and use". (2009). Retrieved from <https://mshp.gov.by/ru/>.
10. Kammoun, M., Ayeb, H., Bettaie, T., and

- Richel, A. (2020). Chemical characterisation and technical assessment of agri-food residues, marine matrices, and wild grasses in the South Mediterranean area: A considerable inflow for biorefineries. *Waste Management*, 118, 247-257.
11. Kharitonov, E. L. and Hotmirova, O. V. (2009). Digestion processes in cows at different levels of fibre in the diet. In: *Actual problems of the procurement, storage and rational use of feed* (pp. 181-189). Moscow, Russian Federation: FGU RCSK.
 12. Kharitonov, E. L., Agafonov, V. I., and Kharitonov, L. V. (2008). *Methodological recommendations for improving and using the feed base in dairy cattle breeding in the Kaluga region (practical recommendations)*. Kaluga, Russian Federation: All-Russian Research Institute of Physiology, Biochemistry and Nutrition of Farm Animals.
 13. Khudyakova, E. V., Gorbachev, M. S., and Nifontova, E. A. (2019). Improving the efficiency of agro-industrial complex management based on digitalisation and system approach. In: *Materials of the AGEGL: "Agrarian Economy in the Era of Globalisation and Integration"*. London, UK: IOP Publishing.
 14. Kirilov, M. P. (Ed.). (2009). *Feed resources of livestock. Classification, composition and nutritional value of feed*. Moscow, Russian Federation: Federal State Institution "Rosinformagroteh".
 15. Leto, J., Perčulija, G., Bošnjak, K., Kutnjak, H., Vranić, M., and Čačić, I. (2013). Effects of genotype, inoculation and maturity stage at harvest on red clover (*Trifolium pratense* L.) yield and chemical composition, *Mljekarstvo*, 63, 98-108.
 16. Levakhin, G., Duskaev, G., and Dusaeva, H. (2015). Assessment of chemical composition of grain crops depending on vegetative stage for feeding. *Asian Journal of Crop Science*, 7, 207-213.
 17. Levakhin, G. I., Airich, V. A., Duskeyev, G. K., and Breus, D. A. (2007). The degree of digestion of substances in the rumen of gobies, taking into account structural carbohydrates in the diet. *Bulletin of the Russian Academy of Agricultural Sciences*, 4, 79-81.
 18. Mertens, D. R. (2002). Measuring fiber and its effectiveness in ruminant diets. Retrieved from: <https://www.researchgate.net/publication/252771141>.
 19. Mertens, D. R. (2010). NDF and DMI – has anything changed? In: *Proceedings of the Cornell Nutrition Conference for Feed Manufacturers*, 72nd Meeting (pp. 160-174). Ithaca, USA: Cornell University.
 20. Pan, X. -H., Yang, L., Yves, B., Xiong, B. -H., and Jiang, L.-S. (2017). Accuracy comparison of dry matter intake prediction models evaluated by a feeding trial of lactating dairy cows fed two total mixed rations with different forage source. *Journal of Integrative Agriculture*, 16(4), 921-929.
 21. Rinne, M., Huhtanen, P., and Jaakkola, S. (2002). Digestive processes of dairy cows fed silages harvested at four stages of grass maturity. *Journal of Animal Science*, 80, 1986–1998.
 22. Rocha-Meneses, L., Ferreira, J.A., Mushtaq, M., Karimi, S., Orupöld, K., and Kikas, T. (2020). Genetic modification of cereal plants: A strategy to enhance bioethanol yields from agricultural waste. *Industrial Crops and Products*, 150, article number 112408.
 23. Rohweder, D. A., Barnes, R. F., and Jorgensen, N. A. (1978). Proposed hay grading standards based on laboratory analyses for evaluating quality. *Journal of Animal Science*, 47, 747-759.
 24. Schroeder, J. W. (2008). Forage nutrition for ruminants. NDSU extension dairy specialist. Retrieved from <https://fliphtml5.com/vopz/zhvi/basic>.
 25. Stanton, T. L. (2010). *Feed composition for cattle and sheep*. Fort Collins, USA: Colorado State University Extension.
 26. Subaeva, A. K., Nurullin, A. A., Vodyannikov, V. T., Khudyakova, E. V., and Sorokin, V. S. (2018). Sustainable development of dairy cattle breeding in different regions of the Russian Federation. *The Journal of Social Sciences Research*, 5, 290-295.
 27. Van-Soest, P. J., Robertson, J. B., and Lewis, B. A. (1991). Methods for dietary fiber, neutral detergent fiber, and nonstarch polysaccharides in relation to animal nutrition. *Journal of Dairy Science*, 74, 3583-3597.
 28. Van-Soest, P. J. (1963a). Use of detergents in the analysis of fibrous feeds. I. Preparation of fiber residues of low nitrogen content. *Journal of the AOAC*, 46, 825-829.
 29. Van-Soest, P. J. (1963b). Use of detergents in

the analysis of fibrous feeds. II. A rapid method for the determination of fiber and lignin. *Journal of the AOAC*, 46, 829-835.

30. Vasiljević, S., Milić, D., and Mikić, A. (2009). Emical attributes and quality improvement of forage legumes. *Biotechnology in Animal Husbandry*, 25, 493-504.
31. Vorobiev, E. S., Khudyakova, H. K., and Garist, A. V. (Eds.). (1984). *Guidelines for determining the carbohydrate nutrition of plant foods for ruminants*. Moscow, Russian Federation: VASKHNIL.
32. Vorobyova, S. V. (2002). *Guidelines for the use of neutral and acid-detergent fiber in the feeding of farm animals and methods for their determination in zootechnical analysis*. Dubrovitsy, Russian Federation: All-Russian Research Institute of Animal Husbandry named after L.K. Ernst.
33. Weiss, W. P. (1998). Estimating the available energy content of feeds for dairy cattle. *Journal of Dairy Science*, 81, 830-839.
34. West, J. (1998). *Factors which influence forage quality and effectiveness in dairy rations*. Tifton, Georgia: University of Georgia.
35. White, R. R., Beth Hall, M., Firkins, J. L., and Kononoff, P. J. (2017). Physically adjusted neutral detergent fiber system for lactating dairy cow rations. II: Development of feeding recommendations. *Journal of Dairy Science*, 100(12), 9569-9584.
36. Zadoks, C., Chang, T. T., and Konzak, C. F. (1974). A decimal code for the growth stages of cereals. *Weed Research*, 14, 415-421.

$$\text{NFE (by Veende), \%} = 100 - (\text{crude protein} + \text{crude fibre} + \text{crude fat} + \text{crude ash}) \quad (\text{Eq. 1})$$

$$\text{ADF} = 1.0764\text{CF} + 6.3265 \quad (n = 64, R^2 = 86.5, s = 2.43) \quad (\text{Eq. 2})$$

$$\text{NDF} = 1.5986\text{CF} + 7.9237 \quad (n = 64, R^2 = 75.7, s = 4.36) \quad (\text{Eq. 3})$$

$$\text{ADF} = 6.89 + 0.5\text{NDF}, \quad (n = 722, R^2 = 0.62, s = 3.1) \quad (\text{Eq. 4})$$

$$\text{ADF} = -0.73 + 0.82\text{NDF} \quad (n = 2899, R^2 = 0.84) \quad (\text{Eq. 5})$$

Table 1. Results of the analysis for the content of NDF, ADF and ADL, % in dry matter

Herbs	Growth phases	NDF	ADF	ADF-lignin
<i>Bromus inermis</i>	shooting	45.24	26.97	5.47
	earing	52.50	32.09	6.32
	flowering	65.24	40.14	7.53
<i>Festuca pratensis</i>	shooting	42.70	26.50	4.26
	earing	62.54	36.01	6.32
	flowering	72.00	45.76	7.86
<i>Phleum pratense</i>	shooting	48.84	30.08	6.94
	earing	59.02	36.40	7.80
	flowering	72.20	42.70	10.62

Table 2. Contents of structural carbohydrates and lignin in fresh herbage of *Medicago varia* and *Trifolium pratense*, % in dry matter

Structural substances	<i>Medicago varia</i>			<i>Trifolium pratense</i>		
	shooting	budding	flowering	shooting	budding	flowering
ADF	28.9	34.3	41.0	25.4	38.2	45.1
NDF	37.0	40.6	48.8	35.7	46.7	52.3
CF	21.7	26.4	32.9	15.8	26.1	32.1
HC	8.1	6.3	7.8	10.3	8.6	7.2
C	22.8	27.4	31.1	19.3	29.4	32.6
L	6.1	6.9	10.0	6.1	8.8	12.5

Table 3. The composition of cell walls, % in NDF

Crop cultures	The proportion of cell wall components in % of NDF			
	ADF	HC	C	ADL
<i>Bromus inermis</i>				
– shooting	52.6	47.4	41.6	11.1
– earing	55.8	39.2	44.8	11.0
– flowering	61.4	38.6	49.8	11.5
<i>Festuca pratensis</i>				
– shooting	43.6	56.4	34.5	9.1
– earing	57.6	42.4	47.5	10.1
– flowering	63.6	36.4	52.6	10.9
<i>Phleum pratense</i>				
– shooting	51.1	48.9	39.3	11.8
– earing	52.7	47.3	41.4	11.3
– flowering	59.1	40.8	44.4	14.7
<i>Trifolium pratense</i>				
– shooting	71.1	28.9	54.2	17.0
– budding	83.0	18.3	62.8	18.9
– flowering	86.2	13.4	62.4	23.8
<i>Medicago varia</i>				
– shooting	78.1	22.1	61.7	16.4
– budding	84.5	15.5	67.6	16.9
– flowering	84.1	15.9	63.6	20.4

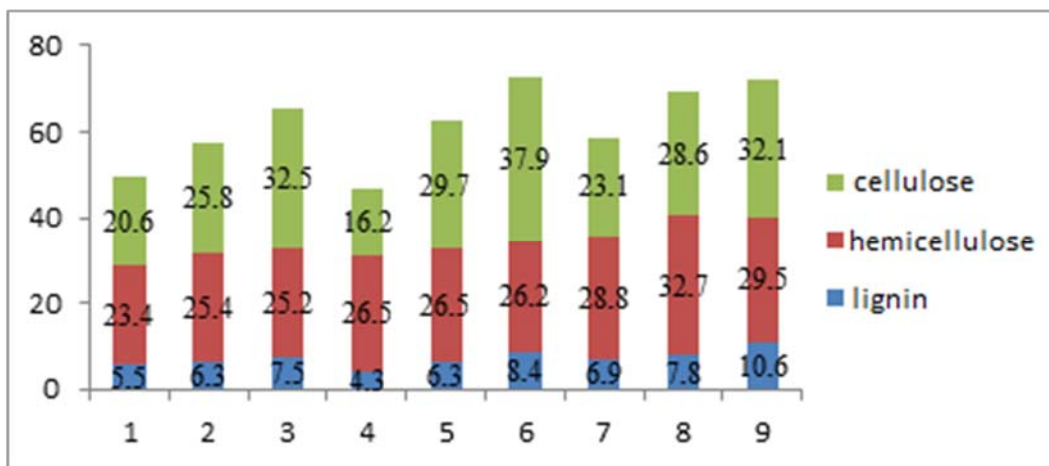


Figure 1. Contents of structural carbohydrates and lignin in grasses at different vegetation phases, % dry matter: 1, 2, 3 – *Bromus inermis* at vegetative, earing and flowering, respectively; 4, 5, 6 – the same for *festuca pratense*; 7, 8, 9 – the same for *Phleum pratense*

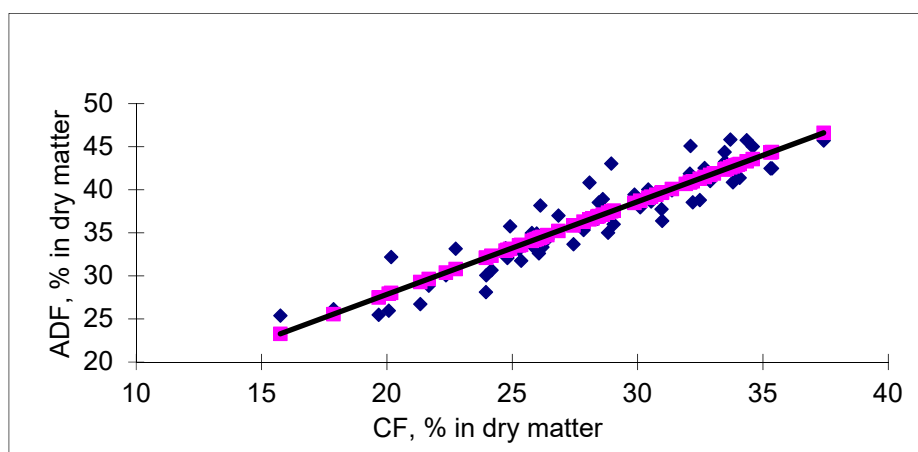


Figure 2. The relationship CF to ADF

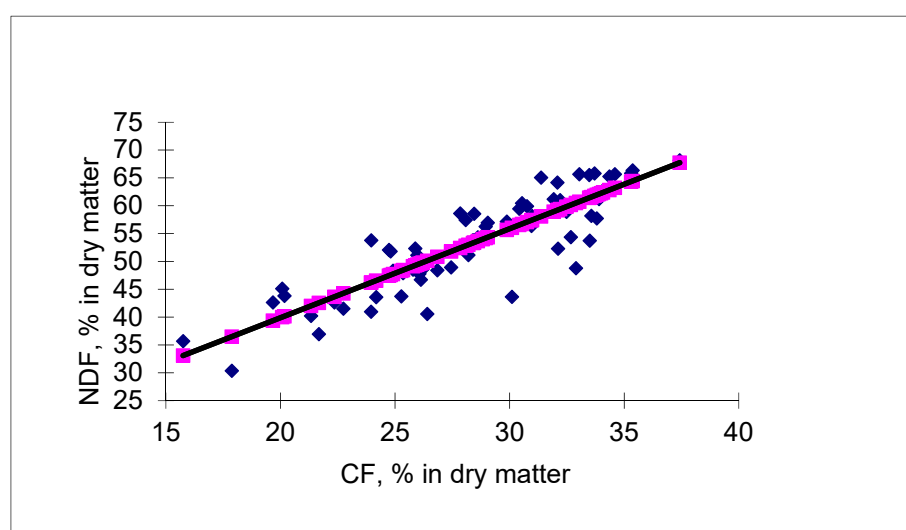


Figure 3. The relationship CF to NDF

PRODUTIVIDADE POTENCIAL DAS CULTURAS DE INVERNO NA REGIÃO DO VOLGA CENTRAL

POTENTIAL PRODUCTIVITY OF WINTER CROPS IN THE MIDDLE VOLGA REGION

ПОТЕНЦИАЛЬНАЯ ПРОДУКТИВНОСТЬ ОЗИМЫХ КУЛЬТУР В СРЕДНЕВОЛЖСКОМ РЕГИОНЕ

GORYANINA, Tatiana A.^{1*};

¹ Samara Federal Research Scientific Center of the Russian Academy of Sciences, Samara Scientific Research Agriculture Institute named after N. M. Tulaykov, Laboratory of Gray Bread Selection, 41 Karl Marx Str., zip code 446254, Bezenchuk – Russian Federation.

* Corresponding author
e-mail: tatyanaag@yandex.ru

Received 29 September 2020; received in revised form 28 October 2020; accepted 10 November 2020

RESUMO

A pesquisa dedicada ao estudo do rendimento das culturas de inverno foi realizada em 2002-2019 nos campos de reprodução do Instituto de Pesquisa Agrícola de Samara, localizado na zona de estepe da região do Transvolga Médio. O experimento envolveu 5 variedades de centeio de inverno, 6 variedades de tritcale de inverno e 2 variedades de trigo de inverno. Foi calculada a produtividade potencial (R_t), o rendimento potencial realmente possível (R_{prp}), o rendimento máximo realmente possível (R_{mrp}), o potencial bioclimático (PBC), análise de correlação. O objetivo do trabalho é: identificar o potencial das culturas de inverno, comprovar cientificamente os dados obtidos. O rendimento máximo do tritcale foi obtido em 2017 – 7,48 t/ha, centeio – 5,88 t/ha, em 2016 – 4,65 t/ha de trigo. Calculado, levando em consideração que $\sum T > 10$ °C para o período de cultivo da cultura, o rendimento potencial para o tritcale em 2017 é de 3,02 t/ha, para o centeio de inverno em 2005 – 6,83 t/ha, para o trigo de inverno em 2005 – 2,79 t/ha. O indicador (PBC) variou significativamente ao longo dos anos: de 0,62 a 1,16 pontos para o centeio de inverno, de 0,30 a 0,60 para o tritcale de inverno e trigo. A análise de correlação mostrou que a produtividade está interligada com a duração do período de cultivo, com um complexo de condições climáticas para o período primavera-verão. O ciclo de vida do tritcale depende da precipitação em maio e do complexo de condições em junho, do centeio de inverno – depende das temperaturas durante o período de semeadura-germinação, da soma das temperaturas ativas durante o período de cultivo.

Palavras-chave: *centeio, tritcale, trigo, rendimento real e potencial.*

ABSTRACT

The study of winter crop cultivars was carried out in the breeding fields of the Samara Agricultural Research Institute, located in the steppe zone of the Middle Volga region, in the nursery of competitive testing in 2002-2019. For calculations, 5 varieties of winter rye, 6 varieties of winter tritcale, and 2 varieties of winter wheat were taken. For scientific justification, the authors calculated the potential productivity (Y_p), the actual possible potential yield (Y_{pp} a), the maximum possible potential yield (Y_{pp} m), the bioclimatic potential (BCP), and correlation analysis. The study aims to calculate the possible yield of winter crops to substantiate the data obtained scientifically. In the dry conditions of Bezenchuk, the maximum yield of tritcale was obtained in 2017 – 7.48 t/ha, rye – 5.88 t/ha, and in 2016 for wheat – 4.65 t/ha. Potential productivity, taking into account $\sum T > 10$ °C for the vegetation period of the crop, for tritcale in 2017, 3.02 t/ha, for winter rye in 2005, 6.83 t/ha, for winter wheat in 2005-2.79 t/ha. The variation of the indicator (BCP) over the years reached significantly higher values from 0.62 to 1.16 points for winter rye, from 0.30 to 0.60 for winter tritcale and winter wheat. The trend of the interrelations between yield is observed with the length of the vegetation period, with a set of climatic conditions for the spring-summer period. The tritcale vegetation duration depends on the precipitation in May and on the set of conditions in June. The winter rye vegetation duration depends on the temperatures during the sowing-germination period and on the sum of active temperatures during vegetation.

Keywords: *rye, tritcale, wheat, actual, potential yield.*

АННОТАЦИЯ

Исследования по изучению урожайности сортов озимых культур проводилось в 2002-2019 годах на селекционных полях Самарского НИИСХ, расположенных в степной зоне Среднего Заволжья. В эксперименте участвовали 5 сортов озимой ржи, 6 сортов озимого тритикале и 2 сорта озимой пшеницы. Производили подсчёт потенциальной продуктивности (Ут), действительно возможного потенциального урожая (Удву п), действительно возможного максимального урожая (Удву м), биоклиматического потенциала (БКП), корреляционного анализа. Цель работы: выявить потенциальные возможности озимых культур, научно обосновать полученные данные. Максимальный урожай тритикале был получен в 2017 году – 7.48 т/га, ржи-5.88 т/га, в 2016 году пшеницы 4.65 т/га. Рассчитанный, с учётом $\sum T > 10^{\circ}\text{C}$ за вегетацию культуры, потенциальный урожай для тритикале в 2017 году 3.02 т/га, для озимой ржи в 2005 году 6.83 т/га, для озимой пшеницы в 2005 году – 2.79 т/га. Существенно варьировал показатель (БКП) по годам: от 0.62 до 1.16 баллов для озимой ржи, от 0.30 до 0.60 для озимых тритикале и пшеницы. Корреляционный анализ показал, что урожайность взаимосвязана с продолжительностью вегетационного периода, с комплексом климатических условий за весенне-летний период. Жизненный цикл тритикале зависит от осадков мая месяца и от комплекса условий в июне, озимой ржи зависит от температур в период посева-всходов, от суммы активных температур за вегетацию.

Ключевые слова: *рожь, тритикале, пшеница, фактическая, потенциальная урожайность.*

1. INTRODUCTION:

At present, all over the territory of the Russian Federation and all over the world, unfavorable conditions for winter crops are developing (Kirchev *et al.*, 2016). There is a sharp increase in the continentality of the climate (Grabovets and Fomenko, 2015; Tuktarova, 2019; Goryanina and Medvedev, 2019). With traditional cultivation technology, more nutrients, and water required to bring crop yields to their climatic potential (Licker *et al.*, 2010; Ray *et al.*, 2012). The potential productivity is interconnected with the bioclimatic potential based on the regularity of changes in plant productivity, depending on climatic factors – heat and moisture. Traditional winter crops have a wide range of ecological plasticity in relation to a complex of environmental factors (Lonbani and Arzani, 2011; Fayaz and Arzani, 2011; Khalifeie and Mohammadi Nejad, 2012).

A theoretically estimated maximum yield is nothing more than potential productivity. The potential productivity must be measured by the number of fertile tillers, and the actual yield – by the number of grains per ear of a plant (Nasrallah *et al.*, 2020). Potential and actual yield depends on the number of productive stems, their grain size, and the mass of 1000 grains. The actual possible yield, in theory, is provided by the genetic potential of the varieties and limiting factors. In real conditions, an actual possible yield can only be obtained in fields with a sufficiently high fertility level (Williams *et al.*, 2020). On less fertile soils, yields will be, accordingly, lower than actually possible. One of the main factors limiting the

growth of crop productivity is the moisture supply of plants. Consequently, the yield value must be predicted by moisture in the meter layer of soil and the amount of precipitation during the vegetation period, taking into account the water consumption coefficient (Kukal and Irmak, 2020).

The insufficient number of new domestic crop varieties, in market conditions, is why a slow changing of seed variety and, accordingly, a limited choice. The created and cultivated varieties react rather weakly to improving the farming standards and the use of intensive cultivation technologies. It is not possible to fulfill its potential. This situation is due to the weak genetic protection against climatic stress factors. The development of new competitive cultivars, their comprehensive evaluation for targeted use is relevant, economically, and environmentally beneficial (Mahmood *et al.*, 2020; Vasco Silva *et al.*, 2020).

Domestic and foreign selectionists have created many highly productive cultivars, but their potential is revealed only with favorable thermal and moisture conditions (Wang *et al.*, 2020; Yang *et al.*, 2020). The situation is deteriorating sharply due to climate change. In the conditions of the Samara region, with the return of favorable years 3 times less frequently than dry years, it is challenging to fulfill the productivity potential. As a result, the elements of productivity vary greatly from year to year. Thus, the problem of counteracting unfavorable environmental factors and adaptability is highly relevant.

When planning and making management decisions, the main thing is the input parameters of the predicted values. Therefore, it is imperative

to provide a high-quality information base for decision-making by building sound forecasts of the main input parameters (Lichko and Shumskaya, 2007). It is possible to guarantee the objectivity of the reflection and the reality of the planned targets and the adoption of real management decisions, only under a reasonable forecast of the yield of crops. At present, it can be affirmed with mathematical precision that an integrated system for forecasting the development of agricultural production in the country does not exist. Research conducted by K.P. Lichko and E.V. Shumskaya (2007) indicates that the Russian Federation has not yet established strict terms for the development of forecasts at various government levels, there are no unified forecasting methods. As a biological property, productivity contains information about the optimal and actual values of many factors for the growing cycle phases (Khvorova and Gavrilovskaya, 2008).

For the arid conditions of the Middle Volga region, the topic of scientific programming of productivity is of particular relevance. In the Samara region, A.A. Vyushkov, S.N. Shevchenko (2008) studied the bioclimatic potential of spring crops. In their papers, the authors revealed the issues of the actual and potential formation of crop yields in the central zone of the Samara region. Potential and actual yield depend on the number of productive stems, their grain size, and the mass of 1000 grains (Kuperman *et al.*, 1980).

Purpose of the study, to calculate the possible yield of winter crops and scientifically substantiate the obtained data.

2. MATERIALS AND METHODS:

The Middle Volga region belongs to the zone of "risky farming". The sum of temperatures was more than 10 °C – 2563.5 ... 3061.7 °C, annual precipitation – 290.3 ... 596.7 mm (Goryanina, 2020). Severely arid conditions of spring-summer vegetation were observed in 2004, 2005, and 2006. (hydrothermic coefficient (HTC) = 0.23-0.34), spring vegetation April-May 2002, 2008, 2010, 2012 (HTC = 0.41-0.57) vegetation in the May in 2004, 2005, 2007, 2008, 2009, 2010, 2012, 2013, 2014, 2016, 2018 and 2019. (HTC = 0.12-0.58). Thus, the arid growing conditions for May were observed in 12 out of 18 studied years. Thus, for the triticale culture, unfavourable growing conditions developed in 2002, 2006, 2007, 2011, 2012, 2013, 2015, 2019, the average (normal growing conditions) – 2003, 2004, 2005, 2008, 2010 and 2018, favourable – in 2009, 2014, 2016 and 2017. For winter rye, since the culture

ripens earlier than triticale and, accordingly, a shift in the development phases was observed, unfavorable growing conditions developed in 2005, 2006, 2007, and 2019, the average (normal growing conditions) – 2002, 2003, 2004, 2008, 2010, 2012, 2013 and 2018, favorable – 2009, 2014, 2015, 2016 and 2017. In the medium term, there was no positive climate change. The calculation of the potential productivity of cultivars was carried out for 18 years (2002-2019).

Bioclimatic potential (BCP) indicates the productivity of plants under the conditions of the experiment. Productivity is the total biomass synthesized during the vegetation period [unit of mass/ (unit of area · unit of time)]. Coefficients of biological productivity by cultivars were calculated based on indicators of maximum and a minimum yield of crops (Equation 1). For winter rye $C_{bp} = 0.35-0.47$, wheat $C_{bp} = 0.24-0.28$, triticale $C_{bp} = 0.14-0.42$. Bioclimatic potential (BCP) was calculated taking into account the coefficients according to the formula of P.I. Koloskov (1963) (Equation 2), where: T – the average daily air temperature (the summation of its values for a calendar year was made for those days when it exceeds 10 °C); C_{bp} – coefficient of biological productivity of the cultivar, depending on moisture availability. Basic conditions for calculation: $\sum T > 10$ °C, the sum of the effective temperatures at the northern border of field agriculture was 1000 °C.

Potential productivity (Y_p) was a yield climatically provided by heat, dt/ha, calculated according to Equation 3, of M. K. Kayumov (1989), where: β – the maximum yield of cultivars, reflects the level of farming standards and the use of active photosynthetic radiation by crops. The main limiting factor that prevents obtaining high yields in the Samara region was the provision of crops with moisture. The actual possible potential yield (Y_{pp}) in terms of moisture supply was calculated taking into account the actual moisture reserves by the years of research and the optimal moisture requirement according to the formula of M.K. Kayumov (1989) (Equation 4), where: W – actual available moisture in the soil, m³/ha; R_w – water-use ratio, m³; C_{eff} – coefficient of plant ear efficiency.

Water-use ratio (R_w), i.e., moisture consumption for the formation of a unit of commodity weight of the crop at standard humidity. It was determined by the actual harvests for several years and was an integrated indicator that included effective soil fertility and the level of agricultural technology. High R_w values indicated a low agrotechnical level. With the growth of

agricultural technology, the introduction of farming intensification, the values of the indicator decreased and stabilized at a certain value (Equation 5), where: Y_a – actual yield of the main product at standard humidity, dt/ha; E – total water-use of crops during the vegetation period, mm. The maximum possible potential yield (Y_{pp} m) in terms of moisture supply was calculated using the same formula as the actual possible potential yield (Y_{pp} a), but according to the long-term annual average moisture reserves (W) in the soil 453.8 mm (Goryanin *et al.*, 2019) and the optimal moisture requirement according to M. K. Kayumov (1989). The optimal moisture requirement for winter crops (R_w) was 326 mm (Bykov, 1968). Correlation analysis of yield and elements of bioclimatic potential was calculated using Excel 2019 program.

To determine the yield of crops by the combination of the interaction of heat, light, and moisture, a model for determining the biohydrothermal potential (Equation 6) was used, where: K_p – biohydrothermal productivity potential, point; W – reserves of productive moisture before sowing, mm; T_v – growing season in decades; R – total PAR for the growing season, kJ/cm². This coefficient was calculated for each cultivar for each year of study. Further, in the aggregate of 18 years, favorable and unfavorable years were selected, and the average values were calculated. These indicators were taken as the basis for calculating the biological productivity of cultivars.

The research was carried out in the Samara Research Institute of Agriculture fields located in the chernozem steppe of the Samara Trans-Volga region. In the experiments, 5 varieties of winter rye, 2 varieties of winter soft wheat, 6 varieties of winter triticale were studied (Table 1). Rye (*Secale cereale* L.) has a fibrous root system that penetrates the soil to a depth of 1.5 m, more powerful than that of wheat. The stem is a hollow straw up to 1-1.5 m high, with 5-7 internodes. Leaves are linear, wider than wheat. The uvula is short, rounded at the top. Ears are short without cilia. Inflorescence – an ear, includes a rod on one two-flowered (rarely three-flowered) spikelet on the ledges. The awns are serrated. The grain is bare, elongated, narrowed towards the grain kernel, with a deep groove and tuft. The grain is greenish, yellow, light brown, gray. The mass of 1000 grains is from 28 to 40 g.

The peculiarity of winter rye is strong tillering in the fall, with the formation of up to 4-5 stems and rapid spring regrowth. Cross-pollinated (wind-pollinated) plant. Ripens 8-10 days earlier

than winter wheat. Winter rye is a relatively drought-resistant plant due to its powerful root system. The transpiration coefficient was from 265 to 420. The maximum moisture consumption occurs during the period of intensive growth – autumn earing and from tube to earing. Lack of moisture during this period leads to the formation of small and unproductive ears.

Winter wheat bushes in autumn and spring. Enhanced tillering is noted at sufficient humidity and a temperature of 8-10 °C. At temperatures less than 3-4 °C and moisture deficit, tillering stops. The toughness increases with the introduction of nitrogen fertilizers and when sowing with large seeds. Before leaving for winter, winter wheat forms 4-8 shoots, and the length of germinal roots on chernozem soils reaches 100-120 cm. The increased temperature and moisture deficit in the soil in the spring have a negative effect on tillering. Late formed stems are late with earing and form a fit, which causes uneven maturation.

The root system is capable of penetrating to a depth of 1.5 m. It makes good use of the moisture of the root layer. In the south of the country, soil moisture during the germination and autumn tillering period is the main factor for the normal growth and development of plants. When the moisture content in the 10 cm soil layer is higher than 10 mm, seedlings, appear evenly. Tillering occurs more vigorously if there is at least 30 mm of available moisture in the 20 cm soil layer. Autumn precipitation increases grain yields compared to straw yields. Spring precipitation leads to increased vegetative mass growth and creates favorable conditions for the emergence of new shoots. During spring awakening to earing, winter wheat spends about 70% of the total water requirement for the growing season, during the period from flowering to the gold ripeness of grain – 20%. The highest productivity was observed at a soil moisture content of 70-75% of the lowest (field) moisture capacity in the zone of the location of the main mass of roots, that is, up to 60 cm. The transpiration coefficient was 250-500.

Winter wheat is more drought-resistant than spring crops due to earlier grain formation and better use of autumn-spring precipitation. However, with dry spring, moisture deficit is possible, which occurs at the stage from entering the tube to hatching, during intensive growth. From the beginning of spring growth to hatching, wheat plants consume 70% of all water consumed during the growing season, from flowering to waxy ripeness – 20%. The total bushiness at the optimal sowing time for the autumn period is 3-6. Triticale

is a self-pollinating plant, but cross-pollination is possible. Ripening occurs 3-5 days later than winter wheat. The growing season is 250-325 days. Winter forms of triticale are relatively winter-hardy, withstand frosts down to -18 ... -20 °C in the zone of tillering node.

For the swelling and germination of triticale seeds, 50-60% of water is consumed from the mass of dry seeds. The highest productivity is noted when soil moisture is 65-75% of the lowest moisture capacity. The maximum moisture consumption occurs during the period of intensive growth – in the phase of tubing and during the formation and filling of the caryopsis. The critical temperature for winter forms in the tillering node zone was up to 18-20°C. In winter and spring, triticale was less sensitive to low temperatures than winter wheat. Triticale bushes more in autumn and continues in spring. The total bushiness in autumn at the optimum sowing time was 3-6. The optimum temperature for seed germination is 20 °C, the minimum is 5 °C and the maximum is 35 °C. Triticale seedlings appear on the 5-7th day after sowing.

Sowing was carried out at the optimal time for the research area (2nd decade of August for winter rye, 3rd decade of August-1st decade of September for wheat and triticale), the area of the plots is 20m², fourfold replication, the predecessor was pure fallow. In the spring, on the sowing of the studied crops, the harrowing of the crops was carried out, the application of fertilizers (ammonium nitrate, 30 kg a.i. each), the treatment with the herbicide Disulam 0.5 l/ha. The standard of winter triticale is Krokha variety, zoned for the Middle Volga region. The standard of winter rye is Antares variety, zoned for the Middle Volga region. The standard of winter wheat is Malakhit variety, zoned for the Middle Volga region.

Sowing was carried out with a CH 10c seeder, the seeding rate was calculated for each crop and variety separately according to the formula. The seeding rate was set by weight (weight of 1000 seeds) and the number of seeds sown per hectare. The weight seeding rate (WSR) is determined by the formula (Equation 7), where: M – the mass of 1000 seeds, N – the number of millions of clean and viable seeds sown per 1 ha in a certain zone of Russia. The coefficient for the Volga region was 4.0-4.5 million viable seeds per hectare for wheat and triticale and 4.5-5.0 million viable seeds per hectare for rye. In reality, the seed material has a seed yield below 100%. Therefore, the growing rate must be adjusted for the actual sowing capacity. The correction for the actual seed yield was calculated using the formula

(Equation 8). Next, the seeding rate was determined, taking into account the germination ability (Equation 9). Mineral fertilizers were not used. Harvesting was carried out by direct combining Sampo 130. The research was carried out in the nursery of competitive variety trials in 4 repetitions, the location of plots was randomized.

3. RESULTS AND DISCUSSION:

Based on the indicators of the maximum and minimum yield of crops, the coefficients of biological productivity were determined for studied cultivars. For winter rye Cbp = 0.35-0.47, winter wheat Cbp = 0.24-0.28, winter triticale Cbp = 0.14-0.42. Taking these factors into account, the bioclimatic potential (BCP) was calculated (Table 2). The variation of the indicator (BCP) over the years reached significantly higher values from 0.62 to 1.16 points for winter rye, from 0.30 to 0.60 for winter triticale and winter wheat. The effects of climate and the consequences of its changes have not been equally reflected in cultures. In arid conditions of the urban-type settlement Bezenchuk, the maximum yield of triticale was obtained in 2017 – 7.48 t/ha, rye – 5.88 t/ha, and in 2016 – 4.65 t/ha for wheat. Potential productivity, taking into account $\sum T > 10$ °C for the vegetation period, for triticale in 2017 is 3.02 t/ha, for winter rye in 2005 6.83 t/ha, for winter wheat in 2005 – 2.79 t/ha. The actual crop yields varied greatly and differed from the potential. The potential of the cultivars was revealed only under extreme conditions. The same conclusions were reached by A. A. Fedotov *et al.* (2014), S. Asseng *et al.* (2011).

In dry and average years, the potential productivity prevailed over the actual yield: for rye, the potential productivity was 4.06-6.83 t/ha, the actual yield was 1.92-4.31 t/ha, and for wheat, the potential productivity was 1.91-2.79 t/ha, and the actual yield was 0.93-1.97 t/ha. For the triticale crop in dry years, the potential productivity prevailed (2.01-2.99 t/ha) over the actual (1.28-2.39 t/ha). The actual yield is higher for the triticale crop than the potential in average and favorable years (2.56-7.48 t/ha and 2.13-3.02 t/ha). For wheat (1.74-4.65 t/ha and 1.58-2.18 t/ha) and rye (4.52-5.88 t/ha and 4.19-4.97 t/ha), respectively, the actual yield prevails over the potential in favorable years. However, for winter rye in favorable 2015 and 2016 years, the potential productivity (5.24-5.34 t/ha) prevailed over the actual yield (4.39-4.58 t/ha). During these years, not all resources were used.

The main limiting factor that prevents the

high yields in the Samara region is the provision of crops with moisture. Potential grain yield, calculated based on actual moisture reserves, is higher in almost all years than the actual yield (Table 3). From this, it was concluded that crops do not consume all moisture during the vegetation period. The taxonomy is observed only for winter wheat. The potential yield (1.78-9.64 t/ha) prevailed over the actual (0.93-3.86 t/ha) in all study years. The potential yield in dry years prevailed over the actual yield in rye and triticale in terms of moisture supply. So, for winter rye, the potential yield was 3.46-8.21 t/ha, and the actual 1.92-2.88 t/ha, for triticale, respectively 2.92-6.95 t/ha and 1.28-2.39 t/ha. In the average statistical and favorable years, there was no taxonomy for triticale and rye crops. In some years (2003, 2004, 2005, 2008, 2014, 2017, 2018) for triticale, there was an excess of potential yields (4.60-9.61 t/ha) over the actual (2.70-7.48 t/ha), and in some (2009, 2010, 2016), the actual yield (2.56-5.59 t/ha) prevailed over the potential (1.68-3.19 t/ha). For winter rye, the actual yield (2.81-4.58 t/ha) prevailed over the theoretical (1.98-3.98 t/ha) in 2002, 2010, 2015, and 2016. Based on the data obtained, these crops do not use moisture sufficiently during the vegetation period. The maximum yield was obtained based on the average annual moisture reserves in all years. Thus, it is theoretically possible to obtain a significantly higher grain yield.

Correlation analysis of yield with climate elements and bioclimatic potential for 2002-2019 revealed significant differences in the influence of growing conditions on crops. According to the data obtained, the triticale yield is significantly correlated with the HTC for April-June ($r=0.63^{**}\pm 0.15$) (** – favorable conditions growing season). At a low level, a correlation is observed with the total precipitation in April ($r=0.27\pm 0.22$), May ($r=0.24\pm 0.23$), May-June ($r=0.32\pm 0.22$), precipitation during the vegetation period ($r=0.23\pm 0.24$), air temperature in May-June ($r=-0.32\pm 0.22$), HTC for May ($r=0.36\pm 0.21$), for June ($r=0.28\pm 0.22$). For winter rye, there is a significantly greater number of interrelations with yield. The duration of the vegetation period ($r=0.61^{**}\pm 0.15$) is observed significant at the 001% level. The average yield of rye depends on air temperatures during the sowing-germination period ($r=-0.40\pm 0.20$), on the sum of active temperatures ($r=0.46\pm 0.19$), HTC of April-June ($r=0.45\pm 0.19$). At a low level, a correlation is observed with the bioclimatic potential ($r=-0.31\pm 0.22$), the total precipitation for August-September ($r=0.31\pm 0.22$), for November-March ($r=-0.28\pm 0.22$), for April ($r=0.28\pm 0.22$), May

($r=0.24\pm 0.23$), temperature in May ($r=-0.25\pm 0.23$), HTC for August-September ($r=0.30\pm 0.22$), and for May ($r=0.21\pm 0.22$).

Studies of the dependence of yield on climatic conditions have revealed a much bigger dependence between yield and vegetation conditions in the autumn for winter rye. The triticale yield is much more interrelated with the climatic conditions of the vegetation period in the spring and summer. The potential productivity (Y_p) for triticale is significantly correlated with the bioclimatic potential ($r=0.61^{**}\pm 0.15$) and the sum of temperatures for the vegetation period ($r=0.85^{**}\pm 0.07$) for winter rye with bioclimatic potential ($r=0.97^{**}\pm 0.01$).

Actual possible yield calculated from the moisture content significantly correlates for the triticale cultivar with the amount of precipitation for August-September ($r=0.59^{**}\pm 0.16$), May-June ($r=0.79^{**}\pm 0.09$), during the vegetation period ($r=0.97^{**}\pm 0.0$), air temperature in May-June ($r=-0.50\pm 0.18$), HTC in August-September ($r=0.57^{**}\pm 0.16$), April-June ($r=0.63^{**}\pm 0.15$), June ($r=0.60\pm$). For winter rye, this indicator shows significantly less interrelations with the total precipitation in May-June ($r=0.78^{**}\pm 0.09$), precipitation during the vegetation period ($r=0.91^{**}\pm 0.04$), and the temperature in May-June ($r=-0.49\pm 0.18$), November-March ($r=0.55\pm 0.17$), HTC in June ($r=0.69^{**}\pm 0.13$). The yield of rye, calculated from the average long-term moisture supply, significantly correlates with the November-March temperature ($r=0.55\pm 0.17$). The grain yield calculated for the rye crop is interrelated with the duration of the vegetation period ($r=0.51\pm 0.18$) (* – arid conditions of spring-summer vegetation). The duration of the triticale vegetation period depends on the amount of precipitation in May ($r=0.51\pm 0.18$), HTC in June ($r=0.51\pm 0.18$). In winter rye, the duration of the vegetation depends on the air temperatures of the autumn ($r=-0.63^{**}\pm 0.15$), the entire vegetation period ($r=0.76^{**}\pm 0.10$). For the triticale culture, the dependence of the HTC on the temperatures of August-September ($r=0.47\pm 0.19$) and the sum of temperatures for the vegetation period ($r=0.78^{**}\pm 0.09$).

The tendency for the interrelation of productivity for both rye and triticale is observed throughout the vegetation period ($r=-0.20-0.66^{**}$), with a complex of climatic conditions for the spring-summer period ($r=0.45-0.63^{**}$). The duration of the triticale vegetation period depends on the precipitation in May ($r=0.51\pm 0.18$) and on the complex of conditions in June ($r=0.51\pm 0.18$). The duration of the rye vegetation period depends on

the temperatures during the sowing-germination period ($r=-0.63^{**}\pm 0.18$), on the sum of active temperatures during the vegetation period ($r=0.76^{**}\pm 0.10$). The data obtained indicate that the reason for the insufficient crop yields is not a low BCP, but its critically weak implementation, reaching in some years 40% of the potential. An important role also belongs to introducing adapted highly productive cultivars and the improvement of cultivation technology.

However, with this calculation, it is necessary to consider the unpredictability of the number of precipitations for the following agricultural year. Moreover, suppose the attention is focused on the average long-term moisture reserves in the soil, then in years with precipitation above the norm. In that case, significant losses in the yield are possible because other factors may appear in the first minimum. Therefore, when programming yields, the author suggests focusing not on average long-term reserves but on moisture reserves corresponding to climatically optimal ones. This means that the yield should be estimated by such a level of moisture supply, which will make it possible to benefit from an increase in yield in favorable years and cover losses from the cost of fertilizing and the formation of a sowing structure in unfavorable years. Thus, the gain from additional annual harvest costs in favorable years should be higher than the sum of these costs in unfavorable years.

Over the exploration period, noticeable climate changes were revealed. In studies, $t^{\circ}\text{C}$ in May 2002 was 11.4°C , in 2018 – 16.3°C . The average temperature of this month over 18 years is 15.9°C . The temperature rise during the period was 0.28°C per year. The air temperature in May-June in 2002 was 14.3°C ; in 2018 – 17.2°C . Average over 18 years, during this period – 17.6°C . The increase is 0.21°C per year. The temperature in April-May in 2002 was 8.2°C ; in 2018 – 10.9°C . The average temperature over 18 years over this period is 11.5°C . Based on this, the increase is 0.21°C . The authors noted an increase in air temperature during the sowing of winter crops in August-September. If in 2002 and 2003 it was 15.8°C , then by 2018 it was 17.5°C . The average over 18 years, during this period, is 17.3°C . The increase is 0.09°C per year.

The time of active vegetation of plants is from April to June. From an agricultural standpoint, the manifestation of droughts in these months is important. Drought trends can be monitored using the hydrothermic coefficient (a comprehensive indicator of the provision of plants with moisture and heat). Of the years analyzed, during the

sowing-germination period, severely arid conditions were observed for 4 years (2006, 2011, 2016, and 2018), with hydrothermic coefficient = 0.13-0.34. At the same time, dry conditions were noted in 9 out of 18 years ($\text{HTC} = 0.13-0.59$).

On average, over the years of the study, the duration of the winter period was 176 days, ranging from 151 days (2014) to 199 days (2010). Modern cultivars created in the Samara Research Institute of Agriculture are distinguished by high winter hardiness. However, low air temperatures, in the absence of snow cover, negatively affect the crops. The average long-term sum of winter temperatures below 0°C (November-March) was -107.4°C . Thus, winters with a sum of negative temperatures for November-March of -73°C and less are warm, $-81-92^{\circ}\text{C}$ is the norm, more than -119°C are cold. The height of the snow cover, on average, over 17 years, amounted to 27.9 cm. Proceeding from this, the winters before 2003, 2005, 2006, 2008, 2010, 2011, 2012, 2017, and 2018 harvest were favorable (the height of the snow cover is 26.5-37.1 cm, $\Sigma t^{\circ}\text{C} = -106.0-154.3^{\circ}\text{C}$).

Warm winters preceded the 2002, 2004, 2007, 2009, 2013 and 2019 harvests (snow depth 11.5-18.1 cm, $\Sigma t^{\circ}\text{C} = -69.4-98.9^{\circ}\text{C}$). Abnormally warm winters preceded 2014, 2015, and 2016 harvests (snow depth 21.0-33.8 cm, $\Sigma t^{\circ}\text{C} = -55.1-99.7^{\circ}\text{C}$). Severely arid spring-summer conditions were observed in 2004, 2005 and 2006, $\text{HTC} = 0.23-0.34$. In the spring period April-May, dry conditions were in 2002, 2008, 2010, 2012 $\text{HTC} = 0.41-0.57$. In 2004, 2005, 2007, 2008, 2009, 2010, 2012, 2013, 2014, 2016, 2018, and 2019, the driest month of May was observed in 12 years out of 18 studied. The mean annual precipitation for April-May was 55.6 mm. A severely arid spring period was observed in 2002, 2005, 2008, 2010 ($\Sigma o = 20.1-27.4$ mm). An analysis of the summer period (May-June) indicated a lack of precipitation in 13 years out of 18 considered (11.4-74.7% of the norm).

It is advisable to associate the manifestation of droughts with the level of productivity. The yield level is significantly related to the level of moisture supply and temperature regime. Studies have shown that the grain yield was largely determined by the growing conditions of May and June. The low yield in 2002 is explained by the lack of precipitation in the spring ($\text{HTC} = 0.57$). During this period, the laying of the future harvest takes place. In 2006, the dry conditions of the autumn period ($\text{HTC} = 0.02$) and June ($\text{HTC} = 0.33$). In June, flowering and formation of caryopses take place. In 2007, the

lack of precipitation ($\Sigma o = 10.3$) and increased temperatures (16.7°C), $\text{HTC} = 0.22$, led to a decrease in yield. In 2011, the dry conditions of the autumn period ($\text{HTC} = 0.26$) contributed to uneven germination. In the spring, the crops have not leveled off. In 2012, the yield was reduced by the dry conditions of May ($\text{HTC} = 0.41$). In 2013, the decline in yields was due to the dry conditions in May ($\text{HTC} = 0.36$) and June ($\text{HTC} = 0.27$). In 2015, the dry conditions of the autumn period ($\text{HTC} = 0.48$) and June ($\text{HTC} = 0.21$) reduced yields. The average duration of the spring-summer period (April-July), over the years of research, was 100 days. A significant fluctuation in the duration of this period from 113-119 days (2002 and 2006) to 88-90 days (2010, 2013, 2018) was established.

To obtain preplanned yields, it is necessary to know the potential of the cultivar (variety). In natural conditions, the potential of the same cultivar varies depending on the growing area. Such data can be obtained by conducting direct experiments or using the materials of state variety sections. With such data, it is possible to select varieties that will make better solar energy use during the growing season. Thus, one of the principles of yield planning is to determine the potential of the variety concerning the conditions where the variety is supposed to be cultivated. Productivity is determined not only by the biological characteristics of the crop but also by its cultivation conditions. When preplanning the yield, it is necessary to take into account and correctly apply the basic laws of agriculture and crop production.

Agricultural science has accumulated a large amount of experimental material on the water consumption of various cultivated plants. The optimal soil moisture has been established at different stages of development of any type of field crop. The critical periods in the development of various crops concerning moisture are clearly defined. Based on the foregoing, the principle of planning yields is to meet the needs of plants for water in optimal sizes in irrigated agriculture and in rainfed conditions to determine the yield level based on the prevailing climatic conditions.

In the conditions of rainfed agriculture, it seems possible to determine the probable water regime of plants based on meteorological data and calculate the water balance and yield level. The accumulation of reliable experimental data on obtaining a pre-calculated yield allows us to approach mathematical modeling of the yield. The obtained data are mathematically processed to determine the optimal variant of the complex of agricultural practices, which will ensure the receipt

of the planned harvest. Thus, crop programming covers three main aspects – agrometeorological, agrophysical, and agrotechnical. Factors reasonably taken into account and applied in a complex combination make it possible to grow planned yields.

With an increase in photosynthetic productivity and solar radiation utilization, it is possible to increase the yield. The implementation of photosynthetic activity in grain harvest depends on its distribution and use by plants. Figures 1 and 2 show the distribution of photosynthetic energy. To construct the scheme, averaged data on crops for favorable and unfavorable years were used. Organic products formed during photosynthesis are distributed, in addition to grain, respiration, root system, leaves, and stems. According to the data obtained, the photosynthesizing surface distribution in drought and favorable years is different. In unfavorable years, the plant spends much energy on breathing. The ratio of grain to straw is 1:4. In terms of moisture supply, a significantly larger biomass is formed before harvesting in favorable years, and the ratio of grain to straw is 1:2.5.

Thus, when plants are deficient in moisture and nutrients, an unsatisfactory absorption of PAR occurs. Varieties of triticale, wheat, and rye differ in height, size of leaf surface, but in dry conditions, these differences are not compensated. At any rate, it cannot develop a large mass of leaves if moisture and nutrients are absent. Nevertheless, in favorable conditions, the leaf surface develops as much as possible. The yield is then influenced by the properties of the plants themselves, their ability to efficiently use thermal and water resources. And thus, the role of the variety increases. The calculations used the average grain: straw ratio for winter rye 1:1.5 ($L = 2.5$), for triticale 1:2 ($L = 3$), for wheat 1:2 ($L = 3$). The highest rate of PAR arrival was noted in 2009 and 2017 (161.15 and 163.7 kJ/cm^2). The minimum arrival of PAR was noted in 2011 and 2018 (122.21 and 129.29 kJ/cm^2). Based on the indicator of the arrival of PAR, years can be conditionally divided into dry ($Q \text{ PAR} = 122.21\text{-}138.65 \text{ kJ/cm}^2$) and favorable ($Q \text{ PAR} = 140.69\text{-}161.15 \text{ kJ/cm}^2$). Thus, it turns out that 2003, 2004, 2005, 2006, 2010, 2011, 2012, 2015, 2018, and 2019 were dry years, and 2002, 2007, 2008, 2009, 2013, 2014, 2016, and 2017 were favourable.

4. CONCLUSIONS:

Based on the data obtained, it can be concluded that winter crops do not use moisture

sufficiently during the vegetation period. The maximum yield was obtained based on the average annual moisture reserves in all years. Thus, it is theoretically possible to obtain a significantly higher grain yield in dry years. The indicator (BCP) varied significantly over the years for winter rye from 0.62 to 1.16 points, much less for winter triticale and winter wheat 0.30 to 0.60.

Thus, the high-performance potential of the cultivars of the Samara Research Institute of Agriculture has been revealed. In some years, low productivity is caused not by the low BCP, but by its critically weak implementation, reaching 40% of the potential. With the improvement of the cultivation technology, the cultivars can grow intensively with a lack of moisture, form a good strong root system, a well-developed conductive stem system, and a large ear that can intensively use the flow of thermal energy.

Another significant factor that needs to be taken into account is the irregularity of precipitations in the agro-climatic regions of a certain region. In this regard, the calculation of actual possible yields based on the average annual moisture supply and climatically optimal moisture supply should be carried out differentially for each specific region and for each field, taking into account the soil characteristics and terrain. Calculation of the potential productivity of winter cereal crops allows to foresee possible options for the production structure of the enterprise, the size of the branches of agricultural production, analyze the current situation and coordinate the results with the strategic goals and objectives of the agricultural facility, i.e., determine the development strategy of the organization.

5. REFERENCES:

1. Asseng, S., Foster, I., and Turner, N. C. (2011). The impact of temperature variability on wheat yields. *Global Change Biology*, 17(2), 997-1012.
2. Bykov, N. I. (1968). *Agro-climatic resources of the Kuibyshev region*. Leningrad, Russian Federation: Hydrometeoizdat.
3. Fayaz, N., and Arzani, A. (2011). Moisture stress tolerance in reproductive growth stages in triticale (X Triticosecale Wittmack) cultivar under field conditions. *Crop Breeding Journal*, 1(1), 1-12.
4. Fedotov, A. A., Likhodievskaya, S. A., and Khripunov, A. I. (2014). Influence of droughts on the productivity of winter wheat. *Achievements of Science and Technology of Agriculture*, 28(11), 19-21.
5. Goryanin, O. I., Chichkin, A. P., Dzhangabaev, B. Z., and Shcherbinina, E. V. (2019). Scientific bases of stabilization of humus in ordinary chernozem in Russia. *Polish Journal of Soil Science*, 52(1), 113-128.
6. Goryanina, T. A. (2020). Comparative evaluation of cultivars of winter triticale for adaptive capacity and stability. *Achievements of Science and Technology of the Agro-Industrial Complex*, 34(1), 37-41.
7. Goryanina, T. A., and Medvedev, A. M. (2019). The influence of climate on the yield and quality of grain of triticale varieties in the Volga region. *Agrarian Science Magazine*, 12, 9-14.
8. Grabovets, A. I., and Fomenko, M. A. (2015). Climate change and methodology for creating new varieties of wheat and triticale with broad ecological plasticity. *Achievements of Science and Technology of the Agro-Industrial Complex*, 29(12), 16-19.
9. Kayumov, M. K. (1989). *Programming harvests of agricultural crops*. Moscow, Russian Federation: Agropromizdat.
10. Khalifeie, N., and Mohammadi Nejad, G. (2012). Evaluation of salt tolerance of new Tritiporum lines, Triticale and Iranian wheat lines. *Advances in Natural and Applied Sciences*, 6(2), 206-212.
11. Khvorova, L. A., and Gavrilovskaya, N. V. (2008). Grain crop yield Forecasting: Methods and calculations. *News of the Altai state University*, 1(57), 65-68.
12. Kirchev, H., Perchev, E., and Georgieva, R. (2016). Yield plasticity and stability of triticale varieties (X Triticosecale wittm.) under increasing nitrogen fertilization norms. *Research Journal of Agricultural Science*, 48(2), 65-68.
13. Koloskov, P. I. (1963). About the bioclimatic potential and its distribution on the territory of the USSR. *Proceedings of the NIIAC*, 23, 90-111.
14. Kukal, M. S., and Irmak, S. (2020). Characterization of water use and productivity dynamics across four C₃ and C₄ row crops under optimal growth conditions. *Agricultural Water Management*, 227, Article number 105840.
15. Kuperman, F. M., Murashev, V. V., and

- Shcherbina, I. P. (1980). *Methodological recommendations for determining the potential and real productivity of wheat*. Moscow, Russian Federation: VASKHNIL Publishing House.
16. Lichko, K. P., and Shumskaya, E. V. (2007). Grain crop yield Forecast as the basis for forecasting agricultural production volumes. *Problems of Forecasting*, 3, 60-67.
 17. Licker, R., Foley, J., and Johnston, M. (2010). Mind the gap: how do climate and agricultural management explain the "yield gap" of croplands around the world? *Global Ecology and Biogeography*, 19, 769-782.
 18. Lonbani, M., and Arzani, A. (2011). Morphophysiological traits associated with terminal drought-stress tolerance in triticale and wheat. *Agronomy Research*, 9(1-2), 315-329.
 19. Mahmood, F., Khokhar, M.F., and Mahmood, Z. (2020). Examining the relationship of tropospheric ozone and climate change on crop productivity using the multivariate panel data techniques. *Journal of Environmental Management*, 272, Article number 111024.
 20. Nasrallah, A., Belhouchette, H., Baghdadi, N., Mhawej, M., Darwish, T., Darwish, S., and Faour, G. (2020). Performance of wheat-based cropping systems and economic risk of low relative productivity assessment in a sub-dry Mediterranean environment. *European Journal of Agronomy*, 113, Article number 125968.
 21. Ray, D., Ramankutty, N., and Mueller, N. (2012). Recent patterns of crop yield growth and stagnation. *Nature Communications*, 3, 1293-1301.
 22. Tuktarova, N. G. (2019). Influence of modern trends in climate change on the productivity of winter crops. *Perm Agrarian Bulletin*, 1(25), 80-86.
 23. Vasco Silva, J., Tenreiro, T.R., Späthjens, L., Anten, N.P.R., van Ittersum, M.K., and Reidsma, P. (2020). Can big data explain yield variability and water productivity in intensive cropping systems? *Field Crops Research*, 255, Article number 107828.
 24. Vyushkov, A. A., and Shevchenko, S. N. (2008). Bioclimatic potential of spring wheat culture and its implementation in the Middle Volga region. In: *Proceedings of the Samara scientific center of the Russian Academy of Sciences. Special issue: "Development of the scientific heritage of academician N.M. Tulaykov" (to the 105th anniversary of the Samara research Institute of S.-H. named after N. M. Tulaykov) (pp. 63-70)*. Samara, Russian Federation: Samara scientific center of the Russian Academy of Sciences. Presidium of the SNC RAS.
 25. Wang, W., Yuan, J., Gao, S., Li, T., Li, Y., Vinay, N., Mo, F., Liao, Y., and Wen, X. (2020). Conservation tillage enhances crop productivity and decreases soil nitrogen losses in a rainfed agroecosystem of the Loess Plateau, China. *Journal of Cleaner Production*, 274, Article number 122854.
 26. Williams, J. D., Long, D. S., and Reardon, C. L. (2020). Productivity and water use efficiency of intensified dryland cropping systems under low precipitation in Pacific Northwest, USA. *Field Crops Research*, 254, Article number 107787.
 27. Yang, X., Li, Zh., Cui, S., Cao, Q., Deng, J., Lai, X., and Shen, Y. (2020). Cropping system productivity and evapotranspiration in the semiarid Loess Plateau of China under future temperature and precipitation changes: An APSIM-based analysis of rotational vs. continuous systems. *Agricultural Water Management*, 229, Article number 105959.

$$C_{bp} = Y_{min} / Y_{max} \quad (\text{Eq. 1})$$

$$BCP = C_{bp} \times \frac{\sum t > 10^{\circ}C}{1000^{\circ}C} \quad (\text{Eq. 2})$$

$$Y_p = \beta \times BCP \quad (\text{Eq. 3})$$

$$Y_{ppa} = \frac{W \times 100}{R_w} \times C_{eff} \quad (\text{Eq. 4})$$

$$R_w = \frac{E}{Y_a} \quad (\text{Eq. 5})$$

$$Kp = \frac{W \times Tv}{8.595 \times R} \quad (\text{Eq. 6})$$

$$\text{WSR} = M \times N \quad (\text{Eq. 7})$$

$$\text{PG} = \text{Purity} \times \text{Germination} / 100 \quad (\text{Eq. 8})$$

$$\text{SAR} = \frac{M \times N \times 100}{GA} \quad (\text{Eq. 9})$$

Table 1. Cultivars used in research

No.	Cultivars of crops	Year of zoning	Region	Yield 2014-2019, t/ha
1	Antares, winter rye	2002	7	44.5
2	Bezenchukskaya 87, winter rye	1993	4,5,7	44.0
3	Olga, winter rye	-	-	47.9
4	Roxana, winter rye	-	-	42.3
5	Bezenchukskaya 110, winter rye	2019	7	43.6
6	Malakhit, winter wheat	2000	7	32.6
7	Biryuza, winter wheat	2008	4,5,7	31.1
8	Krokha, winter triticale	2014	7	36.1
9	Capella, winter triticale	2019	7	39.7
10	Spica, winter triticale	-	-	43.0
11	Arcturus, winter triticale	-	-	42.4
12	Vasilisa, winter triticale	-	-	45.3
13	Stepanida, winter triticale	-	-	42.3

Table 2. Actual and potential productivity

Years*	Cultivar	Vegetation, days	$\sum T > 10^{\circ}\text{C}$ during vegetation	Grain yield, t/ha	BCP, score	Yp, t/ha
2006	rye	166	2349.6	2.68	0.93	5.45
	triticale	158	2349.6	1.80	0.56	2.68
	wheat	155	2106.9	1.29	0.47	2.18
2007	rye	156	1746.3	2.39	0.69	4.06
	triticale	152	1757.3	2.09	0.42	2.01
	wheat	152	1757.3	2.30	0.35	1.63
2016	rye	124	2252.4	4.58	0.89	5.24
	triticale	126	2067.2	5.59	0.42	2.57
	wheat	123	1826.3	4.65	0.45	2.09
2017	rye	145	1797.8	5.88	0.72	4.19
	triticale	147	2422.5	7.48	0.49	3.02
	wheat	148	2197.8	3.76	0.36	2.05

Note: * the table includes years with contrasting moisture supply.

Table 3. Actual possible potential yield by moisture consumption

Years*	Cultivar	Precipitation during the vegetation, mm	Ceff, %	Grain yield, t/ha	Ypp a, t/ha	Ypp m, t/ha
2006	rye	154.3	0.82	2.68	3.83	11.35
	triticale		0.71	1.80	3.32	9.83
	wheat		0.73	1.29	3.44	10.17
2007	rye	339.8	0.79	2.39	8.21	10.97
	triticale		0.67	2.09	6.95	9.29
	wheat		0.69	2.30	7.23	9.66
2016	rye	130.4	0.78	4.58	3.14	10.91
	triticale		0.76	5.59	3.04	10.56
	wheat		-	4.65	-	-
2017	rye	398.0	0.82	5.88	7.88	11.47
	triticale		0.79	7.48	9.61	10.95
	wheat		0.79	3.76	9.64	10.98

Note: * the table includes years with contrasting moisture supply.

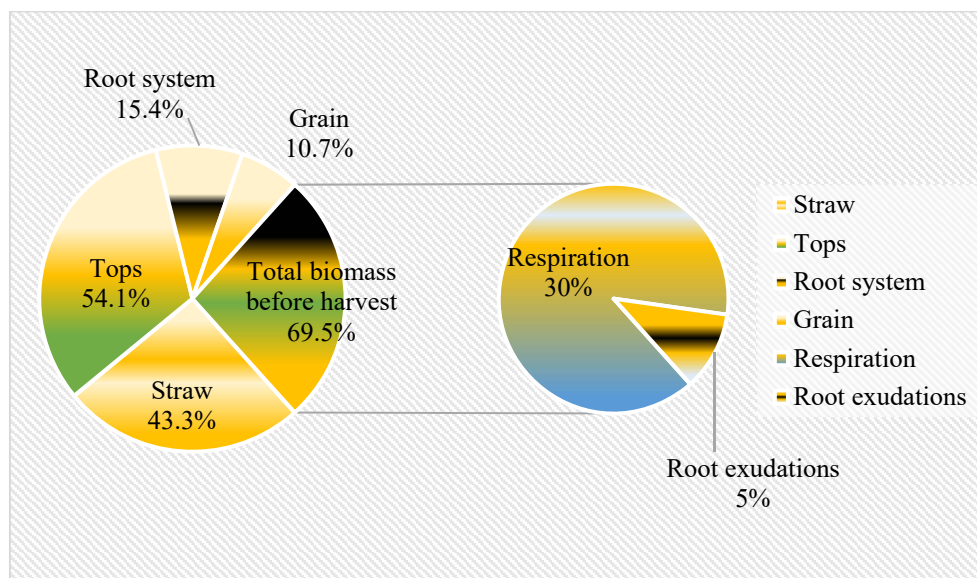


Figure 1. The distribution diagram of the photosynthesis elements in unfavorable years

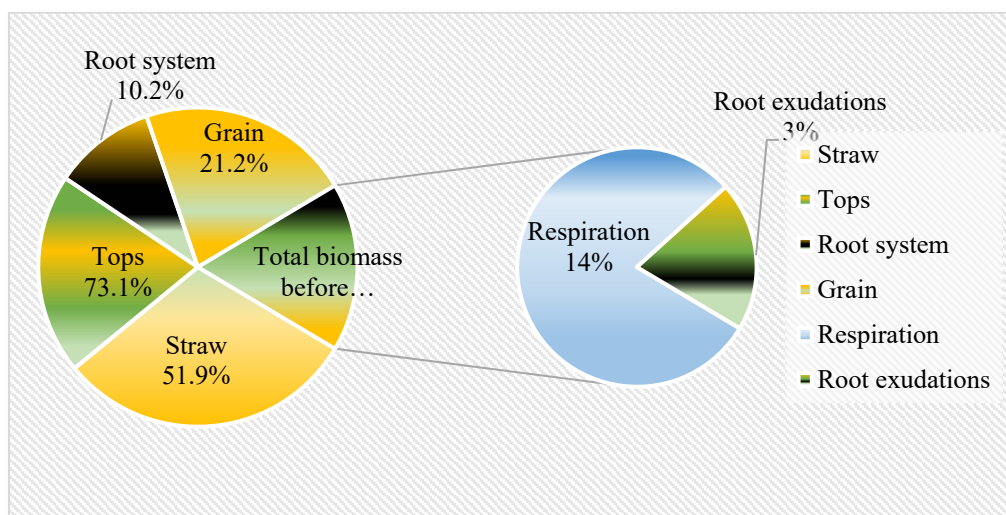


Figure 2. The distribution diagram of the photosynthesis elements in favorable years

DISTRIBUIÇÃO DE RADIONUCLÍDEOS EM ÁGUAS NATURAIS DO NORTE DO CAZAQUISTÃO E AVALIAÇÃO DAS DOSES DE RADIAÇÃO DA ÁGUA USA PELA POPULAÇÃO**DISTRIBUTION OF RADIONUCLIDES IN NATURAL WATERS OF NORTHERN KAZAKHSTAN AND ASSESSMENT OF WATERBORNE DOSES IRRADIATION OF POPULATION****РАСПРЕДЕЛЕНИЕ РАДИОНУКЛИДОВ В ПРИРОДНЫХ ВОДАХ СЕВЕРНОГО КАЗАХСТАНА И ОЦЕНКА ВОДОУСЛОВЛЕННЫХ ДОЗ ОБЛУЧЕНИЯ НАСЕЛЕНИЯ**

SALIKOVA, Natalya S.^{1*}; TLEUOVA, Zhulduz O.²; KURMANBAYEVA, Aigul S.³;
KHUSSAINOVA, Razya K.⁴; KAKABAYEV, Anuarbek A.⁵;

^{1,2} Abay Myrzakhmetov Kokshetau University; Department of Ecology, Life Safety and Environmental Protection; 189A Auezov Str., zip code 020000, Kokshetau – Republic of Kazakhstan

^{3,4,5} Sh. Ualikhanov Kokshetau State University; Department of Geography, Ecology and Tourism; 76 Abay Str., zip code 020000, Kokshetau – Republic of Kazakhstan

* Corresponding author
e-mail: natsal66@mail.ru

Received 20 September 2020; received in revised form 26 October 2020; accepted 10 November 2020

RESUMO

A população da Terra está diariamente exposta à radiação externa e interna. Suas doses variam em uma ampla faixa, dependendo dos níveis de radiação cósmica e do conteúdo de radionuclídeos naturais e antropogênicos na litosfera, hidrosfera, atmosfera e biosfera. A radiação ionizante e os radionuclídeos de origem natural e artificial inevitavelmente causam a exposição humana, o que aumenta a probabilidade de consequências negativas para a saúde. Se a dose de radiação for baixa e a exposição durar por um longo período de tempo (baixa potência), o risco é significativamente reduzido, pois neste caso a probabilidade de reparo dos tecidos danificados aumenta. No entanto, existe o risco de consequências de longo prazo, como o câncer, que pode se manifestar em anos ou mesmo décadas. O objetivo do estudo é estudar os fatores naturais da formação de radioatividade em águas naturais do norte do Cazaquistão e avaliar as doses de exposição da população relacionadas à água. O principal método para estudar este problema é o método radiométrico através da utilização do radiômetro. A análise radioquímica seletiva foi usada para determinar os radionuclídeos de urânio, tório, rádio, chumbo, cério e estrôncio. No decorrer do estudo, 166 fontes de água foram estudadas e sistematizadas nos últimos 5 anos. O objeto do estudo abrange as fontes de água potável para a população das regiões de Ayyrtau, Tayinshinsky, Esilsky, bem como a área de Musrepov, região do Norte do Cazaquistão. Foram investigados 4 tipos de fontes de água potável: água de furos, água de poços, água da torneira, água de furos usados para abastecimento de água centralizado. Ao calcular a dose de exposição interna, usamos os dados da análise radioquímica anual de várias fontes de água doce em quatro distritos da região do Norte do Cazaquistão de 2011 a 2016. Também foram realizadas conservação e recultivo de minas e depósitos de rochas nas áreas de Musrepov e Ayyrtau.

Palavras-chave: fontes de água potável, monitoramento de radiação, atividade específica, dose de radiação interna.

ABSTRACT

The population of the Earth is exposed to external and internal radiation every day. Radiation doses differ over a wide range of cosmic radiation levels and the content of natural and anthropogenic radionuclides in the lithosphere, hydrosphere, atmosphere and biosphere. Ionizing radiation and radionuclides of natural and artificial origin inevitably causes exposure, increasing the probability of adverse health effects. Suppose the dose of radiation is low and is exposed for a long period of time (low power). In that case, the risk is significantly reduced, since the likelihood of repair of damaged tissues increases. However, there is a risk of long-term consequences, such as cancer, which can manifest in years or even decades. The paper aims to research the

natural factors in the formation of radioactivity in the natural waters of Northern Kazakhstan and assess water-related doses to the population. The leading research methods for this issue are radiometric and radiochemical methods of analysis. Selective radiochemical analysis was used to determine the radionuclides of uranium, thorium, radium, lead, cesium and strontium, and a radiometer was used to determine radonucleides. During the study, 166 water sources over the past 5 years were analysed and systematized. The research object was drinking water sources of the population of Ayrtau, Tayinsha, Yesil districts, and Musirepov district of the North Kazakhstan region. Four types of drinking water sources were investigated: well water, borehole water, spring water, borehole water used for centralized water supply. When calculating the dose of internal exposure, the data of the annual radiochemical analysis of various fresh water sources of four districts of the North Kazakhstan region from 2011 to 2016 were used.

Keywords: *drinking water sources, radiation monitoring, specific activity, internal radiation dose.*

АННОТАЦИЯ

Население Земли ежедневно подвергается как внешнему, так и внутреннему облучению. Его дозы различаются в широком диапазоне в зависимости от уровней космического излучения и содержания естественных и антропогенных радионуклидов в литосфере, гидросфере, атмосфере и биосфере. Ионизирующие излучения и радионуклиды естественного и искусственного происхождения неизбежно вызывают облучение человека, увеличивающее вероятность возникновения негативных для здоровья последствий. Если доза облучения является низкой и воздействует длительный период времени (низкая мощность), риск существенно снижается, поскольку в этом случае увеличивается вероятность восстановления поврежденных тканей. Тем не менее риск долгосрочных последствий, таких как рак, который может проявиться через годы и даже десятилетия, существует. Цель исследования заключается в изучении природных факторов формирования радиоактивности природных вод Северного Казахстана и оценке водообусловленных доз облучения населения. Ведущим методом исследования данной проблемы является радиометрический метод с использованием радиометра. Для определения радионуклидов урана, тория, радия, свинца, цезия и стронция применили селективный радиохимический анализ. В ходе исследования было изучено и систематизировано 166 источников воды за последние 5 лет. Объектом исследования стали источники питьевой воды населения Айыртауского, Тайыншинского, Есильского района, а также района г. Мусрепова Северо-Казахстанской области. Было исследовано 4 типа источников питьевой воды: вода скважин, вода колодцев, водопроводная вода, вода скважин, используемая для централизованного водоснабжения. При расчете дозы внутреннего облучения были использованы данные ежегодного радиохимического анализа различных источников пресной воды четырех районов Северо-Казахстанской области с 2011 г. по 2016 г.

Ключевые слова: *источники питьевой воды, радиационный мониторинг, удельная активность, доза внутреннего облучения.*

1. INTRODUCTION:

Every day from water and food people receive certain doses of radiation. On average, approximately 2/3 of the effective equivalent dose of radiation received by a person from natural sources of radiation comes from radionuclides that enter the body with food, water and air. Only a small part of this dose falls on radioactive isotopes such as carbon-14 and tritium, formed under the influence of cosmic radiation (Wilson *et al.*, 2015; World Health Organization, 2017). Everything else comes from sources of terrestrial origin. On average, a person receives about 180 mSv/year due to potassium-40, which is absorbed by the body along with non-radioactive potassium isotopes necessary for the life of the body. However, a person receives a more substantial dose of internal radiation from the

nuclides of the radioactive series of uranium and, to a lesser extent, from the radionuclides of the thorium series. One of the most important sources of natural radioactivity in exposure of the population is the radioactivity of drinking water, determined by the content of uranium, thorium, radium, lead and radon (Grobe *et al.*, 2009; Berdymbaeva, 2012; Vogianis and Nikolopoulos, 2015; Yan, 2019).

The territory of Kazakhstan is the world's largest uranium-ore geochemical province. Two uranium provinces – North Kazakhstan and Betpak-Dala, are located in Northern, Central and Southern Kazakhstan and are characterized by outcrops of pre-Mesozoic formations on the surface. Among the latter, rocks with high uranium and thorium contents are widespread, as well as local near-surface insolation-evaporitonal accumulations of uranium typical of arid zones.

The lack of necessary information on the specific activity of drinking water can lead to the use of water sources in these areas with increased radioactivity as sources of drinking water (World Nuclear Association, 2020).

The formation of the radionuclide composition of groundwater in Northern Kazakhstan depends on natural factors: on the type of water (river, underground); lithologic-petrographic composition of rock complexes; the nature of groundwater circulation in areas of intense and difficult water exchange; ion-salt composition of water; from acid-base and reductive-oxidative conditions. The content of radionuclides in groundwater depends not only on their content in rocks, but also to a small extent is determined by their physicochemical properties that determine the migration ability of the radionuclide (degree of ionization, ability to complexation, solubility of the compounds formed by them, the form of the nuclide associated with ions) (Likhodumova and Salikova, 2013; Kaz *et al.*, 2016; Liu *et al.*, 2020). Granitoids are among the natural factors affecting the radioecological state of Northern Kazakhstan; their massifs contain elevated dispersed concentrations of radionuclides of uranium, thorium and daughter products of their decay. Almost a quarter of the country's uranium reserves are concentrated in the region. In the region, the uranium content, according to Volkovgeologiya (1994), ranges from less than 0.5 to 12.4 mg/kg with a background content of 2.1 mg/kg. The largest anomalies of uranium are located in the south of the region, where massifs of the Kokshetau low mountains are located, composed mainly of granitoids – the most radioactive rocks in nature.

As of the beginning of 1992, 17 deposits of uranium ore were explored in the North Kazakhstan region, which constitute the bulk of the resources of the North Kazakhstan uranium ore province (NKUOP) by reserves. For uranium deposits development, the Tselinnyy Mining and Chemical Complex was formed with its main base in Stepnogorsk, Akmola Region. Of the 17 deposits, 15 belong to hydrothermal and 2 to infiltration in the sediments of the Mesozoic palaeovalleys (Sofronova, 2012; Karibayev, 2014). As of 01.01.2001, there were 9 deposits on the state balance. Grachevka and Semizbai deposits are classified as exploited, and Kosachin, Shokpak, Kamyshovo, Akkan-Burlyk, Viktorovskoe, Fevral'skoe, Burlyk deposits are being used. As of the beginning of 1992, 17 deposits of uranium ore were explored in the North Kazakhstan region, which constitutes the

bulk of the resources of the North Kazakhstan uranium ore province (NKUOP) by reserves. For uranium deposits development, the Tselinnyy Mining and Chemical Complex was formed with its main base in Stepnogorsk, Akmola Region. Of the 17 deposits, 15 belong to hydrothermal and 2 to infiltration in the sediments of the Mesozoic palaeovalleys (Gavrylko, 2014; Karibayev, 2014). As of 01.01.2001, there were 9 deposits on the state balance. Grachevka and Semizbai deposits are classified as exploited, and Kosachin, Shokpak, Kamyshovo, Akkan-Burlyk, Viktorovskoe, Fevral'skoe, Burlyk deposits are being used.

Granitoids are among the natural factors affecting the radioecological state of the North Kazakhstan region, their massifs contain increased dispersed concentrations of uranium radionuclides and daughter products of its decay (Panin, 2005). As a result of the desalination of rocks containing radioactive elements, the hydrosphere of the region is saturated with radionuclides, therefore, there is a danger of increased radiation risk for the population of the North Kazakhstan region. In this regard, the study of drinking water as a source of internal radiation factor, additional to external, and, accordingly, additional radiation risk to the health of the population of Northern Kazakhstan, is relevant (Bersimbaev and Bulgakova, 2015).

A comprehensive research of the environmental situation in the territory of Northern Kazakhstan and analyzing the possible causes of high morbidity and mortality in the region's population is impossible without researching the radiation factor. In this regard, investigating the content and mechanisms of radionuclide intake into various natural components and environments is of particular interest. Natural sources of ionizing radiation to the total radiation doses to people in most cases are the main (Bersynbaev and Bakhtin, 2012; Mazhitova and Pashkov, 2017). In this regard, there is a need to analyze the content of natural radionuclides in natural environments and, in particular, in groundwater used as drinking water. One of these quality indicators is the content (specific activity) of radionuclides (Yapiyev *et al.*, 2019).

Therefore, the aim of this study was to study radionuclides in the natural waters of Northern Kazakhstan, as well as to assessment of waterborne doses irradiation of population.

2. MATERIALS AND METHODS:

To establish the conformity of the quality

of drinking groundwater with the current standards in the field of radiation safety, 726 samples of groundwater were analyzed by the content of ^{238}U , ^{232}Th , ^{226}Ra , ^{210}Pb , ^{137}Cs , ^{90}Sr , ^{222}Rn (Appendices No. 1-4 to the Order..., 2011; Decree of the Government..., 2015a; Decree of the Government..., 2015b; Order of the Minister of Health..., 2019). Water sampling was carried out following Appendix No. 1-4 to the Order of the Chairman of the State Sanitary and Epidemiological Surveillance Committee dated 08.09.2011, No. 194 "On approval of guidelines for radiation hygiene" (Methodological recommendations for sanitary control ... 2011): when using standard containers made of polymeric materials, it is necessary to rinse with water from the source at least 3 times before use (Appendices No. 1-4 to the Order..., 2011). When calculating the required volume of water, it is necessary to rely on the approved indicators in the normative documentation, which considers the method for determining a specific indicator and the number of determined indicators. According to the Appendices No. 1-4 to the Order of the Chairman of the State Sanitary Doctor of the Republic of Kazakhstan No. 194 "On approval of guidelines for radiation hygiene" (2011) the recommended volume of water sampling from surface and underground sources of drinking water is 10 liters. This volume includes the required amount of water needed during the re-analysis, the type of analysis, the volume of water taken. Evaluation of the total indicators of α - or β -activity required at least 1 liter of samples. To assess the radionuclide composition and specific activity of natural radionuclides (^{226}Ra , ^{224}Ra , ^{238}Ra , ^{238}U , ^{234}U , ^{210}Pb , ^{210}P , ^{210}Bi , ^{230}Th , ^{232}Th , ^{228}Th) at least 11 liters were required. To check the specific activity of ^{137}Cs , ^{90}Sr and ^{40}K (if necessary, ^{238}Ru and ^{241}Am) minimum 4 liters were required. To determine the specific activity of ^{222}Rn 1 liter of sample was required.

When sampling, it is necessary to drain the water for a certain time to establish constant characteristics. If the current water source is operational, regardless if it is artesian water or tap water, then the drain time is set within 5 minutes. For newly introduced sources or sources after repair, this time was set individually and depended on the degree of contamination of the water supply channel. There were no established time frames for draining, since the fixation of the stability of water characteristics is only visually recognized. Water can be taken traditionally from wells and open reservoirs, such as rivers, lakes, water storage reservoirs and other bodies of water. After selection, water was

placed in an airtight container for the time required for the deposition of small fragments of sand, soil, silt. Again, the time was set subjectively in each case, but not less than 2-3 hours. After the required time, nitric acid was added to the sample in an amount necessary to achieve a pH of 1. This allowed to eliminate the process of sorption of trace amounts of radionuclides on the inner surface of the container. The container was labeled and a selection certificate was added, which indicated the date, time of selection, and all the necessary information about the source. Appendix 1 to the guidelines contains recommended information for display in the certificate. The analysis period should not exceed 14 days for the selected samples. The test report indicated the shelf life of the sample. If this conditions were violated, analysis was not carried out.

For determining ^{222}Rn , a radiometric method was applied to water with the use of a Ramon-02 radiometer. Selective radiochemical analysis was used to determine the radionuclides of uranium, thorium, radium, lead, cesium, and strontium. Specific activity of ^{238}U , ^{232}Th was determined by the photometric method with the use of a KFK-3 photocolimeter, ^{226}Ra , ^{210}Pb , ^{137}Cs , ^{90}Sr – sedimentation analysis with the use of the low-background setup UMF-2000, entered in the register of the State Automotive Inspection of the Republic of Kazakhstan. All measurements were performed according to the methods included in the register of the GSI RK, the latest edition is presented in (Order of the Chairman of the State Sanitary ... 2011).

The methodology for assessing the internal doses of radionuclides entering the human body with drinking water E_{water} (mSv/year) was calculated according to the Decree of the Government of the Republic of Kazakhstan "On approval of hygiene standards" Sanitary and epidemiological requirements for radiation safety" (Decree of the Government of the Republic of Kazakhstan ... 2015a) according to the formula (Equation 1):

$$E_{\text{water}} = \sum (\epsilon_{\text{wateri}} \cdot C_{\text{wateri}} \cdot 2 \cdot 365) \quad (\text{Eq. 1})$$

Where ϵ_{wateri} is the dose coefficient of the i isotope for water, mSv/Bq; C_{wateri} is the specific activity of the i radionuclide in a water sample, Bq/kg; 2 is the statistically average amount of water consumed by a person per day, kg/day; 365 is the conversion factor, days/year.

3. RESULTS AND DISCUSSION:

3.1. Characteristics of radiation hazardous areas

Considering all radiation factors, 5 radioecological potentially hazardous zones were identified: Priyesil, Zerendy-Balkashino, Chagaly, Akkol-Schuchinsk and Stepnogorsk-Zaozernyy. Exploration of uranium deposits was carried out in the region and it was mined until the middle of 1990s. During mining and evaluation of ore occurrences, extensive dumps of radioactive rocks were formed, most of which are currently reclaimed.

There are five radiation hazardous zones on the territory of Northern Kazakhstan (Beletskaya, 1974, Abdulkabirova, 1975): Priyesil; Zhalgyztau (Zerendy-Balkashino); Saumalkol (Chagaly); Taldykol (Akkol-Schuchinsk); Aisary (Stepnogorsk-Zaozernyy). On the map of dose loads in the southern part of the region there are areas with increased (up to 5.6 mSv/year) radiation dose values.

To calculate the exposure amount, the dose factors were used (Table 1). In terms of the degree of possible technogenic radiation load, the Akmola region is the most dangerous in Kazakhstan (along with the East Kazakhstan and Pavlodar regions, where this danger is caused by the presence of the Semipalatinsk Test Site). Currently, the degree of radiation hazard within it is determined by the following main regional and local factors:

- high content of uranium and thorium in rocks;
- the high content of radon in groundwater, in the surface layer of atmospheric air (and, accordingly, in residential buildings);
- increased groundwater radioactivity;
- the formation of areoles of technogenic radioactivity in places of mining.

There is a small amount of total thorium in the region, averaging 7 mg/kg; its increased content (49 mg/kg) was noted near the highly active, rare-metal Orlinogorsk granitoid massif. Radium is in a diffuse state in the region. In very low concentrations, it is found in aqueous solutions, from which it is extracted as a result of adsorption, coprecipitation and capture by living matter. Some researchers consider the accumulation of radium to be a species trait of plants. The highest concentration of strontium-90 (30 Bq/kg, or 0.093 Ci/km²) within the study area was noted in the largest (2000 km²) Volodarsk anomalous zone.

Alpha radiation within the studied area ranges from 100 to 18025 imp/s·kg. The largest anomalies – with high alpha activity – are recorded in the southern part of the region, to the north of alpha activity is much less. The intensity of beta radiation within the study area ranges from 0 to 781 imp/s·kg. There are 9 anomalies and 3 anomalous points. An analysis of the obtained materials allows us to conclude that the radiation pollution of the territory is mainly due to natural sources (Salikova *et al.*, 2011). The most dangerous objects are those from which the human dose norm from anthropogenic radiation should not exceed 1 mSv/year. These objects include industrial enterprises that involve radioactive natural materials (radioactive ore) in their technological process.

An unfavorable radiological condition is noted in the city of Sergeyevka, in Ornek village and other settlements located in the near-valley part of Ishim, where there are outcrops of indigenous acidic magmatic rocks. A relatively unfavorable radiological situation is also noted in the areas of development of fracture of the platform cover, in the vicinity of Yavlenka village, near the northern border of the ancient platform (Lipchanskaya, 2014). However, as already noted, so far there are few works devoted to the results of the research of radiation intensity or safety of the territory of Northern Kazakhstan. Based on the research results and taking into account the data of other authors, a radiation intensity map was compiled (Bensman *et al.*, 2012).

The territory of the eastern half of the republic, especially the territory of the Akmola and North Kazakhstan regions, is characterized by the greatest radon emanations. About 30 anomalies and 15 anomalous points with an increased concentration of uranium, thorium, ²²⁶Ra, ²²⁸Ra, ⁴⁰K and other elements, were found in the northern half of the region. 2 anomalies of strontium and 2 anomalous cesium points of unknown origin were located. Perhaps they were formed due to global western disturbance and the deposition of products of the Kyshtym accident in the Urals. In general, anomalies of radionuclides characterize a satisfactory ecological state of almost the entire water catchment area of small rivers in the region.

In the predominant part of the region, the annual dose level is 2-3 mSv/year. The zone territories located in the southern border zone (Saumal, Priyesil, Zerenda-Balkashino) include areas with a dose load of up to 4 mSv/year. In the northern part of the region, granites and other

crystalline rocks of a folded basement are overlain by the thickness of aleuric-clay deposits, which increases in the northern and northeastern directions 1000-1500 m or more. The absence of acidic magmatic rocks on the surface, the sluggish tectonic regime and the thick stratum of sedimentary rocks of the platform cover play the role of a protective shield against emanation of the decay products of the radioactive elements of the folded basement. Table 2 describes radiation hazardous areas.

In the city of Petropavlovsk, the gamma background is low, it ranges from 3 $\mu\text{R/h}$ to 45-50 $\mu\text{R/h}$. The increased background radiation (17 anomalies with gamma activity from 50 $\mu\text{R/h}$ to 800 $\mu\text{R/h}$) is created by granite slabs lining the steps near some shops, granite blocks embedded in the foundation of multi-storey buildings and other elements. The presence of natural radioactive objects in these zones, creates an increase of radiation risk. Most of these zones do not pose a real radiation hazard, since on average the radiation dose does not exceed 1 mSv/year. Only in certain local areas can it exceed the annual dose load of 1 mSv/year. The total area of such zones is 489.1 thousand km² or 57.1 of the total area of all zones. These low radiation hazard areas are mainly located in the western region of Kazakhstan. Areas of medium radiation hazard are also identified here.

The most significant concentrations of radionuclides were found in the Orlinogorsk granite massif in the Zhaman-Sopka area. According to the analysis results conducted by Stepgeology JSC, the most critical radiological condition is noted in the village of Gorny, located in the vicinity of the granite quarry at the foot of Orlinaya. There is no homogeneous gamma background and ranges from 18-25 $\mu\text{R/hour}$ to 40-80 $\mu\text{R/hour}$. 25 points with an abnormally high gamma-ray background were detected – approximately of 60-80 $\mu\text{R/hour}$. High levels of radiation were detected inside some rooms.

Of the radioactive elements contained in groundwater, the most hazardous to health is the presence of emanations of radon and its daughter decay products (Isupov *et al.*, 2016). An increased radon content is noted in groundwater near the village of Gorny at the foot of Zhaman-Sopka. The highest content was 2795 Bq/kg, which is more than 45 times the maximum permissible value, and 1663.9 Bq/kg was recorded in the central well, which exceeds the MPC (1100 Bq/kg) by 15.1 times. In other wells, radon concentrations range from 113.7 to 1037.0

Bq/kg (1.03-9.43 MPC). High ²²²Rn activities are also recorded in Saumalkol village of the Ayyrtau region, where the concentrations are 506-1073 Bq/kg, in the wells of Raisovka village – 333 Bq/kg (Musirepov district), Ikobercy village – 303 Bq/kg (Akzhar district), and some other settlements in the North Kazakhstan region (the village of Ruzayevka, the village of Urnek, the town of Strelnikovo, the sanatorium Arka). The content of ²²²Rn in the water of the listed settlements exceeds the established intervention level of 60 Bq/kg. In the waters of open reservoirs, the radon content is much lower and ranges from 0.29 to 0.59 Bq/kg (0.003-0.005 MPC) (Vodopyanova and Mazhitova, 2012).

Radionuclides in high concentrations are also contained in other drinking wells located in the southern part of the region. In the northern part of the region, radioactive groundwater was discovered in the Petropavlovsk region. The radium concentration and radon concentration is of therapeutic value and allows their use in balneological purposes (Larikova, 2012). Thus, the variety of natural conditions contributed to the formation of zones with different levels of radiation conditions in the region: in a significant part of the region (northern regions), the radiological situation is approaching normal; Some territories in the south of the region have increased radiation background due to the wide development of granite massifs and numerous deposits of uranium ores.

3.2. Description of the specific activity of drinking water in the reservoirs of Northern Kazakhstan

Researches have shown that the underground waters in Northern Kazakhstan are distinguished by a variety of chemical composition and content of radioactive elements, which is due to the location of the region on the border of the northern part of the Kazakh small hills and the southern part of the West Siberian plain (Panin, 2005). The radionuclide composition of natural waters varies over a wide range (Table 3).

The absence of the effect of artificial radioactivity on the formation of the radioactive background of groundwater has been established. Technogenic radionuclides are detected in single samples and do not exceed 0.05 IL for ¹³⁷Cs and 0.02 IL for ⁹⁰Sr. Excess levels of intervention are observed in the content of ²³⁸U (Aiyrtau and Ualikhanov districts), in the content of ²²⁶Ra (Yesil and Timiryazev districts), in the content of ²²²Rn (areas: Aiyrtau, Akzhar,

Yesil, G. Musirepov, Shal akyn).

Radon is highly soluble in water and its content in groundwater is unlimited. The formation of aquifers washing uranium-containing granitoids in the zones of fracture and karst contributes to its increased groundwater content in the south of the North Kazakhstan region. Groundwater sedimentary rocks of uranium of the northern part of the North Kazakhstan region have minimal radon content. However, in the northern region of the region, granites and other crystalline rocks of a folded basement are overlain by the thickness of aleuric-clay deposits, the thickness of which increases in the northern and northeastern directions to 1,500 m or more. The thick stratum of sedimentary rocks prevents the emanation of radon to the Earth surface and contribute to its concentration in groundwater.

When calculating the dose of internal exposure, we used the data of the annual radiochemical analysis of various freshwater sources of four regions of the North Kazakhstan from 2011 to 2016. The sources of drinking water such as wells, boreholes, springs, and water supply were calculated. The values of specific activities of drinking water of various sources of the G. Musirepov district for 2011 are presented in the Table 4.

The values of specific activities of drinking water of various sources of the G. Musirepov district for 2012 are presented in the Table 5. As can be seen from the data of Table 5, the specific activity of radionuclides (^{238}U , ^{232}Th , ^{226}Ra , ^{210}Pb) in drinking water of all investigated sources does not exceed the established levels of intervention (IL). Table 6 shows the specific activity of drinking water in the G. Musirepov district for 2013.

The highest specific activity is inherent in uranium-238, with the maximum value of the radionuclide observed in the water of the boreholes. The second place in the specific activity of uranium-238 is water wells. A rather high specific activity is noted for lead-210 in water wells. Table 7 shows the specific activity of drinking water in the G. Musirepov district for 2014. Table 8 presents the specific activity of drinking water in G. Musirepov district for 2015.

The highest specific activity is typical for well water for all analyzed radionuclides. A low specific activity was noted for the thorium-232 isotope in all samples of the analyzed water from various drinking water sources. Despite the absence of obvious sources of anthropogenic interference, the presence of lead-210 isotope in all water samples is observed. Table 9 shows the

specific activity of drinking water in the G. Musirepov district for 2016. During this period, the water of wells, boreholes, and the water of springs was examined. The presence of radioactivity in the water of springs and other water samples of all the analyzed radionuclides is noted. Approximately equal concentrations of radium-226 are observed in all sources of drinking water. Despite strict sanitary and epidemiological control and borehole water used for centralized water supply, it contains radionuclides radium-226, uranium-238, and lead-210. The presence of granite uranium-containing radionuclides naturally explains the presence in the analyzed waters of the isotopes of uranium-238 and its decay product – radium-226. Thorium-232, as less mobile in natural waters, exhibits low radioactivity in all water samples.

Based on the data presented in Tables 4-9, the effective equivalent dose of the population exposure from radionuclides in drinking water of G. Musirepov district was calculated, mSv/year (Table 10). As we can see from the data of Table 10, the drinking water of all the analysed sources does not significantly irradiate the population of the G. Musirepov region for the entire studied period of 2011-2016. According to the calculated data, the exposure of the population to the drinking water consumption of the considered region ranged from 0.024 mSv/year (borehole water used for centralized water supply, 2016) to 0.123 mSv/year (borehole water, 2013). In Tables 11-14, the presented data of radiation monitoring of drinking water of the Yesil district for 2011-2016.

As can be seen from the data, the specific activity of radionuclides (^{238}U , ^{232}Th , ^{226}Ra , ^{210}Pb) in drinking water of all the studied sources does not exceed the established IL. The highest specific activity of uranium-238, radium-226 radionuclides, is observed in water samples from wells and boreholes in Yavlenka, Pokrovka. Noted low specific activity of thorium-232 radionuclide in all water samples from all sources of water supply. In tap water, the highest specific activity is characteristic of the uranium-238 radionuclide. Among all drinking water sources, the highest specific activity for radionuclides is ^{238}U , ^{232}Th , ^{226}Ra , ^{210}Pb , which is typical for water samples from wells. In 2016, in one of the wells of Korneyevka village, the ^{238}U radionuclide content is almost 3 times higher than the specific activity of this radionuclide in the water of other wells, selected at other sampling points of this settlement. In the whole region, borehole water

shows the highest radioactivity.

The effective equivalent dose of exposure to the Yesil district population from radionuclides from drinking water, mSv/year, is presented in Table 15. As can be seen from the data of Table 15, the drinking water from all the analysed sources does not have a significant internal exposure of the population of the Yesil district for the entire studied period 2011, 2014-2016. According to the calculated data, the exposure of the population to the consumption of drinking water in the considered district ranged from 0.024 mSv/year (well water used for centralized water supply, 2015) to 0.084 mSv/year (well water, 2015). Radiological research in the Ayyrtau region was carried out starting in 2012 (Tables 16-19).

As can be seen from the Tables, the specific activity of radionuclides (^{238}U , ^{232}Th , ^{226}Ra , ^{210}Pb) in drinking water of all the analysed sources does not exceed the established IL. The highest radioactivity of drinking water was found in the waters of boreholes in the villages of Saumalkol, Lobanovo, Yeletskoye, Daukara, located in the zone of uranium deposition. The effective equivalent dose of radiation exposure, E_w , of the Ayyrtau region population from radionuclides from drinking water, mSv/year, is presented in Table 20. As can be seen from the data of Table 20, the drinking water of all analysed sources does not have a significant internal exposure of the population of the Ayyrtau region for the entire studied period 2012, 2014-2016. According to the calculated data, the exposure of the population to the drinking water consumption of the considered region ranged from 0.024 mSv/year (borehole water, 2014) to 0.078 mSv/year (borehole water, 2015) (Table 21).

As can be seen from the data of Table 25, the specific activity of radionuclides (^{238}U , ^{232}Th , ^{226}Ra , ^{210}Pb) in drinking water of all the analysed sources does not exceed the established IL. Calculation of the value of the effective equivalent exposure dose for the consumption of water from borehole (Equation 2):

$$E_{\text{water}} = 0.26 \cdot 0.000045 \cdot 2 \cdot 365 + 0.00023 \cdot 0.01 \cdot 2 \cdot 365 + 0.00028 \cdot 0.016 \cdot 2 \cdot 365 + 0.00069 \cdot 0.0355 \cdot 2 \cdot 365 = 0.031 \text{ mSv/year.} \quad (\text{Eq. 2})$$

The values of specific activities of drinking water of various sources of the Taiynsha district for 2013 are presented in Table 22. As can be seen from the data of Table 22, the specific activity of radionuclides (^{238}U , ^{232}Th , ^{226}Ra , ^{210}Pb) in drinking water of all the analysed

sources does not exceed the established IL. Water from these wells is suitable for drinking and domestic purposes. The highest radioactivity in drinking water was found in a borehole used for centralized water supply in Petrovka. Thorium-232 radionuclide is practically not found in most of the water samples.

As can be seen from the data in Table 23, the specific activity of radionuclides (^{238}U , ^{232}Th , ^{226}Ra , ^{210}Pb) in drinking water of all the analysed sources does not exceed the established IL. Water from these sources is suitable for use in domestic and drinking purposes. On average, drinking water sources showed the greatest radioactivity in well water (almost 3 times the specific activity in wells exceeds the average value of specific activity in wells).

As can be seen from the data in Table 24, the specific activity of radionuclides (^{238}U , ^{232}Th , ^{226}Ra , ^{210}Pb) in drinking water of all the studied sources does not exceed the established IL. Water from these sources is suitable for use in domestic and drinking purposes. In this work it was found that the greatest radioactivity was shown by samples of drinking water from boreholes used for drinking water supply (almost 2 times higher than the specific activity of water samples of wells and 3 times higher than the specific water samples of boreholes) (Table 25). We noticed that the greatest radioactivity was shown by samples of drinking water taken from wells.

As can be seen from the data of Table 26, the drinking water of all the analysed sources does not have a significant internal exposure of the population of the Taiynsha district for the entire studied period of 2012-2016. Water from the examined sources can be used for domestic and drinking purposes. According to the calculated data, the irradiation of the population with drinking water consumption in the considered region ranged from 0.026 mSv/year (borehole water, 2014) to 0.099 mSv/year (well water used for centralized water supply in 2013).

3.3. The content of individual radionuclides in groundwater of the North Kazakhstan region

The main sources of radionuclides entering groundwater are acidic magmatic rocks of the Kokshetau massif, widely developed in the south of the region and in the regions adjacent to it. Particularly high enrichment with rare metals is distinguished by granites of the Zolotonosha massif located at the junction of the Ishim

disjunctive zone with the Saumalkol split. Along with potassium and flint, also tantalum, tin, beryllium, niobium, rubidium, zirconium, and uranium enter the water along this zone. On this territory, local accumulations of natural radionuclides develop and uranium deposits form, in which uranium minerals are represented by uraninite, coffinite, brannerite, and nasturan (Karibayev, 2014). These minerals belong to 4-valent form uranium compounds, which are considered inactive (Kulikov, 1990).

The areas of Ayyrtau, Ualikhanov, Shal akyn, and Yesil located within the indicated granitoid massifs are characterized by increased values of groundwater radioactivity (Figures 1-3).

Thorium, even if it is contained in rocks exceeds the uranium content, will be detected in groundwater in concentrations several orders of magnitude lower than uranium. Due to the tendency to hydrolysis and adsorption on suspended particles and colloids, a significant part of thorium is deposited from the water column in the form of suspensions and colloids, as a result of which the thorium migration capacity is small and isotope is found in groundwater in small quantities (Langmuir and Herman, 1980). The oxidizing groundwater conditions contribute to the transition of uranium from a 4-valent sparingly soluble form to a 6-valent migratory active (Federal-Provincial-Territorial..., 2017), which leads to the detection of uranium in groundwater in activities exceeding the established IL. In the underground waters of Northern Kazakhstan, the Th/U ratio ranges from 0.001 to 0.07.

The acid-alkali conditions of groundwater are important, in acidic waters the content of uranium and radium will be significantly higher (by 3 orders of magnitude) than in near-neutral ones. The content of radium and uranium is also limited by the concentration of sulfate ions, the lower their concentration relative to the total mineralization, the more radium and uranium will be detected in groundwater. The results of our previous research confirm this: the ratio of sulfate to total mineralization in groundwaters of Yesil, Ayyrtau, Ualikhanov districts is lower (0.09-0.14) than this ratio in the regions of Akzhar and G. Musirepov (0.2) (Yapiyev *et al.*, 2017).

According to (Chalov, 1975), the $^{226}\text{Ra}/^{238}\text{U}$ ratio is a qualitative indicator of the migration ability of radionuclides in natural waters. In our case, the ratio $^{226}\text{Ra}/^{238}\text{U}$ significantly exceeds the equilibrium one and varies between 0.01-0.8, which indicates a

predominant migration of radium and possible complexation of uranium with related elements.

4. CONCLUSIONS:

Granitoids are among the natural factors influencing the radioecological state of Northern Kazakhstan, their massifs contain increased dispersed concentrations of radionuclides of uranium, thorium and daughter products of their decay in all objects of the environment, including in surface and underground waters. There is a potential danger of increasing the total dose of the population exposure from natural sources due to the intake of natural and man-made radionuclides with drinking water into the human body.

The content of radionuclides in the analysed water bodies used for drinking water supply, in most cases, do not exceed the established levels of intervention and do not exceed the values of the total alpha and beta activity established by the requirements of radiation safety. Such a content of radionuclides does not pose a radiation hazard when drinking water. It was found that the population of the considered regions of the North-Kazakhstan region receives the largest dose of radiation when drinking water from wells (0.123 mSv/year), the lowest dose – when drinking tap water (0.024 mSv/year), which is (1-13%) from the total exposure dose to the population of Northern Kazakhstan.

The researched area population does not use sources with increased radioactivity that were conserved and banned for use. In accordance with the principles of radiation safety – the principle of regulation and the principle of optimization, systematic radiation monitoring of underground drinking water sources is necessary to timely identify and eliminate sources with increased radioactivity from drinking water supply.

5. REFERENCES:

1. Abdulkabirova, M. (1975). *Roof-block structures and endogenous deposits of Northern Kazakhstan*. Alma-Ata: Nauka.
2. Appendices No. 1-4 to the Order of the Chairman of the State Sanitary Doctor of the Republic of Kazakhstan No. 194 "On approval of guidelines for radiation hygiene". (2011). Retrieved from

- https://online.zakon.kz/Document/?doc_id=31249142
3. Beletskaya, N. (1974). *The relief of the Petropavlovsk Priisimye and the history of its development in the Cenozoic*. Moscow: Moscow State University.
 4. Bensman, V., Bragin, A., and Yakovleva, N. (2012). *Development of design solutions and schemes for environmental protection, improving the ecological status of settlements and software for environmental monitoring and zoning of the territory of the Republic of Kazakhstan*. Almaty: KazNII OIR.
 5. Berdymbaeva, D. (2012). Radon safety problems in the Northern regions of Kazakhstan. *International scientific and practical conference "Radioecology of the XXI century"*. Retrieved from <http://elib.sfu-kras.ru/bitstream/handle/2311/8978/Berdimbaeva.pdf?sequence=1&isAllowed=y>
 6. Bersimbaev, R., and Bulgakova, O. (2015). The health effects of radon and uranium on the population of Kazakhstan. *Genes and Environment*, 37, 18.
 7. Bersynbaev, D., and Bakhtin, M. (2012). Radon safety issues in the northern regions of Kazakhstan. *Materials of the International Scientific and Practical Conference "Radioecology of the XXI Century"*, 104-108, Krasnoyarsk, Russian Federation.
 8. Chalov, P. (1975). *Isotopic fractionation of natural uranium*. Frunze: Ilim.
 9. Decree of the Government of the Republic of Kazakhstan No. 202 "On the approval of the Sanitary Rules" Sanitary and Epidemiological Requirements for Ensuring Radiation Safety". Retrieved from (2015b). <http://adilet.zan.kz/rus/docs/P1200000202>
 10. Decree of the Government of the Republic of Kazakhstan No. 754 "On the approval of hygienic standards" Sanitary and epidemiological requirements for radiation safety". (2015a). Retrieved from https://online.zakon.kz/document/?doc_id=31129210#pos=8;-114
 11. Federal-Provincial-Territorial Committee on Drinking Water. (2017). Uranium in Drinking Water. Retrieved from <https://www.canada.ca/content/dam/hc-sc/documents/programs/consultation-uranium-drinking-water/consultation-uranium-drinking-water-eng.pdf>
 12. Gavrylko, V. (2014). North Kazakhstan scientists have announced the reasons for the high incidence of cancer. *Petropavlovsk regional information portal*. Retrieved from <https://pkzsk.info/severokazaxstankie-uchenye-ozvuchili-prichiny-vysokoj-zabolevaemosti-rakom/>
 13. Grobe, A., Renn, O., and Jaeger, A. (2009). The impact of anthropogenic environmental changes on public health. *Russian Academy of Sciences: All-Russian Institute of Scientific and Technical Information*, 5, 3-80.
 14. Isupov, V., Kolpakova, M., Borzenko, S., Shatskaya, S., Shvartsev, S., Dolgushin, A., Arzamasova, G., and Borodilina, I. (2016). Uranium-bearing salt lakes of the Altai territory. *Materials of the V International conference*, 262-266, Ufa, Russian Federation.
 15. Karibayev, E. (2014). State and problems of the mineral resource base of Kazakhstan. *Mine surveying and subsoil use*, 4(72), 3
 16. Kayukov, P., Fedorov, G., and Bensman, V. (2014). Radon risk in Kazakhstan and ways to reduce it. *Materials of the Scientific and Practical Conference*, 64-71, Petropavlovsk, Republic of Kazakhstan.
 17. Kaz, V., Dutova, E., Roldugin, V., and Vtorushina, O. (2016). Uranium in underground waters of the Altai republic. *Materials of the V International conference*, 262-266, Ufa, Russian Federation.
 18. Kulikov, I. (1990). *Isotopes and properties of elements*. Moscow: Metallurgya.
 19. Langmuir, D., and Herman, J. (1980). The mobility of thorium in natural waters at low temperatures. *Geochimica et Cosmochimica Acta*, 44(11), 1753-1766.
 20. Larikova, N. (2012). Genotoxicological assessment of drinking water and some indicators of the incidence of the population of the North Kazakhstan region. *Environmental Genetics*, 4(10), 40-50.
 21. Likhodumova, I., and Salikova, N. (2013).

- Features of the formation of the elemental composition of groundwater in the Kokshetau hydrogeological region within the North Kazakhstan region. *Materials of the VIII Biogeochemical School "Biogeochemistry and Biochemistry under the Conditions of the Biosphere Technogenesis"*, 125-129, Moscow, Russian Federation.
22. Lipchanskaya, M. (2014). Water quality as a risk factor for cancer incidence in the population of the SKO. *Materials of the Scientific and Practical Conference*, 77-83, Petropavlovsk, Republic of Kazakhstan.
 23. Liu, Y., Wang, P., Ruan, H., Wang, T., Yu, J., Cheng, Y., and Kulmatov, R. (2020). Sustainable Use of Groundwater Resources in the Transboundary Aquifers of the Five Central Asian Countries: Challenges and Perspectives. *Water*, 12, 2101
 24. Mazhitova, G., and Pashkov, S. (2017). Assessment of the impact of natural conditions on the standard of living in North Kazakhstan region. *Materials of the IV All-Russian scientific-practical conference with international participation*, 558-561, Tomsk, Russian Federation.
 25. Methodological recommendations for sanitary control over the content of radioactive substances in environmental objects (Appendix No. 6 to the order of the Chairman of the Committee for State Sanitary and Epidemiological Supervision dated September 8, 2011 No. 194 "On approval of" Methodological recommendations on radiation hygiene"). (2011). Retrieved from https://online.zakon.kz/Document/?doc_id=31249938
 26. Order of the Chairman of the State Sanitary and Epidemiological Surveillance Committee dated September 8, 2011 No. 194 "On approval of the" Methodological Recommendations on Radiation Hygiene". (2011). Retrieved from https://online.zakon.kz/Document/?doc_id=31249142&mlink=1002586023&status=0&excludeArcBuh=0#pos=0;0&sel_link=1002586023
 27. Order of the Minister of Health of the Republic of Kazakhstan No. K DSM-97 "On the approval of sanitary rules" Sanitary and epidemiological requirements to ensure radiation safety". (2019). Retrieved from <http://adilet.zan.kz/rus/docs/V1900018920/history>
 28. Panin, M. (2005). *Ecology of Kazakhstan*. Semipalatinsk: SemGPU.
 29. Salikova, N., Petushkov, P., Saraeva, N., Mazik, E., and Mikheeva, T. (2011). Studying the radioactive background of groundwater in the North Kazakhstan region. *Independent Kazakhstan and the Scientific Heritage of Academician M. Kozybaev*, Petropavlovsk, Republic of Kazakhstan.
 30. Sofronova, L. (2012). *Impact of waste from uranium processing enterprises in Northern Kazakhstan on the state of ecosystem components*. Kokshetau: Kokshetau State University.
 31. Vodopyanova, S., and Mazhitova, G. (2012). *Radiation pollution of surface and groundwater in the territory of the North Kazakhstan region*. Retrieved from <http://human.snauka.ru/2012/06/1400>
 32. Vogianis, E., and Nikolopoulos, D. (2015). Radon sources and associated risk in terms of exposure and dose. *Environ Health*, 2, 1–10.
 33. Wilson, J., Zuniga, M., Yazzie, F., Stearns, D. (2015). Synergistic cytotoxicity and DNA strand breaks in cells and plasmid DNA exposed to uranyl acetate and ultraviolet radiation. *Journal of Applied Toxicology*, 35(4), 338–49.
 34. World Health Organization. (2017). Guidelines for drinking-water quality: fourth edition incorporating the first addendum. Retrieved from <https://www.who.int/publications/i/item/9789241549950>
 35. World Nuclear Association. (2020). Uranium and Nuclear Power in Kazakhstan. Retrieved from <https://www.world-nuclear.org/information-library/country-profiles/countries-g-n/kazakhstan.aspx>
 36. Yan, W. (2019). The nuclear sins of the Soviet Union live on in Kazakhstan. Retrieved from <https://www.nature.com/articles/d41586-019-01034-8>

37. Yapiyev, V., Sagintayev, Z., Verhoef, A., Kassymbekova, A., Baigaliyeva, M., Zhumabayev, D., Malgazhdar, D., Abudanash, D., Ongdas, N., and Jumassultanova S. (2017). The changing water cycle: Burabay National Nature Park, Northern Kazakhstan. *Wiley Interdisciplinary Reviews: Water*, 4(5), e1227.

38. Yapiyev, V., Samarkhanov, K., Tulegenova, N., Jumassultanova, S., Verhoef, A., Saidaliyeva, Z., Umirov, N., Sagintayev, Z., and Namazbayeva, A. (2019). Estimation of water storage changes in small endorheic lakes in Northern Kazakhstan. *Journal of Arid Environments*, 160, 42-55.

Table 1. Intervention level and the values of dose factors when radionuclides enter the human body with water

Radionuclide	ϵ_{water}	IL^{water} Bq/kg
^{238}U	$4.5 \cdot 10^{-5}$	3.1
^{232}Th	$2.3 \cdot 10^{-4}$	0.6
^{226}Ra	$2.8 \cdot 10^{-4}$	0.5
^{210}Pb	$6.9 \cdot 10^{-4}$	0.2

Table 2. Characteristics of radiation hazardous areas

Name of region, zone	Area of the zone, ths. km ²	The number of deposits of ore occurrences U and Th	Types of formations rocks *	The area of radioactive formations, ths. km ²	Radium areolas, ths. km ²	Exceeding doses relative to the background, mSv/year	Rank
North-Kazakhstan region							
Priyesil	5.5	10	G, S	0.85	1.0	0.1	III
Zhalgyztau	0.9	-	G, V	0.15	0.16		I
Saumalkol	6.4	9	-	-	0.5	1.2 (>3.0)	II
Taldykol	1.0	1	-	-	0.24		II
Aisary	3.1	1	-	-	-		II
Akmola region							
Priyesil	7.4	4	G, S	3.2	1.8		III
Zerendy-Balkashino	11.2	15	G, V	4.0	3.14	>3.0 (>4.1)	I
Chagaly	2.9	6	G, V	2.7	0.08		
Akkol-Schuchinsk	8.5	9	G, V, S	2.3	1.3	0.9 (2.0)	II
Stepnogorsk-Zaozernyy	6.8	8	G, V	1.5	0.2	1.3 (2.4)	II

Note: * G – granites, granitoids and weathering crust, S – shale rocks, V – volcanic (effusive) acidic rocks

Source: Kayukov et al., 2014

Table 3. The specific activity of radionuclides in groundwater, Bq/kg

Administrative district	²³⁸ U	²³² Th	²²⁶ Ra	²¹⁰ Pb	¹³⁷ Cs	⁹⁰ Sr	²²² Rn
Intervention Level, IL	3	0.6	0.49	0.2	11	4.9	60
Ayyrtau	0.2-10.4	0.01-0.16	0.006-0.38	0.018-0.14	0.07-0.53	0.01-0.04	4-1073
Akzhar	0.3	0.009	-	-	-	-	3-303
Akkayin	0.4-2.19	0.01-0.08	0.04-0.19	0.01-0.04	0.007-0.04	0.007-0.09	3-58
G. Musirepov	0.01-2.92	0.005-0.014	0.008-0.13	0.025-0.1	-	0.03	3-333
Yesil	0.007-2.6	0.002-0.08	0.008-1.98	0.004-0.07	-	-	2-2795
Zhambyl	0.59-0.88	0.03-0.12	0.027-0.04	0.038	-	-	4-20
Kyzylzhar	0.18-3	0.01-0.03	0.018-0.13	0.003-0.04	-	-	3-22
Mamlyut	0.95-2.65	0.02-0.07	0.03-0.05	0.013-0.06			3-31
M. Zhumbayev	0.1-1.7	0.01-0.023	0.014-0.2	0.01-0.05	-	-	4-31
Taiynsha	0.1-1.54	0.004-0.05	0.05-0.44	0.033-0.2	-	-	3-65
Timiryazev	0.11-1.3	0.01-0.014	0.04-0.64	0.045-0.056	-	-	8-42
Ualikhanov	0.01-5.45	0.01-0.1	0.01-0.34	0.01-0.041	0.01-0.05	0.01-0.05	4-31
Shal akyn	0.2-1.13	0.0023-0.018	0.012-0.08	0.02-0.04	-	-	4-136

Note: the values of specific activities are presented in the range from minimum to maximum for the period 2011-2016.

Table 4. Specific activity of drinking water in the G. Musirepov district for 2011.

Sampling point	Source	The specific activity of radionuclides, Bq/kg			
		²³⁸ U	²³² Th	²²⁶ Ra	²¹⁰ Pb
Birlik	water supply	0.4	0	0.09	0.05
Zolotonosha	well	0.49	0.014	0.04	0.03
Saradyr	borehole	0.45	0.02	0.03	0.03
Saradyr	borehole	0.33	0.012	0.13	
Shukurkol	borehole	0.18	0.005	0.064	
Starobelka	borehole	0.94	0.005	0.03	0.04
Druzhba	borehole	1.01	0	0.08	
Peski	borehole – water supply	0.18	0.014	0.2	0.04
average value for boreholes		0.582	0.0084	0.067	0.035
average value for water supply		0.4	0	0.09	0.05
average value for wells		0.49	0.014	0.04	0.03
average value for boreholes, used for centralized water supply		0.18	0.014	0.2	0.04

Table 5. The specific activity of drinking water in the G. Musirepov district for 2012

Sampling point	Source	The specific activity of radionuclides, Bq/kg			
		²³⁸ U	²³² Th	²²⁶ Ra	²¹⁰ Pb
Zharkol	well	2.92	0.01	0.026	0.04
Berezovka	borehole	0.45	0	0.01	0.057
Novoishimskoe	borehole	0.47	0	0.01	0.067
Novoselovka	borehole	0.28	0	0.008	0.025
Kyrymbet	borehole	1.15	0	0.04	0.1
average value for boreholes		0.5875	0	0.017	0.062
average value for wells		2.92	0.01	0.026	0.04

Table 6. The specific activity of drinking water in the G. Musirepov district for 2013

Sampling point	Source	The specific activity of radionuclides, Bq/kg			
		²³⁸ U	²³² Th	²²⁶ Ra	²¹⁰ Pb
Zolotonosha	well	1.18	0.01	0.003	0.04
Chernozubovka	well	1.2	0.02	0.05	0.01
Vozvyshenka	well	1.58	0.02	0.3	0.01
Nezhenka	well	1.15	0	0.12	0.05
Chernozubovka	well	0.82	0.02	0.04	0.47
Shak pak	borehole	1.4	0.018	0.19	0.07
Privolnoe	borehole – water supply	0.05	0	0.05	0.08
average value for wells		1.186	0.014	0.1026	0.116
average value for boreholes		1.4	0.018	0.19	0.07
average value for boreholes, used for centralized water supply		0.05	0	0.05	0.08

Table 7. The specific activity of drinking water in the G. Musirepov district for 2014

Sampling point	Source	The specific activity of radionuclides, Bq/kg			
		²³⁸ U	²³² Th	²²⁶ Ra	²¹⁰ Pb
Birlik	borehole	0.23	0.009	0.026	0.07
Chervonnoye	water supply	0.12	0.014	0.031	0.013
Budennoye	water supply	0.24	0.014	0.009	0.07
Nezhenka	borehole	0.26	0.07	0.25	0.1
Peski	borehole	0.28	0.02	0.16	0.013
Stavropolka	borehole	0	0	0.018	0.026
Peski	borehole – water supply	0.09	0.012	0.2	0.05
Birlik	borehole – water supply	0.26	0.016	0.01	0.07
Kokozhar	borehole – water supply	0.13	0.022	0.1	0.08
Sarybulak	borehole – water supply	2.25	0.03	0.04	0.11
Salkynkul	borehole – water supply	0.15	0.016	0.06	0.05
Yalty	borehole – water supply	0.2	0.012	0.027	0.06
average value for boreholes		0.1925	0.02475	0.1135	0.052
average value for water supply		0.18	0.01	0.02	0.04
average value for boreholes, used for centralized water supply		0.51333	0.018	0.0728	0.07

Table 8. The specific activity of drinking water in the G. Musirepov district for 2015

Sampling point	Source	The specific activity of radionuclides, Bq/kg			
		²³⁸ U	²³² Th	²²⁶ Ra	²¹⁰ Pb
Shukyrkol	borehole	0.38	0.02	0.08	0.04
Sarybulak	borehole	1.3	0.02	0.18	0.04
Raisovka	borehole	1.22	0.03	0.19	0.09
Golopyatovo	borehole	0.58	0.04	0.04	0.07
Zhanasu	borehole	0.2	0.05	0.14	0.07
Yalty	borehole	0.32	0.02	0.04	0.01
Mukur	well	0.49	0.02	0.03	0.022
Kyrymbet	borehole	0.22	0.021	0.04	0.026
Budennoye	water supply	0.37	0.03	0.09	0.08
Novoishimskoye	water supply	0.32	0.01	0.04	0.07
average value for water supply		0.345	0.02	0.065	0.075
average value for boreholes		0.6029	0.0287	0.10143	0.0494
average value for wells		0.49	0.02	0.03	0.022

Table 9. The specific activity of drinking water in the G. Musirepov district for 2016

Sampling point	Source	The specific activity of radionuclides, Bq/kg			
		²³⁸ U	²³² Th	²²⁶ Ra	²¹⁰ Pb
Andreyevka	well	0.24	0.023	0.05	0.07
Yefimovka	well	0.2	0.025	0.05	0.07
Chernobayevka	well	0.47	0.018	0.04	0.014
Chernobayevka	spring	0.54	0.025	0.04	0.08
Tselinnoe	borehole – water supply	0.25	0.028	0.03	0.009
Druzhba	borehole	0.09	0	0.03	0.009
Toksan bi	borehole	0.13	0.018	0.04	0.07
Litvinovka	borehole	0.6	0.013	0.04	0.09
Chistopole	borehole	0.37	0.016	0.04	0.09
Sivkovka	borehole	0.31	0.018	0.04	0.023
average value for wells		0.30333	0.022	0.0467	0.0513
average value for springs		0.54	0.025	0.04	0.08
average value for boreholes, used for centralized water supply		0.25	0.028	0.03	0.009
average value for boreholes		0.3	0.013	0.038	0.0564

Table 10. Effective equivalent dose of radiation exposure, E_w , of the population of G. Musirepov district from radionuclides in drinking water, mSv/year

Year	Water sources				
	boreholes	borehole – water supply	springs	water supply	Wells
2011	0.052	0.069	-	0.057	0.042
2012	0.054	-	-	-	0.123
2013	0.123	0.052	-	-	0.121
2014	0.060	0.070	-	0.033	-
2015	0.070	-	-	0.066	0.037
2016	0.048	0.024	0.070	-	0.049

Table 11. The specific activity of drinking water in the Yesil district for 2011

Sampling point	Source	The specific activity of radionuclides, Bq/kg			
		²³⁸ U	²³² Th	²²⁶ Ra	²¹⁰ Pb
Yesilskoye	water supply	0.007	0	0.016	0.07
Gornoye	spring	0.9	0.002		
Yavlenka	borehole	0.74	0.08	0.07	
Yavlenka	borehole	0.33	0.023	0.034	0.014
Gornoye	borehole	1.9	0.005		
Gornoye	borehole	1.06	0.002		
Zarechnoye	borehole	0.23	0	0.008	0.004
Yasnovka	borehole – water supply	0.06	0.002	0.046	0.07
Amangeldinskoye	borehole – water supply	0.17	0	0.018	0.026
average value for boreholes		0.852	0.022	0.0373	0.009

Table 12. The specific activity of drinking water in the Yesil district for 2014

Sampling point	Source	The specific activity of radionuclides, Bq/kg			
		²³⁸ U	²³² Th	²²⁶ Ra	²¹⁰ Pb
Yavlenka	water supply	0.13	0.012	0.013	0.04
Yavlenka	water supply	0.2	0.009	0.014	0.026
average value for water supply		0.165	0.0105	0.014	0.033

Table 13. The specific activity of drinking water in the Yesil district for 2015

Sampling point	Source	The specific activity of radionuclides, Bq/kg			
		²³⁸ U	²³² Th	²²⁶ Ra	²¹⁰ Pb
Pokrovka	borehole	0.34	0.02	0.18	0.02
Yavlenka	well	1.22	0.04	0.04	0.09
Yavlenka	well	0.34	0.04	0.05	0.08
Amangeldinskoye	borehole – water supply	0.34	0.01	0.03	0.01
Yavlenka	water supply	0.3	0.02	0.03	0.05
Yavlenka	water supply	0.32	0.02	0.03	0.04
Yavlenka	water supply	0.32	0.02	0.03	0.03
Petrovka	water supply	0.17	0.01	0.05	0.04
Tarangul	water supply	0.36	0.01	0.04	0.02
average value for boreholes		0.34	0.02	0.18	0.02
average value for wells		0.78	0.04	0.045	0.085
average value for boreholes, used for centralized water supply		0.34	0.01	0.03	0.01
average value for water supply		0.294	0.016	0.036	0.036

Table 14. The specific activity of drinking water in the Yesil district for 2016

Sampling point	Source	The specific activity of radionuclides, Bq/kg			
		²³⁸ U	²³² Th	²²⁶ Ra	²¹⁰ Pb
Maltsevo	spring	0.69	0.02	0.04	0.04
Amangeldinskoye	borehole	0.13	0.028	0.03	0.021
Korneevka	borehole	0.49	0.016	0.15	0.05
Yasnovka	borehole	0.51	0.018	0.03	0.018
Korneyevka	borehole	1.58	0.03	0.04	0.09
Sovetskoye	borehole	0.107	0.02	0.03	0.07
Novo-Uzenka	borehole	0.3	0.02	0.04	0.07
Korneevka	borehole	2.3	0.023	0.04	0.05
average value for spring		0.69	0.02	0.04	0.04
average value for boreholes		0.774	0.022	0.051	0.053

Table 15. Effective equivalent dose of radiation exposure, E_w , of the population of the Yesil district from radionuclides coming from drinking water, mSv/year

Year	Watersources				
	boreholes	borehole – water supply	springs	water supply	wells
2011	0.044	0.035	0.030	0.039	-
2012	-	-	-	-	-
2013	-	-	-	-	-
2014	-	-	-	0.027	-
2015	0.061	0.024	-	0.038	0.084
2016	0.066	-	0.054	-	-

Table 16. The specific activity of drinking water in the Ayyrtau district for 2012

Sampling point	Source	The specific activity of radionuclides, Bq/kg			
		²³⁸ U	²³² Th	²²⁶ Ra	²¹⁰ Pb
Aryk-Balyk	borehole	0.68	0	0.14	0.03
Aryk-Balyk	borehole	0.68	0	0.17	0.04
Arka resort	borehole	0.23	0.014	0.018	0.13
Arka resort	borehole	0.32	0.023	0.006	0.09
Rodniki	borehole	0.44	0.016	0.012	0.07
Kumtuken	borehole	0.66	0	0.016	0.01
Krasnogorka	borehole	0.06	0	0.008	0.018
Aryk-Balyk	borehole - water supply	0.63	0	0.14	0.04
average value for boreholes		0.438571 4	0.00757 1	0.05285 7	0.05542 9
average value for boreholes, used for centralized water supply		0.63	0	0.14	0.04

Table 17. The specific activity of drinking water in the Ayyrtau district for 2014

Sampling point	Source	The specific activity of radionuclides, Bq/kg			
		²³⁸ U	²³² Th	²²⁶ Ra	²¹⁰ Pb
Orlovka	borehole	0	0.016	0.026	0.0013
Kirillovka	borehole	0	0	0.026	0.026
Alzhanka	borehole	0.035	0	0.026	0.05
Yeletskoye	borehole	0.046	0	0.007	0.04
N.Burluk	borehole	0.035	0	0.004	0.05
N.Burluk	borehole	0.023	0	0.011	0.026
Yakshi-Yangistau	borehole	0.08	0.009	0.001	0.04
Lobanovo	borehole	0	0	0.026	0.05
Saumalkol	borehole	0	0.007	0.013	0.07
Kirillovka	borehole - water supply	0.53	0.035	0.038	0.04
Saumalkol	borehole - water supply	0.023	0.014	0.018	0.12
Gorny	borehole - water supply	0.014	0.012	0.023	0.03
average value for boreholes		0.02433	0.00356	0.016	0.0393
average value for boreholes, used for centralized water supply		0.189	0.02033	0.026	0.0633

Table 18. The specific activity of drinking water in the Ayyrtau district for 2015

Sampling point	Source	The specific activity of radionuclides, Bq/kg			
		²³⁸ U	²³² Th	²²⁶ Ra	²¹⁰ Pb
Saumalkol	borehole	2.24	0.03	0.03	0.05
Saumalkol	borehole	0.85	0.02	0.02	0.09
Saumalkol	borehole	0.87	0.03	0.04	0.14
Saumalkol	borehole	0.45	0.02	0.12	0.09
Saumalkol	borehole	0.26	0.02	0.04	0.03
Saumalkol	borehole	0.85	0.05	0.04	0.04
Saumalkol	borehole	0.68	0.03	0.08	0.04
Saumalkol	borehole	1.02	0.02	0.03	0.05
Zarya	borehole - water supply	0.59	0.04	0.13	0.05
Karlygash	borehole - water supply	0.22	0.03	0.03	0.09
average value for boreholes		0.9025	0.0275	0.05	0.0663
average value for boreholes, used for centralized water supply		0.405	0.035	0.08	0.07

Table 19. The specific activity of drinking water in the Ayyrtau district for 2016

Sampling point	Source	The specific activity of radionuclides, Bq/kg			
		²³⁸ U	²³² Th	²²⁶ Ra	²¹⁰ Pb
Yeletskoye	borehole	0.15	0.018	0.03	0.005
Kumtuken	borehole	0.4	0.03	0.04	0.03
Kumtuken	borehole	0.21	0.016	0.04	0.07
Daukara	borehole	0.69	0.02	0.03	0.07
Lobanovo	borehole	1.45	0.02	0.04	0.09
Novoukrainka	borehole	0.4	0.028	0.03	0.04
Kirillovka	borehole	0.2	0	0.03	0.003
Yeletskoye	borehole	0.15	0.018	0.03	0.022
Yeletskoye	borehole	0.64	0.028	0.03	0.03
average value for boreholes		0.477	0.0198	0.033	0.04

Table 20. Effective equivalent dose of radiation exposure, E_w , of the population of the Ayyrtau region from radionuclides coming from drinking water, mSv/year

Year	Water sources				
	boreholes	borehole – water supply	springs	water supply	wells
2011	-	-	-	-	-
2012	0.054	0.069	-	-	-
2013	-	-	-	-	-
2014	0.024	0.047	-	-	-
2015	0.078	0.071	-	-	-
2016	0.046	-	-	-	-

Table 21. The specific activity of drinking water of the Tayinsha district for 2012

Sampling point	Source	The specific activity of radionuclides, Bq/kg			
		^{238}U	^{232}Th	^{226}Ra	^{210}Pb
Madeniyet	borehole	0.32	0.01	0.027	0,033
Letovochnoye	borehole	0.2	trace	0.005	0,038
average value for boreholes		0.26	0.01	0.02	0.04

Table 22. The specific activity of drinking water of the Tayinsha district for 2013

Sampling point	Source	The specific activity of radionuclides, Bq/kg			
		^{238}U	^{232}Th	^{226}Ra	^{210}Pb
Petrovka	borehole - water supply	1.41	0.014	0.05	0.08
Chkalovo	borehole	0.38	0	0.05	0.05
Kellerovka	borehole	0.39	0.01	0.03	0.05
Podlesnoye	borehole	0.36	0	0.03	0.04
Madeniet	borehole	0.45	0	0.03	0.04
Akkuduk	well	0.45	0	0.01	0.05
average value for boreholes		0.395	0.0025	0.035	0.045
average value for wells		0.45	0	0.01	0.05
average value for boreholes, used for centralized water supply		1.41	0.014	0.05	0.08

Table 23. The specific activity of drinking water of the Tayinsha district for 2014

Sampling point	Source	The specific activity of radionuclides, Bq/kg			
		^{238}U	^{232}Th	^{226}Ra	^{210}Pb
Bolshoy Izyum	well	0.18	0.007	0.04	0.05
Ivan-gorod	well	0.20	0.018	0.29	0.03
Kellerovka	well	0.24	0.022	0.013	0.06
Ozernoye	well	0.24	0.022	0.025	0.028
Kalinovka	well	0.08	0.009	0.04	0.029
Amandyk	well	0.17	0.012	0.04	0.003
Zolotorunnoye	well	0.20	0.008	0.04	0.008

Taldykul	well	0.12	0.01	0.026	0.01
Bolshoy Izyum	well	0.10	0.002	0.026	0.05
Kozashar	well	0.20	0.002	0.04	0.039
Lyubimovka	borehole	0.08	0.012	0.0013	0.07
Makashevka	borehole	0.046	0.007	0.004	0.026
Letovochnoye	borehole	0.046	0.007	0.04	0.05
Podlesnoye	borehole	0.07	0.012	0.026	0.04
Ilichevka	borehole	0.08	0	0.018	0
average value for wells		0.173	0.0112	0.058	0.0307
average value for boreholes		0.0644	0.0076	0.0179	0.0372

Table 24. The specific activity of drinking water of the Tayinsha district for 2015

Sampling point	Source	The specific activity of radionuclides, Bq/kg			
		²³⁸ U	²³² Th	²²⁶ Ra	²¹⁰ Pb
Amandyk	well	0.63	0.02	0.04	0.09
Petrovka	well	0.49	0.03	0.07	0.08
Amandyk	well	0.66	0.03	0.04	0.01
Petrovka	well	0.75	0.04	0.1	0.005
Petrovka	well	0.68	0.02	0.03	0.05
Ak-kuduk	well	0.32	0.01	0.04	0.07
Petrovka	well	0.51	0.02	0.07	0.09
Vishnevka	water supply	0.58	0.03	0.14	0.02
Petrovka	water supply	1.28	0.02	0.08	0.013
Ilichevka	borehole	0.84	0.02	0.04	0.017
Ilichevka	borehole	0.66	0.02	0.05	0.08
Ilichevka	borehole	0.4	0.02	0.04	0.08
Ilichevka	borehole	0.1	0.02	0.04	0.07
Krasnokamenka	borehole	0.2	0.01	0.03	0.02
Kellerovka	borehole	0.13	0.005	0.05	0.02
Dragomirovka	borehole	0.41	0.02	0.06	0.01
average value for wells		0.58	0.02	0.06	0.06
average value for water supply		0.93	0.025	0.11	0.0165
average value for boreholes		0.391	0.0164	0.044	0.0424

Table 25. The specific activity of drinking water of the Tayinsha district for 2016

Sampling point	Source	The specific activity of radionuclides, Bq/kg			
		²³⁸ U	²³² Th	²²⁶ Ra	²¹⁰ Pb
Bolshoy Izyum	well	0.28	0.04	0.05	0.01
Petrovka	well	0.29	0.03	0.05	0.005
Aymak	borehole	0.32	0.03	0.06	0.012
Aymak	borehole	0.21	0.03	0.05	0.003
Letovochnoye	borehole	0	0.04	0.05	0.017
Letovochnoye	borehole	0.22	0.04	0.05	0.008
Ilichevka	borehole	0.02	0.04	0.05	0.03
Ilichevka	borehole	0.24	0.03	0.05	0.01
average value for boreholes		0.168	0.035	0.052	0.0133
average value for wells		0.285	0.035	0.05	0.0075

Table 26. Effective equivalent dose of radiation exposure, E_w , of the population of the Tayinsha district of radionuclides from drinking water, mSv/year

Year	Water sources				
	boreholes	borehole – water supply	springs	water supply	wells
2011	-	-	-	-	-
2012	0.031	-	-	-	-
2013	0.043	0.099	-	-	0.042
2014	0.026	-	-	-	0.035
2015	0.046	-	-	0.066	0.063
2016	0.029	-	-	-	0.029

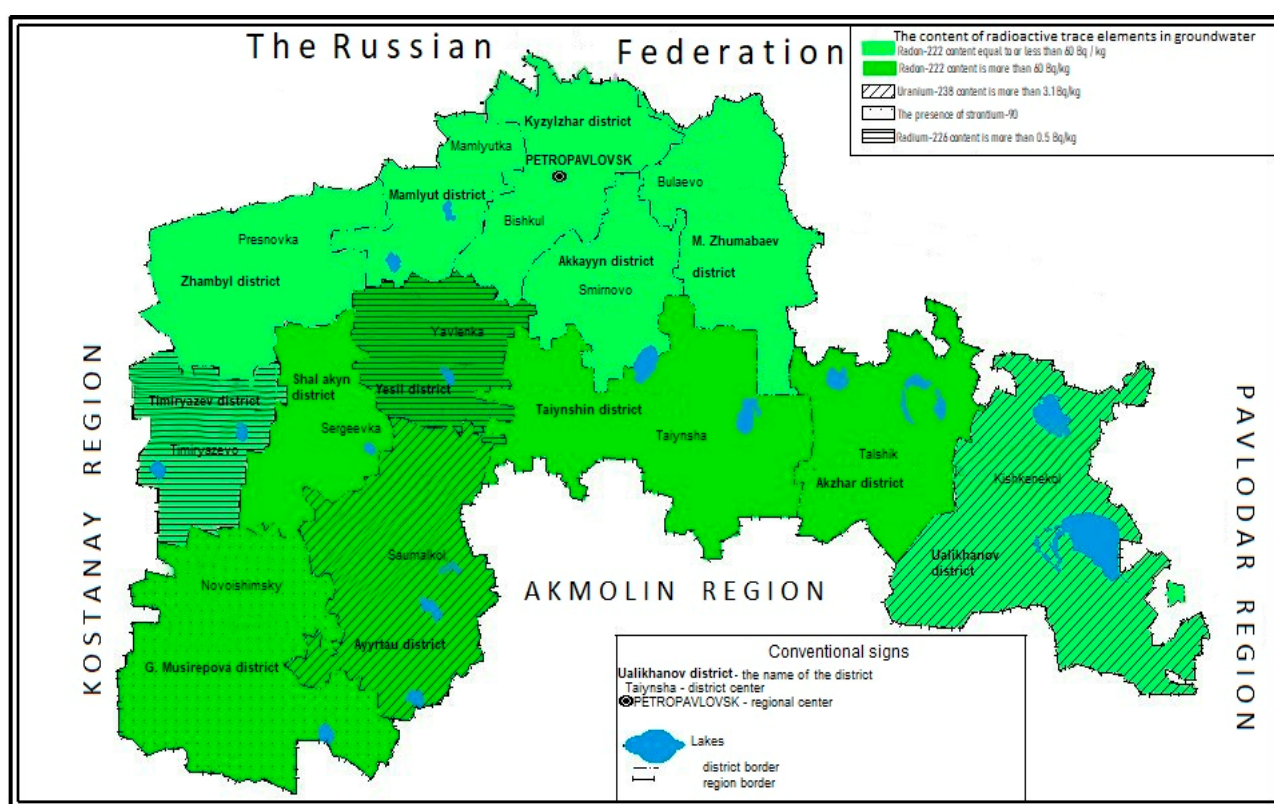


Figure 1. The content of radioactive trace elements in groundwater

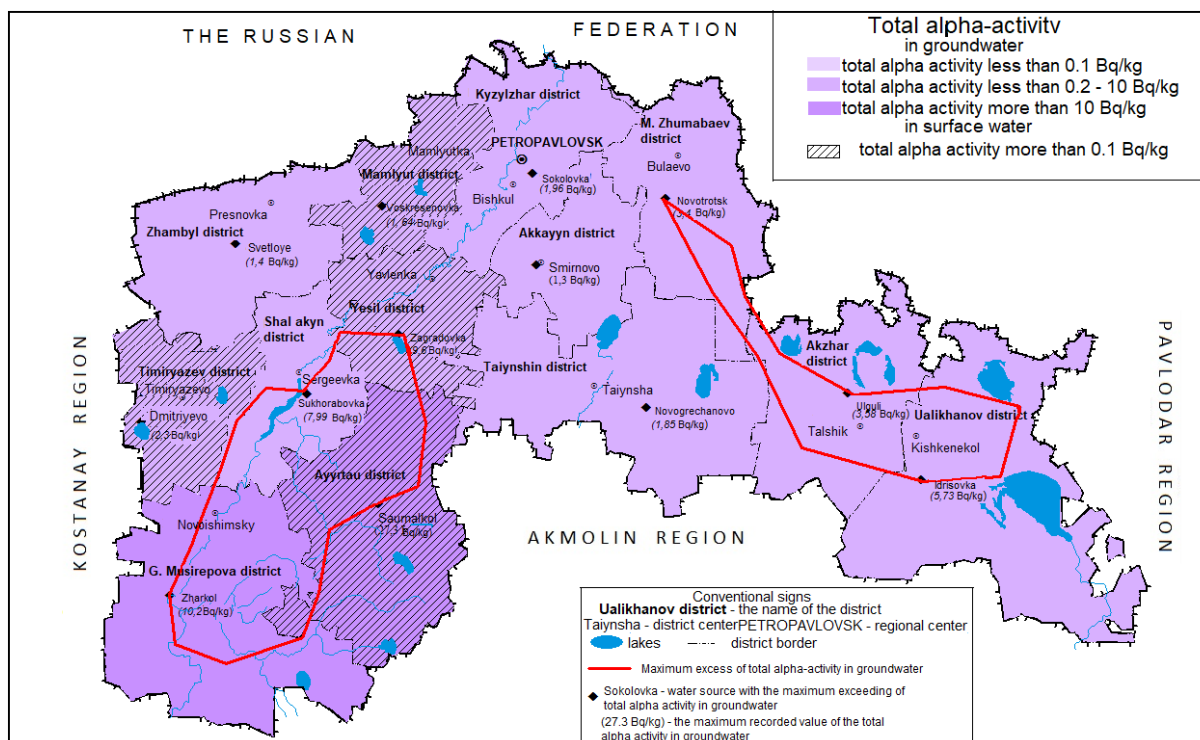


Figure 2. Total alpha-activity in groundwater



Figure 3. Total beta-activity in groundwater

MÉTODOS COSMOGEOLÓGICOS PARA IDENTIFICAR DEPÓSITOS MINERAIS**REMOTE SENSING TECHNIQUES FOR IDENTIFICATION OF MINERAL DEPOSIT****КОСМОГЕОЛОГИЧЕСКИЕ МЕТОДЫ ДЛЯ ВЫЯВЛЕНИЯ ПЕРСПЕКТИВНЫХ МЕСТОРОЖДЕНИЙ ИСКОПАЕМЫХ**

BAIBATSHA, Adilkhan B.^{1*}; KEMBAYEV, Maxat K.²; MAMANOV, Erkhosha Zh.³;
SHAIYAKHMET, Tanirbergen K.⁴;

¹ Kazakh National Research Technical University named after K.I. Satpayev (Satbayev University); K. Turysov Institute of Geology, Oil, and Mining; Innovative Geological and Mineralogical Laboratory; 22a Satpaev Str.; zip code 050013; Almaty – Republic of Kazakhstan

^{2,3,4} Kazakh National Research Technical University named after K.I. Satpayev (Satbayev University); K. Turysov Institute of Geology, Oil, and Mining; Department of Geological Mapping, Mineral Deposits Search and Exploration; 22a Satpaev Str.; zip code 050013; Almaty – Republic of Kazakhstan

* Correspondence author
e-mail: baibatsha48@mail.ru

Received 24 June 2020; received in revised form 29 October 2020; accepted 10 November 2020

RESUMO

Foram realizados os estudos sobre o uso de sensoriamento remoto da Terra para detectar estruturas geológicas de controle de minério. Os resultados da pesquisa foram obtidos usando um banco de dados de sensoriamento remoto baseado em imagens de satélites Landsat e ASTER. Como resultado deste trabalho, foram construídos esquemas de estrutura espacial de regiões individuais do Cazaquistão, determinados os principais fatores de controle de minério e determinadas as áreas de detecção de mineralização endógena. As imagens de satélite digitais selecionadas fornecem uma determinada escala de pesquisa e têm a resolução espectral máxima; portanto, cobrem a área de pesquisa em todas as faixas espectrais possíveis. Os diagramas de estrutura espacial mostram que de acordo com a morfologia as estruturas lineares são falhas, zonas de maior perturbação, limites geológicos, elementos de folheações, corpos de diques e outros elementos de natureza geológica. Sob condições de um relevo fracamente dissecado, métodos de gradiente multidirecional e vários métodos de filtragem provaram ser eficazes na interpretação de estruturas lineares. Ao identificar estruturas de anéis e arcos dentro das áreas estudadas, foram utilizadas as seguintes características: os limites de arcos e anéis entre blocos com diferentes texturas de materiais espaciais; limites da heterogeneidade da paisagem, morfologia de arcos e anéis. Em termos de escala, as estruturas de anel são subdivididas condicionalmente em estruturas de segunda ordem e pequenas. Estruturas com um raio de 3 a 50 km pertencem às estruturas de anel de segunda ordem, e estruturas com um raio inferior a 3 km pertencem a estruturas pequenas. Os complexos estratificados nas áreas estudadas são claramente divididos em cominuídos e litificados. Depósitos de neogeno quaternários, proluviais e aluviais, aluviais, eólicos e depósitos de origem indiferenciada são interpretados como cominuídos. Os complexos em camadas litificadas são dobrados e têm proliferação predominantemente noroeste. Na identificação de corpos de rochas intrusivas, foram utilizadas bibliotecas espectrais, características de textura das imagens de satélite e a experiência dos autores.

Palavras-chave: *sensoriamento remoto, interpretação digital de imagens de satélite, fatores de controle de minério, esquemas cosmogeológicos, áreas prospectiva.*

ABSTRACT

Studies on the use of Remote Sensing to highlight ore-controlling geological structures were performed. The research findings were obtained using a remote sensing database created from Landsat and ASTER data. As a result of this work, space-structural schemes of individual regions of Kazakhstan were built, and the main ore-controlling factors were determined. Besides, the areas for the detection of endogenous mineralization were identified accordingly. The selected digital satellite imageries provide a given research scale and have the maximum spectral resolution; therefore, they covered the research area in all possible spectral ranges. In space-structural diagrams, the lineament morphology represents the faults, areas of increased fracture, geological

boundaries, litter elements, dam bodies, and other elements of a geological nature. Under conditions of a weakly dissected relief, the multidirectional gradient methods and various filtering methods proved to be useful for distinguishing linear structures. When identifying ring and arc structures within the study area, the following functions were used: the boundaries of arcs and rings between blocks with different textures of space materials, boundaries of landscape heterogeneity, the morphology of arcs and rings. According to the scale, ring structures are conventionally divided into second-order and small structures. Structures with radius from 3 to 50 km belong to second-order ring structures, and small structures with a radius less than 3 km belong to small structures. Stratified complexes in the studied areas are divided into loose and lithified. Neogene-Quaternary proluvial, alluvial-proluvial, alluvial, aeolian and undifferentiated sediments are classified as loose. The lithified layered complexes fold into folds with a predominance of the northwestern strike. When identifying bodies of intrusive rocks, spectral libraries, texture features of satellite images, and the experience of the authors were used.

Keywords: *digital image interpretation, ore-controlling factors, cosmogeological schemes, promising areas.*

АННОТАЦИЯ

Проведены исследования по использованию дистанционного зондирования Земли для выделения рудоконтролирующих геологических структур. Результаты исследований получены с использованием базы данных дистанционного зондирования, созданной на основе космических снимков Landsat и ASTER. В результате этой работы были построены космоструктурные схемы отдельных регионов Казахстана и определены основные рудоконтролирующие факторы, а также определены площади обнаружения эндогенной минерализации. Выбранные цифровые спутниковые изображения обеспечивают заданный масштаб исследования и имеют максимальное спектральное разрешение, поэтому они охватывают область исследования во всех возможных спектральных диапазонах. На космоструктурных схемах линейные структуры по морфологии представляют собой разломы, зоны повышенной нарушенности, геологические границы, элементы слоистости, дайковые тела и другие элементы геологического характера. В условиях слабо расчлененного рельефа для интерпретации линейных структур оказались эффективными методы разнонаправленного градиента и различные методы фильтрации. При идентификации кольцевых и дуговых структур в пределах исследованных областей использовались следующие признаки: границы дуг и колец между блоками с различными текстурами космических материалов; границы ландшафтной неоднородности, морфология дуг и колец. По масштабам кольцевые структуры условно подразделяются на второго порядка и малые. Структуры с радиусом от 3 до 50 км относятся к кольцевым структурам второго порядка, а небольшие структуры с радиусом менее 3 км - к малым. Стратифицированные комплексы на изучаемых участках четко делятся на рыхлые и литифицированные. Неоген-четвертичные пролювиальные, аллювиально-пролювиальные, аллювиальные, золотые и отложения недифференцированного происхождения интерпретируются как рыхлые. Литифицированные слоистые комплексы сложены в складки и имеют преимущественно северо-западные простирания. При идентификации тел интрузивных пород использовались спектральные библиотеки, текстурные особенности космоснимков и опыт авторов.

Ключевые слова: *дистанционное зондирование, цифровая интерпретация космоснимков, рудоконтролирующие факторы, космогеологические схемы, перспективные площади.*

1. INTRODUCTION

Existing traditional technologies for targeting and detecting minerals is limited by depth, visibility, and heterogeneity. The work is mainly carried out on the Earth surface and is characterized by discrete data. Deeply occurring geological structures often remain uncharacteristic and undervalued. The underestimation of the phenomena associated with the profound effects of space sounding reduces the effectiveness of the completeness of research and the discovery of deep minerals. Geological studies using remote sensing data provide new material for developing science and practice in this area. The study

attempts to develop a method of analyzing ore-controlling geological structures in exploration areas based on Remote sensing data. The described technology was tested in practice for mineral exploration in Kazakhstan (Galvão *et al.*, 2008; Blaschke, 2010; Mars and Rowan, 2010; Chemin and Ducati, 2011; Khorram *et al.*, 2013; Barrachina *et al.*, 2015; Khorram *et al.*, 2016).

Along with the advances in technology, there has been a rapid and growing social acceptance of remote sensing. At first, remote sensing was a concern to the public with the "eye in the sky" and "Big Brother" concept. This perception, however, has eroded to a

considerable extent (but may be returning). Today, many sensors are deployed on numerous satellites and airborne platforms that collect vast amounts of remotely sensed data around the globe and around the clock. These data of various characteristics in spectral, spatial, radiometric, and temporal resolutions are commonly utilized in environmental and natural resource management, climate change, disaster management, law enforcement, military, and military intelligence gathering. Remote sensing has permeated daily human lives through Google Earth; global positioning systems (GPS); weather forecasting, wildland fire, hurricane, and disaster management; precision agriculture; and natural resources inventory and monitoring. People cannot live without it (Khorram *et al.*, 2016).

2. MATERIALS AND METHODS

2.1. Selection of Satellite Imageries

The possibilities of using Remote Sensing were not limited to those listed. The article used data Remote Sensing data for targeting and determination of minerals. In this study, Landsat ETM+ and ASTER (the Advanced Spaceborne Thermal Emission and Reflection Radiometer), Digital Elevation Models (DEM) – data from SRTM (Shuttle Radar Topographic Mission) and AsterGDEM (Aster Global Digital Elevation Model) were used. Landsat ETM+ archival data were obtained from the satellite imagery library of the University of Maryland (USA) (Galvão *et al.*, 2008). The data of this space system were characterized by the following spectral ranges for multispectral channels: 1) 450-515 nm; 2) 525-605 nm; 3) 630-690 nm; 4) 750-900 nm; 5) 1550-1750 nm; 6) 10400-12500 nm; 7) 2090-2350 nm; 8) PAN channel – 520-900 nm. The spatial resolution of the images was: for 1, 2, 3, 4, 5, and 7 channels – 30 m for six channels – 60 m for the PAN channel – 14.25 m (Figure 1). Two Landsat scenes were used – p147r028_7dk19990826 and p148r028_7dk19990817.

ASTER data were obtained from the satellite imagery library of the American Geological Society (USGS) (EarthExplorer, 2020). The spectral and spatial resolutions of Aster data are shown in Tables 1 and 2. The spectral characteristics of the images of this space system are 1-3 channels (VNIR range) 520-860 nm, 4-9 channels (SWIR range) 1600-2430 nm, 10-14 channels (TIR range) 8125-11650 nm. The spatial resolution of images: 1-3 channels – 15 m, 4-9 channels – 30 m, 10-14 channels – 90 m. DEM (Digital Elevation Model) of AsterGDEM was

obtained from the same library. These data have a spatial resolution of 25 m. Preprocessing digital satellite images, preparation of distance bases and space-structural schemes were performed using licensed software ERDAS Imagine 10.0 and ArcGIS 9.3 in the Scientific-Innovative and geological Remote sensing research Center “Cosmogeology” at the Tomsk Polytechnical University, Russia.

Upon the completion of Landsat and ASTER, data space-structured schemes were obtained for the targeted area. In these areas, the main ore-controlling factors were identified, and the promising areas for detection of mineralization were identified relatively. The general scheme of the study includes the following main stages:

- 1) Selection of Remote Sensing data.
- 2) Preprocessing and processing of digital satellite images;
- 3) Preparation of distance basics based on Landsat and ASTER data;
- 4) Interpretation and compilation of space-structural schemes in the study area.

To support the work stipulated by the research plan (which was presented in the four paragraphs above), medium spatial resolution imageries, including Landsat ETM+ and ASTER, were selected, as well as Digital Elevation Models (DEM) of SRTM and AsterGDEM data were targeted for structure analysis. The selected digital satellite images provided the specified research scale and the maximum spectral resolution, i.e., they made it possible to cover the research area in all possible spectral ranges. The images were selected considering the climate during the period of vegetation cover, lack of snow cover, and minimal humidity. These conditions met the requirements for research of the selected objects (Akoveckij, 1983; Beloborodov and Kogen, 1984; Poceluev *et al.*, 2007; Poceluev *et al.*, 2010; Poceluev *et al.*, 2012; Baibatsha, 2018).

2.2. Data analysis and interpretation

The processing of remotely sensed data for geological interpretation was divided into two main stages. The first stage was preprocessing. It is intended to calibrate and atmospherically correct the satellite data and was mainly required for further interpretation. The preprocessing stage includes the following types of transformations: 1) geometric correction of satellite images; 2) radiometric calibration of images; 3) correction of the influence of the atmosphere; 4) recovery of missing pixels; 5) contrasting; 6) filtration;

7) recalibration of the multispectral image to a higher spatial resolution. The second stage was processing carried out for the purpose of geological interpretation. In this regard, the main point of the procedures of the second processing unit was to identify the features of the earth's surface that have a direct or indirect geological nature (Mamanov *et al.*, 2016).

Details of the and interpretation and modeling of geological and ore systems were considered in works of Akoveckij (1983); Beloborodov and Kogen (1984); Poceluev *et al.* (2007); Poceluev *et al.* (2010); Poceluev *et al.* (2012), and Gohman (2015). The most acceptable can be recognized as the technological scheme for deciphering digital satellite imagery data, Figure 2, (Kalmykov and Serokurov, 1991). In the given scheme, the more traditional approach in geology was visual interpretation. The classification of methods for visual interpretation of Remote Sensing data was generally based on the two approaches: direct (direct interpretation) – a geologist carried out recognition of target objects; preprocessing and processing; and formal (indirect interpretation) was conducted with the allocation of point, linear, arc, ring and plane elements on the earth's surface according to color, texture, brightness and other characteristics, followed by their sorting, statistical processing, qualitative and quantitative assessment, related to geological structures and objects. Direct interpretation involved knowledge of the geology of the studied area by the specialist-interpreter. It often came down to clarifying the boundaries of geological objects mapped by other methods (mainly ground-based) (Lyubimova and Spiridonov, 1999).

Formal visual interpretation of the first stage was limited to recognition and fixation of landscape or thermal heterogeneities. It thus freed the operator from the ideological framework of geological models adopted in the area or its organization. However, as a rule, formal interpretation in its pure form did not occur (it seems that the rule is known to many geologists: "see what you know" worked here), the experience and knowledge of a specialist played a decisive role (Lyubimova and Spiridonov, 1999). In this regard, the possibility of fully formal interpretation in the computer version raises great doubts, although this direction looks attractive since it allows us to exclude the subjective factor.

In interpretation, as a rule, both approaches were used. In addition to this, the interpretation of the source and derivative data was usually made by highly qualified geologists

with approximately the same level of training and experience. In this case, the focus was not on finding out the percentage of integration of the interpretation results but on the possibility of obtaining additional information. The assessment of integration in percentages or points, the results of which are often given in the literature devoted to this topic, in the authors' opinion, was either formal-statistical or subjective. Especially in cases where lineament interpretation was performed, since the lineament could reflect an area object, for example, a straightened section of a river valley and a dividing ridge along with it. Identifying geological structures as lineaments in the processing stage revealed more essential to make sense for achieving g of maximum integration of results (Mamanov *et al.*, 2016).

As practice shows, the analysis of satellite images and digital elevation models revealed many differently oriented lineaments, which were a dense network and numerous ring structures of different sizes. Provided mapped showing lineaments can be generated by various factors, including layering, streakiness, the fracturing of rocks, facies of igneous and metamorphic rocks, fault zones, which are reflected in the features of the soil and vegetation cover, temperature fields, and relief. In some cases, ring and arc structures were directly related to the deep origin rocks or have a deep source, such as bodies of intrusive and volcanic rocks, over-intrusive domes. However, often such a relationship was not detected or was very indirect. The discussion was the nature of large ring structures with a diameter of tens and hundreds of kilometers (Poceluev *et al.*, 2010).

Since the grid of lineaments and ring structures is currently mapped to one degree or another and is confused with line structures on the earth surface, it identified specific structures. It established their relative age and metallogenic value, additional processing of primary data was required. To solve these problems, there were qualitative and quantitative methods for the analysis of primary data (Poceluev *et al.*, 2012).

Qualitative methods for analyzing the lineaments were widely described in the literature and were quite useful in the metallogenic analysis (Crowley *et al.*, 1989; Dolivo-Dobrovol'skij *et al.*, 1980; Kac *et al.*, 1986; Kac *et al.*, 1989; Kalmykov and Serokurov, 1991; Percov, 2000). Specialists carried them out and, together with the data of direct interpretation, allowed revealing structure-forming elements. Quantitative methods for analyzing the spatial relationships of lineaments, arc, and ring structures made it possible to obtain

digital estimates, establish correlation dependencies, and filter information.

Various techniques and methods for preliminary processing of raster images were used to identify mineralization control factors and create predictive-search models. Raster image analyzes were based on the next features: direct interpretations of heterogeneous objects to define its type and scale; qualitative and quantitative analyses of data; interpretation of data, and its correlation with available geological and geophysical data.

The use of digital processing of imagery data with formal interpretation at the first stage, followed by deciphering the data, made it possible to recognize weakly anomalous objects of both linear and arc and ring morphology and elements of a geological character – intrusive formations, paleo-valleys. The results of the interpretation of raster images at the last stage were filtered out based on available geological and geophysical data. The set of reporting information included layers of decryption results containing the entire set of linear, circular, and areal elements of the geological structure. The geological nature of some of them can be clarified if complete information was available on the geology of the area (Mars and Rowan, 2010).

2.3. Indicators of identification and interpretation of linear structures

Traditionally, linear morphology objects on space structural diagrams show intermittent faults, zones of increased fracturing, various cleats, geological boundaries, bedding elements, dike bodies, and other elements of a geological nature. The entire complex of initial and derivative space data was used to identify linear structures in the studied areas. In poorly divided relief conditions, methods of differently oriented gradients and various filtering methods have proven to be especially useful for emphasizing linear structures. In some cases (for example, in the southern part of the Usharal site), linear structures were distinguished due to directed differentiation of digital relief models. The followings are used as indicators of linear structure in this study (Poceluev *et al.*, 2007; Poceluev *et al.*, 2010; Poceluev *et al.*, 2012):

- gradient areas of the filtered image;
- rectilinear fragments of the boundaries between blocks with different image texture;
- linear boundaries underlined by oppressed vegetation;

- straight sections of the elements of river valleys of a high order;

- landscape heterogeneities of linear morphology;

- gradient sections of the first derivative of a digital elevation model.

During the interpretation and processing of space-structural schemes, lineaments having a geological nature were distinguished. Their interpretation was carried out using open geological information. Linear structures were discontinuous disturbances, geological boundaries; bedding elements of sedimentary rocks; dikes of various composition. Indicators of revealing ring and arc structures and their interpretation. Ring and arc structures were traditionally distinguished during the visual interpretation of aerial and satellite imageries. The literature noted the spatial relationship of ring structures and mineral deposits (Lyubimova and Spiridonov, 1999; Percov, 2001; Labutina, 2004; Baibatsha *et al.*, 2016). Simultaneously, various mechanisms of the formation of ring structures (endogenous, exogenous, cosmogenic) were discussed. When highlighting the ring and arc structures in the study area, the following features were used:

- arc and annular boundaries between blocks and different texture of space materials;

- boundaries of landscape heterogeneities of arc and ring morphology.

To identify ring and arc structures, the entire complex of primary and secondary satellite imageries was used. For instance, in East Balkhash and Usharal areas, more than 30 ring and arc structures with a radius of the hundred meters to 48 km were mapped. The radius of the ring structure is conditionally divided into structures of the second-order and small. The second-order ring structures include structures with radius from 4 to 48 km and small ones with a radius of less than 4 km.

It is assumed that all structures were associated with endogenous processes and magmatism. In particular, for the Yenisei Ridge, it was shown (Anan'ev *et al.*, 2012) that first-order ring structures reflect deep facies of granitization during the continental crust formation. Ring structures of the second-order were associated with intermediate intrusive bodies, both blind and exposed by erosion. Higher-order structures can record traces of the interaction of hydrothermal fluid systems with host rocks. According to possible formation mechanisms, all mapped

structures were divided into magmatogenic, hydrothermal-metasomatic, and unknown origins.

2.4. Features (Extraction) of planar bodies and Paleovalleys

An analysis of the entire complex of primary and secondary satellite imageries made it possible to distinguish stratified complexes and bodies of intrusive rocks of various compositions and forms of occurrence (Mamanov *et al.*, 2016). Stratified complexes in the studied areas were divided into loose and lithified. Neogene-Quaternary proluvial, alluvial proluvial, alluvial, aeolian and undivided sediments were classified as loose. The lithified Paleozoic stratified complexes occupy a significant part of the area plots. They were wrinkled in folds with a predominant northwestern strike of the axes.

To extract the bodies of intrusive rocks, the authors used the Johns Hopkins University Rock Library (2020) and the USGS Spectroscopy Laboratory (2020), texture features of satellite images. ASTER satellite images distinguish the vast majority of the bodies of intrusive rocks. Based on mineralogical composition, intrusive rocks were divided into ultrabasic, essential, and intermediate following spectral characteristics. Areas with traces of hydrothermal-metasomatic changes, which possibly control the position of ore mineralization, were also classified as planar bodies.

In the exocontact parts of acidic intrusions, thermal exposure traces are often found, which can be represented by keratinization, skarning. Such traces indicate active intrusive contact and can be considered as a criterion for mineralization. In some local areas of the studied areas, similar exocontact changes were also established by spectral characteristics without a visible connection with magmatism. This may indicate the presence of blind acidic intrusions that do not reach the surface (Barrachina *et al.*, 2015).

3. RESULTS AND DISCUSSION:

The geological remote sensing for detection and exploring of minerals has been tested in various structural and geological zones and areas of Kazakhstan (Baibatsha, 2018): Torgai district, Karsakpai-Ulytau zone, Shu-Ile belt, North Balkhash, East Balkhash, and Usharal (Figure 3). Ore areas were characterized by varying degrees of knowledge. It should be noted that all the covered areas were poorly studied to depth, especially the territories covered by

sediments. The tested techniques are effective for areas such as separate sections of the Valeryanov structural-formation zone, characterized by difficult natural conditions for work – extremely low exposure, poorly divided relief, significant areas of allochthonous deposits, very high agronomic “noisiness” and wide development of hydrological objects (Figure 4). It should be noted that the research area is geologically quite well studied and explored. Therefore, ore mineralization could be explored mainly in considerable depth and buried by loose deposits. This requires the use of new technologies to determine and explore mineral deposits, which allow, at the initial stage, to optimize the size of promising areas for setting up exploratory work in a short time at a minimum cost.

An analysis of Landsat satellite images of the near-IR and thermal channels reveals extended ribbon-like bodies interpreted as buried paleo-valleys (Figure 5). When interpreting satellite images, especially their infrared and thermal channels were found useful for distinguishing buried paleo-valleys and planar bodies of acidic intrusions. Their total length is 228 linear kilometers. According to the manifestation of remotely sensed data, the paleo-valleys are divided into two types: the first type is quite wide (600-3500 m) fragmentary-ribbon-like, read-only in satellite imagery; the second type is narrow (300-900 m), long ribbon-like ones are read in satellite imagery and are emphasized by a network of small lakes (Figure 6). By the nature of the relationship, it was found that the second type of river paleo-valleys crosses the first. Based on this, it is proposed to distinguish two different-age river paleo systems (Poceluev *et al.*, 2010).

Within the area described above, two systems of buried paleo-valleys of the pre-Paleogene age are distinguished. The most ancient paleovalleys are believed to be erosion-karst erosive from Cretaceous and Carboniferous deposits. By age, they are closest to the time of the formation of the Shaimerden and Krasnooktyabrsk deposits, the position of which is controlled by one of these valleys. The direction of the paleo-valleys is variable, but in general, they have a north-northeast orientation. Thus, they can be considered as a search criterion.

The position of mineralization is controlled on the one hand by the development of these valleys, and on the other hand, by tectonic zones of the basement. These zones determine both the location of the paleodolines themselves and the position of the Karst cavities in the interface with structures of a different orientation. The

confinement of mineralization to Karst cavities in the paleo-valleys channels makes it possible to generally represent the conditions for the formation of mineralization and classify it as the "Niagara" type. The term, obviously, most fully reflects the formation mechanism of these ores.

At the same time, deposits of paleo-valleys may include mineralization of a different composition. They may be associated with infiltration-type uranium mineralization in the Upper Jurassic-Lower Cretaceous paleo stream deposits, known in the depressive structures of the northern slope of the Kostanai rampart. There, the paleo-valleys also have a north-north-east direction and merge to the north.

It is possible to identify buried gold placers in the Paleostream deposits, which is indicated by the presence of high metal concentrations (0.2-0.7 to 5 g / t) in deposits 6a of the Aiat deposit and sub-bauxite "clay" clays of the East Aiat deposit. Similar placers in ancient (buried) valleys are known in the Jitigara district of the Kostanai region. In the paleo-valleys, it is also possible to identify zircon-ilmenite placers.

Prospects for the Arganaty area. According to the methodology described above, space-structural schemes of the Arganaty area (East Balkhash) were compiled due to the work. The diagrams show the whole complex of selected elements. The scheme of covering the area of the work with space materials is shown in Figure 7. On the area, linear, ring, and planar space geological structures are distinguished. More than 900 linear structures were identified, among which about 640 received geological interpretation. Discontinuous disturbances, geological boundaries, and layering elements of lithified stratified complexes were attributed to such structures.

Faults on the Arganaty area are predominantly northwestern and sub-latitudinal strikes. The primary fault violation is a right-shift displacement located at the northeast border of the area. It has a north-eastern strike, and it is not possible to determine the amplitude of the displacement due to the wide development of modern sediments and the laid-out relief near the area. Sublatitudinal faults associated with the main structure are classified as second-order faults disturbances. The amplitudes of right-and-right strike-slip faults in such structures reach 16 km. Other faults have a predominantly north-eastern strike.

Ring structures with a radius of 0.13 to 48 km were mapped in the Arganaty area and its immediate vicinity. It should be noted right away

that the site is located in the central part of the second-order magmatogenic ring structure with a radius of 48 km. Ring structures with a smaller radius are "embedded" in this ring structure. The presence of such a complex of ring structures usually indicates the multi-tiered position of the intermediate magma foci.

According to possible formation mechanisms, all annular sections are conditionally divided into magmatogenic and hydrothermal-metasomatic. The reasons for this separation were the spatial combination of ring structures with single manifestations of intrusive magmatism, signs of thermal effects on the host rocks in the north-eastern part of the area, and traces of metasomatic changes. All these facts suggest the presence of a not deeply lying blind magmatic body of considerable size, with which the manifestations of minerals are possibly associated.

Aeolian and undivided Neogene-Quaternary sediments, lithified complexes, an erosion-exposed intrusive body of the presumably medium composition, and a blind intrusive body presumably acidic composition, areas with traces of thermal effects and hydrothermal-metasomatic changes in the host rocks were identified as areal bodies in the area. Stratified formations occupy almost the entire area. Modern aeolian sediments occupy depression in the central part of the area, and undivided Neogene-Quaternary formations are located in the north-eastern, central, and southern parts of the site. The lithified complexes of the presumably Middle Paleozoic age are exposed to elevations in the eastern, northern, and western parts of the area. A single stock of intrusions of presumably medium composition is mapped in the eastern part of the area. Its size is 1.8x0.67 km. Traces of thermal effects are found in his exocontact – contact hornfelses are assumed here. The same hornfelses are recorded in the northern and eastern parts of the area.

A blind intrusive body, presumably of an acidic composition, is mapped in the central part of the area. Signs of its isolation were traces of weak thermal effects on the host rocks and a system of telescopic ring structures. Such systems of ring structures not only indicate the position of the magma chamber but can also indicate its formation and occurrence conditions. Based on the experience gained, it can be argued that the blind acidic intrusive body in the central part of the site has a southeastern declination.

Of particular interest are traces of hydrothermal-metasomatic changes. Spectral

analysis of the ASTER data in these areas indicates mineralization of muscovite, chlorite, carbonate, and epidote. All these areas of hydrothermally altered rocks gravitate toward discontinuous disturbances in the northwestern and sublatitudinal orientations.

The prospects of the Arganaty area are associated with the manifestation of endogenous mineralization and the possible detection of groundwater. Endogenous mineralization can be associated with the manifestation of intrusive magmatism. The signs of which (a single stock, thermal action areas on the host rocks, magmatogenic ring structures) are found within the area. Au, Cu, Mo, Pb, Zn, Sn, W are expected in the area. It is proposed to consider the following mineralization factors within the area:

- ring structures, or rather their arc segments and especially the conjugation sections of such arc segments with multidirectional discontinuous faults;
- multidirectional discontinuous violations;
- intrusive body;
- the blind intrusive body;
- areas with traces of thermal effects on the host rocks;
- areas with signs of hydrothermal-metasomatic changes.

Based on the mineralization factors within the Arganaty area and its immediate vicinity, new promising areas for detecting endogenous mineralization were identified (Figure 8).

4. CONCLUSIONS:

The results of this study are the collection and analysis of a remote sensing database and diagrams for the area of interest. The main cosmogeological factors of mineralization were revealed. Directions for organizing a complex of prospecting work in promising areas were determined. The prospects for the studied territories are related to the possibility of detecting endogenous mineralization (mainly gold, copper, PGM, nickel, lead, zinc, tin, tungsten, chrysotile asbestos) and groundwater. The application of space geological studies results is informative for new or poorly studied territories and geologically concerning fairly well-studied areas. In this regard, in such areas, one can identify mainly hidden and unconventional mineralization, which requires new forecasting and prospecting technologies. This is also true for an area characterized by a significant

development of unconsolidated loose sediments, many hydrological objects, a poorly divided relief, a multi-storey geological structure with access to the day surface, and the identification of paleo-valleys where potential placers can develop.

In buried paleo-valleys, the position of mineralization is controlled on the one hand by the development of these valleys, and on the other, by tectonic zones of the basement. These zones are defined as the location of the paleo-valleys themselves and the position of the Karst cavities in the mating areas of multidirectional structures. The paleo-valleys position can control the mineralization of the area, and alluvial deposits of the valleys include uranium mineralization of the infiltration type and placers of gold. Paleo-valleys may include significant groundwater resources for both drinking and technical purposes.

Currently, a draft of prospecting works has been drawn upon selected prospective sites. Geological and geophysical works have been planned to select the location of the prospecting boreholes, conduct testing, and a complex of laboratory studies of the selected samples.

5. ACKNOWLEDGMENTS:

The research was funded by the Science Committee of the Ministry of Education and Science of the Republic of Kazakhstan (the program-targeted financing theme No. 2018/BR05233713 "Integrated geological study of the subsurface for the development of the resource base and new sources of ore raw materials in Kazakhstan").

The authors are grateful to the Cosmogeology Research and Innovation Center of "Cosmogeology" of the National Research Tomsk Polytechnic University (Russia), who took part in the work and processing of satellite images.

6. REFERENCES:

1. Akoveckij, V. I. (1983). *Photo Interpretation*. Moscow, Russian Federation: Nedra.
2. Anan'ev, Yu. S., Poceluev, A. A., and Zpitkov, V. G. (2012). Cosmostructural positions of gold ore objects of the trans-Angara part of the Yenisei Ridge. *Izvestiya TPU*, 320(1), 38-47.
3. Baibatsha, A. B. (2018). *Innovative technologies for the forecast of minerals*. Almaty, Republic of Kazakhstan: LAP LAMBERT Academic Publishing.

4. Baibatsha, A. B., Mamanov, E. Zh., and Bekbotayev, A. T. (2016, June-July). *Allocation of perspective ores on the areas Shu-Ile belt on the materials remote sensing*. Paper presented at the SGEM2016, Albena, Bulgaria. DOI:10.5593/SGEM2016/B11/S01.005.
5. Barrachina, M., Cristobal, J., and Tulla, A.F. (2015). Estimating above-ground biomass on mountain meadows and pastures through remote sensing. *International Journal of Applied Earth Observation and Geoinformation*, 38, 184-192.
6. Beloborodov, M. A., and Kogen, V. S. (1984). Principles and methods of modeling ore objects in forecasting and metallogenic works (using space information). In *Earth exploration from space*. Moscow, Russian Federation: VIEMS.
7. Blaschke, T. (2010). Object-based image analysis for remote sensing. *ISPRS Journal of Photogrammetry and Remote Sensing*, 65, 2-16.
8. Chemin, G., and Ducati, J. R. (2011). Spectral discrimination of grape varieties and a search for terroir effects using remote sensing. *Journal of Wine Research*, 22(1), 57-78. DOI:10.1080/09571264.2011.550762.
9. Crowley, J. K., Brickey, D. W., and Rowan, L. C. (1989). Airborne imaging spectrometer data of the Ruby Mountains, Montana: mineral discrimination using relative absorption band-depth images. *Remote Sensing of Environment*, 29(2), 121-134.
10. Dolivo-Dobrovol'skij, A. V., Percov, A. V., and Skublova, N. V. (1980). *Using remote sensing methods for forecasting and prospecting for mineral deposits*. Moscow, Russian Federation: Nauka.
11. EarthExplorer. 2020. Retrieved from <https://earthexplorer.usgs.gov>.
12. Galvão, L. S., Formaggio, A. R., Couto, E. G., and Roberts, D. A. (2008). Relationships between the mineralogical and chemical composition of tropical soils and topography from hyperspectral remote sensing data. *ISPRS Journal of Photogrammetry & Remote Sensing*, 63, 259-271.
13. Gohman, V. (2015). GIS in mining and geology. *ArcReview*, 3(74), 145-161.
14. Johns Hopkins University Rock Library. (2020). Retrieved from <http://speclib.jpl.nasa.gov/search-1>.
15. Kac, Ya. G., Kozlov, V. V., Poletaev, A. I., and Sulidi-Kondrat'ev, E. D. (1989). *Ring structures of the Earth: Myth or reality*. Moscow, Russian Federation: Nauka.
16. Kac, Ya. G., Poletaev, A. I., and Rumyansev, E. F. (1986). *The basics of lineament tectonics*. Moscow, Russian Federation: Nedra.
17. Kalmykov, V. D., and Serokurov, Y. N. (1991). Techniques for isolating ore-controlling linear structures based on satellite image interpretation materials. *Geology and Exploration*, 9, 75-79.
18. Khorram, S., van der Wiele, C. F., Koch, F. H., Nelson, S. A. C., and Potts, M. D. (2016). *Principles of applied remote sensing*. New York City, New York: Springer Science+Business Media.
19. Khorram, S., Nelson, S. A. C., Cakir, H. I., and van der Wiele, C. F. (2013). Digital image acquisition, preprocessing, and data reduction. In J. N. Pelton, S. Madry, & S. Camacho-Lara (Eds.), *Handbook of Satellite Applications* (p. 250). New York City, New York: Springer-Verlag.
20. Labutina, I. A. (2004). *Decoding aerospace imagery*. Moscow, Russian Federation: Aspekt-Press.
21. Lyubimova, A. V., and Spiridonov, V. A. (1999). Methodology for processing remote sensing materials in environmental management problems. *Geoinformatics*, 3, 18-21.
22. Mamanov, E. Zh., Baibatsha, A. B., and Muszynski, A. (2016, June-July). *Mapping of ore controlling structures Ulytau-Karsakpai zone according to remote sensing*. Paper presented at the SGEM2016, Albena, Bulgaria.
23. Mars, J. C., and Rowan, L. C. (2010). Spectral assessment of new ASTER SWIR surface reflectance data products for spectroscopic mapping of rocks and minerals. *Remote Sensing of Environment*, 114, 2011-2025.
24. Percov, A. V. (2000). *Aerospace methods of geological research*. St. Petersburg,

- Russian Federation: VSEGEI Publishing House.
25. Percov, A. V. (2001). Requirements for the remote base of the state geological map of the Russian Federation on a scale of 1: 200 000 (third generation). In *Aerospace methods of geological research* (pp. 304-313). St. Petersburg, Russian Federation: VSEGEI Publishing House.
 26. Poceluev, A. A., Anan'ev, Yu. S., and Zhitkov, V. G. (2010). Mapping of buried paleo-valleys and weathering crusts based on modern satellite imagery. In *Materials of the XIV of the international meeting "Placers and deposits of weathering crust: Modern problems of research and development"* (pp. 570-574). Novosibirsk, Russian Federation: Apelsin.
 27. Poceluev, A. A., Anan'ev, Yu. S., and Zhitkov, V. G. (2012). *Remote methods for geological research, forecasting, and prospecting for mineral deposits*. Tomsk, Russian Federation: STT.
 28. Poceluev, A. A., Anan'ev, Yu. S., Zhitkov, V. G., Nazarov, V. N., and Kuznecov, A. S. (2007). *Remote methods of geological research, forecasting, and mineral exploration (on the example of the Ore Altai)*. Tomsk, Russian Federation: STT.
 29. USGS Spectroscopy Laboratory. (2020). Retrieved from <http://speclab.cr.usgs.gov/spectral-lib.html>.

Table 1. Aster satellite image characteristics

Survey regime	VNIR	SWIR	TIR
Channel number and spectral range, nm	1: 520-600	4: 1600-1700	10: 8125-8475
	2: 630-690	5: 2145-2185	11: 8475-8825
	3: 760-860	6: 2185-2225	12: 8925-9275
		7: 2235-2285	13: 10250-10950
		8: 22- 95-2365	14: 10950-11650
		9: 2360-2430	
Spatial Resolution, m	15	30	90

Note: VNIR – visible-to-near-infrared, SWIR – short-wave infrared, TIR – the thermal infrared.

Table 2. Used Aster Images

Image Nomenclature	Survey date
AST_L1T_00304162005060149_20150509025419_21847	16.04.2005
AST_L1T_00304222007060222_20150519050231_7719	22.04.2007
AST_L1T_00304242007054959_20150519054503_44651	24.04.2007
AST_L1T_00306092007060200_20150519203835_40386	09.06.2007
AST_L1T_00311182007054930_20150522024610_15537	18.11.2007
AST_L1T_00304132007060828_20150519021401_31111	13.04.2007
AST_L1T_00304132007060837_20150519021405_34433	13.04.2007
AST_L1T_00306242001061013_20150417225959_93408	24.06.2001
AST_L1T_00306252007060215_20150520011602_22932	25.06.2007

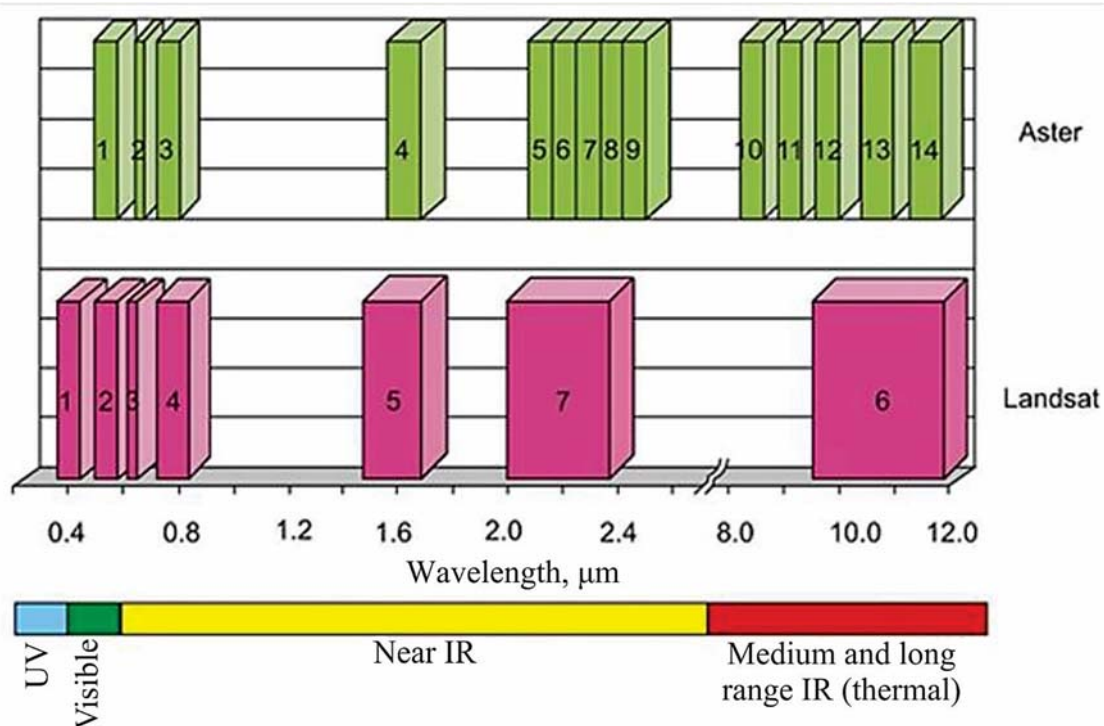


Figure 1. Spectral characteristics of the Landsat and ASTER (the Advanced Spaceborne Thermal Emission and Reflection Radiometer) space systems

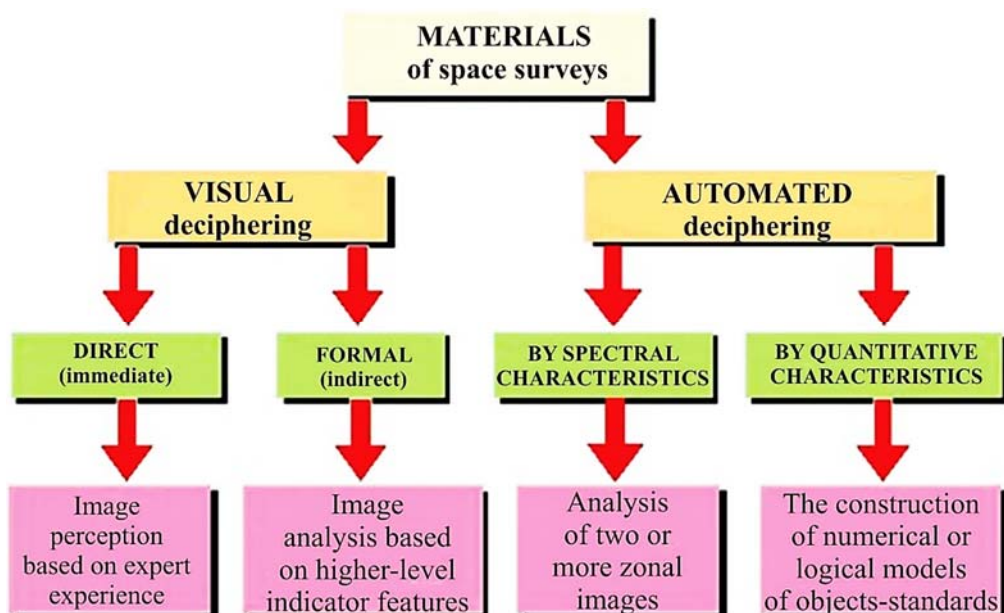


Figure 2. Technological scheme for Deciphering digital satellite images

Source: Kalmykov and Serokurov (1991).

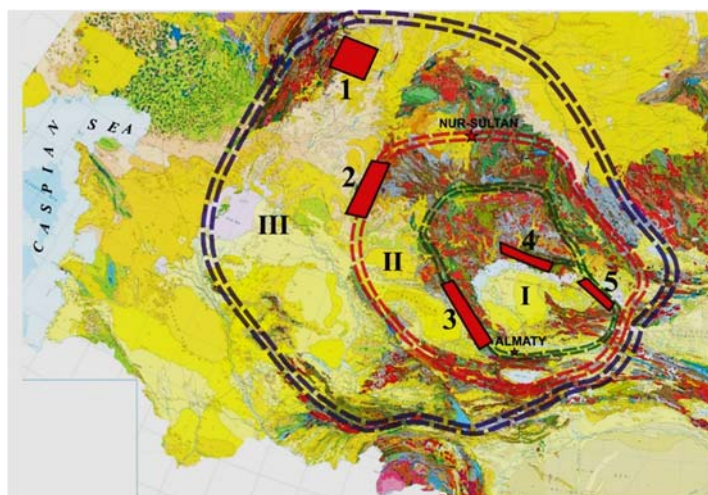


Figure 3. Space geological exploration areas on the tectonic scheme of Kazakhstan: 1 – Torgai; 2 – Karsakpay-Ulytau; 3 – Shu-Ile; 4-5 – North (4) and East (5) Balkhash

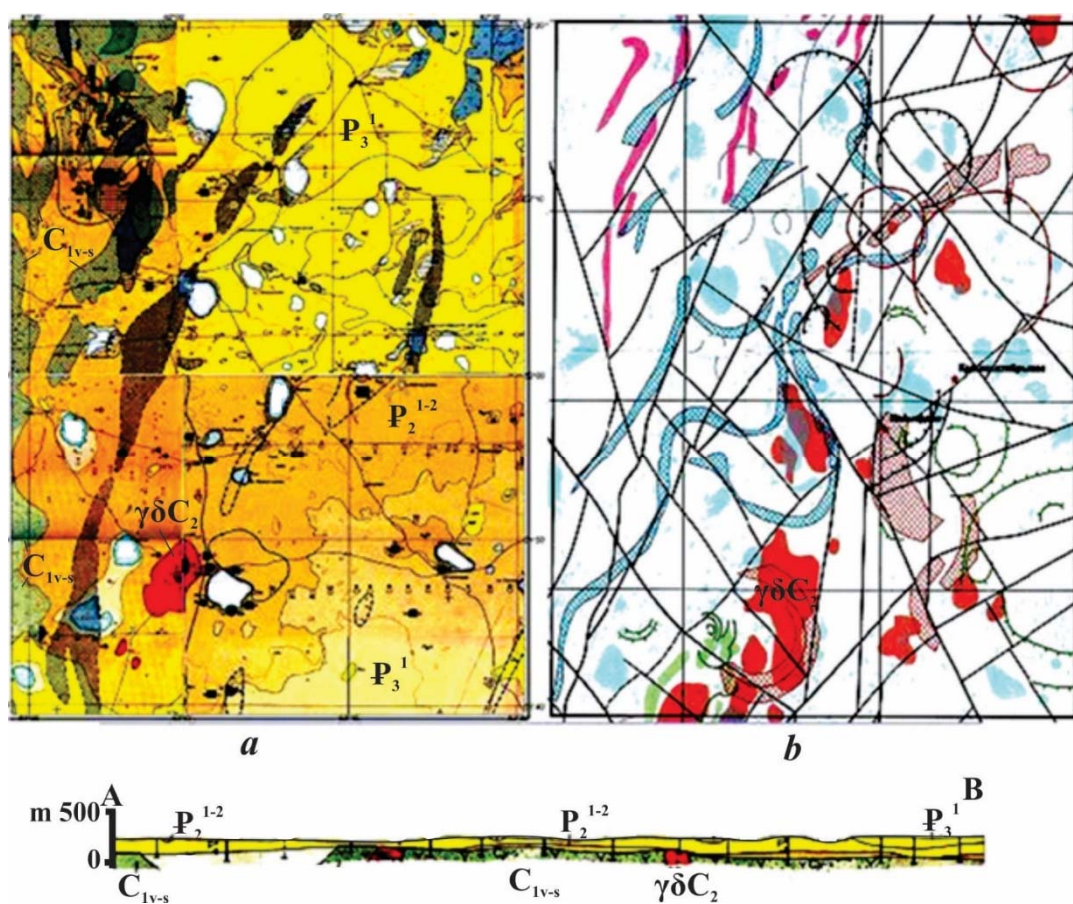


Figure 4. Geological map of the Valeryanov zone closed by sediments (a) and its cosmostructural diagram with the interpretation of hidden structures, areal bodies, and paleodolines at a depth of 40-60 m (b)



Figure 5. An example of the selection of paleovalleys. The raster is obtained as a result of thematic filtering with subsequent indexing of infrared and thermal channels

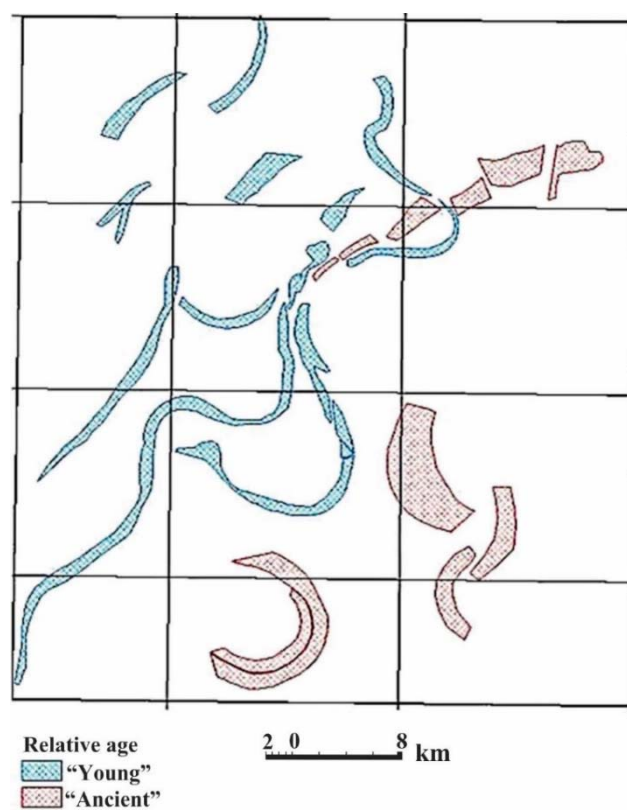


Figure 6. The development pattern of buried Cenozoic paleo-valleys of the Torgai area

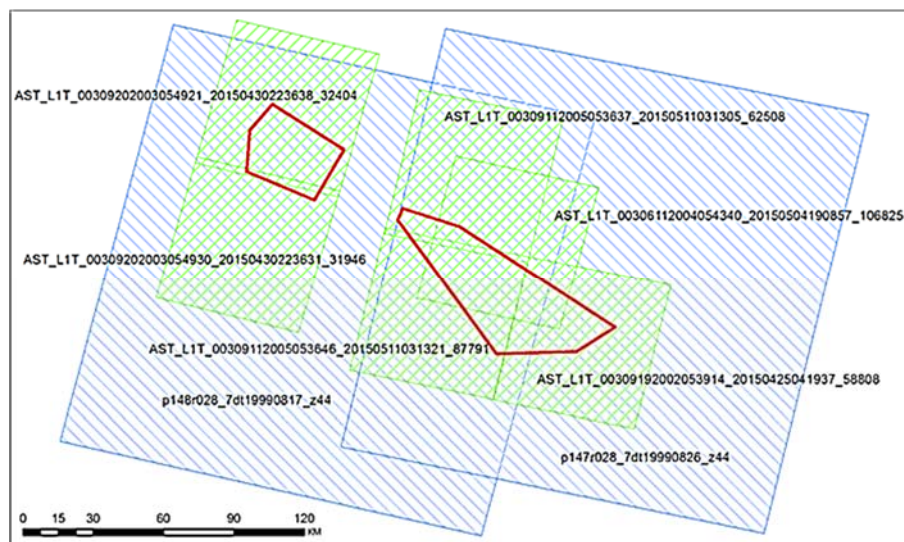


Figure 7. The scheme of covering the work area with space materials

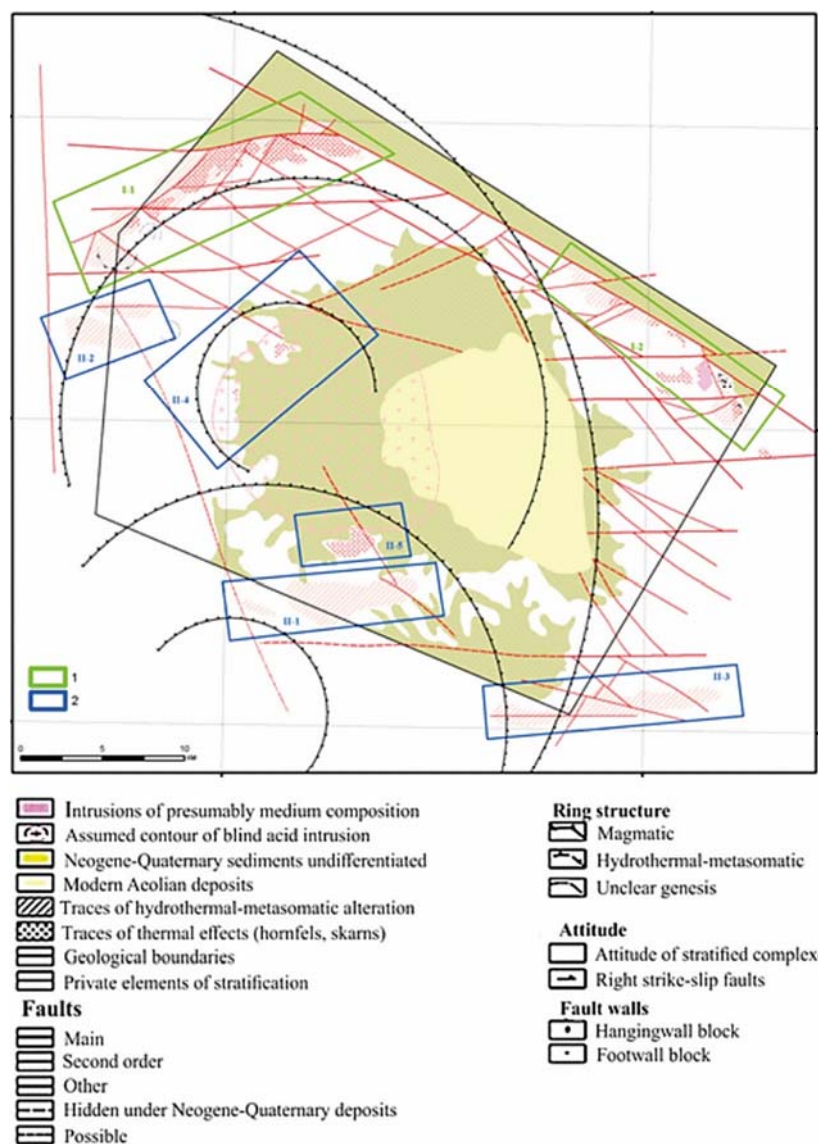


Figure 8. Prospective blocks of the Arganaty area (East Balkhash) for the detection of endogenous mineralization: 1 – blocks of the first stage; 2 – blocks of the second stage

AVALIAÇÃO DE ALGUNS PARÂMETROS HEMATOLÓGICOS DE PACIENTES
INFECTADOS POR *HELICOBACTER PYLORI*

EVALUATING SOME OF THE HEMATOLOGICAL PARAMETERS FOR *HELICOBACTER
PYLORI* INFECTED PATIENTS

تقييم بعض المعلمات الدموية للمرضى المصابين بعدوى الملوية البوابية

HASHIM, Nidhal Abdullah^{1*}; ABDULLAH, Younus Jasim¹; SHAWI, Hasan Rahman²

¹ Amara Technical Institute, Southern Technical University, Misan, Iraq.

² Central Blood Bank, Misan Health Directorate, Ministry of Health, Iraq.

* Correspondence author
e-mail: Nidhal.abdullah@stu.edu.iq

Received 01 June 2020; received in revised form 28 August 2020; accepted 04 September 2020

RESUMO

Helicobacter pylori são bastonetes curvos Gram-negativos que habitam a mucosa gástrica e são considerados as principais causas de úlceras estomacais e duodenais em humanos. O objetivo principal deste estudo foi avaliar as influências da bactéria nos diversos parâmetros hematológicos. Foram incluídos neste estudo 60 pacientes com idades entre 15-40 anos (30 homens e 30 mulheres) e 30 indivíduos saudáveis de mesma idade que foram considerados como o grupo de controle. O sangue venoso (4 ml) foi obtido da população estudada e analisado para hemograma completo utilizando um analisador hematológico automatizado. Os resultados revelaram que há uma diminuição substancial ($p < 0,01$) na hemoglobina (Hb), hemoglobina corpuscular média (HCM) e na largura de distribuição de células vermelhas (RDW) nos pacientes em comparação ao grupo de controle. No entanto, nenhuma diferença significativa nos glóbulos vermelhos (RBC), hematócritos (HCT), volume corpuscular médio (MCV) e na concentração de hemoglobina corpuscular média (MCHC) nos pacientes em comparação com o grupo de controle. Além disso, nenhuma diferença significativa foi encontrada nos glóbulos brancos (WBC) entre pessoas infectadas e não infectadas por *H. pylori*. Caso contrário, existem diferenças significativas ($p < 0,01$) nos linfócitos, monócitos, granulócitos entre os pacientes e os indivíduos saudáveis. Os resultados também descobriram que existem diferenças estatísticas significativas em alguns dos parâmetros hematológicos entre os grupos de estudo de acordo com o sexo. O estudo concluiu que Hb, RDW, linfócitos, monócitos, granulócitos estão reduzidos em pacientes infectados com *H. Pylori*, sugerindo que a infecção pode ter efeitos diretos nos parâmetros sanguíneos.

Palavras-chave: *Helicobacter pylori*, Parâmetros hematológicos, HB, WBC.

ABSTRACT

Helicobacter pylori are Gram-negative curved rods that habitats the gastric mucosa and considered as the leading causes of stomach ulcers and duodenal ulcers in humans. The main object of this study was to evaluate the influences of the bacteria on several hematological parameters. A total of 60 patients aged between 15 to 40 years were included in this study (30 male and 30 female) in addition to 30 healthy individuals from the same ages who were considered as a control group. Venous blood (4 ml) was obtained from the study population and investigated for complete blood count (CBC) using an automated hematology analyzer. The results revealed that there is a substantial decrease ($p < 0.01$) in Hemoglobin (Hb), Red cell distribution width (RDW), and mean corpuscular hemoglobin (MCH) in patients compared to control. However, no significant difference in Red blood cells (RBCs), Hematocrit (HCT), mean corpuscular volume (MCV) and mean corpuscular hemoglobin concentration (MCHC) in patients compared to control. Also, no significant differences were found in the white blood cell (WBC) between *H. pylori* infected and non-infected persons. Otherwise, there are significant differences ($p < 0.01$) in lymphocytes, monocytes, granulocytes in the patients and healthy individuals. The results also found that there are significant statistical differences in some of the hematologic parameters among study groups according to their gender. The study concluded that Hb, RDW, lymphocytes, monocytes, granulocytes are decreased in *H. Pylori* infected patients suggesting that infection may have direct

effects on blood parameters.

Keywords: *Helicobacter pylori*, Hematology parameters, HB, WBC.

المخلص

الملوية البوابية هي بكتريا عصوية سالبة لصبغة كرام توطن الغشاء المخاطي في المعدة وتعتبر من الأسباب الرئيسية لقرحة المعدة وقرحة الاثني عشر في البشر. الهدف الرئيسي من هذه الدراسة هو تقييم تأثير البكتيريا على العديد من المعايير الدموية. تضمنت هذه الدراسة (60) مريضاً كعدد كلي منقسم الى (30 رجلاً و30 أنثى) تتراوح أعمارهم بين (15-40 سنة) بالإضافة إلى (30) من الأفراد الأصحاء من نفس الأعمار الذين اعتبروا مجموعة السيطرة. تم اخذ عينة دم وريدي (4 مل) من مجتمع الدراسة وتم قياس تعداد الدم الكامل CBC باستخدام محلل الدم الآلي. أظهرت النتائج أن هناك انخفاضاً كبيراً (P < 0.01) في مستوى الهيموكلوبين ومتوسط هيموكلوبين الكرية وعرض توزيع الكريات الحمراء في المرضى مقارنة بمجموعة السيطرة. ومع ذلك، لا يوجد فرق كبير في الكريات الحمراء، والهيماتوكرايت، ومتوسط حجم الكرية الحمراء ومتوسط تركيز الهيموكلوبين بالكريات الحمراء في المرضى مقارنة مع السيطرة أيضاً، لم يتم العثور على اختلافات كبيرة في إجمالي الخلايا البيض بين المصابين ببكتيريا الملوية البوابية. خلاف ذلك، هناك اختلافات كبيرة (P < 0.01) في الخلايا اللمفاوية، الخلايا وحيدة النواة والخلايا الحبيبية في المرضى والأفراد الأصحاء. كما وجدت النتائج وجود فروق ذات دلالة إحصائية في بعض المعايير الدموية بين مجموعات الدراسة حسب الجنس. خلصت الدراسة إلى أن الهيموكلوبين، متوسط تركيز الهيموكلوبين بالكرية، وعرض توزيع الكريات الحمراء، الخلايا اللمفاوية، الخلايا وحيدة النواة والخلايا الحبيبية تنخفض في المرضى المصابين بالبكتيريا الحلزونية مما يشير إلى أن العدوى قد يكون لها تأثير مباشرة على معايير الدم.

الكلمات المفتاحية: الملوية الحلزونية، معايير دموية، الهيموكلوبين، الخلايا البيض.

1. INTRODUCTION

Helicobacter pylori (*H. pylori*) is a spiral-shaped, microaerophilic, Gram-negative curved rods, measuring approximately 3–5 µm in length. Their main habits, the gastric mucosa of humans, were considered the leading cause of stomach ulcers, duodenal ulcers, gastritis, and gastric malignancies (Tamokou *et al.*, 2017; Yahya *et al.*, 2017). There specialized traits allowing this organism to flourish in the harsh environment of the stomach include Elaboration of urease, Motility, and Binding of *H. pylori* to gastric epithelial cells via bacterial adhesins; *Helicobacter pylori* elaborate a significant amount of urease (10–15% of total proteins by weight), which produces ammonia and carbon dioxide resulting from endogenous urea hydrolysis, thus buffering (neutralizing) gastric acid in the organism's immediate vicinity. *Helicobacter pylori* possess numerous long flagella, whose flailing movements allow them to swim through viscous gastric mucus with powerful screw-like movements, much like a drill bit spinning. The bacterium colonizes the gastric mucosa by adhering to mucous epithelial cells and the mucus layer lining the gastric epithelium. *Helicobacter pylori* have adhesives that improve the adhesion of gastric epithelial cells by recognizing specific carbohydrate structures, such as the Lewis b blood group antigen and sialyl dimeric Lewis X. Also, Virulence factors such as the cytotoxin-associated pathogenicity island-encoded protein CagA and the vacuolating cytotoxin VacA help in this gastric mucosa colonization (Kusters *et al.*, 2006; Kamerling and Boons 2007). Besides, it could cause Mucosa-associated-lymphoid-type lymphoma and non-

ulcer dyspepsia (Hajimahmoodi *et al.*, 2011; Quaglia *et al.*, 2020). Infections with *H. pylori* are usually more frequent in older people than in children (Hashim *et al.*, 2019). Although several persons have asymptomatic *H. pylori* infection, peptic ulcers may develop in (10 – 20% as lifetime risk), while (1 – 2% risk) of patients may develop stomach cancer (Kusters *et al.*, 2006). An oral-oral, fecal-oral, and a common environmental source has been proposed as possible transmission routes, with familial transmission associated with *H. pylori* infections (Smith *et al.*, 2019; Quaglia *et al.*, 2020).

H. pylori were proposed to be associated with conditions extra-gastrointestinal effects, including those from metabolic, cardiopulmonary, gynecological, dermatologic, endocrinal, pneumatology, and neurologic disorders. *H. pylori* may also be connected with hematological aspects as low serum iron or low serum vitamin B12 levels being defined as having iron or vitamin B12 deficiency (Eledo *et al.*, 2018). Moreover, Idiopathic thrombocytopenic purpura (ITP) is a widespread autoimmune hematologic disease that affecting persons of different ages *H. Pylori* was offered to be correlated with ITP (Ibrahim *et al.*, 2018; Rahman *et al.*, 2019). Also, their associations between *H. pylori* and serum IL-8 production; Belaia *et al.* (2020) found the majority of patients of peptic ulcer disease (90%) have elevated levels of IL-8.

Anemia is a condition featured by reduced oxygen-carrying capacity and count of red blood cells (RBCs), hemoglobin Hb < 12 g/d in females, and (Hb) < 13 g/d in males. It concerns 50% of all anemia conditions caused by low iron intake, increased iron requirement, iron deficiency,

chronic blood loss, and poor absorption (Elamin *et al.*, 2018).

The working by which *H. Pylori* causes iron-deficiency anemia is not abundantly settled. Studies law go preventative hepcidin is increased in patients (Rahman *et al.*, 2019).

In Iraq, no study has considered the effects of *H. pylori* infection on the hematological parameters (Humeida and Abdalla, 2017). Therefore, this study aimed to estimate the effect of *H. pylori* infection on hematological parameters such as hemoglobin (Hb) concentration, Red blood cells (RBCs), Hematocrit (HCT), platelet count, white blood cell (WBCs) and the association of this effect with changes in red blood indices which include mean corpuscular volume (MCV), mean corpuscular hemoglobin concentration (MCHC), mean corpuscular hemoglobin (MCH), red cell distribution width (RDW), in the local population of Maysan province).

2. MATERIALS AND METHODS

2.1. Study Population and Design:

A total of 60 subjects suffering from *H. Pylori* infection (30 women and 30 men) and aging between (15-40) besides, 30 of the same ages and gender healthy persons (control group) are involved in the current study. All subjects were attended in the Hematology Unit of the Al-Sadder Teaching Hospital/Amara, where they were diagnosed and followed-up prospectively between October 2018 and April 2019.

All subjects with *H. Pylori* infection and control group succumbed to complete history taking (particularly age, gender, area, diabetes, hypertension, previous Iron therapy, blood transfusion as well as upper endoscopy state). The exclusion criterion contains patients with malignant hypertension, hepatic, and renal diseases. Over more, those on non-steroidal anti-inflammatory drugs (NSAIDs), proton pump inhibitors (PPI), cytotoxic drugs, or steroids, pregnant women were also excluded. Also, patients with immune thrombocytopenia due to any other causes were excluded.

2.2 Ethical clearance:

Permission to conduct this study is issued by the Health institutional, and the collection of

Blood samples of individuals carried out by under public health technician supervision.

2.3. Sampling Procedure:

A 4mL of venous blood is obtained from every patient and healthy case, then separated into two containers, the first container with ethylene diamine tetraacetic acid (EDTA) was used for hematology estimation, and the rested 2 mL was centrifuged for *H. pylori* screening method (Hashim *et al.*, 2019).

2.4. Hematology estimation:

The automated hematology analyzer Sysmex KX-21 (Sysmex Corporation, Kobe, Japan) was calibrated according to the instructions of the manufacturer, as the followings:

- 3 fresh blood samples were collected from seemingly healthy individuals known to have an MCV 86 fL – 96 fL, and an MCHC 330 g/L – 345 g/L (33.0 g/dL – 34.5 g/dL).
- The samples were anticoagulated with 1.4 mg/mL - 1.6 mg/mL of K2EDTA or K3EDTA.
- (Note: K3EDTA leads to cells to shrink, resulting in an approximate 2 percent decrease in packed (red) cell volume (PCV) or called Hematocrit (HCT).
- The samples were kept at room temperature and checked within 4 hours. The micropipette used was a Class A, standardized; the volumetric flasks were Class A, calibrated, created of borosilicate glass; the unique capillary tubes used to evaluate the PCV must comply with the requirements of the American Society for Testing and Materials, the plastics or glass cell counting vials must have a minimum volume of 10 mL (American Society for Testing and Materials, 1980; International Committee for Standardization in Haematology, 1988).
- Soon after, the evaluation of hematological parameters, Hb, HCT, MCV, MCH, MCHC, platelet count, WBCs count, and the differential count was managed. The hemoglobin concentration of the samples (two dilutions) was measured using the International Committee for Standardization in Haematology (ICSH) haemoglobinocyanide reference method (Zwart, *et al.*, 1996; Bull

et al., 2000a). The PCV (hematocrit) was measured (four capillary tubes) using the ICSH selected method for microhematocrit measurement (International Committee for Standardization in Haematology, 1989; Bull *et al.*, 2000b).

- The red cell count was achieved using a semi-automated single-channel counter. It was used to count all cells in a specified displaced volume of the diluted blood sample through electronic means. At the moment, only particle counters with an aperture impedance follow this specification.
- The diluent was a sterile, non-toxic, buffered saline solution. The diluent included $< 5 \times 10^4$ particles/L within a size range of 20 fL = 120 fL, must not crenate or lysis red blood cells, or change the MCV by > 2 fL more than a period of 30 minutes.
- The main dilution of 0.05 mL of blood, plus 25 mL of diluent, was produced, followed by a second dilution of 0.2 mL of main diluted sample + 20 mL of diluent; this resulted in a total dilution of 50 601 times.
- The sample was transferred to the counting vial with diluted and counts completed within five minutes of completing the final dilution stage. There were two dilutions; each was counted twice (International Council for standardization in Haematology, 1994).
- The count of white cells was achieved using an instrument for measuring red cells. The lytic agent used should be capable of lysing red cells completely, leaving no residual material able to contribute to the count. The leukocyte count signal should fall into the size range equal to 45 fL-450 fL, and the count should be stable after preparation for 15 minutes. There were two dilutions produce for each, and it was counted at least twice.
- The platelet count was measured using ICSH selected methods for the determination of the RBC/platelet (PLT) ratio (International Council for Standardization in Haematology, 2001).

Two dilutions were made. For medical facilities, direct whole blood testing of automated hematology analyzers was rarely, if ever, used. This was, however, the cornerstone of the

recommended system for assigning values to stable blood calibrators and, as such, was used by those calibrator manufacturers.

2.5. *Helicobacter Pylori* diagnosis

H. pylori were diagnosed by using enzyme-linked immunosorbent assay (ELISA) test for the detection of *H. pylori* IgG antibodies in serum supplied by (Monobind Inc., USA) following the procedure supplied by kits as the following:

1. It was pipetted 25 μ L of the appropriate serum reference calibrator, control, or diluted patient specimen into the assigned well for IgG determination.
2. It was added 100 μ L of *H. Pylori* Biotin Reagent Solution.
3. The microplate was swirled gently for 20-30 seconds to mix and cover.
4. It was incubate 60 minutes at room temperature.
5. The contents of the microplate were discarded by decantation or aspiration. If decanting, blot the plate dry with absorbent paper.
6. It was added 350 μ L of wash buffer decant (blot) or aspirate. It was repeated two additional times for a total of three washes.
7. It was added 100 μ L of *H.Pylori* Enzyme Reagent to all wells.
8. It was covered and incubated for thirty (30) minutes at room temperature.
9. Steps 6 and 7 were repeted, as explained above.
10. It was added 100 μ L of working substrate solution to all wells.
11. Incubate at room temperature for fifteen minutes.
12. It was added 50 μ L of stop solution to each well and swirled the microplate gently for 15-20 seconds to mix.
13. The absorbance was read in each well at 450 nm in a microplate reader.

2.6. Statistics

SPSS package version 20 software was applied for statistical analysis of data obtained in this study. Results are analyzed using an independent T-test, form comparing means. $P < 0.05$ was considered statistically significant,

the Chi-square test was used to compare percentages (Ott and Longnecker, 2015).

3. RESULTS AND DISCUSSION:

3.1. RESULTS

The results revealed that the concentrations of hemoglobin (HB g/dl) and MCH were decreased significantly (P-value = 0.003, 0.011, respectively) in *H. pylori* patients against healthy subjects, as seen in Table 1. Also, the percent of RDW is significantly higher (P-value > 0.000) in patients. No significant differences were seen in the other parameters listed in Table 1.

Although no statistically significant difference was found in total WBC between patients and control, numbers of lymphocytes, monocytes, and granulocytes were significantly raised in *H. pylori*-infected subjects against healthy groups, as shown in Table (2). Besides, non-significant variations were found between *H. pylori* patients and the control group in MPV concentration and platelet count, as seen in Table 3. The results also found that hemoglobin concentration was significantly lower in females and males infected with *H. pylori* as compared with healthy women and men (P value=0,040, 0.050, respectively). Differences in the total RBC count and HCT % were not statistically significant between both sexes of patients and control, as showed in Table (4).

Accordingly, Table 5 showing statistically significant differences in the concentrations of MCV, MCH, and the RDW percent in infected females (P-value=0.007, 0.001 and 0.003 respectively), while the differences were significant only in RDW% in infected males when compared with healthy control. Dissension to females patients, *H. pylori*-infected males have a significant increase in WBC counts, lymphocytes, monocytes, and decreased granulocytes percent in comparison with healthy males, see Table 6. On the other hand, Table 7 showed a statistically significant difference in platelet counts and MPV concentration between patients diagnosed with *H. pylori* infection and the control group concerning gender.

3.2. DISCUSSION

The results found that the concentrations of hemoglobin (HB g/dl) and MCH decreased significantly in *H. pylori* patients, while the percent of RDW is higher than the control group. Ibrahim *et al.* (2018) found no significant difference between hematological parameters, platelet counts, White Blood Cell counts of

patients diagnosed with *H. pylori*, and those without infection. On the other hand, Elamin *et al.*, 2018 revealed that parameters of red blood corpuscles (Hb, PCV, MCV, and MCH) were decreased, while the platelet and reticulates count was significantly increased in patients with positive anti-*H. pylori* antibodies compared to those without. Otherwise, the differences of MCHC, total differential, and leukocytes count were non-significant and are in line with the results mentioned in tables 2 and 3. The reason for that perhaps due to the immunity that is generated against *H. pylori* infection. Xu *et al.* (2017) reported that hemoglobin level was reduced in persons with *H. pylori* infection than in healthy groups indicating that *H. pylori* infection may cause a case of anemia.

The results also found that all RBC, MCV, MCH, and MCHC levels are different significantly between infected and healthy subjects (all P < 0.05). However, these differences were small and had no considerable biologic effects, as mentioned by (Mwafy and Afana, 2018).

Rahman *et al.* (2019), mentioned that no difference in white blood cells was found between control and cases, which could be explained by the presence of inflammation in the study control group. Also, most control population may be complaining of inflammation at the time of diagnosis, which may narrow the difference in WBCs count between control and cases. In contrast, Linz *et al.* (2007) and Kodaman *et al.* (2014) described that infected patients had significantly elevated WBC counts compared with healthy persons, which showed raised total WBC, neutrophil, and monocyte counts. This could elucidate the overstated systemic inflammatory response in cases with *H. pylori* infection. This disagrees with Gupta *et al.* (2002), who observed that infection with *H. pylori* caused autoimmune neutropenia.

Papadaki *et al.* (2005) found a slight decrease in hemoglobin (Hb) (g/dl) level and mean of the corpuscular volume (MCV) in cases versus control, no difference in the mean of corpuscular hemoglobin (MCH) between control and cases, and no statistically significant relationship between cases and control in the number of platelet count.

It is reported that *H. pylori* affect red blood cells by causing extra gastric complications like vitamin B12 deficiency, Iron deficiency anemia (IDA), and some hematological parameters. Patients with *H. pylori* infection are more likely to have anti-parietal cell antibodies and anti-intrinsic

factor antibodies (Annibale *et al.*, 2000; Ayeshe *et al.*, 2013).

Ciacchi *et al.* (2004), proposed a potential pathogenic effect of anemia and interpreted it by blood loss occurring after persistent erosive gastritis and low iron intake secondary to chronic gastritis and hypochlorhydria. The results also found that all RBC, MCV, MCH, and MCHC levels are different significantly between infected and healthy subjects (all $P < 0.05$). However, these differences were small and had no considerable biologic effects, as mentioned by (Mwafy and Afana, 2018).

Similarly, Eledo *et al.* (2018) found that infection with *H. pylori* caused significant differences between patients and the control group (Hb, PCV, ESR) parameters between males and females. The authors suggested that the pathogen has not an additional impact on a particular gender through patients in a prescribed geographic location. However, among the *H. pylori* patients, the hemoglobin content decreased significantly.

4. CONCLUSIONS:

The infection with *H. pylori* has led to a decrease in MCH, RDW levels, and LYM, MON, GRA counts. In addition to significant differences in MCV, MCH, total WBC, LYM, MON, and GRA according to gender. The results suggest that infection with *H. pylori* has pathogenic effects on blood components.

5. REFERENCES:

1. American Society for Testing and Materials. (1980). Standard specification for disposable glass blood sample capillary tube (microhematocrit) designation. E734-780.
2. Ayeshe, M. H., Jadalalah, K., Awadi, E. A., Alawneh, K., and Khassawneh, B. (2013). Association between vitamin B12 level and anti-parietal cells and anti-intrinsic factor antibodies among adult Jordanian patients with *Helicobacter pylori* infection. *Brazilian Journal of Infectious Diseases*, 17(6), 629-632.
3. Annibale, B., Capurso, G., Martino, G., Grossi, C., and Delle Fave, G. (2000). Iron deficiency anaemia and *Helicobacter pylori* infection. *International journal of antimicrobial agents*, 16(4), 515-519.
4. Belaia, O. F., Gutkin, D. S., Kareva, E. N., Volchkova, E. V., and Vakhrameeva, M. S. (2020). Serum levels of il-8 in patients with chronic active gastritis and peptic ulcer disease. *Periódico Tchê Química*. 17(34), 826-834.
5. Bull, B. S., Houwen, B., Koepke, J. A., Simson, E., and van Assendelft, O. W. (2000^a). Reference and selected procedures for the quantitative determination of hemoglobin in blood. *Approved standard-*, 20, 1-29.
6. Bull, B. S., Koepke, J. A., Simson, E., and van Assendelft, O. W. (2000^b). Procedure for determining packed cell volume by the microhematocrit method; approved standard. *NCCLS Document H7-A3*, 20(18), 1-18.
7. Ciacchi C, Sabbatini F, Cavallaro R, Castiglione F, Di Bella S, Iovino P, and Mazzacca, G. (2004). *Helicobacter pylori* impairs iron absorption in infected individuals. *Digestive and liver disease*, 36(7), 455-460.
8. Elamin, E. A. I., Suliman, M. A., Azoz, M. E., Ali, E. W., Olerile, L. D., Jiao, Y., and Zhao, Y. (2018). Effect of *Helicobacter pylori* Infection on Haematological Parameters in Kosti Teaching Hospital, Sudan. *Iranian Red Crescent Medical Journal*, 20(2).
9. Eledo, B. O., Allagoa, D. O., Onuoha, E. C., Okamgba, O. C., Ihedioha, A. U., and Ugwu, I. M. (2018). Evaluation of Some Haematological Parameters Among *Helicobacter pylori*-infected students in a Nigerian tertiary educational institution. *Biotechnological Research*, 4(1), 34-39.
10. Gupta V, Eden A. J, Mills M. J. (2002). *Helicobacter pylori* and autoimmune neutropenia. *Clinical and Laboratory Haematology*, 24(3), 183-185.
11. Hajimahmoodi M., Shams-Ardakani, M., Saniee, P., Siavoshi, F., Mehrabani, M., Hosseinzadeh, H., Foroumadi, P., Safavi, M., Khanavi, M., Akbarzadeh, T., Shafiee, A., Foroumadi, A. (2011). *In vitro* antibacterial activity of some Iranian medicinal plant extracts against *Helicobacter pylori*. *Natural Products Research*, 25(11), 1059-1066.
12. Hashim, N. A., Jumaah, M. G., and Abdullah, Y. J. (2019). Prevalence of *Helicobacter pylori* infection in diabetic and nondiabetic patients. *Drug Invention*

- Today, 11(10).
13. Humeida, A. T., and Abdalla, M.H.A. (2017). Association of *Helicobacter pylori* Infection and Vitamin B12 Level among Sudanese Patients. *IOSR Journal of Dental and Medical Sciences*, 16(3): 12-14.
 14. Ibrahim N.K., Fatin Mohammad Al-Sayes F.M., F. A. Alidrous; Alahmadi M.M.; S. H. Bakor, and Aljohani A.F.(2018). *Helicobacter Pylori*: Prevalence and Relationship to Hematological Parameters of Symptomatic Patients who Conducted Gastrosocopy at King Abdulaziz University Hospital, Jeddah. *Journal of Advances in Medicine and Medical Research*, 28(9), 1-9.
 15. International Committee for Standardization in Haematology. (1988). Expert Panel on Cytometry. The assignment of values to fresh blood used for calibrating automated blood cell counters. *Clin Lab Haemat*, 10:203-212.
 16. International Committee for Standardization in Haematology. (1989).; Expert Panel on Cytometry. Recommended method for the determination of packed cell volume by centrifugation. World Health Organization, WHO LAB/89.1.
 17. International Council for standardization in Haematology. (1994). Expert Panel on Cytometry. Reference method for the enumeration of erythrocytes and leukocytes. *Clin Lab Haemat* 1994; 16:131-138.
 18. International Council for Standardization in Haematology. (2001). Expert Panel on Cytometry and International Society of Laboratory Hematology; Task Force on Platelet Counting. Platelet counting by the red blood cell/platelet ratio method: a reference method. *Am J Clin Path*; 115: 460-464.
 19. Kodaman N., Pazos A, Schneider B.G., Piazuelo M.B., Mera R., Sobota R.S., and Harder, R. H. (2014). Human and *Helicobacter pylori* coevolution shapes the risk of gastric disease. *Proceedings of the National Academy of Sciences*, 111(4), 1455-1460.
 20. Kusters, J. G., van Vliet, A. H., and Kuipers, E. J. (2006). Pathogenesis of *Helicobacter pylori* infection. *Clinical Microbiology Reviews*, 19(3):449–490.
 21. Linz B., Balloux F., Moodley Y., Manica A., Liu H, Roumagnac P., and Yamaoka, Y. (2007). An African origin for the intimate association between humans and *Helicobacter pylori*. *Nature*. 445(7130),15–918
 22. Mwafy, S. N., and Afana, W. M. (2018). Hematological parameters, serum iron, and vitamin B12 levels in hospitalized Palestinian adult patients infected with *Helicobacter pylori*: a case-control study. *Hematology, transfusion, and cell therapy*, 40(2), 160-165.
 23. Ott, R. L., and Longnecker, M. T. (2015). *An introduction to statistical methods and data analysis*. Nelson Education.
 24. Papadaki H.A, Pontikoglou C, Stavroulaki E, Minadakis G, Eliopoulos DA, Pyrovolaki K, and Eliopoulos, G. D (2005). High prevalence of *Helicobacter pylori* infection and monoclonal gammopathy of undetermined significance in patients with chronic idiopathic neutropenia. *Annals of hematology*, 84(5), 317-320.
 25. Quaglia, N. C., Storelli, M. M., Scardocchia, T., Lattanzi, A., Celano, G. V., Monno, R., and Dambrosio, A. (2020). *Helicobacter pylori*: Survival in cultivable and non-cultivable form in artificially contaminated *Mytilus galloprovincialis*. *International journal of food microbiology*, 312, 108363.
 26. Rahman, Y. A., Wahid Ahmed, L. A., Mahmoud Hafez, R. M., and Ahmed, R. M. M. (2019). *Helicobacter pylori* and its hematological effect. *The Egyptian Journal of Internal Medicine*, 31(3), 332.
 27. Smith, S., Fowora, M., and Pellicano, R. (2019). Infections with *Helicobacter pylori* and challenges encountered in Africa. *World journal of gastroenterology*, 25(25), 3183.
 28. Tamokou, J., Guimtsop, Y. A. T., Ndebi, M. E., Nzesseu, V. L., Djokge, A. K., and Kuate, J. (2017). Effect of *Helicobacter pylori* Infection on Selected Biochemical Parameters of Hypertensive Patients at Dschang District Hospital in Cameroon. *International Journal of Tropical Disease and Health*, 26(1), 1-8.
 29. Xu, M. Y., Cao, B., Yuan, B. S., Yin, J., Liu, L., and Lu, Q. B. (2017). Association of anaemia with *Helicobacter pylori* infection: a retrospective study. *Scientific reports*, 7(1), 1-7.
 30. Yahya, R. Z., Rudainee, M. H. A., Alshammari, S. A., Alshammari, A., and Ahmari, A. S. A. (2017). *Helicobacter*

- pylori* and Upper Gastrointestinal Diseases. EC Microbiology, SI.1: P23-P30.
31. Zwart, A., Van Assendelft, O. W., Bull, B. S., England, J. M., Lewis, S. M., and Zijlstra, W. G. (1996). Recommendations for reference method for haemoglobinometry in human blood (ICSH

standard 1995) and specifications for international haemoglobinocyanide standard. *Journal of clinical pathology*, 49(4), 271.

Table 1. Effect of *H. pylori* on (RBC, HB, HCT, MCV, MCH, MCHC, and RDW%) in total patients.

parameters	RBC($10^6/\text{mm}^3$)	HB(g/dl)	HCT(%)	MCV(μM)	MCH(p g)	MCHC(g /dl)	RDW(%)
Patients	4.99 ± 4.99	12.67 ± 1.94	39.56 ± 4.77	79.96 ± 8.08	25.64 ± 3.58	31.95 ± 1.99	14.00 ± 1.99
Control	5.03 ± 5.03	13.75 ± 1.12	43.44 ± 3.41	87.51 ± 3.61	27.44 ± 1.84	31.70 ± 1.49	12.94 ± 0.66
P value	0.124^{NS}	0.003*	0.087^{NS}	0.08^{NS}	0.011*	0.232^{NS}	0.000**

NS: Non-Significant. *: Significant at 0.05. **: Significant at 0.001

Table 2. Effect of *H. pylori* on (WBC, LYM, MON, GRA) in total patients.

Parameters	WBCs ($10^3/\text{MM}^3$)	LYM(%)	MON(%)	GRA(%)
Patients	7.92 ± 2.74	35.10 ± 11.43	8.92 ± 4.17	56.27 ± 12.60
Control	8.40 ± 1.90	33.53 ± 6.68	6.72 ± 1.79	57.77 ± 7.37
P value	0.069^{NS}	0.004*	0.001**	0.018*

NS: Non-Significant. * (P<0.05). ** (P<0.01)

Table 3. Effect of *H. pylori* on (MPV and PLT) in total patients.

Parameters	MPV (μM^3)	PLT($10^3/\text{MM}^3$)
Patients	7.06 ± 0.78	290.03 ± 56.322
Control	7.39 ± 1.08	264.94 ± 68.79
P value	0.066 ^{NS}	0.275 ^{NS}

NS: Non-Significant

Table 4. Effect of *H. pylori* on Red blood cells (RBC), Hemoglobin (HB), Hematocrit (HCT) in patients and control according to sex

Parameters		RBCs ($10^6/\text{mm}^3$)	HB(g/dl)	HCT(%)
Female	Patient	4.72 ± 0.59	11.87 ± 0.97	37.43 ± 2.36
	Control	4.78 ± 0.32	12.73 ± 0.55	40.71 ± 1.87
	P value	0.262 ^{NS}	0.040*	0.233 ^{NS}
Male	Patient	5.40 ± 0.35	13.92 ± 2.41	42.83 ± 5.75
	Control	5.21 ± 0.38	14.46 ± 0.84	45.49 ± 2.90
	P value	0.702 ^{NS}	0.050*	0.298 ^{NS}

NS: Non-Significant,*(P<0.05)

Table 5. Effect of *H. pylori* on Red blood cells indices (MCV, MCH, MCHC, RDW) in patients and control according to sex

Parameters		MCV(μ M)	MCH(pg)	MCHC(g/dl)	RDW(%)
Female	Patient	80.00 \pm 7.13	25.42 \pm 3.22	31.70 \pm 1.45	14.03 \pm 1.53
	Control	86.06 \pm 2.86	27.73 \pm 0.87	31.72 \pm 1.28	12.71 \pm 0.70
	P value	0.007**	0.001**	0.322 ^{NS}	0.003**
Male	Patients	79.90 \pm 9.75	25.96 \pm 4.22	32.34 \pm 2.66	13.94 \pm 2.21
	Control	88.77 \pm 3.67	27.18. \pm 2.32	31.56 \pm 1.59	12.71 \pm 0.70
	P value	0.101 ^{NS}	0.388 ^{NS}	0.175 ^{NS}	0.005**

** (P<0.01), NS: Non-Significant.

Table 6. Effect of *H. pylori* on (WBC, LYM, MON, GRA) in patients and control according to sex

Parameters		WBCs (10^3 /MM ³)	LYM(%)	MON(%)	GRA(%)
Female	Patient	7.46 \pm 2.20	34.32 \pm 9.18	8.87 \pm 4.28	57.29 \pm 9.43
	Control	8.75 \pm 2.45	35.63 \pm 6.12	6.06 \pm 1.51	57.30 \pm 6.36
	P value	0.322 ^{NS}	0.093 ^{NS}	0.086 ^{NS}	0.252 ^{NS}
Male	Patients	8.64 \pm 3.42	36.30 \pm 14.66	9.00 \pm 4.19	54.69 \pm 16.78
	Control	8.26 \pm 1.32	32.59 \pm 6.46	7.10 \pm 1.87	57.52 \pm 7.83
	P value	0.001**	0.05*	0.000**	0.01*

** (P<0.01), NS: Non-Significant.

Table 7. Effect of *H. pylori* on (PLT, MPV) in patients according to sex

Parameters		PLT(10^3 /MM ³)	MPV(μ M ³)
Female	Patients	295.17 \pm 63.35	7.30 \pm 0.83
	Control	303.50 \pm 76.17	7.30 \pm 1.12
P value		0.404 ^{NS}	0.063 ^{NS}
Male	Patients	282.09 \pm 45.04	6.70 \pm 0.57
	Control	238.13 \pm 48.80.35	7.450 \pm 1.07
P value		0.850 ^{NS}	0.104 ^{NS}

NS: Non-Significant

JUSTIFICATIVA EXPERIMENTAL DO RENDIMENTO DE PROTEÍNA DE SOJA NO EXTRATANTE DURANTE O ESMAGAMENTO DO GRÃO DE SOJA NA FORMA ENCHARCADA**EXPERIMENTAL STUDY OF THE YIELD OF SOY PROTEIN IN THE EXTRACTANT WHILE THE ABRASION-RESISTANT SOYBEANS IN SOAKED FORM****ЭКСПЕРИМЕНТАЛЬНОЕ ОБОСНОВАНИЕ ВЫХОДА СОЕВОГО БЕЛКА В ЭКСТРАГЕНТ ПРИ ИСТИРАНИИ ЗЕРНА СОИ В ЗАМОЧЕННОМ ВИДЕ**KLASNER, Georgy Georgievich^{1*}; SPIRIDONOV, Alexandr Maximovich²

Kuban State Agrarian University named after I. T. Trubilin, Faculty of Mechanization, Department of livestock breeding mechanization and life safety, Russia

Correspondence author
e-mail: egor.klasner.91@mail.ru

Received 12 June 2020; received in revised form 3 August 2020; accepted 12 October 2020

RESUMO

Atualmete cada agricultor se depara com a tarefa de fornecer ao seu gado alimentos de alta qualidade que contribuam para asua saúde e crescimento rápido. Também é do conhecimento geral que as grandes propriedades têm mais oportunidades de implementar seus projetos e colocar em operação novas tecnologias e dispositivos. O dispositivo apresentado possibilita a obtenção de um produto de transformação de grãos de soja em leite de soja, queijo de soja "tofu", ou em uma base protéica de soja para preparação de rações para animais de fazenda e aves em pequenas propriedades. Este artigo explica o método experimental para encontrar os valores ótimos da velocidade de rotação do disco móvel, a temperatura do extrator, a lacuna entre os discos móvel e estacionário do triturador e a proporção do hidromódulo. Os valores ideais são aqueles que contribuem para o máximo rendimento de extração de proteína. Fatores experimentais: temperatura ambiente de 17 °C a 22 °C, pressão barométrica de 93325 PA a 96658 PA, umidade relativa de 65% a 85%. A extração de proteínas em uma emulsão é baseada nas propriedades físicas e químicas da difusão de compostos orgânicos dissolvidos, tendo a água como extratante. Como resultado, foram encontrados métodos para a produção eficaz de proteína de grãos de soja, o que pode aumentar o rendimento da suspensão para 24-28 Gr. Esta é a maneira mais eficiente de produzir proteína para modificação da alimentação usando este dispositivo.

Palavras-chave: *soja embebida em grão, abrasão de grão, curva de run-out, característica mecânica.*

ABSTRACT

Nowadays, every farmer is faced with the task of providing their livestock with high-quality food that will contribute to their rapid growth and health. It is also common knowledge that large farms have more opportunities to implement their projects and put new technologies and gadgets into operation. The presented device makes it possible to obtain a product of processing soy grain into soy milk, soy cheese "tofu", soy protein base for preparing feed for farm animals and poultry in small farms. This article explains the experimental method for finding the optimal values of the speed of rotation of the movable disk, the temperature of the extractant, the gap between the movable and stationary disks of the shredder, and the ratio of the hydromodule. Optimal values are those that contribute to the maximum protein yield. Experimental factors: ambient temperature from 17°C to 22 °C, barometric pressure from 93325 PA to 96658 PA, relative humidity from 65% to 85%. Protein extraction in an emulsion is based on the physical and chemical properties of the diffusion of dissolved organic compounds, with water as the extractant. As a result, methods have been found for the effective production of protein from soy grains, which can increase the yield of the suspension to 24-28 Gr. This is the most productive way to produce protein for feed modification using this device.

Keywords: *soybean soaked in the grain form, grain abrasion, run-out curve, mechanical characteristic.*

АННОТАЦИЯ

В наше время перед каждым фермером стоит задача давать своему поголовью качественное питание, которое будет способствовать их скорому росту и здоровью. Также, общеизвестно, что большие хозяйства имеют больше возможностей для реализации своих проектов и введения в эксплуатацию новых технологий и гаджетов. Представленное устройство позволяет получать продукт переработки зерна сои в соевое молоко, соевый сыр "тофу", соевую белковую основу для приготовления кормов для сельскохозяйственных животных и птицы в условиях небольших ферм и хозяйств. В данной статье разъяснён экспериментальный метод нахождения оптимальных значений скорости вращения подвижного диска, температуры экстрагента, зазора между подвижным и неподвижным дисками измельчителя, соотношения гидромодуля. Оптимальными значениями считаются те, что способствуют максимальному выходу белка. Факторы проведения экспериментов: температура окружающей среды от 17°C до 22 °C, барометрическое давление от 93325 Па до 96658 па, относительная влажность воздуха от 65% до 85%. Экстракция белка в эмульсии основана на физико-химических свойствах диффузии растворенных органических соединений, в качестве экстрагента выступает вода. В результате найдены методы эффективного получения белка из соевого зерна, с помощью которых можно повысить выход суспензии до 24-28 гр. Это наиболее продуктивный способ выработки белка для модификации кормов с помощью данного доступного устройства.

Keywords: соевые бобы в замоченной форме, измельченное зерно, кривая биения, механические характеристики.

1. INTRODUCTION

That soya is a significant supplier of vegetable protein, while the soy is rich in essential composition and content of amino acids, and feed value reaches of 1.45 units (Bortnikov, S. 2005. efficiency of using full-fat extruded soy / S. Bortnikov // Mixed fodder.- - No. 1.- Pp. 51-52.). Soy is a typical crop and is used both in pure form after treatment and in animal feed for feeding almost all farm animals. The main value of soybean in comparison with other forage crops is the lowest cost protein, which composition is an analog to expensive animal protein (Dotsenko S.M., Tilba V.A., Skripko O.V. 2012. Problems of the Soya Processing for Food. Food Manufacturing Industry. No. 7, Pages 18-21.).

Scientists come to a consensus that the most promising direction for the preparation of soybeans for feeding to agricultural animals is a liquid preparation of the protein suspensions, which is soy milk, which by its biological value, is not inferior to the whole, cow milk (Baturin, A. K. 2006 Chemical composition and energy value of food products: Handbook of Mccans and Widdowson. under the General editorship of A. K. Baturin. Saint Petersburg: Profession, - 416). However, the use of soybeans in the diet of farm animals in the conduct of personal subsidiary farm or small farm animals is not large, in the absence of a universal small-sized and low

power consuming equipment for processing grain for animal feed.

Thus, there is a need to develop a universal technology of preparation of a protein emulsion applicable in the conditions of private farming.

In this regard, the purpose of this research is the justification of constructive-regime parameters of the chopper soaked soybeans to improve the efficiency of the cooking process of protein-rich feed.

2. MATERIALS AND METHODS

The analysis of methods of processing soybeans to prepare soybean fundamentals has shown that using crushed dry grain more finely ground (0,35 to 0,5 mm) is the most significant yield of protein extraction because processing technology "dry method" (energy-intensive, their use for small volumes of production in the livestock enterprises of small farms are not economically profitable. The energy consumption of the grinding process can be reduced if its strength is reduced by pre-soaking "wet method" (Frolov V.Ju., Sysoev D.P., Klasner G.G. 2015. Optimization of Parameters of the Chopper of the Soaked Soya Grain No.3. P 24-25. Farm Machinery Operator; M. SH. Begeulov, 2006 sh. Fundamentals of soy processing. M.: Delhi print). To implement the processes of the preparation of food products based on soybeans (substitute for

whole milk, curd and whey, and add insoluble soy residue in concentrated feed, with the aim increase their nutritional value) the technological scheme (Figure 1) waste-free production.

Was made a prototype (Figure 2), which conducted a series of multi-factorial experiments with the aim of experimental substantiation of constructive-regime parameters of the chipper.

A priori ranking of the factors concerning previously conducted research allowed to identify the most relevant factors (Table 1).

The study was divided into two phases and was carried out on the experimental setup chopper soaked soybeans in laboratory and production conditions:

- the first stage was conducted to study the physicomachanical properties of the swollen soybeans after soaking in water. It is necessary to establish the dependency of the density (ρ), the strength of the swollen grain of the material (J) to change the moisture content (W) and the mass (m) of the degree of swelling, as well as the completeness and quality output of the soy protein in extent (G) from the hydraulic module (h) (the number of water servings supplied when the grain was abrasive) and the water supply temperature (t).

- the second stage was devoted to studying the process of soy milk production and optimization of the main factors that influence the PA process. So the second stage of the research task was to determine the optimal constructive-regime parameters of the chopper, soybean grain, determination of the main characteristics of the developed device.

In experimental studies, the following tasks were solved:

- determined the physical and mechanical properties of soaked soybeans which is a raw material;

- studied the quality indicators of the process, namely extraction of the protein in the emulsion.

The experimental setup adequately allows the required limits to vary the values of selected factors influencing the process of grinding soaked soybeans, followed by separation of the soy protein.

The frequency of rotation of the lower disk coated with an abrasive coating changed the switching speed of the installation. The switch operates in three modes as it was made

replaceable abrasive discs with curved grooves. Curved grooves has different angles of intersection (α -60°, α -90°, α -120°). The clearance between the abrasive discs was exhibited by putting washers between the top of the abrasive cone and the housing cover of the chipper (therefore, in the course of the experiment asked the clearance between the abrasive discs 3, 4, and 5 mm). The roughness of the abrasive surface of the disk is achieved by applying adhesive to the abrasive stone, corundum, the value of roughness was selected $R_a = 50$, $R_a = 250$, $R_a = 450 \mu m$ (Frolov V.Ju., Sysoev D.P., Klasner G.G. 2015. Optimization of Parameters of the Chopper of the Soaked Soya Grain No.3. P 24-25. Farm Machinery Operator).

To measure the energy characteristics of the used device To-505. For quantitative measurement of protein, the yield was used for laboratory flasks and scales VLTK-500. To change the speed of the motor was used in a dimmer built into the experimental setup. The temperature of fluid supplied to the chopper was measured using an electronic non-contact thermometer. Through the use of a measuring Cup was held the volume of the resulting liquid protein suspension.

The experiments were carried out in common in Krasnodar Krai grade soybeans "VILANA". Of grain, the material was taken 6 small servings, each of which consisted of 10 grains. The length of soybean grain was 6 mm. the mass of 10 grains of soybeans 1,767, and the amount of 10 grains was 1.4 ml (volume of grain was calculated at the displaced fluid from the measuring Cup after you're immersed in it). The pilot study took place at room temperature (20-22 °C), and the initial moisture content of the grains was 10 %. According to the experimental data (next Chapter) was built following dependencies: mass change (m), scope (v), and length (L) grain length of soaking (picture 3.5 – 3.6).

The essence of pressing from a physical point of view is the convergence and compaction of loose parts fodder. The increasing mechanical compression of the grain material eliminates air pores and voids. Further increase in pressure is not effective, because swollen grains mainly consist of compressible material is water.

Geometric size, particle shape, and internal structure of the grain material determine its physical and mechanical properties, to measure which is necessary to apply different methods and equipment. So to determine density, one of the main characteristics of the

grain material, knowing that the density is the ratio of the mass of substance (kg) contained in the volume of the substance (kg/m^3), can be applied micro metrically method.

3. RESULTS AND DISCUSSION

The experimental research was conducted on the Barra soya variety. 6 experimental samples with 10 grains in each sample were selected out of the whole batch of the soya grain. The grain's average length is made up of 6 mm. The mass of 10 grains was 1.767, the volume of 10 grains made up 1.4 ml when the grain's absolute humidity was 10%. The experiment was carried out with the room temperature (20-22 °C). According to the obtained values, the graph of dependence of increase in mass (m), volume (v), and length (L) of the grain on the soaking time was constructed (Picture 6).

Analysis of the graph (Figure 6) showed that the optimal time (T) of the soya grain soaking makes up 6-7 hours (the knock point in Figure 3). During the 6-hour soaking, the grain's length, mass, and volume make up $L = 13$ mm, $m = 0.36$ gr., $V = 0.34 \cdot 10^{-6} \text{ m}^3$. Further increase in time of soaking the soya grain is inefficient since when the grain is soaked for 24 hours, $m = 0.434$ gr., $V = 0.38 \cdot 10^{-6} \text{ m}^3$, and no change of the geometrical dimensions of soya is changed.

When knowing the change of the grain's mass and volume depending on the soaking time, we can calculate the change of the grain density (Figure 4). As the soaking time increases up to 7 hours, the grain density is lowered and makes up $\rho = 1.088$ g/ml. It is not reasonable to continue increasing the soaking time since later on, and the density reduction becomes somewhat stable.

While optimizing the operating process of the chopper of the soaked grain, the quality of the finished product, as well as the technical parameters of the process of obtaining the soya milk and curd, were studied.

While processing the results of the experiment, the dependencies of the suspense water duty with the extracting agent temperature of 55-70°C were constructed (Figure 7).

Dependence of the protein yield into the extract is based on the physical and chemical properties of solving the high-molecular organic compounds in the offered technology, and the extracting agent is potable water.

Analysis of the graph (Figure 8) makes it possible to conclude that the extracting agent is actively saturated to the water duty value of 1:10. When the water duty continuous to increase, the saturation becomes somewhat stable.

Grinding soaked soybeans were selected by these optimization criteria: output protein in the extractant – G (the response Y_3), the performance of the chopper – Q (the response Y_2), and power – kW N (the response Y_1). The results of the research were chosen as optimal values.

To substantiate its assessment of the influence of factors on the results of the experiment were calculated the regression equation of the second-order (program Statistica), which are in coded form (Equation 1):

$$Y_3 = -83,4565 + 0,0236 \omega + R 0,017367a - 8,61847 \alpha - 3,9973 h + 0,000006 \omega Ra - 0,000032 \omega \alpha + 0,001 \omega h + 0,0007 Ra \alpha - 0,016 Ra h - 0,0261 \alpha h - 0,00007 Ra^2 + 1,0806 \alpha^2 + 1,11143 h^2 \quad (\text{Eq. 1})$$

and the decoded form (Equation 2):

$$G = 21,35202 + 3,9244 \omega + R 5,452133a + 4,831567 \alpha - 5,29423 h + 0,0009 \omega Ra + 0,0005 \omega \alpha - 0,000086 \omega h + 0,0015 Ra \alpha - 0,0007 Ra h + 0,000089 \alpha h - \omega 0,0379^2 - 0,05217 Ra^2 - 0,04760 \alpha^2 + 0,0514 h^2 \quad (\text{Eq. 2})$$

After obtaining adequate mathematical models of the process, determined the coordinates of the optimum and studied by the response surface.

From the analysis of the dependence presented in figure 10, it can be concluded that the protein yield (G) in the extractant increased from 14 Gy to 24 Gy by increasing the speed of ω . From the analysis of the dependence presented in figure 12, it can be concluded that for maximum protein yield (G) in the extractant, the angle of inclination of the abrasive groove should lie in the range $\alpha=80...105^\circ$.

Analyzing the graph of is shown in figure 13, we can conclude that the maximum protein yield (G) from 24 g to 28 g is observed with decreasing gap width (h) between the abrasive discs from 3.7 mm to 3 mm. The angle of inclination of the curved groove should lie in the range $\alpha=80...105^\circ$.

4. CONCLUSIONS:

The optimum soaking time interval was 6 to 7 hours. The force required to fracture the grain was 0.01 MPa, the density of the grain during the 7 hour soaking was $\rho = 1,088 \text{ g/ml}$; the moisture content was $W = 65\%$, and the average grain mass was $m = 0.37 \text{ g}$, and the volume $V = 0,34 \cdot 10^{-6} \text{ m}^3$.

To achieve the highest protein yield (G) in extent values of the rotation speed (ω) of the lower grinding wheel must be within $\omega = 157...172 \text{ rad/s}$. The clearance between the abrasive discs was $h = 3... 3.26 \text{ mm}$, the magnitude of the applied abrasive must be within $R_a = 260...450 \text{ }\mu\text{m}$, and the angle of curvature of the curved grooves was equal to $\alpha = 80^\circ...105^\circ$. The obtained experimental dependencies and the selected rational values of hydraulic module $\eta = 1:10$; the temperature of the extractant was $t = 55...60^\circ\text{C}$.

5. REFERENCES:

1. G G Klasner, V Yu Frolov, and V F Kremyanskiy. Experimental and Theoretical Substantiation of Device Performance in Soy Milk Production for Animal Feed. International scientific and practical conference AgroSMART - Smart solutions for agriculture, KnELife Sciences, pages 808-819. DOI 10.18502/kl.v4i14.5678
2. S. M. Dotsenko, I. V. Bibik. 1997. Making the Preparation of Concentrated Fodders for Feeding the Animals more Efficient. Collection of scientific papers "Technology and Mechanization of Production and Processing of the Agricultural Products".
3. Dotsenko S.M. Skripko O.V., Tilba V.A. 2014. The Use of Soya in Technology of the Protein - Vitamin and Protein - Carbohydrate Products. Storage and Processing of the Agricultural Raw Materials. No. 4. Pages 45-49
4. Dotsenko S.M., Tilba V.A., Skripko O.V. 2012. Problems of the Soya Processing for Food. Food Manufacturing Industry. No. 7, Pages 18-21
5. Dotsenko S.M., Ivanov S.A., Filonov R.F. 2004, Improvement of the Soya Chopping Process. Journal "Mechanization and Electrification of the Agriculture" No. 5, pages 19-20.
6. V. Ju. Frolov, D. P. Sysoev. 2014. Analytical Aspects of Making the High-Protein Fodders. Scientific Journal of Kuban State Agrarian University [Digital resource]. Krasnodar: Kuban State Agrarian University, 2014. –No. 99(05). – Information register cipher: IDA [article ID]: 0991405058. –Access mode: <http://ej.kubagro.ru/a/viewaut.asp?id=3699>
7. Konakov A. P. 2001. Equipment for Small Livestock Farms. Manual. – M.: PtofObrlzdad, – 208 p.
8. S. V. Melnikov, V. R. Alyoshkin, P. M. 1980. Roschin Planning of the Experiment in the Agricultural Processes Research. the 2nd revised and enlarged edition. – L.: Kolos. Liningrad department, ,168 p, illustration.
9. V. Ju. Frolov, S. M. Dotsenko. V. V. Samuilo, S. V. Varaksin, A. S. Kataev . 1998. A Way of Obtaining the Soya Product. Patent (invention) No. 6 2105494 RU
10. V. Ju. Frolov, D.P. Sysoev. 7 10.03.2013. A Way of Obtaining the Milk and Protein Products Patent (invention) No. 2477179 RU.
11. Pilipenko A. M., Timapovsky L.V. 1989. Mechanization of Processing and Making the Fodders in the Small Holdings. – M.: Rosagropromizdat,. 145 p
12. V. G. Ryadchikov. 2008. Amino Acids and Ideal Protein in the Pigs and Birds' Rations. Efficient Livestock Sector. No. 7. -. –P.48-51
13. Solntsev R. V. 2000. Improvement of the Chopping Process and Substantiation of Design and Standard Parameters of the Grain Centrifugal Chopper: Thesis of Candidate of Technical Sciences.
14. Frolov V. Ju., Dotsenko S. M., Kataev A. S. 1996. Substantiation of Design of the Activator's Operating Device to Make the Soya Milk. Collection of scientific papers. Far Eastern State Agricultural University.
15. Frolov V. Ju., Sysoev D. P., Klasner G. G. 2015. Optimization of Parameters of the Chopper of the Soaked Soya Grain No.3. P 24-25. Farm Machinery Operator.

16. Frolov V. Ju., Sysoev D.P. 2016. The Evaluation of Efficiency of Using Technologies for Preparation and Distribution of Fodder at Small. Research Journal of Pharmaceutical, Biological and Chemical Sciences.
17. S. G. Furtsev, T. A. Sayapina. 1991. Installation to Make the Soya Milk in Farms. Paper of Far Eastern Research, Design and Technology Institute of Mechanization and Electrification of Agriculture.
18. M. SH. Begeulov, 2006 sh. Fundamentals of soy processing. M.: Delhi print,
19. Bortnikov, S. 2005. efficiency of using full-fat extruded soy / S. Bortnikov // Mixed fodder.- - No. 1.- Pp. 51-52
20. Ivanov, S. A. Novosibirsk, 2005 «Improving the technology and technical means of preparing feed for livestock based on soy grain» / S. A. Ivanov. 36 p.
21. Kurkov, Yu. B. 2013 «Perspective technology of preparation and distribution of high-protein complete feed mixes to cattle» / Yu. b. Kurkov, T. A. Krasnoshchekova, V. V. Epifantsev, A. Yu. Kurkov, T. P. Kulagina. – Achievements of science and technology in the agro – industrial complex, no. 12-P. 62-66.

Table 1. Factors and levels of their variation

Level	Factors			
	The angular velocity of rotation of the lower disc coated abrasive ω , rad/s	Grain size of abrasive R_a microns	The direction angle α of the grooves	The gap between the discs hmm
	X_1	X_2	X_3	X_4
The upper (+1)	172	50	α -120°	5
Main (0)	169	250	α -90°	4
Lower (-1)	141	450	α -60°	3

Table 2. Change of the grain density resulting from time of keeping it in water

Index	Time of the soya grain soaking in water Th								
	0	1	2	3	4	5	6	7	24
m, gr	0.18	0.28	0.317	0.32	0.34	0.34	0.36	0.37	0.43
V, ml	0.14	0.24	0.26	0.3	0.3	0.32	0.34	0.34	0.38
ρ . Gr/ml	1.26	1.14	1.22	1.07	1.12	1.08	1.06	1.08	1.14

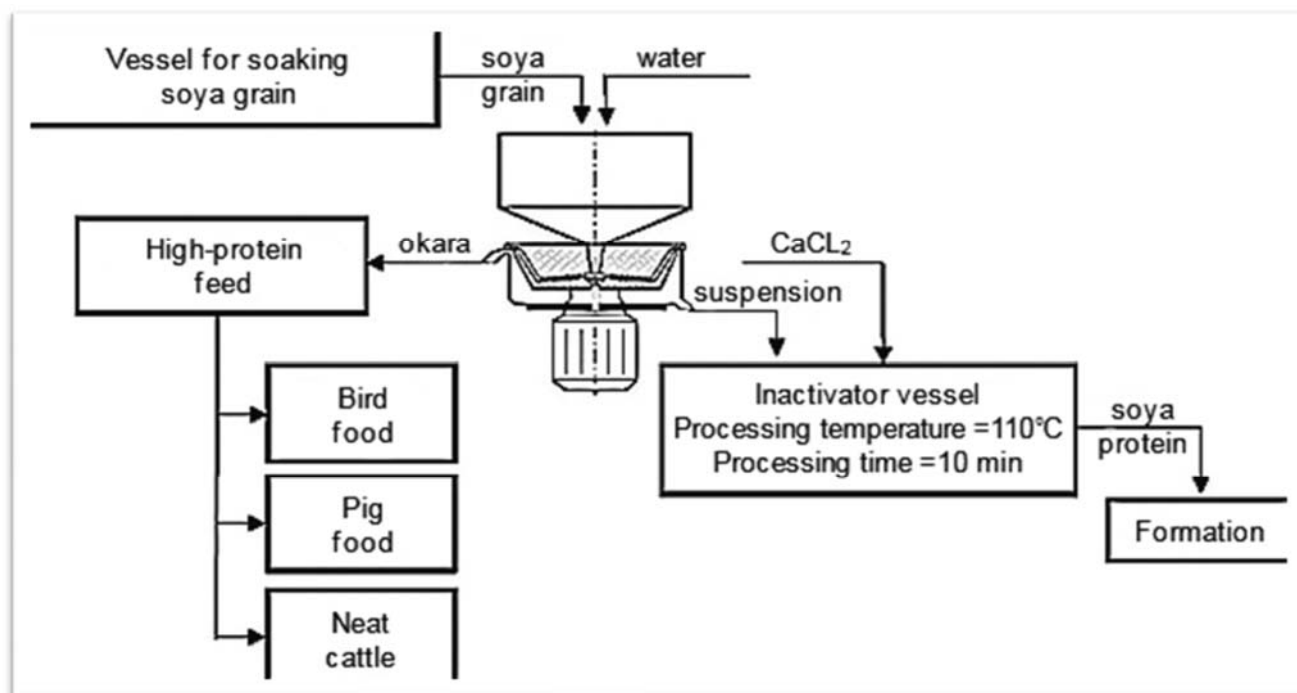


Figure 1. Technology of making the soya milk and protein base for concentrated fodders



Figure 2. Scheme and general view of the experimental complex for the study of processes of production of feed products based on soy protein.



Figure 3. – The dependence of the mass change (m), scope (v) and length (L) grain length of soaking



Figure 4. Dependence of the change of the geometrical sizes of soybean from (time) degree of swelling



Figure 5. The relationship of the destruction of the swollen grains by means of pressure being applied

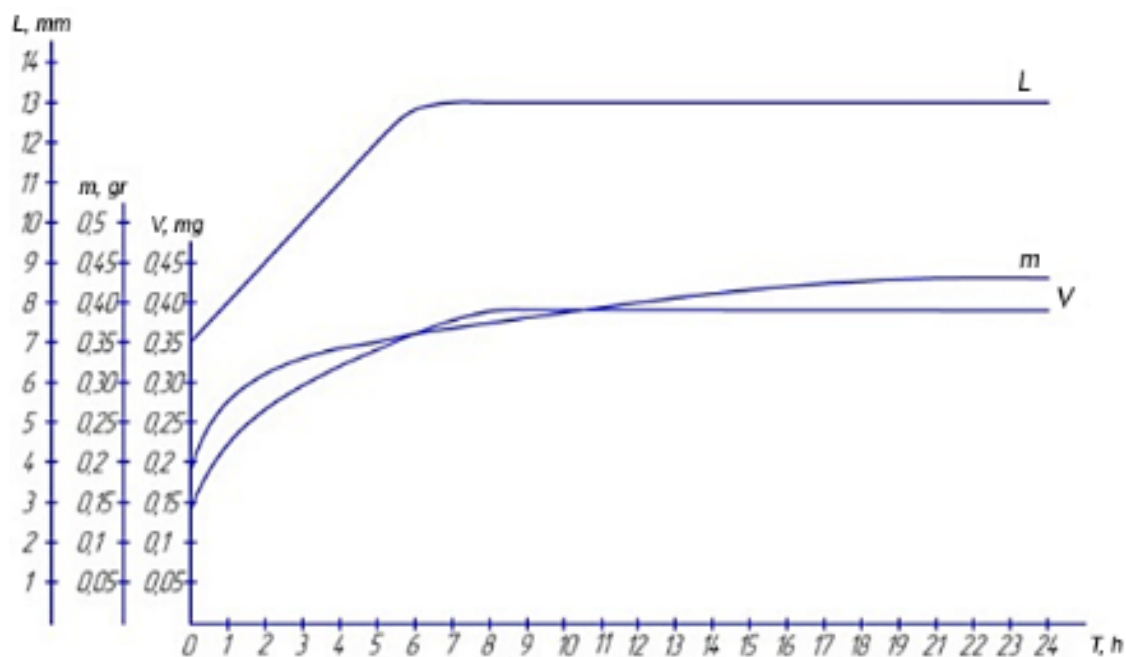


Figure 6. Dependence of increase in mass (m), volume (v) and length (L) of grain on soaking time

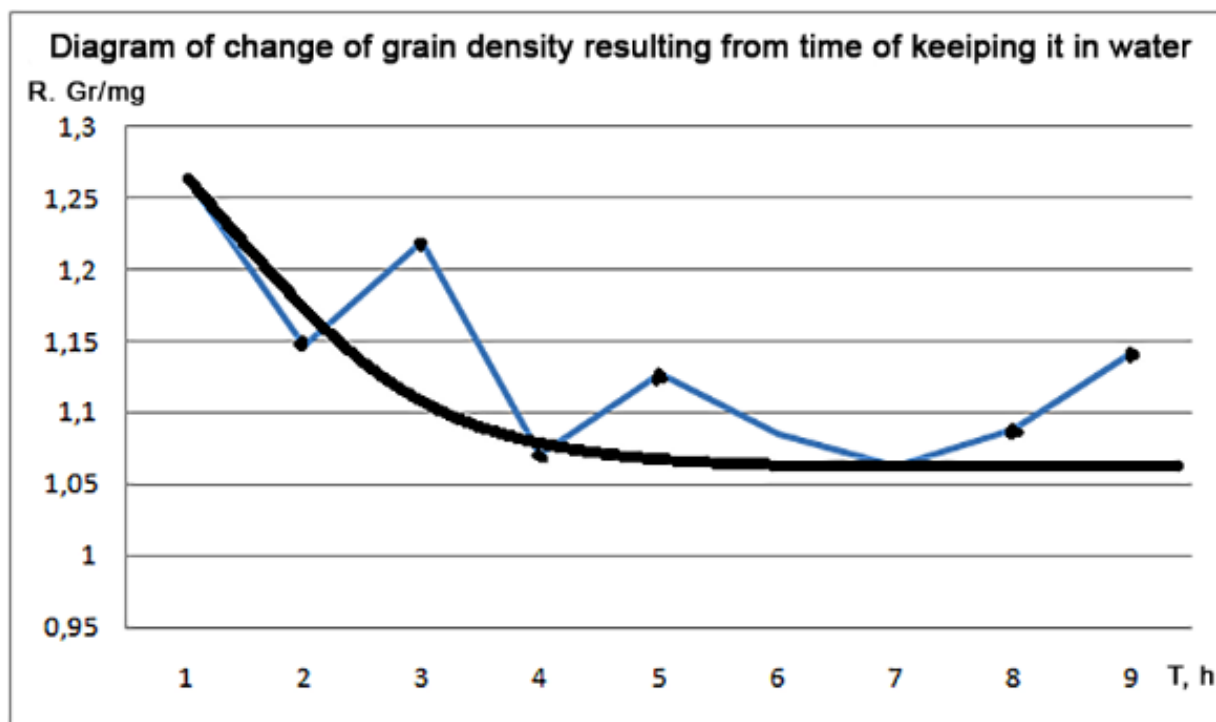


Figure 7. Graph of the dependence of density change on the soaking time

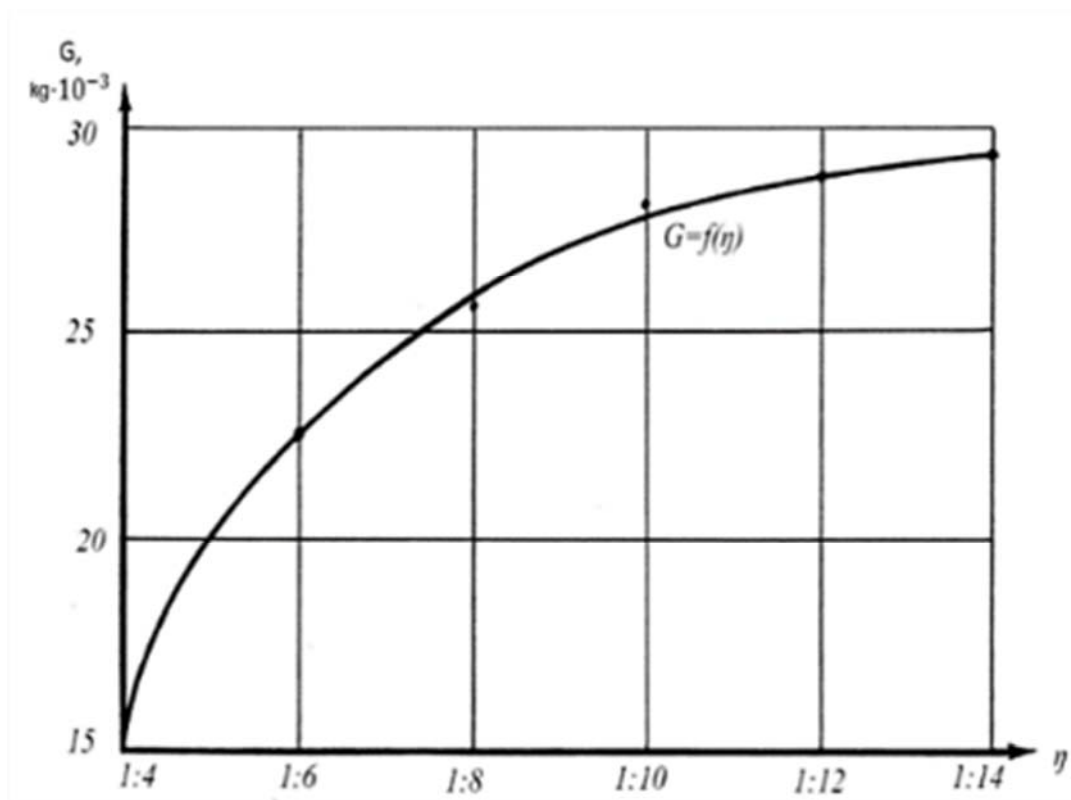


Figure 8. Dependence of protein yield G into the extracting agent on water duty η

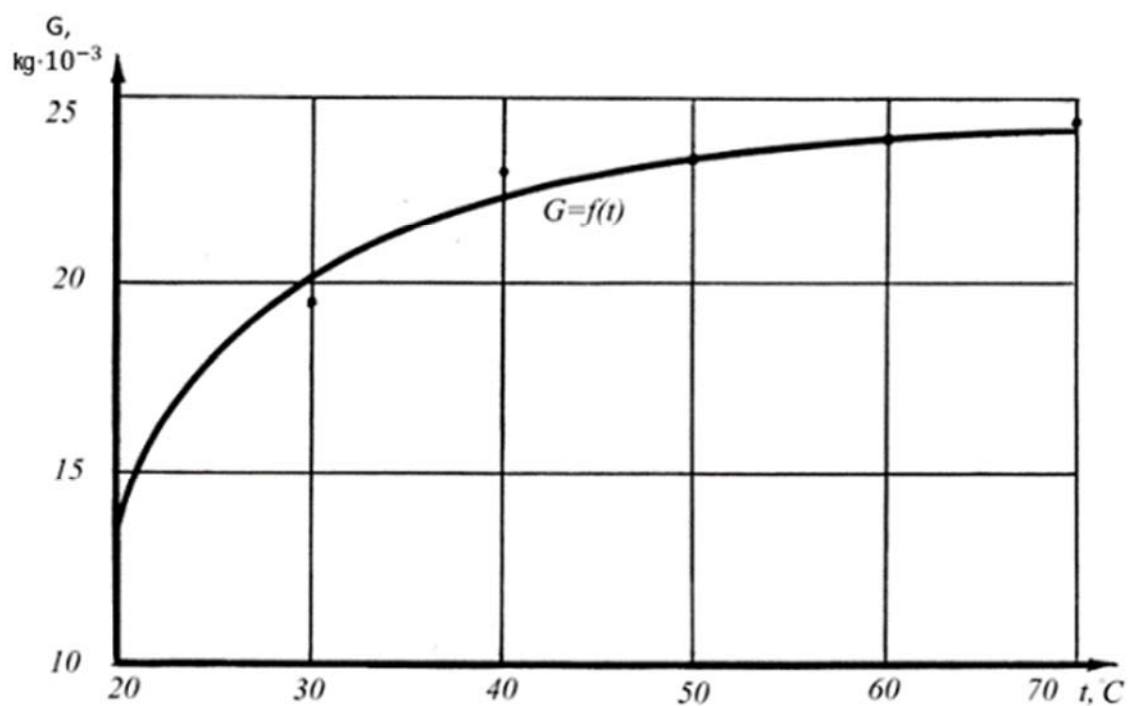


Figure 9. Dependence of protein yield into the extracting agent G on temperature t

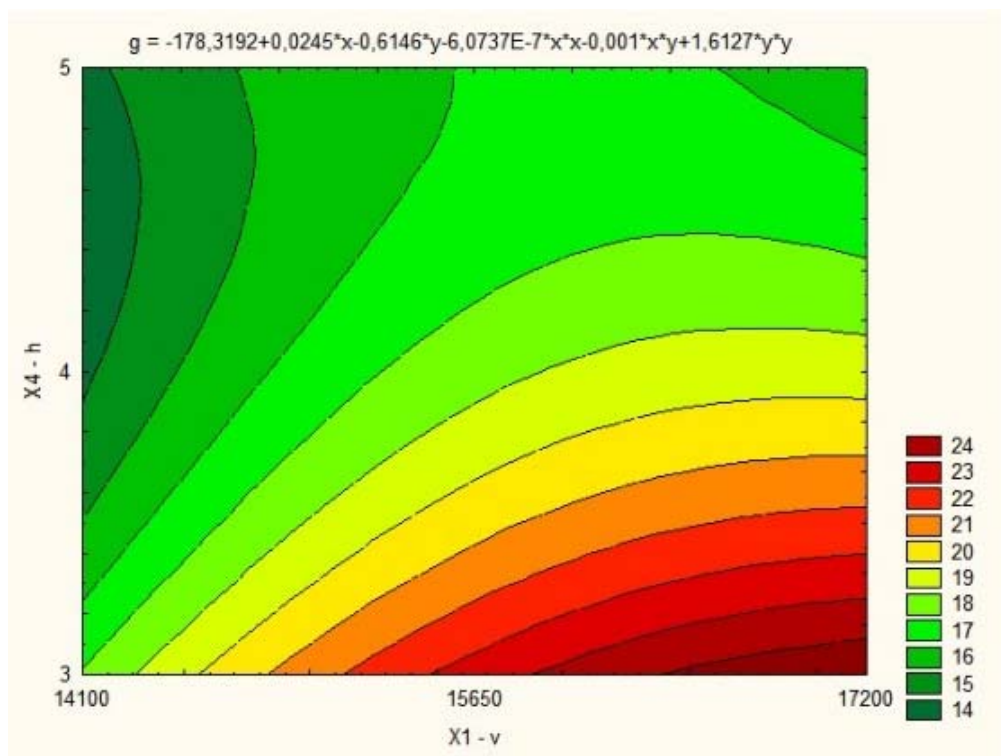


Figure 10. a cross-section of the surface of the protein yield in the extractant on a plane $X_1(\omega)$ from $X_4(h)$

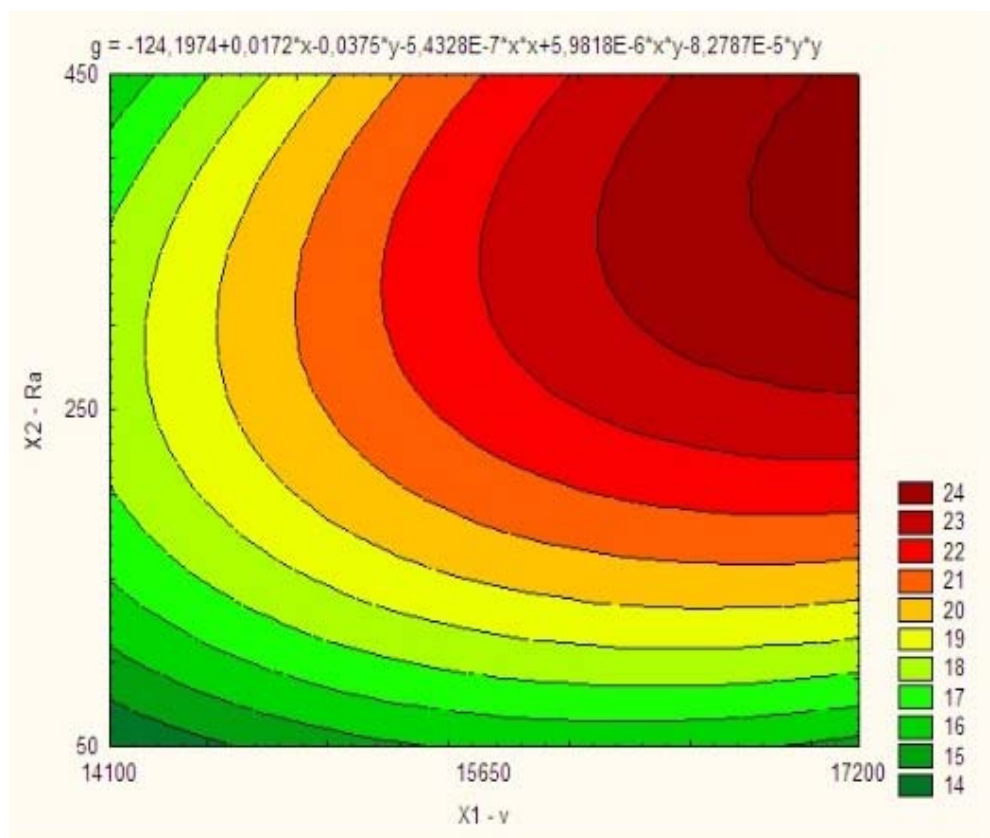


Figure 11. a cross-section of the surface of the protein yield in the extractant on a plane $X_1(\omega)$ from $X_2(Ra)$

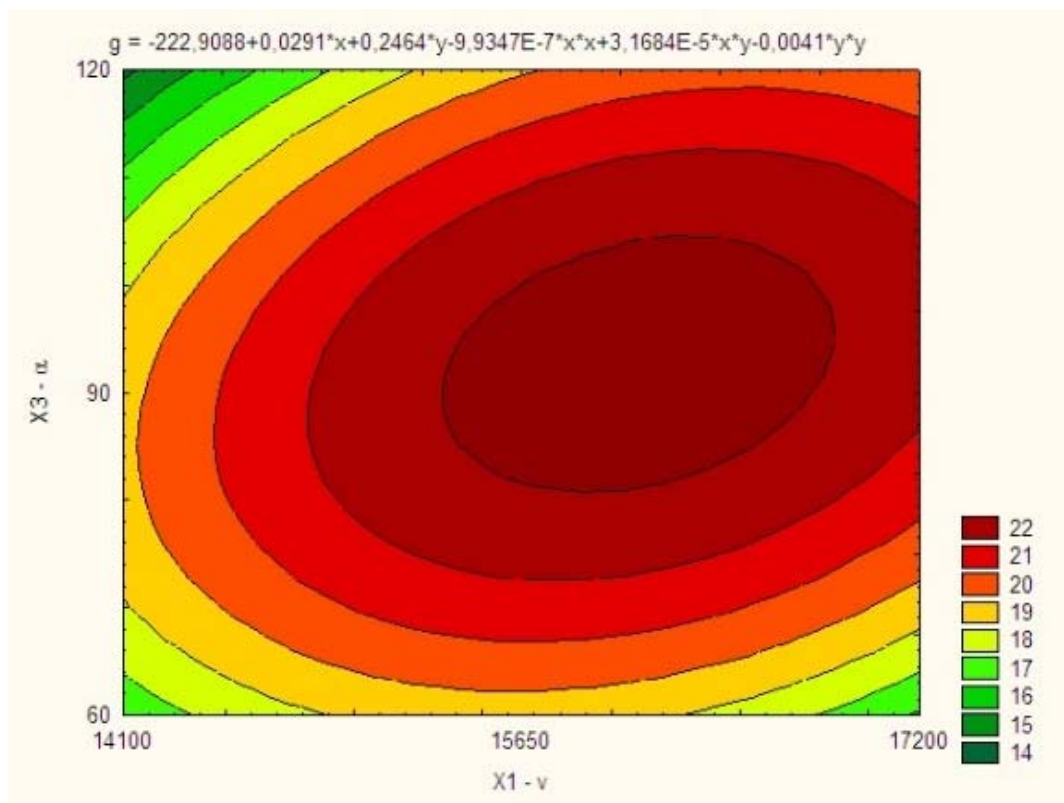


Figure 12. a cross-section of the surface of the protein yield in the extractant on a plane $X_1(\omega)$ from $X_3(\alpha)$

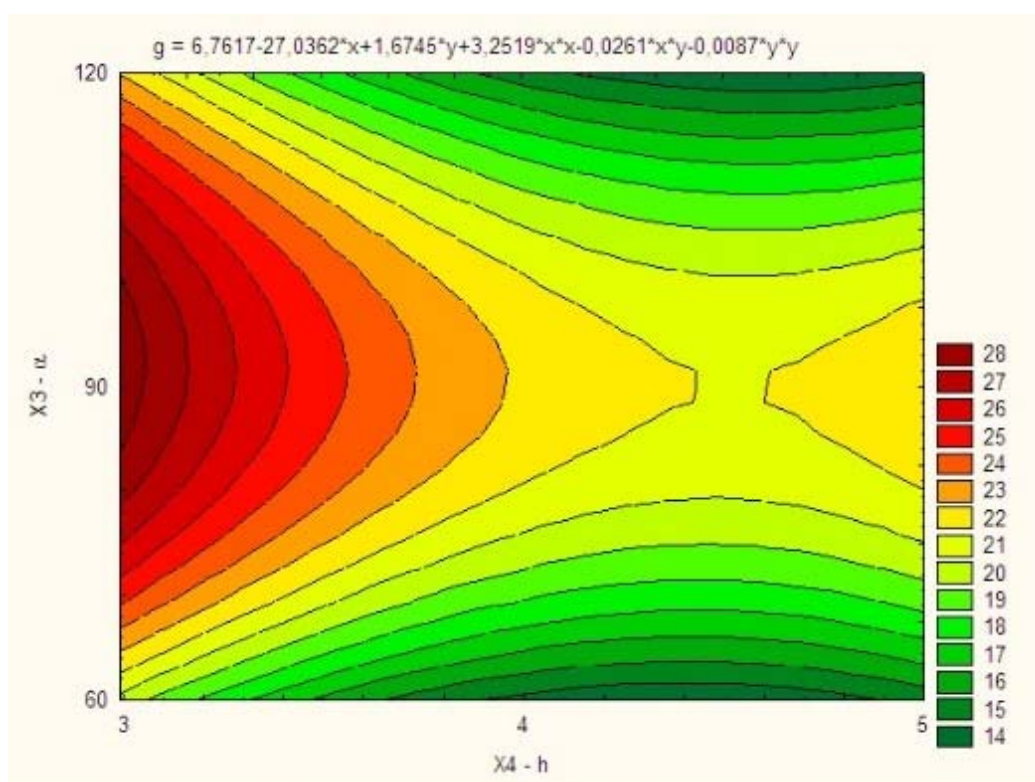


Figure 13. a cross-section of the surface of the protein yield in the extractant on a plane $X_4(h)$ from $X_3(\alpha)$

HIPERMETILAÇÃO DO PROMOTOR DE SOMATOSTATINA (SST) EM ASSOCIAÇÃO COM CÂNCER COLORRETAL

SOMATOSTATIN (SST) PROMOTER HYPERMETHYLATION IN ASSOCIATION WITH COLORECTAL CANCER

فرط المثيلة في حفاز جين السوماتوستاتين بالتزامن مع سرطان القولون والمستقيم

FAWZI, Mohammed^{1*}; TAIFI, Ahmed²; LAWI, Zahraa Kamil Kadhim³

^{1,2} AL-Manara College For Medical sciences, Department of Pharmacy, Maysan, Iraq.

³ Department of Biology, Faculty of Science, University of Kufa, Najaf, Iraq.

* Corresponding author

e-mail: m.fawzi@uomanara.edu.iq

Received 17 August 2020; received in revised form 23 October 2020; accepted 30 October 2020

RESUMO

O câncer colorretal (CCR) é uma das neoplasias malignas mais comuns com diversos fatores de risco, incluindo ambientais e genéticos. Vários genes, chamados genes supressores de tumor, desempenham um papel essencial na inibição desses fatores de risco, impedindo o desenvolvimento de tumores. Um desses genes é a somatostatina (SST). A somatostatina é um peptídeo antiproliferativo com efeitos pró-apoptóticos que aumentam a morte celular para prevenir o crescimento do tumor. Este estudo teve como objetivo investigar a relação entre a metilação do DNA no promotor SST e a progressão do câncer colorretal. Após a conversão do bissulfato de DNA, a metilação do promotor SST foi examinada usando PCR quantitativo específico de metilação (qMSP) em 71 casos (19 metástases CRC, 28 CRC em estágio inicial e 24 controles saudáveis). O PCR específico de metilação quantitativa (qMSP) é um método de PCR em tempo real usado para determinar os resíduos de citosina metilada e não metilada usando um conjunto específico de primers. A porcentagem de hipermetilação no promotor SST foi de 17%, 60% e 79%, em média, para os controles saudáveis, grupos de CRC em estágio inicial e metástase. Os resultados mostraram uma associação significativa entre a hipermetilação do DNA do promotor SST e a progressão do CRC. Os valores de P foram 0,0364 para o grupo de estágio inicial e 0,0138 para o grupo de metástases. Os resultados também confirmaram que a hipermetilação do DNA bloqueia a expressão de SST, que por sua vez induz a carcinogênese. A detecção da hipermetilação do promotor SST no estágio inicial do câncer pode ser usada como um biomarcador para a triagem e prognóstico de CRC.

Palavras-chave: *câncer colorretal, metilação do DNA, gene supressor de tumor.*

ABSTRACT

Colorectal cancer (CRC) is one of the most common diagnosis malignancies with different risk factors, including environmental and genetic. Several genes, called tumor suppressor genes, play an essential role in inhibiting these risk factors by preventing tumor development. One of these genes is somatostatin (SST). Somatostatin is an antiproliferative peptide with pro-apoptotic effects that enhance cell death to prevent tumor growth. This study aimed to investigate the association relationship between DNA methylation in SST promotor and colorectal cancer progression. After DNA bisulfite conversion, SST promoter methylation was examined using quantitative methylation-specific PCR (qMSP) in 71 cases (19 metastasis CRC, 28 early-stage CRC, and 24 healthy controls). Quantitative methylation-specific PCR (qMSP) is a real-time PCR method used to determine the unmethylated and methylated cytosine residues using a specific set of primers. The percentage of hypermethylation in SST promoter was 17%, 60%, and 79% for healthy controls, early-stage, and metastasis CRC groups. The results showed a significant association between DNA hypermethylation of SST promoter and CRC progression. P-values were 0.0364 for the early-stage group and 0.0138 for the metastasis group. The results also supported that the DNA hypermethylation block the expression of SST, which in turn induce carcinogenesis. The detection of SST promoter hypermethylation at early stage of cancer could be used as a biomarker for screening and prognosis of CRC.

Keywords: *colorectal cancer, DNA methylation, tumor suppressor gene.*

يعد سرطان القولون والمستقيم أحد أكثر الأورام الخبيثة شيوعاً التي تم تشخيصها والتي لها عوامل خطر مختلفة، بما في ذلك البيئة والوراثة. تلعب العديد من الجينات دوراً مهماً في تثبيط تأثير عوامل الخطر هذه عن طريق منع تطور السرطان، وهو ما يسمى الجينات الكابتة للورم. أحد هذه الجينات هو السوماتوستاتين السوماتوستاتين هو ببتيد يثبط انقسام الخلايا وتكاثرها وله تأثيرات محفزة للموت الخلوي المبرمج ليمنع نمو الورم. تحاول الدراسة الحالية إيجاد علاقة ارتباط بين مثيلة الحمض النووي في حفاز جين السوماتوستاتين وتطور سرطان القولون والمستقيم. تم فحص المثيلة لحفاز جين السوماتوستاتين باستخدام تفاعل البلمرة الكمي في 71 عينة (19 عينة تمثل مراحل متقدمة من سرطان القولون والمستقيم و 28 عينة مرحلة مبكرة منه و 24 عينة لحالات سليمة). كانت النسبة المئوية لفرط المثيلة في حفاز جين السوماتوستاتين هي 17% و 60% و 79% في العينات السليمة و عينات المراحل المبكرة والمتقدمة من سرطان القولون والمستقيم على التوالي. بينت النتائج أن هناك ارتباط كبير بين فرط مثيل الحمض النووي لحفاز جين السوماتوستاتين وتطور سرطان القولون والمستقيم، إذ كانت القيمة الاحصائية الاحتمالية 0.0364 لمجموعة المرحلة المبكرة و 0.0138 لمراحل المتقدمة من السرطان. وهذا يدعم حقيقة أن فرط مثيل الحمض النووي يمنع تشفير جين السوماتوستاتين، والذي بدوره يؤدي إلى تطور السرطان. يمكن استخدام الكشف عن فرط مثيل حفاز جين السوماتوستاتين في المرحلة المبكرة من السرطان كمؤشر حيوي لفحص سرطان القولون والمستقيم والتنبؤ به.

الكلمات المفتاحية: سرطان القولون والمستقيم، مثيلة الحامض النووي، الجينات الكابتة للورم.

1. INTRODUCTION:

Colorectal cancer (CRC) is a third cancer type in terms of incidence around the world. In the Global Cancer Observatory database (GLOBOCAN), 1.8 million new cases were registered in 2018, according to the International Agency for Research on Cancer (IARC) (Bray *et al.*, 2018). Globally, the incidence and mortality rates of CRC have been increased 10-fold in 10 years. Specifically, low and middle-income countries show a rapid increase in CRC-related mortality (Arnold *et al.*, 2016). Age is the main risk factor of sporadic CRC; the chance of colorectal cancer developing is increased in patients with age more than 50 years old (Levin *et al.*, 2008). Moreover, patients who have Crohn's disease and/or inflammatory bowel disease have more chance to develop CRC by 2.5% to 3.7% than healthy people. The formation of dysplasia, which considered abnormal growth of mucosal cells could induce the CRC after many years of chronic inflammation (Eaden *et al.*, 2001; Canavan *et al.*, 2006). Other CRC risk related to lifestyle and patient habits a sedentary, obesity (Martinez and Garcia, 2016), unhealthy nutrition (Willett, 2005; Bastide *et al.*, 2011; Santarelli *et al.*, 2008), smoking and alcohol consumption (Pöschl, and Seitz, 2004; Botteri *et al.*, 2008) all of these factors have been elucidated as a risk factor for colorectal cancer.

CRC can be classified depending on genetic alteration as sporadic, inherited, and familial colorectal carcinomas (Mármol *et al.*, 2017; Fearon and Vogelstein, 1990; Smith *et al.*, 2002). Sporadic cancer account for 70% of all CRC cases. Most of this type is caused by point mutations and DNA methylation in specific genes, including oncogene, tumor suppressor genes, and DNA repair genes (Hagggar and Boushey, 2009; Kuipers *et al.*, 2015; Lao and Grady, 2011;

Sameer and Nissar, 2016). Polyposis and nonpolyposis forms of inherited mutations in specific genes lead to colorectal cancer responsible for only 5% of all CRC cases. The polyposis group recognizes as a formation of potentially malignant polyps in the colon, including familial adenomatous polyposis (FAP) (Lynch and Chapelle, 2003).

In contrast, inherited nonpolyposis CRC is related to mutations in DNA repair genes. This type of malignant primary derived from Lynch syndrome, caused by inherited mutations in DNA repair genes such as *MLH1*, *MLH6*, *PMS1*, and *PMS2* (Umar *et al.*, 2004). An inherited mutation in different alleles cannot be included in any inherited cancer variant called familial colorectal cancer, which accounts for 25% of all CRC cases (Stoffel *et al.*, 2014).

During carcinogenesis, mechanisms of genetic alterations and epigenetic aberration modifications affected the normal functions of the oncogene, tumor suppressor genes, cell adhesion molecules, and telomerase activity. All these events induce malignant cell growth (Choi and Lee, 2013). Epigenetics studies have confirmed that DNA methylation in the promoter region of a tumor suppressor gene leads to transcriptional inactivation and is correlated with the carcinogenesis of CRC. DNA methylation is a signature including a panel of methylated CpGs that could show the potential in the screening and prognosis, early diagnosis, or therapy response prediction (Jin *et al.*, 2008; Puccini *et al.*, 2017; Ou *et al.*, 2007). The detection of DNA methylation sheds light on the potential of using methylated CpGs as a biomarker for CRC diagnosis and monitoring (Puccini *et al.*, 2017; Ma *et al.*, 2019). Recently, the U.S. Food and Drug Administration (FDA) approves using methylated septin 9 (*SEPT9*) for a screening of CRC (Ma *et al.*, 2019).

Somatostatin (SST) is a peptide that suppresses tumor growth through distinct mechanisms that involve inhibition of growth factors and hormones, reduction in vascularization, and regulation of the immune system (Misawa *et al.*, 2015; Reubi and Laissue, 1995). SST is released in different tissues and organs, including the central nervous system, gastrointestinal tract, pituitary, pancreas, and thyroid (Kumar and Grant, 2010; Patel, 1999). It plays an essential role as an endocrine hormone and neurotransmitter (Reichlin, 1995). SST is released by luminal acid stimulation in the gastrointestinal tract and regulates gastric acid (Goo and Kaunitz, 2010). SST inhibits cell proliferation by its antiproliferative and apoptotic effects and induces apoptosis via somatostatin receptor (SSTR) signaling (Grimberg, 2004). Several studies described the CpG hypermethylation of SST promotor in colon cancer (Leiszter *et al.*, 2015), esophageal cancer (Jin *et al.*, 2008), renal cancer (Ricketts *et al.*, 2012), and gastric cancer (Jackson *et al.*, 2010). SST is produced in different tissue and synthesized from a large precursor molecule called (preproSST) (Leiszter *et al.*, 2015).

This study aimed to elucidate SST promoter hypermethylation associated with CRC progression from early-stage to metastasis, which revealed considerable assay to prognosis or early diagnosis.

2. MATERIALS AND METHODS:

2.1. Tissues samples

After informed consent, 71 fresh biopsy tissue samples were collected from the endoscopy unit of Al Hillah Teaching Hospital in Babylon, and Digestive Disease Education Hospital in Bagdad, Iraq. CRC patients were diagnosed clinically, and specialist physicians evaluated the disease. Samples were divided into three groups, including 19 metastasis, 28 early-stage, and 24 healthy controls (Table 1).

2.2. Bisulfite Conversion

According to the manufacturer protocol, the Genomic DNA was extracted from the biopsies by Promega Wizard® Genomic DNA Purification Kit. A total of 30 mg of fresh tissue was added to 700µl of chilled nuclei lysis solution and homogenized for 15 seconds. Following that, 3µl of RNase solution and 200µl of protein precipitation solution was added to the tissue and incubated for 20–30 minutes at 37°C. Then, the

content was submitted to a vortex and chilled on ice 10 minutes before centrifuged at 15.000 rpm for 5min. The supernatant was transferred to a fresh tube containing 800µl of isopropanol. After second centrifugation at 15.000 rpm for 5min, the supernatant was removed, and 600µl of 70% ethanol was added. After the final centrifugation, the DNA rehydration was in 100µl of DNA rehydration solution for 1 hour at 65°C. The next step was to manage all the genomic DNA by DNA methylation modification using spin-column EZ DNA Methylation™ Kit (ZYMO RESEARCH) according to the manufacturer instructions. The protocol included converting the unmethylated cytosine to uracil, while methylated cytosine protected by methyl group from bisulfite conversion. Unmethylated cytidine residues that convert to uridine residues during bisulfite conversion convert to thymidine by PCR (Herman *et al.*, 1996; Lapeyre *et al.*, 1979). The positive methylated controlled DNA has incubated with CpG methyltransferase for 1-2 h at 37°C and terminated following an incubation period at 65°C for 20 min. The modified DNA was then used as a template for downstream analyses, including quantitative methylation-specific PCR.

2.3. Quantitative Methylation Specific PCR (qMSP)

Quantitative methylation-specific PCR (Q-MSP) was used to measured SST promoter methylation as described previously (Misawa *et al.*, 2015; SHI *et al.*, 2013) using Techne PrimeQ Real-Time PCR System. The PCR amplification of modified DNA samples consisted of initial denaturation at 94 °C for 6 min, 40 cycles of denaturation at 94 °C for 45 s, primer annealing at 58.8 °C for 45 s, primer extension at 72 °C for 45 s. the PCR product is 102 bp length, Q-MSP primers for methylated SST promoter were Q-MSP-SST- forward primer (5'- GGG GCG TTT TTT AGT TTG ACG T-3') and Q-MSP-SST-reverse (5'-AAC AAC GAT AAC TCC GAA CCT CG-3').

2.4. Statistical Analysis

The association relationships were carried out by Fisher's exact test using GraphPad Software(<http://graphpad.com/quickcalcs/contingency1.cfm>). *P*-value was calculated with Two-tailed Fisher's exact test as recommended in this software. It was considered significant when the recorded value was less than 0.05.

3. RESULTS AND DISCUSSION:

The DNA methylation status of SST promoter in the three groups (healthy controls, early-stage, and metastasis) of CRC was detected using qMSP. A single graphic peak elucidated the primer's high quality. When the reaction reached the concentration threshold (CT), the CT value was 15-20 reaction cycles in the amplification curves, demonstrating that the amplification was adequate. The results show that methylated cases were 4 vs. 20, 17 vs. 11, and 19 vs. 4 in healthy controls, early-stage, and metastasis cases, respectively, as shown in Table (2).

The methylation status of SST promoter in the early stage and metastasis CRC group was higher compared with healthy controls. The percentage of methylation for healthy controls, early-stage, and metastasis groups was 17%, 60%, and 79%, respectively (Figure 1).

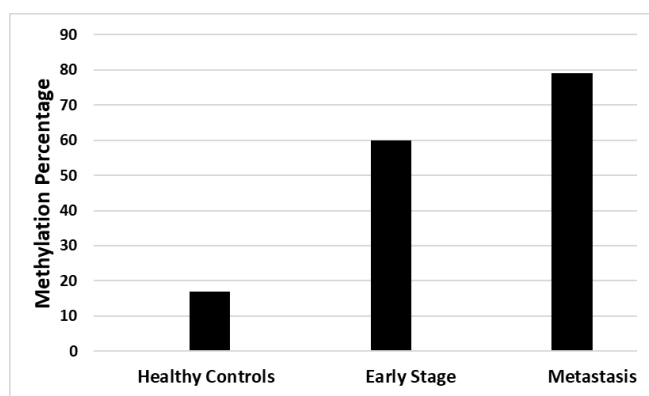


Figure 1. The percentage of methylation for healthy controls, early-stage, and metastasis

The two-tailed *P*-values given by the association between methylation status of early-stage and metastasis groups with healthy controls were 0.0364, 0.0138, respectively (Table 2). This association is considered to be statistically significant. Furthermore, a strong association between healthy controls methylation status and all CRC patients (early-stage and metastasis) with a 0.0115 *P*-value.

Somatostatin is a peptide produced in different tissues, including the gastrointestinal tract. This peptide could act as a neurotransmitter or an inhibitory hormone that blocks cell proliferation (Gorden, 1989). SST directly inhibits cell growth autocrine mechanism via SST receptor type 2. This means that SST has antiproliferative and pro-apoptotic effects (Rauly *et al.*, 1996, Calabró *et al.*, 2002). Several findings involved *in vitro* and *in vivo* studies have suggested that SST functions as a tumor suppressor gene in human cancers (Jin *et al.*, 2008).

Epigenetic surveys based on the detection

of DNA methylation revealed that the hypermethylation of SST in CRC patients was high at an early-stage compared to healthy controls. These findings support that the inactivation of the somatostatin gene by promoter CpG methylation played an essential role in CRC progression (Tariq and Ghias, 2016). Epigenetic silencing of SST promoter could lead to downregulation and silencing of several tumor suppressor genes that enhance more mistakes in cell proliferation (Peng *et al.*, 2008; Clément *et al.*, 2006). Furthermore, the results show an increased percentage of DNA methylation levels with the progression of carcinogenesis. It revealed the maximum DNA methylation in metastasis, which confirmed previous studies (Misawa *et al.* 2015; SHI *et al.*, 2013; Mori *et al.*, 2006).

The present findings suggested that DNA methylation could be the main mechanism of silencing SST expression in CRC. Several previous findings elucidate that SST promoter hypermethylation corresponding with loss of expression of SST in association with cancer progression (Jin *et al.*, 2008). This means that the inactivation of SST may be a critical step in CRC carcinogenesis (Mori *et al.*, 2006).

Modern molecular biology shed the light on the possibility of using epigenetic alteration for new medical strategies in cancer diagnosis and treatment (Hama *et al.*, 2009; Baylin and Ohm, 2006). Several studies attempt to use many methylated genes as biomarkers for CRC diagnosis and monitoring. U.S. Food and Drug Administration (FDA) approves of using methylated septin 9 (*SEPT9*) for a screening of CRC (Ma *et al.*, 2019). This experiment corroborates with the previous results, which show high methylated SST percentage in primary colorectal tumors compared with normal colon mucosa (Patai *et al.*, 2015). CpG methylated penal printed in the early stage of cancer could reveal useful assay to cancer prediction.

4. CONCLUSIONS:

It can be concluded the DNA hypermethylation is the epigenetic mechanism that prevents the expression of SST and other types of tumor suppressor genes, which, in turn, induce carcinogenesis. In case other studies confirm these results, the detection of SST promoter hypermethylation at the early-stage of cancer could be used as a biomarker for CRC screening and prognosis.

5. ACKNOWLEDGMENTS:

We would like to express our profound thanks to AL-Manara College For Medical sciences for providing us with all requirements and laboratories to perform this study; our thanks extend to Al Hillah Teaching Hospital in Babylon, and Digestive Disease Education Hospital in Bagdad staff for the facilities in collecting samples.

6. REFERENCES:

1. Arnold, M., Sierra, M., Laversanne, M., Soerjomataram, I., Jemal, A., and Bray, F. (2016). Global patterns and trends in colorectal cancer incidence and mortality. *Gut*, 66(4), 683-691.
2. Bastide, N. M., Pierre, F. H., and Corpet, D. E. (2011). Heme iron from meat and risk of colorectal cancer: a meta-analysis and a review of the mechanisms involved. *Cancer prevention research (Philadelphia, Pa.)*, 4(2), 177-184.
3. Baylin, S. B., and Ohm, J. E. (2006). Epigenetic gene silencing in cancer - a mechanism for early oncogenic pathway addiction? *Nature reviews. Cancer*, 6(2), 107-116.
4. Botteri, E., Iodice, S., Bagnardi, V., Raimondi, S., Lowenfels, A. B., and Maisonneuve, P. (2008). Smoking and colorectal cancer: a meta-analysis. *JAMA*, 300(23), 2765-2778.
5. Bray, F., Ferlay, J., Soerjomataram, I., Siegel, R., Torre, L., and Jemal, A. (2018). Global cancer statistics 2018: GLOBOCAN estimates of incidence and mortality worldwide for 36 cancers in 185 countries. *CA: A Cancer Journal For Clinicians*, 68(6), 394-424.
6. Calabró, A., Raggi, C., Renzi, D., Orlando, C., Brigati, V., Messerini, L., and Maggi, M. (2002). 4 OP Quantitative evaluation of somatostatin reception subtype 2 expression in sporadic colorectal tumor and in the corresponding normal mucosa. *Digestive And Liver Disease*, 34, A64.
7. Canavan, C., Abrams, K. R., and Mayberry, J. (2006). Meta-analysis: colorectal and small bowel cancer risk in patients with Crohn's disease. *Alimentary pharmacology and therapeutics*, 23(8), 1097-1104.
8. Choi, J., and Lee, J. (2013). Interplay between Epigenetics and Genetics in Cancer. *Genomics and Informatics*, 11(4), 164.
9. Clément, G., Braunschweig, R., Pasquier, N., Bosman, F., and Benhattar, J. (2006). Alterations of the Wnt signaling pathway during the neoplastic progression of Barrett's esophagus. *Oncogene*, 25(21), 3084-3092.
10. Eaden, J. A., Abrams, K. R., and Mayberry, J. F. (2001). The risk of colorectal cancer in ulcerative colitis: a meta-analysis. *Gut*, 48(4), 526-535.
11. Fearon E.R. and Vogelstein B. (1990). A genetic model for colorectal tumorigenesis. *Cell*, 61:759-767.
12. Goo, T., Akiba, Y., and Kaunitz, J. D. (2010). Mechanisms of intragastric pH sensing. *Current gastroenterology reports*, 12(6), 465-470.
13. Gorden, P. (1989). Somatostatin and Somatostatin Analogue (SMS 201-995) in Treatment of Hormone-Secreting Tumors of the Pituitary and Gastrointestinal Tract and Non-Neoplastic Diseases of the Gut. *Annals Of Internal Medicine*, 110(1), 35.
14. Grimberg A. (2004). Somatostatin and cancer: applying endocrinology to oncology. *Cancer biology and therapy*, 3(8), 731-733.
15. Hagggar, F. A., and Boushey, R. P. (2009). Colorectal cancer epidemiology: incidence, mortality, survival, and risk factors. *Clinics in colon and rectal surgery*, 22(4), 191-197.
16. Hama, T., Yuza, Y., Saito, Y., O-uchi, J., Kondo, S., Okabe, M., Yamada, H., Kato, T., Moriyama, H., Kurihara, S., and Urashima, M. (2009). Prognostic significance of epidermal growth factor receptor phosphorylation and mutation in head and neck squamous cell carcinoma. *The oncologist*, 14(9), 900-908.
17. Herman, J., Graff, J., Myohanen, S., Nelkin, B., and Baylin, S. (1996). Methylation-specific PCR: a novel PCR assay for methylation status of CpG islands. *Proceedings Of The National Academy Of Sciences*, 93(18), 9821-9826.

18. Jackson, K., Soutto, M., Peng, D., Hu, T., Marshal, D., and El-Rifai, W. (2010). Epigenetic Silencing of Somatostatin in Gastric Cancer. *Digestive Diseases And Sciences*, 56(1), 125-130.
19. Jin, Z., Mori, Y., Hamilton, J. P., Olaru, A., Sato, F., Yang, J., Ito, T., Kan, T., Agarwal, R. and Meltzer, S. J. (2008). Hypermethylation of the somatostatin promoter is a common, early event in human esophageal carcinogenesis. *Cancer: Interdisciplinary International Journal of the American Cancer Society*, 112(1), 43-49.
20. Kuipers, E. J., Grady, W. M., Lieberman, D., Seufferlein, T., Sung, J. J., Boelens, P. G., van de Velde, C. J., and Watanabe, T. (2015). Colorectal cancer. *Nature reviews. Disease primers*, 1, 15065.
21. Kumar, U., and Grant, M. (2010). Somatostatin and somatostatin receptors. *Results and problems in cell differentiation*, 50, 137-184.
22. Lao, V. V., and Grady, W. M. (2011). Epigenetics and colorectal cancer. *Nature reviews. Gastroenterology and hepatology*, 8(12), 686-700.
23. Lapeyre, J. N., and Becker, F. F. (1979). 5-Methylcytosine content of nuclear DNA during chemical hepatocarcinogenesis and in carcinomas which result. *Biochemical and biophysical research communications*, 87(3), 698-705.
24. Leiszter, K., Sipos, F., Galamb, O., Krenács, T., Veres, G., Wichmann, B., Fűri, I., Kalmár, Patai, Á., V., Tóth, K., Valcz, G., Tulassay, Z., and Molnár, B. (2015). Promoter hypermethylation-related reduced somatostatin production promotes uncontrolled cell proliferation in colorectal cancer. *PLoS One*, 10(2), e0118332.
25. Levin, B., Lieberman, D. A., McFarland, B., Andrews, K. S., Brooks, D., Bond, J., Dash, C., Giardiello, F. M., Glick, S., Johnson, D., Johnson, C. D., Levin, T. R., Pickhardt, P. J., Rex, D. K., Smith, R. A., Thorson, A., Winawer, S. J., American Cancer Society Colorectal Cancer Advisory Group, US Multi-Society Task Force, and American College of Radiology Colon Cancer Committee (2008). Screening and surveillance for the early detection of colorectal cancer and adenomatous polyps, 2008: a joint guideline from the American Cancer Society, the US Multi-Society Task Force on Colorectal Cancer, and the American College of Radiology. *Gastroenterology*, 134(5), 1570-1595.
26. Lynch, H. T., and de la Chapelle, A. (2003). Hereditary colorectal cancer. *The New England journal of medicine*, 348(10), 919-932.
27. Ma, Z., Williams, M., Cheng, Y., and Leung, W. (2019). Roles of Methylated DNA Biomarkers in Patients with Colorectal Cancer. *Disease Markers*, 2019, 1-8.
28. Mármol, I., Sánchez-de-Diego, C., Pradilla Dieste, A., Cerrada, E., and Rodriguez Yoldi, M. J. (2017). Colorectal Carcinoma: A General Overview and Future Perspectives in Colorectal Cancer. *International journal of molecular sciences*, 18(1), 197.
29. Martinez-Useros, J., and Garcia-Foncillas, J. (2016). Obesity and colorectal cancer: molecular features of adipose tissue. *Journal of translational medicine*, 14, 21.
30. Misawa, K., Misawa, Y., Kondo, H., Mochizuki, D., Imai, A., Fukushima, H., Uehara, T., Kanazawa, T., and Mineta, H. (2015). Aberrant methylation inactivates somatostatin and somatostatin receptor type 1 in head and neck squamous cell carcinoma. *PLoS One*, 10(3), e0118588.
31. Mori, Y., Cai, K., Cheng, Y., Wang, S., Paun, B., Hamilton, J. P., Jin, Z., Sato, F., Berki, A. T., Kan, T., Ito, T., Mantzur, C., Abraham, J. M., Meltzer, S. J. (2006). A genome-wide search identifies epigenetic silencing of somatostatin, tachykinin-1, and 5 other genes in colon cancer. *Gastroenterology*, 131(3), 797-808.
32. Ou, J. N., Torrisani, J., Unterberger, A., Provençal, N., Shikimi, K., Karimi, M., Ekström, T. J., and Szyf, M. (2007). Histone deacetylase inhibitor Trichostatin A induces global and gene-specific DNA demethylation in human cancer cell lines. *Biochemical pharmacology*, 73(9), 1297-1307.
33. Patai, Á. V., Valcz, G., Hollósi, P., Kalmár, A., Péterfia, B., Patai, Á., Wichmann, B., Spisák, S., Barták, B. K., Leiszter, K., Tóth, K., Sipos, F., Kovalszky, I., Péter, Z., Miheller, P., Tulassay, Z., and Molnár, B. (2015). Comprehensive DNA methylation

- analysis reveals a common ten-gene methylation signature in colorectal adenomas and carcinomas. *PloS one*, 10(8), e0133836.
34. Patel Y. C. (1999). Somatostatin and its receptor family. *Frontiers in neuroendocrinology*, 20(3), 157–198.
 35. Peng, D., Razvi, M., Chen, H., Washington, K., Roessner, A., Schneider-Stock, R., and El-Rifai, W. (2008). DNA hypermethylation regulates the expression of members of the Mu-class glutathione S-transferases and glutathione peroxidases in Barrett's adenocarcinoma. *Gut*, 58(1), 5–15.
 36. Pöschl, G., and Seitz, H. K. (2004). Alcohol and cancer. *Alcohol and alcoholism (Oxford, Oxfordshire)*, 39(3), 155–165.
 37. Puccini, A., Berger, M. D., Naseem, M., Tokunaga, R., Battaglin, F., Cao, S., Hanna, D. L., McSkane, M., Soni, S., Zhang, W., and Lenz, H. J. (2017). Colorectal cancer: epigenetic alterations and their clinical implications. *Biochimica et Biophysica Acta (BBA)-Reviews on Cancer*, 1868(2), 439–448.
 38. Raully, I., Saint-Laurent, N., Delesque, N., Buscail, L., Estève, J., Vaysse, N., and Susini, C. (1996). Induction of a negative autocrine loop by expression of SST2 somatostatin receptor in NIH 3T3 cells. *Journal Of Clinical Investigation*, 97(8), 1874–1883.
 39. Reichlin S. (1995). Somatostatin and its receptor. Introduction. *Ciba Foundation symposium*, 190, 1–6.
 40. Reubi, J. C., and Laissue, J. A. (1995). Multiple actions of somatostatin in neoplastic disease. *Trends in pharmacological sciences*, 16(3), 110–115.
 41. Ricketts, C. J., Morris, M. R., Gentle, D., Brown, M., Wake, N., and Woodward, E. R., Clarke, N., Latif, F., and Maher, E. R. (2012). Genome-wide CpG island methylation analysis implicates novel genes in the pathogenesis of renal cell carcinoma. *Epigenetics*, 7(3), 278–290.
 42. Sameer, A. S., and Nissar, S. (2016). Epigenetics in diagnosis of colorectal cancer. *Molecular biology research communications*, 5(1), 49–57.
 43. Santarelli, R. L., Pierre, F., and Corpet, D. E. (2008). Processed meat and colorectal cancer: a review of epidemiologic and experimental evidence. *Nutrition and cancer*, 60(2), 131–144.
 44. SHI, X., LI, X., CHEN, L., and WANG, C. (2013). Analysis of somatostatin receptors and somatostatin promoter methylation in human gastric cancer. *Oncology Letters*, 6(6), 1794–1798.
 45. Smith, G., Carey, F. A., Beattie, J., Wilkie, M. J., Lightfoot, T. J., Coxhead, J., Garner, R. C., Steele, R. J., and Wolf, C. R. (2002). Mutations in APC, Kirsten-ras, and p53--alternative genetic pathways to colorectal cancer. *Proceedings of the National Academy of Sciences of the United States of America*, 99(14), 9433–9438.
 46. Stoffel EM, Kastrinos F. Familial colorectal cancer, beyond Lynch syndrome. *Clin Gastroenterol Hepatol*. 2014 Jul;12(7):1059-68.
 47. Tariq, K., and Ghias, K. (2016). Colorectal cancer carcinogenesis: a review of mechanisms. *Cancer biology and medicine*, 13(1), 120–135.
 48. Umar, A., Boland, C. R., Terdiman, J. P., Syngal, S., Chapelle, A. D. L., Rüschoff, J., Fishel, R., Lindor, N. M., Burgart, L. J., Hamelin, R., Hamilton, S. R., Hiatt, R. A., Jass, J., Lindblom, A., Lynch, H. T., Peltomäki, P., Ramsey, S. D., Rodriguez-Bigas, M. A., Vasen, H. F. A., Hawk, E. T., Barrett, J. C., Freedman, A. N., and Srivastava, S. (2004). Revised Bethesda Guidelines for hereditary nonpolyposis colorectal cancer (Lynch syndrome) and microsatellite instability. *Journal of the National Cancer Institute*, 96(4), 261–268.
 49. Willett, W. C. (2005). Diet and cancer: an evolving picture. *Jama*, 293(2), 233–234.

Table 1. Demographic characteristics of studies patients

Demographic characteristics		Patients	Healthy control
No.		47	24
Gender	Male	29	16
	Female	18	8
Age	Mean age	61	51
	<55	24	19
	>55	23	5
Stage	Early-stage	28	
	metastasis	19	

Table 2. The association between methylation status of early-stage and metastasis groups with healthy controls

Biopsies	No. of cases	Methylated cases	<i>P-value</i>
Healthy controls	24	4	
Early-stage	28	17	0.0364
Metastasis	19	15	0.0138
Early-stage + Metastasis	47	32	0.0115

APLICAÇÃO DE SISTEMAS ROBÓTICOS MÓVEIS VOADORES PARA DETECÇÃO PRECOCE DE UMA FONTE DE IGNIÇÃO**APPLICATION OF PORTABLE FLYING ROBOTIC SYSTEMS FOR EARLY DETECTION OF AN IGNITION SOURCE****ИСПОЛЬЗОВАНИЕ МОБИЛЬНЫХ ЛЕТАТЕЛЬНЫХ РОБОТОТЕХНИЧЕСКИХ СРЕДСТВ ДЛЯ РАННЕГО ОБНАРУЖЕНИЯ ИСТОЧНИКА ВОЗГОРАНИЯ**POLYAKOV, R. Yu.^{1*}¹ Bunin Yelets State University, Russia.** Corresponding author
e-mail: ryu.polyakov@bk.ru*

Received 03 August 2020; received in revised form 30 September 2020; accepted 24 October 2020

RESUMO

Recentemente, o desenvolvimento de modernos equipamentos e métodos de detecção precoce de fontes de ignição tornou-se relevante devido ao grande número de incêndios, bem como aos danos materiais e humanos por eles causados. Este estudo teve como objetivo desenvolver um método de busca da fonte de ignição pelo movimento de um analisador móvel de gases em direção ao aumento da concentração de monóxido de carbono (CO) emitido nos estágios iniciais de incêndio. Foi utilizado um algoritmo baseado no método de detecção espacial e definição de trajetória garantida para mover o analisador de gás móvel em direção a um aumento na concentração de acordo com o método simplex e Kiefer. A dependência da velocidade do motor com a tensão de alimentação, a velocidade angular do motor com a tensão de alimentação, a força de tração na frequência de batimento das asas, a tensão de alimentação bem como a energia consumida pelo motor durante a propulsão foram calculadas. Para determinar a direção do azimute em direção ao movimento de aumento da concentração de CO, foi obtida uma equação que tornou possível determinar a concentração de CO em função da distância da fonte de monóxido de carbono. Um diagrama da dependência do gradiente na distância ao ponto de ignição foi traçado e o número de pontos na trajetória na qual a concentração de CO é medida foi determinado. Uma das formas de aprimorar ainda mais os métodos de detecção precoce de incêndio é a utilização de analisadores móveis de gás, na movimentação até a fonte de ignição, e na determinação de suas coordenadas com o aumento da concentração de CO. No entanto, o desenvolvimento posterior é restrito devido à pesquisa insuficiente de métodos de design de analisadores de gás móveis, análise de comunicação entre subsistemas e métodos de cálculo baseados em modelos matemáticos que descrevem adequadamente os modos básicos de movimento dos analisadores de gás móveis.

Palavras-chave: monóxido de carbono, simulação de movimento, analisador de gases.

ABSTRACT

Recently, the development of modern equipment and early detection of ignition sources has become relevant due to many fires and the material and human damage caused by them. This study aimed to develop a method of searching for the ignition source by moving a mobile gas analyzer towards increasing the concentration of carbon monoxide (CO) emitted in the initial stages of fire. According to the simplex and Kiefer method, an algorithm based on the spatial detection method and guaranteed trajectory definition was used to move the mobile gas analyzer towards increasing concentration. The dependence of the engine speed on the supply voltage, the angular speed of the engine with the supply voltage, the tractive force at the wing flap frequency, the supply voltage as well as the energy consumed by the engine during propulsion were calculated. To determine the direction of the azimuth towards the movement of increasing the concentration of CO, an equation was obtained that made it possible to determine the concentration of CO as a function of the distance from the carbon monoxide source. A diagram of the gradient dependence on the distance to the ignition point was plotted, and the number of points on the trajectory on which the CO concentration is measured was determined. One way to further improve early fire detection methods is to use mobile gas analyzers in the ignition source movement and determine their coordinates with the increase in CO concentration. However, further development is restricted due to insufficient research on design methods for

mobile gas analyzers, communication analysis between subsystems, and calculation methods based on mathematical models that adequately describe the basic modes of movement of mobile gas analyzers.

Keywords: *carbon monoxide, movement simulation, gas analyzer.*

АННОТАЦИЯ

В последнее время разработка современных средств и методов раннего обнаружения источников возгорания стала актуальной в связи с большим количеством пожаров, а также материальным ущербом и человеческими жертвами, причиняемыми ими. Целью настоящего исследования являлась разработка метода поиска источника возгорания по движению мобильного газоанализатора в сторону увеличения концентрации монооксида углерода (СО), выделяющегося на начальных стадиях пожара. Был использован алгоритм, основанный на методе зондирования пространства и определения траектории, гарантирующий перемещение мобильного газоанализатора в сторону увеличения концентрации в соответствии с симплексом и методом Кифера. Рассчитана зависимость частоты вращения двигателя от напряжения питания, угловой скорости двигателя от напряжения питания, тягового усилия от частоты взмаха крыла, напряжения питания, а также мощности, потребляемой двигателем при движении вперед. Для определения направления азимута движения в сторону увеличения концентрации СО получено уравнение, позволяющее определить концентрацию СО в зависимости от расстояния от источника монооксида углерода. Построена диаграмма градиентной зависимости от расстояния до точки воспламенения и определено количество точек на траектории, в которых измеряется концентрация СО. Одним из путей дальнейшего совершенствования методов раннего обнаружения пожара является использование мобильных газоанализаторов, перемещающихся к источнику возгорания, и определение его координат с увеличением концентрации СО. Однако дальнейшее развитие сдерживается недостаточными исследованиями методов проектирования мобильных газоанализаторов, анализа связей между подсистемами и методов расчета на основе математических моделей, адекватно описывающих основные режимы движения мобильных газоанализаторов.

Ключевые слова: *угарный газ, моделирование движения, газовый анализатор.*

1. INTRODUCTION:

Recently, the development of modern equipment and methods of early detection of ignition sources has become relevant because of the massive number of fires and the material damage and human casualties caused by them (Sudhakar *et al.*, 2020; Estrada and Ndomab, 2019; Beck, Teacy, Rogers, and Jennings, 2018). Thus, in 2019, 471.537 cases of fire were registered in Russia. During them, 226,319 people and pieces of material assets to 62.2 billion rubles have been saved. Unfortunately, 8,567 people, including 406 children, could not avoid deaths, 9,477 people were injured, and material damage from the fires amounted to 18.2 billion rubles. Compared to the last year, the number of fires increased by 257%, deaths - by 8.3%, the amount of material damage increased by 17.1%, and the number of injured decreased by 1.8%. There were 1292 fires on average daily. Twenty-three people died, twenty-six people were injured on average, and the daily damage was 49.8 million rubles (Russian Ministry for Emergency Situations, 2020).

Fire detectors are used to prevent fire at an early stage in most cases. Such sensors are

based on three parameters: the concentration of smoke particles in the air, ambient temperature, and the radiation of the open flame. Depending on the detection principle, fire detectors are divided into smoke detectors (optical, spot, linear, ionization), thermal detectors (contact, power cables), flame detectors (ultraviolet and infrared), and gas analyzers. Thermal and flame detectors are in many ways inferior to smoke and gas analyzers, which indicates their obvious choice (Fyodorov, Lukyanchenko, and Sokolov, 2005, 2006; Poroshin and Surkov, 2016; Goremykin, Lukashevich, and Alekseev, 2017; Sychev, Sitnikov, and Rakityansky, 2018; Chlenov, Menkeev, Darbakov, Kiselev, and Chernenko, 2018).

However, plural studies have shown that smoke can be released to a level that triggers the smoke detector (Saidulin, 2009; Tamura, 2008; Chew, Wong, and Ho, 2001; Kolodyazhny and Kolosova, 2015; Bogomaz, 2017; Malashkina and Lobaznov, 2011; Betting *et al.*, 2019). This fact significantly reduces the effectiveness of such devices.

Carbon monoxide (CO) is a toxic gas formed in connection with burning any carbon-containing products and materials, the

concentration of which reaches 20-80 ppm at an early stage. Even at low concentrations, CO can already cause dizziness, disorientation and prevent conscious action of people when taking priority measures during a fire (Kozubovsky, Misevich, and Ivanchuk, 2015; Jasim, Hamed, and Abid, 2020; Mohammed, Kamal, Resheq, and Alabdraba, 2019). It is known that when the CO concentration increases up to 0.08%, there is a slight degree of carbon monoxide poisoning, the symptoms of which are headache, dizziness, suffocation, and general weakness. The intermediate severity of poisoning comes at a concentration of 0.32%, which causes motor paralysis and faintness. At a CO concentration of 1.2% and above, a fulminating form of poisoning develops when a person gets a lethal dose for a couple of breaths; in this case, the mortality occurs within 3 minutes (Heightman, 2010; Basharin et al., 2015; Kazantsev and Krasilnikov, 2019; Basharin, Halimov, Tolkach, and Kuzmich, 2018).

Therefore, 80% of deaths accounted for carbon monoxide poisoning. Transition to the application of gas-sensitive CO concentration sensors in fire protection systems allows for the detection of a hazardous fire situation at an early stage when it is possible to take measures to stop the dangerous process and prevent fire (for example, to switch off the power supply and stop the dangerous overheating of the wiring insulation). At the initial stage, when a small amount of material smolders, the carbon monoxide dissolves in the room volume, and its concentration is low. Hence the requirement for the sensitivity threshold of the sensors is formulated. The appearance of high-sensitivity semiconductor sensors that can detect CO concentration starting from 10 ppm can improve fire early detection efficiency.

This study aimed to develop a method of finding the fire source by moving the portable gas analyzer towards a rise in carbon monoxide concentration emitted during the initial stages of fire.

2. MATERIALS AND METHODS:

One way to improve the fire protection effectiveness is the transition from permanently fixed GA to portable gas analyzers (MGAs). It is a new direction in developing and creating fire protection systems based on the application of portable aerial vehicles that perform the ignition source search and detection with the required degree of accuracy. Simultaneously, algorithms for the movement control of the MGA to the

ignition source start to play a crucial role in such systems (Semiz and Polat, 2020; Babel, 2014).

As it has been analyzed earlier by Efimov, Polyakov, and Yatsun, 2017; Polyakov, Efimov, and Yatsun, 2015, special attention should be paid to the solution of the scientific and technical problem on the development of methods for planning the movement trajectory of the MGA to the ignition source, simulation of movement modes of the devices associated with measuring the concentration of CO, which are currently insufficiently studied.

The transition to portable gas analyzers makes it possible to simplify the fire alarm system in many ways because one portable sensor can replace dozens of permanently fixed gas analyzers. Consequently, the MGA development has required small units with flapping wings that allow a long time to stay in the air. In this case, the airflows generated by the flapping wings practically do not affect the gas-air mixture when measuring CO concentration (McKinnon and Schoellig, 2020).

It is reasonable to use aerial vehicles with vertical-takeoff-and-landing functions as a portable platform, hovering at a specific point and horizontal flight. The primary flight criterion is the MGA movement in the direction of increasing carbon monoxide concentration, taking into account external disturbances and obstacles (Polyakov, 2019). The ignition source search problem and planning the movement trajectory to it will be considered taking into account the environment. As the primary criterion, the authors use the level of CO concentration in the air registered by the MGA. The increase in concentration is a determining feature for the portable gas analyzer movement towards the ignition source (Figure 1).

The MGA takes off from any horizontal surface to a specific height H according to the flight assignment. Then, to select the direction of movement, the device starts the movement in a circle of the radius R , according to the following law:

$$Z = H, \quad (\text{Eq. 1})$$

$$X = R \cos(\Omega t), \quad (\text{Eq. 2})$$

$$Y = R \sin(\Omega t), \quad (\text{Eq. 3})$$

R is the radius of the flight area, ΩR is the maximum speed of the MGA center of masses along its trajectory. The trajectory equation is as follows:

$$X^2 + Y^2 = R^2 \quad (\text{Eq. 4})$$

For the simulation of the MGA movement along a specified trajectory, it is proposed to use a model of the three-link electromechanical system with the oscillatory movement of external links, leading to the formation of both lifting force and thrust force, implemented by the application of the "asymmetry" effect of wing shape and speed. An ultrasonic distance measurement device is also installed on the body, which determines the distance to the obstacle, the information from which allows you to correct the MGA trajectory. When approaching the ignition source, the temperature t° of the environment increases, which the onboard sensor monitors. If the condition that

$$t^\circ < t_0^\circ, \quad (\text{Eq. 5})$$

Where t_0° is the limit temperature, is fulfilled, the other flight towards the ignition source is stopped.

The gradient of CO concentration and measuring this parameter with a portable sensor allows for the accurate ignition source. Even at a distance of 60-90 meters, there is an increased CO concentration, which helps the MGA move along the concentration gradient towards increasing the concentration.

An algorithm based on space sensing and trajectory definition has been developed to select the direction of movement. This algorithm guarantees the movement of MGA towards increasing CO concentration following simplex and Kiefer methods (Figures 2 and 3), according to paper (Emelianova, Poliakov, Efimov, and Yatsun, 2018).

The movement in space begins with the application of two-dimensional simplexes. As the MGA approaches the ignition source, it is proposed to search based on planning the straight-line segments, which allows for moving towards the increasing CO concentration with fixation of one of the coordinates, according to papers (Tang and Kumar, 2018; González-Sieira, Cores, Mucientes, and Bugarín, 2020). As illustrated by Figure 4, the position of the ignition source A (the point with the maximum concentration of CO) is set by an unknown radius-vector r_A , and the position of the MGA at the initial moment is set by the radius-vector r_B , respectively. The objective is to determine the position of point A from the values of CO concentration measured by the onboard sensor, from the predetermined initial position of MGA,

defined by the vector r_B under the known coordinates of obstacles C, represented by the vector r_C in the minimum time, according to thesis (Polyakov, 2019).

The search process is completed if the MGA falls into the point A^1 defined by the radius vector r_{A^1} . Herein the position of the point A^1 is determined by the value of the radius vector.

$$r_{A^1} = r_A + r_{eA} \quad (\text{Eq. 6})$$

The point A^1 is located inside the sphere with radius r_C , whose position is determined by the value of the radius-vector

$$r_C = r_A + r_e \quad (\text{Eq. 7})$$

The radius-vector r_e module determines the permissible error occurring when determining the position of the point A in space.

The MGA is considered as a controlled electromechanical system consisting of three links. The calculation scheme of the device is illustrated in Figure 5. The considered electromechanical system has 12 degrees of freedom. Six generalized coordinates describe the central link 2; simultaneously, two generalized coordinates have external links 1 and 3 (wings). It is assumed that the wings are attached to the body through cylindrical joints. In these joints, controlled electric drives are mounted, making it possible to rotate the wings relative to the body at predetermined angles by two coordinates. Therefore, currents received by the windings of electric motors that drive the external links, are also generalized coordinates.

Since the cylindrical joints can rotate relative to the body at a specific angle, this property of the joints makes it possible to simulate the external links intricate movement pattern. The movement of such an object takes place in the absolute OXYZ coordinate system. With the body (the second link of the triplet), the relative portable system of coordinates $C_2X_2Y_2Z_2$ is associated, the beginning of which coincides with the gravity center of the body C_2 . Axis C_2X_2 of this coordinate system is produced parallel to the longitudinal axis of the body, the axis C_2Y_2 is directed perpendicular to the plane $C_2X_2Z_2$, and the axis C_2Z_2 is directed perpendicular to the plane $C_2X_2Y_2$. The $C_2X_2Z_2$ plane is the symmetry plane of the body.

The coordinate systems $O_iX_iY_iZ_i$ ($i = 1, 3$) are associated with links 1 and 3, and the axes O_iX_i coincide with the axes of rotation of the

external links, and the axes $O_i Y_i$ belong to the wing plane and pass through the points C_i . For all changes in the MGA position relative to the absolute OXYZ coordinate system, both linear and angular, the associated coordinate systems move with it.

The radius-vector unambiguously determines the position of the mass center of the body (link 2) of the transport platform in space relative to a fixed coordinate system $R_{C_2} = (X, Y, Z)^T$. The orientation of the body in space is defined by the plane angles defining the vector $\theta = (\varphi, \psi, \theta)^T$. The gas analyzer 4 is installed in the front part of the fuselage. Here rangefinders 5 are also installed, which determine the distance to obstacle 6. It is accepted that the mass center of the body moves in space with the velocity \bar{v} , and the robot body rotates around the mass center with angular velocity $\bar{\omega}$. The MCA moves in space under the action of distributed forces arising from the interaction of system elements with the environment F_i , resulting in the tractive force T and lifting force Q . The force R_2 arising because of the interaction of tail assembly and relative airflow. This force magnitude and direction depend on flight control surfaces speed and angles β_1, β_2 . Besides, weight forces $m_i g$ act on the vehicle.

Differential equations in vector form, describing the movement of the mass center in a fixed coordinate system is as follows:

$$(m_1 + m_2 + m_3) \frac{d\bar{v}}{dt} + m_1 \left(\dot{T}_{20} \dot{T}_{12} \bar{r}_{C_2 C_1}^{(1)} + T_{20} \ddot{T}_{12} \bar{r}_{C_2 C_1}^{(1)} \right) + m_3 \left(\dot{T}_{20} \dot{T}_{32} \bar{r}_{C_2 C_3}^{(3)} + T_{20} \ddot{T}_{12} \bar{r}_{C_2 C_3}^{(3)} \right) = \sum m_i g + T_{12} T_{20} F_1^{(1)} + T_{32} T_{20} F_3^{(3)} \quad (\text{Eq. 8})$$

To describe the rotational movement, it was used the theorem of angular momentum change, as shown in equation 9.

$$\frac{d\bar{L}}{dt} = \sum \bar{M}_C^e \quad (\text{Eq. 9})$$

Moreover, the angular momentum of the considered mechanical system is described by equation 10.

$$\bar{L} = L_{C_2} + \sum \bar{L}_i \quad (\text{Eq. 10})$$

Where L_{C_2} the angular momentum of the body relative to the mass is center of the body;

\bar{L}_i is the angular momentum of the i -wing relative to the mass center; $\sum \bar{M}_C^e = (M_{x_2}, M_{y_2}, M_{z_2})^T$ is the resultant vector of moments of external forces.

Substituting the values of the angular momentum of the system in the assumption of low masses of the external links, it is found the corresponding relations reflecting the theorem of angular momentum change in projections to the associated coordinate system. As a result, a system of differential equations describing the rotational movement of MGA can be obtained.

$$\begin{cases} J^x \dot{\omega}_x + \omega_y \omega_z (J^z - J^y) = M_{x_2} \\ J^y \dot{\omega}_y + \omega_x \omega_z (J^x - J^z) = M_{y_2} \\ J^z \dot{\omega}_z + \omega_x \omega_y (J^y - J^x) = M_{z_2} \end{cases} \quad (\text{Eq. 11})$$

where $J^x, J^y, J^z, \omega_x, \omega_y, \omega_z$ are axial moments of inertia and projections of angular velocity.

Eqs (8) and (11), taking into account the Euler kinematic equations, form a differential equations system describing MGA movement in space. The theoretical studies carried out make it possible to propose a method for determining the ignition source; however, due to the complexity of the considered MGA, it is necessary to supplement mathematical modeling results with experimental data.

One of the primary tasks to be solved in experimental research is verifying the azimuth definition concept by the onboard computer, which provides MGA movement towards a rise in the CO concentration. This task is solved using the onboard control system of the portable gas analyzer. It is necessary to check how useful in terms of accuracy and processing speed the calculation of the movement direction, determined by the azimuth angle, read from the north direction of the meridian, and the direction of the reference point with the maximum content of CO.

For the experimental study of the primary aerodynamic characteristics of the MGA based on the university, a multifunctional test-bed was developed to study the possibilities of CO registration in different modes of movement along a circular trajectory, the general view of which is presented in Figure 6. In Figure 6, the positions of the primary structural elements of the mechanism represented as: 1 – the base; 2 – the rack; 3 – the encoder; 4 – the accelerometer; 5 – rods; 6 – the MGA mounting bracket; 7 – the servo-machine; 8 – the electronics module; 9 – batteries.

In the course of the research, the test-bed design was improved to increase the functionality and accuracy of the measurements.

3. RESULTS AND DISCUSSION

With the help of the experimental test-bed, the values of angular velocity for the minimum angular velocity of 119 rpm and the maximum angular velocity of 190 rpm have been determined, which corresponds to the linear speed of MGA when moving in a circle of 1.5 m/s and 3.0 m/s. Angular velocity values were obtained at different voltages, namely at 2.5 V, 3 V, 3.5 V, and 4 V, as illustrated in Figure 7.

The dependencies of motor speed on the power supply voltage and the dependencies of motor angular velocity on power supply voltage have been determined (Polyakov, 2019). Special attention was paid to determining the propulsion created by the flapping wing. With the help of this test-bed, an experiment has been conducted, because of which the dependence of tractive force on the flapping frequency and power supply voltage has been determined. In addition, the dependence of the power consumed by the electric motor during propulsion has been determined. To experiment, a precision balance and photo strobe tachometer are used, making it possible to measure the rotation speed of the wing. The results of experimental studies are presented in Table 1.

Studies have demonstrated that the speed of MGA depends on the frequency of wing flapping, which in turn is determined by the angular velocity of the motor. Thus, this dependence makes it possible to change the flying speed of the platform, being especially essential when moving the MGA on a circular trajectory during CO concentration measurement. The data obtained makes it possible to determine the time spent in the air by the flying platform. At average speed, angular velocity equals 40-50 rad/s, which corresponds to ≈ 8.5 -10.5 W/N. Currents in the motor winding are equal to 0.12-0.16 A. Thus, for the operation of the air for more than 1 hour, it is necessary to have a battery capacity of at least 0.2 A/h.

Determination of the relative concentration of CO at a distance from a toxic gas source is carried out by formula: $C = C_x/C_{max}$, where C is the relative CO concentration; C_x is the CO concentration at a distance x from the source; C_{max} is the CO concentration in the source. The velocity of air masses influences the distribution of CO in

space in the ignition source area. At zero velocity of air masses, the CO concentration decrease depending on the distance can be determined by the diagram in Figure 8, obtained experimentally.

The problem of approximation of this dependence by a polynomial of the second order has also been solved:

$$C = a_2x^2 + a_1x + a_0 \quad (\text{Eq. 12})$$

To find the constants a_0 , a_1 , and a_2 , boundary conditions have been formulated.

- 1) When $x=0$, $C=1$, then:

$$a_2x^2 + a_1x + a_0 = 1$$

$$a_0 = 1$$

- 2) When $x=40$, $C=0.3$, then:

$$1600a_2 + 40a_1 = -0,7$$

- 3) When $x=15$, $C=0.6$, then:

$$225a_2 + 15a_1 = -0,4$$

- 4) Solving a system of equations:

$$\begin{cases} 1600a_2 + 40a_1 = -0,7 \\ 225a_2 + 15a_1 = -0,4 \end{cases}$$

$$\begin{cases} a_2 = 0,00037 \\ a_1 = -0,0325 \end{cases}$$

As a result, an equation has been obtained that allows for determining the CO concentration as a function of distance from the carbon monoxide source:

$$C = 0,00037x^2 - 0,0325x + 1 \quad (\text{Eq. 13})$$

The formula has also determined the dependence of the concentration gradient on the x coordinate:

$$\frac{dC}{dx} = 0,00037x - 0,0325 \quad (\text{Eq. 14})$$

Using the obtained expression, a diagram of gradient dependence on the distance to the ignition point has been plotted (Figure 9). The maximum gradient value equals 0.00325, and at a distance of 80-90 m from the source, the gradient tends to zero.

The conducted studies have demonstrated that the concentration gradient varies depending on the distance to the toxic gas source. At least two areas can be distinguished: I – the area with the high gradient level (0-40 m);

II – the area with the low gradient level (40-80 m).

For effective sounding of space to find concentration values at predetermined points, the most optimal is a circle located in the horizontal plane. When conducting experimental studies, it is essential to determine the number of points on the trajectory in which the CO concentration is measured. The number of control points varied in the range of 2, 4, and 8. The circle radius varied from 1 m to 10 m. The scheme of the experiment is presented in Figure 10. The determination of the distance from the point where the CO concentration measurement is achieved by the equation 15.

$$L_i = \sqrt{(x_a + R \sin \varphi_i)^2 + (y_a - R \cos \varphi_i)^2} \quad (\text{Eq. 15})$$

R is the radius of the MGA trajectory; x_a and y_a are coordinates of the ignition source; (i) the central angle determines the position of measurement points.

The formula shall determine the CO concentration in the points:

$$C_i = 1 - 0,0325L_i + 0,00037L_i^2 \quad (\text{Eq. 16})$$

The results of several calculations for different radii are presented in Tables 2 and 3. Based on the research results, a methodology has been developed to determine the azimuth for the MGA movement towards a rise in CO concentration. The onboard computer analyzes the data array obtained in Table 1 and Figure 8, and the coordinates of the point with maximum x_1 , y_1 , and minimum x_2 , y_2 concentrations are determined. The coordinates of these points are then used to calculate the equation of a straight line passing through these two points:

$$(y_1 - y_2)x + (x_2 - x_1)y + (x_1y_2 - x_2y_1) = 0 \quad (\text{Eq. 17})$$

In other words, it was obtained the general equation of a straight line on a plane in Cartesian coordinates:

$$Ax + By + C = 0 \quad (\text{Eq. 18})$$

Where A and B are not equal to zero simultaneously.

The formula can determine the tangent of the angle determining the movement vector towards the maximum concentration:

$$\text{tg } \varphi = \frac{(x_1 - x_2)}{(y_1 - y_2)} \quad (\text{Eq. 19})$$

If the maximum concentration is measured in the point C_8 with coordinates $x_1 = 3.54$; $y_1 = 3.54$, and the minimum concentration is measured in the point C_5 with coordinates $x_2 = 0$; $y_2 = -5$, then:

$$\text{tg } \varphi = \frac{(x_1 - x_2)}{(y_1 - y_2)} = \frac{3,54}{(3,54+5)} = 0,41 \quad (\text{Eq. 20})$$

hence $\varphi = \arctg(0,41) = 0,39$ or $\varphi = 22,2^\circ$.

The resulting angle determines the straight position of the line relative to the North and makes it possible to find the azimuth of the direction of further MGA movement. In the course of experiments, the issue of choosing the circle radius, at which the concentration gradient can be guaranteed determined, was solved:

$$R = R\left(\frac{dC}{dL}\right) \quad (\text{Eq. 21})$$

When conducting experimental studies of the concentration gradient, it was calculated using the approximate formula:

$$\frac{dC}{dL} = \frac{\Delta C}{L} \quad (\text{Eq. 22})$$

Where $L^2 = (x_1 - x_2)^2 + (y_1 - y_2)^2$

$\Delta C = CO_1 - CO_2$ is the difference between the maximum and minimum concentration.

The following formula can be applied to determine the circle radius:

$$R = \frac{R_0}{a + \frac{\Delta C}{L}} \quad (\text{Eq. 23})$$

Parameters R_0 and a are determined experimentally. The circle radius depends on the concentration of the gradient value, which increases as the MGA approaches the ignition point. The conducted researches have shown that for the confident determination of the azimuth, the circle radius should be not less than 5 meters, and the difference between the maximum and minimum concentration equals $\Delta C = 0,09$ of standard units at $L = 9$ m or approximately 2-3 ppm, confidently registered by the onboard recorder.

Further increase in radius makes it possible to increase the sensitivity and accuracy of measurements; however, a significant increase in the circle radius leads to a rise in the flight time and, consequently, to a decrease in the measurement of the method processing speed. Therefore, the optimal radius should be considered the radius $R = 5-7$ m. This radius determines the error with which the coordinates of the ignition source are determined. Since the selected sensor, measuring the CO concentration, registers the concentration at the distance of $L = 50-70$ meters, then the relative error of measurement can be estimated as a ratio:

$$\lambda = \left(\frac{R}{L}\right) \cdot 100\% = 10\% \quad (\text{Eq. 24})$$

The climatic and mechanical factors and modes of electrical power supply of sensors and electric drives of the portable platform affect the accuracy of the measurement. In this case, the research was carried out under the following climatic conditions: air temperature was equal to 23-26 °C, the pressure was equal to 750-760 mm Hg, and the wind was equal to 1-3 m/s. Mechanical factors and electric power supply modes, did not change.

The second question, which was to be answered during the experiments, was how fast it was necessary to move along the trajectory so that the onboard measuring system could register the concentration at the point. It was experimentally determined that the speed of the apparatus along the trajectory could vary from the minimum angular velocity of 0.3 1/s, which for a radius of 5 m corresponds to a linear velocity of 1.5 m/s to the maximum angular velocity of 2.0 1/s, which corresponds to a linear velocity of 10 m/s. Thus, the maximum flight time of the whole trajectory in case of 5 m radius equals $T = L/V = 31.4/1.5 = 20.9$ sec, and the minimum flight time equals $T = L/V = 31.4/10 = 3.1$ s.

Since the sensor measuring CO concentration has a processing speed of approximately 1.5 seconds, this factor limits the movement speed of the MGA along the trajectory. In case it is considered that CO concentration measurements take place in n points on the trajectory, the movement time should exceed $n \cdot 1.5$. When measuring the CO concentration in 8 points, the sensor flight time along the 1/8 of the circle will be equal to 2.6 s for the minimum speed and 0.39 s for the maximum speed, respectively. Therefore, the

maximum speed should be limited by the sensor processing speed of 1.5 s. Accordingly, the flight time along the trajectory will be 12 s, and the speed, in this case, will be $V = L/T = 31.4/12 = 2.6$ m/s.

Another issue to be solved by experiments - it is the number of points on a circle in which the CO concentration should be registered. A small step makes it possible to increase the accuracy of azimuth determination. Still, it will require many experiments, and a massive step reduces the probability of accurate azimuth finding. Again, the processing speed of the sensor is a decisive factor in this case. As it has been determined, the movement time along the trajectory T should be greater than $n \cdot 1.5$. Hence, the number of points growth leads to the fact that the minimum movement time increases, and the speed along the trajectory decreases. So when $n = 12$, the authors have $T = 18$ s, which corresponds to the speed $V = L/T = 31.4/18 = 1.74$ m/s, close to the minimum speed of MGA and corresponds to 1.5 m/s. Therefore, it is further accepted that $n = 8$.

According to the accepted in this method step-by-step principle of movement in space along the response surface, the steepest ascent can be performed many times until an almost stationary area where the concentration gradient is close to zero is reached.

4. CONCLUSION:

Thus, the article has considered general fire safety issues, namely, the early detection of the ignition source by determining the azimuth for the MGA movement towards a rise in CO concentration. The schemes of MGA movement towards the ignition source have been studied, and the three-link electromechanical system has been considered to achieve this goal. By experimental methods, there have been found the dependencies of the electrical motor speed of rotation on the power supply voltage and the dependencies of the motor angular velocity on the power supply voltage, the dependence of the tractive effort on the wing flapping frequency and power supply voltage, the dependence of the power consumed by the electric motor during propulsion. An equation has been obtained to determine the direction of azimuth towards the movement of CO concentration increase to determine the CO concentration depending on the distance from the carbon monoxide source, a graph of gradient dependence on the distance to the fire point has been drawn, the number of points on the trajectory in which the CO

concentration is measured has been determined, the optimal speed and the radius along which the CO concentration is measured has been determined. However, subsequent development is constrained by insufficient research of MGA design methods, the analysis of links between subsystems, and calculation methods based on mathematical models that adequately describe the primary modes of the MGA movement.

5. REFERENCES:

1. Babel, L. (2014). Flightpath planning for uncrewed aerial vehicles with landmark-based visual navigation. *Robotics and Autonomous Systems*, 62(2), 142-150.
2. Basharin, V.A., Grebenyuk, A.N., Markizova, N.F., Preobrazhenskaya, T.N., Sarmanaev, S.H. and Tolkach, P.G. (2015). Chemical substances as affecting the factor of fires. *Military Medical Journal*, 336(1), 22-28.
3. Basharin, V.A., Halimov, Yu.S., Tolkach, P.G. and Kuzmich, V.G. (2018). Acute carbon monoxide intoxication. *Military Medical Journal*, 339(4), 12-18.
4. Beck, Z., Teacy, W.T.L., Rogers, A. and Jennings, N.R. (2018). Collaborative online planning for automated victim search in disaster response. *Robotics and Autonomous Systems*, 100, 251-266.
5. Betting, B., Varea, E., Gobin, C., Godard, G., Lecordier, B. and Patte-Rouland, B. (2019). Experimental and numerical studies of smoke dynamics in a compartment fire. *Fire Safety Journal*, 108, 102855.
6. Bogomaz, A.M. (2017). Filling the premises with smoke during fires. *Bulletin of the Civil Defense Academy*, 4(12), 6-11.
7. Chew, M.Y., Wong, N.H. and Ho, J.C. (2001). Smoke control in confined space. *Journal of Applied Fire Science*, 10(2), 109-125.
8. Chlenov, A.N., Menkeev, A.I., Darbakov, D.V., Kiselev, K.V. and Chernenko, S.A. (2018). The current state and prospects of development of fire detectors. In *Historical Experience, Modern Problems, and Prospects of Educational and Scientific Activity in the Field of Fire Safety*. Papers presented at the International Scientific and Practical Conference (pp. 375-379).
9. Efimov, S.V., Polyakov, R.Yu. and Yatsun, S.F. (2017). Method of early fire detection with the help of portable gas fire detectors. *Proceedings of Federal State Budgetary Educational Institution of Higher Education «Southwest State University»*, Series: *Technique and Technology*, 4(25), 81-89.
10. Emelianova, O.V., Poliakov, R.Yu., Efimov, S.V. and Yatsun, S.F. (2018). Portable flying complex for early detection of the fire sources. *Fundamental and Applied Problems of Technique and Technology*, 3(329), 136-141.
11. Estrada, M. and Ndomab, A. (2019). The uses of uncrewed aerial vehicles –UAV's (or drones) in social logistics: Natural disasters response and humanitarian relief aid. *Procedia Computer Science*, 149, 375-383.
12. Fedorov, A.V., Lukyanchenko, A.A. and Sokolov, A.V. (2006). Experimental Studies of hydrogen and carbon oxide concentration fields at the early stage of fire at the premises and determine safe installation places of gas fire detectors. *Fire and Explosion Safety*, 15(3), 74-84.
13. Fyodorov, A.V., Lukyanchenko, A.A. and Sokolov, A.V. (2005). Analytical review of gas fire detectors. *The technology of Technosphere Safety*, 1(1), 5.
14. González-Sieira, A., Cores, D., Mucientes, M. and Bugarín, A. (2020). Autonomous navigation for UAVs managing movement and sensing uncertainty. *Robotics and Autonomous Systems*, 126, 103455.
15. Goremykin, A.A., Lukashevich, N.D. and Alekseev, V.F. (2017). Principles of fire detectors selection for premises protection. In A.A. Savochkina (Ed.), *Modern Problems of Radio Electronics and Telecommunications "RT-2017."* Papers presented at the 13th

- International Youth Scientific and Technical Conference, Sevastopol, 20-24 November. Sevastopol, Russia: Sevastopol State University.
16. Heightman, A.J. (2010). *The silent killers. CO monitoring adds a new dimension to firefighter rehab and emergency care*. San Diego, CA: Elsevier.
 17. Jasim, O.Z., Hamed, N.H. and Abid, M.A. (2020). Urban air quality assessment using integrated artificial intelligence algorithms and geographic information system modeling in a highly congested area, Iraq. *Journal of Southwest Jiaotong University*, 55(1). Retrieved from <http://jsju.org/index.php/journal/article/view/517>
 18. Kazantsev, S.Y. and Krasilnikov, V.I. (2019). Medical and biological aspects of carbon monoxide damage to the body. *Actual Problems of Medicine and Biology*, 1, 13-16.
 19. Kolodyazhny, S.A. and Kolosova, N.V. (2015). Calculation of parameters of combined extract-and-input ventilation for the protection of buildings from smoke spreading during a fire. *Scientific Journal Engineering Systems and Structures*, 3(20), 68-76.
 20. Kozubovsky, V.R., Misevich, I.Z. and Ivanchuk, M.M. (2015). Comparative analysis of gas detectors for early fire detection. *Bezpieczenstwo Technika Pozarnicza*, 40(4), 107-122.
 21. Malashkina, V.A. and Lobaznov, A.V. (2011). Intercomparison of methods of fire early stage detection. *Mining Information-Analytical Bulletin (Scientific and Technical Journal)*, S7, 79-89.
 22. McKinnon, C.D. and Schoellig, A.P. (2020). Estimating and reacting to forces and torques resulting from common aerodynamic disturbances acting on quadrotors. *Robotics and Autonomous Systems*, 123, 103314.
 23. Mohammed, Z.B., Kamal, A.A.K., Resheq, A.S. and Alabdraba, W.M.Sh. (2019). Assessment of air pollution over Baghdad City using fixed annual stations and GIS techniques. *Journal of Southwest Jiaotong University*, 54(6). Retrieved from <http://jsju.org/index.php/journal/article/view/428>
 24. Polyakov, R.Yu. (2019). *A portable instrumental platform for the ecological monitoring system of the atmospheric air pollution by the toxic gases*. Kursk, Russia: Southwest State University.
 25. Polyakov, R.Yu., Efimov, S.V. and Yatsun, S.F. (2015). Robot-insekokter for environmental monitoring. *Bulletin of Voronezh Institute of the State Fire Service of State Ministry of Emergency Situations of Russia*, 3(16), 48-51.
 26. Poroshin, A.A. and Surkov, S.A. (2016). Development directions for testing methods of gas fire detectors. *The Problems of Risk Management in the Technosphere*, 2(38), 33-37.
 27. Russian Ministry for Emergency Situations. (2020, April 17). *Reports with a summary and analysis of compliance practices, standard, and mass violations of mandatory requirements*. Retrieved from http://www.consultant.ru/document/cons_doc_LAW_355636/6727b4a58823f036bde5f951f6715d6f8b9dee5e/
 28. Saidulin, E.N. (2009). Gas fire detectors: Detection of fire at an early stage. *Safety Algorithm*, 6, 32-34.
 29. Semiz, F. and Polat, F. (2020). Solving the area coverage problem with UAVs: A vehicle routing with time windows variation. *Robotics and Autonomous Systems*, 126, 103435.
 30. Sudhakar, S., Vijayakumar, A.V., Kumar, C.S., Priya, V., Ravi, L. and Subramaniaswamy, V. (2020). Uncrewed aerial vehicle (UAV) based forest fire detection and monitoring for reducing false alarms in forest-fires. *Computer Communications*, 149, 1-16.
 31. Sychev, I.V., Sitnikov, A.I. and Rakityansky, A.A. (2018). Application of gas fire detectors upon detection of fire. *Fire Safety: Problems and Perspectives*, 1(9), 864-866.

33. Tang, S. and Kumar, V. (2018). Autonomous flight. *Annual Review of Control, Robotics, and Autonomous Systems*, 1, 29-52.

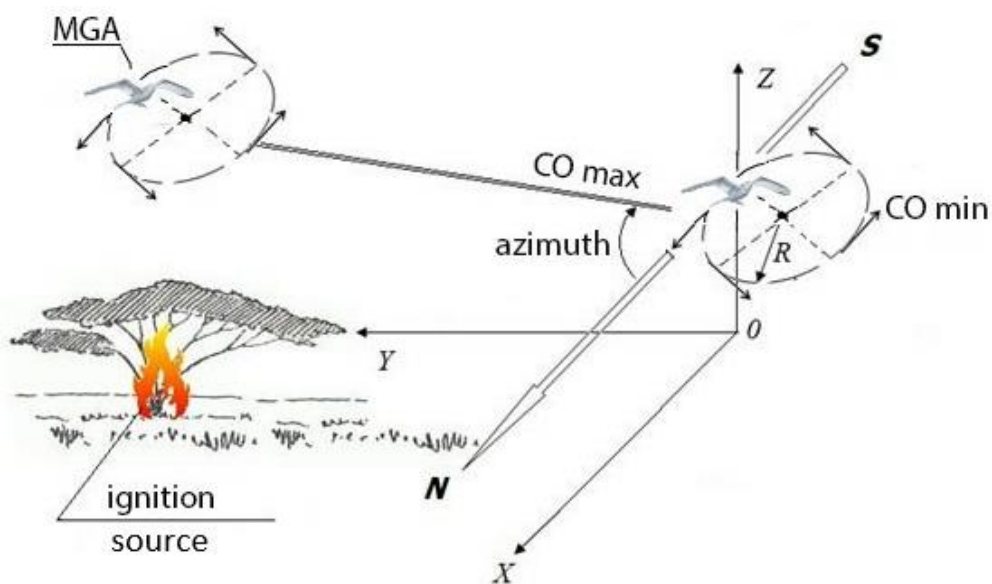


Figure 1. The movement scheme of the portable gas analyzer (MGA) to the ignition source

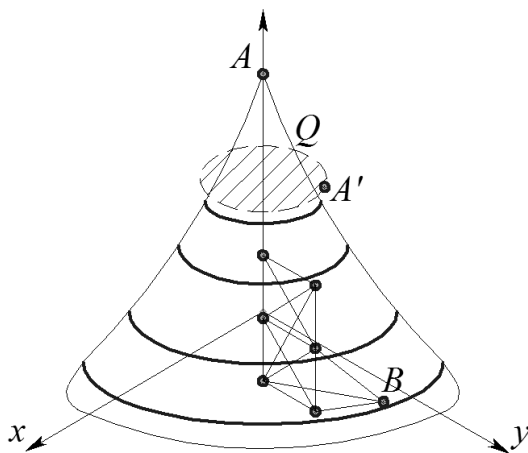


Figure 2. Spatial scheme of the portable gas analyzer (MGA) movement to the ignition source by the simplex method. A is the point with the maximum concentration of CO; B is the initial position of the MGA; Q is the concentration of CO.

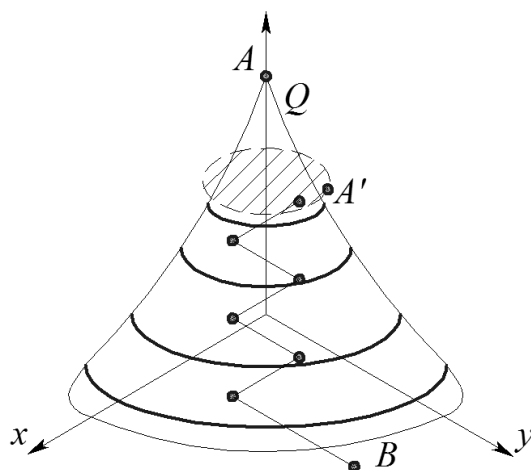


Figure 3. Spatial scheme of the portable gas analyzer (MGA) movement to the ignition source by Kiefer's method. A is the point with the maximum concentration of CO; B is the initial position of the MGA; Q is the concentration of CO

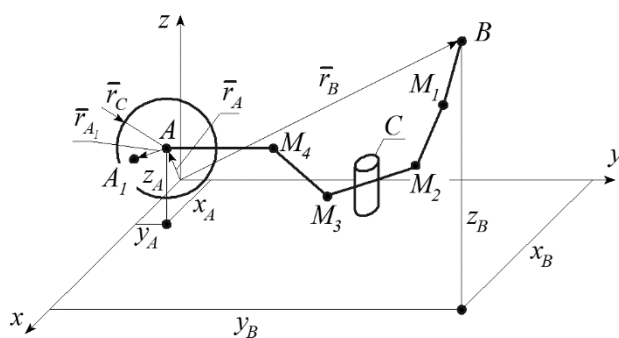


Figure 4. Scheme of portable gas analyzer (MGA) movement to the ignition source. A is the ignition source; B is the initial position of the MGA; C is the obstacle; M_i is the intermediate position of the MGA

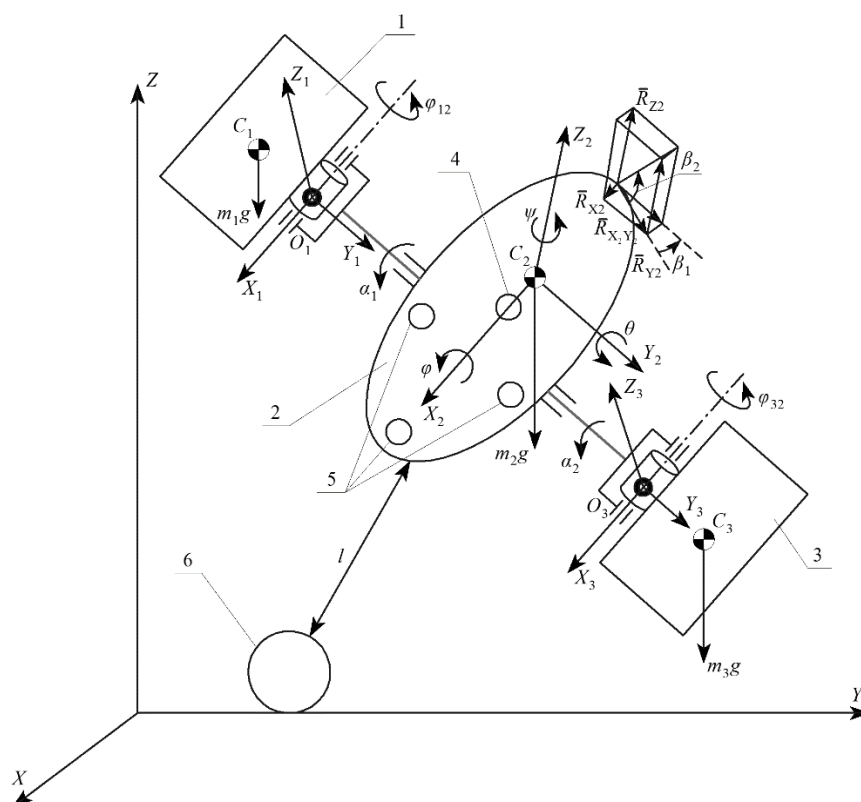


Figure 5. Calculation scheme of the portable gas analyzer

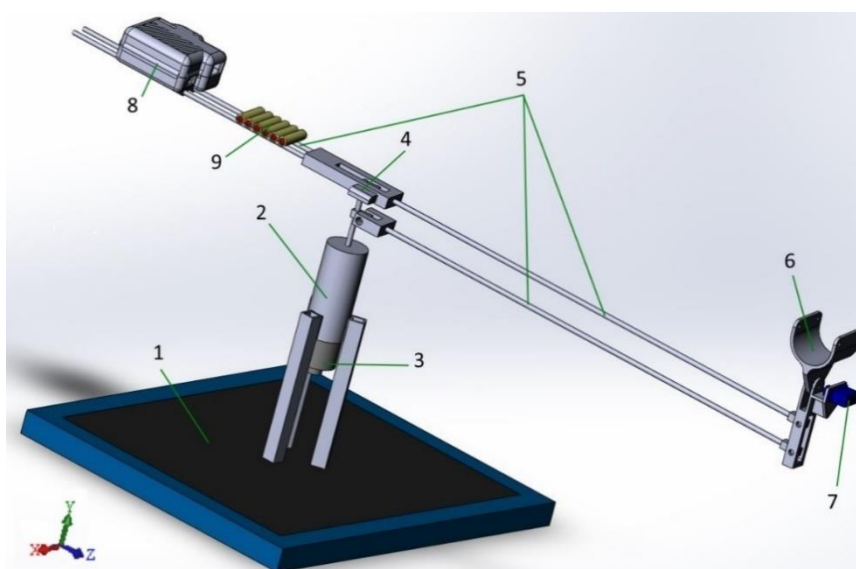


Figure 6. General view of the 3D model of the test-bed

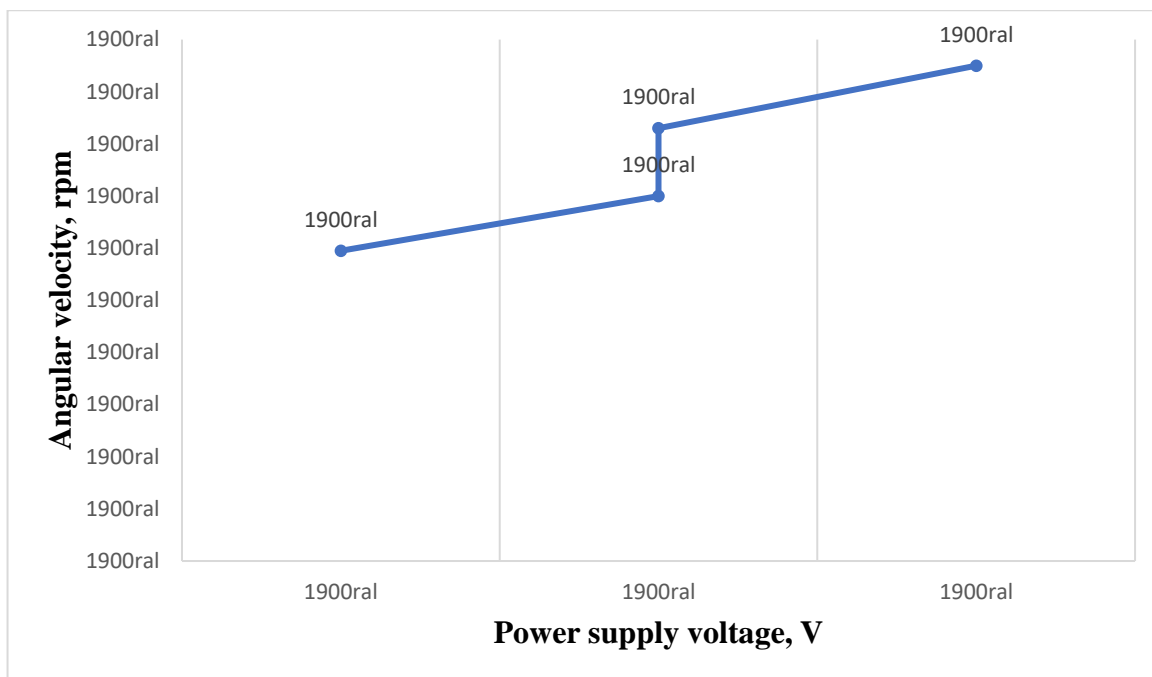


Figure 7. Dependency diagram of the electrical motor angular velocity on the power supply voltage

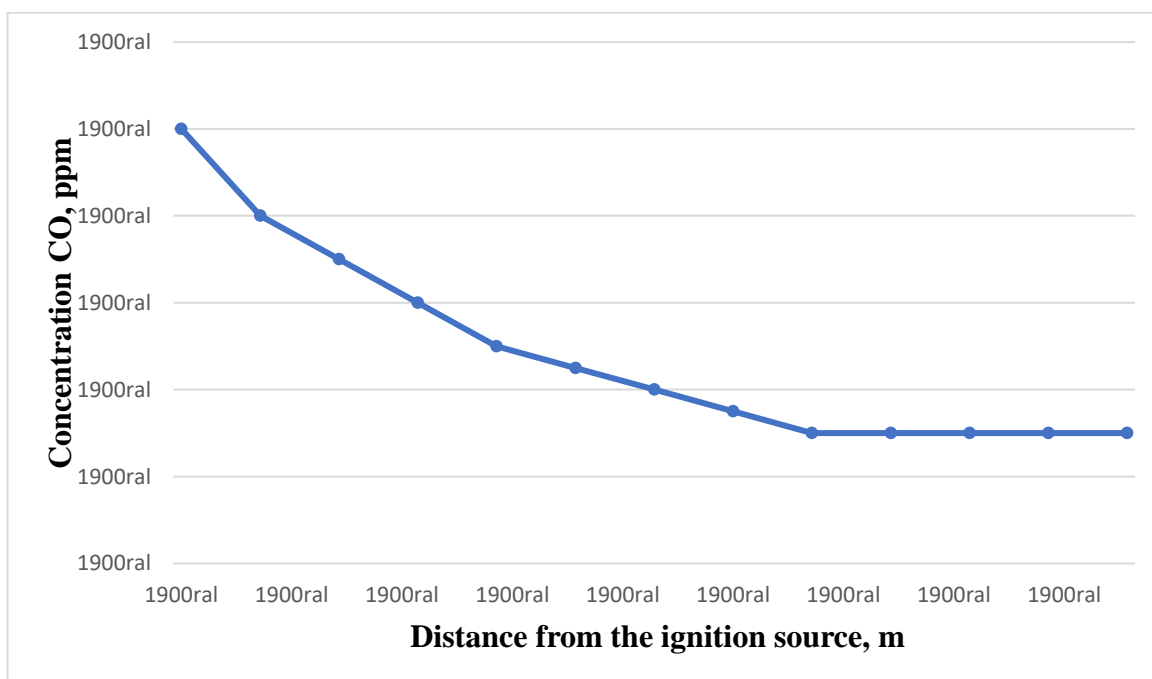


Figure 8. Change in the relative CO concentration as a function of distance from the ignition source

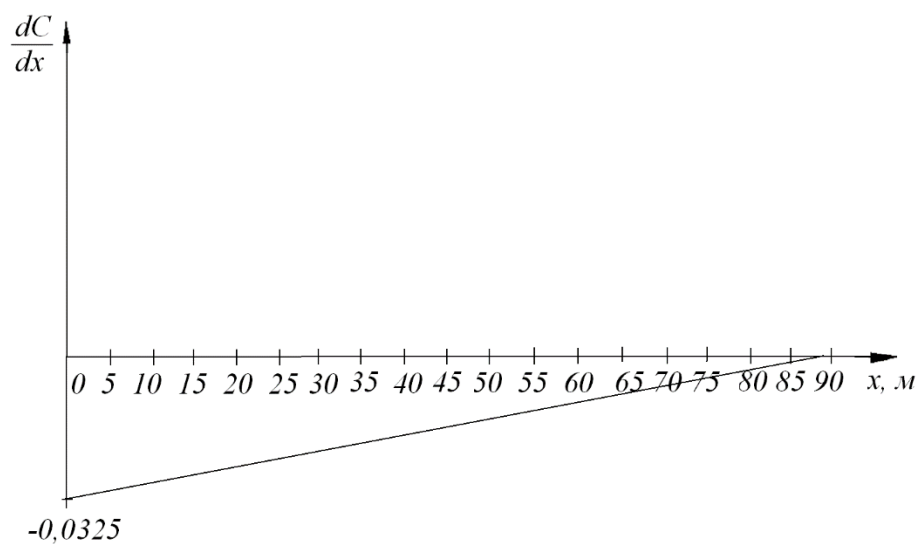


Figure 9. Change in the gradient of CO concentration as a function of distance from an ignition source

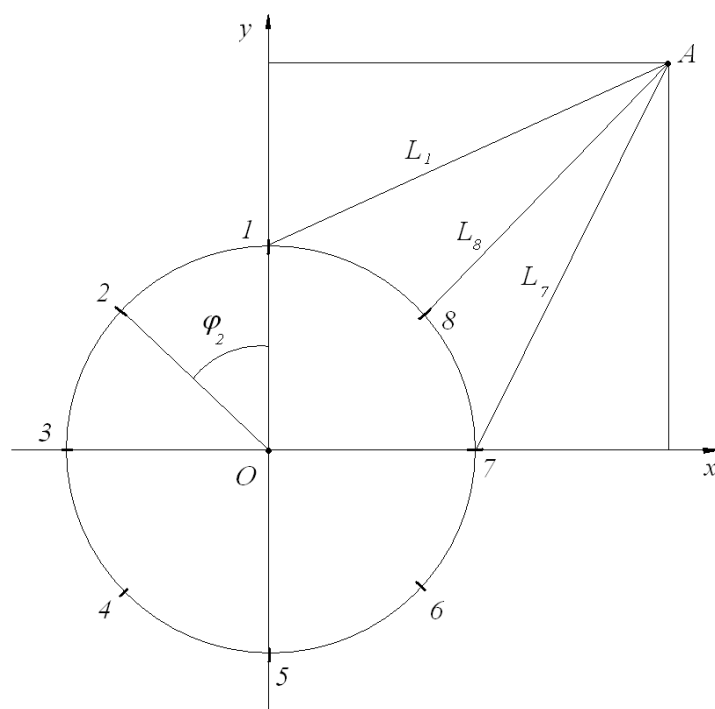


Figure 10. Experimental design for determination of CO concentration during MGA movement in a circumferential direction

Table 1. Results of experimental research

ω , rad/s	T, h	I, A	N, B _T	λ , W/H
15.70	0.00	0.02	0.01	-
28.26	0.01	0.06	0.06	6.75
37.68	0.02	0.10	0.15	8.44
48.15	0.03	0.15	0.30	10.21
56.52	0.04	0.21	0.53	12.81
64.89	0.05	0.26	0.78	14.36
72.64	0.07	0.31	1.09	16.29
80.59	0.08	0.36	1.44	18.33

Table 2. CO concentration for $R = 3$ m

Point number									
Name		C ₁	C ₂	C ₃	C ₄	C ₅	C ₆	C ₇	C ₈
Calculation	C _P	0.33	0.31	0.301	0.30	0.30	0.31	0.32	0.33
Experiment	C ₉	0.34	0.32	0.29	0.29	0.28	0.31	0.33	0.34
Distance to the ignition point	L. m	33.6	35.6	37.8	39.0	37.8	36.8	34.91	33.1

Table 3. CO concentration for $R = 5$ m

Point number									
Name		C ₁	C ₂	C ₃	C ₄	C ₅	C ₆	C ₇	C ₈
Calculation	C _P	0.34	0.31	0.29	0.288	0.29	0.3	0.34	0.35
Experiment	C ₉	0.36	0.33	0.30	0.29	0.28	0.31	0.35	0.37
Distance to the ignition point	L. m	32.02	35.42	39.05	40.97	40.31	37.36	33.54	31.7

O PAPEL DA VITAMINA D COMO UM NOVO MARCADOR NA INFERTILIDADE DAS MULHERES

THE ROLE OF VITAMIN D AS A NEW MARKER ON THE WOMEN INFERTILITY

دور فيتامين D كعلامة دالة جديدة لعقم النساء

MOHAMMED, Najla Salim¹; AL-JAWADI, Zena Abdul Monim^{2*}

^{1,2} University of Mosul, College of Science, Department of Chemistry, Mosul, Iraq.

* Corresponding author

e-mail: zena_aljawadi@uomosul.edu.iq

Received 25 Aug. 2020; received in revised form 10 October 2020; accepted 30 October 2020

RESUMO

O colecalciferol (vitamina D) é essencial para o bom funcionamento do corpo humano. Esta vitamina pertence a uma vitamina lipossolúvel, responsável por estimular a absorção intestinal de cálcio e fosfato. Recentemente, foi observado que a vitamina D pode estar relacionada a casos de infertilidade feminina. Este estudo teve como objetivo examinar o efeito da vitamina D na infertilidade feminina analisando parâmetros hormonais e bioquímicos. Estrogênio, progesterona, FSH, LH, colesterol total, triglicerídeo, HDL, LDL, VLDL, vitamina D e IMC foram testados em 60 mulheres com infertilidade e 40 mulheres férteis como grupo controle. Os resultados mostraram uma elevação altamente significativa na concentração de LH, triglicerídeo, LDL e IMC em mulheres inférteis em comparação com as mulheres saudáveis com um significativo $P=0,025$, $P=0,01$, $P=0,05$ e $P=0,001$, respectivamente. Além disso, uma baixa elevação significativa na concentração de estrogênio, progesterona, FSH, HDL e vitamina D em mulheres inférteis quando comparadas às mulheres saudáveis em um nível significativo de $P=0,01$, $P=0,039$, $P=0,05$, $P=0,05$ e $P=0,001$, respectivamente, também foi observada. Essa vitamina teve uma forte relação positiva com a progesterona, FSH, colesterol total, HDL e LDL. Também foi comprovada uma correlação inversa significativa para LH, estrogênio, TG, VLDL e IMC. Pode-se concluir que existe uma diminuição significativa do nível de vitamina D em mulheres inférteis em comparação com o grupo de mulheres saudáveis, principalmente com IMC elevado. Também pode ser deduzido que a vitamina D pode ser um novo marcador de aumento de infertilidade e risco de aborto.

Palavras-chave: *infertilidade, vitamina D, aborto, hormônios femininos.*

ABSTRACT

Cholecalciferol (Vitamin D) is essential to the proper functioning of the human body. This vitamin belongs to fat-soluble vitamins, responsible for stimulating the intestinal absorption of calcium and phosphate. It has been recently observed that vitamin D may be related to cases of female infertility. This study aimed to examine the effect of vitamin D on female infertility by analyzing hormonal and biochemical parameters. Estrogen, progesterone, FSH, LH, total Cholesterol, Triglyceride, HDL, LDL, VLDL, vitamin D, and BMI were tested in 60 women with infertility and 40 fertile women as a control group. The results showed a highly significant elevation in LH concentration, Triglyceride, LDL, and BMI in infertile women, compared to the healthy women at a significant $P=0.025$, $P=0.01$, $P=0.05$, and $P=0.001$, respectively. Also, a significant low elevation in the concentration of estrogen, progesterone, FSH, HDL, and vitamin D in infertile women when compared to the healthy women at a significant level of $P=0.01$, $P=0.039$, $P=0.05$, $P=0.05$, and $P=0.001$, respectively was observed. This vitamin had a strong positive relationship with progesterone, FSH, total cholesterol, HDL, and LDL. It was also proved a significant inverse correlation to LH, estrogen, TG, VLDL, and BMI. It could be concluded that there is a significant decrease in the level of vitamin D in infertile women compared with the group of healthy women, especially with high BMI. It could also be deduced that vitamin D can be a new marker of increasing infertility and miscarriage risk.

Keywords: *Infertility, Vitamin D, Miscarriage, Female hormones.*

يعتبر الكولكالسيفيرول (فيتامين D) ضرورياً لتنظيم سير عمل جسم الإنسان. ينتمي هذا الفيتامين إلى مجموعة الفيتامينات القابلة للذوبان في الدهون و هو المسؤول عن تحفيز امتصاص الأمعاء للكالسيوم و الفوسفات. لقد لوحظ مؤخراً أن فيتامين D قد يكون مرتبطاً بحالات العقم عند النساء. هدفت هذه الدراسة إلى قياس تأثير فيتامين D على العقم لدى النساء من خلال قياس المتغيرات الهرمونية و الكيموحيوية. حيث تم قياس هورمون الاستروجين و هورمون البروجسترون و FSH و LH و الكوليستيرول الكلي و ثلاثي أسيل كليسيرول و HDL و LDL و VLDL و فيتامين D و مؤشر كتلة الجسم في 60 امرأة مصابة بالعقم و 40 امرأة سليمة كمجموعة سيطرة. أظهرت النتائج ارتفاعاً معنوياً في تركيز LH و ثلاثي أسيل كليسيرول و LDL و مؤشر كتلة الجسم لدى النساء المصابات بالعقم، مقارنة بالنساء السليمات عند مستوى احتمالية $P=0.025$ ، $P=0.01$ ، $P=0.05$ ، $P=0.001$ على التوالي. أيضاً، ظهر إنخفاض معنوي في تركيز هورمون الاستروجين و هورمون البروجسترون و FSH و HDL و فيتامين D لدى النساء المصابات بالعقم مقارنة بالنساء السليمات عند مستوى احتمالية $P=0.01$ ، $P=0.039$ ، $P=0.05$ ، $P=0.05$ ، $P=0.001$ على التوالي. كان لهذا الفيتامين علاقة ارتباط إيجابية قوية بهورمون البروجسترون و FSH و الكوليستيرول الكلي و HDL و LDL. كما تم إثبات وجود علاقة ارتباط عكسية معنوية مع كل من LH و هورمون الاستروجين و TG و VLDL و BMI. يمكن الإستنتاج أن هناك انخفاضاً ملحوظاً في مستوى فيتامين D لدى النساء المصابات بالعقم مقارنة مع النساء السليمات، خاصة مع ارتفاع مؤشر كتلة الجسم. يمكن أيضاً إستنتاج أن فيتامين D يمكن أن يكون علامة دالة جديدة لزيادة مخاطر العقم والإجهاض.

الكلمات الدالة: العقم، فيتامين D، الإجهاض، الهورمونات الإنثوية

1. INTRODUCTION:

Infertility is a common health problem all over the world. It is defined as the inability to conceive after 12 months or more of marriage, even after treatment or in the case of using fertility aids outside the body (Miyashita *et al.*, 2016; Jungwirth *et al.*, 2013; Gurunat *et al.*, 2011). Vitamin D is essential to the proper functioning of the human body. This vitamin is a fat-soluble steroid group responsible for stimulating the intestinal synthesis of calcium and phosphate (Pludowski *et al.*, 2018; Holick, 2007).

The pregnant woman requires a healthy bone and muscles to retain this one of the most important vitamins. Therefore, the appropriateness of a vitamin D requirement of a pregnant woman healthy and complete their pregnancy (Webb, 2006). Iron, folic acid, or zinc deficiency, as well as vitamin B12, affects fertility in women. It has been recently observed that vitamin D may be related to female infertility cases, and studies are still very few to clarify its role. Most of the daily requirements for vitamin D3 are formed from the biosynthesis of vitamin D3 under the skin. Many environmental factors affect skin production with vitamin D3, such as lack of exposure to sunlight caused by season, clouds, or air pollution. The condition of the skin and its pigmentation are also significant factors (Ranjana, 2017).

The production of vitamin D3 by the skin is often insufficient to ensure that the recommended daily amount is met. Especially in industrialized countries where the World Health Organization has defined vitamin D deficiencies as having a serum level of less than (20 ng/dl) (Ranjana, 2017; Gaskins *et al.*, 2017), over the past couple of years, a growing interest in researching the relationship between the deficiency and sterility of

vitamin D. And studies are still very few to clarify its role. Further studies are required to urgently use quantitative methods to explicitly measure vitamin D to check its functionality in the treatment of infertility in women. And investigate the possible therapeutic benefits of vitamin D addition (Cie'slińska *et al.*, 2018; Ranjana, 2017).

The risk of sterility is also proportional to age. As a result of the work defect in the uterus and poor quality of the eggs, it was noted that the infertility rate exceeds (20.3%) in pairs over 40 years in addition to the vast increase in the female fertility rate after 37 years of age (Feichtinger *et al.*, 2019). As with age, eggs with an abnormal genetic structure are created by defects in the splitting and lack of adhesion between structural chromosomes. That prevents natural fertilization and chromosome in aborted women. Obesity also plays an essential role in reproductive disorders, especially in women. It is associated with ovulation, menstrual disorders, infertility, and multiple abortions. Pregnancy changes differ depending on the origin and duration of infertility, the woman's age, pregnancy history, and availability of different therapies for unexplained infertility (Feichtinger *et al.*, 2019; Rodrigu *et al.*, 2018). As for Iraq, there are no accurate statistics on infertility.

Due to the lack of documented records, infertility significantly impacts the psychological and social point of view. Due to changes in lifestyle and environmental stress, the rate of infertility has increased considerably. This disease has become the third most dangerous disease after contracting diseases, Cardiovascular, and cancer diseases (Cong *et al.*, 2016; Jangir *et al.*, 2014).

This research aimed to examine the effect of vitamin D on female infertility by analyzing hormonal and biochemical parameters for early

diagnosis. It can improve treatment response and prevent female infertility by maintaining vitamin D levels at a normal level.

2. MATERIALS AND METHODS:

2.1. Sample collection

2.1.1 Group of Infertile Patients

Sixty infertile women have been registered in this research. Specialists in Hospitals diagnosed it, and a laboratory test was carried out in the laboratories of the hospitals and external laboratories for the period from 13/4/2019 to 17/5/2020. Their ages ranged from 18-45 years, and the BMI is between (17-37.5 kg/m²). Clinical data as age, sex, weight, height, the number of years of marriage, and the number of abortions were obtained for each case in a questionnaire prepared for this purpose. Excluded conditions included diabetes, high blood pressure, and thyroid disease.

2.1.2 Control Group (Reference Group)

This study was attended by forty young fertile women (control group), ages ranging from 17-45 years, and the BMI is between (24-26.1 kg/m²).

2.1.3 Blood Collection

Two groups were tested for blood over 12-hour fasting (values for 5ml), early follicular cycles (cycle days two or three) for estrogen (E2), progesterone, follicle-stimulating hormones (FSH) and lutein's hormone (LH) and vitamin D. Luteal prolactin (cycle day 21). Into the test tube (gel and clot activator tube for serum separation) by drawing (5ml), and centrifuged for serum separation within an hour of blood collection, and the serum was stored in a deep freezer at a temperature of 70°C for subsequent analysis. Samples were analyzed in batches of 100 to be omitted between analytical variations. Samples were permitted to reach room temperature before the study.

2.1.3.1. Materials

This study was performed using a special kit for each variable from the German company Cobas to estimate the following hormonal and chemical variables: Estrogen hormone E2, progesterone, follicle-stimulating hormone (FSH), ovulation hormone, or called luteinizing hormone

(LH), vitamin D, and lipid profile were also measured, which include total cholesterol, triacylglycerol TG, and high-density lipoprotein (HDL) cholesterol.

2.1.3.2. Procedures

The commercial kits (Roche kits) were then measured by Cobas E411. The lipid profile also included Total Cholesterol, Triglyceride (TG), High-Density-Lipoprotein (HDL) analysis, and was measured using commercial kits (Roche Kits) by Cobas C311.

2.1.3.3. Hormones and vitamin D measurement methods

The reagents used are ready and available in the device. After separating the serum in a centrifuge for five minutes at 4000 rpm, it put the separated serum into a type test tube. Hitachi tube then, we put the tube on the required number inside the E411 Cobas device, then the clinical information was entered. The required tests, and the number in which the serum was placed, then press the STAR button, and then the results appear automatically.

2.1.3.4. Lipid profile measurement methods

The reagents used are ready and available in the device. After separating the serum in a centrifuge for five minutes at 4000 rpm, we put the separated serum into a Hitachi tube. After that, the test tube was put on the required number inside the C311 Cobas device, then entered the clinical information, the required tests, and the number in which the serum was placed; then pressed the START button, and then the results appeared automatically.

2.1.3.5. Indirect Procedures

Low-Density-Lipoprotein (LDL) and Very-Low-Density-Lipoprotein (VLDL) were determined indirectly using the Friedewald equations.:

$$\text{LDL Con. (mg/dl)} = \text{Cholesterol Con.} - \text{HDL Con.} - \text{TG/5} \quad (\text{Eq.1})$$

$$\text{VLDL Conc. (mg/dl)} = \text{Triglyceride/5} \quad (\text{Eq. 2})$$

2.1.3.6. BMI Procedures

BMI was calculated using the following

equation:

$$\text{BMI (Kg/m}^2\text{)} = \text{Weight (Kg)} / \text{Height (m}^2\text{)}.$$

(Eq. 3)

2.1.3.7. Statistical analysis

SPSS software has been used to analyze the data. The T-test and Duncan-tests were already used to compare parameters between the total control number and patients based on occupancy at $p \leq 0.05$, $p \leq 0.01$, and $p \leq 0.001$, respectively, and the test of Pearson correlation coefficients. The Duncan-tests is used to indicate the differences when comparing more than two groups of the same chemical parameter (a, b, ab means the difference, and if all are the same, it indicates no significant statistical difference), which is identical to the p-value (Kirkpatrick and Feeney, 2012).

2.1.4 Ethical approval

The research has been carried out and agreed upon by the author's Institutional Review Board following all applicable national legislation, institutional policy, and the values of the Helsinki Declaration.

2.1.5 Informed Consent

All participants rights were protected, and oral informed consent was obtained according to the Helsinki Declaration.

3. RESULTS AND DISCUSSION:

3.1. The level of hormonal and biochemical parameters of infertile women (primary and secondary) compared with the control group

The findings in Table 1 indicate that hormone and biochemical variables were significantly lower estrogen hormone (E2), causing menstrual disruptions and ovulation in women who had infertility than in healthy women (Dag and Dilbaz, 2015). The explanation for this may be due to the presence of a pituitary gland defect (Taraborrelli *et al.*, 2015), which affects the ovaries. Therefore, it may cause any loss of ovarian function or harm to the decrease in the estrogen hormone and adversely affect the female ovulation process. Thus, decreasing the probability of pregnancy and the probability of infertility. Cortisol and sex hormone-bound globulin is increased by the estrogen hormone (Li *et al.*, 2017; Gilbert, 2019).

Also, progesterone hormone concentration revealed a significant decrease, which could lead to an increase in the risk factor of infertility and an increased risk of endometrial cancer. Was found in women who had infertility compared with healthy females, possibly due to lack of ovulation (Dosouto *et al.*, 2019; Momenimovahed *et al.*, 2019). Similarly, women who have low progesterone hormone levels and who are successful in conceiving are more likely to have a miscarriage. Irregular uterine bleeding, or to have an ectopic pregnancy and fetal death (Taraborrelli *et al.*, 2015). With a highly significant level of the ovulation hormone (LH) occurring in women with infertility relative to healthy women, a significant decrease in the concentration of the follicle-stimulating hormone (FSH), because long-term loss of ovulation due to hyperandrogenemia, which could contribute to premature action on granulocytes in the mid-Follicular process through early cessation of follicle growth and development, leading to the absence of ovulation and sterility (Gilbert *et al.*, 2019; Kesmodel, 2012).

Also, the TG, LDL, and BMI concentrations were considerably increased and the high-density lipoprotein (HDL) concentration in infertile women was decreased significantly compared to healthy women. Maybe because of the connection between the abnormal metabolism of lipids and the infertility of women as the high body mass index is linked to the high triglyceride level and the high-level of free fatty acids in the follicular fluid is harmful and not suitable for egg maturity in this fat-rich environment. Dyslipidemia is also seen in obese women by a high concentration of triglycerides, free fatty acid concentration, higher concentration of lipoprotein (LDL) density, and low concentration of lipoprotein (HDL) (Fontana and Torre, 2016).

Vitamin D levels in infertile women was decreased significantly compared to healthy women. The reason may be that disorder in vitamin D is associated with early ovarian failure. It is characterized by menopausal disorder, metabolic deficiency, and increased genital serum levels in women younger than 40 years of age or miscarriage (Voulgaris *et al.*, 2017; Wasim, 2015; Stanford, 2013). In addition to vitamin D deficiency, it is normally responsible for stimulating sexual appetite in women who suffer from primary ovarian insufficiency (Wasiewicz *et al.*, 2018).

3.2. A comparison of the level of hormonal, biochemical parameters, and Vit. D in infertile women with different BMI

Table 2 shows decreased LH and FSH levels in infertile women, depending on BMI, as the higher BMI. Obesity is linked to higher leptin blood levels (Broughton and Moley, 2017; Al-Turki *et al.*, 2017). The leptin hormone inhibits the process of steroidogenesis in granulosa cells in obese women. This deficiency may affect the level of sexual hormones (LH and FSH). This leads to an imbalance in the central nervous system (CNS), leading to the recruitment of inactive ovarian follicles. A small number of them enter the maturity stage. And the resulting egg is of low quality in addition to the effect on follicle growth (Al-Taie and Al-Jawadi, 2019; Baig *et al.*, 2019; Hill and Elias, 2018; Ranjana, 2017).

Besides, the follicle-stimulating hormone decreases as BMI increases. This is because, as well as being a risk factor for multiple metabolic disorders. Obesity affects the fertility of women and the rise in obesity has hormonal changes that may disrupt the sub glands function. The hypothalamus is directly affecting ovarian function and impair ovarian follicle growth, the production, and fertilization of qualitative and quantitative Oocysts (Kamyabi *et al.*, 2015). Significant increases in cholesterol and TG concentrations with increased body mass index in sterile women with BMI (39.9-35 Kg/m²) as shown in Table (2). The reason may be that dietary fat may affect the follicular fluid or the ovarian cell lipid composition. Higher body mass index is associated with a high triglyceride level and free fatty acid in the follicular fluid. That reflects changes in the blood and correlates with the body mass index, meaning that the increased fatty acid associated with the egg quality (Poor Cumulus Oocyte Morphology) (Benjamin *et al.*, 2017; Valckx *et al.*, 2012). No significant difference in the concentrations of estrogen, progesterone, HDL, LDL, and VLDL statistically. However, there has been a substantial decrease in vitamin D levels in women with infertility with an increase in BMI.

The low vitamin D levels are because obese women have a lower level of vitamin D relative to normal-weight patients since the level of vitamin D in follicular fluid is strongly associated with BMI and may play a major role in females infertility. This is primarily due to the presence of VDR (Vitamin D (1,25-dihydroxy vitamin D₃) receptor) and ((CYP27B) Cytochrome P450, family 27 subfamily B member1) in various tissues of the female reproductive system (Blomberg *et al.*, 2018), leading to impaired follicle development and ovulation impairment (Oostingh *et al.*, 2019; Kokanalij *et al.*, 2019).

3.3. Number of miscarriage with Vitamin D

The results in Figure (1) showed a significant decrease in the level of Vit. D in infertile women with repeated miscarriages compared to the control group at ($P = 0.001$), highlighting that Vit. D can be an essential regulator of an immune reaction for the body during pregnancy, as it's supposed that Vit. D stimulates the immune changes necessary to prevent pregnancy loss and strengthen the mother's immune system, and it does not happen. It might harm an unborn baby and end the pregnancy by abortion, as vitamin D receptors are found in the ovaries, uterus, placenta, hypothalamus, and pituitary gland (Li *et al.*, 2017; Zhang *et al.*, 2015; Barragan *et al.*, 2015).

As normal vitamin D levels, reduce the incidence of miscarriage, especially in pregnancy during the first trimester, women who have more likely low levels of Vit. D would have antibodies to phospholipids and antinuclear antibodies and increased natural killer cells (NK) than of women with a normal vitamin D level, which confirms the immune role of the vitamin in preserving the fetus. And that the presence of vitamin D receptors and enzymes responsible for vitamin D hydroxylation work to determine localized vitamin D synthesis in the human placenta; Thus will shed light on the possible mechanism between the vitamin state D and persistence of pregnancy (Grieger and Norman, 2020; Samimi *et al.*, 2017).

3.4. The correlation of vitamin D for infertile women with hormonal and biochemical parameters

Correlation between infertility and vitamin D is shown in Table 3, which confirms that vitamin D, is a sign that increases risk factors of infertility. The correlation between infertility and vitamin D positively correlated with estrogen, progesterone, FSH, total cholesterol, HDL, and LDL, especially in FSH. On the other hand, the correlation between infertility and vitamin D has a significant negative correlation with LH, TG, VLDL, and BMI. Especially in BMI, where the higher the body mass index, the decreased the level of vitamin D in women with infertility. The reason may be that obese people are less able to convert vitamin D into its active form. Vitamin D is synthesized or absorbed in the skin upon exposure to sunlight. Or absorbed by the body from its food sources or nutritional supplements, it is distributed in the fatty tissues. However, its blood levels are low because it is distributed in the fats accumulated in the body and did not reach the blood.

4. CONCLUSIONS:

The study proved a significant decrease in vitamin D levels in infertile women compared with the healthy women's group. Also, when comparing the level of hormonal variables for infertile women, of both types (primary and secondary), with healthy women, there was a significant decrease in the level of estrogen hormones, progesterone hormones, and follicle-stimulating hormones, as well as a significant decrease in the level of high-density lipoprotein (HDL). At the same time, it showed a significant increase in triglyceride levels, LDL, and BMI. Studies have also shown that the level of vitamin D in infertile women with a high BMI; is much lower than the level of vitamin D in infertile women with a normal body mass index. As it has been proven that there is an inverse relationship between BMI and vitamin D. Also, there is a strong inverse correlation between miscarriage times in infertile women and vitamin D levels compared to healthy women.

This study found vitamin D is a new risk factor to increase women infertility and miscarriage. It is associated with hormonal derangements and dyslipidemia, responsible for infertility and impaired ovarian follicular development, qualitative and quantitative development of the Oocyte. Hence it should be primarily targeted in managing these women before starting any therapy to correct their hormonal imbalance; by measuring the level of vitamin D and treating vitamin deficiency through nutritional and drug supplements under medical supervision.

5. CONFLICT OF INTERESTS:

The authors declare that there is no conflict of interest regarding the publication of this article.

6. ACKNOWLEDGMENTS:

The researchers are grateful the Mosul University, the management, and the medical staff of Hospitals for their helping.

7. REFERENCES:

1. Al-Taie F.Kh., Al-Jawadi Z.AM. (2019). The Impact of Obesity on Infertile Women with Polycystic Ovaries in Iraq. *Rafidain journal of science*, 28 (2E: Chem.): 1-9.
2. Al-Turki HA. (2015). Prevalence of primary and secondary infertility from a tertiary center in eastern Saudi Arabia. *Middle East Fertil Soci J.*, 20(4), 237–240.
3. Baig M., Azhar A., Rehman R., Syed H., Tariq S. and Gazzaz Z.J. (2019). Relationship of Serum Leptin and Reproductive Hormones in Unexplained Infertile and Fertile Females, *Cureus*, 11(12), e6524.
4. Barragan M., Good M. and Kolls J.K. (2015). Regulation of Dendritic Cell Function by Vitamin D. *Nutrients.*, 7(9), 8127-8151.
5. Benjamin EJ, Blaha MJ, Chiuve SE, Cushman M, Das SR, Deo R, de Ferranti SD, Floyd J, Fornage M, Gillespie C and Sasi CR. (2017). Heart disease and stroke statistics—2017 update: a report from the American Heart Association. *Circulation*, 135(10), e146–e603.
6. Blomberg J.M, Lawaetz J.G, Petersen J.H, Juul A and Jorgensen N. (2018). Effects of Vitamin D Supplementation on Semen Quality, Reproductive Hormones, and Live Birth Rate: A Randomized Clinical Trial. *J. Clin. Endocrinol. Metab.*, 103, 870–881. DOI: 10.1210/jc.2017-01656.
7. Breton G. (2015). Origin and development of human dendritic cells. *Med Sci (Paris)*, 31(8-9), 725-727.
8. Broughton D.E. and Moley K.H. (2017). Obesity and female infertility: potential mediators of obesity's impact, *Fertility, and Sterility*, 107(4), 840–847.
9. Cie'slinska A., Kostyra E., Fiedorowicz E., Snarska J., Kordulewska N., Kiper, K. and Savelkoul H.F.J. (2018). Single Nucleotide Polymorphisms in the Vitamin D Receptor Gene. *Int. J. Mol. Sci.*, 19(7), 1919.
10. Cong J, Li P, Zheng L and Tan J. (2016). Prevalence and risk factors of infertility at a rural site of Northern China. *PloS One.*, 11(5), e0155563.
11. Dag Z.O. and Dilbaz B. (2015). Impact of obesity on infertility in women, *J. Turk Ger Gynecol Assoc.*, 16(11), 1-7.
12. Dosouto C., Haahr T. and Humaidan P. (2019). Advances in ovulation trigger strategies, *Panminerva Med.*, 61(1), 42-51.
13. Feichtinger M, Nordenhök E, Olofsson J, Hadziosmanovic N and Rodriguez-Wallberg K. (2019). Endometriosis and cumulative live birth rate after fresh and

- frozen IVF cycles with single embryo transfer in young women: no impact beyond reduced ovarian sensitivity—a case-control study, *J Assist Reprod Genet.*, 36(8), 1649–1656.
14. Fontana R. and Torre S.D. (2016). The Deep Correlation between Energy Metabolism and Reproduction: A View on the Effects of Nutrition for Women Fertility, *Nutrients J.*, 8, 1-34.
 15. Gaskins A and Chavarro J. (2017). Diet and fertility: a review. *Am J Obstet Gynecol*, 218, 379–389.
 16. Grieger JA. and Norman RJ. (2020). Menstrual Cycle Length and Patterns in a Global Cohort of Women Using a Mobile Phone App: Retrospective Cohort Study *J Med Internet Res.*, 22(6), e17109.
 17. Gilbert RO. (2019). Symposium review: Mechanisms of disruption of fertility by infectious diseases of the reproductive tract, *J. Dairy Sci.*, 102(4), 3754-3765.
 18. Gurunat HS, Pandian Z, Anderson RA and Bhattacharya S. (2011). Defining infertility—a systematic review of prevalence studies. *Hum Reprod Update.*, 17(5), 575-588.
 19. Hill JW. and Elias CF. (2018). Neuroanatomical Framework of the Metabolic Control of Reproduction, *Physiological Reviews*, 98(4), 2349-2380.
 20. Holick MF. (2007). Vitamin D deficiency, *N Engl J Med.*, 357(3), 266–281.
 21. Jangir RN and Jain GC. (2014). Diabetes mellitus induced impairment of male reproductive functions: a review. *Curr Diabetes Rev.*, 10(3), 147-57
 22. Jungwirth A, Diemer T, Dohle G.R, Giwercman A, Kopa Z and Krausz C, (2012). Tournaye Guidelines for the investigation and treatment of male infertility. *Eur Urol.*, 61(1), 159-163.
 23. Kamyabi Z and Gholamalizade T. (2015). A comparative study of serum and follicular fluid leptin concentrations among explained infertile, unexplained infertile, and fertile women. *Int J Fertil Steril.*, 9, 150-156
 24. Kesmodel U.S. (2012). Fertility and Obesity, pp: 13, Springer-Verlag, Berlin Heidelberg. DOI 10.1007/978-3-642-25023-1_2.
 25. Kirkpatrick L. and Feeney B.C. (2012). A Simple Guide to IBM SPSS Statistics for Version 18.0 and 19.0 11th Edn., pp:115, Wadsworth Cengage Learning, Belmont, ISBN-10:1111352550.
 26. Kokanalij D., Karaca M., Ozakşit G., Elmas B. and Üstün Y.E. (2019). Serum Vitamin D Levels in Fertile and Infertile Women with Polycystic Ovary Syndrome, *Geburtshilfe Frauenheilkd*, 79(5), 510–516.
 27. Li HWR, Cheung TM, Yeung WSB, Ho PC and Ng EHY. (2017). The relative importance of the different components of the Bologna criteria for predicting poor ovarian response in assisted reproduction. *Maturitas*, 100, 170
 28. Li N., Wu H.M, Hang F., Zhang Y.S. and Li M.J. (2017). Women with recurrent spontaneous abortion have decreased 25(OH) vitamin D and VDR at the fetal-maternal interface, *Braz J Med Biol Res.*, 50(11), e6527.
 29. Miyashita M., Koga K., Izumi G., Sue F., Makabe T., Taguchi A, Nagai M., Urata Y., Takamura M., Harada M., Hirata T., Hirota Y., Hiraike O.W., Fujii T., Osuga Y. (2016) Effects of 1,25-Dihydroxy Vitamin D 3 on Endometriosis. *The Journal of Clinical Endocrinology and Metabolism.*, 101(6), 2371–2379.
 30. Momenimovahed Z., Taheri S., Tiznobaik A., and Salehiniya H. (2019). Do the Fertility Drugs Increase the Risk of Cancer? A Review Study. *Frontiers in endocrinology*, 10, 313.
 31. Oostingh EC, Hall J, Koster MPH, Grace B, Jauniaux E and Steegers-Theunissen RPM. (2019). The impact of maternal lifestyle factors on preconception outcomes: a systematic review of observational studies. *Reproduce Biomed Online*, 38, 77–94.
 32. Pludowski, P., Holick, M. F., Grant, W. B., Konstantynowicz, J., Mascarenhas, M. R., Haq, A., Povoroznyuk, V., Balatska, N., Barbosa, A. P., Karonova, T., Rudenka, E., Misiorowski, W., Zakharova, I., Rudenka, A., Łukaszewicz, J., Marciniowska-Suchowierska, E., Łaszczyńska, N., Abramowicz, P., Bhattoa, H. P., and Wimalawansa, S. J. (2018). Vitamin D supplementation guidelines. *The Journal of steroid biochemistry and molecular biology*, 175, 125–135.
 33. Ranjana H. (2017). Role of vitamin D in

- infertility, *Journal of Public Health Policy and Planning*, 1(1), 20.
34. Rodriguez-Purata J and Polyzos NP. (2018). The endometrium during and after ovarian hyperstimulation and the role of segmentation of infertility treatment. *Best Pract Res Clin Endocrinol Metab.*, 33(1), 61-75.
 35. Samimi M, Foroozanfard F, Amini F and Sehat M. (2017). Effect of vitamin D supplementation on unexplained recurrent spontaneous abortion: a double-blind randomized control trial. *Glob J Health Sci.*, 9(3), 95-102.
 36. Stanford JB. (2013). What is the true prevalence of infertility? *Fertil Steril.*, 99, 1201-1202.
 37. Taraborrelli S. (2015). Physiology, production, and action of progesterone. *Acta Obstet Gynecol Scand*, 11, 94:8-16.
 38. Valckx S.D.M., Pauw I., Neubourg D., Inion I., Berth M., Fransen E., Bols P.E.J. and Leroy J.L.M.R. (2012). BMI-related metabolic composition of the follicular fluid of women undergoing assisted reproductive treatment and the consequences for oocyte and embryo quality, *Human Reproduction*, 27(12), 3531–3539.
 39. Voulgaris N, Papanastasiou L, Piaditis G, Angelousi A, Kaltsas G, Mastorakos G Mastorakos G and Kassi E. (2017). Vitamin D and aspects of female fertility. *Hormones (Athens, Greece)*, 16(1), 5-21.
 40. Wasiewicz, T. Piotrowska, A, Wierzbicka, J, Slominski, A.T. and Zmijewski, M.A. (2018). Antiproliferative Activity of Non-Calcemic Vitamin D Analogs on Human Melanoma Lines in Relation to VDR and PDIA3 Receptors *Int. J. Mol. Sci.*, 19, 2583.
 41. Wasim M. (2015). Obesity and Leanness Caused by Mutations in the Leptin Gene: Already 6 Pathogenic Mutations Reported in this Gene, *J Obes Weight Loss Ther.* 5: 276.
 42. Webb AR. (2006). Who, what, where, and when-influences on cutaneous vitamin D synthesis. *Prog Biophys Mol Biol.*, 92(1), 17–25.
 43. Zhang, X., Zhou, M., Guo, Y., Song, Z. and Liu, B. (2015). 1,25-dihydroxy vitamin D (3)

Promotes High Glucose-Induced M1 Macrophage Switching to M2 via the VDR-PPARgamma Signaling Pathway. *Biomed Res Int*, 157834., 2015, Article ID 157834.

Table 1. The level of hormonal and biochemical parameters of infertile women (primary and secondary) compared with the control group.

Hormonal and biochemical parameters	Control Group Mean \pm SD	Infertility group Mean \pm SD		P-value
		Primary	Secondary	
Estrogen (E2) (pg/mL)	84.43 \pm 10.03b	53.30 \pm 9.23a	44.68 \pm 7.68a	0.01**
Progesterone (ng/mL)	11.604 \pm 3.52b	8.54 \pm 8.33a	7.86 \pm 10.51a	0.039*
FSH (mIU/mL)	8.434 \pm 2.65b	6.70 \pm 2.66a	7.25 \pm 2.96a	0.05*
LH (mIU/mL)	5.48 \pm 1.72b	7.19 \pm 3.04a	7.00 \pm 3.83a	0.025*
Total cholesterol (mg/dL)	158.85 \pm 24.93a	160.08 \pm 36.68a	157.46 \pm 23.39a	N
Triglyceride (TG) (mg/dL)	90.28 \pm 31.38a	95.50 \pm 35.84b	100.22 \pm 45.74ab	0.01**
HDL (mg/dL)	50.70 \pm 6.74a	48.40 \pm 7.72ab	46.39 \pm 8.20b	0.05*
LDL (mg/dL)	83.01 \pm 21.79b	90.58 \pm 32.71a	88.73 \pm 20.37a	0.05*
VLDL (mg/dL)	19.61 \pm 8.63a	18.94 \pm 7.57a	22.44 \pm 9.06a	N
Vit. D (ng/dL)	39.94 \pm 6.46a	11.94 \pm 5.82b	11.83 \pm 5.78b	0.001***
BMI (Kg/m ²)	25.28 \pm 0.39b	26.46 \pm 3.23b	30.25 \pm 4.54a	0.001***

*Significant differences at $P \leq 0.05$; **Significant differences at $P \leq 0.01$; ***Significant differences at $P \leq 0.001$, N=No significant differences; a, b, ab denote Duncan-test

Table 2. A comparison of the level of hormonal, biochemical parameters, and Vit. D in infertile women with different BMI

Hormonal and biochemical parameters	BMI (Kg/m ²) (Number of Women) Mean± SD				P-value
	20-24.9 (13)	25-29.9 (27)	30-34.9 (14)	35-40 (6)	
Estrogen (E2) (pg/mL)	52.4±13.4a	51.6±11.70a	46.70±18.62a	51.55±10.21a	N
Progesterone (ng/mL)	8.64±5.00a	9.27±9.65a	9.42±12.62a	9.64±8.52a	N
LH (mIU/mL)	8.65±0.72ab	6.42±1.18a	6.90±0.17a	7.14±1.65b	0.05*
FSH (mIU/mL)	5.82±1.17ab	4.70±2.67a	4.25±3.43a	6.64±3.56b	0.05 *
Total cholesterol (mg/dL)	139.52±35.65b	166.83±31.78a	158.70±16.61ab	163.5±25.19ab	0.01**
Triglyceride (TG) (mg/dL)	94.11±13.87b	100.13±21.56a	102.29±29.14a	110.50±29.72ab	0.05*
HDL (mg/dL)	43.08 ±6.06a	49.73±7.84a	48.28±9.34a	43.67±3.20a	N
LDL (mg/dL)	77.47±31.92a	95.42±28.05a	90.13±18.15a	97.73±22.56a	N
VLDL (mg/dL)	18.76±6.79a	21.66±8.55a	20.52±9.95a	22.10±7.94a	N
Vit. D (ng/dL)	11.26±3.23b	10.30±0.89a	9.75±7.52a	9.33±0.61ab	0.05*

*Significant differences at P≤0.05; **Significant differences at P≤0.01, N=No significant differences; a, b, ab denote Duncan-test.

Table 3. The correlation of vitamin D for infertile women with hormonal and biochemical parameters.

Hormonal and biochemical parameters	r-value	p-value
LH (mIU/mL)	-0.0766	0.05*
FSH (mIU/mL)	0.36975	0.003**
Progesterone (ng/mL)	0.00832	0.05*
Estrogen (E2) (pg/mL)	0.03875	0.05*
Total cholesterol (mg/dL)	0.09434	0.05*
Triglyceride (TG) (mg/dL)	-0.13496	0.03*
HDL (mg/dL)	0.19880	0.01**
LDL (mg/dL)	0.09583	0.05*
VLDL (mg/dL)	-0.14995	0.02*
BMI (Kg/m ²)	-0.04446	0.01**

*Significant differences at P≤0.05; **Significant differences at P≤0.01

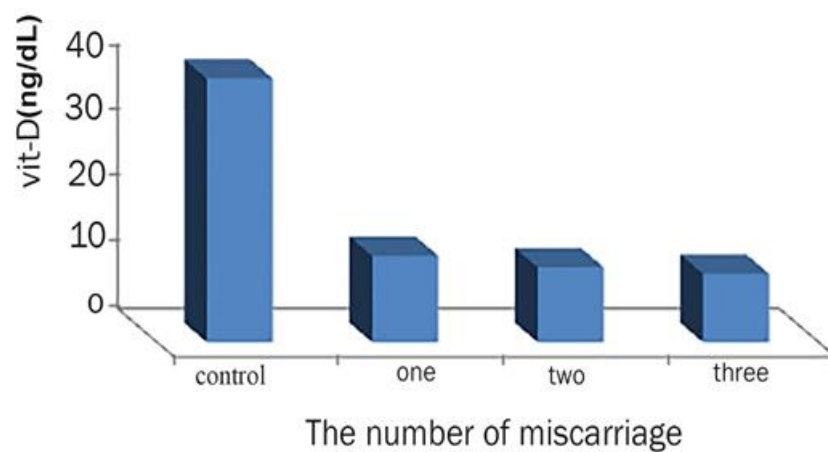


Figure 1. Number of miscarriage with Vitamin D.

DERIVATIZAÇÃO DE CLOROFILA DE FOLHAS DE PANDAN (*Pandanus amaryllifolius* Roxb.) E SUA ATIVIDADE ANTIOXIDANTE**DERIVATIZATION OF CHLOROPHYLL FROM PANDAN (*Pandanus amaryllifolius* Roxb.) LEAVES AND THEIR ANTIOXIDANT ACTIVITY****DERIVATISASI KLOOROFIL DAUN PANDAN (*Pandanus amaryllifolius* Roxb.) DAN AKTIVITAS ANTIOKSIDANNYA**

SURYANI, Chatarina Lilis^{1,2}; WAHYUNINGSIH, Tutik Dwi³; SUPRIYADI⁴; SANTOSO, Umar^{4*}

¹ Doctoral Program of Food Science, Department of Food and Agricultural Products Technology, Faculty of Agricultural Technology, Gadjah Mada University, Yogyakarta 55281, Indonesia

² Department of Food and Agricultural Products Technology, Faculty of Agroindustry, Mercuru Buana University, Yogyakarta 55753, Indonesia.

³ Department of Chemistry, Faculty of Mathematics and Natural Sciences, Gadjah Mada University, Yogyakarta 55281, Indonesia.

⁴ Department of Food and Agricultural Products Technology, Faculty of Agricultural Technology, Gadjah Mada University, Yogyakarta 55281, Indonesia.

*Corresponding author
e-mail: umar_s@ugm.ac.id

Received 09 July 2020; received in revised form 09 September 2020; accepted 30 October 2020

RESUMO

A clorofila é um corante natural com atividade antioxidante. Durante o processo de extração e processamento de alimentos, a clorofila é facilmente degradada e derivatizada. O processo de derivatização resulta em mudanças na estrutura química da clorofila que podem resultar em uma mudança na cor e na sua atividade antioxidante. Os outros compostos secundários extraídos podem afetar sua atividade antioxidante. Este estudo teve como objetivo identificar as alterações na estrutura química da clorofila extraída das folhas de pandan (*Pandanus amaryllifolius* Roxb) afetadas pelo processo de derivatização e avaliar a atividade antioxidante dos extratos e frações de clorofila e seus derivados. A clorofila foi extraída das folhas de pandan com acetona, derivatizada e purificada por fracionamento por cromatografia em coluna. O extrato de clorofila e seus derivados foram analisados quanto aos teores de carotenóides totais, fenólicos totais e flavonóides. A atividade antioxidante do extrato e da fração foi medida pela inibição da peroxidação do ácido linoléico, atividade sequestrante de radical 2,2-difenil-1-picrilhidrazil (DPPH), capacidade de redução férrica / poder antioxidante (FRAP) e ensaio quelante de metais. Com base nos espectros de FTIR e MS/MS, foi observado que os primeiros derivados eram feofitina e clorofilida, enquanto o segundo derivado era feoforbida. Os outros compostos extraídos, incluindo compostos fenólicos, flavonóides e carotenóides, podem aumentar a atividade antioxidante dos derivados da clorofila. A taxa de inibição da peroxidação do ácido linoléico pela clorofila, clorofilida e extrato de feoforbida não foi significativamente diferente do BHT, onde o extrato de feofitina foi menor. A atividade de eliminação de radicais do ensaio DPPH e FRAP mostrou que os extratos de clorofila e clorofilida exibiram a maior atividade, seguidos por feofitina e feoforbideo. Enquanto isso, o ensaio quelante de metal mostrou que a fração clorofilida exibiu a menor atividade. Portanto, a atividade antioxidante dos primeiros derivados da clorofila foi maior do que os segundos derivados. Em geral, o extrato de clorofila e seus derivados exibiram maior atividade antioxidante do que sua fração.

Palavras-chave: Clorofila, *Pandanus amaryllifolius* Roxb, atividade antioxidante.

ABSTRACT

Chlorophyll is a natural coloring agent that has antioxidant activity. During the extraction and food processing process, chlorophyll is easily degraded and derivatized. The derivatization process results in changes in the chemical structure of chlorophyll which can result in a change in color and its antioxidant activity. The other extracted minor compounds can affect its antioxidant activity. This study aimed to identify the chemical structure

changes of chlorophyll extracted from pandan (*Pandanus amaryllifolius* Roxb) leaves as affected by the derivatization process and evaluate the antioxidant activity of the extracts and fractions of chlorophyll and its derivatives. Chlorophyll was extracted from pandan leaves with acetone, derivatized, and then purified by fractionation using column chromatography. Chlorophyll extract and its derivatives were analyzed for total carotenoid, total phenolic, and flavonoid contents. The antioxidant activity of extract and fraction was measured by the inhibition of peroxidation of linoleic acid, radical scavenging activity of 2,2-diphenyl-1-picrylhydrazyl (DPPH), ferric reducing/ antioxidant power (FRAP) ability, and metal chelating assay. Based on the FTIR and MS/MS spectra, it was observed that the first derivatives were pheophytin and chlorophyllide, while the second derivative was pheophorbide. The other extracted compounds, including phenolic compounds, flavonoids, and carotenoids, might enhance the antioxidant activity of the chlorophyll derivatives. The inhibition rate of linoleic acid peroxidation by chlorophyll, chlorophyllide, and pheophorbide extract was not significantly different from BHT, where pheophytin extract was lower. The radical scavenging activity of DPPH and FRAP assay showed that chlorophyll and chlorophyllide extracts exhibited higher activity, followed by pheophytin and pheophorbide. Meanwhile, the metal chelating assay showed that chlorophyllide fraction exhibited the lowest activity. Therefore, the antioxidant activity of the first derivatives of chlorophyll was higher than the second derivatives. In general, the extract of chlorophyll and its derivatives exhibited higher antioxidant activity than that of their fraction.

Keywords: *Chlorophyll, Pandanus amaryllifolius* Roxb, antioxidant activity.

ABSTRAK

Klorofil merupakan pewarna alami yang memiliki aktivitas antioksidan. Selama proses ekstraksi dan pengolahan makanan, klorofil mudah terdegradasi dan terderivatisasi. Proses derivatisasi mengakibatkan perubahan struktur kimiawi klorofil sehingga terjadi perubahan warna dan aktivitas antioksidannya. Keberadaan senyawa minor terekstrak juga dapat mempengaruhi aktivitas antioksidannya. Penelitian ini bertujuan untuk mengidentifikasi perubahan struktur kimia klorofil daun pandan (*Pandanus amaryllifolius* Roxb) akibat proses derivatisasi dan mengevaluasi aktivitas antioksidan ekstrak dan fraksi klorofil dan turunannya. Klorofil diekstraks dari daun pandan dengan aseton, diderivatisasi, kemudian dimurnikan dengan cara fraksinasi menggunakan kromatografi kolom. Ekstrak klorofil dan turunannya dianalisis kandungan karotenoid, fenolik dan flavonoid total. Aktivitas antioksidan diukur dengan menggunakan metode penghambatan peroksidasi asam linoleat, daya tangkap radikal 2,2-diphenyl-1-picryl hydrazyl (DPPH), *Ferric reducing/antioxidant power* (FRAP) ability dan uji aktivitas mengkhelat logam. Berdasarkan spektra FTIR dan MS/MS diketahui bahwa turunan pertama klorofil adalah feofitin dan klorofilid, sedangkan turunan kedua adalah feoforbid. Keberadaan bahan ikutan seperti fenolik, flavonoid dan karotenoid meningkatkan aktivitas antioksidan ekstrak klorofil dan turunannya. Kemampuan menghambat peroksidasi asam linoleat ekstrak klorofil, klorofilid, dan feoforbid tidak berbeda dengan BHT, sedangkan ekstrak feofitin lebih rendah. Hasil uji daya tangkap radikal DPPH dan FRAP menunjukkan bahwa ekstrak klorofil dan klorofilid mempunyai aktivitas yang lebih tinggi diikuti dengan feofitin dan feoforbid. Sedangkan hasil uji mengkhelat logam menunjukkan bahwa fraksi klorofilid mempunyai aktivitas mengkhelat logam yang paling rendah. Oleh karena itu dapat disimpulkan bahwa aktivitas antioksidan turunan pertama klorofil lebih tinggi dibanding turunan kedua. Secara umum ekstrak klorofil dan turunannya mempunyai aktivitas antioksidan yang lebih tinggi dibanding masing-masing fraksinya.

Kata kunci : *Klorofil, Pandanus amaryllifolius* Roxb., aktivitas antioksidan

1. INTRODUCTION:

Currently, the use of natural food colorants is increasing because synthetic colorants in food can cause negative health effects (El-Wahab and Moram, 2012; Dafallah *et al.*, 2015). One of the natural food colorants is chlorophyll. Chlorophylls are chlorin-type tetrapyrrole with a coplanar system conjugated double bonds that form an aromatic structure with the delocalization of electron density in π -orbitals. In general, chlorophylls bind magnesium as the central metal ion and a phytol (C₂₀) esterified with the propionic acid moiety at C₁₇, although there are exceptions to these characteristics. Structurally, they differ on the side-chain substituent at C₇, a methyl group in

the *a*-series and a formyl group in the *b*-series. Chlorophyll *a* (C₅₅H₇₂O₅N₄Mg) is found in all photosynthetic organisms, except some groups of bacteria. Chlorophyll *b* (C₅₅H₇₀O₆N₄Mg) is present in all higher plants and algae of the divisions (Roca *et al.*, 2016).

As a food coloring agent, chlorophyll has an advantage because it has antioxidant activity. Chlorophyll can prevent autoxidation of vegetable oils stored in the dark. Chlorophyll can donate hydrogen ions to break the chain reaction of radical formation during lipid oxidation (Endo *et al.*, 1985a; 1985b). Meanwhile, Cahyana *et al.* (1992) stated that π -cation radicals can donate electrons to break the chain reaction during the oxidation

process. Chlorophyll can also capture free radicals (Lanfer-Marquez *et al.*, 2005; Ferruzzi *et al.*, 2002). Free radicals result from initial lipid oxidation, which has roles in the lipid oxidation chain reaction. If the numbers of free radicals are reducing, the process of lipid oxidation will be reduced too.

In the preparation of chlorophyll as a coloring agent, the chlorophyll is extracted from its source. Other compounds, including flavor components, carotenoids, phenolic compounds, and flavonoids, are also extracted during the extraction process. Various research results show that besides containing chlorophyll, leaves also contain carotenoid, phenolic, and flavonoid compounds (Fasakin *et al.*, 2011; Aryal *et al.*, 2019). Fasakin *et al.* (2011) showed that the phenolic component was soluble in acetone, which is one of the chlorophyll solvents. These substances are expected to enhance the stability of chlorophyll and its activity as an antioxidant. Kim *et al.* (2012) stated that phenolic compounds are capable of inhibiting the photooxidation reaction due to the chlorophyll photosensitizer. Chlorophyll is a pigment that functions to capture light energy during the photosynthesis process. In the use of chlorophyll as food coloring, it is impossible to be free from light so that chlorophyll can act as a sensitizer so that singlet oxygen can be formed. B-carotene compounds can reduce the lipid oxidation process because it can capture singlet oxygen (Lee and Min, 1988) and scavenge free radicals (Lee *et al.*, 2003). Meanwhile, flavonoids should protect lipid from light-induced quality deterioration through deactivation of (triplet-) excited states of chlorophyll, quenching of singlet oxygen, and scavenging of radicals (Huvaere and Skibsted, 2014).

However, chlorophyll is easily damaged by heat, light, acid, and base, leading to its derivatives. Roca *et al.* (2016) explained that four chemical modifications could occur during the storage and cooking process, which resulted in the formation of chlorophyll derivative compounds. The first is the pheophytinization reaction, where the central atom of magnesium of tetrapyrrole replaces with two hydrogen atoms due to acidic conditions or heat treatment. This reaction causes a brownish color change. If this reaction starts with chlorophyll, it will form pheophytin. When starting from chlorophyllide, it will form pheophorbide reaction de-esterification of the phytol branched-chain, which produces components without changing color due to enzymatic reactions by the enzyme chlorophyllase or due to alkaline conditions. If the reaction starts with chlorophyll, a

chlorophyllide compound will be formed, whereas if it starts with pheophytin, a pheophorbide will be formed. The third reaction is a reaction that occurs due to a very high temperature. It induces a loss of the carboxymethoxy C-13², which produces pyro derivatives, most of which are formed pyropheophytin and pyropheophorbide than pyrochlorophyll. The last reaction is under medium temperature conditions, which result in the formation of epimers at C-13² atoms from natural chlorophyll.

The changes in the chemical properties of chlorophyll may affect its antioxidative properties. Lanfer-Marquez *et al.* (2005) examined the antioxidant activity of chlorophyll and its derivatives. The derivatization process was carried out on spinach leaf chlorophyll. The results showed that the ability to inhibit β -carotene bleaching from pheophorbide b was higher than pheophorbide a, pheophytin, and chlorophyll, which led to a functional role of the aldehyde group. Meanwhile, the DPPH radical scavenging assay spinach leaf chlorophyll was higher than pheophytin (Kang *et al.*, 2018). Ferruzzi *et al.* (2002) stated that the chlorophyll a derivative has a more effective DPPH radical scavenging power than the chlorophyll b derivative, and pheophorbide derivative has the same ability as chlorophyll a. It was further stated that metal-free derivatives such as chlorine, pheophytins, and pyropheophytins showed lower antiradical capacity than metal derivatives such as Mg-chlorophyll, Zn-pheophytins, Zn-pyropheophytins, Cu-pheophytin a, and Cu-chlorophyllins.

It can be seen that the results of the analysis of the antioxidant activity of chlorophyll and its derivatives differ between methods of measuring antioxidant activity. The mechanisms of the antioxidants are based on the fact they slow down the oxidation rates of foods by a combination of scavenging free radicals, chelating prooxidative metals, quenching singlet oxygen and photosensitizers, and inactivating lipoxygenase (Choe and Min, 2009). In this study, various methods of measuring antioxidant activity were used, including the ability to inhibit the oxidation of linoleic acid with the ferric thiocyanate (FTC) method, the measurement of the free radical scavenging capacity of 2,2-diphenyl-1-picrylhydrazyl (DPPH), the ability of antioxidants to reduce ferric ions by using The ferric reducing/antioxidant power (FRAP) method, the ability to capture metal ions which can act as prooxidants with the chelation of metal ion assay. In contrast, the ability to capture singlet oxygen

and lipoxygenase inactivation will be discussed in the next publish.

Fragrant pandanus (pandan) from *Pandanus amaryllifolius* Roxb. plant (Figure 1) is a leaf that is commonly used as a food colorant in Indonesia. Pandan leaves have advantages than other leaves because it has a specific scent with a very low odor threshold of 0.1 µg/kg (Wakte *et al.*, 2016) and a relatively high phenolic and flavonoid content (Suryani *et al.*, 2017). It was expected that the existence of phenolic, flavonoids, and carotenoids can increase the total antioxidant activity of the chlorophyll extracted from pandan leaves.

Therefore, this study aimed to identify the chemical structure changes of chlorophyll extracted from pandan (*Pandanus amaryllifolius* Roxb) leaves as affected by the derivatization process and to evaluate the antioxidant activity of the extract and fractions of chlorophyll and its derivatives.

2. MATERIALS AND METHODS:

2.1. Materials

Pandanus leaves were obtained from plants grown in the district of Bantul, Indonesia. This study used mature leaves or leaves at the section numbers of 13-18. The solvents and chemicals used in the extraction of chlorophyll, derivatization, and fractionation by column chromatography were acetone, hexane, petroleum ether, HCl, NaOH and silica gel (silica gel 60, Merck, 0063-0200 mm), all were laboratory grade, butylated hydroxytoluene (BHT), ascorbic acid, and ethylene diamine tetraacetate (EDTA) were from Sigma-Aldrich (Germany). The process of extraction, derivatization and analysis was conducted in a room with controlled lighting.

2.2. Preparation of chlorophyll and its derivatives extract

2.2.1 Preparation of chlorophyll extract

The pandan leaves were taken from the tree in the morning and wrapped with black plastic, then put into a cooling box while being transported to the laboratory. The extraction of chlorophyll from pandan leaves followed the Lanfer-Marquez *et al.* (2005) method. Fresh pandan leaves were cut crosswise at 1-2 cm, weighed as much as 30 g, and dry-milled for 3 min. The slurry (25 g) was put in a 500 mL Erlenmeyer,

mixed with acetone in the ratio 1:5 (w/v), and stirred with a magnetic stirrer for 15 min. A cloth filter filtered the slurry, and the pulp was squeezed with a mini screw press. The extract was re-filtered with Whatman filter paper number 1. The chlorophyll extract was separated using petroleum ether and cold distilled water with a volume ratio of extracts: petroleum ether: distilled water (80/60/30). The mixture was put into a separating funnel, then shaken and separated. The chlorophyll extract in petroleum ether was stored in dark bottles prior to analysis. The total chlorophyll (Chl) content of the extract was determined by the method described by Vernon (1960) using Eq. 1 with A_{645} and A_{663} showed absorbance values of extract at wavelengths of 645 and 663 nm, and DF dilution factor, respectively.

$$\text{Chl (mg/L)} = (20.8A_{645} + 8.02A_{663}) \times \text{DF} \quad (\text{Eq. 1})$$

2.2.2 Preparation of pheophytin extract

Preparation of pheophytin extracts was performed according to the Ngo and Zhao (2007) method. Chlorophyll extract in petroleum ether (30 mL) was slowly added with 10 mL of acetone containing 15 µL of concentrated HCl and stirred to form a brownish yellow-olive oil-like color. Afterward, the HCl excess was removed by washing it with cold distilled water (extract: distilled water = 30:30) and transferred into a separating funnel. The water-acetone layer was separated from petroleum ether containing pheophytin.

The content of pheophytin (Pht) was determined by the Vernon (1960) method as in Eq. 2 with A_{666} , and A_{655} showed absorbance values of the extract at wavelengths of 666 and 655 nm, respectively.

$$\text{Pht(mg/L)} = (6.75A_{666} + 26.03A_{655}) \times \text{DF} \quad (\text{Eq. 2})$$

2.2.3 Preparation of chlorophyllide extracts

Chlorophyllide extract was prepared using the Van Breemen *et al.* (1991) method through an enzymatic process. A slurry (25 g) of fresh pandan leaves was stored in the Erlenmeyer and incubated at 40°C for 2 h in the dark to activate the enzyme chlorophyllase. Chlorophyllide was then extracted with acetone (1:6 w/v), stirred for 15 min, and filtered by a cloth filter. The pulp was squeezed with a mini screw press. The extract was re-filtered with Whatman filter paper number 1. Chlorophyllide extract was purified with hexane in a volume

ratio of chlorophyllide extract: hexane = 150:30. After being stirring with a magnetic stirrer for 2 min, the mixture was separated using a separating funnel. The hexane layer was separated from the chlorophyllide extract. The chlorophyllide extract in acetone was stored in the dark bottles and at cold temperatures before being used. The content of chlorophyllide (Chd) was determined by using the method described by Yang *et al.* (1998) using Eq. 3 with A_{667} , and A_{650} showed absorbance values of extract at wavelengths of 667 and 650 nm, respectively.

$$\text{Chd (mg/L)} = (8.22A_{667} + 13.05A_{650}) \times \text{DF} \quad (\text{Eq. 3})$$

2.2.4 Preparation of pheophorbide extract

The preparation of the pheophorbide extract was in accordance with the Van Breemen *et al.* (1991) method. Chlorophyllide extract in 60 mL of acetone was added with 20 mL acetone containing 15 μL of concentrated HCl dropwise while being stirred with a magnetic stirrer for 10 min to form a blackish color. The pheophorbide extract was concentrated by being blow with nitrogen gas and stored in dark bottles and at a cold temperature before being used. The pheophorbide (Phb) was determined by the total pheopigment content (Arar, 1997) as in Eq. 4. A_{665a} showed the absorbance value at a wavelength of 665 nm from the resulting pheophorbide extract. In comparison, A_{665b} showed the absorbance value at a wavelength of 665 nm from the resulting chlorophyllide extract before conversion into pheophorbide derivatives.

$$\text{Phb(mg/L)} = 26.7[1.7 \times (A_{665a} - A_{665b})] \times \text{DF} \quad (\text{Eq. 4})$$

The content of other extracted compounds from the chlorophyll extract and its derivatives was analyzed for the total carotenoids (Hendry and Grime, 1993), total phenolic by Folin-Ciocalteu method total flavonoid (Chandra *et al.*, 2014). Total phenolic contents in the pandan leaf extracts in terms of gallic acid equivalent (mg EGA/L of extract) and total flavonoid in terms of quercetin equivalent (mg QE/L of extract).

2.3. Chlorophyll and its derivatives fractionation

The fractionation of chlorophyll and its derivatives was carried out using the method of Milenković *et al.* (2012). The fractionation was conducted by column chromatography on silica gel with an eluent mixture of n-hexane/acetone in a ratio of 1:0 to 1:5. Preliminary experiments

revealed that chlorophyll fractions were obtained in the eluent mixture ratio of 1:0.1, pheophytin fraction of 1:1, chlorophyllide fraction of 1:3.3, and pheophorbide fraction of 1:5. Chlorophyll and its derivative fractions were stored in dark bottles at a low temperature before being used. Analysis of the chlorophyll and its derivative content was carried out in Eq. 1-4.

2.4. Identification of chlorophyll and its derivatives

2.4.1 Fourier Transform Infrared (FTIR) spectral analysis

Spectra analysis of fractions of chlorophyll and its derivatives was carried out using FTIR iS 10 (Thermo Fisher Scientific). FTIR analysis was carried out at room temperature with a concentration of chlorophyll and its derivatives fraction of 200 mg/L with acetone and wavelength of 4000-400 cm^{-1} .

2.4.2 MS/MS spectral analysis

Chemical structure changes were identified by using mass spectrometry (MS/MS) Triple Q (quadrupole) (TSQ Quantum Access Max from Thermo Finnigan) with a source of ionization Electro Spray Ionization (ESI), controlled by TSQ Tune software, and operated by positive mode. The evaporation temperature was set at 50°C, the capillary temperature was 270°C, the spray voltage was 3000 volts, and 5 unit gas sheets were used. The operating condition of mass spectrometry was at a low flow with a flow rate of 5 $\mu\text{L}/\text{min}$.

2.5 Antioxidant activity of the chlorophyll and its derivatives

2.5.1 Determination of inhibition of linoleic acid oxidation

The determination of antioxidant activity in a linoleic acid emulsion system was measured by using the FTC method (Mathew and Abraham, 2006). A 4.0 mL extract or fraction of chlorophyll or its derivatives at a concentration of 100 ppm was mixed with linoleic acid emulsion. The linoleic acid emulsion was prepared as follows: 1.0 mL of 2.5% linoleic acid was mixed with 0.1 mL of Tween 20, sample 4.0 mL and potassium phosphate buffer (0.02 M) to reach a volume of 10.0 mL. The mixture was incubated at $37 \pm 1^\circ\text{C}$ in a dark room. A 0.1 mL aliquot was taken daily during 6 days of incubation. The degree of oxidation was measured by adding 5.0 mL of ethanol (75% v/v), 0.1 mL of ammonium thiocyanate (30% w/v), and 0.1 mL of FeCl_2 (0.02 M in 3.5% HCl v/v), and then

homogenized. The absorbance was measured at 500 nm with triplicate. Solution without extract was used as a blank solution, while BHT at 100 ppm concentration was used as a comparison. The percentage inhibition of lipid peroxidation was determined by following Eq. 5 with A_0 absorbance control and A_1 absorbance of the sample at a wavelength of 500 nm.

$$\text{LPI (\%)} = 100 - [(A_1 / A_0) \times 100] \quad (\text{Eq. 5})$$

2.5.2 Determination of radical scavenging activity

DPPH free radical scavenging activity was determined by the Xu and Chang (2007) method. The sample and BHT concentrations were 100 ppm. A 0.2 mL of the extract or fraction of chlorophyll and its derivatives was added to 3.8 mL of 0.1 mM DPPH solution in methanol and mixed via vortex for 1 min. The filtrate was incubated in a dark room at room temperature for 30 min. The control was made by using methanol as a substitute sample and BHT. After incubation, the absorbance of the filtrate was read with UV-Vis spectrophotometry at λ 515 nm. The data obtained was A_0 : absorbance at 515 λ of DPPH without sample, A_s : absorbance at λ 515 nm of samples with DPPH, and A_b : absorbance at λ 515 nm of the sample without DPPH. Radical Scavenging Activity (RSA) was expressed in percent (%). The RSA value showed the ability of the samples in DPPH discoloration and was calculated by the Eq. 6 (Kang *et al.*, 2018).

$$\text{RSA(\%)} = [(A_0 - (A_s - A_b)) / A_0] \times 100 \quad (\text{Eq. 6})$$

2.5.3 Ferric Reducing/Antioxidant Power (FRAP) ability

The determination of antioxidant activity with the FRAP method was carried out as described by Benzie and Devaki (2018). FRAP reagent was prepared by mixing 10 mL of acetate buffer (300 mM, pH 3.6), 1 mL of tripyridyltriazine (TPTZ) (10 mM in 40 mM HCl), and 1 mL of $\text{FeCl}_3 \cdot 6\text{H}_2\text{O}$ (200 mM). A FRAP reagent (3 mL) was put in a test tube and heated at 37 °C for 10 min, then added with extracts or fractions of chlorophyll and its derivatives (100 μL) (extracts or fractions at concentrations of 50 ppm) and 300 μL of distilled water, mixed for 1 min and allowed to stand for 4 min. Then, the absorbance was measured at a λ 593 nm. Ascorbic acid was used as a comparison at the same concentration. The reducing ability (mol/L Fe^{2+}) was calculated based on the standard curve $\text{FeSO}_4 \cdot 7\text{H}_2\text{O}$ (concentration range from 0 to 500 mol/L).

2.5.4 Chelation of metal ion assay

The chelating ability of cation Fe (II) was determined by Dinis *et al.* method (Mathew and Abraham, 2006). It used a sample with a concentration of extract or fractions of 5 ppm, aimed at reducing the interference color of the sample. Extracts or fractions of chlorophyll and its derivatives (3 mL) with 5 ppm concentration were added to 1 mM FeCl_2 (0.3 mL), then incubated for 30 min at room temperature. The reaction was initiated by the addition of 1 mM ferrozine (0.3 mL). Once the mixture reached equilibrium (10 min), the absorbance was measured at 562 nm. EDTA at the same concentration was used for comparison. The percentage inhibition of ferrozine- Fe^{2+} complex formation was determined using Eq. 7 with A_0 absorbance control and A_1 absorbance of the sample at a wavelength of 562 nm.

$$\text{Chelating effect (\%)} = \left[1 - \frac{A_1}{A_0} \right] \times 100 \quad (\text{Eq. 7})$$

3. RESULTS AND DISCUSSION:

3.1. Structural analysis of chlorophyll and its derivatives

3.1.1 FTIR spectral analysis

The FTIR spectra of the chlorophyll and its derivatives fractions in acetone are shown in Figure 2. The FTIR spectra showed significant differences between chlorophyll compared to its derivatives. The spectra of chlorophyll were characterized primarily by the presence of phytol group at a wavelength of 2922 cm^{-1} and in pheophytin that detected the presence of the phytol group. Pheophytin was also detected in the spectra peak at a wavelength of 3392 cm^{-1} , indicating the presence of the N-H bond. The existence of the N-H bond on pheophytin and pheophorbide derivatives indicated that the derivatization with acid caused Mg^{2+} ions to be released and replaced by two H^+ ions.

Chlorophyllide and pheophorbide compound were characterized mainly by the loss of the phytol group on the spectra indicated by the loss of the peak at a wavelength of 2922 cm^{-1} , and the appearance of a new peak at a wavelength of 3318 cm^{-1} , indicating the presence of the O-H group due to the release of phytol. In the pheophorbide spectra, a peak was detected at a wavelength of 3392 cm^{-1} , wherein chlorophyllide was invisible. Pheophorbide fractions were detected on the peak at a wavelength of 3392 cm^{-1} .

¹, indicating the presence of ion H, which replaced Mg²⁺ ions. Pheophorbide has the simplest structure, shown by the lowest number of absorbance peaks that were related to the lowest number of the group. This was in accordance with the pheophorbide structure (Figure 3), which showed that all groups in R2 and R3 were the H ion and the R4 was still bonding -CO₂CH₃ group (Roca *et al.*, 2016).

3.1.2 MS/MS spectral analysis

The result of MS/MS analysis of chlorophyll fragmentation is shown in Figure 4 and Table 1. Based on the chlorophyll structure (Figure 3) and the spectra of ions [M⁺] of chlorophyll and its derivatives, it can be seen the possibility of compounds in each fraction and its results fragmentation. There were two types of chlorophyll compounds in the chlorophyll fraction of the pandan leaf: chlorophyll *a* and *b*. The chlorophyll *a* with a molecular weight (m/z) of 892.680 was fragmented with a loss of the phytol group (R3: -C₂₀H₃₈) and subsequent ester keto group (R4: -CO₂CH₃). Chlorophyll *a* could also be fragmented with the loss of Mg²⁺ ions (R2) and then bound two H⁺ ions, which was the pheophytin *a*. The fraction of chlorophyll was also detected chlorophyll *b* having a molecular weight (m/z) of 906.908. Chlorophyll *b* could be fragmented, indicated by the loss of the phytol group or the keto ester group (R4: -CO₂CH₃).

The spectra of the pheophytin fraction indicated that pheophytin *a* with a molecular weight of 870.569 underwent fragmentation with the loss of the phytol group and keto ester group (R4:-CO₂CH₃) (Table 1). In this study, pheophytin *b* was undetectable, and this is consistent with the results of chlorophyll *b* fragmentation, which did not indicate the loss of Mg²⁺ ions. Similarly, in the chlorophyllide fraction, chlorophyllide *a* with a molecular weight of 614.559 was detected, but chlorophyllide *b* was undetectable. Unlike pheophytin and chlorophyllide, the pheophorbide fragmentation produced pheophorbide *a* and *b* with molecular weights of 592.865 and 606.670, respectively. This fragmentation is indicated by the loss of the keto ester group (R4:-CO₂CH₃). This is consistent with the research reported by Zvezdanovic *et al.* (2014), which showed that chlorophyll fragmentation from spinach leaves did not yield pheophytin *b*, although pheophorbide *b* was detected in pheophorbide derivative.

Based on the data in Table 1, it could be concluded that the derivatization of chlorophyll produced the first derivative of chlorophyll, which

was pheophytin *a*, while enzymatic derivatization produced chlorophyllide *a*, but chlorophyllide *b* was undetectable. The derivatization of chlorophyllide with acidic reaction produced the second derivative, i.e. pheophorbide *a* and *b*. This was following the scheme of the chlorophyll derivatization explained by Simpson *et al.* (2012) and Roca *et al.* (2016).

3.2. The content of carotenoids, phenolics, and flavonoids

The results revealed that chlorophyll derivatization also affected the total carotenoid content, total phenolic content and total flavonoid content. Figure 5 shows that the total carotenoid content in chlorophyll extracts was the highest, followed by pheophorbide extract, and the lowest were in chlorophyllide and pheophytin extract. Carotenoid is soluble in non-polar solvents and, thus, is largely lost during refining chlorophyllide and pheophytin extract. In contrast, the total phenolic and flavonoid content was higher in chlorophyllide and pheophytin extract than in others, allegedly due to a decrease in the proportion of carotenoids and chlorophyll in both types of extracts as they were dissolved in hexane.

3.3. Antioxidant activity

3.3.1. The inhibitory activity of lipid peroxidation

The inhibitory activity of lipid peroxidation of chlorophyll extract and its derivatives from pandan leaves is presented in Figure 6. Based on the result of regression analysis, it is known that the slope of BHT was 7.32, chlorophyll extract was 7.67, pheophytin extract was 6.35, chlorophyllide extract was 7.66, and pheophorbide extract was 7.65. The slope of the chlorophyll, chlorophyllide and pheophorbide were not significantly different from the slope of BHT, whereas the slope of pheophytin is significantly different (*P* < 0.05). It shows that the inhibition rate of lipid peroxidation by extract of chlorophyll, chlorophyllide and pheophorbide was not significantly different from that BHT, whereas the pheophytin was lower. According to Endo *et al.* (1985b), chlorophyll is more effective to inhibit lipid peroxidation than pheophytin, because the presence of Mg may activate the antioxidant activity of chlorophyll.

Furthermore, Lanfer-Marquez *et al.* (2005) reported that the high antioxidant activity of pheophorbide was related to the lowest degree of decolorization. However, in this study, the effectiveness of linoleic acid peroxidation inhibition is allegedly associated with higher levels of total

phenolic, flavonoid, and carotenoid content (Cervantes-Paz *et al.*, 2014; Sarker *et al.*, 2018; Zeb and Imran, 2019). This was supported by results of the correlation, which indicated that the inhibition of lipid peroxidation was highly correlated with the levels of total phenolic content ($r = 0.96$, $P < 0.01$) and the levels of total carotenoid ($r = 0.98$, $P < 0.01$) but negatively correlated with total flavonoid ($r = -0.533$, $P < 0.05$). Chlorophyllide and pheophorbide had a higher total phenolic and total flavonoid content than chlorophyll and pheophytin extract, while chlorophyll extract had the highest carotenoid content (Figure 5). The content of total phenolic and flavonoid was one of the advantages of pandan leaves as a source of chlorophyll over other types of leaves as a food colorant. These results agree with previous studies that showed that the phenolic and flavonoid component of pandan leaves was able to inhibit the formation of lipid peroxides (Suryani *et al.*, 2017).

3.3.2. DPPH radical scavenging activity

DPPH radical scavenging activity was one of the most widely used methods of measuring the antioxidant activity because it was relatively simple and rapid. The DPPH method described by Xu and Chang (2007) was chosen because the sample volume is much smaller than the DPPH solution; thus, the effect of the color of chlorophyll and its derivatives could be minimized. The evaluation of DPPH radical scavenging activity by chlorophyll extracts or fractions and its derivatives is presented in Figure 7. It is known that chlorophyll and its derivatives exhibited antioxidant activity that varied within a range between 36.98-96.78% compared to BHT. According to Endo *et al.* (1985b), the antioxidant activity of chlorophyll and its derivatives is mainly affected by the presence of porphyrin ring, not because of phytol, metal, and isocyclic rings. The formation of n-cation porphyrin compound during oxidation was able to reduce free radicals, including DPPH.

The results showed that the DPPH radical scavenging activity of extracts and fractions of chlorophyll and its derivatives was in the order as follows: chlorophyll extract = chlorophyllide extract > chlorophyll fraction > chlorophyllide fractions and pheophorbide extracts > pheophytin extract > pheophytin fraction > pheophorbide fraction. These results were consistent with the studies of Ferruzzi *et al.* (2002) and Kang *et al.* (2018). Furthermore, Ferruzzi *et al.* (2002) reported that metal-free derivatives such as pheophytin had lower antiradical capacity than chlorophyll

derivatives. The DPPH radical scavenging activity of chlorophyll, pheophytin, chlorophyllide, and pheophorbide extracts were higher than that of the fractions. This might be because of the presence of other antioxidant compounds, such as phenolic and carotenoids. Similar results were toward in the case of antioxidant activity by the FTC method.

3.3.3. Ferric Reducing/ Antioxidant Power (FRAP)

The FRAP method was chosen because it is a direct method for analyzing the combined total antioxidant activity and the ability to reduce (electron donor) antioxidants in the sample simultaneously (Benzie and Devaki, 2018). Figure 8 shows that the extract and fractions of chlorophyll and its derivatives could reduce between 7.26 to 100% compared to ascorbic acid. The FRAP value of ascorbic acid was 592.13 $\mu\text{mol/L Fe}^{2+}$. Similar to the result of DPPH radical scavenging activity, FRAP assay results indicated that the chlorophyll and chlorophyllide extract had a higher reducing ability than chlorophyll fractions. The lowest FRAP values were the extract and fraction of pheophytin and pheophorbide. The high FRAP value of chlorophyll and chlorophyllide extract can be associated with the high total phenolic content.

Chlorophyllide fraction had the highest reducing ability than any other fraction and was not different from ascorbic acid. Chlorophyllide is a derivative of chlorophyll with loss of the phytol group, chlorophyllide is more hydrophilic similar to ascorbic acid. Pheophorbide fraction had the lowest FRAP value. The reducing agent (electron donor) is part of a redox couple with a redox potential that is relatively lower under reaction conditions (Halliwell, 2012). Ohashi *et al.* (2008) stated that oxidation potential was influenced by the inductive effect of substituent groups on the π -electron conjugated system in the macrocycle. Furthermore, Kobayashi *et al.* (2007) stated that the oxidation potential rank was chlorophyll *b* > chlorophyll *d* > chlorophyll *a*, while pheophytin *a*, *b*, and *d* had a higher oxidation potential than chlorophyll. This is because derivatization decreased the electron density in the π -system due to the replacement of magnesium with hydrogen, which was more electronegative.

3.3.4. Metal chelating activity

The results of the evaluation of metal chelating activity are presented in Figure 9. Metal chelating activity, was in the order as follows: chlorophyll fraction extract = pheophytin extract > chlorophyll and chlorophyllide extract > pheophorbide extract > pheophytin and

pheophorbide fraction > chlorophyllide fraction. Chlorophyll fraction had the highest metal chelating activity, while chlorophyllide fraction the lowest. Metal chelating activity of chlorophyll and its derivatives was affected by a lone pair electron from nitrogen and oxygen atoms and bound with empty orbitals of the metal cations. Nitrogen and oxygen atoms are very effective as sources of a free electron pair that played a role as a chelating agent (Hargreaves, 2003). In the chlorophyll molecule, the free electron pair was bound to Mg^{2+} , but Fe^{2+} had a higher reactivity than Mg^{2+} (Cheng *et al.*, 1992), such that Mg^{2+} was replaced by Fe^{2+} and was indicated to have a high metal chelating ability. Pheophytin, pheophorbide, and chlorophyllide extracts had also a metal chelating ability that was higher than its fractions. The metal chelating ability was also related to the flavonoid content of phenolic compounds in the extract. Phenolic and flavonoid compounds can chelation Fe^{2+} (Niciforovic *et al.*, 2010; Benjakul *et al.*, 2014; Taroreh *et al.*, 2015) because they have the hydroxyl and carboxyl group (Cherrak *et al.*, 2016).

Contrary to the antioxidant activity evaluation by DPPH radical scavenging activity, FRAP and FTC methods showed that chlorophyllide had high antioxidant activity, the metal chelating ability chlorophyllide fraction was the lowest. Chlorophyllide is a chlorophyll derivative that loses the phytol group so that it becomes more polar. These results agreed to Shim (2012) that chlorophyll had a higher ability to chelate metal than its more polar derivatives. Besides, to chelate Fe^{2+} ions, chlorophyllide releases Mg^{2+} ions into pheophorbide (Suzuki *et al.*, 2014). This reaction required higher energy or heat (Roca *et al.*, 2016) or an acidic condition (Simpson *et al.*, 2012).

4. CONCLUSIONS:

Based on the FTIR and MS/MS spectra, it was revealed that the result of the derivatization process in the research was pheophytin *a*, pheophytin *b*, chlorophyllide *a*, pheophorbide *a*, and pheophorbide *b*. Other extracted compounds, including phenolics, flavonoids, and carotenoids, enhanced the antioxidant activity of chlorophyll extract and its derivatives. The chlorophyllide and pheophorbide extract exhibited the inhibition rate of lipid peroxidation, which is not significantly different from that of BHT, whereas pheophytin extract is lower. The assay of radical scavenging activity of DPPH and FRAP shows that chlorophyll and chlorophyllide extracts exhibited higher activity, followed by pheophytin and

pheophorbide. The fraction of chlorophyllide showed the lowest metal chelating activity. Thus, it can be concluded that, in general, the first derivatives of chlorophyll had antioxidant activity higher than the second derivative. Chlorophyll and its derivatives extract were better in antioxidant activity than each fraction.

5. ACKNOWLEDGMENTS:

The author would like to thank the Indonesia Endowment Fund for Education (LPDP) for financial support through the Research Grant scholarship BUDI-DN 2019.

6. REFERENCES:

1. Arar, E. J. (1997). In Vitro Determination of Chlorophylls *a*, *b*, *c*₁ + *c*₂ and Pheopigments in Marine And Freshwater Algae by Visible Spectrophotometry. National Exposure Research Laboratory Office of Research and Development U.S. Environmental Protection Agency, Cincinnati, Ohio 45268.
2. Aryal, S., Baniya, M. K., Danekhu, K., Kunwar, P., Gurung, R. and Koirala, N. (2019). Total Phenolic Content, Flavonoid Content and Antioxidant Potential of Wild Vegetables from Western Nepal. *Plants*. 8, 1-12. DOI: 10.3390/plants 8040096
3. Benjakul, S.; Kittiphattanabawon, P; Sumpavapol, P; Maqsood, S. (2014). Antioxidant activities of lead (*Leucaena leucocephala*) seed as affected by extraction solvent, prior dechlorophyllisation and drying methods. *J. Food Sci. Technol.* 51, 3026–3037. DOI: 10.1007/s13197-012-0846-1.
4. Benzie, I.F.F. and Devaki, M. (2018). The ferric reducing/antioxidant power (FRAP) assay for non-enzymatic antioxidant capacity: concepts, procedures, limitations and applications. In R. Apak, E. Capanoglu, and F. Shahidi, (Eds.). *Measurement of Antioxidant Activity and Capacity: Recent Trends and Applications*. (pp. 77–106). Hongkong: John Willey and son, Ltd.
5. Cahyana, A. H., Shuto, Y., and Kinoshita, Y. (1992). Pyropheophytin *a* as an Antioxidative Substance from the Marine Alga, Arame (*Eisenia bicyclis*). *Biosci.*

- Biotechnol. Biochem.* 56, 1533–1535. <https://doi.org/10.1271/bbb.56.1533>.
6. Cervantes-Paz, B; Yahia, E. M., Ornelas-Paz, J. D. J., Victoria-Campos, C.I., Ibarra-Junquera, V., Pérez-Martínez, J.D. and Escalante-Minakata, P. (2014). Antioxidant activity and content of chlorophylls and carotenoids in raw and heat-processed Jalapeño peppers at intermediate stages of ripening. *Food Chem.* 146, 188–196. DOI: 10.1016/j.foodchem.2013.09.060.
 7. Chandra, S; Khan, S., Avula, B; Lata, H., Yang, M. H., Elsohly, M. A. and Khan, I. A. (2014). Assessment of Total Phenolic and Flavonoid Content, Antioxidant Properties, and Yield of Aeroponically and Conventionally Grown Leafy Vegetables and Fruit Crops: A Comparative Study. Evidence-Based Complement. Altern. Med. 2014, 1–9.
 8. Cheng, K, L., Ueno, K. and Imamura, T. (1992). *Handbook of Organic Analytical Reagents* (2nd ed). Boca Raton: CRC Press.
 9. Cherrak, S. A., Mokhtari-Soulimane, N., Berroukeche, F., Bensenane, B., Cherbonnel, A., Merzouk, H. and Elhabiri, M. (2016). In Vitro Antioxidant versus Metal Ion Chelating Properties of Flavonoids: A Structure-Activity Investigation. *PLoS One*. 11, 1–21. <https://doi.org/10.1371/journal.pone.0165575>.
 10. Choe, E. and Min, D, B. (2009). Mechanisms of Antioxidants in the Oxidation of Foods. *Comprehensive Reviews In Foods Science and Food Safety*. 8, 345-358.
 11. Dafallah, A. A., Adellah, A. M., Abdel-Rahim, E., M. and Ahmed, S., H. (2015). Physiologigal Effects of Some Artificial and Natural Food Coloring on Young Albino Rats. *Journal of Food Technology Research.* 2(2). 21-32. DOI: 10.18488/journal.58/2015.2.2/58.2.21.32.
 12. Delgado-Vargas, F. and Paredes Lopez, O. (2003). *Natural Colorants for Food and Nutraceutical Uses*. CRC Press, Boca Raton.
 13. El-Wahap, H. M.F.A. and Moram, G.S.E.D. (2012). Toxic effects of some synthetic food colorants and/or flavor additives on male rats. *Toxicology and Industrial Health.* 29(2). 224-232. DOI: 10.1177/0748233711433935
 14. Endo, Y., Usuki, R. and Kaneda, T. (1985a). Antioxidant Effects of Chlorophyll and Pheophytin on the Autoxidation of Oils in the Dark. I. Comparison of the Inhibitory Effects. *J. Am. Oil Chem. Soc.* 62, 1375–1376.
 15. Endo, Y., Usuki, R. and Kaneda, T. (1985b). Antioxidant Effects of Chlorophyll and Pheophytin on the Autoxidation of Oils in the Dark. II. The Mechanism of Antioxidative Action of Chlorophyll. *J. Am. Oil Chem. Soc.* 62, 1387–1390.
 16. Fasakin, C. F., Udenigwe, C. and Aluko, R.E. (2011). Antioxidant properties of chlorophyll-enriched and chlorophyll-depleted polyphenolic fractions from leaves of *Vernonia amygdalina* and *Gongronema latifolium*. *Food Reseach International.* 44. 2435 - 2441. DOI: 10.1016/j.foodres. 2010.12.019
 17. Ferruzzi, M.G., Bohm, V., Courtney, P.D. and Schwartz, S.J. (2002). Antioxidant and Antimutagenic Activity of Dietary Chlorophyll Derivatives Determined by Radical Scavenging and Bacterial Reverse Mutagenesis Assays. *J. Food Sci.* 67, 2589–2595.
 18. Halliwell, B. (2012). Free radicals and antioxidants: updating a personal view. *Nutr. Rev.* 70, 257–265. DOI:10.1111/j.1753-4887.2012.00476.x.
 19. Hargreaves, T. (2003). Chemical Formulation: An Overview of Surfactant-based Preparations Used in Everyday Life. Retrieved from <https://www.globalspec.com/reference/55565/203279/chelating-agents-sequestrants/>.
 20. Hendry, G, A, E. and Grime, J. (1993). *Methods Comparatives Plant Ecology. Laboratory Manual* (1st. ed.). Hongkong: Chapman and Hall.
 21. Huvaere, K. and Skibsted, L. H.(2014). Flavonoids protecting food and beverages against light. *J Sci Food Agric*, 95: 20–35.

22. Kang, Y.R., Park, J., Jung, S.K. and Chang, Y.H. (2018). Synthesis, characterization, and functional properties of chlorophylls, pheophytins, and Zn-pheophytins. *Food Chem.* 245, 943–950. <https://doi.org/10.1016/j.foodchem.2017.11.079>.
23. Kim, T.S., Decker, E.A. and Lee, J. (2012). Effects of chlorophyll photosensitisation on the oxidative stability in oil-in-water emulsions. *Food Chem.* 133, 1449–1455. <https://doi.org/10.1016/j.foodchem.2012.02.033>.
24. Kobayashi, M., Ohashi, S., Iwamoto, K., Shiraiwa, Y., Kato, Y. and Watanabe, T. (2007). Redox potential of chlorophyll d in vitro. *Biochim. Biophys. Acta* 1767, 596–602. DOI: 10.1016/j.bbabi.2007.02.015.
25. Lanfer-Marquez, U. M., Barros, R. M. C. and Sinnecker, P. (2005). Antioxidant activity of chlorophylls and their derivatives. *Food Res. Int.* 38, 885–891. <https://doi.org/10.1016/j.foodres.2005.02.012>.
26. Lee, E.C. and Min, B. (1988). Quenching Mechanism of p-Carotene on the Chlorophyll Sensitized Photooxidation of Soybean Oil. *Journal of Food Science*, 53(6), 1894–1895.
27. Lee, J.H., Ozcelik, B. and Min, D.M. (2003). Electron Donation Mechanisms of Carotene as a Free Radical Scavenger. *Journal of Food Science*, 69(3), 861–865.
28. Mathew, S. and Abraham, T.E. (2006). In vitro antioxidant activity and scavenging effects of *Cinnamomum verum* leaf extract assayed by different methodologies. *Food Chem. Toxicol.* 44, 198–206. DOI: 10.1016/j.fct.2005.06.013.
29. Milenković, S.M., Zvezdanović, J.B. and Anđelković, T.D. (2012). The Identification of Chlorophyll and Its Derivatives in The Pigment Mixtures: HPLC-Chromatography, Visible and Mass Spectrophotometry Studies. *Adv. Technol.* 1, 16–24.
30. Ngo, T. and Zhao, Y. (2007). Formation of zinc-chlorophyll-derivative complexes in thermally processed green pears (*Pyrus communis* L.). *J. Food Sci.* 72, 397–404. <https://doi.org/10.1111/j.1750-3841.2007.00465.x>.
31. Niciforovic, N., Mihailovic, V., Maškovic, P., Solujic, S., Stojkovic, A. and Pavlovic, D. (2010). Antioxidant activity of selected plant species; potential new sources of natural antioxidants. *Food Chem. Toxicol.* 48, 3125–3130. DOI:10.1016/j.fct.2010.08.007.
32. Ohashi, S., Kasahara, M., Fukuyo, S., Nakazato, M., Iwamoto, K., Shiraiwa, Y., Kato, Y., Watanabe, T. and Kobayashi, M. (2008). Redox Potential of Chlorophyll d. In J. Allen, E. Gantt, J.H. Golbeck, and B. Osmond (Eds.). *Photosynthesis. Energy from the Sun: 14th International Congress on Photosynthesis*. (pp. 105–106). Springer.
33. Roca, M., Chen, K. and Pérez-Gálvez, A., 2016. Chlorophylls. In R. Carle, and R. M., Schweiggert (Eds.). *Handbook on Natural Pigments in Food and Beverages*. (p. 508) Cambridge: Elsevier Ltd. <https://doi.org/10.1016/B978-0-08-100371-8.00006-3>.
34. Sarker, U., Islam, T., Rabbani, G. and Oba, S. (2018). Variability in total antioxidant capacity, antioxidant leaf pigments and foliage yield of vegetable amaranth. *J. Integr. Agric.* 17, 1145–1153. [https://doi.org/10.1016/S2095-3119\(17\)61778-7](https://doi.org/10.1016/S2095-3119(17)61778-7).
35. Shim, S. (2012). Chelating Effect of Leek (*Allium tuberosum* Rottler ex Sprengel) Containing Chlorophyll on Cd, Pb, and As. *J. Korean Soc. Appl. Biol. Chem.* 55, 311–315. DOI: 10.1007/s13765-012-1151-4.
36. Simpson, B.K., Benjakul, S. and Klomklao, S. (2012). Natural Food Pigments. In B.K, Simpson (Ed.). *Food Biochemistry and Food Processing*. (p.901). Ames, Iowa: Wiley-VCH Publisher.
37. Suryani, C.L., Tamaroh, S., Ardiyan, A. and Setyowati, A. (2017). Antioxidant activity of pandan (*Pandanus amaryllifolius*) leaf ethanol extract and its fractions. *Agritech* 37, 271–279. DOI: 10.22146/agritech.11312.

38. Suzuki, T., Inoue, M. and Shioi, Y. (2014). Purification and properties of metal-chelating substance in chlorophyll degradation. *J. Trop. Plant Physiol.* 6, 35–49.
39. Taroreh, M., Raharjo, S., Hastuti, P. and Murdiati, A. (2015). Antioxidant Activities of Sequentially Extracted Gedi (*Abelmoschus manihot* L) Leaves. *Agritech* 35, 280–287.
40. Van Breemen, R.B., Canjura, F.L. and Schwartz, S.J. (1991). Identification of Chlorophyll Derivatives by Mass Spectrometry. *J. Agric. Food Chem.* 39, 1452–1456.
41. Vernon, L.P., 1960. Spectrophotometric Determination of Chlorophylls and Pheophytins in Plant Extracts. *Anal. Chem.* 32, 1144–1150.
42. Wakte, K., Zanan, R., Hinge, V., Khandagale, K., Nadaf, A. and Henry, R. (2016). Thirty-three years of 2-acetyl-1-pyrroline, a principal basmati aroma compound in scented rice (*Oryza sativa* L.): a status review. *J. Sci Food Agric.* July, 1–14. DOI: 10.1002/jsfa.7875.
43. Xu, B.J. and Chang, S.K.C. (2007). A Comparative Study on Phenolic Profiles and Antioxidant Activities of Legumes as Affected by Extraction Solvents. *J. Food Sci.* 72, S159–S166. DOI: 10.1111/j.1750-3841.2006.00260.x.
44. Yang, C.M., Chang, K.W., Yin, M.H. and Huang, H.M. (1998). Methods for the Determination of the Chlorophylls and their Derivatives. *Taiwania* 43, 116–122.
45. Zeb, A. and Imran, M. (2019). Carotenoids, pigments, phenolic composition and antioxidant activity of *Oxalis corniculata* leaves. *Food Biosci.* 32, 1–9. DOI: 10.1016/j.fbio.2019. 100472.
46. Zvezdanovic, J.B., Petrovic, S.M., Markovic, D.Z., Andjelkovic, T.D. and Andjelkovic, D.H. (2014). Electrospray ionization mass spectrometry combined with ultra high-performance liquid chromatography in the analysis of in vitro formation of chlorophyll complexes with copper and zinc. *J. Serbian Chem. Soc.* 79, 689–706.



Figure 1. *Pandanus amaryllifolius* Roxb. plant

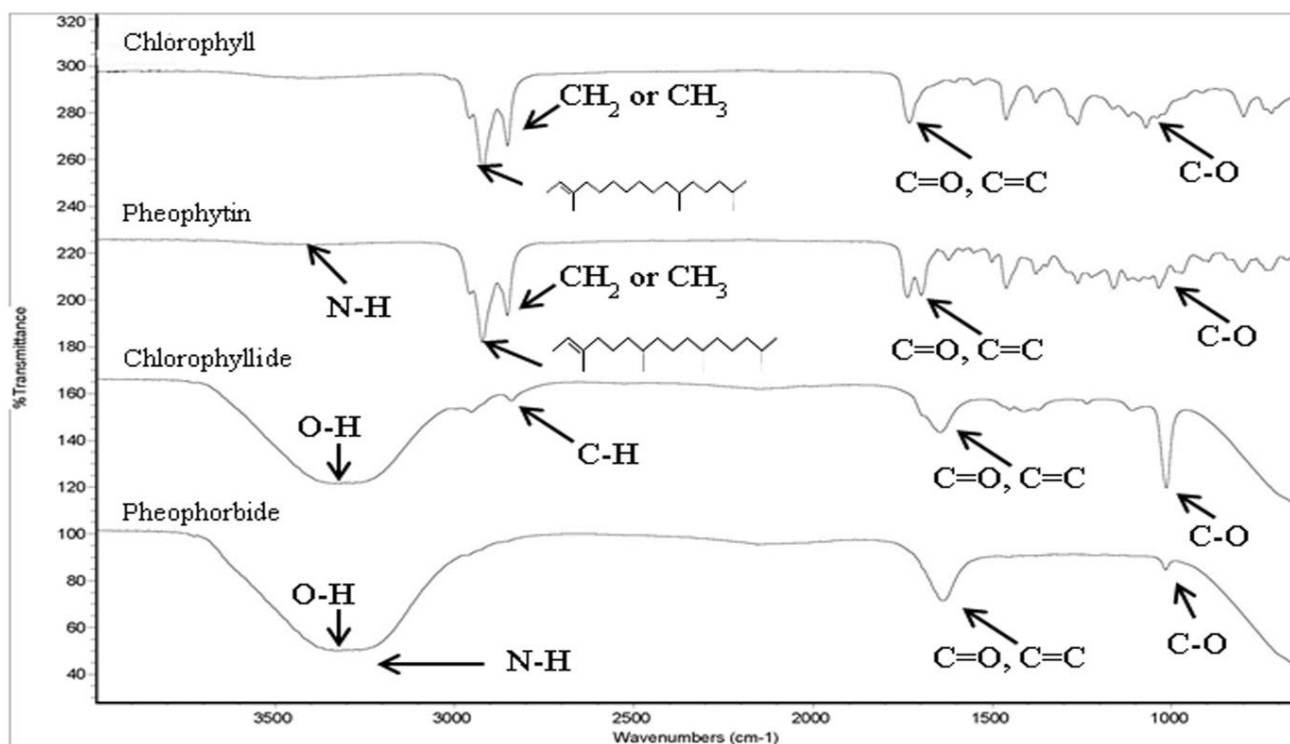
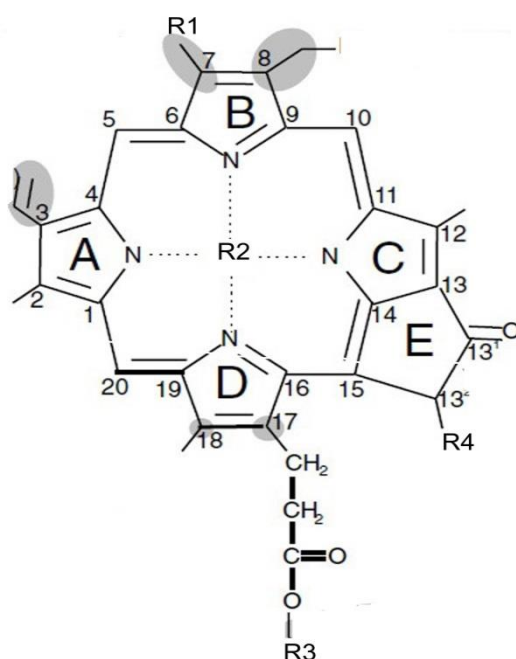


Figure 2. FTIR spectra of chlorophyll, pheophytin, chlorophyllide, and pheophorbide fractions from pandan leaves.



Name	R1*	R2	R3	R4
Chlorophyll a	CH ₃	Mg	Phytol	CO ₂ CH ₃
Pheophytin a	CH ₃	H	Phytol	CO ₂ CH ₃
Chlorophyllide a	CH ₃	Mg	H	CO ₂ CH ₃
Pheophorbide a	CH ₃	H	H	CO ₂ CH ₃

*R1 is CHO in series b

Figure 3. Chemical structure of chlorophyll a and its derivatives (Adapted from Delgado-Vargas and Paredes Lopez (2003)).

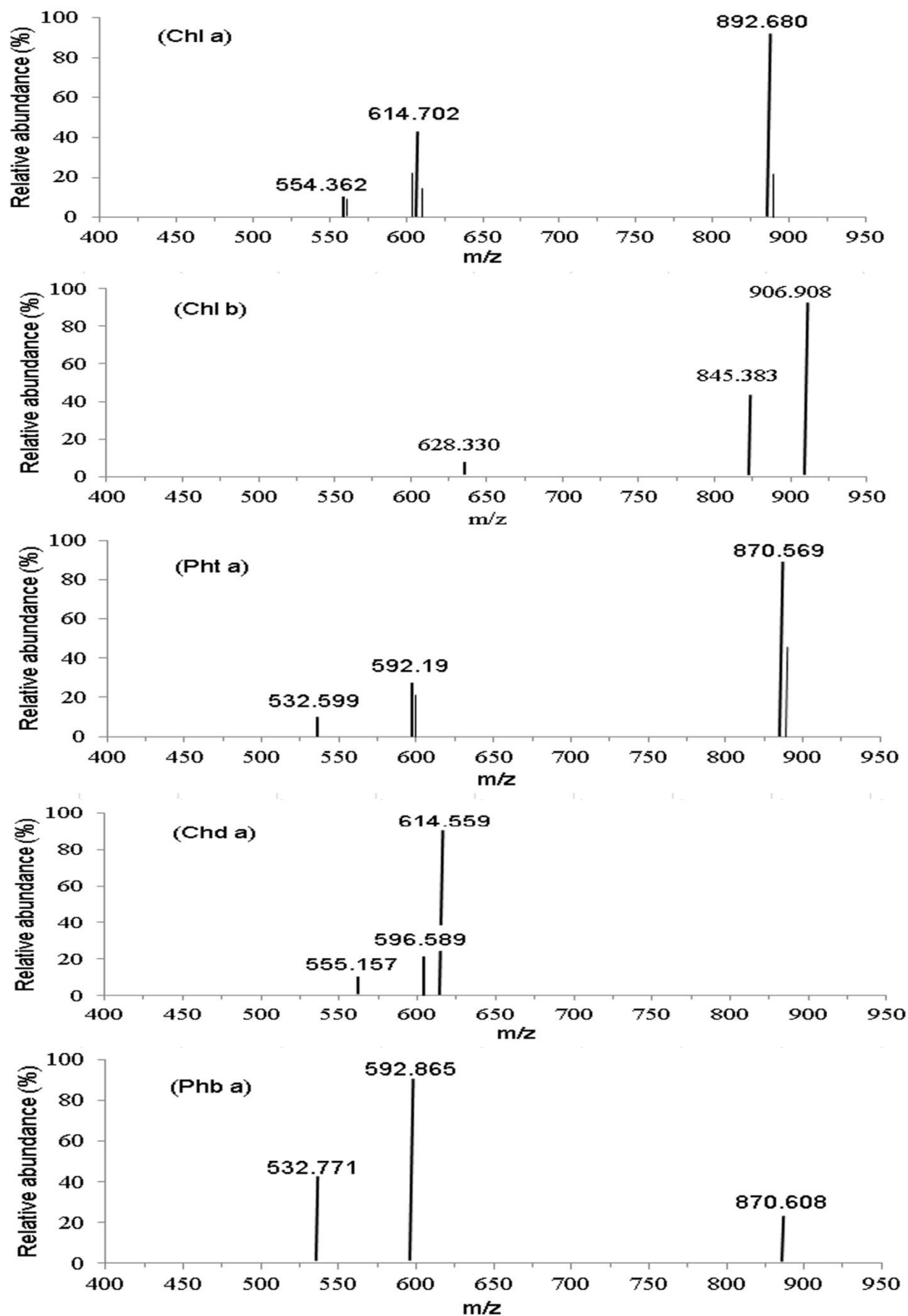


Figure 4. Full scan MS/MS spectra of $[M +]$ ion of chlorophyll a (Chl a), chlorophyll b (Chl b), pheophytin a (Pht a), chlorophyllide a (Chd a), and pheophorbide a (Phb a) taken from their MS spectra of chlorophyll and its derivatives fraction from pandan leaves.

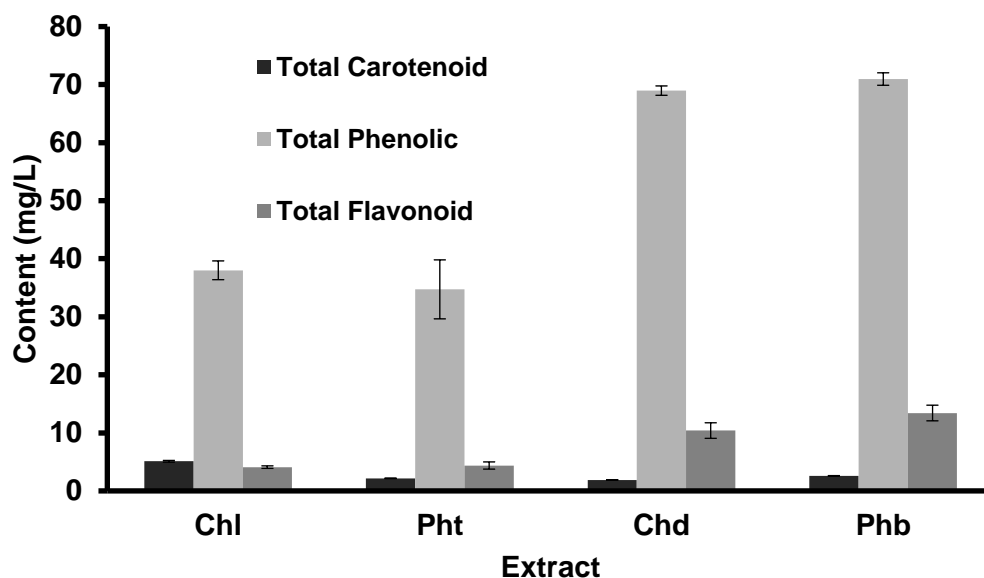
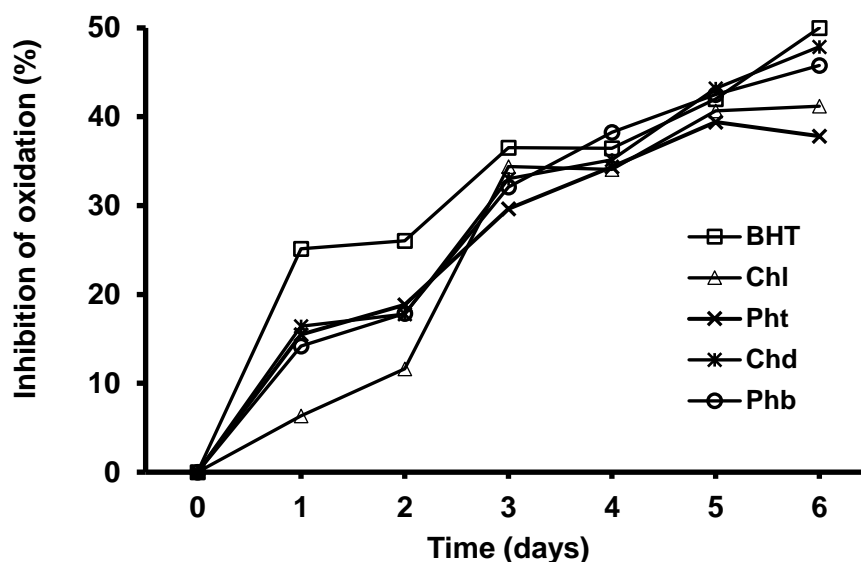


Figure 5. Total carotenoid (mg/L), phenolics (GAE mg/L), and flavonoid (QE mg/L) content in chlorophyll and its derivatives extract from pandan leaves. Chl: chlorophyll extract, Pht: pheophytin extract, Chd: chlorophyllide extract, Phb: pheophorbide extract.



Linear regression equation:

$$Y_{\text{BHT}} = 7.32 X + 9.75 \quad Y_{\text{Chd}} = 7.66 X + 4.65$$

$$Y_{\text{Chl}} = 7.67 X + 1.90 \quad Y_{\text{Phb}} = 7.65 X + 4.28$$

$$Y_{\text{Pht}} = 6.35 X + 6.18$$

Figure 6. Antioxidant activity of chlorophyll and its derivatives extract by FTC method. Chl: chlorophyll extract, Pht: pheophytin extract, Chl: chlorophyllide extract, and Phb: pheophorbide extract. The concentration of extract and BHT was 100 ppm.

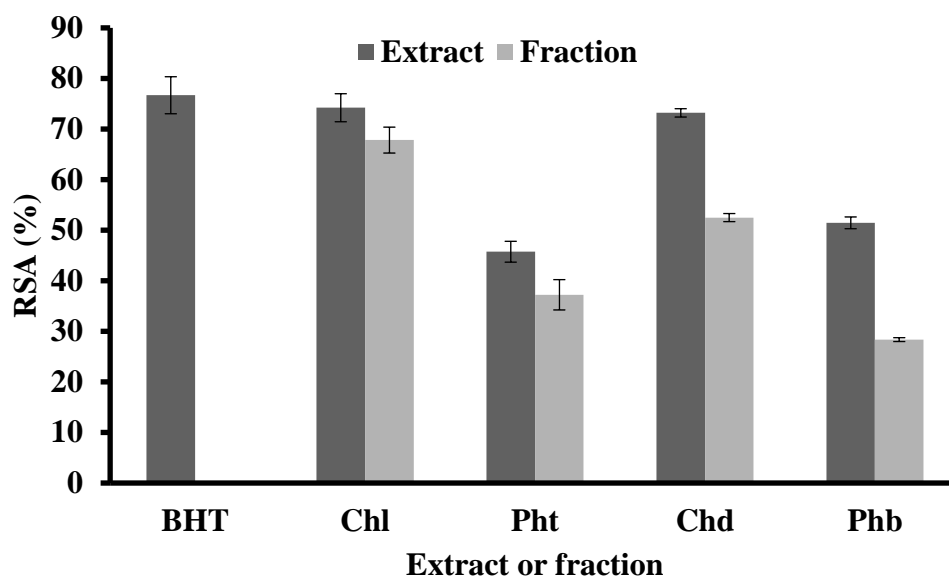


Figure 7. Radical scavenging activity of extract or fraction of chlorophyll and its derivatives from pandan leaves on DPPH radicals. Chl: chlorophyll, Pht: pheophytin, Chl: chlorophyllide, and Phb: pheophorbide at a concentration of extract, fraction, and BHT was 100 ppm.

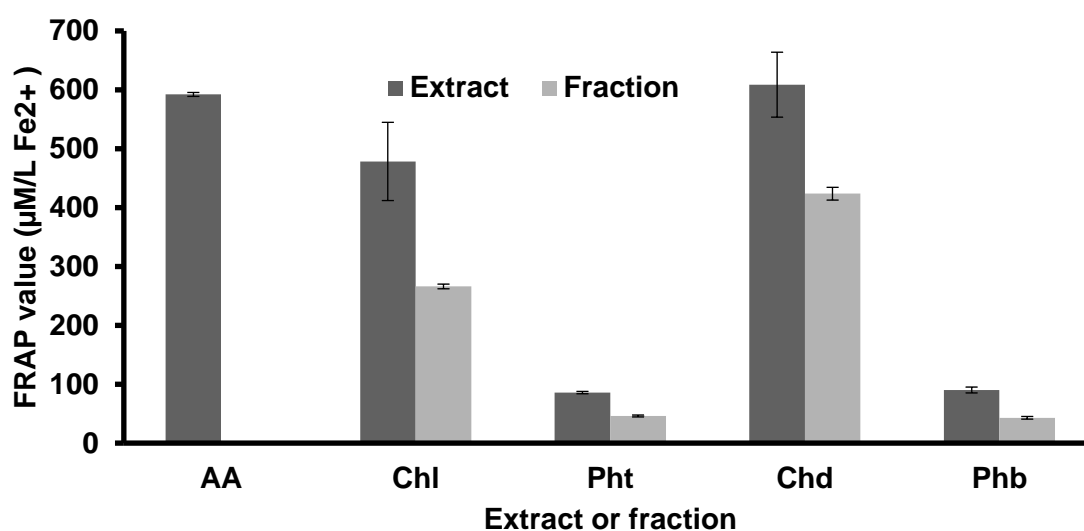


Figure 8. FRAP value of chlorophyll and its derivatives extract or fraction from pandan leaves. Chl: chlorophyll, Pht: pheophytin, Chl: chlorophyllide, Phb: pheophorbide and AA: ascorbic acid at a concentration of extract, fraction, and ascorbic acid 50 was ppm.

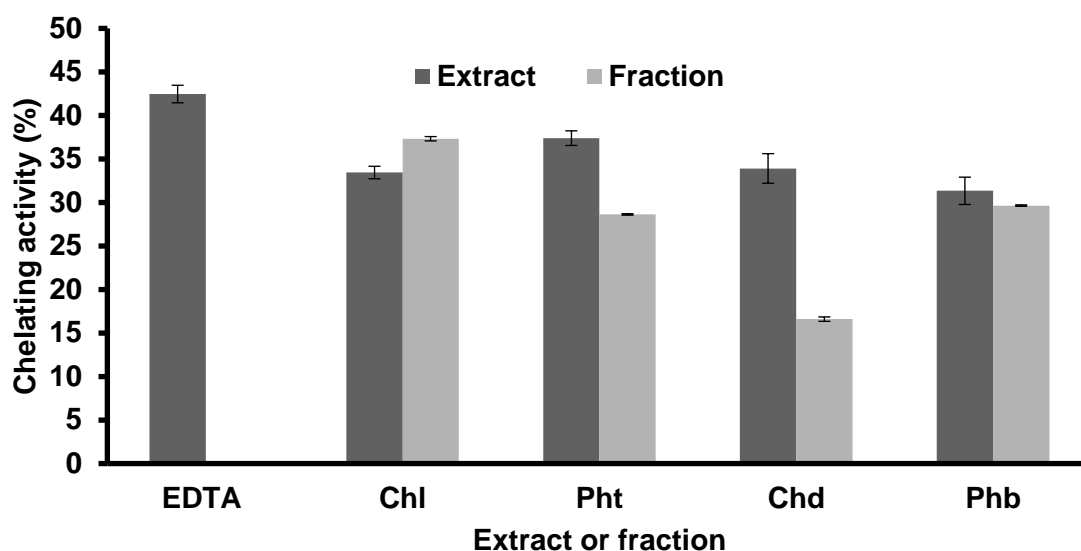


Figure 9. Metal chelating activity of extract or fraction of chlorophyll and its derivatives from pandan leaves. Chl: chlorophyll, Pht: pheophytin, Chl: chlorophyllide and Phb: pheophorbide at a concentration of extract, fraction, and EDTA was 5 ppm.

Table 1. MS/MS fragmentation pattern of chlorophyll and its derivatives from pandan leaves

Main Compound (M)	Founds MW/(m/z)	Average calculated MW/(m/z) ¹	Main observed fragment ions (m/z)	Structure of the fragment ion ^{1,2}
Chlorophyll a	892.680 (100%)	893.50	615[M-278] ⁺ 555[M-338] ⁺	[M-C ₂₀ H ₃₈] ⁺ [M-C ₂₀ H ₃₉ CO ₂ CH ₃] ⁺
	892.135* (25%)	893.50	874[M-24+2] ⁺	[M-Mg+2H] ⁺
Chlorophyll b	906.908 (100%)	907.52	846[M-60] ⁺ 628[M-278] ⁺	[M-CO ₂ CH ₃] ⁺ [M-C ₂₀ H ₃₈] ⁺
Pheophytin a	870.569 (100%)	871.21	593[M-278] ⁺ 533[M-278-60] ⁺	[M-C ₂₀ H ₃₈] ⁺ [M-C ₂₀ H ₃₉ CO ₂ CH ₃] ⁺
Chlorophyllide a	614.559 (100%)	614.30	596[M-17] ⁺ 555[M-59] ⁺	[M-CH ₃] ⁺ [M-CO ₂ CH ₃] ⁺
Pheophorbide a	592.865 (100%)	592.10	533[M-59] ⁺	[M-CO ₂ CH ₃] ⁺
Pheophorbide b	606.670* (100%)	606.70	547[M-59] ⁺	[M-CO ₂ CH ₃] ⁺

Reference: ¹Van Breemen *et al.* (1991) and ²Roca *et al.* (2016).

*MS/MS fragmentation pattern not shown.

DESENVOLVIMENTO DE HABILIDADES ESPECIAIS EM QUÍMICA NO SISTEMA DE FORMAÇÃO PROFISSIONAL UNIVERSITÁRIA DOS ALUNOS**DEVELOPMENT OF SPECIAL CHEMISTRY SKILLS IN THE UNIVERSITY VOCATIONAL TRAINING SYSTEM OF THE STUDENTS****ФОРМИРОВАНИЕ СПЕЦИАЛЬНЫХ УМЕНИЙ В ОБЛАСТИ ХИМИИ В СИСТЕМЕ ПРОФЕССИОНАЛЬНОЙ ПОДГОТОВКИ СТУДЕНТОВ ВУЗА**

MASLENNIKOVA, Nadezhda N.^{1*}; GIBADULINA, Ilzira I.²; GAFIYATULLINA, Elvira A.³;

^{1,2,3} Kazan Federal University, Department of Biology and Chemistry, 18 Kremlevskaya Str., zip code 420008, Kazan – Russian Federation

** Corresponding author
email: m-nadine@yandex.ru*

Received 10 August 2020; received in revised form 11 October 2020; accepted 28 October 2020

RESUMO

A preparação dos estudantes para o trabalho na área de educação contribui para o desenvolvimento da educação escolar. A base de ensino dos estudantes é constituída por técnicas, métodos e formas de ensino a partir do exemplo da atividade prática e da execução de ações profissionais. A utilização de tecnologias informáticas de informação (TIC) no ensino superior promove: divulgação, preservação e desenvolvimento dos interesses individuais; a formação de interesses cognitivos, o desejo de autoaperfeiçoamento e autorrealização dos alunos; assegurar a complexidade do estudo dos fenômenos da realidade, a continuidade da relação entre as ciências naturais, a tecnologia, as humanidades e a arte; atualização dinâmica constante de conteúdos, meios, formas e métodos de ensino e educação. O objetivo do artigo é identificar o nível de formação de competências em informação e comunicação dos futuros professores da química. No início, foi realizado um inquérito a 24 professores das disciplinas de formação profissional geral e das disciplinas de formação profissional que leccionavam para estudantes da direção de formação “Tecnologia Química”. A pesquisa foi direcionada; foram utilizados questionários tanto na forma eletrônica (*Google Form*) quanto impressa. O artigo mostra como se forma a competência informacional dos futuros professores de química. O significado prático do estudo é determinado pela necessidade de combinar o nível de educação escolar com as tendências tecnológicas modernas. Mostra-se a necessidade de formação do interesse individual dos estudantes pela atividade científica. Verificou-se que a aquisição de competências, experiência em sistemas abertos de formação, na opinião de todos os respondentes, é condição necessária para a implementação de novas atividades educacionais, cognitivas e profissionais eficazes. A etapa de verificação da experiência pedagógica estabeleceu a necessidade de seleção e implementação de tecnologias móveis, informáticas e de nuvem no currículo para a resolução de problemas de orientação profissional. A novidade da pesquisa é determinada pela necessidade de aprimorar a competência dos estudantes em uma universidade pedagógica no ensino de disciplinas químicas.

Palavras-chave: *ambiente de informação, tecnologias de informação e comunicação, processo educacional, questionamento.*

ABSTRACT

Preparing students for work in the field of education contributes to the development of school education. The basis for teaching students is made up of techniques, methods, and forms of learning by practical activity and the implementation of professional actions. The use of information and communication technology (ICT) in higher education contributes to the disclosure, preservation, and development of individual interests; the motivation; the desire for self-improvement and self-realization of students; ensuring the complexity of studying the phenomena of reality, the inextricability of the relationship between science, technology, the humanities, and art; a constant dynamic update of the content, means, forms, and methods of training and education. This study aimed to identify the level of future chemistry teachers through ICT competence development. A survey was conducted among 24 teachers of general professional and subject-vocational training, who taught “Chemical Technology” to their students. The questionnaire was targeted; the questionnaires were used both in electronic format (*Google form*) and in print. The article shows how information competence for future chemistry teachers is developed. The

practical significance of the study is determined by the need to match the level of school education with modern technological trends. It is shown that there is a necessity for the motivation of students in scientific activity. It was established that the acquisition of competencies and the experience in open training systems, according to all respondents, is a prerequisite for the implementation of further effective educational, cognitive, and professional activities. The ascertaining stage of the pedagogical experiment established the need to choose and introduce the disciplines of mobile, computer, and cloud technologies into the curriculum for solving professionally-oriented problems. The novelty of the study is determined by the necessity to increase the competence of the pedagogical university students in training how to teach chemical disciplines.

Keywords: *information environment, information and communication technologies, educational process, questionnaires.*

АННОТАЦИЯ

Подготовка студентов для работы в области образования способствует развитию школьного образования. Основу для обучения студентов составляют приемы, методы и формы научения на примере практической деятельности и выполнения профессиональных действий. Использование информационных компьютерных технологий (ИКТ) в высшем образовании способствует: раскрытию, сохранению и развитию индивидуальных интересов; формированию познавательных интересов, стремлению к самосовершенствованию и самореализации студентов; обеспечению комплексности изучения явлений действительности, неразрывности взаимосвязи между естествознанием, техникой, гуманитарными науками и искусством; постоянному динамическому обновлению содержания, средств, форм и методов обучения и воспитания. Целью статьи является выявление уровня сформированности ИКТ-компетентности будущих учителей химии. В начале был проведен опрос 24 преподавателей дисциплин общепрофессиональной и предметно-профессиональной подготовки, которые преподавали для студентов направления подготовки «Химическая технология». Анкетирование было адресное, использовались анкеты, как в электронной (Google форме), так и в печатной форме. В статье показано как формируется информационная компетентность у будущих преподавателей химии. Практическая значимость исследования определяется необходимостью соответствия уровня школьного образования современным технологическим тенденциям. Показано, что существует потребность в формировании также интереса у учащихся к научной деятельности у отдельных учащихся. Установлено, что приобретение компетенций, опыт работы в открытых системах обучения, по мнению всех респондентов, является необходимым условием для осуществления дальнейшей эффективной учебно-познавательной и профессиональной деятельности. Констатирующий этап педагогического эксперимента установил потребность в выборе и внедрении в учебные программы дисциплин мобильных, компьютерно- и облачных технологий для решения профессионально ориентированных задач. Новизна исследования определяется необходимостью повышения компетентности у студентов педагогического вуза при обучении преподавания химических дисциплин.

Ключевые слова: *информационная среда, информационно-коммуникационные технологии, образовательный процесс, анкетирование.*

1. INTRODUCTION:

The use of information and communication technology (ICT) in higher education contributes to the disclosure, preservation, and development of individual interests; the motivation; the desire for self-improvement and self-realization of students; ensuring the complexity of studying the phenomena of reality, the inextricability of the relationship between science, technology, the humanities, and art; a constant dynamic update of the content, means, forms, and methods of training and education (Cai *et al.*, 2014; Viera *et al.*, 2017; Wang *et al.*, 2019; Wei Wen Wong *et al.*, 2020). The main pedagogical goals of using ICTs are (1) the development of the students

personality, his/her preparation for a comfortable life in an informational (digital) society: the development of various types of thinking and communication skills; the formation of an aesthetic culture through the visualization of information using computer graphics programs, multimedia technologies; the development of skills to find optimal solutions in unforeseen difficult situations; the development of skills to carry out experimental research activities – computer modeling, research of the latest ICT tools; building an information culture, and the ability to process diverse information through appropriate software; (2) the implementation of the social order following the needs of the information society and the stage of its informatization: training of specialists in the field of ICT; training of users in PC hardware and

software; (3) the intensification of all levels of the educational process: improving the efficiency and quality of the educational process through the implementation of the entire didactic potential of ICT; providing increased motivation for learning through computer visualization of information, the ability to manage students, the interaction of the educational process of subjects; the expansion and deepening of intrasubject communications through the use of modern means of processing text, graphic, audiovisual information in solving problems from various subject areas and the like (Stromov *et al.*, 2018; Rootman-le Grange and Retief, 2018; Guseinova, 2018; Oreshkina and Dvulichanskaya, 2019; Shcherbakova and Ilina, 2019).

The ICT-based lessons are fundamentally different from the traditional teaching system (Kondo and Fair, 2017). This difference is in changing the role of the teacher: he/she is no longer the main source of knowledge, his/her function is reduced to an advisory and guiding figure (Tomaszewski, 2016). It is due to modern electronic textbooks, virtual chemical laboratories, the Internet, and new teaching aids. The task of the teacher is to select these tools following the content of the educational material, age, and psychological characteristics of the students, as well as the ability of students to use a computer (Sigmann, 2018). The purpose of using a computer in a chemistry lesson is to create a didactically active environment that promotes productive cognitive activity while mastering new material, developing the students thinking, and increasing the motivation for the subject being studied. (Jones and Seybold, 2016; Álvarez-Chávez *et al.*, 2019).

There are the following forms of ICT in chemistry lessons: multimedia presentations, video experiments; testing; distance learning; multimedia laboratory and practical work; research and project activities, use of electronic textbooks (Martin *et al.*, 2020). Besides, computer technologies contribute to as follows: finding additional sources of information for teachers and students; making wider use of audiovisual means to increase the clarity of the material, for better understanding by the students; accompanying educational material with dynamic pictures; simulating processes that cannot be reproduced under normal conditions; reproducing chemical experiments with hazardous, toxic, and explosive reagents; conducting quick and effective testing of students. It also helps to carry out an individual trajectory of teaching students, the possibility of their growth and development; to organize

individual work of students with information, their ability to self-prepare for laboratory and practical work, final control of knowledge, preparation of their own research; to conduct distance training of students in case of their illness or other reasons; to organize post methodological works of the teacher and creative works of students on various sites (Devitt *et al.*, 2020; Zinn *et al.*, 2020; Pekdağ, 2020).

This study aimed to identify the level of future chemistry teachers in ICT competence development.

2. LITERATURE REVIEW:

The development of information and communication technologies (ICT) has led to qualitative changes in the information environment surrounding an individual, which in turn has caused a chain of qualitative changes in all areas of his/her existence (Fernández De Aránguiz *et al.*, 2014). In the field of education, these changes are classified as a shift in the main paradigm: while in the past, a teacher was the main source of professional information for the students, which made the reproductive teaching methodology the leading one, now a student has many available sources (McCollum *et al.*, 2016; Maslennikova and Gibadulina, 2019). A teacher's function becomes different: he/she must teach students to navigate in the information environment, develop their creative and intellectual abilities, including the capacity for self-instruction (Muravyeva *et al.*, 2015; Sazhina *et al.*, 2017; Sazhina *et al.*, 2019).

Significant trends in the development of education in the information society include as follows: continuity of education; the interdependence of education, science, and culture; strengthening the prognostic orientation of education; creation of an educational information environment; creation of a single information educational space of a country and its integration into the global information educational space; personal orientation of education; humanization of education; humanization of the educational process; fundamentalization of education; integrity of education; priority of the moral component; finding the right combination of students freedom, responsibility and self-restraint as the main regulators of their activities; the formation of a personality with value orientations; cultural integrity of education; the natural integrity of education; the formation of chemistry as a meta-subject; deepening the worldview function of chemistry in education (Muravyeva *et al.*, 2018;

Sigmann, 2018).

The integration of ICTs in education can occur as follows: a tool for cognition; an object of study; teaching aids (Peters, 2014), personality development, communication, automation of diagnostic processes for the results of educational and cognitive activities, automation of experimental results, and organization of intellectual leisure (Nunes-Da-Cunha and Fernandez-Llimos, 2019). To implement the tasks of educational informatization, considering the stages and trends of its development, one should look for new approaches to building and organizing the educational process (Tornee *et al.*, 2019), building appropriate pedagogical systems that reflect the effective training of the future generation, in particular, future chemistry teachers, to livelihoods in the information society (Yokono and Mitsuishi, 2012).

The ideological level of informatization should be supported by developing the scientific foundations of the methodology (Emde and Emmett, 2007). These include a systematic analysis of the development and implementation of information technologies, the development of new principles for organizing the educational process (Ovchinnikov *et al.*, 2018), the creation of descriptions of subject areas and chemical models that arise from the formalized functional tasks and the ones that are difficult to formalize, and the development of basic information technologies in the form of interactive tools (Kirova, 2015).

The activities of the Higher School in the information society should be based on a modern educational paradigm: student and information resources, student and technologies, as well as student and teacher (MacDonald, 2018). The implementation ensures the construction of the educational process based on the activity approach (Lou, 2012), which involves the use of active and interactive teaching methods to provide students with an understanding of “where?” and “how?”. It is possible to apply the acquired knowledge to professional activities (Šumiga, 2015); to introduce the modern pedagogical technologies of personality-oriented and humanistic approaches; to integrate the information (computer and telecommunication) technologies into the existing and future innovative pedagogical technologies (Peters, 2011; Nunes-da-Cunha *et al.*, 2019).

The introduction of information technology as a means of innovative development of education is not only positive but also

controversial (and in some aspects, negative), which should be considered to avoid the deformation not only of a specific result but of the entire education system (Jones and Seybold, 2016). There are the following negative aspects (problems): the lack of proper investment by some leaders in the process of implementing the information technologies; higher education institutions inappropriate use of forms and methods of cooperation with the organizations that produce educational services to improve the quality of students training and teachers qualifications; insufficient equipment, often outdated material and technical base in many universities; the inappropriate, sometimes excessive use of certain technologies (e.g., hypertext links, media texts) in the educational process, as the unlimited access to educational resources often scatters and prevents students from focusing on educational material (Tzvetko and Boiadjev, 2013).

In addition to the above-mentioned problems on the effective use of ICTs in education, requiring in-depth analysis and solutions, there are also ontological problems (the coexistence of the real and virtual worlds and ways to distinguish them; artificial intelligence, its impact on personality development); epistemological problems (identification of information and knowledge; the search for new ways to build knowledge using ICTs; the definition of network systems that facilitate the dissemination of knowledge); identity issues (online security; online identity) (Falicoff *et al.*, 2014).

3. MATERIALS AND METHODS:

First, a survey was conducted among 24 teachers of general professional and subject-vocational training disciplines who taught “Chemical Technology” to their students. (Kazan Federal University, Kazan, Russian Federation). The questionnaire was targeted and used in electronic format (Google form) and in print (APPENDIX 1). Among the teachers who took part in the questionnaire, 8 were under 35, 10 – from 35 to 44 years old, 3 people each – from 45 to 54, and more than 55 years old. In the second part of the ascertaining stage of the pedagogical experiment, 22 chemistry teachers took part.

To identify the level of the future chemistry teachers ICT competence development at the end of 2017/2018 and the beginning of 2018/2019, the pedagogical experiment (a survey) was conducted. The purpose of which was to clarify

the motives that encourage students to study and use ICTs in educational and cognitive activities and solving professional problems; the conditions of preparation for the use of ICT for solving professional problems, the availability of educational and methodological support for solving professional problems; the willingness of future chemistry teachers to study ICTs for solving professionally-oriented tasks, which envisages the development of diverse types of electronic educational resources and their testing in a simulated educational environment.

The ascertaining stage of the pedagogical experiment included the following stages: to learn from the teachers, who have trained future chemistry teachers, the level of integration of ICT into professional activities, their ICT competence self-assessment with a focus on the integration of ICT during the educational activities and in the teaching of disciplines in their subject area; the determination of ICT competence for chemistry teachers based on an adapted methodology proposed by UNESCO; the level of ICT competence and students attitudes towards the use of ICT, in particular, multimedia tools, electronic educational resources, subject-oriented tools (mobile, computer-oriented, and cloud-based mathematical systems) in the process of educational and cognitive activity, and solving professional problems.

The formative stage of the pedagogical experiment was carried out according to the developed research methodology among 2nd and then 3rd-year students of the "Chemistry" training direction. That is, the formative stage of the pedagogical experiment started in the 4th semester with the subject "Multimedia Fundamentals" (Stage 1) and ended in the fifth semester with the subject "Packages of Chemical Programs" (Stage 2). It is worth to note that due to a decrease in the enrolment of students in the studied years and almost identical changes in the results before the start of the experimental work, for the purity of the experiment, it was decided to form three experimental (EG) and one control (CG) groups. That is, two experimental groups were studied: EG1, which consisted of 57 students of the 2nd year of study in the 4th semester of 2018/2019 and the 5th semester of 2019/2020; EG2 – 61 students of the 4th semester of 2019/2020 and the 5th semester of 2016/2017. In the experiment, it was decided that students of the "Chemistry" direction who studied in 2019/2020 would comprise the control group CG1 (63 students), and students of 2016/2017 – the experimental group EG3 (70 students), in

which the developed methodology was partially introduced in the second year in the framework of the discipline "Informatics" (the materials of the disciplines "Multimedia Fundamentals" and "Packages of Chemical Programs"), and the materials of the educational and methodical manual "Packages of Chemical Programs in the Training of Future Chemistry Teachers" were used in the educational process by the teachers of chemical disciplines. Besides, the students participated in training and consultation webinars.

In the final part of the ascertaining experiment with 217 1-4-year full-time mode students educated in Chemistry Teaching and those of the 5th year of study on specialty "Chemistry Teacher", it was planned to identify the attitude and ability of future chemistry teachers to use multimedia technologies, computer, cloud, mobile technologies, in particular, chemical systems, in educational, cognitive, and professional activities.

At the beginning of the formative stage of the pedagogical experiment in the experimental and control groups, the level of ICT competence development and its influence on the solution of professionally oriented problems by future chemistry teachers were diagnosed. To determine the dynamics of all the components of ICT competence according to the selected criteria, levels, various methods were used by the authors and adapted to study ICT competence.

The verification of the cognitive criterion consisted of the verification of technological (T), general professional (GP), and subject-professional (SP) components of ICT competence. To test the criterion, different types of questions and tasks were used, constructed by the objectives of the cognitive sphere by B. Blooms taxonomy (structure of the cognitive process), modified by L. Andersen and D. Kratvol. In particular, some tasks required students to independently choose the technologies for their solution since it did not indicate which ICT tools should be used to solve a given task. Similarly, verifying the operational-technological criterion includes verifying the technological, general professional, and subject-professional components of ICT competence. It was built on the solution of professional problems: competence-based tasks and a set of chemical tasks (test), to identify practical skills in using ICT in solving them and surveying.

The determination of the criteria formation level, which implied the use of several diagnostic methods, is calculated as the

arithmetic means of the Equation (Equation 1), where n – the number of techniques used x_i – the result of the i -th technique. The indicator of the general development of ICT competence is calculated similarly as an average sample value for all individual criteria. To determine the homogeneity of the sample in terms of the level of ICT competence development, the following hypotheses were formed at the beginning of the formative stage of the pedagogical experiment:

1. Null hypothesis N –: the distribution of indicators of the levels of ICT competence development in EG1, EG2, EG3 does not differ from the indicators of the level of ICT competence development in the CG. That is, they belong to the same general population.

2. Alternative hypothesis $H1$: the distribution of indicators of the levels of ICT competence development in EG1, EG2, EG3 differs from the indicators of the level of ICT competence development in the CG, respectively, that is, they do not belong to the same population.

To test the statistical hypotheses the Pearson criterion χ^2 is used, since all the requirements necessary for its use are fulfilled (Equation 2), where n_1 , n_2 – the number of students in the experimental and control groups; Q_{1i} and Q_{2i} – the number of students in the experimental and control groups, respectively, who have the i -th level of knowledge ($n=1$ – “low”, $n=2$ – “medium”, $n=3$ – “sufficient”, $n=4$ – “high”)

To determine the Pearson criterion, all 251 students of the EG and the CG were involved, and the data are presented in Table 2. For example, the calculation of the χ^2_{emp} criterion according to Equation (2), for EG2 and CG before the start of the experiment, where $n_1=61$ (EG1), $n_2=63$ (CG), is performed as follows (Equation 3). Similarly, all 5 possible results of pairwise comparisons of groups (experimental and control groups before the start) that are left are calculated. To automate the calculations, MS Excel was used. The calculation results for the experimental and control groups are shown in Table 3.

Having chosen the significance levels $\alpha \leq 0.01$ and $\alpha \leq 0.05$, the empirical values of the statistical criterion χ^2_{emp} in the studied groups with the critical value are compared (Equation 4), which is found in the table of critical values of the χ^2 criterion considering the degree of freedom $v=(k-1)(c-1)=(4-1)(2-1)=3$ (k – the number of categories of the sign: “high”, “sufficient”, “medium”, “low”; c – the number of subsections that are compared). In all 6 cases $\chi^2_{cr} > \chi^2_{exp}$ for significance level and $\alpha = 0.05$, therefore, the null

hypothesis is confirmed that, before the beginning of the formative stage of the pedagogical experiment, students of EG1, EG2, EG3, and CG had the same level of ICT competence development, coinciding at a significance level of 0.05, that is, they are statistically the same and belong to the same general population.

All the experiments performed in the studies involving human participants corresponded to the ethical standards of the institutional and national research committee and the 1964 Helsinki Declaration and its later amendments or comparable ethical standards. Informed consent was obtained from all individual participants included in the study.

4. RESULTS AND DISCUSSION:

4.1 Analysis of the Results of the Survey among Teachers and Students

The frequency of the ICT use by teachers in the educational process is shown in Figure 1. It was found that 65.4% of teachers constantly use general-purpose software in their professional activities, 7.7% – often, 26.9% and 0% – sometimes and rarely, respectively. Hardware, basically, multimedia devices, is used by 50% of teachers in their classes. However, it should be noted that some of the respondents (40%) are also teachers of computer disciplines. That is, the percentage of the use of software and hardware in the educational process by teachers of non-computer disciplines will decrease by almost half. This is primarily due to the logistics problems, where teachers often need to use their laptops, mobile devices, sometimes portable projectors, and the like, in classrooms.

Teachers use communication tools (email, social networks, instant messaging, Facebook, Twitter) quite actively, in particular, 42.3% and 34.6% of teachers use them constantly and often, respectively. Cooperation/brainstorming tools (discussion forums, Wikis, Google Docs, Wikispaces, Mind Maps, Skype, and Google Drive) are constantly used by 15.4% of teachers, often – 42.3%, sometimes – 15.4%, rarely – 0%, and never – 26.9%. Cloud-based file storage/note-taking applications (Google Drive, Dropbox, Evernote) are constantly used by 34.6% of teachers, often – 15.4%, sometimes – 34.6%, rarely – 0%, and never – 15.4%.

However, to achieve the educational goals of the educational process and their professional development, more than 70% of teachers never,

rarely or sometimes use as follows: course management systems/content management systems/feed systems/learning management systems (WhiteBoard, Google Classroom, Moodle, and Sakai); mobile applications and devices (smartphones, tablets, iPad, and digital whiteboards); blogs and RSS feeds (Blogger, WordPress.); educational networks; free online courses/content (open training programs, open training resources, MOOCs, Prometheus, Udacity, and Edx); interactive student response systems or survey tools (synchronous tools, Plickers, Doodle, Learning Analytics, Socrative, Google Calendar, and the like); modeling, and educational games. The authors believe that the mediocre results of the ICT use in the educational process are associated with a rather large load on a teacher, the number of hours, and the number of students. For example, the total number of students, with whom a teacher works for a semester is as follows: 0-30 students – 8.3% of teachers, 30-60 students – 33.3%, 60-120 – 41.7%, 120 and more – 16.7%. The effectiveness of teaching using ICTs requires a large investment of a teachers time and intellectual resources to facilitate the in-depth training of each student, considering their individual characteristics, needs, motives, abilities, and the like.

The survey showed that the average value of the level of the ICT competence self-assessment is 4.33 out of 5. As the questionnaires' analysis shows, a sufficiently high score indicates a high level of competence of teachers in pedagogy and the subject they teach. Most teachers share the view that ICTs allow students to work together efficiently (76.9%), help optimize the time students spend on assignments, develop creativity and creative thinking, and deepen their knowledge of the discipline (92.3%).

The survey results based on the adapted methodology of UNESCO showed that absolutely all teachers have a computer and Internet access at home. Although 68.2% use it daily, 18.2% weekly, 9.1% monthly, and 4.5% of the respondents – once every 2-3 months. The last two indicators are typical for teachers aged 40 years and above. The question: "Do you use a computer at school?" was answered positively by 86.4% of chemistry teachers surveyed. The question "Do you have access to the Internet at school?" was answered positively by 71.8% of them.

The study showed that not all schools have the appropriate software and hardware. Thus, 12.9% of teachers have access to a

multimedia board. Moreover, they use it "always in the classroom, when they consider that the tool will help students learn". However, a multimedia system, which includes a projector, a projection screen, and a computer, can be used by 91.6% of chemistry teachers in the educational process. However, only 36.4% continuously use it in the classroom when they believe this tool will help students learn, and 50.0% only use it during open classes. This indicates a lack of desire and appropriate skills to use ICT for educational purposes.

In particular, 77% of teachers use ICT at a basic level (computer literacy). That is, they are capable of selecting and using ready-made training and game programs in their work, various web resources, simulators for practicing skills; organizing work in a computer classroom or using ICT tools that are available in other classrooms; applying ICTs to achieve the educational results that are implied by the educational standards, to conduct assessment activities, to implement thematic plans and traditional teaching methods; using ICT for current reporting and their professional development.

A total of 68% of teachers can deepen their knowledge and use them in educational activities. This level provides the ability to handle information, structure problems, and set tasks, to combine the use of chemistry software tools with the methods of personality-oriented educational work, with the students completing common educational projects; to use network resources for the implementation of group (joint) educational projects that allow students to work in concert, gain access to information and communicate with external experts in the analysis and solution of their chosen problems; the use of ICT to develop plans and evaluate their realization in the implementation of individual projects.

And only 55% of teachers believe that they are capable of producing new knowledge; that is, they can be as the exemplary students, masters of learning and creating new knowledge, who are constantly involved in educational experiments and innovations; produce new knowledge about the learning process and teaching methods together with colleagues and external experts; use network devices, digital resources, and electronic environments to create and support (anywhere, anytime) communities of people, who learn and generate knowledge together. One of the main conditions for effective ICT competence development is the creation of sustainable motivation for students educational and cognitive activities and their professional development. The

results of the study of the motivation for professional teaching of students, presented by the corresponding data in Table 1, allowed stating that there is a tendency to a decrease in the motivation when moving to senior courses.

Notably, in the interpretation of the methodology, three levels out of four are used: high (4), normal (3) (in this study, this is sufficient), and medium (2). Since it is believed that a low (1) level is not typical for students. However, as the study showed, when moving to senior courses, an insignificant percentage of students with a low level of motivation appears – these are students who either find it difficult to study in specialized subjects or they realize that they are studying in the wrong specialty, they have completely different professional interests and preferences. Therefore, it was decided to keep all four levels for analysis of the obtained empirical data.

The authors briefly describe the students by their level of motivation. A steady professional interest in learning characterizes students with a high and sufficient level of motivation, particularly in using ICT in the educational process by a chemistry teacher, self-development, and self-instruction. However, a high level also shows the students ability to improve professional activities, particularly through the study of new ICTs and the development of their software products. Regarding students with a medium level of motivation, they have a formed positive attitude and desire to acquire knowledge, skills, but are not able to systematically independently deepen and expand professional knowledge, in particular, with the use of ICT, and show educational and cognitive activity at the request of a teacher to demonstrate the results of their training activities. And, as noted above, students with a low level of motivation have a weak motivation to learn, often due to a lack of understanding of the educational material, the realization that they do not see themselves as chemistry teachers in the future, but have a positive attitude towards the use of ICT in teaching and personal development.

Regarding the actual motives for choosing a profession (answers 1–4 to question 1. “What prompted you to choose a profession?”), considering answers “rather yes than no” and “definitely yes”, the results are shown in (Figure 2): 29.5% of students are afraid to be out of a job in the future, students seeking to find themselves in the profession – 69.7%, some subjects are interesting – 76%, and it is interesting to study here – 70%. Regarding the motives of educational and cognitive activity (answers 5-8 to question 1) (Figure 3), answers “rather yes than no”,

“definitely yes”, to the questions are distributed as follows: “I study because it is required” – 39.6% of the respondents, “I study to keep up with my comrades (classmates)” – 26.7%, “I study because most of the subjects are necessary for the profession I chose” – 71%, “I believe that it is necessary to study all subjects” – 48%.

Among the motives that students mentioned when creating their portfolio, there are the following: love for children and the desire to help them learn chemistry using modern ICTs; chemistry and physics are your favorite school subjects; a dream from childhood to be a teacher; in-depth study of chemistry; the desire to devote himself/herself to teaching children; the opportunity to educate children and apply new methods so that they contribute to learning; the desire to raise and educate children; the chance to use your abilities; to improve your moral character and spiritual world; the satisfaction that work brings; communication opportunity; leadership by other people; changing the education system to develop the personality of a student; it is interesting to study at a university and the like.

The analysis of educational and work programs to prepare the recipients of bachelors degree in chemistry and questionnaires indicated the study of mainly chemical packages such as ChemOffice, ChemGraph. Moreover, the students specializing in Chemistry, who were enrolled in 2017-2018, were taught chemistry. They were offered to study computer-oriented systems for use in the educational process in the 3rd semester. The frequency of using heterogeneous ICTs in educational and cognitive activities by students is presented in Figure 4.

As shown in Figure 4, more than 50% of 2-4-year students rarely use ICT in their educational activities. Besides, the question “Are you ready to use multimedia, in particular, a multimedia board, in chemistry classes at school at this stage of training?” was answered positively by the students in the following percentage terms: 2nd year – 27.1% of students, 3rd year – 42.7%, and 4th year – 50%. The analysis of answers to the question: “Are you ready to use multimedia and create electronic educational resources (didactic and methodological materials) to ensure the educational process at school at this stage of training?” demonstrated that 28.6%, 37% and 50% of 2nd, 3rd and 4th-year students respectively gave a positive answer.

More than 97% of all students indicated that the use of diverse types of electronic

educational resources, multimedia, chemical systems in the educational process increases the intensity of studying educational material, helps to better understand and remember educational material, increases the activity of learning objects in the lesson, and helps to focus on educational material. Only 3% noted that this interferes with educational material perception, drains focus, and does not play any role. The students also noted that the most effective form of presentation of materials for educational and cognitive activities, in particular, when studying chemical systems, is as follows: fragments of material from academic disciplines (chemical and computer); electronic files designed for one or more practical exercises, which describe means for solving chemical problems and examples of their use; free work in the environment; open educational resources based on Moodle, Google Classroom.

4.2. Results of the Formative Stage of the Pedagogical Experiment

Since the students of the experimental groups EG1 and EG2 at the time of transition to the formative stage of the pedagogical experiment of the studied years did not differ in the level of ICT competence development. Therefore their data can be combined for further analysis in the group EG1_2. To identify the dynamics of changes in the levels of ICT competence, in particular, the general professional and subject-professional components of ICT, for the group EG1_2, three control cross-sections were conducted: at the stage of entrance control (Table 4), the weekend after studying the discipline "Multimedia Fundamentals" (Table 5) and at the stage of exit control after completing the study of the discipline "Packages of Chemical Programs" (Table 6) according to the updated methodology. In particular, the significance of the levels of ICT competence development according to all criteria for implementing the designed model and the methodology developed based on students of the EG1_2 group is given in Table 4.

According to the data, the technological component of ICT competence is the best-formed, which indicates appropriate training with ICT at the average user level. In particular, only 5.1% and 8.5% of students found a low level of development of this component of ICT competence. In contrast, at a sufficient and high level, together, the indicators of these criteria are 65.1% and 60.1%, respectively. This indicates the quality training of students in the courses "Information and Communication Technologies", "Informatics", "Fundamentals of the Internet",

which were taught to students in the first and second years of study. Also, a value-motivational criterion is well-formed and, as the ascertaining stage of the pedagogical experiment has shown, the main thing is to ensure stability, which will increase the indicator of this component at higher levels. Regarding the personality-reflexive criterion, the students under the applied diagnostic methods have the following results on the level of self-assessment and ability to self-development and self-instruction: high level – 3.3%, sufficient level – 26.3%, medium – 37.3%, and low – 33.1%. The authors believe that this depends on the personality of a student. Besides, students of the second year of study are not yet sufficiently adapted to the educational and cognitive activities at the university.

The second control cross-section was conducted after the students studied the academic discipline "Multimedia Fundamentals", the results of which are presented in Table 5. Since the methodological system of the discipline "Multimedia Fundamentals" was aimed at the development of a general professional component of ICT competence, the indicators of the relevant criteria have changed most of all. An important aspect is that the values of the levels of value-motivational and personality-reflexive criteria also increased. This is evidenced by rather high activity of the students during the execution of different types of tasks in the Moodle system at the laboratory and lecture classes.

The second control cross-section (after studying the course "Multimedia Fundamentals") showed that the percentage of students who have ICT competence at a high and sufficient level increased by 5.9% and 6.8%, respectively, at a medium level – only 1.7%, and the low one decreased by 11.0%. This is explained by the fact that the level of the subject-professional component of ICT competence increased at a high level only by 1.7% of students, at a sufficient level – by 3.9%, at medium – at 7.7%, but at a low level, it decreased by 4.3%. Then, as the value increased only at a sufficient level by 1.7%, and decreased at medium and low, respectively, by 2.6% and 0.9%. The growth of this component is since the preparation and development of didactic materials in mathematics, students had the opportunity to get acquainted with various types of experimental work, in particular methodological developments, for teaching chemistry, in which it is often proposed to solve problems using appropriate chemical systems, online services. Students who had a higher level of self-instruction and self-organization used these services to solve

chemical problems during the control cross-section after the 2nd stage of the formative experiment. Besides, most students first worked in the Moodle system and needed a longer adaptation to the conditions of changing educational activity when switching from full-time to an audience under the guidance of a teacher, online, when a student must organize his/her work for the relevant instructions.

The third control cross-section was conducted after the students studied the discipline "Packages of Chemical Programs", the results of which are presented in Table 6. Compared with the second stage, there is an increase in indicators by all criteria. However, the greatest increase is characteristic of such criteria as personal and general professional, since this stage of the formative experiment was aimed at the development of a subject-professional component of ICT competence.

Upon completion of the study of the disciplines "Multimedia Fundamentals" and "Packages of Chemical Programs", a questionnaire was conducted, which made it possible to determine the attitude of students to the learning process in the Moodle learning management system, the study of the corresponding software for the disciplines, and self-assessment of their ICT competence development. The students evaluated the disciplines, in particular, electronic training courses corresponding to them, according to criteria such as topic and curriculum, theoretical information, practical tasks, teacher competence, a variety of course tools, didactic and methodological support, software, hardware, relevance, essence and the innovativeness of the course, and the use of learning outcomes in the future. For example, the use of the obtained learning outcomes in the future after studying the disciplines "Multimedia Fundamentals" and "Packages of Chemical Programs" in the format of mixed learning for themselves was at a high level – 54.8% and 57.9%, at a sufficient level – 37.3% and 33.4%, at a medium – 7.9% and 8.7%, respectively. Table 7 presents the general results of forming the criteria for ICT competence: value-motivational, cognitive, operational-technological, and personality-reflexive.

The data obtained after the experiment confirmed the positive dynamics in the formation of ICT competence in the experimental group for each criterion. In particular, according to the motivational criterion, there was an increase in high and sufficient levels by 13.4% and 2.6%, in cognitive – by 21.1% and 19.7%, by operational-

technological – by 14.5% and 22.9%, and by personality-reflexive – by 16.5% and 21.2%, respectively. Moreover, the differences in the distribution of indicators of the levels of each criterion for ICT competence in the EG and the CG are different. This is confirmed at the significance level $\alpha=0.05$. In particular, χ^2_{emp} for the value-motivational criterion is 15.172, for the cognitive – 21.581, for the operational-technological – 17.719, for the personality-reflexive – 20.469. That is, in all cases $\chi^2_{\text{emp}} > \chi^2_{\text{crit}}$.

The comparison of empirical data on the levels of a generalized indicator of future chemistry teachers by ICT competence development in the EG and CG before and after completing the formative stage of the pedagogical experiment is shown in Figure 5. As can be seen from Figure 5, the formation of ICT competencies at high and sufficient levels for all EGs has improved qualitatively, and the indicators for the CGs have remained virtually unchanged. In particular, for the CG, the increase occurred at a high level of only 4.1%, and at a sufficient level – 6.7%. This only indicates an improvement in the quality of training students in forming the technological component of ICT competence, which is a prerequisite for the formation of a general professional (pedagogical) and subject-professional (chemical) component of ICT competence.

To identify the presence of differences in quantitative and qualitative indicators of the levels of ICT competence development in the EG and CG after the introduction of the model and experimental methods, the Pearson criterion χ^2 was used. It was established that after the experiment: the value of the Pearson criterion χ^2_{emp} for EG and CG is $\chi^2_{\text{em}} \approx 17.855 > 7.815 \approx \chi^2_{\text{crit}}$ at a significance level of 0.05. This means that the reliability of differences in ICT competence development in the EG and the CG after the experiment is 95%. It can be stated that the increase in the level of ICT competence development is due to the introduction of the developed model and convincingly testifies to its effectiveness in terms of future chemistry teachers by ICT competence development.

The variance analysis also confirmed the effectiveness of the developed model and the corresponding methodology for future chemistry teachers by ICT competence development. In particular, before the beginning of the formative stage of the pedagogical experiment, the coefficient of ICT competence development in the EG and CG was practically the same and amounted to 2.20 and 2.19, respectively, whereas

after the experiment – 2.94 and 2.48. The coefficient of ICT competence development is higher in EG, which indicates the effectiveness of the implemented model. The initial (before the start of the experiment) states of the experimental and control groups coincide, and the final (after the end of the experiment) states are different, which is mathematically confirmed using the Pearson criterion χ^2 and the variance analysis. Therefore, it can be stated that the effect of changes is due precisely to the testing of the designed model, the identified pedagogical conditions, and under the developed methodology.

5. CONCLUSIONS:

It was established that the acquisition of competencies, experience in open training systems, according to all respondents, is a prerequisite for the implementation of further effective educational, cognitive, and professional activities. The ascertaining stage of the pedagogical experiment established the need to choose and introduce the disciplines of mobile, computer, and cloud technologies for solving professionally-oriented problems. The bulk of the students surveyed noted the need to acquire knowledge, multimedia technologies, mobile, computer, and cloud chemical systems to solve professional problems and their further use in academic work.

1. The use of computers in chemistry lessons facilitates the development of the material, contributes to an increase in cognitive interest in chemistry, the development of the desire and ability to learn makes it possible to carry out an individual approach to teaching. It allows objectively assessing the knowledge of students. The learning process observations revealed that in lessons using ICTs, even “weak” students work more actively, are not distracted, and perform tasks with interest. Computer technology enhances perception, facilitates the assimilation and memorization of the material, and affects several information channels of the student at once. At the same time, students' interest in chemistry lessons increases.

2. The introduction of new information and communication technologies in the educational process makes it possible to activate the learning process, implement the ideas of developing education, and increase the lesson's pace, which significantly affects the motivational sphere of the educational process and its activity structure. But their use in the lesson should be thoughtful,

expedient, and competent.

6. REFERENCES:

1. Álvarez-Chávez, C.R., Marín, L.S., Perez-Gamez, K., Portell, M., Velazquez, L., and Munoz-Osuna, F. (2019). Assessing college students' risk perceptions of hazards in chemistry laboratories. *Journal of Chemical Education*, 96(10), 2120-2131. DOI: 10.1021/acs.jchemed.8b00891
2. Cai, S., Wang, X., and Chiang, F.-K. (2014). A case study of augmented reality simulation system application in a chemistry course. *Computers in Human Behavior*, 37, 31-40.
3. Devitt, A., Hsu, D., van den Eijnde, J., Blayney, M.B., and Dicken, R.D. (2020). Literature highlights. *ACS Chemical Health & Safety*, 27(2), 83-85. DOI: 10.1021/acs.chas.0c00023
4. Emde, J., and Emmett, A. (2007). Assessing information literacy skills using the ACRL standards as a guide. *Reference Services Review*, 35(2), 210–229. <https://doi.org/10.1108/00907320710749146>
5. Falicoff, C.B., Odetti, H.S., and Domínguez Castiñeiras, J.M. (2014). Science competency of students enrolling and graduating at University. *Ensenanza de Las Ciencias*, 32(3), 133–154. <https://doi.org/10.5565/rev/ensciencias.1020>
6. Fernández De Aránguiz, M.Y., Berraondo, M.R., Fernández De Aránguiz, A., Lecea, B., Ayerbe, M., Ruiz-Ortega, J.A., and Hernández, R.M. (2014). Gradual development of cross-curricular competencies in the Pharmacy Degree. Methodologies and evaluation tools for the “professional in training”. *Ars Pharmaceutica*, 55(4), 19–28.
7. Guseinova, E.E. (2018). Organizational and Pedagogical Conditions for the Development of Professional Competencies in the Technical Students' Individual Work through the Example of Studying the Discipline “Hydraulics and Fluid Mechanics”. *European Journal of Contemporary Education*, 7(1), 118-126. DOI: 10.13187/ejced.2018.1.118.
8. Jones, M.L.B., and Seybold, P.G. (2016). Combining chemical information literacy, communication skills, career preparation, ethics, and peer review in a team-taught chemistry course. *Journal of Chemical*

- Education*, 93(3), 439–443. DOI: 10.1021/acs.jchemed.5b00416
9. Kirova, M. (2015). Application of information and communication technologies in chemical education: Opinions of teachers in chemistry from one region of Bulgaria. *Chemistry*, 24(5), 776–793.
 10. Kondo, A.E., and Fair, J.D. (2017). Insight into the chemistry skills gap: the duality between expected and desired skills. *Journal of Chemical Education*, 94(3), 304–310.
 11. Lou, B.-S. (2012). Applying principles from “Scientific Foundations for Future Physicians” to teaching chemistry in the department of medicine at Chang Gung University. *Kaohsiung Journal of Medical Sciences*, 28(2), 36–40. DOI: 10.1016/j.kjms.2011.08.007
 12. MacDonald, K.I. (2018). The business of chemistry: Opportunities for interdisciplinary collaboration in information literacy. *Science and Technology Libraries*, 37(4), 323–331. DOI: 10.1080/0194262X.2018.1515689
 13. Martin, J.A., Miller, K.A., and Pinkhassik, E. (2020). Starting and sustaining a laboratory safety team (LST). *ACS Chemical Health & Safety*, 27(3), 170–182. DOI: 10.1021/acs.chas.0c00016
 14. Maslennikova, N.N., and Gibadulina, I.I. (2019). The position of environmental competence in the structure of the practice-oriented preparation of engineering students. *Periodico Tchê Química*, 16(32), 168–185.
 15. McCollum, B., Sepulveda, A., and Moreno, Y. (2016). Representational technologies and learner problem-solving strategies in chemistry. *Teaching and Learning Inquiry*, 4(2), 1–14.
 16. Muravyeva, E.V., Romanovsky, V.L., Sirazetdinov, R.T., and Zabiroy, D.D. (2015). Application of graph-analytical method of risk analysis “The tree structures” for the study of complex systems survivability by the example of liquid rocket thrusters. *Journal of Life Sciences Research*, 2(2), 34–39.
 17. Muravyeva, E.V., Sibgatova, K.I., Khismatova, A.T., Golovko, M.V., and Maslennikova, N.N. (2018). Risk-thinking forming in the aspect of the sendai risk-thinking forming in the aspect of the sendai program requirements. *Modern Journal of Language Teaching Methods*, 8(5), 328–337.
 18. Nunes-Da-Cunha, I., and Fernandez-Llimos, F. (2019). Misuse of competencies in pharmacy curriculum: The Spain case study. *Indian Journal of Pharmaceutical Education and Research*, 53(4), 620–628. DOI: 10.5530/ijper.53.4.123
 19. Nunes-da-Cunha, I., Martinez, F., and Fernandez-Llimos F. (2019). A global comparison of internationalization support characteristics available on college of pharmacy websites. *American Journal of Pharmaceutical Education*, 83(3), article number 6592.
 20. Oreshkina, O.A., and Dvulichanskaya, N.N. (2019). Development of special competencies in hearing impaired students in conditions of inclusive environment of technical university. *Vysshee Obrazovanie v Rossii*, 28(10), 140–151. DOI: 10.31992/0869-3617-2019-28-10-140-151
 21. Ovchinnikov, A.A., Gitman, M.B., and Gitman, Y.K. (2018). An algorithm of an automatic information system to estimate the level of university student’s competencies formation. *Izvestiya Vysshikh Uchebnykh Zavedenii, Seriya Tekhnologiya Tekstil’noi Promyshlennosti*, 2018-January(3), 300–304.
 22. Pekdağ, B. (2020). Video-based instruction on safety rules in the chemistry laboratory: its effect on student achievement. *Chemistry Education Research and Practice*, 21(3), 953–968. DOI: 10.1039/D0RP00088D
 23. Peters, M.C. (2011). Beyond Google: Integrating chemical information into the undergraduate chemistry and biochemistry curriculum. *Science and Technology Libraries*, 30(1), 80–88. DOI: 10.1080/0194262X.2011.545671
 24. Peters, M.C. (2014). Information competencies for chemistry undergraduates and related collaborative endeavors. *Issues in Science and Technology Librarianship*, 16(3/4), 31–43. DOI: 10.5062/F408639D
 25. Rootman-le Grange, I., and Retief, L. (2018). Action research: Integrating chemistry and scientific communication to foster cumulative knowledge building and scientific communication skills. *Journal of Chemical Education*, 95(8), 1284–1290. DOI: 10.1021/acs.jchemed.7b00958
 26. Sazhina, O.P., Glazkova, O.V., and Tarasova, O.V. (2019). Interactive education as a basis for implementation of competency-oriented programs on chemistry disciplines. *Izvestiya*

Vysshih Uchebnykh Zavedenii, Seriya Khimiya i Khimicheskaya Tekhnologiya, 62(8), 155–161. DOI: 10.6060/ivkkt.20196208.5871

27. Sazhina, O.P., Glazkova, O.V., and Tarasova, O.V. (2017). Use of modern education techniques at “Philosophical Issues in Chemistry” lessons. *Koncept*, 4, 34–39.
28. Shcherbakova, I.A., and Ilina, M.S. (2019). Foreign language communicative competence of university students by using interactive teaching methods. *The New Educational Research*, 57(3), 173-183.
29. Sigmann, S. (2018). Chemical safety education for the 21st century — Fostering safety information competency in chemists. *Journal of Chemical Health and Safety*, 25(3), 17–29. DOI: 10.1016/j.jchas.2017.11.002
30. Stromov, V.Yu., Sysoev, P.V., and Zavyalov, V.V. (2018). “Competency school” – new approach to form extra competencies for students of classic university. *Vysshee Obrazovanie Rossii*, 5, 20-29.
31. Šumiga, B. (2015). Understanding and use of information literacy in the industrial project management. *Communications in Computer and Information Science*, 552, 90–98. DOI: 10.1007/978-3-319-28197-1_10
32. Tomaszewski, R. (2016) The concept of the imploded Boolean search: A case study with undergraduate chemistry students. *Journal of Chemical Education*, 93(3), 527-533.
33. Tornee, N., Bunterm, T., Lee, K., and Muchimapura, S. (2019). Examining the effectiveness of guided inquiry with problem-solving process and cognitive function training in a high school chemistry course. *Pedagogies*, 14(2), 126–149. DOI: 10.1080/1554480X.2019.1597722
34. Tzvetko, V., and Boiadjev, E. (2013). Forming key competencies by problem-based learning of chemistry in secondary school. *Chemistry*, 22(5), 662–675.
35. Viera, L.I., Ramírez, S.S., and Fleisner, A. (2017). The Organic Chemistry laboratory: A propose to the promotion of scientific technological competences. *Educacion Quimica*, 28(4), 262–268. DOI: 10.1016/j.Equation2017.04.002
36. Wang, X., Thorarinsdottir, A.E., Bachrach, M., and Blayney, M.B. (2019). Building a sustainable student-led model to promote research safety in academic laboratories. *ACS Central Science*, 5(12), 1900-1903. DOI: 10.1021/acscentsci.9b00562
37. Wei Wen Wong, C., Yi Goh, H., and Ong, Y.Y. (2020). Understanding the specific technical requirements needed for successful transitioning to a workplace and the chemistry undergraduate course syllabi: a case study. *Journal of Chemical Education*, 97(1), 72-79. DOI: 10.1021/acs.jchemed.9b00376
38. Yokono, Y., and Mitsuishi, M. (2012). Education program for Ph.D. Course students to cultivate literacy and competency. *Journal of Japanese Society for Engineering Education*, 60(2), 245-250.
39. Zinn, S.R., Slaw, B.R., Lettow, J.H., Menssen, R.J., Wright, II, J.H., Mormann, K., and Ting, J.M. (2020). Lessons learned from the creation and development of a researcher-led safety organization at The University of Chicago. *ACS Chemical Health & Safety*, 27(2), 114-124. DOI: 10.1021/acs.chas.9b00001

$$X = \frac{\sum_{i=1}^n x_i}{n} \quad (\text{Eq. 1})$$

$$\chi_{emp}^2 = \frac{1}{n_1 n_2} \sum_{i=1}^4 \frac{(n_1 Q_{2i} - n_2 Q_{1i})^2}{Q_{1i} + Q_{2i}} \quad (\text{Eq. 2})$$

$$\chi_{emp}^2 = \frac{1}{61 \cdot 63} \sum_{i=1}^4 \frac{(61 Q_{2i} - 63 Q_{1i})^2}{Q_{1i} + Q_{2i}} = \left(\frac{1}{61 \cdot 63} \frac{(61 \cdot 6 - 63 \cdot 6)^2}{6+6} + \frac{(61 \cdot 6 - 63 \cdot 6)^2}{6+6} + \frac{(61 \cdot 6 - 63 \cdot 6)^2}{6+6} + \frac{(61 \cdot 6 - 63 \cdot 6)^2}{6+6} \right) \approx 0.426286 \quad (\text{Eq. 3})$$

$$\chi_{emp}^2 = \begin{cases} 7.815 (\alpha \leq 0.05) \\ 11.345 (\alpha \leq 0.01) \end{cases} \quad (\text{Eq. 4})$$

Table 1. Dynamics of the Levels of Motivation for Vocational Training of 1-5-Year Students at the Ascertaining Stage of the Pedagogical Experiment

Motivation level	1 year		2 year		3 year		4 year		5 year	
	pers.	%	pers.	%	pers.	%	pers.	%	pers.	%
High	27	56.3	20	47.6	10	25.0	12	27.2	17	39.5
Sufficient	16	33.3	9	21.4	17	42.5	9	20.5	9	20.9
Medium	5	10.4	12	28.6	8	20.0	16	36.4	14	32.6
Low	0	0.0	1	2.4	5	12.5	7	15.9	3	7.0
Total	48	100.0	42	100.0	40	100.0	44	100.0	43	100.0

Table 2. Value of ICT Competence Development

Groups	Levels				Total
	High	Sufficient	Medium	Low	
EG1	Q ₁₁ =8	Q ₁₂ =16	Q ₁₃ =18	Q ₁₄ =15	n ₁ =57
EG2	Q ₂₁ =6	Q ₂₂ =17	Q ₂₃ =22	Q ₂₄ =16	n ₂ =61
EG3	Q ₃₁ =7	Q ₃₂ =18	Q ₃₃ =25	Q ₃₄ =20	n ₃ =70
CG	Q ₄₁ =6	Q ₄₂ =18	Q ₄₃ =24	Q ₄₄ =15	n ₄ =63

Table 3. Empirical Values of the χ^2 Criterion for the data in Table 2

	EG1	EG2	EG3	CG
EG1	0	1.029226	0.45807	1.924949
EG2	1.029226	0	1.427069	0.426286
EG3	0.45807	1.427069	0	1.974865
CG	1.924949	0.426186	1.974865	0

Table 4. Results of the First Control Cross-Section of ICT Competence Development for Students from EG1_2 before the Start of the Formative Stage of the Pedagogical Experiment

Criterion	Scale	Levels				Total
		High	Sufficient	Medium	Low	
Value-motivational (before)	persons	37	41	23	17	118
	%	31.4	34.7	19.5	14.4	100.0
Technological (before)	persons	29	48	35	6	118
	%	24.5	40.7	29.7	5.1	100.0
General professional (before)	persons	0	25	52	41	118
	%	0.0	21.2	44.1	34.7	100.0
Subject-professional (before)	persons	0	23	49	46	118
	%	0.0	19.5	41.5	39.0	100.0
Technological (after)	persons	23	48	37	10	118
	%	19.4	40.7	31.4	8.5	100.0
General professional (after)	persons	0	23	54	41	118
	%	0.0	19.5	45.8	34.7	100.0
Subject-professional (after)	persons	0	15	50	53	118
	%	0.0	12.7	42.4	44.9	100.0
Personality-reflexive (after)	persons	4	31	44	39	118
	%	3.3	26.3	37.3	33.1	100.0
ICT competence	persons	14	31	43	31	118
	%	10.2	27.1	36.4	26.3	100.0

Table 5. Results of the Second Control Cross-Section of ICT Competence Development for Students from EG1_2 at the Formative Stage of the Pedagogical Experiment

Criterion	Scale	Levels				Total
		High	Sufficient	Medium	Low	
Value-motivational (before)	persons	46	43	23	6	118
	%	39.0	36.4	19.5	5.1	100.0
Technological (before)	persons	31	54	29	4	118
	%	26.3	45.8	24.6	3.4	100.0
General professional (before)	persons	17	48	46	7	118
	%	14.4	40.7	39.0	5.9	100.0
Subject-professional (before)	persons	2	17	58	41	118
	%	1.7	14.4	49.2	34.7	100.0
Technological (after)	persons	25	52	33	8	118
	%	21.2	44.1	28.0	6.8	100.0
General professional (after)	persons	29	44	39	6	118
	%	24.6	37.3	33.1	5.1	100.0
Subject-professional (after)	persons	0	17	47	54	118
	%	0.0	14.4	39.8	45.8	100.0
Personality-reflexive (after)	persons	8	41	50	19	118
	%	6.8	34.7	42.4	16.1	100.0
ICT competence	persons	19	40	41	18	118
	%	16.1	33.9	34.7	15.3	100.0

Table 6. Results of the Third Control Cross-Section of ICT Competence Development for Students from EG1_2 of the Formative Stage of the Pedagogical Experiment

Criterion	Scale		Levels				Total
		High	Sufficient	Medium	Low		
Value-motivational (before)	persons	52	44	18	4		118
	%	44.1	37.3	15.2	3.4		100.0
Technological (before)	persons	43	56	19	0		118
	%	36.4	47.5	16.1	0.0		100.0
General professional (before)	persons	19	64	29	6		118
	%	16.1	54.2	24.6	5.1		100.0
Subject-professional (before)	persons	35	46	27	10		118
	%	29.7	39.0	22.9	8.5		100.0
Technological (after)	persons	31	62	23	2		118
	%	26.3	52.5	19.5	1.7		100.0
General professional (after)	persons	15	64	31	8		118
	%	12.7	54.2	26.3	6.8		100.0
Subject-professional (after)	persons	35	44	29	10		118
	%	29.7	37.3	24.6	8.5		100.0
Personality-reflexive (after)	persons	27	56	21	14		118
	%	22.9	47.5	17.8	11.9		100.0
ICT competence	persons	33	55	24	6		118
	%	28.0	46.6	20.3	5.1		100.0

Table 7. Results of ICT Competence Development Criteria for Future Chemistry Teachers (%)

Group	Levels	Criteria							
		Value-motivational		Cognitive		Operational-technological		Personality-reflexive	
		before	after	before	after	before	after	before	after
EG	High	31.3	44.7	8.0	27.1	6.4	22.9	8.0	24.5
	Sufficient	33.0	35.6	27.1	46.8	24.4	47.3	24.5	45.7
	Medium	19.7	15.4	37.8	21.3	39.9	23.4	36.1	18.1
	Low	16.0	4.3	27.1	4.8	29.3	6.4	31.4	11.7
CG	High	19.0	20.3	8.0	11.7	8.5	13.6	9.5	11.9
	Sufficient	46.1	42.4	19.0	30.0	22.5	28.8	25.4	28.8
	Medium	25.4	23.7	47.6	43.3	35.3	37.3	49.2	45.7
	Low	9.5	13.6	25.4	15.0	33.7	20.3	15.9	13.6

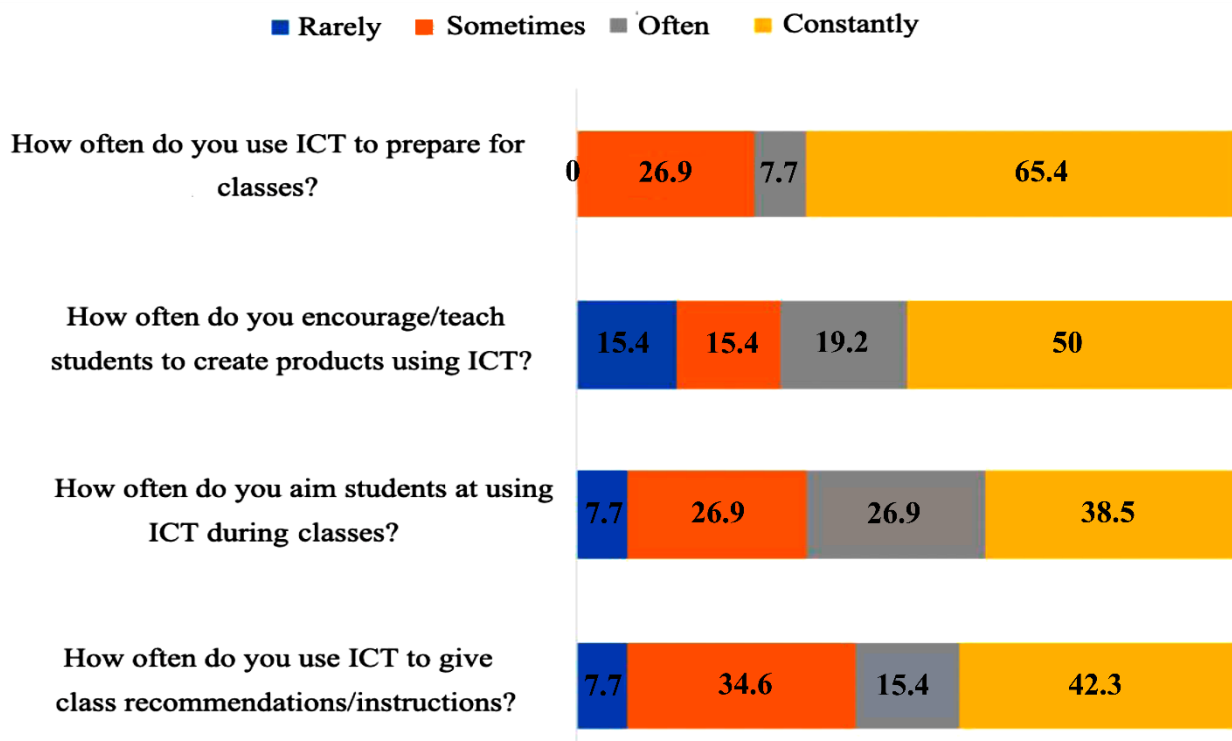


Figure 1. Use of ICT in the Educational Process by Teachers (%)

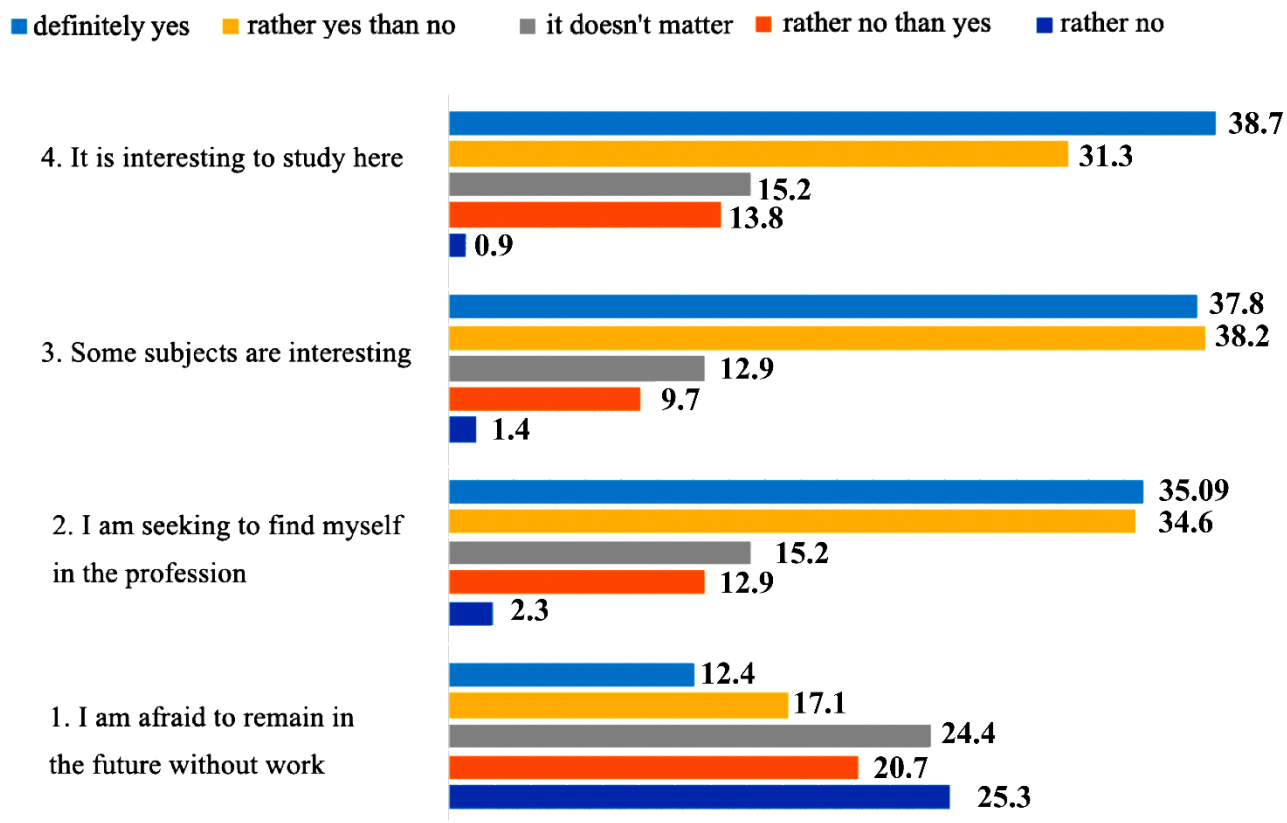


Figure 2. Future Chemistry Teachers' Motives for Choosing the Profession (%)

■ definitely yes ■ rather yes than no ■ it doesn't matter ■ rather no than yes ■ rather no

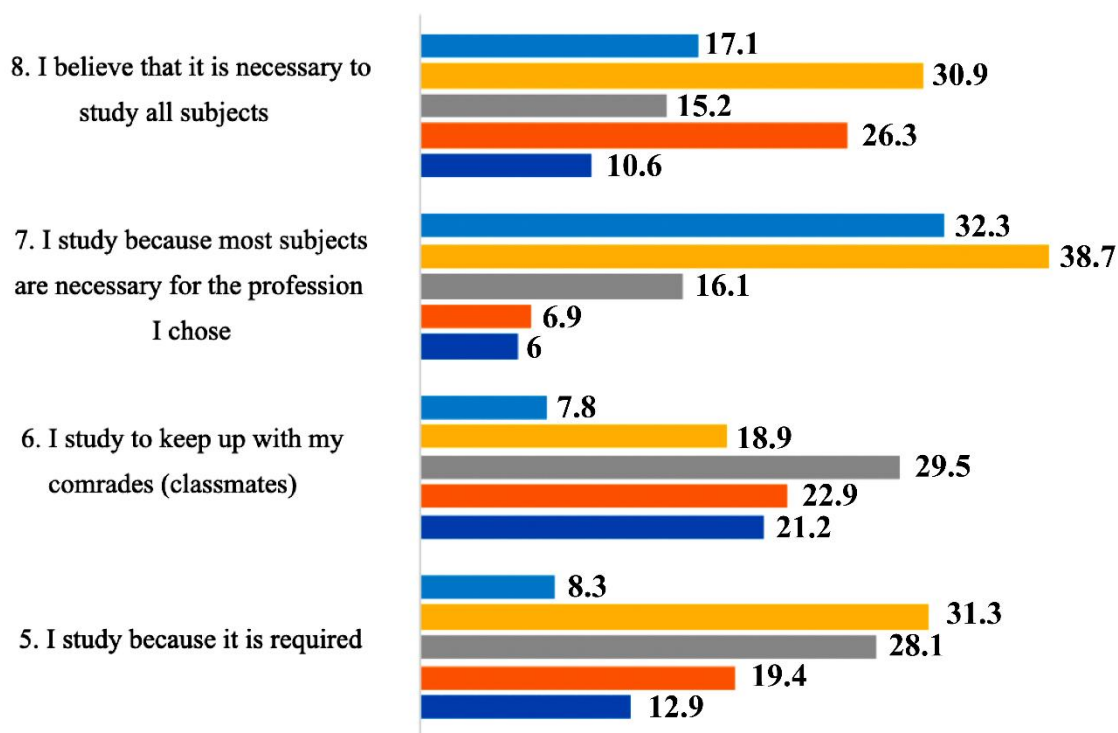


Figure 3. Motives of Educational and Cognitive Activities of Students (%)

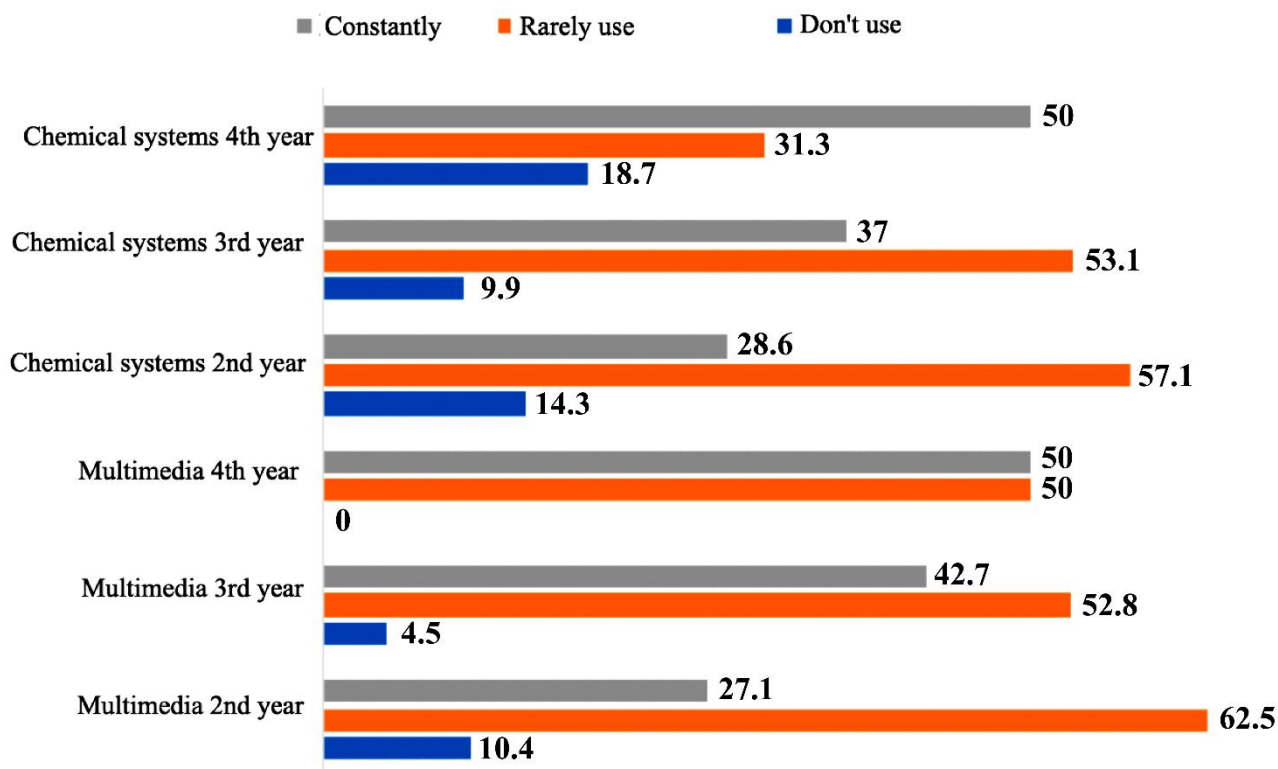


Figure 4. Frequency of Students using ICT in Educational Activities (%)

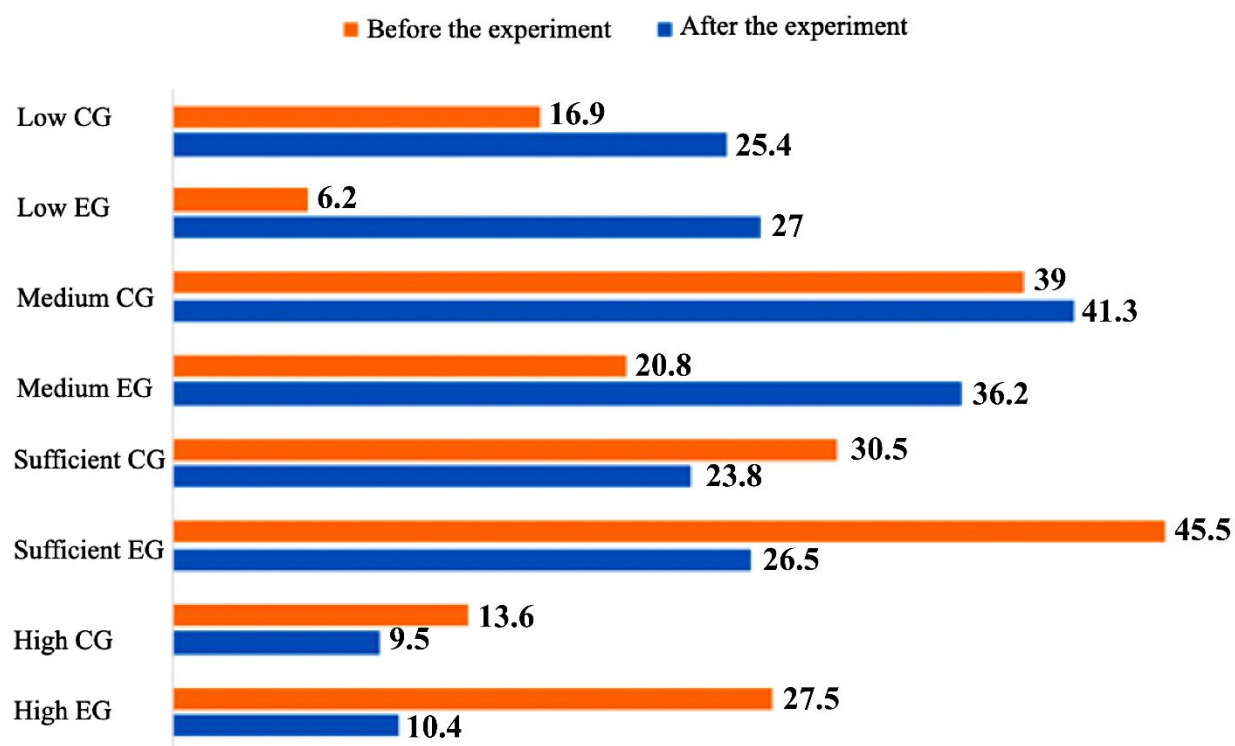


Figure 5. Levels of Future Chemistry Teachers' ICT Competence Development from the EG and CG before and after the Completion of the Formative Stage of the Pedagogical Experiment (%)

APPENDIX 1.

Survey Questions for Teachers:

1. How often do you use ICT to prepare for classes?
2. How often do you encourage/teach students to create products using ICT?
3. How often do you aim students at using ICT during classes?
4. How often do you use ICT to give class recommendations/instructions?
5. How often do you use general-purpose professional software?
6. How often do you use communication tools (email, social media, instant text messaging, Facebook, Twitter.)?
7. How often do you use cooperation/brainstorming tools (discussion forums, Wikis, Google Docs, Wikispaces, Mind Maps, Skype, Google Drive)?
8. How often do you use cloud-based file storage/note-taking applications (Google Drive, Dropbox, Evernote.)?
9. How often do you use course management systems/content management systems/feed systems/learning management systems, mobile applications and devices, blogs and RSS feeds, educational networks, interactive student response systems or survey tools, modeling and educational games to achieve the educational goals of the educational process and their professional development?
10. Do ICTs allow students to work together efficiently, in your opinion?
11. Do ICTs help optimize the time students spend on assignments, develop creativity and creative thinking, and deepen their knowledge of the discipline, in your opinion?
12. How often do you use the Internet?
13. Do you use a computer at school?
14. Do you have access to the Internet at school?
15. How often do you use multimedia equipment?
16. What is your ICT level?
17. Are you able to deepen your knowledge and use it in educational activities?
18. Are you capable of producing new knowledge?

Survey Questions for Students:

1. What prompted you to choose a profession?
2. Are you ready to use multimedia, in particular, a multimedia board, in chemistry classes at school at this stage of training?
3. Are you ready to use multimedia and create electronic educational resources (didactic and methodological materials) to ensure the educational process at school at this stage of training?
4. How often do you use ICT in educational activities?
5. Do you agree that using diverse types of electronic educational resources, multimedia, chemical systems in the educational process increases the intensity of studying educational material, helps to better understand and remember educational material, increases the activity of learning objects in the lesson, and helps to focus on educational material?
6. What is the most effective form of presentation of materials for educational and cognitive activities, in your opinion?

MUDANÇA NA QUÍMICA SANGUÍNEA, CITOCINAS PRO-INFLAMATÓRIAS E GENES APOPTÓTICOS APÓS O USO DE METAFETAMINA EM RATOS EXPERIMENTAIS

CHANGE IN BLOOD CHEMISTRY, PRO-INFLAMMATORY CYTOKINES, AND APOPTOTIC GENES FOLLOWING METHAMPHETAMINE USE IN EXPERIMENTAL RATS

صحرایی موشهای در متامفتامین از استفاده دنبال به که آپوپتوتیک ژنهای و التهابی پیش سینوکینه های ، خون شیمی در تغییر شوند می استفاده آزمایشی

GOUDARZI, Zahra¹; HOSEINI Seyed Ebrahim^{1*}; MEHRABANI, Davood^{2,3,4,5}; HASHEMI, Seyedeh Sara³

¹ Department of Biology, Shiraz Branch, Islamic Azad University, Shiraz, Iran

² Stem Cell Technology Research Center, Shiraz University of Medical Sciences, Shiraz, Iran

³ Burn and Wound Healing Research Center, Shiraz University of Medical Sciences, Shiraz, Iran

⁴ Center of Comparative and Experimental Medicine, Shiraz University of Medical Sciences, Shiraz, Iran

⁵ Department of Oncology, University of Alberta, Edmonton, Alberta, Canada

* Corresponding author
e-mail: mehrabad@outlook.com

Received 20 August 2020; received in revised form 29 October 2020; accepted 14 November 2020

RESUMO

A metanfetamina (METH) é uma substância ilícita abusada globalmente com níveis epidêmicos em todo o mundo. Este estudo teve como objetivo investigar as alterações na química do sangue e citocinas pró-inflamatórias após o uso de metanfetamina em ratos experimentais. Um total de quarenta e cinco ratos fêmeas foram aleatoriamente dedicados a três grupos iguais de experimental recebendo METH por via subcutânea (0,4 mg / kg, em 0,6 mL de volume) por 21 dias, o sham recebeu 0,6 mL de solução salina normal e o controle recebeu 0,6 mL destilado água, de forma idêntica. O teste do labirinto em cruz elevado foi usado para confirmar mudanças cognitivas e de ansiedade após o uso de METH até três semanas. Química do sangue e citocinas inflamatórias foram avaliadas após o uso de METH até 21 dias. Os resultados mostraram um aumento da ansiedade. Os níveis séricos de fator de crescimento transformador beta (TGF-β), interleucinas de IL-15, IL-17 e níveis de adenosina desaminase xantina oxidase foram anotados. No entanto, a contagem de leucócitos (leucócitos) demonstrou uma tendência decrescente. Não houve outras alterações na química do sangue após o uso de METH. Pôde-se observar, entretanto, que a metanfetamina aumenta a ansiedade e faz algumas alterações na química do sangue e nas citocinas pró-inflamatórias. Este estudo pode ajudar a tomar melhores decisões sobre a prevenção e até mesmo o tratamento de pessoas que tomam metanfetamina.

Palavras-chave: metanfetamina, ansiedade, química do sangue, apoptose, citocinas inflamatórias.

ABSTRACT:

Methamphetamine (METH) is a globally heavily abused illicit substance with epidemic levels worldwide. This study aimed to investigate changes in blood chemistry and pro-inflammatory cytokines following methamphetamine use in experimental rats. A total of forty-five female rats were randomly devoted to three equal groups of experimental receiving METH subcutaneously (0.4 mg/kg, in 0.6 mL volume) for 21 days, sham received similarly 0.6 mL normal saline, and the control received 0.6 mL distilled water, identically. The elevated plus-maze test was used to confirm cognitive and anxiety changes following METH use until three weeks. Blood chemistry and inflammatory cytokines were evaluated after METH use until 21 days. The results showed an increase in anxiety. The serum levels of transforming growth factor-beta (TGF-β), interleukins of IL-15, IL-17, and adenosine deaminase xanthine oxidase levels were noted. However, white blood cell (WBC) count demonstrated a decreasing trend. There were no other changes in blood chemistry after METH use. It could be observed, however, that methamphetamine increases anxiety and makes some changes in blood chemistry and pro-

inflammatory cytokines. This study can help make better decisions about the prevention and even treatment of people taking methamphetamine.

Keywords: *methamphetamine, anxiety, blood chemistry, apoptosis, inflammatory cytokines*

چکیده:

مت آمفتامین (METH) یک ماده غیرقانونی است که در سطح جهانی به شدت مورد سوء استفاده قرار گرفته و دارای سطح اپیدمی در سراسر جهان است. این مطالعه با هدف بررسی تغییرات شیمیایی خون و سیتوکین های پیش التهابی به دنبال استفاده از مت آمفتامین در موش های آزمایشگاهی انجام شد. در مجموع چهل و پنج موش ماده به طور تصادفی به سه گروه مساوی از آزمایش تجویز زیر جلدی (0.4 میلی گرم در کیلوگرم ، در حجم 0.6 میلی لیتر) به مدت 21 روز اختصاص داده شد ، شش به طور مشابه 0.6 میلی لیتر نرمال سالین دریافت کرد و شاهد 0.6 میلی لیتر مقطر دریافت کرد. آب ، به طور یکسان. برای افزایش تغییرات شناختی و اضطرابی بدنبال استفاده از METH تا سه هفته ، از آزمایش ماز بعلاوه پیچ و خم استفاده شد. شیمی خون و سیتوکین های التهابی پس از استفاده از METH تا 21 روز مورد بررسی قرار گرفت. نتایج افزایش اضطراب را نشان داد. سطح سرمی تبدیل فاکتور رشد بتا (TGF- β)، اینترلوکینهای IL-15 ، IL-17 و آدنوزین دی آمیناز گرانانتین اکسیداز مشخص شد. با این حال ، تعداد گلبول های سفید (WBC) روند کاهشی را نشان می دهد. پس از استفاده از METH هیچ تغییر دیگری در شیمی خون مشاهده نشد. با این وجود می توان مشاهده کرد که مت آمفتامین اضطراب را افزایش می دهد و برخی تغییرات را در شیمی خون و سایتوکاین های پیش التهاب ایجاد می کند. این مطالعه می تواند به تصمیم گیری بهتر در مورد پیشگیری و حتی درمان افرادی که مت آمفتامین مصرف می کنند ، کمک کند.

واژه های کلیدی: مت آمفتامین ، اضطراب ، شیمی خون ، آپوپتوز ، سیتوکین های التهابی

1. INTRODUCTION:

Amphetamine type stimulants include amphetamine, methamphetamine (METH), and 3,4-methylenedioxymethamphetamine (MDMA, ecstasy). METH is easily manufactured in clandestine drug laboratories and is available as a ground, whitish powder; pills; sticky, waxy base; and crystalline shards (Ice) (McKetin *et al.*, 2005). It was first synthesized in 1893 in Japan (Suwaki, 1991). METH can be used orally, nasally, or intravenously to produce a euphoric high for the consumer and causes inhibition of fatigue, enhancement of mental acuity, mood, social and sexual function, and a reduction in appetite (Shin *et al.*, 2017). Prolonged use at high levels results in independence. METH is a spinoff of amphetamine, which used to be widely prescribed in the 1950s and 1960s as a medicine for depression and obesity, achieving a height of 31 million prescriptions in the United States in 1967. Until the late 1980 ser (Anglin *et al.*, 2000). Methamphetamine-associated psychosis (MAP) represents an intellectual sickness precipitated with the aid of chronic methamphetamine use in a subset of users. The prevalence of the ailment has multiplied in quite a few countries in Europe and Asia, the place methamphetamine use has increased. MAP stays challenging to distinguish from main psychiatric disorders, mainly schizophrenia, growing issues in prescribing remedy plans to sufferers (Chiang *et al.*, 2019). Nonetheless, the prevalence of METH use has increased in both Europe and Asia, including Iran, too (Wang *et al.*, 2016). It was robustly illustrated to produce psychotic symptoms as a condition known as METH-associated psychosis (MAP) (Glasner-Edwards and Mooney, 2014;

Schwarzbach *et al.*, 2020).

There is no pharmacotherapy for METH use disorder to be approved by the Food and Drug Administration (Chan *et al.*, 2019). Accurate identification of exposure to METH can have important implications for the care of the abuser. Sampling blood is one of the first types of biological material analyzed in METH abusers to detect drug complications (Plotka *et al.*, 2014). METH abuse is related to activation of the innate immune response, the concerning cellular and chemical elements, and inflammatory cytokines. The literature collectively displays an association of METH use with innate immune response activation in CNS with neurotoxicity (Clark *et al.*, 2013).

The innate immune response activation is an early stage of neuroinflammatory reaction to insult that can cause migration of inflammatory cells through the blood-brain barrier (BBB) into the CNS parenchyma (Clark *et al.*, 2013). Microglial activation is linked to the production of several pro-inflammatory molecules, including chemokines, cytokines, and nitric oxide (Minagar *et al.*, 2002). Although the negative effects of METH abuse are considered significant problems, few studies have been conducted on changes in blood cells and blood chemistry and pro-inflammatory cytokines.

This study aimed to assess the anxiety and changes in blood chemistry and pro-inflammatory cytokines following methamphetamine use in experimental rats.

2. MATERIALS AND METHODS

2.1. Ethics

The Ethics Committee for Animal Use of Islamic Azad University, Shiraz Branch, approved the study protocol on September 30, 2018 (7-E-IR-MIAU.REC.80-B-2018), and all experiments were undertaken according to Iran Veterinary Organization guidelines.

2.2 Chemicals and Reagents

Except where otherwise stated, all chemicals were obtained from Sigma (Sigma Chemical Co., St. Louis, MO, USA).

2.3. Preparation of METH

METH (Sigma-Aldrich, USA) was a donation by the Shiraz Branch of Islamic Azad University in Shiraz, Iran, with written permission for research purposes. Before use in experiments, Methamphetamine solution in normal saline was prepared with a concentration of 66.6%. To make METH, we dissolved 66.6 mg of METH in 100 cc of normal saline.

2.4 Animals and grouping

A total of forty-five females, with 8 weeks old Wistar rats, weighing from 200 to 220 g were purchased from the Comparative and Experimental Medicine Center of Shiraz University of Medical Sciences, Shiraz, Iran. The animals were kept under controlled environmental conditions of 22 °C, 70 % humidity, a 12-h light and dark cycle (lights on at 8:00 a.m.), and free access to a standard diet and tap water. Before the experiments, the accommodation to their condition was carried out.

The rats were randomly divided into three equal groups (Table 1) of experiments receiving 0.4 mg/kg of METH subcutaneously in 0.6 mL volume for 21 days. The sham group received subcutaneously 0.6 mL normal saline for 21 days, and the control group received 0.6 mL distilled water identically. Daily interventions were performed from 08:00 a.m. to 12:00 a.m.

2.5. Confirming METH addiction by anxiety assessment

A plus-maze with two 50×10 cm opposite open arms confined by 40 cm height walls was

applied, while the arms were connected by a 10×10 cm central square, shaped like a “plus”, and elevated 50 cm from the floor was lit by a dim light. The interventions were video-recorded, while the camera was at a 50° angle above the maze, and the anxiety scores were recorded in an adjacent room. The number of entries, together with the percent time spent in open arm (OAT), closed arm (CAT), and central parts of the maze, were collected. Head dipping for the exploratory movement of the head/shoulders of the rats over the side of the maze was also investigated (Holmes *et al.*, 2000).

When all four paws were inside the arm, an arm entry was registered; and exit from an arm was when the forepaws were outside that arm. On test day before starting experiments, the animals were transferred undisturbed to a dimly illuminated room for 1 h. As rats are usually reactive to man's direct handling, a cylindrical cardboard tube was used for individual transportation of the animals from the cage to the plus-maze. Scoring was conducted for 5 min by an observer who was blind to the protocol, and the data were directly entered into a PC computer. All tests were carried out between 8.00 a.m. and 12.00 a.m., and the maze was thoroughly cleaned (wet and dry cloths) between successive experiments.

2.6. Hematological assessment

A capillary glass tube was inserted into the medial canthus of the right eye above the lacrimal duct under deep anesthesia, and 2.5 ml of blood was collected from the orbital sinus. Aliquots were prepared and dispensed in tubes with EDTA or sodium citrate or without any anticoagulant for hematological assessment of transforming growth factor-beta (TGF-β), interleukins of IL-15, and IL-17, adenosine deaminase (ADA), xanthine oxidase (XO), white blood cells (WBC), red blood cells (RBC), hemoglobin (Hb), hematocrit (HCT), platelet (PLT), triglycerides (TG), cholesterol, high-density lipoprotein cholesterol (HDL), blood urea nitrogen (BUN), total bilirubin, creatinine, uric acid, albumin, total protein, alkaline phosphatase (ALK), aspartate aminotransferase (AST) and alanine aminotransferase (ALT) levels.

Blood urea nitrogen (BUN) levels, creatinine, uric acid, triglycerides (TG), cholesterol, high-density lipoprotein cholesterol (HDL), Total bilirubin, albumin, total protein, alkaline phosphatase (ALK), aspartate aminotransferase (AST), and alanine aminotransferase (ALT) were measured biochemically by an autoanalyzer (Permium24i,

Japan) and Bionic assay kit.

By using an electronic cell counter (Baker 9000 Automated Cell Counter, Biochem Immunosystems, Inc., Allentown, PA), a complete blood count was done. A Coulter Dacos Chemistry Analyzer (Coulter, Miami, FL) was employed to evaluate uric acid levels. RBC count was carried out with a hemocytometer using a solution of 3.13% trisodium citrate as diluents applying standard hemocytometer protocol was used to count the RBC.that integrated the number of RBC counted, dilution factor, as well as area and depth of the chamber. A hemocytometer conducted the platelet count after 1 in 20 dilutions of the sample in 1% ammonium oxalate. WBC count was undertaken identically. Hemoglobin concentration was detected using 1 in 20 dilutions and at a wavelength of 540 nm (Baker *et al.*, 2000).

The adenosine deaminase (ADA, ZellBio GmbH, Germany) assay kit quantitatively assessed rat ADA in serum based on the biotin double antibody sandwich technology. Xanthine oxidase activity (XOX, ZellBio GmbH, Germany) assay kit evaluated XOX activity in serum samples. All tests except leukocyte differential counts were done on the day of blood collection, while all biochemical and hematological experiments were duplicated. TGF- β , IL-15, IL-17, ADA, and XO levels were assessed by ELISA (Stat Fax® 4200 - Awareness Technology, USA – Florida)

2.7. Statistical analysis

The effect of METH on the number of entries and the percent time spent in OAT, CAT, central parts of the maze, and head dipping were investigated between the three groups at the end of the first, second, and third week. The obtained data were exhibited as mean \pm SEM and statistically analyzed using SPSS software (Version 21, Chicago, IL, USA) by one-way ANOVA, Post-hoc Tukey's, and independent Student t-tests. P values \leq 0.05 were defined as statistically significant.

3. RESULTS AND DISCUSSION:

3.1 METH addiction

METH could significantly increase the anxiety level after METH use ($p < 0.05$) based on OAT findings denoting a significant difference between the experimental and the control group (Figure 1). Regarding CAT after METH use, there

was a significant difference between the experimental and the control group ($p < 0.0005$), revealing that METH could significantly increase the anxiety level in experimental rats (Figure 2). Considering the effect of METH on percent time spent in central parts of the maze after METH consumption, there was a significant difference between the experimental and the control group, demonstrating that the METH use could significantly increase the amount of anxiety in the experimental group ($p < 0.05$, $p < 0.0005$) (Figure 3). Evaluation of METH effect on head dipping of the animals revealed a significant difference between the experimental and the control group of rats treated with METH ($p < 0.001$, $p < 0.0005$, $p < 0.0005$) (Figure 4).

3.2. Hematological assessment

The effects of methamphetamine on hematological factors including white blood cells, red blood cells, hemoglobin, hematocrit, platelets, triglycerides, HDL and cholesterol in female rats are shown in Table 2. The results of the effect of methamphetamine on the white blood cell count of female rats indicate that the white blood cell count in the first and second treatments and the Sham group were significantly different from the control group ($P < 0.05$). But there was no significant difference between the number of white blood cells in the third treatment and the control group ($P > 0.05$). For the other factors studied in this study, including red blood cells, hemoglobin, hematocrit, and platelets, no significant differences were observed between the treatment and control groups ($P > 0.05$).

The results related to the effect of methamphetamine on TG level showed a significant difference between the Sham group with the control group and the treatment group in the first week with the control group ($P < 0.05$). The amount of TG in different periods of treatment with methamphetamine and control group and Sham numerically shows an irregular increase trend. The highest rate is related to Sham group and the lowest is related to treatment in the first week. The effect of methamphetamine on Chol and HDL did not show a significant difference ($P > 0.05$). Regarding TGF- β , IL-15, IL-17, ADA, and XO levels, a significant increase was noted following METH use ($p < 0.001$) (Table 4). For WBC count, there was a decrease ($p = 0.009$). However, regarding RBC count, Hb, HCT, PLT, BUN, creatinine, uric acid, TG, cholesterol, HDL, total bilirubin, albumin, total protein, and ALK, no changes in the values were noticed following METH administration. Furthermore, the levels of

AST and ALT were increased in the METH groups in comparison with Control and Sham groups Table 3.

3.3. Discussion

During the past two decades, there has been a tremendous expansion of knowledge regarding how the central nervous system responds to noxious stimuli such as psychostimulants of abuse (methamphetamine, cocaine, ecstasy) by immune response including inflammatory cytokines (IL-1b, IL-6, TNF- α), blood chemistry and gene expression. It was shown that the pro-inflammatory cytokines active in the innate immune process are keys to injury response, extended or amplified production (Clark *et al.*, 2013). Substance use, such as METH, can cause behavioral modifications such as anxiety (Kamali-Sarvestani *et al.*, 2020; Sadeghi Bimorgh *et al.*, 2020). In this study, similarly, an increasing trend for anxiety level was noted following METH use.

Pro-inflammatory cytokines are involved in the maintenance and homeostasis of the immune system, inflammation, and host defense (Li *et al.*, 2020). METH abuse results in severe dysregulation in the peripheral immune response and causes an imbalanced expression in chemokines, cytokines, and other molecular factors due to neuronal injury (Tran *et al.*, 2018). In this study, pro-inflammatory cytokines of IL-15, IL-17, and TGF- β demonstrated a significant increase following METH use.

There has been markedly increased expression of TNF- α (Mahajan *et al.*, 2006) and ultimately induced apoptosis (Shen *et al.*, 2020), leading to an elevated expression of IL-1 β resulting in neurotoxic activity (Du *et al.*, 2017), and exacerbated IL-2 secretion (Bortell *et al.*, 2015), and up-regulated IL-6 level (Wang *et al.*, 2017), a rise in IL-8 to be a significant marker of anxiety and depression (Huckans *et al.* 2015), a considerable enhancement of IL-10 (Burns and Ciborowski, 2016), a significantly increased expression of IL-12 (Peerzada *et al.*, 2013) and a greatly enhanced expression of IFN- α (Li *et al.*, 2020).

There were no data available in the literature regarding changes in IL-15, IL-17, and TGF- β after METH use. However, an increased IL-15, IL-17, and TGF- β expression were shown in patients with inflammatory diseases (Chen *et al.*, 2018). Several studies revealed that TGF- β is the quintessential cytokine of Th17 cell differentiation. It was found that in the presence of TGF- β , polarization to the Th17 cells happens and make

these cells secrete IL-17A, IL-17F, IL-21, and IL-22, that leads to inflammation, tissue remodeling, metaplasia, and hyperplasia modifications in the tissue (Chen *et al.*, 2018), that can explain the rise in TGF- β and as a consequence the increase in IL-17.

Up-regulation of pro-inflammatory cytokines, including IL-17, has been previously reported during allergic inflammation (Vanvalkenburgh *et al.*, 2011), which is in line with our results following METH use. A high expression level of TGF- β , IL-15, and IL-17 was detected in mice with chronic inflammatory diseases (Salehi *et al.*, 2016; Wang *et al.*, 2018) in agreement with our findings METH consumption too. The study provides in vivo evidence for the involvement of the IL-15, IL-17, and TGF- β after METH use with significantly up-regulated IL-15, IL-17, and TGF- β .

These findings denoted an increase in the ADA level following METH use, which was time-dependent. The extracellular adenosine level is regulated by uptake into cells and by metabolism undertaken by adenosine kinase (AKA) and ADA (Meghji, 1991). Adenosine as a neuromodulator is released from metabolically active or stressed cells, and adenosine analogs were demonstrated to exert a neuroprotective effect in METH neurotoxicity in mice (Delle Donne and Sonsalla, 1994; Gołembiowska and Zylewska, 2000). These findings are in agreement with the results of this study.

XO, as the enzyme responsible for the catabolism of purines and their conversion into uric acid, was illustrated can be overexpressed after stress, which eventually can lead to inflammation in the tissue (Maimaiti *et al.*, 2019). It was shown that multiple doses of METH could dramatically raise extracellular concentrations of dopamine and serotonin, with significant behavioral and neurochemical consequences. These neurotransmitters can, in turn, increase cytotoxic quinones and reactive oxygen species (Kokoshka *et al.*, 1998). METH also creates an environment disturbing the balance between oxidative stress and antioxidant defense (McDonnell-Dowling, 2017). Therefore, the increase in xanthine oxidase in our study can be explained by the inflammatory effect of METH administered in rats too. As METH has significant effects on both the innate and adaptive immune responses (Peerzada *et al.*, 2013; Sriram *et al.*, 2015), it can lead to a reduction in the numbers of leukocytes rendering individuals susceptible to certain diseases and infections (Mahajan *et al.*, 2006). This decline in WBC count was also noted in this study in line with the METH effect.

4. CONCLUSIONS:

It was concluded that there was an increase in anxiety following methamphetamine use in animal model. Also, it could be observed that the use of methamphetamine led to an increase in inflammation, ALT, AST, ADA and xanthine oxidase after consumption. The results of the present study also showed that methamphetamine has an effect on the white blood cell and TG where the lowest rate of TG is related to treatment in the first week. Further research is required to confirm these findings and determine involved mechanisms in other animals, and humans.

5. ACKNOWLEDGMENTS:

This work was supported by the Shiraz Branch of Islamic Azad University. The authors would like to thank the Comparative and Experimental Medicine Center of Shiraz University of Medical Sciences, providing the laboratory facility. The authors declare that they have no competing interests.

6. REFERENCES

1. Anglin, M. D., Burke, C., Perrochet, B., Stamper, E., Dawud-Noursi, S. (2000) History of the methamphetamine problem. *J Psychoactive Drugs*, 32, 137-41.
2. Baker, F. J., Silverton, R. E., Pallister, C. J. (2000). Baker and Silverton's Introduction to Medical Laboratory Technology. BH, 7th Edition, Available at: <https://www.amazon.com/Silvertons-Introduction-Medical-Laboratory-Technology/dp/0750621907>.
3. Bortell, N., Morsey, B., Basova, L., Fox, H. S., Marcondes, M. C. (2015). Phenotypic changes in the brain of SIV-infected macaques exposed to methamphetamine parallel macrophage activation patterns induced by the common gamma-chain cytokine system. *Front Microbiol*, 6, 900.
4. Burns, A., Ciborowski, P. (2016). Acute exposure to methamphetamine alters TLR9-mediated cytokine expression in human macrophage. *Immunobiology*, 221, 199-207.
5. Chan, B., Freeman, M., Kondo, K., Ayers, C., Montgomery, J., Paynter, R., Kansagara, D. (2019). Pharmacotherapy for methamphetamine/amphetamine use disorder-a systematic review and meta-analysis. *Addiction*, 114, 2122-36.
6. Chen, S., Han, Y., Chen, H., Wu, J., Zhang, M. (2018). Bcl11b Regulates IL-17 Through the TGF- β /Smad Pathway in HDM-Induced Asthma. *Allergy Asthma Immunol Res*, 10, 543-54.
7. Chiang, M., Lombardi, D., Du, J., Makrum, U., Sitthichai, R., Harrington, A., Shukair, N., Zhao, M., Fan, X. (2019). Methamphetamine-associated psychosis: Clinical presentation, biological basis, and treatment options. *Hum Psychopharmacol*, 34, e2710.
8. Clark, K. H., Wiley, C.A., Bradberry, C.W. (2013). Psychostimulant abuse and neuroinflammation: emerging evidence of their interconnection. *Neurotox Res*, 23, 174-88.
9. Delle Donne, K. T., Sonsalla, P. K. (1994). Protection against methamphetamine-induced neurotoxicity to neostriatal dopaminergic neurons by adenosine receptor activation. *J Pharmacol Exp Therap*, 27, 1320-6.
10. Du, S. H., Qiao, D. F., Chen, C. X., Chen, S., Liu, C., Lin, Z., Wang, H., Xie, W. B. (2017). Toll-Like Receptor 4 Mediates Methamphetamine-Induced Neuroinflammation through Caspase-11 Signaling Pathway in Astrocytes. *Front Mol Neurosci*, 10, 409.
11. Glasner-Edwards, S., Mooney, L. J. (2014). Methamphetamine psychosis: epidemiology and management. *CNS Drugs*, 28, 1115-26.
12. Gołembiowska, K., Zylewska, A. (2000). Effect of adenosine kinase, adenosine deaminase, and transport inhibitors on striatal dopamine and stereotypy after methamphetamine administration. *Neuropharmacology*, 39, 2124-32.
13. Holmes, A., Parmigiani, S., Ferrari, P. F., Palanza, P., Rodgers, R. J. (2000). Behavioral profile of wild mice in the elevated plus-maze test for anxiety. *Physiol Behav*, 71, 509-16.
14. Huckans, M., Fuller, B.E., Chalker, A. L., Adams, M., Loftis, J. M. (2015). Plasma Inflammatory Factors Are Associated with Anxiety, Depression, and Cognitive Problems in Adults with and without Methamphetamine Dependence: An Exploratory Protein Array Study. *Front Psychiatry*, 6, 178.

15. Kamali-Sarvestani, A., Hoseini, S. E., Mehrabani, D., Hashemi, S. S., Derakhshanfar, A. (2020). Effects in rats of adolescent exposure to Cannabis sativa on emotional behavior and adipose tissue. *Bratisl Lek Listy*, 121, 297-301.
16. Kokoshka, J. M., Metzger, R. R., Wilkins, D. G., Gibb, J. W., Hanson, G. R., Fleckenstein, A. E. (1998). Methamphetamine treatment rapidly inhibits serotonin, but not glutamate, transporters in rat brain. *Brain Res*, 799, 78-83.
17. Li, Y., Li, S., Xia, Y., Li, X., Chen, T., Yan, J., Wang, Y. (2020). Alteration of liver immunity by increasing inflammatory response during co-administration of methamphetamine and atazanavir. *Immunopharmacol Immunotoxicol*, 6, 1-9. [Epub ahead of print]
18. Mahajan, S. D., Hu, Z., Reynolds, J. L., Aalinkeel, R., Schwartz, S. A., Nair, M. P. N. (2006). Methamphetamine modulates gene expression patterns in monocyte-derived mature dendritic cells. *Mol Diagn Ther*, 10, 257-69.
19. Maimaiti, Y., Aikebaier, A., Maimaitiali, A., Wubulikasimu, W., Li, Y.L., Aziguli, A., Yan, J., Kelimu, A. (2019). Effects of psychological stress on xanthine oxidase expression, activity, and related markers in adipose tissue of mice. *Zhongguo Ying Yong Sheng Li Xue Za Zhi*, 35, 537-42.
20. McDonnell-Dowling, K.J.P.K. (2017). The role of oxidative stress in methamphetamine-induced toxicity and sources of variation in the design of animal studies. *Curr Neuropsychopharmacol*, 15, 300-14.
21. McKetin, R., McLaren, J., Kelly, E. (2005). *The Sydney Methamphetamine Market: Patterns of Supply, Use, Personal Harms and Social Consequences*; University of New South Wales: Kensington, NSW, Australia; National Drug and Alcohol Research Centre: Randwick, NSW, Australia, 98.
22. Meghji, P. (1991). Adenosine production and metabolism. In: Stone T. (Ed.), *Adenosine in the Nervous System*. Academic Press, London, 25-42.
23. Minagar, A., Shapshak, P., Fujimura, R., Ownby, R., Heyes, M., Eisdorfer, C. (2002). The role of macrophage/microglia and astrocytes in the pathogenesis of three neurologic disorders: HIV-associated dementia, Alzheimer disease, and multiple sclerosis. *J Neurol Sci*, 202, 13-23.
24. Peerzada, H., Gandhi, J. A., Guimaraes, A. J., Nosanchuk, J. D., Martinez, L. R. (2013). Methamphetamine administration modifies leukocyte proliferation and cytokine production in murine tissues. *Immunobiology*, 218, 1063-8.
25. Płotka, J., Narkowicz, S., Polkowska, Z., Biziuk, M., Namieśnik, J. (2014). Effects of addictive substances during pregnancy and infancy and their analysis in biological materials. *Rev Environ Contam Toxicol*, 227, 55-77.
26. Sadeghi Bimorgh, M., Omid, A., Ghoreishi, F.S., Rezaei Ardani, A., Ghaderi, A., Banafshe, H.R. (2020). The effect of transcranial direct current stimulation on relapse, anxiety, and depression in patients with opioid dependence under methadone maintenance treatment: A pilot study. *Front Pharmacol*, 11, 401. Published April 3.
27. Salehi, M., Bagherpour, B., Shayghannejad, V., Mohebi, F., Jafari, R. (2016). Th1, Th2, and Th17 Cytokine Profile in Patients with Multiple Sclerosis Following Treatment with Rapamycin. *Iran J Immunol*, 13, 141-7.
28. Schwarzbach, V., Lenk, K., Laufs, U. (2020). Methamphetamine-related cardiovascular diseases. *ESC Heart Fail*, 7, 407-14.
29. Shen, S., Zhao, J., Dai, Y., Chen, F., Zhang, Z., Yu, J., Wang, K. (2020). Methamphetamine-induced alterations in intestinal mucosal barrier function occur via the microRNA-181c/ TNF- α /tight junction axis. *Toxicol Lett*, 321, 73-82.
30. Shin, E.J., Dang, D.K., Tran, T.V., Tran, H.Q., Jeong, J.H., Nah, S.Y., Jang, C.G., Yamada, K., Nabeshima, T., Kim, H.C. (2017). Current understanding of methamphetamine associated dopaminergic neurodegeneration and psycho toxic behaviors. *Arch Pharm Res*, 40, 403-28.
31. Sriram, U., Haldar, B., Cenna, J.M., Gofman, L., Potula, R. (2015). Methamphetamine mediates immune dysregulation in a murine model of chronic viral infection. *Front Microbiol*, 6, 793.
32. Suwaki, H. (1991). Methamphetamine abuse in Japan. *NIDA Res Monogr*, 115, 84-98.
33. Tran, T. V., Shin, E. J., Nguyen, L. T. T., Lee, Y., Kim, D. J., Jeong, J.H., Jang, C. G., Nah, S.Y., Toriumi, K., Nabeshima, T.,

- Yamada, K., Kim, H. C. (2018). Protein Kinase C δ Gene Depletion Protects Against Methamphetamine-Induced Impairments in Recognition Memory and ERK1/2 Signaling via Upregulation of Glutathione Peroxidase-1 Gene. *Mol Neurobiol*, 55, 4136-59.
34. Vanvalkenburgh, J., Albu, D.I., Bapanpally, C., Casanova, S., Califano, D., Jones, D.M., Ignatowicz, L., Kawamoto, S., Fagarasan, S., Jenkins, N.A., Copeland, N.G., Liu, P., Avram, D. (2011). Critical role of Bcl11b in suppressor function of T regulatory cells and prevention of inflammatory bowel disease. *J Exp Med*, 208, 2069-81.
35. Wang, G., Zhang, Y., Zhang, S., Chen, H., Xu, Z., Schottenfeld, R.S., Hao, W., Chawarski, M.C. (2016). Aripiprazole and risperidone for treatment of methamphetamine-associated psychosis in Chinese patients. *J Subst Abuse Treat*, 62, 84-88.
36. Wang, J., Li, H. Y., Wang, H. S., Su, Z. B. (2018). MicroRNA-485 Modulates the TGF- β / Smads Signaling Pathway in Chronic Asthmatic Mice by Targeting Smurf2. *Cell Physiol Biochem*, 51, 692-710.
37. Wang, Q., Wei, L. W., Xiao, H. Q., Xue, Y., Du, S. H., Liu, Y. G., Xie, X. L. (2017). Methamphetamine induces hepatotoxicity via inhibiting cell division, arresting cell cycle, and activating apoptosis: In vivo and in vitro studies. *Food Chem Toxicol*, 105, 61-72

Table 1. Groups of study

Group	Description	Number of animals
METH	0.4 mg/kg of METH subcutaneously in 0.6 mL volume for 21 days	15
Sham	subcutaneously 0.6 mL normal saline for 21 days	15
Control	0.6 mL distilled water for 21 days	15
Total		45

Table 2: Blood chemistry profile after METH use (Mean± Standard deviation)

Variable		Group
		Control
		Sham
		METH 1 st week
		METH2 nd week
		METH 3 rd week
7.05±1.03	5.55±0.46	7.63±1.81
0.95	0.03	0.004
6.94±0.41	6.73±1.35	6.97±0.63
0.99	0.44	0.91
14.12±1.28	14.04±0.64	14.00±0.84
0.07	0.16	0.29
39.45±2.94	37.07±15.66	40.78±2.97
0.56	0.07	0.43
636.00±332.1	738.25±38.14	717.75±101.3
0.57	0.84	0.36
85.00±4.35	46.75±17.19	95.75±22.42
0.94	0.08	0.003
69.50±9.67	90.25±44.52	69.00±10.98
1.00	0.82	0.53
44.00±6.00	35.00±2.94	39.00±5.35
0.07	0.91	0.36
		WBC
		P-v ¹
		RBC
		P-v
		HB
		P-v
		HCT
		P-v
		PLT
		P-v
		TG
		P-v
		CHOL
		P-v
		HDL
		P-v

1- P-value

Table 3: Liver and renal function tests after METH use (Mean± Standard deviation).

METH weeks	3 rd	METH weeks	METH 2 nd weeks	METH week	1 st	Sham	Control	Variable
27.50±4.50		24.00±3.91		25.67±2.30		29.00±6.05	27.00±1.00	BUN
1.00		0.87		0.99		0.54	N/A	P-V ¹
0.48±0.09		0.53±0.50		0.633±0.057		0.50±0.00	0.56±0.05	CRT ²
0.33		0.894		0.67		0.03	N/A	P-V
6.50±1.02		4.90±0.49		5.90±0.52		7.03±0.095	6.6±0.11	UA ³
0.99		0.01		0.56		0.002	N/A	P-V
6.51±0.26		6.38±0.37		6.83±0.057		6.40±0.133	6.46±0.14	T-PRO ⁴
0.99		0.99		0.348		0.163	N/A	P-V
166.50±019.22		138.75±20.41		107.00±22.60		107.50±11.09	112.33±2.51	AST
0.008		0.304		0.995		0.001	N/A	P-V
61.00± 24.38		5275±7.63		46.00±4.58		50.75±7.63	51.67±2.08	ALT
0.87		1.00		0.98		0.64	N/A	P-V
329.75±63.17		286.00±74.97		362.00±153.189		394.00±8.04	374.67±14.29	ALK
0.93		0.57		0.84		0.36	N/A	P-V

¹- P- value

²- CREATININE

³- URIC ACID

⁴- TOTAL PROTEIN

Table 4: Pro-inflammatory cytokines following METH use (Mean± Standard deviation).

METH 3 rd weeks	METH 2 nd weeks	METH 1 st week	Sham	Control	Variable	
					Group	
514.50±13.89	672.25±23.51	764.66±25.54	153.50±18.41	262.00±208.71	IL-15	
0.012	0.0001	0.0001	0.0001	N/A	P-v ¹	
504.00±8.36	654.25±22.76	763.66±14.04	193.00±9.12	179.66±9.01	IL-17	
0.0001	0.0001	0.0001	0.0001	N/A	P-v	
844.50±19.22	1001.75±56.59	1079.33±58.79	210.00±7.07	209.66±2.30	TGF-β	
0.0001	0.0001	0.0001	0.0001	N/A	P-v	
5651.00±80.51	4420.75±48.35	257.33±58.22	199.25±4.64	196.33±6.42	ADA	
0.0001	0.0001	0.0001	0.0001	N/A	P-v	
135.25±3.86	112.50±1091	72.00±3.60	5.25±0.50	5.33±1.52	XO	
0.0001	0.0001	0.0001	0.0001	N/A	P-v	

¹- P-value

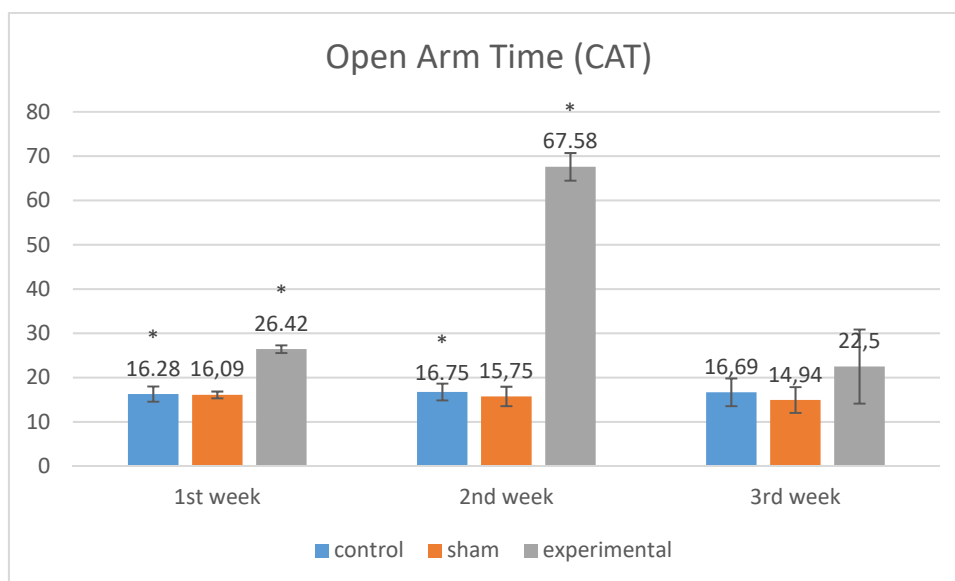


Figure 1. The effect of METH at the end of the first, second, and third week on the mean percentage of open arm time (OAT) between the three groups (* $p < 0.05$).

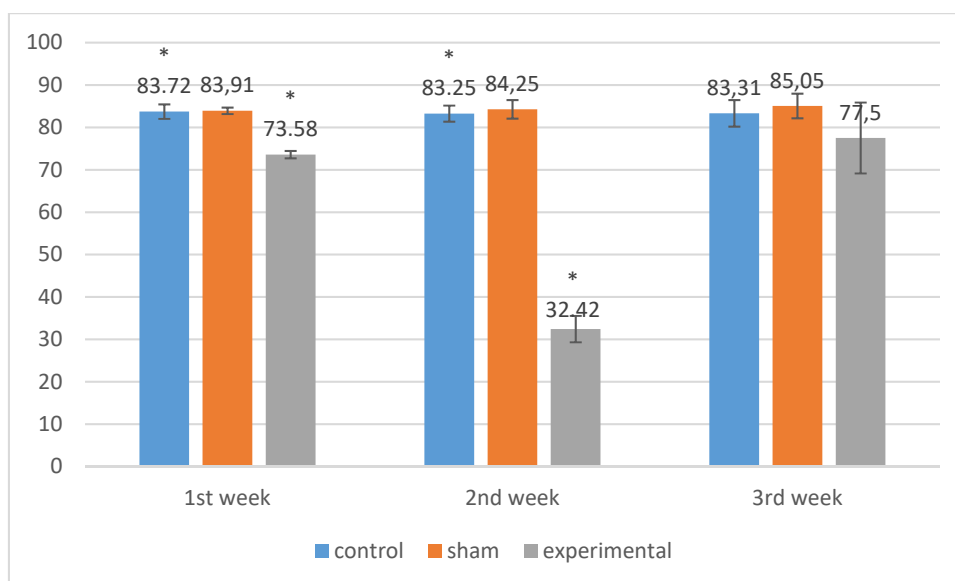


Figure 2. The effect of METH on the mean percentages of time spent in the closed arm time (CAT) at the end of the 1st, 2nd, and 3rd week between the three groups (* $p < 0.0005$).

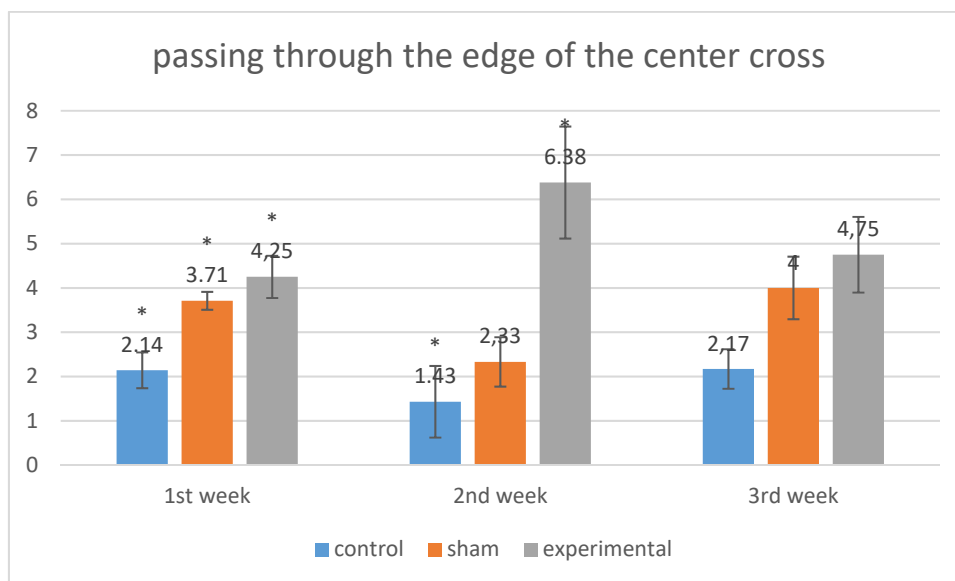


Figure 3. The effect of METH on the mean number of times rats passing through the edge of center cross at the end of the first (* $p < 0.05$), second (* $p < 0.0005$), and third week between the three groups.

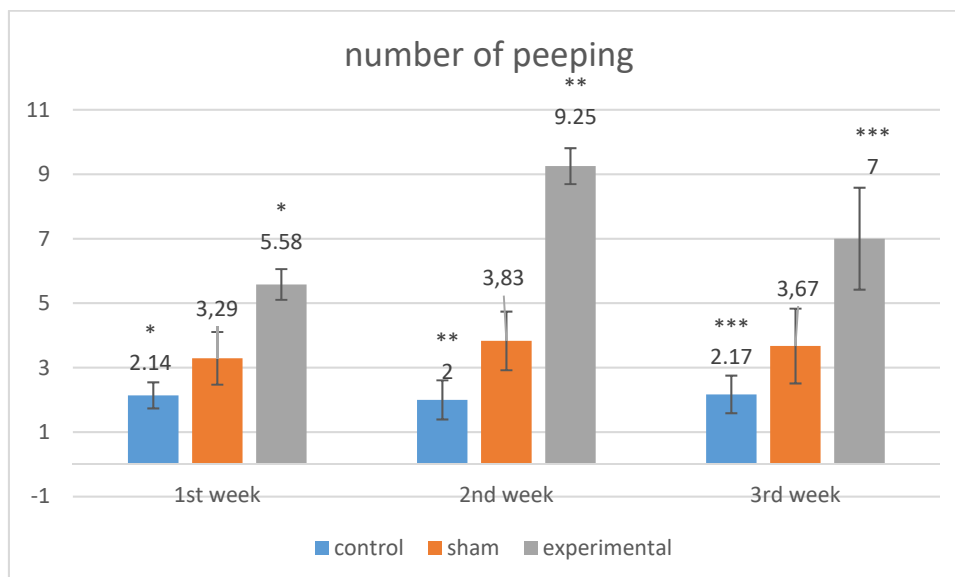


Figure 4. The effect of METH on the mean number of head dipping at the end of the first (* $p < 0.001$), second (** $p < 0.0005$), and third week (** $p < 0.0005$) between the three groups.

PROTOTIPAGEM DE TURBINA MALHA COM SISTEMA DE CONTROLE DE JATO**PROTOTYPING MESH TURBINE WITH THE JET CONTROL SYSTEM****РАЗРАБОТКА ПРОТОТИПА СЕТЧАТОЙ ТУРБИНЫ СО СТРУЙНОЙ СИСТЕМОЙ УПРАВЛЕНИЯ**SAZONOV, Yu.A.¹; MOKHOV, M.A.^{2*}; TUMANYAN, Kh.A.³; FRANKOV, M.A.⁴; BALAKA, N.N.⁵^{1,2,3,4} Gubkin Russian State University of Oil and Gas. Russian Federation.⁵ CJSC "Russian Company for Shelf Development". Russian Federation.

* *Corresponding author*
e-mail: mikhal.mokhov@mail.ru

Received 16 July 2020; received in revised form 30 October 2020; accepted 12 November 2020

RESUMO

Nas condições de instabilidade do mercado de petróleo e gás, é necessário intensificar a pesquisa científica exploratória para o desenvolvimento de equipamentos avançados e baratos de bombeamento e compressores destinados a uma produção mais eficiente de hidrocarbonetos. O trabalho de pesquisa em andamento está sendo realizado com o objetivo de pesquisar e estudar novas oportunidades técnicas para o desenvolvimento de equipamentos avançados de bombeamento e compressores adaptados às complicadas condições de produção de óleo e gás na presença de partículas sólidas abrasivas no escoamento do meio bombeado. Uma nova tecnologia de compressão de gás foi desenvolvida e patenteada usando uma unidade de compressor a jato quando o ejetor é ligado em modo cíclico. O ciclo liga-desliga do ejetor em vez de sua operação contínua torna possível aumentar a multiplicação da razão de compressão do gás. Para aumentar a eficiência energética da unidade de compressor a jato, a tecnologia de recuperação de energia com a aplicação de uma turbina especial tendo a estrutura de malha da parte de fluxo foi proposta e patenteada. Foram realizados trabalhos de pesquisa e desenvolvimento, a caminho do desenvolvimento de turbinas inteligentes e unidades compressoras inteligentes. Modelos 3D com a aplicação do sistema CAD SOLIDWORKS 3D foram desenvolvidos. O pacote de software FloEFD de dinâmica de fluidos computacional tem sido usado para modelagem de computador. Em condições de laboratório, o desempenho do protótipo de turbina de malha equipado com o sistema de controle de jato foi testado com sucesso. O desenvolvimento de unidades compressoras eficientes e mais baratas tornará possível resolver os problemas atuais de produção ao extrair hidrocarbonetos em condições complicadas, bem como no estágio final de desenvolvimento dos campos de petróleo e gás. Certos resultados de pesquisas científicas realizadas podem ser usados em outros ramos de produção, incluindo energia, transporte e robótica.

Palavras-chave: *modelo 3D, modelagem computacional, produção de petróleo.*

ABSTRACT

The oil and gas market is unstable, which requires intensification of the exploratory research for working advanced and inexpensive pumping and compressor equipment out. Such equipment is crucial for more efficient hydrocarbon production. The ongoing research work is being undertaken to search and study new technical opportunities to develop advanced pumping and compressor equipment adapted to the complicated conditions of oil and gas production in solid abrasive particles in the flow of the pumped medium. New technology for gas compression has been evolved and further patented. The technology utilized a jet compressor unit to assist a turned on ejector while in the cyclic mode. Pulsed cycling of the ejector in contrary to continuous operation, increases the compression ratio of the multiplied gas. The energy recovery technology has been evolved, and further patented to increase the energy efficiency in the jet compressor unit. This technology applies a particular mesh turbine located at the flow part. The evolution of smart turbines and compressor units was thoroughly researched. 3D-models have been developed in SOLIDWORKS 3D CAD system. The FloEFD software package of computational fluid dynamics has been used for computer modeling. In laboratory conditions, the performance of the mesh turbine prototype

equipped with the jet control system has been successfully tested. Efficient and cheap compressor units solve many urgent issues in production connected with hydrocarbons extraction in harsh environments and those, which occur at the later stages of developing oil and gas fields. Specific research results can be used in other domains, including energy, transport, and robotics.

Keywords: *3D-model, computer modeling, oil production.*

АННОТАЦИЯ

Рынок нефти и газа нестабилен, что требует интенсификации поисковых исследований для отработки современного и недорогого насосного и компрессорного оборудования. Такое оборудование имеет решающее значение для более эффективной добычи углеводородов. Ведутся постоянные исследовательские работы по поиску и изучению новых технических возможностей для разработки передового насосного и компрессорного оборудования, адаптированного к сложным условиям добычи нефти и газа в виде твердых абразивных частиц в потоке перекачиваемой среды. Была разработана и запатентована новая технология сжатия газа. В технологии использовался струйный компрессор для помощи включенному эжектору в циклическом режиме. Импульсное переключение эжектора в отличие от непрерывного режима увеличивает степень сжатия попутного газа. Технология рекуперации энергии была усовершенствована и запатентована, чтобы повысить энергоэффективность струйного компрессора. В этой технологии применяется конкретная сетчатая турбина, расположенная в проточной части. Разработка интеллектуальных турбин и компрессорных агрегатов была тщательно исследована. 3D-модели разработаны в системе SOLIDWORKS 3D CAD. Программный пакет вычислительной гидродинамики FloEFD был использован для компьютерного моделирования. В лабораторных условиях успешно испытана работоспособность опытного образца сетчатой турбины с системой управления струей. Эффективные и дешевые компрессорные агрегаты решают многие актуальные производственные вопросы, связанные с добычей углеводородов в суровых климатических условиях и возникающие на поздних этапах разработки нефтяных и газовых месторождений. Конкретные результаты исследований могут быть использованы в других областях, включая энергетику, транспорт и робототехнику.

Ключевые слова: *3D-модель, компьютерное моделирование, добыча нефти.*

1. INTRODUCTION:

As reservoir pressure drops at the late stage of oil and gas field development, there is a need for additional pumping and compressor equipment. However, the well-known compressor and turbine machines do not yet fully solve such urgent tasks because the working conditions for the equipment are complicated by the presence of solid abrasive particles in the flow of the pumped media (Chen, Li, Li, and Zhao, 2015).

There are known technologies for developing oil and gas fields, where jet pumps and compressors are used for liquid and gas pumping at high mechanical impurities content, as described in papers by Brink (2014), Singh, Prasad, Singh, Jha, and Tandon (2013). Adjustable ejectors are also used, and most frequently, the adjustment is made by changing the cross-section area in the channel at the nozzle, as described in the patent (Morishima, 2008).

The information on new developments where flow direction is periodically changed in

hydraulic system channels is published in our previous work (Sazonov *et al.*, 2019). Scientific research studies in this area are developing. However, the specific features of reversible pumps and reversible compressors have not yet been studied sufficiently. The technological capabilities of such machines in the area of hydrocarbon extraction under complicated conditions have not been fully realized.

Special pumps and turbines have been developed for severe operational conditions, and each such hydraulic machine is equipped with a rotor made in the form of the mesh. This rotor structure can withstand higher loads, and here the authors can refer to the experience of the development and application of grid-like wings described in by Bilotserkovskiy *et al.* (1985).

In oil and gas fields, the active application of compressor and turbine technologies is currently being hampered by rather high prices for such equipment, especially in falling oil and gas prices. In this regard, the development of new efficient and affordable pump, compressor and turbine units can be fully attributed to the relevant objectives.

The known turbine designs are not adapted to the operating conditions in the oil and gas production system. At present, energy-saving turbine technologies are practically not used in oil fields. This situation is associated with an uncontrolled change in the density of the gas-liquid mixture in the flow channels of the turbine. This density varies in a wide range of values from 1 to 1,000 kilograms per cubic meter. There is a need to create new compressor technology for complicated conditions of use in oil and gas fields.

The purpose of the ongoing research work is to find and study new technical opportunities to develop promising pumping and compressor equipment adapted to the complicated operating conditions of oil and gas production in the presence of solid abrasive particles in the flow of the pumped medium (of liquid, gas or gas-liquid mixture).

The following main tasks were set to create a new turbine technology: 1) development of a reliable jet control system based on advanced scientific developments, including in the field of gas dynamics and hydrodynamics (Abugov and Bobylev, 1987); 2) development of a new turbine design capable of operating in conditions with an uncontrolled change in the density of the gas-liquid mixture in the flow channels, when this density changes in a wide range of values from 1 to 1,000 kilograms per cubic meter; 3) creation of the simplest and cheapest turbine design and control system, to reduce costs and to reduce the payback period of investments.

The specialists of the Gubkin Russian State University of Oil and Gas have developed and patented a new technology for compressing gas through a jet compressor, which implies that the ejector works in a pulse mode (Sazonov *et al.*, 2019). When creating new equipment, reliable technical solutions and methods were used that have successfully passed a long test (Trabold, Esen, and Obot, 1988; Shamanov, Dyadik, and Labinsky, 1989; Croft, Williams, and Tay, 1978; Coleman, Kim, and Spalart, 2003; Gao and Zhuang, 2004), including methods for creating nozzle devices, multiphase jet devices using computer calculation programs. According to preliminary estimates, this technology will make it possible to realize single-stage isothermal gas compression to pressures at the level of 10...40 MPa. Pulse operation of the ejector compared to continuous operation reduces energy consumption for gas compression multiply. The

energy recovery technology, which requires a special mesh turbine of the flow part, has been proposed and subsequently patented to increase the energy efficiency of the jet compressor unit. This scientific field of research is at the initial stage today. In this connection, the study and improvement of energy recovery technology and technology for a jet compressor unit are relevant scientific and practical objectives.

2. MATERIALS AND METHODS:

For computer modeling and computational research, the FloEFD computational fluid dynamics software package developed by the Mentor Graphics company was used. The 3D model was created using the SolidWorks CAD system. In the process of modeling, the complete system of averaged Navier – Stokes equations was solved, described by mathematical expressions of the laws of conservation of mass, energy, and momentum. In the entire computational domain, the system automatically performed the transition between laminar and turbulent states. By default, the turbulence parameters were set automatically. To calculate the turbulent parameters for the closure of the Navier – Stokes system of equations, the authors used the model of turbulent viscosity modified by Lamb – Bremhorst. For the calculation, a structured Cartesian grid was generated. FloEFD uses sliding mesh technology to simulate rotation.

Two well-known additive technologies were used to manufacture a prototype of a mesh turbine and a jet control system: "Material Extrusion", "Sheet Lamination". Material Extrusion technology provides for the "extrusion of material" or layering of molten material through an extruder, which is the main unit of a 3D printer. "Sheet Lamination" technology provides for "joining sheet materials" or layer-by-layer formation of a product from sheet materials. In the presented work, sheet plastic and sheet steel were used to manufacture parts that make up the turbine prototype and the jet control system. For laboratory tests, samples of a mesh turbine with rotor diameters of 30 mm, 60 mm, 100 mm, 120 mm were made. Were also prepared samples of nozzles with a channel diameter from 1 mm to 10 mm.

In the course of laboratory hydraulic tests, the properties of the new turbine were

investigated. During the measurements, the values of physical quantities were found using special technical means, including the use of an infrared frequency meter "Testo 465" with a measurement range from 1 to 99999 rpm with a measurement error of 0.02% (Testo, Germany), weight scale "CAS SWN" with a measurement error of 1 gram at a measurement range of 0.04 kg to 5 kg (manufactured by CAS Corporation, Republic of Korea), frequency converter "Altivar 312-ATV312HU75N4" (Schneider Electric, France), radial pressure gauge ROSMA TM-510P.00 1/2" 10 bar (CJSC ROSMA, Russia), Casio HS-3V-1R stopwatch (Casio, Japan).

The scheme of the laboratory bench installation is shown in Figure 1.

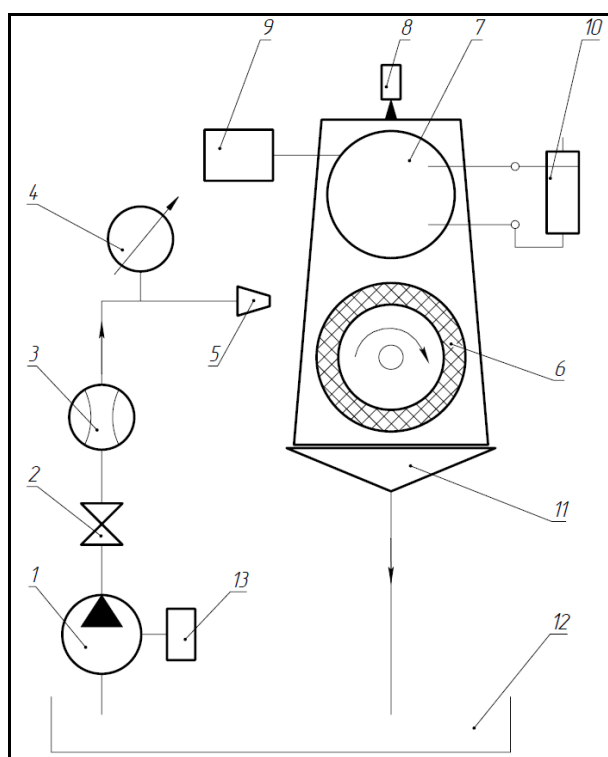


Figure 1. The scheme of laboratory bench installation: 1 - pump; 2 – gate valve; 3 - flowmeter; 4 – pressure gauge; 5 - nozzle; 6 - turbine; 7 - electric generator; 8 - tachometer; 9 - weight scale; 10 - electrical resistance; 11 - casing; 12 - vessel; 13 - frequency converter

Turbine 6 and electric generator 7 were mounted on a common shaft. In the process of testing the turbine, a direct method of measuring the power on the turbine was used. The direct method of measuring the power on the shaft of a hydraulic machine is to measure the torque and speed and is used, as a rule, when testing low-power installations. In this case, an electric braking device was used to

determine the torque. The torque control was carried out by changing the electrical resistance 10 in the electrical circuit of the electric generator 7. To determine the torque by means of the braking device, the following values were measured: length of the brake lever; the weight of the brake lever; force on the brake lever.

When carrying out hydraulic tests of the turbine, it was used pump 1 with a nominal head of 100 meters and a flow rate of 5 to 50 liters per minute, the pump brand Pedrollo PQ-3000 (manufactured by the Italian firm Pedrollo).

3. RESULTS AND DISCUSSION:

Up to the present moment, the scientific and technological capabilities of hydrodynamic and gas-dynamic systems, which have wide opportunities to control the processes associated with changing the direction of the flow of liquid or gas, have not been completely realized. As the direction of liquid or gas flow changes, the operating mode of a pump or compressor unit radically changes. Within the framework of ongoing scientific research, the typical and the most straightforward scheme of a compressor unit is considered, represented in Figure 2.

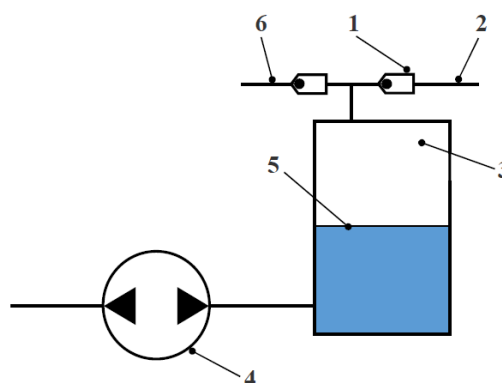


Figure 2. Schematic diagram of a compressor unit equipped with a reversible pump

The valve actuating gear 1 contains the suction valve and the discharge valve, making it possible to periodically connect the working chamber 3 to either the low-pressure gas pipeline 6 or the high-pressure gas pipeline 2. In the working chamber 3, a force impact is applied to the pumped gas, making it possible to compress the gas and direct it to the high-pressure gas pipeline 2. Such a force impact on the gas is provided by the liquid pumped by the

reversible pump 4 into the working chamber 3. The interface between liquid and gas is marked on the diagram by position 5. When the liquid is pumped, the boundary surface 5 is displaced upwards, and the gas pressure increases in the working chamber 3 while the compressed gas is pushed out through the discharge valve into the high-pressure gas pipeline 2. The direction of flow is then changed through the reversible pump 4, and the liquid is pumped out from the working chamber 3. In this case, the boundary surface 5 is displaced downwards, and the pressure in the working chamber 3 is reduced, and the gas from the low-pressure gas pipeline 6 is fed through the suction valve into the working chamber 3. The described operation cycle is repeated.

In the reversible pump, as a rule, the direction of flow is changed due to the change of the rotation direction of the rotor. The area of the practical application of such systems is very limited due to inertial processes. Practical and scientific interest represents the issue of technical possibilities for developing a special switch-gear, which will make it possible to generate reverse flows when using any type of pump, and without changing the rotation direction of the rotor.

For illustration purposes, Figures 3 and 4 represent the connection diagram of the switch-gear 1 to the centrifugal pump 4. The pump 4 has an input channel 3 and an output channel 5. The flow of pumped media is directed from channel 2 to channel 6.

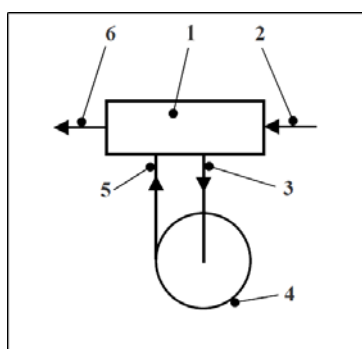


Figure 3. Connection diagram of the switch-gear

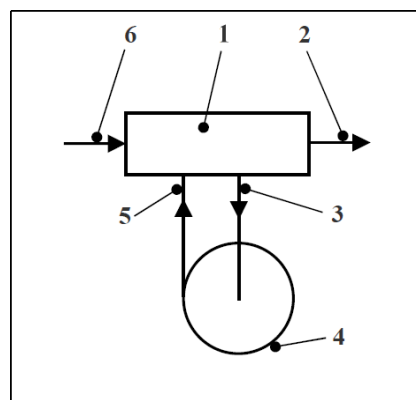


Figure 4. Connection diagram of the switch-gear after switching the flow direction to the opposite one

Figure 4 represents a diagram that corresponds to the operating mode after switching the switch-gear 1.

According to the diagram in Figure 4, the pumped media flow is already directed opposite from channel 6 to channel 2. After this switching, the pump 4 does not change its operating mode while the fluid flow in the pump keeps the same flow direction from inlet channel 3 to outlet channel 5, as shown by the arrows in Figures 3 and 4.

Within the framework of solving practical problems for the oil and gas industry, the complicated working conditions for switch-gears, pumping, and compressor equipment are considered. Complications are related to solid abrasive particles in the flow of liquid, gas, or gas-liquid mixture. At this stage of research work, switch-gear options are considered, which provide a relatively short time interval for switching – at the level of 0.1 seconds. It is known from the state of the art that such a time interval for switching is quite achievable using electromagnetic devices. To solve practical problems, particular interest variants of systems with the pump (or compressor) unit from several dozens to several hundreds of kW.

To improve energy efficiency in hydrocarbon production, turbine technologies are also being considered, which, among other things, ensure more rational use of reservoir energy. As the most interesting scientific perspective, multi-mode turbine units with wide opportunities for practical application in oil and gas fields have been considered.

Figure 5 represents the switch-gear variant of connection with possibilities to change (control) the flow direction. In this

example, the liquid flow is fed to the pump 4 through the inlet channel 3. The liquid is fed into the switch-gear 1 at high pressure through the output channel 5. At the outlet of the switch-gear 1, one (or two) liquid jets 2 and 6 are formed, flowing into the surrounding space. In this case, the surrounding space can be filled with liquid or gas. The diagram shows the centerline 7 and angles " α " and " β " to quantify the jet direction.

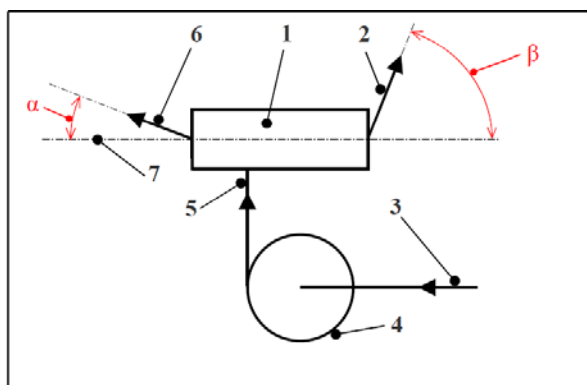


Figure 5. Switch-gear connection diagram with possibilities for changing (regulating) the flow direction

According to Figure 5, gas or a gas-liquid mixture can be used in the technical system instead of the liquid, and the compressor, gas generator, or another source of compressed gas can be used instead of the pump.

For illustration purposes, Figure 6 shows the option of connecting the switch-gear to the conical turbine with possibilities for changing the flow direction. In this example, the conical turbine 1 is connected to the electrical generator 2. The liquid (or gas) is fed into the switch-gear 4 through the inlet channel 3. The switch-gear 4 makes it possible to change the direction of the downstream flow. This may be an option with the direction marked in the diagram as position 5. Other variants, according to positions 6 or 7 are also possible. In this case, the liquid (or gas) jet impacts the conical turbine 1 and brings this turbine into the rotary movement.

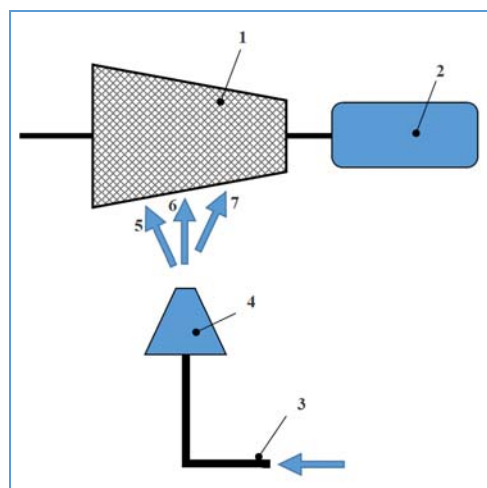


Figure 6. Diagram of connecting the switch-gear to the conical turbine with possibilities for changing the flow direction

For illustration purposes, Figure 7 shows the option of connecting the switch-gear to the disk turbine, with possibilities to change the flow direction. In this example, disk turbine 1 is connected to the electric generator 2. Inlet channel 3 supplies liquid (or gas) to the switch-gear 4. The switch-gear 4 allows the direction of the outgoing flow to be changed; this may be the option with the direction marked in the diagram as position 5. Other options, according to position 6 or 7, are also possible. In this case, the liquid (or gas) jet impacts the disc turbine 1 and brings this turbine into the rotary movement.

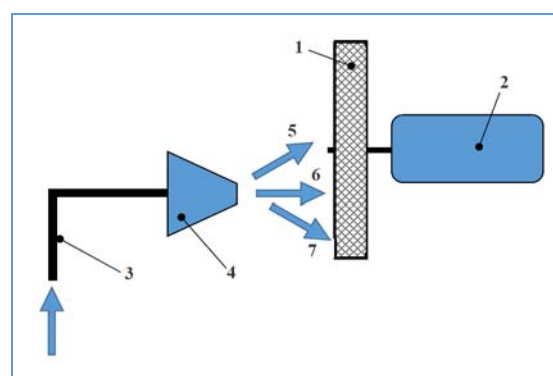


Figure 7. Diagram of connecting the switch-gear to the disc turbine with possibilities for changing the flow direction

In the examples, according to Figures 6 and 7, as the flow direction changes, the point at which the force is applied to the turbine rotor will also change. In this case, the working radius – the distance from the rotor axis of rotation of the turbine to the point of force application, will change. In this case, the

rotational moment on the turbine shaft will also change. The specific feature of this control system is that when the flow rate of the working fluid (or gas) increases, it is possible to slow down the rotor speed of the turbine or even to force the turbine to rotate backward. For well-known power plants, such modes of turbine operation are not considered at all. However, for energy-saving technologies in oil and gas production, such modes can be useful because the turbine can perform several technological functions simultaneously.

At the present stage of research works, certain basic principles have been considered for the development of the multi-mode mesh turbine with possibilities to control the flow of the working medium and with possibilities to change the distance from the revolution axis of the turbine rotor to the point of force application, where the force interaction of the liquid flow with the hard wall of the vane on the turbine rotor is carried out.

Within the ongoing research framework, special designs of turbines, pumps, and compressors have been considered. The specific feature consists of using the mesh structure when profiling the rotor and stator flow. Figure 8 illustrates the mesh vane prototype manufactured on a 3D printer to investigate impeller machines with the mesh structure of channels.



Figure 8. Experimental prototype of the mesh vane manufactured on a 3D printer for investigation of impeller machines with the mesh structure of channels

In design and engineering works, the term “prototype” is usually understood as the

working model developed to demonstrate the working capacity and substantiation of the product being developed. The technology of fast prototyping provides the fast implementation of the basic functionality of the future product. At present, the fast development of the “prototype” became possible for a wide range of researchers and experts due to various additive technologies, including 3D-printers' application.

Figure 9 illustrates the variant of the computer model for carrying out numerical experiments when investigating impeller machines with the mesh structure of channels. Various variants with the application of liquids and gases have been considered. In this example, the ejector, as an element of the switch-gear, is used. For the oil and gas industry, ejector switch-gears are of special scientific and practical interest because of their universality. The ejector can operate both in jet pump mode and in jet compressor mode, and multiphase pump mode.

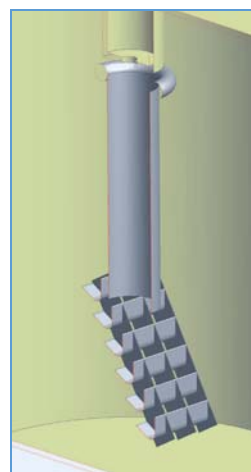


Figure 9. Variant of a computer model for carrying out numerical experiments when investigating impeller machines with the mesh structure of channels

In the example, the flow conditions of one vane in the gas medium have been considered. Figure 10 graphically illustrates the velocity diagrams based on the results of numerical experiments carried out following the model represented in Figure 9.

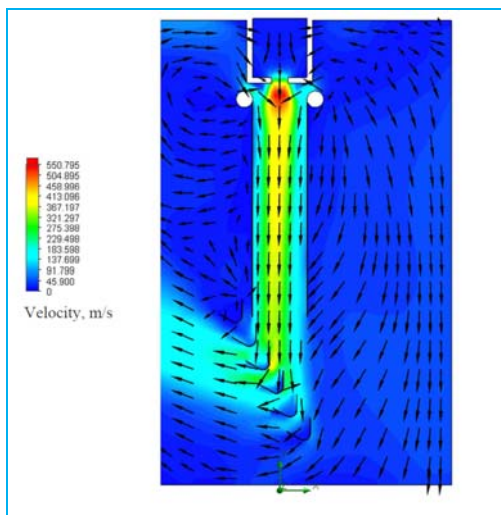


Figure 10. Example with the results of numerical experiments when investigating impeller machines with the mesh structure of channels

Computer modeling results have been used for design engineering within the framework of developing experimental models of new equipment.

For conducting laboratory tests, prototypes of turbines (experimental prototypes and turbines) have been developed. For example, Figures 11 and 12 demonstrate photographs of some experimental prototypes manufactured using additive technologies. As illustrated in Figure 11, the model (prototype) of the turbine was placed directly on the shaft of an electric generator for a faster transition to laboratory testing.



Figure 11. Experimental prototype (pre-production model) of the disk turbine manufactured on a 3D printer for investigating impeller machines with the mesh structure of channels



Figure 12. Experimental prototype (pre-production model) of the conical turbine manufactured on a 3D printer for investigating impeller machines with the mesh structure of channels

Laboratory tests of the created mesh turbine prototypes have been carried out. When testing the turbine prototype, the rotor speed was brought to the level of 20,000 to 30,000 rpm. To simulate the change in the density of the working medium, compressed air and water were used during the turbine tests. In the course of laboratory tests, the efficiency of the created turbine equipment was confirmed. During hydraulic tests of the turbine prototype, the efficiency values were fixed at the level of 50%, the ways were outlined for solving the optimization problem and for increasing the efficiency of the new technology being created, taking into account the capabilities of the jet control system.

Several special experiments have been carried out with a mesh turbine prototype. The jet control system was used to brake the turbine rotor and spin the turbine rotor in the opposite direction. The rotor in such reversible turbines can rotate both forward and backward. Such reversible turbines open up new opportunities for developing technologies for the extraction and treatment of oil and gas.

Figure 13 demonstrates the photograph of the switch-gear prototype. This switch-gear prototype is based on the diagram shown in Figure 5. For pneumatic testing, the blowing machine (and compressor) was used instead of the pump.



Figure 13. Experimental prototype (pre-production model) of the switch-gear manufactured with the application of additive technologies

During switch-gear testing, photography and video recording were made in order to capture the specific performance features of the developed prototype. To observe the change in angle " α " (as illustrated in Figure 5), the indicator thread (or interweaving of several threads) illustrated in Figure 14 was used. One end of the indicator thread was attached at the output channel to the wall of the switch-gear. Another end of the indicator thread was left free. Under these conditions, the indicator thread has always been drawn into the moving air current coming out of the switch-gear. This allows the researcher to observe the change in the flow direction without using complex laboratory equipment. This monitoring system was given the working name "ponytail". This system can also be used in the training process.



Figure 14. Experimental prototype of the switch-gear with the indicator thread ("ponytail") when the air current is cut off

Figure 15 illustrates the experimental prototype of the switch-gear equipped with an indicator thread ("ponytail") when air flows through the outlet channel for the conditions

when the angle " α " is equal to zero degrees according to the diagram in Figure 5.



Figure 15. Experimental prototype of the switch-gear equipped with the indicator thread ("ponytail") when the air flows through the outlet channel for the conditions when the angle " α " is equal to zero degrees

Figure 16 illustrates the experimental prototype of the switch-gear equipped with an indicator thread ("ponytail") when the air flows through the outlet channel for the conditions when the angle " α " is more than zero degrees but less than ninety degrees according to the diagram in Figure 5.



Figure 16. Experimental prototype of the switch-gear equipped with the indicator thread ("ponytail") when air flows through the outlet channel for the conditions when the angle " α " is more than zero degrees but less than ninety degrees

Figure 17 illustrates the experimental prototype of the switch-gear equipped with an indicator thread ("ponytail") when the air flows through the outlet channel for the conditions when the angle " α " is equal to ninety degrees according to the diagram in Figure 5.



Figure 17. Experimental prototype of the switch-gear equipped with the indicator thread ("ponytail") when air flows through the outlet channel for the conditions when the angle " α " is equal to ninety degrees

During the laboratory tests, the working capacity of the impeller machine prototype with the mesh structure of the channels has been confirmed (Figures 11 and 12). During the tests, the process of electricity generation using the mesh turbine was simulated. A set of diode lamps was used as a load for the electric generator. Besides hydraulic tests, pneumatic testing with compressed air at pressure up to 0.5 MPa has been performed. Pilot testing with water vapor for the mesh turbine rotation has also been carried out. Tests of the turbine prototype have been carried out using the switch-gear prototype (Figure 13) that enables changing (adjusting) the direction of the working fluid (gas) flow.

There is an urgent problem restraining the introduction of many technologies to improve the efficiency of oil and gas production. This problem is related to the high price of high-pressure compressors with pressure from 10 to 40 MPa. Due to the high cost of these compressors, the practical application of such technologies as the compressor-assisted gas lift technology, the technology of gas injection into the productive formation for enhanced oil recovery, the technology of air injection into the productive formation for the implementation of oxidizing processes as part of work to improve the oil recovery factor, and technology of pumping gas-liquid mixtures is limited. The

reservoir energy in oil and gas production due to the lack of reliable turbine equipment capable of operating in complicated conditions is weakly used. To solve this urgent problem, it is necessary to develop a new compressor and turbine equipment, which will ensure the profitability of hydrocarbon field development.

Jet control systems performed using ejectors are of scientific and practical interest. Control systems for ejectors are known to be used when a conical needle is placed in the nozzle cavity. The conical needle can be moved along the longitudinal axis of the nozzle, and the cross-sectional area of the passage channel at the nozzle is controlled, which in turn makes it possible to regulate the flow of the working fluid passing through the nozzle into the ejector mixing chamber. The well-known ejector regulation circuit can be improved if the conical needle can move not only along the longitudinal axis of the nozzle but also in a radial direction relative to this longitudinal axis of the nozzle, as demonstrated in our previous publication (Sazonov *et al.*, 2019). In this case, the more mobile conical needle significantly increases the possibilities for ejector regulation. In these conditions, it is possible to regulate the hydraulic fluid flow rate and control the direction of the hydraulic fluid flowing through the nozzle. For the time being, there are still some new issues regarding the ejector's adjustment taking into account the changes in the direction of the working fluid jet. With the use of modern computer technologies, additional opportunities have been added to study the working process of the ejector, taking into account changes in the direction of the jet of the working fluid (gas or gas-liquid mixture). In the case of radial displacement of the conical needle, the jet of the working fluid, flowing through the nozzle, changes. In this case, there are additional possibilities for independent regulation of the ejector operation mode and the power pump operation mode. There are opportunities to adjust the ejector's operating mode while maintaining the same operating mode of the power pump.

The results of research activities demonstrate that expensive positive displacement compressors can be replaced with jet compressor units, which differ by high reliability and low price (Sazonov *et al.*, 2019). The developed turbines can help to solve the problem of improving the energy efficiency of equipment under complicated conditions of oil and gas production.

With the development of computer technology, new opportunities open up for the automation of turbine technology and the progress towards developing intelligent turbines and intelligent compressor units. Jet control systems can be easily adapted to computerized control systems.

With modern computer technologies, many expensive physical experiments can be abandoned while replacing physical experiments with numerical ones. Jet elements from the field of science called “pneumatics” are relatively poorly studied. Modern computer programs make it possible to expand this research field due to more large-scale application of numerical experiments. Known developments in aviation and automation systems seem to represent only a fraction of the enormous potential that jet technology and the science of “pneumatics” have. Our research work deals with jet elements in combination with multi-threaded ejectors of various designs and combinations with electromagnetic control systems when solving control tasks for liquid and gas flows, according to our previous paper (Sazonov *et al.*, 2019).

The results of ongoing research can develop technologies for compressing and pumping various gases, such as methane, associated petroleum gas, nitrogen, carbon dioxide, air, hydrogen, or another gas, depending on the technology applied. The prospect of applying new turbines and compressors to develop particular internal combustion engines, where the combustion of the fuel-air mixture is carried out at a constant volume or constant pressure, is outlined. The development of cheaper and more economical turbines and compressors will make it possible to solve urgent problems of supplying electric and thermal energy to enterprises, including those in remote Arctic oil and gas fields.

Specific findings of the work performed can be used to develop jet control systems for air-based and sea-based unmanned aerial vehicles, which are used in research, rescue operations, or prospecting works, including the development of offshore oil and gas fields. Certain gas (liquid) flow control principles at the nozzle outlet have been considered in the presented work. For example, the same principles can be used to control the thrust vector on unmanned aerial vehicles. Part of the presented research work has been conducted at the junction of two scientific directions: 1 – turbine technologies and jet control systems,

and 2 – rocket and aviation control systems. Typical thrust vector control systems are known from available digital information sources (“Missile Control Systems”, n.d.) and printed publications like the monograph (Chanut, 1961; Bailey, 1982). This published information has been evaluated for applying certain known technical solutions in developing the jet control system for our mesh turbine under development. To save time and reduce financial costs, the verification of the selected published data was performed only using computer simulation and rapid prototyping technologies. Working capacity of the developed microlevel models and the basic known principles of thrust vector control has been tested in laboratory conditions during hydraulic and pneumatic tests using fast prototyping technologies for manufacturing new models and already known models. When using rapid prototyping technology and following accepted terminology (Karasev, 2000), the following methods of thrust vector control were tested in laboratory conditions: “Liquid Injection”, “Jet Vane”, “Axial Plate”, “Jet Tab”, “Movable Nozzle”.

The published data follows that for the known control systems, the largest deviation angle of the thrust vector can vary in the range from plus 20 degrees to minus 20 degrees. According to the published data, the angle “ α ” could vary from plus 20 degrees to minus 20 degrees based on the diagram demonstrated in Figure 5 in this paper. Somewhat different numerical values have been obtained in laboratory tests, according to which the angle “ α ” can vary from plus 90 degrees to minus 90 degrees in any direction within the hemisphere. Therefore, it is possible to draw a preliminary conclusion that the adjustment range by the angle of deviation of the thrust vector can be significantly extended compared to the published data. Besides, it should be noted that with a more complex approach to design, the adjustment range could be extended even further. When designing multi-mode and universal turbine technologies, the authors have set a goal to achieve an extensive adjustment range. The authors are interested in the following adjustment range for changing the angle “ α ” – from plus 180 degrees to minus 180 degrees in all directions. Preliminary design studies and laboratory tests of microlevel models have shown that this goal is achievable since the angle “ α ” can indeed vary in the range from plus 180 degrees to minus 180 degrees in any direction, within a full three-dimensional sphere. The authors plan to publish more

detailed information on this subject after further additional patent research.

The system approach to analyzing the accumulated and incoming scientific information developed by the authors have been used according to our previous publications (Sazonov *et al.*, 2019). The following interrelated issues and processes are always considered in close integration: vane and vortex working processes; the pumping and turbine working process; coalescence and dispersion; cavitation in liquid and gas-liquid mixture; separation in multiphase media; presence of solid particles in the flow; point or distributed energy supply; sequential and parallel connection of machines; single or multistage machines; hydraulic losses due to friction and shock losses with the process of partial pressure recovery; constant and variable resistance coefficients; the development or attenuation of certain processes in different points of the working chamber of the machine at changes in the flow rate of the working fluid; changes in the physical properties of liquid or gas-liquid mixture in different points of the flow part of the machine; the presence of axial symmetry for solid walls and for the flow; used methods of the machine adjustment; and steady-state and impulse flow modes in certain areas. Considering the variety, interrelationships, and complexity of the listed issues, it is possible to speak about great opportunities to apply computer technologies in designing new machines and equipment. This list of questions and processes expands depending on the design or scientific task being solved. Given the possible prospects for the development of the intelligent computerized turbine, the following additional issues should be included in the presented list of interrelated issues: the switch-gear can be equipped with an additional electromagnetic, hydraulic, pneumatic, or hybrid control system; the flow regime through the mesh turbine channels can be at subsonic or supersonic velocities; in the capacity of the working body gas, steam, steam-gas mixture, liquid or gas-liquid mixture with the inclusion of abrasive solid particles can be used; continuous or periodic operation can be assigned to the mesh turbine. Besides, the energy from the mesh turbine can be used to drive one machine or several different machines (including an electric generator, pump, compressor, ventilator, separator, propeller, and air screw). In energy recovery mode, the mesh turbine can be connected to the shaft of an electric engine or the shaft of an

internal combustion engine, including for the primary engine afterburning operation mode implementation.

The literature data analysis made it possible to outline a promising research direction concerning urgent problems in the oil and gas industry. This direction is associated with impulse turbines with a mesh structure of flow channels. Moreover, to control these turbines, it is advisable to use jet control systems. Within the framework of the well-known classification (Glaznev, Zapryagaev, and Uskov, 2000), either the interaction of a jet with an obstacle or the interaction of several jets with each other is considered. In both cases, the jet of gas or liquid is called an "impact jet". The impact jet structure is significantly complicated if a flow chamber of the ejector is placed between the nozzle and the mesh turbine rotor. Such a complicated scheme will be considered within the framework of a separate research work to study in more detail the features of the ejection flow and flow along curved surfaces, taking into account the heat transfer between flows and solid surfaces.

To solve urgent oil and gas production problems, it is advisable to create special stationary gas turbine engines with a constant volume heat supply. An integral part of such an engine is a pulse turbine (Tarasov, 2009), which makes it possible to improve the specific performance of the engine in comparison with a traditional gas turbine engine, where heat is supplied at constant pressure.

It is known that the heat transfer process can be activated in the flow of an impact jet (Pakhomov and Terekhov, 2011; Sadin, Lyubarskiy, and Gravchenko, 2017). The impact jet in the ejector also makes it possible to solve the problem of a controlled decrease in temperature before the hot gas enters the channels of the mesh pulse turbine.

A hybrid scheme is of practical and scientific interest, which combines the properties of the developed grid turbine and the Wales turbine described in the work by Dovgyallo and Shimanov (2015). In this case, the direction of rotation of the turbine rotor does not change when the direction of flow in the turbine rotor changes to the opposite direction.

When discussing gas-dynamic and hydrodynamic processes occurring in a mesh turbine, it is necessary to take into account the process of ventilation of the blades in a pulsed mode of gas or liquid supply (Konchakov,

2001). Usually, this ventilation process is associated with vortex processes, which somewhat reduce the efficiency of the turbine. However, in the preparation of oil and gas, this ventilation process can play a positive role, for example, in a turbine separator. This area of science and technology, associated with supersonic flows in rotating systems, has not lost its relevance for many years (Volov, 2011).

The question of the interaction of a gas (or liquid) jet with a solid wall can also be considered from new positions. An impenetrable solid wall is usually considered (Mordasov, Savenkov, and Chechetov, 2015). However, in problems with mesh turbines, the model of a semi-permeable solid wall can be additionally considered. In this case, it is necessary to consider in more detail the issues of designing individual jet elements intended for the jet control system as a whole. Modern computer technologies make it possible to consider tasks to calculate and design jet elements at a new and higher technical level (Ilyina and Prodan, 2015). Simultaneously, due to such computer technologies, for well-known technical solutions (Rekhten, 1980; Znamensky, Sokolov, and Chekmasov, 1996; Coanda, 1936), a new field of application can be opened, including in the production of hydrocarbons in oil and gas fields. The combination of the Coanda effect (Rekhten, 1980; Coanda, 1936) with deflectors for deflecting the jet may well be considered a new direction in creating jet control systems for pulsed turbines, including mesh turbines. For computer modeling and computational studies, the FloEFD computational fluid dynamics software package can be used. To create 3D models, for example, SolidWorks CAD systems are used. In the process of modeling, the complete system of averaged Navier – Stokes equations is solved, described by mathematical expressions of the laws of conservation of mass, energy, and momentum. All this allows using the results of classical works in the field of gas dynamics and hydrodynamics at a new technical level (Drozdov, 2011; Demyanova, 1998; Borovykh, 2003; Karambirov and Chebaevsky, 2005; Spiridonov, 2005; Temnov, 2003), axisymmetric and plane-parallel jets, free jets, and jets in a concurrent flow are considered.

In some cases, especially in the presence of abrasive solid particles in the flow, it is advisable to reduce the flow rate at the turbine inlet. In such cases, a stream of gas or

liquid is passed through an ejector. The efficiency or efficiency of energy transfer through the ejector ranges from 50% to 90%, depending on the ratio of the nozzle and mixing chamber diameters (Brudny-Chelyadinov, 1971). The solution of optimization problems, when determining the geometric dimensions of the ejector, is performed, taking into account the composition of the multiphase working medium (Kabdesheva, Verbitsky, Dengae, and Lambin, 2003; Verbitsky, Goridko, Fedorov, and Drozdov, 2016). It should be noted that the calculation of an ejector for multiphase media is still a complex theoretical problem, even with modern computer programs. In this regard, published experimental data on ejection processes remain in demand regardless of the publication date, since only a physical experiment is the most accurate source of scientific information in the field of gas dynamics and hydrodynamics. The results of physical experiments (Pavlechko, 2020) have established a scientific foundation for inkjet technology that is applied across a variety of industries. The creation of a new mesh turbine and jet control system is planned to take into account the peculiarities of ejection processes described in classical works (Drozdov, 2008).

In contrast to the known turbines, the developed turbine prototype was developed for complicated application conditions, with a possible uncontrolled change in the density of the gas-liquid mixture in the flow channels. This density varies in a wide range of values from 1 to 1,000 kilograms per cubic meter. In contrast to the known turbines, the developed mesh turbine allows changing and adjusting the torque by changing the distance from the axis of rotation to the point of application of forces (to the point at which the jet interacts with the solid wall of the turbine blade).

Considering the issues mentioned above, it is possible to draw an intermediate conclusion that some of the results of scientific research performed can be used in various industries, including energy, transport, and robotics.

4. CONCLUSIONS:

As a result of the current scientific research, the following main conclusions can be drawn:

1) a prototype of a mesh turbine with a jet control system was developed, capable of

effectively solving the problem of energy conversion when a multiphase flow moves through the flow channels of an impeller machine;

2) the operability of the created turbine equipment was confirmed both when performing numerical experiments and during laboratory tests;

3) during laboratory tests of the prototype of the jet system, it was shown that the angle of deflection of the working jet can be increased to 90 degrees for any direction within the geometric hemisphere;

4) the results of pneumatic and hydraulic tests confirmed the suitability of the mesh turbine for its operation under conditions of changing the density of the working medium, in a wide range - 1 to 1000 kilograms per cubic meter;

5) during the prototyping process, it was shown that a disk (or conical) mesh turbine can be manufactured on the basis of additive technologies using commercially available 3D printers.

5. ACKNOWLEDGMENTS:

The work has been performed with the financial support of the Ministry of Education and Science of the Russian Federation within the framework of the state contract in the sphere of scientific activities, topic number FSZE-2020-0006.

6. REFERENCES:

1. Abugov, D. I., and Bobylev, V. M. (1987). *Theory and calculation of solid-propellant rocket engines. Textbook for mechanical engineering higher education institutions*. Moscow, Russia: Mechanical Engineering.
2. Bailey, J. M. (1982). *United States patent No. 4355949. Control system and nozzle for impulse turbines*. Retrieved from <https://patents.google.com/patent/US4355949>
3. Bilotserkovskiy, S. M., Odnovol, L. A., Safin, Yu. Z., Tyulenev, A. I., Frolov, V. P., and Shitov, V. A. (1985). *Grid-like wings*. Moscow, Russia: Mechanical Engineering.
4. Borovykh, A. E. (2003). One-dimensional theory of a water-jet pump with isobaric mixing in the receiving chamber. *Higher School Proceedings. Engineering Industry*, 12, 20-29.
5. Brink, M. (2014). Jet pump technology for artificial lift in oil and gas production. *The Elomatic Magazine*, 1, 40-43.
6. Brudny-Chelyadinov, S. Yu. (1971). *Theoretical and experimental studies of turbodrills with jet multipliers of flow rate (with jet devices) for drilling deep wells*. Moscow, Russia: VNIIBT.
7. Chanut, P. L. J. (1961). *United States patent No. 3013494. Guided missile*. Retrieved from <https://patents.google.com/patent/US3013494/en>
8. Chen, W., Li, Y., Li, Y., and Zhao, X. (2015). Temperature control strategy for water-cooled proton exchange membrane fuel cells. *Journal of Southwest Jiaotong University*, 50(3). Retrieved from <http://jsju.org/index.php/journal/article/view/162>
9. Coanda, H. (1936). *United States patent 2052869. Device for deflecting a stream of elastic fluid projected into an elastic fluid*. Retrieved from <https://patents.google.com/patent/US2052869A/en>
10. Coleman, G. N., Kim, J., and Spalart, P. R. (2003). Direct numerical simulation of a decelerated wall-bounded turbulent shear flow. *Journal of Fluid Mechanics*, 495, 1-18.
11. Croft, D. R., Williams, P. D., and Tay, S. N. (1978). Numerical analysis of jet pump flows. In C. Taylor, J. A. Johnson, and W. R. Smith. (Eds.), *Numerical Methods in Laminar and Turbulent Flow*. Papers presented at the International Conference, Seattle, WA (pp. 741-753). Swansea, United Kingdom: Pineridge Press.
12. Demyanova, L. A. (1998). Influence of the distance from the working nozzle to the mixing chamber on the characteristics of the jet apparatus when pumping gas-liquid mixtures. *Oil Industry*, 9, 84-85.
13. Dovgyallo, A. I., and Shimanov, A. A. (2015). Possibility of using a pulse two-directional turbine in a thermoacoustic engine. *Bulletin of the Samara State*

- Aerospace University*, 14(1), 132-138.
14. Drozdov, A. N. (2008). *Technology and technique of oil production by submersible pumps in difficult conditions*. Moscow, Russia: MAKSPress.
 15. Drozdov, A. N. (2011). Investigation of the characteristics of pumps when pumping out gas-liquid mixtures and the use of the results obtained for the development of technologies for water-gas treatment. *Oil Industry*, 9, 108-111.
 16. Gao, Z., and Zhuang, F. (2004). Multi-scale equations for incompressible turbulent flows. *Journal of Shanghai University*, 8(2), 113-116.
 17. Glaznev, V. N., Zapryagaev, V. I., and Uskov, V. N. (2000). *Jet and unsteady flows in gas dynamics*. Novosibirsk, Russia: Publishing House of the Siberian Branch of the Russian Academy of Sciences.
 18. Ilyina, T. E., and Prodan, N. V. (2015). Designing an element of a jet control system for a gas-static bearing. *Scientific and Technical Bulletin of Information Technologies, Mechanics and Optics*, 15(5), 921-929.
 19. Kabdesheva, Zh. E., Verbitsky, V. S., Dengaev, A. V., and Lambin, D. N. (2003). research of characteristics of high-pressure jetting apparatus when pumping out a gas-liquid mixture liquid jet. *Oil Industry*, 3, 81-83.
 20. Karambirov, S. N., and Chebaevsky, V. F. (2005). Possibilities of improving the characteristics of jet pumps. *Chemical and Oil and Gas Engineering*, 2, 26-28.
 21. Karasev, V. N. (2000). *Investigation of the influence of the dynamic properties of the power plant and thrust vector control programs on the characteristics of a short takeoff / vertical landing aircraft*. Moscow, Russia: Moscow State Aviation Institute.
 22. Konchakov, E. I. (2001). *Improvement of ship's partial turbomachines on small models*. Vladivostok, Russia: Far Eastern State Technical University.
 23. Missile Control Systems. (n.d.). Retrieved from <http://www.aerospaceweb.org/question/weapons/q0158.shtml>
 24. Mordasov, M. M., Savenkov, A. P., and Chechetov, K. E. (2015). On the refinement of the calculated dependences of the force action of a turbulent gas jet. *Journal of Technical Physics*, 85(10), 141-144.
 25. Morishima, S. (2008). *United States patent No. 7,438,535. Structure of ejector pump*. Retrieved from <http://www.freepatentsonline.com/7438535.pdf>
 26. Pakhomov, M. A., and Terekhov, V. I. (2011). Intensification of turbulent exchange in the interaction of a fog-like axisymmetric impact jet with an obstacle. *Applied Mechanics and Technical Physics*, 52(1), 119-131.
 27. Pavlechko, V. N. (2020). Variation of tangential pressure of process fluid on blade in channels of radial-axial turbine. *Chemical and Petroleum Engineering*, 11-12(55), 888-895.
 28. Rekhten, A. V. (1980). *Inkjet technology: basics, elements, schemes*. Moscow, Russia: Mechanical Engineering.
 29. Sadin, D. V., Lyubarskiy, S. D., and Gravchenko, Yu. A. (2017). Peculiarities of an underexpanded impulse gas-dispersed jet with a high concentration of particles. *Journal of Technical Physics*, 87(1), 22-26.
 30. Sazonov, Yu.A., Mokhov, M.A., Tumanyan, Kh.A., Frankov, M.A., Mun, V.A. & Osicheva, L.V. (2019). Development of technologies for increase the ejector units' efficiency. *Journal of Computational and Theoretical Nanoscience*, 16(7), 3087-3093.
 31. Shamanov, N.P., Dyadik, A.N. & Labinsky, A.Yu. (1989). *Two-phase jet devices*. Leningrad, Russia: Shipbuilding.
 32. Singh, M.K., Prasad, D., Singh, A., Jha, M. & Tandon, R. (2013). *Large scale jet pump performance optimization in a viscous oil field*. Richardson, TX: Society of Petroleum Engineers.
 33. Spiridonov, E. K. (2005). Calculation of a jet pump for hydraulic systems of drainage and emptying of tanks. *Chemical and Oil and Gas Engineering*, 2, 21-25.
 34. Tarasov, V.N. (2009). *Development of rational methods for the design of partial-pulse turbines*. Moscow, Russia: Bauman Moscow State Technical University.
 35. Temnov, V. K. (2003). Questions of efficiency of liquid ejectors. In *Science and Technology: Proceedings of the*

- XXIII Russian School - A Special Issue Dedicated to the 60th Anniversary of the South Ural State University* (pp. 432-438). Miass, Russia: The Russian Academy of Sciences.
36. Trabold, T.A., Esen, E.B. & Obot, N.T. (1988). *The entrainment of the surrounding liquid by turbulent jets flowing out of round nozzles with sharp leading edges. Proceedings of the American Society of Mechanical Engineers. Theoretical foundations of engineering calculations.* Moscow, Russia: Mir.
 37. Verbitsky, V.S., Goridko, K.A., Fedorov, A.E. & Drozdov, A.N. (2016). Study of characteristics of electric centrifugal pump with ejector at the inlet when pumping gas-liquid mixtures. *Oil Industry*, 9, 106-109.
 38. Volov, V.T. (2011). *Modeling of energy exchange processes in strongly swirled compressible flows of gas and plasma.* Kazan, Russia: Kazan (Volga Region) Federal University.
 39. Znamensky, V.P., Sokolov, S.V. & Chekmasov, V.D. (1996). *United States patent No. 5524827. Method and nozzle for producing thrust.* Retrieved from <https://patents.google.com/patent/GB2282854A/en>

PREVALÊNCIA E FATORES DE RISCO PARA OCORRÊNCIA DE ANOMALIAS
CONGÊNITAS EM NEONATOS EM HOSPITAL PARA CRIANÇA E MATERNIDADE NA
PROVÍNCIA DE MISAN

PREVALENCE AND RISK FACTORS FOR OCCURRENCE OF CONGENITAL
ANOMALIES IN NEONATES AT HOSPITAL FOR CHILD AND MATERNITY IN MISAN
PROVINCE

معدل انتشار وعوامل الخطر لحدوث التشوهات الخلقية عند الولادة في مستشفى الطفل والولادة في محافظة ميسان

ALI, Esraa Abd Almuhsen¹; ALJAWADI, Hussein Fadhil^{2*}

^{1,2} Department of Pediatrics, College of Medicine, University of Misan, Misan, Iraq.

* Corresponding author

e-mail: husseinaljawadi.mcm@uomisan.edu.iq

Received 29 June 2020; received in revised form 23 August 2020; accepted 25 October 2020

RESUMO

As anomalias congênitas afetam uma proporção notável de recém-nascidos e têm papel significativo na admissão hospitalar, morbidade e mortalidade em pediatria. Além disso, a morbidade e incapacidade a longo prazo causadas por defeitos congênitos podem ter um efeito significativo no desenvolvimento da criança, bem como nos sistemas de saúde e família. Em Misan, os defeitos congênitos são uma terceira causa comum de mortalidade neonatal. Este estudo teve como objetivo estimar a prevalência, tipos e fatores de risco de defeitos congênitos, a fim de ter um plano de ação para prevenir a ocorrência desses defeitos. Estudo transversal realizado na unidade de cuidados neonatais do Hospital Misan de Criança e Maternidade durante o período de dois anos (2018 e 2019). A província de Misan está localizada no sudeste do Iraque. As informações foram coletadas dos arquivos dos pacientes e dos registros cadastrais. Qualquer recém-nascido com defeito de nascença foi inscrito em nosso estudo. Esses casos foram diagnosticados dependendo da história, do exame clínico apoiado por outras investigações e de estudos radiográficos sempre que necessário. As taxas de prevalência de defeitos congênitos foram de 7,1/1000 e 6,6/1000 nascidos vivos em 2018 e 2019, respectivamente. O envolvimento do sistema nervoso central foi o padrão mais comum. Defeitos de nascimento foram mais frequentes em bebês masculinos, solteiros e a termo, com idade materna entre 18 e 35 anos, residentes em área urbana com histórico de consanguinidade. Assim, a taxa de prevalência de defeitos congênitos foi notavelmente alta em Misan. Esforços para a prevenção, bem como para melhorar o diagnóstico pré-natal, seriam essenciais.

Palavras-chave: *unidade neonatal, anomalias congênitas, Iraque.*

ABSTRACT

Congenital disabilities affect a remarkable proportion of neonates and have a significant role in hospital admission, morbidity, and pediatrics mortality. Besides, the long-term morbidity and disability caused by birth defects may have a considerable effect on the development of the child and family and health care systems. In Misan, congenital disabilities are considered a third common cause of neonatal mortality. This study aimed to estimate the prevalence, types, and risk factors of congenital disabilities to have an action plan toward preventing the occurrence of these defects. A cross-sectional study performed in the neonatal care unit in Misan Hospital for Child and Maternity during the period of two years (2018 and 2019). Misan province is located in the South East of Iraq. The information was collected from the files of patients and registration records. Any delivered a live neonate with birth defects was enrolled in this study. These cases were diagnosed depending on history, clinical examination supported by other investigations, and radiographic studies whenever needed. The prevalence rates of congenital disabilities were 7.1/1000 and 6.6/1000 live birth in 2018 and 2019, respectively. Central nervous system involvement was the most typical pattern. Congenital disabilities were more frequent in male, single, and term babies of maternal age 18-35 years living in an urban area with a consanguinity history. Thus, the prevalence rate of congenital disabilities was notably high in Misan. Efforts toward prevention, as well as improving the prenatal diagnosis, would be essential.

Keywords: *neonatal care unit, congenital anomalies, Iraq.*

تؤثر الإعاقات الخلقية على نسبة ملحوظة من الولدان ولها دور كبير في دخول المستشفى، وفي معدلات الاعتلال ووفيات الأطفال. إلى جانب ذلك، قد يكون للمرض والعجز طويل الأمد الناجمين عن العيوب الخلقية تأثير كبير على نمو الطفل والأسرة وأنظمة الرعاية الصحية. في ميسان، تعتبر العيوب الخلقية السبب الثالث الشائع لوفيات الأطفال حديثي الولادة. هدفت هذه الدراسة إلى تقدير مدى انتشار، أنواع، وعوامل الخطر للإعاقات الخلقية لوضع خطة عمل تجاه منع حدوث هذه العيوب. أجريت دراسة مقطعية في وحدة رعاية الأطفال حديثي الولادة في مستشفى ميسان للأطفال والأمومة خلال فترة سنتين (2018 و2019). تقع محافظة ميسان في جنوب شرق العراق. تم جمع المعلومات من ملفات المرضى وسجلات التسجيل. تم تسجيل أي مولود حي مصاب بعيوب خلقية في هذه الدراسة. تم تشخيص هذه الحالات اعتماداً على التاريخ والفحص السريري المدعوم بالاستقصاءات الأخرى والدراسات الشعاعية عند الحاجة. كانت معدلات انتشار الإعاقات الخلقية 7.1 / 1000 و 6.6 / 1000 ولادة حية في عامي 2018 و2019 على التوالي. كانت إصابة الجهاز العصبي المركزي هي النمط الأكثر شيوعاً. كانت الإعاقات الخلقية أكثر شيوعاً في الذكور، الوليد المفرد لأمهات تتراوح أعمارهن بين 18 و 35 عاماً والذين يعيشون في منطقة حضرية لها تاريخ زواج قرابة. وبالتالي، كان معدل انتشار العيوب الخلقية مرتفعاً بشكل ملحوظ في ميسان. وبالتالي سيكون من الضروري بذل الجهود للوقاية، وكذلك تحسين التشخيص ما قبل الولادة.

الكلمات المفتاحية: وحدة رعاية الاطفال حديثي الولادة، التشوهات الخلقية، العراق.

1. INTRODUCTION:

Congenital anomalies, also generally referred to as birth defects, congenital disorders, congenital malformations, congenital disabilities, or congenital abnormalities, are conditions of fetal origin present at birth affecting the health, growth, and/or survival of an infant (KHOURY, 1989). It affects a remarkable proportion of neonates and has a significant role in hospital admission, morbidity, and mortality in pediatrics (Dastgiri *et al.*, 2011). The more severe congenital disabilities were reported to occur more in the low and middle-income countries in which more than 90% of these cases would die because of the serious defects (Sharma, 2013; Vatankhah *et al.*, 2017).

The entire family is affected by a child with a congenital disability. Parents whose children are affected by birth defects face notable struggles and want to make the lives of their children more comfortable. They also want to contribute to preventing potential congenital disabilities. Parents face obstacles such as contact with health practitioners, quality of life concerns, awareness-raising, and research activism (Lemacks *et al.*, 2013). A global disease study burden reported approximately 510.400 deaths caused mainly by birth defects (Lozano *et al.*, 2012). According to the World Health Organization report, about 3 million fetuses and infants are born with significant malformations every year. Many extensive population-based studies indicate that in 2–3 % of live births that significant malformations occur (Shawky and Sadik, 2011).

Congenital abnormalities contribute a large proportion of child morbidity and mortality, as well as fetal mortality. Birth defects can be classified into three main categories: structural/metabolic, congenital infections, and other conditions. The most common disorders include congenital heart defects, orofacial clefts, Down syndrome,

craniofacial anomalies, and neural tube defects (Al-Alaiyan and AlFaleh, 2012; Irvine *et al.*, 2015; Farhan *et al.*, 2020). The pattern and the prevalence of congenital disabilities vary in population according to the social (Consanguineous marriage), environmental, economic factors, and racial/ethnic disparities (Shawky and Sadik, 2011; Wang *et al.*, 2015).

The racial/ethnic was changed to more specific categories in 1981, from "White or Other", into six different types. The groups are now covered in the racial/ethnic classifier as white, black, Hispanic, American, Asian, and other. The racial/ethnic classification of the baby is derived from the medical records. Mixed race/ethnicity children are coded as "other," and unclear origin children are coded as "unknown." Chavez *et al.*, (1988) found that Americans had the highest overall scores, followed by whites, blacks, Asians, and Hispanics, for their study of 18 major birth defects by race /ethnic group (Chavez *et al.*, 1988). Low socioeconomic levels are at greater risk for congenital disabilities (Yu *et al.*, 2014; Morales-Suárez Varela *et al.*, 2009). Additionally, the pattern of birth defects may be affected by the geographical area (Liu *et al.*, 2020).

In comparison to non-consanguineous marriages, the occurrence of congenital anomalies was mainly seen in consanguineous marriages (Tayebi *et al.*, 2010). The geographic disparities in the prevalence of congenital anomalies in the region might be attributed to the highly polluted air and water or Polluted landfills, hazardous waste, and manufacturing facilities included in the vicinity of residential areas (Kihal-Talantikite *et al.*, 2017).

In the United States, about 3% of all births had congenital disabilities reported by the Center for Disease Control and Prevention (Martin *et al.*, 2005). Moreover, EUROCAT, the European

Surveillance of Congenital Anomalies, is the European network of congenital anomaly population and recorded approximately 23.9 cases per 1000 births of significant congenital disabilities in 2003-2007 (Dolk *et al.*, 2010). Birth defects causing early death or permanent lifelong disability can have a prevalence of up to 45 in 1000 live births in low-income countries, three times higher than in rich countries. (WHO, 1985).

It is estimated that around 7.9 million babies (6% of all global birth) are born with significant congenital disabilities every year. Although specific congenital abnormalities can be controlled and treated, about 3.2 million of these children are life-long disabled. Some congenital disabilities are hereditary. Others result from toxic environmental causes (toxic metal contamination), known as teratogens. There are also others that emerge from complex interactions between genes and environmental influences. These are known as multifactorial. However, the causes are unknown in about half of all cases of birth defects (Lobo and Zhaurova, 2008; Sahar *et al.*, 2008; Mihaileanu *et al.*, 2019). Notably, genetic disorders associated with congenital disabilities reached up to 5% of total live births in the developed countries (Dastgiri *et al.*, 2010; Loughna, 2008).

There are various risk factors for birth defects such as hereditary, the gender of the baby, old-aged parents, complications during pregnancy, unprescribed drugs and excessive vitamin A intake during pregnancy, exposure to chemicals and pesticides during pregnancy, malnutrition, poverty, and living near mobile strengthening stations (Abdou *et al.*, 2019). The causes of only about 30% of congenital disabilities are relatively well known, and awareness even of those is often spotty. On the other hand, 70% still unknown and leaves open the possibility that environmental factors may play a significant role. So, recognizing and managing these risk factors would help reduce the rate of birth defects (Weinhold, 2009). Congenital disabilities can be classified based on their pathogenetic mechanism, severity, or whether they involve a single system or multiple systems (Tanteles and Suri, 2007). A cross-sectional retrospective study by (Obu *et al.*, 2012) was performed in which a four years (January 2007–April 2011) examination was conducted on the registries of all babies admitted to the Newborn Special Care Unit (NBSCU) at the Teaching Hospital of the University of Nigeria (UNTH), Ituku/Ozalla, Enugu. Mainly surgical congenital disabilities and cleft lip/cleft palate and neural tube defects were demonstrated as the commonest types.

In Misan province (South East Iraq), it is worth mentioning that birth defects were found to be the fourth one in the causes of neonatal respiratory distress and the third sequence in its mortality (6.6%) as reported by a study conducted in the same hospital of the current study (Aljawadi and Ali, 2019). Furthermore, another study in Misan considered birth defects, a third common cause of neonatal mortality (Ali, 2016). Additionally, the Iraqi annual statistical report in 2017 recorded that congenital anomalies were forming the second most typical cause of stillbirth in Iraq (Ministry of Health and Environment Iraq, 2017). Although different studies focused on congenital disabilities were conducted in some Iraq provinces, there was no similar study in Misan.

Therefore, this study aimed to estimate the prevalence, types, and risk factors of birth defects to have an action plan toward preventing the occurrence of these congenital anomalies.

2. MATERIALS AND METHODS:

2.1. Study design

The present study is cross-sectional. It was conducted in the neonatal care unit in Misan Hospital for Child and Maternity during the period of 2018 and 2019. Misan province is located in the South East of Iraq. Data were collected from the files of patients (153 files) and records of the neonatal care and the obstetrical unit (22.406 total live births of two years were recorded).

2.2. Ethics

All procedures performed in this study involving data from human participants are per the ethical standards of the institutional and national research committee, the 1964 Helsinki Declaration, and its later amendments or comparable ethical standards. Ethical approval was obtained from the hospital (number 1879 of 1st of June 2020) to carry out this study, which allowed the researchers to have all the rights to check the records and files of patients.

2.3. Inclusion and exclusion criteria

Any delivered alive neonate with congenital disabilities was enrolled in this study. These cases were diagnosed depending on history, clinical examination supported by other investigations, and radiographic studies whenever needed. Stillbirth (dead fetus) was excluded.

2.4. Data analysis

The total number of birth defects and total live birth were recorded each year. Then the prevalence rate was calculated per 1000 live births. The types of congenital disabilities were classified according to the system involvement as (1) central nervous system (hydrocephaly, anencephaly, microcephaly, and neural tube defects); (2) gastrointestinal system (cleft lip and/or palate, trachea-esophageal fistula and/or esophageal atresia, duodenal atresia, diaphragmatic hernia, omphalocele, gastroschisis, and imperforated anus); (3) chromosomal (Down, Patau, Edward, Pierre Robin, and Russel Silver syndrome); (4) musculoskeletal system (polydactyly, syndactyly, chondrodysplasia, and limb deformities); (5) genitourinary system (polycystic kidney, ambiguous genitalia, Potter syndrome, and hypospadias); (6) cardiovascular system (ventricular septal defect, atrial septal defect, transposition of great arteries, and complex heart disease); (7) sensory (ichthyosis, and cutis aplasia); (8) respiratory system (pulmonary hypoplasia, and choanal atresia); and (9) unclassified birth defects (multiple systems involvement).

2.5. General information on the records of the patients

The collected information included gender, gestational age, maternal age, residence, parity, antenatal care, history of chronic maternal illness, type of pregnancy, history of intrauterine exposure (fever, drug, and radiation), consanguinity, and family history of birth defects.

2.6. Statistical Analysis

Data were analyzed using Microsoft Excel 2010 (Winston, 2011).

3. RESULTS AND DISCUSSION:

The total number of birth defects and the prevalence rate in 2018 were 80 cases and 7.1/1000 live births, respectively, while in 2019, there were 73 cases and 6.6/1000 live births, as shown in Table 1. The most typical pattern of congenital disabilities involved the central nervous system, followed by the gastrointestinal system. In contrast, the least pattern was involving the respiratory system, as shown in Table 2. In studying the association between birth defects and their different risk factors, congenital disabilities were more frequent in male, single, and term babies of maternal age 18-35 years living in urban

areas. History of consanguinity was more predominant in babies with congenital disabilities, as shown in Table 3.

The prevalence rate of birth defects was 7.1, and 6.6 per 1000 live birth in two successive years. These results were much less than the total prevalence rate in Ramadi (West of Iraq), which recorded a prevalence rate of about 41/1000 live birth (Al-Ani *et al.*, 2012), but this cannot be considered as low rates that should be neglected. Also, it was less than Saudi Arabia (27/1000 live birth) and Iran (165.5 per 10000 births) (Fida *et al.*, 2007; Dastgiri *et al.*, 2007). In the present study, the stillbirths were excluded, increasing the prevalence rate of birth defects in total birth. A study by (Penchaszadeh, 2002) clarified that the prevalence rate would be underestimated in developing countries. On the contrary, Misan rate was higher than Duhok (North of Iraq) (4.65/1000 live birth), Beijing Obstetrics and Gynecology Hospital, China (5/46), British Columbia (0.5/1000 live birth), and Egypt (2.5/1000 live birth) (Mohammed, 2015; Sun *et al.*, 2015 ;Trimble and Baird, 1978; El Koumi *et al.*, 2013). These variations in the prevalence rates may be attributed to the different risk factors like social, environmental, and geographical distribution.

This study showed the prevalence of congenital anomalies in the central nervous system was the first as the most commonly affected organ system which agreed with studies in Duhok, British Columbia, and Sarajevo (Mohammed, 2015; Trimble and Baird, 1978; Hadžagić-Ćatibušić *et al.*, 2008) followed by the gastrointestinal system to be the second sequence as seen in Karbala (Hussein, 2017). This sequence differs from Ramadi and Saudi Arabia, in which the cardiovascular system was the first most standard involved system (Al-Ani *et al.*, 2012; Fida *et al.*, 2007). These discordant data may be attributed to the early or severe clinical presentation at birth if the central nervous system or gastrointestinal system was involved and the urgent need for interference. Hence, a definite recording of these cases would be applied. Meanwhile, the folic acid role in central nervous anomalies should be studied in future research. The involvement of the cardiovascular system is the seventh congenital disabilities in this study. It might be related to the delayed echocardiographic appointment, especially in asymptomatic cases. Thus, further prospective research is recommended.

In studying the characteristics and risk factors of congenital disabilities, there was more predominance in male babies, agreed by Karbala

(Hussein, 2017), and neonatal outcome in the Netherlands for type 1 diabetic pregnancy (Evers *et al.*, 2009). Moreover, in Ramadi, a significant role of the male gender in congenital disabilities was observed (Al-Ani *et al.*, 2012). Until now there is no definitive cause for male predominance but the genetic or X-linked roles may partially explain this. Besides, more frequent birth defects in term than preterm neonates were detected in the current study. On the contrary, different studies in Egypt and Iran found a significant association between prematurity and congenital disabilities (El Koumi *et al.*, 2013; Woday *et al.*, 2019). A larger sample size and a longer period may be needed to explain this discordance.

The current study revealed more congenital disabilities in multiparous mothers age 18-35 years. These findings were compatible with Karbala (Hussein, 2017) and Alexandria in Egypt (Shawky and Sadik, 2011). Another study in Egypt disagree with these results and found that mothers age more than 35 years were more prone to have babies with congenital anomalies (Abdou *et al.*, 2019). In Misan province, the social, cultural, and tribal attitudes encourage early marriages and large families. So most of the childbearing women are in the twentieth of age and vulnerable to have more kids.

The present study showed that urban residence and regular antenatal care were more frequent in birth defects than in Karbala (Hussein, 2017), which may be due to the lack of education and family planning awareness. This would need a further study about maternal and health provider partnership status in preventing congenital disabilities. More consanguinity association with congenital disabilities was seen in this study. This is in agreement with other research in Ramadi, Erbil (North of Iraq), Egypt, and Iran, which recorded a significant increase in birth defects when it is linked with consanguinity (Al-Ani *et al.*, 2012; Ameen *et al.* 2018; El Koumi *et al.*, 2013; Kaviany *et al.*, 2016). Misan people belong to tribes that prefer consanguineous marriage.

Furthermore, different studies in Ramadi, Erbil, and Egypt revealed a significant relationship between recurrence of congenital disability and previous birth defects (Al-Ani *et al.*, 2012; Ameen *et al.*, 2018; El Koumi *et al.*, 2013). Nevertheless, this study did not find any relationship between congenital disability and the family history of previous congenital disabilities. This might be addressed to the small sample size.

In the current study, congenital disability occurred less frequently in mothers with a chronic

disease that disagrees with Erbil study (Ameen *et al.*, 2018). Mothers aged 18-35 were more frequent in this study; hence, they were less likely to have a chronic disease like hypertension and diabetes mellitus. Birth defects were less frequent in the multiple types of pregnancy, and this needs expanded study in this issue.

Recent studies in Fallujah city (west of Baghdad, Iraq) by (Alaani *et al.*, 2011) have drawn attention to rises in congenital birth abnormalities and cancer blamed on teratogenic, genetic, and genomic stress thought to result from depleted Uranium contamination following the battles in the town in 2004. Their results indicate the enriched uranium exposure is either a primary cause or linked to the cause of the congenital anomaly and cancer increases. This might cause a congenital anomaly in Misan province because the concentration of Uranium in the soil (Al-Ani *et al.*, 2011) reached 2.158 ± 0.631 ppm in some areas. According to the world health organization (WHO), the tolerable intake (TI) for Uranium is 0.0006 mg per kg (ppm) of body weight per day (WHO, 2001).

High rates of mortalities in Maysan province for Neonatal (age: 0-28 day), infants (age: less 1 year), and under 5 years (10.4, 12.6 and 17 per 1000 live births, respectively) were recorded by the Iraqi annual statistical report in 2017 (Ministry of Health and Environment Iraq, 2017). So it is necessary to consider these factors (age and parity of the mother and consanguinity) to correct or act whenever possible, such as more focus on antenatal care, education, and pre-marriage counseling. Subsequently decline in congenital disability would be achieved, leading to more reduction in neonatal and infant mortality rate.

4. CONCLUSIONS:

The prevalence rate of congenital disorders was notably high in Misan. Central nervous system involvement was the most typical pattern followed by the gastrointestinal system. More concentration about the role of folic acid supplements before conception is required. Congenital disabilities were more frequent in male, single, and term babies of maternal age of 18-35 years living in urban areas and a history of consanguinity. Social education using different media types focusing on family planning, consanguineous marriage, and genetic counseling is important.

Furthermore, improvement in the primary health care system leads to the early detection of high-risk pregnancies. So, efforts toward

prevention, as well as improving the prenatal diagnosis, would be essential.

5. ACKNOWLEDGMENTS:

I would like to thank the medical staff working in the neonatal care unit of Misan hospital for child and maternity.

6. REFERENCES:

1. Abdou, M. S. M., Sherif, A. A. R., Wahdan, I. M. H., and El din Ashour, K. S. (2019). Pattern and risk factors of congenital anomalies in a pediatric university hospital, Alexandria, Egypt. *Journal of the Egyptian Public Health Association*, 94(1), 3.
2. Alaani, S., Tafash, M., Busby, C., Hamdan, M., and Blaurock-Busch, E. (2011). Uranium and other contaminants in hair from the parents of children with congenital anomalies in Fallujah, Iraq. *Conflict and Health*, 5(1), 15.
3. Al-Alaiyan, S., and AlFaleh, K. M. (2012). Aborting a malformed fetus: A debatable issue in Saudi Arabia. *Journal of clinical neonatology*, 1(1), 6.
4. Al-Ani, N. H., Qasim, R. Y., and AL-Hussein, Z. A. (2011). Measuring Uranium in the soil of some area in Missan Governorate/Iraq. *Baghdad Science Journal*, 8(1), 39-43.
5. Al-Ani, Z. R., Al-Haj, S. A., Al-Ani, M. M., Al-Dulaimy, K. M., Al-Maraie, A. K., and Al-Ubaidi, B. K. (2012). Incidence, types, geographical distribution, and risk factors of congenital anomalies in Al-Ramadi Maternity and Children's Teaching Hospital, Western Iraq. *Saudi Medical Journal*, 33(9), 979-989.
6. Ali, E. A. A. (2016). Neonatal Mortality Rate in Aseptic Neonatal Care Unit of Al-Sadder Teaching Hospital in Missan Province From 2011 to 2014. *ESJ*, 12(27), 55-62. <https://doi.org/10.19044/esj.2016.v12n27p55>
7. Aljawadi, H. F. M., and Ali, E. A. A.-M. (2019). Neonatal Respiratory Distress in Misan: Causes, Risk Factors, and Outcomes. *Iranian Journal of Neonatology IJN*, 10(4), 53-60.
8. Ameen, S. K., Alalaf, S. K., and Shabila, N. P. (2018). Pattern of congenital anomalies at birth and their correlations with maternal characteristics in the maternity teaching hospital, Erbil city, Iraq. *BMC Pregnancy and Childbirth*, 18(1), 501.
9. Chavez, G. F., Cordero, J. F., and Becerra, J. E. (1988). Leading major congenital malformations among minority groups in the United States, 1981-1986. *Morbidity and Mortality Weekly Report: Surveillance Summaries*, 17-24.
10. Dastgiri, S., Imani, S., Kalankesh, L., Barzegar, M., and Heidarzadeh, M. (2007). Congenital anomalies in Iran: a cross-sectional study on 1574 cases in the North-West of country. *Child: care, health and development*, 33(3), 257-261.
11. Dastgiri, S., Mizani, T., and Bonyadi, M. (2010). The prevalence of genetic disorders in East Azerbaijan province. *J Urmia Univ Med Sci.*, 21(4), 339-346.
12. Dastgiri, S., Sheikhzadeh, Y., and Dastgiri, A. (2011). Monitoring of congenital anomalies in developing countries: a pilot model in Iran. *ITCH*, 164, 157-161.
13. Dolk, H., Loane, M., and Garne, E. (2010). The prevalence of congenital anomalies in Europe. *Advances in Experimental Medicine and Biology*, 686, 349-364.
14. El Koumi, M. A., Al Banna, E. A., and Lebda, I. (2013). Pattern of congenital anomalies in newborn: a hospital-based study. *Pediatric Reports*, 5(1), 20-23.
15. Evers, I. M., De Valk, H. W., and Visser, G. H. (2009). Male predominance of congenital malformations in infants of women with type 1 diabetes. *Diabetes Care*, 32(7), 1194-1195.
16. Farhan, T. M., Al-Abdely, B. A., Abdullateef, A. N., and Jubair, A. S. (2020). Craniofacial Anomaly Association with the Internal Malformations in the Pediatric Age Group in Al-Fallujah City-Iraq. *BioMed Research International*, 2020.
17. Fida, N. M., Al-Aama, J., Nichols, W., and Alqahtani, M. (2007). A prospective study of congenital malformations among live born neonates at a University Hospital in Western Saudi Arabia. *Saudi Medical Journal*, 28(9), 1367.
18. Hadžagić-Ćatibušić, F., Maksić, H., Užicanin, S., Heljić, S., Zubčević, S., Merhemić, Z., Čengić, A., & Kulenović, E.

- (2008). Congenital malformations of the central nervous system: clinical approach. *Bosnian Journal of Basic Medical Sciences*, 8(4), 356.
19. Hussein, A. A. (2017). A Five Years Retrospective Study of Congenital Anomalies at Karbala City, Iraq. *Karbala Journal of Medicine*, 10(1), 2620–2627.
 20. Irvine, B., Luo, W., and León, J. A. (2015). Congenital anomalies in Canada 2013: a perinatal health surveillance report by the Public Health Agency of Canada's Canadian Perinatal Surveillance System. *Health promotion and chronic disease prevention in Canada: research, policy and practice*, 35(1), 21.
 21. Kaviany, N., Sedehi, M., Golalipour, E., Aryaie, M., and Golalipour, M. J. (2016). Birth defects and parental consanguinity in the north of Iran. *Journal of Advances in Medicine and Medical Research*, 1-7.
 22. KHOURY, M. J. (1989). Epidemiology of birth defects. *Epidemiologic reviews*, 11(1), 244-248.
 23. Kihal-Talantikite, W., Zmirou-Navier, D., Padilla, C., and Deguen, S. (2017). Systematic literature review of reproductive outcome associated with residential proximity to polluted sites. *International journal of health geographics*, 16(1), 20.
 24. Lemacks, J., Fowles, K., Mateus, A., and Thomas, K. (2013). Insights from parents about caring for a child with birth defects. *International journal of environmental research and public health*, 10(8), 3465-3482.
 25. Liu, Y., Zhang, H., Li, J., Liang, C., Zhao, Y., Chen, F., Wang, D. and Pei, L. (2020). Geographical variations in maternal lifestyles during pregnancy associated with congenital heart defects among live births in Shaanxi province, Northwestern China. *Scientific reports*, 10(1), 1-10.
 26. Lobo, I., and Zhaurova, K. (2008). Birth defects: causes and statistics. *Nature Education*, 1(1), 18.
 27. Loughna, P. (2008). Congenital abnormalities: failure to detect and treat. *The Obstetrician and Gynaecologist*, 10(1), 33–37.
 28. Lozano, R., Naghavi, M., Foreman, K., Lim, S., Shibuya, K., Aboyans, V., Ahn, S. Y. (2012). Global and regional mortality from 235 causes of death for 20 age groups in 1990 and 2010: a systematic analysis for the Global Burden of Disease Study 2010. *The Lancet*, 380(9859), 2095–2128.
 29. Martin, J. A., Kochanek, K. D., Strobino, D. M., Guyer, B., and MacDorman, M. F. (2005). Annual summary of vital statistics—2003. *Pediatrics*, 115(3), 619-634.
 30. Mihaileanu, R., Neamtiu, I. A., Bloom, M., and Stamatian, F. (2019). Birth defects in Tarnaveni area, Romania—preliminary study results. *Medicine and pharmacy reports*, 92(1), 59.
 31. Ministry of Health and Environment. Iraq. Annual Statistical Report 2017, Directorate General of Planning. Department of Information and statistics, 2018. Available at: <http://www.moh-planning.com/pdf/2017.pdf>
 32. Mohammed, B. M. A. (2015). Congenital Malformation Pattern in Duhok City. *J of Biology*, 5(8), 120–125.
 33. Morales-Suárez Varela, M. M., Nohr, E. A., Llopis-Gonzalez, A., Andersen, A.-M. N., and Olsen, J. (2009). Socio-occupational status and congenital anomalies. *European Journal of Public Health*, 19(2), 161–167.
 34. Obu, H. A., Chinawa, J. M., Uleanya, N. D., Adimora, G. N., and Obi, I. E. (2012). Congenital malformations among newborns admitted in the neonatal unit of a tertiary hospital in Enugu, South-East Nigeria—a retrospective study. *BMC Research Notes*, 5(1), 1–6.
 35. Penchaszadeh, V. B. (2002). Preventing congenital anomalies in developing countries. *Public Health Genomics*, 5(1), 61–69.
 36. Sahar, M., Maisa, N., and Ahmad, R. (2008). Approaching a Dysmorphic Newborn Egypt. *J. Hum. Genet*, 9, 121–137.
 37. Sharma, R. (2013). Birth defects in India: Hidden truth, need for urgent attention. *Indian Journal of Human Genetics*, 19(2), 125.
 38. Shawky, R. M., and Sadik, D. I. (2011). Congenital malformations prevalent among Egyptian children and associated

- risk factors. *Egyptian Journal of Medical Human Genetics*, 12(1).
39. Sun, L., Wu, Q., Jiang, S. W., Yan, Y., Wang, X., Zhang, J., Liu, Y., Yao, L., Ma, Y., and Wang, L. (2015). Prenatal diagnosis of central nervous system anomalies by high-resolution chromosomal microarray analysis. *BioMed research international*, 2015.
 40. Tanteles, G. A., and Suri, M. (2007). Classification and aetiology of birth defects. *Paediatrics and Child Health*, 17(6), 233–243.
 41. Tayebi, N., Yazdani, K., and Naghshin, N. (2010). The prevalence of congenital malformations and its correlation with consanguineous marriages. *Oman medical journal*, 25(1), 37.
 42. Trimble, B. K., & Baird, P. A. (1978). Congenital anomalies of the central nervous system incidence in British Columbia, 1952-72. *Teratology*, 17(1), 43-49.
 43. Vatankhah, S., Jalilvand, M., Sarkhosh, S., Azarmi, M., and Mohseni, M. (2017). Prevalence of congenital anomalies in Iran: A review article. *Iranian journal of public health*, 46(6), 733.
 44. Wang, Y., Liu, G., Canfield, M. A., Mai, C. T., Gilboa, S. M., Meyer, R. E., Anderka, M., Copeland, G. E., Kucik, J. E., Nembhard, W. N., Kirby, R. S. and National Birth Defects Prevention Network (2015). Racial/ethnic differences in survival of United States children with birth defects: a population-based study. *The Journal of pediatrics*, 166(4), 819-826.
 45. Weinhold, B. (2009). Environmental factors in birth defects: what we need to know. *Environ Health Perspect.* 117(10): A440–A447.
 46. Winston, W. (2011). *Microsoft Excel 2010 Data Analysis and Business Modeling: Data Analysis and Business Modeling*. Pearson Education.
 47. Woday, A., Muluneh, M. D., & Sherif, S. (2019). Determinants of preterm birth among mothers who gave birth at public hospitals in the Amhara region, Ethiopia: A case-control study. *PloS one*, 14(11), e0225060.
 48. World Health Organization (WHO). Advisory Group on Hereditary Diseases. 1985. Community approaches to the control of hereditary diseases. Unpublished WHO document HMG/WG/85.10. Geneva: WHO.
 49. Yu, D., Feng, Y., Yang, L., Da, M., Fan, C., Wang, S., and Mo, X. (2014). Maternal socioeconomic status and the risk of congenital heart defects in offspring: a meta-analysis of 33 studies. *PLoS One*, 9(10), e111056.
 50. World Health Organization (WHO). Depleted uranium: Sources, Exposure and Health Effects. Department of Protection of the Human Environment (2001). Retrieved August 23, 2020, from https://apps.who.int/iris/bitstream/handle/10665/66930/WHO_SDE_PHE_01.1.pdf

Table 1. Frequency and prevalence rate of congenital disorders

Year	Number of congenital disorders	Total live birth	Prevalence of congenital disorders per 1000 live birth
2018	80	11343	7.1
2019	73	11063	6.6

Table 2. Types of congenital disorders according to the system involvement

System involvement	Number and percent of congenital disorders	
	2018	2019
Central nervous system	25 (31.2%)	26 (35.6%)
Gastrointestinal system	19 (23.8%)	14 (19.2%)
Chromosomal	8 (10.0%)	12 (16.5%)
Musculoskeletal system	7 (8.8%)	7 (9.6%)
Unclassified (multiple system involvement)	6 (7.5%)	5 (6.8%)
Genitourinary system	5 (6.2%)	0 (0.0%)
Cardiovascular system	4 (5.0%)	5 (6.8%)
Sensory	4 (5.0%)	4 (5.5%)
Respiratory system	2 (2.5%)	0 (0.0%)
Total	80 (100%)	73 (100%)

Table 3. General characteristics and risk factors of congenital disorders

Characteristics and risk factors	2018	2019
Gender:		
Male	44 (55.0%)	41 (56.2%)
Female	36 (45.0%)	32 (43.8%)
Gestational age:		
Term	59 (73.8%)	53 (72.6%)
Preterm	21 (26.2%)	20 (27.4%)
Maternal age:		
< 18 years	5 (6.2%)	13 (17.8%)
18-35 years	60 (75.0%)	52 (71.2%)
> 35 years	15 (18.8%)	8 (11.0%)
Residence:		
Urban	55 (68.8%)	44 (60.3%)
Rural	25 (31.2%)	29 (39.7%)
Parity:		
Primiparous	26 (32.5%)	15 (20.5%)
Multiparous	54 (67.5%)	58 (79.5%)
Antenatal care:		
Regular	40 (50.0%)	45 (61.6%)
Irregular	40 (50.0%)	28 (38.4%)
History of maternal chronic illness:		
Present	8 (10.0%)	12 (16.4%)
Absent	72 (90.0%)	61 (83.6%)
Type of pregnancy:		
Single	75 (93.8%)	69 (94.5%)
Twin	5 (6.2%)	4 (5.5%)
History of intrauterine exposure to (fever, drug, radiation):		
Yes	14 (17.5%)	11 (15.1%)
No	66 (82.5%)	62 (84.9%)
Consanguinity:		
Related	45 (56.2%)	56 (76.7%)
Not related	35 (43.8%)	17 (23.3%)
History of birth defects:		
Yes	20 (25.0%)	20 (27.4%)
No	60 (75.0%)	53 (72.6%)

MODELAGEM DINÂMICA DE USO DE DADOS DE SÉRIE DE TEMPO MODELO BEKK-GARCH

DYNAMIC MODELING OF TIME SERIES DATA USING BEKK-GARCH MODEL

PEMODELAN DINAMIS DATA DERET WAKTU MENGGUNAKAN BEKK-GARCH MODEL

USMAN, Mustofa^{1*}; INDRYANI N¹; WARSONO¹; AMANTO¹, WAMILIANA¹

¹ Universitas Lampung, Faculty of Mathematics and Natural Science, Department of Mathematics, Indonesia

* Corresponding author

e-mail:usman_alfha@yahoo.com

Received 19 August 2020; received in revised form 25 October 2020; accepted 17 November 2020

RESUMO

O modelo de média móvel autorregressiva vetorial (VARMA) é um dos modelos usados com frequência na modelagem de dados de séries temporais multivariadas. Nas séries temporais, os dados econômicos, especialmente o retorno de dados, geralmente apresentam altas flutuações em alguns períodos de tempo, de modo que a volatilidade do retorno é instável. No processo de modelagem do retorno de dados dos preços das ações ADRO e ITMG, será considerado o comportamento de alta volatilidade. Os objetivos deste estudo são encontrar o melhor modelo adequado ao retorno de dados do preço das ações das empresas de energia da PT Adaro Energy Tbk (ADRO) e PT Indo Tambangraya Megah Tbk (ITMG), para analisar o comportamento da resposta ao impulso de os dados das variáveis retornam ADRO e ITMG, para analisar o teste de causalidade de granger e para prever os próximos 12 períodos. Com base na seleção do melhor modelo utilizando os critérios AICC, HQC, AIC e SBC, verificou-se que o modelo VARMA (2.2) -GARCH (1.1) é o melhor para os dados deste estudo. Com base no melhor modelo selecionado, são discutidas a resposta ao impulso, o teste de causalidade maior e a previsão para os próximos 12 períodos.

Palavras-chave: *média móvel autorregressiva vetorial, heterocedasticidade condicional autorregressiva generalizada, Modelo BEKK-GARCH, previsão*

ABSTRACT

The Vector Autoregressive Moving Average (VARMA) model is one of the models that is often used in modeling multivariate time series data. In time-series data of economics, especially data return, they usually have high fluctuations in some periods, so the return volatility is unstable. In modeling data return of share prices ADRO and ITMG, the behavior of high volatility will be considered. This study aims to find the best model that fits the data return of share price of the energy companies of PT Adaro Energy Tbk (ADRO) and PT Indo Tambangraya Megah Tbk (ITMG), to analyze the behavior of impulse response of the variables data return ADRO and ITMG, to analyze the granger causality test, and to forecast the next 12 periods. Based on the selection of the best model using the criteria of AICC, HQC, AIC, and SBC, it was found that the VARMA (2.2) -GARCH (1.1) model is the best one for the data in this study. The model VARMA(2,2)-GARCH (1,1) is then written as a univariate model. For the univariate ADRO model, the test statistics $F=4,73$ and $P\text{-value}=0,0084$, which indicates the model is very significant; and for the univariate ITMG model, the test statistics is $F= 5,82$ and $P\text{-value} < 0,0001$, which indicates the model is significant. Based on the best model selected, the impulse response, Granger causality test, and forecasting for the next 12 periods are discussed.

Keywords: *vector autoregressive moving average, general autoregressive conditional heteroscedasticity, BEKK-GARCH model, forecasting*

ABSTRAK

Model Vektor Autoregresif Moving Average (VARMA) merupakan salah satu model yang sering digunakan dalam pemodelan data deret waktu multivariat. Pada data deret waktu ekonomi, khususnya data return, biasanya memiliki fluktuasi yang tinggi dalam beberapa periode waktu tertentu, sehingga volatilitas return tidak stabil. Dalam pemodelan data return harga saham ADRO dan ITMG, akan diperhatikan perilaku volatilitas yang tinggi. Penelitian ini bertujuan untuk menemukan model terbaik yang sesuai dengan data return harga saham perusahaan energi PT Adaro Energy Tbk (ADRO) dan PT Indo Tambangraya Megah Tbk (ITMG), untuk menganalisis perilaku impulse response dari variabel data return ADRO dan ITMG, untuk menganalisis uji kausalitas granger, dan untuk meramalkan 12 periode berikutnya. Berdasarkan pemilihan model terbaik dengan menggunakan kriteria AICC, HQC, AIC, dan SBC, didapatkan model VARMA (2,2) -GARCH (1,1) yang terbaik untuk data dalam penelitian ini. Model VARMA (2,2) -GARCH (1,1) kemudian ditulis sebagai model univariat. Untuk model ADRO univariat diperoleh statistik uji $F = 4,73$ dan $P\text{-value} = 0,0084$ yang menunjukkan model tersebut sangat signifikan; dan untuk model ITMG univariat diperoleh statistik uji $F = 5,82$ dan $P\text{-value} < 0,0001$ yang menunjukkan model tersebut signifikan. Berdasarkan model terbaik yang dipilih, respon impuls, uji kausalitas Granger, dan peramalan untuk 12 periode berikutnya didiskusikan.

Kata Kunci: vektor autoregressif moving average, bentuk umum autoregresif heteroskedastik bersyarat, model BEKK-GARCH, peramalan.

1. INTRODUCTION:

The time-series data is an observation that is collected over time. Over time, observation data is commonly conducted in economics, finance, capital market, business, climates, and the environment. One of the interesting applications of time series data analysis is in the capital market. In the process of buying and selling in the capital market to get profits, investors must carry out a stock price analysis by looking at the return data of these stock prices to decide whether to buy or to sell in investing (Aspara and Indriani, 2017). Investors are interested in entering the Indonesian capital market because Indonesia is known as a country that is rich in natural resources, including mining resources. Therefore, the mining industry is playing an important role in supporting the development of the Indonesian economy.

In multivariate time series analysis, several models can be used, for example, vector autoregressive model (VAR), vector moving average (VMA), or a combination of both models, namely vector autoregressive moving average (VARMA). However, the data return of stock price analysis is usually conducted on several observations from several variables simultaneously, such as for an investor who not only invests in one company but in several companies. The investor needs to know the movement of return shares of all the companies he invests. In this case, the univariate time series analysis can no longer be relied upon, but multivariate time series analysis will be used instead.

Multivariate time series analysis was developed by Tiao and Box (1981). This analysis has been discussed in several works of literature and is often used to forecast in various fields such as finance, economics, earth science, and capital markets (Lutkepohl, 2005; Reinsel, 1993). The commonly used and effective model for forecasting multivariate time series data is the Vector Autoregressive moving average (VARMA) (Tsay, 2014). The VARMA model is an extension of the ARMA model in univariate time series data (Lutkepohl, 2005; Wei, 1990). This VARMA model can be used to predict more than one variable simultaneously and see the interrelationships between variables and predict macroeconomic data (Dufour and Pelletier, 2002).

The VARMA modeling process can be carried out if it meets the assumptions of stationary. If the stationary assumptions are not met, then the data must be transformed using a differencing process to make them stationary (Brockwell and Davis, 2002; Wei, 2006; Gujarati and Porter, 2009). The multivariate time series analysis was first used by Quenouille (1957) which was then widely used by researchers such as Hillmer and Tiao (1979), Tiao and Box (1981), Tiao and Tsay (1989), Tsay (1991), Kascha and Trenckler (2011), and Warsono *et al.* (2019a, 2019b).

Stock returns are the profits enjoyed by investors from the investment they do (Ang, 2001). Stock returns can also mean the results obtained from stock investment, either profit or loss. Investors will get a profit or capital gain if the return value is positive; by contrast, the investor will get

a loss or capital loss if the return value is negative. Volatility has been widely used in various studies, especially in the economic and financial fields, for example, studies by Mascaro and Meltzer (1983), Belongia (1984), Engle, and Susmel (1993), Karolyi (1995), and Engel and Gizycki (1999). Lopez and Walter (2000) evaluate the Value at Risk (VaR) covariance matrix using the constant, historical, EWMA, GARCH, and applied volatility models.

The volatility of the stock returns depicts the fluctuations in the stock return and shows the risk. High fluctuations in stock return will cause the variance not to be homogeneous but heterogeneous instead. Autoregressive Conditional Heteroscedasticity (ARCH) method in analyzing heterogeneous data can be used to cope with this situation. For multivariate time series data with ARCH properties or ARCH effects, the model used is Multivariate Autoregressive Conditional Heteroscedasticity (Multivariate-ARCH), which was introduced by Engle, Granger, and Kraft (1984) and it can be used more efficiently in modeling. Multivariate-ARCH was later generalized by Bollerslev (1986, 1990) to Multivariate-GARCH. This model is a development of time series analysis, which models the mean and involves modeling variance. The Multivariate-GARCH model is practical and relatively easy to use in estimating volatility and considering the basis of a dynamic volatility model (Alexander and Lazar, 2006).

The multivariate GARCH model can dynamically describe the correlation of fluctuation of stock price data. Studies using Multivariate GARCH, among others, were conducted by Francq and Zakoian (2010), researching the price of assets and management risk crucially depending on the conditional covariance structure of the asset portfolio. Further development of the CCC-GARCH model was introduced by Bollerslev (1990).

The BEKK GARCH model was introduced by Baba, Engle, Kraft, and Kroner (1990) and further developed by Engle and Kroner (1995). Engle and Kroner (1995) propose parametric BEKK GARCH models, which provide an effective model for modeling volatility. BEKK GARCH is known for its ease of obtaining a positively definite variance-covariance matrix and its efficiency in reducing the estimated number of parameters. Compared to GARCH in general, BEKK -GARCH is more profitable in analyzing the volatility of return stocks.

BEKK-GARCH is used to estimate conditional covariance and indirectly estimate conditional correlations. Caporin and McAleer (2011) compared the BEKK GARCH and DCC GARCH methods in estimating volatility, where it was concluded that BEKK GARCH provides a more optimal model in volatility modeling. Xinjun and Minhui (2011) used the BEKK GARCH model (1,1) in modeling the volatility effect of the Hu, Shenzhen, and United States (US) stock markets, and the results showed that the risk of the US stock market affected the Hu, Shenzhen stock market. Still, Shenzhen shares do not affect the US stock market. Also, Hongfei and Lou (2010) used the BEKK GARCH model to model global oil prices on industrial output in China with monthly data from January 2001 to December 2009. The research shows that international oil has a significant fluctuating effect on the oil and gas industry. However, it negatively affects the utility industry, tourism, and entertainment industry shares.

This study aims to model the data return of stock price from an Indonesian mining company, PT. Adaro Energy Tbk. (ADRO) and Indo Tambangraya Megah Tbk. (ITMG) from April 2009 to December 2019. Also, this research will apply the BEKK-GARCH model to data modeling and to find the best model that can describe the dynamic model of the two variables.

2. MATERIALS AND METHODS:

2.1 Statistical Models

The Time series analysis method is useful for forecasting future conditions. However, if several observations from several variables will be analyzed simultaneously, the Multivariate Time Series analysis is used. The model frequently used in Multivariate Time Series analysis is Vector Autoregressive Moving Average (VARMA). The VARMA model explains the relationship between observations and errors of-variables at a certain time with observations and errors in the variable itself and other variables at a previous time. Here are some classifications of the VARMA model,

2.1.1 Vector Autoregressive Model (VAR)

The general form of the VAR model with order p , VAR(p) model, or VARMA($p,0$) model with K variable can be written as Equation 1.

$$\Gamma_t = \delta + \sum_{i=1}^p \Phi_i \Gamma_{t-i} + \varepsilon_t \quad (\text{Eq.1})$$

where δ is a constant vector of dimension $k \times 1$, Φ_i is the i^{th} coefficient of the square matrix of order k of autoregressive parameters, and p is the lag length. According to Tsay (2005), ε_t is $k \times 1$ random vector and is assumed to have a multivariate normal distribution.

2.1.2 Vector Moving Average Model (VMA)

Model VMA with order q , $\text{VMA}(q)$, or $\text{VARMA}(0,q)$ can be written as Equation 2.

$$\Gamma_t = \delta + \varepsilon_t - \sum_{j=1}^q \theta_j \varepsilon_{t-j} \quad (\text{Eq. 2})$$

where δ is $k \times 1$ vector constant, ε_t is $k \times 1$ random vector and uncorrelated, and θ_j is the j^{th} coefficient of a square matrix of order k of moving average.

2.1.3 Vector Autoregressive Moving Average Model (VARMA)

The VARMA model for multivariate time series data is an extension of the ARMA model used for univariate time series data (Lutkepohl, 2005; Wei, 1990). According to Warsono *et al.* (2019a), the combination of the VAR model with the order p and the VMA model with the order q forms the $\text{VARMA}(p, q)$ model. Based on the equations (1) and (2) of multivariate time series data with a dimension k is $\text{VARMA}(p, q)$ and can be written as Equation 3:

$$\Gamma_t = \delta + \sum_{i=1}^p \Phi_i \Gamma_{t-i} + \varepsilon_t - \sum_{j=1}^q \theta_j \varepsilon_{t-j} \quad (\text{Eq. 3})$$

where δ is a constant vector with k dimension, ε_t is $k \times 1$ random vector and uncorrelated, and θ_j is the j^{th} coefficient of a square matrix of order k of moving average, Φ_i is the i^{th} coefficient of a square matrix of order k of autoregressive parameters, and p and q are the lag length for the autoregressive and moving average.

2.1.4. Generalized Autoregressive Conditional Heteroscedastic (GARCH)

The Generalized Autoregressive Conditional Heteroscedasticity (GARCH) model

develops the Autoregressive Conditional Heteroscedasticity (ARCH) model. This model was developed to avoid high orders of the ARCH model, and make a model simpler, thus ensuring that variance is always positive. The GARCH model can be written as Equation 4:

$$\begin{aligned} X_t &= \delta + \sum_{i=1}^p \phi_i X_t + \varepsilon_t - \sum_{i=1}^q \theta_i \varepsilon_t \\ \varepsilon_t &= N(0, \sigma_t^2) \\ \sigma_t^2 &= \lambda_0 + \sum_{i=1}^q \lambda_i \varepsilon_{t-i}^2 + \sum_{j=1}^p \beta_j \sigma_{t-j}^2 \end{aligned} \quad (\text{Eq.4})$$

Where X_t is a conditional mean (Brooks, 2014). The multivariate GARCH model is defined as Equation 5 (Tsay, 2014, Wei, 2019):

$$X_t = \mu_t + a_t \quad (\text{Eq.5})$$

where, X_t : $n \times 1$ vector process at time t , $\mu_t = E(X_t | F_{t-1})$ is the conditional expectation of X_t given the past information, F_{t-1} , up to time $(t-1)$. and the innovation a_t is given in Equation 6.

$$a_t = H_t^{1/2} \varepsilon_t \quad (\text{Eq.6})$$

where $\{\varepsilon_t\}$ is a sequence of an independent identically distributed random vector such that $E(\varepsilon_t) = 0$ and $\text{Cov}(\varepsilon_t) = I_n$ and $H^{1/2}$ denote the positive-definite square root matrix of H_t , where H_t is the conditional covariance matrix X_t given information up to time $(t-1)$.

2.2. BEKK GARCH

BEKK-GARCH model was first introduced by Baba *et al.* (1990) then developed further by Engle and Kroner (1995). Engle and Kroner (1995) propose a new parameterization that is easily given a restriction. The conditional covariance H_t can be written as in Equation 7.

$$H_t = C'C + \sum_{i=1}^q A_i' \varepsilon_{t-i} \varepsilon_{t-i}' A_i + \sum_{i=1}^p G_i' H_{t-i} G_i \quad (\text{Eq.7})$$

Where C is a $m \times m$ triangular matrix, A_i and G_i are $m \times m$ parameter matrices (Tsay, 2014; Wei, 2019).

The model in Equation 7 is called BEKK(p,q) model.

3. RESULTS AND DISCUSSION:

In this study, the data used is the weekly data return of the stock price of Indonesian mining companies, namely PT Adaro Energy Tbk (ADRO) and PT Indo Tambangraya Megah Tbk (ITMG) from April 2009 to December 2019 obtained from <https://www.idnfinancial.com> and the Indonesia Stock Exchange (BEI) in the form of a series plot distribution of the two variables that can be seen in Figure 1. However, what is used in the analysis is not in the form of stock price data but return stock prices because the return data better illustrates the risk of changes in stock prices. Therefore, the stock price data is changed into the form of stock price return to form a series of ADRO and ITMG return data series, as shown in Figure 2.

In Figure 2, it can be seen that both ADRO and ITMG return data have high fluctuation so that the application of the GARCH model might be appropriate. However, in conducting time series analysis, some assumptions must be met first, namely stationarity. To check the stationarity of the data, the Dickey-Fuller test is used, and the results of the test given in Table 1.

In the Augmented Dicky-Fuller test, H_0 is rejected if the p-value < 0.05 , and based on Table 1, the p-value < 0.0001 is obtained for both ADRO and ITMG data, respectively. Therefore, the null hypothesis is rejected; or in other words, stationary data are attained (Dickey and Fuller, 1979; Brockwell and Davis, 2002). The decision is also following the trend graph of ADRO and ITMG presented in Figure 3; the trend graph shows that the ACF and PACF values of ADRO and ITMG decay very past, which means that the data used in the study are stationary.

From Figure 4, we can see the volatility of the ADRO and ITMG from their conditional variances. Figure 4(a) shows that ADRO has high volatility at some periods and the highest trend changes are around observations 350 and 400. Likewise, for ITMG data presented in Figure 4(b), it appears that there is high volatility in several periods, but the changing ITMG trend tends to be more extreme than ADRO.

From the ARCH effect test results, based on Table 2, the p-value values are 0.0449 and 0.0130 for the ADRO and ITMG data, respectively. Therefore, the null hypothesis is rejected; in other words, ADRO and ITMG data have ARCH effects. Thus, the GARCH model is included in the

VARMA modeling formed, and it is, namely as the BEKK-GARCH model. Furthermore, in the process of selecting the best model, the data analysis is performed using several models: VARMA (1,1) -GARCH (1,1), VARMA (1,2) -GARCH (1,1), VARMA(2,1) -GARCH (1,1), and VARMA (2,2) -GARCH (1,1).

Based on the model criteria information presented in Table 3, the AICC and HQC model selection criteria indicate that VARMA (2,2) -GARCH (1,1) has the smallest criterion value, which means the best model. By contrast, based on the AIC criteria, the VARMA (2,1) -GARCH (1,1) model is the best model, and based on the SBC criteria, the VARMA (1,1) -GARCH (1,1) model is the best model. Because there are three best model candidates, these models will be compared using the schematic representation of parameters and GARCH parameters presented in Table 4. and Table 5. From Tables 4 and 5 the best model for ADRO and ITMG stock return data is the model VARMA (2,2) -GARCH (1,1).

Table 2. Univariate Model White Noise Diagnostic

Variables	Durbin Watson	Normality		ARCH	
		Chi- Square	P- value	F- Value	p- value
ADRO	1.99970	132.15	<.0001	4.04	0.0449
ITMG	1.92441	18.44	<.0001	6.21	0.0130

Based on the criterion of selecting the best model by using Information criteria AICC, HQC, AIC, and SBC, the best model that fits the data is VARMA(2,2)-GARCH(1,1) model. The estimated model VARMA(2,2)-GARCH(1,1) is as Equation 8.

$$\Gamma_t = \begin{bmatrix} 0.00379 \\ 0.00782 \end{bmatrix} + \begin{bmatrix} 0.00285 & -0.30001 \\ 0.86976 & -1.19455 \end{bmatrix} \Gamma_{t-1} + \begin{bmatrix} -0.73639 & 0.03952 \\ -3.75264 & 0.65400 \end{bmatrix} \Gamma_{t-2} - \begin{bmatrix} 0.04314 & -0.34157 \\ 0.85100 & -1.14980 \end{bmatrix} \varepsilon_{t-1} - \begin{bmatrix} -0.72864 & 0.02755 \\ -3.88199 & 0.80782 \end{bmatrix} \varepsilon_{t-2} + \varepsilon_t \quad (\text{Eq.8})$$

Model VARMA(2,2)-GARCH(1,1) can also be written as two univariate regression models as Equations 9 and 10.

$$\begin{aligned} \text{ADRO}_t = & 0.00379 + 0.00285 \text{ADRO}_{t-1} - \\ & 0.30001 \text{ITMG}_{t-1} - \\ & 0.73639 \text{ADRO}_{t-2} + \\ & 0.03952 \text{ITMG}_{t-2} - 0.04314 \varepsilon_{1t-1} + \end{aligned}$$

$$0.34157\varepsilon_{2t-1} + 0.072864\varepsilon_{1t-2} - 0.02755\varepsilon_{2t-2} + \varepsilon_{1t} \quad (\text{Eq.9})$$

$$\begin{aligned} \text{ITMG}_t = & 0.00782 + 0.86976 \text{ADRO}_{t-1} - \\ & 1.194551 \text{ITMG}_{t-1} - \\ & 3.75264 \text{ADRO}_{t-2} + \\ & 0.65400 \text{ITMG}_{t-2} - 0.85100\varepsilon_{1t-1} + \\ & 1.14980\varepsilon_{2t-1} + 3.88199\varepsilon_{1t-2} - \\ & 0.807825\varepsilon_{2t-2} + \varepsilon_{12t} \end{aligned} \quad (\text{Eq.10})$$

The conditional variance and covariance-based on the BEKK parameterization of model GARCH (1,1) is as Equations 11, 12, and 13.

$$\begin{aligned} h_{11t} = & 0.00280 + \\ & (0.34203)^2 \varepsilon_{1(t-1)}^2 + (-0.25866)^2 h_{11(t-1)} + \\ & 2(0.34203)(-0.47961) \varepsilon_{1(t-1)} \varepsilon_{2(t-1)} + \\ & (-0.47961)^2 \varepsilon_{2(t-1)}^2 + \\ & 2(-0.25866)(0.01295) h_{12(t-1)} + \\ & (0.01295)^2 h_{22(t-1)} \end{aligned} \quad (\text{Eq.11})$$

$$\begin{aligned} h_{12t} = & 0.00241 + (0.34203)(0.12135) \varepsilon_{1(t-1)}^2 + \\ & (0.03160)(-0.47961) \varepsilon_{2(t-1)}^2 + \\ & (-0.25866)(-0.00595) h_{11(t-1)} + \\ & (0.98885)(0.01295) h_{22(t-1)} + (-0.25866)^2 h_{11(t-1)} + \\ & \{(-0.47961)(0.12135) + \\ & (0.34203)(0.03160)\} \varepsilon_{1(t-1)}^2 \varepsilon_{2(t-1)}^2 + \\ & \{(0.01295)(-0.00595) + \\ & (-0.25866)(0.98885) h_{12(t-1)} \end{aligned} \quad (\text{Eq.12})$$

$$\begin{aligned} h_{22t} = & 0.00003 + \\ & (0.03160)^2 \varepsilon_{2(t-1)}^2 + (0.98885)^2 h_{22(t-1)} + \\ & 2(0.03160)(0.12135) \varepsilon_{1(t-1)} \varepsilon_{2(t-1)} + \\ & (0.12135)^2 \varepsilon_{1(t-1)}^2 + \\ & 2(-0.00595)(0.98885) h_{12(t-1)} + \\ & (-0.00595)^2 h_{11(t-1)} \end{aligned} \quad (\text{Eq.13})$$

Statistical tests of the ADRO_t and ITMG_t models are presented in Table 6. Based on these statistical tests, the ADRO_t model has a value of $F = 4.73$ and $P\text{-Value} = 0.0084$, which means significant and has a coefficient of R-square determination 0.0616. While ITMG_t has a value of $F = 5.82$ and $P\text{-Value} < 0.0001$, which means significant and has a coefficient of determination of R-square of 0.0781. Also, based on Table 7, it is known that the F-test of AR (1), AR (1,2), AR (1,2,3), and AR (1,2,3,4) produces a $P\text{-value} < 0.05$ or in other words, we reject H_0 . So we

conclude that the residuals are not correlated.

Next, a Granger Causality Test is administered, aiming to determine the causal relationship between variables (Tsay, 2014; Warsono *et al.*, 2019a). Granger Causality test is based on a Wald test in which the Chi-square distribution or F-test is used as an alternative. The results of the Granger Causality test analysis presented in Table 8 show that the first test in which ADRO as Group 1 and ITMG as Group 2 obtained Chi-square value = 2.35 and $P\text{-value} = 0.3081$ where the data do not reject H_0 . Therefore, it was concluded that the ITMG return value did not influence the ADRO return value. The second test with ITMG as Group 1 and ADRO as Group 2, Chi-square = 0.74, and $P\text{-value} = 0.6906$; consequently, there is not enough evidence to reject H_0 . In other words, it can be concluded that the ADRO return value does not influence the ITMG return value. Therefore, it is identified that ADRO and ITMG return values are only influenced by themselves.

Table 6. Univariate Model Anova Diagnostics

Variable	R-square	Standard Deviation	F-value	p-value
ADRO	0.0616	0.06036	4.73	0.0084
ITMG	0.0781	0.05999	5.82	<0.0001

Based on Figure 5, it appears that the distribution of prediction error data return ADRO and ITMG tends to approach the normal distribution. Meanwhile, if seen from the form of prediction error, it can be seen that both ADRO and ITMG have unstable prediction errors throughout the year. However, in ADRO prediction errors, there was a high instability compared to other years, namely during 2015 and 2016.

Figures 6 (a) and 6(b) display the Impulse Response of each variable. The Impulse response itself is commonly used in economics to describe the economic reaction from time to time to the exogenous impulse. Figure 6(a) shows the impulse of ADRO. The shock from the ADRO standard deviation causes the response to fluctuating until the 15th week, and then the response goes to zero or stability. Whereas in Figure 6(b), it can be seen that fluctuations in the standard deviation tend to decrease after being shocked in ADRO, and since the 13th week started moving towards 0. This indicates that ITMG fluctuates following shock in ADRO.

Figure 6(a) illustrates the shock response implant in ITMG. The shock from the ITMG standard deviation causes ADRO to fluctuate until the 10th week and then move towards stability. Whereas in Figure 6(b), the shock from the ITMG standard deviation causes ITMG to stabilize or move towards zero after the 18th week.

The purpose of time series analysis is to forecast future conditions based on previous observational data. Therefore, ADRO and ITMG return forecasting will be formed in the next 12 weeks based on the VARMA (2,2) -GARCH (1,1) model, estimated and presented in Table 9. Based on forecasting results, it is seen that the return values of both ADRO and ITMG still quite volatile but ITMG experienced higher fluctuation compared to ADRO. Hence, the risk of investment is higher than ADRO in the next 12 weeks. Also, based on Figures 7 and 8, it appears that ADRO and ITMG have predictive values and observational data approaching each other; this indicates that the model fits the data.

Meanwhile, the forecasts for ADRO and ITMG plots show that the confidence interval tends to be constant. Even in the ADRO forecast, there is a slight decrease in the confidence interval. This shows that the model used is suitable for data analysis and forecasting.

4. CONCLUSION:

Based on the results of the analysis, the best model for data return of PT Adro Energy Tbk (ADRO) and PT Indo Tambangraya Megah Tbk (ITMG) is VARMA(2,2) -GARCH (1,1). Also, based on the Granger causality test, it is known that ADRO and ITMG do not directly influence each other. In line with forecasting results obtained based on the best model, it is found that the prediction value is close to the observation data, which means that the model fits the data. Thus, it can be concluded that VARMA (2,2) -GARCH (1,1) is suitable for modeling the data return of ADRO and ITMG. It can also be seen that confident intervals forecasting of data return ADRO and ITMG for the next 12 weeks tend to be stable, which means that the model provides good forecasting results.

5. ACKNOWLEDGMENTS:

This research was funded by the Directorate of Research and Community Service, Deputy of

Research and Development, The Ministry of Research and Technology Republic of Indonesia / National Research and Innovation Agency under the Research Contract No: 044 / SP2H / LT / DRPM /2020. The data in this study have been provided by idnfinancial.com and the Indonesia Stock Exchange (IDX). The authors thank for the funding and the data provided. Moreover, the authors also want to thank anonymous reviewers for their valuable comments and improvement.

6. REFERENCES:

1. Alexander, C., and Lazar, E. (2006). Normal Mixture GARCH (1,1): Application to Exchange Rate Modeling. *Journal of Applied Econometrics Economic Review*, 39: 885-905.
2. Ang, R. (2001). *Buku Pintar Pasar Modal Indonesia*. Mediasoft, Jakarta.
3. Aspara, R. H., and Indriani, A. (2017). Analisis Pengaruh Crude Oil Price, Earning per Share, price to book value, return on assets and debt to equity ratio terhadap harga saham perusahaan batubara yang terdaftar di Bursa Efek Indonesia Periode 2012-2016. *Diponegoro Journal of Management*, 6(4): 1-13.
4. Baba Y., Engle, R.F., Kraft, D.F., and Koner, K.F. (1990). Multivariate Simultaneous Generalized ARCH. Unpublished Manuscript. University of California, San Diego.
5. Belongia M. (1984). Money growth variability and GNP. *Federal Reserve Bank of St. Louis Review*. 66. pp. 23-31.
6. Bollerslev, T. (1986). Generalized Autoregressive Conditional Heteroscedasticity, *Journal of Econometrics*, 31: 307-327.
7. Bollerslev, T. (1990). Modelling The Coherence in Short-Run Nominal Exchange Rates: A Multivariate Generalized ARCH Model. *Review of Economics and Statistics*, 72: 498-505.
8. Bollerslev, T., Engle, R.F., and Wooldridge, J.M. (1988). A Capital asset pricing model with time-varying covariances. *Journal of Political Economy*, 96: 116-131.
9. Brockwell P.J., and Davis R.A., (2002). *Introduction to Time Series Analysis and*

- Forecasting. Springer, New York.
10. Brooks, C. (2014), *Introductory Econometrics for Finance*. New York: Cambridge University Press.
 11. Caporin, M., and McAleer, M. (2011). Do we really need both BEKK and DCC? A tale of two multivariate GARCH model. *Journal of Economic Surveys*, 10: 1-20.
 12. Dickey, D. A., and Fuller, W. A. (1979). Distribution of the Estimator for Autoregressive Time Series with a Unit Root. *Journal of the American Statistical Association*, 74: 427-431.
 13. Dufour, J. M., and Pelletier, D. (2002) Linear Methods for Estimating VARMA models with Macroeconomic Applications. *Join Statistical Meeting-Business and economic Statistics Section*.
 14. Engel, J., and Gizycki, M. (1999). Value at Risk: On the stability and forecasting of the variance-covariance matrix. *Reserve Bank of Australia Research Discussion Paper*, 1999-04.
 15. Engle, R. F., and Kroner, K. F. (1995). Multivariate Simultaneous Generalized ARCH. *Econometric Theory*. 11: 122-150.
 16. Engle, R. F., Granger C. W. J., and Kraft D. (1984). Combining Competing forecast of inflation based on a bivariate ARCH model. *Journal of Economic Dynamics and Control*, 8: 151-165.
 17. Engle, R. F., and Susmel, R. (1993). Common volatility in international equity markets. *Journal of Business and Economic Statistics*, 11, 167–176.
 18. Francq, C., and Zakoian, J-M. (2010). *GARCH Models*, John Wiley, New York.
 19. Gujarati, D. N., and Porter, D.C. (2009). *Basic Econometrics*. (5th ed.), McGraw-Hill Irwin, New York.
 20. Hillmer, S. C., and Tiao, G. C. (1979). Likelihood Function of Stationary Multiple Autoregressive Moving Average Models. *Journal of the American Statistical Association*, 74: 652-660.
 21. Hongfei, J., and Luo, K. (2010). The shadow of international oil price on Chinese stock market-empirical analysis based on industry data. *Financial Research*, 356(2), 173–187.
 22. Karolyi, A. (1995). A multivariate GARCH model of international transmission of stock returns and volatility. *Journal of Business and Economic Statistics*, 13, pp. 11–25.
 23. Kascha, C., and Trenkler, C. (2011). Cointegrated VARMA Models and forecasting US interest rates. *Social Science Research Network*, 33: 1-18.
 24. Lopez, J.A., and Walter, C.A. (2000). Evaluating covariance matrix forecasts in a Value-at-Risk framework. *Working Paper*, Federal Reserve Bank of San Francisco.
 25. Lutkepohl, H. (2005). *New Introduction to Multiple Time Series Analysis*. Berlin: Springer-Verlag.
 26. Mascaro, A, and Meltzer, A.H. (1983). Long and short-term interest rates in a risky world. *J Monet Econ* 12, pp. 485–518.
 27. Quenouille, M. H. (1957). *The Analysis of Multiple Time Series*. Griffin, London.
 28. Reinsel, G.C. (1993). *Elements of Multivariate Time Series Analysis*. New York: Springer-Verlag.
 29. Tiao, G. C., and Box, G. E. P. (1981). Multiple time series modeling with application. *Journal of the American Statistical Association*, 76: 802-816.
 30. Tiao, G. C., and Tsay, R. S. (1989). Model specification in multivariate time series (with discussion). *Journal of the Royal Statistical Society, Series B*, 51: 157-213.
 31. Tsay, R. S. (1991). Two canonical forms for Vector ARMA processes. *Statistica Sinica*, 1: 247-269.
 32. Tsay, R. S. (2005). *Analysis of Financial Time Series*. Hoboken, New Jersey: John Wiley & Sons, Inc.
 33. Tsay, R. S. (2014). *Multivariate Time Series Analysis: With R and Financial Applications*. Hoboken, New Jersey: John Wiley & Sons, Inc.
 34. Warsono, Russel, E., Wamiliana, Widiarti, and Usman, M. (2019a), Vector Autoregressive with Exogenous Variable Model and its Application in Modeling and Forecasting Energy Data: Case Study of PTBA and HRUM Energy. *International Journal of Energy Economics and Policy*, 9(2): 390-398.
 35. Warsono, Russel, E., Wamiliana, Widiarti, and Usman, M. (2019b), Modeling and Forecasting by the Vector Autoregressive Moving Average Model for Export of Coal and Oil Data. *International Journal of Energy Economics and Policy*, 9(4): 240-247.
 36. Wei, W. W. S. (1990), *Time Series Analysis*:

Univariate and Multivariate Methods. Redwood City, California: Addison-Wasley Publishing Company.

37. Wei, W. W. S.(2006). Time Series Analysis: Univariate and Multivariate Methods. Second Edition. Pearson, New York.
38. Wei, W. W. S.(2019). Multivariate Time Series Analysis and Applications, John Wiley

and Sons, New York.

39. Xinjun, W., and Minhui, L. (2011). Shanghai, deep, the US stock market volatility spillover relationship based on ternary BEKK–GARCH (1,1) model. Shandong Social Sciences, 24(11), 158–162.

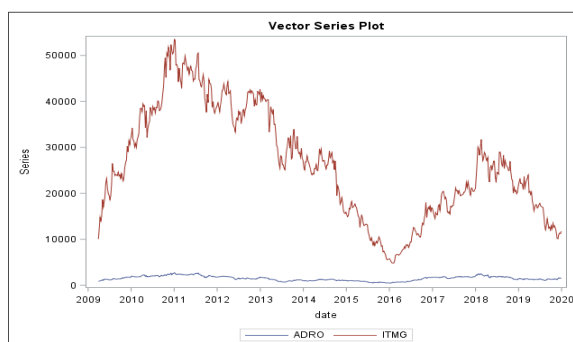


Figure 1. Plot data stock price of ADRO and ITMG April 2009 to December 2019

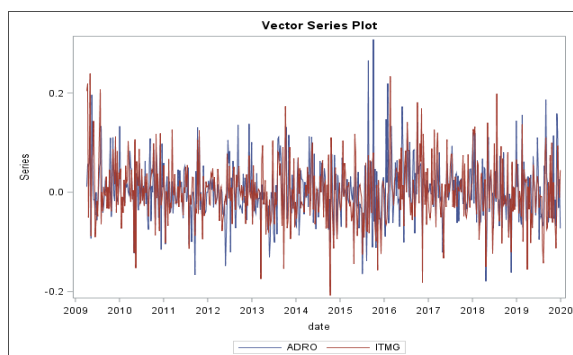


Figure 2. Plot data return stock price of ADRO and ITMG from April 2009 to December 2019

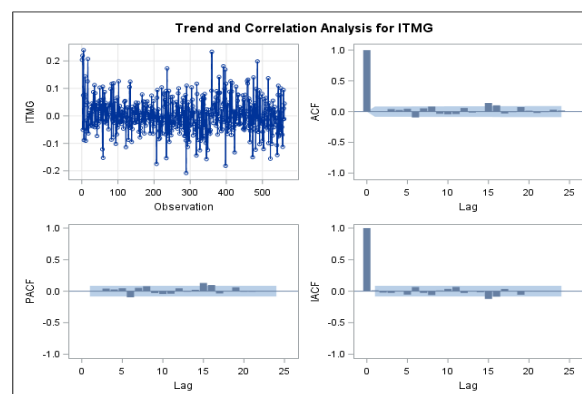
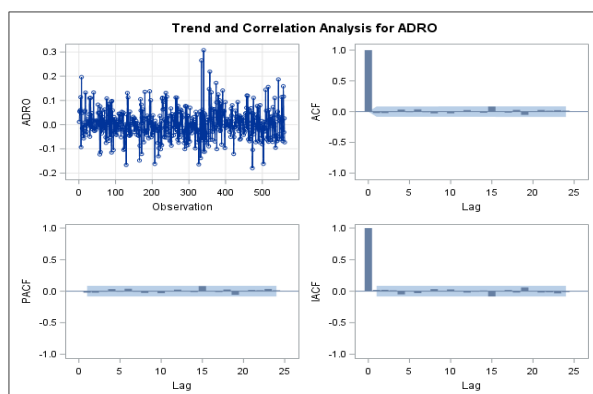


Figure 3. Plot Trend and Correlation Analysis for (a) ADRO and (b) ITMG

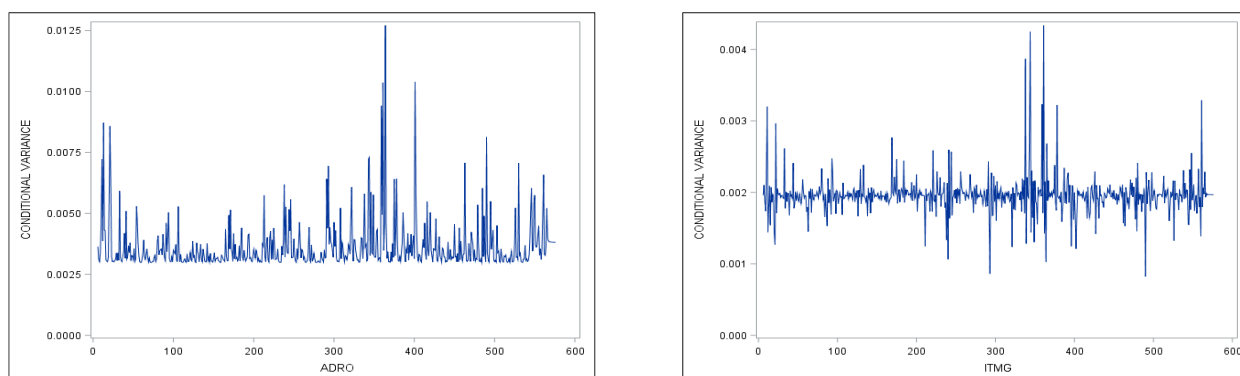


Figure 4. Plot Conditional Variance ADRO (a) and ITMG (b)

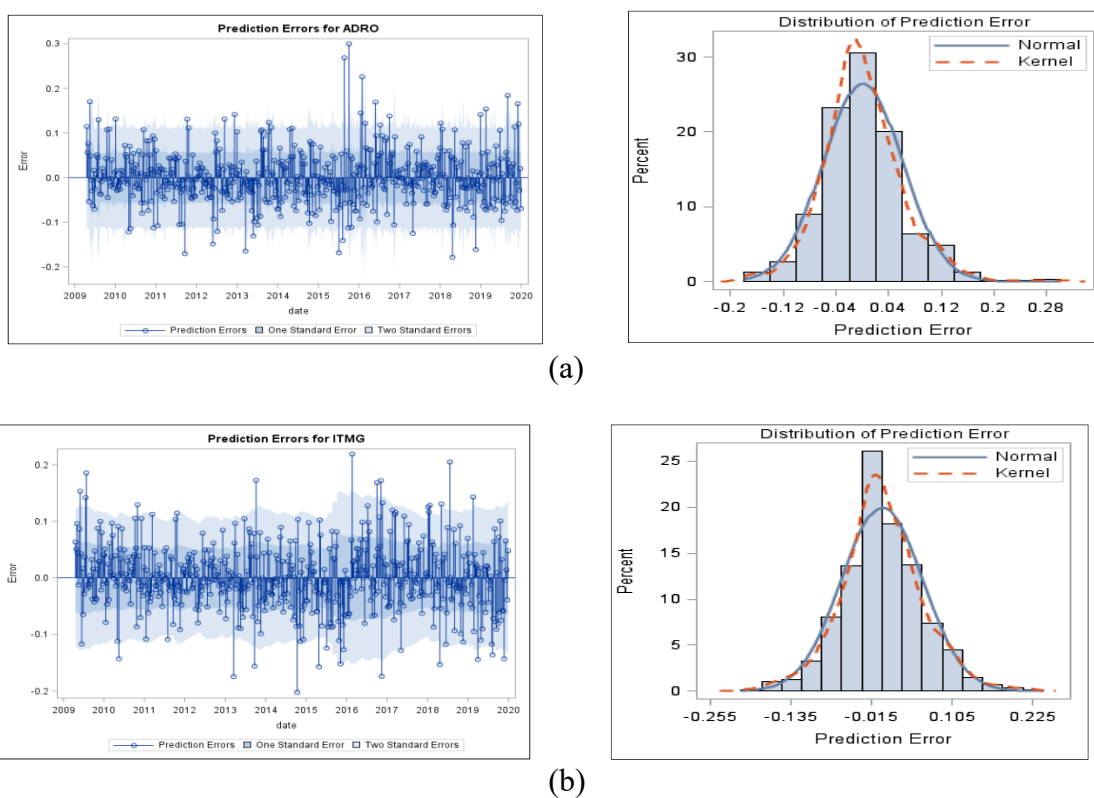


Figure 5. Prediction and Distribution of Errors base on the model for data of ADRO (a) and ITMG (b)

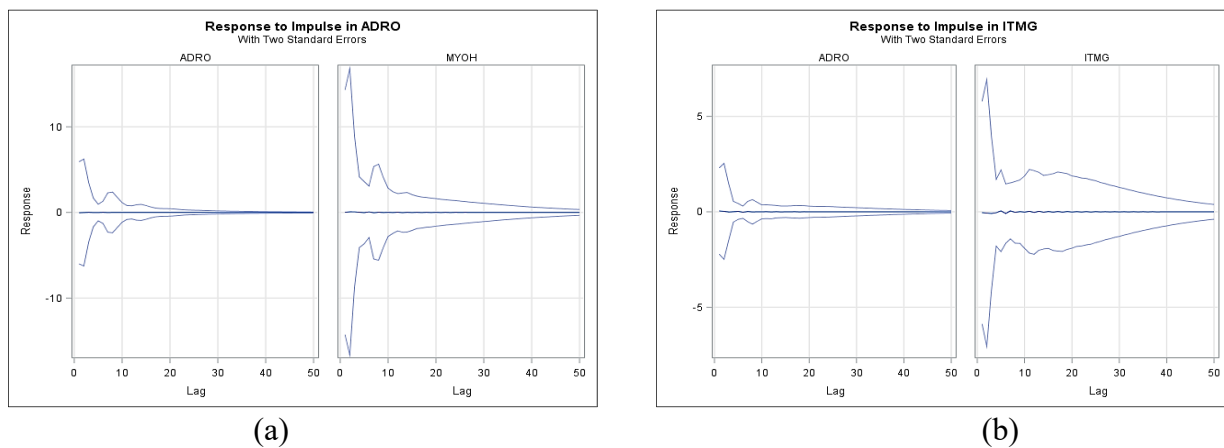


Figure 6. Respond to Impulse in ADRO (a) in ITMG (b)

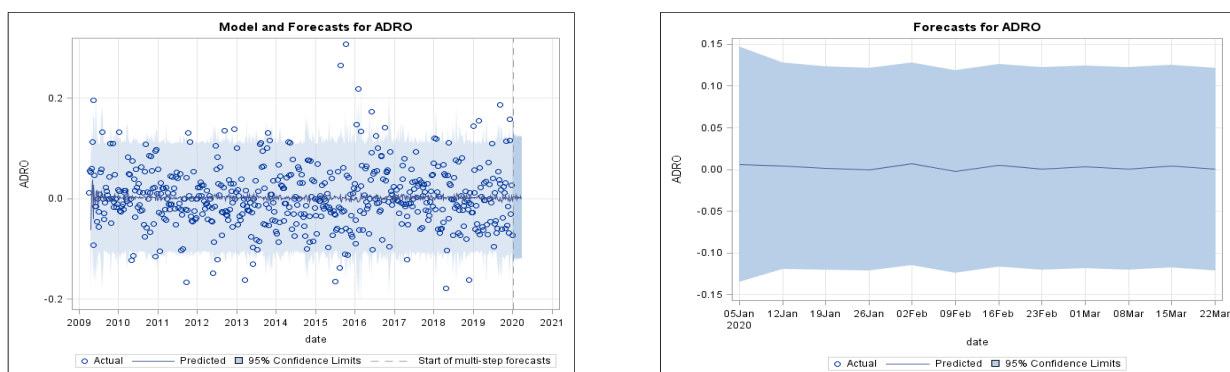


Figure 7. Model and forecast of data return ADRO for the next 12 weeks.

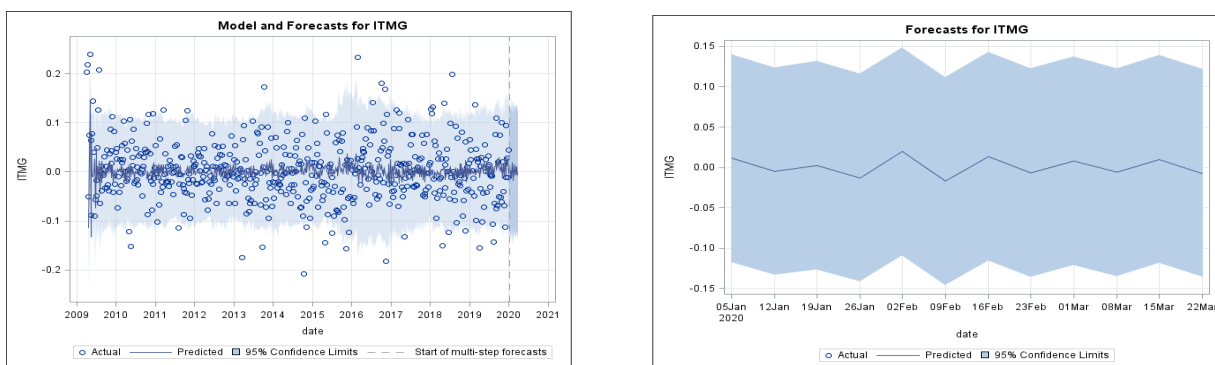


Figure 8. Model and forecast of data return ITMG for the next 12 weeks.

Table 1. Dickey-Fuller Unit Root Test

Variable	Type	Rho	P-value	Tau	P-value
ADRO	Zero Mean	-597.04	0.0001	-17.25	<.0001
	Single Mean	-600.74	0.0001	-17.28	<.0001
	Trend	-601.06	0.0001	-17.27	<.0001
ITMG	Zero Mean	-574.97	0.0001	-17.37	<.0001
	Single Mean	-576.30	0.0001	-17.37	<.0001
	Trend	-583.21	0.0001	-17.43	<.0001

Table 3. Information Criteria of Models

Criterion	VARMA(1,1)- GARCH(1,1)	VARMA(1,2)- GARCH(1,1)	VARMA(2,1)- GARCH(1,1)	VARMA(2,2)- GARCH(1,1)
AICC	-5345.11	-5337.36	-5359.50	-5368.11
HQC	-5311.34	-5297.57	-5319.70	-5322.40
AIC	-5346.82	-5339.80	-6361.94	-5371.40
SBC	-5255.94	-5231.65	-5253.78	-5245.94

Table 4. Schematic Representation of Parameter Estimates

Model	Variable/Lag	C	AR1	AR2	MA1	MA2
VARMA(1,1)- GARCH(1,1)	ADRO	•	+		+	
	ITMG	•	**		**	
VARMA(2,1)- GARCH(1,1)	ADRO	•	••	•	••	
	ITMG	•	•*	••	••	
VARMA(2,2)- GARCH(1,1)	ADRO	•	••	•	••	++
	ITMG	•	••	••	••	-+

Note: + is $> 2 \times \text{std error}$, - is $< -2 \times \text{std error}$, • is between, * is N/A

Table 5. Schematic Representation of GARCH Parameter Estimates

Model	Variable/Lag	GCHC	ACH1	GCH1
VARMA(1,1)- GARCH(1,1)	H1	++	+•	**
	H2	*+	-•	**
VARMA(2,1)- GARCH(1,1)	H1	++	++	••
	H2	*•	-•	•-
VARMA(2,2)- GARCH(1,1)	H1	++	++	••
	H2	••	-•	•+

Notes: + is > 2*std error, - is < -2*std error, • is between, * is N/A

Table 7. Univariate Model AR Diagnostics

Variable	AR1		AR2		AR3		AR4	
	F-value	p-value	F-value	p-value	F-value	p-value	F-value	p-value
ADRO	0.01	0.9175	0.22	0.8003	0.26	0.8575	0.45	0.7752
ITMG	0.73	0.3924	0.41	0.6658	0.78	0.5060	0.77	0.5442

Table 8. Granger Causality Wald Test

Test	Group	DF	Chi-Square	p-value
1	Group 1 Variable: ADRO Group 2 Variable: ITMG	2	2.35	0.3081
2	Group 1 Variable: ITMG Group 2 Variable: ADRO	2	0.74	0.6906

Table 9. Forecasts for the return value of ADRO and ITMG

Variable	Obs.	Time	Forecast	Standard Error	95% Confidence Interval	
ADRO	562	Sun, 5 Jan 2020	0.00593	0.07218	-0.13554	0.14740
	563	Sun, 12 Jan 2020	0.00417	0.06318	-0.11966	0.12801
	564	Sun, 19 Jan 2020	0.00137	0.06236	-0.12085	0.12359
	565	Sun, 26 Jan 2020	-0.00020	0.06204	-0.12179	0.12140
	566	Sun, 2 Feb 2020	0.00671	0.06202	-0.11484	0.12826
	567	Sun, 9 Feb 2020	-0.00235	0.06199	-0.12385	0.11914
	568	Sun, 16 Feb 2020	0.00473	0.06198	-0.11674	0.12621
	569	Sun, 23 Feb 2020	0.00077	0.06196	-0.12067	0.12221
	570	Sun, 1 Mar 2020	0.00286	0.06193	-0.11853	0.12425
	571	Sun, 8 Mar 2020	0.00067	0.06191	-0.12067	0.12201
	572	Sun, 15 Mar 2020	0.00383	0.06189	-0.11747	0.12512
	573	Sun, 22 Mar 2020	0.00007	0.06186	-0.12118	0.12132
ITMG	562	Sun, 5 Jan 2020	0.01113	0.06555	-0.11733	0.13960
	563	Sun, 12 Jan 2020	-0.00497	0.06565	-0.13364	0.12371
	564	Sun, 19 Jan 2020	0.00242	0.06576	-0.12647	0.13131
	565	Sun, 26 Jan 2020	-0.01277	0.06587	-0.14188	0.11633
	566	Sun, 2 Feb 2020	0.01935	0.06582	-0.10965	0.14836
	567	Sun, 9 Feb 2020	-0.01708	0.06579	-0.14603	0.11188
	568	Sun, 16 Feb 2020	0.01364	0.06594	-0.11560	0.14289
	569	Sun, 23 Feb 2020	-0.00669	0.06592	-0.13590	0.12252
	570	Sun, 1 Mar 2020	0.00765	0.06586	-0.12143	0.13673
	571	Sun, 8 Mar 2020	-0.00611	0.06577	-0.13503	0.12280
	572	Sun, 15 Mar 2020	0.00999	0.06570	-0.11878	0.13876
	573	Sun, 22 Mar 2020	-0.00730	0.06564	-0.13595	0.12136

NANOPARTÍCULAS DE METAIS NOBRES NA SUPERFÍCIE DE FLOCOS DE GRAFENO

NANOPARTICLES OF NOBLE METALS ON THE SURFACE OF GRAPHENE FLAKES

НАНОЧАСТИЦЫ БЛАГОРОДНЫХ МЕТАЛЛОВ НА ПОВЕРХНОСТИ ЧЕШУЕК ГРАФЕНА

IONI, Yulia V.^{1,2,3*}

¹ N.S. Kurnakov Institute of General and Inorganic Chemistry of the Russian Academy of Sciences, Department of Exchange Clusters, 31 Leninsky Ave., zip code 119991, Moscow – Russian Federation

² Moscow Aviation Institute (National Research University), Department of Physical Chemistry, 4 Volokolamskoe shosse, zip code 125993, Moscow – Russian Federation

³ P.N. Lebedev Physical Institute of the Russian Academy of Sciences, Department of Luminescence, 53 Leninsky Ave., zip code 119991, Moscow – Russian Federation

* Corresponding author
e-mail: acidladj@mail.ru

Received 01 October 2020; received in revised form 22 October 2020; accepted 14 November 2020

RESUMO

O carbono é um elemento comum que possui muitas combinações diferentes de reações. A preparação de novos materiais compósitos à base de nanopartículas é um tema muito urgente e promissor, uma vez que as nanopartículas possuem propriedades únicas. Essas propriedades são mantidas e até mesmo aumentadas quando as nanopartículas estão localizadas em matrizes diferentes. Além disso, atualmente a criação de compósitos à base de grafeno e estruturas a partir dele é uma direção promissora na síntese de nanomateriais compósitos. Pesquisas anteriores mostraram que o grafeno tem um conjunto único de propriedades eletrofísicas, térmicas, ópticas e mecânicas. O objetivo principal deste trabalho é a síntese de nanocompósitos, que são nanopartículas de metais nobres (Au, Pd, Rh) na superfície de flocos de grafeno; estudo da sua composição, estrutura, propriedades físico-químicas e possíveis aplicações em catálise. Neste trabalho, foi realizada a síntese de nanocompósitos, que são nanopartículas de metais nobres (Au, Pd, Rh) na superfície de flocos de grafeno, bem como o estudo de sua composição, estrutura, propriedades físicas e químicas e possíveis aplicações em catálise. Um método para imobilizar nanopartículas na superfície de óxido de grafeno e grafeno foi desenvolvido e foi criado um método original para a síntese de nanopartículas nanocompósitos de metais nobres na superfície de flocos de grafeno usando isopropanol supercrítico como um agente redutor para a conversão de óxido de grafeno em grafeno. Os resultados do estudo das propriedades físico-químicas dos nanocompósitos obtidos e os resultados do estudo dos nanocompósitos obtidos como catalisadores para modelos de reações orgânicas de acoplamento cruzado e hidroformilação têm mostrado a possibilidade de criar nanoestruturas à base de grafeno como nanomateriais funcionais eficazes. Os trabalhos dedicados à síntese de compostos de grafeno e no estudo de suas propriedades físicas únicas formam uma das áreas promissoras da química e física de novos materiais funcionais inorgânicos. Os nanocompósitos resultantes podem ser usados em aplicações como eletrodos para LEDs e células solares, transistores de efeito de campo, supercapacitores, sensores, células de combustível.

Palavras-chave: grafeno, óxido de grafeno, nanopartículas, metais nobres, nanocompósitos.

ABSTRACT

Carbon is a spread element that has many different reaction combinations. Obtaining new composite materials based on nanoparticles is a very actual and perspective topic because nanoparticles possess unique properties. These properties are retained and even amplified when nanoparticles are located in various matrixes. Furthermore, nowadays, the creation of graphene-based composites and graphene-related structures is a promising area of synthesis of composite nanomaterials. Previous research has determined that graphene has a unique set of electrophysical, thermal, optical, and mechanical properties. In this study, the synthesis of nanocomposites representing nanoparticles of noble metals (Au, Pd, Rh) on the surface of graphene flakes

were carried out, and the study of their composition, structure, physical and chemical properties, and possible applications in catalysis. The immobilization of nanoparticles on the surface of graphene oxide and graphene was developed, and the original method of synthesis of nanocomposite noble metal nanoparticles on the graphene flakes surface using supercritical isopropanol as a reduction agent for the transformation of graphene oxide into graphene was created. The study of physical and chemical properties of the obtained nanocomposites and results of the study of obtained nanocomposites as catalysts for model organic reactions of cross-coupling and hydroformylation showed that it is possible to create the graphene-based nanostructures as effective functional nanomaterials. Research on the synthesis of graphene compounds and its unique physical properties form a promising direction in the chemistry and physics of new inorganic functional materials. The resulting nanocomposites can be used in such branches as electrodes for LEDs and solar cells, field-effect transistors, supercapacitors, sensors, fuel cells.

Keywords: *graphene, graphene oxide, nanoparticles, noble metals, nanocomposites.*

АННОТАЦИЯ

Углерод – распространенный элемент, который имеет множество различных комбинаций реакций. Получение новых композиционных материалов на основе наночастиц является очень актуальной и перспективной темой, поскольку наночастицы обладают уникальными свойствами. Эти свойства сохраняются и даже усиливаются, когда наночастицы расположены в различных матрицах. Кроме того, в настоящее время создание композитов на основе графена и структур на его основе является перспективным направлением синтеза композитных наноматериалов. Предыдущие исследования показали, что графен обладает уникальным набором электрофизических, тепловых, оптических и механических свойств. Основная цель данной работы – синтез нанокомпозитов, представляющих собой наночастицы благородных металлов (Au, Pd, Rh) на поверхности чешуек графена; изучение их состава, структуры, физико-химических свойств и возможных применений в катализе. В данной работе был проведен синтез нанокомпозитов, представляющих собой наночастицы благородных металлов (Au, Pd, Rh) на поверхности чешуек графена, а также изучение их состава, структуры, физических и химических свойств и возможных применений в катализе. Разработан метод иммобилизации наночастиц на поверхности оксида графена и графена и создан оригинальный метод синтеза нанокомпозитных наночастиц благородных металлов на поверхности чешуек графена с использованием сверхкритического изопропанола в качестве восстановителя для превращения оксида графена в графен. Результаты исследования физико-химических свойств полученных нанокомпозитов и результаты исследования полученных нанокомпозитов в качестве катализаторов модельных органических реакций кросс-сочетания и гидроформилирования показали возможность создания наноструктур на основе графена как эффективных функциональных наноматериалов. Работы по синтезу соединений графена и исследованию его уникальных физических свойств образуют одно из перспективных направлений химии и физики новых неорганических функциональных материалов. Полученные нанокомпозиты могут быть использованы в таких областях применения, как электроды для светодиодов и солнечных батарей, полевые транзисторы, суперконденсаторы, сенсоры, топливные элементы.

Ключевые слова: *графен, оксид графена, наночастицы, благородные металлы, нанокомпозиты*

1. INTRODUCTION:

A topical research topic is producing new composite materials based on nanoparticles (Bulychev, 2019; Bulychev and Ivanov, 2019; Kirichenko *et al.*, 2019; Wani *et al.*, 2020). These properties are retained and even amplified when nanoparticles are located in various matrixes (Kretinin *et al.*, 2014; Erokhin *et al.*, 2018; Bulychev *et al.*, 2019). The creation of graphene-based composites and graphene-related structures is a promising area of synthesis of composite nanomaterials. Graphene is a unique two-dimensional material; the thickness of graphene is only one sp^2 - carbon atom. Despite

this, graphene has a wide range of unusual peculiar properties. Besides, there are substances similar to graphene structures such as fullerenes, nanotubes, nanographite, graphene oxide, and modified graphene (Tan *et al.*, 2013; Xu *et al.*, 2013).

Graphene has high mechanical, thermal, and chemical resistance. It is a simple element with one carbon atom tightly packed into a crystal lattice of a cellular structure. Graphene nanoribbons (GNRs) and nanoflakes (GNFs) that are finite in both dimensions can be considered as fragments or molecular subunits of graphene. Since their initial successful fabrication, GNRs and GNFs have rapidly reduced from the

microscale down to nanometer sizes either by top-down or bottom-up approaches. Based on size and shape, GNFs can form ordered columnar mesophases. It is important to understand the properties of HNF and its saturated analogs, polycyclic aromatic hydrocarbons (PAHs), since the main functional components of future electronic and spiroelectronic devices should be nanoscale.

Graphite and graphene are uninterrupted semiconductors. Large deviations in energy can occur when the size of the carbon particles is reduced to a level where the quantum effect becomes noticeable. For clusters with a small number of carbon atoms, the energy gaps are approximately 8.5 eV, and for carbon frameworks consisting of 80 carbon atoms, gaps below 2 eV have been found. Research on sized carbon particles will make them interesting candidates for nanotechnology applications (Neri *et al.*, 2019).

Nanoparticles of noble metals (Au, Pd, Rh) existing both in the dispersions and surrounded by various matrixes are among the most studied classes of nano-objects. Nanoparticles of noble metals have outstanding optical and catalytic properties. Gold nanoparticles act as a uniform model objects for studying various properties of noble metals nanoparticles (Heinsalu *et al.*, 2019). The palladium black or colloidal palladium is known for a long time, but the structure and properties of the palladium particles have been studied only recently. Furthermore, palladium and rhodium are catalytically active metals (Jastrzebska *et al.*, 2017). So, palladium and rhodium nanoparticles are promising candidates for application as catalysts in various organic reactions to synthesize new substances. Materials based on graphene with noble metals nanoparticles attached to its surface can find their application in catalysis, manufacturing of fuel cells, chemical sensors, and other applications (Duan *et al.*, 2015; Zhang *et al.*, 2015; Ioni *et al.*, 2016). The main objective of this work was the synthesis of nanocomposites representing nanoparticles of noble metals (Au, Pd, Rh) on the surface of graphene flakes; study of their composition, structure, physical and chemical properties, and possible applications in catalysis.

2. MATERIALS AND METHODS:

Graphene oxide used in this work was obtained by the modified Hammer's method (Ioni *et al.*, 2016). Synthesis of graphene was carried

out by the original method of reduction of graphene oxide by supercritical isopropanol (SCI) (Figure 1). The developed method for obtaining graphene by reducing supercritical isopropanol is distinguished by the reproducibility of results and manufacturability (it uses off-the-shelf equipment). Isopropanol in the supercritical state can reduce oxygen-containing functional groups on graphene oxide surface, leading to graphene production in gram quantities. The method does not use explosive and toxic reagents. Obtaining graphene in appreciable quantities made it possible to start creating composites based on graphene with high mechanical properties. Obtained graphene oxide and graphene have been characterized by physical and chemical methods of analysis (elemental analysis, XRD, TEM, IR- and Raman spectroscopy). Elemental analysis of the samples was carried out on a EA1108 C/H/N analyzer by CarloEbraInstruments (Italy). A sample weighing up to 1 mg was burned automatically in the reaction tube of the analyzer at $T = 980\text{ }^{\circ}\text{C}$ with a pulsed oxygen supply. A complete analysis of combustion products was carried out using a thermal conductivity detector with processing of the obtained chromatographic data on a computer. The phase composition of the samples was determined by X-ray phase analysis on a Bruker D8 Advance spectrometer operating in the reflection mode on $\text{CuK}\alpha$ radiation (35 kV, 30 mA, $\lambda = 1.54056\text{ \AA}$) with a scanning step of 4 deg/min^{-1} .

Raman spectra of graphene and graphene oxide samples were recorded on a RenishawInVia Raman spectrometer. The laser wavelength was 514 nm (Ar, 20 mW), the power was varied in the range 0.00005–100% using ND filters. The study of the samples was carried out at room temperature in air in the backscattering geometry using a Leica DMLM confocal microscope (100' objective), focal length 250 mm, the laser beam size was changed from 1 to 300 μm .

Nanocomposites based on graphene oxide with noble metal nanoparticles on its surface were reduced using supercritical isopropanol. According to the original method, the powder of nanocomposite NM NPs/GO (100 mg) was dispersed in isopropanol by ultrasound and was placed in a quartz container at the autoclave and kept at $\sim 300\text{ }^{\circ}\text{C}$ for 24 hours. Ultrasonic treatment was carried out using a 500 W generator and a 20.4 kHz transducer. Ultrasonic exposure parameters: specific power - 0.1–1 W/cm^3 , exposure time - 20 min until a stable dispersion of graphene oxide is obtained (pH =

7). The transition into a supercritical state was performed by simultaneous increasing the temperature and the inner pressure of the autoclave. After cooling the autoclave to room temperature, the resulting solid product was washed with isopropanol, acetone, and water, centrifuged (6000 rpm, 10 min.), and dried at room temperature. Series of experiments (on the reduction in supercritical isopropanol of nanocomposites Au/graphene oxide, NPs/graphene oxide and Rh/graphene oxide, and study of samples of initial and obtained nanocomposites) shown that graphene oxide was reduced to graphene, but the nanoparticles are retained on the graphene surface after reduction (Averyushkin *et al.*, 2017; Baskakov *et al.*, 2017).

Chloroauric acid was used as a precursor for obtaining gold nanoparticles on the surface of graphene oxide. 100 μ L of a 0.05 M $\text{HAuCl}_4/\text{HCl}$ solution was added to 10 mL of an aqueous dispersion of graphene oxide (1 mg/mL) with stirring. One hour after decolorization of the solution, 300 μ L of a 0.05 M freshly prepared $\text{NaBH}_4/\text{NaOH}$ solution in water was added to the system, and the mixture was stirred for 10 minutes. To isolate a solid precipitate, the system was centrifuged (6000 rpm, 15 min.), washed with water, and dried in air at a temperature of 60 $^{\circ}\text{C}$. H_2PdCl_4 and RhCl_3 were used for a similar synthesis of nanocomposites containing Pd and Rh nanoparticles, respectively. HAuCl_4 was added to the dispersion of graphene oxide in water, then the reducing agent sodium tetrahydroborate was added to the brown solution. The resulting dispersion was cooled, centrifuged (6000 rot./min., 15 min.) for precipitation of the solid phase, washed several times with water, and dried in air. So, nanocomposite Au NPs/GO was obtained. In the second stage, the reduction of the resulting nanocomposite Au NPs/GO was carried out using isopropanol in supercritical conditions. The synthesis was carried out in a steel autoclave, the volume of isopropanol was 5.2 mL, $T \sim 270^{\circ}\text{C}$ for 24 hours, the working pressure of the autoclave was 54 atm. The transition to the supercritical state was carried out by increasing the temperature of the reactor and, at the same time, the internal pressure in the autoclave. The final product was nanocomposite Au NPs/Graphene. Both nanocomposites Au NPs/GO and Au NPs/Graphene were studied by complex analytical methods. Samples of nanocomposites were characterized by elemental and X-ray structural analysis, IR and Raman spectroscopy, and transmission electron microscopy. The method of X-ray diffraction analysis was used to

study the phase content of nanocomposite (Baskakov *et al.*, 2017; Bravo *et al.*, 2018; Parnianchi *et al.*, 2018 Yang *et al.*, 2019; Wu *et al.*, 2020; Gao *et al.*, 2020).

The purpose of the further study was to propose a fairly simple, convenient, and one-step method for producing nanographite, subsequently, graphene, without its preliminary chemical activation. Natural graphite was used to accomplish this task. It is known that the crystal structure of graphite has defects of various types (vacancies, bulges, and fine structure defects) (Lee *et al.*, 2019). Under the action of intense ultrasound, the splitting of the crystal structure presumably occurs, mainly along the defects of the crystal matrix. Various dispersed systems "graphite-solvent" and "graphite-solvent-surfactant" have been studied. Ultrasonic treatment is a very convenient way to obtain dispersed systems. The method is universal and does not require significant economic costs (Proa-Coronado *et al.*, 2018). In order to increase the stability of dispersed systems, various types of surfactants were used (sodium salt of dodecylbenzene sodium sulfonate (DBSS), sodium bis (2-ethylhexyl) sulfosuccinate (AOT), octadodecylamine (ODA), ethylhexadecyldimethylammonium bromide (EHDAB)), which were directly added to the initial graphite-solvent system (Beniwal *et al.*, 2017; Zhang *et al.*, 2019). To study the morphology and particle size of the nanographite dispersion, various types of microscopic studies were used: interference, transmission, scanning, and atomic force (Araújo *et al.*, 2018). The morphology of the samples was studied using transmission electron microscopy on a JEOL JEM 1011 setup at an accelerating voltage of 80–100 kV. Before recording, the sample was deposited on a copper mesh with a diameter of ~ 3.5 mm covered with a polymer film. Images in transmission mode were acquired at magnifications of up to 500000.

3. RESULTS AND DISCUSSION:

Figure 2 shows XRD data of initial graphite, graphene oxide, and reduced graphene oxide (graphene). Graphite has a sharp peak at $2\theta = 26.5^{\circ}$. The graphene oxide phase corresponds to a distinct peak at $2\theta = 12^{\circ}$, which disappears after a reduction towards graphene. The synthesized graphene oxide and graphene were examined using transmission electron microscopy (Figure 3). IR-spectroscopy analysis has been applied for the investigation of surfaces of graphene oxide and graphene flakes as well.

The process of immobilization of noble metals nanoparticles was performed in several stages. In the first step, the graphene oxide was dispersed by ultrasonification in water. Then, the precursor of the corresponding metal was added to graphene dispersion (Figure 4). As precursors for nanoparticles synthesis, $\text{HAuCl}\cdot 3\text{H}_2\text{O}$, $\text{H}_2[\text{PdCl}_4]$, and $\text{RhCl}_3\cdot 3\text{H}_2\text{O}$ were used.

Graphene oxide was found to have oxygen-containing functional groups on its surface (Figure 4A). It is assumed that metal ions coordinate with various functional groups on the surface of the oxide graphene (Figure 4B). Further on, in the second stage, the reduction agent was introduced for nanoparticles formation (Figure 4C). As a reduction agent, NaBH_4 was used. Since metal ions coordinate with the functional groups of the graphene oxide, these functional groups could act as the centers of crystallization of the new phase to form and grow nanoparticles. The third stage is the reduction of graphene oxide with nanoparticles of noble metals located on its surface to graphene by supercritical isopropanol (Figure 4C). The final result of this reaction is nanocomposite NM NP/Graphene.

The resulting graphene oxide and graphene have a transparent, flake-like structure; the number of graphene layers does not exceed 10. The content of the graphene oxide elements before and after reduction by supercritical isopropanol has been determined by elemental C, H, N – analysis (Table 1). Figure 5 shows the Raman spectra of the initial graphite, graphene oxide, and graphene after the reduction of graphene oxide by supercritical isopropanol. It was found that the spectra of graphite oxide, graphene, and graphene are consisting of two peaks: G – line, which is related to sp^2 - carbon bonds ($\sim 1580\text{ cm}^{-1}$), and 2D – line ($\sim 2700\text{ cm}^{-1}$), which is an overtone of D – lines ($\sim 1330\text{ cm}^{-1}$). The presence of D – lines for graphene and graphene oxide samples indicates the formation of defect structure compared to the original structure of graphite, and the changing of 2D-peak shape is related to a small number of layers in the graphene structure. There are different oxygen-containing functional groups in the graphene oxide spectrum: hydroxyl, epoxy- and carbonyl groups. After reduction by SCI, the content of these functional groups in samples is decreased, as shown in the IR-spectra (Figure 6).

The novel method for synthesizing nanocomposite of Noble Metal Nanoparticles on the graphene surface (NM NP/Graphene) has been developed. In contrast to graphene oxide,

graphene has only a monolayer of carbon atoms in the sp^2 - hybridized state and has no functional oxygen groups, which could act as nucleation sites for nanoparticles formation. That is why, in this work, it was necessary to develop an original method of immobilization of nanoparticles of noble metals (Au, Pd, Rh) on the graphene surface through the formation of an intermediate nanocomposite of Noble Metal Nanoparticles on the graphene oxide surface (NM NP/GO).

The transmission electron microscope was used for studying the size distribution and morphology of gold nanoparticles on the surface of graphene and graphene oxide (Figure 7). Also, for comparison, the dispersion of gold nanoparticles in water was obtained. In the picture of Au NPs in water dispersion (Figure 7a) and the sample of nanocomposite Au NPs/GO (Figure 7b), it is shown that gold nanoparticles have a shape close to spherical. The distribution of the size of the nanoparticles of both samples was 6-10 nm. The average size is near 8 nm. After reducing the nanocomposite Au NPs/GO by SCI, gold nanoparticles on the graphene surface becomes larger due to the disappearance of oxygen-containing functional groups, and distribution of the size of the nanoparticles became 6-19 nm, and the average size is 13.5 nm (Figure 7c).

Figure 8a shows the XRD pattern of the synthesized nanocomposite Au NPs/GO indicating that Au nanoparticles were formed at the graphene oxide surface. The peak at $2\theta=12^\circ$ is related to the graphene oxide phase. Figure 8b shows the XRD pattern of nanocomposite Au NPs/Graphene after reduction by SCI of nanocomposite Au NPs/GO. Diffraction peak $2\theta=12^\circ$ related to graphene oxide has disappeared, which means the reduction of graphene oxide to graphene occurs. However, in Figure 8b, it is obvious that Au nanoparticles are retained on the graphene surface after reduction by SCI.

Gold nanoparticles have a strong band of surface plasmon resonance in the range 500 to 580 nm; its position and intensity depend on the size and shape of the particles. Figure 9A shows the absorption spectra of Au NPs dispersion, graphene oxide dispersion, and Au NPs/GO dispersion in water. Au NPs, both “naked” and in the graphene oxide surface, have a pronounced sharp surface plasmon absorption at 520 nm, corresponding to 10 nm size. Figure 9B shows the absorption spectra of graphene dispersion in water and Au NPs/Graphene in water. It should be noted that the band of surface plasmon

resonance of the gold nanoparticles disappeared in the resulting nanocomposite Au NPs/Graphene.

Dispersed systems of nanographite in various solvents were obtained by the action of ultrasonic cavitation. It was found that graphite powder is dispersed by ultrasound to graphite plates, which are stable as a suspension in a number of solvents. The output of the dispersed phase, depending on the process conditions, is 2-5% (for 7-10 minutes of ultrasonic treatment). The time of graphite dispersion in various solvents was selected using a qualitative assessment of the time of 50% sedimentation of suspensions in a capillary. From the dependences of the sedimentation of nanographite suspension in various solvents on the time of ultrasonic treatment, it follows that nanographite particles precipitate in organic solvents faster than in water, that is, nanographite dispersions in organic solvents are characterized by a shorter stability time than dispersions in water. It has been shown that an increase in the dispersion time (over 7 – 10 min.) does not affect the stability of suspensions.

It was found that ortho-xylene nanographite suspensions are stable for 1-2 days, in acetonitrile and toluene – for 203 days. After the indicated time, there was no absorption in the UV spectra of the suspensions. After centrifugation, the nanoparticles aggregate, and according to X-ray phase analysis, the residue phase corresponds to the phase of graphite. The aqueous dispersion of nanographite is stable for 12-14 days, the particles do not agglomerate with each other. It was shown that in the systems "graphite–organic solvent–surfactant" in comparison with the system "graphite–organic solvent," there is no increase in the stability of dispersions and a decrease in the time of sedimentation of particles, which is associated with the hydrophobicity of solvents. However, when using water as a hydrophilic solvent, the opposite result is observed. It was shown that the greatest stability of nanographite dispersed systems is achieved when using anion-active stabilizers as surfactants. It is likely that stabilization by surfactant molecules occurs along the boundaries of defects in the graphite crystal matrix. Because of the highest stability of dispersions, the systems "graphite–water" and "graphite–water–anion-active stabilizers" were selected for further research.

In the size distribution diagrams of a nanographite dispersion in water (with and without a surfactant), two peaks of the size

distribution are visible. Presumably, the first refers to the thickness of the nanographite plates, and the second is their lateral size. In the case of an aqueous dispersion of nanographite without surfactants, these dimensions were found to be 30 ± 10 nm and 350 ± 50 nm, respectively; in the second case – in the presence of anionic stabilizers – 35 ± 15 nm and 400 ± 75 nm. Microscopic data also confirm this assumption.

The product isolated from the aqueous dispersion without and with the addition of surfactants was identified by XRF. Graphite has two characteristic reflections – at 26.5° and 54.5° . After its dispersion in water under powerful ultrasound action, nanographite with a phase identical to that of graphite was obtained. The X-ray diffraction pattern of a nanographite sample obtained by dispersing the initial graphite under the action of high-power ultrasound in water in the presence of anion-active stabilizers shows that the structure of the crystal lattice is preserved, a slight broadening of the peaks and a significant decrease in their intensity are observed, which indicates a decrease in the particle size. Also, another low-intensity reflex appears, corresponding to the formation of a graphite oxide phase. To compare the changes in the structure of the graphite dispersion product with the initial graphite, the method of Raman spectroscopy was used. However, it is not possible to determine the exact number of graphene layers based on Raman spectra. However, the number of layers is significantly reduced compared to the initial structure of graphite (by 1.5–2 orders of magnitude).

The image obtained by interference microscopy shows and confirms that when graphite is dispersed using powerful ultrasound, the graphite structure is thinned by several orders of magnitude – the resulting nanographite flakes deposited on a silicon oxide substrate are combined into film structures. Such film structures are rather thin, which allows them to be viewed through an optical microscope using the interference contrast method.

It is not possible to see the structure of graphite with a transmission electron microscope. However, samples of nanographite dispersion in water with the addition of anion-active stabilizers deposited on a carbon grid give a clear image. It shows a layered structure of nanographite, which is rather thin in contrast to graphite. According to the data of scanning electron microscopy, the structure of graphite nanoparticles is practically the same for both samples. Nanographite is a layered structure with transparent plates. The

particle size of nanographite in some layers can reach 400-500 nm. However, on the surface of the nanographite plates, smaller structures are visible, the length of which is much less than 100 nm. Such plates can then be fractionally separated by centrifugation.

The atomic force microscopy analysis showed that nanographite plates obtained from an aqueous dispersed system without the addition of surfactants with a surface profile along the scanning line have a lateral plate size of 200-300 nm, the surface height is 20-30 nm. The surface of the nanographite plate is inhomogeneous – the difference in surface heights is about 10 nm. Nanographite plates obtained from an aqueous dispersion with the addition of anionic surfactants and their surface profile along the scanning line have a lateral plate size of 200-300 nm and a surface height of 20-35 nm. The difference in surface heights is about 15 nm.

From the data obtained, it can be noticed that dispersed systems of nanographite in water (with and without the addition of surfactants) contain nanographite plates, the lateral size of which is 200-500 microns, and the thickness is 20-40 nm. Presumably, these plates contain from 30 to 50 graphene layers. Thus, an original one-stage method for dispersing graphite in various solvents using powerful ultrasound has been developed. A stable disperse system of nanographite was obtained in organic solvents (toluene, acetonitrile, ortho-xylene) and in water. The possibility of stabilization of dispersed systems of nanographite using various surfactants has been investigated. It has been shown that the most stable is the dispersed system of nanographite in water with the addition of the sodium salt of dodecyl sulfobenzoic acid. A complex of methods of physicochemical analysis (DLS, XRF, Raman spectroscopy, AFM, SEM, TEM) has established that the resulting disperse system consists of nanographite plates, the lateral size of which is 200-500 nm, the thickness is 20-50 nm.

Thus, direct (without any preliminary activation of the initial graphite) dispersion of graphite by means of ultrasound leads to the production of nanometer-sized plates. Using well-known techniques (spin-coating, Langmuir-Blodgett techniques, and others), dispersed systems of nanographite can be used to create thin films on various substrates, which opens up new possibilities for creating materials based on graphite nanoparticles.

It is known that carbon nanostructures can possess biological activity, which determines their application in various biomedical fields. In experiments with the osteoblasts cultivation, it was found that mono- and multilayer carbon nanostructures noticeably affect the size and other features of growing cells. The comparison was carried out with similar cultures grown on a borosilicate glass substrate. It has been shown that a decrease in the thickness of carbon nanolayers enhances the proliferation of osteoblasts and the synthesis of alkaline phosphatase, and also causes calcium deposition. When studying the dependence of the characteristics of cultured cells of different types (osteoblasts, fibroblasts, chondrocytes) on the size of carbon nanoparticles, an increase in osteoblast adhesion caused by a decrease in the size of the plates was noted. Microscopic studies have revealed cell shape modifications caused by the binding of carbon nanostructures to cell membranes.

The resulting nanocomposites can be used in numerous applications such as catalysis, supercapacitors, (bio)sensors.

4. CONCLUSIONS:

As a result of this study, the following problems were solved. Development of a method for fixation of nanoparticles of noble metals (NM) – gold, palladium, and rhodium on the graphene oxide surface (GO), exploration of the samples by the complex of physical and chemical analyses. Study of the interaction of nanocomposites – nanoparticles of noble metals/graphene oxide (NM NP / GO) with supercritical isopropanol (SCI) in order to reduce graphene oxide to graphene with nanoparticles of noble metals fixed on the graphene flakes surface. Development of procedures for the preparation of nanocomposites – nanoparticles of noble metals on the graphene surface (NM NP / Graphene) and explore physical and chemical properties of nanocomposites. An original method of synthesis of nanocomposite materials based on graphene has been developed.

5. ACKNOWLEDGMENTS:

This work has been partially supported by Ministry of Science and Higher Education of Russian Federation, projects No. MK-893.2020.8 and No. 2020-1902-01-288 (Agreement No. 075-15-2020-775) and by RFBR, project No. 19-08-01023.

6. REFERENCES:

1. Araújo, M. P., Nunes, M., Rocha, I. M., Pereira, M. F. R., and Freire, C. (2018). Co₃O₄ Nanoparticles anchored on selectively oxidized graphene flakes as bifunctional electrocatalysts for oxygen reactions. *ChemistrySelect*, 3(35), 10064-10076.
2. Averyushkin, A. S., Bulychev, N. A., Efimkov, V. F., Erokhin, A. I., Kazaryan, M. A., Mikhailov, S. I., Saraeva, I. N., and Zubarev, I. G. (2017). Stimulated scattering in ag nanoparticles colloids. *Russian Laser Journal*, 27(5), article number 055041.
3. Baskakov, A. O., Starchikov, S. S., Lyubutin, I. S., Avilov, A. S., Solov'eva, A. Y., Ioni, Y. V., Gubin, S. P., and Khodos, I. I. (2017). Magnetic and interface properties of the core-shell fe₃o₄/au nanocomposites. *Applied Surface Science*, 422, 638-644.
4. Beniwal, S., Hooper, J., Miller, D. P., Costa, P. S., Chen, G., Liu, S.-Yu., Dowben, P. A., Charles, E., Sykes, H., Zurek, E., and Enders, A. (2017). Graphene-like boron-carbon-nitrogen monolayers. *ACS Nano*, 11(3), 2486-2493.
5. Bravo, S., Correa, J., Chico, L., and Pacheco, M. (2018). Tight-binding model for opto-electronic properties of penta-graphene nanostructures. *Scientific Reports*, 8, Article number 11070.
6. Bulychev, N. A. (2019). Experimental studies on hydrogen production in plasma discharge in a liquid-phase medium flow. *International Journal of Hydrogen Energy*, 44(57), 29933-29936.
7. Bulychev, N. A., and Ivanov, A. V. (2019). Effect of vibration on structure and properties of polymeric membranes. *International Journal of Nanotechnology*, 16(6/7/8/9/10), 334-343.
8. Bulychev, N. A., Kazaryan, M. A., Kirichenko, M. N., and Ivanov, A. V. (2019). Study of acoustoplasma discharge as a technique for synthesis of optically active materials. *International Journal of Nanotechnology*, 16(1/2/3), 34-41.
9. Duan, J., Chen, S., Jaroniec, M., and Zhang Qiao, S. (2015). Heteroatom-doped graphene-based materials for energy-relevant electrocatalytic processes. *ACS Catalysis*, 5(9), 5207-5234.
10. Erokhin, A. E., Smetanin, I. V., Mikhailov, S. M., and Bulychev, N.A. (2018). Spectral shifts of stimulated Rayleigh – Mie scattering in Ag nanoparticle colloids. *Optics Letters*, 43(7), 1570-1573.
11. Gao, Zh., Zhao, M.-Q., Alam Ashik, M.M., and Johnson, A. T. C. (2020). Recent advances in the properties and synthesis of bilayer graphene and transition metal dichalcogenides. *Journal of Physics: Materials*, 3(4), Article number 042003.
12. Heinsalu, S., Fesenko, O., Treshchalov, A., Kovalchuk, S., Yaremkevych, A., Kavelin, V., and Dolgov, L. (2019). Silver nanoparticles with reduced graphene oxide for surface-enhanced vibrational spectroscopy of DNA constituents. *Applied Nanoscience (Switzerland)*, 9(5), 1075-1083.
13. Ioni, Y., Buslaeva, E., and Gubin, S. (2016). Synthesis of graphene with noble metal nanoparticle on its surface. *Materials Today: Proceedings*, 2016, S209-S213.
14. Jastrzebska, A. M., Karcz, J., Karwowska, E., Fiedorczuk, A., and Olszyna, A. (2017). Synthesis and bioactivity of RGO/TiO₂-noble metal nanocomposite flakes. *Journal of Nano Research*, 47, 33-48.
15. Kirichenko, M. N., Chaikov, L. L., Krivokhiza, S. V., Kirichenko, A., Burkhanov, I. S., Bulychev, N. A., and Kazaryan, M. A. (2019). Effect of iron oxide nanoparticles on fibrin gel formation and its fractal dimension. *Journal of Chemical Physics*, 150(15), Article number 155103.
16. Kretinin, A. V., Cao, Y., Tu, J.S., Yu, G.L., Jalil, R., Novoselov, K.S., Haigh, S.J., Gholinia, A., Mishchenko, A., Lozada, M., Georgiou, T., Woods, C.R., Withers, F., Blake, P., Eda, G., Wirsig, A., Hucho, C., Watanabe, K., Taniguchi, T., Geim, A.K., and Gorbachev, R.V. (2014). Electronic properties of graphene encapsulated with different two-dimensional atomic crystals. *Nano Letters*, 14(6), 3270-3276.
17. Lee, H.-K., Lee, J. H., Seo, J. H., Chun, D. H., Kang, S. W., Lee, D. W., Yang, J.-I., Rhim, G. B., Youn, M. H., Jeong, H.-D., Jung, H., and Park, J. C. (2019). Extremely productive iron-carbide nanoparticles on graphene flakes for CO hydrogenation reactions under harsh conditions. *Journal of Catalysis*, 378, 289-297.
18. Neri, G., Fazio, E., Mineo, P. G., Scala, A., and Piperno, A. (2019). SERS sensing properties of new graphene/gold

- nanocomposite. *Nanomaterials*, 9(9), article number 1236.
19. Parnianchi, F., Nazari, M., Maleki, J., and Mohebi, M. (2018). Combination of graphene and graphene oxide with metal and metal oxide nanoparticles in fabrication of electrochemical enzymatic biosensors. *International Nano Letters*, 8, 229-239.
 20. Proa-Coronado, S., Vargas-García, J. R., Manzo-Robledo, A., Mendoza-Acevedo, S., Villagómez, C. J., Mercado-Zúñiga, C., Muñoz-Aguirre, N., Villa-Vargas, L. A., and Martínez-Rivas, A. (2018). Platinum nanoparticles homogenously decorating multilayered reduced graphene oxide for electrical nanobiosensor applications. *Thin Solid Films*, 658, 54-60.
 21. Tan, C., Huang, X., and Zhang, H. (2013). Synthesis and applications of graphene-based noble metal nanostructures. *Materials Today*, 16, 29-36.
 22. Wani, A.A., Khan, A.M., Manea, Y.K., Shahadat, M., Ahammad, S.Z., and Ali, S.W. (2020). Graphene-supported organic-inorganic layered double hydroxides and their environmental applications: a review. *Journal of Cleaner Production*, 273, Article number 122980.
 23. Wu, T., Wang, X., Emrehan Emre, A., Fan, J., Min, Yu., Xu, Q., and Sun, S. (2020). Graphene-nickel nitride hybrids supporting palladium nanoparticles for enhanced ethanol electrooxidation. *Journal of Energy Chemistry*, 55, 48-54.
 24. Xu, M., Liang, T., Shi, M., and Chen, H. (2013). Graphene-like two-dimensional materials. *Chemical Reviews*, 113(5), 3766-3798.
 25. Yang, B., Chen, Yu., and Shi, J. (2019). Mesoporous silica/organosilica nanoparticles: Synthesis, biological effect, and biomedical application. *Materials Science and Engineering: R: Reports*, 137, 66-105.
 26. Zhang, L., Li, X., Shao, Y., Yu, J., Wu, Y., Hao, X., Yin, Zh., Dai, Yu., Tian, Yu., Huo, Q., Shen, Y., Hua, Zh., and Zhang, B. (2015). Improving the quality of gan crystals by using graphene or hexagonal boron nitride nanosheets substrate. *ACS Applied Materials and Interfaces*, 7(8), 4504-4510.
 27. Zhang, N., Xing, Y.-H., and Bai, F.-Y. (2019). A Uranyl-Organic Framework Featuring Two-Dimensional Graphene-like Layered Topology for Efficient Iodine and Dyes Capture. *Inorganic Chemistry*, 58(10), 6866-6876.

Table 1. Results of elemental analysis of graphene oxide and graphene

Sample	Elements content, %		
	C	H	O
Graphene oxide	58.0 ± 1.0	1.5 ± 0.5	39.0 ± 1.0
Graphene	91.0±1.0	1.5±0.5	6.0±1.0

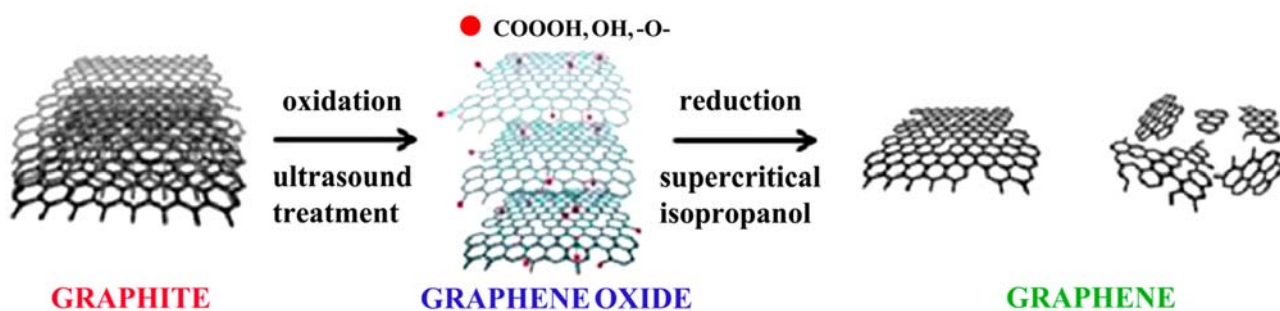


Figure 1. Scheme of graphene synthesis

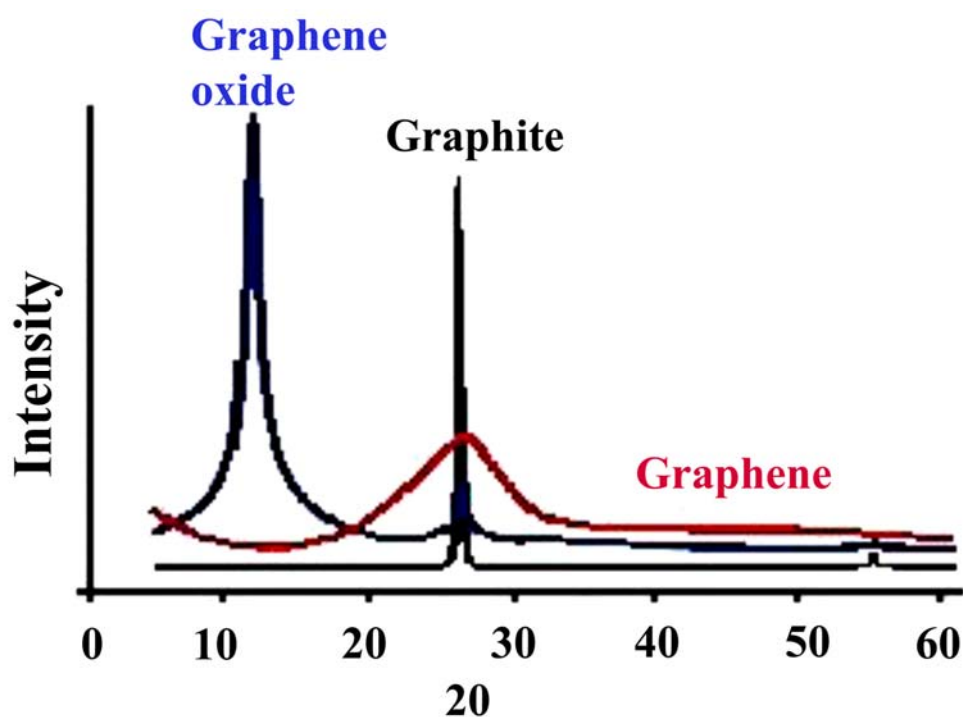


Figure 2. XRD of graphite, graphene oxide, and graphene

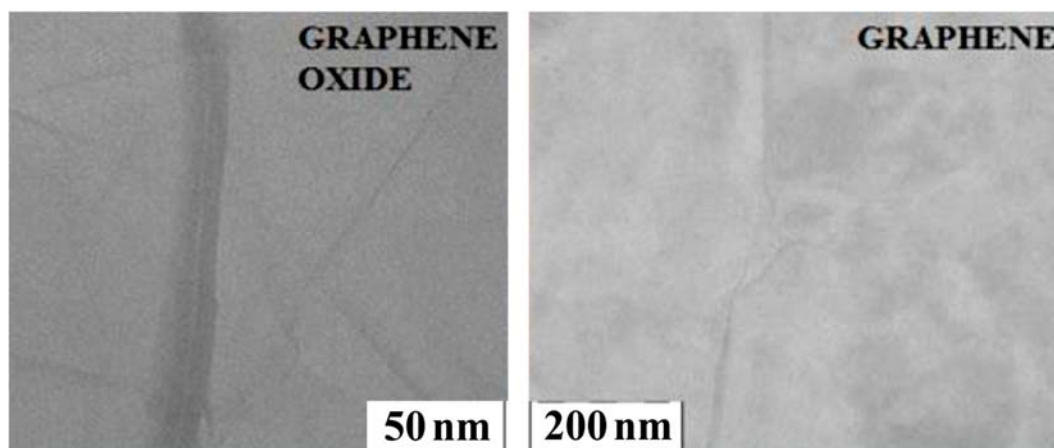


Figure 3. TEM image of graphene oxide and graphene

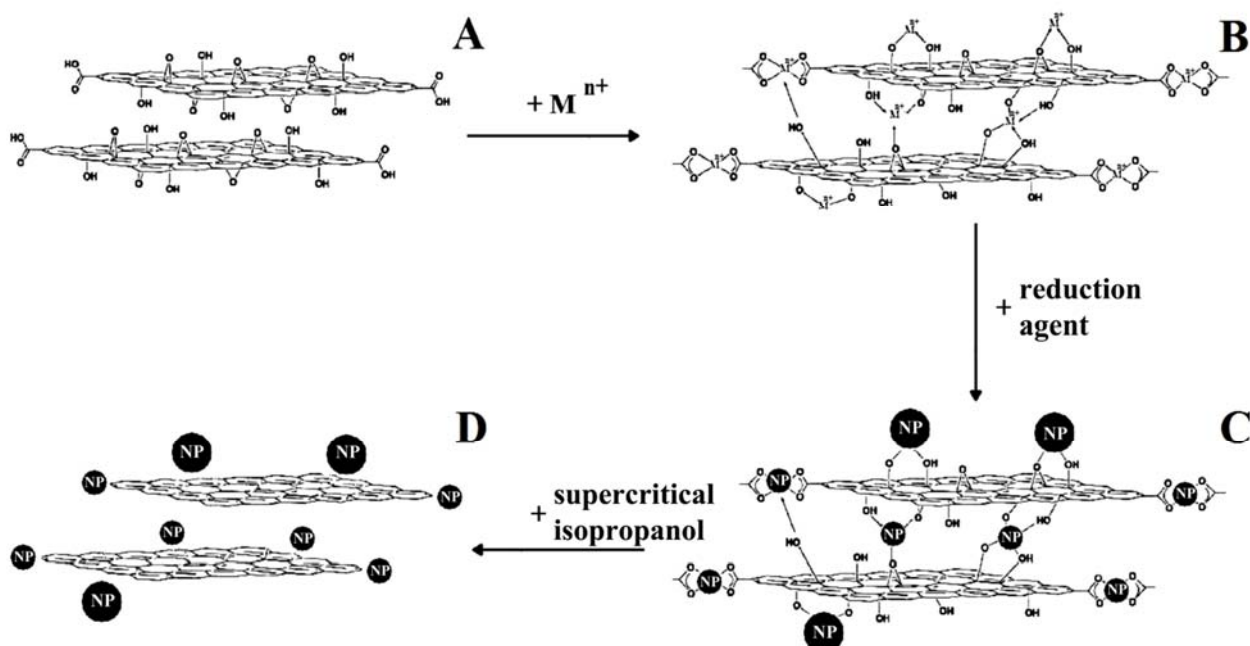


Figure 4. Scheme of the immobilization of noble metals nanoparticles on the surface of graphene: A – initial graphene oxide; B – coordination of metal ions with the functional groups on the surface of graphene oxide; C – formation of nanoparticles on the surface of graphene oxide; D – reduction of the nanocomposite NB NP/GO to nanocomposite NB NP/Graphene by the supercritical isopropanol

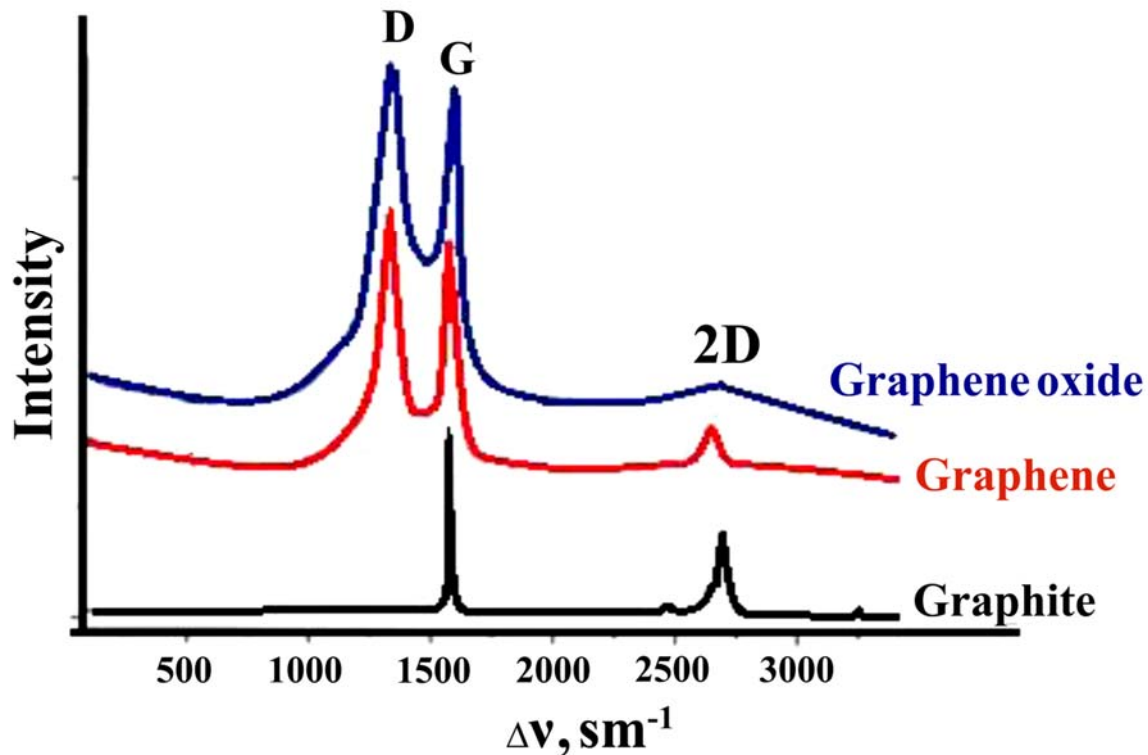


Figure 5. Raman-spectra of graphite, graphene oxide, and graphene

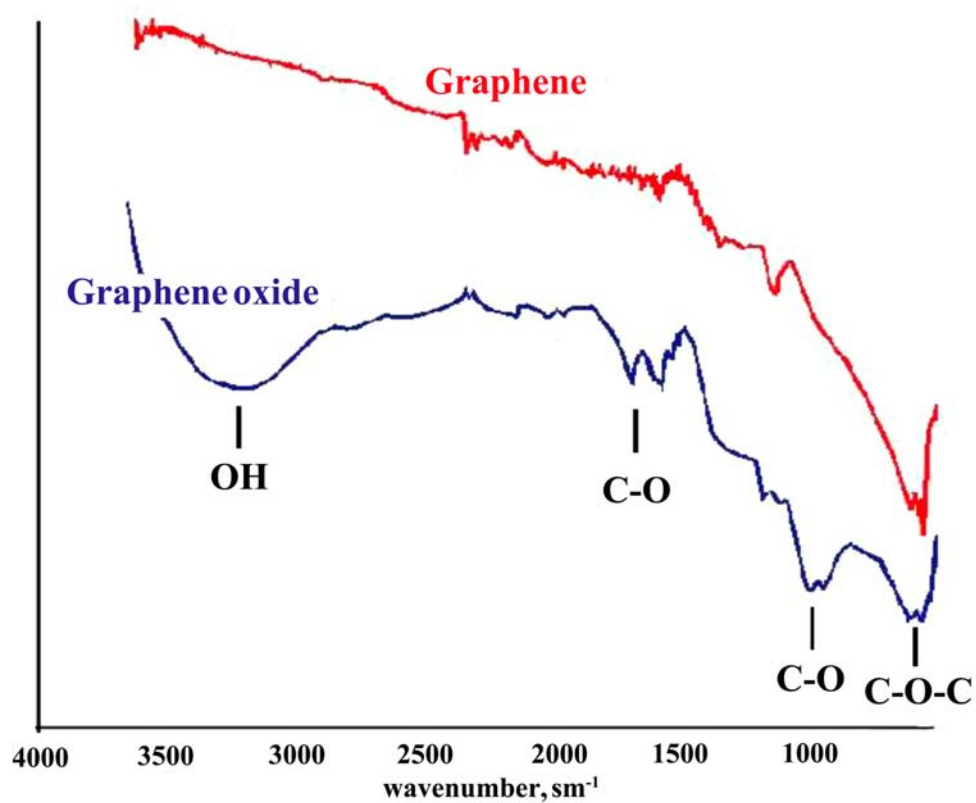


Figure 6. IR-spectra of graphene oxide and graphene

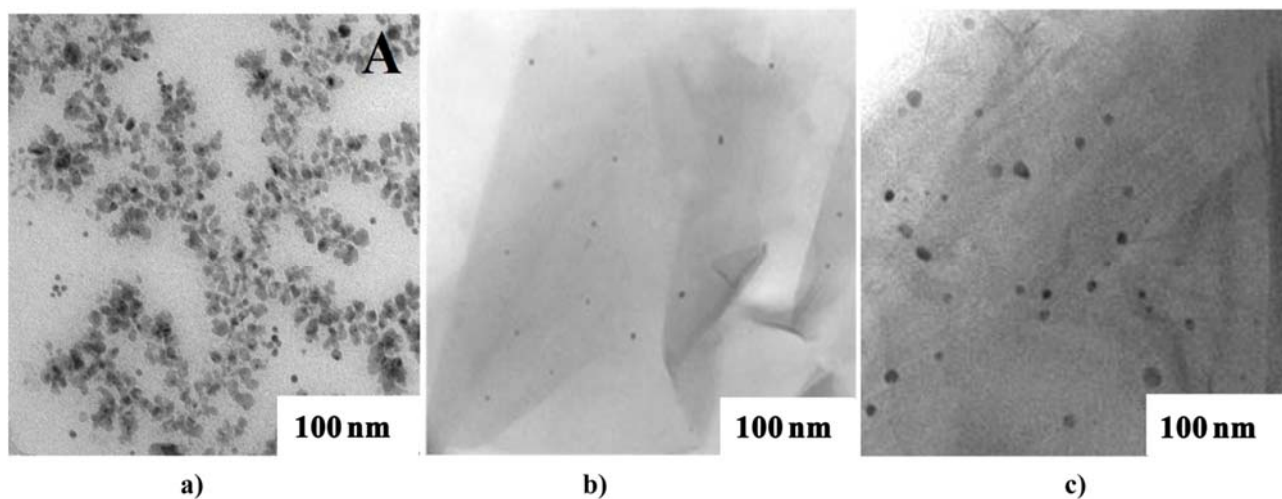


Figure 7. TEM images: a) Au NPs dispersion in water; b) Au NPs/GO; c) Au NPs/Graphene

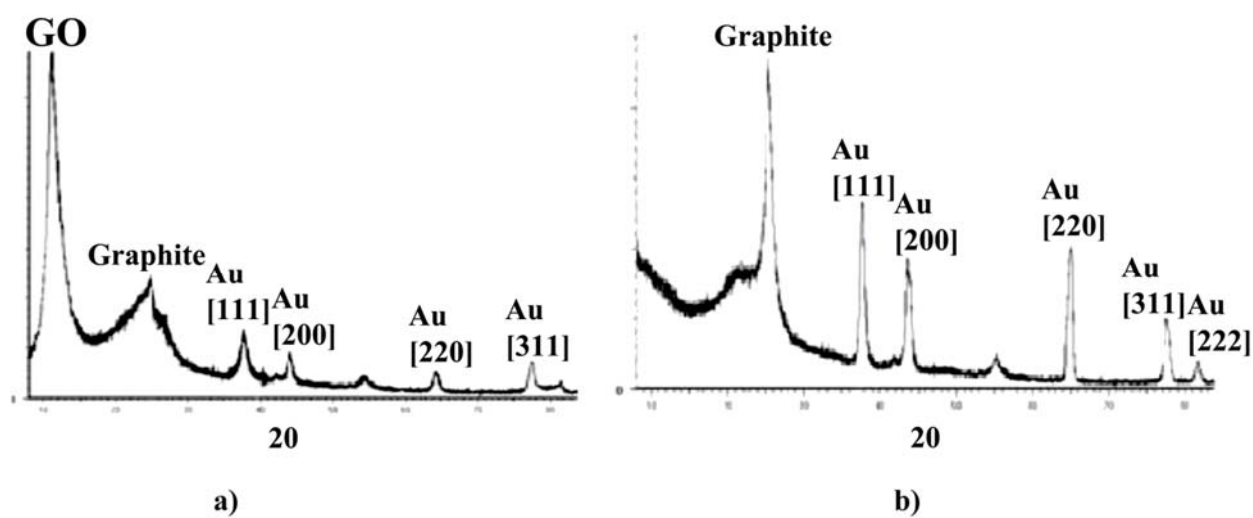


Figure 8. XRD data: a) Au NPs/GO; b) Au NPs/Graphene

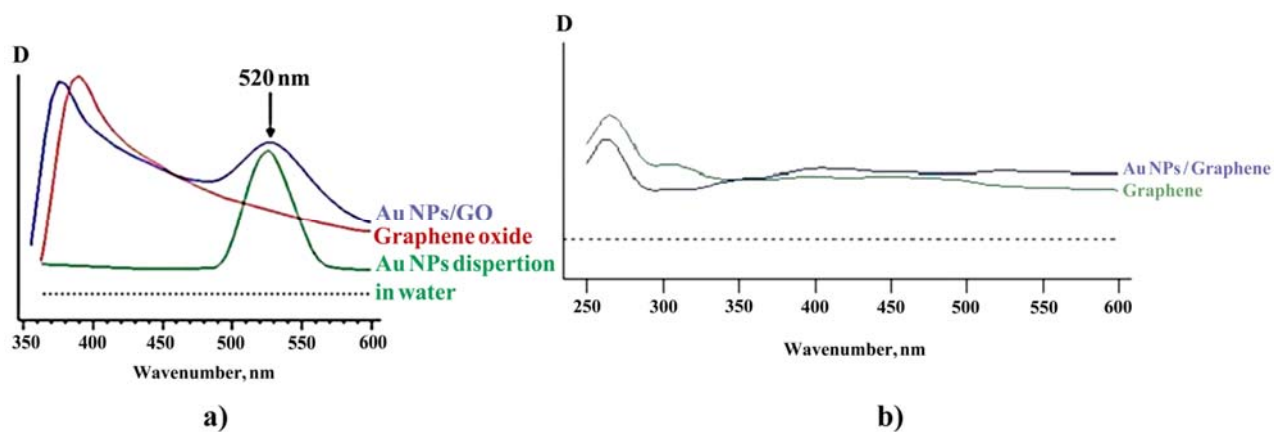


Figure 9. UV/vis-spectra: a) Au NPs/GO; b) Au NPs/Graphene

ESTUDO EXPERIMENTAL DE RESISTÊNCIA HIDRÁULICA DE FLUXO TURBULENTO EM UMA CAMADA COMPACTADA**EXPERIMENTAL STUDY OF THE HYDRAULIC RESISTANCE OF TURBULENT FLOW IN THE PACKED BED****ЭКСПЕРИМЕНТАЛЬНОЕ ИССЛЕДОВАНИЕ ГИДРАВЛИЧЕСКОГО СОПРОТИВЛЕНИЯ ТУРБУЛЕНТНОГО ПОТОКА В УПЛОТНЕННОМ СЛОЕ**

KULYMBAYEVA, Marzhan Sh.¹; ORUMBAYEV, Rakhimzhan K.^{2*}; SEIDALIYEVA, Aiganym B.²; OTYNCHIYEVA, Marzhan T.²; MUNTS, Vladimir A.³;

¹ Kazakh-German University; Faculty of Engineering and Information Technology; 111 Pushkin Str., zip code 050010, Almaty – Republic of Kazakhstan

² Almaty University of Power Engineering and Telecommunications named after Gumarbek Daukeyev; Institute of Heat Power Engineering and Control Systems; Department of Thermal Power Plants; 126/1 Baytursynuli Str., zip code 050013, Almaty – Republic of Kazakhstan

³ Ural Federal University named after the First President of Russia B.N. Yeltsin; Ural Power Engineering Institute; Department of Thermal Energy and Engineering; 19 Mira Str., zip code 620002, Ekaterinburg – Russian Federation

* Correspondence author
e-mail: r.orumbayev@au.es.kz

Received 01 October 2020; received in revised form 28 October 2020; accepted 15 November 2020

RESUMO

Vários dispositivos com inserções porosas e peneiras são amplamente usados em processos de produção modernos. Esses dispositivos são usados para desativar as emissões industriais e substâncias tóxicas e nocivas na indústria de energia térmica e automotiva, bem como para eliminar gases de exaustão na metalurgia de metais não ferrosos. A eficiência do funcionamento de tais dispositivos depende em grande parte do movimento bem organizado de um meio gasoso ou líquido, que tem grande influência nos processos de transferência de calor e massa dentro do reator e determina o seu grau de eficiência. Este artigo é dedicado à resistência hidráulica do movimento do fluido incompressível (ar) no tubo redondo com inserções porosas feitas de pacotes de cartuchos com pequenas células. Novos resultados e dados foram obtidos sobre a resistência hidráulica das inserções porosas representadas por uma malha fina, alinhamento do perfil da velocidade média na frente da malha e alteração do componente longitudinal da intensidade de turbulência da estrutura de fluxo turbulento. Para o cálculo da pressão estática, foram utilizados orifícios de drenagem com diâmetro de 5×10^{-4} m, localizados em diferentes partes da área de trabalho do tubo, dentro das inserções porosas entre as malhas e após as inserções na área de saída de estabilização do bloco. A medição das características médias de velocidade e impulso do fluxo de ar foi realizada por meio do anemômetro de perda de calor, regulado em uma temperatura constante. Foi demonstrado experimentalmente que existe um equilíbrio local entre os processos de geração e dissipação de energia de turbulência dentro das inserções porosas representadas por uma malha fina. Como resultado, foi estabelecido que existe um equilíbrio local entre os processos de geração e dissipação de energia de turbulência dentro de insertos porosos feitos de malhas finas. Verificou-se que a intensidade da turbulência permanece no mesmo nível e depende das características geométricas das grades e da vazão de ar.

Palavras-chave: *cartuchos, energia de turbulência, pressão, fluido incompressível.*

ABSTRACT

Modern production processes widely involve various apparatus with porous inserts and screens. Similar devices are used to decontaminate industrial emissions or the neutralization of toxic and harmful substances in heat energetics and automotive industries and the utilization of exhaust gases in the non-ferrous metal industry. The operational efficiency of such devices vastly depends on the correctly organized movement of gas or liquid medium, which has a significant influence on heat and mass exchange processes within the reactor and defines

Its efficiency rate. This article is about the hydraulic resistance movement of incompressible liquid (air) in a circular tube with porous inserts made from cartridge packs with fine meshes. There were obtained new results and data on hydraulic resistance of porous inserts represented by fine mesh, leveling out the profile of averaged speed before the mesh, and change of longitudinal constituent of the turbulence intensity turbulent flow structure. To calculate the static pressure, some 5×10^{-4} m diameter drainage holes were used, located in different parts of a tube operating area, within the porous inserts between meshes and after inserts at the unit's stabilizing output region. Measurement of an average speed and impulse characteristics of airflow was performed with a heat loss anemometer set to the constant temperature value. It was shown by the experiment that there is a local balance existing between turbulence energy generation and dissipation processes within the porous inserts represented by fine mesh. As a result, it was found that there is a local balance between the processes of generation and turbulence energy dissipation inside porous inserts made of fine meshes. It was determined that the intensity of turbulence remains at the same level and depends on the geometric characteristics of the meshes and airflow rate

Keywords: *cartridge packs, turbulence energy, pressure, incompressible liquid.*

АННОТАЦИЯ

В современных производственных процессах широко используются различные аппараты с пористыми вставками и ситами. Подобные устройства используются для обезвреживания промышленных выбросов или для нейтрализации токсичных и вредных веществ в теплоэнергетике и автомобильной промышленности, а также для утилизации выхлопных газов в цветной металлургии. Эффективность работы таких устройств в значительной степени зависит от правильно организованного движения газовой или жидкой среды, что оказывает большое влияние на процессы тепло- и массообмена внутри реактора и определяет степень его эффективности. Эта статья посвящена гидравлическому сопротивлению движения несжимаемой жидкости (воздуха) в круглой трубе с пористыми вставками, выполненными из пачек картриджей с мелкими ячейками. Получены новые результаты и данные по гидравлическому сопротивлению пористых вставок, представленных мелкой сеткой, выравнивание профиля усредненной скорости перед сеткой и изменение продольной составляющей интенсивности турбулентности структуры турбулентного потока. Для расчета статического давления использовались дренажные отверстия диаметром 5×10^{-4} м, расположенные в разных частях рабочей области трубки, внутри пористых вставок между сетками и после вставок в стабилизирующей выходной области блока. Измерение средней скорости и импульсных характеристик воздушного потока проводилось с помощью анемометра потери тепла, установленного на постоянное значение температуры. Экспериментом было показано, что существует локальный баланс между процессами генерации энергии турбулентности и диссипации внутри пористых вставок, представленных тонкой сеткой. В результате установлено, что между процессами генерации и рассеивания энергии турбулентности внутри пористых вставок из мелких сеток существует локальный баланс. Установлено, что интенсивность турбулентности остается на одном уровне и зависит от геометрических характеристик сеток и скорости воздушного потока.

Ключевые слова: *картриджи, энергия турбулентности, давление, несжимаемая жидкость.*

1. INTRODUCTION

Modern production processes widely involve various apparatus with porous inserts and screens. Chemical oil and chemical industry, heat energetics, and other related industries have experienced widespread reactors with immovable grain or a mesh layer of catalyst. Similar devices are used to decontaminate industrial emissions or the neutralization of toxic and harmful substances in heat energetics and automotive industries and the utilization of exhaust gases in the non-ferrous metal industry. As a rule, such units are represented by two side-by-side channels connected via a common passable wall. The most vivid example of such a unit is a

displacement reactor, which consists of a direct flow channel with a porous insert. The working principle of such units may be described as follows: oncoming movement of liquid with certain speed onto the passable insert. The liquid continues its movement further down the free portion of a channel being filtered through this insert. Simultaneously, the flow that moves through the porous structure is slowing down, and therefore part of the liquid goes from the central area of the channel to its sides (peripheral area), where the flow speed is lower. Afterward, coming through the porous insert, and depending on the characteristics of the porous insert itself, the liquid continues to distribute in a radial direction. Having passed through the porous

insert, the flow then starting to increase speed again due to the direct flow portion of a channel. However, one may observe significant inconsistencies in speed values, causing further degradation down the flow.

The operational efficiency of such devices vastly depends on the correctly organized movement of gas or liquid medium, which has a great influence on heat and mass exchange processes within the reactor and defines its efficiency rate. First of all, it requires the creation of a more stable and balanced distribution of flow within the active layer of devices with high unit capacity, because along with the growth of geometric sizes of the reactor, all the relative values between separate elements of the device will be changed as well. The overall volume of the device, the volume of the reactive area, the section area of the holes through which the reaction mixture is supplied, and the receiving surface of the catalytic layer. All this leads to the change of the aerodynamic scheme of the medium movement and causes a high risk of spatial nonuniformity, which decreases the efficiency of the technological process. Research of efficiency matters referred to studies on features of liquid flow can be divided into several sections. The flow of the liquid within the direct flow portion of the unit was studied well already because they can be accurately described using Navier-Stokes equations for laminar flow (Sergeev *et al.*, 1974; Ershin *et al.*, 1990; Vlasov, 1991; Astanovskii and Astanovskii, 2005). Research of operating modes of turbulent flow units currently is of a much bigger interest.

So, it can be said that the task of optimal control and operational efficiency increase for units with porous layers will be solved if one would know for sure a consistent pattern of liquid and gas flows within the mentioned units. Generally, basic mathematic models for the operation of such units are represented in one measuring dimension (Vaisman and Goldshtik, 1978; Goldshtik, 1985; Esakov and Kotelkin, 1986; Evtushenko and Kotelkin, 1991). However, such an approach does not allow to perform complete research of different features of liquid or gas flows of the real-life unit (McSherry *et al.*, 2016; Wałowski and Filipczak, 2017; Maciel and Camara, 2019). This influence may be researched by the creation of a two-dimension flow model. However, solving the task in such a manner, the most difficult problem would be the accurate definition of the relation between the units operation mode and Reynolds number as the main hydrodynamic parameter (Zhizhkin *et*

al., 2018). Thus, the priority task is to research flow modes of actual liquid within units with porous structures of a certain shape (Vortmeyer and Schuster, 1983; Genbach *et al.*, 2016; Zhizhkin *et al.*, 2018). Simultaneously, one has to consider the location and structure of a porous environment as a whole factor without division into the research of the direct flow section and research of a porous layer itself. The research interest area goes beyond the study of the laminar movement of liquid based on solving accurate equations of Navier-Stokes and involves studying turbulent movement within units with the stationary porous layer. The last task in particular – research of turbulent movement – suggests, in the first place, a creation of a two-dimension measuring model based on a sufficient amount of research material concerning the flow within a channel equipped with passable porous walls or inserts.

The majority of studied research works on flow hydrodynamics after porous layer (Showkat Ali *et al.*, 2017; Wałowski and Filipczak, 2017; Bhattacharjee *et al.*, 2019; Maciel and Camara, 2019) mention macroscopic flow inconsistencies at the moment of porous layer exit – an increase of flow speed next to channel walls and decrease of flow speed in the middle. Interestingly enough, lots of research works were focused on studying the structure within the stationary porous layer itself. Simultaneously, it was believed that speed profiles beyond the porous layer are identical to flow distribution within that layer. However, several studies (Kirillov *et al.*, 1979; Volkov *et al.*, 1984) showed that in matching average flow speed profiles within the porous layer and beyond, local speed profiles would differ heavily. Research on tightly packed and dispersed sets of meshes showed equal result values of hydraulic resistance. It has brought the opportunity to establish an experiment within a direct flow channel with a porous insert and to measure flow characteristics inside the porous layer of the unit.

2. MATERIALS AND METHODS

The study of the hydraulic resistance of turbulent flow in the packed bed were carried out on an experimental installation (Figure 1). A profiled jet 1 named after Vitoshinskiy was installed in the water intake area (Yushko, 2015), which had nine stages of contraction connected with the main channel 2, a 0.05 m and on a 0.1mm distance from the jet itself there was also installed a shaped honeycomb 3. To measure the static pressure, some drainage holes of 5×10^{-4} m in diameter were used, which were located in

different sections of the operating area of the tube, inside the porous inserts between the mesh and after inserts, at the unit's output stabilizing area. The working part of the installation included a system of several small-mesh grids 4 (the number varied from 1 to 10). The operational area had a diameter of 0.05m and was transferring into a stabilizing area with the same diameter and then was connecting to the intake portion of centrifugal fan 5.

In the working area between the grids, the probe moves in the Diametric direction perpendicular to the channel wall. The electrical signal is transmitted from the thread to the secondary voltage measuring device. Measurements of averaged velocities with a heat loss anemometer were compared in the available cross-section with the speed measurement with a Pitot tube. The resistance in the experimental section was measured by the difference in static pressure on the channel walls using micromanometers. Drainage holes of 5×10^{-4} m in diameter were used to measure the static pressure, which were located in different sections of the operational area of a tube, inside the porous inserts in between meshes and after inserts at the output stabilizing area of the unit. With the help of the hydraulic press, metal meshes made from L-68 brass were equally pulled onto the base represented by steel rings with an inner diameter of 0.05 m and then were glued to the base.

All materials and tools, including the experimental setup, embedded grid, Pitot tube, micro manometers, Vitoshinskiy nozzle (profiled jet) and traverse gear, with gauges with needles and wollastonite threads of different diameters of platinum, including heat loss-anemometer – assembled and made in the laboratory of mechanics and mathematics faculty of Al-Farabi Kazakh-National University (Almaty, Kazakhstan).

Measurement of an average speed and impulse characteristics of airflow was performed with a heat loss anemometer set to the constant temperature value. A constant temperature anemometer was used. The linearizing chain was based on the principle of nonlinear resistances. This method was developed at al-Farabi Kazakh-National University (Almaty) and is more accurate. The thermoanemometric method used is based on measuring the dependence of the heat transfer of a heated filament on the gas velocity, temperature, and composition. During forced convection, the intensity of heat transfer was determined by gas flow speed around the

heated sensor thread (Wałowski *et al.*, 2017). Anemometer's gauge's body is a brass cylinder of 2×10^{-4} m in diameter and length of 0.115 m. From the body of a gauge, stems are coming out at 0.015-0.018 m distance, made of ordinary steel needles, and with platinum Wollaston wires of 6×10^{-6} soldered to their ends. Heat loss anemometer was put into the channel through special holes inside the measuring rings made from 0.10 m thick acrylic glass and a micrometer screw with a 1×10^{-5} m movement rate. This screw was steadily secured to the acrylic glass ring via two bolts. Two steel needles protrude from the sensor housing at 0.015 – 0.018 m. a Wollaston platinum wire with a diameter of 6×10^{-6} m was soldered to the points of these needles. (6 microns). In experiments with background noise elimination to a minimum (the measurement of ripple derivatives, the study of spectra), the filament diameter was 1×10^{-6} m (1 - micron with a 40-micron shell). The working section of the thread with a length of 1.5×10^{-3} m was located perpendicular to the sensor body, pre-etched with 80 % nitric acid solution, and served as a sensitive element of the sensor. In the experiments, were used threads from the removal of internal stress when examining in the microscope were straight with no tension. Immediately before the measurements, the sensor with a thread was calibrated on a separate installation with a low degree of turbulence, and the dependence of E (mV) on the value of h (torr) was determined, i.e., the speed of the averaged flow. Direct calibration of the sensor with the thread does not require knowledge of the law of heat exchange between the thread and the airflow. It is not necessary to assume that the thread is cooled by a normal (perpendicular) component of the airflow, and the measurements are free from systematic error. The sensitivity of the thread is the same as that determined in the calibration nozzle with a low turbulence level. But there are still a number of sources of measurement errors that are characteristic of this thread and related electrical circuits of the secondary device. The unit was located inside the laboratory and operating in drain mode. Air was fed directly from the room environment and purified from various mechanical particles through a small-cell volume filter that was immediately connected with the nozzle. The operation of a unit assembled using the scheme mentioned above allowed to exclude the margin of measurement error for a gauge of heat loss anemometer, which was present due to the heating of an operating fan and excluding the airflow.

Pressure differences within the Vitoshinskiy nozzle defined the average consumption speed of airflow. At the inlet, the widest section of a nozzle, the pressure was considered equal to atmospheric pressure. The diameters between the widest and the narrowest (equal to pipe diameter) sections of the nozzle were equal to three. The nozzle for average airflow speed within the direct flow pipe was calibrated at the distance of 0.10 m away from the nozzle. Calibration is the comparison of measurement values delivered by a device under test with those of a calibration standard of known accuracy (Faison *et al.*, 2004). Simultaneously, the pressure difference within the nozzle was measured utilizing the inclined micro manometer, whereas average speed profiles within the pipe were measured by heat loss anemometer gauge. Throughout the experiment, consistency of flow rate and flow temperature remained the same, controlled by a 0.1 K precision thermometer. Each time before initiation of the experiment, heat loss anemometer gauges were calibrated within the potential flow. The field of speed was uniform, and the level of impulses was not exceeding 0.5%. The degree of research data repetition was checked in all cases of every experiment, maintaining a highly isobaric and isometric process.

Meshes within sets were installed in a parallel manner, one after another, maintaining a certain distance in between. Values of geometric characteristics of the meshes and packs used within the operational area of the experimental unit, as well as pore volume ε and specific surface area a calculated according to Equation 1, are presented in Table 1. Digit in the first column describes the amount of meshes for a specific model marked with a Greek letter. Digit in the third column describes the distance between meshes within a pack.

3. RESULTS AND DISCUSSION:

3.1 Hydraulic Resistance of Porous Inserts

According to the results of processing data obtained from experiments on single mesh resistance and resistance of packs with identical meshes in terms of values of equivalent resistance coefficient (Equation 2), where Δp – pressure difference on a mesh or pack of mesh with h thickness; pore amount ε and specific surface area " a " are according to Equation 1 and Reynolds equivalent criteria (Equation 3). During the study (Kukes *et al.*, 1981), universal dependence was obtained using Equation

(Equation 4). Proportionality coefficients for meshes considered a regular system were defined in (Kukes *et al.*, 1981) and equal to $C_1 = 44.2$ and $C_2 = 0.35$.

Figure 2 shows the dependence of pressure difference present at meshes under the flow feed speed above average. The resistance of $9\alpha. 5$; $9\alpha. 15$; $9\beta. 5$; $9\beta. 15$. Fifteen packs with the same amount of meshes almost do not depend on the distance between them, corresponding with conclusions on the experiment (Kukes *et al.*, 1981; Yershin and Khadieva, 1988). The conversion of this data into hydraulic resistance values is shown in Figure 3. A continuous line is described using dependence (Equation 4). The maximum deviation of experiment points from the calculated curve I do not exceed $\pm 9\%$. Relative errors in defining the equivalent Re is not more than 4%. Figure 4 shows the pressure distribution within a tube with a porous insert consisting of ten fine meshes accordingly $10\alpha. 15$ and $10\beta. 15$, whereas the Re value equals 49800. Comparing pressure gradients with similar dense pack (continuous straight lines) confirms that the distance between meshes has almost no influence on pressure drop within the pack.

3.2. The Flow Structure in the Channel with Porous Insert Made of Fine Meshes

Figures 5 and 6 show profiles of the longitudinal element of averaged speed referred to as an average feed speed of flow, and distribution of intensity for longitudinal turbulent speed impulses within various sections of a tube with a porous insert made from fine meshes $10\alpha. 15$ and Re value = 49800. It is clear that the initial, rather sharp shaped, speed deforms profile and becomes less sharp as it comes closer to the insert. It happens due to the deceleration of flow before the local resistance, created by a pack of fine meshes. Having completely verified the theory, flattening of the flow was performed due to deceleration of a flow within the axis area and redistribution of some portion of flow towards the outer area because of the transverse gradient of pressure before the fine mesh pack. It should be noted that the porous insert represented by the fine meshes pack used during the experiment has rather low hydraulic resistance necessary for flattening the flow speed profile before the meshes pack, which was mentioned in paper Min *et al.* (2017).

Decrease of turbulence impulses intensity near the wall of a tube, according to Figure 6b, is based on the acceleration of flow within this area of a channel, whereas in the middle portion of a

tube, it decreases rather slower due to flow deceleration. In all experiments with no exception, measurements were taken from two set distances between meshes ($15 \times 10^{-3} \text{ m}$ from two set distances ($5 \times 10^{-3} \text{ m}$ and $1 \times 10^{-2} \text{ m}$ accordingly) from each of ten meshes. That is why two profiles obtained demonstrate the situation immediately after a mesh and flow condition reaching the next mesh.

Figure 6 shows data of measurements taken after the first and the second meshes. This and the following figures have profiles of the longitudinal component illustrated in the top section and distribution of turbulence intensity in the bottom section (Equation 5). It is still possible to define signs of initial nonuniformity of flow field in the profile of the average speed of the flow coming through the first mesh (Figure 6a). However, these profiles were heavily deformed at that moment. Impulse components behind the first mesh are close in their values to those of an approaching flow. However, with the increase of distance to a mesh, turbulence decrease, as shown in Figure 6b). After the second mesh (Figure 6c), the average turbulence value was equal to 5-6%, and after the third mesh (Figure 6d), it went down to 3%. Profiles of averaged speed after the second mesh are considered to be almost uniform and equal.

Performed experiments show that during the passage of the flow through the first mesh, mesh turbulence with a much smaller scale is placed at the top of the initial large-scale turbulence, even though the first mesh, due to its high degree of pore volume, which also means lower resistance, is not capable of making sufficient changes to the turbulence structure of the flow, generates a larger amount of low-scale turbulence. After the second mesh, such isotropy increases, but some residual effects can still be observed. After the third mesh, there is almost none left from initial large-scale turbulence, and the flow is defined by low scale mesh turbulence, which tends to vanish. Starting from the third mesh and up to the tenth mesh, the distribution character of averaged and impulse speeds is not changing. Profile of averaged speed remains flat "stem", and impulse speed has periodic nature: after each mesh, the degree of impulse was equal to 4-5% and was defined by mesh characteristics. The mesh turbulence tends to vanish and drops down to 3% before the next mesh.

The fact that low scale mesh turbulence trends to vanish can be observed well in sections behind a porous insert. The comparison of

averaged speed profile and turbulence distribution profile within a mesh pack and after the last tenth mesh insert looks identical in the first two sections. In the following sections, profiles of averaged speed are rather flattened already and do not change much, whereas low scale isotropic turbulence continues to vanish and decreases to 0.9%, which means that the flow is cleaning gradually. In this portion of a channel, the generation of turbulence and further development of the border layer on inner tube walls takes place.

There were obtained similar experiment results data for 10α . 15 pack under $Re = 15120$ and average speed of $UAV = 4.9 \text{ m/s}$. Hydraulic resistance of 10α . 15 mesh pack is much lower, almost 10 times lower than the one under $Re = 4980$. A comparison of experimental results for both flow modes ($Re = 4980$ and 15120) shows the similarity of flow development trends, but with the decrease of ΔP . Simultaneously, it is clear that averaged speed profiles have a rather non-uniform nature. However, their mesh turbulence is still prevailing, leading to the growth of flow isotropy. After the third mesh, averaged profiles of longitudinal speed components become almost uniform, and turbulence intensity changes as periodically as under $Re = 4980$.

One of the peculiarities of turbulence behavior within the porous layer of meshes is that turbulence intensity decreases as the flow comes closer to the insert and significantly decreases in immediate proximity to meshes connected with the "cleaning" effect of fine mesh. A fast drop of turbulence intensity also verifies such phenomena after the first two meshes due to the stabilizing effect of fine meshes and suppressing the overall swirling of the flow. What happens is the division of initial large-scale turbulence and simultaneous generation of its mesh turbulence. Simultaneously, a turbulent state of the flow that can be observed after the first mesh depends on turbulence level before this mesh. And only starting from the third mesh and all the way to the tenth mesh, the nature of turbulence changes is stabilizing. Each mesh increases the degree of impulses by 4-5% on average, but this value drops to 3% before the next mesh since turbulence created by the structure are vanishing as they grow distance from it. Based on the studied experiment results, it was considered that the distance between meshes has virtually no influence on pressure drop. Therefore, the complete pressure difference within the meshes set is equal to the sum of pressure difference within composing meshes. One of the biggest

advantages of airflow measurement using heat loss anemometer is the possibility of studying the flow characteristics on rather low speed and the low margin of error (Khintse, 1963; Kukes *et al.*, 1981).

Vanishing of large-scale turbulence on porous insert made of ten smaller meshes 10α . 15 happens faster due to its dense netting. After the third mesh flow stabilizes itself and after each mesh, the degree of turbulence increases and then decreases before the upcoming mesh and equals about 1%. Measurements results under lower Reynolds values have shown similar peculiarities of flow within the porous layer of meshes. Thus, based on obtained experimental results, it can be said that within the porous layer made of fine meshes after the third mesh system reaches the balance between generation and dissipation of turbulence energy. On average, turbulence intensity remains at the same level, which depends on the speed of airflow (Re value) and geometric characteristics of meshes (M/d parameters). Such behavior of turbulence energy takes place in the case of the grainy layer, which was shown in work (Kreindel' *et al.*, 1984), where authors were measuring averaged speed and turbulence intensity in gaps between each of 10 rows of spheres packed in the form of the cube. The measurements give a reason to think that turbulence characteristics generated by each mesh depend on its coefficients of resistance, Equation 6.

Indeed, turbulence energy appears due to work performed by airflow and strives to overcome this resistance. It should be noted that if mesh would be considered as the unit, which transforms intake turbulence (before mesh) (Equation 7) into exhaust turbulence (after mesh) (Equation 8), then the turbulence transformation coefficient (Equation 9) for each mesh in the pack, starting from the third mesh would be equal to Equation 10. According to Dryden and Schubauer theory (Van der Merwe and Gauvin, 1971). In that case, the decrease of longitudinal turbulence (Equation 8) using mesh happens under the following Equation 11. Experiments confirmed such a theoretical conclusion by these very authors (Van der Merwe and Gauvin, 1971). Table 2 contains ξ values and turbulence transfer coefficients, which were calculated using our experiment data. As is seen from Table 2, values Equations 9 and 10 differ from one another by not more than 6%.

Based on the experiments performed, the following conclusion could be made: when liquid moves within the porous environment, there

appears some isotropic turbulence, characteristics of which are defined by flow conditions and size of pores. Analysis of obtained data, with a high degree of validity, shows that turbulence created by mesh, vanish within the space between meshes and do not continue its movement towards the mesh located further down the flow. A similar conclusion can be made due to the results of experimental researches performed by other authors (Manshadi, 2011; Wałowski and Filipczak, 2017). These researches also state that the formation of swirls in some pore cells do not travel to neighboring cells but completely vanishes in the initial cell. Therefore, it may be said that the generation of turbulence energy and its dissipation within the isotropic porous environment is in the local balance.

4. CONCLUSIONS:

Thus, they were obtained from experimental data and results on hydraulic resistance of incompressible liquid (air) movement in a circular tube with porous inserts made from cartridge packs with fine meshes. Experiments carried out show that, during the passage of the flow through the first mesh, mesh turbulence with much less size is put on top of the initial large-scale turbulence, while the first mesh is not capable of making significant changes in the turbulence structure of a flow due to its high pore volume, which also means lower resistance, it produces a greater amount of low-scale turbulence.

Starting from the third mesh and up to the tenth mesh, the distribution character of averaged and impulse speeds is not changing. Immediately before fine meshes, the speed profile becomes flatter. Profile of averaged speed remains flat "stem", and impulse speed has periodic nature: after each mesh, the degree of impulse was equal to 4-5% and was defined by mesh characteristics, then the mesh turbulence trends to vanish and drops down to 3% before the next mesh. After porous inserts and fine meshes, the turbulent structure of flow changes itself. The experiment shows a local balance between generation and dissipation processes within porous inserts made from fine meshes. On average, turbulence intensity remains at the same level, which depends on the speed of airflow (Re value) and geometric characteristics of meshes (M/d parameters).

5. ACKNOWLEDGMENTS:

This research is funded by the Science Committee of the Ministry of Education and Science of the Republic of Kazakhstan (Grant No. AP05133388).

6. REFERENCES:

1. Astanovskii, D., and Astanovskii, L. (2005). Reactor for catalytic processes under optimal temperature conditions. *Chemical and Petroleum Engineering*, 41, 513-521. <https://doi.org/10.1007/s10556-006-0011-7>
2. Bhattacharjee, S., Roy, D., and De, S. (2019). *Hydrodynamics of electroosmotic flow in a microchannel with porous wall*. Retrieved from <https://arxiv.org/abs/1902.04068>
3. Ershin, Sh. A., Zhabbasbaev, U. K., Kulymbaeva, M.Sh., and Khadieva, L.G. (1990). Investigation of aerodynamics of apparatus with a stationary packed bed. *Applied Mechanics and Technical Physics*, 4, 124-232.
4. Esakov, Y. P., and Kotelkin, V. D. (1986). Hydrodynamic model of a reactor with a stationary catalyst bed. *Doklady. Chemical Technology*, 289–291, 106–109.
5. Evtushenko, A. I., and Kotelkin, V. D. (1991). Modelling of transport processes in fixed granular bed. *Teoreticheskie Osnovy Khimicheskoi Tekhnologii*, 25, 511–523.
6. Faison, C. Douglas; Brickenkamp, and Carroll S. (2004). Calibration Laboratories: Technical Guide for Mechanical Measurements. In *NIST Handbook 150-2G*. Gaithersburg: National Institute of Standards and Technology.
7. Genbach, A., Olzhabaeva, K., and Iliev, I. (2016). Boiling process in oil coolers on porous elements. *Thermal Sciences*, 20(5), 1777-1789. <https://doi.org/10.2298/TSCI150602166G>.
8. Goldshtik, M. A. (1985). Variational model of a turbulent rotating flow. *Fluid Dynamics*, 20, 353–362.
9. Khintse, I. O. (1963). *Turbulence*. Moscow: Fizmatgiz.
10. Kirillov, V. A., Kuz'min, V. A., P'yanov, V. I., and Khanaev, V. M. (1979). Velocity profile in a fixed granular bed. *Reports of the Academy of Sciences of the SSSR*, 245, 159-167.
11. Kreindel', I. Y., Sergeev, S. P., Dil'man, V. V., and Nazarov, A.S. (1984). Spreading of a gas stream before a granular catalyst bed. *Theoretical Foundations of Chemical Engineering*, 18(5), 415-419.
12. Kukes, V. I., Ufimtsev, A. A., and Yarin, L. P. (1981). Optimizing a thermoanemometric experiment at low and high turbulence intensities. *Journal of Engineering Physics*, 40, 581–584.
13. Maciel, H. E., and Camara, L. D. T. (2019). Non-darcy flow evaluation of unconsolidated porous media in a closed-loop permeameter. *Revista da Engenharia Térmica*, 18(2), 78-84.
14. Manshadi, M. (2011). The Importance of Turbulence Reduction in Assessment of Wind Tunnel Flow Quality. Retrieved from <https://www.intechopen.com/books/wind-tunnels-and-experimental-fluid-dynamics-research/the-importance-of-turbulence-reduction-in-assessment-of-wind-tunnel-flow-quality>
15. McSherry, R., Chua, K., Stoesser, T., and Falconer, R. A. (2016). Large eddy simulations of rough bed open channel flow with low submergence and free surface tracking. *River Flow - Proceedings of the International Conference on Fluvial Hydraulics, RIVER FLOW, 2016*, 85-90.
16. Min, J. H., Jeong, W. L., Kwak, H. M., and Lee, D. S. (2017). High-performance metal mesh/graphene hybrid films using prime-location and metal-doped graphene. *Scientific Reports*, 7, Article number 10225.
17. Sergeev, S. P., Dil'man, V. V., and Genkin, V. S. (1974). Distribution of streams in channels with porous walls. *Journal of Engineering Physics*, 27, 1180–1185 <https://doi.org/10.1007/BF00864011>
18. Showkat Ali, S. A., Azarpeyvand, M., and Ilário da Silva, C. R. (2017). Boundary layer flow interaction with porous surfaces. In *Proceedings of the 24th International Congress on Sound and Vibration (ICSV 2017)*. London: International Institute of Acoustics and Vibration.
19. Vaisman, A. M., and Goldshtik, M. A. (1978). Dynamic model of liquid motion in a porous medium. *Fluid Dynamics*, 13, 864–869.
20. Van der Merwe, D. F., and Gauvin, W. H. (1971). Velocity and turbulence measurements of airflow through a packed

bed. *AIChE Journal*, 17(3), 519-528.

21. Vlasov, O. A. (1991). Investigation of the aerothermochemical process in a fixed-bed catalytic reactor. *Fluid Dynamics*, 26, 252-258.
22. Volkov, S. A., Reznikov, V. I., Zel'venskii, V. Y., and Khalilov, K. F. (1984). Cross-sectional nonuniformity in a fixed granular bed and linear diffusion. *Theoretical Foundations of Chemical Engineering*, 18, 394-401.
23. Vortmeyer, D., and Schuster, J. (1983). Evaluation of steady flow profiles in rectangular and circular packed beds by a variational method. *Chemical Engineering Science*, 38, 1691-1699.
24. Wałowski, G., and Filipczak, G. (2017). Klinkenberg effect in hydrodynamics of gas flow through anisotropic porous materials. *E3S Web of Conferences*, 19, Article number 03008.
25. Yershina, Sh. A., and Khadieva, L. G. (1988). Hydraulic resistance and refracting effect of a fine-mesh screen. *Fluid Dynamics*, 23, 249-254.
26. Yushko, S. V. (2015). Turbulent stationary gas flow in the Vitoshinsky nozzle, results of studies of integral flow characteristics. *Technological University Bulletin*, 19, 125-126.
27. Zhizhkin, A., Lazutkin, G., Davydov, D., and Volkova, T. (2018). Influence of Porous Material MR Structure on its Flow Characteristics. *IOP Conference Series: Materials Science and Engineering*, 302, Article number 012074.

$$\varepsilon = 1 - \frac{\pi d}{4(b+d)}, a = \frac{\pi}{b+d}. \quad (\text{Eq. 1})$$

$$\xi_e = \frac{\Delta p}{h} \left(\frac{a}{\varepsilon^3} \frac{\rho u_{cp}^2}{2} \right)^{-1}, \quad (\text{Eq. 2})$$

$$\text{Re}_e = \frac{u_3 d_3}{\nu} = \frac{4 u_{cp}}{\nu a}. \quad (\text{Eq. 3})$$

$$\xi_e = \frac{C_1}{\text{Re}_e} + C_2. \quad (\text{Eq. 4})$$

$$\sqrt{u'^2}/u \quad (\text{Eq. 5})$$

$$\xi = 2\Delta P/(\rho u_{av}^2), \quad (\text{Eq. 6})$$

$$(\sqrt{u'^2}/u), \quad (\text{Eq. 7})$$

$$(\sqrt{u'^2}/u)_+, \quad (\text{Eq. 8})$$

$$(\sqrt{u'^2}/u)_+ / (\sqrt{u'^2}/u_-), \quad (\text{Eq. 9})$$

$$\sqrt{1 + \xi}. \quad (\text{Eq. 10})$$

$$1/\sqrt{1 + \xi}. \quad (\text{Eq. 11})$$

Table 1. Geometric parameters of meshes

Mesh amount	Wire diameter $d \times 10^3$, m	Distance in between meshes, mm	Distance in between wires, $b \times 10^3$, m	Mesh cell size, $m \times 10^3$	Pore amount, ε	Spec. surf. area, a , m^{-1}	Equiv. diam., $d_3 \times 10^3$, m
α	0.40		0.88	1.28	0.755	2453	1.23
3 α	0.40	5	0.88	1.28	0.755	2453	1.23
9 α	0.40	5	0.88	1.28	0.755	2453	1.23
9 α	0.40	15	0.88	1.28	0.755	2453	1.23
10 α	0.40	15	0.88	1.28	0.755	2453	1.23
β	0.15		0.25	0.40	0.706	7850	0.36
3 β	0.15	5	0.25	0.40	0.706	7850	0.36
9 β	0.15	5	0.25	0.40	0.706	7850	0.36
9 β	0.15	15	0.25	0.40	0.706	7850	0.36
10 β	0.15	15	0.25	0.40	0.706	7850	0.36

Table 2. ξ values and turbulence transfer coefficients

Porous insert code	Re	u_{av} , m/s	ξ	$\sqrt{1 + \xi}$	$(\sqrt{u'^2}/u) + / (\sqrt{u'^2}/u) -$
10 α . 15	49800	15.9	1.73	1.65	1.56
10 α . 15	15120	4.9	1.87	1.69	1.60
10 β . 15	49800	15.9	3.03	2.01	1.95
10 β . 15	15120	4.9	4.02	2.24	2.18

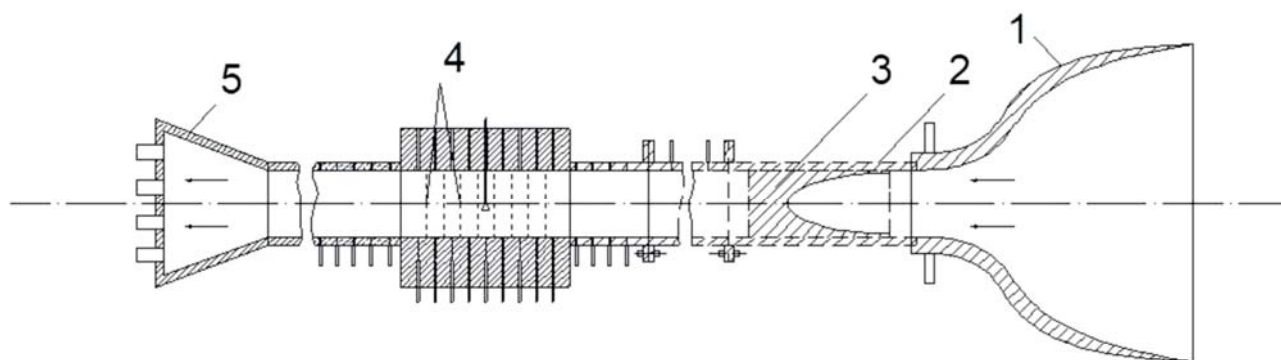


Figure 1. Experimental setup: 1 – vitoshinskiy profiled jet, 2 – main channel, 3 – shaped honeycomb, 4 – system of several small-mesh grids, 5 – centrifugal fan

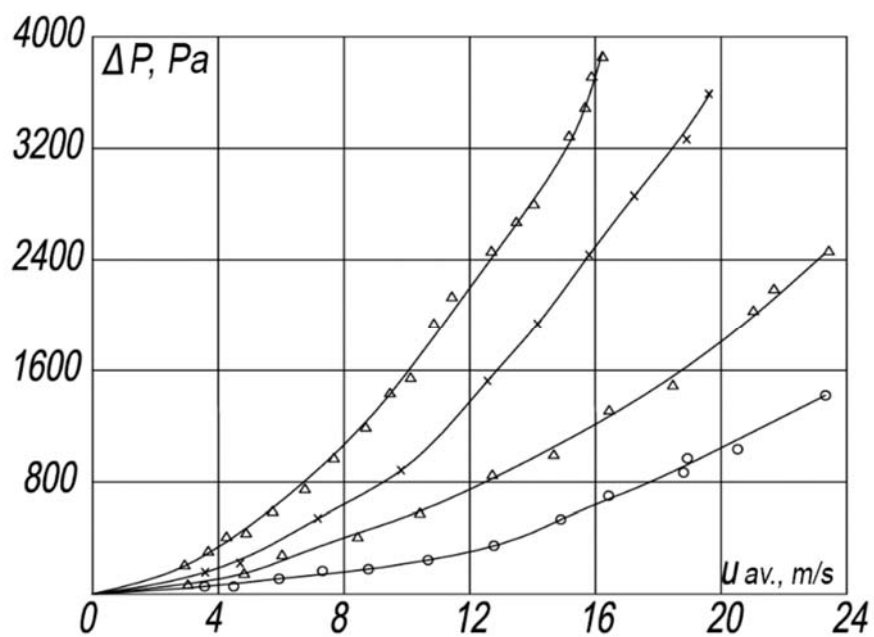


Figure 2. Dependence of pressure difference in a pack with identical meshes on average flow feed speed

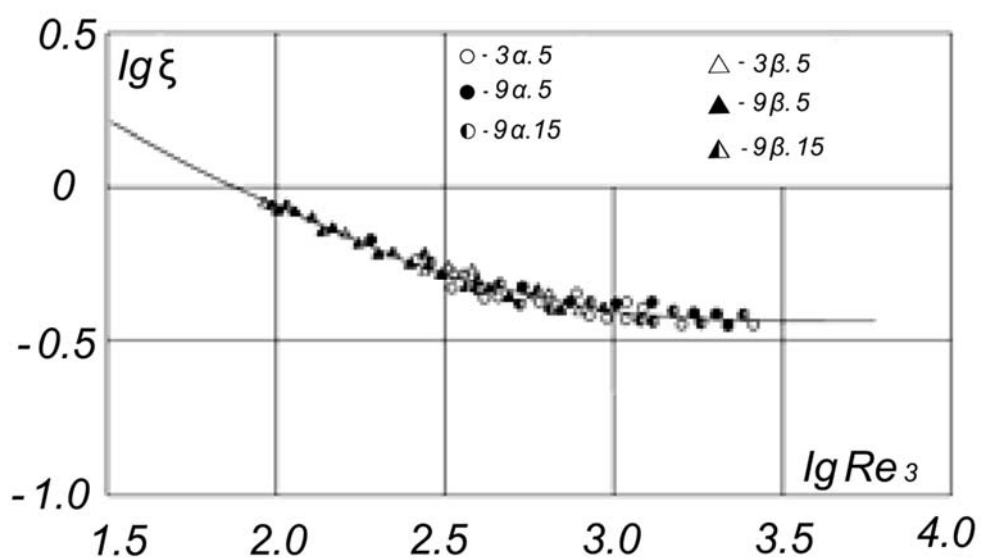


Figure 3. Dependence of equivalent resistance coefficient on Reynolds value for packs with identical meshes

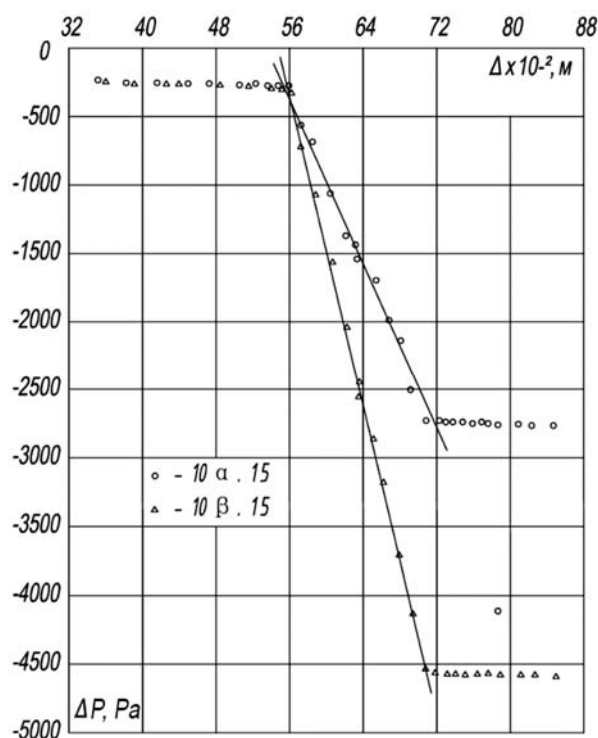


Figure 4. Distribution of pressure along the tube with a porous insert made from ten fine meshes with $Re = 49800$

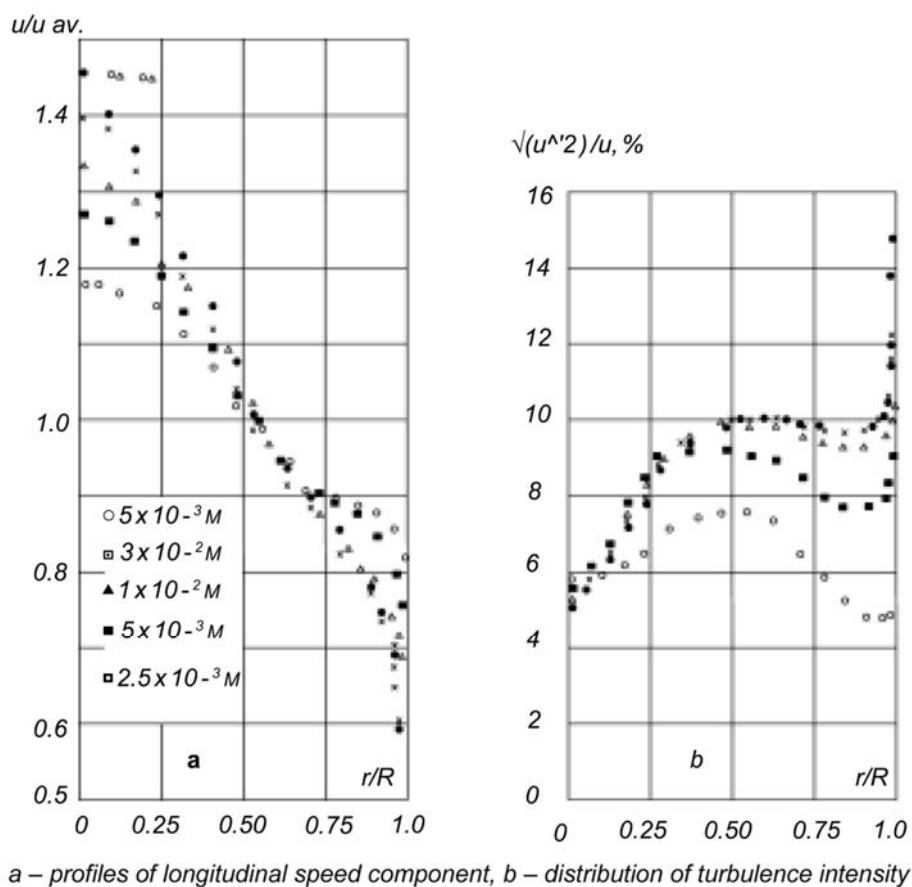
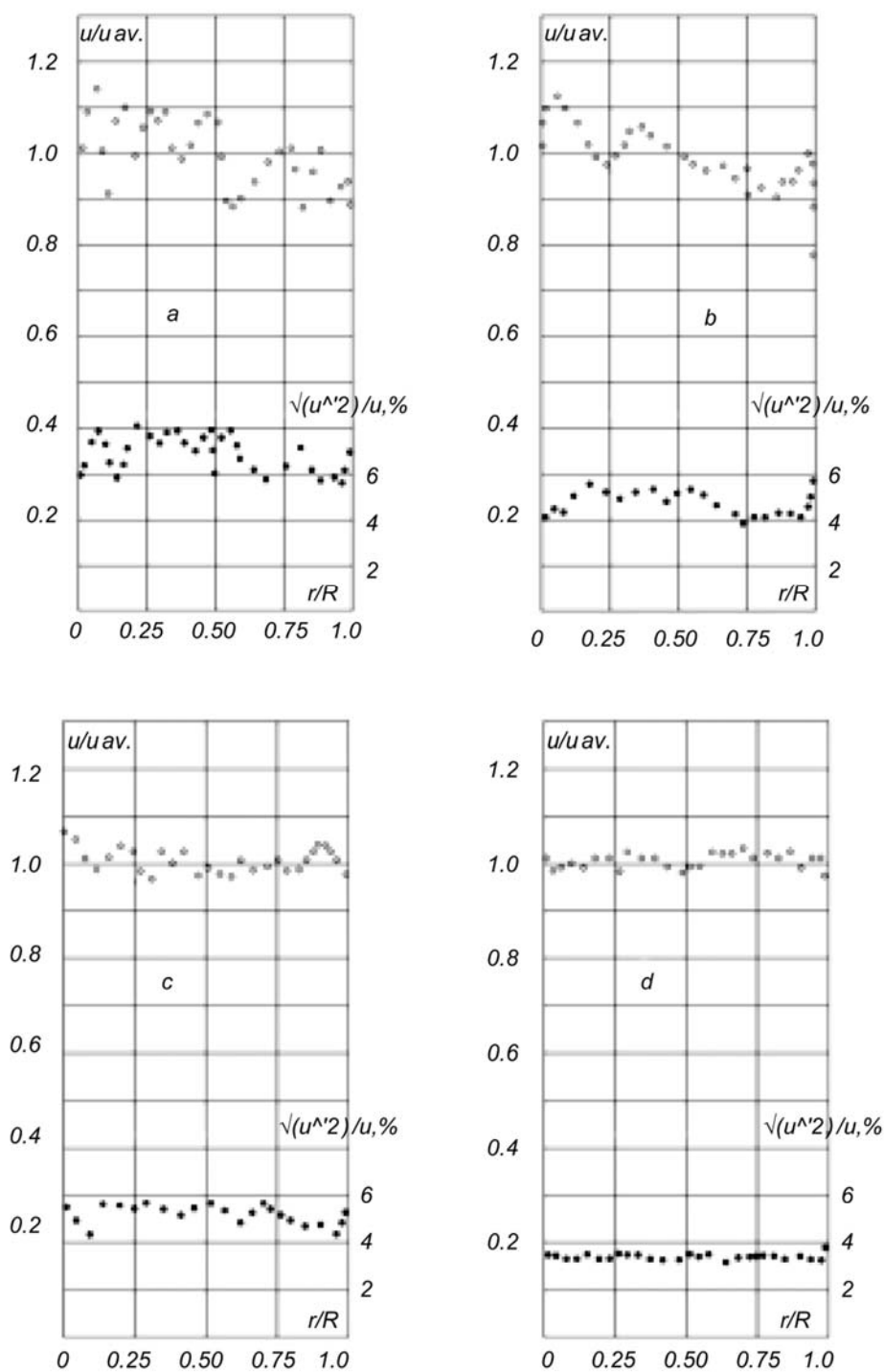


Figure 5. Illustrates the flow speed and turbulence intensity of a porous insert made of ten fine meshes 10α 15 located on a different distance from one another under $Re = 49800$



The first (a,b) and the second (c,d) meshes at the distance of: a,b – 5×10^{-3} m, c,d – 1×10^{-2} m under $Re=49800$

Figure 6. Profiles of longitudinal speed component and distribution of turbulence intensity inside the porous insert $10\alpha. 15$

INSTRUCTIONS FOR AUTHORS

We ask authors always to visit the online instructions for the use of the latest instructions available. Manuscripts must be submitted using the template available on the Journal's website.

PREPARATION OF MANUSCRIPTS

1. PREPARATION OF MANUSCRIPTS
 2. THE FIRST PAGE OF THE MATERIAL
 3. THE CENTRAL TEXT PART OF THE MATERIAL
 4. GUIDELINES FOR REFERENCES
 5. FIGURES
 6. TABLES
 7. MATHEMATICAL EXPRESSIONS
 8. SUPPLEMENTARY MATERIAL
-

1. PREPARATION OF MANUSCRIPTS (TEMPLATE):

Please, observe the following points in preparing manuscripts. Papers not conforming strictly to these instructions may be returned to their authors for appropriate revision or may be delayed in the review process.

READABILITY: Manuscripts should be written in clear, concise, and grammatically correct English (British or American English throughout). The editors can not undertake wholesale revisions of poorly written papers. Every paper must be free of unnecessary jargon and readable by any specialist in the related field. The Abstract should be written in an explanatory style that will be comprehensible to readers who are not experts in the subject matter.

PROOFREADING: Please proofread carefully for both errors and inconsistencies in the following: spelling (especially of scientific terminology, proper names, and foreign words), mathematical notation, numerical values in tables and text, and accuracy of quotations. The Journal will evaluate the file seeking English grammatical issues, correctness, clarity, and engagement errors. There will be a tolerance of up to 100 errors in all manuscripts. In case more errors were found, editors will allow the authors to resubmit again and, in case these errors persist, a proofreading fee will be charged.

GENERAL FORMAT: The completed paper has to be written in English and submitted as a **Word document only** using the template of the Journal. Page size: A4, line spacing: single, font type: Arial. Please leave headers and footers unchanged since the editors should fill it. Please check guidelines for accurate information based on all different categories (review articles and technical notes). A single file of the whole manuscript should then be submitted through TCHE QUIMICA JOURNAL's e-mail (journal.tq@gmail.com) along with the COVER LETTER. **The Journal no longer accepts submissions in any other form than by E-MAIL** (journal.tq@gmail.com).

FORMAT FOR INITIAL SUBMISSION: Title, Author(s), Abstract (maximum 300 words), Keywords (at least 3, maximum 6), Main text (Introduction, Review of Literature, Definitions (if any), Materials and Methods or Methodology, or Development, or Background, Results and Discussion or Findings, Conclusions), Acknowledgements (if any), References, Appendix (if any). This structure of

the main text is not obligatory, but the paper must be logically presented. Footnotes should be avoided. The main text must be written with font size 11, justify. Within each main section, three levels of subheadings are available, and the titles must be bold, bold, and italic, italic, respectively. The manuscript should contain the whole text, figures, tables, and explanations. For more details, please check the template of the Journal.

2. THE FIRST PAGE OF THE MATERIAL SHOULD BE AS FOLLOWS:

TITLE: PORTUGUESE, ENGLISH, and the third language if the author's native language is not English or Portuguese. The editors can provide the title in Portuguese for those whose Portuguese is not the first language. It should be brief and informative. The title should reflect essential aspects of the article, in a preferably concise form of not more than 100 characters and spaces: font size 12, capital letters, center alignment.

BY-LINE: Names (size 12, Arial, small capital) of the authors. No inclusion of scientific titles is necessary. In the case of two or more authors, place their names in the same row, separate them with a semicolon (;) and please indicate the corresponding author with * in superscript. The corresponding author should be the one submitting the article online and an e-mail given (only one e-mail) below the addresses of all authors. Authors from different institutions must be labeled with numbers in superscript after the names. The affiliation of the authors should also be given (size 10).

ABSTRACT: PORTUGUESE, ENGLISH, and a third language if the author's native language is not English or Portuguese. The editors can provide the title in Portuguese for those whose Portuguese is not the first language. Required for all manuscripts in which the problem, the principal results, and conclusions are summarized. The abstract must be self-explanatory, preferably typed in one paragraph, and limited to 300 words. It should not contain formulas, references, or abbreviations. The name ABSTRACT should be written in capital letters, Arial, size 12, bold, left alignment. The Abstract should be written font Arial, size 10, justify.

KEYWORDS: PORTUGUESE, ENGLISH, and a third language if the author's native language is not English or Portuguese. The editors can provide the title in Portuguese for those whose Portuguese is not the first language. Authors should provide appropriate and short keywords that encapsulate the principal topics of the paper. The maximum number of keywords is 5 not including items appearing in the title. The keywords should be supplied, indicating the scope of the paper. Size 10, italic, justify, only the word Keywords must be bold, left alignment.

The authors should include Abbreviations and Nomenclature listings when necessary.

3. THE CENTRAL TEXT PART OF THE MATERIAL SHOULD BE AS FOLLOWS:

The words Introduction, Review of Literature, Definitions (if any), Materials and Methods or Methodology, or Development, or Background, Results and Discussion of Findings, Conclusions must be written in capital letters, Arial, font size 12, left alignment, bold.

INTRODUCTION: The introduction must clearly state the problem, the reason for doing the work, the hypotheses or theoretical predictions under consideration, and the essential background. It should not contain equations or mathematical notation. A brief survey of the relevant literature so that

a non-specialist reader could understand the significance of the presented results. A good introduction should ideally have 3-5 well-explained paragraphs and should finishing pointing out the AIM of the study.

MATERIALS AND METHODS OR METHODOLOGY, OR DEVELOPMENT, OR BACKGROUND: Provide sufficient details to the reader to understand how the study was performed. The technical description of methods should be given when such methods are new. It is generally recommended that the materials and methods should be written in the past tense, preferably in the passive voice. In this section, ethical approval, study dates, number of subjects, groups, evaluation criteria, exclusion criteria and statistical methods should be described sequentially. The following questions should be absolutely provided: the beginning, and termination dates of the study period; number of subjects/patients/experimental animals etc. enrolled in the study; has the approval of the ethics committee been obtained? Study design (prospective, retrospective or other); still additional features of the study design (cross-sectional) should be indicated. Apart from this, other types of study designs (randomized, double-blind, placebo-controlled or double-blind, parallel control etc.) should be revealed. Before you finish your manuscript, ask yourself the following questions about your Materials and Methods section to ensure that you have included all important information. Is there sufficient detail so that the experiments can be reproduced? Is there excess information that could be removed without affecting the interpretation of the results? Are all the appropriate controls mentioned? Are all appropriate citations included? Is the source of each reagent listed? The Materials and Methods section is a vital component of any manuscript. This section of the report gives a detailed account of the procedure that was followed in completing the experiment(s) discussed in the paper. Such an account is very important, not only so that the reader has a clear understanding of the experiment, but a well written Materials and Methods section also serves as a set of instructions for anyone desiring to replicate the study in the future. Considering the importance of "reproducible results" in science, it is very relevant why this second application is so vital. Some general rules for Methods sections are:

- It should be clear from the Methods section how all of the data in the Results section were obtained.
- The study system should be clearly described. In medicine, for example, researchers need to specify the number of study subjects; how, when, and where the subjects were recruited, and that the study obtained appropriate 'informed consent' documents; and what criteria subjects had to meet to be included in the study.
- In most cases, the experiments should include appropriate controls or comparators. The conditions of the controls should be specified.
- The outcomes of the study should be defined, and the outcome measures should be objectively validated.
- The methods used to analyze the data must be statistically sound.
- For qualitative studies, an established qualitative research method (e.g. grounded theory is often used in sociology) must be used as appropriate for the study question.
- If the authors used a technique from a published study, they should include a citation and a summary of the procedure in the text. The method also needs to be appropriate to the present experiment.
- All materials and instruments should be identified, including the supplier's name and location.
- The Methods section should not have information that belongs in another section (such as the Introduction or Results).
- You may suggest if additional experiments would greatly improve the quality of the manuscript. Your suggestions should be in line with the study's aims. Remember that almost any study could be strengthened by further experiments, so only suggest further work if you believe that the manuscript is not publishable without it.

RESULTS AND DISCUSSION OR FINDINGS: Results should be presented concisely. Also, point out the significance of the results, and place the results in the context of other work and theoretical

background. The results and discussion sections are one of the challenging sections to write. It is important to plan this section carefully as it may contain a large amount of scientific data that needs to be presented in a clear and concise fashion. The purpose of a Results section is to present the key results of your research. Results and discussions can either be combined into one section or organized as separate sections. Use subsections and subheadings to improve readability and clarity. Number all tables and figures with descriptive titles. Present your results as figures and tables and point the reader to relevant items while discussing the results. This section should highlight significant or interesting findings along with P values for statistical tests. Be sure to include negative results and highlight potential limitations of the paper. The results and discussion section of your research paper should include the following: Findings; Comparison with prior studies; Limitations of your work; Casual arguments; Speculations; Deductive arguments.

Sources:

<https://www.ref-n-write.com/trial/research-paper-example-writing-results-discussion-section-academic-phrasebank-vocabulary/>

<https://www.ncbi.nlm.nih.gov/pmc/articles/PMC4548564/>

CONCLUSION: Summarize the data discussed in the Results and Discussion or Findings section showing the relevance of the work and how different it is from other researches. Also, point out the benefits and improvements that can be observed to develop new science standards that can change something in the related field.

ACKNOWLEDGMENTS: (if any) These should be placed in a separate paragraph at the end of the text, immediately before the list of references. It may include funding information too.

REFERENCES: References should be cited in the text using the **name-and-year system (Author, year) (APA FORMAT)**. Alternatively, the author's surname may be integrated into the text, followed by the year of publication in parentheses. **Examples:** Grasslands are regarded as important foraging areas for many insectivores in Europe, such as birds (Vichery, 2001; Barnet et al., 2004), bats (Guttinger, 1997) or amphibians and reptiles (Langton and Burton, 1997). However, the knowledge of the overall arthropod availability in such grasslands is scarce, since many studies about insect populations concentrate on extensive grasslands on poor, dry or wet soils include only few species or systematic groups (Ellgsen *et al.*, 1997; Gibson *et al.*, 1992; Hansel and Plachter, 2004; Manhart *et al.*, 2004; Kruess and Tschardtke, 2002a, b; Wingerden *et al.*, 1992; Sjodin, 2007a, b; Perner *et al.*, 2005). Carbon dioxide produced by the combustion of biodiesel can be recycled by photosynthesis, thereby minimizing the impact of biodiesel combustion on the greenhouse effect (Korbitz, 1999; Agarwal and Das, 2001).

- *Cite only essential resources, avoid citing unpublished material. References to papers "in press" must mean that the article has been accepted for publication. At the end of the paper list references alphabetically by the last name of the first author. Please, list only those references that are cited in the text and prepare this list as an automatically numbered list. The word References with size 12, bold, capital letters, left alignment*

4. GUIDELINES FOR REFERENCES:

- The Journal uses the APA (American Psychological Association) FORMAT CITATION as follows:

Author's surname, initial(s). (Date Published). Title of Source. Location of publisher: publisher. Retrieved from URL

Author Rules:

1. Initials are separated and ended by a period.

Examples: Goldani, E.
De Boni, L.A.B.

2. Multiple authors are separated by commas and an ampersand.

Examples: Goldani, E. & De Boni, L.A.B.
Goldani, E., De Boni, L.A.B. & Casanova, K.

3. Multiple authors with the same surname and initial: add their name in square brackets.

Example: Goldani, E. [Eduardo]

Date Rules:

- 1. Date refers to date of publishing**
- 2. If the date is unknown 'n.d' is used in its place.**

Example: De Boni, L.A.B (n.d)

Title Rules:

- 1. The format of this changes depending on what is being referenced**

Publisher Rules:

- 1. If in the US: the city and two letter state code must be stated.**

Examples: San Diego, CA
Houston, TX
New York, NY

- 2. If not in the US: the city and country must be stated.**

Examples: Sydney, Australia
Lisbon, Portugal
Rome, Italy

Retrieved from URL: This is used if the source is an online source

GENERAL RULE FOR ACADEMIC PAPERS:

Author's surname, initial(s). Year of publication after the name of the authors (between parentheses). Title of the paper. Name of the journal in italic, number of the edition also in italic, volume between parentheses and finally initial and final page, and, if the case, retrieved from (what website) or DOI

For example:

1. Nikolaeva, L.P., Cherdantsev DV., Titiv K.S. (2017). Characteristics of bone marrow stem cells in patients with complicated diabetes mellitus. *The Russian biotherapeutic journal*, 16(1): 47-50.
2. Mitchell, J.A. (2017). Citation: Why is it so important. *Mendeley Journal*, 67(2), 81-95. Retrieved

from <https://www.mendeley.com/reference-management/reference-manager>

3. Karthiga, N., Rajendran, S., Prabhakar, P., Rathish, R.J. (2015). Corrosion inhibition by plant extracts - An overview. *Int. J. Nano. Corr. Sci. Eng*, 2(4):31-49.
4. Akbulut, S., and Bayramoglu, M.M. (2013). The Trade and Use of Some Medical and Aromatic Herbs in Turkey. *Ethno Med*, 7(2): 67-77.

✓ **The Journal recommend to visit the websites below for a more detailed information.**

< <https://www.mendeley.com/guides/apa-citation-guide> >

< <https://libguides.murdoch.edu.au/APA6/all> >

< <https://aut.ac.nz/libguides.com/APA6th/referencelist> >

5. FIGURES:

The number of pictures (including graphs, diagrams, etc.) should not exceed 10 and should be submitted either in JPG or PNG formats. All photographs, charts, and diagrams should be numbered consecutively (e.g., Figure 1, Figure 2, Figure 3,...) in the order in which they are referred in the text. Caption must appear below the figure (size 11, bold, italic) and should be sufficiently detailed to enable us to understand apart from the text. Explanation of lettering and symbols should be also given in the caption and only exceptionally in the figures. Figures should be of good quality and preferably in black and white. (Color figures will appear in the downloadable files, but all papers will be printed in black and white.) Scanned figures should be at a resolution of 800 dpi/bitmap for line graphs. Diagrams containing chemical structures should be of high graphical quality and always be of the same size so that they can be uniformly reduced. Figures should have a maximum width of one Journal column (8.5 cm) to be inserted on the body of the text so that they can be applied to the standards of the Journal. If the figures exceed 8.5 cm, they will be placed at the end of the article. Also, authors may be requested to submit each figure also as an image file in one of the following formats: jpg or png. For pictures, graphs, diagrams, tables, etc., identical to material already published in the literature, authors should seek permission for publication from the companies or scientific societies holding the copyrights and send it to the editors of Tche Quimica Journal along with the final form of the manuscript.

6. TABLES:

Tables should be self-explanatory. They should be mentioned in the text, numbered consecutively (e.g., Table 1, Table 2, Table 3,...), and accompanied by a title at the top (size 11, bold, italic). Please insert all the tables in the text and do not enclose huge tables that can not fit within the page margins.

7. MATHEMATICAL EXPRESSIONS:

In general, minimize unusual typographical requirements, use solidus, built-up fractions. Avoid lengthy equations that will take several lines (possibly by defining the terms of the equation in separate displays). For drawing equations, please use the Equation Editor of Word, if possible. Make subscripts and superscripts clear. Display only those mathematical expressions that must be numbered for later reference or that need to be emphasized. The equations displayed should be consecutively numbered throughout the paper. The numbers should be placed in parentheses on the right of the equation, e.g. (Eq. 1).

8. SUPPLEMENTARY MATERIAL:

Any Supplementary material (other figures, tables, diagrams, etc.) should be placed at the end of the manuscript and indicated (APPENDIX, for example). A single.PDF - document, including the supplementary material, should be submitted.

Editors may ask authors to split off part of the manuscript at any time of the editing process, presenting it as supplementary material.

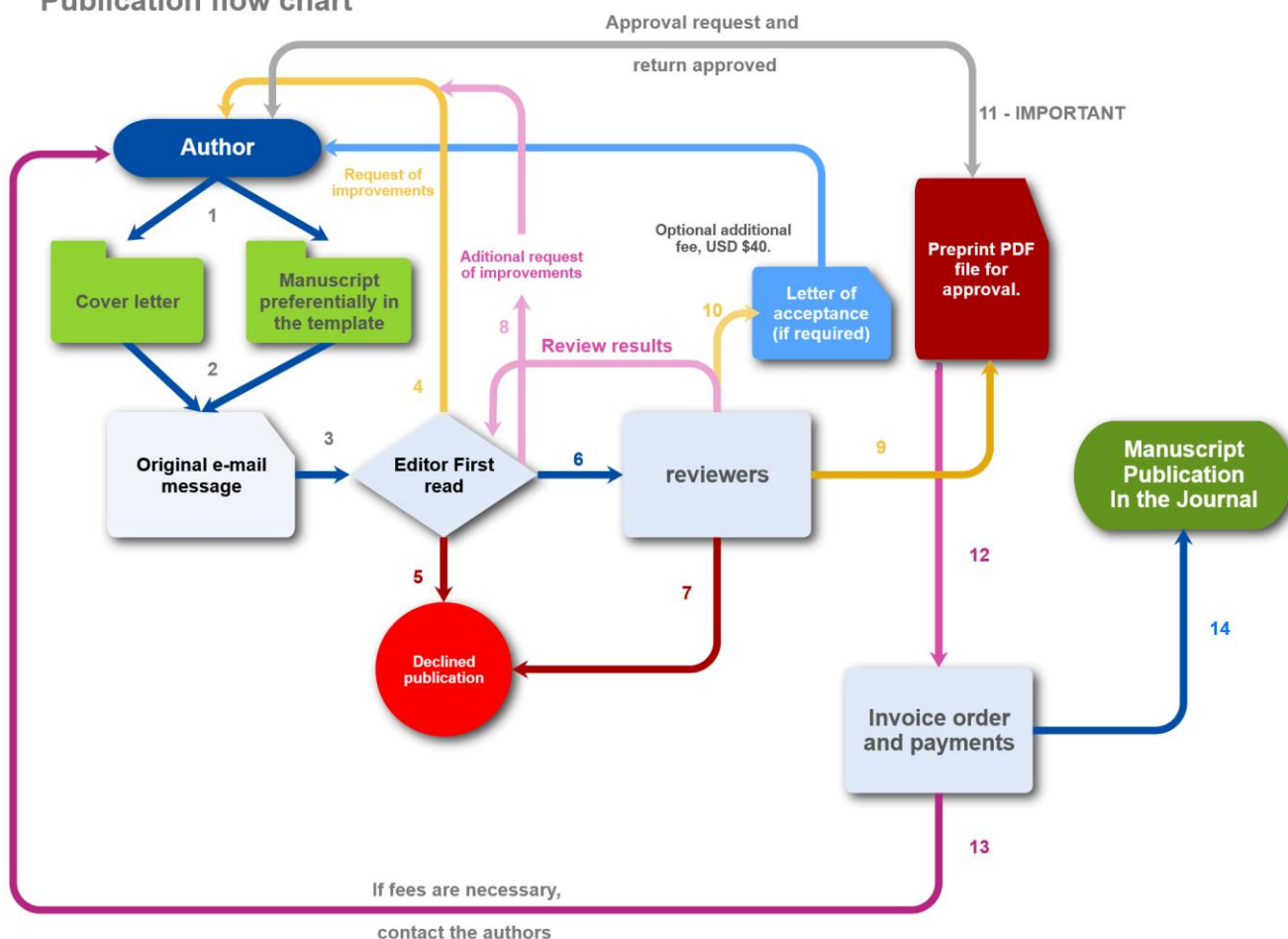
ARTICLE PROCESSING CHARGES (APC)

PUBLICATION FEES (1), ADDITIONAL FEES FOR PUBLICATION (2), DISCOUNTS (3), AND FREE PUBLICATION OPPORTUNITIES (4)

Authors are required to pay a publication fee to share in the costs of production. The fee will be asked **if, and only if, the article is accepted for publication**. Once full payment has been made (PayPal, Bank Transfer, or Western Union Services), the paper will be published at the Ahead of Print and scheduled for the next available issue. All waivers (and the publication fee requests) are **applied to the accepted papers after successful peer-review only**.

Please observe the flowchart below to understand how the Journal works.

Publication flow chart



1. PUBLICATION FEES

*Brazilian authors, USD 200

*Other countries income groups:

High income and **Israel, India, Pakistan, United Kingdom, China, France, United States, Russia, North Korea, and Iran** (nuclear-capable countries) - USD 300

Upper middle-income USD 250

Lower middle-income USD 120

Lower middle income (Heavily indebted poor countries (HIPC)) USD 100

Low-income USD 100

Low income (Heavily indebted poor countries (HIPC)) USD 80

- ✓ (*) Classification according to the World Bank list of economies (June 2020). Please check <https://datahelpdesk.worldbank.org/knowledgebase/articles/906519-world-bank-country-and-lending-groups>

2. ADDITIONAL FEES FOR PUBLICATION

a) Proofreading and/or plagiarism

If the submitted manuscript has more than 100 grammatical errors or plagiarism greater than 5%, **an additional fee of USD 200** will be charged. This fee does not guarantee publication of the manuscript and is non-refundable.

b) Changing PDF pre-printing files

After the final verification of the manuscript and the generation of the PDF pre-print file, **a fee of USD 100** will be charged to authors who wish to make any changes. For each new change, the fee is charged again.

c) Acceptance Letter for article publication

The acceptance letter is an **optional service** of the Journal. If the authors need a document to prove that their article has been peer-reviewed and accepted for publication, they may request, upon payment of **an additional fee of USD 40**, an acceptance letter for publication of the article.

NOTE 1: THE LETTER OF ACCEPTANCE may be issued **if, and only if**, the article has undergone a complete peer-review and is considered ACCEPTED for publication. Letters will NOT be issued for newly sent articles that have not yet been appropriately evaluated and peer-reviewed.

NOTE 2: The Journal does not agree with the trade-in documents that can attest to the publication of articles that have not gone through peer-review due process and are legitimately considered approved for publication in the subsequent edition.

NOTE 3: Bearing in mind that the pre-printing PDF is generally already considered as proof of publication, authors must, via e-mail, justify the request for a letter of acceptance for purposes of general registration by the Journal.

d) Formatting the manuscript according to the template of the Journal

The use of the template is mandatory. All authors must submit their papers according to the official model of the Journal available at www.journal.tchequimica.com (Downloads >> Templates and Instructions). In case the authors do not have time or proper conditions to execute the formatting of the manuscript, we can provide all the adaptation to the template of the Journal. However, this is an **optional service**, and **an extra fee of USD 80** will be charged on top of the Article Processing Charges.

If there is no need, additional fees are not charged.

3. DISCOUNTS

- a) **50% discount** for authors who support other journals from the team (*Southern Brazilian Journal of Chemistry* - this is a 100% free journal), **with 1 manuscript approved** for publication;
- b) **100% discount** for authors who support other journals from the team (*Southern Brazilian Journal of Chemistry* - this is a 100% free journal), **with 2 manuscripts approved** for publication;
- c) **Volume discount.** If you are an author/collaborator of the Journal that has **published with us 4 manuscripts** (paid your full corresponded price), your fifth manuscript will be free of charge. Later the counting cycle restart.

4. FREE PUBLICATION OPPORTUNITIES

- a) Young scientists that are publishing the first manuscript of their career. **Requirements:** Copy of the curriculum without publications; maximum of 2 authors; one manuscript previously accepted in the ***Southern Brazilian Journal of Chemistry*** (the manuscript may be from the author or from colleagues, provided that the extra purpose of the collaboration is notified at the time of submission), or two manuscripts previously accepted in the ***Journal of Law, Public Policies, and Human Sciences*** (manuscripts may be from the author or from colleagues, provided that the extra purpose of the collaboration is notified at the time of submission). (Last revision of the rule: 15th of October 2020);
- b) All personal related to the production of the journals, from Brazil and abroad;
- c) Longtime collaborators. Authors who have published four (4) articles with us during the past decade will be rewarded with one (1) free publication. After that, this cycle starts again, that is, for every five (5) articles published, one will be free of publication fees. Thank you for choosing and trusting the Journal to publish your research.
- d) Paper considered by the Editors of high quality, priority, and relevance for the development of the society shall pay no fees. Note that this condition is a small recognition prize, not something that you may request. Thank you for your comprehension.

Thank you very much for choosing Tche Química Journal to publish your paper! We would be happy if you consider the Journal to submit any further paper in the near future.

Kind Regards,

Editorial Team

Dr. Luis Alcides Brandini De Boni

Dr. Eduardo Goldani



ЮЖНО-БРАЗИЛИЙСКИЙ ЖУРНАЛ ХИМИИ
ВИРТУАЛЬНАЯ КОНФЕРЕНЦИЯ 2021

НАУЧНАЯ КОНФЕРЕНЦИЯ

ДЕКАБРЬ 2021

КОНФЕРЕНЦИЯ ЮЖНО-БРАЗИЛЬСКОГО ЖУРНАЛА ХИМИИ 2021 ГОДА - культурное мероприятие, организованное Южно-бразильским журналом химии (SOUTHERN BRAZILIAN JOURNAL OF CHEMISTRY), Периодическим журналом химии (Periódico Tchê Química) и другими партнерами, чтобы отметить 30-летний юбилей Южно-бразильского журнала химии.

Цель конференции - предоставить авторам возможность представить различные формы научной коммуникации, такие как стендовая презентация, полная публикация статьи, расширенная публикация тезисов и предварительно записанная стендовая презентация.



www.sbjchem.com

Официальные языки английский и португальский

مجلة الكيمياء البرازيلية الجنوبية
المؤتمر الافتراضي 2021

مؤتمر علمي

كانون الأول 2021

يُعد مؤتمر مجلة الكيمياء البرازيلية الجنوبية لعام 2021 حدثًا ثقافيًا تنظمه مجلة الكيمياء البرازيلية الجنوبية، Periódico Tchê Química، وشركاء آخرون للاحتفال بمرور 30 عامًا على مجلة Southern Brazil Journal of Chemistry.

الهدف من المؤتمر هو تزويد الباحثين بمنصة علمية متنوعة، مثل عرض بوستر، والنشر الكامل للمخطوطة، ونشر الملخصات الموسعة، وعرض البوستر المسجل مسبقًا (المدة تصل إلى 5 دقائق).



www.sbjchem.com

اللغة الرسمية الإنكليزية والبرتغالية

SOUTHERN BRAZILIAN JOURNAL OF CHEMISTRY
2021 VIRTUAL CONFERENCE

SCIENTIFIC CONFERENCE

DECEMBER 2021

The 2021 SOUTHERN BRAZILIAN JOURNAL OF CHEMISTRY CONFERENCE is a cultural event organized by the Southern Brazilian Journal of Chemistry, the Periódico Tchê Química, and other partners to celebrate the almost 30 years of the Southern Brazilian Journal of Chemistry.

The goal of the conference is to provide the authors a place to present multiple forms of scientific communications, such as poster presentation, the full manuscript publication, expanded abstract publication, and a pre-recorded poster presentation (up to 5 min long).



www.sbjchem.com

Official languages: English (USA), and Portuguese (BRA).

სამხრეთ ბრაზილიის ქიმიური ჟურნალი
ვირტუალური კონფერენცია 2021

სამეცნიერო კონფერენცია

დეკემბერი 2021

სამხრეთ ბრაზილიის ქიმიური ჟურნალის 2021 წლის კონფერენცია კულტურული ღონისძიებაა, რომლის მიზანაც გახლავთ სამხრეთ ბრაზილიის ქიმიური ჟურნალის თითქმის 30 წლის იუბილის აღნიშვნა. კონფერენციის ორგანიზატორები არიან სამხრეთ ბრაზილიის ქიმიური ჟურნალი (SOUTHERN BRAZILIAN JOURNAL OF CHEMISTRY), ქიმიის პერიოდული ჟურნალი (Periódico Tchê Química) და სხვა პარტნიორები.

კონფერენციის მიზანია ავტორებს გამოუყოს სივრცე სხვადასხვა მიმართულების სამეცნიერო კომუნიკაციების წარსადგენად. ნაშრომის წარდგენის ფორმა მრავალგვარია, პოსტერის პრეზენტაცია, სტატიის სრული გამოცემა, გაფართოებული

აბსტრაქტის პუბლიკაცია და წინასწარ ჩაწერილი პოსტერის ვიდეო პრეზენტაცია (5 წთ-მდე).



www.sbjchem.com

ოფიციალური ენა ინგლისური და პორტუგალიური

GÜNEY BREZİLYA KİMYA DERGİSİ

SANAL KONFERANS 2021

BİLİM KONFERANSI

ARALIK 2021

2021 GÜNEY BREZİLYA KİMYA DERGİSİ KONFERANSI Güney Brezilya Kimya Dergisi, Periódico Tchê Química ve diğer ortaklar tarafından Güney Brezilya Kimya Dergisi'nin neredeyse 30. yılını kutlamak için düzenlenen kültürel bir etkinliktir.

Konferansın amacı, bilim yazarlara poster sunumu, tam makale yayını, genişletilmiş özet yayını ve önceden kaydedilmiş bir poster sunumu (5 dakikaya kadar) gibi çeşitli bilimsel iletişim biçimlerini sunabilecekleri bir yer sağlamaktır.



www.sbjchem.com

Resmi diller İngilizce ve Portekizce

SOUTHERN BRAZILIAN JOURNAL OF CHEMISTRY
CONFERÊNCIA VIRTUAL 2021

CONFERÊNCIA CIENTÍFICA

DEZEMBRO 2021

A CONFERÊNCIA 2021 do SOUTHERN BRAZILIAN JOURNAL OF CHEMISTRY é um evento cultural organizado pelo SOUTHERN BRAZILIAN JOURNAL OF CHEMISTRY, o Periódico Tchê Química, e outros parceiros para comemorar os quase 30 anos do SOUTHERN BRAZILIAN JOURNAL OF CHEMISTRY.

O objetivo da conferência é fornecer aos autores um local para apresentar diversas formas de comunicação científica, como a apresentação de pôster, a publicação do manuscrito completo, a publicação de resumos expandidos e uma apresentação pré-gravada do pôster (de até 5 minutos).



www.sbjchem.com

Idiomas oficiais: Inglês (USA) e Português (BRA).

CONFERENȚA JURNALULUI DE CHIMIE DIN SUD-BRAZILIA
DIN 2021 CONFERINTA ON LINE

STIINTIFIC CONFERINTA

DEZ / 2021

CONFERENȚA JURNALULUI DE CHIMIE DIN SUD-BRAZILIA din 2021 este un eveniment cultural organizat de Jurnalul de Chimie din Brazilia de Sud, Periódico Tchê Química și alți parteneri pentru a sărbători cei aproape 30 de ani ai Jurnalului de Chimie din Brazilia de Sud.

Scopul conferinței este de a oferi autorilor un loc de prezentare a mai multor forme de comunicări științifice, cum ar fi prezentarea posterelor, publicația completă a articolelor, publicația abstractă extinsă și o prezentarea posterelor preînregistrate (până la 5 minute).



www.sbjchem.com

Limba oficiala la engleza si portugheza.

CONFERENCIA VIRTUAL 2021 DE LA
REVISTA DE QUÍMICA DEL SUR DE BRASIL

CONFERENCIA CIENTÍFICA

DICIEMBRE DE 2021

La CONFERENCIA VIRTUAL 2021 DE LA REVISTA DE QUÍMICA DEL SUR DE BRASIL es un evento cultural organizado por la Revista de Química del Sur de Brasil, el Periódico Tchê Química y otros socios, para celebrar los casi 30 años de la Revista de Química del Sur de Brasil.

El objetivo de la conferencia es proporcionar a los autores un lugar para presentar sus comunicaciones científicas en múltiples formas, como la presentación de pósters, la publicación de un manuscrito completo, la publicación de un resumen ampliado y/o presentación de un póster pregrabado (hasta 5 minutos de duración).



www.sbjchem.com

Lenguajes oficiales: Inglés y Portugués